

# PROCEEDINGS

OF THE

# PHYSICAL SOCIETY

JANUARY TO JUNE 1958

VOLUME 71



Published by  
THE PHYSICAL SOCIETY  
1 Lowther Gardens, Prince Consort Road,  
London S.W.7

# OFFICERS AND COUNCIL 1958-59

## PRESIDENT

J. A. RATCLIFFE, O.B.E., M.A., F.R.S.

## VICE-PRESIDENTS

who have filled the office of President

Sir FRANK SMITH, G.C.B., G.B.E., D.Sc., LL.D., F.R.S. (1924-26)  
Sir OWEN RICHARDSON, M.A., D.Sc., F.R.S. (1926-28)  
W. H. ECCLES, D.Sc., M.I.E.E., F.R.S. (1928-30)  
T. SMITH, M.A., F.R.S. (1936-38)  
Sir CHARLES DARWIN, K.B.E., M.C., M.A., Sc.D., F.R.S. (1941-43)  
E. N. DA C. ANDRADE, Ph.D., D.Sc., LL.D., F.R.S. (1943-45)  
Sir DAVID BRUNT, M.A., Sc.D., F.R.S. (1945-47)  
G. I. FINCH, M.B.E., D.Sc., F.R.S. (1947-49)  
S. CHAPMAN, M.A., D.Sc., F.R.S. (1949-50)  
L. F. BATES, D.Sc., Ph.D., F.R.S. (1950-52)  
R. WHIDDINGTON, C.B.E., M.A., D.Sc., F.R.S. (1952-54)  
H. S. W. MASSEY, B.A., M.Sc., Ph.D., F.R.S. (1954-56)  
N. F. MOTT, M.A., D.Sc., F.R.S. (1956-58)

## VICE-PRESIDENTS

F. LLEWELLYN JONES, M.A., D.Phil., D.Sc.      R. W. DITCHBURN, M.A., B.Sc., Ph.D.  
K. MENDELSSOHN, M.A., D.Phil., F.R.S.      A. J. PHILPOT, C.B.E., M.A., B.Sc.

## HONORARY SECRETARIES

C. G. WYNNE, B.A., Ph.D. (*Business*)      H. H. HOPKINS, D.Sc. (*Papers*)  
A. G. PEACOCK, B.Sc. (*Exhibition*)

## HONORARY FOREIGN SECRETARY

E. N. DA C. ANDRADE, Ph.D., D.Sc., LL.D., F.R.S.

## HONORARY TREASURER

D. A. WRIGHT, D.Sc.

## HONORARY LIBRARIAN

R. W. B. PEARSE, D.Sc., Ph.D.

## ORDINARY MEMBERS OF COUNCIL

D. W. FRY, M.Sc.      M. H. L. PRYCE, M.A., Ph.D., F.R.S.  
V. E. COSSLETT, M.A., M.Sc., Ph.D.      E. W. H. SELWYN, B.Sc.  
D. GABOR, Dr. Ing., F.R.S.      W. E. BURCHAM, Ph.D., F.R.S.  
J. G. WILSON, M.A., Ph.D.      N. KEMMER, Dr. Phil., M.A., F.R.S.  
B. H. FLOWERS, M.A., D.Sc.      G. B. B. M. SUTHERLAND, M.A., Ph.D., F.R.S.  
F. C. FRANK, O.B.E., B.A., B.Sc., D.Phil., F.R.S.      W. H. GEORGE, M.Sc., Ph.D.

## OFFICERS OF THE SPECIALIST GROUPS

### COLOUR GROUP

#### Chairman

J. W. PERRY

#### Honorary Secretary

R. A. WEALE, M.Sc., Ph.D.

### LOW TEMPERATURE GROUP

#### Chairman

P. H. SYKES, M.Sc., Ph.D.

#### Honorary Secretary

R. W. POWELL, Ph.D., D.Sc.

### OPTICAL GROUP

#### Chairman

W. D. WRIGHT, D.Sc., Ph.D.

#### Honorary Secretary

W. T. WELFORD, B.Sc., Ph.D.

### ACOUSTICS GROUP

#### Chairman

T. SOMERVILLE, B.Sc.

#### Honorary Secretaries

G. G. PARFITT, B.Sc., Ph.D., and  
R. W. B. STEPHENS, B.Sc., Ph.D.

## SECRETARY-EDITOR

Miss A. C. STICKLAND, M.Sc., Ph.D.

1 Lowther Gardens, Prince Consort Road, London, S.W.7

(Telephone : KENsington 0048, 0049)



# CONTENTS

Part 1

January 1958

	PAGE
Editorial . . . . .	1
Dr. C. CARTER, Dr. N. H. MARCH and Mr. D. VINCENT. X-ray and Electron Scattering by Molecular Hydrogen . . . . .	2
Mr. P. D. EDMONDS and Dr. J. LAMB. A Method for Deriving the Acoustic Absorption Coefficient of Gases from Measurement of the Decay-time of a Resonator . . . . .	17
Mr. R. S. LEIGH. Crystal Field Effects in Metals . . . . .	33
Prof. H. S. W. MASSEY and Mr. A. H. A. MOUSSA. The Elastic Scattering of Positrons by Atoms and Molecules . . . . .	38
Dr. G. S. BARLOW and Dr. K. J. STANDLEY. Microwave Resonance in Nickel at 35 Gc/s (kMc/s) . . . . .	45
Dr. S. HINDS, Dr. R. MIDDLETON and Dr. G. PARRY. An Investigation of the Reactions $^{24}\text{Mg}(\text{d}, \text{p})^{25}\text{Mg}$ and $^{26}\text{Mg}(\text{d}, \text{p})^{27}\text{Mg}$ by Magnetic Analysis . . . . .	49
Dr. R. F. BARROW, Dr. D. PREMASWARUP, Mr. J. WINTERNITZ and Prof. P. B. ZEEMAN. Rotational Analysis of Bands of the $\text{c}^3\Sigma$ , $\text{b}\Sigma^3\text{-a}^3\Pi$ System of Boron Monofluoride, BF. . . . .	61
Mr. M. ASLAM KHAN. AlH Bands at 2173 Å and 2101 Å . . . . .	65
Dr. P. T. LANDSBERG. Magnetic Field Effects on Electron Populations in Semiconductors . . . . .	69
Mr. A. C. KNIPPER. Excited Levels of Cadmium 110 . . . . .	77
Mr. J. E. PARROTT. The Theory of the Nernst Effect in Semiconductors . . . . .	82
Mr. T. C. TOYE and Miss E. R. JONES. Physical Properties of Certain Liquid Binary Alloys of Tin and Zinc . . . . .	88
Dr. J. VARMA and Mr. W. JACK. The Reaction $^{24}\text{Mg}(\text{p}, \gamma)^{25}\text{Al}$ at the 418 kev Resonance . . . . .	100
Dr. R. W. WRIGHT and Mr. J. A. BASTIN. The Characteristic Temperature and Effective Electron Mass for Conduction Processes in Cadmium Oxide . . . . .	109
Dr. D. F. BREWER and Dr. D. O. EDWARDS. Measurements of the Heat of Transport of Liquid Helium II . . . . .	117
Research Notes :	
Mr. B. A. ROBSON. The Mean Free Path of Alpha Particles in Nuclear Matter . . . . .	126
Dr. R. F. BARROW, Mr. H. F. K. CHEALL, Mr. P. M. THOMAS and Prof. P. B. ZEEMAN. Rotational Analysis of Bands of the $\text{A}^3\Pi_{0+}$ , $\text{B}^3\Pi_1\text{-X}^1\Sigma^+$ Systems of Thallous Fluoride . . . . .	128
Mr. J. PETERS and Dr. K. J. STANDLEY. The Dielectric Behaviour of Magnesium Manganese Ferrite . . . . .	131
Letters to the Editor :	
Mr. T. H. E. BRYANT and Dr. E. H. GRANT. Ionic Conductivity of Potassium and Rubidium Chloride Solutions at Microwave Frequencies . . . . .	134
Dr. A. N. HUNTER, Mr. R. D. LEGGE and Dr. E. MATSUKAWA. Loss Factor Measurements in Dry Sand . . . . .	135
Mr. N. L. SVENSSON. Experiments on Controlled Fractures . . . . .	136
Reviews of Books . . . . .	139

	PAGE
Dr. F. BERENCZ and Dr. R. PAUNCZ. Construction of $S^2$ Eigenfunctions by the Method of Spin Operators. I: General Theory . . . . .	145
Dr. F. BERENCZ. Construction of $S^2$ Eigenfunctions by the Method of Spin Operators. II: Six-electron Systems . . . . .	152
Mr. A. ASHMORE, Mr. R. NORDHAGEN, Dr. K. STRAUCH and Mr. B. M. TOWNES. The Gamma-Rays from Muon Catalysed Fusion of Hydrogen and Deuterium . . . . .	161
Mr. S. SEN GUPTA and Mr. H. MUKHOPADHYAY. Problem of Perturbed Boundary Condition in Quantum Mechanics . . . . .	173
Dr. F. MANDL. The Theory of Angular Correlations with Polarization . . . . .	177
Dr. V. KNAPP. Nuclear Gamma Ray Resonance in $^{48}\text{Ti}$ . . . . .	194
Mr. B. N. C. AGU, Mr. T. BURDETT and Dr. E. MATSUKAWA. Transmission of Electrons through Aluminium Foils . . . . .	201
Dr. J. W. C. SHERWOOD. Elastic Wave Propagation in a Semi-Infinite Solid Medium . . . . .	207
Dr. F. E. HOARE and Dr. J. C. MATTHEWS. Heat Capacity between 1.8 and 4.2°K of an Iron-Chromium Alloy in the Alpha and Sigma Phases . . . . .	220
Mr. K. G. BANSIGIR and Dr. K. S. IYENGAR. The Stress Birefringence Relation in some Alkali Halides . . . . .	225
Mr. N. S. BROMILOW. Geometrical-Optical Calculation of Frequency Response for Systems with Spherical Aberration . . . . .	231
Mr. H. N. V. TEMPERLEY. The Equation of State of a Gas of Elastic Spheres . . . . .	238
Mr. F. C. FLACK and Mr. P. MASON. Angular Correlations of Gamma Rays in $^{103}\text{Rh}$ . . . . .	247
Mr. A. W. DALTON, Dr. S. HINDS and Dr. G. PARRY. An Investigation of the $^{16}\text{O}(\text{d}, \alpha)^{14}\text{N}$ Reaction by Magnetic Analysis . . . . .	252
Dr. E. WOLF. Reciprocity Inequalities, Coherence Time and Bandwidth in Signal Analysis and Optics . . . . .	257
Research Notes :	
Mr. K. S. IRANI, Dr. A. P. B. SINHA and Dr. A. B. BISWAS. Entropy of Hausmannite to Spinel Transformation . . . . .	270
Mr. J. S. BELL and Dr. F. MANDL. The Polarization-Asymmetry Equality . . . . .	272
Dr. G. W. SERIES and Mr. K. WILLIS. Note on the Li II Spectrum . . . . .	274
Dr. F. BERZ. On the Theory of Surface Recombination in Semiconductors for Large Potential Differences between Surface and Bulk . . . . .	275
Prof. R. V. JONES. A Possible Infra-Red Detector using Thermal Expansion . . . . .	280
Letters to the Editor :	
International Union of Pure and Applied Physics . . . . .	284
Reviews of Books . . . . .	287



	PAGE
Dr. N. E. BOOTH, Dr. G. W. HUTCHINSON and Dr. B. LEDLEY. Nuclear Cross Sections for 765 mev Neutrons	293
Dr. T. C. GRIFFITH, Mr. A. P. BANFORD, Mr. M. Y. UPPAL and Mr. W. S. C. WILLIAMS. Neutron-Proton Scattering in the Energy Range 70 to 170 mev	305
Dr. D. L. BOOTH, Dr. F. V. PRICE, Dr. D. ROAF and Mr. G. L. SALMON. The Differential Cross Sections for the Reactions $^{14}\text{N}(\text{d}, \text{p})^{15}\text{N}$ and $^{14}\text{N}(\text{d}, \alpha)^{12}\text{C}$ between 600 and 1000 kev	325
Mr. R. K. GUPTA. On the Determination of the Electron Capture Decay Energy: $^{196}\text{Au}$	330
Mr. B. H. ARMITAGE and Dr. W. G. V. ROSSER. The $\beta$ -decay of $^{185}\text{W}$	335
Dr. T. H. Y. YEUNG. Recombination Coefficients for Positive and Negative Ions	341
Dr. G. W. GREENLEES, Dr. L. G. KUO, Mr. J. LOWE and Mr. M. PETRAVIC. The Elastic and Inelastic Scattering of Protons by Silicon	347
Dr. R. L. F. BOYD and Dr. G. W. GREEN. Electron Ionization Cross Sections using Chopped Beams	351
Mr. E. HOLØIEN. The $(2s)^2\ ^1\text{S}$ State Solution of the Non-relativistic Schrödinger Equation for Helium and the Negative Hydrogen Ion	357
Mr. W. N. ASAAD and Dr. E. H. S. BURHOP. The K Auger Spectrum	369
Prof. S. L. ALTMANN and Dr. N. V. COHAN. Cellular Eigenvalues for Titanium Metal	383
Mr. T. R. OPHEL and Mr. I. F. WRIGHT. Photodisintegration of Sodium by $^7\text{Li}$ ( $\text{p}, \gamma$ ) Radiation	389
Mr. A. M. SAYIED. The Čerenkov Effect in Composite (Isotropic) Media	398
Dr. A. R. BRAY, Dr. P. W. M. JACOBS and Dr. L. YOUNG. Ionic Conduction at High Electric Field Strengths in Tantalum Pentoxide	405
Dr. W. N. REYNOLDS, Mr. M. T. LILBURNE and Dr. R. M. DELL. Some Properties of Semiconducting Indium Phosphide	416
Dr. J. R. COOK. Trap Distributions in Calcium Tungstate Single Crystals	422
Mr. J. R. DRABBLE, Mr. R. D. GROVES and Mr. R. WOLFE. Galvanomagnetic Effects in n-type Bismuth Telluride	430
Dr. N. LOUAT. A Theory of Delayed Yielding in the Presence of Cottrell Atmospheres of Solute Atoms	444
Dr. R. A. BUCKINGHAM, Mr. A. R. DAVIES and Mr. D. C. GILLES. Symmetry Effects in Gas Kinetics: II—Ortho- and Para-hydrogen	457
Mr. R. F. BROOM. Magnetoresistance of n-type InSb at 4.2°K	470
Mr. J. W. C. JOHNS and Dr. R. F. BARROW. The Band Spectrum of Silicon Monofluoride, SiF	476
Dr. M. J. STEPHEN. The Infra-red Spectrum of Diamond	485
Dr. E. W. KELLERMANN, Dr. T. SHAW and Mr. G. O. WALKER. On the Structure of Extensive Cosmic Ray Air Showers: Lateral Structure of the Ionizing Component	491
Research Notes:	
Dr. J. G. POWLES. The Adiabatic Fast Passage Experiment in Magnetic Resonance	497
Mr. R. F. BROOM. A Source of Error in Magnetoresistance Measurements	500
Dr. W. HAYES and Dr. D. A. JONES. Paramagnetic Impurities in NaF	503
Dr. P. WRIGHT and Mr. K. F. GODDARD. The Resistivity of Ordered $\text{Au}_3\text{Cu}$	506
Dr. SAMPOORAN SINGH. A Note on Penetration by Rotating Shaped Charges	508
Prof. K. STIEGLER. On the Deduction of the Lorentz-Einstein Transformation from Maxwell's Electromagnetic Field Equations	512
Dr. N. R. TAWDE and Mr. M. I. SAVADATTI. A Note on Ta-You Wu's Method of Calculating Overlap Integrals for Morse Oscillator	514
Letters to the Editor:	
Mr. E. KUFFEL. A Note on the Cross Sections for Electron Attachment in Air	516
Dr. A. H. COOKE and Mr. D. T. EDMONDS. Nuclear Magnetic Interaction in an Antiferromagnetic Crystal	517
Professor N. F. MOTT. International Union of Pure and Applied Physics	519
Corrigenda	519
Reviews of Books	520



	PAGE
Mr. J. M. COWLEY and Mr. A. F. MOODIE. A New Formulation of Scalar Diffraction Theory for Restricted Aperture . . . . .	533
Dr. A. K. HEAD. A Class of Aplanatic Optical Systems . . . . .	546
Mr. A. ASHMORE, Mr. D. S. MATHER and Dr. S. K. SEN. The Elastic Scattering of 350 mev Neutrons by Complex Nuclei . . . . .	552
Mr. G. E. BROWN, Mr. A. ASHMORE and Mr. R. NORDHAGEN. Elastic Scattering of 350 mev Neutrons by Complex Nuclei . . . . .	565
Mr. S. KHASHABA and Prof. H. S. W. MASSEY. The Excitation of the 2p State of Hydrogen by Slow Electrons—Distorted Wave Treatment . . . . .	574
Mr. D. A. GREENWOOD. The Boltzmann Equation in the Theory of Electrical Conduction in Metals . . . . .	585
Dr. C. A. SHIFFMAN. The Thermal Conductivity of Tin-Indium Alloys in the Normal State . . . . .	597
Mr. D. Y. HSIEH and Dr. H. KOLSKY. An Experimental Study of Pulse Propagation in Elastic Cylinders . . . . .	608
Dr. J. H. CARVER and Dr. W. TURCHINETZ. The ( $\gamma$ , 2n) and ( $\gamma$ , 3n) Reactions in $^{181}\text{Ta}$ . . . . .	613
Dr. J. H. CARVER and Dr. W. TURCHINETZ. Radioactivity of $^{178}\text{Ta}$ , $^{179}\text{Ta}$ and $^{180}\text{Ta}$ . . . . .	618
Mr. H. C. NEWNS and Mr. M. Y. REFAI. Polarization in Stripping Reactions . . . . .	627
Dr. H. J. GOLDSMID. The Electrical Conductivity and Thermoelectric Power of Bismuth Telluride . . . . .	633
Dr. C. A. HOGARTH and Mr. A. C. BAYNHAM. Electrical Methods for Determining the Positions of Dislocation Regions in Germanium . . . . .	647
Mr. B. DURNEY. Distorted Wave Approximation in the Reaction $P + P \rightarrow \pi^+ + D$ . . . . .	654
Dr. J. DABROWSKI. On the Binding Energy of the $^{16}\text{O}$ Nucleus . . . . .	658
Dr. E. RABINOWICZ. The Intrinsic Variables affecting the Stick-Slip Process . . . . .	668
Mr. C. HILSUM and Mr. R. BARRIE. Properties of p-type Indium Antimonide : I—Electrical Properties . . . . .	676
Research Notes :	
Dr. F. MANDL. Double Scattering Experiments as a Test for Invariance under Time-reversal in Strong Interactions . . . . .	686
Dr. R. COOPER and Mr. A. FERNANDEZ. Directional Electric Breakdown of KCl . . . . .	688
Dr. J. S. BLAKEMORE. The Fermi Level in Germanium at High Temperatures . . . . .	692
Mr. R. B. CAIRNS and Prof. K. G. EMELÉUS. The Longitudinal Pressure Gradient in Discharge Tubes . . . . .	694
Letters to the Editor :	
Mr. F. W. G. ROSE. On the Mass-Action Laws in Degenerate Semiconductors . . . . .	699
Mr. T. F. JOHNS. Vapour Pressure Ratios of $^{14}\text{N}^{14}\text{N}$ , $^{14}\text{N}^{15}\text{N}$ and $^{15}\text{N}^{15}\text{N}$ . . . . .	701
Prof. H. E. FARNSWORTH. Comments on the Paper by J. C. Rivière : 'Contact Potential Difference Measurements by the Kelvin Method' . . . . .	703
Reviews of Books . . . . .	705



	PAGE
Dr. C. B. O. MOHR. Direct Interaction in the Inelastic Scattering of High Energy Protons in Carbon . . . . .	717
Dr. R. D. BROWN and Mr. I. M. BASSETT. A Method for Calculating the First Order Perturbation of an Eigenvector of a Finite Matrix, with Applications to Molecular-orbital Theory . . . . .	724
Dr. G. E. BROWN and Dr. J. S. LEVINGER. Dispersion Theory of the Direct Photoeffect . . . . .	733
Mr. S. SHIVANANDA TOLPADI. Equation of State of Zinc, Cadmium and Magnesium . . . . .	742
Dr. T. B. GRIMLEY. The Electronic Structure of Crystals having the Sodium Chloride type of Lattice . . . . .	749
Dr. M. BLACKMAN and Mr. E. GRÜNBAUM. Magnetic Effects on the Electron Diffraction Patterns from a Cobalt Crystal. . . . .	758
Dr. J. H. SIMPSON. On the Thermal and Optical Excitation of Colour Centres	761
Mr. D. HARTING, Dr. J. R. HOLT and Mr. J. A. MOORE. The Elastic Scattering of 380 mev Protons by Protons : I—At Angles greater than 30° (c.m.) . . . . .	770
Dr. J. R. HOLT, Dr. J. C. KLUYVER and Mr. J. A. MOORE. The Elastic Scattering of 380 mev Protons by Protons: II—At Angles less than 30° (c.m.) . . . . .	781
Prof. L. F. BATES, Mr. D. J. CRAIK and Mr. P. M. GRIFFITHS. Domain Patterns on a Single Crystal of Manganese Ferrite . . . . .	789
Dr. H. H. G. JELLINEK. The Influence of Imperfections on the Strength of Ice	797
Prof. C. A. COULSON and Mr. P. D. ROBINSON. Wave Functions for the Hydrogen Atom in Spheroidal Coordinates: I—The Derivation and Properties of the Functions . . . . .	815
Mr. P. D. ROBINSON. Wave Functions for the Hydrogen Atom in Spheroidal Coordinates: II—Interaction with a Point Charge and with a Dipole . . . . .	828
Research Notes :	
Mr. J. A. BIRCH, Mr. W. R. G. KEMP and Dr. P. G. KLEMENS. The Lattice Thermal Conductivity of a Gold-Platinum Alloy . . . . .	843
Dr. F. A. RAAL. A New Absorption Band in Diamond and its Likely Cause	846
Dr. A. N. HUNTER. Some Observations on the Debye Effect in Electrolytes	847
Dr. BIPIN KUMAR AGARWAL. Variation of Secondary Emission with Primary Electron Energy . . . . .	851
Mr. J. EWLES, Dr. S. C. JAIN and Mr. R. V. JOSHI. Electron Traps Produced in KCl Crystals by Quenching or Pressure . . . . .	852
Dr. A. S. MELIGY. Expansion of the Regular Coulomb Wave Function in terms of Bessel Functions . . . . .	856
Dr. J. N. LYNESS. Polarization in Nuclear Reactions . . . . .	858
Dr. A. FRANKS and Mr. K. THOMAS. Low-Angle X-Ray Scattering from Cold-Worked Metals . . . . .	861
Dr. G. G. MACFARLANE, Mr. T. P. MCLEAN, Mr. J. E. QUARRINGTON and Mr. V. ROBERTS. Direct Optical Transitions and Further Exciton Effects in Germanium . . . . .	863
Letters to the Editor :	
Dr. J. S. BELL and Dr. F. MANDEL. The Polarization-Asymmetry Equality	867
Mr. L. LEWIN. A Physical Interpretation of Impedance for Rectangular Waveguides . . . . .	868
Reviews of Books . . . . .	870

	PAGE
Dr. B. H. BRANDSEN, Dr. A. DALGARNO, Mr. T. L. JOHN and Dr. M. J. SEATON. The Elastic Scattering of Slow Electrons by Hydrogen Atoms . . . . .	877
Mr. G. P. McCAULEY and Dr. G. E. BROWN. Inelastic Scattering of High Energy Nucleons by Complex Nuclei : I—Semi-classical Formalism . . . . .	893
Dr. G. W. GREENLEES, Mr. J. LOWE, Dr. A. B. ROBBINS and Dr. P. M. ROLPH. The Inelastic Scattering of 9.8 mev Protons by Medium Weight Nuclei . . . . .	904
Dr. P. A. EGELSTAFF. Fluctuations in Slow Neutron Average Cross Sections . . . . .	910
Mr. R. D. EDGE and Mr. D. S. GEMMELL. Gamma Rays from the 6.89 mev Level in $^{10}\text{B}$ . . . . .	925
Dr. E. W. LAING. Elastic Scattering of Pions at a Bound Nucleon . . . . .	932
Dr. C. A. CAINE. Configurational Mixing in $\beta$ -Decay Theory . . . . .	939
Dr. D. ROBINSON and Dr. R. W. NICHOLLS. Intensity Measurements on the $\text{O}_2^+$ Second Negative, CO Angström and Third Positive and NO $\gamma$ and $\beta$ Molecular Band Systems . . . . .	957
Dr. G. G. E. LOW. Acoustomagnetolectric Effects in Metal and Semiconductor Filaments . . . . .	965
Dr. N. B. TERRY. The Behaviour of a Vibrating Visco-elastic Cylinder . . . . .	973
Miss B. E. SABEY. Pressure Distributions beneath Spherical and Conical Shapes pressed into a Rubber Plane, and their Bearing on Coefficients of Friction under Wet Conditions . . . . .	979
Mr. J. A. GREENWOOD and Dr. D. TABOR. The Friction of Hard Sliders on Lubricated Rubber : The Importance of Deformation Losses . . . . .	989
Mr. D. J. SANDIFORD. Temperature Dependence of Carrier Lifetime in Silicon . . . . .	1002
Mr. S. K. SHARMA. Anomalous Variation of Total Absorption of Radio Waves reflected from the F2 Region of the Ionosphere around Mid-day . . . . .	1007
Dr. A. J. COCHRAN and Dr. M. A. S. ROSS. Crystal Reflectivity in Bent Crystal Spectrometers . . . . .	1011
Research Notes :	
Mr. B. K. GUPTA and Mr. V. S. R. RAO. Configuration Interaction in the Ground State and two Excited States (1s, 2s) $^1\text{S}$ and (1s, 3s) $^1\text{S}$ of He Atom. . . . .	1015
Dr. A. S. MELIGY. Simple Method of Interpolation for Coulomb Wave Functions . . . . .	1017
Letters to the Editor :	
Dr. R. G. EADES, Dr. D. G. HUGHES and Prof. E. R. ANDREW. The Nuclear Quadrupole Coupling Constant of $^{23}\text{Na}$ in Sodium Nitrate . . . . .	1019
Mr. G. A. BARNES and Dr. P. C. BANBURY. Electrical Properties of clean Germanium Surfaces . . . . .	1020
Reviews of Books . . . . .	1022
Subject Index, Vol. 71 . . . . .	1029
Index of Authors (with Titles), Vol. 71 . . . . .	1035
Index to Reviews of Books, Vol. 71 . . . . .	1043



# PROCEEDINGS OF THE PHYSICAL SOCIETY

---

VOL. 71, PART 1

1 January 1958

No. 457

---

## EDITORIAL

For the past eight years *Proceedings of the Physical Society* has been published in two sections sub-divided according to subject matter. In the light of the experience of this period, it has now been thought advisable to recombine these two sections into a single book, and this opinion has been confirmed by a majority vote of the Fellowship of the Society.

In future, therefore, the *Proceedings* will be published as a single issue on the first day of each month, the papers included in it covering the same range as has previously been covered by both Section A and Section B of the *Proceedings* together. For ease of reference and binding, Indexes will be published in June covering January–June and in December covering July–December.

## X-ray and Electron Scattering by Molecular Hydrogen

By C. CARTER†, N. H. MARCH‡ AND D. VINCENT‡

† Atomic Energy Research Establishment, Harwell, Berks.

‡ Department of Physics, The University, Sheffield

*MS. received 3rd July 1957*

*Abstract.* A theoretical study has been made of the x-ray and electron scattering to be expected from molecular hydrogen. The methods of calculation have the common feature that they are based on expansions of the wave function, density and potential in Legendre polynomials. Simple self-consistent field wave functions having spherical symmetry are presented and, while the binding energy thereby obtained is poor, it is found nevertheless that they may be utilized with success in both the x-ray and the electron scattering calculations. The x-ray scattering is also discussed on the basis of an LCAO molecular-orbital function and the 'floating' function of Gurnee and Magee. It is found that the results of the various approximations used agree well among themselves and also with experiment, and some conclusions regarding the charge distribution in the hydrogen molecule may be drawn. For the elastic scattering of slow electrons, it is found that there is good agreement between the present results and earlier work of Massey and Ridley if exchange is neglected in both cases. However, it is found that electron exchange markedly affects the scattering cross sections, thus confirming the essential conclusions of Massey and Ridley, although the method employed in the present work is probably not sufficiently reliable to enable the precise effect of exchange to be determined.

### § 1. INTRODUCTION

MANY approximate wave functions for the hydrogen molecule are now available, and for a fairly full list of references the reader may consult Callen (1955). While the approximate wave functions have been obtained almost exclusively by the variational method, it is nevertheless true that the energy criterion, useful guide though it is, gives no assurance that the approximate function yielding the lowest energy is necessarily the best function for the calculation of another physical quantity under discussion. Particularly difficult to assess are the merits of functions in which correlation effects are introduced. Karplus (1956) has recently examined certain moments of the charge distribution in the hydrogen molecule and has made a comparison with experiment, and such calculations undoubtedly give insight into the way in which the various functions describe the size and shape of the molecule. In the present work, we have made a theoretical study of the x-ray and electron scattering to be expected from molecular hydrogen. This study has intrinsic interest since experimental results on the x-ray scattering are available from the work of Wollan (1931), and both theoretical and experimental results on elastic scattering of slow electrons by molecular hydrogen have previously been obtained (see especially Massey



and Ridley 1956). It has the further interest that it throws light on the distribution of charge and the potential field in the hydrogen molecule, and we shall place some emphasis on this aspect of the investigation.

The common method employed throughout the paper is to expand the wave function, density, and potential in the molecule in Legendre polynomials. Thus, in § 2, we work out the 'best' spherical molecular orbital in the sense of the variation method, this then representing an approximation to the first term in an expansion in Legendre polynomials, while in § 3 we consider the s and d terms in the expansion of the densities obtained on the basis of three approximate wave functions. Then in § 4 we use these results to discuss the x-ray scattering by molecular hydrogen, while in § 5 the elastic scattering of slow electrons is examined using the field obtained in § 2.

## § 2. SELF-CONSISTENT FIELD METHOD WITH SPHERICAL FUNCTIONS

Not much attention has been given to the calculation of molecular orbitals by a one-centre expansion in spherical harmonics until quite recently (see especially Carter 1956). It seemed probable at the outset that this method would be less useful in the case of  $H_2$ , at least for the ground state, than for more symmetrical molecules such as  $CH_4$  and  $SiH_4$ . However, a preliminary calculation of the coefficients in the harmonic expansion of the LCAO molecular orbital (the mid-point between the nuclei being taken as origin) showed that the square of the coefficient of the s term was about 0.98, and that of the d term 0.02, indicating that even for  $H_2$  in the ground state there is some justification for trying this method. We were particularly interested to see whether, with a single term in the harmonic expansion, a useful account would be given of the s term in the density (in this connection see Banyard and March 1956, 1957).

The nuclear potential is therefore expanded in spherical harmonics and only the spherical term retained. We have then a self-consistent field problem for two electrons moving in the field of a uniform surface distribution of charge on a sphere of radius  $R$ ,  $2R$  being the internuclear separation. Using this spherical approximation, the molecular orbital may be written

$$\phi_{1s}(r) = \frac{1}{(4\pi)^{1/2}} \frac{P(r)}{r}. \quad \dots\dots(1)$$

The Hartree self-consistent field equation, which yields the best function  $P(r)$  is

$$\left[ \frac{d^2}{dr^2} + 4v_0(r, R) - \frac{2Z_p(r)}{r} - \epsilon \right] P(r) = 0 \quad \dots\dots(2)$$

where

$$v_k(r, R) = \begin{cases} r^k/R^{k+1}, & r \leq R \\ R^k/r^{k+1}, & r \geq R \end{cases} \quad \dots\dots(3)$$

and the effective nuclear charge for potential  $Z_p(r)$  is the solution of

$$\frac{d^2 Z_p}{dr^2} = - \frac{P^2(r)}{r} \quad \dots\dots(4)$$

with

$$Z_p(0) = 0, \quad Z_p(\infty) = 1. \quad \dots\dots(5)$$

The LCAO functions were used to give an initial estimate for  $Z_p(r)$  and equations (2) and (4) were then solved (with  $R=0.7$  atomic unit) in turn until a self-consistent function  $Z_p(r)$  was obtained. Only three iterations were required to give  $Z_p(r)$  self-consistent to within 0.0004. The final values for  $P(r)$  and

Table 1. Self-consistent Field Wave Functions and Effective Nuclear Charges for the Hydrogen Molecule. (Bond length,  $2R=1.40$  atomic units).

$r$	$P(r)$	$Z_p(r)$	$r$	$P(r)$	$Z_p(r)$
0.1	0.1277	0.0947	1.8	0.6048	0.9344
0.2	0.2520	0.1878	2.0	0.5412	0.9543
0.3	0.3694	0.2777	2.2	0.4792	0.9683
0.4	0.4767	0.3630	2.4	0.4209	0.9781
0.5	0.5709	0.4428	2.6	0.3671	0.9849
0.6	0.6489	0.5160	2.8	0.3184	0.9897
0.7	0.7084	0.5822	3.0	0.2747	0.9929
0.8	0.7471	0.6413	3.2	0.2360	0.9952
0.9	0.7689	0.6935			
1.0	0.7769	0.7390	3.6	0.1724	0.9978
1.1	0.7740	0.7786	4.0	0.1245	0.9990
1.2	0.7627	0.8127	4.4	0.0890	0.9995
1.3	0.7447	0.8420	4.8	0.0632	0.9998
1.4	0.7221	0.8670	5.2	0.0446	0.9999
1.5	0.6957	0.8882	5.6	0.0313	1.0000
1.6	0.6668	0.9063	6.0	0.0218	1.0000

$\epsilon=1.1261$ ,  $F_0=0.6319$ ,  $E=-1.0437$ . Binding energy  $=0.0437$  atomic units  $=1.19$  electron volts.

$Z_p(r)$  are given in table 1. Also given in this table are the eigenvalue  $\epsilon$ , the interelectronic potential,

$$F_0 = \int_0^\infty \frac{P^2(r) Z_p(r)}{r} dr$$

and the total molecular energy,  $E = -\epsilon + (1/2R) - F_0$ . It can hardly be expected that a good binding energy will thus be obtained, in fact it is only 0.044 atomic unit (1.2 ev), compared with the LCAO value of 3.6 ev and the experimental value of 4.7 ev. We might mention here that a cruder approximation of product form with spherical one-electron wave functions has been reported recently by Huzinaga† (1956; see also in this connection Funabashi and Magee 1957).

### § 3. DENSITIES FROM APPROXIMATE WAVE FUNCTIONS

#### (a) Wave Function of § 2

Having discussed in § 2 the best form of wave function which is a simple product of spherical molecular orbitals, we can immediately use it to obtain an approximation to the  $s$  term in the expansion of the correct density in the hydrogen molecule in spherical harmonics. We show the result

$$\rho_{00}(r) = 2\phi_{1\sigma}^2(r) \quad \dots\dots(6)$$

in curve 1 of figure 1, and the radial charge distribution in curve 1 of figure 2.

#### (b) Product Wave Function Formed by LCAO Method

Secondly, we make use of another wave function formed as a simple product of molecular orbitals, but this time we assume an LCAO form for the molecular orbitals. The density may then be written

$$\rho(\mathbf{r}) = \frac{1}{1+S_{ab}} [\phi_{1s}(r_a) + \phi_{1s}(r_b)]^2 \quad \dots\dots(7)$$

† It should be remarked, however, that Huzinaga also considers much better approximations in the one-centre method than spherical molecular orbitals.



where  $S_{ab}$  is the overlap integral  $\int \phi_{1s}(r_a) \phi_{1s}(r_b) d\tau$ ,  $\phi_{1s}$  is a normalized hydrogen-like 1s orbital with effective nuclear charge  $Z' = 1.193$  (Coulson 1937), while  $r_a$  and  $r_b$  are distances measured from the two nuclei a and b respectively. The averaging of the density (7) over all orientations yields the s term shown in curve 2 of figure 1 and the radial charge distribution given in curve 2 of figure 2. Also it seemed of interest to obtain the d term in the density and the radial part of this is

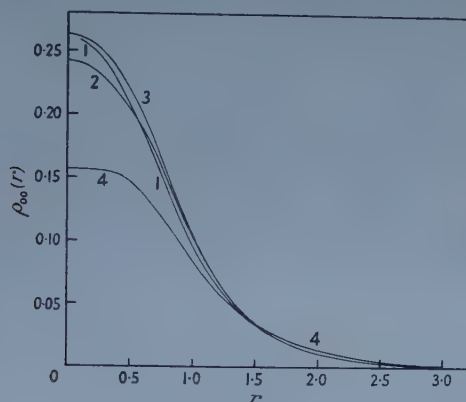


Figure 1. s term in electron density for hydrogen molecule (atomic units used). 1, From 'best' spherical molecular orbital wave function; 2, from LCAO molecular orbital wave function; 3, from Gurnee and Magee wave function; 4, from superposition of densities due to two unperturbed H atoms.

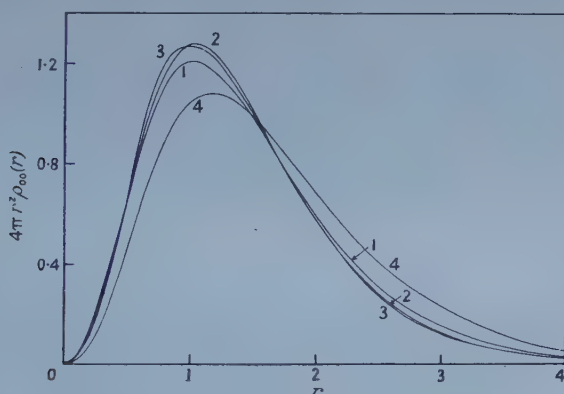


Figure 2. Radial charge distribution ( $4\pi r^2 \rho_{00}$ ) for hydrogen molecule (atomic units used). 1, From 'best' spherical molecular orbital wave function; 2, from LCAO molecular orbital wave function; 3, from Gurnee and Magee wave function; 4, from superposition of densities due to two unperturbed H atoms.

shown in curve 1 of figure 3. These results will be discussed later when we have considered the densities obtained from a wave function in which some electronic correlation is introduced.

### (c) Gurnee and Magee Wave Function

Gurnee and Magee (1950, see also Hurley 1954) proposed the use of a Heitler-London type wave function for the hydrogen molecule, but with the positions on which the 1s orbitals are centred as a parameter to be determined by the variation method. This function leads to a good binding energy (about 4.2 eV) considering its simplicity.

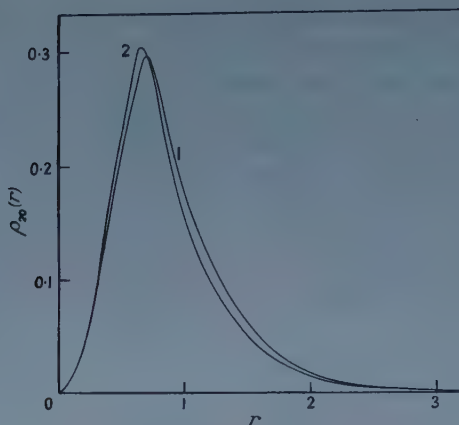


Figure 3. *d* term in electron density for hydrogen molecule (atomic units used). 1, From LCAO molecular orbital wave function; 2, from Gurnee and Magee wave function.

Apart from a normalizing factor, the wave function of Gurnee and Magee may be written

$$\Psi(\mathbf{r}_1, \mathbf{r}_2) = \phi_{1s}(r_{1c})\phi_{1s}(r_{2d}) + \phi_{1s}(r_{1d})\phi_{1s}(r_{2c}) \quad \dots\dots(8)$$

where *c* and *d* denote the points on which the orbitals are centred, and  $r_1$  and  $r_2$  are the coordinates of electrons 1 and 2 respectively. We take the distance between *c* and *d* to be 1.28 atomic units and *Z'* as 1.185. In this approximation the density is given by

$$\rho(\mathbf{r}) = \frac{1}{1 + S_{cd}^2} [\phi_{1s}^2(r_c) + 2S_{cd}\phi_{1s}(r_c)\phi_{1s}(r_d) + \phi_{1s}^2(r_d)] \quad \dots\dots(9)$$

where  $S_{cd}$  is the overlap integral  $\int \phi_{1s}(r_c)\phi_{1s}(r_d)d\tau$ . The *s* term in the density obtained from (9) is shown in curve 3 of figure 1, the corresponding radial charge distribution in curve 3 of figure 2, and the radial part of the *d* term in curve 2 of figure 3.†

#### § 4. X-RAY SCATTERING BY MOLECULAR HYDROGEN

##### 4.1. Coherent Scattering

We proceed now to the calculation of the coherent scattering to be expected from a gas of hydrogen molecules. This will, of course, depend to some extent on the results assumed for the electron distribution, and we shall have to discuss separately cases (*a*), (*b*) and (*c*) of § 3.

With case (*a*), the problem reduces essentially to one of an atomic kind and the scattering factor can be calculated in the usual way. The results obtained numerically from the wave function given in table 1 are shown in curve 1 of figure 4.

For cases (*b*) and (*c*), the densities are not spherical, and the formulation of Banyard and March (1957) may be used. Following their notation, it was shown by these authors that the general expression

$$\frac{\bar{I}_s}{\bar{I}_e} = f^2(\kappa) = \iint \rho(\mathbf{r}_1)\rho(\mathbf{r}_2) \frac{\sin \kappa r_{12}}{\kappa r_{12}} d\tau_1 d\tau_2 \quad \dots\dots(10)$$

† We thought it of interest to calculate the *s* term obtained by superposing the densities of two unperturbed hydrogen atoms separated by the experimental internuclear distance and this is shown for purposes of comparison in curve 4 of figure 1. The corresponding radial charge distribution is shown in curve 4 of figure 2.



for the mean coherent scattering (see, for example, Pirene 1946, p. 57) as a function of  $\kappa = (4\pi/\lambda) \sin \frac{1}{2}\theta$  may be reduced to the form

$$f^2(\kappa) = \sum_{n=0}^{\infty} \sum_{m=-n}^{+n} f_{nm}^*(\kappa) f_{nm}(\kappa) \quad \dots\dots (11)$$

where

$$f_{nm}(\kappa) = (2\pi)^{3/2} \int_0^{\infty} \rho_{nm}(r) \frac{J_{n+1/2}(\kappa r)}{(\kappa r)^{1/2}} r^2 dr \quad \dots\dots (12)$$

and

$$\rho(\mathbf{r}) = 2^{1/2} \sum_{n=0}^{\infty} \sum_{m=-n}^{+n} \rho_{nm}(r) \Theta_{nm}(\theta) e^{im\phi}. \quad \dots\dots (13)$$

Using this method we have investigated the scattering assuming densities (b) and (c), and the results are shown in curves 2 and 3 of figure 4. It turns out that the d

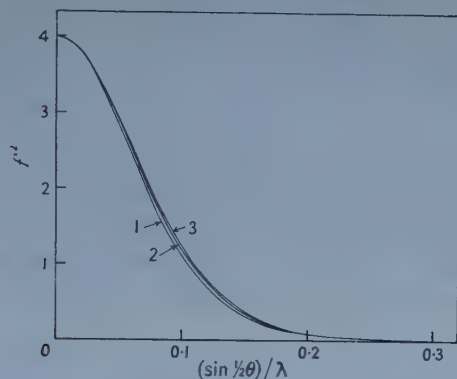


Figure 4. Coherent intensities for x-ray scattering by molecular hydrogen (atomic units used). 1, From 'best' spherical molecular orbital wave function; 2, from LCAO molecular orbital wave function; 3, from Gurnee and Magee wave function.

term in each case makes only a very small difference to the scattering, this being predominantly due to the first, s, term in the density.

#### 4.2. Incoherent Scattering and Total Intensities

Much less attention has been given to the problem of calculating incoherent intensities but, while it is of considerable importance in a two-electron problem, we shall show that the results we obtain by rather different methods agree to within the sort of accuracy we require.

We first of all calculate the scattering on the assumption that we may simply add the incoherent intensities due to two unperturbed hydrogen atoms and the result is shown in curve 1 of figure 5.† Next we have calculated the incoherent scattering using the spherical self-consistent field wave function of § 2. We have then just a two-electron problem of atomic form, and with a simple product wave function we can use for the scattering the formula (see, for example, Herzog 1931)

$$I_{inc}/I_e = 2 - \frac{1}{2}f^2 \quad \dots\dots (14)$$

where  $f$  is the 'atomic' scattering factor. Equation (14) is actually just the classical formula given by Compton and Raman. It will be seen from curve 2 of figure 5 that the incoherent scattering thus obtained is only slightly different from that shown in curve 1.

† The usual relativistic correction (see, for example, Pirene 1946, p. 34) has been applied to all the curves shown in figure 5.

We have also considered the more realistic LCAO case in some detail, and starting from the expression for the total scattering from a particular molecule (see, for

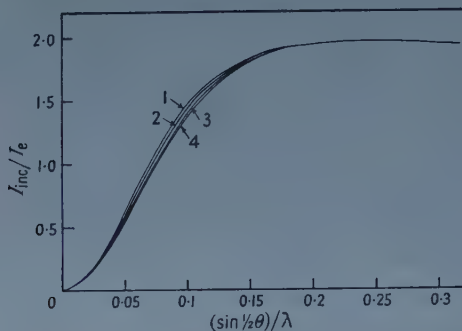


Figure 5. Incoherent intensities for x-ray scattering by molecular hydrogen (atomic units used). 1, From superposition of intensities for two H atoms; 2, from 'best' spherical molecular orbital wave function; 3, from LCAO molecular orbital wave function; 4, from Gurnee and Magee wave function.

example, James 1948), averaging over all possible orientations of the molecules, and using equation (10) for the coherent scattering, the formula (14) again results, where  $f(\kappa)$  is now, however, the 'molecular' scattering factor of equation (10), obtained using the LCAO product wave function. The result is shown in curve 3 of figure 5.

It appears to be a more formidable task to use the Gurnee and Magee function in the calculation of the incoherent scattering, and we have not thought it necessary to do so in view of the agreement between curves 1, 2 and 3 of figure 5. Rather, we have assumed the approximate validity of equation (14) also in this case, and by inserting  $f(\kappa)$  as calculated in § 4.1 from the Gurnee and Magee function, curve 4 of figure 5 has been obtained.

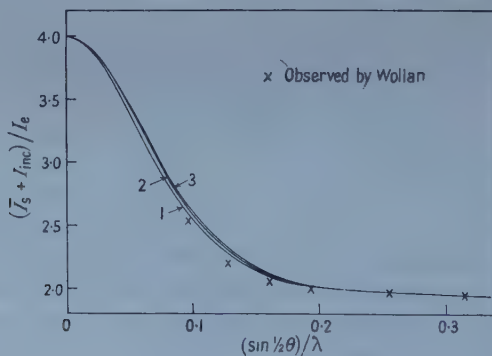


Figure 6. Comparison of observed and calculated total intensities for x-ray scattering by molecular hydrogen (atomic units used). 1, Calculated from 'best' spherical molecular orbital wave function; 2, calculated from LCAO molecular orbital wave function; 3, calculated from Gurnee and Magee wave function.

The total intensities are easily obtained from the separate intensities given in figures 4 and 5, and the results corresponding to wave functions (a), (b) and (c) of § 3 are shown in curves 1, 2 and 3 of figure 6 respectively. The experimental



results of Wollan (1931) are also shown for comparison and it can be seen that there is quite good agreement between theory and experiment in all cases.† Figure 6 would seem to suggest that the wave function (*a*) is giving rather better agreement with experiment than (*b*) or (*c*), although we feel that too much significance should not be attached to this at present, as the deviations between the various theoretical curves are probably comparable with the experimental error. Certainly, from the point of view of energy calculations, the Gurnee and Magee function (*c*) is much to be preferred but, in keeping with our remarks in § 1, we do not think it will necessarily give the most realistic description of the electron distribution.

We conclude from our results, however, that from the point of view of x-ray scattering results, the densities given by the wave functions (*a*), (*b*) or (*c*) are fairly satisfactory, all three leading to a rather similar description of the *s* term which, we find, is dominant in determining the x-ray scattering. It would certainly be very interesting from a theoretical point of view if Wollan's measurements, made more than twenty-five years ago, could be repeated with the increased accuracy which can presumably be obtained with modern techniques.

Little or no information concerning the *d* term can be obtained from the present work as it scarcely contributes to the x-ray scattering, but it is interesting that there is quite good agreement between the results calculated from wave functions (*b*) and (*c*).‡ However, while we do not expect that the use of more refined wave functions will change the *s* term in the density very much, the possibility that the *d* term may change considerably should not be entirely discounted.

## § 5. ELASTIC SCATTERING OF SLOW ELECTRONS BY HYDROGEN MOLECULES

Having seen that the x-ray results can be understood fairly well on the basis of the approximate wave functions used here, we turn now to a discussion of electron scattering.

Previous calculations of the total elastic collision cross section of the hydrogen molecule for scattering of slow electrons have been made by Fisk (1936), Nagahara (1953, 1954), and more recently by Massey and Ridley (1956). By constructing a potential field for the molecule which allowed separation of the variables in spheroidal coordinates, Fisk was able to obtain good agreement with the experimental measurements. In the most recent work by Massey and Ridley, a variational method was used to calculate the zero-order phase shift and it was found that the cross section for scattering by a static potential field becomes much too large at low energies. Their essential conclusion was that it is only by allowing for electron exchange that agreement with observation can be obtained. These workers point out that Fisk's empirical potential field could have included allowance for exchange. On the other hand, Nagahara has obtained reasonable agreement with observation without including exchange effects.

It is well known that exchange effects become important in atomic scattering for light atoms and slow electrons. Thus, Morse and Allis (1933) found that electron exchange reduces the low energy elastic cross section of helium in much the same way as Massey and Ridley have found for molecular hydrogen. In the

† Some estimates we have made show the effect of temperature on the theoretical scattering curves to be insignificant.

‡ Wave function (*a*) leads of course to zero for the *d* term and is obviously unrealistic in this respect.

present work, we follow the general method of expanding in Legendre polynomials, that is, we use spherical polar rather than spheroidal coordinates. When only the spherical potential is included, and using an approximate method for dealing with exchange effects, we obtain a cross section in fair agreement with that of Massey and Ridley. We also show that the quadrupole field of the molecule gives a finite contribution to the cross section for zero-energy electrons, but this contribution appears to be small compared with that from the spherical field. All other multipole fields give a vanishing contribution at zero energy.

### 5.1. Scattering by Static Potential Field

Considering first the scattering by a static molecular potential field expressed as an expansion in Legendre polynomials, namely

$$2V(\mathbf{r}) = \sum_n U_{2n}(r) P_{2n}(\cos\theta), \quad \dots\dots(15)$$

the theory can be developed in a similar way to that used for atomic collisions (Mott and Massey 1949, p. 19). The Schrödinger equation for an electron of energy  $\frac{1}{2}k^2$  is

$$\nabla^2\psi + [k^2 - 2V]\psi = 0 \quad \dots\dots(16)$$

and the wave function  $\psi$  for the scattered electron may be written

$$\psi(\mathbf{r}) = \sum_{lm} A_{lm} P_l^m(\cos\theta) \cos m\phi \frac{1}{r} f_{lm}(r). \quad \dots\dots(17)$$

The coefficients  $A_{lm}$  are determined by the condition that asymptotically  $\psi(\mathbf{r})$  represents the incident wave  $\exp(ikz)$  plus an outgoing wave of the form  $r^{-1}\exp(ikr)$ . Due to the angular dependent terms in the potential field, the differential equations for the  $f_{lm}(r)$  are coupled, and the asymptotic phase shifts  $\eta_{lm}$ , which determine the scattering cross section, are not necessarily real. In addition,  $A_{lm}$ ,  $f_{lm}(r)$  and  $\eta_{lm}$  are dependent on the angle  $\alpha$  between the molecular axis and the direction of the incident electron beam. The observed scattering cross section is obtained by averaging over  $\alpha$ . We then find that the total elastic scattering cross section for an electron of energy  $\frac{1}{2}k^2$  is given by

$$Q = \frac{4\pi}{k^2} \sum_{l=0}^{\infty} \sum_{m=-l}^{+l} \frac{2l+1}{2} \frac{(l-m)!}{(l+m)!} \int_0^\pi |\sin\eta_{lm}|^2 [P_l^m(\cos\alpha)]^2 \sin\alpha d\alpha. \quad \dots\dots(18)$$

Due to the coupling and the dependence on  $\alpha$ , it is at present impracticable to solve the differential equations for the  $f_{lm}(r)$  directly. If, however, the effect of the non-spherical potential field is small, it should be possible to determine this effect by a perturbation technique, and even if the non-spherical potential field is not small, it seems possible that its effect under certain circumstances could be small after averaging over all orientations of the molecule. Thus, we shall first consider the scattering using a spherical approximation for the field and later attempt to discuss the effect of the angular dependent multipole fields as a correction.

### 5.2. The Spherical Approximation

When only the central field  $U_0$  is included, the problem is equivalent to an atomic scattering problem. Then  $f_{lm}(r) \rightarrow g_l(r)$  and

$$\left[ \frac{d^2}{dr^2} - \frac{l(l+1)}{r^2} + k^2 - U_0 \right] g_l = 0 \quad \dots\dots(19)$$



where  $g_l$  has asymptotic form

$$g_l(r) \sim \sin\left(kr - \frac{l\pi}{2} + \sigma_l\right). \quad \dots\dots(20)$$

The total scattering cross section becomes

$$Q = \frac{4\pi}{k^2} \sum (2l+1) \sin^2 \sigma_l = \sum Q_l. \quad \dots\dots(21)$$

As  $k \rightarrow 0$ , it can be shown that  $Q_l$  behaves as  $k^{4l}$ . Thus the series for  $Q$  converges rapidly and only a few  $\sigma_l$  need be calculated.

Equation (19) has been integrated numerically for  $l=0$  and 1, using the central field  $U_0$  obtained from the self-consistent field calculations discussed in §2.  $\sigma_2$  has been determined from the first Born approximation formula

$$\sin \sigma_l \simeq -\frac{1}{k} \int_0^\infty U_0(r) j_l^2(kr) dr. \quad \dots\dots(22)$$

No other  $\sigma_l$  contribute to the total cross section in the range of  $k$  considered. The calculated values of  $\sigma_l$ ,  $Q_l$  and the total cross section  $Q$  are given in table 2.

Table 2.

$k$	$\sigma_0$	$\sigma_1$	$\sigma_2$	$Q_0$	$Q_1$	$Q_2$	$Q$
0.3	1.763			42.82			42.8
0.4	1.561			25.00			25.0
0.5	1.435	0.048		15.71	0.11		15.8
0.7	1.241	0.108		7.31	0.28		7.6
1.0	1.026	0.219	0.021	2.93	0.56	0.01	3.5
1.3	0.854	0.311	0.055	1.35	0.66	0.04	2.1

$Q$  in units of  $\pi a_0^2$ .

### 5.3. Attempt to Allow for Exchange in the Spherical Approximation

Equation (16) for  $\psi$  is obtained when the total wave function  $\Psi(1, 2, 3)$  for the three-electron system is approximated by

$$\Psi_0(1, 2, 3) = \Phi_0(1, 2) \psi(3) \quad \dots\dots(23)$$

where  $\Phi_0(1, 2)$  is the wave function for the ground state of the hydrogen molecule. However, a better approximation to the total wave function is given by

$$\Psi_x(1, 2, 3) = \Psi_0(1, 2, 3) + \Psi_0(2, 3, 1) + \Psi_0(3, 1, 2). \quad \dots\dots(24)$$

This function allows for the exchange of a free electron and a bound electron and is usually called the exchange approximation. If we now use the orbital approximation for  $\Phi_0(1, 2)$  and take  $\psi$  orthogonal to  $\Phi_0$ , that is

$$\iint \psi(1) \Phi_0(1, 2) d\tau_1 d\tau_2 = 0,$$

then in place of the differential equation (16) for  $\psi$ , we obtain the integro-differential equation

$$\nabla^2 \psi(1) + [k^2 - 2V(1)] \psi(1) = -2\phi_0(1) \int \frac{\phi_0(2) \psi(2)}{r_{12}} d\tau_2. \quad \dots\dots(25)$$

$$\dagger j_l(x) \text{ is defined as } \left(\frac{\pi x}{2}\right)^{1/2} J_{l+1/2}(x).$$

Neglecting the non-spherical components of  $V$  and  $\phi$ , that is, writing

$$\phi_0(\mathbf{r}) = \frac{1}{(4\pi)^{1/2}} \frac{P(r)}{r},$$

the equation for  $g_0(r)$  becomes

$$\left[ \frac{d^2}{dr^2} + k^2 - U_0 \right] g_0^\times(r) = -2P(r) \int_0^\infty P(r') v_0(r, r') g_0^\times(r') dr' \quad \dots\dots(26)$$

with asymptotic form

$$g_0^\times(r) \sim \sin(kr + \sigma_0^\times). \quad \dots\dots(27)$$

Then, from equations (19) and (26), we have

$$\sin(\sigma_0^\times - \sigma_0) = \frac{2}{k} \int_0^\infty \int_0^\infty P(r) g_0(r) v_0(r, r') P(r') g_0^\times(r') dr dr' \quad \dots\dots(28)$$

and this equation will be made the basis for our estimates of the effect of exchange.

We note first that if  $\delta_0 = \sigma_0^\times - \sigma_0$  is small, an approximation to  $\sin \delta_0$  can be obtained by putting  $g_0^\times = g_0$  in the right-hand side of equation (28). However, such a procedure fails completely in the present case, illustrating immediately that the effect of exchange is very marked. We ought, therefore, to solve equation (26), but this is a formidable task and we have contented ourselves with a relatively rough attempt to estimate the effect of exchange from equation (28). To this end, we write

$$g_0^\times(r) \simeq \cos \delta_0 g_0(r) + \sin \delta_0 N(r) \cos(kr + \sigma_0), \quad \dots\dots(29)$$

an approximation which is suggested by the type of trial functions used previously in variational methods (see Massey and Moiseiwitsch 1950). This function has then the correct behaviour for small and for large  $r$  if  $N(r)$  varies from 0 at  $r=0$  to 1 outside the scattering molecule. A suitable function is the effective nuclear charge,  $Z_p(r)$ , already calculated from  $P(r)$ . Then, substituting equation (29) into (28) and writing

$$G = \int_0^\infty \int_0^\infty P(r) g_0(r) v_0(r, r') P(r') g_0(r') dr dr', \quad \dots\dots(30)$$

$$X = \int_0^\infty \int_0^\infty P(r) g_0(r) v_0(r, r') P(r') Z_p(r') \cos(kr + \sigma_0) dr dr' \quad \dots\dots(31)$$

we obtain

$$\tan \delta_0 = 2G/(k + 2X). \quad \dots\dots(32)$$

The values of  $\delta_0$  and  $\sigma_0^\times$ , calculated from equation (32) are given in table 3. The total cross section shown in the last column is calculated using the values of  $\sigma_1$  and  $\sigma_2$  given in table 2 for the calculations without exchange.

Table 3. Scattering with Electron Exchange

$k$	$\delta_0$	$\sigma_0^\times$	$Q (\pi a_0^2)$
0.3	0.803	2.566	13.2
0.4	0.815	2.376	12.0
0.5	0.755	2.190	10.7

In figure 7, the total cross sections, without and with exchange, are compared with the calculations of Massey and Ridley and with the experimental results given in Massey and Ridley's paper. When exchange is neglected in both sets of calculations, the agreement is evidently very good. However, the effect of



exchange is clearly considerable, and our estimates of this confirm the essential conclusions of Massey and Ridley, although, as we have already pointed out, it

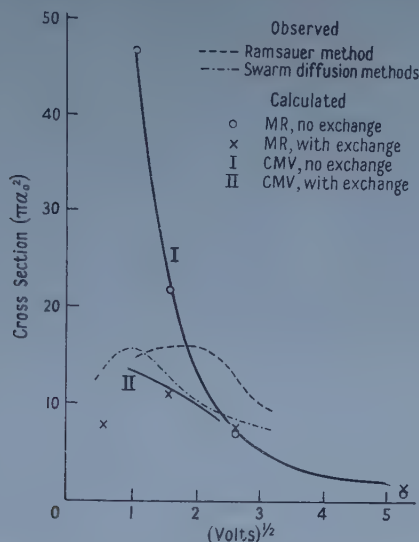


Figure 7. Comparison of observed and calculated cross sections for scattering of electrons by molecular hydrogen.

MR, Massey and Ridley, CMV, present paper.

should not be expected that the very approximate procedure based on equations (28) and (29) can give the precise effect of exchange. Particularly is this the case since  $\delta_0$  is seen from table 3 to be far from small. In view of this, the agreement between the two different theoretical approaches seems quite satisfactory.

#### 5.4. Scattering by a Multipole Field

Finally, we shall briefly consider here the effect of the angular dependent terms in the potential field, electron exchange being neglected. We give the detailed argument in the Appendix, where it is shown that as  $k \rightarrow 0$ , only the quadrupole term gives a contribution to the cross section  $Q$ . If  $q_2$  is the quadrupole moment of the hydrogen molecule as defined by Hirschfelder *et al.* (1954), then it turns out that the contribution to the zero energy cross section from the quadrupole potential field is  $4\pi q_2^2/45$ . The best theoretical and experimental values for  $q_2$  quoted by Hirschfelder *et al.* are  $0.248 \text{ \AA}^2$  and  $0.220 \text{ \AA}^2$  respectively, and thus the contribution is about  $0.06 \pi a_0^2$ . We see that this is small compared with the central field cross section of  $13 \pi a_0^2$  given in table 3 for  $k=0.3$ .†

Throughout this calculation, we have assumed that the molecule is at rest during the collision and that all orientations of the molecular axis are equally probable. When  $k < 0.001$  the collision time becomes comparable to the period of rotation of the molecule. Then the above theory becomes invalid. When  $k \ll 0.001$  it would seem to be reasonable to average the potential field over all orientations, in which case the quadrupole cross section would vanish. Thus the term zero energy cross section used above should be interpreted strictly as the cross section when  $k \ll 1$ , but  $> 0.001$ .

When  $k \sim 1$ , the effect of the quadrupole term is more difficult to assess.

† It should be remarked, however, that as  $k \rightarrow 0$  the results of Massey and Ridley become considerably smaller than ours, and are probably more reliable.

However, the order of magnitude seems unlikely to change as  $k$  varies, and it seems probable that the spherical approximation is quite good throughout the range  $0 < k < 1.3$  considered in this paper.

## APPENDIX

### EFFECT OF THE MULTIPOLE POTENTIAL

The scattering by a multipole field can be dealt with either by analysis into angular momentum states, or alternatively by the three-dimensional Born approximation. We shall confine ourselves here to the treatment based on the Born approximation. Following Mott and Massey (1949; see especially p. 116), we may write Born's first approximation as

$$f(\theta) = -\frac{1}{4\pi} \int \exp[ik(\mathbf{n}_0 - \mathbf{n}) \cdot \mathbf{r}] U(\mathbf{r}) d\tau \quad \dots\dots (A1)$$

where  $\mathbf{n}_0$  is a unit vector along the  $z$  axis, the direction of the incident electron beam,  $\mathbf{n}$  is a unit vector in direction  $(\theta, \phi)$ ,  $\mathbf{r}$  has direction  $(\beta, \gamma)$  with respect to  $(\mathbf{n}_0 - \mathbf{n})$ , and  $\mathbf{n}_0 - \mathbf{n}$  has magnitude  $2 \sin \frac{1}{2}\theta$  and direction  $(\frac{1}{2}\pi - \frac{1}{2}\theta, -\phi)$ . Let the molecular axis  $Oz'$  make an angle  $\alpha$  with  $(\mathbf{n}_0 - \mathbf{n})$ . Then we have

$$\begin{aligned} U(\mathbf{r}) &= \sum_n U_n(r) P_n(\cos \theta') \\ &= \sum_n \sum_{m=-n}^{+n} U_n(r) \frac{(n-m)!}{(n+m)!} P_n^m(\cos \alpha) P_n^m(\cos \beta) \cos m\gamma. \quad \dots\dots (A2) \end{aligned}$$

Then, taking  $d\tau = r^2 dr \sin \beta d\beta d\gamma$ , we have

$$\begin{aligned} f(\theta) &= -\frac{1}{4\pi} \int_0^{2\pi} d\gamma \int_0^\pi \sin \beta d\beta \int_0^\infty r^2 dr \exp(i2k \sin \frac{1}{2}\theta r \cos \beta) U(\mathbf{r}) dr \\ &= -\frac{1}{2} \sum_n P_n(\cos \alpha) \int_{-1}^{+1} \exp(i\kappa r \mu) P_n(\mu) d\mu \int_0^\infty U_n(r) r^2 dr, \quad \dots\dots (A3) \end{aligned}$$

where  $\kappa = 2k \sin \frac{1}{2}\theta$ . Using the expansion

$$\exp(i\kappa r \mu) = \sum_{n=0}^{\infty} (2n+1) i^n \frac{j_n(\kappa r)}{\kappa r} P_n(\mu) \quad \dots\dots (A4)$$

we find

$$f(\theta) = -\frac{1}{\kappa} \sum_n P_n(\cos \alpha) i^n \int_0^\infty r j_n(\kappa r) U_n(r) dr.$$

Now for  $n > 0$  we may write

$$\begin{aligned} U_n(r) &\sim r^n && \text{for } r \rightarrow 0 \\ &\simeq \frac{q_n}{r^{n+1}} && \text{outside the molecule.} \end{aligned}$$

To be definite, let us approximate  $U_n(r)$  by

$$\begin{aligned} U_n(r) &= \frac{q_n r^n}{R^{2n+1}}, && r \leq R \\ &= \frac{q_n}{r^{n+1}}, && r \geq R. \end{aligned}$$

Then

$$\int_0^\infty r j_n(\kappa r) U_n(r) dr = \frac{\kappa^{n-1}}{(\kappa R)^n} q_n [j_{n+1}(\kappa R) + j_{n-1}(\kappa R)], \quad \dots\dots (A5)$$



the first term being the contribution from  $r < R$  and the second term that from  $r > R$ . Since  $j_n(x) \sim x^{n+1}$  for  $x \rightarrow 0$  the contribution from the outer region dominates as  $k \rightarrow 0$ . Using the recurrence relations between spherical Bessel functions, equation (A 5) may be written

$$\int_0^\infty r j_n(\kappa r) U_n(r) dr = \frac{(2n+1) j_n(\kappa R) \kappa^{n-1}}{(\kappa R)^{n+1}} q_n \quad \dots\dots (A 6)$$

and

$$f(\theta) = - \sum_n i^n P_n(\cos \alpha) q_n (2n+1) \frac{j_n(\kappa R)}{(\kappa R)^{n+1}} \kappa^{n-2}. \quad \dots\dots (A 7)$$

Averaging equation (A 7) over  $\alpha$  and integrating over  $\theta$ , we find

$$\begin{aligned} Q &= 2\pi \int_0^\pi |f(\theta)|^2 \sin \theta d\theta \\ &= \frac{4\pi}{k^2} \sum_n \frac{2n+1}{2} \frac{q_n^2}{R^{2n-2}} \int_0^{2\kappa R} \frac{j_n^2(x)}{x^5} dx. \quad \dots\dots (A 8) \end{aligned}$$

For  $k \rightarrow 0$ , we have

$$\frac{j_n^2(x)}{x^5} \rightarrow \left[ \frac{2^n n!}{(2n+1)!} \right] x^{2n-3}$$

and

$$Q \rightarrow 4\pi \sum_n \frac{16q_n^2}{(n-1)(2n+1)} \left[ \frac{n!}{(2n)!} \right]^2 (4k)^{2n-4}. \quad \dots\dots (A 9)$$

We see from (A 9) that at  $k=0$ , only  $q_2$  contributes to  $Q$ , the contribution being  $4\pi q_2^2/45$ .

A more detailed consideration of the higher Born approximations (see Morse and Feshbach 1953) shows that for  $n \geq 2$ , the first Born approximation does give the correct low-energy cross section. When the potential field  $U(\mathbf{r})$  also contains a central field  $U_0(r)$ , the Born approximation is not valid for low-energy scattering. In this case it seems probable that the total zero-energy scattering cross section, after averaging over all orientations of the molecule, is the sum of the contributions from  $U_0$  and  $U_2$  considered separately, but we have been unable to prove this rigorously.

#### REFERENCES

- BANYARD, K. E., and MARCH, N. H., 1956, *Acta Cryst., Camb.*, **9**, 385; 1957, *J. Chem. Phys.*, **26**, 1416.  
 CALLEN, E., 1955, *J. Chem. Phys.*, **23**, 360.  
 CARTER, C., 1956, *Proc. Roy. Soc. A*, **235**, 321.  
 COULSON, C. A., 1937, *Trans. Faraday Soc.*, **33**, 1479.  
 FISK, J. B., 1936, *Phys. Rev.*, **49**, 1951.  
 FUNABASHI, K., and MAGEE, J. L., 1957, *J. Chem. Phys.*, **26**, 407.  
 GURNEE, E. F., and MAGEE, J. L., 1950, *J. Chem. Phys.*, **18**, 142.  
 HERZOG, G., 1931, *Z. Phys.*, **70**, 590.  
 HIRSCHFELDER, J. O., CURTISS, C. F., and BIRD, R. B., 1954, *Molecular Theory of Gases and Liquids* (New York: Wiley), pp. 839, 1028.  
 HURLEY, A. C., 1954, *Proc. Roy. Soc. A*, **226**, 179.  
 HUZINAGA, S., 1956, *Prog. Theor. Phys., Japan*, **15**, 501.  
 JAMES, R. W., 1948, *Optical Principles of the Diffraction of X-rays* (London: Bell).  
 KARPLUS, M., 1956, *J. Chem. Phys.*, **25**, 605.  
 MASSEY, H. S. W., and MOISEWITSCH, B. L., 1950, *Proc. Roy. Soc. A*, **205**, 483.

- MASSEY, H. S. W., and RIDLEY, R. O., 1956, *Proc. Phys. Soc. A*, **69**, 659.
- MORSE, P. M., and ALLIS, W. P., 1933, *Phys. Rev.*, **44**, 269.
- MORSE, P. M., and FESHBACH, H., 1953, *Methods of Theoretical Physics* (New York : McGraw Hill), p. 1073.
- MOTT, N. F., and MASSEY, H. S. W., 1949, *Theory of Atomic Collisions*, 2nd edition (Oxford : University Press).
- NAGAHARA, S., 1953, *J. Phys. Soc. Japan*, **8**, 165; 1954, *Ibid.*, **9**, 52.
- PIRENNE, M. H., 1946, *The Diffraction of X-rays and Electrons by Free Molecules* (Cambridge : University Press).
- WOLLAN, E. O., 1931, *Phys. Rev.*, **37**, 862.



# A Method for Deriving the Acoustic Absorption Coefficient of Gases from Measurement of the Decay-time of a Resonator

BY P. D. EDMONDS† AND J. LAMB

Electrical Engineering Department, Imperial College, London

*MS. received 24th May 1957, and in final form 28th August 1957*

**Abstract.** A unique result for the absorption coefficient is obtained from calculations based on measurement of the decay-time using longitudinal and radial modes of propagation. Expressions are given for the energy losses in the viscous and thermal boundary layers at the walls of the resonator.

The method is applicable in the range of frequency divided by pressure of 1 to 45 kc/s per atmosphere. Calibration measurements have been made using argon and nitrogen: the relaxational contribution to the absorption has been evaluated in the case of cyclopropane.

## § 1. INTRODUCTION

INFORMATION concerning molecular relaxation processes in gases and their association with mechanisms of internal energy transfer can be obtained from a study of the variation of the absorption and velocity of propagation of ultrasonic waves with frequency and temperature.

The majority of previous ultrasonic measurements on polyatomic gases has been obtained by employing an acoustic interferometer at fixed frequency and variable pressure (e.g. Fogg, Hanks and Lambert 1953, Fogg and Lambert 1955, Ener *et al.* 1955, Rao and Hubbard 1955, Sette *et al.* 1955, Rossing and Legvold 1955, Byers 1943). Although this method permits accurate measurements to be made of the velocity dispersion associated with a relaxation process, the accuracy with which the absorption in the gas may be determined is poor unless this is greater than about  $0.1 \text{ cm}^{-1}$  (Markham, Beyer and Lindsay 1951).

The present work is aimed specifically at the direct measurement of the absorption coefficient. The technique stems from the reverberation method of Knudsen (1933) and from the continuous-wave method employed by Knötzel (1948) to measure the bandwidth of a cylindrical resonator excited at a specific resonance.

A cylinder containing the gas to be investigated is excited intermittently at one of its *eigenfrequencies* and the decay-time of the sound field is recorded during the periods when the source of sound is quiescent. This method therefore differs from the normal reverberation technique in which a diffuse sound field is established.

The direct measurement of the decay-time associated with a known resonant condition can be related to the 'Q'-factor of the resonator and thence to the total

† Now with the Mullard Research Laboratories, Salfords, Surrey.

acoustic power loss due to the various absorption mechanisms. Power loss, arising from 'classical' processes, can be calculated on the basis of the kinetic theory of gases and subtracted from the total measured loss to yield the contribution due to molecular relaxation processes. To any power loss,  $P_i$ , arising from mechanism  $i$  there may be assigned a contributory term  $T_i$  to the measured decay-time  $T_M$ . The various  $P_i$ 's are additive. If  $E$  represents the energy stored in the resonator at frequency  $f$  and it can be assumed that  $4\pi/\omega T_i \ll 1$ , then

$$P_i = Ef\{1 - \exp(-4\pi/\omega T_i)\} \simeq 2E/T_i. \quad \dots\dots(1.1)$$

If  $v_0$  is the velocity of plane wave propagation and  $\alpha_i$  is the contribution to the equivalent spatial amplitude absorption coefficient  $\alpha_M (= \Sigma \alpha_i)$  then it follows that for any form of sound field

$$T_i = 1/\alpha_i v_0 \quad \text{and hence} \quad \alpha_i = P_i/2Ev_0. \quad \dots\dots(1.2)$$

Expressions are given in §3 for those power losses  $P_i$  which have to be considered in order to derive the relaxational contribution to the absorption  $\alpha^{(r)}$  from  $T_M$ .

The essential requirements of an apparatus which can be employed for the measurement of absorption coefficient by the method outlined above are: (i) the resonator shall be of simple geometrical form so that the individual resonant conditions can be identified, thus ensuring that the system is amenable to calculation; (ii) the exciting and receiving transducers shall be loosely coupled to the resonator in order not to influence the decay-time appreciably; (iii) the exciting transducers shall be essentially aperiodic so that a sharp cut-off of the source is achieved at the commencement of the decay period; (iv) the bandwidth of the receiver shall be such that it is capable of faithful transmission of the shortest decay to be recorded; (v) both exciting and receiving transducers shall operate over a continuous range of frequency since the resonant frequencies of the system depend upon the gas employed and the selected mode of propagation.

## § 2. EXPERIMENTAL SYSTEM

A block diagram of the experimental system is given in figure 1 together with a photograph of the acoustic section in figure 2 (Plate I). The semi-continuous excitation consists of bursts of sound produced by a ribbon loud-speaker (suggested by Angona's (1953) use of the device) loosely coupled to the cylindrical resonator by a probe tube. The frequency of excitation  $f$  is adjusted to coincide with that of a resonant condition, designated  $(lmn)$ , in the cylinder. The exponential decay of the excess pressure in the resonator, subsequent to the removal of the excitation, is detected by means of a condenser microphone which is also loosely coupled by a probe tube. The received signal is amplified and displayed on one trace of a double-beam oscilloscope. When making a measurement the amplification of the signal and the velocity of the linear time-base are adjusted until the decaying envelope of the trace coincides with an exponential curve drawn on a graticule covering the oscilloscope screen. Two 'trigger' pulses of adjustable position and separation are displayed on the second beam and are arranged to coincide with two known amplitude levels on the graticule which have the ratio  $1:e^{-1}$ . The time interval between these two pulses is equal to the decay time  $T_M$ , and is measured by a crystal-controlled electronic counter for  $T_M < 130$  msec: for decay times greater than about 130 msec it is more



convenient to use a logarithmic pen recorder (Brüel and Kjaer level recorder) to register the amplitude of the received signal as a function of time. A band-pass one-third octave filter, the  $Q$ -factor of which is considerably less than that of the resonator, is inserted in the receiving channel in order to improve the signal-to-noise ratio.

The low-impedance ribbon loudspeaker is energized through step-down transformers from a power amplifier consisting of two 6V6 valves operating in push-pull, preceded by a tone-burst generator (Mayo *et al.* 1951), which provides the master trigger control for the repetitive operation of the system. The tone-burst generator gates the output of a continuous-wave oscillator operating at the frequency  $f$  which can also be measured by the counter.

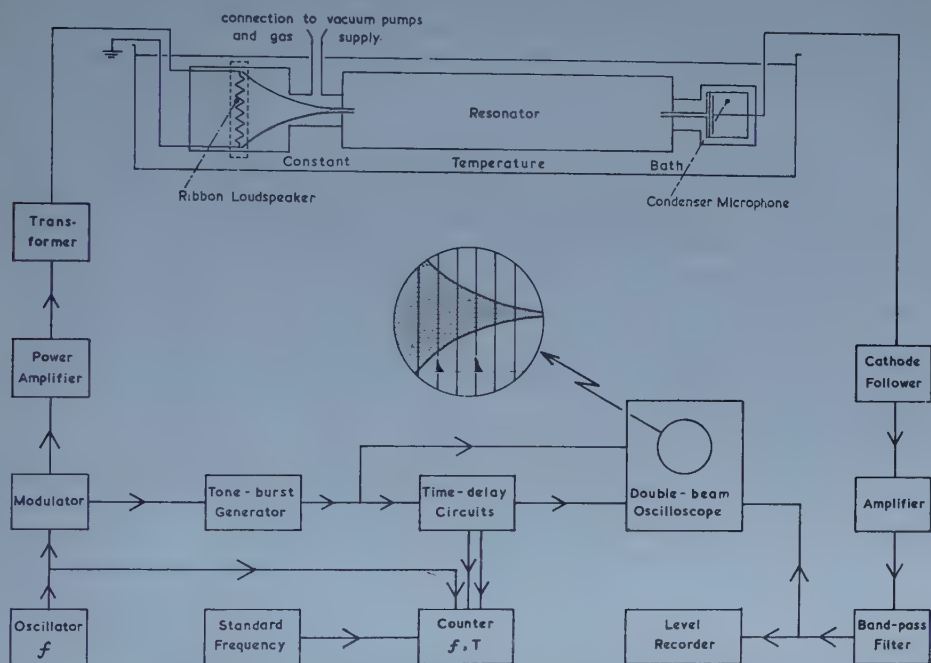


Figure 1. Block diagram of experimental system.

The resonator employed in the work is a precision bore Pyrex tube supplied by the Rotameter Manufacturing Company; the internal diameter is  $(9.80 \pm 0.01)$  cm, the length is 60.1 cm and the wall thickness 6.5 mm. The ends have been ground normal to the axis and end plates of Pyrex are cemented to the tube with Araldite resin type 101. The interior surfaces of the end plates are polished and central holes drilled to accommodate the probe tubes which are of stainless steel (internal diameter 0.042 in. and external diameter 0.058 in.). At one end of the resonator the probe tube leading to the loudspeaker is attached to a flared horn, the mouth of which is situated in front of the ribbon of the loudspeaker. The aluminium ribbon is 0.005 in. thick  $\times$  2 in. wide  $\times$  4 in. long and is mounted inside a piece of waveguide section in the transverse field of a Ticonal magnet fitted with 35% cobalt steel pole pieces having a saturation magnetization of 25 000 gauss. The function of the horn is to enable a probe tube of small diameter to be energized by a transducer of conveniently large dimensions.

The condenser microphone, coupled to the opposite end of the resonator, is constructed from duralumin and P.T.F.E. and provided with a pressure release to equalize the pressure on both sides of the diaphragm.

Both the loudspeaker and microphone assemblies are situated in gas-tight enclosures which are attached to the end faces of the resonator. A number of brass bellows is used to permit alignment and to avoid undue strain on the glass connections to the apparatus from which the gas is obtained. Adjacent sections are joined either by Araldite resin or by P.T.F.E. 'O' ring seals. Several coats of Dulux paint have been applied to the outside of the metal surfaces in order to secure gas tightness.

All measurements have been made at a temperature of  $(25 \pm 0.1)^\circ\text{C}$  by immersing the resonator assembly in a temperature-controlled bath of water or transformer oil. The range of frequency which it is possible to cover with the system is limited at its lower end to about 1 kc/s by the maximum permissible movement of the ribbon of the loudspeaker. The upper frequency is limited by the combined effects of increasing absorption in the resonator and decreasing sensitivity of the transducers. For gases of comparatively low absorption, the upper limit is in the region of 25 kc/s at 1 atmosphere pressure although in practice all necessary information concerning the absorption is obtained from measurements made in the frequency range 1 to 10 kc/s. A pressure range from 1 atm to 0.1 atm has been employed, the lower limit being determined by the fall in sensitivity of the acoustic system resulting from the lowering of the acoustic impedance of the gas with decreasing pressure. The highest value of  $f/p$  attainable is approximately 45 kc/s atm<sup>-1</sup>, since the lower pressures cannot be used at the higher frequencies.

Measured decay times range from 20 msec to 1.5 sec.

Before making measurements, the apparatus was evacuated by a mercury diffusion pump attached to the gas handling system. The objections, from the point of view of high vacuum technique, to evacuating through a tube of small diameter were considered over-ruled by acoustic requirements. After pumping for at least 4 hours the apparatus was flushed once or twice with the gas to be measured and re-evacuated before being filled for measurement purposes.

### § 3. PROPAGATION AND ENERGY LOSSES IN A CLOSED CIRCULAR CYLINDER

#### 3.1. Conditions for Resonance

The wave equation which describes the propagation of sound in a gas with phase velocity  $v$  at a frequency  $f$  ( $=\omega/2\pi$ ), is

$$\nabla^2\phi = \frac{1}{v^2} \frac{\partial^2\phi}{\partial t^2} = -k^2\phi \quad \dots\dots(3.1)$$

where the velocity potential  $\phi = \Phi \exp(i\omega t)$  and  $k = \omega/v$ . The general solution of this equation (3.1) in cylindrical coordinates ( $r, \theta, z$ ) is

$$\phi = [A \cos n\theta + B \sin n\theta][J_n(k_{0mn}r) + N_n(k_{0mn}r)] \exp i[\omega t + k\psi_{mn}z] \quad \dots\dots(3.2)$$

where  $m, n = 0, 1, 2, 3, \dots$

The suffix  $(0mn)$  refers to the cut-off frequency of the  $(mn)$  mode of propagation in an infinitely long cylinder of radius  $r_0$ . The propagation constant is defined by

$$k\psi_{mn} = k[1 - (\omega_{0mn}/\omega)^2]^{1/2}, \quad \dots\dots(3.3)$$

The solutions of (3.2) applicable to the present work necessitate the following restrictions: (i) Bessel functions of the second kind ( $N_n$ ) are not admissible since finite solutions of the wave equation are required on the axis ( $r=0$ ); (ii) for the longitudinal (plane wave) mode,  $m \equiv 0$ ,  $n \equiv 0$ ; (iii) for other modes only those having axial symmetry ( $n=0$ ) are considered for purposes of measurement.

The following terminology will be adopted.

A *mode* is specified by particular values of  $m$  and  $n$  ( $l=0, 1, 2, 3 \dots$ ).

A *resonant condition* is specified by particular values of  $l$ ,  $m$  and  $n$ . It occurs at the resonant frequency or eigenfrequency  $f_{lmn}$ .

The abbreviation 'radial' is to be taken as referring to the axially symmetrical radial modes specified by  $n=0$ .

### 3.1.1. Longitudinal mode (00).

Equation (3.2) reduces to

$$\phi = A \exp i(\omega t + kz). \quad \dots\dots (3.4)$$

The parameters of the sound field are related by the expressions

$$\begin{aligned} p &= \mathcal{R}\{-\rho_0 \partial \phi / \partial t\}; & u_r &= \mathcal{R}[\partial \phi / \partial r] \\ u_\theta &= \mathcal{R}[\partial \phi / \partial \theta]; & u_z &= \mathcal{R}[\partial \phi / \partial z] \end{aligned}$$

where  $p$  is the excess pressure,  $u$  is the particle velocity and  $\rho_0$  is the mean gas density.

The difference in acoustic impedance between the gas and the solid cylindrical shell is sufficiently large for the walls to be considered as rigid. It readily follows that the frequencies of the longitudinally resonant conditions of a closed cylinder of length  $L$  are determined by

$$f_{l00} = \frac{v_0}{2L} l \quad (l=0, 1, 2, 3 \dots). \quad \dots\dots (3.5)$$

The tube correction for the velocity of propagation  $v_0$  is negligible under the conditions of the experiments. The corresponding expressions for the pressure and particle velocity become

$$\left. \begin{aligned} |p_{l00}| &= (2A)\rho_0\omega \cos(l\pi z/L) \\ |(u_z)_{l00}| &= (2A) \left[ \frac{l\pi}{L} \right] \sin\left(\frac{l\pi z}{L}\right). \end{aligned} \right\} \quad \dots\dots (3.6)$$

### 3.1.2. Radial modes ( $m0$ ).

When  $n=0$ :

$$\phi = AJ_0(k_{0m0}r) \exp i(\omega t \pm k\psi_{m0}z). \quad \dots\dots (3.7)$$

The boundary conditions at a rigid wall surface give

$$|u_r|_{r=r_0} = 2Ak_{0m0}J_1(k_{0m0}r_0) \cos(k\psi_{m0}z) = 0 \quad \text{for all } z.$$

Therefore

$$J_1(k_{0m0}r_0) = 0. \quad \dots\dots (3.8)$$

The solutions of this equation are designated  $j_{1m}$  and are given in table 1.

Table 1. First Roots of the Equation (3.8)

$m$	1	2	3
$j_{1m} (=k_{0m0}r_0)$	3.832	7.016	10.16



In addition

$$|u_z|_{z=L} = (2A)k\psi_{m0}J_0(k_{0m0}r)\sin(k\psi_{m0}L) = 0 \quad \text{for all } r.$$

Therefore

$$\sin(k\psi_{m0}L) = 0, \quad \dots\dots(3.9)$$

and the solutions are

$$l\pi = k\psi_{lm0}L = \frac{2\pi L}{\lambda} \left\{ 1 - \left( \frac{\omega_{0m0}}{\omega_{lm0}} \right)^2 \right\}^{1/2} \quad \dots\dots(3.10)$$

where  $\lambda$  is the free-space wavelength. Thus, resonance in the  $(m0)$  modes occurs at the series of frequencies  $f_{lm0}$  ( $=\omega_{lm0}/2\pi$ ) where

$$\begin{aligned} f_{lm0} &= v_0 \left\{ \left( \frac{f_{0m0}}{v_0} \right)^2 + \left( \frac{l}{2L} \right)^2 \right\}^{1/2} \\ &= v_0 \left\{ \left( \frac{j_{1m}}{2\pi r_0} \right)^2 + \left( \frac{l}{2L} \right)^2 \right\}^{1/2}. \end{aligned} \quad \dots\dots(3.11)$$

At a resonant condition, where  $f=f_{lm0}$ , the expressions for the excess pressure and the non-zero components of the particle velocity are

$$\left. \begin{aligned} |p_{lm0}| &= (2A)\rho_0\omega J_0(j_{1m}r/r_0)\cos(l\pi z/L) \\ |(u_r)_{lm0}| &= (2A)\left(\frac{j_{1m}}{r_0}\right)J_1(j_{1m}r/r_0)\cos(l\pi z/L) \\ |(u_z)_{lm0}| &= (2A)\left(\frac{l\pi}{L}\right)J_0(j_{1m}r/r_0)\sin(l\pi z/L). \end{aligned} \right\} \quad \dots\dots(3.12)$$

### 3.2. Energy Storage and Dissipation

#### 3.2.1. General expressions for power losses in thermal and viscous boundary layers.

R. F. Lambert (1953) has shown that the power losses occurring in the thermal and viscous boundary layers at a rigid (isothermal) surface of area  $S$  are given by the following expressions, respectively

$$\left. \begin{aligned} P_S^{(s)} &= \frac{1}{2p_0} \left[ \frac{\omega\kappa}{2\rho_0 C_p} \right]^{1/2} \left( \frac{\gamma-1}{\gamma} \right) \int_S [p(\sigma)]^2 d\sigma \\ P_S^{(v)} &= \frac{1}{2} \left\{ \frac{\omega\rho_0\eta}{2} \right\}^{1/2} \int_S [u_t(\sigma)]^2 d\sigma. \end{aligned} \right\} \quad \dots\dots(3.13)$$

Here  $p(\sigma)$  and  $u_t(\sigma)$  are the amplitudes of excess pressure and tangential particle velocity expressed as functions of the elemental area  $\sigma$  of  $S$ . The associated power losses corresponding to any given resonance can be evaluated from the above equations.

The stored energy in the resonator is found from

$$E = \frac{1}{2\rho_0 v_0^2} \int_{V_R} [p(V)]^2 dV \quad \dots\dots(3.14)$$

where  $V_R$  is the volume of the resonator.

The power losses,  $P^{(1)}$  in the 'body'† of the gas due to the 'classical' processes of shear viscosity and thermal conduction are obtained from equation (1.2) in terms of the 'classical' amplitude absorption coefficient, which in turn is given by (Kirchhoff 1868):

$$\alpha^{(cl)} = \frac{2\pi^2 f^2}{\rho_0 v_0^3} \left\{ \frac{4}{3}\eta + (\gamma-1)K/C_p \right\}. \quad \dots\dots(3.15)$$

† The term 'body' of the gas is used to denote the region remote from the boundary layers.

There may be a further power loss,  $P^{(\tau)}$ , due to possible molecular relaxation processes in the body of the gas, so that the quantity  $\alpha_M (= 1/T_M v_0)$  derived from the measured decay time ( $T_M$ ) is given by

$$\begin{aligned} (p_0 \alpha_M / f^2) &= \frac{p_0 [P_S^{(\kappa)} + P_S^{(\eta)} + P^{(C1)}]}{2f^2 v_0 E} + \frac{p_0 P^{(\tau)}}{2f^2 v_0 E} \\ &= \frac{p_0 \alpha_{\text{calc}}}{f^2} + \frac{p_0 \alpha^{(\tau)}}{f^2} \end{aligned} \quad \dots\dots(3.16)$$

where  $p_0$  is the gas pressure. It is the purpose of this work to evaluate  $p_0 \alpha^{(\tau)} / f^2$  for various gases.

### 3.2.2. Stored energy and boundary layer losses in the longitudinal mode.

Insertion of relationships (3.6) in (3.13) yields

$$[P_w^{(\kappa)}]_{l00} = (2A)^2 \frac{2\rho_0^2 \pi^3 r_0 L}{p_0} \left( \frac{\pi \kappa}{\rho_0 C_p} \right)^{1/2} \left( \frac{\gamma - 1}{\gamma} \right) f_{l00}^{5/2} \quad \dots\dots(3.17)$$

for the power loss in the thermal boundary layer at the cylindrical wall surface  $w$ , and

$$2[P_e^{(\kappa)}]_{l00} = (2A)^2 \frac{4\rho_0^2 \pi^3 r_0^2}{p_0} \left( \frac{\pi \kappa}{\rho_0 C_p} \right)^{1/2} \left( \frac{\gamma - 1}{\gamma} \right) f_{l00}^{5/2} \quad \dots\dots(3.18)$$

for the sum of the power losses in the thermal boundary layers at the two end surfaces  $e$  of the resonator.

The corresponding losses in the viscous boundary layers are

$$\left. \begin{aligned} [P_w^{(\eta)}]_{l00} &= (2A)^2 \frac{\pi^3 r_0}{2L} (\pi \rho_0 \eta)^{1/2} l^2 f_{l00}^{1/2} \\ [P_e^{(\eta)}]_{l00} &= 0. \end{aligned} \right\} \quad \dots\dots(3.19)$$

The stored energy is given from equation (3.14) by

$$E = (2A)^2 \frac{\pi^3 \rho_0 r_0^2 L}{v_0^2} f_{l00}^2. \quad \dots\dots(3.20)$$

### 3.2.3. Stored energy and boundary layer losses in radial modes.

Insertion of the relationships (3.12) in (3.13) yields

$$[P_w^{(\kappa)}]_{lm0} = \frac{(2A)^2}{2p_0} \left[ \frac{\pi \kappa}{\rho_0 C_p} \right]^{1/2} \left( \frac{\gamma - 1}{\gamma} \right) \pi r_0 L [2\pi \rho_0 J_0(j_{1m})]^2 f_{lm0}^{5/2} \quad \dots\dots(3.21)$$

$$2[P_e^{(\kappa)}]_{lm0} = \frac{(2A)^2}{p_0} \left[ \frac{\pi \kappa}{\rho_0 C_p} \right]^{1/2} \left( \frac{\gamma - 1}{\gamma} \right) \frac{\pi}{f_{0m0}^2} [\rho_0 v_0 j_{1m} J_0(j_{1m})]^2 f_{lm0}^{5/2} \quad \dots\dots(3.22)$$

$$[P_w^{(\eta)}]_{lm0} = \frac{(2A)^2}{2} (\pi \rho_0 \eta)^{1/2} \frac{r_0 \pi^3}{L} [J_0(j_{1m})]^2 l^2 f_{lm0}^{1/2} \quad \dots\dots(3.23)$$

$$2[P_e^{(\eta)}]_{lm0} = (2A)^2 (\pi \rho_0 \eta)^{1/2} \pi [j_{1m} J_0(j_{1m})]^2 f_{lm0}^{1/2}. \quad \dots\dots(3.24)$$

The stored energy is

$$E_{lm0} = (2A)^2 \rho_0 L \pi^3 [J_0(j_{1m})]^2 \left[ \frac{r_0}{v_0} \right]^2 f_{lm0}^2. \quad \dots\dots(3.25)$$

## § 4. DISCUSSION OF BOUNDARY LAYER LOSSES

The relationships (3.13) for the power losses in the viscous and thermal boundary layers are general expressions given by R. F. Lambert (1953). Since some difficulty has been found in attempts to reconcile previous work published on this topic, it is considered worth while to summarize the methods of approach. Two separate lines have been followed, namely:

(1). One concept follows from the original treatments of Stokes (1845) and Kirchhoff (1868) who considered the viscous and thermal boundary layers which arise when sound waves are propagated in the neighbourhood of a wall.

The boundary conditions are taken to be that no slip occurs at the wall surface, which being assumed rigid and also thermally perfectly conducting, is at constant temperature. These conditions require that the resultant tangential particle velocity and incremental temperature shall be zero at the wall. Hence transition, or boundary, layers exist between the wall surface and the region 'remote' from the wall where the free-field values of temperature ( $\theta$ ) and tangential particle velocity ( $u_t$ ) apply. The net effect mathematically is that superimposed upon the free-field are compensating fields ( $u_t^{(v)}$  and  $\theta^{(v)}$ ) such that  $u_t^{(v)} + u_t = 0$ , and  $\theta^{(v)} + \theta = 0$  at the wall surface.  $u_t^{(v)}$  and  $\theta^{(v)}$  decay exponentially with distance in the direction perpendicular to the wall and reach a negligible amplitude within a distance which is small in comparison with the sound wavelength. The energy associated with the compensating fields must be derived from the original sound field and is eventually dissipated as heat. Hence a loss of energy occurs in the boundary layers. These arguments underlie the analytical treatments of Nielsen (1949) and R. F. Lambert (1953), the latter quoting expressions applicable to any mode of propagation (see § 3.2.1.)

(2). An alternative derivation introduced by Cremer (1948) for the plane wave case employs the concept of 'wall admittance'. The method was generalized by Beatty (1950) whose work is also generally applicable to any mode of propagation in rectangular or circular tubes. Campbell (1953) has applied the theory to a spherical resonator. These authors apply the same boundary conditions to introduce the compensating fields  $u_t^{(v)}$  and  $\theta^{(v)}$ . The equation of continuity is then considered, assuming an incompressible fluid medium, to obtain expressions for the associated components of particle velocity  $u_N^{(v)}$  and  $u_N^{(v)}$  perpendicular to the wall. The effective admittances of the rigid wall are then given by  $Y^{(v)} = u_N^{(v)}/p$  and  $Y^{(v)} = u_N^{(v)}/p$  where  $p$  is the free-field pressure at the wall. The definition of  $Y^{(v)}$  involves the assumption that the pressure associated with the compensating thermal field can be neglected (Cremer 1948).  $Y^{(v)}$  depends only on the properties of the fluid and the frequency, whilst  $Y^{(v)}$  depends also on the mode of propagation. It follows that the ratio  $\nu$  of the power loss in the viscous layer to that in the thermal layer is dependent upon the form of the sound field. The establishment of a net wall admittance  $Y = Y^{(v)} + Y^{(v)}$  implies that energy is lost from the sound field leading to an associated absorption coefficient, as if in the absence of boundary layers the walls were non-rigid.

Values of the absorption coefficient attributable to boundary layer losses derived by these two methods are in agreement.

Voelz (1952) derived an expression for the thermal loss in the special case when the particle velocity is entirely normal to the wall. Since  $Y^{(v)}$  is independent of the form of the sound field Voelz's final expression for his ' $\epsilon$ ' is, in fact, generally



valid, provided that the square of velocity potential at the surface,  $(\Phi_F^*)^2$ , is integrated over the surface area to take account of the possible variation of  $\Phi_F$  over the surface  $F$ . In the present terminology the expression becomes

$$P_S^{(K)} = E(\gamma - 1) \left[ \frac{\omega \kappa}{2\rho_0 C_p} \right]^{1/2} \frac{\int_S [\phi_S(\sigma)]^2 d\sigma}{\int_{V_R} [\phi(V)]^2 dV} \quad \dots\dots(4.1)$$

which is equivalent to the expression for  $P_S^{(K)}$  in equation (3.13).

### § 5. EVALUATION OF THE RELATIVE LOSSES FOR LONGITUDINAL AND RADIAL RESONANT CONDITIONS

In determining the power losses for a resonant condition it is convenient for purposes of numerical calculation to refer all losses to a chosen 'standard' loss. In the case of the longitudinal mode the thermal loss at the cylindrical surface for the fundamental length resonance  $[P_w^{(K)}]_{100}$  is taken as the standard. For radial

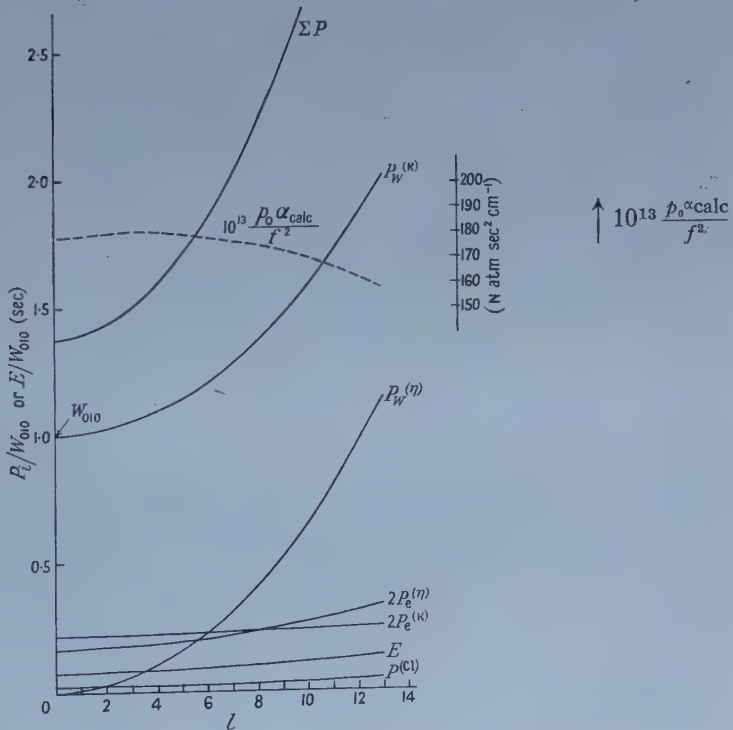


Figure 3. Comparison of the contributory power losses for the (10) mode in argon at 25°C and a pressure of 1 atm.

modes the thermal loss at the cylindrical surface at the cut-off frequency  $[P_w^{(K)}]_{0m0}$  is selected. It then follows from equations (3.17) to (3.25) that the relative losses and the stored energy can be expressed as in table 2.

A numerical comparison is given in figure 3 for the (10)-mode in argon, showing  $P_w^{(K)}$  to be the predominant loss.

Table 2. Relative Power Losses in a Cylindrical Resonator

Longitudinal mode	Axially symmetrical radial mode
Standard ( $W_{100}$ ) = [ $P_w^{(\kappa)}$ ] $_{100}$ (eqn 3.17; $l=1$ )	Standard ( $W_{0m0}$ ) = [ $P_w^{(\kappa)}$ ] $_{0m0}$ (eqn 3.21; $l=0$ )
[ $P_w^{(\kappa)}$ ] $_{100} = W_{100} \times l^{5/2}$	[ $P_w^{(\kappa)}$ ] $_{lm0} = W_{0m0} \times [f_{lm0}/f_{0m0}]^{5/2}$
$2[P_e^{(\kappa)}]_{100} = W_{100} \times \frac{2r_0}{L} l^{5/2}$	$2[P_e^{(\kappa)}]_{lm0} = W_{0m0} \times \frac{2r_0}{L} [f_{lm0}/f_{0m0}]^{5/2}$
[ $P_w^{(\eta)}$ ] $_{100} = W_{100} \times \left(\frac{\eta C_p}{\kappa}\right)^{1/2} \frac{1}{(\gamma-1)} l^{5/2}$	[ $P_w^{(\eta)}$ ] $_{lm0} = W_{0m0} \times \frac{\left(\frac{\eta C_p}{\kappa}\right)^{1/2} v_0^2}{4L^2(\gamma-1)f_{0m0}^2} l^2 \left[\frac{f_{lm0}}{f_{0m0}}\right]^{1/2}$
[ $P_e^{(\eta)}$ ] $_{100} = 0$	$2[P_e^{(\eta)}]_{lm0} = W_{0m0} \times \frac{2r_0}{L(\gamma-1)} \left(\frac{\eta C_p}{\kappa}\right)^{1/2} \left[\frac{f_{lm0}}{f_{0m0}}\right]^{1/2}$

## § 6. EXPERIMENTAL PROCEDURE

Measurements were made at as many eigenfrequencies as possible within specific frequency ranges. As discussed in § 2 the lower limit of frequency was restricted to 1 kc/s. Readings were taken using the following modes:

- (1) the (00) mode between 1 kc/s and the first cut-off frequency,  $f_{011}$ , of a non-planar mode;
- (2) the (10) mode between  $f_{010}$  and  $f_{021}$ ;
- (3) the (20) mode between  $f_{020}$  and  $f_{031}$ .

In the latter cases the appropriate radial mode was predominant and the propagation of modes having lower cut-off frequencies did not disturb the measurements. By locating the two probe tubes on the axis of the cylinder, the experimental conditions were arranged to discriminate against modes having a pressure node on the axis.

A frequency spectrum of the resonator filled with nitrogen is shown in figure 4 (Plate II). It will be seen that in the two series of resonant frequencies  $f_{110}$  and  $f_{120}$  the peaks lie so close together that the resonance curves overlap at low values of  $l$ . Reliable measurements could not be made under these conditions since adjacent resonant frequencies were sufficiently close for beating to occur during the time of decay (figure 5 (a)) (Plate I). This resulted in a non-exponential envelope of the decay curves. Measurements made for  $l \leq 4$  at  $m=1$  or 2 were therefore excluded from further consideration. It would have been possible to separate the resonance curves for low values of  $l$  by using a shorter resonator. However, in this case the relative contribution of the molecular to the total absorption would have decreased to the detriment of the accuracy of the final result. A typical decay curve used in the evaluation of results is shown in figure 5 (b).

The procedure employed to derive the desired contribution to the total absorption which was due to relaxation processes was as follows. A reading of the measured decay time  $T_M$  corresponding to a known eigenfrequency was obtained in the manner described in § 2. The boundary layer losses and 'classical' body loss were calculated from the equations of § 3.2 making use of known or measured physical constants of the gas and the known sound field in

the resonator. The measured and calculated values of  $p_0\alpha/f^2$  were plotted as a function of  $p_0$  for each resonant condition ( $lm0$ ). The value of  $p_0\alpha^{(r)}/f^2$  was obtained by subtracting the total calculated values,  $p_0\alpha_{\text{calc}}/f^2$ , from the measured values  $p_0\alpha_M/f^2$  according to equation (3.16). A unique value of  $p_0\alpha^{(r)}/f^2$  has been obtained for each gas investigated. This justifies the procedure of selecting any convenient mode for determining the relaxational contribution to the absorption of the gas.

The above procedure requires that the sound velocity  $v_0$  shall be known. In gases for which no independent measurements of  $v_0$  were available this was determined from the measured cut-off frequencies  $f_{010}$  and  $f_{020}$  which are easily identified.

## § 7. TYPICAL EXPERIMENTAL RESULTS

The present technique has been used to determine the absorption in a number of gases, the results for which will be analysed in a separate paper. Typical results for argon, nitrogen and cyclopropane are given below to illustrate the use of the method.

### 7.1. Argon and Nitrogen

In examining the accuracy of the method measurements were first made in argon which is known to exhibit only 'classical absorption' (Parker *et al.* 1953) and for which the absorption coefficient can be calculated from the known physical constants of the gas. The agreement between measured and calculated values of  $p_0\alpha/f^2$  as a function of pressure is illustrated by the typical curves of figures 6 to 8.

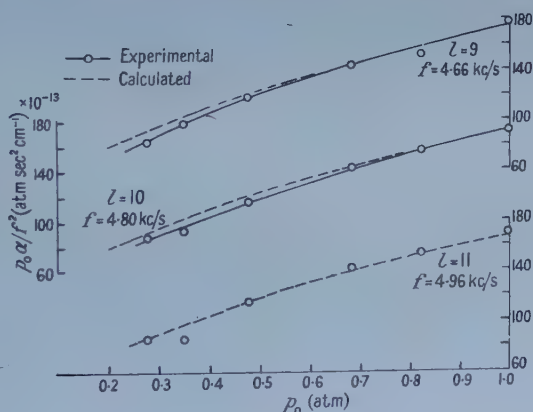


Figure 6. Calculated and measured losses for argon ( $l10$  mode).

The curves for the higher  $l$  values demonstrate the validity of the calculations of boundary layer losses according to § 3: the 'classical' body loss in the gas has been included in the calculated curves but only contributes approximately 1% of the total.

The divergence obtained at lower  $l$  values is illustrated and is attributed to the unreliability of the measurements under these conditions as discussed in § 6.

Similar results were obtained for measurements in nitrogen in which the body loss in the gas is known to be 1.25 times the 'classical' absorption (Parker *et al.* 1953).



This excess arises from the relaxational contribution of the rotational specific heat (Zmuda 1951) but the combined body losses are still only of the order of 1.5% of the total loss. The agreement found for these 'calibration' gases justifies the general use of this method for calculating boundary layer losses.

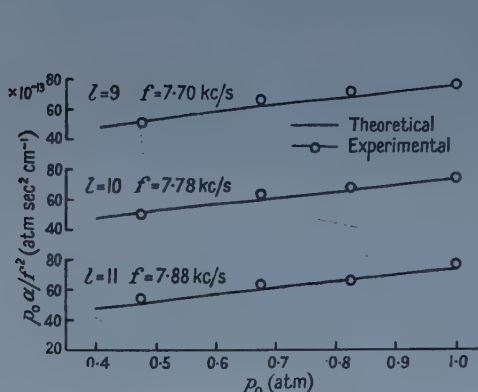


Figure 7. Calculated and measured losses for argon ( $l_{20}$ ).

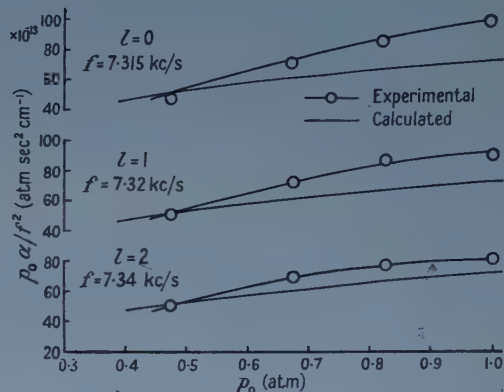


Figure 8. Calculated and measured losses for argon ( $l_{20}$ ). As discussed in the text such measurements are unreliable owing to interference between close resonances.

## 7.2. Cyclopropane

The third example which has been selected to illustrate the method is cyclopropane in which there is an appreciable contribution to the total loss from molecular processes: In this case  $P^{(r)}$  of equation (3.16) is significant (figures 9 and 10).

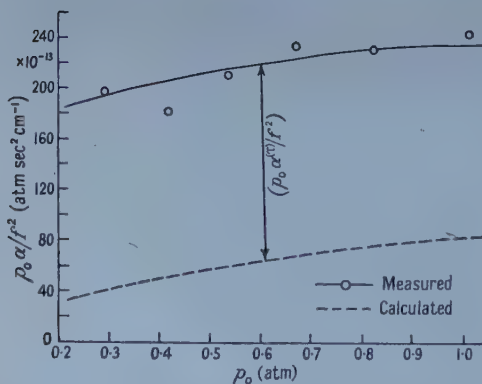


Figure 9. Measured and calculated absorption values in cyclopropane.  $l=7$ ,  $m=1$ ,  $n=0$ ;  $f=3.56$  kc/s. The constant difference between the two curves gives the absorption due to molecular relaxation processes,  $(p_0 \alpha^{(r)} / f^2) = 151 \times 10^{-13}$  atm sec<sup>2</sup> cm<sup>-1</sup>.

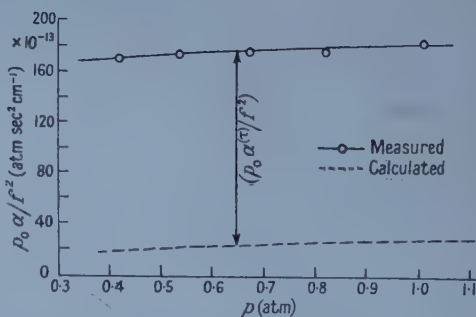


Figure 10. Measured and calculated absorption values in cyclopropane.  $l=10$ ,  $m=2$ ,  $n=0$ ;  $f=6.27$  kc/s. The constant difference between the two curves again gives  $(p_0 \alpha^{(r)} / f^2) = 151 \times 10^{-13}$  atm sec<sup>2</sup> cm<sup>-1</sup>.

The difference between the measured points and the calculated curves is independent of pressure and of the particular resonance for which the measurement is made. This difference  $p_0\alpha^{(r)}/f^2$  which is theoretically independent of  $p_0$  and  $f$  in  $(f/p_0)$  regions remote from the relaxation region represents the contribution from the molecular relaxation processes. Figure 9 and 10 are typical of the results recorded for the complete range of measurement ( $l=5$  to  $7$  for  $m=0$ ,  $l=5$  to  $14$  for  $m=1$  and  $2$ ). The arithmetical mean value of  $p_0\alpha^{(r)}/f^2$  derived from all measured points, according equal weight to each, is

$$151 \times 10^{-13} \text{N atm sec}^2 \text{cm}^{-1}.$$

The method of purifying the cyclopropane is described in the next section. Further measurements were made, however, on cyclopropane taken directly from the original cylinder. These yielded a mean value of  $p_0\alpha^{(r)}/f^2$  which was 5% lower than that for the distilled sample. Since the error of the final result is estimated at  $\pm 5\%$ , it is concluded that in the case of this sample of cyclopropane, no significant effect was produced by the purification procedure.

### 7.3. Sources of Gases and Physical Constants

Supplies of argon, nitrogen and cyclopropane were obtained from the British Oxygen Co. Ltd., who gave the following analyses:

- (i) Argon (Lead Seal): purity 99.95%  
*Impurities:*  $N_2$  < 500 volumes per million  
 $CO_2$  and  $O_2$  < 5 v.p.m.,  
 $H_2$  < 0.5 v.p.m.
- (ii) Nitrogen (Oxygen free): purity 99.9%  
*Impurities:*  $O_2$  < 10 v.p.m.,  
 $CO_2$  and other carbon compounds < 5 v.p.m.
- (iii) Cyclopropane (B.P. anaesthetic grade): assay 99.8%  
*Impurities:* unsaturated substances 0.07%,  
aldehydes < 5 v.p.m.

The gas samples used for flushing and filling the resonator were obtained from the cylinders in the following manner:

#### *Argon and Nitrogen.*

The cylinder was connected by rubber vacuum tubing to a cold trap filled with glass wool and cooled externally by liquid nitrogen. The trap was joined to a glass reservoir of 5 litre capacity which was attached to the all-glass inlet system of the measuring apparatus. Having evacuated the system, the trap and reservoir were flushed and filled with gas at an equilibrium pressure slightly above 1 atm by adjustment of the pressure regulator on the gas cylinder. Gas was admitted slowly to the resonator from the reservoir which was in turn replenished from the cylinder so that the pressure in the filling system did not fall below 1 atm during the operation.

#### *Cyclopropane.*

The gas from the cylinder was passed through a tower containing potassium hydroxide pellets and liquefied in a glass receiver cooled by a mixture of solid carbon dioxide and alcohol. The flow of gas was adjusted to maintain a pressure slightly above 1 atmosphere.

The cooled receiver was transferred to a crude low temperature vacuum distillation apparatus. The sample was degassed and fractionally distilled twice. The frozen middle fraction was transferred to the measuring apparatus and then allowed to distil into the resonator.

Silicone grease was used throughout on taps and cone joints.

The physical constants used in the calculation of boundary layer losses are listed in table 3.

## § 8. ACCURACY

### 8.1. Measuring Errors

The major contribution to the error in the value of  $p_0\alpha_M/f^2$  derived from measurement of a particular decay curve arises from the procedure of aligning the trace with the exponential curve drawn on the graticule. This is estimated to be  $\pm 12\%$ . A probable error of  $\pm 0.5\%$  occurs in each of the following: (i) in reading the pressure  $p_0$ , (ii) in tuning to a resonant frequency  $f_{lm0}$ , (iii) in the measured dimensions of the resonator  $r_0$  and  $L$ , (iv) in the value of the velocity of sound  $v_0$ , when this is derived from measurements of selected resonant frequencies. The error in  $v_0$  is negligible when reliable interferometric measurements are available in the literature.

Table 3. Physical Data

	Cyclopropane at 25°C and 1 atm.	Source	Correction procedure for temperature and pressure
Viscosity ( $\mu P$ )	89.8	Lambert, Cotton <i>et al.</i> (1955)	Graphical extrapolation
Thermal conductivity ( $\text{cal cm}^{-2} \text{sec}^{-1}(\text{deg. cm}^{-1})^{-1}$ )	$42.1 \times 10^{-6}$	<i>Ibid.</i>	Sutherland's equation
Sutherland's constant $C$	203	<i>Ibid.</i>	Derived from viscosity data
Specific heat $C_p$ ( $\text{cal g}^{-1}(\text{deg})^{-1}$ )	0.309	Kistiakowsky and Rice (1940)	Berthelot's equation
$\gamma = C_p/C_v$	1.187	Calculated	<i>Ibid.</i>
Density $\rho_0$ ( $\text{g cm}^{-3}$ )	$1.744 \times 10^{-3}$	Timmermans (1950)	None
Velocity of sound $v_0$ ( $\text{cm sec}^{-1}$ )	$258.5 \times 10^3$	Measured	None
Critical constants	$T_c(^{\circ}\text{K})$ $p_c(\text{atm.})$	397.8 54.2	Stull (1943)
			None

The inaccuracy of measurements and variation of the temperature of the thermostat is less than  $\pm 0.1^{\circ}\text{C}$ . In view of the above considerations it is estimated that an individual value of  $p_0\alpha_M/f^2$  may be in error by  $\pm 15\%$ . On the other hand when smooth curves are drawn through a number of experimental points the final accuracy of absorption determination represents a considerable improvement on this figure. Thus the standard deviation of all experimental points for argon is  $\pm 5\%$  and this represents the final error in the *measured* value



of  $p_0\alpha/f^2$ . The ultimate error in  $p_0\alpha^{(r)}/f^2$  depends also upon the calculated value of  $p_0\alpha/f^2$  which, in turn, is governed by the reliability of the physical constants employed in its derivation.

### 8.2. Other Possible Sources of Energy Loss

In addition to the mechanisms of absorption which have already been considered, energy may also be lost from the sound field in the following ways: (1) by transmission of mechanical energy to the material of the resonator wall; (2) by subsequent radiation of energy from the outer surfaces of the resonator to the ambient medium. This loss might be expected to acquire significance at resonant frequencies of the cylindrical shell; (3) by propagation of sound through the probe tubes.

The close agreement between measurements and calculations obtained for all modes considered in the cases of nitrogen and argon shows that losses from the above sources, (1), (2) and (3) are sufficiently small to be neglected in the present calculations. Appreciable losses by these means may, however, occur at particular frequencies and have, in fact, been observed at rather lower frequencies than those considered here. If such behaviour is found consistently, the measurements taken at these particular frequencies can be discarded.

### 8.3. Effects of Gas Imperfection

The contribution to  $p_0\alpha_M/f^2$  due to boundary layer absorption has been assumed to vary as  $\sqrt{p_0}$ . This is strictly true only in the case of a perfect gas. For imperfect gases the dependence on pressure is given by  $[p_0(1 + Bp_0)]^{1/2}$  where  $B$  is the 2nd virial coefficient. Within the accuracy of the present measurements on cyclopropane the correction can be neglected.

In addition the velocity of sound is affected by considerations of gas imperfection. Corrections to  $p_0\alpha^{(r)}/f^2$  due to this effect are less than 1% and have been neglected.

## § 9. CONCLUSIONS

A method has been investigated for the measurement of the acoustic absorption coefficient of gases in the frequency/pressure range between 1 and 45 kc/s per atmosphere at a temperature of 25°C.

In comparison with the continuous-wave method of delineating the resonance curve, the present method shows the following advantages: (1) The requirement on the frequency stability of the electrical oscillator is not as severe since it is only necessary for the latter to remain tuned at the peak of a resonance curve for the time required for the observation of a few excitation and decay cycles of the system. (2) It is not required to measure very small frequency deviations about resonance. (3) Interference due to direct electrical or acoustical transmission between transmitter and receiver is avoided since a recording is only made whilst the exciting transducer is quiescent. In comparison with the reverberation method there is a loss of sensitivity since resonant transducers cannot be employed. On the other hand the present system employs a specific resonant condition which is more readily produced than the diffuse sound field required for the theoretical analysis of reverberation measurements.

No results have yet been published of pulse measurements made by the pulse method (Parker *et al.* 1953) in highly absorbing gases but there seems to be no reason, in principle, why this method should not be used. Indeed it would appear to have several advantages over other techniques.

The continuous-wave method of Angona (1953), a description of which appeared after the present work had commenced, possesses marked advantages for highly absorbing gases since none of the restrictions on the apparatus listed in § 1 apply in this case.

The validity of the means by which allowance is made for boundary layer losses has been established by calibration measurements in argon and nitrogen.

In the case of cyclopropane, which exhibits an appreciable relaxational contribution to the absorption, it is confirmed that the latter is independent of the mode of propagation employed for its measurements.

The method has been used to determine the relaxational behaviour of other polyatomic gases, the results for which will be reported separately. The measured absorption will then be related to the relaxation time for energy exchange between molecular translation and vibration.

#### ACKNOWLEDGMENTS

This work was supported by a grant from the Department of Scientific and Industrial Research, to whom the authors are indebted. The logarithmic pen recorder was provided by the Scientific Investigations Grant-in-aid administered by the Royal Society and this assistance is gratefully acknowledged.

The authors wish to thank Professor Dr. H. O. Kneser and L. Fritsche of the Technische Hochschule, Stuttgart, for very helpful discussions concerning the losses in the boundary layers. One of us (P. D. E.) is indebted to the Department of Scientific and Industrial Research for the provision of a maintenance grant and to the Worshipful Company of Clothworkers for further support.

#### REFERENCES

- ANGONA, F. A., 1953, *J. Acoust. Soc. Amer.*, **25**, 1111, 1116.  
 BEATTY, R. E., 1950, *J. Acoust. Soc. Amer.*, **22**, 850.  
 BYERS, W. H., 1943, *J. Chem. Phys.*, **11**, 348.  
 CAMPBELL, I. D., 1953, *Acustica*, **3**, 395.  
 CREMER, L., 1948, *Arch. elektr. Übertr.*, **2**, 136.  
 ENER, C., BUSALA, A., and HUBBARD, J. C., 1955, *J. Chem. Phys.*, **23**, 155.  
 FOGG, P. G. T., HANKS, P. A., and LAMBERT, J. D., 1953, *Proc. Roy. Soc. A*, **219**, 490.  
 FOGG, P. G. T., and LAMBERT, J. D., 1955, *Proc. Roy. Soc. A*, **232**, 537.  
 KIRCHHOFF, G., 1868, *Ann. Phys., Lpz.*, **134**, 177.  
 KISTIAKOWSKY, G. B., and RICE, W. W., 1940, *J. Chem. Phys.*, **8**, 610.  
 KNÖTZEL, H., and KNÖTZEL, L., 1948, *Ann. Phys., Lpz.*, **2**, 393.  
 KNUDSEN, V. O., 1933, *J. Acoust. Soc. Amer.*, **5**, 64.  
 LAMBERT, J. D., *et al.*, 1955, *Proc. Roy. Soc. A*, **231**, 280.  
 LAMBERT, R. F., 1953, *J. Acoust. Soc. Amer.*, **25**, 1068.  
 MARKHAM, J. J., BEYER, R. T., and LINDSAY, R. B., 1951, *Rev. Mod. Phys.*, **23**, 353.  
 MAYO, C. G., BEADLE, D. G., and WHARTON, W., 1951, *Electron. Engng*, 424.  
 NIELSEN, A. K., 1949, *Trans. Danish Acad. Tech. Sci.*, No. 10.  
 PARKER, J. G., ADAMS, C. E., and STAVSETH, R. M., 1953, *J. Acoust. Soc. Amer.*, **25**, 263.  
 RAO, S. T., and HUBBARD, J. C., 1955, *J. Acoust. Soc. Amer.*, **27**, 321.  
 ROSSING, T. D., and LEGVOLD, S., 1955, *J. Chem. Phys.*, **23**, 1118.  
 SETTE, D., BUSALA, A., and HUBBARD, J. C., 1955, *J. Chem. Phys.*, **23**, 787.  
 STOKES, Sir G. G., 1845, *Trans. Camb. Phil. Soc.*, **8**, 287.  
 STULL, D. R., 1943, *Industr. Engng Chem. (Industr.)*, **36**, 1303.  
 TIMMERMANS, J., 1950, *Physico-Chemical Constants of Pure Organic Compounds* (Amsterdam: Elsevier).  
 VOELZ, K., 1952, *Z. angew. Phys.*, **3**, 67; 1952, *Ibid.*, **4**, 18.  
 ZMUDA, A. J., 1951, *J. Acoust. Soc. Amer.*, **23**, 472.

## Crystal Field Effects in Metals

By R. S. LEIGH

Atomic Energy Research Establishment, Harwell, Berks.

*Communicated by B. H. Flowers ; MS. received 26th September 1957*

IN this note we estimate the errors made in calculations of one-electron energy levels in metals by using a potential which is spherically symmetric inside the inscribed spheres of the atomic polyhedra and constant between these spheres. This approximation has been used up till now both in the augmented plane wave method (Slater 1937, 1953, Saffren and Slater 1953, Howarth 1955), and in methods of the 'spherical scatterer' type (Korringa 1947, Kohn and Rostoker 1954, Morse 1956), though in the former it is not necessary to make this approximation. We consider an idealized case in which the true crystal potential may be regarded as the sum of the electrostatic potentials of non-overlapping ion cores and a uniform neutralizing distribution of electrons. We consider only body-centred and face-centred cubic lattices.

Suppose that an approximate potential is constructed by taking the spherical average of the true potential inside the inscribed spheres, and by taking a constant, continuous with this, between the spheres. It may be noted that this is a different approximation from that of Howarth (1955), who took the potential inside the sphere to be that of the ion core alone. Between the spheres, our approximate potential, as seen by an electron, is everywhere lower than the true potential, so that its mean value is lower by an amount which we denote  $U(0)$ . Inside an inscribed sphere the true potential differs from the approximate one only to the extent that it is not spherically symmetric. This deviation from spherical symmetry may be expressed in terms of cubic harmonics of order  $l=4$  and higher. Suppose that the net charge of the ions in our model is  $+ze$ , so that the charge density of the uniform distribution of electrons is  $-ze/\Omega$ , where  $\Omega$  denotes the atomic volume. It is convenient to introduce a potential  $V(\mathbf{r})$  which is that of an electron in the field of point charges  $+ze$  at the lattice points and a uniform charge distribution of density  $-ze/\Omega$ . We suppose that the zero of  $V(\mathbf{r})$  is chosen so that its mean value is zero. Since the potential of the non-overlapping ion cores contributes equally to the true and approximate potentials, we need only discuss the potential  $V(\mathbf{r})$ .

Consider first states of the conduction band type. Suppose that each wave function deviates from a single combination of plane waves, with coefficients determined by symmetry, only in a region well inside the ion cores where the difference between the true and approximate potentials is negligible, and that this deviation is such as not to affect the normalization of the wave function appreciably. Estimates of the effect on the eigenvalues of the approximation to the potential may then be made using first order perturbation theory, the results being expressed in terms of the coefficients  $U(h)$  of the Fourier terms  $\exp(i\mathbf{h} \cdot \mathbf{r})$  in the difference between the true and approximate potentials.



To compute the  $U(h)$  we first note that the Fourier coefficients of  $V(\mathbf{r})$  are  $-4\pi ze^2/\Omega h^2$  ( $h \neq 0$ ) (see, for example, Wilson 1936, p. 91). We also have that the spherical average of  $V(\mathbf{r})$  inside the inscribed sphere is  $-ze^2[1/r - \phi_0 + 2\pi r^2/3\Omega]$ , where  $\phi_0$  is a constant whose value is given by Fuchs (1935) as  $3.6392/a$  for a body-centred cubic lattice and  $4.5848/a$  for a face-centred cubic lattice, where  $a$  denotes the lattice constant. We find that

$$U(h) = -\frac{4\pi ze^2}{\Omega} \frac{1}{h^2} \left[ \left(1 - \frac{4\pi r_0^3}{3\Omega}\right) j_0(hr_0) + \frac{4\pi r_0^3}{\Omega} \frac{j_1(hr_0)}{hr_0} \right] \quad (h \neq 0)$$

and

$$U(0) = \frac{ze^2}{r_0} \left[ 1 - r_0\phi_0 + \frac{4\pi r_0^3}{3\Omega} - \frac{1}{5} \left( \frac{4\pi r_0^3}{3\Omega} \right)^2 \right],$$

where  $r_0$  denotes the radius of the inscribed sphere, and the  $j_l(x)$  are spherical Bessel functions. Values of the first few coefficients  $U(h)$  for body-centred cubic and face-centred cubic lattices are given in the table in units of  $ze^2/a$ .

Also given in the table are the coefficients of the  $U(h)$  in the energy shifts of a few selected states. The notation for symmetry types is that of Howarth and Jones (1952) and Howarth (1953). The combinations of plane waves  $\exp(i\mathbf{k} \cdot \mathbf{r})$  used are those with the lowest available  $k$  for each symmetry type. These values of  $k$  are given in the table. Numerical values, in eV, for shifts relative to that of the state  $\Gamma_8$  are quoted for the lattice constants of body-centred cubic sodium and iron, and face-centred cubic copper and aluminium, and for the  $z$  values shown. That the value 6 for  $z$  in iron may be relevant is suggested by the work of Weiss (private communication). The estimates for aluminium are perhaps the most interesting. These indicate, for example, a change in the energy gap at the point L (centre of a hexagonal face of the Brillouin zone) of about 0.4 eV, and a change in the separation of two of the states at the point W (corner of the zone) of about 0.8 eV. In the case of copper there is an additional effect, not considered here, due to the overlapping of the d shells.

The above way of estimating energy shifts is clearly inappropriate for d-like states in metals like iron and copper where the d radial function is strongly peaked near the nucleus. (Strictly, this applies to all states in these metals whose symmetry is compatible with a d function.) In these cases the crystal wave function inside the inscribed sphere is predominantly like an atomic d function, with a low amplitude at the surface of the sphere. We make estimates of energy shifts as follows. We assume that the wave function is equal to an appropriate combination of plane waves, except that, inside the inscribed sphere, the d part of the plane waves is modified by replacing  $j_2(kr)$  by the atomic d radial function  $R_2(r)$  scaled so as to be continuous with  $j_2(kr)$  at the surface of the sphere. There are then two contributions to the energy shift: (i) from the plane waves, calculated as above except that, since their amplitude is less, the effect is reduced; and (ii) from the excess of charge density, inside the sphere, over that of the plane wave combination. The fact that in (i) the contribution from  $U(0)$  is reduced leads to the major part of the shift relative to  $\Gamma_8$  in these levels.

Suppose that the plane wave combination is normalized over a single atomic polyhedron. The normalization integral  $I$  of the above wave function over a polyhedron is then given by

$$I = 1 + \frac{4\pi\eta}{\Omega} \int_0^{r_0} \left\{ \left[ \frac{j_2(kr_0)}{R_2(r_0)} R_2(r) \right]^2 - [j_2(kr)]^2 \right\} r^2 dr,$$

where  $\eta$  for the states  $2\Gamma_d^1$  and  $3\Gamma_d^2$  takes the values  $15/2$  and  $15$  respectively in a body-centred cubic lattice, and  $15$  and  $40/3$  in a face-centred cubic lattice for the plane wave combinations of the previous table. Energy shifts taken from this table have therefore to be divided by the appropriate value of  $I$ . The second contribution to the energy shift comes entirely from the  $l=4$  part of  $V(\mathbf{r})$  inside the sphere. Let  $S_4(\omega)$  denote the cubic harmonic

$$P_4(\cos \theta) + (1/168)P_4^1(\cos \theta) \cos 4\phi.$$

## Body-centred Cubic Lattice

$(a/2\pi)h$	0	$\sqrt{2}$	2	$\sqrt{6}$	$2\sqrt{2}$	$\sqrt{6}$	$2\sqrt{2}$		
$(a/ze^2)U(h)$	+0.0273	-0.0088	+0.0158	+0.0024	-0.0032				
Symmetry type	$(a/2\pi)h$	0	$\sqrt{2}$	2	$\sqrt{6}$	$2\sqrt{2}$	Na	Fe	Fe
	$(a/2\pi)k$	Coefficients of $U(h)$					$z=1$	$z=1$	$z=6$
$\Gamma_s$	0	1						Datum	
$N_s$	$\sqrt{2}/2$	1	1				-0.03	-0.04	-0.27
$N_p^1$	$\sqrt{2}/2$	1	-1				+0.03	+0.04	+0.27
$P_s$	$\sqrt{3}/2$	1	3				-0.09	-0.13	-0.80
$3P_p$	$\sqrt{3}/2$	1	-1				+0.03	+0.04	+0.27
$H_s$	1	1	4	1			-0.07	-0.10	-0.59
$3H_p$	1	1		-1			-0.05	-0.08	-0.48
$2H_d^1$	1	1	-2	1			+0.11		
$2\Gamma_d^1$	$\sqrt{2}$	1	-2	2	-2	1	+0.14		See text
$3\Gamma_d^2$	$\sqrt{2}$	1		-2		1	-0.12		

## Face-centred Cubic Lattice

$(a/2\pi)h$	0	$\sqrt{3}$	2	$2\sqrt{2}$	$\sqrt{11}$	$2\sqrt{3}$	4		
$(a/ze^2)U(h)$	+0.0278	-0.0192	+0.0162	+0.0090	-0.0020	-0.0034	-0.0032		
Symmetry type	$(a/2\pi)h$	0	$\sqrt{3}$	2	$2\sqrt{2}$	$2\sqrt{3}$	4	Al	Cu
	$(a/2\pi)k$	Coefficients of $U(h)$					$z=3$	$z=1$	
$\Gamma_s$	0	1						Datum	
$L_s$	$\sqrt{3}/2$	1	1				-0.21	-0.08	
$L_p^1$	$\sqrt{3}/2$	1	-1				+0.21	+0.08	
$X_s$	1	1		1			+0.17	+0.06	
$X_p^1$	1	1		-1			-0.17	-0.06	
$W_s$	$\sqrt{5}/2$	1	2	1			-0.24	-0.09	
$W_p^1$	$\sqrt{5}/2$	1	-2	1			+0.58	+0.22	
$2W_p^2$	$\sqrt{5}/2$	1		-1			-0.17	-0.06	
$2\Gamma_d^1$	2	1		-2		1	-0.23	See text	
$3\Gamma_d^2$	$\sqrt{3}$	1		-1	-1	1	-0.31		

This table gives, for body-centred cubic and face-centred cubic lattices,

(i) values of the Fourier coefficients  $U(h)$  of the correction to the potential (see text), in units of  $ze^2/a$ ;

(ii) coefficients of  $U(h)$ , in first order perturbation theory, for energy shifts of plane wave combinations of the symmetry type and  $k$  value shown, and

(iii) numerical values in ev of these shifts for the lattice constants of two metals of each structure and for the  $z$  values shown.

The  $l=4$  part of  $V(\mathbf{r})$  is then given by  $B_4 r^4 S_4(\omega)$ , where  $B_4$  may be expressed in the form  $-ze^2 \Sigma P_4(\cos \psi)/R^5$ , where  $R$  and  $\cos \psi$  denote the length and direction cosine, relative to a given cube axis, of a lattice vector, and the summation extends over all non-zero lattice vectors. This formula for  $B_4$  is too slowly

convergent to be suitable for accurate computation, but is adequate for our purposes. We find that  $B_4$  is  $+3ze^2/a^5$  for a body-centred cubic lattice and  $+8ze^2/a^5$  for a face-centred cubic lattice. The energy shift is given by

$$\frac{1}{\bar{r}} \frac{4\pi\xi}{\Omega} B_4 \int_0^{r_0} \left\{ \left[ \frac{j_2(kr_0)}{R_2(r_0)} R_2(r) \right]^2 - [j_2(kr)]^2 \right\} r^6 dr,$$

where  $\xi$  for the states  $2\Gamma_d^1$  and  $3\Gamma_d^2$  takes the values  $+15/7$  and  $-20/7$  respectively in a body-centred cubic lattice, and  $+30/7$  and  $-160/63$  in a face-centred cubic lattice, for the same plane wave combinations as before.

Using the d radial function of Manning and Goldberg (1938), we find for body-centred cubic iron, with  $z=6$ , shifts in  $2\Gamma_d^1$  and  $3\Gamma_d^2$  of  $+0.4$  ev and  $-0.03$  ev respectively from the plane wave part of the charge density, and of  $+0.06$  ev and  $-0.04$  ev from the excess d charge density. Since  $U(0)$  is  $+0.83$  ev in this case, we have total energy shifts relative to  $\Gamma_s$  of  $-0.4$  ev and  $-0.9$  ev respectively. For comparison we give the corresponding results for face-centred cubic iron with  $z=6$ , though there is no evidence that this value of  $z$  is relevant to that case. We find 'plane wave' shifts of  $+0.03$  ev and  $-0.002$  ev for  $2\Gamma_d^1$  and  $3\Gamma_d^2$  respectively, and 'excess d' shifts of  $+0.04$  ev and  $-0.04$  ev. In this case  $U(0)$  is  $+0.67$  ev, so that we have total shifts of  $-0.6$  ev and  $-0.7$  ev relative to  $\Gamma_s$ .

Kohn and Rostoker (1954) have suggested that the constant potential between the spheres be chosen equal to the average value of the true potential in this region, rather than continuous with the spherical average at the surface of the sphere. If we denote the Fourier coefficients of the correction to this approximate potential by  $U'(h)$ , we find that  $U'(0)=0$ , and

$$U'(h) = U(h) + \frac{4\pi r_0^3}{\Omega} \left(1 - \frac{4\pi r_0^3}{3\Omega}\right)^{-1} U(0) \frac{j_1(hr_0)}{hr_0} \quad (h \neq 0).$$

Because of the introduction of a step in the approximate potential, the  $U'(h)$  decrease more slowly with increasing  $h$  than do the  $U(h)$ , for sufficiently large  $h$ . One may expect, however, a tendency for the lower Fourier coefficients to be smaller. For our model of the true potential, we find, for those values of  $h$  appearing in the table, that the values of  $(a/ze^2)U'(h)$  are respectively 0,  $-0.0019$ ,  $+0.0111$ ,  $-0.0011$ ,  $-0.0033$  for a body-centred cubic lattice, and 0,  $-0.0096$ ,  $+0.0168$ ,  $+0.0029$ ,  $-0.0035$ ,  $-0.0035$ ,  $-0.0005$  for a face-centred cubic lattice. For the energies of conduction band states relative to that of  $\Gamma_s$  there would seem to be little to favour either choice of approximate potential. The situation as regards the shifts in the energies of the d-band states relative to that of  $\Gamma_s$  is, however, quite different in the two cases. For the continuous potential, the actual estimated shift in the  $\Gamma_s$  eigenvalue was responsible for the major part of the shift in the d-band eigenvalues relative to it. For the Kohn and Rostoker potential, the estimated correction to the  $\Gamma_s$  eigenvalue is, of course, zero. For that potential, we find 'plane wave' shifts in body-centred cubic iron, with  $z=6$ , of  $+0.15$  ev in  $2\Gamma_d^1$  and  $-0.09$  ev in  $3\Gamma_d^2$ . The 'excess d' shifts are the same as before, so that we have total shifts of  $+0.2$  ev and  $-0.1$  ev respectively. For face-centred cubic iron, with  $z=6$ , we find 'plane wave' shifts of  $-0.03$  ev in  $2\Gamma_d^1$  and  $-0.07$  ev in  $3\Gamma_d^2$ , giving total shifts of  $+0.01$  ev and  $-0.1$  ev respectively.

It should be emphasized that the effect discussed here may readily be taken into account exactly in a full augmented plane wave calculation, including the



change in the wave functions produced by the change in potential. Our purpose has been only to investigate the size of the effect. The details may be quite wrong, particularly in the case of the d-like levels in iron, where our arbitrary assumption that the wave functions behave like a single symmetry combination of plane waves between the atoms may be far from the truth.

## ACKNOWLEDGMENTS

The author is indebted to Dr. W. M. Lomer for several discussions, and to Dr. E. C. Ridley for assistance in checking parts of the calculation.

## REFERENCES

- FUCHS, K., 1935, *Proc. Roy. Soc. A*, **151**, 585.  
HOWARTH, D. J., 1953, *Proc. Roy. Soc. A*, **220**, 513 ; 1955, *Phys. Rev.*, **99**, 469.  
HOWARTH, D. J., and JONES, H., 1952, *Proc. Phys. Soc. A*, **65**, 355.  
KOHN, W., and ROSTOKER, N., 1954, *Phys. Rev.*, **94**, 1111.  
KORRINGA, J., 1947, *Physica*, **13**, 392.  
MANNING, M. F., and GOLDBERG, L., 1938, *Phys. Rev.*, **53**, 662.  
MORSE, P. M., 1956, *Proc. Nat. Acad. Sci. U.S.A.*, **42**, 276.  
SAFFREN, M. M., and SLATER, J. C., 1953, *Phys. Rev.*, **92**, 1126.  
SLATER, J. C., 1937, *Phys. Rev.*, **51**, 846 ; 1953, *Ibid.*, **92**, 603.  
WILSON, A. H., 1936, *The Theory of Metals* (1st Edn) (Cambridge : University Press).

## The Elastic Scattering of Positrons by Atoms and Molecules

By H. S. W. MASSEY AND A. H. A. MOUSSA

University College, London

*MS. received 27th September 1957*

*Abstract.* The information available concerning the cross sections for elastic scattering of slow positrons by helium, neon, argon and hydrogen is analysed in terms of collision theory. Evidence is found that the polarization of the neutral atom or molecule by the incident positron is important in these collisions. A variational calculation of scattering by atomic hydrogen does not support this conclusion. Further methods of investigating the problem are suggested.

### § 1. INTRODUCTION

UNTIL recently it would have seemed to be of little interest to examine theoretically the scattering of slow positrons by atoms and molecules, the possibility of experimental test being extremely remote. The remarkable developments of experimental technique associated with the study of positronium formation has changed this situation completely. Provisional values of cross sections for elastic scattering of positrons of energy about 20 eV in helium, neon and argon have been given by Teutsch and Hughes (1956). These have been derived from an experimental study of the effects of electrical fields on the formation of positronium by slowing down of positrons in the different rare gases (Marder, Hughes, Wu and Bennett 1956). Similar experiments have also been carried out in molecular gases, but the interpretation is complicated by the possibility of energy loss by vibrational excitation. Nevertheless, even in these cases, some information is available about total cross sections.

It is the purpose of the present note to examine the possibilities from the theoretical viewpoint. The elastic scattering of positrons differs from that of electrons in two important aspects—the mean scattering potential is repulsive instead of attractive and no exchange effects occur. The latter difference considerably simplifies the theoretical treatment and suggests that the use of slow positrons for probing atomic and molecular fields, if experimentally practicable, would have advantages in that interpretation would be much simplified. On the other hand, with a repulsive scattering potential, the cross section is much less sensitive to details of the shape than for an attractive potential.

Furthermore, although one is relieved of the necessity of including exchange effects in discussing the scattering of slow positrons by atoms, the need to include the effect of polarization of the scatterer by the incident positron still remains.

We shall find that the experimental data for helium, neon and argon do suggest that polarization is quite important and this may be supported by elementary theoretical arguments. To pursue the matter further we have carried out a variational calculation for scattering by atomic hydrogen in which polarization is allowed for as done by Massey and Moiseiwitsch (1950) for

electron scattering. This leads to the contrary result as no appreciable effect is found to arise from inclusion of polarization. This leaves the matter open for investigation by more elaborate methods.

We also include finally the results of a variational calculation for scattering by molecular hydrogen in which polarization is ignored. Comparison with the observed results again indicates that polarization may be important.

## § 2. ELASTIC SCATTERING BY HELIUM, NEON AND ARGON

If polarization is ignored, the total cross section for elastic scattering of a positron of wave number  $k$  by an atom is given by

$$Q = \frac{4\pi}{k^2} \sum (2n+1) \sin^2 \eta_n \quad \dots\dots(1)$$

where the phase shift  $\eta_n$  is such that the solution of the equation

$$\frac{d^2 f_n}{dr^2} + \left[ k^2 - \frac{8\pi^2 m}{h^2} V(r) - \frac{n(n+1)}{r^2} \right] f_n = 0 \quad \dots\dots(2)$$

which vanishes at the origin, has the asymptotic form

$$f_n \sim \sin(kr - \frac{1}{2}n\pi + \eta_n). \quad \dots\dots(3)$$

The interaction energy  $V(r)$  is simply that of the positron with the undisturbed atom. Thus in the notation of self-consistent field theory, if  $Z_p$  is the effective nuclear charge of the atom for potential

$$V(r) = Z_p e^2 / r. \quad \dots\dots(4)$$

Detailed calculations were carried out for  $k=0.2, 0.5, 1.0$  and  $1.5$  atomic units corresponding to positive energies of  $0.54, 3.4, 13.5$  and  $30.4$  ev. The interaction energies were obtained from the self-consistent field calculations of Wilson and Lindsay (1935) for helium, Brown (1933) for neon and Hartree and Hartree (1936) for argon. The equations (2) were solved using the electronic computer in the Physics Department at University College, London, for the necessary values of  $n$  in each case. Results obtained are given in table 1.

The cross sections† derived from the experiments (Marder *et al.* 1956) refer to a mean positron energy of about 18 ev for which  $k$  is about 1.2 and have the values  $0.023, 0.12$  and  $1.5\pi a_0^2$  for helium, neon and argon respectively. These are much smaller than the theoretical values given in table 1, either for  $k=1$  or  $1.5$ , even though these are already considerably smaller than for electrons of the same energy.

It is very unlikely that the discrepancy is due to inaccuracy in the assumed interaction energy. As remarked earlier the sensitivity of the cross section to the interaction is less for a repulsive than for an attractive field.

It is natural to turn to polarization as the source of the discrepancy. This will certainly exert an effect of the correct sense. Polarization leads to an effective attraction which will therefore tend to reduce the absolute magnitude of the negative phase shift due to the repulsive form of  $V(r)$ . We may examine the matter a little further for helium.

Castellejo, Percival and Seaton (to be published) have shown that, for incident energies below the excitation threshold, polarization introduces an additional

† These cross sections are strictly not elastic but momentum loss cross sections. At the energies concerned the differences between these are unimportant for the arguments presented in this paper.



effective potential which has the asymptotic form  $-\frac{1}{2}\alpha e^2/r^4$  where  $\alpha$  is the polarizability of the scattering atom. The effect on phase shifts for  $n$  greater than 2 can probably be estimated quite accurately by supposing that the additional potential is represented by its asymptotic form throughout. For these values of  $n$  the function  $f_n$  is so small near the origin that this is a sufficient approximation. For the important phases  $\eta_0$  and  $\eta_1$  this procedure is grossly incorrect, but as a first attempt one may attempt to estimate the polarization effect as arising from an additional interaction  $-\frac{1}{2}\alpha e^2/(r^2+l^2)^2$  where  $l$  is of the order of magnitude of atomic dimensions. We now examine the effect of this for positrons in helium. For convenience we shall carry out the detailed analysis for  $k=1$ . It is true that this is above the excitation potential so the polarization effect cannot be strictly considered in terms of an additional real potential but it is not far above the threshold and we are seeking here only to examine possibilities.

Table 1. Phase Shifts and Cross Sections for Elastic Scattering of Positrons by He, Ne and A, ignoring Polarization. (Positron wave number  $k$  in atomic units so positron energy =  $13.5k^2$  ev.)

Phase Shifts (radians)					Partial Cross Sections (in units $\pi a_0^2$ )				
$n=0$					$Q_0=4 \sin^2 \eta_0/k^2$				
Atom \ $k$	0.2	0.5	1.0	1.5	Atom \ $k$	0.2	0.5	1.0	1.5
He	-0.084	-0.203	-0.364	-0.471	He	0.709	0.653	0.506	0.366
Ne	-0.173	-0.419	-0.769 <sub>5</sub>	-1.039	Ne	2.950	2.652	1.936	1.321
A	-0.268	-0.649 <sub>5</sub>	-1.191	-1.606	A	7.000	5.853	3.449	1.776
$n=1$					$Q_1=12 \sin^2 \eta_1/k^2$				
Atom \ $k$	0.2	0.5	1.0	1.5	Atom \ $k$	0.2	0.5	1.0	1.5
He	-0.0006	-0.008 <sub>4</sub>	-0.046	-0.097	He	0.0001	0.003 <sub>4</sub>	0.025	0.050
Ne	-0.0025	-0.033	-0.162	-0.320	Ne	0.002	0.052 <sub>5</sub>	0.310	0.527
A	-0.0077	-0.090	-0.376	-0.686	A	0.018	0.389	1.620	2.139
$n=2$					$Q_2=20 \sin^2 \eta_2/k^2$				
Atom \ $k$	0.2	0.5	1.0	1.5	Atom \ $k$	0.2	0.5	1.0	1.5
A	—	-0.006	-0.083	-0.244	A	—	0.003	0.138	0.499
Total Cross Section (in units $\pi a_0^2$ )									
Atom \ $k$	0.2	0.5	1.0	1.5					
He	0.709	0.656	0.531	0.416					
Ne	2.952	2.704	2.247	1.848					
A	7.018	6.244	5.208	4.413					

We first examine the phase shifts  $\zeta_0, \zeta_1$  which would be produced by a small attractive potential  $v(r) = -\frac{1}{2}\alpha e^2/(r^2+l^2)^2$  alone. Using the formula

$$\zeta_n = -\frac{4\pi^3 m}{h^2} \int_0^\infty v(r) [J_{n+1/2}(kr)]^2 r dr \quad \dots\dots (5)$$

we obtain, in atomic units,

$$\zeta_0 = \frac{\alpha\pi}{8kl^3} [1 - (1+2kl)e^{-2kl}], \quad \dots\dots (6)$$

$$\zeta_1 = \frac{\alpha\pi}{8k^3l^3} [(k^2l^2-3) + e^{-2kl}(3+6kl+5k^2l^2+2k^3l^3)]. \quad \dots\dots (7)$$

As a rough approximation we now take  $\eta_0 + \zeta_0$ ,  $\eta_1 + \zeta_1$  as the true zero and first order phase shifts,  $\eta_0$ ,  $\eta_1$  being as given in table 1 and having opposite signs to  $\zeta_0$  and  $\zeta_1$  respectively. If the 'observed' cross section of  $0.023\pi a_0^2$  is assumed, the magnitude of the first order phase shift for helium must be less than 0.085 radian. Taking the observed value of  $\alpha$  (1.37) for helium we find the values of  $\zeta_0$  and  $\zeta_1$ , for helium for  $l=1, 2$  and 3 which are given in table 2.

Table 2. Values of 'Polarization' Phase Shifts  $\zeta_0$  and  $\zeta_1$  for Helium

$l$	$\zeta_0$ (rad)	$\zeta_1$ (rad)
1	0.320	0.0890
2	0.061	0.0325
3	0.0196	0.0139

To be within the correct limit for  $|\eta_1 + \zeta_1|$  it is seen that  $l$  cannot be taken much smaller than 1. For  $l=1$ , however, the value of  $\zeta_0$  is comparable with that of  $|\eta_0|$  which appears in table 1. It is possible therefore that, while the first order phase shift remains of magnitude less than 0.085 radian, the net zero phase shift due to the opposing effect of the repulsive re-modified atomic field and the polarization is very much smaller in magnitude than when polarization is ignored—the discrepancy between the required theoretical and 'observed' values could then largely disappear. It may readily be verified that for  $k=l=1$ , the contribution to the total cross section from higher order phase shifts  $\zeta_2$ , etc. would be negligible.

It may be objected that the phase shifts estimated from the effective polarization potential are much too large because the positron wave has a much smaller amplitude for small  $r$  than the partial plane wave  $(\pi/2kr)^{1/2}J_{1/2}(kr)$ , because of the repulsion by the main atomic field. This is not really a serious objection. Even if we replace the plane wave in (5) with  $n=0$  by the solution  $(kr)^{-1}f_0(r)$  of the equation (2) the value of  $\zeta_0$  for  $k=1$  is not reduced by a factor of more than 2. Furthermore, if the effect of the mean and polarization fields nearly cancel out the best estimate for  $\zeta_0$  is probably obtained by using plane waves in (5).

A similar situation might well occur in neon and argon. For neon the observed data require for the phase shifts  $|\eta_0 + \zeta_0| < 0.2$ ,  $|\eta_1 + \zeta_1| < 0.11$  and for argon  $|\eta_0 + \zeta_0| < 0.6$ ,  $|\eta_1 + \zeta_1| < 0.35$ . These conditions might well be satisfied for a reasonable value of  $l$  in (6) and (7) in each case.

In view of these considerations one is encouraged to attempt to allow for polarization in a less empirical manner. The first thing to try is an application of the variational method to the scattering of positrons by atomic hydrogen. In anticipation of the results of this calculation it may be said that it provides no evidence of any important contribution at all from polarization even though this should be larger in hydrogen than in helium. This leaves the problem open for further investigation—possible methods are discussed in § 4.

### § 3. VARIATIONAL TREATMENT OF ELASTIC SCATTERING OF POSITRONS BY HYDROGEN ATOMS WITH INCLUSION OF POLARIZATION

We consider only the calculation of the zero-order phase shift.

Distinguishing the coordinates of the atomic electron and the positron by suffixes 1 and 2 respectively, the wave equation for the system can be written

$$(H - E)\Psi = 0,$$

where

$$H = -\frac{\hbar^2}{8\pi^2 m} (\nabla_1^2 + \nabla_2^2) - \frac{e^2}{r_1} + \frac{e^2}{r_2} - \frac{e^2}{r_{12}}, \quad \dots\dots(8)$$

$m$  being the mass of an electron or positron, and the proton is taken as the origin of polar coordinates. The energy  $E = -E_0 + k^2\hbar^2/8\pi^2 m$  where  $E_0$  is the binding energy of the ground state of hydrogen.

The variational method is based on the integral

$$L = \iint \Psi_t^* (H - E) \Psi_t d\tau_1 d\tau_2 \quad \dots\dots(9)$$

where the  $\Psi_t$  are suitable proper trial functions chosen to have the asymptotic form for large  $r_2$

$$\Psi_t \sim r_2^{-1} \psi_0(r_1) [\sin kr_2 + a \cos kr_2] \quad \dots\dots(10)$$

where  $\psi_0$  is the wave function for the ground state of hydrogen. The  $\Psi_t$  are chosen to include a number of parameters  $c_1, c_2, \dots$ . According to Hulthén's method an approximation  $\eta_0^t$  to the zero-order phase shift is given by

$$L(c_1, c_2, \dots, c_n, a) = 0$$

$$\frac{\partial L}{\partial c_r} = 0 \quad (r = 1, \dots, n), \quad \eta_0^t = \arctan a. \quad \dots\dots(11)$$

An alternative method, due to Kohn uses

$$\frac{\partial L}{\partial a} = 4\pi k, \quad \frac{\partial L}{\partial c_r} = 0 \quad (r = 1, \dots, n), \quad \eta_0^t = \arctan(a - L/4\pi k). \quad \dots\dots(12)$$

If  $\Psi_t$  takes the form  $\psi_0(r_1)F_0(r_2)$  the variational method gives an approximation to the phase shift  $\eta_0$  obtained from the equation (2) with  $V(r)$  the interaction energy between a positron and the mean field of a hydrogen atom:

$$V(r) = e^2 \left( \frac{1}{r} + \frac{1}{a_0} \right) \exp(-2r/a_0). \quad \dots\dots(13)$$

In their calculations for electron scattering by atomic hydrogen Massey and Moiseiwitsch (1950) used a trial function of this form with

$$F_0(r_2) = r_2^{-1} [\sin kr_2 + \{a + b \exp(-r_2/a_0)\} \cos kr_2] \quad \dots\dots(14)$$

$b$  being the adjustable parameter. To allow for polarization they replaced this, following a suggestion by Huang (1949), with a function depending on  $r_{12}$ , the interelectronic separation. This function was of the form

$$F_0(r_2, r_{12}) = r_2^{-1} [\sin kr_2 + \{a + (b + cr_{12}) \exp(-r_2/a_0)\} \cos kr_2]. \quad \dots\dots(15)$$

We have carried out calculations for positron scattering using trial functions of the same forms. The results are given in table 3.

Table 3. Zero-order Phase Shifts for Scattering of Positrons by Hydrogen Atoms

$k$ (A.U.)	Phase Shifts (radians)			
	Polarization ignored		Polarization included	
	Exact	Variational		Variational
		H	K	
0.2	-0.114	-0.115	-0.115	-0.098
0.5	-0.264	-0.264	-0.264	-0.251
1.0	-0.421	-0.420	-0.418	-0.417

The letters H and K distinguish results obtained by Hulthén's and Kohn's methods respectively.

It will be seen that the results obtained with the trial function (15) which is supposed to include polarization are not very different from those obtained with



(14) in which polarization is completely ignored. On the other hand, the trial function (14) gives a very good approximation to the phase shift obtained from numerical integration of the equation (2) with  $V$  as given by (13). Moreover, it agrees quite closely with the exact solution. The trial functions seem to be certainly as appropriate for positron as for electron scattering.

Before regarding these results as too strong evidence against the expirical considerations of the preceding section it must be remembered that the trial function (15) may not be really adequate for dealing with polarization effects even though, when polarization is ignored, the corresponding function (14) is fully adequate. The question must be left as still an open one, but we may examine briefly what further investigations may be made to try to settle the matter.

#### § 4. FURTHER METHODS OF INVESTIGATING POLARIZATION EFFECTS

One possibility which occurs immediately is that of using the Schwinger variational method in the same way as has been done by Newstein (1955) for electron scattering by hydrogen. If a plane wave trial function is employed in the Schwinger method a formula is obtained for the scattered amplitude which may be written in the form

$$f(\theta) = \frac{f_{B1}^2}{f_{B1} - f_{B2}} \quad \dots\dots(16)$$

where  $f_{B1}$  and  $f_{B2}$  are the scattered amplitudes given by the first and second Born approximation respectively. There is no difficulty in employing the data given by Newstein to carry out the calculations for positrons. Unfortunately it is not possible to obtain any decisive results in this way. Thus if no account is taken of excited states in calculating  $f_{B2}$  an approximation is obtained for the scattering by the mean undistorted atomic field, which may be calculated exactly by the method of partial cross sections as in § 2. For neither electron nor positron scattering does Newstein's method give very good results, so that it is very doubtful what significance can be attached to the results it gives for the scattering with polarization, in which excited states are allowed for in calculating  $f_{B2}$ .

Moreover, it has been pointed out to us by Dr. Percival that, although there is no effect in positron collisions which is strictly comparable with that of electron exchange in electron collisions, the possibility of real or virtual positronium formation is in some ways similar. The size of the maximum cross section for real positronium formation in atomic hydrogen, as calculated by Massey and Mohr (1954) using Born's approximation, is so large that the coupling between purely elastic scattering and positronium formation is probably strong and may well make a major contribution to the polarization. It should certainly be included in the calculation of  $f_{B2}$  in (16), but a better method of determining its importance in modifying the elastic scattering is to set up the coupled integro-differential equations for the process and solve them on a high-speed computer. This is now in progress and will also be carried out for the excitation of the 2-quantum states. A large part of the polarization should be allowed for in this way and a good estimate obtained of its importance.

It is also possible to use these considerations to guide the choice of more suitable trial functions for use with the Hulthén variational method—a method which does have the advantage of giving good results for scattering by the mean static field of the atom.

The resolution of the difficulties for positron scattering may well prove of importance in relation to electron scattering. It should be easier to disentangle the polarization effects for positrons. A method which gives this correctly can then be applied with some confidence to electrons. In view of the rather confused theoretical situation, it is clear that further experimental investigations would be valuable.

### § 5. POSITRON SCATTERING BY MOLECULAR HYDROGEN

The scattering of slow electrons has been investigated by Massey and Ridley (1956). They used the same variational method as that outlined in § 3 but with appropriate modifications for the axially symmetrical problem. Because of the complexity of the calculation, polarization was ignored. Quite good results were obtained at electron energies less than about 10 eV when electron exchange was allowed for.

It is possible to carry out the same analysis for positron scattering by merely reversing the signs of certain of the terms in their calculations in which electron exchange was not included. In this way cross sections of  $1.90$  and  $1.52\pi a_0^2$  are found for positrons of  $2.3$  and  $6.8$  eV energy respectively. For the higher energy,  $27$  eV, studied by Massey and Ridley the variational method is not so satisfactory as judged by the fact that the Kohn and Hulthén methods do not give results which agree very well. However,  $0.73\pi a_0^2$  can be taken as a rough value for this energy. Interpolation then gives about  $1.1\pi a_0^2$  for positrons of wave number unity.

The observations of Marder *et al.* (1956) give, according to the analysis of Teutsch and Hughes (1956) the value  $0.4\pi a_0^2$  for a cross section which in the atomic gases is the elastic, or more correctly, the momentum loss cross section. For diatomic gases this must be interpreted as an energy loss cross section which includes contributions from the excitation of inner molecular motions. The true elastic cross section according to the experiment must therefore be still less than  $0.4\pi a_0^2$ . There is therefore some evidence that for  $H_2$  also the elastic cross section is reduced by polarization effects.

### ACKNOWLEDGMENTS

We are indebted to Mr. Lawson for his skilled technical assistance in the operation of the electronic computer, to Mrs. Lawson for assistance in some of the numerical computations and to Mr. R. O. Ridley for permission to use numerical data obtained in the course of the joint work with one of us (H. S. W. M.) on electron scattering in molecular hydrogen.

### REFERENCES

- BROWN, F. W., 1933, *Phys. Rev.*, **44**, 214.  
 HARTREE, D. R., and HARTREE, W., 1936, *Proc. Roy. Soc. A*, **166**, 450.  
 HUANG, S. S., 1949, *Phys. Rev.*, **76**, 477, 1878.  
 MASSEY, H. S. W., and MOHR, C. B. O., 1954, *Proc. Phys. Soc. A*, **67**, 695.  
 MASSEY, H. S. W., and MOISEWITSCH, B. L., 1950, *Proc. Roy. Soc. A*, **205**, 483.  
 MASSEY, H. S. W., and RIDLEY, R. O., 1956, *Proc. Phys. Soc. A*, **69**, 659.  
 MARDER, S., HUGHES, V. W., WU, C. S., and BENNETT, W., 1956, *Phys. Rev.*, **103**, 1258.  
 NEWSTEIN, M. C., 1955, *Tech. Rep. No. 4*, M.I.T.  
 TEUTSCH, W. B., and HUGHES, V. W., 1956, *Phys. Rev.*, **103**, 1266.  
 WILSON, W. S., and LINDSAY, R. B., 1935, *Phys. Rev.*, **47**, 681.

## Microwave Resonance in Nickel at 35 Gc/s (kMc/s)

By G. S. BARLOW† AND K. J. STANDLEY

Department of Physics, University of Nottingham

*MS. received 13th September 1957, and in final form 4th November 1957*

**Abstract.** From microwave resonance measurements at 35 Gc/s ( $\lambda = 0.86$  cm) on a nickel single crystal, the anisotropy constants  $K_1$  and  $K_2$  have been determined from 20 to 150°C. At 20°C,  $K_1 = K_2 = -6.06 \times 10^4$  ergs cm<sup>-3</sup> gives the best fit with the experimental data.  $g$ -values of  $2.19 \pm 0.02$  were obtained for the nickel single crystal and for polycrystalline nickel and nickel-copper alloys containing up to 26 atomic per cent of copper. For nickel-manganese alloys, a decrease in  $g$ -value with increase in manganese content occurred, reaching 2.12 for the 13.5 atomic per cent manganese alloy.

### § 1. INTRODUCTION

A STUDY has been made of the microwave resonance absorption at a wavelength of 0.86 cm in a single crystal of nickel, and in polycrystalline nickel, nickel-copper and nickel-manganese alloys. Measurements were made in the temperature range 20–200°C and the object of the investigation was primarily to determine the spectroscopic splitting factor  $g$  and, in the case of the single crystal, the anisotropy constants  $K_1$  and  $K_2$ . Results on similar materials at the longer wavelength of 1.22 cm have already been reported (Standley and Reich 1955, Reich 1954) and it is therefore possible to assess the degree of frequency dependence of these parameters in nickel.

The experimental method was generally similar to that already described by Standley and Reich (1955), and the 8 mm microwave system differed only in minor details from the 1.22 cm equipment. The 8 mm cavity, which resonated in an  $H_{112}$  mode was made of such a diameter that the actual specimens employed in the former investigation could be used without further grinding or re-shaping. The parameters  $g$ ,  $K_1$  and  $K_2$  were determined from the equation (Kittel 1948)

$$h\nu = g\beta \{ [H_z^{\max} + (N_y - N_z)M + \phi] [H_z^{\max} + (N_x - N_z)M + \psi] \}^{1/2}. \quad \dots (1)$$

Here  $\beta$  is the Bohr magneton,  $N_x$ ,  $N_y$  and  $N_z$  are the demagnetization factors in the three coordinate directions,  $H_z^{\max}$  is the applied magnetic field in which maximum power absorption occurs in the specimen, and  $M$  is the magnetization in the specimen which is assumed to be saturated in the field  $H_z^{\max}$ .  $\phi$  and  $\psi$  are algebraic functions which take account of the magnetocrystalline anisotropy of the (single crystal) material and for a cubic crystal, when the surface of the specimen is a (110) face, as in these measurements, Healy (1951) has shown that

$$\begin{aligned} \phi &= (1 - 2 \sin^2 \theta - 3/8 \sin^2 2\theta) 2K_1/M - \sin^2 \theta \cos^2 \theta (3 \sin^2 \theta + 2) K_2/2M \\ \psi &= (2 - \sin^2 \theta - 3 \sin^2 2\theta) K_1/M \\ &\quad + \sin^2 \theta (6 \cos^4 \theta - 11 \sin^2 \theta \cos^2 \theta + \sin^4 \theta) K_2/2M. \quad \dots (2) \end{aligned}$$

The angle between  $H_z$  and the cube edge is  $\theta$ .

† Now at The Gateway School, Leicester.



In the single crystal measurements  $H_z^{\max}$  was determined for a series of values of  $\theta$  and thus, knowing  $M$  and the demagnetization coefficients,  $g$  and  $K_1$  and  $K_2$  were found from equations (1) and (2). With polycrystalline specimens, equation (1) was applied to obtain the  $g$ -values, assuming that both  $\phi$  and  $\psi$  average to zero (see §3 below).

The polycrystalline specimens used in the previous investigation and new specimens punched from thin sheet were polished on fine emery paper, annealed carefully *in vacuo* and then electrolytically polished. A final annealing *in vacuo* was occasionally found necessary.

The single crystal disc was cut from the ingot used by Reich. The orientation of the surface was checked by examination of the x-ray diffraction pattern obtained by reflection, using Cu  $K\alpha$  radiation. The surface finally used was very close to a (110) plane; the [110] direction appeared to lie in the surface, while the [100] direction was inclined at an angle not greater than  $1^\circ$ . The polishing of this surface was carried out as described above.

## § 2. EXPERIMENTAL RESULTS

### 2.1. The Nickel Single Crystal

The experimental results are summarized in table 1 while the figure shows the variation of the resonance field with orientation found at room temperature.

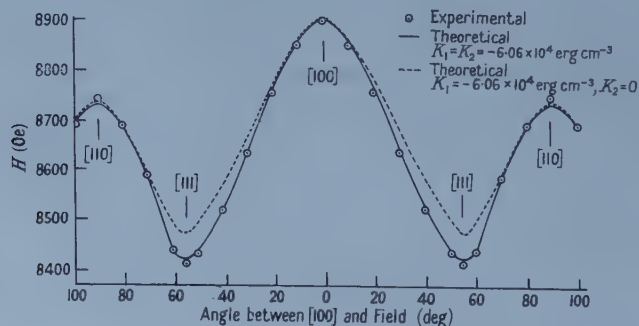
Table 1. Nickel Single Crystal Data

Temp. (°C)	$g$	$K_1$ (erg cm $^{-3}$ )	$K_2$ (erg cm $^{-3}$ )
20	2.17 <sub>3</sub>	$-6.06 \times 10^4$	$-6.06 \times 10^4$
50	2.17 <sub>7</sub>	-1.83	not determined
100	2.17 <sub>4</sub>	-0.49	+0.49
150	2.17 <sub>4</sub>	+0.25	+1.95

The circled points represent the experimental observations and the full line was calculated from equations (1) and (2) using the parameters

$$K_1 = K_2 = -6.06 \times 10^4 \text{ erg cm}^{-3}, \quad g = 2.17_3.$$

The agreement is good and is to be contrasted with the broken line drawn for  $K_1 = -6.06 \times 10^4 \text{ erg cm}^{-3}$  but with  $K_2 = 0$ . The fit is poor in the region of the



Resonance fields for the nickel single crystals.

[111] direction where  $K_2$  makes its greatest contribution and a positive value for  $K_2$  would make the agreement worse. It is not possible to obtain a set of parameters with positive  $K_2$  which represent adequately the experimental results.

The data obtained by Standley and Reich at a wavelength of 1.22 cm yielded  $K_1 = -5.83 \times 10^4$ ,  $K_2 = -6.3 \times 10^4$  erg cm<sup>-3</sup> and  $g = 2.17_5$ , while later room temperature measurements by Reich (1956) on a somewhat impure nickel specimen gave  $K_1 = -4.6 \times 10^4$ ,  $K_2 = -3.6 \times 10^4$  erg cm<sup>-3</sup>,  $g = 2.20$ .

It will be seen that  $K_1$  changes sign between 100 and 150°C and that  $K_2$  does so between 20 and 100°C. The experimental errors prevent an accurate determination of the temperatures at which the anisotropy constants are zero. It is estimated that the values of  $K_1$  and  $K_2$  at room temperature are in error by not more than 5% and 15% respectively. At the higher temperatures the experimental error increases to about 25% at 150°C for  $K_1$ , and to somewhat greater values (40%) for  $K_2$  at the same temperature.

## 2.2. Polycrystalline Nickel, Ni-Cu and Ni-Mn Alloys

Measurements on the nickel and nickel-copper alloys at a wavelength of 0.86 cm, from 20–200°C, yielded the same temperature-independent  $g$ -value as that found at 1.22<sub>2</sub> cm, namely  $2.19 \pm 0.02$ . Data obtained on four nickel-manganese alloys at room temperature are presented in table 2 and confirm the previous finding that the  $g$ -value decreases with increase in manganese content up to 13.5 atomic per cent Mn.

Table 2. Results obtained with Ni-Mn Alloys

atomic % Mn	$\lambda = 0.86$ cm	$\lambda = 1.22$ cm (a)
	$g$	$g$
1.2	2.21	2.17
5.1	2.18	2.14
10.1	2.14 <sub>5</sub>	2.14
13.5	2.13 <sub>5</sub>	2.12

(a)—Standley and Reich (1955)

## § 3. DISCUSSION

The magnetic field was measured either directly using a proton resonance system or indirectly using a search coil and fluxmeter checked against the proton resonance. Further check points of the field calibration were the resonances of the free radical, diphenyl picryl hydrazyl, at wavelengths of 0.86 and 1.22 cm. The estimated error in  $H_z^{\max}$  arising from field calibration and peak location is less than  $\pm \frac{1}{2}\%$  in the most favourable cases and should not exceed  $\pm 1\%$ . The main uncertainty in the measured  $g$ -values thus arises from the determination of  $M$  which may be in error by  $\pm 2\%$ . It seems likely therefore that the absolute values of  $g$  may be in error by  $\pm 1$  to  $\pm 1\frac{1}{2}\%$  or about  $\pm 0.02$  in values close to 2.00.

Referring to the figure,  $H_z^{\max}$  for the individual experimental points should be absolutely correct to within  $\pm 40$  oersteds and within  $\pm 20$  oersteds relative to other experimental resonance fields shown. The error in angle is thought to have been less than  $\pm 1^\circ$ . Thus it may fairly be claimed that the full theoretical line of the figure is a good representation of the experimental data and that the broken line calculated for  $K_2 = 0$  is in error by considerably more than the experimental error. For this material, as had previously been found at a longer wavelength, a negative value of  $K_2$  is clearly indicated.

The value of  $K_1$  agrees in magnitude and sign with recent determinations by torque methods (see for example Bozorth 1951). Usually  $K_2$  has been considered

to be zero, since the positive value reported by McKeehan (1937) from an analysis of Honda, Masumoto and Shirakawa's (1935) results was not a thoroughly reliable estimate. However, a modified torque method employed by Sato and Chandrasekhar (1956), specifically designed to measure  $K_2$ , yielded a positive value,  $+2.34 \times 10^4 \text{ erg cm}^{-3}$  at room temperature. There seems no satisfactory explanation of this discrepancy. A possible objection to the microwave method is that only surface layers are examined and these may differ from the bulk material. This is certainly true but it should be noted that  $K_2$  for iron obtained by Sato and Chandrasekhar is identical in sign and similar in order of magnitude to that obtained by Barlow and Standley (1956) for 2.5% silicon iron, by the microwave method. It has been found that the greatest care must be taken in annealing and subsequently handling the nickel single crystal specimen if reproducible microwave resonance results, relating to unstrained nickel, are to be obtained.

The  $g$ -values obtained confirm the results reported by Standley and Reich (1955), (a) that for nickel and nickel-copper alloys the  $g$ -value is  $2.19 \pm 0.02$  and is independent of frequency and temperature in the ranges 24–32 Gc/s and 20–200°C, and (b) that for nickel-manganese alloys a decrease in  $g$ -value occurs with increasing manganese content—the explanation offered previously still appears to hold. The constancy of the  $g$ -value against changes in frequency and changes from single to polycrystalline form shows that the peak shift in the polycrystalline case due to anisotropy (Standley and Stevens 1956) and any shift due to the finite penetration of the specimen by the microwave field (Kittel and Herring 1950, Rado and Weertman 1954, Ament and Rado 1955) must be small, i.e. within the experimental error of about 1%.

#### ACKNOWLEDGMENTS

The authors wish to thank Professor L. F. Bates for his continued interest and advice. One of us (K. J. S.) is indebted to the Government Grant Committee of the Royal Society for a grant which made possible the purchase of the 8 mm microwave apparatus, while the other (G. S. B.) wishes to thank the Department of Scientific and Industrial Research for a maintenance award.

#### REFERENCES

- AMENT, W., and RADO, G. T., 1955, *Phys. Rev.*, **94**, 1386.
- BARLOW, G. S., and STANDLEY, K. J., 1956, *Proc. Phys. Soc. B*, **69**, 1052.
- BOZORTH, R. M., 1951, *Ferromagnetism* (New York: Van Nostrand).
- HEALY, D. W., 1951, *Harvard University, Cruft Laboratory, Tech. Rep.*, 135.
- HONDA, K., MASUMOTO, H., and SHIRAKAWA, Y., 1935, *Sci. Rep. Tohoku Imp. Univ.*, **24**, 391.
- KITTEL, C., 1948, *Phys. Rev.*, **73**, 155.
- KITTEL, C., and HERRING, C., 1950, *Phys. Rev.*, **77**, 725.
- McKEEHAN, L. W., 1937, *Phys. Rev.*, **51**, 136.
- RADO, G. T., and WEERTMAN, J. R., 1954, *Phys. Rev.*, **94**, 1386.
- REICH, K. H., 1954, *Ph.D. Thesis*, Nottingham University; 1956, *Phys. Rev.*, **101**, 1647.
- SATO, H., and CHANDRASEKHAR, B. S., 1956, *J. Phys. Chem. Solid State*, **1**, 228.
- STANDLEY, K. J., and REICH, K. H., 1955, *Proc. Phys. Soc. B*, **68**, 713.
- STANDLEY, K. J., and STEVENS, K. W. H., 1956, *Proc. Phys. Soc. B*, **69**, 993.



# An Investigation of the Reactions $^{24}\text{Mg}(\text{d}, \text{p})^{25}\text{Mg}$ and $^{26}\text{Mg}(\text{d}, \text{p})^{27}\text{Mg}$ by Magnetic Analysis

By S. HINDS†, R. MIDDLETON† AND G. PARRY

Nuclear Physics Research Laboratory, University of Liverpool

*Communicated by H. W. B. Skinner ; MS. received 31st July 1957, and in final form 2nd October 1957*

**Abstract.** Angular distributions have been measured of some protons groups emitted from targets of natural magnesium and  $^{26}\text{MgO}$  when bombarded by 8.9 mev deuterons. These distributions have been fitted with curves calculated from the deuteron stripping theories enabling assignments of parities and possible spins to be made to the states of the residual nuclei. The reduced level widths of these states have been calculated in absolute units.

Several proton groups were observed corresponding to previously unreported levels in  $^{25}\text{Mg}$  and  $^{27}\text{Mg}$ .

## § 1. INTRODUCTION

THE energy levels of  $^{25}\text{Mg}$  have been determined by Endt, Enge, Haffner and Buechner (1952) up to an excitation energy of 4.42 mev from an investigation of the  $^{24}\text{Mg}(\text{d}, \text{p})^{25}\text{Mg}$  reaction, and up to 3.97 mev from the  $^{27}\text{Al}(\text{d}, \alpha)^{25}\text{Mg}$  reaction. Several proton groups leading to levels having a higher excitation have been observed by Holt and Marsham (1953 a) from the (d, p) reaction. Freier, Fulk, Lampi and Williams (1950) and Fields and Walt (1951) have observed many levels with an excitation above the neutron binding energy of 7.324 mev by neutron resonance scattering.

The reaction  $^{26}\text{Mg}(\text{d}, \text{p})^{27}\text{Mg}$  has been investigated by Endt, Haffner and Van Patter (1952), who reported the first excited state to be at 0.987 mev, and by Holt and Marsham. The latter observed another excited state at 3.50 mev.

Holt and Marsham (1953 a) have measured the angular distributions of some proton groups from the  $^{24}\text{Mg}(\text{d}, \text{p})$  reaction leading to several of the levels of  $^{25}\text{Mg}$  lying below an excitation of 3.5 mev, and they were able to assign parities and possible spins to these levels. Unique spin assignments have been made for some of these levels by Gove, Bartholomew, Paul and Litherland (1956) from an investigation of the  $^{25}\text{Mg}(\text{p}, \text{p}'\gamma)$  reaction.

Angular distributions have been measured by Goldberg (1953) of some neutron groups from the  $^{24}\text{Mg}(\text{d}, \text{n})$  reaction leading to states of the mirror nucleus,  $^{25}\text{Al}$ . Some properties of these states with an excitation energy between 2.29 and 5.8 mev have been determined from proton scattering measurements (Koester 1952) and also the spins and parities of most of the states below 5.3 mev excitation have been determined by Litherland, Paul, Bartholomew and Gove (1956) from the  $^{24}\text{Mg}(\text{p}, \gamma)$  reaction. The latter authors have attempted an explanation of the low-lying level structure of  $^{25}\text{Mg}$  and  $^{25}\text{Al}$  on the basis of the collective model of the nucleus (Bohr and Mottelson 1955).

†Now at the Atomic Weapons Research Establishment, Aldermaston, Berks.

In the present investigation several proton groups from the  $^{24}\text{Mg}(\text{d}, \text{p})$  and  $^{26}\text{Mg}(\text{d}, \text{p})$  reactions have been observed leading to previously unreported levels of  $^{25}\text{Mg}$  and  $^{27}\text{Mg}$ . Angular distributions of many of these groups have been measured, together with those leading to established levels, so enabling parities, possible spins and reduced widths, to be determined on the basis of the deuteron stripping theories.

## § 2. EXPERIMENTAL TECHNIQUE

The results reported here from the bombardment of  $^{24}\text{Mg}$  with 8.9 mev deuterons, accelerated in the Liverpool 37 in. cyclotron, incorporate measurements obtained with two different targets of natural magnesium. The first target was bombarded in the magnetic spectrograph designed by Green and Middleton (1956) and the second in the modified apparatus described by Dalton, Hinds and Parry (1957). The latter exposure, although resulting in poorer resolution, enabled absolute cross sections to be measured and gave better statistical accuracy on the angular distributions.

The targets were prepared by evaporating natural magnesium, in a vacuum, on to polished sheets of stainless steel. On flexing the latter it was possible to peel off very thin foils of magnesium to make self-supporting targets. Natural magnesium contains 78.6%  $^{24}\text{Mg}$ , 10.1%  $^{25}\text{Mg}$ , and 11.3%  $^{26}\text{Mg}$  so that protons arising from the reactions with the rarer isotopes were observed. These were identified by exposing separated isotope targets of  $^{25}\text{MgO}$  and  $^{26}\text{MgO}$ . As only small amounts of these substances were available, the targets were prepared by depositing a drop of a slurry of the oxide in water, on to one leaf gold ( $0.2 \text{ mg cm}^{-2}$ ) supported in the target frame. Unfortunately the  $^{25}\text{MgO}$  target was very thick so that a complete analysis of the  $^{25}\text{Mg}(\text{d}, \text{p})^{26}\text{Mg}$  reaction was not possible, although many proton groups were identified as resulting from this reaction.

Absolute cross sections for the  $^{24}\text{Mg}(\text{d}, \text{p})$  reaction were calculated from the number of protons observed in the group, the charge of deuterons collected in the Faraday cup situated behind the target, the known acceptance solid angle of the spectrograph ( $2.3 \times 10^{-5}$  steradian) and the weight of the target ( $0.6 \text{ mg cm}^{-2}$ ). The estimated error on these absolute cross sections is about  $\pm 25\%$ . The cross section measurements made with the  $^{26}\text{MgO}$  target were converted to absolute units by comparing the intensities of the  $^{27}\text{Mg}$  ground state group which was observed in the spectra obtained from both the separated isotope and natural magnesium targets. The error on these absolute cross sections is estimated to be  $\pm 50\%$ .

## § 3. IDENTIFICATION OF GROUPS

A typical proton spectrum obtained at an angle of observation of  $15^\circ$  from the 8.9 mev deuteron bombardment of natural magnesium is shown in figure 1. Proton groups arising from impurities of carbon and oxygen in the target were identified from their known  $Q$ -values and energy shift with angle and are labelled C or O respectively with a suffix denoting the particular excited state of the residual nucleus. The strong group with an energy of about 7.4 mev is due to recoil protons from the elastic scattering of hydrogen in the target.

Protons were observed from the bombardment of  $^{26}\text{MgO}$  corresponding to transitions to previously unreported levels in  $^{27}\text{Mg}$  at excitations of 3.56, 3.76, 4.13 and 4.76 mev (all  $\pm 0.07$  mev). Most of these groups were observed from





the bombardment of natural magnesium, together with those from transitions to the ground state and levels at 0.987, 1.66 and 3.50 mev. The level at 1.66 mev excitation has previously been reported by Haling, Peck and Eubank (1957) from an investigation of the  $^{27}\text{Al}(n, p)^{27}\text{Mg}$  reaction. These groups are indicated on the spectrum by the symbol  $^{27}\text{Mg}$  and the particular final energy level in mev. The group arising from a transition to the 3.56 mev level of  $^{27}\text{Mg}$  was previously assigned to correspond to a level of  $^{25}\text{Mg}$  at 4.421 mev by Endt, Enge *et al.* (1952) from an investigation using a natural magnesium target. These authors did not rule out the possibility that in fact the group might correspond to a level in  $^{27}\text{Mg}$ . The present assignment was obtained by comparing the ratios of the intensities of this group to other groups from the  $^{26}\text{Mg}(d, p)$  reaction, measured from both the natural magnesium target and the  $^{26}\text{MgO}$  target. All the intensity of this group from the natural magnesium target could be explained on the assumption that there was a negligible yield due to a transition from  $^{24}\text{Mg}$  to a level at 4.421 mev of  $^{25}\text{Mg}$  at all angles of observation.

Several weak groups from the  $^{25}\text{Mg}(d, p)^{26}\text{Mg}$  reaction were observed both from the natural magnesium and  $^{25}\text{MgO}$  targets. These all corresponded to known levels of  $^{26}\text{Mg}$  (Endt and Kluver 1954) except for a group to a new level at 6.86 mev. All of the remaining groups in the spectrum from the natural magnesium target have been assumed to be due to levels of  $^{25}\text{Mg}$ . On this basis new levels have been assigned to  $^{25}\text{Mg}$  at excitations of 4.72, 5.27, 5.79, 6.80, 6.85, 7.18, 7.23 and 8.05 mev (all  $\pm 0.07$  mev), but there is a possibility that the group assigned to a level at 5.27 mev is due to the  $^{25}\text{Mg}(d, p)^{26}\text{Mg}$  reaction. The  $^{25}\text{Mg}(d, p)^{26}\text{Mg}$  reaction may also be responsible for a background in some of the groups. In particular a group due to a level of  $^{26}\text{Mg}$  with an excitation of about 9 mev may be contributing to the doublet arising from the 4.75 mev level of  $^{27}\text{Mg}$  and the 5.79 level of  $^{25}\text{Mg}$ . Similarly, the doublet due to the 6.80/6.85 mev levels may have a background from levels at about 11 mev excitation of  $^{26}\text{Mg}$ .

The  $^{25}\text{Mg}$  level at 4.72 mev excitation probably corresponds to the level at 4.62 mev reported by Holt and Marsham. They also found levels at 5.05, 5.49 and 6.40 mev excitation. Proton groups leading to the last two of these levels were observed, although that to the last level was masked at all angles of observation except  $5^\circ$  by carbon groups. The group corresponding to the level at 5.05 mev was not observed. The small group appearing at this position in the spectrum shown in figure 1 is due to the 4.13 level of  $^{27}\text{Mg}$  with possibly a small background due to levels in  $^{26}\text{Mg}$ . The states of  $^{25}\text{Mg}$  at an excitation of 7.40, 7.58 and 7.73 have been reported by Fields and Walt.

#### § 4. ANGULAR DISTRIBUTIONS FOR THE $^{24}\text{Mg}(d, p)^{25}\text{Mg}$ REACTION

The angular distribution of the proton groups from the  $^{24}\text{Mg}(d, p)$  reaction are shown in figure 2. The distributions are labelled by the excitation energy in mev of the final state of  $^{25}\text{Mg}$ . The stripping curves shown were calculated from the theory of Butler (1951) using a radius of interaction of  $5.2 \times 10^{-13}$  cm, which is the Gamow-Critchfield (1949) radius. Curves were also calculated from the theory of Bhatia, Huang, Huby and Newns (1952) for a radius of  $6.2 \times 10^{-13}$  cm, but these have only been shown where a significant departure was observed between the two theories.

In table 1 are listed the values of  $l$  used in the calculation of the theoretical curves. In the fourth column are the parities and possible spins  $J_f$  of the final states deduced from the stripping selection rules for a target having zero spin. Column (d) contains values of the neutron capture probability  $\Lambda$  deduced from

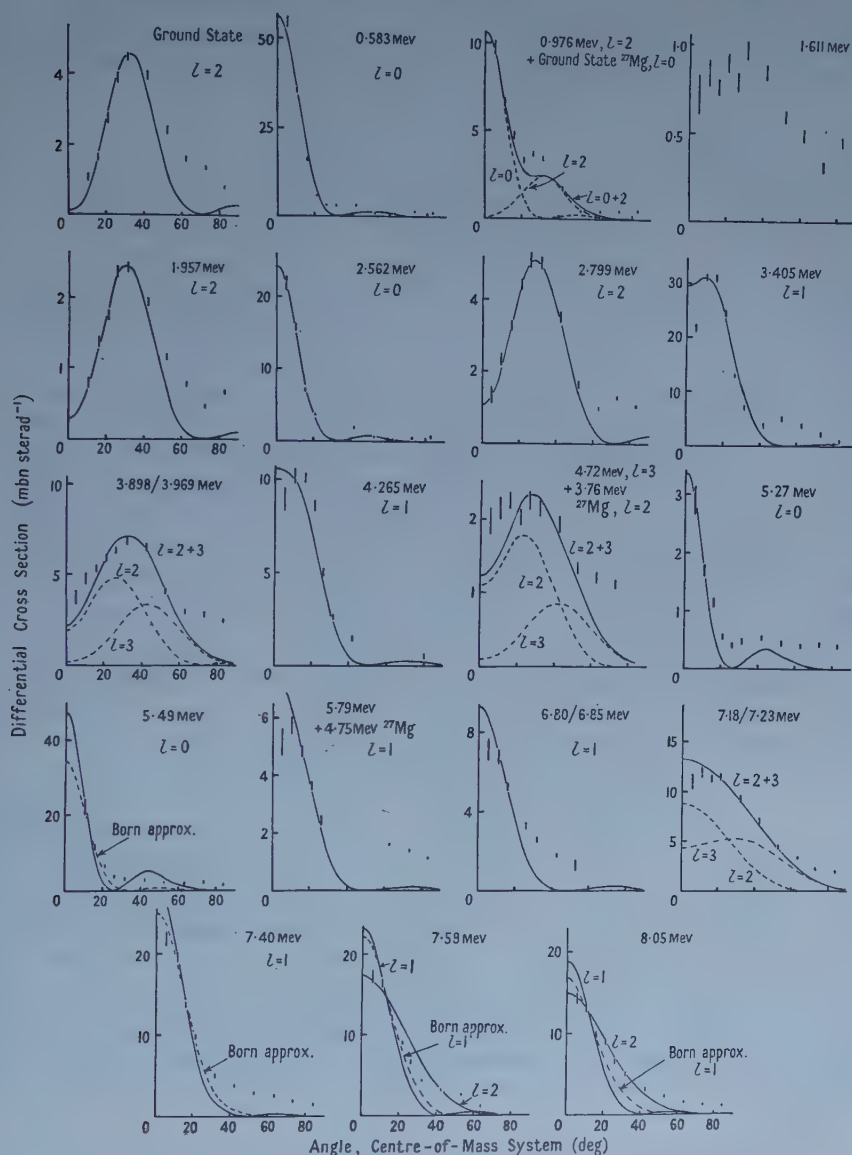


Figure 2. Angular distributions of some proton groups from the  $^{24}\text{Mg}(d, p)^{25}\text{Mg}$  reaction. The distributions are labelled by the excitation energy of the corresponding final state.

the theory of Bhatia *et al.* These are in relative units, chosen to give the same value for the ground state transition as the results of Holt and Marsham, which are tabulated in the previous column (c). Where comparison is possible the corresponding values are in agreement.

Also in the table we give absolute values for the reduced width of the final level,  $\gamma^2$ , multiplied by  $(2J_f+1)$ , deduced from the theory of Butler, and in column (f) values for the ratio of  $\gamma^2$  to the sum rule limit  $3\hbar^2/2MR$ . This column compares with (e), which are the values of  $\theta^2$  obtained by Fujimoto, Kikuchi and Yoshida (1954) from the results of Holt and Marsham. The results of Fujimoto *et al.* have been amended to allow for the numerical correction given by Holt and Marsham (1953 b). It should be noted that the values for  $\gamma^2$  have

Table 1. $^{24}\text{Mg}(d, p)^{25}\text{Mg}$								
Energy levels (MeV)		$l$	$J_f$	$\Lambda$ (rel. units)	$(2J_f+1)\gamma^2$ (erg cm $\times 10^{-20}$ )	$\theta^2$		
(a)	(b)		(c)	(d)	(e)	(f)		
						or (g)		
0		2	$\frac{5}{2}^+$	15.4	15.4	15.5	0.01 (e)	0.013
0.583		0	$\frac{1}{2}^+$	6.2	5.8	11.4	0.02 (e)	0.030
0.976		2	$\frac{3}{2}^+$	6.2	$\sim 6.3$	$\sim 8.0$	0.009 (e)	$\sim 0.01$
1.611		?	$(\frac{7}{2}^+)$	—	—	—	—	—
1.957		2	$\frac{5}{2}^+$	5.5	5.5	7.0	0.004 (e)	0.006
2.562		0	$\frac{1}{2}^+$	—	2.2	5.5	—	0.014
2.736		—	—	—	—	—	—	—
2.799		2	$\frac{3}{2}, \frac{5}{2}^+$	—	10.3	13.4	—	0.017, 0.012
3.405		1	$\frac{3}{2}^-$	8.7	11.2	21.8	0.019 (e)	0.028
3.898	}	2	$\frac{3}{2}, \frac{5}{2}^+$	$\sim 7$	$\sim 10$	—	—	$\sim 0.012, 0.008$
		and	and	—	—	—	—	—
		3	$\frac{5}{2}, \frac{7}{2}^-$	$\sim 25$	$\sim 22$	—	—	$\sim 0.019, 0.014$
3.969		1	$\frac{1}{2}, \frac{3}{2}^-$	2.8	6.1	—	—	0.016, 0.008
4.265		3?	$\frac{5}{2}, \frac{7}{2}^-$	$\sim 5$	$\sim 6$	—	—	$\sim 0.005, 0.004$
4.72		0	$\frac{1}{2}^+$	0.3	2.0	—	—	0.005
5.27		0	$\frac{1}{2}^+$	3.3	$\sim 29$	—	—	$\sim 0.076$
5.49		1	$\frac{1}{2}, \frac{3}{2}^-$	$< 1.1$	$< 3.3$	—	—	$< 0.009, 0.004$
5.79		1	$\frac{1}{2}, \frac{3}{2}^-$	1	4.6	—	—	0.012, 0.006
6.80		$> 1$	—	—	—	—	—	—
6.85		2	$\frac{3}{2}, \frac{5}{2}^+$	$\sim 4$	$\sim 8$	—	—	$\sim 0.011, 0.007$
7.18	}	and	and	—	—	—	—	—
7.23		3	$\frac{5}{2}, \frac{7}{2}^-$	$\sim 16$	$\sim 25$	—	—	$\sim 0.022, 0.017$
7.40		1	$\frac{1}{2}^-$	2.7	18	0.09 (g)	—	0.048
7.58		1	$\frac{1}{2}^-$	2.3	18	0.11 (g)	—	0.046
8.05		2 (or 1)	$\frac{3}{2}, \frac{5}{2}^+$	4.5	12	—	—	0.015, 0.010

a, Endt, Enge *et al.* (1952); b, present investigation; c, neutron capture probability from Holt and Marsham (1953 a); d, neutron capture probability, present investigation; e,  $\theta^2 = \gamma^2(3\hbar^2/2MR)^{-1}$  from Fujimoto *et al.* (corrected values); f,  $\theta^2$  from present investigation; g,  $\theta^2$  from neutron resonance scattering, calculated from the results of Fields and Walt (1951).

been obtained by the usual method of directly fitting the Butler curves to the experimental distributions. These values of  $\gamma^2$  are smaller than would be obtained if allowance were made for Coulomb and other effects (Tobocman and Kalos 1955). Thus the value of  $\gamma^2$  obtained by the analysis of Bowcock (1955) using the results of Holt and Marsham for the 3.405 mev level is  $41 \times 10^{-20}$  erg cm, whereas our result using direct fitting is  $5.5 \times 10^{-20}$  erg cm.

The angular distributions obtained by Holt and Marsham, at a bombarding energy of 8 mev, for the ground state and first two excited state transitions are



in agreement with those presented here. The absolute cross sections also agree with the corrected values of Holt and Marsham (1953 b). It should be noted that the cross section scale in figure 2 for the combined distribution of the groups leading to the 0.976 mev level of  $^{25}\text{Mg}$  and the ground state of  $^{27}\text{Mg}$  refers only to the former group. For the latter group the scale must be corrected for the abundance ratio, i.e. multiplied by 6.9. This also applied to other combined distributions where one member is from the  $^{26}\text{Mg}(d, p)^{27}\text{Mg}$  reaction.

The angular distribution of the group leading to the 1.611 mev level of  $^{25}\text{Mg}$  was not observed to be isotropic, as found by Holt and Marsham, although the magnitude of the cross section is approximately the same. This might be explained by the fact that the bombarding energies differed by about 1 mev. The groups corresponding to levels at 2.562, 2.736 and 2.799 mev were resolved and  $l=0$  and 2 assigned to the transitions leading to the 2.562 and 2.799 mev states. The middle member of the triplet was observed to be weak. This result agrees with the combined distribution of the three groups obtained by Holt and Marsham.

The combined distribution of the groups corresponding to the 3.898 and 3.969 mev levels of  $^{25}\text{Mg}$  was fitted with a combination of curves calculated for  $l=2$  and 3 transitions. The reduced width,  $\gamma_2^2$  for the  $l=2$  part has been calculated from the value of the peak cross section of the  $l=2$  contribution shown. The value of  $\gamma_3^2$  for the  $l=3$  contribution was similarly calculated. This procedure has been followed to calculate  $\gamma^2$  for all combined distributions.

The combined angular distribution of the proton groups leading to the 4.72 mev level of  $^{25}\text{Mg}$  and the 3.76 mev level of  $^{27}\text{Mg}$ , which could not be resolved clearly at all angles, probably corresponds to  $l=2$  and 3 transitions. From the  $^{26}\text{MgO}$  target exposure the transition to the 3.76 mev level of  $^{27}\text{Mg}$  has  $l=2$  so that the transition to the 4.72 mev level of  $^{25}\text{Mg}$  may possibly be assigned as  $l=3$ .

The combined distribution of the groups leading to the 5.79 mev state of  $^{25}\text{Mg}$  and the 4.75 mev state of  $^{27}\text{Mg}$ , has been fitted with an  $l=1$  transition. At angles where these two groups are resolved they have about the same intensity, so that it is probable that  $l=1$  assignments may be made for both transitions. Also from the  $^{26}\text{MgO}$  target exposure an approximate assignment of  $l=1$  could be made to the transition to the  $^{27}\text{Mg}$  level, but this distribution was very poor due to interference from carbon groups. At angles where the doublet leading to the 6.80 and 6.85 mev levels is resolved there are indications that the  $l$ -value of the transition to the 6.85 mev level is greater than one, an assignment of  $l=1$  may therefore be made to the 6.80 mev level transition. The stripping curves with different  $l$ -values are rather similar for  $Q$ -values about  $-3$  mev so that the  $l$ -value assignment for the 8.05 mev level transition is uncertain, although  $l=2$  is preferred.

## § 5. ANGULAR DISTRIBUTIONS FOR THE $^{26}\text{Mg}(d, p)^{27}\text{Mg}$ REACTION

These distributions, shown in figure 3, were all measured from the exposure using the  $^{26}\text{MgO}$  target, except for that corresponding to the 3.56 mev level of  $^{27}\text{Mg}$ . This distribution was obtained from the natural magnesium target exposure, from which an  $l=1$  assignment may be made. Using the separated isotope target the 3.50 and 3.56 mev levels could not be resolved but the combined distribution, shown in figure 3, may be fitted with  $l=0+1$ , and hence the 3.50 mev level transition probably has  $l=0$ .

Holt and Marsham have previously measured the angular distributions of the protons from the ground state and 0.987 Mev transitions and these are in agreement with those reported here, but we observed the cross sections to be about twice as large. It is notable that the distribution for the group leading to the 0.987 Mev level may best be fitted with a Butler curve having  $R = 5.8 \times 10^{-13}$  cm, this is  $0.5 \times 10^{-13}$  cm larger than the Gamow-Critchfield radius which was used for all the other distributions. This is not in disagreement with the distribution observed by Holt and Marsham. The protons leading to the 1.66 Mev level were combined, at most angles, with those arising from carbon. Similarly, the group leading to the 4.75 Mev excited state was obscured at some angles by another group from carbon, so that the angular distribution was difficult to interpret. But it is possible that the 4.75 Mev level transition has  $l = 1$ .

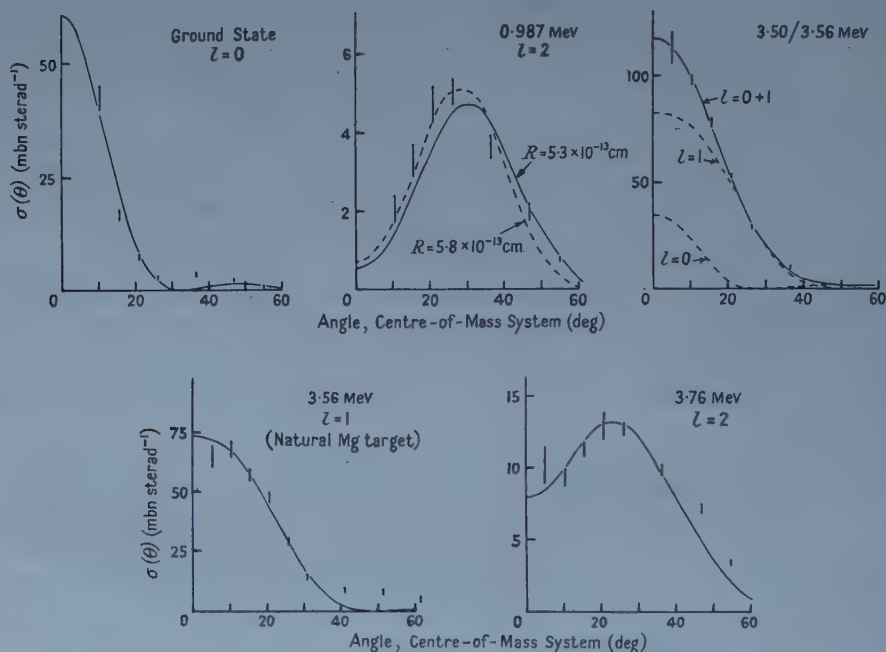


Figure 3. Angular distributions of some proton groups from the  $^{26}\text{Mg}(d, p)^{27}\text{Mg}$  reaction. The distributions are labelled by the excitation energy of the corresponding final state.

The differences between the corrected values of  $\theta^2$  obtained by Fujimoto *et al.*, and our values, shown in the table 2, are due to our cross sections being about a factor two larger than those found by Holt and Marsham.

## § 6. DISCUSSION

A feature of the angular distributions is that all the  $l = 1$  transitions show dips below the theoretical curves in the forward direction. This behaviour has been discussed in a previous paper (Dalton, Hinds and Parry 1958).

The  $l$ -value assignments obtained for the states of  $^{25}\text{Mg}$  agree with the spins and parities found by Gove *et al.* for the states up to 1.957 Mev excitation. These authors have shown that the spin and parity of the 1.611 level is probably

Table 2.  $^{26}\text{Mg}(d,p)^{27}\text{Mg}$ 

Energy level (mev)	$l$	$J_f$	$(2J_f+1) \gamma^2$ (erg cm $\times 10^{-20}$ )	$\theta^2$
(a)	(b)			(c) (d)
0	0	$\frac{1}{2}^+$	12.1	0.009 0.032
0.987	2	$\frac{3}{2}, \frac{5}{2}^+$	10.6	0.006, 0.004 0.014, 0.009
	1.66	—	—	—
3.50	0	$\frac{1}{2}^+$	$\sim 13$	$\sim 0.03$
	3.56	1 $\frac{1}{2}, \frac{3}{2}^-$	35	0.093, 0.047
	3.76	2 $\frac{3}{2}, \frac{5}{2}^+$	25	0.033, 0.022
	4.13	—	—	—
	4.75	1? —	—	—

$a$ , Endt, Haffner and Van Patter (1952) and Holt and Marsham (1953a);  $b$ , present investigation;  $c$ ,  $\theta^2 = \gamma^2 (3\hbar^2/2MR)^{-1}$  from Fujimoto *et al.* (corrected values);  $d$ , present investigation.

$\frac{7}{2}^+$  which is not inconsistent with our observed angular distribution. The formation of this state by stripping would require an  $l=4$  transition which would give a proton group of small intensity so that the major part of the cross section probably arises from compound nucleus formation and decay. The assignment of  $\frac{3}{2}^-$  to the 3.405 mev level of  $^{25}\text{Mg}$  by Kinsey and Bartholomew (1954) from an investigation of the reaction  $^{24}\text{Mg}(n,\gamma)$  is in agreement with the present results. Fields and Walt (1951) have assigned  $\frac{1}{2}^-$  to both the 7.40 and 7.58 mev levels, from an investigation of neutron resonance scattering, which is in agreement with our results. From their data we have calculated the reduced widths  $\gamma^2$  for these virtual levels and also  $\theta^2$ . As may be seen from table 1 the values for  $\theta^2$  obtained from the work of Fields and Walt are only about twice as large as those found from the present stripping investigation. This is surprising since the values of  $\theta^2$  obtained from stripping reactions by fitting Butler curves directly to the experimental points are usually much smaller than the values obtained from resonance scattering, as is shown by Bowcock's analysis. An example of this may be seen by comparing the values of  $\theta^2$  obtained by Koester for certain states of  $^{25}\text{Al}$ , with those reported here for the corresponding mirror levels of  $^{25}\text{Mg}$ , as shown in table 3.

Table 3

$^{25}\text{Mg}$		$^{25}\text{Al}$	
Level (mev)	$\theta^2$ from stripping (direct fitting)	Level (mev)	$\theta^2$ from resonance scattering
3.405	0.028	3.08	0.18
$l=3$ part of 3.898/3.969	0.019 ( $\frac{3}{2}$ ), 0.014 ( $\frac{7}{2}$ )	3.72	0.22
$l=2$ part of 3.898/3.969	0.012 ( $\frac{3}{2}$ ), 0.008 ( $\frac{5}{2}$ )	3.88 ?	0.001
4.265	0.016 ( $\frac{1}{2}$ ), 0.008 ( $\frac{3}{2}$ )	3.85	0.14

It is seen that for three out of the four levels in the table the values obtained from stripping are much smaller than those from resonance scattering. The discrepancy between the values for the  $l=2$  part of the 3.898/3.969 doublet and the 3.88 level of  $^{25}\text{Al}$  is not understood. It is unlikely that a mirror level



of  $^{25}\text{Al}$  having a large value of  $\theta^2$  was missed in the measurements on the resonance scattering of protons. On the other hand if the contribution of an  $l=2$  pattern to the combined distribution corresponding to the 3.898 and 3.969 levels is actually very small, the shape of the distribution is difficult to explain.

There are many states with appreciably reduced widths which cannot be explained by a simple shell model. These may be explained on the independent particle model by assuming the ground state configuration of  $^{24}\text{Mg}$  to be impure. The large values of  $\theta^2$  for the ground, 0.583 and 3.405 mev states suggest that these could be the most predominantly single particle states formed by the addition of a  $d_{5/2}$ ,  $s_{1/2}$  and  $p_{3/2}$  neutron respectively. The assignment of the single particle  $d_{3/2}$  and  $f_{7/2}$  states is uncertain.

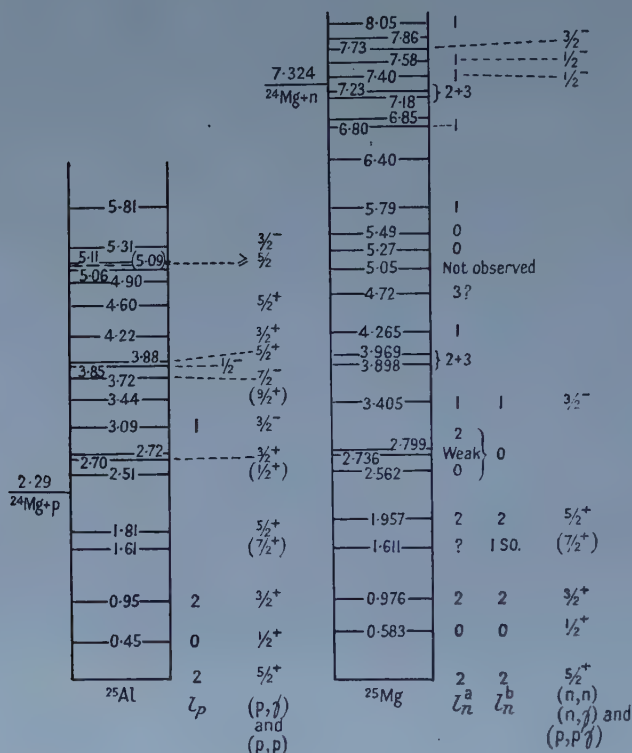


Figure 4. Comparison of the energy level schemes of the mirror nuclei  $^{25}\text{Mg}$  and  $^{25}\text{Al}$ .  $l_n^a$ —value assignments for the ingoing neutron from the  $^{24}\text{Mg}(d, p)^{25}\text{Mg}$  reaction, present investigation.

$l_n^b$ —value assignments from the  $^{24}\text{Mg}(d, p)^{25}\text{Mg}$  reaction, reported by Holt and Marsham (1953).

$l_p$ —value assignments for the ingoing proton from the  $^{24}\text{Mg}(d, n)^{25}\text{Al}$  reaction, reported by Goldberg (1953).

It has been shown by Litherland *et al.* (1956) and Gove *et al.* (1956) that the ideas of the collective model may be applied to nuclei in the region of  $A=25$  to explain their states in terms of rotational bands. Figure 4 is a diagram of the levels of  $^{25}\text{Mg}$  and of its mirror nucleus  $^{25}\text{Al}$ . The above authors have suggested that the states of  $^{25}\text{Al}$  up to 3.88 Mev can be explained in terms of four rotational

bands, and that the 0.583, 0.976 and 1.957 Mev states of  $^{25}\text{Mg}$  can be attributed to a rotational band with  $K=\frac{1}{2}$ . Further similarities to the rotational bands in  $^{25}\text{Al}$  states possibly exist in the  $^{25}\text{Mg}$  states. Thus the level at 3.405 Mev, one of the states of the 3.898/3.969 Mev doublet corresponding to an  $l=3$  transition and the 4.265 Mev level, could form a negative parity band with  $K=\frac{1}{2}$ , the spins of these states being  $\frac{3}{2}^-$ ,  $\frac{7}{2}^-$  and  $\frac{5}{2}^-$ , which are possible from our  $l$ -value assignments. Also by analogy with the  $^{25}\text{Al}$  band having  $K=\frac{1}{2}$  and members at 2.51 ( $\frac{1}{2}^+$ ), 2.70 ( $\frac{3}{2}^+$ ) and 3.88 Mev ( $\frac{5}{2}^+$ ), a further  $K=\frac{1}{2}$  band of  $^{25}\text{Mg}$  would be expected with members 2.562, 2.799 Mev, and the  $l=2$  component of the 3.898 and 3.969 Mev levels. As mentioned above there is some uncertainty associated with the third member of this band.

If there is a fourth rotational band in  $^{25}\text{Mg}$  corresponding to a band in  $^{25}\text{Al}$ , the first two states are the ground state and 1.611 Mev state, assuming its spin to be  $\frac{7}{2}^+$ . The third member would be at about 3.44 Mev excitation with spin  $\frac{9}{2}^+$ . We would not expect to detect a state in  $^{25}\text{Mg}$  with these properties as the transition would result in an  $l=4$  pattern, and the weak group corresponding to it would be obscured by the strong group arising in the transition to the nearby 3.405 Mev level.

The properties of the levels of  $^{27}\text{Mg}$  may be explained by assuming an impure configuration for  $^{26}\text{Mg}$  on the basis of the independent particle model. There is not sufficient information about the levels to attempt an interpretation on the basis of the collective model.

#### ACKNOWLEDGMENTS

The authors are grateful to Professor H. W. B. Skinner for his encouragement and advice. We are also indebted to Dr. H. C. Newns for discussion on the interpretation of the results. We are grateful to Miss P. M. P. Robinson, and the late Mr. E. C. Hewitt for assistance in measuring and processing the plates. One of us (S. H.) wishes to make acknowledgment to the Department of Scientific and Industrial Research for a maintenance grant. The oxides of  $^{25}\text{Mg}$  and  $^{26}\text{Mg}$  were obtained from the Atomic Energy Research Establishment, Harwell.

#### REFERENCES

- BHATIA, A. B., HUANG, K., HUBY, R., and NEWNS, H. C., 1952, *Phil. Mag.*, **43**, 485.  
 BOHR, A., and MOTTELSON, B. R., 1955, *Beta and Gamma Ray Spectroscopy*, edited by K. Siegbahn. (Amsterdam: North-Holland Publishing Co.)  
 BOWCOCK, J. E., 1955, *Proc. Phys. Soc. A*, **68**, 512.  
 BUTLER, S. T., 1951, *Proc. Roy. Soc. A*, **208**, 559.  
 DALTON, A. W., HINDS, S., and PARRY, G., 1957, *Proc. Phys. Soc. A*, **70**, 586.  
 ENDT, P. M., ENGE, H. A., HAFNER, J. W., and BUECHNER, W. W., 1952, *Phys. Rev.*, **87**, 27.  
 ENDT, P. M., HAFNER, J. W., and VAN PATTEN, P. M., 1952, *Phys. Rev.*, **86**, 518.  
 ENDT, P. M., and KLUYVER, J. C., 1954, *Rev. Mod. Phys.*, **26**, 95.  
 FIELDS, R. E., and WALT, M., 1951, *Phys. Rev.*, **83**, 479 (L).  
 FREIER, G., FULK, M., LAMPI, E. E., and WILLIAMS, J. H., 1950, *Phys. Rev.*, **78**, 508.  
 FUJIMOTO, Y., KIKUCHI, K., and YOSHIDA, S., 1954, *Prog. Theor. Phys., Japan*, **11**, 264.  
 GAMOW, G., and CRITCHFIELD, C. L., 1949, *Theory of the Atomic Nucleus* (Oxford: University Press).  
 GOLDBERG, E., 1953, *Phys. Rev.*, **89**, 760.  
 GOVE, H. E., BARTHOLOMEW, G. A., PAUL, E., and LITHERLAND, A. E., 1956, *Nuc. Phys.*, **2**, 132.

- GREEN, T. S., and MIDDLETON, R., 1956, *Proc. Phys. Soc. A*, **69**, 16.  
HALING, R. K., PECK, R. A., and EUBANK, H. P., 1957, *Phys. Rev.*, **106**, 971.  
HOLT, J. R., and MARSHAM, T. N., 1953 a, *Proc. Phys. Soc. A*, **66**, 258 ; 1953 b, *Ibid*,  
**66**, 1032.  
KINSEY, B. B., and BARTHOLOMEW, G. A., 1954, *Phys. Rev.*, **93**, 1260.  
KOESTER, L. J., 1952, *Phys. Rev.*, **85**, 643.  
LITHERLAND, A. E., PAUL, E., BARTHOLOMEW, G. A., and GOVE, H. E., 1956, *Phys. Rev.*,  
**102**, 208.  
TOBOCMAN, W., and KALOS, M. H., 1955, *Phys. Rev.*, **97**, 132.



## Rotational Analysis of Bands of the $c^3\Sigma, b^3\Sigma - a^3\Pi$ System of Boron Monofluoride, BF

By R. F. BARROW, D. PREMASWARUP†, J. WINTERNITZ  
AND P. B. ZEEMAN†

Physical Chemistry Laboratory, Oxford University

*MS. received 23rd September 1957*

**Abstract.** Rotational analyses have been made of six bands of the  $b^3\Sigma - a^3\Pi$  system and of the 0, 0 band of the  $c^3\Sigma - a^3\Pi$  system of BF. Contrary to an earlier analysis, appreciable  $\Lambda$ -type doubling is found in the  $^3\Pi$  state; its magnitude and sign show that this state is regular and not inverted. No predissociations or interactions with the singlet states have been observed.

### § 1. INTRODUCTION

THE halides of the typical elements of group III all have ground states which may be represented:  $(w\pi)^4 (x\sigma)^2, ^1\Sigma^+$ . Their lowest excited states are triplets, and in a number of cases it has been demonstrated that these first excited states are  $^3\Pi_{\text{reg}}$ , presumably from  $(w\pi)^4 (x\sigma) (v\pi), ^1\Pi, ^3\Pi_{\text{reg}}$  (AlCl, AlBr, Sharma 1951 a, b; GaF, Barrow, Dodsworth and Zeeman 1957; InF, Barrow, Glaser and Zeeman 1955).

Two triplet band-systems of BF have been observed (Strong and Knauss 1936); three bands of the system  $b^3\Sigma - a^3\Pi$  were the subject of a rotational analysis by Paul and Knauss (1938). Two of their conclusions, namely that the  $\Lambda$ -type doubling in the state  $a^3\Pi$  is negligibly small and that this state is inverted, are difficult to accept: (for a discussion of electron configurations in the states of BF, see Chrétien 1950).

We have therefore studied the rotational structure of these bands again, using the somewhat higher resolving power available in the third and fourth orders of the 21-ft grating at the University of Stellenbosch. We had also in mind the possibility that this might throw light on the relative heights of singlet and triplet levels in BF, and on the dissociation energy of this molecule. Neither hope has been fulfilled, but what are believed to be correct analyses of bands of the  $c$ - $a$  and  $b$ - $a$  systems show unequivocally that the state  $a^3\Pi$  is regular and not inverted.

### § 2. ANALYSIS: $\Lambda$ -TYPE DOUBLING

Experimental details have been given in earlier papers in this series. The bands were excited in a hollow-cathode discharge through a stream of gaseous boron trifluoride.

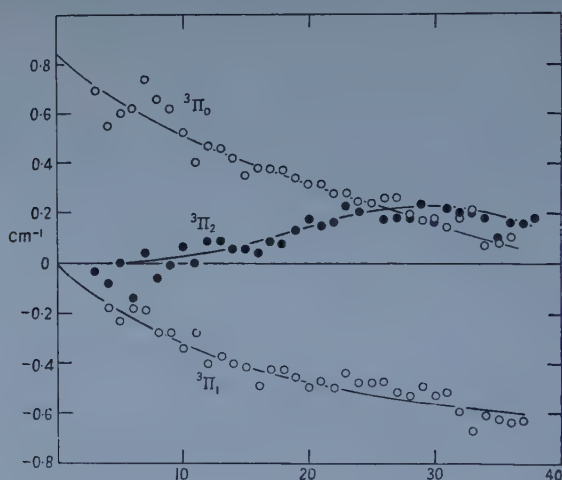
The general structure of the bands has been described by Paul and Knauss (1938). Far from the heads, six branches, three Q branches and three somewhat weaker R branches, both showing the small splitting characteristic of case- $b$ , are observed. The strongest heads are formed by P branches, beyond which lie

† Merensky Institute for Physics, Stellenbosch University.

‡ Now at Physics Department, Andhra University.

two weaker,  $^0P$ , head-forming, branches. A search for common combination differences in the 2, 0, 1, 0, 0, 0, 1, 0, 2 and 1, 4 bands of the b-a system yielded only one acceptable arrangement. The branches could be followed to sufficiently low values of  $K$  for the absolute numbering in this arrangement to be determined by making  $\Delta_2 F'(K)/K + \frac{1}{2}$  linear in  $(K + \frac{1}{2})^2$ .

The triplet-splittings in the upper states  $b^3\Sigma$ ,  $a^3\Sigma$  prove to be negligibly small, but the  $\Lambda$ -doubling in a  $^3\Pi$  is significant. The variation of the  $\Lambda$ -doubling with  $J$ , averaged over all bands studied, since the variation with  $v$  was too small to be detected, is shown in the figure. No simple relations are expected for the  $\Lambda$ -type doubling, for the state tends towards Hund's case- $a$  for low  $J$  values, and shows uncoupling towards case- $b$  at moderate values of  $J$ : however, the fact that at low  $J$  one component ( $^3\Pi_0$ ) shows comparatively large doubling, while the other extreme component ( $^3\Pi_2$ ) shows a doubling tending towards zero, identifies these components of the multiplet, and demonstrates that the state  $a^3\Pi$  is a regular state. It may be remarked that the pattern of



$\Lambda$ -type doubling in the state  $a^3\Pi$  of BF.  $\delta_{J+\frac{1}{2}}$  is plotted against  $J$ .

the  $\Lambda$ -doubling shown in figure 1 is, although on a slightly smaller scale, closely similar to these shown by the states  $a^3\Pi_r$  of CO (Rao 1949) and  $B^3\Pi_g$  of  $N_2$  (Carroll 1952). If it is now assumed that the order of the c and d sub-levels is the same in BF as it is in these states of CO and  $N_2$ , then the upper states b and c of BF are both  $^3\Sigma^+$  states.

### § 3. DETERMINATION OF MOLECULAR CONSTANTS: DISCUSSION

The constants  $B$  and  $D$  were determined from mean values of  $\Delta_2 F''(J)/(J + \frac{1}{2})$  and of  $\Delta_2 F'(K)/(K + \frac{1}{2})$  in the usual way. The expressions for  $F_i''(J)$  given by Budó (1935, 1936) (see Herzberg 1950) were used to determine values of the coupling constant  $Y_v = A_v/B_v$ , and thence of the band-origins  $\nu_0$ . The results are collected in tables 1 and 2.

The values of the constants for states a and b do not differ very greatly from those given originally by Paul and Knauss (1938): the value of  $B_0$  for  $c^3\Sigma^+$  shows that, as for AlF (Dodsworth and Barrow 1955), the excited  $^3\Sigma^+$  states are very similar.

Some of the most interesting questions about the spectrum of BF remain. No irregularities in the rotational structure of the triplet bands have been observed, such as could arise either from perturbations or predissociation, and the height of  $a^3\Pi$  above  $x^1\Sigma^+$  is still unknown. It is possible that the failure to observe bands with  $v' \geq 1$  in  $c^3\Sigma^+$  arises from a predissociation, but since the dissociation energy can as yet be established only by a rather uncertain extrapolation of the levels in  $A^1\Pi$ , this possibility does not lead to a very precise estimate of the excitation energy of  $a^3\Pi$ .

Table 1. Results of Rotational Analysis

	$v', \quad v''$	$\nu_0$ (cm <sup>-1</sup> )		
System b-a	2, 0	35165.45		
	1, 0	33625.19		
	0, 0	32040.42		
	0, 1	30735.12		
	0, 2	29448.65		
	1, 4	28518.10		
System c-a	0, 0	38011.97		
Rotational constants (cm <sup>-1</sup> ).				
	$v$	$B$	$10^6 D$	$Y$
State a	0	1.4056	6.29	17.15
	1	1.3904	6.4	17.12
	2	1.3741	6.5	17.16
	4	1.3424	6.7	17.09
State b	0	1.6294	7.3 <sub>4</sub>	
	1	1.6065	7.6 <sub>5</sub>	
	2	1.5824	7.6 <sub>0</sub>	
State c	0	1.6052	8.2 <sub>2</sub>	

Table 2. Constants for the Triplet States of BF

State	$\omega_e$	$x_e\omega_e$	$y_e\omega_e$	$A$
$c^3\Sigma^+$	—	—	—	—
$b^3\Sigma^+$	1629.28	22.25 <sub>5</sub>	—	—
$a^3\Pi_{reg}$	1323.8 <sub>6</sub>	9.20	0.047	24.2 <sub>5</sub>
State	$B_e$	$\alpha_e$	$D$	$r_e$
$c^3\Sigma^+$	(1.605 <sub>2</sub> ) §	—	$8.2 \times 10^{-6}$	(1.227 <sub>4</sub> ) §
$b^3\Sigma^+$	1.640 <sub>7</sub>	0.0222 †	$7.4 \times 10^{-6}$	1.213 <sub>8</sub>
$a^3\Pi_{reg}$	1.413 <sub>5</sub>	0.0158	$6.3 \times 10^{-6}$	1.307 <sub>9</sub>

†  $-0.0004_5 (v + \frac{1}{2})^2$

§ constants for  $v=0$ .

#### ACKNOWLEDGMENTS

We should like to thank the Commissioners for the Exhibition of 1851 for the award of a Scholarship and Andhra University for a grant to one of us (D.P.) and the Department of Scientific and Industrial Research for a maintenance grant (J.W.).



## REFERENCES

- BARROW, R. F., DODSWORTH, P. G., and ZEEMAN, P. B., 1957, *Proc. Phys. Soc. A*, **70**, 34.  
BARROW, R. F., GLASER, D. V., and ZEEMAN, P. B., 1955, *Proc. Phys. Soc. A*, **68**, 962.  
BUDÓ, A., 1935, *Z. Phys.*, **96**, 219; 1936, *Ibid.*, **98**, 437.  
CARROLL, P. K., 1952, *Proc. Roy. Irish Acad. A*, **54**, 369.  
CHRÉTIEN, M., 1950, *Helv. Phys. Acta*, **23**, 259.  
DODSWORTH, P. G., and BARROW, R. F., 1955, *Proc. Phys. Soc. A*, **68**, 824.  
HERZBERG, G., 1950, *Molecular Structure: I: Spectra of Diatomic Molecules* (New York : van Nostrand).  
PAUL, F. W., and KNAUSS, H. P., 1938, *Phys. Rev.*, **54**, 1072.  
RAO, K. N., 1949, *Astrophys. J.*, **110**, 304.  
SHERMA, D., 1951 a, *Astrophys. J.*, **113**, 210; 1951 b, *Ibid.*, **113**, 219.  
STRONG, H. M., and KNAUSS, H. P., 1936, *Phys. Rev.*, **49**, 740.

# AlH Bands at 2173 Å and 2101 Å

By M. ASLAM KHAN

Department of Physics, Imperial College of Science and Technology, London

Communicated by R. W. B. Pearse; MS. received 5th April 1957, and in revised form 17th September 1957

**Abstract.** Two new bands of aluminium hydride have been found in the far ultra-violet region of the spectrum at 2173 Å and 2101 Å. The rotational analysis shows that they are the (1, 0) and (0, 1) bands of the systems  $c^1\Sigma \rightarrow A^1\Sigma$  and  $D^1\Sigma \rightarrow A^1\Sigma$  respectively. The (0, 1) band at 2101 Å shows perturbation as well as predissociation. The rotational constants for the (0, 1) band and the (1, 0) band are calculated as follows:

$$\begin{array}{l}
 D^1\Sigma \rightarrow A^1\Sigma, (0, 1) \text{ band} \quad \left\{ \begin{array}{ll} B'_r = 6.56 \text{ cm}^{-1} & D'_v = 6.1 \times 10^{-4} \text{ cm}^{-1} \\ B''_r = 6.16 \text{ cm}^{-1} & D''_v = 3.3 \times 10^{-4} \text{ cm}^{-1} \end{array} \right. \\
 \nu_0 = 47665.6 \text{ cm}^{-1} \\
 c^1\Sigma \rightarrow A^1\Sigma, (1, 0) \text{ band} \quad \left\{ \begin{array}{ll} B'_v = 5.87 \text{ cm}^{-1} & D'_v = 13 \times 10^{-4} \text{ cm}^{-1} \\ B''_v = 6.33 \text{ cm}^{-1} & D''_v = 3.2 \times 10^{-4} \text{ cm}^{-1} \end{array} \right. \\
 \nu_0 = 45922.45 \text{ cm}^{-1}
 \end{array}$$

## § 1. INTRODUCTION

MANY systems of bands in the visible and ultra-violet regions of the emission spectrum of aluminium hydride are now well known. They are the  $B^1\Pi \rightarrow A^1\Sigma$ ,  $E^1\Sigma \rightarrow B^1\Pi$ ,  $C^1\Sigma \rightarrow B^1\Pi$ ,  $b^3\Sigma \rightarrow a^3\Pi$ ,  $F^1\Pi \rightarrow B^1\Pi$ ,  $C^1\Sigma \rightarrow A^1\Sigma$ , and  $D^1\Sigma \rightarrow A^1\Sigma$  systems. The last two of these have been reported by Bengtsson (1928) and Grabe and Hulthén (1939) respectively, and consist of single P and single R branches. The band at 2033 Å (0, 0) shows perturbation and predissociation in the breaking off of the P branch after P (11) and the R branch after R (9). These bands have been produced in a vacuum arc in an atmosphere of hydrogen at a pressure of a few cm of mercury. In view of the important part played by the hydrides in the study of astrophysical phenomena and the correlation of molecular and atomic electronic energy levels and the predissociation of diatomic molecules, the present investigation of aluminium hydride was undertaken. It was during such investigation that two new bands at 2173 Å and 2101 Å, which form the subject of this paper, were observed and analysed. The study of deuteride bands is under investigation and the results will be set out in a subsequent paper.

## § 2. EXPERIMENTAL

The source used for production of the spectrum was a special type of discharge tube operated with hydrogen at low pressures. The apparatus employed was very similar in principle to that described by Pearse and Gaydon (1938) but in a highly modified form and proved to be a very intense and economical source for studying hydrides. Hydrogen from a commercial cylinder was allowed to pass

through the tube and the flow was regulated through a needle valve at one end. The other end of the discharge tube was connected to a Hyvac pump to remove impurities produced during the discharge. The pressure was kept at a few mm of mercury. The power supply used was a 5000 v, 7 kva transformer. The spectroscopically pure aluminium piece was placed in the capillary held firmly between two insulating discs. The capillary was made of graphite with a 6 mm internal bore. In order to be sure that the aluminium hydride spectrum was free from impurities arising from graphite, the latter was baked at a high temperature by passing a heavy current discharge through the tube for some time. It was also found possible to line the inside of the capillary with an aluminium deposit. This was done by placing a piece of aluminium in the capillary and running the discharge at a high current. The element vaporized and formed a thin layer about 1 mm thick all along the inside walls of the capillary and thereby covered completely the exposed graphite surface. This procedure proved extremely helpful as no traces of any impurity due to carbon have been recorded on the plate.

For the purpose of measurement, the photographs were taken on a quartz spectrograph of the Littrow type having a dispersion of about  $1.5 \text{ \AA mm}^{-1}$  in the region  $2100 \text{ \AA}$ . The current used for these was 2.5 A and the time for exposure ranged from 2 to 3 minutes for Ilford Q2 plates.

### § 3: MEASUREMENTS

The wavelengths of the lines were determined by using an iron arc and copper arc comparison spectrum. A complete list of the wavelengths and the wave-numbers *in vacuo* of the lines of the bands is given in tables 1 and 2. The reductions to wave numbers *in vacuo* were made with the help of Kayser's *Tabelle der Schwingungszahlen*.

Table 1.  $2173 \text{ \AA}$  (1, 0) Band

<i>J</i>	P Branch		R Branch	
	$\lambda_{\text{air}}$	$\nu_{\text{vac}}$	$\lambda_{\text{air}}$	$\nu_{\text{vac}}$
1			2175.81	45945.45
2	2178.21	45894.83	2175.40	45954.11
3	2178.81	45882.19	2174.92	45964.25
4	2179.56	45866.40	2174.63	45970.37
5	2180.32	45850.42	†	
6	2181.19	45832.13	†	
7	2181.82	45818.90	2173.79	45988.14
8	2182.86	45797.07	2173.68	45990.46
9	2183.90	45775.27		
10	2185.02	45751.81		
11	2187.15	45707.26		
12	2188.57	45677.60		

† Obscured by atomic line.

### § 4. THE STRUCTURE OF THE BAND

The band (0, 1) shown in figure 1 (*b*) (Plate) resembles the one at  $2033 \text{ \AA}$ , figure 1 (*a*) in possessing single P and single R branches only. It also shows predissociation of the P and R branches after P (11) and R (9). The lines P (6) and R (4) show strong perturbations. They are displaced to the right. The band at  $2173 \text{ \AA}$  is a simple band (figure 1 (*d*)) consisting of P and R branches and degraded to the red.



Table 2. 2101 Å (0, 1) Band

<i>J</i>	P Branch		R Branch	
	$\lambda_{\text{air}}$	$\nu_{\text{vac}}$	$\lambda_{\text{air}}$	$\nu_{\text{vac}}$
0			2096.68	47679.24
1	2097.79	47654.02	2096.09	47692.66
2	2098.31	47642.21	2095.46	47706.99
3	2098.78	47631.54	2094.78	47722.48
4	2099.22	47621.55	2094.09	47738.20
5	2099.61	47612.71	2093.31	47755.99
6	2100.05	47602.74	2092.52	47774.02
7	2100.26	47597.98	2091.67	47793.43
8	2100.55	47591.41	2090.85	47812.17
9	2100.74	47587.10	2089.95	47832.76
10	2100.98	47581.67		
11	2101.12	47578.50		

### § 5. ANALYSIS OF THE BAND STRUCTURE

In tables 3 and 4 are shown the combination differences relating to the initial and final states.

Table 3

Rotational Term Differences for Initial States of the Bands 2173 Å (1, 0) and 2229 Å (1, 1)

<i>J</i>	2173 Å (1, 0)	2229 Å (1, 1)
0		
1		
2	59.3	59.0
3	82.1	81.1
4	103.9	103.9
5	†	132.7
6	†	152.2
7	169.2	168.2
8	193.4	192.6
9		215.9

† Obscured by atomic line.

Rotational Term Differences for Final States

<i>J</i>	Ground state			<sup>1</sup> Σ-Ground state	
	2173 Å (1, 0)	<sup>1</sup> Π → <sup>1</sup> Σ (0, 0)	<sup>1</sup> Π → <sup>1</sup> Σ (1, 0)	<sup>1</sup> Σ* → <sup>1</sup> Σ (0, 0)	<sup>1</sup> Σ** → <sup>1</sup> Σ (0, 0)
0					
1					
2	63.3	62.94	63.2	63.1	62.9
3	87.7	88.09	88.0	88.1	88.7
4	113.8	113.15	113.3	113.0	112.1
5	138.2	138.08	137.8	138.3	138.3
6	—	162.76	—	162.9	162.8
7	—	187.78	187.8	188.0	187.2
8	212.9	212.54	212.5	213.5	211.8
9	238.6	236.83	237.0	237.2	237.3

Table 4

Comparison of the Rotational Term Differences for the Initial State of the 2101 Å (0, 1) and 2033 Å (0, 0) Bands

$J$	2101 Å (0, 1)	2033 Å (0, 0)
0		
1	38.6	39.9
2	64.8	64.8
3	90.9	90.5
4	116.7	116.5
5	143.3	143.3
6	171.3	170.3
7	195.5	195.0
8	220.7	219.7
9	245.6	244.5

## Final States

$J$	Ground state :		Ground state, $v=1$	
	2101 Å (0, 1)	$^1\Pi \rightarrow ^1\Sigma$ (1, 1)	$^1\Pi \rightarrow ^1\Sigma$ (0, 1)	$^1\Sigma \rightarrow ^1\Sigma$ (1, 1)
0				
1				
2	37.0	36.24	—	37.5
3	61.1	61.09	60.4	61.5
4	85.4	85.45	85.5	86.5
5	109.7	109.66	109.2	109.9
6	135.5	134.1	134.1	133.8
7	158.0	158.27	158.2	158.1
8	182.6	182.24	182.4	182.3
9	206.3	206.2	206.5	205.9
10	230.5	230.1	230.1	229.8
11	254.2	253.6	253.6	

Examination of the combination differences confirms that the new bands are the (0, 1) and (1, 0) bands of the 2033 Å and 2229 Å systems respectively.

The rotational constants for these bands have been calculated by the help of the relations:

$$\frac{\Delta_2 F(J)}{J + \frac{1}{2}} = 4B_v - 8D_v(J + \frac{1}{2})^2.$$

The rotational constants thus calculated are given below:

$$\begin{aligned} \text{D}^1\Sigma \rightarrow \text{A}^1\Sigma, (0, 1) \text{ band} \quad & \begin{cases} B'_v = 6.56 \text{ cm}^{-1} & D'_v = 6.1 \times 10^{-4} \text{ cm}^{-1} \\ B''_v = 6.16 \text{ cm}^{-1} & D''_v = 3.3 \times 10^{-4} \text{ cm}^{-1} \end{cases} \\ & \nu_0 = 47665.6 \text{ cm}^{-1} \\ \text{C}^1\Sigma \rightarrow \text{A}^1\Sigma, (1, 0) \text{ band} \quad & \begin{cases} B'_v = 5.87 \text{ cm}^{-1} & D'_v = 13.0 \times 10^{-4} \text{ cm}^{-1} \\ B''_v = 6.33 \text{ cm}^{-1} & D''_v = 3.2 \times 10^{-4} \text{ cm}^{-1} \end{cases} \\ & \nu_0 = 45922.45 \text{ cm}^{-1} \end{aligned}$$

## ACKNOWLEDGMENTS

The author wishes to express his thanks to Dr. R. W. B. Pearse for his valuable suggestions, and to Mr. W. R. S. Garton for his help and encouragement.

## REFERENCES

- BENGTTSSON, E., 1928, *Z. Phys.*, **51**, 889.  
 GRABE, B., and HULTHÉN, E., 1939, *Z. Phys.*, **114**, 470.  
 NILSSON, B. E., 1948, *Thesis*, University of Stockholm.  
 PEARSE, R. W. B., and GAYDON, A. G., 1938, *Proc. Roy. Soc. A*, **50**, 201.

## Magnetic Field Effects on Electron Populations in Semiconductors

By P. T. LANDSBERG

Marischal College, University of Aberdeen

*MS. received 6th August 1957, and in revised form 1st October 1957*

**Abstract.** This paper gives a calculation of the change in population of the states of the conduction band when a magnetic field is applied. It is based on two main suppositions: first, that the conduction band states are shifted up or down by an energy  $d$  due to the interaction of their spins with the magnetic field; secondly, that the donor states are also shifted up or down in energy by the same amount  $d$ . The more important general properties of the model are discussed, and a numerical example is worked out in some detail. It is also shown that different results are obtained according to which of two different pictures of the nature of the donor levels one adopts. The first of these pictures is the usual one, which excludes the possibility of having more than one electron on a given donor ('localized' states). The second assumes as before that the levels of either spin are sharp in energy, but postulates that these levels can be populated in any manner consistent with the exclusion principle, as in the ordinary theory of metals ('non-localized' impurity states).

### § 1. INTRODUCTION

WHEN a magnetic field is applied to a semiconductor, the concentration of electrons in the conduction band is changed. This phenomenon is of importance for the interpretation of data such as the magnetoresistive ratio or the magnetic field dependence of the Hall coefficient. A quantitative theory of the effect is faced by the difficulty that it is a consequence of several co-operating causes. (a) A paramagnetic effect due to the electron magnetic moment  $\mu$ , which causes a displacement  $\pm\mu H$  in energy of both conduction and impurity electron states. This effect has been considered by Mackintosh (1956), but his considerations need to be extended, since the splitting of the conduction band was neglected, and the effect of the correct statistics for localized impurities in a magnetic field was not investigated. (b) Diamagnetic effects, in particular the quantization of the orbits of the conduction band electrons. This effect has been considered by Appel (1956), though the effect of the correct statistics for localized impurity states was again not investigated. (c) An increase of the impurity activation energy due to a compression of the electron cloud centred on an impurity atom in a plane normal to the magnetic field. This effect, which becomes important only in very strong fields, has been considered theoretically by Yafet *et al.* (1956) and experimentally by Keyes and Sladek (1956), but a quantitative explanation of the experimental data has not yet been published.

The purpose of this note is to investigate the paramagnetic effect (a) on the basis of a simple model in which the other mechanisms are neglected. The



spread in energy of the impurity levels has also been neglected. The model cannot be expected, therefore, to give any more than a semi-quantitative guide to conditions in a semiconductor crystal in which the effect (*a*) dominates. The population changes which are found here appear to be of the correct order of magnitude for InSb, but other factors such as mobility changes in the magnetic field have to be taken into account before a satisfactory comparison can be made with experiments on the magnetoresistive ratio. A reliable theory of this effect for InSb does not appear to be available so far. In common with the other theoretical papers cited, attention is therefore restricted here to an investigation of the properties of the model, leaving comparison with experiments to a more comprehensive theory.

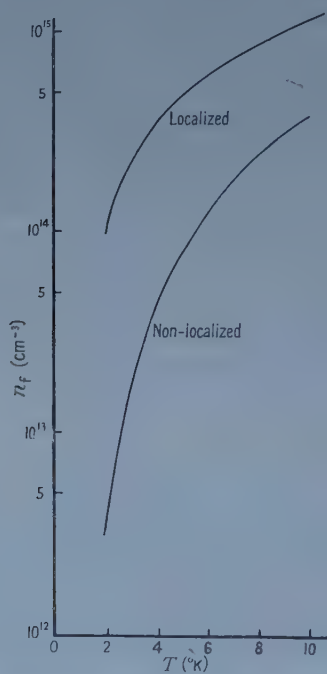


Figure 1. Concentration of conduction band electrons in the absence of a field for a sample specified in § 3.

The donors will be regarded as either neutral or singly ionized. Each ionized donor is regarded as presenting two trapping levels, one for 'positive' spin, the other for 'negative' spin. Two different statistical assumptions for these impurity states will be made. In the first, electrons trapped by impurities are regarded as 'localized', i.e. if one electron has been trapped by a donor the donor is regarded as electrically neutral, and the possibility that another electron of opposite spin will also be trapped by the same donor is neglected. The second picture regards impurity electrons as 'non-localized'. In this picture the impurity levels of either spin may be populated in any manner consistent with the exclusion principle and electrical neutrality, as in an ordinary conduction band of a monovalent metal. Both trapping levels of a donor are therefore regarded as active at all times. Owing to the requirement of electrical neutrality, however, no more than half of these trapping levels can be occupied by electrons at any one time.

A qualitative difference between these two statistical assumptions can be seen as follows. If the trapping levels of a donor are  $g$ -fold ( $g \geq 1$ ) degenerate for each direction of spin, and if there are  $N$  donors per  $\text{cm}^3$ , there are in principle  $2gN$  trapping levels. If  $r$  ( $< N$ ) electrons are in the impurity states, then  $2gN - r$  states can trap additional electrons if the states are non-localized; but only  $2g(N - r)$  are available if the states are localized. Hence, for a given set of conditions, the non-localized statistics may be expected to lead to higher occupation probabilities of the impurity states than the localized statistics; it therefore leads to a smaller concentration of electrons in the conduction band (see figure 1).

The need to distinguish between the two statistical assumptions just discussed is due to the fact that at low temperatures delocalization of impurity levels is by now a well-known phenomenon (Hung 1950, Fritsche 1955 and references given there for germanium, Fritsche and Lark-Horovitz 1955 for InSb).

## § 2. ASSUMPTIONS

The simplest reasonable model of a semiconductor will be used, i.e. one in which only the conduction band and  $N$  identical donors per unit volume need be considered. Let  $E_c$  be the energy at the bottom of the conduction band,  $E$  the energy of the donor levels (both in the absence of a field). Upon application of a field  $H$ , let  $2d(H)$  be the energy separation of corresponding levels. An electron whose energy is lowered is regarded as having a negative spin and a positive magnetic moment. Let  $N_e$  be the number of electrons available in donor and conduction levels at the absolute zero of temperature,  $E_F$  the Fermi level, and let  $n = n_+ + n_-$  be the number of electrons per unit volume in the donor levels. The sign of the magnetic moment will be indicated by a suffix where necessary. We shall write

$$N_0 = 4\pi(2m^*kT/\hbar^2)^{3/2}, \quad \eta_c \equiv E_c/kT, \quad \eta \equiv E/kT, \quad \delta \equiv d/kT, \quad \dots\dots(1)$$

$$F(a) \equiv \int_0^\infty \frac{\sqrt{x} dx}{1 + \exp(x - a)}. \quad \dots\dots(2)$$

The equation for the Fermi level is

$$\frac{1}{2}N_0[F(\eta_F - \eta_c + \delta) + F(\eta_F - \eta_c - \delta)] + n = N_e. \quad \dots\dots(3)$$

The concentration of conduction band electrons is

$$n_i = n_{i+} + n_{i-} = \frac{1}{2}N_0[F(\eta_F - \eta_c + \delta) + F(\eta_F - \eta_c - \delta)]. \quad \dots\dots(4)$$

The contribution to the magnetic moment per unit volume is

$$M = |\mu|(n_{i+} + n_+ - n_{i-} - n_-). \quad \dots\dots(5)$$

As regards the donors, it will be assumed that they are in a non-degenerate state when ionized, and that a neutral donor can be in any one of  $2g$  degenerate states, which are split into two groups of  $g$  degenerate states each by the application of a magnetic field. For the 'localized' model of a centre the ratio of the partition function of a neutral to that of an ionized centre may be taken as (Landsberg 1957, Appendix I),

$$Z_1/Z_0 = 2g \exp(-\eta) \cosh \delta.$$

Hence the concentration of trapped electrons is

$$n = \frac{2gN}{2g + y/\cosh \delta} \quad [y \equiv \exp(\eta - \eta_{FH})] \quad \dots\dots(6)$$

where  $\eta_{FH}$  is the value of  $\eta_F$  in the presence of a field. In the case of 'non-localized' impurity levels one has

$$n_{\pm} = gN / \{1 + \exp [\eta \mp \delta - \eta_{FH}]\},$$

whence

$$n = \frac{2gN[1 + y \cosh \delta]}{1 + 2y \cosh \delta + y^2} \quad \dots\dots (7)$$

By (3), (4), (6) and (7), the population changes due to the Zeeman splitting can be investigated as a function of magnetic field, and the properties of localized and non-localized impurity levels can be contrasted.

### § 3. NUMERICAL EXAMPLE

The properties of the model have been worked out for the following numerical example

Concentration of impurity centres:  $N = N_e = 10^{16} \text{ cm}^{-3}$ .

Impurity activation energy in the absence of a field:  $E_c - E = 5 \times 10^{-4} \text{ ev}$ .

Degeneracy of trapping levels of an ionized impurity in the absence of a field:  $2g = 2$ .

$m^* = 0.03m$ .

The data may apply to certain samples of InSb.† Half the splitting in energy of corresponding levels is given by  $|\mu| \equiv e\hbar/2mc \sim 0.58 \times 10^{-8} \text{ ev oersted}^{-1}$ . Thus the quantity  $d(H)$  introduced in the preceding section is given by  $d = |\mu|H$ , and  $\delta \sim 0.67(H/T)10^{-4}$ , where  $H$  is in oersteds and  $T$  in degrees Kelvin. The equations of § 2 lead to the results given in figures 1 to 3.

The curves show that the difference between the localized and the non-localized statistics for the impurities has an important bearing on the change in the conduction band electron concentration produced by a magnetic field. In the non-localized case the change is positive; in the localized case it is negative and numerically smaller. In both cases the effect increases with  $H$  and  $1/T$ .

If  $r$  be the current carried by the donor states (no suffix), expressed as a fraction of the current carried by the conduction band (suffix  $f$ ), the magnetoresistive ratio is

$$\frac{\Delta \rho}{\rho} = - \frac{1}{1+r} \left[ \frac{\Delta \mu_f}{\mu_f} + \frac{\Delta n_f}{n_f} \right] - \frac{1}{1+r^{-1}} \left[ \frac{\Delta \mu}{\mu} + \frac{\Delta n}{n} \right].$$

Using figure 2, the contribution to it due to electron population changes is seen to be *positive* in the following two cases: (a) If most of the current is carried in an impurity band, when  $-\Delta n/n > 0$ ; and (b) in the case of localized impurity states, when  $-\Delta n_f/n_f > 0$ . The contribution can, however, be *negative*,  $-\Delta n_f/n_f < 0$ , if there is an impurity band, but most of the current is carried by the conduction band (this is the corrected form of statements by Mackintosh 1956). The contribution then found is in fact of the correct order of magnitude for the observed negative magnetoresistive ratio in InSb. But the experiments suggest that this ratio is negative when most of the current flows in the impurity band. If this is so, then the term  $-\Delta/n$  will dominate  $-\Delta n_f/n_f$ , and the contribution to the magnetoresistive ratio from population changes becomes again positive. Although the splitting of conduction and impurity levels can therefore

† According to recent values, the effective mass is high by perhaps a factor of two, but this does not affect the curves appreciably.



not account for a negative ratio on the basis of the present simple model, nonetheless, it is seen that the onset of conduction in an impurity band has important consequences on purely statistical grounds.

#### § 4. GENERAL DISCUSSION OF THE MODEL

It may be of interest to explain this numerical information by some general statements about the properties of the present model.

(i) If the isothermal application of a magnetic field causes a fall of the Fermi level, the concentration of conduction band electrons may still rise; it falls only if the drop in the Fermi level exceeds a certain minimum.

(ii) The isothermal application of a magnetic field causes a drop in the Fermi level if the donor states are localized. In the approximation in which classical statistics is applied to the conduction band, this drop is of just the amount required to leave the conduction band electron concentration unaffected by the application of the field.

(iii) In the case of non-localized donor states, isothermal application of a field causes a lowering of the Fermi level if  $N_e \leq 3gN/2$ . In the physically far less important cases when this inequality is violated, the Fermi level may be either raised or lowered by the field. (Mackintosh's analysis (1956), which appears to imply the assumption  $N_e = 2gN$  falls into this latter class of cases.) In general, the conduction band electron concentration is changed by the application of a magnetic field, even in the classical approximation.

Note that at  $T=0$  the application of a field need not cause any change of the conduction band electron concentration, but this limiting situation is not under consideration here.

The proofs of these statements are as follows.

(i) The Fermi integral (2) is a convex function, i.e.

$$\frac{1}{2}[F(\eta + \delta) + F(\eta - \delta)] \geq F(\eta). \quad \dots\dots(8)$$

Thus, if the application of a field causes a rise of the Fermi level,  $\eta_{FH} > \eta_{F0}$ , then, using (8),

$$n_t(H) > N_0 F(\eta_{FH} - \eta_c) > N_0 F(\eta_{F0} - \eta_c) = n_t(0).$$

The statement (i) follows from this consideration.

(ii) By (6), the concentration of trapped electrons would increase upon application of a magnetic field if the Fermi level were unaffected by it. This would, however, lead to a violation of (3). The same contradiction is produced if the Fermi level were raised by the field. It must therefore fall. If now classical statistics are used in the Fermi level equation (3), so that

$$F(a) \text{ is replaced by } (\sqrt{\pi}/2)e^a, \quad \dots\dots(9)$$

one finds that  $\delta$  occurs only in terms of the form  $\exp(\eta_{FH} - \eta_c) \cosh \delta$ . This quantity is therefore expressible in terms of parameters other than  $\delta$  by solving the Fermi level equation. It follows that  $n_t = N_0 \exp(\eta_{FH} - \eta_c) \cosh \delta$  is independent of  $\delta$ , and therefore of the magnetic field.

(iii) This assertion may be proved by writing the Fermi level equation in the form

where 
$$\frac{1}{2}N_0[F(\eta_{FH} - \eta_c + \delta) + F(\eta_{FH} - \eta_c - \delta)] = Nz, \quad \dots\dots(10)$$

$$z \equiv \frac{\theta y^2 + 2(\theta - g)y \cosh \delta + \theta - 2g}{y^2 + 2y \cosh \delta + 1} \quad \text{and} \quad \theta \equiv \frac{N_e}{N}. \quad \dots\dots(11)$$

It is easily shown that

$$\left(\frac{\partial z}{\partial y}\right)_\delta > 0, \quad \dots\dots(12)$$

and 
$$\left(\frac{\partial z}{\partial(\cosh \delta)}\right)_y \text{ has the sign of } \frac{2\theta}{g} - 3 - y^2. \quad \dots\dots(13)$$

If  $N_e \leq 3gN/2$ , the last expression in (13) is negative. Thus, if the Fermi level were raised by a magnetic field the changes in  $y$  and  $\delta$  would by (12) and (13) cause a decrease of  $z$  and hence of the conduction band electron concentration. By (i) this implies a lowering of the Fermi level, in contradiction with hypothesis. Hence the effect of the field is such that  $z$  is decreased by the rise in  $\delta$ , and increased by a drop in the Fermi level (increase of  $y$ ). If, however, the inequality  $N_e \leq 3gN/2$  is violated, the differential coefficient (13) can have either sign, depending on the position of the Fermi level in the absence of a field. The last statement under (iii) follows from the fact that for a non-degenerate semiconductor with non-localized impurity levels, the Fermi level equation is the cubic

$$y^3 - \alpha y^2 - \beta y - \gamma = 0, \quad \dots\dots(14)$$

where

$$\alpha \equiv \gamma - (2/\theta)(\theta - g) \cosh \delta, \quad \beta = 2\gamma \cosh \delta - (\theta - 2g)/\theta,$$

and

$$\gamma = [\sqrt{\pi}N_0 \cosh \delta]/2N_e.$$

It follows that, in contrast with the case of localized levels, the concentration of conduction band electrons will in general depend on the magnetic field, even if the semiconductor is non-degenerate.

The statement (ii) shows that, in the case of localized impurity levels, the drop in the concentration of conduction electrons upon application of a field, illustrated in figure 2, may be regarded as a consequence of the fact that the semiconductor is degenerate under these conditions. In the case of the numerical example of §3 with non-localized levels, on the other hand, the Fermi level lies close to the impurity level in the absence of a field so that one has a non-degenerate semiconductor at the temperatures envisaged here. The field causes a drop in the Fermi level, but this is too small to prevent a rise in the conduction band electron concentration as a result of the field.

It is easy to verify that the condition for a drop in the conduction band electron concentration as a result of the application of a magnetic field is, on the present model,

$$\eta_{F0} - \eta_{FH} > \begin{cases} \ln(\cosh \delta) & \text{(non-degenerate conduction band),} \quad \dots\dots(15a) \\ \delta^2/4\eta_{FH} & \text{(degenerate conduction band).} \quad \dots\dots(15b) \end{cases}$$

In the numerical example of §3, (15b) holds for the case of localized impurity levels, and (15a) is violated in the case of non-localized impurity levels.

As regards figure 3, the unbalance of electron spins shown there is dominated by the unbalance of spins in the impurity states (which are much more heavily populated than the conduction states). Although the total number of trapped electrons is greatest for *non-localized* impurity states, the excess population in

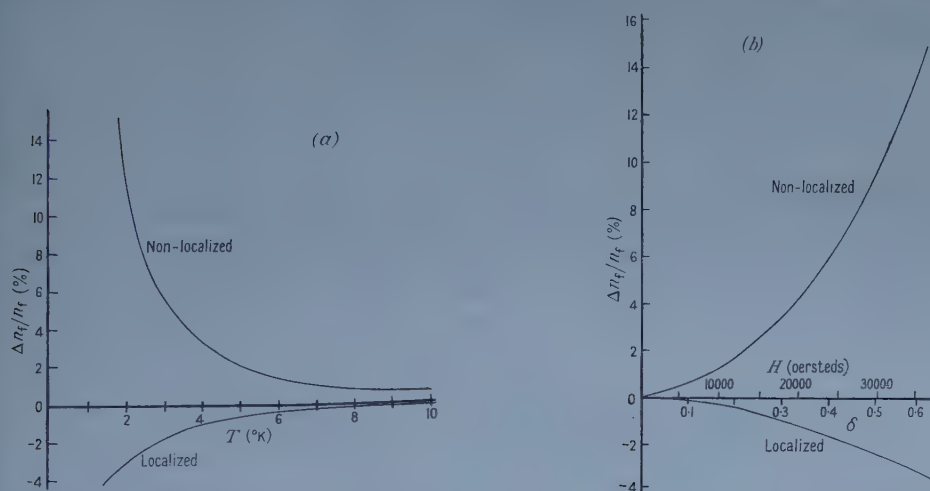


Figure 2. Percentage change in the conduction band electron concentration upon application of a field for a sample specified in § 3. (a) As a function of temperature when  $H \sim 17\,900$  oersteds, (b) As a function of field when  $T \sim 4^\circ\text{K}$ .

the impurity states which have been lowered by the magnetic field over those which have been raised, is greater for *localized* impurity states. This is in the main due to the non-availability of certain states on the localized model, as explained in the introduction. As a consequence, the raised impurity states trap less electrons on the localized model than they do on the non-localized model; while the lowered states trap more electrons (or only slightly less) on the localized model than they do on the non-localized model.

It remains to explain the approximately straight lines shown in figure 3(b). In the case of the non-localized model one finds from § 2 for the contribution, *by the donors only*, to the paramagnetic susceptibility  $M/H$  (cf. also Mooser 1955)

$$\chi_{nt} = \frac{y \sinh \delta}{1 + y \cosh \delta} \frac{|\mu|n}{H} \sim \frac{y}{1 + y} \frac{\mu^2 n}{kT} \quad (\text{if } |\mu|H \ll kT). \quad \dots\dots(16)$$

In the case of the localized model,

$$\chi_l = \frac{2g \sinh \delta}{y + 2g \cosh \delta} \frac{|\mu|N}{H} \sim \frac{\mu^2 N}{kT} \quad (\text{if } |\mu|H \ll kT). \quad \dots\dots(17)$$

In the numerical example of § 3,  $y$  in (16) is of order unity. In this instance  $n_t \ll n$ ,  $|\mu|H \ll kT$ , so that the approximate expressions (16) and (17) represent the contribution by donors *and conduction electrons* quite well. Thus  $M/|\mu|$  is approximately proportional to  $|\mu|H/kT$ . The resulting susceptibility contributions, evaluated for InSb, are approximately  $1.2 \times 10^{-6}$  and  $2.3 \times 10^{-6}$  emu  $\text{gm}^{-1}$  for the non-localized and the localized model respectively. As in the case of the magnetoresistive ratio, the purely statistical effects which accompany the onset of impurity band conduction are also here seen to be quite large.



Suppose in conclusion that the transition to impurity band conduction is fairly sharp, and occurs when the conduction band electron concentration drops below a critical value (Mott 1956). Figure 1 shows that this delocalization of impurity states should be accompanied by a drop in the conduction band electron concentration owing to the statistical effect discussed here. This effect should therefore enhance the sharpness of any transition which may exist.

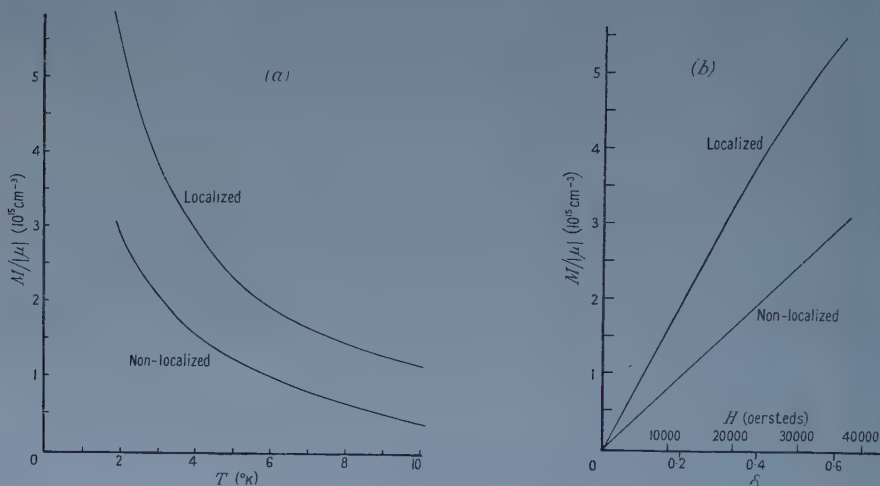


Figure 3. Excess concentration of positive electron spins over negative electron spins in the conduction band and the impurity states for a sample specified in § 3. (a) As a function of temperature when  $H \sim 17\,900$  oersteds. ( $M/|\mu|$  increases more rapidly than  $1/T$  when plotted against  $1/T$ ). (b) As a function of field when  $T \sim 4^\circ\text{K}$ .

#### REFERENCES

- APPEL, J., 1956, *Z. Naturforsch.*, **11a**, 689.  
 FRITSCHÉ, H., 1955, *Phys. Rev.*, **99**, 406.  
 FRITSCHÉ, H. and LARK-HOROVITZ, K., 1955, *Phys. Rev.*, **99**, 400.  
 HUNG, C. S., 1950, *Phys. Rev.*, **79**, 727.  
 KEYES, R. W., and SLADECK, R. J., 1956, *J. Phys. Chem. Solids*, **1**, 143.  
 LANDSBERG, P. T., 1957, *Proc. Phys. Soc. B*, **70**, 282.  
 MACKINTOSH, I. M., 1956, *Proc. Phys. Soc. B*, **69**, 403.  
 MOOSER, E., 1955, *Phys. Rev.*, **100**, 1589.  
 MOTT, N. F., 1956, *Canad. J. Phys.*, **34**, 1356.  
 YAFET, Y., KEYES, R. W., and ADAMS, E. N., 1956, *J. Phys. Chem. Solids*, **1**, 137.

## Excited Levels of Cadmium 110

By A. C. KNIPPER†

Clarendon Laboratory, Oxford

*Communicated by H. Halban; MS. received 6th August 1957, and in final form 23rd September 1957*

**Abstract.** The  $\gamma$ -rays in the decay of  $^{110}\text{Ag}$  have been observed using scintillation counters. A simplified decay scheme is presented. Spin assignments for the levels of  $^{110}\text{Cd}$  and mixing ratios of the  $\gamma$ -rays are obtained from the comparison of angular correlations in the double and triple cascades.

### § 1. INTRODUCTION

The present paper deals with observations on the  $\gamma$ -rays emitted in the decay of 270-day  $^{110}\text{Ag}$ , particularly with the view of determining angular correlations between successively emitted  $\gamma$ -rays. Siegbahn (1950) studied  $\beta$ - and  $\gamma$ -rays in this decay, and proposed a level scheme. His results were essentially confirmed by many authors. However, Cork *et al.* (1950) proposed a slightly different level scheme, in which 18  $\gamma$ -rays had been fitted. Bleuler *et al.* (1953) investigated the decay of  $^{110}\text{In}$ , and collecting previously published data, they were able to make tentative spin assignments and definite parity assignments for several levels of  $^{110}\text{Cd}$ .

### § 2. APPARATUS

THE scintillation coincidence spectrometer described by Bishop and Perez y Jorba (1955) was modified to suit our requirements. The fast coincidence circuit ( $\tau \sim 10^{-8}$  sec) was adapted to Dumond 6292 photomultipliers. Pulses from the Harwell type 1049 linear amplifiers were fed directly to the single channel kicksorters, and a fast-slow coincidence arrangement was set up together with a  $0.3 \mu\text{sec}$  Harwell type 1036 triple coincidence unit. One inch cube NaI(Tl) crystals were used throughout; they subtended a solid angle of  $0.8\%$  of  $4\pi$ .

Stability of the linear channels was found to require particular attention. Single channel counting allowed precise monitoring of their overall stability during the long angular correlation runs. In addition, periodic pulse height analysis of the spectra was made. Amplifiers and discriminator biases were checked with a stable pulse generator. The resolving time of the fast coincidence circuit was frequently determined.

### § 3. $\gamma$ -RAY SPECTROSCOPY

Figure 1 shows a typical spectrum of the  $\gamma$ -rays emitted by  $^{110}\text{Ag}$ . This spectrum was broken upon into several components, listed in table 1. All components relate to well established  $\gamma$ -rays; however, the peaks  $L_2$  and  $L_3$  are displaced due to inaccuracies in the subtraction procedure.

† Now at Institut de Recherches Nucléaires, 1, Place de l'Hôpital, Strasbourg, France.

The relative intensities, also listed in table 1, are evaluated from the area under the full energy peaks, assumed of Gaussian shape. The photopeak efficiency-energy relation for our spectrometer was obtained by calculating the total efficiency as a function of  $\gamma$ -ray energy, and measuring the ratio of peak area to total area for the spectra of five well known calibration  $\gamma$ -rays.

Biases and kicksorter channels used in the angular correlation experiments are also shown in figure 1.

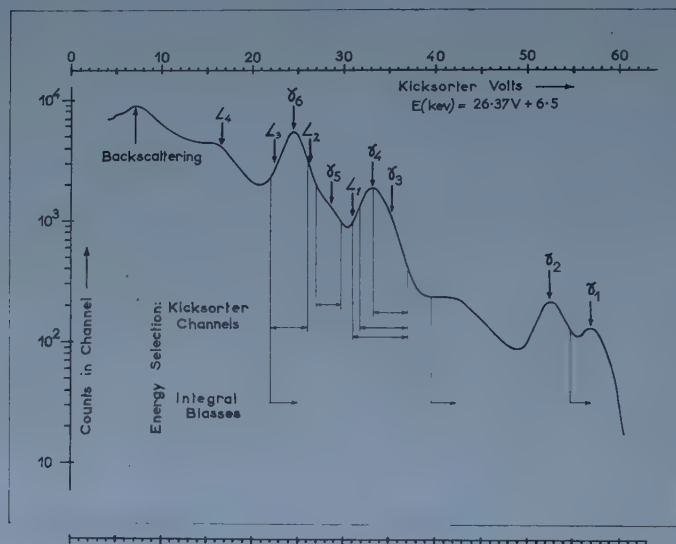


Figure 1. Spectrum of  $\gamma$ -rays from  $^{110}\text{Ag}$ , taken with  $\text{NaI(Tl)}$  crystal. Note that two spectra have been fitted at 40 v; channel width is about 0.75 v below 40 v, and 1.40 v above 40 v.

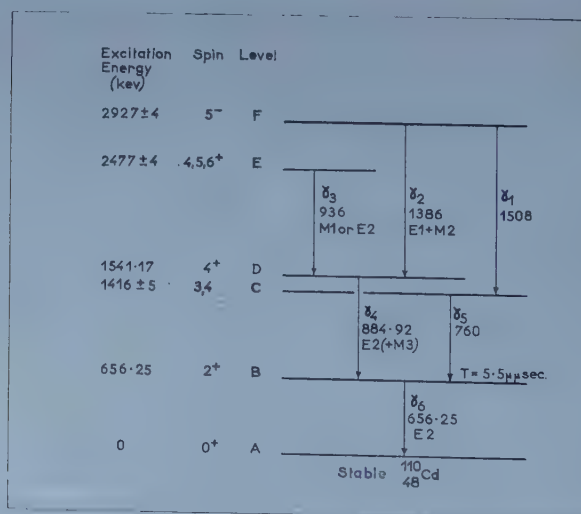


Figure 2. Simplified level scheme for  $^{110}\text{Cd}$  (energies of  $\gamma$ -rays are in kev). Only the lines giving rise to coincidences with the energy selections used in the angular correlation experiments are shown. Accurate energy measurements for  $\gamma_4$  and  $\gamma_6$  are from Marmier and Boehm (1957).



Table 1.  $\gamma$ -Rays Emitted by  $^{110}\text{Ag}$ 

Lines	$L_4$	$L_3$	$\gamma_6$	$L_2$	$\gamma_5$
Energy (kev)	$445 \pm 15$	(600)	$655 \pm 3$	(700)	$760 \pm 5$
Relative intensities (a)	(7)	(10)	100	32 (b)	24

Lines	$L_1$	$\gamma_4$	$\gamma_3$	$\gamma_2$	$\gamma_1$
Energy (kev)	$824 \pm 15$	$884 \pm 4$	$936 \pm 4$	$1386 \pm 5$	$1508 \pm 7$
Relative intensities (a)	(6)	75	25	20	13

(a) Probable error :  $\pm 50\%$  if in brackets,  $\pm 25\%$  otherwise.

(b) Complex line. Using energies of 678, 706 and 723 kev for its components, relative intensities are (12), (18) and (2) with respect to 100 for  $\gamma_6$ .

Cascade relations of lines  $\gamma_1$  to  $\gamma_6$  have been obtained from coincidence experiments, and are summarized in the simplified level scheme of figure 2. Other lines are not included, and it has been checked that they do not give rise to coincidences with the energy selections used in the angular correlation runs.

#### § 4. ANGULAR CORRELATION EXPERIMENTS

A series of observations was made with different energy selections. Since the spectra of most lines overlap, a given energy selection can give rise to coincidences between various  $\gamma$ -rays. Angular correlations involving the most energetic  $\gamma$ -rays could be singled out; for this, the relative intensities were not needed, only the shapes of the spectra of some  $\gamma$ -rays had to be known. The results are displayed in table 2, in the form of coefficients of Legendre polynomial expansions; the correction for finite angular resolution is included.

Table 2. Experimental Angular Correlation Functions

$$W(\theta) = \sum_{k=0, 2, 4} A_k P_k(\cos \theta)$$

Angular correlation between	$A_0$	$A_2$	$A_4$
$\gamma_2$ and $\gamma_4$	$1 \pm 0.006$	$-0.288 \pm 0.012$	$-0.018 \pm 0.014$
$\gamma_2$ and $\gamma_6$	$1 \pm 0.03$	$-0.37 \pm 0.05$	$+0.06 \pm 0.06$
$\gamma_1$ and $\gamma_5$	$1 \pm 0.014$	$-0.16 \pm 0.02$	$+0.01 \pm 0.03$
$\gamma_1$ and $\gamma_6$	$1 \pm 0.07$	$-0.34 \pm 0.07$	$-0.12 \pm 0.09$
$\gamma_3$ and $\gamma_4$	$1 \pm 0.02$	$+0.14 \pm 0.03$	$-0.02 \pm 0.03$

The spin and parity assignments  $J_A = 0^+$ ,  $J_B = 2^+$ ,  $J_D = (?)^+$ ,  $J_E = (4, 5, 6)^+$ ,  $J_F = (4, 5, 6)^-$  suggested by Bleuler *et al.* (1953) have been used for the interpretation of the results. The values 2, 3, 4 and 5 have been tested for both spins  $J_C$  and  $J_D$ . Calculations were made assuming all  $\gamma$ -rays (except  $\gamma_6$ ) to be mixed transitions.

The most informative results are the angular correlations  $W_{24}(\theta)$  and  $W_{26}(\theta)$  between the  $\gamma$ -rays of energies 1386 kev ( $\gamma_2$ ) and respectively 885 kev ( $\gamma_4$ ) and 656 kev ( $\gamma_6$ ). The spin sequence  $J_F = 5$ ,  $J_D = 4$ ,  $J_B = 2$ ,  $J_A = 0$  is required to explain the observed values. From known parities, the  $\gamma_2$ -radiation is a mixture of electric dipole and magnetic quadrupole radiations; the  $\gamma_4$ -radiation is mainly

electric quadrupole (E2) with 0.3 to 2% M3-radiation admixture. Their mixing ratios are listed in table 3.

Table 3. Mixing Ratios of  $\gamma$ -Rays as deduced from angular Correlation Experiments

	$\gamma_1$		$\gamma_2$	$\gamma_3$			$\gamma_4$	$\gamma_5$	
	$J_C=3$	$J_C=4$		$J_F=4$	$J_F=5$	$J_F=6$		$J_C=3$	$J_C=4$
Lowest allowed multipole	$L=2$	$L=1$	E1	M1	M1	E2	E2	$L=1$	$L=2$
Upper limit of $\delta$	6.86	5.92	0.835	1.42	-0.334	-0.050	-0.0571	0.338	-0.180
Lower limit of $\delta$	0.720	0.255	0.413	-0.199	-2.33	-1.89	-0.150	0.273	-0.314

The results have been analysed as follows. The theoretical angular correlation functions can be written as

$$W_{24}(\theta) = \sum_k A_k^{(2)} A_k^{(4)} P_k(\cos \theta) \quad (k=0, 2, 4)$$

$$W_{26}(\theta) = \sum_k A_k^{(2)} U_k^{(4)} A_k^{(6)} P_k(\cos \theta)$$

where each  $A_k^{(i)}$  and  $U_k^{(j)}$  refers to one transition only (Biedenharn and Rose 1953, Rose 1953, Rose 1954, Ferentz and Rosenzweig 1955); for convenience, the coefficients of  $P_0$  were normalized equal to unity. The unknown spin  $J_F$  and mixing ratio  $\delta_2$  of the  $\gamma_2$ -radiation can be provisionally eliminated by considering the ratio  $Y$  of the coefficients of  $P_2(\cos \theta)$  of the two formulae. Indeed,  $Y = A_2^{(4)} A_2^{(6)} U_2^{(4)}$ , where  $A_2^{(6)}$  is numerically known and both  $A_2^{(4)}$  and  $U_2^{(4)}$  involve only the unknown spin  $J_D$  and mixing ratio  $\delta_4$  of the  $\gamma_4$ -radiation. Comparing  $Y$  with its experimental equivalent leads, for given  $J_D$ , to possible values of  $\delta_4$ . These can then be brought in the formula giving  $W_{24}(\theta)$ , and the latter compared with the experimental angular correlation function. Thus, compatible values of  $J_F$ ,  $J_D$ ,  $\delta_2$ ,  $\delta_4$  are found if agreement is obtained.

The angular correlations involving the 1508 keV ( $\gamma_1$ ) radiation have been analysed in a similar way. It is concluded that the level C has spin  $J_C=3$  or 4; both  $\gamma_1$  and  $\gamma_3$  (760 keV) are found to be mixed multipoles, and limits on their mixing ratios have been deduced (see table 3).

The angular correlation  $W_{34}(\theta)$  between  $\gamma$ -rays of energies 936 keV ( $\gamma_3$ ) and 885 keV ( $\gamma_4$ ) is fairly well approximated by the correlation function of the pure cascade  $6^-(E2)4^-(E2)2^-$ , which has  $A_2=0.1020$ ; however, the  $\gamma_4$ -radiation has been shown to be a mixed transition. The measured angular correlation  $W_{34}(\theta)$  is compatible with  $J_E=4, 5, 6$ , provided both  $\gamma$ -rays are mixed multipoles. Corresponding mixing ratios of the  $\gamma_3$ -radiation have been calculated and are included in table 3.

## § 5. CONCLUSION

The analysis of angular correlation results was based essentially on the fact that the ground level and first excited level of  $^{110}\text{Cd}$  have spins  $0^+$  and  $2^+$  respectively. This agrees with even-even nuclei systematics, with the conversion coefficient of  $\gamma_6$  (Rohr and Birkhoff 1955) and Coulomb excitation results (Temmer and Heydenburg 1956, Stelson and McGowan 1956). Internal conversion experiments (quoted by Bleuler *et al.* 1953) suggest that  $\gamma_4$  (885 keV) is probably E2-radiation, and that  $\gamma_3$  (936 keV) might be M1- or E2-radiation, or a mixture thereof.

Presently known information concerning the levels of  $^{110}\text{Cd}$  is summarized in the level scheme of figure 2.

A remarkable analogy exists between some levels of  $^{110}\text{Cd}$  and the levels of  $^{130}\text{Xe}$ : the pattern of levels A, B, D, E, F is reproduced with energies about 15% lower than in  $^{110}\text{Cd}$ . Spin values  $J_A = 0^+$ ,  $J_B = 2^+$ ,  $J_D = 4^+$ ,  $J_E = 6^+$ ,  $J_F = 5^-$  for the levels of  $^{130}\text{Xe}$  have been deduced by Caird and Mitchell (1954) from internal conversion experiments on five  $\gamma$ -rays, and these authors suggest that the levels of  $^{130}\text{Xe}$  with even parity belong to a modified rotational band.

Scharff-Goldhaber and Weneser (1955) pointed out that the second excited level of the type due to collective quadrupole excitation for medium heavy even-even nuclei was usually at an excitation energy of  $2.2 \pm 0.3$  times the energy of the first excited level, and that it had generally a spin  $2^+$  (more rarely  $4^+$ ,  $0^+$ , odd  $J^\pi$ ). From energy considerations, level C or level D in  $^{110}\text{Cd}$  might be such a vibrational level. The possibilities  $J_C = 2$  and  $J_D = 2$  were therefore carefully investigated, and they were found incompatible with the angular correlation results.

The present experiments were limited by time, and it is hoped to extend them elsewhere.

#### ACKNOWLEDGMENTS

It is a pleasure to acknowledge help by Dr. G. R. Bishop and Dr. J. P. Perez y Jorba, for suggesting the problem and for many interesting discussions. Dr. P. F. D. Shaw and Mr. J. C. Lisle should be thanked for the loan of their best pairs of crystals and photomultipliers, and the Electronic Workshop of Mr. Frater for continuous help. Mr. C. F. M. Cacho took part in the early measurements. The author is much indebted to Professor H. Halban for his continued interest and support during the experiment, and wishes to acknowledge the help given by the late Professor Lord Cherwell and the late Professor Sir Francis Simon in extending him the facilities of the Laboratory. The work was supported by a scholarship of the Commissariat à l'Energie Atomique, Saclay, France.

#### REFERENCES

- BIEDENHARN, L. C., and ROSE, M. E., 1953, *Rev. Mod. Phys.*, **25**, 729.  
 BISHOP, G. R., and PEREZ Y JORBA, J. P., 1955, *Phys. Rev.*, **98**, 89.  
 BLEULER, E., BLUE, J. W., CHOWDARRY, S. A., JOHNSON, A. C., and TENDAM, D. J., 1953, *Phys. Rev.*, **90**, 464.  
 CAIRD, R. S., and MITCHELL, A. C. G., 1954, *Phys. Rev.*, **94**, 412.  
 CORK, J. M., RUTLEDGE, W. C., BRANYAN, C. E., STODDARD, A. E., CHILDS, W. J., and LE BLANC, J. M., 1950, *Phys. Rev.*, **80**, 286.  
 FERENTZ, M., and ROSENZWEIG, N., 1955, *A.N.L. Report No. 5324*.  
 MARMIER, P., and BOEHM, F., 1957, N.R.C. card No. 57-4-89.  
 ROHR, R. C., and BIRKHOFF, R. D., 1955, *Phys. Rev.*, **98**, 1266.  
 ROSE, M. E., 1953, *Oak Ridge National Laboratory Report No. 1555*; 1954, *Phys. Rev.*, **93**, 477.  
 SCHARFF-GOLDBABER, G., and WENESER, J., 1955, *Phys. Rev.*, **98**, 1186.  
 SIEGBAHN, K., 1950, *Phys. Rev.*, **77**, 233.  
 STELSON, P. H., and MCGOWAN, F. K., 1956, *Oak Ridge National Laboratory Report No. 2076*.  
 TEMMER, G. M., and HEYDENBURG, N. P., 1956, *Phys. Rev.*, **104**, 967.

*Note added in proof.* A previously unknown level at 1476 keV has been revealed by the Coulomb excitation with 10 MeV  $\alpha$ -particles (Stelson and McGowan, to be published). This is the second vibrational  $2^+$  level.



## The Theory of the Nernst Effect in Semiconductors

By J. E. PARROTT

Research Laboratory, Associated Electrical Industries, Ltd., Aldermaston Court,  
Aldermaston, Berkshire

*MS. received 13th September 1957*

*Abstract.* The effects of phonon-electron drag on the Nernst effect are examined using general methods described in an earlier paper. Following an account of the physical processes involved in this effect, there is a calculation of the Nernst coefficient in some simple cases. It is shown that the sign of the Nernst coefficient can be altered by a phonon current as has been found experimentally in germanium. Furthermore, a quantitative comparison of the theory with these experiments shows satisfactory agreement.

### § 1.

IN a recent paper (Parrott 1957, to be referred to as I) the author has given an account of the effects of 'electron-phonon drag' on the electrical conductivity, thermal conductivity and thermoelectric coefficients of semiconductors. Other papers on the same subject have been published by Frederikse (1953), Herring (1954), Sondheimer (1956), and ter Haar and Neaves (1956), amongst others. It has been shown by Price (1956) and Herring (1957) that 'electron-phonon drag' will also modify the theoretical expressions for the thermomagnetic coefficients, in particular the Nernst coefficient. It is therefore proposed to apply the general methods described in the earlier paper to the calculation of the Nernst coefficient.

The Nernst effect is observed in the following circumstances. Consider a rectangular bar of some conducting material along which a heat current flows in response to a temperature gradient. If we call the long dimension of the bar the  $x$  direction, the heat current  $W_x = -\kappa \partial T / \partial x$  where  $\kappa$  is the thermal conductivity. If we now apply an external magnetic field  $H$  in the  $z$  direction, we shall measure an e.m.f.  $\Delta V_y$  in the  $y$  direction. This is the Nernst voltage and the Nernst coefficient  $P$  is defined by

$$\Delta V_y = -tPH_z \frac{\partial T}{\partial x}$$

where  $t$  is the thickness of the bar in the  $y$  direction. In addition, we shall have another e.m.f. in the  $x$  direction caused by the thermoelectric effect and we can combine both effects in the following vector equation

$$\frac{1}{e} \text{grad } \zeta = Q \text{grad } T - P[\mathbf{H} \times \text{grad } T]. \quad \dots\dots(1)$$

Here we have introduced the electrochemical potential  $\zeta$ ; the measured electromotive forces correspond to differences in  $\zeta/e$ .  $Q$  is the absolute thermoelectric

power. This equation enables us to define a Nernst angle  $\theta_N$  analogous to the Hall angle  $\theta_H$ .† We shall write

$$\tan \theta_N = -PH/Q \quad \dots\dots(2)$$

and  $\theta_N$  is the angle between the direction of  $-\text{grad } \zeta$  and  $\text{grad } T$ .

Callen (1948, 1952) has shown that the Nernst coefficient also arises in a different experimental situation in which there is no temperature gradient. This last point makes it more convenient for theoretical calculation, and this is the approach which will be used later in the paper. Callen shows that

$$\mathbf{w} = TQ\mathbf{j} - TP[\mathbf{H} \times \mathbf{j}] \quad \dots\dots(3)$$

where  $\mathbf{w}$  is the heat current and  $\mathbf{j}$  is the electric current. The meaning of the equation is that in a magnetic field the heat current associated with  $\mathbf{j}$  is modified by the addition of a flow at right angles to  $\mathbf{H}$  and  $\mathbf{j}$ . The total heat current is inclined at an angle to the electric current which is the same as the Nernst angle defined above.

It is worth stating here that there is a thermodynamic relation between the Nernst coefficient, Ettinghausen coefficient‡  $U$  and thermal conductivity  $\kappa$ :

$$\kappa U = TP. \quad \dots\dots(4)$$

This corresponds to the situation where we have a temperature gradient in the  $[\mathbf{H} \times \mathbf{j}]$  direction which compensates the Nernst heat flow in equation (3).

The kinetics of the Nernst effect can be seen most clearly by considering the effect of a normal magnetic field on an electric current (in the  $x$  direction) and its associated heat current. We will maintain  $\partial T/\partial y = 0$  so that there will be (a) a Hall voltage, and (b) a transverse Nernst heat current. The Hall voltage will prevent any net transverse electric current and we can describe the situation in terms of the Hall angle

$$\theta_H = \frac{\partial \zeta/\partial y}{\partial \zeta/\partial x},$$

when  $\theta_H$  is small. Consider the case of positive holes where  $R$  and  $Q$  are positive, and let us make  $P$  positive also. Figure 1 shows the situation; the magnetic field is directed towards the reader in the  $z$  direction, so that, if  $\mathbf{j}$  is in the  $x$  direction, the  $y$  direction is vertically upwards. The tendency of the magnetic field is to deflect the holes in the negative  $y$  direction, so the compensating Hall field gives a resultant  $-\text{grad } \zeta$  as shown. The Hall angle is positive:

$$\theta_H = RH/\rho. \quad \dots\dots(5)$$

† In the Hall effect we have an electric current, a magnetic field and a Hall e.m.f. at right angles to each other. Written in the same form as (1), we have:

$$\frac{1}{e} \text{grad } \zeta = -\rho \mathbf{j} - R[\mathbf{H} \times \mathbf{j}] \quad \dots\dots(1a)$$

where  $\rho$  is the electrical resistivity,  $R$  the Hall constant,  $\mathbf{j}$  the electric current density. The Hall angle, defined as the angle between  $-\text{grad } \zeta$  and the electric current, is given by

$$\tan \theta_H = RH/\rho \quad \dots\dots(2a)$$

which may be compared with (2). Both the Hall angle and the Nernst angle can be measured by determining the change in the equipotential lines across a conductor when the magnetic field is applied.

‡ The Ettinghausen effect is the production of a temperature gradient by an electric current and a magnetic field, all at right angles to one another. The Ettinghausen coefficient is defined by the equation  $\partial T/\partial y = -UH_z j_x$ .

The deflection of the holes by the magnetic field is described as a function of relaxation time  $\tau$  and therefore of energy by

$$\theta = \theta_H - \frac{eH\tau}{mc} \quad \dots\dots(6)$$

i.e. those with larger relaxation times are deflected downwards and those with shorter relaxation times upwards. If  $P$  is positive, there is a component of heat current in the negative  $y$  direction which requires that the more energetic electrons

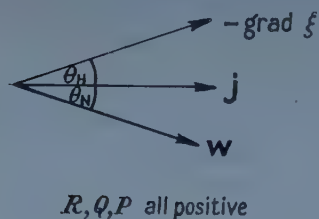


Figure 1. Nernst effect in a p-type semiconductor.

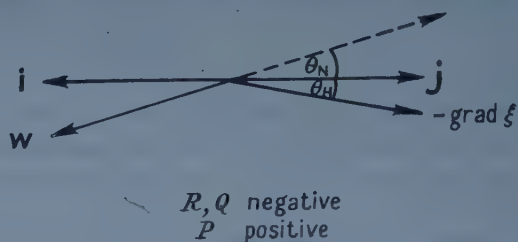


Figure 2. Nernst effect in a n-type semiconductor.

have the longer relaxation times and conversely. This is the case where we have impurity scattering of electrons; lattice scattering,  $\tau \propto \epsilon^{-1/2}$ , gives a negative Nernst coefficient. We must also note that the Nernst coefficient does not change sign with the sign of the current carrier. In figure 2 we have the electric current  $\mathbf{j}$  and the electron particle current  $\mathbf{i}$ . With  $\mathbf{H}$  directed towards the reader, the electrons tend to be deflected downwards and the compensating voltage gives a component of  $-\text{grad } \zeta$  in the same direction. This gives our negative Hall angle. If electrons have a positive Nernst coefficient, the Nernst angle will be positive because for electrons  $Q$  is negative. A deflection of the heat current in this sense will be seen to mean that the more energetic holes are deflected most, i.e. have the longer relaxation times. This is exactly the same as the situation described above for holes.

The effect of phonon disequilibrium will be seen to reverse the sign of the Nernst coefficient, since the phonons are more strongly coupled to slow than to fast electrons. We shall see that the magnitude of the phonon current is frequently large enough to change the sign of the Nernst coefficient.

## § 2.

We shall calculate the Nernst coefficient using equations (3) and (4), making  $\mathbf{j} = (j, 0, 0)$  and  $\mathbf{H} = (0, 0, H)$ . The calculation of the electron perturbation from equilibrium will be carried out as if the phonons were in equilibrium, and this electron perturbation will be used to calculate the phonon perturbation which in fact exists. This method is only approximate but is as good for this case as it is in the theory of thermoelectric power where it is known to be reasonably adequate. The notation used will be that used in I. The electron perturbation  $c(x)$  becomes a vector  $\mathbf{c}(x)$  with  $x$  and  $y$  components and the generalization of (37) of that paper is

$$\left. \begin{aligned} \frac{m}{\hbar\tau_e} c_x(x) + \frac{eH}{\hbar c} c_y(x) &= -\frac{\partial \zeta}{\partial x} \\ -\frac{eH}{\hbar c} c_x(x) + \frac{m}{\hbar\tau_e} c_y(x) &= -\frac{\partial \zeta}{\partial y} \end{aligned} \right\} \cdot \quad \dots\dots(7)$$



The solution is

$$\begin{aligned} c_x(x) &= -\frac{\hbar\tau_e}{m} \left( \frac{\partial\zeta}{\partial x} - \frac{eH\tau_e}{mc} \frac{\partial\zeta}{\partial y} \right) / \left\{ 1 + \left( \frac{eH\tau_e}{mc} \right)^2 \right\} \\ c_y(x) &= -\frac{\hbar\tau_e}{m} \left( \frac{\partial\zeta}{\partial y} + \frac{eH\tau_e}{mc} \frac{\partial\zeta}{\partial x} \right) / \left\{ 1 + \left( \frac{eH\tau_e}{mc} \right)^2 \right\}. \end{aligned} \quad \dots\dots(8)$$

If we restrict ourselves to small magnetic fields, the  $H$ -dependent term in the denominator can be neglected. We then determine  $\mathbf{c}(x)$  under the condition that  $j_y=0$ . We obtain the usual expression for the Hall angle:

$$\tan \theta_H = \frac{\partial\zeta/\partial y}{\partial\zeta/\partial x} = -\frac{eH}{mc} \frac{\langle x^4\tau_e^2 \rangle}{\langle x^4\tau_e \rangle} = -\frac{3\pi}{8} \mu H$$

where the last expression is the explicit value for lattice scattering. Still neglecting terms in  $H^2$  we get for  $\mathbf{c}(x)$

$$c_x(x) = -\frac{\hbar\tau_e}{m} \frac{\partial\zeta}{\partial x}, \quad \dots\dots(9)$$

$$c_y(x) = +\frac{\hbar eH\tau_e}{m^2c} \left( \frac{\langle x^4\tau_e^2 \rangle}{\langle x^4\tau_e \rangle} - \tau_e \right) \frac{\partial\zeta}{\partial x}. \quad \dots\dots(10)$$

The phonon perturbation  $b(y)$  likewise becomes a vector  $\mathbf{b}(y)$  and can be obtained from  $c(x)$  by using (38) of I. We find

$$b_x(y) = -\frac{32\pi n e \lambda^5 s^2 \tau_p y}{3\mu_0 \hbar} \frac{\partial\zeta}{\partial x} \int_y^\infty \exp(-x^2) x \tau_e dx \quad \dots\dots(11)$$

$$\begin{aligned} b_y(y) &= \frac{32\pi n e^2 H \lambda^5 s^2 \tau_p y}{3\mu_0 \hbar m c} \frac{\partial\zeta}{\partial x} \\ &\times \left[ \frac{\langle x^4\tau_e^2 \rangle}{\langle x^4\tau_e \rangle} \int_y^\infty \exp(-x^2) x \tau_e dx - \int_y^\infty \exp(-x^2) x \tau_e^2 dx \right]. \end{aligned} \quad \dots\dots(12)$$

The electron heat current is calculated from

$$\mathbf{w}_e = -\frac{8n}{3\pi^{1/2}\hbar} \left[ \zeta_0 \langle x^4 \mathbf{c}(x) \rangle - kT \langle x^6 \mathbf{c}(x) \rangle \right] \quad \dots\dots(13)$$

and the phonon heat current from

$$\mathbf{w}_p = \frac{8kT}{3\pi^2 \hbar \lambda^3} \int_0^\infty y^2 \mathbf{b}(y) dy. \quad \dots\dots(14)$$

Adding these together to give the total heat current and substituting the expressions for  $\mathbf{c}(x)$  and  $\mathbf{b}(y)$  derived above we obtain

$$\mathbf{w}_x = \frac{8n}{3\pi^{1/2}m} \frac{\partial\zeta}{\partial x} \left[ \zeta_0 \langle x^4\tau_e \rangle - kT \langle x^6\tau_e \rangle - \frac{16es^2}{3\pi^{1/2}\mu_0} \langle x\tau_e(y^3\tau_p) \rangle \right] \quad \dots\dots(15)$$

$$\begin{aligned} \mathbf{w}_y &= \frac{-8n}{3\pi^{1/2}m} \frac{eH}{mc} \frac{\partial\zeta}{\partial x} \left\{ -kT \left[ \frac{\langle x^4\tau_e^2 \rangle \langle x^6\tau_e \rangle}{\langle x^4\tau_e \rangle} - \langle x^6\tau_e^2 \rangle \right] \right. \\ &\quad \left. - \frac{16es^2}{3\pi^{1/2}\mu_0} \left[ \frac{\langle x^4\tau_e^2 \rangle \langle x\tau_e(y^3\tau_p) \rangle}{\langle x^4\tau_e \rangle} - \langle x\tau_e^2(y^3\tau_p) \rangle \right] \right\}. \end{aligned} \quad \dots\dots(16)$$

This gives us

$$\tan \theta_N = \frac{eH}{mc} \times \frac{\left\{ kT \left[ \frac{\langle x^4 \tau_e^2 \rangle \langle x^6 \tau_e \rangle}{\langle x^4 \tau_e \rangle} - \langle x^6 \tau_e^2 \rangle \right] - \frac{16es^2}{3\pi^{1/2}\mu_0} \left[ \frac{\langle x^4 \tau_e^2 \rangle \langle x \tau_e (y^3 \tau_p) \rangle}{\langle x^4 \tau_e \rangle} - \langle x \tau_e^2 (y^3 \tau_p) \rangle \right] \right\}}{\left[ \zeta_0 \langle x^4 \tau_e \rangle - kT \langle x^6 \tau_e \rangle - \frac{16es^2}{3\pi^{1/2}\mu_0} \langle x \tau_e (y^3 \tau_p) \rangle \right]} \quad \dots\dots(17)$$

Since the thermoelectric power is

$$Q = \frac{k}{e} \left[ \frac{\zeta_0}{kT} - \frac{\langle x^6 \tau_e \rangle}{\langle x^4 \tau_e \rangle} - \frac{16es^2}{3\pi^{1/2}\mu_0 kT} \frac{\langle x \tau_e (y^3 \tau_p) \rangle}{\langle x^4 \tau_e \rangle} \right],$$

the Nernst coefficient is

$$P = -\frac{e}{mc} \frac{k}{e} \left\{ \left[ \frac{\langle x^4 \tau_e^2 \rangle \langle x^6 \tau_e^2 \rangle}{\langle x^4 \tau_e \rangle^2} - \frac{\langle x^6 \tau_e^2 \rangle}{\langle x^4 \tau_e \rangle} \right] + \frac{16es^2}{3\pi^{1/2}\mu_0 kT} \left[ \frac{\langle x^4 \tau_e^2 \rangle \langle x \tau_e (y^3 \tau_p) \rangle}{\langle x^4 \tau_e \rangle^2} - \frac{\langle x \tau_e^2 (y^3 \tau_p) \rangle}{\langle x^4 \tau_e \rangle} \right] \right\}. \quad \dots\dots(18)$$

It is instructive to note the following:

- (a)  $\frac{e}{m} \frac{\langle x^4 \tau_e^2 \rangle}{\langle x^4 \tau_e \rangle}$  is the Hall mobility  $\mu_H$  determined by combining the Hall constant and conductivity.
- (b)  $\frac{k}{e} \frac{\langle x^6 \tau_e \rangle}{\langle x^4 \tau_e \rangle}$  is the negative of the kinetic energy contribution to the thermoelectric power  $Q_k$ .
- (c)  $\frac{16es^2}{3\pi^{1/2}\mu_0 T} \frac{\langle x \tau_e (y^3 \tau_p) \rangle}{\langle x^4 \tau_e \rangle}$  is the negative of the phonon portion of the thermoelectric power  $Q_p$  so we can write

$$P = \frac{\mu_H}{c} \left[ Q_k \left( 1 - \frac{\langle x^6 \tau_e^2 \rangle \langle x^4 \tau_e \rangle}{\langle x^6 \tau_e \rangle \langle x^4 \tau_e^2 \rangle} \right) + Q_p \left( 1 - \frac{\langle x \tau_e^2 (\tau_p y^3) \rangle \langle x^4 \tau_e \rangle}{\langle x \tau_e (\tau_p y^3) \rangle \langle x^4 \tau_e^2 \rangle} \right) \right]. \quad \dots\dots(19)$$

The evaluation of the terms in round brackets can be carried out for certain simple cases, as can the ratio  $\mu_H/\mu$ . For lattice scattering of electrons and phonon scattering of phonons we find

$$P = -\frac{3\pi\mu_0 k}{16ce} \left[ 1 - \frac{8}{3} \left( \frac{4}{\pi} - 1 \right) \frac{es^2}{BT^4\mu_0 kT} \right]. \quad \dots\dots(20)$$

Here we have used (see I)

$$(i) \tau_e = \frac{3\pi^{1/2}\mu_0 m}{4ex}, \quad (ii) \tau_p = (BT^4 y^2)^{-1}.$$

The normal electronic term is negative and the phonon term positive in agreement with the qualitative arguments of § 1.

If we assume that impurities dominate in the scattering of the electrons we get a somewhat different result:

$$P = \frac{945\pi\mu_1 k}{1024ce} \left[ 1 - \frac{5}{9} \left( 1 - \frac{4096}{1575\pi} \right) \frac{es^2}{BT^4\mu_0 kT} \right] \quad \dots\dots(21)$$

( $\mu_1$  is the mobility due to impurity scattering). As was suggested by qualitative considerations, the electronic contribution is positive in this case, whilst the phonon contribution has become negative. This example is perhaps a little unrealistic, however, because it takes no account of scattering of phonons by electrons; this has the result of diminishing  $Q_p$ .

A numerical check on the theory can be obtained from data on an n-type germanium specimen, given by Herring (1957):

1. The Nernst coefficient passes through zero at 175°K, being positive at lower temperatures. The phonon contribution to the thermoelectric power is given as  $1.9 \times 10^{-4} \text{ v deg}^{-1}$  and we find that using this figure

$$\frac{8}{3} \left( \frac{4}{\pi} - 1 \right) \frac{es^2}{BT^4 \mu_0 kT} = 1.19$$

rather than the predicted value of 1.

2. The power of the temperature variation of  $P$  is about  $-4.2$  between 50 and 100°K whilst that of  $Q_p$  is about  $-2.5$  over the same temperature range; since  $P/Q_p \propto \mu$  and  $\mu$  for n-germanium has a power of about  $-1.66$ , the results are certainly self-consistent, and in general agreement with the theory.

The effects of boundary scattering of the phonons on the Nernst effect are likely to be complicated. A particular difficulty is that under these conditions the two approaches to the Nernst effect described in §1 are no longer equivalent, since in one case there is a transverse heat flow, but in the other there is not,

Herring (1957) has discussed the dependence of the Nernst effect on magnetic field strength, and concludes that  $P$  tends to zero as the field increases. This is because the dependence of the deflection of the electrons on relaxation time decreases as the field increases, so the magnetic field is no longer able to separate electrons of different energies to give a Nernst effect.

#### ACKNOWLEDGMENT

I wish to thank Dr. T. E. Allibone, Director of the Research Laboratory, Associated Electrical Industries, for permission to publish this paper.

#### REFERENCES

- CALLEN, H. B., 1948, *Phys. Rev.*, **73**, 1349; 1952, *Ibid.*, **85**, 16.  
 FREDERIKSE, H. P. R., 1953, *Phys. Rev.*, **92**, 248.  
 TER HAAR, D., and NEAVES, A., 1956, *Advanc. Phys. (Phil. Mag. Suppl.)*, **5**, 241.  
 HERRING, C., 1954, *Phys. Rev.*, **96**, 1163; 1957, *Proceedings of the International Colloquium on Semiconductors and Phosphors, Garmisch-Partenkirchen, Germany*, to be published.  
 PARROTT, J. E., 1957, *Proc. Phys. Soc. B*, **70**, 590.  
 PRICE, P. J., 1956, *Phys. Rev.*, **102**, 1245.  
 SONDHEIMER, E. H., 1956, *Proc. Roy. Soc. A*, **234**, 391.



## Physical Properties of Certain Liquid Binary Alloys of Tin and Zinc †

BY T. C. TOYE AND E. R. JONES

The British Iron and Steel Research Association, South Wales Laboratories, Swansea

*MS. received 5th March 1957, and in revised form 30th September 1957*

**Abstract.** The viscosity, density and specific resistance of a number of tin based and zinc based binary alloys have been determined over various temperature ranges starting at a few degrees above the liquidus and extrapolated back to the melting point. The variation of these properties with increasing alloy additions has been found to be non-linear and minima have been observed near eutectics and limits of solid solubility.

The paper gives the results of these measurements on Zn-Al, Zn-Pb, Zn-Sn, Sn-Zn, Sn-Ag, Sn-Cu, Sn-Ni and Sn-Pb systems.

### § 1. INTRODUCTION

**F**OLLOWING the determination of the viscosity of pure zinc already described in a previous paper (Hopkins and Toye 1950), a study was made of the effect of small additions of Al upon the viscosity of liquid zinc. This was undertaken in answer to a current commercial problem in hot dip galvanizing, namely that a very viscous zinc bath could be effectively rendered fluid by the addition of small quantities of Al of the order of 0.1%. While the results showed that small quantities of Al do, in fact, reduce the viscosity of the zinc, the effect would certainly not be observed by eye. It was therefore assumed that the reduction of the ever present zinc oxide in the galvanizing bath by the Al might be the real cause of the 'cleaning' up of the bath.

In addition the interesting fact emerged that the viscosity of the parent zinc did not decrease linearly but instead fell to a very sharp minimum at approximately 1.14 weight % Al. Careful repetition and consideration of the observations proved that the effects were real and the work was accordingly extended to cover Zn-Fe, Zn-Pb, Zn-Sn, and also Sn-Cu, Sn-Ni, Sn-Ag, Sn-Pb, and Sn-Zn. All the systems showed similar non-linear behaviour and it was decided to investigate other properties to see whether they too behaved in a similar manner to viscosity. The density and specific resistance of a selected number of the above mentioned alloys were, therefore, measured at temperatures above the liquidus and the results compared with those for the viscosity.

### § 2. DESCRIPTION OF THE EXPERIMENTAL METHODS

#### 2.1. Viscosity

The apparatus and the method for measuring the viscosity have been described in the paper (Hopkins and Toye 1950) to which reference has already been made. The metal is contained in a cylindrical alumina crucible which is suspended in

† Report No. MW/C/4/57 of the Coatings Committee of the British Iron and Steel Research Association.

a furnace through which hydrogen is passed. The cylinder is allowed to oscillate under the control of the torsion in the suspension wire. The damping of the oscillations depends upon the viscosity of the metal. Two methods were given for determining the coefficient of viscosity from the observed damping; one, a calibration method in which certain constants were determined by using liquids of known viscosity and density, and the other an absolute method which requires only a knowledge of the moment of inertia of the oscillating system with an empty crucible, the radius of the crucible and the density of the liquid metal. The viscosity can be calculated from a relationship which was derived between the viscosity and the logarithmic decrement of the oscillating system determined when the crucible is filled with liquid metal. Experience has shown that the latter method is more convenient and satisfactory. For example, the breaking of a crucible—a misfortune which sometimes occurs—does not involve the repetition of a lengthy series of calibration experiments. This latter method was, therefore, used in all the results quoted here. A description of the method employed in calculating  $\eta$  from the formula mentioned above is given in the Appendix.

The quantities which were measured experimentally were the logarithmic decrement  $\delta$  of the oscillations, the times of oscillation  $T$  and  $T_0$  of the crucible containing the liquid metal and the empty crucible respectively, the moment of inertia  $I$  of the oscillating system and the radius of the crucible. The depth  $c$  of the metal in the crucible was fixed by putting a weighed quantity of the metal in the crucible, the density at the temperature of the experiment being known.  $T$ ,  $T_0$  and  $\delta$  were determined by observing the graduated disc attached to the suspension system. The observed value of  $\delta$  was corrected by subtracting from it the value of logarithmic decrement for the (hot) empty crucible. The moment of inertia  $I$  was calculated from the times of oscillation of the system with the empty crucible and then with the crucible filled with a known weight of  $\frac{1}{8}$  in. diameter steel balls. It was found that when the system is hot, the moment of inertia differs slightly from that when it is cold. This difference is practically constant for different crucibles, so that after changing a crucible it was only necessary to determine  $I$  at room temperature and to add a small correction to obtain  $I$  at the temperature of the experiment. The radius of the crucible must be measured as accurately as possible. The method that was adopted was to put successively increasing weighed quantities of mercury into the crucible, and to take readings of the depth of mercury surface below the mouth of the crucible. This was done with a depth micrometer.

Contact between the tip of the micrometer and the surface was indicated by the lighting of a flash lamp bulb, the circuit being completed by a very thin wire dipping into the mercury. The mean of several values of the radius determined with different depths of mercury was taken.

It should be mentioned that similar care was again taken (Hopkins and Toye 1950) to ensure uniformity of temperature while in addition the possibility of segregation was avoided by the initiation of large amplitude oscillations immediately prior to each observation.

A second viscometer of the same type but with a bifilar suspension was built in order to double the rate of observation but it was found that the unifilar suspension was much more convenient for visual observation. This second viscometer was, therefore, modified to unifilar suspension. The accuracy of measurement of viscosity in the experiments was to between  $\pm \frac{1}{4}\%$  and  $\pm \frac{1}{2}\%$ .

## 2.2. Density

After a study of a number of methods the most suitable was considered to be the simple method of weighing a Pyrex glass sphere containing mercury suspended in the liquid metal from one arm of a balance by means of a thin tungsten wire. The balance base was suitably heat insulated and situated about 18 in. from the top of the furnace. In no case was there any increase in temperature inside the balance during an experiment. Adequate air space for safety purposes was provided above the mercury in the Pyrex sphere, the walls of which were also thickened for the same purpose. These precautions, however, had the disadvantage of limiting the maximum resulting density of the sphere to  $8.5 \text{ g cm}^{-3}$  which served perfectly for all the alloys examined except the high Pb, Pb-Sn alloys for which use had to be made of a small solid cylinder of tungsten in place of the Hg filled glass sphere. Care had to be taken to remove trapped air bubbles from below the tungsten cylinder but no such trouble occurred with the glass sphere.

The method was found to be very simple since it was only necessary to weigh the sphere (or cylinder) in air and in water to determine its density at one temperature and then to proceed to the liquid metals.

Allowance was made for the expansion of the Pyrex glass and of course the tungsten cylinder but not for the effect of surface tension on the supporting wire because the very small circumference (diameter 0.0035 in.) of the latter ensured that the effect was smaller than the limit of experimental error. The Pyrex sphere, after preheating above the melt, was lowered slowly through the surface which was quickly skimmed free of oxide immediately prior to the immersion. The temperature of the melt was then lowered and weighings made as the temperature fell. Adequate lagging ensured that the fall in temperature was not too fast and immediately prior to each weighing the surface of the melt was cleaned as for immersion of the sphere. Cleaning the surface prior to a weighing was necessary because the known value of surface tension (the effect of which is negligible) was then very closely approached, a very small non-wetting meniscus being observed. Failure to clean the surface ultimately resulted in the formation of a tenacious oxide film which caused excessive damping.

In only one experiment did the sphere burst and although that particular alloy had to be discarded, there was no other damage. The accuracy of measurement of density in the experiments was to  $\pm 0.05\%$ .

## 2.3. Specific Resistance

Whereas viscosity and density were both measured to a high degree of accuracy, it was decided that purely comparative values of specific resistance would suffice and the method used was, therefore, a relative one.

A helical Pyrex tube was wound and enlarged at its upper end into a large well. The helix was lowered carefully into a crucible of the liquid melt whereupon the liquid metal filled the helix and formed a pool in the enlarged top tube. One contact was placed in this pool and the other in the crucible and effectively, therefore, contact was made at each end of a long filament of liquid metal. The contacts were of stainless steel. The resistance of the filament was compared with a standard resistance by means of a Callender and Griffiths bridge using a.c. and a vibration galvanometer to eliminate the effect of thermal e.m.f.'s.



The constant of the helix was first determined using mercury as the filling liquid. No allowance for expansion of the helix was made and the values obtained were not accurate therefore. The fact that they were consistent, however, was considered to be sufficient for the purpose.

#### 2.4. *Purity of Metals Employed*

The highest purity metals were used for both solvents and solute additions. The solvent metals used were as follows: Tin: Pass S from Capper Pass & Sons; 99.998% pure; impurities mostly in fourth decimal place. Lead: purest lead from Capper Pass & Sons; min. 99.97% pure; max. impurities Bi 0.01%, Ag 0.005%. Zinc: from Imperial Smelting Corporation; analysis Pb 0.0005%, Cd 0.0001%, Cu 0.0001%, Fe 0.0005%, Ca trace.

### § 3. EXPERIMENTAL OBSERVATIONS

Following the observation of the minimum in the viscosity-composition relation of Zn-Al the work was extended to cover Zn-Fe, Zn-Pb, Zn-Sn, Sn-Ag, Sn-Cu, Sn-Ni and Sn-Pb. The variation of viscosity with composition for all the systems was at first investigated over a wide range of composition and attention then concentrated on the systems Sn-Cu, Sn-Ni and Sn-Pb. The results of viscosity and density at the melting point for these three systems are given in tables 1 to 3 respectively, but since the other systems were not examined in such detail, only the curves of viscosity-composition are given for them (see figures 1 to 6). In the case of viscosity, approximately 15 observations of logarithmic decrement were made at each temperature, the standard deviation being about 0.0005 poise.

A typical viscosity-temperature curve is shown in figure 16; it being found that the relationship is well represented by the expression

$$\eta = Ae^{B/kt}$$

In no case has any anomalous increase near the melting point been detected as has been reported by other workers (Yao and Kondic 1952).

The curves of viscosity-composition at the liquidus temperature, at 200°A above the respective liquidus points and at 700°A (isothermal) are given in figures 7 to 9 for the systems Sn-Cu, Sn-Ni and Sn-Pb respectively. These curves show that the viscosity does not change uniformly with composition but tends to minimum values at points which can be associated with eutectics and with solid solubility limits. Furthermore, the minima do not disappear at temperatures immediately above the liquidus points but persist to quite high temperatures as the plots at high isothermals and at standard superheats show. (Standard superheat is here defined as a definite temperature interval above the respective m.p. The superheat used, see figures 7, 8 and 9, is 200°A.) The variation in liquidus temperatures with composition for the systems Sn-Cu and Sn-Ni are not sufficiently large to show much difference between isothermal and constant superheat plots but in the case of the Sn-Pb system there is a wide variation of liquidus temperature with composition. The retention of the shape of the curves for this latter system proves, therefore, that the observations are more than just temperature effects.

The liquid state is not, as yet, sufficiently well understood to provide complete theoretical explanation of these observations; at the same time it is as well to obtain as much information as possible from the observations.



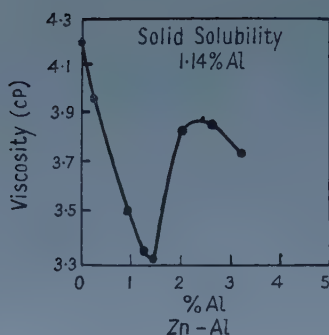


Figure 1

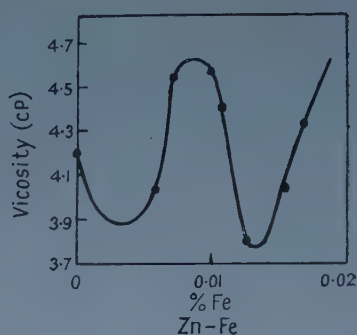


Figure 2

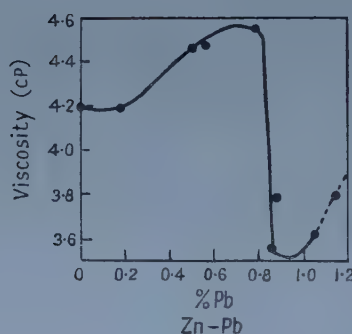


Figure 3

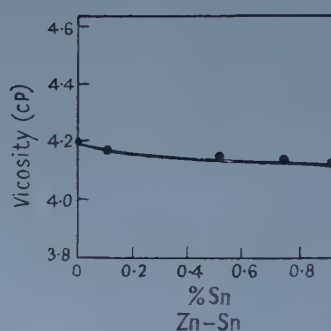


Figure 4

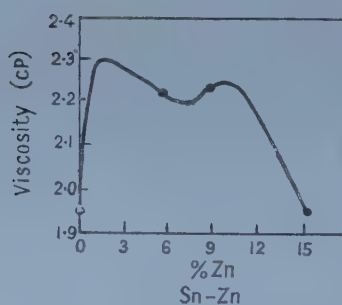


Figure 5

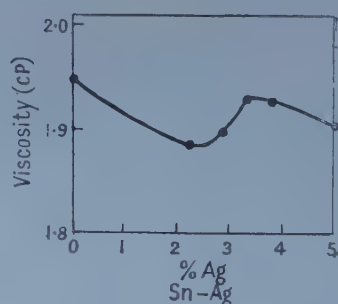


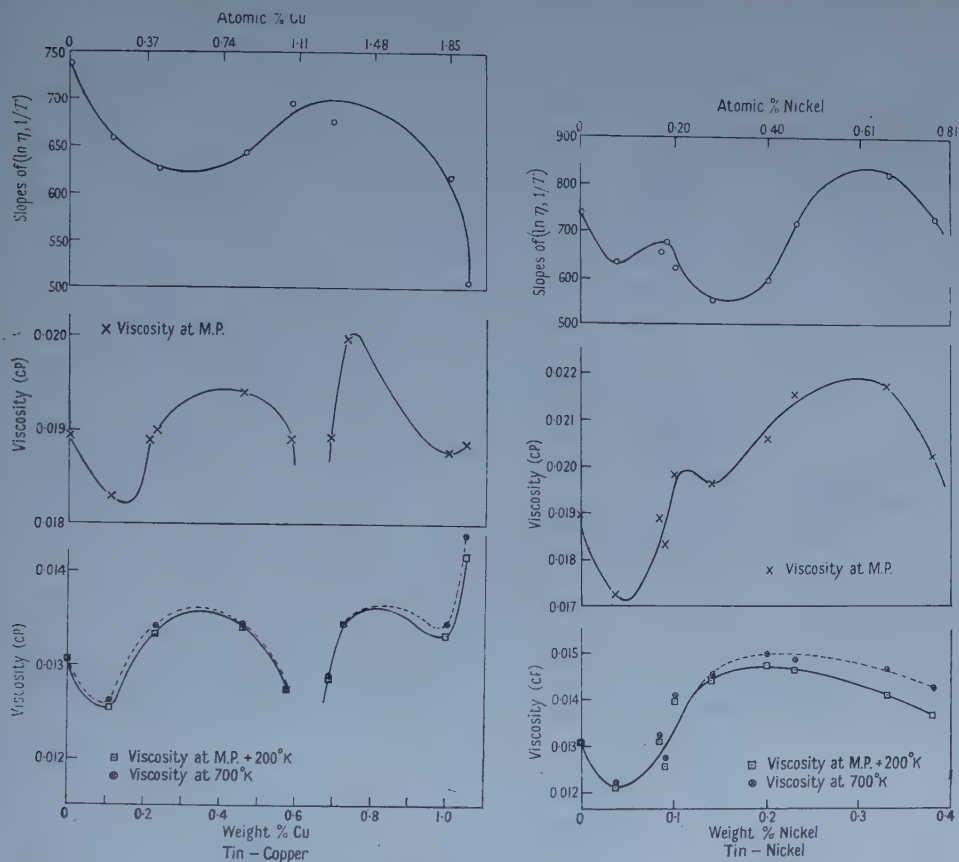
Figure 6

Figures 1-6. Various viscosity-composition curves.

To this end the values of the slopes at each composition of the  $(\ln \eta, 1/T)$  relations have been plotted with the viscosity-composition diagrams (see figures 7 to 9). Inspection of the way in which the slopes vary with composition shows straight away that the shape of the viscosity-composition curves cannot be radically changed at any but very large superheats and one is led to conclude from this that the retention of the minimal behaviour to high superheats must be some short range order effect. The term  $B$  in the viscosity temperature relation of equation (1) represents the activation energy for atomic migration (Andrade 1934). Further, if these are structure effects, then they must start at a very

much higher temperature above the melting point than has previously been thought.

The second interesting feature of the observations is the very existence of minima at all. Thus at the eutectic for example it is possible that there is competition between the two phases which might be the cause of the low viscosity at the points referred to.



Figures 7 and 8. Viscosity-composition curves at melting points and at higher temperatures and variation of slope of  $(\ln \eta, 1/T)$  with composition for Sn-Cu (figure 7) and Sn-Ni (figure 8).

Figures 10 to 15 show the curves for density-composition and specific resistance-composition for Sn-Cu, Sn-Ni and Sn-Pb. In all cases the points are plotted for the respective liquidus temperature, the values at these temperatures being obtained from the respective property-temperature relations by extrapolation over a few degrees. Plots at high superheats and isothermals have not been given for these since due to the restricted temperature range over which the observations were made, wide extrapolation would have been necessary at the high temperature end to compare with the high temperature viscosity curves of figures 7 to 9 for which no extrapolation was needed. Minimal behaviour of density and specific resistance with composition is again seen to occur though except for the Sn-Pb system at about 2.5%Pb the density appears only to possess well defined minima at eutectics and it is thought that this observation requires further investigation. For instance (see figure 8), there may be a minimum below 0.005%Ni but the observations do not show this conclusively.

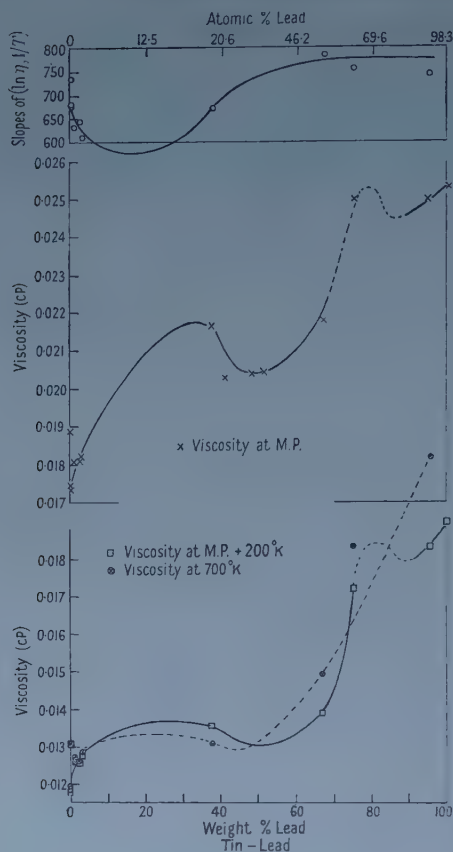


Figure 9. Viscosity-composition curves at melting points and at higher temperatures and variation of slope of  $(\ln \eta, 1/T)$  with composition for Sn-Pb.

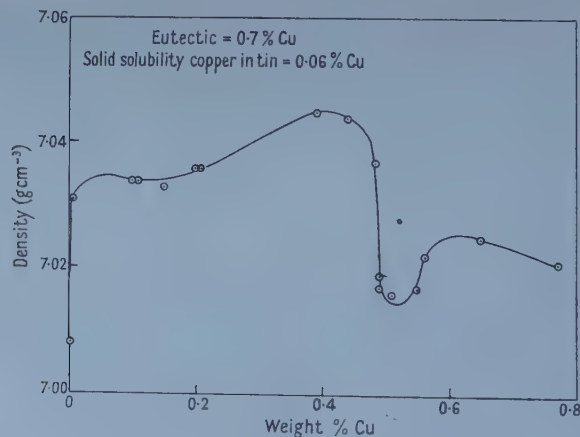


Figure 10. Density-composition curve Sn-Cu.

#### § 4. CONCLUSIONS

The viscosity, density and specific resistance of certain liquid binary alloys do not vary uniformly with composition but fall to minimum values at points which can be associated with eutectics and solid solubility limits. Although this



has not been established in every case, it is thought that sufficient has been done to justify the assumption that further work would show it to be generally true.

It is thought that the observations indicate the existence of short range order at temperatures much above the melting point while the existence of minima

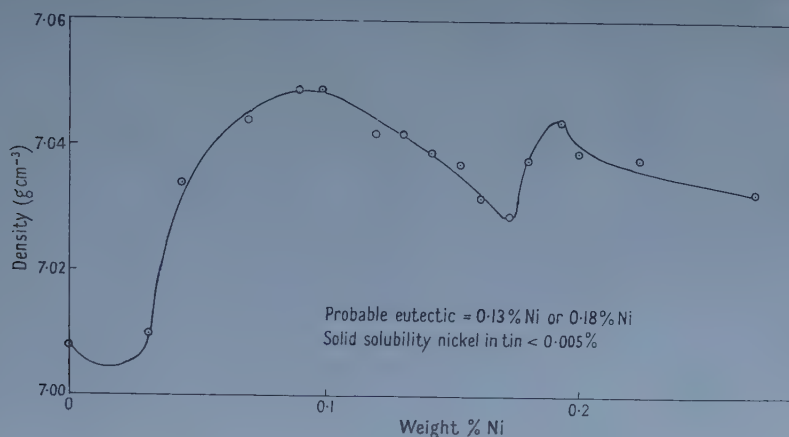


Figure 11. Density-composition curve Sn-Ni.

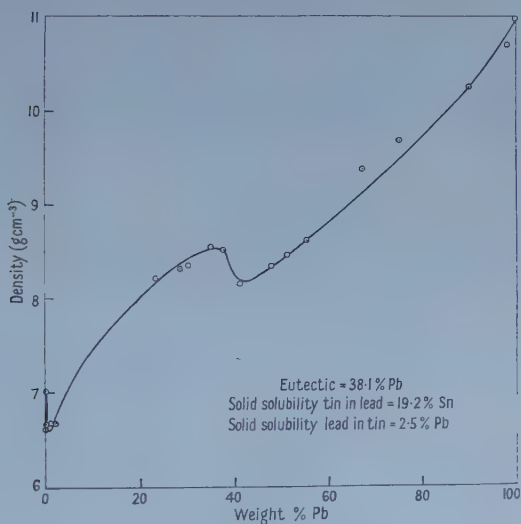


Figure 12. Density-composition curve Sn-Pb.

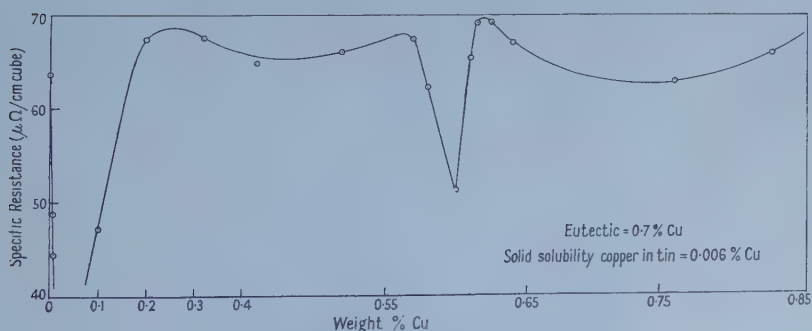


Figure 13. Specific resistance-composition curve Sn-Cu.

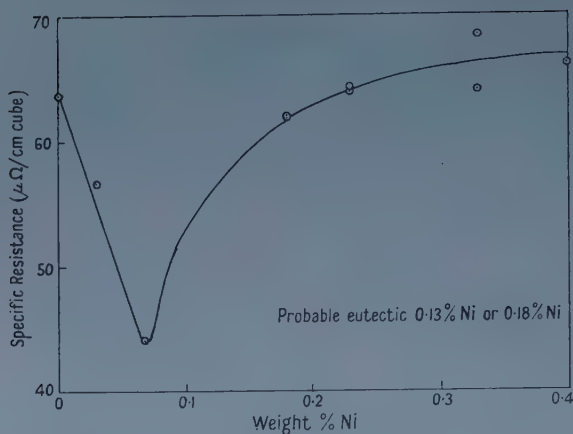


Figure 14. Specific resistance-composition curve Sn-Ni.

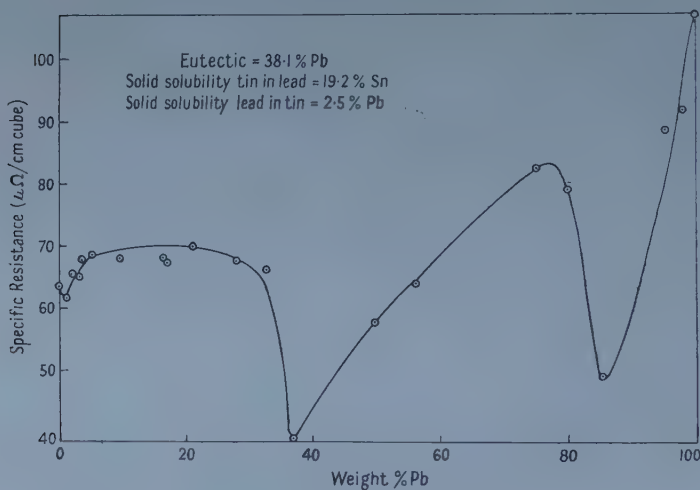


Figure 15. Specific resistance-composition curve Sn-Pb.

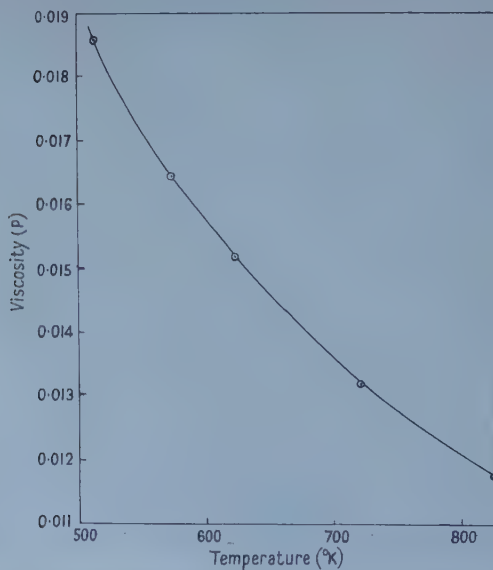


Figure 16. A typical curve showing the variation of viscosity with temperature for a Sn 99%-Cu 1% alloy.

at all is thought to be due to the presence of some competition between phases as might be expected at the eutectic for example.

It is suggested that further experimental work should include low angle x-ray diffraction measurements and also the measurement of the work function of liquid metal surfaces, particularly in the vicinity of minimal points since these two properties, it is thought, should throw further light upon the structure of liquid metals.

#### ACKNOWLEDGMENTS

The authors are indebted to the Imperial Smelting Corporation for the supply of the pure zinc used in their experiments.

They are grateful to Mr. D. G. B. Thomas for his help in performing a large amount of computation work, including all that given in Appendix I. They wish to thank Mr. S. S. Carlisle, Head of the Swansea Laboratories, for his most useful guidance in the preparation of the paper, and finally they wish to record their very sincere appreciation of the active encouragement and continued inspiration given by their Director of Research, Sir Charles Goodeve and their Deputy Director, Mr. W. C. F. Hessenberg.

#### REFERENCES

- ANDRADE, E. N. DA C., 1934, *Phil. Mag.*, **17**, 497, 698.  
 FISHER, H. J., 1953, *Research Reports No. PM153*, 154, 155, Canadian Department of Mines, Ottawa.  
 HOPKINS, M. R., and TOYE, T. C., 1950, *Proc. Phys. Soc. B*, **63**, 773.  
 YAO, T. P., and KONDIC, V., 1952, *J. Inst. Metals*, **81**, 17.

#### APPENDIX

##### THE DETERMINATION OF VISCOSITY

By D. G. B. Thomas

The equation from which the viscosity is calculated is equation (15) on page 776 of Hopkins and Toye (1950), viz.

$$\frac{2I\delta}{T} \left( \frac{T^2}{T_0^2} + 1 \right) = R \left[ 2\pi\eta \left\{ -\xi c a^2 \frac{J_2(\xi)}{J_1(\xi)} + 2\xi^4 \sum_{n=1}^{\infty} \frac{\tanh l_n c}{l_n^2 k_n^2 (k_n^2 a^2 - \eta^2)} \right\} \right] \quad \dots\dots(1)$$

which may be rewritten, using the asymptotic expansions to the Bessel functions, and neglecting terms in  $1/\xi^2$ ,

$$[2\pi c a^2 - K(\mu)]\eta - \pi c a^2 \sqrt{\eta} \mu \phi(\mu) \eta^{1/2} + \frac{I\delta}{T} \left( \frac{T^2}{T_0^2} + 1 \right) = 0 \quad \dots\dots(2)$$

where

$$k(\mu) = R \left[ 2\pi\xi^4 \sum_{n=1}^{\infty} \frac{\tanh l_n c}{l_n^2 k_n^2 (a^2 k_n^2 - \xi^2)} \right] \quad \dots\dots(3)$$

$$\simeq -8\pi\mu^4 a^3 R \left[ \sum_{n=1}^{\infty} (a l_n)^{-3} (a k_n)^{-2} \right], \quad \dots\dots(4)$$

$$\phi(\mu) \simeq R \frac{(256\mu^2 - 9) - (256\mu^2 + 32\mu + 9)i}{(48\mu + 15) - (256\mu^2 - 48\mu)i} \quad \dots\dots(5)$$

where  $a^2 l_n^2 = a^2 k_n^2 + 2i\mu^2$ ,  $ak_n$  is a root of  $J_1(ak_n) = 0$ ,  $\xi = \mu(1-i)$ ,  $\mu = (\pi a^2 \rho / T \eta)^{1/2}$ ,  $\delta$  = logarithmic decrement of the oscillations,  $I$  = moment of inertia of the oscillating system (without melt),  $T$  = time of oscillation when the crucible contains the molten metal,  $T_0$  = time of oscillation when the crucible is empty,  $c$  = height of liquid in the crucible,  $a$  = radius of crucible,  $\eta$  = viscosity and  $\rho$  = density.

There are two features in the calculation of  $K(\mu)$  which should be mentioned. Firstly,  $\tanh l_n c$  in (3) is unity to the necessary degree of accuracy. Secondly, the complex part of (4) is independent of  $a$ , the radius of the crucible, by virtue of the definition of the  $ak_n$  as the roots of  $J_1(ak_n) = 0$ . The series can therefore be calculated once and for all.

Values of  $K(\mu)/a^3$  and of  $\phi(\mu)$  are given in table 1. The quantity  $M''$  is a second difference modified to take into account all the available higher differences.

Table 1

$\mu$	$K(\mu)/a^3$	$+M''$	$\phi(\mu)$	$+M''$	$\mu$	$K(\mu)/a^3$	$+M''$	$\phi(\mu)$	$+M''$
6	1.304 79	3356	1.088 52	534	16	8.787 41	174	1.031 982	259
7	2.004 64	2064	1.075 242	3298	17	9.559 79	144	1.030 060	216
8	2.726 26	1375	1.065 422	2186	18	10.333 62	122	1.028 356	182
9	3.462 17	969	1.057 866	1518	19	11.108 67	104	1.026 835	154
10	4.208 04	710	1.051 872	1099	20	11.884 76	88	1.025 469	131
11	4.961 15	529	1.047 002	819	21	12.661 73	77	1.024 235	114
12	5.719 66	411	1.042 967	628	22	13.439 47	66	1.023 113	98
13	6.482 34	319	1.039 570	490	23	14.217 87	59	1.022 093	88
14	7.248 26	257	1.036 670	391	24	14.996 86	49	1.021 159	75
15	8.016 78	209	1.034 166	317					

From table 1, the equation (2) can be solved quite quickly for  $\sqrt{\eta}$ , by successive approximations.

Table 2. Tin-Copper

Alloy				Density at		Viscosity at
Weight % Sn	Cu	Atomic % Sn	Cu	M.P. (°K)	M.P. (g cm <sup>-3</sup> )	M.P. (poise)
100	0	100	0	505.1	7.008	0.01894
99.994	0.006	99.990	0.010	505.1	7.031	
99.900	0.100	99.810	0.190	504.4	7.034	
99.892	0.108	99.799	0.201	504.4	7.034	0.01830
99.850	0.150	99.720	0.280	504.1	7.033	
99.800	0.200	99.630	0.370	503.7	7.036	
99.792	0.208	99.612	0.388	503.7	7.036	0.01888
99.770	0.230	99.571	0.429	503.5		0.01898
99.610	0.390	99.270	0.730	502.4	7.045	
99.560	0.440	99.180	0.820	502.0	7.044	
99.540	0.460	99.144	0.856	501.9		0.01939
99.516	0.484	99.100	0.900	501.7	7.037	
99.510	0.490	99.090	0.910	501.7	7.019	
99.510	0.490	99.090	0.910	501.7	7.017	
99.490	0.510	99.050	0.950	501.5	7.016	
99.450	0.550	98.980	1.020	501.2	7.017	
99.440	0.560	98.960	1.040	501.2	7.022	
99.420	0.580	98.922	1.078	501.0		0.01891
99.350	0.650	98.790	1.210	500.5	7.025	
99.310	0.690	98.719	1.281	500.2		0.01893
99.270	0.730	98.645	1.355	501.0		0.01998
99.230	0.770	98.570	1.430	502.1	7.021	
99.000	1.000	98.149	1.851	508.3		0.01878
98.951	1.049	98.059	1.941	509.7		0.01887



Table 3. Tin-Nickel

Alloy				M.P. (°K)	Density at M.P. (g cm <sup>-3</sup> )	Viscosity at M.P. (poise)
Weight % Sn	Ni	Atomic % Sn	Ni			
100	0	100	0	505.1	7.008	0.01894
99.969	0.031	99.937	0.063	504.9	7.010	
99.963	0.037	99.925	0.075	504.8		0.01723
99.956	0.044	99.911	0.089	504.8	7.034	
99.930	0.070	99.860	0.140	504.6	7.044	
99.916	0.084	99.830	0.170	504.7		0.01889
99.910	0.090	99.818	0.182	504.4	7.049	0.01832
99.901	0.099	99.800	0.200	504.4	7.049	
99.900	0.100	99.798	0.202	504.4		0.01980
99.880	0.120	99.760	0.240	504.3	7.042	
99.869	0.131	99.740	0.260	504.3	7.042	
99.860	0.140	99.717	0.283	504.7		0.01960
99.858	0.142	99.710	0.290	504.8	7.039	
99.847	0.153	99.690	0.310	505.3	7.037	
99.839	0.161	99.670	0.330	506.2	7.032	
99.828	0.172	99.650	0.350	507.2	7.029	
99.820	0.180	99.640	0.360	508.2	7.038	
99.807	0.193	99.610	0.390	509.2	7.044	
99.800	0.200	99.596	0.404	510.2	7.039	0.02057
99.776	0.224	99.550	0.450	512.2	7.038	
99.770	0.230	99.536	0.464	513.2		0.02152
99.730	0.270	99.460	0.540	517.2	7.033	
99.670	0.330	99.335	0.665	523.2		0.02171
99.620	0.380	99.234	0.766	527.2		0.0202

Table 4. Tin-Lead

Alloy				M.P. (°K)	Density at M.P. (g cm <sup>-3</sup> )	Viscosity at M.P. (poise)
Weight % Sn	Pb	Atomic % Sn	Pb			
100	0	100	0	505.1	7.008	0.01894
99.94	0.06	99.964	0.036	505.0	6.612	0.01742
99.87	0.13	99.924	0.076	504.8	6.643	0.01735
99.01	0.99	99.430	0.570	503.9	6.670	0.01810
97.96	2.04	98.820	1.180	502.5	6.668	0.01817
97.01	2.99	98.270	1.730	501.3		0.01812
76.80	23.20	85.250	14.750	475.3	8.208	
71.80	28.20	81.630	18.370	468.9	8.314	
70.00	30.00	80.290	19.710	466.6	8.352	
65.00	35.00	76.430	23.570	460.2	8.548	
62.59	37.41	74.490	25.510	457.0		0.02171
62.50	37.50	74.420	25.580	456.9	8.516	
59.21	40.79	71.700	28.300	462.4	8.150	0.02028
52.20	47.80	65.590	34.410	478.7	8.336	0.02042
48.70	51.30	62.370	37.630	486.9	8.456	0.02046
44.80	55.20	58.620	41.380	495.9	8.608	
33.04	66.96	46.280	53.720	523.3	9.373	0.02182
24.84	75.16	36.590	63.410	542.4	9.673	0.02505
10.00	90.00	16.250	83.750	576.9	10.238	
4.73	95.27	7.980	92.020	589.2		0.02505
1.50	98.50	2.590	97.410	596.7	10.691	
0	100	0	100	600.4	10.966	0.02535

## The Reaction $^{24}\text{Mg}(p, \gamma)^{25}\text{Al}$ at the 418 keV Resonance†

By J. VARMA AND W. JACK

Natural Philosophy Department, University of Glasgow

*M.S. received 1st January 1957 and in final form 2nd September 1957*

**Abstract.** The  $421 \pm 4$  keV proton capture resonance in  $^{24}\text{Mg}$  has been studied employing scintillation counters. The resonance has a width of less than one kilovolt, and the relative intensities of the resulting gamma-radiations of energies 2.71, 2.26, 1.81, 1.36 and 0.89 mev are as 1:1.5:0.4:0.5:2.2 respectively. Coincidence experiments show that the 2.71 mev level in  $^{25}\text{Al}$  decays to the ground, 0.453 and 1.81 mev states. The 1.81 mev level decays to the ground and first two excited states. The second excited state at 0.94 mev decays in part through the emission of a 0.49–0.45 mev  $\gamma$ -ray cascade.

Measurements of the angular distribution of the gamma rays establish the spin of the resonance level to be  $\frac{3}{2}^+$ , and the ground state transition to be a mixture of M1 and E2 radiations. The 2.26 mev transition to the first excited state is probably pure M1. The spin of the 1.81 mev state is indicated to be  $\frac{5}{2}^-$ , which is consistent with the results of triple angular correlation measurements of the 0.90–1.36 mev gamma-ray cascade.

### § 1. INTRODUCTION

THE levels of  $^{25}\text{Al}$  have been studied by various workers (Endt and Kluyver 1954). The measurements on the reaction  $^{24}\text{Mg}(d, n)^{25}\text{Al}$  (Goldberg 1953) indicated the spin values for the ground and first excited state at 0.45 mev to be  $\frac{5}{2}^+$  and  $\frac{1}{2}^+$  respectively. From the study of the reaction  $^{24}\text{Mg}(p, \gamma)^{25}\text{Al}$  at the 418 keV and 2.40 mev resonances, Bartholomew *et al.* (1955) reported the spin values of both the 0.95 and 2.70 mev states to be  $\frac{3}{2}^+$ . From similar studies at the 222 keV resonance (Casson 1953, Craig 1956, Varma 1956) the spin values of the levels at 0.45, 0.94 and 2.51 mev are reported to be  $\frac{1}{2}^+$ ,  $\frac{3}{2}^-$  and  $\frac{1}{2}^-$  respectively. The 418 keV proton capture resonance in  $^{24}\text{Mg}$  corresponding to the 2.71 mev state of  $^{25}\text{Al}$  was reported by Grötdal *et al.* (1950) and Hunt and Jones (1953); but due to low intensity, and the proximity of the strong resonance in the reaction  $^{12}\text{C}(p, \gamma)^{13}\text{N}$ , the resonance has not been studied satisfactorily.

The pattern of spacing, and the spin values of the various levels of  $^{25}\text{Al}$ , led to the belief that these may be due to the collective motion of the nucleus (Bohr 1956, private communication.) In such a case, one expects a fair competition between M1 and E2 transitions among these levels. Angular distribution and angular correlation measurements in  $(p, \gamma)$  reactions provide a sensitive means of determining the spins of the various levels involved, and also the mixing ratios of the M1 and E2 multipoles in different transitions. With this view in mind, and also to determine the mode of decay of the 2.71 mev state of  $^{25}\text{Al}$ , the 418 keV proton capture resonance in  $^{24}\text{Mg}$  has been studied.

† The results of these measurements were first reported to the International Conference on Nuclear Reactions, Amsterdam, July 2–7, 1956.

Since the present work was started, Ager-Hanssen *et al.* (1956) have reported the energies of the gamma rays from different proton capture resonances in  $^{24}\text{Mg}$ . From  $\gamma$ -ray intensity measurements, these workers assign a spin of  $\frac{3}{2}^-$  to the 1.81 mev level of  $^{25}\text{Al}$ . Litherland *et al.* (1956) have reported the study of the various proton capture resonances in  $^{24}\text{Mg}$ , and have established the presence of various levels predicted by Bohr model. These workers suggest the width of the 418 kev resonance to be less than 10 kev. From the angular distribution measurements, the spin assignment to the 2.71 and 1.81 mev levels is  $\frac{3}{2}^+$  and  $\frac{5}{2}^+$  respectively. The mixtures of M1 and E2 radiations in the ground and first excited state transitions have also been reported.

## § 2. APPARATUS

Two NaI (Tl) crystals, each 1.75 inches in diameter and 2 inches long, were mounted on Du Mont 6292 photomultiplier tubes. The pulses from these phototubes were amplified in IDL wideband amplifiers, and after proper lengthening were fed to a 80 channel pulse height analyser (Hutchinson and Scarrott 1951). A linear output coincidence circuit of resolving time  $3\mu\text{sec}$  was employed in coincidence measurements.

The  $^{24}\text{Mg}$  targets, approximately  $30\mu\text{g cm}^{-2}$  thick, were obtained from the Electromagnetic Separation Division of the Atomic Energy Research Establishment, Harwell. The resolved proton beam of up to  $100\mu\text{A}$  was available from the Glasgow University high voltage set.

## § 3. MEASUREMENTS

Figure 1 shows the pulse height spectra produced by the  $\gamma$ -rays from the reaction  $^{24}\text{Mg}(p, \gamma)^{25}\text{Al}$  at  $E_p = 430\text{ kev}$  when the detecting counter was placed at  $90^\circ$  and  $0^\circ$  to the proton beam. The two spectrograms were obtained for

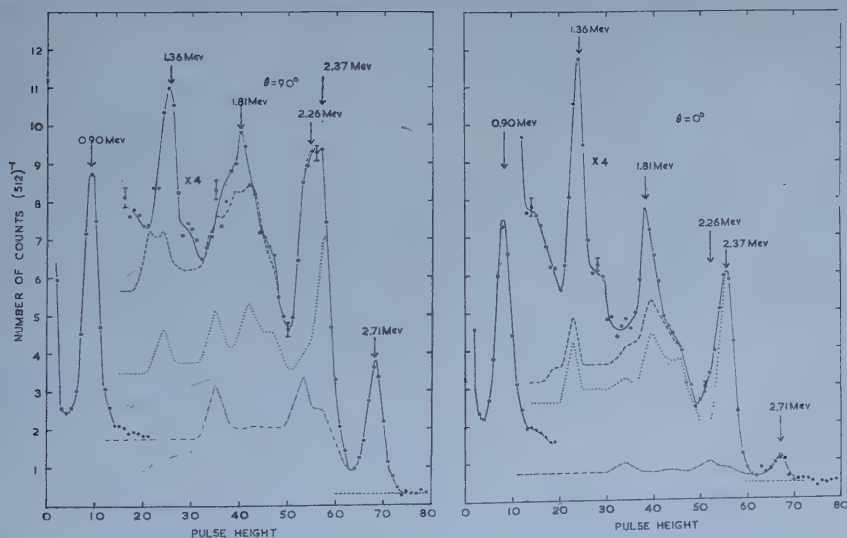


Figure 1. Pulse height spectra in a NaI(Tl) crystal due to gamma rays from the reaction ( $E_p = 430\text{ kev}$ ) at  $90^\circ$  and  $0^\circ$  to the proton beam; about equal charge being delivered to the target in each case.

The chain curve represents the distribution due to the 2.71 mev gamma ray and the background. The top broken curve shows the combined distribution due to the 2.26, 2.37 and 2.71 mev gamma rays and the background.

approximately the same amount of charge delivered to the target. Evidently there are present gamma rays of energies 2.71, 2.37, 2.26, 1.81, 1.36 and 0.89 mev. The spectrum below 0.8 mev consisted of the annihilation radiation peak at 0.51 mev with a slight asymmetry on the lower energy side. The 2.37 mev peak showing the excitation curve similar to that of the reaction  $^{12}\text{C}(p, \gamma)^{13}\text{N}$  arises from the carbon deposited on the target by the beam. The peak at 0.89 mev has a width more than that expected for a single  $\gamma$ -ray and should, therefore, arise from two or more gamma radiations of approximately the same energy. The pulse height distributions due to 2.71, 2.37 and 2.26 mev  $\gamma$ -rays, shown in the figure, were obtained by observing the pulse spectrum due to the 2.62 mev  $\gamma$ -ray from  $^{210}\text{Th}$  and the 2.37 mev  $\gamma$ -ray from the reaction  $^{12}\text{C}(p, \gamma)^{13}\text{N}$ . After taking into consideration the cross section for the interaction with sodium iodide, and the angular distributions of the different  $\gamma$ -rays, the relative intensities of the 2.71, 2.26, 1.81, 1.36 and 0.89 mev radiations from the reaction are found to be as 1:1.5:0.4:0.5:2.2. The excitation curve for the reaction showed that the proton capture resonance takes place at the bombarding energy of  $421 \pm 4$  kev. It is also observed that the resonance is less than one kilovolt in width.

To determine the decay scheme of the 2.71 mev resonance level of  $^{25}\text{Al}$ , coincidences between the various gamma rays were studied. In these measurements a single channel analyser was fixed at the full energy peak of a  $\gamma$ -ray in one counter, and the coincident spectrum in the other counter was recorded on an 80-channel pulse height analyser. Figure 2(a, b) shows the coincidence spectra when the window of the single channel kicksorter was fixed at the 2.26 and 1.81 mev peaks respectively. The broken curve in figure 2(a) is the annihilation radiation peak

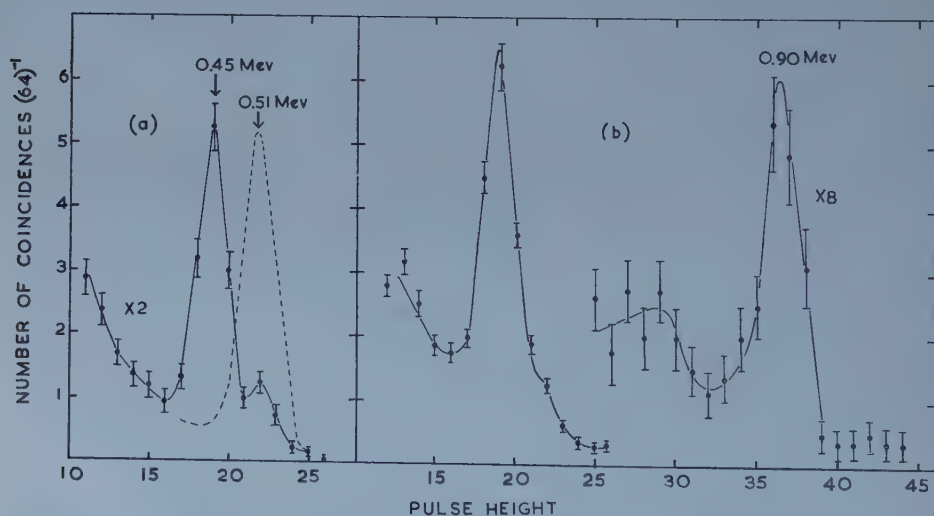


Figure 2. (a) Gamma-ray spectrum in coincidence with the 2.26 mev radiations. The broken curve represents the coincidences due to annihilation radiations. (b) Spectrum in coincidence with the 1.81 mev  $\gamma$ -ray. The low energy peak arises from the detection of the 2.26 mev radiations.

observed under similar circumstances. The 2.26 mev  $\gamma$ -ray is in coincidence with the 0.45 mev  $\gamma$ -ray, and the 1.81 mev radiations are in coincidence with a  $\gamma$ -ray of energy 0.90 mev. The low energy peak in this figure arises from the detection of



the 2.26 mev  $\gamma$ -ray while detecting the 1.81 mev radiations. The width of the 0.90 mev peak suggests that it represents a single  $\gamma$ -ray.

Figure 3(a) shows the  $\gamma$ -spectrum coincident with the 1.36 mev peak. Figure 3(b) shows the low energy spectrum when the channel of the single channel analyser was fixed at the higher energy slope of the 0.89 mev radiation peak. A comparison of figures 2 (b) and 3 (a) shows that both 1.81 and 1.36 mev  $\gamma$ -rays are in coincidence with the same gamma ray of energy 0.90 mev. In addition, the

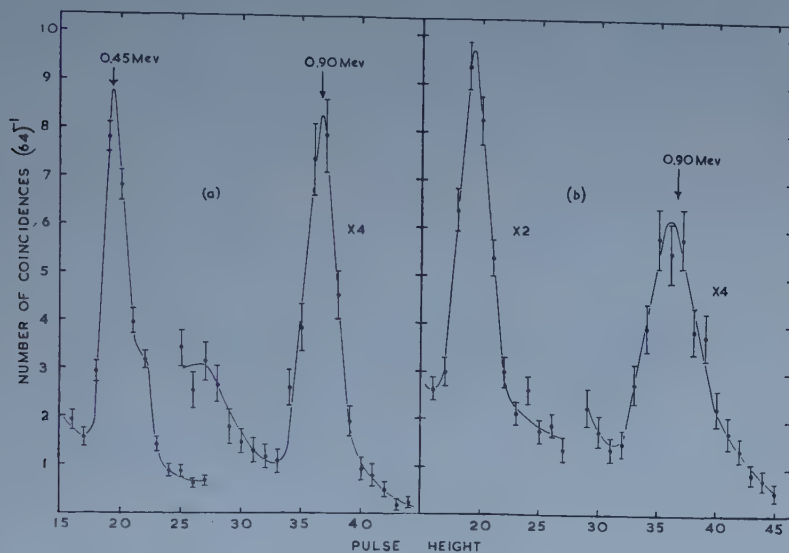


Figure 3. (a) Spectrum in coincidence with the 1.36 mev  $\gamma$ -ray. (b) Low energy spectrum in coincidence with the radiations of energy about 0.9 mev.

1.36 mev radiation is in coincidence with the 0.45 mev  $\gamma$ -ray. From the shape of the peak at approximately 0.90 mev in figure 3 (b), it is evident that the 0.9 mev  $\gamma$ -ray is in cascade with at least one more  $\gamma$ -ray of about the same energy. One concludes from these observations that the 1.81 and 1.36 mev  $\gamma$ -rays arise from the same level in  $^{25}\text{Al}$  at 1.81 mev, which is fed by the 0.90 mev transitions from the 2.71 mev state. The 1.81 mev transitions terminate at the ground state, and the 1.36 mev  $\gamma$ -rays lead to the first excited state at 0.45 mev. As there exists an excited state of  $^{25}\text{Al}$  at 0.94 mev, the transitions from the 1.81 mev state to this level give rise to three  $\gamma$ -rays in cascade having energies 0.90, 0.87 and 0.94 mev. These  $\gamma$ -rays satisfactorily explain the width of the peak at 0.90 mev in figure 3 (b). The slightly larger width of the 0.45 mev peak in figure 3 (b) supports the observation (Craig 1956, Varma 1956) that the 0.94 mev state decays partially through the emission of a 0.49–0.45 mev  $\gamma$ -ray cascade.

To obtain the spin values of the different lower excited states of  $^{25}\text{Al}$ , and the mixing ratios of M1 and E2 radiations in the transitions involved, the angular distributions of the gamma rays from the reaction were studied. In these measurements, the pulse spectra in a NaI (Tl) counter due to all the  $\gamma$ -rays from the reaction were recorded at various angles on the 80-channel pulse height analyser. The crystal was surrounded by a lead collimator one inch thick, and subtended a half angle of  $5^\circ$  at the target. The reaction was monitored employing a current integrator connected to the target, and also by a counter recording all pulses in the

energy region 0.7 to 2.0 mev. The spectrograms obtained at various angles were analysed in a way similar to those of figure 1, and the number of counts in each full energy peak was determined. It was found that as the carbon on the target built up, the number of monitor counts changed, making it impossible to monitor the reaction in this way. As the target did not show any sign of deterioration, and the beam current was fairly constant at  $40\mu\text{A}$  throughout, the reaction in these measurements was monitored by the current integrator counts. The asymmetry of the angular distribution apparatus was measured by observing the angular distribution of the 2.37 mev  $\gamma$ -ray from the reaction  $^{12}\text{C}(\text{p}, \gamma)^{13}\text{N}$  and also of the gamma rays from radioactive sources  $^{22}\text{Na}$  and  $^{210}\text{Th}$  placed in the same geometry

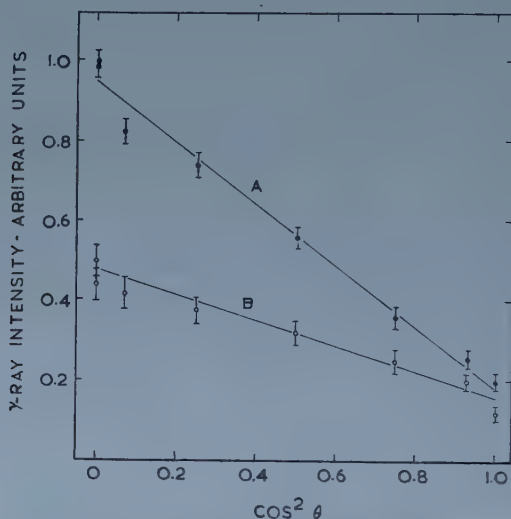


Figure 4. Least squares fit of the data of angular distribution of the 2.71 mev gamma ray (curve A), and the 2.26 mev gamma ray (curve B).

as the target. Figure 4 shows the angular distribution data for the 2.71 and 2.26 mev  $\gamma$ -rays, after correcting for the asymmetry of the apparatus. The least squares fit of the data, after correcting for the finite angular resolution, gives the angular distribution function for the 2.71 and 2.26 mev  $\gamma$ -rays to be :

$$W_{2.71}(\theta) = 1 - (0.75 \pm 0.04) P_2$$

and

$$W_{2.26}(\theta) = 1 - (0.55 \pm 0.04) P_2$$

respectively. In comparison the distribution functions obtained by Litherland *et al.* are as follows :

$$W_{2.71}(\theta) = 1 - (0.5 \pm 0.1) P_2$$

$$W_{2.26}(\theta) = 1 - (0.4 \pm 0.1) P_2$$

Figure 5 shows the angular distributions of the 1.36 and 1.81 mev gamma rays. The vertical bars at each point show the statistical errors. These errors are large because of the fact that a large contribution due to higher energy  $\gamma$ -rays has to be subtracted from the observations to obtain the counts in the full energy peaks of these gamma rays. No errors due to the analysis of the spectrograms are taken

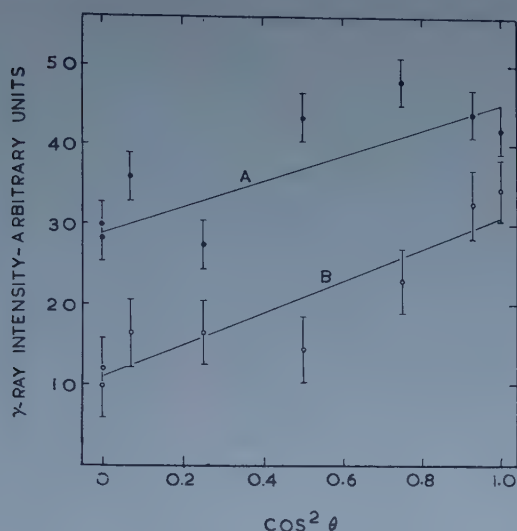


Figure 5. Least squares fit of the data of angular distribution of the 1.36 MeV gamma ray (curve A) and the 1.81 MeV gamma ray (curve B).

into consideration. The least squares fit of the data of figure 5 after angular resolution correction gives:

$$W_{1.36}(\theta) = 1 + (0.32 \pm 0.06) P_2$$

$$W_{1.81}(\theta) = 1 + (0.78 \pm 0.20) P_2$$

Using the tables of Sharp *et al.* (1953), it is found that the angular distribution of the 2.71 MeV  $\gamma$ -ray can be explained only if the 2.71 MeV resonance level of  $^{25}\text{Al}$  has a spin value  $\frac{3}{2}^+$ , and the transition is a mixture of M1 and E2 such that  $E2/M1 = 0.39 \pm 0.10$  or  $8.0 \pm 2.5$  with a phase difference  $0^\circ$ . No mixture of M1 and E2 could give the observed angular distribution for the 2.71 MeV  $\gamma$ -ray if the resonance level is assumed to have a spin of  $\frac{5}{2}$ . This measurement, therefore, fixes the spin of the level to be  $\frac{3}{2}^+$  unambiguously. The angular distribution of the 2.26 MeV radiation indicates that this transition is either pure M1 ( $E2/M1 < 0.003$ ) or a mixture of M1 and E2 such that  $E2/M1 = 2.6 \pm 0.3$  with a phase difference of  $180^\circ$ .

The angular distribution of the 1.36 MeV  $\gamma$ -ray is explained if the spin of the 1.81 MeV level is  $\frac{5}{2}^+$ , and the 0.90 MeV transition is a mixture of  $(17 \pm 13)\%$  of E2 with M1. The 1.36 MeV  $\gamma$ -ray would then be pure E2 radiation. The maximum value of the coefficient of  $P_2$  in the distribution function for the 1.81 MeV  $\gamma$ -ray is predicted to be 0.53 when the transition  $\frac{5}{2}^+ \rightarrow \frac{5}{2}^+$  is a mixture of about 24% E2 with M1 with phase difference of  $180^\circ$ . In view of the fact that the errors in the intensity of the 1.81 MeV  $\gamma$ -ray due to analysis could be appreciable, the agreement between the expected and observed distribution function is regarded as satisfactory.

The triple angular correlation function for the 0.90–1.36 MeV gamma-ray cascade was studied employing two sodium iodide counters, each subtending a half angle of  $17^\circ$  at the target. The single channel analyser selected the 0.90 MeV peak in the counter fixed at  $90^\circ$  to the beam, and the coincidence spectrum in the

† As pointed out by Litherland *et al.* (1956) and Huby (1954), the phase differences reported here differ from those obtained from tables of Biedenharn and Rose (1953) by  $180^\circ$ .

movable counter was observed at five angles. In this experiment the coincidence spectrum had to be recorded for a long time, and a beam current as high as  $90\text{ }\mu\text{A}$  had to be employed. The spectrograms which consisted of peaks at 1.81, 1.36, 0.9 and 0.45 mev were analysed, and the counts in the full energy peaks of the different  $\gamma$ -rays determined. As the reaction could not be monitored by the current integrator counts or the counting rate in the single channel analyser, the number of counts in the 1.36 mev peak was normalized to the number of counts in the peak at 0.45 mev. This normalization corrects for any asymmetry of the apparatus. As the 0.45 mev  $\gamma$ -ray has an isotropic distribution, and the contribution from the 0.49 mev  $\gamma$ -ray is small, normalizing in this fashion should not introduce large

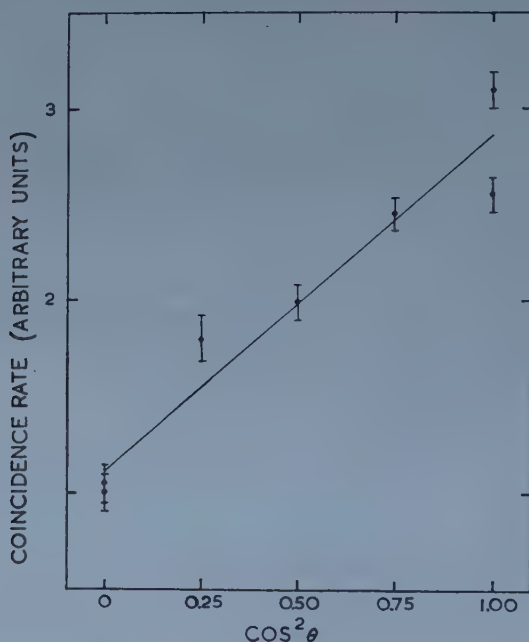


Figure 6. Triple correlation data and their least squares fit for the 0.90-1.36 mev gamma ray cascade.

errors in the correlation data. Figure 6 shows the correlation function as observed and its least square fit. After angular resolution correction, the correlation function was found to be

$$W(\theta) = 1 + (1.85 \pm 0.3) \cos^2 \theta.$$

As the triple correlation function for the transition sequence

$$l=2 \quad L=1 \quad L=2 \\ 0 \longrightarrow \frac{3}{2}^+ \longrightarrow \frac{5}{2}^+ \longrightarrow \frac{1}{2}^+$$

is given by

$$W(\theta) = 1 + 0.449 P_2 - 0.061 P_2^2 \\ = 1 + 1.48 \cos^2 \theta$$

the results of the measurements are consistent with the assignment of spin value  $\frac{5}{2}^+$  to the 1.81 mev state of  $^{25}\text{Al}$ . Any mixing of E2 and M1 in the  $\frac{3}{2}^+ \rightarrow \frac{5}{2}^+$  transition reduces the asymmetry further. The spin assignment of  $\frac{3}{2}$  to the 1.81 mev level does not explain the observed correlation function.



Figure 7 shows the lower energy levels of  $^{25}\text{Al}$  along with their spin assignments as obtained from these measurements, and the values of K quantum numbers

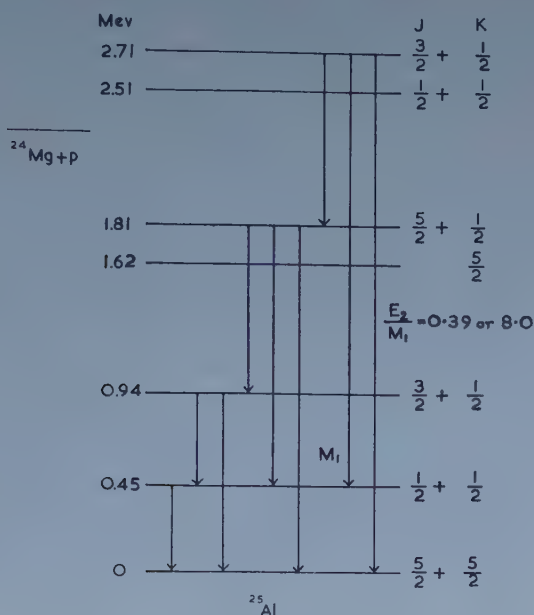


Figure 7. Lower excited state of  $^{25}\text{Al}$ .

(Bohr and Mottelson 1955) as suggested by Litherland *et al.* (1956) and Bohr (1956).

#### § 4. DISCUSSION

The spin and parity assignments for the lower excited states of  $^{25}\text{Al}$ , as obtained by the measurements described here, are in agreement with the results of Litherland *et al.* (1956). The mixing ratios of M1 and E2 multipoles in the various transitions measured in these experiments do not agree with previous reports. The comparable intensities of M1 and E2 transitions among the levels of  $^{25}\text{Al}$  suggest the origin of these levels in the collective motion of the nucleus. A few observations should be made about the selection rules regarding the change in the value of K. According to these selection rules the 2.71 mev transition ( $\Delta K = 2$ ) should be forbidden through M1 emission and should, therefore, be weaker than the 2.27 mev transition ( $\Delta K = 0$ ) which is allowed to take place through the emission of both M1 and E2 multipoles. In fact, the two transitions are of comparable intensity. It is also not possible to explain why the transition from the 2.71 mev state ( $J = \frac{3}{2}^+$ ,  $K = \frac{1}{2}$ ) to the 0.94 mev level ( $J = \frac{3}{2}^+$ ,  $K = \frac{1}{2}$ ) is too weak to be observed. Similar difficulties arise in explaining the branching ratio of the 1.81 mev state ( $J = \frac{5}{2}^+$ ,  $K = \frac{1}{2}$ ). After taking into consideration the transition probabilities of the 0.87 and 1.81 mev  $\gamma$ -rays from Weisskopf's relations, it appears that the K-forbidden nature of the 1.81 mev transition retards it by a factor of about ten. These observations indicate a rather large flexibility in the selection rules governing the changes in the values of K quantum number in the transitions between the levels of  $^{25}\text{Al}$ .

## ACKNOWLEDGMENTS

The authors wish to express their gratitude to Professor P. I. Dee and Dr. P. J. Grant for their interest in the present work. One of the authors (J. V.) wishes to acknowledge the award of an Imperial Chemical Industries Research Fellowship, and the other (W. J.) a Sir James Caird Travelling Scholarship.

## REFERENCES

- AGER-HANSEN, H., LÖNSJÖ, O. M., and NORDHAGEN, R., 1956, *Phys. Rev.*, **101**, 1779.  
BARTHOLOMEW, G. A., GOVE, H. E., LITHERLAND, A. E., and PAUL, E. B., 1955, *Phys. Rev.*, **99**, 1649(A).  
BIEDENHARN, L. C., and ROSE, M. E., 1953, *Rev. Mod. Phys.*, **25**, 729.  
BOHR, A., and MOTTELSON, B. R., 1955, *Beta and Gamma-ray Spectroscopy*, edited by Kai Siegbahn (Amsterdam : North-Holland).  
CASSON, H., 1953, *Phys. Rev.*, **89**, 809.  
CRAIG, D. S., 1956, *Phys. Rev.*, **101**, 1479.  
ENDT, P. M., and KLUYVER, J. C., 1954, *Rev. Mod. Phys.*, **26**, 95.  
GOLDBERG, E., 1953, *Phys. Rev.*, **89**, 760.  
GRÖTDAL, T., LÖNSJÖ, O. M., TANGEU, R., and BERGSTRÖM, I., 1950, *Phys. Rev.*, **77**, 296(L).  
HUBY, R., 1954, *Proc. Phys. Soc. A*, **67**, 1103.  
HUTCHINSON, G. W., and SCARROTT, G. G., 1951, *Phil. Mag.*, **42**, 792.  
HUNT, S. E., and JONES, W. M., 1953, *Phys. Rev.*, **89**, 1283.  
LITHERLAND, A. E., PAUL, E. B., BARTHOLOMEW, G. A., and GOVE, H. E., 1956, *Phys. Rev.*, **102**, 208.  
SHARP, W. T., KENNEDY, J. M., SEARS, B. J., and HOYLE, M. G., 1953, Atomic Energy of Canada Limited, Chalk River, Project A.E.C.L. No. 97.  
VARMA, J., 1956 *Proc. Phys. Soc. A*, **69**, 641.

# The Characteristic Temperature and Effective Electron Mass for Conduction Processes in Cadmium Oxide

By R. W. WRIGHT and J. A. BASTIN†

University College, Ibadan, Nigeria

*MS. received 24th June 1957, and in revised form 29th September 1957*

**Abstract.** Measurements of the Hall effect, resistance, magnetoresistive effect, and thermoelectric power have been made for in all over fifty specimens prepared by sintering compressed powder blocks of cadmium oxide. For all specimens the Hall effect has been measured at room temperature, and this provides a fairly accurate estimate of the conduction electron density. The results are compared in each case with the theoretical expressions for conduction in polar crystals given by Howarth and Sondheimer (1953) and Lewis and Sondheimer (1955). Of particular interest is the variation with temperature of the Hall coefficient. Changes are observed which are not ascribed to changes of electron concentration. The complete comparison gives values of the effective electron mass  $m$  and the characteristic temperature for longitudinal optical vibrations  $\Theta_E$ .

## § 1. INTRODUCTION

CADMIUM oxide has been shown by x-ray analysis to have a NaCl type cubic structure (Davey and Hoffmann 1920, Scherrer 1922). Previous measurements on polycrystalline specimens show an approximately constant Hall coefficient in the temperature range 100–600°K, and a resistance which tends rapidly to a constant value at temperatures below about 20°K (Wright 1953, Bastin and Wright 1955). These results indicate that in such specimens there is a temperature independent conduction electron density. Hall coefficient measurements show this density to be of the order of  $10^{19} \text{ cm}^{-3}$ . The origin of these conduction electrons is thought to be a non-stoichiometric excess of interstitial cadmium atoms, although oxygen vacancies could account for most of the observed electrical properties of specimens. However no assumptions concerning the cause of the conduction electrons are necessary for the comparisons to be made in this paper.

Unfortunately it is as yet impossible to obtain single crystals of cadmium oxide, and the comparison of measurements on polycrystalline specimens with theoretical expressions must of course be treated with caution. However, because of the relatively high conductivity of the specimens used ( $10^2 \text{ ohm}^{-1} \text{ cm}^{-1}$ ) it seems unlikely that surface effects within the polycrystalline specimen would be appreciable when compared with the conduction within each microcrystal. If this is the case then measurements of such properties as the Hall effect and the thermoelectric effect will be substantially the same for polycrystalline specimens as for single crystal specimens.

Fortunately in the case of cadmium oxide, it has been found possible by various heat treatments to produce specimens with a wide range of Hall coefficient,

† Now at Physics Department, University of Reading.

By this means a comparison can be made with the theory, not only of the magnitude of any property, but also of its variation with degeneracy. Finally the assumption of a temperature independent electron concentration (which can be made in the case of the specimens considered) considerably simplifies comparison especially when the temperature variation of a particular electrical property is to be considered.

In the present investigations measurements were made on over 50 specimens produced by sintering blocks of cadmium oxide powder at temperatures between  $600^{\circ}\text{K}$  and  $1200^{\circ}\text{K}$ . By varying the rate of cooling after sintering it has been found possible to produce specimens whose Hall coefficients vary by a factor of over 20. It is hoped to discuss the origin of this variation in a later paper. The values of the Hall coefficients of the specimens produced correspond to electron concentrations from  $2 \times 10^{18}$  to  $4 \times 10^{19} \text{ cm}^{-3}$ .

The results will be compared in each case with the expressions derived for conduction in polar crystals by Howarth and Sondheimer (1953) and by Lewis and Sondheimer (1955). These expressions have been derived from a theory based on the wave mechanical treatment of polar scattering by Fröhlich (1937). This theory gives solutions of the Boltzmann transport equation which do not require an assumption of a time of relaxation. However, the theory only takes into account the scattering of the electrons by the optical modes of the lattice vibrations, and the neglect of the effect of the acoustical modes may be serious, particularly at low temperatures. Despite this restriction, the theory is at present the most comprehensive of the treatments of conduction in polar crystals and we have compared our experimental results to it. The comparison gives an effective electron mass  $m$  for electrons in the conduction band and a characteristic temperature  $\Theta_E$  for lattice vibrations. With regard to the former it is convenient to introduce the numeric  $G$  defined as the ratio of the effective electronic mass  $m$  to the true mass  $m_0$ . The temperature parameter  $\Theta_E$  involved in conduction phenomena is the temperature corresponding to the characteristic frequency for longitudinal waves of the optical branch only. The assumption that this frequency is constant for waves of differing wave number is a good approximation in the case of cadmium oxide, because of the large ratio of the masses of cadmium and oxygen.

## § 2. MEASUREMENTS

The measurements of temperature variation of resistance, of Hall effect and of thermoelectric effect were all made in the usual manner.

In measuring the magnetoresistive effect several precautions were necessary since the change of resistance never exceeded  $5 \times 10^{-5}$  of the total resistance even for the largest field and most favourable specimen. A rise in temperature of  $10^{-2}^{\circ}\text{C}$  gave as great a resistance change as the application of the largest available magnetic field. Careful lagging was therefore necessary and no attempt was made to measure the effect except at room temperature. A switch in the electromagnet current circuit enabled the field to be reduced to zero by reversing the current in one set of magnet coils. In this way the heating effect of the magnet current was kept constant throughout any one set of measurements. Because of the large area of the current and potential contacts the effective points of contact are in general not exactly in line. Thus, on changing the magnetic field, the change in



voltage across the potential probes in general includes a Hall effect term. This effect was so often several times larger than that due to the magnetoresistive change, and in order to eliminate it, it was necessary to make measurements with the magnetic field in opposite directions.

### § 3. DISCUSSION

#### 3.1. Hall Effect Measurements

The Hall coefficient was measured at room temperature for all the specimens considered in this paper. In addition the following measurements were made:

(i) The Hall coefficient was measured for several specimens as a function of field for fields up to  $6 \times 10^3$  oersted. A constant value was found in each case for the coefficient, thus agreeing with the theoretical expression deduced by Lewis and Sondheimer. Values of the specific Hall effect (Hall effect per unit current density per unit distance at right angles to the current flow), for three specimens are shown as a function of field in figure 1.

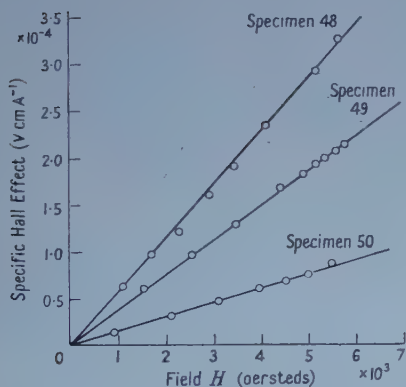


Figure 1. The variation of the specific Hall effect with magnetic field for three specimens of cadmium oxide.

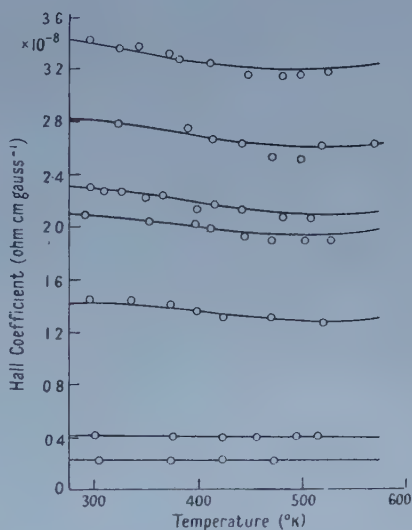


Figure 2. The variation with temperature of the Hall coefficient for specimens of differing electron concentration. The solid lines show the predicted variations given by the theory assuming  $G=0.3$  and  $\Theta_E=500^\circ\text{K}$ .

(ii) The temperature variation of the Hall coefficient was measured from  $300^\circ\text{K}$  to about  $550^\circ\text{K}$ . Above the latter temperature the electrical properties of specimens were found to change with time, and by heat treatment above this temperature permanent changes in the Hall coefficient at room temperature could be produced. Results of measurements made on specimens kept always below  $550^\circ\text{K}$  are shown in figure 2. All the measurements could be easily reproduced. With the exception of the specimen of highest conduction electron concentration (highest degeneracy) the results show signs of a minima at about  $500^\circ\text{K}$ ,

In the case of arbitrary degeneracy Lewis and Sondheimer give the following expression for the Hall coefficient:

$$R = - \frac{3e^2 \hbar^2 \alpha^2}{16a^3 M \nu_0} \mathcal{J} \left( \frac{D}{D_{\alpha\alpha}} \right) \dots\dots (1)$$

where  $a$  is the interionic distance,  $1/M$  is the sum of the reciprocals of the masses of the lattice atoms,  $\alpha e$  is the charge on each lattice ion, and  $\mathcal{J}(D/D_{\alpha\alpha})$  is the imaginary part of the determinant quotient:—

$$\frac{D}{D_{\alpha\alpha}} = \frac{1}{k^2 T^2 (e^z - 1)} \cdot \frac{\begin{vmatrix} D_{00} - i D_{00}\beta & D_{01} - \frac{5}{3} i \left( \frac{F_{3/2}(\eta)}{F_{1/2}(\eta)} \right) D_{00}\beta & \dots \\ D_{10} - \frac{5}{3} i \left( \frac{F_{3/2}(\eta)}{F_{1/2}(\eta)} \right) D_{00}\beta & D_{11} - \frac{7}{3} i \left( \frac{F_{5/2}(\eta)}{F_{1/2}(\eta)} \right) D_{00}\beta & \dots \\ \cdot & \cdot & \\ \cdot & \cdot & \\ \cdot & \cdot & \end{vmatrix}}{\begin{vmatrix} 0 & \frac{3}{2} F_{1/2}(\eta) & \frac{5}{2} F_{3/2}(\eta) & \dots \\ \frac{3}{2} F_{1/2}(\eta) & D_{00} - i D_{00}\beta & D_{01} - \frac{5}{3} i \left( \frac{F_{3/2}(\eta)}{F_{1/2}(\eta)} \right) D_{00}\beta & \dots \\ \frac{5}{2} F_{3/2}(\eta) & D_{10} - \frac{5}{3} i \left( \frac{F_{3/2}(\eta)}{F_{1/2}(\eta)} \right) D_{00}\beta & D_{11} - \frac{7}{3} i \left( \frac{F_{5/2}(\eta)}{F_{1/2}(\eta)} \right) D_{00}\beta & \dots \\ \cdot & \cdot & \cdot & \\ \cdot & \cdot & \cdot & \\ \cdot & \cdot & \cdot & \end{vmatrix}}$$

where  $\beta$  and the constants  $F_n(\eta)$  and  $D_{nm}$  (Fermi-Dirac and collision integrals) are defined by Lewis and Sondheimer. In the second order approximation the expression for the Hall effect reduces to

$$R = \frac{9}{4} F_{1/2}^2(\eta) \left[ \frac{B}{D} - \frac{AE}{D^2} \right] \dots\dots (3)$$

where

$$A = D_{00} D_{11} - D_{10}^2 \dots\dots (4)$$

$$B = \frac{10}{3} \frac{D_{10} F_{3/2}(\eta)}{F_{1/2}(\eta)} - \frac{7}{3} \frac{D_{00} F_{5/2}(\eta)}{F_{1/2}(\eta)} - D_{11} \dots\dots (5)$$

$$D = \frac{15}{2} D_{10} F_{1/2}(\eta) F_{5/2}(\eta) - \frac{9}{4} F_{1/2}^2(\eta) D_{11} - \frac{25}{4} D_{00} F_{3/2}^2(\eta) \dots\dots (6)$$

$$E = \frac{21}{4} F_{1/2}(\eta) F_{5/2}(\eta) - \frac{25}{4} F_{3/2}^2(\eta) \dots\dots (7)$$

Expression (3) can be written as:

$$R = K / ne\epsilon \dots\dots (8)$$

where  $K$  is a very complicated function of temperature and degeneracy.  $K$  is unity as a minimum value at the temperature  $T = \Theta_E$  and its maximum value is only about 1.2. As the degeneracy increases the variation of  $K$  with temperature decreases.

If we assume that the concentration of free electrons in our specimens is independent of temperature, then any variation of Hall coefficient can be ascribed to variations of  $K$ . Definite signs of a minimum value of  $R$  are seen for each specimen in figure 2 indicating that the temperature  $\Theta_E = 500^\circ\text{K}$ . Also in keeping with the theory is the experimental result that the variation becomes less marked as the electron concentration increases, i.e. as the degeneracy increases. The solid lines in figure 2 are the variations of  $R$  predicted theoretically from equation (3) assuming a value of  $G = 0.3$ , and  $\Theta_E = 500^\circ\text{K}$ , and assuming a constant free electron density for each specimen.

The value of  $G = 0.3$  is chosen for all specimens since this value gives best agreement with the experimental results. As will be seen later the values of  $G$  deduced from other measurements are considerably less than 0.3. This apparently high value of  $G$  deduced from Hall effect measurements is almost certainly due to approximations in the theory. The value of  $G$  chosen depends mainly on the difference between  $R$  at say  $300^\circ\text{K}$  and that at  $500^\circ\text{K}$ . The comparison made here uses the first approximation. A much larger value of  $R_{300} - R_{500}$  is to be expected using the second approximation as is shown by Lewis and Sondheimer in the non-degenerate case. If the second approximation could be calculated for all  $\eta$  then a considerably lower value of  $G$  would be required.

We have in this section ascribed the slight changes with temperature of the Hall coefficient, not to changes in the electron concentration, but to changes in the constant  $K$  in the equation

$$R = K/nec \quad \dots\dots(8)$$

The manner in which the variation of  $K$  with temperature depends upon the electron concentration is in remarkable agreement with the theory.

### 3.2. Resistance Measurements

#### 3.2.1. Low temperature measurements.

These have been previously reported and compared with the relevant expression deduced by Howarth and Sondheimer (Bastin and Wright 1953). In particular it was shown that the resistivity can be written as

$$\rho = \rho_0 + \frac{1}{AT \sinh^2(\Theta/2T)} \quad \dots\dots(9)$$

where

$$A = \frac{3^{1/3}}{2} \frac{a^3 M k h}{\alpha^2 m^2 e^2} \left( \frac{n}{\pi} \right)^{4/3} \quad \dots\dots(10)$$

$\rho_0$  being a temperature independent residual resistance. Measurements in the temperature range  $20$ – $250^\circ\text{K}$  on two specimens gave values of  $\Theta_E$  of  $560^\circ\text{K}$  and  $450^\circ\text{K}$ . The mean of these is seen to be in good agreement with the value of  $\Theta_E$  deduced from Hall effect measurements. It must be stressed however that this treatment disregards the effects of acoustical mode scattering. Fröhlich (1937) has shown that, because of its polarization, an optical wave is much more efficient

at electron scattering than an acoustical wave. However when  $T < \Theta_E$  the ratio of the number of optical to acoustical phonons will become small. Thus the *total* scattering by acoustical waves may become important.

### 3.2.2. Room temperature measurements.

Measurements of the temperature coefficient of resistance at room temperature and also of the Hall coefficient were made for 36 specimens. For the specimens of high conduction electron density the assumption of high degeneracy may be made, and equation (9) gives on differentiation

$$\frac{\partial \rho}{\partial T} = \frac{1}{AT^2 \sinh^2(\Theta/2T)} \cdot \left\{ 2 \left( \frac{\Theta}{2T} \right) \frac{\cosh(\Theta/2T)}{\sinh(\Theta/2T)} - 1 \right\} \quad \dots\dots(11)$$

whence:—

$$G = \frac{\left( \frac{\partial \rho}{\partial T} \right)^{1/2} T \sinh(\Theta/2T)}{\left\{ 2 \left( \frac{\Theta}{2T} \right) \frac{\cosh(\Theta/2T)}{\sinh(\Theta/2T)} - 1 \right\}^{1/2}} \cdot \left\{ \frac{3^{1/3} a^3 M k h}{2 \alpha^2 e^2 m_0^2} \right\}^{1/2} \left( \frac{n}{\pi} \right)^{2/3} \quad \dots\dots(12)$$

The value of  $n$  is obtained from the Hall coefficient using equation (3). Strictly this requires a knowledge of  $G$  but as the Hall coefficient depends only slightly on the value of  $G$  assumed, a method of successive approximations can clearly be applied when calculating the best value of  $G$  from equation (12). Table 1 shows

Table 1

Specimen No.	36	22	15	7	20	35
Sintering time (hrs.)	0.5	0.5	0.5	24.0	0.5	0.5
Sintering temperature ( $^{\circ}\text{K}$ )	1200	1000	930	920	1100	1200
Hall coeff. at 300 $^{\circ}\text{K}$ (ohm cm $\text{G}^{-1}$ ) $R \times 10^9$	14.5	17.0	20.5	3.6	2.5	5.6
Concentration of free electrons $n \times 10^{-18}$	4.3	3.6	3.1	17.4	25.0	11.2
Temperature derivative of resistance (ohm $\text{cm}^{-1} \text{deg}^{-1}$ ) $(\partial \rho / \partial T) \times 10^5$	11.3	18.0	13.9	3.7	1.4	4.3
$G = m/m_0$	0.05	0.08	0.05	0.08	0.06	0.06

the values of  $G$  calculated for six typical specimens. For all specimens there is a mean value of  $G = 0.07$  although the actual results vary from 0.04 to 0.09. A large spread of values of  $G$  would be expected since the constriction of current flow at intercrystalline boundaries affects the resistivity, and hence the temperature derivative of resistivity. The magnitude of this effect (which should not affect Hall coefficient and thermoelectric measurements) will clearly depend on the degree of sintering. In addition it should be noted that equation (12) assumes complete degeneracy, and this assumption is not strictly valid for specimens of the lowest electron concentration.

### 3.3. Thermoelectric Power Measurements

For each of four specimens investigated the thermoelectric power was found to increase approximately proportionally to the absolute temperature. The values of the thermoelectric power at 500 $^{\circ}\text{K}$  for each specimen are shown in table 2 together with the values of  $n$  deduced from Hall coefficient measurements as previously described. The values of  $G$  given in table 2 are such as to make the



measured thermoelectric power agree with the theoretical expressions given by Howarth and Sondheimer. The values, whilst showing some dispersions, are in fair agreement with those found from resistance and Hall effect measurements.

Table 2

Specimen No.	55	56	57	50
Hall coefficient (ohm cm G <sup>-1</sup> ) $R \times 10^9$	2.4	3.7	16.5	30.3
Thermoelectric power (v deg <sup>-1</sup> ) $(dE/dT) \times 10^4$	0.90	1.03	1.74	2.14
$G=m/m_0$	0.10	0.11	0.15	0.15

### 3.4. Transverse Magnetoresistive Measurements

The conductivity in a magnetic field is given theoretically by Lewis and Sondheimer as

$$\sigma = - \frac{16a^3 M \nu_0}{3e^2 h^2} \frac{1}{\mathcal{R}(D/D_{\alpha\alpha})} \quad \dots\dots(13)$$

where  $\mathcal{R}(D/D_{\alpha\alpha})$  represents the real part of the expression given in equation (2).

For the second order approximation it may readily be shown that the fractional change in resistance when the specimen is in a magnetic field is given by

$$\frac{\Delta\rho}{\rho} = \frac{9}{1024} \frac{a^6 M^2 \nu_0^2 (\exp(z) - 1)^2 h^8 n^2 H^2}{\alpha^4 e^6 C^2 \pi^4 m_0^6 k^2 T^2} \frac{H^2}{G^6} \left\{ \frac{CD + BE - AE^2/D}{AD} \right\} \quad \dots\dots(14)$$

where

$$C = \frac{25}{9} \frac{F_{3/2}^2(\eta)}{F_{1/2}^2(\eta)} - \frac{7}{3} \frac{F_{5/2}(\eta)}{F_{1/2}(\eta)} \quad \dots\dots(15)$$

and  $A$ ,  $B$ ,  $D$  and  $E$  have already been defined.

Measurements on one specimen (specimen 50) show that for the fields available the effect is proportional to the square of the magnetic field as is shown in figure 3. The results for all three specimens given in table 3 show a decrease of

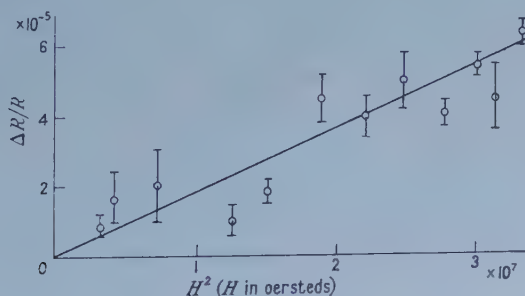


Figure 3. The variation of the magnetoresistance effect with the square of the magnetic field in cadmium oxide. Each point represents the mean of 20 observations.

the effect with increasing electron concentration (increasing degeneracy). Both of these results are in agreement with equation (14). There is however no quantitative agreement between the experimental results and the theoretical expression. The calculated values of  $\Delta\rho/\rho$  for each specimen are shown in table 3. These calculations use values of  $n$  determined from individual Hall

Table 3

Specimen No.	60	61	48
Exptl. values of $(\Delta\rho/\rho) \times 10^5$ at $H = 5.8 \times 10^3$ Oe	5.2	4.7	2.9
Hall coefficient (ohm cm g <sup>-1</sup> ) $R \times 10^9$	24.0	17.0	5.5
Theor. values of $(\Delta\rho/\rho) \times 10^5$ at $H = 5.8 \times 10^3$ Oe	0.062	0.019	0.003

coefficient measurements and a value of  $G$  of 0.12. The marked deviation cannot be rectified (as might be expected from equation (14)) by a choice of a smaller value of  $G$ . This is because the value of  $G$  affects the degeneracy and the expression in brackets in equation (14) varies with degeneracy tending rapidly to zero for  $\eta > 0$ . It may be noted that in many other substances the measured effect is considerably greater than that predicted theoretically assuming an electron energy band of standard form.

#### § 4. CONCLUSIONS

Measurements of various electrical properties of sintered specimens of cadmium oxide are in satisfactory agreement with the theoretical expressions derived by Howarth, Lewis and Sondheimer, except for the magnitude of the magnetoresistive effect. The value of the effective electron mass is found to be of the order of  $0.1 m_0$ . The characteristic temperature for longitudinal optical vibrations is found to be about 500°K.

#### REFERENCES

- BASTIN, J. A., and WRIGHT, R. W., 1955, *Proc. Phys. Soc. A*, **64**, 312.  
 DAVEY, W. P., and HOFFMAN, E. O., 1920, *Phys. Rev.*, **15**, 333.  
 FRÖHLICH, H., 1937, *Proc. Roy. Soc. A*, **160**, 230.  
 HOWARTH, D., and SONDHEIMER, E., 1953, *Proc. Roy. Soc. A*, **219**, 253.  
 LEWIS, B., and SONDHEIMER, E., 1955, *Proc. Roy. Soc. A*, **227**, 241.  
 SCHERRER, P., 1922, *Z. Kristallogr.*, **57**, 186.  
 WRIGHT, R. W., 1953, *Proc. Phys. Soc. B*, **66**, 273.

## Measurements of the Heat of Transport of Liquid Helium II

By D. F. BREWER AND D. O. EDWARDS

Clarendon Laboratory, Oxford

*Communicated by K. Mendelssohn; MS. received 7th August 1957*

**Abstract.** The heat of transport of helium II has been measured accurately from  $1.15^{\circ}\text{K}$  to  $2.1^{\circ}\text{K}$  in order to compare it with the calorimetric entropy data. The measurements were made with a thermally isolated glass vessel, which was connected to an isothermal liquid helium bath by a tube packed with fine powder. The heat of transport was determined (i) from the temperature and hydrostatic pressure changes in the vessel during thermomechanical flow, and (ii) from the heat input necessary to produce a measured flow rate. The results agree well with the indirect measurements of the fountain effect by van den Meydenberg, Taconis, Beenakker and Wansink and with the calorimetric data of Kramers, Wasscher and Gorter. The agreement with Kramers *et al.* is within the experimental error up to  $1.8^{\circ}\text{K}$  but at higher temperatures the present measurements are slightly higher.

Oscillations in the temperature of the vessel were observed even during thermomechanical flow, provided that the rate was subcritical. As expected, the oscillations were damped out above the critical rate. When the flow was just critical, a pronounced peak in the temperature-time graph was observed at the beginning of the flow, which appears to be due to an unexplained irreversible process.

### § 1. INTRODUCTION

THE theory of the thermomechanical effect in liquid helium II has been derived by H. London (1939). When two vessels, A and B, containing liquid helium II at pressures  $p$ ,  $p_0$  and temperatures  $T$  and  $T_0$  are connected by a superleak, then

$$\left(\frac{\partial p}{\partial T}\right)_{p_0, T_0} = \frac{Q^*}{T}.$$

The heat of transport  $Q^*$  is the heat reversibly absorbed in vessel B when unit volume of liquid is transferred to it from A. With the additional assumption that the liquid transferred is in the lowest energy state, London showed that

$$Q^* = \rho ST$$

where  $\rho$  and  $S$  are the density and specific entropy at temperature  $T$ . The entropy  $S$  may be calculated from calorimetric measurements as well as from the thermomechanical effect, permitting a direct test of the equations.

Although the measurements of Kapitza (1941) demonstrated the reversibility of the thermomechanical effect and verified the equations to within 10%, further experiments have not much improved the agreement between the calorimetric and the thermomechanical data. One difficulty was that until recently (Hill and Lounasmaa 1957) the specific heat was uncertain, since the measurements

of Hercus and Wilks (1954) are consistently about 10% higher than the earlier ones of Kramers, Wasscher and Gorter (1952). Older determinations of the specific heat were not accurate enough to resolve this discrepancy, but experiments on  $^3\text{He}$ - $^4\text{He}$  mixtures by Dokoupil, van Soest, Wansink and Kapadnis (1954) include measurements of the specific heat of pure  $^4\text{He}$  which favour the values of Kramers *et al.*

Similar disagreement exists within the thermomechanical measurements (figure 4). For example, Kapitza's results lie between the two sets of entropy data while other fountain pressure measurements by Peshkov (1954) agree with Kramers *et al.* below  $1^\circ\text{K}$  but are rather scattered at higher temperatures. Indirect measurements of the fountain pressure by van den Meydenberg, Taconis, Beenakker and Wansink (1954) also agree with Kramers *et al.* On the other hand, direct measurement of the heat of transport by Chandrasekhar and Mendelssohn (1955) gave values nearly 20% higher.

With this situation in mind, the present experiments were undertaken in order to obtain more accurate measurements of the heat of transport, and if possible, to differentiate between the two sets of calorimetric data by assuming H. London's equations to be correct.

Two methods for determining  $Q^*$  can be used: measurement of the temperature difference accompanying a measured fountain pressure (i.e.  $dp/dT$ ), and measurement of the amount of liquid drawn into a reservoir by a known quantity of heat (i.e. direct measurement of  $Q^*$ ). The first method is more difficult because it requires the measurement of very small temperature differences. Both have been used in the present experiments, but the direct measurement of  $Q^*$  has given more accurate results.

## § 2. METHOD

A thermally insulated reservoir R (figure 1) containing a thermometer T and heater H was connected by a powder-packed tube P to the surrounding bath of liquid helium. Two different cross-sectional areas of R ( $0.257\text{ cm}^2$  and  $1.283\text{ cm}^2$ )

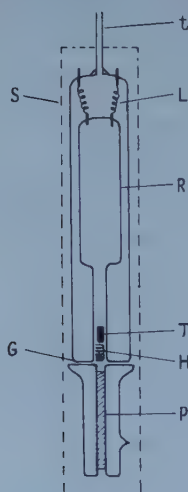


Figure 1. The flow apparatus.



allowed the accurate measurement of a wide range of flow rates. The thermometer was a 'LAB' carbon resistor of nominal resistance  $33\ \Omega$  at room temperature. The constantan heater had a resistance of about  $500\ \Omega$ . Leads passed through the glass walls of the Dewar reservoir by means of platinum wire seals which were connected in the vacuum space by thin tantalum wires L. Contact between platinum and tantalum was made by spot-welding both to small pieces of nickel foil.

To simplify the assembly of the apparatus, the reservoir and superleak were constructed separately as shown in the figure. They were held tightly together by springs and were sealed at the ground glass surfaces G with a mixture of glycerine and white soap which is fairly stiff at room temperature and forms a vacuum-tight glass when cold. The German silver tube t emerged through a gland at the top of the cryostat and was connected to a vacuum system by a flexible tube, so that the flow apparatus could be moved up or down. The superleak had its own permanently sealed vacuum jacket. A tube filled with compressed jewellers' rouge (machine packed) was chosen as a superleak because of its simple construction and because it allows very high rates of superflow with small heat conduction. The whole assembly was surrounded by a copper radiation shield S with narrow viewing slits, and suspended in a helium bath.

During measurements, the temperature of the helium bath was controlled within  $3 \times 10^{-5}^\circ\text{K}$  using an electronic regulator of the type described by Boyle and Brown (1954). Since the regulator was not able to deal sufficiently rapidly with the large heat inputs used, the following procedure was used to ensure constancy of temperature. The heater current was first passed through a compensating heater in the bath, which had the same resistance as the reservoir heater, then after a few seconds when the temperature was steady, the current was switched into the reservoir heater. Since nearly all the heat developed in the reservoir immediately appeared in the bath, the net heat influx to the bath remained constant.

Changes in the resistance of the reservoir thermometer were measured with a Lindeck potentiometer connected to a photocell galvanometer amplifier with variable feed-back (Preston 1946). Short term fluctuations in this system produced an uncertainty of roughly  $3 \times 10^{-5}^\circ\text{K}$  in the temperature change.

The method of measuring  $Q^*$  was quite standard. With the bath temperature stabilized, a constant heat input was switched into the reservoir, and the liquid level was observed with a vernier cathetometer every ten or fifteen seconds. The position of the bath level was also determined at the beginning and end of the measurement, together with the position of the flow apparatus relative to a fixed point. Provided that the rate of rise of level  $dh/dt$  was constant (as it was above  $1.3^\circ\text{K}$ ), it could be determined to within 1%. The observed heat of transport,  $Q_{\text{obs}}^*$  was then calculated from

$$a \frac{dh}{dt} Q_{\text{obs}}^* = W$$

where  $W$  is the rate of heat input and  $a$  the cross-sectional area of the flow reservoir. Values obtained from measurements in the two sections of the reservoir did not differ significantly.

Below  $1.3^\circ\text{K}$  the graphs of  $h$  versus  $t$  were slightly curved, showing a progressive decrease in the rate of rise as the height increased. This effect is due to the

increasing temperature of the reservoir, which is accompanied by an increase in the heat of transport in accordance with London's equation, and by an increase in the heat loss. Both effects are significant only at the lowest temperatures, where  $Q^*$  is small and  $dT/dp$  is large. As a consequence of the curvature, appreciable error results from a wrong choice of the height at which  $dh/dt$  is determined. The correct height is that where the heat loss from the reservoir just balances the heat influx due to radiation and the thermometer measuring current. This cannot be determined by allowing the system to reach a steady state with the heater switched off, since in the steady state, the reservoir must lose more heat than it receives if its level is to descend at the same rate as that of the bath (which loses liquid by evaporation). The method of finding the correct height is illustrated in figure 2, which shows the movement of the reservoir and bath levels during a measurement (the curvature of the graph has been greatly exaggerated). Let  $h$  be the height of the reservoir level above some fixed point and  $\Delta h$  its height above the bath. We wish to find  $\Delta h_0$ , the instantaneous difference in levels which will produce no rise or fall of the reservoir level. If  $\Delta h_1$  and  $\Delta h_2$  are the average level differences over a period just before and just after the measurement, and  $dh_1/dt$ ,  $dh_2/dt$  the corresponding rates of rise and fall of the reservoir relative to a fixed point, then consideration of the energy balance shows that

$$\Delta h_0 = \frac{\Delta h_1 \frac{dh_2}{dt} + \Delta h_2 \frac{dh_1}{dt}}{\frac{dh_1}{dt} + \frac{dh_2}{dt}}.$$

The value of  $\Delta h_0$  was usually one or two centimetres.

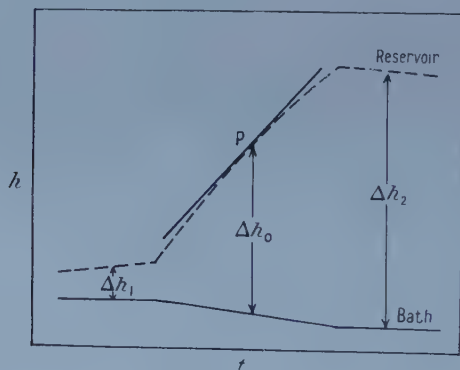


Figure 2. Height of reservoir level plotted against time.

The heat of transport calculated in this way is appropriate to a temperature slightly higher than that of the bath. The small temperature correction was calculated from London's equation. An uncertainty of a few per cent remained owing to the difficulty of drawing a tangent accurately. This random error was considerably reduced by taking the mean of a large number of measurements.

During each heating period, readings of the galvanometer in the thermometer circuit were made simultaneously with observations of the reservoir level. The graphs of  $h$  against galvanometer deflection  $\theta$  were straight lines within the

experimental error. Using London's equation we can relate the slope  $dh/d\theta$  to the specific entropy of the liquid by the equations

$$\left(\frac{dT}{d\theta}\right)^{-1} \left(1 + \frac{a}{A}\right) \frac{dh}{d\theta} = \frac{d(\Delta h)}{dT} = \frac{S}{g}$$

where  $g$  is the acceleration due to gravity,  $A$  the cross-sectional area of the bath, and  $dT/d\theta$  is the thermometer calibration factor. No measurements of  $dp/dT$  were taken above  $1.7^\circ\text{K}$  because of the difficulty of measuring the extremely small temperature differences with sufficient accuracy.

### § 3. RESULTS AND DISCUSSION

The observed heat of transport  $Q_{\text{obs}}^*$  must be corrected for the following effects: (i) as the liquid enters the reservoir, an equal volume of vapour condenses and gives up its latent heat, and (ii) some of the heat input is used in raising the temperature of the liquid in accordance with London's equation. The condensation correction is about 8%, and the second correction is very small except at the lowest temperatures where it is about 4%. Other corrections, such as those due to the heat capacity of reservoir and vapour, expansion coefficients, and increase in the vapour density, are negligible. The corrected heat of transport is

$$Q^* = Q_{\text{obs}}^* + \rho_v L - \rho_l g V \frac{A + a}{Aa} \frac{C}{S}$$

where  $\rho_v, \rho_l$  are vapour and liquid densities,  $V$  the volume of liquid in the vessel, and  $C$  the specific heat of the liquid.

In the measurement of  $dp/dT$  a correction was applied for the difference in vapour pressure due to the fountain temperature difference. It varied from 5% to 8% of the total pressure difference.

The corrected experimental data are given in figure 3. The full circles represent the heat of transport per  $\text{cm}^3$  derived from the flow measurements,† and the open circles represent values derived from measurement of  $dp/dT$ . The results have been plotted as percentage deviations from the values of  $\rho ST$  derived from the smoothed data of Kramers, Wasscher and Gorter (1952). This method of plotting has an advantage over a simple  $(Q^*, T)$  graph since it shows much more clearly the significant differences between the various sets of data.

Each point in the diagram represents the mean of a least three separate measurements, and for the flow measurements the deviations from the mean were never more than 3%. Figure 3 also gives the smoothed calorimetric data of Hercus and Wilks (1954) which are roughly 10% higher than the Leyden entropies. In figure 4 we collect the heat of transport data given by Kapitza (1941) Peshkov (1954), Chandrasekhar and Mendelssohn (1955) and van den Meydenberg *et al.* (1954). We have omitted from this figure the results of

† The values of  $Q^*$  presented in figure 3 are slightly different from those in a preliminary report of this work (Brewer, Edwards and Mendelssohn 1955). As was mentioned there, there was some uncertainty in the values of  $Q^*$  at the lowest temperatures which was due to the difficulty of determining the absolute temperature sufficiently accurately. An experimental determination of the thermo-molecular pressure gradients in the measuring system has removed most of this uncertainty and the new results are in somewhat better agreement with the entropy data of Kramers, Wasscher and Gorter (1952).

Meyer and Mellink (1947) since they show too much scatter. It is clear that our measurements agree rather well with Kramers *et al.*, especially below  $1.8^\circ\text{K}$  where the differences are less than the combined estimated errors of the two experiments. There is also close agreement with the results of van den Meydenberg *et al.*

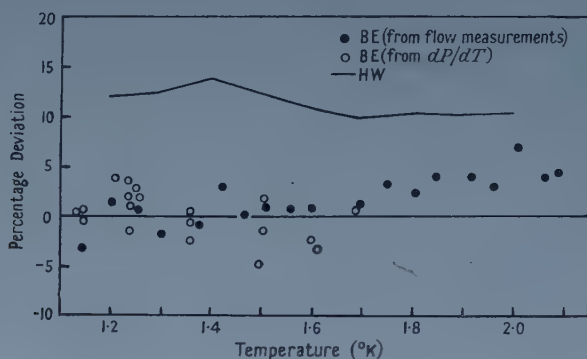


Figure 3. Deviation of  $Q^*$  from values of  $\rho^*ST$  calculated from the data of Kramers *et al.* (see text). HW, Hercus and Wilks, BE, present results.

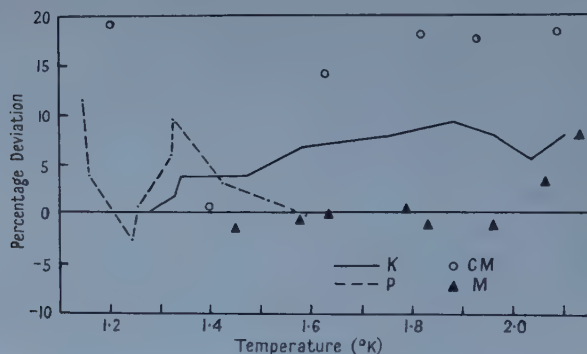


Figure 4. Deviation of  $Q^*$  from the values of  $\rho^*ST$  calculated from the data of Kramers *et al.* (see text). K, Kapitza, P, Peshkov, CM, Chandrasekhar and Mendelssohn, M, van den Meydenberg *et al.*

The largest deviations from Kramers' entropy values are shown by the results of Chandrasekhar and Mendelssohn, who used the film as superleak. The only other experiment using the film is that of van den Meydenberg *et al.* who, although using an indirect method, obtained results which deviate below  $2.1^\circ\text{K}$  by less than 3%. It therefore seems unlikely that the heat of transport depends on the form of superleak used. More probably, there were undetected sources of error in the experiments of Chandrasekhar and Mendelssohn, whose entropy values are appreciably higher even than those of Hercus and Wilks (1954).

Apart from these and the early experiments of Kapitza, there is therefore good agreement between the heat of transport measurements and the entropy values of Kramers *et al.* between  $1.1^\circ\text{K}$  and  $1.8^\circ\text{K}$ . The agreement is extended down to  $0.8^\circ\text{K}$  by the measurements of Peshkov (1954), whose accuracy becomes very much better below  $1.1^\circ\text{K}$  than is indicated by his results at higher temperatures, shown in figure 4. Since other recent calorimetric experiments (Dokoupil



*et al.* 1954, Hill and Lounasmaa 1957) also favour the specific heats of Kramers *et al.*, the most likely conclusion is that the Leyden entropy data are substantially correct and, together with London's equations, may be used to calculate the heat of transport. It has already been pointed out (Brewer, Edwards and Mendelssohn 1956) that this also confirms that the phonons do contribute to the heat of transport, as shown by many experiments including those of Bots and Gorter (1956) and Peshkov (1954) in the temperature region below  $1^\circ\text{K}$ .

There still remains the small systematic discrepancy above  $1.8^\circ\text{K}$  between the present measurements and these calculated values of  $Q^*$ . This discrepancy is rather difficult to explain. We have looked for possible systematic errors which could occur in our measurements at high temperatures and have not found anything which could account for it.

#### § 4. CRITICAL AND SUPERCRITICAL FLOW

For all the measurements to determine the heat of transport the rate of flow through the superleak was subcritical, that is, less than the critical rate at which irreversible effects begin. This was shown by the agreement between measurements made at different flow rates, and, with greater sensitivity, by the absence of any sudden change in the temperature difference at the beginning and end of the flow. The critical flow rate  $R$  at which such a change first appeared is plotted against temperature as the full curve (figure 5). The broken line represents  $R/(1-x)$  (where  $(1-x)$  is the superfluid fraction), which is proportional to the average velocity of the superfluid. It varies little with temperature but has a maximum in the region of  $1.7^\circ\text{K}$ , and the curve is generally similar in shape to that found by Winkel *et al.* (1955) for narrow channels between glass plates.

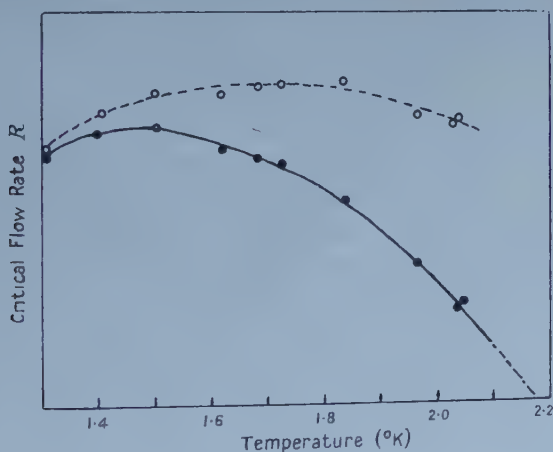


Figure 5. Critical flow rate through the superleak plotted against temperature.

Further observations of the behaviour of the reservoir temperature during both subcritical and supercritical flow were made with a much more sensitive and stable thermometer system. The essential difference was the replacement of the galvanometer amplifier by a d.c.-a.c. 'chopper' amplifier which was connected to a recording potentiometer. Typical results, given in figure 6, show clearly the adiabatic oscillations of the helium in the superleak predicted

by Robinson (1951) and London (1951). The frequency increased rapidly with temperature in rough agreement with Robinson's calculations, but the fairly long time constant of the thermometer system prevented measurement of the frequency over a wide temperature range so that the theory could not be tested in detail. The small damping present can be attributed to irreversible heat conduction across the superleak.

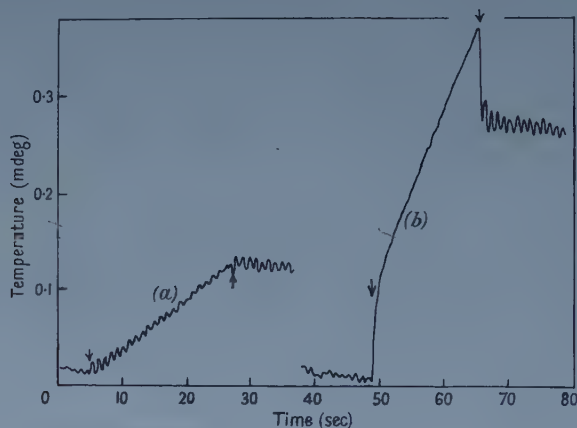


Figure 6. Temperature of the reservoir as a function of time in a flow experiment.  $T=1.346^{\circ}\text{K}$ . (a)  $W=0.18$  mw, subcritical, (b)  $W=0.36$  mw, supercritical.

Oscillations occur even when the helium is flowing into the reservoir provided that the flow is subcritical (figure 6(a)). During the heating period the oscillations are superimposed on the steady rise in temperature of the reservoir. At this temperature ( $1.346^{\circ}\text{K}$ ) and heat input, they correspond to oscillations in the height whose amplitude is less than  $0.01$  cm, which is too small to affect the accuracy of the heat of transport measurements. At higher temperatures, the corresponding amplitude is even less.

With a supercritical flow rate (figure 6(b)) the temperature behaviour is again as expected. When the heat input is switched on, a large temperature difference must be built up to overcome the resistance in the superleak. The amount by which this exceeds the fountain temperature difference is constant for a fixed flow rate, and gives a measure of the frictional forces. When a constant flow rate has been reached the temperature increases steadily and the oscillations are completely damped out by friction in the superleak. When the heat is switched off the excess temperature difference disappears and oscillations occur. The sudden drop in the excess temperature difference is accompanied by the familiar 'overshoot' of the liquid level.

For a heat input close to the critical value a new unexplained feature appears. In figure 7(a) the heat input must be just subcritical since oscillations are maintained during the heating period. There is nevertheless a pronounced peak in the temperature-time graph just at the beginning of the flow. The peak becomes even larger at a slightly higher heat input (figure 7(b)). Here the oscillations are damped out during the heating period, but the additional temperature difference necessary to maintain the rate of flow appears to be extremely small. The initial peak, which was observed over a large range of absolute temperature, does not seem to be a reversible effect since it does not recur when the heater is switched

off. It disappears at flow rates appreciably in excess of the critical, as shown in figure 6(b). Definite conclusions about this effect must await the results of a more thorough investigation.

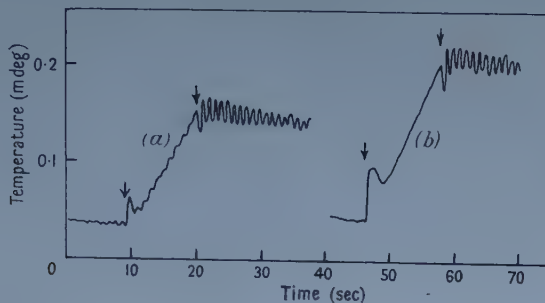


Figure 7. Temperature of the reservoir as a function of time in a flow experiment.  $T=1.346^{\circ}\text{K}$ . (a)  $W=0.25$  mw, just subcritical, (b)  $W=0.32$  mw, just supercritical.

#### ACKNOWLEDGMENTS

Our thanks are due to Dr. K. Mendelssohn for his constant interest in this work. We are indebted to the Nuffield Foundation for a Research Fellowship (D. F. B.) and to Brasenose College for a Senior Hulme Scholarship (D. O. E.).

#### REFERENCES

- BOTS, G. J. C., and GORTER, C. J., 1956, *Physica, 's Grav.*, **22**, 503.  
 BOYLE, W. S., and BROWN, J. B., 1954, *Rev. Sci. Instrum.*, **25**, 359.  
 BREWER, D. F., EDWARDS, D. O., and MENDELSSOHN, K., 1955, *Conference de Physique des Basses Températures, Paris*, p. 40; *Proc. Phys. Soc. A*, **68**, 939.  
 CHANDRASEKHAR, B. S., and MENDELSSOHN, K., 1955, *Proc. Phys. Soc. A*, **68**, 857.  
 DOKOUPIL, Z., VON SOEST, G., WANSINK, D. H. N., and KAPADNIS, D. G., 1954, *Physica, 's Grav.*, **20**, 1181.  
 HILL, R. W., and LOUNASMAA, O. V., 1957, *Phil. Mag.*, **2**, 143.  
 HERCUS, G. R., and WILKS, J., 1954, *Phil. Mag.*, **45**, 1163.  
 KAPITZA, P. L., 1941, *Ź. Phys., Moscow*, **5**, 59.  
 KRAMERS, H. C., WASSCHER, J. D., and GORTER, C. J., 1952, *Physica, 's Grav.*, **18**, 329.  
 LONDON, F., 1951, *Proceedings of the International Conference on Low Temperature Physics* (Oxford: Clarendon Laboratory), p. 5.  
 LONDON, H., 1939, *Proc. Roy. Soc. A*, **121**, 484.  
 MEYER, L., and MELLINK, J. H., 1947, *Physica, 's Grav.*, **13**, 197.  
 PESHKOV, V. P., 1954, *Ź. Exp. Theor. Phys.*, **29**, 351.  
 PRESTON, J. S., 1946, *Ź. Sci. Instrum.*, **23**, 173.  
 ROBINSON, J. E., 1951, *Phys. Rev.*, **82**, 440.  
 VAN DEN MEYDENBERG, C. J. N., TACONIS, K. W., BEENAKKER, J. J. M., and WANSINK, D. H. N., 1954, *Physica, 's Grav.*, **20**, 157.  
 WINKEL, P., DELSING, A. M. G., and POLL, J. D., 1955, *Physica, 's Grav.*, **21**, 331.

## RESEARCH NOTES

## The Mean Free Path of Alpha Particles in Nuclear Matter

BY B. A. ROBSON

Physics Department, University of Melbourne

*Communicated by L. H. Martin ; MS. received 19th August 1957*

THE elastic scattering of  $\alpha$ -particles in the energy range 10–40 mev has been treated theoretically in two different ways, which appear to give conflicting results.

A classical model has been used (Porter 1955), which would seem justified by the fact that the wavelength of the  $\alpha$ -particle is small compared with the nuclear radius for the energies considered. The observed drop in the ratio of the scattering to Coulomb scattering  $\sigma/\sigma_R$  is ascribed to absorption of the  $\alpha$ -particle along a Coulomb orbit through the nucleus. These paths are assumed to be straight lines for simplicity. Take the nuclear density to be

$$\rho(r) = \frac{1}{2}\rho_0\{1 - \tanh[(r-R)/d]\} \quad \dots\dots(1)$$

where  $r$  is the distance between the nuclear and  $\alpha$ -particle centres,  $d$  is a measure of the nuclear boundary diffuseness, and  $\rho_0$  is the nuclear density near the centre of the nucleus. The mean free path is given by

$$l(r) = 2l_0\{1 - \tanh[(r-R)/d]\}^{-1} \quad \dots\dots(2)$$

where  $l_0$  is the mean free path of an  $\alpha$ -particle near the nuclear centre. Taking the transmission factor to be of the form

$$\sigma/\sigma_R = T = \exp\left\{-\int dx/l(x)\right\} \quad \dots\dots(3)$$

where  $x = (r^2 - D^2)^{1/2}$  and  $D$  is the apsidal distance, it may be shown that

$$T = \exp\{- (R/\delta l_0)h(\xi, \delta)\}, \quad \dots\dots(4)$$

where

$$h(\xi, \delta) = \int_{\xi}^{\infty} (v^2 - \xi^2)^{1/2} \operatorname{sech}^2[(v-1)/\delta] dv, \quad \dots\dots(5)$$

and  $\xi = D/R$ ,  $v = r/R$ ,  $\delta = d/R$ .

Porter gives and uses the incorrect expression

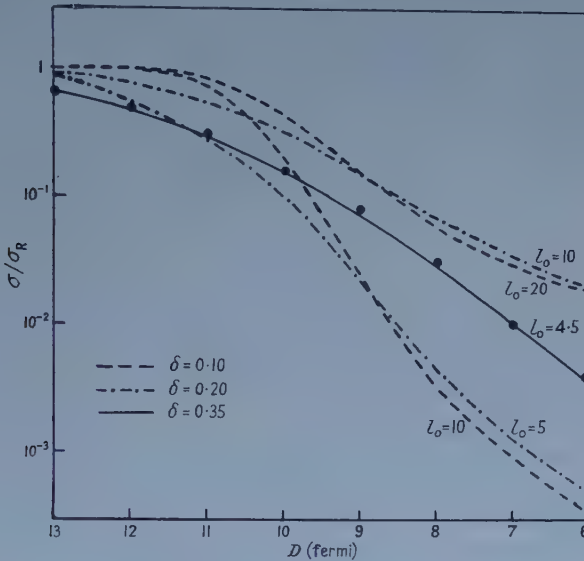
$$T = \exp\{-(2R/l_0)h(\xi, \delta)\}. \quad \dots\dots(6)$$

It therefore seemed worth while to recalculate the results and compare them with the recent optical model calculations (Igo and Thaler 1957, Cheston and Glassgold 1957).

The figure shows the ratio  $\sigma/\sigma_R$  plotted as a function of apsidal distance for  $\alpha$ -particles in gold. The points represent the experimental results. Also shown



are the theoretical curves for  $\delta = 0.10, 0.20$  and  $0.35$  for various values of  $l_0$ . It is seen that (i) an increase in  $\delta$  causes the exponential decrease to take place at larger apsidal distances; (ii) for small apsidal distances ( $\sim 6$  fermi ( $10^{-13}$  cm)),  $\sigma/\sigma_R$  depends only upon  $R/\delta l_0$ ; (iii) a smaller value of  $l_0$  causes the slope of the curve to increase; it was also found that (iv) increasing  $R$  causes a shift of the curve to larger apsidal distances, without changing the slope.



The mean free path of  $\alpha$ -particles in nuclear matter. Points denote experimental data. Units of  $l_0$ ,  $D$  and  $R$  are fermi.  $R = 10.0$ .

The experimental data may be fitted with  $R = 10.0$  f,  $\delta = 0.35$  and  $l_0 = 4.5$  f. This value of  $l_0$  is nearly the same as obtained by Porter but requires a very diffuse nuclear density distribution in disagreement with the optical model calculations which give  $\delta \sim 0.10$ .

Examination of the figure shows that the large value of  $\delta$  is required in order to fit the experimental data at large apsidal distances. If this portion of the graph is ignored, then a fit may be obtained for smaller values of  $\delta$ . Assuming  $\delta = 0.10$  one may test the validity of the Porter model by correlating the corresponding mean free path, namely  $l_0 = 16$  f, with that obtained from the optical model calculations. The mean free path is related to the absorption potential  $W$  by

$$l_0^{-2} = 4\mu\hbar^{-2}(E - V)\{[W^2(E - V)^{-2} + 1]^{1/2} - 1\}, \quad \dots\dots(7)$$

where  $\mu$  is the reduced mass of the  $\alpha$ -particle,  $E$  the incident energy and  $V$  the real component of the optical potential. The optical model calculations indicate that  $7.5 \leq -W \leq 25$  mev and  $-V \sim 40$  mev for incident energies of 20–40 mev so that  $1 \leq l_0 \leq 3$  f. Thus the classical model predicts considerably larger values of  $l_0$ , for the same diffuseness parameter, than the optical model. A mean free path as small as 2 f would require a very diffuse nucleus in the classical model. Thus a reconciliation does not seem possible and the classical description seems of doubtful validity.

The author wishes to thank Associate-Professor C. B. O. Mohr for several helpful discussions on the subject.

## REFERENCES

- CHESTON, W. B., and GLASSGOLD, A. E., 1957, University of Minnesota, Linear Accelerator Laboratory, Annual Progress Report.  
 IGO, G., and THALER, R. M., 1957, *Phys. Rev.*, **106**, 126.  
 PORTER, C. E., 1955, *Phys. Rev.*, **99**, 1400.

## Rotational Analysis of Bands of the $A^3\Pi_{0+}$ , $B^3\Pi_1 - X^1\Sigma^+$ Systems of Thallous Fluoride

By R. F. BARROW†, H. F. K. CHEALL†, P. M. THOMAS†  
 AND P. B. ZEEMAN†

*MS. received 16th October 1957*

### § 1. INTRODUCTION

THE spectrum of thallous fluoride was first observed by Boizova and Butkow (1936), and was later studied by Howell (1937) who gave vibrational analyses. Quite recently the microwave spectra of  $^{205}\text{TlF}$  and  $^{203}\text{TlF}$  have been observed by Mandel and Barrett (1955).

We have now carried out rotational analyses of bands of the two longer wavelength systems,  $A^3\Pi_{0+}$ ,  $B^3\Pi_1 - X^1\Sigma^+$ , with the object of improving the information about the vibrational levels of the upper states and thus deriving a reliable value for the dissociation energy of this molecule. The  $C^1\Pi - X^1\Sigma^+$  system at shorter wavelengths appears to be completely predissociated and does not appear in emission (Howell 1937).

### § 2. EXPERIMENTAL

The spectrum was excited in a hollow cathode discharge with helium as carrier gas. The cathode contained compressed pellets of thallium fluoride,  $\text{TlF}_3$ . The analyses were carried out on 6th order plates taken at the University of Stellenbosch.

### § 3. ANALYSIS

Most of the intensity of the two systems is concentrated into two 0, 0 sequences, and in these the 0, 0 bands are much the strongest. The structure of some of the bands is a little unusual, for  $B' \sim B''$ , but  $D' > D''$ , so that in the 0, 0 band of  $A-X$  are formed two P heads and one R head, while the 0, 0 band of  $B-X$  appears degraded to longer wavelengths although  $B' > B''$ . However, a starting point for the analysis was provided by the 2, 2 and 3, 3 bands of the  $A-X$  system, for which  $F'(J) \sim F''(J)$ , and which therefore consist of rather closely spaced series of R and P lines spreading out in opposite directions from well marked origin gaps. In both bands, lines could be measured at sufficiently low values of  $J$  for unequivocal assignments to be made. The remainder of the analysis followed by conventional routes: it was greatly facilitated by the fact that precise values of the rotational constants for the ground state were available (Mandel and Barrett 1955). The agreement between the values of  $\Delta_2 F''(J)$  found in the present work and those calculated from the microwave spectrum is illustrated in table 1.

† Physical Chemistry Laboratory, Oxford University

‡ Merensky Institute for Physics, Stellenbosch University

Table 1. Values of  $\Delta_2 F''(J)$ 

$v'' =$	0			1		2			3	
$J$	C	A	B	C	B	C	A	B	C	A
5	4.89					4.83	4.92		4.79	4.70
10	9.34		9.45			9.21	9.22		9.15	9.14
15	13.78		13.86			13.60	13.57		13.50	13.44
20	18.22		18.24			17.98	17.98		17.85	17.86
25	22.66		22.73			22.35			22.20	22.23
30	27.09		27.13			26.72		26.74	26.54	26.54
35	31.51		31.55			31.08			30.87	30.83
40	35.92		35.91			35.44		35.52	35.19	35.15
45	40.33		40.33			39.78		39.83	39.51	39.52
50	44.72								43.81	43.87
55	49.10								48.10	48.14
60	53.47	53.48							52.38	52.43
65	57.82	57.88		57.43	57.48				56.65	56.71
70	62.16	62.25		61.74	61.83				60.89	60.94
75	66.48	66.66		66.03	66.08				65.13	65.19
80	70.79	70.91		70.30	70.35				69.34	69.50
85	75.07	75.16		74.56	74.68				73.54	73.70
90	79.33	79.35								
95	83.58	83.70								
100	87.80	87.86								

c—calculated from microwave data.

Values of  $B'-B''$ ,  $D'-D''$  and of  $\nu_0$  were derived from  $R(J-1)+P(J)$  in the usual way. The results are given in table 2, and the constants are summarized in table 3.

Table 2. Results of Rotational Analysis

System A-x				
$v', v''$	$\nu_0$	$B'$	$10^7 D'$	
0, 0	35164.3 <sub>1</sub>	0.2295 <sub>1</sub>	2.8 <sub>5</sub>	
2, 2	35049.0 <sub>4</sub>	0.2232 <sub>2</sub>	3.4 <sub>3</sub>	
3, 3	34973.9 <sub>9</sub>	0.2196 <sub>7</sub>	3.5 <sub>7</sub>	
System B-x				
$v', v''$				
0, 0	36805.6 <sub>3</sub>	0.2231 <sub>6</sub>	3.9 <sub>2</sub>	
1, 1	36675.4 <sub>6</sub>	0.2182 <sub>8</sub>	5.2 <sub>2</sub>	
2, 2	36518.9 <sub>6</sub>	0.2115 <sub>9</sub>	6.7 <sub>3</sub>	

Table 3. Summary of Constants for  $^{205}\text{TlF}$ 

State	$T_0$	$\omega_e$	$x_e \omega_e$	$y_e \omega_e$			
$B^3\Pi_1$	36805.6 <sub>3</sub>	366.6 <sub>4</sub>	10.2 <sub>2</sub>	-1.15 <sub>5</sub>			
$A^3\Pi_0+$	35164.3 <sub>1</sub>	436.3	7.1	-0.1			
$X^1\Sigma+$	0	477.3	2.3	—			
State	$B_e$	$\alpha_1$	$\alpha_2$	$10^7 D_e$	$10^7 \beta_1$	$10^7 \beta_2$	$r_e$
B	0.2249 <sub>2</sub>	0.0030 <sub>7</sub>	0.00090 <sub>5</sub>	3.3 <sub>5</sub>	1.09	0.10 <sub>5</sub>	2.076 <sub>2</sub>
A	0.2309 <sub>1</sub>	0.0027 <sub>4</sub>	0.00013 <sub>5</sub>	2.8 <sub>1</sub>	0.2 <sub>2</sub>	—	2.049 <sub>1</sub>
X	0.22315 <sub>2</sub>	0.00150 <sub>0</sub>	—	1.9 <sub>7</sub>	—	—	2.0844

## Notes :

1. The signs of the different terms are given as follows :

$$G_v = \omega_e(v + \frac{1}{2}) - x_e \omega_e(v + \frac{1}{2}) + y_e \omega_e(v + \frac{1}{2})^3$$

$$B_v = B_e - \alpha_1(v + \frac{1}{2}) - \alpha_2(v + \frac{1}{2})^2$$

$$D_v = D_e + \beta_1(v + \frac{1}{2}) + \beta_2(v + \frac{1}{2})^2$$

2. The rotational constants for the ground state are from the microwave data of Mandel and Barrett (1955). The value of  $D_v''$  is that calculated from the Kratzer formula,  $D = 4B^3/\omega^2$ .

## § 4. DISCUSSION

We may proceed to a brief consideration of the energy of dissociation of this molecule. The head-origin separations in the bands are often large, and the positions even of the Q heads in the B-x system do not always mark the origins, as the direction of degradation in the Q branch sometimes changes within a band. The derivation of good vibrational constants is therefore a matter of some difficulty, and no great precision can be claimed for the values given in table 3. However, it is quite clear that the vibrational levels in  $B^3\Pi_1$  converge rather rapidly. A short extrapolation (of about  $600\text{ cm}^{-1}$ ) leads to a limit at  $38310 \pm 200\text{ cm}^{-1}$  above  $v''=0$ . If it is assumed that the products are unexcited atoms,  $\text{Tl}(^2P_{1/2}) + \text{F}(^2P_{3/2})$ , then  $D_0'' = 109.5 \pm 0.6\text{ kcal}$ .

A second estimate of  $D_0''$  may be derived from thermochemical information. The standard heat of formation of thallous fluoride is  $-76.8\text{ kcal}$  (Caunt and Barrow 1950), its heat of sublimation is  $33.9_5\text{ kcal}$  (Barrow, Jeffries and Swinstead 1955), the heat of sublimation of thallium is  $43.4\text{ kcal}$  (Coleman and Egerton 1935, recalculated Jeffries 1952) and the heat of formation of atomic fluorine is  $18.7\text{ kcal}$  (Doescher 1952, Barrow and Caunt 1953). Thus  $D''(298^\circ\text{K}) = 104.9\text{ kcal}$ , or  $D_0'' = 104.1\text{ kcal}$ .

The agreement with the estimate from the extrapolation in  $B^3\Pi_1$  is not good, but it suffices to show that  $B^3\Pi_1$  is certainly to be correlated with  $\text{Tl}(^2P_{1/2}) + \text{F}(^2P)$ : the separation,  $^2P_{1/2} - ^2P_{3/2}$  in F is only  $1.15\text{ kcal}$ , so that it may be concluded from the extrapolation in  $B^3\Pi_1$  that  $D_0''$  lies within the range  $107.7$  to  $110.1\text{ kcal}$ . Evidence from the similar states of other molecules suggests that in fact  $\text{TlF}(B^3\Pi_1) \rightarrow \text{Tl}(^2P_{1/2}) + \text{F}(^2P_{3/2})$ , so that the most probable spectroscopic value is  $D_0'' = 109.5 \pm 0.6\text{ kcal}$ .

It must be concluded that there is either (i) an unsuspected error in one or more of the quantities entering the thermochemical cycle, or (ii) that the extrapolated limit in  $B^3\Pi_1$  corresponds to a potential maximum rather than to a true dissociation limit. The latter alternative seems here to be unlikely, for acceptance of the low value of  $D_0''$  would require in addition the postulate of a potential maximum in  $C^1\Pi$ . It is more probable that the heat of formation of thallous fluoride is some 5 or 6 kcal higher than is now believed: a new calorimetric study is obviously desirable.

## REFERENCES

- BARROW, R. F., and CAUNT, A. D., 1953, *Proc. Roy. Soc. A*, **219**, 120.  
 BARROW, R. F., SWINSTEAD, J. M., and JEFFRIES, E. A. N. S., 1955, *Trans. Faraday Soc.*, **51**, 1650.  
 BOIZOVA, Z. V., and BUTKOW, K. V., 1936, *Phys. Z. Sowjet.*, **5**, 765.  
 CAUNT, A. D., and BARROW, R. F., 1950, *Trans. Faraday Soc.*, **46**, 154.  
 DOESCHER, R. N., 1952, *J. Chem. Phys.*, **20**, 330.  
 HOWELL, H. G., 1937, *Proc. Roy. Soc. A*, **160**, 242.  
 JEFFRIES, E. A. N. S., 1952, *Thesis*, University of Oxford.  
 MANDEL, M., and BARRETT, A. H., 1955, *Phys. Rev.*, **98**, 1159 (A).



## The Dielectric Behaviour of Magnesium Manganese Ferrite

By J. PETERS AND K. J. STANDLEY

Department of Physics, The University, Nottingham

MS received 7th October 1957

THIS note reports measurements of the dielectric properties of a magnesium manganese ferrite in the frequency range 30 c/s to 100 Mc/s and in the temperature range 20–220°C. The high resistivity ferrite had the approximate composition 0.9 MgO, 0.1 MnO, 0.8 Fe<sub>2</sub>O<sub>3</sub> and its magnetic Curie point was close to 300°C. Samples were in the form of discs 2.5 cm diameter and 1 mm thick and contacts were formed either by rubbing carbon on to the ground surfaces or by evaporating, *in vacuo*, a thin film of silver or gold. Electrical contact with this conducting layer was made by clamping on brass discs to which leads had been soldered. Measurements were made of the capacity and effective parallel resistance of the assembly either by a substitution method or a Schering bridge at the lower frequencies and by a Wayne Kerr v.h.f. admittance bridge at the higher frequencies.

The results are summarized in figures 1 to 3. Figure 1 shows the variation of dielectric constant and effective parallel resistivity with frequency at 20 and 200°C. At room temperature the dielectric constant was almost independent of frequency and close to 15, but at 200°C, a high value ( $\sim 1000$ ) was found at 100 c/s and this

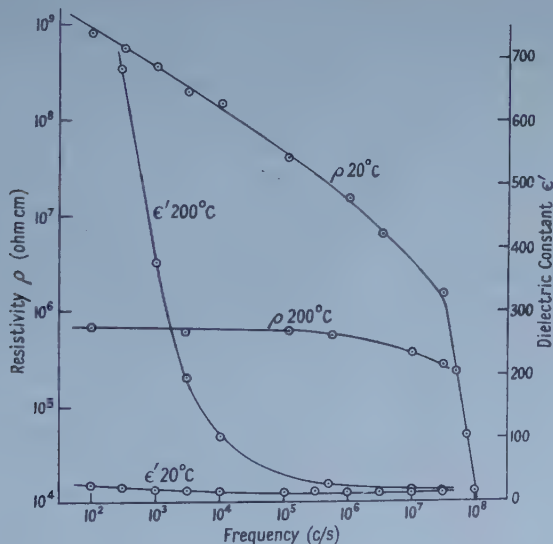


Figure 1. The variation of effective parallel resistivity and dielectric constant with frequency at 20°C and 200°C.

decreased towards 15 again at high frequencies. The effective parallel resistivity  $\rho$  at 20°C followed roughly the law  $\rho\nu^{1/2} = k$  up to a frequency  $\nu = 10$  Mc/s but at higher frequencies  $\rho$  fell much more rapidly. Microwave measurements by MacBain (1957) on this material suggest that the resistivity must pass through a

minimum value between 100 and 10 000 Mc/s. The magnitude of the resistivity was less and its variation with frequency considerably diminished at 200°C. The change of resistivity and dielectric constant with frequency and temperature are shown in figures 2 and 3 respectively. The three figures relate to samples whose density was about 92% of the x-ray density.

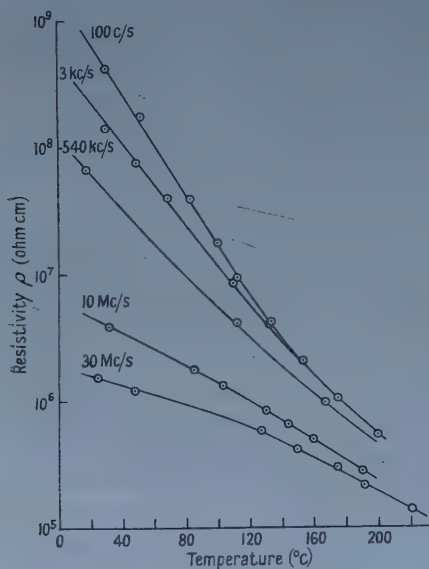


Figure 2. The variation of resistivity with temperature at frequencies from 100 c/s to 10 Mc/s.

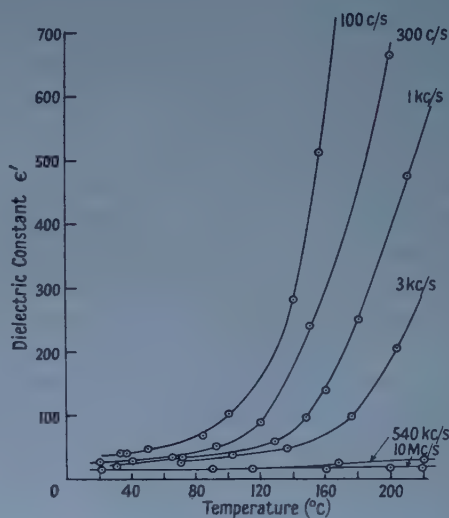


Figure 3. The variation of dielectric constant with temperature at frequencies from 100 c/s to 10 Mc/s.

The interpretation of these data presents some difficulty. Ferrites of this kind with low ferrous iron content are properly classed as semiconductors, and the porous nature of the material formed by a sintering process must be taken into consideration. Koops (1951) explained the dispersion of dielectric constant and resistivity which he found in a nickel zinc ferrite, using as a simple model a material composed of relatively well conducting grains of ferrite separated by poorly conducting layers, which may be, for example, inter-grain contacts or oxide layers at grain surfaces. Koops' analysis shows that a simple relation exists between the relaxation times of the dielectric constant and resistivity and that these two parameters should be similar in order of magnitude in most cases. Data recently published by Van Uitert (1956) do not follow Koops' formulae nor do the measurements shown in figures 1 and 2. If this type of dispersion is in fact still present at room temperature, the capacity measurements show that it is confined to the frequency region below 30 c/s (high dielectric constants in this material have been found by d.c. methods). The dielectric constant-frequency curve at 200°C is not accompanied by a resistivity-frequency curve of similar type and is unlikely to be due to the Koops' mechanism.

The temperature and frequency dependence of the dielectric constant is very similar to that found when true dielectric relaxation is occurring (see, for example, the data for ice of Smyth and Hitchcock (1932)) and an explanation of the results shown in figure 3 in terms of the relaxation of permanent dipoles within the ferrite is envisaged. An order of magnitude calculation suggests that the high dielectric

constant at low frequencies found at 200°C may be explained by the presence of permanent dipole moments of the order of 0.5 debye, indicating an effective charge separation of the order of 0.1 Å. The dipole moment is unlikely therefore to arise from the 'jumps' of an electron between ions of the same material in different valence states (de Boer and Verwey 1937) but might be due to the asymmetry of the field experienced by either oxygen or metallic ions. This might well arise in the case of the oxygen ion which has 3 B-site and 1 A-site neighbours, or in the case of the A-site ion, through a distortion of the tetrahedron at the corners of which the neighbouring oxygen ions are sited.

The measurements reported above demonstrate again that the low frequency behaviour of a ferrite does not necessarily indicate its high frequency performance, especially at elevated temperatures. The possible occurrence and effects of permanent electric dipoles within ferrite materials do not appear to have been widely considered and it is desirable therefore to extend the range of the present measurements. The porosity of the sintered specimen is a complicating factor and it is hoped to carry out further investigations on samples of very high relative density.

#### ACKNOWLEDGMENT

The work described here forms part of an investigation carried out for the Admiralty to whom acknowledgement is made for permission to publish this note.

#### REFERENCES

- DE BOER, J. H., and VERWEY, E. J. W., 1937, *Proc. Phys. Soc. A*, **49**, 59.
- KOOPS, C. G., 1951, *Phys. Rev.*, **83**, 121.
- MACBEAN, I. G., 1957, *Proc. Instn elect. Engrs.*, Part B, Suppl. No. 6, 296.
- SMYTH, C. P., and HITCHCOCK, C. S., 1932, *J. Amer. chem. Soc.*, **54**, 4631.
- VAN UITERT, L. G., 1956, *Proc. Inst. Radio Engrs, N.Y.*, **44**, 1294.

## LETTERS TO THE EDITOR

**Ionic Conductivity of Potassium and Rubidium Chloride Solutions at Microwave Frequencies**

It has been proposed by Little and Smith (1955) that dilute aqueous solutions of sodium and potassium chloride exhibit a dispersion in their conductivities at microwave frequencies. Their measurements were carried out at a wavelength of 10 cm with concentrations down to 0.005 normal. They interpreted their results in terms of the interaction of an ion with its surrounding sheath of water molecules and developed the following relation.

$$R = \frac{1 + \omega^2 \tau^2 - 0.035n}{(1 + \omega^2 \tau^2)(1 - 0.035n)} \quad \dots\dots(1)$$

where  $\tau$  is the relaxation time of the  $n$  molecules in the third shell surrounding the ion and  $\omega$  the angular frequency of the applied field. The factor 0.035 is slightly temperature dependent.

The purpose of this note is to report work carried out at a different wavelength from that used by Little and Smith in order to test the validity of their conclusions. The present measurements were carried out at 16.7 cm on 0.05 normal solutions of potassium chloride and rubidium chloride at a temperature of 20°C. The low frequency ionic conductivity  $\sigma_0$  was measured using a 1000 c/s conductivity bridge with dipping electrodes, and the high frequency value obtained by the coaxial line phase and amplitude balance method as described by Buchanan and Grant (1955). The high frequency ionic conductivity ( $\sigma_\omega$ ) was determined by measuring the total absorption due to the salt solution and subtracting the dipolar contribution of the water. The results are given in the table where  $R = \sigma_\omega / \sigma_0$ .

Solution	RbCl	KCl
Wavelength (cm)	16.7	16.7
$R$	1.05	1.04

The experimental error in  $R$  is  $\pm 0.06$ . This error is almost entirely statistical, the systematic error being very small due to the fact that the measurements for the salt solutions and water were carried out on the same apparatus thus making the method a differential one.

In order to calculate  $R$  from equation (1) it is necessary to know  $\tau$ , the relaxation time of the water molecules in the third shell. Little and Smith assumed  $\tau$  to be about 10% less than that of pure water and this procedure has been adopted in the present work. Hence a value of  $\tau$  corresponding to a relaxation wavelength of 1.57 cm has been chosen, the relaxation wavelength of pure water at 20°C being 1.74 cm (Grant, Buchanan and Cook 1957). This value of the relaxation wavelength for water in the third shell is difficult to deduce accurately, but must be several percent lower than that for pure water due to the effect of the ions. Its actual value is not critical when calculating  $n$  from equation (1).

Substituting the relevant parameters into equation (1), the result  $n = 22$  molecules is obtained for potassium chloride, with an upper limit of 26 molecules.



This may be compared with a value of  $n = 27$  molecules obtained by Little and Smith from their measurements at 10 cm wavelength.

Hence it may be concluded that the present results give a measure of support to the previous work of Little and Smith although the actual magnitude of the increase of the ionic conductivity at 17 cm remains somewhat uncertain.

Thanks are due to Dr. H. F. Cook for his interest and advice concerning this work.

Department of Physics Applied to Medicine,  
The Middlesex Hospital Medical School,  
London, W.1.

T. H. E. BRYANT.  
E. H. GRANT.

10th September 1957

BUCHANAN, T. J., and GRANT, E. H., 1955, *Brit. J. Appl. Phys.*, **6**, 64.

GRANT, E. H., BUCHANAN, T. J., and COOK, H. F., 1957, *J. Chem. Phys.*, **26**, 156.

LITTLE, V. I., and SMITH, V., 1955, *Proc. Phys. Soc. B*, **68**, 65.

---

### Loss Factor Measurements in Dry Sand

Measurements are being carried out on the variation of attenuation and velocity of sound with stress in dry sand and some results showing the change in velocity with stress have already been published (Matsukawa and Hunter 1956). The purpose of this note is to present additional results for attenuation and velocity and to suggest a practical rule for the description of the propagation over a wide range of stress and frequency.

In general, it has been found impossible to obtain accurately reproducible results, particularly for attenuation, in the frequency range 10–30 kc/s used. This is because the propagation is very sensitive to small changes in packing and boundary conditions and in addition, the non-uniformity of the medium distorts the wave front to produce interfering effects at the receiving transducer. Several different pulse and continuous wave experimental schemes have been tried without appreciable improvement in accuracy. The experimental points inevitably show a large scatter and the mean attenuation cannot be estimated to an accuracy closer than 10%.

It is convenient to consider the attenuating medium as having a complex elastic modulus in the form  $E(1 + i\eta)$  where the loss factor  $\eta$  is fairly small compared with unity. It follows that the attenuation coefficient is approximately related to the loss factor by the expression

$$\alpha = 27 \cdot 3 \eta f / c \text{ dB cm}^{-1}$$

where  $f$  is the frequency and  $c$  the phase velocity. Table 1 gives results for attenuation coefficient and the phase velocity at various stresses and a frequency of 20 kc/s. These results were obtained with vertical propagation through a specimen of sand between two transducers, placed one above the other. The stress was applied by loading the top transducer and the thickness of the layer of sand was

increased in stages. The values quoted were obtained from the slopes of linear graphs of attenuation and phase against the path in the sand.

Table 1.

Stress (lb in <sup>-2</sup> )	0.28	0.57	0.85	1.13	2.84	4.26
Attenuation $\alpha$ (dB cm <sup>-1</sup> )	2.14	1.88	1.81	1.70	1.38	1.27
Velocity $c$ (m sec <sup>-1</sup> )	273	310	335	350	418	440
Loss Factor $\eta$	0.104	0.104	0.108	0.106	0.103	0.100

In addition, as shown in table 2, measurements taken at various frequencies show an approximate proportionality of attenuation coefficient with frequency.

Table 2. Constant Load of 5 kg on Dry Sand

Attenuation Coefficient $\alpha$ (dB cm <sup>-1</sup> )	0.9	1.1	1.5	1.7
Frequency $f$ (kc/s)	7.6	12.7	22.9	27.9

Bearing in mind the large experimental error in the attenuation coefficient, the loss factor appears for all practical purposes to be independent of stress and frequency. The value of about 0.1 for  $\eta$  with a linear relation between  $\alpha$  and  $f$  is also supported by the results of Schmidt (1954). Schmidt used a sand bar method so that direct comparison between the results of the two experiments is not really permissible. However, he obtained values between 0.06 and 0.12, depending on the dimensions of the bar, for the frequency range 50 to 2000 c/s. The agreement is sufficiently good to suggest that the proposed working rule holds at lower frequencies as well. The rule presumably fails at wavelengths approaching the average particle size, when dispersive effects become appreciable. Up to the present, it has not proved possible to measure any dispersion, owing to the large attenuation at high frequencies.

In conclusion, all the experiments tried with different experimental arrangements agree in giving a loss factor of about 0.1 for dry sand independent of frequency and pressure. Experiments are being continued on the loss factor for other heterogeneous media.

University of Leicester  
September 1957

A. N. HUNTER.  
R. D. LEGGE.  
E. MATSUKAWA.

MATSUKAWA, E., and HUNTER, A. N.; 1956, *Proc. Phys. Soc. B*, **69**, 847.  
SCHMIDT, H., 1954, *Acustica*, **4**, 639.

### Experiments on Controlled Fractures

A method for the determination of fracture energy has recently been described by Benbow and Roesler (1957). In this method, the fracture energy is determined by the slope of a line which is asymptotic to the mean curve through experimental results. Since the experimental results tend to show some scatter this technique is open to errors of interpretation. However, by considering a more complete expression for the strain energy of the system, the experimental results should fall on a straight line.

The strain energy of a beam subjected to shearing forces is the sum of the energy due to flexure and shearing stresses. Assuming a parabolic distribution of shearing stress over the depth of the beam, and using the notation of Benbow and Roesler, the total strain energy is

$$U(P, s) = \frac{P^2 s^3}{24EI} + \frac{P^2 b^2 s}{32GI} \quad \dots\dots(1)$$

where  $G$  is the modulus of rigidity which may be determined from

$$G = \frac{E}{2(1 + \mu)} \quad \dots\dots(2)$$

where  $\mu$  is Poisson's ratio.

Equation (1) can then be expressed as

$$U(P, s) = \frac{P^2 s^3}{24EI} \left[ 1 + \frac{3}{2}(1 + \mu) \frac{b^2}{s^2} \right] \quad \dots\dots(3)$$

Comparison of this equation with Benbow and Roesler's equation (4) shows that the effect of shear stress is to introduce the factor  $1 + \frac{3}{2}(1 + \mu)b^2/s^2$  say  $S$ . In order to demonstrate the effect of shear stress, this factor is plotted in figure 1.

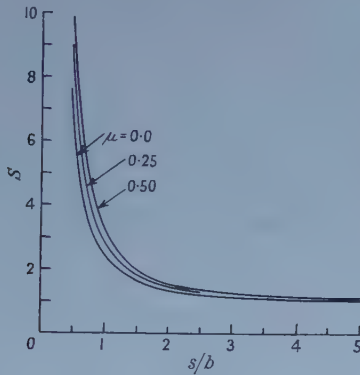


Figure 1

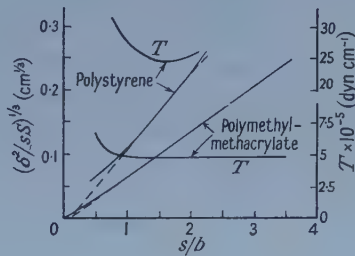


Figure 2.

Using the Griffith energy balance for crack growth, the expression for fracture energy becomes

$$\frac{T}{E} = \frac{3}{64} \frac{\delta^2 b^3}{s^4} \frac{1}{S} \quad \dots\dots(4)$$

Assuming values for  $\mu$  of 0.35 for polymethylmethacrylate and 0.28 for polystyrene, the results obtained by Benbow and Roesler have been replotted in figure 2. The fracture energy computed from the slope of each of these graphs is  $T = 4.8 \times 10^5$  dyn cm<sup>-1</sup> for polymethylmethacrylate and  $T = 24.6 \times 10^5$  dyn cm<sup>-1</sup> for polystyrene.

The curves shown in figure 2 indicate a departure from the straight line when  $s/b < 1$ . This could be explained in terms of St Venant's principle regarding stress distribution. When  $s/b$  is small the nature of the distribution of shear stress is indeterminate and consequently the shear strain energy. As  $s/b$  increases, however, the influence of the loading system has progressively less effect on the stress distribution and the calculated strain energy rapidly approaches the true value. It is generally regarded that theory and fact agree when, in this case,  $s/b \geq 1$ .

The results for polystyrene also show an increase in fracture energy for values of  $s/b > 1.5$ . Whilst definite conclusions cannot be drawn from the limited results available, there does appear a tendency for the fracture energy to vary with  $s/b$ . The fact that such a trend only becomes evident when shear strain energy is also considered is demonstration of the need for greater accuracy in analysis. The variation of  $T$  is also of interest and is therefore worthy of further study.

Department of Mechanical Engineering,  
Imperial College,  
London.  
8th October 1957.

N. L. SVENSSON.

BENBOW, J. J., and ROESLER, F. C., 1957, *Proc Phys. Soc. B*, **70**, 201.



## REVIEWS OF BOOKS

*Advances in Electronics and Electron Physics*, Volume 8. Edited by L. MARTON. Pp. xi+562. (New York: Academic Press, 1956.) 13.00.

This eighth volume of this series provides a further nine reviews which will be of considerable interest and use to those working in this field. Two of the reviews depart from the usual practice in being concerned entirely with electronic circuit applications rather than devices and basic physics. The first review, entitled 'Some New Applications and Techniques of Molecular Beams' by J. G. King and J. R. Zacharias, includes a rather brief description of the applications of molecular beams, followed by considerable detail concerning the techniques involved.

The second review, 'Field Emission', by W. P. Dyke and W. W. Dolan, gives an excellent review of the present state of this art, particularly the theory in its modern form.

'Mass Spectroscopy', by L. Kerwin, is the second review on this subject to appear in the series. It gives a rather general description of instrumental matters and applications with a comprehensive bibliography.

'Amplitude and Time Measurements in Nuclear Physics', by E. Baldinger and W. Franzen, gives a very good description of the factors limiting the accuracy of nuclear pulse measurements and the methods of analysis.

'Pulse Amplitude Analysis', by J. L. W. Churchill and S. C. Curran, describes methods of detecting nuclear events and deals in detail with methods of application such as pulse height analysis.

'Electron Guns and Focusing for High-Density Electron Beams', by C. Süsskind, gives a general description of the developments of space charge compensated high-density electron guns and their application.

'On the Electrical Life of an Oxide-Cathode Receiving Tube', by G. H. Metson, gives an excellent description of the largely empirical work carried out mainly at the British Post Office Research Laboratory on the factors affecting the lines of oxide-cathodes in valves.

'Viewing Storage Tubes', by M. Knoll and B. Kazan, gives a comprehensive review of the published work on this subject.

The final paper 'Magnetron Mode Transitions', by E. C. Okress, reviews the subject rather briefly but effectively, and gives a comprehensive bibliography.

It is difficult to make any general remarks on so varied a collection of papers. It is regrettable that many of them tend to be very uncritical, a fault all too common in this type of paper. However, the Volume represents a further valuable contribution to the electronics library, and is generally adequately comprehensive in bibliographical detail.

M. E. HAINE.

*The Physics of Electrical Contacts*, by F. LLEWELLYN JONES. Pp. xi+219. (Oxford: Clarendon Press, 1957.) 35s.

The importance of electrical contacts in power and communication engineering cannot be overestimated. But since users of contacts have so often been content merely to find electrode materials best suited to their own particular purposes, the numerous investigations of the last quarter of a century have been for the most part uncoordinated.

This treatise on the physics of the subject arose originally from a wish to fill the gap by providing in this country a standard work, in which the physical processes involved in the operation of contacts were described and serious attempts made to elucidate them. Professor Llewellyn Jones from his work on electrical discharges with his collaborators at Swansea was a fitting person to embark upon the task. He produced a Report on the subject for the Radio Research Board which appeared in 1953. But the present work discusses the physical aspects more fully and contains also an account of investigations completed or still in progress since that date.

In an Introductory Chapter the author deals with the nature of contact problems and the scope of their treatment. Then follows a chapter on fundamental concepts with special reference to restrictive resistance and contact temperature.

Chapter 3 describes, in interesting detail, the phenomenon of the formation and ultimate rupture of microscopic molten metal bridges, a subject on which much work has been done in Germany, U.S.A. and in this country. A significant feature of theories of this phenomenon is an asymmetric temperature distribution in a contact due to the Thomson effect. The next chapter is also mainly concerned with this subject and how it may lead to metal transfer on rupture.

In the second half of the book these matters are developed further and an account is included of recent experimental work at Swansea on bridge formation and rupture.

Reference may also be made to Chapter 6 devoted to the properties of metals with which contact theory is concerned almost up to their boiling points. Here there is clearly room for more research in which this technique can play an essential role.

Of the final two chapters one is concerned with the arc discharge and the other surface film phenomena in problems of light contact.

The subject is clearly and attractively presented throughout and the volume is a valuable contribution to the literature.

A. M. TYNDALL.

*Photoconductivity Conference*, edited by R. G. BRECKENRIDGE, B. R. RUSSELL and the late E. E. HAHN. Pp. xiii+653. (New York: Wiley; London: Chapman and Hall, 1956.) 108s.

This volume is the published version of the collected papers presented at the three day conference on photoconductivity held at Atlantic City in November, 1954.

The most serious criticism of the book is that it has taken so long to appear. No doubt this was largely due to the unfortunate death of one of the editors, but the fact remains that in such a rapidly moving field of research, speed of publication is of paramount importance—if necessary at the expense of some imperfections in presentation.

On the latter point the editors have done well to produce a coherent volume of 650 pages from thirty individual papers by workers in several countries. A useful and uncommon feature is the inclusion of most of the spontaneous discussion following each paper—achieved by the joint use of stenographers and tape recorders.

The first section gives a phenomenological discussion of photoconductive theory, particularly stressing the importance of carrier lifetimes, by Rose and by Petritz.

The second section covers the fundamental theory of absorption processes, including the first treatment of indirect (non-vertical) transitions by Bardeen and his co-workers. Dexter discusses the theory of absorption edges in insulators, Lax and Herring consider imperfections and trapped carriers, James discusses electron-vibration coupling in semiconductors and Fan compares his short wave length absorption measurements on Si and Ge with Herman's energy band calculations.

The third part of the book on electron processes treats the behaviour of the photo-electrons and photoholes. A comprehensive paper by Rittner gives the formal carrier transport equations and solves them for specific cases. Ranges of carriers are discussed by Stockman, surface trapping effects by Garrett and Brattain and by Miller and bulk trapping in Si by Haynes and Hornbeck. Pincherle covers the theory of the photo-electro-magnetic effect.

The fourth section reviews the properties of some of the more interesting photoconductors, beginning with a valuable paper by Burstein, Picus and Sclar on absorption and photo-effects in both pure and doped Ge and Si over the whole wavelength range 1-40  $\mu$ . Intermetallic compounds in general are discussed by Frederikse and Blunt and InSb in particular by this reviewer. Krumhansl describes photo-excitation in ionic crystals, Mollwo deals with zinc oxide, and the lead sulphide group of photoconductors are covered by Chasmar and by Mahlman, Nottingham and Slater.

The last section contains shorter papers describing current work on specific topics. Kurnick and Zitter describe PEM measurements on InSb, both Dunlap and Morton deal with impurity photoconduction in Ge, and Redfield discusses intrinsic photocurrents in Te. Photocurrents that increase more rapidly than linearly are described by Bube, and there are four papers on photo-effects in PbS and PbTe by Dutton, Levinstein, Woods, and Scanlon and co-workers.

Although, as the editors admit, such a book cannot give the coherent planned presentation of a subject achievable by a single author, it is equally valid to state that this book could not have been written by a single author. It contains a great deal of both general and specific information which will be particularly useful to anyone actively working on optical or photoelectric effects in semiconductors.

T. S. MOSS.

*A History of Luminescence*, by E. N. HARVEY. Pp. 597. (Philadelphia : American Philosophical Society, 1957.) \$6.

The author is well known for his publications in the field of bioluminescence. In the present volume he has provided an encyclopaedic survey of historical records of all aspects of luminescence. The book has three main sections. In the first the references to luminescence over the great ages from classical antiquity to the nineteenth century are presented in connected form. However, it is from the seventeenth century onwards that the subject benefits from the parallel growth of systematic scientific attack in the observation of natural phenomena. Over this later period the author considers in section two the



various attentions paid to specific classes of luminescence, e.g. electroluminescence, thermoluminescence, triboluminescence, chemi- and bioluminescence, etc. In his detailed description of the observations of various notable men of science one can see the effect of the growing unity of knowledge in physics and chemistry on the different theories of luminescence and its decay. Perhaps the most interesting reading in the book is that part of the text in which we find those pioneers of the nineteenth century such as Becquerel and Stokes, at least for those who now try to probe the phenomena of luminescence for information or possible application.

The last section of the book covers the author's special interest, bioluminescence. Although the earliest of luminescence phenomena in historical records, the occurrence of luminescence in biological systems remains the least understood. The book is completed by a set of copious references and good author and subject indices. There is no doubt that it provides a chronological perspective to a subject which is as aesthetically pleasing as it is scientifically interesting.

G. F. J. GARLICK.

*Microphotography, Photography at Extreme Resolution*, by G. W. W. STEVENS. Pp. xvi + 326. (London: Chapman and Hall, 1957.) 50s.

There is a fascination about things that are small, as, for example, model trains. I suppose that it was this which led J. B. Dancer and those who soon followed him to make tiny photographs—microphotographs—for viewing under a microscope or with a magnifier on which the photograph was cemented in the end of a pencil or a piece of jewellery. But a more serious purpose developed in the 1870–71 Franco-Prussian war when minute copies of printed messages on collodion pellicles were regularly sent by pigeon post into Paris while it was besieged. A single pigeon carried the equivalent of over 200 newspaper pages. This may have been the first, but by no means the last use of microphotographs for the surreptitious conveyance of information.

Today cheques and football pool coupons are recorded as a routine as small photographs and the tendency to use microphotographic copies of books and scientific papers, for the sake of low cost and ease of transport and storage, seems to be increasing. These are important aspects, but the manufacture of graticules is no less important and probably more interesting technically. All this and the technique of microphotography are discussed in Dr. Stevens' book. It is the first on the subject and for that reason alone is likely to be read by those interested in the subject. But it is well worth explicit recommendation for it is pleasantly written at an easy level of intelligibility by one with sufficient experience in the subject to know what he is writing about. The information given about the practical aspects of microphotography is, to a very large extent, that gained by the author in his own work and many of the points made are of sufficient interest to suggest that the book is worth reading by anyone with an interest in laboratory techniques generally. The most attractive feature to many readers will, in fact, be the discussion of the photographic and optical phenomena peculiar to the problem of recording extremely fine detail by photography.

The usual custom has been followed of looking for omissions and things which might be changed, but with meagre results. All that I can suggest (with adequate reasons) is that in a new edition something should be included about reciprocity failure. If the intensity of illumination is changed



considerably then the necessary change in exposure time can be very different from what is calculated by assuming that the effective exposure is the product of intensity and time.

E. W. H. SELWYN.

*Laboratory Glass Working for Scientists*, by A. J. B. ROBERTSON, D. J. FABIAN, A. J. CROCKER and J. DEWING. Pp. xiv + 184. (London : Butterworths Scientific Publications, 1957.) 22s. 6d.

In his *History of Electricity*, published in 1767, Priestley gave the following advice regarding the desirable accomplishments of a physicist (an 'electrician' to Priestley) :

" With respect to glass, he ought, by all means, to learn the use of a blow pipe, the method of drawing out and bending glass tubes, and performing, with some degree of dexterity, other operations upon glass, which he will want to use in a great variety of forms. An electrician, thus furnished, will be able, upon any occasion, to serve himself : and the slowness and blunders of mechanicks do but ill suit with the ardour of persons engaged in philosophical inquiries ".

While the average research worker today can get much of his constructional work done by technicians (unless, perhaps, he works in a University), there are two advantages to him if he becomes skilled in their crafts. First, he will be better able to understand their potentialities and difficulties, and to plan his apparatus accordingly ; and secondly he will not be held up completely if a technician is not available.

The book under review sets out to give the research worker an introduction to glass-blowing in such a way that he can learn from it to make apparatus for himself by methods which are not necessarily those used by professional glass-blowers, but which will nevertheless result in serviceable constructions. The early chapters cover the working techniques and basic properties of glass ; they might well have included a section on the parts played by surface tension, viscosity, gravity, centrifugal force, and delayed blowing after heating, in the process of smoothing out irregularities in joints. All this is summarized on p. 60 as 'alternate heating and blowing', but there is a good deal more to it than that, and it should be more readily explicable to research workers than to professional glassblowers. There are useful chapters on the construction of typical pieces of glassware, such as vapour pumps, and on the assembly of complex equipment.

The authors have compiled a handy volume, with good diagrams and helpful references. There would probably be difficulty in learning to blow glass from the book alone, but it would well supplement a few lessons from an accomplished glass-blower ; and it would help a research worker to instruct a glassblower who knows no science in some of the more unusual operations of his craft.

R. V. JONES.

*The Mechanism of Phase Transforms in Metals*. (Institute of Metals, Monograph and Report Series, No. 18.) Pp. 346. (London : The Institute of Metals, 1956.) 50s.

This book contains eighteen papers written for a Symposium held in November 1955, together with a very full account of the discussion. The theory of how a phase transformation occurs includes many fundamental topics

(fluctuation theory, diffusion, lattice defects, crystallography, etc.), and in recent years, progress has been rather more apparent than in the concomitant question of why it occurs. Current interest in the solid state, and particularly in the role of structural imperfections, is very evident throughout the book, and all the contributors confined themselves to changes in solids.

The usual division into 'nucleation and growth' and 'martensitic' transformations was made, discussion in each case being based on an invited review paper and a number of shorter research papers. On re-reading the contributions, one is impressed by the present ascendancy of the experimentalists in precipitation reactions, and of the theorists in martensitic reactions. Precipitation phenomena inevitably dominated the nucleation and growth session, and it is encouraging to find that the many exhaustive x-ray investigations, supplemented by electron microscopy, are at last beginning to produce agreed results on what happens in the early stages. The outstanding recent progress in martensitic transformations has been in formal crystallography, but there is no well developed theory of the atomic processes, and an experimental approach has yet to be found; perhaps the new methods of observing dislocations will provide some answers.

The popularity of the conference may be judged from the discussion, the edited version of which occupies nearly one quarter of the book. This publishing policy is heartily commended to other organizers; it enhances the value of the papers very considerably. Papers and discussion together provide a comprehensive and well balanced survey of the current position in this interesting field, and may be read with profit by anyone with an interest in the solid state.

J. W. CHRISTIAN.

*Elasticity, Fracture and Flow with Engineering and Geological Applications*, by J. C. JAEGER. Pp. viii + 152. (London: Methuen's Monographs on Physical Subjects, 1956.) 10s. 6d.

The aim of this monograph is to discuss the mechanics and physics of the equilibrium and motion of deformable solids and liquids. It consists of three long chapters. The first deals with the analysis of stress and of strain, the second with the behaviour of actual materials and the third with the equations of equilibrium and motion and with specific applications of these equations.

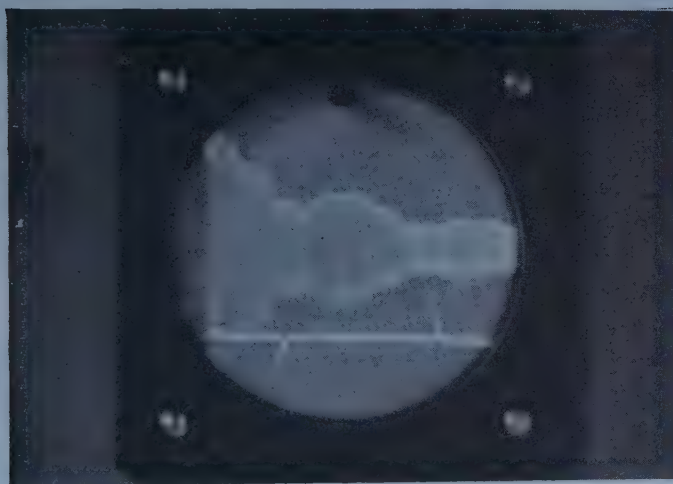
In a book limited in size to some 150 pages, the author must pick and choose, particularly when he elects to write on a wide and highly developed subject like elasticity, fracture and flow. In the present case, the selection of material is excellent and one commendable feature of this monograph is the breadth of outlook and the balance of the treatment. There is, for example, in the first chapter, a discussion of finite homogeneous strain in two and three dimensions as well as infinitesimal strain. Again, the second chapter includes a thorough treatment of theories of fracture and failure and yield criteria.

The book can be recommended without hesitation as a concise, reliable and up-to-date account of the subject.

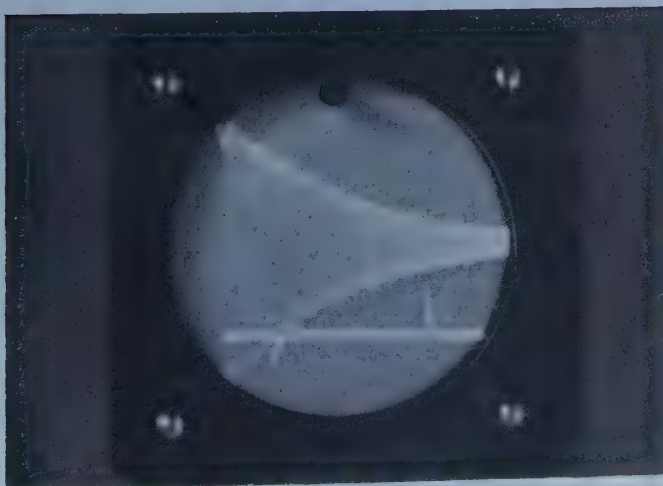
R. M. D.



Figure 2. Photograph of the Acoustic System. The exciting system on the right is shown without the permanent magnet in position; the detection system is on the left.



(a)



(b)

Figure 5. (a) Non-exponential decay curve due to 'overlapping' of the resonance curves at low values of  $l$ . (b) Typical decay curve selected for measurement.

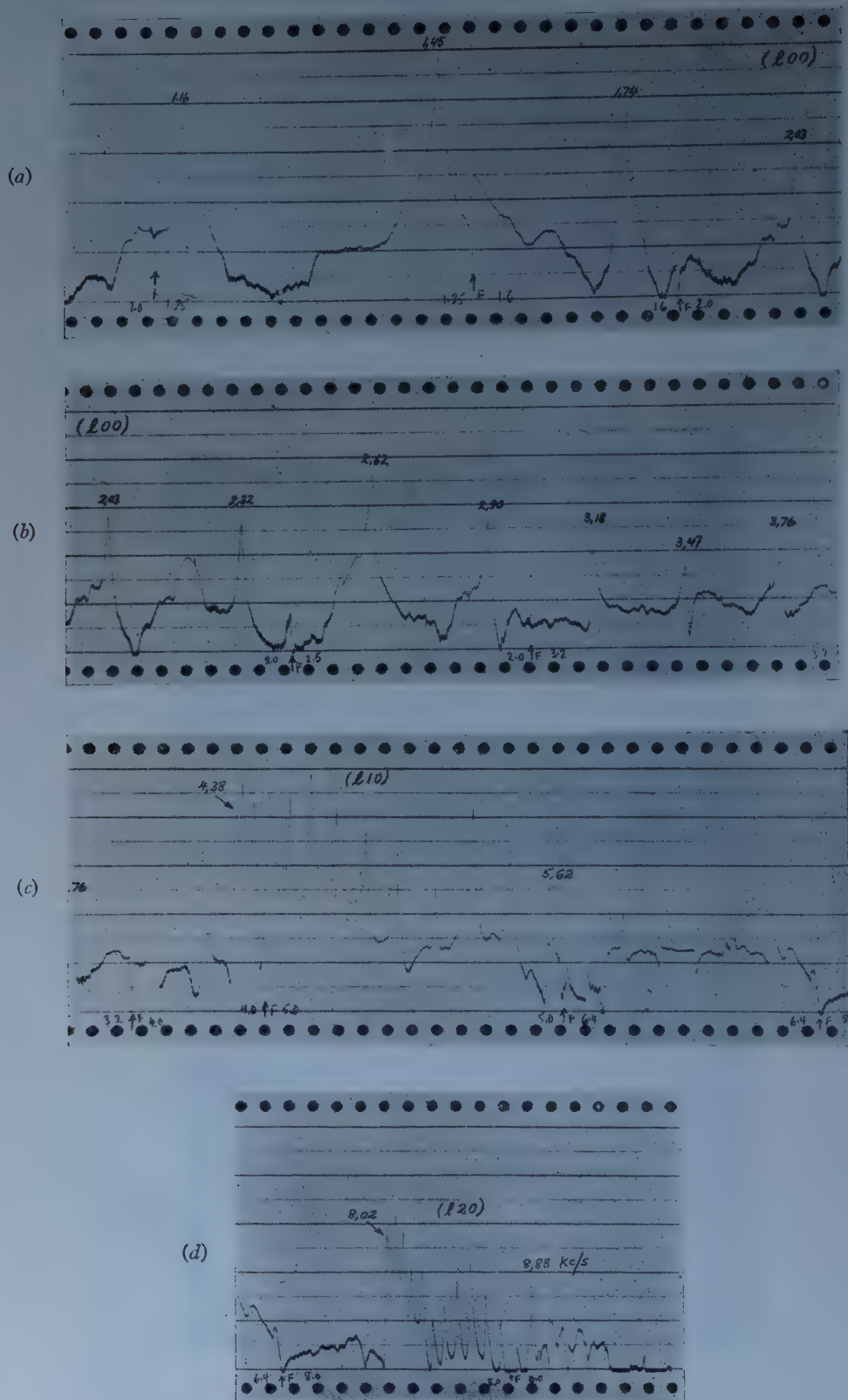


Figure 4. Frequency spectrum of the resonator filled with nitrogen at atmospheric pressure. The figures shown against the peaks represent the frequency in kc/s.



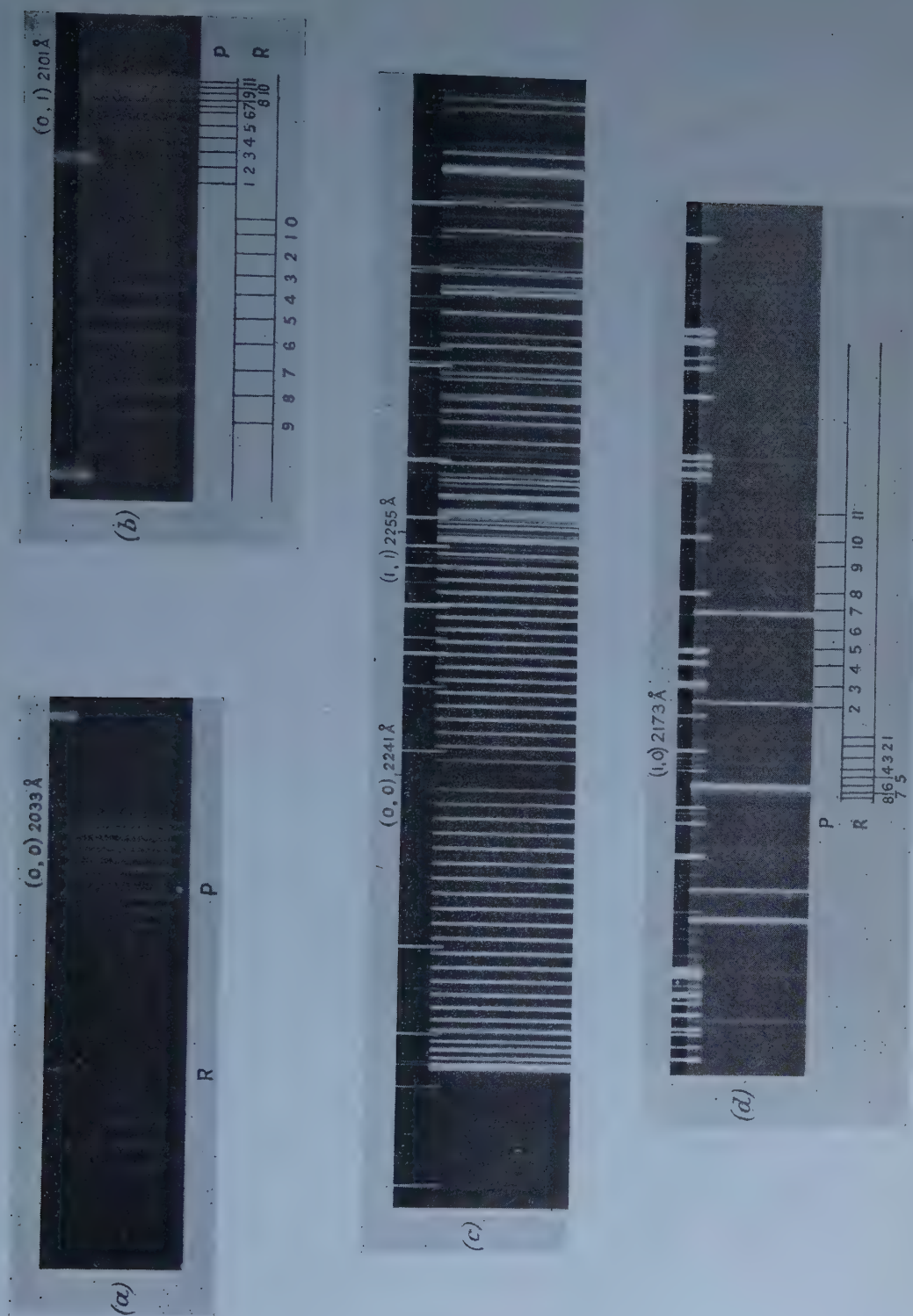


Figure 1. An enlargement from a plate taken on a large quartz spectrograph. (a) (b):  $D^1\Sigma \rightarrow A^1\Sigma$  system, (a) (0, 0) 2033 Å, (b) (0, 1) (2101) Å; (c) (d):  $C^1\Sigma \rightarrow A^1\Sigma$  system, (c) (0, 0) 2241 Å, (1, 1) 2255 Å, (d) (1, 0) 2173 Å.



# Construction of $S^2$ Eigenfunctions by the Method of Spin Operators I: General Theory

BY F. BERENCZ AND R. PAUNCZ†

Department of Theoretical Physics, University of Szeged, Szeged, Hungary

*Communicated by C. A. Coulson; MS. received 14th October 1957*

**Abstract.** A general spin operator, a function of the so-called step-up and step-down operators, is suggested which when operating on the eigenfunctions of the total  $S_z$  operator related to maximal, minimal and zero projections of the total spin creates each eigenfunction of the total  $S^2$  corresponding to its different eigenvalues.

## § 1. INTRODUCTION

ONLY for certain rather special forms of the potential function is the wave equation completely soluble in closed terms; in general, and especially in the field of quantum chemistry, different approximate methods must be applied. The central problem of both well-known approximate methods of quantum chemistry usually denoted as the molecular-orbital and valence-bond approximation, as well as that of the general methods of configuration interaction in the first step to the determination of a suitable zero-order eigenfunction, can be reduced. As is well known, the linear combination of Slater determinants (which will be denoted in the following by  $\phi$ ) containing also an implicit correlational interaction of electronic motion, can be regarded as the best zero-order eigenfunction. Then, the energy, to first order, is given by the roots of the usual secular equation. For the  $n$ -electron problem however, the order of this equation is  $2^n$ , so that the problem will be tractable only if the secular determinant can be broken down into a product of determinants of lower order.

In the atomic problem this can be done by means of the operators  $M^2$ ,  $M_z$ ,  $S^2$ ,  $S_z$ , all of which commute with the Hamiltonian. Owing to the lack of spherical symmetry of most molecular systems, the operators of the orbital momentum, i.e.  $M^2$  and  $M_z$ , will no longer commute with the Hamiltonian, and so they lose their usefulness. Therefore, to the approximation in which spin interactions are neglected, the operators of spin momentum, i.e.  $S^2$  and  $S_z$ , must be considered; these commute with the Hamiltonian and may be used to reduce the order of the secular determinant.

Each term of the Slater determinant  $\phi$  is already, in the case of an  $n$ -electron system, a product of orbital eigenfunctions  $a(1)b(2)\dots n(n)$ , as well as of spin functions of the type  $\alpha(1)\beta(2)\dots\alpha(n)$ . Since each column may contain either  $\alpha$  or  $\beta$  (where by  $\alpha$  the spin eigenfunction corresponding to  $s=\frac{1}{2}$ , and by  $\beta$  the spin eigenfunction corresponding to  $s=-\frac{1}{2}$  are denoted) the degree of degeneracy of the corresponding energy level is  $2^n$ .

Let us denote the number of columns of  $\alpha$ 's by  $n_\alpha$ , and that of  $\beta$ 's by  $n_\beta$ , respectively, then the eigenvalue of any  $\phi$  for  $S_z$  is found from the relation

$$S_z\phi = (n_\alpha - n_\beta)\frac{1}{2}\hbar\phi. \quad \dots\dots(1.1)$$

† Present address, Institute of Organic Chemistry, Technion, Haifa.

Further simplification is, however, possible if the  $\phi$ 's are combined into linear combinations which are eigenfunctions of  $S^2$  as well as of  $S_z$ . Therefore, it is already an almost classical problem of quantum chemistry to construct these linear combinations of eigenfunctions based on the knowledge of the eigenfunctions of  $S_z$ , and for such a construction very different heuristical methods are reviewed in all text books of quantum chemistry too.

Some years ago Pratt (1953) proposed a method of spin operators for setting up all the orthogonal singlets of the  $S^2$  operator. He has analysed the five orthogonal singlets corresponding to a six-electron system in detail and from this analysis he derives a spin operator  $O$  which is a function of step-up and step-down operators. This operator  $O$  when operating on a single Slater determinant creates an eigenfunction of  $S^2$ .

In this paper a spin operator is suggested which when operating on the eigenfunctions of the total  $S_z$  operator related to maximal, minimal and zero projection of the total spin creates each eigenfunction of the total  $S^2$  corresponding to its different eigenvalues.

## § 2. RELATIONS BETWEEN THE EIGENFUNCTIONS OF $S_z$

Let us take an  $n$ -electron system with total spin  $s$ , the state of which is described by the eigenfunction  $\psi(s, m_s)$ . This state is, however, degenerate and the eigenfunctions  $\psi(s, m_s)$  corresponding to different projections of spin are given in  $\hbar$  units by

$$m_s = s, s-1, \dots, s-i, \dots, -s+i, \dots, -s+1, -s.$$

The corresponding eigenfunctions

$$\psi(s, s), \psi(s, s-1), \dots, \psi(s, s-i), \dots, \psi(s, -s+i), \dots, \psi(s, -s+1), \psi(s, -s)$$

will be denoted as the maximal,  $i$ th and minimal components.

Usually the operators

$$S^+ = S_x + iS_y; \quad S_x = \sum S_{xk}, \quad S_y = \sum S_{yk}, \quad \dots \quad (2.1)$$

and

$$S^- = S_x - iS_y \quad \dots \quad (2.2)$$

are called the step-up and step-down operators, respectively, and as is well known these operators operating on the  $i$ th component transform it into the  $(i+1)$ th component and into the  $(i-1)$ th component, respectively:

$$S^+ \psi(s, \mu) = [(s-\mu)(s+\mu+1)]^{1/2} \psi(s, \mu+1) \quad \dots \quad (2.3)$$

$$S^- \psi(s, \mu) = [(s+\mu)(s-\mu+1)]^{1/2} \psi(s, \mu-1). \quad \dots \quad (2.4)$$

Owing to these relations it is obvious that the  $i$ th component can be derived from the maximal and minimal ones by iteration, i.e.

$$\psi(s, s-i) = \frac{1}{i!} \binom{2s}{i}^{-1/2} (S^-)^i \psi(s, s) \quad \dots \quad (2.5)$$

$$\psi(s, -s+i) = \frac{1}{i!} \binom{2s}{i}^{-1/2} (S^+)^i \psi(s, -s). \quad \dots \quad (2.6)$$

If the system contains  $n$  electrons,  $n$  being an even number, then the  $S_z$  operator has also the eigenvalue zero and it is obvious that the  $k$ th component can be derived by means of the above iteration from the zero component too, i.e.

$$\psi(s, k) = \left[ \frac{(s-k)!}{(s+k)!} \right]^{1/2} (S^+)^k \psi(s, 0) \quad \dots \quad (2.7)$$

$$\psi(s, -k) = \left[ \frac{(s-k)!}{(s+k)!} \right]^{1/2} (S^-)^k \psi(s, 0). \quad \dots \quad (2.8)$$



## § 3. SPIN SUMMATION

Let  $\psi_A(s, m_s)$  and  $\psi_B(s, m_s)$  be the eigenfunctions of the  $S_z$  operator, i.e.:

$$\begin{aligned} S_z \psi_A(s, m_s) &= m_s \psi_A(s, m_s) \\ S_z \psi_B(s', m_{s'}) &= m_{s'} \psi_B(s', m_{s'}), \end{aligned} \quad \dots\dots(3.1)$$

then it is known (according to the results of van der Waerden (1932)) that the eigenfunction corresponding to the resulting spin  $S = s + s' - \lambda$ , and to the resulting projection of the spin  $M_s = m_s + m_{s'} = s + s' - \lambda$  is given by

$$\psi(S, M_s) = \binom{2s+2s'-\lambda+1}{\lambda}^{-1/2} \sum_{i=0}^{\lambda} \left[ \binom{2s-i}{\lambda-i} \binom{2s'+i-\lambda}{i} \right]^{1/2} \times \psi_A(s, s-i) \psi_B(s', s'+i-\lambda) \quad \dots\dots(3.2)$$

*Theorem.* The eigenfunction (3.2) is an eigenfunction of  $S^2$  corresponding to the eigenvalue  $(s+s'-\lambda)(s+s'-\lambda+1)$ .

*Proof.* Owing to the relation

$$S^2 = S^+ S^- - S_z + S_z^2$$

having now the explicit form

$$S^2 = (S_A^+ + S_B^+)(S_A^- + S_B^-) - (S_{Az} + S_{Bz}) + (S_{Az}^2 + S_{Bz}^2)$$

and taking into account the relations (2.3) and (2.4)

$$\begin{aligned} S^2 \psi(S, M_s) &= \binom{2s+2s'-\lambda+1}{\lambda} \sum_{i=0}^{\lambda} \left\{ (-1)^i \left[ \binom{2s-i}{\lambda-i} \binom{2s'+i-\lambda}{i} \right]^{1/2} \right. \\ &\quad \times [(2s-i)(i+1) + (2s'+i-\lambda)(\lambda-i+1)] \\ &\quad + (-1)^{i+1} \left[ \binom{2s-i-1}{\lambda-i-1} \binom{2s'+i-\lambda+1}{i+1} \right]^{1/2} \\ &\quad \times [(i+1)(2s-i)(2s'+i-\lambda+1)(\lambda-1)]^{1/2} \\ &\quad + (-1)^{i-1} \left[ \binom{2s-i+1}{\lambda-i+1} \binom{2s'+i-\lambda-1}{i-1} \right]^{1/2} \\ &\quad \times [(2s-i+1)i(\lambda-i+1)(2s'+i-\lambda)]^{1/2} \\ &\quad \left. - (-1)^i \left[ \binom{2s-i}{\lambda-i} \binom{2s'+i-\lambda}{i} \right]^{1/2} [s+s'-\lambda - (s+s'-\lambda)^2] \right\} \\ &\quad \times \psi_A(s, s-i) \psi_B(s', s'+i-\lambda) \\ &= \binom{2s+2s'-\lambda+1}{\lambda}^{-1/2} \sum_{i=0}^{\lambda} (-1)^i \left[ \binom{2s-i}{\lambda-i} \binom{2s'+i-\lambda}{i} \right]^{1/2} \\ &\quad \times [(2s-i)(i+1) + (2s'+i-\lambda)(\lambda-i+1) - (\lambda-i)(2s'+i-\lambda+1) \\ &\quad - i(2s-i+1) - (s+s'-\lambda) + (s+s'-\lambda)^2] \psi_A(s, s-i) \psi_B(s', s'+i-\lambda). \end{aligned}$$

We can obtain finally

$$S^2 \psi(S, M_s) = (s+s'-\lambda)(s+s'-\lambda+1) \psi(S, M_s). \quad \dots\dots(3.3)$$

In this manner it is proved that  $\psi(S, M_s)$  is really an eigenfunction of  $S^2$  corresponding to the eigenvalue  $(s+s'-\lambda)(s+s'-\lambda+1)$ .

This means, however, that the linear combination of the  $S_z$  eigenfunctions (3.2) is just the expected eigenfunctions of the operators  $S^2$ . Furthermore, owing to van der Waerden's (1932) formula of spin summation, equation (3.2) has an immediate physical meaning. If one combines two systems having the spins  $s$  and  $s'$ , respectively, a system with the resulting spin  $s + s' - \lambda$  is obtained, where  $\lambda$  runs from 0 to  $2s'$  and from 0 to  $2s$ , respectively, according to  $s > s'$  or  $s' > s$ .

The formula (3.2) has two interesting special cases, namely  $\lambda=0$  and  $\lambda=2s'$ , respectively.

If  $\lambda=0$ , then  $S=s+s'$  and

$$\psi(S=s+s', M_s=s+s') = \psi_A(s, s) \psi_B(s', s') \quad \dots\dots (3.4)$$

is obtained, i.e. if one combines the two systems with spin  $s$  and  $s'$ , respectively, then the resulting system has the spin  $s+s'$ .

In the case  $\lambda=2s'$  the resulting spin is  $S=s-s'$  with the eigenfunction

$$\psi(S=s-s', M_s=s-s') = \left( \frac{2s+1}{2s'} \right)^{-1/2} \sum_{i=0}^{2s'} (-1)^i \binom{2s-i}{2s'-i}^{1/2} \psi_A(s, s-i) \psi_B(s', -s'+i), \quad \dots\dots (3.5)$$

i.e. the spin of the resulting system is the difference of the two original ones.

#### § 4. THE OPERATORS OF SPIN SUMMATION

In this paragraph the formulae of spin summations discussed above will be put in their operator form. Owing to (2.5) and (2.6), this can be realized quite easily, only the components  $\psi_A(s, s-i)$  and  $\psi_B(s', s'-(\lambda-i))$  of equation (3.2) must be substituted by the eigenfunctions derived from the maximal component by the step-down operators. Based on (2.5) the equation (3.2) can be written in the form

$$\begin{aligned} \psi(S=s+s'-\lambda, M_s=s+s'-\lambda) &= \left( \frac{2s+2s'-\lambda+1}{\lambda} \right)^{-1/2} \sum_{i=0}^{\lambda} (-1)^i \left[ \binom{2s-i}{\lambda-i} \binom{2s'+i-\lambda}{i} \right]^{1/2} \\ &\times \frac{1}{i!} \binom{2s}{i}^{-1/2} \frac{1}{(\lambda-i)!} \binom{2s'}{\lambda-i} (S_A^-)^i (S_B^-)^{\lambda-i} \psi_A(s, s) \psi_B(s', s') \\ &= \left( \frac{2s+2s'-\lambda+1}{\lambda} \right)^{-1/2} [(2s)!(2s')!(2s-\lambda)!(2s'-\lambda)!]^{-1/2} \\ &\times \sum_{i=0}^{\lambda} (-1)^i \frac{(2s-i)!(2s'+i-\lambda)!}{i!(\lambda-i)!} (S_A^-)^i (S_B^-)^{\lambda-i} \psi_A(s, s) \psi_B(s', s'). \end{aligned}$$

Now, let the operator

$$\begin{aligned} O(S=s+s'-\lambda, M_s=s+s'-\lambda) &= \left( \frac{2s+2s'-\lambda+1}{\lambda} \right)^{-1/2} [(2s)!(2s')!(2s-\lambda)!(2s'-\lambda)!]^{-1/2} \\ &\times \sum_{i=0}^{\lambda} (-1)^i \frac{(2s-i)!(2s'+i-\lambda)!}{i!(\lambda-i)!} (S_A^-)^i (S_B^-)^{\lambda-i} \quad \dots\dots (4.2) \end{aligned}$$

be introduced; then, when (4.2) operating on the product eigenfunction  $\psi_A(s, s) \psi_B(s', s')$  which corresponds to the maximal eigenvalue of the operator  $S_z$ , the eigenfunction of the operator  $S^2$  is obtained.

In the special cases of  $\lambda=0$  and  $\lambda=2s'$  the equation (4.2) reduces obviously into

$$O(S=s+s', M_s=s+s') = 1 \quad \dots\dots (4.3)$$

and

$$O(S=s-s', M_s=s-s') = \left( \frac{2s-2s'+1}{2s+1} \right)^{1/2} \sum_{i=0}^{2s'} (-1)^i \frac{(2s-i)!}{(2s)!(2s'-i)!} (S_A^-)^i (S_B^-)^{2s'-i} \quad \dots\dots (4.4)$$

respectively.

Owing to (2.5) and (2.6) an alternative form of (4.4) can be obtained, namely

$$\begin{aligned}\psi(S=s-s', M_s=s-s') &= \left( \frac{2s+1}{2s'} \right)^{-1/2} \sum_{i=0}^{2s'} (-1)^i \binom{2s-i}{2s'-i}^{1/2} \frac{1}{i!} \binom{2s}{i}^{-1/2} (S_A^-)^i \psi(s, s) \\ &\quad \times \frac{1}{i!} \binom{2s'}{i}^{-1/2} (S_B^+)^i \psi(s', -s') \\ &= \left( \frac{2s-2s'+1}{2s+1} \right)^{1/2} \sum_{i=0}^{2s'} (-1)^i \frac{(2s-i)!}{(2s)! i!} (S_A^- S_B^+)^i \psi_A(s, s) \psi_B(s', -s'),\end{aligned}$$

or rather

$$O(S=s-s', M_s=s-s') = \left( \frac{2s-2s'+1}{2s+1} \right)^{1/2} \sum_{i=0}^{2s'} (-1)^i \frac{(2s-i)!}{(2s)! i!} (S_A^- S_B^+)^i. \quad \dots\dots(4.5)$$

Taking the equations (4.2)–(4.5) into account such eigenfunctions of  $S^2$  can be obtained which correspond to the maximal eigenvalue of  $S_z$ . However, considering the equation (2.5) the eigenfunctions related to other eigenfunctions of  $S_z$  can also be derived.

In the case when the eigenfunctions  $\psi_A(s, m_s)$  and  $\psi_B(s', m_{s'})$  correspond to a system containing even numbers of electrons, the spin operator  $O$  can be put in a form which derives the eigenfunctions of  $S^2$  from the eigenfunctions of  $S_z$  related to the eigenvalue zero. Then, one may start from the well known rules of spin summation and spin subtraction as follows

$$\begin{aligned}\psi(S=s+s', M_s=s+s'-i) &= \left[ \frac{(2s)!(2s')!}{(2s+2s')!} \right]^{1/2} \sum_{m_s=-s'}^{s'} \left[ \frac{(S+M_s)!(S-M_s)!}{(s+m_s)!(s-m_s)!(s'+m_{s'})!(s'-m_{s'})!} \right]^{1/2} \\ &\quad \times \psi_A(s, m_s = M_s - m_{s'}) \psi_B(s', m_{s'}) \quad \dots\dots(4.6)\end{aligned}$$

$$\begin{aligned}\psi(S=s-s', M_s=s-s'-i) &= \left[ \frac{(2s-2s'+1)!(2s')!}{(2s+1)!} \right]^{1/2} \sum_{m_{s'}=-s'}^{s'} (-1)^{s'+m_{s'}} \\ &\quad \left[ \frac{(s+m_s)!(s-m_s)!}{(S+M_s)!(S-M_s)!(s'+m_{s'})!(s'-m_{s'})!} \right]^{1/2} \times \psi_A(s, m_s = M_s - m_{s'}) \psi_B(s', m_{s'}) \\ &\quad \dots\dots(4.7)\end{aligned}$$

This means that the eigenfunction of the system derived by the unification of the two systems A and B corresponding to the zero eigenvalue of the operator  $S_z$ , owing to  $M_s = m_s + m_{s'} = 0 \rightarrow m_s = -m_{s'}$ , as follows

$$\begin{aligned}\psi(S=s+s', M_s=0) &= \left[ \frac{(2s)!(2s')!}{(2s+2s')!} \right]^{1/2} \sum_{m_{s'}=-s'}^{s'} (s+s')! [(s-m_{s'})!(s+m_{s'})!(s'+m_{s'})!(s'-m_{s'})!]^{-1/2} \\ &\quad \times \psi_A(s, -m_{s'}) \psi_B(s', m_{s'}), \quad \dots\dots(4.8)\end{aligned}$$

or

$$\begin{aligned}\psi(S=s-s', M_s=0) &= \left[ \frac{(2s-2s'+1)!(2s')!}{(2s+1)!} \right]^{1/2} \sum_{m_{s'}=-s'}^{s'} (-1)^{s'+m_{s'}} \frac{1}{(s-s')!} \left[ \frac{(s-m_{s'})!(s+m_{s'})!}{(s'-m_{s'})!(s'+m_{s'})!} \right]^{1/2} \\ &\quad \times \psi_A(s, -m_{s'}) \psi_B(s', m_{s'}). \quad \dots\dots(4.9)\end{aligned}$$

Finally, taking the equations (2.7) and (2.8) into account, these equations can be transformed in terms of the spin operators into the form

$$\begin{aligned} \psi(S=s+s', M_s=0) \\ = \left[ \frac{(2s)!(2s')!}{(2s+2s')!} \right]^{1/2} \sum_{m_{s'}=-s'}^{s'} \frac{(s-s')!}{(s+m_{s'})!(s'+m_{s'})!} (S_A - S_B^+)^{m_{s'}} \psi_A(s, 0) \psi_B(s', 0), \end{aligned} \quad \dots\dots(4.10)$$

and

$$\begin{aligned} \psi(S=s-s', M_s=0) \\ = \left[ \frac{(2s-2s'+1)!(2s')!}{(2s+1)!} \right]^{1/2} \sum_{m_{s'}=-s'}^{s'} (-1)^{s'+m_{s'}} \frac{(s-m_{s'})!}{(s-s')!(s'+m_{s'})!} (S_A - S_B^+)^{m_{s'}} \\ \times \psi_A(s, 0) \psi_B(s', 0), \end{aligned} \quad \dots\dots(4.11)$$

or rather

$$\begin{aligned} O(S=s+s', M_s=0) \\ = \left[ \frac{(2s)!(2s')!}{(2s+2s')!} \right]^{1/2} \sum_{m_{s'}=-s'}^{s'} \frac{(s+s')!}{(s+m_{s'})!(s'+m_{s'})!} (S_A - S_B^+)^{m_{s'}}, \end{aligned} \quad \dots\dots(4.12)$$

and

$$\begin{aligned} O(S=s-s', M_s=0) \\ = \left[ \frac{(2s-2s'+1)!(2s')!}{(2s+1)!} \right]^{1/2} \sum_{m_{s'}=-s'}^{s'} (-1)^{s'+m_{s'}} \frac{(s-m_{s'})!}{(s-s')!(s'+m_{s'})!} (S_A - S_B^+)^{m_{s'}} \end{aligned} \quad \dots\dots(4.13)$$

respectively.

#### REFERENCES

- PRATT, G. W., 1953, *Phys. Rev.*, **92**, 278.  
 VAN DER WAERDEN, B. L., 1932, *Die Gruppentheoretische Methode in der Quantummechanik* (Berlin: Springer).

#### APPENDIX

In this appendix some theorems will be justified which have been used in §2.

*Theorem.*  $\psi(s, s-i) = \frac{1}{i!} \binom{2s}{i}^{-1/2} (S^-)^i \psi(s, s). \quad \dots\dots(2.5)$

*Proof.* From (2.3)

$$\begin{aligned} S^- \psi(s, s) &= (2s)^{1/2} \psi(s, s-1), \\ \psi(s, s-1) &= \frac{1}{1!} \binom{2s}{1}^{-1/2} S^- \psi(s, s), \\ S^- \psi(s, s-1) &= [(2s-1)2]^{1/2} \psi(s, s-2), \\ \psi(s, s-2) &= \frac{1}{2!} \binom{2s}{2}^{-1/2} (S^-)^2 \psi(s, s). \end{aligned}$$

Therefore, it is obvious that the theorem is valid for  $i=1$  and  $i=2$ . It may be supposed that is also valid for  $i=n-1$ :

$$\psi(s, s-(i-1)) = \frac{1}{(i-1)!} \binom{2s}{i-1}^{-1/2} (S^-)^{i-1} \psi(s, s).$$



Then, operating by  $S^-$  on both sides of this equation

$$S^-\psi(s, s-(i-1)) = [(2s-i+1)i]^{1/2} \psi(s, s-i) = \frac{1}{(i-1)!} \binom{2s}{i-1}^{-1/2} \psi(s, s)$$

$$\psi(s, s-i) = \frac{1}{i!} \binom{2s}{i}^{-1/2} (S^-)^i \psi(s, s)$$

is obtained and in this manner the proof is complete by means of total induction. The proof of equation (2.6) can be carried out similarly.

*Theorem.* 
$$\psi(s, k) = \left[ \frac{(s-k)!}{(s+k)!} \right]^{1/2} (S^+)^k \psi(s, 0). \quad \dots\dots (2.7)$$

*Proof.* From (2.3)

$$S^+\psi(s, 0) = [s(s+1)]^{1/2} \psi(s, 1),$$

$$\psi(s, 1) = \left[ \frac{(s-1)!}{(s+1)!} \right]^{1/2} S^+\psi(s, 0),$$

$$S^+\psi(s, 1) = [(s-1)(s-2)]^{1/2} \psi(s, 2),$$

$$\psi(s, 2) = \left[ \frac{(s-2)!}{(s+2)!} \right]^{1/2} (S^+)^2 \psi(s, 0).$$

The relation (2.7) is also valid for  $k=1$  and for  $k=2$ . Let us suppose that it is also valid for  $k$ , then

$$\psi(s, k) = [(s-k+1) \dots (s+k)]^{-1/2} (S^+)^k \psi(s, 0)$$

is obtained. Operating with  $S^+$  on both sides of this equation

$$S^+\psi(s, k) = [(s-k)(s+k+1)]^{1/2} \psi(s, k+1)$$

$$\psi(s, k+1) = \left[ \frac{(s-k-1)!}{(s+k+1)!} \right]^{1/2} \psi(s, 0)$$

is obtained and in this way the proof is also finished by means of total induction. The proof of equation (2.8) can be obtained quite similarly.

## Construction of $S^2$ Eigenfunctions by the Method of Spin Operators II: Six-electron Systems

By F. BERENCZ

Department of Theoretical Physics, University of Szeged, Hungary

*Communicated by C. A. Coulson; MS. received 14th October 1957*

**Abstract.** In the first part of this paper a spin operator was introduced which when operating on the eigenfunctions of the total  $S_z$  operator related to maximal, minimal and zero projections of total spin creates each eigenfunction of the total  $S^2$  corresponding to its different eigenvalues. In this second part a brief discussion of the proposed operator technique developed for the problem of six-electron system is presented.

### § 1. INTRODUCTION

IN the investigation of molecules by configuration interaction one is usually faced with the problem of setting up the states of definite multiplicity for the various configurations. In the first part of this paper a simple and direct method was suggested to construct the suitable eigenfunctions for an  $n$ -electron system fulfilling the operator equations of both operators  $S^2$  and  $S_z$  simultaneously. In this second part a brief discussion is presented of the proposed operator technique developed for the problem of a six-electron system. The reader is referred to the first part for a more general treatment of these problems.

### § 2. METHOD OF BRANCHING DIAGRAM

For a set of six electrons occupying six distinct orbitals it is possible to form many states of a given multiplicity by associating either  $\alpha$  and  $\beta$  spin (where by  $\alpha$  the spin eigenfunction corresponding to  $\frac{1}{2}$  and  $\beta$  the spin eigenfunction corresponding to  $-\frac{1}{2}$  are denoted) with the collection of orbitals in a variety of ways. It is well known that the number of independent spin states is in fact

$$N(s) = \binom{n}{\frac{1}{2}n-s} - \binom{n}{\frac{1}{2}n-s-1}.$$

This result may be justified easily, e.g. by using the so-called branching diagram, a pictorial description of adding the spin angular momenta of electrons one by one (figure 1, after Corson 1951). This diagram not only shows how many states of a given multiplicity there are for the six electrons (in general  $n$  electrons), but applying the methods of vector addition of angular momentum shows immediately how the states are actually constructed.

Owing to the branching diagram the state with the resulting spin  $s$  of an  $n$ -electron system can be constructed by unification of the spin angular momenta of part systems containing certain numbers of spin  $\alpha$  and  $\beta$ , respectively. Now, taking the equations (4.3) and (4.5) of the first part of this paper† into account for the construction of the eigenfunctions of  $S^2$  a direct method can be given if the states of the part systems are described by Slater determinants. The suggested

† This will be abbreviated by (I, 4.3) and (I, 4.5).

method is nothing else than the abstract formulation of the method of branching diagrams.

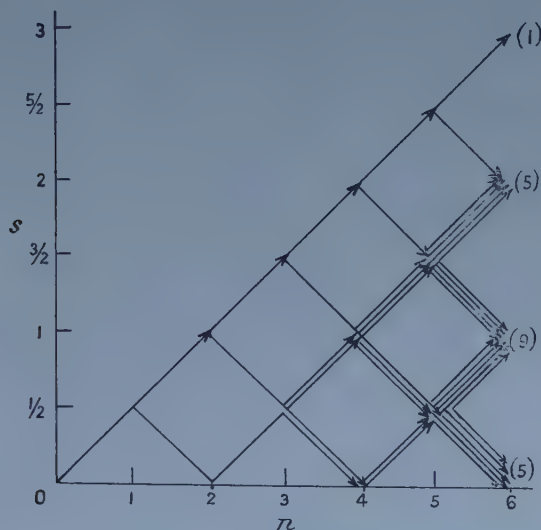


Figure 1.

### § 3. OPERATOR OF SPIN ADDITION

The explicit form of Slater determinants of an  $n$ -electron system characterizing a spatial state, in other words a configuration of the molecule, may be given in the form

$$\phi = \frac{1}{\sqrt{(n!)}} \begin{vmatrix} (a\alpha)_1 & (b\alpha)_1 & (c\beta)_1 & \dots & (n\alpha)_1 \\ (a\alpha)_2 & (b\alpha)_2 & (c\beta)_2 & \dots & (n\alpha)_2 \\ \vdots & \vdots & \vdots & \ddots & \vdots \\ (a\alpha)_n & (b\alpha)_n & (c\beta)_n & \dots & (n\alpha)_n \end{vmatrix}$$

or rather abbreviated by

$$\phi(s, m_s) = |\alpha\alpha\beta\dots\alpha|. \quad \dots\dots(3.1)$$

In the first step let us take  $x$  electrons with parallel spin  $\alpha$ . By uniting these electrons to a system A with the resulting spin  $s = x/2$  the state of the system is described by the so-called maximal component

$$\phi_A(s = x/2, m_s = x/2) = |\alpha^1\alpha^2\dots\alpha^x|. \quad \dots\dots(3.2)$$

In the second step let us consider  $y$  electrons with parallel spin  $\beta$ . By uniting them a system B is obtained with the minimal component

$$\phi_B(s' = y/2, m_{s'} = -y/2) = |\beta^1\beta^2\dots\beta^y|. \quad \dots\dots(3.3)$$

In the third step both systems A and B may be united to a system AB with the resulting spin  $s - s' = x/2 - y/2$ . The maximal component of the united system is given by

$$\phi_{AB} = \left( \frac{x-y+1}{x+1} \right)^{1/2} \sum_{i=0}^y (-1)^i \frac{(x-i)!}{x! i!} (S_A - S_B)^i |\alpha^1\alpha^2\dots\alpha^x\beta^1\beta^2\dots\beta^y|, \quad \dots\dots(3.4)$$

hence it is obvious that also in the case of systems of a certain number of electrons the formulae

$$\phi(s, s-i) = \frac{1}{i!} \binom{n}{i}^{-1/2} (S^-)^i |\alpha^1 \alpha^2 \dots \alpha^n|, \quad \dots (3.5)$$

and

$$\phi(s', -s'+i) = \frac{1}{i!} \binom{n}{i}^{-1/2} (S^+)^i |\beta^1 \beta^2 \dots \beta^n| \quad \dots (3.6)$$

introduced in the first part, can be used (for further particulars see the Appendix). This means, however, that the spin operator, by which the eigenfunctions of the operator  $S^2$  can be obtained, has the form

$$O_{AB} = \left( \frac{x-y+1}{x+1} \right)^{1/2} \sum_{i=0}^y (-1)^i \frac{(x-i)!}{x! i!} (S_A^- S_B^+)^i. \quad \dots (3.7)$$

By adding to the system AB a further system C containing  $z$  electrons with the resulting spin  $z/2$  a system ABC with the resulting spin  $(x-y+z)/2$  is obtained having the maximal component

$$\phi_{ABC} = O_{AB} |\alpha^1 \alpha^2 \dots \alpha^x \beta^1 \beta^2 \dots \beta^y \alpha^1 \alpha^2 \dots \alpha^z|. \quad \dots (3.8)$$

In this manner if one adds to the system ABC in order of succession further systems D, E, F, etc. containing  $u$  electrons with spin  $\beta$ ,  $v$  electrons with spin  $\alpha$  and  $w$  electrons with spin  $\beta$ , respectively, a united system ABCDEF will be constructed with the resulting spin  $(x-y+z-u+v-w)/2$  having the maximal component

$$\begin{aligned} \phi_{ABCDEF} = & \left( \frac{x-y+z-u+v-w+1}{x-y+z-u+v+1} \right)^{1/2} \left( \frac{x-y+z-u+1}{x-y+z+1} \right)^{1/2} \left( \frac{x-y+1}{x+1} \right)^{1/2} \\ & \times \sum_{k=0}^w (-1)^k \frac{(x-y+z-u+v-k)!}{(x-y+z-u+v)! k!} (S_{ABCDE}^- S_F^-)^k \\ & \times \sum_{j=0}^u (-1)^j \frac{(x-y+z-j)!}{(x-y+z)! j!} (S_{ABC}^- S_D^+)^j \\ & \times \sum_{i=0}^y (-1)^i \frac{(x-i)!}{x! i!} (S_A^- S_B^+)^i |\alpha^1 \alpha^2 \dots \alpha^x \beta^1 \beta^2 \dots \beta^y \alpha^1 \alpha^2 \dots \alpha^z \beta^1 \beta^2 \dots \\ & \dots \beta^u \alpha^1 \alpha^2 \dots \alpha^v \beta^1 \beta^2 \dots \beta^w|. \quad \dots (3.9) \end{aligned}$$

This means, however, that in this case the spin operator has the form

$$\begin{aligned} O_{ABCDEF} = & \left( \frac{x-y+z-u+v-w+1}{x-y+z-u+v+1} \right)^{1/2} \left( \frac{x-y+z-u+1}{x-y+z+1} \right)^{1/2} \left( \frac{x-y+1}{x+1} \right)^{1/2} \\ & \times \sum_{k=0}^w (-1)^k \frac{(x-y+z-u+v-k)!}{(x-y+z-u+v)! k!} (S_{ABCDE}^- S_F^+)^k \\ & \times \sum_{j=0}^u (-1)^j \frac{(x-y+z-j)!}{(x-y+z)! j!} S_{ABC}^- S_D^+ \sum_{i=0}^y (-1)^i \frac{(x-i)!}{x! i!} (S_A^- S_B^+)^i. \quad \dots (3.10) \end{aligned}$$

In general this method of construction must be continued until all electrons are taken into account.

#### § 4. MULTIPLETS OF THE SIX-ELECTRON SYSTEM

In the case of a six-electron system the degree of degeneration, i.e. the number of Slater determinants, is  $2^6 = 64$ . In terms of the theory of Hilbert space this means that the linear independent eigenfunctions of the system corresponding



to a given state of energy span a 64-dimensional Hilbert space. This space is, however, reducible, i.e. can be obtained as a direct product of subspaces. Owing to the branching diagram of the system it is obvious that this direct product contains  $5 \times 1$ -dimensional,  $9 \times 3$ -dimensional  $5 \times 5$ -dimensional and  $1 \times 7$ -dimensional subspaces being invariant against the operator  $S^2$  which corresponds to 5 singlet, 9 triplet, 5 quintet and 1 septet spin states.

In this paragraph the eigenfunctions will be presented as they correspond to the different multiplets.

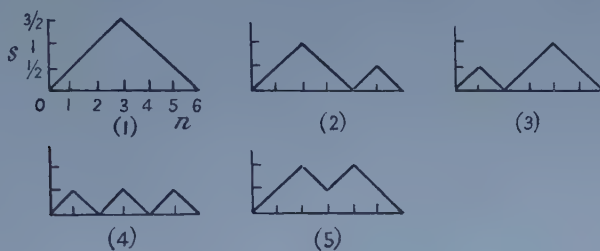


Figure 2.

(a) The singlet spin state of the six-electron system can be constructed in terms of the branching diagram in five ways (figure 2). Owing to the branching

Table 1

Singlets	$x \alpha$	$y \beta$	$z \alpha$	$u \beta$	$v \alpha$	$w \beta$
1	3	3	—	—	—	—
2	2	2	1	1	—	—
3	1	1	2	2	—	—
4	1	1	1	1	1	1
5	2	1	1	2	—	—

diagram the system can be decomposed to part systems as is presented by table 1 in terms of the previous paragraph. The relating eigenfunctions are as follows:

$$\begin{aligned}
 \phi_1 &= \frac{1}{2}[1 - \frac{1}{3}(S_A^- S_B^+) + \frac{1}{12}(S_A^- S_B^+)^2 - \frac{1}{36}(S_A^- S_B^+)^3]|\alpha\alpha\alpha\beta\beta\beta| \\
 &= \frac{1}{6}[3|\alpha\alpha\alpha\beta\beta\beta| - (|\beta\alpha\alpha\alpha\beta\beta| + |\alpha\beta\alpha\alpha\beta\beta| + |\alpha\alpha\beta\alpha\beta\beta| + |\beta\alpha\alpha\beta\alpha\beta| \\
 &\quad + |\alpha\beta\alpha\beta\alpha\beta| + |\alpha\alpha\beta\beta\alpha\beta| + |\beta\alpha\alpha\beta\beta\alpha| + |\alpha\beta\alpha\beta\beta\alpha| + |\alpha\alpha\beta\beta\beta\alpha|) \\
 &\quad + |\alpha\beta\beta\beta\alpha\alpha| + |\beta\alpha\beta\beta\alpha\alpha| + |\beta\beta\alpha\beta\alpha\alpha| + |\alpha\beta\beta\beta\alpha\alpha| + |\beta\alpha\beta\beta\alpha\alpha| \\
 &\quad + |\beta\beta\alpha\beta\alpha\alpha| + |\alpha\beta\beta\alpha\alpha\beta| + |\beta\alpha\beta\alpha\alpha\beta| + |\beta\beta\alpha\alpha\alpha\beta| - 3|\beta\beta\beta\alpha\alpha\alpha|]. \\
 \phi_2 &= \frac{1}{\sqrt{6}}[1 - (S_{AB}^- S_D^+)] [1 - \frac{1}{2}(S_A^- S_B^+) + \frac{1}{4}(S_A^- S_B^+)^2]|\alpha\alpha\beta\beta\alpha\beta| \\
 &= \frac{1}{2\sqrt{6}}[2(|\alpha\alpha\beta\beta\alpha\beta| + |\beta\beta\alpha\alpha\alpha\beta|) - (|\beta\alpha\alpha\beta\alpha\beta| + |\alpha\beta\alpha\beta\alpha\beta| + |\beta\alpha\beta\alpha\alpha\beta| \\
 &\quad + |\alpha\beta\beta\alpha\alpha\beta| + |\alpha\beta\beta\alpha\beta\alpha| + |\beta\alpha\beta\alpha\beta\alpha| + |\alpha\beta\alpha\beta\beta\alpha| + |\beta\alpha\alpha\beta\beta\alpha| \\
 &\quad - 2(|\beta\beta\alpha\alpha\beta\alpha| + |\alpha\alpha\beta\beta\beta\alpha|)].
 \end{aligned}$$

$$\begin{aligned}
\phi_3 &= \frac{1}{\sqrt{6}} [1 - \frac{1}{2}(S_{ABC}^- S_D^+) + \frac{1}{4}(S_{ABC}^- S_D^+)^2] [1 - (S_A^- S_B^+)] |\alpha\beta\alpha\alpha\beta\beta| \\
&= \frac{1}{2\sqrt{6}} [2(|\alpha\beta\alpha\alpha\beta\beta| + |\alpha\beta\beta\beta\alpha\alpha|) - (|\alpha\beta\beta\alpha\alpha\beta| + |\alpha\beta\alpha\beta\alpha\beta| + |\alpha\beta\beta\alpha\beta\alpha| \\
&\quad + |\alpha\beta\alpha\beta\beta\alpha|) + |\beta\alpha\alpha\beta\beta\alpha| + |\beta\alpha\beta\alpha\beta\alpha| + |\beta\alpha\alpha\beta\alpha\beta| + |\beta\alpha\alpha\beta\alpha\beta| \\
&\quad - 2(|\beta\alpha\beta\beta\alpha\alpha| + |\beta\alpha\alpha\alpha\beta\beta|)]. \\
\phi_4 &= \frac{1}{\sqrt{8}} [1 - (S_{ABCDE}^- S_F^+)] [1 - (S_{ABC}^- S_D^+)] [1 - (S_A^- S_B^+)] |\alpha\beta\alpha\beta\alpha\beta| \\
&= \frac{1}{\sqrt{8}} [|\alpha\beta\alpha\beta\alpha\beta| + |\beta\alpha\beta\alpha\alpha\beta| + |\beta\alpha\alpha\beta\beta\alpha| + |\alpha\beta\beta\alpha\beta\alpha| \\
&\quad - (|\beta\alpha\beta\alpha\beta\alpha| + |\alpha\beta\alpha\beta\beta\alpha| + |\alpha\beta\beta\alpha\alpha\beta| + |\beta\alpha\alpha\beta\alpha\beta|)]. \\
\phi_5 &= \frac{\sqrt{2}}{3} [1 - \frac{1}{2}(S_{ABC}^- S_D^+) + \frac{1}{4}(S_{ABC}^- S_D^+)^2] [1 - \frac{1}{2}(S_A^- S_B^+)] |\alpha\alpha\beta\alpha\beta\beta| \\
&= \frac{1}{6\sqrt{2}} [4|\alpha\alpha\beta\alpha\beta\beta| - 2(|\beta\alpha\alpha\alpha\beta\beta| + |\alpha\beta\alpha\alpha\beta\beta| + |\alpha\alpha\beta\beta\alpha\beta| + |\alpha\alpha\beta\beta\beta\alpha|) \\
&\quad - (|\beta\alpha\beta\alpha\alpha\beta| + |\alpha\beta\beta\alpha\alpha\beta| + |\beta\alpha\beta\alpha\beta\alpha| + |\alpha\beta\beta\alpha\beta\alpha|) + |\alpha\beta\alpha\beta\beta\alpha| \\
&\quad + |\beta\alpha\alpha\beta\beta\alpha| + |\alpha\beta\alpha\beta\alpha\beta| + |\beta\alpha\alpha\beta\alpha\beta| + 2(|\alpha\beta\beta\beta\alpha\alpha| \\
&\quad + |\beta\alpha\beta\beta\alpha\alpha| + |\beta\beta\alpha\alpha\alpha\beta|) - 4|\beta\beta\alpha\beta\alpha\alpha|].
\end{aligned}$$

These results are in agreement with the results of Pratt (1953).

(b) The triplet spin state can be constructed in terms of the branching diagram

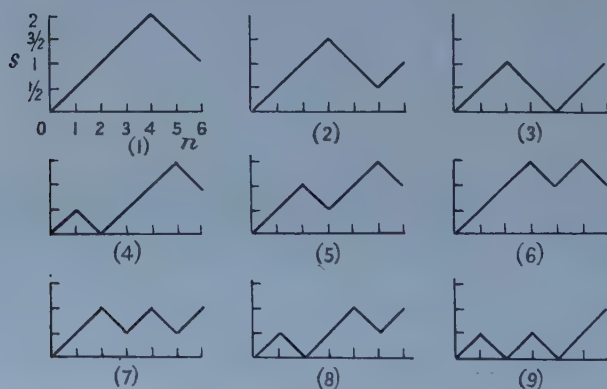


Figure 3.

Table 2

Triplets	$x \alpha$	$y \beta$	$z \alpha$	$u \beta$	$v \alpha$
1	4	2	—	—	—
2	3	2	—	—	—
3	2	2	2	—	—
4	1	1	3	1	—
5	2	1	2	1	—
6	3	1	1	1	—
7	2	1	1	1	1
8	1	1	2	1	1
9	1	1	1	1	2

in nine ways (figure 3) and the system can be decomposed into part systems as it is presented by table 2. The corresponding eigenfunctions are as follows:

$$\begin{aligned}\phi_1 &= \sqrt{\frac{3}{5}} [1 - \frac{1}{4}(S_A^- S_B^+) + \frac{1}{24}(S_A^- S_B^+)^2] |\alpha\alpha\alpha\alpha\beta\beta| \\ &= \frac{1}{2\sqrt{60}} [12|\alpha\alpha\alpha\alpha\beta\beta| - 3(|\beta\alpha\alpha\alpha\alpha\beta| + |\alpha\beta\alpha\alpha\alpha\beta| + |\alpha\alpha\beta\alpha\alpha\beta| + |\alpha\alpha\alpha\beta\alpha\beta| \\ &\quad + |\beta\alpha\alpha\alpha\beta\alpha| + |\alpha\beta\alpha\alpha\beta\alpha| + |\alpha\alpha\beta\alpha\beta\alpha| + |\alpha\alpha\alpha\beta\beta\alpha|) + 2(|\alpha\alpha\beta\beta\alpha\alpha| \\ &\quad + |\alpha\beta\alpha\beta\alpha\alpha| + |\alpha\beta\beta\alpha\alpha\alpha| + |\beta\beta\alpha\alpha\alpha\alpha| + |\beta\alpha\beta\alpha\alpha\alpha| + |\beta\alpha\alpha\beta\alpha\alpha|)].\end{aligned}$$

$$\begin{aligned}\phi_2 &= \frac{1}{\sqrt{2}} [1 - \frac{1}{3}(S_A^- S_B^+) + \frac{1}{12}(S_A^- S_B^+)^2] |\alpha\alpha\alpha\beta\beta\alpha| \\ &= \frac{1}{12\sqrt{2}} [12|\alpha\alpha\alpha\beta\beta\alpha| - 4(|\beta\alpha\alpha\alpha\beta\alpha| + |\alpha\beta\alpha\alpha\beta\alpha| + |\alpha\alpha\beta\alpha\beta\alpha| + |\beta\alpha\alpha\beta\alpha\alpha| \\ &\quad + |\alpha\beta\alpha\beta\alpha\alpha| + |\alpha\alpha\beta\beta\alpha\alpha|) + 4(|\alpha\beta\beta\alpha\alpha\alpha| + |\beta\beta\alpha\alpha\alpha\alpha| + |\beta\alpha\beta\alpha\alpha\alpha|)].\end{aligned}$$

$$\begin{aligned}\phi_3 &= \frac{1}{\sqrt{3}} [1 - \frac{1}{2}(S_A^- S_B^+) + \frac{1}{4}(S_A^- S_B^+)^2] |\alpha\alpha\beta\beta\alpha\alpha| \\ &= \frac{1}{2\sqrt{3}} [2|\alpha\alpha\beta\beta\alpha\alpha| - (|\beta\alpha\alpha\beta\alpha\alpha| + |\alpha\beta\alpha\beta\alpha\alpha| + |\beta\alpha\beta\alpha\alpha\alpha| \\ &\quad + |\alpha\beta\beta\alpha\alpha\alpha|) + 2|\beta\beta\alpha\alpha\alpha\alpha|].\end{aligned}$$

$$\begin{aligned}\phi_4 &= \sqrt{\frac{3}{8}} [1 - \frac{1}{3}(S_{ABC}^- S_D^+)] [1 - (S_A^- S_B^+)] |\alpha\beta\alpha\alpha\alpha\beta| \\ &= \frac{1}{2\sqrt{6}} [3(|\alpha\beta\alpha\alpha\alpha\beta| - |\beta\alpha\alpha\alpha\alpha\beta|) - (|\alpha\beta\beta\alpha\alpha\alpha| + |\alpha\beta\alpha\beta\alpha\alpha| \\ &\quad + |\alpha\beta\alpha\alpha\beta\alpha|) + |\beta\alpha\alpha\beta\alpha\alpha| + |\beta\alpha\beta\alpha\alpha\alpha| + |\beta\alpha\alpha\alpha\beta\alpha|].\end{aligned}$$

$$\begin{aligned}\phi_5 &= \frac{1}{\sqrt{2}} [1 - \frac{1}{3}(S_{ABC}^- S_D^+)] [1 - \frac{1}{2}(S_A^- S_B^+)] |\alpha\alpha\beta\alpha\alpha\beta| \\ &= \frac{1}{6\sqrt{2}} [6|\alpha\alpha\beta\alpha\alpha\beta| - 3(|\beta\alpha\alpha\alpha\alpha\beta| + |\alpha\beta\alpha\alpha\alpha\beta|) - 2(|\alpha\alpha\beta\beta\alpha\alpha| + |\alpha\alpha\beta\alpha\beta\alpha| \\ &\quad - (|\beta\alpha\beta\alpha\alpha\alpha| + |\alpha\beta\beta\alpha\alpha\alpha|) + 2|\beta\beta\alpha\alpha\alpha\alpha| + |\beta\alpha\alpha\beta\alpha\alpha| + |\beta\alpha\alpha\alpha\beta\alpha| \\ &\quad + |\alpha\beta\alpha\beta\alpha\alpha| + |\alpha\beta\alpha\alpha\beta\alpha|)].\end{aligned}$$

$$\begin{aligned}\phi_6 &= \frac{3}{4} [1 - \frac{1}{3}(S_{ABC}^- S_D^+)] [1 - \frac{1}{3}(S_A^- S_B^+)] |\alpha\alpha\alpha\beta\alpha\beta| \\ &= \frac{1}{12} [9|\alpha\alpha\alpha\beta\alpha\beta| - 3(|\beta\alpha\alpha\alpha\alpha\beta| + |\alpha\beta\alpha\alpha\alpha\beta| + |\alpha\alpha\beta\alpha\alpha\beta| + |\alpha\alpha\alpha\beta\alpha\beta|) \\ &\quad - 2(|\beta\alpha\alpha\beta\alpha\alpha| + |\alpha\beta\alpha\beta\alpha\alpha| + |\alpha\alpha\beta\beta\alpha\alpha|) + 2(|\beta\beta\alpha\alpha\alpha\alpha| + |\beta\alpha\beta\alpha\alpha\alpha| \\ &\quad + |\alpha\beta\beta\alpha\alpha\alpha|) + |\beta\alpha\alpha\alpha\beta\alpha| + |\alpha\beta\alpha\alpha\beta\alpha| + |\alpha\alpha\beta\alpha\beta\alpha|].\end{aligned}$$

$$\begin{aligned}\phi_7 &= \frac{2}{3} [1 - \frac{1}{2}(S_{ABC}^- S_D^+)] [1 - \frac{1}{2}(S_A^- S_B^+)] |\alpha\alpha\beta\alpha\beta\alpha| \\ &= \frac{1}{6} [4|\alpha\alpha\beta\alpha\beta\alpha| - 2(|\beta\alpha\alpha\alpha\beta\alpha| + |\alpha\beta\alpha\alpha\beta\alpha| + |\alpha\alpha\beta\beta\alpha\alpha|) - (|\beta\alpha\beta\alpha\alpha\alpha| \\ &\quad + |\alpha\beta\beta\alpha\alpha\alpha|) + |\beta\alpha\alpha\beta\alpha\alpha| + |\alpha\beta\alpha\beta\alpha\alpha| + 2|\beta\beta\alpha\alpha\alpha\alpha|].\end{aligned}$$

$$\begin{aligned}\phi_8 &= \frac{1}{\sqrt{3}} [1 - \frac{1}{2}(S_{ABC}^- S_D^+)] [1 - (S_A^- S_B^+)] |\alpha\beta\alpha\alpha\beta\alpha| \\ &= \frac{1}{2\sqrt{3}} [2(|\alpha\beta\alpha\alpha\beta\alpha| - |\beta\alpha\alpha\alpha\beta\alpha|) - (|\alpha\beta\beta\alpha\alpha\alpha| + |\alpha\beta\alpha\beta\alpha\alpha|) \\ &\quad + |\beta\alpha\alpha\beta\alpha\alpha| + |\beta\alpha\beta\alpha\alpha\alpha|].\end{aligned}$$

$$\begin{aligned}\phi_0 &= \frac{1}{2}[1 - (S_{ABC}^- S_D^+)] [1 - (S_A^- S_B^+)] |\alpha\beta\alpha\beta\alpha\alpha| \\ &= \frac{1}{2}[|\alpha\beta\alpha\beta\alpha\alpha| + |\beta\alpha\beta\alpha\alpha\alpha| - (|\beta\alpha\alpha\beta\alpha\alpha| + |\alpha\beta\beta\alpha\alpha\alpha|)].\end{aligned}$$

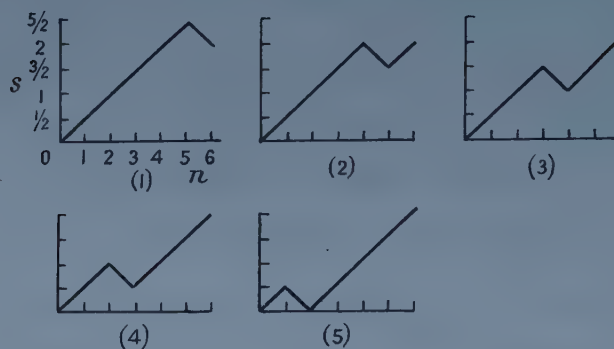


Figure 4.

Table 3

Quintets	$x \alpha$	$y \beta$	$z \alpha$
1	5	1	—
2	4	1	1
3	3	1	2
4	2	1	3
5	1	1	4

(c) The quintet spin state can be constructed in terms of the branching diagram in five ways (figure 4) and the system can be decomposed into part systems as is presented by table 3. The relating eigenfunctions are as follows:

$$\begin{aligned}\phi_1 &= \sqrt{\frac{5}{6}} [1 - \frac{1}{5}(S_A^- S_B^+)] |\alpha\alpha\alpha\alpha\beta| \\ &= \frac{1}{\sqrt{30}} [5|\alpha\alpha\alpha\alpha\beta| - (|\beta\alpha\alpha\alpha\alpha| + |\alpha\beta\alpha\alpha\alpha| + |\alpha\alpha\beta\alpha\alpha| \\ &\quad + |\alpha\alpha\alpha\beta\alpha\alpha| + |\alpha\alpha\alpha\alpha\beta\alpha|)].\end{aligned}$$

$$\begin{aligned}\phi_2 &= \sqrt{\frac{4}{5}} [1 - \frac{1}{4}(S_A^- S_B^+)] |\alpha\alpha\alpha\alpha\beta\alpha| \\ &= \frac{1}{\sqrt{20}} [4|\alpha\alpha\alpha\alpha\beta\alpha| - (|\beta\alpha\alpha\alpha\alpha| + |\alpha\beta\alpha\alpha\alpha| + |\alpha\alpha\beta\alpha\alpha| + |\alpha\alpha\alpha\beta\alpha\alpha|)].\end{aligned}$$

$$\begin{aligned}\phi_3 &= \sqrt{\frac{3}{4}} [1 - \frac{1}{3}(S_A^- S_B^+)] |\alpha\alpha\alpha\beta\alpha\alpha| \\ &= \frac{1}{\sqrt{12}} [3|\alpha\alpha\alpha\beta\alpha\alpha| - (|\beta\alpha\alpha\alpha\alpha| + |\alpha\beta\alpha\alpha\alpha| + |\alpha\alpha\beta\alpha\alpha|)].\end{aligned}$$

$$\phi_4 = \sqrt{\frac{2}{3}} [1 - \frac{1}{2}(S_A^- S_B^+)] |\alpha\alpha\beta\alpha\alpha\alpha| = \frac{1}{\sqrt{6}} [2|\alpha\alpha\beta\alpha\alpha\alpha| - (|\beta\alpha\alpha\alpha\alpha| + |\alpha\beta\alpha\alpha\alpha|)].$$

$$\phi_5 = \frac{1}{\sqrt{2}} [1 - (S_A^- S_B^+)] |\alpha\beta\alpha\alpha\alpha\alpha| = \frac{1}{\sqrt{2}} (|\alpha\beta\alpha\alpha\alpha\alpha| + |\beta\alpha\alpha\alpha\alpha\alpha|).$$



(d) In the case of the septet spin state there exists only one way of construction as can be seen directly in figure 1. The corresponding eigenfunction is given by

$$\phi = [\alpha\alpha\alpha\alpha\alpha\alpha].$$

Finally, let us mention that all Slater determinants have been assumed to be normalized.

Taking also the suggested method of spin operators into account one can count the number of eigenfunctions corresponding to the zero eigenvalue of  $S_z$  as follows. It is obvious that there exist in the case of the singlet state five such eigenfunctions. For the triplet state the eigenvalues of  $S_z$  are  $+1, 0, -1$ , respectively. Nine eigenfunctions of  $S^2$  spanning a 27-dimensional subspace of the Hilbert space correspond to each eigenvalue. This means that in this manner there exist nine eigenfunctions related to the zero eigenvalue of  $S_z$ . For the quintet state the eigenvalues are  $+2, +1, 0, -1, -2$ , respectively. Five eigenfunctions of  $S^2$  spanning a 25-dimensional subspace correspond to each eigenvalue. This means that in this way there exist five eigenvalues related to the zero eigenvalue of  $S_z$ . Finally, in the case of the septet state one eigenfunction spanning a 7-dimensional subspace corresponds to each eigenvalue  $+3, +2, +1, 0, -1, -2, -3$ , of the  $S_z$  operator; i.e. only one eigenfunction corresponds to the zero eigenvalue of  $S_z$  too. Owing to these considerations the six-electron system has 20 independent eigenfunctions related to the zero eigenvalue of  $S_z$ .

As matters stand, we have 20 independent eigenfunctions related to the zero eigenvalue of the operators  $S_z$  and  $S^2$ . This 20-row secular determinant reduces again into the product of one nine-row, two five-row and one one-row determinants, respectively. This does not mean, however, that the reduction of the secular determinant is complete. For example in the case of the benzene molecule, on account of the presence of symmetry in the geometrical configuration of the system one may reduce the determinant by the aid of group theory. But such a final reduction of the problem is occasionally not needed. In the case when one investigates only the ground state of the system related to the zero eigenvalue of the  $S^2$  operator corresponding to the so-called paired state of the system, for example, the true linear combinations of the Slater determinants is directly given by the method of spin operator. This means that the energy of the ground state of the 6-electron system should be given by one of the roots of the five-row determinant corresponding to the maximal number of bond pairs.

Finally, owing to the equation (I, 4.4), another form of the spin operator can also be presented, being a function of the step-down operators only; e.g. in the case of four united systems this operator may be written as follows:

$$\begin{aligned} O_{ABCD} = & \left( \frac{x-y+z+1}{x-y+z+1} \right)^{1/2} \left( \frac{x-y+1}{x+1} \right)^{1/2} \\ & \times \sum_{j=0}^u (-1)^j \frac{(x-y+z-j)!}{(x-y+z)! (u-j)!} (S_{ABC}^-)^j (S_D^-)^{n-j} \\ & \times \sum_{i=0}^y (-1)^i \frac{(x-i)!}{x! (y-i)!} (S_A^-)^i (S_B^-)^{y-i}, \quad \dots\dots (4.1) \end{aligned}$$

Furthermore, another form of the spin operator can be of interest too, namely,

which when operating on the zero component of  $S_z$  traces the eigenfunctions of  $S^2$ ; e.g. in the case of three united systems this operator has the form

$$O_{ABC}^{\circ} = \left[ \frac{(x-y)!z!}{(x-y+z)!} \right]^{1/2} \sum_{i=-z/2}^{z/2} \frac{(x-y+z)!/2}{(\frac{1}{2}[x-y]+i)!(\frac{1}{2}z+i)!} (S_{AB}^{-} S_C^{+})^i \\ \times \left[ \frac{(x-y+1)!y!}{(x+1)!} \right]^{1/2} \sum_{j=-y/2}^{y/2} (-1)^{y/2+j} \frac{(x/2-j)!}{(x/2-y/2)!(y/2+j)!} (S_A^{-} S_B^{+})^j. \\ \dots\dots(4.2)$$

This operator has, however, the disadvantage that it contains twice as much summation as the operator (3.8) by which its practical applications are limited.

## APPENDIX

Here the proof of some formulae of § 3 will be presented.

*Theorem.* 
$$\phi(s, s-i) = \frac{1}{i!} \binom{n}{i}^{-1/2} (S^{-})^i |\alpha^1 \alpha^2 \dots \alpha^n|. \quad \dots\dots(3.5)$$

*Proof.* Obviously the statement is true for  $n=1$  and for  $n=2$ .

For $n=1$ if $s=\frac{1}{2}$ and $M_s=\frac{1}{2}$	then	$\phi(\frac{1}{2}, \frac{1}{2}) =  \alpha $
$M_s = -\frac{1}{2}$	then	$\phi(\frac{1}{2}, -\frac{1}{2}) = S^{-} \alpha  =  \beta $
For $n=2$ if $s=1$ and $M_s=1$	then	$\phi(1, 1) =  \alpha\alpha $
$M_s=0$	then	$\phi(1, 0) = 2^{-1/2}( \alpha\beta  +  \beta\alpha )$
$M_s=-1$	then	$\phi(1, -1) =  \beta\beta $

Assuming the validity of the statement for  $n$  electrons the system may be completed by one further electron, then the  $i$ th component of the system of  $n+1$  electrons with  $s=(n+1)/2$  can be obtained by the formula of spin addition:

$$\phi(S, M_s) = \left[ \frac{(2s)!(2s')!}{(2s+2s')!} \right]^{1/2} \sum_{m_s'=-s'}^{s'} \left[ \frac{(S+M_s)!(S-M_s)!}{(s+m_s')!(s-m_s')!(s'+m_s')!(s'-m_s')!} \right]^{1/2} \\ \times \phi_A(s, M_s - m_s') \phi_B(s', m_s').$$

This means, however, that

$$\phi(\frac{1}{2}(n+1), \frac{1}{2}(n+1)-i) = \left[ \frac{n!}{(n+1)!} \right]^{1/2} \left\{ \left[ \frac{(n-i+1)!i!}{(n-i)!i!} \right]^{1/2} \phi_A(n/2, n/2-i) \phi_B(\frac{1}{2}, \frac{1}{2}) \right. \\ \left. + \left[ \frac{(n-i+1)!i!}{(n-i+1)!(i-1)!} \right]^{1/2} \phi_A(\frac{1}{2}n, \frac{1}{2}n-(i-1)) \phi_B(\frac{1}{2}, -\frac{1}{2}) \right\} \\ = (n+1)^{-1/2} \left\{ (n-i+1)^{1/2} \frac{1}{i!} \binom{n}{i}^{-1/2} (S^{-})^i |\alpha^1 \alpha^2 \dots \alpha^n| |\alpha| \right. \\ \left. + i^{1/2} \frac{1}{(i-1)!} \binom{n}{i-1}^{-1/2} (S^{-})^{i-1} |\alpha^1 \alpha^2 \dots \alpha^n| |\beta| \right\} \\ = \frac{1}{i!} \binom{n+1}{i}^{-1/2} \{ (S^{-})^i |\alpha^1 \alpha^2 \dots \alpha^n| |\alpha| + i (S^{-})^{i-1} |\alpha^1 \alpha^2 \dots \alpha^n| |\beta| \} \\ = \frac{1}{i!} \binom{n+1}{i}^{-1/2} (S^{-})^i |\alpha^1 \alpha^2 \dots \alpha^{n+1}|$$

is obtained; hereby the proof is complete too. The relation (3.6) can be justified analogously.

## REFERENCES

- CORSON, E. M., 1951, *Perturbation Methods in the Quantum Mechanics of  $n$ -electron Systems* (London and Glasgow: Blackie).  
 PRATT, G. W., 1953, *Phys. Rev.*, **92**, 278.

## The Gamma-Rays from Muon Catalysed Fusion of Hydrogen and Deuterium

By A. ASHMORE, R. NORDHAGEN, K. STRAUCH† AND B. M. TOWNES  
Nuclear Physics Research Laboratory, University of Liverpool

*Communicated by J. M. Cassels ; MS. received 20th September 1957,  
and in final form 24th October 1957*

**Abstract.** The fusion of hydrogen and deuterium catalysed by muons was observed by Alvarez *et al.* Events were seen in a bubble chamber in which the muon was re-emitted with the energy released in the fusion process. In the experiments described here the  $\gamma$ -rays from the fusion process were detected and a measurement made of their time distribution. The yield of  $\gamma$ -rays was found to be  $0.34 \pm 0.06$  per muon stopping in liquid hydrogen enriched with 1.8% of deuterium. A comparison with the results of Alvarez *et al.* gives an internal conversion coefficient of  $0.066 \pm 0.014$ . The analysis of the time distribution enables the following limits to be set on the two reaction rates involved:

$$0.19 \times 10^6 \text{ sec}^{-1} < \lambda_{\text{slow}} < 0.88 \times 10^6 \text{ sec}^{-1}$$

$$0.55 \times 10^6 \text{ sec}^{-1} < \lambda_{\text{fast}} < 2 \times 10^7 \text{ sec}^{-1}.$$

A comparison with theory shows that it is not possible to assign them to particular processes in the chain of events following a muon stopping in the enriched mixture.

### § 1. INTRODUCTION

ALVAREZ *et al.* (1957) have found that the stopping of negative muons in mixtures of hydrogen and deuterium is followed by a fusion reaction. Events were observed in a bubble chamber in which the energy released in the fusion is given to the muon. The frequency of these events was measured for different deuterium concentrations. The number of events for each muon undergoing normal decay was  $0.6 \times 10^{-2}$  for 0.016%,  $2 \times 10^{-2}$  for 0.3% and  $2.5 \times 10^{-2}$  for 4.3% concentration. The reaction is seen to be near saturation already at 0.3% concentration.

The reaction is assumed to proceed in the following steps (Skyrme 1957, Jackson 1957, Zeldovich 1954, Frank 1947): (i) The stopped negative muon is captured to form either a hydrogen or deuterium mesic atom. (ii) The neutral hydrogen mesic atoms drift around and can exchange their muons with deuterium atoms. The exothermic nature of this exchange makes it highly probable. (iii) The mesic atoms form mesic molecular ions with normal hydrogen and deuterium atoms.  $\text{HH}^+$ ,  $\text{HD}^+$  and  $\text{DD}^+$  ions will be present. To obtain observable rates for the subsequent fusion of the  $\text{HD}^+$  and  $\text{DD}^+$  systems it is necessary to assume that the particles are confined in a mesic molecule. (iv) The  $\text{HD}^+$  and  $\text{DD}^+$  mesic molecular ions fuse. The  $\text{DD}^+$  fusion will be ignored here, as the concentrations of deuterium considered are too small to give any appreciable

† On leave of absence from Harvard University.

number of  $DD^+$  systems.  $HD^+$  fuses to  $^3\text{He}$ , and the excess energy, 5.5 mev, leaves the excited  $^3\text{He}$  system by the emission of a  $\gamma$ -ray or by internal conversion to the muon bound in the system. The muon emitted in the internal conversion process can recycle the reaction. No appreciable number of muons are believed to be shaken off from the  $^3\text{He}$  de-excited by the radiative process, due to the small recoil velocity of the product nucleus. (v) At all times the muon can undergo normal decay to an electron and two neutrinos. The frequency of fusion found by Alvarez *et al.* (1957) suggests that the lifetime of the reaction is comparable with the lifetime of the muon.

The efficiency of hydrogen bubble chambers for observing  $\gamma$ -rays is low, and only fusion with internal conversion of the muon was observed by Alvarez *et al.* (1957). In the present work the yield of  $\gamma$ -rays from the fusion reaction was measured, and an estimate of the internal conversion coefficient obtained.

The work was done by using the negative meson beam of the Liverpool 156 in. synchrocyclotron. Mesons from the beam were stopped in a liquid hydrogen target. First efforts were aimed at measuring  $\gamma$ -rays from this target by their expected energy distribution, a method that proved to be useless in the background encountered. It was then found that the identification could be based on a knowledge of the lifetime of the reaction. The  $\gamma$ -rays were found as delayed uncharged secondaries from the target, and the identification was based on their time distribution and on a pronounced increase in yield with a small increase in deuterium concentration. The decay electrons were measured to test the apparatus and to give the number of muons stopping in the target. The use of counters for measuring the radiation lent itself readily to the study of time distributions, and a discussion is given of the distribution observed from a 1.8% enriched mixture of hydrogen and deuterium.

## § 2. EXPERIMENTAL DETAILS AND PROCEDURE

### 2.1. *Experimental Arrangement*

The general layout of the experiment is shown in figure 1. After leaving the cyclotron and being focused by two quadrupole lenses, the negative meson beam was slowed down in 10 in. of paraffin wax before entering a bending magnet. Only the muons, left with about 130 mev/c momentum, were bent into the experimental area. By slowing down the beam before bending, the pions and most of the electrons in the original beam did not find their way into the experimental area. A relatively clean muon beam of low intensity was thus produced. After bending, the muons passed through another 5 in. of paraffin wax. This amount of wax gave the maximum number stopping in the hydrogen target. Before reaching the target, the muon beam was collimated to 4 in. by 4 in. with blocks of iron-loaded concrete, and had to pass through a triple coincidence counter telescope.

The counters in this telescope, 1, 2 and 3, were 3 in. diameter circular scintillators, all  $\frac{1}{4}$  in. thick with aluminium foil caps, and viewed by E.M.I. 6260 photomultipliers. An anti-coincidence counter, 4, was mounted behind the target in the beam direction. It consisted of a scintillator, 8 in. in diameter and  $\frac{3}{16}$  in. thick, viewed from behind by an E.M.I. 6099 photomultiplier. A  $4\frac{1}{2}$  in. by  $4\frac{1}{2}$  in. cylindrical NaI(Tl) crystal, counter 6, was mounted to view the target at  $90^\circ$  to the beam direction. The crystal was viewed from behind by an E.M.I. 6099 photomultiplier. An anti-coincidence counter, 5, was inserted between the target



and the NaI crystal. This counter was a  $5\frac{1}{2}$  in. diameter,  $\frac{1}{4}$  in. thick scintillator viewed from the side by an E.M.I. 6260 photomultiplier. The scintillators for counters 1 to 5 were all made from polystyrene containing 2% terphenyl and 0.03%

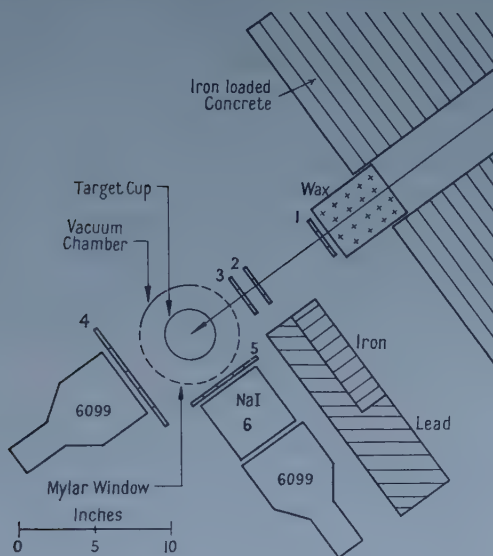


Figure 1. Experimental arrangement.

tetraphenyl butadiene. The last counter of the telescope, the two anti-coincidence counters and the NaI counter were all placed as close to the target as possible. A 4 in. thick shield of lead and iron was placed between the NaI counter and the cyclotron wall. The target is described in § 2.3.

## 2.2. Electronic Equipment

A block diagram of the electronic equipment is shown in figure 2. The numbers of the counters are used to denote the signals they provide, and a barred

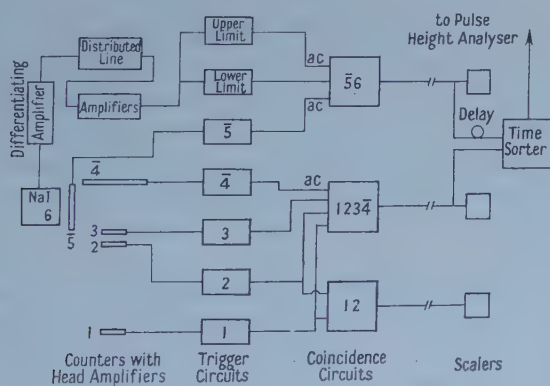


Figure 2. Block diagram of the electronic equipment.

number indicates that the counter is used in anti-coincidence. The coincidence and associated circuits are basically as described by Collinge *et al.* (1956). The resolving time  $\tau$  is of the order of 20  $\mu$ sec.

A count  $123\bar{4}$ , indicating a charged particle stopping in the target, started an electronic circuit for analysing time intervals. This will be referred to as the time-sorter. After being stopped by a count  $\bar{5}6$ , indicating the detection of uncharged radiation in 6, the time-sorter gave an output pulse whose height was proportional to the delay between the two counts. When studying electrons, only 6 was used for stopping the time-sorter. The output from the time-sorter was fed to a Hutchinson-Scarrott multichannel pulse height analyser. Thus the counts were displayed in channels showing the distribution of time intervals between  $123\bar{4}$  and  $\bar{5}6$ . The  $\bar{5}6$  counts were obtained by taking fast output pulses from one of the last dynodes of the photomultiplier in counter 6. These pulses were amplified and fed into a fast differential discriminator. The outputs from the upper limit circuit and from counter 5 were in anti-coincidence with the output from the lower limit circuit. The limits could be set to accept only a chosen part of the energy spectrum from counter 6. The 12 counts were used for monitoring.

### 2.3. Target

The target was a 4 in. high,  $3\frac{5}{8}$  in. diameter cylindrical cup filled with liquid natural hydrogen or liquid hydrogen enriched with deuterium. The cup was isolated by a vacuum and connected to a reservoir, the condenser. By the use of a small heating element the target cup could be emptied into the condenser for background measurements. The condenser was cooled by a surrounding container of liquid hydrogen, again cooled by a collar of liquid nitrogen.

The enrichment was done by letting deuterium gas into the condenser system already filled with hydrogen. The deuterium condensed, and the heat of condensation boiled off some of the hydrogen in the cooling container. By knowing this amount and the amount boiled off when the hydrogen was condensed, a rough estimate of the concentration was obtained. In this way the liquid hydrogen target was enriched with at least 1% and below 2%, probably 1.8% of deuterium. This was sufficient to ensure that the reaction was studied near saturation.

### 2.4. Experimental Procedure

The available running time, 8 days, was roughly divided in two. For the first half, the target was filled with natural hydrogen, for the second half with enriched hydrogen. A first short run on natural hydrogen was used to measure the decay electrons from the target. With the  $\bar{5}$  counter out of operation and the upper discriminator level removed, the lower limit was set at 7.5 Mev to avoid measuring any 5.5 Mev  $\gamma$ -rays.

Uncharged radiation was next measured for both natural and enriched target fillings. Short runs of two hours were interspaced with background runs of one hour to reduce the effect of drifts in the apparatus. The background runs were done with an empty target cup. With  $\bar{5}$  in operation, the discriminators were set to admit signals from counter 6 above 3 Mev and below 7.5 Mev. This energy discrimination helped in identifying the observed neutral radiation and produced a considerable reduction in background and random counts. The experiment ended with another short run on decay electrons, this time with enriched hydrogen in the target.

The experimental data were obtained in the form shown in figure 3. The total number of counts from the runs on enriched hydrogen and the associated background are shown as displayed by the pulse height analyser. By delaying the 56 counts for  $0.45 \mu\text{sec}$ , the counts displayed in the first few channels of the analyser were only due to random counts. The instantaneous counts then appeared in channel 7 on the pulse height analyser. These might be due to

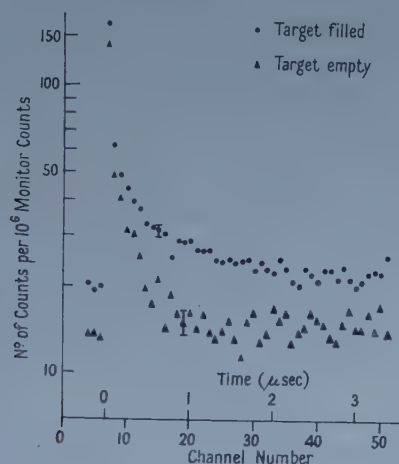


Figure 3. The time distribution of uncharged secondaries from enriched hydrogen, and the associated background.

particles scattered into the NaI counter outside  $\bar{5}$ , or to mesic x-rays from muons stopping in the material surrounding the target. To avoid these, channel 7 was omitted in the final analysis. This corresponds to omitting the first  $0.039 \mu\text{sec}$  of the time distribution. The remaining channels from 8 to 51 were added up in groups of 4. This corresponds to dividing the time interval from  $0.039$  to  $3.46 \mu\text{sec}$  into 11 groups  $0.311 \mu\text{sec}$  wide. The result of this grouping with background subtracted and normalized to  $10^6$  monitor counts, are given for both natural and enriched hydrogen in figure 4.

### 2.5. Background, Counting Rates and Random Counts

Decay electrons and star products from muons stopping in the iron and copper near the hydrogen target, could miss  $\bar{5}$  and find their way into 6. The lifetimes of the negative muon in these metals are  $0.163$  and  $0.116 \mu\text{sec}$  (Keuffel *et al.* 1952). Such events explain the sharp rise towards zero time seen in figure 3, as shown by their disappearance in the results of figure 4 where the background (empty target) has been subtracted.

The  $1234$  counting rate, at the beam rate used, averaged  $23 \text{ sec}^{-1}$  with the target filled, and  $16 \text{ sec}^{-1}$  with the target empty. The counting rate  $\bar{56}$  was high, of the order of  $80 \text{ sec}^{-1}$ , and due to general cyclotron background. It was found to be roughly proportional to the internal beam of the cyclotron. The primary source of random counts was coincidences between unrelated  $1234$  and  $\bar{56}$  events.

The ratio of the random rate for the target filled to that for target empty was roughly as  $0.11 \text{ sec}^{-1}$  to  $0.07 \text{ sec}^{-1}$  in the first  $2.8 \mu\text{sec}$  of the time distribution.

With the target filled with enriched hydrogen, the background rate and  $\gamma$ -ray rate were both  $0.017 \text{ sec}^{-1}$ . A beam rate was chosen to give a practical real rate without too many random counts. The difference in random counts between the runs with the target filled and empty is clearly seen in figures 3 and 4.

### § 3. EXPERIMENTAL RESULTS AND CALCULATIONS

#### 3.1. Results

The final data of the experiment are presented in figure 4(a) for enriched hydrogen and in figure 4(b) for natural hydrogen. It is clearly seen how a small percentage of deuterium added to the hydrogen gives a pronounced difference in the yield of  $\gamma$ -rays.

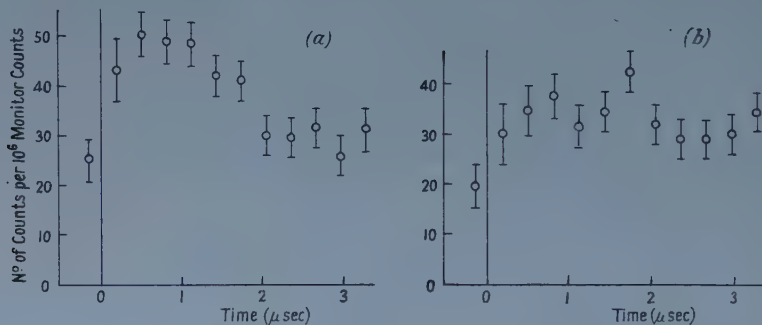


Figure 4. The time distribution of uncharged secondaries from muons stopping in (a) hydrogen enriched with 1.8% of deuterium, (b) natural hydrogen.

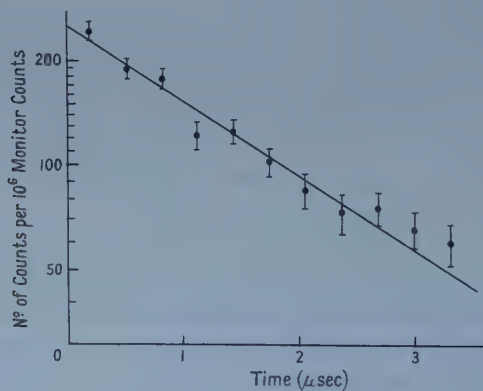


Figure 5. The time distribution of decay electrons. Straight line is the best fit by the least squares method, giving a muon lifetime of  $2.07 \pm 0.20 \mu\text{sec}$ .

The mean results of the two electron runs are given in figure 5. The two runs agreed with each other within the statistical error. A least squares fit to the data gives the value for the lifetime of the negative muon as  $2.07 \pm 0.20 \mu\text{sec}$ , which is consistent with the value of  $2.22 \pm 0.09 \mu\text{sec}$  found by Bell and Hincks (1952). Using the latter value of the lifetime and the measured number of electrons in the time range between 0.039 and  $3.46 \mu\text{sec}$ , the total observable emission of electrons was found to be  $1656 \pm 52$  per  $10^6$  monitor counts.



### 3.2. Identification of the $\gamma$ -rays

That the neutral events growing and decaying in time as shown in figure 4 are indeed the 5.5 mev  $\gamma$ -rays from the  $\text{HD}^+$  fusion is supported by the following arguments: (i) The number of neutral events depends on the deuterium concentration in a manner consistent with the results of Alvarez *et al.* (1957). (ii) They are counted by a detector with a high efficiency for  $\gamma$ -rays between 3 and 7.5 mev. (iii) They have a characteristic time distribution after the muons stop.

The possibility was considered that some other radiation, charged or uncharged, could give rise to the observed effect. Any decay electrons from the hydrogen should be effectively screened out by the  $\bar{5}$  counter. Some decay electrons from other parts of the target reach 6 without traversing  $\bar{5}$  and about 0.8% of them have energies below 7.5 mev and will be detected. But these are removed by the background subtraction. In any case decay electrons would be unable to give the observed difference between natural and enriched hydrogen.

Neutrons from deuterons disintegrating by muon absorption were also considered. Assuming that the  $Z^4$  dependence of the capture probability holds down to  $Z=1$ , capture in deuterium is too small by a factor of the order of  $10^4$  to give the observed result. In any case, no such events were observed by Alvarez *et al.* (1957).

### 3.3. Calculations

The ratio of the efficiency for counting electrons from the target to the efficiency for counting  $\gamma$ -rays is  $\Omega_e \epsilon_e / \Omega_\gamma \epsilon_\gamma$ , where  $\Omega$  and  $\epsilon$  are the solid angle and efficiency of the sodium iodide crystal. The suffixes e and  $\gamma$  refer to the detection of electrons and  $\gamma$ -rays respectively. As the standard deviations of the numbers of electrons and  $\gamma$ -rays detected are rather large, an approximate method will give a sufficiently good estimate of  $\Omega$  and  $\epsilon$ . The detector was assumed to be the cross section of the NaI crystal at the plane of mean detection efficiency. This assumption has been found to be satisfactory for this crystal. A good approximation to the solid angle subtended by a circular disc at a distance comparable with the radius can be found by using Gegenbauer functions. In this way  $\Omega_e / \Omega_\gamma$  was calculated for different parts of the target and found not to vary by more than 2% from the value at the centre of the target.

The electrons have to lose 7.5 mev in the crystal to be detected. Their mean loss of energy going through the material in front of the NaI counter is 2.5 mev. From the values of electron ionization losses given by Sternheimer (1952) the thickness of NaI corresponding to a mean energy loss of 7.5 mev was found. This thickness is the same for a 10 mev and a 50 mev electron within 3%. It has to be corrected for multiple scattering (Yang 1951, Goldwasser *et al.* 1952). The plane of mean detection was then taken at this thickness of 0.53 inch. It was assumed that the shape of the Landau distribution of the electrons does not vary appreciably with thickness in the region considered. The electrons in the decay spectrum of the muon falling below 10 mev were not detected. The spectrum given by Michel (1957) was used with  $\rho=0.64$ , and gave a value of 98.5% for  $\epsilon_e$ .

The detection efficiency and mean plane of detection for  $\gamma$ -rays were found from the stopping power of NaI for 5.5 mev  $\gamma$ -rays (Davisson 1955). Because of the lower discriminator limit, only  $66 \pm 4\%$  of the counts in the spectrum from a 5.5 mev  $\gamma$ -ray were observed. This was established from an independent

measurement with the NaI crystal. An uncollimated beam of  $\gamma$ -rays of 5.36 MeV from the 414 keV resonance in the reaction  $^{29}\text{Si}(p, \gamma)^{30}\text{P}$  was used. The measurement was done with the Liverpool 1 MeV generator. The calculated value of the efficiency ratio was  $\Omega_e \epsilon_e / \Omega_\gamma \epsilon_\gamma = 3.0 \pm 0.17$ .

#### § 4. THE TIME DISTRIBUTION

Figure 6(a) shows schematically the assumed mechanism of muon catalysed fusion of H and D already outlined in the introduction. The reaction rates are indicated in each branch using the following symbols:  $\lambda_s$  = slowing down rate of muons in hydrogen,  $\lambda_0$  = decay rate of muons,  $\lambda_m$  = mesic molecular formation rate, assumed to be the same for all molecules considered,  $\lambda_e$  = exchange rate of muon from hydrogen atom to deuterium atom in pure deuterium,  $\lambda_1$  = rate of

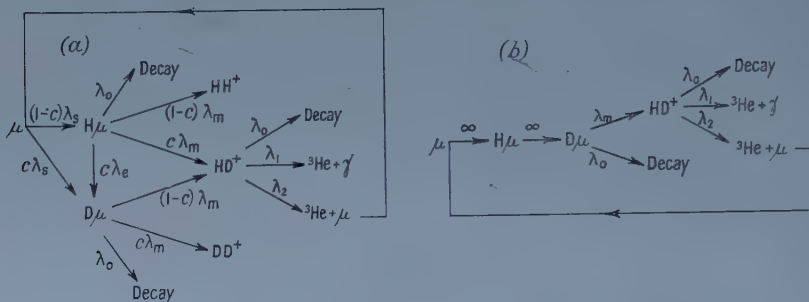


Figure 6. Assumed reaction schemes for muon catalysed fusion of hydrogen and deuterium.

fusion with  $\gamma$ -ray emission,  $\lambda_2$  = rate of fusion with internal muon conversion,  $c$  = deuterium concentration in hydrogen. The slowing down rate  $\lambda_s$  is known to be faster ( $\sim 10^9 \text{ sec}^{-1}$ ) (Wightman 1950) than the other relevant rates and will be ignored from now on. The rapid saturation of the number of fusions with increasing deuterium concentration indicates that the exchange rate  $\lambda_e$  must be very large so that even at a deuterium concentration of the order of 1% nearly every muon gets attached to a deuterium atom (Alvarez *et al.* 1957). Skyrme (1957) has inferred from the Berkeley results that  $\lambda_e \sim 10^3(\lambda_0 + \lambda_m)$ . Thus for the enriched mixture  $c\lambda_e \sim 20(\lambda_0 + \lambda_m)$ . Little error is therefore made by neglecting the alternate methods of transformation of the mesic hydrogen atom and assuming that every muon effectively forms a mesic deuterium atom upon capture. This also agrees with the observation by Cresti *et al.* (1957) that at 0.3% deuterium concentration about 80% of the muons are transferred to a deuteron. This simplified mechanism is shown in figure 6(b). The formation of  $\text{DD}^+$  is also neglected compared with the  $\text{HD}^+$  formation because of the small deuterium concentration.

It follows from this simplified scheme that

$$\frac{dn^{\text{D}}}{dt} = \lambda_2 n^{\text{HD}} - \lambda_b n^{\text{D}}, \quad \frac{dn^{\text{HD}}}{dt} = \lambda_m n^{\text{D}} - \lambda_c n^{\text{HD}}, \quad \frac{dn^\gamma}{dt} = \lambda_1 n^{\text{HD}}, \quad \dots (1)$$

where  $n^{\text{D}}$  = number of mesic deuterium atoms present at time  $t$  after capture of one muon,  $n^{\text{HD}}$  = number of mesic  $\text{HD}^+$  molecular ions present at time  $t$  after capture of one muon,  $n^\gamma$  = number of  $\gamma$ -rays from fusion process at time  $t$  after capture of one muon,  $\lambda_b = \lambda_0 + \lambda_m$  = transformation rate of mesic deuterium atoms,  $\lambda_c = \lambda_0 + \lambda_1 + \lambda_2$  = transformation rate of mesic  $\text{HD}^+$  molecular ions.

Solving these simultaneous equations and utilizing the proper boundary conditions the number of  $\gamma$ -rays emitted per unit time per stopped muon at a time  $t$  is given by

$$\frac{dn^i}{dt} = \frac{\lambda_1 \lambda_m}{\lambda_y - \lambda_x} [\exp(-\lambda_x t) - \exp(-\lambda_y t)] \quad \dots\dots(2)$$

where

$$\lambda_x = \frac{1}{2}(\lambda_b + \lambda_c) - [\frac{1}{4}(\lambda_b - \lambda_c)^2 + \lambda_2 \lambda_m]^{1/2},$$

$$\lambda_y = \frac{1}{2}(\lambda_b + \lambda_c) + [\frac{1}{4}(\lambda_b - \lambda_c)^2 + \lambda_2 \lambda_m]^{1/2}.$$

The total number of  $\gamma$ -rays emitted per stopped muon  $n_T$  is given by

$$n_T = (\lambda_b \lambda_c / \lambda_m \lambda_1 - \lambda_2 / \lambda_1)^{-1}. \quad \dots\dots(3)$$

Assuming that the recycling of the muons can be ignored,

$$n_T = \lambda_m \lambda_1 / \lambda_b \lambda_c. \quad \dots\dots(4)$$

The analysis was made on this assumption. The value obtained for  $\lambda_2 / \lambda_T$  was  $0.066 \pm 0.014$  (§5), which is 1.5% of  $\lambda_b \lambda_c / \lambda_m \lambda_1$ . The error due to ignoring the recycling is then seen to be small. The time distribution for  $\lambda_2 \ll \lambda_1$  is again given by equation (2), but now  $\lambda_x = \lambda_b$  and  $\lambda_y = \lambda_c$ . Equation (2) for  $dn^i/dt$  is symmetrical in  $\lambda_x$  and  $\lambda_y$ , so that they cannot be distinguished by the subsequent analysis.

The results were then fitted to equation (2). The data consist of the twelve groups in the time distribution on figure 4(a). The number of counts in the groups are  $N_0, N_1$ , etc. to  $N_{11}$ . These can be written

$$n_i = N_R + \epsilon n_i, \quad i = 0, \dots, 11,$$

where  $N_R$  is the mean number of random counts in  $0.311 \mu\text{sec}$ .  $\epsilon$  is the experimental efficiency for registering a  $\gamma$ -ray, multiplied by the number of muons stopped in the hydrogen for  $10^6$  monitor counts.  $n_i$  is the number of genuine counts in the  $i$ th channel estimated from equation (2). Measured numbers are denoted by a capital  $N$ , theoretical estimates by a small  $n$ .

$\lambda_x$  and  $\lambda_y$  have to be chosen to give a good estimate of the random counts and the total number of observed counts. The available data can be made to provide two numbers for this test by finding the number of counts in the first  $k$  groups:

$$N_T^k = \sum_1^k N_i = k N_R + \epsilon \sum_1^k n_i, \quad \dots\dots(5)$$

and using the remaining groups for estimating  $N_R$ :

$$(12 - k)N_R = N_0 + \sum_{k+1}^{11} N_i - \epsilon \sum_{k+1}^{11} n_i. \quad \dots\dots(6)$$

Eliminating  $N_R$  between (5) and (6),

$$\sum_1^k N_i = \frac{k}{12 - k} (N_0 + \sum_{k+1}^{11} N_i) + \epsilon \left( \sum_1^k n_i - \frac{k}{12 - k} \sum_{k+1}^{11} n_i \right).$$

Grouping measured and theoretical quantities together,

$$n_T^k - \sum_{k+1}^{11} n_i - \frac{k}{12 - k} \sum_{k+1}^{11} n_i = \frac{1}{\epsilon} \left[ \sum_1^k N_i - \frac{k}{12 - k} \left( N_0 + \sum_{k+1}^{11} N_i \right) \right]. \quad \dots\dots(7)$$

The values of  $\lambda_x$  and  $\lambda_y$  leaving the left-hand side of (7) within the errors of the right-hand side were then found. The values obtained depended to some extent on the value of  $k$ . An investigation showed that the range of possible values could be adequately covered by taking  $k=6$  and  $k=9$ . The area covered

by  $\lambda_x$  and  $\lambda_y$  to give a fit within the errors is plotted in figure 7. The value of  $0.45 \times 10^6 \text{ sec}^{-1}$  found by Bell and Hincks (1952) was used for  $\lambda_0$ .

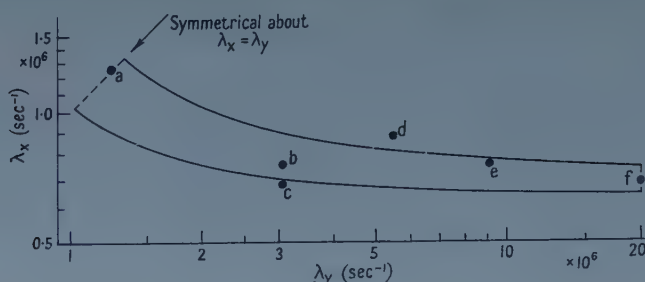


Figure 7. Region of values for  $\lambda_x$  and  $\lambda_y$  giving a fit to the experimental points for enriched hydrogen (equation (7)). The time distributions given by values marked with letters are shown in figure 8.

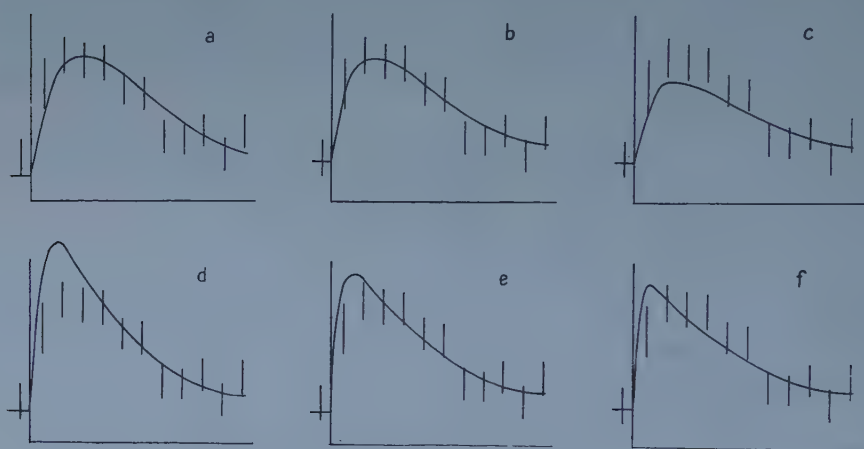


Figure 8. The time distributions given by values of  $\lambda_x$  and  $\lambda_y$  marked with letters in figure 7, with the experimental points.

Some of the fits to the time distribution are shown in figure 8.  $\lambda_x$  and  $\lambda_y$  for the fits a and b lie well inside the region covered, and give good agreement. Fits c and d are just outside the region and give obvious misfits. Fits e and f are still in the region but with large values of  $\lambda_y$ . These fits are not very good and any further increase in  $\lambda_y$  was found to give definite misfits. The values of  $\lambda_x$  and  $\lambda_y$  for the above fits are indicated by the dots on figure 7.

The values of  $\lambda_x$  and  $\lambda_y$  yield limits for the reaction rates when  $\lambda_0$  is subtracted. It is seen that a slow rate is fairly well defined,

$$0.19 \times 10^6 \text{ sec}^{-1} < \lambda_{\text{slow}} < 0.88 \times 10^6 \text{ sec}^{-1}$$

and a faster rate can vary within wide limits:

$$0.55 \times 10^6 \text{ sec}^{-1} < \lambda_{\text{fast}} < 2 \times 10^7 \text{ sec}^{-1}.$$

This is to be expected from the time distribution observed (figure 4). The fast rise of the curve in the region below  $1 \mu\text{sec}$  must clearly be badly determined.

$n_T'$  estimated from (7) gives the number of  $\gamma$ -rays emitted per stopped muon. Its value, which was not too dependent on the values of  $\lambda_x$  and  $\lambda_y$ , was found to be

$$n_T' = 0.34 \pm 0.06.$$



A similar analysis of the time distribution observed from natural hydrogen was not considered worth while in view of the statistical errors. It is seen that  $c\lambda_e$  has become sufficiently small to slow the reaction down and reduce the yield of  $\gamma$ -rays.

### § 5. DISCUSSION

Skyrme (1957) has shown that to explain the data of Alvarez *et al.* (1956) first announced, it must be assumed that the internal conversion coefficient

$$\lambda_2/\lambda_1 = \alpha \geq 0.03.$$

The lower limit of  $\alpha = 0.03$  is obtained when both  $\lambda_1$  and  $\lambda_m$  are large compared with the normal decay rate  $\lambda_0$ . The low yield observed by Alvarez *et al.* (1957) for the internal conversion process might be due to either a fast process with a small amount of recycling (i.e. small value of  $\alpha$ ) or to a slow process with heavy recycling (i.e. large value of  $\alpha$ ). Clearly, the smallest value of  $\alpha$  gives the largest yield of  $\gamma$ -rays. The observed yield of  $\gamma$ -rays is fairly large. The mean of the yield for internal conversion found by Alvarez *et al.* (1957) for 0.3% and 4.3% enrichment is  $0.022 \pm 0.003$ . Compared with the experimental estimate of  $n_1^{\gamma}$  for 1.8% enrichment this gives  $\alpha = 0.066 \pm 0.014$  which is somewhat larger than the lower limit set by Skyrme (1957).

Skyrme (1957) has also discussed the various modes of transition which the fused system might undergo. The major contribution to the interaction is due to S-wave formation of the  $^3\text{He}$  nucleus. The  $^3\text{He}$  is formed in a  $s_{1/2}^+$  and a  $s_{3/2}^+$  state in the ratio 1 : 2 and might undergo either M1 or E2 radiative transitions to the  $s_{1/2}^+$  ground state. The M1 radiation has not sufficient internal conversion, and the E2 radiation not sufficient intensity (Austern 1952) to explain the observed value of  $\alpha$ . Skyrme (1957) assumes the presence of totally internally converted, forbidden monopole transitions between the  $s_{1/2}^+$  states, and finds  $\alpha = 0.17$  by comparison with the M1 radiation. As this value is stated to be too high because of the approximations used for its derivation, it offers a reasonable explanation of the internal conversion coefficient given by this experiment.

Skyrme (1957) and also Jackson (1957) and Gallone *et al.* (1957) have made estimates of the rate of fusion. These estimates might be compared with the rates  $\lambda_{\text{slow}}$  and  $\lambda_{\text{fast}}$  whose experimental limits were calculated in §4. The estimate of Skyrme (1957) giving  $\sim 10^6 \text{ sec}^{-1}$ , might indicate either of these two rates. Jackson (1957) and Gallone *et al.* (1957) both find values of the order of  $0.3 \times 10^6 \text{ sec}^{-1}$ , suggesting that the slow rate might be the fusion rate.

No satisfactory estimate of the molecular ion formation rate has been made. Zeldovich (1954) has suggested that a resonance to a rotational level of the molecular ion is needed to give a sufficiently high rate. The splitting associated with the alignment of the spins of the deuteron and proton would be so small that it would not affect the 1 : 2 ratio for the formation of the  $^3\text{He}$  in the  $s_{1/2}^+$  and  $s_{3/2}^+$  states.

It is thus not possible to assign the experimental values of the reaction rates to a particular step in the fusion process. It is clear, however, that the slowest rate has to be faster than  $0.22 \times 10^6 \text{ sec}^{-1}$ , about half that of the normal decay rate of the muon.

### ACKNOWLEDGMENTS

We wish to thank Professor H. W. B. Skinner for his interest and encouragement. Professor J. M. Cassels suggested the experiment to us and has helped us in many valuable discussions and with the loan of his time-sorter. A most

important contribution was made by Dr. S. G. F. Frank who lent us his target and carried out the filling and the enrichment. The  $4\frac{1}{2}$  in. NaI crystal was lent to us by Dr. L. L. Green, and Dr. J. C. Willmott. Their associates, Dr. J. J. Singh and Mr. E. E. Baart did the calibration run for us on the Cockcroft-Walton generator. We are indebted to Mr. D. N. Edwards for the method of estimating solid angles by using Gegenbauer functions, and to the cyclotron crew for their willing co-operation. K. S. is grateful for the hospitality extended to him during his stay in the laboratory, and to the Alfred P. Sloan foundation for making this stay possible. During the course of this work R. N. was the holder of a CERN Fellowship, and B. M. T. was in receipt of a maintenance grant from the Department of Scientific and Industrial Research.

## REFERENCES

- ALVAREZ, L. W., *et al.*, 1956, UCRL—3620 (University of California) ; 1957, *Phys. Rev.*, **105**, 1127.  
AUSTERN, N., 1952, *Phys. Rev.*, **85**, 147.  
BELL, W. E., and HINCKS, E. P., 1952, *Phys. Rev.*, **88**, 1424.  
COLLINGE, B., MERRISON, A. W., and ECCLESHALL, D., 1956, *J. Sci. Instrum.*, **33**, 72.  
CRESTI, M., GOTTSTEIN, K., ROSENFELD, A. H., and TICHO, H. K., 1957, UCRL—3782 (University of California), p. 8.  
DAVISSON, C. M., 1955, *Beta and Gamma ray Spectroscopy* (Ed. K. Siegbahn), (Amsterdam : North-Holland), Appendix I.  
FRANK, F. C., 1957, *Nature, Lond.*, **160**, 525.  
GALLONE, S., PROSPERI, G. M., and SCOTTI, A., 1957, *Nuovo Cim.*, **6**, 168.  
GOLDWASSER, E. L., MILLS, F. E., and HANSON, A. O., 1952, *Phys. Rev.*, **88**, 1137.  
JACKSON, T. D., 1957, *Phys. Rev.*, **106**, 330.  
KEUFFEL, J. W., HARRISON, F. B., GODFREY, T. N. K., and REYNOLDS, G. T., 1952, *Phys. Rev.*, **87**, 942.  
MICHEL, L., 1957, *Rev. Mod. Phys.*, **29**, 223.  
SKYRME, T. H. R., 1957, *Phil. Mag.*, **2**, 910.  
STERNHEIMER, R. M., 1952, *Phys. Rev.*, **88**, 851.  
WIGHTMAN, A. S., 1950, *Phys. Rev.*, **77**, 521.  
YANG, C. N., 1951, *Phys. Rev.*, **84**, 599.  
ZELDOVICH, Y. B., 1954, *Doklady Akad. Nauk, S.S.S.R.*, **95**, 493.

## Problem of Perturbed Boundary Condition in Quantum Mechanics

BY S. SEN GUPTA<sup>†</sup> AND H. MUKHOPADHYAY<sup>‡</sup>

<sup>†</sup> Physics Department, Darjeeling Government College, Darjeeling, West Bengal, India

<sup>‡</sup> Physics Department, Coochbehar Government College, Cooch Behar, West Bengal, India

*MS. received 10th September 1957*

**Abstract.** Problem of perturbed boundary condition is reduced to an equivalent problem of perturbation potential with the introduction of a deformed coordinate system. The method is applied to determine the energy of a nucleon in a rigid ellipsoidal box.

### § 1. INTRODUCTION

PROBLEM of perturbed boundary condition has been studied by many authors [Fröhlich (1938), Brillouin (1937), Feshbach (1944), Wasserman (1946) and (1948)]. We give in the following a new and much simpler approach to the same problem. Our basic assumption is that the perturbed boundary is expressible as an analytic function of the coordinates and that it is derivable as a small perturbation on a certain arbitrary spherical boundary. We shall introduce the concept of deformed coordinate system and reduce the problem to one with a perturbed potential. Expression for the perturbed potential operator is given for arbitrary deformation of the boundary. Application is shown in the case of an ellipsoidal boundary with rigid walls.

### § 2. PERTURBATION PROBLEM WITH DEFORMED COORDINATES

Let the deformed boundary be given by the equation

$$R = R_0 \{1 + \sum e_\alpha f_\alpha(\theta, \phi)\}, \quad \dots\dots(1)$$

where  $R_0$  is the radius of the sphere on which the deformed boundary may be considered as a small perturbation, the  $e_\alpha$  are the small deformation parameters and summation in (1) includes all such parameters necessary to describe the deformation. We have restricted ourselves to the first order terms only. In general, however, expansion (1) will include higher powers of  $e_\alpha$ .

Let us introduce a set of deformed coordinate system  $(\rho, \theta, \phi)$  defined by the equation

$$\rho = \frac{r}{1 + \sum e_\alpha f_\alpha(\theta, \phi)} \quad \dots\dots(2)$$

$\theta, \phi$  being the same as the corresponding quantities in radial coordinates. For  $\rho = R_0$  the surface traced out by  $(\rho, \theta, \phi)$  is the deformed surface (1). We now consider the quantum mechanical problem of a particle moving in a potential field and satisfying a certain boundary condition at the spherical surface  $R_0$ . We suppose that the solution for this case is known. We now investigate the corresponding solutions when the spherical boundary is deformed into the surface given by (1).

Transforming  $\nabla^2$  in the new coordinate system we get, retaining only first order terms in  $e_\alpha$ ,

$$\nabla_{\rho\theta\phi}^2 = \nabla_0^2 - 2 \sum e_\alpha f_\alpha \nabla_0^2 - \left\{ \sum \left( e_\alpha \frac{\partial^2 f_\alpha}{\partial \theta^2} + e_\alpha \cot \theta \frac{\partial f_\alpha}{\partial \theta} + \frac{e_\alpha}{\sin^2 \theta} \frac{\partial^2 f_\alpha}{\partial \phi^2} \right) \right\} \frac{1}{\rho} \frac{\partial}{\partial \rho} \\ - \frac{2}{\rho} \sum e_\alpha \frac{\partial f_\alpha}{\partial \theta} \frac{\partial^2}{\partial \rho \partial \theta} - \frac{2}{\rho \sin^2 \theta} \sum e_\alpha \frac{\partial f_\alpha}{\partial \phi} \frac{\partial^2}{\partial \rho \partial \phi} \dots \dots (3)$$

$\nabla_0^2$  is the same operator as in spherical coordinates.

Potential energy which is assumed to be a function of  $r$  only takes the form

$$V(r) = V(\rho) + \sum e_\alpha f_\alpha \rho \frac{\partial V}{\partial \rho} \dots \dots (4)$$

The wave equation therefore can be written in the form

$$\nabla_0^2 \psi + \frac{2m}{\hbar^2} (E - V(\rho) - V_{0p}) \psi = 0, \dots \dots (5)$$

where

$$V_{0p} = \frac{\hbar^2}{2m} \sum e_\alpha \left[ 2f_\alpha \nabla_0^2 + \left\{ \frac{\partial^2 f_\alpha}{\partial \theta^2} + \cot \theta \frac{\partial f_\alpha}{\partial \theta} + \frac{1}{\sin^2 \theta} \frac{\partial^2 f_\alpha}{\partial \phi^2} \right\} \frac{1}{\rho} \frac{\partial}{\partial \rho} \right. \\ \left. + \frac{2}{\rho} \frac{\partial f_\alpha}{\partial \theta} \frac{\partial^2}{\partial \rho \partial \theta} + \frac{2}{\rho \sin^2 \theta} \frac{\partial f_\alpha}{\partial \phi} \frac{\partial^2}{\partial \rho \partial \phi} - \frac{2m}{\hbar^2} f_\alpha \rho \frac{\partial V}{\partial \rho} \right] \dots \dots (6)$$

Since  $V_{0p}$  is small, we can treat the equation (5) by ordinary perturbation methods and the change in energy and wave function are easily calculated.

### § 3. APPLICATION

We shall apply the result to calculate the energy of a nucleon moving within a rigid ellipsoidal box. We consider the ellipsoid to be a perturbation of a sphere of radius  $R_0$  having same volume as the ellipsoid. Let the three axes of the ellipsoid be  $R_0 + a$ ,  $R_0 + b$  and  $R_0 + c$ . Deformation parameters are defined by

$$e_1 = \frac{c-a}{R_0}; \quad e_2 = \frac{c-b}{R_0} \dots \dots (7)$$

and the condition of constant volume gives  $a + b + c = 0$ . The ellipsoidal surface is described by the equation

$$R = R_0 [1 + \frac{1}{3} e_1 (1 - 3 \sin^2 \theta \cos^2 \phi) + \frac{1}{3} e_2 (1 - 3 \sin^2 \theta \sin^2 \phi)] \dots \dots (8)$$

Thus  $V_{0p}$  for this case is found to be

$$V_{0p} = - \frac{\hbar^2}{2m} \left[ - \frac{2}{3} e_1 (1 - 3 \sin^2 \theta \cos^2 \phi) \nabla_0^2 - \frac{2}{3} e_2 (1 - 3 \sin^2 \theta \sin^2 \phi) \nabla_0^2 \right. \\ \left. + \left\{ 2 \left( 3 \cos^2 \theta - 1 + \sin 2\theta \frac{\partial}{\partial \theta} \right) (e_1 \cos^2 \phi + e_2 \sin^2 \phi) - 2(e_1 - e_2) \cos 2\phi \right. \right. \\ \left. \left. - 2(e_1 - e_2) \sin 2\phi \frac{\partial}{\partial \phi} \right\} \frac{1}{\rho} \frac{\partial}{\partial \rho} \right] \dots \dots (9)$$

The diagonal matrix element of this operator in the  $lmsm_s$  scheme can be easily determined. Using the result

$$\int_0^\pi (3 \cos^2 \theta - 1) y_{lm}^2 \sin \theta d\theta = - \int_0^\pi \sin 2\theta y_{lm} \frac{\partial y_{lm}}{\partial \theta} \sin \theta d\theta \\ = \frac{2[l(l+1) - 3m^2]}{(2l+3)(2l-1)}, \dots \dots (10)$$



where  $y_{lm}$  are normalized Legendre polynomials, we get

$$\langle lmsm_s | V_{0p} | lmsm_s \rangle = \frac{2}{3} E_{\text{kin}} (e_1 + e_2) \frac{[l(l+1) - 3m^2]}{(2l+3)(2l-1)}. \quad \dots\dots(11)$$

$E_{\text{kin}}$  is the kinetic energy of the nucleons within the rigid spherical box of radius  $R_0$ . If  $e_1 = e_2$  our case reduces to that of a spheroidal box and equation (11) becomes identical with Rosenfeld's (1951) expression derived from Rainwater's (1950) calculation.

Comparing expression (9) with the interaction energy of a nucleon in an ellipsoidal nucleus as given by Bohr (1952), in his equation (74), we notice that the two expressions are not identical. Substituting  $\nabla_0^2 \psi = -(2m/\hbar^2)(E - V)\psi$  in (9) we get for the first two terms in (9),

$$V_{0p}^{-1} = -2 E_{\text{kin}} (R - R_0)/R_0. \quad \dots\dots(12)$$

This is identical with equation (74) of Bohr. Extra terms in (9) (those within braces) may be written in the form

$$\begin{aligned} V_{0p}^{-2} = & (e_1 + e_2) \left\{ 3 \cos^2 \theta - 1 + \sin 2\theta \frac{\partial}{\partial \theta} \right\} \frac{1}{\rho} \frac{\partial}{\partial \rho} \\ & + (e_1 - e_2) \left\{ -3 \sin^2 \theta \cos 2\phi + \sin 2\theta \cos 2\phi \frac{\partial}{\partial \theta} - 2 \sin 2\phi \frac{\partial}{\partial \phi} \right\} \frac{1}{\rho} \frac{\partial}{\partial \rho} \quad \dots\dots(13) \end{aligned}$$

This operator does not contribute anything to the diagonal matrix either in the  $lmsm_s$  scheme or in the  $lsjm$  scheme. Evidently first term in (13) also does not contribute to the non-diagonal elements. That the total contribution from the second term to the non-diagonal elements also vanishes in both the schemes is shown in the Appendix. Thus the interaction energy operator (9) of the nucleon in the ellipsoidal box reduces to the simple form (12) as given by Bohr.

## APPENDIX

We shall determine the non-diagonal matrix elements of the second term in (13) in the  $lmsm_s$  scheme. Since it contains  $\cos 2\phi$  or  $\sin 2\phi$  all matrix elements vanish if  $\Delta m$  is not  $\pm 2$ . For these cases matrix elements are easily calculated by using following results:

$$\begin{aligned} \int_0^\pi y_{l,m+2} y_{lm} \sin \theta d\theta &= - \left\{ \frac{(l-m)(l-m-1)}{(l+m+2)(l+m+1)} \right\}^{1/2} \\ \int_0^\pi y_{l+2,m} y_{l,m+2} \sin \theta d\theta &= 0 \\ \int_0^\pi y_{l-2,m} y_{l,m+2} \sin \theta d\theta &= 2(m+1) \left\{ \frac{(2l+1)(2l-3)}{(l+m+2)(l+m+1)(l+m)(l+m-1)} \right\}^{1/2} \\ \frac{1}{2} \sin 2\theta \frac{\partial y_{lm}}{\partial \theta} &= \left\{ \frac{(2l+1)(l+m+1)(l-m+1)}{2l+3} \right\}^{1/2} \cos \theta y_{l+1,m} - (l+1) \cos^2 \theta y_{lm}. \end{aligned}$$

Here  $m \geq 0$  and  $y_{lm}$  are the normalized Legendre polynomials with phases as defined by Condon and Shortley (1953, p. 52). Equation (21) on page 53 of the

above book may now be used to obtain all the necessary matrix elements. The results are

$$\begin{aligned}\langle lm+2 | \sin^2\theta \cos 2\phi | lm \rangle &= - \frac{\{(l+m+2)(l+m+1)(l-m)(l-m-1)\}^{1/2}}{(2l-1)(2l+3)} \\ \langle lm+2 | \sin 2\phi \frac{\partial}{\partial \phi} | lm \rangle &= - \frac{m}{2} \left\{ \frac{(l-m)(l-m-1)^{1/2}}{(l+m+2)(l+m+1)} \right\} \\ \langle lm+2 | \sin 2\theta \cos 2\phi \frac{\partial}{\partial \theta} | lm \rangle \\ &= - \frac{3(l+1)(l+2)+2m(l+1)(2l+3)+3m^2}{(2l-1)(2l+3)} \left\{ \frac{(l-m)(l-m-1)}{(l+m+2)(l+m+1)} \right\}^{1/2}.\end{aligned}$$

From (13) we obtain

$$\langle lm+2 | V_{op}^2 | lm \rangle = 0.$$

Similar calculations show that  $\langle lm-2 | V_{op}^2 | lm \rangle$  also vanishes.

The result will evidently be the same in the  $lsjm$  scheme, as each wave function in this scheme is a linear combination of two functions in the  $lmsm_s$  scheme. Since our operator (13) does not connect states differing in  $m_s$  the matrix of  $V_{op}^2$  in the  $lsjm$  scheme will include two separate matrices in the  $lmsm_s$  scheme. Since the latter will vanish individually we get the result

$$\langle jm \pm 2 | V_{op}^2 | jm \rangle = 0$$

#### REFERENCES

- BOHR, A., 1952, *Dan. Mat. Fys. Medd.*, **26**, No. 14.  
 BRILLOUIN, L., 1937, *C. R. Acad. Sci., Paris*, **204**, 1863.  
 CONDON, E. U., and SHORTLEY, G. H., 1953, *Theory of Atomic Spectra* (Cambridge : University Press).  
 FESHBACH, H., 1944, *Phys. Rev.*, **65**, 307.  
 FRÖHLICH, H., 1938, *Phys. Rev.*, **54**, 945.  
 RAINWATER, J., 1950, *Phys. Rev.*, **79**, 432.  
 ROSENFELD, L., 1951, *Physica*, **17**, 461.  
 WASSERMAN, G. D., 1946, *Phil. Mag.*, **37**, 563 ; 1948, *Proc. Camb. Phil. Soc.*, **44**, 251.

*Note added in proof.* Dr. S. A. Moszkowski has kindly pointed out a similar work by himself (*Phys. Rev.*, 1955, **99**, 803) which unfortunately escaped the authors' notice. He used a coordinate transformation to obtain spherical symmetry in the wave equation for the case of a spheroidal boundary. Instead of expanding the kinetic energy in powers of the deformation parameter he used the direct diagonalization method of the energy matrix.

# The Theory of Angular Correlations with Polarization

By F. MANDL

Atomic Energy Research Establishment, Harwell, Berks.

*Communicated by B. H. Flowers; MS. received 26th August 1957*

**Abstract.** The theory of angular correlations is reformulated using the algebra of tensor operators. This has important advantages resulting in considerable simplifications : (1) It enables us to deal in a uniform manner with all polarization problems for both particles and photons, leading automatically to expansions in terms of the most natural functions for any particular problem. (2) We expand the intensity directly in terms of spherical harmonics, rather than 'squaring' the expanded amplitude. (3) We avoid the quite unnecessary explicit introduction of sums over magnetic quantum numbers of products of Wigner coefficients and their subsequent elimination by means of cumbersome algebra. (4) In this procedure, the reduced matrix elements of certain tensor operators (formed from the polarization tensors) are calculated once and can then be used in all problems, since any angular correlation can be expressed simply in terms of these reduced matrix elements.

## § 1. INTRODUCTION

THE modern theory of angular correlations is essentially due to two fundamental contributions by Racah. He recognized how to separate out the purely geometrical factors, which occur as sums over magnetic quantum numbers of products of Wigner coefficients, from the physical factors (Racah 1951). Using techniques he had developed earlier (Racah 1942) he could write these sums in closed form†. These latter calculations lead to very heavy algebraic manipulation of Wigner coefficients (even quite simple problems involve sums of products of six or more of these) which become rapidly more cumbersome with the complexity of the problem.

In the spirit of Racah's work we shall, in this paper, achieve a considerable further simplification by applying the algebra of tensor operators (Racah 1942, Edmonds 1957) to angular correlation theory. In this way, the explicit introduction of Wigner coefficients and sums over magnetic quantum numbers will be avoided altogether‡. Our formulation of the theory will enable us to deal in a natural and unified manner with polarization problems of photons and particles. Furthermore, we shall see that the expressions for the angular correlations naturally subdivide into certain standard quantities referring to different radiations, spins, etc., permitting more complicated problems to be calculated easily in terms of these.

† These methods are discussed exhaustively by A. R. Edmonds (1957).

‡ A different method, which also avoids the explicit evaluation of these geometrical expressions, is based on the use of the statistical operator (Fano 1951, Coester and Jauch 1953). Comprehensive references to papers, etc., dealing with the various approaches to angular correlation theory are given by Siegbahn (1955), chap. 19.

No new results are derived in this paper, but problems involving the emission of radiation (photons or non-relativistic particles) are treated in sufficient generality to explain clearly how our formalism is to be applied to other cases. The emission of particles and photons from oriented nuclei will be treated in § 2 and § 3 respectively. These problems already involve all necessary steps. As an example of a more complicated problem, the double correlation will be treated in § 4. For convenience of the reader, the necessary results concerning angular momenta, rotation matrices, tensor operators and multipole radiations are stated in four appendices.

## § 2. RADIATION FROM ORIENTED NUCLEI : PARTICLES

Let us consider the decay of an oriented nucleus of spin  $J_0$ , decaying to a state of spin  $J_1$  and emitting a non-relativistic particle of spin  $s$ . The polarization of the initial nucleus is given by a weight function  $w(M_0)$  which gives the relative populations of the  $(2J_0 + 1)$  magnetic substates, referred to a fixed coordinate system  $\Gamma_0$ . Let  $|J_0 M_0\rangle$  denote the wave function of the initial nucleus in the state with  $z$ -component of spin equal to  $M_0$ . The development of the system, i.e. the decay of the initial nuclear level, can then formally be written in terms of the  $T$ -matrix

$$\begin{aligned} \Psi(J_0 M_0) \\ \equiv T |J_0 M_0\rangle = \sum |J_1(l)sj; J_0 M_0; \mathbf{r}\rangle \langle J_1(l)sj; J_0 M_0; \mathbf{r} | T | J_0 M_0\rangle, \quad \dots\dots(1) \end{aligned}$$

i.e.  $\Psi(J_0 M_0)$  represents the total decaying state, and we are interested in picking out the intensity corresponding to one particular final state (emission of the particle in the direction  $(\theta, \phi)$ ). In equation (1)  $|J_1(l)sj; J_0 M_0; \mathbf{r}\rangle$  represents a state with a final nucleus of spin  $J_1$ , having emitted a particle of spin  $s$  and orbital angular momentum  $l$  with resultant angular momentum  $j$ . The angular momenta  $J_1$  and  $j$  are combined to give a state whose total angular momentum is specified by  $(J_0, M_0)$ . The position vector of the emitted particle is denoted by  $\mathbf{r} = (r, \theta, \phi)$ . We have not stated explicitly other quantum numbers required to specify the nucleus or the emitted particle. The summation in equation (1) is over all final states. The  $T$ -operator is a scalar, i.e. the elements of the  $T$ -matrix are independent of the magnetic quantum number  $M_0$  and are diagonal in  $J_0$ . (In fact we assumed this already in writing equation (1).) Omitting the labels  $J_0, J_1$  and  $s$  we can simply write

$$\Psi(J_0 M_0) = \sum_{l,j} t(lj) |J_1(l)sj; J_0 M_0; \mathbf{r}\rangle. \quad \dots\dots(2)$$

The values of  $l$  and  $j$  which occur here are of course restricted by conservation of angular momentum, the parity of the nuclear levels, etc.

We can now write down the intensity per unit solid angle  $I(\theta, \phi)$  of particles emitted in the direction  $(\theta, \phi)$ . It is given by

$$I(\theta, \phi) = \sum_{M_0} w(M_0) \{ R^2 \sum \int |\Psi(J_0 M_0)|^2_{\mathbf{R}} \}, \quad \dots\dots(3)$$

where  $\mathbf{R} = (R, \theta, \phi)$  denotes the position vector of the emitted particle at a large distance  $R$  and  $\sum \int$  represents summation or integration over all coordinates except the position vector  $\mathbf{R}$ .

Expanding the angular distribution in spherical harmonics

$$I(\theta, \phi) = \sum_{\alpha=0}^{\infty} \sum_{\alpha=-\alpha}^{\alpha} A_{\alpha}^{\alpha} Y_{\alpha}^{\alpha}(\theta, \phi), \quad \dots\dots(4)$$



one at once obtains the expansion coefficients  $A_a^\alpha$  from equation (3) :

$$A_a^\alpha = \sum_{M_0} w(M_0) \int d\Omega Y_{\alpha}^{a*}(\theta\phi) \{ R^2 \sum \int |\Psi(J_0 M_0)|_{\mathbf{R}}^2 \} \\ = \sum_{M_0} w(M_0) R^2 \langle \Psi(J_0 M_0) | Y_{\alpha}^{a*}(\theta\phi) | \Psi(J_0 M_0) \rangle_{\mathbf{R}}, \quad \dots\dots(5)$$

where  $d\Omega = \sin\theta d\theta d\phi$ , and the matrix element in the last expression is with respect to all coordinates except the radial coordinate of the emitted particle which is held fixed at a large value  $R$ . It is convenient to separate out the radial dependence of the wave function in the asymptotic region of large  $R$  :

$$|J_1(ls)j; J_0 M_0; \mathbf{R}\rangle = |J_1(ls)j; J_0 M_0\rangle \frac{\exp\{i(\kappa R - l\pi/2)\}}{\kappa R}, \quad \dots\dots(6)$$

where  $\kappa$  is the wave number of the emitted particle. We can now write equation (5), with the aid of equation (2), as

$$A_a^\alpha = \frac{1}{\kappa^2} \sum_{lj} \sum_{l'j'} t^*(lj) t(l'j') i^{l-l'} \\ \times \sum_{M_0} w(M_0) \langle J_1(ls)j; J_0 M_0 | Y_{\alpha}^{a*}(\theta\phi) | J_1(l's)j'; J_0 M_0 \rangle, \quad \dots\dots(7)$$

which gives the angular distribution explicitly.

Before turning to the evaluation of expressions such as equation (7), let us consider the state of polarization of the beam of particles emitted in a given direction  $(\theta, \phi)$ . This is specified by the expectation values in the beam of a set of polarization tensors  $T_p^k$ . For a particle of spin  $s$  there are  $2s+1$  irreducible tensors of rank  $k=0, 1, \dots, 2s$  ( $k=0$  corresponds to the angular distribution without reference to polarization), each with  $2k+1$  components, labelled by  $p = -k, -k+1, \dots, k$ . (e.g. for spin  $\frac{1}{2}$ , we have the operators  $\sigma_x, \mp(\sigma_x \pm i\sigma_y)/\sqrt{2}$ . For spin 1, there is, in addition to the angular momentum operators, also a second rank tensor (cf. Appendix D, equations (D13-14).) The components of polarization tensors are here referred to the fixed coordinate system  $\Gamma_0$ . Let  $T_p^k(\alpha\beta\gamma)$  denote the components referred to a different coordinate system  $\Gamma(\alpha\beta\gamma)$ , obtained by rotating the system  $\Gamma_0$  through Eulerian angles  $(\alpha\beta\gamma)$ †. The new tensor components are then given by

$$T_p^k(\alpha\beta\gamma) = \sum_q T_q^k \mathfrak{D}_{qp}^k(\alpha\beta\gamma) \quad \dots\dots(8)$$

where the  $\mathfrak{D}_{qp}^k(\alpha\beta\gamma)$  are the matrices of the irreducible representations of the rotation group (Appendix B). In equation (8) the angles  $(\alpha\beta\gamma)$  may be constant or they may depend on  $(\theta\phi)$  corresponding to coordinate axes whose orientation is related to the direction in which the particle is emitted. The latter case is the more important one, since one is usually interested in the polarization relative to the direction of propagation, i.e. in the transverse (linear) or longitudinal (circular) polarization of the emitted particle (photon). This means choosing the direction of propagation as the new polar axis, i.e. taking Eulerian angles  $(\phi \theta 0)$ .

† For the components in the original system  $\Gamma_0$ , which should now be written  $T_p^k(000)$ , we shall always omit the arguments and write  $T_p^k$ .

The polarization intensity in the direction  $(\theta, \phi)$ , i.e. the product of the intensity  $I(\theta, \phi)$  and the expectation value of  $T_p^k(\alpha\beta\gamma)$  in the direction  $(\theta, \phi)$ , is given, using equation (8), by

$$I(\theta, \phi) \langle T_p^k(\alpha\beta\gamma) \rangle_{\theta\phi} = \sum_{M_0} w(M_0) \{ R^2 \langle \Psi(J_0 M_0) | \sum_q T_q^k \mathfrak{D}_{qp}^k(\alpha\beta\gamma) | \Psi(J_0 M_0) \rangle_{\mathbf{R}} \}, \quad \dots\dots (9a)$$

where, as indicated by the suffixes  $\mathbf{R}$ , the matrix elements are again taken at a constant value of  $\mathbf{R}$ . On this account we can take the rotation matrices outside the matrix element even if  $(\alpha\beta\gamma)$  depend on  $(\theta, \phi)$ , giving the alternative expression

$$I(\theta\phi) \langle T_p^k(\alpha\beta\gamma) \rangle_{\theta\phi} = \sum_q \mathfrak{D}_{qp}^k(\alpha\beta\gamma) \{ I(\theta\phi) \langle T_q^k \rangle_{\theta\phi} \} \\ = \sum_q \mathfrak{D}_{qp}^k(\alpha\beta\gamma) \sum_{M_0} w(M_0) \{ R^2 \langle \Psi(J_0 M_0) | T_q^k | \Psi(J_0 M_0) \rangle_{\mathbf{R}} \}. \quad \dots\dots (9b)$$

We now obtain different forms for the polarization intensity according as to whether we expand equation (9a) directly in spherical harmonics or expand  $I(\theta\phi) \langle T_q^k \rangle_{\theta\phi}$  and use equation (9b). The former method generally leads to difficulties (matrix elements which cannot easily be evaluated) and is of use only in special cases. For the coordinate system  $\Gamma(\phi\theta 0)$  and  $p=0$ , equation (8) reduces, on account of equations (B2) and (C4), to the scalar product

$$T_0^k(\phi\theta 0) = \left( \frac{4\pi}{[k]} \right)^{1/2} \mathbf{T}^k \cdot \mathbf{Y}^k(\theta\phi), \quad \dots\dots (10)$$

where

$$[k] = (2k+1). \quad \dots\dots (11)$$

Since this is invariant under rotations, the direct evaluation of equation (9a) is simple compared with decomposing the scalar product and using equation (9b). Hence for the case  $p=0$ , which corresponds to circular polarization, the direct evaluation of equation (9a) is preferable and we shall consider it in this connection in §3.

In this section, we want to give the generally applicable method of evaluating equation (9b) for the coordinate system  $\Gamma(\phi\theta 0)$ , the only case of practical interest (other than fixed axes which are always trivial). Expanding  $I(\theta\phi) \langle T_q^k \rangle_{\theta\phi}$  in spherical harmonics, equation (9b) becomes

$$I(\theta\phi) \langle T_p^k(\phi\theta 0) \rangle_{\theta\phi} = \sum_q \mathfrak{D}_{qp}^k(\phi\theta 0) \sum_{\alpha, \alpha'} Y_\alpha^q(\theta\phi) \{ R^2 \sum_{M_0} w(M_0) \\ \times \langle \Psi(J_0 M_0) | Y_\alpha^{a*} T_q^k | \Psi(J_0 M_0) \rangle_{\mathbf{R}} \} \\ = \sum_{a, \nu} \{ \sum_{\alpha, q} \mathfrak{D}_{qp}^k(\phi\theta 0) Y_\alpha^q(\theta\phi) (-1)^\alpha C_{-\alpha, q, q-\alpha}^{ak\nu} \} \\ \times \{ R^2 \sum_{M_0} w(M_0) \langle \Psi(J_0 M_0) | (\mathbf{Y}^a \cdot \mathbf{T}^k)_{q-\alpha}^\nu | \Psi(J_0 M_0) \rangle_{\mathbf{R}} \} \quad \dots\dots (12)$$

where  $C_{\alpha\beta\gamma}^{abc}$  is the Wigner coefficient (Appendix A) and the tensor product  $(\mathbf{Y}^a \cdot \mathbf{T}^k)_{q-\alpha}^\nu$  in the last line was introduced by means of equation (C2).

To evaluate the second curly bracket in equation (12) we use the Wigner-Eckert theorem, equation (C6), to extract the  $M_0$ -dependent terms, which are

$$\sum_{M_0} w(M_0) C_{M_0, q-\alpha, M_0}^{J_0^\nu J_0} = \delta_{\alpha q} \sqrt{\frac{[J_0]}{[\nu]}} F_\nu(J_0) \quad \dots\dots (13)$$

which defines Fano's statistical tensor  $F_\nu(J_0)$  (Fano 1951). Thus this term becomes

$$\delta_{\alpha q} R^2 F_\nu(J_0) [\nu]^{-1/2} \langle \Psi(J_0) | (\mathbf{Y}^a \cdot \mathbf{T}^k)^\nu | \Psi(J_0) \rangle_{\mathbf{R}}. \quad \dots\dots (14)$$

In calculating the first curly bracket in equation (12) we note that only terms with  $\alpha = q$  contribute on account of the  $\delta_{\alpha q}$  in equations (13-14). We replace the spherical harmonic  $Y_q^a$  by  $\mathfrak{D}_{-q,0}^a(\phi\theta)$  [equation (B2)], and successively apply equation (B4) and the ortho-normality relation of the Wigner coefficients, equation (A2), giving

$$\sqrt{\frac{[a]}{4\pi}} \mathfrak{D}_{0p}^v(\phi\theta) C_{0pp}^{akv} \dots \dots (15)$$

We rewrite  $\mathfrak{D}_{0p}^v(\phi\theta)$ , using equations (B3) and (B2) and the symmetry relation  $\mathfrak{D}_{qp}^v(0\theta) = (-1)^{q-p} \mathfrak{D}_{pq}^v(0\theta)$ , and rewrite  $C_{0pp}^{akv}$  in terms of  $C_{-p,p,0}^{vka}$  to obtain

$$\sum_q \mathfrak{D}_{qp}^k(\phi\theta) Y_q^a(\theta\phi) (-1)^q C_{-q,q,0}^{akv} = (-1)^{k+p} Y_{-p}^v(\theta) C_{-p,p,0}^{vka} \dots \dots (16)$$

Substituting equations (14) and (16) into equation (12), using also equations (2) and (6) to replace  $|\Psi(J_0 M_0)\rangle$ , we obtain

$$I(\theta\phi) \langle T_p^k(\phi\theta) \rangle_{\theta\phi} = \frac{(-1)^{k+p}}{\kappa^2} \sum_v F_v(J_0) [\nu]^{-1/2} Y_{-p}^v(\theta) \sum_{lj} \sum_{l'j'} t^* t' i^{l-l'} \times \sum_a C_{-p,p,0}^{vka} \langle J_1(ls)j; J_0 \| (\mathbf{Y}^a \cdot \mathbf{T}^k)^v \| J_1(l's)j'; J_0 \rangle, \dots \dots (17)$$

where  $t = t(lj)$  and  $t' = t(l'j')$ . The reduced matrix element (17) is given by equation (C9) since  $(\mathbf{Y}^a \cdot \mathbf{T}^k)^v$  operates on the wave functions of the emitted particle only:

$$\langle J_1(ls)j; J_0 \| (\mathbf{Y}^a \cdot \mathbf{T}^k)^v \| J_1(l's)j'; J_0 \rangle = (-1)^{J_1 + v - j - J_0} [J_0] W(jJ_0j'J_0; J_1\nu) \langle (ls)j \| (\mathbf{Y}^a \cdot \mathbf{T}^k)^v \| (l's)j' \rangle \dots \dots (18)$$

and substituting this into equation (17) gives

$$I(\theta\phi) \langle T_p^k(\phi\theta) \rangle_{\theta\phi} = \frac{(-1)^{k+p+J_1-J_0}}{\kappa^2} [J_0] \sum_v F_v(J_0) [\nu]^{-1/2} (-1)^v Y_{-p}^v(\theta) \times \sum_{lj} \sum_{l'j'} t^* t' i^{l-l'} (-1)^{-j} W(jJ_0j'J_0; J_1\nu) \times \langle (ls)j \| \sum_a C_{-p,p,0}^{vka} (\mathbf{Y}^a \cdot \mathbf{T}^k)^v \| (l's)j' \rangle. \dots \dots (19)$$

Thus the calculation of the angular distribution reduces to that of the last reduced matrix element. Furthermore, for a particle of given spin  $s$  and a particular polarization tensor, this matrix element need only be calculated once and for all and can then be fed into any other problem.

The reduced matrix element in equation (19) can be written, using equations (C7) and (C11):

$$\langle (ls)j \| \sum_a C_{-p,p,0}^{vka} (\mathbf{Y}^a \cdot \mathbf{T}^k)^v \| (l's)j' \rangle = \frac{(-1)^{l'}}{\sqrt{4\pi}} \{ [l][l'][j][j'][v] \}^{1/2} \langle s \| \mathbf{T}^k \| s \rangle \sum_a C_{-p,p,0}^{vka} C_{000}^{ll'a} \left\{ \begin{matrix} l & s & j \\ l' & s & j' \\ a & k & v \end{matrix} \right\} \dots \dots (20)$$

where the reduced matrix element  $\langle s \| \mathbf{T}^k \| s \rangle$  is of course easily calculated for a particular tensor  $\mathbf{T}^k$ , using the Wigner-Eckert theorem. Due to its generality, the evaluation of equation (20) may appear rather complicated at first sight. However, in practical cases, where one only deals with a few channels with small angular momenta and particles of small spin ( $s=0, \frac{1}{2}$  or 1, say) it simplifies greatly. We shall return to the case of spin 1 in § 3 in treating photons. Using

the properties of  $6j$  and  $9j$ -symbols one can write the  $a$ -summation in equation (20) as

$$\frac{(-1)^{p+2s}}{\{[k][\nu][j][j']\}^{1/2}} \sum_m C_{0mm}^{ksj} C_{0,p-m,p-m}^{l'sj'} C_{m,p-m,p}^{jj'\nu} C_{p-m,m,p}^{ssek} \dots\dots (21)$$

The usefulness of this formula is merely due to the fact that in many practical cases the sum over  $m$  reduces to a single term (cf. § 3).

The unpolarized angular distribution follows at once from equation (19). For  $k=p=0$ , the reduced matrix element of this equation reduces to  $\langle (ls)j \| \mathbf{Y}^\nu \| (l's)j' \rangle$  and this is the only quantity required for calculating unpolarized distributions. It is given by equation (C10). From equation (C11) and since  $\langle s \| 1 \| s \rangle = [s]^{1/2}$ , the unpolarized angular distribution becomes

$$I(\theta\phi) = \frac{(-1)^{J_1-J_0+s}}{\kappa^2 \sqrt{4\pi}} [J_0] \sum_{\nu \text{ even}} F_\nu(J_0) [\nu]^{-1/2} Y_0^\nu(\theta\phi) \sum_{lj} \sum_{l'j'} t^* t' i^{l-l'} (-1)^{2j} \\ \times \{[l][l'][j][j']\}^{1/2} W(jJ_0j'J_0; J_1\nu) C_{000}^{ll'\nu} W(lj l' j'; s\nu), \dots\dots (22)$$

where the restriction to even values of  $\nu$  follows from equation (A7), since conservation of parity implies that  $l-l'$  is even. This formula could of course have been obtained more easily directly from equation (7). Due to the special relations for  $C_{000}^{ll'\nu} W(lj l' j'; s\nu)$  given in Appendix A, equations (A4-6) and (A8), it simplifies further for spin  $\frac{1}{2}$  and 1 (cf. § 3). For  $s=\frac{1}{2}$ , equation (22) becomes

$$I(\theta\phi) = \frac{(-1)^{J_1-J_0-\frac{1}{2}}}{\kappa^2 \sqrt{4\pi}} [J_0] \sum_{\nu \text{ even}} F_\nu(J_0) [\nu]^{-1/2} Y_0^\nu(\theta\phi) \sum_{lj} \sum_{l'j'} t^* t' i^{l-l'} \\ \times \{[j][j']\}^{1/2} C_{\frac{1}{2},-\frac{1}{2},0}^{jj'\nu} W(jJ_0j'J_0; J_1\nu), \dots\dots (23)$$

where the second summation is over  $l$  and  $l'$  and  $j=l\pm\frac{1}{2}$ ,  $j'=l'\pm\frac{1}{2}$  (for  $l=0$ ,  $j=\frac{1}{2}$ , etc., as usual).

The angular distribution given by equation (19) is axially symmetric, as expected on physical grounds for this problem. This also explains why the alternative treatment based on equation (9a) is in general not satisfactory. It corresponds to an expansion in terms of  $Y_0^\nu(\theta\phi)$  instead of  $Y_{-p}^\nu(\theta\phi)$  which has turned out to be the natural set of polynomials. For  $p=0$ , the sets are identical, explaining why in this case either procedure is possible, as mentioned above.

Equations (19) and (20) contain all the usual parity and angular momentum selection rules; they follow from the triangle relations of the angular momenta in the  $6j$  and  $9j$ -symbols from equation (A7), etc.

### § 3. RADIATION FROM ORIENTED NUCLEI : PHOTONS

We shall now consider the emission of photons from oriented nuclei, using the same formalism as in the last section.

In Appendix D we give explicit expressions for electric and magnetic multipole fields, taken from Blatt and Weisskopf (1952, Appendix B) whose notation we follow. Blatt and Weisskopf show that in the wave-zone, where electric field  $\mathbf{E}$ , magnetic field  $\mathbf{H}$  and position vector  $\mathbf{R}$  are mutually orthogonal, the energy radiated per unit time into an element of solid angle  $d\Omega$  in the direction  $(\theta, \phi)$  is given by

$$R^2 d\Omega \frac{c}{2\pi} \mathbf{E}^*(\mathbf{R}) \cdot \mathbf{E}(\mathbf{R}) = R^2 d\Omega \frac{c}{2\pi} \mathbf{H}^*(\mathbf{R}) \cdot \mathbf{H}(\mathbf{R}). \dots\dots (24)$$



Similarly to equations (1) and (2), we can now specify the possible transitions from the initial nuclear state  $|J_0 M_0\rangle$  in terms of the  $T$ -matrix:

$$\begin{aligned}\Psi(J_0 M_0) &= T|J_0 M_0\rangle \\ &= \sum |J_1(\pi l); J_0 M_0; \mathbf{r}\rangle \langle J_1(\pi l); J_0 M_0; \mathbf{r} | T | J_0 M_0\rangle \\ &= \sum t(\pi l) |J_1(\pi l); J_0 M_0; \mathbf{r}\rangle. \quad \dots\dots (25)\end{aligned}$$

Here  $\pi$  labels the electric ( $\pi=E$ ) or magnetic ( $\pi=M$ ) nature of the radiation. We think of the 'wave function'  $|J_1(\pi l); J_0 M_0; \mathbf{r}\rangle$  as built up from the nuclear wave function and the electric field of the emitted multipole radiation. We can think of it as the electric field at the point  $\mathbf{r}$ , being an appropriately weighted superposition of the individual multipole fields. The use of the vector  $\Psi(J_0 M_0)$  is to indicate the vector character of this field. The intensity of the emitted radiation is again given by equations (3) to (5) (with  $\Psi$  replaced by  $\Psi$ ). We write the asymptotic form of the wave functions for large  $R$  as

$$|J_1(\pi l); J_0 M_0; \mathbf{R}\rangle = \Delta(\pi) |J_1 \mathbf{F}(\pi l); J_0 M_0\rangle \frac{\exp\{i(\kappa R - l\pi/2)\}}{\kappa R}, \quad \dots\dots (26)$$

where  $\Delta(\pi) = \mp 1$ , according as to whether  $\pi=E$  or  $\pi=M$  and the  $\mathbf{F}(\pi l)$  (which depend of course on the angles  $\theta, \phi$ ) are the multipole fields defined in Appendix D. We obtain the coefficients of the angular distribution, equation (4), analogously to the derivation of equation (7). Dropping a factor  $c/2\pi\kappa^2$  throughout the following, one finds that

$$\begin{aligned}A_\alpha^\alpha &= \sum_{\pi l} \sum_{\pi' l'} t^* t' \Delta(\pi) \Delta(\pi') i^{l-l'} \\ &\quad \times \sum_{M_0} w(M_0) \langle J_1 \mathbf{F}; J_0 M_0 | Y_\alpha^{a*}(\theta\phi) | J_1 \mathbf{F}'; J_0 M_0 \rangle, \quad \dots\dots (27)\end{aligned}$$

where  $\mathbf{F} = \mathbf{F}(\pi l)$ ,  $\mathbf{F}' = \mathbf{F}(\pi' l')$ ,  $t = t(\pi l)$  and  $t' = t(\pi' l')$ .

To evaluate equation (27) we again eliminate the  $M_0$ -dependence by means of the Wigner-Eckert theorem and by introducing the statistical tensor. Only terms with  $\alpha=0$  contribute, giving

$$\begin{aligned}A_a^0 &= F_a(J_0) [a]^{-1/2} \sum_{\pi l} \sum_{\pi' l'} t^* t' \Delta(\pi) \Delta(\pi') i^{l-l'} \langle J_1 \mathbf{F}; J_0 \| \mathbf{Y}^a \| J_1 \mathbf{F}'; J_0 \rangle \\ &= (-1)^{J_1 - J_0 + a} F_a(J_0) [a]^{-1/2} [J_0] \sum_{\pi l} \sum_{\pi' l'} t^* t' \Delta(\pi) \Delta(\pi') i^{-l-l'}, \\ &\quad \times W(l J_0 l' J_0; J_1 a) \langle \mathbf{F} \| \mathbf{Y}^a \| \mathbf{F}' \rangle, \quad \dots\dots (28)\end{aligned}$$

where the last line follows from equation (C9). These reduced matrix elements of  $\mathbf{Y}^a$  between any two multipole fields are given in Appendix D and it follows from equations (D10-12) that only even values of  $a$  occur if parity is conserved in the transition. In equation (28) the summation indices are varied independently. It is more convenient to write the angular distribution as a sum of terms each of which refers to the interference between two definite multipoles. For this purpose we define the real quantities

$$T(\pi l, \pi' l') = \left\{ \begin{array}{ll} |t(E l)|^2, & \text{if } \pi = \pi' = E, l = l', \\ i^{l-l'} \{ t^*(E l) t(E l') + t^*(E l') t(E l) \}, & \text{if } \pi = \pi' = E \\ |t(M l)|^2, & \text{if } \pi = \pi' = M, l = l' \\ i^{l-l'} \{ t^*(M l) t(M l') + t^*(M l') t(M l) \}, & \text{if } \pi = \pi' = M \\ i^{l-l'+1} \{ t^*(E l) t(M l') + t^*(M l') t(E l) \}, & \text{if } \pi = E, \pi' = M. \end{array} \right\} \quad (29)$$

Substituting equations (D10-12) and reordering terms with the help of equation (29), equation (28) becomes

$$A_a^0 = \frac{(-1)^{J_1-J_0+1}}{\sqrt{(4\pi)}} [J_0] F_a(J_0) [a]^{-1/2} \\ \times \sum T(\pi l, \pi' l') \{[l][l']\}^{1/2} C_{1,-1,0}^{ll'a} W(lJ_0 l' J_0; J_1 a), \quad (a=\text{even}), \quad \dots\dots(30)$$

with the individual terms in the summation corresponding to pairs of definite multipoles.

We next consider the general polarization tensor  $T_p^k(\phi\theta\theta)$ . For  $k=p=0$ , this will again reduce to the angular distribution. The appropriate tensor operators for circular and linear polarization are given in Appendix D. Proceeding as in § 2, one finds that

$$I(\theta\phi) \langle T_p^k(\phi\theta\theta) \rangle_{\theta\phi} = (-1)^{k+p+J_1-J_0} [J_0] \sum_{\nu} F_{\nu}(J_0) [\nu]^{-1/2} (-1)^{\nu} Y_{-\nu}^{\nu}(\theta\theta) \\ \times \sum_{\pi l} \sum_{\pi' l'} t^* t' \Delta(\pi) \Delta(\pi') i^{-l-l'} W(lJ_0 l' J_0; J_1 \nu) \\ \times \langle \mathbf{F} || \sum_a C_{-p,p,0}^{vka} (\mathbf{Y}^a \cdot \mathbf{T}^k)^{\nu} || \mathbf{F}' \rangle. \quad \dots\dots(31)$$

Taking  $k=p=0$ , equation (31) becomes equivalent to equations (28).

In Appendix D it is shown that the tensor operators corresponding to circular and linear polarization are  $T_0^1(\phi\theta\theta)$  and  $\{T_2^2(\phi\theta\theta) + T_{-2}^2(\phi\theta\theta)\}$  respectively. Correspondingly, we define operators

$$C_{\mu}^{\nu} = \sum_a C_{000}^{v1a} (\mathbf{Y}^a \cdot \mathbf{T}^1)_{\mu}^{\nu} \quad \dots\dots(32)$$

and

$$L_{\mu}^{\nu} = \sum_a (C_{2,-2,0}^{v2a} + C_{-2,2,0}^{v2a}) (\mathbf{Y}^a \cdot \mathbf{T}^2)_{\mu}^{\nu} \quad \dots\dots(33)$$

which are seen from equation (31) to be the operators we need. The reduced matrix elements of these operators between any two multipole fields are given in Appendix D, equations (D23-24) and (D26-27), and these enable us generally to deal with any polarization problem. Substituting these equations into equation (31) and again writing the distribution in terms of interference terms between definite multipoles with the aid of equation (29), one obtains :

(i) for circular polarization :

$$I(\theta\phi) \langle T_0^1(\phi\theta\theta) \rangle_{\theta\phi} = \frac{(-1)^{J_1-J_0}}{\sqrt{(4\pi)}} [J_0] \sum_{\nu=\text{odd}} F_{\nu}(J_0) [\nu]^{-1/2} Y_0^{\nu}(\theta\phi) \\ \times \sum T(\pi l, \pi' l') \{[l][l']\}^{1/2} C_{1,-1,0}^{ll'\nu} W(lJ_0 l' J_0; J_1 \nu), \quad \dots\dots(34)$$

where individual terms in the sum correspond to pairs of definite multipoles ;

(ii) for the linear polarization :

$$I(\theta\phi) \cdot \langle T_2^2(\phi\theta\theta) + T_{-2}^2(\phi\theta\theta) \rangle_{\theta\phi} \\ = \frac{(-1)^{J_1-J_0}}{\sqrt{(4\pi)}} [J_0] \sum_{\nu=\text{even}} F_{\nu}(J_0) [\nu]^{-1/2} Y_2^{\nu}(\theta\theta) \\ \times \sum_{l,l'} \{ -T(El, El') + T(Ml, Ml') - T(El, Ml') \} \{[l][l']\}^{1/2} C_{112}^{ll'\nu} W(lJ_0 l' J_0; J_1 \nu) \\ \dots\dots(35)$$

where we have written out explicitly the terms with different multipole character because of the changes in signs. These results, equations (30) and (34-35), agree with previously derived expressions, (cf. for example, Tolhoek and Cox (1953) who consider pure multipoles).

We consider briefly the alternative method of calculating the circular polarization, mentioned in § 2. The appropriate operator is now the spin component in the direction  $(\theta, \phi)$ , i.e. from equation (10) :

$$\left(\frac{4\pi}{3}\right)^{1/2} \mathbf{Y}^1(\theta\phi) \cdot \mathbf{S} \quad \dots\dots (36)$$

where we put  $\mathbf{S} \equiv \mathbf{T}^1$ . Expanding the angular distribution, equation (9a), in spherical harmonics,

$$\text{now gives} \quad I(\theta\phi) \langle S_0(\phi\theta 0) \rangle_{\theta\phi} = \sum_{a, \alpha} B_a^\alpha Y_\alpha^a(\theta\phi), \quad \dots\dots (37)$$

$$B_a^\alpha = \delta_{\alpha 0} \left(\frac{4\pi}{3}\right)^{1/2} (-1)^{J_1 - J_0 - a} F_a(J_0) [a]^{-1/2} [J_0] \sum_{\pi} \sum_{\pi'} t^* t' \Delta(\pi) \Delta(\pi') i^{-l-l'} \\ \times W(lJ_0 l' J_0; J_1 a) \langle \mathbf{F} \| (\mathbf{Y}^1 \cdot \mathbf{S}) \mathbf{Y}^a \| \mathbf{F}' \rangle. \quad \dots\dots (38)$$

Now

$$\langle \mathbf{F}(\pi l 0) | (\mathbf{Y}^1 \cdot \mathbf{S}) Y_0^a | \mathbf{F}(\pi' l' 0) \rangle \\ = \langle \mathbf{F}(\pi l 0) | \mathbf{Y}^1 \cdot \mathbf{S} | \mathbf{F}(\tilde{\pi} l 0) \rangle \langle \mathbf{F}(\tilde{\pi} l 0) | Y_0^a | \mathbf{F}(\pi' l' 0) \rangle, \quad \dots\dots (39)$$

where  $\tilde{\pi}$  means radiation of the opposite type to  $\pi$  (i.e. if  $\pi = E$ , then  $\tilde{\pi} = M$ , and *vice versa*). Equation (39) follows from the pseudo-scalar character of  $(\mathbf{Y}^1 \cdot \mathbf{S})$ , so that this is the only non-vanishing term in the expansion of the left-hand side. Using equation (D29), we can write

$$\langle \mathbf{F}(\pi l) | (\mathbf{Y}^1 \cdot \mathbf{S}) \mathbf{Y}^a | \mathbf{F}(\pi' l') \rangle = -i \Delta(\pi) \left(\frac{3}{4\pi}\right)^{1/2} \langle \mathbf{F}(\tilde{\pi} l) | \mathbf{Y}^a | \mathbf{F}(\pi' l') \rangle. \quad \dots\dots (40)$$

Thus this polarization distribution is also reduced to the matrix elements (D11-12). By means of equations (D11-12), (40) and (29), equation (38) can be completely evaluated, the distribution, equation (37), agreeing with our previous result, equation (34).

#### § 4. THE DOUBLE CORRELATION

The methods developed in the last two sections can easily be applied to more general problems. This merely involves writing down the correlation coefficients and successively decoupling angular momenta. As an example we consider briefly the well known directional correlation of two gamma rays successively emitted in the nuclear decay scheme  $J_0 \rightarrow J_1 \rightarrow J_2$  from an initially unpolarized nucleus.

Writing the angular distribution as

$$I(1, 2) = \sum A_{ab}^{\alpha\beta} Y_\alpha^a(1) Y_\beta^b(2) \quad \dots\dots (41)$$

where 1 and 2 specify the directions of emission  $(\theta_1\phi_1)$  and  $(\theta_2\phi_2)$ , the expansion coefficients are given by

$$A_{ab}^{\alpha\beta} = \sum_{\pi_1 l_1} \sum_{\pi_1' l_1'} \sum_{\pi_2 l_2} \sum_{\pi_2' l_2'} t_1^* t_1' t_2^* t_2' \Delta_1 \Delta_1' \Delta_2 \Delta_2' i^{l_1 - l_1' + l_2 - l_2'} X \quad \dots\dots (42)$$

where  $t_i' = t_i(\pi_i' l_i')$ ,  $t_i^* = t_i^*(\pi_i l_i)$ ,  $\Delta_i = \Delta(\pi_i)$ ,  $\Delta_i' = \Delta(\pi_i')$ , and, assuming the initial nucleus unpolarized ( $w(M_0) = [J_0]^{-1}$ ),  $X$  is given by

$$X = \sum_{M_0} [J_0]^{-1} \langle J_2 \mathbf{F}_2; J_1 \mathbf{F}_1; J_0 M_0 | Y_\alpha^{a*}(1) Y_\beta^{b*}(2) | J_2 \mathbf{F}_2'; J_1 \mathbf{F}_1'; J_0 M_0 \rangle \quad \dots\dots (43)$$

where  $\mathbf{F}_i = \mathbf{F}(\pi_i l_i)$ ,  $\mathbf{F}_i' = \mathbf{F}(\pi_i' l_i')$ . Substituting equation (C2) :

$$Y_{\alpha}^{a*}(1) Y_{\beta}^{b*}(2) = (-1)^{\alpha+\beta} \sum_{c, \gamma} C_{-\beta, -\alpha, \gamma}^{bac} (\mathbf{Y}^b(2) \cdot \mathbf{Y}^a(1))_{\gamma}^c \quad \dots\dots (44)$$

we can apply the Wigner-Eckert theorem, whence

$$\gamma = 0, \quad \text{i.e. } \beta = -\alpha, \quad \dots\dots (45)$$

and

$$X = \sum_c C_{\alpha, -\alpha, 0}^{bac} \langle J_2 \mathbf{F}_2; J_1 \mathbf{F}_1; J_0 \| (\mathbf{Y}^b(2) \cdot \mathbf{Y}^a(1))^c \| J_2 \mathbf{F}_2'; J_1 \mathbf{F}_1'; J_0 \rangle \\ \times [J_0]^{-3/2} \sum_{M_0} C_{M_0 0 M_0}^{J_0 c J_0}. \quad \dots\dots (46)$$

Since

$$[J_0]^{-3/2} \sum_{M_0} C_{M_0 0 M_0}^{J_0 c J_0} = [J_0]^{-1/2} \delta_{0c}, \\ X = C_{\alpha, -\alpha, 0}^{aa0} [J_0]^{-1/2} \langle J_2 \mathbf{F}_2; J_1 \mathbf{F}_1; J_0 \| (\mathbf{Y}^a(2) \cdot \mathbf{Y}^a(1))^0 \| J_2 \mathbf{F}_2'; J_1 \mathbf{F}_1'; J_0 \rangle. \quad \dots\dots (47)$$

Substituting equations (47) and (42) into equation (41) and using equation (C4) and the spherical harmonics addition theorem, equation (C5), one obtains for the angular correlation

$$I(\theta_{12}) = \sum_a A_a P_a(\cos \theta_{12}), \quad \dots\dots (48)$$

where

$$A_a = \sum t_1^* t_1' t_2^* t_2' \Delta_1 \Delta_1' \Delta_2 \Delta_2' i^{l_1 - l_1' + l_2 - l_2'} \\ \times \langle J_2 \mathbf{F}_2; J_1 \mathbf{F}_1; J_0 \| \mathbf{Y}^a(2) \cdot \mathbf{Y}^a(1) \| J_2 \mathbf{F}_2'; J_1 \mathbf{F}_1'; J_0 \rangle. \quad \dots\dots (49)$$

Here, as also in the following, we omit irrelevant constant factors. Equations (47) to (49) depend only on  $\theta_{12}$ , the angle between the directions of emission of the two gamma rays, as expected. We must now evaluate the reduced matrix element in equation (49). This is easily done using equations (C8) and (C9); one obtains

$$[J_0]^{1/2} (-1)^{J_0 - J_1 - l_1' + 2a} W(J_1 l_1 J_1 l_1'; J_0 a) \langle \mathbf{F}_1 \| \mathbf{Y}^a(1) \| \mathbf{F}_1' \rangle \\ \times \langle J_2 \mathbf{F}_2; J_1 \| \mathbf{Y}^a(2) \| J_2 \mathbf{F}_2'; J_1 \rangle \quad \dots\dots (50)$$

and

$$\langle J_2 \mathbf{F}_2; J_1 \| \mathbf{Y}^a(2) \| J_2 \mathbf{F}_2'; J_1 \rangle \\ = [J_1] (-1)^{J_1 + a - l_1 - J_1} W(J_1 l_2 J_1 l_2'; J_2 a) \langle \mathbf{F}_2 \| \mathbf{Y}^a(2) \| \mathbf{F}_2' \rangle. \quad \dots\dots (51)$$

Combining equations (49) to (51)

$$A_a = (-1)^{-a} \sum t_1^* t_1' t_2^* t_2' \Delta_1 \Delta_1' \Delta_2 \Delta_2' i^{l_1 + l_1' - l_2 - l_2'} \\ \times W(J_1 l_1 J_1 l_1'; J_0 a) W(J_1 l_2 J_1 l_2'; J_2 a) \langle \mathbf{F}_1 \| \mathbf{Y}^a(1) \| \mathbf{F}_1' \rangle \langle \mathbf{F}_2 \| \mathbf{Y}^a(2) \| \mathbf{F}_2' \rangle. \quad \dots\dots (52)$$

We proceed as in §2. With the aid of equation (29), we write the sum in equation (52) as a sum of terms each of which refers to a definite interference term  $(\pi l, \pi' l')$  for each transition and substitute equations (D10-12) for the reduced matrix elements  $\langle \mathbf{F}_i \| \mathbf{Y}^a(i) \| \mathbf{F}_i' \rangle$ .  $A_a$  is non-zero only for even  $a$  and is then given by

$$A_a = \sum (-1)^{l_1 + l_1'} T(\pi_1 l_1, \pi_1' l_1') T(\pi_2 l_2, \pi_2' l_2') \{ [l_1] [l_1'] [l_2] [l_2'] \}^{1/2} \\ \times C_{l_1 - 1, -1, 0}^{l_1 l_1' a} C_{l_2 - 1, -1, 0}^{l_2 l_2' a} W(J_1 l_1 J_1 l_1'; J_0 a) W(J_1 l_2 J_1 l_2'; J_2 a), \quad (a = \text{even}). \quad \dots\dots (53)$$



The factor  $(-1)^{l+l'}$  is equal to  $(-1)$  for terms arising from the interference of a magnetic and an electric multipole in the *first* transition  $J_0 \rightarrow J_1$ . It can be eliminated by a suitable redefinition of the transition amplitudes  $t(\pi l)$  (Biedenharn and Rose 1953).

## § 5. CONCLUSIONS

In this paper a method of calculating angular correlation problems is given which, we believe, has many advantages. It admits a uniform treatment of problems involving emission of particles or gamma rays, including polarization correlations. As we have seen, it automatically 'selects' the appropriate set of functions in terms of which to expand the distribution. In §2 and §3, for example, we dealt with problems possessing axial symmetry, and thus one might have expected an expansion in terms of the Legendre polynomials, i.e. the spherical harmonics  $Y_0(\theta\phi)$ . In fact, for a polarization tensor  $T_p^k(\phi\theta 0)$  we found the natural set of functions for the expansion to be the  $Y_{-p}^v(\theta, 0)$ , i.e. the associated Legendre polynomials.

By a reformulation of the basic equations of correlation theory, the angular distributions are expressed in a form which admits direct application of the algebra of tensor operators. In this way, one avoids the quite unnecessary introduction and subsequent laborious elimination of sums over magnetic quantum numbers of products of Wigner coefficients. This seems the more satisfactory, as one knows on general grounds that these geometrical factors can be expressed in closed form.

The method derived in this paper is of general applicability. The basic quantities are the reduced matrix elements of certain tensor operators (formed from the polarization tensors and characteristic of the state of polarization) with respect to single-particle states. These reduced matrix elements, referring to single particles, need only be calculated once; any correlation can be expressed in terms of them, using the algebra of tensor operators.

## ACKNOWLEDGMENTS

I should like to acknowledge several stimulating discussions with members of the Theoretical Physics Division, Atomic Energy Research Establishment, particularly with Dr. J. P. Elliott.

## APPENDIX A

### 3j, 6j and 9j Symbols

(i) The Wigner coefficient  $C_{\alpha\beta\gamma}^{abc}$  is defined in terms of the addition of the angular momenta of two independent systems. If these have total angular momenta  $a$  and  $b$  whose  $z$ -components are  $\alpha$  and  $\beta$  and the composite system is similarly specified by  $c$  and  $\gamma$ , then

$$\phi(c, \gamma) = \sum_{\alpha+\beta=\gamma} C_{\alpha\beta\gamma}^{abc} \phi(a, \alpha) \phi(b, \beta) \quad \dots\dots (A1)$$

where  $\phi(a, \alpha)$  is the wave function of the first system, etc. Equation (A1) defines the Wigner coefficients except for normalization and a phase factor. We choose these to agree with Condon and Shortley (1951), who denote these coefficients by

$$\langle ab\alpha\beta | abc\gamma \rangle \equiv C_{\alpha\beta\gamma}^{abc}$$

The Wigner coefficients satisfy numerous symmetry relations (cf. Edmonds. 1957) and the ortho-normality relation

$$\sum_{\alpha} C_{\alpha, \gamma-\alpha, \gamma}^{abk} C_{\alpha, \gamma-\alpha, \gamma}^{abl} = \delta_{kl}. \quad \dots\dots (A2)$$

(ii) The Racah coefficient  $W(abcd; ef)$  is defined by

$$\begin{aligned} C_{\alpha, \gamma-\alpha, \gamma}^{afc} \{[e][f]\}^{1/2} W(abcd; ef) \\ = \sum_{\beta} C_{\alpha, \beta, \alpha+\beta}^{abe} C_{\alpha+\beta, \gamma-\alpha-\beta, \gamma}^{edc} C_{\beta, \gamma-\alpha-\beta, \gamma-\alpha}^{bdf} \end{aligned} \quad \dots\dots (A3)$$

In the theory of multipole radiation certain special cases of equation (A3) are needed :

$$C_{000}^{LL'v} W(LL'L'; 1\nu) = \{[L][L']\}^{-1/2} C_{1,-1,0\frac{1}{2}}^{LL'v} \{1 + (-1)^{L+L'-v}\} \quad \dots\dots (A4)$$

$$C_{000}^{L, L'-1, v} W(L_2 L, L'-1, L'; 1\nu) = \left\{ \frac{L'+1}{[L][L'][L'-1]} \right\}^{1/2} C_{1,-1,0\frac{1}{2}}^{LL'v} \{1 + (-1)^{L+L'-1-v}\} \quad \dots\dots (A5)$$

$$C_{000}^{L, L'+1, v} W(L, L, L'+1, L'; 1\nu) = \left\{ \frac{L'}{[L][L'][L'+1]} \right\}^{1/2} C_{1,-1,0\frac{1}{2}}^{LL'v} \{1 + (-1)^{L+L'+1-v}\}. \quad \dots\dots (A6)$$

Equations (A4-6) follow from equation (A3), using the symmetry relations of the Wigner coefficients, the relation

$$C_{000}^{abc} = 0, \quad \text{if } a+b+c = \text{odd integer} \quad \dots\dots (A7)$$

and the explicit expression for the Wigner coefficient  $C_{\alpha\beta\gamma}^{ab1}$  (Condon and Shortley 1951, p. 76).

In the same way, one obtains the corresponding relation for spin  $\frac{1}{2}$  particles :

$$C_{000}^{LL'v} W(LJL'J'; \frac{1}{2}\nu) = \{[L][L']\}^{-1/2} C_{\frac{1}{2}, -\frac{1}{2}, 0\frac{1}{2}}^{JJ'v} \{1 + (-1)^{L+L'+v}\}. \quad \dots\dots (A8)$$

(In writing equations (A4-6) and (A8) we have suppressed 'Kronecker' deltas corresponding to the triangle relations for the angular momenta involved ; e.g. equation (A8) vanishes unless  $(L, J, \frac{1}{2})$  and  $(L', J', \frac{1}{2})$  satisfy triangle relations.)

(iii) The  $9j$ -symbol is defined in terms of the Racah coefficients by the equation

$$\left\{ \begin{matrix} abc \\ def \\ ghi \end{matrix} \right\} = \sum_{\lambda} [\lambda] W(abif; c\lambda) W(dfhb; e\lambda) W(adih; g\lambda). \quad \dots\dots (A9)$$

With one of the arguments zero, the  $9j$ -symbol reduces to a Racah coefficient. In particular,

$$\begin{aligned} \left\{ \begin{matrix} edc \\ eba \\ 0ff \end{matrix} \right\} &= \left\{ \begin{matrix} ced \\ aeb \\ f0f \end{matrix} \right\} = \left\{ \begin{matrix} abe \\ cde \\ ff0 \end{matrix} \right\} \\ &= \{[e][f]\}^{-1/2} (-1)^{e+f-a-d} W(abcd; ef). \end{aligned} \quad \dots\dots (A10)$$

## APPENDIX B

### Rotation Matrices

The rotation matrices  $\mathfrak{D}_{qp}^k(\alpha\beta\gamma)$  are defined in terms of the transformations of spherical harmonics under rotations of axes. If the point P has coordinates  $(r, \theta, \phi)$  in the coordinate system  $\Gamma_0$  and coordinates  $(r, \theta', \phi')$  referred to the

system  $\Gamma(\alpha\beta\gamma)$ , obtained by rotating the system  $\Gamma_0$  through Eulerian angles  $(\alpha, \beta, \gamma)^\dagger$ , then

$$Y_p^k(\theta' \phi') = \sum_q Y_q^k(\theta \phi) \mathcal{D}_{qp}^k(\alpha\beta\gamma). \quad \dots\dots(B1)$$

These rotation matrices are discussed fully by Edmonds (1957). We shall require these properties :

$$(i) \quad \mathcal{D}_{q0}^k(\phi \theta 0) = \left( \frac{4\pi}{2k+1} \right)^{1/2} Y_q^{k*}(\theta \phi) \quad \dots\dots(B2)$$

$$(ii) \quad \mathcal{D}_{qp}^k(\alpha\beta\gamma) = e^{-iq\alpha} \mathcal{D}_{qp}^k(0\beta 0) e^{-ip\gamma} \quad \dots\dots(B3)$$

$$(iii) \quad \mathcal{D}_{\lambda\mu}^a(\alpha\beta\gamma) \mathcal{D}_{\sigma\tau}^b(\alpha\beta\gamma) \\ = \sum_c C_{\lambda, \sigma, \lambda+\sigma}^{abc} C_{\mu, \tau, \mu+\tau}^{abc} \mathcal{D}_{\lambda+\sigma, \mu+\tau}^c(\alpha\beta\gamma). \quad \dots\dots(B4)$$

## APPENDIX C

### Tensor Operators

A set of  $(2k+1)$  quantities  $T_q^k$ , ( $q = -k, -k+1, \dots, k$ ), defines an irreducible tensor operator of rank  $k$  if, under rotations, it transforms like the spherical harmonics  $Y_q^k(\theta \phi)$  [cf. equation (B1)].

(i) From two commuting tensor operators  $T_{q_1}^{k_1}(1), U_{q_2}^{k_2}(2)$  (e.g. they refer to two independent systems, labelled 1 and 2) we can form tensor products of rank  $k$  :

$$(\mathbf{T}^{k_1} \cdot \mathbf{U}^{k_2})_q^k = \sum_{q_1+q_2=q} C_{q_1 q_2 q}^{k_1 k_2 k} T_{q_1}^{k_1} U_{q_2}^{k_2}, \quad \dots\dots(C1)$$

whence

$$T_{q_1}^{k_1} U_{q_2}^{k_2} = \sum_k C_{q_1 q_2 q}^{k_1 k_2 k} (\mathbf{T}^{k_1} \cdot \mathbf{U}^{k_2})_q^k \quad \dots\dots(C2)$$

In particular for  $k_1 = k_2 = K$  we can form a scalar product ( $k=0$ ) :

$$(\mathbf{T}^K \cdot \mathbf{U}^K)_0^0 = \sum_q C_{q, -q, 0}^{KK0} T_q^K U_{-q}^K. \quad \dots\dots(C3)$$

Racah (1942) defined the scalar product slightly differently. We shall write his definition in the form

$$\mathbf{T}^K \cdot \mathbf{U}^K = \sum_q (-1)^q T_q^K U_{-q}^K = (-1)^K [K]^{1/2} (\mathbf{T}^K \cdot \mathbf{U}^K)_0^0. \quad \dots\dots(C4)$$

The spherical harmonics addition theorem is a special case of equation (C4) :

$$\mathbf{Y}^K(\theta_1 \phi_1) \cdot \mathbf{Y}^K(\theta_2 \phi_2) = \frac{[K]}{4\pi} P_K(\cos \theta_{12}) \quad \dots\dots(C5)$$

where  $\theta_{12}$  is the angle between the unit vectors  $(\theta_1 \phi_1)$  and  $(\theta_2 \phi_2)$ .

(ii) The Wigner-Eckert theorem gives the dependence on magnetic quantum numbers of a matrix element  $\langle \alpha j m | T_q^k | \alpha' j' m' \rangle$  where  $|\alpha j m\rangle$  is a state with angular momentum  $j$ ,  $z$ -component of angular momentum  $m$  and  $\alpha$  specifies all other quantum numbers. Then

$$\langle \alpha j m | T_q^k | \alpha' j' m' \rangle = (-1)^{2k} [j]^{-1/2} C_{m' q m}^{j' k j} \langle \alpha j || \mathbf{T}^k || \alpha' j' \rangle \quad \dots\dots(C6)$$

which is the definition of the reduced matrix element  $\langle \alpha j || \mathbf{T}^k || \alpha' j' \rangle$ .

† We define these rotations as successively : (i) through  $\alpha$  about the  $z$ -axis, (ii) through  $\beta$  about the new  $y$ -axis, (iii) through  $\gamma$  about the new  $z$ -axis.

(iii) Consider two independent systems, specified completely by the two sets of quantum numbers  $\alpha_i, j_i, m_i$ , ( $i=1, 2$ ), which combine to a single system specified by  $\alpha, j, m$ . Then the reduced matrix element of the tensor product  $(\mathbf{T}^{k_1} \cdot \mathbf{U}^{k_2})_q^k$  is given by (Edmonds 1957)

$$\langle \alpha j_1 j_2 j \| (\mathbf{T}^{k_1} \cdot \mathbf{U}^{k_2})_q^k \| \alpha' j_1' j_2' j' \rangle = \{[j][j']\}^{1/2} \begin{Bmatrix} j_1 & j_2 & j \\ j_1' & j_2' & j' \\ k_1 & k_2 & k \end{Bmatrix} \times \sum_{\alpha''} \langle \alpha j_1 \| \mathbf{T}^{k_1} \| \alpha'' j_2 \rangle \langle \alpha'' j_2 \| \mathbf{U}^{k_2} \| \alpha' j_2' \rangle. \quad \dots (C7)$$

For the case of the scalar product, equation (C4), this gives, using equations (C6) and (A10) :

$$\begin{aligned} \langle \alpha j_1 j_2 j m | \mathbf{T}^K \cdot \mathbf{U}^K | \alpha' j_1' j_2' j' m' \rangle \\ = \delta_{j_1' m_1' m} (-1)^{j-j_1-j_2'+2K} W(j_1 j_2 j_1' j_2' ; j K) \\ \times \sum_{\alpha''} \langle \alpha j_1 \| \mathbf{T}^K \| \alpha'' j_1' \rangle \langle \alpha'' j_2 \| \mathbf{U}^K \| \alpha' j_2' \rangle. \quad \dots (C8) \end{aligned}$$

From equation (C7) we can derive two special important cases by taking  $\mathbf{T}^{k_1} \equiv 1$  or  $\mathbf{U}^{k_2} \equiv 1$ . Using equations (A10),

$$\begin{aligned} \langle \alpha j_1 j_2 j \| \mathbf{U}^k \| \alpha' j_1' j_2' j' \rangle = \delta_{j_1 j_1'} (-1)^{j_1+k-j_2-j'} \{[j][j']\}^{1/2} \\ \times W(j_2 j_2' j' ; j_1 k) \langle \alpha j_2 \| \mathbf{U}^k \| \alpha' j_2' \rangle, \quad \dots (C9) \end{aligned}$$

$$\begin{aligned} \langle \alpha j_1 j_2 j \| \mathbf{T}^k \| \alpha' j_1' j_2' j' \rangle = \delta_{j_2 j_2'} (-1)^{j_2+k-j_1-j'} \{[j][j']\}^{1/2} \\ \times W(j_1 j_1' j' ; j_2 k) \langle \alpha j_1 \| \mathbf{T}^k \| \alpha' j_1' \rangle. \quad \dots (C10) \end{aligned}$$

(iv) If we write  $|\lambda \mu\rangle = Y_\mu^\lambda(\theta \phi)$ , then

$$\langle \lambda \| \mathbf{Y}^a \| \lambda' \rangle = \frac{(-1)^{\lambda'}}{\sqrt{(4\pi)}} \{[\lambda][\lambda']\}^{1/2} C_{000}^{\lambda \lambda' a}. \quad \dots (C11)$$

If  $|\frac{1}{2}\mu\rangle$  denote the spin wave functions of a particle of spin  $\frac{1}{2}$ , ( $\mu = -\frac{1}{2}, \frac{1}{2}$ ), and  $\sigma_q$ , ( $q = -1, 0, 1$ ), the Pauli spin matrices (these form a tensor of the first rank, i.e. a vector), then

$$\langle \frac{1}{2} \| \boldsymbol{\sigma} \| \frac{1}{2} \rangle = \sqrt{6}. \quad \dots (C12)$$

The corresponding reduced matrix elements for photons ('spin' 1) will be given in Appendix D.

## APPENDIX D

### Multipole Radiation

(i) With  $(\mathbf{e}_x, \mathbf{e}_y, \mathbf{e}_z)$  unit vectors in the directions of the coordinate axes, let

$$\boldsymbol{\chi}_0 = \mathbf{e}_z, \quad \boldsymbol{\chi}_{\pm 1} = \mp \frac{1}{\sqrt{2}} (\mathbf{e}_x \pm i\mathbf{e}_y). \quad \dots (D1)$$

Define

$$|(\lambda 1)lm\rangle = \sum_{\mu} C_{m+\mu, -\mu, m}^{\lambda 1 l} Y_{m+\mu}^{\lambda}(\theta \phi) \boldsymbol{\chi}_{-\mu}. \quad \dots (D2)$$

Electric and magnetic  $2^l$ -pole fields are then defined in the wave zone by

$$\mathbf{E}_M = \mathbf{H}_E = \frac{\exp \{i(\kappa r - l\pi/2)\}}{\kappa r} \mathbf{F}(Mlm), \quad \dots (D3)$$

$$-\mathbf{E}_E = \mathbf{H}_M = \frac{\exp \{i(\kappa r - l\pi/2)\}}{\kappa r} \mathbf{F}(Elm), \quad \dots (D4)$$

where  $\kappa$  is the wave number of the emitted photon and

$$\mathbf{F}(Mlm) = \mathbf{L} Y_m^l(\theta \phi) / \{l(l+1)\}^{1/2} = |(l1)lm\rangle \quad \dots (D5)$$



$$\begin{aligned}\mathbf{F}(Elm) &= ir \text{grad } Y_m^l(\theta \phi) / \{l(l+1)\}^{1/2} \\ &= [l]^{-1/2} i \{ \sqrt{l} | (l+1, 1)lm \rangle + \sqrt{l+1} | (l-1, 1)lm \rangle \}. \quad \dots\dots (D6)\end{aligned}$$

(ii) Denoting the three components of the three unit vectors

$\chi_\mu$ , ( $\mu = -1, 0, 1$ ), by  $\chi_\mu^i$ ,  $i = 1, 2, 3$  :

$$\langle \chi_\mu | \chi_{\mu'} \rangle = \sum_i \chi_\mu^{i*} \chi_{\mu'}^i = \delta_{\mu\mu'} \quad \dots\dots (D7)$$

and

$$\langle \chi | \chi \rangle = \sum_i \langle \chi^i | \chi^i \rangle = \sqrt{3}. \quad \dots\dots (D8)$$

Using equations (C10-11) :

$$\langle (\lambda 1)l || \mathbf{Y}^a || (\lambda' 1)l' \rangle = \frac{(-1)^{1+a-l}}{\sqrt{(4\pi)}} \{ [l][l'][\lambda][\lambda'] \}^{1/2} C_{000}^{\lambda\lambda a'} W(\lambda\lambda' l' ; 1a) \quad \dots\dots (D9)$$

Equations (D5-9), together with equations (C10) and (A4-6), give the reduced matrix elements  $\langle \mathbf{F}(\pi l) || \mathbf{Y}^a || \mathbf{F}(\pi' l') \rangle$  where  $\pi$  stands for electric ( $\pi = E$ ) or magnetic ( $\pi = M$ ) radiation :

$$\left. \begin{aligned} \langle \mathbf{F}(El) || \mathbf{Y}^a || \mathbf{F}(El') \rangle \\ \langle \mathbf{F}(Ml) || \mathbf{Y}^a || \mathbf{F}(Ml') \rangle \end{aligned} \right\} = \frac{(-1)^{1+a-l}}{\sqrt{(4\pi)}} \{ [l][l'] \}^{1/2} C_{1,-1,0}^{ll'a} \frac{1}{2} \{ 1 + (-1)^{l+l'+a} \} \quad \dots\dots (D10)$$

$$\left. \begin{aligned} (-1) \langle \mathbf{F}(El) || \mathbf{Y}^a || \mathbf{F}(Ml') \rangle \\ \langle \mathbf{F}(Ml) || \mathbf{Y}^a || \mathbf{F}(El') \rangle \end{aligned} \right\} = \frac{(-1)^{1+a-l}}{\sqrt{(4\pi)}} i \{ [l][l'] \}^{1/2} C_{1,-1,0}^{ll'a} \frac{1}{2} \{ 1 + (-1)^{l+l'+1+a} \}, \quad \dots\dots (D11)$$

$$\text{and} \quad \langle \mathbf{F}(\pi l) || \mathbf{Y}^a || \mathbf{F}(\pi' l') \rangle = (-1)^{l'-l} \langle \mathbf{F}(\pi' l') || \mathbf{Y}^a || \mathbf{F}(\pi l) \rangle. \quad \dots\dots (D12)$$

(iii) Let  $\mathbf{S}$  be the angular momentum vector for a particle of spin 1, operating in the spin space spanned by the three vectors  $\chi_\mu$ , ( $\mu = -1, 0, 1$ ). We then define the tensor operators :

$$T_0^1 = S_z, \quad T_{\pm 1}^1 = \mp \frac{1}{\sqrt{2}} (S_x \pm iS_y) \quad \dots\dots (D13)$$

and

$$T_{\pm 2}^2 = \left\{ \mp \frac{1}{\sqrt{2}} (S_x \pm iS_y) \right\}^2, \quad \dots\dots (D14)$$

so that

$$T_2^2 + T_{-2}^2 = (S_x^2 - S_y^2). \quad \dots\dots (D15)$$

(We shall not require the other second-rank tensors; they are given in Mandl and Regge (1955).) Operating on the basis vectors  $\chi_\mu$  these operators have the properties

$$S_z \chi_\mu = \mu \chi_\mu \quad \dots\dots (D16)$$

and

$$(T_2^2 + T_{-2}^2) \chi_\mu = |\mu| \chi_{-\mu} \quad \dots\dots (D17)$$

so that from equation (D1)

$$\left. \begin{aligned} (\mathbf{e}_x, (T_2^2 + T_{-2}^2) \mathbf{e}_x) &= -1 \\ (\mathbf{e}_y, (T_2^2 + T_{-2}^2) \mathbf{e}_y) &= +1. \end{aligned} \right\} \quad \dots\dots (D18)$$

It follows that the expectation value of the operator  $S_z$  with respect to the electric field, of a photon propagating in the direction of the  $z$ -axis, gives the circular polarization, a positive (negative) value corresponding to left-circular (right-circular) polarization. Similarly, the operator  $(T_2^2 + T_{-2}^2)$  will give the linear polarization for such a photon, positive and negative values corresponding to linear polarizations in the directions of the  $y$ - and  $x$ -axis respectively. For a photon emitted in the direction  $(\theta, \phi)$  the appropriate operators, obtained by a rotation of axes, are  $T_0^1(\phi, \theta, 0)$  and  $\{T_2^2(\phi, \theta, 0) + T_{-2}^2(\phi, \theta, 0)\}$ , cf. equation (8). The expectation values of these operators now give the corresponding polarizations referred to the new coordinate system  $\Gamma(\phi, \theta, 0)$ .

We require now the reduced matrix elements of the operators  $C_\mu^\nu$  and  $L_\mu^\nu$ , equations (32–33), between any two multipole fields  $\mathbf{F} = \mathbf{F}(\pi l m)$  and  $\mathbf{F}' = \mathbf{F}(\pi' l' m')$ . We consider first the quantity

$$\langle (\lambda 1) l \| \sum_a C_{-p, p, 0}^{\nu k a} (\mathbf{Y}^a \cdot \mathbf{T}^k)^\nu \| (\lambda' 1) l' \rangle \quad \dots (19)$$

from which the multipole matrix elements can be derived (on account of equations (D5–6)). Using equations (C7) and (C11), this can be written

$$\frac{(-1)^{\lambda'}}{\sqrt{(4\pi)}} \langle 1 \| \mathbf{T}^k \| 1 \rangle \{ [l] [l'] [\lambda] [\lambda'] [\nu] \}^{1/2} \\ \times \left\{ \sum_a C_{-p, p, 0}^{\nu k a} C_{000}^{\lambda \lambda' a} \begin{Bmatrix} \lambda & 1 & l \\ \lambda' & 1 & l' \\ a & k & \nu \end{Bmatrix} \right\} \quad \dots (D20)$$

The summation over  $a$  can be rewritten, using the properties of the  $6j$  and  $9j$ -symbols, in the form of equation (21) of § 2.

For circular polarization the  $m$ -summation in equation (21) reduces to a single term. In this case  $k=1$ ,  $p=0$ , and the last Wigner coefficient in equation (21),  $C_{-m, m, 0}^{111}$ , vanishes for  $m=0$  (equation (A7)), and the terms with  $m = \pm 1$  are equal since

$$C_{\alpha\beta\gamma}^{abc} = (-1)^{a+b-c} C_{-\alpha, -\beta, -\gamma}^{abc} \quad \dots (D21)$$

From equations (32) and (D19–20) one then finds that

$$\langle (\lambda 1) l \| \mathbf{C}^\nu \| (\lambda' 1) l' \rangle \\ = C_{1, -1, 0}^{l' \nu} \frac{(-1)^{\lambda'}}{\sqrt{(4\pi)}} \{ [\lambda] [\lambda'] \}^{1/2} C_{011}^{\lambda 1 l} C_{011}^{\lambda' 1 l'} \{ 1 + (-1)^{\lambda + \lambda' + 1 - \nu} \}. \quad \dots (D22)$$

The required reduced matrix elements now follow from equations (D5–6). Assuming conservation of parity for the transition, it follows that for an electric–electric or magnetic–magnetic interference term  $l-l'$  and  $\lambda-\lambda'$  are both even integers, whereas for an electric–magnetic interference term  $l-l'$  is odd but  $\lambda-\lambda'$  is still even. It follows from equation (D22) that only odd values of  $\nu$  contribute to the circular polarization. For the allowed values of  $l-l'$  (i.e.  $l-l'$  is even (odd) for  $EE$  and  $MM$  ( $EM$  and  $ME$ ) terms), one then finds that

$$\left. \begin{aligned} & \langle \mathbf{F}(El) \| \mathbf{C}^\nu \| \mathbf{F}(El') \rangle \\ & \langle \mathbf{F}(Ml) \| \mathbf{C}^\nu \| \mathbf{F}(Ml') \rangle \\ & -i \langle \mathbf{F}(El) \| \mathbf{C}^\nu \| \mathbf{F}(Ml') \rangle \\ & i \langle \mathbf{F}(Ml) \| \mathbf{C}^\nu \| \mathbf{F}(El') \rangle \end{aligned} \right\} = C_{1, -1, 0}^{l' \nu} \frac{(-1)^{\lambda'}}{\sqrt{(4\pi)}} \{ [l] [l'] \}^{1/2}, \quad \dots (D23)$$

and (again for odd  $\nu$ )

$$\langle \mathbf{F}(\pi l) \| \mathbf{C}^\nu \| \mathbf{F}(\pi' l') \rangle = (-1)^{l-l'} \langle \mathbf{F}(\pi l') \| \mathbf{C}^\nu \| \mathbf{F}(\pi' l) \rangle. \quad \dots (D24)$$

For the case of linear polarization,  $k=2$ ,  $p=\pm 2$ , the  $m$ -summation in equation (21) again reduces to one term, since the last Wigner coefficient in that expression vanishes unless  $|p-m|\leq 1$ . Equation (21) then gives, in close similarity to equation (D22):

$$\langle (\lambda 1) l \| \mathbf{L}^v \| (\lambda' 1) l' \rangle = C_{112}^{ll'v} \frac{(-1)^{\lambda'}}{\sqrt{(4\pi)}} \{ [\lambda][\lambda'] \}^{1/2} C_{011}^{\lambda 1 l} C_{011}^{\lambda' 1 l'} \{ 1 + (-1)^{\lambda+\lambda'-v} \}. \dots (D25)$$

It now follows that for transitions permitted by conservation of parity,  $v$  is necessarily even and for such transitions

$$\left. \begin{aligned} & - \langle \mathbf{F}(El) \| \mathbf{L}^v \| \mathbf{F}(El') \rangle \\ & \langle \mathbf{F}(Ml) \| \mathbf{L}^v \| \mathbf{F}(Ml') \rangle \\ & - i \langle \mathbf{F}(El) \| \mathbf{L}^v \| \mathbf{F}(Ml') \rangle \\ & - i \langle \mathbf{F}(Ml) \| \mathbf{L}^v \| \mathbf{F}(El') \rangle \end{aligned} \right\} = C_{112}^{ll'v} \frac{(-1)^v}{\sqrt{(4\pi)}} \{ [l][l'] \}^{1/2}, \dots (D26)$$

and (again for even  $v$ )

$$\langle \mathbf{F}(\pi l) \| \mathbf{L}^v \| \mathbf{F}(\pi' l') \rangle = \langle \mathbf{F}(\pi' l') \| \mathbf{L}^v \| \mathbf{F}(\pi l) \rangle. \dots (D27)$$

In deriving these expressions we have required, in equation (D20), the reduced matrix elements of  $\mathbf{T}^k$ . These are easily found to be

$$\langle 1 \| \mathbf{T}^k \| 1 \rangle = \begin{cases} \sqrt{3}, & \text{if } k=0, \\ \sqrt{6}, & \text{if } k=1, \\ \sqrt{5}, & \text{if } k=2. \end{cases} \dots (D28)$$

With the aid of equations (D5-6), (C8), (C11) and (D28) one easily derives

$$\left. \begin{aligned} & \langle \mathbf{F}(El0) | \mathbf{Y}^1 \cdot \mathbf{S} | \mathbf{F}(Ml0) \rangle \\ & - \langle \mathbf{F}(Ml0) | \mathbf{Y}^1 \cdot \mathbf{S} | \mathbf{F}(El0) \rangle \end{aligned} \right\} = i \left( \frac{3}{4\pi} \right)^{1/2} \dots (D29)$$

which is required in the derivation of equation (40).

# REFERENCES

- BIEDENHARN, L. C., and ROSE, M. E., 1953, *Rev. Mod. Phys.*, **25**, 729.  
 BLATT, J. M., and WEISSKOPF, V. F., 1952, *Theoretical Nuclear Physics* (New York : Wiley).  
 COESTER, F., and JAUCH, J. M., 1953, *Helv. Phys. Acta*, **26**, 3.  
 CONDON, E. U., and SHORTLEY, G. H., 1951, *Theory of Atomic Spectra* (Cambridge : University Press).  
 EDMONDS, A. R., 1957, *Angular Momentum in Quantum Mechanics* (Princeton : University Press).  
 FANO, U., 1951, *Nat. Bur. Standards (Wash., D.C.)*, *Rep. No.* 1214.  
 MANDL, F., and REGGE, T., 1955, *Phys. Rev.*, **99**, 1478.  
 RACAH, G., 1942, *Phys. Rev.*, **62**, 438; 1951, *Ibid.*, **84**, 910.  
 SIEGBAHN, K., 1955, *Beta and Gamma-Ray Spectroscopy* (Amsterdam : North-Holland Publishing Co.).  
 TOLHOEK, H. A., and COX, J. A. M., 1953, *Physica*, **19**, 101.

# Nuclear Gamma Ray Resonance in $^{48}\text{Ti}$

By V. KNAPP†

Department of Physics, University of Birmingham

*Communicated by P. B. Moon: MS. received 16th September 1957,  
and in final form 28th October 1957*

**Abstract.** The resonance scattering of the  $^{48}\text{V}$  990 kev gamma rays in titanium was observed using the recoil of the previous transition to restore the recoil losses. From the measured scattering cross section, the mean life of the 990 kev level was found to be  $(6 \pm 2) \times 10^{-12}$  sec, which is rather shorter than the Coulomb excitation value.

Extending the comparison of mean lives as obtained by the two methods to other even-even nuclei, the same discrepancy is found in all available cases.

## § 1. INTRODUCTION

THE lifetimes of excited levels of nuclei can be measured directly when longer than about  $2 \times 10^{-11}$  sec. Shorter lifetimes must be inferred from phenomena that depend upon the width of the excited level, and in the last few years many lifetimes have been deduced from the Coulomb excitation experiments and several from measurements of the resonant scattering of gamma rays. Since the first excited states of even-even nuclei in the vicinity of closed shells generally lie at several hundreds of kev above the ground state, their lifetimes, especially in medium and light weight nuclei, are usually too short for direct measurements, and their energies often too high for study by those forms of the resonance method that depend on mechanical motion (Moon 1951) or on heating the source (Malmfors 1952).

The Doppler effect of previous recoil of the emitting nucleus, as used by Ilakovac (1954) for a liquid source and by Metzger (1956 *a*) for a gaseous source, enables gamma rays of higher energy to be studied, and, so far, several instances are available of lifetimes measured both by resonance and by Coulomb excitation. Since the two methods give appreciably different results (see § 6) it seemed interesting to investigate by the resonance method another transition that had already been studied by Coulomb excitation. The 990 kev  $2^+$  level in  $^{48}\text{Ti}$  seemed to be a good choice; the scattering isotope is abundant (73.4%), strong sources of  $^{48}\text{V}$  are obtainable and several compounds of vanadium have a low boiling point, so that the preparation of a gaseous source seemed feasible.

## § 2. EXPERIMENTAL TECHNIQUE

The essential features of  $^{48}\text{V}$  decay are shown in figure 1 (Casson *et al.* 1953).  $^{48}\text{V}$  sources were produced by bombardment of Ti metal with 8 mev protons in the 60 in. Nuffield cyclotron.

The Ti metal sheet was first spot-welded to nickel, and the nickel then hard-soldered to a copper target. In a preliminary experiment, the vanadium activity

† On leave from Institut Ruder Bošković, Zagreb.



was in a mixture of vanadium and titanium tetrachlorides obtained by passing chlorine over the heated titanium scrapings containing the  $^{48}\text{V}$  activity. It was attempted later to prepare a high specific activity source in the form of  $\text{VOCl}_3$ , but as chemical difficulties were encountered, the experiment was finally performed with the  $\text{VCl}_4$  source, the amount of  $\text{TiCl}_4$  being determined by the specific activity of  $^{48}\text{V}$  in a thin surface layer of Ti targets. A 10 mc source was sealed in an evacuated ampoule of rather large volume ( $\sim 17 \text{ cm}^3$ ) in order to reduce the vapour density. After repeated and prolonged heating of the source, up to  $250^\circ\text{C}$ , no chemical reaction was observed.

The experimental arrangement is shown in figure 1. A titanium scatterer, total weight about 3600 g was used. Iron scatterers were used for comparison purposes. The detector, consisting of a NaI (Tl) crystal 1 in.  $\times$  1½ in. in diameter mounted on the E.M.I. 6260 photomultiplier, was heavily shielded against the direct radiation. The scattered radiation was filtered through 0.2 cm of lead in

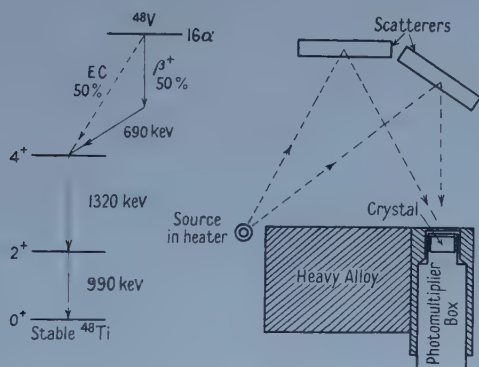


Figure 1. Decay of  $^{48}\text{V}$  and the horizontal section of experimental arrangement.

front of the crystal in order to reduce the strong Compton scattering, which, though of much lower energy, could cause the pile-up counts in the higher energy regions of the spectrum. Pulses from the detector were sorted in a single channel pulse height analyser with the admittance window set in the region of 990 keV gamma rays photopeak, the channel limits corresponding to the energies 910 and 1070 keV. Observations were taken exchanging the titanium and iron scatterers every 3 minutes, and to ensure that the pulses corresponding to the correct energy are admitted, the energy calibration of the counter was checked every 45 minutes, and the channel of the pulse height analyser set accordingly. The counting rates of scattered radiation were measured in alternation with the source in liquid form at room temperature and with the vaporized source at increased temperatures.

The source strength, in terms of the counting rate in the 910–1070 keV region of the spectrum, was measured accurately with the source about 8 feet from the crystal. The absolute strength was not required. In view of the extended scatterers, the geometrical factor of the arrangement was determined experimentally; a small  $^{48}\text{V}$  source was moved across the scatterer and the counting rate and distance from oven measured for each position. So determined, the geometrical factor accounts also for any change of crystal efficiency, relative to that at the perpendicular incidence of 990 keV gamma rays.

### § 3. THE LINE SHAPE OF THE EXCITING GAMMA RAYS

The cross section for the scattering of a gamma ray of energy  $E$  by a level of width  $\Gamma$  and energy  $E_0$  is given by a single level dispersion formula:

$$\sigma(E) = \sigma_{\max} g \frac{\frac{1}{4}\Gamma^2}{[E_0 + (E^2/2Mc^2) - E]^2 + \frac{1}{4}\Gamma^2} \quad \dots\dots(1)$$

where  $\sigma_{\max} = \lambda^2/2\pi$ ,  $g$  is the spin statistical factor and  $E^2/2Mc^2$  is the energy lost to the recoiling nucleus of mass  $M$  in the process of absorption of the gamma ray.

If the energy distribution of the incident gamma ray is given by the function  $P(E)$ , assumed normalized to unity, the average cross section is

$$\sigma_{\text{av}} = \int_0^\infty \sigma(E) P(E) dE.$$

As the level widths of the low lying bound states are very narrow,  $10^{-4}$  ev or less for quadrupole radiation, the resonances are extremely sharp, generally much sharper than the energy spectrum of the incident gamma rays and the integration is simplified, assuming the function  $P(E)$  to be constant in the very narrow region where  $\sigma(E)$  is large. Then

$$\sigma_{\text{av}} = \sigma_{\max} g P(E_0 + E_0^2/2Mc^2) \frac{1}{2}\pi \Gamma. \quad \dots\dots(2)$$

To determine the energy spectrum  $P(E)$  of the 990 kev gamma rays incident to the titanium scatterer, a break up of the  $\text{TiCl}_4$  molecule and the free recoil of the  $^{48}\text{Ti}$  nuclei after  $\beta^+$  and electron capture decay was assumed. If the  $^{48}\text{V}$  nucleus decays by electron capture, the recoiling  $^{48}\text{Ti}$  nucleus receives the momentum of  $3.35 mc$  because of the emission of the neutrino and further  $2.59 mc$  after the emission of the 1320 kev gamma ray. The resultant momenta of  $^{48}\text{Ti}$  nuclei prior to the emission of 990 kev gamma rays will range from  $0.76 mc$  to  $5.94 mc$ . A Doppler energy increase  $\Delta E$  of the 990 kev gamma ray depends on the angle of its emission, relative to the direction of motion of the  $^{48}\text{Ti}$  nucleus. Neglecting the angular correlation between the gamma rays, the Doppler energy increase spectrum will have a trapezoidal form extending from  $\Delta E = -66.6$  ev to  $\Delta E = +66.6$  ev.

The positron decay of  $^{48}\text{V}$  gives to the recoiling  $^{48}\text{Ti}$  nuclei a continuous momentum spectrum obtained from the positron and neutrino momentum distributions and reaching up to  $2.1 mc$ .

The combined recoils of the positron decay and of 1320 kev gamma ray finally result in the Doppler energy increase spectrum extending from  $\Delta E = -50$  ev to  $\Delta E = +50$  ev. This Doppler energy increase spectrum gives the energy spectrum  $P(E)$  of the 990 kev gamma rays incident upon the scatterer, its origin  $\Delta E = 0$  corresponding to the gamma ray energy  $E = E_0 - E_0^2/2Mc^2$  or to  $E = E_0 - 10.95$  ev, 10.95 ev being the numerical value of the recoil energy loss of the 990 kev gamma ray.

Figure 2 shows the energy spectrum  $P(E)$  obtained by numerical integration assuming a 50-50 branching ratio of  $\beta^+$  and electron capture decay of  $^{48}\text{V}$ . The 50-50 branching ratio is adopted on the basis of information given by Casson *et al.* (1953). The resonant energy  $E_R = E_0 + E_0^2/2Mc^2$ , at which the Doppler energy increase  $\Delta E$  amounts to  $2 \times E_0^2/2Mc^2 = 21.9$  ev and compensates for the recoil losses of energy in emission and in absorption, is indicated. The value of the function  $P(E)$  at the resonant energy, i.e.  $P(E_0 + E_0^2/2Mc^2)$  is equal to  $0.0114 \text{ ev}^{-1}$ . The error of this value due to the neglect of the angular correlations is estimated to be smaller than 5%. As the values of  $P(E_0 + E_0^2/2Mc^2)$  for pure  $\beta^+$  decay and for

pure electron capture decay differ only by about 20%, the effect of the error in the branching ratio on the above value of  $P(E_0 + E_0^2/2Mc^2)$  is also small.

We must now discuss the free recoil assumption on the basis of which the function  $P(E)$  was obtained. The assumption is plausible for the electron capture decay, the recoil energy of the Ti nucleus being 32 ev, 75% of which is available for the excitation of internal motions in the  $\text{TiCl}_4$  molecule.

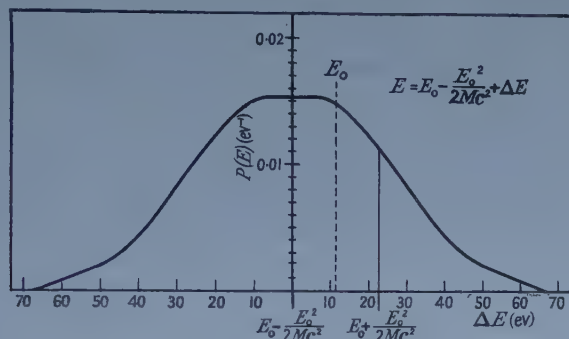


Figure 2. Line shape of 990 keV gamma rays emitted from a  $\text{VCl}_4$  source, as calculated on the basis of 50–50 branching ratio of electron capture and positron decay.

Owing to the central position of the Ti nucleus in the  $\text{TiCl}_4$  molecule, only a small fraction of the recoil energy is spent on the molecular rotational excitation. Thus more than 20 ev remains available for the radial relative motion which is ample to break the bonds. The assumption is probably correct for most of the positron decays. It is more likely to be so, when the largest part of the decay energy is given to positron or to neutrino, though also in the case of equal sharing it is supported by the tendency of neutrino and positron to be emitted in the same direction.

Further, molecules excited but not broken after the positron decay are unlikely to escape a break-up when the 1320 keV gamma ray is emitted giving the Ti nucleus the recoil energy of 19.5 ev. Should the molecules break up only after the emission of the 1320 keV gamma ray in as much as 50% of positron decays the value  $P(E_0 + E_0^2/2Mc^2)$  would increase by about 10%. We thus conclude that the total error of our value  $P(E_R) = 0.0114 \text{ ev}^{-1}$  could be up to 10–15%. The assumptions about the break up of the  $\text{TiCl}_4$  molecule may, at first sight, seem to be at variance with the findings of Metzger (1956*a*) that the  $\text{As}_4$  molecule did not break in the 17% of decays in which an As nucleus received the recoil energy of about 26 ev. But in the  $\text{As}_4$  molecule the recoiling nucleus is not in the central position and thus on average 2/3 of the energy given to internal motion will be the rotational energy and only 1/3 the energy of radial motion effective for the breaking of the bonds (Steinwedel and Jensen 1947).

#### § 4. INFLUENCE OF COLLISIONS

In order to establish whether the resonance is affected by the collisions of the nuclei recoiling in the vapour, experiments were performed at different vapour densities, varying the source temperature. The presence of the collision effect was found, as the resonant scattering counting rate did not increase linearly with the vapour phase activity. From the observed deviation from linearity, it was possible



to make an approximate correction for the collision effect. For this purpose a 'collision time'  $t_c$  was introduced, assuming that the recoiling  $^{48}\text{Ti}$  nuclei move undisturbed for time  $t_c$ , after which time they collide, with the result that their speeds become insufficient for the resonant Doppler broadening.

If  $\tau$  is the mean life of the 990 keV excited state, only the fraction  $(1 - \exp(-t_c/\tau))$  of excited nuclei recoiling in the vapour phase will emit the 990 keV gamma ray in time  $t_c$ . Further, if  $\rho$  is the relative density, showing the fraction of total activity in the vapour phase (measured by admitting the gamma rays from the upper point of the ampoule containing the source into the counter through a narrow slit in a heavy alloy shielding), the 990 keV gamma rays will be emitted before the collision in a fraction  $f = \rho[1 - \exp(-t_c/\tau)]$  of all decays.

The resonance counting rate  $N_R$  will be directly proportional to this fraction, i.e.  $N_R \propto \rho[1 - \exp(-t_c/\tau)]$ ; a non-linear increase relative to the increase in the source density  $\rho$  being due to the exponential term.

Writing  $t_c = a\tau/\rho$ , where  $a$  is a constant, the fraction  $f$  becomes a function of the density only, i.e.  $f = \rho(1 - e^{-a/\rho})$ . This treatment is of course only approximate, but the error actually involved depends on the vapour density  $\rho$  determining the collision correction term.

We therefore calculate the mean life from the lowest density data, only 40% of  $^{48}\text{V}$  activity being in the vapour phase, while the data for higher densities serve for determination of the collision correction term. In figure 3 the relative source density and the resonant scattering counting rate  $N_R$  are shown as a function of temperature. A fit of the curve  $\rho(1 - e^{-a/\rho})$  to the observed variation of the counting rate is also shown in the figure and gives the value for  $a = 0.55$ . With this value for  $a$ , at density  $\rho = 0.4$ , the collision correction term  $e^{-a/\rho}$  is 0.25 corresponding to a 25% decrease in the experimental cross section.

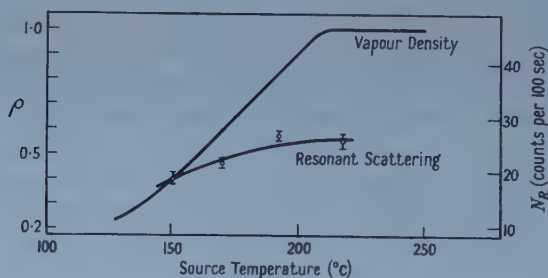


Figure 3. Vapour fraction of the source and the resonant scattering counting rate as a function of temperature.

## § 5. RESULTS

With the source in a liquid state, both scatterers gave almost the same counting rate, about 90 counts in 100 seconds. With the source partly vaporized the counting rate with the Ti scatterer increased by 18–26 counts, depending on the source temperature (figure 3), while the counting rate with the Fe scatterer remained unchanged. With the measured source strength and geometrical factor, the resonance scattering cross section at the scattering angle of  $120^\circ$ ,  $\sigma_{120} = \sigma_{av} f_{120}$ , was calculated for the lowest vapour density data. The resonance scattering angular distribution function  $f(\theta)$  for the spin sequence 0–2–0 and pure E2



radiation being  $f(\theta) = (5/4)(1 - 3\cos^2\theta + 4\cos^4\theta)$ , the average resonant scattering cross section  $\sigma_{\text{av}} = 24 \text{ mbn}$  was obtained. By equating this value with the theoretical cross section  $\sigma_{\text{av}} = 2.2 \times 10^{-22} \text{ cm}^2$  as obtained from expression (2), inserting the values for  $P(E_0 + E_0^2/2Mc^2) = 0.0114 \text{ ev}$ ,  $\sigma_{\text{max}} = 24.9 \times 10^{-22} \text{ cm}^2$  and  $g = 5$ , we obtain the level width of the 990 keV excited state  $\Gamma = 1.08 \times 10^{-4} \text{ ev}$ . The corresponding gamma mean life of the level is  $\tau_\gamma = 6.1 \times 10^{-12} \text{ sec}$ .

To allow for the uncertainties of collision correction and in the value of  $P(E_R)$ , we put the result finally with a standard deviation rather larger than that which would be due to the statistical variation (figure 3) as

$$\tau_\gamma = (6 \pm 2) \times 10^{-12} \text{ sec}.$$

The experiment also gives evidence for the accepted gamma ray order in the decay of  $^{48}\text{V}$ . Observing the gamma ray energy spectrum in the region of the 1320 keV gamma ray photo-peak, no change in the counting rate was found in the conditions that produced an increase in the region of 990 keV gamma ray photopeak.

## § 6. DISCUSSION

From the Coulomb excitation of the 990 keV level in  $^{48}\text{Ti}$ , Temmer and Heydenburg (1956) deduced the mean life  $\tau_\gamma = 14 \times 10^{-12} \text{ sec}$ . There is a significant difference in the results obtained by the two methods. The other two cases of medium weight even-even nuclei for which the two methods can be compared are  $^{72}\text{Ge}$  and  $^{74}\text{Ge}$  (Metzger 1956 *a*, Temmer and Heydenburg 1956). In all three cases, the mean life as measured by the nuclear resonance method is shorter, the discrepancy being largest in the case of the lightest nucleus  $^{22}\text{Ti}^{48}$  which, with 22 protons and 26 neutrons, is nearest to the closed shell configurations.

A Coulomb excitation study of the 1330 keV level in  $^{60}\text{Ni}$ , which has a closed proton shell, could provide further evidence, as the nuclear resonance lifetime measurement has been performed (Metzger 1956 *b*).

The levels investigated in the above cases are of collective vibrational character (Alder *et al.* 1956). Comparison is also possible on levels of this character in the heavy even-even nuclei  $^{198}\text{Hg}$  and  $^{202}\text{Hg}$ , revealing the same trend. (Resonance measurements,  $^{198}\text{Hg}$ : Davey and Moon 1953, Metzger and Todd 1954,  $^{202}\text{Hg}$ : Metzger 1956 *c*, Coulomb excitation measurements, see Alder *et al.* 1956). The table summarizes the cases of even-even nuclei in which the lifetimes of vibrational levels have been measured by both methods.

(1)	(2)	(3)	(4)
$^{22}\text{Ti}^{48}$	990	$14 \pm$	$6 \pm 2$
$^{32}\text{Ge}^{72}$	830	$6.2 \pm 0.5$	$4.6 \pm 1.2$
$^{32}\text{Ge}^{74}$	595	$23 \pm 2$	$19 \pm 3$
$^{78}\text{Pt}^{196}$	354	$50 \pm$	$34 \pm 7$
$^{80}\text{Hg}^{198}$	411	$43 \pm$	$31 \pm 3$
$^{80}\text{Hg}^{202}$	439	$55 \pm$	$34 \pm 7$

(1) Nucleus; (2) energy (keV); (3), (4) gamma mean lives ( $10^{-12} \text{ sec}$ ): (3), Coulomb excitation, (4), resonance scattering.

The lifetime of the 354 keV level in  $^{196}\text{Pt}$  was measured in a preliminary resonance experiment heating the  $^{196}\text{Au}$  source, and the mean life of

$$\tau_\gamma = (34 \pm 7) \times 10^{-12} \text{ sec}$$

was obtained, to be compared with the Coulomb excitation value of  $50 \times 10^{-12} \text{ sec}$ ,

obtained by Stelson and McGowan (1955). An account of this experiment will be published separately.

#### ACKNOWLEDGMENTS

It is a pleasure to thank Professor P. B. Moon for his interest and advice. The author also wishes to express his gratitude to Dr. P. Reasbeck for assistance in the rather unpleasant chemical work, to Mr. B. S. Sood for help in taking the data and to the Nuffield cyclotron operators for preparation of sources. He is indebted to the Institut Ruder Bošković for a maintenance grant.

#### REFERENCES

- ALDER, K., BOHR, A., HUUS, T., MOTTELSON, B., and WINTHER, A., 1956, *Rev. Mod. Phys.*, **28**, 432.  
CASSON, H., GOODMAN, L. S., and KROHN, V. E., 1953, *Phys. Rev.*, **92**, 1517.  
DAVEY, W. G., and MOON, P. B., 1953, *Proc. Phys. Soc. A*, **66**, 956.  
ILAKOVAC, K., 1954, *Proc. Phys. Soc. A*, **67**, 601.  
MALMFORS, K. G., 1952, *Ark. Fys.*, **6**, 49.  
METZGER, F. R., 1956 a, *Phys. Rev.*, **101**, 286; 1956 b, *Ibid.*, **103**, 983; 1956 c, *J. Franklin Inst.*, **261**, 219.  
METZGER, F. R., and TODD, W. B., 1954, *Phys. Rev.*, **95**, 853.  
MOON, P. B., 1951, *Proc. Phys. Soc. A*, **64**, 76.  
STEINWEDEL, H., and JENSEN, H., 1947, *Z. Naturf.*, **2a**, 125.  
STELSON, P. H., and MCGOWAN, F. K., 1955, *Phys. Rev.*, **99**, 112.  
TEMMER, G. M., and HEYDENBURG, N. P., 1956, *Phys. Rev.*, **104**, 967.

## Transmission of Electrons through Aluminium Foils

By B. N. C. AGU, T. BURDETT AND E. MATSUKAWA

Department of Physics, University of Leicester

*Communicated by E. A. Stewardson ; MS. received 23rd July 1957,  
and in final form 16th October 1957*

**Abstract.** Measurements have been made of the transmission through aluminium foils of an electron beam of initially monochromatic energy in the range 0.25–0.75 mev. The current of transmitted electrons was measured directly, with a collecting cup and a galvanometer, this procedure yielding transmission curves of different shape from those obtained using Geiger counters or ionization chambers. The extrapolated range–energy relationship under these conditions also departs considerably from the generally accepted curve.

### § 1. INTRODUCTION

THE relatively few published measurements of monochromatic electron beam attenuation by aluminium foils do not show very close agreement. Differences in the shape of measured transmission curves are attributed to variations in collector geometry. The nature of the measuring device may, however, be of significance in determining transmission, although this aspect has received little criticism. The initially monochromatic beam emerges from the foil with a modified energy distribution, dependent upon the foil thickness, so that the measured transmission will depend upon the energy response of the detecting device.

The early work of Varder (1915) and Madgwick (1927), and that of Marshall and Ward (1937) employed an intermediate size ionization chamber for electron detection, while in the work of Eddy (1929), who investigated effects of geometry upon the transmission curve, and in the recent careful experiments of Seliger (1955) on electron and positron transmission, a Geiger counter was employed. Only in the experiments of Schonland (1926) has the actual number of emerging electrons, that is the current, been measured. Schonland's investigations, however, extended up to only 87 kv and are therefore not directly comparable with the other work, quoted above, which covers the range from about 0.15 mev up to several mev.

### § 2. METHOD

A well collimated electron beam of a few microamperes obtained from the Leicester 1 mev electrostatic generator (Matsukawa, Rose and Wilson 1957) was allowed to fall on the foil and collector arrangement shown schematically in figure 1(a). The collector current  $i_C$ , the foil current  $i_F$  and the reflected current  $i_R$  were measured independently by galvanometers. The reflected current was in fact measured as the current to the insulated vacuum tank housing the foil and the collector system. The incident beam current  $i_0$  was computed as the sum of the currents  $i_C$ ,  $i_F$  and  $i_R$ . For the transmission measurements

reported here, all three electrodes were operated at zero bias ; subsidiary experiments to examine the effect of small bias voltages on the collector or foil have also been carried out. In practice, current transmission measurements were taken for any one foil thickness over the complete energy range 0.25–0.75 mev.

### § 3. EXPERIMENTAL DETAILS

#### 3.1. Foil and Collector System

An ideal collector would behave as a black body to incident electrons of all energies, and further, would accept all electrons emerging from the foil into the solid angle  $2\pi$ . The collector used in the present measurements represents a practical compromise. The experimental foil is held, in an aluminium ring clamp, at a distance of 0.1 cm above the aperture of the collector. The solid angle subtended at the centre of the foil by the aperture is then 93% of  $2\pi$ . Part of the foil assembly and collector is shown in figure 1(b), which is drawn to scale. The top mica ring insulates the foil clamp from the collector, while the lower mica ring serves to locate the assembly centrally.

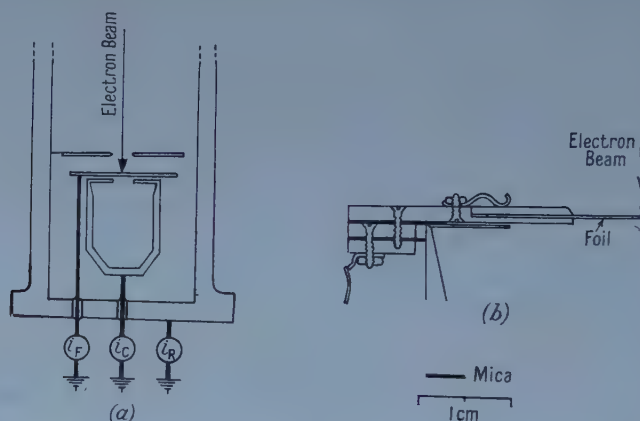


Figure 1. (a) Foil and collector arrangement, schematic ; (b) detail of foil assembly, to scale.

Some information on the extent to which the collector departs from a black body was obtained by firing the beam  $i_0'$  through a hole, 1.0 cm in diameter, in a dummy foil. Under these conditions, electrons reflected back from the collector through the collector aperture were recorded as foil current  $i_F'$  and as tank current  $i_R'$ .

It was found that the coefficients  $R' = i_R'/i_0'$  and  $A' = i_F'/i_0'$  were constant over the energy range 0.25–0.75 mev and each amounted to approximately 1%. A small correction to the measured current values with a foil in position in the holder, may be made by making the reasonable assumption that the reflection from the collector remains the same fraction  $R' + A'$  of the collector current. This assumption is not wholly correct since the collecting efficiency of the cup presumably depends somewhat upon the angular distribution of the entering electrons. However the above procedure will indicate the order of magnitude of the reflection, and since this is fairly small (approximately 2%), no serious error



can be introduced. A more correct transmission coefficient  $T$  is therefore given in terms of the apparent transmission coefficient  $T_a = i_c/i_0$ , by  $T_a [1 + (R' + A')]$ . This correction will be approximately 2% of the apparent transmission value.

### 3.2. Voltage Calibration

The generator potential was indicated by a linear characteristic generating voltmeter, calibrated against a resistance column and sphere spark gap up to 290 kv and 212 kv respectively. Extrapolation of the linear calibration curve beyond this value was then necessary. From the published figures for sphere spark gap voltages (N.P.L. Symposium on Precision Electrical Measurements, Section 20, 1 (1954)), the nature of the extrapolation, and the reproducibility of calibrations, it is estimated that the generator voltage measurement could be made with an accuracy of about 1%.

## § 4. EXPERIMENTAL RESULTS

Transmission coefficient as a function of aluminium foil thickness in  $\text{mg cm}^{-2}$ , is shown in figure 2 for various initial energies. The curves exhibit a reasonably linear central portion, as found by other investigators and one may extrapolate this to the thickness axis to define an extrapolated range. These curves show, however, a new feature compared with those obtained by ion chamber or counter

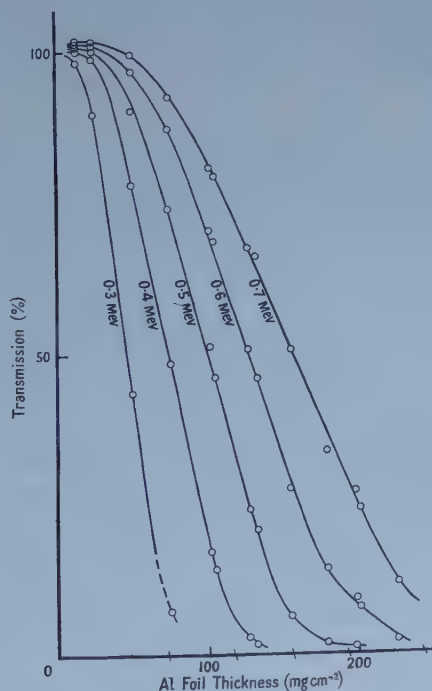


Figure 2. Current transmission coefficients for various initial beam energies.

methods, in that for small foil thicknesses, a transmission greater than 100% is obtained. This is presumably due to the relatively large number of secondary electrons that can emerge from a foil which is too thin to absorb or backscatter

any appreciable amount. This feature is even more pronounced in measurements we are taking on beryllium foils. Under these conditions the foil absorption coefficient is, of course, negative.

The extrapolated range values from measurement of current are smaller than those obtained by ion chamber or counter methods. This is clearly shown in figure 3 where the range values have been plotted as a function of energy. On the same diagram is shown the Katz and Penfold (1952) empirical range-energy relationship (a best fit through the results of Schonland, Eddy, Madgwick, Marshall and Ward and others, of the form  $R_e = 412 E_0^n$  where  $n = 1.265 - 0.0854 \ln E_0$ ). Extrapolated range values from Seliger's results fit closely to this curve.

Under the experimental conditions described above, the reflection coefficient is found to increase with foil thickness, at first linearly from the origin, and then to approach a horizontal asymptote at 11%, which is independent of incident beam energy.

For bias voltages up to  $\pm 100$  volts applied to collector or foil, fractional changes in transmission up to about 10% were observed. Some detailed bias measurements have actually been carried out, and these will be reported in a later note. It appears that most of the secondaries suppressed by 100 volts have, in fact, energies of about 15 eV, and that their intensity is approximately proportional to the transmitted current. Extrapolated range values derived from transmission measurements in which these low energy secondaries have been suppressed do not, therefore, differ significantly from the zero bias extrapolated range values reported here.

## § 5. DISCUSSION

It has not been possible, unfortunately, to obtain a theoretical expression with which to compare the present transmission curves. This circumstance arises from complexity, rather than any lack of knowledge concerning the interactions involved in the slowing down and scattering processes. For the purposes of the present note, however, it is sufficient to make a direct comparison of the present transmission results with a previous set obtained with a different measuring device. The results of Seliger, obtained under carefully defined conditions are particularly suitable for this comparison.

Seliger has shown that his counter transmission curves can be normalized, such that a universal (independent of energy) transmission curve is obtained if transmission is plotted as a function of the dimensionless parameter  $m/R_0$ , where  $m$  is the foil thickness, and  $R_0$  the true range of the incident electrons. Values of  $R_0$  were derived from the theoretical treatment of electron penetration by Spencer (1955). In fact, since Seliger's values for extrapolated range fall close to the Katz and Penfold empirical relationship for range  $R_e$ , it follows from the unique extrapolation intercept  $k_s$  of the universal curve, that  $R_0 = R_e/k_s$ . From Seliger's curve,  $k_s = 0.755$ .

In figure 4, we show the present transmission results plotted, with Seliger's curve, against the convenient parameter  $m/R_0$ . For the present curves also the normalizing property is exhibited, but this universal curve is clearly not coincident with the Seliger curve. Since a unique extrapolation intercept  $k_L = 0.712$  is obtained from the present results also, then extending a previous argument slightly, it follows that the range-energy relationship from the present

measurements yields a range value  $R_L$  simply related to the Katz and Penfold value  $R_e$ . Thus,  $R_L = (k_L/k_S) R_e = 0.94 R_e$ .

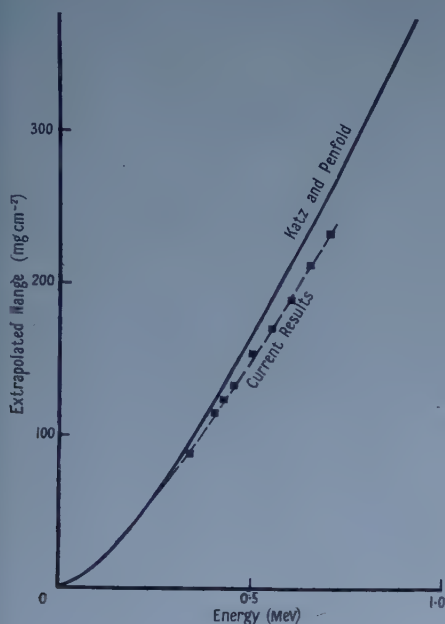


Figure 3. Extrapolated range as a function of energy.

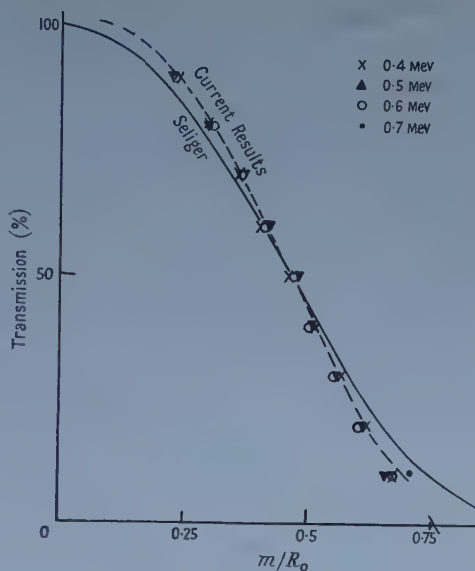


Figure 4. Transmission as a function of fractional range.

The divergence between the present results and the Katz and Penfold range-energy relationship is too great to be accounted for by inaccuracy of voltage measurement, but must be considered as resulting from the difference in characteristics of the measuring devices. As described in an earlier section, this divergence cannot be accounted for in terms of low energy (less than 100 eV) secondaries. The small departure of the collecting aperture from  $2\pi$  may be expected to influence slightly the shape of the transmission curve, as the angular distribution of the transmitted electrons changes with increasing foil thickness. In fact, in a subsidiary series of experiments we obtained range values approximately 4% higher with a much poorer geometry, collecting over 75% of  $2\pi$ . This suggests that the error due to the geometry in the present results is very small, and further, its direction is such that 100% collection geometry, would yield slightly shorter range values.

The relatively close agreement between the ion chamber results of Marshall and Ward and the counter results of Seliger is rather puzzling. However, the geometrical conditions of the former work are not clearly defined, and further, the energy response and directional sensitivity of an intermediate size ion chamber are difficult to assess for the purposes of comparison. It may be noted finally, that the transmission curve from a sufficiently large ion chamber should lie always below the current measurement transmission curve, and hence yield an extrapolated range value even smaller than the current measurement result.

Work on this topic has now been extended to examine in detail the effects of bias voltages on the shape of the transmission curve, and also to cover a range of foil atomic number.

## REFERENCES

- EDDY, C. E., 1929, *Proc. Camb. Phil. Soc.*, **25**, 50.  
KATZ, L., and PENFOLD, A. S., 1952, *Rev. Mod. Phys.*, **24**, 28 (summary of results up to 1952).  
MADGWICK, E., 1927, *Proc. Camb. Phil. Soc.*, **23**, 970.  
MARSHALL, J. S., and WARD, A. G., 1937, *Canad. J. Res.*, **15**, 39.  
MATSUKAWA, E., ROSE, P. H., and WILSON, J. E., 1957, *Research* **10**, 280.  
SCHONLAND, B. J. F., 1926, *Proc. Roy. Soc. A*, **108**, 187.  
SELIGER, H. H., 1955, *Phys. Rev.*, **100**, 1029.  
SPENCER, L. V., 1955, *Phys. Rev.*, **98**, 1599.  
VARDER, R. W., 1915, *Phil. Mag.*, **29**, 725.



# Elastic Wave Propagation in a Semi-Infinite Solid Medium

By J. W. C. SHERWOOD

Physics Department, Imperial College, London  
and

Applied Physics Division, National Research Council, Ottawa

*Communicated by R. W. B. Stephens; MS. received 13th September 1957, and in final form 5th November 1957*

**Abstract.** A simple physical picture is given of plane waves possessing complex angles of propagation, which play an important role in the theory of elastic wave radiation. Their utility is illustrated by studying continuous sinusoidal wave propagation parallel to the unstressed, plane boundary of a semi-infinite, homogeneous and isotropic solid medium, the Rayleigh and head waves being particular features of the investigation. A novel study of the field due to an impulsive force acting at a line in the surface of a semi-infinite medium indicates a general method of solving important transient propagation problems encountered in seismology. The equivalent problem of an impulsive force acting at the edge and in the plane of a semi-infinite thin sheet has been simulated experimentally by detonating small explosive charges at the edge of an aluminium sheet. The displacements detected by a condenser microphone technique are in excellent agreement with the theoretical determinations.

## § 1. INTRODUCTION

THE problem of elastic pulse transmission through the earth has been steadily gaining in interest, from the earlier investigation of earthquake waves to the more recent use of controlled explosions in the search for oil and ore bodies. The interpretation of the elastic disturbances, which are complicated by the effects of multiple reflections, refraction, diffraction and scattering arising from the heterogeneous nature of the medium, depends upon associating the salient features with familiar propagation characteristics. Until recent years detailed knowledge of such characteristics has been restricted in two ways: firstly by the involved mathematical analyses required for all but the simplest elastic wave problems and secondly by the difficulty of performing controlled experiments. The advent of laboratory model seismology techniques (e.g. Levin and Hibbard 1955, Oliver *et al.* 1954) has eliminated the latter limitation, but theoretical difficulties still remain. In this study emphasis is placed on the theoretical attack, novel model seismology techniques being employed to substantiate the work.

## § 2. PLANE WAVE THEORY

It is well known that elastic disturbances can propagate with slower velocities than those associated with simple dilatation, P, and rotation, S, waves. Plane waves possessing this very property are simple solutions of the equation of motion for an infinite, isotropic and homogeneous medium. They are of vital

importance in the general theory of radiation, as they may be superposed to synthesize any wave field, just as in Fourier synthesis sine waves may be superposed to construct any arbitrary wave. These plane waves will be discussed here in some detail, as an adequate description does not appear to exist in the present literature.

The equation of motion, in the absence of external forces, may be expressed in the form

$$(\lambda + 2\mu) \nabla (\nabla \cdot \mathbf{s}) - \mu \nabla \times \nabla \times \mathbf{s} = \rho \partial^2 \mathbf{s} / \partial t^2, \quad \dots (1)$$

where  $\lambda, \mu$  are the Lamé constants,  $\rho$  is the density,  $t$  is the time and  $\mathbf{s}$  is the vector displacement. For a plane dilatation or rotation wave generality is not lost by taking the  $y$  axis to lie perpendicular to the displacement  $\mathbf{s}$ . The dilatation  $\Delta$  and the rotation  $W$  (strictly speaking  $W$  is twice the rotation) may then be defined as

$$\Delta = \nabla \cdot \mathbf{s} = \frac{\partial u}{\partial x} + \frac{\partial w}{\partial z}, \quad W \mathbf{j} = \nabla \times \mathbf{s} = \left( \frac{\partial u}{\partial z} - \frac{\partial w}{\partial x} \right) \mathbf{j}, \quad \dots (2)$$

where  $\mathbf{j}$  is the unit vector in the  $y$  direction, and  $(u, w)$  are the displacement components in the  $x, z$  directions. Assuming sinusoidal time dependence, the equation resulting from the substitution of definitions (2) in equation (1) is

$$(\lambda + 2\mu) \nabla \Delta - \mu \nabla \times \mathbf{j} W = -\rho \omega^2 \mathbf{s}, \quad \dots (3)$$

where  $\omega$  is the pulsance. Successively eliminating  $W$  and  $\Delta$ , by taking the divergence and curl of equation (3) and manipulating, we obtain the two independent scalar wave equations

$$\nabla^2 \Delta + k_1^2 \Delta = 0; \quad \nabla^2 W + k_2^2 W = 0, \quad \dots (4)$$

where

$$k_1 = \frac{\omega}{\alpha} = \omega \left( \frac{\rho}{\lambda + 2\mu} \right)^{1/2}, \quad k_2 = \frac{\omega}{\beta} = \omega \left( \frac{\rho}{\mu} \right)^{1/2}, \quad \dots (5)$$

$\alpha$  and  $\beta$  being the velocities associated with dilatation and rotation waves, respectively. Equations (3) and (4) indicate that the plane wave solution for the dilatation and its associated displacement components may, omitting the time factor  $\exp(i\omega t)$ , be expressed by

$$\begin{bmatrix} \Delta \\ u \\ w \end{bmatrix} = A \exp \{ -ik_1(x \sin \theta + z \cos \theta) \} \begin{bmatrix} -ik_1 \\ \sin \theta \\ \cos \theta \end{bmatrix}, \quad \dots (6)$$

where  $\theta$  is defined as the propagation angle. When  $\theta$  is real it denotes the angle between the direction of propagation and the  $z$  axis. The wave travels with a velocity  $\alpha$  and possesses a uniform amplitude of motion, with the displacement in the direction of propagation. However  $\theta$  may be complex and the imaginary term imparts some interesting properties to the plane wave. We may investigate these properties by assuming  $\theta = i\theta'$ , where  $\theta'$  is real. Then equation (6) becomes

$$\begin{bmatrix} \Delta \\ u \\ w \end{bmatrix} = A \exp \{ -ik_1 z \cosh \theta' + k_1 x \sinh \theta' \} \begin{bmatrix} -ik_1 \\ i \sinh \theta' \\ \cosh \theta' \end{bmatrix}.$$

This describes a plane wave propagating parallel to the  $z$  axis with velocity and wave number given respectively by

$$c = \alpha \operatorname{sech} \theta' < \alpha; \quad k' = k_1 \cosh \theta'. \quad \dots (7)$$

The amplitude of the wave varies along the wave front as  $\exp(k'x \tanh \theta')$  and at any point the particle motion is elliptical with the major axis in the direction of propagation.

In general it is seen that the real part of  $\theta$  gives the direction of propagation of the dilatation wave, while the imaginary part specifies the physical characteristics of the wave. Analogous results may be obtained for plane rotation waves.

### 2.1. Propagation Parallel to a Stress Free Boundary

The problem of plane wave propagation parallel to a stress-free boundary has received considerable attention in recent years (see Ewing *et al.* 1957, chap. 2, Roesler 1955). This particular analysis is being presented as it clearly illustrates the utility of the preceding plane wave concepts and provides a refined treatment of the problem.

A dilatation wave  $\Delta_1$  incident on a plane stress free boundary  $z=0$  will generate reflected dilatation,  $\Delta_2$ , and rotation,  $W_3$ , waves (Kolsky 1953, p. 24). If  $\theta$  is the complex angle of incidence and reflection of the dilatation waves and  $\psi$  is the angle of reflection of the rotation wave

$$\left. \begin{aligned} \Delta_1 &= A_1(-ik_1) \exp \{-ik_1(x \sin \theta - z \cos \theta)\} \\ \Delta_2 &= A_2(-ik_1) \exp \{-ik_1(x \sin \theta + z \cos \theta)\} \\ W_3 &= A_3(-ik_2) \exp \{-ik_2(x \sin \psi + z \cos \psi)\} \end{aligned} \right\}, \quad \dots\dots(8)$$

where

$$\sin \theta / \sin \psi = \alpha / \beta = k_2 / k_1. \quad \dots\dots(9)$$

Since both the tangential and normal surface stresses are zero, two relationships exist between  $A_1$ ,  $A_2$ ,  $A_3$ ,  $\theta$  and  $\psi$  (Kolsky 1953, p. 27), namely

$$\left. \begin{aligned} 2(A_1 - A_2) \cos \theta \sin \psi - A_3 \cos 2\psi &= 0 \\ (A_1 + A_2) \cos 2\psi \sin \theta - A_3 \sin \psi \sin 2\psi &= 0 \end{aligned} \right\}. \quad \dots\dots(10)$$

Interest here is restricted to propagation parallel to the boundary and this may be obtained by expressing  $\theta$  in the form

$$\theta = \frac{1}{2}\pi + i\theta' \quad \dots\dots(11)$$

where  $\theta'$  is real. The complete wave system is equivalent to a combined dilatation disturbance  $\Delta_1 + \Delta_2$  travelling along the boundary with velocity  $c$  and wave number  $k'$  (see equation (7)), together with an associated rotation disturbance  $W_3$  propagated in the direction designated by  $\psi$ . Equations (7) and (10) in conjunction with equation (9) indicate that when the dilatation velocity  $c$  is between  $\alpha$  and  $\beta$ ,  $\psi$  is real and the rotation travels away from the boundary at an angle  $\arcsin(\beta/c)$  and with a velocity  $\beta$ . On the other hand, when the dilatation velocity  $c$  is less than  $\beta$ ,  $\psi$  is complex, with the real part equal to  $\frac{1}{2}\pi$  radians, and the rotation then propagates along the boundary with the velocity  $c$ .

Equation (8) also indicates that the dilatation  $\Delta_1 + \Delta_2$  and the rotation  $W_3$  only have the same simple exponential form if  $A_1$  is zero. For equation (10) to be consistent this requires that

$$\begin{vmatrix} -2 \cos \theta \sin \psi & -\cos 2\psi \\ \cos 2\psi \sin \theta & -\sin \psi \sin 2\psi \end{vmatrix} = 0. \quad \dots\dots(12)$$

Using equations (7), (9) and (11), the variables  $\theta$  and  $\psi$  may be eliminated from equation (12) in favour of the variable velocity  $c$  and the known velocities



$\alpha$  and  $\beta$ . This yields the well-known Rayleigh wave velocity equation. Further investigation shows that the individual dilatation and rotation parts of the disturbance decrease or increase exponentially with increasing  $z$ , according to whether  $\theta'$ ,  $\psi'$  assume positive or negative values, respectively. The solution yielding a disturbance that decreases with increasing  $z$  is generally termed the Rayleigh wave.

This brief analysis shows that a dilatation wave system can propagate along a stress-free boundary with a velocity  $c$ , between  $\alpha$  and  $\beta$ , continuously generating a simple rotation wave (this is often called the von Schmidt or head wave for the particular case where  $c = \alpha$ ) into the medium at an angle  $\arcsin(\beta/c)$ . Combined dilatation and rotation disturbances can also propagate parallel to the boundary with velocities less than  $\beta$ . The Rayleigh wave is the particular system which does not increase in amplitude at large distances from the boundary.

### § 3. THE RADIATION FROM LOCALIZED TRANSIENT FORCES

In the preceding account only plane waves possessing sinusoidal time dependence have been considered, whereas in seismology interest lies mainly in the diverging disturbances created by localized transient forces. The extensive bibliography compiled by Ewing, Press and Jardetzky (1957) lists the diverse theoretical contributions to this wide field of study up to the year 1955. Various methods of solution have been employed in these investigations and there is a consequent demand for a standard system of development consisting of a number of major steps, each step being clearly related to a basic physical process. It is considered that a suitable method can be provided by a combination of the work of Eason, Fulton and Sneddon (1955) and Sauter (1950). The proposed technique will be broadly indicated in the following section by a novel investigation of an impulsive force acting on a line in the surface of a semi-infinite solid medium, a problem which was initially considered by Lamb (1904) and again by Sauter (1950). The technique provides an alternative to the methods employed in the many relevant investigations listed by Ewing *et al.* (1957) and in several more recent works, including those of Garvin (1956), Jeffreys and Lapwood (1957) and Pekeris (1955).

### § 4. THE FIELD RADIATED BY AN IMPULSIVE FORCE ACTING ON A LINE IN THE SURFACE OF A SEMI-INFINITE MEDIUM

The general nature of the field generated by an impulsive force acting on a line in the surface of a semi-infinite, homogeneous and isotropic medium can be conceived from the simple analysis contained in §2.1. Dilatation and rotation disturbances radiate from the force with velocities ranging from  $\alpha$  to 0 and  $\beta$  to 0, respectively. In addition, the dilatation disturbances travelling along the surface with velocities between  $\alpha$  and  $\beta$  generate rotation waves into the medium. At a time  $t$  after the initiation of the impulsive force, dilatation exists in the regions a, b and c shown in figure 1, while rotation exists in regions b and c.

In the detailed analysis Cartesian  $(x, y, z)$  and cylindrical  $(R, \phi, y)$  coordinates are employed, the  $y$  axis being coincident with the source while the positive  $z$  axis and  $\phi = 0$  half-plane lie in the medium, perpendicular to the surface. As a first step the radiation from the impulsive line force into an infinite medium is expressed



as an integral superposition of plane waves possessing complex angles of propagation. The stress free boundary is then introduced, causing the plane waves radiating into the negative  $z$  half-space to be completely reflected into the positive  $z$  half-space. In this manner the required field is expressed as an integral superposition of plane waves radiating only into the positive  $z$  domain, and is finally evaluated using standard integration techniques.

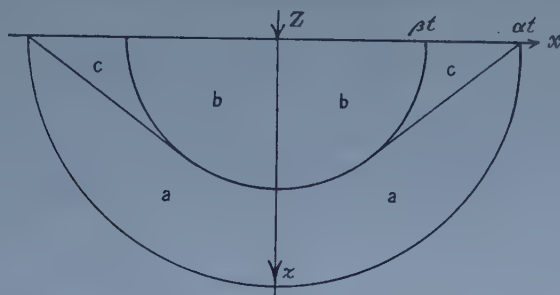


Figure 1. The field radiated by an impulsive force acting on a line in a surface of a semi-infinite solid.

#### 4.1. Radiation into an Infinite Medium

The equation of motion for a medium upon which forces per unit volume  $\mathbf{F}$  are being exerted is

$$(\lambda + 2\mu) \nabla(\nabla \cdot \mathbf{s}) - \mu \nabla \times \nabla \times \mathbf{s} + \mathbf{F} = \rho p^2 \mathbf{s} \quad \dots\dots(13)$$

where  $p$ , for the present moment, may be considered as the operator  $\partial/\partial t$ . If the dilatation and rotation potentials  $\Delta'$  and  $\mathbf{W}'$  are defined as

$$\nabla \cdot \mathbf{s} = \Delta = p^2 \Delta' / \alpha^2 = h^2 \Delta'; \quad \nabla \times \mathbf{s} = \mathbf{W} = p^2 \mathbf{W}' / \beta^2 = k^2 \mathbf{W}', \quad \dots\dots(14)$$

equation (13) becomes

$$\nabla \Delta' - \nabla \times \mathbf{W}' + \mathbf{F} / \rho p^2 = \mathbf{s}. \quad \dots\dots(15)$$

Taking the divergence and then the curl of equation (15) we obtain

$$\nabla^2 \Delta' + \nabla \cdot \mathbf{F} / \rho p^2 = h^2 \Delta' \quad \dots\dots(16)$$

and

$$-\nabla \times \nabla \times \mathbf{W}' + \nabla \times \mathbf{F} / \rho p^2 = k^2 \mathbf{W}'. \quad \dots\dots(17)$$

With the vector identity  $-\nabla \times \nabla \times \mathbf{W}' + \nabla(\nabla \cdot \mathbf{W}') = \nabla^2 \mathbf{W}'$  and the fact that, by definition,  $\nabla \cdot \mathbf{W}' = \nabla \cdot (\nabla \times \mathbf{s}) / k^2 = 0$ , equation (17) becomes

$$\nabla^2 \mathbf{W}' + \nabla \times \mathbf{F} / \rho p^2 = k^2 \mathbf{W}'. \quad \dots\dots(18)$$

Equations (16) and (18) are the inhomogeneous wave equations for the dilatation and rotation wave potentials. The problem now is to solve these equations for the particular force that is being considered, and then substitute in equation (15) to obtain the displacement field. The components of the impulsive force acting in the  $x$  and  $z$  directions can be treated independently. Consider first the component acting in the  $z$  direction, with a strength  $Z$  per unit length of the  $y$  axis; the force per unit volume becomes

$$\mathbf{F} = Z \delta(x) \delta(z) \delta(t) \mathbf{k}, \quad \dots\dots(19)$$

where  $\mathbf{k}$  is the unit vector in the  $z$  direction and  $\delta(x)$  is the Dirac delta function which will be loosely defined here as

$$\lim_{\epsilon \rightarrow 0} \int_0^\epsilon \delta(x) dx = 1.$$

Since symmetry considerations show that there is no  $y$  component of displacement, the rotation must be in the  $y$  direction and may be written as

$$\mathbf{W}' = W'\mathbf{j}. \quad \dots\dots(20)$$

Substitution of equations (19) and (20) in equations (16) and (18) yields

$$\left. \begin{aligned} \nabla^2 \Delta' + Z \frac{\partial}{\partial z} \delta(x) \delta(z) \delta(t) / \rho p^2 &= h^2 \Delta', \\ \text{and} \quad \nabla^2 W' - Z \frac{\partial}{\partial x} \delta(x) \delta(z) \delta(t) / \rho p^2 &= k^2 W' \end{aligned} \right\} \dots\dots(21)$$

The solution of these equations can be effected by reducing them to simple algebraic form, using standard integral transformation techniques. Now  $p$  has previously been considered as the operator  $\partial/\partial t$ , but it also corresponds to the parameter involved in the direct and inverse Laplace transformations (McLachlan 1953)

$$g\langle p \rangle = p \int_0^\infty g(t) \exp(-pt) dt, \quad g(t) = \int_{\text{Br}} g\langle p \rangle \exp(pt) dp / 2\pi i p,$$

where  $g\langle p \rangle$  is defined as the Laplace transformation of  $g(t)$  and Br denotes the Bromwich integration contour from  $c - i\infty$  to  $c + i\infty$ ,  $c \geq 0$ . It is thus convenient to employ Laplace transformations for the  $x$ ,  $z$  and  $t$  coordinates, giving three-dimensional transformations defined by

$$g\langle \xi, \eta, p \rangle = \xi \eta p \int_0^\infty dt \int_0^\infty dz \int_0^\infty dx g(x, z, t) \exp(-\xi x - \eta z - pt)$$

$$\text{and} \quad g(x, z, t) = \int_{\text{Br}} dp \int_{\text{Br}} d\eta \int_{\text{Br}} d\xi g\langle \xi, \eta, p \rangle \exp(\xi x + \eta z + pt) / (2\pi i)^3 \xi \eta p. \quad \dots\dots(22)$$

Applying the direct transformation to equations (21) we have

$$\left. \begin{aligned} (\xi^2 + \eta^2) \Delta' \langle \xi, \eta, p \rangle + Z \xi \eta^2 / \rho p &= h^2 \Delta' \langle \xi, \eta, p \rangle \\ \text{and} \quad (\xi^2 + \eta^2) W' \langle \xi, \eta, p \rangle - Z \xi^2 \eta / \rho p &= k^2 W' \langle \xi, \eta, p \rangle, \\ \text{or} \quad \Delta' \langle \xi, \eta, p \rangle &= -Z \xi \eta^2 / \rho p (-h^2 + \eta^2 + \xi^2) \\ \text{and} \quad W' \langle \xi, \eta, p \rangle &= Z \eta \xi^2 / \rho p (-k^2 + \eta^2 + \xi^2) \end{aligned} \right\} \dots\dots(23)$$

Performing the inverse Laplace transformations for the  $x, z$  coordinates,

$$\left[ \begin{array}{c} \Delta' \langle p \rangle \\ W' \langle p \rangle \end{array} \right] = \frac{Z}{\rho p (2\pi i)^2} \int_{\text{Br}} d\xi \int_{\text{Br}} d\eta \left[ \begin{array}{c} -\eta / (-h^2 + \eta^2 + \xi^2) \\ \xi / (-k^2 + \eta^2 + \xi^2) \end{array} \right] \exp(\xi x + \eta z). \quad \dots(24)$$

Each integral with respect to  $\eta$  possesses simple poles at  $\pm \sqrt{(m^2 - \xi^2)}$ , as indicated in figure 2, where  $m$  has the values  $h$  and  $k$  for the  $\Delta' \langle p \rangle$  and  $W' \langle p \rangle$

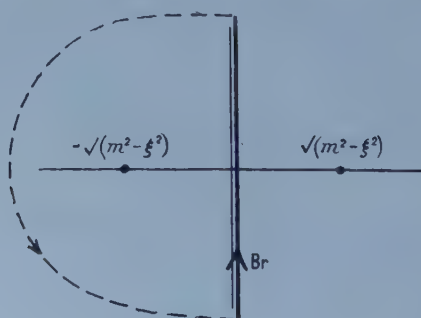


Figure 2. Complex  $\eta$  integration plane.

expressions, respectively. When  $z > 0$ , each integral around the dotted contour from  $+i\infty$  to  $-i\infty$  is zero. Thus, from the theorem of residues, the value of each integral along the Br contour is  $2\pi i$  times the residue at the pole  $-\sqrt{(m^2 - \xi^2)}$ . Equations (24) then become

$$\left[ \frac{\Delta' \langle p \rangle}{W' \langle p \rangle} \right] = - \frac{Z}{4\pi i \rho p} \int_{\text{Br}} d\xi \left[ \frac{\exp \{ \xi x - z \sqrt{(h^2 - \xi^2)} \}}{\xi \exp \{ \xi x - z \sqrt{(k^2 - \xi^2)} \} / \sqrt{(k^2 - \xi^2)}} \right]. \quad \dots\dots (25)$$

Complex angles are now introduced by performing the coordinate transformations

$$\xi = -h \sin \theta = -k \sin \psi, \quad d\xi = -h \cos \theta d\theta = -k \cos \psi d\psi \quad \dots\dots (26)$$

giving

$$\left[ \frac{\Delta' \langle p \rangle}{W' \langle p \rangle} \right] = \frac{Z}{4\pi \rho p} \int_{i\infty}^{-i\infty} i \left[ \frac{-h \cos \theta \exp \{ -h(x \sin \theta + z \cos \theta) \} d\theta}{k \sin \psi \exp \{ -k(x \sin \psi + z \cos \psi) \} d\psi} \right], \quad \dots\dots (27)$$

since  $p$  (and thus  $h$  and  $k$ ) may be treated as a real and positive parameter.

The introduction of the inverse Laplace transformation for the time coordinate  $t$  yields the potentials

$$\left[ \frac{\Delta'}{W'} \right] = \frac{Z}{8\pi^2 \rho} \int_{\text{Br}} \frac{dp}{p} \int_{i\infty}^{-i\infty} \left[ \frac{-\cos \theta \exp \{ pt - h(x \sin \theta + z \cos \theta) \} d\theta / \alpha}{\sin \psi \exp \{ pt - k(x \sin \psi + z \cos \psi) \} d\psi / \beta} \right]. \quad \dots\dots (28)$$

The potentials propagating into the half-space  $z > 0$  have now been expressed as double integral superpositions of plane waves possessing complex angles of propagation and angular frequencies of  $-ip$ . Due to the symmetry of the problem, the potentials propagating into the half-space  $z < 0$  may be written as

$$\left[ \frac{\Delta'}{W'} \right] = \frac{Z}{8\pi^2 \rho} \int_{\text{Br}} \frac{dp}{p} \int_{i\infty}^{-i\infty} \left[ \frac{\cos \theta \exp \{ pt - h(x \sin \theta - z \cos \theta) \} d\theta / \alpha}{\sin \psi \exp \{ pt - k(x \sin \psi - z \cos \psi) \} d\psi / \beta} \right]. \quad \dots\dots (29)$$

#### 4.2. Normal Impulsive Force on a Semi-Infinite Medium

The introduction of the stress free boundary at  $z = 0$  results in the generation of reflected dilatation and rotation potential waves by each of the incident plane waves contributing to the dilatation potential in equation (29), the reflection coefficients being  $A$ ,  $B$  and the propagation angles  $\theta$ ,  $\psi$  respectively. Reflected dilatation and rotation potential waves are also generated by each incident rotation potential wave, the reflection coefficients in this case being given by  $C$ ,  $D$  and the propagation angles by  $\theta$ ,  $\psi$ . An extension of the analysis in §2.1 yields the following expressions for the reflection coefficients

$$\left. \begin{aligned} A &= D = (4 \sin^3 \psi \cos \theta \cos \psi - \sin \theta \cos^2 2\psi) / E \\ B &= (4 \sin^2 \psi \cos \theta \cos 2\psi) / E \\ C &= (-4 \sin \theta \sin \psi \cos \psi \cos 2\psi) / E \end{aligned} \right\}, \quad \dots\dots (30)$$

where

$$E = 4 \sin^3 \psi \cos \theta \cos \psi + \sin \theta \cos^2 2\psi.$$

The combination of these reflected waves with the waves specified in equations (28) gives the complete disturbance propagating into the half-space  $z > 0$ , the relevant

potentials becoming (with the aid of definitions (26))

$$\left[ \frac{\Delta'}{W'} \right] = \frac{Z}{8\pi^2\rho} \int_{\text{Br}} \frac{dp}{p} \int_{i\infty}^{-i\infty} \left[ \begin{aligned} &\cos\theta\{(A-1)+C\sin\psi/\cos\psi\} \\ &\times \exp\{pt-h(x\sin\theta+z\cos\theta)\} d\theta/\alpha \\ &\{(A+1)\sin\psi+B\cos\psi\} \\ &\times \exp\{pt-k(x\sin\psi+z\cos\psi)\} d\psi/\beta \end{aligned} \right].$$

When the reflection coefficients (30) are inserted into the expressions for the potentials it is evident that the integrands of the double integrals over  $p$  and  $\theta$  or  $\psi$  are real functions (i.e.  $i$  does not occur explicitly). The following indicated steps

$$\left[ \frac{\Delta'}{W'} \right] = \int_{\text{Br}} \int_0^{-i\infty} - \int_{\text{Br}} \int_0^{i\infty} = \int_{\text{Br}} \int_0^{-i\infty} + \int_{(\text{Br})^*} \int_0^{i\infty} = 2\mathcal{R} \left\{ \int_{\text{Br}} \int_0^{-i\infty} \right\},$$

plus a transformation to cylindrical coordinates ( $y, R, \phi$ ) then yield the potentials

$$\left[ \frac{\Delta'}{W'} \right] = \frac{Z}{2\pi^2\rho\beta} \mathcal{R} \left\{ \int_{\text{Br}} \frac{dp}{p} \int_0^{-i\infty} F(\theta, \psi) \left[ \begin{aligned} &-\cos 2\psi \exp\{pt-hR\cos(\theta-\phi)\} d\theta \\ &\sin 2\psi \exp\{pt-kR\cos(\psi-\phi)\} d\psi \end{aligned} \right] \right\} \quad \dots\dots(31)$$

where

$$F(\theta, \psi) = \cos\theta \sin\psi / E(\theta, \psi). \quad \dots\dots(32)$$

The poles  $r$  and branch points  $p, s$  of the integrands of equations (32) are shown in figure 3. The poles occur at the values of  $\theta, \psi$  that make  $E(\theta, \psi)$  zero and correspond physically to the Rayleigh wave propagated along the free surface (see equation (12)). Inspection of equations (25) and (26) indicates that branch points ( $p, s$ ) occur when  $\cos\theta$  and  $\cos\psi$  are respectively zero.

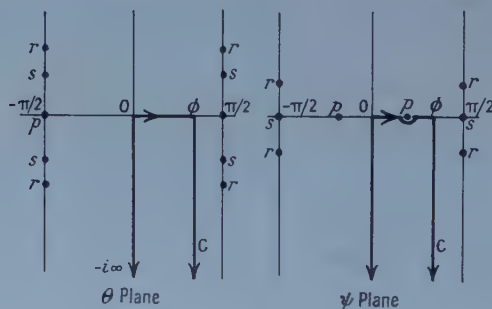


Figure 3. Complex  $\theta$  and  $\psi$  integration planes.

It is evident that  $\cos(\theta-\phi)$  and  $\cos(\psi-\phi)$  may be made real throughout the  $\theta$  and  $\psi$  integrations by replacing the imaginary axis integration contour with a contour  $C$  from 0 to  $\phi$  and  $\phi$  to  $\phi-i\infty$ , a step that is justified because the integration from  $\phi-i\infty$  to  $-i\infty$  is zero. It is now valid to interchange the order of the  $p$  and  $\phi, \psi$  integrals and the subsequent execution of the  $p$  integration yields

$$\left[ \frac{\Delta'}{W'} \right] = \frac{Z}{\pi\rho\beta} \mathcal{R} \left\{ \int_C iF(\theta, \psi) \left[ \begin{aligned} &-\cos 2\psi H\{t-R\cos(\theta-\phi)/\alpha\} d\theta \\ &\sin 2\psi H\{t-R\cos(\psi-\phi)/\beta\} d\psi \end{aligned} \right] \right\}, \quad \dots\dots(33)$$



where  $H$  denotes the unit step function. The displacements corresponding to these potentials are, from equation (15),

$$\begin{bmatrix} s_R^\Delta \\ s_\phi^\Delta \end{bmatrix} = \frac{Z}{\pi\rho\beta} \mathcal{R} \left\{ \int_C iF(\theta, \psi) \cos 2\psi \delta\{t - R \cos(\theta - \phi)/\alpha\} \begin{bmatrix} \cos(\theta - \phi) \\ \sin(\theta - \phi) \end{bmatrix} \frac{d\theta}{\alpha} \right\}$$

and

$$\begin{bmatrix} s_R^W \\ s_\phi^W \end{bmatrix} = \frac{Z}{\pi\rho\beta} \mathcal{R} \left\{ \int_C iF(\theta, \psi) \sin 2\psi \delta\{t - R \cos(\psi - \phi)/\beta\} \begin{bmatrix} \sin(\psi - \phi) \\ -\cos(\psi - \phi) \end{bmatrix} \frac{d\psi}{\beta} \right\}, \quad \dots\dots(34)$$

where the subscripts  $R, \phi$  denote radial and tangential displacement components, and the superscripts  $\Delta, W$  indicate whether the disturbance is due to the dilatation or rotation.

Finally, the evaluation of the integrations along the contour  $C$  gives

$$\begin{bmatrix} s_R^\Delta \\ s_\phi^\Delta \end{bmatrix} = \frac{-Z}{\pi\rho\beta R} \mathcal{R} \left\{ iF(\theta, \psi) \cos 2\psi \begin{bmatrix} \cot(\theta - \phi) \\ 1 \end{bmatrix} \right\}_{\theta=\phi-i\theta'}, \quad \frac{\alpha t}{R} > \cos \phi \quad \dots\dots(35)$$

$$\begin{bmatrix} s_R^W \\ s_\phi^W \end{bmatrix} = \frac{-Z}{\pi\rho\beta R} \mathcal{R} \left\{ iF(\theta, \psi) \sin 2\psi \begin{bmatrix} 1 \\ -\cot(\psi - \phi) \end{bmatrix} \right\}_{\psi=\phi-i\psi'}, \quad \frac{\beta t}{R} > \cos \phi \quad \dots\dots(36)$$

where  $\theta' = \text{arc cosh}(\alpha t/R)$ ,  $\psi' = \text{arc cosh}(\beta t/R)$  and, as indicated, the expressions are to be evaluated at  $\theta = \phi - i\theta'$  or  $\psi = \phi - i\psi'$ .

In equation (35) the displacement components when  $\alpha t/R < 1$  are zero, since  $\theta$  and  $\psi$  are both real. When  $\alpha t/R > 1$  the displacement due to the dilatation becomes

$$\begin{bmatrix} s_R^\Delta \\ s_\phi^\Delta \end{bmatrix} = \frac{Z}{\pi\rho\beta R} \mathcal{R} \left\{ F(\theta, \psi) \cos 2\psi \begin{bmatrix} \coth \theta' \\ -i \end{bmatrix} \right\}_{\theta=\phi-i\theta'}. \quad \dots\dots(37)$$

When  $\beta t/R > 1$ , expression (36) corresponds to the direct rotation wave and yields

$$\begin{bmatrix} s_R^W \\ s_\phi^W \end{bmatrix} = \frac{Z}{\pi\rho\beta R} \mathcal{R} \left\{ F(\theta, \psi) \sin 2\psi \begin{bmatrix} -i \\ -\coth \psi' \end{bmatrix} \right\}_{\psi=\phi-i\psi'}. \quad \dots\dots(38)$$

When  $\beta t/R < \cos(\phi - \gamma)$ , where  $\gamma$  is the critical angle  $\text{arcsin}(\beta/\alpha)$ ,  $\theta$  and  $\psi$  in equation (36) are real and the displacements consequently zero. However,  $\theta$  becomes complex when  $1 > \beta t/R > \cos(\phi - \gamma)$  and expressions (36) then correspond to the displacements of the rotation disturbance that is generated by the dilatation propagating along the surface of the semi-infinite solid, giving

$$\begin{bmatrix} s_R^W \\ s_\phi^W \end{bmatrix} = \frac{Z}{\pi\rho\beta R} \mathcal{R} \left\{ -iF(\theta, \psi) \sin 2\psi \begin{bmatrix} 1 \\ \cot \psi'' \end{bmatrix} \right\}_{\psi=\phi-i\psi''}, \quad \dots\dots(39)$$

where  $\psi'' = \text{arc cos}(\beta t/R)$ .

### 4.3. Tangential Impulsive Force on a Semi-Infinite Medium

In §§ 4.1 and 4.2 only the impulsive force component in the  $z$  direction was considered. A similar analysis involving only the  $x$  component  $x$  of the impulsive force per unit length of the  $y$  axis yields the following field. The displacement components due to the dilatation disturbance are

$$\begin{bmatrix} s_R^\Delta \\ s_\phi^\Delta \end{bmatrix} = \frac{X}{\pi\rho\beta R} \mathcal{R} \left\{ G(\theta, \psi) \sin 2\theta \frac{\beta^2}{\alpha^2} \begin{bmatrix} \coth \theta' \\ -i \end{bmatrix} \right\}_{\theta=\phi-i\theta'}. \quad \dots\dots(40)$$

where  $G(\theta, \psi) = \cos \psi \sin \theta / E(\theta, \psi)$ . The direct rotation wave displacements are

$$\begin{bmatrix} s_R^W \\ s_\phi^W \end{bmatrix} = \frac{X}{\pi \rho \beta R} \mathcal{R} \left\{ G(\theta, \psi) \cos 2\psi \begin{bmatrix} i \\ \coth \psi' \end{bmatrix} \right\}_{\psi = \phi - i\psi'} \quad \dots (41)$$

The disturbance with which the head wave is connected is given by

$$\begin{bmatrix} s_R^W \\ s_\phi^W \end{bmatrix} = \frac{X}{\pi \rho \beta R} \mathcal{R} \left\{ iG(\theta, \psi) \cos 2\psi \begin{bmatrix} 1 \\ \cot \psi'' \end{bmatrix} \right\}_{\psi = \phi - \psi''} \quad \dots (42)$$

The expressions (37) to (42) provide the complete theoretical solution to the problem under consideration in this section. The displacements in the directions  $\phi = 0, 9, 18, 27, 31.5, 36, 40.5, 45, 49.5, 54, 58.5, 63, 67.5, 72, 76.5, 81, 84, 86, 88, 89, 90$  degrees have been numerically evaluated as a function of normalized time

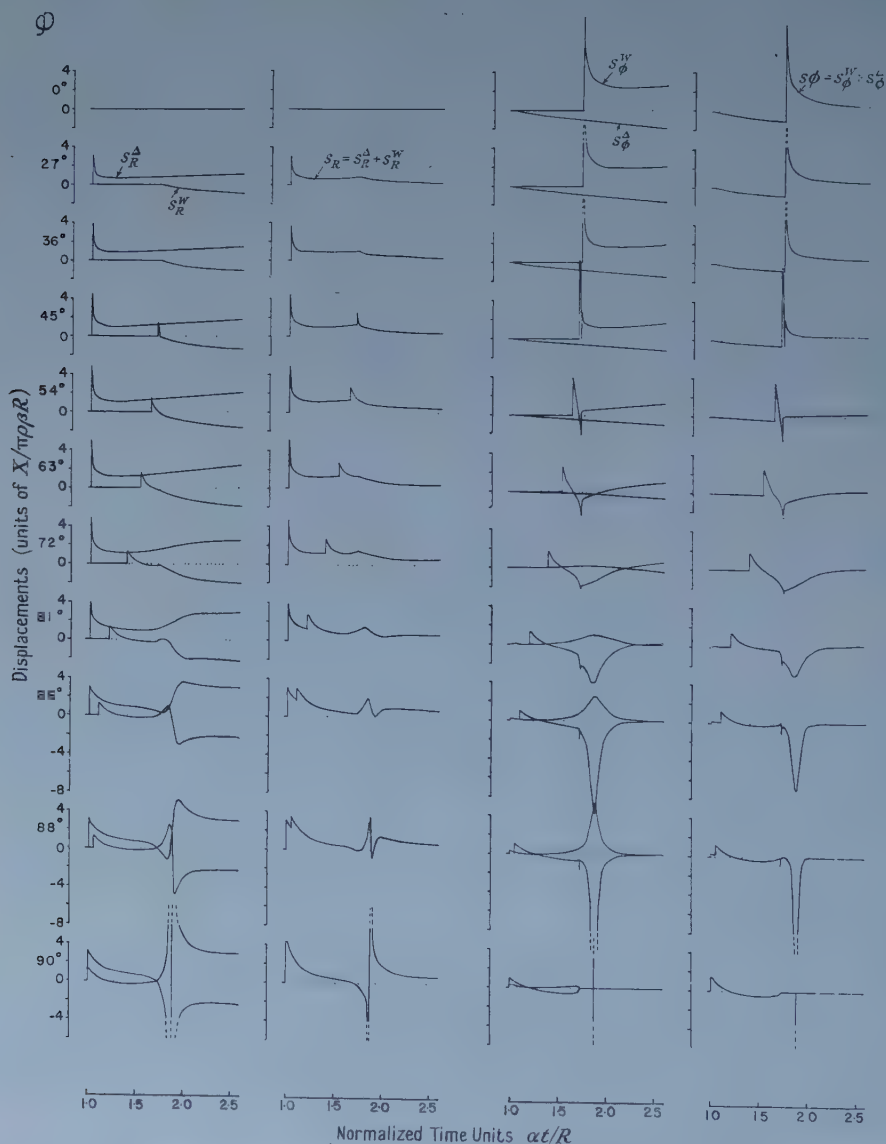


Figure 6. Theoretical radial and tangential displacements due to an impulsive force acting along the surface of the semi-infinite medium.

$\alpha t/R$ , using the specific velocity ratio  $\alpha/\beta = \sqrt{3}$ . The dilatation, rotation and total radial and tangential displacement components in several of these directions are plotted in figures 4, 5 and 6. Also shown in figures 4 and 5 are the displacement recordings obtained in an experimental simulation (described in §5) of the impulsive force acting normally to the surface, the symbols P, S and H indicating the discontinuities occurring at the arrival times of the direct dilatation and rotation waves and the head wave, respectively.

It is of interest to note that, by the general theory of reciprocity (Rayleigh 1877), the solution developed here also yields the surface disturbance of a semi-infinite medium due to a directional impulsive force which acts on an internal line lying parallel to the surface. Pekeris (1955) has solved an analogous three-dimensional problem of a transient force acting at an internal point in a direction perpendicular to the surface. When his detailed computations are published it will be interesting to compare them with the results presented here.

### § 5. EXPERIMENTAL INVESTIGATION

An experimental investigation of the problem examined in §4.2 was assisted by means of an analogy which avoided the difficulties of simulating a line source and detecting displacements in the interior of a bulky medium. Since the problem is two-dimensional in nature it appears that it might be equivalent to an impulsive force acting at the edge and in the plane of a thin sheet. Oliver, Press and Ewing (1954) have rigorously established this equivalence, subject to the replacement of the infinite medium dilatation wave velocity  $\alpha$  by the thin sheet dilatation wave velocity.

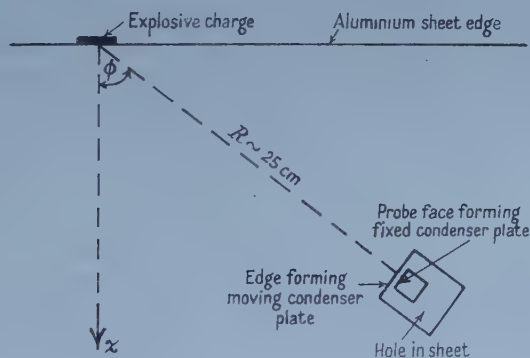


Figure 7. Experimental technique.

Two criteria must be satisfied in order clearly to resolve the rapid displacement variations in the plane of the thin sheet. Firstly, the linear dimensions of the force and the displacement detector must be small compared with the distance separating them and secondly, the time duration of the force must be much smaller than the time taken for the main disturbance to travel to the detector. The experimental system finally adopted is indicated in figure 7. The explosive cap, about 1.3 mm in diameter, of a Christmas cracker was placed symmetrically at the straight edge of a 0.5 mm thick aluminium sheet and detonated by means of a heated nichrome wire. This provided an impulsive force with a time duration of about 2 microseconds (Kolsky 1953, p. 189). The radial and tangential displacements in a specific direction were detected by a condenser

microphone technique. A square hole, of side 1.0 mm, was formed in the aluminium sheet, the edges being parallel and perpendicular to the line connecting the hole to the explosive about 25 cm away. One edge was used as the moving condenser plate, the parallel stator plate being provided by a face of a probe (0.6 mm square) inserted into the hole. A fixed 500 pF condenser was placed in parallel with the condenser detector, whose plate separation was about 0.1 mm, and a polarizing voltage of 200 volts provided from a source of 0.5 M $\Omega$  output impedance. This gave a circuit with a time constant ( $CR \simeq 250 \mu\text{sec}$ ) sufficiently long to maintain the condenser charge tolerably constant over a time of 40  $\mu\text{sec}$ , which was the approximate duration of the significant elastic disturbance. The voltage variation of the condenser was amplified by a 1.5 Mc/s wide-band amplifier and displayed on the single stroke time base of a high speed oscilloscope, this being initiated by the pulse from a photocell irradiated with the light flash from the explosive. The oscilloscope display corresponded directly to the time variation of the relevant displacement in the aluminium sheet, the displacement amplification factor  $A$  being

$$A \simeq SGEk_0a/Cd^2 \sim 1.6 \times 10^3 \quad \dots\dots (43)$$

where  $S$  is the deflection sensitivity of the cathode-ray tube ( $4.0 \times 10^{-4}$  m/v),  $G$  is the overall gain of the electronic amplifier ( $4.0 \times 10^4$ ),  $E$  is the condenser microphone polarizing voltage ( $2.0 \times 10^2$  volts),  $k_0$  is the permittivity of free space ( $8.85 \times 10^{-12}$  F),  $a$  is the effective area of the condenser plates ( $3.0 \times 10^{-5}$  m $^2$ ),  $C$  is the total capacity of the microphone circuit ( $5.0 \times 10^{-10}$  F), and  $d$  is the gap between the condenser plates (approximately  $0.1 \times 10^{-3}$  m).

Photographs of the oscilloscope display, corresponding to the radial and tangential displacements for various values of  $\phi$ , are shown in figures 4 and 5 (Plates). The rapid variations corresponding to the arrival times of the various disturbances are clearly resolved, and the initial displacement features are in excellent agreement with those resulting from the theoretical analysis. Features occurring in later parts of the experimental records are due to disturbances reflected from various edges of the aluminium sheet.

### 5.1. Quantitative Analysis

The orders of magnitude of the physical characteristics of an explosive cap were determined by comparing the theoretical and experimental observations. The theory predicted that an impulsive force would initiate an impulsive radial displacement travelling along the edge of the sheet with Rayleigh wave velocity (see the radial displacement for  $\phi = 90^\circ$ , in figure 4, also Lamb 1904). Since the explosive impulse duration (about 2  $\mu\text{sec}$ ) was considerably greater than the time of passage (about 0.4  $\mu\text{sec}$ ), of a Rayleigh wave across the face of an explosive cap this meant that the experimentally observed Rayleigh wave displacement had approximately the same time variation as the explosive force. The display of this displacement on a 20  $\mu\text{sec}$  time base indicated that the impulsive force had a roughly Gaussian dependence on time and was equivalent to the maximum force operating for about 1.5  $\mu\text{sec}$ .

The experimental displacement record was calibrated by means of the displacement amplification factor estimated in equation (43). Then from a direct comparison with the theoretical displacement expressed in units of  $Z/\pi\rho\beta R$  (see figure 4), the impulse per centimetre sheet width  $Z$  was determined to be  $7 \times 10^4$  g sec $^{-1}$ . As this typical explosive cap extended over a length of 1.3 mm



along the edge of the aluminium sheet, the impulse per unit area was  $5.4 \times 10^5 \text{ g cm}^{-1} \text{ sec}^{-1}$ . Then, since the impulse was found to be equivalent to the maximum force operating for  $1.5 \mu\text{sec}$ , the value of the maximum explosive pressure must have been about  $4 \times 10^{11} \text{ dyn cm}^{-2}$ , a value that is fairly typical of high explosives (Pack, Evans and James 1948).

As a result of this high pressure plastic flow of the aluminium occurred in the immediate vicinity of an explosive cap, causing a permanent indentation at the edge of the sheet. Since this violates the theoretical assumption of linear elastic processes, it is perhaps surprising that such excellent agreement exists between the theoretical and experimental displacement fields. This is of direct interest in connection with exploration seismology, where the elastic behaviour around the source (usually an explosive charge) is also generally non-linear.

### § 6. CONCLUSION

The solution of a particular transient elastic wave problem has been derived here using simple physical concepts, the results being substantiated by an experimental analogue. The technique may clearly be adapted to provide a method of solution for similar but more complex studies, including the particular case where a localized impulsive force is situated in a stratified medium. This is the basic problem encountered in seismic prospecting and it will be the subject of a subsequent publication.

### ACKNOWLEDGMENTS

The author wishes to express his deep appreciation of the invaluable aid and encouragement of Dr. R. W. B. Stephens during the course of this research, the main part of which was performed in the Physics Department of the Imperial College of Science and Technology, with the financial assistance of the Department of Scientific and Industrial Research. The author is also indebted to the National Research Council of Canada for the award of a Postdoctorate Fellowship and the provision of facilities enabling both refinements in the theoretical analysis and the computation of expressions (40) to (42) in the text.

### REFERENCES

- EASON, G., FULTON, J., and SNEDDON, I. N., 1955-56, *Phil. Trans. Roy. Soc. A*, **248**, 575.  
 EWING, W. M., JARDETZKY, W. S., and PRESS, F., 1957, *Elastic Waves in Layered Media* (New York: McGraw-Hill).  
 GARVIN, W. W., 1956, *Proc. Roy. Soc. A*, **234**, 528.  
 JEFFREYS, H., and LAPWOOD, E. R., 1957, *Proc. Roy. Soc. A*, **241**, 455.  
 KOLSKY, H., 1953, *Stress Waves in Solids* (Oxford: Clarendon Press).  
 LAMB, H., 1904, *Phil. Trans. Roy. Soc. A*, **203**, 1.  
 LEVIN, F. K., and HIBBARD, H. C., 1955, *Geophysics*, **20**, 19.  
 McLACHLAN, N. W., 1953, *Complex Variable Theory and Transform Calculus* (Cambridge: University Press).  
 OLIVER, J., PRESS, F., and EWING, W. M., 1954, *Geophysics*, **19**, 20.  
 PACK, D. C., EVANS, W. M., and JAMES, H. J., 1948, *Proc. Phys. Soc.*, **60**, 1.  
 PEKERIS, C. L., 1955, *Proc. Nat. Acad. Sci. U.S.A.*, **41**, 469, 629.  
 RAYLEIGH, Lord, 1877, *The Theory of Sound*, **1**, §107 (New York: Dover).  
 ROESLER, F. C., 1955, *Phil. Mag.*, **46**, 517.  
 SAUTER, F., 1950, *Z. angew. Math. Mech.*, **30**, 203.

## Heat Capacity between 1·8 and 4·2°K of an Iron–Chromium Alloy in the Alpha and Sigma Phases

By F. E. HOARE AND J. C. MATTHEWS†

Physics Department, The University of Leeds

*MS. received 26th September 1957*

**Abstract.** The alloy contained 44·1 atomic per cent chromium, where the pure sigma phase may be precipitated by prolonged annealing.

In the alpha phase the specific heat is almost identical with that of pure iron.

In the sigma phase however, a larger specific heat appears which is linear with temperature, and this is assumed to be electronic in origin giving for  $\gamma$ ,  $26\cdot8 \times 10^{-3} \text{ J deg}^{-2} \text{ mole}^{-1}$ , which is greater than has been observed for any other metal or alloy.

### § 1. INTRODUCTION

THE sigma phase can be precipitated as a single phase in the iron–chromium system between 41 and 51 atomic per cent chromium and is stable at temperatures below about 800°C. It is distinguished from the alpha phase of the same composition by an increase in hardness, brittleness and density and by its zero intrinsic magnetization at room temperature. It is of interest to learn as much as possible of the structure of the electronic energy bands in the two phases since this might elucidate the conditions which lead to sigma phase precipitation as well as helping towards a fuller understanding of the electronic structure of metals in general. With this object in view the heat capacity of one iron–chromium alloy has been determined in the composition range where 100% sigma phase can be formed. The measurements were all below 4·2°K as it is more probable that an unambiguous separation of the electronic and lattice contributions can be made in this temperature range.

### § 2. PREPARATION OF THE SPECIMEN

The alloy used in these measurements was prepared from spectrographically standardized iron and chromium supplied by Johnson, Matthey and Co. Ltd., these having laboratory numbers 4954 and 10163 respectively. The alloy was melted and cast in a vacuum induction furnace, as described by Matthews (1957), and a chemical analysis of turnings from the specimen showed the composition to be 44·1 atomic % chromium and 55·9 atomic % iron.

In the chill cast state the specimen was in the pure alpha phase and could be easily machined to the exact dimensions demanded by the calorimeter, i.e. outside diameter 0·4 in. and length 1·58 in. After completing the heat capacity measurements on the specimen in the alpha phase, it was annealed at 700°C to form the sigma phase, the transformation being followed by a magnetic method described by Nevitt and Beck (1955, private communication). When the room temperature magnetic moment had been reduced to zero after 100 hours it was assumed that

† Now at Physics Department, University of Nottingham.

the specimen was entirely in the sigma phase; this was confirmed by an x-ray examination made by Dr. Goldschmidt of B.S.A. Research Centre, Sheffield. The increase in density of the alloy during this transformation caused deformation cracks to appear at the surface of the specimen but these were insufficient to cause disintegration.

### § 3. METHOD OF MEASUREMENT

The cryostat, calorimeter and the method of measurement have been described by Hoare and Yates (1957). Heat capacity measurements on the specimen in the alpha phase were made on two days using helium as exchange gas while those on the sigma phase specimen were made on two days using helium as exchange gas and on one subsequent day using hydrogen as exchange gas. In the experimental arrangement employed the exchange gas, whether helium or hydrogen, was removed at 20°K and the reason for using the hydrogen as exchange gas was to confirm that the unusual results obtained could not be attributed to absorption effects which if present would vary with the exchange gas used.

### § 4. RESULTS

The measured heat capacities of the specimen in the alpha and sigma phases are given in tables 1 and 2 and are shown graphically in figures 1 and 2. If the usual assumptions are made regarding the temperature dependence of the lattice and electronic contributions to the specific heat  $C_v$ , then

$$C_v = \gamma T + \beta T^3.$$

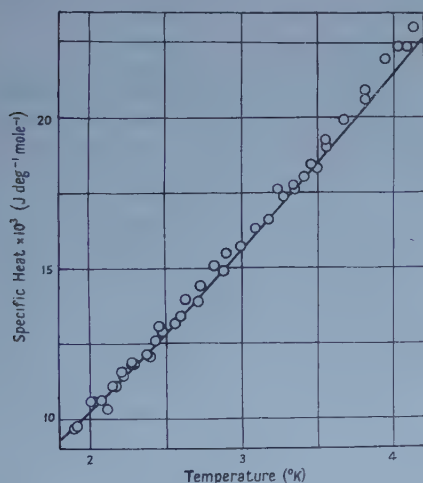


Figure 1. Measured specific heat of iron-chromium alloy in alpha phase. The full line represents results of Keesom and Kurrelmeyer (1939) for pure iron.

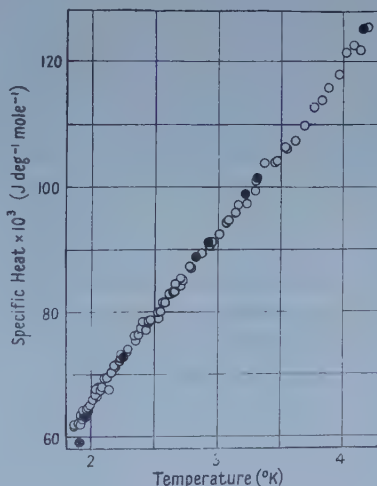


Figure 2. Measured specific heat of same iron-chromium alloy as for figure 1 when transformed to the sigma phase. Open circles, results using helium as initial exchange gas, full circles, check results using hydrogen as initial exchange gas.

The values of  $\gamma$  and  $\theta_D$ , the Debye temperature, may be found in the usual way by plotting  $C_v/T$  against  $T^2$ . This method of treating the results appears to be valid in the case of the alpha phase data in the present set of measurements and gives the

Table 1. Heat Capacity of the Iron-Chromium Alloy in the Alpha phase  
(J mole<sup>-1</sup> deg<sup>-1</sup> × 10<sup>3</sup>)

<i>T</i> (°K)	<i>C<sub>p</sub></i>	<i>T</i> (°K)	<i>C<sub>p</sub></i>	<i>T</i> (°K)	<i>C<sub>p</sub></i>
1·889	9·71	3·552	19·27	3·177	16·63
2·004	10·60	3·674	91·93	3·262	17·39
2·074	10·63	3·809	20·90	3·342	17·66
2·145	11·12	4·027	22·36	3·418	18·05
2·199	11·59	4·123	22·97	3·488	18·31
2·268	11·79	2·102	10·36	3·556	19·02
2·388	12·08	2·202	11·47	3·815	20·62
2·465	13·09	2·273	11·88	3·943	21·96
2·624	13·98	2·364	12·15	4·085	22·35
2·725	14·42	2·473	12·88	1·906	9·80
2·806	15·10	2·592	13·41	2·020	10·60
2·884	15·50	2·703	13·89	2·147	11·12
3·232	17·63	2·870	14·90	2·296	11·78
3·335	17·79	2·984	15·73	2·426	12·60
3·450	18·47	3·085	16·31	2·553	13·13

Table 2. Heat Capacity of the Iron-Chromium Alloy in the Sigma phase  
(J mole<sup>-1</sup> deg<sup>-1</sup> × 10<sup>3</sup>)

<i>T</i> (°K)	<i>C<sub>p</sub></i>	<i>T</i> (°K)	<i>C<sub>p</sub></i>	<i>T</i> (°K)	<i>C<sub>p</sub></i>
<i>Helium as exchange gas</i>					
1·874	61·7	1·926	62·5	3·834	113·9
1·905	63·4	1·887	62·2	3·878	115·7
1·933	64·2	1·934	63·7	3·963	117·8
1·959	64·7	1·978	65·0	4·024	121·5
1·992	65·1	2·028	67·6	4·083	122·5
2·021	66·0	2·073	67·4	4·140	121·7
2·052	68·1	2·121	69·4	4·196	125·4
2·085	67·9	2·165	70·3	1·911	62·0
2·128	69·3	2·219	72·0	1·952	64·2
2·177	71·4	2·282	73·4	1·990	64·2
2·229	72·4	2·343	75·3	2·024	66·7
2·295	74·0	2·404	78·4	2·052	66·4
2·375	76·2	2·461	78·5	2·080	67·7
2·446	78·5	2·540	80·0	2·113	69·4
2·517	79·8	2·659	84·5	2·137	67·5
2·586	81·5	2·709	85·4	2·189	71·1
2·651	83·5	2·780	87·0	2·226	73·4
2·717	84·8	2·871	89·3	2·265	72·7
2·784	87·0	2·964	91·2	2·340	76·2
2·850	89·3	3·059	94·1	2·382	77·2
2·930	90·2	3·141	95·8	2·420	77·1
3·008	92·4	3·223	98·9	2·457	78·0
3·081	94·6	3·299	100·8	2·530	78·8
3·155	96·9	3·375	103·8	2·565	81·5
3·227	97·3	3·475	104·1	2·606	82·8
3·295	99·3	3·551	106·3	2·640	83·1
3·459	103·8	3·623	107·3	2·674	84·1
3·544	106·4	3·692	109·8	2·707	84·0
1·875	62·3	3·766	112·7		
<i>Hydrogen as exchange gas</i>					
1·903	59·2	2·821	88·8	3·309	101·3
1·951	63·2	2·917	91·0	4·165	125·1
2·258	72·8	3·219	98·7		



values  $\gamma = 5.02 \times 10^{-3} \text{ J deg}^{-2} \text{ mole}^{-1}$  and  $\theta_D = 400^\circ\text{K}$ . These values are to be compared with  $\gamma = 1.20 \times 10^{-3} \text{ cal deg}^{-1} \text{ mole}^{-1}$  ( $5.02 \times 10^{-3} \text{ J deg}^{-2} \text{ mole}^{-1}$ ) and  $\theta_D = 462^\circ\text{K}$ , found for pure iron by Keesom and Kurrelmeyer (1939). If the results for the sigma phase are treated similarly, it is found that the  $(C_v/T, T^2)$  curve has a negative slope and therefore yields negative values of the Debye temperature. This corresponds to a  $(C_v, T)$  curve concave towards the temperature axis. Whilst this may possibly be seen in figure 2 the evidence is not so convincing as in the alternative form of plotting the results as shown in figure 3.

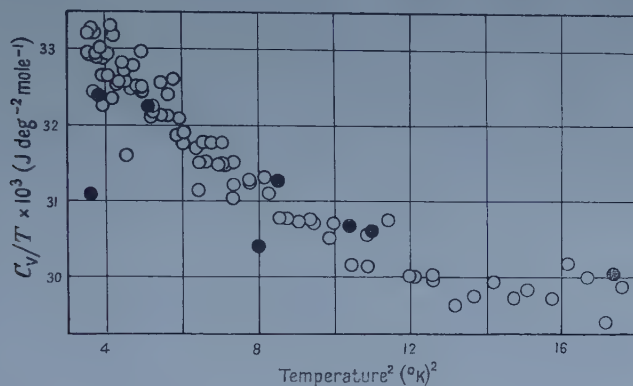


Figure 3. Plot of  $C_v/T$  against  $T^2$  for sigma phase alloy. Points distinguished as in figure 2.

### § 5. DISCUSSION OF THE RESULTS

The results for pure iron and for the iron-chromium alloy shown in figure 1 indicate that the lattice contribution to the specific heat is small and that the difference between the pure iron and the alloy in the alpha phase is but slight.

For the sigma phase material however the method ordinarily employed for distinguishing the electronic and lattice components cannot be used. If it is assumed that the whole of the observed specific heat is electronic in origin it is then apparent that its magnitude is greater than has previously been observed for any metal or alloy. According to the simple electron theory this indicates that the electrons responsible for the heat capacity occupy a portion of an electronic energy band where there exists a very high density of states. From the slope of the  $(C_v, T)$  curve, approximately  $26.8 \times 10^{-3} \text{ J deg}^{-2} \text{ mole}^{-1}$ , the density of states at the Fermi level may be deduced to be of the order of 5.7 per electron volt per atom. This high density of states is not the only interesting feature of these results for there is also the departure from linearity which has to be accounted for. Elcock *et al.* (1953) have considered the effect of confining the electrons in a narrow band and have shown that for such a band the heat capacity of the electrons may be expected to exhibit curvature in the direction observed in the present measurements on the sigma phase. They show that for a narrow closed band the heat capacity rises to a maximum at a temperature depending on the width of the band and then falls slowly to zero.

There are reasons for supposing that the linear term in the specific heat is of more complex origin than is suggested by the simple theory and its obvious modifications as outlined above (Pines 1954, Buckingham and Schafroth 1954, Jones 1957). Whether these modifications to the theory will account for the

observed effects in sigma phase alloys cannot be established without more detailed examination. Meanwhile similar measurements on a series of sigma phase alloys are now in hand to determine whether such behaviour is characteristic of the phase.

## REFERENCES

- BUCKINGHAM, M. J., and SCHAFROTH, M. R., 1954, *Proc. Phys. Soc. A*, **67**, 828.  
ELCOCK, E. W., RHODES, P., and TEVIOTDALE, A., 1953, *Proc. Roy. Soc. A*, **221**, 53.  
HOARE, F. E., and YATES, B., 1957, *Proc. Roy. Soc. A*, **240**, 42.  
JONES, H., 1957, *Proc. Roy. Soc. A*, **240**, 321.  
KEESOM, W. H., and KURRELMAYER, B., 1939, *Physica, 's Grav.*, **6**, 633.  
MATTHEWS, J. C., 1957, *J. Sci. Instrum.*, **34**, 62.  
PINES, D., 1954, *Phys. Rev.*, **92**, 626.

# The Stress Birefringence Relation in some Alkali Halides

By K. G. BANSIGIR AND K. S. IYENGAR

Department of Physics, Osmania University, Hyderabad, Deccan

*Communicated by Professor E. G. Richardson; MS. received 4th July 1957,  
and in revised form 30th August 1957*

**Abstract.** The stress birefringence relation in the alkali halides KBr, KCl and NaCl has been studied employing for the purpose a modified form of Filon's spectrometer method. A linear law is found to hold for stresses ranging from zero to  $25 \text{ kg cm}^{-2}$ . Curves are given showing the photo-elastic dispersion of these solids.

## § 1. INTRODUCTION

THE birefringence introduced by stress in cubic crystals has been the subject of several investigations. Systematic work in this field was begun by Pockels (1889, 1906) who gave the phenomenological theory and determined the photo-elastic coefficients of rocksalt, sylvite and fluorite. Since then many crystals have been investigated.

The experimental method of quantitatively studying this phenomenon consists in applying a known stress to the crystal either along a cube-axis or a cube diagonal and observing in a direction perpendicular to the stress the relative retardation for a beam of light polarized respectively parallel and perpendicular to the stress direction. If  $\Delta$  is the relative retardation in a length  $t$  of the crystal for a stress  $p$ , the following relation is assumed to hold good:

$$\Delta = C_{\lambda} t p \quad \dots\dots(1)$$

where  $C_{\lambda}$  is the retardation for unit stress in unit length, a function only of the wavelength of light. This relation is known to hold for most glasses. In cubic crystals however, the only attempt so far made to test the validity of expression (1) appears to be due to Maris (1927) who experimented with the crystals NaCl, KCl and  $\text{CaF}_2$  at three wavelengths of light. His experiments show that  $C_{\lambda}$  depends both on wavelength and stress. According to him in NaCl, for example, the variation in  $C_{\lambda}$  is as much as 500% when the stress is varied from zero to  $2.5 \text{ kg cm}^{-2}$ . He therefore arrived at the conclusion that 'no crystal showed a direct proportionality between photo-elastic effect and stress for all stresses below elastic limits'. The object of the work described here is to examine how far the above stated conclusion is justified and to determine the dependence of  $C_{\lambda}$  on  $\lambda$  and  $p$ .

## § 2. EXPERIMENTAL METHOD AND RESULTS

### 2.1. Apparatus

The experimental arrangement used for this purpose is shown in figure 1. Light from a bright source S (usually the straight glowing filament of an electric lamp) is focused in a rectangular glass block Q by means of a lens  $L_1$ . Another

lens  $L_2$  forms an image of  $Q$  on the slit of a constant deviation spectrometer  $M$ .  $N_1$  and  $N_2$  are nicols used as polarizer and analyser and  $R$  the specimen under

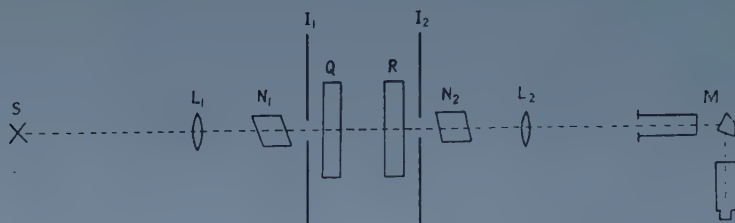


Figure 1. Experimental arrangement.

investigation. The slits  $I_1$  and  $I_2$  allow light to pass through narrow regions of  $Q$  and  $R$ . The arrangement is essentially the same as the one described by Filon and Harris (1931). However it differs in two respects. In the first place the nicols are arranged with their polarizing planes parallel to each other and secondly the block  $Q$  which is under stress takes the place of the quartz compensator used in their experiments. These modifications enable accurate measurements of small changes in birefringence to be made.

## 2.2. Direct and Indirect Methods

Initially  $R$  is omitted and the block  $Q$  of optical glass which is free from residual strains is placed between  $I_1$  and  $I_2$ . This is supported between two knife-edge blocks and a uniform vertical stress is applied with the usual lever arrangement (Filon and Jessop 1922). The nicols are set with their polarizing planes at an angle of  $45^\circ$  to the vertical. Whenever the condition

$$n\lambda/2 = C_\lambda tp \quad \dots\dots(2)$$

is satisfied a dark band with its centre at  $\lambda$  appears in the spectrum. The integer  $n$  is even when the nicols are crossed and odd when they are parallel. The stress  $p$  is then varied in equal steps and the corresponding position of the band is noted. The observations reported here were made with the band for which  $n=1$  and figure 2 shows the variation of  $C_\lambda$  with wavelength for one of the glass blocks studied in this manner. This is the direct method of studying the variation of  $C_\lambda$  with  $\lambda$ . In the indirect method the solid  $R$  under investigation is placed next to the block  $Q$ , the  $(C_\lambda, \lambda)$  variation of which is known. The slits are adjusted

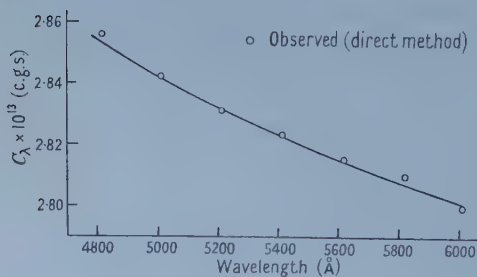


Figure 2.  $C_\lambda$ - $\lambda$  glass.

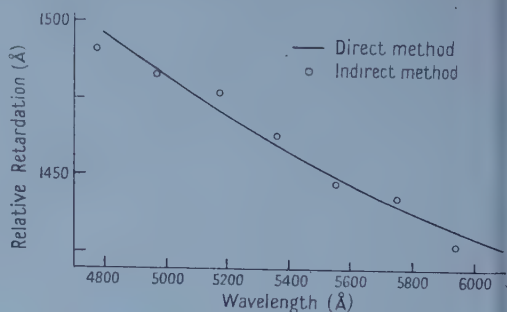


Figure 3. Relative retardation in glass.



so that the beam of light traverses the central homogeneous portions of Q and R. A steady load is applied to R while the load on Q is varied and the corresponding positions of the band are noted. From expression (1) the relative retardation in Q is obtained and since the total relative retardation in the combination Q, R is  $\lambda/2$ , the relative retardation in R is determined. From a knowledge of the stress in R the  $(C_\lambda, \lambda)$  relation may be derived for the solid. The relative retardation in glass as obtained by both methods are shown in figure 3. The points on the smooth curve refer to the direct method while the circles represent the values obtained indirectly.

### 2.3. Application to Cubic Crystals

The direct method is applicable only to solids which are photo-elastically soft like glasses. The cubic crystals KBr, KCl and NaCl cannot withstand large stresses and the maximum relative retardations produced in them are of the order of  $\lambda/4$ . The only way therefore, of studying them is by the indirect method. In table 1 the dimensions and orientations of the rectangular bars of crystals

Table 1

Crystal		Length (dir <sup>n</sup> of stress)		Breadth		Thickness (dir <sup>n</sup> of obs <sup>n</sup> )	
		cm	to	cm	to	cm	to
KBr	A	1.556	[001]	0.635	[010]	0.564	[100]
KBr	B	1.395	[110]	0.801	[110]	0.558	[001]
KCl	C	1.337	[001]	0.865	[010]	0.540	[100]
KCl	D	1.280	[110]	0.796	[110]	0.735	[001]
NaCl	E	1.680	[001]	0.794	[010]	0.605	[100]
NaCl	F	1.095	[110]	0.615	[110]	0.490	[001]

employed are given. All of them showed a small amount of initial birefringence, when examined between crossed nicols. Only those which showed a single colour over a large area were finally selected for investigation. Before introducing one of these at R the load on Q is adjusted until the centre of the dark band occupies

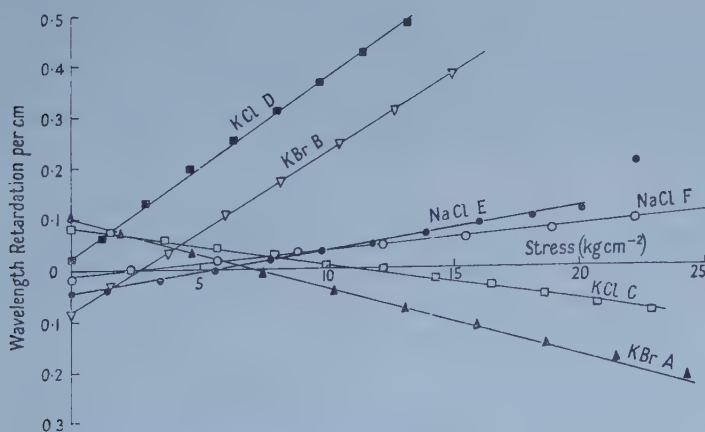


Figure 4. Relative retardation in crystals at 5890 Å.

in the spectrum the position of a known wavelength. The crystal is then introduced at R. Owing to the presence of residual birefringence the position of the dark band is slightly disturbed. It is brought back to its original place by adjusting the load on Q. R is then loaded by a known amount and the displaced band is restored to its old position by adjusting once again the load on Q. From a knowledge of the retardation in Q, the retardation in R is calculated. A plot of retardation in unit length against stress obtained in this manner at one wavelength is shown in figure 4 for all the crystals. Similar curves have been obtained at other wavelengths.

### § 3. DISCUSSION AND CONCLUSIONS

The accuracy of the experimental method rests upon two factors: (1) the accuracy with which the wavelength corresponding to the centre of the black band can be determined, (2) the magnitude of relative retardations produced in Q and R. The band appears narrow in the red region of the spectrum and increases in width towards the violet end. It had an average width of 40 Å in the present work when Q alone was used. With the introduction of R the average value increased to 70 Å. However, with the use of a scale in the eye-piece of the spectrometer telescope, it was always possible to locate the centre of the band to within  $\pm 5$  Å in the spectral region 4800–6000 Å. Outside this the band becomes diffuse and the accuracy rapidly falls. Figure 5 (Plate) is a photograph showing the successive positions occupied by the dark band when the load on the specimen is varied. A comparison iron arc spectrum is also shown superposed and the wavelengths of some identified lines are marked.

As has been remarked earlier, the maximum relative retardation in the crystals is of the order of  $\lambda/4$  (see figure 4). If this retardation is to be measured with some accuracy it is necessary that the retardation in Q should also be of the same order. In other words the total retardation should remain in the neighbourhood of  $\lambda/2$ . This is possible only when the nicols are set with their polarizing planes parallel to each other and measurements are made on the band  $n=1$ .

The curve of figure 2 follows closely the pattern of most glasses and may be shown to fit the formula  $C=C_0/(1-\lambda_0/\lambda)$  when  $C_0=2.609 \times 10^{-13}$  c.g.s. and  $\lambda_0=411$  Å.

It is evident from equation (1) that  $C_\lambda$  is given by the slope of each of the lines of figure 4.  $C_\lambda$  is positive when the crystal is compressed in the direction [110] and light is observed in the direction [001]. Its value in KCl and KBr is negative and in NaCl positive when the compression takes place along [001] and observation is made along [100]. These signs agree with the results reported by other workers.

The variation of  $C_\lambda$  with  $\lambda$  may be obtained from the slopes of the lines of figure 4 drawn for each wavelength in the manner described in §2.3. Alternatively  $C_\lambda$  at different wavelengths may be obtained by maintaining a steady load on R and varying in equal steps the load on Q as described in §2.2. This latter method was employed to study the dispersion in  $C_\lambda$ . From the theory of photoelasticity of cubic crystals (Pockels 1889, 1906) it may be shown that for crystals A, C and E,  $C_\lambda = -\frac{1}{2}\nu^3(q_{11}-q_{12})$  and for crystals B, D and F,  $C_\lambda = -\frac{1}{2}\nu^3q_{44}$ , where  $\nu$  is the refractive index of the undeformed crystal and  $q_{ik}$  are the stress optical coefficients.  $q_{11}-q_{12}$  and  $q_{44}$  may be calculated at each wavelength using known values of refractive index (Radhakrishnan 1948, Ramachandran 1947) and  $C_\lambda$ .

They are shown in figures 6 and 7. In table 2 their values for sodium light are given and compared with the results of other workers (Burstein and Smith 1948, West and Makas 1948).

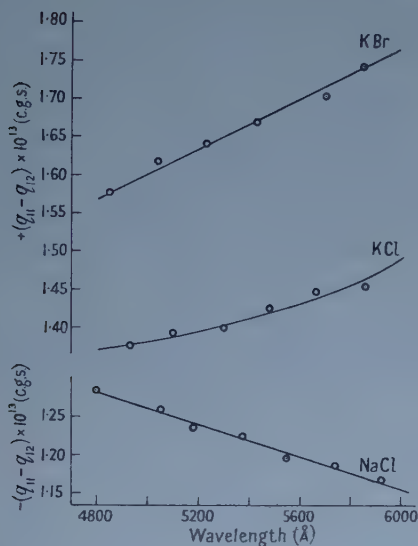


Figure 6. Photo-elastic dispersion.

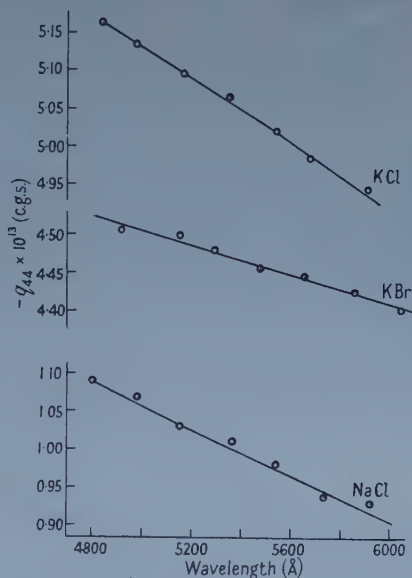


Figure 7. Photo-elastic dispersion.

Mueller (1935) has shown that the photo-elastic effect in cubic crystals can be explained satisfactorily on the assumption that in addition to the anisotropy of the Lorentz and the Coulomb forces caused by elastic deformations, optical anisotropy of the ions also occurs. On this basis he has been able to account for the signs of the elasto-optic constants. Although it is not possible to test this theory quantitatively it may nevertheless be argued (Iyengar 1953) that the optical anisotropy will alter the dispersion frequencies of the optical electrons and thus partly account for the observed photo-elastic dispersion.

Table 2

Crystal	$q_{11} - q_{12}$			$q_{44}$		
	Authors	Others	Dispersion	Authors	Others	Dispersion
KBr	+1.76	+1.70 BS	%	-4.42	-5.14 BS	
		+1.58 WM	12		-4.67 WM	2.3
KCl	+1.47	+1.85 P		-4.94	-4.24 P	
		+1.37 BS	7.8			4.6
NaCl	-1.17	-1.18 BS	10.6	-0.92	-0.83 BS	18.5

(BS, Burstein and Smith (1948); WM, West and Makas (1948); P, Pockels (1906)).

The main conclusions may be stated as follows:

(a) The stress birefringence relation at each wavelength of light is linear from zero to the maximum stress employed in the present investigation ( $25 \text{ kg cm}^{-2}$ ).

In NaCl alone relation (1) does not appear to hold beyond a stress of  $20 \text{ kg cm}^{-2}$  applied in the direction of the cube-axis. This could be due to plastic deformation or to planes of failure occurring in the crystal.

(b) The birefringence initially present appears to arise mostly from strains of a tensional type. Since the crystals were obtained from melt the method of cooling presumably has some bearing on the nature of the strains present.

(c) The magnitude and direction of photo-elastic dispersion is not the same in all crystals.  $q_{11}-q_{12}$  increases with increasing wave-length in KBr and KCl and decreases in NaCl.  $q_{44}$  decreases with increasing wave-length in all crystals. The ratio of the total change in  $q_{11}-q_{12}$  and  $q_{44}$  over the range of wavelengths studied to their value at the mean wavelength, may be taken as a measure of the photo-elastic dispersion. This is given in columns 4 and 7 of table 2. It is of interest to note that while the dispersion is less than 2% in glass it is much larger in these crystals.

#### ACKNOWLEDGMENT

We wish to express our thanks to Professor S. Bhagavantam for providing the alkali halide crystals on which these measurements were made.

#### REFERENCES

- BURSTEIN, E., and SMITH, P. L., 1948, *Phys. Rev.*, **74**, 229.  
FILON, L. N. G., and HARRIS, F. C., 1931, *Proc. Roy. Soc. A*, **130**, 410.  
FILON, L. N. G., and JESSOP, H. T., 1922, *Phil. Trans. A*, **223**, 89.  
IYENGAR, K. S., 1953, *Ph.D. Thesis*, Osmania University.  
MARIS, H. B., 1927, *J. Opt. Soc. Amer.*, **15**, 194.  
MUELLER, H., 1935, *Phys. Rev.*, **47**, 947.  
POCKELS, F., 1889, *Ann. Phys., Lpz.*, **37**, 151 ; 1906, *Lehrbuch der kristall Physik* (Leipzig, Berlin).  
RADHAKRISHNAN, T., 1948, *Proc. Indian Acad. Sci.*, **27**, 165.  
RAMACHANDRAN, G. N., 1947, *Proc. Indian Acad. Sci.*, **25**, 481.  
WEST, W., and MAKAS, A. S., 1948, *J. Chem. Phys.*, **16**, 427.



# Geometrical-Optical Calculation of Frequency Response for Systems with Spherical Aberration

By N. S. BROMILOW†

Department of Physics, Imperial College, London

*MS. received 14th October 1957*

**Abstract.** The usefulness of the geometrical-optical treatment of frequency response is considered. With this treatment calculations have been made, using numerical integration, for several cases of defect of focus, primary and secondary spherical aberration. The results are compared with those obtained from diffraction treatments of the same cases. Provided the wave front aberration exceeds about 1 wavelength, it appears that geometrical optics will give an accuracy in the calculated frequency response of about 5% of its value for zero frequency, over the range of frequencies encountered in many photographic objectives.

## § 1. INTRODUCTION

THE method of frequency response for the specification of the image quality of optical systems is becoming well established. This method allows all aspects of the optical-recording process to be treated within the framework of a single theory, in that it links up the constructional data of the lens, the appearance of the image and testing techniques. In the application of this new approach to practical problems there is a need for a method of obtaining a quick and reliable estimate of the influence of aberration on the frequency response of optical systems. The tolerance theory given by Hopkins (1957 a), provides a satisfactory account of the influence of aberration for cases where the frequency response is not less than 80% of its value in the absence of aberration. For lenses intended for use with television systems, for example, the detector responds to only a small band width of frequencies, so that a tolerance of this order is frequently imposed. In photography, however, a wider range of frequencies is recorded by the emulsion and the above criterion is then not necessarily suitable.

A satisfactory estimate of image quality in such cases requires information about the response curve of the system over the whole range of frequencies of interest, and for these higher frequencies the response will then, usually, have decreased to a value smaller than 80% of its value in the absence of aberration. To obtain the form of the frequency response curve by means of a diffraction treatment requires rather lengthy calculations in all but the simple cases of defect of focus and astigmatism. Even with an electronic computer the cost might be too great to allow the full diffraction calculation to be made as a routine step in lens designing.

## § 2. GEOMETRICAL-OPTICAL APPROXIMATION FOR FREQUENCY RESPONSE

In a recent paper Hopkins (1957 c) has given a treatment of the frequency response of optical systems according to geometrical optics. This leads to an

† Now at Weapons Research Establishment, Department of Supply, South Australia.

expression for the frequency response of the form

$$D(s) = \frac{1}{A} \iint_A [\tau(x, y)]^2 \exp \{iks W_x(x, y)\} dx dy \quad \dots\dots (1)$$

where  $(x, y)$  are pupil coordinates with the  $y$  axis parallel with the direction of the line structures considered,  $W_x(x, y)$  is the first derivative with respect to  $x$  of the wave front aberration and  $\tau(x, y)$  denotes the amplitude over the wave front; the integration is taken over the total area of the pupil  $A$ . The spatial frequency variable  $s$  is given by  $s = (\lambda/n' \sin \alpha') R'$  where  $R'$  is the number of (sine wave) cycles per unit length in the image,  $\alpha'$  is the angular semi-aperture of the optical system and  $\lambda$  is the wavelength of the light.

In the diffraction treatment, the above expression is replaced by

$$D(s) = \frac{1}{A} \iint_S \tau(x + \frac{1}{2}s, y) \tau(x - \frac{1}{2}s, y) \exp \{iks W(x, y; s)\} dx dy \quad \dots\dots (2)$$

where

$$W(x, y; s) = W_x(x, y) + \frac{1}{3!} \left(\frac{s}{2}\right)^2 W_x^{\text{III}}(x, y) + \frac{1}{5!} \left(\frac{s}{2}\right)^4 W_x^{\text{V}}(x, y) + \dots\dots (3)$$

and the region of integration  $S$  is that common to two pupils centred on the points  $(\pm \frac{1}{2}s, 0)$ .

It will be seen that the calculation of frequency response using geometrical optics is appreciably simpler than, and may therefore offer a useful alternative to, the diffraction treatment.

In many cases it appears to be useful to employ the frequency response averaged over, say, a given frequency band. Some kind of averaging over azimuths is also necessary in the general case, though not when, as here, the aberrations are radially symmetrical. The calculation of such averaged values is greatly facilitated by the use of the geometrical optical formula, since the region of integration  $A$  is independent of  $s$ , and this latter merely appears as a simple factor in the argument of the exponential function. A further advantage of the geometrical optical treatment is that the wavelength of the light only appears explicitly in the argument of the exponential function on account of the dependence of aberration,  $W_x(x, y)$ , on the wavelength. This fact simplifies the study of the influence of chromatic aberration on frequency response in white light.

Apart from the above factors, which may help in analytical studies, the notable simplification in computing would itself justify the use of the geometrical treatment. The usefulness of this method will clearly depend on the accuracy of the results obtainable. The present work was undertaken in order to assess this accuracy in practical cases. It may be useful, however, to comment first on the conditions under which the geometrical optical treatment is likely to be satisfactory. By comparing the expressions (1) and (2) above, it is easily seen that as  $s$  tends to zero the region of integration  $S$  degenerates to the region  $A$ , and also  $W(x, y; s)$  tends to  $W_x(x, y)$ . It follows that geometrical optics will be valid in the limit  $s$  tending to zero. This occurs when either  $\lambda$  or  $R'$  tend to zero. It is the latter case, that of low frequencies, that arises in practical systems. It will therefore be for the low frequency range that one will expect the approximation of geometrical optics to be of use. The accuracy of this approximation depends also on the powers of the pupil variables which occur in the aberration function, for as these powers increase so do the magnitudes of the successive terms in the expression  $W(x, y; s)$ , and the

difference between this quantity and  $W_x(x, y)$  becomes greater. In the case of defect of focus, the wave front aberration has the simple form  $W(x, y) = w_{20}(x^2 + y^2)$ , and therefore  $W_x(y, x) = W(x, y; s)$  exactly, so that no error arises from this part of the approximation. The same is true for astigmatism. Clearly the difference between  $W(x, y; s)$  and  $W_x(x, y)$  will be significant, if at all, in cases such as spherical aberration, in which the fourth, sixth and occasionally higher powers of the variables occur. For systems in which the pupil is of uniform transparency  $\tau(x, y) = 1$  and therefore  $\tau(x + \frac{1}{2}s, y)\tau(x - \frac{1}{2}s, y) = [\tau(x, y)]^2$ , so that this factor gives rise to no error. This case, which is that most commonly met in practice, is the one to be considered here.

For systems with relatively large amounts of aberration, as distinct from highly corrected microscope and telescope objectives, only low values of  $s$  are of interest, because the response is small for the higher frequencies. For most photographic lenses, which are a case in point, the aberrations may be expressed to sufficient accuracy by polynomials of degree not greater than six in the aperture variables. For example, the terms present in the wave front aberration for an axial image point are  $w_{20}(x^2 + y^2)$ ,  $w_{40}(x^2 + y^2)^2$  and  $w_{60}(x^2 + y^2)^3$ , where  $w_{20}$ ,  $w_{40}$  and  $w_{60}$  are the coefficients of defect of focus, primary and secondary spherical aberration respectively. Curves for the response in the presence of pure defect of focus have been given by Hopkins (1955). The results using geometrical optics are in good agreement with those obtained by the diffraction treatment for values of  $s$  less than about 0.10. These results were obtained analytically, but an analytical treatment for cases in which  $w_{40}$  and  $w_{60}$  are not zero does not appear to be practicable. Hopkins (1957 b), has given a calculation of the frequency response, based on diffraction theory, for a single case involving these aberration terms, and Goodbody (1957, private communication) has subsequently calculated a whole series of curves using an electronic computer. In the present work calculations have been made using the geometrical-optical treatment of frequency response for cases of spherical aberration, for which

$$W(x, y) = w_{20}(x^2 + y^2) + w_{40}(x^2 + y^2)^2 + w_{60}(x^2 + y^2)^3. \quad \dots\dots (4)$$

With  $w_{60} = 0$ , this represents primary spherical aberration with different planes of focus; where  $w_{60}$  is finite a higher order spherical aberration term is included. The pupil is taken to be a circle of unit radius. The simplification resulting from the geometrical-optical approximation made the use of an ordinary desk computer quite feasible.

The geometrical optical formula (1) for the above case takes the form:

$$D(s) = \frac{1}{\pi} \iint_{x^2 + y^2 \leq 1} \cos \{ks W_x(x, y)\} dx dy \quad \dots\dots (5)$$

where

$$W_x(x, y) = 2x \{w_{20} + 2w_{40}(x^2 + y^2) + 3w_{60}(x^2 + y^2)^2\} \quad \dots\dots (6)$$

the imaginary part in (1) vanishing because  $W_x(x, y)$  is an odd function of  $x$ .

### § 3. COMPUTING PROCEDURE

The diffraction integral corresponding to (5), for defect of focus and primary spherical aberration alone (i.e.  $w_{60} = 0$ ), has been evaluated by Black and Linfoot (1957) employing a method based on Simpson's rule. An alternative method, due to Hopkins (1957 b) and used by Goodbody (1957, private communication) on



the diffraction integral gives results which show good agreement with those of Black and Linfoot. Hopkins' method, which reduces the amount of computation, was used in the work described here. The  $(x, y)$  plane is considered to be divided into small rectangles having sides of length  $2\epsilon_x, 2\epsilon_y$ . The centre of the rectangle  $(p, q)$  then has coordinates  $x_p = (2p-1)\epsilon_x, y_q = (2q-1)\epsilon_y$ . For the case of symmetrical aberrations and pupil shape, the above method gives the following expression for the frequency response:

$$D(s) = \frac{1}{N} \sum_p \sum_q \cos Z_{p,q} \frac{\sin X_{p,q}}{X_{p,q}} \frac{\sin Y_{p,q}}{Y_{p,q}} \quad \dots\dots (7)$$

in which

$$\left. \begin{aligned} Z_{p,q} &= 2ks x_p \{w_{20} + 2w_{40}(x_p^2 + y_q^2) + 3w_{60}(x_p^2 + y_q^2)^2 + \dots\} \\ X_{p,q} &= 2k\epsilon_x \{w_{20} + 2w_{40}(3x_p^2 + y_q^2) + 3w_{60}(x_p^2 + y_q^2)(5x_p^2 + y_q^2) + \dots\} \\ Y_{p,q} &= 8k\epsilon_y x_p y_q \{w_{40} + 3w_{60}(x_p^2 + y_q^2) + \dots\} \end{aligned} \right\} \quad \dots\dots (8)$$

and  $N$  is the number of rectangles whose contributions are included in the double summation.

Numerical results obtained by Goodbody using different sizes of interval suggest that, where errors of less than 0.01 in  $D(s)$  are of little importance, a mesh size of  $2\epsilon_x = 2\epsilon_y = 0.10$  is sufficiently small. Any rectangle is included in the summation or not according as its centre lies inside or outside the region of integration. Only the first quadrant of the circle  $x^2 + y^2 = 1$  need be considered in the summation, since the expression (7) represents the mean value of the sum of the contributions of all rectangles included, and this mean value is the same for all four quadrants when the aberrations are axially symmetrical. For any given combination of aberrations the calculation of the response for a given frequency then involves the summation of the contributions of 79 squares of sides  $2\epsilon_x = 2\epsilon_y = 0.10$ . Because the sum in (7) is divided by the number of squares included,  $N$ , the accuracy required in calculating each term is simply equal to that required in the final result. Five places of decimals were used in the computations, and the final result rounded off to three places. Even this is, of course, superfluous accuracy because an error of  $\pm 0.01$  can easily arise from the approximate method of integration.

For the case of defect of focus with primary spherical aberration alone, we put  $w_{60} = 0$  in (4) above. Making the substitution  $\beta = w_{20}/w_{40}$ , the three expressions (8) take the forms,

$$\left. \begin{aligned} Z_{p,q} &= 2k x_p \{\beta + 2(x_p^2 + y_q^2)\} (sw_{40}) \\ X_{p,q} &= 2k \epsilon_x \{\beta + 2(3x_p^2 + y_q^2)\} (sw_{40}) \\ Y_{p,q} &= 8k \epsilon_y x_p y_q (sw_{40}) \end{aligned} \right\} \quad \dots\dots (9)$$

which are more convenient for use in computation. A given value  $\beta$  then corresponds to a particular form of wave front relative to the chosen focal plane. What is more, the amount of aberration, indicated by the magnitude of  $w_{40}$ , occurs only in the factor  $(sw_{40})$ . Thus  $(sw_{40})$  may be taken as the variable, and one computation then applies to any value of  $w_{40}$ , merely requiring the appropriate scale of  $s$  to be taken.

When secondary spherical aberration is present the parameters

$$\beta_{26} = \frac{w_{20}}{w_{60}}, \quad \beta_{46} = \frac{w_{40}}{w_{60}}$$



are used to denote the plane of focus and amount of primary aberration respectively.  $\beta_{46}$  then denotes a given state of correction of the system relative to the paraxial focus, and the two parameters together specify a given form of wave front relative to the chosen focal plane. In place of (9) we now obtain

$$\left. \begin{aligned} Z_{p,q} &= 2k x_p \{ \beta_{26} + 2\beta_{46} (x_p^2 + y_q^2) + 3 (x_p^2 + y_q^2)^2 \} (sw_{60}) \\ X_{p,q} &= 2k \epsilon_x \{ \beta_{26} + 2\beta_{46} (3x_p^2 + y_q^2) + 3 (x_p^2 + y_q^2) (5x_p^2 + y_q^2) \} (sw_{60}) \\ Y_{p,q} &= 8k \epsilon_y x_p y_q \{ \beta_{46} + 3 (x_p^2 + y_q^2) \} (sw_{60}) \end{aligned} \right\} \dots\dots(10)$$

and, in this case, the product  $(sw_{60})$  is employed as variable, and again one computation applies to any value of  $w_{60}$  provided only that the scale of  $s$  is appropriately chosen.

#### § 4. RESULTS

##### *Primary Spherical Aberration*

Figure 1 (a), (b) and (c) show the results of calculations carried out for the three values  $\beta = -\frac{1}{2}$ ,  $-1$  and  $-1\frac{1}{2}$ . In each case five values of  $(sw_{40})$  were used, giving five points on each of the corresponding frequency response curves. For comparison, the curves obtained by Goodbody for these cases using a diffraction treatment and the same mesh size are given. In the geometrical treatment the frequency response appears as a function of the product  $(sw_{40})$ , so that only one curve is needed for each value of  $\beta$ . On the other hand, the diffraction treatment leads to results which depend on the magnitude of  $w_{40}$  itself. For this reason, corresponding to each value of  $\beta$ , five curves are given for the cases  $w_{40} = 1, 2, 3, 4$  and  $8\lambda$  respectively. The spread of these curves relative to that of the geometrical optical treatment serves as a criterion of the usefulness of the latter.

It will be seen from these curves that, for constant  $\beta$ , the geometrical optical treatment gives greater accuracy for larger amounts of aberration, this being a consequence of the smaller values of  $s$  involved. Except for the case  $w_{40} = 1\lambda$  the errors in  $D(s)$  are much less than 0.10 within the range of values of  $(sw_{40})$  considered.

It will be seen from expression (5) that  $\{(\partial/\partial s)[D(s)]\}_{s=0} = 0$  for the case of geometrical optics, whereas in the diffraction treatment this slope is equal to  $(-2/\pi)$ . It is to be expected, therefore, that for small  $s$ , values of  $D(s)$  greater than those given by the diffraction treatment will be obtained from the geometrical treatment. In figure 1 (a), (b) and (c) it will be seen that the first point calculated by this latter does, in fact, lie above all the diffraction curves. As the value of  $(sw_{40})$  increases, the geometrical optical curve oscillates about the corresponding diffraction curves and, for a constant value of  $w_{40}$ , the value of  $s$  at which the two curves cross increases as  $\beta$  decreases algebraically. This may be explained qualitatively by the following considerations. The errors of the geometrical treatment arising from the difference in the two regions of integration are  $O(s)$ , whereas those arising from the approximation in the integrand are  $O(s^3)$ . In the geometrical optical treatment all squares whose centres lie in the interior of the whole pupil area are included in the summation, but in the diffraction treatment the contributions of squares in the neighbourhood of  $x = 1, y = 0$  are omitted. The sign of the contribution of a given square at  $x = 1, y = 0$  may, therefore, be used as an indication of the direction of the errors in  $D(s)$ . The value of the integrand at this point is  $\cos\{2ks(w_{20} + 2w_{40})\}$ . The point of first cross over of the curves is to be expected when the integrand at  $x = 1, y = 0$  changes sign. This occurs when

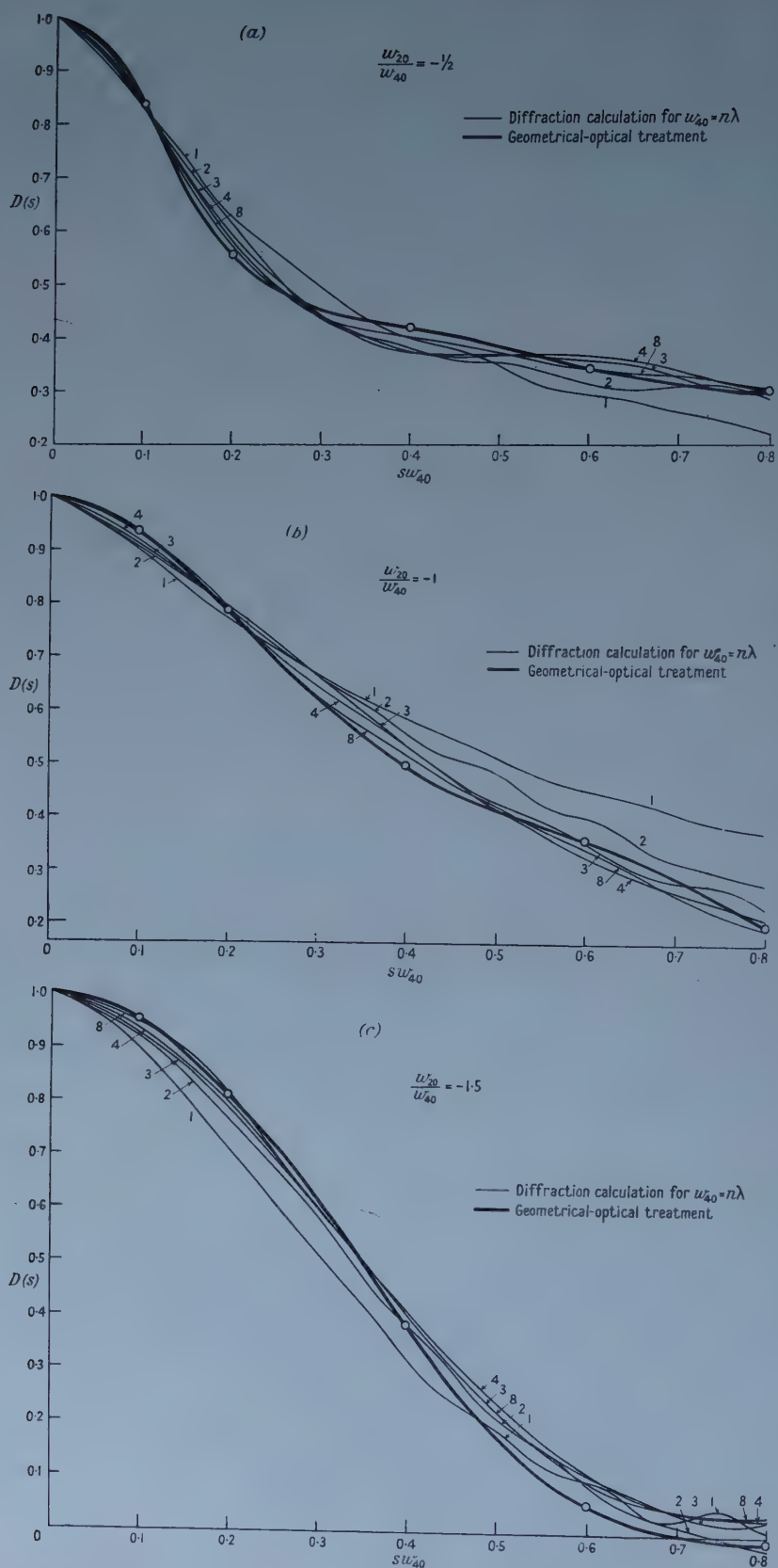


Figure 1. Comparison of frequency response according to diffraction and geometrical optics for defect of focus and primary spherical aberration.

$2ks w_{40}(\beta + 2) = \pi/2$ , and for  $w_{40} = n\lambda$  the value of  $s$  at this crossover is  $s = 1/8n(\beta + 2)$ , and clearly this increases with decreasing values of  $\beta$  in the practical range of values of  $s$ ,  $n$  and  $\beta$ .

### Secondary Spherical Aberration

In view of the satisfactory agreement obtained between the results of the geometrical and diffraction treatments in the case of primary spherical aberration, it seemed sufficient to treat a single case of higher order spherical aberration. For this purpose the parameters were given the values  $\beta_{26} = 0.75$  and  $\beta_{46} = -1.50$ . Figure 2 shows the results obtained for five values of the product  $(sw_{60})$  plotted together with four curves obtained by Goodbody using the diffraction treatment. Again satisfactory agreement is obtained, the maximum error in  $D(s)$  being less than 0.05.

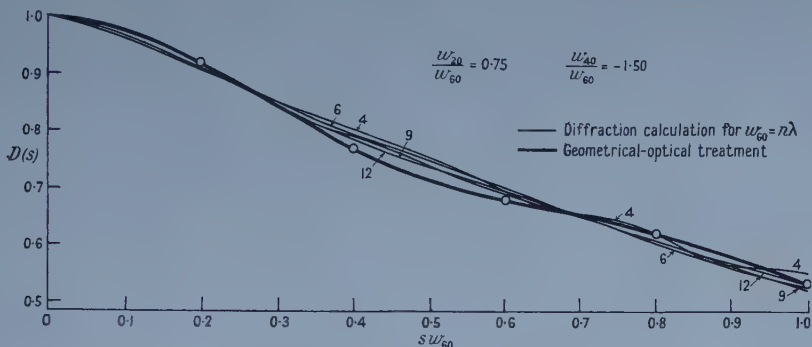


Figure 2. Comparison of frequency response according to diffraction and geometrical optics for defect of focus, primary and secondary spherical aberration.

These results have shown that useful information regarding frequency response may be obtained using the geometrical optical treatment. Indeed, provided accuracy not better than about 5% is required, it would appear that this treatment will usually be adequate. This will often be the case for photographic lenses, and it is precisely here, with a large number of off-axis points to consider, that the reduction in computation is most needed.

### ACKNOWLEDGMENTS

I am grateful to Dr. H. H. Hopkins for suggesting the subject of this paper and for useful discussions. My thanks are due also to Mr. A. M. Goodbody of Imperial College, for allowing me to use some of his results prior to publication. I am indebted to the Chief Scientist, Department of Supply, Australia, for the opportunity of studying in England.

### REFERENCES

- BLACK, G., and LINFOOT, E. H., 1957, *Proc. Roy. Soc. A*, **239**, 522.  
 HOPKINS, H. H., 1955, *Proc. Roy. Soc. A*, **231**, 91; 1957 a, *Proc. Phys. Soc. B*, **70**, 449;  
 1957 b, *Ibid.*, **70**, 1002; 1957 c, *Ibid.*, **70**, 1162.

## The Equation of State of a Gas of Elastic Spheres

By H. N. V. TEMPERLEY

Atomic Weapons Research Establishment, Aldermaston, Berks.

*MS. received 26th August 1957, and in revised form 28th October 1957*

**Abstract.** A study is made of the 'Gaussian' model of an imperfect gas used by Ford, which assumes the Mayer function  $\exp(-\epsilon/kT) - 1$  to be a Gaussian function of the interatomic distance and is, at any fixed temperature, practically equivalent to an elastic sphere model though it could not give the temperature variation of the virial coefficients. The problem is shown to be closely related to one of 'restricted random-walk' type, which can be solved almost completely, the combinatorial problems being similar to those of circuit theory. It is concluded that the virial series is analytic for all positive  $V$  and that the high-order virial coefficients probably alternate in sign, though this limiting behaviour may well be approached very slowly, because of various 'small number effects' that influence the early terms. The model is not directly comparable with that of rigid spheres, because it can be compressed to zero volume.

### § 1. INTRODUCTION

IN a former paper, referred to as I, Temperley (1957) has exhibited some relationships between the problem of obtaining a closed form for the equation of state of an imperfect gas and that of enumerating the configurations of a polymer chain (or of a domain boundary) that is not allowed to cross itself. It was shown that the latter problems could be handled by a slight modification of the Mayer Cluster technique, and that the mathematics was considerably simpler. For any specified interaction there will exist both an 'equation of state' and a 'chain' problem, the condition for the latter being, roughly, that neighbouring molecules in a chain must 'overlap', but other pairs of molecules are not to 'overlap'. In the equation of state problem, no two molecules may overlap.

In this paper we study a very simple, but not unrealistic, model, the so-called Gaussian one in which the Mayer function  $\exp(-\epsilon_{12}/kT) - 1 = f_{12}$  is represented by the Gaussian function  $-A \exp(-r_{12}^2/a^2)$ . This interaction, with  $A=1$  implies that two molecules cannot coincide and that their centres are unlikely to approach to a distance small compared with  $a$ . It thus resembles the familiar 'elastic sphere' repulsion but the 'radius' of the spheres is a complicated function of temperature. (For the rigid sphere we have  $f_{12} = -1$ ,  $r_{12} < a$ ,  $f_{12} = 0$  otherwise.) This model was used by Ford (1954) who made an important step by showing that, in any number of dimensions, either problem can be made to depend on a combinatorial one that occurs in circuit theory. The 'chain' problem in three or more dimensions can be solved subject to one very plausible approximation. An allowance for steric effects can be computed for a long chain as a reduction of the 'entropy per chain link', though the simple limiting behaviour is probably approached rather slowly. These conclusions are in line with numerical evidence obtained by Wall and others (1954, 1955) on various simple chain models. The position in two dimensions is less clear.



Our method can also be applied to the 'equation of state problem' at a fixed temperature, and in three dimensions it is probable that the limiting behaviour and signs of the virial coefficients are correctly given by applying a steric correction to the 'ring' approximation for the cluster integrals, which ignores all diagrams except those corresponding to simple polygons, (Riddell and Uhlenbeck 1953, Rushbrooke and Scoins 1953). Here again, there is evidence of the existence of several 'small-number effects', so that the *limiting* behaviour of the virial coefficients is approached quite slowly and it is known that the 'ring' approximation fails badly for virial coefficients beyond the third. For this purely repulsive model it seems probable that the equation of state is analytic for all positive  $V$ .

Throughout this paper, we shall take  $A=1$ , which implies that the repulsive energy is infinite when two molecules coincide.  $A>1$  would imply a negative Boltzmann factor for close approaches, while  $A<1$  implies that there is a finite probability of coincidence. However, it is possible to draw valuable qualitative conclusions by considering the effect of small changes in  $A$ , as we shall see below.

As in I, the 'chain' problem is to obtain asymptotic estimates of quantities like :

$$f_{12}f_{23}f_{34}\dots f_{N1}(1+f_{13})(1+f_{24})\dots \dots \dots (1)$$

integrated over all possible positions of molecules 2, 3, 4, ... molecule 1 being held fixed. For our special model we take

$$f_{12} = -\exp(-r_{12}^2/a^2). \dots \dots (2)$$

We suppose expression (1) to be expanded, each term then corresponding to a certain Mayer diagram, one line corresponding to each  $f$  factor in the term. The integrations over the  $x, y$  and  $z$  coordinates can clearly be carried out independently and, as shown by Ford (1954), the result of an integration over the  $x$  coordinates keeping molecule 1 fixed is readily expressed in terms of the 'complexity' of the corresponding Mayer diagram

$$I = \frac{(a\sqrt{\pi})^{N-1}}{C^{1/2}} \dots \dots (3)$$

where we obtain the complexity  $C$  of any diagram by writing down a certain determinant according to a simple rule. The rows and columns are numbered to correspond with the molecules and if, for example, the line 13 is present in the diagram we enter  $-1$  in the positions 13 and 31 in the determinant and  $+1$  in each of the positions 11 and 33. We make corresponding entries for each line that is present in the diagram. The complexity of the diagram is then defined as the value of any principal minor of the determinant (all of which are readily shown to be equal). Equation (3) then follows by making a principal axis transformation in terms of the variables  $x_{12}, x_{13}, x_{14}$ , etc. Actually  $C$  has a combinatorial significance of its own, it being a well-known result of circuit theory that it represents the number of different 'trees' that can be obtained from the Mayer diagram by deleting one or more lines, this being always done in such a way as to leave the  $N$  points simply connected with one another by  $N-1$  lines. Our problem is then solved if we can estimate the asymptotic dependence of  $C$  on  $N$  and on the numbers of added lines. According to (1), the  $N$  'sides' connecting points 1, 2, 3 ... in succession into a ring, are always present in the Mayer diagram, while we may also include any  $L-N$  of the lines between non-neighbours in the ring. We shall call the latter lines the 'diagonals', and we shall distinguish between diagonals of different lengths, e.g. 13 and 24 being of the same length.

## § 2. CRITIQUE OF VARIOUS APPROXIMATE TREATMENTS

In I we made a fundamental assumption, that for  $N$  and  $L$  large, we could safely work with mean values of our cluster integrals for a given  $N$  and  $L$ . This appeared to be adequate for  $N = 5$  or  $6$ , but we shall find that the 'spread' increases unacceptably when  $N$  is large. Various other 'small number effects' have come to light in this investigation, emphasizing once again the difficulties of making valid deductions from series expansions of a partition function, even if a good many terms are available.

With our present model, the effect of this 'spread' can be seen very easily. Consider our first-order correction to the 'ring' approximation, obtained by considering diagrams with only one added line. The complexity of the empty ring is just  $N$ , while the mean complexity of a diagram with one extra line is approximately  $N^2/6$ , and there are approximately  $N^2/2$  such diagrams. Since, in a space of  $k$  dimensions, the cluster integral is proportional to the inverse  $\frac{1}{2}k$ th power of the complexity, we would be tempted to conclude that, in a space of five or more dimensions, steric effects would be negligible, the ring integral being proportional to  $N^{-5/2}$  and the first order correction to  $N^{-3}$ . But now consider the contribution to the correction from the diagrams containing any one of the shortest possible diagonals, joining points like 1 and 3. There are  $N$  such diagrams, each of a complexity  $3N - 4$ , the correction due to which is never negligible. Truly a case of the 'tail wagging the dog', and another example of the care necessary in averaging processes. The Rushbrooke and Scoins (1953) approximation is equivalent to considering a selection of such diagrams involving only these shortest diagonals. As stated in I, an apparently better treatment of the 'chain' problem, including the effect of *all* diagrams with non-crossing diagonals, in fact gives worse results.

For the Gaussian model, we can improve considerably on the crude approximation discussed in I, in that we can classify separately all diagrams according to the lengths of the diagonals and only average over diagrams that have the same numbers of diagonals of each length. Two such diagrams will be said to have the same 'structure'. We introduce successively longer and longer diagonals but now allow them to cross. If we confine ourselves to the shortest diagonals, the approximation is still rather crude. Its significance is best seen from the 'square lattice' models used in I in which the successive links of a chain are constrained to lie along the bonds of the lattice. In the linear chain, if we bring any two points like 1 and 3 into contact, we divide the number of possible configurations by exactly two, irrespective of whether or not 2 is in contact with 4. In two and three dimensions it is easily found that the retention of only the shortest diagonals reduces the number of configurations from  $4^N$  ('ring' approx.) to  $4 \cdot 3^{N-1}$  and from  $8^N$  to  $8 \cdot 7^{N-1}$ , corresponding simply to the removal of backward steps. The progressive introduction of longer diagonals should now eliminate closed loops of larger and larger sizes.

## § 3. ESTIMATES OF COMPLEXITIES

To assist in the calculation of complexities of diagrams containing given numbers of diagonals, we introduce an auxiliary quantity  $D_r$ . Consider first a diagram containing  $r$  diagonals all of the same length (the extension to the more general case is immediate).  $D_r$  is defined as the mean number of trees that can be

formed from the lines in the diagram, each such tree being known to contain *all* the *r* diagonals, i.e. the lines to be deleted must all come from the polygon. We can establish a rigorous relation between  $C_r$  and  $D_r$  by repeated application of the self-evident principle that, if we fix our attention on a definite line in the diagram, the complexity is the sum of the numbers of constituent trees that do contain this line and of those that do not. Thus, for a polygon with one diagonal:

$$C_1 = D_1 + D_0$$

with two diagonals

$$C_2 = D_2 + 2C_1 - C_0 = D_2 + 2D_1 + D_0$$

since there are two ways of omitting one out of two diagonals, hence the term  $2C_1$ , but  $C_0$  is now included twice. By repeated application of this argument, we can show generally that

$$C_l = \sum_0^l \binom{l}{r} D_r \quad \dots\dots(4)$$

If now, *l*, *r* and *m*, *s* refer respectively to diagonals of lengths 13 and 14, we can generalize this further to

$$C_{l,m} = \sum_r \sum_s \binom{l}{r} \binom{m}{s} D_{r,s} \quad \dots\dots(5)$$

and so on for more lengths of diagonal. The behaviour of the  $D$ 's is simpler mathematically than that of the  $C$ 's, first because the former vanish whenever  $r+s+\dots \geq N$ . (This happens because, if we draw  $N$  diagonals in a polygon of  $N$  sides, the diagonals alone cannot fail to form at least one cycle.) Secondly, it seems easier to 'separate out' the dependence of  $D$  on  $N$  and on the numbers of diagonals. For small *r*, we can readily write down exact expressions for  $D_r$ , for example

$$D_0 = N \quad \dots\dots(6)$$

because we can form a tree by omitting any one of the  $N$  sides of the polygon,

$$D_{1,0,0} = 2(N-2); \quad D_{0,1,0} = 3(N-3) \text{ etc.} \quad \dots\dots(7)$$

because a diagonal which has *q* sides to its left and  $N-q$  to its right forms a tree if any one of the *q* sides is omitted, together with any one of the  $N-q$  sides. These arguments can be carried much further, but the number of cases to be considered increases rapidly with *r*, *s*. However, the following generalization of the complexity matrix already mentioned at once gives a generating function for the  $D$ 's. Consider the matrix

$$\left\| \begin{array}{cccc} 2x+2y+2z+\dots-x, & -y, & -z, & \dots \\ -x & \dots, & 2x+2y+2z\dots-x, & -y, & -z, & \dots \\ -y & , & -x, & 2x+2y+2z, & -x, & -y, & \dots \\ -z & , & -y & \dots\dots\dots \end{array} \right\| \quad \dots\dots(8)$$

the (11) minor determinant  $G(x,y,z)$  of which can be evaluated by fairly straightforward processes. The quantity

$$a_2 \sin 2j\theta + a_3 \sin 4j\theta + a_4 \sin 6j\theta, \dots\dots$$

where *j* is an integer and  $\theta = \pi/N$  is readily found to be an eigen-function of this (11) minor. After some manipulations we find, for odd  $N=2n+1$

$$G(x,y,z) = N \prod_{j=1}^n \left( x + \frac{y \sin^2 2j\theta}{\sin^2 j\theta} + \frac{z \sin^2 3j\theta}{\sin^2 j\theta} + \dots \right)^2 \quad \dots\dots(9)$$



where  $\theta = \pi/N$ , which has been checked for  $N=5$  and  $N=7$  by direct evaluation of the determinant. We shall show that (9) can be used as a generating function for the  $D$ 's, in the form

$$G(1, y, z) = \sum_{r,s} \binom{N}{r} \binom{N}{s} \dots D_{r,s} \dots y^r z^s \dots \quad (10)$$

(8) is simply the complexity matrix for the 'full polygon' with  $N$  sides and  $N$  diagonals of each length, factors  $x, y, z$  referring respectively to sides, and diagonals of length 13, 14 etc. Since the structure of the matrix is known to be such that all products involving cycles cancel, leaving only products associated with trees, we conclude that, for example, the coefficient of  $yz^3$  in (10) counts the total number of trees of order  $N$  that can be formed from any 1 diagonal of length 13, and any three diagonals of length 14, the remaining  $N-5$  lines in the tree coming from the sides. We have to divide by the number of ways of selecting such a set of diagonals from the  $N$  possible diagonals of length 13 and the  $N$  possible diagonals of length 14 in order to get the mean value of  $D_{r,s}$ , hence the factor  $\binom{N}{r} \binom{N}{s}$  in (10). (There are slight complications when  $N$  is even, one set of diagonals containing only  $\frac{1}{2}N$  lines.)

#### § 4. APPROXIMATIONS USED

To estimate the cluster integrals, we substitute the mean values  $\bar{D}_{r,s}$  obtained from equations like (9) and (10) in rigorous equations typified by (5), that is, we are averaging over all diagrams of the same structure, i.e. that have the same numbers of diagonals of each length, when we calculate  $D$ , and the linearity of equation (5) shows us that our expression for  $C$  involves an averaging of analogous type, but no other approximation is involved so far. The values of  $C$  so obtained then give us the cluster integrals by (3). (This approximation could be avoided only by introducing into (8) a separate selector variable for each individual diagonal, which would make the matrix non-cyclic.) Since expression (9) cannot be put into simpler form we use, in practice, only the lowest order terms in the variables  $y, z, \dots$  which lead to mathematically and physically sensible results, and higher terms could be computed quite readily.

Finally, there is a departure from rigour when we compare (1) with the corresponding expression for the  $N$ th virial coefficient. We have to proceed tentatively since the numbers of irreducible clusters occurring in the equation of state problem are not accurately known. However (1), *as it stands*, implies a much better approximation to the virial coefficient than does the 'ring' or similar approximations, and takes account of a much more representative selection of the diagrams (see table 1 and the discussion that follows).

#### § 5. SMALL NUMBER EFFECTS

Results (4) to (10) are exact, and permit us to work out the consequences of our model for any  $N$ , subject only to the assumption that, for given  $r, s$  etc. the 'spread' of values of the  $C$ 's is small. In I we proposed the more drastic approximation of assigning a mean value to the complexity of all clusters with the same *total* number of lines  $L$ . Direct enumeration of diagrams is not practicable beyond  $N=7$  (see Ford 1954), and examination of the data up to this  $N$  did seem to show that the spread is reasonably small. However, we have shown above that the more drastic approximation fails for high  $N$ , so that we have here another 'small number effect'. Yet others cropped up during the course of this investigation, for example diagrams with  $L > 2N$  are absent for  $N < 6$ , but form the huge



majority for  $N > 6$ . Again, if we examined Ford's data we should conclude that, 'other things being equal', one gets a higher complexity if two diagonals cross than if they do not. For large  $N$  this trend is reversed. Suppose, for example, that we have just two diagonals of length 13. If they do not cross the value of  $D$  is  $4(N-4)$ , whereas if they do it is  $3N-8$  the reversal in trend not occurring until  $N=8$ . The feature that certain selections of diagonals themselves form cycles, for example (13, 35, 51), thus leading to zero contributions to the corresponding  $D$ , does not begin until  $N=6$ .

### § 6. DEDUCTIONS FROM OUR APPROXIMATIONS

We consider first the simple case in which we take account only of diagrams made up of the sides of the polygon and the shortest diagonals, which approximation is very similar to that of Rushbrooke and Scoins (1953). In (9) and (10) we retain only the selector variable  $y$ , putting  $x=1$  and  $z$  and all other selector variables equal to zero. Then we have

$$\sum_r \binom{N}{r} D_r y^r = N \prod_{j=1}^n \left( 1 + 4y \cos^2 \frac{j\pi}{N} \right)^2. \quad \dots\dots(11)$$

For  $N$  large, this approaches the form  $N(1+2y+O(y^2))^{N-1}$  leading to the estimate  $D_r \sim (N-r)2^r$ , the effect of the term  $O(y^2)$  being to contribute terms of lower order in  $N$ . From (4) we conclude that  $C_l \sim N3^l$ . There are  $\binom{N}{l}$  different diagrams with a given  $N$  and  $l$ , so that by the same arguments as those used in I, the total contribution to the integral of expression (1) when just these diagrams are considered is, by (3), proportional to

$$(a\sqrt{\pi})^{k(N-1)} \sum_l \binom{N}{l} (C_l)^{-k/2} (-1)^l \quad \dots\dots(12)$$

where  $k$  is the number of dimensions. If steric effects were neglected altogether, we should have just the term  $l=0$  in (12). Using the estimate for  $C_l$ , we conclude that, to this approximation, steric effects reduce the number of configurations by a factor  $(1-3^{-k/2})^N$  that is, the steric correction takes the familiar form of a reduction of the 'entropy per link of chain'. The factor  $2^r$  in  $D_r$  arises simply from the fact that the complexity is practically doubled each time we introduce another short diagonal that does *not* cut any of these already present. If it *does*, the increase in  $D$  is less, and the effect of such crossings is allowed for by introducing the terms  $O(y^2)$  that would give a more accurate expansion of the right hand side of (11). The resulting estimate of  $D_r$  is only modified by terms of lower order in  $N$ , and the reason for this is simple; there are approximately  $N^2/2$  diagrams with two short diagonals that do not cross, but only  $N$  with two short diagonals that do cross.

If we now take all the possible lengths of diagonal into account, our approximate expansion of (9) is now

$$N(1+2y+3z+4w\dots + \text{second order terms})^{N-1}$$

instead of (11). Carrying out an analogous process for each pair of quantities  $l, r; m, s$  etc., we conclude that

$$C_{l,m} \sim N3^l 4^m \dots \quad \dots\dots(13)$$

so that the whole correction for steric effects should be a factor

$$(1-3^{-k/2})(1-4^{-k/2})(1-5^{-k/2}) \quad \dots\dots(14)$$

per link in the chain,

For  $k=2$ , (14) approaches zero as  $N \rightarrow \infty$ , but for  $k > 2$  the entropy per link of chain rapidly approaches a limiting value in the way that has been found for other models—the corrections for closure of loops of various sizes becoming rapidly smaller as the size of loop increases. Expression (13) could have been got from quite elementary considerations on the complexities of diagrams with non-crossing diagonals, the value of the generating function (9) and (10) is that it permits us, for any given value of  $N$ , to estimate the error that would be caused by omitting 'interaction effects' due to the crossing of diagonals.

It is easy to see that bringing in our second order terms in  $y, z, w \dots$  would not change the qualitative form of (14). It would change each of the factors by a term of the order  $1/N$  and consideration of the sign shows that this can only *increase* the magnitudes of the steric correction. (We have already noted that diagrams with crossing diagonals tend to have smaller complexities, therefore larger cluster integrals.) The tendency of the correcting factor to approach zero for  $k=2$  is therefore accentuated. We already know that steric effects are abnormally heavy in two-dimensional models, but the possibility that the unexpected result is a consequence of our process of averaging over all diagrams with the same structure cannot be ruled out.

### § 7. THE 'EQUATION OF STATE' PROBLEM

The generating function (9) actually includes *all* trees than can be made by joining up  $N$  points by  $N-1$  lines. We are now interested in all the Mayer clusters, that is, in the complexities of connected diagrams of all possible structures, whereas, in the former problem, the only structures that interested us were those in which all  $N$  'sides' were present always. We introduce another auxiliary quantity  $E_{p,r,s}$  which is the mean number of trees of order  $N$  that can be drawn using exactly  $p$  sides,  $r$  diagonals of length 13,  $s$  diagonals of length 14 etc., where we must clearly have  $p+r+s \dots = N-1$ . We now write, instead of (10)

$$G(x, y, z) = \sum_{p,r,s} \binom{N}{p} \binom{N}{r} \binom{N}{s} \dots E_{p,r,s} x^p y^r z^s \dots \quad (15)$$

$G$  is still given by (9). The  $E$ 's are all necessarily unity or less, each representing the chance of forming a tree by selecting  $N-1$  lines completely at random, prescribing only the numbers  $p, r, s$  of lines of the various lengths. We clearly have

$$D_{r,s} = \sum_p \binom{N}{p} E_{p,r,s} \dots \quad (16)$$

so that (10) could have been obtained from (15) by summing over  $p$ , and, in (15), the sides and diagonals are all treated on the same footing, as they should be. We could also write, for the mean complexity of a diagram including  $h$  sides,  $l$  diagonals of length 13,  $m$  diagonals of length 14, the obvious generalization of (5) to the case  $h < N$

$$C_{h,l,m} = \sum_{p,r,s} \binom{h}{p} \binom{l}{r} \binom{m}{s} \dots E_{p,r,s} \dots \quad (17)$$

A combination of (15) and (17) leads to the elegant result

$$\sum \binom{N}{h} \binom{N}{l} \binom{N}{m} C_{h,l,m} \dots a^h b^l c^m \dots = (1+a)^N (1+b)^N (1+c)^N \dots G(x, y, z \dots) \quad (18)$$

with  $x = a/(1+a)$ ,  $y = b/(1+b)$  etc.

This, however, is not so useful as expression (5) because this average value of  $C$  includes unconnected diagrams, the complexity of which is zero. (Our former

problem corresponds to the case  $h=N$  and any diagram including all  $N$  sides is necessarily connected.)

Unfortunately, we do not yet possess a formula which tells us the chance that a random selection of lines gives us a connected diagram, without which we cannot safely use (17) in conjunction with (3), because the latter equation breaks down for unconnected diagrams. However, the information already obtained on the 'chain' problem enables us to draw some conclusions about the 'equation of state' problem. We have already (Temperley 1956) shown that there is both physical and mathematical evidence of a close connection between these two problems, and we shall now give some reasons for thinking that, for  $N$  large, the probability of a non-crossing ring  $N$  units long should 'mimic' fairly closely the behaviour of the  $N$ th virial coefficient.

We notice first that both quantities are entirely made up of irreducible cluster integrals of order  $N$ , though some that occur in the virial coefficient are absent for the ring. In physical language, we have, in effect, two estimates of the probable number of configurations of  $N$  molecules, each being known to overlap at least two others. Secondly, although we do not know the number of irreducible diagrams for a given  $h, l, m$ , we do know the number of such diagrams if we specify the total number of lines  $L = h + l + m + \dots$ , at least we possess this information in the form of generating functions (see Riddell and Uhlenbeck 1953, Ford 1954). The correspondence is very close when  $L$  exceeds  $N \log N$  (and  $L$  must be at least  $N$  to get an irreducible cluster at all.) In these two cases, our estimates for the number of diagrams with a total of  $L$  lines are

$$\binom{N(N-3)/2}{L-N} \text{ (chain problem) and } \binom{N(N-1)/2}{L} \text{ (virial coefficient),}$$

which means that the chain calculation gives *relatively more* weight to the cluster with a large number of lines than does the virial calculation. As  $L$  increases, the two numbers approach equality. The following data for  $N=6$ , in which the number of irreducible clusters is tabulated against  $L$  for the two problems, shows this trend to be smooth but not monotonic. The data for the virial coefficient are taken from Ford (1954), while those for the chain problem are just the binomial coefficients for  $N=9$ .

Numbers of irreducible diagrams for  $N=6$

$L$	6	7	8	9	10	11	12	13	14	15
Virial coefficient:	60	720	2445	3635	2697	1335	455	105	15	1
Chain problem :	1	9	36	84	126	126	84	36	9	1
Ratio :	60	80	68	43.3	21.4	10.5	5.4	2.9	1.67	1

It will be seen from this table that almost all these discrepancies can be removed by an alteration of the parameter  $A$  occurring in the definition of the  $f$ -factors, which modifies the weight given to clusters containing  $L$  lines by a factor  $A^L$ . Thus for  $N=6$ , we could compare the virial problem with a chain problem in which  $A$  is reduced by a factor of the order of 1.7–1.8 to compensate for the larger relative weight given to clusters of large  $L$  in the chain problem. The effect of using an  $A$  different from unity is simply that the factors in (14) are changed to  $(1 - A \cdot 3^{-k/2})$  etc. In using the table, one must also remember the existence of the factor  $1/(N-1)!$  in the definition of the cluster integrals occurring in the virial series



No such normalizing factor occurs in the 'chain' problem because the arrangement of molecules in the basic ring is fixed (see I).

The ratio in the table passes through a maximum instead of being monotonic, and it is important to know its approximate height and position. On the basis of some unpublished work on the enumeration of irreducible clusters with  $L$  slightly greater than  $N$ , I have concluded that, for large  $N$ , this maximum ratio occurs for  $L = 10N/9$ , ( $N/9$  extra lines) and attains a value approximately  $\exp(N/9)$  times the well known value of  $(N-1)!/2$  for  $L = N$ , corresponding to the number of distinguishable rings of  $N$  atoms. Thus, the appropriate modification of  $A$  is by a factor of the order of  $(N!)^{2/N^2}$ , which approaches unity for large  $N$ .

The expression (14) implies that, for the chain problem, the sign of the first term persists in the final result, in spite of large cancellations of much larger terms, and such a result is, of course, required by the physics of the problem, because the number of non-crossing paths cannot possibly be negative for any model. Comparison of the two problems suggests the possibility of an analogous behaviour for the virial series—that is its terms should alternate in sign just like the result of the 'ring' approximation, but the effect of the higher cluster integrals could be allowed for by applying a steric factor of the type (14) to the 'ring' approximation. Because of the 'small number effects' we have found, this limiting behaviour may well be approached very slowly, though Ford (1954) has already shown that the fourth and seventh virial coefficients are negative for this model.

Such behaviour of the virial coefficients would imply that the nearest singularity of the virial series would be on the *negative* real axis of  $1/v$ , and this probably implies that, for this model, the virial series shows *no* 'condensation' effect. For  $A \leq 1$  there is no excluded volume effect, and it is easy to show that  $Pv$  must be finite as  $v \rightarrow 0$ . For the form (2) for  $f_{12}$  implies the following form for the potential energy, as  $r$ , the mean distance between molecules, tends to zero

$$\epsilon(r) = -kT \log \left( 1 - A + \frac{Ar^2}{a^2} \right)$$

which implies that  $\partial\epsilon/\partial r$  vanishes when  $A < 1$ , but gives a finite contribution to  $Pv$  when  $A = 1$ .

Very recently, W. W. Wood (1957) and Alder (1957) have reported that the *rigid* sphere model *does* show a transition, using a Monte Carlo and a dynamical method. The present model is not comparable, since it can be compressed to *zero* volume, the repulsion being 'soft'. A 'hard' repulsion can be roughly represented by taking  $A > 1$ , which *could* lead to a transition by altering the sign of (14).

#### ACKNOWLEDGMENTS

I wish to thank Dr. W. W. Wood and Prof. J. G. Kirkwood for helpful discussions, and the Director, Atomic Weapons Research Establishment, for permission to publish this paper.

#### REFERENCES

- ALDER, B. J., 1957, Varenna Conference on the Condensed State.  
 FORD, G. W., 1954, *Thesis*, University of Michigan. (To be published shortly in book form, *Progress of Statistical Physics*.)  
 RIDDELL, R. J., and UHLENBECK, G. E., 1953, *J. Chem. Phys.*, **21**, 2056.  
 RUSHBROOKE, G. S., and SCOINS, H. I., 1953, *Proc. Roy. Soc. A*, **216**, 203.  
 TEMPERLEY, H. N. V., 1956, *Phys. Rev.*, **103**, 1; 1957, *Trans. Farad. Soc.*, **53**, 1065. referred to as I in the text.  
 WALL, F. T., *et al.*, 1954, *J. Chem. Phys.*, **22**, 1036; 1955, *Ibid.*, **23**, 913, 2314.  
 WOOD, W. W., 1957, Varenna Conference on the Condensed State.



## Angular Correlations of Gamma Rays in $^{103}\text{Rh}$

By F. C. FLACK AND P. MASON

Physics Department, Washington Singer Laboratories, University of Exeter, Exeter

Communicated by G. K. T. Conn ; MS. received 27th August 1957 and in revised form 16th October 1957

**Abstract.** Lifetime measurements indicate that the 55 keV transition in  $^{103}\text{Rh}$  is mostly dipole in character. Angular correlation measurements involving this transition rule out  $\frac{5}{2}^+$  for the spin of the level at 538 keV, but allow  $\frac{7}{2}^+$  or  $\frac{9}{2}^+$ , the former being preferred. The spin of the 650 keV level is not determined by these results.

### § 1. INTRODUCTION

THE recent work of Saraf (1955) and de Raad *et al.* (1954) on the  $\beta$ -decay of 40-day  $^{103}\text{Ru}$ , together with that of Rietjens *et al.* (1954), Rietjens (1956) and Saraf (1955) on the electron capture nucleus  $^{103}\text{Pd}$  (17 days) has led to an improved understanding of the energy level scheme of the common daughter nucleus  $^{103}\text{Rh}$ . In particular Saraf, using  $^{103}\text{Ru}$  sources, has shown that the well known gamma rays of 610 and 498 keV are the cross-overs for two weak cascade transitions of 555–55 and 440–55 keV, and that all these transitions terminate on the 56-min isomeric state at 40 keV above ground. The 55 keV radiation was already known, Saraf giving a conversion coefficient  $\alpha_K$  of approximately unity (M1 or E2 radiation). Avignon (1956) however measured  $\alpha_K$  for a photoelectron line corresponding to a 55 keV transition after the decay of  $^{103}\text{Pd}$ . His value of  $\alpha_K > 10^4$  corresponds to E5 or M5 radiation. If these two estimates of  $\alpha_K$  refer to the same transition they are in marked disagreement.

The present paper describes angular correlation measurements of the gamma rays emitted following the  $\beta$ -decay of  $^{103}\text{Ru}$  and discusses the spins of some of the excited states of  $^{103}\text{Rh}$ . It also reports an experiment on the lifetime of the state responsible for the 55 keV gamma ray from which independent evidence is obtained about the multipolarity of this transition.

### § 2. SOURCE AND APPARATUS

The source was prepared from 'Specpure' ruthenium metal sponge which was irradiated in a Harwell pile and then aged for one month to allow short period activities to decay. The material was then purified by distillation of  $\text{RuO}_4$  to remove an impurity which was found to be  $^{192}\text{Ir}$ . Finally, a fine powder of black ruthenium oxides (amorphous) was obtained. This was mounted in a small distrene container with very thin walls.

The apparatus consisted of two conventional scintillation counters, using NaI crystals and EMI 5359 photomultipliers, connected for coincidence work. They were constrained to move on a circle at the centre of which was placed the source. The larger of the two crystals ( $1\frac{1}{2}$  in. diam.  $\times$   $1\frac{1}{2}$  in.) resolved the higher energy radiations while the other ( $\frac{1}{2}$  in.  $\times$   $\frac{1}{2}$  in.  $\times$   $\frac{1}{8}$  in.) was used to examine soft gamma rays

and x-rays. The latter was inefficient above a few hundred kev but had good energy resolution and efficiency in the 50 kev region. Perspex absorbers prevented beta rays from entering the detectors. The coincidence circuit was of the 'fast-slow' type with a resolving time set at  $2\tau = 20 \text{ m}\mu\text{sec}$  for the correlation measurements, but reduced to  $2\tau = 7 \text{ m}\mu\text{sec}$  for the lifetime experiments. The slow line pulses were examined with single channel analysers.

### § 3. EXPERIMENTAL PROCEDURE

The existence of the cascade radiations was first confirmed by mounting the source, together with a graded lead, tin and copper Compton shield, between the two crystals. One single channel analyser accepted pulses from 55 kev gamma rays while the other scanned the region above 350 kev for coincident radiations. Two peaks were found corresponding to gamma rays of energies  $440 \pm 10$  and  $555 \pm 10$  kev, in good agreement with the results of Saraf.

For the angular correlation measurements the pulse analyser on the large crystal detected the appropriate one of these two high energy rays. The coincidence counting rate, and random coincidences, were measured as a function of the angle  $\theta$  between the counters at intervals of  $30^\circ$  from  $+90^\circ$  to  $-90^\circ$ . The effective angular window of the counting arrangement was determined by annihilation radiation coincidence measurements using  $^{22}\text{Na}$ . The full width at half height was  $30^\circ$ .

Lifetime measurements were made using the arrangement described in the first paragraph of this section, but with the resolving time of the coincidence circuit as small as was consistent with a reasonable coincidence efficiency (viz.  $2\tau = 7 \text{ m}\mu\text{sec}$ ). With the high energy counter accepting all pulses corresponding to energies greater than about 350 kev delay curves were plotted and compared with similar curves obtained using prompt coincidences from  $^{22}\text{Na}$  annihilation radiation. Allowance must be made for the longer time taken by small pulses (55 kev radiation) than by large pulses to rise to the cut-off voltage for the limiter valve in the fast line. The resultant effect is an overall shift of the delay curve from the position occupied when both pulses are large (Gerholm 1956). Both kicksorters therefore accepted the same pulse heights in the ruthenium and sodium experiments, the Compton plateau being used in the latter case.

### § 4. RESULTS

#### 4.1. Angular Correlations

The coincidence counting rates were fitted by the least squares procedure of Rose (1953) to a function of the usual form, containing terms up to the fourth Legendre polynomial in  $\cos \theta$ . The result was then corrected for finite solid angle of the counters by the method of Lawson and Frauenfelder (1953). The values obtained were, for the 555-55 kev cascade

$$W(\theta) = 1 - 0.129 (\pm 0.02) P_2(\cos \theta) - 0.00 (\pm 0.03) P_4(\cos \theta),$$

and for the 440-55 kev cascade

$$W(\theta) = 1 + 0 (\pm 0.02) P_2(\cos \theta) + 0 (\pm 0.04) P_4(\cos \theta).$$

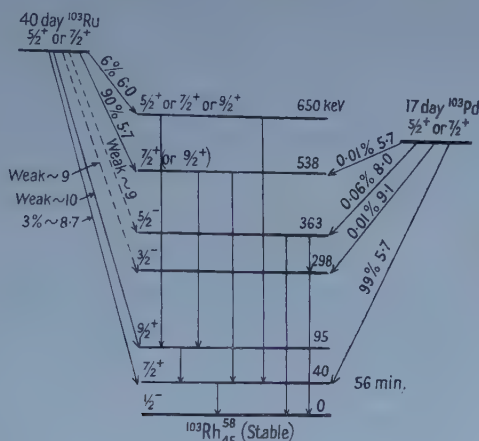
The latter figures include a correction for a small contribution from the 'tail' of the 550 kev peak which fell in the window of the analyser observing the 440 kev peak.

## 4.2. Lifetime Measurement

No change in the slope of the edge of the delay curves for annihilation radiation and  $^{103}\text{Rh}$  could be detected. Centroid shift measurements in this case would appear somewhat unreliable because of the small pulse effect mentioned, but it seems possible, on such a basis, to put the lifetime of the level responsible for the 55 kev radiation as less than or equal to  $10^{-9}$  sec. Three separate experiments all yielded shifts of less than half this amount.

## § 5. DISCUSSION

The arguments leading to most of the spin assignments shown in the figure were given originally by Saraf (1955) and with some changes, which have been



Decay scheme of  $^{103}\text{Ru}$  ( $\beta$ - and capture transition figures are the relative intensity and  $\log ft$  values respectively).

incorporated in the diagram, by Rietjens (1956). The level responsible for the 55 kev gamma ray is assigned  $\frac{9}{2}^+$  by these workers and by Avignon (1956), though the latter requires the transition to go direct to the  $\frac{1}{2}^-$  ground state to explain his large value of  $\alpha_K$ . The measured lifetime supports the scheme of the figure the transition being classified as chiefly magnetic dipole. If it were pure E2, the expected lifetime, using single particle estimates, is  $10^{-5}$  sec.

The shell model predicts the  $^{103}\text{Ru}$  ground state as either  $g_{7/2}$  (preferred by Saraf) or  $d_{5/2}$  (preferred by Rietjens). The value chosen affects the range of spins it is necessary to consider for the levels at 538 and 650 kev in  $^{103}\text{Rh}$ , reached via allowed beta decays ( $\log ft = 5.7$  and 6 respectively). Both the authors mentioned limit the spin of the 538 kev level to  $\frac{5}{2}^+$  or  $\frac{7}{2}^+$ . Saraf rejects a possible  $\frac{9}{2}^+$  on theoretical grounds.

Consider first the 538 kev level, which decays both by an M1 or E2 transition ( $\alpha_K \sim 10^{-2}$ ,  $K/L \sim 8$ ) of 498 kev and by a weaker (0.5%) 440 kev radiation. On intensity grounds the latter has generally been considered to be E2 in character. The angular correlation for the 440-55 kev cascade  $\frac{5}{2}^+$  (E2)  $\frac{9}{2}^+$  (M1 + E2)  $\frac{7}{2}^+$  can be fitted by assuming a mixing ratio  $\delta_{55} = 0.16$  ( $\delta^2 = \text{intensity of E2}/\text{intensity of M1}$ ). This choice of  $\delta_{55}$  must also fit the 555-55 kev cascade. In fact, the value quoted makes all the calculated correlation functions for these transitions much more



isotropic than experiment indicates, no matter what value of spin is chosen for the 650 keV state or the mixing ratio in the 555 keV radiation. An assignment of  $\frac{7}{2}^+$  is therefore indicated for the 538 keV level and one can also eliminate the possibilities that the 440 keV transition is E2 or M3 because a similar value of  $\delta_{55}$  is needed. The observed correlations are thus fitted by the cascade  $\frac{7}{2}^+ (M1 + E2) \frac{9}{2}^+ (M1 + E2) \frac{7}{2}^+$ . The mixing ratio  $\delta_{440} = 0.16$  gives the necessary isotropy to the correlation, the result being little affected by the value chosen for  $\delta_{55}$ . Unfortunately, the experimental results do not rule out the cascade beginning  $\frac{9}{2}^+ (M1 + E2)$ , since suitable mixing ratios can again be chosen. If one accepts the views of the authors quoted then the  $\frac{7}{2}^+$  assignment is preferred.

It is not possible to determine a spin value for the level at 650 keV from the results presented here. The 555 keV radiation may be M1 in character as indicated by its relative intensity to the 610 keV gamma ray, so that two mixing parameters are available and a fit to experimental data may easily be made. Even if this radiation is only quadrupole or octupole  $\frac{9}{2}^+$ ,  $\frac{7}{2}^+$  and  $\frac{5}{2}^+$  possibilities can be made to agree with experiment, the appropriate values of  $\delta_{55}$  being consistent with the indication from the lifetime measurements that the contribution of E2 in the 55 keV transition is probably not large.

#### §.6. CONCLUSIONS

The gamma ray of energy 55 keV in  $^{103}\text{Rh}$  is mostly magnetic dipole in character. The level at 538 keV in the same nucleus has, probably, a spin  $\frac{7}{2}^+$  or, less likely  $\frac{9}{2}^+$ . A value  $\frac{5}{2}^+$  is ruled out by the experimental data. No conclusions can be drawn about the spin of the 650 keV level from these data.

It should perhaps be pointed out that the spins of the 40 and 95 keV levels are explained, on the shell model, as  $G_{7/2}$  and  $G_{9/2}$  states respectively, the responsible protons of orbital  $g_{9/2}$  being five in number. One might expect the level at 538 keV to be a  $G_{7/2}$  or  $G_{9/2}$  state also. In that case the shell model selection rule  $\Delta l = 0$  for allowed beta decay is not in accordance with a  $d_{5/2}$  ground state for  $^{103}\text{Ru}$ . If, therefore,  $g_{7/2}$  is taken as the appropriate neutron orbital for  $^{103}\text{Ru}$  then the allowed,  $l$ -forbidden nature of the 700 keV beta transition (Goeppert-Mayer 1955) with  $\Delta l = 2$ , is no longer an explanation of the  $\log ft$  value of 8.7 for this beta group.

Similar difficulties arise in the decay of  $^{103}\text{Pd}$ . Professor P. M. Endt has pointed out to the authors that the non-appearance of the 55 keV transition in this decay gives a value of  $\log ft$  greater than 10.3 for a branch of electron capture feeding the 95 keV level. This would indicate  $\Delta J = 2$  and so gives  $\frac{5}{2}^+$  for the  $^{103}\text{Pd}$  ground state, which is expected to be  $d_{5/2}$  or  $g_{7/2}$ .

#### ACKNOWLEDGMENTS

The authors are deeply grateful to Professor P. M. Endt for valuable suggestions which have been incorporated in this paper. They would also like to thank Mr. L. R. Jenkin for help with the electronic equipment and Mr. J. V. Wills for aid in the chemical processing of the source.

One of us (P. M.) would like to acknowledge the receipt of a maintenance grant from the Department of Scientific and Industrial Research during the course of this work.



REFERENCES

- AVIGNON, P., 1956, *Ann. Phys., Paris*, **1**, 10.  
DE RAAD, B., MIDDELKOOP, W. C., VAN NOOYEN, B., and ENDT, P. M., 1954, *Physica*, **20**, 1278.  
GERHOLM, T. R., 1956, *Arkiv Fys.*, **10**, 523.  
GOEPPERT-MAYER, M., 1955, *Beta and Gamma-Ray Spectroscopy* (Amsterdam : North Holland.)  
LAWSON, J. S., and FRAUENFELDER, H., 1953, *Phys. Rev.*, **91**, 649.  
RIETJENS, L. H., 1956, *Ph.D. Thesis*, University of Utrecht.  
RIETJENS, L. H., VAN DEN BOLD, H. J., and ENDT, P. M., 1954, *Physica*, **20**, 107.  
ROSE, M. E., 1953, *Phys. Rev.*, **91**, 610.  
SARAF, B., 1955, *Phys. Rev.*, **97**, 715.

## An Investigation of the $^{16}\text{O}(\text{d}, \alpha)^{14}\text{N}$ Reaction by Magnetic Analysis

By A. W. DALTON, S. HINDS† AND G. PARRY

Nuclear Physics Research Laboratory, University of Liverpool

*Communicated by Professor H. W. B. Skinner; MS. received 20th August 1957, and in revised form 4th November 1957*

**Abstract.** The  $^{16}\text{O}(\text{d}, \alpha)^{14}\text{N}$  reaction has been investigated at bombarding energies of 6.8, 7.1, 7.2 and 8.9 MeV. At these energies the intensity of the transition to the 2.31 MeV,  $T=1$  state of  $^{14}\text{N}$  has been measured. Angular distributions have been obtained for the alpha particles leading to the ground state and the 3.95 MeV level of  $^{14}\text{N}$  for bombarding energies of 6.8 and 8.9 MeV.

### § 1. INTRODUCTION

THE  $^{16}\text{O}(\text{d}, \alpha)^{14}\text{N}$  reaction has been studied by Freemantle, Gibson, Prowse and Rotblat (1953) at a deuteron bombarding energy of 19 MeV. More recently Browne (1956) has measured the angular distributions and excitation functions of the alpha-particle groups leading to the ground, first and second excited states of  $^{14}\text{N}$  for bombarding energies up to 7.5 MeV. His measurements show that there is a minor breakdown of the isotopic spin selection rule governing transitions to the first excited state at 2.31 MeV which has  $T=1$ . Preliminary measurements here using deuterons of about 9 MeV energy indicated only a very weak transition to this state. Further measurements have been made with lowered beam energies for comparison with Browne's results.

### § 2. EXPERIMENTAL TECHNIQUE

The deuterons were accelerated to 9 MeV energy in the Liverpool 37 in. cyclotron. For the measurements at 7 MeV the deuterons were reduced in energy by using absorbers of aluminium foil. The majority of the measurements on the alpha particles were made using the magnetic spectrograph described by Green and Middleton (1956a). A modification was made using a vacuum-tight sliding seal surrounding the target, so that the range of angles of observation was increased to  $135^\circ$  (Dalton, Hinds and Parry 1957). Some measurements were also made using a scattering camera technique with small photographic plates distributed round the inside of the target chamber.

### § 3. THE TRANSITION TO THE 2.31 MeV, $T=1$ LEVEL OF $^{14}\text{N}$

For these measurements the target was  $0.7 \text{ mg cm}^{-2}$  Melinex film supplied by I.C.I. The target is essentially  $\text{C}_5\text{H}_4\text{O}_2$  and the alpha-particle group under investigation is not contaminated with alpha particles of the same energy from reactions of other constituents. Unfortunately this substance is not absolutely permanent under bombardment so that a new target was required for each exposure and comparison of yields for different bombarding energies is not possible. Observations were made at beam energies of 8.9, 7.2, 7.1 and 6.8 MeV. These energies were determined by measuring the ranges in the photographic emulsion of groups of particles from reactions with well-known  $Q$ -values. The

† Now at Atomic Weapons Research Establishment, Aldermaston, Berks.

angle of observation was  $35^\circ$  except at 7.1 Mev when an additional observation was made at  $20^\circ$ .

Two of the spectra are shown in figure 1 and the results are listed in the table, which gives the intensities of the transitions to the  $T=1$  state expressed as a percentage of the transitions to the ground state and second excited state at 3.95 Mev.

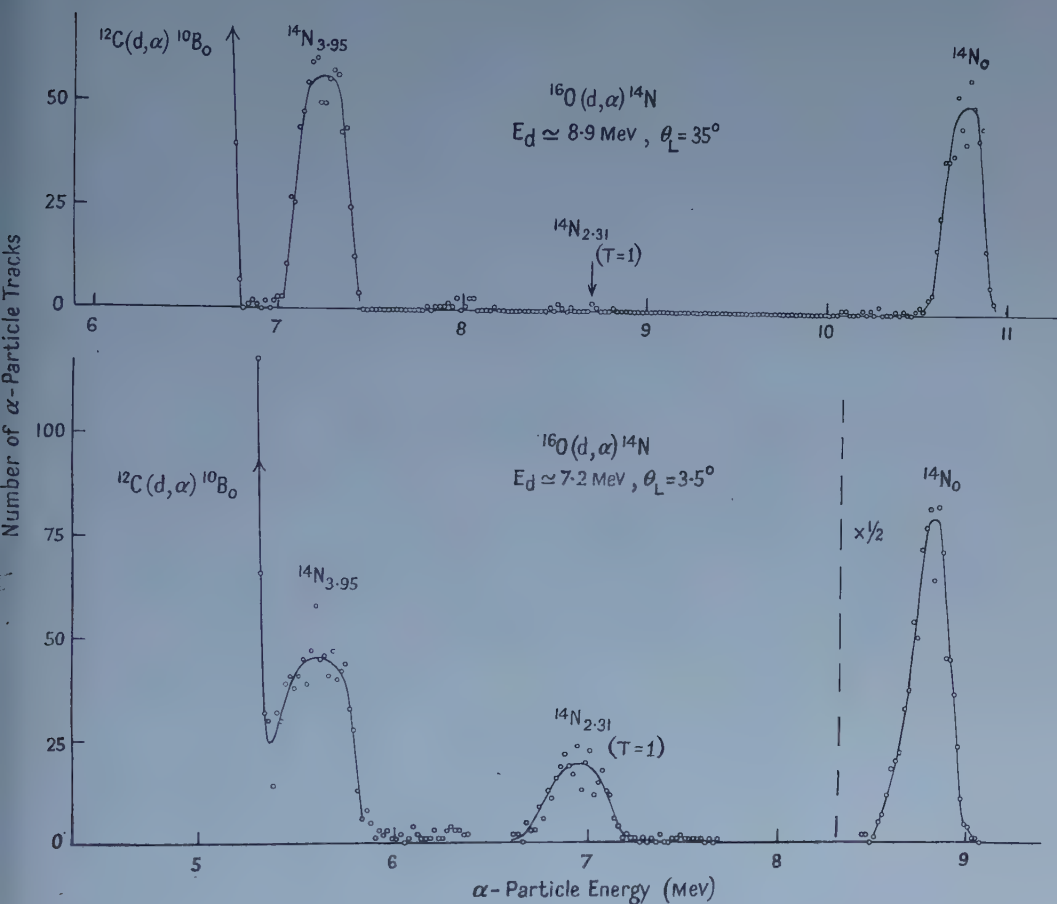


Figure 1. Alpha-particle energy spectrum obtained at an angle of observation of  $35^\circ$  resulting from the bombardment of an oxygen target (Melinex) by 8.9 and 7.2 Mev deuterons.

Table 1			
Beam energy (Mev)	Angle of Obs <sup>n</sup> ( $^\circ$ )	Intensity Ratios (percentages)	
		<i>a</i>	<i>b</i>
$6.8 \pm 0.1$	35	6	5
$7.1 \pm 0.1$	35	6	9
$7.2 \pm 0.1$	35	16	37
$8.93 \pm 0.03$	35	2	1
$7.1 \pm 0.1$	20	3	10

*a*, Ratio of intensities of transitions to 2.31 Mev and ground states.

*b*, Ratio of intensities of transitions to 2.31 Mev and 3.65 Mev states.

In all cases, except for that at 7.2 mev, the percentages represent an upper limit to the transition since the small background is included. At a bombarding energy of  $7.2 \pm 0.1$  mev the yield shows a 'resonance', and here the respective percentages are 16 and 37 at  $35^\circ$ , which agree approximately with Browne's observations at  $30^\circ$  at about this energy. At 8.9 mev the intensity is exceedingly small. The small violation of the isotopic spin selection rule has been explained by Browne on the basis of Coulomb forces admixing isotopic spin impurities into the initial, intermediate and final state configurations.

#### § 4. ANGULAR DISTRIBUTIONS

The angular distributions have been measured, at deuteron bombarding energies of 8.9 and 6.8 mev, for the alpha particles from transitions to the ground and 3.95 mev states of  $^{14}\text{N}$ . These are shown in figure 2. A stable target of quartz,  $1.1 \text{ mg cm}^{-2}$ , was used so that all cross sections are given in absolute units, with an error of about  $\pm 25\%$ .

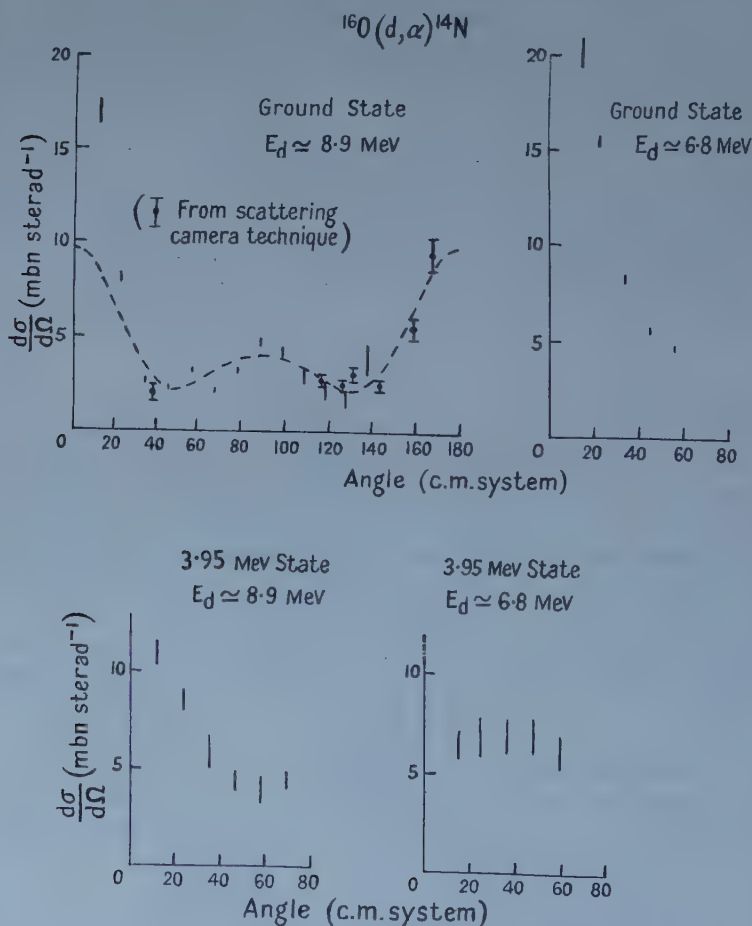


Figure 2. Angular distributions of the alpha-particle groups from the  $^{16}\text{O}(d, \alpha)^{14}\text{N}$  reaction leading to the ground and 3.95 mev excited states of  $^{14}\text{N}$  at bombarding energies of 8.9 and 6.8 mev.

In the first distribution the curve shown is a least squares fit to the points excluding those at  $11^\circ$  and  $23^\circ$ .



In general the angular distributions were only measured up to an angle of about  $60^\circ$ , mainly due to loss of resolution at larger angles, but in the case of the group to the ground state for 8.9 Mev bombarding energy, it was possible to extend the angular range to about  $135^\circ$  using the magnetic spectrograph. Further points up to  $167^\circ$  were obtained by using the target chamber as a scattering camera with a Melinex target, the particular alpha particles required being identified by their ionization and range. This technique is similar to that of Burrows, Powell and Rotblat (1951). Because of interference from elastically scattered deuterons and the inelastically scattered deuteron group from carbon it was only possible to obtain observations at the angles shown. The absolute cross sections for the two sets of observations from the spectrograph measurements and the range measurements were calculated independently and are plotted as shown. There is possibly an error in the relative magnitudes of the two sets of cross sections, but the agreement between them at angles between  $118^\circ$  and  $144^\circ$  and at  $38^\circ$  suggests that this error is probably small.

The angular distributions for a bombarding energy of 8.9 Mev show a forward peak. For the transition to the 3.95 Mev level the forward peak is suppressed when the bombarding energy is reduced to 6.8 Mev, whereas for the transition to the ground state of  $^{14}\text{N}$  the forward peak is maintained when the bombarding energy is reduced. The more complete angular distribution for the ground state transition at  $E_d = 8.9$  Mev is essentially symmetrical about  $90^\circ$  with probably a small additional forward peak superimposed, which possibly arises from a direct interaction. To estimate the part symmetrical about  $90^\circ$ , the experimental points in figure 2, excluding those at  $11^\circ$  and  $23^\circ$ , are fitted by a least squares curve containing even Legendre polynomials up to  $P_6$ . This curve is given by

$$y = (3.58 \pm 0.08)P_0 + (1.35 \pm 0.20)P_2 + (3.76 \pm 0.25)P_4 + (0.97 \pm 0.30)P_6.$$

It seems that the part symmetrical about  $90^\circ$  can be fitted adequately without the use of higher polynomials.

### § 5. DISCUSSION

The suppression of the forward peak in the distribution relating to the 3.95 Mev level when the bombarding energy is reduced suggests that this transition proceeds via a compound nucleus, since this change could be due to the reduced penetrability of the low-energy alpha particles emitted.

The mechanism governing the transition to the ground state of  $^{14}\text{N}$  is not at all clear. Preliminary angular distribution measurements by Green and Middleton (1956b) for this transition at  $E_d = 8.9$  Mev had shown a forward peak, and on the assumption that this suggested some form of direct interaction El Nadi (1957) made calculations based on a double pick-up process. However Browne using a bombarding energy of 7.03 Mev and with observations up to  $140^\circ$  did not observe a forward peak and his angular distribution was not symmetrical about  $90^\circ$ . The distribution reported here for  $E_d = 8.9$  Mev is essentially symmetrical about  $90^\circ$  with probably a small additional forward peak superimposed. The distribution observed by Freemantle *et al.*, at the much higher bombarding energy of 19 Mev, was much less intense and was symmetrical about  $90^\circ$  but did not possess a forward peak.

If the symmetry of the distribution for  $E_d = 8.9$  Mev is attributed to contributions from a large number of compound states with random phases, then these are present although the excitation of the compound nucleus is only

15.4 mev. A second possibility is that of exciting a single resonance level but it is seen that over the limited range of its observation the angular distribution for  $E_d = 6.8$  mev seems similar to that for  $E_d = 8.9$  mev. If this is so it would have to be due to the fortuitous excitation of similar resonances in the two cases.

A third possibility resulting in symmetry about  $90^\circ$  can be realized without direct discussion of the way the reaction proceeds. If the deuteron and alpha particle are considered to move in a nuclear field represented by a cloudy crystal ball potential it is possible that one partial wave can resonate and so predominate over the other partial waves taking part in the reaction. This means essentially only one partial wave in either the ingoing or outgoing channels, which is sufficient to ensure symmetry about  $90^\circ$ . In the case of the  $^{16}\text{O}(d, \alpha)^{14}\text{N}$  reaction such a resonance could not occur in the deuteron wave functions since this would imply that all deuteron reactions at this energy would give products with angular distributions symmetrical about  $90^\circ$ . This is not the case. Such a resonance would therefore be attributable to one of the alpha-particle waves. If such an explanation were correct it could be checked experimentally by measurements on the outgoing particles produced by alpha particle bombardment at this energy (14 mev). Their angular distributions should all be symmetrical about  $90^\circ$ .

#### ACKNOWLEDGMENTS

We wish to thank Professor H. W. B. Skinner for his interest in this work and Dr. H. C. Newns for helpful discussion. We are indebted to Miss M. Elmslie for assistance with the numerical calculations. Two of us (A. W. D. and S. H.) are grateful to the Department of Scientific and Industrial Research for maintenance grants.

#### REFERENCES

- BROWNE, C. P., 1956, *Phys. Rev.*, **104**, 1598.  
BURROWS, H. B., POWELL, C. F., and ROTBLAT, J., 1951, *Proc. Roy. Soc. A*, **209**, 461.  
DALTON, A. W., HINDS, S., and PARRY, G., 1957, *Proc. Phys. Soc. A*, **70**, 586.  
EL NADI, MOHAMMED, *Proc. Phys. Soc. A*, 1957, **70**, 62.  
FREEMANTLE, R. G., GIBSON, W. M., PROWSE, D. J., and ROTBLAT, J., 1953, *Phys. Rev.* **92**, 1268.  
GREEN, T. S., and MIDDLETON, R., 1956 a, *Proc. Phys. Soc. A*, **69**, 16; 1956 b, *Ibid.*, **69**, 28.

# Reciprocity Inequalities, Coherence Time and Bandwidth in Signal Analysis and Optics †

By E. WOLF

Institute of Mathematical Sciences, New York University‡

**Abstract.** This paper is concerned with establishing a rigorous reciprocity relation of the Heisenberg type between the coherence time and the bandwidth of polychromatic radiation. Following upon an observation of Gabor (1946) that the usual formulation of the reciprocity inequality which relates the effective duration of a signal and its effective bandwidth is unsatisfactory for signals that are intrinsically real (e.g., an electric signal) a modified version is here presented. Our analysis is closely related to that of Gabor and supplements it in several respects. In particular we show that his formulation, like our own, is restricted to signals with zero mean value. Contrary to general belief, there is no evidence that the inequality holds when this restriction is removed.

A definition of the coherence time of light is then proposed in terms of the (measurable) correlation function that plays a central part in the theory of partial coherence. The coherence time obeys rigorously a reciprocity inequality of the required type and is shown to have a simple interpretation in terms of averages involving the correlations in fluctuations of the instantaneous intensity. It is also shown that the coherence time may be determined experimentally from Michelson's visibility curve of interference fringes.

## § 1. INTRODUCTION

WHEN two beams of light originating in the same source are allowed to interfere, the visibility of the interference fringes decreases (in general not monotonically) as the path difference between them is increased and eventually the fringes disappear altogether. It is well known (Born 1933, § 42) that under usual experimental conditions, the time  $\Delta t = \Delta l/c$  ( $c$  = velocity of light) that corresponds to the path difference  $\Delta l$  at which the fringes disappear, and the effective spectral frequency range  $\Delta \nu$  are connected by the order of magnitude relation  $\Delta t \Delta \nu \sim 1$ .  $\Delta t$  is called the *coherence time* and  $\Delta l$  the *coherence length* of the light.

In analogy with the well-known mathematical inequality that is intimately connected with the quantum mechanical uncertainty relation of Heisenberg, one might suspect that the coherence time and the effective bandwidth could be defined more precisely so as to yield a rigorous reciprocity inequality of the form

$$\Delta t \Delta \nu \geq a, \quad \dots\dots (1.1)$$

where  $a$  is a constant of the order of unity.

† The research reported in this document has been sponsored by the Air Force Cambridge Research Center, Air Research and Development Command, under Contract No. AF 19(604)1717.

‡ On leave of absence from the Physical Laboratories, University of Manchester, England.



When one tries to apply to the present problem an argument similar to that which leads to the usual inequality, two unsatisfactory features are revealed. In the first place, unlike the wave functions of quantum mechanics, the basic functions that characterize an optical field (components of the electric and magnetic field vectors) are intrinsically real; hence if such a function is represented by a Fourier integral, say

$$V(t) = \int_{-\infty}^{+\infty} v(\nu) \exp(-2\pi i \nu t) d\nu.$$

then, because of the 'reality condition'  $v(-\nu) = v^*(\nu)$  (asterisks denoting the complex conjugate), the mean frequency

$$\bar{\nu} = \int_{-\infty}^{+\infty} \nu v(\nu) v^*(\nu) d\nu / \int_{-\infty}^{+\infty} v(\nu) v^*(\nu) d\nu \quad \dots\dots (1.2)$$

turns out to be zero. In consequence the root mean square spectral width  $\Delta\nu$ , defined by the formula

$$(\Delta\nu)^2 = \int_{-\infty}^{+\infty} (\nu - \bar{\nu})^2 v(\nu) v^*(\nu) d\nu / \int_{-\infty}^{+\infty} v(\nu) v^*(\nu) d\nu \quad \dots\dots (1.3)$$

is centred on a mean value ( $\bar{\nu}$ ) that is quite different from what is normally understood by the mean frequency of a real signal; moreover  $\Delta\nu$ , as defined by (1.3), represents the normalized radius of gyration of the spectral energy density about the origin  $\nu=0$  and not the effective bandwidth. In the domain of classical physics, only positive frequencies are considered to have a physical significance and the mean frequency and the r.m.s. width ought to be defined by formulae of the type (1.2) and (1.3) but with the lower limit  $-\infty$  replaced by zero. However, when this modification is made, the symmetry between the time representation and the frequency representation is destroyed and the usual argument leading to the reciprocity inequality no longer applies. This fact appears to have been first noted by Gabor (1946) in an interesting paper on communication theory. Gabor suggested that an inequality of the type (1.1) lies at the root of a fundamental principle of communication theory and he showed that a more satisfactory formulation of the inequality is obtained if the averages  $\bar{\nu}$  and  $\Delta\nu$ , and the corresponding averages  $\bar{t}$  and  $\Delta t$  in the time domain, are formally defined in terms of the so-called *complex analytic signal*, which is a certain linear transform (see § 2) containing only positive spectral frequencies of the real signal  $V(t)$ . Unfortunately, Gabor's discussion does not reveal the physical significance of the quantities  $\bar{t}$  and  $\Delta t$  introduced in this way.

The second unsatisfactory aspect, of significance for optics rather than for communication theory in general arises from the fact that the 'signal'  $V(t)$  is never measured in an optical experiment. Only certain averages over time intervals that are very large compared to the basic period are measurable†. Hence an inequality involving quantities that are defined directly in terms of  $V(t)$  cannot, at optical frequencies at any rate, be tested experimentally.

In this paper a rigorous inequality of the required type free of these objections is established. This is achieved by defining  $\Delta t$  in terms of the auto-correlation function of the disturbance  $V$  and  $\Delta\nu$  in terms of its Fourier transform, the power spectrum of  $V$ . The former may be determined from the measurements of the

† We may recall that the optical periods are of the order of  $10^{-15}$  sec, whereas the best photomultipliers that are at present available have resolving time of the order of  $10^{-9}$  sec,



Michelson visibility curve, the latter from measurements of the spectral energy function. The 'coherence time'  $\Delta t$  defined in this way has a simple interpretation in terms of an average relating to the correlation between intensity fluctuations, rather than in terms of amplitude fluctuations.

As a preliminary, Gabor's proof is completed and it is shown that the quantity  $\Delta t$  defined by him (to be denoted  $\Delta't$  here) may be interpreted as the normalized r.m.s. of the squared amplitude of the *envelope* belonging to the real signal. Moreover, it will be shown that if  $\Delta't$  exists, it is equal to the normalized r.m.s. width  $\Delta t$  of the square of the real signal itself. However, the requirement of the existence of  $\Delta't$  is found to be a rather strong one. For example, if the real signal  $V(t)$  is zero outside a finite interval  $-T \leq t \leq T$ , then  $\Delta t$  exists but  $\Delta't$  does not exist unless the average value of the signal is zero, or what amounts to the same thing, unless the signal has no spectral components of zero frequency. This condition is satisfied in the application discussed in this paper, but the need for imposing it raises doubts about the validity of the inequality (1.1) for an arbitrary real signal when  $\bar{v}$  and  $\Delta v$  are redefined in accordance with our intuitive notion of these quantities.†

## § 2. THE ANALYTIC SIGNAL AND GABOR'S FORMULATION OF THE INEQUALITY FOR REAL SIGNALS

Let  $V(t)$  ( $-\infty < t < \infty$ ) be a real signal, assumed to possess a Fourier integral representation

$$V(t) = \int_{-\infty}^{+\infty} v(\nu) \exp(-2\pi i \nu t) d\nu. \quad \dots\dots(2.1)$$

Then, by the Fourier inversion formula

$$v(\nu) = \int_{-\infty}^{+\infty} V(t) \exp(2\pi i \nu t) dt. \quad \dots\dots(2.2)$$

Since  $V(t)$  is real,

$$v(-\nu) = v^*(\nu). \quad \dots\dots(2.3)$$

The *complex analytic signal*‡  $\hat{V}(t)$  associated with  $V(t)$  is defined by the equation

$$\hat{V}(t) = 2 \int_0^{\infty} v(\nu) \exp(-2\pi i \nu t) d\nu, \quad \dots\dots(2.4)$$

i.e.,  $\hat{V}$  is obtained from  $V$  by suppressing all the negative frequency terms and multiplying the amplitude of the positive terms by two.

Let  $|v(\nu)|$  be the amplitude and  $\phi(\nu)$  the phase of  $v(\nu)$  :

$$v(\nu) = |v(\nu)| \exp[i\phi(\nu)]. \quad \dots\dots(2.5)$$

Using (2.3) it is easily seen that  $V$  and  $\hat{V}$  may also be written in the form

$$\hat{V}(t) = 2 \int_0^{\infty} |v(\nu)| \cos[\phi(\nu) - 2\pi \nu t] d\nu, \quad \dots\dots(2.6)$$

$$\hat{V}(t) = 2 \int_0^{\infty} |v(\nu)| \exp(i[\phi(\nu) - 2\pi \nu t]) d\nu. \quad \dots\dots(2.7)$$

Evidently

$$\hat{V}(t) = V(t) + iW(t), \quad \dots\dots(2.8)$$

where

$$W(t) = 2 \int_0^{\infty} |v(\nu)| \sin[\phi(\nu) - 2\pi \nu t] d\nu. \quad \dots\dots(2.9)$$

† See footnote† on p. 263.

‡ Also called 'the half-range complex function'.

$V(t)$  and  $W(t)$  are *allied Fourier integrals*, and it is well known (Titchmarsh 1948, p. 119) that they are Hilbert transforms of each other:

$$W(t) = \frac{1}{\pi} P \int_{-\infty}^{+\infty} \frac{V(t')}{t' - t} dt', \quad V(t) = -\frac{1}{\pi} P \int_{-\infty}^{+\infty} \frac{W(t')}{t' - t} dt', \quad \dots (2.10)$$

where  $P$  denotes the Cauchy principal value at  $t' = t$ . From (2.8) we see that the real part of the analytic signal associated with a real signal  $V$  is this signal itself, while the imaginary part is its Hilbert transform.

In terms of the improper function

$$\delta_-(x) = \int_0^{\infty} \exp(2\pi i \nu x) d\nu, \quad \dots (2.11)$$

well known in quantum mechanics (Heitler 1954, p. 69), the relation between  $V$  and  $\hat{V}$  may be expressed in the form of a linear transform

$$\hat{V}(t) = 2 \int_{-\infty}^{\infty} V(t') \delta_-(t' - t) dt', \quad \dots (2.12)$$

which follows on substituting from (2.2) into (2.4) and inverting the order of integration.

In Gabor's formulation of the reciprocity inequality for real signals, the mean frequency  $\bar{\nu}$  and the r.m.s.  $\Delta\nu$  are defined not by the customary formulas (1.2) and (1.3) but by the more appropriate formulas†

$$\bar{\nu} = \frac{\int_0^{\infty} \nu v(\nu) v^*(\nu) d\nu}{\int_0^{\infty} v(\nu) v^*(\nu) d\nu}, \quad (\Delta\nu)^2 = \frac{\int_0^{\infty} (\nu - \bar{\nu})^2 v(\nu) v^*(\nu) d\nu}{\int_0^{\infty} v(\nu) v^*(\nu) d\nu}. \quad \dots (2.13)$$

The corresponding averages  $\bar{t}'$  and  $\Delta't$  are defined by Gabor in terms of the analytic signal:

$$\bar{t}' = \frac{\int_{-\infty}^{+\infty} t \hat{V}(t) \hat{V}^*(t) dt}{\int_{-\infty}^{+\infty} \hat{V}(t) \hat{V}^*(t) dt}, \quad (\Delta't)^2 = \frac{\int_{-\infty}^{+\infty} (t - \bar{t}')^2 \hat{V}(t) \hat{V}^*(t) dt}{\int_{-\infty}^{+\infty} \hat{V}(t) \hat{V}^*(t) dt}. \quad \dots (2.14)$$

Now according to (2.7),  $\hat{V}(t)$  and the function

$$v(\nu) = 2v(\nu) \quad \text{when } \nu \geq 0, \\ = 0 \quad \text{when } \nu < 0, \quad \dots (2.15)$$

are (complex) Fourier transforms of each other. Consequently, the well-known argument of Weyl and Pauli (Weyl 1931, pp. 77, 393) leading to the usual inequality may be applied without change and one obtains

$$\Delta't \Delta\nu \geq 1/4\pi. \quad \dots (2.16)$$

This is essentially Gabor's formulation of the inequality when the signal is real.

The quantities  $\bar{\nu}$  and  $\Delta\nu$  represent correctly the mean and the r.m.s. width of the spectral energy function of the real signal  $V$ . However, as  $\bar{t}'$  and  $\Delta't$  are defined not in terms of  $V$  but in terms of the associated analytic signal  $\hat{V}$ , the physical significance of these quantities is not clear; nor is it clear how they are related to

† Actually Gabor uses a slightly different normalization. Our  $\Delta\nu$  and  $\Delta t$  correspond to  $(2\pi)^{-1/2}$  times Gabor's.

the corresponding averages  $\bar{t}$  and  $\Delta t$  defined in terms of  $V$  itself. Further, since  $\hat{V}\hat{V}^* = V^2 + W^2$ , it follows that  $\bar{t}'$  and  $\Delta' t$  are only defined if, in addition to the appropriate moments of  $V^2$ , the corresponding moments of the square of the Hilbert transform  $W$  of  $V$  also exist. This evidently imposes some restrictions on the real signal. We shall now investigate these questions.

### § 3. THE PHYSICAL SIGNIFICANCE OF $\bar{t}'$ AND $\Delta' t$ AND A CONDITION FOR THEIR EXISTENCE

Let  $\nu_0$  be any frequency and let us rewrite (2.7) in the form ( $A, \Psi$  real),

$$\hat{V}(t) = A(t) \exp[i\{\Psi(t) - 2\pi\nu_0 t\}] \quad \dots\dots(3.1)$$

where

$$\begin{aligned} A(t) \exp[i\Psi(t)] &= 2 \int_0^\infty |v(\nu)| \exp i[\phi(\nu) - 2\pi(\nu - \nu_0)t] d\nu \\ &= \int_{-\nu_0}^\infty g(\mu) \exp(-2\pi i\mu t) d\mu, \quad \dots\dots(3.2) \end{aligned}$$

and

$$g(\mu) = 2|v(\nu_0 + \mu)| \exp[i\phi(\nu_0 + \mu)] = 2v(\nu_0 + \mu). \quad \dots\dots(3.3)$$

The functions  $V$  and  $W$ , being the real and imaginary parts of  $\hat{V}$ , may, according to (3.1), be written in the form

$$V(t) = A(t) \cos[\Psi(t) - 2\pi\nu_0 t], \quad W(t) = A(t) \sin[\Psi(t) - 2\pi\nu_0 t]. \quad \dots\dots(3.4)$$

Suppose that  $V$  is a high-frequency narrow-band signal, and let  $\nu_0$  be a mean frequency of the signal. Then the spectral amplitudes  $|v(\nu)|$  differ appreciably from zero only when  $\nu$  is in a relatively small neighbourhood of the mean frequency. Consequently  $|g(\mu)|$  will have appreciable values only in a small neighbourhood around  $\mu = 0$ . Hence the integral (3.2) represents a superposition of harmonic components of low frequencies so that  $A(t)$  and  $\Psi(t)$  will vary slowly in comparison with the periodic term  $\exp(-2\pi i\nu_0 t)$ . Evidently  $A(t)$  represents an *envelope* of the real signal, and it follows from (3.4) and (2.8) that

$$A(t) = \sqrt{V^2(t) + W^2(t)} = \sqrt{\hat{V}(t)\hat{V}^*(t)} = |\hat{V}(t)|, \quad \dots\dots(3.5a)$$

$$\Psi(t) = 2\pi\nu_0 t + \tan^{-1} \frac{W(t)}{V(t)} = 2\pi\nu_0 t + \tan^{-1} \left( i \frac{\hat{V}^* - \hat{V}}{\hat{V}^* + \hat{V}} \right). \quad \dots\dots(3.5b)$$

Since  $\hat{V}\hat{V}^* = A^2$ , it follows that:  *$\bar{t}'$  and  $\Delta' t$  defined by (2.14) may be interpreted as the mean epoch and the (normalized) r.m.s. width of the square of the envelope belonging to the real signal  $V$ .* However, as will now be shown, whenever these quantities exist they will also be equal to the mean epoch and to the r.m.s. width of the square of the signal itself.

Let  $F(x)$  by any function of a real variable  $x$  and let  $M_n(F)$  be its  $n$ th moment,

$$M_n(F) = \int_{-\infty}^{+\infty} x^n F(x) dx. \quad \dots\dots(3.6)$$

The equations (2.14) may be written in the form

$$\bar{t}' = \frac{M_1(\hat{V}\hat{V}^*)}{M_0(\hat{V}\hat{V}^*)}, \quad (\Delta' t)^2 = \frac{M_0(\hat{V}\hat{V}^*)M_2(\hat{V}\hat{V}^*) - M_1^2(\hat{V}\hat{V}^*)}{M_0^2(\hat{V}\hat{V}^*)}. \quad \dots\dots(3.7)$$

Consider now the corresponding moments of  $V^2$ . Since according to (2.6) and (2.4)

$$V(t) = 2\Re \int_0^\infty v(\nu) \exp(-2\pi i\nu t) d\nu, \quad \dots\dots(3.8)$$

where  $\mathcal{R}$  denotes the real part,  $M_n(V^2)$  may formally be expressed in the form

$$\begin{aligned} M_n(V^2) &= \int_{-\infty}^{+\infty} t^n V(t) \left[ 2\mathcal{R} \int_0^{\infty} v(\nu) \exp(-2\pi i \nu t) d\nu \right] dt \\ &= 2\mathcal{R} \int_0^{\infty} v(\nu) d\nu \int_{-\infty}^{+\infty} t^n V(t) \exp(-2\pi i \nu t) dt \\ &= 2\mathcal{R} \int_0^{\infty} v(\nu) d\nu \left( -\frac{1}{2\pi i} \frac{\partial}{\partial \nu} \right)^n \int_{-\infty}^{+\infty} V(t) \exp(-2\pi i \nu t) dt \\ &= 2\mathcal{R} \left( -\frac{1}{2\pi i} \right)^n \int_0^{\infty} v(\nu) \left( \frac{\partial}{\partial \nu} \right)^n v^*(\nu) d\nu, \end{aligned} \quad \dots\dots(3.9)$$

where (2.1) and (2.2) were used.

Next we consider the corresponding moments of  $W^2$ . Comparison of the real representations (2.6) and (2.9) shows that  $V$  may be transformed into  $W$  simply by changing the phase  $\phi(\nu)$  of each Fourier component to  $\phi(\nu) - \pi/2$  ( $\nu \geq 0$ ). It follows that if  $M_n(W^2)$  exists, its value is given by (3.9), with  $v(\nu) = |v(\nu)| \exp(i\phi)$  replaced by  $w(\nu) = |v(\nu)| \exp[i(\phi - \pi/2)] = -iv(\nu)$ . But (3.9) remains invariant under this transformation. Noting also that

$$M_n(\hat{V}\hat{V}^*) = M_n[(V+iW)(V-iW)] = M_n(V^2) + M_n(W^2), \quad \dots\dots(3.10)$$

we have the following theorem:

Let  $V(t)$  be any real function. If  $W(t)$  is the Hilbert transform of  $V(t)$  and  $\hat{V}(t)$  the analytic signal associated with  $V(t)$  and if, moreover, for any particular value of  $n$  (non-negative integer) the moments  $M_n(V^2)$  and  $M_n(W^2)$  both exist, then  $M_n(\hat{V}\hat{V}^*)$  also exists and moreover

$$M_n(\hat{V}\hat{V}^*) = 2M_n(V^2) = 2M_n(W^2). \quad \dots\dots(3.11)$$

Let us now introduce the mean epoch  $\bar{t}$  and the r.m.s. width  $\Delta t$  of the square of the real signal  $V$ :

$$\left. \begin{aligned} \bar{t} &= \frac{\int_{-\infty}^{+\infty} t V^2(t) dt}{\int_{-\infty}^{+\infty} V^2(t) dt} = \frac{M_1(V^2)}{M_0(V^2)} \\ (\Delta t)^2 &= \frac{\int_{-\infty}^{+\infty} (t - \bar{t})^2 V^2(t) dt}{\int_{-\infty}^{+\infty} V^2(t) dt} = \frac{M_0(V^2) M_2(V^2) - M_1^2(V^2)}{M_0^2(V^2)} \end{aligned} \right\} \dots\dots(3.12)$$

Assuming that the moments of  $V^2$  and  $W^2$  of orders  $n=0, 1, 2$  exist, it follows from the theorem just established that  $V^2$  may be replaced by  $\hat{V}\hat{V}^*$  in (3.12), and we see on comparison with (3.7) that

$$\bar{t}' = \bar{t}, \quad \Delta' t = \Delta t. \quad \dots\dots(3.13)$$

Thus the mean epoch of the squared amplitude of the envelope belonging to the real signal is equal to the mean epoch of the squared signal itself, and the r.m.s. widths are also equal, and (2.16) gives

$$\Delta t \Delta \nu \geq 1/4\pi. \quad \dots\dots(3.14)$$



We shall not investigate here the general conditions which must be imposed on  $V(t)$  in order that the required moments should exist. We only confine ourselves to the case of great practical importance when  $V(t)$  is zero outside a finite interval  $-T \leq t \leq T$ . Then  $M_0(V^2)$ ,  $M_1(V^2)$  and  $M_2(V^2)$  exist, but as shown in the Appendix, the corresponding moments involving  $W^2$  do not all exist unless

$$\int_{-T}^T V(t) dt = 0.$$

According to (2.2) this condition may also be written as  $v(0) = 0$ . For such signals the relations (3.13) and the inequality (3.14) hold.†

#### § 4. A DEFINITION OF THE COHERENCE TIME OF A LIGHT BEAM

The results of the preceding sections will now be used to introduce a satisfactory definition of coherence time of polychromatic radiation. We shall discuss in detail only the case of light, but similar considerations apply for other noise-like signals, such as microwaves from a radio star, the fluctuating field of an electron stream, etc.

Let us consider a simple interference experiment. A beam of light from a source O is divided into two beams of the same intensity and the beams are brought together after a path difference  $l = c\tau$  ( $c$  = vacuum velocity of light), has been introduced between them, for example in a Michelson interferometer. For simplicity we shall consider the light disturbance to be a real scalar, e.g. a Cartesian component of the electric field vector. We assume that the field exists only for a finite time interval  $-T \leq t \leq T$  which is large compared to the basic optical period  $(1/\bar{\nu})$  and to the reciprocal of the effective bandwidth.

Apart from inessential multiplying factors, the disturbance  $V_P$  at the point P of superposition is related to the disturbance  $V$  at the point O where the beam is divided by

$$V_P(t) = [V_0(t - t_1) + V_0(t - t_1 - \tau)], \quad \dots\dots(4.1)$$

where  $t_1$  and  $t_1 + \tau$  are the times in which the light travels from O to P along the two paths. The intensity  $I_P$  observed at P is the time average of  $V_P^2(t)$ , and we may, for convenience, take the averaging interval equal to the interval  $2T$  during which the field is assumed to exist:‡

$$I_P = \frac{1}{2T} \int_{-T}^T V_P^2(t) dt. \quad \dots\dots(4.2)$$

Denoting the time average by angular brackets, it follows from (4.1) and (4.2) that

$$I(P) = \langle V_0^2(t - t_1) \rangle + \langle V_0^2(t - t_1 - \tau) \rangle + 2\langle V_0(t - t_1) V_0(t - t_1 - \tau) \rangle.$$

Assuming the field to be stationary, we may shift the origin of time. Setting

$$J(\tau) = \langle V_0(t + \tau) V_0(t) \rangle, \quad \dots\dots(4.3)$$

the intensity at P may be expressed in the form

$$I_P = 2[J(0) + J(\tau)]. \quad \dots\dots(4.4)$$

† Since this investigation was carried out Kay and Silverman (1957) have obtained a more general inequality, which holds for all real signals for which  $\Delta t$  and  $\Delta \nu$  exist (irrespective of the existence of  $\Delta' t$ ). They also showed that signals exist for which the product  $\Delta t \Delta \nu$  is smaller than  $1/4\pi$ .

‡ Under normal experimental conditions the averaging interval is large compared to  $1/\bar{\nu}$  and  $1/\Delta' \nu$ , and provided that, as here assumed,  $T$  is much larger than either of these quantities its exact value is evidently immaterial.

$J(0) = \langle V_0^2(t) \rangle = I_0$  is the intensity of each beam and  $J(\tau)$  is an *interference term*. Equation (4.3) defines  $J$  in terms of the rapidly fluctuating function  $V_0(t)$ , but it represents a measurable quantity since according to (4.4) it may be obtained from the measurements of the intensities at O and P.

We now represent  $V_0(t)$  as a Fourier integral of the form (2.1). It then follows from the convolution theorem and the 'reality condition' (2.3) that  $J(\tau)$  may also be expressed in the form

$$J(\tau) = \int_0^\infty j(\nu) \cos 2\pi\nu\tau \, d\nu, \quad \dots\dots(4.5)$$

where

$$j(\nu) = (1/T) |v(\nu)|^2 \quad \dots\dots(4.6)$$

is the average spectral energy density. According to (4.7),  $J(\tau)$  and  $j(\nu)$  are Fourier cosine transforms of each other.<sup>†</sup>

Since  $V_0(t)$  was assumed to be zero when  $|t| > T$ , it follows from (4.3) that  $J(\tau) = 0$  when  $|\tau| > T$ ; moreover, since we are dealing with a pure radiation field,  $j(0) = 0$ . Hence, if quantities  $\Delta\tau$  and  $\Delta\nu$  are defined by<sup>‡</sup>

$$(\Delta\tau)^2 = \frac{\int_{-\infty}^{+\infty} \tau^2 J^2(\tau) \, d\tau}{\int_{-\infty}^{+\infty} J^2(\tau) \, d\tau} = \frac{\int_0^\infty \tau^2 J^2(\tau) \, d\tau}{\int_0^\infty J^2(\tau) \, d\tau}, \quad \dots\dots(4.7a)$$

$$(\Delta\nu)^2 = \frac{\int_0^\infty (\nu - \bar{\nu})^2 j^2(\nu) \, d\nu}{\int_0^\infty j^2(\nu) \, d\nu}, \quad \bar{\nu} = \frac{\int_0^\infty \nu j^2(\nu) \, d\nu}{\int_0^\infty j^2(\nu) \, d\nu}, \quad \dots\dots(4.7b)$$

it follows from the results established in § 3 that

$$\Delta\tau \Delta\nu \geq 1/4\pi. \quad \dots\dots(4.8)$$

The quantity  $\Delta\tau$  has an interesting interpretation in connection with the well-known method of Michelson (1891, 1892) for determining the energy distribution in spectral lines from measurements of the visibility of fringes. Let

$$\hat{J}(\tau) = \int_0^\infty j(\nu) \exp(-2\pi i\nu\tau) \, d\nu \quad \dots\dots(4.9)$$

be the analytic signal associated with  $J(\tau)$ . Then, according to (3.4) and (3.5),  $J$  may be written in the form

$$J(\tau) = B(\tau) \cos [\Phi(\tau) - 2\pi\bar{\nu}\tau],$$

where

$$B(\tau) = |\hat{J}(\tau)|, \quad \Phi(\tau) = 2\pi\bar{\nu}\tau + \tan^{-1} \left( i \frac{\hat{J}^* - \hat{J}}{\hat{J}^* + \hat{J}} \right),$$

and the expression (4.4) for the intensity at the point P becomes

$$I_P = 2 \{ \hat{J}(0) + |\hat{J}(\tau)| \cos [\Phi(\tau) - 2\pi\bar{\nu}\tau] \}.$$

<sup>†</sup> In the limit as  $T \rightarrow \infty$  this result reduces to the Wiener-Khinchine theorem (Wang and Uhlenbeck 1945, p. 326, Rice 1944, § 2.1). We do not proceed to the limit here, since we shall make use of our theorem concerning moments of squares of Hilbert transforms, established on the assumption that the real signal is zero outside a finite interval.

<sup>‡</sup> Since  $J(\tau)$  is an even function of  $\tau$ ,  $\int_{-\infty}^{+\infty} \tau J^2(\tau) \, d\tau = 0$  so that  $\bar{\tau} = 0$ .

If  $\Delta\nu/\bar{\nu} \ll 1$ , then  $|\hat{J}(\tau)|$  and  $\Phi(\tau)$  will vary slowly with  $\tau$  in comparison with  $\cos(2\pi\bar{\nu}\tau)$  and  $\sin(2\pi\bar{\nu}\tau)$  and we see that the minima and maxima of the intensity near P are approximately given by

$$I_{\max} = 2[\hat{J}(0) + |\hat{J}(\tau)|], \quad I_{\min} = 2[\hat{J}(0) - |\hat{J}(\tau)|].$$

Hence the *Michelson visibility of the fringes*  $\mathcal{V}(\tau)$  is given by

$$\mathcal{V}(\tau) = \frac{I_{\max} - I_{\min}}{I_{\max} + I_{\min}} = \frac{|\hat{J}(\tau)|}{|\hat{J}(0)|}, \quad \dots\dots(4.10)$$

i.e. it is proportional to the absolute value of the complex interference function  $\hat{J}(\tau)$ . Now according to (4.9) and the Fourier inversion formula, the energy distribution  $j(\nu)$  (defined to be zero for  $\nu < 0$ ) is the Fourier transform of  $\hat{J}(\tau)$ , so that as first shown by Michelson,  $j(\nu)$  may be determined from measurements of the visibility curve, provided that suitable assumptions are made about the phase†  $\Phi(\tau)$ .

Now according to § 3, we may replace  $J^2(\tau)$  by  $|\hat{J}(\tau)|^2$  in (4.7a); then using equation (4.10) it follows that

$$(\Delta\tau)^2 = \int_0^\infty \tau^2 \mathcal{V}^2(\tau) d\tau \bigg/ \int_0^\infty \mathcal{V}^2(\tau) d\tau.$$

Thus  $\Delta\tau$  is equal to the normalized r.m.s. width of the square of the *Michelson visibility function*, and it is evidently reasonable to regard  $\Delta\tau$  as the *coherence time* of the light. Of course, the visibility is in general not zero when the path difference between the beams exceeds the length  $\Delta l = c\Delta\tau$ , but is then, as a rule, small compared with the visibility at the centre ( $\tau = 0$ ) of the pattern. Other definitions of the coherence time are, naturally, possible. For example, we could define it as the  $\tau$ -value beyond which  $J(\tau)$  is smaller than  $\epsilon J(0)$ , where  $\epsilon$  is some prescribed number which is small compared to unity. It appears, however, that only when  $\Delta\tau$  is defined as a simple average such as (4.7a) may a rigorous reciprocity relation of the required type be formulated. It is to be noted that both  $\Delta\tau$  and  $\Delta\nu$  can be determined from experiment;  $\Delta\tau$  from the visibility curve  $\mathcal{V}(\tau)$  and  $\Delta\nu$  from the spectral energy curve  $j(\nu)$ .

It is often convenient to describe an interference experiment in terms of mutually incoherent 'elementary wave trains' of finite length, rather than in terms of the random function  $V(t)$ , or its auto-correlation function  $J(\tau)$ . The coherence time as here defined may evidently be interpreted as the duration of an elementary wave train.

Since our definition of the coherence time involves the second power of  $J$  and therefore the fourth power of  $V$ , it may not be expected at first sight that a physical interpretation could be given to this quantity. However, if we write  $V_0(t) = V_1$ ,  $V_0(t + \tau) = V_2$  and denote by  $P(V_1, V_2) dV_1 dV_2$  the probability that for any  $t$  ( $\tau$  fixed),  $V_1$  will be found in the interval  $V_1, V_1 + dV_1$  and  $V_2$  in the interval  $V_2, V_2 + dV_2$ , then under usual circumstances  $P(V_1, V_2)$  may be assumed to be Gaussian and it may then be shown‡ that

$$J^2(\tau) = \frac{1}{2} \langle \Delta I(t + \tau) \Delta I(t) \rangle, \quad \dots\dots(4.11)$$

†  $\Phi(\tau)$  may in principle be determined from measurements of the position of the fringes, but such measurements are extremely difficult to carry out.

‡ See Wolf (1957). Blanc-Lapierre and Dumontet (1955) pointed out that  $P$  may not be Gaussian for points close enough to the source, or with light of very low intensity.

where

$$\Delta I(t) = I(t) - \langle I(t) \rangle = V^2(t) - \langle V^2(t) \rangle.$$

Thus  $J^2(\tau)$  is proportional to the correlation that exists between the fluctuations in the intensity at O, at two instants of time separated by an interval  $\tau$ , and it follows that (4.7a) may also be written in the form

$$(\Delta\tau)^2 = \frac{\int_0^\infty \tau^2 \langle \Delta I(t+\tau) \Delta I(t) \rangle d\tau}{\int_0^\infty \langle \Delta I(t+\tau) \Delta I(t) \rangle d\tau}. \quad \dots\dots(4.12)$$

Returning to the basic relation (4.8) it is not difficult to see that with the type of spectral distributions normally encountered in optics, the inequality may be replaced by the order of magnitude sign. To see this, consider the spectrum which has the form of a truncated Gaussian function

$$j(\nu) = \exp[-(\nu - \nu_0)^2/2\sigma^2] \quad (\nu \geq 0). \quad \dots\dots(4.13)$$

Now, strictly speaking, this is not a function of the class that we are considering, since it does not obey the condition  $j(0) = 0$ . However, if  $\sigma/\nu_0 \ll 1$ ,  $j(0)$  will be negligible in comparison with  $j(\nu_0)$  and we may assume that the corresponding value of the product  $\Delta t \Delta \nu$  will be a fairly representative one.

On substituting from (4.13) into (4.5) and setting  $\mu = (\nu - \nu_0)/\sigma\sqrt{2}$ , we obtain for the interference function the expression

$$J(\tau) = \sigma\sqrt{2} \int_{-\nu_0/\sigma\sqrt{2}}^\infty e^{-\mu^2} \cos[2\pi(\nu_0 + \sigma\sqrt{2}\mu)\tau] d\mu.$$

Now since  $\nu_0/\sigma \gg 1$ , the lower limit may be replaced by  $-\infty$  without introducing an appreciable error and it follows that

$$J(\tau) \sim \sqrt{(2\pi)\sigma} \exp(-2\pi^2\sigma^2\tau^2) \cos 2\pi\nu_0\tau. \quad \dots\dots(4.14)$$

From (4.14) and (4.7) we obtain, if terms of order  $\exp(-\nu_0^2/\sigma)$  are neglected in comparison with unity,  $(\Delta\tau)^2 \sim 1/8\pi^2\sigma^2$ . With a similar approximation,  $(\Delta\nu)^2 \sim \sigma^2/2$ , and it follows that

$$\Delta\tau\Delta\nu \sim 1/4\pi. \quad \dots\dots(4.15)$$

Finally, it should be noted that the effective width  $\Delta\nu$  is not the usual r.m.s. width of the spectral energy function  $j(\nu) = (1/T)|v(\nu)|^2$ , but rather the r.m.s. width of the *square* of this function. As a rule the two r.m.s. widths are, however, of the same order of magnitude. For the Gaussian function, for example, they differ by a multiplying factor  $\sqrt{2}$ .

## § 5. A GENERALIZATION

In the preceding section we considered interference between two beams obtained by the division of a single beam at a particular point O. The interference effects were then characterized by the function  $J(\tau)$  which depends on the coordinates of O and on the time delay  $\tau$  introduced between the beams.

In the general theory of partially coherent fields it is necessary to employ a more general correlation function (Blanc-Lapierre and Dumontet 1955, Wolf 1955

$$J_{12}(\tau) = \langle V_1(t+\tau) V_2(t) \rangle \quad \dots\dots(5.1)$$

which depends on the coordinates of two points  $O_1$  and  $O_2$  and on a time delay  $\tau$ . This correlation function may be determined from a Young interference experiment



with a small opening at each of these two points (Wolf 1955, Thompson and Wolf 1957). We shall now formulate a reciprocity relation appropriate to experiments in which the interference effects are characterized by  $J_{12}(\tau)$ .

We again assume that the field exists only for a finite time interval  $-T \leq t \leq T$ , and we represent the (real) disturbance at the points  $O_1$  and  $O_2$  as Fourier integrals

$$V_1(t) = \int_{-\infty}^{+\infty} v_1(\nu) \exp(-2\pi i \nu t) d\nu, \quad V_2(t) = \int_{-\infty}^{+\infty} v_2(\nu) \exp(-2\pi i \nu t) d\nu. \quad \dots\dots(5.2)$$

Then, using the convolution theorem and the reality conditions  $v_1(-\nu) = v_1^*(\nu)$ ,  $v_2(-\nu) = v_2^*(\nu)$ , (5.1) can readily be expressed in the following 'spectral form':

$$J_{12}(\tau) = \int_0^{\infty} |j_{12}(\nu)| \cos[\phi_{12}(\nu) - 2\pi\nu\tau] d\nu, \quad \dots\dots(5.3)$$

where

$$j_{12}(\nu) = |j_{12}(\nu)| \exp[i\phi_{12}(\nu)] = [v_1(\nu) v_2^*(\nu)]/T. \quad \dots\dots(5.4)$$

Formulae (5.3) and (5.4) are generalizations of the relations (4.5) and (4.6).

We now define the quantities

$$\bar{\tau}_{12} = \frac{\int_{-\infty}^{+\infty} \tau J_{12}^2(\tau) d\tau}{\int_{-\infty}^{+\infty} J_{12}^2(\tau) d\tau}, \quad (\Delta\tau_{12})^2 = \frac{\int_{-\infty}^{+\infty} (\tau - \bar{\tau})^2 J_{12}^2(\tau) d\tau}{\int_{-\infty}^{+\infty} J_{12}^2(\tau) d\tau}, \quad \dots\dots(5.5a)$$

$$\bar{\nu}_{12} = \frac{\int_0^{\infty} \nu j_{12}(\nu) j_{12}^*(\nu) d\nu}{\int_0^{\infty} j_{12}(\nu) j_{12}^*(\nu) d\nu}, \quad (\Delta\nu_{12})^2 = \frac{\int_0^{\infty} (\nu - \bar{\nu})^2 j_{12}(\nu) j_{12}^*(\nu) d\nu}{\int_0^{\infty} j_{12}(\nu) j_{12}^*(\nu) d\nu}. \quad \dots\dots(5.5b)$$

Since  $J_{12} = 0$  when  $|\tau| > T$ , and since  $j_{12}(0)$  may again be assumed to be zero, we have, in accordance with §3

$$\Delta\tau_{12} \Delta\nu_{12} \geq 1/4\pi. \quad \dots\dots(5.6)$$

It also follows from §3 that in (5.5a) we may replace  $J_{12}^2$  by  $\hat{J}_{12} \hat{J}_{12}^*$ , where  $\hat{J}_{12}$  is the analytic signal associated with  $J_{12}$ , i.e.†

$$\hat{J}_{12}(\tau) = \int_0^{\infty} |j_{12}(\nu)| \exp(i[\phi_{12}(\nu) - 2\pi\nu\tau]) d\nu.$$

In a similar manner as in §4, (4.10), it is possible to relate  $|J_{12}(\tau)|$  to the visibility of fringes. If the intensity of the beams proceeding from the openings at  $O_1$  and  $O_2$  are equal and if  $\mathcal{V}_{12}(\tau)$  represents the visibility of the fringes in the neighbourhood of a point P such that  $\overline{O_2 P} - \overline{O_1 P} = c\tau$ , then

$$\mathcal{V}_{12}(\tau) = \frac{|\hat{J}_{12}(\tau)|}{|\hat{J}_{12}(0)|}.$$

† It was shown elsewhere (Wolf 1955, p. 262) that in terms of the analytic signals  $\hat{V}$  of  $V$ ,

$$\hat{J}_{12}(\tau) = \frac{1}{2} \langle \hat{V}_1(t + \tau) \hat{V}_2^*(t) \rangle.$$

It follows that (5.5a) may also be written in the form

$$\bar{\tau}_{12} = \frac{\int_{-\infty}^{+\infty} \tau \mathcal{V}_{12}^2(\tau) d\tau}{\int_{-\infty}^{+\infty} \mathcal{V}_{12}^2(\tau) d\tau}, \quad (\Delta\tau_{12})^2 = \frac{\int_{-\infty}^{+\infty} (\tau - \bar{\tau}_{12})^2 \mathcal{V}_{12}^2(\tau) d\tau}{\int_{-\infty}^{+\infty} \mathcal{V}_{12}^2(\tau) d\tau}.$$

Further, by analogy with (4.11),  $\Delta\tau_{12}$  may be expressed in terms of the intensity fluctuations

$$\Delta I_1(t) = I_1(t) - \langle I_1(t) \rangle = V_1^2(t) - \langle V_1^2(t) \rangle,$$

$$\Delta I_2(t) = I_2(t) - \langle I_2(t) \rangle = V_2^2(t) - \langle V_2^2(t) \rangle,$$

at the points  $O_1$  and  $O_2$  by means of the formula

$$J_{12}^2(\tau) = \frac{1}{2} \langle \Delta I_1(t+\tau) \Delta I_2(t) \rangle.$$

Thus in (5.5a) the function  $J_{12}^2(\tau)$  may be replaced by  $\langle \Delta I_1(t+\tau) \Delta I_2(t) \rangle$ , which expresses the correlation between the intensity fluctuations at  $O_1$  and  $O_2$ .

Evidently  $\Delta\tau_{12}$  may be interpreted as the 'mutual coherence time' of the light vibrations at  $O_1$  and  $O_2$ , and  $\Delta\nu_{12}$  as their 'effective mutual spectral width.'

## APPENDIX

### *Conditions for the Existence of Certain Moments Involving Hilbert Transforms*

Let  $V(t)$  be a real function which is zero for all values of  $t$  outside the range  $-T \leq t \leq T$ , and let  $W(t)$  be its Hilbert transform:

$$W(t) = \frac{1}{\pi} P \int_{-\infty}^{+\infty} \frac{V(t')}{t' - t} dt',$$

where  $P$  denotes the Cauchy principle value at  $t' = t$ . We shall examine the existence of certain moments involving  $W$ .

We have, for all values of  $|t|$  greater than  $T$ ,

$$\begin{aligned} W(t) &= \frac{1}{\pi} \int_{-T}^T \frac{V(t')}{t' - t} dt' = -\frac{1}{\pi t} \int_{-T}^T \frac{V(t')}{1 - t'/t} dt' \\ &= -\frac{1}{\pi t} \int_{-T}^T V(t') \sum_{n=0}^{\infty} \left(\frac{t'}{t}\right)^n dt' = -\frac{1}{\pi} \sum_{n=0}^{\infty} \frac{M_n(V)}{t^{n+1}} dt, \end{aligned}$$

where

$$M_n(V) = \int_{-T}^T t'^n V(t') dt'$$

is the  $n$ th moment of  $V$ . Hence for large values of  $|t|$ ,

$$W(t) \sim -\frac{1}{\pi} \frac{M_{n_0}(V)}{t^{n_0+1}},$$

where  $n_0$  is the lowest integer for which  $M_{n_0}(V) \neq 0$ .

It follows that the integral

$$M_n(W^2) = \int_{-\infty}^{+\infty} t^n W^2(t) dt$$

is convergent only if  $n < 2n_0 + 1$ . We have thus the following theorem:

If  $V(t)$  is zero outside the range  $-T \leq t \leq T$ , and  $W(t)$  is the Hilbert transform of  $V$ , then the  $n$ th moment of  $W^2$  will exist only if  $n$  is smaller

than  $2n_0 + 1$ , where  $n_0$  is the lowest integer for which  $M_{n_0}(V) \neq 0$ . In particular the moments of  $W^2$  up to and including the second order ( $n \leq 2$ ) will exist only if  $n_0 > 0$ , i.e. if

$$M_0(V) = \int_{-T}^T V(t) dt = 0.$$

## ACKNOWLEDGMENT

I am obliged to Dr. F. Kahn for advice relating to the existence of moments of Hilbert transforms; the analysis given in the Appendix is substantially due to him. I also wish to acknowledge stimulating discussions with Drs. I. Kay, G. C. Rota and R. A. Silverman.

## REFERENCES

- BLANC-LAPIERRE, A., and DUMONTET, P., 1955, *Rev. Opt. (théor. instrum.)*, **34**, 1.  
 BORN, M., 1933, *Optik* (Berlin : Springer).  
 GABOR, D., 1946, *J. Instn Elect. Engrs*, **93**, Part III, 429.  
 HEITLER, W., 1954, *The Quantum Theory of Radiation* (Oxford : Clarendon Press), 3rd Edn.  
 KAY, I., and SILVERMAN, R. A., 1957, *Information and Control*, **1**, 64.  
 MICHELSON, A., 1891, *Phil. Mag.*, **31**, 338 ; 1892, *Ibid.*, **34**, 280.  
 RICE, S. O., 1944, *Bell Syst. Tech. J.*, **23**, 282.  
 THOMPSON, B. J., and WOLF, E., 1957, *J. Opt. Soc. Amer.*, **47**, 895.  
 TITSCHMARCH, E. C., 1948, *Introduction to the Theory of Fourier Integrals* (Oxford : Clarendon Press), 2nd Edn.  
 WANG, M. C., and UHLENBECK, G. E., 1945, *Rev. Mod. Phys.*, **17**, 323.  
 WEYL, H., 1931, *The Theory of Groups and Quantum Mechanics* (Translated from German). (London : Methuen; New York : Dover Publications.)  
 WOLF, E., 1955, *Proc. Roy. Soc. A*, **230**, 246.  
 WOLF, E., 1957, *Phil. Mag.*, **2**, 351.

## RESEARCH NOTES

## Entropy of Hausmannite to Spinel Transformation

By K. S. IRANI, A. P. B. SINHA AND A. B. BISWAS

National Chemical Laboratory, Poona, India

*MS. received 15th November 1957*

THE crystal structure of hausmannite ( $\text{Mn}_3\text{O}_4$ ) at room temperature is known to be tetragonally distorted from the cubic spinel type (Aminoff 1926) with a 'normal' distribution of cations  $\text{Mn}^{2+}[\text{Mn}_2^{3+}]\text{O}_4$  (Romeijn 1953, Sinha, Sanjana and Biswas 1957); and on heating, it transforms reversibly to the cubic symmetry at  $1170^\circ\text{C}$  (McMurdie and Golovato 1948).

The tetragonal distortion is explained on the basis of the formation of four square, coplanar  $\text{dsp}^2$  bonds parallel to the  $a$  and  $b$  axes and two longer ionic bonds parallel to the  $c$  axis by  $\text{Mn}^{3+}$  ions at the octahedral sites (Goodenough and Loeb 1955). The crystal field theory also gives similar results (Dunitz and Orgel 1957). According to Goodenough and Loeb, the transition to the cubic form at higher temperature is due to the thermal excitation of electrons from the covalent band, which make the bonds ionic and resonating among the three biaxial planes of the octahedral interstice. Finch, Sinha and Sinha (1957), however, viewed this transition as a randomization of the orientation of the distorted octahedra surrounding the  $\text{Mn}^{3+}$  ions. A calculation of the entropy of this transition is presented below, which agrees well with the reported value.

At lower temperatures the longer bonds in the crystal are aligned parallel to the long axis ( $c$  axis), as this condition will be one of minimum elastic energy. However, with rise in temperature, due to increase in energy, some of the long bonds will get oriented parallel to the  $a$  or  $b$  axes, with a consequent decrease in  $c/a$ . In contrast to the monotonic decrease of  $c/a$  with temperature observed for tetragonal  $\text{CuFe}_2\text{O}_4$  (Bertaut 1951), which was due to the removal of the distorting cations ( $\text{Cu}^{2+}$ ) from the octahedral sites, we found that in the case of  $\text{Mn}_3\text{O}_4$  the change is inappreciable before the transition temperature is reached, as is shown by the constancy of  $c/a$  but it rapidly decreases to  $c/a=1$  at the transition temperature (Irani, Sinha and Biswas, to be published). The octahedral bonds are, after transition, randomly orientated and the probability of the longer bond being parallel to the  $a$ ,  $b$  or  $c$  axis will be equal.

It is reasonable to assume that at the transition temperature the partition function attributable to other ions is unchanged before and after the transition. We thus consider the partition function due to the  $\text{Mn}^{3+}$  ions only. If the number of  $\text{Mn}^{3+}$  ions at the octahedral sites in a gramme-mole of  $\text{Mn}_3\text{O}_4$  is  $x$  and if there is no disorder in the system the partition function will be of the form

$$Z = \left[ \left( \frac{2\pi m k T}{h^2} \right)^{3/2} V_i^* \exp \left( - \frac{W_0}{k T} \right) \right]^x$$

(Lennard Jones and Devonshire 1939) where the symbols have the usual significance. In a disordered state let  $x_a$ ,  $x_b$ , and  $x_c$  ( $x_a + x_b + x_c = x$ ) denote the number of  $\text{Mn}^{3+}$  ions having their longer bonds parallel to the crystal  $a$ ,  $b$  and  $c$  axes respectively in a gramme-mole of  $\text{Mn}_3\text{O}_4$ . If  $x_a \neq x_b$ , the crystal symmetry



will fall to orthorhombic, but since this was not observed,  $x_a = x_b$  at any stage of disorder and in a state of complete disorder  $x_a = x_b = x_c$ . On rotation of the longer bond from the  $c$  axis to the  $a$ , or  $b$  axis direction, there is an increase in the energy of the system; let this increase per manganese ion be denoted by  $W$ . The total increase in energy due to disorder will be  $(x_a + x_b)W = 2x_a W$ . Now the number of possible arrangements in which  $x_a$   $\text{Mn}^{3+}$  ions have the longer bonds parallel to the  $a$  axis,  $x_b$  ions have those parallel to the  $b$  axis and  $x_c$  ions parallel to the  $c$  axis is given by  $\gamma = x! / x_a! x_b! x_c!$ . Thus an extra factor  $\gamma \exp(-2x_a W/kT)$  has to be introduced into the partition function to account for the disorder, giving the new partition function

$$Z' = Z \left\{ \gamma \exp \left( - \frac{2x_a W}{kT} \right) \right\}.$$

The increase in entropy when disorder sets in is

$$\begin{aligned} \Delta S &= kT \frac{\partial}{\partial T} \log \frac{Z'}{Z} + k \log \frac{Z'}{Z} \\ &= k \log \gamma \\ &= k \log \frac{x!}{x_a! x_b! x_c!}. \end{aligned}$$

Using Stirling's approximation this reduces to

$$\Delta S = k[x \log x - 2x_a \log x_a - x_c \log x_c].$$

In the case of complete disorder  $x_a = x_b = x_c = x/3$  and thus  $\Delta S = xk \log 3$ .  $x = 2N$  for a 'normal' spinel and  $x = N$  for an 'inverse' spinel; where  $N$  is Avogadro's number. Thus the value of  $\Delta S$  should lie between 4.32 and 2.16 cal deg<sup>-1</sup> mole<sup>-1</sup> depending on the degree of inverseness. It is not possible to determine the cationic distribution in  $\text{Mn}_3\text{O}_4$  at the transition temperature. However, the high temperature x-ray study of other 'normal' manganites (to be published) indicates that the distribution is unchanged at elevated temperatures. Thus it is reasonable to assume that in  $\text{Mn}_3\text{O}_4$  most of the  $\text{Mn}^{3+}$  ions still occupy the octahedral sites and thus  $\Delta S$  should be only slightly lower than 4.32 cal deg<sup>-1</sup> mole<sup>-1</sup>.

Kelly (1949) has reported a value of  $5.0 \pm 0.3$  kcal g mole<sup>-1</sup> for the heat of transformation and thus the increase in entropy  $\Delta S$  is  $3.47 \pm 0.20$  cal deg<sup>-1</sup> mole<sup>-1</sup> which is close to expectations.

#### ACKNOWLEDGMENT

The authors thank the Director, National Chemical Laboratory, for the continued interest in the work.

#### REFERENCES

- AMINOFF, G., 1926, *Z. Kristallogr.*, **64**, 475.  
 BERTAUT, E. F., 1951, *J. Phys. Radium*, **12**, 252.  
 DUNITZ, J. D., and ORGEL, L. E., 1957, *J. Phys. Chem. Solids*, **3**, 20.  
 FINCH, G. I., SINHA, A. P. B., and SINHA, K. P., 1957, *Proc. Roy. Soc. A*, **242**, 28.  
 GOODENOUGH, J. B., and LOEB, A. L., 1955, *Phys. Rev.*, **98**, 391.  
 KELLEY, K. K., 1949, *Bull. U.S. Bur. Mines* No. 476, quoted in 'Metallurgical Thermochemistry' by Kubaschewski and Evans (London: Pergamon Press, 1956), p. 294.  
 LENNARD-JONES, J. E., and DEVONSHIRE, A. F., 1939, *Proc. Roy. Soc. A*, **170**, 464.  
 MCMURDIE, H. F., and GOLOVATO, E., 1948, *J. Res. Nat. Bur. Stand.*, **41**, 589.  
 ROMEIJN, F. C., 1953, *Philips Res. Rep.*, **8**, 304, 321.  
 SINHA, A. P. B., SANJANA, N. R., and BISWAS, A. B., 1957, *Acta Cryst., Camb.*, **10**, 439.

## The Polarization-Asymmetry Equality

BY J. S. BELL AND F. MANDL

Atomic Energy Research Establishment, Harwell, Berks.

*Communicated by B. H. Flowers; MS. received 14th November 1957*

**D**ALITZ (1952) and Wolfenstein and Ashkin (1952) have shown that the equality

$$\text{polarization} = \text{asymmetry} \quad \dots\dots(1)$$

in double scattering experiments of spin  $\frac{1}{2}$  particles follows from the assumption of invariance under time reversal of the theory. These proofs, based on the explicit construction of the  $S$ -matrix from the available spin and momentum vectors, assumed parity conservation.

Recent demonstrations of parity non-conservation in weak interactions raise the question whether parity non-conservation in strong interactions would affect the above result. Although parity is almost certainly conserved in strong interactions (experiments by D. H. Wilkinson (1958) suggest that the strength of the parity non-conserving force is less than  $10^{-3.5}$  of the parity conserving force), it is of interest to note that relation (1) holds even if parity is not conserved, provided the theory is invariant under time reversal.

This can be proved by the explicit construction of the appropriate  $S$ -matrix but it can also be seen more directly as follows.

Consider an incident unpolarized beam of spin  $\frac{1}{2}$  particles with momentum  $\mathbf{k}$  scattered through an angle  $\theta$  by an unpolarized target, the final momentum being  $\mathbf{k}'$ , where all quantities will throughout be referred to the centre-of-mass system.

The polarization  $P$  of the scattered beam is given by

$$P = \frac{\sum_m \{\sigma_\theta(+|m) - \sigma_\theta(-|m)\}}{\sum_m \{\sigma_\theta(+|m) + \sigma_\theta(-|m)\}} \quad \dots\dots(2)$$

Here spins are quantized along the axis  $\mathbf{k} \times \mathbf{k}'$ , i.e. at right angles to the plane of scattering.  $\sigma_\theta(m'|m)$  is the cross section for scattering through an angle  $\theta$  from the spin state  $m$  ( $= \pm$ ) to  $m'$  ( $= \pm$ ). In equation (2) the spin states of the target have already been averaged and summed over, assuming it initially unpolarized.

Correspondingly, the asymmetry due to scattering a fully polarized incident beam (in the  $+$  state) is

$$A = \frac{\sum_m \{\sigma_\theta(m|+) - \sigma_{-\theta}(m|+)\}}{\sum_m \{\sigma_\theta(m|+) + \sigma_{-\theta}(m|+)\}} \quad \dots\dots(3)$$

Time reversal means interchanging initial and final states and changing the signs of all spins and momenta, i.e. under time reversal

$$\sigma_\theta(m'|m) \rightarrow \sigma_{-\theta}(-m|-m'). \quad \dots\dots(4)$$

Assuming invariance under time reversal, equation (2) can be written

$$P = \frac{\sum_m \{\sigma_{-\theta}(-m|-) - \sigma_{-\theta}(-m|+)\}}{\sum_m \{\sigma_{-\theta}(-m|-) + \sigma_{-\theta}(-m|+)\}} \quad \dots\dots (5)$$

We now carry out a rotation through  $180^\circ$  about the axis defined by  $\mathbf{k}'$ . This changes  $+\theta$  into  $-\theta$ , and all spins  $m$  normal to the plane of scattering into  $-m$ , i.e. under this operation

$$\sigma_\theta(m'|m) \rightarrow \sigma_{-\theta}(-m'|-m). \quad \dots\dots (6)$$

Hence assuming invariance under rotations only (but not necessarily under reflections), equation (5) becomes

$$P = \frac{\sum_m \{\sigma_\theta(m|+) - \sigma_{-\theta}(-m|+)\}}{\sum_m \{\sigma_\theta(m|+) + \sigma_{-\theta}(-m|+)\}} \quad \dots\dots (7)$$

and this agrees with the asymmetry, equation (3), if we replace the summation index  $-m$  by  $m$  in the two right-hand terms.

When parity is not conserved, the polarization need no longer be perpendicular to the scattering plane. In this case the above result can be generalized. Above, spins were quantized along the direction of the vector  $\mathbf{k} \times \mathbf{k}'$ : however, all that is required for equation (6) to hold is that we consider components of spin orthogonal to  $\mathbf{k}'$ . Thus we could equally well have taken an axis of quantization defined by the vector  $\mathbf{n}$ , obtained by rotating the vector  $\mathbf{k} \times \mathbf{k}'$  through an angle  $\alpha$  about  $\mathbf{k}'$  in a right-hand sense. This would mean that in the polarization experiment, equation (2), the 'up-down' difference in spins of the scattered beam is measured along  $\mathbf{n}$  and in the asymmetry experiment, equation (3), we use an incident beam fully polarized along an axis  $\mathbf{n}'$ , obtained from  $\mathbf{k} \times \mathbf{k}'$  by a right-handed rotation about  $\mathbf{k}$  through an angle  $-\alpha$ . (As above,  $\mathbf{k}$  denotes in both cases the momentum of the incident particle,  $\mathbf{k}'$  that of the scattered particle.) Hence for polarization and asymmetry measured under these conditions

$$P(\theta, \alpha) = A(\theta, \alpha) = I(\theta) \cos[\alpha - \alpha_0(\theta)] \quad \dots\dots (8)$$

where the last step follows since the polarization, and hence the asymmetry, satisfy a cosine law,  $\alpha_0(\theta)$  being the angle at which the maximum projected polarization occurs in the first experiment and the maximum asymmetry in the second.

In the asymmetry experiment we treated the incident beam as fully polarized transversely. If parity is not conserved, this beam which is usually itself prepared by a scattering, may contain a longitudinal component of polarization. The asymmetry in this case measures the transverse component since, as is easily seen, the longitudinal component does not affect an asymmetry measurement.

Strictly speaking the relation (4) depends on reciprocity (Blatt and Weisskopf 1952) rather than on reversibility. These are of course equivalent for a unitary theory. But consider, for example, the scattering of spin  $\frac{1}{2}$  particles by a complex potential well of the form

$$V_c(\mathbf{r}) + V_{s0}(\mathbf{r})\boldsymbol{\sigma} \cdot \mathbf{r} \times \mathbf{p}.$$

This process is not reversible when  $V_c$  and  $V_{s0}$  are complex, but it is reciprocal and the relation (4) is valid.

## REFERENCES

- BLATT, J. M., and WEISSKOPF, V. F., 1952, *Theoretical Nuclear Physics* (New York : Wiley).  
DALITZ, R. H., 1952, *Proc. Phys. Soc. A*, **65**, 175.  
WILKINSON, D. H., 1958, *Phys. Rev.*, in the press.  
WOLFENSTEIN, L. and ASHKIN, J., 1952, *Phys. Rev.*, **85**, 947.

---

Note on the Li II Spectrum

BY G. W. SERIES AND K. WILLIS

Clarendon Laboratory, Oxford

*MS. received 26th November 1957*

THE visible and ultra-violet lines in the spectrum of Li II were photographed by Schöler (1926) and by Werner (1925, 1926). The analysis of the spectrum did not allow the location of the level  $1s2s\ ^1S_0$  whose value is known only by extrapolation (Moore 1949). From the extrapolated values the line  $1s2p\ ^1P_1-1s2s\ ^1S_0$  should lie at  $8517.7\ \text{\AA}$  (air wavelength).

A line has now been observed at  $8517.1 \pm 1.5\ \text{\AA}$  which we identify with this transition. The light source was a hot hollow cathode of stainless steel. A close-fitting cap with a central hole prevented too rapid loss of the lithium metal by evaporation. The pressure of the carrier gas, helium, was reduced when the lithium vapour pressure became sufficient to sustain the discharge. A neon spectrum from a different source was used for wavelength calibration. Dispersion in the region  $8500\ \text{\AA}$  was about  $250\ \text{\AA}\ \text{mm}^{-1}$ .

The line at  $8517\ \text{\AA}$  appeared only when other lines of the Li II spectrum (in particular the strong triplet line  $5485\ \text{\AA}$  deriving from the analogous transition) were present. The new line was overlaid by bands which formed part of a system extending from  $7350$  to  $8750\ \text{\AA}$ , possibly the LiH system reported by Crawford and Jorgensen (1934). The hydrogen atomic lines were present. Also present as impurities were sodium and potassium indicated by their resonance lines. Since one of the caesium resonance lines lies at  $8521\ \text{\AA}$ , the plates were carefully scrutinized for traces of caesium. No signs were found, either of caesium or of rubidium. The line  $8517\ \text{\AA}$  was not only stronger than the sodium and potassium resonance lines, but in its distribution across the cathode it followed the lithium spark line  $5485\ \text{\AA}$  rather than the arc lines of the impurities.

## ACKNOWLEDGMENT

We are grateful to the Atomic Energy Research Establishment, Harwell, for financial support.

## REFERENCES

- CRAWFORD, F. H., and JORGENSEN, T., 1934, *Phys. Rev.*, **45**, 737.  
MOORE, C. E., 1949, *Atomic Energy Levels*, Vol. I. (Washington, D.C. : Nat. Bur. Stand.).  
SCHÖLER, H., 1926, *Z. Phys.*, **37**, 568.  
WERNER, S., 1925, *Nature, Lond.*, **116**, 574 ; 1926, *Ibid.*, **118**, 154.



## On the Theory of Surface Recombination in Semiconductors for Large Potential Differences between Surface and Bulk

By Dr. F. BERZ

Mullard Research Laboratories, Salfords, Redhill, Surrey

*MS. received 4th June 1957, and in revised form 24th September 1957*

### § 1. INTRODUCTION

It is usually assumed in the theories dealing with surface recombination that, for the non-degenerate case, the electrons and holes follow the Maxwell-Boltzmann distribution law (to be referred to as the MB law).

According to a fundamental result of statistical mechanics such a law holds for carriers in equilibrium. For injected carriers it can be considered at best as an approximation which breaks down in the following two cases.

Case A. When the carriers which recombine at the surface form an appreciable proportion of the injected carriers which fall on the surface during the same interval of time.

Case B. When over a part of the space charge layer near the surface the potential variation over a carrier mean free path is of the order of  $kT/e$  or above.

In Case A there are appreciably more injected carriers falling on the surface than are returning from it, and the velocity distribution cannot therefore be represented by the isotropic MB distribution which corresponds to no drift. This case will not be considered in the present note. It is of no practical importance for the values of the surface potential reported up to now in etched Ge at room temperature, when the surface recombination velocity is of the order of  $1000 \text{ cm sec}^{-1}$  or below.

In Case B the carriers which are accelerated towards the surface by the potential drop in the space charge layer acquire an extra momentum of the order of the mean thermal value, which is neither scattered in direction nor partly dissipated through collisions with the lattice. Under equilibrium conditions the distributions are maintained Maxwellian, through the combined effect of the reflection of the carriers at the surface, and their emission and absorption by the surface recombination centres. These mechanisms may, however, prove insufficient to maintain a Maxwell-Boltzmann distribution near the surface when the equilibrium is disturbed. More precisely, in such a case the relation between the density of the carriers in the surface recombination centres and their density in the bulk is altered since the corresponding quasi Fermi levels do not coincide. Hence the effect of the recombination centres on the carriers distribution is changed, and the distribution in the space charge layer becomes non-Maxwellian, provided that the energy interchange of the carriers and the surface during reflection is sufficiently weak.

The effect is significant even for small densities  $\delta n$  of injected carriers. Due to it the net rate of recombination  $\delta U$  of the carriers at the surface is altered by an

amount proportional to  $\delta n$ , and therefore the velocity of recombination  $s = \delta U / \delta n$  changes by a finite amount, independent of  $\delta n$ , to a first approximation.

Case B forms the subject of the present note. It is of practical importance in Ge, as illustrated by the two examples of figure 1, taken from the experiments at room temperature  $T_0$ , of Many *et al.* (1956), and Brattain and Garrett (1956). In this figure the horizontal segments represent the range of variation of the potential  $V_s$  of the surface with respect to the bulk. The point O shows the surface potential for which the conductance of the surface layer is minimum. Each division corresponds to a potential increment  $2kT_0/e$ . The heavy lines show the range for which the potential variation is between  $kT_0/2e$  and  $kT_0/e$  over a distance under the surface equal to half of an electron mean free path, and the shaded lines show the range where this variation is larger than  $kT_0/e$ . For these data, the electron mean free path  $l$  has been taken equal to  $0.9 \times 10^{-5}$  cm (Kingston 1955), and the potential variations in the space charge layer have been calculated from the theory of Garrett and Brattain (1955).

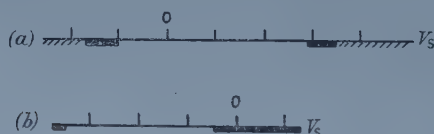


Figure 1. (a) n-type Ge sample,  $25 \Omega \text{ cm}^{-1}$ , used by Many *et al.* (1956). (b) p-type Ge sample,  $8.1 \Omega \text{ cm}^{-1}$ , used by Brattain and Garrett (1956).

## § 2. OBJECT OF THIS INVESTIGATION AND MAIN ASSUMPTIONS

As mentioned above it is proposed to consider what are the changes to the standard results on surface recombination obtained by Stevenson and Keyes (1954), which are introduced by the large variations of the electric potential in the surface layer, and by the consequent invalidity of the MB law.

A complete treatment of the question presents great difficulties, and the following simplified model has been used.

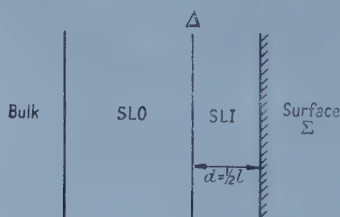


Figure 2.  $V_1$  is the potential drop across SLI.  $V_s$  is the potential drop across SLO + SLI.

The space charge layer is divided in two parts SLO and SLI by a plane  $\Delta$  parallel to the surface  $\Sigma$ , and at a distance  $d$  from it equal to half of an electron mean free path  $d = \frac{1}{2} l$  (see figure 2). In the part SLO adjacent to the bulk the potential

variations are assumed to be sufficiently small for the MB law to be satisfied up to  $\Delta$ . In the part SLI adjacent to the surface no collisions are supposed to occur. Both these assumptions are somewhat drastic, but the errors introduced thereby tend to balance, and it seems reasonable to expect that this simple picture will give the right order of value for the overall effect.

Besides this basic simplification, some assumptions have to be made regarding the unknown law governing the reflection at  $\Sigma$  of the carriers coming from SLI, which are not captured by the surface states. It will be assumed that the kinetic energy of the carriers is substantially unchanged by the collision with the surface. As for the direction of the reflection, two cases corresponding to specular reflection and to random scattering will be considered.

The other assumptions are the same as in the usual theory of surface recombination, limited to the case of a single trapping energy level. The trapping cross sections are taken to be either constant or inversely proportional to the velocity of the incident carriers.

### § 3. METHOD OF DERIVATION

The basic concepts concerning the traps and the method of derivation are essentially the same as developed by Shockley and Read (1952) and Stevenson and Keyes (1954). The fundamental difference is that the carriers are not assumed to follow the MB law up to  $\Sigma$ , but that their distribution there is derived using the model described in § 2.

The carriers of each sign are divided into two categories according to the mode of their first appearance in SLI. In the first group are the carriers which have come from SLO, across  $\Delta$ , and in the second those which are emitted by the surface traps. The velocity distribution of the carriers at  $\Sigma$ , and their density, are derived by following in SLI the to-and-fro motion of the carriers belonging to each category, until they are captured by the surface traps, or pass across  $\Delta$  into SLO. The full derivation has been carried out (Berz 1957) but would be too long to give here. It is found that the carriers moving towards  $\Sigma$  and decelerated in SLI satisfy the MB law. The carriers accelerated towards  $\Sigma$  show a deviation from this law, which is due, as expected, to the difference between the quasi Fermi level of the free carriers in the material, and of the carriers in the recombination centres. The effects of this deviation on the recombination velocity are summed up below.

### § 4. RESULTS

Let us first consider the surface recombination velocity  $s$ , in the case when the MB law is valid up to the surface  $\Sigma$ . In that case, both for constant cross sections and for cross sections inversely proportional to the velocity of the carriers,

$$s = \frac{1}{2} N_t \left( \frac{2kT}{\pi(m_n m_p)^{1/2}} \right)^{1/2} [\sigma_n] [\sigma_p] \frac{n_0 + p_0}{[\sigma_n][n_s + n_1] + [\sigma_p][p_s + p_1]} \dots (1)$$

where  $N_t$  is the density of the surface traps,  $k$  the Boltzmann constant,  $T$  the absolute temperature,  $m_n$ ,  $m_p$  the effective masses of the electrons and holes,  $n_0$  and  $p_0$  their bulk densities,  $n_s$  and  $p_s$  their densities at the surface, and  $n_1$ ,  $p_1$  the densities they would have if the Fermi level passes through the energy level of the traps. The symbols  $[\sigma_n]$  and  $[\sigma_p]$  stand for the 'average' cross sections of the traps for the

capture of electrons and holes, defined as

$$\begin{aligned} [\sigma_n] &= \left(\frac{m_p}{m_n}\right)^{1/4} \sigma_n(c_n), & c_n &= \left(\frac{8kT}{\pi m_n}\right)^{1/2} \\ [\sigma_p] &= \left(\frac{m_n}{m_p}\right)^{1/4} \sigma_p(c_p), & c_p &= \left(\frac{8kT}{\pi m_p}\right)^{1/2} \end{aligned} \quad \dots\dots(2)$$

where  $\sigma_n(c_n)$  and  $\sigma_p(c_p)$  are the traps cross sections for  $c=c_n$  and  $c=c_p$  ( $c$ =carrier velocity). Formulae (1) and (2) correspond to standard results for  $s$ , which have been derived by previous authors (see Stevenson and Keyes 1954, Kingston 1956).

The curves defined by (1) and (2) giving the variation of  $s$  with the potential  $V_s$  of the surface with respect to the bulk, are symmetrical and have a single maximum  $s_M$  (see curve 0 of figure 4, referred to later). If  $V_s^M$ ,  $V_s^{(1)}$  and  $V_s^{(2)}$  are the values of  $V_s$  for  $s=s_M$ , and  $s=\frac{1}{2}s_M$  respectively, one has

$$\begin{aligned} \ln \frac{[\sigma_p]}{[\sigma_n]} &= \frac{2}{kT} (F - E_i + e V_s^M) \\ &= \frac{2}{kT} [F - E_i + \frac{1}{2} e (V_s^{(1)} + V_s^{(2)})] \end{aligned} \quad \dots\dots(3)$$

and if  $\frac{e}{kT} (V_s^M - V_s^{(1)}) \gg 1$

$$E_T^{(1)} \simeq F + e V_s^{(1)} \quad E_T^{(2)} \simeq F + e V_s^{(2)} \quad \dots\dots(4)$$

where  $F$  is the Fermi level,  $E_i$  the intrinsic Fermi level, and  $E_T^{(1)}$  and  $E_T^{(2)}$  are the alternative values of the energy  $E_T$  of the trapping centres, which would both give the same observed variation of  $s$  with  $V_s$ .

Expressions (3) and (4) are used to derive the characteristics of the trapping centres from experimental data (see Many *et al.* 1956).

Let us now return to the case of large potential gradients, when the MB law no longer holds in the space charge layer near  $\Sigma$ . The value of  $s$  is derived as outlined in §§2 and 3. One then finds that (1) and (2) can be retained with the following modifications:

1. For  $V_s > 0$   $[\sigma_n]$  must be replaced by  $[\sigma_n]/K \left( \frac{eV_1}{kT} \right)$ .
2. For  $V_s < 0$   $[\sigma_p]$  must be replaced by  $[\sigma_p]/K \left( \frac{eV_1}{kT} \right)$ .

where  $V_1$  is the potential drop across SLI, and  $K(|eV_1/kT|)$  is a function whose variations with  $|eV_1/kT|$  are shown in figure 3. Equations (3) and (4) are no longer justified.

The practical effect of  $K$  on the shape of the  $(s, V_s)$  curve depends on the characteristics of the trapping centres and on the laws of reflection.

Figure 4 shows its influence in the case of the Ge sample, referred to in (a) of figure 1, with  $[\sigma_p]/[\sigma_n] = 150$ , and  $(E_T - E_i)/kT_0 = -1$ . It is seen from figure 4 that the introduction of the factor  $K$  has modified quite appreciably the right-hand half of the curves. The unjustified application of (3) and (4) to these curves would lead to erroneous values of  $[\sigma_p]/[\sigma_n]$  and  $E_T^{(2)}$ , as shown in the table.

Curve	0	I	I*	II	II*
$\frac{[\sigma_p]}{[\sigma_n]}$ from (3)	150	34	21	90	64
$\frac{E_T^{(2)} - E_i}{kT_0}$ from (4)	6.20	4.70	4.25	5.70	5.35



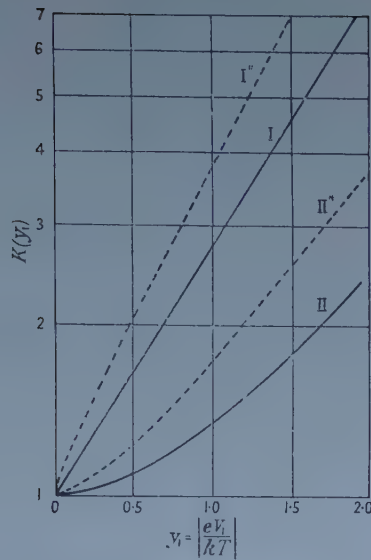


Figure 3. Curve I. Specular reflection. Constant cross sections,  $K = \exp y_1$ .

Curve I\*. Specular reflection. Cross sections  $\sim 1/c$ .

$$K = \left[ \frac{2}{\sqrt{\pi}} \sqrt{y_1} \exp(-y_1) + (1 - \operatorname{erf} \sqrt{y_1})(1 - 2y_1) \right]^{-1}.$$

Curve II. Random scattering. Constant cross sections  $K = \exp(y_1)/(1 + y_1)$ .

Curve II\*. Random scattering. Cross sections  $\sim 1/c$ .

$$K = \left[ \frac{2}{\sqrt{\pi}} \sqrt{y_1} \exp(-y_1) + (1 - \operatorname{erf} \sqrt{y_1}) \right]^{-1}.$$

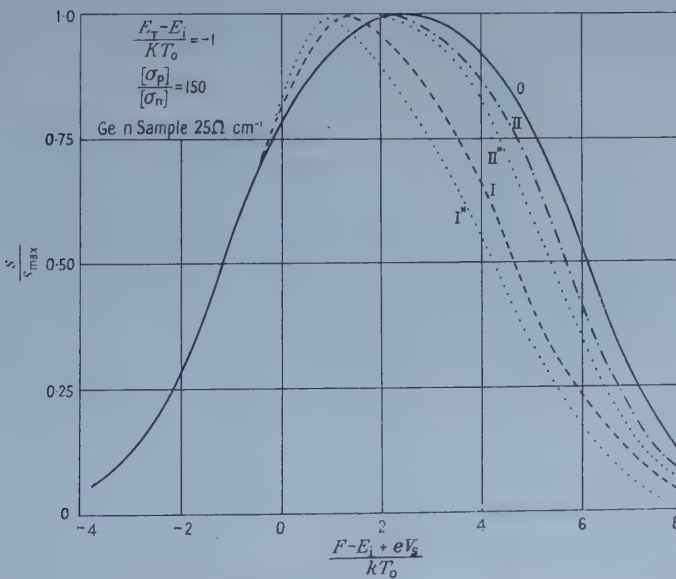


Figure 4. Curve 0. Curve for the Maxwell-Boltzmann distribution. Curve I. Specular reflection. Constant cross sections. Curve I\*. Specular reflection. Cross sections  $\sim 1/c$ . Curve II. Random scattering. Constant cross sections. Curve II\*. Random scattering. Cross sections  $\sim 1/c$ .

## § 5. CONCLUSIONS

It is seen that the invalidity of the Maxwell-Boltzmann law for injected carriers, in the case of strong potential gradients in the space charge layer, may have an appreciable effect on the surface recombination. This fact must be kept in mind when interpreting experimental results concerned with the variation of  $s$  width with the potential drop across the surface layer.

## ACKNOWLEDGMENTS

The author wishes to thank Dr. F. H. Stieltjes for an informative preliminary discussion, and Dr. K. Hoselitz and Mr. T. B. Watkins for their interest and encouragement. Acknowledgment is made to the Directors of Mullard Research Laboratories for the permission to publish this note.

## REFERENCES

- BERZ, F., 1957, Mullard Research Report No. 2141.  
 BRATTAIN, W. H., and GARRETT, C. G. B., 1956, *Bell Syst. Tech. J.*, **35**, 1019, 1041.  
 GARRETT, C. G. B., and BRATTAIN, W. H., 1955, *Phys. Rev.*, **99**, 376.  
 KINGSTON, R. H., 1955, *Phys. Rev.*, **98**, 1766 ; 1956, *J. Appl. Phys.*, **27**, 101.  
 MANY, A., HARNIK, E., and MARGONINSKI, Y., 1956, *Semiconductor Surface Physics*, ed. R. H. Kingston (Philadelphia : University of Pennsylvania Press).  
 SHOCKLEY, W., and READ, W. T., 1952, *Phys. Rev.*, **87**, 835.  
 STEVENSON, D. T., and KEYES, R. J., 1954, *Physica*, **20**, 1041.

## A Possible Infra-Red Detector using Thermal Expansion

By R. V. JONES

Department of Natural Philosophy, University of Aberdeen

*MS. received 18th October 1957*

**T**HERMAL infra-red detectors generally measure the temperature rise in a thin receiver warmed by the incident radiation. Since the rise is small ( $10^{-6}$  to  $10^{-3}$  deg c), the measurement techniques have customarily made use of phenomena with high temperature dependence, such as electrical resistance change, thermoelectric effect, or gaseous expansion. It may, however, be worth considering phenomena with lower temperature coefficients, if they offer promise of less disturbance from accidental fluctuations.

The sensitivity of any thermal radiation detector is fundamentally limited by the spontaneous fluctuations in temperature of the receiver, caused by the random exchange of photons between the receiver and its surroundings. If the receiver and its surroundings are at an absolute temperature  $T$ , the root mean square of the fluctuations, for an observation bandwidth of  $B$  c s, is equal to the temperature rise which would be caused by an amount of radiation  $I_q$  (the noise equivalent signal), where

$$I_q^2 = 16AB\sigma kT^5.$$

Here  $\sigma$  is Stefan's constant and  $k$  is Boltzmann's constant.  $A$  is the area of the receiver, which is assumed to be perfectly black on the side receiving the radiation and perfectly reflecting on the other, and also to lose no heat by

conduction (Lewis 1947). A typical receiving area is  $1 \text{ mm}^2$ , and for this at  $290^\circ\text{K}$  with an observing bandwidth of  $1 \text{ c/s}$ ,

$$I_q = 5 \times 10^{-12} \text{ watt.}$$

The best thermal detectors hitherto reported have shown fluctuations with an r.m.s. value about seven times the theoretical value, owing to other sources of noise in the detector (Fellgett 1949).

Perhaps the simplest of all thermal effects is linear expansion; a detector using this phenomenon would employ a thin foil whose length would change upon irradiation. Edison, incidentally, made such a detector (the 'thermophone') in which the length change altered the pressure on a carbon microphone. The present author once made a detector using the curvature of a bimetallic foil receiver, but neither this device nor Edison's was as good as conventional detectors. Recently, however, it has become feasible to develop a sensitive expansion detector by converting the length change to an angular one, and then using an optical lever and photoelectric amplifier. The simplicity of the system offers the hope of locating and minimizing the sources of noise; and the fact that the receiver need have no thermal losses other than those due to radiation (in contrast, for example, to the thermoelement) suggests that an expansion detector might have a higher efficiency than other devices.

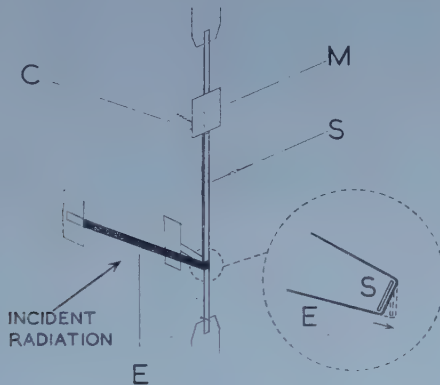


Figure 1. E: Expansion strip,  $0.2 \text{ mm}$  wide,  $0.1 \mu$  thick, length on side receiving radiation  $5 \text{ mm}$ , length on other side  $5 \text{ mm}$  (for best thermal compensation) or less than  $1 \text{ mm}$  (for minimum noise). S: Suspension strip,  $50 \mu$  wide,  $5 \mu$  thick, total length  $11 \text{ mm}$ , length above mirror  $2 \text{ mm}$ , length below expansion strip  $2 \text{ mm}$ , intermediate length of  $5.5 \text{ mm}$  between M and E copperplated to thickness of  $50 \mu$ . M: Mirror,  $1.5 \text{ mm} \times 1.5 \text{ mm} \times 0.06 \text{ mm}$ . C: Counterpoise for mirror,  $4 \text{ mm}$  of manganin wire,  $20 \mu$  diameter.

The temperature fluctuations corresponding to the radiation  $I_q$  are of the order of  $10^{-6} \text{ deg C}$ , and so, with a typical strip of material  $5 \text{ mm}$  long with an expansion coefficient  $10^{-5} \text{ deg}^{-1}$ , the measuring system must be capable of detecting a length change of  $5 \times 10^{-12} \text{ cm}$ , or about the diameter of an atomic nucleus. Optical levers with photoelectric amplifiers capable of detecting changes in angle of  $10^{-9}$  radian have been available for some years (Jones 1951), and so the outstanding difficulties to be overcome are the production of (1) a foil about  $0.1 \text{ micron}$  thick of constantan or some other material having poor thermal conductivity and high mechanical stability, (2) a frictionless lever system to

convert expansion into rotation with an effective arm of 50 to 100  $\mu$ , and (3) a suspension carrying the optical lever mirror which is sufficiently well balanced against mechanical disturbances.

An optical lever system capable of detecting changes of  $10^{-10}$  radian has now been developed, with a time constant of about 0.1 second, using principles previously described (Jones 1951). The minimum size of mirror giving sufficient resolution to work with this system is about 1.5 mm  $\times$  1.5 mm, and to minimize its mass it is made from specially thin (60  $\mu$ ) glass sheet kindly supplied by Messrs. Chance Brothers. The lever system is sketched in figure 1. The expansion strip E acts as a pair of reins pulled tight around a thin taut suspension strip S of the type used in galvanometers; when radiation falls on one side of the 'reins', this side expands, and allows the corresponding edge of the suspension to move forward, thus causing a rotation of the suspension. The mirror M is placed on the suspension some distance away from the expansion

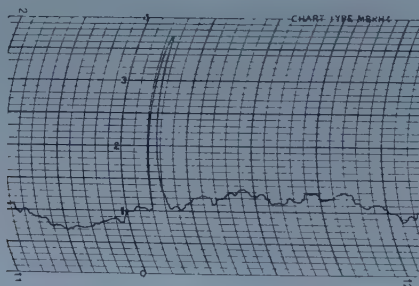


Figure 2. Record of deflection caused by a signal of about  $1.5 \times 10^{-9}$  w. Each small horizontal division = 2 sec, each small vertical division =  $5 \times 10^{-11}$  w, or  $4 \times 10^{-11}$  cm, or  $5 \times 10^{-6}$  deg c. Optical lever amplifier operating at one-twentieth maximum gain; bandwidth about 1.5 c/s.

strip, to minimize thermal disturbance by light from the optical lever. The suspension strip is stiffened by electroplating between the expansion strip and the mirror. Despite its small mass the mirror must be counterpoised by a few millimetres length (C) of 20  $\mu$  diameter wire to immunize the system against external vibration; the counterpoising has to be better than 1  $\mu$ g 1 mm off axis. The effective lever arm used is about 100  $\mu$ , although values down to 50  $\mu$  have been obtained. Constantan foil down to 0.06  $\mu$  thickness has been made by rolling 7  $\mu$  diameter wire, and it has been blackened by depositing about  $1.5 \times 10^{-4}$  g cm $^{-2}$  of gold black by evaporation in nitrogen. The complete detector is mounted in a vacuum of about  $10^{-4}$  mm mercury pressure, and has a thermal time constant of about 0.1 second. The output of the optical lever, which uses Schwarz photoconductive cells, is amplified electronically and recorded; the electronic equipment was designed by Dr. J. C. S. Richards. At maximum sensitivity an expansion of about  $10^{-12}$  cm gives a movement of one division on the final record, and the amplifier is quiet enough with a fixed mirror for such a displacement to be detectable against the noise background.

A record of the deflections of the detector system using a constantan strip receiver 5 mm long by 0.2 mm wide is shown in figure 2, when a signal of about  $1.5 \times 10^{-9}$  w of incident energy from a black body at 200°C is used to indicate



the sensitivity; ignoring long term drifts, the fluctuations in the zero have a root mean square value corresponding to between  $1.0$  and  $1.5 \times 10^{-11}$  w of incident energy for a bandwidth of 1 c/s. There are periods when the fluctuations are lower than this value, and it is possible that the inherent fluctuations are of r.m.s. value less than  $1.0 \times 10^{-11}$  w, the additional fluctuations being due to some external cause which is not always present. From the record of figure 2 and similar ones it appears that the device is potentially not more than a factor of two in sensitivity from an ideal detector of this area, and that some of the fluctuations in the quieter part of the record are caused by spontaneous temperature fluctuations in the strip. While it is far from being an operational instrument, the device thus compares well in sensitivity with other detectors of thermal radiation.

## REFERENCES

- LEWIS, W. B., 1947, *Proc. Phys. Soc.*, **59**, 34.  
FELLGETT, P. B., 1949, *Proc. Phys. Soc. B*, **62**, 351.  
JONES, R. V., 1951, *Proc. Phys. Soc. B*, **64**, 469.

## LETTERS TO THE EDITOR

## International Union of Pure and Applied Physics

## Ninth General Assembly

The International Union of Pure and Applied Physics, founded in 1922, held its Ninth General Assembly in Rome from 17th to 20th September, 1957. The National Committees of the U.S.S.R., Austria and Bulgaria were formally admitted to the Union, that from the U.S.S.R. having been provisionally agreed by the Executive Committee at its meeting in 1956. The number of countries now adhering to the Union is thirty.

For the period 1957-1960, the Executive Committee of the Union has the following members:

President	E. Amaldi (Rome).
Former Presidents	N. F. Mott (Cambridge, U.K.), M. Siegbahn (Stockholm).
Vice-Presidents	J. de Boer (Amsterdam), R. B. Brode (Berkeley), M. Kotani (Tokyo), J. H. Van Vleck (Cambridge, Mass.), G. Herzberg (Ottawa), A. Joffe (Leningrad), E. Rasmussen (Copenhagen), H. Staub (Zurich), F. C. A. Trendelenburg (Erlangen), J. Weyssenhoff (Cracow).
Secretary General	P. Fleury (Paris).

Eight specialized Commissions were authorized to develop international cooperation in the following fields. (Names of Presidents (P) and Secretaries (S) are indicated below, with the addresses of the Secretaries.)

*Symbols, Units and Nomenclature*: (P): H. H. Nielsen (Columbus, Ohio);  
(S): J. de Boer, Finsensstraat 28, Amsterdam, Netherlands.

*Thermodynamics and Statistical Mechanics*: (P): J. Yvon (Paris);  
(S): G. Careri, Università degli Studi, Rome.

*Cosmic Rays*: (P): B. Rossi (Cambridge, Mass.);  
(S): C. F. Powell, H. H. Wills Physical Laboratory, Royal Fort, Bristol, 8.

*Very Low Temperatures*: (P): C. J. Gorter (Leiden);  
(S): D. Shoenberg, Cavendish Laboratory, Cambridge, U.K.

*Publications*: (P): J. H. Awbery (London);  
(S): G. A. Boutry, 292 rue Saint-Martin, Paris 3e.

*Acoustics*: (P): W. Furrer (Berne);  
(S): C. W. Kosten, Mijnboulevard 11, Delft, Netherlands.

*Solid State Physics*: This Commission is composed of three sub-groups.

A. (General) (P): J. C. Slater (Cambridge, Mass.);

(S): C. Kittel, Department of Physics, University of California, Berkeley 4, California, U.S.A.

B. (Semiconductors) (P): A. Joffe (Leningrad);

(S): R. A. Smith, Royal Radar Establishment, Malvern, U.K.

C. (Magnetism) (P): L. Néel (Grenoble);

(S): L. F. Bates, Department of Physics, University of Nottingham, U.K.

*High Energy Physics*: (P): C. J. Bakker (CERN, Geneva);

(S): R. E. Marshak, University of Rochester, U.S.A.

The formation of a Commission for Low Energy Nuclear Physics and of a Commission for Electronics are under consideration.

In addition the International Commission on Optics is affiliated to IUPAP and its Officers are as follows:

(P): S. S. Ballard (San Diego, U.S.A.);

(S): W. D. Wright, Department of Physics, Imperial College, London, S.W.7.

The Union is also represented in the International Council of Scientific Unions and in the Joint Commissions of this Council for Spectroscopy, Applied Radioactivity and the Ionosphere.

The decision was made that the Union should sponsor the following meetings planned for 1958. The names and addresses in brackets are those of persons or organizations able to give information about these meetings.

The meeting on Magnetism, planned at New Delhi in January 1958, is postponed.

1. 6-9 May 1958, Brussels 'Optics in Metrology'.

(Comité Belge d'Optique, 128 rue de Sport, Ghent.)

2. 19-26 May, Leningrad 'Mechanical Properties of Non-Metallic Solids'.

(Professor M. V. Volkenstein, Head of the Laboratory of the Institute of Polymers of the Academy at Leningrad.)

3. 2-7 June, Brussels 'Physics of the Solid State and its applications to Electronics and Telecommunications'.

(Société Belge de Physique, Loverval, Belgium.)

4. 23-28 June, Leiden 'Very Low Temperatures'.

(Professor C. J. Gorter, Nieuwsteeg, Leiden, Netherlands.)

5. 30 June-5 July, Geneva (Switzerland) 'High Energy Nuclear Physics'.

(CERN, Aéroport de Cointre-Clessin, Geneva.)

6. 2-5 July, Grenoble 'Ferro- and Antiferromagnetism'.

(Professor L. Néel, Institut Fourier, Place du Doyen Gosse, Grenoble.)

7. 7-12 July, Paris 'Radioactivity and Nuclear Physics' (provisional title).

(M. F. Netter, C.E.N., B.P. N° 2, Gif-sur-Yvette, Seine-et-Oise, France.)

8. 25-29 July, Paris 'Chromatic Discrimination' in co-operation with the Unions of Biology (organizer of the Conference), of Physiology and Biochemistry.

(Professor H. Pieron, Collège de France, Place M. Berthelot, Paris V°.)

9. 18–22 August, Rochester (N.Y.) ‘Semiconductors’.  
(Dr. Malcolm H. Hebb, General Electric Research Laboratory,  
P.O. Box 1088, Schenectady, N.Y., U.S.A.)
10. 25–29 August, Geneva (N.Y.) ‘Electronic Properties of Metals at Low  
Temperatures’.  
(M. D. Fiske, Planning Committee, P.O. Box 1088, Schenectady,  
N.Y., U.S.A.)

The General Assembly discussed the role of the Union in respect to the progress of physics in under-developed countries. The matter is under consideration. It also recognizes the great importance of international summer schools in physics.

For all further information application may be made to the Secretaries of the conferences mentioned above. For information about the general activities of the Union, application may be made to its Secretary General: 3 Boulevard Pasteur, Paris XV<sup>e</sup>.



## REVIEWS OF BOOKS

*Handbuch der Physik*, Vol. XX. *Electrical Conductivity II*, edited by S. FLÜGGE. Pp. vii+491. (Berlin : Springer, 1957.) 112 DM.

Volume XX of the new *Handbuch der Physik* contains four articles on the properties of non-metallic solids, differing widely in scope and method of treatment but each valuable in its own way. The most ambitious contribution is that on semiconductors by O. Madelung (in German), which occupies the first half of the volume and forms, in effect, a new and welcome monograph on the subject. It is an indication of how vast the subject of semiconductors has grown nowadays that, in spite of the length of the article, a considerable amount of selection has been necessary. Taking as his excuse, perhaps, the title of the volume, the author has subordinated the treatment of the optical and magnetic properties to the discussion of conductivity questions, which are considered at a length that at times seems a little excessive in the pursuit of the predictions of particular models and the preoccupation with formulae for particular geometrical configurations. However, in a subject that has not always been free from slipshod argument and idle speculation, it is good to see the mathematical consequences of the basic assumptions clearly and fully set out and the implications pursued to their logical conclusion. In this respect the article forms a worthy successor to a number of illustrious predecessors among German *Handbuch* articles. The main chapters deal, in turn, with general conductivity theory, non-equilibrium processes in homogeneous semiconductors, the properties of p-n junctions and of surfaces and contacts. (It is interesting to see that the different types of transistor now seem to fall quite naturally into their rightful places in the general development of semiconductor theory.) Two useful concluding chapters review the determination of the most important semiconductor parameters and the properties of the most important semiconducting substances.

The second article is by A. B. Lidiard on ionic conductivity, and represents a remarkable achievement of a different sort. In dealing at shorter length with a much more circumscribed topic, the author has (to quote his words) "aimed to expose the principles which lie behind the elucidation of the mechanism of ionic conduction and the determination of the concentration and properties of isolated lattice defects". This programme is carried out in three main parts, the first dealing briefly with the classical experiments on the transport of matter to the electrodes, the second describing the work on the magnitude of the conductivity of pure salts and of salts containing small known amounts of aliovalent impurities, and the third discussing measurements of diffusion coefficients and their relation to electrical conductivities. Topics such as mechanical effects and the influence of high energy radiations have been deliberately excluded, as being insufficiently well understood to add anything significant to the main theme of the article. In showing, in a beautifully clear, tightly argued and elegantly phrased account, how our understanding of the properties of lattice defects in solids has been advanced by studies of the sort described, the author has performed a valuable service to a subject which in clarity and coherence have not hitherto been particularly conspicuous features,

In a short third article J. M. Stevels discusses the electrical properties of glass. The concern here is with a type of ionic conduction whose great technological importance is matched by the imperfection of our understanding of the processes at work. Even so, the author succeeds in showing that many of the complications of the observed behaviour can be understood in principle in terms of the simple 'network' picture of the glassy state; but it is clear that there will have to be much further effort in this interesting field before the subject can become the theme of an article like that by Lidiard.

The last article, by E. Darmon (in French), deals with electrochemistry. It is concerned partly with the properties of electrolytes and partly with the double layer, including electrocapillarity and electrokinetic phenomena. The treatment is scholarly and deals, almost in textbook fashion, primarily with well-established facts and theories; it should serve as an excellent introduction to topics of current interest such as the importance of electrochemistry for biological processes.

The volume concludes with a *Sachverzeichnis* (Deutsch-Englisch), coupled with a Subject Index (English-German). These useful glossaries are followed by a 'Table des matières pour la contribution écrite en français'. It can only be hoped that the strange exclusion of French from the Anglo-German embrace does not represent a disquieting symptom of any kind. E. H. SONDEHEIMER.

*Progress in Semiconductors*, Volume 2, by A. F. GIBSON, P. AIGRAIN and R. E. BURGESS. Pp. vii+280. (London: Heywood, 1957.) 63s.

The first volume of the series has been reviewed in this journal (*Proc. Phys. Soc. B*, **70**, 632). The second volume follows essentially the same lines. There is again one article on luminescence, this time on the theories of electroluminescence by D. Curie of the Laboratoire de Luminescence, Faculté des Sciences, Paris. All other articles deal with semiconduction in the narrower sense.

F. Herman, M. Glicksman and R. H. Parmenter (R.C.A.) present a paper on Semiconductor Alloys, such as Si-Ge and ZnS-ZnSe alloys. Intermetallic compounds are covered by a report by F. A. Cunnell and E. W. Saker of the Services Electronics Research Laboratory, Baldock, on the Properties of the III-V Compound Semiconductors. Recent work on radiation damage is reviewed by J. H. Crawford, Jr. and J. W. Cleland of the Oak Ridge National Laboratory in a paper entitled Radiation Effects in Semiconductors. A. Rose, now in the R.C.A. Laboratories in Zurich, has contributed a paper on Lifetimes of Free Electrons and Holes in Solids, in which he attempts to present a unified theory. The Production of High-Quality Germanium Single Crystals is explained by L. G. Cressell and J. A. Powell of the Marconi's Wireless Telegraph Company Ltd. in Chelmsford; the authors give preference to horizontal growth as against the more usual Czochralski technique. An article by W. Crawford Dunlap, now with Bendix Aviation Corporation Research Laboratories, Detroit, on Impurities in Germanium, deals mainly with the less well-known impurities. Finally, J. B. Gunn, now at the University of British Columbia in Vancouver, in a paper on High Electric Field Effects in Semiconductors discusses the

important effects, and their causes, which arise if the electric fields inside semiconductors are higher than the first order theory allows for.

The reports are very much up-to-date: most contributions have references up to 1957, in addition to references to private communications and work in the press or to be published. (The reviewer also noted some omissions.) As a result, the reports will greatly assist any worker in catching up with the literature in his special field. On the other hand the volume makes neither inspiring, nor easy reading, even for a physicist with a good general background in semiconductors. He will find many passages obscure, and will often feel ashamed of his ignorance. He will also find a good deal of theorizing without obvious relation to either facts or basic ideas. But, presumably, this is unavoidable in a book aimed at the specialist who has to keep abreast of the developments but cannot read more than a small fraction of the hundreds of papers on semiconductors and allied subjects published every year. The volume thus has a strictly professional appeal, which in fact is very strong. But the 'general reader' will barely profit by perusing it.

W. E.

*Physical Properties of Crystals*, by J. F. NYE. Pp. xi + 322. (Oxford: Clarendon Press, 1957.) 50s.

The basic approach of this textbook on crystal properties is indicated by the subsidiary title 'Their representation by tensors and matrices'. It has developed from a course given by the author to second-year undergraduates studying crystallography at Cambridge, but in its present form it will also be useful to more advanced students entering the domain of solid state physics.

The book is neatly divided into four parts. In the first the groundwork is laid in an account of the properties of tensors, up to those of second rank (not all readers are likely to support the author when he replaces the usual term 'order' by 'rank', which already has a specialized meaning in relation to matrices, but this is a minor criticism). This introduction, though not lengthy, is admirably clear and well suited to the subject, and among other things it is pleasing to find a lucid distinction being made between polar and axial vectors. The mathematical background is not complete, in the sense that the reader is expected, or well advised, to know something about point and space groups and the symmetry classes of crystals, although a great deal of information about these is summarized in appendices.

Part 2 deals with the equilibrium properties of crystals, starting with magnetic susceptibility and electric polarization, proceeding to the stress and strain tensors and thermal expansion, and then with the introduction of third and fourth order tensors, to piezoelectricity and elasticity. The value of rectangular matrices as an alternative to the higher order tensors is discussed and illustrated by examples, and the relevant thermodynamics briefly presented. In part 3, transport properties, thermal and electrical conductivity and thermoelectricity are covered; and in part 4, crystal optics, including optical activity.

There are many things which commend this book to the reviewer, not himself an expert in crystallography. Not the least is Dr. Nye's very clear and pleasant style of writing, but there are also the economy of mathematics, the summaries



after each chapter, the numerical examples, and the exercises, with brief notes on the solutions. Altogether, it is an elegant and orderly introduction to what is, from the structural aspect, an elegant and orderly subject. R. A. BUCKINGHAM.

*Applied Probability*, edited by L. A. MACCOLL (Proceedings of the Seventh Symposium in Applied Mathematics). Pp. vi+104. (New York: McGraw-Hill, 1957.) \$5.00.

This book contains a very valuable collection of papers presented at the Seventh Symposium in Applied Mathematics, held at the Polytechnic Institute of Brooklyn in 1955. Its present title is, however, somewhat misleading, for probability has important applications in industry, electrical engineering, and biology that are not considered; moreover, some of the papers, especially those classified under diffusion theory, come more under the title of 'mathematical probability', part of the original title of the symposium, than under 'and its applications', the rest of the original title. The three principal themes are, however, explained in the editor's preface, these being, in addition to diffusion theory (treated in an abstract sense), the theory of turbulence and probability in classical and modern physics. The individual titles and authors are sufficiently imposing to be listed in full. They are: 'Brownian motion depending on  $n$  parameters: the particular case  $n=5$ ', by P. Lévy; 'A new look at the first boundary value problem', by J. L. Doob; 'On boundaries defined by stochastic matrices (abstract)', by W. Feller; 'On the application of functional calculus to the statistical theory of turbulence', by E. Hopf; 'Stochastic processes of astronomical interest', by G. Münch; 'The singularity in the spectrum of homogeneous turbulence', by G. K. Batchelor; 'Probability in classical physics', by M. Kac; 'Infinite models in physics', by S. M. Ulam; 'Quantum theory and the foundations of probability', by B. O. Koopman.

The papers classified under the last two of the three main themes are of special interest to applied mathematicians and theoretical physicists, those which the reviewer found particularly informative being the turbulence paper by Batchelor and the statistical mechanics paper by Kac. The latter paper was more of a general survey of its field than Batchelor's, but both combined the presentation of definite results with a clear explanation of their physical meaning. Survey volumes of the present kind seem very useful in looking at topics rather farther back than research workers sometimes manage to do, and also in introducing a subject to those not actively researching in it. However, for the latter purpose especially, bibliographies or at least references to bibliographies, are important, and these did not always seem adequate. Ulam, for example, was concerned with possible infinite physical systems not classifiable under the usual dichotomy of particulate or continuous systems, but it would surely have been of some relevance to refer to some of the more orthodox models discussed in recent years by other writers (for example, models known as one-dimensional fluids and the like). The concluding paper by Koopman was a very clear, though rather 'negative', exposition of the logical relation of probability laws to the events of quantum mechanics; no discussion of *why* the events are governed, by, say, the wave equation, in the way they are, was attempted.

M. S. BARTLETT.



*Particulate Clouds—Dusts, Smokes and Mists*, by H. L. GREEN and W. R. LANE.  
Pp. xv+425. (London: Spon, 1957.) 70s.

There can be few industries in which the subject matter of this book is of no concern. The properties and behaviour of particulate clouds, their production, sampling and measurement, deposition and filtration, and their transport in the atmosphere are of interest and importance in so many fields of science and technology that it is not surprising that they have been investigated from many rather different points of view and that the considerable advances made in the last thirty years are scattered in a wide range of publications. The literature of the subject, vast, sprawling with little shape or coherence has become impossible.

The authors of this splendid book have therefore performed a valuable service in providing an integrated and synthesized account of the physics and physical chemistry of aerosols, and of the techniques used for their production and investigation.

The book is divided into two parts. The first part deals with the basic physics of individual suspended particles in gases, and of clouds of particles, with special reference to their formation, stability, optical properties, measurement and aerodynamics. The second part deals with the industrial and environmental aspects of aerosols such as the health hazards of industrial dusts, atmospheric pollution, the dispersal of insecticides and the formation of natural clouds and rain. Here the aim is not to give an exhaustive account of these topics, each of which requires a book in itself, but to illustrate the practical applications of the scientific principles established in Part I.

The text, which is lucidly written, carries the authority of two scientists who have themselves made major contributions to the subject over many years and who have brought to the task first-hand knowledge of the many diverse problems with which they deal.

This book, which is well produced, at a reasonable price, is likely to serve as a standard text for many years. It is highly recommended. B. J. MASON.

*Colloque National sur l'Optique Moléculaire et la Physicochimie Structurale*, report of meetings arranged by LA SOCIÉTÉ FRANÇAISE DE PHYSIQUE ET LA FACULTÉ DES SCIENCES DE BORDEAUX. Pp. 95. (Paris: Éditions de la Revue D'Optique Théorique et Instrumentale, 1956.) 500 fr.

This book of 95 pages is a collection of 39 papers delivered at meetings held in Bordeaux in May 1956. The meetings were arranged by la Société Française de Physique et la Faculté des Sciences de Bordeaux. The papers form two main groups dealing with molecular optics and structural physical chemistry respectively. In the first group are papers on ultra-violet and infra-red absorption, scattering of light (Rayleigh and Raman effects) and molecular luminescence: some aspects of magnetism and x-rays are included in the second group. The papers are short but the subject matter will be readily intelligible to those well acquainted with such work and much of value will be found by the careful and interested reader. Possibly the most valuable aspect of the book is that it gives the reader who was not able to be present at the conference an opportunity of learning about some of the recent work of French scientists in these fields. All

the papers are in French, each paper contains a number of recent references and there are subject and author indexes. In a few cases the graphs suffer in clarity by the omission of the units of the quantities plotted but in general the book is well produced with clear diagrams and tables.

H. G. JERRARD.

*Transducers and Magnetic Amplifiers*, by A. G. MILNES. Pp. ix + 286. (London: Macmillan, 1957.) 63s.

A 'transducer' is a coil with an iron core, the inductance of which may be varied by changing the saturation of the iron by means of a separate control winding. This simple possibility has been the basis for the development during the last two decades of a large variety of devices for the regulation and control of electric currents. A main group of these are the 'magnetic amplifiers' that are making an important and increasing contribution in the development of automatic control systems.

Analysis of the behaviour of such devices presents great difficulties, since their action depends essentially on the non-linear relationship between flux and m.m.f. in iron including saturation, hysteresis and the effects of eddy currents. No general analysis of much use has been devised, but each of the multitude of possible arrangements must be considered separately and its possibilities explored by detailed examination, often guided by experimental observation. Once the general mode of operation has been clarified, useful quantitative relationships emerge by the use of quite elementary mathematics.

Dr. A. G. Milnes has made many contributions to such developments and his own papers are an important item in the extensive and scattered literature on the subject. He has acquired both a remarkable insight into the possibilities and also the knack of presenting the principles with as much clarity as their complexity permits. He has now produced a well-written book in which the large number of related but distinct circuits and devices are described and discussed. In this he has succeeded in being clear without using excess of words and with the help of abundant well-arranged diagrams. The book will be valued both as an excellent textbook and as a work of reference.

Early chapters develop an account of magnetic amplifiers, progressively introducing the effects of finite permeance, feeds back, load characteristics, smoothing devices and push-pull combinations. There are chapters on three-phase magnetic amplifiers and on combinations of magnetic amplifiers with valves and transistors, and brief accounts of many representative applications.

The book is excellently produced, and includes many full-page photographic plates illustrating arrangements of elements, panels and devices of various kinds. No doubt these have contributed to the rather high cost of the book, but are justified in that they are well chosen to be of use to designers besides introducing a flavour of engineering reality to the work as a textbook.

Dr. Milnes' book will meet a need that has been felt by teachers, research workers and designers. He is to be congratulated in success in the difficult task of giving a lucid, orderly and compact exposition of such extensive and complex material.

A. TUSTIN.

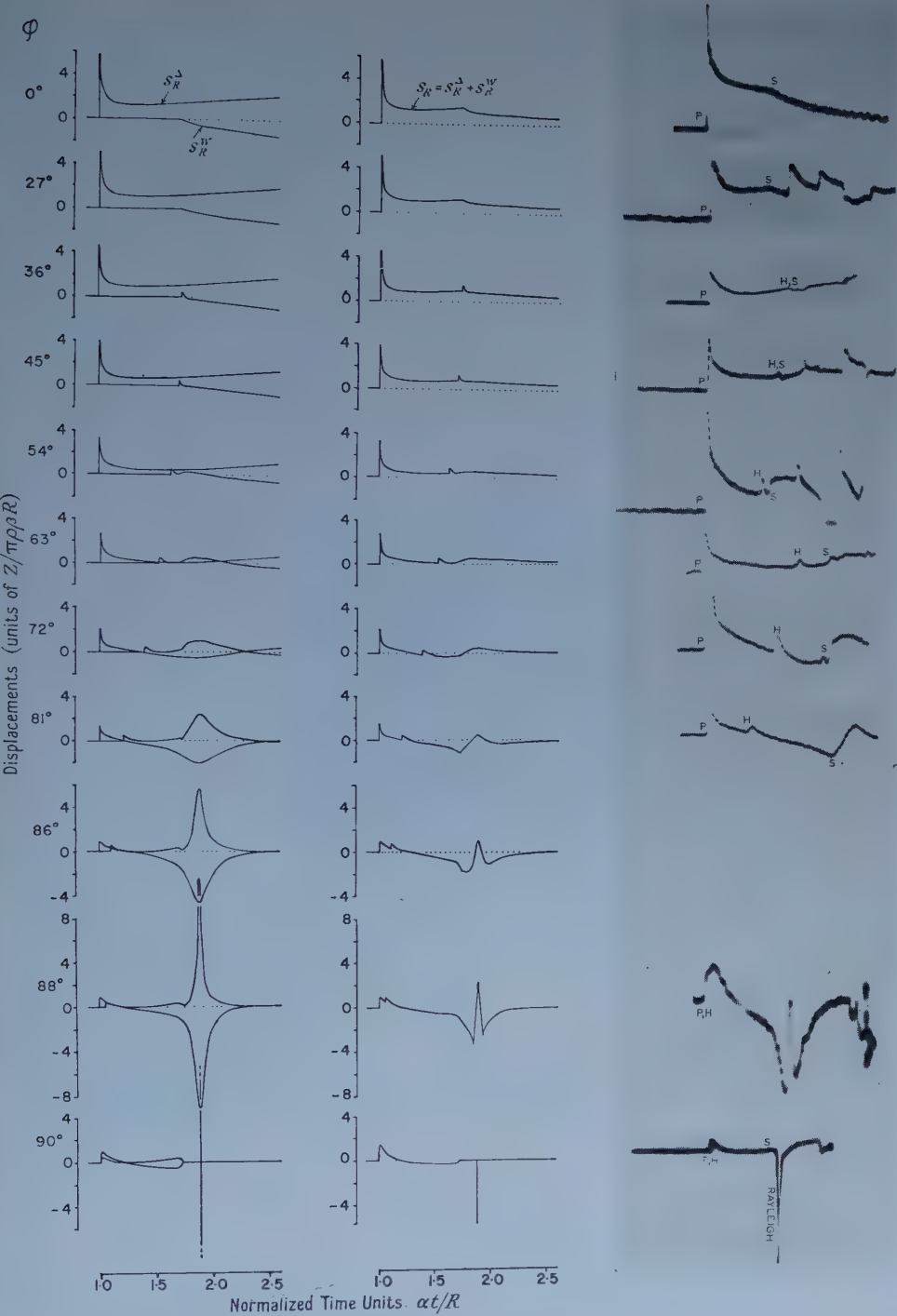


Figure 4. Theoretical and analogous experimental radial displacements due to an impulsive force acting normally to the surface of the semi-infinite medium.

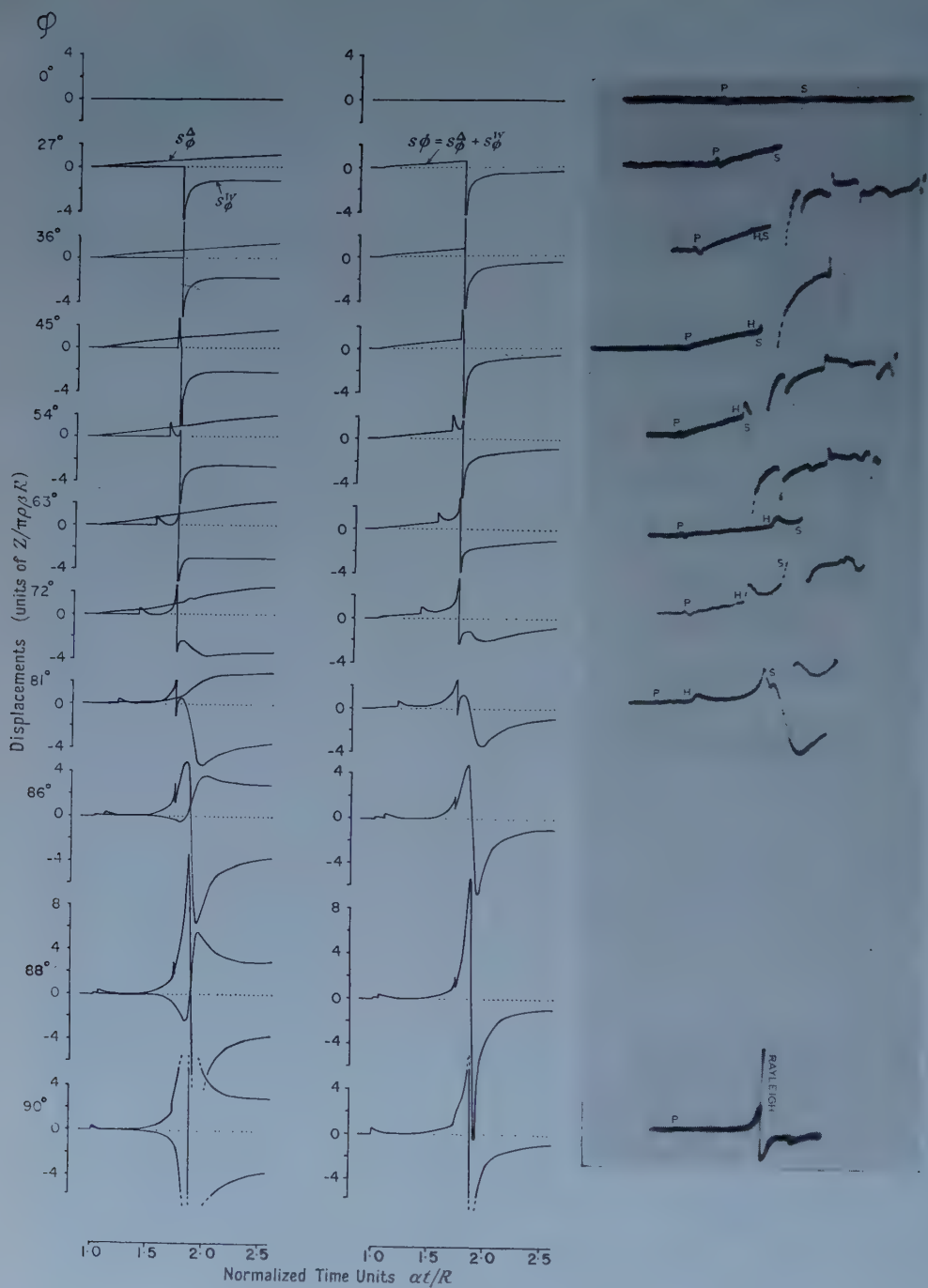


Figure 5. Theoretical and analogous experimental tangential displacements due to an impulsive force acting normally to the surface of the semi-infinite medium.



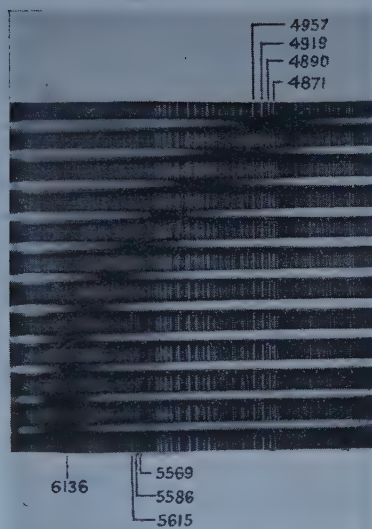


Figure 5. Position against load of dark band  $n=1$ .



## Nuclear Cross Sections for 765 Mev Neutrons

By N. E. BOOTH, G. W. HUTCHINSON AND B. LEDLEY

Department of Physics, University of Birmingham

*Communicated by P. B. Moon; MS. received 8th October 1957, and in final form  
14th November 1957*

**Abstract.** Total cross sections have been measured for the elements H, D, Li, C, O, Al, Cu, Sb and Pb and absorption cross sections for C, Al, Cu and Pb for neutrons of an effective energy of  $765 \pm 30$  Mev. The neutrons were detected by observing the Čerenkov light from charged secondaries produced in a cylinder of Perspex. Large corrections must be applied to the measured absorption cross sections and these are strongly dependent upon the differential cross section assumed. The results are compared with an optical model with a potential distribution indicated by electron scattering measurements, and with an imaginary central potential and a real spin-orbit potential. The results can be adequately represented by assuming that at this energy the imaginary potential is given by the free nucleon-nucleon total cross sections and that the nuclear potential size and shape agree with the charge density size and shape. The spin-orbit coupling parameter required to fit the results is somewhat less than that found at lower energies.

### § 1. INTRODUCTION

THE measurement of total and absorption cross sections for high energy nucleons is mainly of interest for the information obtainable concerning nuclear size and transparency and their relation to nuclear forces. The results have been generally interpreted in the light of the uniform optical model of Fernbach, Serber and Taylor (1949) or one of its later modifications. The uniform optical model of the nucleus is a homogeneous sphere of nuclear matter with an absorption coefficient  $K$  and an index of refraction  $n = (k + k_1)/k$  where  $k$  is the wave number of an incident nucleon outside the nucleus and  $k + k_1$  is its wave number inside. This is equivalent to describing the interaction by means of a complex potential. The index of refraction is given by the real part and the absorption coefficient by the imaginary part of the potential.

The physical basis of the optical model for complex nuclei has been considered by Watson (1957) and others and it is shown that multiple scattering of an incident wave by the individual nucleons leads to such an interaction potential. The optical model is only the first step in the theory of nuclear reactions. It attempts to predict only the elastic and absorption parts of the nuclear reactions and tells us nothing of the details following an absorption event.

The uniform optical model gives reasonable fits to experimental data on a series of elements at a given bombarding energy (for example, Booth, Ledley, Walker and White 1957) but there seems to be little correlation between the nuclear radii obtained at different energies and with different bombarding particles.

Furthermore, recent electron scattering and other results have shown that the square well is unrealistic and that the potential should have a tapered edge of thickness of the order of  $2$  to  $3 \times 10^{-13}$  cm (Hofstadter 1956).

The proton density distributions indicated by the electron scattering results (i.e. for the heavier elements the Fermi distribution) have been used to fit experimental data. An analysis by Williams (1955) of neutron absorption cross sections at 1400 mev and proton absorption cross sections at 860 mev indicates that at these energies the nuclear potential distribution has the same size as the charge distribution. On the other hand, even with the Fermi distribution, the nuclear radii obtained from the low energy nucleon scattering (Woods and Saxon 1954) are considerably larger than the charge distribution radii indicated by the electron scattering measurements. However, Harris and Jastrow (paper read at the Physical Society Nuclear Physics Conference 1957) have found that the charge distribution radii fit the nuclear scattering results both at 310 mev and at low energies. It is not clear whether there is an actual discrepancy although arguments have been put forward that a genuine difference should be expected (see, for example, Johnson and Teller 1954, Drell 1955 and Brueckner 1956).

With regard to the situation at high energies Brown (1957) has developed a high energy approximation which indicates that at approximately 1 gev the nucleon density and nuclear potential distributions are the same, the corrections for the finite range of nuclear forces being negligible. Brown has further shown that at high energies the central part of the potential should be mainly imaginary. In addition a real spin-orbit potential with radial dependence  $(1/r)[dV_c(r)/dr]$  should be assumed, where  $V_c(r)$  is the central potential. This is required to fit polarization data (Levintov 1956) and, as will be seen, is required to fit our measured total cross sections if we assume that the central potential has no real part.

The present paper describes the measurement of total and absorption cross sections of complex nuclei for neutrons of an effective energy of 765 mev and attempts to consider the results in terms of the optical model picture.

Similar experiments in the gev range have included the measurement of total and absorption cross sections for 1400 mev neutrons (Coor, Hill, Hornyak, Smith and Snow 1955) and for 650 mev (Moskalev and Gavrilovskii 1956), 860 mev (Chen, Leavitt and Shapiro 1955) and 895 mev protons (Booth, Ledley, Walker and White 1957). Total cross sections have also been measured by Dzhelepov, Satarov and Golovin (1955) with 500, 590 and 630 mev neutrons.

## § 2. NEUTRON BEAM AND APPARATUS

The neutrons were produced by allowing the circulating proton beam of the Birmingham synchrotron to strike a 3 in. thick Be target placed near the inside wall of the vacuum chamber. Two neutron beams, at  $3^\circ$  and  $6^\circ$  to the direction of the circulating beam, were collimated with lead and concrete as shown in figure 1. The  $6^\circ$  beam was used only for monitoring and had a cross section of 5 cm by 5 cm. The  $3^\circ$  beam was used for the cross section measurements and was usually 5.1 cm in diameter at the emergent end of the collimator, although for some experiments a 2.5 cm diameter beam was used. Filters of up to  $80 \text{ g cm}^{-2}$  of Pb were placed in the beams to absorb  $\gamma$ -rays produced in the Be target.



$C_1$  and  $C_3$  are plastic scintillators  $\frac{1}{2}$  in. thick and 3 in. and 5 in. diameter and are connected in anticoincidence with  $C_2$  and  $C_4$  respectively.  $C_2$  consists of a polished cylinder of Perspex 5 cm in diameter by 30 cm long, the farther end of which is viewed by a Du Mont 6292 multiplier.  $C_4$  is a similar cylinder of Perspex 10 cm in diameter by 50 cm long viewed by a Du Mont 6364 multiplier and has been described fully elsewhere (Booth and Ledley 1957). High energy incident neutrons produce energetic charged secondary particles in the Perspex, and some of the Čerenkov light produced is detected by the photomultipliers.

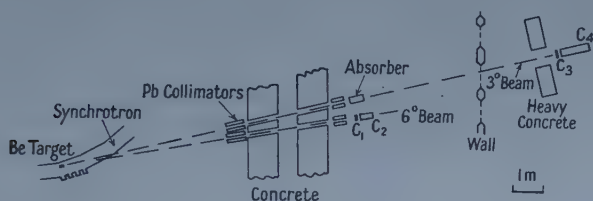


Figure 1. Experimental arrangement for the total cross section measurements.

The ends of both cylinders facing the beam were roughened and blackened to reduce the light collection efficiency for background particles.

The threshold energy in Perspex for Čerenkov light from protons is about 325 mev but, by setting a discrimination level so as to accept only those pulses above a given height, the effective threshold may be made considerably higher. The dependence of the efficiency of the neutron detector  $C_4$  on neutron energy and discrimination level have been determined (Booth and Ledley 1957). The discrimination level was checked before each run by gating the pulses from  $C_4$  with the anticoincidence  $\overline{C}_3C_4$  and measuring the cut-off voltage on a kicksorter. With the particular discrimination level used the effective neutron energy was 765 mev if the neutron spectrum was assumed to be peaked at the high energy end, as has been indicated by spectrum measurements at lower energies (Goodell, Loar, Durbin and Havens 1953, Flyagin 1954). If a flat spectrum is assumed, the effective neutron energy, weighted by the detector efficiency and by the variation of cross section with energy ( $\sim 8\%$  increase between 500 and 900 mev), is 745 mev. Since the first assumption is probably more valid we have taken the effective neutron energy to be  $765 \pm 30$  mev.

The outputs of the counters were amplified by 100 Mc/s amplifiers. The anticoincidences  $\overline{C}_1C_2$  and  $\overline{C}_3C_4$  were formed and scaled with resolving times of 0.25 microsecond.

### § 3: MEASUREMENT OF TOTAL CROSS SECTIONS

The experimental arrangement for the total cross section measurements is shown in figure 1. The distance from the absorber to the detector  $C_4$  was about 7.5 m. Before each run horizontal and vertical plots were made across the beam and the detector was positioned on the beam centre. To obtain zero delay for the anticoincidence and to check its operation the lead filters were removed from the  $3^\circ$  beam and a 1 cm thickness of lead was placed directly in front of  $C_3$  in order to convert a large fraction of the  $\gamma$ -rays and increase the charged particle

contamination in the beam. A typical anticoincidence delay curve is shown in figure 2. The background, determined by placing a 50 cm thickness of heavy alloy (density  $18 \text{ g cm}^{-3}$ ) in front of the collimator of the  $3^\circ$  beam was about 3% of the unattenuated beam.

The transmission through a given absorber is given by

$$T = \frac{I - I_b}{I_0 - I_b}$$

where  $I$  is the ratio of the number of counts  $\bar{C}_3 C_4$  to  $\bar{C}_1 C_2$  with the absorber in position,  $I_0$  with no absorber present and  $I_b$  with the heavy alloy blocking the collimating channel. Each day's run consisted of a series of cycles; no absorber,

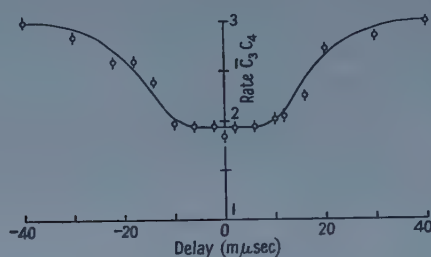


Figure 2. Delay curve for  $\bar{C}_3 C_4$  anticoincidence.

absorber in, background, no absorber, absorber in, etc. This procedure minimized the effect of any systematic drifts of the electronic equipment. At least six cycles were taken for each absorber. The relative counting times for  $I$ ,  $I_0$  and  $I_b$  were chosen so as to minimize the statistical uncertainty of  $T$  for a given overall counting time. In each cycle about 2500 counts  $\bar{C}_3 C_4$  were recorded for  $I$ . With the lead filters in position the charged particle contamination, determined by disconnecting  $C_3$ , was less than 3%. Thus it is not important that the anticoincidence counter  $C_3$  should be 100% efficient, although its efficiency was measured and found to be not less than 98%.

The  $\gamma$ -ray contamination of the beam was checked by measuring the transmission of lead as a function of thickness. A semi-log plot of transmission against absorber thickness was linear within the experimental error of 2% indicating that there was no significant contribution to the counting rate from  $\gamma$ -rays.

The hydrogen cross section was obtained from carbon-polythene difference and the deuterium cross section from heavy water-ordinary water difference. The oxygen cross section was obtained from the hydrogen cross section and the cross section for water. In other cases the absorbers were pure elements. The absorber thickness ranged from one quarter to one mean free path and were measured to 0.2%.

The measured cross section is given by

$$\sigma = - \frac{A}{Nx} \ln T \text{ cm}^2 \quad \dots\dots(1)$$

where  $x$  is the absorber thickness in  $\text{g cm}^{-2}$ ,  $A$  is the atomic weight and  $N$  is Avogadro's number. Table 1 shows the measured cross sections. The errors quoted are standard deviations. The r.m.s. deviations of the results of the individual cycles from their collective means were always less than 1.5 times

and usually less than 1.2 times the deviations expected from the individual internal errors.

Table 1. Total Cross Sections

Element	Corrected $\sigma_t$ (mbn)
H	$34.4 \pm 1.6$
D	$68.8 \pm 2.8$
Li	$221.2 \pm 4.7$
C	$342.1 \pm 3.7$
O	$460.7 \pm 6.0$
Al	$660.2 \pm 7.3$
Cu	$1310 \pm 24$
Sb	$2149 \pm 74$
Pb	$3106 \pm 45$

The cross sections tabulated in table 1 contain two small corrections. The first is due to the fact that the detector subtends a finite effective solid angle ( $\sim 1.0 \times 10^{-4}$  steradian) at the centre of the absorber and neutrons diffracted into this solid angle do not miss the detector. The second correction is due to the fact that an estimated 16% of the unattenuated beam normally misses the detector due to the divergence of the beam and scattering inside the walls of the collimator. However, this 16% is intercepted by the absorbers and some of the neutrons diffracted there reach the detector. Both these corrections were made by using the optical relation

$$\mathcal{I}f(0) = (k/4\pi)\sigma_t$$

where  $\mathcal{I}f(0)$  is the imaginary part of the forward scattering amplitude and  $k$  is the incident neutron wave number. It was assumed that  $\mathcal{I}f(0) = f(0)$ , so that the first correction is given by

$$\Delta\sigma = (k/4\pi)^2 \sigma_t^2 \Delta\Omega$$

where  $\Delta\Omega$  is the solid angle subtended by the detector at the centre of the absorber. The second correction is just 0.16 times this. In all cases the corrections are less than the statistical uncertainty, and they are negligible for the lighter elements.

#### § 4. MEASUREMENT OF ABSORPTION CROSS SECTIONS

For the measurement of absorption cross sections, one would like, ideally, to detect all the diffraction scattered neutrons and exclude all inelastically scattered neutrons. A separation is possible firstly because of the nature of the inelastic processes and secondly because of the relatively small angular spread of the diffraction scattered neutrons. However, even at the energy of this experiment, part of the diffraction patterns for the light elements extends beyond the acceptance angle of the detector. A further complication arises because, even for small angles, the efficiency of the neutron detector depends upon angle, and to correct accurately for this one must know the shape of the diffraction pattern.

'Poor-geometry' measurements were made in one or two positions for the elements C, Al, Cu and Pb. The uncorrected cross sections are shown in table 2.

Large corrections have been applied to these results to take account of the above-mentioned effects.

Measurements of the diffraction scattering of protons on carbon performed in this laboratory (Batty and Goldsack 1957) indicate that the differential cross section may be fitted by a suitably normalized black disc diffraction pattern, at least as far as the first diffraction minimum. We have therefore assumed for the corrections that

$$\frac{d\sigma_d}{d\Omega} = \frac{\sigma_d}{\pi} \left[ \frac{J_1(kR \sin \theta)}{\sin \theta} \right]^2.$$

For  $R$  we have used the values given by  $(\sigma_t/2\pi)^{1/2}$ . These values should be sufficiently accurate for the corrections. Since we know  $\sigma_a$  approximately, we can find  $\sigma_d = \sigma_t - \sigma_a$ , make the correction and continue by successive approximations to find the corrected values of  $\sigma_a$  and  $\sigma_d$ .

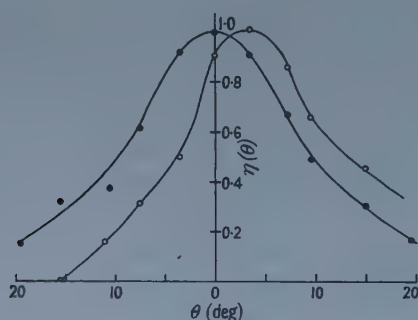


Figure 3. Angular dependence of the efficiency  $\eta(\theta)$  of  $C_4$  for 765 mev neutrons, measured with a 2.5 cm diameter beam. The open circles are for the case when the beam enters  $C_4$  at 2.5 cm off axis.

Table 2. Absorption and Diffraction Cross Sections (mbn)

(1)	(2)	(3)	(4)	(5)	(6)
			$\sigma_a$	$\sigma_d$	
C	9	$278 \pm 25$	$172 \pm 25$	$170 \pm 25$	$197 \pm 25$
	16	$270 \pm 18$	$198 \pm 18$	$144 \pm 19$	$220 \pm 18$
Al	14	$501 \pm 10$	$392 \pm 10$	$268 \pm 12$	$435 \pm 10$
Cu	16	$906 \pm 23$	$742 \pm 23$	$568 \pm 33$	$822 \pm 23$
Pb	7	$2118 \pm 62$	$1679 \pm 62$	$1427 \pm 77$	$1888 \pm 62$
	16	$2035 \pm 62$	$1771 \pm 62$	$1335 \pm 77$	$1923 \pm 62$
					$145 \pm 25$
					$122 \pm 18$
					$225 \pm 12$
					$488 \pm 33$
					$1218 \pm 77$
					$1183 \pm 77$

(1) Element; (2)  $\theta'$  (deg); (3) uncorrected cross sections, determined directly from equation (1); (4) cross sections corrected by black disc diffraction patterns; (5) cross sections corrected assuming no elastic scattering beyond first diffraction minimum; (6) calculated cross sections  $\sigma_a$ .

In order to find the angular dependence of the efficiency of  $C_4$ , the neutron beam was collimated to 2.5 cm diameter and the counting rate in  $C_4$  was measured as a function of angle as  $C_4$  was rotated about the centre of its front face. Figure 3 shows the results of two such sets of measurements. In one case the beam entered at the centre of the front face of  $C_4$  and in the other case  $C_4$  was displaced 2.5 cm horizontally. It would have been advisable to use even finer collimation but this was not feasible with the low beam intensity available.



The correction  $\delta\sigma$  to  $\sigma_a$  is given by

$$\delta\sigma = 2\sigma_d \int_0^R [1 - \eta(d, \theta)] \left\{ \frac{J_1(kR \sin \theta)}{\sin \theta} \right\}^2 \sin \theta d\theta \quad \dots\dots (2)$$

where  $\eta(d, \theta)$  is the counting efficiency relative to  $\eta(0, 0) = 1$  for neutrons entering the front face of  $C_4$  at a distance  $d$  from the centre and at an angle  $\theta$  to the axis. This correction was about 12% for lead and 35% for carbon. The correction for double diffraction scattering was negligible for the geometry and absorber thicknesses used. Inelastically scattered neutrons also had a negligible effect.

The corrected cross sections are shown in columns (4) of table 2 together with the statistical errors.  $\theta'$  is the half-angle subtended at the centre of the absorber by the front face of  $C_4$ .

## § 5. DISCUSSION OF RESULTS

### 5.1. Total Cross Sections

Figure 4 shows our total cross sections for H, D, C, Al, Cu and Pb compared with other measurements at 410 mev (Nedzel 1954), 590 mev (Dzhelepov, Satarov and Golovin 1955) and 1400 mev (Coor, Hill, Hornyak, Smith and Snow 1955).

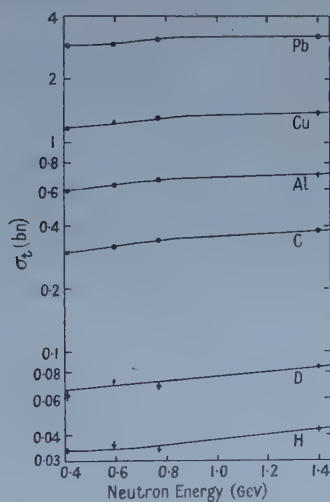


Figure 4. Total cross sections for neutrons as a function of energy: 0.410 gev (Nedzel 1954), 0.590 gev (Dzhelepov, Satarov and Golovin 1955), 0.765 gev (present experiment), 1.40 gev (Coor, Hill, Hornyak, Smith and Snow 1955).

The cross sections increase with energy due to the increase in the free nucleon-nucleon cross sections. The effect is less marked for the heavier elements as they are already considerably opaque and less sensitive to changes in the elementary cross sections.

### 5.2. Nucleon-Nucleon Cross Sections

The value  $\sigma_{np} = 34.4 \pm 1.6$  mbn measured at 765 mev indicates that the n-p total cross section is essentially constant between 400 and 800 mev. This has also been observed by Chen, Leavitt and Shapiro (1956), who measured the difference cross section, ' $\sigma_{pn}$ ' =  $\sigma_{pd} - \sigma_{pp}$ , between  $D_2O$  and  $H_2O$  using incident protons.

Similarly, the difference between our D and H cross sections gives us the neutron-neutron total cross section ' $\sigma_{nn}$ ' =  $\sigma_{nd} - \sigma_{np} = 34.4 \pm 2.6$  mbn. However, it is necessary to correct this cross section for the shielding of one nucleon by the other in the deuteron (Glauber 1955). The shielding corrections for incident neutrons and incident protons are in the ratio  $\sigma_{nn}/\sigma_{pp}$ . Since  $\sigma_{pp}$  and  $\sigma_{nn}$  are approximately equal, we have (Chen, Leavitt and Shapiro 1956)

$$\sigma_{np} - \sigma_{pn} = \sigma_{nn} - \sigma_{nn}.$$

Interpolation of the results of Chen, Leavitt and Shapiro at 740 and 830 mev gives ' $\sigma_{pn}$ ' =  $29.0 \pm 1.3$  mbn at 765 mev. Using our values  $\sigma_{np} = 34.4 \pm 1.6$  mbn and ' $\sigma_{nn}$ ' =  $34.4 \pm 2.6$  mbn we have  $\sigma_{nn} = 39.8 \pm 3.4$  mbn. This agrees within statistical error with the value  $\sigma_{pp} = 44.4 \pm 2.7$  mbn measured by Chen, Leavitt and Shapiro at 740 mev.

### 5.3. Absorption Cross Sections

Because of the large corrections to the measured absorption cross sections (discussed in §4), the corrected cross sections are sensitive to the diffraction pattern assumed, particularly to the amount of large angle scattering. This will be discussed more fully in §6, where it is noted that the black disc pattern gives too much large angle scattering for the light elements.

## § 6. OPTICAL MODEL ANALYSIS

As indicated earlier, the results of nuclear scattering experiments at high energies give nuclear radii in agreement with the electron scattering values. Furthermore, at these energies we expect the real part of the central potential to be small and the imaginary part to be determined by the free nucleon-nucleon cross sections with negligible correction for the Pauli exclusion principle (Glauber 1956). On this basis we have calculated the cross sections for C, Cu and Pb.

Following Brown (1957, and private communication) we have assumed a potential of the form

$$V(r) = V_c(r) + \alpha \mathbf{L} V_s(r) \quad \dots\dots(3)$$

where the central potential is purely imaginary, i.e.  $V_c(r) = iW(r)$ , and  $W(r) = -W_0\rho(r)/\rho_0$ , where  $\rho(r)/\rho_0$  is the density distribution given by the electron scattering results and  $-W_0$  is the potential at the origin. We take  $V_s(r) = (c_e/r)[dW(r)/dr]$  where  $c_e$  is the effective spin-orbit coupling parameter (Levintov 1956), which we have assumed to be real. The assumptions for the model are clearly rather special: however, calculations based on them may be easily generalized to include a real central potential and an imaginary spin-orbit term.

The complex phase changes, due to the two parts of the potential (3), of a neutron wave travelling parallel to the  $z$ -axis with impact parameter  $b$  are

$$\chi_1 = -\frac{E}{k} \int_{-\infty}^{\infty} V_c dz \quad \text{and} \quad \chi_2 = -\frac{E}{k} kb \int_{-\infty}^{\infty} V_s dz$$

where  $E$  and  $k$  are the incident total energy and momentum. Thus, we have

$$\sigma_a = 2\pi \int_0^{\infty} \{1 - |\exp(i\chi_1 + i\chi_2)|^2\} b db = 2\pi \int_0^{\infty} \{1 - \exp(-2\mathcal{J}\chi_1)\} b db \quad \dots\dots(4)$$

and

$$\sigma_t = \frac{4\pi}{k} \mathcal{J} f(0) = 4\pi \int_0^{\infty} \{1 - \exp(-\mathcal{J}\chi_1) \cos \chi_2\} b db. \quad \dots\dots(5)$$

Calculations were performed for C, Cu and Pb using the density distributions (Fregeau 1956, Hahn, Ravenhall and Hofstadter 1956)

$$(1) \text{ for C; } \frac{\rho(r)}{\rho_0} = \left(1 + \frac{4}{3} \frac{r^2}{a^2}\right) \exp\left(-\frac{r^2}{a^2}\right), \quad a = 1.635 \times 10^{-13} \text{ cm}$$

and

$$(2) \text{ for Cu and Pb; } \frac{\rho(r)}{\rho_0} = \left\{1 + \exp\left[\frac{(r-R)}{a}\right]\right\}^{-1}, \quad a = 0.535 \times 10^{-13} \text{ cm}$$

and  $R = 4.27 \times 10^{-13} \text{ cm}$  for Cu and  $6.38 \times 10^{-13} \text{ cm}$  for Pb.

For the nucleon-nucleon cross sections we have used our value of 34 mbn for  $\sigma_{np}$ . For  $\sigma_{nn}$  we have taken the weighted mean of our value of 39.8 mbn and the value of  $\sigma_{pp} = 45.3 \text{ mbn}$  interpolated from the measurements of Chen, Leavitt and Shapiro (1956), i.e.  $\sigma_{nn} = 43 \text{ mbn}$ .

### 6.1. Absorption Cross Sections

Our calculated values of  $\sigma_a$  for C, Cu and Pb are shown in table 2. These calculated values may be in error by 3–4% due to uncertainties in the density distribution parameters and, to a less important extent, due to the errors in the nucleon-nucleon cross sections. Considering these uncertainties the agreement in the case of Pb is satisfactory. However, the agreement for Cu is less satisfactory and for C there is a discrepancy of 20%. This discrepancy would be largely removed if, for the correction, we assumed a smaller proportion of elastic scattering beyond the first diffraction minimum than that predicted by the black disc. Calculations made by Brown (private communication) for C at 350 MeV with the present model indicate that the fraction of elastic scattering beyond the first minimum is in fact less than approximately 5% while the black disc predicts 15–20%. On very general grounds one would expect little large angle scattering from a nucleus such as C which is mainly edge, i.e. in which the surface thickness is comparable with the r.m.s. radius. In the Born approximation for the scattering there are few high momentum transfer components in this case. Thus, although the black disc pattern is a good approximation for Pb it gives too much large angle scattering for light elements.

For this reason we have recalculated the corrections to our measured absorption cross sections assuming that there is no diffraction scattering beyond the first minimum. This involves renormalizing equation (2) and integrating only to the first diffraction minimum. The cross sections corrected in this way are 10–12% larger than the cross sections corrected with the complete black disc pattern. The results are given in columns (5) of table 2 and are presented in figure 5 as a plot of  $(\sigma_a/\pi)^{1/2}$  against  $A^{1/3}$ . The lower straight line is drawn through the points corrected by the black disc patterns, while the upper line is drawn through the points calculated assuming no large angle scattering. The three points calculated from the model show the transition from the black disc approximation for the heavy elements to the situation for the lighter elements where there is little large angle scattering.

We have also calculated  $\sigma_a$  by the same model for 650, 860 and 895 MeV protons and for 1400 MeV neutrons for which measurements have been made (Moskalev and Gavrilovskii 1956, Chen, Leavitt and Shapiro 1955, Booth, Ledley, Walker and White 1957, Coor, Hill, Hornyak, Smith and Snow 1955). The values are given in table 3. In eight out of the twelve cases the measured and calculated

cross sections differ by less than 1.4 times the quoted standard deviations for the experimental results. The large differences between the values for C and Cu for 1400 mev neutrons can be explained by the fact that large corrections for diffraction scattering were made in that experiment using diffraction patterns like those from black discs. If more realistic diffraction patterns had been used for the corrections, the derived experimental values would have been higher. The discrepancies of 2.5 standard deviations for Pb at 650 mev and 4.7 standard deviations for Cu at 860 mev are unexplained.

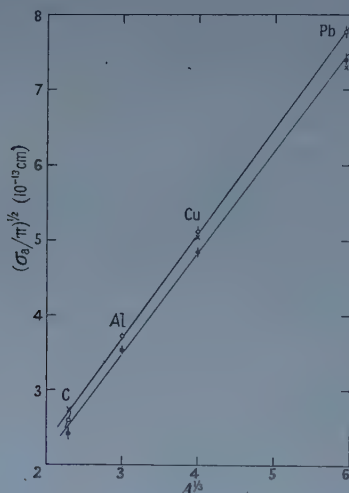


Figure 5. Plot of  $(\sigma_a/\pi)^{1/2}$  as a function of  $A^{1/3}$ . The closed circles are the values of  $\sigma_a$  corrected with black disc diffraction patterns: the open circles are the values assuming no scattering beyond the first diffraction minimum: the crosses represent the calculated values.

Table 3. Absorption Cross Sections (mbn)

Element	650 mev protons		860 mev protons		895 mev protons		1400 mev neutrons	
	Calc.	Meas.	Calc.	Meas.	Calc.	Meas.	Calc.	Meas.
C	227	$227 \pm 12$	242	$209 \pm 22$	243	$230 \pm 20$	252	$201 \pm 13$
Cu	790	$850 \pm 50$	808	$728 \pm 17$	808	$740 \pm 52$	833	$674 \pm 34$
Pb	1650	$1930 \pm 110$	1673	$1680 \pm 40$	1673	$1660 \pm 50$	1712	$1727 \pm 45$

We may conclude that at approximately 800 mev the experimental results can be adequately represented by assuming that the Pauli principle has a negligible effect on the value of the absorption coefficient and that the nuclear potential distribution is not far different from the charge density distribution obtained by electron scattering.

With these assumptions the values of  $\mathcal{J}f_i(0) = k\bar{\sigma}/4\pi$ , the imaginary part of the average nucleon-nucleon forward scattering amplitude, and of  $K_0 = \rho_0\bar{\sigma}$  and  $W_0$  can be calculated and are shown in table 4.

Table 4

Element	$\rho_0(\text{cm}^{-3})$	$K_0(\text{cm}^{-1})$	$W_0(\text{mev})$	$\mathcal{J}f_i(0)(\text{cm})$
C	$1.65 \times 10^{38}$	$6.3 \times 10^{12}$	52	$2.2 \times 10^{-13}$
Cu	$1.69 \times 10^{38}$	$6.6 \times 10^{12}$	54	$2.2 \times 10^{-13}$
Pb	$1.78 \times 10^{38}$	$7.0 \times 10^{12}$	58	$2.3 \times 10^{-13}$



## 6.2. Total Cross Sections

Since we have assumed the spin-orbit potential to be mainly real it does not affect the absorption cross sections, but it has a strong effect on the total cross sections. Levintov (1956) found that a spin-orbit parameter  $c_e \sim 3.3 \times 10^{-27} \text{ cm}^2$  fits a wide range of phenomena in the energy range 0–315 mev. However, we find this value to be too large at 765 mev. The calculation of the total cross sections involves only the parameter  $c_e$  in addition to those used for the calculation of the absorption cross sections. We have therefore evaluated  $c_e$  to make the calculated total cross sections agree with the measured ones. The results are shown in table 5.

Table 5. Spin-Orbit Parameter

Element	C	Cu	Pb
$c_e (10^{-27} \text{ cm}^2)$	$0.90 \pm 0.05$	$0.91 \pm 0.15$	$1.25 \pm 0.06$

Although we have taken  $c_e$  to be real, it may in fact have an imaginary part. For C and Cu where  $\chi_2$  is always less than 1 we may write  $\cos \chi_2 \sim 1 - \chi_2^2/2$ . In this case if the parameter is complex,  $c = \alpha + i\beta$ , the value of the effective coupling parameter  $c_e$  found from the total cross section is approximately equal to  $(\alpha^2 - \beta^2)^{1/2}$ . The angle of maximum polarization of the elastically scattered neutrons determines  $|c| = (\alpha^2 + \beta^2)^{1/2}$ . Thus the two quantities, total cross section and angle of maximum polarization, together determine  $\alpha$  and  $\beta$ .

## § 7. CONCLUSIONS

Our results indicate that no correction is needed to  $K$  to take account of the Pauli exclusion principle and that the nuclear potential distribution follows the proton density distribution. The assumption of a negligible real part to the central potential gives agreement with experiment provided a real spin-orbit term is taken into account. The strength of the spin-orbit potential is less than that found at lower energies.

## ACKNOWLEDGMENTS

The authors wish to extend their thanks to Dr. G. E. Brown for many helpful discussions. One of us (N. E. B.) wishes to thank Imperial Oil Limited for the award of a Graduate Research Fellowship.

## REFERENCES

- BATTY, C. J., and GOLDSACK, S. J., 1957, *Proc. Phys. Soc. A*, **70**, 165.  
 BOOTH, N. E., and LEDLEY, B., 1957, *Nuc. Instrum.*, **1**, 345.  
 BOOTH, N. E., LEDLEY, B., WALKER, D., and WHITE, D. H., 1957, *Proc. Phys. Soc. A*, **70**, 209.  
 BROWN, G. E., 1957, *Proc. Phys. Soc. A*, **70**, 361.  
 BRUECKNER, K. A., 1956, *Phys. Rev.*, **103**, 1121.  
 CHEN, F. F., LEAVITT, C.-P., and SHAPIRO, A. M., 1955, *Phys. Rev.*, **99**, 857; 1956, *Ibid.*, **103**, 211.  
 COOR, T., HILL, D. A., HORNYAK, W. F., SMITH, L. W., and SNOW, G., 1955, *Phys. Rev.*, **98**, 1369.  
 DRELL, S. D., 1955, *Phys. Rev.*, **100**, 97.  
 DZHELEPOV, V. P., SATAROV, V. I., and GOLOVIN, B. M., 1955, *Doklady Akad. Nauk S.S.S.R.*, **104**, 717.

- FERNBACH, S., SERBER, R., and TAYLOR, T. B., 1949, *Phys. Rev.*, **75**, 1352.  
FLYAGIN, V. B., 1954, *Report Inst. Nuc. Problems, Acad. Sci., U.S.S.R.*  
FREGEAU, J. H., 1956, *Phys. Rev.*, **104**, 225.  
GLAUBER, R. J., 1955, *Phys. Rev.*, **100**, 242; 1956, *Physica, 's Grav.*, **22**, 1185.  
GOODELL, W. F., JR., LOAR, H. H., DURBIN, R. P., and HAVENS, W. W., JR., 1953, *Phys. Rev.*, **89**, 724.  
HAHN, B., RAVENHALL, D. G., and HOFSTADTER, R., 1956, *Phys. Rev.*, **101**, 1131.  
HOFSTADTER, R., 1956, *Rev. Mod. Phys.*, **28**, 214.  
JOHNSON, M. H., and TELLER, E., 1954, *Phys. Rev.*, **93**, 357.  
LEVINTOV, I. I., 1956, *Doklady Akad. Nauk. S.S.S.R.*, **107**, 240.  
MOSKALEV, V. I., and GAVRILOVSKII, B. V., 1956, *Doklady Akad. Nauk S.S.S.R.*, **110**, 972.  
NEDZEL, V. A., 1954, *Phys. Rev.*, **94**, 174.  
WATSON, K. M., 1957, *Phys. Rev.*, **105**, 1388.  
WILLIAMS, R. W., 1955, *Phys. Rev.*, **98**, 1387.  
WOODS, R. D., and SAXON, D. S., 1954, *Phys. Rev.*, **95**, 577.

# Neutron-Proton Scattering in the Energy Range 70 to 170 MeV

By T. C. GRIFFITH, A. P. BANFORD†, M. Y. UPPAL‡  
AND W. S. C. WILLIAMS§

Physics Department, University College London

*MS. received 18th October 1957*

**Abstract.** The angular distributions of neutrons scattered by protons at effective energies of 96, 130 and 137 mev and at angles between  $19.3^\circ$  and  $78.1^\circ$  in the centre-of-mass system have been measured using photographic emulsions.

The differential cross sections have been normalized to the absolute scale by deducing the energy spectrum of the neutrons. The results confirm that at 130 and 137 mev the cross sections for scattering at angles within  $60^\circ$  of the forward direction in the centre-of-mass system are less than those for a similar range of angles in the backward direction.

## § 1. INTRODUCTION

DURING recent years numerous measurements on the angular distributions of neutrons scattered by protons at various energies from 40 to 400 mev have been reported. Hadley *et al.* (1949) measured the distributions at neutron energies of 40 and 90 mev; Brueckner *et al.* (1949), Fox (1950), Wallace (1951), Selove *et al.* (1953), Chamberlain and Easley (1954), Stahl and Ramsey (1954) and Chung (1954), at 90 mev; Randle *et al.* (1952), at 153 mev; Guernsey *et al.* (1952), Kelly *et al.* (1950) and Easley (1954), at energies between 180 and 300 mev; and finally Hartzler *et al.* (1954), Dzhelepov and Kazarimov (1954) and De Pangher (1955) at energies between 300 and 400 mev. All these workers, with the exception of Wallace (1951), have used either cloud chamber or counter techniques for their investigations. The established features of the angular distributions are that they are anisotropic and are not symmetrical about  $90^\circ$  in the centre-of-mass system, except at energies below 100 mev. An angular distribution symmetrical about  $90^\circ$  would favour an interpretation of the scattering in terms of the Serber force for which interactions between nucleons in states of odd parity are excluded.

When the present experiment was commenced there were no measurements of the angular distributions at angles less than  $60^\circ$  in the centre-of-mass system for energies between 100 and 200 mev. It was, therefore, of the utmost importance to measure the distribution for this range of angles and energies in order to establish whether the approximate symmetry obtained at 90 mev persisted to this region. With this end in view three independent investigations, those of Thresher *et al.* (1955) at 105 and 137 mev, Randle *et al.* (1956) at 130 mev, and the present work (the preliminary results for which were first reported by Massey

† Now at the Atomic Energy Research Establishment, Harwell, Berks.

‡ Now at Government College, Lahore, West Pakistan.

§ Now at the Department of Natural Philosophy, University of Glasgow.

(1955)), were conducted using the neutron beam from the Harwell synchro-cyclotron. All three measurements are in agreement with one another and provide, between them, definite evidence that the angular distributions at 130 and 137 mev are not symmetrical about  $90^\circ$  in the centre-of-mass system.

In the experiment described the scattering of neutrons with effective energies 96, 130 and 137 mev was measured in the range  $19.3^\circ$  to  $78.1^\circ$  (centre-of-mass scattering angles) using a photographic emulsion technique. A collimated beam of neutrons was allowed to traverse in succession three thin extended target films of polythene, deuterium wax, and carbon respectively. Recoil particles from collisions in these targets were detected in photographic emulsions of thickness and orientation so chosen that at the recoil angles investigated the particles were brought to rest in the emulsion. The number of recoil protons from n-p collisions in the polythene was obtained by the conventional polythene-carbon difference method. The measurements on n-d scattering from the deuterium wax target will not be discussed in this communication.

## § 2. EXPERIMENTAL DETAILS

### 2.1. The Neutron Beam

The internal proton beam in the cyclotron (maximum energy 170 mev) was allowed to strike a beryllium target of thickness  $\frac{1}{4}$  in. Neutrons ejected in the forward direction were collimated, as shown in figure 1, by holes in the concrete shielding to give a beam of diameter 2 in. at the entrance port of the scattering chamber.

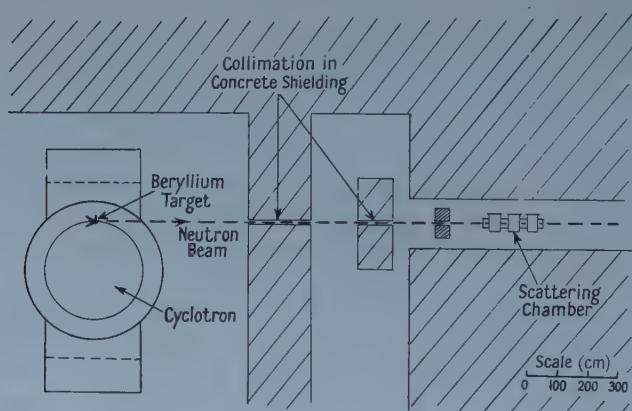


Figure 1.

Radial oscillations of the proton beam, multiple traversals of the target and the internal momentum distribution of the nucleons in the beryllium nuclei lead to a broad neutron spectrum with maximum intensity at about 145 mev (Randle *et al.* 1951, 1953). The spectrum can be sharpened, at the expense of intensity, by the insertion of polythene filters which decrease the relative number of low energy neutrons in the beam. As a compromise between sharpness and intensity a polythene filter of  $40 \text{ g cm}^{-2}$  was used.

### 2.2. The Scattering Chamber

Three steel cylinders 12 in. long and  $12\frac{1}{4}$  in. in diameter, closed at one end, were welded to another cylinder 6 ft long and  $6\frac{1}{2}$  in. in diameter passing through



the centre of each at right angles to its axis as shown in figure 2. Lids fitting on to flanges on the open ends of the three cylinders carried the scattering cameras in which the target films and plates were mounted. The cameras projected

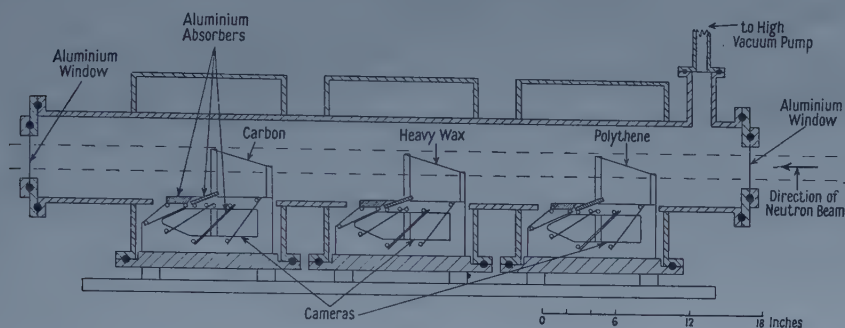


Figure 2.

through rectangular openings in the wall of the long cylinder so that the targets intercepted the neutron beam which passed along the axis of this cylinder. The lids carrying the cameras were rigidly connected together to form a single unit which allowed accurate positioning of the cameras relative to one another. The neutron beam entered and left the chamber through aluminium windows of thickness 0.013 cm mounted on the lids which closed the ends of the long cylinder. O-ring seals on all the removable lids together with vacuum-tight

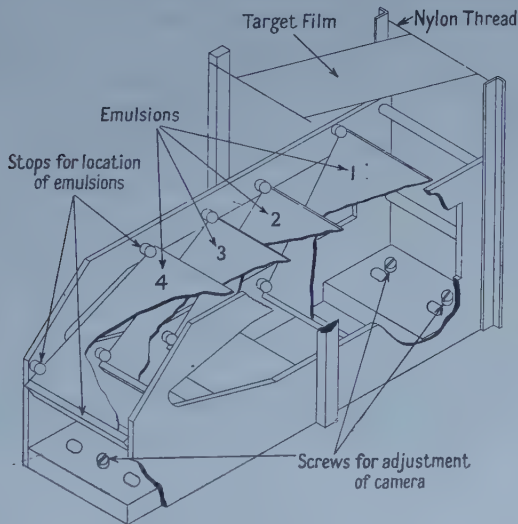


Figure 3.

weldings between the cylinders allowed the entire chamber to be evacuated and maintained at a pressure of  $10^{-2}$  cm of mercury. This low pressure was essential in order to avoid the background of recoil particles from neutron interactions with the air in the chamber and also to avoid the energy loss of the recoils between the target and plates.

The three identical scattering cameras (figures 2 and 3) were constructed so that correct relative alignment of the plates and target films with respect to each other was ensured. The cameras, when clamped to the lids of the scattering chamber, were so adjusted that they would be correctly orientated and positioned with respect to a common axis when assembled in the chamber. This common axis was the axis of the scattering chamber and was arranged to be coincident with the central axis of the neutron beam. The alignment was checked at the end of the run by means of photographic emulsions, one at each end of the chamber, exposed to the neutron beam for one hour in positions perpendicular to the axis. Recoil tracks produced in the emulsions by the neutrons gave circular patches defining the beam. Measurements on these circles indicated that the alignment had been accomplished to better than  $0.2^\circ$ .

### 2.3. *The Target Films*

The target films were 5 in. long,  $1\frac{1}{2}$  in. wide and 100 to  $200\mu$  thick. The polythene target was cut from a sheet of polythene of thickness about  $100\mu$ . The carbon target was prepared by the drying out of aquadag, which had been diluted with water, in a metal mould; removal of the dry carbon film from the mould was facilitated by the use of a wet sheet of 'Cellophane' tightly stretched over the base of the mould. The thickness of the carbon film was chosen so as to give the same energy loss for particles (of the same energy) traversing it as did the polythene target.

The targets were suspended symmetrically between the four pillars of each camera by means of thin nylon threads glued along the ends of the films. During the exposure the targets were in a vertical plane at  $15^\circ$  (angle  $\lambda$  in figure 4) to the axis of the neutron beam. This arrangement avoided distortion of the films due to sagging and enabled particles at large recoil angles to leave the targets with the minimum loss of energy. The targets were entirely within the neutron beam, the only foreign material intercepted by the neutrons being the nylon thread; any tracks originating in these threads were rejected by geometrical tests applied during scanning.

The thickness uniformity of the target films was investigated by weighing and measuring small sections of each target. The surface densities were  $10.54 \pm 0.01 \text{ mg cm}^{-2}$  for polythene and  $13.62 \pm 0.03 \text{ mg cm}^{-2}$  for carbon.

Chemical analysis of the target materials showed that the polythene was pure  $(\text{CH}_2)_n$  whilst the carbon film was 93.4% carbon, 1% hydrogen and 5.6% nitrogen and oxygen. The interaction of fast neutrons with oxygen and nitrogen nuclei is almost the same as with carbon nuclei so that it is not necessary to treat them as impurities in the carbon.

### 2.4. *Photographic Emulsions*

The emulsions were coated on glass plates of thickness 1.5 mm, length 4 in. and width 3 in. The length and width were accurate to better than  $1/64$  in. and were a close fit in the plate holders in which they were held by springs against four metal stops which were accurately machined to accommodate them. The emulsions were 600 micron thick layers of Ilford C2 with a supercoat of G5 emulsion of thickness 25 microns. Extra plasticizers (glycerine) added to the emulsions together with the thick glass provided a safeguard against any distortion

and flaking of the emulsion when the moisture was removed under the vacuum in the scattering chamber.

The use of the composite emulsion enabled the tracks of fast particles to be easily picked up in the sensitive G5 supercoat and then followed down into the C2 where the grain density was better suited for the ionization measurements that had to be made on tracks from the deuterium wax target. Moreover, the thickness of the G5 supercoat proved to be so uniform that it provided a rapid method of measuring the dip of the tracks in the emulsion.

Each of the three cameras carried four plates. Plate 1 (figure 3) was at an angle of  $54^\circ$  to the axis of the neutron beam and detected all the recoil particles at angles between  $57.5^\circ$  and  $90^\circ$ ; over this range of angles the recoil protons from neutrons of energy 170 Mev or less reached the end of their range in the emulsion. Plates 2, 3 and 4 were at angles of  $44^\circ$ ,  $34^\circ$  and  $24^\circ$  respectively to the neutron beam and had aluminium absorbers of suitable thickness interposed between the target and the plates in order to bring most of the recoils to rest within the emulsions. Unfortunately, multiple scattering of the recoils in the aluminium was too large for the measurements on the plates at  $34^\circ$  and  $24^\circ$  to be reliable.

The emulsions were processed using amidol bisulphite developer (Dainton *et al.* 1951); the usual precautions with thick emulsions were taken to avoid reticulation and to ensure uniform development with depth. No difficulties were experienced through the use of composite emulsions since optimum development of tracks in the G5 was not essential. The development times were chosen to give tracks of good quality in the C2 emulsion.

The shrinkage factor of the emulsion was determined by measuring the thickness of the plates with a micrometer immediately after their removal from the vacuum and after processing. Six points well in from the edge of each plate were considered and the glass thickness was obtained by stripping a small portion of the emulsion off the glass at these points. Test plates coated with C2 and G5 emulsions from the same batch were measured in a similar manner and the difference in shrinkage between the two emulsions was found to be within the experimental errors of measurements. The mean value of the shrinkage factor  $s$  was found to be  $2.75 \pm 0.03$ , the high value being due to the extra plasticizers in the emulsion.

### § 3. MEASUREMENT OF THE TRACKS

The emulsions were scanned using Cooke, Troughton and Simms M. 4004 microscopes with  $\times 15$  eyepieces and  $\times 45$  oil immersion objectives. An eyepiece graticule calibrated at this magnification was used for length measurements. All the depth measurements were taken with a  $\times 95$  oil immersion objective. The two reference lines OX and OY, shown in figure 4, were drawn on the emulsions in order to facilitate accurate location of the areas scanned on each plate. OX was parallel to the reference edge QT of the plate and about 1 cm from the opposite edge RS. The median line OY, perpendicular to OX, represented the projection of the direction of the neutron beam (and the centre line of the target film) on the plane of the emulsion. Equal areas on each side of OY were scanned in strips of width  $103 \mu$  and total length 2.5 cm parallel to OX. A distance of  $10 \mu$  was missed between successive strips in order to avoid overlapping. An area of  $2.32 \text{ cm}^2$  was scanned on the polythene plate at  $54^\circ$  and



1.03 cm<sup>2</sup> on the plate at 44°. Areas of 1.69 cm<sup>2</sup> and 0.75 cm<sup>2</sup> respectively were scanned on the corresponding carbon plates.

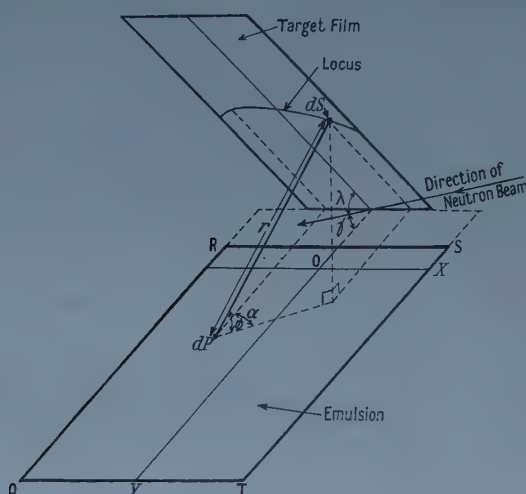


Figure 4. Line marked 'locus' is the locus (hyperbola) of scattering centres for tracks of constant  $\theta$  entering the emulsion at  $dP$ .

The recoil angle  $\theta$  of each particle entering the emulsions, and originating on the target films, was deduced from the measurements using the relation

$$\cos \theta = \cos \alpha \cos \phi \cos \gamma - \sin \phi \sin \gamma \quad \dots\dots(1)$$

where  $\phi$  is the angle of dip of the track,  $\alpha$  the angle between  $OY$  and the projection of the track on the surface of the emulsion and  $\gamma$  the angle between the plane of the emulsion and the direction of the neutron beam (viz. 54° and 44° respectively for the two sets of plates examined). In the range of recoil angles investigated the values of  $\phi$  were between 3.5° and 27.5° and those of  $\alpha$  between +26° and -26° (see figure 6).

The angle  $\alpha$  was measured directly, for the first straight portion of each track, using a goniometer eyepiece. Two methods were used for the determination of  $\phi$ : (a) in the case of particles either ending in the G5 layer or being appreciably scattered in traversing it into the C2 underneath,  $\phi$  was obtained by the usual method of measuring the dip,  $\delta$ , over the first straight projected length  $l$  of the track. (b) For particles traversing the G5 layer without being visibly scattered therein the projected length  $L$  of that portion of the track in the G5 together with the processed thickness  $d$  of this layer were used to evaluate  $\phi$ . Since  $d$  was nearly constant over the surface of the emulsion, it only had to be measured accurately at a few suitably spaced positions on the scanned areas; this could be done rapidly thus obviating any corrections arising from variations in the humidity of the emulsion which occur over prolonged periods of scanning. The method, when applied to fast particles, proves to be rapid, accurate and much less susceptible to subjective errors than the first method; when, however, the particles have low energy and a long track length in the G5 layer, the accuracy is decreased due to the effect of multiple scattering in the emulsion.



The effect of errors in the measurement of  $\alpha$  and  $\phi$  on the determination of  $\theta$  has been examined using the relation

$$\sigma_{\theta}^2 = \left( \frac{\partial \theta}{\partial \phi} \right)^2 \sigma_{\phi}^2 + \left( \frac{\partial \theta}{\partial \alpha} \right)^2 \sigma_{\alpha}^2 \quad \dots\dots (2)$$

where  $\sigma_{\theta}$ ,  $\sigma_{\alpha}$  and  $\sigma_{\phi}$  are the mean errors in  $\theta$ ,  $\alpha$  and  $\phi$  respectively and  $\partial\theta/\partial\alpha$  and  $\partial\theta/\partial\phi$  are deduced from equation (1). It can be shown that the contribution to  $\sigma_{\theta}$  from  $\sigma_{\phi}$  is much larger than that from  $\sigma_{\alpha}$ . Any systematic error in  $\theta$  arising either from an error in  $\gamma$  (which is certainly less than  $0.2^\circ$ ), or from an error in the shrinkage factor  $s$  is considerably smaller than  $\sigma_{\phi}$ .

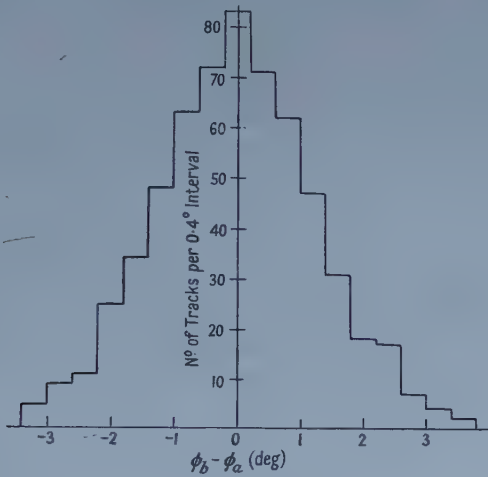


Figure 5.

The error in  $\phi$  measured by the first method results entirely from measurement errors. In the second method the measurement errors are small but, since many of the particles had only moderate energy, the multiple scattering errors were relatively large thus offsetting some of the advantages of the method. Most of the tracks traversing the G5 were measured by both methods and the distribution of  $\phi_b - \phi_a$ , where  $\phi_a$  and  $\phi_b$  are the values of  $\phi$  obtained by the first and second method respectively, is shown in figure 5. This distribution is symmetrical about zero thus showing that if there is any systematic error in the measurement of  $\phi$  it must be of the same magnitude and common to both methods. If the mean errors in  $\phi_a$  and  $\phi_b$  are  $\sigma_a$  and  $\sigma_b$ , then the mean error in  $\phi_b - \phi_a$  is  $\sigma = (\sigma_a^2 + \sigma_b^2)^{1/2}$ . The error  $\sigma_b$  arises from the multiple scattering error  $\beta$  and to a much lesser extent from the measurement error  $\sigma_m$ .  $\sigma_a$  is almost entirely due to the measurement error, the length of track involved in the measurement being short enough for multiple scattering to have a negligible effect.

Estimates of the errors, given in table 1, show that  $\sigma_a$  can be assumed to be equal to  $\sigma_b$  and that the values of  $\sigma$  are in agreement with the mean width of the distribution shown in figure 5. The errors were evaluated for recoil protons from 120 mev neutrons, at each value of  $\theta$ , assuming that  $d$  could be measured to  $\pm 0.15 \mu$ ,  $\delta$  to  $\pm 0.4 \mu$  and both  $l$  and  $L$  to  $\pm 1\%$ . The average of the two values of  $\phi$  measured for tracks traversing the G5 layer, used in the final analysis, has an error  $\sigma_{\phi}$  given approximately by  $0.5\sigma$  (since  $\sigma_a \simeq \sigma_b$ ). This error, together with an error  $\sigma_{\alpha} = \pm 0.25^\circ$ , was used in the estimation of  $\sigma_{\theta}$ .

Table 1

$\phi$ (°)	$\theta$ (°)	$\beta$ (°)	$\sigma_m$ (°)	$\sigma_b$ (°)	$\sigma_a$ (°)	$\sigma$ (°)	$\sigma_\phi$ (°)	$\sigma_\theta$ (°)	$\sigma_{E_n}$ (MeV)
6	60	0.60	0.10	0.61	0.55	0.82	0.41	0.46	4.0
11	65	0.55	0.15	0.57	0.75	0.94	0.47	0.51	5.0
16	70	0.75	0.23	0.78	0.80	1.12	0.56	0.59	7.5
21	75	0.90	0.25	0.93	0.95	1.33	0.66	0.69	10.0
26	80	—	—	—	1.20	—	1.20	1.21	30.0

The energy  $E_p$  of the recoil particles was obtained from their range  $R_p$  using the range-energy relations for protons in the emulsion and assuming all the tracks to be due to protons. This procedure cannot lead to any error in the final grouping of the recoil protons from n-p scattering, because all the  $\alpha$ -particles from carbon are automatically cancelled when taking the polythene-carbon difference (§ 5). Because of the extra plasticizers in the emulsions it was necessary to check the validity of the normal C2 range-energy relations for protons. Following the method of Vigneron (1953) the parameters in the range-energy relations, involving the composition of the emulsion (with plasticizers) were derived. The values of these parameters were almost the same as those given by Vigneron for normal dry C2 and therefore his range-energy relations, which agree with the available experimental data to better than 2%, were used in all the calculations.

The range  $R_p$  was obtained with accuracy to about 1% from the total projected length of the track and its mean angle of dip. On the average, the value of  $R_p$  obtained in this manner was not found to be significantly different from the value obtained when due allowance was made for the scattering along the tracks. About 3% of the protons at recoil angles less than  $67.5^\circ$  from collisions with neutrons of energy near 170 MeV were found to be scattered into the glass below the emulsion before reaching the end of their range. These tracks were easily distinguished from those of fast cosmic-ray particles and their residual range was estimated by grain counting. The number of particles scattered in such a way as to emerge through the surface of the emulsion was negligible.

The energy  $E_n$  of a neutron involved in an elastic n-p collision giving a recoil proton of energy  $E_p$  at an angle  $\theta$  was calculated using the relativistic relation between  $E_n$ ,  $E_p$  and  $\theta$ . The mean error  $\sigma_{E_n}$  in  $E_n$  given in table 1, was calculated for  $E_n = 120$  MeV using the estimated values of  $\sigma_\theta$  and assuming an overall error of  $\pm 2\%$  in the determination of  $E_p$ .

#### § 4. THE SELECTION OF TRACKS

The values of  $\phi$  and  $\alpha$  for tracks recorded at a given point on the emulsion have definite limiting values within which all tracks at recoil angles between  $57.5^\circ$  and  $87.5^\circ$  from the target film must lie. Tracks outside these limits were background tracks which could be rejected with the aid of tables indicating the maximum permitted values of  $\phi$  and  $\alpha$  as a function of position on the plate. All tracks with values of  $\alpha$  less than  $-26^\circ$  or greater than  $+26^\circ$  were rejected during scanning and about 3% of those actually measured were discarded when the tables were consulted.

Assuming uniform target thickness and uniform neutron flux across the beam the distribution of accepted tracks as a function of  $\alpha$  was computed from geometrical considerations. The distribution of tracks from the polythene target is shown in figure 6 and is seen to be in good agreement with the experimental distribution to which it has been normalized. The symmetry of the histogram about  $\alpha=0$  shows that the relative alignment of the target and plate was correct. A symmetrical distribution was also obtained for the carbon target thus indicating a correct alignment of the apparatus to the neutron beam.

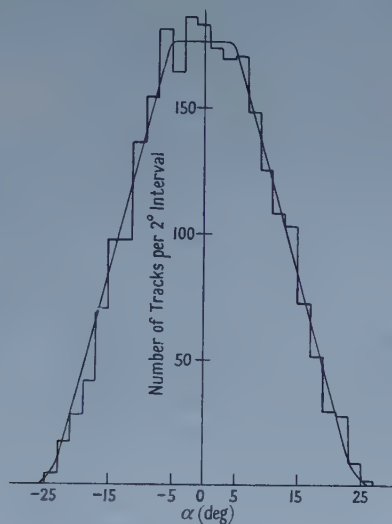


Figure 6.

In addition to the  $\phi$  and  $\alpha$  selection criteria the fact that the recoil protons from *n-p* collisions at any particular angle  $\theta$  have a limited range of energies (dictated by the energy spectrum of the incident neutrons) permitted a further rejection of undesirable tracks. Graphs of the range  $R_p$  of the recoil protons in the emulsion as a function of the recoil angle  $\theta$  with the incident neutron energy  $E_n$  as parameter were used to reject all the recoils that appeared to be due to neutrons of energies greater than 170 mev or less than 50 mev.

## § 5. CORRECTIONS FOR BACKGROUND TRACKS

### 5.1. Carbon Background

The most serious source of background was that arising from interactions between the incident neutrons and the carbon atoms in the polythene. This was cancelled by obtaining the difference between the number of tracks measured on the emulsions exposed, at the same angle  $\gamma$ , opposite the polythene and carbon targets. The ratio of the areas scanned on the two plates to effect this cancellation was obtained from the relation

$$(\Omega_c A_c)_\theta = (\Omega_p A_p)_\theta \left( \frac{N_p D_c^2}{N_c D_p^2} \right) \dots\dots (3)$$

where the suffixes *c* and *p* refer to the carbon and polythene respectively,  $A$  is the scanned area on the emulsion,  $N$  the number of carbon atoms per  $\text{cm}^2$  of the

target and  $D$  the distance from the target film to the beryllium target in the cyclotron. The solid angle  $\Omega$  is defined by the equation

$$(\Omega A)_\theta = \iint \frac{\sin \phi dS dP}{r^2} \quad \dots\dots(4)$$

where, referring to figure 4,  $dS$  is an elementary area on the target film from which the recoil particles detected in an elementary area  $dP$  of the emulsion, at a distance  $r$  from  $dS$ , have originated. The limits of integration are defined by the 'effective' area on the target film and the scanned area  $A$  of the emulsion (see §7).

The ratio  $A_c/A_p$  obtained from these calculations was 0.728, the ratio  $(\Omega_c A_c)_\theta/(\Omega_p A_p)_\theta$ , for the range of recoil angles considered being 0.700.

## 5.2. General Background

This second source of background arises from neutron-induced stars in the material around the cameras and from cosmic-ray particles. The background tracks which appear to originate on the target films were only rejected if their range was beyond the acceptable limits of the selection criteria. Since the intensity of general background tracks that were not rejected during scanning was found to be the same on both the polythene and carbon plates, it was not completely cancelled by the carbon subtraction because of the unequal areas that had to be considered on the two plates.

The general background was measured by scanning parts of the carbon and polythene plates, applying the usual selection criteria, but confining the scanning to areas where the tracks of particles from the target films could only have azimuthal angles  $\alpha$  all of the same sign. Only the background tracks with values of  $\alpha$  of the opposite sign to those expected for tracks from the target were measured in these areas. An area equivalent to  $0.272A_p$  was scanned in this manner and the tracks added to the carbon background from an area of  $0.728A_p$ . This sufficed to correct for the background from all the known sources. The magnitude of the general background added to the carbon data amounted to 1% of the total number of particles from the polythene target with energies below 20 Mev and to 6% for energies above 20 Mev; in the region where only protons from n-p collisions were expected the amount added was only about 1 to 2%.

The energy distribution of particles from the polythene and carbon targets for a sample of tracks in which the range-angle ( $R, \theta$ ) selection criteria were not applied during scanning is shown in figure 7. The ratio  $A_c:A_p$  of the areas in which these tracks were measured was 0.728, the correct amount of general background being included with the carbon data. All the tracks were assumed to be due to protons (see §3), the shortest range considered being  $8\mu$ . Particles entering the glass below the emulsions are shown with energies which only correspond to the observed length of their tracks in the emulsion. A satisfactory cancellation of tracks is obtained everywhere except in the regions where proton recoils from n-p collisions are expected. This is particularly noticeable in the case of particles entering glass and also for particles in the angular interval  $82.5^\circ$  to  $87.5^\circ$  where all the genuine proton recoils have ranges less than  $20\mu$ . The shape of the energy distributions of particles from carbon (after allowing for the general background) does not appear to vary with  $\theta$  in the interval  $57.5^\circ$  to  $87.5^\circ$ . It is also found to be in good agreement with the distribution given by Hodgson (1954).



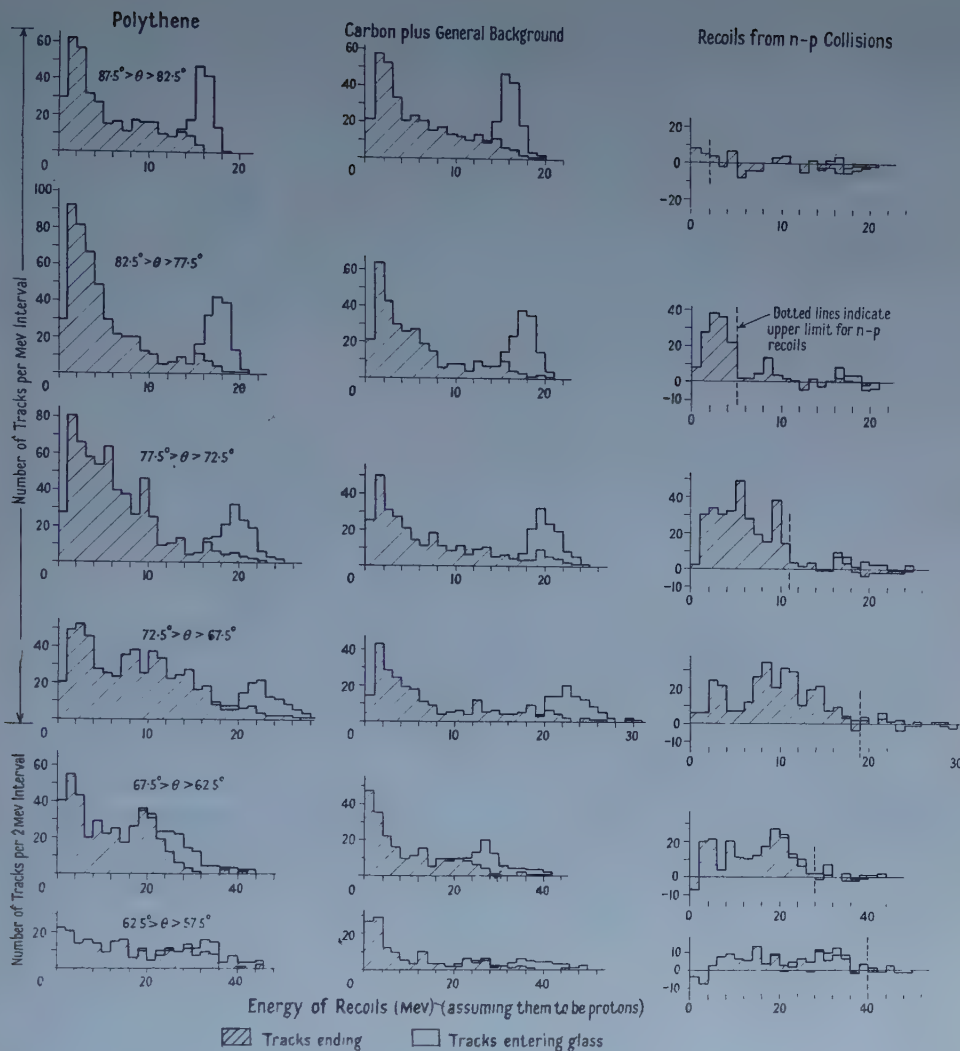


Figure 7.

§ 6. THE GROUPING OF PROTON RECOILS FROM  $N$ - $P$  COLLISIONS

The recoil protons were considered in two broad groups of incident neutron energies, one extending from 70 to 120 mev and the other from 120 to 170 mev. All the acceptable tracks measured in a given area of the polythene plate were plotted on the  $(R, \theta)$  graphs (§ 4) and the tracks falling between the curves defining the two energy groups were counted in angular intervals of width 5° from 57.5° to 82.5°. The tracks from the appropriate area of the carbon plate were counted in a similar manner and the difference between the two counts, for each angle and energy interval, gave the number of protons from  $n$ - $p$  scattering used in evaluating the differential cross sections. In obtaining these differences it was noted that, as expected, a complete cancellation of tracks occurred in the region above the  $(R, \theta)$  curve for 170 mev neutrons at angles less than 77.5°. At greater angles, where the errors of measurement were significant, the cancellation was not complete. Consequently, in this region, the 170 mev curve was not used for

grouping the tracks and the higher energy group included all the tracks above the 120 mev curve.

It can be shown that since the angle and energy intervals of  $5^\circ$  and 50 mev are large in comparison with the measurement errors (table 1) the effect of these errors on the number of recoils counted in any group tends to cancel itself out everywhere except at the 170 mev boundary where the tracks are only expected on one side. The net effect of the measurement errors is, therefore, considered to be much smaller than the statistical error. This conclusion was confirmed by grouping tracks using the two independent series of measurements obtained from the alternative methods of measuring  $\phi$  (§ 3); in both cases the number of tracks finally counted in each group was the same.

### § 7. NORMALIZATION OF THE DIFFERENTIAL CROSS SECTIONS

The differential cross sections  $\sigma(\bar{E}_n, \theta)$ , for n-p scattering in the laboratory system, at the mean recoil angle  $\theta$  in the interval  $\theta_1$  to  $\theta_2$ , and in the energy group with effective energy  $\bar{E}_n$  were calculated from the relation

$$n = N T t n_0(\bar{E}_n) \sigma(\bar{E}_n, \theta) (\Omega_p A_p)_\theta \quad \dots\dots (5)$$

where  $n$  is the number of recoil protons, in each energy group, recorded in an area  $A_p$  of the emulsion in an exposure of duration  $t$  sec,  $N$  the number of scattering centres per  $\text{cm}^3$  of the target of thickness  $T$ , and  $n_0(\bar{E}_n)$  the total number of incident neutrons  $\text{cm}^{-2} \text{sec}^{-1}$  with energies between  $E_{n1}$  and  $E_{n2}$ . The geometrical factor,  $(\Omega_p A_p)_\theta$ , defined in equation (4) had to be evaluated for each of the angular intervals under consideration. In each interval the extreme values of  $\theta$  defined the 'effective' area on the target from which the recoils detected at any given point on the emulsion had originated. Assuming  $T$  to be negligible in comparison with  $r$  the problem is that of scattering from one plane area and detection on another plane area. The factors  $(\Omega_p A_p)_\theta$  were therefore evaluated by successive graphical integration over the appropriate areas on the target film and the emulsion.

Since  $n_0(\bar{E}_n)$  was not directly known for the two energy groups under consideration, only relative values of  $\sigma(\bar{E}_n, \theta)$  were obtained. These values were placed on an absolute scale by suitable normalization using known values of the cross sections  $\sigma(E_n, \theta)$  as a function of  $E_n$  for  $\theta = 62.5^\circ$ . This normalization involved a determination of the neutron energy spectrum given in figure 8. The tracks of recoil protons in the interval  $57.5^\circ$  to  $67.5^\circ$  were plotted on the  $(R, \theta)$  graphs and the number,  $dn$ , of tracks lying between the  $(R, \theta)$  curves drawn for values of  $E_n$  in steps of 10 mev from 50 to 170 mev, were counted. The neutron flux  $n_0(E_n)$ , viz. the number of neutrons  $\text{cm}^{-2} \text{sec}^{-1} (\text{mev})^{-1}$ , was then calculated for each of the 10 mev steps. In this calculation the density of the polythene target was taken to be  $10.54 \text{ mg cm}^{-2}$ ,  $t$  was  $6.18 \times 10^4$  sec, and the factor  $(\Omega_p A_p)_\theta$ , for the interval  $57.5^\circ$  to  $67.5^\circ$ , was  $28.9 \times 10^{-3} \text{ cm}^2$ . The values of  $\sigma(E_n, \theta)$  at  $62.5^\circ$ , given in table 2, were interpolated from the results of Hadley *et al.* (1949), at 40 mev; Stahl and Ramsey (1954) (collected data), at 90 mev; Thresher *et al.* (1955), at 105 and 137 mev; Randle *et al.* (1952, 1956), at 156 and 130 mev; and Kelly *et al.* (1950), at 260 mev. The errors assigned to the values of  $\sigma(E_n, \theta)$  include the errors arising from the interpolation as well as the errors quoted by the authors.

The neutron energy spectrum in figure 8 is compared with the spectrum given by Randle *et al.* (1953) for neutrons produced at Harwell under the same conditions as those used in the present experiment. The Harwell spectrum has been normalized to that obtained from the present work and has also been modified,

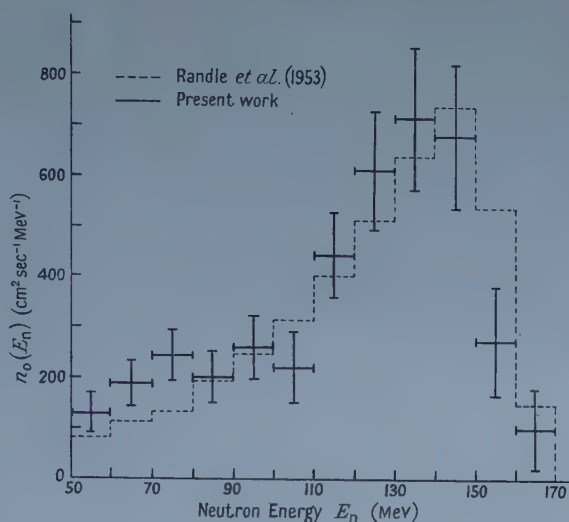


Figure 8.

using known values of the neutron total cross sections in carbon and hydrogen (Taylor and Wood 1953), to allow for the attenuation produced in passing the neutrons through 40 g cm<sup>-2</sup> of polythene filter. There is good agreement between the shapes of the two spectra.

Table 2

$E_n$ (MeV)	55	65	75	85
No. of tracks from the polythene target	75	77	78	63
No. of background tracks	38	30	25	25
$dn$	37	47	53	38
$\sigma(E_n, \theta)$ (mbn sterad <sup>-1</sup> )	$18.0 \pm 2.0$	$15.6 \pm 1.5$	$13.5 \pm 1.0$	$11.7 \pm 0.7$
$n_0(E_n)$ (cm <sup>-2</sup> sec <sup>-1</sup> (MeV) <sup>-1</sup> )	$128 \pm 39$	$187 \pm 45$	$243 \pm 50$	$200 \pm 51$
$E_n$ (MeV)	95	105	115	125
No. of tracks from the polythene target	69	67	68	91
No. of background tracks	27	36	14	23
$dn$	42	31	54	66
$\sigma(E_n, \theta)$ (mbn sterad <sup>-1</sup> )	$10.1 \pm 0.5$	$8.8 \pm 0.6$	$7.6 \pm 0.7$	$6.7 \pm 0.7$
$n_0(E_n)$ (cm <sup>-2</sup> sec <sup>-1</sup> (MeV) <sup>-1</sup> )	$258 \pm 62$	$219 \pm 72$	$442 \pm 84$	$610 \pm 117$
$E_n$ (MeV)	135	145	155	165
No. of tracks from the polythene target	90	71	40	18
No. of background tracks	22	16	19	11
$dn$	68	57	21	7
$\sigma(E_n, \theta)$ (mbn sterad <sup>-1</sup> )	$5.9 \pm 0.7$	$5.2 \pm 0.7$	$4.8 \pm 0.7$	$4.4 \pm 0.8$
$n_0(E_n)$ (cm <sup>-2</sup> sec <sup>-1</sup> (MeV) <sup>-1</sup> )	$713 \pm 140$	$678 \pm 144$	$271 \pm 107$	$99 \pm 79$

The neutron fluxes,  $n_0(\bar{E}_n)$ , and effective energies,  $\bar{E}_n$ , for the two energy groups under consideration were determined from the data given in table 2 using the two relations

and

$$n_0(\bar{E}_n) = \int_{E_{n1}}^{E_{n2}} n_0(E_n) dE_n$$

$$\sigma(\bar{E}_n, \theta) n_0(\bar{E}_n) = \int_{E_{n1}}^{E_{n2}} \sigma(E_n, \theta) n_0(E_n) dE_n. \quad \dots, (6)$$

The values obtained were  $1.36 \pm 0.14 \times 10^4$  neutrons  $\text{cm}^{-2} \text{sec}^{-1}$  at  $96 \pm 4$  mev and  $2.37 \pm 0.27 \times 10^4$  neutrons  $\text{cm}^{-2} \text{sec}^{-1}$  at  $137 \pm 5$  mev. The magnitudes of the fluxes compare favourably with the values of  $1.26 \times 10^4$  and  $2.33 \times 10^4$  neutrons  $\text{cm}^{-2} \text{sec}^{-1}$  obtained (without normalization of the spectra) for the same energy intervals from the results of Randle *et al.* (1951). The errors in the final differential cross sections arising from normalization to the absolute scale may therefore be much less than the errors suggested by those assigned to the values of  $n_0(\bar{E}_n)$ . The values of the effective energies obtained using the Harwell spectrum (figure 8) and the total n-p cross sections of Taylor and Wood (1953), instead of the differential cross sections, were  $97 \pm 2$  mev and  $140 \pm 3$  mev respectively.

### § 8. CORRECTIONS FOR ENERGY LOSS IN THE TARGET FILM

At recoil angles greater than  $72.5^\circ$  protons from neutrons with energies between 70 and 170 mev originating inside the target lose an appreciable fraction of their energy before entering the emulsion. It was therefore necessary to apply corrections to allow for those tracks which, when plotted on the  $(R, \theta)$  graphs, fall below the lower boundary line of the group to which they belong.

The total range  $R(E_n, \theta)$  of a recoil proton at angle  $\theta$  from a neutron of energy  $E_n$  is given by the relation  $R(E_n, \theta) = R_p(E_n, \theta) + L(E_n, \theta)$  where  $R_p(E_n, \theta)$  is the observed range in the emulsion and  $L(E_n, \theta)$  the range in the target film (expressed in terms of the equivalent range in emulsion). If  $E_{n1}$  represents the neutron energy defining the boundary between the high and low energy neutron groups then the range  $R_p(E_n, \theta)$  for recoil protons at angle  $\theta$  from neutrons of energy  $E_n \geq E_{n1}$  has to be greater than  $R_m(E_{n1}, \theta)$  to be counted in the higher energy group,  $R_m(E_{n1}, \theta)$  being the observed range of recoil protons at angle  $\theta$  from neutrons of energy  $E_{n1}$  in the emulsion when  $L(E_n, \theta) = 0$ . Recoils due to neutrons of energy  $E_n \geq E_{n1}$  fall into the lower energy group if they originate in the target at a thickness greater than  $L_i(E_n, \theta)$  which is defined by

$$L_i(E_n, \theta) = R(E_n, \theta) - R_m(E_{n1}, \theta)$$

and represents the effective thickness within which all the recoils counted in the higher energy group have originated.  $L_i(E_n, \theta)$  was assumed to be normal to the plane of the target (the average angle between the tracks and the normal being less than  $10^\circ$ ) and was calculated using the kinematic equation (relativistic) relating  $E_n$ ,  $E_p$  and  $\theta$  and the range-energy relations for protons in the polythene and emulsion.

The correction factor  $F$  for the loss of recoil proton tracks from neutrons with energies between  $E_{n1}$  and  $E_{n2}$  at angles between  $\theta_1$  and  $\theta_2$  is given by  $F = n_p/n_p'$  where  $n_p'$  and  $n_p$  are respectively the numbers of recoils expected in these intervals with and without energy loss. Using equation (5) it can be shown that

$$n_p' = Nt \int_{\theta_1}^{\theta_2} \int_{E_{n1}}^{E_{n2}} L_i(E_n, \theta) \sigma(E_n, \theta) n_0(E_n) (\Omega A)_\theta dE_n d\theta$$

$$\text{and} \quad n_p = Nt \int_{\theta_1}^{\theta_2} \int_{E_{n1}}^{E_{n2}} \sigma(E_n, \theta) n_0(E_n) (\Omega A)_\theta dE_n d\theta. \quad \dots, (7)$$



Table 3

	High Energy Group (120 to 170 mev)				Low Energy Group (70 to 120 mev)			
	Effective Energy $137 \pm 5$ mev				Effective Energy $96 \pm 4$ mev			
Range of recoil angles (lab. system)	57.5° to 62.5°	62.5° to 67.5°	67.5° to 72.5°	72.5° to 77.5°	77.5° to 82.5°	57.5° to 62.5°	62.5° to 67.5°	67.5° to 72.5°
Scattering angle (c.m. system)	58.3°	48.4°	38.7°	29.0°	19.3°	58.8°	48.9°	39.1°
No. of tracks from polythene target	105	205	265	299	255	118	229	309
No. of background tracks	33	58	59	90	150	42	88	95
<i>n</i>	72	147	206	209	105	76	141	214 (2)
<i>F</i>	1.0	1.0	1.01	1.22	2.45	1.0	1.0	1.01
$(\Omega_p A_p)_\theta \times 10^{-3} \text{ cm}^2$	9.92	18.96	27.85	36.54	44.97	9.92	18.96	27.85
$\sigma(E_n, \theta)$ (mbn sterad <sup>-1</sup> )	$5.5 \pm 0.9$	$5.85 \pm 0.65$	$5.65 \pm 0.50$	$5.27 \pm 0.51$	$4.30 \pm 0.85$	$10.1 \pm 1.6$	$9.8 \pm 1.2$	$10.1 \pm 0.90$
Conversion of $\sigma(E_n, \theta)$ from lab. to c.m. system	0.518	0.619	0.771	1.026	1.537	0.513	0.611	0.759
$d\sigma/d\Omega$ (mbn sterad <sup>-1</sup> )	$2.85 \pm 0.45$	$3.63 \pm 0.40$	$4.35 \pm 0.40$	$5.41 \pm 0.52$	$6.65 \pm 1.30$	$5.2 \pm 0.85$	$6.00 \pm 0.75$	$7.65 \pm 0.70$

(The numbers in the brackets represent tracks from the high energy group included in the lower energy group.)

1.008

9.0 ± 1.3

Table 4

(1)	(2)	(3)	(4)	(5)	(6)	(7)	(8)	(9)	(10)	(11)
44	47.5 to 52.5	78.1	85	43	42	1.0	3.76	6.60 $\pm$ 1.8	0.394	2.60 $\pm$ 0.70
44	52.5 to 57.5	68.2	131	53	78	1.0	7.12	6.50 $\pm$ 1.1	0.446	2.89 $\pm$ 0.51
54 & 44	57.5 to 62.5	58.4	350	153	197	1.0	20.35	5.72 $\pm$ 0.66	0.517	2.96 $\pm$ 0.34
54 & 44	62.5 to 67.5	48.6	566	223	343	1.0	32.73	6.19 $\pm$ 0.52	0.617	3.82 $\pm$ 0.32
54	67.5 to 72.5	38.8	383	107	276	1.01	27.85	5.92 $\pm$ 0.48	0.768	4.55 $\pm$ 0.37
54	72.5 to 77.5	29.1	437	134	303	1.11	36.54	5.44 $\pm$ 0.44	1.022	5.56 $\pm$ 0.45
54	77.5 to 82.5	19.3	367	200	167	1.90	44.97	4.17 $\pm$ 0.60	1.530	6.40 $\pm$ 0.90
Comparison of data from the 54° and 44° plates										
54	57.5 to 62.5	58.4	148	51	97	1.0	9.92	5.78 $\pm$ 0.85	0.517	3.00 $\pm$ 0.44
44	57.5 to 62.5	58.4	202	102	100	1.0	10.43	5.70 $\pm$ 1.00	0.517	2.93 $\pm$ 0.52
54	62.5 to 67.5	48.6	300	94	206	1.0	18.96	6.42 $\pm$ 0.63	0.617	3.96 $\pm$ 0.39
44	62.5 to 67.5	48.6	266	129	137	1.0	13.77	5.90 $\pm$ 0.90	0.617	3.63 $\pm$ 0.53

(1) Plate angle (°); (2) range of recoil angles (lab. system) (°); (3) scattering angle (c.m. system) (°); (4) no. of tracks from polythene target; (5) no. of background tracks; (6)  $n$ ; (7)  $F$ ; (8)  $(\Omega_1 A_1)_{10} \times 10^{-3}$  (cm<sup>2</sup>); (9)  $\sigma(E_n, \theta)$  (mbn sterad<sup>-1</sup>); (10) conversion of  $\sigma(E_n, \theta)$  from lab. to c.m. system; (11)  $d\sigma/d\Omega$  (mbn sterad<sup>-1</sup>).

These integrals were evaluated numerically using the values of  $L_1(E_n, \theta)$  calculated for  $E_n$  every 5 meV from 70 to 170 meV and  $\theta$  every  $0.5^\circ$  from  $72.5^\circ$  to  $82.5^\circ$ , and the values of  $(\Omega A)_\theta$  calculated for  $0.5^\circ$  intervals over the same range of angles. The relative values of  $\sigma(E_n, \theta)n_0(E_n)$  as a function of  $E_n$  were assumed to be independent of  $\theta$  and were obtained directly by counting the tracks in 5 meV intervals on the  $(R, \theta)$  graphs at angles between  $57.5^\circ$  and  $67.5^\circ$  (§7), this being a region where the energy loss in the target is negligible. The values of  $F$  only changed by about 2% when various other assumptions concerning the variation of  $\sigma(E_n, \theta)n_0(E_n)$  as a function of  $E_n$  were made. Since a number of assumptions concerning the variation of  $\sigma(E_n, \theta)$  as a function of  $\theta$  were found to give similar results, the final values of  $F$  were calculated assuming  $\sigma(E_n, \theta)$  to be constant over the angular intervals of width  $5^\circ$  under consideration.

The correction factors are given in tables 3 and 4. Since the total thicknesses of the polythene and carbon targets were such that particles with the same energy experience equal energy loss in traversing them,  $F$  had to be evaluated for only one target, the value obtained being directly applied to the final numbers of recoil protons from *n*-*p* collisions. The corrections were negligible at angles less than  $72.5^\circ$  but, at angles greater than  $82.5^\circ$  for the higher energy group and greater than  $77.5^\circ$  for the lower energy group, they were so large that the corrected number of recoils had no useful significance. For the lower energy group, at all angles, a correction was made for tracks from the higher energy group falling between 70 and 120 meV.

#### § 9. ANALYSIS OF THE DATA FROM THE EMULSIONS AT $44^\circ$

Since the recoil protons are more energetic at smaller recoil angles the surface of the emulsions at  $44^\circ$  to the neutron beam was covered with an aluminium absorber of uniform thickness  $350\mu$ , so that all the recoil protons from neutrons with energy less than about 125 meV reached the end of their range in the emulsion. The path length,  $350 \csc \phi$ , of each particle in the absorber was converted to an equivalent path length in emulsion and added to the actual observed track length in the emulsion. The resultant length  $R_t$  representing the total equivalent range of the particle in emulsion was plotted against  $\theta$  on the  $(R, \theta)$  graphs as was done for tracks from the  $54^\circ$  plates. This was done for the data from both the polythene and carbon targets and the number of recoil protons from neutrons with incident energies between 100 and 170 meV was obtained for each  $5^\circ$  interval between  $47.5^\circ$  and  $67.5^\circ$ .

At the extreme angles,  $47.5^\circ$  and  $67.5^\circ$ , the path length of the recoil particles in the aluminium was so long that the errors in  $\theta$  due to multiple scattering were appreciable. Approximate estimates of the effect of these errors suggested that about 5% more particles would be counted at the extreme angles than at the median angle  $57.5^\circ$ , where the scattering was smaller and its effect would tend to be self-cancelling. The effect was minimized by choosing an absorber thickness ( $350\mu$ ) such that at the extreme angles the recoil protons from 170 meV neutrons reached the end of their range very near to the glass. As a consequence of this restriction proton recoils at  $57.5^\circ$  from neutrons of energy 125 meV or greater would enter the glass before reaching the end of their range. In practice, because of the scattering both in the aluminium and the emulsion, the limiting value of  $E_n$  for particles entering glass was less than 120 meV. The tracks could not, therefore,

be grouped according to the same energy intervals as was used for the  $54^\circ$  plate and only one group, which included all the tracks above the  $(R, \theta)$  curve for 100 mev, was considered. Since the majority of the tracks in this group entered the glass it was not possible to apply any  $(R, \theta)$  selection criteria and the proportion of general background tracks which had to be cancelled with the carbon background was therefore much higher than for the data from the  $54^\circ$  plate. It was verified that the ratio of polythene to background (carbon plus general background) tracks in the interval  $57.5^\circ$  to  $67.5^\circ$  was the same for the data from both the  $44^\circ$  and  $54^\circ$  plates when no  $(R, \theta)$  selection criteria had been applied with the latter.

The neutron flux  $n_0(\bar{E}_n)$ , estimated from figure 8 for the energy interval 100 to 170 mev, was  $3.03 \pm 0.29 \times 10^4$  neutrons  $\text{cm}^{-2} \text{sec}^{-1}$  at an effective energy of  $130 \pm 5$  mev. The corresponding values obtained using the Harwell spectrum were  $3.03 \times 10^4$  neutrons  $\text{cm}^{-2} \text{sec}^{-1}$  at  $133 \pm 3$  mev.

### § 10. RESULTS AND CONCLUSIONS

The differential cross sections  $d\sigma/d\Omega$  in the centre-of-mass system for n-p scattering for the two groups of neutrons with effective energies 96 and 137 mev respectively, considered on the  $54^\circ$  plate, are given in table 3. The values are on an absolute scale, the errors shown being the standard deviations which arise mainly from the statistical error in the number of tracks counted in each group; the error involved in the normalization (see § 7) has not been included here.

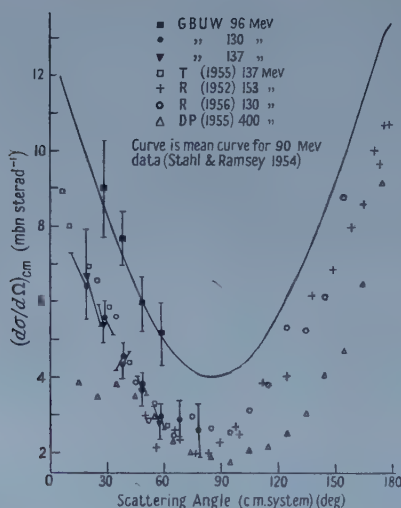


Figure 9. GBUW, present work; T, Thresher *et al.*; R, Randle *et al.*; DP, De Pangher.

The plate at  $\gamma = 54^\circ$  covers a range of scattering angles extending from  $19.3^\circ$  to  $58.8^\circ$  in the centre-of-mass system. Inclusion of the measurements on the  $44^\circ$  plate increased this angular range so as to cover from  $19.3^\circ$  to  $78.1^\circ$ . In combining the measurements made on the two plates the tracks measured on the  $54^\circ$  plate had to be regrouped so as to correspond to the same range of neutron energies as that used on the  $44^\circ$  plate, viz. 100 to 170 mev. In the recoil angular interval  $57.5^\circ$  to  $67.5^\circ$ , for this energy group, the cross sections obtained from



the independent measurements made on the  $44^\circ$  and  $54^\circ$  plates are in good agreement with one another. These values together with the combined cross sections at the effective energy of  $130 \pm 5$  mev are given in table 4.

The final results are shown graphically in figure 9, where it is seen that the angular distributions are in good agreement with those obtained by other workers using different techniques of measurement. This is so for neutron energies near 95 mev as well as those near 130 mev. The results of De Pangher (1955) at 400 mev are shown in order to demonstrate the change obtained in the distribution as the energy is increased. The differential cross sections at angles within  $60^\circ$  of the forward direction measured in the present experiment for neutrons with energies between 130 and 140 mev are definitely smaller than those measured at the supplementary angles by Randle *et al.* (1952, 1956). It is therefore concluded that the results of the present work confirm that the angular distributions at energies between 130 and 140 mev are asymmetrical about  $90^\circ$  in contrast to the approximate symmetry of the distributions obtained at 90 mev. This asymmetry provides evidence in favour of the view that states with unit angular momenta contribute appreciably to the scattering of 130 to 140 mev neutrons by protons. The experiments of Hillman and Stafford (1956) and Roberts *et al.* (1954) using polarized neutrons also lead to similar conclusions.

#### ACKNOWLEDGMENTS

Throughout the course of this work we have been encouraged by the keen interest and advice given by Professor H. S. W. Massey. We have also had the benefit of many discussions with Dr. T. G. Pickavance and Professor J. M. Cassels (now at Liverpool) at Harwell, and with Dr. E. H. S. Burhop, Dr. W. E. Duncanson and Mr. L. Castillejo at University College.

We wish to thank the Director of the Atomic Energy Research Establishment for the use of the facilities at Harwell, and members of the cyclotron group for their kind co-operation and hospitality. We are greatly indebted to Dr. C. Waller, Ilford Ltd., for his invaluable advice concerning the use and processing of the emulsions and for checking our shrinkage factors; to Dr. A. Maccoll, Chemistry Department, University College London, for arranging for the chemical analysis of the target films, and to Miss E. McKenzie and Mr. F. W. Bullock for their assistance with the scanning and routine calculations.

Two of us (A. P. B. and W. S. C. W.) wish to thank the Department of Scientific and Industrial Research for the award of maintenance grants, and another (M. Y. U.) is grateful to the Department of Education, West Pakistan, for the grant of two years' study leave.

#### REFERENCES

- BRUECKNER, K., HARTSOUGH, W., HAYWARD, E., and POWELL, W. M., 1949, *Phys. Rev.*, **75**, 555.  
CHAMBERLAIN, O., and EASLEY, J. W., 1954, *Phys. Rev.*, **94**, 208.  
CHUNG, YING CHIH, 1954, University of California UCRL—2575.  
DAINTON, A. D., GATTIKER, A. R., and LOCK, W. O., 1951, *Phil. Mag.*, **42**, 396.  
DE PANGHER, J., 1955, *Phys. Rev.*, **99**, 1447.  
DZHELEPOV, V. P., and KAZARINOV, YU. M., 1954, *Doklady Akad. Nauk S.S.S.R.*, **99**, 939.  
EASLEY, J. W., 1954, University of California UCRL—2693.  
FOX, R. H., 1950, University of California UCRL—867.

- GUERNSEY, G., MOTT, G., and NELSON, B. K., 1952, *Phys. Rev.*, **88**, 15.  
HADLEY, J., KELLY, E., LEITH, C., SEGRÈ, E., WIEGAND, C., and YORK, H., 1949, *Phys. Rev.*, **75**, 351.  
HARTZLER, A. J., SIEGEL, R. T., and OPITZ, W., 1954, *Phys. Rev.*, **95**, 591.  
HILLMAN, P., and STAFFORD, G. H., 1956, *Nuovo Cim.*, Ser. 10, **3**, 633.  
HODGSON, P. E., 1954, *Phil. Mag.*, **45**, 190.  
KELLY, E., LEITH, C., SEGRÈ, E., and WIEGAND, C., 1950, *Phys. Rev.*, **79**, 96.  
MASSEY, H. S. W., 1955, *Proceedings of the 1954 Glasgow Conference on Nuclear and Meson Physics* (London : Pergamon Press).  
RANDLE, T. C., CASSELS, J. M., PICKAVANCE, T. G., and TAYLOR, A. E., 1951, *Phil. Mag.*, **42**, 215; 1953, *Ibid.*, **44**, 425.  
RANDLE, T. C., SKYRME, D. M., SNOWDEN, M., TAYLOR, A. E., URIDGE, F., and WOOD, E., 1956, *Proc. Phys. Soc. A*, **69**, 760.  
RANDLE, T. C., TAYLOR, A. E., and WOOD, E., 1952, *Proc. Roy. Soc. A*, **213**, 392.  
ROBERTS, A., TINLOT, J., and HAFNER, E. M., 1954, *Phys. Rev.*, **95**, 1099.  
SELOVE, W., STRANCH, K., and TITUS, F., 1953, *Phys. Rev.*, **92**, 724.  
STAHL, R. H., and RAMSEY, N. F., 1954, *Phys. Rev.*, **96**, 1310.  
TAYLOR, A. E., and WOOD, E., 1953, *Phil. Mag.*, **44**, 95.  
THRESHER, J. J., VOSS, R. G. P., and WILSON, R., 1955, *Proc. Roy. Soc. A*, **229**, 492.  
VIGNERON, L., 1953, *J. Phys. Radium*, **14**, 145.  
WALLACE, R., 1951, *Phys. Rev.*, **81**, 493.

# The Differential Cross Sections for the Reactions $^{14}\text{N}(\text{d}, \text{p})^{15}\text{N}$ and $^{14}\text{N}(\text{d}, \alpha)^{12}\text{C}$ between 600 and 1000 kev

By D. L. BOOTH, F. V. PRICE, D. ROAF AND G. L. SALMON

Clarendon Laboratory, Oxford

*MS. received 2nd October 1957, and in final form 23rd November 1957*

**Abstract.** Using a thin gas target, the differential cross sections for the two most energetic proton and alpha groups have been measured; an expansion in the form  $\Sigma a_n P_n(\cos \theta)$  has been fitted to the results. In no case was the value of  $a_n$  significant for  $n > 3$ , indicating that deuteron stripping is not important below 1 mev bombarding energy.

## § 1. INTRODUCTION

NUCLEAR reactions induced by deuterons are usually considered as proceeding through a combination of compound nucleus formation and deuteron stripping. The latter process predominates at bombarding energies greater than a few mev, but at lower energies compound nucleus formation becomes more important. Experiments in this energy region cannot easily be interpreted, but there is a need for reliable experimental data on absolute differential cross sections and angular distributions if the relative importance of the two mechanisms is to be studied.

The residual nuclei in the reactions considered may be left in their ground states, or in several possible excited states. Protons produced by the  $^{14}\text{N}(\text{d}, \text{p})^{15}\text{N}$  reaction corresponding to the formation of  $^{15}\text{N}$  in its ground state are referred to in this paper as group  $p_0$ . The first two excited states in  $^{15}\text{N}$  differ in energy by only 25 kev, so that the corresponding proton groups were not resolved in the present experiment and will be referred to as group  $p_{1,2}$ . A similar notation will be used for the various groups,  $\alpha_0$ ,  $\alpha_1$  and  $\alpha_2$  of alpha particles from the  $^{14}\text{N}(\text{d}, \alpha)^{12}\text{C}$  reaction, as shown in table 1. The energy-level data are given by Ajzenberg and Lauritsen (1955).

Table 1

Group	$p_0$	$p_{1,2}$	$p_3$	$\alpha_0$	$\alpha_1$	$\alpha_2$
$Q$ value (mev)	8.61	3.31	2.28	13.57	9.14	5.92
Excitation energy of residual nucleus (mev)	0	5.30	6.33	0	4.43	7.65

The angular distributions of the various proton groups from  $^{14}\text{N}(\text{d}, \text{p})^{15}\text{N}$  have been investigated at bombarding energies at 14.8 mev by Warburton and McGruer (1957) and above 8 mev by Green and Middleton (1956), and the results analysed using the stripping theory. Wyly (1949) using a gaseous target found that, between 1.5 and 3.0 mev bombarding energy, group  $p_0$  has an angular distribution with a maximum in the forward direction, whereas group  $p_{1,2}$  is approximately isotropic. Jongerius, Valckx and Endt (1954), using deuteron energies between 400 and 600 kev, found group  $p_0$  to have a strong forward

maximum, which they attributed to stripping. Stanley (1954) obtained similar results with 620 keV deuterons and a thick target.

The angular distributions of the first two alpha-particle groups from  $^{14}\text{N}(\text{d}, \alpha)^{12}\text{C}$  have been studied by Gibson and Thomas (1952) at 8 MeV, and by Warburton and McGruer (1957) at 14.8 MeV and that of group  $\alpha_1$  by Green and Middleton (1956) at 9 MeV. At lower energies Cartwright, Green and Willmott (1954), and Stanley (1954) found that the angular distribution of group  $\alpha_0$  has a strong forward maximum between 600 and 730 keV. Group  $\alpha_1$  appeared to have a maximum in the backward direction.

The present experiment gives information about the angular distributions of groups  $p_0$ ,  $p_{1,2}$ ,  $\alpha_0$  and  $\alpha_1$  at higher bombarding energies than were used by Jongerius *et al.* and Cartwright *et al.* The use of a windowless thin gaseous target has enabled the cross sections of these groups to be determined in absolute units.

## § 2. APPARATUS

A deuteron beam from the laboratory's 1.1 MeV cascade generator was passed through a gas target which has been described by Booth, Hill, Price, Roaf and Salmon (1958). The  $\text{D}^+$  ions were selected by an  $11^\circ$  magnetic analyser whose field was provided by a permanent magnet with a variable soft-iron shunt. To keep the background of neutrons low, the beam was initially collimated with a 5.5 mm diameter molybdenum stop. The perimeter of this hole was maintained by the beam at a gentle red heat, thus reducing the occlusion of deuterium.

The beam was everywhere enclosed in a thick-walled tube except for a gap 5 mm long which determined a reaction volume. To detect the protons and  $\alpha$ -particles, glass-backed nuclear emulsions were placed on either side of the gap, parallel to the axis of the beam. A sliding tubular shutter was used to control the duration of the exposure.

The beam current was determined by measuring the h.t. voltage and the heat delivered to a calorimeter at the far end of the target assembly similar to that described by Sanders (1949). The beam was stopped in a thick copper block, and the heat conducted down a copper tube to the water-cooled base of the instrument. Two constantan wires were soldered inside the copper tube, forming the junctions of a thermocouple which measured the temperature gradient in the tube.

## § 3. THE EXPOSURES

Exposures were made at 990, 805 and 595 keV effective bombarding energy. The data of Reynolds, Dunbar, Wenzel and Whaling (1953) were used when calculating the energy loss of the beam before reaching the reaction volume (between  $10\frac{1}{2}$  and  $27\frac{1}{2}$  keV). The target thickness, or energy loss in crossing the reaction volume, was between 0.25 and 0.7 keV depending on the bombarding energy and the target gas pressure.

The accelerating voltage was measured by comparing it with a standard cell by means of a resistance chain. The ratio of the resistance was determined from measurements on resonances in  $^{19}\text{F}(\text{p}, \alpha\gamma)^{16}\text{O}$ . The estimated error on the bombarding energy was 0.5%. The accelerating voltage was maintained within 1 kV of its nominal value during exposures, the 300 cycle ripple being approximately 1.4 kV peak to peak.



To reduce the partial pressure of deuterium in the target, beam currents of only 2 to  $8\mu\text{A}$  were used, with target gas pressures of 0.7 to 1.8 mm Hg. The estimated proton yield from  $\text{D}(d, p)^3\text{H}$  due to deuterium accumulated in the target gas as an impurity was calculated to be less than  $\frac{1}{8}\%$  of that from the  $p_0$  group. Errors in the duration of the exposure, variation in beam current and target pressure affect neither the shape of the angular distribution, nor the relative cross sections of groups studied on the same plates.

#### § 4. TRACK COUNTING

Ilford C2 emulsions  $200\mu$  thick were used for detecting the long range proton groups. Thick aluminium absorbers were placed in front of the plates to reduce the range in the emulsion of the  $p_0$  group and to exclude all the other groups of charged particles. Different thicknesses of absorber were placed in front of various parts of the plates so that the oblique path of the protons in the absorber was such that the residual projected range of a particle in the nuclear emulsion was about  $70\mu$ .

Ilford  $100\mu$  E1 emulsions, in which it is possible readily to distinguish between proton and alpha particle tracks, were used for detecting the shorter-ranged particles. Thin aluminium absorbers, sufficient only to exclude scattered deuterons and ultra-violet light, were placed in front of these plates.

The  $p_0$  tracks in the C2 plates under the thick foil were readily recognizable, and they could be rapidly counted as there were no other groups present. The proton range distributions on the E1 plates under the thin foils showed peaks corresponding to groups  $p_{1,2}$  and  $p_3$ . The groups showed a spread in projected range, due to the scattering in the absorber or in the emulsion.

The alpha-particle tracks on the E1 plates showed peaks due to groups  $\alpha_0$ ,  $\alpha_1$  and  $\alpha_2$ . The  $\alpha_0$  tracks were quite unmistakable, because of their length and thickness, and group  $\alpha_1$  was well resolved from the shorter groups.

Two background exposures were made at 990 keV, one with the shutter open and no gas in the target, the other with the shutter closed and 1.6 mm Hg of nitrogen in the target. The background tracks were found to be negligibly few in number.

#### § 5. RESULTS

The measured values of the differential cross section are shown in figures 1 to 3, together with the standard deviation of the number of tracks counted at each point (usually 2000). A least squares analysis in terms of Legendre polynomials gave the coefficients and standard deviations which are given in table 2; these coefficients determine the angular distribution irrespective of the uncertainties discussed below.

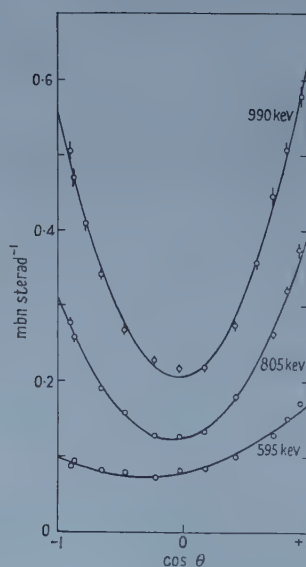
The precision of absolute value of the total cross section is affected not only by the statistical error mentioned above (always  $<2\frac{1}{2}\%$ ) but also by uncertainties in the nature and size of the target and in the intensity of the beam. The estimated uncertainty in the calibration of the manometer and in the size of the reaction volume, which were common to all exposures, was 2%. Uncertainties in the calorimeter readings, and in the bombarding energy, contributed a possible error of 2 to 4% in the intensity of the beam. The errors in the total cross section ( $\sigma_{\text{TOT}}$ ) shown in table 2 are the sum of the estimated uncertainties due to these various factors.

Table 2. Coefficients in the Expansion for the Differential Cross Section

$$\frac{d\sigma}{d\Omega} = \frac{\sigma_{TOT}}{4\pi} \{1 + a_1 P_1(\cos \theta) + a_2 P_2(\cos \theta) + a_3 P_3(\cos \theta)\}$$

Particle group	Energy (keV)	Total cross section (mbn)	$a_1$	$a_2$	$a_3$
$p_0$	990	$4.21 \pm 0.23$	$0.096 \pm 0.019$	$0.767 \pm 0.025$	—
	805	$2.52 \pm 0.13$	$0.198 \pm 0.018$	$0.764 \pm 0.023$	—
	595	$1.23 \pm 0.07$	$0.365 \pm 0.032$	$0.381 \pm 0.032$	—
$p_{12}$	990	$13.63 \pm 1.29$	—	—	—
	805	$4.52 \pm 0.36$	—	—	—
	597	$1.20 \pm 0.10$	—	—	—
$\alpha_0$	990	$3.92 \pm 0.33$	$1.261 \pm 0.053$	$0.810 \pm 0.042$	—
	805	$1.99 \pm 0.12$	$1.204 \pm 0.039$	$0.833 \pm 0.036$	—
	597	$0.82 \pm 0.04$	$1.044 \pm 0.018$	$1.094 \pm 0.021$	—
$\alpha_1$	990	$19.37 \pm 1.70$	$0.125 \pm 0.034$	$0.581 \pm 0.042$	—
	805	$8.47 \pm 0.56$	$-0.072 \pm 0.028$	$0.574 \pm 0.038$	$0.163 \pm 0.042$
	597	$2.57 \pm 0.15$	$-0.144 \pm 0.014$	$0.420 \pm 0.019$	$0.129 \pm 0.025$

The angular distributions of the group  $p_0$  and group  $\alpha_1$  become more symmetrical in the centre-of-mass system as the deuteron energy increases; that of the group  $\alpha_0$  becomes less symmetrical. The groups  $p_1$  and  $p_2$  are not resolved but combine to give an isotropic distribution.

Figure 1. The differential cross section of group  $p_0$ .

The overlapping of the energy levels of the compound nucleus could account for these variations, and it is concluded that the contribution to these reactions of deuteron stripping is small at energies from 600 keV to 1 MeV.

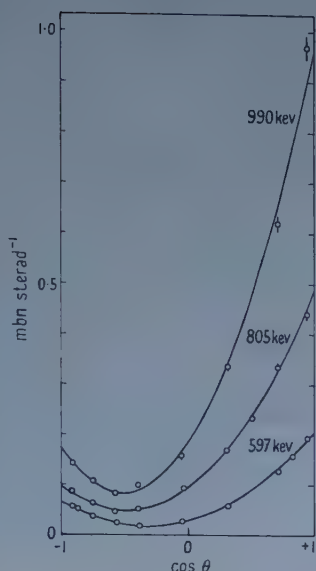


Figure 2. The differential cross section of group  $\alpha_0$ .

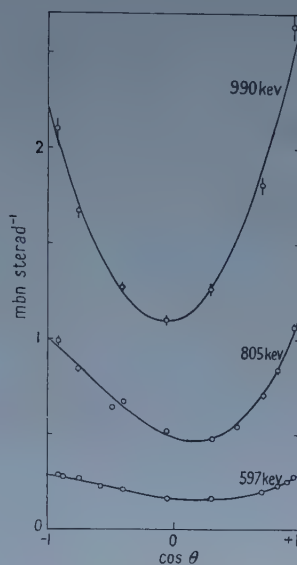


Figure 3. The differential cross section of group  $\alpha_1$ .

#### ACKNOWLEDGMENTS

The authors acknowledge with gratitude a maintenance grant to D. L. Booth from the Department of Scientific and Industrial Research, and a scholarship to G. L. Salmon from the Rhodes Trustees.

#### REFERENCES

- AJZENBERG, F., and LAURITSEN, T., 1955, *Rev. Mod. Phys.*, **27**, 77.  
 BOOTH, D. L., HILL, R. S., PRICE, F. V., ROAF, D., and SALMON, G. L., 1958, *J. Sci. Instrum.*, **43**, 24.  
 CARTWRIGHT, D., GREEN, L. L., and WILMOTT, J. C., 1954, *Phil. Mag.*, **45**, 742.  
 GIBSON, W. M., and THOMAS, E. E., 1952, *Proc. Roy. Soc. A*, **210**, 543.  
 GREEN, T. S., and MIDDLETON, R., 1956, *Proc. Phys. Soc. A*, **69**, 28.  
 JONGERUS, H. M., VALCKX, F. P. G., and ENDT, P. M., 1954, *Physica, 's Grav.*, **20**, 29.  
 REYNOLDS, H. K., DUNBAR, D. N. F., WENZEL, W. A., and WHALING, W., 1953, *Phys. Rev.*, **92**, 742.  
 SANDERS, J. H., 1949, *J. Sci. Instrum.*, **26**, 36.  
 STANLEY, A. G., 1954, *Phil. Mag.*, **45**, 807.  
 WARBURTON, E. K., MCGRUE, J. N., 1957, *Phys. Rev.*, **105**, 639.  
 WYLY, L. D., 1949, *Phys. Rev.*, **76**, 104.

# On the Determination of the Electron Capture Decay Energy: $^{196}\text{Au}$

By R. K. GUPTA

Tata Institute of Fundamental Research, Apollo Pier Road, Bombay 1

*MS. received 24th September 1957, and in revised form 20th November 1957*

**Abstract.** A single crystal scintillation spectrometer has been utilized to detect the triple summing, in the crystal, of three coincidence radiations. It has been shown that in an electron capture isotope the triple sum of two cascade  $\gamma$ -rays and K x-ray, which precedes the emission of  $\gamma$ -rays, can be used to calculate the ratio  $P_L/P_K$  for the transition to the second excited state of the daughter isotope. The ratio  $P_L/P_K$  can also be calculated by recording triple coincidence rate with two coincidence spectrometer units, by detecting the sum of two  $\gamma$ -rays in one and K, x-rays in the other unit. These methods have been used to calculate the decay energy of  $^{196}\text{Au}$ . The decay energy has been found to be  $911^{+55}_{-25}$  kev.

## § 1. INTRODUCTION

THE decay energy of an isotope decaying by electron capture can be calculated in terms of  $\beta$ -decay theory if  $P_L/P_K$ , the ratio of L-electron capture to K-electron capture, can be deduced from experimental observations. If the capture decay is to the ground state of the daughter isotope, and the observations involve the relative intensities of the K x-rays and L x-rays, then it is necessary to know the K- and L-fluorescence yields in order to deduce the capture branching ratio  $P_L/P_K$ . If the capture decay is to an excited state of the daughter nucleus, it is necessary in addition to know the values of K- and L-internal conversion coefficients with some accuracy. On the other hand, if one measures the number of K x-rays in coincidence with the  $\gamma$ -ray, either by the summing technique or with a conventional coincidence set-up, the ratio  $P_L/P_K$  (the ratio of the probabilities of the L- and K-electron capture) does not involve either the conversion coefficients or the L-fluorescence yield (Gupta and Jha 1956, 1957, Bisi *et al.* 1956). The situation, however, is complicated when the electron capture leads to the second excited state of the daughter isotope which de-excites by the emission of two cascade  $\gamma$ -rays without any appreciable cross-over transition. In such a case, the coincidences between one of the  $\gamma$ -rays and the K x-rays either by the summing technique or in a conventional coincidence set-up does not yield the ratio  $P_L/P_K$  without accurate knowledge of the conversion coefficients of the  $\gamma$ -rays. For finding out the decay energy of such an isotope, one needs to measure the triple coincidences among the two  $\gamma$ -rays and the Kx-rays.

A single crystal scintillation spectrometer has been used in this laboratory to detect the summing in the crystal of the two cascade  $\gamma$ -rays and the K x-rays from the K-electron capture which precedes the emission of the  $\gamma$ -rays. The area under the triple sum peak is the measure of the number of the triple coincidences. The triple coincidence studies have also been made in a conventional set-up. The sum peak of the two  $\gamma$ -rays is accepted in one channel and the K x-rays are detected in the other channel.



## § 2. TRIPLE COINCIDENCE BY THE SUMMING TECHNIQUE

If a source of electron capture isotope, emitting two  $\gamma$ -rays  $\gamma_1$  and  $\gamma_2$  of energy  $E_1$  and  $E_2$  respectively in cascade (no cross-over transition) is placed directly on the top of a NaI crystal of the scintillation spectrometer, one gets, in addition to the three peaks corresponding to the x-ray and the two  $\gamma$ -rays, a peak corresponding to the energy  $E_1 + E_2$  and another corresponding to the energy  $E_1 + E_2 + E_K$  ( $E_K$  being the energy of the K x-rays from the source). Let the area of the double sum peak be  $A_{12}$  and that of triple sum peak be  $A_{123}$ . Then the number of  $\gamma$ -rays,  $\gamma_1$  and  $\gamma_2$  detected simultaneously in the crystal is given by

$$I_{\gamma_1\gamma_2} = N\epsilon_{\gamma_1}\epsilon_{\gamma_2}S_1^2(1-X_1)(1-X_2) \propto (A_{12} + A_{123}) \quad \dots\dots(1)$$

where  $N$  is the number of disintegrations reaching the second excited state,  $\epsilon_{\gamma_1}$  and  $\epsilon_{\gamma_2}$  are the efficiencies of detection of  $\gamma_1$  and  $\gamma_2$  respectively,  $S_1$  is the fractional solid angle subtended by the source at the crystal, and  $X_1$  and  $X_2$  are the total conversion probabilities of transitions 1 and 2 respectively, where conversion probability is related to conversion coefficient by the relation

$$X = \alpha/(1 + \alpha).$$

Similarly, the triple sum peak area  $A_{123}$  due to the simultaneous detection of the two  $\gamma$ -rays and the K x-rays is given by

$$I_{\gamma_1\gamma_2X} = N_K\epsilon_{\gamma_1}\epsilon_{\gamma_2}\epsilon_XS_1^3\omega_K(1-X_1)(1-X_2) \propto A_{123} \quad \dots\dots(2)$$

where  $N_K$  is the number of K-electron captures leading to the second excited state, and  $\omega_K$  is the K-fluorescence yield in the daughter product. Also

$$\left(\frac{I_{\gamma_1\gamma_2X}}{I_{\gamma_1\gamma_2}}\right) = \left(\frac{N_K}{N}\right)\omega_K\epsilon_XS_1 = \frac{A_{123}}{A_{12} + A_{123}} \quad \dots\dots(3)$$

or

$$(N_K/N) = (I_{\gamma_1\gamma_2X}/I_{\gamma_1\gamma_2})(1/\omega_K\epsilon_XS_1)$$

and

$$\frac{P_L}{P_K} = \frac{(1 - N_K/N)}{N_K/N}.$$

From the value of the ratio  $P_L/P_K$ , one can calculate the decay energy to the second excited state (Marshak 1942, Brysk and Rose 1955). The value of  $P_L/P_K$  found by this method does not involve the conversion coefficient of  $\gamma$ -rays, nor the photoelectric efficiencies of the  $\gamma$ -rays in the crystal. This method will not work when the K x-ray energy is small, and the  $\gamma$ -ray energies relatively large. In that case, the sum peak of the two  $\gamma$ -rays cannot be resolved from the triple sum peak of the two  $\gamma$ -rays and the K x-rays.

The determination by the triple summing technique of the electron capture decay energy of an isotope, where the electron capture is followed by two  $\gamma$ -rays in cascade, is not very accurate when the  $P_L/P_K$  ratio is large, because in such a case the triple sum peak cannot be measured accurately. This difficulty, however, can be avoided if one uses a conventional coincidence set-up with two coincidence spectrometer units. The source is placed on the top of one of the crystals, and the other spectrometer crystal is placed at a sufficiently large distance that the x-ray pulses do not get summed up. The first channel accepting the sum peak pulses serves as the gate, and the number of x-ray pulses in coincidence

is found in the second spectrometer. The area of the sum peak or the number of counts in the gate is given by the relation (1). If the channel of the scanner spectrometer is made wide enough to cover all the K x-rays pulses and their escape peak pulses, the number of counts of K x-rays in coincidence with the two  $\gamma$ -rays is given by

$$I_{\gamma_1\gamma_2\text{X}} = N_K \epsilon_{\text{X}} \epsilon_{\gamma_1} \epsilon_{\gamma_2} S_1^2 S_2 \omega_K (1 - X_1)(1 - X_2) \quad \dots\dots(4)$$

where  $S_2$  is the fractional solid angle subtended by the source at the crystal of the second spectrometer. The ratio of (4) and (1) gives

$$\frac{I_{\gamma_1\gamma_2\text{X}}}{I_{\gamma_1\gamma_2}} = \frac{N_K}{N} \omega_K \epsilon_{\text{X}} S_2. \quad \dots\dots(5)$$

The relation (5) is the same as relation (3) with this difference that whereas in the relation (3) all the rays are counted in the same fractional solid angle  $S_1$ , in the second experiment (relation (5)), the K x-rays are counted in fractional solid angle  $S_2$ . From the relation (5) the ratio  $P_L/P_K$  can be calculated and so one can get the decay energy to the second excited state exactly as in the triple summing technique. It may be stated here that the quantities  $I_{\gamma_1\gamma_2}$  and  $I_{\gamma_1\gamma_2\text{X}}$  can be determined in a two-spectrometer coincidence method much more accurately than by the summing technique alone. One could do these triple coincidence measurements with three spectrometers, but one would need a much stronger source. This method has been used to calculate decay energy of  $^{133}\text{Ba}$  (to be published). The two methods described above have been used to determine the decay energy of  $^{196}\text{Au}$ .

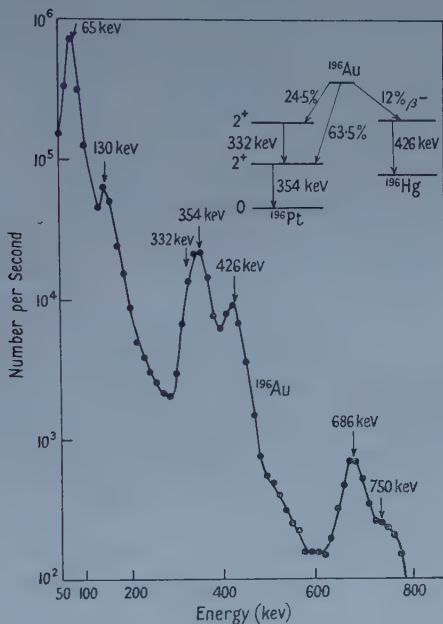
### § 3. THE DECAY SCHEME OF $^{196}_{79}\text{Au}$

It was shown by Steffen *et al.* (1949) for the first time that this isotope decays by electron capture with a half-life of 5.6 days to the excited states of  $^{196}\text{Pt}$  at 358 keV and at 686 keV and also by  $\beta^-$ -emission to  $^{196}\text{Hg}$ . The intensity of the 686 keV cross-over transition  $\gamma$ -ray was estimated to be less than 5%. Later Staehelin (1952) found a  $\gamma$ -ray of 426 keV energy associated with the  $\beta^-$ -decay branch, the maximum beta energy being  $270 \pm 20$  keV. More recently Thieme *et al.* (1956) have made a thorough study of  $^{196}\text{Au}$ . The decay scheme suggested by them is given in the inset of the figure.

### § 4. SUMMING TECHNIQUE MEASUREMENTS ON $^{196}\text{Au}$

A mixed source of  $^{195}\text{Au}$  (half-life 180 days) and  $^{196}\text{Au}$  was supplied by Philips-Roxane, Amsterdam, in a carrier free state in a dilute HCl solution. The presence of  $^{195}\text{Au}$  did not interfere with the studies on  $^{196}\text{Au}$  as the former emits all low energy  $\gamma$ -rays. The spectrum of the  $\gamma$ -rays from the  $^{196}\text{Au}$  source, deposited on an aluminium source holder with a mylar backing ( $600 \mu\text{g cm}^{-2}$ ), taken with a scintillation spectrometer with a NaI(Tl) crystal  $1\frac{3}{4}$  in. diameter and 2 in. high, is reproduced in the figure. The peak at 65 keV is due to K x-rays of Pt from ( $^{196}\text{Au}$  and  $^{195}\text{Au}$ ) and at 130 keV is due to simultaneous detection of two x-rays (capture and conversion). The peak at 354 keV is due to two  $\gamma$ -rays, unresolved, one of energy 332 keV and another of energy 354 keV. The peak

at 686 keV is due to the simultaneous detection of the 332 keV and the 354 keV  $\gamma$ -rays. The last peak, not very well resolved, is at 750 keV, which is due to the triple sum of the two  $\gamma$ -rays and the K x-rays of platinum. The total area under the 686 keV peak (the double sum peak) and 750 keV peaks was broken into two by making a Gaussian fit for the 686 keV peak and subtracting it from the total.



The difference plot gave only the 750 keV peak. The spectrum was taken for two different solid angles. The results are summarized below. The value of the K-fluorescence yield of platinum  $\omega_K$  has been taken to be 0.95. The value of  $\epsilon_X$  (inclusive of absorption in the cover of the crystal) has been calculated to be 0.94.

Fractional solid angle	$I_{\gamma_1\gamma_2}$	$I_{\gamma_1\gamma_2X}$	$(I_{\gamma_1\gamma_2X}/I_{\gamma_1\gamma_2})$	$(P_L/P_K)$
0.412	168	44	$0.260 \pm 0.02$	$0.41^{+0.13}_{-0.11}$
0.310	225	44	$0.195 \pm 0.015$	$0.41^{+0.13}_{-0.11}$

### § 5. COINCIDENCE MEASUREMENTS

For this work, a conventional coincidence set-up with two scintillation spectrometers having a resolving time of  $5 \times 10^{-7}$  sec was used. The source was put on the top of the crystal of one of the spectrometers and the entire peak under the 686 keV and 750 keV peaks was used as a gate. The other spectrometer crystal viewing the same source was placed at a distance of 29 mm, 49 mm and 56 mm. The channel of this detector was made wide enough to cover the entire K x-rays peak along with its escape peak. The results of different

measurements are summarized below. From these values of  $P_L/P_K$  and taking the value of  $(\psi_{L1}/\psi_K)^2$  for  $^{79}\text{Au}$  to be 0.147 (Rose and Jackson 1949), the values of the decay energy have been calculated. The mean value of the decay energy of  $^{196}\text{Au}$  to the 686 keV state comes out to be  $225 \pm_{27}^{55}$  keV. The total decay energy from the ground state of  $^{196}\text{Au}$  to the ground state of  $^{196}\text{Pt}$  is thus  $911 \pm_{27}^{55}$  keV.

Fractional solid angle	Gate counts	Coincidence counts	$\left(\frac{I_{\gamma_0\gamma_2X}}{I_{\gamma_1\gamma_2}}\right)$	$P_L/P_K$
$S_2$	$I_{\gamma_1\gamma_2}$	$I_{\gamma_1\gamma_2X}$		
0.08	4879	268.0	0.0550	$0.315 \pm 0.05$
0.035	4811	118.8	0.0246	$0.30 \pm 0.05$
0.027	3698	70.0	0.0189	$0.315 \pm 0.05$

The  $\log ft$  values for electron capture transitions to the first and second excited states of  $^{196}\text{Pt}$  (Major and Biedenharn 1954) calculated from the above results are 6.1 and 6.5 respectively. Both of the  $\log ft$  values are consistent with first forbidden transition of the type  $\Delta J = 0, \pm 1$ , yes. The ground state of even-even nuclei of  $^{196}\text{Pt}$  is  $0^+$ . The first and second excited states of  $^{196}\text{Pt}$  have been assigned  $2^+$  and  $2^+$  respectively from angular correlation experiments and measurement of conversion coefficient (Steffen *et al.* 1949, Steffen and Roberts 1951, Steffen 1953). The ground state of  $^{196}\text{Au}$ , in analogy with the ground state of  $^{198}\text{Au}$  (Elliott *et al.* 1955) can be assigned  $2^-$  or  $3^-$ . With either of the assignments, the electron capture to both of the excited states is of the type  $\Delta J = 0, \pm 1$ , yes. This is consistent with the values of  $\log ft$  calculated using decay energies determined here.

#### ACKNOWLEDGMENTS

My thanks are due to Dr. S. Jha for helpful discussions and to Dr. B. V. Thosar for keen interest and encouragement.

#### REFERENCES

- BISI, A., GERMAGNOLI, E., and ZAPPA, L., 1956, *Nuclear Phys.*, **1**, 593.  
 BRYSK, H., and ROSE, M. E., 1955, Oak Ridge National Laboratory, Report 1830.  
 ELLIOTT, L. G., PRESTON, M. A., and WOLFSON, J. L., 1955, *Canad. J. Phys.*, **33**, 607.  
 GUPTA, R. K., and JHA, S., 1956, *Nuovo Cim.*, **4**, 88 ; 1957, *Ibid.*, **5**, 1524.  
 MAJOR, J. K., and BIEDENHARN, L. C., 1954, *Rev. Mod. Phys.*, **26**, 321.  
 MARSHAK, R. E., 1942, *Phys. Rev.*, **61**, 431.  
 ROSE, M. E., and JACKSON, J. L., 1949, *Phys. Rev.*, **76**, 1540.  
 STAEHELIN, P., 1952, *Phys. Rev.*, **87**, 374.  
 STEFFEN, R. M., 1953, *Phys. Rev.*, **89**, 665.  
 STEFFEN, R. M., HUBER, O., and HUMBEL, F., 1949, *Helv. Phys. Acta*, **22**, 167.  
 STEFFEN, R. M., and ROBERTS, D. M., 1951, *Phys. Rev.*, **83**, 222.  
 THIEME, M. T., and BLEULER, E., 1956, *Phys. Rev.*, **101**, 1031.



## The $\beta$ -decay of $^{185}\text{W}$

By B. H. ARMITAGE AND W. G. V. ROSSER

Physics Department, University of Exeter

*Communicated by G. K. T. Conn; MS. received 16th October 1957, and in final form 3rd December 1957*

**Abstract.** It is shown that the 56 keV  $\gamma$ -ray observed from natural tungsten irradiated in the pile does not arise from the decay of  $^{185}\text{W}$  as was suggested by Bisi, Terrani and Zappa (1955). The  $\gamma$ -ray peak at 125 keV probably arises from a 0.005% branching ratio to the 125 keV excited level in  $^{185}\text{Re}$ . The continuous photon spectrum is interpreted quantitatively as internal plus external bremsstrahlung.

### § 1. INTRODUCTION

IT has been known for some time that  $^{185}\text{W}$  decays by  $\beta^-$  emission to  $^{185}\text{Re}$ , mainly direct to the ground state. The maximum  $\beta$ -ray energy is  $426 \pm 3$  keV. Some of the early workers also reported a weak  $\gamma$ -ray at 134 keV. However, in 1955 Bisi, Terrani and Zappa suggested that 10% of the  $\beta$ -rays decayed to an excited level at 55.6 keV in  $^{185}\text{Re}$ . The main purpose of the present work was to try and confirm this result by  $\beta$ - $\gamma$  coincidence measurements. Whilst the work was in progress Bhattacharjee and Raman (1956), using two scintillation spectrometers found coincidences between  $\beta$ -rays and  $\gamma$ -rays of energy 55.6 keV. They reported a branching ratio of 15%. On the other hand Marty and Vergnes (1956) found no  $\beta$ - $\gamma$  coincidences apart from those which they attributed to coincidences between  $\beta$ -rays and 28 keV iodine x-rays. They compared the 55.6 keV  $\gamma$ -ray with tantalum x-rays and concluded that they had the same energy, and suggested that these  $\gamma$ -rays were emitted following electron capture in  $^{181}\text{W}$ . Dubey, Mandeville, Mukerji and Potnis (1957) also come to this conclusion from measurements with enriched isotopes.

### § 2. INVESTIGATION OF THE DECAY SCHEME

The single  $\gamma$ -ray spectrum of ordinary  $\text{WO}_3$  exposed in the pile at Harwell is shown in curve A of figure 1. The  $\gamma$ -rays were detected using a NaI(Tl) crystal and an E.M.I. Type 6097 photomultiplier. There is a large peak at about 56 keV and a smaller peak at about 125 keV. The intensity then decreases to approximately zero at about 400 keV.

A search for  $\beta$ - $\gamma$  coincidences was made. The  $\beta$ -rays were detected using a Naton 11 crystal and an E.M.I. Type 6262 photomultiplier. A coincidence circuit of the Bell, Graham and Petch (1952) type was used with a resolving time of  $0.02 \mu\text{sec}$ . Coincidences between  $\beta$ -rays and photons with energy in the region of 56 keV were observed, but they corresponded to a very much smaller branching ratio than reported by Bisi *et al.* Furthermore, the  $\beta$ - $\gamma$  coincidences were not confined to photons within this energy region only; the spectrum

of photons in coincidence with all  $\beta$ -rays greater than about 50 keV is shown in curve B of figure 1. The momentum spectrum of  $\beta$ -rays in coincidence with all photons is shown in figure 2. The momentum of the  $\beta$ -rays was determined with a magnetic lens spectrometer. The results showed that the coincident  $\beta$ -ray spectrum is displaced from the single  $\beta$ -ray spectrum by an amount approximately equivalent to the mean energy of the  $\gamma$ -rays in coincidence with  $\beta$ -rays (curve B, figure 1). This showed from energy considerations that most of the  $\beta$ - $\gamma$  coincidences observed with the unseparated isotope were associated

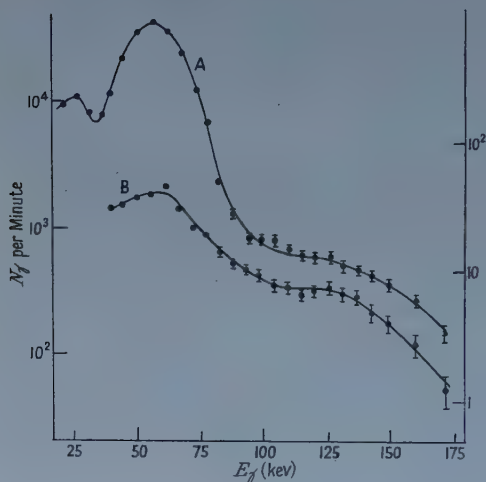


Figure 1. Energy spectra of photons from natural tungsten aged after irradiation in the pile: A, all photons; B, photons in coincidence with  $\beta$ -rays.

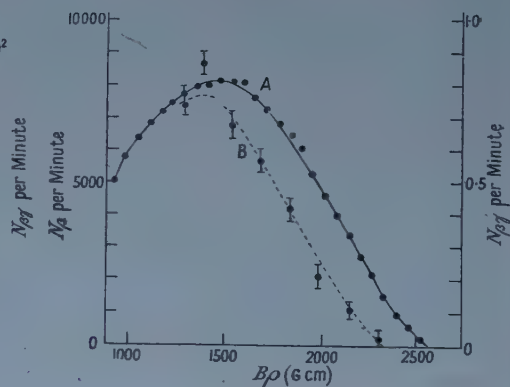


Figure 2. Momentum spectra of  $\beta$ -rays from natural tungsten aged after irradiation in the pile: A, all  $\beta$ -rays; B,  $\beta$ -rays in coincidence with photons.

with the decay of  $^{185}\text{W}$ . The large peak at 56 keV, present in curve A, figure 1, did not appear to be in coincidence with  $\beta$ -rays. It will be shown in §3 that apart from the small peaks at about 60 keV and about 125 keV all the  $\beta$ - $\gamma$  coincidences shown in curve B of figure 1 can be accounted for as internal and external bremsstrahlung accompanying the  $\beta$ -decay of  $^{185}\text{W}$ . These results suggested that the large 56 keV  $\gamma$ -ray peak did not arise during the decay of  $^{185}\text{W}$ .

As further confirmation an enriched tungsten source containing 94%  $^{184}\text{W}$  was exposed in the pile at Harwell. The single  $\gamma$ -ray and  $\beta$ - $\gamma$  coincidence spectra obtained with this source are shown in figure 3. The results showed conclusively that the strong 56 keV  $\gamma$ -ray did not occur in the decay of  $^{185}\text{W}$ . They are in agreement with curve B, figure 1. Superimposed on the continuous bremsstrahlung spectrum were additional  $\gamma$ -ray peaks at approximately 300 and 610 keV. These did not appear in the unseparated source, though they would have been detectable if they were present in the same proportion. Furthermore, the  $\beta$ -rays in coincidence with these peaks could penetrate more than  $125\text{ mg cm}^{-2}$  of aluminium and were too energetic to be associated with  $\beta$ -rays from the decay of  $^{185}\text{W}$  to  $^{185}\text{Re}$ . These  $\gamma$ -rays were probably due to minute traces of impurities (mainly  $^{192}\text{Ir}$ ) present in the enriched isotope only.

It can be seen from figures 1 and 3 that the  $\gamma$ -ray at about 125 keV was in coincidence with  $\beta$ -rays. It was present in about the same proportion relative to bremsstrahlung in both the ordinary and the enriched isotopes, when sources of the same thickness were used. A study of the range of  $\beta$ -rays in coincidence with photons in the energy range 115 to 135 keV suggested that all the  $\beta$ -rays had a range of about  $75 \text{ mg cm}^{-2}$ . This was consistent with a maximum  $\beta$ -ray energy of about 300 keV for all such  $\beta$ -rays. However,  $\beta$ -rays going direct to the ground state but which gave bremsstrahlung photons in the energy range 115–135 keV would have the same maximum energy as  $\beta$ -rays which decayed via the excited level at 125 keV in  $^{185}\text{Re}$ . As the number of photons in the 125 keV peak was always smaller than the bremsstrahlung background it was difficult to be absolutely sure from the experimental results that there is a branching to a 125 keV in  $^{185}\text{Re}$ .

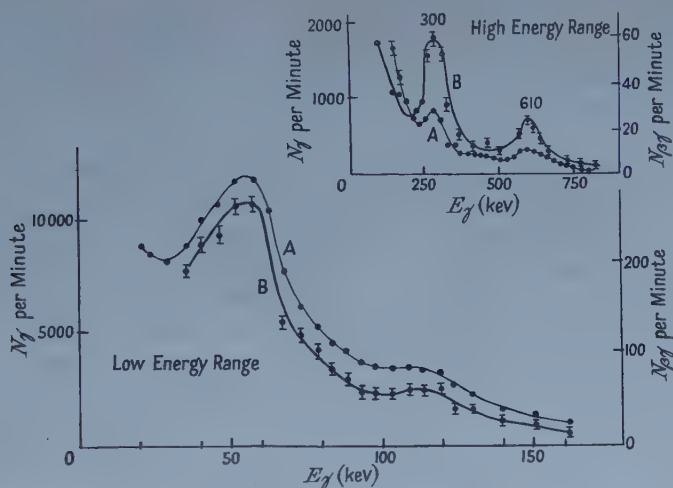


Figure 3. Energy spectra of photons from enriched  $^{185}\text{W}$  with ordinates plotted on a linear scale: A, all photons; B, photons in coincidence with  $\beta$ -rays.

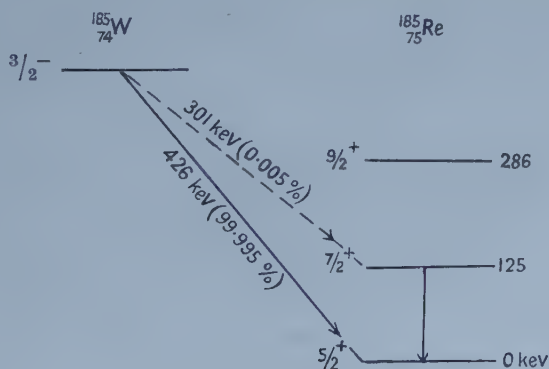


Figure 4. Energy levels of  $^{185}\text{Re}$  and the decay scheme proposed for  $^{185}\text{W}$ .

Several workers have observed rotational levels at 125 keV and 286 keV in  $^{185}\text{Re}$  by Coulomb excitation (Alder, Bohr, Huus, Mottelson and Winther 1956). The spins and parities of the levels are shown in figure 4. The ground state spin of  $^{185}\text{Re}$  has been measured as  $5/2$ . The  $\beta$ -transition to the ground state

of  $^{185}\text{Re}$  is first forbidden ( $\Delta J=1$ ; 'yes';  $\log ft=7.4$ ). A  $\beta$ -transition to the excited level at 125 keV in  $^{185}\text{Re}$  would be  $\Delta J=2$ ; 'yes' and should be first forbidden. However, the change in angular momentum would be 3 so that the transition would be  $l$ -forbidden. The intensity observed in the 125 keV peak corresponded to  $5 \times 10^{-5}$  photons per  $\beta$ -disintegration. Neglecting any internal conversion this would correspond to a  $\log ft$  of 11.1. A branching ratio of this amount could be consistent with an  $l$ -forbidden transition. It is therefore suggested tentatively, that there is a branching ratio of 0.005% to the 125 keV excited level in  $^{185}\text{Re}$ .

For  $\beta$ -decay to the 286 keV level in  $^{185}\text{Re}$  we would have  $\Delta J=3$ ; 'yes', which would make the transition third forbidden. The intensity expected in this case would be too low to be observed experimentally. The decay scheme proposed for  $^{185}\text{W}$  is shown in figure 4.

### § 3. INVESTIGATION OF THE CONTINUOUS PHOTON SPECTRUM

The experiments were carried out using an enriched  $^{185}\text{W}$  source. The source strength was determined with a magnetic lens spectrometer of known transmission. Due to the impurities present in the enriched isotope it was not possible to extend the measurements for photon energies above 250 keV. The photons were detected with a NaI(Tl) crystal placed at a fixed distance from the source. The  $\beta$ -rays were stopped by a Perspex absorber placed between the source and the crystal. The experimental results were corrected for the efficiency of the scintillation spectrometer and for the attenuation of photons in the absorbers between the source and the crystal. The corrected results for the single photon spectrum are shown in figure 5.

Due to the low specific activity of the sources available it was necessary to use a tungsten source  $2 \text{ mg cm}^{-2}$  thick. This led to the production of an

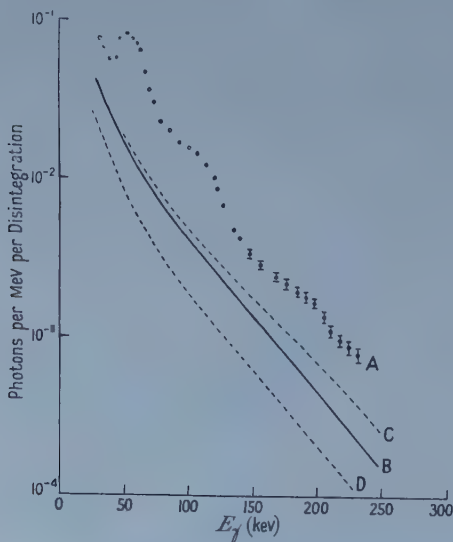


Figure 5. The continuous photon spectrum from enriched  $^{185}\text{W}$ : A, experimental results; B, intensity of internal plus external bremsstrahlung calculated using the Knipp-Uhlenbeck theory for internal bremsstrahlung; C, intensity of internal plus external bremsstrahlung calculated using the Nilsson theory for internal bremsstrahlung; D, calculated intensity of external bremsstrahlung from the source and absorber.



appreciable amount of external bremsstrahlung in the tungsten source. It was also necessary to place the source near the crystal so that a large fraction of the external bremsstrahlung produced by the  $\beta$ -rays in the Perspex absorber was detected by the crystal. The external bremsstrahlung produced in both the source and the absorber was calculated using the Elwert-Sommerfeld formula (Heitler 1954); the results are shown by curve D of figure 5, approximately 50% of the total being produced in the source. The results of Lidén and Starfelt (1955) and Starfelt and Svantesson (1955) have shown that the theory of external bremsstrahlung is fairly reliable for light elements, but for heavy elements such as tungsten the experimental values are generally up to 50% higher than calculated. It was therefore not possible to estimate the experimental internal bremsstrahlung accurately with the sources available at present.

The intensity of internal bremsstrahlung calculated on the basis of the Knipp-Uhlenbeck (1936) theory and using the Nilsson (1956) modification are shown by curves B and C of figure 5, respectively. The estimated external bremsstrahlung has been added in each case.

Superimposed on the continuous spectrum there was, in addition to the peak at about 125 keV, another small peak at about 60 keV, corresponding to an intensity of  $(6 \pm 2) \times 10^{-4}$  photons per  $\beta$ -disintegration. Photons with energies of about 60 keV might have arisen in several ways. The emission of a  $\beta$ -ray occasionally leads to the internal ionization of the transforming atom (auto-ionization), leading to the emission of  $^{185}\text{Re}$  x-rays. According to the theory developed by Midgal (1941) we would expect  $1.3 \times 10^{-4}$  K x-rays per  $\beta$ -disintegration. Levinger (1953) has suggested corrections which might have increased this calculated intensity by a factor of the order of two. Part of the peak might have been due to the emission of characteristic K x-rays following the ionizing collisions of the  $\beta$ -rays as they passed through the tungsten source. A trace of  $^{181}\text{W}$  in the enriched isotope would also have contributed to the peak in the single photon spectrum, as tantalum x-rays would have been emitted following electron capture in  $^{181}\text{W}$ .

These results show that the continuous spectrum after subtracting the peaks can be interpreted quantitatively as internal plus external bremsstrahlung. The uncertainties in the calculated external bremsstrahlung did not allow us to make a reliable comparison of internal bremsstrahlung with theory.

#### § 4. CONCLUSIONS

The large peak at 56 keV in the photon spectrum from natural tungsten which has been irradiated in a pile does not arise in the decay of  $^{185}\text{W}$  as was suggested by Bisi *et al.* (1955).

The small peak at about 60 keV present in this energy region in the decay of the enriched isotope can be accounted for as auto-ionization leading to the emission of Re x-rays together with tungsten x-rays due to the ionizing collisions of the  $\beta$ -rays as they pass through the tungsten source. The photon peak at about 125 keV probably arises from a 0.005% branching ratio to the 125 keV excited level in  $^{185}\text{Re}$ . The continuous photon spectrum can be interpreted quantitatively as internal plus external bremsstrahlung.

## ACKNOWLEDGMENTS

The authors would like to thank Professor H. O. W. Richardson for the loan of a  $\beta$ -ray spectrometer and Mr. N. J. Freeman for his help in the construction of the electronic apparatus. One of us (B. H. A.) would like to acknowledge the award of a scholarship by the University of Exeter.

## REFERENCES

- ALDER, K., BOHR, A., HUUS, T., MOTTELSON, B., and WINTHER, A., 1956, *Rev. Mod. Phys.*, **28**, 432.  
BELL, R. E., GRAHAM, R. L., and PETCH, H. E., 1952, *Canad. J. Phys.*, **30**, 35.  
BHATTACHERJEE, S. K., and RAMAN, S., 1956, *Nuovo Cim.*, **3**, 1131.  
BISI, A., TERRANI, S., and ZAPPA, L., 1955, *Nuovo Cim.*, **1**, 295.  
DUBEY, V. S., MANDEVILLE, C. E., MUKERJI, A., and POTNIS, V. R., 1957, *Phys. Rev.*, **106**, 785.  
HEITLER, W., 1954, *The Quantum Theory of Radiation*, 3rd Edn (Oxford: Clarendon Press).  
KNIPP, J. K., and UHLENBECK, G. E., 1936, *Physica*, **3**, 425.  
LEVINGER, J. S., 1953, *Phys. Rev.*, **90**, 11.  
LIDÉN, K., and STARFELT, N., 1955, *Phys. Rev.*, **97**, 419.  
MARTY, N., and VERGNES, M., 1956, *J. Phys. Radium*, **17**, 1013.  
MIDGAL, A., 1941, *J. Phys.*, (*Moscow*), **4**, 449.  
NILSSON, S. B., 1956, *Ark. Fys.*, **10**, 467.  
STARFELT, N., and SVANTESSON, N. L., 1955, *Phys. Rev.*, **97**, 708.

## Recombination Coefficients for Positive and Negative Ions

By T. H. Y. YEUNG

Electron Physics Department, University of Birmingham

*Communicated by J. Sayers ; MS. received 4th October 1957*

**Abstract.** The dielectric constant of an ionized medium is decreased not merely by the presence of electrons but also by that of other free carriers, the positive and negative ions. In a highly electronegative gas discharge, the effect of the ions cannot be neglected and sometimes their contributions may swamp that of the electrons.

Under such conditions, measurements of the recombination coefficient between positive and negative ions have been made in the afterglow following pulsed radio-frequency discharges in iodine and bromine vapours. The recombination coefficient  $\alpha_i$  was found to be  $1.47 \times 10^{-8} \text{ cm}^3 \text{ sec}^{-1}$  for iodine molecular ions and  $1.85 \times 10^{-8} \text{ cm}^3 \text{ sec}^{-1}$  for bromine at room temperature.  $\alpha_i$  was constant over an extended pressure range and was found to be temperature dependent.

### § 1. INTRODUCTION

As is well known, the dielectric constant of an ionized medium is a function of all types of free charged particles present in the medium, and of the applied frequency. If we neglect the effects of collisions and there is no magnetic field, the general equation for the real part of the dielectric constant is given by

$$\epsilon' = 1 - \frac{4\pi e^2}{\omega^2} \left( \frac{n_e}{m} + \frac{N^-}{M^-} + \frac{N^+}{M^+} \right) \quad \dots\dots(1)$$

where  $e$  is electronic charge,  $\omega$  is the applied angular frequency,  $n_e$ ,  $N^-$  and  $M^+$  are electron, negative and positive ion concentrations, and  $m$ ,  $M^-$  and  $M^+$  are their respective masses. Since the ionic mass  $M$  is very much greater than the electronic mass  $m$  and in a normal ionized plasma  $n_e \simeq N^+$ , the ion terms  $N^-/M^-$  and  $N^+/M^+$  in the equation are usually neglected. Against this usual condition, if  $n_e \ll (N^-/M^-)m$  or  $(N^+/M^+)m$ , then the ion contributions become predominant in the equation and in this case the electron contribution can be neglected. Therefore equation (1) becomes

$$\epsilon' = 1 - \frac{4\pi e^2}{\omega^2} \left( \frac{N^-}{M^-} + \frac{N^+}{M^+} \right) \quad \dots\dots(2)$$

and if the charge carrier concentrations of both signs are equal and of the same mass then we have

$$\epsilon' = 1 - \frac{8\pi e^2}{M\omega^2} N. \quad \dots\dots(3)$$

In the afterglow plasma of a highly electronegative gas discharge, with the source of ionization removed, the electrons will encounter attachment collisions with neutral molecules or dissociated atoms to form negative ions. The plasma

will thus approach a state in which it consists of positive and negative ions of equal concentration and in thermal equilibrium with the neutral gas. For high ion densities, the deionization process will proceed mainly by mutual recombination between these ions; finally, at lower ion densities, diffusion will be the main process to complete the deionization.

Iodine and bromine vapours were used in the present experiment and the coefficients of ionic recombination of the two-body process were measured.

## § 2. FACTORS UNDER CONSIDERATION

### 2.1. *The Effect of Collisions*

In equations (1) to (3), we neglected the effect of collisions of the electrons or ions with neighbouring neutral particles. When we take collisions into consideration, the plasma behaves as an absorbing medium; and these collisions will affect both the real part of the dielectric constant and the imaginary part which is the conductivity. It is possible, in principle, to measure the components of the complex dielectric constant and, provided sufficient information is available on the collision cross section and angular distribution, to calculate the electron or ion density from the above measurement. It was, however, possible in these experiments to choose conditions such that the collision frequency was small compared with the angular frequency of the test signal. This ensures that the imaginary part of the dielectric constant is small compared with the real part and, to a first approximation, the former may be neglected.

If the pressure and temperature of the medium are known we may write for the collision frequency

$$\nu = \frac{\bar{c}}{l} \text{ and } c = \sqrt{\frac{8kT}{\pi M}}, \quad l = \frac{1}{nA} \quad \dots\dots(4)$$

where  $c$  is the mean thermal velocity of electrons or ions,  $l$  is the corresponding mean free path,  $n$  is the number of neutral particles per  $\text{cm}^3$  and  $A$  is the molecular (or atomic) collision cross section. By a rough estimate from the experimental results given by Healey and Reed (1941), the collision cross section of halogens for low energy electrons will be of the order of  $100 Q$  where  $Q$  is the area of the first Bohr orbit of the hydrogen atom. This would give a value for collision frequency of the order of  $10^7 \text{ sec}^{-1}$  for both iodine and bromine molecular ions, at 1 mm Hg pressure, which was the highest pressure used in the present experiments. The angular frequency chosen for the test signal was  $9 \times 10^7 \text{ sec}^{-1}$ .

### 2.2. *The Disappearance of Electrons*

The electron attachment cross section for halogens is about  $5 \times 10^{-18} \text{ cm}^2$  or larger (Yeung and Sayers 1957, Healey and Reed 1941). According to this value, at a pressure 0.05 mm Hg which was the lowest pressure used, free electrons with an initial density of  $10^{13}$  per  $\text{cm}^3$  should have almost disappeared within 300 microseconds after the discharge.

In figure 1, the straight lines represent on a logarithmic scale the calculated rates of decay of the electron density at different pressures, due to the attachment process with an assumed cross section of  $5 \times 10^{-18} \text{ cm}^2$ . The curves at the top of the diagram represent the rates of change of the ion density, due to recombination between positive and negative ions, for four different values of the recombination coefficient. Another similar set of curves in the lower part of the diagram,



which is plotted with a factor of mass ratio between electronic mass and that of molecular ion of iodine, shows us the region to be chosen where measurements can be carried out. Taking a simple example, if the ion-ion recombination

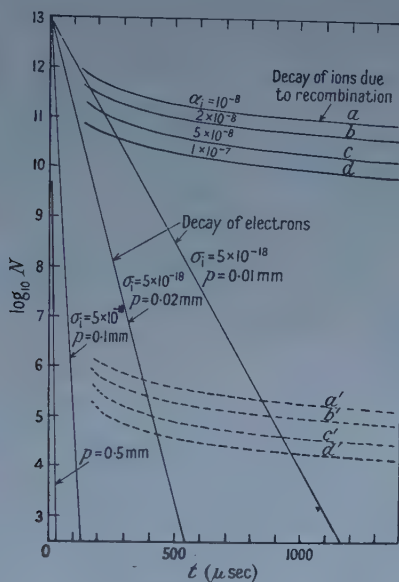


Figure 1. Decay of electrons and ions in the afterglow of an electronegative gas.

coefficient  $\alpha_i$  is  $10^{-8} \text{ cm}^3 \text{ sec}^{-1}$  and the pressure is  $0.02 \text{ mm Hg}$ , then  $400$  microseconds after the discharge the ion density will be of the order of  $2 \times 10^{11}$  per  $\text{cm}^3$  but the electron density will be only  $2 \times 10^5$  per  $\text{cm}^3$ . Obviously, after that time the contribution of electrons to the dielectric constant can be neglected.

### 2.3. The Effect of Diffusion

One further point which needs clarification is diffusion. No experimental study has been made to investigate this effect. However, in the present work the lowest pressure used is  $0.05 \text{ mm Hg}$  and the longest measuring time after the glow is  $700$  microseconds; according to a study of diffusion correction by Sayers (1952), the effect of diffusion under such conditions will be insignificant.

## § 3. EXPERIMENTAL DETAILS AND RESULTS

Discharge afterglows in iodine and bromine vapours were chosen for study as, with these gases, the conditions mentioned in the previous section are most readily realized. Figure 2(a) illustrates the type of discharge tube used for most of the measurements. The tube was made of Pyrex  $8 \text{ cm}$  in diameter and about  $25 \text{ cm}$  in length. One meshed cylindrical electrode  $1.5 \text{ cm}$  in diameter and  $8 \text{ cm}$  in length (made of nickel gauze for the iodine vapour tube and platinum for the bromine one) was inserted in the centre of the tube. This electrode together with the outside copper screen, as shown, formed a cylindrical capacitor with iodine or bromine vapour as the dielectric.

It was thoroughly outgassed by baking the tube in an electric oven for over ten hours and running a continuous radio-frequency discharge for several hours

before distilling over a small quantity of solid iodine or bromine and sealing off. The vapour of iodine or bromine was controlled by regulating the condensation temperature in the reservoir which formed an appendage to the main tube.

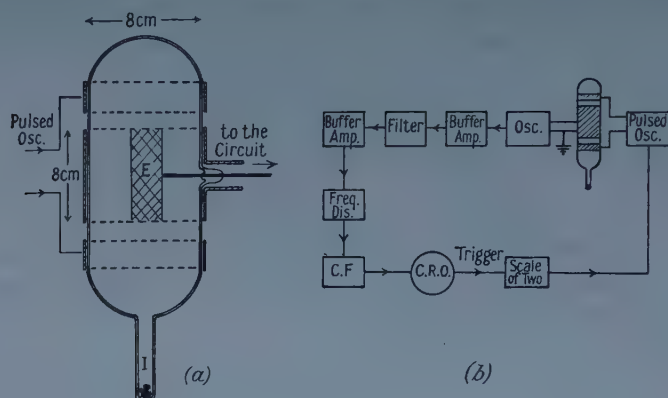


Figure 2. (a) The discharge tube ; (b) the block diagram.

The vapour pressure of iodine corresponding to the condensation temperature was determined according to the values given by Giles<sup>1</sup> and Fraser (1936), and that of bromine was taken from the values given by Henglein (1922).

The source of ionization was a 2 microsecond pulsed power oscillator operating at 200 Mc/s and 25 c/s repetition frequency.

The coaxial capacitor of the discharge tube with plasma as its dielectric material, formed part of the small test LC circuit. This circuit was made to oscillate at its resonance frequency by a weakly coupled driver valve. In order to prevent both the ions being swept out due to the applied external field and the effect of damping due to the conductivity of the discharge plasma introduced, this oscillator was so designed that the output voltage was less than 0.3 volt r.m.s. and a damping resistor of 1.5 k $\Omega$  was connected across the tuned circuit.

Figure 2(b) illustrates the experimental arrangement. The dielectric change due to the decay of ions in the discharge tube introduced a frequency shift in the

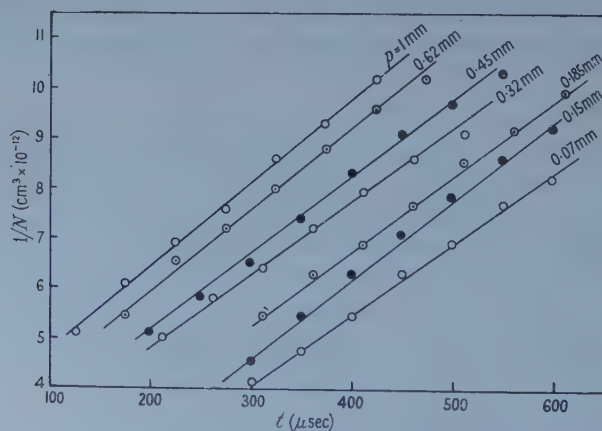


Figure 3. The reciprocal values of ion concentrations plotted against the times after the discharge in iodine.

main oscillator. By converting this frequency shift, through amplifier, filter and discriminator, into a voltage variation displayed on the screen of an oscillograph, appropriate records were made of its variation with time.

Except when otherwise stated, the frequency chosen in this experiment was 15 Mc/s. This gave a satisfactory range of pressure variation up to 1 mm Hg with precautions outlined in the previous section.

Figure 3 shows typical characteristic curves obtained in the recombination study, in which the reciprocal values of ion concentrations were plotted against the times after the discharge over an extended range of pressures.

Again the table shows the values of  $\alpha_i$  and the corresponding cross sections  $\sigma_i$  at various pressures and at room temperature (i.e. ion temperature). This represents a mean value of  $1.47 \times 10^{-8} \text{ cm}^3 \text{ sec}^{-1} \pm 5\%$  for iodine molecular ions

#### Variation of $\alpha_i$ and $\sigma_i$ with Pressure

Iodine			Bromine		
$p$ (mm Hg)	$\alpha_i$ ( $\text{cm}^3 \text{ sec}^{-1} \times 10^{-8}$ )	$\sigma_i$ ( $\text{cm}^2 \times 10^{-13}$ )	$p$ (mm Hg)	$\alpha_i$ ( $\text{cm}^3 \text{ sec}^{-1} \times 10^{-8}$ )	$\sigma_i$ ( $\text{cm}^2 \times 10^{-13}$ )
0.07	1.4	8.3	0.05	1.9	8.75
0.095	1.4	8.3	0.07	1.85	8.5
0.15	1.6	9.3	0.1	1.8	8.3
0.185	1.45	8.5	0.5	1.8	8.3
0.32	1.46	8.5	0.7	1.85	8.5
0.45	1.52	8.85	1.0	2.0	9.3
0.62	1.5	8.7			
1.00	1.55	9.1			
†0.2	1.45	8.5			
†0.33	1.4	8.3			

† With oscillator frequency of 19 Mc/s.

and  $1.85 \times 10^{-8} \text{ cm}^3 \text{ sec}^{-1} \pm 3\%$  for bromine, or in other words,  $\alpha_i$  is independent of pressure in the range 0.07 to 1.0 mm Hg; furthermore, the reaction cross sections in both gases are practically the same with an average value  $8.7 \pm 0.4 \times 10^{-13} \text{ cm}^2$ .

In order to study the effect of ion temperature on the recombination coefficient, the main body of the discharge tube was enclosed in an electric oven with a temperature control device adjusted to give the required bulb temperature.

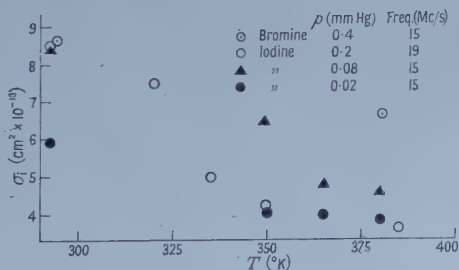


Figure 4. Variation of recombination cross section with ion temperature.

Figure 4 shows the superimposed relation between the measured values of recombination cross section and ion temperature for several different pressures. The general result is that the cross section falls as the temperature rises.

## § 4. DISCUSSION

The results indicate clearly that within experimental error the ionic recombination coefficient is constant over a considerable range of pressure. Thus it is evident that the recombination is a two-body process. Furthermore, the coefficient  $\alpha_1$  is a function of ion temperature as we expect (Bates and Lewis 1955).

Although in the present work it has not been possible to identify the types of ions in the afterglow plasma, mass spectrograph studies by Spencer-Smith (1935) lead to the conclusion that the ions are molecular and this identification has been adopted. The recombination coefficient is within the range of the estimated values given by previous workers (Bates and Massey 1943, Bates and Lewis 1955).

The present method could be extended with minor modifications to study the discharge afterglows in other gases besides halogens, possibly atmospheric gases like oxygen.

In view of the difficulties connected with any theoretical estimate of two-body charge exchange recombination for gases other than hydrogen, experimental values will probably have to be relied upon for some time to come.

## ACKNOWLEDGMENT

The author acknowledges with thanks the many helpful discussions with Professor J. Sayers in the course of this work.

## REFERENCES

- BATES, D. R., and LEWIS, J. T., 1955, *Proc. Phys. Soc. A*, **68**, 173.  
BATES, D. R., and MASSEY, H. S. W., 1943, *Phil. Trans. Roy. Soc. A*, **239**, 269.  
GILESPIET, L. J., and FRASER, L. H. D., 1936, *J. Amer. Chem. Soc.*, **58**, 2260.  
HEALEY, R. H., and REED, J. W., 1941, *The Behaviour of Slow Electrons in Gases* (London: Amalgamated Wireless), p. 54.  
HENGLEIN, F. A. V., ROSENBERG, G., and MUCHLINSKI, H., 1922, *Z. Phys.*, **11**, 1.  
SAYERS, J., 1952, *Geophys. Res. Papers*, No. 11A, 124 (Cambridge: U.S. Air Force Res. Centre).  
SPENCER-SMITH, J. L., 1935, *Phil. Mag.*, **19**, 806, 1016.  
YEUNG, T. H. Y., and SAYERS, J., 1957, *Proc. Phys. Soc. B*, **70**, 663.



## The Elastic and Inelastic Scattering of Protons by Silicon

By G. W. GREENLEES, L. G. KUO, J. LOWE AND M. PETRAVIC

Physics Department, University of Birmingham

*MS. received 28th October 1957*

**Abstract.** Absolute differential cross sections are given for the elastic scattering by silicon of 9.45 mev, 9.28 mev, 8.96 mev, 8.55 mev and 7.97 mev protons for an angular range of  $15^\circ$ – $156^\circ$  (centre-of-mass coordinates). The angular distributions show characteristic maxima and minima, the patterns varying slowly with energy as might be expected for scattering by a complex potential. Absolute differential cross sections for the inelastic scattering of protons at these five energies from the 1.78 mev level of  $^{28}\text{Si}$  are also given. All the inelastic angular distributions are asymmetric about  $90^\circ$  with a forward peaking. The magnitude of the asymmetry varies with energy and is greatest at 8.96 mev.

### § 1. INTRODUCTION

AN earlier paper (Greenlees *et al.* 1957a) presented results on the elastic and inelastic scattering of protons by magnesium at five energies between 7.86 and 9.55 mev. The angular distributions for elastic scattering by this element showed marked variations with incident energy. These variations could not easily be explained by the optical model type of analysis. Similar measurements on the elastic scattering of protons by the neighbouring element aluminium (Greenlees *et al.* 1957b) showed only small variations with incident energy.

The magnesium inelastic angular distributions also varied sharply with incident energy and showed a strong forward peaking at 8.83 mev. At this energy the corresponding elastic angular distribution shows maxima and minima less pronounced than at other energies. Optical model analyses (Glassgold *et al.* 1957, Melkanoff *et al.* 1957) have shown that suppression of the maxima and minima is indicative of large absorption effects, a conclusion which is probably correct whether or not it is reasonable to represent the data completely by such a model. The magnesium results thus show a marked anomaly in the inelastic scattering at an incident energy where the elastic results indicate strong absorption. This variation of absorption with incident energy suggests that the effects observed with magnesium may be due to variations in the level density of the compound system and that compound elastic scattering will need to be considered in an analysis of the data. The present experiments with silicon were undertaken to see whether the compound nucleus  $^{25}\text{Al}$  formed from magnesium was exceptional in this respect.

### § 2. APPARATUS AND PROCEDURE

The 9.8 mev proton beam from the Nuffield 60 in. cyclotron passed through a Si target at the centre of a scattering chamber and was collected in a Faraday cup and integrated. The scattered beam was detected by a CsI(Tl) crystal and photomultiplier and the spectra were displayed on a 60-channel pulse analyser.

Laboratory angles between  $15^\circ$  and  $165^\circ$  were available with an angular definition of  $\pm 1^\circ$ . A more detailed description of the apparatus and experimental procedure is given elsewhere (Greenlees *et al.* 1957 a).

The Si target used had a thickness of  $9.35 \text{ mg cm}^{-2}$ . To prepare these targets, pieces of pure Si were lapped to approximately 0.002 in. thick, mounted in a holder of gold and etched down to the final thickness with a solution consisting of 5 volumes of concentrated  $\text{HNO}_3$ , 3 volumes of  $\text{HF}$  and 3 volumes of  $\text{CH}_3\text{COOH}$  at  $25^\circ\text{C}$ . The surface density was determined by comparison of the scattering with that obtained from a thicker piece which was weighed directly.

Figure 1 shows a typical spectrum taken at  $53^\circ$  (c.m.) for a known charge collected by the Faraday cup. The two well-resolved groups are attributed respectively to elastic scattering from the three isotopes of silicon ( $^{28}\text{Si}$ ,  $^{29}\text{Si}$ , and  $^{30}\text{Si}$ ) and to inelastic scattering from the 1.78 Mev level of  $^{28}\text{Si}$  (cf. Endt and Kluyver 1954). Similar spectra were obtained at other angles and angular distributions for the elastic and inelastic groups were plotted. Absolute differential cross sections were obtained from the observed spectra together with knowledge of the charge collected, the target thickness and the solid angle subtended by the detector.

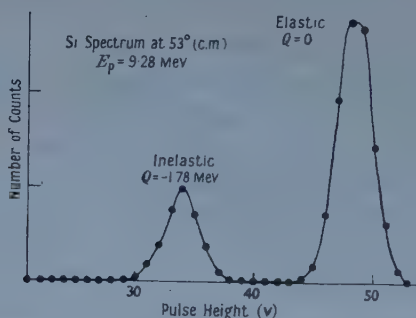


Figure 1. Pulse-height spectrum on the kicksorter for the scattering of 9.28 Mev protons by Si at  $53^\circ$  (c.m.).

The maximum beam energy was found by measurement of the range of protons elastically scattered from a thin gold foil into a photographic emulsion. Reduced energies were obtained by placing Al absorbers in front of the collimator used to define the beam. Angular distributions were obtained for energies (at the centre of the target foil) of 9.45 Mev, 9.28 Mev, 8.96 Mev, 8.55 Mev and 7.97 Mev, all  $\pm 0.07$  Mev.

### § 3. RESULTS

Figure 2 shows the elastic differential cross sections at five energies plotted as the ratio of the observed cross section to the corresponding Rutherford scattering cross section. The errors in the absolute cross sections are  $\pm 3\%$  in general, and the errors in the angles  $\pm 30'$ . This angular error is important in computing the Rutherford cross sections at forward angles and in figure 2 the ordinate and abscissa errors are not independent. Figure 3 shows the inelastic differential cross sections at the five incident energies; the errors are also estimated at  $\pm 3\%$  in general. In both figure 2 and figure 3 the errors in the cross sections exceed  $3\%$  for some parts of the curves particularly at forward and backward angles. This is shown in figure 4 which gives the elastic and inelastic curves at 8.96 Mev with the ordinate errors included.

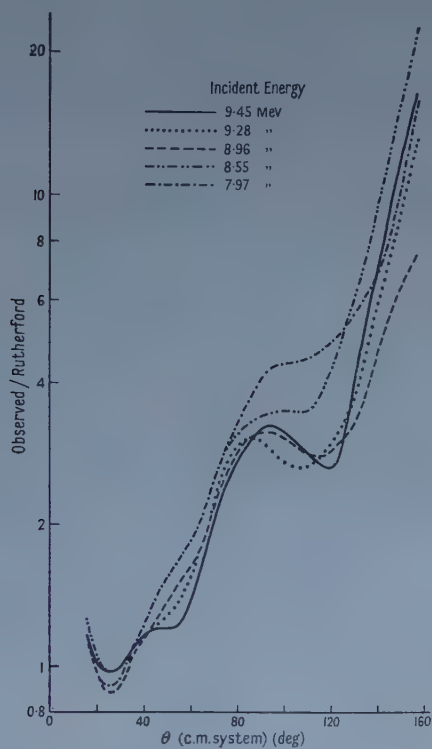


Figure 2. Ratio of observed to Rutherford elastic scattering cross sections of protons of various energies by Si.

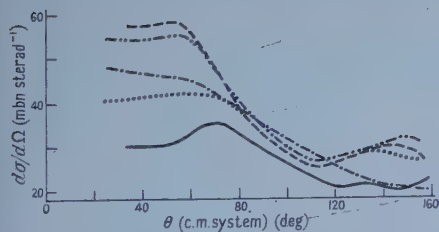


Figure 3. Differential cross sections for inelastic scattering ( $Q = -1.78$  MeV) of protons of various energies by  $^{28}\text{Si}$ . (For key see figure 2.)

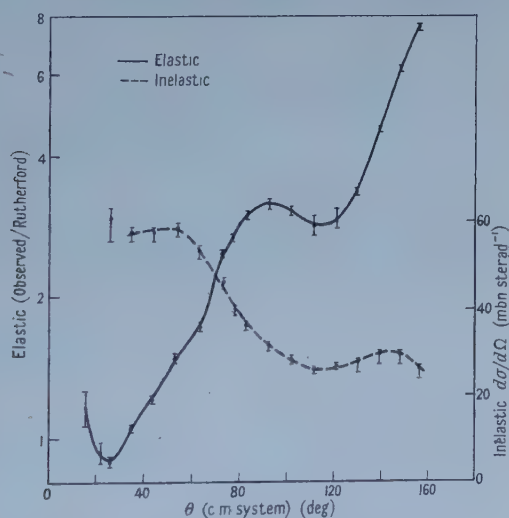


Figure 4. Differential cross sections for elastic and inelastic scattering at 8.96 MeV.

## § 4. DISCUSSION

Elastic scattering curves similar to those given in figure 2 are well known and can be interpreted for one element and one energy in terms of scattering from a complex potential of the form

$$V(r) = \frac{V + iW}{1 + \exp[(r - R_0)/a]}$$

(cf. Glassgold *et al.* 1957, and Melkanoff *et al.* 1957). The parameters of this model are expected to vary only slowly with energy and hence the angular distributions would be expected to vary slowly with incident energy. Small systematic variations are observed in figure 2 but the positions of the maxima and minima remain approximately independent of energy. The curves can therefore probably be fitted by making small variations in the parameter  $W$  (cf. Glassgold *et al.* 1957). This is in contrast with the corresponding Mg results (Greenlees *et al.* 1957a) and similar to the Al results (Greenlees *et al.* 1957b).

The Si inelastic results (figure 3) are asymmetric about  $90^\circ$  at all energies but show a smoother energy variation than the similar results with Mg. In the case of Si, the target was about 400 kev thick, so that sharp variations with energy of the type observed with the thinner Mg target (100 kev) for both elastic and inelastic scattering would be less noticeable in the Si experiments. It is therefore not clear that the two elements are markedly different in their behaviour in inelastic scattering although it seems probable.

The forward peaking of the inelastic distributions found with both Mg and Si is suggestive of the direct interaction mechanism discussed by Butler (1957) but this mechanism does not predict a rapid enough variation of angular distribution with energy to explain either case. A complete description of the present results presumably includes features of both direct interaction and compound nucleus processes; the general method of formulating such a description has recently been discussed by Brown and De Dominicis (1957a, b).

## ACKNOWLEDGMENTS

The authors wish to thank Dr. D. E. Mason for supplying the original Si and suggesting the procedure used to prepare the target from this. They also wish to thank Drs. P. M. Rolph and R. A. Peck, Jr. for help in recording the results. Three of us (L. G. K., J. L. and M. P.) wish to thank various bodies for financial support as follows: L. G. K. the University of Birmingham, J. L. the Department of Scientific and Industrial Research, M. P. the Institute "Ruder Bošković", Zagreb.

## REFERENCES

- BROWN, G. E., and DE DOMINICIS, C. T., 1957 a, *Proc. Phys. Soc. A*, **70**, 668; 1957 b, *Ibid.*, **70**, 686.  
 BUTLER, S. T., 1957, *Phys. Rev.*, **106**, 272.  
 ENDT, P. M., and KLUYVER, J. C., 1954, *Rev. Mod. Phys.*, **26**, 95.  
 GLASSGOLD, A. E., CHESTON, W. B., STEIN, M. L., SCHULTZ, S. B., and ERICKSON, G. W., 1957, *Phys. Rev.*, **106**, 1207.  
 GREENLEES, G. W., HAYWOOD, B. C., KUO, L. G., and PETRAVIĆ, M., 1957 a, *Proc. Phys. Soc. A*, **70**, 331.  
 GREENLEES, G. W., KUO, L. G., and PETRAVIĆ, M., 1957 b, *Proc. Roy. Soc. A*, **243**, 206.  
 MELKANOFF, M. A., NODVIK, J. S., SAXON, D. S., and WOODS, R. D., 1957, *Phys. Rev.*, **106**, 793.



## Electron Ionization Cross Sections using Chopped Beams

By R. L. F. BOYD AND G. W. GREEN

Department of Physics, University College London

*MS. received 15th October 1957*

**Abstract.** The paper describes the development of a crossed beam method suitable for measuring ionization cross sections of unstable gases such as atomic hydrogen.

Results obtained in He and  $H_2$  are compared with those of Tate and Smith. The method makes use of a narrow band amplifier associated with a beam chopper and phase sensitive detector, to eliminate the current due to ionization of the background gas. The electric field in the collision region is such that limitation of the beam crossover volume can make the uncertainty in electron energy much smaller than is otherwise possible, without resorting to magnetic collimation or pulsed collection. An analysis of the sources of error due to the collection of spurious currents at signal frequency is given.

### § 1. INTRODUCTION

**T**HIS paper describes a method for studying the ionization (and other) cross sections of unstable atomic gases such as atomic hydrogen, and gives the results of some preliminary measurements made in helium and molecular hydrogen.

When measurements of collision cross sections must be made in vapours and unstable gases the problem of avoiding the effects of the containing chamber and electrodes may be solved by employing the method of crossed atom and electron beams. Using this method Funk (1930) carried out measurements in mercury, sodium and potassium. Because of the high mass of the atoms the impinging electrons caused negligible deflection of ions from the beam so that it was possible to collect the ions alone without much distortion of the field in the impact region. The use of condensable vapours also made it possible to maintain a very high pumping speed and correspondingly good vacuum. In spite of this, however, there was an appreciable contribution to the ionization current from the residual gas and so accuracy was poor.

In the present work a chopped beam technique has been employed to eliminate the errors due to residual gas. Because it is required to measure the ionization cross sections for light gases, whose atoms may receive appreciable momentum from the impinging electrons, a carefully designed collecting field is required. A further problem encountered in past work on the ionization cross sections of gases has been that of the scattered electrons. In the early work of Compton and Van Voorhis (1925), the electric field, required to prevent the collection of scattered electrons, resulted in a large uncertainty in the beam energy. Tate and Smith (1932) employed a magnetic field to prevent scattered electrons from leaving the beam, but by so doing introduced uncertainty as to the true path length of the electrons in the beam.

In the present method by delimiting the impact region suitably the uncertainty in the electron energy may be made small.

The principle employed in the method reported here is similar to that used by Branscomb and Fite (1954) in their measurements of photo-detachment and the authors are glad to acknowledge the valuable collaboration and assistance rendered by Dr. Fite during the early part of the work. The effectiveness of the method is such that it has been found possible to operate satisfactorily when the background ionization signal exceeds the beam signal by a factor of over 1000.

## § 2. PRINCIPLE OF THE EXPERIMENT

A collimated beam of electrons is passed through a collimated beam of atoms or molecules in a strongly evacuated region. The geometry is such that the density in the atom beam may be assumed to be uniform over the width of the electron beam. The atom beam is chopped by a shutter and the collision region is arranged to lie in a saddle-shaped field such that the ions produced can only escape by passing to a collector ring. The current to the collector is amplified in a parallel T feedback amplifier and passed to a phase-sensitive detector synchronized to the chopping frequency.

Contributions to the signal frequency arise both from the wanted ionization signal and from statistical and coherent fluctuations in the background current.

The statistical fluctuations are chiefly due to the d.c. current flowing in the input grid resistor of the pre-amplifier. If  $I_1 + I_2$  is the value of this current, composed of background ionization  $I_1$  together with the grid current  $I_2$  then the r.m.s. shot noise current is given by  $\delta I_s = (2e(I_1 + I_2)B)^{1/2}$  where  $B$  is the band width of the system. There is in addition the r.m.s. resistor noise of value equivalent to a current  $\delta I_R = (4kTB/R)^{1/2}$  where  $R$  is the value of the grid resistor and  $T$  its temperature. The total noise current  $\delta I = (\delta I_s^2 + \delta I_R^2)^{1/2}$ .

The amplifier used gave a band width of 2 c/s. However, by adding a phase-sensitive detector the band width becomes approximately equal to the reciprocal of the integrating time constant and could thus readily be made 0.1 c/s or less. It is not satisfactory to attempt to use simply a feedback amplifier with so narrow a band width owing to the difficulty of keeping it sharply tuned to the chopping frequency.

Typical values of the relevant parameters are: wanted ionization signal  $I > 10^{-14}$  A, d.c. background signal  $I_1 = 10^{-10}$  A, grid current (assumed entirely ionic)  $I_2 = 3 \times 10^{-10}$  A and input resistor  $R = 10^{11}$  ohms.

Under these circumstances a signal-to-noise ratio of about 30 to 1 is obtained. This will be much improved in future by some simple modifications of the vacuum system and by employing a valve with smaller grid current.

## § 3. THE BEAM AND ELECTRODE SYSTEMS

The apparatus consists of two chambers separately pumped—the source chamber and the collision chamber (see figure 1). Particles emerge from a 1 mm orifice in the source. They pass a shutter, which can be opened and closed magnetically from outside the vacuum, and enter the second chamber through a slit. Next they pass through a slotted disc mounted on a synchronous motor

which chops the beam. Externally, a second identical motor drives a phase-sensitive detector from the same supply. Finally, the beam passes through the electrode system shown.

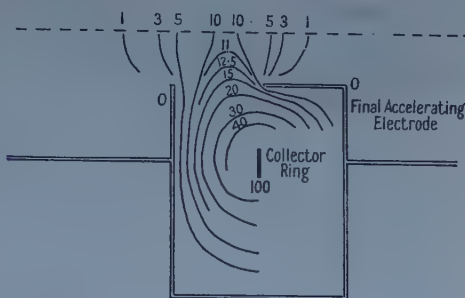
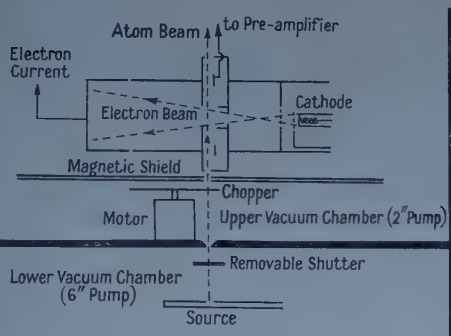


Figure 1. Arrangement of electrodes and beams.

Figure 2. Section of ion collecting system showing equipotentials. The numbers give the percentage of the collector potential (referred to the final accelerator as zero) existing around the collision region.

The form of the electric field due to the applied potentials is given in figure 2. The atom and electron beams cross in the centre of the region bounded by the 10% equipotentials. Scattered electrons are unable to reach the collector ring because of its large retarding potential, but ions formed are unable to reach any other electrode than the collector.

The cathode is oxide coated and heated indirectly. Electrons are accelerated by a pair of grids and carefully collimated by a 5 mm diameter hole so that the whole electron beam passes through the atom beam which, in the collision region, is a ribbon 10 mm wide and 3 mm thick. The electron current entering the final collector is measured.

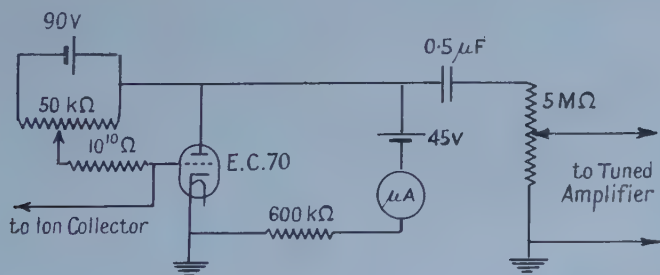


Figure 3. Preamplifier circuit showing 100% feedback arrangement and means for backing off voltage due to the d.c. component of collector current.

The ion current is measured by a miniature electrometer pre-amplifier inside the vacuum. The circuit is shown in figure 3. The anode current of the electrometer was maintained at a fixed value by the bias potentiometer. The bias voltage provided a measure of the steady ion current whilst the a.c. component was measured after amplification and detection.



## § 4. CONTRIBUTIONS TO THE ION CURRENT

The ion current collected by the collector arises basically either from ionization of the background gas or of the beam. However, it is not sufficient to assume that the former is entirely unmodulated and that the latter represents the whole of the modulated signal.

Unmodulated currents may arise by: (i) direct ionization of the background, (ii) collection of scattered electrons scattered by the background, (iii) ionization of the background by electrons scattered by the background.

Significant modulated signals might be due to: (i) direct ionization of the beam, (ii) direct ionization of a pressure modulated background, (iii) collection of electrons scattered by the beam, (iv) ionization of the beam by scattered electrons, (v) ionization of the background by electrons scattered by the beam, (vi) direct ionization of atoms scattered from the beam, (vii) electrostatic or magnetic pick-up from the motor or shutter. The unmodulated currents are only significant as a means of monitoring and as a source of noise. In this connection it is worth mentioning that early in the work much difficulty was experienced from sudden bursts of current which, though very small compared with the steady value, still gave a large noise component at low frequencies. This was eventually traced to very small pressure fluctuations. These no longer occurred when the original oil pumps were replaced by mercury pumps.

The unwanted sources of modulated signal were investigated one by one and allowed for (or eliminated) as follows: The pressure modulation of the background is only a small fraction of one per cent but is sufficient to cause a significant error if no correction is applied. It arises from the modulation by the shutter of the random flux of gas from the source chamber, where the pressure is higher, into the collision chamber, where it is less. It is unaffected by intercepting the beam by the small magnetically operated shutter just above the source, and can therefore be allowed for by subtracting from the measured signal the signal obtained when the beam is so intercepted.

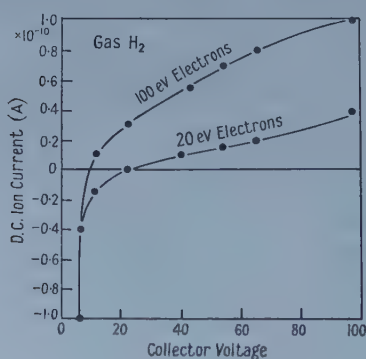


Figure 4. Plot of d.c. component of collector current as function of collector potential, showing collection of scattered electrons at low collector potentials and of ions from beyond the collision region for higher potentials.

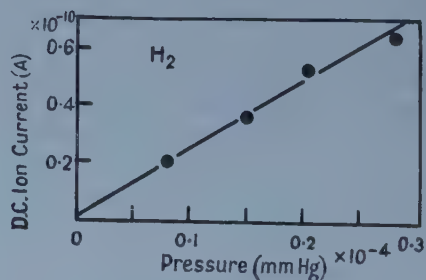


Figure 5. Plot of d.c. component of collector current as function of collision chamber pressure, showing linear relationship. Electron energy 170 ev. Collector potential  $-60$  v relative to final accelerator.



The collection of scattered electrons was studied by measurements on the unmodulated signal. Typical curves are shown in figure 4, for electron beams of 20 ev and 100 ev respectively. When the potential difference between the ion collector ring and its surroundings is less than about 20 volts a large reverse current flows due to the collection of scattered electrons. As the collector voltage is raised these electrons are prevented from reaching the collector. However, the ion current does not saturate, as the rising collecting field collects ions from an ever increasing length of electron beam. In fact, the ion current for the 20 ev case in figure 4 is almost entirely due to ionization occurring after the beam has been accelerated somewhat by the voltage on the electron collector.

Ionization of the beam by scattered electrons will, because of the low density in the beam, be less probable than ionization of the background by scattered electrons. However, if this were to occur a plot of ion current against background pressure would be non-linear. Figure 5 shows that this is not the case. It follows therefore that both ionization of the background by electrons scattered from the beam and ionization of the beam by scattered electrons are negligible.

Direct ionization of atoms scattered from the beam has not been investigated in detail, though it could be studied by examining the dependence of the modulated signal on the background pressure. Error introduced by this effect is likely to be of a small order since it merely represents a small contribution to the ionization from outside the region of accurately defined potential. Figure 6 shows the

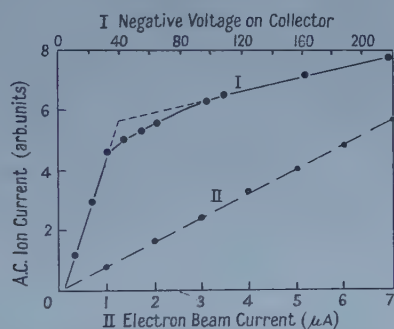


Figure 6. I. Extent of saturation of a.c. ion signal with increase of collector field. II. Linear relationship between a.c. ion signal and beam current.

modulated ion current as a function of collector voltage. It is probable that the absence of complete saturation is due to the ionization of scattered atoms and their collection from greater distances along the electron beam as the collecting field is increased. The figure also shows a satisfactory linear relationship between ion current and electron beam current.

Pick-up signals were eliminated by electrostatic and magnetic shielding.

## § 5. RESULTS OF MEASUREMENTS ON $H_2$ AND He

Ionization cross sections observed for molecular hydrogen and for helium up to electron energies of 260 volts are plotted in figure 7. Two normalizations have been introduced. The observed energy scale is in error due to contact potentials and the collector field penetration. This has simply been corrected by normalizing to the known appearance potentials of the ions. The cross sections

as measured are in arbitrary units. The curves have therefore been normalized to those of Tate and Smith at 256 volts. It is felt that the agreement of the forms of the ionization functions obtained with those of Tate and Smith is satisfactory and justifies the immediate application of the method to the more difficult case of atomic hydrogen.

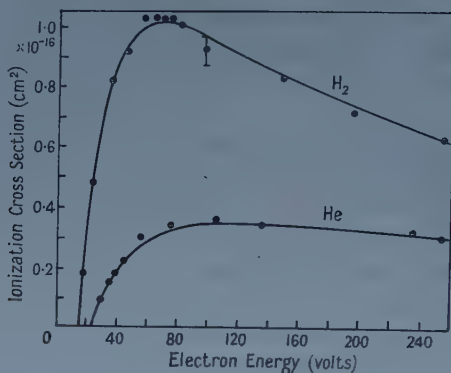


Figure 7. Results of ionization cross section measurements in  $H_2$  (upper curve) and He (lower curve). The full lines give Tate and Smith's results for comparison, to which the energy scale of the present results are normalized at the threshold and the ordinates at 256 volts.

The equipment has already been modified to include a discharge source of atomic hydrogen, while microcalorimetric techniques suitable for determining the degree of dissociation have been successfully developed in this laboratory.

Preliminary values for the ionization function of atomic hydrogen have already been obtained and it is hoped that these may be published shortly, together with an account of the assaying technique.

#### REFERENCES

- BRANSCOMB, L. M., and FITE, W. L., 1954, *Phys. Rev.*, **93**, 651.  
 COMPTON, K. T., and VAN VOOHRIS, 1925, *Phys. Rev.*, **26**, 436.  
 FUNK, H., 1930, *Ann. Phys., Lpz.*, **4**, 651.  
 TATE, J. T., and SMITH, P. T., 1932, *Phys. Rev.*, **39**, 270.

# The $(2s)^2\ ^1S$ State Solution of the Non-relativistic Schrödinger Equation for Helium and the Negative Hydrogen Ion

By E. HOLØIEN

Institute of Theoretical Physics, University of Oslo, Norway

*MS. received 6th August 1957, and in revised form 4th November 1957*

**Abstract.** A finite set of possible Slater determinants with spatial part constructed from an orthonormal complete one-electron set of associated Laguerre functions in the radial coordinates, and Legendre functions in the angular coordinates, has been introduced into the minimal sequence of the Ritz variational principle applied to the  $(2s)^2$  state solution ( $L=0$ ) of the two-electron wave equation for infinite nuclear mass. The sequence converges on a certain limiting eigenfunction of the energy state. The numerical solution of the function and the corresponding energy value are given for helium as well as the negative hydrogen ion. The identification of certain helium lines in the vacuum ultra-violet is discussed.

## § 1. INTRODUCTION

THE recent calculations of auto-ionization probabilities for double excited helium in connection with the identification of certain corona lines in the vacuum ultra-violet by Bransden and Dalgarno (1953) have renewed the interest in solving the non-relativistic two-electron wave equation to a higher degree of accuracy for doubly excited states. Approximate solutions involving only a single Slater determinant built up from one-electron products (Fender and Vinti 1934, Wu 1934, Wu and Ma 1936) and solutions derived by the self-consistent field method (Wilson 1935) have been carried through. All these solutions are subject to the same uncertainty, namely their lack of orthogonality to the exact eigenfunctions of the infinitely many lower states of the same multiplicity. It is worth noting that these orthogonality restrictions have been approximately taken into account in a rather elaborate work by Wu and Kou (1945) using the conventional Hylleraas expansion in the eigenfunction, but the minimal sequence constructed for the  $(2s)^2$  state is not necessarily convergent.

In the present paper the method of configurational interaction is employed using a linear combination of a finite set of Slater determinants constructed from configurations of an orthonormal one-electron set of radial associated Laguerre functions and angular Legendre functions. On investigating the radial configurational interaction such a simple physical interpretation of the orbitals has been proved successful in the ground state solution (Löwdin and Shull 1956, Holøien 1956). When it became known to us that Shull at Indiana University had carried out similar calculations using additional angular configurations (private communication), we decided not to proceed to higher orders of approximation in the ground state solution.

We shall only be concerned with the  $(2s)^2\ ^1S$  state solution of helium and the negative hydrogen ion. This investigation was not done so much in order to obtain a more accurate solution of this energy state, but rather in order to gain experience in some aspects of attacking systematically the correlation effects in

three- and four-electron problems. For comparison of the solution with the ground state solution we also present the results of the latter at the 20-parameter stage.

This very extensive programme has been rendered possible by the availability of an electronic computer (NUSSE) for solving the secular equations.

## § 2. THEORY

We first make the assumption that an exact solution of the wave equation may be expanded in any infinite sum of configurations of a complete one-electron set of orbitals. An infinite sum of terms which satisfy the wave equation formally has been assumed (Bartlett *et al.* 1935, Fock 1954, Pluinage 1956, Pluinage and Munchy 1957, Kinoshita 1957). The method most frequently used to determine approximately the lowest energy value and the corresponding eigenfunction of a bound system is the Ritz variational method. A trial eigenfunction depending on a number of variable parameters is assumed. The expectation value of the energy is then an upper limit of the lowest energy of the system. The parameters are varied until the expectation value is a minimum. The variational principle can also be used to obtain an upper limit of the higher energy levels provided the eigenfunction used is orthogonal to the exact eigenfunctions of all the lower states. The  $(2s)^2^1S$  state solution must therefore be orthogonal to the infinitely many lower singlet  $S$  states, i.e. the  $(1sns)^1S$  states when  $n=1, 2, \dots \infty$ . As is known, this mutual orthogonality is automatically realized by the solution of the secular equation. It is thus clear that the eigenfunction identified with the  $(2s)^2$  level is indeed orthogonal to all the eigenfunctions which correspond to the lower roots of this particular secular equation, but, it is not orthogonal to the entire infinity of  $(1sns)^1S$  states. The exact solution could be obtained if the corresponding infinite matrix problem could be solved. Since there is no other practical method in the theory to ensure this orthogonality, we have decided to proceed to higher orders of approximation in the finite matrix problem. Some uncertainty, of course, will exist with regard to the results obtained. Will the convergence limit be too low or too high in any given approximation? Will the introduction of the remaining  $1sns$  terms into the eigenfunction raise or lower this limit? However, by careful choice of trial wave function, the effect of this departure from orthogonality can be rendered unimportant. The results of the investigation on this point are discussed more fully in § 6.

There is a very fundamental condition in the treatment of eigenvalue problems that the minimal sequence in the Ritz variational principle applied to the non-relativistic wave equation must be constructed from a complete system of functions. Otherwise, using a non-complete system the convergence limit is found to be incorrect. It is also important to include all the members of the complete set. The literature contains many examples of the appearance of a false convergence limit, presumably due to systematic omission of particular members of the set.

We consider an approximate solution obtained by varying the coefficients of a linear combination of a finite set of Slater determinants. The determinants are constructed from a complete one-electron set of three-dimensional space functions (radial associated Laguerre functions and angular Legendre function) together with the single-electron spin functions. The superpositions of the states



of configurations can only occur between those of the same  $L$  and  $S$  values (Russel-Saunders coupling) and the same parity (Condon and Shortley 1935). The solution must be symmetric for interchange of the electronic space coordinates.

The spatial part of the orbitals may be written

$$X(mq, \mathbf{r}_1 | nq, \mathbf{r}_2)_{\eta}^{\nu} = R_{\eta}^{N, +\nu}(mq | \mathbf{r}_1) R_{\eta}^{N, -\nu}(nq | \mathbf{r}_2) P_q^N(\cos \vartheta) \dots (1)$$

$$P_q^N(\cos \vartheta) = \frac{(2q+1)^{1/2}}{4\pi} P_q(\cos \vartheta)$$

where  $\vartheta$  is the angle between the electronic vectors  $\mathbf{r}_1$  and  $\mathbf{r}_2$ , and  $P_q$  is the Legendre polynomial. To accelerate the convergence of the energy expectation value, it is customary to introduce a scale parameter and define a new set of orbitals

$$R_{\eta}^{N, \pm \nu}(|\mathbf{r}) = \phi^{N, \pm \nu}(|\eta \mathbf{r}) \dots (2)$$

where  $\eta$  is the scale parameter and  $\nu$  is a splitting parameter.

The secular equation is

$$\text{Det} \{ \eta^2 M(i|j) - \eta Z L(i|j) + \eta L'(i|j) - E \epsilon(i|j) \} = 0 \dots (3)$$

with the matrix elements of the kinetic, nuclear potential, electronic repulsion energy operators and the unit matrix respectively.

It is found most convenient to present the radial orbitals as follows

$$\begin{aligned} \phi^N(\alpha q | r) &= N(\alpha, q) (2r)^q L_{\alpha+q+1}^{(2q+2)}(2r) \times \exp(-r)/(\alpha+q+1)! \\ &= \frac{N(\alpha, q)}{2\pi i} \int_C dt \times (2r)^q t^{-\alpha+q}(1-t)^{-2q-3} \times \exp\left(-\frac{r(1+t)}{1-t}\right) \end{aligned}$$

with the normalization factor

$$N(\alpha, q) = 2 \left[ \frac{2}{(\alpha-q)(\alpha-q+1) \dots (\alpha+q+1)} \right]^{1/2} \dots (4)$$

The  $(2q+2)$ -order Laguerre polynomials may conveniently be written

$$L_{\alpha+q+1}^{(2q+2)}(2r) = \sum_{s=0}^{\alpha+q-1} \frac{\{(\alpha+q+1)!\}^2}{(\alpha-q-1-s)!(2q+2+s)!s!} (-2r)^s \dots (5)$$

and the corresponding Laguerre functions are mutually orthogonal in ordinary space. Restricting ourselves to positive integral values of  $\alpha$  and  $q$ , the contour  $C$  can be taken to include the origin ( $t=0$ ) only. For the  $(\alpha q)^2 1S$  states we found it most convenient to put  $\nu$  (the splitting parameter) equal to zero. The determinantal equation (3) must be solved for several values of  $\eta$  until  $E$  is minimized with respect to the scale parameter. A check on the correctness of  $\eta$  and  $E$  is obtained by ascertaining whether the relations

$$\eta = \frac{ZL - L'}{2M}, \quad -E = \frac{(ZL - L')^2}{4MN} \dots (6)$$

are fulfilled, where

$$L = \sum_i \sum_j L(i|j) c_i c_j, \quad L' = \sum_i \sum_j L'(i|j) c_i c_j, \quad M = \sum_i \sum_j M(i|j) c_i c_j$$

and

$$N = \sum_i \sum_j \epsilon(i|j) c_i c_j$$

are computed from the matrix elements and the coefficients derived from the secular determinant with the best energy.

## § 3. THE MATRIX ELEMENTS

The matrix elements of the kinetic, nuclear potential and electronic repulsion energy operators (3) are given separately

$$\left. \begin{aligned} M(ab|pq|cd) &= \frac{1}{16} [A(ab|q)\lambda_{cd} + A(cd|q)\lambda_{ab} + A(ad|q)\lambda_{bc} + A(bc|q)\lambda_{ad}]\lambda_{pq} \\ L(ab|pq|cd) &= \frac{1}{4} [B(ab|q)\lambda_{cd} + B(cd|q)\lambda_{ab} + B(ad|q)\lambda_{bc} + B(bc|q)\lambda_{ad}]\lambda_{pq} \\ L'(ab|pq|cd) &= \frac{1}{16} \sum_{k=|p-q|}^{p+q} C_{2s}(p|k|q) [D_{2s}(ab|pq|cd) + D_{2s}(ad|pq|bc)] \cdot \lambda_{p+q+k, 2s} \end{aligned} \right\} \dots\dots(7)$$

where

$$C_{2s}(p|k|q) = \frac{(2p+1)^{1/2}(2q+1)^{1/2}\{s!\}^2(p+q-k)!(k+p-q)!(k+q-p)!}{(2s+1)!(s-k)!^2(s-p)!^2(s-q)!^2}$$

and

$$\lambda_{\alpha\beta} = \begin{cases} 1, & \alpha = \beta, \\ 0, & \alpha \neq \beta, \end{cases} \quad \lambda_{p+q+k, 2s} = \begin{cases} 1, & p+q+k=2s, \\ 0, & p+q+k \neq 2s, \end{cases} \quad s=0, 1, 2, \dots,$$

that is the integers  $p$ ,  $q$  and  $k$  must be equal to the sides of a triangle of even parameter. Explicit expressions for the integrals  $A(\alpha\beta|q)$ ,  $B(\alpha\beta|q)$  and  $D_{2s}(\alpha\beta|pq|\gamma\omega)$  are given in the Appendix.

The diagonal matrix of the unity may be written

$$\epsilon(ab|pq|cd) = \frac{1}{2}(\lambda_{ab}\lambda_{cd} + \lambda_{ad}\lambda_{bc})\lambda_{pq}. \quad \dots\dots(8)$$

Since the matrix elements of the  $(2q+2)$ -order Laguerre functions may conceivably be of use in other calculations involving configurational interaction (they are not available elsewhere), we found it wise to quote them numerically in the present paper.

§ 4. THE PROCEDURE OF CHECKING THE  $L'$  ( $i|j$ ) ELEMENTS

The matrix elements of both the kinetic and nuclear energy operators are easy to compute numerically. On the other hand, the numerical computation of the elements of the electronic repulsion operator is very lengthy, but the general expression derived for this matrix  $D_{2s}(\alpha\beta|pq|\gamma\omega)$  is very suitable for checking the numerical computations. All the elements off the diagonal can be checked very carefully.†

It is worth while giving an illustration of this checking procedure. With reference to notations given in the Appendix we may give this briefly as follows. The computations were carried out in three stages.

(a) The basic matrix ( $Q_{ij}$ ) was computed ( $i=0, 1, 2, \dots, j=0, 1, 2, \dots$ ). From this matrix the matrices ( $Q_{ij}^{2s}$ ) and the symmetrical matrices ( $Z_{ij}^{2s}$ ) were formed.

(b) the next stage consisted in computing the matrices ( $Y(\alpha|\beta)_{uz}^{2s}$ ) where

$$Y(\alpha|\beta)_{uz}^{2s} = \sum_x f_{\alpha,p}(x) \sum_y f_{\beta,q}(y) Z_{ij}^{2s}$$

to every combination of  $\alpha$  and  $\beta$  ( $u=0, 1, 2, \dots, z=0, 1, 2, \dots$ ).

† All the elements have been checked by Dr. Shull and the author (private communication). At first more discrepancies were found, but all these were cleared up by the discovery of an error,

(c) Finally, from these matrices again we form the main matrix

$$D_{2s}(\alpha\beta|pq|\gamma\omega) = \sum_u^{\gamma} f_{\gamma,p}(u) \sum_z^{\omega} f_{\omega,q}(z) Y(\alpha|\beta)_{uz}^{2s}. \quad \dots\dots(9)$$

The results can then be checked by the identities

$$\begin{aligned} D_{2s}(\alpha\beta|pq|\gamma\omega) &= D_{2s}(\gamma\omega|pq|\alpha\beta) & \text{when } p \geq q \\ D_{2s}(\alpha\beta|pq|\gamma\omega) &= D_{2s}(\beta\alpha|pq|\gamma\omega) = D_{2s}(\alpha\beta|pq|\omega\gamma) & \text{when } p = q. \quad \dots\dots(10) \end{aligned}$$

When  $\alpha = \beta = \gamma = \omega$  (the diagonal elements) this checking procedure no longer holds good.†

## § 5. RESULTS

It is most convenient to present the numerical solution as follows

$$\begin{aligned} \Psi(\mathbf{r}_1, \mathbf{r}_2) &= \sum_{m=n,q} c(m, m, q|\eta) \phi^N(mq|\mathbf{r}_1) \phi^N(mq|\mathbf{r}_2) P_q^N(\cos\vartheta) \\ &+ 2^{-1/2} \sum_{m < n, q} c(m, n, q|\eta) [\phi^N(mq|\mathbf{r}_1) \phi^N(nq|\mathbf{r}_2) \\ &+ \phi^N(nq|\mathbf{r}_1) \phi^N(mq|\mathbf{r}_2)] P_q^N(\cos\vartheta) \quad \dots\dots(11) \end{aligned}$$

with the normalization condition

$$\sum_{m=n,q} |c(m, m, q|\eta)|^2 + \sum_{m < n, q} |c(m, n, q|\eta)|^2 = 1. \quad \dots\dots(12)$$

The matrix elements, however, are obtained by using the eigenfunction

$$\begin{aligned} \Psi(\mathbf{r}_1, \mathbf{r}_2) &= \phi^N(1s|\mathbf{r}_1) \phi^N(1s|\mathbf{r}_2) + \sum_{m=2} \zeta(m, m, q|\eta) \phi^N(mq|\mathbf{r}_1) \phi^N(mq|\mathbf{r}_2) P_q^N(\cos\vartheta) \\ &+ \frac{1}{2} \sum_{m < n, q} \zeta(m, n, q|\eta) \\ &\times [\phi^N(mq|\mathbf{r}_1) \phi^N(nq|\mathbf{r}_2) + \phi^N(nq|\mathbf{r}_1) \phi^N(mq|\mathbf{r}_2)] P_q^N(\cos\vartheta) \quad \dots\dots(13) \end{aligned}$$

without any normalization condition.

The elements of the energy determinant (3) and the subsequent solution of a matrix equation of finite order were obtained by means of a programme written for NUSSE, the electronic computer at the Institute of Industrial Research, Oslo. The coefficients  $\zeta(m, n, q|\eta)$  were thus obtained by the computer from the secular determinants using the final  $E$  and  $\eta$  values. The quantities  $L$ ,  $L'$ ,  $M$  and  $N$  (6) were also obtained at the same time. The expansion coefficients of the numerical solution (11 and 12)  $c(m, n, q|\eta)$  are then obtained by the following relations

$$c(1s, 1s|\eta) = \xi^{-1/2}, \quad c(m, n, q|\eta) = \zeta(m, n, q|\eta) \xi^{-1/2}$$

when  $m = n$  and

$$c(m, n, q|\eta) = \zeta(m, n, q|\eta) (2\xi)^{-1/2}$$

when  $m < n$ , where

$$\xi = 1 + \sum_{m=2,q} |\zeta(m, m, q|\eta)|^2 + \frac{1}{2} \sum_{m < n, q} |\zeta(m, n, q|\eta)|^2. \quad \dots\dots(14)$$

† The process of checking our results with those of Dr. Shull showed the efficiency of the method when all the elements off the diagonal were found to be correct, whereas a slight error was indicated in the diagonal element (4p 4p | 4p 4p).

The coefficients of the original Slater determinantal set may easily be deduced by

$$c_s(m, m, q|\eta) = c(m, m, q|\eta) \quad \text{and} \quad c_s(m, n, q|\eta) = 2^{-1/2}c(m, n, q|\eta). \quad \dots (15)$$

The eigenvalues, the coefficients  $c(m, n, q|\eta)$  and the corresponding quantities  $L$ ,  $L'$ ,  $M$  and  $N$  are given for various approximations of the  $(2s)^2 1S$  state solution in table 1, and the 20-parameter approximation of the ground state solution in table 2. The input values of  $\eta$  and  $E$  together with the best values derived from the formulae (6) are also included in the tables. A comparison with previous results obtained by using other wave functions is finally quoted in table 3.

### § 6. DISCUSSION

In the first place some comments may be given on the figures listed in table 1. Proceeding from an estimated value of  $\eta$  (the correct interpretation of the  $(2s)^2$ -root) NUSSE computes the determinantal values for a sufficient number of  $E$ -values in order to interpolate the correct  $E$ -value which makes the determinant equal to zero. Thereupon  $\eta$  is varied until the lowest eigenvalue is obtained. The minimum point on the energy curve  $E(\eta)$  identified with the  $(2s)^2$ -root can thus easily be found, but, unfortunately, in three cases (denoted by \* in the table) this point coincides with the intersecting point between the  $(2s)^2$ -curve and another minimum curve belonging to a lower root of the secular equation. In these cases it is quite impossible to check the correctness of the minimum point by using the formulae (6). The optimum  $\eta$ -value and the corresponding eigenvalue differ now very much from the input values because the minimum condition with

Table 1. The Eigenvectors and the Eigenvalues (Ryd)  
of the  $(2s)^2 1S$  State Solution

Terms	He, $Z=2$					$H^-$ , $Z=1$	
$(1s)^2$	+0.2337	+0.3691	+0.2409	+0.2686	+0.31124	+0.2656	+0.38132
$1s2s$	-0.5553	-0.5024	-0.5518	-0.5395	-0.45217	-0.5458	-0.50726
$(2s)^2$	+0.6331	+0.5995	+0.5923	+0.5827	+0.53835	-0.5237	+0.38524
$(2p)^2$	-0.4860		-0.5202	-0.51745	-0.48741	-0.5606	-0.51957
$1s3s$		-0.1611	+0.0046	-0.0138	-0.16227	+0.0081	-0.21097
$2s3s$		-0.1705	+0.0786	+0.0355	-0.09445	+0.1363	-0.06074
$(3s)^2$		-0.1107	-0.0065	-0.0390	-0.07385	-0.0178	-0.11652
$2p3p$			+0.0931	+0.0738	+0.06258	+0.1328	+0.02337
$(3p)^2$			+0.0281	+0.0188	-0.00233	+0.0653	+0.01887
$(3d)^2$			+0.0194	+0.0192	+0.01380	+0.0464	+0.03407
$1s4s$		-0.3788		-0.0703	-0.30553		-0.29485
$2s4s$		-0.1427			-0.13597		-0.08935
$3s4s$		-0.1224			-0.10306		-0.12274
$(4s)^2$		-0.0765			-0.06208		-0.07452
$2p4p$					-0.09535		-0.00612
$3p4p$					+0.00064		+0.01544
$(4p)^2$					+0.00139		+0.01391
$3d4d$					+0.00781		+0.01526
$(4d)^2$					+0.00131		+0.00327
$(4f)^2$					+0.00050		+0.00219
$1s5s$				-0.0951			
$1s6s$				-0.0030			
$1s7s$				+0.0798			
Input							
$\eta$	0.8906	0.9375*	0.8828	0.8828	0.9375*	0.3828	0.390625*
$-E$	1.53547	1.48344*	1.54732	1.56096	1.597039*	0.29018	0.3096527*
$L$	1.95557	3.17694	1.98886	2.026975	2.0816241	1.98016	3.0133914
$L'$	0.48780	0.87532	0.47291	0.45846	0.6408257	0.46548	0.7377155
$M$	1.90801	4.15597	1.98467	2.07013	3.4761752	1.97660	3.7963894
$N$	1.00000	1.00000	1.00000	1.00000	1.00000	1.00000	1.00000
From (6)							
$\eta$	0.8971		0.8830	0.8684		0.3832	
$-E$	1.53555		1.54732	1.561196		0.29018	



respect to  $\eta$  is no longer applicable to the upper curve, only to the lower. In the other approximations listed in table 1, the optimum values derived from equations (6) are slightly different from the input values indicating the correctness of the energy minimum. In order to see what influence on the energy the addition of still more  $1sns$ -terms might have, the terms  $1s4s$ ,  $1s5s$ ,  $1s6s$  and  $1s7s$  were added to the 10-parameter function listed in the fourth column. The resulting 14-parameter function is shown in the fifth column. The resultant effect of these terms in that particular approximation is a marked lowering of the energy (0.01388 rydberg). As is well known, the importance of the various terms is ascertained by the squares of the corresponding weighting constants, and these squares are surprisingly large for three of the terms ( $1s4s$ ,  $1s5s$  and  $1s7s$ ). One needs to make a rough estimate of the influence on the energy when the remaining

Table 2. The Eigenvectors and the Eigenvalues (Ryd)  
of the Ground State Solution

He Z=2	{	Eigenvector	+0.92349, -0.35312, +0.00669, -0.06208, +0.13228, -0.01142, -0.00342, -0.00556, -0.01017, -0.01085, -0.02235, +0.00656, -0.00115, -0.00201, +0.00238, -0.00423, -0.00433, -0.00627, -0.00547, -0.00358		
		Input			
		$\eta=2.2220$	$L=3.0388478$ , $L'=0.8547598$	From formulae (6) $\eta=2.2219$	
		$-E=5.8024629$	$M=1.17532235$ , $N=1.00000$	$-E=5.8024631$	
H Z=1	{	Eigenvector	+0.91433, -0.26065, -0.16089, -0.10679, +0.23530, +0.01392, +0.00662, -0.03362, -0.01627, -0.01247, -0.02540, -0.01308, -0.00384, -0.00376, -0.00894, -0.01390, -0.00880, -0.01197, -0.00863, -0.00319		
		Input			
		$\eta=0.7560$	$L=3.6234738$ , $L'=0.8410404$	From formulae (6) $\eta=0.7558$	
		$-E=1.05146826$	$M=1.84074385$ , $N=1.00000$	$-E=1.05146835$	

The order of the states of configuration is equivalent to the 20-parameter approximation of the (2s)<sup>2</sup>-state solution.

infinity of  $1sns$ -terms is included. To illustrate this, we may consider the diagonal elements ( $1s\ 1s|ns\ ns$ ) and the elements of the main row ( $2s\ 1s|2s\ ns$ ) of the infinite energy determinant. These elements are the most important ones in affecting the energy. The diagonal elements run from negative to positive values when the order of the  $1sns$ -terms increases, and the main row elements are always positive. When the order approaches infinity the first elements are growing continually whereas the latter are approaching zero. The remaining infinity of the terms should therefore lower the energy only, and the best eigenvalue (-1.597039 rydberg for He and -0.3096527 rydberg for H-) obtained by the 20-parameter function (the sixth column) must be an upper limit to the true energy.

Let us consider the behaviour of the coefficients in the various approximations listed in table 1. The coefficients of the configurations (2s)<sup>2</sup>,  $1s2s$  and (2p)<sup>2</sup> come out very strongly, with the (2s)<sup>2</sup>-term as the leading term in He, whereas in H- the (2p)<sup>2</sup>-term is the leading one. In the 20-parameter approximation several terms seem to be unimportant, but, nevertheless, it is to be remembered that the resultant effect on the energy of these terms is not negligible. At this stage of investigation it may be predicted certainly that the inclusion of higher angular terms will turn out to be unimportant, but, conversely, some higher radial terms will still give considerable contributions to the energy. The computations also indicate that the radial correlation energy defined as the difference between the Hartree-Fock energy and the energy obtained by using

the best radial function, is at least 0.0229 rydberg in the He  $(2s)^2 1S$  state (the Hartree-Fock energy is  $-1.4605$  rydberg (Wilson 1935)), and that the angular correlation energy amounts surprisingly to as much as 0.11460 rydberg which is more than twice the corresponding energy in the ground state.

Table 3. Comparison of Different Approximations to the Energy Values ( $\text{cm}^{-1}$ ) obtained in the  $(2s)^2$  State and Ground State Solution

	(1)	(2)	(3)	(4)	(5)
He					
$(1s)^2 1S$		197770.4	189088.8	197939.0	198317.0
$(2s)^2 1S$		65508.5	50527.1	59381.7	
H <sup>-</sup>					
$(1s)^2 1S$		5645.0 (6081.8)			
$(2s)^2 1S$		6542.7			

(1) Ion and states; (2) 20-parameter approximation; (3) self-consistent field approximation; (4) 6-parameter approximation (Wu and Kou); (5) 39-parameter approximation (Kinoshita).

The result obtained by the 24-parameter approximation by Hylleraas and Midtdal (1956) is given in brackets. Recently a slight error in this work has been found.

As can be seen from table 2, the substitution of  $L$ ,  $L'$ ,  $M$  and  $N$  in (6) gives a very satisfactory check of the energy minimum, namely to better than 1 part in  $10^4$  for  $\eta$  and 3 parts in  $10^7$  for  $E$  in the case of He. The energy so obtained differs very much from the best eigenvalue obtained with functions of the Hylleraas type (table 3, Kinoshita 1957). This difference is essentially due to the rather slow energy convergence from our angular terms. The rate of the convergence is initially rapid ( $q=0$ ,  $q=1$ ) but becomes rather slow for higher angular terms ( $q>1$ ) as might have been expected since the potential energy is expanded in the Legendre functions of  $\vartheta$ .

The most striking feature about the results summarized in table 3 is that the electron affinity in the  $(2s)^2 1S$  state of H<sup>-</sup> is greater than in the ground state. This doubly excited state of the negative ion is therefore highly closed, not metastable, since the state is capable of auto-ionization. It may seem strange to find out that the 6-parameter approximation by Wu and Kou (1945) gives an eigenvalue for the ground state ( $-5.804$  rydbergs) which is so much better than our 21-parameter approximation, whereas, conversely, our 20-parameter approximation improves the Wu and Kou energy ( $-1.5412$  rydbergs) considerably in the  $(2s)^2 1S$  state solution. Provided no numerical errors have crept into their work, this means that an eigenfunction formed by a superposition of states of configurations of a complete one-electron set is more advantageous in the  $(2s)^2$  state solution than the Hylleraas function containing the interelectronic distance explicitly.

## § 7. IDENTIFICATION OF HELIUM LINES

Compton and Boyce (1928) observed emission lines in the vacuum ultra-violet of He with wave numbers 279 715, 312 118 and 323 206  $\text{cm}^{-1}$ . The first one which Kruger (1930) identified with the transition  $(2s)^2 1S-1s2s 1S$ , is the most interesting in our case. We have therefore listed in table 4 all the possibilities of quantum transitions from the  $(2s)^2$ -level to singly excited levels which can be important in connection with this corona line. The frequencies ( $\text{cm}^{-1}$ ) are calculated by using the total energy ( $-1.597039$  rydbergs) obtained with our

20-parameter approximation for the (2s)<sup>2</sup>-level and experimental values for the singly excited states.

Table 4. Possibilities of Quantum Transitions between the (2s)<sup>2</sup>-Level and Singly Excited States in He

Transitions	Frequencies (calculated in cm <sup>-1</sup> )
(2s) <sup>2</sup> <sup>1</sup> S-1s2s <sup>1</sup> S	295 692
(2s) <sup>2</sup> <sup>1</sup> S-1s2p <sup>1</sup> P	290 834
(2s) <sup>2</sup> <sup>1</sup> S-1s3s <sup>1</sup> S	277 104
(2s) <sup>2</sup> <sup>1</sup> S-1s3p <sup>1</sup> P	275 760
(2s) <sup>2</sup> <sup>1</sup> S-1s2p <sup>3</sup> P	292 882
(2s) <sup>2</sup> <sup>1</sup> S-1s3p <sup>3</sup> P	276 505

As can be seen from table 4 the transition (2s)<sup>2</sup> <sup>1</sup>S-1s2s <sup>1</sup>S originally identified by Kruger (1930) with the observed line, differs most from the observed value 279 715 cm<sup>-1</sup>. From a theoretical analysis, it is clear that there are no dipole or quadrupole radiation transitions between the (2s)<sup>2</sup> <sup>1</sup>S state and the two singly excited states 1s2s <sup>1</sup>S and 1s3s <sup>1</sup>S, while, on the other hand, the remaining transitions in table 4 involving two electron jumps comply with the selection rules of electric dipole radiation. It seems therefore at least possible that both (2s)<sup>2</sup> <sup>1</sup>S-1s3p <sup>1</sup>P and (2s)<sup>2</sup> <sup>1</sup>S-1s3p <sup>3</sup>P may be identified with the observed line even if the transition (2s)<sup>2</sup> <sup>1</sup>S-1s2p <sup>1</sup>P which may be expected to be stronger, has not yet been observed, and the observed sharpness of the line does not agree with the width expected in that case where the initial state (2s)<sup>2</sup> <sup>1</sup>S of the transition is subject to auto-ionization. The identification of the line is thus still in doubt, and the problem is even more difficult since the line may also correspond to one of the transitions 2s2p <sup>3</sup>P-1s4s <sup>3</sup>S, 2s2p <sup>3</sup>P-1s5s <sup>3</sup>S and 2s2p <sup>3</sup>P-1s4d <sup>3</sup>D with wave numbers (calculated) 281 639, 278 590 and 280 493 cm<sup>-1</sup> respectively (Bransden and Dalgarno 1953).

#### ACKNOWLEDGMENTS

This work has been financed largely by grants from the Norwegian Research Council for Science and Humanities, Oslo, and the author acknowledges his gratitude for this support. The author is greatly indebted to Dr. H. Shull for checking the matrix elements of the two-electron problem and for information concerning recent results of the ground state solution. Acknowledgment is also made of the computing assistance rendered by Mr. J. Midtdal in the solution of the secular equations by means of NUSSE, and thanks are due to the Computation Center at the Institute of Industrial Research, Oslo, for the availability of the electronic computer. The author is further indebted to Professor E. A. Hylleraas for the great hospitality he has enjoyed at the Institute for Theoretical Physics, Oslo.

#### APPENDIX

EVALUATION OF THE INTEGRALS  $A(\alpha\beta|q)$ ,  $B(\alpha\beta|q)$  and  $D_{2s}(\alpha\beta|pq|\gamma\omega)$

Using the contour integral representation of the radial orbitals (4), no difficulties emerge in the evaluation of the matrix elements of the kinetic and nuclear potential operators (3) when  $\nu=0$ . In this way we easily deduce

$$A(\alpha\beta|q) = N(\alpha, q)N(\beta, q) \sum_{w=1}^{\sigma} g_w(\alpha|q)g_w(\beta|q)(2q+w+1)!/(w-1)!$$

$$B(\alpha\beta|q) = N(\alpha, q)N(\beta, q) \sum_{w=1}^{\sigma} (2q+w)!/(w-1)! \quad \dots\dots (16)$$







## Matrix Elements of the Nuclear Potential Energy Operator

$|(1s)^2|4, 2/\sqrt{3}, 0, 0, 2/\sqrt{6}, 0, 0, 0, 0, 0, 2/\sqrt{10}, 0, 0, 0, 0, 0, 0, 0, 0, 0,$   
 $|1s2s|2, 2/\sqrt{3}, 0, 1/\sqrt{2}, 1/\sqrt{6}, 0, 0, 0, 0, 3/\sqrt{30}, 1/\sqrt{10}, 0, 0, 0, 0, 0, 0, 0, 0,$   
 $|(2s)^2|4, 0, 0, 2/\sqrt{2}, 0, 0, 0, 0, 0, 6/\sqrt{30}, 0, 0, 0, 0, 0, 0, 0, 0, |(2p)^2|2, 0, 0, 0,$   
 $1/\sqrt{5}, 0, 0, 0, 0, 0, 0, 1/\sqrt{15}, 0, 0, 0, 0, 0, 0, |1s3s|2, 1/\sqrt{3}, 2/\sqrt{6}, 0, 0, 0, 3/\sqrt{15},$   
 $0, 1/\sqrt{10}, 0, 0, 0, 0, 0, 0, 0, |2s3s|2, 2/\sqrt{2}, 0, 0, 0, 0, 3/\sqrt{15}, 3/\sqrt{30}, 0, 0, 0,$   
 $0, 0, 0, 0, |(3s)^2|4, 0, 0, 0, 0, 0, 6/\sqrt{15}, 0, 0, 0, 0, 0, 0, 0, 0, |2p3p|1, 1/\sqrt{5}, 0,$   
 $0, 0, 0, 0, 1/2\sqrt{3}, 1/2\sqrt{15}, 0, 0, 0, 0, |(3p)^2|2, 0, 0, 0, 0, 0, 0, 1/\sqrt{3}, 0, 0, 0,$   
 $0, |(3d)^2|4/3, 0, 0, 0, 0, 0, 0, 2/3\sqrt{7}, 0, 0, 0, |1s4s|2, 1/\sqrt{3}, 1/\sqrt{6}, 2/\sqrt{10}, 0, 0,$   
 $0, 0, 0, 0, |2s4s|2, 1/\sqrt{2}, 6/\sqrt{30}, 0, 0, 0, 0, 0, 0, |3s4s|2, 6/\sqrt{15}, 0, 0, 0, 0, 0,$   
 $0, |(4s)^2|4, 0, 0, 0, 0, 0, 0, 2p4p|1, 1/2\sqrt{5}, 1/\sqrt{15}, 0, 0, 0, |3p4p|1, 1/\sqrt{3}, 0,$   
 $0, 0, |(4p)^2|2, 0, 0, 0, |3d4d|2/3, 2/3\sqrt{7}, 0, |(4d)^2|4/3, 0, |(4f)^2|1.$

## Matrix Elements of the Electronic Repulsion Energy Operator

$|(1s)^2|5/4, 5/8\sqrt{3}, 1/4, 7/16\sqrt{3}, 1/4\sqrt{6}, 3/16\sqrt{2}, 7/64, 21/32\sqrt{15}, 9/32\sqrt{3},$   
 $9/64\sqrt{5}, 1/16\sqrt{10}, 5/16\sqrt{30}, 35/128\sqrt{15}, 1/16, 13/64\sqrt{5}, 15/128, 3/16\sqrt{3},$   
 $45/128\sqrt{35}, 5/32\sqrt{5}, 11/256\sqrt{7}, |1s2s|5/8, 1/2\sqrt{3}, -7/96, 4/8\sqrt{2}, 7/16\sqrt{6},$   
 $27/128\sqrt{3}, 7/48\sqrt{5}, 5/64, -27/128\sqrt{15}, 9/16\sqrt{30}, 11/32\sqrt{10}, 25/128\sqrt{5},$   
 $15/128\sqrt{3}, 45/128\sqrt{15}, 19/128\sqrt{3}, 5/64, -27/128\sqrt{105}, -5/128\sqrt{15},$   
 $-55/512\sqrt{21}, |(2s)^2|7/8, 17/96\sqrt{3}, 9/16\sqrt{6}, 15/32\sqrt{2}, 1/4, -25/192\sqrt{15},$   
 $1/6\sqrt{3}, 17/96\sqrt{5}, 15/32\sqrt{10}, 13/16\sqrt{30}, 75/128\sqrt{15}, 1/8, -7/192\sqrt{5}, 31/384,$   
 $23/128\sqrt{3}, 7/128\sqrt{35}, 1/24\sqrt{5}, 61/512\sqrt{7}, |(2p)^2|111/128, -17/192\sqrt{2},$   
 $17/384\sqrt{6}, 7/96\sqrt{3}, 111/256\sqrt{5}, 51/320, 121/128\sqrt{15}, -17/128\sqrt{30},$   
 $-13/192\sqrt{10}, 7/192\sqrt{5}, 11/256\sqrt{3}, 9/256\sqrt{15}, 153/1280\sqrt{3}, 179/2560,$   
 $363/256\sqrt{105}, 915/1792\sqrt{15}, 3991/10240\sqrt{21}, |1s3s|31/64, 41/128\sqrt{3},$   
 $37/128\sqrt{6}, -73/384\sqrt{10}, -1/64\sqrt{2}, -7/128\sqrt{30}, 117/128\sqrt{15}, 5/16\sqrt{5},$   
 $73/256\sqrt{10}, 21/128\sqrt{6}, 9/64\sqrt{30}, 17/256\sqrt{6}, 13/256\sqrt{2}, -129/256\sqrt{210},$   
 $-25/128\sqrt{30}, 37/1024\sqrt{42}, |2s3s|65/128, 13/32\sqrt{2}, 85/384\sqrt{30}, -41/384\sqrt{6},$   
 $-17/384\sqrt{10}, 45/128\sqrt{5}, 61/64\sqrt{15}, 269/256\sqrt{30}, 51/256\sqrt{2}, -43/768\sqrt{10},$   
 $13/384\sqrt{2}, 55/512\sqrt{6}, 217/768\sqrt{70}, -1/256\sqrt{10}, -183/2048\sqrt{14},$   
 $|(3s)^2|355/512, 5/96\sqrt{15}, 115/768\sqrt{3}, 37/512\sqrt{5}, 45/128\sqrt{10}, 165/128\sqrt{30},$   
 $1187/1024\sqrt{15}, 121/512, 35/1536\sqrt{5}, -71/3072, 91/1024\sqrt{3}, -161/3072\sqrt{35},$   
 $187/1536\sqrt{5}, 335/4096\sqrt{7}, |2p3p|111/256, 453/1280\sqrt{5}, -121/1280\sqrt{3},$   
 $-17/128\sqrt{30}, 1/64\sqrt{2}, 1/64, 23/512\sqrt{15}, 657/2560\sqrt{3}, 963/2560\sqrt{15},$   
 $687/5120\sqrt{5}, 121/320\sqrt{21}, 2337/17920\sqrt{3}, -11973/20480\sqrt{105}, |(3p)^2|261/400,$   
 $431/1280\sqrt{5}, -33/128\sqrt{30}, -5/96\sqrt{10}, 65/1536\sqrt{5}, 17/256\sqrt{3}, 687/1280\sqrt{15},$   
 $4353/12800\sqrt{3}, 2089/12800, -779/2560\sqrt{105}, 4073/8960\sqrt{15}, 17811/51200\sqrt{21},$   
 $|(3d)^2|1651/2560, 1/80\sqrt{2}, -37/640\sqrt{6}, 37/5120\sqrt{3}, 101/2560\sqrt{5}, -431/7680,$   
 $431/15360\sqrt{5}, 2333/15360\sqrt{15}, 1651/5120\sqrt{7}, 1979/17920, 5163/4096\sqrt{35},$   
 $|1s4s|53/128, 1/4\sqrt{3}, 55/256\sqrt{6}, 53/256\sqrt{10}, -19/256\sqrt{2}, -1/16\sqrt{10},$   
 $3/512\sqrt{30}, -19/1280\sqrt{14}, -7/256\sqrt{2}, 109/2048\sqrt{70}, |2s4s|13/32, 9/32,$   
 $97/128\sqrt{30}, 9/128\sqrt{30}, 9/128\sqrt{6}, -27/128\sqrt{30}, -7/128\sqrt{10}, -49/640\sqrt{42},$   
 $11/640\sqrt{6}, -19/128\sqrt{210}, |3s4s|443/1024, 533/512\sqrt{15}, 13/1024\sqrt{3},$   
 $165/1024\sqrt{15}, -125/2048\sqrt{5}, 259/5120\sqrt{21}, -29/1280\sqrt{3}, -335/8192\sqrt{105},$   
 $|(4s)^2|595/1024, 1/128\sqrt{5}, 1/64, 267/2048\sqrt{3}, 21/1280\sqrt{35}, 329/5120\sqrt{5},$   
 $325/8192\sqrt{7}, |2p4p|881/2560, 227/1024\sqrt{5}, 269/1280\sqrt{15}, -1883/15360\sqrt{7},$   
 $61/8960, -973/10240\sqrt{35}, |3p4p|9497/25600, 15323/51200\sqrt{3}, 3017/15360\sqrt{35},$   
 $-4763/53760\sqrt{5}, -5937/204800\sqrt{7}, |(4p)^2|55431/102400, 2839/30720\sqrt{105},$

63157/215040 $\sqrt{15}$ , 60531/409600 $\sqrt{21}$ , |3d4d|1651/5120, 4789/17920 $\sqrt{7}$ ,  
 -5163/57344 $\sqrt{5}$ , |(4d)<sup>2</sup>|126563/250880, 3379/8192 $\sqrt{35}$ , |(4f)<sup>2</sup>|236317/458752.

## REFERENCES

- BARTLETT, J. H., GIBBONS, J. J., and DUNN, C. G., 1935, *Phys. Rev.*, **47**, 679.  
 BRANDEN, B. H., and DALGARNO, A., 1953, *Proc. Phys. Soc. A*, **66**, 904, 911.  
 COMPTON, K. T., and BOYCE, J. C., 1928, *J. Franklin Inst.*, **205**, 497.  
 CONDON, E. U., and SHORTLEY, G. H., 1935, *Theory of Atomic Spectra* (Cambridge : University Press), p. 371.  
 FENDER, F. G., and VINTI, J. P., 1934, *Phys. Rev.*, **46**, 78.  
 FOCK, V., 1954, *Izvest. Akad. Nauk, S.S.S.R.*, **18** (2), 161.  
 HOLØIEN, E., 1956, *Phys. Rev.*, **104**, 1301.  
 HYLLERAAS, E. A., and MIDTDAL, J., 1956, *Phys. Rev.*, **103**, 829.  
 KINOSHITA, T., 1957, *Phys. Rev.*, **105**, 1490.  
 KRUGER, P. G., 1930, *Phys. Rev.*, **36**, 853.  
 LÖWDIN, P. O., and SHULL, H., 1956, *Phys. Rev.*, **101**, 1730.  
 PLUVINAGE, P., 1955, *J. Phys. Radium*, **16**, 675; 1956, *C.R. Acad. Sci., Paris*, **242**, 2109.  
 PLUVINAGE, P., and MUNCHY, G., 1957, *J. Phys. Radium*, **18**, 157.  
 WILSON, W. S., 1935, *Phys. Rev.*, **48**, 536.  
 WILSON, W. S., and LINDSAY, R. B., 1935, *Phys. Rev.*, **47**, 638, 681.  
 WU, T. Y., 1934, *Phys. Rev.*, **46**, 239.  
 WU, T. Y., and KOU, T. T., 1945, *J. Chin. Phys.*, **6**, 50.  
 WU, T. Y., and MA, S. T., 1936, *J. Chin. Chem. Soc.*, **4**, 345.

## The K Auger Spectrum

By W. N. ASAAD AND E. H. S. BURHOP

University College, London

*MS. received 24th October 1957*

**Abstract.** The fine structure of the K Auger spectrum is discussed and the positions and intensities of the K-LL and K-LM Auger lines calculated for different values of  $Z$  using a non-relativistic theory and assuming intermediate coupling between the two inner shell vacancies of the atom in the final states. In regions of intermediate atomic number the usual six-line K-LL spectrum expected on the basis of  $j$ - $j$  coupling is modified into a nine-line spectrum and the relative intensity of the various lines varies markedly with  $Z$ . The effect of inter-configuration terms on the K-LL spectrum is also discussed. The observed position and relative intensities of the K-LL lines can be understood when reasonable allowance is made for relativistic effects but the interpretation of the rather meagre experimental data on the K-LM spectrum is less clear, although there is qualitative agreement with the theoretical predictions.

### § 1. INTRODUCTION

MANY measurements have been made of the K series fluorescence yield of atoms of a wide range of atomic numbers, and the results obtained are in reasonably good agreement with those expected theoretically (Burhop 1952, 1955, Broyles, Thomas and Haynes 1953). With the development of high resolution beta-ray spectrometers in recent years, it has been possible to determine the positions and intensities of the lines of the K Auger electron spectrum with considerable accuracy, and it has been found that they are not in good agreement with existing calculations using either non-relativistic or relativistic theory. Previous calculations have usually estimated only the total Auger transition probability to a certain configuration of the doubly ionized atom, without considering in detail the different possible terms within a given final configuration. Where different terms have been considered, these have been expressed either in terms of  $j$ - $j$  coupling,<sup>†</sup> or, for light elements, Russell-Saunders coupling.<sup>‡</sup>

It is not clear, however, over what part of the range of atomic numbers the assumption of extreme  $j$ - $j$  coupling is applicable. A non-relativistic calculation of these terms on the basis of intermediate coupling is described in this paper; values of the relative K Auger electron intensities are obtained in markedly better agreement with experiment than those derived from pure  $j$ - $j$  coupling, although some discrepancies remain which, presumably, must be attributed to the neglect of relativity.

<sup>†</sup> Such estimates (unpublished) have been made by Burhop, and are quoted by Mladjenovic and Slätis (1954). An attempt to separate out the different terms in  $j$ - $j$  coupling made much earlier (Burhop 1935) was incorrect.

<sup>‡</sup> Rubinstein and Snyder, as described in thesis of Rubinstein (1955, University of Illinois).

## § 2. INTERMEDIATE COUPLING THEORY

After an Auger transition an atom is left doubly ionized in inner shells. For the K-LL and K-LM Auger spectra considered in this paper, atoms in the final state may have the following configurations involving non-closed L and M shells:

$$\left. \begin{aligned} (2s)^0(2p)^6, (2s)(2p)^5, (2s)^2(2p)^4, (2s)(3s), (2s)(3p)^5, \\ (2s)(3d)^9, (3s)(2p)^5, (2p)^5(3p)^5, (2p)^5(3d)^9. \end{aligned} \right\} \dots\dots(1)$$

The electrons in these non-closed shells are considered to be moving in an effective central field of the nucleus screened by the other electrons in the atom. The degeneracy of the motion in the central field is removed by the perturbation

$$\sum_{i,j(i \neq j)} \frac{e^2}{r_{ij}} + \sum_i \xi(r_i) \mathbf{L}_i \cdot \mathbf{S}_i$$

arising from the electrostatic interaction of pairs of electrons, and the coupling between spin and orbital motion of electrons, in the non-closed shells, where

$$\xi(r) = \frac{e}{2m^2c^2} \frac{1}{r} \frac{\partial V}{\partial r},$$

$V$  being the potential in the central field.

The states of the above nearly closed shell configurations can be expressed in terms of those of completely closed shell configurations together with the two-electron configurations,

$$\left. \begin{aligned} (2s)^2, (2s)(2p), (2p)^2, (2s)(3s), (2s)(3p), \\ (2s)(3d), (3s)(2p), (2p)(3p), (2p)(3d). \end{aligned} \right\} \dots\dots(2)$$

It can be shown (Condon and Shortley 1953, p. 295 ff.) that the states of the two systems are equivalent, provided the sign of the spin-orbit coupling term is reversed and certain additional terms added to the diagonal elements of the matrix of the electrostatic interaction. Since these additions are the same for all diagonal elements for a given configuration, they will not affect the relative positions of terms within a given configuration but only the total energy of the whole configuration.

The required matrices for the two-electron configurations can be obtained from the electrostatic energies given by Condon and Shortley (1953, p. 197 ff.), the spin-orbit matrices given in the same book (pp. 268 and 269) for different values of the total angular momentum  $J$ , the unperturbed system being expressed in the representation ( $SLJM$ ) appropriate to Russell-Saunders coupling. Solutions of the corresponding secular equations then enable the energy of the various terms in intermediate coupling to be obtained, and corresponding to each of these energy values  $E_i(J)$  the appropriate mixing parameters which give the eigenfunctions of the system in intermediate coupling in terms of the Russell-Saunders eigenfunctions. The notation  $C_i^n(L, J)$  is used for these mixing coefficients where  $n$  is the multiplicity,  $L, J$  the orbital and total angular momenta respectively of the basic  $\psi$  with which the coefficient is associated, and  $i$  ( $= 1, 2, 3$ , etc.) specifies the particular solution of the secular equation. For example, for the term  $J = 1$  of the configuration  $(2p)^5(3d)^9$  the wave functions of the three possible terms in intermediate coupling can be written

$$\psi_i(1) = C_i(^3D_1)\psi(^3D_1) + C_i(^3P_1)\psi(^3P_1) + C_i(^1P_1)\psi(^1P_1) \quad (i = 1, 2, 3) \dots\dots(3)$$

and the corresponding energy values are  $E_i^{(2p)(3d)}(1)$ .



## § 3. THE AUGER TRANSITION AMPLITUDES

The Auger transition probabilities are expressed in terms of the amplitudes

$$\{(nl), (n'l'), \nu, k\} = \frac{4\pi^2 e^2}{h^2} \int \int_{r_1, r_2=0}^{\infty} \gamma_{\nu} R_{10}(r_1) R_{nl}(r_1) R_{n'l'}(r_2) R_{\infty^k}(r_2) \cdot r_1^2 r_2^2 dr_1 dr_2 \quad \dots\dots\dots (4)$$

where  $R_{10}(r)$ ,  $R_{nl}(r)$ ,  $R_{n'l'}(r)$ ,  $R_{\infty^k}(r)$  are the radial parts of the wave functions of an electron in the (1s),  $(nl)$ ,  $(n'l')$ , bound states and a positive energy state of orbital angular momentum quantum number  $k$  respectively, in the central field of the nucleus screened by the appropriate other electrons in the atom. The positive energy state, which has the energy of the ejected Auger electron, is normalized to represent one ejected electron per unit time and

$$\gamma_{\nu} = \begin{cases} r_1^{\nu}/r_2^{\nu+1}, & (r_1 < r_2), \\ r_2^{\nu}/r_1^{\nu+1}, & (r_2 < r_1). \end{cases} \quad \dots\dots\dots (5)$$

In Russell-Saunders coupling the following expressions are obtained for the Auger transition probabilities for the possible final states:

$$\begin{aligned} (2s)^0(2p)^6 : & {}^1S_0 \dots | \{(2s)^2, 0, 0\} |^2 = K \{(2s)^2 {}^1S_0\} \\ (2s)(2p)^5 : & {}^1P_1 \dots \frac{3}{2} | \{(2s)(2p), 0, 1\} + \frac{1}{3} \{(2p)(2s), 1, 1\} |^2 = K \{(2s)(2p) {}^1P_1\} \\ & {}^3P_{0,1,2} \dots (J + \frac{1}{2}) | \{(2s)(2p), 0, 1\} - \frac{1}{3} \{(2p)(2s), 1, 1\} |^2 \\ & = K \{(2s)(2p) {}^3P_{0,1,2}\} \\ (2s)^2(2p)^4 : & {}^1S_0 \dots \frac{1}{3} | \{(2p)^2, 1, 0\} |^2 = K \{(2p)^2 {}^1S_0\} \\ & {}^3P_{0,1,2} \dots 0 \\ & {}^1D_2 \dots \frac{2}{3} | \{(2p)^2, 1, 2\} |^2 = K \{(2p)^2 {}^1D_2\} \\ (2s)(3s) : & {}^1S_0 \dots \frac{1}{2} | \{(2s)(3s), 0, 0\} + \{(3s)(2s), 0, 0\} |^2 = K \{(2s)(3s) {}^1S_0\} \\ & {}^3S_1 \dots \frac{3}{2} | \{(2s)(3s), 0, 0\} - \{(3s)(2s), 0, 0\} |^2 = K \{(2s)(3s) {}^3S_1\} \\ (2s)(3p)^5 : & {}^1P_1 \dots \frac{3}{2} | \{(2s)(3p), 0, 1\} + \frac{1}{3} \{(3p)(2s), 1, 1\} |^2 = K \{(2s)(3p) {}^1P_1\} \\ & {}^3P_{0,1,2} \dots (J + \frac{1}{2}) | \{(2s)(3p), 0, 1\} - \frac{1}{3} \{(3p)(2s), 1, 1\} |^2 \\ & = K \{(2s)(3p) {}^3P_{0,1,2}\} \\ (2s)(3d)^9 : & {}^1D_2 \dots \frac{5}{2} | \{(2s)(3d), 0, 2\} + \frac{1}{5} \{(3d)(2s), 2, 2\} |^2 = K \{(2s)(3d) {}^1D_2\} \\ & {}^3D_{1,2,3} \dots (J + \frac{1}{2}) | \{(2s)(3d), 0, 2\} - \frac{1}{5} \{(3d)(2s), 2, 2\} |^2 \\ & = K \{(2s)(3d) {}^3D_{1,2,3}\} \\ (3s)(2p)^5 : & {}^1P_1 \dots \frac{3}{2} | \frac{1}{3} \{(2p)(3s), 1, 1\} + \{(3s)(2p), 0, 1\} |^2 = K \{(3s)(2p) {}^1P_1\} \\ & {}^3P_{0,1,2} \dots (J + \frac{1}{2}) | \frac{1}{3} \{(2p)(3s), 1, 1\} - \{(3s)(2p), 0, 1\} |^2 \\ & = K \{(3s)(2p) {}^3P_{0,1,2}\} \\ (2p)^5(3p)^5 : & {}^1S_0 \dots \frac{1}{6} | \{(2p)(3p), 1, 0\} + \{(3p)(2p), 1, 0\} |^2 = K \{(2p)(3p) {}^1S_0\} \\ & {}^3S_1 \dots \frac{1}{2} | \{(2p)(3p), 1, 0\} - \{(3p)(2p), 1, 0\} |^2 = K \{(2p)(3p) {}^3S_1\} \\ & {}^1P_1 \dots 0 \\ & {}^3P_{0,1,2} \dots 0 \\ & {}^1D_2 \dots \frac{1}{3} | \{(2p)(3p), 1, 2\} + \{(3p)(2p), 1, 2\} |^2 = K \{(2p)(3p) {}^1D_2\} \\ & {}^3D_{1,2,3} \dots \frac{(2J+1)}{15} | \{(2p)(3p), 1, 2\} - \{(3p)(2p), 1, 2\} |^2 \\ & = K \{(2p)(3p) {}^3D_{1,2,3}\} \end{aligned}$$

$$\begin{aligned}
(2p)^5(3d)^9: & \quad {}^1P_1 \dots \frac{1}{3} \left| \{ (2p)(3d), 1, 1 \} + \frac{2}{3} \{ (3d)(2p), 2, 1 \} \right|^2 = K \{ (2p)(3d) {}^1P_1 \} \\
& \quad {}^3P_{0,1,2} \dots \frac{(2J+1)}{9} \left| \{ (2p)(3d), 1, 1 \} - \frac{3}{5} \{ (3d)(2p), 2, 1 \} \right|^2 \\
& \quad \quad \quad = K \{ (2p)(3d) {}^3P_{0,1,2} \} \\
& \quad {}^1D_2 \dots 0 \\
& \quad {}^3D_{1,2,3} \dots 0 \\
& \quad {}^1F_3 \dots \frac{1}{2} \left| \{ (2p)(3d), 1, 3 \} + \frac{2}{3} \{ (3d)(2p), 2, 3 \} \right|^2 = K \{ (2p)(3d) {}^1F_3 \} \\
& \quad {}^3F_{2,3,4} \dots \frac{(2J+1)}{14} \left| \{ (2p)(3d), 1, 3 \} - \frac{3}{5} \{ (3d)(2p), 2, 3 \} \right|^2 \\
& \quad \quad \quad = K \{ (2p)(3d) {}^3F_{2,3,4} \}.
\end{aligned}
\tag{6}$$

For intermediate coupling the Auger transition probabilities are given in terms of the above by the expressions

$$J_i \{ (nl), (n'l'), J \} = \frac{\sum \{ C_i({}^n L_J) \}^2 K \{ (nl)(n'l')({}^n L_J) \}}{\sum \{ C_i({}^n L_J) \}^2} \tag{7}$$

where the  $C$ 's (which also depend on the configuration) are the mixing coefficients defined earlier, and  $i$  specifies a particular root of the secular equation for a given  $J$  value within the configuration  $(nl)(n'l')$ .

Calculations of the Auger transition amplitudes  $\{ (nl), (n'l'), \nu, k \}$ , have been carried out by Burhop (1935), Pincherle (1935), Ramberg and Richtmyer (1937), and by Rubinstein and Snyder (1955). Pincherle used hydrogenic wave functions, Burhop used screened hydrogenic functions, Ramberg and Richtmyer used wave functions for a Fermi-Thomas field and Rubinstein and Snyder for a self-consistent field. Discrepancies exist between these calculations which seem larger than might have been expected from the differences between the wave functions employed. For the K-LL spectrum the transition amplitudes calculated by Burhop are generally used in the present paper, although those of Rubinstein and Snyder are quoted for comparison. For the K-LM spectrum the Rubinstein and Snyder transition amplitudes are used.

#### § 4. THE ELECTRON ENERGIES OF THE K-AUGER SPECTRUM

The energies of the electrons in the K Auger spectrum can be calculated in terms of the matrix elements of the electrostatic interaction between two electrons,  $F^\nu(nl, n'l')$ ,  $G^\nu(nl, n'l')$  defined by

$$\left. \begin{aligned} F^\nu(nl, n'l') &= e^2 \int \int_{r_1, r_2=0}^{\infty} \gamma_\nu R_{nl}^2(r_1) R_{n'l'}^2(r_2) r_1^2 r_2^2 dr_1 dr_2 \\ G^\nu(nl, n'l') &= e^2 \int \int_{r_1, r_2=0}^{\infty} \gamma_\nu R_{nl}(r_1) R_{n'l'}(r_1) R_{nl}(r_2) R_{n'l'}(r_2) r_1^2 r_2^2 dr_1 dr_2. \end{aligned} \right\} \dots \tag{8}$$

For the K-LL spectrum the following expressions are obtained:

$$\left. \begin{aligned} (2s)^0(2p)^6: & \quad 2I(2s) - F^0(20, 20) - 6[2F^0(21, 20) - \frac{1}{3}G^1(21, 20)] \\ (2s)(2p)^5: & \quad I(2s) + I(2p) - F^0(20, 20) - 4[2F^0(21, 20) - \frac{1}{3}G^1(21, 20)] \\ & \quad - 3[\frac{5}{3}F^0(21, 21) - \frac{2}{15}F^2(21, 21)] + E_i^{(2s)(2p)}(J) \\ (2s)^2(2p)^4: & \quad 2I(2p) - 2[2F^0(21, 20) - \frac{1}{3}G^1(21, 20)] \\ & \quad - 6[\frac{5}{3}F^0(21, 21) - \frac{2}{15}F^2(21, 21)] + E_i^{(2p)^4}(J) \end{aligned} \right\} \dots \tag{9}$$

where the terms  $E_i^{(2s)(2p)}(J)$ , etc., depend on the particular term within the final state, and  $I(2s)$ ,  $I(2p)$  are the energies of  $2s$ ,  $2p$  electrons respectively in the field due to the nucleus and the electrons other than those in the  $L$  shell.

The energy required to move a single  $L$  electron from an atom can be calculated using these same quantities:

$$\left. \begin{aligned} (2s)(2p)^6. \quad L_1: \quad & I(2s) - 3[F^0(21, 20) - \frac{1}{3}G^1(21, 20)] - F^0(20, 20) = E(L_1) \\ (2s)^2(2p)^5(J = \frac{1}{2}). \quad L_2: \quad & I(2p) - [2F^0(21, 20) - \frac{1}{3}G^1(21, 20)] \\ & - 3[\frac{5}{3}F^0(21, 21) - \frac{2}{15}F^2(21, 21)] + \zeta_{21} = E(L_2) \\ (2s)^2(2p)^5(J = \frac{3}{2}). \quad L_3: \quad & E(L_2) - \frac{3}{2}\zeta_{21} = E(L_3) \end{aligned} \right\} \dots\dots (10)$$

where

$$\zeta_{nl} = \hbar^2 \int_0^\infty R_{nl}^2(r) \xi(r) r^2 dr.$$

In the following we shall sometimes need to refer to the ionization energy of the  $(2s)^2(2p)^5$  state without taking account of spin-orbit splitting. We refer to the quantity as

$$E(2p)(=E(L_2) - \zeta_{21} = E(L_3) + \frac{1}{2}\zeta_{21}). \quad \dots\dots (11)$$

#### § 5. CALCULATION OF THE TERM ENERGIES, MIXING COEFFICIENTS AND AUGER TRANSITION PROBABILITIES

The secular determinants from which the term energies,  $E_i^{nl, n'l'}(J)$  and the mixing coefficients,  $C_i^{(n)L_J}$ , are determined involve the quantities  $F^v(nl, n'l')$ ,  $G^v(nl, n'l')$ , and  $\zeta_{nl}$ . In general, screened hydrogenic wave functions were

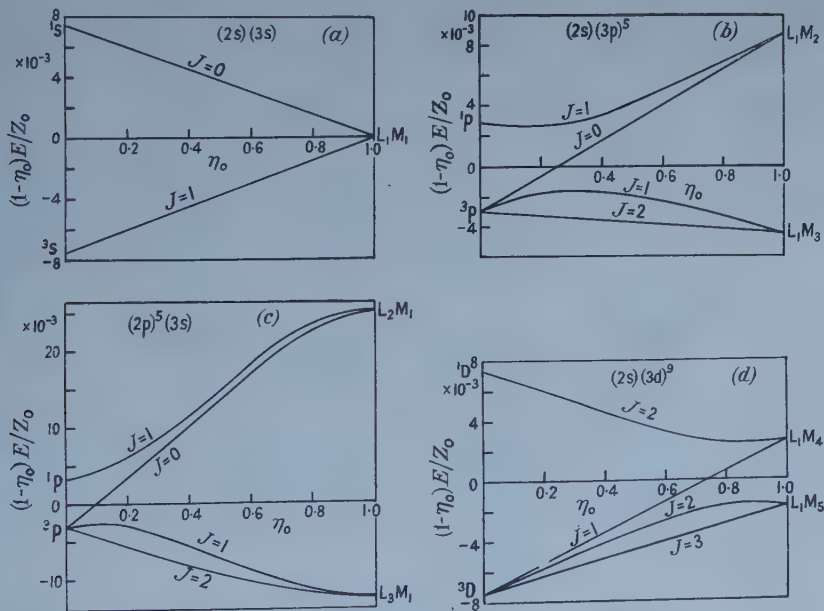


Figure 1. Energies of lines expected in the K-LM Auger spectrum for different  $Z$  showing the transition from  $L$ - $S$  to  $j$ - $j$  coupling. The ordinates are  $(1-\eta_0)E/Z_0$  where  $\eta_0$  and  $Z_0$  are defined in the text and  $E$  is the energy expressed in A.U. (1 A.U. = 27.09 eV). The final state configurations are (a)  $(2s)(3s)$ , (b)  $(2s)(3p)^5$ , (c)  $(2p)^5(3s)$ , (d)  $(2s)(3d)^9$ .

employed for the calculation of these quantities, the screening constant being derived from Slater's rules. Simple closed expressions are then obtained for them. A difficulty arose as to the best value of the screening constant to take in the K-LM case since Slater's rules give different values for  $R_{nl}$  and  $R_{n'l'}$ . In this case, in order to preserve orthogonality, the effective nuclear charge was taken as the geometric mean of that given by Slater's rules for the L and M shells. The value of the effective nuclear charge was different for the  $M_{4,5}$  shells from that for the  $M_{1,2,3}$  shells.

As a check on the applicability of screened hydrogenic functions in the calculation of these quantities they were also evaluated for mercury ( $Z=80$ ) using wave functions calculated for a self-consistent field. The effective value of the screening constant that would make these values agree with those calculated using screened hydrogenic wave functions are as follows:  $F^0(20,20)$ , 3.8;  $F^0(21,21)$ , 4.5;  $F^2(21,21)$ , 5.1;  $F^0(21,20)$ , 4.0;  $G^1(21,20)$ , 2.6;  $\zeta_{21}$ , 2.9. The screening constant given by Slater's rules is 3.3 which is in reasonably good agreement with the above values.

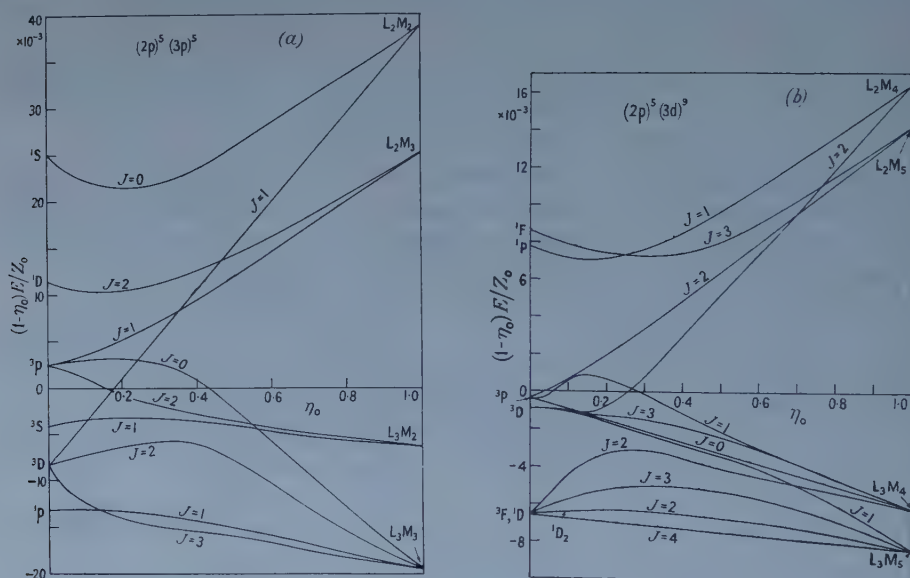


Figure 2. As for figure 1, for final state configurations  
(a)  $(2p)^5(3p)^5$ , (b)  $(2p)^5(3d)^9$ .

The results of the calculations of the energies of the terms of the Auger spectrum within a given configuration are given in figures 1 and 2 for the K-LM case. In exhibiting these results it is difficult to find suitable parameters, on account of the large change of scale involved with change of atomic number  $Z$ . The quantity  $\eta_0$  defined by the relation

$$\eta_0 = \frac{(Z_0/30)^3}{1 + (Z_0/30)^3} \quad \dots\dots(12)$$

has been used as abscissa,  $Z_0$  being the screened nuclear charge. It is taken as  $(Z-3.3)$  for the K-LL spectrum,  $[(Z-3.3)(Z-10.25)]^{1/2}$  for the K-LM<sub>1,2,3</sub> spectrum and  $[(Z-3.3)(Z-20.15)]^{1/2}$  for the K-LM<sub>4,5</sub> spectrum.



Table 1. Calculated Relative Intensities in the K-LL, K-LM Auger Spectrum for Different Z (all intensities relative to K-L<sub>1</sub>L<sub>1</sub>)

Z	25	30	37	47	80
L <sub>1</sub> L <sub>2</sub> ( <sup>1</sup> P <sub>1</sub> )	2.99	2.80	2.40	1.77	1.15
L <sub>1</sub> L <sub>2</sub> ( <sup>3</sup> P <sub>0</sub> )	0.047	0.047	0.047	0.047	0.047
L <sub>1</sub> L <sub>3</sub> ( <sup>3</sup> P <sub>1</sub> )	0.24	0.40	0.80	1.42	2.03
L <sub>1</sub> L <sub>3</sub> ( <sup>3</sup> P <sub>2</sub> )	0.24	0.24	0.24	0.24	0.24
L <sub>2</sub> L <sub>2</sub> ( <sup>1</sup> S <sub>0</sub> )	0.41	0.38	0.32	0.24	0.15
L <sub>2</sub> L <sub>3</sub> ( <sup>1</sup> D <sub>2</sub> )	6.08	5.54	5.08	4.71	4.32
L <sub>2</sub> L <sub>3</sub> ( <sup>3</sup> P <sub>0</sub> )	0.012	0.038	0.096	0.185	0.28
L <sub>3</sub> L <sub>3</sub> ( <sup>3</sup> P <sub>2</sub> )	0.47	0.86	1.30	1.72	2.12
L <sub>1</sub> M <sub>1</sub> ( <sup>3</sup> S <sub>1</sub> )	0.001	0.001	0.001	0.002	0.002
L <sub>1</sub> M <sub>1</sub> ( <sup>1</sup> S <sub>0</sub> )	0.17	0.19	0.20	0.29	0.31
L <sub>1</sub> M <sub>2</sub> ( <sup>3</sup> P <sub>0</sub> )	0.005	0.006	0.007	0.011	0.013
L <sub>1</sub> M <sub>2</sub> ( <sup>1</sup> P <sub>1</sub> )	0.19	0.18	0.17	0.19	0.18
L <sub>1</sub> M <sub>3</sub> ( <sup>3</sup> P <sub>1</sub> )	0.035	0.059	0.114	0.25	0.31
L <sub>1</sub> M <sub>3</sub> ( <sup>3</sup> P <sub>2</sub> )	0.027	0.031	0.037	0.057	0.062
L <sub>2</sub> M <sub>1</sub> ( <sup>3</sup> P <sub>0</sub> )	0.005	0.005	0.005	0.006	0.006
L <sub>2</sub> M <sub>1</sub> ( <sup>1</sup> P <sub>1</sub> )	0.146	0.138	0.118	0.150	0.152
L <sub>3</sub> M <sub>1</sub> ( <sup>3</sup> P <sub>1</sub> )	0.100	0.115	0.170	0.25	0.28
L <sub>3</sub> M <sub>1</sub> ( <sup>3</sup> P <sub>2</sub> )	0.023	0.024	0.024	0.033	0.035
L <sub>1</sub> M <sub>4</sub> ( <sup>3</sup> D <sub>1</sub> )	—	0.001	0.002	0.010	0.010
L <sub>1</sub> M <sub>4</sub> ( <sup>1</sup> D <sub>2</sub> )	—	—	0.001	0.004	0.009
L <sub>1</sub> M <sub>5</sub> ( <sup>3</sup> D <sub>2</sub> )	—	0.001	0.003	0.015	0.010
L <sub>1</sub> M <sub>5</sub> ( <sup>3</sup> D <sub>3</sub> )	—	0.002	0.005	0.022	0.022
L <sub>2</sub> M <sub>2</sub> ( <sup>1</sup> S <sub>0</sub> )	0.080	0.077	0.059	0.087	0.071
L <sub>3</sub> M <sub>2</sub> ( <sup>3</sup> S <sub>1</sub> )	0.001	0.001	0.001	0.001	0.001
L <sub>3</sub> M <sub>3</sub> ( <sup>1</sup> P <sub>1</sub> )	—	—	0.0004	0.001	0.001
L <sub>3</sub> M <sub>3</sub> ( <sup>3</sup> P <sub>0</sub> )	0.020	0.029	0.058	0.125	0.142
L <sub>2</sub> M <sub>3</sub> ( <sup>3</sup> P <sub>1</sub> )	—	0.0002	0.0004	0.0009	0.0010
L <sub>3</sub> M <sub>2</sub> ( <sup>3</sup> P <sub>2</sub> )	0.087	0.34	0.39	0.75	0.80
L <sub>2</sub> M <sub>3</sub> ( <sup>1</sup> D <sub>2</sub> )	1.08	0.93	0.88	1.035	0.93
L <sub>2</sub> M <sub>2</sub> ( <sup>3</sup> D <sub>1</sub> )	0.001	0.001	0.001	0.002	0.002
L <sub>3</sub> M <sub>3</sub> ( <sup>3</sup> D <sub>2</sub> )	0.015	0.016	0.088	0.60	0.70
L <sub>3</sub> M <sub>3</sub> ( <sup>3</sup> D <sub>3</sub> )	—	0.002	0.003	0.005	0.005
L <sub>3</sub> M <sub>4</sub> ( <sup>3</sup> P <sub>0</sub> )	—	—	0.0002	0.0007	0.0014
L <sub>3</sub> M <sub>4</sub> ( <sup>3</sup> P <sub>1</sub> )	—	—	0.0003	0.0012	0.0030
L <sub>2</sub> M <sub>5</sub> ( <sup>3</sup> P <sub>2</sub> )	—	—	0.0006	0.0026	0.0058
L <sub>2</sub> M <sub>4</sub> ( <sup>1</sup> P <sub>1</sub> )	—	—	0.0004	0.0014	0.0023
L <sub>3</sub> M <sub>5</sub> ( <sup>3</sup> D <sub>1</sub> )	—	—	0.0004	0.0019	0.0041
L <sub>2</sub> M <sub>4</sub> ( <sup>3</sup> D <sub>2</sub> )	—	—	0.0049	0.028	0.053
L <sub>3</sub> M <sub>4</sub> ( <sup>3</sup> D <sub>3</sub> )	—	—	0.0099	0.138	0.315
L <sub>3</sub> M <sub>5</sub> ( <sup>1</sup> D <sub>2</sub> )	—	—	0.0014	0.0055	0.0057
L <sub>3</sub> M <sub>4</sub> ( <sup>3</sup> F <sub>2</sub> )	—	—	0.0015	0.0057	0.0146
L <sub>3</sub> M <sub>5</sub> ( <sup>3</sup> F <sub>3</sub> )	—	—	0.0084	0.0225	0.040
L <sub>3</sub> M <sub>5</sub> ( <sup>3</sup> F <sub>4</sub> )	—	—	0.0135	0.070	0.137
L <sub>2</sub> M <sub>5</sub> ( <sup>1</sup> F <sub>3</sub> )	—	—	0.049	0.158	0.263

The parameter  $\eta_0$  tends to 0 as  $Z_0$  tends to 0 and the coupling approaches pure Russell-Saunders. It tends to 1 when  $Z_0$  becomes large and conditions of pure  $j-j$  coupling apply. The quantity  $(1-\eta_0)E/Z_0$  is plotted as ordinate, the energy of the term being expressed in atomic units ( $a_0=e=\hbar=1$ ).

The relative intensities of the various Auger lines relative to the  $K-L_1L_1$  line are given in table 1. The terms in intermediate coupling are specified in terms of the extreme  $j-j$  and  $L-S$  coupling states to which they tend in the limit of large and small  $Z$  respectively.

## § 6. COMPARISON WITH THE MEASURED AUGER SPECTRUM

Detailed studies of the Auger spectrum have been made by Johnson and Foster (1953) for silver and by several authors (Mihelich 1952, Bergstrom and Hill 1954, Ellis 1933, and Mladjenovic and Slätis 1954) for elements near  $Z=80$ . Using expressions (9) above for the energies of the lines of the Auger spectrum, the agreement with observation is poor. The  $K-L_1L_{2,3}$  spectrum overlaps the  $K-L_1L_1$  spectrum and the difference in energy between these two sets of levels is too small. From the calculations referred to above using a self-consistent field for mercury it is possible to estimate the energy required to remove a single 2s or 2p electron from a mercury atom. Since spin-orbit interaction is not taken into account the value found for the 2p ionization energy should correspond to the quantity  $E(2p)$  defined in (11). The calculations give for this quantity for mercury the value  $E(2p)=12.90$  kev. The experimental value taken from the tables of Hill, Church and Mihelich (1952) is 12.92 kev, corresponding to  $E(L_2)=14.21$  kev and  $E(L_3)=12.28$  kev respectively. For the  $L_1$  ionization energy, however, there is a large discrepancy. The calculated value of  $E(L_1)$  using the mercury self-consistent field is 13.26 kev compared with the observed value of 14.84 kev. Evidently then this discrepancy, as well as the related discrepancy in the positions of the lines of the Auger spectrum is associated with relativistic effects in the 2s state.

A comprehensive relativistic investigation of the Auger spectrum of mercury is in progress but until this is completed it is more convenient to relate the observed Auger spectrum directly with the observed single ionization energies. From equations (9) and (10) the following relations may be deduced for the energies of the  $K-LL$  Auger lines in terms of the  $K$  and  $L$  ionization energies,  $E(K)$ ,  $E(L_1)$ , and  $E(2p)$ ,

$$\left. \begin{aligned} K-L_1L_1(^1S_0), & \quad E(K)-2E(L_1)-F^0(20, 20) \\ K-L_1L_2(^1P_1), & \quad E(K)-E(L_1)-E(2p)-F^0(21, 20)-\frac{1}{4}\zeta_{21} \\ & \quad -\{(\frac{1}{3}G^1(21, 20)-\frac{1}{4}\zeta_{21})^2+\frac{1}{2}\zeta_{21}^2\}^{1/2} \\ K-L_1L_3(^3P_1), & \quad E(K)-E(L_1)-E(2p)-F^0(21, 20)-\frac{1}{4}\zeta_{21} \\ & \quad +\{(\frac{1}{3}G^1(21, 20)-\frac{1}{4}\zeta_{21})^2+\frac{1}{2}\zeta_{21}^2\}^{1/2} \\ K-L_1L_2(^3P_0), & \quad E(K)-E(L_1)-E(2p)-F^0(21, 20)+\frac{1}{3}G^1(21, 20)-\zeta_{21} \\ K-L_1L_3(^3P_2), & \quad E(K)-E(L_1)-E(2p)-F^0(21, 20)+\frac{1}{3}G^1(21, 20)+\frac{1}{2}\zeta_{21} \\ K-L_2L_3(^1D_2), & \quad E(K)-2E(2p)-F^0(21, 21)+\frac{2}{25}F^2(21, 21)+\frac{1}{4}\zeta_{21} \\ & \quad -\{(\frac{3}{25}F^2(21, 21)+\frac{1}{4}\zeta_{2,1})^2+\frac{1}{2}\zeta_{21}^2\}^{1/2} \\ K-L_3L_3(^3P_2), & \quad E(K)-2E(2p)-F^0(21, 21)+\frac{2}{25}F^2(21, 21)+\frac{1}{4}\zeta_{21} \\ & \quad +\{(\frac{3}{25}F^2(21, 21)+\frac{1}{4}\zeta_{21})^2+\frac{1}{2}\zeta_{21}^2\}^{1/2} \end{aligned} \right\}$$

$$\left. \begin{aligned} \text{K-L}_3\text{L}_3(^3\text{P}_0), \quad E(\text{K}) - 2E(2\text{p}) - F^0(21, 21) - \frac{1}{10}F^2(21, 21) - \frac{1}{2}\zeta_{21} \\ \quad + \left\{ \left( \frac{3}{10}F^2(21, 21) - \frac{1}{2}\zeta_{21} \right)^2 + 2\zeta_{21}^2 \right\}^{1/2} \\ \text{K-L}_2\text{L}_2(^1\text{S}_0), \quad E(\text{K}) - 2E(2\text{p}) - F^0(21, 21) - \frac{1}{10}F^2(21, 21) - \frac{1}{2}\zeta_{21} \\ \quad - \left\{ \left( \frac{3}{10}F^2(21, 21) - \frac{1}{2}\zeta_{21} \right)^2 + 2\zeta_{21}^2 \right\}^{1/2}. \end{aligned} \right\} \dots\dots (13)$$

From the observed separation of the  $L_2$  and  $L_3$  ionization energies ( $E(L_2) - E(L_3) = \frac{3}{2}\zeta_{21}$ )  $\zeta_{21}$  can be estimated. Then by comparing the observed Auger spectrum with that expected from (13), values of the quantities  $F^0(20, 20)$ ,  $F^0(21, 20)$ ,  $F^0(21, 21)$ ,  $F^2(21, 21)$ ,  $G^1(21, 20)$  can be deduced.

The position of the Auger lines is very insensitive to the last two of these quantities but the first three can be obtained with an accuracy to within about 10% from the measurements of Mladjenovic and Slätis for  $Z=83$ . The values of these quantities obtained in this way have been compared with those calculated using the self-consistent field for  $Z=80$ , suitably adjusted to allow for the slight difference in  $Z$ . The calculated values are found to be between 20 and 25% too large. Assuming this to arise from the neglect of relativity and that these terms can be approximated, in their dependence on  $Z$  by expressions of the form

$$A(Z - Z_s)(1 - \alpha Z^2) \dots\dots (14)$$

where  $Z_s$  is the screening constant and the term  $1 - \alpha Z^2$  takes account of the effect of relativity,† the values of  $A$ ,  $Z_s$  and  $\alpha$  required to give the values of the  $F$ 's and  $G$ 's deduced from the measurements for  $Z=83$  are shown in table 2.

Table 2

	$A$	$Z_s$	$\alpha$
$F^0(20; 20)$	$4.08 \times 10^{-3}$	3.8	$1.76 \times 10^{-5}$
$F^0(21; 20)$	$4.41 \times 10^{-3}$	4.0	$3.25 \times 10^{-5}$
$G^1(21; 20)$	$2.39 \times 10^{-3}$	2.6	—
$F^0(21; 21)$	$4.94 \times 10^{-3}$	4.5	$2.5 \times 10^{-5}$
$F^2(21; 21)$	$2.39 \times 10^{-3}$	5.1	—

The constant  $A$  is expressed in kev in this table to facilitate comparison with experiment. Using expressions (13), values of  $E(\text{K})$ ,  $E(L_1)$ ,  $E(2\text{p})$ ,  $\zeta_{21}$  deduced from measurements of single ionization energies given by Hill, Church and Mihelich (1952), and the  $F$ 's and  $G$ 's derived from table 2, the positions of the K-LL Auger lines to be expected for elements of a wide range of  $Z$  are shown in figure 3. Observed Auger spectra have almost invariably been analysed in terms of  $j-j$  coupling which predicts a six-line K-LL spectrum. This is justified for large  $Z$  but as  $Z$  decreases the spectrum becomes more complicated and nine Auger lines would be expected. For small  $Z$ , when the coupling approaches Russell-Saunders, the spectrum again contains six lines. Measurements under high resolution of the Auger spectrum in the range 30 to 40 of  $Z$  would be of interest because they might reveal the greater complexity of the spectrum, although some of the lines are probably too weak to be detected with available techniques.

The positions of the Auger lines predicted for silver using the  $F$ 's and  $G$ 's of table 2 are compared with the values observed by Johnson and Foster in table 3.

† The justification for approximating the variation of relativistic effects with  $Z$  by an expression of this type is discussed by Burhop (1955).

The three weakest lines were not resolved but the positions of the other lines are in good agreement. Table 3 shows also a similar comparison with the measurements of Bellicard, Moussa and Haynes for copper. The agreement is not so good here, the calculated energies being about 0.04 keV too small. This could be due to a discrepancy in the value taken for  $E(K)$  however. In all these comparisons where there are several unresolved lines in a group, the calculated energy of the stronger line is compared with the observed spectrum.

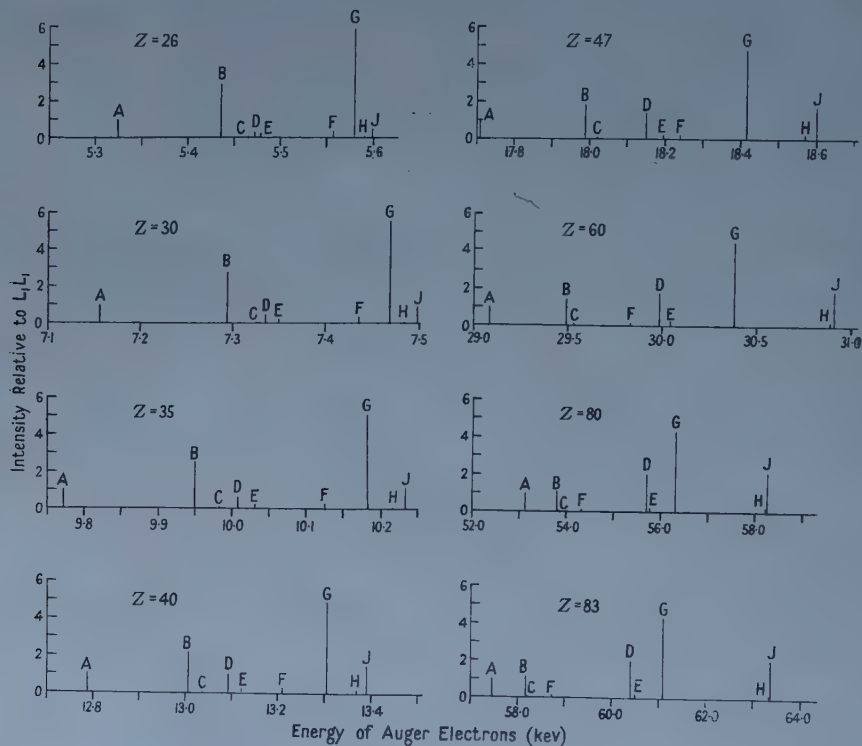


Figure 3. The predicted positions and relative intensities of the lines of the K-LL Auger spectrum. The intensities are relative to the  $K-L_1L_1$  line.

The lines A . . . . J are specified in terms of the limits to which they tend for extreme  $j-j$  and  $L-S$  coupling respectively :

A,  $L_1L_1(^1S_0)$ ; B,  $L_1L_2(^1P_1)$ ; C,  $L_1L_2(^3P_0)$ ; D,  $L_1L_3(^3P_1)$ ; E,  $L_1L_3(^3P_2)$ ; F,  $L_2L_2(^1S_0)$ ; G,  $L_2L_3(^1D_2)$ ; H,  $L_3L_3(^3P_0)$ ; J,  $L_3L_3(^3P_2)$ .

Turning now to the relative intensity of the K-LL Auger lines, the calculations demonstrate the marked change of the relative intensities of the different terms within a given configuration as  $Z$  varies, although the relative intensities of the different configurations as a whole do not change. For example as  $Z$  increases, within the  $(2s)(3p)^5$  configuration the intensity of the  $K-L_1L_2(^1P_1)$  line decreases, while that of  $K-L_1L_3(^3P_1)$  increases, so that the expected relative intensity of these two lines changes from 12.4 at  $Z=25$  to 0.57 at  $Z=80$ . Similarly, in the  $(2s)^2(2p)^4$  configuration the intensity of the  $K-L_3L_3(^3P_2)$  line builds up at the expense of the  $K-L_2L_3(^1D_2)$  line as  $Z$  increases so that the expected relative intensity of these two lines changes from 12.8 for  $Z=25$  to 2.04 for  $Z=80$ .



Table 3. Comparison of Observed and Calculated Auger Spectrum

Transition	Z=29				Z=47				Z=80				Z=83			
	Energy (kev)		Rel. Int.		Energy (kev)		Rel. Int.		Energy (kev)		Rel. Int.		Energy (kev)		Rel. Int.	
	Obs.	calc.	obs.	calc.	obs.	calc.	obs.	calc.	obs.	calc.	obs.	calc.	obs.	calc.	obs.	calc.
K-L <sub>1</sub> L <sub>1</sub>	6.735	6.681	1.00 <sup>+</sup>	1.00	17.70	17.709	1.0	1.00	53.18	53.150	1.0	1.00	57.466	57.465	1.0	1.00
K-L <sub>1</sub> L <sub>2</sub>	6.845	6.811	2.8 (2.2)	3.49	17.98	17.978	1.3	1.82	53.79	53.818	1.2 (1.7)	1.20	58.186	58.177	1.8 (1.8)	1.20
K-L <sub>1</sub> L <sub>3</sub>					18.14	18.142	1.3	1.66	55.71	55.708	0.7 (1.2)	2.27	60.417	60.427	1.1 (1.3)	2.27
K-L <sub>2</sub> L <sub>2</sub>					18.25	18.240	0.5	0.24	54.32	54.347	0.2 (0.3)	0.15	58.746	58.746	0.2 (0.2)	0.15
K-L <sub>2</sub> L <sub>3</sub>	7.015	6.976	9.9 (6.8)	6.80	18.42	18.419	3.2	4.71	56.35	56.317	1.4 (1.4)	4.32	61.090	61.083	1.6 (2.3)	4.32
K-L <sub>3</sub> L <sub>3</sub>					18.61	18.601	1.8	1.90	58.27	58.263	0.6 (0.8)	2.40	63.404	63.389	0.8 (1.3)	2.40
K-L <sub>1</sub> M <sub>1</sub>					20.88		0.8	0.29					70.020		0.4	0.31
K-L <sub>1</sub> M <sub>2</sub>					} 21.02,		0.8	0.51					70.391		0.5	0.19
K-L <sub>1</sub> M <sub>3</sub>							—	0.04								0.37
K-L <sub>1</sub> M <sub>4, 5</sub>																0.05
K-L <sub>2</sub> M <sub>1</sub>					21.17		0.2	0.16					70.761		0.8	0.16
K-L <sub>3</sub> M <sub>1</sub>					—		—	0.28								0.32
K-L <sub>2</sub> M <sub>2</sub>					} 21.31		1.6	1.13					71.553		0.7	0.07
K-L <sub>2</sub> M <sub>3</sub>							—	0.19								0.93
K-L <sub>2</sub> M <sub>4, 5</sub>	7.925		1.9	1.68	—		—									0.32
K-L <sub>3</sub> M <sub>2</sub>					21.47		{ 1.7 { 1.48						73.301		0.7	0.80
K-L <sub>3</sub> M <sub>3</sub>													73.873		1.0	0.85
K-L <sub>3</sub> M <sub>4, 5</sub>					21.68		0.55	0.25								0.52

The experimental values for Z=29 are those of Bellicard, Moussa and Haynes (1957). The values in brackets in this column are those of Moussa, Bellicard (1954) for Z=26. The experimental values for Z=47 are those of Johnson and Foster (1953). The experimental values for Z=80 are those of Bergstrom and Hill (1954). Those in brackets in this column are due to Mihelich (1952) for Z=79. The experimental values for Z=83 are those of Mladjenovic and Stäus (1954). Those in brackets are also for Z=83 and are due to Ellis (1933).

The intensities of the Auger lines of silver relative to the  $K-L_1L_1$  line, observed by Johnson and Foster are also shown in table 3. The agreement with the calculated intensity appears good when one bears in mind the difficulty of the intensity measurements. The biggest discrepancy is in the intensity of the  $K-L_2L_3(^1D_2)$  line which, although the strongest line, still has a considerably smaller intensity relative to  $K-L_1L_1$  than predicted (3.2 observed as against 4.7 predicted). The position would have been even worse if the Rubinstein-Snyder Auger amplitudes had been used since these give a value of 6.5 for this ratio for silver.

The discrepancy is even more marked for heavy elements where it is seen that this ratio drops to 1.7. It appears likely then that this change in relative intensity may be a relativistic effect. The available relativistic calculations (Massey and Burhop 1936) did not deal with the  $(2s)^2(2p)^4$  configuration.

This ratio might also be affected by inter-configuration interaction. The term  $L_1L_1(^1S_0)$  of the  $(2s)^0(2p)^6$  configuration will mix with the terms  $L_2L_2(^1S_0)$  and  $L_3L_3(^3P_0)$  of the  $(2s)^2(2p)^4$  configuration. These last transitions are weaker than the  $L_1L_1(^1S_0)$  transition, however, so that the effect of the inter-configuration terms can only be to increase the probability of the weaker at the expense of the stronger transition, which would further increase the discrepancy in this case.

The secular equation for the  $J=0$  state involving terms from different configurations was set up and solved for silver, using the values of the quantities  $F^0(20, 20)$ ,  $F^0(21, 21)$ ,  $F^2(21, 21)$  of table 2. The relative intensity of transitions to the three final states involved was altered by less than 3% by the inclusion of the inter-configuration terms and the change in energy separation was 0.014 keV—too small to be detected.

The introduction of intermediate coupling accounts for the observed relative intensity of the  $K-L_1L_2$  and  $K-L_1L_3$  groups, of 1.0 for  $Z=47$ . The predicted ratio of these is 1.1 while in extreme  $j-j$  coupling it would be 0.5. Comparison of the intensities of these two lines for heavy elements, however, indicates that the extreme  $j-j$  limiting value is not approached as  $Z$  becomes large. Indeed table 3 indicates that for  $Z$  about 80 the relative intensity, far from approaching 0.5, appears to be more nearly 1.5. The effect of relativity, however, appears to shift this ratio in the required direction. For example, the calculations of Massey and Burhop (1936) for gold gave 1.04 for this ratio. Since these calculations are effectively for  $j-j$  coupling and the influence of the electrostatic interaction of the two vacant final states will, if the non-relativistic calculations are a guide, further increase the intensity of  $K-L_1L_2$  relative to  $K-L_1L_3$ , it looks as though the combined effects of relativity and intermediate coupling can clear up the discrepancy in this ratio. Relative to the  $K-L_1L_1$  line, however, the intensities of both  $K-L_1L_2$  and  $K-L_1L_3$ , calculated using the relativistic theory, are about four times too large. Such a discrepancy would be very difficult to account for. A thorough re-check and extension of the earlier relativistic calculations is at present in progress.

In all these comparisons the Auger transition amplitudes have been calculated assuming the energy of the ejected electron is the same for a whole configuration. Strictly, different energies should have been used for each possible final state within the configuration. The effect of this approximation is not likely to be important, however.

Turning now to the K-LM spectrum, the available experimental data do not permit a very detailed comparison with the calculations. The most extensive measurements are again those of Johnson and Foster for silver shown in table 3. The resolution has not been sufficient to enable a very exhaustive test of the allowance for intermediate coupling in the final state. Where comparison with the calculated values is possible there seem to be a number of discrepancies. For both silver and bismuth the intensity of the K-LM spectrum relative to the K-LL spectrum is greater than the value estimated by Rubinstein and Snyder (1955). For copper these calculations give for the relative intensity of K-L<sub>1</sub>M to K-L<sub>2,3</sub>M a value only about half of that measured by Bellicard, Moussa and Haynes (1957). In the case of silver, for which a more detailed comparison is possible the measurements agree with the theory in showing that transitions involving the M<sub>4,5</sub> levels are weak and that the strongest line is K-L<sub>3</sub>M<sub>2,3</sub>. The intensity of the K-L<sub>2</sub>M<sub>1</sub> line appears to agree well with that expected, but the line K-L<sub>3</sub>M<sub>1</sub> which should be even stronger, was not found. And as in the case of copper, the relative intensity of transitions involving L<sub>1</sub> are stronger than predicted.

### § 7. CONCLUSIONS

It appears that the main features of the K-LL Auger spectrum both as regards the position of the various lines and their relative intensities can be understood when allowance is made for the possibility of relativistic effects and account is taken of the possible terms of the final state of the doubly ionized atom using intermediate coupling theory. The calculation shows it would be interesting to study the K-LL spectrum under conditions of high resolution, particularly in the range of  $Z$  from 30 to 40, to look for the extra lines expected on intermediate coupling theory. On the other hand some of the features of the K-LM spectrum are difficult to interpret and an extension of the experimental measurements would be of considerable interest.

### ACKNOWLEDGMENTS

We are greatly indebted to Professor J. N. Snyder for sending us, in advance of publication, portions of Dr. Rubinstein's thesis, giving their calculated Auger transition amplitudes; to Dr. M. J. Seaton for valuable discussions on configuration interactions; to Mrs. J. Lawson for solving a number of the secular determinants occurring in the intermediate coupling theory and to Mr. W. Lawson for assistance with some of the calculations, using the University College computer. One of us (W. N. A.) acknowledges a study leave from Cairo University and a maintenance grant from the Egyptian Atomic Energy Commission.

### REFERENCES

- BELLICARD, J. B., MOUSSA, A., and HAYNES, S. K., 1957, *Nuclear Physics*, **3**, 307.  
 BERGSTROM, I., and HILL, R. D., 1954, *Ark. Fys.*, **8**, 21.  
 BROYLES, C. D., THOMAS, D. A., and HAYNES, S. K., 1953, *Phys. Rev.*, **89**, 715.  
 BURHOP, E. H. S., 1935, *Proc. Roy. Soc. A*, **148**, 272; 1952, *The Auger Effect and Other Radiationless Transitions* (London, Cambridge: University Press); 1955, *J. Phys. Radium*, **16**, 625.  
 CONDON, E. U., and SHORTLEY, G. H., 1953, *The Theory of Atomic Spectra* (Cambridge: University Press).  
 ELLIS, C. D., 1933, *Proc. Roy. Soc. A*, **139**, 336.  
 HILL, R. D., CHURCH, E. L., and MIHELICH, J. W., 1952, *Rev. Sci. Instrum.*, **23**, 523.

- JOHNSON, F. A., and FOSTER, J. S., 1953, *Canad. J. Phys.*, **31**, 469.  
MASSEY, H. S. W., and BURHOP, E. H. S., 1936, *Proc. Roy. Soc. A*, **153**, 661.  
MIHELICH, J. W., 1952, *Phys. Rev.*, **88**, 415.  
MLADJENOVIC, M., and SLÄTIS, H., 1954, *Ark. Fys.*, **9**, 41.  
MOUSSA, A., and BELLICARD, J. B., 1952, *J. Phys. Radium*, **15a**, 85.  
PINCHERLE, L., 1935, *Nuovo Cim.*, **12**, 81.  
RAMBERG, E. G., and RICHTMYER, F. K., 1937, *Phys. Rev.*, **51**, 913.  
RUBINSTEIN, R. A., and SNYDER, J. N., 1955, *Phys. Rev.*, **97**, 1653.



## Cellular Eigenvalues for Titanium Metal

By S. L. ALTMANN† AND N. V. COHAN†

Mathematical Institute, Oxford

*MS. received 25th September 1957, and in final form 28th October 1957*

**Abstract.** A programme developed by Altmann for a high-speed computer to carry out cellular computations for close-packed hexagonal metals has been applied to titanium. The eigenvalues and eigenfunctions corresponding to all states for  $\mathbf{k}=0$  have been determined and the effect on these results of the type of potential field used has been investigated.

### § 1. INTRODUCTION

THE Wigner-Seitz-Slater cellular method has been found successful in recent years in dealing with increasingly complex metal computations. Schiff (1955) was the first to apply it to a close-packed hexagonal metal, Ti. He calculated the energy eigenvalues for some of the representations corresponding to  $\mathbf{k}=0$ . Unfortunately, some of his results were found to be in error owing to the use of incorrect expansions in spherical harmonics (Altmann 1956, Schiff 1956). Also the boundary conditions that he used were not always the correct ones for all the points of the Wigner-Seitz polyhedron (see Altmann 1958 a).

More recently the theory of the cellular method for a close-packed hexagonal lattice has been re-formulated (Altmann 1958 a), so as to obtain correct expansions and boundary conditions. Also, Altmann has developed a programme for a Ferranti Mk 1\* electronic computer, to obtain the eigenvalues and eigenfunctions for the centre of the Brillouin zone of a close-packed hexagonal lattice. This programme is fully automatic, that is, the whole of the computation is done on the computer in a continuous process and it can deal with any hexagonal close-packed metal. It was first used for Zr (Altmann 1958 b) and it then seemed convenient to apply it to Ti, with a view not only to revise and extend Schiff's work, but also to investigate how sensitive the results are to the atomic potential field used. As is well known, this is a critical problem in the cellular method and one for which Ti was a good example to take, as two potential fields for the ion core are available for it (see § 3).

The details of the method, programme and notation need not be given here, as they can be obtained from the articles mentioned before (Altmann 1958 a, b). A correlation between our notation for the energy states (irreducible representations) and that used by Schiff will also be found there.

The fitting of the boundary conditions has been done throughout by using the set of 16 points called set 1 by Altmann, which comprises 7 points on the edges and corners of the cell and 9 on the intersection of the equivalent sphere with the two faces of the Wigner-Seitz cell considered. The results obtained for Zr indicate that the use of a different set of points to fit the boundary conditions would introduce differences in the eigenvalues of no more than a few thousands of a rydberg unit.

The lattice constants used were derived from the experimental value of  $a=2.950$  A.U. (cf. McQuillan and McQuillan 1956, p. 134) and a rounded-off value of  $c/a$  equal to 1.59 (experimental 1.587).

† Now at Facultad de Ciencias Exactas, Perú 222, Buenos Aires, Argentina.

## § 2. THE MAIN COMPUTATIONS AND RESULTS

The main computations were carried out with the potential field for  $\text{Ti}^+$  given by Schiff (1955), which was obtained as follows: an empirical potential field was derived for  $\text{Ti}^{4+}$  by the method of Prokofjew and the valence electrons were accounted for by adding to this potential that of a uniform charge distribution normalized so as to contain a charge of three electrons inside the equivalent sphere of radius  $R = 3.064$  A.U. This potential function is represented by the curve *a* of figure 1.

The results for all the representations corresponding to  $\mathbf{k} = 0$  are given in the table. The eigenvalues  $\epsilon$  are given in rydberg units. The expansions used, which are of the form  $\psi = \sum_{lm} C_{lm} R_l Y_l^m(\theta, \phi)$ , are specified in the first column for each pair of representations through the values  $l$  and  $m$  of the spherical harmonics that enter in them. The  $\phi$  dependence of the spherical harmonic can be obtained from table 3 of Altmann (1958 a). In the above expansions the  $R_l$ 's are radial solutions of the Schrödinger equation and the  $C_{lm}$ 's are the coefficients obtained through the fitting of the boundary conditions. Their values, normalized to unity, are shown in the table.

As can be seen from the table, we used eight terms in the expansions for the seven representations leading to the lower energy eigenvalues, which are all binding. For the five anti-binding representations, six terms only were used. To terminate the expansions, we used throughout dictionary order in the  $l$  and  $m$  values of the spherical harmonics, as other criteria used in the past have been found to be unsatisfactory (Altmann 1957 b). The minimization procedure was carried out to a precision of  $\pm 0.0005$  Ryd for all the representations† except the three most anti-binding where it is about  $\pm 0.020$  Ryd. However, these eigenvalues are probably correct to about  $\pm 0.005$  Ryd owing to accumulated errors of the truncation of the series and the uncertainties due to the finite number of points used in the fitting of the boundary conditions. The system of terms obtained for the binding representations is shown graphically in figure 2 scheme *a*, where we also identify, in the usual spectroscopic notation, the main spherical harmonics that contribute to the wave function. We include only those whose weight is larger than 1%. It should be noticed that the eigenvalues of figure 2 were obtained with three terms in the expansions instead of eight; therefore, small differences will be found if we compare this figure with the table.

## § 3. THE USE OF ALTERNATIVE POTENTIAL FIELDS

The question of the choice of the potential field for the metal electrons in the Wigner-Seitz cell is one for which a satisfactory answer could only be given if some degree of self-consistency for the field were obtained through the calculation of the wave function. This is certainly a formidable task, although some progress towards it can be expected in the future, when faster electronic computers become available.

On the other hand, the Schiff potential which we have employed in the main computation is one of several possible choices, and by comparing the results obtained with different potentials, some idea about their reliability could be obtained.

† With this precision in the eigenvalues the corresponding error in the eigenfunctions is of two or three units in the fourth decimal place.

Eigenvalues and Expansion Coefficients for all Symmetry Types  
corresponding to  $k=0$  (Schiff's potential field)

$A_{1+}'$			$A_{1-}'$			$A_{2+}'$			$A_{2-}'$		
$l, m$	$C_{lm}$		$l, m$	$C_{lm}$		$l, m$	$C_{lm}$		$l, m$	$C_{lm}$	
0, 0	-0.9999		3, 3	+0.9964		3, 3	+0.9964		3, 3	+0.9505	
2, 0	+0.0034		5, 3	+0.0255		5, 3	+0.0255		5, 3	+0.2936	
3, 3	+0.0099		6, 6	-0.0206		6, 6	-0.0206		6, 6	-0.0063	
4, 0	+0.0018		7, 3	-0.0675		7, 3	-0.0675		7, 3	+0.0993	
5, 3	+0.0086		8, 6	+0.0060		8, 6	+0.0060		8, 6	-0.0129	
6, 0	+0.0027		9, 3	-0.0402		9, 3	-0.0402		9, 3	+0.0176	
6, 6	+0.0057										
7, 3	+0.0020										
$\epsilon$	-0.789		$\epsilon$	+3.358		$\epsilon$	+3.358		$\epsilon$	+3.127	
$A_{1+}''$			$A_{1-}''$			$A_{2+}''$			$A_{2-}''$		
$l, m$	$C_{lm}$		$l, m$	$C_{lm}$		$l, m$	$C_{lm}$		$l, m$	$C_{lm}$	
4, 3	+0.9826		1, 0	-0.9862		1, 0	-0.9862		1, 0	-0.3781	
6, 3	+0.0652		3, 0	+0.1636		3, 0	+0.1636		3, 0	+0.8883	
7, 6	+0.0366		4, 3	-0.0248		4, 3	-0.0248		4, 3	-0.2215	
8, 3	-0.1546		5, 0	-0.0061		5, 0	-0.0061		5, 0	-0.1369	
9, 6	-0.0246		6, 3	+0.0088		6, 3	+0.0088		6, 3	+0.0110	
10, 3	-0.0666		7, 0	+0.0023		7, 0	+0.0023		7, 0	+0.0079	
			7, 6	+0.0054		7, 6	+0.0054		7, 6		
			8, 3	-0.0016		8, 3	-0.0016		8, 3		
$\epsilon$	+5.421		$\epsilon$	-0.344		$\epsilon$	-0.344		$\epsilon$	+1.097	
$E_{+}'$			$E_{-}'$			$E_{+}''$			$E_{-}''$		
$l, m$	$C_{lm}$		$l, m$	$C_{lm}$		$l, m$	$C_{lm}$		$l, m$	$C_{lm}$	
1, 1	-0.0882		2, 1	-0.9978		2, 1	-0.9978		2, 1	+0.9988	
2, 2	-0.9959		3, 2	-0.0577		3, 2	-0.0577		3, 2	+0.0139	
3, 1	-0.0126		4, 1	-0.0230		4, 1	-0.0230		4, 1	-0.0470	
4, 2	-0.0030		5, 2	-0.0203		5, 2	-0.0203		5, 2	+0.0013	
4, 4	+0.0126		5, 4	-0.0041		5, 4	-0.0041		5, 4	-0.0072	
5, 1	-0.0032		6, 1	+0.0027		6, 1	+0.0027		6, 1	-0.0023	
5, 5	+0.0012		6, 5	+0.0096		6, 5	+0.0096		6, 5	-0.0052	
6, 2	+0.0081		7, 2	-0.0035		7, 2	-0.0035		7, 2	-0.0035	
$\epsilon$	-0.462		$\epsilon$	-0.439		$\epsilon$	-0.439		$\epsilon$	-0.340	

There are two main problems about the choice of the potential. The first is the determination of the potential of the ion core,  $Ti^{4+}$  in our case. The second is the potential of the outer electrons, which in the free atom are in the configuration  $3d^2 4s^2$ . In the Schiff potential used in the main computations the first was an empirical potential and the second a uniform charge distribution.

To consider the effect of the ion core potential we first substituted the empirical potential by an interpolated self-consistent field with exchange for  $\text{Ti}^{4+}$ , kindly made available to us by Professor D. R. Hartree. To this we added a uniform charge distribution normalized so as to contain a charge of three electrons inside a sphere of radius  $R$ , the radius of the boundary point more distant from the centre of the cell, namely 3.907 A.U. This potential is represented by curve *b* in figure 1.

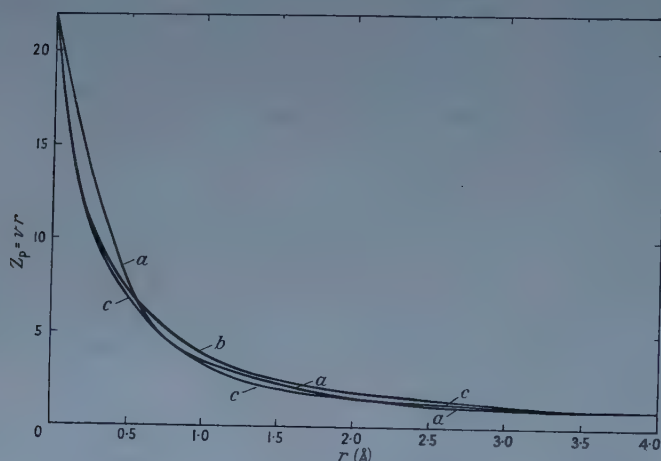


Figure 1. Potential functions. *a*, Empirical  $\text{Ti}^{4+}$  plus uniform charge distribution (three electrons) (Schiff potential). *b*, Self-consistent field with exchange for  $\text{Ti}^{4+}$  plus uniform charge distribution. *c*, Self-consistent field with exchange for  $\text{Ti}^{4+}$  plus distribution of  $3d^2 4s$  configuration.

In the third potential function used we modified the potential due to the outer electrons, by going to the opposite approximation to the one previously used. That is, we fixed three of the four outer electrons in the orbitals they would have in the free atom. We choose a configuration  $3d^2 4s$  and the corresponding potential was obtained by an interpolation procedure (Hartree 1957, Ridley 1955) from a self-consistent field without exchange for Fe (Manning and Goldberg 1938). To have as before the whole charge within the sphere of radius 3.907 A.U. corresponding to the point of the boundary more distant from its centre, we scaled the potential function from  $r = 2$  A.U. outwards so as to make the potential equal to unity at  $r = 3.907$  A.U. This is certainly a very rough procedure, but sufficient for our purposes. The ion core potential used was again the self-consistent field one. The resulting potential is represented in curve *c* of figure 1.

To make the comparison of the three fields the seven binding representations only were considered. It was enough for the present purposes to use three-term expansions, as the differences found in the main computations (§ 2) between 3- and 8-term expansions were of the order of 0.02 Ryd for the binding representations. Also, the minimization procedure was carried out to a lower degree of accuracy than before, about  $\pm 0.02$  Ryd. The results are shown in figure 2.

It should be noted that the degeneracies shown in figure 2 are probably due to the relatively small precision in the determination of the eigenvalues.



## § 4. DISCUSSION

We shall first consider the comparison of the results obtained with the three fields used. In making this comparison, it is only the energies of the levels with respect to the lowest ones that are significant, rather than their absolute values. We then see that, when the empirical ion-core potential is substituted by a self-consistent field one ( $a$  and  $b$  respectively in figure 2; uniform charge for the outer electrons in both cases), the energy levels for the first four representations are altered by no more than 0.06 Ryd, which is certainly a good agreement.

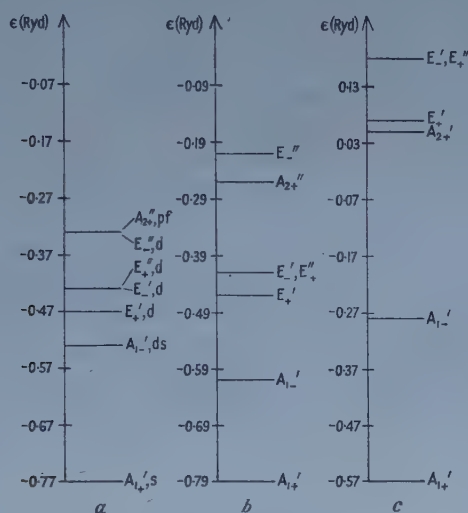


Figure 2. Binding energy levels, using three terms in the expansions, for the three types of potential functions,  $a$ ,  $b$  and  $c$  (see legend to figure 1). The level  $E_{-}'$  has not been included for the potential  $c$ ; its energy is larger than 1.1 Ryd above the ground state.

If we now compare  $b$  with  $c$  in figure 2, the changes are clearly more severe. Of course the change in the potential is now more drastic, as we keep the same self-consistent ion-core potential and change the uniform charge distribution for the outer electrons ( $b$ ) by atomic orbitals ( $c$ ). The agreement for the non-degenerate levels  $A_{1-}'$  and  $A_{2+}''$  is still reasonable, the differences being about 0.10 Ryd. The relative positions of the degenerate levels is still maintained but now all of them are above the  $A_{2+}''$  level.

It is clear from the above that the eigenvalues obtained with any one field must be regarded as provisional. The position of the first excited level can be considered as fairly reliable, although, as no change in the potential more drastic than going from  $b$  to  $c$  in figure 2 can be expected. On the whole, of course, more reliance should be placed in the results obtained with fields  $a$  and  $b$  as we can expect the outer electrons to behave more nearly like free electrons than atomic ones. In what follows, and with the above limitations in mind, we shall therefore consider the results of our main computations (potential field  $a$ , figure 1).

If we first compare these results with those for Zr (Altmann 1958 *b*) we notice that the order of the levels is identical. Whereas in Zr we had four mainly  $d$  states going from 0.16 to 0.35 Ryd above the ground state, they now appear ranging from

0.22 to 0.36 Ryd. In fact, all the binding levels from the first excited state onwards are now rather more crowded, the first  $p$  level appearing now at 0.45 Ryd above the ground state (0.63 Ryd in Zr). The anti-binding levels, on the other hand, are all pushed up by 1 Ryd or so with respect to the corresponding ones in Zr. The results that the  $A_{1+}' - A_{1-}'$  separation is larger in Ti (0.22 Ryd) than in Zr (0.16 Ryd) correlates nicely with the fact that in the free atom of Ti the first state with configuration  $3d^3 4s$  appears 0.60 Ryd above the ground state, which is higher than the similar one in Zr (0.44 Ryd, see Moore 1949). On the other hand, the first  $p$  level appears lowered with respect to that in Zr, whereas in the free atoms the position is reversed (the configuration  $3d^2 4s 4p$  in Ti is 1.45 Ryd above the ground state, whereas the corresponding one in Zr is 1.35 Ryd above the ground state). It might be relevant in this respect that the weight of the  $f$  orbital in this state of Zr is almost twice as much as that in the corresponding state of Ti.

## REFERENCES

- ALTMANN, S. L., 1956, *Proc. Phys. Soc. A*, **69**, 184 ; 1958 a, *Proc. Roy. Soc. A*, in the press ; 1958b, *Ibid.*, in the press.  
 HARTREE, D. R., 1957, *The Calculations of Atomic Structures* (New York : Wiley).  
 MANNING, M. F., and GOLDBERG, L., 1938, *Phys. Rev.*, **53**, 662.  
 MCQUILLAN, A. D., and MCQUILLAN, M. K., 1956, *Titanium* (London : Butterworths Scientific Publications).  
 MOORE, C. E., 1949, *Atomic Energy Levels* (Washington : National Bureau of Standards).  
 RIDLEY, C., 1955, *Proc. Camb. Phil. Soc.*, **51**, 693.  
 SCHIFF, B., 1955, *Proc. Phys. Soc. A*, **68**, 686 ; 1956, *Ibid.*, **69**, 185.

# Photodisintegration of Sodium by ${}^7\text{Li}(\text{p}, \gamma)$ Radiation

By T. R. OPHEL AND I. F. WRIGHT

Research School of Physical Sciences, Australian National University, Canberra

*Communicated by E. W. Titterton; MS. received 7th August 1957, and in revised form 5th November 1957*

**Abstract.** A small thin NaI(Tl) scintillator has been used as both source and detector of photoprotons produced in sodium by  ${}^7\text{Li}(\text{p}, \gamma)$  radiation. This technique provides photoproton energy spectra of good resolution and high statistical precision. Spectra were obtained with both resonance and non-resonance radiation from the  ${}^7\text{Li}(\text{p}, \gamma)$  reaction which permit identification of protons produced by the 17.6 MeV component of the incident radiation. These protons correspond to transitions to states in  ${}^{22}\text{Ne}$  at energies of 0 (0.31 mbn), 1.3 (2.5 mbn), 3.3 (0.6 mbn), 4.4 (0.9 mbn), 5.4 and 5.7 MeV (approximately 2 mbn for both).

This experiment establishes the existence of  ${}^{22}\text{Ne}$  levels at the three highest energies. Previous evidence for a level between 4 and 5 MeV is discussed and is found to be compatible with the present results.

## § 1. INTRODUCTION

MEASUREMENTS made with monochromatic gamma rays are important in the study of photonuclear reactions because they provide unambiguous information on reaction cross sections, the energy spectra of the emitted particles and the corresponding excited states of the residual nuclei. Previous experiments with monochromatic radiation on the photo-emission of charged particles have made use of induced activity (e.g. Hirzel and Wüffler 1947), gas counters (e.g. Barnes *et al.* 1952, Carver *et al.* 1955) and nuclear emulsions (reviewed by Titterton 1955).

The present technique is new in that it employs a scintillation counter in which a phosphor (sodium iodide) acts as both the target and the detector.

## § 2. EXPERIMENTAL METHOD

Gamma rays from the  ${}^7\text{Li}(\text{p}, \gamma)$  reaction were used for this experiment and were produced by bombarding a thick lithium target with a 50–200  $\mu\text{A}$  beam of 500 keV protons from the Canberra 1.2 MeV high tension set. Practically all the photoprotons produced within the 'target' crystal arise from the  ${}^{23}\text{Na}(\gamma, \text{p})$  reaction and can be observed if the magnitude of the pulses due to the electron background is sufficiently reduced.

High energy electron pairs, which will travel almost normally to the crystal, lose approximately 500 keV in traversing a crystal thickness of 0.020 in. so that large pulses can only be produced by electrons scattered along the crystal or by

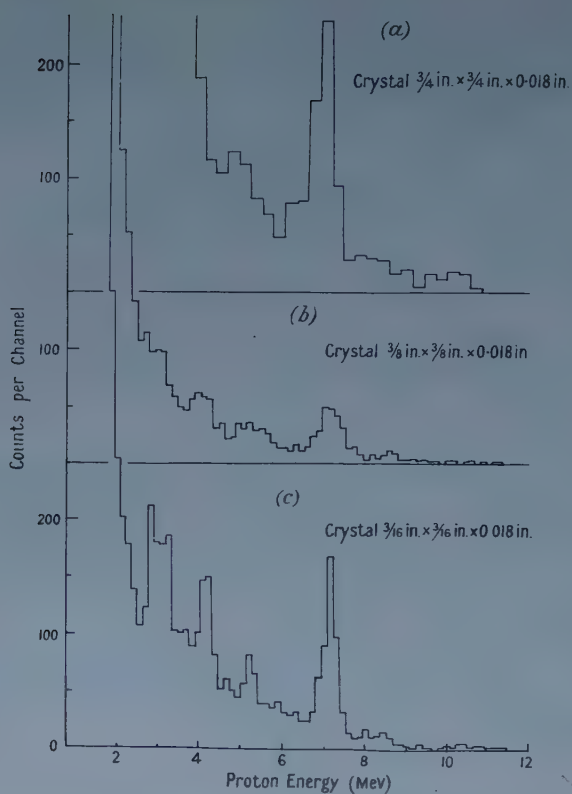


Figure 1. Spectra illustrating the effect of crystal size on electron background.

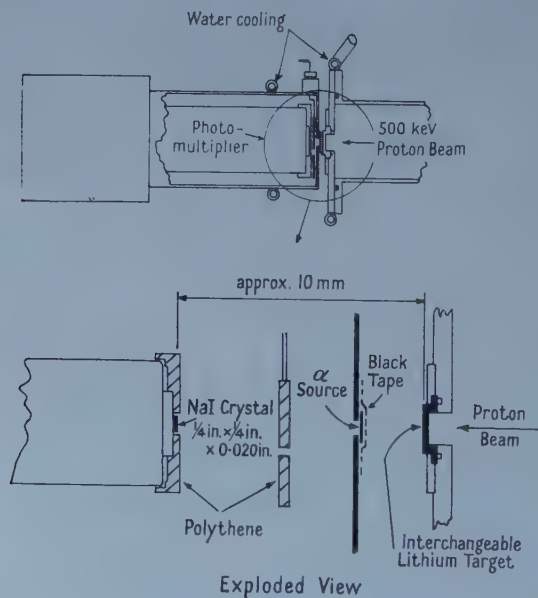


Figure 2. Scintillation counter for studying the  $^{23}\text{Na}(\gamma, p)$  reaction.



'pile up' of a number of these small pulses. The electron backgrounds were examined for crystals of dimensions  $\frac{3}{4}$  in.  $\times$   $\frac{3}{4}$  in.  $\times$  0.018 in.,  $\frac{3}{8}$  in.  $\times$   $\frac{3}{8}$  in.  $\times$  0.018 in. and  $\frac{3}{16}$  in.  $\times$   $\frac{3}{16}$  in.  $\times$  0.018 in. and the spectra obtained are shown in figure 1. In each case the shape of the electron background was unaltered when the gamma-ray intensity was varied by a large factor; thus none of the higher energy electron pulses are due to pile up. Reduction of detector size produces the expected change in the size of the scattered electron pulses and the smallest detector gives a spectrum in which photoproton groups above 3 MeV are clearly resolved.

The counter assembly is shown in figure 2. The sodium iodide detector was mounted on a Perspex disc with Ciba Araldite and was protected from water vapour with a smearing of vaseline and a covering aluminium foil ( $1.5 \text{ mg cm}^{-2}$ ). Pulses from the photomultiplier (E.M.I. type 6097B) and the associated cathode follower were amplified with a linear amplifier and analysed with a Hutchinson-Scarrott type multi-channel analyser. Experiment showed that this analyser was not linear for very short pulses and consequently the pulse rise time was increased to  $2 \mu\text{sec}$  by means of a double integrating circuit between the cathode follower and the amplifier. A constant check on the stability of the total gain of the system was maintained with a ( $\text{ThC} + \text{ThC}'$ ) alpha-particle source mounted behind a polythene shutter. To keep the position of the alpha peak constant, the photomultiplier volts were set so that the counting rates were equal in the two adjacent channels defining the peak position. A drift in gain produced asymmetry in the two channels and it was found that a gain variation of less than 0.25% could be observed and corrected by adjustment of the photomultiplier volts.

Polythene, of a thickness sufficient to stop protons of energy less than 10 MeV, surrounded the crystal so that protons produced externally would not be detected. No high energy protons are produced in the polythene since the threshold of the  ${}^{12}\text{C}(\gamma, p)$  reaction is 15.95 MeV. Reactions occurring in the Perspex and in the aluminium foil over the crystal, mainly  ${}^{16}\text{O}(\gamma, p)$  and  ${}^{27}\text{Al}(\gamma, p)$ , are unavoidable sources of photoprotons but their contribution to the total will be small (approximately 5% from each reaction). This assumes the cross sections for  ${}^{27}\text{Al}(\gamma, p)$  and  ${}^{16}\text{O}(\gamma, p)$  to be twice and half the  ${}^{23}\text{Na}(\gamma, p)$  cross section respectively.

Both the thick lithium targets for the resonance runs and the thin targets for the non-resonance runs were prepared by evaporating lithium metal on to a copper backing 0.040 in. thick and the radiation was monitored with a thick-walled brass geiger counter (Barnes *et al.* 1952).

An energy calibration of the crystal was carried out using protons from the  ${}^{10}\text{B}(d, p)$  reaction employing the procedure described in the Appendix.

### § 3. RESULTS

The following spectra (each representing a summation of a number of individual runs of approximately 45 minutes duration) were recorded using resonance radiation from a thick lithium target.

(a) Sodium iodide crystal  $\frac{3}{16}$  in.  $\times$   $\frac{3}{16}$  in.  $\times$  0.018 in. mounted on glass (figure 1(c)).

(b) Sodium iodide crystal  $\frac{1}{4}$  in.  $\times$   $\frac{1}{4}$  in.  $\times$  0.016 in. mounted on Perspex (figure 3).

(c) Sodium iodide crystal  $\frac{1}{4}$  in.  $\times$   $\frac{1}{4}$  in.  $\times$  0.038 in. mounted on Perspex (figure 4).

(d) Sodium iodide crystal  $\frac{1}{8}$  in.  $\times$   $\frac{1}{8}$  in.  $\times$  0.024 in. mounted on Perspex (figure 5).

Spectrum (c) was intended to cover the region above 7 meV. The range of a 7.2 meV proton in sodium iodide is approximately 0.016 in. so that a large proportion of photoprotons with energies in excess of 7 meV will escape from a crystal 0.018 in. thick.

The observed spectra contain photoprotons from both the sharp 17.6 meV gamma-ray line and the broad 14.8 meV line. Since the intensity ratio of the two components is  $1.7 \pm 0.2$  for the 440 keV resonance radiation (Stearns and McDaniel 1951) and approximately unity for the non-resonance radiation (Devons and Hine 1949, Campbell 1956), a spectrum produced by non-resonance radiation could assist in the identification of photoproton groups due to the 17.6 meV component. Such a spectrum, produced by an 850 keV proton beam incident on a lithium target approximately 100 keV thick, is shown in figure 6.

Comparison of the spectra of figure 6 enables assignments to be made as follows: the 8.4, 7.2 and 5.2 meV groups are due to 17.6 meV gamma rays. Between 3 and 5 meV the position is not so clear. The spectrum of figure 3 shows peaks at 4.15, 3.8, 3.25 and 3.0 meV, with a further probable peak at about 2.5 meV, whereas the spectra of figure 6 show no direct evidence for the 3.8 meV peak or for the doublet structure at about 3 meV (see also figure 1(a)). This difference could be due to the poor statistics of the spectrum of figure 3 or to the slightly inferior resolution of the spectrum of figure 6 and the fact that it occupies fewer channels. The effect of the latter can be appreciated from the insert of figure 3 where the spectrum is replotted with adjacent channels added together.

Figure 5, in which the energy region 2.6–5.5 meV covers the full 80 channels, shows that there is no peak at 3.8 meV and that there are separate peaks at 3.2 and 2.9 meV.

In comparing the two spectra of figure 6 it appears that the number of counts in the groups at 4.2 and 3 meV has been reduced and that the peaks have been lifted by an increase in an underlying broad group centred at about 4 meV. (This energy corresponds to the transition through the 1.28 meV level of  $^{22}\text{Ne}$  for 14.8 meV radiation.) We therefore attribute the protons in the peaks at 4.15, 5.25 and 3.0 meV to 17.6 meV radiation. The upward energy displacement of the peak relative to the resonance spectrum is further evidence for this identification since the energy of peaks produced by the 17.6 meV component will be increased by an amount corresponding to the increase in the gamma-ray energy. On the other hand, the energies of the resulting proton groups would be unaltered by an energy displacement of the 14.8 meV line because this broad component can only produce sharp peaks by selective absorption into narrow levels of  $^{23}\text{Na}$ .

The above data are summarized in table 1 in which are also listed the corresponding excitation energies of the residual  $^{22}\text{Ne}$  nucleus for these transitions.

The cross section of the 7.2 meV group was established by four independent measurements with well defined geometries using crystals of approximately  $\frac{1}{2}$  in.  $\times$   $\frac{1}{2}$  in. and of thickness 0.043 in., 0.037 in., 0.028 in. and 0.021 in. Cross sections for the other groups were estimated from all the appropriate spectra available.

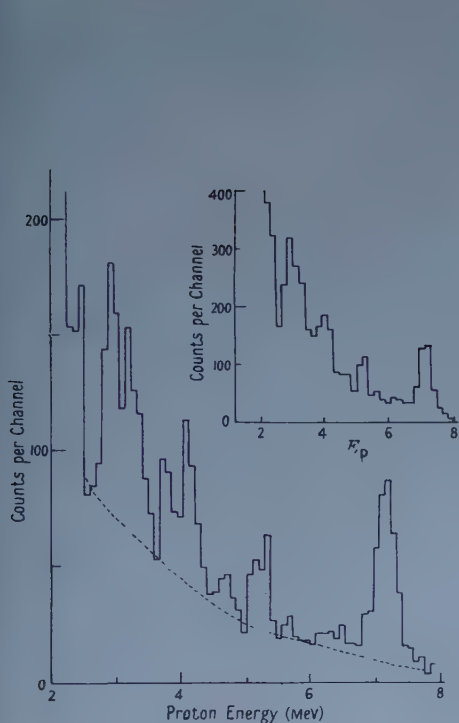


Figure 3. Spectrum for crystal  $\frac{1}{4}$  in.  $\times$   $\frac{1}{4}$  in.  $\times$  0.016 in. Insert: Same spectrum with adjacent channels added together.

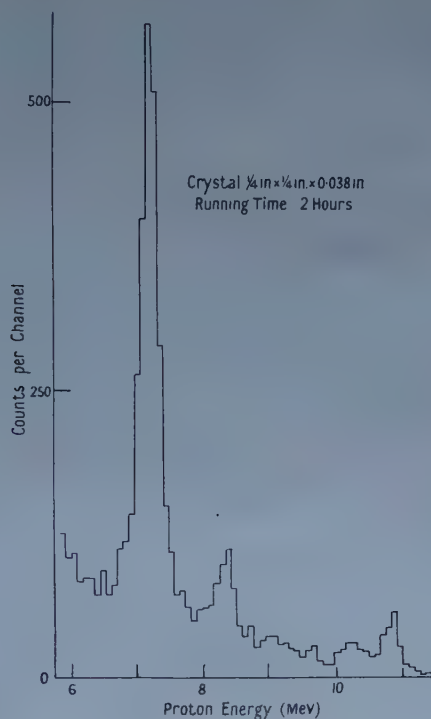


Figure 4. Spectrum showing detail above 6 MeV. Most of the protons beyond the 8.4 MeV group are attributed to the  ${}^{127}\text{I}(\gamma, p)$  reaction. Crystal  $\frac{1}{4}$  in.  $\times$   $\frac{1}{4}$  in.  $\times$  0.038 in.

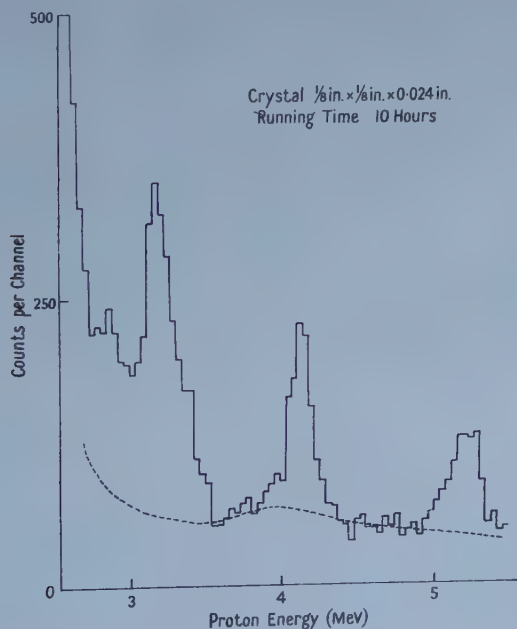


Figure 5. Spectrum showing detail of structure between 2.5 and 5.5 MeV. Crystal  $\frac{1}{8}$  in.  $\times$   $\frac{1}{8}$  in.  $\times$  0.024 in.

Table 1. Proton Groups for the  $^{23}\text{Na}(\gamma, p)$  Reaction

Proton energy (MeV)	8.4	7.2	5.2 <sub>5</sub>	4.1 <sub>5</sub>	3.2	2.9
Excitation energy of $^{22}\text{Ne}$ (MeV)	0	1.3	3.3	4.4	5.4	5.7
Cross section (mbn)	0.31	2.5	0.6	0.9	$\sim 2^\dagger$	

$^\dagger$  Our best estimate of the ratio of the cross sections for the 3.2 and 2.9 MeV peaks is 3:2.

A major source of error in such an estimation is the uncertainty of the background. Electron pulses and photoprotons from iodine contribute in part to the background and between 3 and 6 MeV a portion of it will be photoprotons from the  $^{23}\text{Na}(\gamma, p)$  reaction produced by the 14.8 MeV gamma rays. The contribution from the first two are unknown and an attempt to estimate the latter using the spectra of figure 6 was not successful because the magnitude depends very sensitively on the intensity ratios of the two gamma-ray components. Consequently a smooth background passing through the valleys was assumed (see figures 3, 5 and 7) and, as a result, the estimated cross sections may be considerably in error. Loss corrections were made assuming isotropic angular distributions and using proton ranges in sodium iodide of 0.022 in. ( $E_p = 8.4$  MeV), 0.016 in. (7.2), 0.010 in. (5.25), 0.006 in. (4.15) and 0.004 in. (3.0). The accuracy of the cross section of the 7.2 MeV group can be judged from the internal consistency of the four measurements which gave values of 2.49, 2.46, 2.68 and 2.57 mbn.

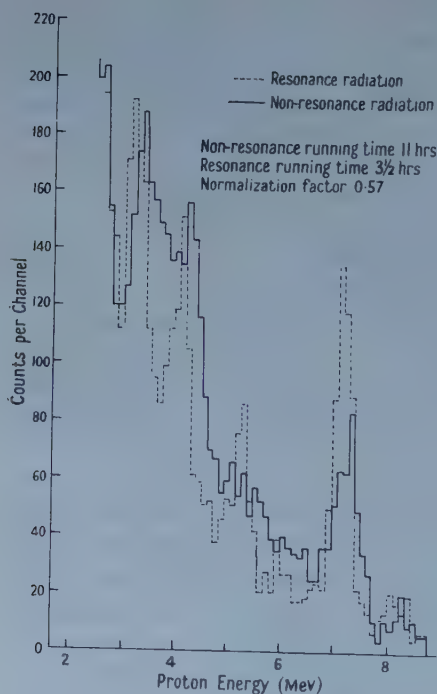


Figure 6. Spectra obtained using resonance and non-resonance radiation. The gamma ray flux was approximately the same for both. Crystal  $\frac{1}{4}$  in.  $\times$   $\frac{1}{4}$  in.  $\times$  0.018 in.

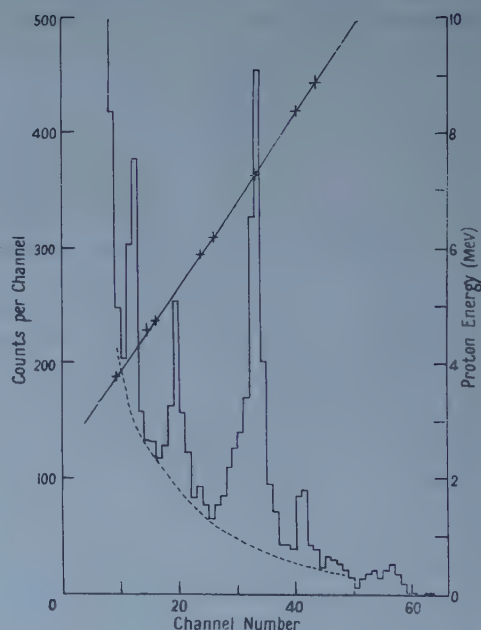


Figure 7.  $^{23}\text{Na}(\gamma, p)$  spectrum and proton calibration curve. Crystal  $\frac{1}{4}$  in.  $\times$   $\frac{1}{4}$  in.  $\times$  0.040 in.



The gamma-ray flux was measured with a thick-walled brass geiger counter of the type described by Barnes *et al.* (1952) using the reported sensitivity of  $2.66 \text{ counts quantum}^{-1} \text{ cm}^{-2}$  for 17.6 mev gamma rays and  $2.1 \text{ counts quantum}^{-1} \text{ cm}^{-2}$  for 14.8 mev gamma rays and a relative gamma-ray intensity of 1.7 for resonance radiation.

The proton groups beyond 8.5 mev cannot be attributed to the  ${}^{23}\text{Na}(\gamma, p)$  reaction. Possible sources for these protons are the  ${}^{127}\text{I}(\gamma, p)$  and  ${}^{27}\text{Al}(\gamma, p)$  reactions, but since the maximum energy of photoprotons from aluminium is 9 mev, it follows that protons beyond this energy are from the  ${}^{127}\text{I}(\gamma, p)$  reaction. From the  ${}^{127}\text{I}(\gamma, n)$  threshold and the energy release in the decay of  ${}^{126}\text{I}$  to  ${}^{126}\text{Te}$  (Sher, Halpern and Mann 1951, Perlman and Welker 1954, and Koerts *et al.* 1955) the expected energy of the ground state protons for 17.6 mev gamma rays is  $11.4 \pm 0.2 \text{ mev}$ . This corresponds to the group at  $11.5 \pm 0.2 \text{ mev}^\dagger$ ; which is therefore identified as these photoprotons. The cross section for this transition is 0.3 mbn.

#### § 4. DISCUSSION

Of the levels listed in table 1, the energies of the lowest two  ${}^{22}\text{Ne}$  levels agree well with the established levels at 1.28 and 3.35 mev (Alburger 1949, Foster *et al.* 1954, and Fader 1954). The only previous results for levels about 3.35 mev are an early report of a level at 4.6 mev (May and Vaidyanathan 1936) and an identification of a level at 4.9 mev (Foster *et al.*). May and Vaidyanathan, from a study of the  ${}^{19}\text{F}(\alpha, p)$  reaction, proposed levels at 1.5, 3.5 and 4.6 mev. Assuming a systematic energy error of 0.2 mev, this level scheme agrees with the established states and the present result (4.4).

Foster *et al.* measured the spectrum of protons from the  ${}^{19}\text{F}(\alpha, p)$  reaction and found that it contained low energy protons corresponding to a state in  ${}^{22}\text{Ne}$  above 3.35 mev but of indeterminate energy. They then used a sodium iodide spectrometer to examine the gamma rays in coincidence with these low energy protons and this latter spectrum assigned a value of 4.9 mev to the excitation energy of the level. However, Foster *et al.* point out that the high energy peaks of the gamma-ray spectrum do not fit exactly with those expected for a 4.9 mev gamma ray and in any case, since the spectrum falls off rapidly from 50 counts per channel in the region above 3.2 mev, identification of peaks in this region is doubtful. Also, the peaks at 3.1 and 2.6 mev, which Foster *et al.* identify as the first and second escape peaks corresponding to the cascade transition from 4.9 mev to 1.28 mev may equally well be the 'photopeak' and the first escape peak of the same transition from a 4.4 mev level. In view of this and the fact that the present experiment gives no evidence of a level at 4.9 mev, it is likely that the level observed by Foster *et al.* was in fact the 4.4 mev level identified in this experiment.

The levels observed at 5.4 and 5.7 mev are in a region which has not been investigated previously.

A study of photonuclear reactions induced by  ${}^7\text{Li}(p, \gamma)$  radiation using nuclear emulsions has been under way in this laboratory for some years (Titterton 1955). This new crystal technique was intended to supplement it in the case of nuclei

$^\dagger$  This values includes an allowance for the fact that in the energy scale used 7.2 mev means 7.2 mev proton + recoil  ${}^{22}\text{Ne}$  nucleus. The contribution from the latter was obtained from the results of Allison and Casson (1953).

such as K, I and Cs, which can be incorporated into scintillating crystals. The results of further experiments by both techniques will be reported shortly.

The interpretation of these measurements in terms of current theories of photonuclear process awaits the assembly of much more data and will be attempted later.

#### ACKNOWLEDGMENT

Dr. A. K. Mann, who was a Visiting Fulbright Fellow in this laboratory during 1955-56, took an active part in the early stages of this experiment and the authors record their appreciation of his generous assistance.

#### APPENDIX

##### *Energy Calibration*

The scintillation counter was calibrated with proton groups from the  $^{10}\text{B}(\text{d}, \text{p})$  reaction. The calibration chamber was designed to measure both  $^{10}\text{B}(\text{d}, \text{p})$  spectra and the  $^{23}\text{Na}(\gamma, \text{p})$  spectrum and changeover from one measurement to the other could be made in 20 minutes. All the electronic apparatus, including the photomultiplier was kept running during the whole of this period.

The arrangement of the scintillation detector was similar to that of figure 2 except that, in this case, the photomultiplier was within the vacuum system and the dimensions of the sodium iodide crystals used were approximately  $\frac{1}{4}$  in.  $\times$   $\frac{1}{4}$  in.  $\times$  0.040 in. To obtain the  $^{10}\text{B}(\text{d}, \text{p})$  spectra, the lithium target was replaced by a boron target ( $1 \text{ mg cm}^{-2}$  of natural  $\text{B}_2\text{O}_3$  on  $1.5 \text{ mg cm}^{-2}$  aluminium foil), which was bombarded with a  $5 \mu\text{A}$  beam of 300 kev deuterons. A foil holder immediately behind the boron target carried aluminium absorber foils which served to increase the number of calibration points.

Four foil thicknesses were used and the total amounts of absorber between the  $\text{B}_2\text{O}_3$  and the crystal were 5.5, 18.5, 45.4 and  $74.2 \text{ mg cm}^{-2}$  of aluminium respectively. Proton energies were obtained from the data of Ajzenberg and Lauritsen (1955) and the range-energy tables of Aron *et al.* (1949). In measuring the  $^{23}\text{Na}(\gamma, \text{p})$  spectrum, a thick lithium target was bombarded with  $100 \mu\text{A}$  of protons at 600 kev. For this proton energy the field of the beam analysing magnet is the same for both the deuteron and proton beams and any corrections for the slight change in photomultiplier gain caused by the leakage field of the magnet were avoided.

The gain of the system was checked with the ( $\text{ThC} + \text{ThC}'$ ) alpha source before and after each individual run for both the  $^{10}\text{B}(\text{d}, \text{p})$  and the  $^{23}\text{Na}(\gamma, \text{p})$  spectrum measurements. The  $^{23}\text{Na}(\gamma, \text{p})$  spectrum measurement was followed by a repeat measurement of the  $^{10}\text{B}(\text{d}, \text{p})$  spectra. The two calibrations were always in excellent agreement, the displacement between corresponding points being generally less than a few tenths of 1%.

The calibration line and photoproton spectrum of a typical set of measurements are shown in figure 7. Because of the increase in the background of electron pulses consequent on the increase in crystal thickness, the lower energy peaks do not appear in the  $^{23}\text{Na}(\gamma, \text{p})$  spectrum but all peaks above 4 mev are resolved. Altogether five sets of measurements were made but the agreement between the five sets of values for the energies of the photoproton peaks is not as good as would be expected from the above consistency between the two calibrations, in an

individual set of measurements. Thus the results for the energy of the '7.2 mev' peak are 7.4<sub>4</sub>, 7.1<sub>0</sub>, 7.0<sub>8</sub>, 7.2<sub>5</sub> and 7.6<sub>1</sub> mev. The cause of this scatter is unknown but it is thought to be due to an unlocated source of gain variation. If the results are normalized by adjusting all the above energies to the one value then the results for the other peaks are in good agreement. The most natural assumption is that the '7.2 mev' proton group represents the transition to the first excited state in  ${}^{22}\text{Ne}$  at 1.28 mev. Therefore the energies have been normalized to 7.2 mev, the photoproton energy for this transition. Corresponding results are listed in table 2 from which we assign energies of 8.4, 7.2, 5.2<sub>5</sub> and 4.1<sub>5</sub> mev to the four  ${}^{23}\text{Na}(\gamma, p)$  peaks. The calibration of the spectra in figures 1 and 3-6 was made by assuming a linear relationship between energy and channel number and using these four points to fix the straight line. From the fit obtained, the experimental error in the calibration is estimated as less than  $\pm 0.1$  mev between 4 and 8.5 mev.

Table 2. Normalized Results of Calibration Runs

Run	Photoproton peak energies (mev)			
16/12/56	8.3	7.2	5.2 <sub>0</sub>	4.1 <sub>6</sub>
13/12/56	8.4	7.2	5.2 <sub>5</sub>	4.2 <sub>6</sub>
12/12/56	8.4	7.2	5.2 <sub>4</sub>	4.1 <sub>3</sub>
27/11/56	8.5	7.2	5.2 <sub>1</sub>	4.1 <sub>2</sub>
25/11/56	8.3	7.2	5.2 <sub>8</sub>	—

## REFERENCES

- AJZENBERG, F., and LAURITSEN, T., 1955, *Rev. Mod. Phys.*, **27**, 77.  
 ALBURGER, D. E., 1949, *Phys. Rev.*, **76**, 435.  
 ALLISON S. K., and CASSON, H., 1953, *Phys. Rev.*, **90**, 880.  
 ARON, W. A., HOFFMAN, B. G., and WILLIAMS, F. C., 1949, *U.S. Atomic Energy Commission Report No. AECU 663*.  
 BARNES, C. A., CARVER, J. H., STAFFORD, G. H., and WILKINSON, D. W., 1952, *Phys. Rev.*, **86**, 359.  
 CAMPBELL, J. G., 1956, *Aust. J. Phys.* **9**, 156.  
 CARVER, J. H., HAY, H. J., and TITTERTON, E. W., 1955, *Phil. Mag.*, **46**, 841.  
 DEVONS, S., and HINE, M. G. N., 1949, *Proc. Roy. Soc. A*, **199**, 56.  
 FADER, W. J., May 1954, M.I.T. Progress Report.  
 FOSTER, B. P., STANDFORD, G. S., and LEE, L. L., 1954, *Phys. Rev.*, **93**, 1069.  
 HIRZEL, O., and WÄFFLER, H., 1947, *Helv. Phys. Acta*, **20**, 373.  
 KOERTS, L., MACKLIN, P., FARRELLY, B., VAN LIESHOUT, R., and Wu, C. S., 1955, *Phys. Rev.*, **98**, 1230.  
 MAY, A. N., and VAIDYANATHAN, R., 1936, *Proc. Roy. Soc. A*, **155**, 519.  
 PERLMAN, M. L., and WELKER, J. P., 1954, *Phys. Rev.*, **95**, 133.  
 SHER, R., HALPERN, J., and MANN, A. K., 1951, *Phys. Rev.*, **84**, 387.  
 STEARNS, M. B., and MCDANIEL, B. D., 1951, *Phys. Rev.*, **82**, 450.  
 TITTERTON, E. W., 1955, *Progress in Nuclear Physics*, Vol. 4.



## The Čerenkov Effect in Composite (Isotropic) Media

By A. M. SAYIED

Institute of Nuclear Physics, Calcutta

*MS. received 12th February 1957, and in revised form 27th June 1957*

**Abstract.** The Čerenkov radiation emitted by a fast charged particle moving through one medium and in the vicinity of another medium has been theoretically investigated, employing the invariance of the phenomenological electrodynamic equations of Maxwell. A simple geometry has been considered, this being the case of two coaxial dielectrics and permeable cylinders with a common cylindrical interface and a charged particle moving along their common axis. The results obtained have been discussed with special reference to the case of Čerenkov radiation at microwave and radio-frequency regions. The effect of the phenomena of coherence on the output of the emitted radiation in these cases has been briefly outlined.

### § 1. INTRODUCTION

GINSBURG (1957 a, b) was the first to consider theoretically the case of Čerenkov type of radiation at microwave frequencies from electrons moving near a dielectric through free space. Abele (1952) has considered similar production of microwave radiation in a cylindrical metallic (ideal conductor) wave guide filled with a lossless and non-dispersive dielectric medium and which has a very fine axial bore through which a charge  $q$  moves axially with a uniform velocity  $v$ .

These investigations were a prelude to the experimental detection of such an effect by Danos, Geschwind, Lashinsky and van Trier (1953). They detected the Čerenkov radiation at microwave frequencies corresponding to the region of wavelength of the order of 1.5 cm emitted from a flat ribbon-like bunched electron beam passing very close to the surface of a dielectric which was polycrystalline  $\text{TiO}_2$  with  $\epsilon = 105$  for  $\lambda = 1.25$  cm.

Recently Danos (1955) and Lashinsky (1956) have investigated theoretically the nature of the Čerenkov radiation from extended electron beams bunched in a sinusoidal form along their direction of motion through free space and very close to the surface of a dielectric. Danos (1955) has considered several geometries which include the cylindrical and plane type of interfaces. Lashinsky (1956) has extended Danos' calculations. However, the investigation of the nature of the Čerenkov radiation emitted by a single charged particle moving through free space and very close to the surface of a dielectric medium is of intrinsic interest and has been investigated by Linhart (1955) in some detail for the case of a plane interface. It is intended in the present paper to investigate theoretically the more generalized case of Čerenkov radiation emitted in the case of composite media following the method of solution along the lines of the treatment of the Čerenkov type of effect in a single media considered by Nag and Sayied (1956, to be referred to as I) based on the invariance of the phenomenological electrodynamic equations of Maxwell. We consider media which have both dielectric



constant  $\epsilon$  and permeability  $\mu$  greater than unity and the results of the previous authors will appear as limiting cases for  $\mu = 1$ . We also consider the case of  $\mu \geq 1$  and  $\epsilon \geq 1$  for both media and the results of the previous authors including the case of a single medium will appear as limiting cases. Finally the radiation from bunched beams are considered taking into account the phenomenon of coherence.

The method of treating the Čerenkov type of effect using the invariance of the phenomenological electrodynamic equations of Maxwell is the calculation of the electromagnetic field produced by a uniformly moving charged particle in material media in two steps. The electromagnetic field seen by an observer at rest with respect to the charges, with the medium moving with a uniform velocity, is first calculated from equations in I.

$$\frac{1}{\lambda} \frac{\partial^2 \phi}{\partial x^2} + \frac{\partial^2 \phi}{\partial y^2} + \frac{\partial^2 \phi}{\partial z^2} = - \frac{4\pi\rho}{\epsilon\lambda} \quad \dots\dots(1a)$$

$$\lambda = \frac{(1-\beta^2)}{(1-\epsilon\mu\beta^2)} = - \frac{1}{\gamma^2} \quad \dots\dots(1b)$$

$$A_x = \frac{v}{c} \phi = \frac{(1-\epsilon\mu)\beta}{(1-\epsilon\mu\beta^2)} \phi \quad \dots\dots(1c)$$

$$A_y = A_z = 0 \quad \dots\dots(1d)$$

$$\mathbf{B} = \text{curl } \mathbf{A} \quad \dots\dots(2a)$$

$$\mathbf{E} = -\text{grad } \phi \quad \dots\dots(2b)$$

$$\mathbf{D} + \frac{1}{c} \mathbf{v} \times \mathbf{H} = \epsilon \mathbf{E} + \frac{\epsilon}{c} \mathbf{v} \times \mathbf{B} \quad \dots\dots(2c)$$

$$\mathbf{B} - \frac{1}{c} \mathbf{v} \times \mathbf{E} = \mu \mathbf{H} - \frac{\mu}{c} \mathbf{v} \times \mathbf{D} \quad \dots\dots(2d)$$

The boundary conditions to be satisfied at the interface of two media in this case are (Møller 1952):

(a) The tangential components of

$$\mathbf{E}^* = \mathbf{E} + \frac{1}{c} \mathbf{v} \times \mathbf{B} \quad \dots\dots(\text{i})$$

$$\mathbf{H}^* = \mathbf{H} - \frac{1}{c} \mathbf{v} \times \mathbf{D} \quad \dots\dots(\text{ii})$$

should be continuous. (b) The normal component of  $\mathbf{B}$  must be continuous at the interface. (c) The change  $\Delta D_n$  in the normal component of  $\mathbf{D}$  should be equal to the surface density of charge on the boundary.

Next, the observer is supposed to move with the medium with the same velocity (i.e. observer at rest with respect to the medium but both moving with respect to the charged particle) and the electromagnetic field as seen by him is calculated using the Lorentz-Minkowski transformation relations for electromagnetic fields in moving media given by the special theory of relativity. The energy radiated as Čerenkov radiation will then be calculated using the Poynting vector theorem.

## § 2. CASE I: COMMON CYLINDRICAL INTERFACE WITH A SINGLE CHARGE MOVING ALONG THE AXIS

Consider an infinitely extended cylindrical medium of radius  $a$ , the medium having a dielectric constant  $\epsilon_1$  and permeability  $\mu_1$ . Let this medium be surrounded

by another medium of dielectric constant  $\epsilon_2$  and permeability  $\mu_2$ , this second medium extending up to infinity. A charged particle of charge  $e$  is considered to be moving with a uniform velocity  $v$  along the axis of symmetry which is considered as the  $x$ -axis of the system of coordinates. To evaluate the electromagnetic field produced, we have to solve equation (1a) satisfying the boundary conditions (a), (b) and (c). These, in cylindrical coordinates  $(r, \theta, x)$  are (assuming no charges at the cylindrical interface),

$$\partial\phi/\partial x \text{ should be continuous at } r=a \text{ for all } x \quad (\text{A})$$

$$\left\{ \frac{\epsilon}{(1-\epsilon\mu\beta^2)} \right\} \left( \frac{\partial\phi}{\partial r} \right) \text{ should be continuous at } r=a \text{ for all } x. \quad (\text{B})$$

We now seek solutions of equation (1a) as  $\phi = \phi_1$  for the inner medium and  $\phi = \phi_2$  for the other medium satisfying the following conditions :

(i)  $\phi_1$ ; has a singularity at the origin and is regular everywhere in the region  $0 < r \leq a$

(ii)  $\phi_2$ ; vanishes as  $r \rightarrow \infty$  and is regular in the region  $a \leq r < \infty$

$$\text{(iii A)} \quad \left( \frac{\partial\phi_1}{\partial x} \right)_{r=a} = \left( \frac{\partial\phi_2}{\partial x} \right)_{r=a},$$

$$\text{(iii B)} \quad \chi_1 \left( \frac{\partial\phi_1}{\partial r} \right)_{r=a} = \chi_2 \left( \frac{\partial\phi_2}{\partial r} \right)_{r=a},$$

where

$$\chi = \frac{\epsilon}{1 - \epsilon\mu\beta^2}. \quad \dots\dots(3)$$

(iv)  $\phi_2$  should be such that it represents an outgoing wave in medium 2.

We now note that the solution  $\phi_{11}$  of equation (1a) for the case of only one medium  $\epsilon_1$ ;  $\mu_1$  being present and filling the entire space as given in I was

$$\phi_{11} = -\frac{ei}{2} \int_{-\infty}^{+\infty} \frac{\gamma_1^2}{\epsilon_1} \exp(ik_1 x) \left\{ \frac{k_1}{|k_1|} J_0(\gamma_1 |k_1| r) + iN_0(\gamma_1 |k_1| r) \right\} dk_1 \dots\dots(4)$$

which has a singularity at the origin. The solution  $\phi_1$  in the present case of two media should be such that a part  $\phi_{12}$  is added to  $\phi_{11}$  to take into account the effect of the second medium.  $\phi_{12}$  must be regular in the region  $0 \leq r \leq a$  and should have no singularity at the origin, that is,  $\phi_{12}$  must be a solution of the homogeneous equation

$$\frac{1}{\lambda} \frac{\partial^2 \phi}{\partial x^2} + \frac{\partial^2 \phi}{\partial y^2} + \frac{\partial^2 \phi}{\partial z^2} = 0. \quad \dots\dots(5)$$

The physical basis for  $\phi_{12}$  satisfying equation (5) is that  $\phi_{12}$  denotes the effect of the difference in the polarization of the two media, and as the polarization effects are due to induced dipole moments which everywhere satisfy the equation  $\text{div } \mathbf{D} = 0$ , the part  $\phi_{12}$  consequently satisfies the homogeneous equation (5). We now write out a solution of (5) in the form of a Fourier-Bessel integral with one undetermined constant as

$$\phi_{12} = \int_{-\infty}^{+\infty} A_{k_1} \exp(ik_1 x) J_0(\gamma_1 |k_1| r) dk_1. \quad \dots\dots(6)$$

Thus, the solution  $\phi_1 = \phi_{11} + \phi_{12}$  for the inner medium is

$$\phi_1 = \int_{-\infty}^{+\infty} \exp(ik_1 x) \left[ \left\{ A_{k_1} - \frac{ei\gamma_1^2 k_1}{2\epsilon_1 |k_1|} \right\} J_0(\gamma_1 |k_1| r) + \frac{e\gamma_1^2}{2\epsilon_1} N_0(\gamma_1 |k_1| r) \right] dk_1. \quad \dots\dots(7)$$

Similarly, we obtain the solution  $\phi_2$  for the outer medium as

$$\phi_2 = \int_{-\infty}^{+\infty} \exp(ik_1 x) B_{k_1} H_0^{(1)}(\gamma_2 | k_1 | r) dk_1. \quad \dots\dots(8)$$

The unknown constants  $A_{k_1}$  and  $B_{k_1}$  are evaluated by matching the boundary conditions (iii A) and (iii B) for each frequency of the spectrum, and thus we get

$$A_{k_1} = \frac{\chi_2 \gamma_2 H_0^{(1)'}(\gamma_2 | k_1 | a) \left\{ \frac{e\gamma_1^2}{2\epsilon_1} N_0(\gamma_1 | k_1 | a) - \frac{e i \gamma_1^2 k_1}{2\epsilon_1 |k_1|} J_0(\gamma_1 | k_1 | a) \right\} - \chi_1 \gamma_1 H_0^{(1)}(\gamma_2 | k_1 | a) \left\{ \frac{e\gamma_1^2}{2\epsilon_1} N_0'(\gamma_1 | k_1 | a) - \frac{e i \gamma_1^2 k_1}{2\epsilon_1 |k_1|} J_0'(\gamma_1 | k_1 | a) \right\}}{\chi_1 \gamma_1 J_0'(\gamma_1 | k_1 | a) H_0^{(1)}(\gamma_2 | k_1 | a) - \chi_2 \gamma_2 J_0(\gamma_1 | k_1 | a) H_0^{(1)'}(\gamma_2 | k_1 | a)} \quad \dots\dots(9)$$

$$B_{k_1} = \frac{e\gamma_1^2 \chi_1 / \pi \epsilon_1 |k_1| a}{\chi_2 \gamma_2 H_0^{(1)'}(\gamma_2 | k_1 | a) J_0(\gamma_1 | k_1 | a) - \chi_1 \gamma_1 H_0^{(1)}(\gamma_2 | k_1 | a) J_0'(\gamma_1 | k_1 | a)} \quad \dots\dots(10)$$

As a check to the correctness of the solutions (7) and (8) we note:

(i) For  $v = \beta c = 0$  the solutions for  $\phi_1$  and  $\phi_2$  must be identical with the well-known solutions for the static case†.

(ii) For  $\epsilon_1 = \epsilon_2$  and  $\mu_1 = \mu_2$ , the solutions for  $\phi = \phi_1$  and  $\phi = \phi_2$  must be identical with the solution  $\phi$  for the case of the single medium given in I.

(iii) For  $a \rightarrow 0$  we must have  $\phi_2$  identical with that for a single medium given in I.

(iv) For  $a \rightarrow \infty$  we must have  $\phi_1$  identical with the solution for a single medium given in I.

The Čerenkov radiation emitted by the system per unit time is obtained using the Poynting vector theorem as (I)

$$-\left(\frac{dW}{dt}\right) = \frac{cr\beta}{2} \int_{-\infty}^{+\infty} \epsilon_2 \lambda_2 \left(\frac{\partial \phi_2}{\partial x}\right) \left(\frac{\partial \phi_2^*}{\partial r}\right) dx \quad \dots\dots(11)$$

substituting for  $\partial \phi_2 / \partial x$  and  $\partial \phi_2^* / \partial r$  from (8) we get on simplification (I)

$$-(dW/dt) = 4v \int_0^\infty \epsilon_2 \lambda_2 B_{k_1} B_{k_1}^* k_1 dk_1 \quad \dots\dots(12)$$

$$-\left(\frac{dW}{dt}\right) = \frac{4e^2 v}{\pi^2}$$

$$\times \int_0^\infty \frac{d\omega'}{\epsilon_2(\omega' a) \left[ J_0^2(\xi_1) \{ J_1^2(\xi_2) + N_1^2(\xi_2) \} + \left( \frac{\epsilon_1^2}{\epsilon_2^2} \right) \left( \frac{\epsilon_2 \mu_2 \beta^2 - 1}{\epsilon_1 \mu_1 \beta^2 - 1} \right) J_1^2(\xi_1) \{ J_0^2(\xi_2) + N_0^2(\xi_2) \} \right]} \quad \dots\dots(13)$$

where

$$k_1 = \frac{\omega}{v} = \frac{(1 - \beta^2)^{1/2} \omega'}{v} \quad \dots\dots(14a)$$

$$\xi = \gamma |k_1| a = (\epsilon \mu \beta^2 - 1)^{1/2} \left( \frac{\omega' a}{v} \right) \quad \dots\dots(14b)$$

$\omega'$  being the circular frequency of the emitted Čerenkov radiation.

† It should be noted that in I this trick could have been suitably employed in obtaining the solution of the equation satisfied by  $\phi$ .

It can be shown at once that for  $a=0$  the expression (13) gives us the generalized Frank and Tamm's formula given in I†. Equation (13) is the expression from which the total output of Čerenkov type of radiation for cylindrical geometries for various media with various values of  $a$  can be evaluated.

For small values of  $a$ , confining our attention to the regions of large wavelengths, i.e.  $|k_1|$  small, we can expand the  $J_n$ 's and  $N_n$ 's for small values of their arguments and obtain,

$$-\left(\frac{dW}{dt}\right) = \frac{e^2 v}{c^2} \int_0^{\omega'_{\max}} \mu_2 \left(1 - \frac{1}{\epsilon_2 \mu_2 \beta^2}\right) \omega' d\omega' \times \left[ 1 + \frac{\pi^2 \epsilon_2^2 \mu_2^2}{16c^4} \left(1 - \frac{1}{\epsilon_2 \mu_2 \beta^2}\right)^2 \omega'^4 a^4 + \frac{\pi^2 \epsilon_1^2 \mu_2^2 \omega'^4 a^4}{16c^4} \left\{ 1 + \frac{4}{\pi^2} \left( \ln \frac{2v}{\Gamma \omega' a (\epsilon_2 \mu_2 \beta^2 - 1)^{1/2}} \right)^2 \right\} \right] \quad \dots\dots(15a)$$

$$-\left(\frac{dW}{dt}\right) = \frac{e^2 v}{c^2} \int_0^{\omega'_{\max}} \mu_2 \left(1 - \frac{1}{\epsilon_2 \mu_2 \beta^2}\right) \frac{\omega' d\omega'}{1 + F(\omega', a, \epsilon_2, \mu_2, \epsilon_1, \beta)} \quad \dots\dots(15b)$$

where

$$F(\omega', a, \epsilon_2, \mu_2, \epsilon_1, \beta) = \frac{\pi^2 \epsilon_2^2 \mu_2^2}{16c^4} \left(1 - \frac{1}{\epsilon_2 \mu_2 \beta^2}\right)^2 \omega'^4 a^4 + \frac{\pi^2 \epsilon_1^2 \mu_2^2 \omega'^4 a^4}{16c^4} \times \left\{ 1 + \frac{4}{\pi^2} \left( \ln \frac{2v}{\Gamma \omega' a (\epsilon_2 \mu_2 \beta^2 - 1)^{1/2}} \right)^2 \right\} \quad \dots\dots(16a)$$

$$(\epsilon_2 \mu_2)_{\omega'_{\max}} \beta^2 = 1 \quad \dots\dots(16b)$$

$$\Gamma = 1.7811. \quad \dots\dots(16c)$$

Equation (15) enables us to draw the following conclusions about the nature of the emitted Čerenkov radiation in such cases.

(1) For  $a=0$  we see that equation (15) becomes

$$-\left(\frac{dW}{dt}\right) = \frac{e^2 v}{c^2} \int_0^{\omega'_{\max}} \mu_2 \left(1 - \frac{1}{\epsilon_2 \mu_2 \beta^2}\right) \omega' d\omega', \quad \dots\dots(17)$$

which is identical to the generalized Frank and Tamm's equation.

(2) The value of the function  $F$  defined in equation (16a) is always positive, for all the variables involved occur as second and fourth powers. Thus, equation (15) shows that the energy of Čerenkov radiation at any frequency  $\omega'$  decreases with increasing  $a$  and is a maximum for  $a=0$ , i.e. the case of a single medium.

(3) At low frequencies (small value of  $\omega'$ ) the value of  $F$  is very small because of the presence of the factor  $(\omega' a/c)^4$ . Thus, the term  $\omega'$  in the numerator of the integrand of equation (15b) practically governs the output of energy as Čerenkov radiation at low frequencies, and consequently at low frequencies the output is practically independent of the presence of  $a$ . The output is zero at  $\omega'=0$  and thus the  $((dW/dt)_{\omega'}, \omega')$  curve passes through the origin.

(4) At high frequencies (large values of  $\omega'$ ) the value of  $F$  increases with increasing  $\omega'$  and is always positive. Thus, the output of energy as Čerenkov radiation does not increase with increasing frequency  $\omega'$  as fast as that for the case

† The generalized Frank and Tamm's formula given in I has also been obtained by Sitenko (1954) and Pafomov (1956).



of a single medium. At very high frequencies when the value of  $F$  becomes much greater than unity, it is the function  $F$  involving  $(\omega')^4$  which practically governs the nature of the output, and thus the output begins to decrease very rapidly with increasing frequency. If the natural cut-off frequency  $\omega'_{\max}$  for Čerenkov radiation due to the dispersive nature of the medium is very high, then we at once see that due to the presence of  $a$  the output at these frequencies becomes negligibly small. Thus, there must exist a frequency  $\omega''_{\max}$  at which the emitted radiation is a maximum. The value of  $\omega'$  corresponding to  $\omega''_{\max}$ , at which the radiation yield is a maximum, can be obtained directly from equation (13). It should be noted that  $\omega''_{\max}$  shall be different from  $\omega'_{\max}$  and shall be a function of the parameters  $\epsilon_1$ ,  $\epsilon_2$ ,  $\mu_2$ ,  $\beta$  and  $a$ . Thus in the composite system considered the expression for  $-(dW/dt)_{\omega'}$  rises less steeply than proportional to  $\omega'$  for  $a=0$ , reaches a maximum at  $\omega''_{\max}$  and subsequently falls to zero, the rate of fall to zero being determined by the function  $F$ .

This presents an interesting possibility of concentrating a large fraction of the total emitted Čerenkov radiation into any desired band of frequencies, different from the band of frequencies near the cut-off frequency and determined by the geometry and the nature of the media.

(5) It may also be noted that the function  $F$  involves only the electric property  $\epsilon_1$  of the inner medium. The magnetic property  $\mu_1$  of the inner medium has no effect on the nature of the radiation for cases when equation (15) is valid. However, both the dielectric property  $\epsilon_2$  and the magnetic property  $\mu_2$  of the outer medium have pronounced effects on the nature of the Čerenkov radiation.

### § 3. CASE II: COMMON CYLINDRICAL INTERFACE WITH A GROUP OF CHARGES MOVING ALONG THE AXIS

If a group of charged particles all moving with the same velocity  $v$  along the  $x$ -axis which is the axis of symmetry of the system is considered, the nature of the coherence effect in the Čerenkov radiation emitted can be easily obtained along the lines of Schiff's (1946) treatment of bremsstrahlung radiation from a group of charges. The Čerenkov radiation emitted by a group of charged particles then takes the form

$$-\left(\frac{dW}{dt}\right) = \frac{e^2 v}{c^2} \int_0^{\omega'_{\max}} \mu_2 \left(1 - \frac{1}{\epsilon_2 \mu_2 \beta^2}\right) \left\{ \left| \sum_{p=1}^f \sum_{q=1}^N \exp(-i\omega' d_{pq}'/v) \right| \right\}^2 \\ \times \frac{\omega' d\omega'}{1 + F(\omega', a, \epsilon_2, \mu_2, \epsilon_1, \beta)} \dots\dots (18)$$

where all the charged particles in the group constituting the pulses are moving with the same velocity  $v$ ,  $d_{pq}'$  being the coordinate of the  $q$ th electron in the  $p$ th pulse and the effect of coherence is the same as in the case of a single medium. One feature of the phenomena of coherence which presents a very interesting possibility is that by suitable modulation of the group of charged particles a large fraction of the emitted radiation can be concentrated into the same frequency band; into which the dimension  $a$  of the system tends to concentrate, and obtain much larger outputs of Čerenkov radiation at the frequency  $\omega''_{\max}$ . However, from equation (18) it is possible to find the value of  $\omega'$  at which the radiation yield has a maximum value, for a pre-assigned charge distribution and geometry of the system.

## ACKNOWLEDGMENTS

The author wishes to express his sincere gratitude to Professor B. D. Nag for encouragement and valuable discussions. He also wishes to thank the Department of Atomic Energy of the Government of India for the award of a Fellowship and to the Institute of Nuclear Physics, Calcutta for facilities provided.

## REFERENCES

- ABELE, M., 1952, *Nuovo Cim. Supplements IX, Series IX*, **3**, 207.  
DANOS, M., GESCHWIND, S., LASHINSKY, H., and VAN TRIER, A., 1953, *Phys. Rev.*, **92**, 828.  
DANOS, M., 1955, *J. Appl. Phys.*, **26**, 2.  
GINSBURG, V. L., 1947 a, *Doklady Akad. Nauk, S.S.S.R.*, **56**, 145; 1947 b, *Izv. Akad. Nauk, S.S.S.R.*, **11**, 165.  
LASHINSKY, H., 1956, *J. Appl. Phys.*, **27**, 631,  
LINHART, J. G., 1955, *J. Appl. Phys.*, **26**, 527.  
MØLLER, C., 1952, *Theory of Relativity* (Oxford : University Press), Chapter VII.  
NAG, B. D., and SAYIED, A. M., 1956, *Proc. Roy. Soc. A*, **235**, 544.  
PAFOMOV, V. E., 1956, *Soviet Physics (J.E.T.P.)* **3**, 597.  
SCHIFF, L. I., 1946, *Rev. Sci. Instrum.*, **17**, 6.  
SITEENKO, A. G., 1954, *Doklady Akad. Nauk, S.S.S.R.*, **98**, 377.

*Note added in proof.* The following references have been brought to the notice of the author since the paper was written :

- BOGDAN KEVICH, L. S., and BOLOTOVSKY, B. M., 1957, *J. Exp. Theor. Phys.*, **32**, 1421.  
PAFOMOV, V. E., 1957, *J. Exp. Theor. Phys.*, **32**, 610.

# Ionic Conduction at High Electric Field Strengths in Tantalum Pentoxide

A. R. BRAY†, P. W. M. JACOBS AND L. YOUNG‡

Department of Chemistry, Imperial College, London S.W.7

*MS. received 26th July 1957 and in final form 5th December 1957*

**Abstract.** Polarization of the cell  $\text{Ta}|\text{Ta}_2\text{O}_5|\text{Solution}|\text{Pt}$  sets up a very high electric field strength in the oxide and ionic conduction (resulting in growth of the oxide film) occurs with negligible electronic conduction. With this cell measurements of field strength and current density have been made in the temperature range  $-63$  to  $+90^\circ\text{C}$ . These results are incompatible with single barrier control in which space charge is neglected but are consistent with a theory proposed by Dewald in 1955 in which space charge due to ions in transit causes the field in the oxide to vary through its thickness, so that barriers near the metal interface and within the oxide both play a part in controlling the rate of oxide formation.

## § 1. INTRODUCTION

WHEN metals such as aluminium, niobium, tantalum, zirconium, etc., are made the anode in an electrochemical cell a coherent film of oxide is deposited on the metal. Metal ions dissolve in the oxide and diffuse through it to the solution interface, where they react with water liberating hydrogen ions and forming new layers of oxide. Although thermodynamically feasible, the reaction soon becomes negligibly slow unless a field is applied across the oxide. In their theory of metal oxidation, Cabrera and Mott (1948) considered the potential barrier  $\phi$  opposing entry into the oxide as rate determining. This may be generalized: if space charge is negligible, the first barrier at which the backwards current may be neglected controls the current at a given applied potential difference. In the presence of a field  $\mathbf{E}$  the barrier is depressed to  $\phi - b\mathbf{E}q$  when  $q$  is the charge on the mobile cation and  $b$  the half jump distance. The rate of oxidation is then

$$\frac{dX}{dt} = N_s \nu_s \Omega \exp \{ -(\phi - b\mathbf{E}q)/kT \} \quad \dots\dots(1)$$

where  $X$  is the thickness of the film at time  $t$ ,  $N_s$  is the number of ions  $\text{cm}^{-2}$  of metal surface,  $\nu_s$  their vibrational frequency normal to the barrier and  $\Omega$  the volume of oxide containing one metal ion, namely  $4.20 \times 10^{-23} \text{ cm}^3$  for  $\text{Ta}_2\text{O}_5$  of density  $8.74 \text{ g cm}^{-3}$  (the bulk value). Cabrera and Mott consider that every ion escaping from the metal is swept right through the oxide by the field, so

† Now at Bell Telephone Laboratories, Murray Hill, N.J., U.S.A.

‡ Now at British Columbia Research Council, University of British Columbia, Vancouver 8, B.C., Canada.

that conduction through the oxide is not an activated process. From equation (1), the ionic current density  $i$  in the oxide is given by

$$\ln i = \ln(N_s \nu_s q) - \frac{\phi}{kT} + \frac{bEq}{kT} \quad \dots\dots(2)$$

and the Tafel slope by

$$\tau = \left( \frac{\partial E}{\partial \ln i} \right)_T = \frac{kT}{bq} \quad \dots\dots(3)$$

Thus the Tafel slope should be proportional to the absolute temperature, a result common to any theory based on current control by a single barrier where no limit is placed on the concentration of ions before the barrier.

The Cabrera-Mott theory was tested by Vermilyea (1953) who determined the thickness of his oxide films on tantalum by comparison with a set of standard specimens and calculated the field (assumed constant, as in the theory) from  $V/X$  where  $V$  is the potential difference across the oxide, viz. the voltage applied to the cell corrected for ohmic drop in the solution and the potential of the electrochemical reaction. Vermilyea found that the plots of  $\ln(dX/dt)$  against field for various temperatures were, within experimental error, parallel, so that

$$\ln(dX/dt) = \ln C + BE \quad \dots\dots(4)$$

with  $B = 5.05 \pm 0.1 \times 10^{-6} \text{ cm v}^{-1}$ , independent of  $T$  between 0 and  $80^\circ\text{C}$ .  $\ln C$  varied with temperature according to the Arrhenius expression,  $C = A \exp(-E/kT)$  the activation energy  $E$  being 0.71 eV. Therefore,

$$\ln i = \ln(qA/\Omega) - E/kT + BE. \quad \dots\dots(5)$$

This result is in disagreement with the Cabrera-Mott theory because  $B$  is constant and therefore  $E$  is a linear function of  $1/T$ , with slope independent of  $\ln i$  but intercept dependent on  $\ln i$ —cf. equation (2) which predicts that  $E$  is a linear function of  $T$  with slope dependent on  $\ln i$ .

Young (1954), using buffed specimens, for which the current efficiency cannot be assumed to be 100%, and manual control of the current, also failed to find a dependence of Tafel slope on temperature between 20 and  $60^\circ\text{C}$ . In later work (in which formations at constant voltage were used exclusively) Vermilyea (1955a) found two activation energies corresponding to zero-field barriers of 2.17 and 1.47 eV with half-widths of 4.8 and  $2.4 \text{ \AA}$  respectively (assuming  $q = 5e$ ).

The existence of two rate-controlling barriers should lead to the setting up of a space charge but, because his results do not reveal any dependence of average field on thickness, Vermilyea rejects the existence of any substantial space charge in the oxide and instead (Bean, Fisher and Vermilyea 1956) associates the two activation energies found with the creation of interstitial ions in the presence of the field. The interaction of vacancy and applied field is postulated to be such as to allow a change in barrier height and jump distance as the field increases. The argument however, cannot be sustained: if there is a barrier controlling the current within the oxide, ions must enter the oxide from the metal at a rate either greater than or less than the rate at which they diffuse through the oxide barrier (in this instance supposed to be that for the escape of interstitial ions from vacancies). Only at one field and temperature will the entrance current be equal to the migration in the initial non-steady state. If the entrance rate is less than the migration rate the current is controlled by the entrance barrier; if the entrance rate exceeds the diffusion rate ions must 'pile up' within the oxide



and constitute a space charge. This space charge reduces the field across the metal-oxide boundary until the rate at which ions enter the oxide is adjusted to that at which they can escape through it and react at the solution interface. This argument is quite general and *any* barrier exercising control within the oxide, before which the number of ions is not allowed to increase without limit, must lead to a space charge and dual barrier control. Generation of conduction ions within the oxide does not evade this point for, since the ionic current is accompanied by growth, ions must continually be entering the oxide from the metal. It is possible that the generated vacancies diffuse to the metal at a rate equal to that at which the interstitial ions migrate to the solution interface, but this seems unlikely on general grounds and is specifically rejected by Dewald (1957) in his application of the Vermilyea theory to transient currents.

The only other accurate measurements of Tafel slopes which have been reported are those of Young (1956) on niobium. His results also show a Tafel slope independent of temperature and hence total disagreement with any single barrier theory.

## § 2. EXPERIMENTAL

Tantalum rolled into sheet 0.005 in. thick from rod of at least 99.9% purity was obtained from Murex Ltd. It was cleaned by chemical polishing in a bath of 5 parts 98%  $\text{H}_2\text{SO}_4$ , 2 parts 70%  $\text{HNO}_3$  and 2 parts 40%  $\text{HF}$ . This mixture dissolved a thick oxide film in a few seconds, leaving a bright unscratched surface. Specimens were cut to about 3 cm  $\times$  1.25 cm and a strip was bent back to form a tab on which oxide to a thickness of 3000 Å was formed, with the exception of the tip to which electrical connection was made. The oxide-coated tab enables the whole specimen to be immersed in the electrolyte without itself undergoing any formation and so introducing any uncertainty in the surface area. The cell used was similar to that described by Young (1956). Water from a thermostat was pumped through the outer jacket, the temperature of the electrolyte being kept constant to 0.5°C. The electrolyte of decinormal  $\text{Na}_2\text{SO}_4$  was stirred by a teflon-coated magnet rotated at high speed by a rotating magnet below the cell. A glass frame supported two large platinum sheets spot welded to the platinum cathode lead; these were, however, used only in impedance measurements to be described in a later paper, a small platinum wire being used in the Tafel slope measurements because it assumes a steady potential more rapidly during polarization.

The polarizing circuit employed the constant-current generator described previously by Young (1956). Currents could be kept constant to 0.25% over the complete formation range. Successive formations were made for 60 sec at 1  $\text{mA cm}^{-2}$ , 140 sec at 0.1  $\text{mA cm}^{-2}$  and 210 sec at 0.001  $\text{mA cm}^{-2}$ . The longer periods at the lower fields were necessary to allow steady state conditions to be reached. Voltage readings were taken at intervals of 10 sec, 20 sec and 30 sec during formations at high, intermediate and low currents respectively. The applied voltage was plotted against time for the three currents used and the voltages read off at 60, 120 and 180 seconds. These voltages were plotted against the charge passed (figure 1), formations being generally continued until five points on each line were obtained. It was observed that some loss of linearity in the voltage-time plots at high and intermediate fields (those for low fields were continued only sufficiently long for steady state conditions to be established)

occurred when the applied voltage exceeded 100 v, indicating a fall in current efficiency. This occurred more readily at higher temperatures, at which a good straight line through four points in the (voltage, charge) plot was accepted. Plots in which any point of the five (or, at higher temperatures, four) were more than 0.3 v off the best straight line were rejected. Under the conditions of formation, 79% of the total charge was passed at the highest current and only 2.8% at the lowest current, thus limiting as much as possible any inaccuracies due to slightly reduced efficiency at the lowest current.

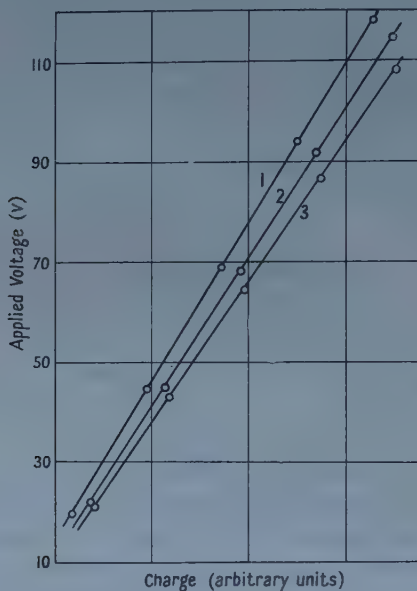


Figure 1. Typical plot of applied voltage against charge passed. 1,  $1.0 \text{ mA cm}^{-2}$ ; 2,  $0.1 \text{ mA cm}^{-2}$ ; 3,  $0.01 \text{ mA cm}^{-2}$ .

In measurements conducted below  $0^\circ\text{C}$ , a small cell which could be inserted in a Dewar flask containing a freezing mixture was used instead. The anode was a Johnson Matthey 'Specpure' rod and the electrolyte a concentrated solution of picric acid in acetone containing a few drops of water. This electrolyte was selected after many attempts to find one with an adequate conductance at temperatures down to  $-78^\circ\text{C}$ . If the electrolyte conductance was poor, the heat dissipated at the higher currents raised the temperature of the whole cell by several degrees. When a large cylindrical platinum cathode, concentric with the specimen, was used no perceptible temperature rise occurred even when a current of 5 mA was passed through the electrolyte used.

Considerable difficulty was experienced in the formation of anodic films at low temperatures. Breakdown, accompanied by profuse bubbling, invariably occurred at potentials of 20 v or even lower, particularly at the edges of the specimen. Considerable improvement was effected by rounding the edges with a file, followed by prolonged etching. The method of determining Tafel slopes used in aqueous solutions could not be followed at low temperatures, since the working range was too small for the necessary number of separate formations to be made. The method was therefore adapted as follows. A formation of 90 seconds duration was made at a low current  $i_2$  ( $0.06 \text{ mA cm}^{-2}$ ) followed by

formation for 60 or 90 seconds at a high current  $i_1$  ( $0.6 \text{ mA cm}^{-2}$ ). A further formation was then made at the low current. If no inefficiency develops during the course of these three formations, the (voltage, time) plots for the low current are parallel. This was used as the criterion for acceptance.

### § 3. RESULTS

#### 3.1. Aqueous Solution

Let the values of the applied voltage  $V$  corresponding to any two arbitrary charges  $Q_1'$ ,  $Q_1$  be  $V_1'$ ,  $V_1$  at current  $i_1$ , etc. and let the charge  $Q_1' - Q_1$  produce a change  $\Delta X$  in the thickness of the film. The mean field over an increase in thickness  $\Delta X$  at constant current  $i_1$  is given by

$$E_1 = -\frac{\Delta V_1}{\Delta X} = \frac{V_1' - V_1}{\Delta X} \quad \dots\dots (6)$$

with similar expressions for currents  $i_2$ ,  $i_3$ . Since  $i_1 = 10i_2 = 100i_3$ , the mean Tafel slope in the current range  $i_1 - i_2$  is

$$\tau = \left( \frac{\Delta E}{\Delta \ln i} \right)_T = \frac{E_1 - E_2}{2.303} \quad \dots\dots (7)$$

It will be noted that in equation (6) the applied voltage may be used instead of the potential difference across the oxide, which is not known, since the voltage drop in the electrolyte and overpotential are independent of the amount of charge passed at constant current.  $\Delta X$  is calculated from  $Q' - Q$ , assuming the bulk density  $8.74 \text{ g cm}^{-3}$  and a current efficiency of unity.<sup>†</sup> The results obtained in the temperature range  $0-90^\circ\text{C}$  are shown in table 1. Where several determinations were made at one temperature, the results have been averaged.

Table 1. Mean Tafel Slopes  $(\Delta E/\Delta \ln i)_T$  as a function of  $T$ , for Anodic Oxidation of Tantalum

$T(^{\circ}\text{K})$	$\tau \times 10^{-5}/\text{V cm}^{-1}$ in current range		
	1-0.1	0.1-0.01	1-0.01
273	1.97	1.78	1.86
283	1.99	1.78	1.88
293	2.01	1.71	1.85
303	1.66	1.82	1.74
313	1.98	1.45	1.71
323	1.43	2.05	1.74
333	1.95	1.79	1.86
343	2.06	1.82	1.94
353	1.85	1.82	1.91
363	2.08	1.71	1.89
Mean 273-323	$1.90 \pm 0.08$	$1.76 \pm 0.05$	$1.83 \pm 0.03$
Mean 333-363	$2.02 \pm 0.06$	$1.78 \pm 0.06$	$1.89 \pm 0.06$
Mean 273-363	$1.95 \pm 0.05$	$1.77 \pm 0.04$	$1.86 \pm 0.03$

Means are means of all results accepted within temperature range specified.

Limits quoted are standard errors of the mean.

It will be observed that there is hardly any increase with temperature between  $0$  and  $90^\circ\text{C}$  in contrast with the Cabrera-Mott theory which predicts an increase of 33% in  $\tau$  over this temperature range. Because of the relatively large errors

<sup>†</sup> Further work by one of us has since indicated that the film density may be as low as  $7.93 \text{ g cm}^{-3}$ . This affects the absolute values of  $\tau$  but not their temperature dependence.



inherent in these measurements, it was decided to try to settle this point by doing two further sets of formations at temperatures of 2°C and 60°C only. The means of nine runs at the lower temperature and six runs at the higher temperature in the current range 1–0.1 mA decreased by 8%, those in the range 0.1–0.01 mA were identical and those in the complete range 1–0.01 mA decreased by 3.5%, for a temperature rise of 58° in contrast to the 25% increase predicted by the Cabrera–Mott theory. It is concluded that there is no substantial net increase in  $\tau$  over the temperature range accessible in aqueous solution.

The same results as led to table 1 are shown graphically in a different form in figure 2, where the experimental field is plotted against the reciprocal of the

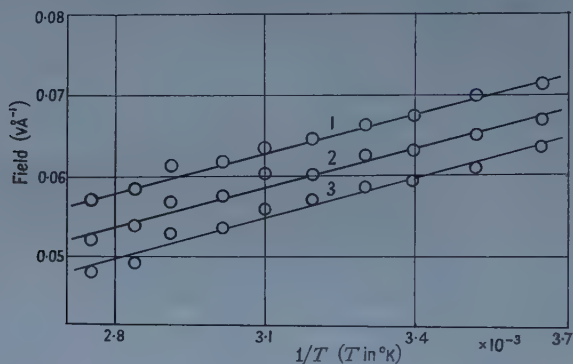


Figure 2. Plot of the experimental field  $-\Delta V/\Delta X$  against reciprocal of the absolute temperature. 1, 1.0 mA cm<sup>-2</sup>; 2, 0.1 mA cm<sup>-2</sup>; 3, 0.01 mA cm<sup>-2</sup>. The straight lines are regression lines through the median values.

absolute temperature, with formation current as a parameter. These data can be represented within experimental error by straight regression lines. If the Tafel slope were independent of temperature, these lines would be parallel; that they are virtually so indicates that  $\tau$  does not vary substantially between 0 and 90°C.

### 3.2. Non-aqueous Solution

Let  $t_1$ ,  $t_2$  denote the times at which the high-current formation began and ceased, and let the charge passed at  $i_1$  cause voltage changes of  $\Delta V_1$  at the high current and  $\Delta V_2$  at the low current  $i_2$ , respectively (see figure 3). A small relative inefficiency in  $i_2$  is unimportant, since the whole charge in the measured growth period is passed at the high current.

The change in thickness corresponding to the charge passed in the interval  $t_2 - t_1$  is calculated in the usual way and  $\tau$  evaluated from equation (7). The results obtained in the non-aqueous electrolyte are shown in table 2. It was considered necessary to establish that the measured Tafel slope was independent of the electrolyte, especially as Vermilyea (1955 b) has reported that an oxide different from Ta<sub>2</sub>O<sub>5</sub> is formed in solutions based on ethylene glycol. Accordingly, the first set of formations refers to 20°C and the mean value found,  $1.82 \pm 0.03 \times 10^5$  v cm<sup>-1</sup>, is in satisfactory agreement with that measured in aqueous Na<sub>2</sub>SO<sub>4</sub> at the same temperature, viz.  $1.85 \times 10^5$  v cm<sup>-1</sup> (1 to 0.01 mA cm<sup>-2</sup>). This shows that the solution interface does not affect appreciably the current-field relation.



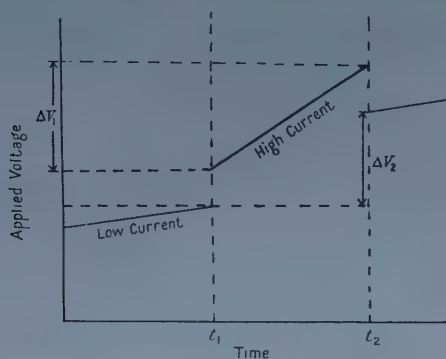


Figure 3. Method of measuring Tafel slopes at low temperatures.

Table 2. Mean Tafel slopes in range  $0.6\text{--}0.06\text{ mA cm}^{-2}$ , for anodic oxidation of tantalum at various temperatures in an electrolyte consisting of picric acid dissolved in acetone. Limits quoted are standard errors of the mean.

Values of $\tau \times 10^{-5}/\text{V cm}^{-1}$			
293°K	230°K	210°K	195°K
1.96	1.69	1.55	1.53
1.95	1.64	1.69	1.76
1.62	1.69	1.81	2.05
1.74	1.61	1.80	2.10
1.73	1.53	1.55	1.93
1.91	1.61	1.22	1.35
1.90		1.45	1.39
1.68	$1.63 \pm 0.03$	1.37	1.77
1.81		1.37	
1.91		1.42	
		1.31	
		1.57	
		1.73	
		1.48	
$1.82 \pm 0.03$		$1.55 \pm 0.05$	

With decreasing temperature satisfactory formations became increasingly difficult to achieve and the results obtained at 195°K are too scattered to have any significance. The results at 230 and 210°K are, however, significantly lower than the mean value in the range 273–363°K which is  $1.86 \pm 0.03$  (table 1). This shows that  $\tau$  is neither a linear function of  $T$  nor independent of  $T$ , and is consistent with the two-barrier theory of Dewald (1955).

#### § 4. DISCUSSION

In Dewald's theory of oxide growth allowance is made for the existence of space charge within the film, arising from the approximate equality of entrance and diffusion barriers. It is shown (Dewald 1955) that the field  $\mathbf{E}$ , as a function of position  $x$  in the oxide, is given by

$$\mathbf{E}(x) = \mathbf{E}_0 + \frac{1}{\beta} \ln(1 + \beta \gamma n_0 x) \quad \dots\dots(8)$$

where  $\beta = aq/kT$ ,  $\gamma = 4\pi q/\epsilon$ ,  $\epsilon$  is the dielectric constant of the oxide and  $n_0$  the

number of mobile ions per  $\text{cm}^3$  at  $x=0$ .  $\mathbf{E}_0$ , the field due to surface charge, is given by equation (2),

$$\mathbf{E}_0 = \frac{kT}{bq} \ln(i/N_s \nu_s q) + \frac{\phi}{bq} \quad \dots\dots(2')$$

The second term in equation (8) is the space charge contribution.  $n_0$  is evaluated by substituting for  $\mathbf{E}_0$  from (2') in the expression for the current in the film at  $x=0$ ,

$$i_0 = 2avqn_0 \exp\{-(U - a\mathbf{E}_0 q)/kT\}. \quad \dots\dots(9)$$

In the steady state  $i_0 = i(x) = i$ ; from (2') and (9) then,

$$n_0 = \frac{(N_s \nu_s q)^{a/b}}{2avq} i^{1-a/b} \exp(-W/kT) \quad \dots\dots(10)$$

where  $W = a\phi/b - U$ . Here  $i$  is the current density in units of  $\text{A cm}^{-2}$  and not in ions  $\text{cm}^{-2} \text{sec}^{-1}$  as in Dewald's paper.

The experimental field is given by

$$\mathbf{E} = -\frac{\Delta V}{\Delta X} = \frac{1}{\Delta X} \int_X^{X'} \mathbf{E}(x) dx \quad \dots\dots(11)$$

Hence, substituting from (8), the theoretical expressions for the experimental field and the derived Tafel slope are

$$\mathbf{E} = \mathbf{E}_0 + \frac{1}{\beta} \left\{ \left( 1 + \frac{1}{\beta \gamma n_0 \Delta X} \right) \ln(1 + \beta \gamma n_0 \Delta X) - 1 \right\} \quad \dots\dots(12)$$

and

$$\tau = \left( \frac{\partial E}{\partial \ln i} \right)_T = \frac{kT}{aq} \left\{ 1 + \left( \frac{a}{b} - 1 \right) \frac{\ln(1 + \beta \gamma n_0 \Delta X)}{\beta \gamma n_0 \Delta X} \right\} \quad \dots\dots(13)$$

or

$$\tau = \frac{kT}{aq} \left\{ 1 + \left( \frac{a}{b} - 1 \right) \frac{\ln(1 + \delta)}{\delta} \right\} \quad \dots\dots(13')$$

with

$$\delta = \beta \gamma n_0 \Delta X = \frac{2\pi q}{v\epsilon kT} (N_s \nu_s q)^{a/b} i^{1-a/b} \exp(-W/kT) \Delta X. \quad \dots\dots(14)$$

Values of  $\delta$  cannot be calculated empirically; instead we find values of the parameters  $a$ ,  $b$ ,  $W$  which allow equation (13') to represent the experimental values of the Tafel slopes.

The change in field for a ten-fold increase in  $i$  at constant temperature is

$$\Delta \mathbf{E} = \Delta \mathbf{E}_0 + \frac{1}{\beta} \{F(\delta)_{i=1} - F(\delta)_{i=0.1}\} \quad \dots\dots(15)$$

where

$$F(\delta) = \left( 1 + \frac{1}{\delta} \right) \ln(1 + \delta). \quad \dots\dots(16)$$

Now if  $\delta$  denotes the values of  $\beta \gamma n_0 \Delta X$  at  $i = 0.1 \text{ mA cm}^{-2}$ ,

$$\delta_{i=1} = \delta \times 10^{1-a/b} = \delta/\theta$$

therefore

$$\Delta \mathbf{E}_0 - \Delta \mathbf{E} = \frac{1}{\beta} \{F(\delta) - F(\delta/\theta)\}. \quad \dots\dots(17)$$

$\Delta \mathbf{E}$  is known from experiment and is (see figure 4) independent of  $T$ , within experimental error, between 0 and  $90^\circ\text{C}$ ;  $\beta = aq/kT$  and  $\Delta \mathbf{E}_0 = 2.303kT/bq$ , therefore equation (17) may be written in the form

$$2.303 \frac{a}{b} - \beta \Delta \mathbf{E} = F(\delta) - F(\delta/\theta). \quad \dots\dots(18)$$

To find  $a$  and  $b$  we (i) assume provisional values for  $a$  and  $b$  and calculate the corresponding value of  $\theta$ , (ii) plot  $F(\delta) - F(\delta/\theta)$  as a function of  $\delta$ , (iii) evaluate the left-hand side of (18) at  $10^\circ$  intervals between 0 and  $90^\circ\text{C}$ , (iv) find  $\delta(T)$  by interpolation, and evaluate  $\tau(T)$  from equation (13'), using the assumed values of  $a$  and  $a/b$ .

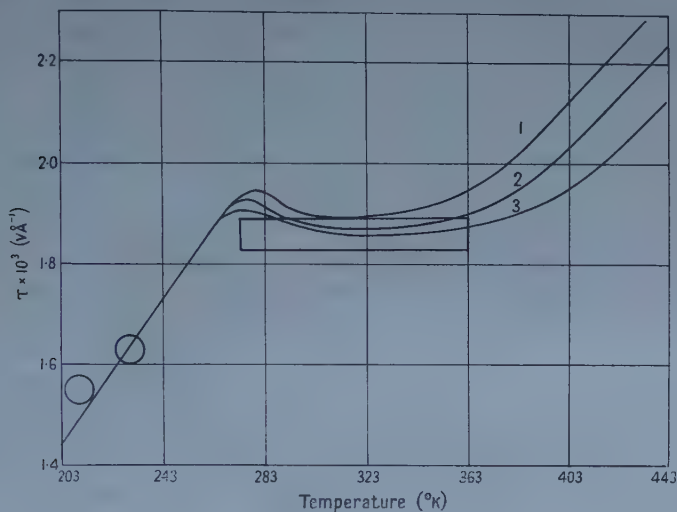


Figure 4. Comparison of calculated values of the Tafel slope  $\tau$  with experiment, using various values of the parameters  $a$ ,  $b$ .

1.  $a = 3.280 \text{ \AA}$ ,  $a/b = 1.350$ .
2.  $a = 3.422 \text{ \AA}$ ,  $a/b = 1.410$ .
3.  $a = 3.592 \text{ \AA}$ ,  $a/b = 1.480$ .

The circles are low temperature points and the rectangle represents the mean of values measured between 273 and 363°K. Size of circles and vertical height of rectangle represent standard error of the mean.

The calculation is repeated until the values of  $a$  and  $b$  are found which give the best agreement with the experimental values for the Tafel slopes. The results of several such calculations are shown in figure 4. The fit using  $a = 3.592 \text{ \AA}$ ,  $b = 2.427 \text{ \AA}$ ,  $a/b = 1.480$  was considered to be adequate. A value of  $4.47 \times 10^{-3} \text{ V \AA}^{-1}$  (figure 2) was used throughout for  $\Delta E$ . The values of  $\delta$  corresponding to this choice of  $a$  and  $b$  appear in table 3.

Table 3. Values of the Parameter  $\delta$  as a Function of Temperature

$T(^{\circ}\text{K})$	283	293	303	313	323	333	343	353	363
$\delta$	0.42	0.98	1.70	2.67	3.97	5.67	8.20	12.20	18.90

Since  $\delta$  depends on  $T$  mainly through the exponential term  $\exp(-W/kT)$ ,  $W$  was evaluated from the plot of  $\log \delta$  against  $1/T$ ; this was sufficiently linear (figure 5, curve I) for the  $1/T$  term in the pre-exponential factor to be ignored. Next  $\phi$  was found by plotting  $E_0/T$  against  $1/T$  (figure 5, curve II); this is linear with slope  $\phi/bq$ .  $E_0$  was evaluated from equation (2') using the values of  $\delta$  from table 3, and values of  $E$  interpolated from figure 2. From these values of  $E$  and  $E_0$  the field due to the space charge is readily found, the calculated values being given in table 4. The values of  $W$  and  $\phi$  found from the slopes of the

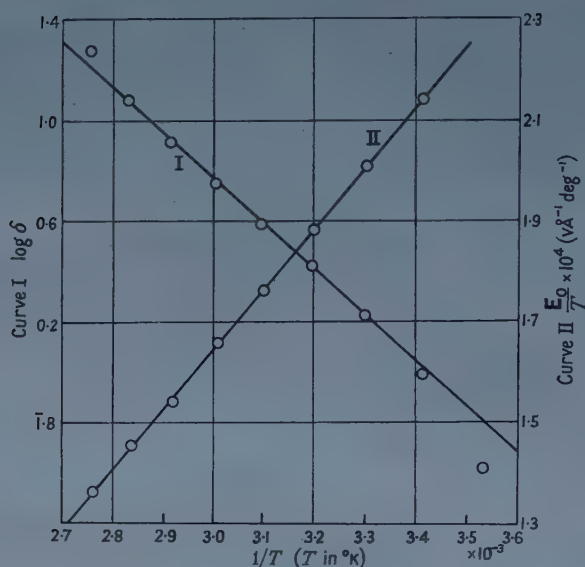


Figure 5. Plot of  $\log \delta$  against  $1/T$  (curve I) and plot of  $E_0/T$  against  $1/T$  (curve II).

Table 4. Comparison of the field due to space charge  $E_{sc}$  with that due to surface charge  $E_0$  in anodically formed tantalum pentoxide, calculated from equation (12) using experimental values of  $\delta$  from table 3.

$T(^{\circ}\text{K})$	293	303	313	323	333	343	353	363
$10^2 E_0 (\text{v } \text{\AA}^{-1})$	6.28	6.09	5.89	5.69	5.52	5.28	5.13	4.93
$10^4 E_{sc} (\text{v } \text{\AA}^{-1})$	5.35	7.98	11.85	15.64	19.71	24.57	30.41	34.83

two lines of figure 5 are  $W = 0.363 \text{ eV}$ ,  $\phi = 1.456 \text{ eV}$ , whence  $U = 1.796 \text{ eV}$ . The value of  $N_s \nu_s$  can also be found from figure 6 since the intercept is

$$(2.303k/bq) \log(i/N_s \nu_s q)$$

and  $i = 0.1 \text{ mA cm}^{-2}$ . The result is

$$N_s \nu_s = 1.1 \times 10^{26} \text{ cm}^{-2} \text{ sec}^{-1},$$

a low, but not impossibly low, figure.

The activation energy for ionic conduction obtained from equation (12) is

$$-k \left( \frac{\partial \ln i}{\partial (1/T)} \right)_E = \frac{\delta(U + kT - aEq) + [(a\phi/b) - U - kT] \ln(1 + \delta)}{\delta - [1 - (a/b)] \ln(1 + \delta)} \quad \dots (19)$$

At low temperatures, where  $\delta$  is small,  $\{\ln(1 + \delta)\}/\delta \simeq 1$  and the activation energy is  $\phi - bEq$ , corresponding to entrance control. At high temperatures, where  $\delta$  is large,  $\{\ln(1 + \delta)\}/\delta \ll 1$  and the activation energy becomes  $U + kT - aEq$ , corresponding to diffusion control within the oxide. Between these two limits, for intermediate values of  $\delta$ , both barriers exercise control and the activation energy is complex being given by the right-hand side of equation (19).

## § 5. CONCLUSION

These measurements of the field in the oxide as a function of temperature and ionic current support the two-barrier theory of oxide growth. The results are in clear disagreement with any theory of single-barrier control, but are fitted by the equations for two-barrier control, with reasonable values of the parameters. The difference between the zero field activation energies  $\phi - U$  is equal to the



energy absorbed in transferring a tantalum ion from the metal into an interstitial position in the oxide. It is unfortunately not possible to calculate the value of  $\phi - U$  at all accurately in an *a priori* manner. Intuitively, one would expect  $\phi$  to be greater than  $U$  and the experimental result that  $\phi - U$  is  $-0.34$  eV is therefore somewhat surprising. The magnitudes of  $a$ ,  $b$  also merit further examination. That of  $a$ ,  $3.6$  Å, represents half the average jump distance of an activated  $\text{Ta}^{5+}$  ion within the oxide film. It is reasonable to suppose that the mobile ions occupy interstitial positions and a total jump distance of  $7.2$  Å seems somewhat too large for a single jump. This may be accounted for, however, if the high-field conduction mechanism is of the interstitialcy type, in which an interstitial ion displaces a normal ion which itself occupies the next interstitial position. Persistence of activation energy could result in successive processes of this type, corresponding to a mild form of cascade, until sufficient de-activation occurs. The experimental value for the jump distance indicates an average number of displacements per activated 'jump'. The value of  $2b$ ,  $4.8$  Å, should represent the jump distance at the barrier opposing entry into the oxide. One would expect the metal-oxide surface barrier to depend on pre-treatment prior to anodization, and yet (Young 1957) the pre-existing film between the metal and the anodic oxide proper does not affect the field appreciably at a given current. There is evidence that with chemically polished tantalum the pre-existing film is chemically different from the anodic oxide film. This seems to indicate that the 'entrance barrier' is actually just within the anodic film and it may be necessary to modify Dewald's original picture, of a single entrance barrier different from later barriers, to one in which there is a gradual change in barrier just within the oxide.

The effect of space charge on the (potential difference, thickness) plot is to cause this to be slightly non-linear to an extent which should be experimentally detectable. This would, however, be readily masked by slight variations in current efficiency, so that failure to find the predicted curvature in the (potential, thickness) plots does not invalidate the dual-barrier theory. The lack of effect of the surface film on the field is a more serious objection and it may be that the results of further experimental work will require some modification of the two-barrier theory. For the present, it provides an adequate basis for the interpretation of our Tafel slope measurements.

#### ACKNOWLEDGMENT

We are indebted to the Director, Atomic Energy Research Establishment, for permission to publish this paper and for financial assistance including the award of a bursary to one of us (A. R. B.).

#### REFERENCES

- BEAN, C. P., FISHER, J. C., and VERMILYEA, D. A., 1956, *Phys. Rev.*, **101**, 551.  
CABRERA, N., and MOTT, N. F., 1948, *Rep. Progr. Phys.*, **12**, 163 (London: Physical Society).  
DEWALD, J. F., 1955, *J. Electrochem. Soc.*, **102**, 1; 1957, *J. Phys. Chem. Solids*, **2**, 55.  
VERMILYEA, D. A., 1953, *Acta Metallurgica*, **1**, 282; 1954, *Ibid.*, **2**, 482; 1955 a, *J. Electrochem. Soc.*, **102**, 655; 1955 b, *Acta Metallurgica*, **3**, 1201.  
VERWEY, E. J. W., 1935, *Physica*, **2**, 1059.  
YOUNG, L., 1954, *Trans. Faraday Soc.*, **50**, 159; 1956, *Ibid.*, **52**, 502; 1957, *Ibid.*, **53**, 841.

## Some Properties of Semiconducting Indium Phosphide

By W. N. REYNOLDS†, M. T. LILBURNE‡ AND R. M. DELL§

Admiralty Research Laboratory, Teddington, Middlesex

*MS. received 26th September 1957*

**Abstract.** Pure polycrystalline samples of indium phosphide have been prepared. Point contact experiments have shown useful rectification on both n- and p-type samples, as well as transistor effects with power gains up to 20 times. The infra-red transmission spectrum has been extended to  $20\mu$ , and the effective mass of electrons has been estimated as  $0.02m$ . Previous work on general properties has been revised and extended.

### § 1. INTRODUCTION

INDIUM PHOSPHIDE is a member of the III-V series of semiconducting compounds to which increasing attention has been paid in recent years. Welker (1953) described observations on point contacts on the material indicating rectification and transistor action, but the evidence for the latter was later shown by Jenny (1955) to be inconclusive. Oswald (1954, 1955) has given transmission curves for the material out to  $15\mu$  showing very low absorption out to  $13\mu$ . Conductivity and Hall effect curves have been given by Folberth and Weiss (1955), together with the carrier mobility values they obtained. It has been the object of the work to be described to prepare the compound in as pure a form as possible and to revise and extend the published data.

### § 2. PREPARATION

Considerable care was taken with the purity of the components. Specpure indium was degreased, etched in HCl and finally reduced in hydrogen at red heat in the same silica vessel in which the reaction was to be performed. Commercial yellow phosphorus was purified by several distillations in a vacuum before being introduced by a further distillation into the reaction vessel. This was a long narrow silica tube suitable for use in a zone-refiner. The reaction was then carried out by the method of Folberth and Weiss, in which the temperature of the hot zone was raised at each pass until it exceeded the melting point of the compound. The rest of the sealed silica tube was meanwhile kept at  $350^{\circ}\text{C}$  by a background heater, in order to maintain the vapour pressure of the phosphorus at a sufficiently high value to prevent the dissociation of the compound.

### § 3. GENERAL PROPERTIES

Indium phosphide is a dark grey crystalline solid. It is fairly brittle, and softer than silicon or germanium, so that it can easily be cut to desired shapes by the same methods. An ultrasonic cutting machine was used to produce the

† Now at Services Electronics Research Laboratory, Baldock, Herts.

‡ Now at G.E.C. Research Laboratories, Wembley, Middlesex.

§ Now at Houdry Process Corporation, Marcus Hook, Pa., U.S.A.

slices and filaments required in our experiments. A sample from which the free unreacted elements had been carefully removed was remelted in an evacuated vessel and found to have a melting point of  $1054 \pm 5^\circ\text{C}$  in good agreement with previous values (Welker 1954). Spectroscopic analysis showed that arsenic and antimony were not present in the material, and that the phosphorus purification process was therefore effective.

X-ray powder photographs were taken of two samples and the results compared with those of Iandelli (1941). Cu  $K_\alpha$  radiation was used with a nickel filter and a 9 cm camera. Some free indium was present in our samples, as it had been in Iandelli's, but it is not believed that this is soluble in the compound to any appreciable extent. Iandelli's sample also contained 2% of germanium, which probably accounts for his estimation of the lattice constant as  $5.86_1 \text{ \AA}$  as compared with our value of  $5.869 \pm 0.001 \text{ \AA}$ . This gives a bond length of  $2.542 \text{ \AA}$  and an x-ray density of  $4.787 \text{ g cm}^{-3}$  for the material.

Pure indium phosphide is quite stable to oxidation, being unattacked in air at  $250\text{--}300^\circ\text{C}$ . It is not hydrolized by water or acetic acid, even on boiling, and is unattacked by NaOH solution or CP4. Dilute HCl and  $\text{H}_2\text{SO}_4$  hydrolize InP on heating, phosphine being liberated. Hot dilute or cold concentrated HCl may be used for cleaning and etching the surface, in which crystallite boundaries are clearly revealed. This behaviour contrasts with that of aluminium phosphide, which is hydrolized even by cold water.

#### § 4. ELECTRICAL MEASUREMENTS

It was found that low-resistance non-rectifying contacts could be made with lead-tin solder, pure zinc chloride being employed as a flux. Indium, however, would not solder or alloy, even when heated to a high temperature in a vacuum. Filaments a few millimetres in length and a few tenths of a millimetre square were soldered at each end, etched and their electrical behaviour studied. This was usually non-ohmic when the specimen was of reasonably high resistivity, but exploration with a voltage probe revealed the existence of appreciable uniform regions of resistivity up to about 30 ohm cm. The size of these regions appeared to be limited by the crystallite size to dimensions of the order of 1 mm. In the case of n-type material, such a resistivity indicates the presence of about  $6 \times 10^{13} \text{ carriers cm}^{-3}$  if the value of electron mobility is taken as  $3400 \text{ cm}^2 \text{ v}^{-1} \text{ sec}^{-1}$ , as given by Folberth and Weiss.

Point contact studies were made of specimens with suitably soldered bases. The circuit used was that employed by Banbury, Gebbie and Hogarth (1951) to study diode and triode action at point contacts, in which the input voltage was swept at 50 c/s from a Variac supply, and suitable biases and loads were inserted. The characteristics were displayed on a calibrated oscilloscope. Figure 1 illustrates a rectification curve taken on p-type material, showing the drastic effect of intense illumination with a Pointolite lamp. Several p-type specimens were found capable of withstanding over 400 v in the blocking direction, as well as n-type specimens withstanding up to 250 v. Rectification ratios as high as  $10^5$  at 100 v were obtained. Both n- and p-type specimens exhibited photo-voltages (of opposite sign), some p-type points giving as much as 1.05 v on open circuit under intense illumination.

A careful study has been made of transistor action, which was shown to occur in high back-voltage p-type regions. Two phosphor-bronze point contacts were



used, placed close together on specimens soldered to a conducting base. These were connected as emitter and collector in a conventional triode circuit. Figure 2(a), (b) and (c) shows curves obtained from a pair of points about 0.1 mm apart, illustrating respectively (collector voltage, emitter voltage), (collector current, emitter current), (collector current, emitter voltage), (collector current, emitter current, emitter voltage).



Figure 1. (Voltage, current) curve for a point contact on p-type indium phosphide, showing the effect of illumination.

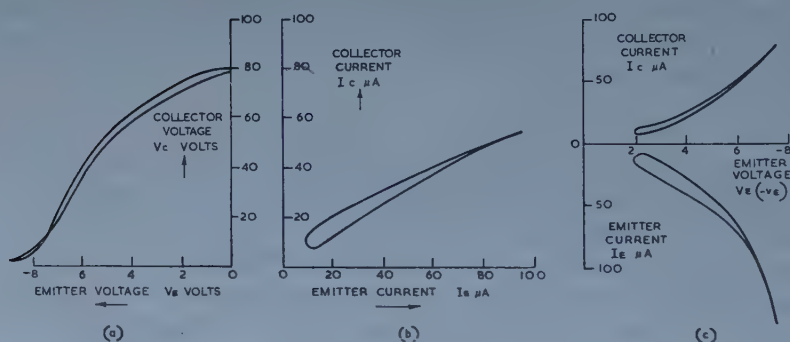


Figure 2. Transistor characteristics obtained on p-type indium phosphide: (a) voltage gain, (b) current gain, (c) (currents, emitter voltage).

emitter current) and (collector and emitter currents, emitter voltage). The maximum voltage gain is about 30, current gain about 0.5 and power gain 15. The best power gain was about 20, but in no case was current gain greater than unity observed. The looping observed in some of the characteristics was partly due to mains pick-up, which was difficult to eliminate with the high circuit resistances, but may also have been partly due to low carrier mobilities. The collector was 'formed' electrically, but not too vigorously as this causes decomposition, bright beads of indium becoming visible and emitter-collector short circuit being observed.

## § 5. OPTICAL MEASUREMENTS

### 5.1. Infra-Red Transmission

Optical transmission was studied as a function of wavelength on specimens about 0.5 mm in thickness. A Leiss double monochromator was used as a source of radiation, the beam being chopped at 10 or 12.5 c/s, and a Schwarz thermopile with a KBr window was used as a detector. The intensity at each wavelength



was compared with the transmitted intensity, and the absorption coefficient calculated with allowance for loss by reflection. The specimen holder was supported in a vacuum cryostat with KRS5 windows, so that measurements could be made below room temperature.

When rock salt prisms were employed in the monochromator, results were obtained which agreed closely with those obtained by Oswald over the range 1 to  $15\mu$ . The value of the gap width  $E_g$  was found by the method of Oswald and Schade (1954), namely by finding the intersection of the extrapolated absorption edge with the extrapolated (almost constant) absorption curve at longer wavelengths. The value found at  $293^\circ\text{K}$  was  $1.27 \pm 0.01\text{ eV}$ , and that at  $109^\circ\text{K}$  was  $1.36\text{ eV}$ . This represents close agreement with Oswald's result, viz.

$$E_g = 1.41 - 4.6 \times 10^{-4}T \text{ eV.}$$

Potassium bromide prisms were next fitted in the monochromator, and it became possible to make a more detailed study of the  $12$  to  $20\mu$  range. Figure 3 shows results obtained for n-type samples at room temperature and at liquid nitrogen temperature. Transmission beyond the  $15\mu$  doublet has not previously been reported.

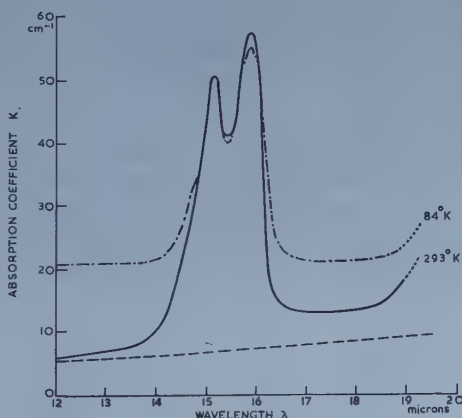


Figure 3. Infra-red absorption curves for n-type indium phosphide at  $293^\circ\text{K}$  and  $84^\circ\text{K}$ . The broken line corresponds to  $K \propto \lambda^{3/2}$ .

The behaviour of the doublet itself is now elucidated. It is insensitive in both magnitude and position to variations in temperature. A similar band is known in type I diamonds (Collins and Fan 1954), but it does not appear to be possible to give a simple explanation in terms of either impurity or lattice absorption. An attempt to observe photoconductivity in the same wavelength region was unsuccessful. The increase in background absorption at low temperatures is also anomalous, although it has also been observed in both n- and p-type indium antimonide (Kaiser and Fan 1955).

The background absorption at room temperature increases with wavelength in a manner characteristic of free carrier absorption. Fan (1956) has shown that this should increase as  $\lambda^{3/2}$  for phonon scattering of the carriers, and as  $\lambda^{7/2}$  for impurity scattering. The broken curve in figure 3 corresponds to the  $\lambda^{3/2}$  law

and has been calculated to fit the experimental results at shorter wavelengths. As it accounts for most of the background absorption at longer wavelengths, where the  $\lambda^{7/2}$  law would give values much too large, it is assumed that phonon scattering of the carriers is the more important. Fan's equation for the wavelength variation of absorption coefficient due to free carriers scattered by phonons is:

$$K = \frac{4}{9\pi^{3/2}} \frac{Ne^3}{nc^3\mu_n} \left( \frac{hc}{kT} \right)^{1/2} \frac{\lambda^{3/2}}{m^{*2}} \quad \dots\dots(1)$$

where  $N$  is the carrier density, estimated at  $10^{15} \text{ cm}^{-3}$  from rectification tests with a point contact on the specimens,  $n$  the refractive index, given as 3 by Oswald and Schade,  $\mu_n$  is the mobility of the carriers and  $m^*$  their effective mass. The dashed curve corresponds to an effective mass of 0.02 electron mass.

## 5.2. Photo-Voltaic Response

The large photo-voltages exhibited by point contacts made it a simple matter to study the response as a function of wavelength. This was compared with that of the Schwarz thermopile, and some results normalized to the same maximum response are shown in figure 4. The  $\lambda_{1/2}$  point, where the response falls to half

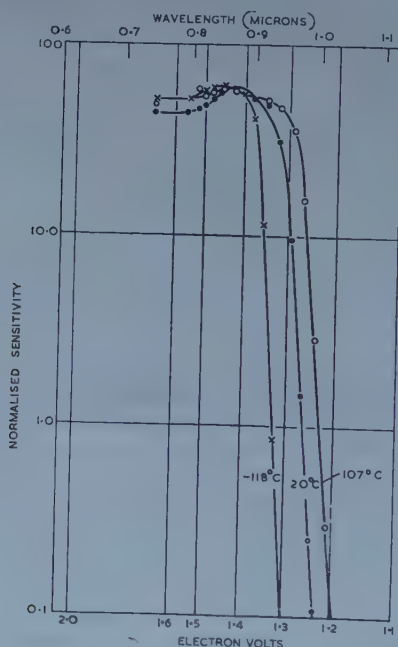


Figure 4. Response curves for a p-type indium phosphide photodiode.

the maximum, may be taken as the photo-voltaic threshold  $E_t$  and most values obtained were found to lie close to the line

$$E_t = 1.44 - 4.5 \times 10^{-4} T \text{ ev.}$$

Moss (1952) suggested that at the threshold, the diffusion length  $L$  of the injected minority carriers must be of the order of  $1/K$ . Such a relationship yields an order of magnitude value of the carrier lifetime, for

$$L = (kT\mu_n\tau/e)^{1/2}. \quad \dots\dots(2)$$

This gives a value of  $5\mu\text{sec}$  for  $\tau$ , at room temperature, corresponding to a diffusion length of 0.2 mm, which is supported by the observation of transistor action at 0.1 mm described in §4.

#### § 6. CONCLUSIONS

Indium phosphide has been shown to exhibit semiconductor effects, including transistor action, to a marked degree. The low effective mass of electrons indicated by the optical transmission measurements suggests that thermoelectric and magnetoelectric effects would be well worth studying. Further work would, however, require the production of uniform single crystal material.

#### ACKNOWLEDGMENTS

The authors would like to express their thanks to Mr. M. Webberley for great assistance with the preparation of the material, and Mr. J. R. Redding who did the glass and silica work. They are indebted to the Admiralty for permission to publish this paper.

#### REFERENCES

- BANBURY, P. C., GEBBIE, H. A., and HOGARTH, C. A., 1951, *Semi-conducting Materials* (London: Butterworths Scientific Publications), p. 78.  
 COLLINS, R. J., and FAN, H. Y., 1954, *Phys. Rev.*, **93**, 674.  
 FAN, H. Y., 1956, *Rep. Progr. Phys.*, **19**, 107 (London: Physical Society).  
 FOLBERTH, O., and WEISS, H., 1955, *Z. Naturforschung*, **10a**, 615.  
 LANDELLI, A., 1941, *Gazzetta Chimica Italiana*, **71**, 58.  
 JENNY, D. A., 1955, *Z. Naturforschung*, **10a**, 1032.  
 KAISER, W., and FAN, H. Y., 1955, *Phys. Rev.*, **98**, 966.  
 MOSS, T. S., 1952, *Photoconductivity in the Elements* (London: Butterworths Scientific Publications).  
 OSWALD, F., 1954, *Z. Naturforschung*, **9a**, 181 ; 1955, *Ibid.*, **10a**, 927.  
 OSWALD, F., and SCHADE, R., 1954, *Z. Naturforschung*, **9a**, 611.  
 WELKER, H., 1953, *Z. Naturforschung*, **8a**, 248 ; 1954, *Physica, 's Grav*, **20**, 893.

## Trap Distributions in Calcium Tungstate Single Crystals†

By J. R. COOK

Department of Physics Applied to Medicine, Middlesex Hospital Medical School,  
London

*Communicated by J. E. Roberts ; MS. received 15th April 1957, and in  
revised form 19th September 1957*

**Abstract.** An investigation has been made of the trap distributions in a single crystal of calcium tungstate as revealed by thermoluminescence and current 'glow' curves. The resulting distribution agrees reasonably well with the results of a theoretical analysis of the photocurrent and phosphorescence decays after irradiation with ultra violet light or gamma rays from a  $^{60}\text{Co}$  source.

### § 1. INTRODUCTION

THE phosphorescent and semiconductive properties of single crystals of calcium tungstate have recently been investigated (Cook and Mahmoud 1954, Cook 1955), and an attempt was made to correlate the photoconductive experiments with a theoretical treatment due to Rose (1951). In view of the unsatisfactory agreement between this theory and experiment it was decided to investigate the specific trap distribution in a calcium tungstate crystal. The present experiments determined the shape of the trap distributions as shown by the decay of long duration photocurrent and phosphorescence coupled with curves of thermoluminescence and 'current glow'.

### § 2. EXPERIMENTAL METHOD

#### 2.1. Photocurrent Decay Curves

The experimental technique was similar to that previously described (Cook 1955). The calcium tungstate crystal of length 0.5 cm and diameter 0.5 cm had carbon contacts and was mounted in a container so that its temperature could be kept constant at selected values from  $-60^{\circ}\text{C}$  to  $+100^{\circ}\text{C}$ . The crystal was then irradiated with ultra-violet light from a mercury lamp and the current decay was measured with a Lindemann electrometer. The present experiments measured the slow decay at various temperatures but in addition the presence of a faster component was shown by photographing the fibre of the Lindemann with a cine camera.

In general a few seconds elapsed between the cutting off of the light and the first visual determination of the slow component, and in this time the fast component had decayed to a small value so that the first points on the long duration decay curves did not contain an appreciable percentage from the fast decay component. The decay curves were measured with approximately the same initial intensity of illumination.

† The subject matter of this paper formed part of a thesis submitted for the Ph.D. degree at London University.



## 2.2. Current Glow Curve

The crystal was cooled to  $-50^{\circ}\text{C}$ , illuminated with ultra-violet light and then allowed to warm up slowly in the dark. The Lindemann electrometer was used to measure the current at various temperatures during warming. The times at which the various temperatures occurred were also noted so that the instantaneous rate of warming could be derived at these temperatures.

## 2.3. Phosphorescence Decay Curves

The crystal used in the above experiments was attached to a Perspex light guide and photomultiplier in order to measure any slow component of phosphorescence decay. A gamma-ray source was used for irradiation so that the window of the photomultiplier was not exposed to any visible light. The source was then removed and the count rate from the photomultiplier recorded as a function of time. The crystal holder could be maintained at various temperatures and the Perspex light guide separated the window of the photomultiplier from the crystal so that a change in temperature of the crystal did not affect the photomultiplier noise level. In these experiments it was possible to record pulses of height smaller than the average pulse height due to single photons incident on the photocathode.

# § 3. EXPERIMENTAL RESULTS

## 3.1. Decay Curves

Figures 1 and 2(a) show the fast and slow current decays at various temperatures. The curves in figure 1 refer to the same initial intensity but, for convenience in drawing, the ordinates of the curves at  $T = +8.5^{\circ}\text{C}$  and  $-13^{\circ}\text{C}$  have been adjusted arbitrarily. At these two temperatures the rise time was less than the time between successive photographs (0.1 sec).

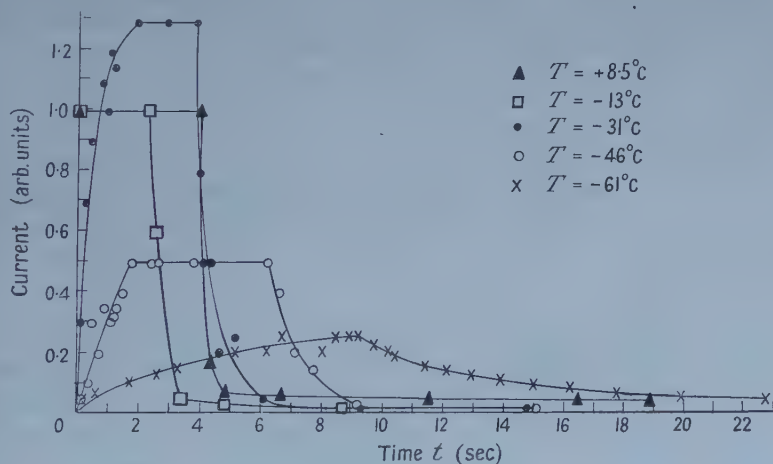


Figure 1. Build up and decay of short duration current.

Figure 2(a) shows a semi-log plot of the slow current component which takes about an hour to decay. The slow component had appreciable magnitude only at higher temperatures and was not measurable at  $-50^{\circ}\text{C}$ . The form of the decay varies with temperature and departs from the simple hyperbolic relation previously found at  $T = +18^{\circ}\text{C}$  (Cook 1955).

Figure 2(b) shows a semi-logarithmic plot of phosphorescence for several temperatures (the background count has been subtracted). The existence of a slow component of phosphorescence is evident, and the form of the decay obviously varies with temperature. The nature of the slow phosphorescence decay will be shown later to be similar to the slow component of current decay but it is evident from figures 2(a) and 2(b) that the decay curves are reasonably similar. Figures 2(a) and 2(b) cannot be compared directly since the rate of decay depended on the initial intensity which was less in the case of  $\gamma$ -ray excitation.

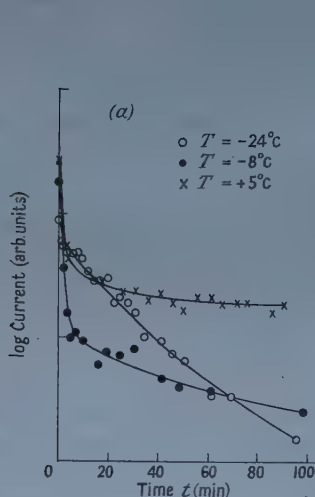


Figure 2(a). Decay of long duration current at various temperatures.

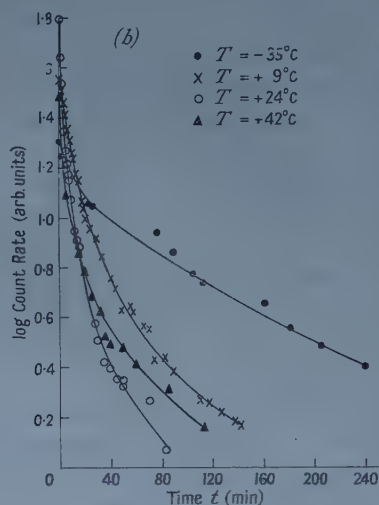


Figure 2(b). Phosphorescence decay at various temperatures.

### 3.2. Glow Curves

Figure 3 shows the presence of thermoluminescence in the region  $-150^{\circ}\text{C}$  to  $+65^{\circ}\text{C}$ . Two separate experiments were carried out by irradiating the crystal at  $-30^{\circ}\text{C}$  and  $-170^{\circ}\text{C}$  and they suggest the existence of three sets of traps.

Figure 4 shows the current glow curve of the same crystal. There was no measurable glow current from  $-50^{\circ}\text{C}$  to  $-60^{\circ}\text{C}$ . Experiments were not made at

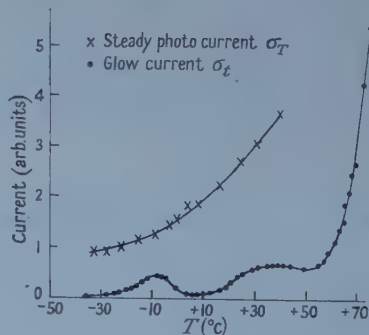
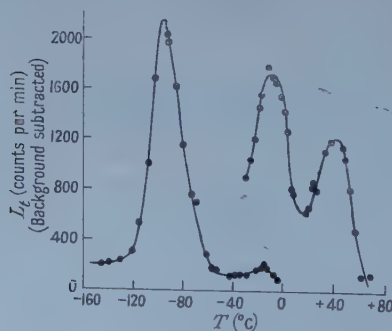


Figure 3. Thermoluminescence curves. Figure 4. Current glow curve and steady photocurrent as a function of temperature.

temperatures less than  $-60^{\circ}\text{C}$  owing to condensation difficulties. A peak is clearly resolved at  $-9^{\circ}\text{C}$  while a partly resolved peak occurs at a temperature about  $+40^{\circ}\text{C}$ . The rapid rise in current for temperatures above  $+50^{\circ}\text{C}$  is due to dark current which has been discussed previously (Cook 1955).

### 3.3. Photocurrent-Temperature Curve

Figure 4 also shows the variation of steady photocurrent as a function of temperature. This curve did not exhibit a peak as with the previous crystals (Cook 1955) at a temperature about  $-15^{\circ}\text{C}$  but the current glow curve in the present case has a peak at  $-9^{\circ}\text{C}$ . This difference is probably due to a difference in the trap concentration.

## § 4. ANALYSIS OF RESULTS

### 4.1. Theoretical Description

It was reasonable to conclude from the above work that the phosphorescence and photocurrent were related to each other and to the trap distributions. An attempt was therefore made to correlate the form of the decay curves with the trap distributions obtained from the glow curves. The fact that the room temperature decay curve previously obtained (Cook 1955) was accurately hyperbolic suggested a simple recombination of the electrons with the positive holes or luminescent centres. Broser and Broser-Warminsky (1955) have analysed the case of recombination in a photoconductor when the positive holes are trapped at the activator centres. In their theory the form of the decay curve is related to the distribution of the number of traps as a function of energy. The general equations relating the decay curves with the crystal properties were so complex that simplifying assumptions were made in order to reach a solution. In the present case the dark current was negligible except at higher temperatures and the observed photocurrents and glow currents were always small, which satisfies two of their assumptions. The application of the theory to the present experiment may be considered in two parts.

#### 4.1.1. Decay curves.

For small current values the decay curve of the current is given by the expression

$$\frac{Z_t}{Z_0} = \frac{1}{1 + (2Z_0 t / S_E k T)} \quad \text{.....(1)}$$

where  $Z_t$  = number of electrons escaping from the traps into the conduction band per second,  $Z_0$  = initial number excited into the conduction band per second,  $k$  = Boltzmann's constant  $T$  = absolute temperature, and  $S_E$  = number of defect levels per unit energy range below the conduction band at depth  $E$  electron volts.

The number of photons emitted per second  $L_t$  is equal to  $Z_t$ , and the conductivity is proportional to  $Z_t$ . It is therefore possible to relate  $S_E$  to the decay curves. Further, there is a correlation between the depth  $E$  of the Fermi level and the time  $t$  on a decay curve, since electrons being raised thermally to the conduction band from the region of the Fermi limit are those influencing the decay process. As time goes on those electrons from deeper traps influence the decay curve. The energy level  $E$  is related to the time  $t$  on the decay curve by the expression

$$E \propto k T \log (F/n_t). \quad \text{.....(2)}$$

If  $T$  is constant then  $F$  is constant and  $E \propto \text{constant} - \log n_t$  where  $n_t$  is the number of electrons at time  $t$  in the conduction band. Therefore  $E \propto \text{constant} - \log i_t$  where  $i_t$  is the decay current at time  $t$ . Let  $R_t = i_t/i_0$  where  $i_0$  = initial value of  $i$ ; then from equation (1),  $S_E$  is a function of time according to the relation  $S_E \propto R_t t / (1 - R_t)$ . A plot of  $R_t t / (1 - R_t)$  against  $\log i_t$  should represent the trap distribution with reasonable accuracy if the assumptions are correct.

#### 4.1.2. Glow curves.

Broser and Broser-Warminsky have also applied their theory to the case of thermoluminescence and current 'glow' curves for a rate of warming equal to  $dT/dt$  degrees per second. The relation between 'glow' conductivity  $\sigma_t$  at time  $t$  and temperature  $T$  during warming and luminescence  $L_t$  is given by

$$\frac{L_t}{Z_0} = \frac{\sigma_t}{\sigma_T} = k \frac{dT}{dt} S_E \log \frac{(F/n_t)}{2Z_0} \quad \dots\dots (3)$$

where  $\sigma_T$  = conductivity under steady illumination at temperature  $T$ . The factor  $\log (F/n_t)$  does not change appreciably for large changes in  $n_t$  as  $F$  is very large and can be assumed constant. For a thermoluminescence curve  $S_E$  is proportional to  $L_t dt/dT$  and for a current glow curve  $S_E$  is proportional to  $\sigma_t dt/dT$ . The physical significance of equation (3) is simple, namely that the phosphorescence and conductivity while warming are proportional to the number of traps in the region of the Fermi limit.

#### 4.2. Application to Experiment

Figure 5 shows the trap distribution obtained by the application of equation (3). The value of  $\sigma_T$  was given by figure 4. The peak obtained by analysis of the current decay curve at  $-24^\circ\text{C}$  should correspond to that observed in the current glow experiment at  $-9^\circ\text{C}$ . The scale of the abscissae for the decay analyses was based on a simple proportionality between the half width of the peak at  $-9^\circ\text{C}$

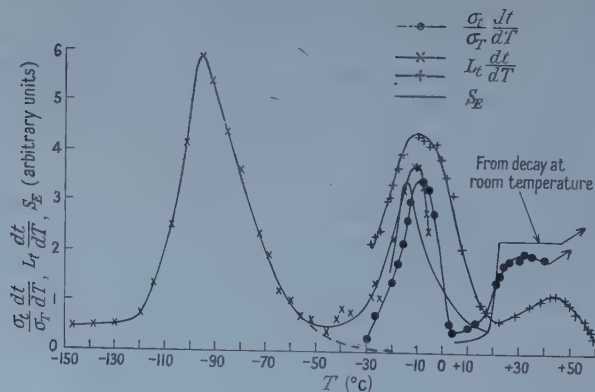


Figure 5. Comparison of trap distributions from glow and decay curves.

(measured in arbitrary units) and temperature (measured in  $^\circ\text{C}$ ). The decay analysis included in figure 5 was not extended to temperatures greater than room temperature in view of the increase of dark current. At room temperature the trap distribution is approximately constant and results in the close fit of the decay



curve to a hyperbolic law. The constant  $C$  previously attributed to a long duration current decay (Cook 1955) was shown by more recent work to be due to a very small leakage across the crystal surface and the equation for the slow decay process is therefore an accurate hyperbolic curve.

The shallow trap distribution obtained from thermoluminescence is shown in figure 5, and figure 6 shows a plot of  $S_E$  against  $(2 - \log L_t)$  obtained from the phosphorescence decay curves. The slopes of the distributions shown in figure 6 correlate fairly well with the thermoluminescence curve. Since the measurement of phosphorescence decay was not as accurate, the results of this analysis are not shown in figure 5. In addition the experimental conditions were such that analysis of the decay curves did not give a peak. The scale of the abscissae could not be determined with confidence. However, the result of analysing the decay curve at  $T = +24^\circ\text{C}$  is a trap distribution which is nearly constant as a function of energy. This agrees with the hyperbolic current decay found at  $T = +18^\circ\text{C}$  and with the glow and thermoluminescence curves.

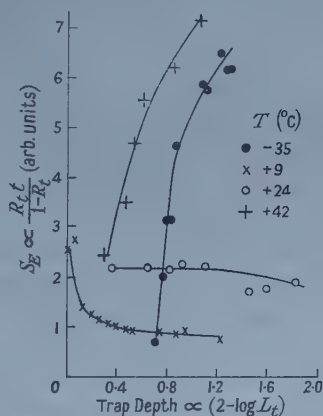


Figure 6. Trap distributions from phosphorescence decay curves at various temperatures.

#### 4.3. Discussion

It is evident from figure 5 that at temperature near  $-30^\circ\text{C}$  the current glow curve has reached a much lower value than the phosphorescence glow curve. Below  $-40^\circ\text{C}$  the glow current was not measurable. Thermoluminescence was however observable at  $-40^\circ\text{C}$  (figure 3), a pronounced peak occurring at  $-95^\circ\text{C}$ . This suggests that at  $-40^\circ\text{C}$  the number of traps responsible for the observed current glow curve had decreased but a shallow set of traps existed which could account for the observed thermoluminescence. The intensity of the thermoluminescence at  $-40^\circ\text{C}$  could consist of two components arising from two sets of traps. The absence of a measurable current glow below  $-40^\circ\text{C}$  can be understood on the basis of the short lifetime of the electrons from the shallow traps in the conduction band. This results from the large difference in rates of recombination from the shallow and deeper traps. A high rate of recombination shortens the lifetime of electrons in the conduction band but does not affect the amount of phosphorescence. The shortened lifetime leads to a smaller relative contribution to the current glow curve from the shallow traps compared with the deeper traps.

The variation of the decay time with temperature of the rapid component of current decay was observed at temperatures from  $-61^\circ\text{C}$  to  $-13^\circ\text{C}$ . From

equation (1)  $1/R_t = 1 + K't/S_E T$  where  $K'$  is a constant for the same initial exciting intensity. The application of this equation to figure 1 shows that  $S_E$  at  $-61^\circ\text{C}$  is about five times  $S_E$  at  $-46^\circ\text{C}$  and about 20 times  $S_E$  at  $-31^\circ\text{C}$ . This suggests a possible distribution for the shallow traps shown dotted in figure 5. A fast phosphorescence decay was expected to accompany the fast current decay and recent experiments have shown this component. The experiments involved the cine photography of the phosphorescence pulses in the region from 0 to 10 seconds but accurate analysis was difficult owing to the presence of a short duration phosphorescence attributed to the photomultiplier window, and the results are not described in detail.

The deep traps which peak about  $+45^\circ\text{C}$  on the thermoluminescence curve (see figure 5) give decay times similar to the middle traps and the current glow curve is in reasonable agreement. The shape of the thermoluminescence curve on the high temperature side of the  $+45^\circ\text{C}$  peak may be influenced by the filling of the positive recombination centres with electrons from the filled band in a direct thermal process.

The energy separation of the peaks can be found with reasonable accuracy from equation (2) since a change of  $n_t$  by 10 gives a change of  $E$  equal to  $2.303 kT$ . The width of the middle trap distribution is then about 0.1 eV. If the factor  $\log(F/n_t)$  is assumed to be about 20 then the middle traps peak at an energy about 0.3 eV below the conduction band. The absolute value of  $S_E$  can be obtained from equation (1) and data on the absolute number of photons emitted after gamma-ray excitation. Single photon calibration gave the number of photons emitted in the  $\alpha$  phosphorescent process (Cook and Mahmoud 1954) at about 650 per pulse when irradiated with  $^{60}\text{Co}$  gamma rays at  $+18^\circ\text{C}$ . The observed secondary electrons from the gamma rays had an average energy about 1.0 MeV and each is assumed to produce a number of electrons of the order of  $10^4$  by secondary ionization in the crystal. These electrons will in general have energies greater than the activation energy of 2.1 eV, and therefore about  $10^4$  electrons can be ejected directly into the conduction band. Their subsequent recombination with the activator centres may lead to the rapid emission of the photons in the  $\alpha$  process. The conversion efficiency of the process is then about 650 in  $10^4$ , i.e. about 6%, some of the electrons losing their energy in other ways such as non-radiative transitions at the activator centres. The assumption is made that the quantum efficiency observed in the  $\alpha$  process is approximately that in the slow decay process. Since the initial count rate of slow phosphorescence at room temperature ( $S_E \sim \text{constant}$ ) was observed to be  $220 \text{ sec}^{-1}$ , and the photo-cathode efficiency was about 5%, the initial excitation rate  $Z_0 \sim 88\,000 \text{ sec}^{-1}$ . The application of equation (1) gives  $S_E \simeq 6 \times 10^9 \text{ eV}^{-1}$  in the total crystal volume.

## § 5. CONCLUSION

The theory of Broser and Broser-Warminsky seems to account reasonably well for the photoconductive and phosphorescent properties of a single crystal of calcium tungstate. The components of the decay process arise from a distribution of trap energy levels containing at least three peaks. The nature of the emitting centre is unknown though Randall (1939) has suggested that the emission is related to the tungstate ion. The number of activator centres seems to be quite small though it is not known whether these centres are due to impurities or excess atoms such as tungsten or to crystal defects.

A hyperbolic decay could perhaps arise from metastable levels discussed by Randall and Wilkins (1945) for a constant trap distribution if retrapping occurs. In the present case however there is no evidence for retrapping since the thermoluminescence curves for widely different initial excitation conditions (i.e. ultra-violet light or gamma rays) are similar.

#### ACKNOWLEDGMENT

I am grateful to Professor J. E. Roberts for encouragement in this investigation.

#### REFERENCES

- BROSER, I., and BROSER-WARMINSKY, R., 1955, *Brit. J. Appl. Phys.*, Suppl. **4**.  
COOK, J. R., 1955, *Proc. Phys. Soc. B*, **68**, 148.  
COOK, J. R., and MAHMOUD, K. A., 1954, *Proc. Phys. Soc. B*, **67**, 817.  
RANDALL, J. T., 1939, *Trans. Faraday Soc.*, **35**, 2.  
RANDALL, J. T., and WILKINS, M. H. F., 1945, *Proc. Roy. Soc. A*, **184**, 347.  
ROSE, A., 1951, *R.C.A. Review*, **12**, 362.

## Galvanomagnetic Effects in n-Type Bismuth Telluride

By J. R. DRABBLE, R. D. GROVES AND R. WOLFE

Research Laboratories, The General Electric Company Limited, Wembley, Middx.

*MS. received 22nd October 1957, and in final form 21st November 1957*

**Abstract.** The resistivity, Hall coefficients and low field magnetoresistance coefficients associated with current flow in the cleavage planes have been measured at 77°K on a number of n-type specimens of bismuth telluride. The resistivity and Hall coefficient measurements were extended up to room temperature. The experimental results are given and are shown to be reasonably consistent with a many-valley model of the band structure in which the energy minima are situated on the reflection planes. The parameters associated with this model are evaluated and used to relate the two Hall coefficients to the density of carriers. These relations are used to obtain the conductivity mobility of electrons for current flow in the cleavage planes. This mobility varies as  $T^{-1.68}$  over the temperature range 150°K to 300°K and has a value of  $1250 \text{ cm}^2 \text{ sec}^{-1} \text{ V}^{-1}$  at room temperature.

### § 1. INTRODUCTION

ALTHOUGH several workers have made measurements of the resistivity and Hall coefficient of bismuth telluride, many of these used either polycrystalline or compressed specimens. The results of measurements on such samples are difficult to interpret since it is known from measurements on single crystal samples that the material is markedly anisotropic. In fact, from the crystal symmetry it may be predicted that there are two independent components of the resistivity tensor and two independent Hall coefficients (Drabble and Wolfe 1956, to be referred to as DW).

It is therefore not immediately apparent that the simple relations connecting the resistivity and Hall coefficient with the density and mobility of the charge carriers which are applicable for isotropic materials, can be used for bismuth telluride. As in the analogous case of anisotropic metals, some model of the band structure and scattering mechanism must be assumed and tested experimentally, in order to develop the corresponding relations. For the measurements on n-type bismuth telluride which are reported in this paper, it seems to be well established that only one type of charge carrier is present whereas the results on metals such as bismuth are usually interpreted in terms of a two-band model.

In DW it was shown that a simple many-valley model of the band structure gives rise to the correct anisotropy with only one type of charge carrier present. Expressions for the resistivity, Hall coefficient and low field magnetoresistance components were derived for a model in which the energy extrema in wave vector space were on the reflection planes. These expressions involve three parameters which characterize the shape and orientation of the surfaces of constant energy round the extrema and other parameters which involve the density of carriers and the scattering mechanism.



In this paper, experimental measurements of the galvanomagnetic effects in single crystals of *n*-type bismuth telluride are reported. The results are shown to be reasonably consistent with the model proposed in DW and the parameters associated with this model are evaluated. This enables the Hall coefficients to be interpreted in terms of the density of carriers and leads to a value of a 'conductivity' mobility for electrons of about  $1250 \text{ cm}^2 \text{ sec}^{-1} \text{ V}^{-1}$  at room temperature. This mobility varies as  $T^{-1.68}$  over the temperature range  $150^\circ$  to  $300^\circ \text{K}$ .

## § 2. EXPERIMENTAL PROCEDURE

### 2.1. Preparation of Single Crystals

The single crystals of bismuth telluride used in the experiments were prepared by Mr. A. Sheard. Zone refined bismuth and tellurium were heated together overnight at  $950^\circ \text{C}$  in a sealed evacuated silica tube. The resulting compound was zone refined and subsequently remelted together with a suitable amount of iodine to produce *n*-type material. This material was then seeded at one end of a horizontal silica boat and a single crystal was grown by a zone melting technique. A typical crystal grown in this way was 12 cm long and 1.5 cm wide. The height, which was perpendicular to the cleavage planes was 1 cm. The thermoelectric power at  $300^\circ \text{K}$  was almost uniform along the length of the crystal and was about  $-200 \mu\text{V deg}^{-1}$ .

### 2.2. Preparation of Specimens

The large crystals prepared in this way were sectioned with a carborundum or a diamond wheel. It was found that the resulting slices usually contained cracks which were propagated parallel to the cleavage planes. These cracks were readily revealed by etching in an acid solution (1 part HCl, 1 part  $\text{HNO}_3$ , 2 parts water). Some of these cracks appeared to be introduced by the sectioning process but others were visible throughout the ingot.

Specimens free from visible cracks were obtained by the following procedure. Bars of about  $6 \text{ mm} \times 6 \text{ mm}$  cross section were given a prolonged etching treatment at  $50^\circ \text{C}$  until the final cross section was about  $2.5 \text{ mm} \times 2.5 \text{ mm}$ . This treatment left the faces reasonably plane and the cross section still remained remarkably square. In this way, specimens about 1 cm in length could be obtained free from cracks but only if the length was parallel to the cleavage planes. So far, it has not been possible to obtain comparable specimens with the long dimension perpendicular to the cleavage planes, by this or any other technique. This fact has restricted the accurate measurements of the transport properties to those associated with current flow in the cleavage planes.

Usually, three or four such specimens were prepared from one large single crystal. These were chosen to be as close to each other in the ingot as possible to avoid possible large scale inhomogeneity and were cut so that the long directions were orientated differently in the cleavage planes as discussed below.

### 2.3. Etch Figures and the Crystal Symmetry

When cleaved surfaces were etched slowly at room temperature in a dilute etch, well-defined etch figures were produced. The type of pattern obtained depended upon the conditions of etching but two types predominated, namely, triangular and hexagonal figures. Typical examples of these are shown in figures 1(a) and 1(b) (Plate).

Bismuth telluride belongs to the crystal class  $R\bar{3}m$  and the etch figures illustrate the symmetry elements associated with this class. In particular, the shallow triangle shown in figure 1(a) may be used to find the direction of the three reflection planes containing the threefold axis and hence to find the direction of the current flow in the sample relative to these planes. Since the current is flowing parallel to the cleavage planes, this direction can be specified by a single angle  $\theta$  and a knowledge of  $\theta$  is necessary for a proper interpretation of the magnetoresistance measurements. The value of  $\theta$  estimated from visual observations of the etch pits was varied from one specimen to another, being chosen to be either as close to zero as possible or as close to  $30^\circ$  as possible.

#### 2.4. Measurement of the Galvanomagnetic Components

The galvanomagnetic coefficients associated with bismuth telluride up to and including quadratic terms in the magnetic induction have been discussed in DW. These coefficients have been defined by the expression

$$E_i = \rho_{ij} J_j - \rho_{ijk} J_j B_k + \rho_{ijkl} J_j B_k B_l$$

which uses the summation convention to relate the components of the electric field  $\mathbf{E}$  to the components of the current density  $\mathbf{J}$  and of the magnetic induction  $\mathbf{B}$ . For bismuth telluride there are twelve independent coefficients. These were listed in DW but it has been discovered subsequently that two of them were wrong. This error and the corrected set of coefficients are discussed in the Appendix.

Three of the twelve independent galvanomagnetic coefficients viz.  $\rho_{33}$ ,  $\rho_{3333}$  and  $\rho_{3311}$ , cannot be measured unless the current is flowing in a direction perpendicular to the cleavage planes (the  $z$  axis). For the reasons discussed previously, measurements are in this case unreliable since the current flow is distorted by the presence of cracks parallel to the cleavage planes. Only one specimen has been obtained so far for which a reasonably reliable estimate of  $\rho_{33}$  could be obtained, but this specimen was unsuitable for making measurements of magnetoresistance.

Two types of experiment were carried out and are described in this paper. In the first type, accurate measurements of the galvanomagnetic coefficients were made at a fixed temperature (liquid nitrogen temperature) in order to test the model of the band structure proposed by DW and hence to relate the measured Hall coefficients to the density of carriers. In the second class of experiments, measurements of the resistivity and Hall coefficients were made over the temperature range  $100^\circ\text{K}$  to room temperature.

Considering the first type of experiment, the nine independent galvanomagnetic coefficients which can be associated with current flow in the cleavage planes can be determined using two different experimental arrangements, to be referred to as I and II respectively. These arrangements are illustrated in figures 2(a) and 2(b). In I, the specimen is mounted so that it can be rotated about the  $z$  axis while in II the specimen is rotated about an axis lying parallel to the cleavage planes. The magnetic field and the current are always perpendicular to the axis of rotation and the angle between them will be denoted by  $\phi$ .

Expressions for the components of the electric field in the crystal can be derived by using the method given by Juretschke (1955). These components are denoted as follows:  $E_J$ , component parallel to the current,  $E_\phi$ , component

along the  $z$  axis,  $E_{z\wedge J}$ , component perpendicular to the  $z$  axis and to the current. Then, if the galvanomagnetic components are referred to crystal axes chosen as

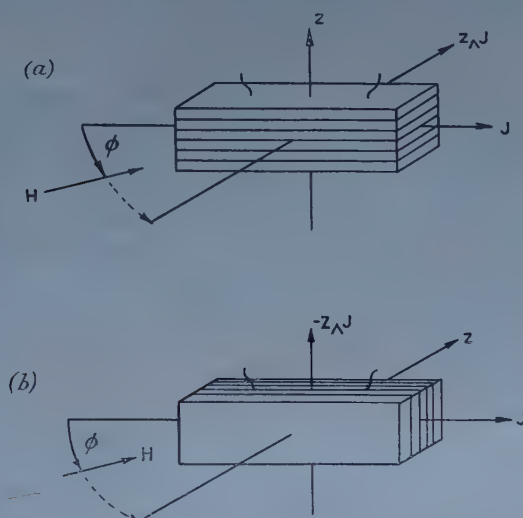


Figure 2. Experimental arrangements.

discussed in the Appendix and the current makes an angle  $\theta$  with one of the three equivalent reflection planes, the following expressions are obtained.

#### Arrangement I.

$$E_J = \rho_{11}J + JB^2[\rho_{1111}\cos^2\phi + \rho_{1122}\sin^2\phi] \quad \dots\dots(1a)$$

$$E_z = -\rho_{312}JB\sin\phi + JB^2\rho_{3111}\cos(3\theta + 2\phi) \quad \dots\dots(1b)$$

$$E_{z\wedge J} = JB^2\sin\phi\cos\phi[\rho_{1111} - \rho_{1122}] \quad \dots\dots(1c)$$

#### Arrangement II.

$$E_J = \rho_{11}J + JB^2[\rho_{1111}\cos^2\phi + \rho_{1133}\sin^2\phi + \rho_{1131}\cos 3\theta\sin 2\phi] \quad \dots\dots(2a)$$

$$E_z = JB^2[\rho_{3111}\cos 3\theta\cos^2\phi + \rho_{3113}\sin 2\phi] \quad \dots\dots(2b)$$

$$E_{z\wedge J} = \rho_{123}JB\sin\phi - JB^2\rho_{1131}\sin 3\theta\sin 2\phi. \quad \dots\dots(2c)$$

In these expressions  $J$  is the current density.

Thus, in principle, all the nine galvanomagnetic coefficients, together with checks on some values, may be obtained by measuring the various components of  $\mathbf{E}$  as a function of the angle  $\phi$  in the two arrangements. In practice, it is not possible to obtain the ideal arrangements illustrated in figure 2 and various corrections have to be applied for this and for other reasons.

In the early stages of these experiments, thermoelectric effects were found to be particularly troublesome and the usual methods of correcting for these were inadequate. This can be accounted for on the basis of the rather exceptional thermoelectric properties of bismuth telluride. A satisfactory solution of this problem was obtained by carrying out the measurements with the specimen immersed in a bath of liquid nitrogen.

The procedure finally used, which was found to give consistent results, was as follows. Current electrodes were attached to the ends of the specimen by first



plating these ends with rhodium and subsequently soldering contacts on to the plating. It was found necessary to avoid the use of copper in any part of the soldering process since copper diffuses very readily into bismuth telluride even at room temperature and changes the electrical properties. Tungsten probe pressure contacts were used for the potential probes and the whole specimen assembly was mounted on a holder so that it could be rotated freely. This was then inserted in a long-necked Dewar vessel containing liquid nitrogen, which was placed between the poles of the electromagnet. Corrections for out of balance voltages due to misalignment of the probes were applied in an obvious way.

The measurements of resistivity and Hall coefficient as functions of temperature were carried out in a standard way apart from the fact that it was necessary to use a compensating arrangement to cancel the temperature gradient associated with the passage of current through the sample. The method used was similar to that described by Putley (1955).

### § 3. RESULTS

#### 3.1. 'Spot' Measurements on Various Samples at 77°K

In order to check the repeatability of the techniques, 'spot' measurements of the principal galvanomagnetic coefficients were made on a number of specimens. For example, using arrangement I, the field  $E_J$  at  $\phi=0$  should yield a value of  $\rho_{1111}$ , and at  $\phi=90^\circ$  should give  $\rho_{1122}$ . The setting for  $\phi=0$  was determined by finding the position of zero Hall voltage and could be determined usually to within  $\frac{1}{2}^\circ$ . In this way, estimates of the coefficients  $\rho_{11}$ ,  $\rho_{123}$ ,  $\rho_{312}$ ,  $\rho_{1111}$ ,  $\rho_{1122}$  and  $\rho_{1133}$  were obtained for six n-type specimens. Four of these had been cut so that the current was flowing in a direction nearly parallel to a reflection plane ( $\theta=0$ ) while in the remaining two  $\theta$  was close to  $30^\circ$ . The magnetic field used was  $10^4$  oersteds.

It would be expected that the values of these coefficients would vary from one specimen to another due to variations in the density of charge carriers. However certain combinations of the coefficients should remain constant independently of such variations, provided that these are not too large, for example, the ratio of the two Hall coefficients and the ratios of the various  $\rho_{ijkl}$ . This was found to be the case within experimental error for the four specimens for which  $\theta$  was close to  $0^\circ$ . The ratio of the two Hall coefficients was the same for all six specimens, but the two for which  $\theta$  was close to  $30^\circ$  showed systematically lower values of  $\rho_{1111}$  and  $\rho_{1122}$  than would have been expected on the basis of the results obtained for the other four. This discrepancy was eventually linked with the variation of the coefficients with magnetic field, which is described in the next section.

#### 3.2. Variation of the Galvanomagnetic Coefficients with Magnetic Field at 77°K

The first measurements of the angular variation of the galvanomagnetic effects were made with a magnetic field of about  $10^4$  oersteds. It was found that the measured variation showed systematic deviations from the behaviour predicted by equations (1) and (2). These appeared to be consistent with a decrease in the coefficients as the appropriate components of the magnetic field increased. Accordingly, detailed measurements of the Hall coefficients  $\rho_{123}$ ,  $\rho_{312}$ , and of the magnetoresistance coefficients  $\rho_{1111}$ ,  $\rho_{1122}$  and  $\rho_{1133}$  were made as a function of field strength.



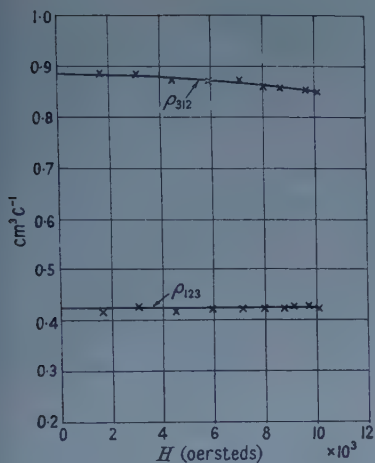


Figure 3. Variation of Hall coefficients with magnetic field.

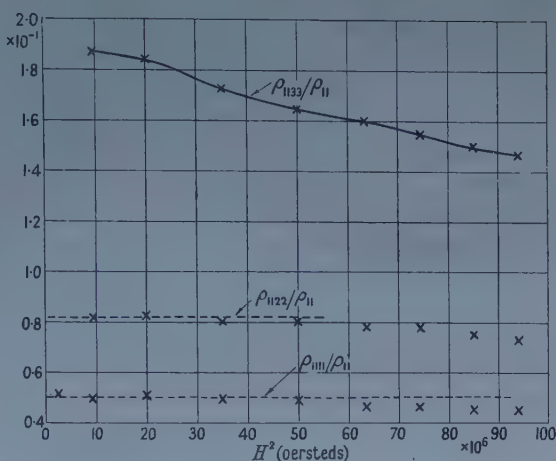


Figure 4. Variation of magnetoresistance coefficients with magnetic field.

Figure 3 shows the variation of  $\rho_{123}$  and  $\rho_{312}$  as a function of  $H$  for a typical sample (SBT6/F) and figure 4 shows the variation of  $\rho_{1111}/\rho_{11}$ ,  $\rho_{1122}/\rho_{11}$  and  $\rho_{1133}/\rho_{11}$  with  $H^2$ . Up to  $10^4$  oersteds, the deviations of the Hall coefficients from a constant value are small. In contrast, the magnetoresistance coefficients all decrease with increasing field and the proportional decrease is different for the different coefficients, being particularly large for  $\rho_{1133}$ . The deviations from the low field value are small up to fields of 6000 oersteds and this field was used in most of the subsequent measurements. It was then found that the angular variation corresponded to that given by equations (1) and (2), with some exceptions which are discussed in the next section.

The above sample (F1) was one of the four specimens for which  $\theta$  was close to zero. In view of the results described in the last section, similar measurements were made on a second specimen (E1) for which  $\theta$  was close to  $30^\circ$ . It was found that the Hall coefficients were again constant up to fields of  $10^4$  oersteds. The coefficients  $\rho_{1111}$  and  $\rho_{1122}$  decreased with increasing magnetic field and, while the low field values were the same, within experimental error, as those observed for specimen F1, the proportional decrease was appreciably larger. The coefficient  $\rho_{1133}$  had practically the same value for all values of magnetic field for both specimens. The discrepancies described in the previous section could therefore be explained by these observations.

### 3.3. Measurements of the Galvanomagnetic Effects as a Function of the Angle between the Magnetic Field and the Current

Three specimens, designated F, C and E, have been studied in some detail in order to observe the variation of the galvanomagnetic effects as a function of the angle between the magnetic field and the current. Specimens F and C had a value of  $\theta$  close to zero while specimen E had a value of  $\theta$  close to  $30^\circ$  as judged from observations on the orientation of the etch pits.

Measurements of this type provide a check on the experimental technique and also on the degree of uniformity of the specimens used, since it is to be expected that distortions in the current flow lines in the specimen would give rise to deviations from the ideal situations discussed in §2.4.

The results on the three specimens have all been of the same general character. The observed variation of  $E_J$  with  $\phi$  in arrangements I and II always agreed closely with the form predicted by expressions (1a) and (2a) respectively. However, the  $H^2$  terms of the other components of the electric field in the two arrangements usually showed systematic deviations from the predicted form, although the Hall component, when present, always followed the theoretical variation exactly. The deviations of the  $H^2$  terms were not large, being only just outside the estimated experimental error, and so far no satisfactory explanation of them has been given. A possible explanation is that the corresponding coefficients vary with magnetic field strength and, since these experiments had to be carried out at high fields because of the small voltages involved, the observed angular variation is different from that to be expected if the coefficients were constant.

The good agreement between the theoretical and experimental variations of  $E_J$  with  $\phi$  in arrangements I and II is illustrated in figures 5 and 6. These are

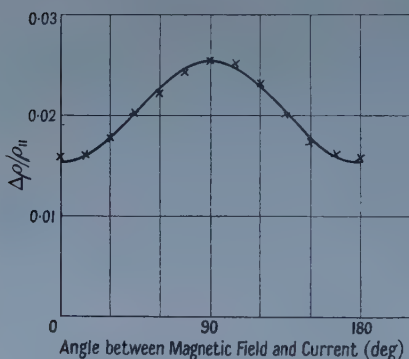


Figure 5. Angular variation of  $\Delta\rho/\rho_{11}$  for arrangement I.

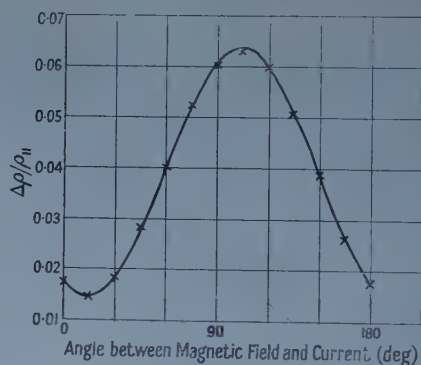


Figure 6. Angular variation of  $\Delta\rho/\rho_{11}$  for arrangement II.

plotted in the form  $\Delta\rho/\rho_{11}$  against  $\phi$ , where  $\Delta\rho$  is the increase in the resistivity due to the magnetic field. According to equation (1a), the experimental points shown in figure 5 should correspond to an angular variation of the form

$$\frac{\Delta\rho}{\rho_{11}} = \frac{E_J/J - \rho_{11}}{\rho_{11}} = a \cos^2 \phi + b \sin^2 \phi$$

where  $a = \rho_{1111}B^2/\rho_{11}$ ,  $b = \rho_{1122}B^2/\rho_{11}$ . The continuous curve shows the best fit of the expected form to the experimental points. The values of  $a$  and  $b$  used were  $a = 0.0154$ ,  $b = 0.0253$ . In the experiment, the magnetic field was 5650 oersteds, and  $\rho_{11}$  was  $1.46 \times 10^{-4}$  ohm cm.

A similar analysis of figure 6, based on an expected variation of the form (equation (2a)):

$$\Delta\rho/\rho_{11} = a \cos^2 \phi + b \sin^2 \phi + c \sin 2\phi$$

with  $a = \rho_{1111}B^2/\rho_{11}$ ,  $b = \rho_{1133}B^2/\rho_{11}$ ,  $c = \rho_{1131}B^2 \cos 3\theta/\rho_{11}$ , gave good agreement with the experimental points using  $a = 0.0175$ ,  $b = 0.0608$  and  $c = 0.0115$ . The magnetic field used was 5950 oersted, so that the value of  $\rho_{1111}$  obtained from this measurement was in good agreement with that deduced from the previous one.

The values of  $E_J$  for the two arrangements on the other specimens corresponded equally well with the predicted angular variation. Specimen E was of particular interest because it was to be expected that the term  $c \sin 2\phi$  in the expression for  $\Delta\rho/\rho_{11}$  obtained from equation (2a) would be small, since the value of  $\cos 3\theta$  should be close to zero. This was found to be the case, the corresponding angular variation being nearly symmetrical about  $\phi = 90^\circ$ .

For the components  $E_z$  and  $E_{zAJ}$  of the electric field, the agreement was not so satisfactory although the general qualitative behaviour observed was as expected. The contributions to  $E_z$  for arrangement I and to  $E_{zAJ}$  in arrangement II which reversed sign on reversing the magnetic field always followed the predicted sinusoidal variation, but the contributions which were even in the magnetic field did not vary with  $\phi$  in the manner predicted by equations (1b) and (2c). Similar discrepancies were found in the  $H^2$  contributions to  $E_z$  in arrangement II. Thus the values of the  $H^2$  terms deduced from these experiments are unlikely to be very accurate.

In principle, checks can be made on several of the magnetoresistance coefficients for a given sample. However, in the present experiments, due to the small magnitude of the effects, it was not possible to do this completely. For example, in order to get the maximum signal from the  $\rho_{1131}$  term in  $E_J$  for arrangement II it was necessary to choose  $\cos 3\theta$  to be close to unity and this prevents the observation of the corresponding term in  $E_{zAJ}$  for arrangement II. Also, in principle, measurements of  $E_J$  and  $E_{zAJ}$  in arrangement I provide a check on  $\rho_{1111}$  and  $\rho_{1122}$ , but the measured voltages in the latter case were very much smaller than in the former. The values of  $\rho_{1111}$  as determined from  $E_J$  in arrangements I and II always agreed very closely. The other coefficient that can be checked is  $\rho_{3111}$ . For specimen F analysis of the  $H^2$  contribution to  $E_z$  in arrangement I gave a value of  $\rho_{3111}$  of  $3.1 \times 10^{-8}$  m.k.s. units while from  $E_z$  in arrangement II a value of  $\rho_{3111} \cos 3\theta$  of  $2.3 \times 10^{-8}$  was obtained. The value of  $\theta$  estimated from observations on the orientation of the etch pits was close to  $4^\circ$ .

The results which have been obtained are summarized in table 1. Included in this table are values of the dimensionless factors  $\rho_{123}^2/\rho_{11}\rho_{ijkl}$  for the principal magnetoresistance components. The spread of values between specimens in this expression for a given component reflects the absolute accuracy of the

Table 1. Experimental Values of the Galvanomagnetic Coefficients for Three Specimens of *n*-type Bismuth Telluride at  $77^\circ\text{K}$

Specimen	F	C	E
$\rho_{11}$ (ohm m) $\times 10^6$	1.46	1.68	1.53
$\rho_{123}$ ( $\text{m}^3 \text{c}^{-1}$ ) $\times 10^6$	0.425	0.505	0.443
$\rho_{312} \times 10^6$	0.874	1.013	0.944
$\rho_{1111}$ (m.k.s. units) $\times 10^8$	7.41	7.75	7.90
$\rho_{1122}$ "	11.9	12.7	11.9
$\rho_{1133}$ "	25.6	29.0	27.2
$\rho_{1131}$ "	4.8	4.2	
$\rho_{3111}$ "	3.1	4.1	
$\rho_{3113}$ "	4	—	2
$\rho_{123}^2/\rho_{11}\rho_{1111}$	1.67	1.96	1.63
$\rho_{123}^2/\rho_{11}\rho_{1122}$	1.04	1.19	1.08
$\rho_{123}^2/\rho_{11}\rho_{1133}$	0.484	0.524	0.472



measurements and is due in part to the difficulty of obtaining ideal geometry of the specimens and also of measuring the dimensions. It will be noted that the relative ratios of the principal magnetoresistance components are reasonably constant for the different specimens.

### 3.4. Measurements of the Hall Coefficients and Resistivity versus Temperature from 100°K to 300°K

The Hall coefficients  $\rho_{123}$  and  $\rho_{312}$  and the resistivity component  $\rho_{11}$  were measured over the temperature range 100°K to room temperature on specimen SBTC/6/G. The results are plotted in figure 7. The coefficient  $\rho_{123}$  is practically

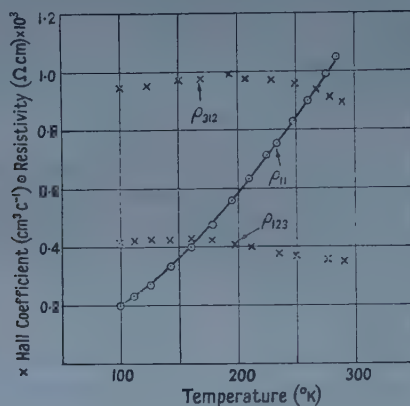


Figure 7. Resistivity and Hall coefficients plotted against temperature for specimen G.

constant in the range 100° to 175°K and thereafter starts to decrease with increasing temperature, but the rate of decrease is small. The coefficient  $\rho_{312}$  increases very slightly over the range 100° to about 230° and thereafter begins to decrease with increasing temperature. The decrease in the coefficients at the higher temperatures cannot be due to the onset of intrinsic behaviour since evidence on the thermoelectric power shows that the specimen was not intrinsic even at room temperature. This conclusion is supported by the behaviour of the resistivity which increases systematically with temperature over the whole range. The results are analysed in the next section.

## § 4. DISCUSSION

In this section, the results are discussed in terms of the model of the band structure proposed in DW which assumes a many-valley model with energy minima on the reflection planes and a relaxation time which is a function of energy only. This model was developed to try to account for the observed anisotropy of the galvanomagnetic coefficients with only one type of charge carrier present. The justification for the assumption of only one type of carrier is based on the variation of the Hall coefficients with temperature, which is so small that it seems impossible to attribute it to a variation in the density of carriers.

It will be assumed that the density of carriers is constant over the temperature range and as a logical consequence that there is only one type of carrier present. Then the expressions for the galvanomagnetic coefficients, derived on the basis of the assumed model of the band structure, involve the usual parameters such



as the density of carriers and those defining the scattering process and, in addition, three other parameters which define the shape and orientation of the surfaces of constant energy in the region of the minima. These last three parameters enter in different ways into the expressions and are assumed to be responsible for the anisotropy. By forming suitable combinations of the coefficients, expressions may be derived which involve only these parameters. One such expression is the ratio of the Hall coefficients, and in the present case, the three other expressions of the form  $\rho_{123}^2/\rho_{11}\rho_{ijk}$  listed in table 1 have been used. On the basis of the theory given in DW these will be functions only of the three parameters provided that the electron gas is degenerate and hence the coefficients  $A$ ,  $B$  and  $C$  occurring in equation (25) of DW satisfy the condition  $B^2 = 2AC$ . It has been estimated from measurements of the thermoelectric power on similar specimens that the specimens used in the present measurements were in fact highly degenerate at 77°K.

The experimentally determined values of the four expressions thus obtained can be used to obtain an estimate of the parameters defining the shape and orientation of the valleys in the proposed model. In doing this, the results on specimen F have been used since these are probably the most accurate ones, but in fact the values of the three parameters giving the best fit to the four experimental values are unlikely to differ greatly for the different specimens. For specimen F all four expressions could be satisfied by a suitable choice of the three parameters. On the basis of these results it was concluded that the shape and orientation of the valleys were defined by

$$\frac{m_1}{m_2} = 1.21, \quad \frac{m_3}{m_2} = 0.093, \quad \cos^2 \theta = 0.0546,$$

where  $m_1$ ,  $m_2$  and  $m_3$  are the three principal effective masses of the valleys and the principal axes of one of the valleys are related to the principal crystal axes by the direction-cosine scheme

$$\begin{Bmatrix} c & 0 & -s \\ 0 & 1 & 0 \\ s & 0 & c \end{Bmatrix} \quad \text{with } c = \cos \theta, \quad s = \sin \theta.$$

Hence the surfaces of constant energy are almost spheroidal and are highly compressed in a direction nearly parallel to the three-fold axis of rotation of the crystal.

Using the above values the remaining galvanomagnetic coefficients can be calculated and compared with experiment where possible. The results are given

Table 2. Calculated Values of the Galvanomagnetic Coefficients for Specimen F

$\rho_{11}$	$1.46 \times 10^{-6}\dagger$	$\rho_{1131}$	$3.4 \times 10^{-8}$
$\rho_{123}$	$0.425 \times 10^{-6}\dagger$	$\rho_{3111}$	$11.0 \times 10^{-8}$
$\rho_{312}$	$0.874 \times 10^{-6}\dagger$	$\rho_{3113}$	$6 \times 10^{-8}$
$\rho_{1111}$	$7.38 \times 10^{-8}$	$\rho_{33}/\rho_{11}$	4.1
$\rho_{1122}$	$11.9 \times 10^{-8}$	$\rho_{3333}$	$7.6 \times \rho_{1111}$
$\rho_{1133}$	$26.0 \times 10^{-8}$	$\rho_{3311}$	$38 \times \rho_{1111}$

† Adjusted to the experimental values.

in table 2, in which the resistivity and Hall coefficient values for specimen F have been used to determine the parameters other than those specifying the shape and orientation of the valleys.

The predicted ratio of the resistivity perpendicular to the cleavage planes to that parallel to the cleavage planes is 4.1. Although no measurements of this ratio have been made in the present experiments, some measurements have been made on a different n-type sample (H. J. Goldsmid, private communication) which appeared to be free from cracks. The estimated ratio of the two resistivities at 77°K was 3.8. It is reasonable to assume that the true value of this ratio should not differ greatly from one specimen to another so that the value predicted on the basis of the magnetoresistance measurements may be regarded as being in good agreement with experiment.

Of the remaining coefficients, it appears that the calculated values of  $\rho_{1131}$  and  $\rho_{3111}$  are outside the range of experimental error of the measured values. However, in view of the approximations involved in the theory and the experimental uncertainty in the measurement of  $\rho_{3111}$ , a new estimate of the parameters taking into account all measurements is unnecessary. It is certain that such a new estimate could be made to give a reasonable fit to all the parameters in the table except perhaps the last two, but these new values would not differ appreciably from those used in the above calculation. It is better to wait for other measurements, in particular the longitudinal and transverse magnetoresistances with current flowing perpendicular to the cleavage planes, before attempting a more refined analysis.

The results may be regarded as confirming the utility of the six-valley model for interpreting the galvanomagnetic effects in bismuth telluride. In particular, the anisotropy of the Hall tensor can be determined with the use of this model and the following expressions can be obtained:

$$\rho_{123} = -\frac{r}{nec} \times 0.326,$$

$$\rho_{312} = -\frac{r}{nec} \times 0.670$$

where  $r$  is the usual factor involving the average over the electron distribution (1 for degenerate statistics,  $3\pi/8$  for non-degenerate statistics and covalent lattice scattering),  $n$  is the density of carriers and the numerical coefficients are the anisotropy factors.

Assuming the above expressions to hold at 77°K, then, for specimen G, on which measurements of the Hall coefficients and resistivity were made over a temperature range, the density of carriers at 77°K is  $4.8 \times 10^{18} \text{ cm}^{-3}$ . Then, taking this density to be constant over the temperature range, it is possible to obtain the values of a 'conductivity' mobility of electrons in the cleavage planes defined by  $\rho_{11} = 1/ne\mu_n$ . The values of mobility obtained in this way are plotted as a function of temperature on a log-log scale in figure 8. Over the range from 150°K to room temperature, the mobility is given by an equation of the form

$$\mu_n = 1.67 \times 10^7 T^{-1.68}.$$

The variation of the mobility with temperature expressed by this equation is the same as that found on a number of n-type samples by Goldsmid (private communication), over the same temperature range. The value of  $\mu_n$  at 286°K is  $1250 \text{ cm sec}^{-1} \text{ V}^{-1} \text{ cm}^{-1}$ .

In a general account of the work of these laboratories on bismuth telluride, Wright (1956) gave a value of  $250 \text{ cm}^2 \text{ sec}^{-1} \text{ V}^{-1}$  for the mobility of electrons parallel to the cleavage planes, and deduced a value of the effective mass of electrons of  $1.3m_0$ . The mobility quoted was the Hall mobility, defined in the present terminology as  $\rho_{123}/\rho_{11}$ , since at that time no estimate had been made of

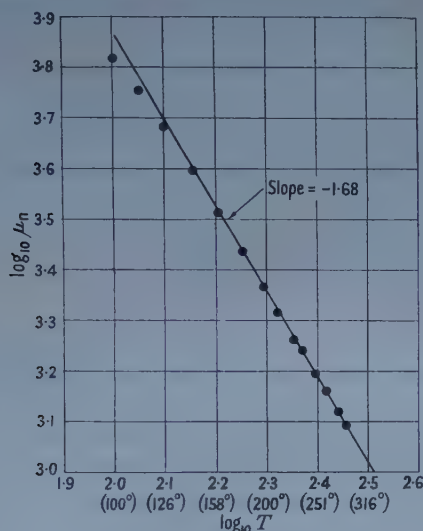


Figure 8.  $\mu_n$  plotted against  $T$  for specimen G.

the effect of the band structure on the relation between the Hall coefficients and the density of carriers. The discrepancy between the Hall mobility and the conductivity mobility given above comes largely from the present interpretation of the Hall effect in terms of the six-valley model of the band structure. Thus, neglect of the anisotropy factors in the expression for the Hall coefficient  $\rho_{123}$  would reduce the conductivity mobility by a factor of three. The value  $\mu_n = 1250$  would modify the value of the effective mass of electrons given by Wright to give  $0.45m_0$ .

The Hall mobility at room temperature in the present experiments was  $330 \text{ cm}^2 \text{ sec}^{-1} \text{ V}^{-1}$ . Other workers have given values of this quantity for *n*-type bismuth telluride. Konorov (1956) gives data from which a value of 375 can be calculated. Although the agreement between this and our value is reasonable, other results for the specimens used by Koronov are completely at variance with ours. Thus, the ratio of conductivities in and perpendicular to the cleavage planes is given in his paper as 50 whereas our measurements indicate a value between 4 and 5. Also the value of the energy gap is given as 0.3 eV, whereas various methods of measurement on our material have given a value of 0.15 eV (Wright 1956).

Vlasova and Stil'bans (1955) quote a value of Hall mobility of about 360 but they used polycrystalline samples and again the rest of the data is not consistent with our experience. The recent value of 800 given by Black *et al.* (1957) was deduced from measurements on a *p*-type sample and must be subject to considerable uncertainty.

In conclusion, it may be stated that although the interpretation of the galvanomagnetic properties in terms of the proposed band structure and scattering



mechanism is fairly successful, some modifications to the theory are necessary for a more detailed investigation. In particular, the assumption of a constant effective mass tensor for the valleys in a partly degenerate material and the use of a relaxation time which is a function of energy only are both open to question. For example, these assumptions lead to the conclusion that the thermoelectric power should be isotropic, while recent measurements by H. J. Goldsmid (private communication—to be published) have shown that there is a small degree of anisotropy in the thermoelectric power over the temperature range 150°K to room temperature. This anisotropy, which is about 25 in  $200 \mu\text{V deg}^{-1}$  at room temperature could be accounted for by modifying the form of the scattering mechanism which has been used in the present analysis of the galvanometric effects. However, in view of the reasonable agreement which has been obtained using the simpler model, it seems unlikely that a more elaborate theory would seriously affect the conclusions of this paper.

## APPENDIX

The independent components of the resistivity tensors for the crystal class  $\bar{3}m$  have been discussed by DW using the results of Juretschke (1955). However, Juretschke (private communication) has pointed out an error in his paper which has led to an error in DW. This error is associated with the choice of coordinate system. The results given in both papers apply when the  $yz$  plane is chosen as one of the three equivalent planes of reflection. Since in DW the analysis on the basis of a many-valley model is based on a coordinate system in which the  $xz$  plane is a plane of reflection, the independent components and their relation to the remaining non-vanishing components are given for this coordinate system:

$$\begin{aligned} \rho_{11} &= \rho_{22} \\ \rho_{33} \\ \left. \begin{aligned} \rho_{123} \\ \rho_{231} &= \rho_{312} \end{aligned} \right\} & \rho_{ijk} = -\rho_{jik} \\ \rho_{1111} &= \rho_{2222} & \rho_{1113} &= -\rho_{2213} = -\rho_{1223} \\ \rho_{3333} & & \rho_{3111} &= -\rho_{3122} = -\rho_{3221} \\ \rho_{1122} &= \rho_{2211} & \rho_{1313} &= \rho_{2323} \\ \rho_{1133} &= \rho_{2233} \\ \rho_{1212} &= \frac{1}{2} \{ \rho_{1111} - \rho_{1122} \} \\ \rho_{3311} &= \rho_{3322} \end{aligned}$$

Generally

$$\rho_{ijkl} = \rho_{jikl} = \rho_{jilk} = \rho_{ijlk}.$$

As a result of this error, two of the independent components of the conductivity tensor were omitted from equation (25) of DW. The expressions for these components are:

$$\begin{aligned} \sigma_{1113} &= \frac{3C}{m_1 m_2 m_3} \left\{ sc \left[ c^2 \frac{m_3}{m_1} - s^2 \frac{m_1}{m_3} + \frac{m_1}{m_2} - \frac{m_3}{m_2} + s^2 - c^2 \right] \right\}, \\ \sigma_{3111} &= \frac{3C}{m_1 m_2 m_3} \left\{ sc \left[ c^2 \frac{m_1}{m_3} - s^2 \frac{m_3}{m_1} + \frac{m_2}{m_1} - \frac{m_2}{m_3} + s^2 - c^2 \right] \right\}. \end{aligned}$$



$\sigma_{1123}$  and  $\sigma_{2311}$  are identically zero because of crystal symmetry and not as a consequence of the six-valley model.

## REFERENCES

- BLACK, J., CONWELL, E. M., SEIGLE, L., and SPENCER, C. W., 1957, *Phys. Chem. Solids*, **2**, 240.
- DRABBLE, J. R., and WOLFE, R., 1956, *Proc. Phys. Soc. B*, **69**, 1101.
- JURETSCHKE, H. J., 1955, *Acta Cryst., Camb.*, **8**, 716.
- KONOROV, P. P., 1956, *Ž. Tech. Phys., Moscow*, **26**, 1400.
- PUTLEY, E. H., 1955, *Proc. Phys. Soc. B*, **68**, 35.
- VLASOVA, R. M., and STIL'BANS, L. S., 1955; *Ž. Tech. Phys., Moscow*, **25**, 569.
- WRIGHT, D. A., 1956, *Proceedings of Garmisch Conference* (to be published in *Halbleiter-Probleme*, **4**, Ed. Schottky).

## A Theory of Delayed Yielding in the Presence of Cottrell Atmospheres of Solute Atoms

BY N. LOUAT

Aeronautical Research Laboratories, Melbourne, Australia

*MS. received 22nd October 1956, and in revised form 19th August 1957*

*Abstract.* A theory of yielding in iron is developed which includes the effect of the continued reduction with time under load of the restraint offered to the motion of dislocations by atmospheres of solute atoms. The manner in which this reduction comes about, namely by decrease in atmosphere density consequent on the bending of the dislocations, is analysed and is shown to lead to the existence of stress and temperature-dependent delay times and to the presence of microstrain prior to yielding. Qualitative and to some extent quantitative agreement is found between the predictions of the theory and the experimental evidence.

### § 1. INTRODUCTION

AT present the dislocation theory of the yield point phenomenon (Cottrell 1948, Cottrell and Bilby 1949, Cottrell 1950, Yokobori 1954, Louat 1956) is not entirely satisfactory, particularly in that it takes insufficient account of the microstrain which occurs prior to yielding (Roberts, Carruthers and Averbach 1952, Vreeland, Wood and Clark 1953). The theory employs models in which the dislocations are considered to be fixed rigidly in position by solute atoms until a combination of applied stress and thermal fluctuations is able to release a short length of one or more of them. This free length then extends rapidly under the action of the applied stress until the dislocation is completely released from its atmosphere and operates as a Frank-Read source.

Assuming that operation of the first source leads immediately to yielding, it is possible to predict the temperature dependence of the yield point (Cottrell and Bilby 1949, Louat 1956) and the delay time for yielding after rapid loading (Fisher 1955) found by several workers (Clark and Wood 1949, Wood and Clark 1951, 1952, Gallagher 1952). However, it is difficult to account for the plastic microstrain which occurs prior to yielding. This difficulty may be overcome if one envisages the release of a Frank-Read source from an atmosphere as a gradual rather than a sudden process, and one which involves the motion of the dislocation together with its solute atoms. This model is now developed and its implications discussed.

### § 2. THE MOVEMENT OF DISLOCATIONS HAVING COTTRELL ATMOSPHERES

Louat (1956) has suggested that the solute atoms near the centre of a dislocation may be disposed in two (for simplicity) energy levels of energy difference  $W$  in which the restraining effect on the dislocation of the atoms in the lower energy group is much greater than that due to atoms in the outer

position which offer little restraint. The solute density in the lower energy group at temperature  $T^\circ\text{K}$  is given by

$$\alpha = \frac{\theta \exp(W/kT)}{\beta + \exp(W/kT)}, \quad \dots\dots(2.1)$$

where  $\theta \leq 1$  is the overall atmosphere density and  $\beta$  the multiplicity of the upper level relative to the lower. Equilibrium should normally be attained quickly because the (interstitial) solute atoms lie in a region of extreme dilatation so that the activation energy for movement of a solute atom from one site to another should be small. The occupation probability for solute atoms in an outer position is  $1 - \alpha$  and it may be shown that in a great length of  $N$  atoms ( $\sim N\mathbf{b}$ , where  $\mathbf{b}$  is the Burgers vector) the number of sequences of lengths  $2l$  or greater in which the solute atoms are either in an outer position or are absent is  $N\alpha(1 - \alpha)^{2l/b}$ .

### 2.1. Dislocation Motion

Dislocation motion is conceived as taking place by the repetition of two processes: namely (a) the formation of a small loop whose central region is solute locked at a distance  $b$  from its original position; (b) the extension of this central region to cover the length of a Frank-Read source.

#### 2.1.(a) Loop formation.

It may be seen from the previous remarks that a length of dislocation in which all the solute atoms are in outer positions will behave much as though the solute atmosphere were not present, and will bend under an applied stress  $\sigma$  into an arc of radius  $R$  given by

$$R = T/\sigma b. \quad \dots\dots(2.2)$$

Here  $T$  is the line tension of the dislocation and has been given by Nabarro (1952) for the case where the amplitude and length of the bend are small (as they are here) as  $\mu b^2/6$  where  $\mu$  is the shear modulus.

From geometry the displacement of the mid-point of such a length is

$$d \simeq l^2/2R \quad \dots\dots(2.3)$$

provided  $R \gg l$ .

Thus from (2.2) and (2.3) we have with the stated value of  $T$  that the condition for the amplitude of the bend to be equal to or greater than  $b$  is

$$2l \geq (4\mu b^2/3)^{1/2}. \quad \dots\dots(2.4)$$

It is generally accepted that the fine structure near the centre of a dislocation varies periodically (period  $b$ ) as the dislocation moves through the crystal lattice. It must therefore be concluded that the distances between a solute atom at the dislocation centre and its neighbouring solvent atoms and hence the solute atom configurational energy vary with this same period. We are thus led to consider a model in which lower energy levels mentioned above (in § 2) exist only when this configurational energy is a minimum or nearly so.

The necessary condition that this model be satisfactory, namely that the variation in configurational energy be significantly greater than  $W$ , is reasonably certain to be satisfied since  $W \sim 0.05$  ev (Louat 1956). Assuming satisfaction we see that if a bend of length defined by equation (2.3) is formed, solute atoms in the upper energy levels near the middle of the bent length can move forward a distance  $\sim b$ , fall to the lower energy levels and then tend to drag the dislocation 'forward' through the small remaining distance to the new position of minimum configurational energy.

It may be seen that atoms falling into low energy levels tend to flatten the bend near its mid-point and thus to produce a straight length displaced a distance  $b$  from its original position. Similarly, solute atoms falling into lower energy positions near the ends of the original bent length tend to shorten this length. This latter process should proceed more slowly since the displacements  $\lambda$  (figure 1) near 0-0 are, due to the applied stress, greater than those near  $b-b$ . Hence some time after the first solute atom falls, the dislocation will have assumed a final configuration as indicated in figure 1 (curve 2).

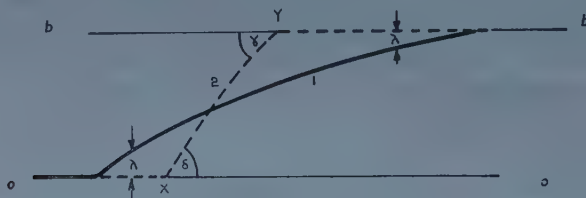


Figure 1.

Here the rate of 'fall' of solute atoms is comparatively slow, i.e. with frequency

$$\nu \exp \{-(X+\Delta)/kT\} < \nu \exp (-X/kT)$$

where  $X$  is the activation energy necessary for the transition from an upper to a lower energy level when the dislocation is at a position of minimum configurational energy,  $\nu$  is the frequency of atomic vibrations and  $\Delta$  is the excess configurational energy.

### 2.1.(b) Loop extension.

To examine the process of extension of the central length, we consider the effect of thermal fluctuations (frequency  $\nu \exp \{-(X+W)/kT\}$ ) which raise the solute atoms from the lower levels. While such an event at  $Y$  (figure 1) leads to a lengthening of the 'free' dislocation ( $X-Y$ ) and a consequent decrease in the angles  $\gamma$  and  $\delta$ , the dislocation is more likely to return subsequently to its new position than it is to move so as to reduce the width of the bend ( $L$ ). On the other hand, an event at  $X$  will probably lead to an extension of the length in the new position. Thus it would seem that the formation of such a bend will be followed by an increase in the length of dislocation in the new position at a rate of the order of  $2\nu b \exp \{-(X+W)/kT\}$  cm sec<sup>-1</sup>. Later considerations will show that the time taken for this transition to cover the whole length of dislocation source is much less than the time between the formation of bends which lead to this extension. Therefore the rate of 'advance' of the dislocation can be equated to the rate of formation of these bands.

### 2.2. Dislocation Velocity

For simplicity, it has been assumed above that a dislocation must bend until its centre advances a distance  $b$ . This probably represents an overestimate since it does not take account of motion of the dislocation relative to the locking solute atoms at the end of the bend. This motion may well be considerable for these atoms must provide a restraining force of the order  $l\sigma b$  whilst according to Cottrell and Bilby (1949) the maximum restraint offered by a solute atom does not occur until the solute atom and dislocation are mutually displaced about 1 Å.



To take some account of this we relax equation (2.4) slightly and have as the condition for appreciable 'forward' motion of the dislocation line that a length

$$2l \geq (\mu b^2 / \sigma)^{1/2} \quad \dots\dots (2.4a)$$

in which all the atoms are in an upper energy level or are absent shall occur with significant frequency.

Now, as stated above, the number of such sequences of length  $2l$  or greater is

$$N\alpha(1-\alpha)^{2l/b} = K = N\alpha(1-\alpha)^{\sqrt{(\mu/\sigma)}} \quad \dots\dots (2.5)$$

from (2.4a). Since the number of these lengths is constant at equilibrium it follows that the rate of creation and destruction must be equal. The former can therefore be evaluated by determining the latter. Thus the life of a single solute atom in an upper level will be of order  $\exp(X/kT)/\nu$  and that of a number  $2l/b$  will be of order  $b \exp(X/kT)/2\nu l$ .

Hence the rate at which stable bends are formed is of order

$$S = \frac{2K\nu l}{b} \exp\left(\frac{-X}{kT}\right) \quad \dots\dots (2.6)$$

and substituting for  $K$  from (2.5), the period between the formation of such bends is

$$\frac{1}{S} = \frac{b}{2N\nu l\alpha} \left(\frac{1}{1-\alpha}\right)^{2l/b} \exp\left(\frac{X}{kT}\right).$$

Taking values reasonable for iron:  $N = 10^3$ ,  $\alpha = 0.7$  at  $T = 300^\circ\text{K}$ ,  $\nu = 10^{12} \text{ sec}^{-1}$ ,  $W = 590k$  and  $2l/b = 20$ , it is clear that the quantity

$$\frac{1}{S} \simeq 10^{-6} \exp\left(\frac{X}{kT}\right) \gg \frac{N}{2\nu} \exp\left(\frac{X+W}{kT}\right) \simeq 10^{-9} \exp\left(\frac{X+W}{kT}\right)$$

which is of the order of the time for a bend to extend the full length of the source. It follows that the forward velocity of the dislocation is  $Sb$ ; a quantity which depends exponentially on  $X$ .

It is apparent from its definition that  $X$  must be closely related to the activation energy for diffusion of the (interstitial) solute near the centre of the dislocation. This energy has not yet been determined but recent measurements (Turnbull and Hoffman 1945, Turnbull 1954) of the rate of self-diffusion along low angle boundaries indicate an activation energy about half that for normal diffusion. Since this result applies to mean behaviour of the material in the neighbourhood of the dislocations making up the boundary, it is apparent that a very considerable reduction in this energy might be expected for the material at or near the dislocation centre.

This conclusion is in accord with that to be drawn from the agreement between the theory and experiment given by previous work (Louat 1956) on the variation of yield strength with temperature. In this work it was required that  $\alpha$  reach an equilibrium value as defined by equation (2.1) in a reasonable time even at very low temperature.

On this basis the experimental results of Eldin and Collins indicate that  $X$  cannot be much greater than  $1200k$  ( $\sim 0.1 \text{ ev}$ ) and we accordingly adopt this value.

### 2.3. Motion of a Frank-Read Source with Cottrell Atmosphere.

It is now necessary to determine the shape which the source assumes after many such 'forward' movements. After one movement the middle of the originally straight source remains straight, and it follows that all the resultant curvature must occur at its ends. A second such operation should lead either to the situation represented in figure 2(a) or to that in figure 2(b) depending on

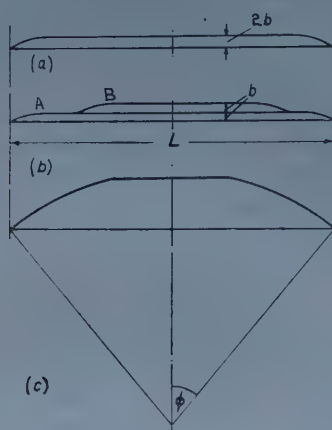


Figure 2.

whether or not important repulsions exist between the bent elements A, B. Notwithstanding these repulsions, it must be expected that, after a few operations, elements will commence to coalesce near the ends of the source. The resultant lengths of bent dislocation will be anchored by their solute atmospheres and bent elements should be able to move along them in much the same way as along the straight portion of the source. Thereafter, the source would appear to deform homogeneously, and we would expect it to satisfy minimum energy requirements by behaving, except for a straight section near its middle, like a Frank-Read source without an atmosphere under the action of an applied stress which increases relatively slowly (vide figure 2(c)).

In conformity with this result we write as the effective stress applied to the dislocation

$$\tau = \sigma - (\mu b \sin \phi) / L = \sigma - c \sin \phi \quad \dots\dots(2.7)$$

where  $\phi$  and  $L$  are as defined in figure 2(c). We have already evaluated the rate of motion of a straight length of dislocation and we can now write an expression for that of the straight section at the middle of the source assuming that the atmosphere continuously redistributes itself so as to remain uniform over the dislocation length. On this basis the atmosphere density is given by

$$\theta(\phi) = \theta \sin \phi / \phi$$

and the velocity of the middle section from (2.5), (2.6) and (2.7) by

$$V = Sb = R(1 - \alpha \sin \phi / \phi)^{\sqrt{(\mu/\tau)}} \quad \dots\dots(2.8)$$

where  $R = 2lN\nu\alpha \sin \phi \exp(-X/kT)/\phi$ , and  $N = L/b$ . Briefly, then, we have examined the manner and rate with which a single dislocation, bound at its ends and having a solute atmosphere, might be expected to bend under the action of an applied stress and thermal fluctuations. We shall consider next the behaviour

of such a length when it is subjected to the various stress conditions appropriate to the available experimental evidence.

### § 3. COMPARISON OF THEORY AND EXPERIMENT

#### 3.1. Delay Time for Yielding

We shall assume that catastrophic operation of a Frank-Read source will commence when a small bend is formed which has sufficient length to permit it to be pulled away from the solute atoms at its ends. Thus the process of yielding is different only in degree from that involved in the bending of the source. Now, it may be verified that, when  $\sigma$  is constant,  $Sb$  decreases with increasing  $\phi$ , passes through a minimum and subsequently increases without limit. Furthermore, if yielding does not occur when  $\phi=0$  (figure 2(c)) it will not occur until after the dislocation velocity has passed through this minimum. It follows that it is the time taken to reach the position of this minimum which principally determines the delay in yielding.

The time for a dislocation of length  $L$  to bend through an angle  $\phi$  may be written as

$$t = \int_0^{\bar{x}} dx/V \simeq L \int_0^{\bar{\phi}} d\phi/4V$$

using the approximation  $x = \frac{1}{2} L \tan \frac{1}{2} \phi \simeq L\phi/4$ . Substituting for  $V$  from (2.8)

$$t \simeq \frac{L}{4R} \int_0^{\bar{\phi}} \left( \frac{1}{1 - \alpha \sin \phi/\phi} \right)^{\sqrt{(\mu/\tau)}} d\phi. \quad \dots\dots (3.1)$$

An exact solution to this integral in a useful form has yet to be obtained and certain approximations are necessary. Thus, it is found by plotting the value of the integrand for reasonable values of the parameters (e.g.  $\alpha=0.7$ ,

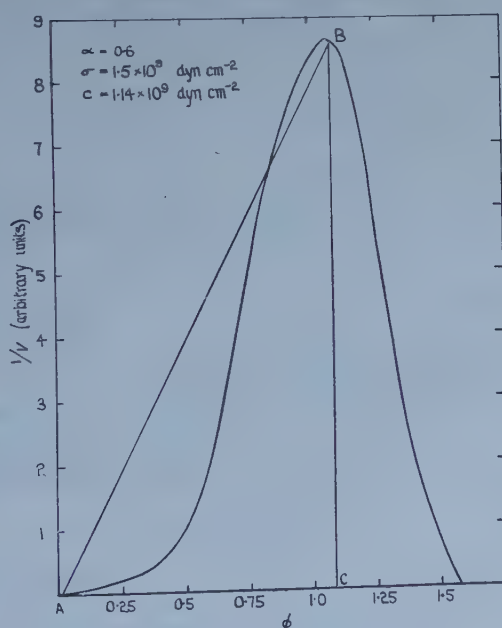


Figure 3.

$c = 1 \times 10^9 \text{ dyn cm}^{-2}$ ,  $\sigma = 1.5 \times 10^9 \text{ dyn cm}^{-2}$  against  $\phi$  that the area obtained beneath the curve up to the maximum ordinate is not very different from half

the area of the triangle ABC (see figure 3). This implies that the time taken for the dislocation to bend to the position of minimum velocity is approximately a quarter of that taken by a hypothetical dislocation to travel the same distance to  $\phi = \phi_m$  at a constant velocity ( $V_m$ ) equal to the minimum. Further the additional time needed for the dislocation to travel from the position  $\phi = \phi_m$  to that at which it will break away from its atmosphere will also be of this order.

Hence

$$t \simeq L\phi_m/8V_m \quad \dots\dots(3.2)$$

$$V_m \simeq R(1 - \alpha \sin \phi_m/\phi_m)^{(\nu/2)(1/\tau_m)}.$$

Now at a given temperature  $R$  is approximately constant so that we can evaluate  $t$  to the correct order of magnitude providing we can determine  $\phi_m$  and  $V_m$ . Differentiating the integrand of equation (3.1) and setting it equal to zero we obtain a relation between the applied shear stress and the angle at which the velocity becomes a minimum, namely

$$\sigma = c \sin \phi_m - c \cos \phi_m (1 - \alpha \sin \phi_m/\phi_m) \ln (1 - \alpha \sin \phi_m/\phi_m) \times \{\phi_m^2/2\alpha(\sin \phi_m - \phi_m \cos \phi_m)\}.$$

Using this expression and equation (2.8) we obtain values for  $\sigma$  and  $V_m$  for particular values of  $\phi_m$ , and substitution in equation (3.2) gives values of  $t$  for particular values of  $\sigma$ . The curves obtained in this manner are shown in figures 4 and 5 for  $\alpha = 0.7$  and  $0.5$  respectively, and  $c = 1.0 \times 10^9$  dyn cm<sup>-2</sup>. This

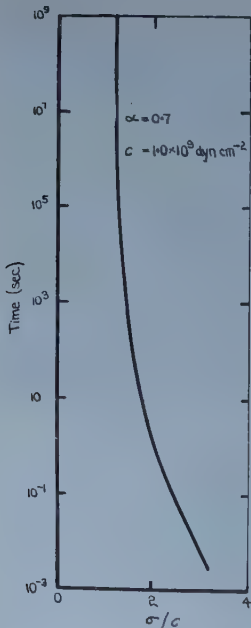


Figure 4. Delay time plotted against  $\sigma/c$ .

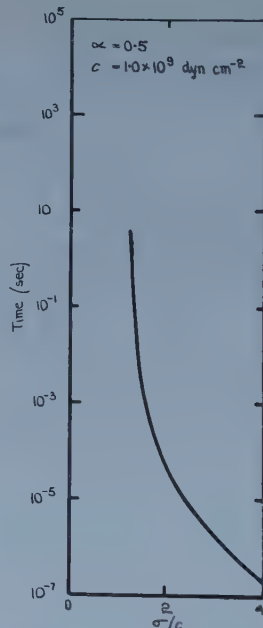


Figure 5. Delay time plotted against  $\sigma/c$ .

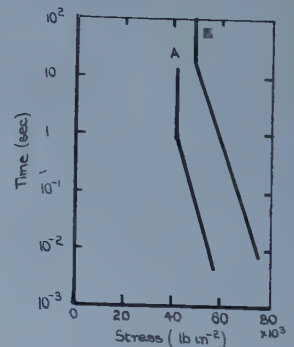


Figure 6. Delay time plotted against stress.

value of  $c$  was chosen to fit the experimental results of Wood and Clark (figure 6) and thus to be rather less than the least value of the yield stress ( $1.3 \times 10^9$  dyn cm<sup>-2</sup>) at the highest temperature they employed. This has been done for consistency with the view that  $c$  represents the restraining stress which would apply in the



absence of an atmosphere, and it is expressed in our results by the fact that the curves shown are asymptotic to  $c$ . Here the present theory differs from the interpretation made by Wood and Clark (1951, 1952) of their results. These authors suggest in effect that the behaviour can be divided into three modes: (a) a range in which the delay time varies inversely with the load; (b) a load for which the delay is indeterminate; and (c) loads for which yielding never occurs. Examination of their results, however, suggest that this interpretation, which involves fitting their results to two straight lines, is not to be preferred above fitting them to a single curved line.

Referring to figures 4 and 5 we see that comparatively small variations in  $\alpha$  and  $c$  produce large changes in the delay time at a given stress. This is particularly so with the delay times at which these curves have their maximum curvature and which we might suppose correspond to the 'knee' in Wood and Clark's results (see figure 6). Thus, by varying  $\alpha$  and  $c$ , we could arrange that these regions of maximum curvature occur at the stresses and times found by Wood and Clark. However, this would not seem to serve any useful purpose in view of the approximations involved in the analysis. Nevertheless, it may be seen that (a) delay times of the correct order of magnitude may be predicted using reasonable values of  $\alpha$  and  $c$ , (b) the temperature dependence is in the correct direction since larger values of  $\alpha$  which result from lower testing temperatures lead to increased delay times, and (c) the slope of the curve in the region of large stresses is of the same order as those found by Wood and Clark.

Finally, it should be noted that if the expression for yield strength given by Louat and Wain (unpublished) be modified to allow for the bending of the dislocation sources, one obtains

$$\sigma = c \sin \phi - \frac{2\sigma_0 \ln(1 - \alpha \sin \phi / \phi)}{\ln(MNt / (1 - \alpha)^2 t_0)}$$

and hence

$$\ln t = -\ln \frac{MN}{(1 - \alpha)^2 t_0} - \frac{2\sigma_0 \ln(1 - \alpha \sin \phi / \phi)}{\sigma - c \sin \phi} - D. \quad \dots\dots(3.3)$$

Here  $t$  could be identified as the delay time for yielding after the application of a constant load  $\sigma$ ,  $\sigma_0$  is the stress equivalent of the maximum restraining force between solute atom and dislocation,  $MN$  is number of atomic lengths of dislocation in a region or regions of the test specimen in which maximum shear stresses occur,  $t_0 = \nu \exp(-X/kT)$  and  $D$  is a constant.

Since with the anticipated values of  $d\phi/dt$ ,  $MN$ , and  $t_0$ ,  $\sigma$  increases with  $\phi$  and hence  $t$  up to a maximum at  $\phi_M > \phi_m$ , these considerations do not invalidate the criterion for delay time we have adopted. However, it is interesting to note that when  $\phi = 0$  equation (3.3) may, in view of the present uncertainty as to the value of  $\beta$  and  $W$  (cf. § 2.1), reduce to a form approximating that derived by Fisher (1955) namely

$$\ln t = -A + B/T\sigma$$

where  $A$  and  $B$  are constants.

### 3.2. Equilibrium Microstrain

It is clear that for stresses less than  $c$  the slow bending of the source will cease altogether. If this criterion were satisfied for every dislocation in the specimen

(whose lengths must be expected to vary) the anelastic microstrain which accompanies the motion would cease also and an equilibrium microstrain characteristic of the applied load would be reached.

It is difficult to express this quantity as a function of applied stress so as to permit comparison with the experimental evidence (Vreeland, Wood and Clark 1953 b) derived from polycrystalline specimens. The analysis is accordingly restricted to the hypothetical case of a uniformly stressed single crystal having all its dislocations of equal length.

We first estimate the amount of strain which would occur if all the dislocations were bent through an angle  $\pi/2$ . Consider  $1 \text{ cm}^3$  of suitably oriented material and suppose as before that  $c \sim 1 \times 10^9 \text{ dyn cm}^{-2}$  so that  $L/b \sim 800$ . If a roughly consistent dislocation density  $\rho = 10^9 \text{ cm}^{-2}$  is assumed, we find that about  $N \sim 10^{14}$  Mott net elements exist in the volume. When each element has bent through an angle  $\pi/2$  the area swept is

$$\pi N L^2 / 8 \simeq 6 \pi b^2 \times 10^{19} / 8 = A$$

and the strain is given approximately by

$$A b / 2 \simeq 3 \times 10^{-4}$$

which is about ten times that found by Vreeland, Wood and Clark (1953 b). That our estimate should be larger than the experimental values was to be expected since only a portion of the volume would contribute to the microstrain of polycrystalline specimens.

Again, consider a single source in a crystal of 'best' orientation and take the stress which must be applied to produce detectable deformation in a reasonable time (a few minutes) as  $6.3 \times 10^8 \text{ dyn cm}^{-2}$  to correspond with the value found by Vreeland, Wood and Clark. One can write an equation for constant terminal velocity,

$$\left( \frac{\mu}{6.3 \times 10^8} \right)^{1/2} \ln(1 - \alpha) = \left( \frac{\mu}{\tau} \right)^{1/2} \ln \left( 1 - \alpha \frac{\sin \phi}{\phi} \right)$$

and hence a relationship between applied shear stress and  $\phi$  for equilibrium microstrain.

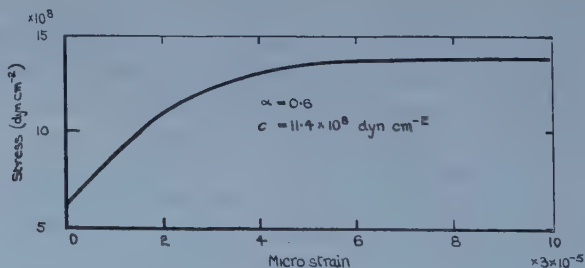


Figure 7. Equilibrium microstrain against stress.

We may then obtain the relation between applied shear stress and equilibrium microstrain (illustrated in figure 7) from the fact that microstrain is here proportional to the area of the segment of a circle swept out by a Frank-Read source.

It is difficult to draw conclusions from a comparison of this result with that obtained by the above authors for polycrystals (figure 8) and we merely note that the two curves are not dissimilar in shape.

## 3.3. Time Dependence of Microstrain

In the same paper Vreeland, Wood and Clark have shown that the rate of microstrain under constant load continuously decreases with time unless yielding occurs. While an attempt to find quantitative agreement with these results would encounter the same difficulties as before, it is interesting to note that the curve predicted (by graphically evaluating the integral  $\int_0^{\bar{\phi}} d\phi/V = t(\bar{\phi})$  for the hypothetical single crystal of the previous section) is similar to that found experimentally (see figures 9 and 10). Both curves are initially steep and

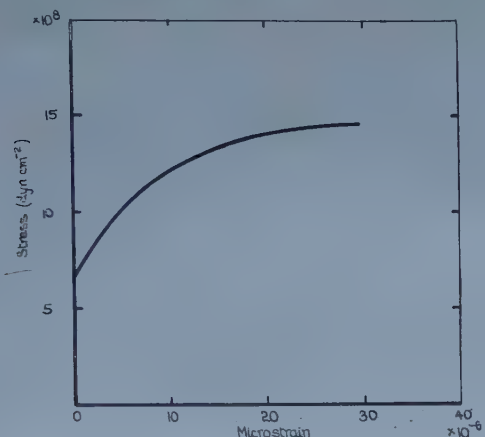


Figure 8. Equilibrium stress plotted against microstrain.

continuously become flatter, but their slope rapidly increases when yielding occurs. On the other hand, the predicted curves show greater deformation than do the experimental results as expected from the considerations of the preceding section.

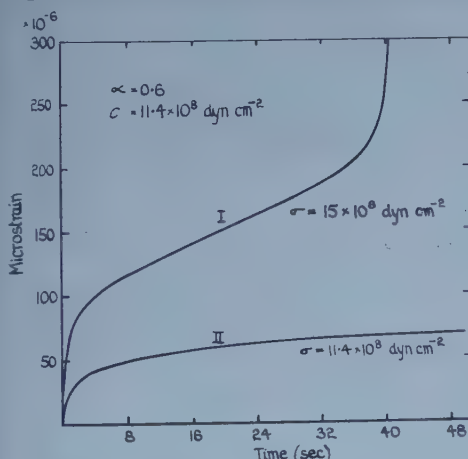
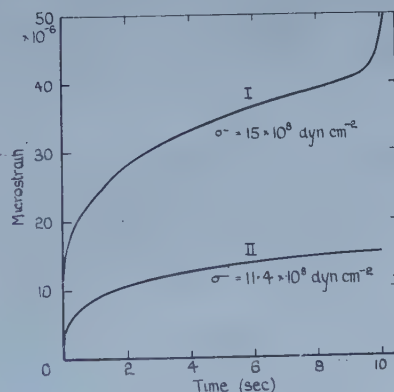


Figure 9. Microstrain plotted against time.

Figure 10. Microstrain plotted against time (after Vreeland *et al.*).

Other points of difference lie in the comparatively long linear portion found in curve 1, figure 9 (cf. curve 1, figure 10) and in the fact that the ratio of the ordinates of curves 1 and 2 for comparable times is not the same in the two cases. This

arises since the volume taking part in the microstrain process does not depend on stress in the same way in both substances.

### 3.4. The Effects of Preloading

Vreeland, Wood and Clark (1953 a) have also subjected specimens to stresses sufficient, but for times insufficient, to cause yielding. The specimens were then unloaded, annealed and reloaded. They found that this cycle could apparently be repeated indefinitely without yielding under appropriate annealing conditions. An activation energy for 'recovery' of  $18\,800\text{ cal mole}^{-1}$  was determined which is close to that for the diffusion of carbon and nitrogen in  $\alpha$ -iron.

Other results from these experiments were that: (a) the amount of microstrain decreased with repetition of the stress-pulse ageing cycle—this effect was more noticeable when ageing conditions induced recovery; (b) about 50% of the microstrain was recovered on unloading; (c) there was no inhomogeneity of strain between the two halves of the specimen nor could slip lines be observed prior to yielding; and (d) there was no systematic correlation of the amount of microstrain with the magnitude of the applied stress.

These results may be predicted from the model developed above. Loading a crystal sufficiently will cause its dislocations to bend giving rise to a microstrain. If the load is removed before yielding occurs the dislocations will attempt to straighten under the action of the stress  $c \sin \phi$ . Hence, some recovery of microstrain should be observed which should proceed at a continually decreasing rate and effectively cease when  $\phi = \phi_1$ , as defined by

$$(1 - \alpha)^{\sqrt{(\mu/6 \cdot 3 \times 10^8)}} = (1 - \alpha \sin \phi_1 / \phi_1)^{\sqrt{(\mu/c \sin \phi_1)}}.$$

Further, both the delay time for yielding and the microstrain in a second loading would be less than those found without preloading.

If, after the application of a stress pulse, the temperature of the specimen were raised,  $\alpha$  would be reduced and recovery of microstrain to an angle  $\phi_2 < \phi_1$  would occur. Prolonged heating would lead to an increase in  $\alpha$  as the result of an increase in  $\theta$  (see equation (2.1)) by the diffusion of carbon and nitrogen to the unoccupied sites in dislocations created when it stretched. On reloading the delay time would increase since the dislocation velocity at an angle  $\phi$  would be less than previously since  $V$  is now proportional to

$$\left\{ 1 - \frac{\alpha \sin (\phi - \phi_2)}{\phi - \phi_2} \right\}^p$$

where  $p = [\mu/(\sigma - c \sin \phi)]^{1/2}$ .

It should be possible to carry out the stress-pulse annealing cycle an indefinite number of times without yielding since the effect of such a process is merely to increase the effective atmosphere density. In addition, the microstrain per stressing should become progressively less as cycling continues.

Since we consider the deformation prior to yielding as purely 'anelastic', it follows that there should be no inhomogeneity of microstrain between the halves of the specimen and that no slip lines would appear.

Finally, we have the observation that microstrain does not vary consistently with applied stress. Referring to figure 11 we see that  $\phi_m$  decreases with increasing  $\sigma$  so that for a uniformly loaded idealized single crystal ( $c = \text{constant}$ ) there should be a consistent variation. It is difficult to decide to what extent



this prediction is applicable to real materials. We can merely observe having regard to figure 11, the slope of the delay time-stress curves, and to the stress

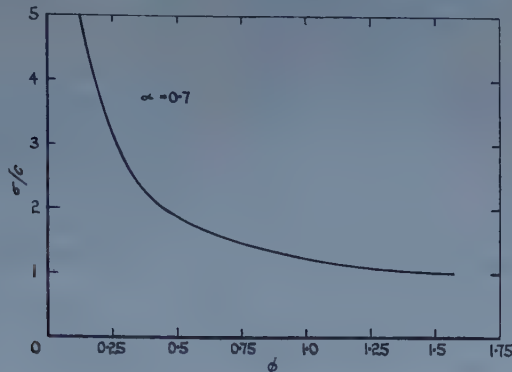


Figure 11.  $\sigma/c$  plotted against  $\phi$  for minimum velocity.

dependence of velocity, that an increase in applied stress would result in a decrease in microstrain in the more highly stressed regions and an increase in the other portions of the specimen.

#### § 4. DISCUSSION

It has been found that the results of a theory of yielding, based on a dislocation model in which Frank-Read sources and their atmospheres bend under the action of an applied stress, are in qualitative agreement with experiment in respect of microstrain and delay time for yielding. The analysis employed is approximate, in particular no account has been taken of the shortening of the straight length along which stable bends are formed as the bending of the source proceeds. This factor may have a considerable influence on the behaviour of the sources at low stresses (i.e.  $\sigma \sim c$ ) and lead to increased delay times in these regions; a result which would tend to be more in conformity with the experiments of Wood and Clark. Again, this effect should modify the exact form of the microstrain-time and equilibrium microstrain-stress curves but not their general appearance. In view of this and the absence of experimental evidence with which the curves could be compared no good purpose would seem to be served by undertaking the additional computations necessary to include the effect. For similar reasons no account has been taken of the interactions between sources which result from their bending and which, it may be shown, tend to reduce the effective value of  $c$  leading to smaller yield stresses for a given delay time and to smaller values of  $\phi$  at yielding.

#### ACKNOWLEDGMENTS

This work forms part of the research programme of the Aeronautical Research Laboratories, Department of Supply, Melbourne, Australia, and thanks are due to the Chief Scientist, Department of Supply, for permission to publish.

#### REFERENCES

- CLARK, D. S., and WOOD, D.S., 1949, *Proc. Amer. Soc. Test. Mater.*, **49**, 717.  
 COTTRELL, A. H., 1948, *Bristol Conference on Strength of Solids* (London: Physical Society);  
 1950, *Plastic Deformation of Crystalline Solids* (Pittsburgh).

- COTTRELL, A. H., and BILBY, B. A., 1949, *Proc. Phys. Soc. A*, **62**, 49.  
FISHER, J. C., 1955, *Trans. Amer. Soc. Metals*, **47**, 451.  
GALLAGHER, C. J., 1952, *Phys. Rev.*, **88**, 721.  
LOUAT, N., 1956, *Proc. Phys. Soc. B*, **69**, 459.  
MOTT, N. F., 1951, *Proc. Phys. Soc. B*, **64**, 729.  
NABARRO, F. R. N., 1952, *Advanc. Phys. (Phil. Mag. Suppl.)*, **1**, 171.  
PETCH, N. J., 1953, *J. Iron St. Inst.*, **174**, 25.  
ROBERTS, C. S., CARRUTHERS, R. C., and AVERBACH, B. L., 1952, *Trans. Amer. Soc. Metals*, **44**, 1150.  
TURNBULL, D., 1954, *Report of the Conference on Defects in Crystalline Solids* (London : Physical Society).  
TURNBULL, D., and HOFFMAN, R. E., 1954, *Acta Metallurg.*, **2**, 419.  
WOOD, D. S., and CLARK, D. S., 1951, *Trans. Amer. Soc. Metals*, **43**, 57 ; 1952, *Ibid.*, **44**, 726.  
VREELAND, T., WOOD, D. S., and CLARK, D. S., 1953 a, *Trans. Amer. Soc. Metals*, **45**, 620 ; 1953 b, *Acta Metallurg.*, **1**, 414.  
YOKOBORI, T., 1954, *J. Appl. Phys.*, **25**, 593.

# Symmetry Effects in Gas Kinetics

## II: Ortho- and Para-hydrogen

By R. A. BUCKINGHAM†, A. R. DAVIES† AND D. C. GILLES†

† Department of Physics, University College London

† Computing Machine Laboratory, University of Manchester; now at Computing Laboratory, University of Glasgow

MS. received 14th October 1957

**Abstract.** The Manchester University Mk I computer has been used to calculate accurately the viscosity cross section for hydrogen molecules, and its dependence on the symmetry of the wave function for binary collisions. The calculations assume a central intermolecular potential of (exp, 6, 8) type, and cover reduced temperatures in the range  $0.05 \leq T^* \leq 2.0$ .

Comparison is made with estimates of the relative difference in viscosity cross sections for para-para and para-ortho collisions derived from Becker and Stehl's measurements. Assuming elastic collisions only, fairly good agreement is found at 15°K, but at higher temperatures the theoretical results become increasingly too small. A central interaction is seemingly inadequate to explain the relatively large ortho-ortho cross sections observed; in this connection the effect of an increased range of interaction is briefly discussed and shown to be unimportant.

### § 1. INTRODUCTION

IN an earlier paper (Halpern and Buckingham 1955, to be referred to as I) the effect of using properly symmetrized wave functions on the viscosity of the He isotopes and their mixtures was discussed and shown to lead to results in good agreement with experimental data below 5°K. Among other things attention was called to the relative magnitude, as a function of temperature, of the averaged viscosity cross section  $\bar{S}_\eta$  for identical particles satisfying Bose statistics and for dissimilar particles of the same mass satisfying classical (Boltzmann) statistics. Thus for atoms of mass corresponding to <sup>4</sup>He, the following inequalities were found,  $T^*$  being the reduced temperature (Figure 1(b) of I):

$$\begin{aligned} T^* < 0.1 \quad \bar{S}_\eta(\text{Bose}) < \bar{S}_\eta(\text{class.}) & \dots\dots(1) \\ T^* > 0.1 \quad \bar{S}_\eta(\text{Bose}) > \bar{S}_\eta(\text{class.}) \end{aligned}$$

For a mass appropriate to <sup>3</sup>He the reversal of the inequality occurs when  $T^*$  is about 0.08.

It was not at all obvious how this effect might depend on the magnitude of the quantal parameter  $\Lambda_m = \hbar / (M\epsilon r_m^2)^{1/2}$  characterizing the collision; in particular, for the smaller value of this parameter appropriate to collisions of H<sub>2</sub> molecules, whether the reversal would persist and at what value of  $T^*$ . From calculations now completed it appears that the result for H<sub>2</sub> molecules is indeed quite different. Thus we find the inequalities

$$\begin{aligned} T^* < 0.2 \quad \bar{S}_\eta(\text{Bose}) > \bar{S}_\eta(\text{class.}) & \dots\dots(2) \\ T^* > 0.2 \quad \bar{S}_\eta(\text{Bose}) < \bar{S}_\eta(\text{class.}) \end{aligned}$$

The reversal here corresponds to an absolute temperature of about 7°K, and the inequality is consistent with the differential viscosity measurements of Becker and

Stehl (1952) at 15°K and above. At 15°K the magnitude of the difference in the cross sections also agrees well with experiment, but becomes progressively too small at higher temperatures.

Independent calculations of this viscosity difference, using a different intermolecular potential, have been published recently by Cohen *et al.* (1956) and their results agree in the main with our own. A detailed comparison is made later in the paper.

It is clearly of interest to know how the transition from the situation represented by (1) to that represented by (2) occurs as  $\Lambda_m$  decreases, and this question is being studied further.

## § 2. VISCOSITY FORMULAE

We use the same notation as in I, whereby the reduced viscosity cross section  $S_\eta$  is given in terms of the usual quantal phase shifts by

$$S_\eta(K, \Lambda_m) = \frac{6}{\lambda^2 K} \sum_L w_L \frac{(L+1)(L+2)}{2L+3} \sin^2(\delta_{L+2} - \delta_L) \quad \dots\dots (3)$$

where  $K$  is the reduced collision energy,  $\lambda (= 2\pi/\Lambda_m)$  the quantal mass-interaction parameter, and  $w_L$  a simple weighting factor depending on the symmetrization of the wave function.

The reduced viscosity  $\eta^*$  is then proportional to  $(T^*)^{1/2}/\bar{S}_\eta$ , where  $T^*$  is the reduced temperature  $\hbar T/\epsilon$  and  $\bar{S}_\eta$  is the averaged cross section

$$\bar{S}_\eta(T^*, \Lambda_m) = \frac{1}{6} \int_0^\infty x^3 e^{-x} S_\eta dx \quad (x = K/T^*). \quad \dots\dots (4)$$

The absolute viscosity  $\eta$  is proportional to  $T^{1/2}/(\bar{S}_\eta r_m^2)$ .  $\epsilon$  and  $r_m$  are parameters which define the minimum in the interaction potential.

For hydrogen gas at low temperatures considered as a mixture of para and ortho molecules, each in their lowest rotational states, we must distinguish three cross sections  $S_p$ ,  $S_{po}$  and  $S_o$  corresponding to binary collisions between para-para, para-ortho and ortho-ortho molecules respectively (the subscript  $\eta$  is here omitted for convenience). If in addition the same centrally symmetrical potential is assumed for all types of collision, and ortho-molecules are assumed to include nine independent and equally abundant subspecies, and then the appropriate values of  $w_L$  are as follows:

	$\bar{S}_p$	$\bar{S}_{po}$	$\bar{S}_o$
$L_{\text{even}}$	$w_L = 2$	1	10/9
$L_{\text{odd}}$	0	1	8/9

For subsequent comparisons it is convenient to introduce the relative differences

$$\Delta_{po} = (\bar{S}_p - \bar{S}_{po})/\bar{S}_p \quad \Delta_{oo} = (\bar{S}_p - \bar{S}_o)/\bar{S}_p \quad \dots\dots (5)$$

It follows from the above table that

$$\Delta_{oo} = \frac{8}{9} \Delta_{po}. \quad \dots\dots (6)$$

This conclusion, however, is not substantiated by the experimental evidence, to be discussed later, which indicates that for temperatures above 15°K at least,  $\Delta_{oo}$  is appreciably greater than  $\Delta_{po}$  in magnitude. It therefore appears that the assumptions made above over-simplify the situation, particularly in respect of collisions between ortho-molecules. For this reason we shall restrict any comparison between theory and experiment to the ratio  $\Delta_{po}$ .



One further point must be discussed at this stage. In order to derive  $\Delta_{po}$  from differential viscosity measurements of ortho-para mixtures it is necessary to use an appropriate mixture formula, and it is important that this should be adequate. With the assumption of independent subspecies it can be shown that the numbers of these do not appear explicitly in the mixture formula, provided  $\bar{S}_p$ ,  $\bar{S}_{po}$  and  $\bar{S}_o$  are derived from correctly symmetrized wave functions. It follows from the general formula for the viscosity of mixtures† that

$$\bar{S}_{mix} = \frac{x_p^2 \bar{S}_p + 2x_p x_o \{\mu \bar{S}_{po} + \bar{S}_p \bar{S}_o / \bar{S}_{po}\} / (1 + \mu) + x_o^2 \bar{S}_o}{x_p^2 + 2x_p x_o \{\mu + (\bar{S}_p + \bar{S}_o) / \bar{S}_{po} - 1\} / (1 + \mu) + x_o^2} \quad \dots\dots(7)$$

where  $x_p$ ,  $x_o (= 1 - x_p)$  are the fractions of para and ortho molecules present in the mixture, and  $\mu$  is the ratio of two collision integrals related to their mutual diffusion. It is convenient to express (7) in terms of cross sections, but translation into viscosities is readily achieved by writing  $\eta_p = CT^{1/2} / \bar{S}_p$  etc.

We may now write

$$\Delta_{mix} = (\bar{S}_p - \bar{S}_{mix}) / \bar{S}_p$$

and, using the symbols  $\Delta_{po}$  and  $\Delta_{oo}$  defined in (5), it follows that

$$\Delta_{mix} = \frac{-2x_p x_o \Delta_{po} \{\mu + 1 / (1 - \Delta_{po})\} / (1 + \mu) + x_o^2 \Delta_{oo}}{1 + 2x_p x_o \{(2\Delta_{po} - \Delta_{oo}) / (1 - \Delta_{po})\} / (1 + \mu)} \quad \dots\dots(8)$$

So far no algebraic approximations have been made, but if it is now assumed that  $\Delta_{po}$  and  $\Delta_{oo}$  are small, and quadratic terms neglected,

$$\Delta_{mix} \simeq x_o \{2x_p \Delta_{po} + x_o \Delta_{oo}\}. \quad \dots\dots(9)$$

This first-order approximation depends linearly on  $\Delta_{po}$  and  $\Delta_{oo}$  and quadratically on the concentration  $x_p$ . For normal- $H_2$ , with  $x_p = \frac{1}{4}$ ,

$$\begin{aligned} \Delta(n-H_2) &\simeq \frac{3}{16} (2\Delta_{po} + 3\Delta_{oo}) \\ &= \frac{7}{8} \Delta_{po} \quad \text{when} \quad \Delta_{oo} = \frac{8}{9} \Delta_{po}. \end{aligned} \quad \dots\dots(10)$$

### § 3. PHASE SHIFT CALCULATIONS

All calculations described here have been carried out using an intermolecular potential of the type introduced by Buckingham and Corner (1948) combining an exponential repulsion with van der Waals attractive terms involving  $r^{-6}$  and  $r^{-8}$ . Thus

$$V = -\epsilon f(\sigma), \quad \sigma = r/r_m \quad \dots\dots(11)$$

where  $f(\sigma) = f_1 \sigma^{-6} (1 + b\sigma^{-2}) - f_2 e^{-a(\sigma-1)}$

$$f_1 = a / \{a(1+b) - 6 - 8b\}, \quad f_2 = -1 + (1+b)f_1.$$

More precisely, this form is used when  $\sigma > 1$ , i.e. beyond the minimum, and when  $\sigma < 1$ ,  $f_1$  is multiplied by an exponential factor which rapidly removes the  $\sigma^{-6}$  and  $\sigma^{-8}$  terms but maintains continuity of  $f$  and several derivatives at the minimum. Numerical values of 13.5 and 0.2 have been allotted to  $a$  and  $b$  respectively. We refer to (11) briefly as a potential of the type (E 13.5, 6, 8).

† Formula (11) of paper I, from which (7) can be derived by the substitutions  $x_1 = x_p$ ,  $2x_2 = x_o$ ,  $s = p = 1$ , contains a misprint; the central term in the numerator should read  $4\gamma_1 x_1 x_2 \{\frac{1}{4}\mu(s+1+1/s) + \alpha_1 \alpha_2' / \gamma_1^2\}$ . The correct form was used in the calculations of that paper. An extensive discussion of mixture formulae for all transport properties, with application to helium isotopes, has been given by Cohen, Offerhaus and de Boer (1954). Unfortunately, we were unaware of this work when paper I was being prepared, and reference to it was therefore omitted.

It is also necessary to assign values to the physical parameters  $\epsilon$  and  $r_m$ . We have assumed here that the parameter  $\lambda^2$  equals 16 and this determines the combination  $\epsilon r_m^2$ . An empirical investigation by Buckingham, Davies and Davies (1958), using viscosity data for  $H_2$  over a wide range of temperature, has led to the values

$$\epsilon/k = 33.6^\circ \quad r_m = 3.380 \times 10^{-8} \text{ cm}$$

as being the most suitable for the chosen  $\lambda$ . These are consistent with a value  $10.9 \times 10^{-60} \text{ erg cm}^2$  for the coefficient of the van der Waals term in  $r^{-6}$ , in good agreement with the value  $10.5 \times 10^{-60}$  suggested on theoretical grounds by Britton and Bean (1955).

The value chosen for  $\lambda^2$  is not necessarily the best, but is unlikely to be seriously in error. More recent calculations suggest that 16.7 is a better value. It is doubtful whether the differential effects we are concerned with depend critically on this choice, but later calculations may decide this point.

It will be noticed that any dependence of the interaction upon angular coordinates is being ignored, together with the possibility of inelastic collisions between para- and ortho-molecules which is introduced by angular dependent forces. For long range forces at least the angular dependence is certainly not marked (Britton and Bean 1955) and it is therefore desirable to determine whether the experimental results can be understood, at least qualitatively, without invoking any such dependence.

All phase shifts exceeding about 0.02 radian in magnitude have been evaluated by numerical integration using the Ferranti Mk I computer at Manchester University, and are thought to be accurate, certainly to 4 decimals and probably to 5 decimals. The values of  $K$  (the relative kinetic energy of collision in units of  $\epsilon$ ) for which the phase shifts were determined are as follows:

$$K = 0.0125(0.0125)0.075(0.025)0.25(0.0625)0.5(0.125)0.75(0.25)3.25.$$

For the larger values of  $K$ , the values of  $L$  covered by these computations extended to 15. Phase shifts of magnitude about 0.02 and less were evaluated by Born's approximate formula, and the largest of these were checked against machine computed values to ensure that the Born approximation was adequate. The largest value of  $L$  it was necessary to cover in this way was 23. Further details of the methods of calculating  $\delta_L$  are given in an Appendix.

#### § 4. VISCOSITY CROSS SECTIONS

From the phase shifts the sums required for  $S_\eta$  were derived for odd and even values of  $L$  separately. Table 1 contains the results of these calculations for  $S_p$  and  $S_{p0}$ . Before proceeding to the integrations for  $\bar{S}_p$  and  $\bar{S}_p - \bar{S}_{p0}$  some interpolation was necessary and was carried out either in  $S_\eta$  itself or through the phase differences  $\delta_{L+2} - \delta_L$ . The resulting values of  $S_\eta$  were in the main accurate to 4 decimal places.

The calculation of  $\bar{S}_p$  presents no further difficulty when  $T^*$  is less than about 0.5. When  $T^* > 0.5$  it is essential to extend the table of  $S_\eta$  beyond  $K = 3.25$ . However, a table of  $S_\eta$  for  $K \geq 6$  was available from the high temperature investigation by Buckingham, Davies and Davies (1958) and the gap could be bridged graphically without serious error. Evaluation of the difference  $\Delta\bar{S} = \bar{S}_p - \bar{S}_{p0}$  is a more difficult matter because of the oscillatory nature of the integrand which leads

Table 1. Reduced Cross Sections for  $H_2$  Molecules

	Viscosity		Diffusion	Elastic Scattering	
16K	$(S_\eta)_p$	$(S_\eta)_{p0}$	$(S_D)_{p0}$	$(S_{sc})_p$	$(S_{sc})_{p0}$
0	29.69	14.84	14.84	29.69	14.84
0.1	26.038	14.077	9.860	25.844	14.670
0.2	22.9686	13.7928	9.028	22.538	15.089
0.3	20.4148	13.4405	9.155	19.751	15.206
0.4	18.1098	12.9280	9.561	17.492	15.107
0.6	14.2202	11.6925	10.838	14.829	14.879
0.8	11.4159	10.5511	12.614	15.792	15.722
1.0	10.5526	10.1381	14.178	21.621	18.613
1.2	11.9586	10.7215	13.860	28.641	21.895
1.6	13.8928	11.2353	9.765	28.064	20.899
2.0	12.7547	10.0825	7.476	21.710	16.973
2.4	11.2662	8.7166	6.4333	17.343	14.173
2.8	9.9796	7.4782	5.7921	14.531	12.372
3.2	8.9006	6.4394	5.2687	12.620	11.274
3.6	7.9780	5.6432	4.7710	11.246	10.652
4.0	7.1688	5.1018	4.3026	10.212	10.289
5	5.4714	4.4915	3.3829	8.497	9.473
6	4.0982	4.0951	2.8595	7.518	8.383
7	3.0342	3.6114	2.5164	7.006	7.416
8	2.3366	3.1551	2.2383	6.778	6.729
10	1.9579	2.5836	1.8321	6.418	5.867
12	2.1312	2.2799	1.5978	5.651	5.215
16	2.0971	1.8330	1.3226	4.015	4.314
20	1.6752	1.5828	1.1662	3.275	3.767
24	1.3523	1.4187	1.0691	3.166	3.381
28	1.2309	1.3035	1.0012	3.205	3.103
32	1.2032	1.2209	0.9521	3.162	2.890
36	1.1780	1.1572	0.9143	3.016	2.721
40	1.1334	1.1072	0.8842	2.810	2.585
44	1.0804	1.0671	0.8597	2.589	2.473
48	1.0331	1.0339	0.8392	2.382	2.379
52	0.9979	1.0061	0.8217	2.206	2.298

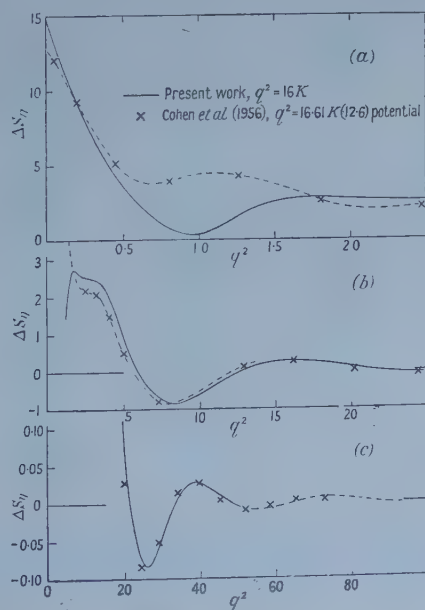


Figure 1. Variation of viscosity cross section,  $\Delta S = S_p - S_{p0}$ , with collision energy. Note the wide differences in scales between (a), (b) and (c).

to considerable cancellation. This is obvious from figure 1 which shows the variation of  $S_p - S_{p0}$  with  $K$ . The last two or three oscillations, however, are extremely regular, and it seems reasonable to extrapolate beyond  $K = 3.25$  by fitting an exponentially damped sine function of the form  $A \exp(-\alpha K^{1/2}) \sin \beta (K^{1/2} - K_0^{1/2})$ . This was in fact done to enable  $\Delta \bar{S}$  to be evaluated beyond  $T^* = 0.5$ .

It must be emphasized that the oscillatory tail of  $\Delta \bar{S}$ , small though it is in amplitude, plays an important part in determining  $\Delta \bar{S}$  as  $T^*$  increases. This is evident from the following table which gives the contributions to  $\Delta \bar{S}$  from the ranges  $K < 3.25$  and  $K > 3.25$ . It must be remembered that each of these contributions is itself the net result of positive and negative parts.

$T^*$	$K < 3.25$	$K > 3.25$	$\Delta \bar{S}$
0.4	-0.00575	-0.00021	-0.00596
0.5	-0.00205	-0.00047	-0.00252
0.6	-0.00056	-0.00071	-0.00127
0.8	+0.00040	-0.00089	-0.00049
1.0	+0.00054	-0.00083	-0.00028
1.5	+0.00035	-0.00047	-0.00012
2.0	+0.00019	-0.00025	-0.00006

Clearly the last few values of  $\Delta \bar{S}$  must be accepted with reserve, and the correct values might well lie anywhere between zero and twice the values given. Nevertheless the values as a whole appear mutually consistent.

Table 2 contains a more complete set of averaged viscosity cross sections,  $\bar{S}_p$ ,  $\Delta \bar{S}$  and  $\Delta_{p0}$  for values of  $T^*$  from 0.05 to 2.0. The crucial feature is the change in sign of  $\Delta_{p0}$  between 0.15 and 0.20. This is also illustrated in figure 2, which shows the substantially different behaviour of  $\Delta_{p0}$  for smaller values of  $\lambda^2$ , corresponding to the mass and interaction of the helium isotopes.

Table 2. Averaged Cross Sections for  $H_2$  Molecules

$T^*$	$T(^{\circ}K)$	Viscosity			Diffusion
		$(\bar{S}_\eta)_p$	$(\Delta \bar{S}_\eta)_{p0}$	$(\Delta \eta)_{p0}$	$(\bar{S}_D)_{p0}$
0.05	1.68	9.387	1.955	0.208	7.983
0.10	3.36	5.145	0.619	0.120	4.791
0.15	5.04	3.418	0.1027	0.0301	
0.20	6.72	2.653	-0.0074	-0.0028	2.685
0.25	8.40	2.243	-0.0196	-0.0087	
0.30	10.1	1.965	-0.0147	-0.0075	1.961
0.35	11.8	1.774	-0.00950	-0.0054	
0.40	13.4	1.631	-0.00596	-0.00366	1.606
0.45	15.1	1.520	-0.00381	-0.00251	
0.50	16.8	1.431	-0.00252	-0.00176	1.396
0.55	18.5	1.359	-0.00174	-0.00128	
0.60	20.2	1.300	-0.00127	-0.00097	1.257
0.8	26.8	1.138	-0.00049	-0.00043	1.085
1.0	33.6	1.043	-0.00028	-0.00027	0.983
1.5	50.4	0.915	-0.00012	-0.00013	0.848
2.0	67.2	0.853	-0.00006	-0.00007	0.780

It is interesting to compare the results of calculations using a more or less realistic potential like (11), with an idealized model such as the rigid sphere potential. For this the phase shifts are simply expressed in terms of spherical Bessel



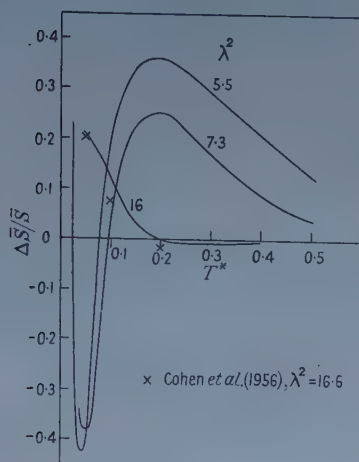


Figure 2. Comparison of viscosity ratio  $\Delta\bar{S}/\bar{S} = (\bar{S}_p - \bar{S}_{p0})/\bar{S}_p$  for  $\lambda^2 = 5.5, 7.3$  and  $16$ .

functions  $(\pi/2q)^{1/2} J_{\pm(L+1/2)}$ , and the calculation of viscosity is facilitated by the fact that

$$S_\eta = \frac{6}{q^8} \sum_L w_L \frac{(L+1)(2L+3)(L+2)}{A_L^2 A_{L+2}^2}$$

where

$$A_L^2(q) = \frac{\pi}{2q} \{[J_{L+1/2}(q)]^2 + [J_{-L-1/2}(q)]^2\}$$

$$q = Mvr_0/\hbar$$

( $v$  = relative collision velocity,  $r_0$  = sphere diameter). Tables of these Bessel functions are available.

Table 3. Viscosity of Gas of Rigid Spheres

$q_0^2$	$T(^{\circ}\text{K})$	$(\bar{S}_\eta)_p$	$(\Delta\bar{S}_\eta)_{p0}$	$(\Delta_\eta)_{p0}$
0.8	2.1	3.194	0.746	0.224
1.6	4.3	2.160	0.139	0.064
2.4	6.4	1.871	0.0324	0.0173
3.2	8.6	1.737	0.0098	0.0056
4.0	10.7	1.655	0.00374	0.00226
4.8	12.8	1.596	0.00172	0.00108
5.6	15.0	1.550	0.00090	0.00058
6.4	17.1	1.514	0.00052	0.00034
7.2	19.3	1.483	0.00032	0.00022
8.0	21.4	1.457	0.00021	0.00014
8.8	23.5	1.432	0.00014	0.00010
9.6	25.7	1.408	0.00010	0.00007

$\bar{S}_p$  and  $\Delta\bar{S}$  have been evaluated for a number of values of  $q_0^2 = (Mr_0^2/\hbar^2)kT$ . (The variable  $x$  in (4) is now  $q^2/q_0^2$ .) The results are given in table 3, and it will be seen that  $\Delta\bar{S}$  and  $\Delta_{p0}$  are always positive for rigid spheres. A rough comparison with the results of table 2 is possible if  $r_0$  is adjusted so that the curves of  $\bar{S}_p$  roughly coincide. This requires that  $r_0 = 3 \times 10^{-8}$  cm, assuming that  $T = 33.6 T^*$ .

## § 5. OTHER COLLISION CROSS SECTIONS

The phase shifts obtained for the (E 13.5, 6, 8) potential have been used to evaluate the following sums:

$$S_D = \frac{4}{\lambda^2 K} \sum_L (L+1) \sin^2(\delta_{L+1} - \delta_L) \quad \dots\dots(12)$$

$$S_{SC} = \frac{4}{\lambda^2 K} \sum_L w_L (2L+1) \sin^2 \delta_L. \quad \dots\dots(13)$$

$S_D$  leads to the coefficient of mutual diffusion of ortho- and para- $H_2$  when the summation includes all integral values of  $L$ . The appropriate integrated cross section mass transfer is

$$\bar{S}_D = \frac{1}{2} \int_0^\infty x^2 e^{-x} S_D dx \quad \dots\dots(14)$$

whence the coefficient of mutual diffusion

$$D = \frac{3(\pi M k T)^{1/2}}{8\rho \bar{S}_D \pi r_m^2} \quad \dots\dots(15)$$

where  $\rho$  is the gas density.  $S_{SC}$  represents the total elastic scattering cross section, and  $w_L$  takes different values for p-p, p-o and o-o collisions as for viscosity.  $S_D$ ,  $\bar{S}_D$  and  $S_{SC}$  are all in units of  $\pi r_m^2$ , and would be unity for rigid spheres of diameter  $r_m$  obeying classical mechanics.

Values of  $S_D$  and  $S_{SC}$  are given in table 1, and of  $\bar{S}_D$  in table 2. These do not call for much comment. There is one measurement of  $D$  by Harteck and Schmidt (1933) at 20.4°K with which comparison can be made, but here the theoretical estimate, using the values of  $\epsilon$  and  $r_m$  given above, is about 1.45 times larger. A similar difference was found by Cohen *et al.* (1956) using a (12,6) potential.

## § 6. VISCOSITY OF ORTHO-PARA MIXTURES

It has already been remarked that experimental data on the variation of viscosity of mixtures of ortho- and para- $H_2$  with the relative concentrations, can be analysed by means of a mixture formula such as (8) or (9). It is true that these formulae assume that the components of the mixture are independent and subject to a spherically symmetrical interaction. Neither assumption is likely to be wholly justified, but it seems reasonable to accept (8) as a basis of analysis in the first instance. Becker and co-workers did in fact use (9) to derive estimates of  $\Delta_{po}$  and  $\Delta_{oo}$  from their differential viscosity measurements, and we have verified that the second-order terms contained in the more accurate formula (8) are quite trivial at the temperatures concerned. We quote their results, denoting them by  $\Delta'_{po}$  and  $\Delta'_{oo}$ :

$T(^{\circ}\text{K})$	$\Delta'_{oo}$	$\Delta'_{po}$
15.0	-0.0099	-0.0042
20.3	-0.0083 <sub>5</sub>	-0.0025 <sub>3</sub>
63.2	-0.00275	-0.00055
77.3	-0.00223	-0.00037
90.1	-0.00187	-0.00028

The most striking feature is the relatively large magnitude of  $\Delta'_{oo}$ , quite inconsistent with (6). Comparison with the theoretical results for  $\Delta_{po}$  also shows a divergence which increases with increasing temperature. Thus figure 3 shows that at 15°K the experimental value is about 30% greater, at 20°K the ratio is about

2 and between 63° and 90°K it is between 6 and 7. The latter value is, however, subject to considerable uncertainty as stressed earlier.

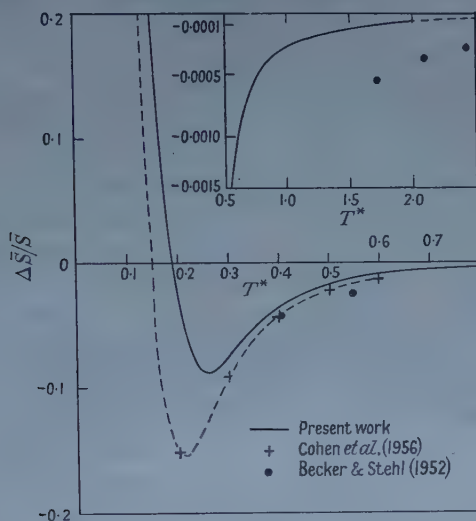


Figure 3. Comparison of theoretical and experimental values of viscosity ratio,  $\Delta\bar{S}/\bar{S}$ . Inset diagram shows tail of curve considerably magnified.

The broken curve is a rough construction through the points of Cohen *et al.*

Figure 3 also shows the curve of  $\Delta_{p0}$  due to Cohen and others (1956) using a (12, 6) potential. Beyond  $T^* = 0.3$  the difference from our curve is not very marked but the minimum is substantially lower, and the reversal of sign is at a lower temperature (about 5.7°K compared with 6.5°K, when appropriate values of  $\epsilon/k$  are used). These differences appear to arise mainly from differences in  $\Delta S_\eta$  in the range of  $K$  from 0.15 to 0.50, which more than compensate for an opposite effect when  $K < 0.15$ . The sensitivity of  $\Delta S_\eta$  for small collision energies may arise from the slightly different values assumed for  $\Lambda_m$ , which affects the disposition of bound state energies, and also from the difference in asymptotic form (for larger  $r$ ) of the two potentials.

To understand the discrepancies with experiment, we should first recall the principal approximations which have been made in the theory:

(1) Any angular dependence of the potential has been ignored, in particular the long range quadrupole-quadrupole interaction (varying as  $r^{-5}$ ), the spherical average of which is zero.

(2) No inelastic collisions, involving exchange of the  $z$ -component of angular momentum between internal and external motions, have been assumed to occur. Such collisions, which could only arise when an ortho-molecule is involved, are implicitly ruled out by the assumption of a central potential. Excitation of higher rotational or vibrational states is also ignored.

(3) Exactly the same interaction potential has been assumed for p-p, p-o and o-o collisions.

The effect of angular dependence on the magnitude of cross sections for elastic collisions is not known with any certainty, although calculations by Takayanagi and Ohno (1955) have suggested that it is not very significant. With regard to (2) we must note that inelastic collisions of the kind envisaged would

certainly tend to bring  $\Delta_{po}$  and  $\Delta_{oo}$  into better agreement with experiment, since they would increase  $(S_\eta)_{po}$  and, to an even greater extent,  $(S_\eta)_{oo}$ . These effects might also be expected to increase with temperature. The difficult problem of calculating the contribution of inelastic collisions to  $(S_\eta)_{po}$  is at present under investigation by Takayanagi and Niblett.

We may conclude with a brief consideration of (3). It has been suggested by Takayanagi and Ohno (1955) that the rotation of the ortho-molecule, which extends the distance between the H nuclei by about 0.03%, might increase the effective diameter of an ortho-molecule relative to a para-molecule without much altering the form of the interaction potential. Thus, if  $r_m$  represents the range for the p-p interaction, we might use  $r_m + \delta r_m$  for the p-o interaction and  $r_m + 2\delta r_m$  for the o-o interaction. The value of  $\delta r_m/r_m$  would, however, not exceed 0.0003 and might be appreciably less. Now since  $\eta \propto T^{1/2}/\bar{S}_\eta r_m^2$  this assumption would be equivalent to an increase in the effective values of  $\bar{S}_{po}$  and  $\bar{S}_{oo}$  in the mixture formula. If this is followed through in detail, we find that (9) should be replaced by

$$\Delta_{\text{mix}} - \delta_{\text{mix}} = x_o \{2x_p(\Delta_{po} - \delta) + x_o(\Delta_{oo} - 4\delta)\}$$

where  $\delta = 2\delta r_m/r_m$ , and  $\Delta_{po}$  and  $\Delta_{oo}$  are as before the quantities calculated assuming the same interaction for all collisions. The quantities derived by analysing the observed data would now represent  $\Delta_{po} - \delta$  and  $\Delta_{oo} - 4\delta$ . (It should be remembered that the observed values,  $\Delta'_{po}$  and  $\Delta'_{oo}$ , are negative). On looking at the observed data again, we see that the value of  $\Delta'_{po}$  at 90°K effectively sets an upper limit to  $\delta$ , i.e.  $\delta < 0.00028$ . Even assuming that  $\delta = 0.00028$ , the difference between  $\Delta'_{po}$  and  $\Delta'_{oo}$  is only partially accounted for by the contribution of  $3\delta$ , even at 90°K. Since the effect of  $\delta$  is independent of temperature, the situation at 15° or 20°K is hardly affected. We must conclude that this particular effect has little importance as an explanation of the relatively large values of  $\Delta'_{oo}$  observed.

#### ACKNOWLEDGMENTS

We should like to express our thanks to Mrs. J. Sida, Mrs. J. Lawson and Mrs. J. Wallace for their able assistance with many of the hand computations involved in this work, also to Mr. Duffy and the maintenance staff of the Manchester Mk I machine for their assistance in running the programme.

It is also a pleasure to thank Dr. Otto Halpern, both for discussions which were largely responsible for starting this investigation, and for his continued interest and encouragement.

#### REFERENCES

- BECKER, E. W., and STEHL, O., 1952, *Z. Phys.*, **133**, 615.  
 BRITTON, F. R., and BEAN, D. W. T., 1955, *Canad. J. Phys.*, **33**, 668.  
 BUCKINGHAM, R. A., and CORNER, J., 1948, *Proc. Roy. Soc. A*, **189**, 118.  
 BUCKINGHAM, R. A., DAVIES, A. E., and DAVIES, A. R., 1958, *Conference on Thermodynamic and Transport Properties of Fluids*, London, in the press.  
 COHEN, E. G. D., OFFERHAUS, M. J., and DE BOER, J., 1954, *Physica, 's Grav*, **20**, 501.  
 COHEN, E. G. D., OFFERHAUS, M. J., VAN LEEUWEN, J. M. J., ROOS, B. W., and DE BOER, J., 1956, *Physica, 's Grav*, **22**, 791.  
 HALPERN, O., and BUCKINGHAM, R. A., 1955, *Phys. Rev.*, **98**, 1626.  
 HARTECK, P., and SCHMIDT, H. W., 1933, *Z. phys. Chem. B*, **21**, 447.  
 TAKAYANAGI, K., and OHNO, K., 1955, *Progr. Theor. Phys.*, **13**, 243.

#### APPENDIX

##### EVALUATION OF PHASE SHIFTS

The numerical integrations required to evaluate phase shifts for the (E 13.5, 6, 8) potential were carried out on the Ferranti Mk. I computer at Manchester



University, using a programme for second order differential equations prepared by one of the authors (D. C. G.) and based on the well-known Gauss-Jackson method. The programme (in its original form) performed the following operations:

(1) The Schrödinger equation with  $L=0$  was integrated outwards from a point at which the repulsive potential is sufficiently large for the solution to be effectively zero. The starting value of  $\sigma$  was usually 0.5 and the integration step 0.01.

(2) At each change of sign, three values of the solution on either side of the zero were used to interpolate the position of the zero itself.

(3) Integration was continued until the intermolecular potential fell below a pre-assigned level relative to the kinetic energy of collision. The last two zeros were recorded.

(4) Similar integrations were carried out with  $L=1, 2$ , etc.

Under this procedure the derivation of  $\delta_L$  was completed by hand computation, a separate estimate being obtained from each of the two recorded zeros by assuming that the solution had reached its asymptotic form, which is a linear combination of the spherical Bessel functions  $j_L(\rho)$  and  $j_{-L}(\rho)$ , where  $\rho = K^{1/2}\lambda\sigma = q\sigma$ . These estimates did not in general agree because of a residual effect due to the attractive tail of the potential. A positive correction was therefore made, based on a continued solution using the Jeffreys (WKB) approximation from the last recorded zero, say at  $\rho_k$ . The correction to  $\delta_L$  then takes the form

$$\Delta\delta_L = \int_{\rho_k}^{\infty} \left\{ 1 - \frac{L(L+1)}{\rho^2} + \frac{1}{K}f \right\}^{1/2} d\rho - \int_{\rho_k}^{\infty} \left\{ 1 - \frac{L(L+1)}{\rho^2} \right\}^{1/2} d\rho.$$

When  $\rho_k$  is large, only the  $f_1$  term in the potential is significant, and it is then an easy matter to expand  $\Delta\delta_L$  in powers of  $t = L(L+1)/\rho_k^2$ . One obtains

$$\begin{aligned} \Delta\delta_L = D \bigg\{ & 1 + \frac{5}{14}t + \frac{5}{24}t^2 + \frac{25}{276}t^3 + \frac{175}{1664}t^4 + \dots \\ & + \frac{5}{7}b\left(\frac{q}{\rho_k}\right)^2 \left( 1 + \frac{7}{18}t + \frac{21}{88}t^2 + \frac{35}{156}t^3 + \dots \right) \bigg\} \\ & - \frac{25}{22}\left(\frac{D^2}{\rho_k}\right) \left\{ 1 + \frac{33}{26}t + \dots + \frac{22}{13}b\left(\frac{q}{\rho_k}\right)^2 (1 + \dots) \right\} \end{aligned}$$

where  $D = \lambda^2 q^4 f_1 / 10 \rho_k^5$ ,  $q^2 = \lambda^2 K$ . Corrections from this source were usually a few units in the fifth decimal.

As mentioned in the main text numerical integration was used only when  $\delta_L$  exceeded about 0.02 radian. With a potential of the form (11) the Born approximation to  $\delta_L$  can be expressed in analytical form, the contribution from the term in  $f_1$  being given by

$$\delta_{LB} = \frac{16c}{(2L-3)(2L-1)(2L+1)(2L+3)(2L+5)} \left\{ 1 + \frac{d}{(2L-5)(2L+7)} \right\}$$

where  $c = 3\pi\lambda^2 q^4 f_1 / 16$ ,  $d = 10bq^2/3$ . The contribution from the exponential term can also be expressed analytically, but is usually negligible.

On comparing this approximate formula with the results of accurate numerical integration, it was found that values of  $\delta_{LB}$  were consistently low, but that a reliable adjustment was possible by assuming that

$$\delta_L = \delta_{LB} + k_L \delta_{LB}^2$$

in which  $k_L$  is an empirical parameter depending on  $L$ . To illustrate this we quote the following examples for  $L=12$ .

$16k$	$\delta_{LB}$	$\delta_{LB} + 0.51\delta_{LB}^2$	$\delta_L$
28	0.02025	0.02046	0.02047
32	0.02657	0.02693	0.02693
36	0.03377	0.03435	0.03436
40	0.04187	0.04276	0.04277
44	0.05088	0.05220	0.05220

The consistency of this correction makes its use for smaller values of  $\delta_L$  very valuable.  $k_L$  was found to vary in a regular way from 0.40 for  $L=15$  to 2.00 for  $L=5$ , but it may depend on the form of the potential.

It should also be noted that the Born approximation enables the contribution to a sum such as  $S_\eta$  from terms with large values of  $L$  ( $\geq L_0$  say) to be evaluated with relative ease. For this purpose we use the Euler-Maclaurin series in the form

$$\sum_{y \geq y_0} u(y + \frac{1}{2}w) = \frac{1}{w} \int_{y_0}^{\infty} u(y) dy - \frac{1}{24} w \left( \frac{du}{dy} \right)_{y_0} + \frac{7}{5760} w^3 \left( \frac{d^3u}{dy^3} \right)_{y_0} - \dots$$

where the sum on the left includes integral values of  $y$  at intervals of  $w$ . Derivatives of  $u(y)$  are assumed to be zero when  $y = \infty$ .

For  $S_\eta$ , it is easily shown that when  $y = 2L + 3$

$$\begin{aligned} \frac{(L+1)(L+2)}{2L+3} \sin^2(\delta_{L+2} - \delta_L) &= \frac{25600c^2q^2}{y^{11}} \left[ 1 + \frac{111}{y^2} + \frac{7728}{y^4} + \dots \right. \\ &\quad \left. + \frac{14d}{5y^2} \left( 1 + \frac{175}{y^2} + \frac{18928}{y^4} + \dots \right) + \frac{49d^2}{25y^4} \left( 1 + \frac{239}{y^2} + \frac{34224}{y^4} + \dots \right) \right]. \end{aligned}$$

One then obtains the following asymptotic series for the contribution to  $S_\eta$  from  $L \geq L_0$ , in which  $\eta = (L_0 + 1)^{-1}$ .

$$\begin{aligned} S_\eta(L_0) &= \frac{15}{2} \frac{c^2\eta^5}{q^2} \left[ 1 + \frac{665}{24} \eta + \frac{11387}{24} \eta^2 + \dots + \frac{7}{12} d\eta \left( 1 + 44\eta + \frac{20083}{16} \eta^2 + \dots \right) \right. \\ &\quad \left. + \frac{7}{80} d^2\eta^2 \left( 1 + \frac{1953}{32} \eta + \frac{9233}{4} \eta^2 + \dots \right) \right]. \end{aligned}$$

Although the coefficients are large, when  $L_0 > 20$  and  $\eta d \gg 1$  the convergence is acceptable.

A similar treatment of the tails of  $S_D$  and  $S_{SC}$  gives results as follows

$$\begin{aligned} S_D(L_0) &= \frac{5}{2} \frac{c^2\zeta^5}{q^2} \left[ 1 + \frac{115}{6} \zeta + \frac{1719}{8} \zeta^2 + \dots + \frac{7}{12} d\zeta \left( 1 + 32\zeta + \frac{4837}{8} \zeta^2 + \dots \right) \right. \\ &\quad \left. + \frac{7}{80} d^2\zeta^2 \left( 1 + \frac{91}{2} \zeta + \frac{7105}{6} \zeta^2 + \dots \right) \right] \end{aligned}$$

where  $\zeta = (L_0 + \frac{1}{2})^{-2}$ .

$$\begin{aligned} S_{SC}(L_0) &= \frac{1}{4} \frac{c^2\zeta^4}{q^2} \left[ 1 + 11\zeta + \frac{1721}{24} \zeta^2 + \dots + \frac{2}{5} d\zeta \left( 1 + \frac{245}{12} \zeta + \frac{4033}{16} \zeta^2 + \dots \right) \right. \\ &\quad \left. + \frac{1}{24} d^2\zeta^2 \left( 1 + \frac{61}{2} \zeta + \frac{9023}{16} \zeta^2 + \dots \right) \right] \end{aligned}$$

where  $\xi = L_0^{-2}$ .

It has been assumed here that in  $S_\eta$  and  $S_{SC}$ , as in  $S_D$ , all integral values of  $L$  are given equal weight. Different weighting for even and odd values of  $L$  presents no difficulty, however.

We conclude with a further reference to the computer programme which has recently been considerably extended so that the evaluation of each phase shift, and the summation for  $S_\eta$  and  $S_D$ , is automatic. In this case the input data consist primarily of a value of  $\lambda^2$  and a sequence of values of  $K$  (or  $q^2$ ).

The integration procedure is precisely the same as before, but facilities are provided for successive doubling of the integration step every 64 values as many times as permissible. For a given value of  $K$  integration for each value of  $L$  proceeds until the contribution to  $S_\eta$  from  $\delta_L - \delta_{L-2}$  is less than a prescribed limit, with the further proviso that this must hold when  $\delta_L$  is estimated from *two* successive zeros of the solution. For the value of  $L$ , the following data are then printed out: (a) the value of  $L$ , (b) the zero of the equation from which  $\delta_L$  is computed, (c) the values of  $j_L(\rho)$  and  $j_{-L}(\rho)$  at this zero, scaled so that  $|j_{\pm L}(\rho)| \leq \frac{1}{4}$ , (d) the value of  $\delta_L$  (defined except for a multiple of  $\pi$ ), (e) the contributions to  $S_\eta$  and  $S_D$ .

The programme then arranges for integration to take place with the next value of  $L$ , terminating when two successive contributions to  $S_\eta$  and  $S_D$  fall below a second prescribed limit, or when  $L > 20$ . The value of  $S_D$ , and the separate contributions to  $S_\eta$  from even and odd  $L$  are then printed, and the machine searches the input tape for a further value of  $K$ . The programme thus designed, with the restart facilities provided, can be run without the presence of anyone familiar with its details.

Although this programme does not aim at a precision quite as high as that thought desirable for the calculation of viscosity differences in ortho- and para- $H_2$ , it is quite adequate for a further investigation of the dependence of these differences on the quantal parameter  $\lambda^2$ . This is in progress.

## Magnetoresistance of n-Type InSb at 4.2°K

By R. F. BROOM

Services Electronics Research Laboratory, Baldock, Herts.

*MS. received 13th August 1957, and in revised form 28th October 1957*

**Abstract.** Negative magnetoresistance in n-type InSb at 4.2°K has been investigated for several specimens prepared by different techniques from single crystals of differing purity. The results indicate that this phenomenon is not a bulk property of the material but is largely due to the method of preparation of the specimens.

Oscillations in the magnetoresistance as a function of magnetic field have been observed in samples having a balanced donor concentration of less than  $10^{16} \text{ cm}^{-3}$  and the results are discussed in detail for two samples.

### § 1. INTRODUCTION

MAGNETORESISTANCE effects in n-type InSb at liquid helium temperatures have been reported by Frederikse and Hosler (1956) and Kanai and Sasaki (1956). These authors have observed an oscillatory behaviour in the magnetoresistance as a function of magnetic field which is believed to be related to the de Haas-van Alphen effect and, at low fields, the former authors have found that the magnetoresistance becomes negative,  $\Delta\rho/\rho_0$  attaining a maximum negative value of  $4 \times 10^{-3}$ . The first part of this paper is concerned with experiments aimed at determining whether the negative magnetoresistance is a bulk property of the material or an experimental effect, since no straightforward theory accounts for it (Wilson 1953). The second part describes the results of measurements on the oscillatory magnetoresistance.

### § 2. NEGATIVE MAGNETORESISTANCE

Magnetoresistance measurements were made initially on samples cut from a crystal of n-type InSb having a donor concentration of  $5 \times 10^{16} \text{ cm}^{-3}$ . The samples were oriented with their current axes in a [110] direction and mounted in the cryostat in such a way that the magnetic field could be applied in a direction parallel or perpendicular to the current axis. The ends of the samples were copper plated and current and potential leads soldered to them with Indium metal. Errors due to having the potential leads at the ends of the specimen were not considered to be of much importance since only the variation of  $\Delta\rho/\rho_0$  with magnetic field was required (Drabble and Wolfe 1957). A pen recorder was used to indicate the change in resistance as the magnetic field was continuously varied, this method being quicker than plotting points and changes of one part in  $10^5$  being easily measurable.

The first samples to be measured were prepared by grinding rectangular pieces of material to dimensions of  $1 \text{ mm}^2$  cross section by 10 mm long. Longitudinal and transverse magnetoresistance was measured at 4.2°K in magnetic fields up to



about 1500 oersteds and in each case  $\Delta\rho/\rho_0$  was negative at the lower fields with a maximum negative value of about  $2 \times 10^{-3}$  at fields in the region of 100 oersteds. At higher fields the change in resistance decreased and  $\Delta\rho/\rho_0$  became positive above 200 oersteds. The form of the curves is typified in curve A, figure 1, which shows the transverse magnetoresistance for one of these samples.

To find out whether this result was connected in any way with the method of preparation of the specimen a rectangular sample of the above dimensions was prepared using an 'Airbrasive' sandblast cutter. In this case  $\Delta\rho/\rho_0$  showed no negative value but instead a smooth curve of parabolic form. The transverse magnetoresistance for this sample is shown by curve B, figure 1. This result suggests that the negative magnetoresistance is not a bulk property of the material but a secondary effect dependent upon the treatment of the sample. Samples prepared by turning cylindrical rods using a small lathe and the 'Airbrasive' cutter (Barbieri and Durand 1956), gave results similar to B, figure 1, indicating that the actual shape of the specimen was unimportant.

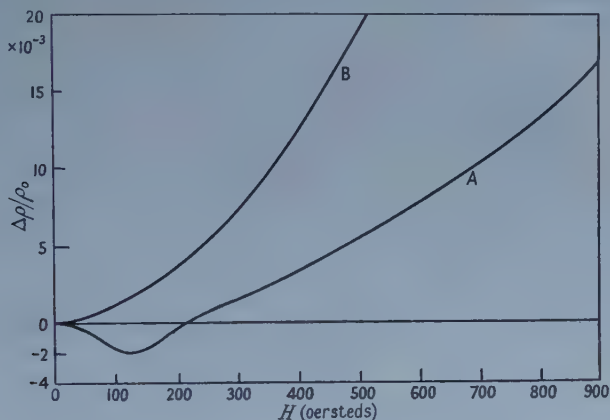


Figure 1. Variation of transverse magnetoresistance with  $H$ . Curve A, rectangular ground sample. Curve B, sample prepared with 'Airbrasive' cutter.

In some cases it was found that samples produced by the 'Airbrasive' cutting technique, and showing no negative magnetoresistance, subsequently showed a negative effect after the sample had been ground on a hard surface using an aqueous suspension of 600 grade carborundum as the abrasive. Heavily etching the sample after this treatment failed to remove the negative magnetoresistance demonstrating that the effect produced by the grinding must penetrate through the bulk of the specimen. It is thought that, due to the presence of large particles in the abrasive, grinding the sample may have introduced small cracks or 'dislocation cracks' similar to those observed by Allen (1957) in InSb crystals subjected to sudden impact.

To provide a closer comparison with the results of Frederikse and Hosler (1956) the experiment was repeated using a cylindrical sample of higher purity ( $N_d - N_a = 7.5 \times 10^{15} \text{ cm}^{-3}$ ), prepared as described above. This sample is subsequently referred to in § 3 as sample 1. The longitudinal magnetoresistance is shown in figure 2, curve A, and indicates a slight negative magnetoresistance which is about eight times smaller than that found by Frederikse and Hosler. The effect

of deliberately bending the material was investigated. A cylindrical sample similar to that used above was bent through an angle of about  $1^\circ$  by supporting it at the ends, hanging a weight of 30 grammes at the centre and heating to  $230^\circ\text{C}$ .† This resulted in a very high dislocation density at the centre of the sample. The longitudinal magnetoresistance after this treatment is shown in figure 2, curve B; the negative magnetoresistance has increased to four times its former value and, at higher fields,  $\Delta\rho/\rho_0$  shows a rapid increase with  $H$  in contrast to curve A for the unbent sample. It must be noted that, as is evident from figure 2, material carefully prepared by the 'Airbrasive' method sometimes showed a small negative magnetoresistance, but for all the samples investigated  $-\Delta\rho/\rho_0$  was increased by bending and, in some cases, by grinding in the manner described. To eliminate the possibility of any experimental errors platinum potential contacts were used for the measurements described in figure 2 (Broom 1958). The effect of the Hall voltage produced across the contacts due to slight misalignment was eliminated by making two traces for each orientation of the sample, reversing the direction of the magnetic field for the second trace, the mean value of the two curves being taken as the true magnetoresistance.

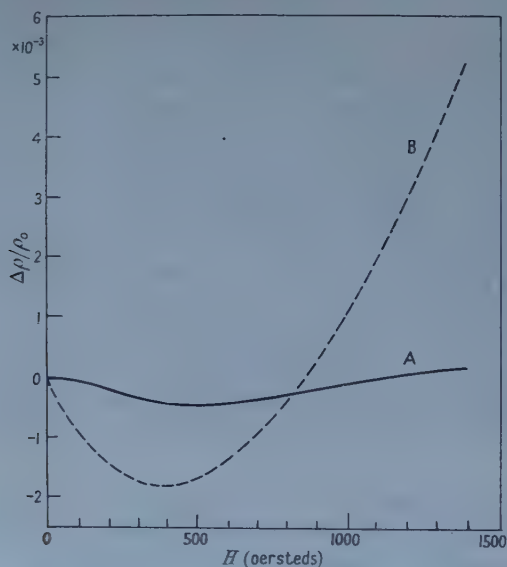


Figure 2. Variation of longitudinal magnetoresistance with  $H$ . Curve A, unstrained sample. Curve B, strained sample.

### § 3. OSCILLATORY MAGNETORESISTANCE

No oscillatory effects were observed at magnetic fields up to 10 000 oersteds in the less pure samples previously described. Sample 1 (figure 2, curve A) showed oscillations at magnetic fields above 2000 oersteds but the results described here in detail are those for another sample, 2, of slightly greater purity, which showed more oscillations. Preparation of the sample and measurement of the magnetoresistance was carried out in the manner described in § 2 for sample 1; platinum potential contacts were again used and the current axis was aligned in a  $[110]$  crystal direction.

† The author is indebted to Mr. J. W. Allen of this laboratory for producing the bent specimen.

This sample showed a very small negative magnetoresistance of about  $2 \times 10^{-4}$  in a longitudinal magnetic field of 560 oersteds.

Figure 3 shows the magnetoresistance of sample 2 as a function of magnetic field, the full curve representing the magnetoresistance obtained in a longitudinal field and the broken curve the magnetoresistance in a transverse field. Oscillations of large amplitude are apparent and four minima can be distinguished on the curves. It will be noticed that the minima in the transverse magnetic field occur at

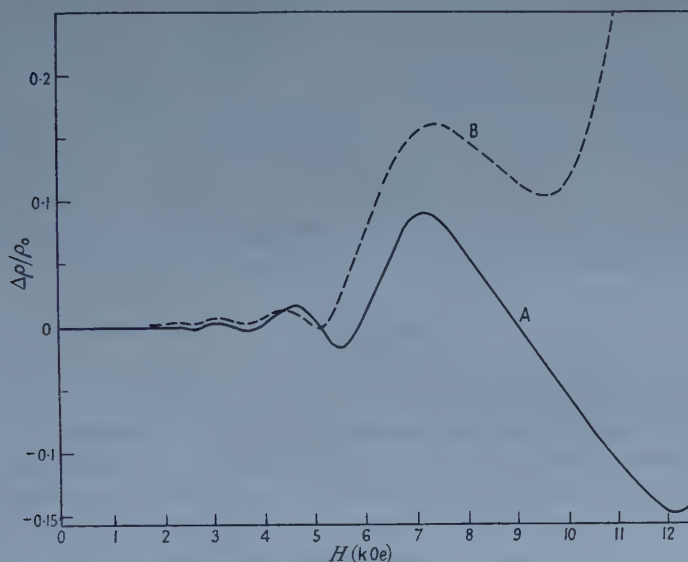


Figure 3. Variation of oscillatory longitudinal (A) and transverse (B) magnetoresistance with  $H$ .

slightly lower values of  $H$ , particularly at the high field end of the curve: this was attributed to the steeper slope of the non-oscillatory component in this orientation causing a displacement of the minima. On this assumption only the values obtained in a longitudinal magnetic field were used in subsequent calculations. The effect of lowering the temperature below 4.2°K is shown in figure 4. The full curve shows the longitudinal magnetoresistance at 4.2°K, the broken curve the values obtained at 1.7°K. In the figure only the low field part of the curve is

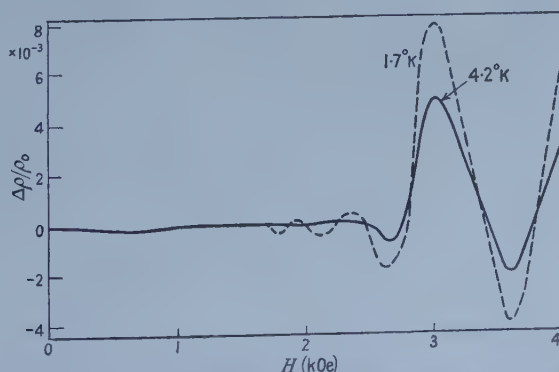


Figure 4. Variation of oscillatory longitudinal magnetoresistance with  $H$ .

traced in order to show the smaller values of  $\Delta\rho/\rho_0$  on a larger scale than in figure 3. It is clear that lowering the temperature increases the amplitude of the oscillations and also enables two more resistance minima to be resolved, at 2120 and 1800 oersteds.

The condition for observing the oscillatory magnetoresistance may be identified with the cyclotron resonance condition, namely, the scattering time should be sufficiently long to enable the electrons to complete at least one orbit before being scattered. This may be expressed by the relation  $\omega_c\tau > 1$  where  $\omega_c/2\pi$  is the cyclotron resonance frequency  $f_c = eH/2\pi m^*c$ , and  $\tau$  is the relaxation time.  $m^*$  is the effective mass of the electrons and  $e$  their electric charge. For the above case  $\omega_c\tau > 1$  may be written as  $\mu H > 1$ , where  $\mu$  is the Hall mobility. Davydov and Pomeranchuk (1940) have predicted that minima occur in the resistance when the Fermi energy  $\zeta$  is equal to a multiple of the cyclotron resonance frequency, viz.

$$\zeta = (n + \frac{1}{2})\hbar\omega_c \quad \dots\dots (1)$$

where  $n$  is an integer  $= 0, 1, 2 \dots$ . Assuming spherical energy surfaces the numerical value of  $\zeta$  is given by

$$\zeta = \frac{h^2}{8m^*} \left( \frac{3N}{\pi} \right)^{2/3} \quad \dots\dots (2)$$

from which it will be seen that  $m^*$  occurs on both sides of equation (1) showing that the values of  $H$  for which the minima occur depend only on the number of carriers  $N$ . It is evident from equation (1) that  $(n + \frac{1}{2}) \propto 1/\omega_c \propto 1/H$  and thus the minima should be equidistant when  $\Delta\rho$  is plotted against  $1/H$ . The minima obtained in a longitudinal magnetic field, from figures 3 and 4, are arbitrarily labelled by  $n' = 1, 2$ , etc., and in figure 5 these numbers are plotted against the corresponding values of  $1/H$ . A similar set of figures obtained from sample 1 are also included and it is evident that the graphs for both these samples are straight lines indicating that the interval  $\Delta(1/H)$ , separating the minima, is constant.

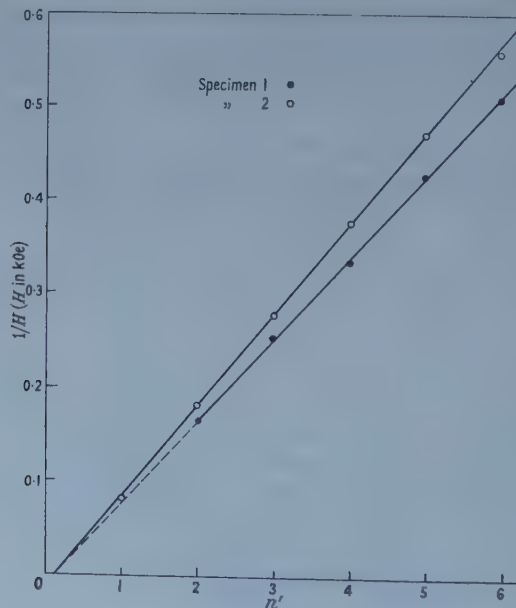


Figure 5.  $1/H$  plotted against resistance minima (arbitrarily numbered 1-6).



On comparing these results with equation (1) it is clear that the minima occur at values approximating to integral multiples of  $\hbar\omega_c$  and the best fit is obtained with equation (1) if the factor  $\frac{1}{2}$  is omitted. At present no explanation can be offered for this disagreement with theory.

From equations (1) and (2) and using the mean value of  $\Delta(1/H)$  for the separation of the resistance minima the number of carriers may be calculated. The results obtained for samples 1 and 2, compared with the values obtained from the Hall coefficient measured at 77°K, are shown in the table and the agreement is seen to be quite good.

	Sample 1	Sample 2
Average $\Delta(1/H)$ from fig. 5 ( $\text{Oe}^{-1}$ )	$0.86 \times 10^{-4}$	$0.94 \times 10^{-4}$
$(N_d - N_a) \text{ cm}^{-3}$ from magnetoresistance	$7.1 \times 10^{15}$	$6.0 \times 10^{15}$
$(N_d - N_a) \text{ cm}^{-3}$ from Hall coefficient	$7.5 \times 10^{15}$	$6.1 \times 10^{15}$

Theory predicts that the Hall voltage should also exhibit an oscillatory behaviour but with the oscillations 180° out of phase with those of the resistance (Zil'berman 1956). To check this the Hall coefficient was measured as a function of magnetic field up to 11 000 oersteds but, in agreement with the results of Frederikse and Hosler (1956), was found to be constant and no modulation could be observed.

#### ACKNOWLEDGMENTS

The author wishes to express his gratitude to Dr. E. H. Rhoderick for his kind assistance with the preparation of the manuscript. Acknowledgment is made to the Admiralty for permission to publish this paper.

#### REFERENCES

- ALLEN, J. W., 1957, *Phil. Mag.*, **2**, 1475.  
 BARBIERI, F., and DURAND, J., 1956, *Rev. Sci. Instrum.*, **27**, 871.  
 BROOM, R. F., 1958, *Proc. Phys. Soc.*, **71**, 500.  
 DAVYDOV, B., and POMERANCHUK, I., 1940, *J. Phys. U.S.S.R.*, **2**, 147.  
 DRABBLE, J. R., and WOLFE, R., 1957, *J. Electronics and Control*, **3**, 259.  
 FREDERIKSE, H. P. R. and HOSLER, W. R., 1956, *Canad. J. Phys.*, **84**, 1377.  
 KANAI, Y. and SASAKI, W., 1956, *J. Phys. Japan*, **11**, 1017.  
 WILSON, A. H., 1953, *The Theory of Metals*, 2nd Edition (Cambridge: University Press), p. 193.  
 ZIL'BERMAN, G. E., 1956, *Soviet Phys., J.E.T.P.*, **2**, 650.

## The Band Spectrum of Silicon Monofluoride, SiF

By J. W. C. JOHNS AND R. F. BARROW

Physical Chemistry Laboratory, University of Oxford

MS. received 2nd October 1957

**Abstract.** The emission spectrum of SiF has been examined in the Schumann and infra-red regions. The system B-A ( $\nu_{0,0} = 11850.8 \text{ cm}^{-1}$ ) is strong, and rotational analysis shows that both states are  $^2\Sigma$ . A new rotational analysis of the 0, 0 band of the  $\alpha$ -system, A- $x^2\Pi$ , although in substantial agreement with earlier work, confirms the view that state A is  $^2\Sigma^+$ , and not  $^2\Pi$  (case-*b*), as had previously been supposed. Violet degraded bands which have tentatively been ascribed to five systems, all with  $x^2\Pi$  as the ground state, are found, partly superimposed, in the region 51 000 to 53 500  $\text{cm}^{-1}$ . Three of the excited states of SiF appear to form a Rydberg series of  $^2\Sigma^+$  states leading to the ground state  $\dots\pi^4\sigma^2, ^1\Sigma^+$  of SiF $^+$ . The ionization potential is found to be 7.2<sub>6</sub> ev. Evidence about the dissociation energy is briefly considered; the best value seems to be  $D_0''(\text{SiF}) \sim 125 \text{ kcal}$ .

### § 1. INTRODUCTION

WITH a few important exceptions, as for example the cases of H<sub>2</sub> and N<sub>2</sub>, comparatively little is yet known about highly excited molecular states. One obvious way to get information is by emission spectroscopy in the Schumann region, but here observations are often limited to wavelengths above about 1300 Å because of the need to use a transparent window between source and spectrograph. This limitation is less important for odd-electron molecules whose ionization potentials will be relatively low: thus the first ionization potential of NO is 9.25 ev, whereas those for CO and O<sub>2</sub> are 14.01<sub>3</sub> and 12.07<sub>5</sub> ev respectively.

One such odd-electron molecule whose longer wavelength spectrum may readily be excited is silicon monofluoride, and we have now investigated its emission spectrum in the Schumann region. A number of bands have indeed been found, which, since they occur as doublets separated by the doublet separation of the ground state of silicon monofluoride, must arise from transitions involving highly excited states of this molecule. In the hope of gaining further information about these states we have investigated the spectrum as far as 9000 Å in the infra-red. No transitions involving the new states have been found. A new system of silicon monofluoride has, however, been discovered which proves to arise from the transition B-A. Since the bands have only P and R branches which are resolved into doublets at high values of *K* the transition must be  $^2\Sigma \rightarrow ^2\Sigma$ . State A must then be  $^2\Sigma$  not  $^2\Pi_r$  (case-*b*) as has been believed up to now. A new rotational analysis of the 0, 0 band of the A- $x$  system has been carried out confirming this view. Further, states B, D, and one of the new states can now be identified as a Rydberg series of  $^2\Sigma^+$  states. The ionization potential of silicon monofluoride is found to be 7.2<sub>6</sub> ev.

## § 2. EXPERIMENTAL

The spectrum was excited in a hollow cathode discharge run in a few millimetres of helium which was circulated through the tube in a closed vacuum system containing traps to keep it in a high state of purity. The steel cathode was filled with a mixture of powdered silicon and barium fluosilicate. To obtain good photographs of the infra-red system the barium fluosilicate had to be replaced by the corresponding potassium compound since the spectrum of barium fluoride was emitted very strongly in this region.

The far ultra-violet bands were photographed in about an hour and a half with a 1 metre grazing incidence vacuum spectrograph. Ilford Q2 plates were used. The bands were measured either against internal lines of Si or against Cu II lines superimposed on the band spectrum by replacing the steel cathode by one lined with copper. In the latter case the two spectra were separated by means of a focal plane shutter.

The infra-red bands were photographed in a first order of a 2.4 metre grating in an Eagle mounting. Hypersensitized Kodak IIaN plates were used. Exposure times were about 45 minutes. The bands were measured against Fe arc lines.

The 0, 0 band of the A-x system was photographed by Professor P. B. Zeeman in a fourth order of the 21 foot grating at the University of Stellenbosch.

## § 3. ANALYSIS AND DETERMINATION OF CONSTANTS

3.1. *The Infra-Red System*  $B^2\Sigma^+ - A^2\Sigma^+$ 

A reproduction of the 0, 0 band is shown in figure 1(a) (Plate). That this system arises from the transition B-A is shown (i) by the agreement between the observed position of the origin of the 0, 0 band,  $11\,850.84\text{ cm}^{-1}$ , and that calculated from the A, B-x systems,  $11\,850.7\text{ cm}^{-1}$ , (ii) by the agreement between the combination differences,  $\Delta_2 F(K)$ , obtained from the rotational analysis of the 0, 0 band of B-A with those obtained from the 0, 0 bands of the A, B-x systems (table 1).

Table 1. Comparison of Combination Differences from the 0, 0 bands of Systems A-x, B-x and B-A

$K$	B-A	A-x	$K$	B-A	B-x
	$\Delta_2 F''(K)$	$\Delta_2 F'(K)$		$\Delta_2 F''(K)$	$\Delta_2 F'(K)$
10	24.0	24.13	22	56.2	55.89
15	—	35.58	23	59.1	58.33
20	47.0	47.01	24	61.1	60.89
25	58.3	58.31	25	63.6	63.43
30	69.6	69.93	26	66.1	65.69
35	80.9	80.85	27	68.5	68.17
40	92.2	92.13	28	70.9	70.73
45	103.2	103.23	29	73.4	73.23
50	114.0	114.29	30	75.8	75.64
			31	78.6	78.07
			32	80.9	80.59
			33	83.4	83.04
			34	85.6	85.62
			35	88.3	87.89
			36	90.8	90.00

The differences for B-x are taken from Eyster. That the agreement here is not very good probably arises from the fact that all the lines involved must be blends.

Reliable constants for  $v''=0$  may be obtained from the 0, 0 band of the A-x system (§ 3.4) so that constants for  $v'=0$  were determined from the relation

$$R(K-1) + P(K) + 2(D' - D'')K^2(K^2 + 1) = 2\nu_0 + 2(B' - B'')K^2 \dots \dots (1)$$

The value of  $2\Delta D$  was adjusted until the left-hand side plotted against  $K^2$  gave a straight line.

The other constants were determined by plotting (i) for bands having a common upper state,  $\Delta R(K) = \Delta P(K)$  against  $K(K+1)$ , (ii) for bands having a common lower state,  $\Delta R(K-1) = \Delta P(K+1)$  against  $K(K+1)$ .

To within the limits of accuracy of measurement it was found that  $D'$  and  $D''$  did not vary with  $v$ . The above procedure could not be used with the 4, 2 band. However, the first four values of  $B'$  can be represented very well by a linear relation so that it seemed safe to use a calculated value for  $B_4'$ .  $B_2''$  was then determined from (1).

In favourable cases the spin doubling was resolved in lines with  $K \geq 35$ .

The constants are summarized in table 2.

Table 2. Constants for the B-A System ( $\text{cm}^{-1}$ )

$v$	$B'$	$B''$	$\Delta G'v, v+1$	$\Delta G''v, v+1$
0	0.62477	0.57375	1001.6 <sub>0</sub>	698.7 <sub>2</sub>
1	0.62015	0.56457	991.9 <sub>0</sub>	679.3 <sub>5</sub>
2	0.61549	(0.55568)	982.3 <sub>0</sub>	
3	0.61091		(972.6 <sub>3</sub> )	
4	(0.60628)			

$D' = 1.0_1 \times 10^{-6}$		$D'' = 1.5_7 \times 10^{-6}$	
$v', v''$	$\nu_0$	$v', v''$	$\nu_0$
0, 1	11152.1 <sub>2</sub>	2, 0	13844.3 <sub>4</sub>
0, 0	11850.8 <sub>4</sub>	3, 1	14127.9 <sub>2</sub>
1, 0	12852.4 <sub>4</sub>	4, 2	14421.2 <sub>0</sub>
2, 1	13145.6 <sub>2</sub>		

### 3.2. The 0, 0 Band of the System $A^2\Sigma - x^2\Pi_r$ (Case-a)

Following an earlier rotational analysis of the 0, 0 band this system was ascribed to the transition  $A^2\Pi$  (case-b) -  $x^2\Pi$  (case-a) (Eyster 1937). However, several features, especially the absence of doubling in the  $^5R_{21}$  and  $R_2$  branches at high  $J$ , strongly support the view that the upper state is  $^2\Sigma$  and not  $^2\Pi$  (case-b). The rotational analysis presented little difficulty, and eleven of the twelve branches predicted for  $^2\Sigma - ^2\Pi$  (case-a) were found. The analysis remains substantially the same as that proposed by Eyster.

### 3.3. The $^2\Sigma$ State

The term values of a  $^2\Sigma$  state are given by:

$$F_1 = BK(K+1) - DK^2(K+1)^2 + 1/2\gamma K$$

$$F_2 = BK(K+1) - DK^2(K+1)^2 - 1/2\gamma(K+1)$$

from which:

$$\frac{1}{2}[\Delta_2 F_1(K) + \Delta_2 F_2(K)] = (4B - 6D)(K + \frac{1}{2}) - 8D(K + \frac{1}{2})^3.$$



$B$  and  $D$  were determined in the usual way by plotting the mean of  $\Delta_2 F_1(K)$  and  $\Delta_2 F_2(K)$  over  $(K + \frac{1}{2})$  against  $(K + \frac{1}{2})^2$ . The spin splitting constant  $\gamma$  was determined directly from the combination relations

$$\begin{aligned} R_1(J = K - 0.5) - {}^R Q_{21}(J = K - 0.5) &= Q_1(J = K + 0.5) - {}^Q P_{21}(J = K + 0.5) \\ &= {}^Q R_{12}(J = K - 0.5) - Q_2(J = K - 0.5) \\ &= {}^P Q_{12}(J = K + 0.5) - P_2(J = K + 0.5) \\ &= \gamma K. \end{aligned}$$

### 3.4. The ${}^2\Pi$ State

It was assumed that the term values in the lower  ${}^2\Pi_r$  state could be expressed by the Hill and Van Vleck formulae

$$F_1 = B[(J + 0.5)^2 - \Lambda^2 + 0.5 \{4(J + 0.5)^2 + Y(Y - 4)\Lambda^2\}^{1/2}] - DJ^4 \pm \phi_1(J)$$

$$F_2 = B[(J + 0.5)^2 - \Lambda^2 - 0.5 \{4(J + 0.5)^2 + Y(Y - 4)\Lambda^2\}^{1/2}] - D(J + 1)^4 \pm \phi_2(J)$$

where  $\phi_1(J)$  and  $\phi_2(J)$  represent the  $\Lambda$ -type doubling. It follows that

$$\frac{1}{2}[\Delta_2 F_1(J) + \Delta_2 F_2(J)] = (4B - 14D)(J + 0.5) - 8D(J + 0.5)^3. \dots\dots (2)$$

The lower state terms were first evaluated with respect to  $K = 0$  in  $A^2\Sigma$  using the upper state term values already derived.

The  $\Lambda$ -type doubling is given directly by the differences  $F_{1d} - F_{1c}$  and  $F_{2d} - F_{2c}$  for the two components of the state.  $\Delta_2 F_1(J)$  and  $\Delta_2 F_2(J)$  were computed from the term values taking care to eliminate  $\Lambda$ -type doubling effects in the process of averaging.  $B$  and  $D$  were determined from (2).

The coupling constant  $A$  was determined from the relation

$$\left\{ \frac{F_1(J) - F_2(J) - D[(J + 1)^4 - J^4]}{B} \right\}^2 - 4(J + 0.5)^2 = Y(Y - 4)$$

where  $Y = A/B$ .

$\nu_0$  was determined using term values already obtained and unblended lines having  $J$  up to 20. The more usual method involving the Q branches was not used since the early Q lines of each sub-band are unresolved blends.

The sign of the  $\Lambda$ -doubling in  $x^2\Pi_{1/2}$  can be determined if the character of the upper state is assumed. It is difficult to see—from considerations of the electron configurations—how this state can be other than  ${}^2\Sigma^+$ . If it is assumed to be  ${}^2\Sigma^+$ , then the sign of the  $\Lambda$ -doubling in  $x^2\Pi_{1/2}$  is found to be the same as that predicted by the case- $a$  formula for a regular  ${}^2\Pi_{1/2}$  state,  $\Delta\nu_{dc} = -p(J + \frac{1}{2})$ , where  $p = 2AB_v l(l + 1)/\nu(\Pi, \Sigma)$ , if the doubling is produced by interaction with an excited  ${}^2\Sigma^+$  state. However, the observed doubling is smaller than that predicted on the assumption of a doubling produced by a pure precession interaction between  $A^2\Sigma^+$  and  $x^2\Pi$ .

The values of the constants are set out in table 3, together with calculated frequencies and values of residuals  $\nu_{\text{obs}} - \nu_{\text{calc}}$  for the first few lines.

### 3.5. The Far Ultra-Violet Bands

A reproduction of the far ultra-violet bands is given in figure 1(c) (Plate), and the measurements are listed in table 4. The most probable assignment is indicated. The system shown as G-x must be regarded as doubtful since all but two of the heads assigned to it are already assigned to other systems. But if the band at 51 938 is not part of such a system it would be difficult to account for the intensities

Table 3. The 0, 0 band of the System A-X

$\nu_0 = 22787.64$

The upper state $A^2\Sigma^+$				The lower state $X^2\Pi_r$		
$B_0' = 0.57372$				$B_0'' = 0.57886$		
$D_0' = 1.57 \times 10^{-6}$				$D_0'' = 1.08 \times 10^{-6}$		
$\gamma = -0.0062_5$				$A = 161.92$		
$\Delta\nu_{dc} (^2\Pi_{1/2}) = +0.002 (J + \frac{1}{2})$						
$J$	$^sR_{21}$	$^sQ_{21}$	$R_1$	$^sP_{21}$	$Q_1$	$P_1$
0.5	22871.47	22869.18	22869.17	—	22868.02	—
1.5	73.18	69.74	69.72	22867.45	67.44	22866.29
2.5	74.90	70.30	70.28	66.86	66.84	64.56
3.5	76.60	70.86	70.83	66.26	66.24	62.80
4.5	78.30	71.41	71.37	65.67	65.64	61.05
5.5	79.98	71.96	71.92	65.05	65.01	59.30
6.5	81.65	72.50	72.45	64.44	64.40	57.49
7.5	83.33	73.02	72.96	63.83	63.78	55.77
8.5	85.00	73.56	73.50	63.21	63.15	54.01
9.5	86.66	74.06	74.00	62.58	62.52	52.21
$J$	$R_2$	$^sQ_{12}$	$Q_2$	$P_2$	$^sPQ_{12}$	$^sOP_{12}$
0.5	—	—	—	—	—	—
1.5	22712.40	22708.94	22708.96	22706.67	22706.66	22705.51
2.5	14.10	09.48	09.50	06.06	06.04	03.76
3.5	15.78	10.01	10.04	05.44	05.42	01.98
4.5	17.44	10.51	10.55	04.81	04.78	00.19
5.5	19.09	11.01	11.05	04.16	04.12	22698.39
6.5	20.70	11.48	11.53	03.49	03.43	96.56
7.5	22.33	11.94	12.00	02.83	02.78	94.75
8.5	23.91	12.39	12.39	02.45	02.12	92.90
9.5	25.49	12.81	12.87	01.41	01.35	91.02
$J$	$^sR_{21}$	$^sQ_{21}$	$R_1$	$^sP_{21}$	$Q_1$	$P_1$
0.5	-0.06*	-0.01*	0*	—	+0.04	—
1.5	+0.33*	-0.03*	0*	-0.01*	0*	-0.05*
2.5	+0.11*	-0.06*	-0.04*	+0.02*	+0.04*	—
3.5	-0.12*	-0.02*	+0.01*	-0.02*	0*	—
4.5	0*	0*	+0.04*	-0.03*	0*	+0.01
5.5	+0.03*	0*	+0.04*	+0.01*	+0.05*	-0.02*
6.5	+0.06*	-0.05*	0*	0*	+0.04*	+0.04
7.5	-0.05*	-0.03*	+0.04*	-0.03*	+0.02*	+0.04*
8.5	+0.05	-0.04*	+0.01*	-0.03*	+0.03*	-0.04
9.5	+0.02	-0.04*	+0.02*	-0.04*	+0.02*	+0.07*
$J$	$R_2$	$^sQ_{12}$	$Q_2$	$P_2$	$^sPQ_{12}$	$^sOP_{12}$
0.5	—	—	—	—	—	—
1.5	—	—	—	-0.01*	0*	-0.03*
2.5	—	—	—	0*	+0.02*	-0.01*
3.5	—	+0.06*	+0.03*	+0.04*	+0.06*	-0.08*
4.5	—	-0.03*	-0.07*	+0.05*	+0.08*	—
5.5	—	—	—	+0.01*	+0.14*	+0.03*
6.5	—	+0.05*	0*	-0.02*	+0.04*	—
7.5	+0.04*	+0.06*	0*	0*	+0.05*	—
8.5	-0.02*	+0.02*	-0.04*	0*	+0.06*	—
9.5	+0.01*	+0.09*	+0.03*	-0.01*	+0.05*	+0.03

\* denotes blended line.

of the group of bands in that region. The upper state vibration frequencies found for the states G (?) and H are a little more than  $1000\text{ cm}^{-1}$  and are thus of the magnitude expected.

Table 4. The Vacuum Ultra-Violet Bands of SiF

<i>I</i>	$\nu$	System	$v', v''$	Head	<i>I</i>	$\nu$	System	$v', v''$	Head
0	51114	?			9	52077	{ G-X	1, 1	P <sub>2</sub>
0	130	E-X	0, 0	P <sub>2</sub>			{ H-X	0, 0	P <sub>2</sub>
0	143	E-X	0, 0	Q <sub>2</sub>			{ G-X	0, 0	P <sub>1</sub>
0	233	{ G-X	0, 1	OP <sub>12</sub>	10	098	{ G-X	1, 1	Q <sub>2</sub>
		{ H-X	0, 1	P <sub>2</sub>			{ H-X	0, 0	Q <sub>2</sub>
4	252	{ G-X	0, 1	P <sub>1</sub>	5	242	{ G-X	1, 1	OP <sub>12</sub>
		{ H-X	0, 1	Q <sub>2</sub>			{ H-X	0, 0	OP <sub>12</sub>
3	286	E-X	0, 0	OP <sub>12</sub>	7	260	{ G-X	1, 1	P <sub>1</sub>
5	302	E-X	0, 0	P <sub>1</sub>			{ H-X	0, 0	P <sub>1</sub>
3	400	H-X	0, 1	OP <sub>12</sub>	4	305	I-X	0, 0	P <sub>2</sub>
6	412	H-X	0, 1	P <sub>1</sub>	6	325	I-X	0, 0	Q <sub>2</sub>
3	601	H-X	1, 2	P <sub>1</sub>	0	468	I-X	0, 0	OP <sub>12</sub>
2	649	F-X	0, 0	P <sub>2</sub>	0	489	I-X	0, 0	P <sub>1</sub>
4	685	F-X	0, 0	Q <sub>2</sub>			{ G-X	1, 0	P <sub>1</sub>
0	829	F-X	0, 0	OP <sub>12</sub>	0	53106	{ H-X	1, 0	P <sub>2</sub>
1	851	F-X	0, 0	P <sub>1</sub>	4	118	H-X	1, 0	Q <sub>2</sub>
5	914	G-X	0, 0	P <sub>2</sub>	4	270	H-X	1, 0	OP <sub>12</sub>
8	938	G-X	0, 0	Q <sub>2</sub>	5	283	H-X	1, 0	P <sub>1</sub>
9	52077	G-X	0, 0	OP <sub>12</sub>	0	455	H-X	2, 1	P <sub>1</sub>

### 3.6. Summary of Molecular Constants

In transitions of the type  $^2\Sigma - ^2\Pi$ , if spin doubling,  $\Lambda$ -doubling, and effects due to  $D$  terms are neglected, the head-head separations can be expressed by

$$\Delta\nu = -\frac{2B'B_{\text{eff}}''}{B' - B_{\text{eff}}''} \quad \text{where} \quad B_{\text{eff}}'' = B_v'' \left[ 1 \pm \frac{B_v''}{A} \right].$$

A value of  $\alpha$  was estimated for the ground state from the head-head separations in the system B-X since the rotational constants for state B are known from the rotational analysis of system B-A. The value of  $\alpha$  was combined with the known value of  $B_0''$  to give  $B_e''$ . Rotational constants were calculated for states c and d using the ground state constants as determined above and the head-head separations in the systems C-X and D-X. (A reproduction of the D-X system is given in figure 1(b)).

The vibrational constants of all the states of SiF have been derived from band origins determined from the rotational constants and the two inner of the four heads observed in each band. Systems B, C and D-X are all violet degraded and these heads are P<sub>1</sub> and Q<sub>2</sub>: their separation from the sub-band origin is given by

$$\Delta\nu = -\frac{(B_{\text{eff}}'')^2}{4(B' - B_{\text{eff}}'')} - \frac{B'}{4},$$

again assuming that spin doubling,  $\Lambda$ -doubling, and  $D$  term effects are small.

However, in system A-X the head-head separations are large. In this case, the positions of the origins were found by finding the maximum value of the difference between the appropriate rotational term values, including  $D$  terms.

The constants for the known states of SiF are arranged in table 5.

Table 5. Summary of Constants of the Known States of SiF

	$T_e^a$	$\omega_e$	$x_e\omega_e$	$B_e$	$\alpha$	$r_e$ (Å)
I	[52409]					
H <sup>2</sup> $\Sigma^+$	[52179]	$\approx 1030$				
G	[52020]	$\approx 1020$				
F	[51770]					
E	[51224]					
D <sup>2</sup> $\Sigma^+$	47418.6	1003.2	5.64	0.625	0.005 <sub>5</sub>	1.54
C	39438.4	891.5	5.8	0.6043	0.0067	1.570
B <sup>2</sup> $\Sigma^+$	34561.5	1011.2 <sub>3</sub>	4.825	0.62707	0.00462	1.5414
A <sup>2</sup> $\Sigma^+$	22858.4	718.5 <sub>8</sub>	10.167 <sup>b</sup>	0.57839	0.00941 <sup>c</sup>	1.6049
X <sup>2</sup> $\Pi_r$	$\pm 80.9_6$	857.6	4.67	0.5817	0.0056 <sub>6</sub>	1.600

Notes. a Values in parentheses are of  $T_0$ , not  $T_e$ .

b  $+0.157(v+\frac{1}{2})^3$

c  $+1.3 \times 10^{-4}(v+\frac{1}{2})^2$

Rotational constants for states C and D were determined from head-head separations.  $\alpha$  for state X was determined from head-origin separations and was combined with  $B_0$  to give the value of  $B_e$  quoted.

## § 4. DISCUSSION

### 4.1. The Electron Configurations of the States of SiF

Possible low-lying configurations (see for example Asundi and Samuel 1936) are set out below:

- (1) KKL  $(z\sigma)^2(y\sigma)^2(w\pi)^4(x\sigma)^2(v\pi)$  —<sup>2</sup> $\Pi_r$
- (2) KKL  $(z\sigma)^2(y\sigma)^2(w\pi)^4(x\sigma)(v\pi)^2$  —<sup>2</sup> $\Sigma^+$ , <sup>2</sup> $\Sigma^-$ , <sup>2</sup> $\Delta$ , <sup>4</sup> $\Sigma^-$
- (3) KKL  $(z\sigma)^2(y\sigma)^2(w\pi)^3(x\sigma)^2(v\pi)^2$  —<sup>2</sup> $\Pi_r$ , <sup>2</sup> $\Pi_r$ , <sup>2</sup> $\Pi$ , <sup>2</sup> $\Phi$ , <sup>4</sup> $\Pi_i$
- (4) KKL  $(z\sigma)^2(y\sigma)^2(w\pi)^4(x\sigma)^2 \dots (ns\sigma)$  —<sup>2</sup> $\Sigma^+$
- (5) KKL  $(z\sigma)^2(y\sigma)^2(w\pi)^4(x\sigma)^2 \dots (np\sigma)$  —<sup>2</sup> $\Sigma^+$

The ground state must have configuration (1). State A is very much less stable than the ground state and must thus involve promotion into an antibonding orbital. Since the transition to A from state B, which is identified as arising from configuration (4) is observed, configuration (2) is the only possibility left for A. In (3) a strongly bonding  $(w\pi)$  electron has been promoted to the less strongly bonding  $(x\sigma)$  orbital and this configuration must therefore be even less strongly bound than (2) and the conclusion is that these states are repulsive.

The evidence about state C is incomplete. The C-X bands show strong Q branches, but the transition C-A seems not to occur. State C may then be

$$(w\pi)^4(x\sigma)^2(3d\delta) - ^2\Delta.$$

### 4.2. Rydberg Series

The states B and D are regarded as Rydberg states according to the arguments above.  $T_e$  for these states can be represented by:

$$T_e = 58566 - \frac{109737}{(m-1.862)^2} \text{ where } m = 4, 5.$$

With  $m=6$ ,  $T_e=52157$  which may be identified with the state H with  $\nu_0 \sim 52179 \text{ cm}^{-1}$ , giving the strongest far ultra-violet bands. The process of ionization can in this case be regarded as the loss of an electron from the silicon



atom since the ionization potential of fluorine is so very much larger than that of silicon. The quantum defect for the corresponding series in silicon might thus be expected to be about the same as that for SiF. This is in fact found to be the case since the quantum defect in the  $3s^2 3p \dots ns$  series of Si is 1.92 at  $n=4$ . States analogous to  $B^2\Sigma^+$  in SiF are known for CF, GeF, and SnF. If it is assumed that these are all the first members of Rydberg series and that the quantum defects follow closely the defects in the atoms it is possible to derive ionization potentials for these molecules. It is of interest to observe that the heats of dissociation of the ionized species, calculated from these ionization potentials, are all, as might be expected, somewhat higher than those of the normal molecules.

Table 6

Molecule	<i>m</i>	$-a$	$T_e$	I.P. (ev)	$D(MX)$ (kcal)	$D(MX^+)$ (kcal)	$D(MX^+)/D(MX)$
CF	3	1.06 <sup>a</sup>	42705 <sup>c</sup>	8.9 <sub>1</sub>	114 <sup>c</sup>	169	1.48
SiF	4	1.86	34562	7.2 <sub>6</sub>	125	146	1.17
GeF	5	2.85 <sup>a</sup>	35007 <sup>d</sup>	7.2 <sub>8</sub>	115 <sup>f</sup>	129	1.12
SnF	6	3.5 <sub>0</sub> <sup>b</sup>	34108 <sup>e</sup>	7.0 <sub>4</sub>	90 <sup>f</sup>	109	1.21

a, Moore (1949), b, Shenstone (1956, private communication), c, Andrews and Barrow (1951), d, Andrews and Barrow (1950), e, Jenkins and Rochester (1937), f, Andrews (1951).

#### 4.3. The Dissociation Energy of SiF

The dissociation energy of SiF as determined from linear Birge-Sponer extrapolation of a number of its states is shown in table 7.

Table 7

State	Products of Dissociation	$D$ (kcal mole <sup>-1</sup> )
$H^2\Sigma^+$	$F(^2P) + Si(6s)$ 59500 cm <sup>-1</sup>	95 <sup>a</sup>
$D^2\Sigma^+$	$F(^2P) + Si(5s)$ 54600 cm <sup>-1</sup>	107
$B^2\Sigma^+$	$F(^2P) + Si(4s)$ 39850 cm <sup>-1</sup>	136
$A^2\Sigma^+$	$F(^2P) + Si(^3P)$ 0	109 <sup>b</sup>
$X^2\Pi_r$	$F(^2P) + Si(^3P)$ 0	113

a, with  $\omega_e \simeq 1030$ ,  $x_e\omega_e \simeq 6$ . b, too low as  $y_e\omega_e$  is fairly large and positive.

It seems probable that the high levels of  $B^2\Sigma^+$  will converge more rapidly than indicated by a linear formula so that we can regard 136 kcal mole<sup>-1</sup> as an upper limit. 115 kcal mole<sup>-1</sup> would seem to be a sensible lower limit, so that the spectroscopic evidence indicates that  $D_0'' = 125 \pm 10$  kcal mole<sup>-1</sup>. Baughan (1953) has recently proposed that the dissociation energy of the diatomic group IVb halides can be expressed by

$$D(MX) = 0.25\{2D(X_2) + \Delta_s H(M) - \Delta H_{\text{formation}}(MX_4)\}/1.079.$$

Honig (1954) has measured the heat of sublimation of silicon as 105 kcal mole<sup>-1</sup> ( $\pm 12$ ) by a second Law treatment of mass-spectroscopic observations. Using  $D(F_2) = 38$ ,  $\Delta H_{\text{formation}}(SiF_4) = -370$ , and  $\Delta_s H(Si) = 105$  (all expressed in kcal mole<sup>-1</sup> and at 298°K) we find  $D_{298^0}(SiF) = 126$  kcal mole<sup>-1</sup> in fortuitously close agreement with the spectroscopic value.

4.4. *Unassigned Bands in the SiF Discharge*

There are still some features of the spectrum of SiF which have so far defied analysis. Among these are two groups which Johnson and Jenkins (1927) named the  $\epsilon$  bands. One group falls in the green and is the most prominent feature observed when the source is viewed through a pocket spectroscope. They are always associated with strong emission of SiF. They have a more complex structure and appear to be triple-headed. They may perhaps be due to a quartet-quartet transition in SiF, or a triplet-triplet transition in SiF<sup>+</sup>.

The appearance of the ultra-violet bands is consistent with the idea that the transition may be  $^1\Pi \leftrightarrow ^1\Sigma$ . The ground state of SiF<sup>+</sup> must be  $^1\Sigma^+$ : further the vibration frequency will be about 1000 cm<sup>-1</sup>. The first excited singlet state of SiF<sup>+</sup> is expected to be  $^1\Pi$ , by analogy with the isoelectronic molecule AlF and would also be expected to have a vibration frequency of about 1000 cm<sup>-1</sup>. It would probably lie at about 35 000 cm<sup>-1</sup> above  $x^1\Sigma^+$ . The two most prominent of the ultra-violet  $\epsilon$  bands are separated by 1021 cm<sup>-1</sup>, but since they lie at about 24 000 cm<sup>-1</sup> they cannot be the  $A^1\Pi \rightarrow x^1\Sigma^+$  transition in SiF<sup>+</sup>; they could however involve a highly excited  $^1\Sigma$  state analogous perhaps to  $B^1\Sigma^+$  in AlF. It is thus suggested that some of the bands may be due to a transition  $^1\Sigma^+ - A^1\Pi$  in SiF<sup>+</sup>.†

The  $\delta$  bands also observed by Johnson and Jenkins are as yet not explained satisfactorily. There are two possibilities. First as was suggested by Asundi and Samuel (1936), they could form the 1, 0 sequence of the system c-x. This system is remarkable in that there are apparently no bands to the violet of the 0, 0 sequence. The rotational constants indicate that bands of the 1, 0 sequence should be almost headless which does at least fit with the appearance of the bands. However, the bands do not appear to be emitted by the hollow cathode source, though it is difficult to be certain since the region is covered by a strong continuum. Their appearance, the facts that they are favoured by passing low current discharges through SiF<sub>4</sub> vapour, and that they do not seem to be excited in the vigorous hollow cathode source, suggest that the emitter may be SiF<sub>2</sub>, analogous to CF<sub>2</sub>. High resolution photographs will be necessary before a decision between the two possibilities can be made.

## ACKNOWLEDGMENTS

We should like to express our thanks to Professor P. B. Zeeman for his kindness in providing the plate of the 0, 0 band of the A-x system.

One of us (J. W. C. J.) is indebted to the Department of Scientific and Industrial Research for the award of a maintenance grant.

## REFERENCES

- ANDREWS, E. B., 1951, *D. Phil. Thesis*, University of Oxford.  
 ANDREWS, E. B., and BARROW, R. F., 1950, *Proc. Phys. Soc. A*, **63**, 185; 1951, *Ibid.*, **64**, 481.  
 ASUNDI, R. K., and SAMUEL, R., 1936, *Proc. Indian Acad. Sci. A*, **3**, 346.  
 BAUGHAN, E. C., 1953, *Quart. Rev. Chem. Soc. Lond.*, **7**, 103.  
 EYSTER, E. H., 1937, *Phys. Rev.*, **51**, 1078.  
 HONIG, R. E., 1954, *J. Chem. Phys.*, **22**, 1610.  
 JENKINS, F. A., and ROCHESTER, G. D., 1937, *Phys. Rev.*, **52**, 1135.  
 JOHNSON, R. C., and JENKINS, H. G., 1927, *Proc. Roy. Soc. A*, **116**, 327.  
 MOORE, C. E., 1949, *Atomic Energy Levels*, National Bureau of Standards, Circular 467 (Washington D.C.).

† *Note added in proof.* Rotational analysis of the  $\epsilon$  band now shows that they are to be assigned to two transitions  $D^1(^2\pi \text{ case-}b) - A^2\Sigma^+$ ,  $C^1(^2\pi, A \sim 16) - A^2\Sigma^+$  in SiF.

## The Infra-Red Spectrum of Diamond

By M. J. STEPHEN†  
Mathematical Institute, Oxford

*Communicated by C. A. Coulson ; MS. received 30th September 1957*

**Abstract.** The contribution of lattice vibrations to the infra-red spectrum of diamond in the 2 to 6  $\mu$  region has been calculated from the vibrational frequency distribution where second nearest neighbour central forces are taken into account. It is assumed that this absorption is associated with two-phonon processes arising from second-order terms in the electric moment. Certain general selection rules are determined. Most of the details of the observed spectrum are reproduced in the calculated spectrum.

### § 1. INTRODUCTION

THE diamond structure consists of two identical interpenetrating face-centred cubic lattices with one of these lattices displaced relative to the other one-quarter of the distance up the main body diagonal. Because of the crystal symmetry the displacement of one sub-lattice relative to another will not result in an electric moment. The fundamental optical vibration is therefore infra-red inactive, although it is Raman active. However, weak absorption bands have been observed in diamond (Robertson, Fox and Martin 1934).

Diamond crystals are found to fall into two types which exhibit different absorption spectra. Type I diamonds exhibit absorption in two regions: from 2 to 6  $\mu$  and from 8 to 13  $\mu$ . Type II diamonds show absorption only in the 2 to 6  $\mu$  region. The absorption in the 8 to 13  $\mu$  region for type I diamonds varies from specimen to specimen and appears therefore to be an impurity or structure sensitive property. The 2 to 6  $\mu$  absorption does not vary from specimen to specimen. Lax and Burstein (1955) suggested that this 2 to 6  $\mu$  absorption is due to lattice vibrations. The absorption coefficients of bands associated with thermal vibrations should be temperature dependent. Collins and Fan (1954) have studied the temperature dependence of absorption in diamond. The absorption in the 8 to 13  $\mu$  region was found to be temperature independent whereas the bands in the 2 to 6  $\mu$  region showed a temperature dependence which was similar to that of corresponding bands in Si and Ge.

The 2 to 6  $\mu$  intrinsic absorption in diamond occurs at higher frequencies than the fundamental optical vibration at 1332  $\text{cm}^{-1}$ . Lax and Burstein (1955) have suggested that this absorption is associated with two-phonon processes arising from second-order terms in the expansion of the electric moment in terms of the atomic displacements. These terms would be produced by charge deformation during vibration. The customary mechanism for explaining summation bands, namely anharmonic forces, is inadequate in diamond structures, since anharmonic forces without charge deformation can produce no electric moment of any order and hence no absorption. Second-order electric moments

† Now at Department of Theoretical Chemistry, University of Cambridge.



are adequate to explain the existence of summation bands without anharmonic terms. The latter may produce additional broadening or side bands. Anharmonic forces in diamond are small as shown by the small thermal expansion coefficient (which would be zero for purely harmonic forces).

In this paper the contribution of two-phonon processes to the absorption coefficient in the 2 to 6  $\mu$  region has been calculated from Smith's (1948) calculations on the vibrational spectrum of diamond. Anharmonic forces have been neglected as being small and the electric moment has been expanded to second order so that these two-phonon processes are allowed. Certain general selection rules for combination bands valid throughout the Brillouin zone have been determined.

## § 2. THEORY

The absorption of radiation of frequency  $\omega$  by a crystal of volume  $V$  may be described by an absorption coefficient  $k(\omega)$  (Lax and Burstein 1955)

$$k(\omega) = \left[ \frac{n}{\epsilon} \left( \frac{E_e}{E} \right)^2 \right] \frac{4\pi^2 \omega}{Vc} I(\omega). \quad \dots\dots (1)$$

The factors in brackets represent a correction for the fact that the absorption process takes place in a medium of dielectric constant  $\epsilon$  and refractive index  $n$ . The factor  $(E_e/E)^2$  describes the fact that in the crystal the effective field  $E_e$  may differ from the macroscopic electric field  $E$ . For vibrational transitions, with which we will be concerned here,

$$I(\omega) = \sum_n \left| \int X_n^*(\mathbf{x}) \mathbf{M}(\mathbf{x}, \mathbf{v}) X_m(\mathbf{x}) d\mathbf{x} \right|^2 \delta(E_m - E_n - \hbar\omega) \quad \dots\dots (2)$$

where  $\mathbf{x}$  denotes a set of nuclear coordinates,  $X(\mathbf{x})$  are vibrational states and  $\mathbf{M}(\mathbf{x}, \mathbf{v})$  is the dipole moment.  $\sum_n$  means a sum over all possible vibrational states weighting each with the usual Boltzmann factor.

As shown by Lax and Burstein for homopolar crystals we may expand the dipole moment in terms of the nuclear displacements  $\mathbf{u}(l)_k$ .  $\mathbf{u}(l)_k$  is the displacement of atom  $k$  in unit cell  $l$ . Thus

$$M_p = M_p^{(0)} + M_p^{(1)} + M_p^{(2)} + \dots \quad \dots\dots (3)$$

$$M_p^{(0)} = 0,$$

$$M_p^{(1)} = \sum_{\mu} \sum_{kl} \exp(i\mathbf{v} \cdot \mathbf{r}^l) M_{p,\mu}(l)_k u_{\mu}(l)_k \quad \dots\dots (4)$$

$$M_p^{(2)} = \sum_{\mu\nu} \sum_{kl} \sum_{k'l'} \exp(i\mathbf{v} \cdot \mathbf{r}^l) M_{p,\mu\nu}(l)_{kk'} u_{\mu}(l)_k u_{\nu}(l')_{k'}. \quad \dots\dots (5)$$

$M_{p,\mu}(l)_k$  and  $M_{p,\mu\nu}(l)_{kk'}$  are the derivatives of the dipole moment taken in equilibrium,  $\mathbf{v}$  is the wave vector of the radiation and  $\mathbf{r}^l$  denotes the position vector of the  $l$ th unit cell. We have regarded the radiation as having wavelength large compared with the unit cell dimensions.

As the dipole moment must be invariant for rigid translations the coefficients in (4) and (5) must satisfy the following invariance relations.

$$M_{p,\mu}(l)_k \text{ is independent of } l. \quad \dots\dots (6)$$

$$\sum_k M_{p,\mu}(l)_k = 0$$

$$M_{p,\mu\nu}(l)_{kk'} = M_{p,\mu\nu}(l-v)_{kk'} = M_{p,\nu\mu}(l-v)_{k'k}, \quad \dots\dots (7)$$

$$\sum_{lk} M_{p,\mu\nu}(l)_{kk'} = 0, \quad \dots\dots (8)$$



It is easily seen that for the diamond lattice  $M_p^{(1)} = 0$  and we will be concerned here only with  $M_p^{(2)}$  which leads to two-phonon processes.

Following Smith we assume that the nuclei form a set of  $6N$  coupled harmonic oscillators and then we may write the nuclear displacements  $\mathbf{u}_k^{(l)}$  in terms of complex normal coordinates  $\xi_j^{(q)}$  where  $j = 1 \dots 6$ . In Smith's notation we have

$$\sqrt{m} \mathbf{u}_k^{(l)} = \sum_{qj} \mathbf{e}(k|j) \exp(i\mathbf{q} \cdot \mathbf{r}^l) \xi_j^{(q)}. \quad \dots\dots(9)$$

The choice of possible wave vectors  $\mathbf{q}$  is restricted by the cyclic lattice condition. the  $\mathbf{e}(k|j)$  are the eigenvectors of the lattice corresponding to the frequency  $\omega_j^{(q)}$ .

We substitute from (9) into (5). The resulting expression may be simplified by replacing  $l-l'$  by  $l$  and performing the sum over  $l'$ . For all practical purposes we may regard the incident photon as having zero momentum, i.e.  $\mathbf{v} = 0$ . From (5) we then obtain

$$M_p^{(2)} = \sum_q \sum_{jj'} M_p(q, jj') \xi_j^{(q)} \xi_{j'}^{*(q)} \quad \dots\dots(10)$$

where

$$M_p(q, jj') = \frac{1}{m} \sum_{\mu\nu} \sum_{lkk'} M_{p, \mu\nu}(l, kk') \exp(i\mathbf{q} \cdot \mathbf{r}^l) e_{\mu}(k|j) e_{\nu}^{*}(k'|j'). \quad \dots\dots(11)$$

Substituting (10) in (2) performing the integration and thermal averaging over all possible initial states we obtain for the second-order effect

$$I^{(2)}(\omega) = \sum_p \sum_{jj'} \sum_q i_p(q, jj') \quad \dots\dots(12)$$

where

$$i_p(q, jj') = 2C(q)C(j') \{M_p(q, jj')M_p^{*}(q, jj') + M_p(q, jj')M_p^{*}(q, jj')\} \delta(\hbar\omega_j^{(q)} - \hbar\omega) \left\{ \exp[\beta(q)] \right\} \quad \dots\dots(13)$$

and

$$C(j) = \frac{\hbar/2\omega(j)}{1 - \exp[-\beta(j)]}; \quad \beta(j) = \frac{\hbar\omega(j)}{kT}.$$

The two cases in (13) correspond to combination and difference bands, i.e.  $\omega_j^{(q)} = \omega_j^{(q)} \pm \omega_{j'}^{(q)}$ . The summation in (12) over all wave vectors  $\mathbf{q}$  may be replaced by an integration and the second-order spectrum will consist of a number of continuous bands each of which has a maximum at a certain frequency. The result of the superposition will be a continuous background with a number of peaks. Thus in the interval  $d\omega$  we have

$$I^{(2)}(\omega) d\omega = \sum_p \sum_{jj'} \int \int \int i_p(q, jj') dq_1 dq_2 dq_3. \quad \dots\dots(14)$$

Owing to the delta function in (13) the range of integration in (14) will extend over the interval  $\omega \leq \omega_j^{(q)} \leq \omega + d\omega$ .

Equation (13) shows that at temperatures low compared with the Debye temperature difference bands will have very small intensity and that the intensity of combination bands will be nearly independent of temperature. If  $kT \simeq \hbar\omega$  the absorption increases with increasing temperature.

In order to determine which branches of the vibrational spectrum will combine we must determine the factors  $M_p(q, jj')$  at a number of points in the Brillouin zone. These factors are given by (11) and require a knowledge of  $M_{p, \mu\nu}(l, kk')$  and the eigenvectors  $\mathbf{e}(k|j)$  of the dynamical matrix.  $M_{p, \mu\nu}(l, kk')$  must transform as a tensor of rank three and it is easily shown using the invariance relations (7) and (8) that the non-zero components for the nearest neighbouring atoms depend on

one parameter only. Following Smith we label the two atoms in the base cell 0 and 0' with nearest neighbours  $\bar{1} \bar{2} \bar{3} \bar{4}$  and 1 2 3 4 respectively. Thus  $(\frac{l}{kk'})$  label bonds between nucleus  $(\frac{0}{k})$  of the base cell and some other nucleus  $(\frac{l}{k'})$  and we write

$$M_{\rho, \mu\nu}(\frac{1}{12}) = M_{\rho, \mu\nu}(1), \quad M_{\rho, \mu\nu}(\frac{\bar{1}}{21}) = M_{\rho, \mu\nu}(\bar{1}).$$

Using the transformation matrices given by Smith it is easily shown

$$M_{\alpha, \alpha\beta}(1) = -M_{\alpha, \beta\alpha}(1) = -M_{\alpha, \alpha\beta}(\bar{1}) = M_{\alpha, \beta\alpha}(\bar{1}) = n \text{ say. } \dots\dots (15)$$

All other non-zero components may be obtained by further application of the transformation matrices. If we extend  $M_{\rho, \mu\nu}(\frac{l}{kk'})$  to second nearest neighbours another six non-zero parameters are required to characterize this tensor. These parameters would be expected to be considerably smaller than for nearest neighbours and for simplicity we will only take nearest neighbours into account.

From the symmetry of the dynamical matrix at a general point in the Brillouin zone we have

$$e_{\alpha}(1|\frac{q}{j}) = \pm e_{\alpha}^*(2|\frac{q}{j}). \quad \dots\dots (16)$$

Using (15) and (16) we easily show that  $M_{\rho}(\frac{q}{jj'}) = 0$  if  $j \neq j'$  so that when we consider only nearest neighbour interactions no summation bands involving the same vibrational modes may occur. Thus we have the following combinations allowed at a general point in the zone:

$$\left. \begin{array}{cccccc} \omega_1 + \omega_2 & & & & & \\ \omega_1 + \omega_3 & \omega_2 + \omega_3 & & & & \\ \omega_1 + \omega_4 & \omega_2 + \omega_4 & \omega_3 + \omega_4 & & & \\ \omega_1 + \omega_5 & \omega_2 + \omega_5 & \omega_3 + \omega_5 & \omega_4 + \omega_5 & & \\ \omega_1 + \omega_6 & \omega_2 + \omega_6 & \omega_3 + \omega_6 & \omega_4 + \omega_6 & \omega_5 + \omega_6 & \end{array} \right\} \dots\dots (17)$$

Allowing for degeneracies these give 11 possible combinations. In addition to the general selection rule  $j \neq j'$  there are others valid at special points or along special lines in the zone. For example at  $q=0$  all combinations are forbidden and at  $q=(\frac{1}{2} \frac{1}{2} \frac{1}{2})$  we may have only combinations of optical and acoustical and transverse and longitudinal modes, i.e.  $\omega_1 + \omega_4$ ,  $\omega_2 + \omega_4$ ,  $\omega_3 + \omega_5$ ,  $\omega_3 + \omega_6$  and along the (111) direction we may only have combinations of transverse and longitudinal modes, i.e.  $\omega_1 + \omega_3$ ,  $\omega_1 + \omega_4$ ,  $\omega_2 + \omega_3$ ,  $\omega_2 + \omega_4$ ,  $\omega_3 + \omega_5$ ,  $\omega_3 + \omega_6$ ,  $\omega_4 + \omega_5$ ,  $\omega_4 + \omega_6$ .

In considering the Raman spectrum of diamond to determine the selection rules Smith only considered the point  $q=(\frac{1}{2} \frac{1}{2} \frac{1}{2})$ . This is a poor approximation as this is a point of high symmetry in the zone. To determine the relative importance of the various combinations (17) would require a knowledge of the eigenvectors  $e(k|\frac{q}{j})$  of the dynamical matrix at a number of points in the zone. The labour involved would be prohibitive and instead we assume for each of the combinations (17) that  $M_{\rho}(\frac{q}{jj'}) = n/m$  at all points in the zone (see (11) and (15)). Thus from (13) and (14) we obtain for a single combination band  $\omega(\frac{q}{j}) + \omega(\frac{q}{j'})$

$$I_{jj'}^{(2)}(\omega) d\omega = \frac{12n^2}{\hbar m^2} \int \int \int C(\frac{q}{j}) C(\frac{q}{j'}) dq_1 dq_2 dq_3. \quad \dots\dots (18)$$

$$\omega \leq \omega(\frac{q}{j'}) \leq \omega + d\omega.$$

The integral (18) diverges for the acoustical modes at  $q=0$ . This arises because of the approximation we have made in replacing  $M_{\rho}(\frac{q}{jj'})$  by  $n/m$  at the point  $q=0$ . Thus in order to evaluate (18) we exclude a small interval around

the origin. Values of  $\omega$  at various points in the zone are given by Smith. Use was made of her results where second nearest neighbours are taken into account. The range of values of  $\omega$  is divided into equal intervals  $d\omega = 0.6 \times 10^{14} \text{ sec}^{-1}$  and then the number of combinations  $\omega(\frac{q}{jj'}) = \omega(\frac{q}{j}) + \omega(\frac{q}{j'})$  of frequencies belonging to the same wave vector  $\mathbf{q}$  is counted in each interval and multiplied by the weighting factor  $C(\frac{q}{j})C(\frac{q}{j'})$ . Three histograms were plotted, each shifted  $0.2 \times 10^{14} \text{ sec}^{-1}$  in the  $\omega$  scale from the other two. These histograms were then smoothed out and give curves of  $I^{(2)}_{jj'}(\omega)$ . In figure 1 curves of the absorption coefficient for the 11 combinations considered are shown. The temperature was taken to be  $300^\circ\text{K}$ . In figure 2 the total absorption coefficient  $k(\omega)$  is compared with the typical spectrum for type I diamonds measured by Blackwell and Sutherland (1949) in the combination region. A similar scale has been used for both curves.

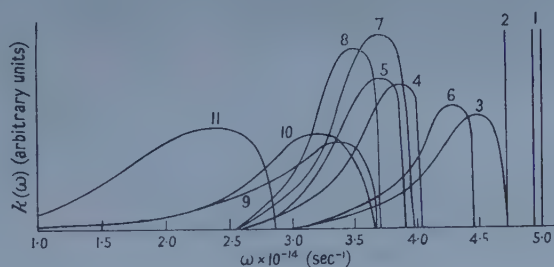


Figure 1. Absorption coefficients of combination bands. 1,  $\omega_1 + \omega_2$ ; 2,  $\omega_1 + \omega_3$ ; 3,  $\omega_1 + \omega_4$ ; 4,  $\omega_1 + \omega_5$ ; 5,  $\omega_1 + \omega_6$ ; 6,  $\omega_3 + \omega_4$ ; 7,  $\omega_3 + \omega_5$ ; 8,  $\omega_3 + \omega_6$ ; 9,  $\omega_4 + \omega_5$ ; 10,  $\omega_4 + \omega_6$ ; 11,  $\omega_5 + \omega_6$ .

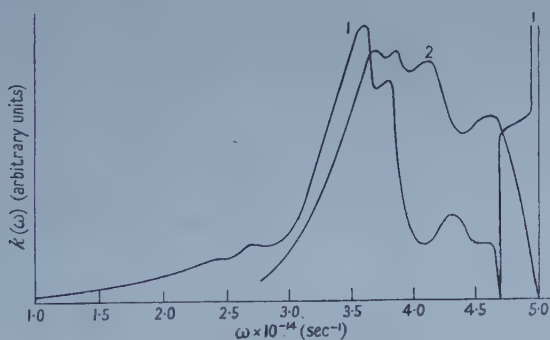


Figure 2. Comparison of calculated infra-red spectrum of diamond with experiment. 1, calculated; 2, observed.

### § 3. CONCLUSIONS

It is seen that the combinations of two acoustical or two optical phonons which give bands in the region  $2.0\text{--}3.0 \times 10^{14} \text{ sec}^{-1}$  and  $4.7\text{--}5.0 \times 10^{14} \text{ sec}^{-1}$  do not appear in the observed spectrum whereas they appear with a large intensity in the calculated spectrum. This disagreement is probably due to the approximation in putting  $M_p(\frac{q}{jj'}) = n/m$  for these combinations and the intensity of these bands would be greatly reduced if a full calculation of the  $M_p(\frac{q}{jj'})$  was made

at a number of points in the zone. This follows because as shown above at certain points these combinations are forbidden and therefore we might expect at intermediate points  $M_p(\frac{g}{j})$  to be much smaller than for combinations allowed at all points in the zone.

Excluding these two bands most of the details of the spectrum are reproduced in the calculated spectrum although the frequencies of the main peaks do not agree exactly. Changing the relative intensities of the different combinations would improve the agreement and this would seem to indicate that the vibrational spectrum as calculated by Smith is essentially correct.

#### ACKNOWLEDGMENTS

The author would like to thank the Ministry of Supply for an appointment as Vacation Consultant at the Royal Radar Establishment, Malvern, and Dr. G. G. Macfarlane and Dr. T. P. McLean of the Royal Radar Establishment for much useful discussion.

#### REFERENCES

- BLACKWELL, D. E., and SUTHERLAND, G. B. B. M., 1949, *J. Chim. Phys.*, **46**, 9.  
COLLINS, R. J., and FAN, H. Y., 1954, *Phys. Rev.*, **93**, 674.  
LAX, M., and BURSTEIN, E., 1955, *Phys. Rev.*, **97**, 39.  
ROBERTSON, R., FOX, J. J., and MARTIN, A. E., 1934, *Phil. Trans. Roy. Soc. A*, **232**, 463.  
SMITH, H. M. J., 1948, *Phil. Trans. Roy. Soc. A*, **241**, 105.



## On the Structure of Extensive Cosmic Ray Air Showers: Lateral Structure of the Ionizing Component

By E. W. KELLERMANN, T. SHAW† AND G. O. WALKER‡

Department of Physics, The University of Leeds

MS. received 18th October 1957

**Abstract.** The lateral distribution of ionizing particles in extensive showers over the approximate range of size  $5 \times 10^4 < N < 5 \times 10^5$  particles has been studied using a core-locating device (already described) to select showers, and unshielded 'probing' counter trays to estimate particle density at measured distances from the located shower axis. The distribution is determined with useful accuracy for four ranges of shower size. For the three greatest size ranges examined, the distribution is generally in accord with that of other workers and confirms the observation that for these showers structure does not vary significantly with shower size. For the range corresponding to the smallest showers, which are of a size for which accurate structure measurements have not previously been reported, it is found that the lateral structure shows evidence of significant ageing of the effective cascade.

### § 1. INTRODUCTION

THE lateral density distribution of particles in extensive air showers remains one of the keys to the understanding of shower development. Measurements of it have been carried out in the immediate core region by Hazen, Williams and Randall (1954), for large counter separations by the Russian School (1955, 1956), by Rossi and his co-workers (cf. Clark *et al.* 1957), by Cranshaw *et al.* (1957), and in the intermediate region by Williams (1948), Cocconi, Tongiorgi and Greisen (1949), Campbell and Prescott (1952), Haddara and Jakeman (1953), Fujioka (1953), and Kasnitz and Sitte (1954). One of the problems in these experiments has been that of locating the shower core with sufficient accuracy, and core detecting devices of varying efficiency have been employed by many of these workers. In a previous communication (Kellermann, Shaw and Dickinson 1957, to be referred to as I), a core sensitive device has been described and its accuracy of core location estimated. The response of this apparatus encouraged us in the hope of determining the lateral electron distribution with an accuracy high enough to present a useful contribution.

### § 2. EXPERIMENTAL METHOD

The experiments described here were carried out 100 m above sea level, and preliminary accounts have been given at the cosmic-ray conferences at Guanajuato 1955, and at Oxford (Kellermann 1956).

The method adopted rested on the comparison of the electron density near the core detecting device with densities registered at various distances from the detector in showers for which core-selection was indicated. Electron density at points remote from the core detectors was estimated using two trays of unshielded counters, 'probing trays'. Figure 1 shows the geometry of the arrangement;

† Now at British Nylon Spinners, Doncaster.

‡ Now at Marconi's Wireless Telegraph Company, Great Baddow, Essex.

at one time density comparisons for four distances of separation of a probing tray and a core detector were made. These distances were varied, and altogether more than 500 000 showers were recorded for distances between probing trays and core detectors of from 4 to 66 metres.

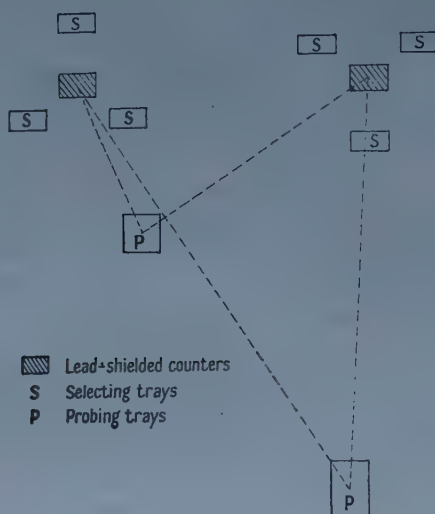


Figure 1. Lay-out of core detectors and probing trays.

The core detectors and their performance have been described in detail in I. It is sufficient to recall here that a detector consists of counter trays shielded in a lead block placed at the centre of a triangle, of side 5 m, formed by three trays of unshielded counters, the 'selecting trays'. A selecting tray contained two counters of area  $140 \text{ cm}^2$  and one counter of area  $35 \text{ cm}^2$ . The core detectors have been shown to respond to shower cores of which more than 50% fall within 3 m of the centre of the lead block. Each of the probing trays contained ten counters (or counter-groups connected in parallel) of 240, 480 or  $960 \text{ cm}^2$  area, the larger counter areas being used at the greater distances from the core detectors. The whole counter arrangement was triggered by a master pulse from the trays of selecting counters incorporated in either of the core detectors, and events were classified according to the particle density at the core detectors as indicated by the discharge of counters in these trays. As in I, a (4.2) event, for example, denotes a discharge of four counters out of the six  $140 \text{ cm}^2$  area counters in one set of selecting trays. For each density group indicated by the selecting trays the counter discharge distribution and hence the density at the probing trays was determined. In I the relative contribution of showers of different densities to the response of the selecting trays for the four groups is given; the average densities correspond to shower sizes extending from about  $5 \times 10^4$  to about  $5 \times 10^5$  particles.

### § 3. ANALYSIS

When either core detector registers a core event, the shower axis falls on average about 3 m from the centre of the detector. The selecting trays are spaced uniformly at a distance of 3 m from the central unit, and together they give a response which describes an average density over the three points at which the trays are placed. This average density will be that at a certain distance from the shower axis which is likely to be somewhat larger than 3 m; no attempt is made

to calculate this distance, but the internal evidence of the work supports the view that it is, in fact, rather greater than 3 m.

If, for any shower of which the core is detected, the density at this distance is taken to be unity that at a probing tray may be written as  $\alpha$ , where  $\alpha < 1$ , and where  $\alpha$  is certainly a very slowly varying function of shower size. Accordingly, a single value of  $\alpha$  is applicable to the range of shower densities included in any one of the density categories defined by the discharges of the counters in the selecting trays, and the response of the probing trays is determined by a calculable density spectrum of incident showers for which  $\alpha$  is the only parameter. For a group of showers falling within a single density category, indicated by the selecting trays, the frequency with which  $\nu$  out of the  $n$  counters in a probing tray are discharged for all values of  $\nu$  may be obtained. That value of  $\alpha$  which in conjunction with the known density spectrum near the shower axis best fits the observed distribution is then determined.

The analysis follows closely that commonly used to describe the simultaneous discharge of counter arrays by showers, with the difference that one considers not the normal shower density spectrum  $S(x)$ , but a spectrum  $S^c(x)$  which includes only those showers for which the detector has registered a core event.

The spectrum  $S^c(x)$  is not known, but an adequate expression for it can be obtained by assuming its form and fitting the rate of certain events calculated with it to the observed rate. For this purpose we choose the distribution of discharges in the small counters of the selecting trays and test the fit of the assumed spectrum by means of the  $\chi^2$ -test.

Since the criterion of core selection which we have used differs between the density groups, the spectrum  $S^c(x)$  of showers with detected cores has to be deduced separately for each of the four density groups. It is found that the spectrum  $S^c(x)$  can be written in the general form

$$S_i^c(x) = R_i(x)S(x)$$

where  $S(x) = dx/x^{\gamma+1}$  is the density spectrum of all air showers with  $\gamma = 1.5$ , and the index denotes the density group.  $R_i(x)$  can be interpreted as the response of the shielded counters of the core detector, which modifies the response band of the counters in the selecting trays very much as would additional counters in coincidence.

A good fit is obtained in the four groups by writing

$$R_i(x) = \{1 - \exp(-a_i x)\}^2$$

with  $a_1 = 0.0175 \text{ m}^2$ ,  $a_2 = 0.0105 \text{ m}^2$ ,  $a_3 = 0.0070 \text{ m}^2$ ,  $a_4 = 0.0175 \text{ m}^2$  and where all densities  $x$  are measured in particles/ $\text{m}^2$ , for the (3.3), (4.2), (5.1), and (6.0) groups respectively. The result that the response functions for the first and last groups are identical, but different from those of the other groups, is at first surprising, but it is clear that the functions have been chosen simply to fit observed events, and that these events depend on several factors all of which do not operate in the same direction.

With this spectrum we can now write down the rate  $\mathcal{R}$  for the discharge of  $\nu$  counters out of ten in the probing tray when, for instance, the (4.2) event has been recorded

$$\mathcal{R}_{(4.2)}(x) \propto \int_0^\infty \{1 - \exp(-A_0 x)\}^4 \exp(-2A_0 x) S_2^c(x) \times \{1 - \exp(-A_1 \alpha x)\}^\nu \exp\{-(10-\nu)A_1 \alpha x\}.$$



Here  $A_0$  is the area of one of the selecting counters,  $A_1$  the area of the counters in the probing trays,  $x$  and  $\alpha x$  the densities prevailing at the respective trays.

The actual determination of  $\alpha$  has been made using a method described by Broadbent, Kellermann and Hakeem (1950). It consists essentially in comparing the frequencies of discharges of a number of counters in the probing trays, calculated for particular values of  $\alpha$ , with the observed number by means of a least square method, i.e. a best fit is obtained for a particular value of  $\alpha$ . This method is not only quite sensitive, but it yields, too, the standard error in the fitted  $\alpha$ . A complete list of the values of  $\alpha$  is given in the table with their standard

The Fitted Values of  $\alpha$ , determined for Distances  $r$  from Shower Axis

Distance $r$ (m)	Shower density group			
	(3.3)	(4.2)	(5.1)	(6.0)
4.0	$0.66 \pm 0.08$	$0.97 \pm 0.11$	$0.85 \pm 0.08$	$0.90 \pm 0.11$
6.0	$0.64 \pm 0.10$	$0.77 \pm 0.17$	$0.64 \pm 0.10$	$0.97 \pm 0.12$
7.0	$0.62 \pm 0.10$	$0.69 \pm 0.07$	$0.54 \pm 0.04$	$0.56 \pm 0.10$
8.0	$0.32 \pm 0.05$	$0.49 \pm 0.09$	$0.39 \pm 0.06$	$0.57 \pm 0.09$
11.0	$0.38 \pm 0.06$	$0.41 \pm 0.04$	$0.40 \pm 0.05$	$0.46 \pm 0.07$
15.5	$0.19 \pm 0.03$	$0.31 \pm 0.03$	$0.19 \pm 0.04$	$0.25 \pm 0.03$
19.7	$0.16 \pm 0.02$	$0.16 \pm 0.01$	$0.20 \pm 0.02$	$0.22 \pm 0.02$
30.2	$0.102 \pm 0.018$	$0.081 \pm 0.015$	$0.101 \pm 0.013$	$0.097 \pm 0.014$
40.1	$0.049 \pm 0.012$	$0.037 \pm 0.012$	$0.038 \pm 0.004$	$0.052 \pm 0.008$
50.9	$0.030 \pm 0.005$	$0.034 \pm 0.004$	$0.028 \pm 0.002$	$0.031 \pm 0.002$
55.0	$0.019 \pm 0.005$	$0.023 \pm 0.004$	$0.023 \pm 0.003$	$0.031 \pm 0.002$
65.7	$0.021 \pm 0.002$	$0.020 \pm 0.003$	$0.017 \pm 0.001$	$0.021 \pm 0.002$

deviations. The employment of large counter areas in the probing trays has resulted in small standard errors, even for the larger separations of these trays from the detector. It should be noted that the (3.3) events, of which there are many more recorded than of (6.0) events, show larger errors for the larger separations than do the (6.0) events. This must be expected, since the (3.3) events are due to smaller showers which will bias the distribution in the probing trays towards 0 events, i.e. no discharge of counters.

#### § 4. DISCUSSION OF RESULTS AND CONCLUSION

The logarithm of the value of  $\alpha$  determined has been plotted in figure 2 against the distance from the centre of the core detector in metres. The curve giving the best fit reaches the value  $\log \alpha = 0$  (that is to say,  $\alpha = 1$ ) at about 3.5 m for the (3.3) events, and at a slightly larger distance for the other groups, 4.5 m in the case of (6.0) events, an increase with shower size which one would expect.

The smooth curves drawn are the lateral distributions calculated by Nishimura and Kamata and communicated by K. Greisen privately in late 1956, they represent results amended from those of these authors in 1952 (cf. Greisen 1956), and have been calculated for a pure cascade, arising from a single electron or photon primary. The theoretical curve decreases initially as  $r^{s-2}$  where  $s$  is the 'age parameter' of the pure electron-photon cascade. The two curves drawn for the age parameters  $s=1.0$  and  $s=1.4$  have been fitted at  $\log \alpha = 0$ . They can thus be thought to provide a rough scale within which the lateral distribution of the real showers can be represented.

It will be seen that the experimental results obtained for all but the smallest shower sizes are compatible with a distribution corresponding to a parameter



$s = 1.25$  and show no appreciable variation with size. In this respect our results agree with those obtained by other workers who have examined the lateral particle distribution as a function of the shower size (Cocconi *et al.* (1949), Kasnitz and Sitte (1954), Abrosimov *et al.* (1955), and Clark *et al.* (1957)). Zatsepin and Khristiansen (1956) in an analysis of the Russian work have published graphs which show that the initial slope for showers of all sizes together is compatible with a Nishimura-Kamata curve with an age parameter  $s$  between 1.2 and 1.3. This agrees with our results better than those of Clark *et al.* (1957) who obtained a result closer to 1.4.

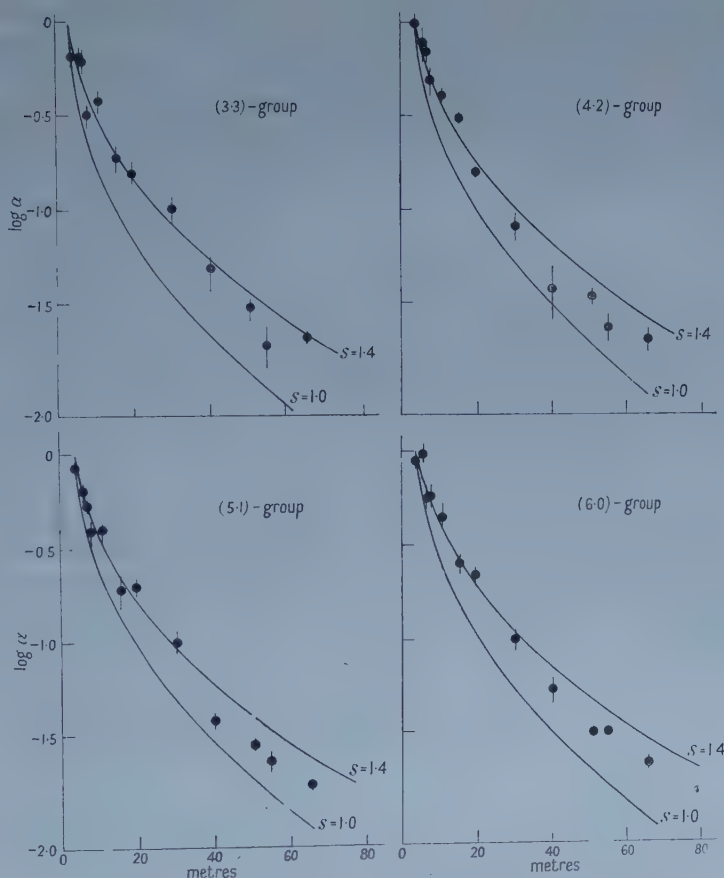


Figure 2. The values of  $\alpha$ , determined in the four density groups, plotted on a semi-logarithmic scale. The curves represent, on the same scale, the Nishimura-Kamata functions  $f(r/r_0, s)$  with  $r_0 = 79$  m.

The slope obtained for the (3.3) group, however, seems to require a value of  $s$  rather larger than that obtained for the other groups. Whereas all our other groups define rather wide density groups, we note that the (3.3) group corresponds to a fairly narrow density band about the average particle density of 25 particles/m<sup>2</sup> at approximately 4 metres from the core, and to a shower size of about  $5 \times 10^4$  particles (cf. I). The next group in our density range (4.2) already contains a very much wider range of densities, and our statistics are not good enough to

decide whether there is a gradual increase of the parameter  $s$  within the rather diffused ranges of density represented by the other groups.

Shower sizes as small as those in our (3.3) group have tended to be neglected in most experiments. They are included in the experiment of Abrosimov *et al.* and in the 'A' group of showers in the experiment of Kasnitz and Sitte. In the Russian work, statistics are insufficient to point to differences in slope for the different shower sizes. Variations found by Kasnitz and Sitte lie just within the limits afforded by the statistics and the indirect method of determination employed; but as far as any variation is indicated by this experiment, it seems that the lowest density, 'A', group has a flatter distribution than the others. In general, one must bear in mind that any uncertainty in the location of the shower axis will make the lateral distribution appear flatter. Such uncertainty will be greater for the larger showers so that any difference in slope of the curve for the larger and smaller showers will tend to be minimized.

By substitution of our value for  $s$  we find that the slope of the density distribution of our smallest size showers varies as  $r^{-0.6}$ , compared with an  $r^{-0.75}$  dependence for our (6.0) group containing the largest showers recorded by us. It is well known (cf. Greisen 1956) that the lateral electron distribution in extensive air showers is not very sensitive to shower size for a range of size from  $10^5$  to well over  $10^8$  particles. Nevertheless, one would expect that there must be limits beyond which a change of shower structure is noticeable, and the flatter distribution found to apply for the group of smallest showers which we have investigated, seems to indicate that for these showers the regenerative process which prevents apparent ageing of larger showers is beginning to fail.

#### ACKNOWLEDGMENTS

The authors wish to express their thanks to Professor E. C. Stoner for the facilities provided. They are indebted to Professor J. G. Wilson for valuable discussions of the manuscript. T. S. wishes to acknowledge a maintenance grant from the Department of Scientific and Industrial Research and G. O. W. grants from the University of Leeds and the Durham County Education Authority.

#### REFERENCES

- ABROSIMOV, A. T., BEDNYAKOV, A. A., ZATSEPIN, V. I., NECHIN, YU. A., SOLO'EVA, V. I., KRISTIANSEN, G. B., and CHIKIN, P. S., 1955, *J. Expt. Theor. Phys.*, **29**, 693.  
 BROADBENT, D., KELLERMANN, E. W., and HAKEEM, M. A., 1950, *Proc. Phys. Soc. A*, **63**, 861.  
 CAMPBELL, I. D., and PRESCOTT, T. R., 1952, *Proc. Phys. Soc. A*, **65**, 258.  
 CLARK, G., EARL, T., KRAUSHAAR, W., LINSLEY, J., ROSSI, B., and SCHERB, F., 1957, *Nature, Lond.*, **180**, 353.  
 COCCONI, G., TONGIORGI, V., and GRISEN, K., 1949, *Phys. Rev.*, **76**, 1020.  
 CRANSHAW, T. E., GALBRAITH, W., and PORTER, N. A., 1957, *Phil. Mag.*, **2**, 891.  
 FUJIOKA, G., 1953, *Proc. of the International Conference of theoretical Physics*, Tokyo and Kyoto, p. 125.  
 GRISEN, K., 1956, *Progr. Cosmic Ray Phys.* Vol. III, Amsterdam, p. 1.  
 HADDARA, S. R., and JAKEMAN, D., 1953, *Proc. Phys. Soc. A*, **66**, 549.  
 HAZEN, W. E., WILLIAMS, R. W., and RANDELL, C. A., JR., 1954, *Phys. Rev.*, **93**, 578.  
 KASNITZ, J. L., and SITTE, K., 1954, *Phys. Rev.*, **94**, 977.  
 KELLERMANN, E. W., 1956, *The Oxford Conference on Extensive Showers* (Harwell: Atomic Energy Establishment), p. 20.  
 KELLERMANN, E. W., SHAW, T., and DICKINSON, N., 1957, *Proc. Phys. Soc. A*, **452**.  
 WILLIAMS, R. W., 1948, *Phys. Rev.*, **74**, 414.  
 ZATSEPIN, G. T., and KRISTIANSEN, G. B., 1956, *The Oxford Conference on Extensive Showers* (Harwell: Atomic Energy Establishment), p. 11.

## RESEARCH NOTES

## The Adiabatic Fast Passage Experiment in Magnetic Resonance

By J. G. POWLES

Queen Mary College, London

*MS. received 27th August 1957 and in revised form 25th November 1957*

A WELL-KNOWN experiment in magnetic resonance is that in which one sweeps through resonance either by variation of field or frequency and, under certain conditions, the macroscopic magnetization after the passage is reversed in direction and is thus opposite to the equilibrium magnetization. The effect was among the first to be observed in magnetic resonance (Bloch 1946, Bloch *et al.* 1946) and has been used in a method of measuring the spin-lattice relaxation time,  $T_1$  (Drain 1949, Chiarotti and Giulotto 1954). It may have some importance in electron resonance in the realization of the solid state masers (Gordon *et al.* 1955, Combrisson *et al.* 1956) because the system after a fast passage is in a suitable excited state for the occurrence of stimulated emission of radiation. The same thing occurs in some molecular beam experiments (Rabi *et al.* 1954). The effect has been explained by Bloch (1946) and others (Rabi *et al.* 1954) but the treatment although straightforward is rather mathematical and I have frequently been asked for a more 'physical' explanation. The following may therefore be of interest.

In the experiment the nuclear or electronic system is allowed to come to equilibrium above or below resonance and so acquires a magnetization  $M_0$  in the direction  $Oz$  of the large field  $H_0$ . (We shall ignore small variations in  $M_0$  with the magnitude of  $H_0$ .) A transverse field of amplitude  $H_1$  and frequency  $\omega$  is applied. The resonant frequency or field is given by  $\omega_r = \gamma H_0$  where  $\gamma$  is the appropriate gyromagnetic ratio. We consider the case where we pass through resonance by variation of  $H_0$  at constant  $\omega$ . For the adiabatic fast passage experiment we must have

$$\frac{H_1}{T_2} \ll \left| \frac{dH_0}{dt} \right| \ll \gamma H_1^2$$

where  $T_2$  is the transverse relaxation time and  $dH_0/dt$  is the rate of variation of the large field near resonance. These conditions are not always possible to satisfy and indeed are usually very difficult to satisfy in the electron resonance case.

The first inequality is soon explained. It is clear that we must pass through resonance in a time less than  $T_2$  since we are going to produce transverse magnetization during the passage. We ignore  $T_1$  since  $T_1 \geq T_2$ . Now if we operate faster than  $T_2$  the 'line width' appropriate to the situation is  $H_1$  and the time  $\tau$  'at or near' resonance is  $H_1/(dH_0/dt)$ , i.e. we require

$$\frac{H_1}{dH_0/dt} \ll T_2 \quad \text{or} \quad \frac{H_1}{T_2} \ll \frac{dH_0}{dt}.$$

The second condition is easily shown to ensure that the magnetization nutates many revolutions during the passage through resonance. The angle of nutation

about  $H_1$  is of magnitude  $\gamma H_1 \tau$  and since  $\tau$  is  $H_1/(dH_0/dt)$  we have an angle of nutation of approximately  $\gamma H_1 \cdot H_1/(dH_0/dt)$  and for large nutation we require  $\gamma H_1^2/(dH_0/dt) \gg 1$ , i.e.  $dH_0/dt \ll \gamma H_1^2$ .

To see physically why a large angle of nutation assures that the magnetization is reversed after the fast passage consider an applied field ( $H_0(t)$ ,  $H_1 \cos \omega t$ ,  $H_1 \sin \omega t$ ). Transform to a coordinate system rotating at  $\omega$  about  $Oz$ , so that the effective field in the rotating coordinate system is (Rabi *et al* 1954) ( $H_0(t) - \omega/\gamma$ ,  $H_1$ , 0). We need now only consider precession about the resultant field  $H_r(t)$  shown in figure 1. Far above resonance the effective field is practically  $H_0(t) - \omega/\gamma$  and

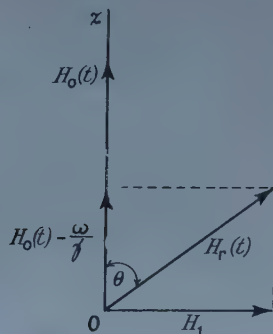


Figure 1.

is along  $Oz$ . As  $H_0$  is reduced,  $H_r$  begins to rotate and tends to leave the magnetization behind (we recall that  $\mathbf{M}$  is constant since for  $\tau \ll T_1, T_2$ , we have  $d\mathbf{M}/dt = \gamma \mathbf{M} \wedge \mathbf{H}$  so that  $\mathbf{M} \cdot (d\mathbf{M}/dt) = 0$  or  $(d/dt)|\mathbf{M}|^2 = 0$ ). However, as soon as this happens  $\mathbf{M}$  begins to precess about  $H_r$  but the angle between  $\mathbf{M}$  and  $H_r$  never gets very big because as  $\mathbf{M}$  gets left behind  $H_r$  the precession tends to swing the magnetization round, provided there is time for this to happen. Thus the magnetization  $\mathbf{M}$  follows  $H_r$  which after the passage through resonance is in the negative  $Oz$  direction. Reverting to the laboratory system does not affect this magnetization which is therefore found to be reversed.

In order for the reversal to occur therefore the rate of precession,  $d\phi/dt$ , about  $H_r$  must be more rapid than the angular velocity,  $d\theta/dt$ , of  $H_r$ , i.e. we require

$$\frac{d\phi}{dt} = \gamma H_r \gg \frac{d\theta}{dt}.$$

But

$$\tan \theta = \frac{H_1}{\{H_0(t) - \omega/\gamma\}} \quad \text{therefore} \quad \frac{d\theta}{dt} = \frac{H_1}{H_r^2} \left( \frac{dH_0}{dt} \right).$$

Hence we require  $\gamma H_r^3/H_1 \gg dH_0/dt$ . But the minimum value of  $H_r$  is  $H_1$  so that

$$\frac{dH_0}{dt} \ll \gamma H_1^2$$

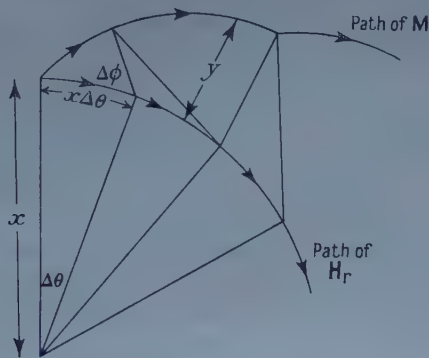
i.e. finally

$$\frac{H_1}{T_2} \ll \frac{dH_0}{dt} \ll \gamma H_1^2.$$

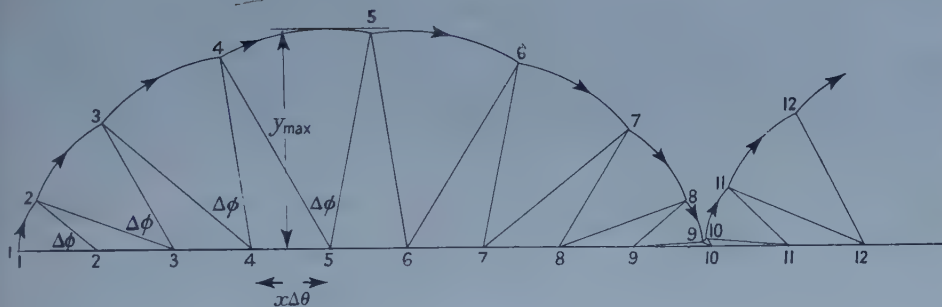
The outer inequality  $1/T_2 \ll \gamma H_1$  is merely a requirement that no decay of transverse magnetization should occur during a period of nutation,



Even so one has the feeling that during a number of rotations of the magnetization about  $\mathbf{H}_r$  during the fast passage the magnetization might well accumulate an appreciable angular displacement from  $\mathbf{H}_r$ . The fact that this is not so is easily illustrated by the diagrams in figure 2 where we have made



(a)



(b)

Figure 2.

the simplifying assumptions that  $\mathbf{H}_r$  is constant in magnitude and rotates in jumps of equal angular increments  $\Delta\theta$  at equal intervals and during any interval the magnetization precesses about  $\mathbf{H}_r$  by  $\Delta\phi$ .  $\mathbf{H}_r$  and  $\mathbf{M}$  are initially collinear. The 'physical' situation is shown in figure 2(a) which gives a perspective view and we are interested in the deviation of  $\mathbf{M}$  from  $\mathbf{H}_r$  marked  $y$ . The motion of the ends of the vectors  $\mathbf{M}$  and  $\mathbf{H}_r$  is shown in figure 2(b) where we have chosen  $x\Delta\theta = 1$  unit and  $\Delta\phi = 40^\circ = 0.7_0$  radian; it turns out that  $y_{\max} = 2.9$  units. If  $\mathbf{M}$  is to remain practically collinear with  $\mathbf{H}_r$  we require  $y_{\max} \ll x$ , i.e.  $x/y_{\max} = (1/\Delta\theta)(1/2.9) \gg 1$ , i.e.  $\Delta\theta \ll 0.3_4$ . But  $\Delta\phi = 0.7_0$  radian so that the condition is in fact  $\Delta\theta \ll \Delta\phi$ , i.e.  $d\phi/dt \gg d\theta/dt$  which is the second adiabatic condition. It is quite immaterial what scale is chosen for  $x\Delta\theta$  or what increment is chosen for  $\Delta\phi$  as the reader will readily discover.

In this way all the other properties of the fast passage effect are easily deduced, for example, the form of the nuclear induction signal, which is simply due to the transverse component of rotating magnetization of the constant magnitude  $M_0$  which is directed, effectively, always along  $\mathbf{H}_r$ .

In the experiment just described we passed through resonance from above, i.e. initially  $H_0 > \omega/\gamma$ . We note that the transverse magnetization was in phase

with  $H_1$ . On the other hand if we pass through resonance from below then initially  $\mathbf{H}_r$  is in the negative  $Oz$  direction and the magnetization tends to remain in the opposite direction to  $\mathbf{H}_r$ . Thus, as we pass through resonance the magnetization is again reversed. However, the transverse magnetization is now always  $180^\circ$  out of phase with  $H_1$ . It is obvious then that the displayed signal, which is obtained by comparing the induction signal with a signal locked in phase to  $H_1$ , is opposite in sign in the two experiments.

It is perhaps not clear why the process is described as adiabatic. Adiabatic in the Ehrenfest sense means in this context that the change in the system during the perturbation is so slow that there is negligible change in the populations of the energy levels. This is manifestly not so in this experiment since we have a resonant perturbation and there is significant change in the populations of the levels. It is just this that gives the reversal of the magnetization. However, in the rotating coordinate system the perturbation becomes non-resonant and we may imagine we have energy levels determined by  $H_r$ , i.e. the energy level separation  $\Delta E$  is  $\hbar\gamma H_r$ . Now for a non-resonant perturbation the adiabatic condition is simply  $1/\tau \ll \Delta E/\hbar$  (Bohm 1951) where  $\tau$  is the time of application of the perturbation and  $\Delta E$  is the energy separation of the levels in question. The  $\tau$  in this case is evidently the time 'at or near resonance' so that we require  $(dH_0/dt)/H_1 \ll \gamma H_r$  and since the minimum value of  $H_r$  is  $H_1$  we require  $dH_0/dt \ll \gamma H_1^2$  as before. In a sense then the populations remain unchanged (and so does the entropy) but the energy levels are reversed and so is the magnetization.

#### REFERENCES

- BLOCH, F., 1946, *Phys. Rev.*, **70**, 460.  
 BLOCH, F., HANSEN, W. W. and PACKARD, M., 1946, *Phys. Rev.*, **70**, 474.  
 BOHM, D., 1951, *Quantum Theory* (New York: Prentice Hall), p. 449.  
 CHIAROTTI, G., and GIULOTTO, L., 1954, *Phys. Rev.*, **93**, 1241.  
 COMBRISSE, J., HONIG, A., and TOWNES, C. H., 1956, *C.R. Acad. Sci., Paris*, **242**, 2451.  
 DRAIN, L. E., 1949, *Proc. Phys. Soc. A*, **62**, 301.  
 GORDON, J. P., ZEIGER, H. J., and TOWNES, C. H., 1955, *Phys. Rev.*, **99**, 1264.  
 RABI, I. I., RAMSEY, N. F., and SCHWINGER, J., 1954, *Rev. Mod. Phys.*, **26**, 167.

### A Source of Error in Magnetoresistance Measurements

By R. F. BROOM

Services Electronics Research Laboratory, Baldock, Herts.

*MS. received 13th August 1957, and in revised form 28th October 1957*

**M**EASUREMENTS of the magnetoresistance of InSb and GaAs using a conventional potentiometer arrangement have been found to yield inconsistent results unless certain conditions are fulfilled with regard to the method of preparation of the specimens and arrangement of contacts. These anomalies were first observed in the magnetoresistance of n-type GaAs, for which the results did not satisfy one of the fundamental requirements of the cubic symmetry applicable to this material; namely that, for a specimen cut with its current axis in a [111] or [110] crystal direction, the low field transverse

magnetoresistance should be constant as the magnetic field is rotated about the current axis. In some samples a modulation of 50% was observed. Subsequent measurements on n- and p-type InSb showed similar results and so a series of experiments was undertaken to try and find the cause of these errors, which was eventually traced to distortion of the current distribution by the potential contacts.

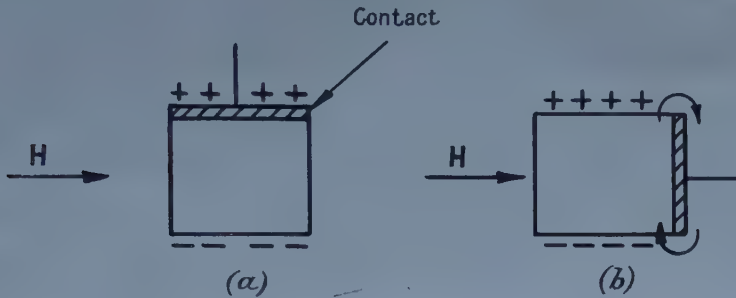


Figure 1. Shorting of Hall field by large area potential contact.

The type of sample used initially consisted of a rectangular rod of dimensions 10 mm long by 1 mm<sup>2</sup> cross section. Current leads were soldered to the ends and potential contacts soldered to the sides of the sample. In the case of GaAs the contact areas were first copper plated. Consider now the effects produced by rotating such a specimen in a transverse magnetic field. Figure 1 shows a cross section of the specimen through one of the potential contacts. The magnetic

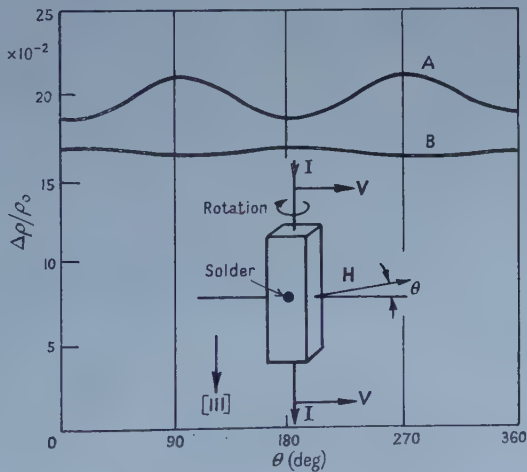


Figure 2. Rotation of specimen in a transverse magnetic field.

field is in the direction  $\mathbf{H}$  and the current flows perpendicular to the paper. In figure 1(a) a Hall field is built up across the specimen as shown. If now the specimen is rotated through 90° to the position shown in figure 1(b) the Hall field rotates through 90° with respect to the specimen but, in this case, the contact partially short circuits the Hall field causing a current to flow in the direction of the arrows. The partial cancellation by the Hall field of the force on the carriers due to the magnetic field is altered so that the effect of the latter is increased,

resulting in an increase in the magnetoresistance. Thus, if the specimen is rotated through  $360^\circ$  in a transverse magnetic field, the contacts will modulate the true magnetoresistance values and show maxima when the contact area is perpendicular to the magnetic field. Such an effect is illustrated in figure 2, in which a sample of InSb, cut with its current axis in a [111] direction, is rotated through  $360^\circ$  in a transverse magnetic field. For this measurement a single pair of contacts, attached to the ends of the sample, was used for both current and potential leads. On one side of the central portion of the sample was attached a small spot of solder, about 1 mm in diameter, to simulate a soldered contact. At  $\theta=0$  and  $180^\circ$  the plane of contact of the solder with the sample was parallel to the magnetic field. Curve A shows the values of  $\Delta\rho/\rho_0$  obtained with this arrangement. It will be seen that the maximum in the curve occurs when the soldered area is perpendicular to  $\mathbf{H}$ . Curve B shows the results obtained when the solder spot was removed: the overall value of  $\Delta\rho/\rho_0$  has fallen and the modulation almost vanished. Although there is no shorting of the Hall field when the plane of the solder spot is parallel to the magnetic field, the curves A and B do not coincide at these positions. This is presumably due to the solder spot causing a distortion of the lines of current flow, the resistivity of the solder being less than that of the sample. However, the most significant point is the almost complete reduction of modulation on removal of the solder.

It should be noted that when a single pair of contacts is used for both current and potential leads, as described above, a short circuiting effect is present all the time if the magnetic field is transverse. This effect, which has been analysed by Wick (1954), leads to an error in the absolute value of the magnetoresistance. In some cases this can be tolerated if one is interested only in the angular dependence of the magnetoresistance, as in the above case. If an absolute value of the magnetoresistance is required, separate potential leads must be used, and it is clear from the foregoing considerations that the area of contact of these leads must be kept to the minimum if errors are to be avoided. For InSb, potential contacts consisting of 0.003 in. platinum wire welded to the specimen by a condenser discharge have been found satisfactory. These contacts must be placed at a distance of the order of the width of the specimen from the ends (Drabble and Wolfe 1957). Dumb-bell-shaped specimens of the type used by Pearson and Suhl (1951) for Ge were found unsatisfactory for InSb and GaAs, presumably because the lower resistivity of the material leads to shorting effects similar to those described above.

#### ACKNOWLEDGMENTS

The author wishes to thank Dr. E. H. Rhoderick for his kind assistance in the preparation of this note. Acknowledgment is made to the Admiralty for granting permission to publish this work.

#### REFERENCES

- DRABBLE, J. R., and WOLFE, R., 1957, *J. Electronics and Control*, **3**, 259.
- PEARSON, G. L., and SUHL, H., 1951, *Phys. Rev.*, **83**, 768.
- WICK, R. F., 1954, *J. Appl. Phys.*, **25**, 741.



## Paramagnetic Impurities in NaF

By W. HAYES † ‡ AND D. A. JONES §

† Clarendon Laboratory, Oxford

§ Department of Natural Philosophy, University of Aberdeen

*Communicated by B. Bleaney; MS. received 19th November 1957.*

THE paramagnetic resonance spectrum of a single crystal of NaF containing iron as an impurity was investigated by Bleaney and Hayes (1957, to be referred to as I); after irradiation with x-rays,  $\gamma$ -rays or electrons, a spectrum was observed which was assigned to  $\text{Fe}^+$ . The spectra of other iron group impurities in NaF have since been examined before and after irradiation, using the irradiation doses described in I. The crystals were grown from melts containing  $\text{Mn}^{2+}$ ,  $\text{Cr}^{3+}$ ,  $\text{Co}^{2+}$  or  $\text{Ni}^{2+}$  ions added in 0.01% molar concentration. The results may be briefly summarized as follows.

### Manganese.

Before irradiation a complex spectrum was observed arising from about  $4 \times 10^{16}$   $\text{Mn}^{2+}$  centres in a crystal of  $0.05 \text{ cm}^3$  volume. There are two sets of magnetic centres each consisting of three magnetic ions with similar spectra and with axial symmetry about each of the cube edges. One set has a stronger axial field and contains only about 1% of the total number of centres. The basic features of the spectrum of each ion are described by the spin Hamiltonian

$$\mathcal{H} = g\beta\mathbf{H}\cdot\mathbf{S} + D\{S_z^2 - \frac{1}{3}S(S+1)\} + A\mathbf{I}\cdot\mathbf{S}$$

with  $S=5/2$  and  $I=5/2$ .

Because of the complexity of the spectrum the parameters  $g$ ,  $D$  and  $A$  could be determined only from measurements along the axis of the crystal field. The constants of the weaker set at  $90^\circ\text{K}$  are  $g=2.00 \pm 0.01$ ,  $A=92 \pm 4 \times 10^{-4} \text{ cm}^{-1}$ ,  $D=225 \pm 8 \times 10^{-4} \text{ cm}^{-1}$ ; the constants of the stronger set are  $g=1.996 \pm 0.006$ ,  $A=91 \pm 4 \times 10^{-4} \text{ cm}^{-1}$ ,  $D=89 \pm 5 \times 10^{-4} \text{ cm}^{-1}$ .

Each of the manganese hyperfine structure lines has a resolved structure due to interaction of the magnetic electrons with the nuclei of fluorine ions; the interaction may be described by adding a term  $\sum_N \mathbf{I}_0^N \cdot \mathbf{A}^N \cdot \mathbf{S}$  to the spin Hamiltonian (Tinkham 1956);  $I_0=1/2$  is the spin of the  $^{19}\text{F}$  nucleus. An analysis of this structure in the stronger spectrum shows that the  $\text{Mn}^{2+}$  ions are on cation sites and are surrounded by a complete octahedron of fluorine ions. Fluorine hyperfine structure components occur at fields displaced from the zero interaction position by

$$\delta H_z = \sum_N I_{0z}^N A_z^N = \sum_N I_{0z}^N \{A_s^N + A_\sigma^N (3 \cos^2 \theta_{z,\sigma} - 1)\}$$

where the summation is over the six nearest neighbour fluorine nuclei (I). The interaction constants are found to be

$$A_s = 14.4 \pm 0.3 \times 10^{-4} \text{ cm}^{-1}, \quad A_\sigma = 2.8 \pm 0.7 \times 10^{-4} \text{ cm}^{-1}.$$

An analysis of the fluorine hyperfine structure in the weaker spectrum was not possible because of insufficient intensity.

‡ Now at the Argonne National Laboratory.

After irradiation, the intensity of the  $\text{Mn}^{2+}$  spectrum is reduced by about 90%. A search by Dr. P. M. Llewellyn with a sensitive spectrometer at 4°K for a spectrum which could be attributed to  $\text{Mn}^+$  was not successful.

### Chromium.

Before irradiation no spectrum is observed down to 20°K but after irradiation a single isotropic line with a resolved fluorine hyperfine structure appears at 90°K; about  $6 \times 10^{15}$  centres are present in a crystal of 0.05 cm<sup>3</sup> volume. A structure due to  $^{53}\text{Cr}$  ( $I=3/2$ , natural abundance 9.5%) is found on the extreme fluorine hyperfine structure lines. A detailed investigation of the spectrum suggests that it arises from  $\text{Cr}^+$  which is isoelectronic with  $\text{Mn}^{2+}$  ( $3d^5$ ,  $^6\text{S}$ ).

The spectrum may be fitted to the spin Hamiltonian

$$\mathcal{H} = g\beta\mathbf{H}\cdot\mathbf{S} + F(a) + A\mathbf{I}\cdot\mathbf{S} + \sum_N \mathbf{I}_0^N \cdot \mathbf{A}^N \cdot \mathbf{S}$$

with  $S=5/2$ ,  $I=3/2$ ,  $I_0=1/2$ ,  $g=2.000 \pm 0.002$ ,  $A=14.0 \pm 0.5 \times 10^{-4} \text{ cm}^{-1}$ .

The term  $F(a)$  represents the effect of the cubic crystal field on the fine structure of the  $^6\text{S}$  ground term; the magnitude of the cubic field splitting parameter  $a$  is found to be  $3.6 \pm 0.6 \times 10^{-4} \text{ cm}^{-1}$ . The measured values of the fluorine interaction constants are

$$A_s = 12.8 \pm 0.2 \times 10^{-4} \text{ cm}^{-1}, \quad A_\sigma = 0.9 \pm 0.7 \times 10^{-4} \text{ cm}^{-1}.$$

### Cobalt.

Before irradiation an extremely complicated spectrum is observed at 20°K arising from about  $8 \times 10^{15}$  centres in a crystal of 0.05 cm<sup>3</sup> volume. There are six types of magnetic ion with similar spectra. Each ion has rhombic symmetry with two face diagonals and a cube edge as principal axes. The spectrum of each ion is described by the following spin Hamiltonian with  $S=1/2$  and  $I=7/2$ :

$$\mathcal{H} = \beta\mathbf{S}\cdot\mathbf{g}\cdot\mathbf{H} + \mathbf{I}\cdot\mathbf{A}\cdot\mathbf{S}.$$

The measured constants are  $g_x=4.3$ ,  $g_y=3.3$ ,  $g_z=5.7$ ,  $A_y=82 \times 10^{-4} \text{ cm}^{-1}$ ,  $A_z=250 \times 10^{-4} \text{ cm}^{-1}$ . Confusion due to overlap prevented the measurement of  $A_x$ . The results are reasonably consistent with the theory of Abragam and Pryce (1951) for  $\text{Co}^{2+}$  in an octahedral cubic field with a rhombic distortion. A well resolved fluorine hyperfine structure was observed but a detailed analysis was not possible.

After irradiation the spectrum described above disappears completely and two isotropic lines are found. One occurs at 20°K with a  $g$ -value of 4.5, is about 400 gauss wide and has no resolved structure; it probably arises from  $\text{Co}^{2+}$  in slightly distorted cubic surroundings. The second line appears at 90°K with a  $g$ -value of  $2.31 \pm 0.02$  and has a flat top about 200 gauss long. The  $g$ -value is close to the value  $2.227 \pm 0.002$  measured for  $\text{Ni}^{2+}$  in  $\text{MgO}$  at 70°K (Low 1956) and suggests that the magnetic centre is  $\text{Co}^+$  which is isoelectronic with  $\text{Ni}^{2+}$  ( $d^8$ ). The absence of a resolved structure may be due to the simultaneous presence of cobalt hyperfine structure ( $A \sim 30 \times 10^{-4} \text{ cm}^{-1}$ ), fluorine hyperfine structure and line broadening due to slight distortions of the crystal field.

### Nickel.

No lines are observed before irradiation down to 20°K but after irradiation a spectrum arising from about  $5 \times 10^{15}$  centres in a crystal of 0.05 cm<sup>3</sup> volume,

appears at 20°K. There are three magnetic ions with similar spectra and with axial symmetry about each of the cube edges. The spectrum may be explained by assuming that the magnetic centres are  $\text{Ni}^+$  ions which are isoelectronic with  $\text{Cu}^{2+}$  ( $d^9$ ). The cubic field leaves a 'non-magnetic' orbital doublet lowest and the degeneracy is raised by a Jahn-Teller distortion of the octahedron (cf. Bleaney, Bowers and Trenam 1955). The  $g$ -values indicate that the octahedron is extended along a cube edge. The spectrum is fitted to the following spin Hamiltonian with  $S=1/2$  and  $I_0=1/2$ :

$$\mathcal{H} = \beta \mathbf{S} \cdot \mathbf{g} \cdot \mathbf{H} + \sum_N \mathbf{I}_0^N \cdot \mathbf{A}^N \cdot \mathbf{S}.$$

The measured  $g$ -values are  $g_{\parallel}=2.766 \pm 0.002$ ,  $g_{\perp}=2.114 \pm 0.002$ . The term  $\sum_N \mathbf{I}_0^N \cdot \mathbf{A}^N \cdot \mathbf{S}$  in the spin Hamiltonian leads to fluorine hyperfine structure components shifted from the zero interaction position by

$$\begin{aligned} \delta H_z &= \sum_N A_z^N I_{0z}^N \\ &= \sum_I I_{0z}^I \{A_s^I + A_{\sigma}^I (3 \cos^2 \theta_{z,\sigma} - 1)\} \\ &\quad + \sum_{II} I_{0z}^{II} \{A_s^{II} + A_{\sigma}^{II} (3 \cos^2 \theta_{z,\sigma} - 1)\}. \end{aligned}$$

The interaction parameters are found to be

$$\begin{aligned} A_s^I &= 41 \pm 2 \times 10^{-4} \text{ cm}^{-1}, & A_s^{II} &= 10 \pm 1 \times 10^{-4} \text{ cm}^{-1}, \\ A_{\sigma}^I &= 16 \pm 2 \times 10^{-4} \text{ cm}^{-1}, & A_{\sigma}^{II} &= 0 \pm 0 \times 10^{-4} \text{ cm}^{-1}. \end{aligned}$$

The superscript I refers to the four fluorines in the plane perpendicular to the symmetry axis and the superscript II to the two fluorines on the axis. Bonding to the latter is not expected unless the excited  $3z^2-r^2$  level is admixed to the  $x^2-y^2$  ground state; in the present case this may result from a rhombic distortion which is not observable, however, in the  $g$ -values.

All the irradiation centres described above may be annealed out by heating at 150°C for 48 hours.

A more detailed discussion is in course of preparation.

We are indebted to Dr. J. M. Baker and Professor B. Bleaney for their interest in the work and to Dr. M. C. M. O'Brien and Dr. J. Owen for valuable discussions. We would like to thank Professor R. V. Jones for making the crystal growing facilities available to us and Mr. J. Orton and the Atomic Energy Research Establishment, Harwell, for the irradiation facilities.

#### REFERENCES

- ABRAGAM, A., and PRYCE, M. H. L., 1951, *Proc. Roy. Soc. A*, **206**, 173.  
 BLEANEY, B., BOWERS, K. D., and TRENAM, R. S., 1955, *Proc. Roy. Soc. A*, **228**, 157.  
 BLEANEY, B., and HAYES, W., 1957, *Proc. Phys. Soc. B*, **70**, 626.  
 LOW, W., 1956, *Phys. Rev.*, **101**, 1827.  
 TINKHAM, M., 1956, *Proc. Roy. Soc. A*, **236**, 535, 549.

# The Resistivity of Ordered $\text{Au}_3\text{Cu}$

By P. WRIGHT AND K. F. GODDARD

University College of North Wales, Bangor

*MS. received 18th November 1957*

X-RAY and electron diffraction studies have now definitely established the existence of the superlattice in the alloy  $\text{Au}_3\text{Cu}$  predicted by statistical theory. The resistivity of the alloy at temperatures between about  $160^\circ\text{C}$  and  $290^\circ\text{C}$  has been observed by Hirabayashi (1951) whose results appeared to indicate a critical temperature of  $280^\circ\text{C}$  for the ordering transition and a higher resistivity in the ordered than in the disordered phase. This interpretation is not supported by the present writers who find an isothermal decrease in resistivity with time at temperatures below  $190^\circ\text{C}$  and an equilibrium resistance-temperature curve showing an increase in resistivity as the temperature approaches  $190^\circ\text{C}$ , followed by a decrease at lower temperatures. The curves (see figure 1) were determined by a pulse-annealing method in which a wire filament of  $\text{Au}_3\text{Cu}$  of stoichiometric composition was heated by an electric current from room temperature to a preset annealing temperature in about 20 sec. The temperature was thermostatically controlled during the anneal and the wire was then quenched to room temperature in a few seconds by a jet of cold nitrogen, and its resistivity  $R_{20}$  at  $20^\circ\text{C}$  determined from measurements near room temperature.

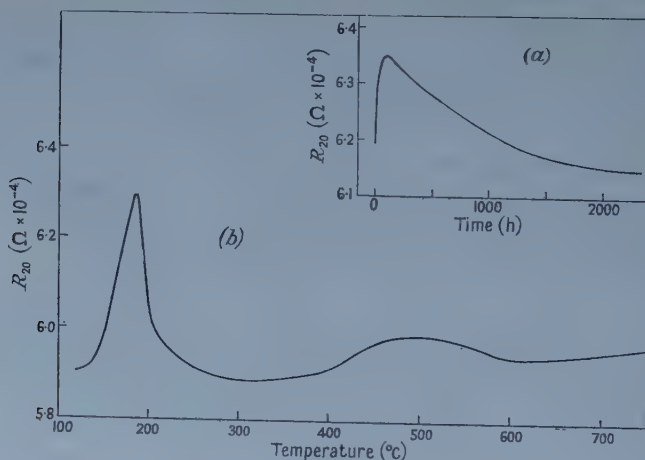


Figure 1. Ordering in  $\text{Au}_3\text{Cu}$ .

- (a) Resistivity plotted against annealing time;  $167^\circ\text{C}$  isothermal  
(b) Equilibrium resistivity plotted against temperature.

Above  $190^\circ\text{C}$ , a few hours of annealing at any temperature sufficed to produce an equilibrium value of  $R_{20}$ . The  $167^\circ\text{C}$  isothermal was determined with the alloy initially in the equilibrium state at  $195^\circ\text{C}$ ; the resistivity after annealing for 100 days at  $167^\circ\text{C}$  is seen to be significantly lower than the initial value. Following this long anneal, annealing periods of several days were adequate to produce equilibrium values of  $R_{20}$  at temperatures from  $190^\circ\text{C}$  to a lower limit at  $120^\circ\text{C}$  below which the alloy was effectively 'frozen'. We have obtained similar results, somewhat masked by the superposed temperature component



of resistivity, when the resistivity measurements were made 'at temperature' on  $\text{Au}_3\text{Cu}$  wire in a furnace. It therefore appears unlikely that the ordering phenomena produced by pulse-annealing and quenching, at temperatures below about  $400^\circ\text{C}$ , are appreciably stimulated by vacancy migration.

Though the relaxation periods are of a different order of magnitude, the behaviour of  $\text{Au}_3\text{Cu}$  in the order-disorder transformation resembles that of its companion alloy  $\text{Cu}_3\text{Au}$  more closely than has been generally supposed. Isothermals similar to that shown in figure 1(a) were obtained by Burns and Quimby (1955) with  $\text{Cu}_3\text{Au}$ . Corresponding to the rise in the equilibrium value of  $R_{20}$  between  $300^\circ\text{C}$  and  $190^\circ\text{C}$  (figure 1(b)), Damask (1956) observed an increase in the resistivity (measured at  $77^\circ\text{K}$ ) of  $\text{Cu}_3\text{Au}$  as the critical temperature for long-range order is approached from higher temperatures. An explanation of these resistivity increases, in both isothermals and equilibrium curves, may be found in terms of ordering by a process of nucleation and growth. In an electron diffraction study using monocrystalline films of  $\text{Cu}_3\text{Au}$ , Raether (1957) observed that above the critical temperature  $T_c$  there occurred a complex diffuse scattering which was most intense at points in reciprocal space where the superlattice reflections appeared below  $T_c$ . This observation was taken by Raether to indicate the presence of small antiphase domains above  $T_c$ . It would, therefore, seem reasonable to attribute the above-mentioned resistivity effects to the scattering of conduction electrons by small domains of nearest-neighbour order. These domains would be expected to increase in size and number as the critical temperature is approached and finally to become stable and coalesce to give a coherent scheme of long-range order. At temperatures below  $190^\circ\text{C}$ , our observations with  $\text{Au}_3\text{Cu}$  are consistent with the more general effect of a resistivity which diminishes with the onset of long-range order; they indicate a value of  $T_c \simeq 190^\circ\text{C}$  for this alloy which agrees with that predicted by Cowley's approximate theory of order (1950).

The small maximum which occurs between  $400^\circ\text{C}$  and  $600^\circ\text{C}$  would appear to indicate a new phase transition in the region where normally a continuous decrease in the degree of short-range order is expected. Anomalies in the properties of disordered  $\text{Cu}_3\text{Au}$  have been reported by Kuczynski and others (1956) who concluded that this alloy undergoes a phase transition between  $550^\circ\text{C}$  and  $600^\circ\text{C}$  and possibly another one near  $850^\circ\text{C}$ . Recent calorimetric studies by Hirabayashi and others (1957) did not, however, reveal any anomalous peaks in the specific heat-temperature curve for  $\text{Cu}_3\text{Au}$ . From further observations with quenched specimens, they conclude that properties measured at room temperature may not reveal the nature of the alloy at high temperatures owing to ordering produced by migration of excess vacancies made available by quenching. We might therefore expect to find, at high temperatures, that the degree of order in the quenched state is greater the higher the quenching temperature. In the case of  $\text{Au}_3\text{Cu}$ , the long relaxation period precludes the possibility of long-range ordering, moreover the resistivity maximum at  $500^\circ\text{C}$  is not comparable with that at  $190^\circ\text{C}$ . It is conceivable that the excess vacancy concentration could induce some short-range order in  $\text{Au}_3\text{Cu}$  quenched from high temperatures. Thus as the temperature, and hence the vacancy concentration, increases, the alloy might be expected to acquire a degree of short-range order corresponding to points on the equilibrium resistivity curve well below the quenching temperature. A process such as this could account satisfactorily for the observed form

of the resistivity curve above 500°C, and with this as a possibility, we cannot be certain that the anomalous 'peak' is associated with a new phase transition.

## REFERENCES

- BURNS, F. P., and QUIMBY, S. L., 1955, *Phys. Rev.*, **97**, 1567.  
 COWLEY, J. M., 1950, *Phys. Rev.*, **77**, 669.  
 DAMASK, A. C., 1956, *J. Phys. Chem. Solids*, **1**, 23.  
 HIRABAYASHI, M., 1951, *J. Phys. Soc. Japan*, **6**, 129; 1955, *Nippon Kink. Gakk.*, **16**, 67.  
 HIRABAYASHI, M., NAGASAKI, S., and KONO, H., 1957, *J. Appl. Phys.*, **28**, 1070.  
 KUCZYNSKI, G. C., DOYAMA, M., and FINE, M. E., 1956, *J. Appl. Phys.*, **27**, 651.  
 RAETHER, H., 1957, *Z. angew. Phys.*, **4**, 53.

## A Note on Penetration by Rotating Shaped Charges

By SAMPOORAN SINGH

Defence Science Laboratory, Ministry of Defence, New Delhi, India

*Communicated by F. C. Auluck; MS. received 16th July 1957 and in final form 6th November 1957*

THE basic theory of penetration by high explosive charges with metal-lined cavities (shaped charges) was developed independently by Mott, Hill and Pack (Pack and Evans 1951) and by Pugh (Birkhoff *et al.* 1948) during World War II. Recently Singh (1953 a), Eichelberger (1956) and Singh (1957) suggested some simple modifications of the theory which appear to account adequately for the discrepancies between experimental observations and the existing theory. The basic equation of the modified theory is (Singh 1957)

$$\Delta P = \epsilon \Delta L \left( \frac{\gamma \rho}{\rho_t} \right)^{1/2} \left[ 1 - \frac{\sigma}{\rho_t V^2} \left\{ \left( \frac{\rho_t}{\gamma \rho} \right)^{1/2} + 1 \right\}^2 \right] \quad \dots\dots (1)$$

where  $\Delta P$  is the depth of penetration,  $\epsilon$  an empirical constant,  $\Delta L$  the length of a jet element that is about to strike a target,  $\rho$  the density of the liner material,  $\rho_t$  the density of the target material,  $V$  the mean velocity of the jet element, and the quantity  $\sigma$  is the difference between two quantities,  $\sigma_t$  and  $\sigma_j$  which represent the resistance of the target and the jet, respectively, to the plastic deformation required by the penetration process. The term  $\gamma$  takes into consideration all corrections for discontinuities within the jet element, i.e. the break-up of the jet element into particles and the waver of the jet element due to imperfections in charge or liner. Let  $U$  be the time rate of change of the depth of the hole by the given jet element and  $\Delta t$  the time taken for a jet element  $\Delta L$  to penetrate  $\Delta P$ ;  $U$  and  $\Delta t$  are given by the expressions

$$U = V \left[ \frac{1}{1 + (\rho_t / \gamma \rho)^{1/2}} - \frac{\sigma}{\rho_t V^2} \left( \frac{\rho_t}{\gamma \rho} \right)^{1/2} \right] \quad \dots\dots (2)$$

$$\Delta t = \Delta P / U. \quad \dots\dots (3)$$

It is well established that when a shaped charge rotates about its axis, there is loss of penetration. As early as 1943, the Germans observed by Kerr cell photography (Simon 1947) the increase of cross sectional area of a jet due to rotation. Recently Schall and Thomer (1954) took x-ray flash photographs of rotating shaped charges

about their axes and showed that rotation brings about a widening of the jet and that the velocity of the jet is not influenced by the rotation. Each element of the rotating liner—as in the case of a spin-stabilized shaped charge projectile—possesses angular momentum and in consequence (Singh 1953 b, 1955) the individual elements do not converge upon the axis as the liner collapses, since each element has both a tangential and a radial velocity; this effect has been shown to be negligible, a calculation of the radius of a jet element that is newly formed showing that it is virtually independent of the angular momentum of the parent element in the original liner. If we assume that each jet element possesses all the angular momentum of the parent element in the original liner, this results in a continuous spreading (i.e. an increase of cross-sectional area) of the jet element as it travels in space. The present note correlates theoretically the depth of penetration and the angular velocity of the liner in a rotating shaped charge and is basically an extension of the author's previous work (1953 b).

Let  $V_0$  represent the velocity with which a liner element travels towards the axis,  $\beta$  the angle between the collapsing element and the axis,  $V_j$  the velocity of the jet element formed, and let  $x$  be the distance measured from the apex along the axis to the plane of the zonal element in the liner. We assume that the direction and magnitude of  $V_0$  are independent of rotation and as such the collapse parameters (i.e.  $V_0$ ,  $\beta$ ,  $V_j$  as functions of  $x$ ) of a conical liner are independent of rotation. When a shaped charge rotates about its axis, we may assume that an angular velocity is imparted to each jet element; this leads to an increase in the cross-sectional area of the element as it travels in space, and the spreading is symmetrical about the axis. Let  $R_j$  represent the initial radius of a jet element and  $R_r$  the increase in radius at any time  $\tau$  due to the angular velocity of the jet element. On the basis of dimensional considerations, we assume that  $R_r$  is given by the expression

$$R_r = \xi v \tau \quad \dots\dots(4)$$

where  $v$  is the 'tangential' velocity (see below) of the jet element and  $\xi$  is an empirical constant. Let  $\omega$  and  $\Omega$  represent the angular velocities of an element in the liner and the corresponding element in the jet, respectively;  $x \tan \alpha$  is the perpendicular distance of the element in the original conical liner from the axis of the liner where  $\alpha$  is the half-angle of the liner. Equating the angular momentum of a finite element on the surface of the liner to that of the corresponding element in the jet, we have

$$\omega x^2 \tan^2 \alpha = \Omega R_j^2 \quad \dots\dots(5)$$

The tangential velocity of the jet element is given by

$$v = \Omega R_j = \omega x^2 \tan^2 \alpha / R_j; \quad \dots\dots(6)$$

substituting the value of  $v$  from equation (6) in equation (4), we have

$$R_r = \xi \omega x^2 \tan^2 \alpha \tau / R_j. \quad \dots\dots(7)$$

Let  $\Delta L'$  represent the length of an element of the jet that is just formed from a finite element in the slant surface of the liner. As the radius of a jet element that is just formed from any finite element of the liner is, for practical purposes, independent of rotation (Singh 1955), we may take the length  $\Delta L'$  of a jet element to be the same for non-rotating and rotating charges. The jet element  $\Delta L'$  (having  $V_j$  and  $V_j'$  as the velocity of the head end and the tail end respectively) stretches like a ductile metal as it travels in space along the axis of the equipment and becomes narrower till its length is  $C\Delta L'$ , where  $C$  is an 'elongation' constant.



Further stretching of the jet element as it travels in space causes it to break into particles and spread (or waver), the result of imperfections in charge or liner. Let  $\Delta L$  be its length when it is about to strike a target. In discussing the penetration, we have to consider two possibilities—case 1:  $\Delta L \leq C\Delta L'$ ; case 2:  $\Delta L > C\Delta L'$ —and both may occur at different stages in the *same* jet element depending on the distance available for the jet element to stretch due to the velocity gradient.

*Case 1.* When a shaped charge rotates, the different elements in the jet have different angular velocities and it may be expected that the increase of the angular velocity of a jet element may decrease the extent of ductile drawing. In the absence of any experimental data we assume that the spreading of a jet element due to its angular momentum is negligible as long as ductile drawing continues and the value of  $C$  for a given jet element is the same for a non-rotating and a rotating shaped charge. For a continuous jet element  $\gamma$  is unity, and  $\Delta P$ ,  $U$  and  $\Delta t$  are given by equations (1) to (3), respectively.

*Case 2.* We now specify  $\tau$ ,  $R_j$  and  $R_r$  in relation to an individual jet element of initial length  $C\Delta L'$ . The time interval  $\tau$  is identified as the time taken for  $C\Delta L'$  jet element to stretch to  $\Delta L$  and is given by the expression

$$\tau = \frac{\Delta L - C\Delta L'}{V_j - V_j'}, \quad \dots\dots(8)$$

$R_j$  is the radius of the jet element when its length is  $C\Delta L'$  and  $R_r$  is the increase of the radius in the time  $\tau$  due to the angular velocity of the jet element. The radius  $R_t$  of the jet element when its length is  $\Delta L$  can now be written in the form

$$R_t = R_j + S_d \tan \phi + R_r \quad \dots\dots(9)$$

where  $S_d$  is the axial distance from the point of normal break-up of an element of the jet to the point of its impingement on the target, and  $\phi$  the angle of spread which the particles subtend with the axis. The term  $S_d \tan \phi$  takes into consideration the spreading or waver of the jet element due to imperfections in charge or liner and the term  $R_r$  takes into account the angular velocity of the jet element. Substituting the value of  $R_r$  from equation (7) and  $\tau$  from equation (8) in equation (9) we have

$$R_t = R_j + S_d \tan \phi + \frac{\xi \omega x^2 \tan^2 \alpha (\Delta L - C\Delta L')}{R_j (V_j - V_j')} \quad \dots\dots(10)$$

The conservation of mass equation is as follows:

$$\Delta m_j = \pi R_j^2 C \Delta L' \rho = \pi R_t^2 \Delta L \gamma \rho \quad \dots\dots(11)$$

where  $\Delta m_j$  is the mass of the jet element. From the above equation, the break-up factor  $\gamma$  is given by the expression

$$\gamma = \frac{C\Delta L'}{\Delta L} \left( \frac{R_j}{R_t} \right)^2 \quad \dots\dots(12)$$

where  $R_j = (\Delta m_j / \pi C \Delta L' \rho)^{1/2}$ . Substituting the value of  $\gamma$  from equation (12) in equations (1) to (3), we have

$$\Delta P = \epsilon \left( \frac{R_j}{R_t} \right) \left( \frac{C\Delta L' \Delta L \rho}{\rho_t} \right)^{1/2} \left[ 1 - \frac{\sigma}{\rho_t V^2} \left\{ \frac{R_t}{R_j} \left( \frac{\Delta L \rho_t}{C\Delta L' \rho} \right)^{1/2} + 1 \right\}^2 \right] \quad \dots\dots(13)$$

$$U = V \left[ \frac{1}{1 + \frac{R_t}{R_j} \left( \frac{\Delta L \rho_t}{C\Delta L' \rho} \right)^{1/2}} - \frac{\sigma R_t}{\rho_t V^2 R_j} \left( \frac{\Delta L \rho_t}{C\Delta L' \rho} \right)^{1/2} \right] \quad \dots\dots(14)$$

$$\Delta t = \Delta P / U \quad \dots\dots(3)$$



The equations (10) and (13) indicate that as  $\omega$  increases,  $R_t$  increases and  $\Delta P$  decreases. Since  $x \tan \alpha$  progressively increases from the apex to the base of a liner, it follows that, for a given rotation of a shaped charge, the deleterious effect of rotation on penetration increases from the head to the tail end of the jet. If the collapse parameters of a conical liner are known, the jet characteristics (i.e.  $\Delta L'$ ,  $\Delta L$ ,  $R_j$ ,  $R_t$ ,  $S_d$ ) can be evaluated and the jet and target characteristics (i.e.  $\epsilon$ ,  $C$ ,  $V$ ,  $\rho$ ,  $\rho_t$ ,  $\sigma$ ,  $\phi$ ) are known, so  $\Delta P$ ,  $U$  and  $\Delta t$  can be calculated.† The only unknown term in equation (10) is  $\xi$  and the value of  $\xi$  is so chosen that the theoretical curve of penetration against angular velocity of liner gives an overall fit with the experimental curve.

Numerical evaluations have been carried out for the standard M9Al steel conical liner in the standard C.I.T. laboratory charge for which experimental results are available (Eichelberger 1955). Figure 1 shows the calculated depth of penetration in a mild steel target as a function of speed of rotation at a stand-off distance of 7.62 cm taking  $\xi$  to be equal to 0.5 and 0.4. This indicates that the depth of penetration decreases rapidly as the speed of rotation increases from zero to 100 revolutions per second; the decrease of penetration becomes very gradual

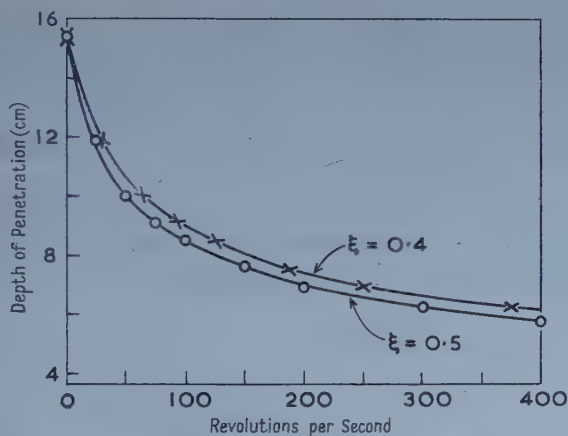


Figure 1. Depth of penetration at 7.62 cm stand-off distance in mild steel targets as a function of the speed of rotation of the standard M9Al steel cones in the standard C.I.T. laboratory charge.

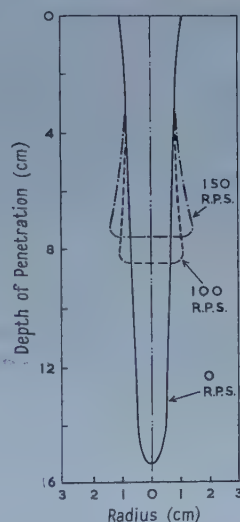


Figure 2. Calculated profiles of holes made in mild steel targets by non-rotating and rotating standard C.I.T. laboratory charges at 7.62 cm stand-off distance.

as the speed of rotation increases beyond 100 revolutions per second. The calculated profiles (taking  $\xi = 0.5$ ) of holes made by non-rotating and rotating shaped charges at 7.62 cm stand-off distance are shown in figure 2. This indicates that the radius near the bottom of the hole increases with increase of the speed of rotation of a shaped charge.

A stringent test of the theory would be to compare the experimental and theoretical curves of jet velocity, penetration velocity and time of penetration as functions of stand-off distance and angular velocity of the liner for a given shaped

† If we put  $\omega$  equal to zero in equation (10), then the equations (10), (13) and (14) reduce to the corresponding expressions for a non-rotating shaped charge.

charge; but the precise experimental data has been not published so far. Basset and Basset (1950) stated that penetration by a shaped charge decreases rapidly with increasing speed of rotation. Hegde and Singh (1955) experimentally observed that the depth of penetration by rotating charges at 160 revolutions per second is about half of its static performance. A comparison of the experimental and theoretically calculated depth of penetration at 160 revolutions per second suggests that the value of  $\xi$  is about 0.4. It is of interest to note that the calculated profile of the hole at 160 revolutions per second is in close agreement with the experimental one.

#### ACKNOWLEDGMENT

The author is grateful to Professor D. S. Kothari, Scientific Adviser to the Minister of Defence, for suggesting this work, for encouragement and interest throughout the course of this investigation, and for permission to publish this paper.

#### REFERENCES

- BASSET, J., and BASSET, J., 1950, *C.R. Acad. Sci. Paris*, **231**, 1440.  
 BIRKHOFF, G., MACDOUGALL, D. P., PUGH, E. M., and TAYLOR, G. I., 1948, *J. Appl. Phys.*, **19**, 563.  
 EICHELBERGER, R. J., 1955, *J. Appl. Phys.*, **26**, 398; 1956, *Ibid.*, **27**, 63.  
 HEGDE, V. S., and SINGH, S., 1955, unpublished.  
 PACK, D. C., and EVANS, W. M., 1951, *Proc. Phys. Soc. B*, **64**, 298; 1951, *Ibid. B*, **64**, 303.  
 SCHALL, R., and THOMER, G., 1954, *Proc. 2nd Int. Congr. High-Speed Photogr.*, Paris: Dunod.  
 SIMON, L. E., 1947, *German Research in World War II* (New York: John Wiley), p. 119.  
 SINGH, S., 1953 a, *Proc. Nat. Inst. Sci. India*, **19**, 583; 1953 b, *Proc. Nat. Inst. Sci. India*, **19**, 665; 1955, *J. Sci. Industr. Res. Delhi B*, **14**, 669; 1957, *Proc. Phys. Soc. B*, **70**, 867.

### On the Deduction of the Lorentz-Einstein Transformation from Maxwell's Electromagnetic Field Equations

By K. STIEGLER

Zagreb

*MS. received 29th August 1957, and in revised form 18th November 1957*

IN this note it is shown that the Lorentz-Einstein transformation can be deduced from Maxwell's electromagnetic field equations by means of the principle of special relativity and the linearity of space-time transformations between two galilean systems of reference.

We suppose that for the transformation of coordinates and the time between two galilean systems of reference S and S' there are relations:

$$x' = a_{11}x + a_{12}t \quad \dots\dots(1) \quad y' = y \quad \dots\dots(2)$$

$$z' = z \quad \dots\dots(3) \quad t' = a_{21}x + a_{22}t \quad \dots\dots(4)$$

$$\frac{dx}{dt} = v \quad \text{when} \quad \frac{dx'}{dt'} = 0 \quad \dots\dots(5) \quad \frac{dx'}{dt'} = -v \quad \text{when} \quad \frac{dx}{dt} = 0 \quad \dots\dots(6)$$

where  $v$  means the constant relative velocity of the systems S and S', and  $a_{11}$ ,  $a_{12}$ ,  $a_{21}$ ,  $a_{22}$  are the coefficients to be determined (Axiom 1). We suppose

further that for the electromagnetic phenomena *in vacuo* Maxwell's field equations

$$\text{rot } \mathfrak{E} = -\frac{1}{c} \frac{\partial \mathfrak{H}}{\partial t}, \quad \text{rot } \mathfrak{H} = \frac{1}{c} \frac{\partial \mathfrak{E}}{\partial t}, \quad \text{div } \mathfrak{E} = 0, \quad \text{div } \mathfrak{H} = 0 \quad \dots\dots(7)$$

are valid, where  $c$  is the velocity of light (Axiom 2) and finally that in all galilean systems of reference the physical laws have the same analytical form (Axiom 3).

From (1), (4), (5) and (6) it follows that

$$a_{11} = a_{22} \quad \dots\dots(8) \qquad a_{12} = -a_{11}v. \quad \dots\dots(9)$$

If we write the Maxwell's electromagnetic field equations (Axiom 2) in their scalar form for the S and S' systems (for the latter according to Axiom 3) and transform by means of (1)–(4) the three scalar equations for the time derivative of the components of the electric and magnetic field vectors  $\mathfrak{E}$  and  $\mathfrak{H}$  into the corresponding equations for the system S', then considering (8), (9) and the two last equations of (7) we get:

$$\frac{1}{c'} \frac{\partial E_x}{\partial t'} = \frac{\partial}{\partial y'} \left[ \frac{H_z - \frac{v}{c} E_y}{a_{11} \frac{c'}{c} + a_{21} \frac{vc'}{c}} \right] - \frac{\partial}{\partial z'} \left[ \frac{H_y + \frac{v}{c} E_z}{a_{11} \frac{c'}{c} + a_{21} \frac{vc'}{c}} \right] \quad \dots\dots(10.1)$$

$$\frac{1}{c'} \frac{\partial}{\partial t'} \left( a_{11} \frac{c'}{c} E_y + a_{21} c' H_z \right) = \frac{\partial H_x}{\partial z'} - \frac{\partial}{\partial x'} \left[ a_{11} \left( H_z - \frac{v}{c} E_y \right) \right] \quad \dots\dots(10.2)$$

$$\frac{1}{c'} \frac{\partial}{\partial t'} \left( a_{11} \frac{c'}{c} E_z - a_{21} c' H_y \right) = \frac{\partial}{\partial x'} \left[ a_{11} \left( H_y + \frac{v}{c} E_z \right) \right] - \frac{\partial H_x}{\partial y'} \quad \dots\dots(10.3)$$

$$-\frac{1}{c'} \frac{\partial H_x}{\partial t'} = \frac{\partial}{\partial y'} \left[ \frac{E_z + \frac{v}{c} H_y}{(a_{11} + a_{21}v) \frac{c'}{c}} \right] - \frac{\partial}{\partial z'} \left[ \frac{E_y - \frac{v}{c} H_z}{(a_{11} + a_{21}v) \frac{c'}{c}} \right] \quad \dots\dots(11.1)$$

$$-\frac{1}{c'} \frac{\partial}{\partial t'} \left( a_{11} \frac{c'}{c} H_y - a_{21} c' E_z \right) = \frac{\partial E_x}{\partial z'} - \frac{\partial}{\partial x'} \left[ a_{11} \left( E_z + \frac{v}{c} H_y \right) \right] \quad \dots\dots(11.2)$$

$$-\frac{1}{c'} \frac{\partial}{\partial t'} \left( a_{11} \frac{c'}{c} H_z + a_{21} c' E_y \right) = \frac{\partial}{\partial x'} \left[ a_{11} \left( E_y - \frac{v}{c} H_z \right) \right] - \frac{\partial E_x}{\partial y'} \quad \dots\dots(11.3)$$

where the constant  $c'$  means the velocity of light in this system for which we do not know *a priori* if it equals the constant  $c$  in the system S. By comparison of equations (10.1), (10.2), (10.3) and (11.1), (11.2), (11.3) with the corresponding Maxwell's field equations for the system S' in its scalar form, in accordance with Axioms 2 and 3, we get the relations for the components of the electric and magnetic field vector from S to S'. Therefrom follows the fundamental relation

$$c = c' \quad \dots\dots(12)$$

and the well-known expressions for the coefficients  $a_{11}$ ,  $a_{12}$ ,  $a_{21}$  and  $a_{22}$  of the Lorentz–Einstein transformation,

## A Note on Ta-You Wu's Method of Calculating Overlap Integrals for Morse Oscillator

BY N. R. TAWDE AND M. I. SAVADATTI

Department of Physics, Karnatak University, Dharwar, India

*MS. received 7th November 1957*

**T**A-YOU WU (1952) has given an approximate analytical method to calculating overlap integrals using Morse potential in the determination of wave functions. While studying his method and its application to  $O_2^+$  bands, we have found some of the fundamental constants used by him to be in error. So we have calculated squares of overlap integrals using the corrected constants with a view to testing their agreement with the results obtained from the numerical integration method. The numerical integration results on  $O_2^+$  are available from Poots (1953) and Nicholls, Jarman and Fraser (1953).

The expression for overlap integral as given by Wu (1952, eqn (7)) is

$$I[n'v', n''v''] = (-1)^{v'+v''} \frac{Nv'Nv''}{a'} \xi^k \sum_{\lambda=0}^{v'} \sum_{\mu=0}^{v''} (-1)^{\lambda+\mu} B(v'\lambda) B(v''\mu) I_{\lambda\mu} \dots (1)$$

where the exponent  $k$  of  $\xi$  is

$$\frac{1}{2} \left( \frac{1}{x_c''} - 1 \right). \dagger$$

(The nomenclature is that used in Wu's paper.)

As  $I_{\lambda\mu}$  cannot be evaluated exactly, an approximate analytical procedure gives

$$I_{\lambda\mu} = \frac{1}{2} \left( \frac{\pi}{\ln 2} \right)^{1/2} \left( \epsilon_1 - \frac{1}{\epsilon_2} \right) z_0^{p+1} \exp \left\{ -\frac{1}{2} (z_0 + \xi z_0') \right\}. \dots (2)$$

For the evaluation of  $\epsilon_1 - 1/\epsilon_2$  in the above expression, Wu has suggested a graphical method, which is rather laborious. Hence we have developed here the analytical expression

$$\epsilon_1 - \frac{1}{\epsilon_2} = 4 \left\{ \frac{\ln 2}{2\gamma p - (\gamma - 1)z_0} \right\}^{1/2}. \dots (3)$$

This saves a good amount of labour and seems adequate for the purpose. Firstly, it agrees with the value obtained graphically up to the fifth place after the decimal and secondly, the  $I_{\lambda\mu}$  determined by using the analytical value of  $\epsilon_1 - 1/\epsilon_2$  agrees with that of  $I_{\lambda\mu}$  determined graphically within one per cent which is of the same order as that given by Wu.

Table 1 records the values of constants calculated from the vibrational analysis data available from Feast (1950) and also for comparison, constants derived by Wu and those given by Nicholls. Table 2 gives the values of squares of overlap

$\dagger$  In the original paper (eqn. 7), the exponent  $k$  of  $\xi$  in equation (1) above has been misprinted as  $(1/2x_c'') - 1$ ; also in equation (14a) of Wu's paper the negative sign in front of  $2p \log \epsilon_2^{-1}$  should be positive. These have since been confirmed by us in a private communication with Dr. Ta-You Wu.



integrals obtained by the present method. These are compared with similar data available from numerical integration.

Table 1.  $O_2^+(A^2\Pi_u \rightarrow X^2\Pi_g)$ 

Molecular constants	Ta-You Wu	Nicholls, Jarman and Fraser	Calculated by present Authors
$r_e'(\text{\AA})$	1.4089	1.4089	1.4089†
$r_e''(\text{\AA})$	1.1227	1.1227	1.1227†
$a'$	$2.56 \times 10^8$	$2.5495 \times 10^8$	$2.5496 \times 10^8$
$a''$	$2.85 \times 10^8$	$2.8005 \times 10^8$	$2.8006 \times 10^8$
$1/x_e'$	65.5738	65.613	65.613
$1/x_e''$	113.3786	113.515	113.515
$D_e'(\text{cm}^{-1})$	14740	—	14744.9
$D_e''(\text{cm}^{-1})$	53200	—	53249.8
$\xi$	0.50	—	0.514512
$\gamma$	1.11	—	1.09845

† The values are taken from Herzberg, *Spectra of Diatomic Molecules*.

Table 2. Squares of Overlap Integrals.  $O_2^+(A^2\Pi_u \rightarrow X^2\Pi_g)$ 

$v'$	$v''$	0	1	2	3	4	5
0	(i)	$2.4 \times 10^{-6}$	$4.2 \times 10^{-5}$	$3.6 \times 10^{-4}$	$1.9 \times 10^{-3}$	$7.4 \times 10^{-3}$	$2.1 \times 10^{-2}$
	(ii)				$2.0 \times 10^{-3}$	$9.0 \times 10^{-3}$	$2.5 \times 10^{-2}$
	(iii)	$3.0 \times 10^{-6}$	$5.8 \times 10^{-5}$	$4.5 \times 10^{-4}$	$2.2 \times 10^{-3}$	$8.0 \times 10^{-3}$	$1.6 \times 10^{-2}$
	(iv)	$3.0 \times 10^{-6}$	$5.2 \times 10^{-5}$	$4.8 \times 10^{-4}$	$3.6 \times 10^{-3}$	$8.1 \times 10^{-3}$	$5.3 \times 10^{-2}$
1	(i)	$1.9 \times 10^{-5}$	$2.8 \times 10^{-4}$	$2.1 \times 10^{-3}$	$9.3 \times 10^{-3}$	$2.8 \times 10^{-2}$	—
	(ii)			$3.0 \times 10^{-3}$	$10 \times 10^{-3}$	$3.2 \times 10^{-2}$	—
	(iii)	$2.8 \times 10^{-5}$	$3.9 \times 10^{-4}$	$2.5 \times 10^{-3}$	$9.8 \times 10^{-3}$	$2.8 \times 10^{-2}$	—
	(iv)	$2.4 \times 10^{-5}$	$3.5 \times 10^{-4}$	$2.3 \times 10^{-3}$	$23 \times 10^{-3}$	$30 \times 10^{-2}$	—

(i) Poots (1953); (ii) Nicholls, Jarman and Fraser (1953); (iii) Wu (1952); (iv) calculated by authors from corrected constants.

The small difference between the first two sets of values (table 2) of numerical integration results may be due to the different methods adopted for evaluation. Since Poots found his values to agree with those of Wu, he was led to believe that Wu's method was, in general, satisfactory. However, the new results as derived by us show, in general, poor agreement although they are fairly satisfactory at low quantum numbers. The individual terms of equation (1) being very large in comparison to the final value of overlap integral, even a slight error in them might lead to wrong results on account of cancellation, which is sometimes up to four significant figures. This factor may contribute to large disagreement seen at high quantum numbers. In general, the disagreement seems to be due to the inadequate approximation adopted in the evaluation of  $I_{\lambda\mu}$ . This view has been confirmed by Wu in a private communication.

## REFERENCES

- FEAST, M. W., 1950, *Proc. Phys. Soc. A*, **63**, 557.  
 HERZBERG, G., 1950, *Spectra of Diatomic Molecules* 2nd Edn (New York: D. Van Nostrand).  
 NICHOLLS, R. W., JARMAIN, W. R., and FRASER, P. A., 1953, Scientific Report No. 8 Contract No. AF 19 (122)-470, Department of Physics, University of Western Ontario.  
 POOTS, G., 1953, *Proc. Phys. Soc. A*, **66**, 1181.  
 WU, TA-YOU, 1952, *Proc. Phys. Soc. A*, **65**, 965.

## LETTERS TO THE EDITOR

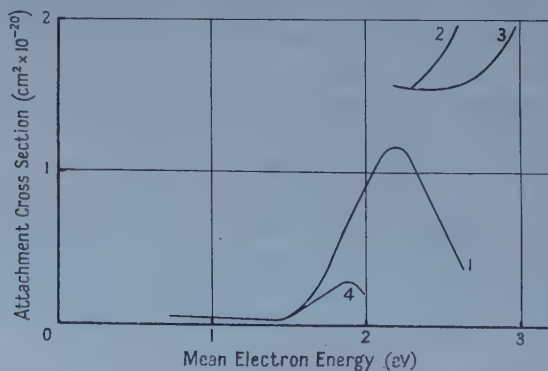
## A Note on the Cross Section for Electron Attachment in Air

The cross sections for electron attachment in oxygen and other gases have been measured directly (Lozier 1934, Craggs, Thorburn and Tozer 1957) but there appears a lack of similar data for air. Measurements of attachment coefficients have been made in mixtures of air and water vapour and in dry air and pure water vapour. An electron filter type apparatus was used (Bradbury 1932). The values for attachment cross sections for dry air derived from the measured attachment coefficients are quoted in this note, and they are in reasonably good agreement with those of Harrison and Geballe (1953). The full results will be published later.

The principle of the method is well known. Let  $\eta$  be the chance that an electron will be attached to a molecule in passing unit distance in the direction of an electric field. Then the loss of electron current in distance  $dx$  is  $dI = -I\eta dx$  where  $I$  is the initial current. Hence the ratio of the electron currents at two points  $x_2$  and  $x_1$  is  $I_2/I_1 = \exp\{-\eta(x_2 - x_1)\}$ . This expression does not allow for the formation of new electrons by ionization processes which become prominent at the higher electron energies. Corrections may be made to account for this effect if the ionization coefficient  $\alpha$  is known. The cross section  $\sigma$  for the formation of negative ions may be calculated from the values of attachment coefficients. The two quantities are related by

$$\sigma = \frac{\eta v_e}{p c n_0}$$

where  $p$  is the experimental pressure in mm Hg,  $v_e$  is the drift velocity of the electrons caused by the field,  $c$  is the mean electron speed of thermal agitation and  $n_0$  is the number of molecules per  $\text{cm}^3$  at a pressure of 1 mm Hg.



Recently Harrison and Geballe (1953) measured simultaneously the ionization and attachment coefficients of dry air and they derived the cross sections for attachment for mean electron energies above 2.2 eV (curve 3 of figure). Bradbury's (1932) results cover an experimental range up to about 2.0 eV (curve 4) and it is evident that the two sets of results will not agree when both curves are extrapolated

to cover a common range even when Bradbury's results are corrected for the  $\alpha$  effect. Curve 1 is calculated from the present work using the data of Townsend and Tizard (1913) for  $v_e$  and  $c$ . This curve, when corrected for ionization (curve 2) meets the lower end of Harrison and Geballe's curve (curve 3) using the latter's values for  $\alpha$  (Loeb 1955). The divergence of curves 2 and 3 is probably due to the uncertainty of the available values of  $\alpha$  in this region.

Despite the difference between the present results and Bradbury's results for air the attachment coefficient measured in pure oxygen gave good agreement with Bradbury's results for oxygen. The latter values are in general agreement with those derived by other workers (Craggs, Thorburn and Tozer 1957). The principal difference between the present and Bradbury's original apparatus was in the size of the chamber. The present chamber was much bigger and it is thought that this permitted the use of higher field gradients before the onset of corona. It was found that corona caused considerable variations in the measured currents. Thus it was possible to cover a wider range of electron energies with the present equipment. The present results (curve 2) are in approximate agreement with those of Harrison and Geballe.

Research Department,  
Metropolitan-Vickers Electrical Co., Ltd.,  
Manchester 17.

E. KUFFEL.

12th December 1957.

BRADBURY, N. E., 1932, *Phys. Rev.*, **44**, 885.

CAGGS, J. D., THORBURN, R., and TOZER, B. A., 1957, *Proc. Roy. Soc. A*, **240**, 473.

HARRISON, M. A., and GEBALLE, R., 1953, *Phys. Rev.* **91**, 1.

LOEB, L. B., 1955, *Basic Electronics*, University of California Press, p. 413.

LOZIER, W. W., 1934, *Phys. Rev.* **46**, 286.

TOWNSEND, J. S., and TIZARD, H. T., 1913, *Proc. Roy. Soc. A*, **88**, 336.

### Nuclear Magnetic Interaction in an Antiferromagnetic Crystal

Manganous fluoride  $\text{MnF}_2$  becomes antiferromagnetic at about  $68^\circ\text{K}$ . Below this temperature, the Mn ions tend to become aligned in two oppositely directed sub-lattices, the ions at the corners of the tetragonal unit cell belonging to one, and the ion at the centre to the other. At low temperatures this alignment is practically complete, and as a result there are very strong internal magnetic fields in the crystal, which interact with the nuclear magnetic moments of the manganese and fluorine nuclei. The effect of the aligned sub-lattices on the fluorine nuclei has been investigated by nuclear magnetic resonance (Bleaney 1956, Jaccarino and Shulman 1957), but no measurements on the manganese nuclei have been reported. We are indebted to Professor Bleaney for pointing out to us that at temperatures below  $1^\circ\text{K}$  the alignment of the sub-lattices produces an appreciable alignment of the Mn nuclei, which could be detected by measurement of the accompanying specific heat anomaly. We have measured the specific heat at temperatures from  $0.5^\circ\text{K}$  to  $2^\circ\text{K}$  by electrical calorimetry.

The specimen used consisted of a single crystal of manganous fluoride and a spherical crystal of iron ammonium alum mounted together on a silver strip on which was wound an electrical heating coil. The specimen was cooled by adiabatic demagnetization of the iron alum, and the temperatures were measured



from its susceptibility. A subsidiary experiment was made with the  $\text{MnF}_2$  crystal removed, in order to find the heat capacity of the rest of the system. We were unable to determine the specific heat of the manganous fluoride below  $0.5^\circ\text{K}$ . Experiments were made down to  $0.2^\circ\text{K}$ , but at the lower temperatures the result obtained was simply the thermal capacity of the iron alum. We attribute this failure of contact to the very rapid rise in the nuclear spin-lattice relaxation time in manganous fluoride at low temperatures (Moriya 1956, van Kranendonk and Bloom 1956, Mitchell 1957). Since the specific heat arises from the re-orientations of the nuclear spins, it cannot be detected if the relaxation time is long compared with the time occupied by the measurements. At the temperatures of our measurements the dominant term in the expression for the transition probability is of the form  $\exp(-T/T_a)$ , where  $T_a$  is the temperature characterizing the magnetic anisotropy, approximately  $13^\circ\text{K}$ . Our observation was that at  $1^\circ\text{K}$  equilibrium between the iron alum and the manganese fluoride was established in a time shorter than we could detect, but at  $0.5^\circ\text{K}$  the equilibrium time was about seven minutes, and at lower temperatures we could not establish equilibrium at all. Irradiation of the crystal with x-rays for 24 hours, a time sufficient to produce a brown discolouration, reduced the relaxation time. This effect is being further investigated.

Over the range  $0.5^\circ\text{K}$  to  $2.0^\circ\text{K}$  the specific heat of manganous fluoride is given by  $c = 0.0032R/T^2$ , with an accuracy to  $\pm 2\%$ . This result can be interpreted very simply in terms of the interaction of the electronic and nuclear moments, which can be represented by an interaction energy  $-AS \cdot I$ , where for the  $\text{Mn}^{2+}$  ion  $S = 5/2$  and  $I = 5/2$ . In the antiferromagnetic state the electronic moments are practically completely aligned, that is  $S_z = \pm 5/2$ , taking the axis of alignment as the  $z$  axis. The interaction with the nuclear moments then gives six equally spaced hyperfine levels with a separation  $5A/2$  between adjacent levels. At temperatures high compared with  $\theta = 5A/2k$ , the specific heat anomaly has a tail given by  $CT^2/R = 35\theta^2/12$ . Our measurements give  $\theta = 0.033^\circ$  or  $A = 0.0092 \pm 0.0002 \text{ cm}^{-1}$ . Tinkham (1956) who measured the paramagnetic resonance spectrum of manganese present in very small amount (5 parts per million) in a crystal of zinc fluoride, obtained  $A = 0.0096 \pm 0.0003 \text{ cm}^{-1}$ , in good agreement with our value for the concentrated salt.

It is to be expected that other antiferromagnetic salts of elements which possess nuclear magnetic moments should show similar effects, and we are now investigating some of these. Such substances may be of value as a kind of thermal ballast in demagnetization work, for example in a magnetic refrigerator, since they possess a considerable heat capacity without having a temperature-dependent magnetic susceptibility. Manganous fluoride has the further advantage of being extremely stable. A promising line of work is the investigation of nuclear alignment in antiferromagnetics. This possibility was suggested by Daunt (1951) and Gorter (1951), but no experimental work has been reported. The system of six hyperfine levels in antiferromagnetic  $\text{MnF}_2$  is a very much simpler one than the system of hyperfine levels in an ordinary paramagnetic salt of manganese, and there is a single axis of alignment. Provided the relaxation time can be sufficiently reduced, manganous fluoride appears to be a suitable substance for alignment experiments.

We have to express our thanks to Dr. Stephenson and Mr. W. Mitchell of the Department of Natural Philosophy of the University of Aberdeen, who



supplied us with the manganous fluoride crystal used in these experiments, and to Mr. C. B. P. Finn, who assisted us in some of the experiments.

The Clarendon Laboratory,  
Oxford.

10th January 1958.

A. H. COOKE.  
D. T. EDMONDS.

- BLEANEY, B., 1956, *Phys. Rev.*, **104**, 1190.  
DAUNT, J. G., 1951, *Proc. Int. Conf. on Low Temperature Physics*, 157.  
GORTER, C. J., 1951, *Proc. Int. Conf. on Low Temperature Physics*, 158.  
JACCARINO, V., and SHULMAN, R. G., 1957, *Phys. Rev.*, **107**, 1196.  
VAN KRAENDONK, J., and BLOOM, M., 1956, *Physica*, **22**, 545.  
MITCHELL, A. H., 1957, *J. Chem. Phys.*, **27**, 17.  
MORIYA, T., 1956, *Progr. Theor. Phys., Japan*, **16**, 23, 641.  
TINKHAM, M., 1956, *Proc. Roy. Soc. A*, **236**, 535.

### International Union of Pure and Applied Physics.

In the February issue of the *Proceedings of the Physical Society*, page 284, an announcement was made concerning the Ninth General Assembly of the International Union of Pure and Applied Physics. This included the names of the Executive Committee, Presidents and Secretaries of the Specialised Commissions, and plans for 1958 meetings.

The *Proceedings of the Physical Society* has been appointed by the British National Committee for Physics as the official British organ for the circulation of information concerning the International Union.

Royal Society,  
Burlington House,  
London, W.1.

N. F. MOTT.  
Chairman,  
British National Committee.

### CORRIGENDA

*The Theory of Angular Correlations with Polarization* by F. MANDL (*Proc. Phys. Soc.*, 1958, **71**, 177).

- Eqn. (13) p. 180  $F_v(J_0)$  should read  $F_r(J_0)$   
Eqn. (34) p. 184 Last bracket should read  $W(lJ_0l'J_0; J_1v)$   
Eqn. (A 5) p. 188 First bracket should read  $W(L, L, L' - 1 \dots)$   
Eqn. (C 4) p. 189  $U_{-q}^k$  should read  $U_{-q}^K$   
Eqn. (C 8) p. 190 First term after equals sign should read  $\delta_{jj'} \delta_{mm'} \dots$   
Eqn. (D 9) p. 191 Superscript to  $C$  should read  $^{\lambda\lambda'a}$   
Eqn. (D 20) p. 192 Last element should read  $v$ , not  $v$

*Expressions for certain Wigner Coefficients*, by A. P. STONE (*Proc. Phys. Soc. A*, 1957, **70**, 908).

P. 909, l. 1. The third factor in the denominator of the first fraction in the expression for  $D$  should read  $(\frac{1}{2}l - m + \frac{1}{2})!$  not  $(\frac{1}{2}l + m + \frac{1}{2})!$

## REVIEWS OF BOOKS

*An Outline of Atomic Physics*, by O. H. BLACKWOOD, T. H. OSGOOD and A. E. RUARK. Third Edition. Pp. x + 501. (New York: Wiley; London: Chapman and Hall.) 60s.

The purpose of this textbook is to provide non-specialists with an elementary treatment of the whole field of modern physics. There are chapters on the kinetic theory of gases, the nature of radiation, atomic structure, atomic and molecular spectra, wave mechanics, nuclear physics, atomic energy, elementary particles, cosmic rays, and the theory of relativity. And all this is done—on the whole, in a very successful manner—without once making use of the calculus. The book bears the mark of the wide teaching experience of the three authors and of the four ‘additional collaborators’ who are named as having shared in the preparation of earlier editions. Each chapter is subdivided into a number of short sections, and there are many diagrams and photographs, while a generous supply of numerical problems (with answers) serves to fix the student’s attention and consolidate his understanding.

Perhaps inevitably, there are occasions when the attempt to simplify complicated issues leads to obscurity. Parity, for instance—a notoriously difficult topic—is allotted one paragraph, and that in connection with the intrinsic parity of elementary particles. It is doubtful whether the paragraph was worth including. On other occasions, the obscurity is of the authors’ own making. In commenting on the fact that free neutrons undergo radioactive decay, whereas neutrons in stable nuclei do not, a reference to the conservation of energy would be more useful than the statement “the detailed understanding . . . is a challenge to theoreticians”. Vague statements of this kind appear in a number of places, and tend to confuse rather than clarify the issues involved. The description of the Rossi transition curve in the chapter on cosmic rays is plainly wrong.

In general, however, the book reads easily, and will give the non-specialist for whom it is intended a lively impression of current physics. First year physics students in this country might find it useful as preparatory reading before they commence their more detailed studies.

H. R. ALLAN.

*Progress in Cosmic Ray Physics*, Vol. 3, edited by J. G. WILSON. Pp. vii + 420. (Amsterdam: North-Holland, 1956.) 76s.

During the past few years the emphasis in cosmic ray physics has gradually changed. The development of high energy particle accelerators has meant that much of the study of fundamental particles can now be carried out using these machines. In this connection, the present volume marks the end of an epoch. Of the four articles it contains, two are on unstable nuclear particles and give an authoritative account of the progress which has been made in the field largely as a result of cosmic ray studies. Of the two remaining articles, one deals with extensive air showers and the other with the processes whereby the incoming cosmic ray energy is degraded and dissipated in the atmosphere. The review dealing with extensive air showers will be particularly welcome because of the growing interest in this field at the present time.

This book will be of great value both to the specialist and to those working in allied fields who require an authoritative account of current problems and achievement in cosmic ray physics.

H. ELLIOT.

*Thermodynamik*, Band III. 1.—*Tabellen*; Band III. 2.—*Graphische Darstellungen und Literatur*, by H. ZEISE. Pp. xi+311; 299. (Leipzig: Hirzel, 1954, 1957.) 20, 22.20 D.M.

Only after Nernst announced his heat theorem in 1906 chemists started, somewhat timidly, to assign definite numerical values to the entropy of the mass unit of any chemical species. These values were derived from direct measurement or from calorimetry. The progress of 50 years consists not only in the increased amount of available data. The main achievement consists in the use of statistical mechanics for deducing theoretically thermodynamical functions from atomic physics, in particular, spectroscopy.

The present work is part of a treatise on thermodynamics. It consists of two volumes in which the thermodynamical functions of numerous substances are compiled. The power of the statistical theories is forcibly demonstrated by displaying the results of theoretical deductions. Of those thermodynamical functions which are arrived at by the older methods only a selection is shown. Preference is hereby given to substances which, like uranium, have only recently attracted interest.

The theoretical approach is essentially restricted to the properties of gases; it applies on the other hand also to free radicals or to molecules of low stability which could not be investigated by conventional experimental methods.

Material presented in this work is arranged in tables and graphs. They include entropies, enthalpies and specific heats of chemical elements and inorganic and organic compounds. A special section is concerned with the equilibrium constants of chemical reactions in gases. The origin of the published material is recorded in an extensive list of references to which critical comments are added.

The methods of statistical thermodynamics are reviewed in an introductory chapter of 40 000 words. As an aid to future research special tables are added. A six-figure table of the thermodynamical functions of harmonic oscillators may be equally useful as a list of the potential barriers of numerous organic molecules which preclude the free rotation about chemical bonds.

The book under review may be very helpful in studies of chemical equilibria whether pursued in scientific research or for the purposes of technology. The subject and its presentation are, however, better adapted to chemical laboratories than to research in physics.

R. EISENSCHITZ.

*Propriétés et Structure des Noyaux*, edited by L. DE BROGLIE, Pp. 0+126. (Paris: Editions de la Revue D'Optique Théorique et Instrumentale, 1956.) 1200 fr.

This is the latest in the annual series of symposia edited by L. de Broglie in each of which leading French physicists survey a field, the present being that of nuclear structure. The basic duality of modern nuclear theory is set out in the articles by Marty on the shell model and Trocheris on the collective model—or



rather the unified nuclear model, which represents individual nucleons in a distorted collective field. The remaining eight articles deal with special theoretical aspects (e.g. isotopic spin by Deutsch), or methods of investigating the theoretical concepts (e.g.  $\beta$ -decay by Nataf, and stripping by Horowitz and Cotton). The level is didactic, comparable to that of Blatt and Weisskopf, rather than that of a comprehensive review article, and the calibre of the authors guarantees a high standard. One notes with regret that, while the nominal date is 1954, which represents roughly the actual date of the material, the cover says 1956, and this review is being written mid-1957. Publishing delays are a wastage in these circumstances of rapid change in research. Nevertheless, this book gives the broadest, most coherent and most up-to-date introduction to current nuclear theory known to the reviewer.

R. HUBY.

*Mathematics and Wave Mechanics*, by R. H. ATKIN. Pp. xv + 348. (London : Heinemann, 1956.) 30s.

This book is an excellent introduction to some parts of wave mechanics. The author first sets out to establish a sufficient mathematical background and then describes modern quantum theory. There are five chapters on pure mathematics, three on applied mathematics and seven on wave mechanics. The book is chiefly to be criticized upon what is omitted from it. Admittedly it is not possible to cover all topics in a book of this kind but surely scattering theory deserves more than three pages, the last three pages of the book. Because of this omission many physicists must find that this book stops short of what they require. But what is selected for discussion is described very well and it is clear that the author is well acquainted with the usual difficulties of students. A notable feature is the large number of examples which are worked through in detail as illustrations.

The author assumes the reader to possess that knowledge of mathematics which is usual on entry to a university and rapidly describes further topics in analysis. Vectors, determinants and matrices are then introduced. Short accounts of curvilinear coordinates and multiple integrals and a chapter on differential equations complete that part of the book devoted to pure mathematics. After a short chapter on classical mechanics and a description of vector field theory, quantum mechanics, the Heisenberg representation and the Schrödinger equation are introduced. The next chapter gives an account of time independent perturbation theory and this is followed by a discussion of the Dirac equation which is applied to the hydrogen atom. The book concludes with chapters on quantum chemistry, statistics and quantized fields.

W. MARSHALL.

*La Diffusion dans les Metaux*, edited by J. D. FAST, H. G. VAN BUEREN and J. PHILIBERT. Pp. 124. (Eindhoven : Philips, 1957.) 37s. 6d.

As a consequence of considerable development over the past five or six years, the study of diffusion in metals is now assuming a position of some importance in metallurgy and solid state physics. The physical meanings of diffusion coefficients measured under different conditions are better understood, and both experimental methods and theoretical reasoning have advanced to the point



where good agreement has been reached in certain problems. For the metallurgist interested mainly in practical behaviour, more reliable data is becoming available to assist in the interpretation of phenomena involving the movement of atoms in metals, and from a more fundamental point of view, experimental and theoretical studies are together making a valuable contribution to our knowledge of the metallic state.

For these reasons it is desirable that current ideas in this subject should be made available in convenient book form to metallurgists and physicists working in related fields. This small volume fulfils this need to some extent, but because of its origin cannot provide the general account which is needed for a balanced introduction to the subject. It is in fact a symposium of the papers read at a colloquium held in Eindhoven in September of last year by a small group of European metallurgists. The subject matter is therefore rather specialized, though the disadvantage of this for the non-specialist reader is partly offset by the inclusion of general reviews of some of the chosen topics, and an adequate selection of references to published work.

An introductory article by A. D. LeClaire provides in a form both concise and clearly illustrative of physical meaning, the definitions of and relationships between diffusion coefficients and mean atomic displacements in different kinds of metallic systems. The Kirkendall effect in chemical diffusion, and methods of measurement are also summarized.

By far the greater part of the following articles is devoted to three problems, grain boundary diffusion, chemical diffusion and the Kirkendall effect, and interstitial diffusion with particular reference to anelastic methods of measurement. Three further articles deal very briefly, all within the space of ten pages, with the diffusion of silver in AgCl, introducing the concept of equivalent electrical circuits to describe the diffusive movement of atoms, the diffusion of helium gas through silicon and germanium by a mass spectrometric method, and the effect of elastic deformation on the mobility of vacancies in copper.

The more detailed articles include a very useful review of grain boundary diffusion in metals by P. Lacombe, in which the theoretical analysis of the problem, experimental methods and results of importance to the nature of grain boundaries are discussed. This is followed by a preliminary report of a study by C. Leymonie and P. Lacombe of grain boundary diffusion in iron using an autoradiographic method with the radioactive isotopes of Fe.

Experimental details of chemical diffusion studies in both monophase and polyphase alloys are illustrated by accounts of work on copper alloys, the zirconium-uranium and gold-platinum systems.

To criticize the subject matter of the book is of course to criticize the scope of the colloquium, but it is unfortunate that the theoretical aspects of diffusion in metals have been somewhat neglected, and that no account is given of the measurement of lattice diffusion coefficients in metals of homogeneous composition with the aid of radioactive tracers. This approach appears to provide the most fundamental kind of data for comparison with theory, and its application to a wide range of metallic systems is undoubtedly a promising path towards a more complete understanding of the elementary diffusion process.

The absence of discussions of the papers is also felt to be an unfortunate omission, for discussion is surely a very important part of a colloquium, and at its present stage of development, the subject is by no means lacking in controversy.

The book is well produced, with clear diagrams and plates, and is written in easily readable French. The specialist reader will find the new experimental data of interest, and his fellows in allied fields will derive an insight into some aspects of an increasingly important branch of metal physics. D. H. TOMLIN.

*Dreidimensionale Überschallprobleme der Gasdynamik*, by K. R. DORFNER.

Pp. viii + 150. (Berlin, Göttingen, Heidelberg: Springer, 1957.) DM.26.

For sixty years since the pioneer work of Sommerfeld, mathematicians have readily fallen for the fascination of the two-dimensional wave equation, and of the problem of seeking out exact solutions of it, together with their physical interpretations. In recent years, it has been possible to combine this pleasant activity with a virtuous feeling that the work was contributing to a great new industry and a great new human adventure—supersonic aerodynamics. This is because the small disturbances to the air, due to the passage through it of a sufficiently slender wing or fuselage, can be treated by means of the approximations of the theory of sound, and these lead in the case of steady supersonic flight to the two-dimensional wave equation, with time replaced by a multiple of the space-coordinate (relative to the aeroplane) in the downwind direction. The ‘light-cones’ of the abstract ‘space-time continuum’ of optics become visible ‘Mach cones’ in supersonic flow. Enormous numbers of mathematicians all over the world have revelled in this new situation, which has called for the development of vast dictionaries of new solutions and has involved many new techniques of mathematical treatment and new principles of physical interpretation. An excellent account of all this work will be found in the book under review, and any mathematical physicist, even though previously concerned only with the optical applications, will find it interesting.

Alas! The effort expended has been less valuable than it appeared. To be sure, the aircraft companies have attached importance to this work, and used it to develop wing and fuselage shapes with satisfactory aerodynamic properties according to the theory. The main reason for this has been the prohibitive cost of testing more than a handful of shapes in supersonic wind tunnels. However, the evidence of such experimentation as has been done is that the qualification ‘sufficiently slender’, noted above as a condition for the theory to be a good approximation, is not satisfied by aerodynamic shapes that are satisfactory on structural grounds. Thus, while in the ordinary theory of sound one is concerned with pressure changes three or more orders of magnitude less than the absolute pressure, it is a question in this field only of half an order of magnitude. As a result, the predicted pressures have some value as very rough approximations, but the theory is altogether too crude to give a sensitive indication of trends to be expected from particular alterations, and is not therefore a suitable tool for seeking optimum configurations.

As a result of these shortcomings (which are not discussed in the book under review) efforts are now being made to develop a practical calculation procedure based on more exact aerodynamic theory. In this work, the resourceful brainpower of the analyst must collaborate with the speed and endurance of the electronic computer. Perhaps the challenge of this new collaboration will at last hold fascination for mathematicians, greater even than that of the theories which Dr. Dorfner has here so ably expounded.

M. J. LIGHTHILL.

*Rectifying Semiconductor Contacts*, by H. K. HENISCH. Pp. xii + 372. (London : Oxford University Press, 1957.) 70s.

Research on semiconductors is proceeding so rapidly that the authors of books on the subject are faced with many difficulties. Perhaps the greatest are to know where to start and to get the book out while it is still up-to-date.

In *Rectifying Semiconductor Contacts* the author does something which is very rare these days—he starts at the beginning. The developments of rectifiers is traced from the first observations of the phenomenon about eighty years ago until the date of going to press (1955). This account includes much material not readily available elsewhere.

It has become customary to include in all books on semiconductors an introductory section in which the elements of solid state theory and the basic properties of the better known semiconductors are briefly described. I did not find this part of the present book particularly satisfying. The result of attempting to cover too much ground has been to include several ambiguous over-simplifications. Thus to discuss the effects of impurities in semiconductors without describing fairly fully the effects of compensation of one type of impurity by another is, in the light of present knowledge, misleading to say the least. Since it is unlikely that anyone completely unacquainted with semiconductors would wish to tackle this work, much of this introductory material could have been left out.

About half the book is devoted to the properties of crystal diodes and a good account is given of the properties of plate rectifiers. While making passing references to p-n junctions the author rules any detailed discussion of them as outside his province. I thought this was a pity in view of the ever growing technical importance of this type of rectifier. Since p-n junctions can be made by an 'alloying' process which bears a resemblance to the older 'forming' process used with catwhiskers, it does not seem wise to draw too sharp a distinction between these different types of rectifiers. Since, also, studies on p-n junctions are much more easy to interpret than those on the older types of rectifier, it would have been better to have devoted most of the space given to the general introduction to a fuller account of this type of rectifier.

In conclusion, it is right to point out that in the task which he set himself, the author has achieved a fair measure of success, but had he set out in a slightly different direction a book of much greater value would have been produced.

E. H. PUTLEY.

*Viscous Flow Theory—II: Turbulent Flow*, by SHIH-I PAI. Pp. xi + 277. (Princeton : Van Nostrand; London : Macmillan, 1957.) 48s.

It is very difficult to write a book on turbulence that will satisfy both engineers and mathematical physicists, and usually an author's own interests will incline him towards one viewpoint or the other. This book, however, is the exception that illustrates the advantages of this; it consists of two practically unrelated sections, of which the first is concerned with the old mixing length theories and the second with some of the aspects of the theory of turbulence developed in the last twenty years. While it is true that modern experimental studies have shown



the basic inadequacy of the mixing length hypotheses and that, until quite recently, they have provided little satisfactory alternative, the number of physically significant results that can be deduced from sound physical principles is by no means as small as this book would lead us to believe.

After an introductory chapter on some basic concepts of turbulent flow, the book deals in some detail with the solutions given by the 'semi-empirical theories' for the flows in pipes and channels, jets and wakes and for the turbulent boundary layer without and with a pressure gradient and in a compressible fluid. The more modern theory is introduced by comparing the basic ideas with those in classical statistical mechanics, leading to a rather inconclusive chapter on probability distributions. A discussion of turbulent diffusion precedes any mention of the dynamics of the problem, which is found in two chapters on the correlation tensor and the spectrum of turbulence. The book concludes with a little on the theory of local similarity, magnetohydrodynamics and turbulence in a compressible fluid.

From a textbook one expects a unity and continuity of treatment and a critical judgment on the relative importance of the many contributions that have been made to the subject, and these criteria the present book fails to satisfy. Many sections consist of almost word-for-word extracts from original papers by various authors, yet often the important and revealing physical discussion is absent and we are presented with merely the formal mathematics. This must lead to a serious lack of understanding on the part of the reader, and results in a patchy, heterogeneous structure of the book. There is a lack of ordered development of the theme, and the significance of important results is often obscured by insufficient emphasis and development. For instance, in the chapter on the local similarity theory, no discussion is given to make the hypothesis plausible, and little development is given to show how the theory can be applied, say, to such problems in diffusion as the relative motion of neighbouring fluid elements. After reading this section, the student might be excused for wondering what has been established and what is the point of it all.

The reviewer also looked with little success for evidence of a critical selection from the vast number of papers that have been published in this subject. This lack of selection has certainly resulted in the compilation of a large bibliography, which may be valuable, but in the text points of cardinal importance are mixed indiscriminately with long and detailed descriptions of theories of debatable validity or relevance.

Technically, the book is well set up and meets the standards one has come to expect from this publishing house, but as a guide to turbulence theory, it suffers from a number of serious defects and shortcomings.

O. M. PHILLIPS.

*Theorie der Riemannschen Flächen*, Volume LXXXIX of the *Grundlehren der Mathematischen Wissenschaften*, by A. PFLÜGER. Pp. xii + 248. (Berlin : Springer, 1957.) DM. 39.20.

The study of Riemann surfaces is about a hundred years old. It started because certain functions such as  $\log z$  and  $\sqrt{z}$  were not one-valued in the plane. Hence Riemann introduced the notion of a surface covering the plane repeatedly and such that the different points of the surface 'lying over' the



same point in the plane correspond to different values of the original many-valued function which now becomes one-valued on the surface.

Since then the subject has grown free of such applications, and, as so often happens, developed in its own right. The Riemann surface is introduced as a one-dimensional complex analytic manifold, an object in which neighbourhoods are defined that can be mapped on to circles in the plane. If two such neighbourhoods intersect, the corresponding mapping is conformal. The key problems concern the existence of various kinds of functions and differentials on such a surface and the corresponding classification of surfaces.

The author gives a very good account of these problems, introducing most of the methods which are used at various times for solving them, and showing when each is most appropriate. Thus the Perron method based on the upper envelope of classes of subharmonic functions is introduced in the first chapter and, following Nevanlinna, is used to construct a function with a non-vanishing gradient throughout the surface. This leads very simply to Rado's theorem that a Riemann surface defined as above has a countable system of neighbourhoods and so is triangulable. The Perron method is also used for solving the Dirichlet problem of finding a harmonic function with given boundary values, and further, for constructing a Green's function on those surfaces which possess one, i.e. those with a positive boundary (chapter 4). On the other hand, the method of orthogonal decomposition, and the Dirichlet minimum principle, is used to construct harmonic differentials with given periods, and later with given singularities in the case of a surface with null boundary (chapter 4).

From these differentials it is not difficult to construct the basic mapping functions from simply connected surfaces on to a circle, open or closed plane, and also the mapping of a multiply connected surface of genus zero on to a plane domain bounded by horizontal or vertical slits (chapter 5).

In chapter 6 we have first the discussion of differentials on closed surfaces including the Riemann-Roch theorem. Then there follows the Behnke-Stein theorem concerning the existence of analytic functions on an arbitrary open surface  $R$  which approximate a function defined on a normal sub-domain of  $R$ . In chapter 7 various criteria are given for a function to have null or positive boundary and the classification of surfaces according to the type of function (positive harmonic, bounded analytic, etc.) which they admit is discussed in detail.

For those wishing to study Riemann surfaces as a subject in its own right, this is probably the best book available. All the fundamental results are here, and the treatment is concise, thoroughly modern, and as clear as the subject permits. There is a good index and bibliography. In several cases, for instance, in his treatment of the Dirichlet principle on page 132, the author introduces new methods which simplify existing proofs. The fundamental Behnke-Stein theorem is also absent from earlier books apart from Behnke and Sommer's monumental work. In spite of its relatively modest size this is a scholarly and comprehensive book, leading the student right up to the modern work in the field. He should be warned, however, that it is on an extremely abstract level. It contains no applications of any kind, even to other branches of function theory, and very few examples of specific surfaces.

W. K. HAYMAN.

*An Introduction to Junction Transistor Theory*, by R. D. MIDDLEBROOK. Pp. xxiv + 296. (New York: John Wiley; London: Chapman and Hall, 1957). 68s.

Recently several books have appeared dealing with semiconductors and their applications. Some are primarily theoretical accounts of the basic physics, some refer mainly to the engineering aspects, and some attempt to combine the two, with varying success. The present volume is restricted to a theoretical account of junction transistors, and is very successful as a result of the limited field of interest. No attempt is made to deal with practical problems of transistor materials and techniques.

The theory of transistors is presented clearly and in considerable detail, and is preceded by an account of semiconductor theory and junction physics which is adequate for the purpose, while avoiding the mathematical complexity inevitable in a treatment intended for students of the solid state. Part I presents in fact a good introductory account of semiconductor physics for any type of reader.

After a brief history of the transistor, Part I gives a qualitative discussion of semiconductor theory followed by a quantitative account of Fermi statistics and factors affecting electron and hole density and electrical conductivity. These considerations are then applied to a p-n junction, and extend the treatment of drift and diffusion currents to the behaviour of injected minority carriers in a forward-biased junction.

In Part II the basic ideas developed in Part I are applied to semiconductor devices, in particular to the rectifier characteristics of a single junction and to the properties of a p-n-p transistor. The treatment is confined to the case of diffusion currents, and does not attempt to deal with fields and currents so high that drift becomes important.

The behaviour at high frequency is next dealt with, and factors affecting frequency cut-off are considered. A generalization of the whole treatment follows, taking account of the effect of collector voltage on base width, and allowing a generalized waveform. The later chapters are concerned with setting up an equivalent circuit, adequate to frequencies of the order of the cut-off frequency, and accounting for the capacitances and resistances inherent in the transistor. The expression first derived is in terms of its physical dimensions and properties. This is then converted into an expression based on measurable parameters of a complete transistor. Much of this material is original, and all of it will be found valuable to circuit engineers.

The treatment has so far assumed an idealized transistor. The final chapter deals briefly with complications introduced at the semiconductor surface, by leakage conductance and by surface recombination, and with the effect of increasing the injected carrier density. All who wish to understand transistor action will find this book of great value.

D. A. WRIGHT.

*Causality and Chance in Modern Physics*, by D. BOHM. Pp. xi + 170. (London: Routledge and Kegan Paul, 1957.) 21s.

*Determinism and Indeterminism in Modern Physics*, by E. CASSIRER. Pp. xxiv + 227. (New Haven: Yale University Press, 1956.) 40s.

The possibility of quantum mechanical prediction of the probable course of atomic events, but not of the precise course of individual events, poses certain particular questions for philosophical discussion. Recent interest has been aroused by Bohm's 'causal interpretation' in which chance at the atomic level is supposed to result from happenings in a sub-atomic domain. In his book Bohm explains his philosophical viewpoint, which he refers to as that of the 'qualitative infinity of nature'. Much of it is better known as dialectical materialism. Bohm criticizes the view that future research will leave unchanged the general form of quantum laws, and gives reasons for believing possible a more precise description of atomic events, but emphatically rejects the view that all happenings can be explained as consequences of the operation of a finite number of quantitative laws.

The weakness of Bohm's philosophy is that sweeping assertions are made without indication of how they can be given a precise meaning and hence how they can be confirmed or infirmed. An interesting exercise in logical analysis would be provided by discussion of his view that "the world as a whole is objectively real, and that, as far as we know, it has a precisely describable and analysable structure of unlimited complexity". How can one decide whether the complexity of the world is limited or unlimited? And if unlimited how does one describe it precisely? Perhaps with the intention of answering the second of these questions Bohm adds that "any specified element can in principle ultimately be discovered" and that "any *given* kind of thing is, in principle, knowable". But to persist: how can an element be specified before it is discovered or a thing be given before it is known?

Bohm's philosophy may be criticized without challenge to his contention that it would be unjustifiable "to restrict *all* research in theoretical physics to those lines that fit into a continuation of the usual interpretation of quantum theory". The 'causal models' are of interest in demonstrating that more precise prediction is not inconceivable. To demonstrate more than this it is necessary that such predictions should be made and verified.

Cassirer's book, translated from a work published in German over twenty years ago, stems from a very different philosophical school which attaches great importance to epistemological precision. The value to physicists of his analysis of the history of the causal concept, and of its relation to the concept of physical reality, is that it lays bare the nature and origin of many of our preconceived ideas. His contention is that the causal principle does not provide a new insight concerning the content of reality but has its significance in the scientific method. He considers the causal principle to be the axiomatic presupposition that results of physical measurements can be "so related and combined with one another that . . . there results a system of physical knowledge and not a mere aggregation of isolated observations". From this standpoint he considers that quantum theory involves no abrogation of the causal principle.

Those primarily concerned with ethical judgments frequently discuss the situation in physics and physicists themselves, in seeking a philosophy of physical



science, are frequently influenced by consideration of ethical questions. This alone provides ample justification for Cassirer's concluding discussion on implications for ethics. He considers that there should be no conflict between the search for ethical judgments and the search for a rational understanding of nature since ethics represents a different type of conformity to law, the requirement that our acts be judged in the light of reason. Cassirer concludes that "ethics would certainly be in a bad way—it would lose all its dignity—if it could maintain its authority and fulfil its particular function in no other way than by keeping a lookout for gaps in the scientific explanation of nature".

M. J. SEATON.

*Excited States in Chemistry and Biology*, by C. REID. Pp. ix + 215. (London: Butterworth Scientific Publications, 1957). 45s.

The purpose of this book is to build a bridge between the theoretical study of the intimate mechanism of chemical reactions, with particular reference to the physical concepts of molecular excitation and interaction, and such biological problems as those of bio-luminescence, the nervous excitation process in visual receptors, and the effects of high energy radiation.

The treatment is largely that of mathematical physics, and there are four appendices on such topics as group theory and perturbation theory. The question may be raised as to whether the book will be of use to more than a rather restricted group of biologists. By the nature of things those who are not familiar already with a great deal of the important but difficult field of molecular physics may not find the book easy to read. On the other hand it is full of suggestive facts and ideas, and valuable bibliographical references, so that it will no doubt fulfil the author's hope, namely to stimulate investigators in the biological sciences to acquire a more detailed knowledge of quantum-chemical ideas than it was possible to present in the book itself.

The book gives a good idea of the considerable advances recently made in the theoretical and experimental study of excitation mechanisms, the triplet state, and inter- and intra-molecular energy exchanges. The discussion of luminescent reactions and of visual excitation from the standpoint of this new knowledge is valuable and interesting. Yet in the latter connection the reviewer, as a student of visual physiology, may perhaps point out that the fact that—even though several photons are required for seeing—nervous excitation can be produced in a retinal rod cell by the absorption of one single photon of visible light, is not explicitly stated or discussed. True enough the mechanism of such action largely remains a mystery, but it is the kind of mystery which, one hopes, progress in the study of the dynamics of quantum-molecular phenomena will help to solve. This minor comment should not be taken as a criticism, but rather as evidence to show that the type of integration sought by the author is very important to achieve.

In any case the book will form an excellent introduction to the subject of excited states for students of physics and chemistry.

M. H. PIRENNE.

*Digital Computers*, by R. K. LIVESLEY. Pp. viii + 52. (Cambridge: University Press, 1957.) 8s. 6d.

This is a short and very readable book which in some 50 pages gives an excellent survey of the logical and engineering structure of electronic digital computers



and of their uses in science and industry. There are four chapters, in an unusual and interesting order: Elements of Programming; Input, Storage and Output; Organisation of Programmes; and Solution of Engineering Problems. The first, basing its arguments on the solution by an iterative method of a set of simultaneous linear algebraic equations, develops most of the essential ideas of programming, including the very important one of the construction of loops or cycles in a calculation. The second is descriptive, concerned with the equipment actually used for conveying information to and from the machine and for holding it inside the machine; there is a delightful photograph of the first machine built in the Manchester Laboratory in 1948, to remind us of what these things looked like in their dark ages, 10 years ago. The third is concerned mainly with the idea of the division of a programme into distinct routines, corresponding to logical divisions of the calculation, and in particular explains the use of 'closed' sub-routines which can be entered from any point in a calculation and so make possible the formation of a library of standard routines—one of the fundamentally important pieces of programme technique. Other points dealt with in this chapter include automatic programming—that is, using the machine itself to construct programmes—and testing and fault-finding in programmes. The last chapter "discusses some of the points which arise in applying computers to engineering calculations and describes some of the problems which have so far been solved"; the latter include the solution of algebraic linear and non-linear equations (specifically, stress calculations and the design of optical lens systems), of ordinary and partial differential equations and the logistics type of problem generally called linear programming. The book concludes with short discussions of the effect of fast computers on the development of mathematical techniques, some economic questions and the probable future developments on computers and their applications.

Dr. Livesley succeeds very well in doing what he sets out to do, that is, to give an account of these machines and their powers mainly in general terms but with sufficient detail to convey real and realistic information; I would find it hard to say how his account could be significantly improved. I have a few minor criticisms; I think Dr. Livesley could have laid still more stress on the importance of the B-register—"the only new idea in computing machines since Babbage", I once heard said by a well-known member of the computing world: it is noticeable that all the newest and most powerful machines are now equipped with these. The discussion on page 18 of the desirable size of the fast store has a rather old-fashioned air for a book published in 1957: even 1000 numbers is now beginning to seem a small capacity and machines are being produced on a large scale with many times this amount of storage. Partial differential equations are dismissed rather summarily: many of the most impressive applications are in this field, as for example in numerical weather forecasting and nuclear reactor design, and the need to solve larger and larger systems has undoubtedly been an important factor in the remarkable new machine projects now being undertaken in America.

The general impression given by the book is one of an exceedingly practical common-sense attitude towards computers and their uses; it is particularly well produced and is very good value indeed for its modest price.

J. HOWLETT.

*Quantum Mechanics*, by H. A. KRAMERS. Pp. xvi + 496. (Amsterdam: North-Holland Publishing Company, 1957). 90s.

This book is a translation of two well-known works, *Die Grundlagen der Quantentheorie* and *Quantentheorie des Elektrons und der Strahlung*, by the late Professor H. A. Kramers, which were first published some twenty years ago. The translation has been undertaken for two reasons, firstly its appearance completes the English edition of all Professor Kramers' published work and secondly both the publishers and Dr. D. ter Haar, the translator, feel that the English speaking world has been the poorer in not having access to this very fine exposition of quantum theory. These are both excellent reasons for a translation and its completion will be widely welcomed.

The author's intention was to give a thorough and complete (at that time) account of quantum theory, and particular emphasis is paid to the fundamentals of the subject. Indeed it is the treatment of these which makes the book so valuable, for while there is no shortage of books in English on quantum theory there are few, if any, which give such a balanced and well-reasoned account of it. At the same time the book is of considerable length, and as it is a work which needs to be studied carefully it will probably not appeal to those who want to get to the stage of using wave mechanics in particular problems, without worrying too much about the underlying ideas. It also presupposes a good deal of mathematical knowledge on the part of the reader, and a willingness to extend this, if necessary, at least to spinors, though not to group theory.

The list of chapter headings reads much like that of any other book on quantum theory, the usual topics of the treatment of free and bound particles, transformation theory, perturbation theory, the electron spin, the exclusion principle and radiation theory being covered. While this list gives some guidance about the contents the great virtue of the book is the way in which each topic is treated. Throughout one is conscious of being under the guidance of someone who has thought very deeply and carefully about all the various aspects of quantum theory, and who is able to express his ideas in a most stimulating and lucid way.

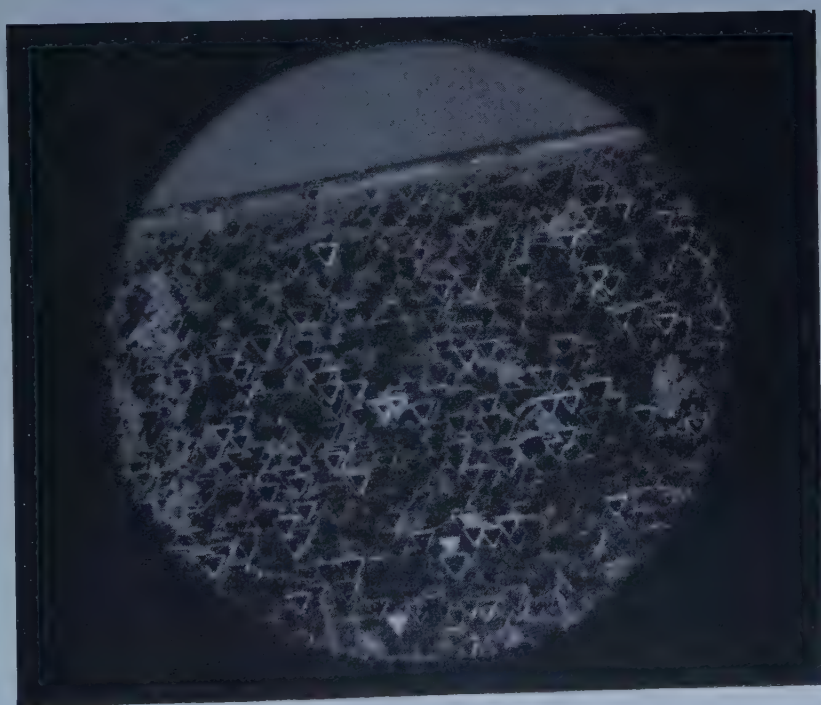
The publisher clearly feels that the first five chapters provide a good introduction to quantum theory, for these chapters have been printed separately under the title of *The Foundation of Quantum Theory* (36s.). While this is true, it is not an elementary treatment and indeed the whole work will probably be of most value to those who have already obtained a good grasp of quantum theory and can appreciate a discussion of the finer points.

The standard of the translation is high and though there are a number of misprints and unusual constructions the meaning is generally clear. The first statement of the uncertainty principle has the inequality the wrong way round, but such errors will only add slightly to the burden of the beginner, for there are no indications which sections should be omitted in a preliminary reading.

K. W. H. STEVENS.



(a)



(b)

Figure 1. (a), (b). Etch pits on cleavage surfaces of bismuth telluride.



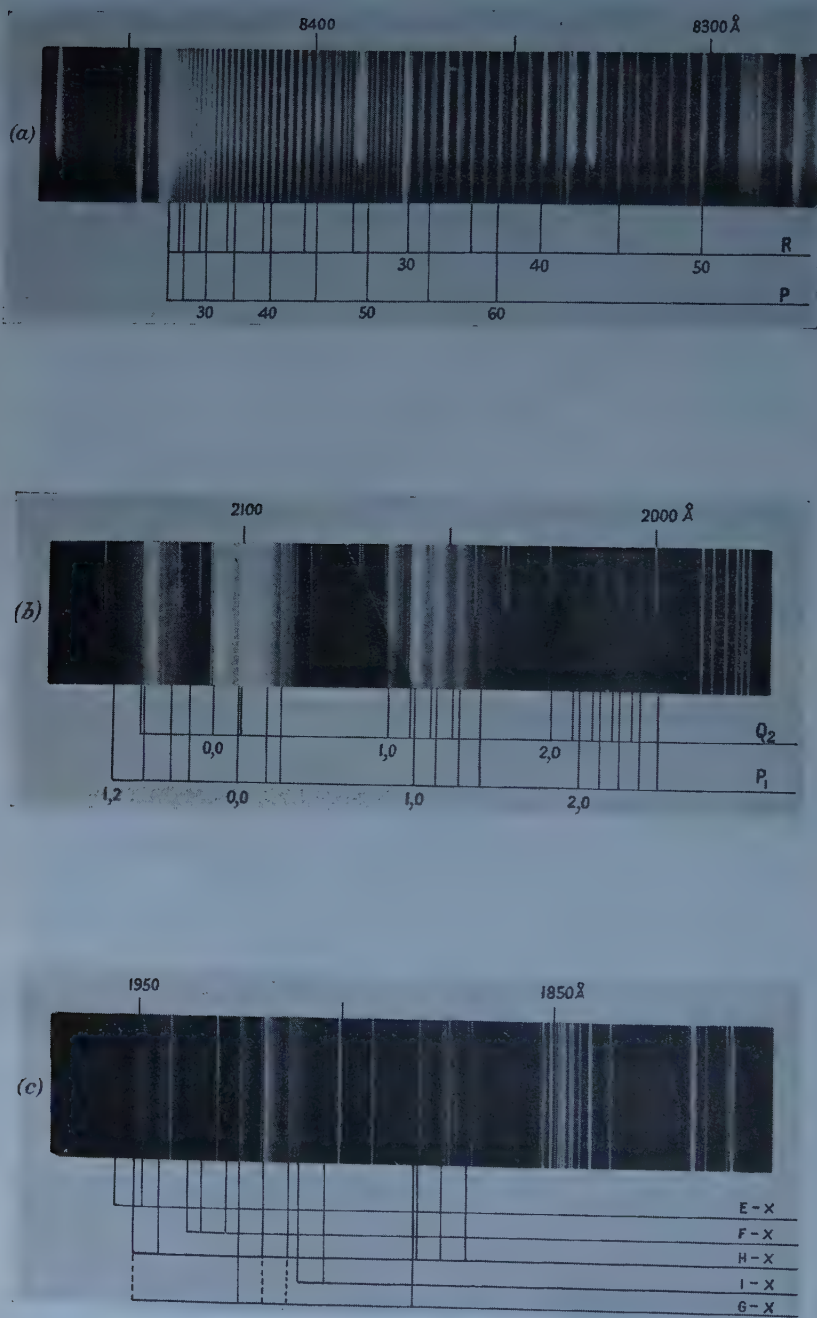


Figure 1. Emission bands of SiF. (a) The 0, 0 band of system B-A; (b) the D-X system; (c) far ultra-violet bands.



# A New Formulation of Scalar Diffraction Theory for Restricted Aperture

By J. M. COWLEY AND A. F. MOODIE

Chemical Physics Section, Division of Industrial Chemistry, Commonwealth Scientific and Industrial Research Organization, Melbourne, Australia

*Communicated by A. L. G. Rees; MS. received 15th July 1957*

**Abstract.** A formulation for scalar problems in physical optics is presented. Approximations involve the neglecting of the obliquity factor and the dependence of amplitude on distance and the replacement of spherical by paraboloidal wavefronts. Expressions are obtained for wave function in a multi-component system in terms of convolution integrals, the components of the system being described by functions of either direct or Fourier space.

The formulation is equally applicable to light optics, electron microscopy or electron diffraction and permits interchange in the techniques of these disciplines. Some elementary examples of the application to thin lenses, and to periodic objects are given.

## § 1. INTRODUCTION

MANY methods have been devised for the solution of problems in scalar diffraction. None of these can, however, be readily adapted to treat certain types of problems encountered in light and electron optics, the transmission of radio waves and so on. These arise mainly in multi-component systems, and systems where the diffracting object is neither a fully transparent aperture nor a wholly opaque stop.

Examples of the first of these two types of problem encountered in light optics are found in the various phase contrast systems. Examples arising in electron diffraction and electron microscopy include successive scattering by a number of crystals, scattering by a thick crystal with prescribed disorder, and scattering by a perfect thick crystal. In all of these systems it is desirable to be able to evaluate the wave function on any plane.

This facility can be even more important in the second type of problem. Thus, since it is not possible to make a direct observation of the structure of an object on the atomic or even molecular level by observing the intensity distribution of the image on the image plane of an electron lens or of the diffraction pattern in the back focal plane of the lens, the question arises as to whether additional useful information may not be obtained on some other plane in the system (Gabor 1949, 1951, Cowley and Moodie 1957a). The examination of such a point given, for example, the tolerances for practical components and prescribed *a priori* information on the object, at once requires a formulation explicitly in terms of Fresnel diffraction.

Attempts to solve such problems rigorously encounter fundamental difficulties. Usually approximations are made in the course of the analysis in an effort to circumvent those difficulties. Very frequently those approximations can be shown to contain assumptions which restrict the range of validity to apertures

or which spherical wavefronts may be treated as paraboloidal surfaces. Since approximations of this type are valid for many problems of practical interest, and in particular, hold to a high accuracy for virtually all of the current problems in electron diffraction and electron microscopy, it would appear worthwhile to enquire whether it is possible to set up a formulation which exploits this from the outset.

Classical procedures still, however, meet formidable difficulties even for relatively simple systems. It is the purpose of this communication to describe an attempt to overcome some of these difficulties by means of a formulation in which more emphasis is placed on the derivation of physically suggestive equations than of analytical solutions in closed form. In particular it is shown that many of the techniques of Fourier transformation can be incorporated in a formulation that describes the phenomena of Fresnel diffraction explicitly, thus permitting direct application of the methods which have proved powerful in crystallography. A comparison may be made with formulations recently described by various authors; for instance those of Duffieux (1946), Hopkins (1953) and Linfoot (1955) which refer to light optical systems in the region of the image plane, this restriction being imposed for mathematical convenience, and that of Ratcliffe (1956) which has application to problems concerned with the propagation of radio waves.

The formulation is approximate in that the paraboloidal approximation to a spherical wavefront is made, the obliquity factor is omitted, and the dependence of amplitude on distance is neglected. It is elementary in that the derivation proceeds from the definition of optical path length rather than from Schrödinger's equation or the equation of wave motions. The formulation can be derived from these equations, but this is avoided since it tends to obscure the simplicity of the approach. Examples of the uses of the method in systems of moderate complexity have already been given (Cowley and Moodie 1957 b, c). The application of the formulation to multiple scattering problems in electron diffraction and electron microscopy affords an example of the use of the method in systems of inherent complexity (Cowley and Moodie 1957 d). It has been found in practice that a substantial advantage accrues only for systems above a certain level of complexity. Thus little is to be gained by the use of this method in the description of diffraction by a simple aperture but a wave theory of the various moiré effects for either light or electrons may be obtained directly. A few particularly simple illustrations are given in this communication.

## § 2. INTRODUCTORY FORMULATION FOR TWO COMPONENTS

It is assumed that all sources present in the system are coherent. Thereby little generality is lost. Should the sources be incoherent the analysis is always simpler and solutions can be obtained by an obvious process. For problems of partial coherence Hopkins' coherence factor is available (Hopkins 1953), and in a form well suited to the formulation. The formulation is set up in this section for a two-component system and the extension to  $n$  components is obtained in § 3.

The two-component system is defined by reference to three parallel planes spaced at distances  $R_1$ ,  $R_2$ , the last plane being taken as the plane of observation. The planes are characterized by coordinates  $(u_1, v_1)$ ,  $(u_2, v_2)$ ,  $(x, y)$ , and their positions chosen to give the most convenient description of the components of the system in terms of the functions  $q_1(u_1, v_1)$ ,  $q_2(u_2, v_2)$ . Multiplication of

the wave function by these functions represents the effects of the components. Thus the functions will in general be complex, and may represent apertures, lenses, phase gratings, planes in a crystal lattice and so on.

In order to simplify the notation the analysis is given in one dimension. The extension to two dimensions is straightforward. Exponential Fourier transforms of the component functions are designated by capitals,  $Q_n(U_n)$ , so that

$$\mathcal{F}_{U_n} q_n(u_n) = \int_{-\infty}^{\infty} q_n(u_n) \exp \{-iU_n u_n\} du_n = Q_n(U_n),$$

and

$$\mathcal{F}_{U_n} Q_n(u_n) = 2\pi q_n(-U_n).$$

The convolution of two functions is defined as

$$q_1(x) \star q_2(x) = \int_{-\infty}^{\infty} q_1(\omega) q_2(x - \omega) d\omega.$$

This process may be interpreted as laying down the second function at every point of the first with the weight of the first, and integrating the whole. Extension to any number of dimensions presents no special difficulties. The transform of the convolution is given by

$$\mathcal{F}[q_1(x) \star q_2(x)] = Q_1(U) Q_2(U).$$

The convolution of a set of functions is then defined as

$$\begin{aligned} q_1(x) \star q_2(x) \star \dots \star q_n(x) &= \int_{-\infty}^{\infty} q_n(\omega_n) d\omega_n \int_{-\infty}^{\infty} q_{n-1}(\omega_{n-1}) d\omega_{n-1} \dots \\ &\quad \times \int_{-\infty}^{\infty} q_2(\omega_2) q_1(x - \omega_1 \dots \omega_n) d\omega_2, \end{aligned}$$

and

$$\mathcal{F}_{U_n}[q_1(x) \star q_2(x) \star \dots \star q_n(x)] = Q_1(U) Q_2(U) \dots Q_n(U).$$

The wave function at a point  $u_1$  on the first plane is given by  $q_1(u_1)$ . To the approximation of parabolic wave fronts, and neglecting the obliquity factor and the dependence of amplitude on distance, the wave function at the point  $u_2$  due to the element at  $u_1$  is

$$A q_1(u_1) q_2(u_2) \exp \left( -\frac{ik}{2R_1} (u_1 - u_2)^2 \right) du_1.$$

The complete wave function at  $u_2$  is then

$$A \int_{-\infty}^{\infty} q_1(u_1) q_2(u_2) \exp \left( -\frac{ik}{2R_1} (u_1 - u_2)^2 \right) du_1.$$

Thus the wave function at a point  $x$  on the plane of observation is given by

$$\psi(x) = A \int_{-\infty}^{\infty} \int_{-\infty}^{\infty} q_1(u_1) q_2(u_2) \exp \left( -\frac{ik}{2R_1} (u_1 - u_2)^2 \right) \exp \left( -\frac{ik}{2R_2} (u_2 - x)^2 \right) du_1 du_2 \dots \dots (2.1)$$

$$= A \int_{-\infty}^{\infty} \left[ q_1(u_2) \star \exp \left( -\frac{ik}{2R_1} u_2^2 \right) \right] q_2(u_2) \exp \left( -\frac{ik}{2R_2} (u_2 - x)^2 \right) du_2$$

$$= A \left[ q_2(x) \right]_2 \left[ q_1(x) \star \exp \left( -\frac{ik}{2R_1} x^2 \right) \right]_1 \star \exp \left( -\frac{ik}{2R_2} x^2 \right) \right]_2 \dots \dots (2.2)$$

This expression could have been written down directly using Huygens' principle and the definition of convolution. We now seek a means of manipulating



the equation in such a way that contact with the underlying physical processes is maintained. In particular, we look for any special properties that the function  $\exp(-i\alpha x^2)$  may possess under the operations of convolution and the Fourier transform, and obtain

$$\mathcal{F} \exp(-\tfrac{1}{2}iu^2) = (1-i)\pi^{1/2} \exp(\tfrac{1}{2}iU^2), \quad \dots\dots(2.3)$$

$$q(u) \star \exp(-i\alpha u^2) = (1-i) \left(\frac{\alpha}{2\pi}\right)^{1/2} \exp(-i\alpha u^2) [Q(-2\alpha u) \star \exp(i\alpha u^2)]. \quad \dots\dots(2.4)$$

These two relations constitute a basis for the manipulation of equation (2.2) and its generalizations. Moreover, a physical interpretation can be obtained for both equations (2.2) and (2.4). To the approximations used, the wave function for a point source is of the form  $\exp(-i\alpha u^2)$ . In the absence of interactions, the wave function at any point due to an arbitrary coherent wavefront  $q(u)$  is then of the form  $q(u) \star \exp(-i\alpha u^2)$ , that is, a superposition of the component and unit excitation functions in direct space. Equation (2.4) shows that an equivalent description may be given in terms of superposition of the transforms of the component and unit excitation functions and multiplication by the unit excitation function. In other words a direct and symmetrical relation is established between the wave functions for Fresnel and Fraunhofer diffraction.

As will be seen later, equation (2.3) can be regarded as defining a fundamental property of a corrected lens.

A set of relations can now be built up from equations (2.3) and (2.4). These can be regarded as the formal rules of an algebra for manipulating the wave function. First we obtain the analogue of equation (2.4) in terms of the transformed functions

$$Q(u) \star \exp(i\alpha u^2) = (1+i)(2\pi\alpha)^{1/2} \exp(i\alpha u^2) [q(-2\alpha u) \star \exp(-i\alpha u^2)]. \quad \dots\dots(2.5)$$

It is then necessary to determine how  $\exp(-i\beta u^2)$  may be 'factored' from a convolution in direct space. We find

$$q(u) \exp(-i\alpha u^2) \star \exp(-i\beta u^2) = (1-i) \left\{ \frac{\beta^2}{2\pi(\alpha+\beta)} \right\}^{1/2} \exp(-i\beta u^2) \times \left[ Q(-2\beta u) \star \exp\left(i \frac{\beta^2}{\alpha+\beta} u^2\right) \right]. \quad \dots\dots(2.6)$$

The right-hand side of equation (2.6) may be manipulated to give a result entirely in direct space, so that

$$q(u) \exp(-i\alpha u^2) \star \exp(-i\beta u^2) = \frac{\beta}{\alpha+\beta} \exp\left(-i \frac{\alpha\beta}{\alpha+\beta} u^2\right) \times \left[ q\left(\frac{\beta}{\alpha+\beta} u\right) \star \exp\left(-i \frac{\beta^2}{\alpha+\beta} u^2\right) \right]. \quad \dots\dots(2.7)$$

Corresponding relations can be obtained for the transformed functions

$$Q(u) \exp\{i\alpha u^2\} \star \exp\{i\beta u^2\} = (1+i) \left(\frac{2\pi\beta^2}{\alpha+\beta}\right)^{1/2} \exp\{i\beta u^2\} \times \left[ q(-2\beta u) \star \exp\left\{-i \frac{\beta^2}{\alpha+\beta} u^2\right\} \right] \quad \dots\dots(2.8)$$

$$= \frac{\beta}{\alpha+\beta} \exp\left\{i \frac{\alpha\beta}{\alpha+\beta}\right\} \left[ Q\left(\frac{\beta}{\alpha+\beta} u\right) \star \exp\left\{i \frac{\beta^2}{\alpha+\beta} u^2\right\} \right]. \quad \dots\dots(2.9)$$



A number of useful special cases arise, the following being typical

$$q(bu) \exp \{-i\alpha u^2\} \star \exp \{i\alpha u^2\} = \frac{1}{b} \exp \{i\alpha u^2\} Q\left(\frac{2\alpha}{b} u\right). \quad \dots\dots(2.10)$$

As an example of the use of the relations (2.3) to (2.10) we derive some formulae required in § 4. The forms to be obtained are: (a) first component described in direct space and second component described in Fourier space, that is, in terms of its Fraunhofer diffraction pattern; (b) both components described in Fourier space; (c) first component described in Fourier space, second component described in direct space.

(a) Applying equation (2.4) to  ${}_1[\dots]_1$  in equation (2.2) there results;

$$\begin{aligned} \psi(x) = & K_2 \left[ q_2(x) \exp \left\{ -\frac{ik}{2R_1} x^2 \right\} \right. \\ & \times \left. {}_1 \left[ Q_1 \left( -\frac{k}{R_1} x \right) \star \exp \left\{ \frac{ik}{2R_1} x^2 \right\} \right]_1 \star \exp \left\{ -\frac{ik}{2R_2} x^2 \right\} \right]_2. \quad \dots\dots(2.11) \end{aligned}$$

Equation (2.6) now gives

$$\begin{aligned} \psi(x) = & K_1 \exp \left( -\frac{ik}{2R_2} x^2 \right) \\ & \times \left[ q_1 \left( -\frac{R_1}{R_2} x \right) \exp \left( -\frac{ikR_1}{2R_2^2} x^2 \right) \star Q_2 \left( -\frac{k}{R_2} x \right) \star \exp \left( i \frac{kR_1 x^2}{2R_2(R_1 + R_2)} \right) \right]. \quad \dots\dots(2.12) \end{aligned}$$

(b) Applying equation (2.4) to  ${}_2[\dots]_2$  in equation (2.2) there results;

$$\begin{aligned} \psi(x) = & K_2 \exp \left( -\frac{ik}{2R_2} x^2 \right) \\ & \times \left[ Q_1 \left( -\frac{k}{R_2} x \right) \exp \left( i \frac{kR_1}{2R_2^2} x^2 \right) \star Q_2 \left( -\frac{k}{R_2} x \right) \star \exp \left( \frac{ik}{2R_2} x^2 \right) \right]. \quad \dots\dots(2.13) \end{aligned}$$

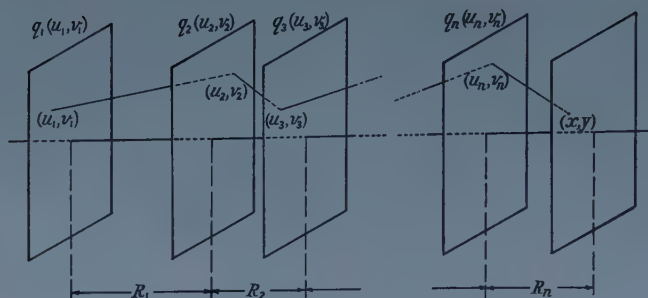
(c) Applying equation (2.7) to equation (2.11),

$$\begin{aligned} \psi(x) = & K_3 \exp \left( -i \frac{k}{2(R_1 + R_2)} x^2 \right) {}_2 \left[ q_2 \left( \frac{R_1}{R_1 + R_2} x \right) {}_1 \left[ Q_1 \left( -\frac{k}{R_1 + R_2} x \right) \right. \right. \\ & \star \exp \left( i \frac{kR_1}{2(R_1 + R_2)^2} x^2 \right) \left. \right]_1 \star \exp \left( -i \frac{kR_1}{2R_2(R_1 + R_2)} x^2 \right) \left. \right]_2. \quad \dots\dots(2.14) \end{aligned}$$

Each of these forms, when interpreted physically, describes the action of the system in terms of a different model. This point is illustrated in § 4 for the special case in which the second component is a lens.

### § 3. THE $n$ -COMPONENT SYSTEM

The system is defined by reference to a set of parallel planes spaced at distances  $R_1, R_2, \dots, R_n$  (figure), the final plane being taken as the plane of observation. The components are described by a set of functions  $q_1(u_1, v_1); q_2(u_2, v_2); \dots, q_n(u_n, v_n)$ . For simplicity in notation the analysis is again given in one dimension.



Coordinate system used in the formulation.

With the same approximations as before the wave function due to  $n$  components and at a point  $x$  on the plane of observation is given by

$$\begin{aligned}
 \psi(x) &= A \int_{-\infty}^{\infty} \dots \int_{-\infty}^{\infty} q_1(u_1) \dots q_n(u_n) \exp\left(-\frac{ik}{2R_1}(u_1-u_2)^2\right) \dots \\
 &\quad \times \exp\left(-\frac{ik}{2R_n}(u_n-x)^2\right) du_1 \dots du_n \\
 &= A \int_{-\infty}^{\infty} \dots \int_{-\infty}^{\infty} \left[ q_1(u_2) \star \exp\left(-\frac{ik}{2R_1}u_2^2\right) \right]_1 q_2(u_2) \dots q_n(u_n) \\
 &\quad \times \exp\left(-\frac{ik}{2R_2}(u_2-u_3)^2\right) \dots \exp\left(-\frac{ik}{2R_n}(u_n-x)^2\right) du_2 \dots du_n \\
 &= A \int_{-\infty}^{\infty} \dots \int_{-\infty}^{\infty} \left[ q_2(u_3) \left[ q_1(u_3) \star \exp\left(-\frac{ik}{2R_1}u_3^2\right) \right]_1 \star \exp\left(-\frac{ik}{2R_2}(u_3)^2\right) \right]_2 \\
 &\quad \times q_3(u_3) \dots q_n(u_n) \exp\left(-\frac{ik}{2R_3}(u_3-u_4)^2\right) \dots \exp\left(-\frac{ik}{2R_n}(u_n-x)^2\right) du_3 \dots du_n \\
 &= A \left[ q_n(x) \dots \left[ q_3(x) \left[ q_2(x) \left[ q_1(x) \star \exp\left(-\frac{ik}{2R_1}x^2\right) \right]_1 \right. \right. \right. \\
 &\quad \left. \left. \star \exp\left(-\frac{ik}{2R_2}x^2\right) \right]_2 \star \exp\left(-\frac{ik}{2R_3}x^2\right) \right]_3 \star \dots \star \exp\left(-\frac{ik}{2R_n}x^2\right) \right]_n.
 \end{aligned}$$

.....(3.1)

This, again, is a statement of Huygens' principle in terms of convolution. In the absence of interaction the relation between the wave functions at different distances from a fixed point is given by convolution with the unit excitation function appropriately scaled. Passage through a component modulates the wave function, possibly both in amplitude and phase, and the combined function is in turn convoluted with the unit excitation function. This process is repeated up to the plane of observation.

The form of the equation is independent of the degree of approximation. More precisely, if the optical path length can be expressed in the form  $f(u_{n-1}-u_n)$  then the wave function can be expressed in the form

$$\psi(x) = A_n [q_n(x) \dots \left[ q_3(x) \left[ q_2(x) \left[ q_1(x) \star g_1(x) \right]_1 \star g_2(x) \right]_2 \star g_3(x) \right]_3 \star \dots \star g_n(x) ]_n,$$

.....(3.2)

where  $g_n(x)$  is the appropriate unit excitation function. Thus, for circular wave fronts, neglecting the obliquity factor and the dependence of amplitude on distance,  $g_n(x) = \exp\{-ik(R_n^2 + x^2)^{1/2}\}$ .



The second form is symmetrical in convolution and multiplication. Equation (3.4) is written in the form

$$\psi(x) = K \exp\left(-\frac{ik}{2R_n} x^2\right) \left[ \mathcal{Q}_n\left(-\frac{k}{R_n} x\right) \star G_{n-1}(x) \exp\left(i\frac{kR_{n-1}}{2R_n^2} x^2\right) \star \exp\left(\frac{ik}{2R_n} x^2\right) \right].$$

Equation (2.9) gives

$$\begin{aligned} \psi(x) &= K \frac{R_n}{R_n + R_{n-1}} \exp\left(-\frac{ik}{2R_n} x^2\right) \left[ \mathcal{Q}_n\left(-\frac{k}{R_n} x\right) \star \left[ G_{n-1}\left(\frac{R_n}{R_n + R_{n-1}} x\right) \star \exp\left(i\frac{k}{2(R_n + R_{n-1})} x^2\right) \right] \exp\left(i\frac{kR_{n-1}x^2}{2R_n(R_n + R_{n-1})}\right) \right]_2 \\ &= K \frac{R_n}{R_{n-1} + R_n} \exp\left(-\frac{ik}{2R_n} x^2\right) \left[ \mathcal{Q}_n\left(-\frac{k}{R_n} x\right) \star \left[ \mathcal{Q}_{n-1}\left(-\frac{k}{R_{n-1} + R_n} x\right) \star G_{n-2}(x) \exp\left(i\frac{kR_{n-2}}{2(R_{n-1} + R_n)^2} x^2\right) \star \exp\left(i\frac{k}{2(R_{n-1} + R_n)} x^2\right) \right]_1 \right. \\ &\quad \left. \times \exp\left(i\frac{kR_{n-1}}{2R_n(R_{n-1} + R_n)} x^2\right) \right]_2. \end{aligned}$$

Repeating the process  $n$  times

$$\begin{aligned} \psi(x) &= \frac{A}{(2\pi)^{n-1}} (1-i)^n \left(\frac{\pi}{k}\right)^{(n/2)-1} \frac{(R_1 R_2 \dots R_n)^{1/2}}{2(R_1 + R_2 + \dots + R_n)} \exp\left(-\frac{ik}{2R_n} x^2\right) \\ &\quad \times \left[ \mathcal{Q}_n\left(-\frac{k}{R_n} x\right) \star \left[ \mathcal{Q}_{n-1}\left(-\frac{k}{R_{n-1} + R_n} x\right) \star \dots \right. \right. \\ &\quad \star \left[ \mathcal{Q}_2\left(-\frac{k}{R_2 + R_3 + \dots + R_n} x\right) \star \left[ \mathcal{Q}_1\left(-\frac{k}{R_1 + R_2 + \dots + R_n} x\right) \star \exp\left(i\frac{k}{2(R_1 + R_2 + \dots + R_n)} x^2\right) \right]_1 \right. \\ &\quad \left. \left. \times \exp\left(i\frac{kR_1}{2(R_2 + R_3 + \dots + R_n)(R_1 + R_2 + \dots + R_n)} x^2\right) \right]_2 \times \dots \right. \\ &\quad \left. \times \exp\left(i\frac{kR_{n-2}}{2(R_{n-1} + R_n)(R_{n-2} + R_{n-1} + R_n)} x^2\right) \right]_{n-1} \\ &\quad \left. \times \exp\left(i\frac{kR_{n-1}}{2(R_{n-1} + R_n)R_n} x^2\right) \right]_n. \end{aligned} \quad \dots (3.5)$$

This expression may be contrasted with equation (3.1). As indicated previously the latter may be regarded as a direct statement of Huygens' principle for a multi-component system in direct space, and takes the form of successive multiplications by component functions and convolutions with unit excitation functions. Equation (3.5), on the other hand, gives an equivalent expression for the wave function in terms of successive convolutions of the transforms of the component functions and multiplications by the transforms of the unit excitation functions. It may therefore be regarded as the fundamental statement of Huygens' principle for a multi-component system when all functions are given in Fourier space.



Reference to the equations given in this and the preceding section illustrates a number of points relevant in the application of this formulation. The wave function on any plane in a multi-component optical system may be written down by inspection. By the application of a few rules the role of any component or group of components in the system may be described in terms of either their direct or Fourier space representations. Usually the co-operative effects of groups of components may be best understood by a comparison of a number of the possible reductions.

It is usually neither necessary nor desirable to insert specific analytical details until the last stages of the calculations since this merely masks the essential processes involved. These processes emerge most clearly if the various terms in the equation are handled in the same manner as the components on an optical bench. For instance, if the Fraunhofer diffraction pattern from a multi-component system is required it is possible to invoke a limiting argument. There is, however, no need to abandon the actual physical situation in this way. The expression for a thin lens may be incorporated in the equations and the wave function on the back focal plane readily calculated by means of the rules given in §2. An example of this process is given in §4.

Having examined the relevant reductions for a system, the detailed analytical result can frequently be obtained by merely consulting a table of Fourier, Hankel or Mellin transforms, for instance Volumes I and II of the Bateman Manuscript Project (Bateman 1954). Difficulties can arise when the transforms are intractable, but such difficulties are readily isolated in this formulation so that approximation is easier.

In any of the expressions the general result for an arbitrary coherent source is always of the same form as the response of the system to a point source; that is the delta function response. It might be noted, however, that the general response is not merely the convolution of the source function with the delta function response so that direct analogy with filter theory can be misleading. Detailed discussion of this point is not given here. It is sufficient to remark that extension from coherent to partially coherent wave fronts involves no formal difficulties for practical systems with the formulation given above.

#### § 4. SPECIAL CASES

The form of such equations as (3.4) and (3.5) invites consideration of special functional types for the  $Q_n(U_n)$ . We shall consider in this communication only the simplest aspects of the two most obvious types; namely (i) the form  $\exp(-ikc_1 U^2)$  and (ii) the set of Dirac delta functions. These refer to the Fourier transforms of a thin lens and a periodic object respectively. It is interesting to note that both of these types can lead to image formation in the strict sense of identity of amplitude and phase distribution on image and object, despite the fact that they are mathematically very dissimilar and that they represent completely different physical processes. These two types are in fact special solutions of integral equations obtained from the equations given in §§2 and 3; the component function being regarded as unknown and a prescribed condition between object and complete wave function being given. This aspect of the formulation is not, however, pursued here.

4.1. The Form  $\exp(-ikc_1U^2)$ 

In equation (3.1) we write

$$q(x) = q_{n-1}(x) \underset{n-2}{\left[ q_{n-2}(x) \dots \underset{1}{\left[ q_1(x) \star \exp\left(-\frac{ik}{2R_1}x^2\right) \right]} \star \dots \star \exp\left(-\frac{ik}{2R_{n-2}}x^2\right) \right]}_{n-2},$$

so that, from equation (2.12),

$$\psi(x) = K_1 \exp\left(-\frac{ik}{2R_n}x^2\right) \left[ q\left(-\frac{R_{n-1}}{R_n}x\right) \exp\left(-\frac{ikR_{n-1}}{2R_n^2}x^2\right) \star \mathcal{Q}_n\left(-\frac{k}{R_n}x\right) \star \exp\left(i\frac{kR_{n-1}}{2R_n(R_{n-1}+R_n)}x^2\right) \right].$$

Form (i) is then introduced by writing  $q_n(u) = \exp(ikc_2u^2)$ . The component function  $q_n(u)$  then describes a thin lens in the sense that the phase change  $kc_2u^2$  is introduced on the plane of the lens.

Now

$$\mathcal{Q}_n\left(-\frac{k}{R_n}x\right) = (1+i)\left(\frac{\pi}{2kc_2}\right)^{1/2} \exp\left(-i\frac{k}{4R_n^2c_2}x^2\right).$$

Hence

$$\psi(x) = K_2 \exp\left(-\frac{ik}{2R_n}x^2\right) \left[ q\left(-\frac{R_{n-1}}{R_n}x\right) \exp\left(-\frac{ikR_{n-1}}{2R_n^2}x^2\right) \star \exp\left(-\frac{ikR_{n-1}}{2R_n\{2R_nR_{n-1}C_2-(R_{n-1}+R_n)\}}x^2\right) \right],$$

so that if the condition  $2c_2 = (1/R_n + 1/R_{n-1})$  is satisfied,

$$\psi(x)\psi\star(x) = K_2K_2\star q\left(-\frac{R_{n-1}}{R_n}x\right)q\star\left(-\frac{R_{n-1}}{R_n}x\right).$$

If the thin lens has a focal length  $f$ , and if the radii of curvature of the surfaces are  $r_1$  and  $r_2$  then

$$2c_2 = (\mu - 1)\left(\frac{1}{r_1} + \frac{1}{r_2}\right) = \frac{1}{f}.$$

If an aperture function  $h(u)$  with Fourier transform  $H(U)$  is associated with the lens we obtain

$$\psi(x) = K_2 \exp\left(-\frac{ik}{2R_n}x^2\right) \left[ q\left(-\frac{R_{n-1}}{R_n}x\right) \exp\left(-\frac{ikR_{n-1}}{2R_n^2}x^2\right) \star \exp\left(-i\frac{kR_{n-1}}{2R_n\{(R_nR_{n-1}/f)-(R_{n-1}+R_n)\}}x^2\right) \star H\left(-\frac{k}{R_n}x\right) \right], \quad \dots (4.1)$$

and on a focal plane,

$$\psi(x) = K_2 \exp\left(-\frac{ik}{2R_n}x^2\right) \left[ q\left(-\frac{R_{n-1}}{R_n}x\right) \exp\left(-\frac{ikR_{n-1}}{2R_n^2}x^2\right) \star H\left(-\frac{k}{R_n}x\right) \right]. \quad \dots (4.2)$$

On setting  $R_n = f$  and applying equation (2.10) to equation (4.1) the wave function on the back focal plane is found to be

$$\psi(x) = K_3 \exp\left(-\frac{ik}{2R_n}x^2\right) \left[ \mathcal{Q}\left(-\frac{k}{f}x\right) \exp\left(\frac{ikR_{n-1}}{2f^2}x^2\right) \star H\left(-\frac{k}{f}x\right) \right]. \quad \dots (4.3)$$

If  $q(u)$  is considered simply as a representation of an object and its illuminating system, equation (4.2) describes the formation of an image according to the Rayleigh theory, in that the wave function appropriate to the object and its illuminating system is convoluted with the transform of the aperture function. The expression is more familiar in the form appropriate to a self-luminous object, that is

$$\psi(x)\psi^*(x) = K_2 K_2^* \left[ q \left( -\frac{R_{n-1}}{R_n} x \right) q^* \left( -\frac{R_{n-1}}{R_n} x \right) \star H \left( -\frac{k}{R_n} x \right) H^* \left( -\frac{k}{R_n} x \right) \right].$$

Equation (4.1) may be regarded as an extension of the Rayleigh treatment for a fully coherent system to any plane in the system. Equations of this type have application in electron diffraction and electron microscopy since additional information on the object may be conveniently obtained in some practical cases on off-focus planes. In the limiting condition in the region of the image plane this expression reduces to conventional form.

The aperture function  $h(u)$  has not been restricted to real values, so that equations (4.1), (4.2) and (4.3) apply to those thick lenses which can be described by the component function for a thin lens multiplied by the aperture function  $h(u) = t(u) \exp \{i\phi(u)\}$  where  $t(u)$  is real.

Equivalent expressions of different form and leading to different interpretations of the physical processes involved may, as is usual in this formulation, be obtained by alternative reductions of the equation chosen as starting point. For instance, expressions corresponding to the Abbe treatment may be obtained starting from equation (2.13). If equation (2.14) is chosen, however, a description of image formation which corresponds to neither of the classical models is obtained.

A more general treatment of thick lenses consists of treating the lens as the limiting case of an assembly of thin plates. This does not represent the most direct attack, but it demonstrates the parallel between the wave optics of thick lenses and the dynamic theory of electron diffraction, where, as is shown in another publication, this approach is both direct and practical (Cowley and Moodie 1957 d).

#### 4.2. The Sets of Delta Functions $Q_n(U_n) = \sum_m F_m \delta(U_n - cm)$

Here the  $F_m$  are in general complex and  $c$  is an arbitrary constant. Since the Fourier transform of a set of equally spaced delta functions is a periodic function, the physical process described by the equations is that of diffraction by periodic objects. The simplest case, for all  $R_n$  finite, is obtained when  $Q_1$  is a constant,  $Q_2$  a set of delta functions and the remaining  $Q_n$  are zero. The only components in the system are then a point source and a grating. As has been shown (Cowley and Moodie 1957 b) the equations immediately reduce to forms which display the characteristics of the system in both direct and Fourier spaces. In particular the formation of a series of images of varying magnification which have been named Fourier images is made apparent. The effects associated with finite source size can also be investigated in the same way (Cowley and Moodie 1957 c).

A particular case of some interest arises when the  $F_m$  are constrained to have the distribution appropriate to a phase grating. This corresponds, for instance, to the elastic scattering of electrons by a 'thin' crystal, and the method described above provides the Fresnel diffraction counterpart of a pseudo-kinematic theory



of diffraction (Hoerni 1956). Briefly, under certain conditions a crystal in a beam of electrons behaves as a phase grating. The results are therefore of some importance in the interpretation of the images of crystals obtained by means of the electron microscope (Menter 1956). While the development from, say, equation (3.4) is straightforward, considerations of practical application require a fairly detailed treatment and this will be given in another publication.

When  $Q_1$  is a constant,  $Q_2$  and  $Q_3$  are each a set of delta functions and the remaining  $Q_n$  are zero, the direct application of either equation (3.4) or equation (3.5) provides a solution. A multiplicity of special cases, a number of which have practical application in electron diffraction and electron microscopy, arises and these will be discussed elsewhere. For the purposes of the present communication, it is relevant to give a brief quantitative treatment of one point. When two or more of the  $Q_n$  consist of a set of delta functions, reduction to the case of the source and screen at infinity is not trivial in that it does not lead to solutions which can be derived directly from the standard Fraunhofer or kinematic theories of diffraction. This is to be expected. Fresnel diffraction is involved within the composite diffracting object although the overall system satisfies the requirements for Fraunhofer diffraction. Referring, as an illustration, to electron diffraction, the diffraction by two crystals, each of which satisfy the conditions for pseudo-kinematic scattering separately, should show the first-order features of a full dynamic theory. This in fact has been observed, although not interpreted from this point of view (Farrant and Rees, in preparation).

In order to derive one of the relevant expressions we consider a system consisting of a source  $q_1(u_1)$  a set of pseudo-kinematic crystals  $q_2(u_2) \dots q_{n-1}(u_{n-1})$ , and a thin lens  $q_n(u_n)$  the plane of observation being located on the back focal plane of this lens. Equation (4.3) is then relevant.

Writing  $x/f = 2\theta$  and expanding  $Q(-2k\theta)$  we obtain

$$\begin{aligned} \psi(\theta) = & K_{4n} [{}_{n-1}[Q_{n-1}(-2k\theta) \star \dots \star {}_2[Q_3(-2k\theta) \star {}_1[Q_2(-2k\theta) \star Q_1(-2k\theta) \\ & \times \exp(2ikR_1\theta^2)]_1 \times \exp(2ikR_2\theta^2)]_2 \times \dots \times \exp(2ikR_{n-2}\theta^2)]_{n-2} \\ & \times \exp(2ikR_{n-1}\theta^2)]_{n-1} \star H(-2k\theta)]_n. \end{aligned}$$

If a plane wave is incident on the set of crystals,

$$\begin{aligned} \psi(\theta) = & K_{4n-1} [{}_{n-2}[Q_{n-1}(-2k\theta) \star \dots \star {}_1[Q_3(-2k\theta) \star Q_2(-2k\theta) \exp(2ikR_2\theta^2)]_1 \\ & \times \dots \times \exp(2ikR_{n-1}\theta^2)]_{n-2} \star H(-2k\theta)]_{n-1}. \end{aligned}$$

This is the diffraction pattern on the back focal plane. The conventional diffraction pattern is obtained when  $f \rightarrow \infty$ . It is readily verified that equation (4.4) reduces to the standard diffraction equation used in electron diffraction and electron microscopy for only one crystal. Thus Bragg's law is satisfied in the approximate form  $2d\theta = \lambda$ , and the diffraction field consists of the reciprocal lattice convoluted with the shape function appropriate to the crystal, the whole being multiplied by a phase factor and convoluted with the Fourier transform of the lens aperture.

As indicated in §4.1 the multi-crystal case may be extended by a limiting process to the case of dynamic diffraction. This development is described elsewhere (Cowley and Moodie 1957 d).

#### REFERENCES

- BATEMAN, H., 1954, *Tables of Integral Transforms* (New York: McGraw-Hill).  
 COWLEY, J. M., and MOODIE, A. F., 1957 a, *Proc. Phys. Soc. B*, **70**, 486; 1957 b, *Ibid.*, **70**, 497; 1957 c, *Ibid.*, **70**, 505; 1957 d, *Acta Cryst., Camb.*, **10**, 609.



- DUFFIEUX, P. M., 1956, *L'integrale de Fourier et ses applications à l'optique* (Paris : Editions de la Revue d'Optique).
- GABOR, D., 1949, *Proc. Roy. Soc. A*, **197**, 454; 1951, *Proc. Phys. Soc. B*, **64**, 449.
- HOERNI, J. A., 1955, *Phys. Rev.*, **102**, 1530.
- HOPKINS, H. H., 1953, *Proc. Roy. Soc. A*, **217**, 408; 1955, *Ibid.*, A, **231**, 41.
- LINFOOT, E. H., 1955, *Recent Advances in Optics* (Oxford : Clarendon Press).
- MENTER, J. W., 1956, *Proc. Roy. Soc. A*, **236**, 119.
- RATCLIFFE, J. A., 1956, *Rep. Prog. Phys.*, **19**, 188 (London : Physical Society).

## A Class of Aplanatic Optical Systems

By A. K. HEAD†

Aeronautical Research Laboratories, Melbourne, Australia

*MS. received 13th August 1957*

**Abstract.** An arbitrary centred optical system is followed by two aspherical mirrors which are such that the complete system is exactly aplanatic. It is shown that the equations specifying these mirrors can be reduced to a first order linear differential equation and so the solution involves two quadratures. If these integrals can be evaluated then the mirrors can be specified exactly. If the arbitrary optical system is axially stigmatic then a particular solution of the differential equation can be found by inspection and the solution then involves only one quadrature. As an example the combination of two aspherical mirrors following a parabolic reflector to form an aplanatic telescope is solved exactly.

### § 1. INTRODUCTION

IT is well known that if two aspherical reflecting or refracting surfaces are added to an arbitrary centred optical system then it is possible to choose these aspherical surfaces so that the complete system is exactly aplanatic, and Wasserman and Wolf (1949) have given a method by which the differential equations specifying the aspherical surfaces may be integrated numerically. The possibility of obtaining an analytical solution will be examined with the restrictions that the aspherical surfaces to be determined are mirrors and that they follow the arbitrary optical system. These restrictions arose naturally in the design by geometrical optics of focusing systems for radio waves and as it has been found (Head 1957a) that highly aspherical surfaces may be necessary to obtain optimum properties an exact solution is desirable. In §2 the general case is considered and in §3 the special case where the arbitrary optical system is axially stigmatic. In §4 this is applied to the case where the arbitrary optical system is a parabolic reflector.

### § 2. GENERAL CASE

To specify the arbitrary optical system we consider (figure 1) a ray which leaves the object O at an angle  $\phi$  to the axis. After passing through the arbitrary system it will intersect the axis at an angle  $\theta(\phi)$ . This point of intersection will be at a distance  $X(\phi)$  from a fixed point on the axis and the optical path length from object to this point of intersection will be  $P(\phi)$ . These three functions  $\theta(\phi)$ ,  $X(\phi)$  and  $P(\phi)$  form the appropriate specification of the arbitrary optical system.† If the object is at infinity then  $\phi$  is replaced by  $h$ , the height of a typical ray from the axis.

Figure 2 shows the path of the ray when the two aspherical mirrors have been added. The final focus is at I and the second mirror will be specified by polar

† Now at Division of Tribophysics, Commonwealth Scientific and Industrial Research Organization, University of Melbourne, Australia.

‡ These three functions are not completely arbitrary but are subject to the relationship  $dP/dX = -\cos \theta$ .

coordinates  $(r, u)$  about I, and will be referred to as the  $r$ -mirror. The distance  $X(\phi)$  will be measured from I and the first mirror will be specified in quasi-polar coordinates  $(\rho, \theta)$  about the variable point  $X$ , and will be referred to as the  $\rho$ -mirror. Finally let the path length of the ray from the  $\rho$ -mirror to the  $r$ -mirror be  $l$  and the angles of incidence and reflection at the  $r$ -mirror be  $i$ .

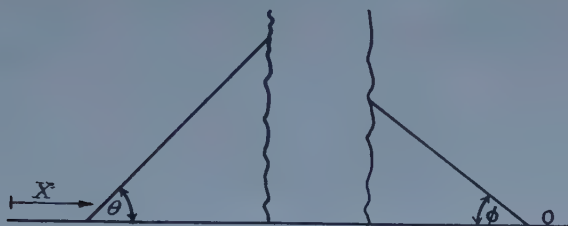


Figure 1.

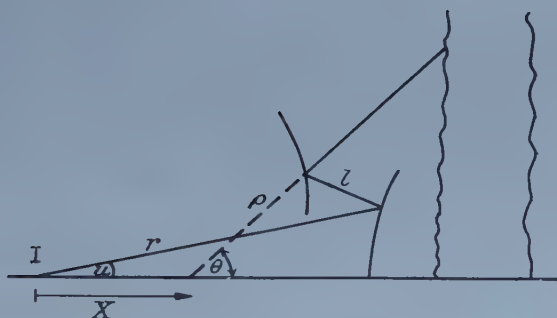


Figure 2.

The system is then specified by the following equations (1)–(5).

Reflection at  $r$ -mirror:

$$\frac{1}{r} \frac{dr}{du} = \tan i. \quad \dots\dots(1)$$

Constant path length:

$$P(\phi) - \rho + r + l = \text{constant} = L \text{ (say)}. \quad \dots\dots(2)$$

Projection of  $l$  parallel and perpendicular to axis:

$$l \cos(2i - u) = r \cos u - \rho \cos \theta - X \quad \dots\dots(3)$$

$$l \sin(2i - u) = \rho \sin \theta - r \sin u. \quad \dots\dots(4)$$

Sine condition:

If the object is at a finite distance and  $m$  is the magnification of the complete system then

$$m \sin u = \sin \phi \quad \dots\dots(5a)$$

or if the object is at infinity and  $F$  is the focal length of the complete system then

$$F \sin u = h. \quad \dots\dots(5b)$$

From equations (1)–(4) we eliminate the variables  $\rho$  and  $l$ , obtaining

$$\frac{\sin(2i + \theta - u)}{1 + \cos(2i + \theta - u)} = \frac{r \sin(\theta - u) - X \sin \theta}{r \cos(\theta - u) - X \cos \theta + L - P - r} = Q \text{ (say),} \quad \dots\dots(6)$$

whence

$$\tan i = \frac{Q - \tan \frac{1}{2}(\theta - u)}{1 + Q \tan \frac{1}{2}(\theta - u)}$$

or, inserting the expression for  $Q$ ,

$$\tan i = -S(u) - rT(u) \quad \dots\dots(7)$$

where

$$S(u) = \frac{(L - P + X) \tan \frac{1}{2}\theta - (L - P - X) \tan \frac{1}{2}u}{(L - P - X) + (L - P + X) \tan \frac{1}{2}\theta \tan \frac{1}{2}u}, \quad \dots\dots(8)$$

$$T(u) = \frac{2(\tan \frac{1}{2}u - \tan \frac{1}{2}\theta)}{(L - P - X) + (L - P + X) \tan \frac{1}{2}\theta \tan \frac{1}{2}u}. \quad \dots\dots(9)$$

In (8) and (9)  $P$ ,  $X$  and  $\theta$  are functions of  $\phi$  but by using the sine condition (5a) it is possible, in principle, to express these as functions of  $u$  alone, and so, as is implied by the notation, it is possible to express  $S(u)$  and  $T(u)$  as functions of  $u$  alone.

From (7) and (1) we see that

$$\frac{d}{du} \left( \frac{1}{r} \right) = \left( \frac{1}{r} \right) S(u) + T(u). \quad \dots\dots(10)$$

Now this is a first order linear differential equation for  $1/r$  and the general solution, involving two quadratures, is

$$\frac{1}{r} = C \exp \left[ \int S(u) du \right] + \exp \left[ \int S(u) du \right] \int T(u) \exp \left[ - \int S(u) du \right] du \quad \dots\dots(11)$$

where the arbitrary constant of integration  $C$  is determined by  $r = r_0$  when  $u = 0$ .

If, in a particular case, the two integrals in (11) can be evaluated then an exact solution of the problem is obtained. If this is not possible then some approximate method such as expansion in series or numerical integration is necessary and it may be preferable to apply these to (11) rather than to the original equations (1)–(5).

If, in a particular case, any particular solution of the differential equation (10) can be found, e.g. by trial and error, then the general solution becomes

$$\frac{1}{r} = C \exp \left[ \int S(u) du \right] + [\text{particular solution}] \quad \dots\dots(12)$$

and only one integral has to be evaluated to obtain an exact solution. Use is made of this in §3.

It is now necessary to find the equation of the  $\rho$ -mirror. From (3) and (4),

$$l^2 = (r \cos u - \rho \cos \theta - X)^2 + (\rho \sin \theta - r \sin u)^2$$

and from (2)

$$l^2 = (L - P + \rho - r)^2.$$



Equating the right-hand sides of these two equations we find that terms involving  $\rho^2$  and  $r^2$  are eliminated and the equation can be written

$$\begin{aligned} & \left[ \frac{1}{r} - 2 \frac{L-P-X \cos u}{(L-P)^2 - X^2} \right] \left[ \frac{1}{\rho} + 2 \frac{L-P-X \cos \theta}{(L-P)^2 - X^2} \right] \\ &= -[(L-P)^2 - X^2]^{-2} [1 + \cos \theta][1 + \cos u] [(L-P-X) + (L-P+X) \tan \frac{1}{2} \theta \tan \frac{1}{2} u]^2 \\ &\text{i.e.} \\ & \frac{1}{\rho} = -2 \frac{L-P-X \cos \theta}{(L-P)^2 - X^2} - [(L-P)^2 - X^2]^{-2} [1 + \cos \theta][1 + \cos u] \\ & \quad \times [(L-P-X) + (L-P+X) \tan \frac{1}{2} \theta \tan \frac{1}{2} u]^2 \left[ \frac{1}{r} - 2 \frac{L-P-X \cos u}{(L-P)^2 - X^2} \right]^{-1} \dots (13) \end{aligned}$$

where  $1/r$  is known from (11). Since  $\rho$  is measured from the moving point  $X$  it may be preferable to specify the  $\rho$ -mirror in cartesian coordinates about  $I$  by  $x = X + \rho \cos \theta$ ,  $y = \rho \sin \theta$ .

### § 3. AXIALLY STIGMATIC SYSTEMS

In the simplest case in which this theory is applicable, that of the two mirror aplanat (Head 1957b), it was found that there was a particular solution of the equivalent of (10) of the form  $A + B \cos u$ . If such a trial solution is substituted in (10) it is found to be a solution if and only if the functions  $P(\phi)$ ,  $X(\phi)$  are constants. This is so if and only if the arbitrary optical system is axially stigmatic, and we will now consider this case.

If  $r_0$ ,  $\rho_0$  and  $l_0$  are the values of  $r$ ,  $\rho$  and  $l$  when  $u=0$  then the two aspherical mirrors are specified by the four constants  $r_0$ ,  $\rho_0$ ,  $l_0$  and  $m$  (or  $F$ ) from the sine condition.

From (2),  $L - P = \text{constant} = r_0 - \rho_0 + l_0$  and from figure 2,  $X = r_0 - \rho_0 - l_0$  and so  $L$ ,  $P$  and  $X$  in the equations of § 2 can be expressed in terms of  $r_0$ ,  $\rho_0$  and  $l_0$ . If this is done and the trial solution  $1/r = A + B \cos u$  substituted in (10), it is found to be a solution if

$$A = \frac{1}{2(r_0 - \rho_0)} + \frac{1}{2l_0} \quad \text{and} \quad B = \frac{1}{2(r_0 - \rho_0)} - \frac{1}{2l_0}.$$

Hence from (12)

$$\frac{1}{r} = \left[ \frac{1}{2(r_0 - \rho_0)} + \frac{1}{2l_0} \right] + \left[ \frac{1}{2(r_0 - \rho_0)} - \frac{1}{2l_0} \right] \cos u - \frac{\rho_0}{r_0(r_0 - \rho_0)} \exp \mathcal{J} \dots (14)$$

where

$$\mathcal{J} = \int_0^u \frac{(r_0 - \rho_0) \tan \frac{1}{2} \theta - l_0 \tan \frac{1}{2} u}{l_0 + (r_0 - \rho_0) \tan \frac{1}{2} \theta \tan \frac{1}{2} u} du \quad \dots (15)$$

and from (13)

$$\begin{aligned} \frac{1}{\rho} = & - \left[ \frac{1}{2(r_0 - \rho_0)} + \frac{1}{2l_0} \right] - \left[ \frac{1}{2(r_0 - \rho_0)} - \frac{1}{2l_0} \right] \cos \theta \\ & + \frac{r_0}{\rho_0(r_0 - \rho_0)} \left[ \frac{1 + \cos \theta}{2} \right] \left[ \frac{1 + \cos u}{2} \right] \left[ 1 + \frac{r_0 - \rho_0}{l_0} \tan \frac{1}{2} \theta \tan \frac{1}{2} u \right]^2 \exp - \mathcal{J}. \quad (16) \end{aligned}$$

In this case, since  $X$  is a constant,  $(\rho, \theta)$  are true polar coordinates about a fixed point, the focus of the arbitrary optical system.

## § 4. PARABOLIC REFLECTOR

As an example we will consider the case where the arbitrary optical system is a parabolic reflector with object at infinity. Since a parabolic reflector is axially stigmatic the analysis of § 3 is applicable.

If the focal length of the parabola is  $f$  then (figure 3) from the geometry of the parabola  $\tan \frac{1}{2}\theta = h/2f$  and the sine condition is  $h = F \sin u$  where  $F$  is the focal length of the complete system.

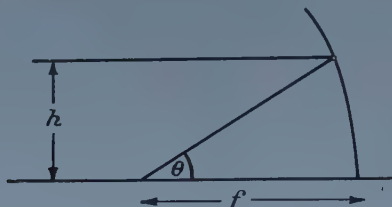


Figure 3.

Thus

$$\tan \frac{1}{2}\theta = (F/2f) \sin u \quad \dots\dots (17)$$

and substituting this in (15)

$$\begin{aligned} \mathcal{J} &= \int_0^u \frac{(r_0 - \rho_0)(F/2f) \sin u - l_0 \tan \frac{1}{2}u}{l_0 + (r_0 - \rho_0)(F/2f) \sin u \tan \frac{1}{2}u} du \\ &= \frac{\alpha}{2+\alpha} \log \left( \frac{1+\cos u}{2} \right) + \frac{2}{2+\alpha} \log \left( \frac{\alpha+1-\cos u}{\alpha} \right) \end{aligned}$$

where  $\alpha = 2l_0 f / (r_0 - \rho_0) F$ .

Hence from (14) the equation of the  $r$ -mirror is

$$\begin{aligned} \frac{1}{r} &= \left[ \frac{1}{2(r_0 - \rho_0)} + \frac{1}{2l_0} \right] + \left[ \frac{1}{2(r_0 - \rho_0)} - \frac{1}{2l_0} \right] \cos u \\ &\quad - \frac{\rho_0}{r_0(r_0 - \rho_0)} \left[ \frac{1+\cos u}{2} \right]^{\alpha/(2+\alpha)} \left[ \frac{\alpha+1-\cos u}{\alpha} \right]^{2/(2+\alpha)} \quad \dots\dots (18) \end{aligned}$$

and from (16) the equation of the  $\rho$ -mirror can be written

$$\begin{aligned} \frac{1}{\rho} &= - \left[ \frac{1}{2(r_0 - \rho_0)} + \frac{1}{2l_0} \right] - \left[ \frac{1}{2(r_0 - \rho_0)} - \frac{1}{2l_0} \right] \cos \theta \\ &\quad + \frac{r_0}{\rho_0(r_0 - \rho_0)} \left[ \frac{1+\cos \theta}{2} \right] \left[ \frac{1+\cos u}{2} \right]^{2/(2+\alpha)} \left[ \frac{\alpha+1-\cos u}{\alpha} \right]^{(2+2\alpha)/(2+\alpha)} \quad \dots (19) \end{aligned}$$

and this equation can be expressed entirely as a function of  $u$  or as a function of  $\theta$  by using (17).

For certain values of the constants (18) and (19) become indeterminate. By suitable limiting processes it can be shown that

(i) if  $\alpha = -2$  then

$$\begin{aligned} \frac{1}{r} &= \left[ \frac{1}{2(r_0 - \rho_0)} + \frac{1}{2l_0} \right] + \left[ \frac{1}{2(r_0 - \rho_0)} - \frac{1}{2l_0} \right] \cos u \\ &\quad - \frac{\rho_0}{r_0(r_0 - \rho_0)} \left[ \frac{1+\cos u}{2} \right] \exp \left[ \frac{\cos u - 1}{\cos u + 1} \right] \quad \dots\dots (18a) \end{aligned}$$

and

$$\frac{1}{\rho} = - \left[ \frac{1}{2(r_0 - \rho_0)} + \frac{1}{2l_0} \right] - \left[ \frac{1}{2(r_0 - \rho_0)} - \frac{1}{2l_0} \right] \cos \theta + \frac{r_0}{\rho_0(r_0 - \rho_0)} \left[ \frac{1 + \cos \theta}{2} \right] \left[ \frac{1 + \cos u}{2} \right]^2 \exp \left[ \frac{1 - \cos u}{1 + \cos u} \right]; \dots (19a)$$

(ii) if  $r_0 = \rho_0$  then

$$\frac{1}{r} = \frac{1 - \cos u}{2l_0} + \left[ \frac{1 + \cos u}{2} \right] \left[ \frac{1}{r_0} + \frac{F}{f l_0} \log \left( \frac{1 + \cos u}{2} \right) \right] \dots (18b)$$

and

$$\frac{1}{\rho} = \frac{\cos \theta - 1}{2l_0} + \left[ \frac{1 + \cos \theta}{2} \right] \left[ \frac{1}{\rho_0} - \frac{F}{f l_0} \log \left( \frac{1 + \cos u}{2} \right) \right] \dots (19b)$$

In all cases the paraxial radius of curvature of the  $r$ -mirror is

$$R_r = \frac{2r_0 l_0}{r_0 + l_0 - \rho_0 F/f}$$

and of the  $\rho$ -mirror is

$$R_p = \frac{2\rho_0 l_0}{l_0 - \rho_0 + r_0 f/F}$$

## § 5. DISCUSSION

The original problem which it was hoped to solve was that of an aplanatic telescope formed by two small aspherical mirrors following a main spherical mirror which might be described as an all-reflecting Schmidt telescope. It has not been possible to perform the necessary integrations in this case and it appears that an exact solution in terms of known functions is not possible.

As was mentioned in § 1 an aspherical lens could be used instead of the two aspherical mirrors to render an arbitrary optical system aplanatic. However even in the simplest case of an aplanatic lens with one focus at infinity (Martin 1944) it does not appear possible to obtain an exact solution.

## ACKNOWLEDGMENT

This paper is published with the permission of the Chief Scientist, Department of Supply.

## REFERENCES

- HEAD, A. K., 1957 a, *Nature, Lond.*, **179**, 692; 1957 b, *Proc. Phys. Soc. B*, **70**, 945.  
MARTIN, L. C., 1944, *Proc. Phys. Soc.*, **56**, 104.  
WASSERMAN, G. D., and WOLF, E., 1949, *Proc. Phys. Soc. B*, **62**, 2.

# The Elastic Scattering of 350 mev Neutrons by Complex Nuclei

By A. ASHMORE, D. S. MATHER†, AND S. K. SEN‡

Nuclear Physics Research Laboratory University of Liverpool

Communicated by H. W. B. Skinner; MS. received 25th November 1957

**Abstract.** Differential cross sections have been measured for the elastic scattering of neutrons with a mean energy of  $351.5 \pm 3$  mev by lead, tin, copper, aluminium and carbon. Measurements were made out to the first diffraction minimum. The total elastic scattering cross sections subtracted from the total cross sections measured previously, give upper limit values for the absorption cross sections. By comparison with other measurements the absorption cross sections are seen to be essentially constant from 140 mev to 1.4 gev. Values of the radius of the black disc, giving an angular distribution which, when normalized, fits the experimental points, are found to be in agreement with those deduced from measurements of high energy electron scattering. From the values of the forward scattering cross sections and the previously measured values of the total cross sections, it is found that within the accuracy of the measurement the forward scattering amplitude is purely imaginary.

## § 1. INTRODUCTION

THE measurements that are described in this paper are part of a series that has been made of the cross sections of complex nuclei for 350 mev neutrons. In previous papers the measurements of the energy spectrum of the neutron beam and of the total cross sections have been described (Ashmore, Jarvis, Mather and Sen 1957 a, b, to be referred to as I and II). In a companion paper (Brown, Ashmore and Nordhagen 1958, to be referred to as IV), the interpretation of the experimental results in terms of the optical model is discussed.

The elastic scattering of high energy neutrons has been studied experimentally by Bratenahl *et al.* (1950) at 84 mev, van Zyl, Voss and Wilson (1956) at 136 mev and Ball (U.C.R.L. report 1938, unpublished) at 290 mev. The results of these experiments have been analysed by Wilson (1956) in terms of the optical model. From the widths of the main peaks of the diffraction patterns, values were deduced for the nuclear radii which were rather larger than those obtained from high energy electron scattering measurements. The experimental values of the forward scattering cross section  $d\sigma/d\omega(0)$  were combined with previously measured values of the total cross section  $\sigma_t$  to derive the real and imaginary parts of the forward scattering amplitude  $f(0)$ :

$$d\sigma/d\omega(0) = |f(0)|^2 \quad \dots\dots (1)$$

and by the optical theorem

$$k'\sigma_t/4\pi = \mathcal{J}f(0) \quad \dots\dots (2)$$

where  $k'$  is the wave number of the neutron in the centre-of-mass system. For

† Now at the Atomic Weapons Research Establishment, Aldermaston, Berks.

‡ Now with Siemens Schuckert Ltd., Erlangen, West Germany.



the light elements the real and imaginary parts of  $f(0)$  were of comparable size, while for the heavy elements the real part was an order of magnitude smaller than the imaginary part. As the energy increased there was a general trend of decreasing real part and increasing imaginary part. From the values of  $\Re f(0)$  the real part of the central nuclear potential was found to be about 15 to 20 meV, with some evidence of a trend towards lower values for heavier nuclei.

It was considered to be useful to carry out similar measurements at 350 meV, particularly as the measurements at 290 meV had been done with rather poor angular resolution. The relative sizes of the real and imaginary parts of the forward scattering amplitude were of particular interest. It was also important to find out whether the observed angular distributions were compatible with the nuclear sizes and density distributions deduced from high energy electron scattering measurements. Measurements were made of the differential cross sections, out to the first diffraction minimum, for the elastic scattering of neutrons with a mean energy of  $351.5 \pm 3$  meV by carbon, aluminium, copper, tin and lead.

## § 2. EXPERIMENTAL DETAILS

### 2.1. Experimental Lay-out

The arrangement for producing the neutron beam described in §2.1 of I was modified to reduce the background of high energy neutrons surrounding the main beam. In order to obtain a better approximation to a point source the beryllium target in the cyclotron was turned so that it was 1 in. long in the direction of the proton beam and 0.25 in. high. The size of the beam in the experimental area was determined by a 2 ft long steel collimator in the entrance to the channel through the main shielding wall. At the exit channel a similar collimator was placed with a hole through it which just cleared the beam defined by the first collimator. Two sets of collimators were available. The first set produced a beam of 1.25 in. diameter at the scatterer and was used for measurements at angles greater than or equal to  $4^\circ$ . For angles equal to or less than  $4^\circ$  a second set was used which produced a beam 0.625 in. wide and 1.25 in. high at the scatterer.

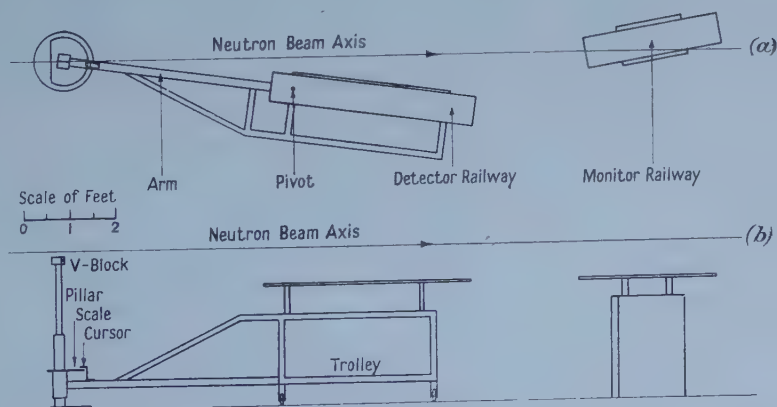


Figure 1. The experimental arrangement: (a) plan, (b) side elevation.

Figure 1 shows the experimental arrangement. The scatterers were placed in the V-block. Height adjustment was provided on the supporting pillar which was bolted to the floor. The detector trolley ran on the floor on four sprung castors and was constrained to rotate about the pillar supporting the V-block by means of the bearing on the end of the long arm. Screws in this bearing were used to clamp the trolley in position. A cursor on the long arm and a scale on the pillar were used to indicate the angular setting, which could be made with an accuracy to better than  $\pm 0.1^\circ$ . The components of the detector were mounted on carriages which could be slid along the detector railway. This railway was pivoted about a vertical axis shown in figure 1 and its height above the trolley was adjustable. The monitor components were mounted on a similar railway on a concrete block bolted to the floor. This was placed so as to be always clear of the detector trolley.

### *2.2. The Scatterers*

The scatterers were accurately machined cylinders of graphite, aluminium, copper, tin and lead. Their lengths were chosen so that approximately 10% of the incident beam was scattered by them. Thus the correction for multiple scattering was an order of magnitude smaller than the single scattering and higher orders than double scattering could be ignored. The diameters of the scatterers were chosen so that for the purpose of calculating the double scattering correction they could be regarded as being of infinite extent. Their surface densities were measured with an error of less than 0.1% using vernier calipers and an accurate balance. As a check on their uniformity their volume densities were also measured. In all cases the amount of impurity was less than 0.1%.

### *2.3. The Detector*

The neutron detector was a modification of that described in §2.3 of I. Recoil protons from the polythene converter were detected in a triple coincidence scintillation counter telescope, with a copper absorber between the last two counters to set the energy threshold. For this experiment an anticoincidence counter was placed in front of the polythene converter to eliminate counts due to charged particles ejected from the scatterer. Different arrangements of the detector were used for angles greater and less than  $4^\circ$ . These arrangements will be referred to as the large angle detector and the small angle detector. The dimensions and separations of the scintillators and the polythene converters are shown in figure 2(a).

Counters 1 and 2 had flat caps of thin brass fitting closely over the scintillators so that these could be placed very close to the faces of the polythene converter. It could thus be arranged that all straight line paths through counters 2 and 3, passed also through the anticoincidence counter 1, without its scintillator being much larger than those in counters 2 and 3. All scintillators were made from polystyrene containing tetraphenyl butadiene. Counters 2 and 3 were viewed from below and counter 1 from the side by E.M.I. 6260 photomultipliers, counter 4 was viewed from behind by an E.M.I. 6099 photomultiplier. The polythene converter was supported on a thin brass V fastened to the casing of counter 1.

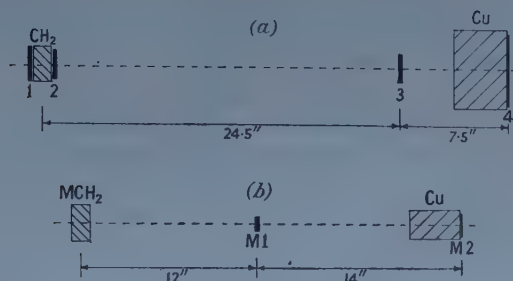


Figure 2. Plan of (a) the detector and (b) the monitor components. Dimensions of the scintillators and polythene converters (in.) :

	Thickness	Diameter	Width	Height
1	$\frac{1}{4}$	$2\frac{3}{8}$ (L.A.)	$1\frac{1}{4}$ (S.A.)	$2\frac{3}{8}$ (S.A.)
CH <sub>2</sub>	$1\frac{1}{4}$	$2\frac{1}{2}$ (L.A.)	$1\frac{1}{4}$ (S.A.)	$2\frac{1}{2}$ (S.A.)
2	$\frac{1}{4}$	2 (L.A.)	1 (S.A.)	2 (S.A.)
3	$\frac{1}{4}$	2		
4	$\frac{1}{8}$	5		
M CH <sub>2</sub>	$1\frac{1}{4}$	$2\frac{1}{2}$	L.A. = Large Angle Detector.	
M 1	$\frac{1}{4}$	1	S.A. = Small Angle Detector.	
M 2	$\frac{1}{8}$	$1\frac{5}{8}$	M = Monitor.	

In the small angle detector the axis of the counter telescope was set at an angle of  $10^\circ$  to the incident neutron direction, so as to keep the casing of counter 4 out of the direct neutron beam. The thickness of the copper absorber between counters 3 and 4 was then made the same ( $78.7 \text{ g cm}^{-1}$ ) as in the total cross section measurements described in II. In the large angle detector the axis of the counter telescope was set along the incident neutron direction. The thickness of the copper absorber was then increased to  $84 \text{ g cm}^{-2}$  to compensate for the difference in energy of protons ejected by 350 MeV neutrons at  $0^\circ$  and  $10^\circ$  in n-p collisions.

The angular resolution of the detector can be judged from the fact that at the distance of 5 ft between the centre of the scatterer and counter 2, 1 inch corresponds approximately to 1 degree. Thus the large angle detector had an angular diameter of about  $2^\circ$ , and the small angle detector was approximately  $1^\circ$  wide and  $2^\circ$  high.

The electronic equipment was the same as that described in § 2.4 of I with the addition of an anticoincidence channel to the coincidence circuit. Counting rates were such that counting losses and random coincidences could be neglected.

#### 2.4. The Monitor

It is particularly important that the energy thresholds of the monitor and the detector should be the same so that monitoring is independent of the changes in the energy spectrum of the neutron beam discussed in § 4 of II. The monitor consisted of a polythene converter with the same dimensions as the one used in the large angle detector, and a double coincidence scintillation counter telescope set with its axis making an angle of  $10^\circ$  with the neutron beam direction. A copper absorber of the same thickness as the one used in the small angle detector was placed between the two counters. The separations and dimensions of the monitor components are shown in figure 2 (b).



When a scatterer was in the neutron beam the monitor measured the beam after attenuation by the scatterer. This is not a disadvantage since the scattered neutrons were attenuated in the same ratio (§5.1).

### § 3. EXPERIMENTAL PROCEDURE

#### 3.1. *Alignment*

A theodolite situated a few feet beyond the monitor block was used for the alignment, which was carried out in a similar way to that described in §3.1 of II. First the V-block carrying the scatterer was aligned and its supporting pillar bolted to the floor. The detector trolley was then rotated until the vertical pivoting axis of the detector railway intersected the line defining the neutron beam direction. The trolley was then clamped in position and the scale set to read  $0^\circ$  angle of scattering. Adjustments to the height and orientation of the railway were made so that the line defining the centres of the counters coincided with the neutron beam direction. The counters were then mounted on the railway and final individual adjustments made to them to bring the centres of the scintillators on to the line of the neutron beam. After counter 1 had been set, the polythene scatterer was placed on its V-support which was adjusted to bring the centre of the scatterer on to the vertical pivoting axis of the railway. The monitor was aligned by a similar procedure, and the concrete block on which it was mounted bolted to the floor. For the large angle detector the railway was fixed in its aligned position, and for the small angle detector it was rotated through  $10^\circ$  and then fixed in position.

#### 3.2. *Check of the Detector Telescope*

The operation of the detector telescope was checked in the external proton beam in the arrangement described in §2.6 of I. Delays between the counters were adjusted and the efficiency of the anticoincidence counter measured. The counts remaining when this counter was brought into operation were no more than would be expected from dead time effects. When operating in the neutron experiment the counting losses in this counter never exceeded 1%. Since the triple coincidence rate was about doubled when the anticoincidence counter was taken out of operation, the effect of the losses was negligible. By reducing the energy of the external proton beam with carbon absorbers a check was made of the energy threshold of the detector telescope.

#### 3.3. *Background*

There was a background of high energy neutrons in the experimental area consisting of a uniformly distributed component due to the leakage through the shielding wall, and a component whose intensity rose sharply near the neutron beam due to scattering from the collimators. For all the scatterers the scattered intensity became indistinguishable from the uniform component of the background near the first diffraction minimum. At the smallest angles for the carbon scatterer the scattered intensity became comparable with the non-uniform component of the background.

Each measurement of the scattered intensity consisted of a run with and without the scatterer in position, the times being approximately apportioned for the best statistical accuracy. Since the monitor was placed beyond the scatterer



the background counts had to be increased in the ratio of the reciprocal of the transmission through the scatterer. This transmission was obtained by using as a monitor the high pressure hydrogen ionization chamber in the cyclotron room which had been used in the measurements described in I and II. The mean value of the transmission taken over all the runs with a given element was used for correcting the background counts. The measured values of the transmission checked within the error of 0.5% with the values of the total cross section given in II.

For the smallest angles the non-uniform component of the background was attenuated by the scatterer. The angle below which this occurred depended on the size of the scatterer, being largest for the lightest element. This attenuation was taken into account when subtracting the background.

### *3.4. Counting Sequence*

Measurements were first completed with the large angle detector, a calibration run then made as described in §3.5, and finally the measurements made with the small angle detector. In order to obtain a value with a reasonably small error for the relative efficiencies of the two detector arrangements measurements were made with both of them for all scatterers at 4°.

Each run, consisting of a measurement with and without the scatterer, had a duration of about an hour. An average of four runs at each angle was needed to give the required statistical accuracy. These runs were intermingled at random with the runs at other angles so as to reduce the effects of drifts in the detector and monitor.

### *3.5. Calibration of the Detector*

To be able to convert the measured scattered intensities to absolute differential cross sections, a calibration run was made with the large angle detector measuring the direct neutron beam. Measurements with the small angle detector were converted in terms of the large angle detector by using the comparative measurements at 4°. With the detector in the direct neutron beam, the path of the beam to the monitor was blocked. The hydrogen ionization chamber was therefore used to compare alternate measurements with the detector and monitor, i.e. with the detector in and then out of the neutron beam. For these measurements the intensity of the neutron beam had to be reduced considerably to avoid appreciable counting losses. This was done by placing a lead absorber in the neutron beam before the first collimator, to avoid varying conditions in the cyclotron and hence the energy spectrum of the neutron beam.

A correction was required for the gradual fall in detector efficiency with distance off the telescope axis. In the measurement of scattered intensity the whole detector was effective, whereas in the calibration run only a circle of 1.25 in. diameter was illuminated. The correction was estimated by numerical integration and found to be 2.5%.

## *§ 4. ENERGY RESOLUTION*

The effective neutron energy spectrum was similar to that for the total cross section measurement deduced in §4 of II. There will be small differences for the following reasons:

(i) The beryllium target in the cyclotron was turned through  $90^\circ$  so that its thickness was 1 in. instead of 0.25 in. This will produce only a small change since the number of traversals of the target by the circulating beam will be reduced almost in proportion to the increase in thickness.

(ii) There will be small changes in the energy resolution curve of the detector due to differences in the dimensions of the neutron beam and the detector counters. These changes will be different for the large and small angle detectors.

(iii) In the large angle detector the angle between the counter telescope axis and the incident neutron direction was  $0^\circ$ , whereas in the small angle detector and the total cross section measurement it was  $10^\circ$ . Although the thickness of the copper absorber was increased to compensate for the change in angle, there will still be small differences in the resolution curves due to different variation with angle of the n-p differential cross section in the region of  $0^\circ$  and  $10^\circ$ .

An estimate showed that all these effects were sufficiently small for the effective spectrum for the total cross section measurements, shown in figure 3 of II, to be taken as an adequate representation of the effective spectrum for the present measurements. To allow for the small differences an extra error was included in the mean neutron energy which was taken to be  $351.5 \pm 3$  mev.

Neutrons elastically scattered through an angle are slightly reduced in energy, and with a threshold detector there is a consequent loss of efficiency. For carbon at the largest scattering angle of  $20^\circ$  the change in energy is about 3 mev, corresponding to a loss of efficiency of about 15%. This is small compared with the statistical error at this angle. For smaller angles and heavier elements the error is always relatively smaller and is never sufficiently large for a correction to be worth while.

The effective neutron spectrum (figure 3 of II) has a half-width of 15 mev. Thus, some inelastically scattered neutrons will be detected. Measurements with protons at 220 mev by Chesnut, Hafner and Roberts (1956) and at 185 mev by Tyrén and Maris (1957) show that the contribution from inelastic scattering will become comparable with that from elastic scattering near the first diffraction minimum. For this reason points near this minimum were not considered in the analysis of the experimental results.

## § 5. TREATMENT OF EXPERIMENTAL RESULTS

### 5.1. Relation between Scattered and Incident Intensities

The number of neutrons  $n_1(\theta)$  singly scattered into a detector subtending a solid angle  $\delta\omega$  at an angle  $\theta$  by a scatterer of thickness  $m$  g cm $^{-2}$  from an incident beam of  $n_0$  neutrons is given by

$$n_1(\theta) = n_0 \exp(-Nm\sigma_t/A) \left\{ Nm \frac{d\sigma}{d\omega}(\theta)/A \right\} \delta\omega.$$

$N$  is Avogadro's number,  $A$  the atomic weight of the scatterer material,  $\sigma_t$  the total cross section, and  $(d\sigma/d\omega)(\theta)$  the differential cross section for elastic scattering through an angle  $\theta$ . The attenuation factor  $\exp(-Nm\sigma_t/A)$  is the same for the scattered and transmitted beams. In the calibration run at  $0^\circ$  the number of neutrons  $n_0'$  passing through the detector was

$$n_0' = n_0 \exp(-Nm\sigma_t/A).$$

Thus, the differential cross section is given by

$$\frac{d\sigma}{d\omega}(\theta) = \frac{n_1(\theta)A}{n_0'Nm\delta\omega} \quad \dots\dots(3)$$

The total cross section for elastic scattering out to the first diffraction minimum  $\sigma_d$  is given by

$$\exp(Nm\sigma_d/A) = 1 + \int_0^{\theta_1} \frac{n(\theta)}{n_0'\delta\omega} 2\pi \sin \theta d\theta. \quad \dots\dots(4)$$

$n(\theta)$  is the total number of neutrons scattered into a solid angle  $\delta\omega$  at an angle  $\theta$ . This number includes all orders of scattering.  $\theta_1$  is the angle of the first diffraction minimum. Since measurements could not be made beyond this angle contributions in this region will subsequently be ignored.

The number of neutrons  $n_2(\theta)$  doubly scattered into a solid angle  $\delta\omega$  at an angle  $\theta$  is given by

$$n_2(\theta) = n_0'^{\frac{1}{2}}(Nm\sigma_d/A)^2 F_2(\theta) \delta\omega. \quad \dots\dots(5)$$

To obtain a simple expression for  $F_2(\theta)$  it was assumed, following Sternheimer (1954), that the main peak of the diffraction pattern was a Gaussian curve so that

$$F_2(\theta) = F_1(\theta/\sqrt{2}). \quad \dots\dots(6)$$

$F_1(\theta)$  is the angular distribution for single scattering and is related to the differential cross section by the equation

$$\frac{d\sigma}{d\omega}(\theta) = \sigma_d F_1(\theta). \quad \dots\dots(7)$$

## 5.2. Finite Angular Resolution

The angular resolution curves of the large and small angle detectors were calculated from the dimensions of the neutron beam at the scatterer and counter 2. For the large angle detector the resolution curve had a half-width of just less than  $2^\circ$ . For the small angle detector the half-width varied from  $1.2^\circ$  at  $\theta = 1.25^\circ$  to  $1.0^\circ$  at  $\theta = 4^\circ$ .

Corrections for finite angular resolution were necessary in the regions of the diffraction pattern where the curvature is large. For this purpose the angular distribution for single scattering was assumed to have the form for a black disc:

$$F_1(\theta) = F_1(0) \{2J_1(kR\theta)/kR\theta\}^2. \quad \dots\dots(8)$$

$k$  is the wave number corresponding to the mean neutron energy, and  $R$  is the nuclear radius. For each element the values of  $kR$  and  $F_1(0)$  were determined which gave the best fit to the experimental points, roughly corrected for double scattering. These values were then used in equation (8) to estimate the corrections for finite angular resolution.

## 5.3. Conversion from Small to Large Angle Detector

The observed numbers of scattered neutrons at angles less than  $4^\circ$  were converted to the numbers that would have been observed with the large angle detector by making use of the ratio of the numbers observed with the large and small angle detectors at  $4^\circ$ . These ratios, corrected for finite angular resolution, are given for the different scattering materials in table 1. The weighted mean was used for the conversion for all the scatterers and its statistical error was included in the errors for angles less than  $4^\circ$ .



Table 1. Ratio of Counts at 4° with Large and Small Angle Detector

Element	Lead	Tin	Copper	Aluminium	Carbon
4° ratio	3.02 ± 0.27	2.87 ± 0.22	2.72 ± 0.28	3.28 ± 0.36	2.69 ± 0.33
		Weighted Mean	2.90 ± 0.13		

#### 5.4. The Effective Solid Angle

For calculating the effective solid angle the size of the detector was assumed to be defined by the scintillator in counter 2. An estimate by numerical integration of the effect of the variation of detector efficiency with distance off the telescope axis, showed that the effective area of the detector was 5% less than that of the scintillator. Careful measurements were made of the radius  $r$  of the scintillator and of the distance  $d$  from the centre of the scatterers to the front face of the scintillator. The effective solid angle is then given by

$$\delta\omega = 0.95\pi r^2/d^2. \quad \dots\dots (9)$$

#### 5.5. The Total Elastic Scattering Cross Sections

The values of the total elastic scattering cross section out to the first diffraction minimum  $\sigma_d$  were calculated from equation (4) with the integral replaced by the sum

$$\sum_0^{\theta_1} \frac{n(\theta)}{n_0 \delta\omega} 2\pi\theta\Delta\theta.$$

All the angles involved were sufficiently small to put  $\sin \theta$  equal to  $\theta$ . To calculate this sum it is not necessary to assume a particular form for the angular distribution. The values obtained for  $Nm\sigma_d/A$  and  $\sigma_d$  are given in table 2. Values are also given of  $\sigma_t - \sigma_d$ , which represents an upper limit to the absorption cross section. The previously measured values of  $\sigma_t$  given in II were used to calculate this difference. Due to the inclusion of some inelastic scattering (§ 4) the values of  $\sigma_d$  will tend to be high, and this will compensate to some extent for the exclusion of elastic scattering beyond the first diffraction minimum. The values of  $\sigma_t - \sigma_d$  should still be slightly higher than the true absorption cross section, by an amount less than 10%.

Table 2. Total Elastic Scattering Cross Sections

Element	$Nm\sigma_d/A$	$\sigma_d$ (mbn)	$\sigma_t - \sigma_d$ (mbn)
Lead	0.132 ± 0.005	979 ± 40	1849 ± 42
Tin	0.124 ± 0.005	589 ± 24	1298 ± 28
Copper	0.107 ± 0.0055	364 ± 16	774 ± 18
Aluminium	0.120 ± 0.007	170 ± 10	395 ± 11
Carbon	0.136 ± 0.007	84.5 ± 4.5	200.8 ± 4.7

#### 5.6. The Differential Cross Sections

For calculating the corrections for double scattering the angular distribution for single scattering was assumed to be that for a black disc given by equation (8). This assumption should be a good one since the theoretical analysis in IV shows that for lead and carbon all the possible fits gave an angular distribution identical with that given by a black disc normalized to give the same forward scattering cross section.

Different values of  $n_1(0)$  and  $kR$  were tried and for each pair of values the corresponding values of  $n_1(\theta)$  calculated for the angles at which measurements



were made. To these numbers corrections  $n_2(\theta)$  were added for double scattering. From equations (3), (5) and (7)  $n_2(\theta)$  is given by

$$n_2(\theta)/n_1(0) = \frac{1}{2} \{ N m \sigma_d / A \} \{ F_2(\theta) / F_1(0) \}. \quad \dots\dots (10)$$

The values of  $N m \sigma_d / A$  are given in table 2. The values of  $F_2(\theta) / F_1(0)$  were calculated from equations (6) and (8). The resulting values of  $n(\theta)$  were compared with the experimental values and a least squares fit obtained giving the best values of  $n_1(0)$  and  $kR$ . For the reasons given in § 4 points near the first diffraction minimum were not included when making this fit.

The best values for  $kR$  give values for the nuclear radii, which are given in table 3. These are the radii of the black disc giving an angular distribution which, when normalized, gives the best fit to the experimental points.

Table 3. Nuclear Radii

Element	$R$ (fermi)	$R/A^{1/3}$ (fermi)
Lead	$7.16 \pm 0.26$	$1.21 \pm 0.04$
Tin	$5.81 \pm 0.28$	$1.18 \pm 0.06$
Copper	$4.77 \pm 0.23$	$1.20 \pm 0.06$
Aluminium	$3.59 \pm 0.20$	$1.18 \pm 0.07$
Carbon	$2.59 \pm 0.16$	$1.13 \pm 0.07$
		Mean value $1.18 \pm 0.03$

Corrections for double scattering, calculated with the best values of  $n_1(0)$  and  $kR$ , were subtracted from the experimental values of  $n(\theta)$ . The values of the differential cross sections  $d\sigma/d\omega(\theta)$  were then calculated from equation (3) and are given in table 4. They are plotted as a function of angle in figure 3 together with the angular distribution curve calculated with the best values of  $n_1(0)$  and  $kR$ .

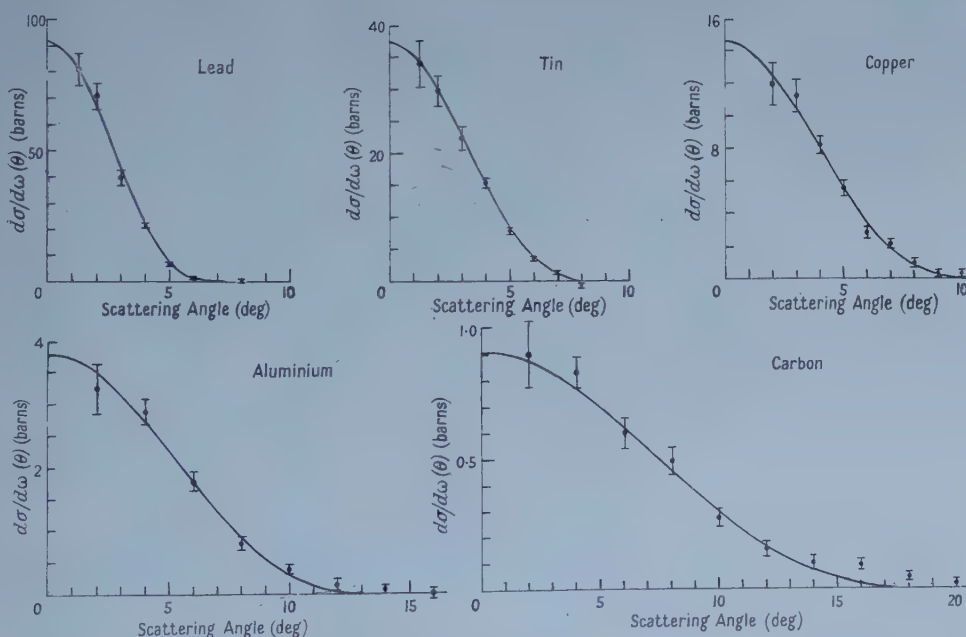


Figure 3. The angular distributions of the elastically scattered neutrons. Points are measured differential cross sections given in table 4. Curves are 'black disc' diffraction patterns with best values of  $d\sigma/d\omega(0)$  and  $kR$ . Note In ordinates, for barns read barns sterad<sup>-1</sup>.

From the best values of  $n_1(0)$  the forward scattering cross sections  $d\sigma/d\omega(0)$  were calculated using equation (3). These are given in table 5 together with the values of  $[\mathcal{J}f(0)]^2$  calculated from the total cross sections  $\sigma_t$  given in II, using equation (2).

Table 4. Differential Cross Sections (barns sterad<sup>-1</sup>)

Element	Lead	Tin	Copper	Aluminium	Carbon
Angle (°)					
1 $\frac{1}{2}$	80.8 ± 6.4	34.1 ± 3.7			
2	70.9 ± 5.1	29.8 ± 2.4	12.0 ± 1.3	3.24 ± 0.39	0.900 ± 0.130
3	39.5 ± 3.2	22.4 ± 1.9	11.2 ± 1.0		
4	21.5 ± 1.15	15.5 ± 0.8	8.25 ± 0.54	2.88 ± 0.20	0.835 ± 0.060
5	7.1 ± 0.85	7.8 ± 0.55	5.58 ± 0.48		
6	1.55 ± 0.7	3.5 ± 0.45	2.83 ± 0.38	1.78 ± 0.15	0.600 ± 0.060
7		1.4 ± 0.30	2.15 ± 0.31		
8	0.35 ± 0.8	-0.8 ± 0.40	0.93 ± 0.28	0.80 ± 0.12	0.493 ± 0.053
9			0.33 ± 0.23		
10			0.28 ± 0.22	0.39 ± 0.08	0.277 ± 0.038
12				0.15 ± 0.10	0.153 ± 0.031
14				0.07 ± 0.08	0.099 ± 0.027
16				0.01 ± 0.10	0.091 ± 0.023
18					0.043 ± 0.019
20					0.017 ± 0.020

Table 5. Forward Scattering Cross Sections (barns sterad<sup>-1</sup>)

Element	$\frac{d\sigma(0)}{d\omega} =  f(0) ^2$	$\left[\frac{k'\sigma_t}{4\pi}\right]^2 = [\mathcal{J}f(0)]^2$	$\frac{[\mathcal{J}f(0)]^2}{ f(0) ^3}$
Lead	91.8 ± 6.0	100 ± 1.4	1.09 ± 0.075
Tin	37.4 ± 3.3	44.2 ± 0.85	1.18 ± 0.105
Copper	14.6 ± 1.5	15.8 ± 0.30	1.08 ± 0.110
Aluminium	3.79 ± 0.43	3.68 ± 0.07	0.97 ± 0.110
Carbon	0.91 ± 0.115	0.839 ± 0.013	0.925 ± 0.120
Mean value			1.05 ± 0.05

## § 6. DISCUSSION

### 6.1. The Absorption Cross Sections

The values obtained for  $\sigma_t - \sigma_d$  given in table 2 are compared in table 6 with the values of the absorption cross sections obtained by Voss and Wilson (1956) at 140 mev, Ball (U.C.R.L. report 1938, unpublished) at 300 mev, and Coor *et al.* (1955) at 1.4 gev.

Table 6. Variation of Absorption Cross Sections with Energy

Element	VW	B	AMS	C <i>et al.</i>
Lead	1704 ± 24	1720 ± 80	1849 ± 42	1727 ± 45
Copper	741 ± 13	755 ± 33	774 ± 18	674 ± 34
Aluminium	418 ± 14	390 ± 23	395 ± 11	415 ± 23
Carbon	221 ± 10	203 ± 33	201 ± 5	201 ± 13

VW, Voss and Wilson, 140 mev; B, Ball, 300 mev; AMS, present measurements, 350 mev; C *et al.*, Coor *et al.*, 1.4 gev.

Within the experimental errors the absorption cross sections remain constant from 140 mev up to 1.4 gev. The total cross sections are constant between 270 and 400 mev (table 2 of II) but increase at energies above and below this range.

At 1.4 GeV (Coor *et al.* 1955) and at 156 MeV (Taylor *et al.* 1951) the total cross sections are considerably higher than at 350 MeV. The increase must be almost entirely an increase in the amount of elastic scattering. This can be explained if the nucleus is almost opaque throughout the energy region. An increase in opacity would then have a much more marked effect on the elastic scattering cross section than on the absorption cross section (Fernbach, Serber and Taylor 1949). The value of the absorption coefficient  $K$  for 350 MeV neutrons in a uniform nucleus of radius  $1.2A^{1/3}$  fermis as calculated from the nucleon-nucleon cross sections is  $0.43 \text{ fermi}^{-1}$ . Thus, at 350 MeV  $KR = 1.2$  for carbon and  $3.1$  for lead. This would just bring carbon into the region where the main effect of an increase in  $K$  would be an increase in the amount of elastic scattering.

### 6.2. The Nuclear Radii

The nuclear radii given in table 3 must be treated with caution. The method of their deduction (§5.6) is such that it is not clear exactly how they are related to the r.m.s. radii of the nuclear charge distribution. However, within the experimental error they are the same as the more accurate values of the r.m.s. radii obtained from high energy electron scattering experiments (Ford and Hill 1955). In the theoretical analysis for lead and carbon in IV it is shown that the experimental angular distributions can be fitted using the charge density distributions obtained from electron scattering experiments.

### 6.3. The Differential Cross Sections

It is shown in IV that the shape of the angular distribution remains almost identical with that given by a black disc over a wide range of optical model parameters. The theoretical fits are distinguished by the differences they give in the forward scattering cross section. From table 5 it is seen that within the experimental error the forward scattering amplitude is purely imaginary. This is in contrast to the situation at 136 MeV (Wilson 1956) where for light elements the real and imaginary parts of the forward scattering amplitude are roughly equal. In the theoretical analysis in IV it is assumed as a first approximation that the central potential is purely imaginary, which is the most natural explanation of the imaginary forward scattering amplitude. A more accurate determination of the real part of the forward scattering amplitude would be useful. This could be done by a more accurate measurement of the neutron forward scattering cross sections, although they are relatively insensitive to the size of the real part when this is small. A better method would be to measure the Coulomb interference at small angles in the elastic scattering of protons which is directly dependent on the real part of the scattering amplitude and relatively insensitive to other parameters.

### ACKNOWLEDGMENTS

The authors wish to thank Professor H. W. B. Skinner for his interest and encouragement. The discussions with Dr. G. E. Brown concerning the theoretical interpretation of the results have been invaluable in the preparation of this paper. Valuable discussions have also been held with Professor J. M. Cassels. Thanks are due to the cyclotron crew for their willing co-operation. During the course of this work D. S. M. was the holder of a University Fellowship, and S. K. S. the holder of a West Bengal State Scholarship.

## REFERENCES

- ASHMORE, A., JARVIS, R. G., MATHER, D. S., and SEN S. K., 1957 a, *Proc. Phys. Soc. A*, **70**, 735; 1957 b, *Ibid.*, **70**, 745.
- BRATENAH, A., FERNBACH, S., HILDEBRAND, R. H., LEITH, C. E., and MOYER, B. J., 1950, *Phys. Rev.*, **77**, 597.
- BROWN, G. E., ASHMORE, A., and NORDHAGEN, R., 1958, *Proc. Phys. Soc.*, **71**, 565.
- CHESNUT, W. G., HAFNER, E. M., and ROBERTS, A., 1956, *Phys. Rev.*, **104**, 449.
- COOR, T., HILL, D. A., HORNYAK, W. F., SMITH, L. W., and SNOW, G., 1955, *Phys. Rev.*, **98**, 1369.
- FERNBACH, S., SERBER, R., and TAYLOR, T. B., 1949, *Phys. Rev.*, **75**, 1352.
- FORD, K. W., and HILL, D. L., 1955, *Ann. Rev. Nucl. Sci.*, **5**, 25.
- STERNHEIMER, R. M., 1954, *Rev. Sci. Instrum.*, **25**, 1070.
- TAYLOR, A. E., PICKAVANCE, T. G., CASSELS, J. M., and RANDLE, T. C., 1951, *Phil. Mag.*, **42**, 751.
- TYRÉN, H., and MARIS, Th. A. J., 1957, *Nucl. Phys.*, **3**, 52.
- VOSS, R. G. P., and WILSON, R., 1956, *Proc. Roy. Soc. A*, **236**, 41.
- WILSON, R., 1956, *Phil. Mag.*, **1**, 1013.
- VAN ZYL, C. P., VOSS, R. G. P., and WILSON, R., 1956, *Phil. Mag.*, **1**, 1003.



# Elastic Scattering of 350 Mev Neutrons by Complex Nuclei

By G. E. BROWN<sup>†</sup>, A. ASHMORE<sup>‡</sup> AND R. NORDHAGEN<sup>‡</sup>

<sup>†</sup> Department of Mathematical Physics, University of Birmingham

<sup>‡</sup> Nuclear Physics Research Laboratory, University of Liverpool

*Communicated by R. E. Peierls; MS. received 24th November 1957, and  
in final form 11th December 1957*

**Abstract.** The scattering of 350 Mev neutrons by lead and carbon is analysed using the optical model. The parameters of the latter are determined as well as possible. The problem of the unambiguous determination of optical model parameters is considered in detail for the high energy region.

## § 1. INTRODUCTION

THE elastic scattering of nucleons by complex nuclei can be described by replacing the nucleus by a complex spin-dependent potential  $V(r) = V_1(r) + \sigma \cdot \mathbf{L} V_2(r)$ . The parameters of this potential are related to the small angle nucleon-nucleon amplitudes and the determination of them gives useful relations between these small angle amplitudes (see, for example, Brown 1957, Bethe 1957).

In recent papers (Wilson 1956, Williams 1955) cross sections have been fitted with theoretical models. Their results are discussed by Ashmore, Mather and Sen (1958).

In the present paper the scattering of 350 Mev neutrons by carbon and lead will be analysed. These two nuclei have been chosen because they have been studied extensively experimentally and a great deal is known about their properties. It seemed appropriate to choose one light and one heavy nucleus, with a view towards investigating them carefully at several energies. Whereas most earlier investigations have employed rough models for  $V_1$  and  $V_2$ , e.g. square wells and simple harmonic oscillator wells, we shall use realistic models as explained in § 2.

The theoretical analysis in this paper will be applied specifically to the results of Ashmore, Mather and Sen (1958) although most of the general arguments made will be applicable to scattering in the range above approximately 300 Mev. A particular aim of this paper is to indicate which experiments are necessary to obtain each parameter more or less uniquely and it will be shown that there is much more ambiguity in the determination than is usually assumed.

In a following article, theoretical and experimental results for carbon and lead in the higher energy range 600–1000 Mev will be discussed. Thus, some indication of the energy dependence of the parameters will be obtained. The energy dependence of the spin-orbit part of the potential is of special interest since this gives some indication of the nature of the spin-dependent part of the nucleon-nucleon potential, as pointed out previously (Brown 1957).

## § 2. DEVELOPMENT

The amplitude for the scattering of a nucleon by a spin-zero nucleus is given by

$$F(\theta, \phi) = A + B \boldsymbol{\sigma} \cdot \mathbf{n}. \quad \dots\dots(1)$$

Although the exact expressions for  $A$  and  $B$  in terms of phase shifts are complicated, simple expressions which are quite accurate for the problem in hand (Shapiro 1955) can be obtained in the semi-classical approximation. These are

$$\left. \begin{aligned} A &= \frac{k}{i} \int b \, db J_0(kb \sin \theta) \left\{ \frac{\exp(i\chi^+) + \exp(i\chi^-)}{2} - 1 \right\} \\ B &= -\frac{1}{2}k \int b \, db J_1(kb \sin \theta) \{ \exp(i\chi^+) - \exp(i\chi^-) \} \end{aligned} \right\} \quad \dots\dots(2)$$

where

$$\chi^\pm = \chi_1 \pm \chi_2 = -\frac{E}{k} \int_{-\infty}^{\infty} dz \{ V_1(r) \pm kb V_2(r) \}. \quad \dots\dots(2a)$$

Here  $r^2 = z^2 + b^2$ ,  $b$  representing the impact parameter;  $J_0$  and  $J_1$  are Bessel functions.

In the approximation in which the range of nucleon-nucleon forces is neglected compared to the nuclear radius (see Brown 1957 for a discussion of this in the semi-classical formalism), the potentials  $V_1$  and  $V_2$  are given by

$$\left. \begin{aligned} V_1 &= -\frac{2\pi}{E} \sum_i \bar{f}_i(0) \rho(r) \\ V_2 &= -\frac{2\pi}{E} \sum_i \bar{g}_i(0) \frac{1}{r} \frac{d\rho}{dr} \end{aligned} \right\} \quad \dots\dots(3)$$

where  $f_i$  and  $g_i$  are components of the  $i$ th nucleon-nucleon scattering amplitude, given by

$$f_i(\theta, \phi) = f_i(\theta) + i\boldsymbol{\sigma} \cdot \mathbf{k}' \times \mathbf{k} g_i(\theta) \quad \dots\dots(4)$$

and the bar indicates that an average over spin and charge states has been carried out. Here  $\rho(r)$  is the nuclear density, normalized to unity.

The imaginary part of  $V_1$  is closely related to the mean free path of the nucleon in nuclear matter, as can be seen by remembering the optical theorem

$$\sigma_i = \frac{4\pi}{k} \mathcal{I} f_i(0) \quad \dots\dots(5)$$

where  $\sigma_i$  is the total cross section and  $\mathcal{I}$  means that the imaginary part must be taken. Thus,

$$\mathcal{I} V_1(r) = -\frac{k}{2E} \sum_i \bar{\sigma}_i \rho(r). \quad \dots\dots(5a)$$

In employing  $f_i(\theta, \phi)$  and  $\sigma_i$  for free nucleons we are neglecting the exclusion principle. The effect of it in preventing certain transitions has been calculated by Goldberger (1948), who finds that the imaginary part of  $V_1$  should be diminished by approximately 12% at this energy from that given by (5a) using the  $\bar{\sigma}_i$  for free nucleons. There, is however, an opposing effect of the exclusion principle; it tends to increase the absorption by preventing nucleons in the same spin and charge state from coming close together, thereby decreasing the shadow effect (Glauber 1956). At 350 mev the net effect of the Pauli principle would appear to be very small, and we shall neglect it,

In optical model calculations one obtains  $V_1$  and  $V_2$  phenomenologically by fitting the experiments, and can then determine  $\overline{f_i(0)}$  and  $\overline{g_i(0)}$ . The results given in (3) indicate that one should consider only  $V_2$ 's satisfying

$$V_2 = \frac{C}{r} \frac{dV_1}{dr} \quad \dots\dots(5b)$$

where  $C$  is a complex constant. Thus  $V_1$  and  $V_2$  are not to be determined independently; once the functional form of  $V_1$  is set, that of  $V_2$  follows, and the only freedom is in the choice of  $C$ , which we shall refer to as the spin-orbit coupling parameter. Clearly,  $C$  has the dimensions of a length squared, and we shall give it in units of  $10^{-27} \text{ cm}^2$  throughout this paper.

The striking feature of the Liverpool experiments is that the real part of  $V_1$  appears to be very small compared with the imaginary part. This can be seen by applying the optical theorem (5) to the scattering by the complex nucleus, in which case one obtains

$$\left. \frac{d\sigma}{d\Omega} \right|_{\theta=0} \geq \left( \frac{k\sigma_T}{4\pi} \right)^2 \quad \dots\dots(6)$$

where  $\sigma_T$  is the total cross section. The equality holds only if the real part of the forward amplitude is zero. Absolute measurements of both the small angle differential cross section and the total cross section were made; within the experimental accuracy to the order of  $10\%$  for the former the equality was found to hold. A purely imaginary forward amplitude can be obtained most naturally by assuming  $V_1 = iV_{1I}$ , i.e.  $V_1$  to be pure imaginary. We shall start from this assumption and will discuss later the effect of introducing a real part  $V_{1R}$ .

Since the experimental data can be explained to a good approximation by a purely imaginary potential, we shall begin from formulae for pure absorption and introduce  $V_{1R}$  later as a perturbation. The resulting  $A$  and  $B$  are

$$A_I = \frac{k}{i} \int b db \{ \exp(-\chi_{1I}) \cos \chi_2 - 1 \} J_0(kb \sin \theta)$$

$$B_I = \frac{k}{i} \int b db \exp(-\chi_{1I}) \sin \chi_2 J_1(kb \sin \theta)$$

where

$$\chi_{1I} = -\frac{E}{k} \int_{-\infty}^{\infty} dz V_{1I}(r). \quad \dots\dots(7)$$

It will be assumed for the moment that  $V_2$ , and therefore  $\chi_2$  is real. Thus  $C$  in (5b) is equal to  $-ic_e$ , where  $c_e$  is real. This  $c_e$  defines an effective real potential which will fit the cross section. We shall show later that we can relate  $c_e$  to the real and imaginary parts of the actual (complex) spin-orbit potential in the case of light nuclei. With a real spin-orbit potential and  $\chi_{1R} = 0$ ,  $A$  and  $B$  are pure imaginary, as indicated by the lower suffix I.

We have data only up to the first diffraction minimum at our disposal. However, even if the experiments went beyond this angle, they would not give much more useful information, since inelastic scattering leaving the nucleus in excited levels becomes important near and beyond the minimum and the experiments do not have sufficient energy discrimination to exclude this. Indeed, the experiments at 220 and 185 mev (Chesnut *et al.* 1956, Tyren and Maris 1957) show that inelastic scattering leaving carbon in the 4.42 mev excited level plays

a large role and it would take an exceptional energy discrimination at approximately 350 MeV to keep these events from being counted as elastic.

We shall now discuss our fits to experiment made under the above assumptions of an imaginary central potential and a real spin-orbit potential. In the next section we shall introduce deviations from these assumptions.

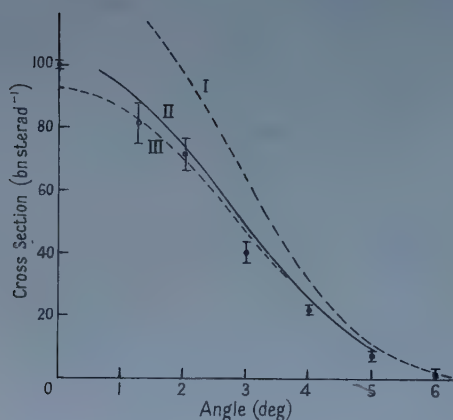


Figure 1. Results for lead. Curve I: black disc. Curve II: potential with linear taper, such that  $R_1/R_2=0.64$ , absorption as for incident protons with  $\sigma_{pp}=24$  mbn,  $\sigma_{np}=34$  mbn and no account is taken of the Pauli principle. Curve III: square potential with absorption  $K=0.43(13)$  cm $^{-1}$ . The point at zero angle is not an experimental point, but is a minimum value deduced from the total cross section by using the equality in (6).

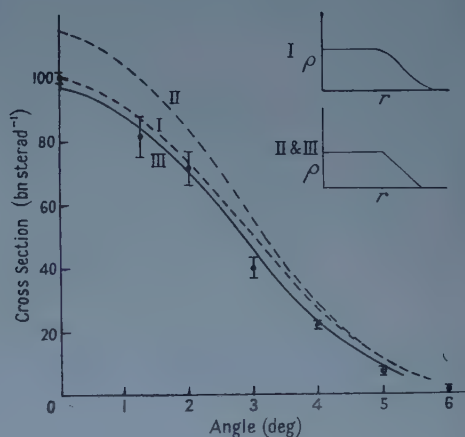


Figure 2. Results for lead. The potentials for I, II and III were chosen to give the r.m.s. radius 7.2 fermis and the transition range  $t=2.35$  fermis, which is found by electron scattering for the charge distribution (Hahn *et al.* 1956). In all three cases the absorption was calculated for incident neutrons, assuming  $\sigma_{nn}=24$  mbn  $\sigma_{np}=34$  mbn. A real spin-orbit force with  $c_e=2.56$  was used for I and II; for III a force with  $c_e=1.65$  was employed.

In figure 1 we show results from rough models for lead. Curves II and III were actually calculated for incident protons, for which the absorption is approximately 15% higher than for neutrons, but the curves from this higher absorption fit the neutron results well. The shape of the curve for the black disc is the same as for the other two. If normalized at the origin to either of curves II or III, it is coincident over the entire range.

In figure 2 we show results from two distributions chosen to reproduce the r.m.s. radius and transition range found for the charge distribution in lead from electron scattering. Curves I and II result from potentials having the same spin-orbit coupling parameter and the same absorption per unit density, but differ markedly. Thus, it is clear that different distributions which reproduce the electron scattering results can give quite different nucleon scattering. However, once again, the shapes of the two are the same and by changing the parameters of II, a fit can be obtained (curve III).



It is clear that fits to the data can be obtained with a variety of functional forms for the potential. To remove this ambiguity, we have assumed in the case of carbon that the nucleon density is the same as the charge density, which is known quite accurately from electron scattering (Fregeau 1956),† i.e.

$$\rho(r) = \rho_0 \left( 1 + \frac{4}{3} \frac{r^2}{a^2} \right) \exp \left( -\frac{r^2}{a^2} \right), \quad \dots (8)$$

with  $a = 1.635$  fermis.

In figure 3 we show that a reasonable fit can be achieved by choosing  $c_e$  appropriately, and illustrate the effect of changing  $c_e$ . In the upper right-hand corner, we compare the predictions for the polarization with the Berkeley proton results at slightly lower energies. The theoretical curve would be expected to reproduce the experimental one only if the experimental curve included no inelastic scattering and the actual spin-orbit potential were real. The fact that the curve for  $c_e = 2.4$ , which fits the cross section, gives the maximum polarization at too large an angle means that the spin-orbit potential has an appreciable imaginary part, as we shall discuss later. Although  $c_e = 2.4$  fits the differential cross section, we see that a value of  $c_e$  of about 2.0 fits the zero angle cross section obtained by taking the equality sign in (6). In line with our previous discussion, this is the value we should choose.

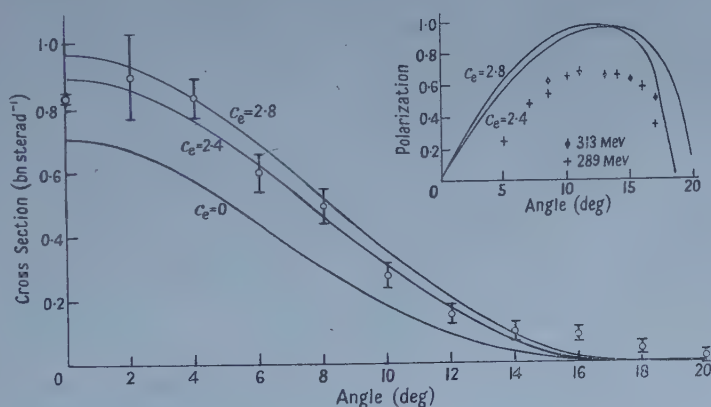


Figure 3. Results for carbon. For all three curves, the potential was assumed to have the same shape as the charge distribution Fregeau 1956, and the absorption was calculated using  $\sigma_{nn} = 24$  mbn,  $\sigma_{np} = 34$  mbn and taking no account of the Pauli principle. Different values of  $c_e$  were used, as indicated. The point at zero angle is a minimum value deduced from the total cross section using the equality in (6).

In figure 4 we show that almost identical fits can be obtained for two different values of  $c_e$  if we relax our assumption that the absorption is computed from (5a) and adjust it to compensate for the change in  $c_e$ . The normalized black disc curve is shown to illustrate that again the shapes of curves from different distributions are the same.

† In Fregeau's work, other distributions were found to give almost as good fits, so this charge distribution should not be considered as unique. This distribution is very suitable for our own work, because its derivatives have no discontinuities which would falsely accentuate the contribution from the spin-orbit potential. Furthermore, it is convenient, in that most of the necessary integrals can be carried out analytically.

In the following analysis we will concentrate now on carbon because the experimental data on polarization are available here, and not for lead, and because the assumption that the nucleon density is the same as the charge density is almost certainly valid here, whereas it is not clear that it is for lead.

### § 3. DISCUSSION

It is clear from the preceding illustrations that a  $V_1$  of almost any reasonable form will reproduce the experimental results as long as the radius is chosen so as to give the diffraction minimum in the right place and the parameters are chosen to give the correct zero-angle cross section (or total cross section, since one cross section determines the other when the forward amplitude is imaginary), i.e. all reasonable potentials give curves of the same shape. Indeed, we obtained a unique value of  $c_e$  only by assuming a definite absorption. If the absorption is also treated as a parameter, then for any reasonable value, a value of  $c_e$  can be found which gives the experimental zero-angle cross section, and hence the entire small-angle cross section since the shapes of the curves for different values of  $c_e$  and different absorptions are the same. This is illustrated in figure 4.

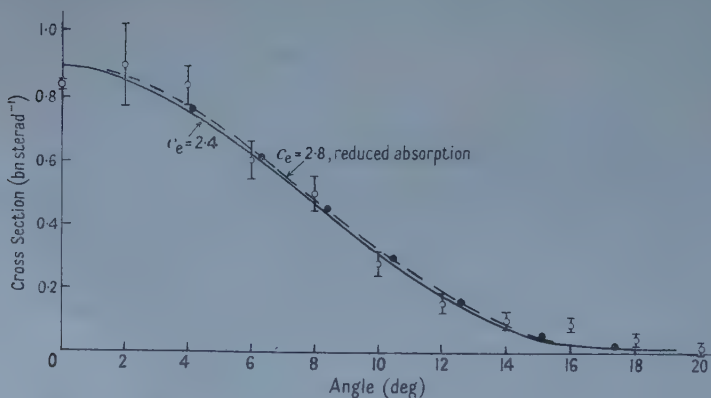


Figure 4. Results for carbon. Curve I is the same as the curve for  $c_e = 2.4$  in figure 3. To obtain II, the absorption in the potential employed for the curve  $c_e = 2.8$  in figure 3 was reduced  $5\frac{1}{2}\%$ . A normalized curve from a black sphere of radius  $2.50(-13)$  cm is shown for comparison (black dots).

From most previous treatments in the literature, one might conclude that it is possible to obtain the absorption from the reaction cross section  $\sigma_R$ . This might be so if we knew the true reaction cross section. However, experimentally at energies in the several hundred MeV range one usually measures the cross section integrated for all angles greater than the first diffraction minimum, which we denote by  $\sigma_R'$ , and then subtracts the estimated elastic scattering for angles greater than the first minimum. But  $\sigma_R'$  is the same for two models which give the same small-angle cross section under our assumptions, since they will also give the same total cross section, this quantity being determined by  $d\sigma/d\Omega$  at  $\theta = 0$ , and  $\sigma_R'$  is just the difference of  $\sigma_T$  and the integrated small-angle cross section. Of course, differing amounts of elastic scattering will be included in predicted values of  $\sigma_R'$  by the two models, but this is not separated experimentally.

Thus, we must assume the absorption; this is not determined by any of the usual experimental measurements.

We now allow the spin-orbit coupling  $C$  to be complex, defining its relative phase  $\gamma$  by  $C = ce^{i\gamma}$ . In this case  $\chi_2$  has a real part  $\chi_{2R}$  and an imaginary part  $\chi_{2I}$ . Since both of these are smaller than unity in the case of carbon, we find that here  $\cos \chi_2$  is given well by the lowest terms in its expansion

$$\cos(\chi_{2R} + i\chi_{2I}) \simeq (1 - \frac{1}{2}\chi_{2R}^2 + \frac{1}{2}\chi_{2I}^2) - i\chi_{2R}\chi_{2I}. \quad \dots\dots(9)$$

Thus,  $A_R(0)$  is seen to be small. Further, the  $A_I(0)$  given by a real spin-orbit potential with  $c_e$ , will be given by a complex one as long as  $c^2(\sin^2\gamma - \cos^2\gamma) = c_e^2$ , i.e. if  $\cos 2\gamma = -c_e^2/c^2$  since in both cases the same values for  $-\frac{1}{2}\chi_{2R}^2 + \frac{1}{2}\chi_{2I}^2$  will result.

We can thus obtain the phase of  $C$  from the zero-angle cross section, knowing its absolute value  $c$ . The latter is determined by the polarization. This is easily seen by employing the approximate formula given by Levintov (1956). He finds that the maximum polarization  $P_m$  is equal to  $\sin\gamma$  and occurs at an angle  $\theta_m$  given by  $\sin\theta_m = 1/ck^2$ . We have checked by our more accurate calculations that this gives good results as long as  $\theta_m$  is well inside the first diffraction minimum. The value of  $\gamma$  cannot be reliably determined from experiments in this way, because they usually include inelastic scattering which alters the apparent  $P_m$ . However, the position of maximum polarization  $\theta_m$  would seem to be less affected by this, and one sees from Levintov's tabulation that the values of  $c$  determined from different nuclei are consistent. He finds  $c = 3.3$ . Using this value, and  $c_e = 2.0$ , we find from the formulae following equation (9) that  $C = -i2.73 - 1.85$ . This is the phase relative to the central potential, thus the ratio of imaginary to real part for the spin-orbit potential is  $-0.68$ . To obtain the sign of the imaginary part we refer to the calculations of Heckrotte (1956), who looked at the small-angle interference between this spin-orbit potential and the Thomas term, which arises from the Coulomb force. Although this was at the slightly lower energy of the Berkeley experiments, we would expect the sign to be the same here. It is interesting to note that our ratio is in the range of ratios found by him ( $-0.5$  to  $-1$ ) which seemed to fit the small-angle Berkeley polarization experiments.

The real part of the potential is relatively small and has only a second-order effect on the quantities considered so far. In fact, adding a real part one-third the size of the imaginary part would change the imaginary part of the forward amplitude  $A_I$  by only 4% in the case of carbon. Thus, a small real part could not be easily determined through considering the quantities discussed above. It can best be obtained from Coulomb interference experiments with protons, such as the Berkeley experiments at 313 MeV (Chamberlain *et al.* 1957). In a fit to these by a rough calculation we found that the real part of the forward amplitude was zero within our accuracy. Bethe (1958) obtained a different result, finding it to be 2.3 fermis, which is still small compared with the imaginary part. His calculation can, however, be criticized because, although he uses the correct zero-angle nuclear amplitude, he employs the angular dependence given by Born approximation. Furthermore, he takes the experimental normalization as given by Chamberlain *et al.* although it should be considered variable since it is quoted as accurate to only 20%.

Because fitting the data is an intricate matter more accurate calculations are now being carried out. It seems reasonable from the above discussion that a



small real part of the central potential will not appreciably change the conclusions obtained here about the other parameters.

#### § 4. CONCLUSIONS

By assuming a functional form of the potential and no effect from the Pauli principle, we have obtained parameters of the optical model at 350 mev by analysing several data for carbon. Since there was not enough information to do this from the Liverpool experiments polarization results were also used. With  $c = 3.3$ , the ratio of imaginary to real parts for the spin-orbit potential was found to be approximately 0.68. The real part of the central potential was found to be small but not accurately determined by the experiments considered here. It could, in principle, be accurately determined from Coulomb interference experiments.

In an analysis of the Berkeley data for several elements Harris and Jastrow (private communication) find about the same value for  $c$ ; however, they employ a purely real spin-orbit potential and, consequently, get a fairly large real part of the central potential. (We have indicated that adding an imaginary part to the spin-orbit potential gives results for the differential cross section similar to those from adding a real part of the potential.) It is reasonable that they should obtain the same value for  $c$ , notwithstanding the different real part of the central potential, because  $c$  is determined by the position of the polarization maximum, which they fitted. Our value of  $c$  is the same as that found by Levintov (1956).

After this work was completed, we received Bethe's (1958) analysis of the Berkeley results. His results for the real part of the potential are noted at the end of the last section. The major difference between his results and ours is that the value of  $c$  obtained by him is only about one-third as large as ours. He rejects Levintov's method of finding  $c$ , pointing out that Levintov's formulae are not valid near the diffraction minimum. For carbon, however, the maximum polarization occurs well within the diffraction minimum, where they should still be valid. Both Harris and Jastrow and the present authors obtained the same result as Levintov using more accurate formulae. Thus, it does not seem that Levintov's results can be dismissed. On the other hand, the value of  $c$  found by Bethe is in the range of those calculated from presents sets of nucleon-nucleon phase shifts by our equation (3), as outlined in his paper. Thus, our value is much too high if equation (3) is correct and the present sets of nucleon-nucleon phase shifts are the only ones.

Fits of the angular distribution in lead indicated that agreement could be obtained for a wide variety of assumed nuclear shapes. Even assuming a particular shape the parameters could not be determined without polarization data.

The present investigation indicates that results derived from fewer experimental data, as is the case with most published treatments, are quite ambiguous. In these analyses, more special assumptions have usually been made to obtain results. For example, the spin-orbit force has been taken to be real, or has been simply neglected. It is clear that the results from such analyses are not reliable.

If future experiments determine the purely elastic scattering beyond the first diffraction minimum, these data will provide a more stringent test. However, an exceptional energy discrimination would be required for this.



*Note added in proof.* An exact phase analysis carried out by Bjorklund, Blandford and Fernbach (1957, *Phys. Rev.*, **108**, 795) for a variety of elements in the range 287–313 MeV gives the absolute value of the spin-orbit coupling parameter as  $c=2.1$ . This lies about half-way between Bethe's value and that of Levintov. Using this value together with our value of  $c_e=2.0$  for carbon gives a very small imaginary part for the spin-orbit potential, in contradiction with Heckrotte's values. Bjorklund *et al.* have used a large imaginary part of the spin-orbit potential in order to depress the maximum polarization to the experimentally observed values. This procedure can, as they point out, lead to large errors. This is because the admixture of inelastic scattering in the experiments could lower the observed maximum from that for the purely elastic scattering considerably, and seems to do so at the lower energies where the separation has been made. However, in so far as the value of  $c$  follows mainly from the angle of maximum polarization, their determination of this parameter should be almost independent of differences in phase of the potentials. Our determination of  $c_e$  is independent of the particular value chosen for  $c$ .

#### ACKNOWLEDGMENTS

We would like to thank Professor R. E. Peierls for several useful discussions. One of us (R. N.) received support from CERN during this work.

#### REFERENCES

- ASHMORE, A., MATHER, D. S., and SEN, S. K., 1958, *Proc. Phys. Soc.*, **71**, 552.  
BETHE, H. A., 1957, *Proc. of Rochester Conference, Section III*; 1958, *Phys. Rev.*, in the press.  
BROWN, G. E., 1957, *Proc. Phys. Soc. A*, **70**, 361.  
CHAMBERLAIN, O., SEGRÈ, E., TRIPP, R. D., WIEGAND, C., and YPSILANTIS, T., 1956, *Phys. Rev.*, **102**, 1659.  
CHESNUT, W. C., HAFNER, E. M., and ROBERTS, A., 1956, *Phys. Rev.*, **104**, 449.  
FOX, R., LEITH, C., WOUTERS, L., and MACKENZIE, K. R., 1950, *Phys. Rev.*, **80**, 23.  
FREGEAU, J. H., 1956, *Phys. Rev.*, **104**, 225.  
GLAUBER, R., 1956, *Physica*, **22**, 1185.  
GOLDBERGER, M. L., 1948, *Phys. Rev.*, **74**, 1269.  
HAHN, B., RAVENHALL, D. G., and HOFSTADTER, R., 1956, *Phys. Rev.*, **101**, 1131.  
HECKROTTE, W., 1956, *Phys. Rev.*, **101**, 1406.  
LEVINTOV, I. I., 1956, *Doklady Akad. Nauk S.S.S.R.*, **107**, 240.  
SHAPIRO, I. I., 1955, *Thesis*, Harvard University.  
TYRÉN, H., and MARIS, TH. A. J., 1957, *Nuclear Physics*, **3**, 52.  
WILLIAMS, R. W., 1955, *Phys. Rev.*, **98**, 1387.  
WILSON, R., 1956, *Phil. Mag.*, **1**, 1003.

## The Excitation of the 2p State of Hydrogen by Slow Electrons—Distorted Wave Treatment

By S. KHASHABA AND H. S. W. MASSEY

University College, London

*MS. received 18th November 1957*

**Abstract.** The distorted wave method is applied to the calculation of the cross sections for excitation of the 2p state of hydrogen by impact of electrons with energies between 13.5 and 54 eV. The polarization of impact radiation emitted from the 2p state when excited by an electron beam is also calculated.

Comparison of results obtained using the Born–Oppenheimer approximation shows that the effect of distortion on the total cross section is not as great as for the excitation of the 2s state. It is pointed out that coupling between the 2s and 2p states which has been neglected in all calculations may be important.

### § 1. INTRODUCTION

THE distorted wave method has been applied to the calculation of cross sections for excitation, by impact of slow electrons, of the 2s state of hydrogen (Erskine and Massey 1952), and the  $2^3S$  and  $2^1S$  states of helium (Massey and Moiseiwitsch 1951). On the whole the results obtained have been very encouraging and represent a great advance on those obtained by the use of the Born or Born–Oppenheimer approximations. This is particularly true for the helium states where the results obtained are in quite good agreement with experiment both as regards the magnitude of the cross section and its variation with electron energy near the threshold. For the 2s level of hydrogen it appears that at electron energies close to the threshold, the exchange coupling between the initial and final states is quite strong (Marriott 1957) and then the distorted wave approximation is not too satisfactory. These discrepancies occur when the zero order cross section (which is by far the most important at the low electron energies concerned), as given by the distorted wave method becomes comparable with the maximum possible value  $\pi/k^2$  where  $k$  is the wave number of the incident electron. In this connection it must be remembered that it by no means follows that when the Born or Born–Oppenheimer approximation to the cross section is small compared with  $\pi/k^2$  it is a good approximation. On the other hand, when the distorted wave method gives a small cross section it will be at least a fair approximation provided the distortion has been allowed for properly (Massey and Mohr 1952).

In this paper we extend the application of the distorted wave method to the excitation of the 2p states of atomic hydrogen. This is of interest for several reasons. Knowledge of the true form of the cross section is important for astrophysical and other applications. It may be that the distorted wave method gives

cross sections at certain electron energies which are close to the maximum possible in which case the result will be suspect, and the indication will be that the coupling is strong. This in itself would be very useful information. There is a further feature of interest which does not arise in the previous cases studied. This concerns the polarization of the resonance radiation excited by electron impact in hydrogen. Although measurements of polarization were carried out a long time ago (cf. Massey and Burhop 1950) for impact radiation in helium and other gases and vapours, there has been little attempt to provide an adequate theory. The polarization depends on the difference between the cross sections for excitation of p states with angular momenta respectively parallel and perpendicular to the incident electron beam. Distortion will affect the relative magnitudes of these two cross sections just as it affects the total cross section, and can be expected to give rather different results than those obtained by use of the Born or Born-Oppenheimer approximations.

## § 2. GENERAL FORMULATION—THE INTEGRO-DIFFERENTIAL EQUATIONS FOR THE PROCESS

The problem is considerably more complicated than for excitation of s states because of the angular dependence of the wave functions for the excited state. We may use the formulae derived by Percival and Seaton (1957, to be referred to as PS) in which a representation in terms of the total angular momentum (quantum number  $L$ ) and its  $z$ -component (quantum number  $M$ ) is employed.

Quantities referring to the atomic and colliding electrons are distinguished by suffices 1 and 2 respectively, while primed quantities refer to initial states and unprimed to final states. To avoid unnecessary generality we shall suppose at the outset that the only two atomic states concerned are the initial 1s state and the final 2p state. The existence of all other atomic states will be ignored as in the corresponding calculations for the excitation of the 2s level. We wish to obtain the cross sections  $Q(0)$  and  $Q(\pm 1)$  for the excitation in which the final value of the  $z$ -component of angular momentum of the atomic electron is 0 or  $\pm 1$  respectively.

When allowance is made for the antisymmetrical property of the electrons we have

$$Q(m_1) = \frac{1}{4}\{Q^+(m_1) + 3Q^-(m_1)\}, \quad \dots\dots(1)$$

the  $\pm$  signs distinguishing symmetrical and antisymmetrical orbital states. We may write now

$$Q^\pm(m_1) = \sum_{l_2} q_{l_2}^\pm(m_1), \quad \dots\dots(2)$$

i.e. in a series of partial cross sections corresponding to different total angular momentum quantum numbers  $l_2$  of the scattered electron. The distortion of the scattered partial waves with different  $l_2$  depends very markedly on  $l_2$ . The field of a hydrogen atom excited to a two-quantum state is only able to produce appreciable distortion for  $l_2=0$  or 1. We may therefore write

$$q_{l_2}^\pm(m_1) = q_{l_2,B}^\pm(m_1), \quad l_2 > 1, \quad \dots\dots(3)$$

$q_{l_2,B}^\pm(m_1)$  being the partial cross section given by the Born-Oppenheimer approximation. This of course supposes that in the cross sections for  $l_2 > 1$  distortion of the incident wave is not important. For atomic hydrogen this

distortion is only important for  $l_2' = 0$  and such incident partial waves do not appear for partial cross sections for  $l_2 > 1$ . It follows that we may write

$$Q^\pm(m_1) = Q_B^\pm(m_1) + q_0^\pm(m_1) - q_{0B}^\pm(m_1) + q_1^\pm(m_1) - q_{1B}^\pm(m_1). \quad \dots\dots (4)$$

The full analysis need therefore only be applied for  $l_2 = 0, 1$ .

Referring to PS, formula (26), we have

$$q_{l_2}^\pm(m_1) = \frac{\pi}{k^2} \left| \sum_{l_1 L} (2l_2' + 1)^{1/2} i^{l_2 - l_1} C_{m_1 m_2}^{l_1 l_2 L} C_{000}^{0 l_2' L} S_L^\pm(l_2, l_2') \right|^2. \quad \dots\dots (5)$$

The coefficients  $C$  are Clebsch-Gordan coefficients and  $S_L^\pm(l_2, l_2')$  is given in terms of the asymptotic forms, for large  $r$ , of certain radial functions.

For the cases  $l_2' = 0, 1$  in which we are concerned the following possibilities arise. Remembering that  $l_1 = 1$  we have

$$\begin{array}{lll} L=0, & l_2'=0, & l_2=1, \\ L=1, & l_2'=1, & l_2=0, 2, \\ L=2, & l_2'=2, & l_2=1, 3. \end{array}$$

For a given  $L$  the radial functions will be given by coupled integro-differential equations equal in number to the possible  $l_2'$  and  $l_2$  values. When  $L=0$  we have the simplest situation which we shall first discuss.

The radial functions for this case satisfy the equations (see PS (29))

$$\begin{aligned} & \left[ \frac{d^2}{dr^2} + \frac{2}{r} + k'^2 - 2y_0(2s, 2s, r) \right] F^\pm(k's, r) \\ & \quad \mp [2y_0(1s, k's, r) - (\tfrac{1}{4} + k'^2)(1s|k's)] P(1s, r) \\ & = -\frac{2}{\sqrt{3}} y_1(1s, 2p, r) F^\pm(kp, r) \mp \frac{2}{\sqrt{3}} y_1(1s, kp, r) P(2p, r), \quad \dots\dots (6) \end{aligned}$$

$$\begin{aligned} & \left[ \frac{d^2}{dr^2} - \frac{2}{r^2} + \frac{2}{r} + k^2 - 2y_0(2p, 2p, r) - \tfrac{4}{3} y_2(2p, 2p, r) \right] F^\pm(kp, r) \\ & \quad \mp [2y_0(2p, kp, r) + \tfrac{4}{3} y_2(2p, kp, r) - (\tfrac{1}{4} + k^2)(2p|kp)] P(2p, r) \\ & = -\frac{2}{\sqrt{3}} y_1(1s, 2p, r) F^\pm(k's, r) \mp \frac{2}{\sqrt{3}} y_1(2p, k's, r) P(1s, r). \quad \dots\dots (7) \end{aligned}$$

The notation is that of self-consistent field theory. Instead of the quantum numbers  $l_1', l_1$  the symbols  $s$  and  $p$  are used.  $r^{-1}P(2p, r)$  denotes the radial atomic function (normalized to unity) for the  $2p$  state.

$$\begin{aligned} y_\lambda(nln'l', r) &= r^{-(\lambda+1)} \int_0^r P(nl, r') P(n'l', r') r'^\lambda dr' \\ & \quad + r^\lambda \int_r^\infty P(nl, r') P(n'l', r') r'^{-(\lambda+1)} dr'. \quad \dots\dots (8) \end{aligned}$$

If  $n'l'$  is replaced by  $k'l'$  the function  $P(n'l', r')$  is replaced by  $F(k'l', r')$ . Finally,

$$(nl|kl) = \int_0^\infty P(nl, r') F(kl, r') dr'. \quad \dots\dots (9)$$

The required quantity  $S_0^\pm(1, 0)$  for this case is such that the proper solutions of (6) and (7) have the asymptotic form for large  $r$

$$F^\pm(k's, r) \sim -2ik'^{-1/2} [\sin k'r + \alpha^\pm \exp(ik'r)], \quad \dots\dots (10)$$

$$F^\pm(kp, r) \sim -k^{-1/2} \exp(ikr) S_0^\pm(1, 0). \quad \dots\dots (11)$$



According to the distorted wave method we have

$$S^{\pm}(1, 0) = \frac{4i}{\sqrt{3}} \int_0^{\infty} \mathcal{F}^{\pm}(kp, r) [\gamma_1(1s\ 2p, r) \mathcal{F}^{\pm}(k's, r) \pm \gamma_1(2p\ k's, r) P(1s, r)] dr, \quad \dots\dots(12)$$

where  $\mathcal{F}^{\pm}(k's, r)$ ,  $\mathcal{F}^{\pm}(kp, r)$  are proper solutions of the equations (6) and (7) respectively with the terms on the right-hand sides put equal to 0. They must have the asymptotic form

$$\mathcal{F}^{\pm}(k's, r) \sim k'^{-1/2} \exp(i\eta_0) \sin(k'r + \eta_0), \quad \dots\dots(13)$$

$$\mathcal{F}^{\pm}(kp, r) \sim k^{-1/2} \exp(i\zeta_1) \sin(kr - \frac{1}{2}\pi + \zeta_1). \quad \dots\dots(14)$$

In (12)  $\gamma_1(2p\ k's, r)$  is calculated from (8) with  $\mathcal{F}^{\pm}(k's, r)$  replacing  $F(k's, r)$ .

For  $L=2$ , in which the outgoing wave with  $l_2=1$  is also involved, the problem is further complicated by the existence of a coupling between the waves with  $l_2=1$  and  $l_2=3$ . We shall ignore this coupling as it is likely to lead to only a very small additional distortion at electron energies quite close to the threshold. This is because, if the reciprocal wave number  $1/k$  is large compared with atomic dimensions the centrifugal force when  $l_2=3$  reduces the wave amplitude near the atom to such small values that the overlap with the wave for which  $l_2=1$  is very small. Neglecting the coupling we have corresponding to (6) and (7) the equations, for  $L=2$ ,

$$\left[ \frac{d^2}{dr^2} - \frac{6}{r^2} + \frac{2}{r} + k'^2 - 2\gamma_0(1s\ 1s, r) \right] F(k'd, r) \mp \frac{2}{5}\gamma_2(1s\ k'd, r) P(1s, r) \\ = 2\sqrt{\frac{2}{15}} [\gamma_1(1s\ 2p, r) F(k2p, r) \pm \gamma_1(1s\ kp, r) P(2p, r)], \quad \dots\dots(15)$$

$$\left[ \frac{d^2}{dr^2} - \frac{2}{r^2} + \frac{2}{r} - k^2 - 2\gamma_0(2p\ 2p, r) - \frac{2}{25}\gamma_2(2p\ 2p, r) \right] F(kp, r) \\ \mp [2\gamma_0(2p\ kp, r) - \frac{2}{5}\gamma_2(2p\ kp, r) - (\frac{1}{4} + k^2)(2p|kp)] P(2p, r) \\ = 2\sqrt{\frac{2}{15}} [\gamma_1(1s\ 2p, r) F(k'd, r) \pm \gamma_1(2p\ k'd, r) P(1s, r)]. \quad \dots\dots(16)$$

The calculation of  $S_2^{\pm}(1, 2)$  then proceeds as for  $S_0^{\pm}(1, 0)$  but there are two further approximations which may be made. Comparing (16) with (7) we see that the distorted wave  $\mathcal{F}^{\pm}(k_{2p}p, r)$  for  $L=2$  only differs from that for  $L=0$  because of interaction terms in  $\gamma_2(2p\ 2p, r)$ ,  $\gamma_2(2p\ kp, r)$ . These terms, which essentially arise because of departures from spherical symmetry in the excited atomic wave function, are in general quite small. If we neglect them consistently then the final distorted waves may be taken the same for both  $L=0$  and  $L=2$ .

The second simplification is that the distortion of the incident wave can be neglected for  $l_2'=2$ , so that for  $L=2$

$$\mathcal{F}(k'd, r) = (\frac{1}{2}\pi r)^{1/2} J_{5/2}(k'r). \quad \dots\dots(17)$$

Referring to a table of Clebsch-Gordan coefficients we have

$$C_{000}^{110} = -\frac{1}{\sqrt{3}}, \quad C_{000}^{112} = \sqrt{\frac{2}{3}}, \quad C_{000}^{022} = 1, \quad C_{1-10}^{110} = \frac{1}{\sqrt{3}}, \quad C_{1-10}^{112} = \frac{1}{\sqrt{6}}, \quad \dots\dots(18)$$

so that

$$q_1^{\pm}(0) = \frac{16\pi}{9} \frac{1}{kk'^3} |I_0^{\pm} - 2I_{\frac{1}{2}}^{\pm}|^2, \quad \dots\dots(19)$$

$$q_1^{\pm}(\pm 1) = \frac{16\pi}{9} \frac{1}{kk'^3} |I_0^{\pm} + I_{\frac{1}{2}}^{\pm}|^2, \quad \dots\dots(20)$$

where

$$I_0^\pm = \int_0^\infty \mathcal{F}^\pm(kp, r) [y_1(1s\ 2p, r) \mathcal{F}^\pm(k's, r) \pm y_1(2p\ k's, r) P(1s, r)] dr, \quad \dots\dots (21)$$

$$I_2^\pm = - \int_0^\infty \mathcal{F}^\pm(kp, r) [y_1(1s\ 2p, r) \mathcal{F}^\pm(k'd, r) \pm y_1(2p\ k'd, r) P(1s, r)] dr. \quad \dots\dots (22)$$

$\mathcal{F}^\pm(kp, r)$  satisfies

$$\left[ \frac{d^2}{dr^2} - \frac{2}{r^2} + \frac{2}{r} + k^2 - 2y_0(2p\ 2p, r) \right] \mathcal{F}^\pm(kp, r) \\ \mp [2y_0(2p\ kp, r) - (\frac{1}{4} + k^2)(2p|kp)] P(2p, r) = 0, \quad \dots\dots (23)$$

vanishes when  $r=0$  and has the asymptotic form

$$\mathcal{F}^\pm(kp, r) \sim k^{-1/2} \exp(i\zeta_1^\pm) \sin(kr - \frac{1}{2}\pi + \zeta_1^\pm). \quad \dots\dots (24)$$

$\mathcal{F}^\pm(k's, r)$  satisfies

$$\left[ \frac{d^2}{dr^2} + \frac{2}{r} + k'^2 - 2y_0(2s\ 2s, r) \right] \mathcal{F}^\pm(k's, r) \\ \mp [2y_0(1s\ k's, r) - (\frac{1}{4} + k'^2)(2s|k's)] P(1s, r) = 0, \quad \dots\dots (25)$$

vanishes when  $r=0$  and has the asymptotic form

$$\mathcal{F}^\pm(k's, r) \sim k'^{-1/2} \exp(i\eta_0^\pm) \sin(k'r + \eta_0^\pm). \quad \dots\dots (26)$$

$\mathcal{F}^\pm(k'd, r)$  is as given in (17).

If  $\mathcal{F}^\pm(kp, r)$ ,  $\mathcal{F}^\pm(k's, r)$  are replaced by the corresponding undistorted functions  $(\pi r/2)^{1/2} J_{3/2}(kr)$ ,  $(\pi r/2)^{1/2} J_{1/2}(k'r)$  respectively, the formulae (19) and (20) reduce to those given by the Born-Oppenheimer approximation.

We must return now to consider  $q_0^\pm(0)$  which is obtained by considering the case  $L=1$ ,  $l_2'=1$ ,  $l_2=0, 2$ . As for  $L=2$  above we neglect the coupling between the  $l_2=0$  and  $l_2=2$  states, the justification being the same as in that case. The equations for the radial functions  $F^\pm(k'p, r)$ ,  $F^\pm(ks, r)$  then become, on appropriate substitution in PS (29),

$$\left[ \frac{d^2}{dr^2} - \frac{2}{r^2} + \frac{2}{r} + k'^2 - 2y_0(1s\ 1s, r) \right] F(k'p, r) \mp \frac{2}{\sqrt{3}} y_1(1s\ k'p, r) P(1s, r) \\ = \frac{2}{3} y_1(1s\ 2p, r) F(ks, r) \pm \{2y_0(1s\ ks, r) - (\frac{1}{4} + k'^2)(1s|ks)\} P(2p, r), \quad \dots\dots (27)$$

$$\left[ \frac{d^2}{dr^2} + \frac{2}{r} + k^2 - 2y_0(2p\ 2p, r) \right] F(ks, r) \mp \frac{2}{\sqrt{3}} y_1(2p\ ks, r) P(2p, r) \\ = \frac{2}{3} y_1(1s\ 2p, r) F(k'p, r) \pm \{2y_0(2p\ k'p, r) - (\frac{1}{4} + k^2)(2p|k'p)\} P(1s, r). \quad \dots\dots (28)$$

Following the same procedure as before we find

$$q_0^\pm(0) = \frac{3\pi}{k'^2} |S_1^\pm(0, 1)|^2 \quad \dots\dots (29)$$

$$S_1^\pm(0, 1) = -2i \int_0^\infty \mathcal{F}^\pm(ks, r) \left[ \frac{2}{3} y_1(1s\ 2p, r) \mathcal{F}^\pm(kp, r) \right. \\ \left. \pm \{2y_0(2p\ k'p, r) - (\frac{1}{4} + k^2)(2p|k'p)\} P(1s, r) \right] dr. \quad \dots\dots (30)$$

$\mathcal{F}^\pm(ks, r)$  is the solution which vanishes at  $r=0$ , of (28) with the right-hand side zero. It has the asymptotic form

$$\mathcal{F}^\pm(ks, r) \sim k^{-1/2} \exp(i\zeta_0^\pm) \sin(kr + \zeta_0^\pm). \quad \dots\dots (31)$$

The function  $\mathcal{F}^\pm(k'p, r)$  which is the appropriate solution of (27) with the right-hand side zero can be represented with sufficient accuracy by the undistorted wave

$$\mathcal{F}^\pm(k'p, r) = (\pi r/2) J_{3/2}(k'r). \quad \dots\dots (32)$$

## § 3. THE BORN-OPPENHEIMER APPROXIMATION

The cross sections  $Q_B^\pm(m_1)$  are given by (Corinaldesi and Trainor 1952),

$$Q_B^\pm(m_1) = \int_0^{2\pi} \int_0^\pi |f_B(m_1, \theta, \phi) \pm g_B(m_1, \theta, \phi)|^2 \sin \theta d\theta d\phi, \quad \dots\dots(33)$$

where

$$\begin{aligned} f_B(m_1, \theta, \phi) &= -768i\sqrt{2} \left\{ k' \delta_{0m_1} - k \sqrt{\left(\frac{4\pi}{3}\right)} Y_{1m_1}(\theta, \phi) \right\} K^{-2} (4K^2 + 9)^{-3}, \\ g_B(m_1, \theta, \phi) &= 8i\sqrt{2} k' \delta_{0m_1} \chi^{-4} (128 - 96C_4 - 32\chi C_3 - \chi^2 C_2) \\ &\quad - 2i\sqrt{2} \left\{ k' \delta_{0m_1} - k \sqrt{\left(\frac{4\pi}{3}\right)} Y_{1m_1}(\theta, \phi) \right\} \chi^{-3} (15\chi^2 D_1 + 48\chi D_2 + 128D_3). \end{aligned} \quad \dots\dots(34)$$

$$C_2 = 128(4K^2 + 9)^{-2},$$

$$C_3 = -\frac{1}{2} K^{-4} (4K^2 - 27)(4K^2 + 9)^{-1} + \frac{1}{8} K^{-5} (4K^2 - 9)X,$$

$$C_4 = \frac{K^{-6}}{192} (144K^4 - 232K^2 - 135) + \frac{K^{-7}}{256} (64K^6 - 112K^4 + 252K^2 + 135)X,$$

$$D_1 = \frac{1024}{5} (4K^2 + 9)^{-3},$$

$$D_2 = -4K^{-4} (4K^2 + 9)^{-2} (20K^2 + 27) + K^{-5} X,$$

$$D_3 = \frac{3}{32} K^{-6} (4K^2 + 9)^{-1} (16K^4 + 160K^2 + 135) + \frac{K^{-7}}{64} (16 - 120K^2 - 135)X,$$

$$X = \sin^{-1} \left( \frac{4K^2 + 3}{(4K^2 + 9)^{1/2} (4K^2 + 1)^{1/2}} \right) + \sin^{-1} \left( \frac{4K^2 - 3}{(4K^2 + 9)^{1/2} (4K^2 + 1)^{1/2}} \right),$$

$$\chi = 4k'^2 + 1,$$

$$K^2 = k^2 + k'^2 - 2kk' \cos \theta.$$

## § 4. THE POLARIZATION OF RESONANCE RADIATION

The relative magnitudes of the cross sections  $Q(0)$  and  $Q(\pm 1)$  is important in determining the degree of polarization of the radiation emitted from atoms excited to the 2p state by electron impact. The percentage polarization of the radiation observed at right angles to the electron beam is defined by

$$P = 100(I^{\parallel} - I^{\perp}) / (I^{\parallel} + I^{\perp}),$$

where  $I^{\parallel}$  and  $I^{\perp}$  are the intensities of the radiation with electric vector parallel and perpendicular to the beam.  $P$  may be expressed in terms of  $Q(0)$  and  $Q(\pm 1)$ , but care must be taken to include the statistical effect of fine and possibly also hyperfine structure. This has been reconsidered in detail by Percival and Seaton (to be published). They give reasons why, for the particular case of the 2p level of hydrogen, it is necessary to allow for fine but not hyperfine structure. This gives

$$P = 100 \frac{3(1-x)}{7+11x}, \quad \dots\dots(35)$$

where

$$x = Q(\pm 1)/Q(0). \quad \dots\dots(36)$$

If fine structure were also neglected the formula would become

$$P = 100(1-x)/(1+x). \quad \dots\dots(37)$$

## § 5. CALCULATION OF THE DISTORTED WAVE FUNCTIONS

For the 1s-2p excitation in hydrogen

$$k^2 = k'^2 - \frac{3}{4} \quad \dots\dots(38)$$

$k'$  and  $k$  being in atomic units. Numerical calculations were carried out for  $k' = 1.000, 1.200, 1.500, 2.000$  which covers a range of incident electron energy from 13.5 to 54 eV.

The functions required are  $\mathcal{F}^\pm(k's, r)$ ,  $\mathcal{F}^\pm(ks, r)$ ,  $\mathcal{F}^\pm(kp, r)$ . Of these the first is already available in approximate analytical form from the calculations of Massey and Moiseiwitsch (1950) on the elastic scattering of electrons by hydrogen atoms. Thus

$$\mathcal{F}^\pm(k's, r) = k'^{-1/2}(1 + (a^\pm)^2)^{-1/2}[\sin k'r + (a^\pm + b^\pm e^{-r})(1 - e^{-r}) \cos k'r], \quad \dots\dots(39)$$

where  $a^\pm$  and  $b^\pm$ , determined by the Hulthén variational method, are given for appropriate values of  $k'$  by Massey and Moiseiwitsch. The values of the phase shifts  $\eta_0^\pm$  are given in table 1.

A similar variational method was used to determine  $\mathcal{F}^\pm(ks, r)$ . This function is very similar to that for the motion of s electrons in the mean direct and exchange fields of a 2s hydrogen atom (Erskine and Massey 1951), so that a similar trial form was assumed.

$$\mathcal{F}^\pm(ks, r) = k^{-1/2}(1 + (c^\pm)^2)^{-1/2}[\sin kr(1 + d^\pm e^{-r}) + c^\pm(1 - e^{-r}) \cos kr]. \quad \dots\dots(40)$$

Table 1 gives the values found for  $c^\pm$ ,  $d^\pm$  and the phase shifts  $\zeta_0^\pm$  for appropriate values of  $k$ , using the Hulthén variational method.

The functions  $\mathcal{F}^\pm(kp, r)$  were calculated numerically by iterative solution of the corresponding integro-differential equations, using desk computation. Use of the variational method in these cases would have involved so much labour that the iterative method was considered the more practical. Table 1 gives the phase shifts  $\zeta_1^\pm$ . It will be seen that these are much smaller than  $\zeta_0^\pm$ , showing that the distortion is much less important. This will be manifest from table 2

Table 2. The Partial Cross Section  $q_0$  (in units  $\pi a_0^2$ )

$k'$ (A.U.)	$k$ (A.U.)	Exchange Neglected		Exchange Included			
		Born	DW	Symmetrical		Antisymmetrical	
				BO	EDW	BO	EDW
1.0	0.5	0.488	$2.45 \times 10^{-3}$	0.023	0.142	1.55	0.224
1.2	0.831	0.256	$1.76 \times 10^{-3}$	0.160	0.0160	0.361	0.051
1.5	1.225	0.0919	$1.50 \times 10^{-3}$	0.120	$8.36 \times 10^{-4}$	0.067	0.0121
2.0	1.803	0.0220	$0.66 \times 10^{-3}$	0.033	$5.03 \times 10^{-5}$	0.013	$1.93 \times 10^{-3}$

DW, distorted wave calculation ignoring all exchange interaction; EDW, distorted wave calculation with full allowance for exchange interaction; BO, Born-Oppenheimer approximation.

which compares the cross sections calculated by the Born-Oppenheimer approximation with those obtained using the distorted wave method. In table 1 data are given for distorted wave functions calculated neglecting exchange interaction.

## § 6. NUMERICAL RESULTS AND DISCUSSION

Having obtained the distorted wave functions the cross sections  $q_0(0)$ ,  $q_1(0)$ ,  $q_1(\pm 1)$  can be calculated without difficulty from the formulae (29), (19) and (20) respectively. Some of the calculations may be carried out analytically, but in many cases numerical integration was employed.



Table 1. Data relating to the Distorted Wave Functions

$k'$ (A.U.)	$k$ (A.U.)	$\mathcal{F}^{\pm}(k's, r)$		$\mathcal{F}^{\pm}(ks, r)$		$\mathcal{F}^{\pm}(kp, r)$										
		$\eta_0$	$\epsilon$	$d$	$\zeta_0$	$\zeta_0$	$\zeta_0$									
		0	0	0	0	0	0									
1.000	0.500	0.904	0.645	1.390	-0.6950	-0.7151	-4.333	-4.301	-4.352	2.545	2.535	2.521	0.67	0.17	1.61	
1.200	0.831	0.851	0.583	1.217	-1.9411	-1.4908	-2.668	-4.639	-4.4334	-5.142	2.047	2.162	1.930	0.90	0.36	0.95
1.500	1.225	0.783	0.546	1.027	-7.366	-6.228	-8.976	-10.174	-5.894	-11.489	1.706	1.731	1.682	0.84	0.81	0.90
2.000	1.803	0.694	0.542	0.826	+4.161	+4.077	+4.249	+2.933	+2.823	+3.050	1.332	1.332	1.329	0.76	0.79	0.72

0, exchange distortion neglected; +, symmetrical case; -, antisymmetrical case. Units are radians in each case.

Table 3. The Partial Cross Sections  $q_1(0), q_1(\pm 1)$  (in units  $\pi a_0^2$ )

$k'$	$k$	Exchange Neglected			Exchange Included								
		Symmetrical			Antisymmetrical								
		Born	DW	EDW	BO	EDW	EDW						
		0	$\pm 1$	0	$\pm 1$	0	$\pm 1$	0	$\pm 1$				
(A.U.)	(A.U.)												
1.0	0.5	0.277	0.041	1.1013	0.130	0.929	0.189	1.174	0.168 <sub>s</sub>	0.0073	0.0008	0.0036	0.0012
1.2	0.831	0.308	0.041	0.371	0.044	0.881	0.153	1.400	0.104	0.029 <sub>s</sub>	0.0002	0.0155	0.0034
1.5	1.225	0.167	0.019	0.117 <sub>s</sub>	0.010	0.381 <sub>s</sub>	0.053	0.305	0.031	0.039	0.0018	0.0211	0.0030
2.0	1.803	0.0519	0.005	0.0205	0.0015	0.090 <sub>s</sub>	0.010 <sub>s</sub>	0.040 <sub>s</sub>	0.0033	0.024	0.0017	0.0075	0.0007

The Born-Oppenheimer total cross sections were calculated by numerical integration from the formulae (33)–(34). The partial cross sections  $q_{0B}(0)$ ,  $q_{1B}(0)$ ,  $q_{1B}(\pm 1)$  were calculated from the formulae (29), (19) and (20), respectively, replacing all the distorted wave functions  $\mathcal{F}$  by the corresponding partial plane wave functions.

Table 2 gives the values for  $q_0$  and  $q_{0B}$  calculated for the various cases which arise. The most noteworthy feature is the almost complete annihilation of this partial cross section by the distortion. For both the symmetric and antisymmetric cases, in which exchange interaction is fully allowed for, and also when exchange is completely neglected,  $q_0$  is very small compared with  $q_{1B}$ . The distortion of the functions is such as to produce strong destructive interference in the integrand of the corresponding integral for the scattered amplitude.

Table 3 gives the values obtained for  $q_1(0)$ ,  $q_{1B}(0)$ ,  $q_1(\pm 1)$  and  $q_{1B}(\pm 1)$  for the various cases. Here the effect of distortion, though marked, is not so great. It will be noted that in all cases  $q_1(\pm 1)$  is small compared with  $q_1(0)$ .

Table 4 gives, for the various cases, the total cross sections  $Q(0)$ ,  $Q_B(0)$ ,  $Q(\pm 1)$ ,  $Q_B(\pm 1)$  for excitation of states with  $m=0$ ,  $m=\pm 1$  respectively and also the total cross sections  $Q(0)+2Q(\pm 1)$ ,  $Q_B(0)+2Q_B(\pm 1)$  for excitation of all states with  $n=2$ ,  $l=1$ . If  $Q^+$  and  $Q^-$  are the cross sections for the symmetrical and antisymmetrical cases, the observed cross section will be the weighted mean  $\frac{1}{4}(Q^++3Q^-)$  and this is also given for the Born-Oppenheimer and distorted wave approximations.

Finally, in table 5, the calculated percentage polarization of resonance radiation due to excitation of the 2p state by electron impact is given for the different approximations. In calculating this the formula (35) has been assumed.

Table 5. Percentage Polarization of Impact Radiation

$k'$ (A.U.)	Born	DW	BO	EDW
1.0	33.6	29.1	37.5	31.3
1.2	24.9	21.3	26.4	24.9
1.5	16.6	13.7	17.7	14.9
2.0	8.0	6.1	8.4	6.8

DW, distorted wave formula, exchange neglected; BO, Born-Oppenheimer; EDW, distorted wave formula including exchange distortion. The formula (35) has been assumed allowing for electron but not nuclear spin.

It will be apparent from tables 4 and 5 that the strong influence of the distortion on the cross section  $q_0$  (see table 2) is markedly diluted in the total cross section even for electron energies as low as 13.5 eV. Thus, referring to the last two columns of table 4 it will be seen that the effect of distortion reduces the Born-Oppenheimer cross section by a factor of about 2.1 for  $k'=1.0$  (13.5 eV) but at  $k'=1.2$  the reduction is only by about 1.2. Comparison of the data in the last two columns with that in the upper half of the table shows that the effect of exchange is comparable with that of distortion. Neither is as marked as for the excitation of the 2s level (Massey and Moiseiwitsch 1951, Erskine and Massey 1952, Marriott 1957). This is partly due to the fact that, for excitation of an optically allowed level, the series of partial cross sections converges very slowly because of the slow fall-off of the direct coupling potential with distance. Exchange and distortion effects are only important in the low order cross sections which contribute a relatively small amount to the whole.

Table 4. Total Cross Sections  $Q(0)$ ,  $Q(\pm 1)$  and  $Q = Q(0) + 2Q(\pm 1)$  (in units  $\pi a_0^2$ )

$k'$ (A.U.)	$k$ (A.U.)	Exchange Neglected				Exchange Included				Mean ( $\frac{1}{4}$ Sym. + $\frac{3}{4}$ Antisym.)			
		Born		Distorted Wave		Symmetrical		Antisymmetrical		BO		EDW	
		$Q(0)$	$Q(\pm 1)$	$Q(0)$	$Q(\pm 1)$	$Q(0)$	$Q(\pm 1)$	$Q(0)$	$Q(\pm 1)$	$Q(0)$	$Q(\pm 1)$	$Q(0)$	$Q(\pm 1)$
1.0	0.500	0.863	0.083	1.029	1.113	0.172	1.457	1.650	0.018	1.686	0.318	0.018	1.354
1.2	0.831	0.907	0.199	1.305	0.716	0.202	1.120	0.648	0.092	0.832	0.324	0.091	0.506
2.0	1.803	0.453	0.275	1.023	0.300	0.281	0.962	0.514	0.191	0.896	0.441	0.191	0.822
								0.390	0.240 <sub>s</sub>	0.871	0.362	0.240 <sub>s</sub>	0.843

The effect of exchange and distortion on the polarization of the resonance radiation is also very small for much the same reason.

More marked effects of distortion may arise in the excitation of optically allowed transitions in heavier atoms. The phase shifts in the incident and scattered partial waves which determine the partial cross sections  $q_1(0)$ ,  $q_1(\pm 1)$  might well be such as to increase  $q_1(\pm 1)/q_1(0)$  very substantially.

A case of special interest to investigate is that of the  $2^3P$  state of helium which can only be excited through exchange. The effect of distortion is likely to be more marked as the convergence of the series of partial cross sections will be much faster than for the case we have considered. Some experimental information is also available with which to check the results. This investigation is in progress.

Unlike the excitation of the  $2s$  level of hydrogen there is no evidence that the coupling between the  $1s$  and  $2p$  states is strong. All the partial cross sections are much smaller than the maximum allowed values. For  $k'=1$  the Born-Oppenheimer antisymmetrical cross section  $q_0(1.55\pi a_0^2)$  is a little more than half the maximum allowed value  $3\pi a_0^2$  but distortion reduces this by a factor of 7. But for one complication we would therefore feel that the final EDW values were a good approximation. The complication is that we have not allowed for the possibility of an important coupling arising via a strong coupling between the  $2s$  and  $2p$  states, nearly equal in energy. This requires examination of the coupled equations corresponding to (6), (7), (15), (16), (27) and (28) in which the  $2s$  state is included. It is not impracticable to deal with these equations using a fast electronic computer and a programme is being prepared to do this.

#### ACKNOWLEDGMENTS

We are indebted to Drs. M. J. Seaton and I. C. Percival for communicating their results to us prior to publication. Grateful acknowledgment must be made of the assistance rendered by Mrs. D. W. Sida, Mrs. Lawson and Mrs. Wallace in the extensive numerical work. In this connection we have also benefited from advice given us by Dr. R. A. Buckingham.

#### REFERENCES

- CORINALDESI, E., and TRAINOR, L., 1952, *Nuovo Cim.*, **9**, 940.  
 ERSKINE, G. A., and MASSEY, H. S. W., 1952, *Proc. Roy. Soc. A*, **212**, 521.  
 MASSEY, H. S. W., and BURHOP, E. H. S., 1950, *Electronic and Ionic Impact Phenomena* (Oxford: University Press), p. 82.  
 MASSEY, H. S. W., and MOHR, C. B. O., 1952, *Proc. Phys. Soc. A*, **65**, 845.  
 MASSEY, H. S. W., and MOISEWITSCH, B. L., 1951, *Proc. Roy. Soc. A*, **205**, 483.  
 MARRIOTT, R., 1957, *Proc. Phys. Soc. A*, **70**, 288.  
 PERCIVAL, I. C., and SEATON, M. J., 1957, *Proc. Camb. Phil. Soc.*, **53**, 654.



# The Boltzmann Equation in the Theory of Electrical Conduction in Metals

By D. A. GREENWOOD

Birkbeck College, University of London

*Communicated by R. E. Peierls; MS. received 14th November 1957, and in final form 6th January 1958*

**Abstract.** The motion of conduction electrons in a metal in an electric field, scattered by an irregular static potential, is considered; this model is applicable to the resistance due to lattice waves at high temperatures, and to imperfections at any temperature. In §2 the Boltzmann equation is re-derived without the customary perturbation theory, avoiding the usual necessity of averaging over phases of different electron states after repeated small time intervals. The assumption that the scattering centres are distributed at random in the crystal is alone sufficient. The theory is, however, still dependent on assuming that  $\hbar/\tau \ll kT$ , where  $\tau$  is the collision time, as is the usual perturbation theory. §3 gives a general formula for the conductivity of the model, not subject to any assumption. This helps to justify an argument by Landau according to which the usual theory is valid provided  $\hbar/\tau \ll \eta$ , where  $\eta$  is the cut-off energy of the Fermi distribution. No direct evaluation of the formula has been achieved.

## § 1. INTRODUCTION

THE Boltzmann equation, on which the quantum theory of electrical conduction in metals depends, is usually obtained by a calculation in which the scattering of electrons by phonons and lattice imperfections is treated as a perturbation. In setting up the equation, assumptions are made analogous to the 'Stosszahlansatz' of the kinetic theory of gases.

In § 2, a new derivation of the Boltzmann equation is given, for the case of scattering centres distributed at random in the metal. The steady-state equation is derived from the equation of motion of the density matrix, using the randomness of the scattering centres; the repeated averaging over phases which appears in the usual derivation is avoided.

This derivation is, however, subject to the same restriction,  $\hbar/\tau \ll kT$  where  $\tau$  is the collision time, which appears in the usual theory (Peierls 1934a). In real metals this condition is not satisfied at high temperatures, when  $\hbar/\tau$  and  $kT$  are of the same order of magnitude, or at low temperatures, when the temperature-independent part of the resistance due to impurity scattering remains. However, in both these cases more general considerations due to Landau apply (Peierls 1934b, 1955, §6.8). These show that, when the scattering is elastic, the condition  $\hbar/\tau \ll kT$  can be replaced by  $\hbar/\tau \ll \eta$  where  $\eta$  is the Fermi energy. Most metals easily satisfy this condition. In view of the detailed theory which has been based on the Boltzmann equation, and the close agreement with experiment it is possible to obtain (Ziman 1954), this argument is important. In § 3 an

explicit formula for the conductivity in an irregular static potential is considered. This elaborates the Landau argument. The formula has so far proved intractable to further calculation.

## § 2. THE DENSITY MATRIX AND THE BOLTZMANN EQUATION

Given the basic model of electrons moving independently in Bloch states  $\psi_{\mathbf{k}} = u_{\mathbf{k}} \exp(i\mathbf{k} \cdot \mathbf{r})$ , the usual approach to the theory of electrical conduction in metals is to set up the Boltzmann equation,

$$\left(\frac{\partial n}{\partial t}\right)_{\text{field}} + \left(\frac{\partial n}{\partial t}\right)_{\text{coll}} = 0, \quad \dots\dots(1)$$

for  $n(\mathbf{k}, t)$ , the number of electrons in the state  $\mathbf{k}$ . The first term on the left is the rate of change of  $n(\mathbf{k}, t)$  due to an applied field  $F$ ; the second term, representing the effect of the scattering of electrons by phonons and lattice imperfections, is calculated by second-order perturbation theory. The equation has a steady-state solution if terms in  $F^2$ , which correspond to the Joule heat, are neglected.

We shall restrict the discussion to the case of a large number of similar scattering centres, distributed at random in the crystal, and take the scattering potential to be

$$W(\mathbf{r}) = \sum_{\nu} \omega(\mathbf{r} - \mathbf{R}_{\nu}), \quad \dots\dots(2)$$

where  $\mathbf{R}_{\nu}$  ( $\nu = 1, 2, \dots, N$ ) are the position vectors of the scattering centres. This is a simple model for the resistance due to impurities. The model is also applicable to the scattering by lattice vibrations at high temperatures, when it is a good approximation to take electron-phonon collisions as elastic. We shall assume that the potential  $\omega(\mathbf{r})$  can be used in perturbation theory: a strong potential can be replaced by an equivalent pseudo-potential, which gives the same scattered wave when treated as a perturbation. (A recent discussion is given by Huang and Yang (1957).) We are concerned in this paper rather with the restrictions which arise from the number of the scattering centres.

The statistical distribution of electrons is properly described by a density matrix  $\rho$  (see, for example, ter Haar 1954) satisfying

$$i\hbar \frac{\partial \rho}{\partial t} = [H, \rho], \quad \dots\dots(3)$$

where  $H$  is the total Hamiltonian. The diagonal elements of  $\rho$  in the  $\mathbf{k}$ -representation give the probability of finding an electron in the state  $\mathbf{k}$ , i.e.  $n(\mathbf{k}, t)$ , so that the calculation of  $(\partial n / \partial t)_{\text{coll}}$  may be set out as a calculation on the matrix elements of  $\rho$ . Averaging over phases at  $t = 0$ ,  $\rho$  is diagonal. The effect of  $W$  over a small time interval  $t$  may then be found by applying second-order perturbation theory to (3). The change in the diagonal elements gives the well-known result

$$n(\mathbf{k}, t) - n(\mathbf{k}, 0) = \sum_{\mathbf{k}'} |(\mathbf{k}'|W|\mathbf{k})|^2 \{n(\mathbf{k}', 0) - n(\mathbf{k}, 0)\} \\ \times 2\{1 - \cos(E - E')t/\hbar\} / (E - E')^2. \quad \dots\dots(4)$$

This is valid for  $t < \tau$  say. The condition  $\hbar/\tau \ll kT$  appears when, in the usual

way, the resonance factor in the right-hand side of (4), which is of width  $\hbar/t$ , is replaced by a  $\delta$ -function, since  $n(\mathbf{k}', 0)$  varies sharply over an energy range  $kT$  near  $E = \eta$ .

At the same time, off-diagonal elements appear in the density matrix. In order to extend the calculation over a further small time interval, these off-diagonal elements must be set equal to zero, and, similarly, after each small time interval over which perturbation theory is applied. This procedure may be regarded as a repeated averaging over phases, or may be justified by the randomness of the potential (2). The off-diagonal elements  $(\mathbf{k}|\rho|\mathbf{k}')$  contain factors of the form  $(\mathbf{k}|W|\mathbf{k}'')(\mathbf{k}''|W|\mathbf{k}')$  and

$$(\mathbf{k}|W|\mathbf{k}'')(\mathbf{k}''|W|\mathbf{k}') = (\mathbf{k}|\omega|\mathbf{k}'')(\mathbf{k}''|\omega|\mathbf{k}') \sum_{\mu, \nu} \exp \{i(\mathbf{k}'' - \mathbf{k}) \cdot \mathbf{R}_\mu - i(\mathbf{k}'' - \mathbf{k}') \cdot \mathbf{R}_\nu\}, \quad \dots\dots (5)$$

Since the  $\mathbf{R}_\mu$  are random, the right-hand side above averages to zero (except when  $\mathbf{k}$  and  $\mathbf{k}'$  differ by a vector of the reciprocal lattice; in this case, however, the states have different energies and are not linked by the perturbation). The expression averages to  $N|(\mathbf{k}|\omega|\mathbf{k}'')|^2$  for  $\mathbf{k} = \mathbf{k}'$ , since then the  $N$  terms with  $\mu = \nu$  contribute.

Accepting this 'Stosszahlansatz' procedure, (4) gives at all times

$$\left(\frac{\partial n}{\partial t}\right)_{\text{coll}} = \frac{2\pi}{\hbar} \sum_{\mathbf{k}'} |(\mathbf{k}'|W|\mathbf{k})|^2 \{n(\mathbf{k}') - n(\mathbf{k})\} \delta(E - E'), \quad \dots\dots (6)$$

provided that  $\hbar/\tau \ll kT$ . In order of magnitude,  $\tau$  is given by

$$\frac{1}{\tau} = \frac{2\pi}{\hbar} \sum_{\mathbf{k}'} |(\mathbf{k}'|W|\mathbf{k})|^2 (1 - \cos \Theta) \delta(E - E'),$$

where  $\Theta$  is the angle between  $\mathbf{k}$  and  $\mathbf{k}'$ .

The other term in (1) is well known (Jones and Zener 1934). For an electric field  $(F, 0, 0)$

$$\left(\frac{\partial n}{\partial t}\right)_{\text{field}} = - \frac{eF}{\hbar} \frac{\partial n}{\partial k_x}.$$

Combining this with (6) we obtain the Boltzmann equation

$$\frac{2\pi}{\hbar} \sum_{\mathbf{k}'} |(\mathbf{k}'|W|\mathbf{k})|^2 \{n(\mathbf{k}') - n(\mathbf{k})\} \delta(E - E) = \frac{eF}{\hbar} \frac{\partial n}{\partial k_x}. \quad \dots\dots (7)$$

It will now be shown that it is possible to obtain the Boltzmann equation directly from (3), avoiding the familiar, but undesirable, 'Stosszahlansatz'. The Hamiltonian for an electron moving in the crystal is

$$H = H_0 + W - eFx,$$

where  $H_0$  is the Hamiltonian for an electron in the periodic lattice, so that (3) becomes

$$i\hbar \frac{\partial \rho}{\partial t} = [H_0, \rho] + [W, \rho] - eF[x, \rho]. \quad \dots\dots (8)$$

We may form matrix elements of (8) between states  $\mathbf{k}, \mathbf{k}'$  of the periodic lattice:

$$i\hbar (\mathbf{k}'|\dot{\rho}|\mathbf{k}) = (\mathbf{k}'|H_0\rho - \rho H_0|\mathbf{k}) + (\mathbf{k}'|W\rho - \rho W|\mathbf{k}) - eF(\mathbf{k}'|x\rho - \rho x|\mathbf{k}). \quad \dots\dots (9)$$

The term  $(\mathbf{k}'|x\rho - \rho x|\mathbf{k})$  may be written

$$\begin{aligned} (\mathbf{k}'|x\rho - \rho x|\mathbf{k}) &= \int u_{\mathbf{k}'}^* \exp(-i\mathbf{k}' \cdot \mathbf{r})(x\rho - \rho x)u_{\mathbf{k}} \exp(i\mathbf{k} \cdot \mathbf{r}) d\mathbf{v} \\ &= i \left( \frac{\partial}{\partial k_x} + \frac{\partial}{\partial k'_x} \right) \int u_{\mathbf{k}'}^* \exp(-i\mathbf{k}' \cdot \mathbf{r}) \rho u_{\mathbf{k}} \exp(i\mathbf{k} \cdot \mathbf{r}) d\mathbf{v} \\ &\quad - i \int \frac{\partial u_{\mathbf{k}'}^*}{\partial k_x} \exp(-i\mathbf{k}' \cdot \mathbf{r}) \rho u_{\mathbf{k}} \exp(i\mathbf{k} \cdot \mathbf{r}) d\mathbf{v} \\ &\quad - i \int u_{\mathbf{k}'}^* \exp(-i\mathbf{k}' \cdot \mathbf{r}) \rho \frac{\partial u_{\mathbf{k}}}{\partial k_x} \exp(i\mathbf{k} \cdot \mathbf{r}) d\mathbf{v}. \end{aligned}$$

At the edge of a band, there is a discontinuity in  $u_{\mathbf{k}}$  with respect to  $\mathbf{k}$ , but one-sided derivatives exist. The last two terms on the right-hand side can (with a suitable choice of phase factors in the  $u_{\mathbf{k}}$ ) be expressed in terms of matrix elements linking different bands. Such inter-band terms we shall everywhere neglect. Then (9) becomes

$$i\hbar(\mathbf{k}'|\dot{\rho}|\mathbf{k}) = (\mathbf{k}'|H_0\rho - \rho H_0|\mathbf{k}) + (\mathbf{k}'|W\rho - \rho W|\mathbf{k}) - ieF \left( \frac{\partial}{\partial k_x} + \frac{\partial}{\partial k'_x} \right) (\mathbf{k}'|\rho|\mathbf{k}). \quad \dots\dots (10)$$

If in (10) terms in  $F^2$  are neglected, a steady state is possible, and periodic boundary conditions can be imposed. We therefore replace  $\rho$  by its equilibrium value in the absence of an electric field,  $\rho_0 = f(H_0 + W)$ , where  $f$  is the Fermi function, in the term containing  $F$ ; then, using the completeness relation, (10) gives

$$\begin{aligned} \mathbf{k} \neq \mathbf{k}': \quad i\hbar\dot{\rho}_{\mathbf{k}'\mathbf{k}} &= (E' - E)\rho_{\mathbf{k}'\mathbf{k}} + \sum_{\mathbf{k}''} (W_{\mathbf{k}'\mathbf{k}''}\rho_{\mathbf{k}''\mathbf{k}} - \rho_{\mathbf{k}'\mathbf{k}''}W_{\mathbf{k}''\mathbf{k}}) \\ &\quad - ieF \left( \frac{\partial}{\partial k_x} + \frac{\partial}{\partial k'_x} \right) (\mathbf{k}'|\rho_0|\mathbf{k}), \quad \dots\dots (11a) \end{aligned}$$

$$\mathbf{k} = \mathbf{k}': \quad i\hbar\dot{\rho}_{\mathbf{k}\mathbf{k}} = \sum_{\mathbf{k}'} (W_{\mathbf{k}\mathbf{k}'}\rho_{\mathbf{k}'\mathbf{k}} - \rho_{\mathbf{k}\mathbf{k}'}W_{\mathbf{k}'\mathbf{k}}) - ieF \frac{\partial}{\partial k_x} (\mathbf{k}|\rho_0|\mathbf{k}). \quad \dots\dots (11b)$$

A subscript notation for matrix elements is used where it is convenient.

The solution of these equations depends on the initial conditions. It is simplest to consider a field  $F' = Fe^{\Gamma t}$ , where  $F$  is constant and  $\Gamma$  is small. Then at  $t = -\infty$  the system is in statistical equilibrium in the absence of a field, and the field is switched on gradually. When  $|t| \ll 1/\Gamma$ ,  $F'$  is essentially constant and equal to  $F$ .

We attempt to find solutions of (11) taking  $\rho = \rho_0 + F'g$  where  $g$  is to be independent of  $F$  and  $t$ , so that

$$\frac{\partial \rho}{\partial t} = \frac{dF'}{dt} g = \Gamma F' g.$$

Since  $[H_0 + W, \rho_0] = 0$ , the equations for  $g$  are

$$\begin{aligned} 0 &= (E' - E - i\epsilon)g_{\mathbf{k}'\mathbf{k}} + \sum_{\mathbf{k}''} (W_{\mathbf{k}'\mathbf{k}''}g_{\mathbf{k}''\mathbf{k}} - g_{\mathbf{k}'\mathbf{k}''}W_{\mathbf{k}''\mathbf{k}}) - ie \left( \frac{\partial}{\partial k_x} + \frac{\partial}{\partial k'_x} \right) (\mathbf{k}'|\rho_0|\mathbf{k}), \\ &\quad \dots\dots (12a) \end{aligned}$$

$$0 = \sum_{\mathbf{k}'} (W_{\mathbf{k}\mathbf{k}'}g_{\mathbf{k}'\mathbf{k}} - g_{\mathbf{k}\mathbf{k}'}W_{\mathbf{k}'\mathbf{k}}) - ie \frac{\partial}{\partial k_x} (\mathbf{k}|\rho_0|\mathbf{k}), \quad \dots\dots (12b)$$

where  $\epsilon = \hbar\Gamma$ . In (12b) a term  $i\epsilon g_{\mathbf{k}\mathbf{k}}$  has been left out; it can be seen to be unimportant. (12a) and (12b) are indeed independent of  $F$  and  $t$ . So far,



no important simplifications have been made. It would be easy, but lengthy, to write in (12) the inter-band terms we have dropped.

These equations we attempt to solve by a process of successive approximation. Let us suppose that, in the sum over  $\mathbf{k}''$  in (12a), the terms involving diagonal elements of  $g$  are most important, so that the sum may be replaced by the terms  $W_{\mathbf{k}\mathbf{k}'}(g_{\mathbf{k}\mathbf{k}} - g_{\mathbf{k}'\mathbf{k}'})$ . Then (12a) gives an expression for the non-diagonal elements of  $g$  in terms of the diagonal elements:

$$g_{\mathbf{k}'\mathbf{k}} = \frac{W_{\mathbf{k}\mathbf{k}'}(g_{\mathbf{k}'\mathbf{k}'} - g_{\mathbf{k}\mathbf{k}})}{E' - E - i\epsilon} + \frac{ie}{E' - E - i\epsilon} \left( \frac{\partial}{\partial k_x} + \frac{\partial}{\partial k_{x'}} \right) (\mathbf{k}' | \rho_0 | \mathbf{k}). \quad \dots\dots (13)$$

Using this for the non-diagonal elements in (12b) we find

$$0 = \sum_{\mathbf{k}'} |W_{\mathbf{k}\mathbf{k}'}|^2 \left\{ \frac{g' - g}{E' - E - i\epsilon} - \frac{g - g'}{E - E' - i\epsilon} \right\} - ie \frac{\partial}{\partial k_x} (\mathbf{k} | \rho_0 | \mathbf{k}) + \sum_{\mathbf{k}'} \frac{ie W_{\mathbf{k}\mathbf{k}'}}{E' - E - i\epsilon} \left( \frac{\partial}{\partial k_x} + \frac{\partial}{\partial k_{x'}} \right) (\mathbf{k}' | \rho_0 | \mathbf{k}) - \sum_{\mathbf{k}'} \frac{ie W_{\mathbf{k}'\mathbf{k}}}{E - E' - i\epsilon} \left( \frac{\partial}{\partial k_x} + \frac{\partial}{\partial k_{x'}} \right) (\mathbf{k} | \rho_0 | \mathbf{k}'), \quad \dots\dots (14)$$

where  $g, g'$  stand for  $g_{\mathbf{k}\mathbf{k}}, g_{\mathbf{k}'\mathbf{k}'}$ .

The first term on the right may be written

$$2\pi i \sum_{\mathbf{k}'} |W_{\mathbf{k}\mathbf{k}'}|^2 (g' - g) \delta(E' - E),$$

where the 'δ-function' comes from the familiar representation

$$\lim_{\epsilon \rightarrow 0} \epsilon / \{(E - E')^2 + \epsilon^2\} = \pi \delta(E' - E).$$

(The interpretation of this depends on the function having a finite width,  $\Delta E$  say, so that a number of  $\mathbf{k}$ -values are included in the sum. This restricts the time  $t$  for which  $\Gamma|t| \ll 1$  by the condition  $|t| \ll \hbar/\Delta E$ . We consider the case of a large crystal, so that  $\Delta E \rightarrow 0$ .)

The other terms in (14) involve matrix elements of  $\rho_0 = f(H_0 + W)$ . In the  $\mathbf{k}$ -representation,  $\rho_0$  is not diagonal, but an expansion of the matrix elements of  $\rho_0$  in terms of the matrix elements of  $W$  can be made:

$$(\mathbf{k}' | f(H_0 + W) | \mathbf{k}) = f(E) \delta_{\mathbf{k}\mathbf{k}'} + (\mathbf{k}' | W | \mathbf{k}) \frac{f(E) - f(E')}{E - E'} + \dots \quad \dots\dots (15)$$

The terms in this expansion can easily be obtained by expanding  $f(H_0 + W)$  as a power series in  $H_0 + W$ , and considering each term separately. The general term is given, for example, by Schafroth (1951). We shall work with the leading terms written down above, and, without important loss of generality, we may take  $(\mathbf{k} | W | \mathbf{k}) = 0$ .

By use of (15) it is possible to estimate the last two terms on the right-hand side of (14). The calculation (Appendix A) shows that they are of order of magnitude  $ieh(\partial f/\partial k_x)/\tau kT$  for  $E$  in the neighbourhood of the Fermi energy, the range of particular importance. They may therefore be neglected compared with the term  $ie(\partial f/\partial k_x)$  provided that  $\hbar/\tau \ll kT$ . Subject to this condition, (14) becomes

$$2\pi \sum_{\mathbf{k}'} |W_{\mathbf{k}\mathbf{k}'}|^2 (g_{\mathbf{k}'\mathbf{k}'} - g_{\mathbf{k}\mathbf{k}}) \delta(E' - E) = e \frac{\partial f}{\partial k_x}. \quad \dots\dots (16)$$

This, to our level of approximation, is equivalent to the Boltzmann equation (7).

On dimensional grounds, we might expect the convergence of the expansion (15) to depend on the factor  $(\hbar/\tau)/kT$ , and a factor related to the shape of the potential  $\omega(\mathbf{r})$ . This is confirmed by a calculation of higher terms in (15), using the model, and methods, of Appendix A. In principle, the latter factor can be handled. It appears therefore, that the effect of higher terms in the expansion is negligible when  $\hbar/\tau \ll kT$ .

A solution of (16), independent of the  $\mathbf{R}_{\nu}$ , may be obtained if  $|W_{\mathbf{k}\mathbf{k}}|^2$  is replaced by its mean value  $N|\omega_{\mathbf{k}\mathbf{k}}|^2$  obtained by averaging over the position vectors of the scattering centres. It is shown in Appendix B that this, in general, will be a good solution. This is not immediately obvious: the statistical deviation of  $|W_{\mathbf{k}\mathbf{k}}|^2$  from its mean value is of the same order as the mean. (The problem is equivalent to that of the 'random walk' in two dimensions.)

Using this solution, (13) gives a value,  $g_{\mathbf{k}'\mathbf{k}}^0$  say, for the non-diagonal matrix elements, i.e.  $g_{\mathbf{k}'\mathbf{k}}^0$  is the right-hand side of (13), with the values found from the Boltzmann equation (16) inserted for the diagonal elements  $g_{\mathbf{k}\mathbf{k}}$ . This is our first approximation. We use it, in the terms previously omitted from the sum in (12a), to obtain a corrected value

$$g_{\mathbf{k}'\mathbf{k}} = g_{\mathbf{k}'\mathbf{k}}^0 - \frac{1}{E' - E - i\epsilon} \sum_{\mathbf{k}''} (W_{\mathbf{k}'\mathbf{k}''} g_{\mathbf{k}''\mathbf{k}}^0 - g_{\mathbf{k}'\mathbf{k}''}^0 W_{\mathbf{k}''\mathbf{k}}). \quad \dots\dots (17)$$

(In the sum over  $\mathbf{k}''$ ,  $g_{\mathbf{k}\mathbf{k}}^0 = 0$ .) The correction terms, within the framework of approximation implied by the use of (15) and the neglect of inter-band effects, contain factors of the form  $W_{\mathbf{k}'\mathbf{k}''} W_{\mathbf{k}''\mathbf{k}}$ . Their mean value, averaged over the position vectors of the scattering centres, is therefore zero, by (5). It can be shown, however, that the deviation of the correction terms from their mean value is large, compared with the remaining terms in the equation. In justifying the method of successive approximation we have used, it is therefore more satisfactory to investigate the effect of the correction terms when (17) is inserted into (12b). It is straightforward, if tedious, to write down the new terms which appear. The model of Appendix A has been used to obtain an order of magnitude estimate of their effect. With this model, the expression simplifies considerably; if the cut-off energy, which in this model is necessary to avoid divergencies, is assumed to be of the order of magnitude of  $\eta$ , it is found that the terms are negligible provided that

$$\left(\frac{\hbar}{\tau}\right) \frac{V k_{\eta}^3}{N} \ll 1, \quad \dots\dots (18)$$

and the condition  $\hbar/\tau \ll kT$  is also satisfied. Here  $V$  is the volume of the crystal and  $k_{\eta}$  the wave-vector at the Fermi edge. If our model is applied at high temperatures, so that  $N$  is the total number of atoms in the crystal, this condition is easily satisfied. In fact, if (18) is rewritten in terms of the scattering cross section of a single centre, it is easily seen to be just the condition for first-order Born approximation to be valid for the scattering by one centre.

The total current is

$$\mathbf{J} = 2e \sum_{\mathbf{k}, \mathbf{k}'} (\mathbf{k}|\rho|\mathbf{k}') (\mathbf{k}'|\mathbf{v}|\mathbf{k}), \quad \dots\dots (19)$$

where  $\mathbf{v}$  is the velocity operator. Since  $(\mathbf{k}'|\mathbf{v}|\mathbf{k})$  vanishes unless  $\mathbf{k}$  and  $\mathbf{k}'$  differ by a vector of the reciprocal lattice, this reduces to

$$\mathbf{J} = 2e \sum_{\mathbf{k}} (\mathbf{k}|\rho|\mathbf{k}) (\mathbf{k}|\mathbf{v}|\mathbf{k}) \quad \dots\dots (20)$$

if inter-band effects are neglected. (20) is the expression for the current in the usual theory. Subject to the condition  $\hbar/\tau \ll kT$ , and neglecting inter-band effects, we have thus been able to derive the equations of the usual theory without a 'Stosszahlansatz' assumption. Instead, we have used directly the randomness of the scattering centres. This result for the steady-state equation is, in some respects, similar to the more general, but less explicit, results of Van Hove (1955, 1957) where the transport equation for the return to equilibrium of a quantum-mechanical system is obtained using the properties of matrix elements of the perturbing potential.

### § 3. GENERAL THEORY

The derivation of the Boltzmann equation given above is still subject to the restriction  $\hbar/\tau \ll kT$ . It has been pointed out that this is unsatisfactory, if the theory is to be applied to experimental results, and that it can be replaced by the condition  $\hbar/\tau \ll \eta$ , following an argument by Landau. If perturbation theory is carried out to fourth order in the potential  $W$  it is in fact found that the new effects are small provided only that  $\hbar/\tau \ll \eta$  (van Wieringen 1954) though this is not, in itself, conclusive.

The Landau argument depends on the fact that, independently of perturbation theory, the expression for the conductivity  $\sigma$  can be written in the form

$$\sigma = \int \phi(E) \frac{\partial f}{\partial E} dE, \quad \dots\dots (21)$$

when the scattering of electrons is elastic.  $\phi(E)$  can then be identified with the corresponding expression obtained by perturbation theory. Landau shows this without calculating  $\phi$  explicitly. It is possible, however, to derive an explicit expression for  $\phi$  starting from the equation of motion (3) of the density matrix. This is due to Peierls (unpublished), but no detailed proof has been given. Equivalent expressions have been obtained by Nakano (1956) and Kubo (1956). We outline below a proof for the independent electron model discussed in § 2, which is directly applicable to the Landau argument.

Introducing a constant external field  $(F, 0, 0)$  by the time-dependent vector potential  $(-cFt, 0, 0)$ , the one-electron Hamiltonian is

$$H(t) = \frac{1}{2m} \left\{ \left( \frac{\hbar}{i} \frac{\partial}{\partial x} + eFt \right)^2 + \left( \frac{\hbar}{i} \frac{\partial}{\partial y} \right)^2 + \left( \frac{\hbar}{i} \frac{\partial}{\partial z} \right)^2 \right\} + V(x, y, z), \quad \dots\dots (22)$$

where  $V$  is the potential function resulting from the periodic potential of the lattice and the random potential of the scattering centres. This choice of Hamiltonian avoids difficulties in imposing periodic boundary conditions.

We shall form matrix elements between eigenfunctions  $u_n(t)$  of the equation

$$H(t)u(t) = E(t)u(t) \quad \dots\dots (23)$$

solved subject to periodic boundary conditions. In (23),  $t$  enters merely as a parameter: the functions  $u_n(t)$  will be used as a convenient complete set. The states  $u_n(0)$ , however, are physically significant, and are just the stationary states of an electron in the crystal in the absence of an electric field. Such states must be strictly non-degenerate, so that the associated flow of charge is zero. The potential  $V$  would not otherwise give a finite resistance.

From (23) we have the well-known result

$$\begin{aligned}\int u_m^* u_n dv &= -\frac{(m|\dot{H}|n)}{E_m - E_n} (1 - \delta_{mn}) \\ &= -\frac{eF(m|v_x|n)}{E_m - E_n} (1 - \delta_{mn}), \quad \dots\dots (24)\end{aligned}$$

where the last step uses (22). (Equation (23) allows an arbitrary time-dependent phase factor in the  $u_n$ , which may be chosen to make  $\int u_n^* \dot{u}_n dv$  vanish.)

It is also easily verified that

$$H(t_1 + t) = \exp(-ieFtx/\hbar) H(t_1) \exp(ieFtx/\hbar)$$

so that

$$H(t_1 + t) \left\{ \exp\left(\frac{-ieFtx}{\hbar}\right) u_n(t_1) \right\} = E_n(t_1) \left\{ \exp\left(\frac{-ieFtx}{\hbar}\right) u_n(t_1) \right\}.$$

The set of functions  $\exp(-ieFtx/\hbar)u_n(t_1)$  satisfy periodic boundary conditions. if  $t = t_r = 2\pi\hbar r/eFL$  ( $r=0, 1, \dots$ ). Hence the eigenfunctions of (23) at times  $t_1 + t_r$  are (apart from phase factors) the set of functions  $\exp(-ieFt_r x/\hbar)u_n(t_1)$  with corresponding eigenvalues  $E_n(t_1)$ . The intervals  $T = 2\pi\hbar/eFL$  between these times will typically be short: if  $L = 1$  cm,  $F = 10^{-2}$  v cm $^{-1}$ , then  $T \sim 10^{-13}$  sec.

We form the matrix elements  $(n|\rho|m)$ , and differentiate with respect to  $t$ . Using the completeness relation,

$$\frac{d}{dt}(n|\rho|m) = \left(n \left| \frac{\partial \rho}{\partial t} \right| m\right) + \sum_l \int \dot{u}_n^* u_l dv (l|\rho|m) + \sum_l (n|\rho|l) \int u_l^* \dot{u}_m dv. \quad \dots (25)$$

With the equation of motion (3), and (24), (25) gives

$$\begin{aligned}\frac{d}{dt}(n|\rho|m) &= \frac{1}{i\hbar} (E_n - E_m)(n|\rho|m) + eF \sum_{l(\neq n)} \frac{(n|v_x|l)}{E_n - E_l} (l|\rho|m) \\ &\quad - eF \sum_{l(\neq m)} (n|\rho|l) \frac{(l|v_x|m)}{E_l - E_m}. \quad \dots\dots (26)\end{aligned}$$

We look now for solutions of this equation with  $\rho$  of the form  $\rho = f(H) + g$ , where  $g$  is of the order  $F$ , and consistently reject terms of order  $F^2$  which appear. The equations for matrix elements of  $g$  are then

$$n \neq m: \quad \frac{d}{dt}(n|g|m) = \frac{1}{i\hbar} (E_n - E_m)(n|g|m) - eF(n|v_x|m) \frac{f_n - f_m}{E_n - E_m}, \quad \dots\dots (27a)$$

$$n = m: \quad \frac{d}{dt}(n|\rho|n) = 0, \quad \dots\dots (27b)$$

where  $f_n = f(E_n)$ , and in (27a) the matrix elements of  $v_x$ , and the  $E_n$ , are taken at  $t=0$ .

Supposing the field to be switched on at  $t=0$ , equations (27) give on integration

$$(n|g|m) = i\hbar eF(n|v_x|m) \frac{f_n - f_m}{(E_n - E_m)^2} [1 - \exp\{(E_n - E_m)t/i\hbar\}],$$

$$(n|\rho|n) = f_n(0).$$



We therefore obtain an expression for the current,

$$\begin{aligned} J_x(t) &= 2e \sum_{m,n} \rho_{nm}(t) v_{mn}(t) \\ &= 2e \sum_n f_n(0) v_{nn}(0) + 2i\hbar e^2 F \sum_{n,m} v_{nm}(0) \left| \frac{f_n - f_m}{(E_n - E_m)^2} [1 - \exp\{(E_n - E_m)t/i\hbar\}] \right|. \end{aligned} \quad (28)$$

(Matrix elements are denoted by subscripts where this is convenient.)

We consider first the part  $2e \sum_n f_n(0) v_{nn}(t)$  of this expression. Using the properties of the eigenfunctions, it may be shown that  $v_{nn}(t)$  is an oscillatory function of  $t$ , period  $T$ , and its time average is zero. The apparent coherence of the 'ripple currents' due to different electrons comes from the sharp switching on of the electric field. If a field  $Fe^{t/\tau}$  is considered, as in § 2, no such coherence is possible, and the ripple current averages to zero at all times. The term has little physical significance in our problem, but is rather a reflection of our use of periodic boundary conditions. The current is therefore given by the last part of (28), i.e.

$$J_x(t) = -2Fe^2\hbar \sum_{m,n} |v_{mn}|^2 \frac{f_n - f_m}{E_n - E_m} \frac{\sin(E_n - E_m)t/\hbar}{E_n - E_m}. \quad (29)$$

We write  $\pi\delta(E_n - E_m)$  for the 'quasi- $\delta$ -function'  $\sin\{(E_n - E_m)t/\hbar\}/(E_n - E_m)$  and suppose the nature of the potential to be such that

$$\sum_n |v_{mn}|^2 \delta(E_n - E_m)$$

is insensitive to the width  $\hbar/t$  of the peak, provided that a large number of energy levels  $E_n$  are included. Then, over times  $\hbar/kT \ll t \ll \hbar/\Delta E$ , (28) gives a time-independent current, and hence a value for the conductivity,

$$\sigma = -2\pi e^2\hbar \sum_{m,n} |v_{mn}|^2 \left( \frac{\partial f}{\partial E} \right)_{E_n} \delta(E_n - E_m), \quad (30)$$

which may be rewritten in the form of (21),

$$\sigma = -2\pi e^2\hbar \int \sum_{m,n} |v_{mn}|^2 \delta(E - E_n) \delta(E - E_m) \frac{\partial f}{\partial E} dE. \quad (31)$$

The restriction  $t \ll \hbar/\Delta E$  is presumably related to the ergodic theorem.

The relation of (31) to the Landau argument makes it clear that the correct condition for the validity of conduction theory, as usually set out, is  $\hbar/\tau \ll \eta$ . One might hope to show, at least in the case  $\hbar/\tau \ll kT$ , that (31) gives a value for  $\sigma$  identical with the value given by the Boltzmann equation. It has not so far been possible to do this. Efforts to find a simple model for which the formula could be evaluated explicitly have not been successful.

#### ACKNOWLEDGMENTS

Much of this work was carried out at the Department of Mathematical Physics, University of Birmingham. I should like to thank Professor R. E. Peierls for his constant guidance and stimulus. I should also like to thank Professor Van Hove for a useful discussion. I am obliged to the Department of Scientific and Industrial Research for a maintenance grant.

## APPENDIX A

Order of magnitude estimates have been obtained by using free-electron states in place of Bloch states, so that  $E = \hbar^2 k^2 / 2m$ , and taking the scattering potential  $\omega(\mathbf{r})$  to be isotropic, i.e. taking  $\omega(\mathbf{r}) = \lambda \delta(\mathbf{r})$ . In fact,  $\omega(\mathbf{r})$  will, typically, extend over a distance of the order of an atomic radius  $R$ . We allow for this by cutting off integrals containing the Fourier transform  $(\mathbf{k}|\omega|\mathbf{k}')$  at an appropriate energy, wherever a cut-off is necessary to avoid a divergent integral. Since  $(\mathbf{k}|\omega|\mathbf{k}')$  will be appreciable only for  $|\mathbf{k} - \mathbf{k}'| \lesssim 1/R$ , the corresponding cut-off energy  $E_c$  will be of the same order of magnitude as the Fermi energy  $\eta$ , except in the case of a nearly empty band. With these simplifications, the expressions become amenable to calculation; it seems reasonable to suppose that the results are correct, in order of magnitude, for less special models.

With free electrons, (15) gives then

$$\left( \frac{\partial}{\partial k_x} + \frac{\partial}{\partial k_{x'}} \right) (\mathbf{k}' | \rho_0 | \mathbf{k}) = (\mathbf{k}' | W | \mathbf{k}) \left( \frac{\partial}{\partial k_x} + \frac{\partial}{\partial k_{x'}} \right) \left( \frac{f-f'}{E-E'} \right).$$

The last two terms on the right of (14) reduce to

$$\begin{aligned} & 2ie \sum_{\mathbf{k}'} |W_{\mathbf{k}\mathbf{k}'}|^2 \frac{E-E'}{(E-E')^2 + \epsilon^2} \left( \frac{\partial}{\partial k_x} + \frac{\partial}{\partial k_{x'}} \right) \left( \frac{f-f'}{E-E'} \right) \\ &= 2ieN\lambda^2 \frac{\partial E}{\partial k_x} \sum_{\mathbf{k}'} \frac{1}{(E-E')^2 + \epsilon^2} \left( \frac{\partial f}{\partial E} - \frac{f-f'}{E-E'} \right), \end{aligned}$$

averaging over the position vectors of the scattering centres; the terms involving  $\partial/\partial k_{x'}$  then cancel.

Replacing the sum by an integral, with a weighting factor  $V/(2\pi)^3$ , in the usual way, we have to evaluate

$$I = \int_0^\infty \frac{(E')^{1/2}}{(E-E')^2 + \epsilon^2} \left\{ \frac{\partial f}{\partial E} - \frac{f-f'}{E-E'} \right\} dE'.$$

The case of particular interest is  $E$  in the neighbourhood of  $\eta$ . We consider

$$I = \int_0^\infty \dots dE' = \int_0^{E-\Delta E} + \int_{E-\Delta E}^{E+\Delta E} + \int_{E+\Delta E}^\infty \dots dE' = I_1 + I_2 + I_3.$$

Taking  $\Delta E$  to be of order  $kT$ , then over most of the ranges  $(0, E-\Delta E)$ ,  $(E+\Delta E, \infty)$ ,  $|(f-f')/(E-E')|$  is small compared with  $|\partial f/\partial E|$ , and  $\epsilon$  is negligible; hence in these ranges we may approximate to the integrand by  $(\partial f/\partial E)(E')^{1/2}/(E-E')^2$ . This is a standard form, and it is easily verified that the two ranges give contributions to the integral of the order of  $(\partial f/\partial E)E^{1/2}/\Delta E$ .

In the range  $(E-\Delta E, E+\Delta E)$  we expand the integrand in powers of  $x = E' - E$  to give

$$I_2 = E^{1/2} \int_{-\Delta E}^{\Delta E} \left\{ \frac{1}{2} \frac{\partial^2 f}{\partial E^2} \frac{x}{x^2 + \epsilon^2} + \left( \frac{1}{6} \frac{\partial^3 f}{\partial E^3} + \frac{1}{4E} \frac{\partial^2 f}{\partial E^2} \right) \left( \frac{x^2}{x^2 + \epsilon^2} \right) + \dots \right\} dx.$$

The first term is odd, and does not contribute. In the higher terms,  $\epsilon$  is negligible. Since for  $E$  near  $\eta$ ,  $\partial^n f/\partial E^n \sim (kT)^{-1} \partial^{n-1} f/\partial E^{n-1}$ , we shall finally obtain

$$I_2 \sim (\partial f/\partial E) E^{1/2} \Delta E / (kT)^2.$$

Since  $\Delta E \sim kT$  the correction terms are thus of the order of

$$ieN\lambda^2 A (\partial f/\partial k_x) E^{1/2} / kT,$$

where, including all factors,  $A = V(2m/\hbar^2)^{-3/2}(2\pi)^{-2}$ . With the same model,

$$\frac{\hbar}{\tau} = \sum_{\mathbf{k}'} N\lambda^2 \delta(E - E') = N\lambda^2 A E^{1/2}.$$

Hence we have the result quoted in the text.

## APPENDIX B

From (5),

$$|W_{\mathbf{k}\mathbf{k}'}|^2 = N|\omega_{\mathbf{k}\mathbf{k}'}|^2 + |\omega_{\mathbf{k}\mathbf{k}'}|^2 \sum_{\mu \neq \nu} \exp\{i(\mathbf{k} - \mathbf{k}') \cdot (\mathbf{R}_\mu - \mathbf{R}_\nu)\}.$$

Averaged over the  $\mathbf{R}_\mu$ , the value of  $|W_{\mathbf{k}\mathbf{k}'}|^2$  is  $N|\omega_{\mathbf{k}\mathbf{k}'}|^2$ ; similarly, the average of  $|\{ |W_{\mathbf{k}\mathbf{k}'}|^2 - N|\omega_{\mathbf{k}\mathbf{k}'}|^2 \}|^2$  is  $N(N-1)|\omega_{\mathbf{k}\mathbf{k}'}|^4$ . This latter average may be interpreted as the square of the deviation, which is, therefore, of the same order as the mean.

We wish to solve (16), which may be written

$$2\pi \sum_{\mathbf{k}'} \{N|\omega_{\mathbf{k}\mathbf{k}'}|^2 + |\omega_{\mathbf{k}\mathbf{k}'}|^2 \sum_{\mu \neq \nu} \exp[i(\mathbf{k} - \mathbf{k}') \cdot (\mathbf{R}_\mu - \mathbf{R}_\nu)]\} (g' - g) \delta(E' - E) = e \frac{\partial f}{\partial k_x}. \quad \dots\dots (B1)$$

The solution of the equation obtained by averaging over the  $\mathbf{R}_\mu$ , i.e. the equation

$$2\pi N \sum_{\mathbf{k}'} |\omega_{\mathbf{k}\mathbf{k}'}|^2 (g' - g) \delta(E' - E) = e \frac{\partial f}{\partial k_x}, \quad \dots\dots (B2)$$

is of the form

$$g = G(E) \cos \theta, \quad \dots\dots (B3)$$

assuming an isotropic crystal, where  $\cos \theta = k_x/|\mathbf{k}|$ . If this solution is inserted in (B1), the terms left over are

$$\alpha = 2\pi G \sum_{\mathbf{k}'} \{ |\omega_{\mathbf{k}\mathbf{k}'}|^2 \sum_{\mu \neq \nu} \exp[i(\mathbf{k} - \mathbf{k}') \cdot (\mathbf{R}_\mu - \mathbf{R}_\nu)] (\cos \theta' - \cos \theta) \delta(E - E') \}.$$

The average value of  $\alpha$  is zero. The dispersion is of order  $\sqrt{(\alpha\alpha^*)}$ , where the bar denotes averaging over the  $\mathbf{R}_\mu$ . We show that (B3) is a good solution of (B1), in the sense that  $\sqrt{(\alpha\alpha^*)}$  is then small compared with the other terms in the equation. We have

$$\begin{aligned} \alpha\alpha^* &= (2\pi G)^2 \sum_{\mathbf{k}'} \sum_{\mathbf{k}''} |\omega_{\mathbf{k}\mathbf{k}'}|^2 |\omega_{\mathbf{k}\mathbf{k}''}|^2 (\cos \theta' - \cos \theta) (\cos \theta'' - \cos \theta) \\ &\quad \times \delta(E - E') \delta(E - E'') \sum_{\mu \neq \nu} \sum_{p \neq q} \exp\{i(\mathbf{k} - \mathbf{k}') \cdot (\mathbf{R}_\mu - \mathbf{R}_\nu) - i(\mathbf{k} - \mathbf{k}'') \cdot (\mathbf{R}_p - \mathbf{R}_q)\}. \end{aligned}$$

The summations over the position vectors average to zero, unless  $\mathbf{k}' = \mathbf{k}''$ , when they average to  $N(N-1)$ , so that

$$\begin{aligned} \overline{\alpha\alpha^*} &= N(N-1)(2\pi G)^2 \sum_{\mathbf{k}'} \sum_{\mathbf{k}''} |\omega_{\mathbf{k}\mathbf{k}'}|^2 |\omega_{\mathbf{k}\mathbf{k}''}|^2 (\cos \theta' - \cos \theta) (\cos \theta'' - \cos \theta) \\ &\quad \times \delta(E - E') \delta(E - E'') \delta_{\mathbf{k}'\mathbf{k}''}. \quad \dots\dots (B4) \end{aligned}$$

This is to be compared with the square of

$$\beta = 2\pi GN \sum_{\mathbf{k}'} |\omega_{\mathbf{k}\mathbf{k}'}|^2 (\cos \theta' - \cos \theta) \delta(E - E').$$

If there are  $n$   $\mathbf{k}$ -values corresponding to the energy shell  $E$ ,  $E + \epsilon$  ( $\epsilon$  is the width of the  $\delta$ -function), the effect of the  $\delta_{\mathbf{k}'\mathbf{k}''}$  in (B4) is to make  $\alpha\alpha^* \sim \beta^2/n$ , and  $n$ , in general, is a large number.

## REFERENCES

- TER HAAR, D., 1954, *Elements of Statistical Mechanics* (New York : Rinehart).  
HUANG, K., and YANG, C. N., 1957, *Phys. Rev.*, **105**, 767.  
JONES, H., and ZENER, C., 1934, *Proc. Roy. Soc. A*, **144**, 101.  
KUBO, R., 1956, *Canad. J. Phys.*, **34**, 1274.  
NAKANO, H., 1956, *Progr. Theor. Phys.*, **15**, 77.  
PEIERLS, R. E., 1934 a, *Z. Phys.* **88**, 786; 1934 b, *Helv. Phys. Acta*, **7**, suppl., 24; 1955, *Quantum Theory of Solids* (Oxford : Clarendon Press).  
SCHAFROTH, M. R., 1951, *Helv. Phys. Acta.*, **24**, 645.  
VAN HOVE, L., 1955, *Physica*, **21**, 517 ; 1957, *Ibid.*, **23**, 441.  
VAN WIERINGEN, J. S., 1954, *Proc. Phys. Soc. A*, **67**, 206.  
ZIMAN, J. M., 1954, *Proc. Roy. Soc. A*, **226**, 436.



# The Thermal Conductivity of Tin-Indium Alloys in the Normal State

By C. A. SHIFFMAN†

The Clarendon Laboratory, Oxford

*Communicated by K. Mendelssohn; MS. received 8th October 1957, and in final form 6th December 1957*

**Abstract.** Measurements have been made of the thermal conductivity in the normal state of ten alloys of tin with from two to eight per cent indium, over the range from 2 to 20°K. The samples with less than 3% indium satisfy the relation  $W = \rho_0/L_0T + \alpha T^2$  except at the lowest temperatures where a small lattice term lowers the thermal resistance. The more impure samples show a large lattice conductivity over the entire range. This is roughly parabolic below 4°K, but is linear in  $T$  from 5 to 16 or 17°K. The linear dependence is ascribed to scattering of phonons either by the local disorder in the lattice at the boundaries of mosaic domains or by stacking faults.

## § 1. INTRODUCTION

SINCE the transition to superconductivity frequently occurs where lattice waves are scattered predominantly by conduction electrons, the effect of the transition is often particularly noticeable in the phonon contribution to the thermal conductivity. Various studies of heat transport in superconductors have been undertaken in recent years with the object of separating and examining this contribution. So far no simple rules of behaviour have been deduced, other than the statement that (except at the lowest temperatures) the phonon conductivity in the superconducting state falls as the temperature rises. It is likewise only recently that most of the experimental work on the thermal conductivity of normal metals has been undertaken. In these cases good qualitative agreement with theory has been found, and accurate estimates of the roles of different conduction and scattering mechanisms have been obtained for many metals and alloys. In particular, increasing attention has been paid to the phonon contribution in alloys. It is the purpose of the present work to examine this component in the normal state of alloys which become superconductive, in order to allow a more exact estimate of the scattering mechanism to be expected for phonons in the superconducting state. In this paper we shall treat the normal state properties only, reserving for a later publication the correlation of normal and superconducting state results.

## § 2. SPECIMENS AND APPARATUS

In pure metals at low temperatures, and in the absence of large magnetic fields, the lattice conductivity  $K_g$  is generally much smaller than the electronic component  $K_e$  (cf. Olsen and Rosenberg 1953). Since  $K_e$  and  $K_g$  are essentially independent however (Hanna and Sondheimer 1957),  $K_g$  will become comparable with  $K_e$  when sufficient impurity has been added to the lattice to lower the

† Now at the National Bureau of Standards, Washington 25, D.C.

electronic term by a few orders of magnitude. If one wishes to preserve the crystal structure of the parent metal and avoid the complications of a mixed-phase system it is necessary to choose an alloy series which has a wide range of solid solubility. It is also desirable that single crystals of the alloys be used, and this puts a further restriction on the choice of system. The tin-indium alloys selected for these experiments satisfy these requirements moderately well. The solubility limit for the tin-rich  $\delta$  phase lies between six and seven per cent indium (Valentiner 1940, Rhines *et al.* 1947, see also Lee and Raynor 1954), high enough to ensure measurable lattice conductivities over a fairly wide range of concentrations. Also, single crystals can be grown in about one-half of the phase, as is discussed below.

Ten specimens with indium concentrations ranging from 2 to 8% were prepared from Johnson Matthey spectroscopically pure tin and 'Analar' (B.D.H.) indium whose purity was stated to be 99.9%. The alloys were melted, homogenized and cast into clean Pyrex tubes under high vacuum to avoid contamination. After the glass had been dissolved each ingot was placed in a simple 'gradient oven' for crystal growth. This process was then repeated with the specimen reversed in the oven, to avoid concentration gradients. The specimens were annealed *in vacuo* for 30 hours at 185°C before mounting in the apparatus. A brief description of each sample is given in the table.

The Sn-In Specimens				
	Number	Concentration (%) <sup>1</sup>	State <sup>2</sup>	Orientation (°) <sup>3</sup>
Group I	Sn-2	2.02	S.C.	90
	Sn-2'	2.02	S.C.	77
	Sn-2.1	2.11	S.C.	70
	Sn-2.5	2.45	S.C.	85
	Sn-2.8	2.84	F.S.	78
Group II	Sn-4	3.96	C.P.	— <sup>4</sup>
	Sn-5	4.97	C.P.	—
	Sn-5.7	5.65	C.P.	—
	Sn-6	5.96	C.P.	—
	Sn-8.2	8.20	F.P.	—

<sup>1</sup> The indium concentrations were determined by neutron activation and spectroscopic analyses. The neutron activation analyses also showed that the specimens were macroscopically homogeneous to within 2% of the indium content, the limit of accuracy of the method.

<sup>2</sup> S.C. single crystal; F.S. single crystal with about 5% of volume being inclusions of foreign orientation; C.P. coarse polycrystal with grain size about 2–3 mm; F.P. fine grained polycrystal, grains not visible to the eye.

<sup>3</sup> Angle between tetragonal axis and specimen axis as determined by optical goniometer methods.

<sup>4</sup> In agreement with the experience of Pippard (1955) and Weintraub (private communication) it was impossible to grow single crystals at these concentrations.

The experiments were done in the cryostat which had previously been used for thermal conductivity measurements by Olsen (1952) and by Rosenberg (1955). The differential gas thermometer method of determining the conductivity and the mean absolute temperature was used. Neglecting form factor considerations, calculation shows that the maximum total error in  $K$  should not exceed about 1%.

This conclusion is supported by the observed scatter in the data and by the good correlation between the electrical and thermal measurements. Whilst inaccuracies of this size are quite invisible in the usual  $(K, T)$  graphs they do become significant when plotting the quantities  $WT$  and  $K/T$  which are used to derive the lattice component of the conductivity. For this reason all data taken in the liquid helium region have been corrected for the non-ideality of the gas thermometers, even though this correction is quite small with the filling pressures used (Keesom 1942).

### § 3. THE EXPERIMENTAL RESULTS

The electrical resistance of each specimen was measured at several temperatures below  $4.2^\circ\text{K}$  and was found to be constant within the experimental error, about  $\frac{1}{2}\%$ . (Superconductivity was quenched by a longitudinal magnetic field of a few hundred gauss where necessary. Magnetoresistance was negligible.) Figure 1 shows the ratio of this residual resistivity  $\rho_0$  to the Lorenz number  $L_0$  as a function of indium concentration. (This ratio converts the resistivity to units of  $T/K$  which we shall find more convenient in what follows.) The graph is linear

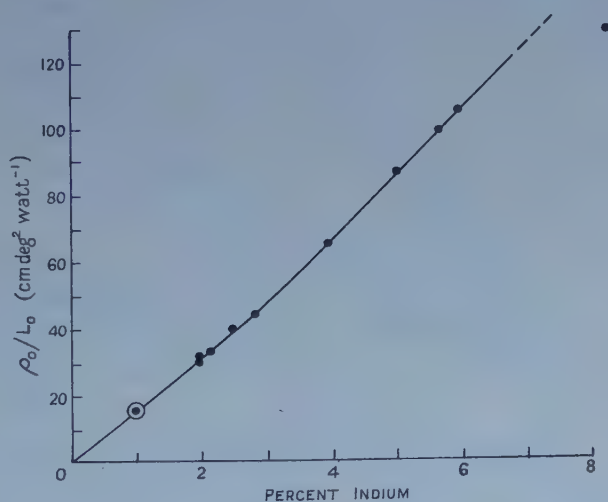


Figure 1. The residual resistivity divided by the Lorenz number, as a function of indium concentration.

through the origin up to 3% indium, where it starts to curve upwards. Between 4% and 6% the plot is once again linear, but no longer through the origin, while the 8.2% point lies well below the extrapolation of the second linear region. Figure 1 also includes the  $\rho_0/L_0$  value of a 1% alloy measured by Rosenberg.<sup>†</sup> This point is indicated by a double circle; evidently there is good agreement with his result.

An overall view of the thermal conductivities is given in figure 2. It is immediately evident that even 2% of indium is sufficient to displace the maximum, characteristic of the conductivity of pure metals, to temperatures well above the normal boiling point of hydrogen. In the case of the more impure specimens it

<sup>†</sup> We are indebted to Dr. Rosenberg for allowing us to use this result prior to publication.

is likely that the maximum does not exist at all. Qualitatively, however, the principal features found in pure metals are also found here. At the lowest temperatures the conductivity is linear through the origin, in accordance with the well-known rule for electronic conduction with scattering by impurities,

$$K = L_0 T / \rho_0. \quad \dots\dots(1)$$

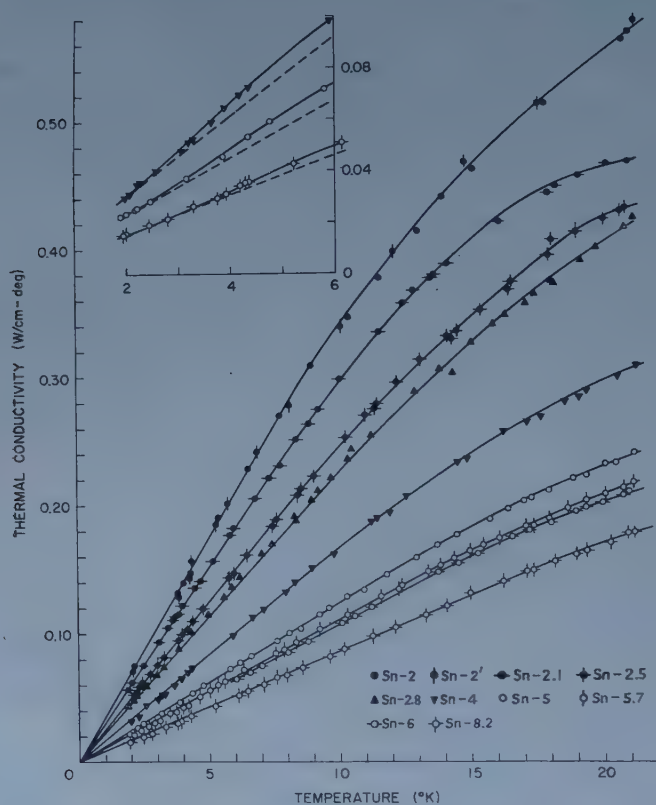


Figure 2. The thermal conductivity of the tin-indium alloys as a function of temperature.

As we shall see in more detail below, substitution of the values of  $\rho_0$  shown in figure 1 into this relation gives the observed slopes, except in the case of the most impure specimens. At higher temperatures the conductivity increases less rapidly, demonstrating that lattice vibrations have become effective in limiting the electronic mean free path.

The principal deviation from this description occurs below 5 or 6°K in the data for the most impure specimens. (The data for Sn-6 have been omitted in this region for the sake of clarity. The behaviour of this specimen closely follows Sn-5.7.) Here the conductivity lies discernibly below the extrapolation of the linear region, down to at least 2°K. The state of affairs is shown more clearly in the inset of figure 2 where, to avoid the confusion of overlap, data are presented for only three specimens. Smooth curves have been drawn through the measured points, while the broken lines represent equation (1) with the appropriate values of  $\rho_0$ . Evidently the conductivity above 5°K is larger than the theoretical prediction, rather than the conductivity below this temperature



lying lower than equation (1) predicts. Since this equation deals only with the electronic contribution, we are led to infer that these positive deviations represent a growing lattice term. The linear dependence observed above 5°K must therefore be connected with this phonon component, at least in part.

Frequently the thermal resistance  $W=1/K$  proves a more valuable quantity in the analysis of conductivity data. In particular, when heat transport is entirely electronic the resistance should have the form (Makinson 1938)

$$W = \rho_0/L_0 T + \alpha T^2 \quad \dots\dots(2)$$

where the first term represents scattering by impurities and the second scattering by lattice vibrations. Accordingly, a plot of  $WT$  against  $T^3$  should be a straight line with intercept  $\rho_0/L_0$  and slope  $\alpha$ . This relationship has been observed for many metals and alloys, although quantitative agreement has not been found. Figure 3 shows this plot for a number of the Sn-In Alloys. The first group, with impurity concentrations less than 3%, shows the expected behaviour over much of the range, but not at the lowest temperatures. A pronounced minimum exists in the  $WT$  values for the two 2% samples, while the more impure members of the group apparently have two linear regions with different slopes in each case. All the curves extrapolate to the measured values of  $\rho_0/L_0$ , and this is also true for the high temperature linear regions.

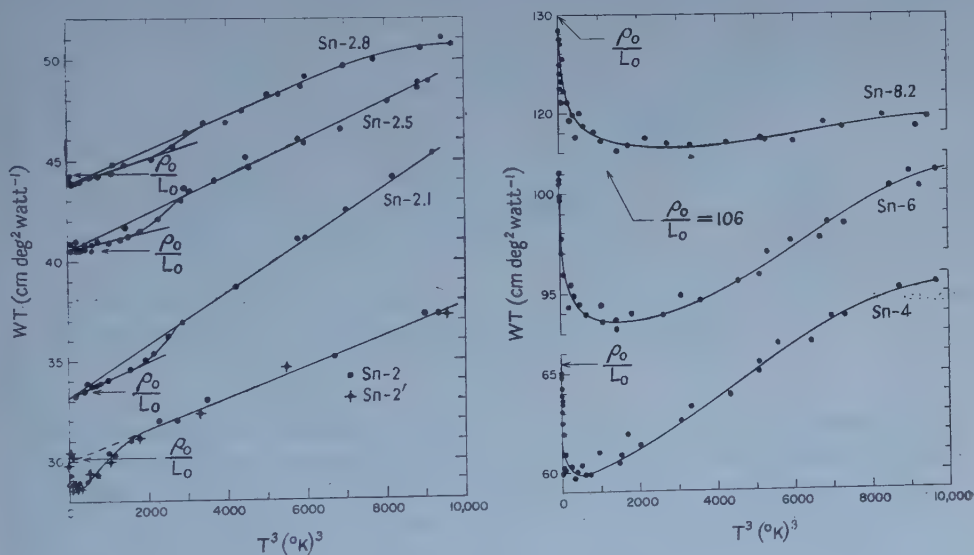


Figure 3.  $WT$  as a function of the cube of the temperature.

The second group presents a more complicated picture. For the specimens with indium concentration greater than about 4% the dominant feature of the  $WT$  curves is the strong minimum at low temperatures and the subsequent rise which becomes less pronounced with increasing impurity. (The curves for Sn-5 and Sn-5.7 follow the same trend; they have been omitted from the figure for the sake of clarity.) The rise at high values of  $T^3$  might be construed as the

linear region predicted by (2), but extrapolation to the  $WT$  axis shows that this interpretation is very tenuous; the intercepts obviously fall far below the experimental values of  $\rho_0/L_0$ . One must conclude that the values of  $WT$  lie considerably lower than equation (2) predicts. These deviations correspond directly with those observed in the  $(K, T)$  plots of the inset to figure 2 and support the conclusion drawn earlier, that the electronic heat conduction is supplemented by an appreciable lattice term.

Over the range of these measurements the dominant scattering mechanism for phonons is expected to be the interaction with conduction electrons, although impurity and *umklapp* scattering must play an increasing role with rising temperature. The electron-phonon interaction alone gives a lattice conductivity  $K_g = AT^2$ , where  $A$  is a constant characteristic of the metal (Makinson 1938; see also Olsen and Rosenberg 1953). On the other hand, the  $(WT, T^3)$  curves for the second group show that as a first approximation the electronic conductivity is limited mainly by the impurities. Then, since these components are additive, we have for the total conductivity

$$K = \frac{L_0 T}{\rho_0} + AT^2. \quad \dots\dots(3)$$

Accordingly, a plot of  $K/T$  against  $T$  should yield a straight line with intercept  $L_0/\rho_0$  and slope  $A$ . Such a graph is shown in figure 4 for Sn-4 as an example.

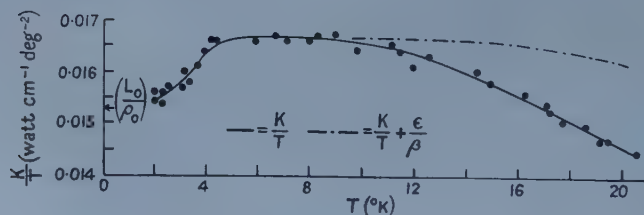


Figure 4.  $K/T$  plotted against  $T$  for Sn-4; an example of the procedure for deriving the lattice conductivity.

With the exception of Sn-8.2, all the specimens of the second group exhibit the same qualitative behaviour. Below 4 or 5°K the curves are conceivably linear, but the scatter does not justify a definite conclusion. In any event, the best straight lines which can be drawn do not intercept the  $K/T$  axis at the corresponding values of  $L_0/\rho_0$ , but much lower. Above 4°K the curves break off sharply and become nearly temperature independent until about 9 or 10°K, beyond which there is a gradual decline. Thus, the agreement with (3) is doubtful. It is interesting to note that Garfinkel and Lindenfeld (1957) have found that  $K_g$  in a 3% In alloy is accurately quadratic with temperature, but in a specimen which was annealed for more than 500 days.

Before pursuing this conclusion further there are two refinements which should be made to equation (3). Obviously, the approximation  $AT^2$  for  $K_g$  is inadequate, and secondly we must take into account the fact that the electronic component should include the small but significant lattice scattering term.

It is easy to show that if the electronic thermal resistance satisfies equation (2) and if  $\alpha T^2$  is small compared with  $\rho_0/L_0$  then (3) becomes

$$K/T = (1 - \epsilon)/\beta + K_g/T. \quad \dots\dots(4)$$

where  $\epsilon = \alpha T^3/\beta$  and  $\beta = \rho_0/L_0$ . From figure 3 it is evident that the required  $\alpha$  values cannot be determined from the results on the Group II specimens. Instead, we make use of the observation by Rosenberg (1955) that for chemically similar metals the quantity  $\alpha K_\infty \theta_D^2 = F$  is constant to within about 10% where  $K_\infty$  is the limiting value of the conductivity when  $T \gg \theta_D$  and where  $\theta_D$  is the Debye characteristic temperature. We note also that our Group I specimens satisfy this relation† and yield values for  $F$  in good agreement with Rosenberg's for pure tin. Accordingly, we have derived values for  $\alpha$  for the more impure specimens, using for  $F$  the average observed for the purer ones. With these it is easily proved that the conditions for (4) are satisfied quite well over most of the temperature range. This equation then shows that in order to interpret the difference between the curve for  $K/T$  and  $L_0/\rho_0$  as  $K_g/T$  it is first necessary to add  $\epsilon/\beta$  to the plotted points. The result of this correction is shown in figure 4 by the broken curve. It is now evident that  $K_g/T$  is substantially constant from 5 to 15°K or more, falling off only very slowly thereafter. In other words, the lattice conductivity is proportional to  $T$  over a range of three to one of the absolute temperature. Similar corrections have been made for the other specimens of the second group. The results are given in the  $(K_g, T)$  graphs of figure 5. Because

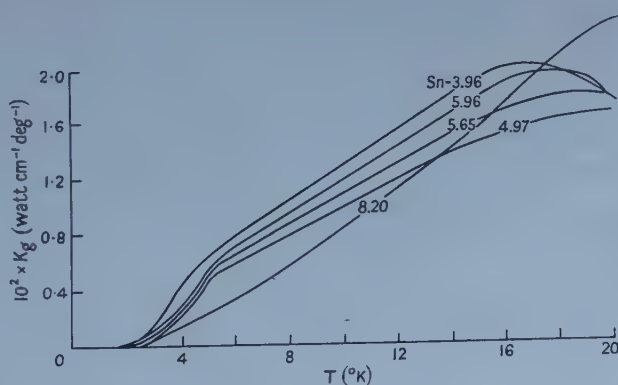


Figure 5. The derived lattice conductivities as a function of temperature.

of the scatter in the data below 5°K the curves shown in that region are not derived in detail from the  $K/T$  plots, but are represented schematically. With the exception of Sn-8.2, each of the samples has a linear  $K_g$  over a wide range followed by a maximum near 18°K. There is no correlation between the magnitude of  $K_g$  and indium concentration, nor any simple rule for the range of linearity. The 8% sample shows quite different behaviour, a consequence of the fact that the  $K/T$  graph for this specimen has no constant region but rises monotonically throughout the range of measurement.

† Except for Sn-2.1 where  $F$  is about 50% too large. This might be due to the complicated zone structure determined by Lee and Raynor (1954). Also, the  $\alpha$  values used in these calculations are taken from the high temperature regions of figure 3. See below for further discussions of this point.



## § 4. DISCUSSION

The first linear region of the residual resistance graph (figure 1) is qualitatively what one expects from a simple gas-kinetic model. Similar results have been obtained for this alloy series by Pippard (1955) and by Doidge (1956). Above 3% In the curve becomes concave upward, however. While the magnitude of this deviation is only about 10% (at 6% In) the direction is the opposite of what one expects at first sight. Nordheim (1931) has shown that in a homogeneous disordered binary alloy  $\rho_0$  should be proportional to  $x(1-x)$ , where  $x$  is the solute concentration. This formula leads to an inclination of the  $\rho_0$  curve towards the concentration axis, and shows that the effect should be quite negligible even at 6% In. Pippard (1953) has shown that the residual resistance of a 3% indium-tin alloy is 14% larger when the direction of current flow is parallel to the tetragonal axis of the crystal than when the current is perpendicular. Examination of the present specimens has shown, however, that most of the visible grains have their tetragonal axis inclined by at least 70% to the specimen axis. It follows from a necessarily crude calculation that the anisotropy correction should not exceed 3% of  $\rho_0$ . Therefore most of the observed deviations from linearity must be due to some additional scattering mechanism which becomes noticeable only after about 3% In is added. It is possible that dislocations, stacking faults or other large scale lattice defects are responsible. Another possibility is that at these high impurity densities large numbers of vacancies or other point defects are created which lead to an increased resistance. When one considers that at 3% In the nearest indium-indium separation is only a little over two unit cell dimensions, and that the indium ion is 20% larger than the tin which it replaces, a rapid multiplication of lattice defects does not seem unreasonable. Doidge's measurements also extend to 6% In, but unfortunately the scatter of his points precludes a comparison with our results in this regard. The remaining feature of interest in figure 1 is the position of the 8.2% point. The residual resistance corresponds to an In concentration of about 7%, i.e. the solubility limit. Similar behaviour has been observed in several other tin alloy systems (Serin and Lohman 1953) and an analogous result has been obtained by Rosenberg (1955) in slightly impure iron.

The principal feature of the lattice conductivities in the second group of specimens is the linear dependence on temperature from 5 to 16 or 17°K. In this range one usually finds (cf. Klemens 1956) first a  $T^2$  dependence, corresponding to electronic scattering and then, as the temperature is raised, an admixture of  $T^{-1}$  and an exponential law, corresponding to scattering by point defects and *umklapp* processes respectively. A mechanism which results in a linear dependence is the scattering of phonons from small angle grain boundaries, as proposed by Pomeranchuk (1942) and further developed by Klemens (1955). Various crystallographic and metallurgical studies lead to the conclusion that real crystals are composed of blocks of the order of microns or less on a side, with adjacent blocks differing slightly in orientation (cf. Hirsch 1956). This system, called a mosaic structure, ensures many small angle boundaries even in 'single crystals' or coarse grained polycrystals. Klemens has calculated the scattering of phonons by such a structure using a model wherein rows of edge dislocations represent the mosaic boundaries. On this basis the scattering is analysed into two parts, (i) scattering by the disorder in the immediate neighbourhood of a boundary and (ii) scattering by the long range strain field, i.e. the



misorientation of adjacent domains. The relaxation times for these processes are

$$\tau_d \simeq \frac{VG_2}{\omega^2 a \gamma^2} \left( \frac{b}{H} \right)^{-2} \quad \dots\dots(5)$$

and

$$\tau_s \simeq \frac{36aG_2}{V\gamma^2} \left( \frac{b}{H} \right)^{-2} \quad \dots\dots(6)$$

where  $\omega$  is the phonon frequency,  $v$  the phonon velocity,  $a$  the average lattice spacing,  $G_2$  a constant indicating the density of boundaries,  $b/H$  essentially the angle of misfit of adjacent domains, and  $\gamma$  is the Grüneisen factor. The strain field gives rise to a relaxation time  $\tau_s$  (eqn (6)) which is independent of  $\omega$ , and hence the conductivity limited by this mechanism alone is proportional to  $T^3$ . The disorder close to the boundary results in a relaxation time  $\tau_d$  (eqn (5)) which varies as  $\omega^{-2}$ . The lattice conductivity limited by disorder scattering along  $\tau$  is then proportional to  $T$ . Which of these terms will dominate is given by the ratio

$$\frac{\tau_d}{\tau_s} \sim \frac{\omega^{-2} V^2}{36a^2} \quad \dots\dots(7)$$

If we use the Debye model and substitute for  $\omega$  the dominant phonon frequency, equation (7) becomes

$$\frac{\tau_d}{\tau_s} \sim 2.3 \times 10^{-4} \left( \frac{\theta_D}{T} \right)^2, \quad \dots\dots(8)$$

that is,  $\tau_d \ll \tau_s$  and scattering by local disorder dominates, unless  $\theta_D/T$  is very large. The condition  $\tau_d \sim \tau_s$  is  $\theta_D/T \sim 63$ . With 185°K as the average value for  $\theta_D$  for tin in the range up to 4°K (Corak and Satterthwaite 1956)† the condition  $\tau_d \sim \tau_s$  is further reduced to  $T \sim 3^\circ\text{K}$ . Therefore for temperatures above 3°K we expect the local disorder to predominate in the scattering of phonons and the conductivity to vary linearly with temperature. More recently Klemens (1957) has shown that stacking faults also result in a linear  $K_g$ . Unfortunately it is impossible to calculate the relaxation times in either case, so no comparison of magnitudes with the experimental results can be made at the present time.‡

There remain a few features of figure 5 which merit attention here. In the region just below 5°K there must be a mixture of electronic and mosaic or stacking fault scattering terms of roughly the same size, a fact which explains the absence of a clear-cut electronic term in the  $(K/T, T)$  graphs. Similarly, at the highest temperatures we must expect a very complex phonon conductivity as the mosaic or stacking fault term becomes progressively subdued by point imperfection and *umklapp* scattering. For this reason the region above 16 to 17°K yields curves which cannot be fitted to any simple scheme of explanation. Secondly, it is significant that the magnitude of  $K_g$  in the linear range does not depend on the indium concentration. Probably there is some connection between the magnitudes and the thermal and mechanical history of each specimen. It is interesting that all samples were subjected to what was presumed to be the same treatment, with the result that the magnitudes differ by no more than 15% from the mean value. Lastly,  $K_g$  for the 8% specimen bears little resemblance to that for the others. Both the residual resistance data and the metallurgical investigations quoted

†  $\theta_D$  varies by  $\pm 10\%$  in this range, but the average value is good enough for the present purpose.

‡ Rosenberg (1955) has found further evidence for linear lattice terms in Ti, Zr, V, Mn and Ce. See also Klemens (1956).

above indicate that this specimen consists of two phases and is therefore *prima facie* distinguished from the others. For Sn-8.2,  $K_g$  has no simple temperature dependence but appears to lie somewhere between a linear and a quadratic law. This might be caused by the large increase in the number of effectively free electrons per atom near the solubility limit. Unfortunately, the situation is too complex and the data too meagre to examine this possibility further.

The small anomalies in the  $(WT, T^3)$  graphs for specimens Sn-2.1, Sn-2.5 and Sn-2.8 of the first group are important in this discussion. Recently, Rosenberg (1957) has discussed deviations of this type in zinc and gallium and has shown that there is a good correlation between the changes in slope and a sharp decrease in the Debye  $\theta$  in these metals. Theoretically, the correlations stem from the fact that the coefficient  $\alpha$  in equation (2) is given by the relation

$$\alpha = \frac{GN^{2/3}}{K_{\infty}\theta_D^2} \quad \dots\dots(9)$$

where  $G$  is a constant and the other symbols have their usual definitions. (This equation is discussed in detail by Olsen and Rosenberg (1953).) Since  $K_{\infty}$  is itself proportional to  $\theta_D^2$ , a change from  $\theta_{D1}$  to  $\theta_{D2}$  will result in a change in slope of the  $(WT, T^3)$  curve from  $\alpha_1$  to  $\alpha_2$ , where  $\alpha_1/\alpha_2 = (\theta_{D2}/\theta_{D1})^4$ . A decrease in  $\theta_D$  will therefore cause a strong increase in  $\alpha$ . Such a decrease does indeed occur in the case of tin near 4°K (Corak and Satterthwaite 1956). However  $\theta_D$  does not remain constant thereafter but rises steadily with increasing temperature (Keesom and v. d. Ende 1932). According to (9) this should result in  $\alpha$  rising sharply at  $T \sim 4^\circ\text{K}$  and then slowly decreasing in a complicated way. By way of contrast, the  $(WT, T^3)$  curves for Sn-2.1, Sn-2.5 and Sn-2.8 have their sharp changes in slope at  $T \sim 13^\circ\text{K}$  and the regions above  $T \sim 14^\circ\text{K}$  ( $T^3 \sim 3000$ ) are quite linear. Moreover, for all but one of the Group I specimens the values of  $\alpha$  in the high temperature region yield values of  $F = \alpha K_{\infty} \theta_D^2$  which agree closely with Rosenberg's (1955) value for pure tin below 6' or 7°K. In view of these facts it seems that the linear regions above  $T^3 \sim 3000$  represent equation (2) and that the deviations at lower temperatures are not connected with the supposed variation of  $\theta_D$ . This suggests that  $\theta_D$  behaves differently in these alloys than in pure tin, provided that the introduction of the Debye  $\theta$  into the equations for the thermal conductivity is justified (see Rosenberg 1957).

These conclusions are supported by the results for Sn-2 and Sn-2' wherein there is a much stronger deviation from the linear law at low values of  $T^3$ . It is evident that all of these anomalies must be ascribed to a small lattice contribution which is quite invisible in the  $(K, T)$  curves of figure 2. Unfortunately this contribution is too small relative to the electronic component to allow an analysis along the lines used in the case of the Group II specimens. However the magnitudes of the lattice conductivities can now be compared for all the specimens, at least at low temperatures. The result for  $T \sim 6^\circ\text{K}$  is that  $K_g$  is largest for specimens Sn-2 and Sn-2' with 0.012 watt unit each, and varies from one-half to two-thirds of that value amongst the remaining eight samples, excepting Sn-8.2 where it is a good deal smaller. Thus the emergence of the linear lattice component in the second group is not connected with a strong increase in the absolute value of  $K_g$ . On the other hand the correlation between the appearance of the linear  $K_g$  and the anomalous rise in residual resistance is clear and it is possible that the scattering mechanisms are the same in both cases.

## ACKNOWLEDGMENTS

The author expresses his gratitude to Drs. K. Mendelssohn, H. Rosenberg and H. Montgomery for many valuable discussions and communications. He would also like to thank Drs. R. A. Allen of the Atomic Energy Research Establishment, Harwell, and S. R. Taylor for carrying out the specimen analyses, and Mr. S. Weintraub of the University of Southampton for supplying the two 2% samples. Finally, he gratefully acknowledges the support of the Rhodes Scholarship Trust during his stay in Oxford.

## REFERENCES

- CORAK, W. S., and SATTERTHWAITE, C. B., 1956, *Phys. Rev.*, **102**, 662.  
DOIDGE, R. P., 1956, *Phil. Trans. Roy. Soc. A*, **248**, 553.  
GARFINKEL, M., and LINDENFELD, P., 1957, *Proc. 5th Int. Conf. Low Temp. Phys. Chem.*, in the press.  
HANNA, I. I., and SONDHEIMER, E. H., 1957, *Proc. Roy. Soc. A*, **239**, 247.  
HIRSCH, P. B., 1956, *Progress in Metal Physics* Vol. 6 (London : Pergamon Press).  
KEESOM, W. H., 1942, *Helium* (Amsterdam : Elsevier).  
KEESOM, W. H., and v. d. ENDE, P. H., 1932, *Leid. Comm.* **219b**, 10.  
KLEMENS, P. G., 1955, *Proc. Phys. Soc. A*, **68**, 1113; 1956, *Handbuch der Physik*, Vol. **14** (Berlin : Springer); 1957, *Canad. J. Phys.*, **35**, 441.  
LEE, J. A., and RAYNOR, G. V., 1954, *Proc. Phys. Soc. B*, **67**, 737.  
MAKINSON, R., 1938, *Proc. Camb. Phil. Soc.*, **34**, 474.  
NORDHEIM, L., 1931, *Ann. Phys., Lpz.*, **9**, 607.  
OLSEN, J. L., 1952, *Proc. Phys. Soc. A*, **65**, 518.  
OLSEN, J. L., and ROSENBERG, H. M., 1953, *Advanc. Phys.*, **2**, 28.  
PIPPARD, A. B., 1953, *Proc. Roy. Soc. A*, **216**, 547; 1955, *Phil. Trans. Roy. Soc. A*, **248**, 97.  
POMERANCHUK, I., 1942, *J. Phys. U.S.S.R.*, **6**, 237.  
RHINES, F. N., URQUHART, W. M., and HOGE, H. R., 1947, *Trans. Amer. Soc. Metals*, **39**, 694.  
ROSENBERG, H. M., 1955, *Phil. Trans. Roy. Soc. A*, **247**, 441; 1957, *Phil. Mag.*, **2**, 541.  
SERIN, B., and LOHMAN, C., 1953, *Proc. 3rd Int. Conf. Low Temp. Phys. Chem.* (Houston), p. 47.  
VALENTINER, S., 1940, *Z. Metallk.*, **32**, 31.



# An Experimental Study of Pulse Propagation in Elastic Cylinders

BY D. Y. HSIEH AND H. KOLSKY

Brown University, Providence, Rhode Island, U.S.A.

MS. received 28th November 1957

**Abstract.** The distortion of longitudinal pulses in elastic cylinders resulting from the effects of lateral inertia is discussed in terms of the Pochhammer treatment. The experimentally observed displacement-time curve produced at one end of a steel cylinder when a small explosive charge is detonated at the opposite end is compared with that obtained theoretically using Fourier synthesis. It is found that only the fundamental mode of propagation need be considered in predicting the pulse shape under such conditions.

## § 1. INTRODUCTION

THE exact theory of the propagation of longitudinal sinusoidal waves along elastic cylinders was first formulated by Pochhammer (1876) and independently by Chree (1889). In recent years the *frequency equations* obtained by these authors have been solved numerically by a number of workers (Field 1931, Bancroft 1941, Czerlinsky 1942, Mindlin 1946, Davies 1948, and Hueter 1949). These solutions show that for a medium of known Poisson's ratio  $\nu$ , the non-dimensional quantity  $c/c_0$  can be calculated for any value of  $a/\lambda$ ;  $c$  is here the phase velocity of waves of wavelength  $\lambda$  in a cylinder of radius  $a$  and  $c_0$  is the velocity given by the simple theory and is equal to  $(E/\rho)^{1/2}$  where  $E$  is Young's modulus and  $\rho$  is the density of the material of the cylinder.

It is found that in addition to the fundamental mode of propagation a number of higher modes involving one or more nodal cylinders are possible. In the fundamental mode the phase velocity approaches  $c_0$  for small values of  $a/\lambda$  (i.e. for wavelengths which are long compared with the radius of the cylinder) and decreases monotonically as  $a/\lambda$  increases, tending asymptotically to  $c_s$ , the velocity of Rayleigh surface waves, for large values of  $a/\lambda$ . For higher modes, the phase velocity tends to infinity as  $a/\lambda$  tends to certain critical cut-off values and approaches the velocity of distortional waves  $(\mu/\rho)^{1/2}$  for large values of  $a/\lambda$  ( $\mu$  denotes the rigidity modulus of the medium). In addition to the above references, the problem of wave propagation in cylinders and the role of lateral inertia to which these dispersive effects are due, are discussed by Davies (1956) and by one of the authors (Kolsky 1953, 1954).

From a knowledge of the phase velocity of infinite trains of sinusoidal waves, it should be possible by means of Fourier synthesis to forecast the way in which a mechanical pulse will change in shape as it travels down a cylinder. The purpose of the present note is to compare an experimental investigation of the problem with the results predicted by the Pochhammer-Chree theory.

Davies (1948, 1956) discusses the nature of the distortion which results from the fact that for the fundamental mode, the high frequency components of a pulse travel with lower group velocities than those of the low frequency



components. This results in the main pulse being followed by a *coda* of high frequency oscillations. Using Kelvin's method of stationary phase, Davies has shown that the times of arrival of the *dominant groups* observed experimentally are in good agreement with those predicted by theory. In the present note, the problem is treated in terms of the phase velocities of the Fourier components, and the changes in pulse shape are investigated by means of numerical Fourier synthesis.

## § 2. METHOD OF ANALYSIS

Consider a cylinder of length  $l$  and radius  $a$  at one end of which a sharp blow is applied. Let  $\sigma(x, t)$  represent the stress a distance  $x$  along the cylinder at time  $t$ . Then the stress at the impact end can be expressed as a Fourier integral

$$\sigma(0, t) = \int_{0-}^{\infty} A \cos(pt - \epsilon) dp \quad \dots\dots (1)$$

where  $A$  and  $\epsilon$  are functions of  $p$  which define the shape of the pulse. The pulse arriving at the other end of the cylinder (which will be called the measuring end) is

$$\sigma(l, t) = \int_0^{\infty} A \cos \left[ p \left( t - \frac{l}{c} \right) - \epsilon \right] dp \quad \dots\dots (2)$$

where  $c$  is the phase velocity of waves of frequency  $p/2\pi$ . For a plane wave the particle velocity produced by a stress  $\sigma$  is  $\sigma/\rho c$  and, if the measuring end is free, the wave reflected back along the cylinder will result in a doubling of the particle velocity; consequently, if  $V$  is the velocity of the measuring end of the bar we have

$$V = \int_0^{\infty} \frac{2A}{\rho c} \cos \left[ p \left( t - \frac{l}{c} \right) - \epsilon \right] dp.$$

The displacement  $u$  at the measuring end is the integral of  $V$  with respect to  $t$  so that

$$u = \int_0^{\infty} \frac{2A}{\rho c p} \sin \left[ p \left( t - \frac{l}{c} \right) - \epsilon \right] dp + A_0 t, \quad \dots\dots (3)$$

where  $A_0$  is the direct current component of the pulse. In order to evaluate (3) numerically, the Fourier integral must be replaced by a Fourier series, and it is also desirable to choose a frame of reference which is moving with the pulse. If we take the velocity of our frame of reference to be  $c'$ , we may write:

$$\begin{aligned} u &= \sum_0^n \frac{2A}{\rho c n p_0} \sin \left[ n p_0 \left( t - \frac{l}{c} + \frac{l}{c'} \right) - \epsilon \right] + A_0 t \\ &= \sum_0^n A_n \sin n p_0 t - \sum_0^n B_n \cos n p_0 t + A_0 t, \quad \dots\dots (4) \end{aligned}$$

where 
$$A_n = \frac{2A}{\rho c n p_0} \cos \left[ n p_0 \left( \frac{l}{c} - \frac{l}{c'} \right) + \epsilon \right]$$

and 
$$B_n = \frac{2A}{\rho c n p_0} \sin \left[ n p_0 \left( \frac{l}{c} - \frac{l}{c'} \right) + \epsilon \right].$$

The basic interval of the summation is  $2\pi/p_0$  and  $p_0$  must be chosen sufficiently small for the pulse to lie entirely within the interval and, if accuracy is to be

achieved,  $p_0$  must be sufficiently large for the pulse to occupy a large part of the interval. The value of  $c'$  is not at all critical and can be taken as  $c_0$ .

If the pulse at the impact end is Fourier-analysed to give  $A$  and  $\epsilon$  for each frequency,  $\pi p_0/2\pi$  and the value of  $c$  at each frequency is obtained from the Pochhammer treatment.  $A_n$  and  $B_n$  in equation (4) can be calculated and hence the displacement produced at the measuring end of the bar can be determined.

In earlier work (Kolsky 1956) on pulses in visco-elastic solids it was shown that, as a result of the large attenuation of the high frequency components by these materials, a sharp pulse could be approximated to by a Dirac  $\delta$ -function, i.e.  $A$  could be taken as constant and  $\epsilon$  as zero for all frequencies. In the present problem, no attenuation is assumed, and although the contribution of each component to the displacement  $u$  is proportional to the reciprocal of its frequency, it is found that if a  $\delta$ -function is employed here, the convergence is too slow for numerical calculations to be carried out and, if the shape of the initial pulse is to be represented analytically, a more realistic approximation must be employed.

The experimental results which were analysed by equation (4) were obtained with small explosive charges which were detonated at the ends of steel cylinders. The displacement at the measuring end was detected with a condenser-unit and an experimental arrangement similar to that used in earlier work (Kolsky 1956). Figure 1 shows the cathode-ray oscillograph trace for the displacement at one

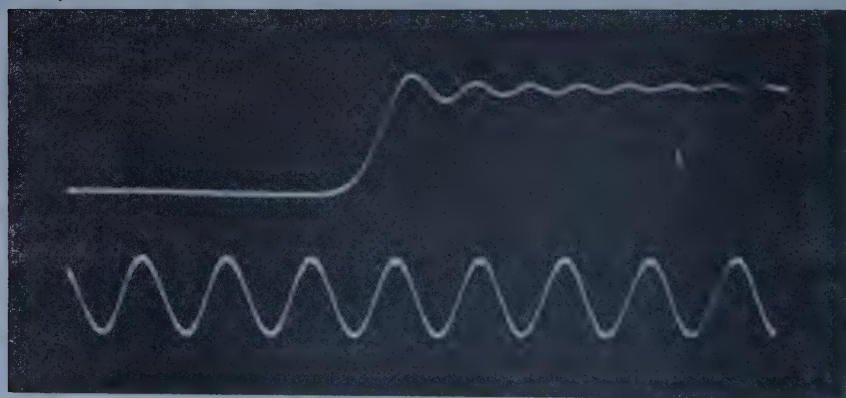


Figure 1. Oscilloscope trace of end displacement of steel bar for 0.01 gramme lead azide charge detonated at other end. Length of bar 22.5 cm. Diameter 0.63 cm. Lower trace: 100 kc/s timing wave.

end of a cylinder 22.5 cm in length and 0.63 cm in diameter when a 0.01 gramme lead azide charge was detonated at the other end. It may be seen that the smooth rise corresponding to the main pulse is followed by a series of oscillations. The exact shape of the pressure-time curve at the impact end is not known, but the duration of the pulse produced by such a charge is about 2 microseconds and since the very high frequency components change only the tail of the displacement-time curve and their effect on the displacement decreases with frequency, inserting an analytic function of the same half-width as the pulse should give a reasonable approximation to the observed displacement-time curve. A convenient function for this purpose is the error function as it has a simple

Fourier transform and corresponds to a fairly steep-sided pulse. Thus we can take

$$\sigma(0, t) = \int_0^{\infty} B \exp(-\alpha^2 p^2) \cos pt \, dp = \frac{1}{2\alpha} \sqrt{\pi} B \exp(-\beta^2 t^2) \quad \dots (5)$$

where  $\beta = \frac{1}{2}\alpha$  so that in equation (4) we have  $A = B \exp(-\alpha^2 n^2 p_0^2)$  and  $\epsilon = 0$ .

Figure 2 shows the results of a numerical synthesis carried out for the steel bar used in the experiment shown in figure 1, i.e.  $l = 22.5$  cm,  $a = 0.315$  cm,  $c_0$  was taken as  $5100$  m sec<sup>-1</sup>, Poisson's ratio  $\nu = 0.29$ , and the fundamental

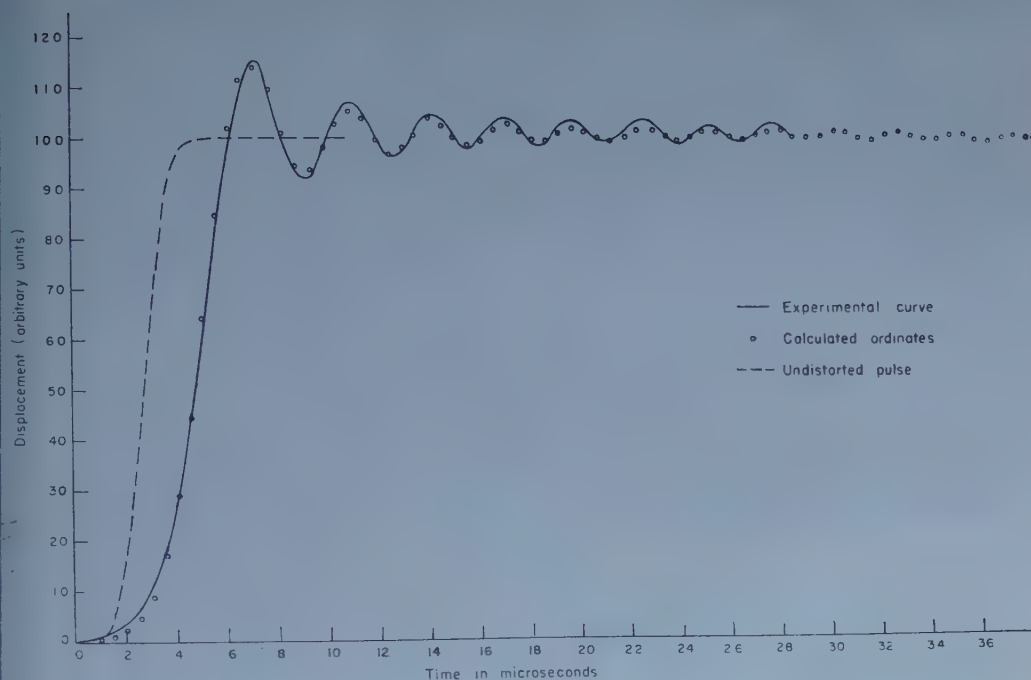


Figure 2.

frequency  $p_0/2\pi$  was 15 kc/s, so that the basic interval of the synthesis is  $66.6 \mu\text{sec}$ . The value  $c$  for each harmonic up to the 64th, i.e. 960 kc/s, was obtained from the paper by Bancroft (1941), interpolating for  $\nu = 0.29$ ;  $\alpha$  was taken as  $5.33 \times 10^{-7}$  sec, as this made  $\alpha p_0$  equal to 0.05 and gave an error curve of  $1.76 \mu\text{sec}$  half-width. The direct current component of the pulse  $A_0$  is given by integrating (5) over the basic interval  $2\pi/p_0 = \tau$ . Thus

$$\begin{aligned} A_0 &= \frac{1}{\tau} \int_0^{\tau} \frac{2\sigma}{pc} \, dt \\ &= \frac{B\sqrt{\pi}}{\alpha pc \tau} \int_0^{\tau} \exp(-\beta^2 t^2) \, dt. \end{aligned}$$

and hence can be calculated from the value of  $\alpha$ . The Fourier synthesis was carried out on an I.B.M. card-programmed calculator to give 64 cosine terms and 64 sine terms in the interval  $0$  to  $\pi/p_0$  and thus 128 ordinates were obtained in the full interval  $2\pi/p_0 = 66.6 \mu\text{sec}$ . Seventy-two of these ordinates are shown in the figure. The calculation was carried out putting  $B = 1$  and the amplitude of the experimental curve has been fitted to it. It may be seen that the agreement

between theory and experiment is remarkably good, the main difference being that the oscillations observed experimentally at the tail of the pulse are rather larger than those predicted theoretically. This is to be expected in that the pressure pulse produced by the explosive is sharper than the error curve used in the calculation and its spectrum will contain a higher proportion of high frequency components which will appear at the tail of the pulse. The broken line of figure 2 shows the displacement-time curve which would be observed in the absence of dispersion, e.g. in an infinitely thin cylinder. This curve has been obtained from the integral of the error function given in equation (5).

### § 3. CONCLUSION

The good agreement between the theoretical and experimental displacement-time curves indicates that a numerical method of Fourier synthesis can be used for quantitatively describing the dispersion produced by lateral inertia effects. In the experiment described there appears to be no evidence of higher modes being excited and whilst the assumption that the separate Fourier components of the pulse travel down the cylinder as plane waves whose amplitude is independent of the distance from the axis is not true for the higher frequency components, the mean displacement of the cross section calculated on this assumption appears to be close to that found experimentally.

### ACKNOWLEDGMENTS

The authors are indebted to the Office of Naval Research, Washington, D.C., for support in this work which was carried out under Contract Nonr-562(14).

### REFERENCES

- BANCROFT, D., 1941, *Phys. Rev.*, **59**, 588.  
 CHREE, C., 1889, *Trans. Camb. Phil. Soc.*, **14**, 250.  
 CZERLINSKY, E. VON, 1942, *Akust. Z.*, **7**, 12.  
 DAVIES, R. M., 1948, *Phil. Trans. A*, **240**, 375; 1956, *Surveys in Mechanics* (Cambridge : University Press).  
 FIELD, G. S., 1931, *Canad. J. Res.*, **5**, 619.  
 HUETER, T. F., 1949, *Z. angew. Phys.*, **1**, 274.  
 KOLSKY, H., 1953, *Stress Waves in Solids* (Oxford : Clarendon Press); 1954, *Phil. Mag.*, **45**, 712; 1956, *Ibid.*, **1**, 693.  
 MINDLIN, J. A., 1946, *Doklady Akad. Nauk., S.S.S.R.*, **1**, 11.  
 POCHHAMMER, L., 1876, *J. reine angew. Math.*, **81**, 324.



## The $(\gamma, 2n)$ and $(\gamma, 3n)$ Reactions in $^{181}\text{Ta}$

By J. H. CARVER AND W. TURCHINETZ

Research School of Physical Sciences, Australian National University, Canberra

*Communicated by E. W. Titterton; MS. received 17th September 1957*

**Abstract.** The  $^{181}\text{Ta}(\gamma, 3n)$  reaction has been studied by measuring the 9.5 min and 150 min activities of  $^{178}\text{Ta}$ . The two  $^{178}\text{Ta}$  isomers are produced in the effectively constant ratio  $A(9.5 \text{ min})/A(150 \text{ min}) = 3.0 \pm 0.6$  by gamma rays of all energies between 24 mev and 32 mev. The experimental results have been combined with previous determinations of the  $^{181}\text{Ta}(\gamma, n)$  cross section and of the photo-neutron yield to obtain the relative cross sections for the  $^{181}\text{Ta}(\gamma, n)$ ,  $(\gamma, 2n)$  and  $(\gamma, 3n)$  reactions from their thresholds to 31 mev. The integrated cross sections for the  $(\gamma, n)$ ,  $(\gamma, 2n)$  and  $(\gamma, 3n)$  reactions to 31 mev are  $(73 \pm 3)\%$ ,  $(24 \pm 3)\%$ , and  $(3.0 \pm 1.2)\%$  of the total integrated cross section,  $(3.3 \pm 1.2)$  mev barns, for these three photo-neutron reactions.

### § 1. INTRODUCTION

THE analysis of total photo-neutron yield measurements (e.g. Montalbetti, Katz and Goldemberg 1953, Nathans and Halpern 1954, Jones and Terwilliger 1953) is complicated by the fact that multiple emission may occur at the higher energies. Even in the case of heavy nuclei, for which neutrons are expected to be the chief disintegration products, the gamma-ray absorption cross section can only be derived if the neutron multiplicity is known. Measurements of the cross sections for the different processes may also indicate the relative importance of direct emission and compound-nucleus formation.

The competition between single and multiple photo-neutron emission from tantalum has been studied previously by Carver, Edge and Lokan (1957) who determined the  $^{181}\text{Ta}(\gamma, n)$  reaction by induced radioactivity and the total neutron yield with a Szilard-Chalmers detector. In order to separate the  $(\gamma, 2n)$  and  $(\gamma, 3n)$  contributions to the multiple yield a direct measurement has now been made on the  $(\gamma, 3n)$  reaction using a scintillation spectrometer to observe the radioactivity of the resulting  $^{178}\text{Ta}$ .

### § 2. EXPERIMENTAL METHOD

A detailed discussion of the scintillation spectrometer results and of the decay schemes of the radioactive isotopes of tantalum is given elsewhere (Carver and Turchinets 1958). The thresholds for the  $^{181}\text{Ta}(\gamma, n)$ ,  $(\gamma, 2n)$  and  $(\gamma, 3n)$  reactions and the half-lives of the product nuclei are listed in the table.

Photo-neutron Reactions in  $^{181}\text{Ta}$

Reaction	Threshold (mev)	Product nucleus	Half- life
$(\gamma, n)$	7.6	$^{180}\text{Ta}$	8.15 h (isomer)
$(\gamma, 2n)$	14	$^{179}\text{Ta}$	600 day
$(\gamma, 3n)$	22	$^{178}\text{Ta}$	9.5 min
		$^{178}\text{Ta}$	150 min

The relative yields for the  $(\gamma, n)$  and  $(\gamma, 3n)$  reactions were obtained by irradiating tantalum foils ( $240 \text{ mg cm}^{-2}$ ) for ten-minute periods with the bremsstrahlung from the Canberra electron synchrotron and measuring the resulting activities with the spectrometer. A series of irradiations was performed at approximately 1 mev intervals between maximum bremsstrahlung energies of 22 and 32 mev, so that the usual yield curves could be obtained.

Despite the fact that the  $(\gamma, 3n)$  activity was only a few per cent of the total induced activity it was possible to distinguish it quite clearly from the much more intense  $(\gamma, n)$  activity owing to its distinctive radioactive properties. The  $(\gamma, n)$  yield was obtained from the intensity of the 8.15 hr component of the 55 kev x-ray line. For  $\gamma$ -ray energies above the  $(\gamma, 3n)$  threshold this x-ray line has in addition a strong 9.5 min component and by analysing the decay curves, the yield of the 9.5 min  $(\gamma, 3n)$  reaction was determined. The yield of the 150 min  $(\gamma, 3n)$  reaction was obtained from the intensities of the  $\gamma$ -ray lines at 215, 325 and 415 kev. These gamma rays form part of a rotational band and decay with a measured half-life of  $150 \pm 10$  min (Carver and Turchinets 1958).

The  $(\gamma, 3n)$  yield was obtained from these measurements in terms of the  $(\gamma, n)$  yield and as the latter had previously been determined in this laboratory (Carver, Edge and Lokan 1957) the shape of the  $(\gamma, 3n)$  yield curve was determined as a function of the maximum bremsstrahlung energy.

### § 3. RESULTS AND ANALYSIS

The yield curve for the  $^{181}\text{Ta}(\gamma, 3n)^{178}\text{Ta}$  reaction is shown in figure 1 in which both the 9.5 min and 150 min results are plotted. Although the absolute yields are different there is no significant difference between the shapes of the curves defined by the 9.5 min and 150 min yield points and the mean curve shown in figure 1 has been fitted to both sets of observations. This yield curve has been analysed by an iterative method (Carver and Lokan 1957) to obtain the relative  $^{181}\text{Ta}(\gamma, 3n)$  cross section also drawn in figure 1.

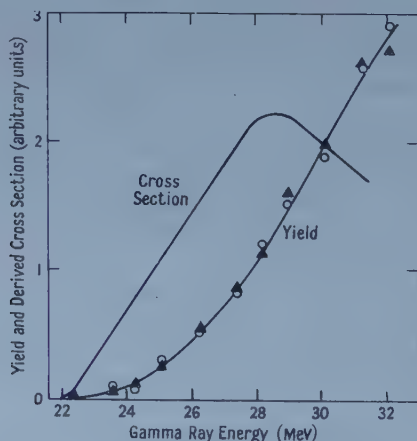


Figure 1. Yield curve and derived cross section for the reaction  $^{181}\text{Ta}(\gamma, 3n)^{178}\text{Ta}$ . The circles and triangles refer to the normalized 9.5 min and 150 min observations.

From the measured activities and the decay scheme data of Carver and Turchinets (1958) the two  $^{178}\text{Ta}$  isomers are found to be produced in the ratio  $A(9.5 \text{ min})/A(150 \text{ min}) = 3.0 \pm 0.6$ . At 30 mev the total  $(\gamma, 3n)$  yield is  $(2.0 \pm 0.6)\%$  of the 8.15 hr  $(\gamma, n)$  yield.

Since  $^{180}\text{Ta}$  is stable (White *et al.* 1955) the present measurement only relates the  $(\gamma, 3n)$  yield to that fraction of the  $(\gamma, n)$  yield which leads to the 8.15 hr isomer. In the earlier  $(\gamma, n)$  measurements the total neutron yield and the 8.15 hr  $(\gamma, n)$  yield† were normalized at bremsstrahlung energies below the  $(\gamma, 2n)$  threshold (14 MeV) so that the cross section for multiple neutron production  $\sigma_m = 2\sigma_2 + 3\sigma_3$  was obtained in terms of the total  $(\gamma, n)$  cross section  $\sigma_1$ .

In order to distribute  $\sigma_m$  between  $\sigma_2$  and  $\sigma_3$  the spectrometer has been used to determine the  $(\gamma, 2n)$  yield by counting the 600 day, 55 keV x-rays associated with the decay of  $^{179}\text{Ta}$ . Tantalum foils were irradiated for eight hours and the 8.15 h  $\text{Ta}(\gamma, n)$  reaction was used as before to monitor the irradiations, the  $(\gamma, 2n)$  yield being determined some 30 days later when all short-lived activities had decayed away. Owing to the length of time which was required for the  $(\gamma, 2n)$  measurements the activation curve was not determined completely in this way. Measurements were made at two bremsstrahlung energies, 18 and 30 MeV, between which the  $(\gamma, 2n)$  yield was found to increase by a factor of three in accordance with the previous multiple neutron yield measurements. The 30 MeV results were used to obtain the relative  $(\gamma, 2n)$  and  $(\gamma, 3n)$  yields,  $A(\gamma, 3n)/A(\gamma, 2n) = (3.6 \pm 1.2)\%$ . This normalization also indicates that the 8.15 hr level is populated in  $(60 \pm 20)\%$  of the  $(\gamma, n)$  disintegrations.

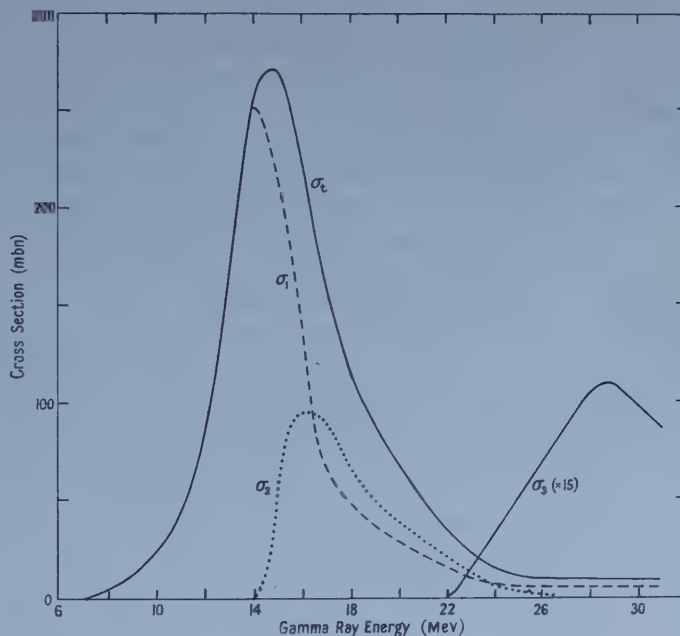


Figure 2. Cross sections  $\sigma_1$ ,  $\sigma_2$  and  $\sigma_3$ , for the reactions  $^{181}\text{Ta}(\gamma, n)$ ,  $(\gamma, 2n)$  and  $(\gamma, 3n)$  and the total cross section  $\sigma_t = \sigma_1 + \sigma_2 + \sigma_3$ .

The  $\text{Ta}(\gamma, n)$ ,  $(\gamma, 2n)$  and  $(\gamma, 3n)$  cross sections shown in figure 2 have been obtained by combining the present results on the  $(\gamma, 3n)$  cross section with the

† In both experiments it is assumed that the 8.15 h activity is proportional to the total  $(\gamma, n)$  yield and that the constant of proportionality is independent of gamma-ray energy. That this assumption is probably reliable except perhaps in the region immediately above the threshold, is shown by direct comparisons of the relative photo-production of two isomers (e.g. Goldemberg and Katz (1953) for  $^{114}\text{In}$  and the present data for  $^{178}\text{Ta}$ ).

previous data on the single and multiple neutron yields using the  $(\gamma, 2n)$  normalization at 30 mev. The total photo-neutron cross section  $\sigma_t = \sigma_1 + \sigma_2 + \sigma_3$  is also drawn in figure 2. The absolute cross section scale has been obtained by comparison of the 8.15 hr and 10 min activities induced in tantalum and copper foils using the absolute  $^{63}\text{Cu}(\gamma, n)$  cross section of Berman and Brown (1954). This measurement was made with end-window Geiger counters and corrections were applied for absorption, for the radioactive decay schemes and for the transitions to stable  $^{180}\text{Ta}$ .

The integrated cross sections to 31 mev for the  $(\gamma, n)$ ,  $(\gamma, 2n)$  and  $(\gamma, 3n)$  reactions are  $(73 \pm 3)\%$ ,  $(24 \pm 2)\%$  and  $(3.0 \pm 1.2)\%$  respectively of the total integrated cross section,  $(3.3 \pm 1.2)$  mev barns, for these three reactions.

A rotational band having almost the same energy levels as those populated in the decay of 150 min  $^{178}\text{Ta}$  could have been excited by means of the  $^{181}\text{Ta}(\gamma, p)^{180}\text{Hf}$  reaction (Mihelich *et al.* 1956). No 5.5 hr components corresponding to this reaction were found and it is estimated that at 30 mev the yield of the 5.5 hr  $^{181}\text{Ta}(\gamma, p)$  reaction is less than 10% of the 150 min  $^{181}\text{Ta}(\gamma, 3n)$  reaction.

#### § 4. DISCUSSION

It has been remarked previously (Carver, Edge and Lokan 1957) that the large  $(\gamma, n)$  cross section beyond about 17 mev indicates that in this energy region the  $(\gamma, n)$  reaction arises almost entirely from direct interactions and only the multiple reactions  $(\gamma, 2n)$  and  $(\gamma, 3n)$  involve the formation of a compound nucleus at some stage. The multiple reactions may arise from interactions in which the photon transfers all, or only a part, of its energy to the statistical motion of the nucleons. The present results indicate that  $\sigma_3$  rises fairly rapidly from a threshold of 22 mev and appears to exhaust the cross section for multiple production above about 25 mev. Such competition between  $\sigma_2$  and  $\sigma_3$  is to be expected on the basis of the statistical theory. If the extreme assumption is made that for these multiple reactions all the incident energy has been transferred to the statistical mode, the calculations of Levinger and Bethe (1952) for the neutron multiplicity suggest that  $\sigma_3$  would equal  $\sigma_2$  at 25 mev and  $\sigma_3$  would rapidly exhaust  $\sigma_2$  at higher energies.

No  $^{181}\text{Ta}(\gamma, p)$  transitions to the 5.5 h level of  $^{180}\text{Hf}$  were found, the yield being less than 10% of the 150 min  $^{181}\text{Ta}(\gamma, 3n)$  yield, i.e. less than 0.03% of the total  $^{181}\text{Ta}(\gamma, n)$  yield. This limit does not, however, imply that the total  $^{181}\text{Ta}(\gamma, p)$  reaction yield is entirely negligible (cf. Hoffman and Cameron 1953) at these energies at which directly emitted protons can surmount the 13 mev Coulomb barrier. Such  $(\gamma, p)$  reactions are more likely to populate the stable ground state of  $^{180}\text{Hf}$  (spin 0) than the 5.5 hr isomer (spin 9), transitions to which are further inhibited by the fact that it has  $K=9$  in the Bohr-Mottelson scheme (Mihelich *et al.* 1956).

The correction to the neutron yield data for neutron multiplicity is directly obtained from the present results. Considering only the  $(\gamma, n)$ ,  $(\gamma, 2n)$  and  $(\gamma, 3n)$  cross sections the ratio of the true integrated cross section to that which would be obtained from the uncorrected neutron yield is

$$\int_0^{31} (\sigma_1 + \sigma_2 + \sigma_3) dE \bigg/ \int_0^{31} (\sigma_1 + 2\sigma_2 + 3\sigma_3) dE = (0.77 \pm 0.05).$$



## REFERENCES

- BERMAN, A. I., and BROWN, K. L., 1954, *Phys. Rev.*, **96**, 83.  
CARVER, J. H., EDGE, R. D., and LOKAN, K. H., 1957, *Proc. Phys. Soc. A*, **70**, 415.  
CARVER, J. H., and LOKAN, K. H., 1957, *Aust. J. Phys.*, **10**, 312.  
CARVER, J. H., and TURCHINETZ, W., 1958, *Proc. Phys. Soc.*, **71**, 618.  
GOLDEMBERG, J., and KATZ, L., 1953, *Phys. Rev.*, **90**, 308.  
HOFFMAN, M. M., and CAMERON, A. G. W., 1953, *Phys. Rev.*, **92**, 1184.  
JONES, L. W., and TERWILLIGER, K. M., 1953, *Phys. Rev.*, **91**, 699.  
LEVINGER, J. S., and BETHE, H. A., 1952, *Phys. Rev.*, **85**, 577.  
MIHELICH, J. W., SCHARFF-GOLDHABER, G., and McKEOWN, M., 1956, *Phys. Rev.*, **94**, 794-(A).  
MONTALBETTI, R., KATZ, L., and GOLDEMBERG, J., 1953, *Phys. Rev.*, **91**, 569.  
NATHANS, R., and HALPERN, J., 1954, *Phys. Rev.*, **93**, 437.  
WHITE, F. A., COLLINS, T. L., and ROURKE, F. M., 1955, *Phys. Rev.*, **97**, 566.

## Radioactivity of $^{178}\text{Ta}$ , $^{179}\text{Ta}$ and $^{180}\text{Ta}$

By J. H. CARVER AND W. TURCHINETZ

Research School of Physical Sciences, Australian National University, Canberra

*Communicated by E. W. Titterton; MS. received 17th September 1957, and in revised form 16th December 1957*

**Abstract.** The neutron deficient isotopes,  $^{178}\text{Ta}$ ,  $^{179}\text{Ta}$  and radioactive  $^{180}\text{Ta}$  have been produced by photodisintegration of  $^{181}\text{Ta}$  and studied with scintillation spectrometers used singly and in coincidence. The identification of each isotope is based on a knowledge of the  $(\gamma, n)$  threshold and an appropriate choice of bremsstrahlung energies. Radioactive  $^{178}\text{Ta}$  is shown to comprise an isometric doublet with half-lives  $9.5 \pm 0.1$  min and  $150 \pm 10$  min. The 9.5 min activity populates levels in  $^{178}\text{Hf}$  at 0, 91 and possibly 1480 keV, the first two by both electron capture and  $\beta^+$  emission and the last by electron capture, while the 150 min activity decays by electron capture to a level of  $^{178}\text{Hf}$  at 1046 keV. A decay scheme is proposed based on the experimental results and the strong coupling collective model of Bohr and Mottelson.

Evidence is presented to support the recent contention that  $^{179}\text{Ta}$  decays by electron capture to the ground state of  $^{179}\text{Hf}$ .

The observed  $\gamma$  radiation from 8.15 hour  $^{180}\text{Ta}$  is in general agreement with the decay scheme of Brown *et al.* except that there is no evidence for gamma radiation in the energy range 175–450 keV.

### § 1. INTRODUCTION

THE photodisintegration of tantalum is a convenient source of the radioactive isotopes  $^{180}\text{Ta}$ ,  $^{179}\text{Ta}$  and  $^{178}\text{Ta}$ , through the  $^{181}\text{Ta}(\gamma, n)$ ,  $(\gamma, 2n)$  and  $(\gamma, 3n)$  reactions† which have thresholds of 7.6, 14 and 22 MeV. This investigation of the radioactive properties of these isotopes is complementary to the cross section measurements described elsewhere (Carver and Turchinets 1958).

Tantalum foils ( $240 \text{ mg cm}^{-2}$ ) were irradiated with the bremsstrahlung from the Canberra electron synchrotron, the length of the irradiations and their energy being chosen to suit the particular activity which was being investigated. The foils were wrapped in cadmium so that slow neutron induced activities were minimized and, in fact, no activity attributable to  $^{182}\text{Ta}$  was observed.

### § 2. EXPERIMENTAL METHOD

Gamma-ray spectra were analysed with a  $1\frac{3}{4}$  in. diameter  $\times$  2 in. thick NaI(Tl) scintillation spectrometer, the resolution of which was 9% for the 662 keV line of  $^{137}\text{Cs}$ . The crystal was enclosed in a 3 in. thick lead castle with a graded shield of cadmium, brass and aluminium to absorb the Pb x-rays. The data were recorded on a multichannel kicksorter of the Hutchinson-Scarrott type.

† Natural tantalum is 99.988%  $^{181}\text{Ta}$  and 0.0123%  $^{180}\text{Ta}$  (White *et al.* 1955). The radioactive yields from the photodisintegration of  $^{180}\text{Ta}$  are negligible.

The following gamma-ray sources (Hollander *et al.* 1953) were used to calibrate the energy scale of the spectrometer over the range 28–1910 keV:  $^{181}\text{W}$ ,  $^{131}\text{I}$ ,  $^{22}\text{Na}$ ,  $^{137}\text{Cs}$ ,  $^{60}\text{Co}$ ,  $^{89}\text{Zr}$  and  $^{57}\text{Ni}$ . These sources were also used to obtain the photofraction as a function of energy for the geometries used. Relative gamma-ray intensities were then estimated from the photo-peaks after corrections were made for (i) the escape peak for low energy radiation, (ii) the total crystal efficiency and (iii) absorption. Correction (i) was obtained from the data of Axel (1954) which was found to agree to within 3% with the measured escape peak for the 57 keV  $^{181}\text{W}$  line. Corrections (ii) and (iii) were calculated for the particular geometries using published absorption coefficients (Davisson 1955).

Beta-ray spectra were investigated with a 1 in. diameter  $\times \frac{1}{2}$  in. thick anthracene crystal having a  $1.5 \text{ mg cm}^{-2}$  Al window. Thick sources ( $240 \text{ mg cm}^{-2}$ ) were used and the energy scale was calibrated in terms of equally thick sources of  $^{11}\text{C}$  (990 keV),  $^{13}\text{N}$  (1240 keV) and  $^{15}\text{O}$  (1680 keV). No intensity data were derived from these measurements.

To investigate  $\gamma$ - $\gamma$  coincidence spectra a single-channel analyser was used to select one feature in the spectrum and to gate the kicksorter for the output from a second crystal. A comparatively slow resolving time ( $2\tau = 5 \mu\text{sec}$ ) was used but at the low counting rates involved the accidental rate, measured by inserting a  $15 \mu\text{sec}$  delay in one line, was less than 10% of the genuine rate in the most unfavourable case.

#### $^{180}\text{Ta}$

The 8.15 hr isomer of  $^{180}\text{Ta}$  (spin  $1^\pm$ ) has been extensively studied (Brown *et al.* 1951) and it is known that 21% of the transitions populate the ground level and the first excited level of  $^{180}\text{W}$  by emission of 705 keV (10%) and 605 keV (11%) electrons and that most of the remainder proceed by electron capture to the ground level and first excited level (93 keV) of  $^{180}\text{Hf}$ . Brown *et al.* also reported low intensity gamma radiation in the energy range 175–450 keV which they tentatively assigned to a weak ( $\leq 1\%$ ) electron capture transition to levels of  $^{180}\text{Hf}$ . If this is so it implies the presence of low-lying levels of  $^{180}\text{Hf}$  other than those associated with the  $K=0^+$  rotational band found by Mihelich *et al.* (1954).† Alternatively, this radiation, if present, might proceed to the ground state of  $^{180}\text{Ta}$  but this is unlikely since the ground state spin of  $^{180}\text{Ta}$  is probably 8 (Mottelson and Nilsson 1955, Eberhardt *et al.* 1955, Petkau 1956).

Substantially pure sources of 8.15 hr  $^{180}\text{Ta}$  were prepared by irradiating tantalum foils for periods of three hours at a maximum bremsstrahlung energy of 18 MeV.‡ Figure 1 shows the gamma-ray spectrum which was obtained with the source sufficiently far (2 in.) from the crystal so that no 'coincidence-sum' lines were observed. Three lines are evident at 27, 55 and 95 keV (with the source only  $\frac{1}{4}$  in. from the crystal a 'coincidence-sum' line was observed at 150 keV). The 55 keV line can be explained as due to (i) Hf x-rays following K-capture in  $^{180}\text{Ta}$ , (ii) K-shell conversion of the 93.3 keV  $^{180}\text{Hf}$  gamma ray and (iii) K-shell conversion of the 102 keV  $^{180}\text{W}$  gamma ray. The 27 keV line is the satellite of the 55 keV line and corresponds to the escape of an iodine K x-ray from the crystal. The observed 95 keV line can be attributed to the unresolved 93.3 keV  $^{180}\text{Hf}$  radiation and the 102 keV  $^{180}\text{W}$  radiation.

† Since  $^{180}\text{W}$  probably has a similar low-lying  $K=0$  band the same arguments apply to  $\beta^-$  emission.

‡ The counting yield from 600 day  $^{179}\text{Ta}$  was negligible.

In addition to these features which may be identified, there is a structureless tail extending to about 220 keV, i.e. somewhat lower in energy than the weak radiation reported by Brown *et al.* (1951). We attribute this radiation to bremsstrahlung from the  $^{180}\text{Ta}$  beta radiation. In agreement with this assignment, it was found that placing 100 mg cm $^{-2}$  of molybdenum between the source and detector increased the magnitude of the tail relative to the 95 keV line by about a factor of four and that the tail then extended to about 350 keV.

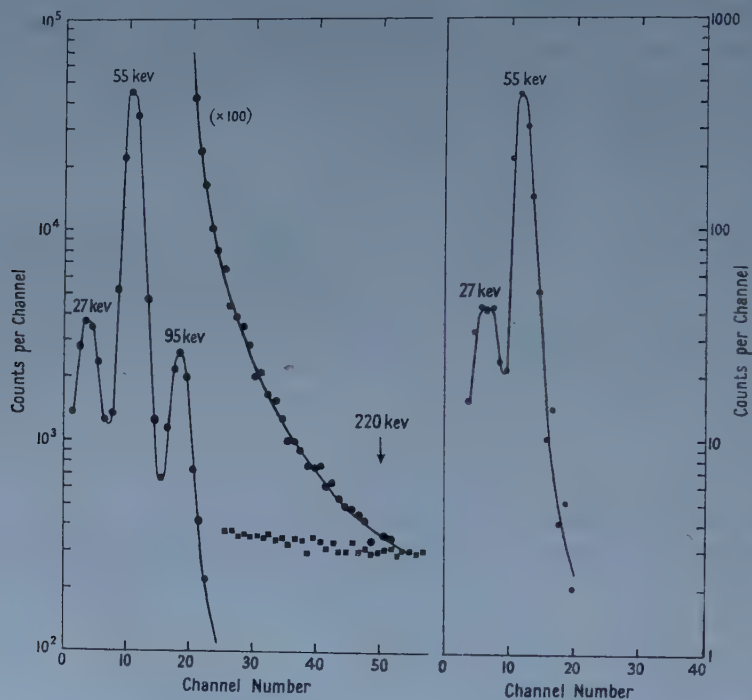


Figure 1. Gamma-ray spectrum of  $^{180}\text{Ta}$ . (The solid squares represent the background.) The low-energy part of the  $^{178}\text{Ta}$  spectrum is similar.

Figure 2. Gamma-ray spectrum of  $^{179}\text{Ta}$ .

Taking as an upper limit to the gamma-ray intensity the area under the bremsstrahlung tail from 175 to 220 keV, plus four times the standard deviation of the background counting rate from 220 to 450 keV, it is estimated that there are fewer than  $5 \times 10^{-5}$  quanta per x-ray in the energy range 175–450 keV.

#### $^{179}\text{Ta}$

A 600 day activity decaying predominately by K-capture was identified by Wilkinson (1950) with  $^{179}\text{Ta}$  produced among the products of the reactions  $\text{Lu}(\alpha, n)$ ,  $\text{Hf}(p, n)$  and  $\text{Ta}(p, pn)$ . Further work by Bisi, Zappa and Zimmer (1956) again based on Wilkinson's identification of the activity, showed that there was no gamma radiation other than the characteristic Hf L and K x-rays. From their measured L/K capture ratio Bisi *et al.* found that the transition energy was  $94 \pm 9$  keV and concluded that  $^{179}\text{Ta}$  decays to  $^{179}\text{Hf}$  in a ground to ground state decay.



Tantalum foils were irradiated for periods of eight hours at bremsstrahlung energies of both 18 and 30 mev. The gamma-ray spectra were observed some 30 days later when all short-lived components had decayed. The yield at 30 mev was three times that at 18 mev as expected from neutron yield data (Carver and Turchinets 1958) and the spectrum obtained at 30 mev, less background, is shown in figure 2. The Hf x-ray at 55 mev and its satellite at 27 mev are clearly evident in the spectrum in agreement with the results of Bisi *et al.* and of Wilkinson.

The production of this activity via the  $^{181}\text{Ta}(\gamma, 2n)$  reaction confirms Wilkinson's identification with  $^{179}\text{Ta}$ .

### $^{178}\text{Ta}$

Two activities of half-lives ( $9.35 \pm 0.03$ ) min and ( $2.1 \pm 0.1$ ) hr have been assigned to  $^{178}\text{Ta}$  by Wilkinson (1950) (see also Nervik and Seaborg 1955) who found that in each case the decay proceeded mainly by electron capture with less than 10% positron branching. Wilkinson's results are summarized in table 1. No detailed decay schemes were proposed.

Table 1. Previous Results for  $^{178}\text{Ta}$  (Wilkinson 1950)

(2.1 $\pm$ 0.1) hr activity		(9.35 $\pm$ 0.05) min activity	
Component	Rel. int.	Component	Rel. int.
$\sim 0.1$ mev $e^-$	$\sim 0.3$	$\sim 0.08$ mev $e^-$	$\sim 0.5$
$\sim 1$ mev $\beta^+$	$\sim 0.02$	1.06 mev $\beta^+$	0.03
L x-ray	1	L x-ray	$\sim 1$
K x-ray	1	K x-ray	1
$\sim 1.4$ mev $\gamma$ -ray	$\sim 0.5$	1.5 mev $\gamma$	0.03

Recent studies of Coulomb excitation (Heydenburg and Temmer 1955) and of the reaction  $^{177}\text{Hf}(n, \gamma)$  (Bockelman *et al.* 1957) have given some information about the low-lying levels of  $^{178}\text{Hf}$  which may be populated† in the decay of  $^{178}\text{Ta}$  and indicate that radiation of 91, 220 and 330 kev is to be expected.

In the present work sources of both short- and long-lived  $^{178}\text{Ta}$  were prepared by means of the  $^{181}\text{Ta}(\gamma, 3n)$  reaction. Tantalum foils were irradiated for periods of 10 minutes to 2 hours, at bremsstrahlung energies of 30 mev. A complex gamma-ray spectrum was observed, which, below 200 kev, was qualitatively indistinguishable from that of the 8 hr  $^{180}\text{Ta}$  activity shown in figure 1. Measurements with a single channel analyser of the decay of the lines at 55 and 95 kev are given in figure 3 (Band C) and show two components with half-lives of 8.15 hr, and  $9.5 \pm 0.1$  min corresponding to  $^{180}\text{Ta}$  and  $^{178}\text{Ta}$ . A 2.1 hr component of the 55 and 95 kev reaction was too weak to be observed in this way but was detected in the coincidence experiments described later.

The observed spectrum at energies above 200 kev is shown in figure 4. Well-defined photo-lines are present at  $215 \pm 5$ ,  $325 \pm 5$ ,  $415 \pm 10$ ,  $511 \pm 10$  and  $1390 \pm 10$  kev. Two further lines are present at  $1160 \pm 20$  and  $1480 \pm 20$  kev, partly confused by the 1390 kev line and its Compton distribution, but clearly seen when the observed spectrum is compared with that of the 1380 kev  $^{57}\text{Ni}$  radiation.

† The decay must proceed in this direction since  $^{178}\text{W}$  is radioactive and decays to  $^{178}\text{Ta}$  (Bisi, Terrani and Zappa 1956).

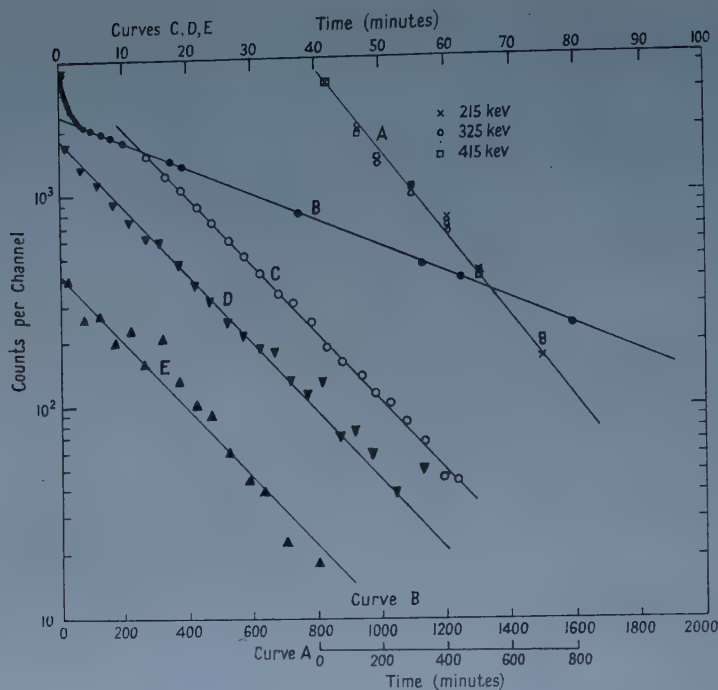


Figure 3. Decay curves: A, rotational band of  $^{178}\text{Ta}$ ; B, x-radiation with components of 8.15 hr and 9.5 min corresponding to  $^{180}\text{Ta}$  and  $^{178}\text{Ta}$  (decay of 95 keV line is similar); C, 9.5 min component of B; D, 900–1550 keV gamma radiation of  $^{178}\text{Ta}$ ; E,  $\beta^+$  annihilation radiation of  $^{178}\text{Ta}$ .

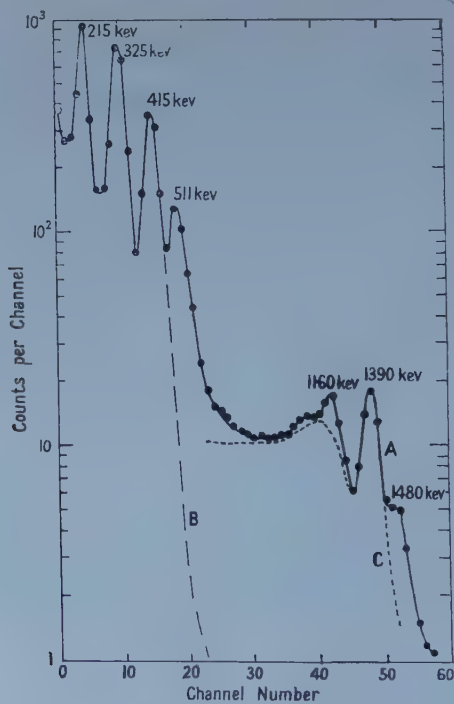


Figure 4. Gamma-ray spectra of  $^{178}\text{Ta}$ . A, spectrum obtained in first 20 min after irradiation; B, spectrum obtained two hours later, normalized to A at the 325 keV line; C, spectrum of 1380 keV  $^{57}\text{Ni}$  radiation normalized to the 1390 keV line of  $^{178}\text{Ta}$ .

Part A of the spectrum of figure 4 was taken in the first 20 minutes following a 15 min irradiation at 30 MeV; part B was taken two hours later and normalized to part A at the 325 keV line. The half-lives of the 511 keV and of the higher energy lines are clearly much less than 2 hours. The 511 keV line was selected with a single channel analyser and found to have a half-life of  $9.5 \pm 0.3$  min (figure 3, E). The radiation between 900 and 1550 keV also had a half-life of 9.5 min (figure 3, D) but owing to their low intensities it was not possible to determine the half-lives of the individual high-energy lines.

The lines at 215, 325 and 415 keV were found to have a half-life of  $150 \pm 10$  min (figure 3, A). If there were any 511 keV radiation of this half-life its intensity was less than 2% of that of the 415 keV line.

### 9.5 min Activity of $^{178}\text{Ta}$

The gamma rays associated with the 9.5 min  $^{178}\text{Ta}$  isomer and their relative intensities as estimated in these experiments are listed in table 2.

Table 2. Gamma Rays from 9.5 min  $^{178}\text{Ta}$

Gamma-ray Energy (keV)	55	95	511	1160	1390	1480
Relative intensity ( $\pm 25\%$ )	3300	300	100	6	75	19
(not corrected for internal conversion)						

Despite the complication arising from the 8.15 hr  $^{180}\text{Ta}$  activity some useful qualitative results were obtained from coincidence measurements. The 55 keV radiation was used to gate the kicksorter spectrum and lines at 55 keV and 95 keV were found with short-lived components showing that the 9.5 min decay populates a level at about 95 keV by K capture. Coincidence measurements made at  $90^\circ$  and  $180^\circ$  showed that the 511 keV radiation was due to positron annihilation but the intensities were insufficient to establish whether or not the annihilation radiation was in coincidence with the 95 keV and 55 keV radiations. No coincidence measurements were made on the higher energy radiation.

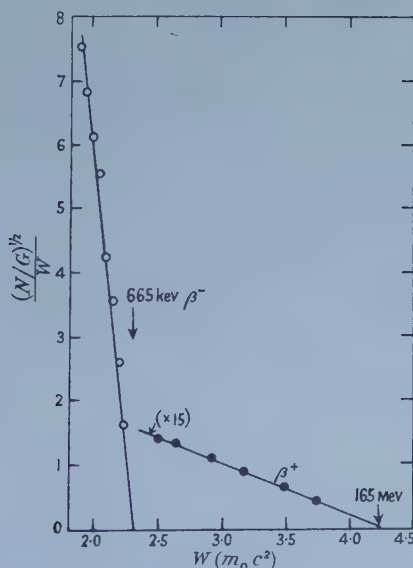


Figure 5. Fermi plots of  $\beta^-$  particles of  $^{180}\text{Ta}$  and  $^{178}\text{Ta}$ .

The positron and point energy was measured with the anthracene crystal using  $240 \text{ mg cm}^{-2}$  sources obtained from a 15 min irradiation at 30 MeV. The observed spectrum, shown in figure 5, is dominated by an 8.15 hr electron component with an end-point of  $665 \pm 25 \text{ keV}$  in fair agreement with the value 705 keV reported by Brown *et al.* for  $^{180}\text{Ta}$ . There is an additional component with an end point of  $1.65 \pm 0.05 \text{ MeV}$  and a half-life of about 10 min. The short half-life and the absence of the radiation at irradiation energies of less than 22 MeV go far to identify it as the positron, indicated by the annihilation radiation in the 9.5 min  $^{178}\text{Ta}$  gamma-ray spectrum.

#### 150 min Activity of $^{178}\text{Ta}$

The gamma-ray spectrum in coincidence with the 325 keV radiation is shown in figure 6; all lines in this spectrum decayed with a 150 min half-life. The coincidence measurements show that the 91, 215, 325 and 415 keV gamma-rays.

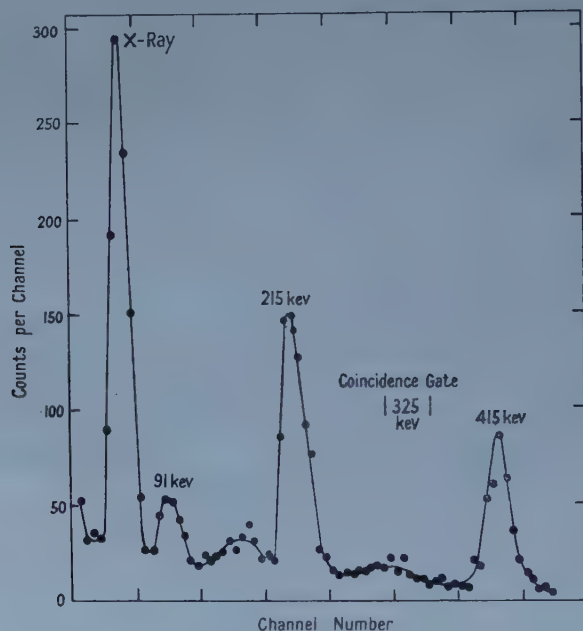


Figure 6.  $\gamma$ - $\gamma$  coincidence spectrum of 150 min  $^{178}\text{Ta}$  gated with the 325 keV line. The abscissae run from 0 to 80.

are in a cascade probably initiated by a K-capture event. The energies and relative intensities of the 150 min gamma rays are listed in table 3.

Table 3. Gamma Rays from 150 min  $^{178}\text{Ta}$

Gamma-ray energy (keV)	55	91	215	325	415	511
Relative intensity ( $\pm 25\%$ )	200	22	94	135	100	<2
(not corrected for internal conversion)						

#### Decay Scheme of $^{178}\text{Ta}$

The decay scheme shown in figure 7 has been constructed on the basis of the present somewhat incomplete experimental results using as a guide the strong coupling model of Bohr and Mottelson (1955) which is known to apply fairly well for nuclei having  $Z$  of the order of 70.





indicated in figure 7. The expected, weak, 9.5 min component in the decay of the 215 keV line could not be definitely established experimentally in the presence of the strong 150 min radiation. If the 1480 keV level is assumed to be the lowest member of a  $K=2^+$  rotational band the branching ratios for its decay to the  $K=0^+$ ,  $I=0, 2, 4$  levels can be calculated from the theory of Alaga *et al.* (1955). This theory predicts that the 1480, 1390 and 1160 keV lines should have intensities in the ratios 0.7:1:0.05. The observed ratios are 0.25:1:0.08 indicating that the 1480 keV line is about 2.5 times weaker than predicted which casts some doubt on the assignment  $K=2^+$  to the 1480 keV level.

The assignment  $I=1^+$  and  $I=8, 9$  or  $10^\pm$  to the 9.5 min and 150 min  $^{178}\text{Ta}$  isomers may be compared with the predictions of Mottelson and Nilsson (1955) and of Gottfried (1956). For deformations somewhat larger than those assumed for the corresponding odd  $A$  nuclides, both theories characterize the proton and neutron configurations by  $g_{7/2}(7/2^+)$  and  $i_{13/2}(9/2^+)$  respectively and predict an  $I=1^+$ ,  $8^+$  doublet for  $^{178}\text{Ta}$  in agreement with the present decay scheme. The  $I=8^+$  level is assumed to lie below the  $I=1^+$  level in accordance with the limited systematics on odd  $Z$ -odd  $N$  nuclei in the region  $Z \sim 70$  (cf.  $^{180}\text{Ta}$ ,  $^{182}\text{Ta}$  and  $^{176}\text{Lu}$ ).

#### REFERENCES

- ALAGA, G., ALDER, K., BOHR, A., and MOTTELSON, B. R., 1955, *K. Danske Vidensk. Selsk., Mat-Fys. Medd.*, **24**, No. 9.
- AXEL, P., 1954, *Rev. Sci. Instrum.*, **25**, 391.
- BISI, A., TERRANI, S., and ZAPPA, L., 1956, *Nuovo Cim.*, **3**, 661.
- BISI, A., ZAPPA, L., and ZIMMER, E., 1956, *Nuovo Cim.*, **4**, 307.
- BOCKELMAN, C. K., FENSTERMACHER, C. A., and DRAPER, J. E., 1957, *Bull. Amer. Phys. Soc.*, **2**, No. 1, 41, NA2.
- BOHR, A., and MOTTELSON, B. R., 1955, *Beta and Gamma Ray Spectroscopy* (Editor K. Siegbahn) (New York: Interscience Publications).
- BROWN, H. N., BENDEL, W. L., SHORE, F. J., and BECKER, R. A., 1951, *Phys. Rev.*, **84**, 292.
- CARVER, J. H., and TURCHINETZ, W., 1958, *Proc. Phys. Soc.*, **71**, 613.
- DAVISSON, C. M., 1955, *Beta and Gamma Ray Spectroscopy* (Editor K. Siegbahn) (New York: Interscience Publications).
- EBERHARDT, P., GEISS, J., LANG, C., HERR, W., and MERZ, E., 1955, *Z. Naturf.*, **10a**, 796.
- FEENBERG, E., and TRIGG, G., 1950, *Rev. Mod. Phys.*, **22**, 399.
- GOTTFRIED, K., 1956, *Phys. Rev.*, **103**, 1017.
- HEYDENBURG, N. P., and TEMMER, G. M., 1955, *Phys. Rev.*, **100**, 150.
- HOLLANDER, J. M., PERLMAN, I., and SEABORG, G. T., 1953, *Rev. Mod. Phys.*, **25**, 469, *Nuclear Level Schemes*, 1955, U.S.A.E.C. TID-5300.
- MIHELICH, J. W., SCHARFF-GOLDHABER, G., and McKEOWN, M., 1956, *Phys. Rev.*, **94**, 794 (A).
- MOSZKOWSKI, S. A., 1951, *Phys. Rev.*, **82**, 35.
- MOTTELSON, B. R., and NILSSON, S. G., 1955, *Phys. Rev.*, **99**, 1615. *See also:* Nilsson, S. G. 1955, *K. Danske Vidensk. Selsk., Mat-Fys. Medd.*, **29**, No. 16.
- NERVIK, W. E., and SEABORG, G. T., 1955, *Phys. Rev.*, **97**, 1092.
- PETKAU, A., 1956, *M.Sc. Thesis*, University of Manitoba.
- SUNYAR, A. W., 1955, *Phys. Rev.*, **98**, 653.
- WHITE, F. A., COLLINS, T. L., and ROURKE, F. M., 1955, *Phys. Rev.*, **97**, 566.
- WILKINSON, G., 1950, *Phys. Rev.*, **80**, 495.

## Polarization in Stripping Reactions

By H. C. NEWNS AND M. Y. REFAI

Department of Theoretical Physics, University of Liverpool

*Communicated by H. W. B. Skinner; MS. received 8th November 1957, and in final form 13th January 1958*

**Abstract.** Recent experimental results make a new discussion of the mechanism of this reaction necessary. A classical discussion is presented and the conclusions confirmed by quantum mechanical calculations at rather low energies. The qualitative features of the reaction seem now to be understood.

THE theory of the stripping reaction (Butler 1951 and subsequent reformulations; see for example Tobocean and Kalos 1955) shows that the differential cross section is proportional to the absolute square of the matrix element

$$\int \psi_p^* \psi_n^* V_{np} \psi_d d\mathbf{r}_n d\mathbf{r}_p$$

where  $V_{np}$  is the neutron-proton interaction,  $\psi_n$  is the wave function representing the neutron bound in the nucleus, and  $\psi_d$  and  $\psi_p$  are the wave functions representing the incident deuteron and outgoing proton respectively. The integration over  $\mathbf{r}_n$  is over the region  $r_n > R_0$  where  $R_0$  is the 'stripping radius'. Butler assumed that in  $\psi_d$  and  $\psi_p$  the interaction of the deuteron and proton with the initial and final nuclei respectively could be neglected and plane waves used. This approximation is perfectly good for the purposes of nuclear spectroscopy. In this approximation, however, the polarization of the outgoing protons is always zero.

If either the proton or deuteron wave functions, or both, are assumed to be distorted by the interaction with the nucleus (this can be simply the Coulomb interaction) then polarization can result. Thus the polarization arises as the result of a weakening of the assumptions of Butler's theory.

So far most of the theoretical treatments of polarization in (d, p) reactions have considered only the interaction of the proton with the nucleus. A classical argument which assumes that the nucleus is completely opaque to protons (Newns 1953) predicts that the polarization should be negative if the neutron is captured with  $j_n = l_n + \frac{1}{2}$  and positive if captured with  $j_n = l_n - \frac{1}{2}$  (the direction  $\mathbf{k}_d \times \mathbf{k}_p$  being positive). Quantum mechanical calculations at low energies (Horowitz and Messiah 1953 a, b) using essentially the same model as the classical theory do not yield such a simple rule, but do mainly confirm the assignments of the classical theory,† and so provide a justification for the classical treatment of this reaction, a reaction already known to be very classical in nature (Huby 1953).

† The exceptions occur in the so-called 'singular' region of Butler's theory, where the predictions of the theory are suspect. For a discussion of this region see, for example, Bhatia, Huang, Huby and Newns (1952).



A calculation by Cheston (1954) modifies previous treatments by introducing a spin-orbit coupling into the proton-nucleus interaction, and also takes into account the deuteron interaction with the nucleus. Unfortunately, these calculations are found to be in error even as regards the sign of the polarization (an error has been pointed out by Sawicki 1957, and in addition Cheston's equations (7) and (8) seem to be in error, although it is difficult to be sure of this in a paper where the theory is only sketched). These calculations have been repeated by the present authors and the results are included in the present paper.

Experimental results have only comparatively recently become available. Measurements of the polarization in the  $^{12}\text{C}(\text{d}, \text{p})^{13}\text{C}$  ground state reaction at 4 meV (Hillman 1956), 11 meV (Juveland and Jentschke 1956) and 9 meV (Bokhari *et al.* 1958) all agree that the sign of the polarization is negative at angles around the stripping peak. Since the neutron is captured with angular momentum  $j_n = l_n - \frac{1}{2}$  one would expect from the classical argument of Newns (1953) and presumably from analogous quantum mechanical calculations that the sign would be positive. Experiments on the  $^{29}\text{Si}(\text{d}, \text{p})^{29}\text{Si}$  reaction to the 4.93 meV and 6.38 meV excited states of  $^{29}\text{Si}$  (Juveland and Jentschke 1956) also indicate the opposite sign to that predicted by Newns (1953).

An important suggestion has been made in this respect by Tobocman (1956). In contrast to Newns (1953), Tobocman considers not the proton but the deuteron interaction with the nucleus. In this way he obtains positive polarization if the neutron is captured with  $j_n = l_n + \frac{1}{2}$  and negative if it is captured with  $j_n = l_n - \frac{1}{2}$ . These signs are opposite to those obtained by Newns and are in agreement with experiment.

In practice, however, both the deuteron and proton interactions have to be considered, and one would then expect a polarization intermediate between that obtained using the separate interactions (classically one would expect it to be the algebraic sum of the polarization from the separate interactions). The precise polarization will depend on the details of the interactions and the fact that the sign of polarization determined experimentally agrees with Tobocman's model indicates that the nucleus is much more opaque to deuterons than to protons. This is, of course, physically very reasonable.

A further point of interest in the experimental results is the occurrence of polarizations as large as 40-50% (Hillman 1956, Juveland and Jentschke 1956). If no spin forces are involved in the deuteron and proton interactions with the nucleus, the maximum polarization which can be obtained is  $33\frac{1}{3}\%$  (Newns 1953, Horowitz and Messiah 1953 b). Consequently, if a detailed description of the experimental results is to be obtained, spin forces must be introduced. Cheston (1954) has used a spin-orbit force in the proton nucleus interaction. Such a force is well substantiated by the analysis of experiments on the elastic scattering of protons and would relieve the restriction of a  $33\frac{1}{3}\%$  maximum for the polarization. This spin-orbit force would not be expected to affect the sign of the polarization in the 'classical' region, i.e. where the stripping amplitude is large. The effect of this force is to introduce different scattering amplitudes for protons having  $j_p = l_p + \frac{1}{2}$  and  $j_p = l_p - \frac{1}{2}$ . Since the spin-orbit force is not of great magnitude compared with the static potential, this difference will be rather small and although it will change the magnitude slightly it should not affect the sign. The conclusions are borne out by calculations to be presented later in the paper.



Before discussing these calculations, it should be mentioned that the Coulomb field of the nucleus has been ignored in all the work mentioned so far in this discussion. In his work on stripping reactions at very low energies, Yoccoz (1954) has shown that if the effect of the Coulomb field on the deuteron and proton is taken into account (no nuclear interactions) then polarization can result and the sign of the polarization depends on the angular momentum of the captured neutron in the same way as in Tobocman's model. Since the Coulomb field cannot be responsible for the results at the higher energies (9 or 11 mev), and since we are interested in the mechanism of the reaction and the validity of the classical model rather than a detailed fit of the experiments, we have ignored its effect altogether.

### CALCULATIONS

The classical arguments which have been presented in the earlier part of this paper throw a great deal of light on the mechanism responsible for the production of polarization in stripping reactions. It is important to confirm these results by quantum mechanical calculations, especially at rather low energies since it is here that the classical arguments are most suspect. Although Cheston's (1954) work contains errors, it has aroused considerable interest. Consequently, it was decided to use the same interactions as assumed by Cheston. The work was extended, however, by investigating the part played by the interactions separately and in various combinations. This facilitates comparison with the classical arguments.

The interactions which Cheston used were as follows: a hard sphere interaction for the deuteron of radius  $R_0 = 6.5 \times 10^{-13}$  cm, and a cloudy crystal ball potential plus spin-orbit interaction for the proton of the form  $-19(1 + 0.05i) - 2\mathbf{LS}$  (mev) when  $r < r_0$  and zero when  $r > r_0$  where  $r_0 = 1.45A^{1/3} \times 10^{-13}$  cm. We discuss the  $^{12}\text{C}(d, p)^{13}\text{C}$  ground state reaction at a deuteron energy of 3.21 mev. We assume that the proton waves with  $l_p = 0, 1, 2$  and deuteron waves with  $l_d = 0, 1$  are distorted by the potentials. Five cases are considered.

(1) Deuteron waves distorted by the hard sphere scattering.† Zero potential for the protons (plane waves).

(2) Proton waves distorted by the cloudy crystal ball potential but without the spin-orbit term. Plane wave deuterons.

(3) Proton waves distorted by the cloudy crystal ball potential including the spin-orbit term. Plane wave deuterons.

(4) Proton and deuteron waves both distorted by the respective potentials but no spin-orbit term in the proton potential.

(5) Proton and deuteron waves both distorted including the spin-orbit term in the proton potential.

† It will be noticed that in the classical treatment we have assumed black-body absorptions of the deuterons, while in the quantum mechanical treatment we follow Cheston in using a hard-sphere reflection. Since only qualitative results are sought in this paper, it is considered by the authors that, provided the deuteron interaction is strong, it does not much matter whether it is strong absorption or strong reflection since both these interactions are effective in removing deuterons from the beam.

The results for the polarization and the angular distribution for these five cases are shown in figures 1 to 5 respectively. The sign of the polarization in figure 1 confirms the classical argument of Tobocman (1956) and the sign in figure 2 confirms the classical argument of Newns (1953). The effect of including the spin-orbit term in the proton potential is seen by comparing figures 2 and 3.

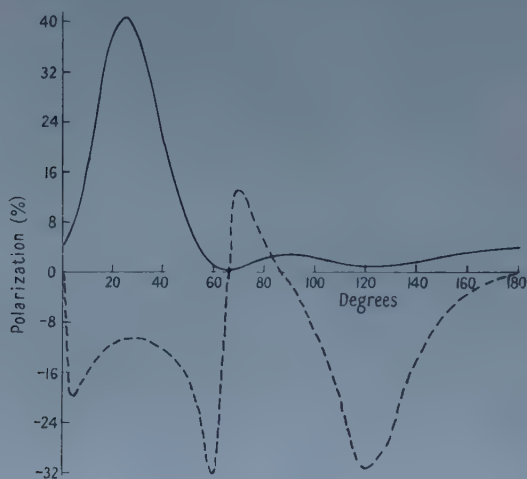


Figure 1.

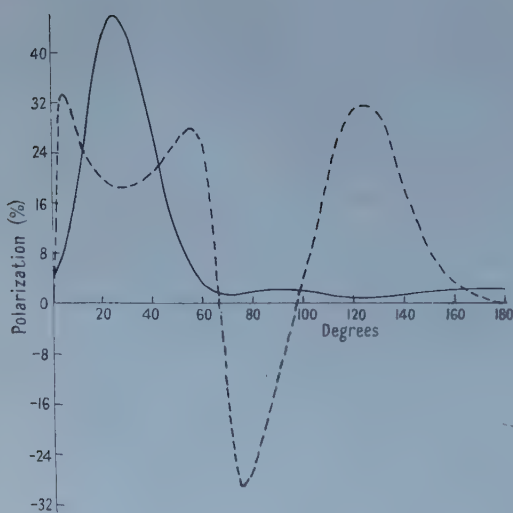


Figure 2.

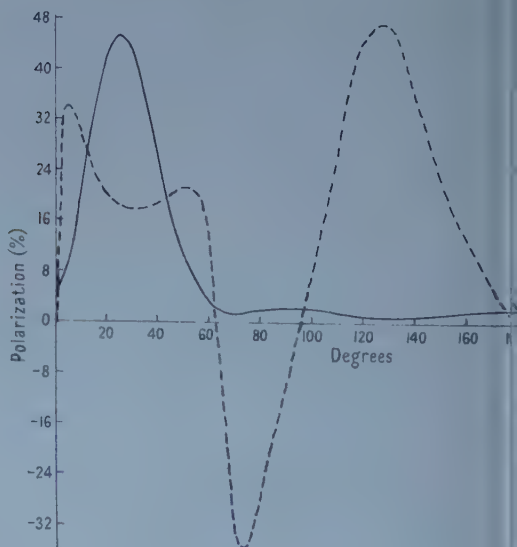


Figure 3.

or 4 and 5. As expected, the effect is small in the 'classical' region of the stripping peak but can give large polarizations where the various amplitudes are small. The calculations with and without the spin-orbit force are very similar but have one essential difference. The spin-orbit force introduces terms which have no

counterpart in the calculations which omit the spin-orbit coupling. These terms represent spin-flip scattering of the proton. This can occur since the plane of scattering of the proton by the final nucleus is not necessarily the plane defined by the (d, p) reaction. These terms, which are in fact those omitted by Cheston (Sawicki 1957), depend on the factor  $\eta(l_p, j_p^+) - \eta(l_p, j_p^-)$  where  $j_p^\pm = l_p \pm \frac{1}{2}$  and the  $\eta$ 's are those defined by Blatt and Weisskopf (1952), and so are negligibly small except where the other amplitudes are also very small. This is also borne out by the fact that the angular distributions in the two cases with and without spin-orbit coupling are practically identical.

Figures 4 and 5 show the result of including both proton and deuteron interactions. Classically one would expect the same polarizations as are obtained by adding together the polarizations in figures 1 and 2, and 1 and 3 respectively, and this is indicated by the dotted line in figures 4 and 5. This result would be strictly correct if only the interference terms between the stripping amplitude and the distorted parts of the deuteron and proton waves respectively were of consequence. It is seen that even at these low energies the classical approximation is surprisingly good although other interference terms do contribute. It would be expected that at higher energies these other terms would be relatively smaller and the classical approximation more accurate. This result may be of practical use as a step in the detailed analysis of experiments at higher energies.

Figure 5 shows the results obtained from the treatment of Cheston's model, and these are in fact quite different from his published results. The internal consistency of the present results gives confidence in their correctness.

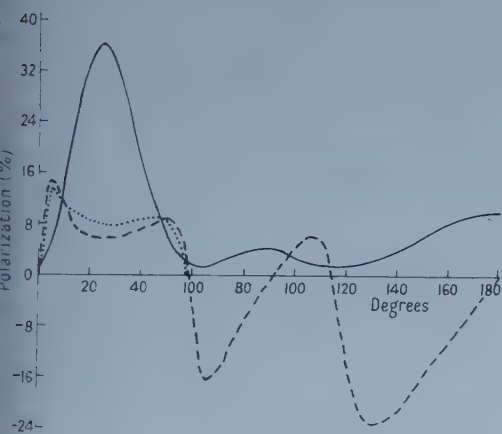


Figure 4.

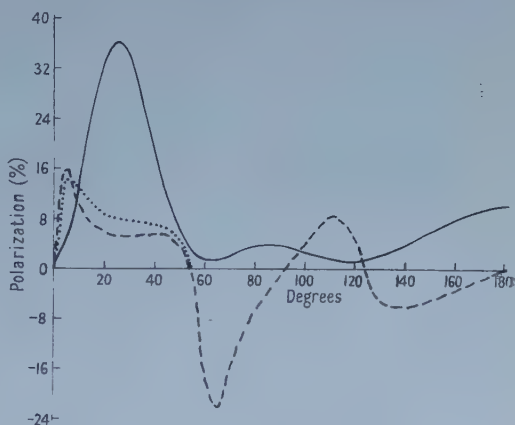


Figure 5.

Some general features not obtainable from classical arguments can also be found in these results. It is seen that the polarization changes sign near the first stripping minimum and it is due to the stripping amplitude changing sign and being large enough to outweigh the other interference terms. The behaviour of the polarization around the stripping peak can also be understood on general grounds. It is seen that the polarization rises rapidly from zero in the forward direction and then decreases at the stripping peak, possibly rising again on the large angle side before changing sign. The smallness of the polarization at the peak is due to the fact that the polarization is a 'correction' to pure stripping theory, which itself would give zero polarization. Near the stripping peak the

corrections are relatively small but as the stripping amplitude diminishes on either side the corrections become more important and larger polarizations result. This behaviour is found also in the experimental results (Juveland and Jentschke 1956).

Finally, it is seen that the particular combination of proton and deuteron interaction which has been used does not agree with the experimental results since it gives polarization of the wrong sign. This combination will have to be adjusted if a detailed fit is to be obtained. We have, however, provided evidence for the validity of the classical arguments which are useful for a qualitative discussion of the experiments and many features of this reaction seem now to be understood.

#### ACKNOWLEDGMENT

We are greatly indebted to Dr. R. Huby for many valuable discussions.

#### REFERENCES

- BHATIA, A. B., HUANG, K., HUBY, R., and NEWNS, H. C., 1952, *Phil. Mag.*, **43**, 485.  
 BLATT, J. M., and WEISSKOPF, V. F., 1952, *Theoretical Nuclear Physics* (New York: Wiley).  
 BOKHARI, M. S., COOKSON, J. A., HIRD, B., and WEESAKUL, B., 1958, *Proc. Phys. Soc.*, **71** (in the press).  
 BUTLER, S. T., 1951, *Proc. Roy. Soc. A*, **208**, 559.  
 CHESTON, W. B., 1954, *Phys. Rev.*, **96**, 1590.  
 HILLMAN, P., 1956, *Phys. Rev.*, **104**, 176.  
 HOROWITZ, J., and MESSIAH, A., 1953 a, *Phys. Rev.*, **92**, 1326 ; 1953 b, *J. Phys. Radium*, **14**, 731.  
 HUBY, R., 1953, *Progr. Nucl. Phys.*, **3**, 177.  
 JUVELAND, A. C., and JENTSCHKE, W., 1956, *Bull. Amer. Phys. Soc. Ser. II*, **1**, 193.  
 NEWNS, H. C., 1953, *Proc. Phys. Soc. A*, **66**, 477.  
 SAWICKI, J., 1957, *Phys. Rev.*, **106**, 172.  
 TOBOCMAN, W., 1956, *Tech. Rep. No. 29, Case Institute of Technology*.  
 TOBOCMAN, W., and KALOS, M. H., 1955, *Phys. Rev.*, **97**, 132.  
 YOCOZ, J., 1954, *Proc. Phys. Soc. A*, **67**, 813.



# The Electrical Conductivity and Thermoelectric Power of Bismuth Telluride†

By H. J. GOLDSMID

Research Laboratories of the General Electric Company Limited, Wembley, Middx.

*MS. received 22nd October 1957, and in revised form 5th January 1958*

**Abstract.** The electrical conductivity and thermoelectric power of the semiconductor  $\text{Bi}_2\text{Te}_3$  have been measured between  $150^\circ\text{K}$  and  $300^\circ\text{K}$ . n-type and p-type samples with a wide range of carrier concentration have been included. Most samples have shown extrinsic conduction and have been partially degenerate over at least part of the temperature range, so it has been necessary to use Fermi-Dirac statistics in interpreting the results. A few samples have exhibited mixed and intrinsic conduction at the higher temperatures. It has been possible to determine the variation of carrier mobility with temperature and to estimate the energy dependence of the relaxation time, as well as a number of the semiconductor parameters.

## § 1. INTRODUCTION

THE first comprehensive electrical measurements, which demonstrated that  $\text{Bi}_2\text{Te}_3$  is a semiconductor, were made by Vlasova and Stil'bans (1955). They measured the electrical conductivity, thermoelectric power and Hall coefficient for sintered, polycrystalline material. The same properties have also been measured for single crystals by Shigetomi and Mori (1956) and by Konorov (1956). A preliminary survey of the properties of  $\text{Bi}_2\text{Te}_3$  has been given by Wright (1956). Recently Harman *et al.* (1957) and Black *et al.* (1957) have published the results of measurements on  $\text{Bi}_2\text{Te}_3$  and similar compounds.

The work to be described here has consisted of the measurement of the electrical conductivity and thermoelectric power of samples of  $\text{Bi}_2\text{Te}_3$  covering a wide range of carrier concentration. All the measurements have been made with the current flow parallel to the cleavage planes, i.e. perpendicular to the  $c$  crystal axis. One of the main objects of the measurements has been the establishment of the parameters from which the electronic component of the thermal conductivity may be calculated. The magnitude of the Lorenz number is dependent on the scattering law for the charge carriers and, over the range of partial degeneracy, on the position of the Fermi level. The application of the results to heat conduction in  $\text{Bi}_2\text{Te}_3$  will be considered separately (Goldsmid 1958).

## § 2. EXPERIMENTAL PROCEDURE

### 2.1. Preparation of Samples

Zone-refined ingots of  $\text{Bi}_2\text{Te}_3$  are generally polycrystalline, but the  $c$  axes of the individual crystals have always been perpendicular to the direction of zone refining. Consequently, samples cut from such ingots have been suitable

† The material contained in this paper forms part of a Ph.D. thesis submitted to the University of London.

for use in measurements with gradients parallel to the cleavage planes. Most of the results, which are reported here, have been obtained with such samples, but some measurements have been carried out using single crystals. No difference between the properties of the single crystals and of the zone-refined material has been found.

$\text{Bi}_2\text{Te}_3$ , when prepared from the pure elements in the atomic proportions 2:3, is always found to be p-type with an electrical resistivity at room temperature of about  $2 \times 10^{-3}$  ohm cm. n-type material may be prepared by the addition of excess tellurium, any of the halogens, or certain metals such as lithium or aluminium (A. R. Sheard, private communication). Although most n-type samples have been doped with iodine, it has been found that the relationship between the thermoelectric power and the electrical conductivity is the same if one of the other donor impurities is employed. Similarly, the relation between these properties for p-type  $\text{Bi}_2\text{Te}_3$  is the same for samples containing excess bismuth or other acceptors, for example, lead or cadmium.

In order to solder contacts to  $\text{Bi}_2\text{Te}_3$  it was first necessary to electroplate the samples. All the results were obtained using nickel-plated specimens. At one stage the use of copper-plating was contemplated but it was found that remarkable changes took place during the plating process. p-type samples became n-type, indicating that copper is a donor impurity with an exceptionally high rate of diffusion in  $\text{Bi}_2\text{Te}_3$  (cf. the diffusion of copper in  $\text{PbTe}$ ) (Bloem and Kröger 1956). Moreover, it was found that copper, dissolved in molten solder, could diffuse through nickel-plating and then into  $\text{Bi}_2\text{Te}_3$ ; precautions against contamination of samples in this way were taken.

## 2.2. Measurement of Conductivity and Thermoelectric Power

The measurement of the electrical conductivity of  $\text{Bi}_2\text{Te}_3$  using direct current is complicated by large thermoelectric effects. These effects have been eliminated by the use of alternating current. A modified Wheatstone bridge has been employed; since all reactances in the circuit were kept to a minimum, the bridge could be treated as a direct current network. The basic circuit diagram is shown in figure 1.

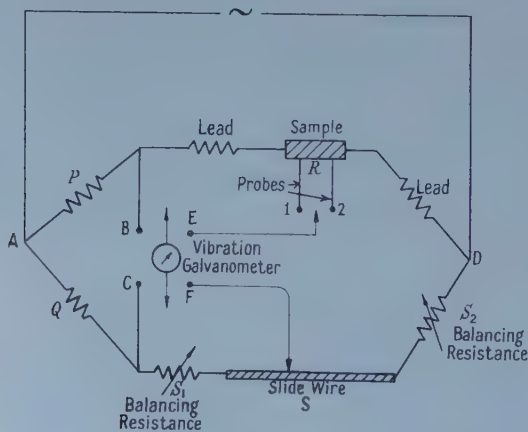


Figure 1. Basic circuit diagram for conductivity apparatus.

The ratio of the standard resistances  $P$  and  $Q$  was of the order of the ratio of the resistance  $R$  of the sample to that  $S$  of the calibrated slide wire.  $S_1$  and  $S_2$  were balancing resistances to compensate for the resistances of the leads to the sample. Before each measurement, balance was obtained with the vibration galvanometer inserted between B and C. The ratio of the current through the sample  $i_R$  to that through the slide wire  $i_s$  was then given by  $i_R/i_s = Q/P$ . Then, with the galvanometer between E and F, the positions of contact on the slide wire, for balance against the potentials at the probes 1 and 2 on the sample, were found. Thus if  $\Delta R$  was the resistance of the sample between the probes, and if  $\Delta S$  was the resistance of the slide wire between the balance points,  $\Delta R/\Delta S = P/Q$ .

The sample was contained in a simple cryostat which enabled measurements to be made over the temperature range  $100^\circ\text{K}$  to  $300^\circ\text{K}$ . Full details of this cryostat and of the electrical circuit have been given elsewhere (Goldsmid 1957). The estimated total error from all sources was no more than about 2%.

The thermoelectric power of  $\text{Bi}_2\text{Te}_3$  against copper was obtained from the potential difference between the source and the sink of the apparatus for the measurement of thermal conductivity which has been described previously (Goldsmid 1956). After allowing for the small thermoelectric power of copper (Borelius 1953), the absolute value was determined. A total error of less than 1.5% in this measurement was estimated.

### § 3. THERMOELECTRIC POWER OF EXTRINSIC $\text{Bi}_2\text{Te}_3$

The thermoelectric power  $\alpha$  of a non-degenerate extrinsic semiconductor, for which the relaxation time of the charge carriers  $\tau$  is related to their kinetic energy  $E$  by

$$\tau(E) \propto E^{q/2}, \quad \dots\dots (1)$$

is given by

$$|\alpha| = \frac{k}{e} \left( \frac{5+q}{2} - \eta \right) \quad \dots\dots (2)$$

where  $\eta$  is the reduced Fermi potential, i.e. the energy at the Fermi level measured from the band edge in units of  $kT$  (Wilson 1953, p. 232). Conventionally, the thermoelectric power is positive for a p-type semiconductor and negative for an n-type semiconductor.

The carrier concentration  $n$  is also related to the reduced Fermi potential by

$$n = 2 \left( \frac{2\pi m^* kT}{h^2} \right)^{3/2} \exp(\eta) \quad \dots\dots (3)$$

where  $m^*$  is the effective mass of the charge carriers and  $T$  is the absolute temperature. Expressions (2) and (3) are valid only for spherical or ellipsoidal equal-energy-surfaces in momentum space.

For many semiconductors there is a range of temperature, the saturation range, in which no further ionization of impurities takes place, and in which intrinsic excitation of carriers is not yet appreciable. In this range the carrier concentration remains constant so, from (2) and (3) it follows that the product of  $T^{3/2}$  and  $\exp(\eta)$  must be constant. The thermoelectric power should then be given by

$$|\alpha| = \frac{3}{2} \frac{k}{e} \ln T + \text{constant}. \quad \dots\dots (4)$$

Thus, in the saturation range, a plot of thermoelectric power against  $\ln T$ , for a particular sample, should be a straight line of slope  $3k/2e$ . In figures 2 and 3, therefore, the results of the experiments have been presented as plots of thermoelectric power against  $\ln T$ . Both the n-type and p-type ingots with the higher thermoelectric powers show a linear variation over a considerable range of temperature so it seems reasonable to suppose that the carrier concentration was constant. The non-linear variation at the higher temperatures is clearly due to the influence of mixed conduction as the intrinsic range is approached. The departures from the linear plots, for thermoelectric powers below about  $-190 \mu\text{V deg}^{-1}$  for n-type  $\text{Bi}_2\text{Te}_3$  and  $+170 \mu\text{V deg}^{-1}$  for p-type  $\text{Bi}_2\text{Te}_3$  are due to the effects of degeneracy.

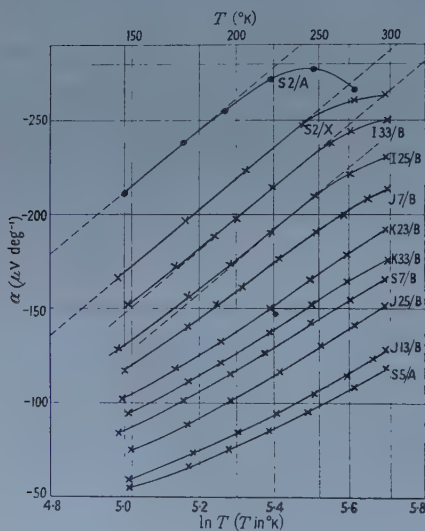


Figure 2. Thermoelectric power plotted against  $\ln$  (temperature) for n-type  $\text{Bi}_2\text{Te}_3$ .

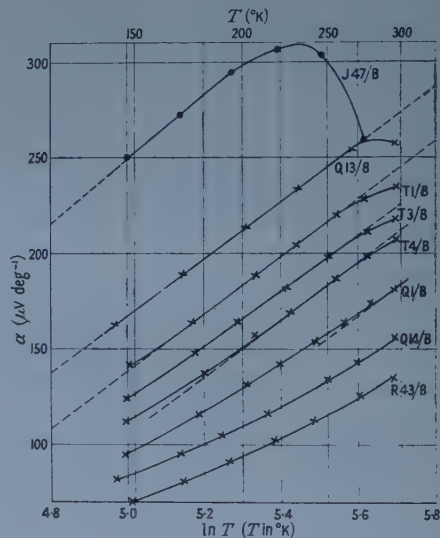


Figure 3. Thermoelectric power plotted against  $\ln$  (temperature) for p-type  $\text{Bi}_2\text{Te}_3$ .

The slope of the plots of thermoelectric power against  $\ln T$ , over the linear range, is not exactly equal to the value  $3k/2e$  predicted by the simple theory, for either n-type or p-type material. The slope for n-type  $\text{Bi}_2\text{Te}_3$  is  $167 \mu\text{V deg}^{-1}$  and for p-type material it is  $150 \mu\text{V deg}^{-1}$  whereas the numerical value of  $3k/2e$  is  $129 \mu\text{V deg}^{-1}$ . There are a number of possible explanations of this discrepancy; three of the most reasonable will be discussed here.

One possibility is that the energy dependence of the relaxation time changes with temperature. However, over the experimental range of temperature, as shown in the next section, there was no evidence of such an effect.

Another possibility is that the effective masses of the charge carriers are temperature dependent. For example, Chasmar and Stratton (1956) have used the assumption of a variable effective mass in explaining the measurements on indium antimonide and indium arsenide. However, the results of the next section suggest that covalent-type lattice scattering of the charge carriers is



predominant and, in this case, the mobility should vary with effective mass according to

$$\mu \propto (m^*)^{-5/2}. \quad \dots\dots (5)$$

Thus, a comparatively slow variation of the effective mass with temperature would have a large effect on the mobility variation and, particularly for n-type material, a much stronger dependence of the mobility on temperature than is observed, might have been expected. Furthermore, the calculation of the Lorenz number based on the assumption of a variable effective mass could not be reconciled with the experimental observations on the thermal conductivity and it is concluded that the inertial effective mass, at least, is not appreciably dependent on temperature.

A further possibility is that the density of states within the energy bands is not proportional to  $E^{1/2}$ . This could be the result of warped energy surfaces such as are supposed to occur for the valence band in germanium (Herman 1955), or it could result from the presence of an overlapping impurity band. In § 5.2 some evidence for such an overlapping impurity band is presented, but there are some difficulties in attributing the departure of the slopes in figures (2) and (3) from the theoretical value to its presence. It might be expected, for example, that the effect of such an impurity band would depend on the carrier concentration. Furthermore, Brooks (1955) has suggested that the assumption of ellipsoidal energy surfaces should always hold true sufficiently close to the band edges.

It is concluded that no really satisfactory explanation of the departure of the experimental variation of thermoelectric power from that predicted by the simple theory can be given at the present time. However, the departure is quite small and it is considered that its bearing on the calculations which follow later should be slight.

Incidentally, the experiments show that there can have been no phonon contribution to the thermoelectric power (Herring 1954), such as has been observed for germanium (Frederikse 1953), at least over the temperature range 150°K to 300°K. The result of such an effect would have been a considerable increase in the thermoelectric power at low temperatures.

#### § 4. ELECTRICAL CONDUCTIVITY OF EXTRINSIC Bi<sub>2</sub>Te<sub>3</sub>

The carrier mobility  $\mu$  of a semiconductor is related to its electrical conductivity  $\sigma$  by

$$\sigma = ne\mu. \quad \dots\dots (6)$$

Also, for lattice scattering of the charge carriers where it is assumed that the mean free path is inversely proportional to the temperature, the mobility varies with temperature according to

$$\mu \propto T^{3/2-1}. \quad \dots\dots (7)$$

The measurements of thermoelectric power have shown that the carrier concentration remained constant over the whole range of temperature, apart from the effects of mixed conduction. Thus, from (6), the variation of electrical conductivity with temperature represents the variation of mobility. Figures 4 and 5 show the results of experiments, for n-type and p-type Bi<sub>2</sub>Te<sub>3</sub> respectively presented as plots of log (conductivity) against log  $T$ .

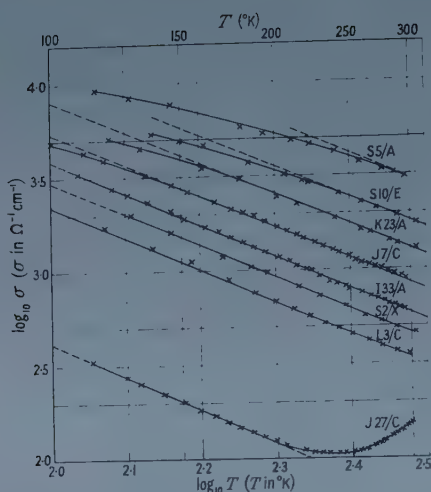


Figure 4. Log (electrical conductivity) plotted against log (temperature) for n-type  $\text{Bi}_2\text{Te}_3$ .

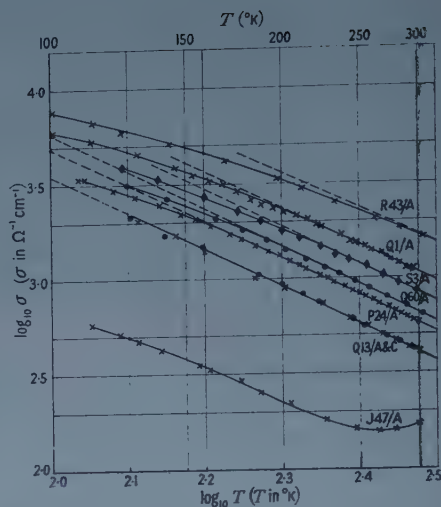


Figure 5. Log (electrical conductivity) plotted against log (temperature) for p-type  $\text{Bi}_2\text{Te}_3$ .

Considering, first of all, n-type  $\text{Bi}_2\text{Te}_3$ , each plot follows one of a series of parallel straight lines for at least some portion of the temperature range. Some samples no longer follow the linear variation at the higher temperatures, due to mixed conduction. At the highest conductivities, also, the plots depart from the straight lines, this being due to degeneracy. For each sample with a reasonably long straight line portion, the slope has been measured, and in no case was it found to depart appreciably from a value of  $-1.72$ . Thus, for non-degenerate  $\text{Bi}_2\text{Te}_3$ , over the range of temperature  $150^\circ\text{K}$  to  $300^\circ\text{K}$ , the variation of the electron mobility is given by

$$\mu_n \propto T^{-1.72}.$$

(The subscripts n and p will be used to denote electron and hole conduction respectively.) Substitution in relation (7) gives  $q_n = -1.44$  which may be compared with the value  $q = -1$  which applies for the simplest form of covalent-type lattice scattering.

The results for p-type  $\text{Bi}_2\text{Te}_3$  are, qualitatively, similar to those for n-type material. Again there are plots which show departures from a series of parallel straight lines due to mixed conduction and degeneracy. However, for p-type  $\text{Bi}_2\text{Te}_3$ , the straight lines have a different slope; the mean experimental value is  $-1.94$ , so the mobility of holes, for non-degenerate  $\text{Bi}_2\text{Te}_3$ , is given by

$$\mu_p \propto T^{-1.94}.$$

The corresponding value of  $q_p$  from expression (7) is

$$q_p = -1.88.$$

It will be noticed that the p-type sample with the lowest conductivity shows a departure from the linear variation of  $\log \sigma$  with  $\log T$  below about  $150^\circ\text{K}$ . The reason for this effect is not understood; it is certainly not due to degeneracy since it is not present for a less pure sample.

## § 5. APPLICATION OF FERMI-DIRAC STATISTICS

### 5.1. Thermoelectric Power

The use of the classical theory of conduction has enabled some important conclusions to be reached but, in order to proceed further, it is necessary to take some degree of degeneracy into account, since the low thermoelectric power of some samples implies that the Fermi level must have been well inside the appropriate energy band. In this sub-section the dependence of thermoelectric power on the reduced Fermi potential will be calculated. It will be assumed that the scattering law remains unchanged by, for example, impurity scattering, even at high carrier concentrations and low temperatures; the results of the next sub-section justify this assumption.

If Maxwell-Boltzmann statistics are replaced by Fermi-Dirac statistics, equation (2), relating the thermoelectric power to the reduced Fermi potential, becomes (Wilson 1953, p. 204)

$$|\alpha| = \frac{k}{e} \left( \frac{1}{kT} \frac{K_2}{K_1} - \eta \right) \quad \dots\dots (8)$$

where

$$K_n = \frac{16\sqrt{2\pi}(m^*)^{1/2}}{3h^3} \int_0^\infty \tau(E) E^{n+1/2} \frac{\partial f_0(\eta)}{\partial E} dE \quad \dots\dots (9)$$

and

$$f_0 = \{1 + \exp(E - \eta)\}^{-1}.$$

Substituting  $\tau(E) \propto E^{q/2}$  and integrating by parts it is found that

$$K_n = \text{const.} \left( n + \frac{1}{2}(q+1) \right) kT^{n+(q+1)/2} \int_0^\infty E^{n+(q-1)/2} f_0 dE. \quad \dots\dots (10)$$

Let

$$\int_0^\infty E^r f_0 dE$$

be represented by  $F_r(\eta)$ . McDougall and Stoner (1938) have given tables of  $F_{3/2}$  and  $F_{1/2}$ , and also  $F_{1/2}'$  which is related to  $F_{-1/2}$  since it may be shown that

$$\frac{\partial}{\partial \eta} F_r = r F_{r-1}. \quad \dots\dots (11)$$

Also, Rhodes (1950) has given tables of  $F_r(\eta)$  for  $r$  equal to 4, 3, 2 and 1 and  $F_0(\eta)$  is merely  $\int f_0 dx$  from 0 to  $\infty$ . However, no tables of  $F_r$  have been published for other than integral or half-integral values of  $r$ .

The expression for the thermoelectric power (8) involves the integrals  $K_1$  and  $K_2$ . Thus, using the results of § 4, these integrals are needed for values of  $q$  equal to  $-1.44$  and  $-1.88$ , for n-type and p-type  $\text{Bi}_2\text{Te}_3$  respectively. The nearest values of  $q$ , leading to integral or half-integral values of  $r$ , are  $-1$  and  $-2$ . For  $q = -1$  the evaluation of  $K_2$  and  $K_1$  involves the integrals  $F_1$  and  $F_0$  respectively, while for  $q = -2$  the integrals  $F_{1/2}$  and  $F_{-1/2}$  are required.

Using equation (8), and the values of  $F_r$  from the tables, the dependence of the thermoelectric power on the reduced Fermi potential has been calculated for  $q = -1$  and  $-2$ . The results are represented by the top and bottom curves,

respectively, of figure 6. Now, in the range where classical statistics are applicable, as will be seen from equation (2), the variation of thermoelectric power with  $q$  is linear. Moreover, at the degenerate limit

$$|\alpha| = (q+3)\pi^2 k/\eta \quad \dots\dots (12)$$

and again the thermoelectric power varies linearly with  $q$ . Thus, in the region of partial degeneracy covered by figure 6, the values of the thermoelectric power in terms of the reduced Fermi potential, corresponding to  $q = -1.44$  and  $-1.88$ , have been obtained by linear interpolation. The results of the interpolation are represented by the two inner curves which, therefore, show how the thermoelectric power is expected to vary with the Fermi potential for n-type and p-type  $\text{Bi}_2\text{Te}_3$ .

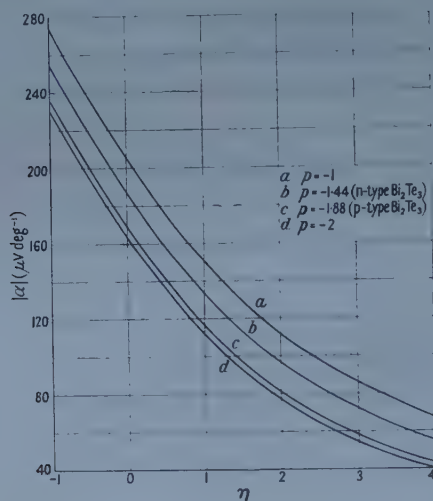


Figure 6. Thermoelectric power plotted against reduced Fermi potential.

### 5.2. Electrical Conductivity

For a non-degenerate semiconductor the use of equations (2), (3) and (6) enables the quantity  $\mu(m^*/m)^{3/2}$  to be determined if the dependence of the electrical conductivity on the thermoelectric power has been measured. An additional measurement of, for instance, the Hall constant is needed in order to obtain the mobility  $\mu$  or the effective mass  $m^*$ , separately. In order to determine  $\mu(m^*/m)^{3/2}$  for partially degenerate  $\text{Bi}_2\text{Te}_3$ , it is necessary to use Fermi-Dirac statistics.

In figures 7, 8, 9 and 10 the thermoelectric power has been plotted against electrical conductivity for n-type and p-type  $\text{Bi}_2\text{Te}_3$  at  $150^\circ\text{K}$  and  $300^\circ\text{K}$ . The carrier concentration has been obtained in terms of the reduced Fermi potential from the expression

$$n = \frac{4}{\sqrt{\pi}} \left( \frac{2\pi m^* kT}{h^2} \right)^{3/2} F_{1/2} \quad \dots\dots (13)$$

and, thus, in terms of the thermoelectric power and the effective mass using figure 6. It has, therefore, been possible to relate the electrical conductivity and the carrier concentration, so, defining the mobility by equation (6), the product  $\mu(m^*/m)^{3/2}$  has been calculated. In figures 11 and 12 this product



has been plotted against the reduced Fermi potential  $\eta$ , for n-type and p-type  $\text{Bi}_2\text{Te}_3$ , respectively. In both cases the product appears to remain constant until  $\eta > 0$ , i.e. until the Fermi level lies within the appropriate band. It may be noted that, even at  $150^\circ\text{K}$ , there appears to be no effect of impurity scattering; the decrease of  $\mu(m^*/m)^{3/2}$  for  $\eta > 1$  is merely the consequence of degeneracy. In fact, as will be shown in the next paragraph, a more rapid fall of this product with rise of  $\eta$  might have been expected.

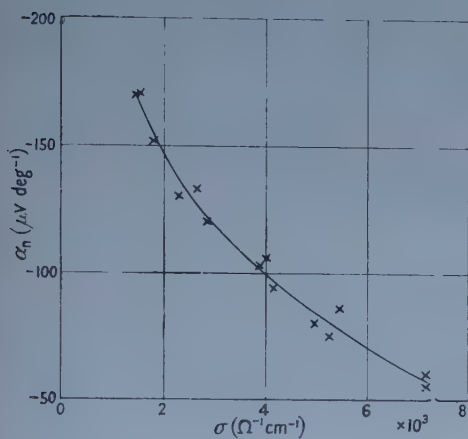


Figure 7. Thermoelectric power plotted against electrical conductivity for n-type  $\text{Bi}_2\text{Te}_3$  at  $150^\circ\text{K}$ .

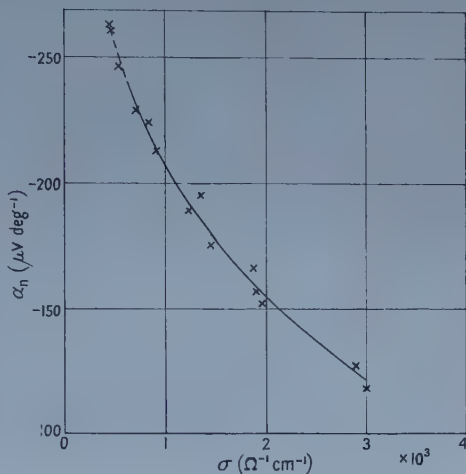


Figure 8. Thermoelectric power plotted against electrical conductivity for n-type  $\text{Bi}_2\text{Te}_3$  at  $300^\circ\text{K}$ .

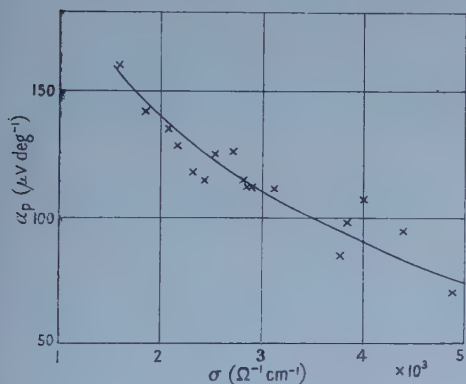


Figure 9. Thermoelectric power plotted against electrical conductivity for p-type  $\text{Bi}_2\text{Te}_3$  at  $150^\circ\text{K}$ .

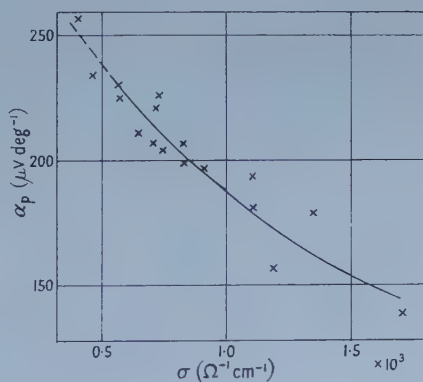


Figure 10. Thermoelectric power plotted against electrical conductivity for p-type  $\text{Bi}_2\text{Te}_3$  at  $300^\circ\text{K}$ .

The theoretical variation of the mobility with the position of the Fermi level will now be calculated, using the assumption that the same scattering law applies throughout the range of concentrations under consideration. The electrical conductivity is given by

$$\sigma = e^2 K_1. \quad \dots\dots (14)$$

Thus, using the definition of mobility as given above,

$$\mu \propto \sigma/n \propto K_1/F_{1/2}. \quad \dots\dots (15)$$

Now, from (10),  $K_1$  is proportional to  $F_{(q+1)/2}$  so,

$$\left. \begin{aligned} \mu_n &\propto F_{-0.22}/F_{1/2} \\ \mu_p &\propto F_{-0.44}/F_{1/2} \end{aligned} \right\} \quad \dots\dots (16)$$

Using the tables mentioned previously the values of  $F_0/F_{1/2}$  and  $F_{-1/2}/F_{1/2}$  have been obtained for a range of values of  $\eta$ , and the ratios  $F_{(q+1)/2}/F_{1/2}$ , for n-type and p-type  $\text{Bi}_2\text{Te}_3$ , have been derived by linear interpolation. Since  $\frac{1}{2}(q+1)$  for p-type  $\text{Bi}_2\text{Te}_3$  is not far from  $-\frac{1}{2}$ , the interpolated values for the ratio of the integrals should be quite reliable in this case. However, for n-type material,  $\frac{1}{2}(q+1)$  is not very close to either  $-\frac{1}{2}$  or zero, so, in this case, the values for the ratio  $F_{(q+1)/2}/F_{1/2}$  can only be regarded as qualitatively correct.

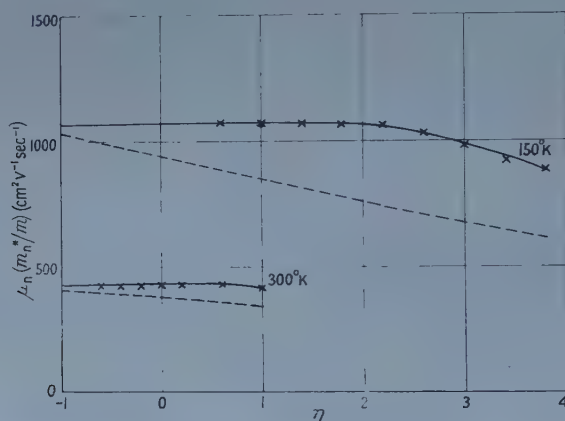


Figure 11. Product  $\mu(m^*/m)^{3/2}$  plotted against reduced Fermi potential for n-type  $\text{Bi}_2\text{Te}_3$  at 150°K and 300°K (broken curves represent the theoretical variation assuming  $m^*/m$  to be constant).

It has been assumed that the values of  $\mu(m^*/m)^{3/2}$ , for non-degenerate  $\text{Bi}_2\text{Te}_3$  may be obtained by extrapolating the experimental values towards  $\eta \rightarrow -\infty$ . Using these extrapolated values the theoretical variation of  $\mu(m^*/m)^{3/2}$  with  $\eta$  has been calculated on the basis of the relations (16), assuming the effective mass to be constant. The results of this calculation are shown by the broken curves of figures 11 and 12. These curves show a more rapid fall of  $\mu(m^*/m)^{3/2}$  with rise of  $\eta$  than do the curves based on the experimental results. In other words, the effective mass appears to increase with the carrier concentration.

For the high carrier concentrations which are encountered in  $\text{Bi}_2\text{Te}_3$ , it is to be expected that the impurity levels should broaden into an impurity band which should overlap the conduction band (Conwell 1956) (cf. Stern and Talley 1955). Now, as the carrier concentration is increased by adding more impurities, the number of states in the impurity band must increase. These extra states must be removed from the conduction band, since the total number of states must remain unchanged. However, the missing states in the conduction

band cover a wide range of energy (Parmenter 1955), so the overall effect is to increase the density of states near the band edge. This increased density of states may be regarded as an apparent increase of effective mass and, thus, the differences between the full and broken curves of figures 11 and 12 appear reasonable.

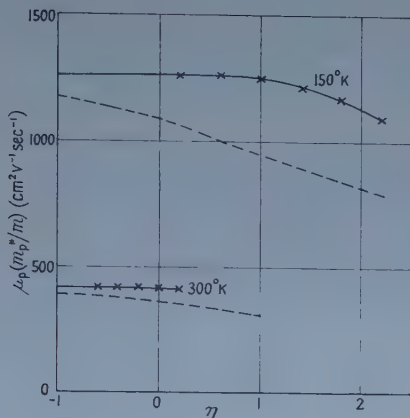


Figure 12. Product  $\mu(m^*/m)^{3/2}$  plotted against reduced Fermi potential for p-type  $\text{Bi}_2\text{Te}_3$  at 150°K and 300°K (broken curves represent the theoretical variation assuming  $m^*/m$  to be constant).

### § 6. INTRINSIC $\text{Bi}_2\text{Te}_3$

Measurements on a semiconductor in the intrinsic range enable the width of the forbidden band and the mobility and effective mass ratios to be determined. Unfortunately, it is not easy to prepare  $\text{Bi}_2\text{Te}_3$  showing intrinsic behaviour at room temperature and only one such ingot was available. This ingot contained just sufficient iodine to compensate for the usual high acceptor concentration.

Since complications due to a large difference between the effective masses of electrons and holes, such as are found for InSb (Austin and McClymont 1954), do not arise for  $\text{Bi}_2\text{Te}_3$ , it is possible to employ classical statistics in the intrinsic range, whence

$$\sigma_i = 2e(\mu_n + \mu_p) \left( \frac{2\pi kT}{h^2} \right)^{3/2} (m_n^* m_p^*)^{3/4} \exp - \left( \frac{\epsilon_g}{2kT} \right) \dots (17)$$

where  $\epsilon_g$  is the width of the forbidden band, and the subscript *i* refers to intrinsic conduction.

It will be supposed that the variation of the energy gap with temperature is linear so that

$$\epsilon_g = \epsilon_g^0 + GT \dots (18)$$

where  $\epsilon_g^0$  is the energy gap extrapolated to the absolute zero.

Further, the exponential term in (17) provides the main contribution to the variation of conductivity with temperature. Thus, since the ratio of the electron to hole mobility in  $\text{Bi}_2\text{Te}_3$  appears to be quite close to unity, it is reasonable to substitute a mean mobility variation,  $\mu \propto T^{-1.83}$ , whence the following expression may be obtained:

$$\ln(\sigma_i T^{0.33}) = -\epsilon_g^0 / 2kT + \text{constant}.$$

Figure 13 shows a plot of  $\ln(\sigma T^{0.33})$  against  $1/T$  for a sample for which the electrical conductivity reached a minimum value at about  $150^\circ\text{K}$ . Above  $250^\circ\text{K}$  the plot is linear with a slope of  $-0.95 \times 10^3 \text{ deg K}$ , the corresponding value for the energy gap being  $\epsilon_g^0 = 0.16 \text{ ev}$ .

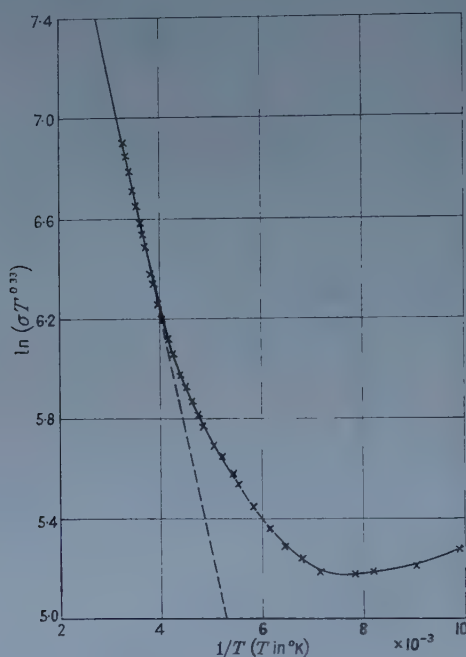


Figure 13.  $\ln(\sigma T^{0.33})$  plotted against  $1/T$  in the transition and intrinsic ranges ( $\sigma$  in  $\Omega^{-1} \text{ cm}^{-1}$ ).

Results obtained from near-intrinsic, but probably non-uniform, samples suggest that the intrinsic thermoelectric power of  $\text{Bi}_2\text{Te}_3$  is close to  $-50 \mu\text{V deg}^{-1}$ . Substituting this value in an expression for the intrinsic thermoelectric power obtained by combining equation (2) for electrons and holes in the form given by Chambers (1952, eqn. (28a)), one may estimate the mobility and effective mass ratios. The values found in this way are  $\mu_n/\mu_p \simeq 1.2$ ,  $m_n^*/m_p^* \simeq 0.9$ .

## § 7. CONCLUSIONS

The measurements of the electrical conductivity and thermoelectric power of  $\text{Bi}_2\text{Te}_3$  have enabled some of the fundamental semiconductor parameters to be obtained. Their values have been listed in table 1 and, for comparison, the results obtained by other workers have been included. The calculations have been based on the assumption of a constant carrier concentration in the extrinsic range, whereas it has been found that the Hall coefficient is not perfectly constant (Wolfe, private communication), a variation which cannot be explained in terms of a change-over from degeneracy to non-degeneracy. The calculated scattering law, based on the above assumption, has been supported by thermal conductivity measurements (Goldsmid 1958), so it appears that a slowly varying Hall coefficient does not exclude the possibility of a constant carrier concentration.



Table 1. Properties of  $\text{Bi}_2\text{Te}_3$

Property	Units	Temp. (°K)	Present values	Previous values	Ref.
Energy gap $\epsilon_g^0$	ev	0	0.16	0.15 (optical)	1
				0.16	2
				0.3	3
				0.21	4
				0.16	6
				0.20	7
Mobility of electrons $\mu_n$	$\text{cm}^2 \text{v}^{-1} \text{sec}^{-1}$	300		800	2
				400	3
				360 (sintered)	5
				270	7
Mobility of holes $\mu_p$	$\text{cm}^2 \text{v}^{-1} \text{sec}^{-1}$	300		400	2
				240	4
				170 (sintered)	5
				420	7
Effective mass of electrons $m_n^*$				1.07 $m$	4
				3.2 $m$	5
				0.32 $m$	6
Effective mass of holes $m_p^*$				1.26 $m$	4
				1.9 $m$	5
				0.46 $m$	6
$\mu_n(m_n^*/m)^{3/2}$	$\text{cm}^2 \text{v}^{-1} \text{sec}^{-1}$	300	430		
$\mu_p(m_p^*/m)^{3/2}$	$\text{cm}^2 \text{v}^{-1} \text{sec}^{-1}$	300	420	340	4
Ratio of electron to hole mobility $\mu_n/\mu_p$		300	1.2	2.0	2
				1.7	4
				2.1 (sintered)	5
				0.65	7
Ratio of electron to hole effective mass, $m_n^*/m_p^*$		300	0.9	0.85	4
				1.7	5
				0.70	6
Mobility variation for electrons ( $\mu_n$ )			$\propto T^{-1.72}$	$\propto T^{-3}$	3
				$\propto T^{-2.7}$	7
Mobility variation for holes ( $\mu_p$ )			$\propto T^{-1.94}$	$\propto T^{-2.3}$	4
				$\propto T^{-2.5}$	5
				$\propto T^{-1.5}$	7
Scattering law for electrons ( $\tau_n$ )			$\propto E^{-0.72}$		
Scattering law for holes ( $\tau_p$ )			$\propto E^{-0.94}$		

Note. All properties measured with the gradient parallel to the cleavage planes.

References: 1, Austin, I. G. (private communication); 2, Black *et al.* 1957; 3, Konorov 1956; 4, Shigetomi and Mori 1956; 5, Vlasova and Stil'bans 1955; 6, Harman *et al.* 1957; 7, Satterthwaite and Ure 1957.

Drabble and Wolfe (1956) have shown that the anisotropy of the Hall coefficient in extrinsic  $\text{Bi}_2\text{Te}_3$  cannot be explained using a single-valley semiconductor model, and galvanomagnetic measurements have indicated that a six-valley model is applicable (Drabble *et al.* 1958). This means that the measured Hall coefficient cannot be related to the carrier concentration without a knowledge of the parameters of the band structure. Thus, if any of the latter parameters are temperature dependent, it is clear that the relation between Hall coefficient and carrier concentration changes with temperature. Furthermore, this relationship is probably different for n-type and p-type  $\text{Bi}_2\text{Te}_3$ . Thus estimations of the ratios of electron to hole mobility and of electron to hole effective mass from Hall effect data may be unreliable. This may be the reason for some of the discrepancies between values calculated for these ratios from the present measurements and those reported previously. Detailed knowledge of the band structure will be necessary to clarify the situation.

#### ACKNOWLEDGMENTS

The author wishes to express his appreciation to Mr. A. R. Sheard, who is responsible for the preparation of bismuth telluride and related materials, and has prepared all the material used in these investigations, and to Dr. D. A. Wright and Dr. J. R. Drabble for helpful discussions.

#### REFERENCES

- AUSTIN, I. G., and MCCLYMONT, D. R., 1954, *Physica*, **20**, 's Grav., 1077.  
 BLACK, J., CONWELL, E. M., SEIGLE, L., and SPENCER, C. W., 1957, *J. Phys. Chem. Solids*, **2**, 240.  
 BLÖEM, J., and KRÖGER, F. A., 1956, in Report of the Physical Society Conference on Semiconductors (London: Physical Society), p. 77.  
 BORELIUS, G., 1953, *Physica*, 's Grav., **19**, 807.  
 BROOKS, H., 1955, *Advances in Electronics and Electron Physics* (New York: Academic Press), **7**, 85.  
 CHAMBERS, R. G., 1952, *Proc. Phys. Soc. A*, **65**, 903.  
 CHASMAR, R. P., and STRATTON, R., 1956, *Phys. Rev.*, **102**, 1686.  
 CONWELL, E., 1956, *Phys. Rev.*, **103**, 51.  
 DRABBLE, J. R., and WOLFE, R., 1956, *Proc. Phys. Soc. B*, **69**, 1101.  
 DRABBLE, J. R., GROVES, R. D., and WOLFE, R., 1958, *Proc. Phys. Soc.*, in the press.  
 FREDERIKSE, H. P. R., 1953, *Phys. Rev.*, **92**, 248.  
 GOLDSMID, H. J., 1956, *Proc. Phys. Soc. B*, **69**, 203; 1957, *Ph.D. thesis*, University of London; 1958, *Proc. Phys. Soc.*, in the press.  
 HARMAN, T. C., MILLER, S. E., and GOERING, H. L., 1957, *J. Phys. Chem. Solids*, **2**, 181.  
 HERMAN, F., 1955, *Proc. Inst. Radio Engrs.*, **43**, 1703.  
 HERRING, C., 1954, *Phys. Rev.*, **96**, 1163.  
 KONOROV, P. P., 1956, *J. Tech. Phys., Moscow*, **26**, 1400.  
 MCDUGALL, J., and STONER, E. C., 1938, *Phil. Trans. Roy. Soc.*, **237**, 67.  
 PARMENTER, R. H., 1955, *Phys. Rev.*, **97**, 587.  
 RHODES, P., 1950, *Proc. Roy. Soc. A*, **204**, 396.  
 SATTERTHWAIT, C. B., and URE, R. W., 1957, *Phys. Rev.*, **108**, 1164.  
 SHIGETOMI, S., and MORI, S., 1956, *J. Phys. Soc., Japan*, **11**, 915.  
 STERN, F., and TALLEY, R. M., 1955, *Phys. Rev.*, **100**, 1638.  
 VLASOVA, R. M., and STIL'BANS, L. S., 1955, *J. Tech. Phys., Moscow*, **25**, 569.  
 WILSON, A. H., 1953, *The Theory of Metals*, 2nd Edition (Cambridge: University Press).  
 WRIGHT, D. A., 1956, Proceedings of Garmisch Conference, *Halbleiter-Probleme*, **4**, in the press.

## Electrical Methods for Determining the Positions of Dislocation Regions in Germanium

By C. A. HOGARTH AND A. C. BAYNHAM

Royal Radar Establishment, Great Malvern

*MS. received 8th November 1957, and in final form 16th December 1957*

**Abstract.** It is shown that the walls of edge dislocations which exist in germanium crystals grown on a deformed seed are regions of high electrical conductivity in both n- and p-type samples. By means of simple plotting of potential against distance at constant current or from point-contact rectification measurements the positions of such dislocation walls may be located, the results agreeing with the positions determined by etch pit examination of the surfaces at which dislocations emerge. Evidence of the p-type character of dislocations in n-type germanium is presented.

### § 1. INTRODUCTION

THE study of dislocations and their resultant electrical effects in germanium crystals is of great importance in transistor technology. Dislocation densities may now be determined with some confidence by x-ray methods (Kurtz, Kulin and Averbach 1956, Bell 1957) or by etch-pit counting (Vogel, Pfann, Corey and Thomas 1953). More recently Dash (1956) has been able to observe the position of dislocation lines by means of infra-red transmission in the range  $1.1$  to  $1.3\ \mu$  through thin silicon samples using a microscope with high magnification and an image converter tube. Since the image converter tube is not sensitive beyond  $1.3\ \mu$  and the absorption edge of germanium is at  $1.8\ \mu$  this technique is not applicable to germanium. It was believed that the dislocations in germanium would probably possess different electrical properties from the bulk of the crystal since it has been shown by Pearson, Read and Morin (1954) that gross deformation of germanium by plastic bending has a marked effect on the electrical properties of crystals. Thus, if localized changes in resistivity for example could be detected, these could probably be correlated with the paths of dislocations. In a high quality single crystal containing perhaps  $10^3\ \text{cm}^{-2}$  edge dislocations distributed at random the determination of the position of an individual dislocation by such means would be virtually impossible. We were fortunate however in having available crystals through which the dislocations ran predominantly in parallel arrays and were highly polygonized (Bell and Hogarth 1957). The crystals were grown in the  $[111]$  direction and the dislocations ran close to  $[111]$ . The chances of determining local changes of conductivity associated with polygonized dislocation walls are much greater than of finding individual dislocations. We have been able to determine the positions of low-resistivity regions in germanium and to correlate these with the positions of dislocation walls, which in our crystals are typically  $20\text{--}30\ \mu$  apart.

## § 2. EXPERIMENTAL METHOD

The general form of the experiment is shown in figure 1. A constant current of order 1 mA was passed through a grown dislocated crystal cut as shown and the potential difference between the fixed and moving probes was measured as a function of distance parallel to the axis of the specimen. In order to ensure that plateaux in the curves obtained were genuine and not due to a change in cross-sectional area of the specimens, great care was taken in the preparation, preliminary examination, and mounting of specimens.

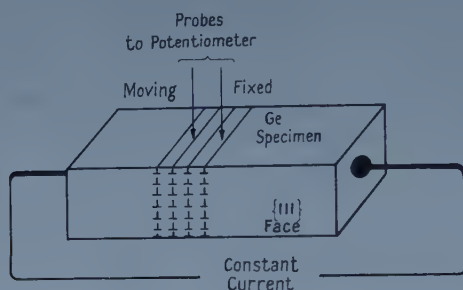


Figure 1. Schematic arrangement of probing experiment.

(i) *Cutting of specimens.* The directions of the parallel array of dislocations and of the appropriate  $\{111\}$  planes were determined for us by x-ray examination and the specimens were then cut as indicated schematically in figure 1. The specimens were then lapped with carborundum of successive grades down to 600, and were washed and etched in CP-4 solution for about 20 seconds when the  $\{111\}$  etch pits were clearly revealed. About sixteen photographs were taken of each side of the specimen using a Vickers projection microscope and from the prints which were carefully dried so as to avoid stretching, a large etch pit map at a magnification of approximately 130 times each vertical side of the crystal could be assembled. Thus a record of the emergence of edge type dislocations on the bounding  $\{111\}$  planes was preserved for use after any subsequent polishing of the specimen.

(ii) *Final preparation of specimens.* The specimens were polished with diamond dust abrasive on photographic paper to produce surfaces with a high quality optical finish, free of scratches, and with final dimensions of order  $15\text{ mm} \times 1\text{ mm} \times 1\text{ mm}$ . The optical polishing served two purposes: (a) it ensured that the sides of the specimen were plane so that the cross section could be accurately determined and (b) it reduced the rectification efficiency of the potential probes and thus increased the accuracy of the potentiometer readings. The end contacts were made by soldering.

(iii) *The manipulator.* The specimen was mounted on the bed of a specially designed manipulator which itself stood on a heavy concrete plinth to reduce vibration and shock. The traversing mechanism operated via two sets of angle spring hinges and reduced 1 cm of micrometer movement to 0.423 mm of lateral movement at the point. The movement was measured by means of a travelling microscope and found to obey a linear law. The fine moving probes were formed by mechanical polishing. The measurements were made in a darkened room so as to reduce any spurious potentials resulting from photovoltaic effects.



## § 3. RESULTS OF MEASUREMENTS

Figures 2(a) and 2(b) (Plate) show two photographs of etch pits on opposite {111} faces of a p-type germanium specimen, in the region over which electrical measurements were made. It is seen that the majority of the dislocations are polygonized into walls and that some regions between these walls are clear and that others contain a few randomly distributed dislocations. Potential difference measurements were made on the surface joining edges AA' and BB'.

Figure 3 shows a part of a typical graph of potential as a function of distance for a current of 1 mA through the p-type sample. It is seen that the general form of curve is approximately linear but that 'plateaux' occur where the potential remains nearly constant. To ensure that these plateaux were genuine features of the experiment and not due to random experimental error one length of crystal was measured on three separate occasions at intervals of two days. The measured potential differences were added and the graph re-plotted as shown in figure 4,

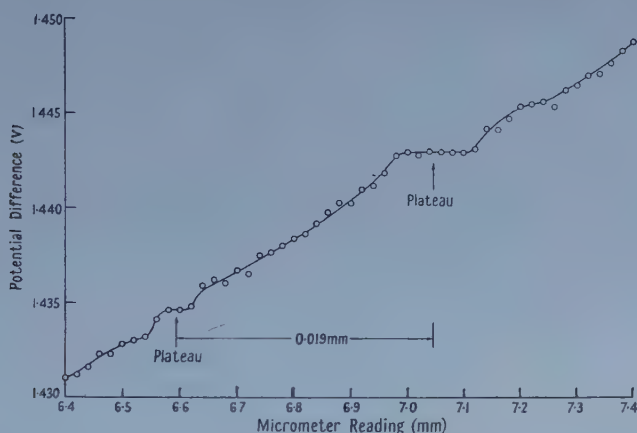


Figure 3. Potential difference as a function of distance along a dislocated p-type germanium specimen.

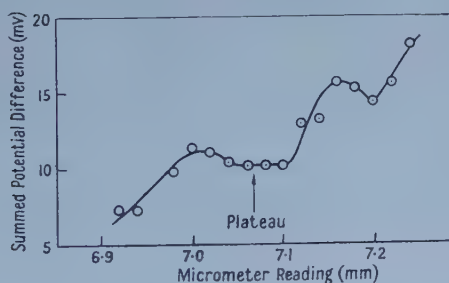


Figure 4. The sum of potential differences measured on three occasions as a function of distance.

when the plateau part of the curve was still flat. It was assumed that the positions of these plateaux represented the positions of dislocation walls and this was confirmed in the following manner. A scale drawing was made as shown in figure 5 where the positions of dislocation walls as indicated by lines of etch pits in figure 2 were marked along AA' and BB' and an attempt was made to sketch in the directions in which the edge dislocations were believed to run. The shape of the

etch pits when examined at high magnification suggested that the dislocations should run nearly perpendicular to the  $\{111\}$  faces and the suggested directions are drawn in figure 5. A transparent sheet with a straight edge was marked to the same scale with arrows indicating the positions of the mid-points of the plateaux determined electrically. By placing this sheet over the sketch of the dislocation paths it was found that the intersections of arrows and dislocation lines fitted exactly at only one position of the sheet. This fit indicated how far across the crystal the electrical plotting had been carried out in this particular experiment and from the diagram a distance of 0.32 mm was obtained. Travelling microscope examination of the crystal gave a distance of 0.33 mm so that agreement was good.

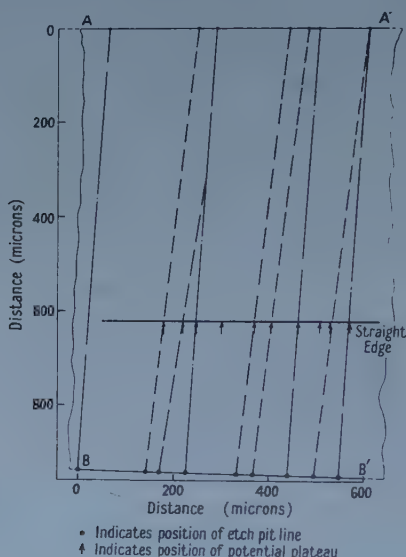


Figure 5. Scale drawing (plan) of the surface of part of a p-type germanium crystal showing the direction in which dislocation walls are believed to run.

The agreement between the positions of the electrically determined plateaux and the tentatively drawn dislocations shown in figure 5 confirms that over the thickness of crystal used the dislocations revealed on the  $\{111\}$  planes do run fairly accurately in straight lines through the crystal. More precise determinations could be made by traversing along the same length of the crystal at different distances across it and from the results the paths of the dislocation walls could be traced out.

Similar though less exhaustive results were obtained with n-type germanium the positions of dislocation walls being correlated with plateaux on the potential plots.

A high-perfection specimen of germanium whose  $\{111\}$  dislocation count was less than  $10 \text{ cm}^{-2}$  was examined. Examination of the  $\{111\}$  etch pits showed no evidence for polygon walls. After plotting over a distance of 200 microns no plateaux of the kind described above were observed.

In general it was found that for regions between dislocation walls relatively free of etch pits the potential-distance curves were good straight lines. For those

in which various odd etch pits were observed the potential-distance curves were 'bumpy'.

#### § 4. RECTIFICATION MEASUREMENTS

It is well known (see, for example, Hensich 1957, p. 133) that the rectification characteristic of an unformed point contact on germanium is a function of the resistivity of the material used and the rectification tends to be better on high resistivity germanium. Thus, it would be expected that the characteristics obtained with the probe accurately located on a dislocation wall would be inferior to those obtained when contact was made to an undislocated region of the crystal. Probing experiments were therefore carried out to determine whether a set of data indicating regions of poor rectification could be obtained consistent with the positions of the potential plateaux described above. In order to measure rectification characteristics it was necessary to etch the specimens, which were carefully removed from the manipulator complete with leads and immersed in hot dilute hydrogen peroxide for about ten minutes. The crystals were then replaced in as close a position as possible to that before the etching, with the aid of a travelling microscope. The subsequent distance zero would be slightly different from that of the previous measurements but relative distances would still be the same. Thus, if rectification data consistent with the potential plotting data could be obtained, the change in zero could be allowed for. It was found that for both n- and p-type germanium the distances between regions of poor rectification agreed exactly with the distances between plateaux. Measurements of rectification characteristics using a point contact were made at different points across the plateaux located from the potential plotting.

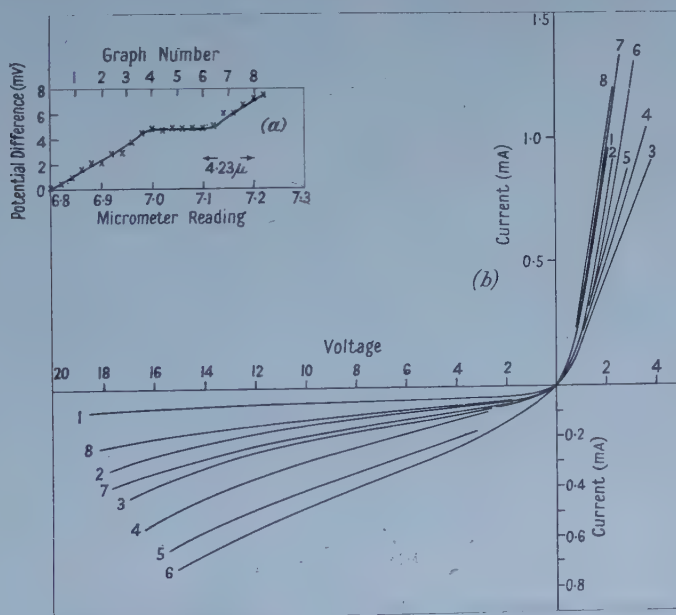


Figure 6. (a) Potential difference as a function of distance demonstrating a dislocation plateau. (b) Rectification characteristics of a point contact at various positions traversing the dislocation wall.

The results of one such experiment are shown in figure 6 where 6(a) shows the potential-distance plot across one such region and 6(b) the rectification

characteristics obtained at various points across the same region. It is observed that the characteristics become inferior as the dislocation region is reached and improve as it is passed.

It was found possible to make some quantitative deductions from the rectification results in the following manner. It is known that at high electric fields the drift velocity of charge carriers in germanium first saturates at a given field  $E_1$  but that at a higher applied field  $E_2$  avalanche ionization takes place (Gunn 1957). This observation was used by Gunn (1952) to explain the form of reverse current-voltage characteristics for point contacts on germanium, arising from the high local fields. Gunn's formula for moderate applied reverse voltages was

$$V = \frac{(E_2 + E_1)I^{1/2}}{(2\pi\sigma E_1)^{1/2}} - E_2 r_0$$

where  $\sigma$  is the local electrical conductivity and  $r_0$  the radius of the contact. Since  $E_1$  and  $E_2$  are constants for the material  $\sigma$  can thus be obtained from a study of the quantity  $dI^{1/2}/dV$ . The above form of relation for contacts of small area on germanium has been accurately verified by Paige (1957). In applying the method to p-type germanium there is some doubt as to the precise values to assume for  $E_1$  and  $E_2$ . Thus although the relative magnitudes of  $\sigma$  obtained will be correct the absolute values will depend on  $E_1$  and  $E_2$  and may thus be somewhat in error. The results obtained from analysis of the curves in figure 6(b) and assuming  $E_1 = 3 \times 10^3 \text{ v cm}^{-1}$  and  $E_2 = 8 \times 10^4 \text{ v cm}^{-1}$  are shown in figure 7. The conductivity

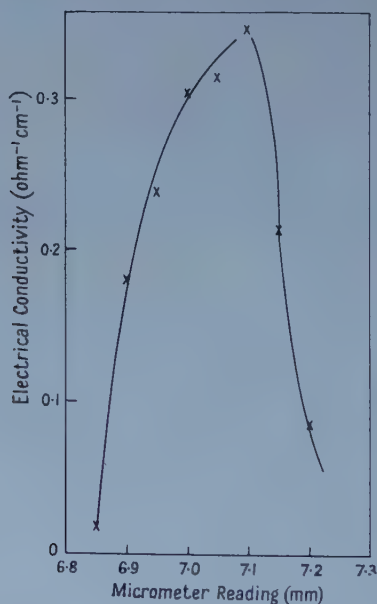


Figure 7. Conductivity derived from rectification measurements as a function of probe position.

calculated from the plateau region of figure 6(a) is obviously indeterminate because of the limited accuracy of the measurements but the mean slope on either side yields a conductivity value of  $0.02 \text{ ohm}^{-1} \text{ cm}^{-1}$ . Thus there is satisfactory



agreement between the direct measurement and that deduced from rectification experiments. We conclude from the above experiments that the dislocation walls in grown p-type germanium are p-type and of low resistivity.

For n-type germanium the rectification characteristics deteriorate as the dislocation region is approached and over a very short interval curves characteristic of low resistivity p-type germanium are obtained. On the application of more than a few volts to such contacts, breakdown takes place, and a poor n-type rectification characteristic is observed. On probing beyond the dislocation the characteristics improve to those typical of bulk germanium. It has often been suggested in the past that dislocations in germanium are of predominantly p-type character and the above result provides some evidence for this belief.

The p-type 'core' does not show up by the potential plotting experiment for the following reason, which was suggested by Dr. A. F. Gibson. When plotting in the vicinity of a p-type core we are effectively studying the potential-distance variation of an n-p-n transistor assembly with a floating base contact. For low applied fields the resistance of such an assembly is low while for higher fields it should increase. Attempts to detect this effect were unsuccessful because of instabilities and heating caused by the higher currents.

#### ACKNOWLEDGMENTS

During the course of these experiments we had the benefit of many valuable discussions with Dr. R. L. Bell. We should like to acknowledge also the help received from other colleagues, in particular Dr. W. Bardsley and Mr. P. J. Hoyland who grew the dislocated crystals and Mr. B. W. Straughan who carried out the crystal orientations. The special micromanipulator was designed by Messrs. Elliott Brothers and constructed in the Engineering Unit, Royal Radar Establishment. The paper is published by permission of the Controller, H.M. Stationery Office.

#### REFERENCES

- BELL, R. L., 1957, *J. Electronics and Control*, **3**, 487.  
BELL, R. L., and HOGARTH, C. A., 1957, *J. Electronics and Control*, **3**, 455.  
DASH, W. C., 1956, *J. Appl. Phys.*, **27**, 1193.  
GUNN, J. B., 1952, *Proc. Phys. Soc. B*, **65**, 908; 1957, *Progress in Semiconductors*, **2**, 211.  
HENISCH, H. K., 1957, *Rectifying Semiconductor Contacts* (Oxford: Clarendon Press).  
KURTZ, A. D., KULIN, S. A., and AVERBACH, B. L., 1956, *Phys. Rev.*, **101**, 1285.  
PAIGE, E. G. S., 1957, *J. Electronics and Control*, **2**, 378.  
PEARSON, G. L., READ, W. T., and MORIN, F. J., 1954, *Phys. Rev.*, **93**, 666.  
VOGEL, F. L., PFANN, W. G., COREY, H. E., and THOMAS, E. E., 1953, *Phys. Rev.*, **90**, 489.

# Distorted Wave Approximation in the Reaction $P + P \rightarrow \pi^+ + D$

BY B. DURNEY

Mathematics Department, University College London

*Communicated by H. S. W. Massey; MS. received 18th November 1957*

**Abstract.** The improvement in the agreement between theory and experiment in the threshold region of  $\pi^+$ -meson production from proton-proton collisions is shown to be independent of any detailed model of the meson-nucleon interaction in the final state. The distorted wave approximation applied to the resonant scattering state gives a marked increase in the production cross section over the cross section calculated in Born approximation.

## § 1. INTRODUCTION

THE cross section for the reaction



is computed by considering the transition matrix  $M$  of Chew, Goldberger and Steinberger (1951) in the form

$$M = \langle \psi_f | T | \psi_i \rangle. \quad \dots\dots(1)$$

In equation (1)  $\psi_f$  and  $\psi_i$  are non-relativistic wave functions describing the two-nucleon system after and before the production of the  $\pi$ -meson. These wave functions are taken to be solutions of the Schrödinger equation with phenomenological potentials and with the appropriate boundary conditions. The potentials are chosen to give a good description of the deuteron wave function  $\psi_f$  and also of the proton-proton scattering cross section at the energies involved in the initial state. The threshold of reaction (a) is 290 mev.  $T$  is linear in the wave function of the pion which is produced in the collision and the calculation in this paper is based on a more accurate choice of this wave function than has been made in previous work.

If s-meson production is neglected, the simplest form for  $T$  which is linear in the meson field  $\phi$ , galilean invariant in space and rotational invariant in isotopic spin space is

$$T = \alpha \sum_{i=1,2} \sigma^{(i)} \cdot \nabla^{(i)} [\tau^{(i)} \cdot \phi(\mathbf{R}_i)]; \quad \dots\dots(2)$$

$\alpha$  can be chosen by experiment and may be energy dependent. The simplest form of  $T$  available from relativistic field theory would make  $\alpha$  vary as  $1/\omega^{1/2}$  where  $\omega$  is the energy of the emitted meson. The form (2) for  $T$  will allow emission of p-wave mesons by each nucleon: mesons of higher angular momenta are not considered.

For the two nucleon wave functions in equation (1) we write

$$\begin{aligned} \psi_i &= \phi_i(\mathbf{r}) \chi_0 \Lambda_1^1 \\ \psi_f &= e^{-i\mathbf{k} \cdot \mathbf{R}} \phi_D(\mathbf{r}) \chi_1^m \Lambda_0 \end{aligned} \quad \dots\dots(3)$$

where  $\mathbf{R} = \frac{1}{2}(\mathbf{R}_1 + \mathbf{R}_2)$  and  $\mathbf{r} = \mathbf{R}_1 - \mathbf{R}_2$ ;  $\chi_0, \chi_1^m$  are singlet and triplet spin wave functions while  $\Lambda_0, \Lambda_1^1$  are singlet and triplet isotopic spin wave functions for

the two nucleon systems respectively.  $\phi_D(\mathbf{r})$  and  $\phi_I(\mathbf{r})$  are the deuteron and initial diproton wave functions in the relative coordinate  $\mathbf{r}$ . That the incident wave is spin singlet is due to the pion emission being considered to be entirely p-wave.

## § 2. CALCULATION

When the isotopic spin matrix element is computed the transition matrix (1) becomes

$$M = \alpha \langle e^{-i\mathbf{k} \cdot \mathbf{R}} \phi_D(\mathbf{r}) \chi_1^m | -\sigma^{(1)} \cdot [\nabla_s \phi^{(1)}(\mathbf{s})]_{\mathbf{s}=\mathbf{R}_1}^\dagger + \sigma^{(2)} \cdot [\nabla_s \phi^{(2)}(\mathbf{s})]_{\mathbf{s}=\mathbf{R}_2}^\dagger | \phi_I(\mathbf{r}) \chi_0 \rangle \quad \dots\dots (4)$$

In (4)  $\phi^{(i)}(\mathbf{s})$  is the wave function of the  $\pi$ -meson created by nucleon  $i$ . Previous calculations by Gunn, Power and Touschek (1951) used expression (4) in relativistic form, taking for  $\phi_I(\mathbf{r})$  and  $\phi(\mathbf{s})$  plane waves. Also Geffen (1955) used (4) taking for  $\phi_I(\mathbf{r})$  a realistic diproton wave function but a plane wave for  $\phi(\mathbf{s})$ . In the approximation of Geffen the reaction (a) can proceed by the two channels

$$^1S_0 \rightarrow ^3S_1 + p \quad \dots\dots (C1)$$

$$^1D_2 \rightarrow ^3D_1 + p. \quad \dots\dots (C2)$$

The observed asymmetry in the production cross section arises then entirely from (C2). That the asymmetry could arise from the pion interaction with the nucleons in the resonant ( $\frac{3}{2}, \frac{3}{2}$ ) state was suggested by Aitken *et al.* (1954). More recently Lichtenberg (1957) and Mandelstam (unpublished: report at Physical Society's Manchester Conference July 1957; see also Dalitz, report at Rochester Conference May 1957) have considered this possibility in greater detail. In order to take into account the presence of nucleon  $i$  in the emission of the meson by nucleon  $j$  ( $i \neq j$ ) we take for  $\phi^{(i)}(\mathbf{s})$  the meson wave function in the potential of nucleon  $j$ . Reaction (a) can now proceed through four channels

$$^1S_0 \rightarrow ^3D_1 + p \quad \dots\dots (C3)$$

$$^1D_2 \rightarrow ^3D_1 + p \quad \dots\dots (C4)$$

$$^1S_0 \rightarrow ^3S_1 + p \quad \dots\dots (C5)$$

$$^1D_2 \rightarrow ^3S_1 + p. \quad \dots\dots (C6)$$

The channel (C6) may be the dominant channel due to the dependence of channels (C3) and (C4) on the D state deuteron amplitude and due to the channel (C5) going through the  $J = \frac{1}{2}$  (non-resonant) state between the nucleon and the produced meson. In this approximation we write for the meson wave function

$$\phi^{(i)}(\mathbf{s}) = \exp(i\mathbf{p} \cdot \mathbf{R}_j) \int \exp\{i\mathbf{q} \cdot (\mathbf{s} - \mathbf{R}_j)\} \phi_p(\mathbf{q}) d\mathbf{q}, \quad \dots\dots (5)$$

where

$$\phi_p(\mathbf{q}) = \sum_{l,m} Y_l^{m*}(\mathbf{p}) Y_l^m(\mathbf{q}) U_l(p, q),$$

and

$$U_l(p, q) = \frac{1}{p^2} \delta(p - q) + \frac{B_l(q)}{pq(p^2 - q^2 - i\epsilon)}. \quad \dots\dots (6)$$

$B_l(q)$  will vanish for  $l \neq 1$  and for  $l = 1$ ;  $B_1(p) = -(2p/\pi) \sin \eta e^{-i\eta}$ ,  $\eta$  being the phase shift in the only scattering channel which is appreciable. The 'incoming wave' boundary condition is a consequence of the meson momentum being measured at  $t = +\infty$  (Mott and Massey 1949).

For the initial state of the diproton system we use the expression  
 $\phi_i(\mathbf{r}) = 2 \exp(i\delta_0)(k_0 r)^{-1} u_0(r) - 10 \exp(i\delta_2)(k_0 r)^{-1} u_2(r) P_2(\cos \theta); \quad \dots\dots (7)$   
 here  $k_0$  is the incident proton momentum in the centre-of-mass system. The deuteron wave function is taken to be

$$\phi_D(\mathbf{r}) = (4\pi)^{-1/2} r^{-1} [u(r) + 8^{-1/2} S_{12} \omega(r)]; \quad \dots\dots (8)$$

$S_{12}$  is the usual tensor operator. Expanding  $\exp(\pm i\mathbf{p} \cdot \mathbf{r}/2)$  in spherical harmonics and neglecting higher angular momenta than one, we obtain for the average sum of the square of the transition matrix

$$\sum |M|^2 = \alpha^2 16\pi (p/k_0)^2 [S^2 + 2S\mathcal{R}(D + F^+) \exp\{i(\delta_2 - \delta_0)\} \cdot (3 \cos^2 \theta - 1) + |D + F^+|^2 (3 \cos^2 \theta + 1)] \quad \dots\dots (9)$$

where  $\theta$  is the angle between the emitted meson and the incident protons,  $\mathcal{R}$  means the real part and  $S$ ,  $D$  are the overlap integrals

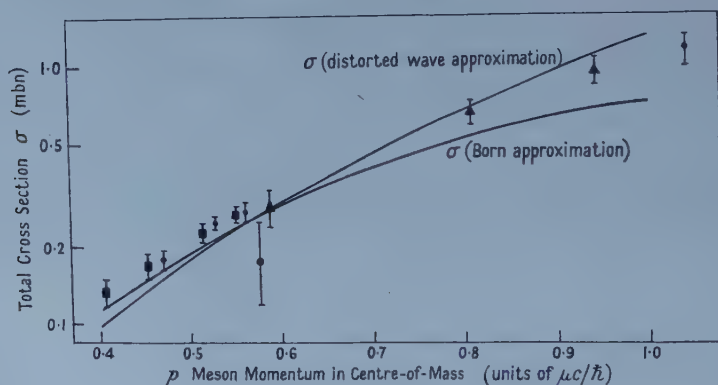
$$\left. \begin{aligned} S &= \int j_0(\tfrac{1}{2}pr) u_0(r) u(r) dr \\ D &= (1/\sqrt{2}) \int j_0(\tfrac{1}{2}pr) u_2(r) \omega(r) dr \end{aligned} \right\} \quad \dots\dots (10)$$

common to the plane wave approximation and the distorted wave approximation. On the other hand  $F$  is due to the final produced meson being scattered in the resonant state and is given by

$$F = \frac{1}{p^2} \int dq dr \frac{q^2 B_1(q)}{p^2 - q^2 - i\epsilon} j_0(\tfrac{1}{2}pr) j_2(qr) u(r) u_2(r). \quad \dots\dots (11)$$

### § 3. CONCLUSION

The numerical calculations were made for incident energies such that  $p \lesssim \mu$  and thus  $j_0(\tfrac{1}{2}pr) \simeq 1$  for those values of  $r$  giving an appreciable contribution to the integrals. The results are shown in the figure. For the diproton system and



Cross sections for the reaction  $p + p \rightarrow \pi^+ + D$  calculated in Born approximation and by the distorted wave approximation compared with the experimental results in the region of incident energies up to 450 mev. Both calculated curves are normalized to 0.269 mbn at 338 mev.

the deuteron wave functions (7) and (8), Gartenhaus potentials (with no spin-orbit force) were used. It cannot be expected that the cross section will be valid at energies exceeding 600 mev without taking into account in some way



the reaction of the pion production process on the pion production itself. Such damping effects are most easily considered, as has been shown by Goldberger, by calculating the transition matrix  $T$  from the reaction matrix  $K$  (Mandelstam, unpublished 1957). The distorted wave approximation does not involve any specific meson-nucleon force but takes  $B_1(q) = B_1(p)$ , i.e. its value on the energy shell determined by meson-nucleon scattering. The effect of the scattering integral  $F$  is to raise the cross section from the Born approximation results of Geffen (1955) in the region of moderate meson momentum where the Born approximation is considerably low. In the region of low meson momentum the distorted wave approximation is slightly smaller than the Born approximation but this is easily accounted for from a small s-wave production. The agreement with the experimental results so obtained is of the same order as that obtained with a more detailed model which predicts the variation of  $B_1(q)$  as for example the calculation of Lichtenberg (1957).

#### ACKNOWLEDGMENT

It is a pleasure to thank Dr. E. A. Power for suggesting this problem and for several discussions.

#### REFERENCES

- AITKEN, A., MAHMOUD, H., HENLEY, E. M., RUDERMAN, M. A., and WATSON, K. M., 1954, *Phys. Rev.*, **93**, 1349.  
 CHEW, G. E., GOLDBERGER, M. L., STEINBERGER, J. M., and YANG, C. N., 1951, *Phys. Rev.*, **84**, 581.  
 GEFFEN, D. A., 1955, *Phys. Rev.*, **99**, 1534.  
 GUNN, J. C., POWER, E. A., and TOUSCHEK, B. F., 1951, *Phil. Mag.*, **42**, 523.  
 LICHTENBERG, D. B., 1957, *Phys. Rev.*, **105**, 1084.  
 MOTT, N. F., MASSEY, H. S. W., 1949, *Theory of Atomic Collisions*, 2nd edn (Oxford : University Press), chap. VI.

## On the Binding Energy of the $^{16}\text{O}$ Nucleus

BY J. DABROWSKI†

Department of Mathematical Physics, University of Birmingham

*M.S. received 30th December 1957*

**Abstract.** A variational calculation of the binding energy of the  $^{16}\text{O}$  nucleus is presented. A two-body central Yukawa interaction with a hard core of radius  $a$ , and with Serber exchange is assumed and the parameters adjusted to fit the low energy data. A two-parameter trial function in the form of a product of harmonic oscillator shell model wave functions and correlation functions is assumed, and the Ursell-Jastrow cluster development is applied. The results show that the assumed two-body interaction with  $0.2 < a < 0.6$  is capable of reproducing the saturation of both binding and density of the  $^{16}\text{O}$  nucleus.

### § 1. INTRODUCTION

THE aim of this paper is to outline a method of calculation of the wave function and energy of the ground state of the  $^{16}\text{O}$  nucleus based on realistic two-body forces. The  $^{16}\text{O}$  nucleus is chosen as an example of a nucleus which is probably large enough to use the independent particle model with a proper average potential as the zero order approximation, and which at the same time is small enough for the actual performance of the calculation.

First of all, we have to decide which method we want to use, bearing in mind that evidently the  $^{16}\text{O}$  nucleus is finite. Although the formal scheme of the Brueckner theory is applicable to the finite nucleus (see for example Eden 1958), the performance of the corresponding calculations would be extremely difficult.‡ Let us then apply the ordinary variational treatment. Now it is well established that the nucleon-nucleon force is strongly repulsive at small distances, a property which can be represented by a hard core, i.e. a potential which becomes infinitely large at a certain distance  $a$ , the hard core radius. The essential problem is then how to treat the hard core in the variational calculation.

One procedure would be to replace the repulsive core by an equivalent pseudopotential, such as that discussed by Huang and Yang (1957) in the case of a low density. Some calculations of this type for a finite nucleus have convinced me, however, that the method using a pseudopotential is not adequate for dealing with such high densities as occur in nuclei.

† On leave of absence from the Institute of Theoretical Physics, Warsaw, Poland.

‡ But it is possible to perform calculations with the Brueckner theory if one makes the simplifying assumption that the local properties of a finite nucleus can be identified with those of infinite nuclear matter of the same density (Brueckner, private communication).

Since we are not able to replace the singular repulsive core potential by the transition operator, the pseudopotential or any other more or less regular quantity, we have to use in the variational principle trial functions which vanish at the relative distances between the nucleons  $r_{ij} \leq a$ . These boundary conditions are evidently satisfied by a function of the form

$$\Psi(1, \dots, A) = \prod_{i < j} f(r_{ij}) \Phi(1, \dots, A) \quad \dots\dots(1)$$

with

$$f(r_{ij}) = \begin{cases} 0 & \text{for } r_{ij} \leq a, \\ 1 & \text{for } r_{ij} \rightarrow \infty, \end{cases} \quad \dots\dots(2.1)$$

where the arguments of the functions denoted by numbers indicate the full set of the space, spin, isotopic-spin co-ordinates of the corresponding nucleons. This form of the wave function, being the product of the Slater determinant function

$$\Phi(1, \dots, A) = (A!)^{-1/2} \det\{\phi_k(l)\} \quad \dots\dots(2.2)$$

and the factorized correlation function  $\prod f$ , has the advantage of admitting a cluster development for any observable quantity. The variational procedure with the wave function (1) and with the cluster development, previously introduced by Ursell (see for example de Boer 1948) in the statistical mechanics, was suggested for nuclear problems by Jastrow (1955). Recently, a systematic derivation of the cluster development for the expectation value of energy, with the explicit expressions for all the terms of order 1 and  $\Omega_c/\Omega$  ( $\Omega$  = the volume of the system,  $\Omega_c$  = the total volume within which the correlations are strong) was given by Iwamoto and Yamada (1957).

There are essentially two methods for determining the wave functions  $\phi_k$  and the correlation function  $f$  satisfying the variational principle

$$\delta \langle \Psi | H | \Psi \rangle / \langle \Psi | \Psi \rangle = 0, \quad \dots\dots(3)$$

where  $H$  is the total Hamiltonian of the system of  $A$  nucleons. The first method consists of deriving from (3) the corresponding differential or integro-differential equations. Progress on this approach was achieved recently by Jastrow and his collaborators (Drachman *et al.* 1957). The second is the direct method followed in the present calculation: we introduce definite forms of  $f$  and  $\phi_i$  containing some free parameters and find the values of these parameters which minimize the energy expectation value.

For the functions  $\phi_i$  in the Slater determinant harmonic oscillator wave functions are used. These functions have the well-known property that  $\phi_i(1)\phi_j(2)$  may be expressed easily as the function of the relative and the centre-of-mass co-ordinates of the two particles. (For the analytical methods dealing with harmonic oscillator functions see Talmi 1952, Thieberger 1956–57.) This property enables one to find simple analytical expressions for the various terms occurring in the cluster development of the energy expectation value.

For the two-body potential it would be desirable to use the phenomenological potential which describes all the two-body experiments in the best way. In this respect, the potential discussed by Gammel, Christian and Thaler (1957) and especially the new potential with the spin-orbit coupling discussed by Gammel†

† The author is indebted to J. L. Gammel for communicating these results before publication.

and Thaler (1957) should be mentioned. But using the wave function of the form (2), one gets no contribution from the tensor and spin-orbit interaction (for the  $^{16}\text{O}$  nucleus). This results in a small value of the mean potential energy. In fact the calculation performed with the potential of Gammel and Thaler (1957) gave much too small a binding energy. This shows that the trial function (2) is too simple for the two-body force with the tensor and the spin-orbit term. The introduction of a more complicated correlation function (spin dependent) would greatly complicate the calculations. On the other hand, it seems reasonable to expect that any potential with a repulsive core of the suitable radius, describing the scattering phenomena at the energies occurring inside the nucleus, should explain the main features of the nuclear structure. In the present calculation we decide to retain the simple form (2) of the wave function and to use the central two-body potential with repulsive core and with the Serber exchange.

The first consideration of the nuclear saturation based on the variational treatment with the correlation function was made by Drell and Huang (1953) who used the Lévy (1952) nuclear potential. They came to the conclusion that only with many-body forces could nuclear saturation be established. Unfortunately, they calculated the potential energy with the help of a correlation function  $f$  of step form and for the kinetic energy they used the small density approximation of Lenz (1929).† But this procedure is completely inadequate. In fact the real minimum of the energy is determined by the competition between the two opposite tendencies: the increase of the negative potential energy and the rapid increase of the positive kinetic energy when the correlation functions get steeper. And indeed an additional calculation with the continuous  $f$  function performed by Drell and Huang with the three-body forces gave a binding energy three times smaller.‡ Further, it is to be mentioned that the calculation with the Lévy potential performed once more by Kerimov (1957) gave no saturation even with the three-body forces. Surely the lack of saturation is caused by the inadequate approximation for the  $f$  function and for the kinetic energy.

Although the  $^{16}\text{O}$  nucleus is treated merely as a convenient example for the calculation of the binding energy of the finite nucleus, this nucleus is in itself not without interest. The previous attempt by Redlich (1955) to calculate the binding energy of the  $^{16}\text{O}$  nucleus with an attractive two-body potential (with a proper exchange) was unsuccessful. In the recent treatment of the  $^{16}\text{O}$  nucleus by Tauber and Wu (1957) an attractive two-body potential of a very simplified form had been used and the experimental value of the binding energy was assumed as an additional condition. It is then difficult to draw a definite conclusion from their results as they could not get simultaneous agreement for the binding energy of the  $^{16}\text{O}$  and either  $^{15}\text{O}$  or  $^{17}\text{O}$  nucleus.

## § 2. THE TWO-BODY POTENTIAL

As mentioned in the introduction we choose for the two-body interaction a central potential with hard core and with Serber exchange. The Yukawa form

† This approximation is essentially equivalent to the calculation of the expectation value of the pseudopotential of Huang and Yang (1957).

‡ Surely this part of the calculation is correct. The fact that the optimum  $f$  function among all those considered was a simple function rising from 0 to 1 is an additional support of our choice in equation (17).



of the radial dependence is assumed. This interaction may be written in the form:

$$V(1, 2) = \begin{cases} \infty & \text{for } r_{12} \leq a, \\ [\frac{1}{2}V^s(r_{12})(1-P_\sigma) + \frac{1}{2}V^t(r_{12})(1+P_\sigma)]\frac{1}{2}(1+P_r) & \text{for } r_{12} > a, \dots\dots (4) \end{cases}$$

where

$$V^{s(t)}(r) = -V^{s(t)} \frac{\exp(-r_{12}/r_{s(t)})}{r_{12}/r_{s(t)}} \dots\dots (5)$$

and where  $P_\sigma$ ,  $P_r$  are the spin and space exchange operators respectively.

For the repulsive core radius  $a$  we choose two values: I,  $a=0.2$ ; and II,  $a=0.6$ .† Evidently the actual value  $a$  for the two-body potential lies between the values I and II. Calculating the binding energy of the  $^{16}\text{O}$  nucleus with the two values of  $a$  we expect to get upper and lower limits for the binding compatible with realistic two-body forces.

For a given value of  $a$  the parameters  $V^s$ ,  $V^t$ ,  $r_s$ ,  $r_t$  are adjusted to fit the following low energy data: (i) the binding energy of the deuteron (2.226 mev), (ii) the  $^3\text{S}$  n-p scattering length (5.378 fermis), (iii) the  $^1\text{S}$  n-p scattering length (-23.68 fermis), (iv) the  $^1\text{S}$  n-p and p-p effective range (2.7 fermis).

The values of the force parameters are given in table 1. For the singlet state interaction we used the force parameters given by Gammel, Christian and Thaler (1957), (actually the values of  $V^s$  given in table 1 are the average values of the  $^1V_c^+(n-p)$  and  $^1V_c^+(p-p)$  given by Gammel *et al.*). The force parameters for the triplet state interaction in table 1 are those calculated by Ohmura *et al.* (1957).

Table 1. The Parameters of the two-body Interactions (4), (5)

$a$	$r_s$	$V^s$	$r_t$	$V^t$
0.2	0.9091	130.3	0.9225	181.1
0.6	0.5	2097.5	0.3517	10396.6

The assumed Serber exchange character of the interaction makes it possible to describe with the help of this potential the main features of the high energy scattering. A further advantage of the Serber exchange is that it simplifies the calculations. Since our potential has a repulsive core we are not concerned with the old saturation conditions which excluded the Serber exchange.

In the case of two protons one has to add to the interaction (4) the Coulomb interaction which is included in all the following calculations.

### 3. THE CALCULATION OF THE BINDING ENERGY

Our main problem is to calculate the expectation value of the energy:

$$\frac{\langle \Psi | H | \Psi \rangle}{\langle \Psi | \Psi \rangle} = \frac{\langle \Psi | \sum_{i=1}^A T(i) + \frac{1}{2} \sum_{i,j=1}^A V(ij) | \Psi \rangle}{\langle \Psi | \Psi \rangle} \dots\dots (6)$$

where  $T(i)$  is the kinetic energy operator of the  $i$ th nucleon,  $V(1, 2)$  is given by equation (4) and  $\Psi$  has the form (2).

To calculate the expectation value of  $H$  we apply the 'cluster development' method following closely the systematic treatment by Iwamoto and Yamada (1957). Their final expression may be written in the form

$$\langle \Psi | H | \Psi \rangle / \langle \Psi | \Psi \rangle = T_0 + \mathcal{V} + O(\Omega_c/\Omega), \dots\dots (7)$$

† Throughout the paper all the lengths are given in fermis and the energies in mev.

where  $T_0$  is the kinetic energy calculated with the help of the Slater determinant function  $\Phi$  and

$$\mathcal{V} = \langle \Phi | \frac{1}{2} \sum_{i,j=1}^A \mathcal{V}(ij) | \Phi \rangle, \quad \dots\dots (8)$$

where

$$\mathcal{V}(ij) = \frac{\hbar^2}{m} \left| \frac{df(r_{ij})}{dr_{ij}} \right|^2 + |f(r_{ij})|^2 V(ij). \quad \dots\dots (9)$$

All the rest of the terms of the cluster development are contained in the quantity  $O(\Omega_c/\Omega)$  which is of the order  $\Omega_c/\Omega$  compared with  $T_0$  and  $\mathcal{V}$  and will be neglected in this calculation. The resulting error will be discussed in §4.

Evidently  $T_0 + \mathcal{V}$  contains the kinetic energy of the nucleus, including the increase of the kinetic energy due to the curvature of the correlation functions  $f$  and the potential energy calculated without taking into account the lack of orthogonality of the single nucleon functions due to the correlation functions.

In the present calculation we restrict ourselves to

$$\langle \Psi | H | \Psi \rangle / \langle \Psi | \Psi \rangle \simeq \mathcal{E} = T_0 + \mathcal{V}. \quad \dots\dots (10)$$

For the Slater determinant wave function  $\Phi$  we use the shell model wave function for the configuration  $(1s^2)_N(1p^6)_N(1s^2)_P(1p^6)_P$  with the harmonic oscillator radial functions.

We introduce two simplifications: (i) the same functions are used for neutrons and protons, (ii) the same value of the harmonic oscillator parameter  $\nu$  is used in both the s and p shells.

As the result of the two simplifications (i) and (ii) the Slater function  $\Phi$  has only one free parameter  $\nu$  which is to be adjusted so as to minimize  $\mathcal{E}$ . It may be mentioned that the introduction of different  $\nu$ 's for different shells would be analogous to the energy dependent average potential in the Brueckner theory.<sup>†</sup>

In accordance with the above remarks we have the functions  $\phi_i(j)$  of the Slater determinant (equation (2.2)) in the form:

$$\phi_i(j) = \eta_{s_i}(\sigma_j) \chi_{t_i}(\tau_j) Y_{l_i m_i}(\Omega_j) N_{l_i}(\nu) R_{l_i}^{\nu}(r_j), \quad \dots\dots (11)$$

where  $\eta$  and  $\chi$  are the spin and isotopic spin wave function of the  $j$ th nucleon respectively.

$$R_{l_i}^{\nu}(r_j) = \begin{cases} \exp(-\frac{1}{2}\nu r_j^2) & \text{for the s shell } (l_i=0), \\ r_j \exp(-\frac{1}{2}\nu r_j^2) & \text{for the p shell } (l_i=1), \end{cases} \quad \dots\dots (12)$$

and

$$N_l(\nu)^2 = 2^{l+2} \nu^{l+\frac{3}{2}} / \pi^{1/2} (2l+1)!! \quad \dots\dots (13)$$

The calculation of  $T_0 + \mathcal{V}$  with the help of the  $\Phi$  function with  $\phi$ 's defined by equations (11)–(13) is a standard procedure. The result of the calculation after applying the well-known technique of the oscillator wave functions (Talmi 1952, Thieberger 1956–7, Tauber and Wu 1957) is

$$\mathcal{E} = \frac{18\hbar^2}{m} \nu + \frac{83}{2\sqrt{2}\pi} e^2 \nu^{1/2} + \frac{93}{4} I_0 + \frac{45}{4} I_2 - \frac{9}{2} I_1 + \frac{93}{2} J_0 + \frac{45}{2} J_2 + 51 J_1, \quad \dots\dots (14)$$

where the first term is the kinetic energy  $T_0$ , the second term is the Coulomb energy<sup>‡</sup>  $C$ , the terms containing  $I$ 's represent the potential energy (later denoted

<sup>†</sup> The author is grateful to Professor Levinger for his interesting remarks concerning this point.

<sup>‡</sup> The expression for the Coulomb energy in (14) is obtained with the help of the  $\Phi$  function since the direct effect of the correlation function on the calculated Coulomb energy is of the order of magnitude of tenths of one mev.

by  $V_0$ ) and those with  $J$ 's give the increase of the kinetic energy due to the curvature of  $f$  (later denoted by  $\Delta_0 T$ ). Explicitly we have

$$I_l = I_l(\nu) = N_l(\nu/2)^2 \int_0^\infty dr [V^s(r) + V^l(r)] f^2(r) \exp(-\frac{1}{2}\nu r^2) r^{2l+2}, \quad \dots\dots (15)$$

$$J_l = J_l(\nu) = N_l(\nu/2)^2 \int_0^\infty dr \frac{\hbar^2}{m} \left( \frac{df}{dr} \right)^2 \exp(-\frac{1}{2}\nu r^2) r^{2l+2}. \quad \dots\dots (16)$$

To perform these integrations we have to choose a definite form for the correlation function  $f$  with the property (2.1). It is found convenient to define  $f$  in the following way:

$$f(r) = \begin{cases} 0 & \text{for } r \leq a, \\ 1 - \exp\{-\beta[(r/a)^2 - 1]\} & \text{for } r > a, \end{cases} \quad \dots\dots (17)$$

where  $\beta$  is the parameter the value of which is to be determined by minimizing  $\mathcal{E}$ . The essential assumption contained in equation (17) is that  $f$  varies monotonically from zero at  $r = a$  to unity at large  $r$  (cf. the footnote in § 1). It is hardly probable that the exact form chosen is of any special importance.

After introducing the form (17) of  $f$  into equations (15) and (16) we may easily obtain simple analytical expressions for the  $I$ 's and  $J$ 's which then combined with equation (14) give finally an essentially simple expression for  $\mathcal{E} = \mathcal{E}(\nu\beta)$ .

To find the minimum value of  $\mathcal{E}$  the function  $\mathcal{E}(\nu\beta)$  was calculated for several values of  $\nu$  and  $\beta$ . The optimum values of  $\nu$  and  $\beta$  together with the values of the different terms contributing to  $\mathcal{E}$  are given in table 2.

Table 2. The Values of the different Terms contributing to  $\mathcal{E}$  for the Optimum Values of  $\nu$  and  $\beta$

$a$	$\beta$	$\nu^{1/2}$	$r_0$	$T_0$	$\Delta_0 T$	$V_0$	$C$	$\mathcal{E}$
0.2	0.75	0.9	0.86	605.4	378.1	-1204.0	21.5	-199.0
0.6	2	0.55	1.40	226.1	425.4	-729.3	13.1	-64.7

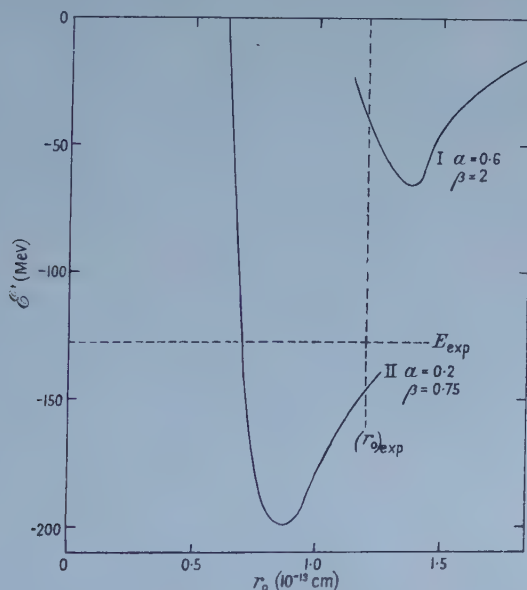


Figure 1.  $\mathcal{E}$  as a function of nuclear radius for the indicated optimum values of  $\beta$ .

The actual determination of the minimum of  $\mathcal{E}(\nu\beta)$  was simplified by the fact that the value of  $\beta$  minimizing  $\mathcal{E}(\nu\beta)$  for the given value of  $\nu$  was found to be practically independent of  $\nu$ . For the optimum value of  $\beta$ ,  $\mathcal{E}(\nu\beta)$  was calculated as a function of  $\nu$ . The result of these calculations is shown by the two curves of figure 1. On the abscissa, instead of  $\nu$  the values of

$$r_0 = [\frac{5}{3} \langle \Phi | r_i^2 | \Phi \rangle]^{1/2} / A^{1/3} = (15/4\nu)^{1/2} / (16)^{1/3} \quad \dots\dots (19)$$

are given.<sup>†</sup>

The results of our calculations are to be compared with the following experimental values of  $r_0$  and of the binding energy of the  $^{16}\text{O}$  nucleus:

$$(r_0)_{\text{exp}} = 1.2, \quad E_{\text{exp}} = -127.56. \quad \dots\dots (20)$$

The two experimental values are indicated in figure 1. We see that

$$\mathcal{E}(a=0.2) < E_{\text{exp}} < \mathcal{E}(a=0.6), \quad \dots\dots (21)$$

and

$$r_0(a=0.2) < (r_0)_{\text{exp}} < r_0(a=0.6). \quad \dots\dots (22)$$

#### § 4. DISCUSSION

First of all let us discuss the inaccuracy of our calculation coming from two sources: (i) the variational treatment, and (ii) the cluster development.

(i) Applying the direct method of the variational calculus we obtain a value of the energy which is greater than the real value. But how much greater is it? In answering this question we restrict ourselves to discussing whether our trial function has the necessary qualitative features to give a reasonable value of the energy. The average gross features of the Slater function  $\Phi$  are probably correct since its form is indicated by the shell model which is especially suitable for the double magic  $^{16}\text{O}$  nucleus. More serious is the question of how far our trial function is able to reproduce the behaviour of the system for small inter-nucleon distances. The impression may arise that with our correlation function  $f$  defined by equation (17) we only take into account the existence of the repulsive core, neglecting completely the attractive correlation caused by the attractive forces. Fortunately, it is not so, since after transforming  $\phi_i(1)\phi_j(2)$  into the relative (and centre-of-mass) co-ordinates we get the attractive correlation from the Slater function  $\Phi$  (see figure 2). Now the wave function with the proper gross behaviour with the attractive as well as the repulsive correlations is surely capable of giving the main part of the binding. In conclusion it seems to us to be hardly possible that an improvement of the trial function might change radically the values obtained in § 3, and in particular displace the value of  $\mathcal{E}$  for  $a=0.6$  below the experimental value (any displacement of  $\mathcal{E}$  for  $a=0.2$  would be of no importance for our conclusions).

(ii) The error connected with the cluster development is caused by the neglect of  $O(\Omega_c/\Omega)$  in equation (10). To evaluate the ratio of the total volume  $\Omega_c$  within which the correlations are strong to the volume of the nucleus  $\Omega$  we put  $\Omega_c/\Omega \simeq (r_c/r_0)^3$  where the radius of the correlation region  $r_c$  is defined by the condition  $f(r_c)^2 = 0.5$ . The quantity  $(r_c/r_0)^3$  is equal to 5% for  $a=0.2$  and to 16% for  $a=0.6$ . Surely an error of this magnitude in  $\mathcal{E}$  would be of small importance for our results. But the situation is not quite so satisfactory. The separate terms in  $O(\Omega_c/\Omega)$  are  $\Omega_c/\Omega$  smaller than  $T_0$  and  $\mathcal{V} = \Delta_0 T + V_0$  and

<sup>†</sup> The fact that we use the function  $\Phi$  instead of  $f\Phi$  in equation (19) is without any importance (see preceding footnote).



the last terms are of the magnitude of several hundred mev for  $a=0.2$  and of a few hundred mev for  $a=0.6$ . The quantity  $O(\Omega_c/\Omega)$  may then reach the magnitude of a few tens of mev. Nevertheless, our main conclusion contained in equations (21) and (22) seems to be well established since we have  $|E - E_{\text{exp}}| > 60$  mev for both the values of  $a$ .

Of course the only way to prove this conclusion about  $O(\Omega_c/\Omega)$  exactly is the actual calculation of the further terms in the cluster development. It is our plan to calculate the terms of order  $\Omega_c/\Omega$  in  $O(\Omega_c/\Omega)$ . In fact, many of these terms have already been calculated in an approximate way. The very provisional results would suggest that the further terms in the cluster development give a contribution to the energy of the order of magnitude of the Coulomb energy. We hope to return to this problem in the future.

The above considerations suggest that even taking into account the eventual corrections, the main result of our calculations expressed in equations (21) and (22) should not change. Then this shows that the realistic two-body force with a repulsive core of radius  $0.2 < a < 0.6$  reproduces the binding energy of the  $^{16}\text{O}$  nucleus and gives the proper value of its radius. This conclusion supports the results of several calculations made by Brueckner† and his collaborators in the case of infinite nuclear matter.

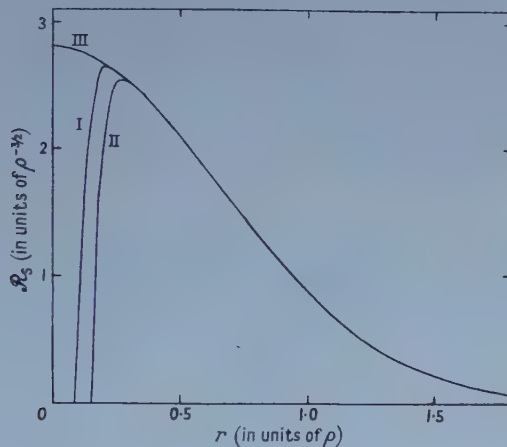


Figure 2. The radial wave function  $\mathcal{R}_S$  of the relative motion in the S state. The unit of length is  $\rho = (\langle r_{ij}^2 \rangle)^{1/2}$ . I,  $a=0.2$ ; II,  $a=0.6$ ; III, the shell model function ( $f=1$ ).

To get an idea of how to reconcile the strong nucleon-nucleon interaction with the shell model, the wave function of the relative motion in the S state is shown in figure 2. As is well known (Talmi 1952) the S part of the relative motion contained in the product of  $\phi_i(1)\phi_j(2)$  of the two harmonic oscillator functions is again given by the harmonic oscillator wave function with the frequency parameter  $\nu/2$ . In our case the function we are interested in, which is shown in figure 2, is

$$\mathcal{R}_S = f(r_{ij}) N_0 (\nu/2) R_0^{\nu/2} (r_{ij}).$$

† We mention only the last publications: Brueckner and Gammel (1958) and Brueckner, Gammel and Weitzner (1958). The author is indebted to K. A. Brueckner for letting him know these results prior to publication.

In figure 2 we use the root of the mean square inter-nucleon distance

$$\rho = (\langle \Phi | r_{ij}^2 | \Phi \rangle)^{1/2} = (23/5\nu)^{1/2}$$

as unit of length (cf. the footnote following eqn (19)). With this unit the shell model wave function  $R_0^{1/2}$  (III) is the same for the two cases  $a=0.2$  (I) and  $a=0.6$  (II). Now this function is changed by the correlation function  $f$  so as to give the real function  $\mathcal{R}_s$  in both cases. The essential point is that the disturbances introduced into  $R_0^{1/2}$  are restricted to distances much smaller than  $\rho$ . This means that when we come to the next particle, the wave function is already the shell model wave function. This is exactly the same situation as that discussed by Weisskopf (lecture at 1957 Pittsburgh Conference) in the case of infinite nuclear matter.

The equations of this paper allow two interpretations. One may think either of the 'true' wave function  $\Psi$  and an exact interaction  $V(ij)$  or else one may include  $f$  in  $V(ij)$  so as to get the 'effective' interaction  $\mathcal{V}(ij)$  acting on the 'model' wave function  $\Phi$ . Evidently  $f$  plays the role of the model operator of the Brueckner theory (see for example Eden 1957).

If we want to preserve the 'model' picture when considering the higher terms of the cluster development involving integrations over the co-ordinates of three or more particles, we are immediately faced with effective many-body interactions. This means that any indications of 'many-body forces' based on the model wave function calculations do not necessarily mean that there are real many-body forces. It may merely indicate effective many-body forces connected with the higher cluster terms. The estimated small magnitude of the 'many-body forces'† is probably a new indication that the higher terms in the cluster development are negligible.

#### ACKNOWLEDGMENTS

The author expresses his deep gratitude to Professor R. E. Peierls for his kind hospitality and his encouragement during the course of this work. Sincere thanks are expressed to my colleagues in the Department of Mathematical Physics of the University of Birmingham, especially to J. Lascoux and W. Tobocman for many helpful discussions. Further, he would like to thank R. Jastrow for his valuable remarks concerning the cluster development method and G. E. Tauber for his interesting remarks concerning his paper. A grant from the Polish Academy of Science is also acknowledged.

† See for example the review article by Pandya and French (1957).

#### REFERENCES

- DE BOER, J., 1948, *Rep. Progr. Phys.* (London: Physical Society), **12**, 305.  
 BRUECKNER, K. A., and GAMMEL, J. L., 1958, *Phys. Rev.*, in the press.  
 BRUECKNER, K. A., GAMMEL, J. L., and WEITZNER, H., 1958, *Phys. Rev.*, in the press.  
 DRACHMAN, R. J., AVILES, J. B., and JASTROW, R., 1957, *Bull. Amer. Phys. Soc.*, **2**, No. 1, 26.  
 DRELL, S. D., and HUANG, R., 1953, *Phys. Rev.*, **91**, 1527.  
 EDEN, R. J., 1958, to be published in *Nuclear Reactions* edited by Endt and Demeur (Amsterdam: North Holland).  
 GAMMEL, J. L., CHRISTIAN, R. S., and THALER, R. M., 1957, *Phys. Rev.*, **105**, 311.  
 GAMMEL, J. L., and THALER, R. S., 1957, *Phys. Rev.*, **107**, 291, 1337.  
 HUANG, K., and YANG, C. N., 1957, *Phys. Rev.*, **105**, 767.  
 IWAMOTO, F., and YAMADA, M., 1957, *Prog. Theor. Phys. Japan*, **17**, 543.  
 JASTROW, R., 1955, *Phys. Rev.*, **98**, 1479.

- KERIMOV, B. K., 1957, *J. Exp. Theor. Phys.*, **32**, 377.  
LENZ, W., 1929, *Z. Phys.*, **56**, 778.  
LÉVY, M. M., 1952, *Phys. Rev.*, **88**, 725.  
OHMURA, T., MORITA, M., and YAMADA, M., 1957, *Prog. Theor. Phys. Japan*, **17**, 326.  
PANDYA, S. P., and FRENCH, J. B., 1957, *Annals of Physics*, **2**, 166.  
REDLICH, M. G., 1955, *Phys. Rev.*, **99**, 1421.  
TALMI, I., 1952, *Helv. Phys. Acta*, **25**, 185.  
TAUBER, G. E., and WU, T. Y., 1957, *Phys. Rev.*, **105**, 1772.  
THIEBERGER, R., 1956-57, *Nuclear Phys.*, **2**, 533.

## The Intrinsic Variables affecting the Stick-Slip Process

By E. RABINOWICZ

Department of Mechanical Engineering, Massachusetts Institute of Technology,  
Cambridge, Massachusetts, U.S.A.

*MS. received 26th November 1957*

**Abstract.** Stick-slip oscillations are normally analysed in terms of the kinetic friction-velocity and the static friction-time of stick characteristics of the rubbing surfaces. It is shown that, in addition, a critical distance, of the order of  $10^{-3}$  cm, enters into the calculations, being the minimum resolving power of the friction process. Stick-slip oscillations must normally have an amplitude greater than the critical distance, and thus increased spring stiffness is often effective in eliminating stick-slip. Using the critical distance concept, it is possible to deduce a simple relationship between the static and kinetic coefficients of friction, and this is confirmed by experimental data.

### § 1. THE INTRINSIC VARIABLES AFFECTING THE STICK-SLIP PROCESS

IT is well known that, if two surfaces are slid together, the motion is in many cases oscillatory rather than smooth. Thus, if the sliding system is represented schematically by figure 1, it is frequently observed that the

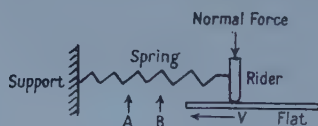


Figure 1. Schematic representation of friction apparatus capable of producing stick-slip oscillations.

rider sticks to the plate and is dragged to A, then slips back to B, sticks to the plate again and is dragged on to A, and continues to repeat this cycle indefinitely (Bowden and Leben 1939, Bowden and Tabor 1954). This mode of behaviour may be denoted as 'regular stick-slip' and, although it is only one of several possible forms of frictional vibrations (Rabinowicz 1958), it is the one that has received the widest consideration:

In practical sliding systems stick-slip is generally considered a serious nuisance, and measures are normally taken to eliminate it if at all possible, or, if not, at any rate to reduce the amplitude of the vibration. In this paper we shall discuss the intrinsic frictional characteristics of the surface which determine whether stick-slip will be present, and, if oscillations do occur, what will be their amplitude.

The stick-slip phenomenon may be studied in two ways. If a mathematical approach is adopted, it is customary to assume simple idealized frictional properties and to derive and solve differential equations for the motion in terms of the inertia, velocity and damping of the system (cf. Dudley and Swift 1949, Lomakin 1957,



Derjaguin, Push and Tolstoi 1957). Since we are here concerned with the physics rather than the mathematics of the phenomenon, we go to the other extreme and choose a system that is as devoid of complications as possible, namely one in which the plate velocity is low (much lower than the maximum rider velocity during the slip stage), the rider inertia so small that the rider can readily keep up with the movement of the plate, and the external damping negligible. Having made these simplifying assumptions, we may now describe the nature of the oscillations at the three levels of sophistication considered in the literature, and show that a further complicating factor must be considered.

## § 2. FIRST ASSUMPTION: $f_k$ CONSTANT, $f_s$ CONSTANT

This is the simplest solution, in which the kinetic coefficient of friction  $f_k$  is independent of the sliding velocity  $v$ , and the static coefficient  $f_s$  is larger than  $f_k$  but independent of the time of stationary contact  $t$ . Plotting the force in the spring as a function of time of sliding we then have the situation shown in figure 2(a), in which the force in the spring increases at a steady rate until it reaches a value  $f_s L$ , where  $L$  is the applied load, and then during the slip stage the force drops to  $(2f_k - f_s)L$ , as far below  $f_k L$  as it started above it. If the frequency of the oscillation is changed, either by raising the sliding velocity or by using a stiffer spring, the amplitude of the oscillations, which we will denote as  $\Delta f$ , remains constant at  $2(f_s - f_k)$ .

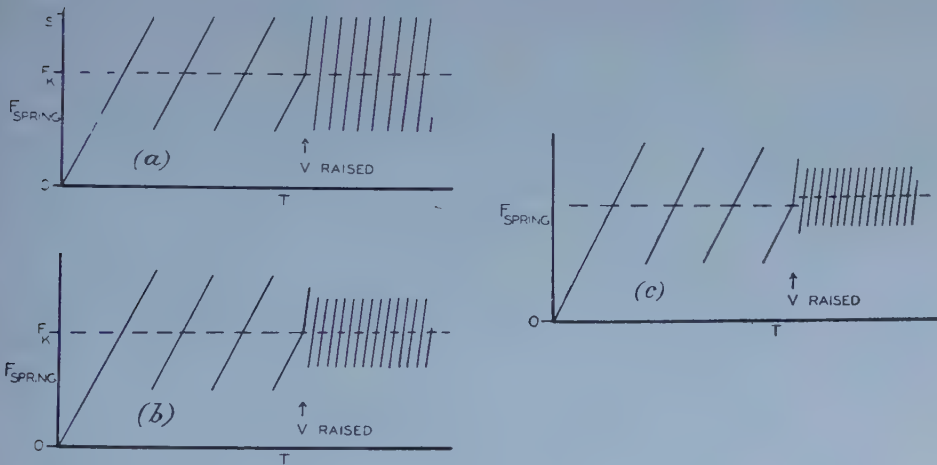


Figure 2. Stick-slip according to the different friction models (for clarity of illustration, only the stick trace is shown): (a)  $f_k$  and  $f_s$  constant, (b)  $f_k$  constant,  $f_s$  a function of time of stick, (c)  $f_k$  a function of sliding velocity,  $f_s$  a function of time of stick; the midpoint of the stick varies with the sliding velocity.

This presentation is essentially that due to Blok (1940), who realized that in actual practice the stick-slip amplitude becomes smaller as  $v$  is raised, and attributed this to damping. Later work, however, suggests that it is rather the dependence of the static coefficient on the time of stick which is responsible for this effect. We consider this next.

### § 3. SECOND ASSUMPTION : $f_k$ CONSTANT, $f_s$ A FUNCTION OF $t$

We assume that the static coefficient of friction is a function of time of contact (Ishlinski and Kragelski 1944), as shown in figure 3, but that the kinetic coefficient remains a constant. As justification for the shape of the curve we note that Sampson, Morgan, Reed and Muskat (1943) have shown that the static coefficient for small times of stationary contact is equal to the kinetic, while the data of Dokos (1946) plotted in figure 4 show that the plot of  $f_s$  against  $\log t$  approximates to a straight line, indicating that for small values of  $t$  the slope of the curve in figure 3 must be very steep, for large values very small.

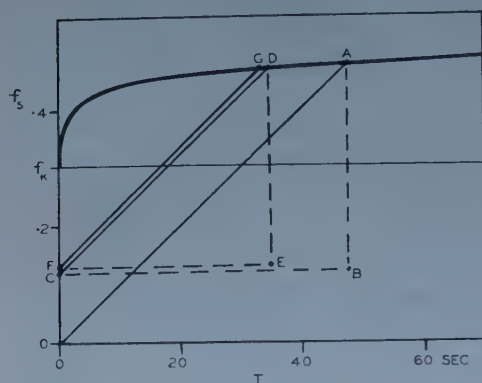


Figure 3. Static coefficient plotted against time of stick.

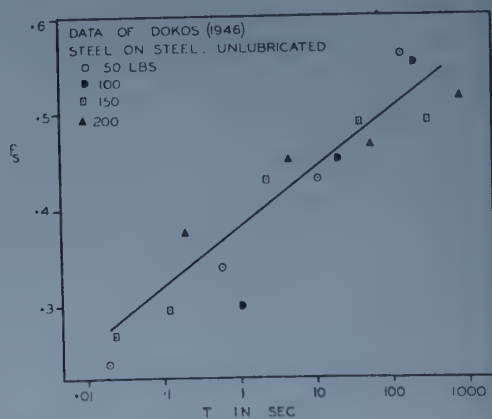


Figure 4. Dokos' data of static coefficient plotted against time of stick.

If we place our surfaces together and set the flat in motion at a velocity  $v$ , the spring force increases with time at a rate  $kvt$ , and this may be plotted in figure 3 as a straight line through the origin with slope  $k v / L$ . At point A slip occurs and, since the kinetic coefficient is assumed constant, we again have a situation where slip continues to point B, as far below the  $f_k$  line as A was above it. At B the rider comes to rest, which we plot as point C, and the next stick-cycle takes us to D, E and F. Finally, a steady state is reached. If we increase  $v$  or  $k$  then our line becomes steeper and the stick-slip will have a smaller amplitude (figure 2(b)).

### § 4. THIRD ASSUMPTION : $f_k$ A FUNCTION OF $v$ , $f_s$ A FUNCTION OF $t$

In general the kinetic coefficient is known to be a function of the sliding velocity, curves such as are shown in figure 5 being typical. The kinetic coefficients plotted as a function of sliding velocity are those for steel sliding on steel unlubricated, perfectly lubricated by a fatty acid derivative, and in intermediate stages of lubrication. It is believed that steel surfaces covered by a long chain organic material will always give a curve keeping a constant ratio between the top and bottom curves, the position of the curve indicating the relative effectiveness of the lubricant expressed as percentage coverage of the total surface.

The existence of the velocity dependence of the kinetic coefficient means that we can no longer determine the amplitude during slip in a simple way, but

rather must evaluate, for the whole slip stage, the instantaneous velocity, thence the instantaneous friction force, thence the instantaneous acceleration, and so on to a subsequent velocity (Dudley and Swift 1949). It seems logical to assume that, provided the  $(f_s, t)$  and  $(f_k, v)$  curves for our system are known, the complete progress of the stick-slip cycle can thus be calculated. It is the purpose of this paper to suggest that this is not the case, that in actual practice the kinetic coefficient is not only velocity dependent, but also displacement dependent.

### § 5. DEPENDENCE OF KINETIC FRICTION COEFFICIENT ON PREVIOUS SLIDING HISTORY

The difficulty arises because the curves of figure 5 were derived from experiments in which a constant velocity was maintained for a long time and then the coefficient of friction measured. The question is whether it is reasonable to expect the same friction values if the rider reaches a certain velocity momentarily during the slip stage, and, if not, what estimate of the friction coefficient can be made under these conditions.

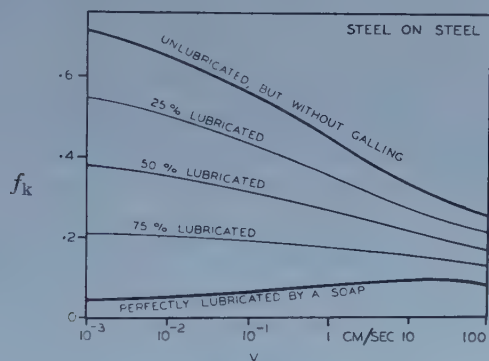


Figure 5. Kinetic coefficient-velocity graphs for steel surfaces in various states of lubrication.

To summarize previously obtained data which bear on this point, we note that tests with a low speed friction apparatus suggest that, if tests are run at one velocity and a new velocity is suddenly imposed, the coefficient changes gradually and reaches a steady value only after a sliding distance of the order of  $10^{-3}$  cm (Heymann, Rabinowicz and Rightmire 1955). Similarly, if sliding tests are carried out at a constant velocity, intrinsic fluctuations of the friction force are noted, and statistical tests show a persistence of the order of  $10^{-3}$  cm (Rabinowicz 1956). Also, when surfaces in stationary contact are suddenly set into motion by an impact, the static coefficient maintains its initial value unchanged for the first  $2 \times 10^{-4}$  cm, and drops to the lower kinetic coefficient only after sliding a distance of the order of  $10^{-3}$  cm (Rabinowicz 1951). Taken together, the three experiments suggest strongly that the friction force is determined, not only by the instantaneous sliding conditions, but by the sliding history of a preceding critical distance, which for our sliding conditions may be taken to be  $10^{-3}$  cm. It seems plausible to assume, therefore, that in a situation in which the velocity is changing rapidly the instantaneous value of the friction coefficient

will be given, on a plot like figure 5, not by the instantaneous sliding velocity but by the average sliding velocity of the previous  $10^{-3}$  cm (i.e. by  $10^{-3}$  divided by the time to slide the previous  $10^{-3}$  cm).

An excellent practical demonstration of a memory effect such as we have postulated is seen in the work of Sampson *et al.* (1943), who obtained experimentally the displacement-time function of a rider during slip, and from it attempted to deduce the friction-velocity curve. Their result is shown in figure 6,

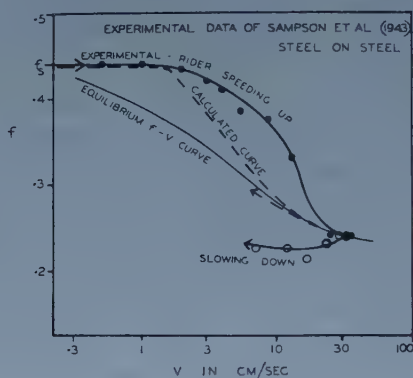


Figure 6. The  $(f_k, v)$  curve computed by Sampson *et al.* (thick continuous line), and comparable  $(f_k, v)$  curve taken from figure 5 (thin continuous line), and the  $(f_k, v)$  curve computed from the latter assuming a critical distance of  $10^{-3}$  cm (broken line).

in which is plotted the effective friction coefficient as a function of velocity both for the first part of the slip stage, while the rider was speeding up, and during the second part, while it was slowing down. In figure 6 is also shown the equilibrium  $(f_k, v)$  curve, from figure 5, for a lubricant effectiveness of 15%. The pattern of the results is precisely what we would expect from the critical distance concept: during the speeding up stage the observed friction coefficient was abnormally high, because during part of the critical distance the velocity had been lower. During the slowing down stage the friction was abnormally low, because during part of the critical distance the speed had been higher.

We can go further, and attempt to calculate the  $(f_k, v)$  curve we might expect for this experiment, using the critical distance concept, the equilibrium  $(f_k, v)$  curve shown in figure 6, and the other data given or calculable from Sampson *et al.* (1943). The result is shown in the broken curve in figure 6, and seems to fit the data much better than does the equilibrium curve from which it was derived.

## § 6. DISPLACEMENT CRITERION FOR STICK-SLIP

The critical distance concept discussed above leads to an important practical deduction, namely that there exists a lower limit to the distance slid during the slip stage, of the order of  $10^{-3}$  cm, and that stick-slip cannot occur if the distance that would be slid is less than this figure. Figure 7 shows stick-slip amplitudes obtained with springs of different stiffness at different sliding velocities. It will be seen that, for any spring, the stick-slip amplitude drops to zero abruptly as the velocity is raised, rather than becomes gradually smaller. This is what we



would expect, given the critical distance concept. For the stiffest spring there are no oscillations whatever; making various plausible assumptions, the distance

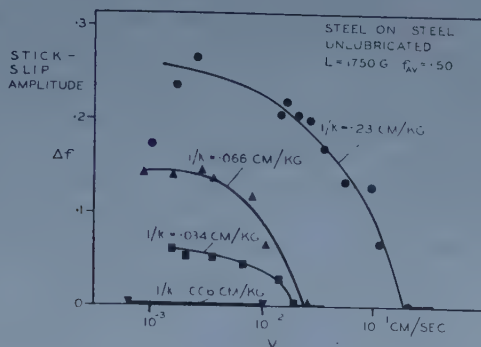


Figure 7. Stick-slip amplitudes obtained with an apparatus of the type shown in figure 1, but with a spring of variable stiffness.

that would have been slid during slip, at the lowest speed tested, turns out to be only  $2 \times 10^{-4}$  cm, well below the limiting value.

## § 7. RELATION BETWEEN STATIC AND KINETIC FRICTION COEFFICIENTS

The critical distance concept, suggesting that the resolving power of the friction process is limited (the limit for steel surfaces being about  $10^{-3}$  cm), raises questions as to whether the  $(f_s, t)$  curve and the  $(f_k, v)$  curve for any system are independent, or whether there is some simple relation between them, arising from the common frictional phenomena responsible for both curves. If we

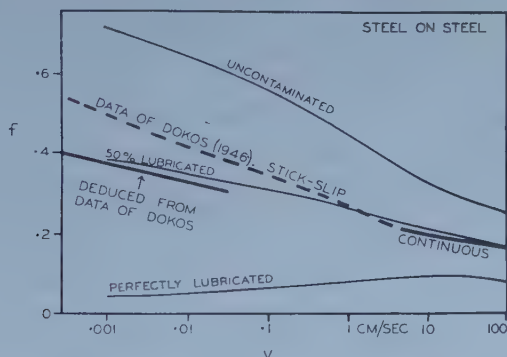


Figure 8. Comparison of Dokos' data (continuous line for steady sliding, broken line for stick-slip) with that of figure 5. Also shown is the  $(f_k, v)$  curve calculated from Dokos' stick-slip data assuming a critical distance of  $10^{-3}$  cm.

maintain stationary contact for  $t$  seconds, then slide a distance  $s$  corresponding to the critical distance, and repeat this cycle indefinitely, we have on the one hand, to within the resolution of the friction process, maintained a steady speed of  $s/t$ , on the other hand performed a series of static friction tests with time of contact  $t$ . Hence, we might expect the same friction coefficient in the two cases.

Experimental evidence in favour of this hypothesis is seen in the work of Dokos (1946), who, at various loads, measured the friction coefficient as a function

of sliding velocity and, if stick-slip occurred, measured the stick frequency also. In figure 8 is plotted his data for friction coefficient as a function of sliding velocity superposed on the author's data, also for steel surfaces. As long as continuous sliding occurs, Dokos' data seem close to my own for 50% contamination, but as soon as stick-slip starts serious discrepancies occur. However, we can still deduce what his  $(f_k, v)$  curve would have been like, had no stick-slip occurred, by using his  $(f_s, t)$  data from figure 4. A time of stick of  $10^{-1}$  sec, for example, is equivalent to a steady sliding velocity of  $10^{-3}/10^{-1} = 10^{-2}$  cm sec $^{-1}$ , and thus figure 4 can be cross-plotted on to figure 8. Thus we obtain the line shown in the left centre of figure 8, and it is seen to be in good agreement with my own line, and a reasonable continuation of Dokos' own non-stick line on the right side of figure 8.

### § 8. DISCUSSION

This paper has been concerned with two points. Firstly, based on earlier work showing that distance effects are an essential part of the friction process, we have postulated that a sliding velocity reached instantaneously during slip gives rise to a friction coefficient characteristic, not of the velocity itself, but of the average velocity over some previous slid distance. This conclusion is supported by consideration of an experimental analysis of an actual stick-slip process, which shows marked discrepancies between the acceleration and deceleration parts of the slip stage, of the kind we would expect given a distance effect; also, by work showing that at low velocities and with a stiff spring, as the sliding velocity or the spring stiffness is raised, stick-slip does not gradually decrease in amplitude down to zero, but rather stops abruptly, a feature characteristic of a critical distance effect.

Secondly, we have postulated a relation between the  $(f_s, t)$  and  $(f_k, v)$  curves, based again on the critical distance concept. This relation explains, for example, the experimental fact that the static coefficient, for very small times of stationary contact, is essentially equal to the kinetic. In addition, light is thrown on the well-known fact that sliding systems which have negative  $(f_k, v)$  curves tend to give rise to regular stick-slip oscillations, when in principle the condition for regular stick-slip to occur is merely that the static coefficient must exceed the kinetic, whether or not the latter decreases as the sliding velocity is raised. According to the critical distance concept, the two conditions are equivalent.

We can be more specific and note that the  $(f_k, v)$  relation for steel quoted by Barwell (1956)  $f_k = c_1 v^{-1/10}$  where  $c_1$  is a constant, is the exact equivalent of one which well represents the  $(f_s, t)$  data for steel of Dokos, namely  $f_s = c_2 t^{1/10}$  where  $c_2$  is again a constant. It is a feature of both functions that the graph of  $(\log f, \log v)$  or  $(\log f, \log t)$  is a straight line, and that the graph of  $(f, \log v)$  or  $(f, \log t)$  is nearly a straight line. These relationships seem characteristic of the behaviour of most sliding systems.

Having seen the link between the  $(f_k, v)$  and the  $(f_s, t)$  curves when the former has a negative characteristic, we may ask what happens when its slope is positive. Under these conditions, it may readily be seen that there can be no such thing as a static coefficient of friction, since any force, however small, will produce some motion (Burwell and Rabinowicz 1953). In fact there is evidence that, at low enough velocities, most if not all  $(f, v)$  curves have a positive slope (Rabinowicz 1958), and hence for these systems there is no true static coefficient,

what is called the static coefficient being some quantity near the maximum of the  $(f, v)$  curve. Thus, what we call the 'stick' stage of the stick-slip process is in fact a slip of very low velocity (Bristow 1950), but this does not invalidate the previous discussion as long as the 'microslip' velocity is much lower than the plate velocity, which is indeed generally the case.

The practical uses of the distance concept are several. On the negative side, it seems that previously published mathematical analyses of stick must be severely modified to allow for the distinction between the instantaneous and equilibrium friction coefficients. On the positive side, however, it becomes possible, if the shape of the  $(f_k, v)$  curve is known, to estimate the  $(f_s, t)$  curve, fundamental in all stick-slip analyses. It should be emphasized that this derived  $(f_s, t)$  curve will only be an approximation to the real one because the critical distance constant used in the conversion should more properly be a critical distance function; also, as figure 6 makes clear, considerable discrepancy between theory and experiment, only partly due to experimental vagaries, still exists.

Three main methods may be used in eliminating stick-slip that is unwanted. Two of these, the introduction of external damping and the application of a lubricant to ensure a positive  $(f_k, v)$  curve, have received much attention. The third, the stiffening of the spring so that the distance slid during slip drops below the critical distance, seems to be entirely independent of the other two and deserves individual consideration.

The critical distance concept may also find application in the design of sliding controls, which are often operated while externally vibrated so as to eliminate sticking. Our analysis suggests suitable values for the vibration amplitude.

#### ACKNOWLEDGMENTS

I wish to acknowledge many helpful discussion with Professors B. G. Rightmire and N. H. Cook, and to thank the U.S. Office of Naval Research for financial support under projects NR-065-335 and Nonr-1841(33).

#### REFERENCES

- BARWELL, F. T., 1956, *Lubrication of Bearings* (London: Butterworths Scientific Publications), p. 19.
- BLOK, H., 1940, *S.A.E. Jl.*, **46**, 54.
- BOWDEN, F. P., and LEBEN, L., 1939, *Proc. Roy. Soc. A*, **169**, 371.
- BOWDEN, F. P., and TABOR, D., 1954, *The Friction and Lubrication of Solids* (Oxford: Clarendon Press).
- BRISTOW, J. R., 1950, *Proc. Phys. Soc. B*, **53**, 964.
- BURWELL, J. T., and RABINOWICZ, E., 1953, *J. Appl. Phys.*, **24**, 136.
- DERJAGUIN, B. V., PUSH, V. E., and TOLSTOI, D. M., 1957, *Conference on Lubrication and Wear, Instn Mech. Engrs*, Paper 13.
- DOKOS, S. J., 1946, *J. Appl. Mech.*, **13**, A148.
- DUDLEY, B. R., and SWIFT, H. W., 1949, *Phil. Mag.*, 6 Ser., **40**, 849.
- HEYMANN, F., RABINOWICZ, E., and RIGHTMIRE, B. G., 1955, *Rev. Sci. Instrum.*, **26**, 56.
- ISHLINSKI, A. Y., and KRAGELSKI, I. V., 1944, *J. Techn. Phys.* (Russian), **14**, 276. This paper was not available to me.
- LOMAKIN, G. D., 1957, *Soviet Physics—Technical Physics*, **1**, 843.
- RABINOWICZ, E., 1951, *J. Appl. Phys.*, **22**, 1373; 1956, *Ibid.*, **27**, 131; 1958, to be published.
- SAMPSON, J. B., MORGAN, F., REED, D. W., and MUSKAT, M., 1943, *J. Appl. Phys.*, **14**, 689.



## Properties of p-type Indium Antimonide: I. Electrical Properties

BY C. HILSUM AND R. BARRIE†

Services Electronics Research Laboratory, Baldock, Herts.

*MS. received 10th December 1957*

**Abstract.** The dependence of electron and hole mobilities on carrier concentration has been determined for p-type indium antimonide with impurity concentrations ranging from  $10^{14}$  to  $2 \times 10^{17} \text{ cm}^{-3}$ . The method used was the analysis of the variation of Hall coefficient and resistivity with a magnetic field. Good agreement was obtained with a simple theory, which assumes that the carrier relaxation time is independent of energy. The decrease of electron mobility with acceptor concentration can be explained by assuming that in pure indium antimonide the important scattering mechanisms are polar scattering and electron-hole scattering.

### § 1. INTRODUCTION

MOST semiconductors of practical interest have a small number of intrinsic carriers at room temperature, and so can be prepared to give either n- or p-type conduction. The carrier concentration and mobility can be found by measuring the Hall coefficient and the resistivity. In indium antimonide, which is of importance theoretically and practically because of its high electron mobility, this is not the case. At room temperature both holes and electrons contribute to the conduction mechanism, and the concentrations and mobilities cannot be found directly. It is generally assumed that the mobility ratio is so high that the effect of holes can be ignored; this is fairly accurate for pure or n-type material, but with p-type specimens there is no simple procedure available for measuring the basic parameters. One method adopted has been to study samples at a temperature sufficiently low that only hole conduction is present, and then to extrapolate the results to room temperature; it is not possible to achieve high accuracy by this method.

We have attempted to find the concentrations and mobilities at room temperature by studying the variation of Hall coefficient  $R$  and resistivity  $\rho$  with an applied transverse magnetic field  $B$ .

### § 2. EXPERIMENTAL PROCEDURE AND RESULTS

Four p-type specimens were used, taken from single crystals pulled by the Kyropoulos method along the  $[111]$  axis, and cut from 1 mm slices perpendicular to this axis. The crystals were grown from purified material doped with pure zinc. Measurements were also made on two pure specimens, one polycrystalline with about  $2 \times 10^{15}$  acceptors per  $\text{cm}^3$ , and the other single crystal with less than  $10^{14}$  donors per  $\text{cm}^3$ .†

† Now at Department of Physics, University of British Columbia, Vancouver.

‡ This material was kindly supplied by Dr. A. C. Beer. The plane of the specimen is a  $(111)$  plane.



The specimens were rectangular blocks, 15 mm × 3 mm × 1 mm. Current electrodes were soldered to the ends, and three platinum wires 0.003 in. in diameter welded to each long side (figure 1). To avoid end errors, all contacts

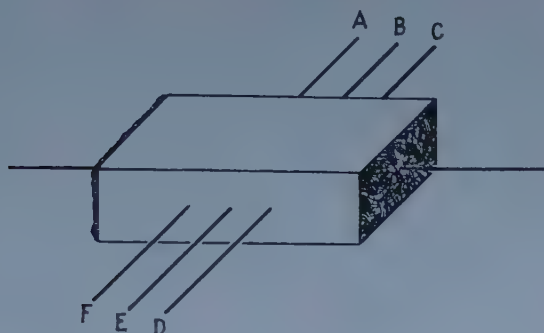


Figure 1. Contact arrangement on specimen.

were kept more than 3 mm from the ends of the specimen. Voltages were measured on a vernier potentiometer accurate to a microvolt; the Hall voltage was taken across probes B and E and magnetoresistance deduced from the average of measurements across A and C, and D and F. The magnetic field was supplied by a Newport Instruments type A electromagnet, fitted with coned vanadium-permendur pole pieces. It was found that consistent results were obtained only if the specimen did not change in temperature during a run, which lasted about 15 minutes. To avoid temperature drifts it was necessary to restrict the specimen current to 20 mA, and the current through the magnet coils to 4 amps, giving a maximum magnetic field of 12 kG. Resistivity was measured by a potential probe at 1 mm intervals along the specimen length. All the specimens had uniform resistivity. The values found for  $R$  and  $\Delta\rho/\rho_0$  as a function of  $B$  are given in table 1.

### § 3. DETERMINATION OF PARAMETERS

#### 3.1. Fundamental Equations

There are four parameters to be found for each specimen; the electron mobility  $\mu$ , the ratio of electron to hole mobility  $b$ , the electron concentration  $n$  and the hole concentration  $p$ . The four equations that we need to find these parameters are the expressions for the Hall coefficient  $R_0$  in zero magnetic field, the resistivity  $\rho_0$  in zero magnetic field, the Hall coefficient  $R$  in arbitrary magnetic field  $B$ , and the magnetoresistance  $\Delta\rho$  due to  $B$ .

Kurnick and Zitter (1956) have shown that the photoelectric effects in InSb at 77°K are best explained by assuming that a time of relaxation for the carriers exists and that it is energy independent. We assume that the same applies at room temperature and, writing  $c$  as the ratio  $n/p$ , the formulae are

$$-R_0 = \frac{b^2c - 1}{pe(1 + bc)^2}, \quad \dots\dots (1) \qquad R = R_0 \frac{1 - Z\mu^2B^2}{1 + Y\mu^2B^2} \quad \dots\dots (2)$$

$$\rho_0 = \frac{b}{pe\mu(1 + bc)}, \quad \dots\dots (3) \qquad \frac{\Delta\rho}{\rho_0} = \frac{X\mu^2B^2}{1 + Y\mu^2B^2} \quad \dots\dots (4)$$

where

$$X = \frac{c(b+1)^2}{b(1+bc)^2}, \quad Y = \frac{(1-c)^2}{(1+bc)^2}, \quad Z = \frac{1-c}{b^2c-1} \quad \dots\dots (5)$$

and  $e$  is the electronic charge.

The data in table I must be used in conjunction with these equations to determine  $\mu$ ,  $b$ ,  $c$  and  $p$ , and hence  $n$  and the intrinsic electron concentration  $n_i = p\sqrt{c}$ .

Table 1

Specimen No.	1	2	3	4	5	6
$B$ (G)			$R$ (cm <sup>3</sup> /coulomb)			
1070	376	405	897	934	701	285
2270	384	410	892	902	680	253
4360	377	412	853	823	572	177
6570	381	408	792	708	435	112
8500	384	410	731	613	348	71
10400	384	410	671	527	271	44
12000	386	411	618	459	219	28
$B$ (G)			$\Delta\rho/\rho_0$			
1070	0.010	0.010	0.025	0.036	0.027	0.012
2270	0.040	0.040	0.120	0.139	0.113	0.054
4360	0.128	0.130	0.406	0.443	0.343	0.146
6570	0.260	0.269	0.807	0.852	0.579	0.222
8500	0.426	0.434	1.25	1.25	0.770	0.275
10400	0.626	0.640	1.73	1.62	0.924	0.311
12000	0.824	0.854	2.15	1.92	1.030	0.329

### 3.2. Analysis of Results for Impure Specimens

A simple method of analysis is possible for specimens 3-6.  $R$  is plotted against  $\Delta\rho/\rho_0$  as in figure 2, and, as predicted by equations (2) and (4) a straight line is obtained. This passes through the points  $(0, R_0)$  and  $(\beta, 0)$  where  $\beta = (b^2c-1)/b(1-c)$ .

The relations

$$\frac{1}{\mu^2 B^2} + \left( \frac{1-c}{1+bc} \right)^2 = \frac{\rho_0}{\Delta\rho} \frac{c(b+1)^2}{b(1+bc)^2} = \frac{R_0}{R_0-R} \frac{c(1-c)(b+1)^2}{(b^2c-1)(1+bc)^2} \dots\dots (6, 7)$$

can now be used, since  $R_0$  is known. Plots of  $1/B^2$  against  $\rho_0/\Delta\rho$  and  $R_0/(R_0-R)$  have the same negative intercept  $1/B_1^2$  on the  $1/B^2$  axis, and the intercepts on the other axis are, respectively,  $\alpha$  and  $\gamma$ , where

$$\alpha = \frac{b(1-c)^2}{c(b+1)^2} \quad \text{and} \quad \gamma = \alpha\beta, \quad \dots\dots (8a, b)$$

This provides a check for  $\beta$ . Since  $c$  is small,  $\beta$  and  $\alpha$  give  $bc$  to within 5%, but  $b$  and  $c$  individually accurate only to about 20%. A good determination of  $\mu$  is possible, since

$$\mu = \frac{1}{B_1} \frac{1+bc}{1-c} \dots\dots (9)$$

Another determination of  $\mu$  can be made from the ratio  $R_0/\rho_0$  which depends on  $\mu$  and  $bc$ , but not critically on  $b$ .

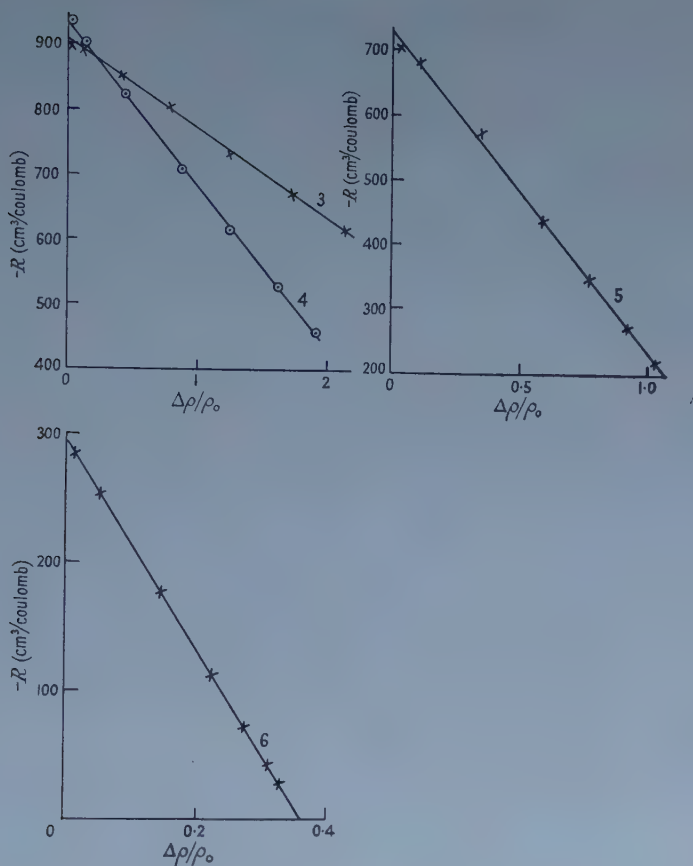


Figure 2. Relationship between Hall constant and magnetoresistance for specimens 3-6.

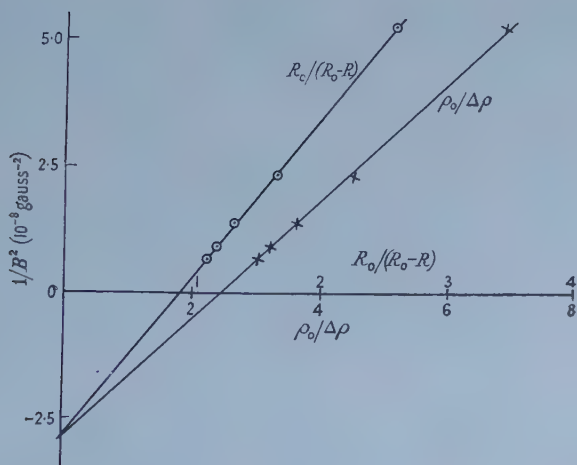


Figure 3. Dependence of Hall constant and magnetoresistance on magnetic field, plotted as for equations (6) and (7) for specimen 6.

The analysis to this point can be illustrated by reference to figure 3 where the results for specimen 6 are given; we measure  $\alpha=2.44$ ,  $\beta=0.366$ ,  $\gamma=0.90$  and  $1/B_1^2=2.85 \times 10^{-8} \text{ gauss}^{-2}$  and deduce  $bc=0.39$ ,  $c$  being less than 0.01 and  $b$  just under 50. From equation (9)  $\mu$  is found to be  $23\,500 \text{ cm}^2 \text{ v}^{-1} \text{ sec}^{-1}$  and from  $R_0/\rho_0$ ,  $\mu$  is given as  $23\,700 \text{ cm}^2 \text{ v}^{-1} \text{ sec}^{-1}$ .

We must now find  $b$  more accurately. A calculation of  $R/R_0$  at one of the higher values of  $B$  gives  $Z$  in terms of  $Y$ , and  $b$  is determined from equation (5). Once  $b$  is known  $p$  can be calculated from either  $R_0$  or  $\rho_0$ , and finally  $n_i$  deduced from  $p$  and  $c$ . Curves for the variation of  $R$  and  $\rho$  with  $B$  can now be computed and the effect of changes in  $b$  studied. It is estimated that the parameters are determined to within  $\pm 5\%$ .

### 3.3. Analysis of Results for Pure Specimens

When only a few impurities are present  $c$ , the ratio of electron to hole concentration, approaches unity, and both  $Y$  and  $Z$  become small. As a consequence  $R$  is invariant with the magnetic field and we have only three equations left from which to determine the four parameters. However, it is now permissible to determine the acceptor concentration  $N_A$  by a Hall effect measurement at  $90^\circ \text{K}$ . This is a consistent procedure only when  $N_A$  is small compared with  $n_i$  since  $c$  does not then depend markedly on the scattering factor used in deducing  $N_A$ . For specimen 1,  $c$  was found to be 1.004 and for specimen 2, about 0.90. The equation

$$\mu = \frac{R_0 bc + 1}{\rho_0 bc} \quad \dots\dots (10)$$

gives  $\mu$  to within 5% since  $bc$  is not very different from 100. For these specimens  $Y$  is extremely small, and  $\Delta\rho/\rho_0$  should be proportional to  $B^2$ ; this graph has a slope  $\mu^2 X$ . For specimen 1,  $X$  is equal to  $1/b$ , and  $p$  can then be found from  $R_0$ . Specimen 2 is not pure enough for this to be true; the measured value of  $c$  must be used with  $X$  to give  $b$ , and hence  $p$ . The accuracy of the determinations for this specimen is probably only half as good as for the other five.

### 3.4. Results

The values found for  $\mu$ ,  $b$ ,  $c$ ,  $p$  and  $n_i$  are assembled in table 2, with the calculated and measured values of resistivity. The consequent dependence

Table 2

No.	$T$	$p$	$n_i \times 10^{16}$	$\mu$	$b$	$c$	Predicted		Meas.
							$R_0$	$\rho_0 \times 10^3$	
1	18	$< 10^{14} \dagger$	1.62	78000	104	1.004	380	4.90	4.97
2	17.5	$2 \times 10^{15} \dagger$	1.60	75000	104	0.90	406	5.45	5.50
3	18	$5.2 \times 10^{16}$	1.62	41000	62	0.097	908	26.6	27.5
4	18	$7 \times 10^{16}$	1.67	37000	60	0.057	940	33.0	34.4
5	21	$1.07 \times 10^{17}$	1.80	28500	52	0.028	720	43.0	43.4
6	19	$1.86 \times 10^{17}$	1.71	24000	46	0.0084	290	46.5	46.0

Units:  $T$  ( $^\circ \text{C}$ ),  $p$  ( $\text{cm}^{-3}$ ),  $n_i$  ( $\text{cm}^{-3}$ ),  $\mu$  ( $\text{cm}^2 \text{ v}^{-1} \text{ sec}^{-1}$ ),  $R_0$  ( $\text{cm}^3 \text{ c}^{-1}$ ),  $\rho_0$  ( $\text{ohm cm}$ ).

$\dagger$  For specimens 1 and 2 the impurity concentration is given in column (c) instead of the hole density.

of  $R$  and  $\Delta\rho/\rho_0$  on  $B$  in accordance with equations (2) and (4) is shown on figure 4, and compared with the experimental data. The agreement is very good, for example for specimen 6 only one point departs from the predicted line by more than 0.5%.



## § 4. VALIDITY OF ASSUMPTIONS

In the derivation of equations (1) to (4), the assumptions were made that a time of relaxation  $\tau$  exists, and that it is independent of the carrier energy  $E$ . Before commenting on this it is necessary to show that if a different scattering law were obeyed, the experimental data would be sensitive enough to detect it.

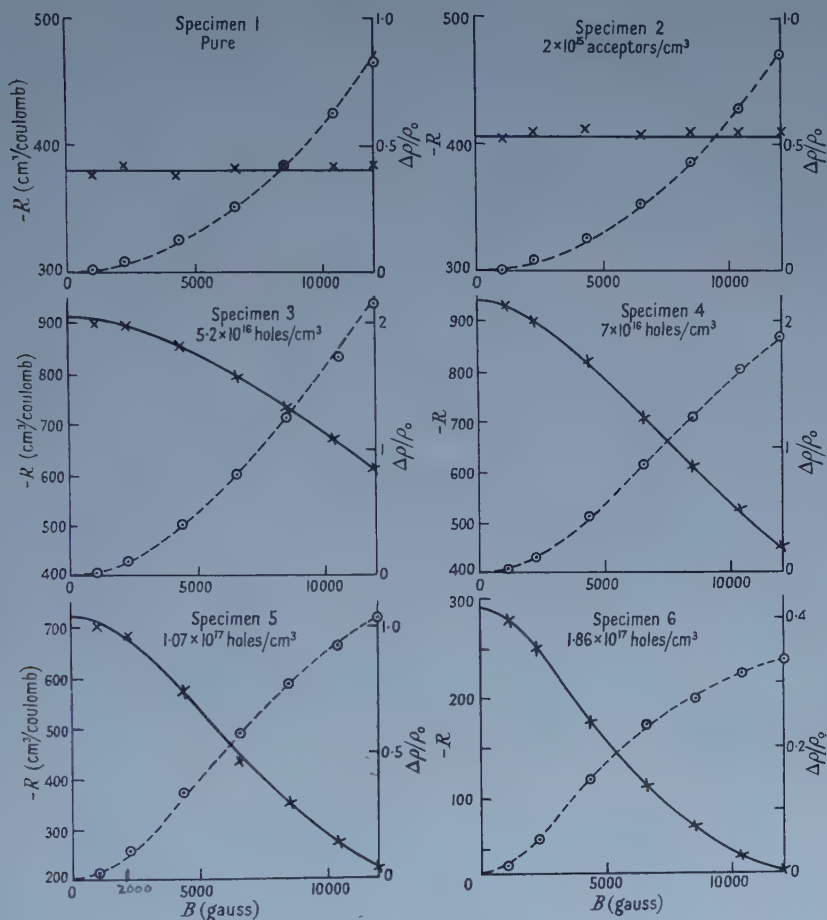


Figure 4. Comparison of theory with experiment.

To test the effect of a relaxation time that does depend on the energy, it was assumed that  $\tau$  could be written in the form  $E^s$ . Equations (1) to (4) then correspond to taking  $s=0$  for both the electrons and holes. Attempts were made to fit the data using certain non-zero values of  $s$ , but as shown now these proved unsuccessful.

Equations (1) to (4) predict straight-line graphs when  $R_0 B^2 / (R - R_0)$  and  $\rho_0 B^2 / \Delta \rho$  are plotted against  $B^2$ , and straight lines were obtained experimentally. When  $s \neq 0$  the equations contain the integrals

$$K_s = \int_0^\infty \frac{x^{(3/2)-s}}{x^{-2s} + g} e^{-x} dx \quad \dots\dots (11)$$

$$L_s = \frac{2}{\sqrt{\pi}} \int_0^\infty \frac{x^{3/2}}{x^{-2s} + g} e^{-x} dx \quad \dots\dots (12)$$

$$g = \frac{9\pi}{16} \frac{1}{[\Gamma(5/2 + s)]^2} \mu^2 B^2. \quad \dots\dots (13)$$

These integrals have been tabulated for  $s = -\frac{1}{2}$  by staff of the Battelle Memorial Institute. It was therefore possible to check if the assumption  $s = -\frac{1}{2}$  could be valid by computing the dependence of  $R$  and  $\Delta\rho/\rho_0$  on  $B$  for specimens with the parameters of table 2 and plotting  $R_0 B^2/(R - R_0)$  and  $\rho_0 B^2/\Delta\rho$  against  $B^2$ . These graphs showed considerable departure from linearity and the position could not be sufficiently improved by varying the parameters. For the impure specimens, a similar procedure was tried, using  $s = +\frac{1}{2}$ . The integrals required can be calculated from the relations

$$K_s(g) = \frac{1}{g} K_{-s} \left( \frac{1}{g} \right), \quad \dots\dots (14)$$

$$L_s(g) = \frac{3}{2g} - \frac{1}{g^2} L_{-s} \left( \frac{1}{g} \right). \quad \dots\dots (15)$$

Again the agreement with experiment was poor.

It is therefore apparent that if  $\tau$  can be written in the form  $E^s$ ,  $s$  must be near zero.

It has been assumed in the derivation of the equations that the relaxation time is independent of the magnetic field. This is normally taken to be the case when  $eB/m^*c \ll 1/\tau$ , a condition not satisfied by the specimens studied. However, it is not clear that this is a necessary condition, and it may be that the assumption is still valid when  $eB/m^*c \ll \hbar/kT$ . This second condition, which is satisfied, arises from the fact that a certain sum appearing in the time of relaxation for an electron in the presence of a magnetic field (see for example Barrie 1957) can then be replaced by an integral. This gives  $\tau$  independent of the magnetic field.

## § 5. VARIATION OF MOBILITIES WITH IMPURITY CONCENTRATION

The values of electron and hole mobilities found experimentally have been plotted against the acceptor concentration in figure 5. It should be noted that the values for specimen (5) are for a slightly higher temperature. In this section we shall outline how the theoretical curves, also shown in the figure, were obtained.

The specimens studied cover a wide range of impurity concentrations, and at room temperature practically all the impurities are ionized. The scattering processes we shall consider are lattice scattering, electron-hole scattering and ionized impurity scattering.

Recently there has been speculation about the nature of lattice scattering in InSb. Keyes (1955) has proved that scattering by the acoustic lattice modes could only reduce the electron mobility at room temperature to  $10^7 \text{ cm}^2 \text{ v}^{-1} \text{ sec}^{-1}$ . Ehrenreich (1957) pointed out that scattering by the optical modes, via the polar interaction, would be much larger than acoustic scattering, and calculated that the lattice mobility due to this mechanism was about  $10^5 \text{ cm}^2 \text{ v}^{-1} \text{ sec}^{-1}$ . It has been shown by Howarth and Sondheimer (1953) that the relaxation time approximation

holds for polar scattering only at high temperatures; however, at temperatures less than that corresponding to the optical-mode frequency the scattering can be formally represented by a relaxation time which is energy independent. In InSb the optical-mode temperature is 290°K, and a rigorous treatment of mobility at room temperature would be quite complicated, so we have assumed that the low temperature approximation holds up to room temperature.

The impurity and electron-hole scattering contributions are combined with the polar scattering by defining an effective relaxation time  $\tau$  in terms of the polar relaxation time  $\tau_L$  and the impurity relaxation time  $\tau_I$  as

$$1/\tau = 1/\tau_L + 1/\tau_I. \quad \dots\dots (16)$$

Holes are treated as additional impurity centres and their effect is included in  $\tau_I$ .

The mobility is now deduced in the usual way (Shockley 1950) from

$$\mu = \frac{e}{m^*} \frac{\langle v^2 \tau \rangle}{\langle v^2 \rangle} \quad \dots\dots (17)$$

$v$  being the velocity of an electron of charge  $e$  and mass  $m^*$ . We may simplify by introducing  $x = v^2/v_T^2$ , where  $m^*v_T^2 = 2kT$ , and treating  $x$  as the variable.

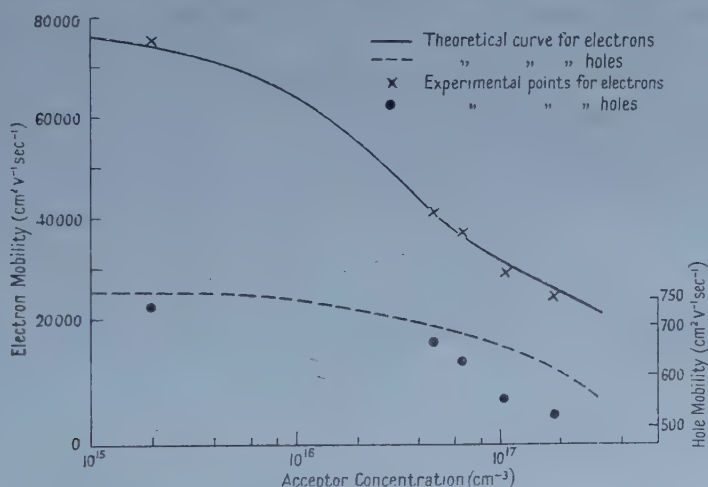


Figure 5. Dependence of electron and hole mobilities on acceptor concentration.

The relaxation time due to impurity scattering by  $N$  impurities/cm<sup>3</sup> is given by Dingle (1955) as

$$\tau_I = \frac{K\sqrt{(2m^*)E^{3/2}}}{\pi N e^4 [\ln(1+\xi) - \xi/(1+\xi)]} \quad \dots\dots (18)$$

where

$$\xi = \frac{8\pi m^* E K k T}{h^2 e^2 (n+p)}, \quad \dots\dots (19)$$

$K$  is the dielectric constant and  $E$  is the electron energy.

We take  $K$  as 15, and  $m^*$  as  $0.02m$ , an average of the values obtained by resonance methods ( $0.013m$ – $0.020m$ ) and by thermoelectric and optical methods ( $0.025m$ – $0.037m$ ). The scattering effect of holes is included by substituting  $N+p$  for  $N$  in equation (18).

Since  $\tau_L$  is independent of energy, the polar mobility  $\mu_L$  is given by

$$\mu_L = e\tau_L/m^* \quad \dots\dots (20)$$

and

$$\mu = \frac{4\mu_L}{3\sqrt{\pi}} \int_0^\infty \frac{x^3 e^{-x} dx}{x^{3/2} + 1.75 \times 10^{-22} \mu_L (N+p) [\ln(1+\xi) - \xi/(1+\xi)]} \quad \dots\dots (21)$$

The value adopted for  $\mu_L$ ,  $107\,000\text{ cm}^2\text{v}^{-1}\text{sec}^{-1}$ , is chosen so that  $\mu$  is  $78\,000\text{ cm}^2\text{v}^{-1}\text{sec}^{-1}$  for pure material ( $N=0$ ,  $n=p=n_i=1.6 \times 10^{16}\text{ cm}^{-3}$ ). Ehrenreich deduces  $\mu_L$  as  $65\,000\text{ cm}^2\text{v}^{-1}\text{sec}^{-1}$  using an effective ionic charge of  $0.18e$ ; if he had used the experimental value (Spitzer and Fan 1955) of  $0.13e$ ,  $\mu_L$  would have been over  $120\,000\text{ cm}^2\text{v}^{-1}\text{sec}^{-1}$ . The value we must take to fit the data for pure specimens is lower, but we expect this since we use a larger effective mass than Ehrenreich.

The integral in (21) converges rapidly, and values of  $x$  larger than 10 can be ignored. The computed values of mobility are shown as the full line in figure 5. Similar calculations may be made for n-type material (Hilsum 1957).

The general agreement between theory and experiment confirms that polar scattering and electron-hole scattering are the important mechanisms in pure InSb, and that the decrease in mobility as impurities are added is predicted by Dingle's impurity scattering formula, with allowance for the change in electron-hole scattering.

Also shown in figure 5 is the curve for hole mobility, obtained by assuming that the lattice scattering for holes is due to the acoustic modes, the relaxation time for this process being proportional to  $E^{-1/2}$ . The integrals occurring in the combination of this with ionized impurity scattering have been evaluated by Mansfield (1956a). The hole effective mass was taken as  $0.18m$  and the hole lattice mobility as  $750\text{ cm}^2\text{v}^{-1}\text{sec}^{-1}$ . The decrease of mobility with impurity concentration is larger than we should expect theoretically.

Throughout the analysis the effect of degeneracy of the electron gas and that of the non-parabolic nature of the conduction band (Ehrenreich 1957) have been ignored. For specimens 3 to 6, the electron gas will be non-degenerate and these effects will be negligible. For specimens 1 and 2 the effect is smaller than the experimental error.

## § 6. DISCUSSION

There appears little doubt that the galvanomagnetic properties of p-type InSb at room temperature are adequately explained by making the assumptions which lead to equations (1) to (4). This seems rather surprising when one considers the results obtained in § 5. It was seen that there is considerable variation in the electron mobility as ionized impurities are added and one would then have expected that the additional impurity scattering would alter the dependence of the relaxation time on energy. The specimens, however, all seemed to satisfy the same simple theory, though for the two pure specimens, it will be noted from figure 4 that  $\Delta\rho/\rho_0$  shows very slight deviations from the predicted curve. Although these were within the experimental error, they were repeatable.

The Hall coefficients of specimens 3, 4 and 6 were measured at  $90^\circ\text{K}$ . (Specimen 5 was not available having been broken during this experiment.) Using the relation  $R = -r/N_A e$  and deducing  $N_A$  from table 2, one finds that  $r$  lies



between 1.33 and 1.43 for these three specimens. For impurity scattering alone, Mansfield (1956 b) gives values between 1.58 and 1.41 for these specimens. For  $\tau \propto E^{-1/2}$  the value would be 1.18 and for  $\tau$  independent of  $E$  it would be 1. At this temperature, and for these impure specimens, it would therefore appear that the relaxation time for holes is not energy independent.

The values we obtain for  $n_i$  should be expected to lie 18% below previous values published since it has generally been assumed that  $\tau \propto E^{-1/2}$  for pure specimens, and the expression for  $n_i$  in terms of  $R$  then includes the scattering factor  $3\pi/8$ ; with the simple model the factor does not occur. Comparing our results with those obtained by other workers, we find that allowing for the different temperatures used, only Madelung and Weiss (1954) give a value about 20% above ours; the other results are more or less the same as our own.

The hole mobility found for pure InSb is lower than previous values quoted. Most other determinations have been made by extrapolation from low temperatures and are of low accuracy, but Kurnick and Zitter (1956) gave  $b$  as 91, using magnetoresistance data. The value they quoted was, however, not  $b$  but  $1/X$ , found from the slope of  $\Delta\rho/\rho_0$  against  $B^2$ . Their procedure was equivalent to assuming  $c=1$ , though they state that the material used had an acceptor concentration of  $10^{15} \text{ cm}^{-3}$ . This indicates that  $c \simeq 0.96$ , and a value for  $b$  of 107 can now be deduced from their data, in good agreement with our results.

#### ACKNOWLEDGMENTS

The authors are glad to acknowledge the assistance of Miss A. Clark throughout the measurements, and that of Dr. O. Simpson during the preparation of the manuscript. The crystals used were provided by Mr. M. A. Coupland and Dr. F. A. Cunnell. Permission to publish has kindly been given by the Admiralty.

#### REFERENCES

- BARRIE, R., 1957, *Proc. Phys. Soc. B*, **70**, 1008.  
 DINGLE, R. B., 1955, *Phil. Mag.*, **46**, 831.  
 EHRENREICH, H., 1957, *J. Phys. Chem. Solids*, **2**, 131.  
 HILSUM, C., 1957, *S.E.R.L. Technical Memo.* No. 366.  
 HOWARTH, D. J., and SONDHEIMER, E. H., 1953, *Proc. Roy. Soc. A*, **219**, 53.  
 KEYES, R. W., 1955, *Phys. Rev.*, **99**, 190.  
 KURNICK, S. W., and ZITTER, R. N., 1956, *J. Appl. Phys.*, **27**, 278.  
 MADELUNG, O. and WEISS, H., 1954, *Z. Naturf.*, **9a**, 527.  
 MANSFIELD, R., 1956 a, *Proc. Phys. Soc. B*, **69**, 76; 1956 b, *Ibid.*, **69**, 862.  
 SHOCKLEY, W., 1950, *Electrons and Holes in Semiconductors* (New York: van Nostrand), p. 275.  
 SPITZER, W. G., and FAN, H. Y., 1955, *Phys. Rev.*, **99**, 1893.

## RESEARCH NOTES

## Double Scattering Experiments as a Test for Invariance under Time-reversal in Strong Interactions

By F. MANDL

Atomic Energy Research Establishment, Harwell, Berks.

*MS. received 20th December 1957*

THE polarization-asymmetry equality in double scattering experiments, derived by Dalitz (1952) and Wolfenstein and Ashkin (1952), depends on invariance under time-reversal (hereafter denoted by  $T$ ) of the scattering matrix. When suitably stated, it is independent of parity conservation (Bell and Mandl 1958). Hence an experimental test of this equality, for proton-proton scattering for example, is a direct test of  $T$ -invariance in strong interactions†.

In order to interpret such an experiment one would like to know to how large an admixture of  $T$ -violating terms an observed polarization-asymmetry difference  $P-A$  corresponds. It is this point we wish to discuss, for pp-scattering.

In this analysis we shall assume that parity is conserved in strong interactions. Experimental evidence that this is the case to a high degree has been obtained by Tanner (1957) and Wilkinson (1958). With this assumption, the parity- and  $T$ -conserving scattering matrix (which we shall write, in the usual notation,  $S = A + B(\sigma^1 \cdot \sigma^2) + C(\sigma^1 \cdot \mathbf{K})(\sigma^2 \cdot \mathbf{K}) + D(\sigma^1 \cdot \mathbf{P})(\sigma^2 \cdot \mathbf{P}) + E(\sigma^1 \cdot \mathbf{N} + \sigma^2 \cdot \mathbf{N})$ )

.....(1)

where  $\mathbf{P}$ ,  $\mathbf{K}$  and  $\mathbf{N}$  are the unit vectors derived from  $\mathbf{k}' \pm \mathbf{k}$  and  $\mathbf{k}' \times \mathbf{k}$  respectively,  $\mathbf{k}$  and  $\mathbf{k}'$  being the relative momenta before and after scattering in the centre-of-mass system) is augmented by only a single term:

$$S' = T\{(\sigma^1 \cdot \mathbf{K})(\sigma^2 \cdot \mathbf{P}) + (\sigma^2 \cdot \mathbf{K})(\sigma^1 \cdot \mathbf{P})\}. \quad \text{.....(2)}$$

This follows since the  $S$ -matrix must be symmetric in the two particles for a pp-system, but it also holds for the np-system if one assumes charge-symmetry.

From equations (1) and (2) one obtains directly, by calculating the polarization-asymmetry difference, that

$$|T| \geq \frac{I_0}{4|D-C|} |P-A| \quad \text{.....(3)}$$

where  $I_0$  is the differential cross section at the angle and energy at which the polarization and asymmetry are measured. If  $\bar{A}$  is the mean of the  $T$ -conserving amplitudes  $A \dots E$  in equation (1), then  $\xi = |T/\bar{A}|$  is a measure of the  $T$ -violating admixture to the  $S$ -matrix.

Assuming this admixture small, one can as a first approximation use the existing phase-shift analyses to calculate  $\xi$  from equation (3) for a given  $|P-A|$ .

† For systems of total spin  $\frac{1}{2}$ , e.g., scattering of protons by a spin zero nucleus, this equality holds independently of  $T$ -invariance. This has also been pointed out by Henley and Jacobsohn (1957). However, this is an exceptional case. Furthermore, their criterion, that in a double scattering experiment  $\sigma(LL) - \sigma(LR) > 0$ , represents an extremely weak test of the polarization-asymmetry equality: it merely requires that polarization and asymmetry have the same sign.

We have done this for pp scattering at 150 mev and a scattering angle of  $45^\circ$  (centre-of-mass), using the analysis of Signell and Marshak (1957), and obtain  $|\bar{A}| = 0.25 \times 10^{-13}$  cm and

$$|T| \geq 0.2 \times 10^{-13} |P - A| \text{ cm} \quad \dots\dots (4)$$

i.e.

$$\xi \geq 0.8 |A - P|. \quad \dots\dots (5)$$

This inequality suggests that the polarization-asymmetry measurement might be used to test  $T$ -invariance to about 1% as a measurement of  $|A - P|$  to this accuracy may be feasible. Since Henley and Jacobson conclude from their analysis that  $T$ -invariance in strong interactions is only confirmed to about 10–20%, this measurement may be worth doing.

Assuming that only partial waves with  $l$  less than or equal to 3 contribute to the scattering at 150 mev, Phillips (1958) has shown that in this case the  $T$ -violating terms of the  $S$ -matrix are specified by one real parameter  $\lambda$ . He then obtains instead of the inequality (4), an equation for  $T$ . For the case considered above this leads to

$$|T| = 0.14 \times 10^{-13} \sin 2\lambda \text{ cm}. \quad \dots\dots (6)$$

Assuming quite a small admixture,  $\lambda = 5^\circ$ , for which  $|P - A| = 0.09$ , equation (6) gives  $|T| = 0.024 \times 10^{-13}$  cm whereas from inequality (4),  $|T| \geq 0.018 \times 10^{-13}$  cm showing that the actual value of  $|T|$  is not much larger than its possible minimum. Similar results have also been found for other cases. Whereas Phillips obtains a definite value for  $T$  from a measurement of  $P - A$ , his analysis neglects partial waves with  $l$  greater than 3 and it may in practice be doubtful (e.g. at 150 mev) whether this is really justified, in particular whether the  ${}^3F_4$ – ${}^3H_4$  coupling can be neglected. On the other hand in deriving the inequality (3) no approximations have been made.

*Note added in proof.* Mr. B. Rose has pointed out to me that one can, in principle, test the polarization-asymmetry equality from the four counts (left-left, left-right, etc.) measured in the triple scattering experiment for the depolarization parameter  $D(\theta)$ . This has the advantage that both  $P$  and  $A$  are actually measured for the same scattering event. In practice, owing to the large targets required to give reasonable counting rates, difficulties are likely to arise from the angular variations of the cross sections.

#### ACKNOWLEDGMENT

I would like to thank Dr. R. J. N. Phillips for helpful discussions.

#### REFERENCES

- BELL, J. S., and MANDEL, F., 1958, *Proc. Phys. Soc.*, **71**, 272; and future paper.
- DALITZ, R. H., 1952, *Proc. Phys. Soc. A*, **65**, 175.
- HENLEY, E. M., and JACOBSON, B. A., 1957, *Phys. Rev.*, **108**, 502.
- PHILLIPS, R. J. N., 1958, *Nuovo Cim.*, in the press.
- SIGNELL, P. S., and MARSHAK, R. E., 1957, *Phys. Rev.*, **106**, 832.
- TANNER, N., 1957, *Phys. Rev.*, **107**, 1203.
- WILKINSON, D. H., 1958, *Phys. Rev.*, in the press.
- WOLFENSTEIN, L., and ASHKIN, J., 1952, *Phys. Rev.*, **85**, 947.

## Directional Electric Breakdown of KCl

By R. COOPER AND A. FERNANDEZ

Electrical Engineering Laboratories, University of Manchester

*MS. received 7th October 1957, and in revised form 16th November 1957*

THE electric breakdown of potassium chloride single crystals is characterized by very large spread in the values of electric strengths obtained from apparently similar specimens (Calderwood, Cooper and Wallace 1953). This phenomenon has been attributed to structural differences caused by plastic deformation and consequently it is believed that the low values of electric strength are the significant ones provided they are obtained from carefully conducted experiments (Cooper and Wallace 1953, 1956). On this basis a recent investigation (Cooper, Grossart and Wallace 1957) has shown that potassium chloride is anisotropic at temperatures below about 200°C. At room temperature, for example, the minimum value of electric strength with the field applied in a (100) direction was  $0.54 \text{ MV cm}^{-1}$  but when the field was in a (110) direction it exceeded  $0.8 \text{ MV cm}^{-1}$ , i.e. about  $\sqrt{2}$  times as great. The possibility therefore exists of the breakdown track following the (100) direction even if the applied field is uniform and in the (110) direction.

We have found no account in the literature of the observation of breakdown track directions during the intrinsic electric breakdown of KCl. In order to do this satisfactorily the discharge current from the generator capacitors must be diverted from the specimen within a few microseconds after it has become conducting. If this is not done the damage to the specimen precludes detection of the initial discharge direction. In recent years a number of circuits have been described (Higham and Watson 1953, Saxe and Lewis 1955) for this purpose. In general, a trigatron spark gap is placed in parallel with the specimen and it is triggered by a thyatron when current flows through the specimen. We have found it possible to dispense with the thyatron and using only a trigatron gap and resistance in series with the specimen, current diversion has been achieved within about 1 microsecond of breakdown. The energy supplied to the discharge in this time comes mainly from the specimen self-capacitance and that of the associated leads.

Initial experiments were performed using 33 annealed specimens. They had been prepared in a way previously described (Calderwood, Cooper and Wallace 1953) and in all cases the electric field was applied in a (110) direction. The specimens were broken down with direct current. The result of this experiment is illustrated in figure 1(a) which shows the distribution of values of electric strength and at the same time it correlates electric strength with breakdown track direction. The track was in a (100) direction in the majority of cases, i.e. at 45° to the applied field. Figure 2(a) (Plate) is a photograph of a typical breakdown track. In a small minority of the specimens the track direction was the same as that of the applied field. These specimens also possessed electric strengths in excess of about  $1.1 \text{ MV cm}^{-1}$ .



The result of breaking down 25 similar but unannealed specimens is illustrated in figure 1 (b). The situation found previously was now reversed. The majority of specimens possessed electric strengths in excess of about  $1.1 \text{ MV cm}^{-1}$  and in most of these specimens the breakdown track followed the direction of the applied field. Nevertheless, the track was in a (100) direction in the few specimens with electric strengths less than about  $1.1 \text{ MV cm}^{-1}$ . Thus in both experiments low values of electric strength are associated with anisotropic behaviour and high values with isotropic behaviour, the transition taking place at a value of electric strength about  $1.1 \text{ MV cm}^{-1}$ .

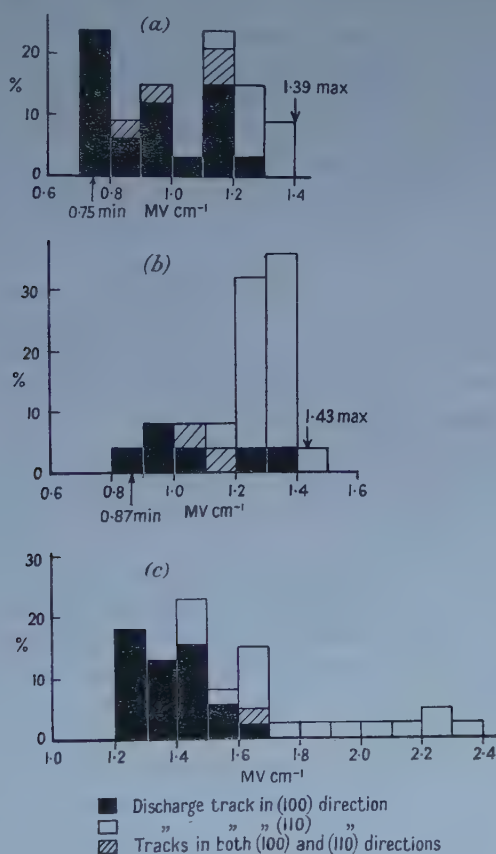


Figure 1. Anisotropy in the breakdown of KCl.

- (a). Breakdown of 33 annealed specimens of KCl. Field in (110) direction.
- (b). Breakdown of 25 unannealed specimens. Field in (110) direction.
- (c). Influence of electric field on discharge direction. Tracks observed in 39 annealed specimens of KCl. Field in (110) direction.

The track shown in figure 2 (a) is clearly a cylindrical channel from which the material has been removed. It is not a crack but when precautions are not taken it is possible for (100) breakdown tracks to be obscured by cracks, and incipient cleavages within the specimen. Figure 2 (b) is of interest in this connection. It is a photograph of a track obtained when the current diverter operated more slowly by a few microseconds than the one used in the case of figure 2 (a). Incipient cracks can be seen starting at one end of the breakdown

track. They lie in (100) planes at  $45^\circ$  to the breakdown channel and extend about half-way across the specimen. From this it follows that mechanical destruction of the specimens occurs at a significantly later stage in the process than does the phenomenon at present under investigation. The fact that we observe in many cases breakdown channels in the direction of easy cleavage, i.e. (100), cannot be explained in terms of mechanical effects.

Some discussion has been given previously of possible differences between annealed and unannealed specimens (Calderwood, Cooper and Wallace 1953). According to these investigators annealing relieves the severe internal strains created in the crystal lattice during the preparation of the specimens. High values of electric strength are associated with strained specimens because of the additional scattering of conduction electrons by the imperfections. Conversely, low values of electric strength are associated with specimens possessing a more perfect lattice. There is always appreciable spread in values of electric strength for two reasons. In the first place the internal strains are not homogeneously distributed within the specimens, and in the second place strains can be induced by the Coulomb force of attraction between the electrode surfaces (Cooper and Wallace 1953, 1956).

The present observations are consistent with the above views. Comparison of figure 1 (*a*) with figure 1 (*b*) shows that annealing has increased both the chance of obtaining low values of electric strength as well as the chance of observing (100) breakdown channels. Anisotropy of electric strength must arise from a property of the periodic crystal lattice. Imperfections, which are likely to be distributed randomly within the lattice, are expected not only to increase the electric strength but also to reduce and possibly to destroy any directional sensitivity possessed by this quantity. Previous investigations (Cooper and Wallace 1956) have shown that any specimen of KCl withstanding more than about  $1.0\text{--}1.2\text{ MV cm}^{-1}$  is certainly strained before breakdown occurs whatever was its state before the application of voltage. The transition between (100) tracks and (110) tracks observed to occur in the present experiments at about  $1.1\text{ MV cm}^{-1}$  is entirely consistent with this. Thus, a connection has been established between anisotropic behaviour and crystal structure. At the same time more evidence is provided in favour of the 'low value' criterion of electric strengths proposed by Calderwood, Cooper and Wallace (1953).

It is perhaps worth mentioning that the investigations described above provide a reason for Caspari's (1955) recent failure to detect any anisotropy in the intrinsic electric strength of NaCl. Previous investigations (von Hippel and Davisson 1940, Cooper, Grossart and Wallace 1957) have shown that with this material any differences are within about 10%. Clearly, great care must be taken with experiments aimed at detecting differences in intrinsic strength as small as this. In particular great care must be taken over the state of strain of the specimens. Caspari's specimens were prepared by grinding and apparently no attempt was made to relieve the severe strains which are set up in the crystal lattice by this treatment (Calderwood, Cooper and Wallace 1953).

The question remains to what extent the anisotropic behaviour of KCl is influenced by (*a*) substitutional impurities, (*b*) temperature, (*c*) overvoltage.

The influence of substitutional impurities was studied using KCl crystal in which some ions of Cl were replaced with ions of Br and also with KCl crystals in which some ions of K were replaced by Na ions. It was established that the

anisotropy was not destroyed by adding up to 15% by weight of KBr to KCl, nor by adding up to 1% by weight of NaCl to KCl. These figures correspond respectively to the replacement of one chlorine ion in every ten by a bromine ion and the replacement of one potassium ion in every 77 by a sodium ion. In carrying out this experiment some difficulty was experienced in preparing recessed specimens. The parent crystals of the mixed salts were brittle and difficult to handle, and when more than the above concentrations of KBr or NaCl were added they became quite unsatisfactory. For this reason experiments with higher concentrations were not performed.

No convincing evidence of an effect of temperature on the anisotropy was found within the temperature range  $-195^{\circ}\text{C}$  to about  $200^{\circ}\text{C}$ .

In a recent paper (Callen and Offenbacher 1953) directional phenomena in the breakdown of alkali halide crystals have been discussed. Although the theory developed is not entirely consistent with the results of experiments on KCl (Cooper, Grossart and Wallace 1957) it seemed worth while to investigate the prediction that breakdown track directions are influenced by the magnitude of the applied electric field. A voltage impulse with a rise time of about  $1/20\ \mu\text{sec}$  to  $90^{\circ}$ , of the peak value was required to carry out this experiment. This was obtained from a conventional single stage impulse generator. Protection of the specimen was achieved by using a generator of very small capacitance and by using a suitably small wave tail and wave front resistances. A single impulse was applied to each of 39 specimens in turn. The amplitude of the impulse was kept constant but as the thickness of the specimens was not the same, the electric fields varied from  $1.2\ \text{MV cm}^{-1}$  to  $2.3\ \text{MV cm}^{-1}$ . In all cases oscillograms showed that breakdown occurred within about  $1/20\ \mu\text{sec}$  after the passage of the peak of the wave. The rate of decay of the wave tail was such that in the above period the voltage across the specimen was constant to within 3% of the peak value. The result of this experiment is illustrated by figure 1(c). At about  $1.6\ \text{MV cm}^{-1}$  there was a change in the track direction. Below  $1.6\ \text{MV cm}^{-1}$  the track was in a (100) direction but above this value of electric field it was in a (110) direction, i.e. in the direction of the field.

In the above experiment the electric field always exceeded the limit of about  $1.1\text{--}1.2\ \text{MV cm}^{-1}$  beyond which sustained fields are known to strain the specimens (Cooper and Wallace 1956). The transition occurring at about  $1.6\ \text{MV cm}^{-1}$  is not believed to be due to modifications of the crystal structure because the time of less than about  $1/10\ \mu\text{sec}$  between application of the voltage and breakdown is too short. In fields of about  $1\ \text{MV cm}^{-1}$  we have found that more than a microsecond must elapse after the application of electric stress and before mechanical deformation of the lattice takes place. We therefore conclude that the directional sensitivity of the breakdown processes in KCl is reduced by the application of overvoltage. As far as we are aware this is the first convincing demonstration of this phenomenon although there has been some speculation about it in the past (Callen and Offenbacher 1953, Davisson 1946, Caspari 1955). During investigations with point electrodes Davisson claims to have observed a definite influence of field only with sodium salts. However, it is not clear how the overvoltages were achieved in this investigation and some doubt must therefore exist about this claim. The fact that overvoltages can be applied depends on the existence of finite time lags in breakdown (Cooper and Grossart 1956). The time lags are normally of the order of microseconds in duration but decrease



with overvoltage. For this reason impulses with very fast fronts must be used, as in the case of our investigation, if breakdown is to occur with any appreciable overvoltage.

It seems reasonable to infer from the above experiment that the breakdown process in KCl will be quite independent of crystal symmetry if electric fields sufficiently in excess of  $1.6 \text{ MV cm}^{-1}$  are applied. It follows, if this is true, that the breakdown tracks observed in the experiments merely mark the path of some precursor that makes the material conducting within the channel. Otherwise the intense radial field about the tip of a narrow, advancing, conducting channel would render its propagation through the material quite independent of the crystal symmetry. The path would wander at random through the material and this was not observed.

#### ACKNOWLEDGMENTS

Mr. A. Fernandez wishes to thank the British Council and the Institute of Physics of the University of Mexico for maintenance grants during the course of the work.

#### REFERENCES

- CALDERWOOD, J. H., COOPER, R., and WALLACE, A. A., 1953, *Proc. Instn. Elect. Engrs.*, 100, Pt. 11A, 105.  
 CALLEN, H., and OFFENBACHER, F. L., 1953, *Phys. Rev.*, 90, 401.  
 CASPARI, M. E., 1955, *Phys. Rev.*, 98, No. 6, 1679.  
 COOPER, R., and GROSSART, D. T., 1956, *Proc. Phys. Soc. B*, 69, 135.  
 COOPER, R., GROSSART, D. T., and WALLACE, A. A., 1957, *Proc. Phys. Soc. B*, 70, 169.  
 COOPER, R., and WALLACE, A. A., 1953, *Proc. Phys. Soc. B*, 66, 1113; 1956, *Proc. Phys. Soc. B*, 69, 1287.  
 DAVISSON, J. W., 1946, *Phys. Rev.*, 70, 685.  
 HIGHAM, J. B., and WATSON, P. K., 1953, *Proc. Instn. Elect. Engrs.*, 100, Pt. 11A.  
 VON HIPPEL, A., and DAVISSON, J. W., 1940, *Phys. Rev.*, 57, 156.  
 SAXE, R. F., and LEWIS, T. J., 1955, *Brit. J. Appl. Phys.*, 6, 211.

### The Fermi Level in Germanium at High Temperatures

By J. S. BLAKEMORE

Honeywell Research Center, Hopkins, Minnesota, U.S.A.

MS. received 8th October 1957

SOME results are given in this note of calculations on the Fermi level  $\phi$  in doped and intrinsic germanium from room temperature to the melting point ( $\sim 1200^\circ\text{K}$ ). Knowledge of the way  $\phi$  deviates for strong doping from its intrinsic position  $\psi$  even at near-melting temperatures was required for the interpretation of diffusion phenomena, but it is published in the expectation that the information will prove useful in other connections. Curves of  $\phi$  against temperature for some impurity densities in germanium have been given before (Hutner *et al.* 1950, Billig 1952), but these were based on a constant intrinsic gap width of 0.75 eV, which is very far from the case at high temperatures.



In this note the separation between the bottom of the conduction band and the top of the valence band is taken to be

$$\epsilon_c - \epsilon_v = 0.77 - 4.0 \times 10^{-4} T \text{ eV.} \quad \dots\dots(1)$$

This forms a smooth extrapolation to the optical gap results of Macfarlane and Roberts (1955) and implies an intrinsic carrier density in general accord with the observations of Morin and Maita (1954). It does not seem possible to write an expression for  $\epsilon_c - \epsilon_v$  which fits the results of all types of measurement; thus high temperature thermoelectric data (Domenicali 1957) suggest a temperature dependence larger than that of (1) if interpreted conventionally.

The densities of free electrons and holes can be expressed as

$$n = 2\pi^{-1/2} N_c F_{1/2} \left( \frac{\phi - \epsilon_c}{kT} \right) \quad \dots\dots(2)$$

and

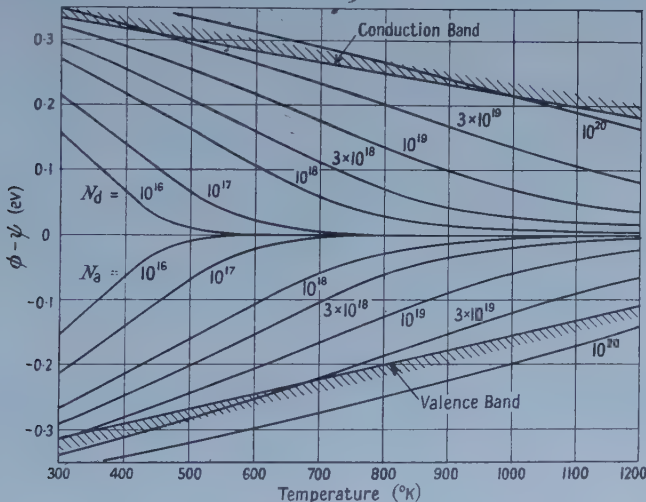
$$p = 2\pi^{-1/2} N_v F_{1/2} \left( \frac{\epsilon_v - \phi}{kT} \right) \quad \dots\dots(3)$$

where

$$F_{1/2}(\eta^*) = \int_0^\infty \frac{\eta^{1/2} d\eta}{1 + \exp(\eta - \eta^*)}$$

and  $N_c = 2(2\pi m_n kT/h^2)^{3/2}$ ,  $N_v = 2(2\pi m_p kT/h^2)^{3/2}$ .

From the results of cyclotron resonance experiments (Dresselhaus *et al.* 1955) the density of states effective masses in these expressions are  $m_n = 0.56m$  and  $m_p = 0.37m$ . The integral  $F_{1/2}(\eta^*)$  reduces to  $\frac{1}{2}\pi^{1/2} \exp(\eta^*)$  when  $\eta^*$  is sufficiently large and negative, but for the partially degenerate conditions encountered in this calculation appropriately modified analytic forms were used (Blakemore 1952).



The edges of the conduction and valence bands in germanium, and the Fermi level for various concentrations of donors or acceptors (in units of  $\text{cm}^{-3}$ ) referred to the intrinsic Fermi level as zero energy.

In the absence of impurities  $n=p$ , a condition which fixes  $\psi$  with respect to  $\epsilon_c$  and  $\epsilon_v$ . In the figure  $\psi$  is used as the zero of the energy scale, and the band edges with respect to this zero are indicated as functions of temperature. The

other curves in this figure show the temperature dependence of  $\phi - \psi$  for various impurity concentrations. For a density  $N_d$  of Group V donors the problem consists in obtaining roots of the equation

$$2\pi^{-1/2} \left[ N_c F_{1/2} \left( \frac{\phi - \epsilon_c}{kT} \right) - N_v F_{1/2} \left( \frac{\epsilon_v - \phi}{kT} \right) \right] = \frac{N_d}{1 + 2 \exp \{ (\phi - \epsilon_c) / kT \}} \quad \dots (4)$$

This is applicable for large impurity densities,  $N_d > 10^{17} \text{ cm}^{-3}$ , when the impurity activation energy vanishes (Debye and Conwell 1954) and the donor levels form part of the bottom of the conduction band. For smaller densities the donor levels are discrete, and we should replace  $\epsilon_c$  in the right-hand term of (4) by the donor energy, some 0.012 eV lower. But the distinction is academic since for these densities all the donors are ionized at the temperatures of interest here and the term reduces to  $N_d$ .

The curves in the upper half of the figure were built up by solving (4) for various donor densities and temperatures. Similar procedures for various densities of Group III acceptors yielded the curves in the lower half of the figure.

It will be noted that  $\phi - \psi$  can be appreciable even up to the melting point for large impurity densities. However, the intrinsic gap is only  $3kT$  wide at  $1200^\circ\text{K}$ , which does not permit a wide range of values for the function  $[1 + \beta \exp \{ (\epsilon - \phi) / kT \}]^{-1}$  describing the degree of occupancy for a set of levels within the gap (the quantity  $\beta$  allowing for possible spin choices in filling a level, Landsberg 1956). Thus level occupancy is not critically dependent on the doping situation at the highest temperatures.

Whereas impurity compensation is all-important at low temperatures,  $\phi$  is not greatly affected at high temperatures by a moderate degree of compensation. Unless the opposing impurity densities are almost equal, the Fermi level is given quite adequately as that corresponding with  $N_d - N_a$ ; and compensation of a few per cent shifts  $\phi$  by a negligible amount.

#### REFERENCES

- BILLIG, E., 1952, *Brit. J. Appl. Phys.*, **3**, 244.  
 BLAKEMORE, J. S., 1952, *Proc. Phys. Soc. A*, **65**, 460.  
 DEBYE, P. P., and CONWELL, E. M., 1954, *Phys. Rev.*, **93**, 693.  
 DOMENICALI, C. A., 1957, *J. Appl. Phys.*, **28**, 749.  
 DRESSELHAUS, G., KIP, A. F., and KITTEL, C., 1955, *Phys. Rev.*, **98**, 368.  
 HUTNER, R. A., RITTNER, E. S., and DUPRE, F. K., 1950, *Philips Res. Rep.*, **5**, 188.  
 LANDSBERG, P. T., 1956, *Proc. Phys. Soc. B*, **69**, 1056.  
 MACFARLANE, G. G., and ROBERTS, V., 1955, *Phys. Rev.*, **97**, 1714.  
 MORIN, F. J., and MAITA, J. P., 1954, *Phys. Rev.*, **94**, 1525.

### The Longitudinal Pressure Gradient in Discharge Tubes

BY R. B. CAIRNS AND K. G. EMELÉUS

Physics Department, Queen's University, Belfast

MS. received 23rd December 1957

A PRESSURE gradient, which may be accompanied by convection, can be produced along the positive column of a discharge tube because of (a) transport of gas as positive ions, (b) action of the longitudinal field on the positive space-charge in the plasma and sheaths, (c) difference in the

momentum given to the wall by positive ions and electrons leading to a compensating reaction on the gas.

The first two effects tend to increase the pressure near the cathode, the last to increase the pressure near the anode (Langmuir 1923, Druyvesteyn 1935). It is found experimentally that the pressure is greatest near the anode at relatively high pressures, and greatest near the cathode at lower pressures. From work described previously it can be inferred that the pressure at which the

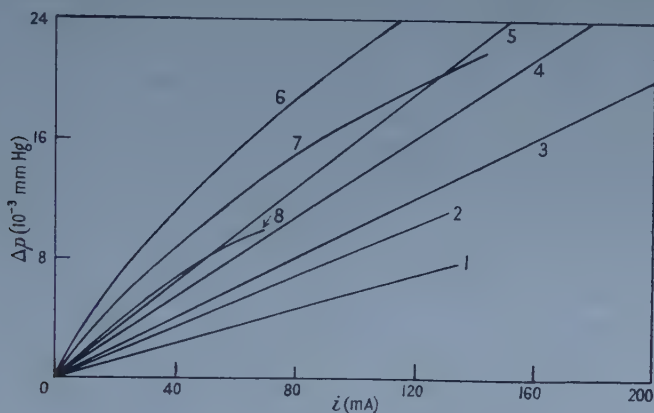


Figure 1. Pressure difference plotted against tube current for discharges in argon in tube I at mean pressures: 1, 2.01 mm Hg; 2, 1.18 mm Hg; 3, 1.08 mm Hg; 4, 0.52 mm Hg; 5, 0.38 mm Hg; 6, 0.25 mm Hg; 7, 0.11 mm Hg; 8, 0.07 mm Hg.

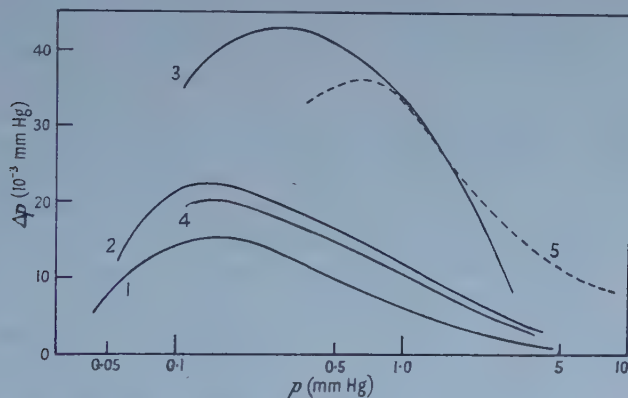


Figure 2. Pressure difference plotted against mean gas pressure on logarithmic scale.

Curves 1, 2 and 3 are for discharges in argon in tube I with  $i$  equal to 60, 120 and 240 mA respectively. Curves 4 and 5 represent data obtained from discharges in tube II with  $i = 240$  mA, 4 in argon and 5 in helium.

change-over occurs is of the order of 0.1 mm Hg (Francis 1956), but it almost certainly depends on the diameter of the tube. The main features of the results obtained at the higher pressures can be accounted for by Langmuir and Druyvesteyn's theory of (c), although (see later) this is incomplete.

In this note, some experiments with tubes of simple geometry are described which provide fresh data for the higher pressure range, and show the beginning of the transition to the lower pressure régime.

Two tubes were used, both mounted horizontally. The first, I, was 110 cm long and had an electrode separation of 91.4 cm. The electrodes were hollow cylinders (2.1 cm in diameter, 6.5 cm long) closed at the base, and mounted axially in tubes 3.1 cm in diameter connected end-on by a tube 0.8 cm in diameter and 81 cm long. The electrode sections were also connected by side tubes to a differential oil manometer read by a microscope. The mean pressure was taken to be that recorded by a McLeod gauge when no current was passing. The second, II, was similar in design and with the same diameters, but the length of the narrow section was 40 cm. The tubes were degassed and protected from oil and mercury vapour by normal techniques. The gas mainly used was the British Oxygen Company's 'spectroscopically pure' argon; a few measurements were made with helium. The current was drawn from a d.c. generator with a maximum output of 4000 v, which allowed discharges in argon to be studied down to a mean pressure of 0.05 mm Hg.

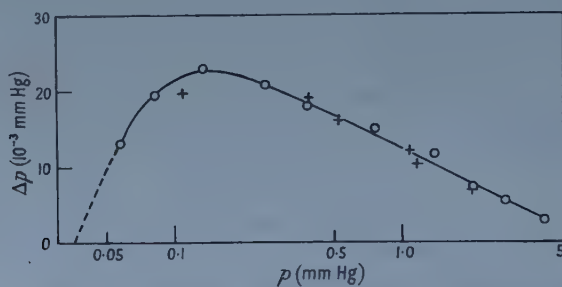


Figure 3. Graph 2 of figure 2 plotted to show the spread of the experimental points. The circled points were obtained by varying the pressure  $p$  at constant current. The crosses represent data transferred from figure 1. The broken line represents a tentative extrapolation to  $\Delta p = 0$ .

With a discharge in argon in tube I, readings were first taken of the pressure difference  $\Delta p$  for various tube currents  $i$ , the mean gas pressure  $p$  remaining constant. Since the tube was symmetrical it was possible to measure  $\Delta p$  by reading the difference in oil levels between the two limbs of the manometer, or by observing the movement in one limb when the electrode polarity was reversed. Both methods were employed with consistent results. Graphs of  $\Delta p$  against  $i$  are shown in figure 1 for values of  $p$  between 2.01 mm Hg and 0.07 mm Hg. For discharges with  $p > 0.3$  mm Hg,  $\Delta p$  is proportional to  $i$ , in agreement with Langmuir and Druyvesteyn's theory of (c). When  $p < 0.3$  mm Hg the rate of increase of  $\Delta p$  decreases as  $i$  increases. In these discharges the slope  $d(\Delta p)/di$  attained a maximum value at a mean pressure of 0.25 mm Hg. At this pressure, the pressure gradient along the tube was  $8 \times 10^{-5}$  mm Hg cm $^{-1}$  when the discharge current was 20 mA, assuming that  $\Delta p$  occurs entirely between the ends of the narrow part of the tube.

The variation of pressure gradient with  $p$  can also be shown by varying  $p$  and measuring  $\Delta p$  for fixed values of  $i$ . Typical results are shown in figure 2, with  $p$  on a logarithmic scale, for discharges through argon and helium in both tubes, for currents of 60, 120 and 240 mA. To illustrate the consistency and reproducibility of the results, the curve for a discharge in argon at 120 mA in tube I is shown separately in figure 3. The circles represent data obtained by varying the pressure  $p$  at constant current, as just described, the crosses data transferred from figure 1 for this value of the current.



$\Delta p$  for argon reaches a maximum in each case at about 0.15–0.25 mm Hg mean pressure.  $\Delta p$  again increased with  $i$ . When  $p < 0.15$  mm Hg,  $\Delta p$  decreased rapidly in argon. Although a discharge could not be maintained at lower pressure with the voltage available, the curves suggest that, in argon, the pressure gradient would reverse for  $p$  less than about 0.03 mm Hg. The maximum in this gas occurs at about the same value of  $p$  for tubes I and II. The values of  $\Delta p$  in tube II are rather less than one-half those in tube I under comparable conditions, in general agreement with previous experiments and theory (Francis 1956). The maximum occurs at a higher value of  $p$ , approximately 0.7 mm Hg, in helium.

The time taken for the pressure gradient to establish itself in these experiments was too short to measure exactly. However, it was much less than the time of 3 minutes allowed by Kenty (1938) for stabilization in a mercury vapour discharge.

The existence of the maxima, and the reversal of the pressure gradient at low mean pressure are almost certainly connected with the ratios of ionic free path  $\lambda_+$  and neutral atom free path  $\lambda$  to tube radius  $R$  (Hamburger 1923, Druyvesteyn 1935). The exact values of  $\lambda_+$  under the conditions existing in tubes I and II are uncertain, but unlikely to be much different from those for  $\lambda$ . The value of  $\lambda$  at the pressure  $p$  of about 0.2 mm Hg at which the pressure gradients are greatest in argon is about 0.5 mm, supposing the gas to be at a temperature of 350°K, giving a ratio  $\lambda/R$  of only 0.12. At the pressure at which the gradient appears to reverse (0.03 mm), the ratio  $\lambda/R$  has increased to nearly 0.8. Further evidence that the ratio  $\lambda/R$  is important is provided by the facts that (i) the pressure gradient at a given current reaches a maximum at about the same value of  $p$  in tube I and tube II, which have different lengths, but the same diameters, (ii) the maximum for helium in figure 2 occurs at a value of  $p$  about four times that at which it occurs for argon; the ratio of  $\lambda$  for helium to  $\lambda$  for argon at the same temperature and pressure is about 3, which is comparable.

No attempt has been made to correlate our results in detail with theory. This is partly because some of the quantities involved, such as free paths, mobility, and longitudinal electric field, are uncertain. We do, however, feel that the existing theory is likely to be inadequate, for two reasons.

First, it is based on the assumption that the positive column is uniform, whereas in our tubes, and probably in many of those studied previously, moving striations were present; an apparently homogeneous column can in fact be inhomogeneous. Not enough is yet known about moving striations (cf. Olesen and Cooper 1957) to say how the pressure gradient theory should be modified to allow for their presence. It is possible that the moving striations may produce a periodic pumping action on the gas, and that there is a reaction of this on the striations themselves. At the lowest pressures used in the present investigation, a form of stationary striation appeared at the cathode end of the positive column.

Second, the theory may not take adequate account of the thermal and mechanical boundary conditions at the anode and cathode ends of the positive column. These are of two kinds: (i) those primarily of electrical origin, allowing for the transitions from the positive column to the anode fall space, and to the Faraday dark space and cathode fall space respectively, (ii) those controlling the behaviour of the gas otherwise through changes in cross section of the tubes near the electrodes, including the effects of side-tubes leading to pressure gauges, etc..

There is some evidence that the pressure varies anomalously near the cathode: (Dauvillier 1926).

It would be of great interest if a direct demonstration could be given of the longitudinal circulation of the gas which is basic to Langmuir's and Druyvesteyn's theories of the higher pressure régime.

## REFERENCES

- DAUVILLIER, A., 1926, *C. R. Acad. Sci., Paris.*, **182**, 575.  
DRUYVESTEYN, M. J., 1935, *Physica, 's Grav.*, **2**, 255.  
FRANCIS, G., 1956, *Handbuch der Physik*, **22**, II, (Berlin : Springer).  
HAMBURGER, L., 1923, *Proc. Acad. Sci. Amst.*, **25**, 463.  
LANGMUIR, I., 1923, *J. Franklin Inst.*, **196**, 751.  
KENTY, C., 1938, *J. Appl. Phys.*, **9**, 765.  
OLESON, N. L., and COOPER, A. W. M., 1957, *Phys. Rev.*, **105**, 1411.

## LETTERS TO THE EDITOR

## On the Mass-Action Laws in Degenerate Semiconductors

In a recent Research Note (Rose 1957) the mass-action laws for the reactions between free carriers and impurities in semiconductors have been derived. In this note it was stated that it was difficult to interpret the results in the degenerate case because in this case, the 'effective' density of the energy levels in the conduction band and valence band respectively was not well defined. The purpose of the present letter is to show that these densities are in fact defined, as can be seen from the following.

The chemical reaction which takes place when an "electron is excited from a donor level into the conduction band" is the transfer of an electron from a donor to an outer term of any lattice point. Since electrons which have been accepted by one lattice point can easily move to other lattice points, they are called 'free' electrons. Thus in the reaction



$D^{\times}$  and  $D^{+}$  are neutral and charged donors respectively,  $v$  is an ordinary lattice point and  $e$  a lattice point which has accepted an electron. From equation (1) the actual 'density of energy levels in the conduction band'  $\bar{N}_e$  (or maximum concentration of  $v$ ) is the concentration of lattice points. However, when most of the lattice points have already accepted an electron further lattice points will accept electrons only at a higher energy level and the mass-action law should be written

$$\frac{\overrightarrow{n_e n_{D^{+}}}}{(\bar{N}_e - n_e) n_{D^{\times}}} = \exp \left[ \frac{-(\mathcal{E}_e - \mathcal{E}_D)}{kT} \right] \quad \dots\dots (2)$$

(cf. Rose 1957, eqn. (5)) where  $\mathcal{E}_e$  is an 'effective' energy level for the spin considered.

It is more convenient to use the lowest level in the conduction band  $\mathcal{E}_e$  (the energy level at which a lattice point accepts an electron if all the other lattice points are empty) and to define instead an 'effective density' of energy levels  $\bar{N}_e$  by

$$\frac{\bar{N}_e - n_e}{\bar{N}_e - n_e} = \exp \left( \frac{\mathcal{E}_e - \mathcal{E}_e}{kT} \right) \quad \dots\dots (3)$$

One has then

$$\frac{\overrightarrow{n_e n_{D^{+}}}}{\overrightarrow{n_{D^{\times}}} (\bar{N}_e - n_e)} = \exp \left[ \frac{-(\mathcal{E}_e - \mathcal{E}_D)}{kT} \right] \quad \dots\dots (4)$$

and similarly all the other equations of Rose (1957) with  $\mathcal{E}_e$  as the lowest level in the conduction band,  $\mathcal{E}_v$  the highest level in the valence band and  $N_c$  and  $N_v$  as effective densities.

In addition, one may define a parameter  $\mathcal{E}_F$  (the electrochemical potential or Fermi level) which satisfies

$$\vec{n}_e = \frac{\vec{N}_c}{1 + \exp[(\mathcal{E}_c - \mathcal{E}_F)/kT]} \quad \dots\dots (5)$$

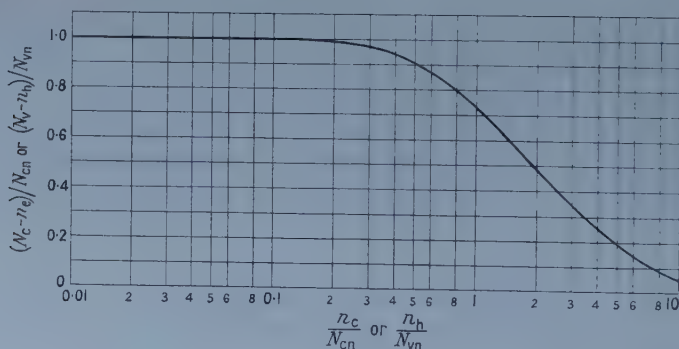
and

$$\vec{n}_{D \times} = \frac{N_D/2}{1 + \frac{1}{2} \exp[(\mathcal{E}_D - \mathcal{E}_F)/kT]}$$

and thus equation (4). The value of  $N_c = \vec{N}_c + \overleftarrow{N}_c$  can be calculated as a function of  $\mathcal{E}_F$  as in Fermi statistics by integrating over the number of lattice points which cover a certain energy difference. From such an integration one finds first the relation between the electron concentration  $n_e$  and  $\zeta \equiv -(\mathcal{E}_c - \mathcal{E}_F)$ . The relation between  $\zeta/kT$  and  $n_e/N_{cn}$ , is given by Spenke (1955, fig. AII 1), where

$$N_{cn} \equiv 2.5 \times 10^{19} \left(\frac{m_e}{m}\right)^{3/2} \left(\frac{T}{300}\right)^{3/2} \text{ cm}^{-3}$$

is the effective density of energy levels in the conduction band for the non-degenerate case. Using this figure and equation (5) one can calculate  $(N_c - n_e)/N_{cn}$  as a function of  $n_e/N_{cn}$ . This relation and the analogous one for holes are plotted in the figure.



$$N_{cn} = 2.5 \times 10^{19} \left(\frac{m_e}{m}\right)^{3/2} \left(\frac{T}{300}\right)^{3/2} \text{ cm}^{-3}$$

$$N_{vn} = 2.5 \times 10^{19} \left(\frac{m_h}{m}\right)^{3/2} \left(\frac{T}{300}\right)^{3/2} \text{ cm}^{-3}$$

An advantage of the mass-action laws is that they enable us to derive the degenerate case from the non-degenerate one by a simple substitution. Thus, for instance, Rose and Sandiford (1955) have calculated the hole lifetime in an n-type semiconductor with acceptor traps for the non-degenerate case. By substituting

$$n_1 \equiv g(N_c - n_e) \exp\left[\frac{-(\mathcal{E}_c - \mathcal{E}_t)}{kT}\right] \quad \dots\dots (6)$$

$$p_1 \equiv \frac{1}{g}(N_v - n_h) \exp\left[\frac{-(\mathcal{E}_t - \mathcal{E}_v)}{kT}\right] \quad \dots\dots (7)$$

their final equation is also valid for the degenerate case. In equations (6) and (7) the same assumptions are made as by Rose (1957) and  $g$  is the ratio of the



degeneracy of neutral traps to the degeneracy of charged traps,  $\mathcal{E}_t$  is the energy level of the traps.

I would like to thank my colleagues in the Research Laboratory of the British Thomson-Houston Co. for helpful discussions.

Research Laboratory,  
The British Thomson-Houston Co. Ltd.,  
Rugby.

F. W. G. ROSE.

29th January, 1958.

ROSE, F. W. G., 1957, *Proc. Phys. Soc. B*, **70**, 801.

ROSE, F. W. G., and SANDIFORD, D. J., 1955, *Proc. Phys. Soc. B*, **68**, 894.

SPENKE, E., 1955, *Elektronische Halbleiter* (Heidelberg : Springer), p. 368.

### Vapour Pressure Ratios of $^{14}\text{N}^{14}\text{N}$ , $^{14}\text{N}^{15}\text{N}$ and $^{15}\text{N}^{15}\text{N}$

Kirshenbaum and Urey (1942) measured the differences between the vapour pressures of two samples of nitrogen, one natural and the other containing 34.6 atom per cent of  $^{15}\text{N}$ . They then proceeded to calculate the differences between the vapour pressures of  $^{15}\text{N}^{15}\text{N}$  and  $^{14}\text{N}^{14}\text{N}$ , on the assumption that the vapour pressure difference is proportional to the atom percentage of  $^{15}\text{N}$  present. The sample containing 34.6 atom per cent  $^{15}\text{N}$  was an equilibrium mixture of  $^{14}\text{N}^{14}\text{N}$ ,  $^{14}\text{N}^{15}\text{N}$  and  $^{15}\text{N}^{15}\text{N}$ , containing about 45%  $^{14}\text{N}^{15}\text{N}$  and 12%  $^{15}\text{N}^{15}\text{N}$ , and Kirshenbaum and Urey made it clear that in making the above assumption they were in effect assuming that the vapour pressure of  $^{14}\text{N}^{15}\text{N}$ ,  $p_1$ , is the mean of the vapour pressures of  $^{14}\text{N}^{14}\text{N}$ ,  $p_0$ , and  $^{15}\text{N}^{15}\text{N}$ ,  $p_2$ .

Measurements of the relative vapour pressures of  $^{12}\text{C}^{16}\text{O}$ ,  $^{13}\text{C}^{16}\text{O}$  and  $^{12}\text{C}^{18}\text{O}$  have, however, shown unexpected relationships between them (Johns, Kronberger and London 1952, Johns 1957).  $^{12}\text{C}^{18}\text{O}$  is intermediate in volatility between  $^{12}\text{C}^{16}\text{O}$  and  $^{13}\text{C}^{16}\text{O}$ , even though it is the heaviest of the three and has the largest moment of inertia. This was explained as being due to the different degrees of asymmetry of the three species, the more asymmetric species being more restricted in their movements and therefore behaving as if they were lighter molecules. It might be expected that similar considerations would apply in the case of the three isotopic species of nitrogen, and it was predicted (London 1957) that  $p_0 - p_2$  may be considerably greater than  $2(p_0 - p_1)$ . Bigeleisen (1957), however, stated that in his opinion the rule of the geometric mean (Bigeleisen 1955) would be found to apply to the nitrogen isotopes. He asserted that the 'anomalous' behaviour of the carbon monoxide isotopes is not due to their asymmetry as such, but due to the fact that the molecule contains two different types of atoms. The effect on the vapour pressure of an isotopic substitution depends on the product of the difference of the reciprocal masses of the atoms concerned by an appropriate energy parameter; hence the vapour pressure ratio of  $^{12}\text{C}^{16}\text{O}$  and  $^{13}\text{C}^{16}\text{O}$  at absolute temperature  $T$  is given by

$$\ln \left( \frac{p_a}{p_b} \right) = \frac{A}{T^2} \left[ \frac{1}{12} - \frac{1}{13} \right] = \frac{A}{156T^2} \quad \dots\dots(1)$$

(for sufficiently high values of  $T$ ), whereas the corresponding ratio for  $^{12}\text{C}^{16}\text{O}$  and  $^{12}\text{C}^{18}\text{O}$  is

$$\ln \left( \frac{p_a}{p_c} \right) = \frac{B}{T^2} \left[ \frac{1}{16} - \frac{1}{18} \right] = \frac{B}{144T^2}, \quad \dots\dots (2)$$

where  $A$  and  $B$  are proportional to the energy parameters of the carbon and oxygen atoms respectively. The observed experimental results can be satisfactorily explained on the assumption that

$$A \simeq 1.46B. \quad \dots\dots (3)$$

For the isotopic species of nitrogen, however, we shall have

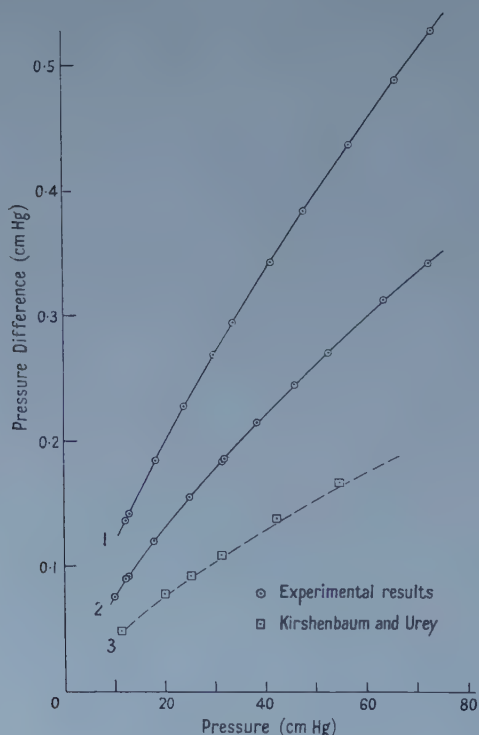
$$\ln \left( \frac{p_0}{p_1} \right) = \frac{C}{T^2} \left[ \frac{1}{14} - \frac{1}{15} \right] = \ln \left( \frac{p_1}{p_2} \right), \quad \dots\dots (4)$$

where  $C$  corresponds to the energy parameter of a nitrogen atom; that is, the rule of the geometric mean will apply:

$$p_1^2 = p_0 p_2 \quad \dots\dots (5)$$

or approximately

$$p_0 - p_2 = 2(p_0 - p_1). \quad \dots\dots (6)$$



Isotopic Content of Samples.			
Experiment	Sample	$^{14}\text{N}^{15}\text{N}$ %	$^{15}\text{N}^{15}\text{N}$ %
1	Enriched	16.89	81.61
	Reference	0.71	0.05
2	Enriched	47.86	35.06
	Reference	0.96	0.19
3	Enriched	(45.26)	(11.97)
	Reference	(0.76)	—

Direct measurements have now been made of the differences between the vapour pressures of samples of nitrogen containing respectively about 60 and 90 atom per cent  $^{15}\text{N}$ , and reference samples of (substantially) natural nitrogen. The apparatus and technique were the same as previously described (Johns 1957). In the figure the measured vapour pressure differences (reference sample—enriched sample) are plotted against the absolute vapour pressure of the reference sample. The isotopic compositions of the materials used are shown in the table. Thus, for example, curve 1 shows the measured vapour pressure differences between a reference sample containing 0.71%  $^{14}\text{N}^{15}\text{N}$  and 0.05%  $^{15}\text{N}^{15}\text{N}$ , and an enriched sample containing 16.89%  $^{14}\text{N}^{15}\text{N}$  and 81.61%  $^{15}\text{N}^{15}\text{N}$ .

The vapour pressure differences are found to be proportional, within experimental accuracy, to the atom per cent  $^{15}\text{N}$  present in the enriched sample (less the atom per cent  $^{15}\text{N}$  in the reference sample); it follows that equation (6) applies. Kirshenbaum and Urey's results are also shown in the figure; their results are seen to be in good agreement with the values predicted from the present measurements if equation (6) applies (these values being indicated by the broken line).

United Kingdom Atomic Energy Authority,  
Harwell, Didcot, Berks.  
18th December, 1957.

T. F. JOHNS.

BIGEISEN, J., 1955, *J. Chem. Phys.*, **23**, 2264; 1957, *Proceedings of the International Symposium on Isotope Separation* (Amsterdam: North-Holland Publishing Company), in the press.

JOHNS, T. F., 1957, *A.E.R.E. Harwell Report* GP/R.2166.

JOHNS, T. F., KRONBERGER, H., and LONDON, H., 1952, *Mass Spectrometry* (London: Institute of Petroleum), p. 141.

KIRSHENBAUM, I., and UREY, H. C., 1942, *J. Chem. Phys.*, **10**, 706.

LONDON, H., 1957, *Proceedings of the International Symposium on Isotope Separation* (Amsterdam: North-Holland Publishing Company), in the press.

---

### Comments on the Paper by J. C. Rivière: 'Contact Potential Difference Measurements by the Kelvin Method'

J. C. Rivière (1957) has made careful measurements of the contact potential differences between several different pairs of metal surfaces condensed from the vapour under excellent vacuum conditions. These values are interpreted to be characteristic of the polycrystalline metals in question and have been obtained with an ultimate objective of an "investigation into the effects of certain reactive gases on the average work functions of clean metallic surfaces". The metal films were deposited on to glass plates coated with a thin film of platinum which appear to have been close to room temperature at the time of deposit.

We wish to call attention to certain characteristics of the work function of metal films, condensed from the vapour *in vacuo*, which must be taken into account in the interpretation of measured values of work function. Experiments in this laboratory (Blackmer and Farnsworth 1950, Chung Fu Ying and Farnsworth 1952) have shown that films of both gold and silver which are condensed from the vapour on to a surface near room temperature have work

functions which are lower than those of the corresponding bulk metals, and that the work functions of the films change to those of bulk metals as a result of annealing in the proper temperature range. This was also found to be true for silver deposited on the (100) face of a silver single crystal, even though the film formed in a crystal lattice with the same orientation as that of the supporting crystal, as observed by low-energy electron diffraction (Clarke and Farnsworth 1952). A change as great as 0.3 eV has been observed. The work function of a silver film has also been shown to be dependent on the type of support, the values for silver films on quartz and molybdenum being different from that for a silver film on bulk silver (Blackmer and Farnsworth 1952).

It is now believed that these differences are due to the presence of large densities of lattice defects in the deposited films which are largely removed on annealing. The differences observed for different supports may be due to different preferred orientations of the small crystallites in the cases in question.

In addition, mention may be made of the influence of density of lattice defects on the adsorption characteristics of solid surfaces. Observations in this laboratory (Farnsworth 1957) show that the chemisorption of oxygen on a clean nickel crystal face is greatly influenced by the density of lattice defects at the surface. Since unannealed films condensed from the vapour contain high densities of defects, it is probable that the adsorption characteristics of such films of many metals are markedly different from those of the corresponding bulk metals in the annealed state.

Brown University,  
Providence, R.I., U.S.A.  
14th November 1957.

H. E. FARNSWORTH.

BLACKMER, L. L., and FARNSWORTH, H. E., 1950, *Phys. Rev.*, **77**, 826.

CLARKE, E. N., and FARNSWORTH, H. E., 1952, *Phys. Rev.*, **85**, 484.

FARNSWORTH, H. E., 1957, *Advances in Catalysis*, Vol. 9, p. 493 (New York : Academic Press).

RIVIÈRE, J. C., 1957, *Proc. Phys. Soc. B*, **70**, 676.

YING, CHUNG FU, and FARNSWORTH, H. E., 1952, *Phys. Rev.*, **85**, 485.



## REVIEWS OF BOOKS

*Relaxation Spectrometry*, by E. G. RICHARDSON. Pp. viii + 140. (Amsterdam : North-Holland, 1957.) 40s.

Mechanical vibrations in materials are damped, to an extent that is often extremely sensitive to their frequency. In the spectrum of acoustical frequencies various peaks appear at places where particular molecular processes, able to relax the stress in the material, come to resonance. The study of these relaxation spectra has grown rapidly in recent years because of its increasing value as a method for examining molecular processes, particularly in solids, and there is undoubtedly now a need for a book to bring the whole subject together. Zener's *Elasticity and Anelasticity of Metals*, published a few years ago, gave an excellent account of the basic theory and of some of the observed effects, but it was restricted to metals.

Professor Richardson is thus to be commended for having attempted a survey of the entire field. The breadth of his approach is shown by listing some of the topics touched upon : for example rheological materials such as gelatine, clay, rubber, wood, glass and sulphur; effects of impurities, grains and structural transformations, in metals and alloys; ferromagnetic, thermoelastic and dielectric relaxations; cross-linking in high polymers; and various aspects of gases and liquids.

Inevitably, in 140 pages these topics have mostly to be treated very briefly. The book will thus be valuable as a guide to the widely scattered literature of the subject. One would wish that it could also serve as an introduction to the subject for the newcomer, but unfortunately the exposition of the basic theory is too sketchy, the style of writing too imprecise, and the misprints too numerous, to enable one to recommend it for this purpose.

A. H. C.

*Physikalisches Taschenbuch*, edited by H. EBERT. Pp. viii + 544. (Brunswick : Vieweg, 1957.) DM 22.80.

In his preface to this book the editor states that it is intended to serve as a reference work for students and teachers of physics in which they can find short and concise formulations of the basic notions and laws of physics, accompanied by numerical tables, and which they can literally carry in their coat pockets. Evidently a book of this type, although bound to be sketchy, can be extremely useful provided it covers the ground uniformly and the reader can find his way easily.

The thirty-eight contributors have certainly succeeded in pressing an enormous amount of information into this really pocket-sized book, but unfortunately the different articles are not sufficiently correlated to each other and are of widely different standards, using different systems of units and different notations (e.g. for vectors). The subject index is not nearly detailed enough, which makes it sometimes difficult to look for a special item, and hardly any references to textbooks are given where more detailed information could be found.

In spite of these and some other shortcomings physicists in this country, who have a knowledge of scientific German, may find the pocket book very useful indeed, but will have to put up with the regrettable recent tendency in German

scientific literature to replace internationally understandable terms by newly created German words which cannot be found in any dictionary. R. FÜRTH.

*Progress in Low Temperature Physics*, Volume 2, edited by C. J. GORTER. Pp. xi + 480. (Amsterdam: North-Holland Publishing Company, 1957.) 84s.

The number of learned journals devoted to physics, together with the size of each issue, has increased rapidly over the last ten years (faster, it would sometimes seem, than the amount of significant work actually done). No physicist could hope to digest for himself more than a small fraction of this literature, so that all collections of review articles, such as this volume and its predecessor, are to be welcomed on principle. There is always a risk, of course, that the articles may be insufficiently homogeneous to make a satisfactory book; nobody wants to have to buy a substantial and expensive tome for the sake of one or two indispensable contributions, if the others are of no interest to him. Professor Gorter's collection does in fact suffer from being rather too miscellaneous.

It contains first of all four articles on liquid helium, by de Boer, Kramers, Winkel and Wansink, and Atkins, which take up between a third and a quarter of the book. These are well written and contain some important material, but much of it will be familiar already to the specialist, while the non-specialist will have to hunt rather hard to isolate the significant advances (he had better confine his attention to the outstanding article by Feynmann in volume 1).

Next comes a short article by Matthias, summarizing his own work on superconducting compounds and alloys. One can hardly agree with the publishers' blurb that in these 12 pages "superconductivity receive(s) ample attention".

Thirdly, one can class together an article by Sondheimer on the theory of transport effects in metals, one by Johnson and Lark-Horovitz on semiconductors at low temperatures, and one by Shoenberg on the de Haas-van Alphen effect, which together account for a further 110 pages or so. All these are excellent.

The remaining 200 pages are devoted to paramagnetic relaxation (Gorter); methods for orienting nuclei (Steenland and Tolhoek—written too soon to contain an account of the celebrated experiment done at the National Bureau of Standards to test the conservation of parity); the behaviour of solid helium (Domb and Dugdale); the rare earth metals (Spedding, Legvold, Daane and Jennings); specific heats and thermal expansion coefficients (de Bijl); and finally the temperature scale in the helium range (van Dijk and Durieux—another article that suffers from having been written a bit too soon).

Altogether it seems unlikely that any one reader will want to study more than a third of the book, and that is rather a small proportion. The truth is, perhaps, that low temperature physics has ceased to be a coherent domain of research, now that experience of cryogenic techniques is no longer confined to a few laboratories.

T. E. FABER.

*Nuclear Reactors for Research*, by C. K. BECK. Pp. xii + 267. (London: Macmillan, 1957). 55s.

The stream of information presented at the Geneva Conference on the Peaceful Uses of Atomic Energy has subsequently been followed by a flood of literature

purporting to give a summary of the proceedings. In order to prevent too much duplication and to justify a further publication it is clear that an author must select and present the information in some characteristic manner. Unfortunately in Dr. Beck's compilation he has merely taken what are essentially verbatim extracts from about twenty papers of the already published proceedings and arranged them into eight chapters. It is unfortunate that errors in the original have not been eliminated and the reader does not gain any further insight than he could obtain by reading Vol. 2 of the *Proceedings* published by the United Nations.

To the general reader the first two chapters which constitute Part I of the book will be of the most interest. A particularly good discussion on the technological factors affecting the choice of a research reactor is given in the first chapter entitled Research Reactor Types. The second chapter on the uses of research reactors in physics, chemistry, engineering and biology includes the results of some experiments which have only become possible with the advent of the large fluxes from reactors.

Part II of the book is devoted to various research reactor projects and contains much factual information on the engineering design, experimental facilities and operating performance of individual reactors. Each of the six chapters in Part II are devoted to a particular reactor type commencing with the natural uranium graphite moderated research reactors which have played such an important role in the historical development of atomic energy. A description of NRX at Chalk River which held the unique position for many years as the world's best research reactor is included in the chapter on Heavy Water Heterogeneous Reactors. By comparison the next chapter discusses a more advanced type of reactor—the highly enriched homogeneous reactors which have become known as 'water boilers'. Following this is a chapter entitled material testing reactors although an alternative and perhaps more descriptive title would have been light water moderated heterogeneous reactors. To keep the political balance, the water moderated reactors of the U.S.S.R. are discussed and in this chapter some editing and rewriting would have been invaluable. Finally there is a chapter on fast neutron reactor research which is a reprint of the excellent paper by the Harwell group. In this last chapter the omission of any American work on the subject is unfortunate.

For the worker actively engaged in the design or operation of a reactor there is already adequate coverage of the Geneva Conference; the scientist who wishes in his general reading to acquaint himself with the information released at Geneva may not find that this book meets his needs.

D. JAKEMAN.

*Jets, Wakes, and Cavities* (Applied Mathematics and Mechanics, Vol. II), by G. BIRKHOFF and E. H. ZARANTONELLO. Pp. xii+353. (New York: Academic Press; London: Academic Books, 1957). \$10.00.

The authors have devoted the greater part of this book to a very thorough treatment of potential flows in ideal fluids. Against a background of the underlying theory, they have given a wide range of solutions to boundary value problems of potential theory for plane flows, and they have included also an interesting account of effective methods for computation. Extensions of the theory which have been treated include compressible flows, flows under gravity and unsteady potential flows.



In the remainder of the book a relatively brief account has been given of viscous laminar, unsteady, and turbulent flow in jets and wakes. This section is short because the authors have attached greater importance to the mathematical structure of model theories than to the significance of the physical systems which they represent, but they have done this openly and in a way which is designed to stimulate further work on some of the absorbing problems that they have mentioned.

I think that the main section on potential methods should provide a valuable source of reference, particularly since the physical limitations of the treatment have been made clear. However, the section on the behaviour of real fluids must be regarded rather as a critical introduction to a field in which much remains to be done.

B. R. MORTON.

*The Relativistic Gas*, by J. L. SYNGE. Pp. xi+108. (Amsterdam: North-Holland, 1957.) 15 guilders.

In developing the relativistic equations to the motion of a fluid, one is led to study the symmetric energy-momentum tensor  $T_{rs}$ , satisfying the four conservation laws  $\partial T_{rs}/\partial x_s = 0$ . The restriction to the case of a perfect fluid reduces the number of unknowns from ten to five. In this book the remaining indeterminacy is removed, for the case of the relativistic gas, by the application of statistical mechanics. The main results are not new: relativistic extensions of the Maxwell theory were obtained by Jüttner in 1911, simply by substituting the relativistic expression for the energy of a particle in the classical formulae. What is new is the rigorous exclusion from the beginning of non-relativistic concepts, even at the cost of restricting the range of the theory.

Collisions between particles must play an essential role in the theory, in that they enable the gas to attain its most probable momentum distribution. Besides the conservation of 4-momentum at each collision, the author assumes for simplicity that particle-number is conserved, and that each particle has a constant proper mass; however, no attempt is made to give a relativistic treatment of collision mechanisms, so that all problems demanding a detailed discussion of collision processes are excluded. In particular, it is assumed that the gas attains its most probable state instantaneously, so that only the adiabatic or isentropic case is covered. In classical language, the mean free path is taken as vanishingly small, so that no transport phenomena occur.

Instead of the conventional gas confined in a fixed box, the author selects as his sample all particles whose world lines cross that part of an arbitrary 3-flat that lies within the null cone into the future. Classical statistics are applied, and the condition of maximum probability for the momentum distribution function is written down, subject to the conservation laws. This function must be Lorentz invariant—i.e. independent of the choice of the 3-flat defining the sample; this suffices to determine the system uniquely.

The theory is developed simultaneously for particles of finite mass and for 'photons' (indestructible particles of zero rest mass, uniform velocity  $c$ , but variable momentum), and for mixtures of both. As in classical theory, the parameter common to all components in a mixture is defined as a generalized temperature. The equation of state of a material gas is deduced, and shown to reduce in the low temperature limit to the familiar adiabatic law for a



monatomic gas; for high temperatures, and for a photon gas at all temperatures, Stefan's law is proved. Theorems are given, analogous to but differing from the classical results on equipartition of energy. The entropy integral from the statistical theory is related to the entropy per particle as defined thermodynamically. There is a discussion of shock waves—non-isentropic discontinuities in a gas otherwise flowing isentropically, irreversibility being secured by the demand that entropy increase across the shock. Finally, there is an Appendix on the radiation field in a moving gas, in which the unplausible assumptions of conservation of proper mass and photon-number are dropped.

The book can be recommended to those interested in relativity, gas dynamics and statistical mechanics, and to all others who enjoy seeing a well-defined problem treated rigorously.

L. MESTEL.

*The Hypercircle in Mathematical Physics*, by J. L. SYNGE. Pp. xii + 424. (Cambridge: University Press, 1957.) 70s.

This book describes a technique for the approximate solution of linear partial differential equations subject to linear boundary conditions. Two linear compounds of convenient functions are used, one compound satisfying the equation and the other the boundary conditions. Using the functional naturally associated with the differential operator to define the 'length' of a function and the 'distance' between two functions, the 'closest' forms of the linear compounds are found. This closest pair of functions defines a hypercircle in function space, on which the solution must lie. Hence upper and lower bounds on the 'length' of the solution can be found. The 'centre' of the hypercircle is the best approximate solution available from the linear compounds used. If a Green's function for the differential operator is known, it is possible to derive bounds on the error of this approximate solution at a point in physical space, though with considerable computation.

The method is presented in geometrical language; the first chapter of the book is an introduction to the theory of linear subspaces in function space without a metric, and the second chapter deals with the elementary geometry of the linear subspace, hypersphere and hypercircle in function space with a positive definite metric, such as that which arises from the Dirichlet integral associated with Laplace's equation. In this chapter the equations for the 'nearest' function of two linear subspaces are derived for use in later chapters, as are the bounds on the length of a function known to lie on a hypercircle.

In chapters three and four these results are applied to the Dirichlet and Neumann problems for Laplace's equation over a simply or multiply connected region of the plane. A convenient set of functions to form the basis of a linear compound satisfying Laplace's equation is the set of functions which are piecewise linear over meshes of a polygonal subdivision of physical space. This leads to a set of equations for the coefficients of the linear compound which closely resemble the usual crude finite difference approximation to Laplace's equation. Several examples are presented in adequate detail. Chapter five contains a brief treatment of several more general topics, such as the more general second order linear partial differential equation, and the biharmonic equation.

In chapters six and seven the geometry of function space with an indefinite metric is considered, in particular the case in which the metric is the difference

of two positive definite forms. The geometry is similar to that of space-time, the hypersphere is no longer a bounded region of function space, so that bounds on the error of the approximate solution are not available. However, a technique of projection on the space-like and time-like directions is described which leads to a process of improving approximation. This type of metric occurs with the wave equation and many vibration problems.

The application of the method leads to large numbers of simultaneous linear equations. The author suggests systematic iteration by single steps as a method of solving these and quotes the results obtained on SEAC for the torsional rigidity of a hollow square prism. Two thousand complete cycles of iteration with a mesh of 430 points in the octant gave the rigidity with an accuracy of about three parts in 1200, which probably corresponds to about the same error in the warping function. This is intolerable for hand work, and the use of relaxation techniques would considerably reduce the labour required. The development of a set of functions which satisfy Laplace's equation but fit together more smoothly than linear functions would be equivalent to the use of a better finite difference approximation to the differential operator (or of the difference correction) would enable many fewer points in the mesh to yield the same accuracy, and would enable the method of the hypercircle to be used with much less work. The author also suggests refining the mesh to overcome the difficulty of poor fitting of a curved boundary by a polygon. The work of Southwell and others has shown that this need only be done near the boundary. This sort of information about the practical techniques available for solving large systems of linear equations is essential if the hypercircle method is to become a really useful tool. It is a great pity, therefore, that the bibliography contains no reference to the work of Allen, Fox, Shaw and Southwell, who have written on this subject.

In spite of this lack the book is a valuable presentation of a very useful method. The author's masterly use of the similarities between function space and ordinary three dimensional space makes his account of the geometry of function space particularly vivid, and his description of the method of the hypercircle becomes in consequence beautifully clear. This book is well worth reading for all who need to use function space as a tool and could well serve as a model of the art of exposition for others who have to present abstract subjects to an audience not already familiar with them.

S. MICHAELSON.

*Handbuch der Physik*, Vol. XXX, *X-Rays*, edited by S. FLÜGGE. Pp. vii + 384. (Berlin : Springer, 1957.) DM. 88.

This volume consists of five almost independent articles :

1. Erzeugung von Röntgenstrahlen. Dr. W. Schaaffs ; pp. 77, figs. 87.
2. Experimental Methods of x-ray Spectroscopy : Ordinary Wavelengths. Dr. A. E. Sandström : pp. 167, figs. 108.
3. The Experimental Methods of Soft x-ray Spectroscopy and the Valence Band Spectra of the Light Elements. Dr. D. H. Tomboulia : pp. 58, figs. 35.
4. x-ray Microscopy. Drs. P. Kirkpatrick and H. H. Pattee, Jr. : pp. 31, figs. 27.
5. The Continuous x-ray Spectrum. Dr. S. T. Stephenson : pp. 33, figs. 27.

There are subject indexes in German-English and English-German, but no author index; and, as is customary in these Volumes, the references are given as footnotes, as well as in the form of general references at the end of each article; which makes any specific reference very difficult to locate.

For those who can read both German and English these articles provide a useful summary of experimental techniques, with a certain amount of overlap. This overlap and the complete, or almost complete, absence of any consideration of certain aspects of the subject, do reflect a basic weakness in the planning of the Encyclopedia as a whole. One might expect an Encyclopedia to cover all aspects of the subject, or at least to provide references to books or papers where a complete treatment may be found. Instead, we have a group of authoritative articles by very specialized experts, but not the kind of book, for example, that might have replaced Compton and Allison's *X-rays in Theory and Experiment*. R. W. James' *Optical Principles of the Diffraction of X-rays* seems not even to be mentioned, although it could well have been referred to as providing excellent accounts of anomalous dispersion (here dismissed in a few lines) and of the diffuse scattering of x-rays by thermal waves (not mentioned at all). The subject of microradiography is discussed under *X-ray Microscopy*, but there is nothing on radiography otherwise, and almost nothing on x-ray diffraction as a subject of interest in itself and not just as a technique. Let us hope that these are discussed elsewhere in the series.

There are some misleading statements. A. E. Sandström defines the x unit, on p. 93, in terms of what he calls 'the conventional lattice constant of calcite:  $d_{180} = 3029.04 \text{ xU}$ '. In Volume XXXV the definition is correctly given by E. R. Cohen and J. W. M. DuMond in terms of 'the grating constant of the cleavage planes of calcite' as ' $d_{180} = 3029.45 \text{ x-units}$ '. The explanation of the discrepancy appears 50 pages later, where Sandström does make it clear that 3029.04 refers only to the uncorrected first order spacing which, however, he still wrongly calls the '100 lattice constant'. Sandström also wrongly states that the xU may be regarded as defined by the equation  $1000 \text{ xU} = 1.00202 \text{ \AA}$ . Here again the reader should consult Cohen and DuMond in Volume XXXV for a correct interpretation of the conversion factor, which is probably nearer to 1.002045, but which is still undergoing experimental investigation.

It is a pity that figures such as those on page 306 (one of which is inverted) and on page 307 should have been separated. And the reviewer is quite sure that Sir Lawrence Bragg would not wish to claim the credit of having first pointed out the relationship between the diffracted x-ray beams and the terms of a Fourier series.

These criticisms, however, must not be allowed to detract from the value of the Volume as a whole. It is written by experts, and contains some excellent material that physicists will wish to have on easy reference although, in view of the price, they will probably be content to consult it from a library.

KATHLEEN LONSDALE.

*H. A. Lorentz, Impressions of His Life and Work*, Edited by G. L. DE HAAS-LORENTZ. Pp. 172. (Amsterdam: North-Holland, 1957.) 20s.

The centenary of the birth of H. A. Lorentz fell in the year 1953. On the occasion of the commemoration it was suggested that some of those who had



known him personally should write down their reminiscences. This book represents the fulfilment of that suggestion.

It is a modest volume of a size that enables it to be slipped into a coat pocket and it is a witness to the fact that when there is something of importance to be said, it can be said simply, convincingly and at the same time briefly.

In its portrayal of Lorentz's personality, genius and contribution to science, it is a remarkable work. It is written 'with reverence and affection' and, had these words not appeared on a page of dedication it would be clear to the reader that the inspiration of each contributor was veneration and high regard.

Lorentz was for the people of Holland what Planck became at the end of his life for the people of Germany. The book contains essays on his scientific work and influence, alternating with reminiscences of his daughter, who gives details of his personal life and portrays his character. A brief essay from Einstein is the first contribution. It is moving in his expression of regard and it goes straight to the point of Lorentz's contribution to electromagnetism. This is the hypothesis that the field is generated by elementary charges, that its seat is empty space and that it is to be described by one electric and one magnetic vector.

Of the discovery of the transformations known by the name of Lorentz, Einstein writes that the situation revealed by this discovery simply had to lead to the special theory of relativity.

Like every other contributor he recognized, through his personal contact with Lorentz, a man of great gifts of character as well as of high quality of mind.

The scientific work of Lorentz is described and discussed in an article by A. D. Fokker, who writes of interests and contributions in other fields as well as of the great contributions to electromagnetism, for example in statistics and thermodynamics.

Balth. van der Pol has written on the bearing of Lorentz's work on electromagnetic communication. It is interesting to read that at the age of 22 he presented a doctorate thesis on the theory of reflection and refraction of light on the basis of Maxwell's equations. The view expressed is that Maxwell's theory is to be preferred in the explanation of these phenomena. This has been so completely absorbed in physics that the name of its discoverer has been dropped. An interesting essay by J. Th. Thijssse tells of Lorentz's work in solving problems raised by the changes in tidal movements consequent upon the construction of a dam across the northern part of the Zuider-Zee. He tells how Lorentz undertook a tedious study and calculations and made original and successful suggestions in what was essentially a problem for engineers, oceanographers and meteorologists.

The last article by H. B. G. Casimir discusses the influence of Lorentz on modern ideas and his attitude to the changes which he saw taking place. One sees here a broad-minded classical physicist who never subscribed to the view, attributed to some of his contemporaries, that the summit of physical knowledge had been reached.

This is a book to be recommended to younger physicists who have perhaps hardly known the source of many of the basic principles of theoretical physics which they have taken almost for granted.

Those who can remember Lorentz will enjoy this reminder of early impressions of him as a kindly figure, a clear, logical lecturer who spoke, as he wrote, in simple language without repetition and without the need of correcting his first thoughts.



All who know him through his writings may well wish, after reading this memorial, that they had had the opportunity of knowing him personally.

H. T. FLINT.

*The Molecular Theory of Solutions*, by I. PRIGOGINE. Pp. xx + 448. (Amsterdam: North-Holland, 1957.) 48 guilders.

This book deals very fully with the modern theory of solutions within a defined range of topics. Nothing is said about electrolytic solutions or surface properties, or about any empirical approaches to the subject. The object rather is to relate the properties of solutions to the properties of the constituent molecules by the use of the methods of statistical mechanics. The important property of the constituent molecules is, of course, the law of force between them.

After a brief introduction on the thermodynamics of solutions and the one-dimensional model of solutions the author discusses the cell model of pure liquids. He then discusses in some detail the average potential model for solutions, which was developed by himself, and a variety of topics, such as solutions of non-spherical molecules, dipolar effects, and solutions of polymers. There are also two chapters on quantum effects in the liquid state.

The whole book gives a useful and detailed account of the present state of the subject. In a subject that is developing so rapidly as this any book must necessarily become out of date in a fairly short time, and the author has taken care that the information given is as up-to-date as possible, a special chapter on the most recent developments being given.

The book is well printed with numerous clear figures. A. F. DEVONSHIRE.

*Handbuch der Physik*, Vol. 35, *Atoms I*, edited by S. FLÜGGE. Pp. 454. (Berlin, Göttingen, Heidelberg: Springer, 1957.) DM. 99.50.

Volume 35 of the *Handbuch der Physik*, the first of the volumes specifically devoted to Atomic Physics, contains articles by E. R. Cohen and J. W. M. DuMond on "The Fundamental Constants of Atomic Physics" (87 pages), and by H. A. Bethe and E. E. Salpeter on "Quantum Mechanics of One and Two Electron Systems" (349 pages).

The evaluation of the best values to be used for the fundamental atomic constants was put on a satisfactory basis in the classical work of R. T. Birge published more than a quarter of a century ago. The article of Cohen and DuMond is a worthy successor to this earlier work. Many of the experiments which we had been taught to regard as model examples of precision work fail to stand up to the searching and critical scrutiny of these authors. In the end, four basic atomic constants, the fine structure constant  $\alpha$ , the electronic charge  $e$ , Avogadro's number  $N$ , and the ratio  $A(=\lambda_g/\lambda_s)$ , of x-ray wavelengths measured by ruled gratings and by a calcite crystal, are estimated from a least squares adjustment of the results of seven different types of experimental investigation capable of sufficient accuracy.

From the values thus obtained for the four basic constants and from other constants such as the velocity of light, the ratio of the atomic mass of H to the mass of the proton, and so on, which are known to much higher accuracy, the 'best' values of all the main atomic constants are estimated. Although comparatively few experiments have been selected to provide material for this analysis, the values given are not inconsistent with the great body of less precise

information accumulated during the first half of the present century. The present article reviews most of these measurements and in addition discusses the theory and application of the method of least squares to the problem of selecting a 'best' series of constants. It represents a contribution of great importance in this field.

Of no less importance is the second article in this volume on the quantum theory of one and two electron systems. It is characterized by the clarity of treatment and intelligent choice of material that one has come to associate with the authors. It will prove of particular value both for students approaching the subject for the first time and for research workers.

After an account of the basic non-relativistic theory of the hydrogen atom, with wave functions expressed in both ordinary and momentum space, the first part goes on to deal with the Dirac theory applied to the hydrogen atom, including the calculation of the Lamb shift. A discussion of the remarkable properties of positronium concludes this part of the article.

The second part deals with the two electron systems He and  $H^-$ . After a full discussion of variation methods applied to the non-relativistic helium problem the article goes on to consider the application of the relativistic Breit equation.

The Stark and Zeeman effects are treated in the third part, while the final part contains an account of the interaction with radiation, including transition probabilities in hydrogen and helium, recombination, photoeffect and bremsstrahlung.

It is impossible in the space of a short review to give any real indication of the wealth of material contained in this chapter. Many will remember the classical article by Bethe on similar topics that appeared in the old *Handbuch*. The present article fully maintains the standard set there and no higher tribute could be paid to it.

E. H. S. BURHOP.

*An Introduction to Semiconductors*, by W. CRAWFORD DUNLAP. Pp. xxi + 417. (London: Chapman and Hall; New York: Wiley, 1957.) 94s.

This book gives a general introduction to semiconductors, covering the relevant solid-state theory, the properties and preparation of elemental and compound semiconductors, the basic experimental measurements, and the main applications, especially of course to rectifiers and transistors. The treatment is at a uniform level, and avoids a highly formalized mathematical approach. Where mathematics are essential, the emphasis is on the physical basis of the analysis. The treatment of energy bands, effective mass and the theory of electron transport processes is inevitably limited with this approach, but will be found useful as an introduction by all who are beginning to specialize in the subject.

After a brief account of crystal structure, energy band theory and crystal imperfections, the Fermi statistics are dealt with, and then the electron transport processes. The technical aspects are then approached via a discussion of semiconductor surfaces and contacts with metals, and general features of p-n junctions. The main physical measurements on semiconductors are then described and some of the precautions are indicated.

The chapter on preparation of materials gives a brief account of crystal growing and zone refining, and of preparing various forms of p-n junction. There follows a fairly detailed account of the properties of germanium, and a

shorter one of silicon and other semiconducting elements. Several semiconducting compounds are then dealt with.

The final chapters describe the main features of rectifiers and transistors, and give a brief description of photoconductive and photovoltaic devices, thermistors, devices based on the Hall effect, phosphors, and other allied applications.

The book on the whole reads well, and provides a useful general introduction to almost all aspects of semiconductors.

D. A. WRIGHT.

*The Physics and Chemistry of Life*, sponsored by the *Scientific American*. Pp. xi+269. (London: Bell, 1957.) 13s. 6d.

In later times it will probably be recognized that the mid-twentieth century was marked by a revolution in fundamental biology as important as the revolution in physics of its earlier years. The two revolutions are not independent but it would be wrong to treat one as the mere consequence of the other. The essence of the biological revolution is in the reduction of previously mysterious vital processes, metabolism, photosynthesis, cell division, the contraction of muscle and the message transmission of nerve, to something like a physico-chemical explanation in terms of molecular structure and quantum chemistry. This in itself would have been quite impossible without the developments in chemical structure analysis due largely to x-ray crystallography and to that of theoretical chemistry, new concepts of the chemical bond and the mechanism of chemical reactions. At the same time many new experimental tools were placed in the hands of the biologist by physical and chemical advances. Radioactive tracers, high amplification electronics, the electron microscope, chromatography, have made measurements possible on far smaller systems and at far faster rates than was ever before possible.

But when all is said and done these are merely tools and it is out of the heads of the new experimental biologists and biophysicists that has come the skill to use them, to set and answer riddles which no physicist would think of for himself. The spearhead of the advance has been formed from two primarily biological disciplines—from the junction of the logic of the geneticist with that of the biochemist where the spirit of Hopkins has been as inspiring as that of Rutherford in physics.

*The Physics and Chemistry of Life* is a record of the advances of the period since the war written largely by those responsible for them. It is a set of eighteen articles divided into six groups ranging from the Origin of Life to the Electrical Activity of the Brain and including discussions on proteins, nucleic acids, viruses, genes and cell division. The authors are all drawn from Britain and America and include such names as Kamen, Pauling, Mirsky, Rabinowitch, Crick, Katz, Waddington and Grey Walter.

Originally the articles appeared in the *Scientific American* and all, with the possible exception of the more severe biochemical ones, are in simple language understandable to a mere physicist. The only criticism of the book is its date. It appeared first in the United States two years ago and much of it deals with researches a year or two earlier still. Unfortunately the speed of research seems to be now much greater than the speed of printing and though little in the articles has been since proved wrong it gives a woefully inadequate picture of present advances in the fields it covers. Thus, for instance, the advances in detailed virus



structure and the vital discovery of the infective power of protein free ribonucleic acid finds no place, nor does the new exciting structural work on cells using the electron microscope in which structure can be seen practically down to the molecular level. This is perhaps too much to ask for no-one can read this collection without getting something of the sense of the great break through in biological knowledge or glimpse something of its possibilities of application to science as a whole and the service of humanity.

J. D. BERNAL.

*Introduction to Solid State Physics*, by C. KITTEL. Pp. xvii + 617. (New York: John Wiley and Son, 1956.) \$12.00.

Professor Kittel's book provides an introduction to solid state physics in the sense that an encyclopaedia provides an introduction to knowledge. At a time when solid state physics is advancing rapidly—stimulated by its impact on technology—it is difficult for the general physicist, or even the specialist in a particular branch of the solid state, to keep abreast of the developments. For such a person this book is invaluable for its lucidity, its emphasis on physical foundations and its full references to more detailed work. For a student with no previous knowledge of the modern theory of solids it would prove rather heavy going.

Professor Kittel has chapters on the well established topics such as the classification of crystal structures, x-ray diffraction, elastic constants, lattice vibrations, thermal properties of crystals, the free-electron model of metals, and band theory. What gives the book its distinctive flavour, however, is the inclusion of so much material on the more modern advances in semiconductors, ferroelectricity, ferromagnetic and antiferromagnetic materials, colour centres and vacancy diffusion, excitons and luminescence, dislocations, and the like. These topics are treated in their more essential aspects, and where the phenomena are not yet fully understood, the experimental facts are related to models which illustrate the lines along which it is possible to reason. The chapter on superconductivity, for instance, gives an excellent résumé of the experimental situation, with hardly any account of the recent, but still controversial, theories as their difficulties are beyond the scope of an introductory book.

Problems are set at the end of each chapter. Appendices at the end of the book deal with points needing more extended mathematical treatment than is allowed in the body of the book.

The great technical importance of such semiconductors as germanium, of ferroelectrics, and of non-conducting ferromagnetic materials like the ferrites has recently directed much research effort into their basic physics, and these topics are naturally well represented in the book. Other topics have been deliberately left out, e.g. solid helium, surface physics, piezoelectricity, molecular crystals. Any selection for a book of this kind must naturally be very difficult to make, and Professor Kittel is to be congratulated on the way in which he has integrated his material into a readable and coherent form.

Most people interested in solid state physics will want to own this book. Unfortunately it is very expensive. And if one extrapolates from this, the second, edition, bearing in mind the frequent reference to works published since 1954 in this one, as an indication of the rate of growth of the subject, one may feel tempted to leave to it institutional libraries to acquire it, as it will probably soon be superseded by an even more expensive and more indispensable third edition—which is a pity.

M. H. L. PRYCE.





Figure 2. Etch pits on opposite {111} faces of a p-type germanium rod. (Crystal No. 4.)

Figure 2. Discharge Tracks in Potassium Chloride. To improve contrast graphite was introduced into the channel.

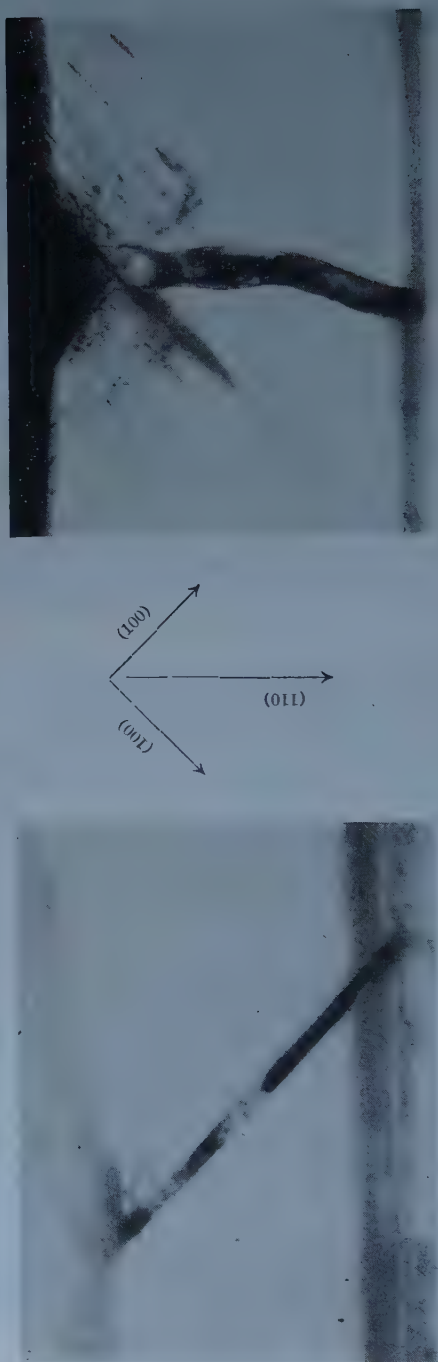


Figure 2 (a). Annealed Specimen  
Thickness = 0.0154 in.  
Diameter of recess = 0.25 in.  
Electric strength = 0.75 mv cm<sup>-1</sup>.  
Field in (110) direction.  
Track in (100) direction.

Figure 2 (b). Un-annealed Specimen  
Thickness = 0.0150 in.  
Diameter of recess = 0.25 in.  
Electric strength = 1.19 mv cm<sup>-1</sup>.  
Field in (110) direction.  
Track in (110) direction.

# Direct Interaction in the Inelastic Scattering of High Energy Protons in Carbon

By C. B. O. MOHR

Physics Department, University of Melbourne

*Communicated by L. H. Martin; MS. received 10th December 1957*

**Abstract.** The angular distribution of elastic and inelastic scattering of 89 MeV protons in carbon is calculated on the distorted wave approximation, assuming direct interaction in inelastic collisions. Different forms of nuclear potential are tried, and it is found that a satisfactory fit with the experimental curves may be obtained, provided direct interaction is assumed to take place throughout the nuclear volume, and not just at the surface. The Born approximation gives diffraction minima which are much too low, at angles which are appreciably too large; and gives far too little scattering at small angles for electric quadrupole excitation.

## § 1. INTRODUCTION

MANY nuclear reactions take place by direct interaction at the nuclear surface (Butler 1957) rather than by compound nucleus formation, especially in the energy range 10–30 MeV. For such cases the Born approximation (or other approximation giving the same form of matrix element) has been used to derive formulae for the differential cross section. For inelastic scattering the theory predicts an angular distribution strongly peaked in the forward direction, at an angle which depends on the number of units of angular momentum transferred to the nucleus by the colliding particle; and also predicts marked diffraction effects at larger angles. In some cases a good fit with experiment seems obtainable by suitable choice of the nuclear radius.

But in the energy range mentioned, distortion of the incident and outgoing waves by the nuclear potential is considerable, and the Born approximation cannot be valid. Furthermore, the form of theoretical angular distributions will be sensitive to the form of the nuclear potential ('giant resonance' effect), and in fact the experimental curves sometimes vary markedly with small changes of energy (e.g. Greenlees and Souch 1956). At lower energies, compound nucleus formation may contribute strongly to the scattering (e.g. Browne and Lamarsh 1956).

The situation will be clearer at higher energies, where the use of the Born approximation may be less questionable, and where the giant resonance and compound nucleus effects will not be important. These advantages outweigh the disadvantage of the much larger number of partial waves needed at high energies in a distorted wave calculation. It was therefore decided to investigate the collision of 89 MeV (centre-of-mass) protons with carbon nuclei, for which experimental data are available on both the elastic and inelastic scattering (Strauch and Titus 1956), thus providing an additional test of the theoretical assumptions and approximations.



## § 2. THEORY

The 4.4 mev loss studied in the experiments corresponds to the transition  $0+ \rightarrow 2+$  in the carbon nucleus, in which—on the independent particle model—a single  $p$  state nucleon changes the direction of its angular momentum vector. The interaction between the incident proton and the bound nucleon is taken to be a  $\delta$ -function, as is frequent in this work, to avoid unduly laborious calculations. Let the transition potential acting on the incident proton at the point  $\mathbf{r}'$  be denoted by  $V_{if}(\mathbf{r}')$ , the suffixes  $i$  and  $f$  referring to the initial and final states respectively. The radial dependence of  $V_{if}(\mathbf{r}')$  has the form of the transition density  $\psi_f^*(r')\psi_i(r')$  of the bound nucleon, and the angular dependence is that of a quadrupole moment,  $Y_2^m(\theta'\phi')$  with  $m=0, \pm 1, \pm 2$ . So

$$V_{if}(\mathbf{r}') = V_{if}(r')Y_2^m(\theta'\phi').$$

We shall also be investigating the nature of the results to be expected for electric dipole and monopole transitions, so we take the general transition potential for electric  $2^l$ -pole transitions

$$V_{if}(\mathbf{r}') = V_{if}(r')Y_l^m(\theta'\phi'). \quad \dots\dots (1)$$

Then, on the distorted wave approximation, the differential cross section for inelastic scattering of the incident proton through an angle  $\theta$  is given (Massey and Mohr 1934) by

$$\sigma_{in}(\theta) = (k'/k)(4\pi^2 M^2/h^4) \sum_{m=-l}^l |f_l^m(\theta)|^2, \quad \dots\dots (2)$$

where  $\mathbf{k} = 2\pi M\mathbf{v}/h$  for proton incident,  $\mathbf{k}'$  for proton outgoing, and  $M$  is the relativistic mass for velocity  $\mathbf{v}$ ; while

$$f_l^m(\theta) = \int F_i^*(\mathbf{r}')V_{if}(\mathbf{r}')F_f(\mathbf{r}')d\mathbf{r}', \quad \dots\dots (3a)$$

with

$$F_i(\mathbf{r}') = \sum_{s=0}^{\infty} (2s+1)i^s \exp(i\eta_s)F_i^s(r')P_s(\cos\theta'). \quad \dots\dots (3b)$$

Here  $\eta_s$  is the phase difference at infinity between the  $s$ th order distorted wave  $F_i^s$  of the incident proton and the corresponding component of the undistorted plane wave, the distortion being due to the nuclear potential.

Using (1) and (3) it may be shown that

$$f_l^m(\theta) = \sum_{s=m}^{\infty} a_{ls}P_s^m(\cos\theta), \quad \dots\dots (4)$$

where the  $a$ 's contain polynomials in  $s$  and products of terms  $r'^2V_{if}(r')$ ,  $\exp(i\eta_l)F_i^l(r')$  and  $\exp(i\eta_u)F_i^u(r')$  integrated over  $r'$ , the values of  $t$  and  $u$  being related to  $s$  by the selection rule for a  $2^l$ -pole transition. The general trend of the detailed procedure for dipole excitation is indicated elsewhere (Massey and Mohr 1934), the necessary modifications for monopole and quadrupole transitions being obvious and readily carried through.

The Born approximation takes plane waves  $F_i(\mathbf{r}') = \exp(i\mathbf{k} \cdot \mathbf{r}')$  and  $F_f^*(\mathbf{r}') = \exp(-i\mathbf{k}' \cdot \mathbf{r}')$ . Putting  $\mathbf{Q} = \mathbf{k} - \mathbf{k}'$  and expanding  $\exp(i\mathbf{Q} \cdot \mathbf{r}')$  in spherical harmonics, we have

$$\sigma_{in}(\theta) = (k'/k)(4\pi^2 M^2/h^4)f_l^2, \quad \dots\dots (5a)$$

with

$$f_l = 4\pi \int_0^{\infty} V_{if}(r')j_l(Qr')r'^2 dr'. \quad \dots\dots (5b)$$



Assuming the incident protons interact with the nucleus only at the nuclear radius  $r' = R$ , we have  $V_{if}(r') = V_{if}\delta(r', R)$ , and hence

$$\sigma_{in}(\theta) \propto \{j_l(QR)\}^2, \quad \dots\dots (6)$$

a simple approximate result which has frequently been used for comparison with experimental angular distributions.

The effect of nuclear spin has so far been neglected. Its effect is merely to introduce a numerical factor of order unity, whose value depends on whether  $j-j$  or  $L-S$  coupling is used (Benoist, Marty and Mayer 1956).

For elastic collisions, the use of distorted waves leads without approximation to the well-known formula involving the phase shifts  $\eta_s$ . In the Born approximation, taking for the nuclear potential a square well of radius  $R$  and depth  $V_0$ , we have

$$\sigma_{el}(\theta) = (4\pi^2 M^2 / h^4) f_0^2, \quad \dots\dots (7a)$$

with

$$\begin{aligned} f_0 &= 4\pi \int_0^R V_0 j_0(Qr') r'^2 dr', \\ &= 4\pi V_0 R^3 j_1(QR) / QR, \end{aligned} \quad \dots\dots (7b)$$

where now

$$Q = 2k \sin \frac{1}{2}\theta, \quad \dots\dots (7c)$$

so that

$$\sigma_{el}(\theta) \propto \{j_1(QR) / QR\}^2. \quad \dots\dots (8)$$

### § 3. CALCULATION

The nuclear potential was chosen to give for the binding energy of the bound p nucleon the experimental value of 16 mev, and this requirement was satisfied by a well of depth 36 mev and mean radius 3.2 fermis, which are values reasonably close to those used in optical model calculations. Three shapes of well were adopted: (a) a real square well, (b) a complex trapezoidal well with a diffuse rim of thickness 1.6 f, (c) a real trapezoidal well with a diffuse rim of thickness 3.2 f, slightly rounded-off at the heel and toe of the trapezoid (see inset diagrams in the figures). The imaginary potential in case (b) was taken to be 12 mev (van der Vegt and Jonker 1957). The Coulomb barrier was neglected, since its height, 2.7 mev at 3.2 f, is unimportant in comparison with the incident energy or the well depth.

The various order waves  $F_i^t$  and  $F_i^u$ , for the incident and outgoing proton, and the corresponding phase shifts  $\eta_t$  and  $\eta_u$  of these waves, were found for the square well by fitting wave functions across the edge of the well, and for the trapezoidal wells by numerical integration of the modified radial wave equation. The wave function  $\psi$  of the bound nucleon was also found for the trapezoidal wells by numerical integration.

The absolute magnitude of the transition potential  $V_{if}$  was fixed approximately by associating the average density distribution due to all the s and p nucleons with the nuclear potential of 36 mev.

The radial integrations necessary for determining the  $a$ 's in (4) were then carried out numerically, and tables of  $P_s^m$  used to sum the series (4). Partial waves up to  $s = 11$  were required for well (a), and up to  $s = 14$  for well (c).

## § 4. RESULTS AND DISCUSSION

## 4.1. Elastic Scattering

The exact phase shift method was used to obtain the three full-line curves in figure 1. We observe the usual result of increasing the diffuseness of the nuclear surface: diffraction maxima and minima are smoothed out, and large angle scattering—due partly to ‘surface reflection’—is reduced. Best fit occurs for the potential well (*c*), which is not far from the shape deduced from various considerations (Elton 1958). The use of an imaginary component for potential (*b*) does not give rise to any characteristic effect other than a decrease in the small angle scattering as a result of absorption (Mohr and Robson 1956). The steep rise in the experimental curve below  $5^\circ$  is due to the Coulomb scattering which, however, falls to 3% of the calculated nuclear scattering at  $10^\circ$ .

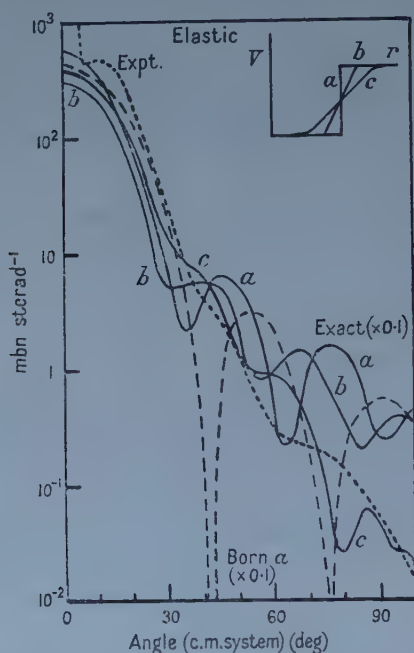


Figure 1. Angular distribution of elastic scattering of 89 MeV (c.m.) protons by carbon nuclei, as calculated by the exact phase shift method for the three potential wells shown in the inset diagram (well depth = 36 MeV, mean radius = 3.2 f), as calculated in the Born approximation for the square well, and as measured.

The Born approximation (8) for a square well gives minima which are far too low and at too large an angle. This is a general result for most energies and all nuclei; thus for the scattering of 30 MeV protons by a wide range of nuclei, fitting the positions of the diffraction minima with the Born approximation gives values of the nuclear radius which are too large by 20–40% (Leahy 1956).

All the theoretical values are greater than the experimental by an order of magnitude. They could be reduced by reducing the magnitude of the nuclear potential  $V$ , since  $\sigma(\theta)$  is proportional to  $V^2$  on the Born approximation; but agreement with experiment could be achieved only by reducing  $V$  to a value seemingly somewhat small to be realistic.

#### 4.2. Inelastic Scattering: Quadrupole Transition

In the direct interaction picture as used at lower energies, it is assumed that the reaction proceeds only at the nuclear surface. This effect is not properly accounted for by the use of an imaginary component of the potential (corresponding to nuclear absorption), for the imaginary potential is not large enough to give a sufficiently rapid fall in the amplitude of the incident wave as it enters the nucleus. The lack of contribution of direct interaction processes in the nuclear interior is best attributed mainly to total internal reflection of the proton waves at the nuclear surface (Elton and Gomes 1957). At 89 mev, however, the refractive index of the nucleus is less, so that total internal reflection is greatly reduced, also the mean free path of the proton in the nucleus is longer, so that one can no longer expect the direct interaction process to take place only at the nuclear surface.

In obtaining the distorted wave curves on the left side of figure 2 for a surface interaction, the radial integration in (3a) was carried out from  $r=R$  (the mean radius) to  $r=\infty$ . Not very different curves were obtained by taking just the value of the integrand at  $r=R$  and not integrating, though the relative scattering is then slightly larger at large angles. The Born approximation curve is for interaction only at  $r=R$ , and is given by (6) with  $l=2$ .

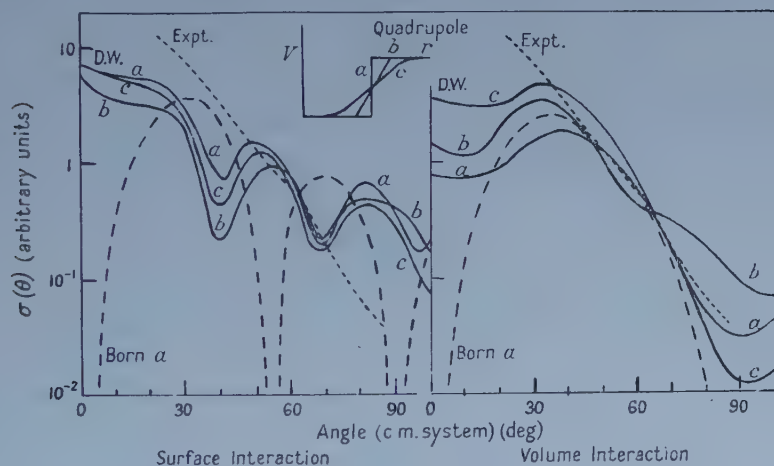


Figure 2. Angular distribution of inelastic scattering of 89 mev (c.m.) protons by carbon nuclei, for the 4.4 mev loss, the nuclear excitation involving an electric quadrupole transition. The calculated curves, obtained by the distorted wave approximation for the three potential wells shown in the inset diagram, and by the Born approximation for a square well, are fitted to the experimental curve at about  $60^\circ$  to facilitate comparison.

The distorted wave and Born approximation curves on the right side of figure 2 were obtained for interaction throughout the nuclear volume, by carrying out the radial integration in (3a) and in (5b) from 0 to  $\infty$ . A volume interaction smoothes out the diffraction minima and reduces the scattering at large angles, and is clearly necessary to account for the observed scattering. The best fit is obtained with the most diffuse nuclear surface, as for the elastic scattering. The experimental curve does not bend over at the smaller angles like the theoretical curves; but experimental curves for 171 mev (centre-of-mass) protons on carbon

(Tyrén and Maris 1957) do bend over at nearly the angle predicted by the Born approximation.

For a surface interaction the Born approximation is seen to give minima which are far too marked and at too large an angle. At lower energies, where the interaction may be largely a surface one, the distorted wave method may give much lower minima than at higher energies, for few partial waves are involved; but the minima will probably still occur at smaller angles than in the Born approximation: such is certainly the tendency for elastic scattering (Mohr and Robson 1956).

The absolute magnitude of the theoretical values at  $40^\circ$ – $70^\circ$  for a volume interaction is only about 0.2 of the observed values, assuming that only one of the  $p$  nucleons is effective in the scattering. The discrepancy may be removed by allowing for co-operative effects: the collective model with surface excitation gives, for a quadrupole deformation, an angular distribution of the same form as the direct interaction theory (Hayakawa and Yoshida 1955).

But even with collective action of several nucleons, it is hard to see how the inelastic scattering can be as strong as the elastic scattering, as is observed above  $40^\circ$ . A surface interaction would of course give less scattering than a volume interaction—by a factor of about 0.2 at the smaller angles. The main contribution to volume interaction comes from the region of the maximum in the radial wave function of the  $p$  nucleon, which occurs at about  $0.6R$ .

#### 4.3. Inelastic Scattering: Monopole and Dipole Transitions

Angular distributions for monopole and dipole transitions were calculated for 89 MeV protons in carbon, since the main features may be expected for protons of similar energy in other elements. The results are shown in figure 3. The

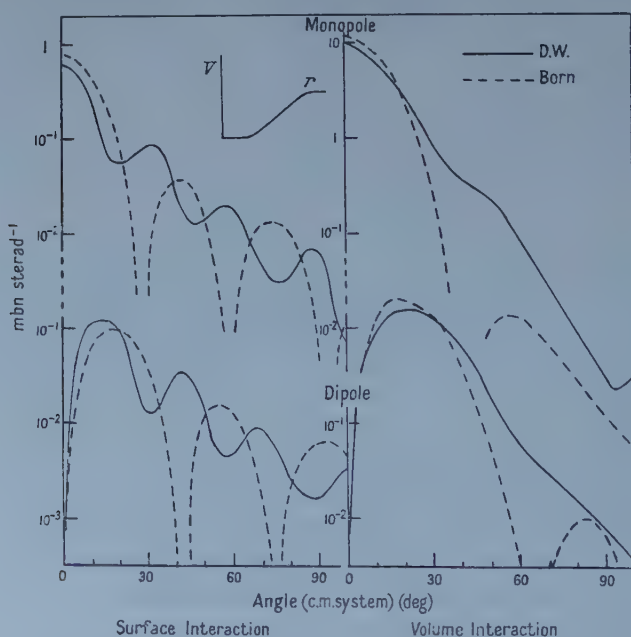


Figure 3. Calculated angular distribution of inelastic scattering of 89 MeV protons by carbon nuclei, for supposed electric monopole and dipole transitions in the nucleus.



same general features occur as for quadrupole transitions, except that whereas in the dipole case the scattering falls to very small values at small angles in both the distorted wave method and the Born approximation, in the quadrupole case this marked drop does not occur in the distorted wave method, but only in the Born approximation. The absolute magnitude is calculated on the assumption of only one  $p$  nucleon effective in the scattering.

## REFERENCES

- BENOIST, P., MARTY, C., and MEYER, PH., 1956, *Proc. International Conference on Nuclear Reactions* (Amsterdam, Netherlands Physical Society), p. 1173.  
BROWNE, C. P., and LAMARSH, J. R., 1956, *Phys. Rev.*, **104**, 1099.  
BUTLER, S. T., 1957, *Phys. Rev.*, **106**, 272.  
ELTON, L. R. B., 1958, *Nuclear Phys.*, **5**, 173.  
ELTON, L. R. B., and GOMES, L. C., 1957, *Phys. Rev.*, **105**, 1027.  
GREENLEES, G. W., and SOUCH, A. E., 1956, *Proc. Phys. Soc. A*, **69**, 686.  
HAYAKAWA, S., and YOSHIDA, S., 1955, *Prog. Theor. Phys.*, **14**, 1.  
LEAHY, J., 1956, *Thesis*, University of California, Radiation Laboratory, UCRL 3273.  
MASSEY, H. S. W., and MOHR, C. B. O., 1934, *Proc. Roy. Soc. A*, **146**, 880.  
MOHR, C. B. O., and ROBSON, B. A., 1956, *Proc. Phys. Soc. A*, **69**, 365.  
STRAUCH, K., and TITUS, F., 1956, *Phys. Rev.*, **103**, 200.  
TYRÉN, H., and MARIS, TH. A. J., 1957, *Nuclear Phys.*, **3**, 52.  
VAN DER VEGT, A., and JONKER, C. C., 1957, *Physica*, **23**, 359.

# A Method for Calculating the First Order Perturbation of an Eigenvector of a Finite Matrix, with Applications to Molecular-orbital Theory

By R. D. BROWN AND I. M. BASSETT

Department of Chemistry, University of Melbourne, Australia

*MS. received 16th August 1957, and in final form 13th January 1958*

**Abstract.** The first-order perturbation,  $\mathbf{c}'$ , of an eigenvector  $\mathbf{c}$  of a symmetric matrix  $\mathbf{H}$  satisfies the inhomogeneous equation

$$(\mathbf{H} - y\mathbf{I})\mathbf{c}' = -(\mathbf{H}' - y'\mathbf{I})\mathbf{c}$$

where  $\mathbf{I}$  is the unit matrix,  $y$  the eigenvalue belonging to  $\mathbf{c}$ , and the prime denotes the appropriate derivative. The derivative  $\mathbf{c}'$  can be determined from  $y$ ,  $y'$ ,  $\mathbf{c}$ , and a particular solution of the inhomogeneous equation; a convenient computational procedure is demonstrated. In contrast, the conventional perturbation theory requires knowledge of a complete set of eigenvectors of  $\mathbf{H}$ . Another advantage of the present method is that arithmetic checks are easily applied in numerical work. The method lends itself to the calculation of polarizabilities in the simple molecular-orbital theory. In this connection a complication associated with partly occupied degenerate orbitals is pointed out; the present method is convenient for dealing with this complication.

A more rapid method of reducing a matrix by use of symmetry than that commonly used is presented. It is useful in the present perturbation problem but it should prove equally convenient in other problems.

The determination of  $\mathbf{c}'$  in certain cases of degeneracy is described and an error in the literature pointed out.

The analysis throughout is general, and may be of interest outside molecular-orbital theory.

## § 1. INTRODUCTION

LET us consider a real symmetric matrix

$$\mathbf{H} = \begin{bmatrix} h_1 & k_{12} & k_{13} & \dots & k_{1n} \\ k_{12} & h_2 & k_{23} & \dots & k_{2n} \\ \cdot & \cdot & \cdot & \cdot & \cdot \\ k_{1n} & k_{2n} & k_{3n} & \dots & h_n \end{bmatrix}$$

with eigenvalues  $y_i$  and corresponding eigenvectors  $\mathbf{c}_i = \{c_{i1}, c_{i2}, \dots, c_{in}\}$ . The determination of the perturbation of an eigenvector owing to variation of the matrix coefficients, or the equivalent determination of the derivatives of the eigenvector with respect to those coefficients, is often called for. For example, it is called for in the calculation of 'polarizabilities' in the simple molecular-orbital theory; the polarizabilities can be expressed in terms of such derivatives of eigenvectors (Coulson and Longuet-Higgins 1947).

## §2. THE METHOD FOR NON-DEGENERATE EIGENVECTORS

The  $i$ th eigenvalue and eigenvector and their derivatives satisfy the inhomogeneous equation

$$(\mathbf{H} - y_i \mathbf{I})\mathbf{c}_i' = -(\mathbf{H}' - y_i' \mathbf{I})\mathbf{c}_i. \quad \dots\dots (1)$$

If  $\mathbf{a}_i$  is a particular solution of (1), the general solution may be written  $\mathbf{a}_i + \lambda \mathbf{c}_i$  where  $\lambda$  is a real number. Hence, if a particular solution of (1) is available, the required derivative is given by

$$\mathbf{c}_i' = \mathbf{a}_i + \lambda \mathbf{c}_i \quad \dots\dots (2)$$

the appropriate numerical value of  $\lambda$  being obtained by substituting (2) in the differentiated normalization condition for the eigenvector. This gives

$$\lambda = - \sum_{\mu=1}^n c_{i\mu} a_{i\mu}. \quad \dots\dots (3)$$

The utility of the present method depends of course on the ease with which a particular solution of (1) can be found. In certain cases, for example if the matrix  $\mathbf{H}$  has few off-diagonal elements differing from zero, such as happens with the Hamiltonian matrices arising in the simple molecular-orbital theory, it is easy to find a particular solution. The procedure and its advantages for numerical work are exemplified in Appendix II.

In order to determine a particular solution it is necessary to know  $y_i'$ . This may be obtained by differentiating the expression  $y_i = \mathbf{c}_i^\dagger \mathbf{H} \mathbf{c}_i / \mathbf{c}_i^\dagger \mathbf{c}_i$  (compare Coulson and Longuet-Higgins 1947). For differentiation with respect to an  $h$  parameter,  $h_1$  say,

$$y_i' = c_{i1}^2 \quad \dots\dots (4)^\dagger$$

while for differentiation with respect to a  $k$  parameter,  $k_{12}$  say,

$$y_i' = 2c_{i1}c_{i2}. \quad \dots\dots (5)^\dagger$$

## §2. COMPARISON WITH CONVENTIONAL PERTURBATION THEORY

In the conventional perturbation theory the calculation of the derivative of an eigenvector calls for knowledge of the complete set of eigenvectors and eigenvalues of the unperturbed matrix. In the present method only the eigenvector whose derivative is sought need be known. The present method has the further advantage of providing an additional equation which may be used as a computational check. Thus only  $n-1$  of the linear equations (1) are needed for obtaining  $\mathbf{c}_i'$ . Incorrect solutions will be obtained if incorrect values are inadvertently used for  $y_i$ ,  $y_i'$  or  $\mathbf{c}_i$  but such errors, or errors arising in the solution of the equations (1), may be detected because the values obtained for  $\mathbf{c}_i'$  will satisfy the remaining equation of (1) only if the calculations are free from the various errors detailed above.

Since the most important application of the present method will probably be for the calculation of polarizabilities in the simple molecular-orbital theory we shall briefly compare the advantages of the new method with those of alternative procedures. These are § the conventional perturbation theory

† When the components are complex these formulae become

$$\bar{y}_i' = \bar{c}_{i1}c_{i1} \quad \dots\dots (4')$$

$$\bar{v}' = \bar{c}_{i1}c_{i2} + c_{i1}\bar{c}_{i2} \quad \dots\dots (5')$$

§ A contour integral formula (Coulson and Languet-Higgins 1947) is not considered here because of the difficulty of comparing a method involving numerical integration with methods involving exact algebraic expressions unless the required accuracy of final values is specified.

formula (Coulson and Longuet-Higgins 1947) and a 'residue' formula (Brown 1956). The conventional formula requires knowledge of both occupied and unoccupied molecular orbitals except in the special case of alternant hydrocarbon systems. It also avoids most of the complications associated with degeneracies. However, it does not avoid the complication which arises when the degenerate orbitals are only incompletely occupied. In such a case the occupancy of the orbitals after perturbation depends upon the sense of the perturbation and the polarizability for such a system becomes two-valued. Although systems of this type have received some attention (e.g. Longuet-Higgins 1950) the fact that their polarizabilities are two-valued does not appear to have been noticed previously. To evaluate such polarizabilities the derivatives of the individual orbitals are required and the present method is convenient for this.

The residue formula for polarizabilities deals only with occupied orbitals but involves other quantities not generally available unless localization energies are simultaneously being computed. For such combined computations the residue formula is arithmetically considerably more convenient than either the conventional formula or the present method. However, when the polarizabilities alone are required the present method, calling for data for occupied orbitals only, is superior to the alternative formulae when applied to non-alternant systems or heterocyclic systems. It has already been used for certain heterocycle calculations (Bassett and Brown 1954, Brown and Heffernan 1956) and has been found to be particularly economic arithmetically when a series of mutual polarizabilities involving one particular atom is required (e.g. Brown and Heffernan 1956).

The present method is also most suitable for calculations of polarizabilities of frontier electrons (Fukui *et al.* 1952) because data for the frontier orbital alone are required. Such polarizabilities have not so far been reported.

#### § 4. FACTORIZATION BY USE OF SYMMETRY

It frequently happens, particularly in molecular-orbital applications, that symmetry relationships exist between the elements of  $\mathbf{H}$  (in the molecular-orbital application, the system under consideration possesses certain symmetry elements). If the symmetry properties are not completely removed by the perturbation then the solution of (1) may be simplified by the application of group theory. Such factorization by use of symmetry is commonly used (often based only on symmetry of reflection in one or more planes) but a rationalization of the procedure does not seem to be readily available. One possible general procedure is to transform from the original basis of the eigenvectors to symmetric base vectors belonging to various irreducible representations of the symmetry group, by the methods outlined for example by Eyring, Walter and Kimball (1944). This transforms the original symmetric matrix into a symmetric diagonal block matrix.

However, an alternative procedure, set out below, seems considerably simpler. It is a generalization of the 'commonsense' procedure based on reflection symmetry alone and it does not call for transformation to symmetrical base vectors. It decomposes the original matrix into a set of matrices of lower order, corresponding to the blocks of the alternative procedure but no longer necessarily symmetric†.

† The loss of symmetry does not call for any change in applying the procedure of § 2 for determining the derivatives of eigenvectors. However, if the original matrix is unsymmetrical then formulae (4) and (5) are not correct.



To describe the symmetry transformations it is convenient to have in mind matrices  $\mathbf{H}$  coming from the molecular-orbital treatment of conjugated systems so that it is the symmetry of the conjugated system which is under discussion. Let the perturbed system belong to the point group  $\mathcal{G}$  and let

$$R = \begin{pmatrix} 1 & 2 & \dots & n \\ \alpha_1 & \alpha_2 & \dots & \alpha_n \end{pmatrix}$$

denote a permutation of the subscript indices of  $\mathbf{H}$ . If there are certain permutations which do not alter  $\mathbf{H}$ , i.e. such that

$$H_{\mu\nu} = H_{\alpha_\mu\alpha_\nu}$$

these permutations must form a representation of  $\mathcal{G}$ . It is possible to find a complete set of independent eigenvectors such that each eigenvector transforms, under these permutations of indices, according to some irreducible representation of this group. The procedure described below is convenient for finding the eigenvectors belonging to every one-dimensional irreducible representation of  $\mathcal{G}$ . If there are any two-dimensional irreducible representations of  $\mathcal{G}$  the eigenvectors belonging to these are readily found by considering a sub-group  $\mathcal{S}$  of  $\mathcal{G}$  such that a two-dimensional irreducible representation of  $\mathcal{G}$  correlates with two one-dimensional irreducible representations of  $\mathcal{S}$  and then finding eigenvectors belonging to these one-dimensional representations by the method set out below. For example, if the perturbed system belongs to the group  $D_3$ , the eigenvectors belonging to the  $E$ -representation are found by considering the two formally non-degenerate representations of  $C_3$  having complex characters. In the case of the molecular-orbital treatment of conjugated systems the factorization achieved by the present method corresponds exactly with that achieved by the method given by Eyring, Walter and Kimball because all possible two-dimensional irreducible representations occur for the groups†  $D_n$  or  $C_{nv}$  and in every case these correlate exactly with pairs of complex one-dimensional irreducible representations of  $C_n$ .

Let  $a_R$  denote the character of  $R$  in the selected one-dimensional representation. If the  $i$ th eigenvector  $\mathbf{c}_i$  of the problem happens to belong to this representation then it will satisfy

$$P_R c_{i\mu} = a_R c_{i\mu}$$

for each  $R$ , where  $P_R$  stands for the appropriate operation on the subscript indices of the vector  $\mathbf{c}_i$ . Then  $P_R c_{i\mu} = c_{i\alpha_\mu}$  so that  $c_{i\alpha_\mu} = a_R c_{i\mu}$  for each  $R$ . That is, there exist certain homogeneous linear relations between the elements of the vector  $\mathbf{c}_i$ . If these relations are substituted in the original equations for the eigenvectors

$$(\mathbf{H} - y_i \mathbf{I})\mathbf{c}_i = 0 \quad \dots\dots (6)$$

the order of the equations is reduced, or, if there is no eigenvector belonging to the chosen representation, the result will be a contradiction. The equations of reduced order are then differentiated to obtain equations analogous to (1) and the procedure of §2 is followed to obtain the derivatives.

† The molecular symmetry would be  $D_{nh}$  rather than  $D_n$  but the  $\sigma_h$  feature is constant for orbitals of a particular kind (e.g.  $\pi$ -orbitals) and so may be ignored.

For example, consider the matrix

$$\mathbf{H} = \begin{bmatrix} r & 1 & 0 & 1 & 0 & 1 & 0 \\ 1 & s & 1 & 0 & 0 & 0 & 0 \\ 0 & 1 & t & 0 & 0 & 0 & 0 \\ 1 & 0 & 0 & s & 1 & 0 & 0 \\ 0 & 0 & 0 & 1 & t & 0 & 0 \\ 1 & 0 & 0 & 0 & 0 & s & 1 \\ 0 & 0 & 0 & 0 & 0 & 1 & t \end{bmatrix}$$

whose symmetry group is  $D_3$  for which the character table is

	$I$	$2C_3$	$3C_2'$
$A_1$	1	1	1
$A_2$	1	1	-1
$E$	2	-1	0

The components of an eigenvector belonging to the  $A_1$  representation satisfy the equations,

$$c_2 = c_4 = c_6 \quad \text{and} \quad c_3 = c_5 = c_7 \quad \dots\dots (7)$$

and the equations (6) are reduced, by substitution according to (7), to the form

$$\begin{aligned} (r-y)c_1 + 3c_2 &= 0 \\ c_1 + (s-y)c_2 + c_3 &= 0 \\ c_2 + (t-y)c_3 &= 0. \end{aligned}$$

The components of an eigenvector belonging to the  $A_2$  representation are required to satisfy the equations

$$c_1 = -c_1, \quad \dots, \quad c_7 = -c_7$$

showing that there are no eigenvectors belonging to this representation.

The  $E$ -representation is two-dimensional, correlating with the following one-dimensional irreducible representations of  $C_3$ :

	$I$	$C_3^+$	$C_3^-$
$\Gamma_2$	1	$\exp(2\pi i/3)$	$\exp(4\pi i/3)$
$\Gamma_3$	1	$\exp(4\pi i/3)$	$\exp(2\pi i/3)$

The components of an eigenvector belonging to the  $\Gamma_2$  representation satisfy the relations

$$\begin{aligned} c_1 &= 0, & c_4 &= \exp(2\pi i/3)c_2, & c_6 &= \exp(4\pi i/3)c_2, \\ c_5 &= \exp(4\pi i/3)c_3, & c_7 &= \exp(2\pi i/3)c_3, \end{aligned}$$

and on substitution of these equations in the equations (6) we obtain

$$\begin{aligned} (s-y)c_2 + c_3 &= 0, \\ c_2 + (t-y)c_3 &= 0. \end{aligned} \quad \dots\dots (8)$$

The  $\Gamma_3$  representation leads to the same reduced equations (8) as are given by the  $\Gamma_2$  representation because, as Mulliken (1933) has pointed out, such pairs of complex representations must lead to degenerate pairs of eigenvectors.

## § 5. DEGENERATE EIGENVECTORS

The procedure set out in §2 may require modification for degenerate eigenvectors. Such degeneracies may be 'essential' (cf. Wigner 1931) in that they correspond to degenerate irreducible representations of the symmetry group, or they may be 'accidental', i.e. not essential.† In the case of essential degeneracies, or of accidentally degenerate eigenvectors belonging to different irreducible representations, the reduction of the matrix by the method of §4 leads to smaller matrices, the eigenvalues of each such sub-matrix being distinct so that the procedure of §2 is applicable without modification.

However, in the case of accidental degeneracies for which the degenerate eigenvectors belong to the same irreducible representation, the symmetry transformations of §4 no longer partition the degenerate eigenvectors singly among the sub-matrices and the procedure described below is required to calculate derivatives of such degenerate eigenvectors. The method applies only to perturbation of an  $h$ -parameter and does not succeed for a  $k$ -parameter.

Consider differentiation with respect to say  $h_1$  and let  $t$  be the value of  $h_1$  for the unperturbed system. The equations (6) can be solved for a range of values of  $h_1$  including the value  $t$ . Let us suppose that the perturbation completely removes the degeneracy in first order. If this degeneracy is of order  $g$  there are  $g$  roots, distinct for  $h_1 \neq t$ , which become equal to  $y_i$  for  $h_1 = t$ . For each of these  $g$  roots, and for each value of  $h_1 \neq t$ , there is only one normalized solution of (6) which joins smoothly with the correct 'zeroth-order solution' which belongs to it. Let us write these  $g$  normalized solutions

$$\mathbf{c}_i^{(1)}, \quad \mathbf{c}_i^{(2)}, \quad \dots, \quad \mathbf{c}_i^{(g)}$$

and let us consider how to determine the derivative of  $\mathbf{c}_i^{(j)}$  with respect to  $h_1$  at  $h_1 = t$ . The general solution of (6) is now

$$\alpha_1 \mathbf{c}_i^{(1)} + \alpha_2 \mathbf{c}_i^{(2)} + \dots + \alpha_g \mathbf{c}_i^{(g)}$$

and the general solution of (1) is

$$\mathbf{a}_i + \lambda_1 \mathbf{c}_i^{(1)} + \lambda_2 \mathbf{c}_i^{(2)} + \dots + \lambda_g \mathbf{c}_i^{(g)}$$

where  $\mathbf{a}_i$  is any particular solution of (1) corresponding to the eigenvalue  $y_i$ .

The  $g$  parameters  $\lambda_1, \lambda_2, \dots, \lambda_g$  can be determined from the  $g$  conditions that the vector  $(d/dh_1)[\mathbf{c}_i^{(j)}]_{h_1=t}$  be orthogonal to each of the vectors  $\mathbf{c}_i^{(1)}, \mathbf{c}_i^{(2)}, \dots, \mathbf{c}_i^{(g)}$ . These  $g$  conditions lead at once to

$$\begin{aligned} \lambda_1 &= - \sum_{\mu} a_{i\mu} c_{i\mu}^{(1)}, & \lambda_2 &= - \sum_{\mu} a_{i\mu} c_{i\mu}^{(2)}, & \dots, \\ \lambda_g &= - \sum_{\mu} a_{i\mu} c_{i\mu}^{(g)}. & & & \dots\dots\dots (9) \end{aligned}$$

The proof of these orthogonality conditions is given in Appendix I.

An analogous procedure for perturbation of a  $k$ -parameter does not seem feasible. In this case the derivative is no longer necessarily orthogonal to every

† It is of interest that the specification of essential degeneracy given here is *not* equivalent to the specification that such degeneracies are not split by a totally symmetric perturbation because the degeneracies associated with complex one-dimensional representations (see § 4) are accidental in our sense but are nevertheless not split by totally symmetric perturbations.

Accidental degeneracies are sometimes specified as those which occur only for particular numerical values of the matrix elements but again the accidental degeneracies associated with complex one-dimensional representations occur for any values of the matrix elements consistent with the symmetry group.

eigenvector belonging to the degenerate level in question (see also Appendix II) and we have not been able to find an expression for the relevant scalar products in terms of the degenerate eigenvectors alone. However summation formulae (involving the complete set of eigenvectors) for the derivatives are of course available (see Appendix II).

## APPENDIX I

The orthogonality relationships required in § 5 may be obtained as follows. Let  $y_i$  be the eigenvalue belonging to the degenerate eigenvector  $\mathbf{c}_i^{(j)}$ . Equation (1) becomes

$$(\mathbf{H} - y_i \mathbf{I}) \mathbf{c}_i^{(j)'} = -(\mathbf{H}' - y_i^{(j)'} \mathbf{I}) \mathbf{c}_i^{(j)}.$$

If we premultiply by  $\overleftarrow{\mathbf{c}_i^{(k)'}}$ , the left-hand side becomes

$$\overleftarrow{\mathbf{c}_i^{(k)'}} (\mathbf{H} - y_i \mathbf{I}) \mathbf{c}_i^{(j)'} = \overleftarrow{\mathbf{c}_i^{(j)'}} (\mathbf{H} - y_i \mathbf{I}) \mathbf{c}_i^{(k)} = 0.$$

Hence

$$\overleftarrow{\mathbf{c}_i^{(k)'}} (y_i^{(j)'} \mathbf{I} - \mathbf{H}') \mathbf{c}_i^{(j)} = 0. \quad \dots\dots (10)$$

Since we are considering differentiation with respect to  $h_1$ ,

$$\mathbf{H}' = \begin{bmatrix} 1 & 0 & 0 & \dots \\ 0 & 0 & 0 & \dots \\ . & . & . & . \end{bmatrix}$$

and (10) becomes

$$y_i^{(j)'} \overleftarrow{\mathbf{c}_i^{(k)'}} \mathbf{c}_i^{(j)} = c_{i1}^{(k)} c_{i1}^{(j)}. \quad \dots\dots (11)$$

But  $\overleftarrow{\mathbf{c}_i^{(k)'}} \mathbf{c}_i^{(j)} = \delta_{jk}$  so that, from (11) with  $j = k$ ,

$$y_i^{(j)'} = [c_{i1}^{(j)}]^2 \quad \dots\dots (12)$$

or, with  $j \neq k$ ,

$$c_{i1}^{(j)} c_{i1}^{(k)} = 0. \quad \dots\dots (13)$$

If one of the quantities  $c_{i1}^{(1)}, c_{i1}^{(2)}, \dots, c_{i1}^{(p)}$  is not zero, say  $c_{i1}^{(h)} \neq 0$ , then (13) shows that all others must be zero and it follows from (12) that  $y_i^{(j)'} = 0$  for  $j \neq h$ . Thus the assumption that the perturbation removes the degeneracy in the first order implies that  $g = 2$ . The formula for the derivative of the vector  $\mathbf{c}_i^{(j)}$ , obtained using conventional perturbation theory, is given in Appendix II. For a matrix which is a linear function of the variables with respect to which the derivative is formed, the formula reduces to

$$\mathbf{c}_i^{(j)'}(\lambda = 0) = \sum_{m \neq j} \sum_{l \neq i} \frac{\mathbf{H}'_{im;l} \mathbf{H}'_{l;j}}{(y_i - y_l)(\mathbf{H}'_{ij;j} - \mathbf{H}'_{im;im})} \mathbf{c}_i^{(m)} + \sum_{l \neq i} \frac{\mathbf{H}'_{l;j}}{y_i - y_l} \mathbf{c}_l \quad \dots\dots (14)$$

where  $\mathbf{H}'_{ik;p}$ , for example, is the scalar product of the vector  $\mathbf{c}_i^{(k)}$  with the vector  $\mathbf{H} \mathbf{c}_p$  and  $\lambda$  represents the quantity  $h_1 - t$ . For differentiation with respect to  $h_1$ ,  $\mathbf{H}'_{ik;ik} = y_i^{(k)'}$ . Furthermore

$$\mathbf{H}'_{im;i} \mathbf{H}'_{i;j} = c_{i1}^{(m)} c_{i1}^{(j)} c_{i1} = 0$$



from equation (13). Thus all terms in  $\mathbf{c}_i^{(k)}$  in the expression (14) vanish, so that the derivative of the degenerate eigenvector is orthogonal to every eigenvector belonging to the degenerate eigenvalue.

It may be noted that the restriction to degeneracies which are split in the first order is necessary owing to the presence of  $\mathbf{H}'_{ij;ij} - \mathbf{H}'_{im;im}$  in the denominator in (14).

## APPENDIX II

In Appendix I it is established that for perturbation to an  $h$ -parameter, and when the degeneracy is split in the first order, the derivative of a degenerate eigenvector is orthogonal to every eigenvector belonging to the degenerate eigenvalue in question. Statements made by Schrödinger (1926) and repeated in textbooks (e.g. Eyring, Walter and Kimball 1944) imply such orthogonality regardless of the restrictions specified above. That this generalization is not true may be shown for example by considering the matrix

$$\begin{pmatrix} \lambda & \lambda^2 \\ \lambda^2 & 0 \end{pmatrix}$$

which has a degeneracy at  $\lambda=0$  of order two which is also the order of the matrix. Therefore, any two-rowed vector can be expressed as a linear combination of the degenerate eigenvectors. Since the derivative of the degenerate eigenvectors do not vanish at  $\lambda=0$ , neither is orthogonal to both degenerate eigenvectors.

If we consider a symmetric matrix  $\mathbf{H}(\lambda)$  in which the matrix elements are functions, not necessarily linear, of  $\lambda$ , an expression for the derivative of a degenerate eigenvector with respect to  $\lambda$  may be found by the methods of conventional perturbation theory. We have preferred to use derivatives in place of the more usual power-series expansion. If we assume that the degeneracy at  $\lambda=0$  is removed in first order the result is

$$\frac{d}{d\lambda} [\mathbf{c}_i^{(j)}]_{\lambda=0} = \sum_{m \neq j} \frac{1}{\mathbf{H}'_{im;im} - \mathbf{H}'_{ij;ij}} \left\{ \sum_{l \neq i} \frac{\mathbf{H}'_{ij;l} \mathbf{H}'_{im;l}}{y_l - y_i} - \frac{1}{2} \mathbf{H}''_{im;ij} \right\} \mathbf{c}_i^{(m)} + \sum_{l \neq i} \frac{\mathbf{H}'_{ij;l}}{y_l - y_i} \mathbf{c}_l.$$

## APPENDIX III

To illustrate the method† by which a particular solution of (1) may be found we consider the Hamiltonian matrix of benzene in the simple molecular-orbital theory:

$$\mathbf{H} = \begin{pmatrix} 0 & 1 & 0 & 0 & 0 & 1 \\ 1 & 0 & 1 & 0 & 0 & 0 \\ 0 & 1 & 0 & 1 & 0 & 0 \\ 0 & 0 & 1 & 0 & 1 & 0 \\ 0 & 0 & 0 & 1 & 0 & 1 \\ 1 & 0 & 0 & 0 & 1 & 0 \end{pmatrix}.$$

† It should be noted that since benzene is an alternant hydrocarbon the Coulson-Longuet-Higgins formula is more convenient in this case. Although a non-alternant or heterocyclic system would better illustrate the advantages of the present method, the eigenvalues and components of eigenvectors of such systems do not have such neatly rounded values as do those of benzene, so that illustrations using such systems could not be presented so compactly as in the benzene case.

If we consider differentiation with respect to  $h_1$  then the perturbed system belongs to the symmetry group  $C_2$  and by the method of §4 equations (6) for benzene are reduced for eigenvectors of the  $B$ -representation to:

$$\begin{aligned} c_1(h_1 - y) + 2c_2 &= 0 \\ c_1 - yc_2 + c_3 &= 0 \\ c_2 - yc_3 + c_4 &= 0 \\ 2c_3 - yc_4 &= 0. \end{aligned}$$

Differentiating with respect to  $h_1$  and setting  $h_1 = 0$ , we obtain

$$\begin{aligned} -yc_1' + 2c_2' &= (y' - 1)c_1 \\ c_1' - yc_2' + c_3' &= y'c_2 \\ c_2' - yc_3' + c_4' &= y'c_3 \\ 2c_3' - yc_4' &= y'c_4 \end{aligned} \quad \dots\dots (15)$$

If we consider the eigenvector of eigenvalue  $y = -2$  belonging to this irreducible representation, its components are

$$c_1 = 1/\sqrt{6}; \quad c_2 = c_6 = -1/\sqrt{6}; \quad c_3 = c_5 = 1/\sqrt{6}; \quad c_4 = -1/\sqrt{6}.$$

If these values are substituted in (15) and also  $y' = c_1^2 = 1/6$ , we have

$$\begin{aligned} 2c_1' + 2c_2' &= -5/6\sqrt{6} \\ c_1' + 2c_2' + c_3' &= -1/6\sqrt{6} \\ c_2' + 2c_3' + c_4' &= 1/6\sqrt{6} \\ 2c_3' + 2c_4' &= -1/6\sqrt{6} \end{aligned} \quad \dots\dots (16)$$

A particular solution  $a_\mu$  of equations (16) may quickly be obtained by setting  $a_2 = 0$ ; it is

$$a_1 = -5/12\sqrt{6}; \quad a_2 = 0; \quad a_3 = 1/4\sqrt{6}; \quad a_4 = -1/3\sqrt{6}; \quad a_5 = 1/4\sqrt{6}; \quad a_6 = 0.$$

It should be noted that the fourth equation of (16) need not be used to obtain this particular solution; the test that  $a_3$  and  $a_4$  satisfy this equation serves as a check on the computations to this point.

The parameter  $\lambda$  is next found from (3):  $\lambda = -5/72$ ; and finally, from (2), the desired derivatives are

$$\begin{aligned} c_1' &= -35/72\sqrt{6}; & c_2' &= 5/72\sqrt{6}; & c_3' &= 13/72\sqrt{6} \\ c_4' &= -19/72\sqrt{6}; & c_5' &= 13/72\sqrt{6}; & c_6' &= 5/72\sqrt{6}. \end{aligned}$$

These may be checked, if desired, by re-substitution in (16).

#### REFERENCES

- BASSETT, I. M., and BROWN, R. D., 1954, *J. Chem. Soc.*, 2701.  
 BROWN, R. D., 1956, *J. Chem. Soc.*, 767.  
 BROWN, R. D., and HEFFERNAN, M. L., 1956, *J. Chem. Soc.*, 3683.  
 COULSON, C. A., and LONGUET-HIGGINS, H. C., 1947, *Proc. Roy. Soc. A*, **191**, 39.  
 EYRING, H., WALTER, J., and KIMBALL, G. E., 1944, *Quantum Chemistry* (New York: Wiley).  
 FUKUI, K., YONEZAWA, T., SHINGU, H., 1952, *J. Chem. Phys.*, **20**, 722.  
 LONGUET-HIGGINS, H. C., 1950, *J. Chem. Phys.*, **18**, 265.  
 MULLIKEN, R. S., 1933, *Phys. Rev.*, **43**, 279.  
 SCHRÖDINGER, E., 1926, *Ann. Phys., Lpz.*, **80**, 437.  
 WIGNER, E., 1931, *Gruppentheorie und ihre Anwendung auf die Quantenmechanik der Atom-spektren*, (Braunschweig: Vieweg).

## Dispersion Theory of the Direct Photoeffect

By G. E. BROWN AND J. S. LEVINGER†

Department of Mathematical Physics, University of Birmingham

*Communicated by R. E. Peierls; MS. received 23rd December 1957*

**Abstract.** The process of direct interaction with photons (the emission of fast particles) is formulated in nuclear dispersion theory. The cross section can be evaluated for energies far from the single particle resonances; an order of magnitude estimate can be made for the region of the resonances. The results are in rough agreement with those from Wilkinson's modified shell model.

The dipole-quadrupole interference is estimated to give an appreciable forward asymmetry for photo protons.

### § 1. INTRODUCTION

THE giant dipole resonance for absorption of gamma rays has been observed in many elements, and it is clear that it is a general feature of nuclei. The energy at which it occurs and the dependence of this energy on atomic number have been reasonably explained by models of Goldhaber and Teller (1948) and of Jensen and Jensen (1950) which view the process as one in which the nuclear fluid as a whole is set in motion. In these models there is no natural mechanism for obtaining the anomalously large number of fast nucleons which are experimentally observed. It has been well established experimentally that several per cent of the emitted particles result from some sort of direct interaction. The first evidence was in the data of Hirzel and Wäffler (1947) who found anomalously high yields of protons following absorption of 17.6 MeV gamma rays. Although these constituted only several per cent of the decay processes, their probability was orders of magnitude above the predictions of the statistical theory, in which proton emission in medium and heavy nuclei is strongly inhibited by the Coulomb barrier. On the other hand, in the models above, in which the gamma-ray energy is distributed among all of the nucleons, the statistical theory would appear to be suitable for describing the decay process.

Wilkinson (1956) has proposed a shell-model interpretation of the giant dipole resonance which seems to account for the fast decay particles. He assumes that photon absorption with a cross section  $\sigma(E)$  leads to a state in which a single nucleon is excited to a state in a potential well. In general this state will be in the continuum. This excited shell-model state can decay by a direct photoeffect with a probability proportional to the escape width  $\Gamma$  given as the product of the kinetic factor  $k\hbar^2/MR$  and the penetration factor  $P$ . However, the excited shell model state can decay with larger width  $2W$  by the nucleon interacting with the imaginary part  $W$  of the cloudy crystal ball potential. He gives the cross section for the direct photoeffect  $\sigma_d = \sigma\Gamma/2W$  where  $\Gamma$  is an average escape width. Wilkinson realizes that this model is a great over-simplification, since at the

† On leave from Louisiana State University; Guggenheim Fellow.

excitation energy of 15–25 mev reached by photon absorption the nucleus possesses millions of compound nucleus levels per mev. He gives, however, reasons to suggest that the compound nucleus model will give something like the above relation. Brink (1957) has pointed out that for a special case, phase relations between shell-model transitions lead to a collective type of oscillation.

In this note we shall show that a model (Brown and De Dominicis 1957 a, b, Bloch 1957 a, b) which has been successful in explaining the optical model of Feshbach, Porter and Weisskopf (1954) and direct interaction in inelastic nucleon scattering, can be extended to describe the giant dipole photoeffect, giving many features of Wilkinson's model. We shall carry through the development in the formalism of Brown and De Dominicis (1957 a, b, to be referred to as I and II).

## § 2. DEVELOPMENT

We shall first extend the formalism of I to treat the absorption of radiation. This extension is similar to that carried out in the framework of the continuum theory of nuclear reactions by Peaslee (1952). In order to avoid inessential complication, we assume that only one definite particle in the nucleus can be emitted, and denote its coordinates by  $\mathbf{r}$ . We use  $\xi$  to denote the totality of co-ordinates of all other nucleons in the nucleus. The wave function of the system is, then, for  $r > R$

$$\Psi(\mathbf{r}, \xi) = \sum_{\alpha'j} S_{\gamma\alpha'j} \chi_j(\xi) \psi_{\alpha'j}^+(\mathbf{r}) \quad \dots\dots(1)$$

where  $S_{\gamma\alpha'j}$  is the amplitude for  $\gamma$ -ray absorption with emission of the nucleon into channel  $\alpha'$ , leaving the residual nucleus in state  $j$ ;  $\chi_j$  is the  $j$ th state of the residual nucleus and  $\psi_{\alpha'j}$  is the state of the emitted particle. The suffix  $j$  on  $\psi_{\alpha'j}$  indicates that it is the wave function at energy  $E - E_j$ , where  $E_j$  is the excitation energy of the state  $\chi_j$ . For  $r < R$  we have

$$\Psi = \Psi_0(\mathbf{r}, \xi) + \sum_p a_p \Phi^{(p)}(\mathbf{r}, \xi) \quad \dots\dots(2)$$

where  $\Psi_0(\mathbf{r}, \xi)$  is the ground state of the initial nucleus (it being understood that a gamma ray is present) and the  $\Phi^{(p)}$  are the eigenstates of the nuclear Hamiltonian  $H_0$ , i.e.

$$H_0(\mathbf{r}, \xi) \Phi^{(p)} = W_p \Phi^{(p)} \quad \dots\dots(2.1)$$

where the  $W_p$  are the complex eigenvalues which occur in the Kapur–Peierls theory. The  $H_0$  contains all of the nuclear interaction; it is the same as the  $H$  employed by Brown and De Dominicis. The interaction with the radiation field (electric field  $\mathcal{E}$  along the  $z$  axis normalized to a flux of one photon  $\text{cm}^{-2} \text{sec}^{-1}$ ) will be described by  $H_1$ , where

$$H_1 = e\mathcal{E}_z = e(2\pi\hbar\omega)^{1/2}z \quad \dots\dots(2.2)$$

if we restrict our considerations to the dipole interaction. Since the coupling to the radiation field is weak, we need obtain the  $a_p$ 's only to first order, which can easily be done by requiring  $\Psi$  to satisfy the Schrödinger equation to that order. We have

$$H_1 \Psi_0 = (E - H_0) \sum_p a_p \Phi^{(p)} = \sum_p a_p (E - W_p) \Phi^{(p)}. \quad \dots\dots(2.3)$$



Here  $E$  is the full energy of the system. If we measure it from the ground state of the initial nucleus,  $E = \hbar\omega$ , where  $\hbar\omega$  is the gamma-ray energy. To obtain  $a_p$  we multiply both sides of the equation by  $\Phi^{(p)}$  and integrate, obtaining

$$a_p = \frac{\int \Phi^{(p)}(\mathbf{r}, \xi) H_I \Psi_0(\mathbf{r}, \xi) d\mathbf{r} d\xi}{E - W_p} \quad \dots\dots (3)$$

We easily obtain  $S_{\gamma\alpha'j}$  by equating  $\Psi$  from equations (1) and (2) at  $r=R$  and using (3), resulting in

$$S_{\gamma\alpha'j} = - \frac{1}{\phi_{\alpha'j}^+(R)} \sum_p \int_0^R d\xi \int d\theta \frac{\Phi^{(p)}(\xi, \mathbf{R}) \chi_j(\xi) \Theta_{\alpha'}(\theta)}{E - W_p} \times \left\{ \int_0^R d\xi \int_0^R d\mathbf{r} \Phi^{(p)}(\xi, \mathbf{r}) H_I \Psi_0(\mathbf{r}, \xi) \right\} \quad \dots\dots (4)$$

where  $\Theta_{\alpha'}(\theta)$  is the angular part and  $\phi_{\alpha'j}^+(r)$  the radial part of the  $\psi_{\alpha'}^+$  function. This equation is analogous to equation (7) of I. The modulus squared of the term in braces is simply the width for photon absorption into the  $p$ th compound state.

In line with the development of I, we consider that the average effect of the nucleons described by coordinates  $\xi$  can be described by a complex potential  $\hat{V}(r)$ . Although  $\hat{V}$  is, strictly speaking, a function of  $j$ , for low excited states of the residual nucleus this dependence is weak, and we will neglect it here. We then expand  $\Phi^{(p)}$  in terms of eigenfunctions of the residual nucleus and of the single nucleon in this well:

$$\Phi^{(p)}(\mathbf{r}, \xi) = \sum_{jm} a_{jm}^p \chi_j(\xi) \hat{\psi}_m^j(\mathbf{r}). \quad \dots\dots (5)$$

The  $\hat{\psi}$ 's depend upon  $j$ , as indicated, because of the boundary condition I (2.3). This dependence is, again, weak for low excited states, and we will neglect it in the following. We denote, as in I, the energies of the core states by  $E_j$  and those of the single nucleon by  $E_m$ . The latter is complex and we denote its real and imaginary parts by  $\epsilon_m$  and  $\alpha_m$  respectively.

In the picture of Lane, Thomas and Wigner (1955), which has been substantiated by Brown (1957), the  $a_{jm}^p$  are large only in the neighbourhood of single particle resonances in the well  $\hat{V}$ . In fact, for the special case of low energies, Brown and De Dominicis (unpublished) have demonstrated that the half-width of the distribution of  $(a_{jm}^p)^2$  about the single particle resonance energy is just  $W$ , where  $W$  is the imaginary part of  $\hat{V}$ . At higher energies the width will contain an additional term equal to the natural width for decay, but this is somewhat smaller than  $W$ , and we shall take the half-width to be equal to  $W$  in our order of magnitude estimates.

We must distinguish two cases:

(1) The energy  $E (= \hbar\omega)$  is far from the single particle resonance energy  $E_j + \epsilon_m$ , i.e.  $E - E_j - \epsilon_m \gg W$ .

(2) The energy is in the neighbourhood of  $E_j + \epsilon_m$ .

In order to utilize the single particle features, we substitute the expansion equation (5) for the  $\Phi^{(p)}$ 's into equation (4), obtaining

$$S_{\gamma\alpha'j} = - \frac{1}{\phi_{\alpha'j}^+(R)} \sum_p \sum_m \sum_{kl} a_{jm}^p a_{kl}^p \int d\theta \hat{\psi}_m(\mathbf{R}) \Theta_{\alpha'}(\theta) \times \int_0^R d\xi \int_0^R d\mathbf{r} \chi_k(\xi) \hat{\psi}_l(\mathbf{r}) H_I(\mathbf{r}) \Psi_0(\mathbf{r}, \xi) \frac{1}{E - W_p} \quad \dots\dots (6)$$

In case (1) we can set  $W_p$  equal to  $E_k + E_l$  when it occurs together with  $a_{kl}^p$ . We can then use completeness in carrying out the sum over  $p$ , i.e.

$$\sum a_{jm}^p a_{kl}^p = \delta_{jk} \delta_{ml} \quad \dots\dots (6.1)$$

to obtain

$$S_{\gamma\alpha'j} = - \frac{1}{\phi_{\alpha'j}^+(R)} \sum_m \int d\theta \hat{\psi}_m(\mathbf{R}) \Theta_{\alpha'}(\theta) \int_0^R d\xi \int_0^R d\mathbf{r} \chi_j(\xi) \hat{\psi}_m(\mathbf{r}) H_I(\mathbf{r}) \Psi_0(\mathbf{r}, \xi). \quad \dots\dots (7)$$

Usually,  $\Psi_0(\mathbf{r}, \xi)$  can be adequately described by a product wave function, in which case

$$\Psi_0 = \Omega(\xi) \psi_0(\mathbf{r}) \quad \dots\dots (7.1)$$

where  $\Omega$  will, in general, represent a shell model state with a hole in it. We can then write

$$S_{\gamma\alpha'j} = - \frac{1}{\phi_{\alpha'j}^+(R)} Q_{\Omega j} \sum_m \int d\theta \hat{\psi}_m(\mathbf{R}) \Theta_{\alpha'}(\theta) \int_0^R d\mathbf{r} \hat{\psi}_m(\mathbf{r}) H_I(\mathbf{r}) \psi_0(\mathbf{r}) \quad \dots\dots (8)$$

where

$$Q_{\Omega j} = \int \chi_j(\xi) \Omega(\xi) d\xi \quad \dots\dots (8.1)$$

and  $Q_{\Omega j}^2$  is just the overlap of the excited state  $j$  and the state  $\Omega$  describing the initial nucleus minus the excited particle. This is related to the 'dissolving' of the nucleus with a hole in it into the excited states of the final nucleus, referred to by Wilkinson. We drop the summation sign, considering only one state  $m$ .

The energy spread of the states  $j$  is produced by the mixing of shell model states in forming low excited states of the residual nucleus, and is small because the Pauli principle inhibits this mixing. From the completeness of the  $\chi_j$ 's and the normalization of  $\Omega$  we see immediately that

$$\sum_j Q_{\Omega j}^2 = 1. \quad \dots\dots (8.2)$$

Thus, if we wish the probability of ending up in any one of the low excited states, we have

$$\begin{aligned} \sigma_{\gamma\alpha'} &= \sum_j \frac{\hbar^2 k_j}{Mc} \left| S_{\gamma\alpha'j} \right|^2 \\ &= \sum_j \Gamma_{\alpha'j} Q_{\Omega j}^2 \frac{1}{\hbar c} \left| \int_0^R d\mathbf{r} \hat{\psi}_m(\mathbf{r}) H_I(\mathbf{r}) \psi_0(\mathbf{r}) \right|^2 \end{aligned} \quad \dots\dots (8.3)$$

where

$$\Gamma_{\alpha'j} = \frac{\hbar^2 k_j}{M} \left| \frac{1}{\phi_{\alpha'j}^+(R)} \right|^2 \left| \int \hat{\psi}_m(\mathbf{R}) \Theta_{\alpha'}(\theta) d\theta \right|^2 \quad \dots\dots (8.4)$$

is the escape width for the channel  $\alpha'j$ . If we neglect  $E_j$  in the denominator compared with  $E - \epsilon_m$ , we can define an average escape width

$$\bar{\Gamma}_{\alpha'} = \sum_j \Gamma_{\alpha'j} Q_{\Omega j}^2 \quad \dots\dots (8.5)$$

and a shell model oscillator strength (to be generalized for many particles in a shell)

$$f_{0m} = (2m\omega/\hbar) \left| \int_0^R d\mathbf{r} \hat{\psi}_m(\mathbf{r}) z \psi_0(\mathbf{r}) \right|^2 \quad \dots\dots (8.6)$$

we obtain

$$\sigma_{\gamma\alpha'} = \bar{\Gamma}_{\alpha'} \frac{1}{\hbar c} \left| \frac{\int_0^R d\mathbf{r} \hat{\psi}_m(\mathbf{r}) H_I(\mathbf{r}) \psi_0(\mathbf{r})}{E - \epsilon_m} \right|^2 = \frac{\pi e^2 \hbar}{Mc} \frac{\bar{\Gamma}_{\alpha'} f_{0m}}{(E - \epsilon_m)^2} \dots \dots (9)$$

Wilkinson (1956) and Rand (1957) give calculations of  $f_{0m}$ . This formula is valid for  $E - \epsilon_m \gg W$ , i.e. for  $E$  far from the single particle resonance. In so far as the width averaged over the various energies  $E - E_j$  for the final particle can be identified with the width at energy  $E - E_\Omega$  where  $E_\Omega$  is the excitation energy of the shell model state  $\Omega$  (which, in general, has a 'hole' in it and is, therefore, an excited state), the above cross section is just that which would be obtained from a pure shell model picture. This latter quantity can easily be obtained from equation (4) by expressing  $\Phi^{(p)}(\xi, \mathbf{r})$  as a pure product wave function, and remembering that the  $\xi$ -dependent part must be equal to that of  $\Psi_0(\mathbf{r}, \xi)$ .

Thus, we see that for energies far from the resonance our formula is equivalent to that obtained from the pure shell model picture after correcting for the fact that the escape width is to be taken for energy  $E - E_j$  rather than  $E - E_\Omega$ .

Equations (8) and (9) can be used to estimate the cross section for direct radiative capture of neutrons or protons. (Similar work has been done by Beck (1956), Lynn and Lane (unpublished) and also by Bloch (unpublished).) The cross sections  $(\gamma, p)$  and  $(p, \gamma)$  leaving the product nucleus in the ground state in each case are clearly related by detailed balance.

For equation (9) we have found the  $(\gamma, p)$  cross section by summing over all members  $j$  of the configuration of the final  $A - 1$  nucleus (see figure 1(a)). The  $(\gamma, p)$  reaction calculated in equation (9) goes from the ground state to all final states  $\chi_j$ . The  $(p, \gamma)$  reaction may go from the ground state  $\chi_0$  to the various final states (see figure 1(b)) which contain an appreciable component of  $\chi_0(\xi)$ .

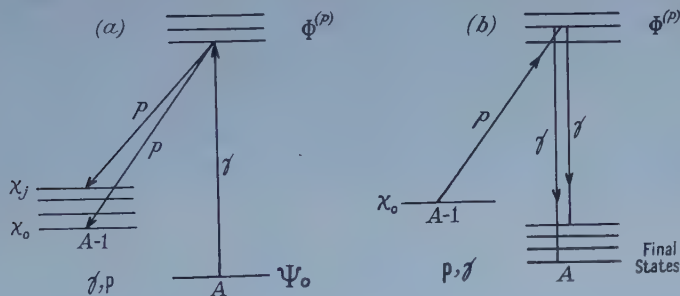


Figure 1.

(The wave function for the particles described by  $\xi$  must remain the same since  $H_I$  is a function only of  $\mathbf{r}$ .) Further, the final state must contain an appreciable component of  $\psi_0(\mathbf{r})$ , the relevant single-particle state in the well. From arguments similar to those used above, we see that the probability of finding  $\chi_0\psi_0$  somewhere in the ground or low excited states is essentially unity. Thus, we find that the cross section for the  $(p, \gamma)$  reaction, summed over the ground and low excited states is given by (9) with two minor changes: (i) we multiply by the usual factor  $k_\gamma^2/k_p^2$  from detailed balance or dispersion theory, where  $k_\gamma$  and  $k_p$  are  $\gamma$ -ray and proton wave-numbers; (ii) we use  $\Gamma_{\alpha'}$  without the averaging of equation (8.5), since the incident particle now has a unique energy.

From the above it is seen that, within the accuracy of our approximations, all absorption in the energy region covered by case (i) leads to the emission of fast particles. Of course, our picture is idealized and even if the energy is well off the single particle resonance, a few compound nucleus levels will be in the neighbourhood of the photon energy. We have effectively neglected these by replacing a small energy denominator by one of several MeV and submerging these levels among the much greater number on the single particle resonance. As discussed in II, these would seem to give mainly compound-nucleus reactions. Thus, although our above treatment has neglected these, it would appear to give the fast particle emission correctly. Our development should not be taken to imply that the compound-nucleus cross section is small; since the energy denominators are small, their total effect can be quite large. In general, the initial beam of photons is a wide one resulting from bremsstrahlung, and covers the region of both cases (i) and (ii). In this case, we can obtain the number of fast particles coming from the region of case (i) by integrating equation (9) over the region of its validity,  $E - \epsilon_m \gg W$ . This gives the proportion of events covered by case (i) to be of the order  $\bar{\Gamma}_\alpha/W$ , roughly that given by Wilkinson.

Whereas case (i) is straightforward to handle, case (ii) is much more difficult because of the variation in the energy denominators when the energy  $E$  is on a single-particle resonance. We shall now give an argument† to suggest that an appreciable number of fast particles are emitted also in this region, equal in order of magnitude to the number predicted by Wilkinson's modified single particle model.

Let us consider the average of  $S_{\gamma\alpha'j}$  over an energy interval  $\mathcal{J}$  covering the whole single-particle resonance. For the moment we will neglect the variation in energy of the quantities in equation (6) other than the energy denominator. (Except for the  $\phi_{\alpha'j}^+(R)$  the terms vary little with incident energy.) If our interval is chosen symmetrically we immediately find that

$$\int_{-\mathcal{J}/2}^{\mathcal{J}/2} (E - W_p)^{-1} dE = i\pi,$$

remembering that  $W_p$  has a small negative imaginary part and that the real part of the integral will go out after averaging over all the levels. Thus,

$$\begin{aligned} \bar{S}_{\gamma\alpha'j} = & -\frac{i\pi}{\mathcal{J}} \frac{1}{\phi_{\alpha'j}^+} \sum_p \sum_{kl} a_{jm}^p a_{kl}^p \int d\theta \hat{\psi}_m(\mathbf{R}) \Theta_{\alpha'}(\theta) \\ & \times \int_0^R d\xi \int_0^R d\mathbf{r} \chi_k(\xi) \hat{\psi}_l(\mathbf{r}) H_1(\mathbf{r}) \Psi_0(\mathbf{r}, \xi) \quad \dots\dots (10) \end{aligned}$$

where we have dropped the sum over  $m$  which occurs in equation (6) because we are considering only the  $m$ th single-particle resonance. We can now carry out the sum over  $p$  using closure, and we find

$$\begin{aligned} \bar{S}_{\gamma\alpha'j} = & -\frac{i\pi}{\mathcal{J}} \frac{1}{\phi_{\alpha'j}^+} \int d\theta \hat{\psi}_m(\mathbf{R}) \Theta_{\alpha'}(\theta) \int_0^R d\xi \int_0^R d\mathbf{r} \chi_j(\xi) \hat{\psi}_m(\mathbf{r}) H_1(\mathbf{r}) \Psi_0(\mathbf{r}, \xi). \\ & \dots\dots (10.1) \end{aligned}$$

Now  $\mathcal{J} |\bar{S}_{\gamma\alpha'j}|^2$  gives a minimum value for the number of direct emission processes occurring on the giant resonance. These are seen to be of the order of  $\bar{\Gamma}_\alpha/\mathcal{J}$

† This argument is due to Professor R. E. Peierls. It shows that the hypothesis of II, where it was assumed that a negligible amount of direct interaction comes from the region of single particle resonance, was incorrect.



of the integrated absorption cross section. Now  $\mathcal{J}$  must be larger than  $2W$  in order to cover the single-particle resonance. Thus, the proportion of processes giving rise to fast particle emission will again be of order  $\bar{\Gamma}_{\alpha'j}/W$  for this case, although it may have a small numerical factor of the order of  $1/4$  or  $1/8$  because of the restriction that  $\mathcal{J}$  must cover the single-particle level. We emphasize that the above estimate which necessitates averaging over a large interval  $\mathcal{J}$  gives a minimum value, and the actual value may be considerably higher, although we would expect the above order of magnitude to be correct.

In the above we assumed that the terms other than the energy denominator were not energy dependent. This is certainly not valid for  $\phi_{\alpha'j}^+$  which can vary considerably over a single particle resonance. However, it varies smoothly and, taking its variation into account, would not be expected to change the order of magnitude of our answer.

We could, in fact, take this variation into account by employing the averaging procedure proposed by Wigner (1951). Since an expression such as the  $S_{\gamma\alpha'j}$  of equation (6) has poles only in the lower half of the energy plane, its average over real values of energy  $E(E_0 - \frac{1}{2}\mathcal{J} < E < E_0 + \frac{1}{2}\mathcal{J})$  can be replaced by the average for complex values of the energy  $E + i\eta$ , where  $E$  covers the same range as before, providing  $\eta \ll \mathcal{J}$ . If we replace  $E$  in equation (6) by  $E + i\eta$  with  $\eta$  satisfying the inequalities  $2W \ll \eta \ll \mathcal{J}$ , we can then replace  $W_p$  by  $E_j + \epsilon_m$  to a good approximation since  $W_p - E_j - \epsilon_m \ll \eta$  for most  $p$ , and then carry out the summation over  $p$ . This gives the same order of magnitude as the above. We note that since the spread in  $W_p - E_j - \epsilon_m$  is the order of the single particle width, the interval  $\mathcal{J}$  must necessarily be larger than this width, and hence we cannot say anything about the detailed behaviour of the scattering amplitude on the single-particle level.

The same result for the average phase over the interval  $\mathcal{J}$  would be obtained if we replaced  $W_p$  by  $E_j + E_m$ , where the  $E_m$  are the complex energy eigenvalues in the complex well, as we mentioned above. This is just what would be obtained from perturbation theory for the average phase (Bloch 1957 b). However, because of the inequalities that must be satisfied in our argument we are unable to check perturbation theory in any detail over the single-particle resonance.

### § 3. ANGULAR DISTRIBUTION

Direct emission due to electric dipole processes has the characteristic  $a + \sin^2 \theta$  angular distribution, where  $\theta$  is the angle between the propagation directions of the photon and emitted particle. The numerical value of  $a$ , as calculated from equation (9) is in rough agreement with Wilkinson's (1956) value.

We can also use equation (9) to estimate the order of magnitude of forward asymmetry in the angular distribution of the direct photoeffect, arising from interference between the dipole transitions and quadrupole transitions of higher energy. (Equation (9) applies in the region between the electric dipole and electric quadrupole resonances, and far from either resonance. Near either resonance we expect the order of magnitude of  $\Gamma/W$  of the corresponding absorption cross section.) The shell-model quadrupole resonances occur at average energy  $\bar{\epsilon}'$  about twice the average energy  $\bar{\epsilon}$  of the dipole resonances (for the harmonic oscillator shell-model the ratio  $\bar{\epsilon}'/\bar{\epsilon}$  is exactly two).

For a harmonic oscillator shell-model potential the dipole cross section  $\sigma^d$  for the direct photoeffect is, from equation (9)

$$\sigma^d = (\pi e^2 \hbar / Mc) \bar{\Gamma} \sum_m f_{0m} / (E - \bar{\epsilon})^2. \quad \dots\dots (11)$$

The summed dipole oscillator strength for proton excitation is  $\sum_m f_{0m} = Z/4$ . (Here, and in the quadrupole sum-rule, we neglect the effects of exchange forces, and further make the approximation  $Z = A/2$ .)

The electric quadrupole cross section  $\sigma^q$  for the direct photoeffect is

$$\sigma^q = (\pi e^2 \hbar / Mc) \bar{\Gamma}' \sum_m f_{0m}' / (E - \bar{\epsilon}')^2 \quad \dots\dots (11.1)$$

where primed quantities refer to quadrupole effects. The quadrupole oscillator strength is (Levinger, Rustgi and Okamoto 1957)

$$f_{0m}' = (\bar{\epsilon} / Mc^2) (n_z + 1) (n_y + 1).$$

Here we have considered a transition from a state with quantum numbers  $(n_x, n_y, n_z)$  to a state  $(n_x, n_y + 1, n_z + 1)$  for a photon polarized along  $y$  and propagated along  $z$ . For  $Z$  protons in a harmonic oscillator potential, filling states up to and including total quantum number  $N$  ( $N = n_x + n_y + n_z$ ), we find

$$\sum_m f_{0m}' = \frac{1}{2} (N + 2) Z \bar{\epsilon} / Mc^2. \quad \dots\dots (11.2)$$

As a rough approximation we assume equal penetrabilities  $\bar{\Gamma}$  and  $\bar{\Gamma}'$  for the different parity waves of direct protons due to dipole and quadrupole absorption respectively. Using the above summed oscillator strengths in equation (9) we have

$$\begin{aligned} \sigma^q / \sigma^d &\simeq 2(N + 2) (\bar{\epsilon} / Mc^2) (E - \bar{\epsilon})^2 / (E - \bar{\epsilon}')^2 \\ &\simeq 0.1 (E - \bar{\epsilon})^2 / (E - \bar{\epsilon}')^2. \quad \dots\dots (12) \end{aligned}$$

The numerical result applies for  $N = 3$  ( $Z = 40$ ); we have chosen  $\bar{\epsilon} = 10$  mev for the level spacing in a velocity-independent harmonic oscillator potential.

Equation (12) should be used with great discretion, due to the approximations made in its derivation, and due to uncertainties in the values to insert for the average *experimental* resonance energies  $\bar{\epsilon}$  and  $\bar{\epsilon}'$ . Equation (12) does give the experimental order of magnitude (e.g. Mann, Halpern and Rothman 1952) of a few per cent for the value of  $\sigma^q / \sigma^d$  as determined by the forward asymmetry of proton emission.

#### § 4. DISCUSSION

Experiments have demonstrated the existence of the direct photoeffect, and have indicated the existence of direct radiative capture. Both the experimental data and knowledge of the values of theoretical parameters are such that at present it seems difficult to verify in detail (i) that equation (9) gives the cross section for the direct photoeffect far from the giant resonance, (ii) that Wilkinson's or our estimate of the direct photoeffect is valid in the resonance region, (iii) that equation (12) gives the experimental forward asymmetry of photoprotons. At least these three statements seem not inconsistent with experimental data: e.g. Hirzel and Wäffler (1947), Ferrero *et al.* (1957 a, b), Cohen (1956), Ball, Fairhall and Halpern (unpublished), Osikina and Ratner (1957).

The existence of the direct photoeffect was the main evidence for the validity of Wilkinson's shell-model calculation of photodisintegration (Levinger 1956).

The integrated absorption cross section and the resonance energy are insensitive to the (shell or collective) model used, while the width of the resonance curve is not calculated from first principles with either the shell or collective models. Both the shell and collective models are idealizations of the complete representation of excited nuclear states in terms of the very many compound nucleus levels.

In this paper we have shown that it is unnecessary to assume a *literal* shell-model wave function for the states excited by photon absorption; the existence of a resonance in the strength function gives us a direct photoeffect similar to that calculated from shell-model wave functions in a complex potential. (The collective model is not useful in calculations of the direct photoeffect; since for this process we are interested in a final state—emitted particle and daughter nucleus with none or low excitation energy—that can only be well represented by shell-model wave functions.) We conclude that the existence of the direct photoeffect is insensitive to the detailed character of the compound nucleus states in the region of the giant dipole resonance.

We are in partial agreement with Brink (1957) who argues that a shell-model and a collective model give *identical* results for the nuclear photoeffect. He argues that both models are correct. We believe that neither the shell or collective model is correct; the compound levels reached by photon absorption are neither good shell model nor good collective model states, but the direct photoeffect may be estimated *as if* the shell model were valid.

#### ACKNOWLEDGMENTS

We are grateful to Professor R. E. Peierls and Dr. A. M. Lane for helpful discussions of these problems.

#### REFERENCES

- BECK, F., 1956, *Physica, 's Grav.*, **22**, 1164.  
 BLOCH, C., 1957 a, *Nuclear Physics*, **3**, 137; 1957 b, *Ibid.*, **4**, 503.  
 BRINK, D. M., 1957, *Nuclear Physics*, **4**, 215.  
 BROWN, G. E., 1957, *Proc. Phys. Soc. A*, **70**, 681.  
 BROWN, G. E. and DE DOMINICIS, C. T., 1957 a, *Proc. Phys. Soc. A*, **70**, 668; 1957 b, *Ibid.*, **70**, 686.  
 COHEN, B., 1955, *Phys. Rev.*, **100**, 206.  
 FERRERO, F., HANSON, A. O., MALVANO, R., and TRIBUNO, C., 1957 b, *Nuovo Cim.*, **6**, 585.  
 FERRERO, F., MALVANO, R., and TRIBUNO, C., 1957a, *Nuovo Cim.*, **6**, 385.  
 FESHBACH, H., PORTER, C. E., and WEISSKOPF, V. F., 1954, *Phys. Rev.*, **96**, 448.  
 GOLDBABER, M., and TELLER, E., 1948, *Phys. Rev.*, **74**, 1046.  
 HIRZEL, O., and WÄFFLER, H., 1947, *Helv. Phys. Acta*, **20**, 373.  
 JENSEN, J. H. D., and JENSEN, P., 1950, *Z. Naturf.*, **5a**, 343.  
 LANE, A. M., THOMAS, R. G., and WIGNER, E. P., 1955, *Phys. Rev.*, **98**, 693.  
 LEVINGER, J. S., 1956, *Rev. Mex. Fis.*, **5**, 177.  
 LEVINGER, J. S., RUSTGI, M. L., and OKAMOTO, K., 1957, *Phys. Rev.*, **106**, 1191.  
 MANN, A. K., HALPERN, J., and ROTHMAN, M., 1952, *Phys. Rev.*, **87**, 146.  
 OSIKINA, M., and RATNER, B. S., 1957, *J. Exp. Theor. Phys.* (Trans.) **5**, 1.  
 PEASLEE, D. C. 1952, *Phys. Rev.*, **88**, 812.  
 RAND, S., 1957, *Phys. Rev.*, **107**, 208.  
 WIGNER, E. P., 1951, *Ann. Math.*, **53**, 36.  
 WILKINSON, D. H., 1956, *Physica, 's Grav.*, **22**, 1039.



## Equation of State of Zinc, Cadmium and Magnesium

By S. SHIVANANDA TOLPADI

X-Ray Section, Physics Department, Banaras Hindu University, India

*MS. received 30th July 1957, and in revised form 2nd December 1957*

**Abstract.** A method of deriving the equation of state of crystals belonging to the hexagonal system from the experimental data on specific heat, thermal expansion and elastic constants has been developed. The method is a modification of the one given by Dayal for cubic crystals. The pressures along the hexagonal axis and those perpendicular to it are divided into two parts, of which the first is the static part due to a non-vibrating lattice and the second due to the thermal vibrations. Two average Grüneisen constants have been calculated from the experimental data and have been used in the calculation of the thermal pressures, along the two axes. The static pressure for a non-vibrating lattice is calculated as a function of the linear dimension from the condition that for the linear dimension measured at zero pressure, the sum of the thermal and static pressures must be zero. In this way the total pressure comes out to be the difference between the thermal pressure at a temperature  $T$  and length  $l$  and the one calculated for a temperature at which the crystal has the same length at  $P=0$ . Detailed calculations have been made for zinc, cadmium and magnesium. It is found that in all cases except in the case of cadmium perpendicular to the hexagonal axis, the calculated results are in good agreement with Bridgman's experimental measurements.

It has been shown that the equation of state derived from the assumption made by Grüneisen about two Debye characteristic temperatures, one perpendicular and the other parallel to the hexagonal axis, does not agree with the experimental observations made by Bridgman.

### § 1. INTRODUCTION

THE methods of statistical thermodynamics have been applied by a number of workers to the derivation of the equation of state of solids of simple structure. The usual starting point in these investigations is the Helmholtz free energy  $A$ , from which pressure can be obtained as a derivative with respect to the volume. There are two terms in the expression for pressure, one of which, the static pressure, is independent of temperature, while the other is expressly dependent on it. The former is calculated from the potential energy of the constituent atoms of the solid obtained as a function of their mutual distances. This is very difficult to obtain rigorously and approximate expressions for the potential energy have been used extensively. Fortunately, due to the small changes of volume suffered by a solid even at the highest pressures obtainable in the laboratory, we are only interested in a narrow region of volume in the neighbourhood of the equilibrium point. It is therefore possible to use an empirical expression for the interatomic force law which may only resemble the real law in this narrow region. The constants for this expression are usually



derived from the observed lattice structure and from other experimental data. Such expressions have been used by Grüneisen (1912, 1926), Born (1939, 1940), Fürth (1945), Bardeen (1938), Huggins and Mayer (1933) and others.

The evaluation of the thermal pressure involves a knowledge of the  $3N$  characteristic vibration frequencies in terms of the interatomic forces. This is not a simple task and here also recourse has been had to the approximate methods. It has been usual to assume the Einstein or the Debye model of a solid, so that one has to deal with only one single frequency for all computational purposes. Grüneisen (1912, 1926) was the leader of this type of work, while later workers included Herzfeld and Mayer (1934) and Kane (1939). Born and Bradburn (1943) and Bradburn (1943) have, however, developed methods based on a simple power law of interatomic forces, in which the thermal pressure can be calculated from the  $3N$  vibration frequencies by the use of the Born lattice dynamics discussed in an article by Born and Kármán (1912). Fürth (1945) has used this method to make an extensive study of the equation of state of solids. These studies, however, suffer from an important limitation inasmuch as they are concerned with the classical statistics and the results only apply above the Debye characteristic temperature.

Dayal (1950, 1950-51) has recently suggested a new approach to the problem in which there is no restriction as regards statistics and the static and thermal pressures are both calculated from the experimentally observed quantities, viz. the specific heat, the coefficient of thermal expansion and the compressibility. On account of the exclusive use of the experimental data, this method also provides an independent check on some of the laws of interatomic force used by earlier workers. Dayal has studied the isotherms of sodium chloride by this method and has obtained results in good agreement with Bridgman's experimental work (1931, p. 160). Similar results have been obtained for a number of metals crystallizing in the cubic system by Sharma (1954). Dayal and Sharma (1955) have used this method to check the exponents of the interatomic force law used by Fürth (1945), and Sharma (1954) has also compared his results with those obtained from the potential functions used by Bardeen (1938) and by Huggins and Mayer (1933).

All the above theoretical studies of the equation of state of solids have generally been concerned with the simple monatomic solids which crystallize in the cubic system. Metals belonging to the hexagonal system come next from the point of view of simplicity of structure, and of interest. It has, therefore, been thought advisable to use Dayal's method for the derivation of the isotherms of such of these metals for which the necessary experimental data are available. The cases of zinc, cadmium and magnesium have accordingly been taken up for study in the present paper. A summary of some preliminary results for zinc only has been reported by Shivananda Tolpadi and Purushottaman (1956).

## § 2. DERIVATION OF EQUATION OF STATE AND MAIN RESULTS

The Helmholtz free energy  $A$  of the solid is given by

$$A = \Phi + \sum_{j=1}^{3N} kT \log [1 - \exp(-h\nu_j/kT)] \quad \dots\dots (1)$$

where  $\Phi$  is the potential energy and the summation is over all the  $3N$  vibration frequencies.

The stress components  $X_x, Z_z, \dots$  are given by the three equations of the type

$$\left. \begin{aligned} X_x &= - \frac{\partial(A/V)}{\partial x_x}, \\ &\dots \dots \dots \end{aligned} \right\} \dots\dots (2)$$

where  $x_x, \dots$  are the strain components and  $V$  is the volume per gramme atom of the solid.

On substituting equation (2) in (1) we get the equation of state in the form

$$\left. \begin{aligned} X_x &= - \frac{\partial(\Phi/V)}{\partial x_x} + \sum_{j=1}^{3N} \frac{\gamma(j)_{xx} E_j}{V}, \\ &\dots \dots \dots \end{aligned} \right\} \dots\dots (3)$$

where  $(\gamma_j)_{xx} = -\partial \log \nu_j / \partial x_x$  is the Grüneisen constant for the  $j$ th frequency,  $E_j$  is the mean energy of an oscillator of frequency  $\nu_j$  given by

$$h\nu_j / [\exp(h\nu_j/kT) - 1].$$

Grüneisen assumed that  $\gamma_{xx}$  is the same for all frequencies. Dayal (1944) and Barron (1957) have shown that this assumption is not correct. We may, however, take an average value of the Grüneisen constant such that the second term on the right-hand side of equation (3) can be written as  $\bar{\gamma}E/V$  where  $E$  is the total thermal energy. We thus get the equation of state in the same form as given by Grüneisen (1926), i.e.

$$\left. \begin{aligned} X_x &= - \frac{\partial(\Phi/V)}{\partial x_x} + \bar{\gamma}_{xx} \frac{E}{V}, \\ &\dots \dots \dots \end{aligned} \right\} \dots\dots (3a)$$

The entropy  $S$  is given by  $-(\partial A/\partial T)_v$  and the principal linear coefficients of thermal expansion parallel to the three crystallographic axes are given by

$$\left. \begin{aligned} V\alpha_x &= -(\partial S/\partial X_x)_T, \\ &\dots \dots \dots \end{aligned} \right\} \dots\dots (4)$$

In the hexagonal system  $\alpha_x = \alpha_y$  so that there are only two principal linear coefficients of thermal expansion  $\alpha_x$  and  $\alpha_z$ , perpendicular and parallel to the hexagonal axis respectively.

Using the expressions for  $A$  and  $S$  and following the procedure given by Grüneisen (1912, 1926), we get the well-known result

$$\left. \begin{aligned} \alpha_x &= (s_{11} + s_{12})q_{xx} + s_{13}q_{zz} \\ \alpha_z &= 2s_{13}q_{xx} + s_{33}q_{zz} \end{aligned} \right\} \dots\dots (5)$$

where  $s_{ik}$  represents the elastic moduli and

$$Vq_{xx} = \sum_{j=1}^{3N} (\gamma_j)_{xx} C(\nu_j) \dots\dots (6)$$

with a similar expression for  $Vq_{zz}$  where  $C(\nu_j)$  is the specific heat function for the frequency  $\nu_j$  and is given by

$$C(\nu_j) = \frac{[(h\nu_j)^2/kT^2] \exp(h\nu_j/kT)}{[\exp(h\nu_j/kT) - 1]^2}.$$

Grüneisen used Debye function for the specific heat and arbitrarily split specific heats into two Debye functions, one along the hexagonal axis and the

other perpendicular to it. We may, however, follow the previous procedure and put  $Vq_{xx} = \bar{\gamma}_c C_v$  where  $C_v$  is the total specific heat at constant volume and  $\bar{\gamma}_c$  is an average Grüneisen constant; the subscript  $c$  has been inserted to show that the averaging process need not necessarily give the same average constant as obtained while deriving equation (3a). In the case when  $\bar{\gamma}_c$  is the same for all frequencies as assumed by Grüneisen or when the temperatures are such that all the frequencies give the classical values of specific heat, the averaging process involved in equations (3a) and (6) will give exactly the same values of Grüneisen constant. Dayal assumed that variation of  $\gamma$  from one frequency to the other is not very large and the two average constants may, therefore, be taken to be sensibly the same under all conditions. This is also justified by the fact that this assumption leads to isotherms in good agreement with experimental data (Sharma 1954). The subscript  $c$  can therefore be dropped and equation (6) is written in the form

$$Vq_{xx} = \bar{\gamma}_{xx} C_v, \quad Vq_{zz} = \bar{\gamma}_{zz} C_v.$$

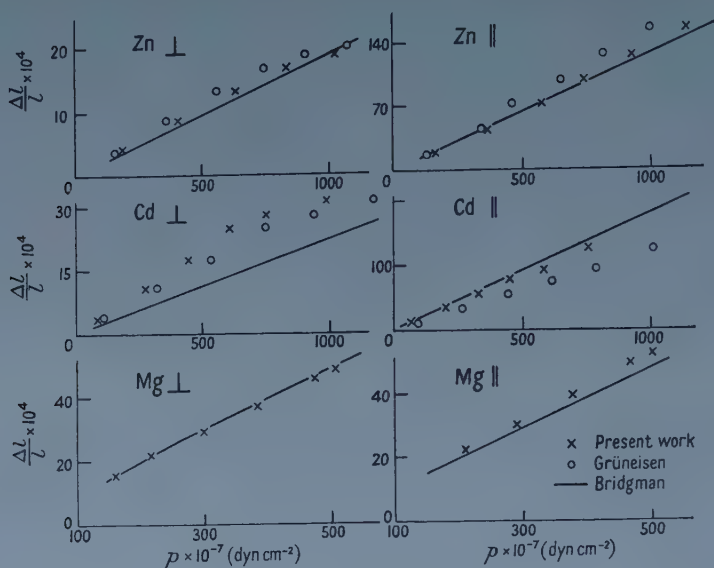
In the present method  $\bar{\gamma}_{xx}$  and  $\bar{\gamma}_{zz}$  are calculated by substituting the experimental linear thermal expansion coefficients and the elastic moduli in equation (5). Their values are shown in the table and it can be seen that Grüneisen's assumption that they are independent of temperature and pressure is not correct. The same conclusion has been reached by Barron (1955). We have assumed that Grüneisen's constants are a function of the linear dimensions only and do not depend on the pressure and temperature as long as the linear dimensions remain constant. The constants given in the table have been taken to refer to linear dimensions corresponding to the temperatures. These values of  $\bar{\gamma}$  are substituted in the second term of the equation of state (3a) and thus the thermal pressures are calculated. The first term in the equation of state is then calculated as a function of the linear dimension by the following process which is the same in principle as those used by Dayal (1950) and by Sharma (1954) in the case of cubic crystals.

Starting from the equilibrium values of the linear dimensions  $l_x$  and  $l_z$  at  $P = T = 0$  and using the thermal expansion data, values of length at various pressures are calculated. These are the lengths measured at room pressure which is practically zero in the scales of pressures involved here. For these lengths, therefore, stresses  $X_x$  etc. are zero and the two terms on the right-hand side of the equation (3a) are equal and opposite in sign to each other. This condition enables the static term to be as calculated as a function of the linear dimension. The total pressures at various lengths, i.e.  $X_x, \dots$  are then calculated by adding the static and thermal pressures. In this way the total pressure is found to be the difference between the thermal pressure at a temperature  $T$  and length  $l$  and that calculated for a temperature at which the crystal has the same length at  $P = T = 0$ . In the figure are plotted the calculated values of

$$\Delta l/l = (l_{PT} - l_{0T})/l_{00}$$

for zinc, cadmium and magnesium at various pressures by the present method, both perpendicular and parallel to the hexagonal axis. The thermal expansion for zinc and cadmium are taken from Grüneisen (1926, table 16, p. 48), and that of magnesium from the work of Goens and Schmid (1936). The specific heat data for zinc are taken from the study made by Keesom and Ende (1932) in the range 3.2°K to 20°K and Clusius and Harteck (1928) in the range 21.9°K

to 201°K, for cadmium from the experimental data of Lange and Simon (1928) and for magnesium from the observations of Clusius and Vaughen (1930).



Graphs connecting  $\Delta l/l$  and  $p$  for zinc, cadmium and magnesium, both parallel and perpendicular to the hexagonal axis.

Metal	$T(^{\circ}\text{K})$	Grüneisen Constants	
		$\perp$ hexag. axis	$\parallel$ hexag. axis
Zinc	53.2	1.66	2.38
	113.2	1.86	2.06
	153.2	1.97	2.03
	193.2	2.04	2.02
	233.2	2.09	2.00
	273.2	2.12	1.99
	303.0	2.15	2.01
Cadmium	53.2	1.99	2.14
	113.2	2.30	2.09
	153.2	2.45	2.09
	193.2	2.54	2.13
	233.2	2.62	2.15
	273.2	2.68	2.16
	293.0	2.72	2.17
Magnesium	49.0	1.33	1.34
	87.0	1.34	1.34
	141.5	1.36	1.37
	182.0	1.43	1.44
	217.2	1.49	1.49
	243.0	1.54	1.51
	274.0	1.55	1.53
	303.0	1.55	1.53

The elastic constant data are from Zwicky (1934, table 1). The calculations have been made at a temperature of 303°K for zinc and magnesium and for cadmium at a temperature of 293°K. These results are compared with the experimental



measurements of Bridgman (1931) in the figure. It can be seen that the calculated values of  $\Delta l/l$  are in good agreement with experimental values except in the case of cadmium perpendicular to the hexagonal axis. In the case of this metal an agreement has only been found for the measurements made parallel to the hexagonal axis. Since the values of  $\Delta l/l$  perpendicular to the hexagonal axis of cadmium are about one-tenth those in the other direction for the same pressure, the possibility of errors in these measurements cannot be ignored.

It may be remarked that even though we have calculated the total pressure as the sum of static and thermal parts, the present method provides a convenient approach of obtaining the static contribution to the pressure and also to the linear compressibility.

### § 3. GRÜNEISEN'S ASSUMPTION OF TWO DEBYE CHARACTERISTIC TEMPERATURES

The equations (3a) are identical with those given originally by Grüneisen (1926). The only difference is that he defined  $q_{xx}$  and  $q_{zz}$  in such a way that the Debye function took the place of the experimental values of  $C_v$ . Grüneisen was more concerned with the derivation of the values of the coefficients of thermal expansion than with the equation of state. Since the experimental values of  $C_v$  did not yield values of the Grüneisen constants  $\bar{\gamma}_{xx}$  and  $\bar{\gamma}_{zz}$  which would remain constant at all temperatures, he split  $C_v$  into two parts. One of these was supposed to be due to the vibrations parallel to the hexagonal axis and the other due to those perpendicular to it. It was postulated that their values were given by two separate Debye functions  $\theta_x$  and  $\theta_z$  the first of which alone appeared in the definition of  $q_{xx}$  and the other in that of  $q_{zz}$ . The values of  $\theta_x$  and  $\theta_z$  were so selected empirically that  $\bar{\gamma}_{xx}$  and  $\bar{\gamma}_{zz}$  remained constant in the temperature region in which he was interested. This process does not seem to be justified so far as the equation of state is concerned, since all the  $3N$  frequencies appear in the definition of  $q_{xx}$  and  $q_{zz}$  and in the equation of state (3a).

It is, however, worth while to find out whether Grüneisen's method of two Debye functions gives a satisfactory equation of state in agreement with the experimental data of Bridgman. We have, therefore, also calculated the equation of state for zinc and cadmium from Grüneisen's values of  $\bar{\gamma}_{xx}$  and  $\bar{\gamma}_{zz}$  and  $\theta_x$ ,  $\theta_z$  as given in the *Handbuch der Physik*, Vol. X (1926), table 17, p. 48. The  $\sum E_j$  occurring in the equation of state (3) have been calculated from the appropriate  $\theta$ . The results are shown in the figure and it can be seen that Grüneisen's method does not yield a satisfactory agreement with Bridgman's data.

### ACKNOWLEDGMENT

The author is indebted to Dr. B. Dayal for suggesting this problem and for his continued interest, encouragement and helpful advice during the progress of this work.

### REFERENCES

- BARDEEN, J., 1938, *J. Chem. Phys.*, **6**, 372.
- BARRON, T. H. K., 1955, *Annals of Physics*, **1**, 77; 1957, *Phil. Mag.*, **46**, 720.
- BORN, M., 1939, *J. Chem. Phys.*, **7**, 591; 1940, *Proc. Camb. Phil. Soc.*, **36**, 160.
- BORN, M., and BRADBURN, M., 1943, *Proc. Camb. Phil. Soc.*, **39**, 104.
- BORN, M., and KÁRMÁN, T. V., 1912, *Phys. Z.*, **13**, 297.
- BRADBURN, M., 1943, *Proc. Camb. Phil. Soc.*, **39**, 113.

- BRIDGMAN, P. W., 1931, *The Physics of High Pressure* (London : Bell), table V, p. 160.
- CLUSIUS, K., and HARTECK, P., 1928, *Z. phys. Chem.*, **134**, 256.
- CLUSIUS, K., and VAUGHEN, J. V., 1930, *J. Amer. Chem. Soc.*, **52**, 4686.
- DAYAL, B., 1944, *Proc. Indian Acad. Sci.*, **A20**, 145; 1950, *J. Chem. Phys.*, **18**, 1302; 1950-51, *J. Sci. Res., Banaras Hindu Univ.*, **1**, 21.
- DAYAL, B., and SHARMA, R. S., 1955, *Proc. Phys. Soc. B*, **68**, 1049.
- FÜRTH, R., 1945, *Proc. Phys. Soc. A*, **183**, 87.
- GOENS, E., and SCHMID, E., 1936, *Phys. Z.*, **37**, 385.
- GRÜNEISEN, E., 1912, *Ann. Phys., Lpz.*, **39**, 257; 1926, *Handbuch der Physik* (Springer : Berlin) **10**, 23-48.
- HERZFELD, K. F., and MAYER, M. G., 1934, *Phys. Rev.*, **46**, 995.
- HUGGINS, M. L., and MAYER, J. E., 1933, *J. Chem. Phys.*, **1**, 643.
- KANE, B. G., 1939, *J. Chem. Phys.*, **7**, 603.
- KEESOM, W. M., and ENDE, J. N., 1932, *Leiden Commun.*, No. 219b.
- LANGE, F., and SIMON, F., 1928, *Z. phys. Chem.*, **134**, 376.
- SHARMA, R. S., 1954, *Ph.D. Thesis*, Banaras Hindu University, India.
- SHIVANANDA TOLPADI, S., and PURUSHOTTAMAN, C., 1956, *Current Sci.*, **25**, 392.
- ZWICKY, P., 1934, *Rev. Mod. Phys.*, **6**, 1934.

# The Electronic Structure of Crystals having the Sodium Chloride type of Lattice

By T. B. GRIMLEY

Department of Inorganic and Physical Chemistry, University of Liverpool

*MS. received 13th December 1957, and in final form 31st January 1958*

**Abstract.** The electronic structure of an ionic crystal is investigated with the assumption that the solutions of Fock's equations for the valence electrons can be expressed as linear combinations of the outer orbitals on the negative ions and the first vacant orbitals on the metal ions. The inclusion of this latter group of orbitals allows for homopolar binding. Numerical calculations are made for LiF and the width of the  $F^- 2p$  band is found to be 5.4 eV of which about 5% is due to homopolar binding. The main homopolar effect is to provide a coupling between ions which are second nearest neighbours in the halide ion lattice.

## § 1. INTRODUCTION

**I**N an ionic crystal, the outer electrons from the negative ions will be shared to some extent with the surrounding metal ions. This sharing of the electrons gives rise to an additional cohesive force which may be called homopolar. In a previous paper (Grimley 1957, to be referred to as I) it has been shown how this homopolar contribution to the lattice energy may be calculated. The calculation was made by assuming that the solutions of Fock's (1930) equations for the valence electrons in the crystal could be expressed adequately as linear combinations of a finite number of orthogonal atomic orbitals. The atomic orbitals were chosen so as to allow for the possibility of the electron sharing referred to above. The problem of solving Fock's equations is now reduced to that of diagonalizing the Fock energy matrix when it is expressed in this finite representation. To calculate the total energy of the system in the ground state, it is not necessary to carry this diagonalization to completion because the total energy is invariant under unitary transformations of the ground state one-electron functions. Complete diagonalization is necessary to discuss the electronic band structure. This problem will be treated in the present paper.

No calculations of the band structures of ionic crystals using this method have so far been published. In previous discussions (Shockley 1936, Ewing and Seitz 1936) attempts were made to solve Fock's equations directly, and to do this several more or less plausible assumptions had to be made.

In this paper, numerical calculations are carried out for LiF, and the results are compared with those of Ewing and Seitz (1936). Our general formulae are applicable, with only trivial modifications to all monovalent metal halides, divalent metal oxides, sulphides, selenides and tellurides having the NaCl structure.

## § 2. BASIC FORMULAE

The fundamental problem in the determination of the electronic structure of a solid in the ordinary Hartree-Fock approximation is to find the eigenvalues  $\epsilon_p(\mathbf{k})$  of the equation

$$F_{\text{op}}\psi_p(\mathbf{x}, \mathbf{k}) = \epsilon_p(\mathbf{k})\psi_p(\mathbf{x}, \mathbf{k}). \quad \dots\dots (1)$$

$\psi_p(\mathbf{x}, \mathbf{k})$  are the one-electron wave functions ( $\mathbf{x}$  stands for both space and spin coordinates),  $\mathbf{k}$  is a vector in the reciprocal lattice and the index  $p$  denotes the Brillouin zone number in  $\mathbf{k}$ -space.  $F_{\text{op}}$  is the effective one-electron Hamiltonian operator in Fock's approximation. We note that for crystals having the NaCl type of lattice, the reciprocal lattice is body-centred cubic.

To obtain an approximate solution of equation (1) we suppose that the  $\psi_p(\mathbf{x}, \mathbf{k})$  may be expressed as linear combinations of atomic orbitals (LCAO). For the valence band of a LiF crystal containing  $N$  molecules, the atomic orbitals selected are the  $8N$  free ion spin-orbitals consisting of  $6N$  2p spin-orbitals on the  $\text{F}^-$  ions and  $2N$  (normally vacant) 2s spin-orbitals on the  $\text{Li}^+$  ions. The inclusion of this latter set of orbitals allows for homopolar binding. These orbitals will be denoted by  $\phi_p(\mathbf{x}, \alpha)$ , where the vector  $\alpha$  specifies the position of the ion, and the index  $p$  goes over all spin-orbitals associated with the ion at  $\alpha$ . For brevity in what follows we condense our indices  $(p, \alpha)$  and  $(p, \mathbf{k})$  into the single symbols  $\alpha$  and  $k$ , and write

$$\Psi = \Phi \mathbf{C}', \quad \dots\dots (2)$$

where  $\Psi$  and  $\Phi$  are row matrices.  $\mathbf{C}'$  is taken as a square ( $8N \times 8N$ ) matrix so that equation (2) defines a set of  $8N$  crystal spin-orbitals. Only  $6N$  of these are occupied in the ground state. We order the row matrix  $\Phi$  such that the first  $6N$  elements are the spin-orbitals on the halide ions, and the last  $2N$  elements are those on the metal ions. Similarly, the first  $6N$  elements of  $\Psi$  are the ground state crystal spin-orbitals. We use the indices  $\mu, \nu$  and  $\lambda$  to denote the halide ion orbitals, and  $m$  and  $n$  to denote the orbitals on the metal ions. The indices  $\alpha, \beta, \gamma, \delta$  will be used to denote *any* orbital, halide or metal.

The set of orbitals  $\Phi$  are not all orthogonal at any finite lattice parameter. We introduce, therefore, an orthonormal set  $\Phi$  by Löwdin's (1950) transformation

$$\Phi = \Phi \mathbf{L}, \quad \dots\dots (3)$$

where

$$\left. \begin{aligned} \mathbf{L} &= (\mathbf{1} + \mathbf{S})^{-1/2}, \\ S_{\alpha\beta} &= \int \phi_\alpha^*(\mathbf{x})\phi_\beta(\mathbf{x}) d\mathbf{x} - \delta_{\alpha\beta}. \end{aligned} \right\} \quad \dots\dots (4)$$

In terms of the set  $\Phi$ , equation (2) becomes

$$\Psi = \Phi \mathbf{C}, \quad \mathbf{C}^\dagger \mathbf{C} = \mathbf{C} \mathbf{C}^\dagger = \mathbf{1}. \quad \dots\dots (5)$$

Using equation (5) in equation (1) our fundamental approximation is expressed as

$$\mathbf{C}^\dagger \mathbf{F} \mathbf{C} = \epsilon, \quad \dots\dots (6)$$

where  $\epsilon$  is a diagonal matrix, and the matrix  $\mathbf{F}$  has elements  $F_{\alpha\beta}$  defined by

$$F_{\alpha\beta} = H_{\alpha\beta} + 2 \sum_{k\gamma\delta} C_{k\gamma}^\dagger G_{\alpha\beta}^{\gamma\delta} C_{\delta k}, \quad \dots\dots (7)$$



where

$$\left. \begin{aligned} H_{\alpha\beta} &= \int \Phi_{\alpha}^*(\mathbf{x}) H \Phi_{\beta}(\mathbf{x}) d\mathbf{x}, \\ G_{\alpha\beta}^{\gamma\delta} &= \int [\Phi_{\alpha}^*(\mathbf{x}_1) \Phi_{\gamma}^*(\mathbf{x}_2) G \Phi_{\beta}(\mathbf{x}_1) \Phi_{\delta}(\mathbf{x}_2) \\ &\quad - \Phi_{\alpha}^*(\mathbf{x}_1) \Phi_{\gamma}^*(\mathbf{x}_2) G \Phi_{\delta}(\mathbf{x}_1) \Phi_{\beta}(\mathbf{x}_2)] d\mathbf{x}_1 d\mathbf{x}_2. \end{aligned} \right\} \dots\dots (8)$$

In equations (8),  $H$  is the Hamiltonian operator for an electron moving in the field of the ion cores, and  $G = 1/2|\mathbf{r}_1 - \mathbf{r}_2|$ .

Let  $F(\alpha, \beta)$  stand for the submatrix consisting of all elements of  $F$  formed between the atomic spin-orbitals centred on the ions at  $\alpha$  and  $\beta$ . Let  $\mathbf{B}$  be a unitary matrix which transforms  $\mathbf{F}$  to a new matrix  $\epsilon'$ , where

$$\epsilon' = \mathbf{B}^{\dagger} \mathbf{F} \mathbf{B}, \quad \dots\dots (9)$$

and let  $\mathbf{B}$  be chosen such that the submatrices  $\epsilon'(\mu, \mathbf{m})$  and  $\epsilon'(\mathbf{m}, \mu)$  are null matrices. The matrix  $\mathbf{B}$  defines a set  $\chi$  of orthonormal atomic spin-orbitals according to

$$\chi = \Phi \mathbf{B}, \quad \dots\dots (10)$$

and  $\epsilon'$  is the Fock energy matrix in the  $\chi$  representation. In terms of the set  $\chi$  we have

$$\psi = \chi \mathbf{V}, \quad \dots\dots (11)$$

where  $\mathbf{V}$  is a unitary matrix. Using our full notation, the wave functions for the occupied states are given by

$$\psi_p(\mathbf{x}, \mathbf{k}) = \sum_{q\mu} \chi_q(\mathbf{x}, \mu) V_{qp}(\mu, \mathbf{k}),$$

and this shows that the wave functions for the valence band can be expressed in terms of the atomic orbitals  $\chi_p(\mathbf{x}, \mu)$  centred on the halide ions. In a similar way, the orbitals  $\chi_p(\mathbf{x}, \mathbf{m})$  centred on the metal ions provide a basis for treating the conduction band. This property of the set  $\chi$  was used in I to calculate the lattice energy. To discuss the electronic structure we need to know more about the matrix  $\mathbf{V}$  in equation (11).

$\mathbf{V}$  is the unitary matrix which reduces  $\epsilon'$  to diagonal form with the eigenvalues  $\epsilon_p(\mathbf{k})$  of equation (1) on the diagonal. Thus

$$\epsilon = \mathbf{V}^{\dagger} \epsilon' \mathbf{V}. \quad \dots\dots (12)$$

To find the eigenvalues we first construct the Bloch functions

$$\eta_p(\mathbf{r}, \mathbf{k}) = N^{-1/2} \sum_{\mu} \chi_p(\mathbf{r}, \mu) \exp(2\pi i \mu \cdot \mathbf{k}),$$

where  $\mathbf{k}$  is a vector in the reciprocal lattice. Then

$$\psi_p(\mathbf{x}, \mathbf{k}) = \sum_q \eta_q(\mathbf{x}, \mathbf{k}) U_{qp}(\mathbf{k}), \quad \dots\dots (13)$$

where

$$U_{qp}(\mathbf{k}) = N^{1/2} \exp(-2\pi i \mathbf{k} \cdot \mu) V_{qp}(\mu, \mathbf{k}). \quad \dots\dots (14)$$

Either by using equation (14) in equation (12) or equation (13) in equation (1), we arrive at the secular equation

$$\det |\mathcal{E}_{pq}(\mathbf{k}) - \delta_{pq} \epsilon(\mathbf{k})| = 0 \quad \dots\dots (15)$$

for the eigenvalues  $\epsilon_p(\mathbf{k})$ . In equation (15)

$$\left. \begin{aligned} \mathcal{E}_{pq}(\mathbf{k}) &= \int \eta_p^*(\mathbf{x}, \mathbf{k}) F_{\text{op}} \eta_q(\mathbf{x}, \mathbf{k}) d\mathbf{x}, \\ &= \epsilon_{pq}'(\mu, \mu) + \sum_{\lambda} \epsilon_{pq}'(\mu, \mu + \lambda) \exp(2\pi i \lambda \cdot \mathbf{k}), \end{aligned} \right\} \dots\dots(16)$$

where  $\lambda$  is a vector which maps out the halide ion lattice from an arbitrarily chosen halide ion at  $\mu$ . Equations (15) and (16) show that the structure of the valence band is determined by the elements  $\epsilon_{pq}'(\mu, \nu)$  of the matrix  $\epsilon'$ . We can show in a similar way that the elements  $\epsilon_{pq}'(\mathbf{m}, \mathbf{n})$  determine the structure of the conduction band.

### § 3. THE MATRIX $\epsilon'$ IN SECOND ORDER

The matrix  $\epsilon'$  is obtained in second order from equation (9) by treating all non-diagonal elements of  $\mathbf{F}$  as first-order small quantities and applying perturbation theory. The results can be written in terms of the matrix elements defined in equation (8) and the matrix  $\mathbf{R}$  with elements  $R_{\alpha\beta}$  defined by

$$R_{\alpha\beta} = \sum_{\nu} B_{\alpha\nu} B_{\nu\beta}^{\dagger}.$$

$\mathbf{R}$  is the charge- and bond-order matrix corresponding to the orthonormal spin-orbitals  $\Phi$ . For convenience we define a new matrix  $\mathbf{P}$  with elements  $P_{\mu\mu}$ ,  $P_{m\mu}$  and  $P_{mn}$  the same as the corresponding elements of  $\mathbf{R}$ , but with  $P_{\mu\nu} = \delta_{\mu\nu} - R_{\mu\nu}$ .  $\mathbf{P}$  represents the homopolar contribution to the charge- and bond-order matrix  $\mathbf{R}$ , and would be a null matrix if we could neglect the sharing of the outer electrons from the halide ions with the surrounding metal ions (see I). In terms of  $\mathbf{P}$  we find that, in second order

$$\begin{aligned} \epsilon_{\mu\nu}' &= K_{\mu\nu} - 2G_{\mu\nu}^{\nu\mu} P_{\mu\nu} - 2 \sum_m G_{\mu\nu}^{m\mu} P_{\mu m} - 2 \sum_m G_{\mu\nu}^{\nu m} P_{m\nu} \\ &\quad + \sum_m P_{\mu m} P_{m\nu} (K_{\mu\mu} - K_{mm}), \end{aligned} \dots\dots(17)$$

where

$$K_{\alpha\beta} = H_{\alpha\beta} + 2 \sum_{\nu} G_{\alpha\beta}^{\nu\nu}. \dots\dots(18)$$

For numerical calculations it is more convenient to express the right-hand side of equation (17) in terms of matrix elements formed with the given non-orthogonal spin-orbitals  $\varphi$ , and the corresponding charge- and bond-order matrix  $\mathcal{R}$  whose elements  $\mathcal{R}_{\alpha\beta}$  are defined by

$$\mathcal{R}_{\alpha\beta} = \sum_{\nu} \mathcal{B}_{\alpha\nu} \mathcal{B}_{\nu\beta}^{\dagger}, \quad \mathcal{B}_{\alpha\beta} = \sum_{\gamma} L_{\alpha\gamma} B_{\gamma\beta}.$$

Again we can separate from  $\mathcal{R}$  a new matrix  $\mathcal{P}$  representing the homopolar contribution. Its elements  $\mathcal{P}_{\mu\mu}$ ,  $\mathcal{P}_{m\mu}$  and  $\mathcal{P}_{mn}$  are the same as those of  $\mathcal{R}$ , but  $\mathcal{P}_{\mu\nu} = T_{\mu\nu} - \mathcal{R}_{\mu\nu}$ , where  $\mathbf{T} = (\mathbf{1} + \mathbf{S}_1)^{-1}$ , and  $\mathbf{S}_1$  is the submatrix of  $\mathbf{S}$  consisting of all elements of the form  $S_{\mu\nu}$ . In terms of these quantities equation (17) becomes

$$\left. \begin{aligned} \epsilon_{\mu\nu}' &= \mathcal{K}_{\mu\nu} - 2\mathcal{G}_{\mu\nu}^{\nu\mu} \mathcal{P}_{\mu\nu} - 2 \sum_m \mathcal{G}_{\mu\nu}^{m\mu} \mathcal{P}_{\mu m} - 2 \sum_m \mathcal{G}_{\mu\nu}^{\nu m} \mathcal{P}_{m\nu} \\ &\quad + \sum_m \mathcal{P}_{\mu m} \mathcal{P}_{m\nu} (\mathcal{K}_{\mu\mu} - \mathcal{K}_{mm}) + \mathcal{K}_{\mu\mu} \sum_{\lambda} S_{\mu\lambda} S_{\lambda\nu} - \sum_{\lambda} S_{\mu\lambda} \mathcal{K}_{\lambda\nu}, \end{aligned} \right\} \dots\dots(19)$$

where  $\mathcal{K}_{\alpha\beta}$  and  $\mathcal{G}_{\alpha\beta}^{\gamma\delta}$  stand for matrix elements like  $K_{\alpha\beta}$  and  $G_{\alpha\beta}^{\gamma\delta}$  in equations (18) and (8) but with the set  $\varphi$  replacing the set  $\Phi$ . The formulae of this section have been derived using a simplified model in which the crystal

is regarded as a system of  $6N$  electrons and  $2N$  ion cores. However, it is easy to include properly the effects of the neglected electrons. To do this, the index  $m$  in equation (19) must go over all inner orbitals on the metal ions as well as the normally vacant  $s$  orbitals. With this modification, equation (19) still gives  $\epsilon_{\mu\nu}'$  in second order, and the structure of the valence band is determined by these elements according to equations (15) and (16).

#### § 4. THE BAND STRUCTURE

The structure of the valence band is determined by the roots of the secular equation (15). This is a sixth-order equation because, so far, we have used one-electron functions depending on both space and spin coordinates. However, because of the orthogonality of the two spin functions involved, the equation factorizes into the product of two third-order equations, one for each spin function. Thus, it will be understood henceforth that the indices  $p$  and  $q$  in  $\epsilon_{pq}'(\mu, \nu)$  go only over the space parts of the atomic orbitals centred on the ions at  $\mu$  and  $\nu$ .

We now classify the various terms on the right in equation (19) according to their 'order of neighbourhood'. Thus, terms are classed as first order, second order, etc., according as they depend upon the overlap between a pair of orbitals of the set  $\phi$  which are centred on ions which are respectively nearest neighbours, second neighbours, etc., in the crystal lattice. In this classification,  $\mathcal{P}_{\mu\mu}$  is at the most a first-order quantity,  $\mathcal{K}_{\mu\nu}$ ,  $\mathcal{P}_{\mu\nu}$  and  $S_{\mu\nu}$  are at the most second order for  $\mu \neq \nu$  whilst  $\mathcal{G}_{\mu\nu}^{vm}$  is at the most third order for  $\mu \neq \nu$ . It will be assumed henceforth that terms on the right in equation (19), of order higher than the second in this order of neighbourhood classification, may be ignored. All elements  $\epsilon_{pq}'(\mu, \nu)$  for which the halide ions at  $\mu$  and  $\nu$  are further away than second neighbours in the halide ion lattice are zero in this approximation.

The space parts of the orbitals  $\phi_p(\mathbf{x}, \mu)$  have the form  $xf(\mathbf{r}-\mu)$ ,  $yf(\mathbf{r}-\mu)$  or  $zf(\mathbf{r}-\mu)$ , and with the axes of quantization orientated to point towards the nearest metal ions, we can express all non-vanishing elements  $\epsilon_{pq}'(\mu, \mu+\lambda)$  in terms of five quantities. Thus

$$\left. \begin{aligned} \epsilon_{xx}'(\mu, \mu) &= \epsilon_{yy}'(\mu, \mu) = \epsilon_{zz}'(\mu, \mu) = A_0, \\ \epsilon_{xx}'(\mu, \mu+\lambda) &= \epsilon_{yy}'(\mu, \mu+\lambda) = A_1, & \lambda &= (r_0, r_0, 0), \\ \epsilon_{zz}'(\mu, \mu+\lambda) &= A_1', & \lambda &= (r_0, r_0, 0), \\ \epsilon_{xy}'(\mu, \mu+\lambda) &= A_1'', & \lambda &= (r_0, r_0, 0), \\ \epsilon_{xx}'(\mu, \mu+\lambda) &= A_2, & \lambda &= (2r_0, 0, 0). \end{aligned} \right\} \dots\dots (20)$$

Here  $r_0$  is the cation-anion distance. Using equations (20) in equation (16) we now have

$$\left. \begin{aligned} \mathcal{E}_{xx}(\mathbf{k}) &= A_0 + 4A_1(\cos 2\pi r_0 k_x \cos 2\pi r_0 k_y + \cos 2\pi r_0 k_x \cos 2\pi r_0 k_z) \\ &\quad + 4A_1' \cos 2\pi r_0 k_y \cos 2\pi r_0 k_z + 2A_2 \cos 4\pi r_0 k_x, \\ \mathcal{E}_{xy}(\mathbf{k}) &= -4A_1'' \sin 2\pi r_0 k_x \sin 2\pi r_0 k_y, \end{aligned} \right\} \dots\dots (21)$$

and the other elements follow from (21) by interchanging  $x$ ,  $y$  and  $z$ . The secular equation (15) is easily solved for several prominent directions in  $\mathbf{k}$ -space.

(100) direction,  $\mathbf{k} = (k, 0, 0)$ . There is a non-degenerate and a two-fold degenerate band,

$$\left. \begin{aligned} \epsilon(\mathbf{k}) &= \epsilon_0 - 16A_1 \sin^2 \pi r_0 k - 4A_2 \sin^2 2\pi r_0 k && \text{(non-degenerate),} \\ \epsilon(\mathbf{k}) &= \epsilon_0 - 8(A_1 + A_1') \sin^2 2\pi r_0 k && \text{(two-fold),} \end{aligned} \right\} \dots\dots (22)$$

where  $\epsilon_0 = A_0 + 8A_1 + 4A_1' + 2A_2$ . The end point of the first Brillouin zone is at  $k = 1/2r_0$ .

(111) direction,  $\mathbf{k} = (k, k, k)$ . There is a non-degenerate and a two-fold degenerate band,

$$\left. \begin{aligned} \epsilon(\mathbf{k}) &= \epsilon_0 - 4(2A_1 + A_1' + 2A_1'' + A_2) \sin^2 2\pi r_0 k && \text{(non-degenerate),} \\ \epsilon(\mathbf{k}) &= \epsilon_0 - 4(2A_1 + A_1' - A_1'' + A_2) \sin^2 2\pi r_0 k && \text{(two-fold).} \end{aligned} \right\} \dots\dots (23)$$

The end point is at  $k = 1/4r_0$ .

(110) direction,  $\mathbf{k} = (k, k, 0)$ . The degeneracy is removed,

$$\left. \begin{aligned} \epsilon(\mathbf{k}) &= \epsilon_0 - 16A_1 \sin^2 \pi r_0 k - 4A_1' \sin^2 2\pi r_0 k, \\ \epsilon(\mathbf{k}) &= \epsilon_0 - 8(A_1 + A_1') \sin^2 \pi r_0 k - 4(A_1 - A_1'' + A_2) \sin^2 2\pi r_0 k, \\ \epsilon(\mathbf{k}) &= \epsilon_0 - 8(A_1 + A_1') \sin^2 \pi r_0 k - 4(A_1 + A_1'' + A_2) \sin^2 2\pi r_0 k, \end{aligned} \right\} \dots\dots (24)$$

and the end point is at  $k = 3/8r_0$ .

We note at this stage that  $A_2$  in equations (22)–(24) is only finite in second order because of the terms involving the matrix  $\mathcal{P}$  on the right-hand side of equation (19).  $A_2$  would be zero if homopolar effects could be neglected, and its actual magnitude will therefore be a measure of the importance of homopolar effects in determining the band structure. The other quantities which involve  $\mathcal{P}$ , namely  $A_0$  and  $A_1''$ , are finite in second order even in the 'ionic approximation' when  $\mathcal{P}$  is a null matrix. Hence, the main homopolar effect is the introduction of a coupling in second order between ions which are actually fourth nearest neighbours in the lattice. This coupling would be a fourth-order effect in the ionic approximation.

## § 5. NUMERICAL RESULTS

We take for the basic set  $\varphi$  of atomic orbitals, the solutions of the Hartree–Fock equations for the free halide ions and metal atoms. In terms of this set

$$\begin{aligned} A_0 &= \lambda_\mu + (6 - \alpha_M)/r_0 + (\mu|V^{\text{nn}\mu}|\mu) + 2|\mathcal{P}_{m\mu}|^2(\lambda_\mu - \lambda_m - 2\alpha_M/r_0), \\ A_2 &= -(1/2r_0)(|\mathcal{P}_{m\mu}|^2 - 2|\mathcal{P}_{m\mu}||S_{m\mu}|) - |\mathcal{P}_{m\mu}|^2(\lambda_\mu - \lambda_m - 2\alpha_M/r_0), \end{aligned}$$

where  $\alpha_M$  is Madelung's constant ( $\alpha_M = 1.7476$  for LiF), and  $\lambda_\mu$  and  $\lambda_m$  are the Hartree–Fock energy parameters for the halide ion 2p orbital and the metal atom 2s orbital respectively.  $V^{\text{nn}\mu}$  is the potential energy of an electron in the Coulomb field of point positive charges at the positions of the six  $\text{Li}^+$  ions which are the nearest neighbours of the halide ion at  $\mu$ .  $m$  and  $\mu$  are nearest neighbours in the lattice.

According to equations (20),  $A_1$ ,  $A_1'$  and  $A_1''$  all involve matrix elements  $\mathcal{H}_{\mu\nu}$  for a pair of ions which are nearest neighbours in the halide ion lattice. From its definition we easily prove that

$$\mathcal{H}_{\mu\nu} = 2\lambda_\mu S_{\mu\nu} - (\mu|T|\nu) + (\mu|V^{(\mu\nu)}|\nu),$$

where  $T$  is the usual kinetic energy operator and  $V^{(\mu\nu)}$  is the potential energy

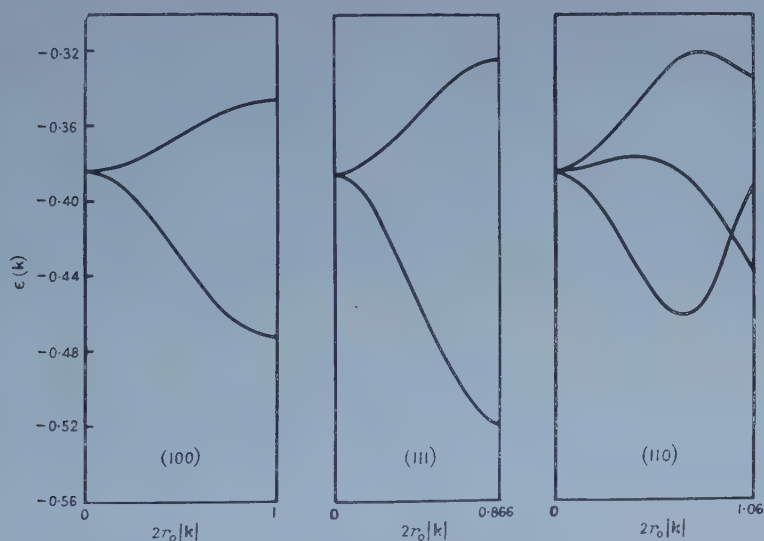


of an electron in the field of all ions in the lattice except those at  $\mu$  and  $\nu$ . Let  $g$  be the value of  $\mathcal{K}_{\mu\nu}$  for neighbouring halide ions  $\mu$  and  $\nu$  when the direction of maximum charge density for the orbitals and the direction of the line joining  $\mu$  and  $\nu$  coincide. Let  $g'$  be its value when these two directions are perpendicular. Thus we have a pair of  $2p\sigma$  orbitals for  $g$  and a pair of  $2p\pi$  orbitals for  $g'$ . All elements  $\mathcal{K}_{\mu\nu}$  can be expressed in terms of  $g$  and  $g'$ . In this way we find

$$A_1 = \frac{1}{2}(g + g'), \quad A_1' = g',$$

$$A_1'' = \frac{1}{2}(g - g') - (1/\sqrt{2}r_0)(|\mathcal{P}_{m\mu}|^2 - 2|\mathcal{P}_{m\mu}||S_{m\mu}|) - |\mathcal{P}_{m\mu}|^2(\lambda_\mu - \lambda_m - 2\alpha_M/r_0).$$

Again, the ions at  $m$  and  $\mu$  are nearest neighbours in the lattice.  $\mathcal{P}_{m\mu}$ ,  $S_{m\mu}$  and  $(\mu|V^{\text{nn}\mu}|\mu)$  have already been calculated for various values of  $r_0$  in connection with the work in I. The integrals  $S_{\mu\nu}$  and  $(\mu|T|\nu)$  were evaluated from the formulae given by Mulliken, Rieke, Orloff and Orloff (1949) and by Roothaan (1951).  $(\mu|V^{(\mu\nu)}|\nu)$  is a three-body potential and was neglected. For  $r_0 = 3.80$  atomic units (the observed distance in LiF) we found (in atomic units)  $A_0 = -0.3882$ ,  $A_1 = 0.00555$ ,  $A_1' = -0.0102$ ,  $A_1'' = 0.0165$ ,  $A_2 = 0.00052$ . In the ionic approximation ( $\mathcal{P}_{m\mu} = 0$ ),  $A_1$  and  $A_1'$  are unaltered but  $A_0 = -0.3872$ ,  $A_1'' = 0.0157$  and  $A_2 = 0$ . Evidently therefore, homopolar effects will play only minor part in determining the structure of the  $F^- 2p$  band. The band structure is shown in the figure.



$\epsilon(\mathbf{k})$  curves for the fluorine  $2p$  band in LiF along three prominent directions in  $\mathbf{k}$ -space. The upper curve in the (100) and (111) directions is double. In the (110) direction two of the curves cross to give a point of accidental degeneracy. The energy is expressed in atomic units.

## § 6. DISCUSSION

In the (100) and (111) directions, the curves of  $\epsilon(\mathbf{k})$  against  $|\mathbf{k}|$  are periodic in  $\mathbf{k}$ -space with the first Brillouin zone covered in one cycle. In the (110) direction, the zone boundary cuts off the  $\epsilon(\mathbf{k})$  curves before one cycle is completed. The energies corresponding to the missing portions of the curves occur again

with wave functions whose  $\mathbf{k}$ -vectors lie in other direction in  $\mathbf{k}$ -space and are contained in the first Brillouin zone. This situation is familiar from work in the ordinary tight-binding approximation.

In the (100) and (111) directions the upper (doubly degenerate) band is concave upwards. This is what the tight-binding approximation would lead one to expect (Seitz 1940, p. 307). On the other hand, Ewing and Seitz (1936), who attempted to construct directly a self-consistent field for the lattice, found all bands to be concave downwards in the (100) and (111) directions. No simple explanation of this discrepancy can be advanced.

The band width, according to the present calculations, is 5.4 eV whereas Ewing and Seitz (1936) found 2.3 eV. The soft x-ray emission spectrum of LiF has been investigated by O'Bryan and Skinner (1940) and the width of the emission band at half the maximum height is 2.7 eV. However, the justification for taking the half-width of the experimental curve as the actual band width is obscure. The actual shape of the emission curve indicates a band width of at least 5 eV, and this is in good agreement with the present calculations. In the (111) direction, homopolar terms alone, i.e. those involving  $\mathcal{P}_{m\mu}$ , would give a band width of 0.26 eV. This is about 5% of the total band width. It appears therefore, that improvements in the approximation are more likely to come from the inclusion of s, d, f, ... functions in the basic set of halide ion orbitals than from any more accurate discussion of the homopolar terms.

It has already been mentioned in §2 that the LCAO method also provides us with a set of functions  $\chi_p(\mathbf{x}, \mathbf{m})$  centred on the metal ions, which might be used as a basis for treating the conduction band. Closer investigation shows however that the problem of the conduction band is a rather difficult one. The trouble is that the overlap integrals amongst the basic set  $\phi(\mathbf{r}, \mathbf{m})$  of metal atom orbitals are so large ( $\sim 0.5$  for nearest neighbours) that it will be quite useless to use an 'order of neighbourhood' classification cut off at second-order terms. The situation in this respect is actually worse for the conduction band of LiF than it would be in a treatment of Li metal along the same lines, because the cation-cation distance in the salt is considerably less than the nearest neighbour distance in the metal.

## APPENDIX

The basic formulae of this paper have been derived using second-order perturbation theory, and the value of our results will depend on whether or not the perturbation series converges. In the calculation of the matrix  $\mathbf{L}$ , perturbation theory is equivalent to using the power series expansion

$$(\mathbf{1} + \mathbf{S})^{-1/2} = \mathbf{1} - \frac{1}{2}\mathbf{S} + \frac{3}{8}\mathbf{S}^2 - \dots$$

For neighbouring metal and halide ions, the submatrix  $S(\mathbf{m}, \mu)$  is

$$\begin{bmatrix} -0.2274 & 0 & 0 \end{bmatrix}$$

and for a pair of neighbouring halide ions  $S(\mu, \nu)$  is

$$\begin{bmatrix} -0.0279 & -0.0770 & 0 \\ -0.0770 & -0.0279 & 0 \\ 0 & 0 & 0.0491 \end{bmatrix}.$$

These elements are so large that the power series expansion is divergent. It

is also likely that perturbation theory leads to a divergent series for the matrix  $\epsilon'$ . The occurrence of these divergent expansions is a major obstacle in the application of the LCAO method to solids. This difficulty is well known but Lundqvist (1954) has obtained useful results for the lattice energy of LiH in spite of the divergent nature of the formulae used. It seems therefore that these divergent series might really have an asymptotic character (Löwdin 1956), and the results in this paper are presented with this possibility in mind.

## REFERENCES

- EWING, D. H., and SEITZ, F., 1936, *Phys. Rev.*, **50**, 760.  
FOCK, V., 1930, *Z. Phys.*, **61**, 126.  
GRIMLEY, T. B., 1957, *Proc. Phys. Soc. A*, **70**, 123.  
MULLIKEN, R. S., RIEKE, C. A., ORLOFF, D., and ORLOFF, H., 1949, *J. Chem. Phys.*, **17**, 1248.  
LÖWDIN, P.-O., 1950, *J. Chem. Phys.*, **18**, 365; 1956, *Advanc. Phys.*, **5**, 126.  
LUNDQVIST, S. O., 1954, *Ark. Fys.*, **8**, 177.  
O'BRYAN, H. M., and SKINNER, H. W. B., 1940, *Proc. Roy. Soc. A*, **176**, 229.  
ROOTHAAN, C. C. J., 1951, *J. Chem. Phys.*, **19**, 1445.  
SEITZ, F., 1940, *Modern Theory of Solids* (New York: McGraw-Hill).  
SHOCKLEY, W., 1936, *Phys. Rev.*, **50**, 754.

## Magnetic Effects on the Electron Diffraction Patterns from a Cobalt Crystal

By M. BLACKMAN AND E. GRÜNBAUM

Department of Physics, Imperial College, London

*MS. received 9th January 1958*

**Abstract.** Electron diffraction patterns taken on the prism face of a cobalt crystal showed a distortion due to the magnetic leakage field. The normal diffraction spots were replaced by a series of arcs. When the primary beam was moved parallel to the edge of the crystal, the distorted pattern changed with a period characteristic of the domain spacing. On heating the crystal, the magnitude of the distortion decreased, and became negligible at about 250°C.

### § 1. INTRODUCTION

IT was shown in previous work (Blackman and Grünbaum 1957 a) that some of the electron diffraction patterns obtained from an unmagnetized single crystal of hexagonal cobalt at room temperature appeared distorted. This was the case when the primary beam was incident at a grazing angle on the hexagonal face in any direction or on the prism face in the direction of the hexagonal axis. This distortion was due to the strong magnetic leakage field which existed close to the surface. This field was due to the magnetic domains, which have their longest axis parallel to the hexagonal axis, adjacent domains being of opposite polarity. The field was therefore periodic in a direction normal to the hexagonal axis.

The leakage field decreased with increasing temperature, becoming negligible at about 260°C (Scheidler 1955, Blackman and Grünbaum 1957 b). This was a consequence of the known decrease with temperature of the magnetic anisotropy, the crystal becoming isotropic between 250°C and 290°C (Bozorth 1951, Sucksmith and Thompson 1954). A decrease with temperature of the distortion of the diffraction pattern was therefore to be expected. Scheidler examined the hexagonal face of cobalt. He found no diffraction patterns at room temperature, but a pattern appeared at the isotropic temperature and above.

In the present work the prism face was studied, because the distorted diffraction patterns were much more clear-cut than on the hexagonal face. Two aspects of these patterns were examined. The first was the observation at room temperature of the changes in the patterns when the restricted primary beam was moved parallel to the crystal edge; the second was the study of the changes when the crystal was heated.

### § 2. EXPERIMENTAL DETAILS AND RESULTS

The crystal used was the same as in previous experiments (Blackman and Grünbaum 1957 a). This had been cut from a single crystal of hexagonal cobalt and a face ground parallel (within 1°) to a (10·0) plane. It had been electro-polished using the method of Elmore (1938).



The experimental arrangement employed was also the same as that described previously. In this arrangement, a conventional electron-diffraction camera with a hot filament gun and a magnetic focusing lens was used. The accelerating potential was 46 kv. The primary beam was limited by an aperture of diameter  $25\mu$ , which could be moved in a plane normal to the primary beam in directions parallel and perpendicular to the edge of the crystal face. The edge of the crystal face referred to here, and subsequently, is the one normal to the primary beam and nearest to the photographic plate.

The temperature of the crystal could be raised by a heater, designed by N. D. Lisgarten, consisting of a metal plate and a flat wire winding on mica. The temperature was measured by means of a thermocouple attached to the metal plate.

The primary beam, limited by an aperture of diameter  $25\mu$  and incident on the prism face in the direction of the hexagonal axis, produced a diffraction pattern consisting of arcs (figure 1, Plate I). These were arranged in a manner roughly corresponding to the normal hexagonal array of the (00.1) reciprocal lattice plane. In the present case the primary beam was incident on the face near the edge and the arcs were all convex in the same direction. The formation of the arcs is explained in terms of the deflection of the diffracted electrons by the leakage field at the edge of the crystal face (Blackman and Grünbaum 1957 a).

When the aperture was moved in a direction parallel to the edge of the crystal all the arcs were seen to rotate continuously. This is shown in figures 1 (a)–(d), obtained with the aperture moved in steps of  $30\mu$  parallel to the edge from left to right. The arcs in these four figures are produced by the diffracted electrons which are deflected by the magnetic field (a) to the right, (b) downwards, (c) to the left and (d) upwards. It can easily be deduced from the direction of the deflections that the electrons are passing over (a) a south pole, (b) a domain wall, (c) a north pole and (d) another domain wall. The periodic character of the magnetic field parallel to the crystal edge is thus clearly shown. The repeat distance of the deflections in a certain direction (e.g. to the right) is deduced from these figures as about  $120\mu$ . This corresponds to a domain width of about  $60\mu$ , which agrees with the values found in magnetic powder patterns.

When the crystal was heated above room temperature, the length of the arcs was found to decrease steadily. At about  $250^{\circ}\text{C}$  the arcs were reduced to spots, and this condition persisted above this temperature. The spots were elongated in a direction normal to the shadow edge, indicating a smooth electropolished surface. On cooling the crystal, the length of the arcs increased again. Figure 2 (a)–(c) (Plate II) shows the diffraction patterns obtained at three different temperatures. The distortion of the primary spot is also seen to decrease with temperature.

The steady decrease of the length of the diffraction arcs and of the distortion of the primary spot is consistent with the decrease of the leakage field found in previous work (Blackman and Grünbaum 1957 b, see also § 1). This is therefore a further proof that the distortion of the diffraction pattern is due to the magnetic leakage field.

#### ACKNOWLEDGMENTS

One of the authors (E. G.) is indebted to the British Council for a scholarship and grant, and to the University of Chile for leave of absence.

## REFERENCES

- BLACKMAN, M., and GRÜNBAUM, E., 1957 a, *Proc. Roy. Soc. A*, **241**, 508; 1957 b, *Nature, Lond.*, **180**, 1189.
- BOZORTH, R. M., 1951, *Ferromagnetism* (New York: van Nostrand).
- ELMORE, W. C., 1938, *Phys. Rev.*, **53**, 757.
- SCHEIDLER, G., 1955, *Arbeitstagung Festkörperphysik 1954 in Dresden* (Leipzig: Barth), pp. 181-5.
- SUCKSMITH, W., and THOMPSON, J. E., 1954, *Proc. Roy. Soc. A*, **225**, 362.

# On the Thermal and Optical Excitation of Colour Centres

By J. H. SIMPSON

National Research Council, Ottawa, Canada

*Communicated by H. Fröhlich; MS. received 11th December 1957*

**Abstract.** A method of calculating the ground state thermal dissociation energy and the electronic part of the optical (1s-2p) absorption energy of a colour centre in an ionic crystal is outlined. The electrostatic energy of interaction of the trapped electron and the lattice is determined by the summation of individual terms due to lattice charges and to dipoles induced at the lattice points. Polarizabilities of these dipoles can be determined readily from the results of Mott and Littleton for NaCl. The calculated thermal dissociation energy for this material is within 10% of the experimental value. A direct comparison with experiment for the optical absorption energy is not possible because of the relatively large lattice oscillator term which is not determined by the present method. A comparison with the results of Huang and Rhys for KBr indicates, however, that the electronic component of the absorption energy for NaCl here calculated is approximately correct.

## § 1. INTRODUCTION

THE theoretical study of the properties of colour centres, particularly the optical excitation process, has advanced considerably in recent years. The most complete investigation known to the writer is that of Huang and Rhys (1950) in which the interaction with the lattice vibrations during the optical (1s-2p) transition is taken into account on the assumption that the lattice may be treated as a continuum having a single optical mode whose frequency can be obtained from the experimentally determined infra-red dispersion frequency. This procedure is not entirely free from objection as Lax has pointed out (1952). It does, however, seem to be the only method at present capable of describing the main features of the F-centre absorption process with reasonable accuracy.

The expression obtained by Huang and Rhys for the peak of the optical absorption curve was

$$h\nu = E + p\hbar\omega_l + B(\bar{n} + \frac{1}{2}) \quad \dots\dots (1)$$

in which  $E$  is the energy of the electronic transition considered separately,  $p$  is the number of lattice vibrational quanta  $\hbar\omega_l$  involved in the transition at the absorption peak,  $\bar{n}(T)$  is the thermal average of the vibrational quantum number and  $B$  is a constant. The values of  $E$  and  $B$  were chosen to make the theoretical absorption curves fit those obtained experimentally for KBr by Mollwo (1933). Correspondence of theoretical and experimental absorption curves was obtained at all temperatures for the same values of  $E$  and  $B$ . The value of  $p$  at the maximum of the theoretical absorption curve is the same ( $\approx 20$  quanta for KBr) at all temperatures.

It is one of the purposes of the present paper to outline a method of obtaining  $E$  theoretically and to show that it can give a numerical result that is approximately correct. The procedure can also be adapted to the determination of the thermal dissociation energy of the colour centre thus yielding an additional result that can be compared with experiment.

## § 2. OUTLINE OF THE METHOD

The procedure used in the determination of the electron wave function and excitation energies (thermal and optical) is based on the Bloch collective electron model which, in its most complete form, may be specified as follows:

(a) The electron wave function shall be of the form  $\psi = f(r)g(r)$  where  $f(r)$  is a slowly varying function of the radius  $r$  measured from the position of the vacant lattice point and  $g(r)$ , which has the periodicity of the lattice, becomes the Bloch wave function at large  $r$ .

(b) The potential energy of the electron shall be determined by the summation of terms involving the interaction of the electron with the nuclei and electronic structures of the surrounding ions, taking into account displacements and distortions due to the field produced by the centre and to the interaction of the ions with each other.

In this complete form this model can probably account for all properties of a colour centre not dependent directly on lattice vibrations. The calculations required would be quite complicated, however, and simplifications, which depend on the property being investigated, are usually introduced. To account for the shape and width of microwave spin resonance lines, for instance, it is apparently sufficient to consider the magnitude of  $g$  at the nearest and next nearest neighbours of the centre (Dexter 1954, Krumhansl 1954).

In the calculation of the thermal dissociation energy and the electronic part of the optical excitation energy, it seems to be sufficiently accurate to use the function  $f(r)$  alone, and to average the effect of  $g(r)$  over a unit cell of the crystal by the use of an effective mass different from that of the free electron. Two approximations then arise depending on different treatments of the electrostatic interaction between electron and lattice. These may be called:

(1) The effective-mass continuum model. In this the trapping centre is treated as a positive charge in a spherical cavity in a continuous medium having the macroscopic dielectric properties of the crystal.

(2) The effective-mass lattice-sum model. In this the energy of interaction of the trapped electron with each ion of the lattice is calculated and the resulting terms summed over all lattice points. This model may be simplified by treating the ions as combinations of point charges and induced dipoles.

The continuum approximation has been applied to the calculation of the energy of the 1s-2p transition (Simpson 1949, Krumhansl and Schwartz 1953) and, on the assumption of an effective electron mass equal to that of the free electron, has given results in apparent agreement with experiment. In view of the results of Huang and Rhys (1950) and those of the present paper, the writer now believes that the energies determined using the continuum model were too large by a substantial amount. Difficulties arise in the application of this model to the calculation of the thermal ionization (dissociation) energy. For this case the radius of the cavity, as determined, for example, by the method



of Mott and Littleton (1938) should be different from that used in the calculation of the optical absorption since the surrounding ions move during the thermal process, but not during the optical one. Further, in the thermal calculation, the radius to be used in the determination of the energy of interaction of the trapped electron and the electronic structure of the surrounding ions should probably be different from that used in the calculation of the interaction with the central positive charge. These considerations show the simple continuum model to be a very artificial one, and make it necessary to resort to the more exact lattice-sum model. In the following sections, this model is used in the determination of the thermal dissociation energy and the electronic excitation energy involved in the optical process. The wave function of the electron is determined by a variational procedure equivalent to that used previously (Simpson 1949) although, as outlined below, the method of applying it is somewhat simpler.

The type of treatment used here has been called a 'static' one by Fröhlich (1954). It does not take account of the interaction of the electron with the lattice vibrations in the determination of the initial (1s) wave function and the thermal dissociation energy. A 'dynamic' calculation, which includes this interaction, has been done for a shallower type of trapping centre consisting of a positive point charge in a polarizable continuum (Simpson 1955) and the static treatment has been shown to give the same result for the alkali halides. It should apply *a fortiori* to colour centres in these materials.

### § 3. APPLICATION OF THE VARIATIONAL PROCEDURE

The usual method of determining the wave function in calculations of this type is a self-consistent one in which a potential initially chosen is used to determine the wave function and the latter is used to calculate a more exact form of the potential. The difference between the more exact form and that initially chosen is then often incorporated into the calculation by perturbation theory.

There are two ways in which the amount of labour involved in this process may be diminished. In the first, due to N. F. Mott, and used earlier (Simpson 1949), the initially chosen potential is of such a form that the first attempt at a solution can be made completely self-consistent. This method can be used to obtain the wave function and the component of optical excitation energy due to the trapped electron. The second method, due to H. Fröhlich (1953, 1954), is somewhat more general and gives the thermal dissociation energy in addition to the above. It consists in minimizing the total energy of the system: electron plus trapping centre plus lattice. In the static approximation, this total energy consists of the kinetic energy of the electron and potential energy equal to the smallest amount of energy to remove the electron from the centre. Together these constitute the thermal dissociation energy. The potential energy  $U$  can be determined quite readily by putting

$$U = - \frac{1}{4\pi} \int_{\text{vol}} \int \mathbf{E} \frac{d\mathbf{D}}{dt} dt d\tau \quad \dots\dots (2)$$

where the first integral is taken over all space and  $d\tau$  is the volume element. The electron is assumed to be in the centre at time zero and to have been removed at time  $t$ ;  $\mathbf{E}$  and  $\mathbf{D}$  are the total electric field and displacement vectors respectively. For the thermal transition here considered,  $t$  will be long enough so that the

surrounding ions can reorient themselves during the process while for an optical transition they will remain stationary. We now write

$$U = -\frac{1}{4\pi} \int_v \int_0^t (\mathbf{D}_m - 4\pi \mathbf{P}_m + \mathbf{D}_- - 4\pi \mathbf{P}_{i-} - 4\pi \mathbf{P}_{o-}) \left( \frac{d\mathbf{D}_m}{dt} + \frac{d\mathbf{D}_-}{dt} \right) dt d\tau \quad \dots\dots (3)$$

$$= \frac{1}{4\pi} \int_v (\mathbf{D}_m \mathbf{D}_- - 4\pi \mathbf{P}_m \mathbf{D}_-) d\tau + \int_v \int_0^t \mathbf{P}_{i-} \mathbf{D}_- dt d\tau + \int_v \int_0^t \mathbf{P}_{o-} \mathbf{D}_- dt d\tau \quad \dots\dots (4)$$

where  $\mathbf{D}_m$  and  $\mathbf{P}_m$  are the electric displacement and polarization produced by the trapping centre (note that  $d\mathbf{D}_m/dt=0$ ) and  $\mathbf{D}_-$  the electric displacement produced by the electron.  $\mathbf{P}_{i-}$ , the infra-red polarization produced by the electron arises from the displacement of the surrounding ions. It can respond only to the mean position of the trapped electron, i.e. to the charge density  $-e\psi^*\psi$  where  $\psi$  is the wave function of the electron.  $\mathbf{P}_{o-}$  the optical (ultra-violet) polarization produced by the electron results from the distortion of the electronic structure of the surrounding ions. It responds to the detailed motion of the trapped electron considered as a point charge.

If  $\phi_m$ ,  $\phi_i$  and  $\phi_o$  are the potentials corresponding to  $\mathbf{D}_m - 4\pi \mathbf{P}_m$ ,  $4\pi \mathbf{P}_{i-}$  and  $4\pi \mathbf{P}_{o-}$  respectively, and  $\rho = -e\psi^*\psi$ , the functional to be minimized becomes

$$\int \psi^* H \psi d\tau = -\frac{\hbar^2}{2m} \int \psi^* \nabla^2 \psi d\tau + \int \rho \phi_m d\tau + \frac{1}{2} \int \rho \phi_i d\tau + \frac{1}{2} \int \rho \phi_o d\tau. \quad \dots\dots (5)$$

In Fröhlich's method,  $\phi_i$  must be expressed in terms of the wave function  $\psi$  and equation (5) minimized with respect to the variable parameter contained in the wave function. The factors  $\frac{1}{2}$  in the last two terms arise because  $\phi_i$  and  $\phi_o$  vary as the electron moves out of the centre during a thermal excitation process.

For the case of an electron interacting with the lattice alone Fröhlich (1953, 1954) has shown that the above procedure gives the same wave function as the self-consistent method. The outline in the 1954 paper is considerably more complicated than that in the 1953 reference which uses the static method. The latter is not readily available and the argument used therein is outlined for the present case as follows.

The field due to the infra-red polarization is  $-4\pi \mathbf{P}_{i-} = -(1/\epsilon_\infty - 1/\epsilon) \mathbf{D}_-$  where  $\epsilon$  is the static dielectric constant and  $\epsilon_\infty$  the high-frequency (ultra-violet) dielectric constant. With  $\mathbf{D}_-$  expressed in terms of the wave function,  $\phi_i(r)$  becomes

$$\phi_i = e(1/\epsilon_\infty - 1/\epsilon) \int \frac{\psi^*(\mathbf{r}_1) \psi(\mathbf{r}_1) d\tau_1}{|\mathbf{r} - \mathbf{r}_1|}. \quad \dots\dots (6)$$

Substitution of this in (5) gives

$$\begin{aligned} \int \psi^* H \psi d\tau = & -\frac{\hbar^2}{2m} \int \psi^* \nabla^2 \psi d\tau - e \int \psi^* \psi \phi_m d\tau \\ & - \frac{e^2}{2} \left( \frac{1}{\epsilon_\infty} - \frac{1}{\epsilon} \right) \iint \frac{\psi^*(\mathbf{r}) \psi(\mathbf{r}) \psi^*(\mathbf{r}_1) \psi(\mathbf{r}_1) d\tau d\tau_1}{|\mathbf{r} - \mathbf{r}_1|} - \frac{e}{2} \int \psi^* \psi \phi_o d\tau. \quad \dots\dots (7) \end{aligned}$$

When  $\psi^*$  is varied using the Lagrange multiplier  $E$  to take care of normalization we obtain

$$-\frac{\hbar^2}{2m} \nabla^2 \psi - e\phi_m \psi - e\phi_i \psi - \frac{1}{2} e\phi_o \psi = E\psi. \quad \dots\dots (8)$$

Equations (6) and (8) taken together define the self-consistent procedure. The functional

$$\int \psi^* H_1 \psi d\tau = -\frac{\hbar^2}{2m} \int \psi^* \nabla^2 \psi d\tau + \int \rho \phi_m d\tau + \int \rho \phi_1 d\tau + \frac{1}{2} \int \rho \phi_0 d\tau \dots\dots (9)$$

derived from (8) on the assumption that  $\phi_1$  is independent of  $\psi$  is minimized and (6) is used to determine the accuracy of the potential function chosen.

It has thus been shown that the wave function  $\psi$  determined from equation (5) when  $\phi_1$  is expressed in terms of  $\psi$  is the same as that obtained using the self-consistent procedure defined by (6) and (9) with  $\phi_1$  held constant when (9) is solved. In view of the simplicity of the former procedure and the fact that it can be readily used to give both the thermal dissociation energy and the electronic component of the optical excitation energy, it will be used in this paper.

Once the wave function has been determined, substitution in equation (5) gives the thermal dissociation energy  $W$  relative to a potential energy zero outside of the crystal. The energy of the lowest level of the conduction band relative to this same energy zero may then be subtracted to give a thermal dissociation energy which may be compared with the experimental value. Substitution of the wave function in equation (9) gives an optical energy  $W_{1s}$  for the 1s state since during an optical transition the electrostatic potential  $\phi_1$  due to displacement of the ions cannot change.

The electronic wave function for the 2p optical state may also be obtained from (9) by a variational calculation. In this case,  $\phi_1$  is a constant and retains its value for the 1s case. The energy  $W_{2p(1s)}$  obtained from (9) using the 2p wave function has  $W_{1s}$  subtracted from it to give  $E$  that part of the energy of the optical absorption transition due to the electron.

#### § 4. CALCULATION OF THE ENERGY

In the detailed evaluation of (5) a hydrogen-like wave function will be used. This is not a particularly good approximation but earlier calculations (Simpson 1949, Gourary and Adrian 1957) indicate that it should give an energy within about 10% of the true value. It also simplifies the outline of the method of calculation.

We first consider the potential  $\phi_m$  produced by the charges and dipoles of the lattice when a negative ion is removed. The energy of interaction of electron and lattice charges is given, for a lattice of monovalent ions, in atomic units (Hartree 1928), by

$$U_1 = - \sum_{n,l} l \int \frac{\psi^* \psi}{r_1} r^2 \sin \theta d\theta d\phi dr \dots\dots (10)$$

where  $r_1 = (r^2 + n^2 a^2 - 2rna \cos \theta)^{1/2}$  is the distance of the electron from a lattice point at distance  $na$  from the centre.  $a$  is the nearest neighbour distance in a lattice of the NaCl type, and  $l$  is the number of ions, multiplied by the sign of their charge, at distance  $na$ . For  $l = +6, -12, +8, -6$ , etc.,  $n$  has the values 1,  $\sqrt{2}$ ,  $\sqrt{3}$ , 2 etc. It will be noted that the effective mass is implicitly contained in  $U_1$ , since the atomic unit of energy is  $me^4/\hbar^2$  where  $m$  is the effective mass of the electron.

Equation (10) can be readily evaluated for a lattice of point charges using spherical harmonics and a hydrogen-like wave function

$$\psi = (\lambda^3/\pi)^{1/2} \exp(-\lambda r).$$



The result is

$$U_1 = -\frac{1}{a} \sum_n \frac{l}{n} [1 - (1 + \frac{1}{2}x)e^{-x}] \quad \dots\dots (11)$$

$$= -\frac{\alpha_m}{a} + \frac{1}{a} \sum_n \frac{l}{n} (1 + \frac{1}{2}x)e^{-x} \quad \dots\dots (12)$$

where  $\alpha_m = 1.7476$  is the Madelung constant and  $x = 2\lambda an$ .

The energy of interaction of the electron with the dipoles produced when a negative ion is removed, can be evaluated in a similar manner giving

$$U_2 = \frac{1}{a} \sum_n \frac{M|l|}{n^4} [1 - e^{-x}(\frac{1}{2}x^2 + x + 1)] \quad \dots\dots (13)$$

$Ma^3$  is a modified polarizability used by Mott and Littleton (1938, p. 495) to take account of the fact that the dipole at a given lattice point is determined by the dipoles of all the other ions as well as the effective positive charge at the centre. For this term the dipoles are considered arising from both ionic and electronic polarizabilities. The Mott and Littleton (ML) 'first approximation', in which the first shell of (positive) ions is considered separately, is used. Thus there are separate  $M$  values for the first shell, for the remaining positive ions and for the negative ions. Point dipoles are assumed since, upon removal of an ion from the lattice, the field at the other lattice sites is accurately known while its value between the sites is much less readily determined.

The third integral of (5) leads to the expression

$$U_3 = -\frac{1}{2a} \sum_n \frac{P|l|}{n^4} [1 - e^{-x}(\frac{1}{2}x^2 + x + 1)]^2 \quad \dots\dots (14)$$

in which  $Pa^3$  is the ionic polarizability of the ion considered, modified by the displacements of the surrounding ions. For all ions but the first shell  $P$  is equal to  $(1/4\pi)(1/\epsilon_\infty - 1/\epsilon)$ . For the displacement of the first shell ions it is necessary to repeat the ML calculation using an assumed value for the wave function and to verify later that this assumed value is approximately correct. In practice, the displacement of the first shell ions must be determined when the effective positive charge and the electron are present together because of the non-linearity of the short range forces. Using the ML value for the displacement produced by the positive charge, it is then possible to determine the displacement produced by the electron cloud for use in the third term of (5).

In the fourth term of (5), the point dipole approximation is not a good one near a lattice point because of the rapid (fourth power) variation of the interaction energy with distance between the F-centre electron and the lattice point. For radii less than the conventional ionic radius the induced dipole is difficult to estimate but it must be considerably reduced. The procedure followed was, therefore, to treat the dipole induced by the electron as a point dipole for  $r_1 \leq r \leq \infty$  and to assume that there is zero interaction for  $0 \leq r \leq r_1$ , where  $r_1$ , a radius characteristic of the ion, is initially made equal to the conventional ionic radius. The fourth term of (5) then becomes

$$U_4 = -\lambda^3 a^2 \sum_n \frac{Q|l|}{n} \left[ \int_0^{x-y} \frac{(1+\omega)e^{-\omega} d\omega}{(x-\omega)^3} + \int_0^\infty \frac{(1+\omega)e^{-\omega} d\omega}{(x+\omega)^3} - \int_{x+y}^\infty \frac{(1+\omega)e^{-\omega} d\omega}{(\omega-x)^3} \right] \quad \dots\dots (15)$$



where  $y = 2\lambda r_i$ ,  $\omega = 2\lambda(na - r)$  and  $Qa^3$  is the electronic polarizability, as modified by the surrounding ions. For large distances between the electron and the dipole induced by it we may put  $Q = \alpha/\epsilon_\infty^2 a^3$  where  $\alpha$  is the polarizability of the type of ion concerned. For smaller distances, the interaction with the surrounding induced dipoles is more complicated but it will be tentatively assumed that the above expression applies for  $r_i \leq r \leq \infty$  where  $r$  is the distance of the electron from the ion considered.

The value of  $\lambda$  obtained by minimizing equation (5), when the above potential energy terms have been introduced, is used in (5) to give the energy  $W$ . The thermal dissociation energy is then  $W_T = W - X$  where  $X$ , the energy to remove an electron from the lowest conduction level of the crystal, is 0.5 ev for NaCl (Mott and Gurney 1940, 1948, p. 97). Substitution of the same value of  $\lambda$  in equation (9) gives an optical energy  $W_{1s}$  for the 1s state.

The optical excitation energy for the 2p state is also obtained from (9) by using the hydrogen-like wave functions

$$\psi_{2z} = Bre^{-\beta r} \cos \theta, \quad \psi_{2x} = Bre^{-\beta r} \sin \theta \cos \phi, \quad \psi_{2y} = Bre^{-\beta r} \sin \theta \sin \phi.$$

Applying the variational procedure in this case leads to a value of  $\beta$  and an optical energy  $W_{2p1s}$ . The 1s-2p optical absorption energy is then  $W_{2p1s} - W_{1s}$ .

### § 5. NUMERICAL RESULTS

Calculations using the wave functions of the preceding section have been completed for NaCl since the values of  $M$  and  $P$  for this material are readily obtained from the results of Mott and Littleton. The following results were obtained:

State	Parameter	Energy (ev)
1s Thermal	$\lambda = 0.320$	$W = -2.35$
1s Optical	$\lambda = 0.320$	$W_{1s} = -3.35$
2p(1s) Optical	$\beta = 0.353$	$W_{2p1s} = -1.58$
Thermal dissociation energy $W_T = 2.35 - 0.5 = 1.85$ ev		
Optical excitation energy $E = 3.35 - 1.58 = 1.77$ ev		

Mott and Gurney have determined (1940, p. 143) a value  $W_T = 1.87$  from Pohl's experimental results using a theoretical value for the energy  $W_0$  to create a lattice vacancy. With the experimental value of  $W_0$ , determined by Etzel and Maurer (1950), the experimental value is 1.95 ev. This may probably be taken as the more accurate value. Thus, if the effective mass of the electron is taken equal to that of a free electron, the theoretical value of  $W_T$  is about 5% smaller than the experimental value. Use of a more accurate wave function would probably increase the calculated energy by about 10% so that the theoretical and experimental values for the thermal dissociation energy are seen to be remarkably close to each other.

An exact comparison of the optical excitation energy with experiment cannot be made since  $E$  is only one component of the total given by equation (1). An estimate of the difference may, however, be made by considering the data on KBr mentioned in the paper of Huang and Rhys:  $E = 1.67$  ev,  $B = -0.1$  ev and  $p = 22$ . For NaCl  $\hbar\omega_l$  is about 0.03 ev and hence  $p\hbar\omega_l \simeq 0.7$  ev. The peak of the absorption would thus be at about 2.5 ev, which compares as favourably as can be expected with the experimental value of 2.7 ev.

## § 6. DISCUSSION

The initial results have indicated that, with some refinements, the method should give the thermal dissociation energy quite accurately. The most important refinement would certainly be the choice of a better but not necessarily very complicated wave function. The work of Gourary and Adrian (1957) has shown that the energy for the 1s state, using a simple hydrogen-like wave function, only differs by 10% from that with a complicated Bessel function. Further, their model which considers lattice point charges only in the initial variational calculation, probably emphasizes the difference between these wave functions to a greater extent than the present one. In view of this, a wave function of the form  $\psi = A(1 + \alpha r)e^{-\alpha r}$  would probably be suitable because in the continuum model (Simpson 1949) it gave a result about 7% lower than the hydrogen-like wave function.

A further improvement might result from refinements of the ML calculation. A suggestion by Brauer (1952) will be considered in future. A refinement of the ML calculation which was taken into account here was the reduction in effective charge discussed by Szigeti (1949, 1950). This led to changes of the order of 10% in  $M$ ,  $P$  and  $Q$ . The terms involving these constants tend to compensate each other and the changes in energy values to this effect were negligible.

A point which merits discussion in connection with the optical excitation is the magnitude of the factor  $p$  of Huang and Rhys. One would expect this to be equal to about 4, the value determined by them from earlier wave functions obtained by the present writer, whereas the value derived from experiment is 22.4. One may possibly account for this discrepancy in the following argument:

The removal of a negative ion from the lattice will introduce new low frequencies of vibration of the ions surrounding the vacant site. This is not taken into account in the model of Huang and Rhys. However, most of the interaction of the F-centre electron with the single lattice mode assumed by them must take place in the neighbourhood of the centre. Thus, in a rough approximation one would expect their characteristic frequency  $\omega_l$  to be reduced and, correspondingly, the factor  $p$  which is inversely proportional to  $\omega_l^3$ , to be increased. To fit the experimental curve it will be necessary, however, to increase the number of vibrational quanta involved, because of the reduction in  $\omega_l$ . A reduction of  $\omega_l$  by a factor of about 2 would probably produce a fit of the experimental data on KBr for a value of  $p$  calculated from the theoretical electronic wave functions.

Several references have been made above to the work of Gourary and Adrian, and it seems desirable at this point to compare their method with that used in the present paper. These authors circumvented some of the complications of the self-consistent procedure by confining their potential energy term to that produced by the point charges of the lattice and treating all other terms as perturbations. The assumption that the electronic structures of the surrounding ions respond to the average charge of the F-centre electron is implied in this procedure. As pointed out by Krumhansl and Schwartz (1953), however, one should consider, when forming the Hamiltonian, that the electronic dipoles can respond to the detailed motion of the electron. The latter assumption introduces a factor  $\frac{1}{2}$  in this term and the cancellation of effects due to the electron and the effective positive charge of the centre no longer applies. It is just this

cancellation which simplifies the Gourary-Adrian procedure and makes possible the direct application of the self-consistent method.

The other major difference between the method of Gourary and Adrian and that of the present paper concerns the use of the polarizabilities of the surrounding ions. In the present paper an attempt has been made, following Mott and Littleton to take account of the effect of the surrounding induced dipoles on the one under consideration. This has not been done in the method of Gourary and Adrian, and their approximation may consequently be somewhat poorer.

If the theory of the present paper is correct, the  $G$  and  $A$  optical energy is too large by about 0.5 eV and the thermal dissociation energy too large by about 1 eV. This difference seems to be chiefly due to the first of the above-mentioned effects.

Two factors, which should be mentioned in this discussion are the approximation used in obtaining  $U_4$  and the importance of short range (exchange) interaction between the F-centre electron and those of the surrounding ions. Intuitively one would expect the latter to be small because of the relatively large spread of the F-centre wave function. The former is quite a rough approximation but concerns a term which does not exceed about 20% of the final result. It is also found to be relatively insensitive to the value chosen for  $r_i$  if this is in the neighbourhood of the conventional ionic radius. Thus, while further investigation of the accuracy of both approximations is desirable, the errors introduced by them are probably not very large.

#### ACKNOWLEDGMENTS

The calculations of this paper required the summation of interaction terms for more than forty shells of ions. They were fortunately amenable to solution on the computer (Ferut) of the University of Toronto Computation Centre. The writer is indebted to N. R. Stewart and R. S. McCullough for programming parts of the problem and especially to Dr. J. F. Hart who set up the programming procedure and supervised it through all its stages.

#### REFERENCES

- BRAUER, P., 1952, *Z. Naturf.*, **7a**, 372.  
DEXTER, D. L., 1954, *Phys. Rev.*, **93**, 244.  
ETZEL, H. W., and MAURER, R. J., 1950, *J. Chem. Phys.*, **18**, 1003.  
FRÖHLICH, H., 1953, *Electrons in Crystals*: Lectures given at Purdue University during the Spring Semester of 1953; 1954, *Advanc. Phys.*, *Phil. Mag. Suppl.*, **3**, 325.  
GOURARY, B. S., and ADRIAN, F. J., 1957, *Phys. Rev.*, **105**, 1180.  
HARTREE, D. R., 1928, *Proc. Camb. Phil. Soc.*, **24**, 105.  
HUANG, K., and RHYS, A., 1950, *Proc. Roy. Soc. A*, **204**, 406.  
KRUMHANSL, J. A., 1954, *Phys. Rev.*, **93**, 245.  
KRUMHANSL, J. A., and SCHWARTZ, N., 1953, *Phys. Rev.*, **89**, 1154.  
LAX, M., 1952, *J. Chem. Phys.*, **20**, 1752.  
MOLLWO, Z., 1933, *Z. Phys.*, **85**, 56, 62.  
MOTT, N. F., and GURNEY, R. W., 1940, 1948. *Electronic Processes in Ionic Crystals* (Oxford: The Clarendon Press).  
MOTT, N. F., and LITTLETON, M. J., 1938, *Trans. Faraday Soc.*, **34**, 485, 495.  
SIMPSON, J. H., 1949, *Proc. Roy. Soc. A*, **197**, 269; 1955, *Ibid.*, **231**, 308.  
SZIGETI, B., 1949, *Trans. Faraday Soc.*, **45**, 155; 1950, *Proc. Roy. Soc. A*, **204**, 51.



## The Elastic Scattering of 380 MeV Protons by Protons I: At Angles Greater than 30° (c.m.)

By D. HARTING,<sup>†</sup> J. R. HOLT AND J. A. MOORE<sup>‡</sup>

Nuclear Physics Research Laboratory, University of Liverpool

*Communicated by Professor H. W. B. Skinner; MS. received 23rd December 1957*

**Abstract.** The proton-proton differential elastic scattering cross section at 380 MeV has been accurately measured over the angular range 30° to 90° (c.m.). Coincidences between scattered and recoil protons were counted, using targets of polyethylene and carbon, and the number of incident protons determined with a calibrated ionization chamber. At 90° the differential cross section is  $3.70 \pm 0.06$  mbnsterad<sup>-1</sup> and increases at smaller angles to a value 9% greater at 30°.

### § 1. INTRODUCTION

WITH the completion of the Liverpool 156 in. synchro-cyclotron a very clean and well focused beam of protons having an energy of 380 MeV became available. It was felt that this circumstance might favour an attempt to measure the differential proton-proton elastic scattering cross section with greater accuracy than is claimed for any of the previous measurements in this energy region.

The most precise measurements have been carried out at Berkeley, Chicago and Pittsburgh (see Sutton *et al.* 1955 for references) and at Moscow (Meščerjakov *et al.* 1956) with quoted accuracies not better than about  $\pm 5\%$ . One of the main sources of error arises in the determination of the number of protons passing through the target. The workers at Chicago used a very small intensity of protons and counted them with a counter telescope; the others made use of measurements with a Faraday cup to determine the charge carried by the beam. The Pittsburgh and Berkeley measurements are not independent since the former used an ionization chamber and related the ionization current to the proton beam passing through it by means of the comparison made at Berkeley between an ionization chamber and a Faraday cup. In the present investigation both direct counting of the beam and Faraday cup measurements were used in conjunction with an ionization chamber.

In the region of energies between 150 MeV and 400 MeV the angular distribution of the scattering in the centre-of-mass system is nearly isotropic between 30° and 90°. At an energy of about 450 MeV measurements at Pittsburgh, Moscow and Brookhaven (Smith *et al.* 1955) show an increasing cross section between 90° and 30°, the values given for the percentage increase ranging between 8 and 26. At higher energies the anisotropy increases rapidly. It is obvious that at 380 MeV measurements of high accuracy are needed to determine any departure from isotropy.

<sup>†</sup> Now at CERN, Geneva, Switzerland.

<sup>‡</sup> Now at Atomic Weapons Research Establishment, Aldermaston, Berks.



## § 2. EXPERIMENTAL DETAILS

The arrangement of the experiment is shown in figure 1. The external proton beam of the cyclotron is focused on to the target T and then passes through the ionization chamber I which is used as a monitor. Plastic scintillation counters (1, 2, 3) detect in coincidence the scattered and recoil protons from either a polyethylene or a carbon target.

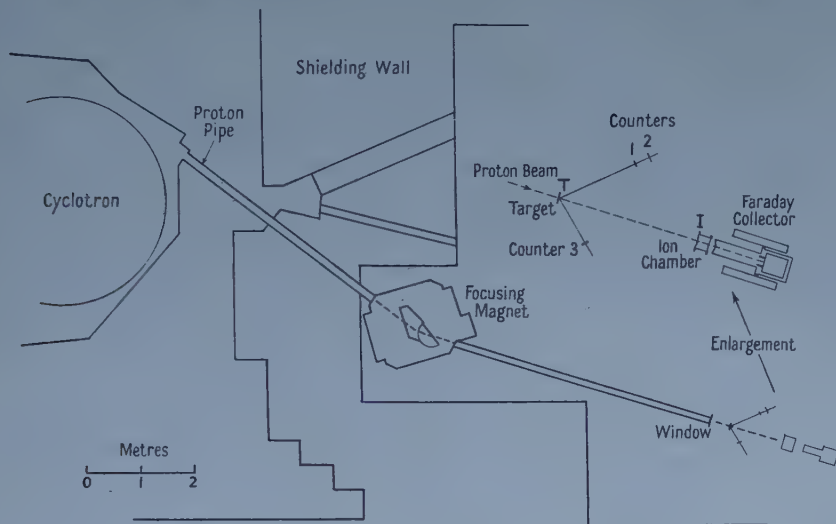


Figure 1. General experimental arrangement.

### 2.1. The Proton Beam

The proton beam, extracted by means of a regenerative magnetic deflector (Crewe and Gregory 1955), is deflected through an angle of  $20^\circ$  by a double focusing magnet of the type investigated by Cross (1951) and emerges into the air at a distance of about twenty feet from the magnet through a window of aluminium foil 0.05 mm in thickness. This method of extraction ensures that the proton beam is unpolarized.

The beam was defined at the cyclotron vacuum chamber by an aperture (6 mm  $\times$  9 mm) in a block of tungsten-copper alloy. This material has a high stopping power and a length of only 4 cm was used. A short length was desirable since the beam is divergent and also appreciably curved in this region. Protons passing through the walls of the aperture were reduced in energy by about 150 mev and removed from the beam by the bending magnet. No additional defining apertures were used and the cross section of the beam at the target was about 10 mm  $\times$  15 mm. From the range in copper the energy of the beam at the centre of the target was found to be  $380 \pm 2$  mev. The geometry of the magnet and the size of the beam at the target set a limit of 4 mev on the total energy spread and a limit of  $0.3^\circ$  on the total angular spread. A beam of  $10^9$  protons per second could be obtained through the above aperture but for the purpose of the present experiment this was reduced by a factor of about 100 by operating the cyclotron ion source with nitrogen and relying on stray hydrogen to provide the beam. The beam was found to be modulated in bursts about 30  $\mu$ sec in duration with the cyclotron repetition frequency of 110 per second.

## 2.2. Geometrical Arrangement

The polyethylene or carbon targets were rectangular sheets  $3.2 \text{ cm} \times 5.0 \text{ cm}$  held in light aluminium frames which could be slid into a holder at the centre of a turntable. The targets were placed at right angles to the beam except for the measurements at  $43^\circ$ ,  $36^\circ$  and  $30^\circ$  (c.m.) when they were placed at about  $45^\circ$  to reduce the energy lost by the recoil proton in emerging from the target. The scattered protons were defined by counter number 1 (figure 1),  $2.5 \text{ cm}$  square and  $0.5 \text{ cm}$  thick, placed about  $75 \text{ cm}$  from the target. Counter number 2,  $5.0 \text{ cm}$  by  $3.7 \text{ cm}$  and the same thickness as the first was mounted  $10 \text{ cm}$  behind it. On the other arm of the turntable counter number 3, the same size as number 2, was arranged to detect the recoil protons. Double coincidences (1, 3) and triple coincidences (1, 2, 3) were counted simultaneously.

In order to reduce the background counting rate from carbon the distance of counter number 3 was made as great as possible consistent with reliable counting of all the recoils. To check that no recoils were in fact being missed the p-p coincidence rate was measured as a function of the angle of the arm carrying the recoil detector (figure 2).

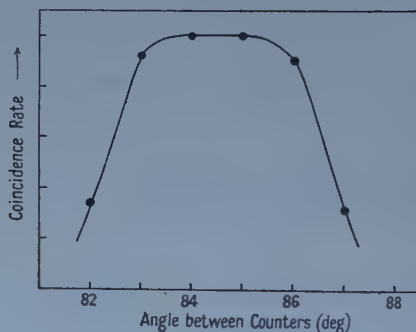


Figure 2. Coincidence rate as a function of angle between proton counters.

## 2.3. The Proton Beam Monitor

The number of protons passing through the target was measured with an air-filled ionization chamber placed about  $1 \text{ metre}$  beyond the centre of the turntable. This has entrance and exit windows  $10 \text{ cm}$  in diameter covered with aluminium foil  $0.03 \text{ mm}$  thick and contains seven parallel plate electrodes with similar windows covered with thin aluminium foil. It was designed so that the sensitive volume is well defined and contains no regions where the collecting field is weak. This is of some importance when calibrating the chamber with a  $\gamma$ -ray source. The length of the proton paths through the sensitive region is  $12.7 \text{ cm}$ . The chamber was filled with dry air at  $68 \text{ cm Hg}$  and  $20^\circ\text{C}$  and sealed off.

The voltage characteristic of the ion chamber with the proton beam passing through it was determined with the help of a Faraday cup beyond the chamber to monitor the beam. It was found that  $1900 \text{ volts}$  was adequate to produce saturation if the proton beam was less than  $10^8$  protons per second.

The current from the chamber was integrated by means of a circuit due to Lewis and Collinge (1953). The charge flowing into the integrator is measured

as a number of counts, each count corresponding in the present case to about  $7 \times 10^{-9}$  coulomb. The calibration of this ionization chamber and integrator is described below and was found to remain constant to better than 0.5% over a period of 6 months and to better than 0.2% over a day. However, in order to be independent of any drift or accident to the system regular checks were carried out with a 60 mc  $^{60}\text{Co}$   $\gamma$ -ray source placed in a standard position on the ionization chamber.

## 2.4. Electronics

The light pulses from the scintillators were detected with EMI 6260 photomultipliers. The pulses developed by the photomultipliers across a 300 ohm resistance were several volts high and of 70  $\mu\text{sec}$  duration. A pre-amplifier stage consisting of a single EFP 60 secondary emitter valve delivered the pulses into a clipping line which reduced their length to 40  $\mu\text{sec}$  and into a 130 ohm cable leading to the coincidence circuit which was of the type described by Garwin (1953). The output pulses, after linear amplification, were counted on a fast scaler having a dead time of 0.3  $\mu\text{sec}$ .

To check the overall performance of the electronic equipment and to determine the settings of the photomultiplier voltages and the bias levels of the scalers the counters were placed in line in a proton beam of very low intensity. The output pulses of the coincidence circuit were fed into a 60-channel pulse height analyser. Pulse height spectra of double or triple coincidences should then show a well defined peak. Figure 3 shows pulse height spectra obtained during actual runs with polyethylene and carbon targets.

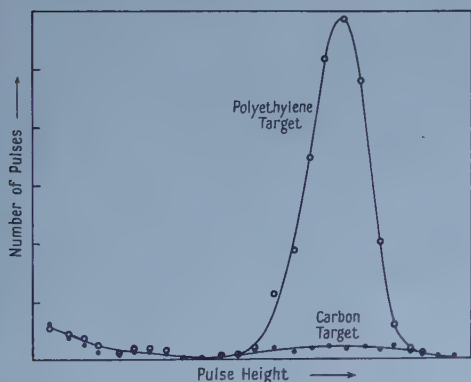


Figure 3. Pulse height spectrum from coincidence circuit with targets of polyethylene and carbon.

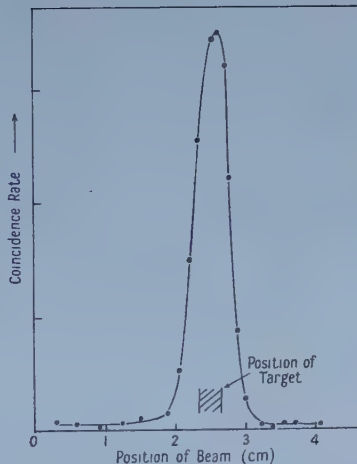


Figure 4. To illustrate the method of centring the beam by adjusting the current through the deflecting magnet.

## 2.5. Alignment of the Apparatus

Before starting a run a strip of polyethylene 3 mm wide was placed vertically in the position of the target, exactly over the centre of the turntable. The arms of the table were set at the angles corresponding to  $90^\circ$  in the centre-of-mass.

system and the current in the bending magnet was adjusted to give the maximum triple coincidence counting rate (figure 4). The centre of the beam then passed exactly over the centre of the turntable.

The polyethylene strip was then replaced by a steel pointer, pointing downwards, the tip being in the same horizontal plane as the centres of the scintillators. A second pointer, but pointing upwards, was mounted on a horizontal bar 50 cm beyond the first in the approximate direction of the beam. Two x-ray films, 10 cm behind each pointer, were simultaneously exposed to the proton beam. The first photograph showed the position of the beam relative to the target centre and could be used to adjust the height of the turntable. On the second photograph the shadows of both pointers appeared, fixing the direction of the beam to within 0.2 degree. The horizontal bar could then be moved exactly into the direction of the beam, and the turntable arms set at the desired angles with respect to this bar.

### § 3. CALIBRATION OF THE IONIZATION CHAMBER

#### 3.1. Faraday Cup Measurement

The Faraday cup consisted of a solid brass cylinder 18 cm in diameter and 18 cm long, with an extension on the front face in the form of a brass ring 12 cm in diameter and 10 cm long. This block was mounted in a vacuum chamber on polyethylene insulators. A second brass ring, placed in front of the extension on the block could be held at a negative potential with respect to the block. The proton beam entered the chamber through a window of copper foil 0.12 mm thick mounted on the end of an extension tube 50 cm long. A magnetic field of 100 oersteds perpendicular to the axis of the tube in the region of the brass rings served to turn back secondary electrons emitted from the block and the entrance window. A potential of several hundred volts applied between the rings had no effect on the charge collected by the cup when the magnetic field was on.

A proton beam of about  $10^7$  particles per second passed through the ionization chamber and into the Faraday cup. The charge collected by the cup flowed to a standard condenser, of which the other terminal was joined to a precision potentiometer. The latter was used to keep the cup at earth potential as indicated by a vibrating reed electrometer; then the charge collected was given in terms of the standard capacity and the potentiometer reading.

At the same time the charge from the ionization chamber was measured with the integrator, so that the number of protons  $N$  corresponding to 100 integrator counts could be found.

The standard  $^{60}\text{Co}$  source was then placed on the ionization chamber and the time for 100 integrator counts measured. This time was corrected for decay of the  $^{60}\text{Co}$  to give the value  $T$  corresponding to the strength of the source at some standard date, that is to say to a standard  $\gamma$ -emission.

The following results were obtained:

	$C$ (pF)	$\delta V$ (mv)	$N$	$T$ (sec)
(1)	1055.4	$631 \pm 2$	$4.15 \times 10^9$	716
(2)	1055.4	$630 \pm 8$	$4.14 \times 10^9$	714

$C$  is the capacity of the standard condenser,  $\delta V$  is the potential change across it corresponding to 100 counts of the integrator and  $N$  is the number of protons



calculated from  $C\delta V$ . There was an interval of six months between the two measurements, during which time the ionization chamber had been refilled. The first measurement of  $\delta V$  is the mean of four determinations and the second the mean of six determinations. The errors are the standard deviations obtained from the variations from the mean value in each case.

### 3.2. *Direct Counting of the Protons*

For this measurement the proton beam intensity was reduced to a few hundred per second by switching off the arc source of the cyclotron. The proton beam passed through two scintillation counters ( $3.8 \text{ cm} \times 5 \text{ cm}$ ) connected in coincidence and then through the ionization chamber mounted in its usual position beyond the turntable.

The current from the ionization chamber was of the order of  $10^{-13}$  amp when the beam was small enough to be counted with the scintillators. This current was too small for the integrator so the number of protons which would give 100 counts on the integrator was determined in two steps. First, the absolute charge collected from the ionization chamber when a certain number of protons passed through it was measured using the method which was applied to the Faraday cup. Then the absolute sensitivity of the integrator was determined by discharging into it, through a high resistance, a known capacity charged up to a known voltage. The final voltage across the condenser was measured with a meter in the integrator circuit, calibrated in terms of voltage at the input and this meter was also used to measure fractions of an integrator count. From these data the value of  $N$  could be got directly.  $T$  was found as usual by connecting the ionization chamber to the integrator and placing the standard  $^{60}\text{Co}$  source in position.

In order to determine accurately the number of protons corresponding to a given charge from the ionization chamber a correction had to be made for counting losses due to the dead time of the fast scaler. This was approximately  $0.3 \mu\text{sec}$ , and led to a loss of about 5% at a counting rate of 1000 per second. A large number of measurements were made at different beam intensities within the range 150 to 1200 per second in order that an extrapolation to zero counting rate could be made. From the counting loss formula it follows that  $1/m = a + bn$  where  $m$  is the multiplication factor of the ionization chamber determined with a counting rate of  $n$  per second and  $a$  and  $b$  are constants. In figure 5 the measured values of  $1/m$  are plotted against the counting rate. The spread of the points is due mainly to errors in the measurement with the reed electrometer of the charge from the ionization chamber. The background drift of this instrument was between 5% and 20% of the drift rate with the proton beam. This was determined before and after each run while the proton beam was stopped by raising a target inside the cyclotron tank. The mean of these two measurements, which usually differed by less than 2% of the measurement with the proton beam, was subtracted from the latter. Another possible cause of spread of the measured points is variation of the beam pulse-width, which would lead to changes in the counting loss.

A straight line was fitted to the points in figure 5 by the method of least squares. By extrapolation to zero counting rate the multiplication factor of the ionization chamber was found to be 1073 with a standard deviation of  $\pm 1\%$ . This figure

has to be increased by 0.7% to allow for the protons which are absorbed in the second scintillator of the counter telescope so that  $m = 1081 \pm 1\%$ .

The integrator sensitivity was  $7.050 \times 10^{-7}$  coulomb per 100 counts so  $N = 4.06 \times 10^9$  protons per 100 counts.  $T$  was found to be 715 seconds per 100 counts, the same as for the previous calibration.

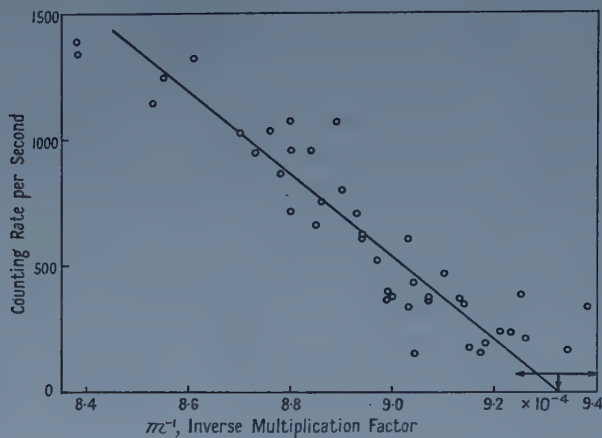


Figure 5. Method of correcting for counting loss in calibrating the ionisation chamber by direct counting of the proton beam.

### 3.3. Discussion of Results of Calibration

The values of  $N$  obtained by the two methods just described differ by 2%. This is a little greater than the estimated experimental errors and probably represents a real discrepancy. There are two effects which could cause such a discrepancy. There might be some recombination of ions in the ionization chamber with the large proton beam used in the comparison with the Faraday cup, but not with the very small beams used in the second case. The beam in the first case was about the same as that used in the scattering experiment and tests in which the voltage on the chamber was reduced by several hundred or the beam increased by a factor of 4 failed to produce any change greater than 1% in the ratio of the currents from the chamber and the Faraday cup.

The second effect concerns the Faraday cup. We feel that the geometrical arrangement and the magnetic field ensure that a negligible number of electrons enter or leave the front face of the block. However, about 50% of the protons make nuclear collisions in the block and the  $\gamma$ -radiation and neutrons so produced can eject electrons and protons from the whole surface of the block. It is possible that the number of these ejected particles might amount to 1 or 2% of the number of incident protons.

For the best value of  $N$  we take the mean of the two determinations and designate an error of 1.3%, i.e.  $4.10 \times 10^9 \pm 1.3\%$ .

The two values for the multiplication factor of the ionization chamber derived from the two experiments are  $1060 \pm 0.4\%$  and  $1081 \pm 1\%$ , with a mean value of  $1071 \pm 1.3\%$ . It is interesting to compare this value with one calculated from the results of Bakker and Segrè (1951) obtained at Berkeley with a similar ionization chamber. They find 33.3 ev for the energy required to produce one ion pair by 340 mev protons in air. The energy loss per centimetre of 380 mev

protons in air at the temperature and pressure at which our chamber was filled can be obtained from the range-energy curves of Rich and Madey (1954). Knowing the depth of the chamber one could calculate the number of ion pairs produced by each proton; this gave the value  $m=1131$ . This differs by 6% from our measured value.

The only explanation we can offer for this discrepancy is to suggest that the proton beam in the measurements of Bakker and Segrè contained a small proportion of heavily ionizing particles. The effect of even a small amount of material in the beam near the ionization chamber was demonstrated in our case by placing a brass plate 3 mm thick in front of the entrance window, when the ionization current increased by 5%.

The discrepancy need not cast doubt on the values of the absolute cross sections measured at Berkeley and Liverpool since in both places absolute calibrations of the ionization chambers were carried out. It does indicate that caution is necessary in attempting to derive an efficiency for an ionization chamber from published figures of the energy needed to produce an ion pair.

#### § 4. CALCULATION OF RESULTS

The number of triple coincidences (1, 2, 3) and the number of double coincidences (1, 3) corresponding to a certain number of counts on the beam integrator were measured simultaneously. This provided a useful continuous check on the operation of the electronic circuits, since, apart from certain small corrections, the results should agree.

The contribution of the carbon to the coincidence rate from the polyethylene was determined by making measurements with a carbon target having the same stopping power as that of polyethylene. This ensured that the probability for the escape of slow particles was the same in the two cases. The coincidence rate due to the carbon actually present in the polyethylene amounted to about 3% of the coincidence rate due to hydrogen. The rate with no target present was also measured.

The accidentals amounted to about 5% of the double coincidence rate with a polyethylene target and to about 2.5% of the triple coincidence rate. The number of accidentals was determined by introducing an extra length of cable into the lead from the recoil proton counter to produce a delay of 50 mμsec, equal to the separation of the proton beam pulses. Thus no genuine coincidences could be counted, whereas the accidental rate should be the same. Since the latter rate varies as the square of the beam intensity, a correction was made for small differences in the mean intensity of the beam during the runs with and without the delay cable.

Let  $C_p$ ,  $C_c$  and  $C_n$  be the number of coincidences with the polyethylene, carbon and no target for 100 counts of the beam integrator. Let  $A_p$ ,  $A_c$  and  $A_n$  be the corresponding numbers of accidental coincidences. The numbers of true coincidences  $T_p$ ,  $T_c$  and  $T_n$  are the differences of these. Then the number of coincidences due to p-p scattering events is  $C' = T_p - T_n - k(T_c - T_n)$ , where  $k$  is the ratio of the number of carbon atoms per unit area of the polyethylene and carbon targets.  $C'$  had to be corrected for absorption of the incident and scattered protons in the target, and in the case of the triple coincidence measurements, for the absorption of the scattered protons in counter number 1. These corrections were about 1% and led to a value  $C$  for the number of protons



scattered from the hydrogen in the target into the defining counter for 100 counts of the beam integrator. To correct for small errors in the centring and alignment of the beam all the measurements were repeated at the same angle on the opposite side of the beam. Table 1 shows the results of one complete run at  $90^\circ$  (c.m.). The total number of coincidences from polyethylene in each run was chosen to be about 10 000. The number of hydrogen atoms in the polyethylene target was calculated from the formula  $\text{CH}_2$  and we were assured by the manufacturers that the error in this should be less than 0.1%.

Table 1

Polyethylene target	$2.852 \times 10^{22}$ H atoms per $\text{cm}^2$
Carbon target	$2.032 \times 10^{22}$ C atoms per $\text{cm}^2$
Area of defining counter	$6.353 \text{ cm}^2$
Distance target centre to centre of defining counter	77.9 cm
Scattering angle	$90^\circ$ c.m. ( $42^\circ 20'$ lab.)
Proton beam intensity	$\sim 1.5 \times 10^7$ protons per second.

		$C_p$	$A_p$	$T_p$	$C_c$	$A_c$	$T_c$	$C_n$	$A_n$	$T_n$	$C'$	$C$	Error
(1)	Doubles	1484	93	1391	154	90	64	19	12	7	1344	1349	1.4%
	Triples	1408	31	1377	85	33	52	6	3	3	1340	1354	1.2%
(2)	Doubles	1481	77	1404	132	91	41	17	11	6	1373	1379	1.4%
	Triples	1418	34	1384	87	49	38	4	2	2	1356	1371	1.2%

(1) Defining counter to left of beam; (2) defining counter to right of beam.

The numbers are the coincidences per 100 integrator counts ( $4 \cdot 10 \times 10^9$  incident protons). The total numbers of integrator counts for this run were 700 for  $C_p$ , 200 for  $A_p$ ,  $C_c$  and  $A_c$  and 100 for  $C_n$  and  $A_n$ . The errors in the last column are the statistical standard deviations.

The main errors in the values of the differential cross sections are those due to counting statistics and the absolute calibration of the beam monitor. Since the latter is common to all angles the relative values of the differential cross sections are more accurately determined than are the absolute values. The relative values were first calculated in the form

$$\left( \frac{d\sigma}{d\Omega} \right)_{\theta(\text{c.m.})} \cdot N = \frac{J \cdot C}{\delta\Omega \cdot n} \cdot \frac{T}{T'},$$

where  $N$  is the proton calibration constant of the ionization chamber ( $N = 4 \cdot 10 \times 10^9$ ) and  $T$  the  $^{60}\text{Co}$  calibration associated with it ( $T = 715$  sec). The remaining quantities on the right of the equation are defined and displayed in table 2.

The results are shown in column (7) of the table where the errors are compounded of the statistical counting errors shown in column (6) together with the errors assigned to  $T'$ ,  $\delta\Omega$  and  $n$ ;  $T'$  was assigned an error of  $\pm 0.2\%$  from its short term reproducibility. The error in  $\delta\Omega$  is due to uncertainty in the area of the defining counter ( $\pm 0.2\%$ ), and in the effective distance from the target to the counter. This distance was measured between centres, but the finite thickness of the counter introduces an uncertainty in the plane of detection which was taken to be plus or minus one half the thickness. The net error in  $\delta\Omega$  was then  $\pm 0.4\%$ . The error in  $n$  ( $\pm 0.3\%$ ) is composed of a  $\pm 0.2\%$  error in the measurement of the target area and a similar error due to variation in target thickness.



Table 2

(1)	(2)	(3)	(4)	(5)	(6)	(7)	(8)
30°	0.2189	711.0	1.053	2.732(45°)	2163 ± 1.0%	1.655 ± 1.2%	1.092 ± 0.010
30°	0.2189	712.2	1.053	2.732(45°)	2187 ± 0.9%	1.671 ± 1.1%	
36°	0.2240	711.0	1.053	2.732(45°)	2123 ± 1.1%	1.662 ± 1.3%	
43°	0.2313	714.1	1.053	1.932	1452 ± 1.0%	1.653 ± 1.2%	1.082 ± 0.010
43°	0.2313	712.2	1.053	2.231(60°)	1661 ± 1.0%	1.642 ± 1.2%	
50°	0.2402	711.9	1.053	1.932	1342 ± 1.0%	1.592 ± 1.2%	
65°	0.2656	711.9	1.053	1.932	1188 ± 0.9%	1.558 ± 1.1%	1.045 ± 0.012
90°	0.3355	714.6	0.999	1.932	874 ± 1.1%	1.520 ± 1.3%	1.000 ± 0.006
90°	0.3355	713.8	1.051	1.932	919 ± 1.3%	1.521 ± 1.4%	
90°	0.3355	713.5	1.048	2.852	1345 ± 0.8%	1.513 ± 1.0%	
90°	0.3355	713.3	1.048	2.852	1364 ± 0.8%	1.535 ± 1.0%	

(1)  $\theta$  c.m.; (2) ratio of c.m. and lab. cross sections  $J$ ; (3) time in seconds for 100 integrator counts with standard  $^{60}\text{Co } T'$ ; (4) solid angle of detection ( $\times 10^3$  sterad),  $\delta\Omega$ ; (5) number  $n$  of protons in target per  $\text{cm}^2$  ( $\times 10^{22}$ ): the target angle is also indicated when other than  $90^\circ$ ; (6) corrected number of p-p coincidences per 100 integrator counts ( $C$ );

$$(7) \left( \frac{d\sigma}{d\Omega} \right)_{\theta \text{ (c.m.)}} N \times 10^{17}; (8) \left( \frac{d\sigma}{d\Omega} \right)_{\theta \text{ (c.m.)}} / \left( \frac{d\sigma}{d\Omega} \right)_{90^\circ \text{ (c.m.)}}$$

In the last column of table 2 the relative cross sections in the previous column have been averaged at each angle where necessary and expressed in terms of the cross section at  $90^\circ$ . The absolute cross section at  $90^\circ$  was obtained from the figures in column (7) after dividing by the value of  $N$  and suitably increasing the error. The result is,

$$\left( \frac{d\sigma}{d\Omega} \right)_{90^\circ \text{ (c.m.)}} = 3.70 \pm 0.06 \text{ mbn sterad}^{-1}.$$

Hess (1956), and Meščerjakov, Bogačev and Neganov (1956) and Taylor (1957) have summarized previous results for this cross section over a wide range of energies. In the region of our proton energy the following results for the differential cross section at  $90^\circ$  (in mbn sterad $^{-1}$ ) have been obtained.

Oxley and Schamberger (1952) find at 240 mev,  $3.54 \pm 0.4$ ; Chamberlain, Segrè and Wiegand (1951) find at 250 mev,  $3.68 \pm 0.2$  and at 345 mev,  $3.80 \pm 0.2$ ; Marshall, Marshall and Nedzel (1955) find at 419 mev,  $3.42 \pm 0.13$ ; Meščerjakov *et al.* (1956) find at 420 mev,  $3.3 \pm 0.2$  and Sutton *et al.* (1955) find at 437 mev,  $3.49 \pm 0.17$ . At higher energies the value decreases rapidly, being about  $2.0 \text{ mbn sterad}^{-1}$  at 650 mev. At lower energies there appears to be little change down to about 150 mev.

Our value is quite consistent with the above results. Between  $90^\circ$  and  $30^\circ$  we find, at our energy of 380 mev, an increase in differential cross section of 9%. In the following paper the investigation of this cross section at smaller angles is described.

#### ACKNOWLEDGMENTS

We wish to record our thanks to Professor H. W. B. Skinner for his close interest in this work and to the operating crew of the cyclotron for their willing co-operation. During their stay in Liverpool D. H. was the holder of a CERN Fellowship and J. A. M. received a grant from the Department of Scientific and Industrial Research.

## REFERENCES

- BAKKER, C. J., and SEGRÈ, E., 1951, *Phys. Rev.*, **81**, 489.  
CHAMBERLAIN, O., SEGRÈ, E., and WIEGAND, C., 1951, *Phys. Rev.*, **83**, 923.  
CREWE, A. V., and GREGORY, J. W. G., 1955, *Proc. Roy. Soc. A*, **232**, 242.  
CROSS, W. G., 1951, *Rev. Sci. Instrum.*, **22**, 717.  
GARWIN, R. L., 1953, *Rev. Sci. Instrum.*, **24**, 618.  
HESS, W. N., 1956, University of California UCRL-4639.  
LEWIS, I. A. D., and COLLINGE, B., 1953, *Rev. Sci. Instrum.*, **24**, 1113.  
MARSHALL, J., MARSHALL, L., and NEDZEL, V. A., 1955, *Phys. Rev.*, **98**, 1513.  
MEŠČERJAKOV, M. G., BOGAČEV, N. P., and NEGANOV, B. S., 1956, *Nuovo Cim., Suppl.*, **3**, 119.  
OXLEY, C. L., and SCHAMBERGER, R. D., 1952, *Phys. Rev.*, **85**, 416.  
RICH, M., and MADEY, R., 1954, University of California UCRL-2301.  
SMITH, L. W., McREYNOLDS, A. W., and SNOW, G., 1955, *Phys. Rev.*, **97**, 1186.  
SUTTON, R. B., FIELDS, T. H., KANE, J. A., MOTT, W. E., and STALLWOOD, R. A., 1955, *Phys. Rev.*, **97**, 783.  
TAYLOR, A. E., 1957, *Rep. Progr. Phys.*, **20**, 86 (London : Physical Society).

## The Elastic Scattering of 380 MeV Protons by Protons II: At Angles less than $30^\circ$ (c.m.)

By J. R. HOLT, J. C. KLUYVER† AND J. A. MOORE‡  
Nuclear Physics Research Laboratory, University of Liverpool

*Communicated by Professor H. W. B. Skinner; MS. received 23rd December 1957*

**Abstract.** Measurements on the proton-proton differential elastic scattering cross section at 380 MeV have been made within the angular range  $4^\circ$  to  $30^\circ$  (c.m.). A target of liquid hydrogen was used and a threshold Čerenkov counter was included in the detecting telescope to eliminate particles from inelastic processes. The total cross section for deuteron production was found to be  $0.57 \pm 0.08$  mbn.

### § 1. INTRODUCTION

IN continuation of the work described in the preceding paper (Harting, Holt and Moore 1958, to be referred to as I) we have extended the measurements of the p-p differential cross section at 380 MeV into the region of small angles. Previous measurements in this region where nuclear and coulomb scattering are of comparable magnitude have shown that there is destructive interference between the two processes (Chamberlain, Pettengill, Segrè and Wiegand 1954, Chamberlain and Garrison 1954, Fischer and Goldhaber 1954). Increased accuracy is desirable since a knowledge of the exact form of the variation of cross section with angle is of importance in the phase shift analysis of the nuclear scattering process.

Below an angle of about  $30^\circ$  (c.m.) it is no longer possible to use the polyethylene-carbon difference method with coincidence selection of the scattered and recoil protons because the energy of the latter becomes too small. A target of liquid hydrogen must be used and the scattered protons alone detected. It is then necessary, with incident protons of our energy, to discriminate against the products of inelastic processes, consisting of pions, deuterons and low energy protons. In previous work this has been accomplished with absorbers; in the present investigation we have been able to employ the selective properties of a simple type of Čerenkov detector.

### § 2. EXPERIMENTAL DETAILS

#### 2.1. Proton Beam and Target

In order to obtain sufficiently good angular resolution at small angles of scattering, where the cross section varies rapidly with angle, the proton beam at the target must be well defined in the plane of scattering and have small angular spread. The beam aperture and focusing magnet were the same as described in I, the most favourable shape of the beam at the target being obtained by adjusting the angle of the emergent pole-edge of the magnet. It was found

† Now at CERN, Geneva, Switzerland.

‡ Now at Atomic Weapons Research Establishment, Aldermaston, Berks.

possible to obtain a smaller spread vertically than horizontally and the best shape was  $0.8 \text{ cm} \times 3.5 \text{ cm}$ .

To make use of this the detecting telescope was mounted on a vertical table placed at a distance of either 4 m or 2 m from the target, depending on the angular range being investigated.

At small angles one of the chief experimental difficulties is the reduction of background counting. This is produced mainly in two ways. Stray protons travelling at the side of the main beam may enter the telescope directly or protons may be scattered into the telescope from the various windows and from any air through which the beam passes. These effects were minimized by a suitable arrangement of stops, by using thin windows and by replacing as much as possible of the air in the path of the beam by hydrogen.

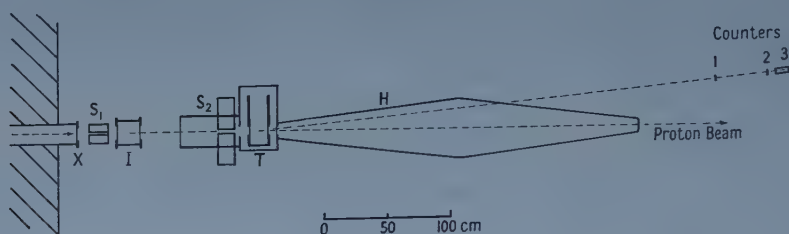


Figure 1. General arrangement of target and counters.

The general arrangement of the apparatus is shown in figure 1 and details of the liquid hydrogen target in figure 2. The target *T* was insulated with a double-walled box of foamed polystyrene, the liquid hydrogen being contained in an aluminium box *A* having windows of Mylar,  $0.05 \text{ mm}$  thick, cemented on with hot-setting Araldite. For the angular range  $6^\circ$  to  $14^\circ$  the box was  $10 \text{ cm}$  long and  $9 \text{ cm}$  wide; for angles less than  $6^\circ$  a box  $17 \text{ cm}$  long was used. The larger box increased the ratio of hydrogen scattering to background and did not seriously impair the angular resolution at these small angles.

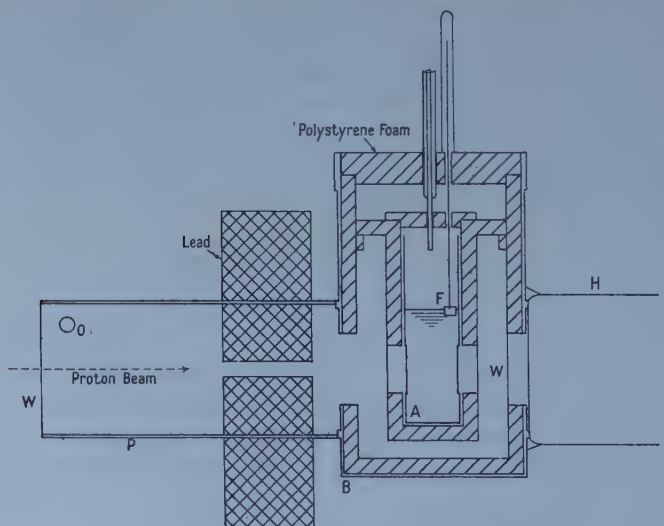


Figure 2. Liquid hydrogen target.



The loss rate of liquid hydrogen from the target was about 3 litres per hour. The escaping hydrogen gas circulated around the outside of the inner target box and then through an extension box P of Perspex to the exhaust pipe O. The seal between this box and the outer container B, which was of plywood, was made with adhesive tape and the outer lid of the target was sealed in the same way. The level of the liquid hydrogen could be determined with the help of the float F.

The windows W on the outer container were of polystyrene film 0.02 mm thick. The hydrogen bag H was held in contact with the exit window by adhesive tape to prevent ice collecting there; the entrance window was sufficiently far from the target box that the water condensed on it did not freeze.

The copper stop  $S_1$  (figure 1) had a rectangular aperture 1.2 cm high which was just sufficient to clear the beam; the lead stop  $S_2$  had an opening 2.5 cm high which just cleared the shadow, produced by stray protons, of the aperture  $S_1$ . These stops were positioned so that protons scattered from the window X, the stop  $S_1$  or the ionization chamber I could not reach the detecting telescope.

The beam was measured with the ionization chamber as described in I. An auxiliary monitor in the form of a double counter telescope at a large angle to the beam in the horizontal plane was also used.

## 2.2. The Proton Detector

Scattered protons were detected with a telescope of three counters used with a coincidence circuit of the Garwin type. Numbers 1 and 2 (figure 1), of plastic scintillator 0.5 cm thick, 2.5 cm  $\times$  3.7 cm and 1.25 cm diameter respectively, were separated by 40 cm. Counter number 2 was the defining counter; close behind it was a Čerenkov counter (number 3) consisting of a glass tube 10 cm

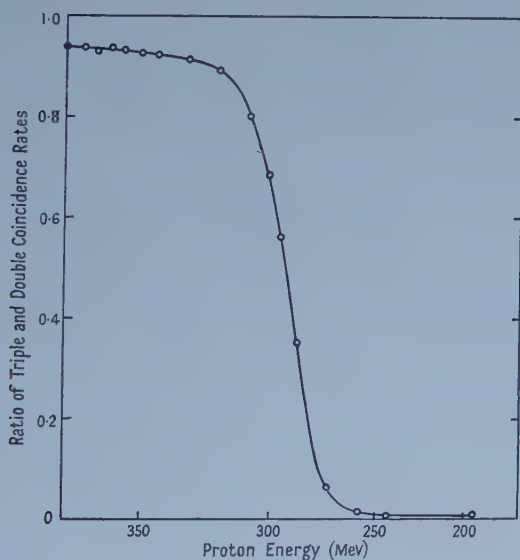


Figure 3. Efficiency of Čerenkov counter as a function of proton energy.

long and 3.5 cm in diameter, filled with carbon bisulphide, having one end in optical contact with a 2 in. diameter EMI 6260 photomultiplier. The refractive index of the carbon bisulphide is about 1.64, corresponding to a threshold for

production of Čerenkov radiation by particles with  $\beta$  equal to 0.61. This is the velocity of 250 mev protons, 500 mev deuterons and 35 mev pions. Thus the counter is not sensitive to the protons and deuterons from the reactions producing pions, but it responds to the great majority of the emitted pions.

However, the pions amount to less than 2.6% of the number of elastically scattered protons and a correction was made for them as described later. The deuterons are concentrated within a cone of semi-angle  $7.6^\circ$  and can amount to as much as 70% of the number of elastic protons.

The performance of the counter was investigated by placing it in the direct proton beam and varying the energy of the latter with carbon absorbers placed about 4 metres in front of the telescope. In figure 3 the ratio of the number of triple coincidences to the number of double coincidences in the first two counters is plotted as a function of the proton energy. It can be seen that the efficiency of the arrangement changes from 94% at full energy to less than 1% at energies below 250 mev.

### § 3. EXPERIMENTAL PROCEDURE

The apparatus was aligned with respect to the beam by exposing x-ray films behind the stops and behind pointers placed at the position of the centre of the target and at that of the defining counter. The height of the vertical table was finally set so that the zero of the angular scale was exactly at beam level by placing an aluminium scatterer at the target position and arranging that the counting rate was the same with the telescope at  $2^\circ$  above and  $2^\circ$  below the zero.

The efficiency of the counter telescope was checked in the direct beam and the target filled with liquid hydrogen through a double-walled glass syphon. Counting was then started at a given angle of the telescope, the number of doubles (1, 2) and triples being noted down at each multiple of 100 counts of the ionization chamber beam monitor.

After about 20 minutes the evaporation of the liquid hydrogen caused the liquid surface to fall below the level of the beam. Then the counting rate dropped abruptly and measurements were continued for a further period of about 12 minutes on the background.

The angle of the telescope was then altered, the target refilled and the procedure repeated. The calibration of the ionization chamber was checked with the standard  $^{60}\text{Co}$  source at the beginning and end of each day.

Measurements were made at intervals of  $0.5^\circ$  between  $2^\circ$  and  $8^\circ$  and at intervals of  $1^\circ$  between  $8^\circ$  and  $14^\circ$ . At all angles below  $11^\circ$  the telescope was positioned both above and below the beam and the two results always agreed within the statistical uncertainty.

The proton beam intensity was kept below about  $8 \times 10^7$  particles per second to avoid any correction for counting loss in the scaler, the counting rate then being always less than 50 per second. The background was about equal to the hydrogen effect at the smallest angles, decreasing to about 10% with increasing angle.

### § 4. CORRECTIONS

The largest correction which had to be made in calculating the differential cross section for elastic scattering was the allowance for pions produced in the reactions  $p + p \rightarrow \pi^+ + d$  and  $p + p \rightarrow \pi^+ + n + p$ . The cross sections for these reactions have not been measured at our energy, but we were able to derive

approximate values during the present experiment. The cross section for the reaction  $p + p \rightarrow \pi^0 + n + p$  is known to be much smaller.

The difference between the double coincidence rate (1, 2) and the triple rate, after backgrounds have been subtracted, is the rate due to deuterons and inelastically scattered protons from the hydrogen. In figure 4 this difference is plotted against angle. The deuteron component, with a sharp cut-off at about  $8^\circ$ , is very evident, the tail beyond this being due to protons. The latter are also expected to be concentrated in the forward direction (Rosenfeld 1954).

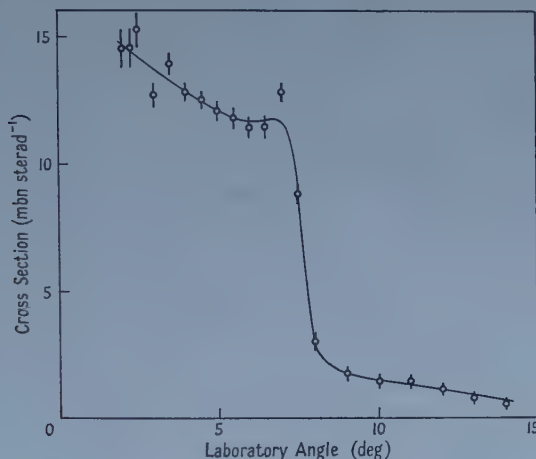


Figure 4. Differential cross section for production of deuterons and inelastic protons.

By extrapolating the tail to  $0^\circ$  and subtracting its contribution the total cross section for deuteron production was found to be  $0.57 \pm 0.08$  mbn, where the error includes an allowance for uncertainty in extrapolation. This value agrees well with the value (0.60 mbn) given by the formula  $0.2\eta + 0.83\eta^3$  ( $\eta$  is the c.m. pion momentum in units of  $\mu c$ ) which fits the measurements at neighbouring energies (Merrison 1956). By extrapolating the tail to larger angles and integrating the whole curve the total cross section for pion production was found to be of the order of 0.90 mbn. This accords with previous observations of Alston *et al.* (1956) that the cross section for producing protons and neutrons is rather less than that for deuteron production.

These workers also measured the angular distribution of the pions and found a form  $0.19 + \cos^2 \theta$  for both production reactions. Using this form and the above total cross section the correction to be applied to the triple coincidence count at each angle of the telescope was worked out. It had a maximum value of 2.6% at  $6^\circ$ .

Careful consideration was given to the problem of determining the effective number of protons in the target. The boiling of the liquid hydrogen means that its effective density is reduced, but a crude estimate indicated that the reduction should be smaller than 1%. During the background measurements the target contains gaseous hydrogen at some temperature near to that of the liquid; the counting rate of the large-angle monitor telescope, in which other sources of background were small, indicated a mean contribution of about 1% from hydrogen gas. Lastly, it was not known whether the Mylar windows on the target bulged outwards when the target contained liquid hydrogen.

In order to check these points, absolute cross sections were first worked out neglecting any corrections due to them, but including all other corrections, and compared with those of Paper I in the region of overlap at  $30^\circ$  (c.m.). Also, the monitor telescope in the horizontal plane was similarly used to determine absolute cross sections at  $90^\circ$  and  $65^\circ$  (c.m.), including corrections for pions and for absorption of the scattered protons in the walls of the target. These measurements with the liquid hydrogen target are compared with the results of the polyethylene-carbon difference method in table 1.

Table 1

	$\theta$ (c.m.)( $^\circ$ )	90	65	30
Polyethylene-carbon difference	$\sigma$ (mbn sterad $^{-1}$ )	3.70	3.76	4.04
Liquid hydrogen target	$\sigma$ (mbn sterad $^{-1}$ )	3.70, 3.64	3.74	3.97

The mean difference between the two sets of results is 1% and is probably due mainly to neglect of the scattering from residual hydrogen gas during the background measurements with the liquid hydrogen target. The results with the two liquid hydrogen containers of different length were compared at the common angle of  $6^\circ$  (lab.) and these agreed to better than 1%. Hence an upward correction of 1% was applied to all the results with both targets to normalize them to the results with the solid target.

Other corrections made in calculating the absolute cross sections were for absorption of the protons in the liquid hydrogen and in the first counter of the telescope and for the efficiency of the Čerenkov counter. The finite angular resolution of the arrangement necessitated a correction to the shape of the angular distribution at angles smaller than  $4^\circ$  (lab.). The r.m.s. width of the resolution curve was  $0.25^\circ$ , made up of contributions from multiple scattering in the hydrogen ( $0.2^\circ$ ), the finite size of the target and detector, and the divergence of the proton beam ( $0.07^\circ$  from each).

Accidental coincidences in the telescope amounted to less than 0.5% except at  $3^\circ$  and  $2^\circ$  where they were 0.5% and 1% respectively.

### § 5. RESULTS

In table 2 the final values for the differential cross sections are given in terms of the value at  $90^\circ$  from Paper I. The errors include the statistical standard deviation and allowances for uncertainty in the efficiency of the Čerenkov counter (0.25%), in the normalization to the measurements at large angles (1%)

Table 2

$\theta$ (c.m.)( $^\circ$ )	$\left(\frac{d\sigma}{d\Omega}\right)_\theta / \left(\frac{d\sigma}{d\Omega}\right)_{90}$	$\theta$ (c.m.)( $^\circ$ )	$\left(\frac{d\sigma}{d\Omega}\right)_\theta / \left(\frac{d\sigma}{d\Omega}\right)_{90}$
4.14	$7.07 \pm 0.30$	14.3	$1.176 \pm 0.022$
4.69	$4.26 \pm 0.17$	15.4	$1.151 \pm 0.018$
5.28	$3.08 \pm 0.12$	16.5	$1.154 \pm 0.016$
6.42	$1.783 \pm 0.054$	17.6	$1.154 \pm 0.015$
7.56	$1.435 \pm 0.040$	19.8	$1.133 \pm 0.020$
8.73	$1.238 \pm 0.028$	21.8	$1.141 \pm 0.016$
9.9	$1.176 \pm 0.027$	24.0	$1.114 \pm 0.016$
11.0	$1.176 \pm 0.020$	26.2	$1.130 \pm 0.018$
12.1	$1.173 \pm 0.027$	28.4	$1.103 \pm 0.017$
13.2	$1.165 \pm 0.015$	30.6	$1.084 \pm 0.017$



and in the correction for finite angular resolution. The error in the ionization chamber calibration was not included since this was the same in all the measurements. To obtain absolute cross sections the figures must be multiplied by the absolute cross section at  $90^\circ$  ( $3.70 \pm 0.06$  mbn sterad $^{-1}$ ) with appropriate increases in the errors.

All the results of both experiments are plotted in figure 5, where the curve has been drawn freely between the points and the triangles at the bottom indicate the angular resolution. By extrapolating the curve from  $10^\circ$  to  $0^\circ$  and integrating, a value for the total cross section of  $24.4 \pm 0.4$  mbn is obtained.

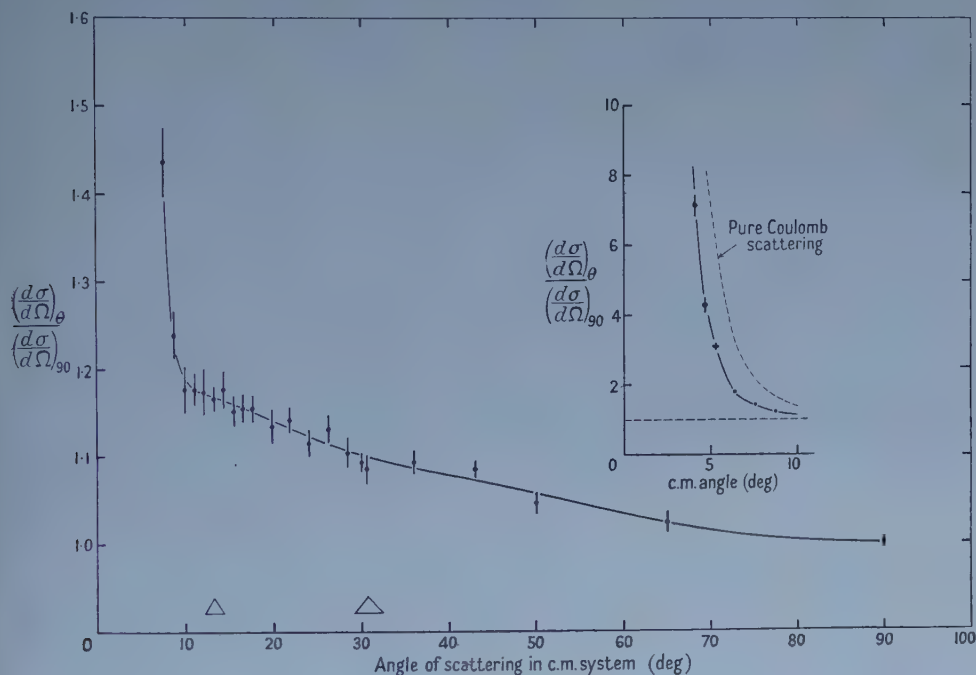


Figure 5. Differential cross section relative to that at  $90^\circ$  for elastic scattering of 380 MeV protons by protons.

The differential cross section rises by 9% between  $90^\circ$  and  $30^\circ$ . At higher energies the forward concentration of the scattering has been attributed to the rising cross section for inelastic processes (Smith, McReynolds and Snow 1955, Meščerjakov, Bogačev and Neganov 1956). At our energy we were able to show that these processes produce only a small effect on the cross section for elastic scattering by the following procedure. In the pion production processes the two protons are known to be mainly in a  $^1D_2$  state (Rosenfeld 1954). We used the known cross section for these processes to introduce a complex component into the D-wave in the various alternative sets of phase shifts given by Stapp *et al.* (1957) for the elastic process. In no case did this increase the cross section at  $30^\circ$  by more than 2%.

The destructive interference between Coulomb and nuclear scattering is demonstrated in figure 5, where the pure Coulomb cross section, added to a constant nuclear cross section of  $3.7$  mbn sterad $^{-1}$ , is plotted at small angles.

The application of the results of the present work to a phase shift analysis of the elastic scattering process must await the completion of experiments on polarization effects at present in progress in this laboratory.

#### ACKNOWLEDGMENTS

We wish to record our thanks to Professor H. W. B. Skinner for his close interest in this work, to Dr. G. E. Brown for helpful discussions of the theoretical aspects of the scattering process and to Mr. D. Harting for his help in the early stages of the experiment. The work was facilitated by the willing cooperation of the cyclotron operating crew under Mr. B. Halliday. J. C. K. was the holder of a CERN Fellowship and J. A. M. received a grant from the Department of Scientific and Industrial Research.

#### REFERENCES

- ALSTON, M. H., CREWE, A. V., EVANS, W. H., and VON GIERKE, G., 1956, *Proc. Phys. Soc. A*, **69**, 691.  
CHAMBERLAIN, O., and GARRISON, J. D., 1954, *Phys. Rev.*, **95**, 1349.  
CHAMBERLAIN, O., PETTENGILL, G., SEGRÈ, E., and WIEGAND, C., 1954, *Phys. Rev.*, **95**, 1348.  
FISHER, D., and GOLDBABER, G., 1954, *Phys. Rev.*, **95**, 1350.  
HARTING, D., HOLT, J. R., and MOORE, J. A., 1958, *Proc. Phys. Soc.*, **71**, 770.  
MERRISON, A. W., 1956, *Proc. CERN Symposium*, 329.  
MEŠČERJAKOV, M. G., BOGAČEV, N. P., and NEGANOV, B. S., 1956, *Nuovo Cim., Suppl.*, **3**, 119.  
ROSENFELD, A. H., 1954, *Phys. Rev.*, **96**, 139.  
SMITH, L. W., McREYNOLDS, A. W., and SNOW, G., 1955, *Phys. Rev.*, **97**, 1186.  
STAPP, H. P., YPSILANTIS, T. J., and METROPOLIS, N., 1957, *Phys. Rev.*, **105**, 302.

## Domain Patterns on a Single Crystal of Manganese Ferrite

By L. F. BATES, D. J. CRAIK † AND P. M. GRIFFITHS

Department of Physics, University of Nottingham

*MS. received 21st January 1958, and in final form 21st February 1958*

**Abstract.** Powder patterns were obtained on the cleaved surface of a single crystal of manganese ferrite by using a modification of the normal powder pattern technique. Two types of patterns were observed, a large scale pattern having a 'fern'-like structure, and an underlying structure of exceptional fineness and unusual configuration.

### § 1. INTRODUCTION

FERRITES of the general formula  $MOFe_2O_3$ , of which manganese ferrite ( $MnFe_2O_4$ ) is typical, have a cubic spinel structure, which may be considered as a cubic close-packed arrangement of the large oxygen ions with 32 in a unit spinel cell, and in the interstices between them are situated the smaller metal ions. The interstices are of two types: tetrahedral (A) and octahedral (B) sites, surrounded by four and six oxygen ions respectively. Of the sixty-four tetrahedral sites eight are occupied, and of the thirty-two octahedral sites sixteen are occupied. In the case of manganese ferrite, which is an inverted ferrite, the  $Mn^{2+}$  ions occupy the sixteen octahedral sites and the  $Fe^{3+}$  ions the eight tetrahedral sites.

The single crystal of  $MnFe_2O_4$  used in the experiments to be described was kindly supplied by the Mullard Research Laboratories, and was prepared by the flame fusion technique. This method results in boules which consist mainly of one crystal. The boule supplied to us was thimble-shaped, approximately 2 cm long with a diameter of 1 cm at its widest cross section.

### § 2. EXPERIMENTAL TECHNIQUE

It was decided to attempt to obtain a crystal face by cleavage, since the Mullard Research Laboratories informed us that the long axis of a boule tended to lie close to a [110] or a [100] direction. It is a well-known phenomenon that the cohesion of any crystal is not the same in all directions, and this generally leads to the existence of crystallographic cleavage planes, which are planes of high reticular density of atomic or molecular packing and large interplanar spacing, the cohesion being strong in the plane and weak perpendicular to it. Thus cleavage planes have simple indices and are often parallel to the principal axes of the crystal.

There were a number of short fine cracks in the end faces of the boule. When a razor blade was held against the surface in line with one of these and tapped smartly with a hammer, the boule split into two roughly equal parts, with their cleaved faces parallel to the long axis. The faces were by no means flat in a

† Now with Boots Pure Drug Co. Ltd., Beeston, Notts.

macroscopic sense, but there were some large flat areas. These areas were examined by means of the optical microscope, and under the highest power available showed no fine structure whatever. However, the flat areas on both cleft faces exhibited arrays of surface clefts or cracks which ran either perpendicular or parallel to the long axis of the original boule. Cracks in the two faces could be brought into register, suggesting that they were not caused during cleavage but were formed during the preparation of the boule. Figure 1† shows an electron-micrograph of the surface, taken by the Bradley (1954) carbon replica technique; running vertically across it is a typical crack, while the rest of the surface shows a very fine and shallow undulatory structure, of period  $0.1\mu$ .

Because of the macroscopic unevenness of the surfaces it was not possible to employ the usual method of observing domain configurations by applying a thin film of colloidal solution of magnetite between the surface and a thin glass coverslip. It was not desired at this stage to attempt to produce a flat surface suitable for this method by grinding and polishing. Hence a new method was developed which is an extension of that employed by Craik (1956) for the study of domain configurations by the electron microscope.

A thin film of a colloid solution was allowed to dry on the surface of the specimen, following all the undulations or irregularities of the surface. For example, figure 2 shows in the centre a flat region of the surface which is crossed by one dagger-shaped region which stands out above it. The colloid deposits are well in focus in the flat region, and are also seen to spread continuously over the raised portion of the surface towards the corners of the figure. The heavy vertical deposits represent cracks. The preparation of the colloid was such that it dried without any aggregation or distortion of the colloid particles. The latter were set in a solid matrix of a soluble plastic, which could later be removed from the specimen by washing gently in soapy water, leaving an unstained surface. While the film is on the surface it may be examined using an optical microscope. For electron microscopy a more dilute colloid is allowed to dry on the surface and is then stripped off for examination in an electron microscope.

In the original technique of Craik for the production of a film suitable for examination in an electron microscope a few drops of a very dilute colloid containing 0.1% sodium carboxy methyl cellulose‡ was applied to the surface, which had previously been covered by a very thin plastic film, which was necessary for the subsequent removal of the colloid film. This method was modified in so far as a heavier suspension of magnetite in 0.5% to 1.0% Celacol, to which glycerine was added as 10% weight for weight of the Celacol, was adopted. A very thin film of this colloid was applied direct to the surface, this dried more quickly and due to the glycerine had less adhesion, and could therefore be stripped easily without the use of an intervening plastic film. The interposition of the plastic film was disadvantageous in that it decreased the effects of very weak localized fields in the surface (Craik and Griffiths 1957).

As used with the optical microscope this method gives a very good resolution, rendering visible structure which was not even formed in a wet colloid film, apart from its essential use on an undulatory surface. A full account of these methods, for both optical and electron microscopy will be published elsewhere (Craik and Griffiths 1958).

† All figures appear as Plates at the end of the issue.

‡ This is distributed as 'Celacol' by J. M. Steele and Co. Ltd., 36 Kingsway, London, W.C.2.



## § 3. EXPERIMENTAL RESULTS

A film of colloid allowed to dry onto one of the cleaved surfaces was examined under an optical microscope. Several distinct straight lines were observed, and were found by comparison with the same region without colloid to be surface cracks along which deposits of colloid had settled. In one particular region, figure 2, some horizontal fine line structure was observed, but it was not related to any visible surface discontinuities. Observation of the remainder of the surface by the electron microscope showed it to be covered with an extremely fine and regular pattern of straight lines, figure 3, whose spacing is approximately  $0.3\mu$ . The crack visible on the left-hand side of the picture is parallel to the vertical lines in figure 2.

In order to intensify the effects of any domain structure in the body of the specimen and to clarify the fine patterns, a vertical field was applied to one of the portions of the boule. The specimen was placed over an iron core projecting from a small solenoid. When a current of 1.2 amp was passed through the latter an external field of about 150 oersteds was found at the pole of the core. The effective field in the specimen would of course be a small fraction of this, due to demagnetization effects. A new film was then dried on the surface while the field was applied. Observation under the optical microscope showed the surface to be covered in part with a 'fern'-like structure as in figure 4, and in part by a heavy line structure, figure 5. Figure 4 appears to be on a negative rather than a positive photograph; this is possibly due to interference effects caused by unevenness in the thickness of the colloid film. A portion of the 'fern' pattern observed at a magnification of 750, figure 6, consisted of two distinct components, viz. large scale heavy deposits which comprise the 'ferns', and an interposed fine line structure with spacing approximately  $1.0\mu$ .

When patterns from the same region and prepared under the same conditions were examined with the electron microscope, the fine structure appeared in greater detail, figure 7, while the 'fern' structure appeared only as a periodic thickening of the regular line deposits, indicated by the arrows. A detailed examination of the fine structure showed it to consist of three distinct types. The first and most extensive, figure 11, was of straight parallel alternate bands, with the colloid uniformly deposited over the dark regions. The spacing of these sharply defined bands is equal to their width,  $0.35\mu$ . In the second, figure 12, the bands are replaced by pairs of fine lines, giving a tubular appearance. The lines are  $0.15\mu$  thick, the width of the tubes is  $0.35\mu$ , and their spacing is  $0.7\mu$ . The third type, figure 8, also consists of a series of fine lines  $0.15\mu$  thick, but these are no longer straight and are less regularly spaced. The wide line on the right in figure 8 is a deposit along a crack; this had a curved appearance due to the flattening of the film when stripped from the specimen.

It was thought that the pattern of straight lines in figure 11 might be due either to flux emergence at regular surface defects due to step formation on cleavage, or to the existence of a corresponding ordered precipitation such as was observed by Heidenreich and Nesbitt (1952) in the case of alnico after heat treatment. However, carbon replicas of several different parts of the surface revealed no such step structure. In figure 1 a portion of one of these is shown; as previously mentioned the only structure observable here has a spacing of  $0.1\mu$  and would therefore not be expected to give a line structure of  $0.35\mu$  by flux emergence. As the presence of precipitation should be revealed by etching,

one portion of the boule was lightly etched in boiling HCl, and the surface re-examined by the carbon replica technique. The etch pattern is shown in figure 9 and bears no relation to the observed powder patterns.

In order to determine whether the fine patterns were unique to this particular cleavage, the crystal was split once more, this time in a plane perpendicular to both the original face and the long axis. The same vertical field was applied and the resulting patterns examined by optical and electron microscopy. Figure 10 shows a fourth type of fine structure on the second of the cleaved surfaces, taken by the optical microscope. It seems to consist of a double 'comb' structure, but it appeared only in one small region. Figure 15 shows an electron micrograph corresponding to figure 10; the bands are again sharply defined but the configuration is in marked contrast to any previously observed in our work, also there is a greater band width and spacing of  $0.7\mu$ .

Larger vertical fields were now applied to the unetched portion of the original cleaved surface along the length of the boule. Over a portion of the surface identified by the lower edge of figure 13 a zigzag configuration of the fine structure, in an applied field of about 25 oersteds, was seen with the optical microscope. The spacing is larger than any previously observed, and from electron microscopy was found to be  $1.0\mu$ . This denotes a regular increase of both the bands and their spacings, and not simply an increase in the separations. The film was removed and another allowed to dry in the presence of a horizontal field of about 180 oersteds applied parallel to the long axis of the portion. The zigzag structure now gave place to a regular straight line array, the colloid lines forming in the direction of the field. Figure 14 shows the same area (see lower edge) in the presence of the horizontal field. When this field was increased to a value of about 300 oersteds, all the fine structure disappeared, as was verified by electron microscopy, and the surface was covered with randomly distributed colloid, which lay heavily over any cracks perpendicular to the long axis.

Since the observed fine structure may have arisen from a modification of the surface layer, due to the effect of cleavage, the etched portion of the boule was examined for domain configuration. Again no structure was visible by the optical microscope in the absence of an applied field. When a small vertical field was applied, a large scale configuration was observed similar to that in figure 5. It is shown with an increased magnification in figure 16, for which the magnification is the same as for figure 6; no fine line structure is present. Electron microscopy of this region, under the same magnetic conditions, also showed the absence of the fine structure, but indicated an overall surface irregularity due to the etching.

The large scale structure of figure 5 has been compared with powder patterns, obtained by Stephan (1955) on the surface of a single crystal of nickel, which he suggested were due to internal stresses. As manganese ferrite has an anisotropy of approximately the same order and the same most easy direction, [111], it was thought that the patterns might have had a similar origin, in which case a change of domain configuration should occur on annealing. The etched portion of the boule was therefore annealed in an open ended furnace, i.e. effectively in an atmosphere of air or oxygen, the temperature being maintained at  $800^{\circ}\text{C}$  for 10 hours and then at  $700^{\circ}\text{C}$  for 20 hours, after which the furnace was allowed to cool slowly to room temperature. When removed from the furnace the surface was heavily coated with a thick, greyish crust. In an attempt to remove this

crust the specimen was re-etched. The etchant had little effect on the crust, but penetrated into surface cracks and caused large irregularities in the surface, and spoiled the surface for re-examination with the optical or electron microscope. For this reason the second cleavage was made. Examination of one of its surfaces showed large structure in the presence of magnetic fields, similar to those already shown for the original cleaved surface, and electron microscopy gave a fine structure as in figure 15.

Due to poor reflecting quality of the surface produced after anneal, a flat was ground upon it as nearly as possible parallel to one of the original faces. This was first done by using a high speed carborundum wheel, which removed the surface in a manner indicating that large grains, of the order of  $10\mu$ , were torn away. The surface was then ground with 000 emery until it was smooth, further polished with 0000 emery, and finally finished on a polishing wheel with emery '305' powder. This resulted in a glass-like surface which was presumably a Beilby layer. It was observed both with and without applied vertical and horizontal fields. Apart from heavy deposits above scratches no pattern was observed. The surface was therefore lightly etched and in some regions the structure of figure 17 was observed. This may be compared with that of figure 10; there is some similarity in the general appearance of the two structures since they both appear to consist of two-edged 'comb' formations. The specimen was subsequently re-etched and coarse line structure appeared over the major part of the surface.

#### § 4. DISCUSSION

The most striking feature of the above observations is the existence of two distinct patterns, one underlying the other. They consist of heavy colloidal structures of the 'fern' and heavy wall types, and the much finer band structures respectively. Their occurrence is most unusual as the fine structure does not merely extend between the powder patterns of the larger structure, but from figure 7 it is seen that the larger structure is formed by regular intensification of the fine bands themselves. If both the coarse and fine patterns represented domain structures characteristic of the whole material, then one would expect them to be continuous one with another. The fact that they are not suggests that they oppose one another from place to place. It is therefore assumed that the patterns represent two independent domain structures, the fine bands being due to a surface effect caused by cleavage and the coarse pattern to the internal domain structure of the ferrite. Thus, where the direction of magnetization in the surface layer has a component in the same sense as the large structure there is an additive effect giving rise to the observed intensification, but where they oppose the larger pattern is suppressed. In figure 17, of the etched specimen, under high magnification we see that not only has the fine structure been removed, but the deposits caused by the large structure have become continuous.

In manganese ferrite, which can be considered as a face-centred cubic lattice, there are eight easy directions. The faces so far investigated being due to cleavage of the face-centred cubic structure, are (100) planes. These crystallographic planes do not contain an easy direction of magnetization so that no ordered large scale surface configuration can be expected. It is hoped in the near future to obtain other suitable faces, such as (110) or (111), on which further observations



will be made using the present technique. The spacing of the heavy line deposits in the 'fern' structure is of the order of  $70\mu$  which is of the order of the domain spacing in large ferromagnetic crystals. The 'leaves' of the 'fern' may be due to magnetic poles appearing in the surface due to internal closure structures, and may be compared with the echelon structure (Martin 1957) found on the (100) surface of iron and silicon-iron.

In the previous section it was noted that the fine structure was of three distinct types, vide figures 8, 11 and 12. Two of these figures, 11 and 12, appear to be related and will now be considered in detail. Figure 11 consists of parallel straight bands of uniform width  $0.35\mu$  and same spacing. They lie at an angle of approximately  $45^\circ$  to the long axis of the crystal. The second related type figure 12 shows very fine, usually parallel, lines  $0.15\mu$  wide and  $0.35\mu$  or  $0.70\mu$  apart, also lying at an angle of approximately  $45^\circ$  to the long axis. These patterns were both observed in the presence of a small normal field. The former was of general occurrence while the latter occurred only over very limited areas.

If it is assumed that figure 12 represents a pattern of domain walls then the wall width is very small compared with the calculated value for manganese ferrite. Taking the wall width  $\delta$  as  $7(A/K)^{1/2}$  cm, and the wall energy  $\sigma$  as  $3(AK)^{1/2}$  ergs  $\text{cm}^{-2}$ , where  $A$  the exchange coupling energy is  $10^{-6}$  erg  $\text{cm}^{-1}$  and  $K$  the crystalline anisotropy given by Smit and Wijn (1954) is  $-3 \times 10^4$  erg  $\text{cm}^{-3}$ , then  $\delta$  is  $0.55\mu$  and  $\sigma$  is  $0.41$  erg  $\text{cm}^{-2}$ . Since the wall width measured from the electron micrographs is smaller than the calculated  $\delta$  by a factor of 3.5, the corresponding wall energy must be  $1.3$  erg  $\text{cm}^{-2}$ . It may be noted that the intensified portions of the fine structure in figure 7 cover a band approximately  $0.8\mu$  wide which corresponds to the calculated value of  $\delta$ .

Since the lines of the fine structure are at an angle of approximately  $45^\circ$  to the long axis of the boule, they are in  $[110]$  directions. It is therefore reasonable to assume that the magnetization in the fine structure still lies in the easiest direction, despite the modification of the properties of the surface layer. Also, the pronounced regularity and straightness of this structure over considerable areas of the surface suggests that it is constrained by the crystal anisotropy. Hence the fine structure will be considered to consist of  $180^\circ$  domain slabs, with their magnetizations in the  $[111]$  directions, which make an angle of  $34^\circ$  with the surface. The structure shown in figure 12 occurs over very limited areas, where it is assumed that the local curvature of the cleaved surface causes it to approximate to a (110) plane containing  $[111]$  directions of easy magnetization, thus allowing little surface divergence.

It is not considered that the fine structure constitutes a closure system, as was assumed by Chikazumi and Suzuki (1955) for the maze pattern on silicon-iron, since this would imply an underlying structure of similar dimensions.

The following considerations indicate that the structure exists near the surface only. The spacing of this pattern is one-tenth of the finest silicon-iron maze pattern. If the walls continue through the specimen, the wall energy density will be  $1.3/0.35 \times 10^{-4}$  or  $4 \times 10^4$  erg  $\text{cm}^{-3}$ , making a total energy of the structure  $8 \times 10^4$  erg  $\text{cm}^{-3}$ . This is less than the energy of a single domain structure which would be the saturation magnetic field energy, approximately  $I_s^2$  or  $16 \times 10^5$  erg  $\text{cm}^{-3}$ . The observed spacing, however, does not correspond to the equilibrium spacing of the whole crystal.



The appropriate expression (Kittel 1949) for the energy per unit surface area is

$$W = \frac{\sigma L}{D} + 1.7 I_s^2 D \text{ erg cm}^{-2}.$$

In this case  $I_s$  must be replaced by its component normal to the surface which is

$$I_s \sin 34^\circ \text{ or } I_s \frac{1}{\sqrt{3}}, \quad \text{i.e. } W = \frac{\sigma L}{D} + \frac{1.7}{3} I_s^2 D \text{ erg cm}^{-2},$$

and this corrected value of the wall energy, namely  $3.5\sigma$ , must now be used.

The energy is a minimum when  $D = (3.5\sigma L)^{1/2} / (0.57 I_s^2)^{1/2} \text{ cm}$ , whence taking  $L = 0.5 \text{ cm}$ ,

$$D = \left( \frac{1.3 \times 0.5 \times 3}{1.7 \times (400)^2} \right)^{1/2} \mu = 25 \mu;$$

$D$  however is greater than the observed spacing by a factor of about 100.

Noting that for equilibrium  $D \propto \sqrt{L}$ , the observed value of  $D$  corresponds to a depth of  $0.5 \times (0.3/25)^2 \mu = 1.0 \mu$ .

Thus, the patterns conform to the usual theory if their depth is of the order of  $1 \mu$ . The energy of the structure per unit area is then  $W = 2(0.57 I_s^2 \sigma L)^{1/2}$  or approximately  $8 \text{ erg cm}^{-2}$ .

If the change in wall thickness is assumed to be due to a change in anisotropy, then since  $\delta \propto 1/\sqrt{K}$  the anisotropy must be changed from its usual value of  $-3 \times 10^4 \text{ erg cm}^{-3}$  to  $-3 \times 10^5 \text{ erg cm}^{-3}$ . If this additional anisotropy is due to strain then effectively  $K = \lambda \epsilon$  where  $\lambda$  is the coefficient of magnetostriction and  $\epsilon$  is the stress. Taking  $\lambda = -5 \times 10^{-6}$  we have  $-3 \times 10^5 = -5 \times 10^{-6} \epsilon$ , or  $\epsilon = 6 \times 10^{10} \text{ dyn cm}^{-2}$  or  $600 \text{ kg mm}^{-2}$ , approximately.

According to A. J. Forty (1957) when perfect cleavage is achieved no dislocations are formed and presumably the resulting surface is strain free. If, however, a crack can be made to travel sufficiently slowly slip takes place. Dislocations are generated along any line at which the crack is temporarily halted, but where the crack travels continuously no such dislocations will appear. In the case of a cleaved surface such as described above, many slip lines appear on the surface indicating that the crystal has been strained.

When the manganese ferrite boule was cleaved, the resultant surface did not show any slip lines, see figure 1, and indeed, since the cleavage occurred almost instantaneously and the material is so hard and brittle such lines are not to be expected according to the above theory. The surfaces appeared very flat and uniform, even to an electron microscope. However, it has been necessary to postulate an extremely uniform strain, in order to account for the observed fine domain structure. The strain which Forty described, occurring in controlled cleavage, may be considered as a bulk effect. In this particular case, it is considered that cleavage has generated a very high strain in the surface layer. From magnetostatic energy considerations this surface layer is found to be approximately  $1 \mu$  in depth.

When a brittle material is cleaved it is generally assumed that a strain-free surface is produced, indeed crystals have been cleaved specifically to produce a strain-free surface for the purpose of examining deformation features, and the distribution of dislocations through the specimen (Holden 1952, Birks and Seal

1957). Cleavage of softer materials has been found to produce a thin amorphous or flowed layer on the cleaved surface (Petch 1954).

It was suggested to us that the fine structure might be due to a ferroelectric effect on the surface. Experiments, performed in an attempt to verify this suggestion, by applying an electric field to the specimen, and also by applying a Celacol colloidal film to a polycrystalline specimen of barium titanate gave negative results.

It is difficult to account for these patterns other than in terms of strain. The comparison of the carbon replica, figure 1, with any of the fine structures revealed by the electron microscope rules out flux emergence phenomena. They cannot be due to ordered precipitation because the patterns change direction under the influence of an applied field, see figures 13 and 14; an etch would have intensified rather than removed effects due to precipitation, see figure 16.

The specimen surface was examined by the back reflection x-ray technique in an attempt to verify the existence of a strained layer. No radical elongation of the spots in the x-ray pattern was found. Failure to manifest the strained layer may be due to penetration of the x-ray beam into the body of the specimen to a depth of about  $10\mu$ , whereas the postulated depth of the surface layer is about  $1\mu$ .

#### ACKNOWLEDGMENTS

The authors express their thanks to the Mullard Research Laboratories and Dr. K. Hoselitz for providing the single crystal boule and for measuring the orientations of the cleaved surfaces; D. J. C. thanks Mr. W. J. Randall and the Directors of Boots Pure Drug Co. Ltd. for permission to use the electron microscope and their interest in the work; P. M. G. thanks the Department of Scientific and Industrial Research for a maintenance grant.

#### REFERENCES

- BIRKS, L. S., and SEAL, R. T., 1957, *J. Appl. Phys.*, **28**, 541.  
 BRADLEY, D. E., 1954, *Brit. J. Appl. Phys.*, **5**, 65.  
 CHIKAZUMI, S., and SUZUKI, K., 1955, *J. Phys. Soc., Japan*, **10**, No. 7.  
 CRAIK, D. J., 1956, *Proc. Phys. Soc. B*, **69**, 647.  
 CRAIK, D. J., and GRIFFITHS, P. M., 1957, *Proc. Phys. Soc. B*, **70**, 1000; 1958, *Brit. J. Appl. Phys.*, in the press.  
 FORTY, A. J., 1957, *Proc. Roy. Soc. A*, **242**, 392-399.  
 HEIDENREICH, R. D., and NESBITT, E. A., 1952, *J. Appl. Phys.*, **23**, 352.  
 HOLDEN, J., 1952, *Phil. Mag.*, **43**, 976.  
 KITTEL, C., 1949, *Rev. Mod. Phys.*, **21**, 541.  
 MARTIN, D. H., 1957, *Proc. Phys. Soc. B*, **70**, 77.  
 PETCH, N. J., 1954, *Progr. Metal Phys.* (London: Pergamon Press), **5**, 1.  
 SMIT, J., and WIJN, H. P. J., 1954, *Advances in Electronics and Electron Physics*, Vol. 6, edited by L. Morton (New York: Academic Press).  
 STEPHAN, W., 1955, *Exp. Tech. Phys.*, **1**, 1.

# The Influence of Imperfections on the Strength of Ice

By H. H. G. JELLINEK†

Snow, Ice and Permafrost Research Establishment, Corps of Engineers,  
U.S. Army, Wilmette, Illinois

*MS. received 24th October 1957*

**Abstract.** Tensile strength measurements on ice cylinders adhering to stainless steel have been made as a function of rate of loading, thickness and cross-sectional area of specimens, and temperature. A rapid increase of tensile strength occurs as the volume is decreased. The data for a temperature of  $-4.5^{\circ}\text{C}$  can be represented over a thousandfold range of volumes by an equation as follows

$$S = 2.74AV^{-0.84} + 9.4 \text{ kg cm}^{-2}$$

where  $S$  is the tensile strength,  $A$  the cross-sectional area in  $\text{cm}^2$  and  $V$  the volume in  $\text{cm}^3$ . The experimental results are interpreted by means of a statistical treatment involving imperfections in the specimens. The statistics for a model consisting of a large number of parallel elements is elaborated. The final equation derived on statistical grounds approximates the equation found empirically, and reads as follows

$$\bar{S}_{r,n} = kA^{1/\beta}V^{-1/\beta} + C$$

where  $\bar{S}_{r,n}$  is the number average of the tensile strength,  $k$ ,  $\beta$  and  $C$  are constants and  $r$  is the number of imperfections in each of  $n$  parallel elements. This result is quite general and not confined to ice.

The conclusion is reached that due to imperfections the tensile strength is a statistical function of the volume and cross-sectional area of the specimens. Superimposed on the statistical effect is a stress distribution effect, which becomes predominant for large volumes.

## § 1. INTRODUCTION

IT is well known that the strength of solids depends to a large extent on various kinds of dislocations or even macroscopic defects such as small cracks. The influence of such imperfections should become apparent when the strength of solids is investigated as a function of the geometrical parameters of the test specimens. Such an influence can be treated on a statistical basis and the part played by the defects on the one hand and stress distribution on the other can be elucidated. In this work, the strength of ice cylinders has been investigated as a function of their cross-sectional area and height. The effect of rate of stress application to the specimens and the temperature dependence of tensile strength have also been studied.

There are numerous data on the bulk tensile strength of ice (Butkovich 1954 and references cited therein). However, tensile strength as a function of geometrical parameters has not yet been extensively investigated. The only works available are the reports on the chemical-physical nature of adhesion of ice to solid surfaces from the University of Cincinnati (1950–55). These workers

† Present address: Applied Science Research Laboratory, University of Cincinnati, Cincinnati, Ohio, U.S.A.



investigated the tensile strength properties of ice films sandwiched between carbon steel plugs at  $-25^{\circ}\text{C}$ . A sharp increase of strength with decreasing ice volume was noted. However, their experimental data show a rather large scatter so that a detailed evaluation is not possible. The data described in this work make such an analysis possible. It appears that the tensile strength of thin ice discs is dependent not only on their volume, but also on such geometrical parameters as cross-sectional area and height of the specimens.

An increase of strength with decreasing thickness is a general phenomenon, which has particularly been noticed in studies of adhesives (DeBruyne 1951). The experimental data are discussed here in terms of theories based on statistical considerations, postulating distributions of imperfections in the ice, and on stress distributions in the specimens (Meissner and Baldauf 1951). Papers concerning the statistics of probability distributions relevant to the present work have been published by Peirce (1926), Weibull (1939 a, b), Daniels (1945), and Epstein (1948). In this paper, the statistics of imperfections, particularly of elements arranged in parallel, which were discussed to some extent in the papers mentioned above, are enlarged and elaborated. These statistics are applicable to solids generally.

## § 2. EXPERIMENTAL

### 2.1. *Materials*

The larger ice cylinders (0.5 cm high and above) were prepared from snow-ice, which came from the same batch as that used in a previous investigation (Jellinek and Brill 1956). It was obtained by sieving snow into water and subsequent freezing. Thin discs of ice, sandwiched between stainless steel cylinders, were prepared by freezing water which was freed of electrolytes by passing through exchange resin. Air was removed by boiling and the water left in a closed container which had been cleaned with benzene of Analar grade.

### 2.2. *Preparation and Mounting of Specimens*

To prepare the larger cylinders, a cube of snow-ice was frozen onto the roughened base of an aluminium cylinder. An ice cylinder of desired dimensions was then turned on a lathe at  $-10^{\circ}\text{C}$ . The aluminium cylinder plus the ice was placed into a mounting apparatus (figure 1), consisting essentially of a stainless steel frame with a stainless steel rod which can be moved vertically up and down, sliding in a ball bearing.

The steel rod was exactly centred above an arrangement into which the aluminium cylinder was inserted. A stainless steel cylinder was attached to the bottom of the steel rod and heated to slightly above  $0^{\circ}\text{C}$  by a heating wire wound around the lower end of the steel rod. The temperature of the steel cylinder was measured by a thermocouple and controlled by a Variac. Then the electric current was turned off and the steel cylinder was lowered and frozen to the snow-ice, forming only a small amount of water in the process. The aluminium cylinder was then cut off from the ice and the specimen turned over so that the stainless steel cylinder was in the position previously occupied by the aluminium cylinder. The process was repeated with a second stainless steel cylinder. The stainless steel was grade 304/A, with polished surface; the finishing polish used was Lapping Compound No. 38-900A, U.S. Products Company. The steel



cylinders were kept in benzene, and were thoroughly cleaned with benzene before each experiment.

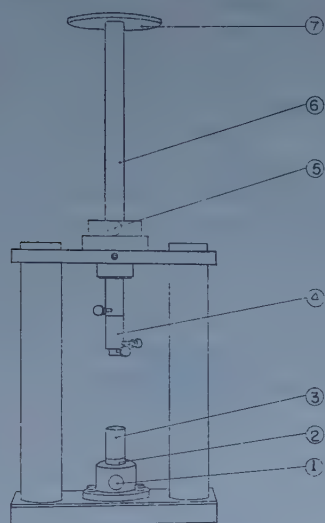


Figure 1. Mounting apparatus for larger ice cylinders. (1) Set screw; (2) Stainless steel disc; (3) Ice specimen; (4) Adapters; (5) Set screw; (6) Stainless steel rod; (7) Platform for weights.

The thin cylinders or discs were prepared in a somewhat different way, using a modification of the previous mounting apparatus (figure 2). In this case, the apparatus is horizontal and the stainless steel rod is operated by turning a screw.

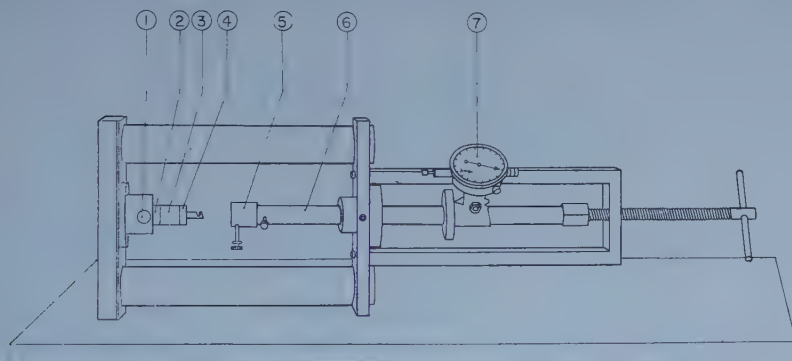


Figure 2. Horizontal mounting apparatus for thin discs of ice. (1) Set screw; (2) and (4) Stainless steel discs; (3) Ice specimen; (5) Adapter; (6) Stainless steel rod; (7) Starrett gauge.

A Starrett dial gauge was rigidly connected to the steel rod, which allowed distances to be measured within  $2.5 \times 10^{-4}$  cm. Two stainless steel cylinders were mounted in the apparatus and adjusted to the desired distance. Water was then introduced between the gap and seeded with ice, so that freezing took place within a few seconds. Any extraneous ice formed from waterdrops was carefully removed, either by a scalpel or on the lathe.

The mountings in either apparatus were carried out at  $-10^{\circ}\text{C}$ . Ten to fifteen minutes were allowed for each newly-frozen interface before proceeding with the operation.

### 2.3. Tensile Strength Apparatus

The apparatus (figure 3) consists of a stainless steel frame and a threaded steel rod, which can be moved only vertically, driven by a three-phase motor through a worm gear and gear wheel. The loading speed can be varied by inserting different gear wheels in the motor. One revolution of the shaft leading from the motor to the apparatus corresponds to a vertical movement of about  $3 \times 10^{-3}$  cm. A Baldwin SR-4, U-1 500-lb load cell was rigidly fixed to the lower end of the threaded steel rod. The ice specimen with its steel cylinders was hung onto the load cell by means of a flexible ball chain; and was hooked by a similar chain to the base of the steel frame.

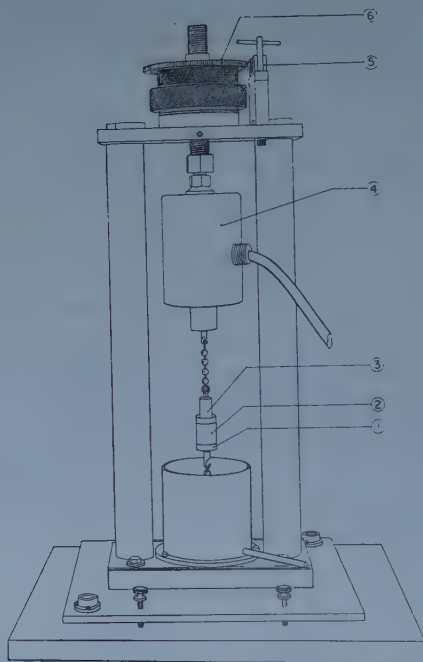


Figure 3. Tensile strength apparatus. (1) and (3) Stainless steel discs; (2) Ice cylinder, 2 cm high; (4) Baldwin load cell, S-R4, U-1, 500 lb.; (5) Worm gear; (6) Gear wheel.

The output of the Baldwin load cell was recorded on a Leeds and Northrup recorder as a (load, time) curve. As specified by the manufacturer, the cell showed a linear relationship between output and load.

## § 3. EXPERIMENTAL RESULTS

### 3.1. Tensile Strength as a Function of Rate of Loading for Large Specimens

Cylinders of snow-ice of 2 cm height and 2 cm diameter were tested at different rates of stress application. All snow-ice samples showed random orientation under polarized light, the grains had 'diameters' not larger than about 1 mm. In most cases, twelve tests were carried out at each rate. The data are given in table 1.

At relatively high rates of loading, the (load, time) curves were straight lines at lower rates, S-shaped curves were obtained. In the latter cases, the rates were derived from the straight portions of the curves.

Table 1. Tensile Strength ( $\text{kg cm}^{-2}$ ) of Snow-Ice Cylinders adhering to Stainless Steel, as a Function of Rate of Stress Application

Temp. =  $-4.5^\circ\text{C}$ ; vol. =  $6.28 \text{ cm}^3$ ; area =  $3.14 \text{ cm}^2$ ; height =  $2 \text{ cm}$

Stress rate, ( $\text{kg cm}^{-2} \text{ sec}^{-1}$ )	0.051	0.11	0.21	0.57	1.10
Mean	14.7	16.7	17.0	15.6	16.1
Standard deviation	$\pm 2.6$	$\pm 2.5$	$\pm 3.9$	$\pm 2.2$	$\pm 2.1$
Standard error of mean	$\pm 0.7$	$\pm 0.7$	$\pm 1.2$	$\pm 0.6$	$\pm 0.8$
Variance	6.8	6.3	15.3	4.9	4.4

Most of the breaks were partly cohesive and partly adhesional, usually exposing 20 to 30% of the metal surface (figure 4, A, B). In most cases, the breaks took place within 1–2 mm of one of the ice-metal interfaces and the rupture plane formed an angle of  $10^\circ$  to  $20^\circ$  with the metal surface. Occasionally the break was completely cohesive but still in the neighbourhood of the interface and forming an angle with it (figure 4, C). In a few instances, the rupture plane was at right angles to the cylinder axis, and, in very rare instances, such a rupture

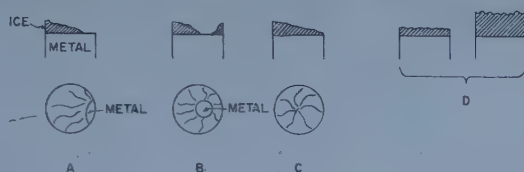


Figure 4. Typical breaks of snow ice. A, B, most frequent; C, occasional, more frequent at high rates of loading; D, rare.

plane was situated near the middle of the cylinder (figure 4, D). It was also observed that the breaks became more cohesive with increasing rates of loading. Figure 5 shows the tensile strength as a function of the rate of stress application

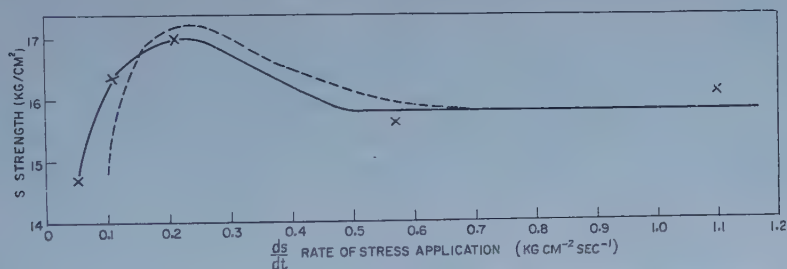


Figure 5. Average tensile strength as a function of rate of stress application for snow ice cylinders (height 2 cm, diameter 2 cm). Broken line is calculated curve according to equation (1).

for the snow-ice cylinders of 2 cm height and 2 cm diameter. It can be seen, that, as the rate of stress application increases, the tensile strength values pass through a maximum and eventually reach a constant value indicating that they become independent of the rate of stress application. Similar curves were found by Komichevskaja (1940) for permafrost and ice. For our specimens, the tensile strength  $S$  as a function of rate of stress application  $v$  can be expressed approximately by the equation

$$S = C \left[ \left( \frac{v\epsilon}{\epsilon v_m - 1} - 1 \right) \exp(-\epsilon v) + 1 \right]; \quad \dots\dots (1)$$

in this particular case,  $\epsilon = 10 \text{ cm}^2 \text{ sec kg}^{-1}$ ,  $v_m = 0.22 \text{ kg cm}^{-2} \text{ sec}^{-1}$  and  $C = 15.8 \text{ kg cm}^{-2}$ .

### 3.2. Tensile Strength as a Function of Geometrical Parameters

Tensile strength experiments were performed on thin discs prepared by freezing water in the manner described previously. In every instance, the breaks were completely cohesive, the rupture planes being situated nearer one of the metal ice interfaces for the thicker specimens. In some instances the rupture surfaces appeared very smooth with only a small rough patch; in other instances the whole rupture surface was rough.

It can be shown that most of the strain was taken up by the chains, as there is only a relatively small increase in loading rate with area; the height of the specimens has no marked effect on the rate of loading. Table 2 shows some tensile strength values for different cross-sectional areas and equal heights at different rates of stress application. It is seen that the tensile strength values appear to be independent of stress rate within the range employed. As all subsequent strength measurements were carried out in this range of areas and rates, the strength values for the thin discs can be considered to be independent of the rate of stress application.

Table 2. Tensile Strength ( $\text{kg cm}^{-2}$ ) for Different Cross-Sectional Areas and Rates of Stress Application

Ice cylinders adhering to stainless steel. Temp = $-4.5^{\circ}\text{C}$ ; height = $7.62 \times 10^{-2} \text{ cm}$				
Volume ( $\text{cm}^3$ )	$1.17 \times 10^{-1}$		$1.49 \times 10^{-2}$	
Area ( $\text{cm}^2$ )	1.54		0.196	
rev./min.	355	89	355	89
Stress rate ( $\text{kg cm}^{-2} \text{ sec}^{-1}$ )	2.81	0.82	13.8	3.22
Mean	35.3	35.3	37.0	32.7
Standard deviation	$\pm 5.4$	$\pm 5.6$	$\pm 5.2$	$\pm 6.3$
Standard error of mean	$\pm 1.6$	$\pm 1.6$	$\pm 1.5$	$\pm 1.8$
Variance	28.8	31.6	26.7	39.5

Many of the fractured discs were observed under polarized light. The grain size varied. Frequently there were one or two larger grains with a number of small ones. In other cases, the whole specimen consisted of relatively small grains. A preferred orientation was often observed, with the  $c$ -axis lying parallel to the cylinder axis.

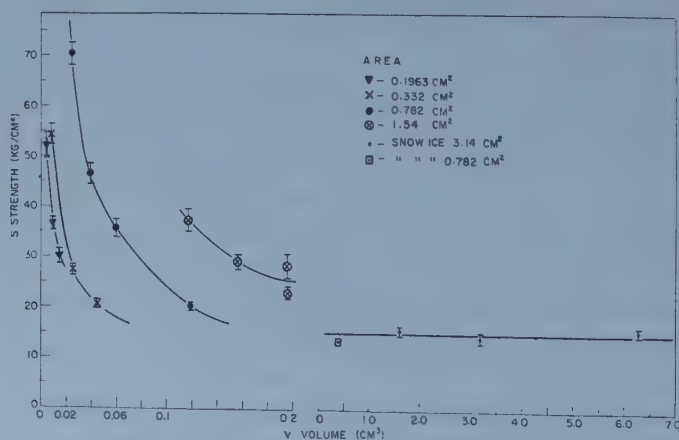


Figure 6. Average tensile strength as a function of ice volume (each point represents the average value of at least 12 tests). Ranges indicated are standard errors of the mean.



Table 3 gives the tensile strength data for ice specimens and snow-ice specimens. Figure 6 shows the average tensile strength values plotted as a function of the volume. Figure 7 shows the logarithms of the tensile strength plotted against the logarithms of the specimen volumes (snow ice values not shown). The

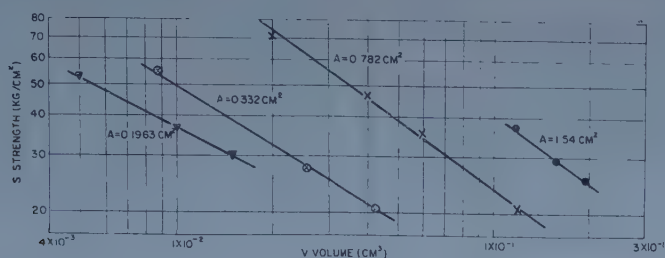


Figure 7. Average tensile strengths as a function of volumes.

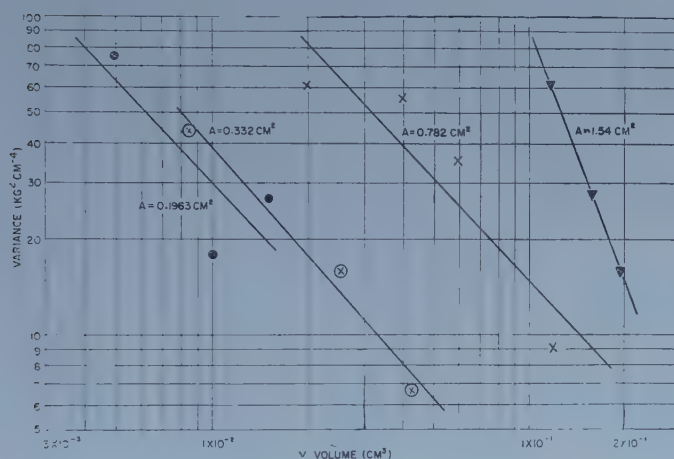


Figure 8. Variances of tensile strength as a function of volumes.

straight lines were obtained by the method of least squares. It is seen that the tensile strength increases very rapidly as the volume decreases. However, only values for any one area lie on a curve, each area forming a separate curve. The variances of the tensile strength are shown in figure 8 as a function of the volumes.

Table 3. Tensile Strength ( $\text{kg cm}^{-2}$ ) as a function of Geometrical Parameters Ice cylinders adhering to stainless steel. The mean represents 12 tests

(a) Snow ice. Temp. =  $-4.5^\circ\text{C}$ ; stress rate =  $0.64 \text{ kg cm}^{-2} \text{ sec}^{-1}$ ; area =  $3.14 \text{ cm}^2$

Volume ( $\text{cm}^3$ )	1.57	3.14	6.28
Height (cm)	0.50	1.00	2.00
Mean	15.5	14.1	15.7
Standard deviation	$\pm 2.9$	$\pm 2.7$	$\pm 2.7$
Standard error of mean	$\pm 0.8$	$\pm 0.9$	$\pm 0.7$
Variance	8.3	7.2	7.0

(b) Ice cylinders. Temp. =  $-4.5^{\circ}\text{C}$ ; stress rate =  $1.26 \text{ kg cm}^{-2} \text{ sec}^{-1}$ ;  
area =  $1.54 \text{ cm}^2$

Volume ( $\text{cm}^3$ )	$1.17 \times 10^{-1}$	$1.57 \times 10^{-1}$	$1.96 \times 10^{-1} \dagger$	$1.96 \times 10^{-1}$
Height (cm)	$7.62 \times 10^{-2}$	$1.02 \times 10^{-1}$	$1.27 \times 10^{-1}$	$1.27 \times 10^{-1}$
Mean	37.3	29.1	28.3	22.9
Standard deviation	$\pm 7.9$	$\pm 5.3$	$\pm 8.1$	$\pm 4.0$
Standard Error of Mean	$\pm 2.3$	$\pm 1.5$	$\pm 2.3$	$\pm 1.2$
Variance	61.6	27.9	65.7	15.9

$\dagger$  This column represents one of the first series of experiments when the technique was not too well established. The mean of the standard deviations for this and the next column has been plotted in figure 7. The variance for this column, however, is not shown in figure 8.

(c) Ice cylinders. Temp. =  $-4.5^{\circ}\text{C}$ ; stress rate =  $2.46 \text{ kg cm}^{-2} \text{ sec}^{-1}$ ;  
area =  $0.782 \text{ cm}^2$

Volume ( $\text{cm}^3$ )	$1.99 \times 10^{-2}$	$3.97 \times 10^{-2}$	$5.96 \times 10^{-2}$	$1.19 \times 10^{-1}$	$0.391 \dagger$
Height (cm)	$2.54 \times 10^{-2}$	$5.08 \times 10^{-2}$	$7.62 \times 10^{-2}$	$1.52 \times 10^{-1}$	0.50
Mean	70.4	46.3	35.8	20.7	13.4
Standard deviation	$\pm 7.8$	$\pm 7.4$	$\pm 6.0$	$\pm 3.0$	$\pm 2.9$
Standard error of mean	$\pm 2.2$	$\pm 2.1$	$\pm 1.8$	$\pm 0.9$	$\pm 0.8$
Variance	60.2	55.1	35.5	9.1	8.4

$\dagger$  Snow ice

(d) Ice cylinders. Temp. =  $-4.5^{\circ}\text{C}$ ; stress rate =  $4.95 \text{ kg cm}^{-2} \text{ sec}^{-1}$ ;  
area =  $0.332 \text{ cm}^2$

Volume ( $\text{cm}^3$ )	$8.43 \times 10^{-3}$	$2.53 \times 10^{-2}$	$4.24 \times 10^{-2}$
Height (cm)	$2.54 \times 10^{-2}$	$7.62 \times 10^{-2}$	$1.27 \times 10^{-1}$
Mean	54.7	27.5	20.6
Standard deviation	$\pm 6.6$	$\pm 4.0$	$\pm 2.6$
Standard error of mean	$\pm 1.9$	$\pm 1.1$	$\pm 0.7$
Variance	43.8	15.7	6.6

(e) Ice cylinders. Temp. =  $-4.5^{\circ}\text{C}$ ; stress rate =  $6.90 \text{ kg cm}^{-2} \text{ sec}^{-1}$ ;  
area =  $0.196 \text{ cm}^2$

Volume ( $\text{cm}^3$ )	$4.99 \times 10^{-3}$	$9.97 \times 10^{-3}$	$1.50 \times 10^{-2}$
Height (cm)	$2.54 \times 10^{-2}$	$5.08 \times 10^{-2}$	$7.62 \times 10^{-2}$
Mean	52.3	36.5	30.0
Standard deviation	$\pm 8.7$	$\pm 4.2$	$\pm 5.2$
Standard error of mean	$\pm 2.5$	$\pm 1.2$	$\pm 1.5$
Variance	75.2	17.8	26.7

Figure 9 shows the tensile strength values derived from the curves of figure 7, plotted as a function of cross-sectional area at constant volume. Straight line relationships are obtained, which intersect the ordinate at finite values. The straight lines were again obtained by the method of least squares. The average value of these intercepts is  $C = 9.4 \text{ kg cm}^{-2}$  with a standard deviation of  $\pm 3.3 \text{ kg cm}^{-2}$ . It appears that the tensile strength values obey an equation of the form

$$S = kAV^{-b} + C. \quad \dots\dots(2)$$

Here,  $S$  is the tensile strength,  $A$  the cross-sectional area,  $V$  the volume, and  $k$ ,  $b$  and  $C$  are constants. Hence, by plotting  $(S-C)/A$  against volume  $V$  on a logarithmic scale a straight line should be obtained. That this is actually the

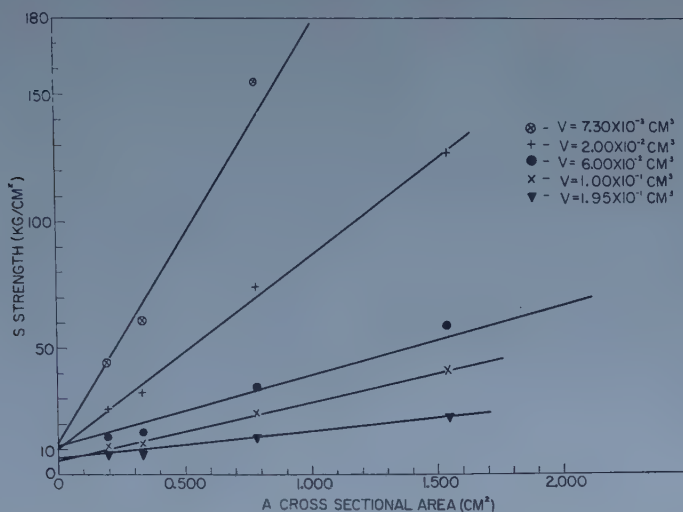


Figure 9. Tensile strength as a function of cross-sectional area at constant volume.

case over an approximately thousandfold range of volumes is shown in figure 10. The straight line was drawn by the method of least squares, not including the snow ice values for volumes 3.14 and 6.28 cm³. The corresponding equation is.

$$S = 2.74AV^{-0.84} + 9.4 \quad \text{.....(3)}$$

where  $S$  is in  $\text{kg cm}^{-2}$ ,  $A$  in  $\text{cm}^2$ , and  $V$  in  $\text{cm}^3$ .

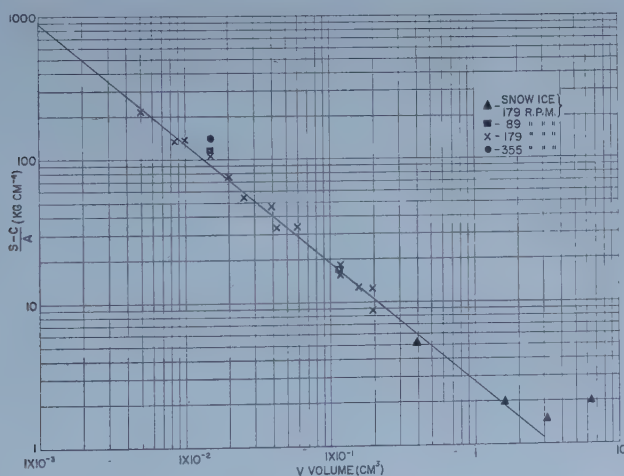


Figure 10.  $(S-C)/A$  as a function of ice volumes ( $S$ , average tensile strength,  $\text{kg cm}^{-2}$ ;  $C=9.4 \text{ kg cm}^{-2}$ ,  $A$ , area,  $\text{cm}^2$ ).

Equation (2) can also be expressed in terms of  $L$  the length or height of the specimens. Thus,

$$S = kA^{1-b}L^{-b} + C \quad \dots\dots (2a)$$

or

$$S = 2.74A^{0.16}L^{-0.84} + 9.4 \quad \dots\dots (3a)$$

These equations will be of importance for the interpretation of the experimental data, as will become apparent in the discussion.

### 3.3. Temperature Dependence

The average tensile strength data for ice films of height  $7.62 \times 10^{-2}$  cm and area  $0.782$  cm<sup>2</sup> as a function of temperature are shown in table 4. Measurements were carried out at  $-4.5$  (see table 3 (c)),  $-11$ ,  $-20$ ,  $-35$  and  $-45^\circ\text{C}$ . There is no appreciable dependence of tensile strength on temperature in this region, only a slight indication that the tensile strength will decrease rather than increase with decreasing temperatures. Butkovich (1954) found a slight increase of tensile strength with decreasing temperatures for commercial ice, which had rather large grains. Moreover, his specimens had cross-sectional areas of  $3$  cm<sup>2</sup> and were about  $9$  cm long with ends of larger cross section. Thus, Butkovich's values are bulk tensile strength values, whereas the present ones are values for thin films constrained by stainless steel surfaces.

Table 4. Tensile Strength (kg cm<sup>-2</sup>) as a function of Temperature  
Ice cylinders adhering to stainless steel

Height = $7.62 \times 10^{-2}$ cm; area = $0.782$ cm <sup>2</sup> ; volume = $5.96 \times 10^{-2}$ cm <sup>3</sup>				
Temperature ( $^\circ\text{C}$ )	-11	-20	-35	-45
Rate of stress appl <sup>n</sup> . (kg cm <sup>-2</sup> sec <sup>-1</sup> )	2.7	2.8	2.7	2.3
Mean	32.2	38.8	34.7	25.9
Standard deviation	$\pm 5.5$	$\pm 9.2$	$\pm 8.7$	$\pm 6.9$
Standard error of mean	$\pm 1.6$	$\pm 2.7$	$\pm 2.5$	$\pm 2.0$
Variance	30.3	84.5	75.3	47.9

## § 4. DISCUSSION

### 4.1. Tensile Strength as a function of Rate of Loading for Snow Ice (large specimens)

The data are shown in table 1 and figure 5. The ruptures always took place in the neighbourhood of one of the metal-snow ice interfaces. This indicates that there is a certain stress concentration near the interface, which is undoubtedly due to the constraint exerted on the ice by the adherence of the ice to the metal plate. A relevant discussion of this point by Alstadt is to be found at the end of a paper on the strength behaviour of adhesive bonds by Meissner and Baldauf (1951). During load application on snow ice, not only elastic deformation but also plastic flow takes place, as was clearly shown by Jellinek and Brill (1956). This deformation and flow cause an additional stress concentration lateral to the interface. This is somewhat counteracted by stress relaxation, which always takes place during plastic flow. Thus, rupture takes place preferably in the vicinity of the interface. The fact that the break is partly cohesive and to a smaller extent adhesive is accounted for as follows: The break starts in the ice near the interface and at an angle of  $10$  to  $20^\circ$  towards it. Thus, in most cases, the rupture has to reach the interface before it is completed. By the time the



rupture has reached the interface, tensile stress and an added torque are active at the interface. Such a torque produces a peeling action. It is well known that adhesive bonds succumb relatively easily to a peeling action. It is almost certain that the rupture is not initiated at the interface, as the adhesional strength of ice to stainless steel is very much larger than the cohesive bulk strength of ice. This will become clear during the subsequent discussion of the rupture of thin ice discs.

The change of tensile strength with the rate of loading can now be explained as follows: At low speeds of loading, an appreciable plastic flow takes place, which is apparent from the non-linearity of the recorded (load, time) curves. Hence, an appreciable lateral stress component will be present in the neighbourhood of the interface, and, though counteracted by a certain amount of stress relaxation, will lead to smaller tensile strength values. At high speeds of loading less plastic flow will take place and the lateral stress component will decrease. Therefore the tensile strength should be higher than at relatively low rates of loading. However, at the high rates, stress relaxation will be small, which in turn will tend to decrease the tensile strength. Hence there will be an optimum region of loading rates where all these effects will combine to give a maximum tensile strength, which is actually observed.

As pointed out previously the rupture of thin ice discs shows characteristics different from those of larger samples. The break is always completely cohesive and the tensile strength is a function of the volume and cross-sectional area or the thickness and cross-sectional area of the cylinders.

#### 4.2. Tensile Strength of Disc-shaped Ice Cylinders as a function of Geometrical Parameters

First, the discussion may be based on the distribution of stresses, as was proposed, for instance, by Meissner and Baldauf (1951). They point out that a quantitative, mathematical analysis of stress distribution in a cylinder has not yet been carried out, but that there should be a general correlation between tensile strength and the ratio of height to diameter of the cylinder. They further

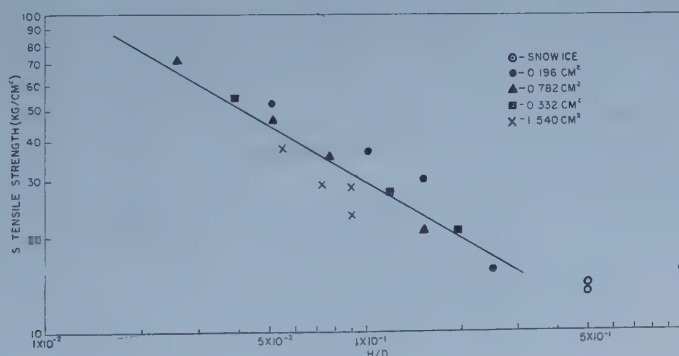


Figure 11. Tensile strengths as a function of ratio  $H/D$  of height to diameter of the ice cylinder.

state, without giving substantial reasons, that the strength should increase with decreasing length or height of the specimens. Berghausen *et al.* (1950-55) set up general equations for stress distributions in a cylinder, but did not solve them. Figure 11 shows an approximate straight-line relationship between the

logarithms of the tensile strength and the logarithms of the ratio of height to diameter of the specimens. However, the points for each area are still clearly discernible as belonging together. The equation for the logarithmic straight line obtained by the method of least squares (excluding the snow ice values) is  $S = 7.6(H/D)^{-0.59} \text{ kg cm}^{-2}$ .

In spite of this approximate correlation between the tensile strength and the ratio of height to diameter, the above assumption that the change in tensile strength with geometrical parameters is due to stress distribution is untenable.

It is well known that all crystalline substances have imperfections (e.g. dislocations). Such imperfections explain the large discrepancies between tensile strength values deduced from theoretical considerations and those found by experiment. An approximate theoretical strength value for ice can be deduced from the equation  $S = 2\gamma/d$  where  $S$  is the strength,  $\gamma$  the free surface energy for unit area, and  $d$  the distance over which the work of rupture has to take place. For water  $\gamma_{\text{H}_2\text{O}} = 76 \text{ erg cm}^{-2}$  and  $d = 2 \times 10^{-8} \text{ cm}$ ; hence one obtains a conservative estimate of  $S = 7600 \text{ kg cm}^{-2}$ . The bulk tensile strength of ice found by experiment is only about  $15 \text{ kg cm}^{-2}$ . Thus, it is clear that imperfections will have to be considered in any theory concerning tensile strength.

It will be assumed here that there is a definable distribution of imperfections in the ice. This distribution is considered in relation to the strength of the imperfections. This means that each imperfection can withstand stresses up to a certain critical value. When this critical stress is reached, the imperfection opens up to a crack and the specimen is ruptured. The spatial distribution of the imperfections is assumed to be random and the number of imperfections proportional to the specimen volume. In large specimens, the whole distribution of imperfections will be represented from the weakest to the strongest. In small specimens, not all types of imperfections will be present; those in the neighbourhood of the distribution maximum will be predominant. The relevant statistics are briefly presented here.

The underlying distribution of imperfections of different strengths is given by  $y = f(S)$ , where  $y$  is the frequency of imperfections of strength  $S$ . As soon as the stress  $S$  is reached, the imperfection opens up and produces rupture of the specimen. The strength of each specimen will be given by its weakest imperfection. The problem is to calculate the frequency distribution for these weakest imperfections, or the distribution of tensile strengths for the specimens. Such a distribution can be obtained experimentally from a large number of tensile strength experiments.

Specimens of volumes which have  $r$  imperfections each will be considered now. The probability of obtaining a specimen whose weakest imperfection corresponds to a tensile strength  $S$  is given by

$$P_r = r f(S) dS \left[ \int_S^\infty f(S) dS \right]^{r-1} \dots\dots (4)$$

$f(S) dS$  is the probability of having an imperfection of strength between  $S$  and  $S + dS$  in the sample, provided that

$$\int_0^\infty f(S) dS = 1.$$

$[\int_0^{\infty} f(S) dS]^{r-1}$  gives the probability that all other imperfections are of strength larger than  $S$ ,  $r$  gives the number of ways in which this particular assembly of imperfections can be achieved. Equation (4) can also be expressed by means of the cumulative or integral distribution of  $f(S)$  since

$$\int_0^S f(S) dS = F(S),$$

where  $F(S)$  is the cumulative distribution. Hence

$$P_r = r f(S) dS [1 - F(S)]^{r-1} \quad \dots\dots (5)$$

and the frequency distribution for the weakest imperfections is

$$f_r(S) = r f(S) [1 - F(S)]^{r-1}. \quad \dots\dots (5a)$$

The cumulative distribution for specimens containing  $r$  imperfections is obtained by integrating equation (5a) and the most probable value by finding the maximum for equation (5a), hence

$$\int_0^S f_r(S) dS = F_r(S) = 1 - [1 - F(S)]^r, \quad \dots\dots (6)$$

$$(r-1)f^2(S_{\max}) = f'(S_{\max})[1 - F(S_{\max})]. \quad \dots\dots (7)$$

The average tensile strength of the specimens is given by

$$\bar{S}_r = \int_0^{\infty} S f_r(S) dS. \quad \dots\dots (8)$$

The variance given by the square of the standard deviation  $\sigma$  is

$$\sigma^2 = \int_0^{\infty} f_r(S) [S - \bar{S}_r]^2 dS. \quad \dots\dots (9)$$

According to the assumptions outlined above,  $r = kV$  where  $k$  is a constant and  $V$  the volume of the specimen containing  $r$  imperfections.

It remains now to introduce for  $f(S)$  a specific distribution. Weibull (1939a, b) introduced a distribution function, which seems to represent experimental data quite satisfactorily in many cases. The relevant equations are collected in table 5 which shows that the average strength value of the samples should depend only on the volume and should be proportional to  $V^{-1/\beta}$  and that the variance should be proportional to  $V^{-2/\beta}$  where  $\beta$  is a constant.

Table 5. Equations based on Weibull's Distribution Function  
 $\alpha$  and  $\beta$  are constants

Underlying distribution function:  $f(S) = \alpha \beta S^{\beta-1} \exp(-\alpha S^\beta)$

Cumulative distribution:  $F(S) = 1 - \exp(-\alpha S^\beta)$

Distribution of weakest imperfections in volumes having  $r$  imperfections

$$f_r(S) = r \alpha \beta S^{\beta-1} \exp(-r \alpha S^\beta)$$

Introducing  $r = kV$ :  $f_r(S) = kV \alpha \beta S^{\beta-1} \exp(-kV \alpha S^\beta)$

Cumulative distribution  $F_r(S) = 1 - \exp(-r \alpha S^\beta)$

Most probable value  $r S_{\max}^\beta + S_{\max}^\beta = \frac{\beta-1}{\alpha \beta}$

Average strength value  $\bar{S}_r = \frac{\Gamma(1/\beta+1)}{(r \alpha)^{1/\beta}} = \frac{\Gamma(1/\beta+1)}{(kV \alpha)^{1/\beta}}$

Variance  $\sigma^2 = \frac{\text{const.}}{(kV \alpha)^{2/\beta}}$



The experimental average tensile strength values are proportional to  $V^{-1/\beta}$  (figure 7). However, a separate curve is obtained for each cross-sectional area, the strength values increasing linearly with the areas at constant volumes. The equations for the straight lines shown in figure 7 (179 rev/min values only) and the equations for the corresponding variances (figure 8), both obtained by the method of least squares, are

Area (cm <sup>2</sup> )	Height (cm)	Tensile strength (kg cm <sup>-2</sup> )	Variance
1.54	0.762 to $1.27 \times 10^{-1}$	$\bar{S} = 5.46 V^{-0.92}$	$\sigma^2 = 0.22 V^{-2.6}$
0.782	0.254 to $1.52 \times 10^{-1}$	$\bar{S} = 4.79 V^{-0.70}$	$\sigma^2 = 1.3 V^{-1.1}$
0.332	0.254 to $1.27 \times 10^{-1}$	$\bar{S} = 3.04 V^{-0.61}$	$\sigma^2 = 0.1 V^{-1.14}$
0.196	0.254 to $0.762 \times 10^{-1}$	$\bar{S} = 3.49 V^{-0.51}$	$\sigma^2 = 0.22 V^{-1.1}$

As can be seen from these data the exponents for the volumes in the expressions for the variances are about twice those in the strength equations. Thus, on the whole, the data fit the statistical theory, except for the marked influence of the cross-sectional area. Berghausen *et al.* (1950-55) found that their data gave approximately a straight line when the tensile strengths were plotted against the logarithms of the volumes. They concluded that the dependence of the strength on the volume is due to a statistical effect involving imperfections. However, they did not attempt a detailed analysis. Their standard deviations are at least two to four times larger than those obtained in this work and the influence of the cross-sectional areas is obscured owing to the large scatter of the experimental values.

It is clear that the dependence of the tensile strength on the specimen volume is due to a statistical effect, most reasonably explained by imperfections. However, the statistical treatment as outlined above only accounts for certain aspects of the experimental data.

An attempt will now be made to account for the influence of the area on a statistical bases. For this purpose, the assumption that the whole specimen ruptures as soon as the strength of the weakest imperfection is reached will be modified. It will be assumed now that, when the strength of an imperfection is reached, a crack is formed which does not grow beyond a certain unspecified average size. Thus, there will be stress relief in the neighbourhood of this crack and the next stronger imperfection will open up; the specimen will rupture when a string of cracks has formed in cascade fashion across the specimen. It is very difficult to treat such a model mathematically on a statistical basis. A simpler problem, which constitutes an approximation to the above model, is treated here. The specimen is considered as a bundle of parallel rods of equal cross section and length. An imperfection which opens into a crack, only 'ruptures' the rod in which it is situated. Thus, the problem reverts to the case of the strength of a bundle of parallel threads encountered with textiles. This problem has been developed to a certain extent by Weibull (1939 a, b). However, as pointed out by Daniels (1945), his probabilities were not chosen correctly. Daniels has elaborated the statistics of such parallel systems, but operated only with cumulative distributions and studied the behaviour of such distributions and their average values for large numbers of parallel elements. The statistics are developed here starting with derivative distributions, which allow average values to be calculated.



In the case of one rod having a volume which contains  $r$  imperfections, the breaking load-frequency distribution is given by equation (5a). Loads are used here in preference to stress. Hence the probability of having such a rod of breaking load  $L$  is given by

$$P_r = rf(L) dL [1 - F(L)]^r$$

(when  $r$  is large). The condition for  $n$  parallel rods to break under exactly a load  $L$ , in terms of  $L$ , is given in table 6. The above scheme for  $n$  parallel rods

Table 6

Rod	1	2	3	4	..	$n-1$	$n$
1	1	1 to $\frac{1}{2}$	1 to $\frac{1}{3}$	1 to $\frac{1}{4}$	..	1 to $\frac{1}{n-1}$	1 to $\frac{1}{n}$
2	$\frac{1}{2}$ to 0	$\frac{1}{2}$	$\frac{1}{2}$ to $\frac{1}{3}$	$\frac{1}{2}$ to $\frac{1}{4}$	..	$\frac{1}{2}$ to $\frac{1}{n-1}$	$\frac{1}{2}$ to $\frac{1}{n}$
3	$\frac{1}{3}$ to 0	$\frac{1}{3}$ to 0	$\frac{1}{3}$	$\frac{1}{3}$ to $\frac{1}{4}$	..	$\frac{1}{3}$ to $\frac{1}{n-1}$	$\frac{1}{3}$ to $\frac{1}{n}$
4	$\frac{1}{4}$ to 0	$\frac{1}{4}$ to 0	$\frac{1}{4}$ to 0	$\frac{1}{4}$	..	$\frac{1}{4}$ to $\frac{1}{n-1}$	$\frac{1}{4}$ to $\frac{1}{n}$
.	.	.	.	.	.	.	.
.	.	.	.	.	.	.	.
.	.	.	.	.	.	.	.
$n-2$	$\frac{1}{n-2}$ to 0	$\frac{1}{n-2}$ to 0	$\frac{1}{n-2}$ to 0	$\frac{1}{n-2}$ to 0	..	$\frac{1}{n-2}$ to $\frac{1}{n-1}$	$\frac{1}{n-2}$ to $\frac{1}{n}$
$n-1$	$\frac{1}{n-1}$ to 0	$\frac{1}{n-1}$ to 0	$\frac{1}{n-1}$ to 0	$\frac{1}{n-1}$ to 0	..	$\frac{1}{n-1}$	$\frac{1}{n-1}$ to $\frac{1}{n}$
$n$	$\frac{1}{n}$ to 0	$\frac{1}{n}$ to 0	$\frac{1}{n}$ to 0	$\frac{1}{n}$ to 0	..	$\frac{1}{n}$ to 0	$\frac{1}{n}$

may be exemplified by discussing the case of two parallel rods. For the two rods to break exactly under the load  $L$ , we have,

Rod 1: case 1,  $L$ ; case 2,  $L$  to  $\frac{1}{2}L$ .

Rod 2: case 1,  $\frac{1}{2}L$  to 0; case 2,  $\frac{1}{2}L$ .

Thus for case 1, rod 1 is able to support a breaking load of  $L$ , whereas rod 2 can support any breaking load from  $\frac{1}{2}L$  to 0. If these conditions are fulfilled, the system will break when a load of  $L$  is applied to it. The probability of having a rod which can maintain a breaking load  $L$  is  $f_r(L) dL$ , the probability of having a rod which can maintain a breaking load from  $\frac{1}{2}L$  to 0 is  $\int_0^{\frac{1}{2}L} f_r(L) dL$ . There are two possible cases: either rod 1 can sustain  $L$  and rod 2  $\frac{1}{2}L$  to 0 or vice versa. Hence, the probability of having two rods satisfying case 1 is

$$2! f_1(L) dL \int_0^{\frac{1}{2}L} f_r(L) dL.$$

Similarly, for case 2

$$2! f_r(\frac{1}{2}L) dL \int_{\frac{1}{2}L}^L f_1(L) dL.$$

Therefore, the total probability for the system of two rods to break exactly under the load  $L$  is

$$P_{r,2} = 2! f_r(L) dL \int_0^{L/2} f_r(L) dL + 2! f_r(\frac{1}{2}L) dL \int_{L/2}^L f_r(L) dL$$

and the corresponding frequency distribution is given by

$$f_{r,2}(L) = 2! f_r(L) \int_0^{L/2} f_r(L) dL + 2! f_r(\frac{1}{2}L) \int_{L/2}^L f_r(L) dL.$$

By extending these considerations to larger numbers of rods, the above scheme was obtained and the general equation for the frequency distribution for  $n$  parallel rods can be deduced. This equation is given by an expression as follows:

$$\begin{aligned} f_{r,n}(L) = & n! f_r(L) \prod_{a=1/n}^{1/2} \int_0^{aL} f_r(L) dL + n! f_r(\frac{1}{2}L) \int_{L/2}^L f_r(L) dL \prod_{a=1/n}^{1/3} \int_0^{aL} f_r(L) dL \\ & + n! f_r(\frac{1}{3}L) \int_{L/3}^{L/2} f_r(L) dL \int_{L/3}^L f_r(L) dL \prod_{a=1/n}^{1/4} f_r(L) dL \\ & + n! f_r(\frac{1}{4}L) \int_{L/4}^{L/3} f_r(L) dL \int_{L/4}^{L/2} f_r(L) dL \int_{L/4}^L f_r(L) dL \prod_{a=1/n}^{1/5} \int_0^{aL} f_r(L) dL + \dots \\ & + n! f_r\left(\frac{1}{n}L\right) \left[ \int_{L/n}^{L/(n-1)} f_r(L) dL \int_{L/n}^{L/(n-2)} f_r(L) dL \dots \int_{L/n}^L f_r(L) dL \right]. \end{aligned}$$

The average breaking load in the case of the Weibull distribution is given by expressions as follows (two rods):

$$\bar{L}_{r,2} = \frac{\Gamma(1/\beta + 1)}{(r\alpha)^{1/\beta}} 2! \{1 - [1 + (\frac{1}{2})^\beta]^{-(1+1/\beta)} [1 + (\frac{1}{2})^{\beta-1}] + 2^{\beta-1/\beta}\}$$

or

$$\bar{L}_{r,2} = \frac{\Gamma(1/\beta + 1)}{(r\alpha)^{1/\beta}} 2! C_2 \quad \dots\dots (11)$$

where  $C_2$  is a constant. The average tensile strength is given by

$$\bar{S}_{r,2} = \frac{\Gamma(1/\beta + 1)}{(r\alpha)^{1/\beta}} \frac{2! C_2}{2A_1} \quad \dots\dots (12)$$

where  $A_1$  is the cross-sectional area of a single rod. The average value for three rods is given by

$$\bar{L}_{r,3} = \frac{\Gamma(1/\beta + 1)}{(r\alpha)^{1/\beta}} 3! C_3.$$

The values for the constants  $C_1$ ,  $C_2$ ,  $C_3$  and  $C_4$  have been calculated for  $\beta=1$  and  $\beta=2$  and are

	$C_1$	$C_2$	$C_3$	$C_4$
$\beta=1$	1.00	1.10	0.79	0.45
$\beta=2$	1.00	1.34	1.01	0.63

It can be seen that the theoretical stress values for specimens of constant height rise rather steeply with the number of parallel rods as long as this number is small. Figure 12 shows the experimental tensile strength values plotted against the cross-sectional areas of the specimens at constant heights; for heights between about  $6 \times 10^{-2}$  to  $2 \times 10^{-1}$  cm, the strengths do not change appreciably with area. However, for smaller heights this increase becomes more appreciable.

The observed increases are not large enough to justify the assumption of a small number of parallel elements.

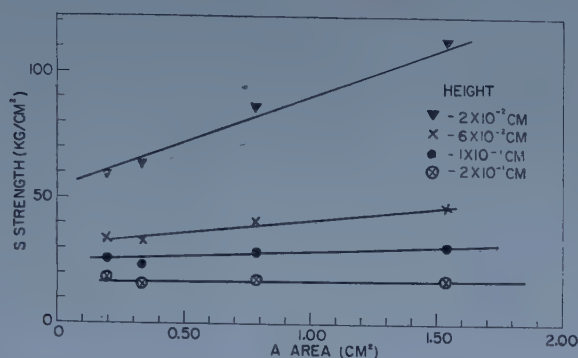


Figure 12. Tensile strength as a function of cross-sectional area at constant height.

Daniels has shown that, as the number of parallel rods  $n$  becomes very large the average breaking load is approximately given by

$$\bar{L}_{r,n} = n \times \text{constant}, \quad \dots\dots (13)$$

At the same time, the strength-frequency distribution approximates a normal distribution. Equation (13) holds if  $1 - F_r(L)$  tends to zero faster than  $1/L$ . This is the case for the Weibull distribution as  $\exp(-r\alpha L)$  for  $(B \geq 1)$  tends to zero faster than  $1/L$ . Hence for large values of  $n$  one obtains

$$\bar{L}_{r,n} = \frac{\Gamma(1/\beta + 1)}{(r\alpha)^{1/\beta}} n! C_n \quad \text{or} \quad \bar{L}_{r,n} = \frac{\Gamma(1/\beta + 1)}{(r\alpha)^{1/\beta}} nc \quad \dots\dots (14)$$

where  $c$  is a constant. The average tensile strength is then given by

$$\bar{S}_{r,n} = \frac{\Gamma(1/\beta + 1)}{(r\alpha)^{1/\beta}} \frac{c}{A_1}. \quad \dots\dots (15)$$

$r$  in this case is proportional to the length of the sample  $r = kL$ , hence equation (15) can be written as  $\bar{S}_{r,n} = kL^{-1/\beta}$ . It was shown by Weibull that if the underlying distribution starts at a finite value, a constant  $C$  has to be added to the equation. Hence the final equation reads

$$S_{r,n} = kL^{-1/\beta} + C. \quad \dots\dots (16)$$

Equation (16) would be identical with the empirical equation (2a) if  $b = 1/\beta = 1$ . The experiments reported here lead to a value for  $b$  of 0.84. Equation (16) can also be written in the form

$$\bar{S}_{r,n} = kA^{1/\beta} V^{-1/\beta} + C. \quad \dots\dots (17)$$

Thus it appears that this statistical treatment accounts well for the experimental results except for a relatively small residual area effect. Equation (17) would be identical with the empirical equation (2):  $S = kAV^{-b} + C$  if the exponent for  $A$  were unity; actually, the exponent  $1/\beta = b = 0.84$ . The variance, following Daniels (1945), can be written as follows†

$$\sigma^2 = \frac{1}{(r\alpha\beta)^{2/\beta}} \{ \exp(-1/\beta) - \exp(-2/\beta) \},$$

†Daniels'  $b(s)$  is  $F_r(S)$  here.

$$\sigma^2 = \frac{A^{2/\beta}}{(\alpha\beta V)^{2/\beta}} \{\exp(-1/\beta) - \exp(-2/\beta)\}.$$

As was seen previously, the variances are approximately proportional to  $V^{-2/\beta}$  (see p. 810).

Though the statistical result represents the experimental data quite well, there is still a noticeable cross-sectional area effect. This is believed to be due to two causes. First, the statistical model is only an approximate one, and second, there is probably a stress distribution effect superimposed on the statistical effect.

As was previously pointed out, the large ice cylinders break predominantly in the neighbourhood of the metal-ice interface, usually in a region of 1 to 2 mm from the interface. This is caused by the combined effect of stress distribution and imperfections. The location of the rupture is due to the stress concentration in the neighbourhood of the interfaces. The magnitude of the tensile strength, however, is largely conditioned by the imperfections. Only occasionally an especially weak imperfection is present outside the interfacial zones, which ruptures before a weak imperfection opens up near the interface. This situation will prevail until the specimens are decreased to a thickness where the stress concentration regions overlap. When this happens, the statistics of the imperfections become more important in determining the tensile strength obtained; this is to be expected theoretically and also is in accordance with the results found experimentally. The stress distribution effect still makes itself felt in the residual observed influence of the cross-sectional area.

#### ACKNOWLEDGMENTS

This work was carried out under a personal service contract with the Corps of Engineers at the Snow, Ice and Permafrost Research Establishment Laboratories. It is the author's pleasure to thank Messrs. J. A. Bender, T. R. Butkovich, and Drs. D. Assur and J. K. Landauer for helpful discussions; Messrs. B. L. Hansen and L. E. Stanley for advice in the construction of the apparatus; and Dr. H. Bader for his interest in this work. The author is also indebted to Mr. G. M. Walker for valuable help in the execution of a large number of the experiments.

#### REFERENCES

- BERGHAUSEN, P. E., GOOD, R. J., KRAUS, F., PODOLSKY, B., and SOLLER, W., 1950-55, Applied Science Research Laboratory, University of Cincinnati, Progress Reports, Army Air Force Contract AF 33 (616)-231; also WADC Technical Report 53-461 and WADC Technical Report 55-44.
- BUTKOVICH, T. R., 1954, Snow, Ice and Permafrost Research Establishment, Corps of Engineers, U.S. Army, Research Paper 11.
- DANIELS, H. E., 1945, *Proc. Roy. Soc. A*, **183**, 405.
- DEBRUYNE, N. D., Editor, 1951, *Adhesion and Adhesives* (Amsterdam: Elsevier).
- EPSTEIN, B., 1948, *J. Appl. Phys.*, **19**, 140.
- JELLINEK, H. H. G., and BRILL, R., 1956, *J. Appl. Phys.*, **27**, 1198.
- KHOMICHEVSKAIA, L. S., 1940, *Trudi Komiteta po vechnoi merzlotе*, X, 37. Translated by St. Anthony Falls Hydraulic Laboratory, University of Minnesota, for St. Paul District, Corps of Engineers, Project Report No. 26, October, 1951.
- MESSNER, H. P., and BALDAUF, G. H., 1951, *Trans. Amer. Soc. Mech. Engrs*, **697**.
- PEIRCE, F. T., 1926, *J. Text. Inst.*, **17**, 355.
- WEIBULL, W., 1939 a, *Ingeniöretsk Akad. Handl.*, **153**; 1939 b, *Ibid.*, **155**.



# Wave Functions for the Hydrogen Atom in Spheroidal Coordinates

## I: The Derivation and Properties of the Functions

By C. A. COULSON AND P. D. ROBINSON

Mathematical Institute, Oxford

*MS. received 30th December 1957*

**Abstract.** The Schrödinger equation is set up for the hydrogen atom using spheroidal coordinates with the nucleus at one focus, and it is solved as completely as possible. An expression is obtained for the wave function in a general excited state, and orthogonality properties are proved. Relations are investigated between spheroidal, spherical polar and parabolic wave functions.

### § 1. INTRODUCTION

THE reasons which prompted this investigation were twofold. Firstly, it was hoped to find some simplification in the complicated wave functions which are known to exist in spheroidal coordinates for the two-centre problem in wave mechanics. The hydrogen atom is a special case of the two-centre problem, and simple wave functions are already known for it both in spherical polar and in parabolic coordinates. Since there are simple relations (see later) between the three sets of coordinates, this implies that there must be elementary solutions of the hydrogenic wave equation in spheroidals also. Secondly, it was hoped that these functions, if convenient, would assist calculations when a hydrogen atom is in the neighbourhood of a point charge, in the same way that the parabolic wave functions are used to investigate the Stark effect in a uniform field (Schrödinger 1926).

Although the expression obtained for the wave functions is not complete in that its coefficients depend on a purely numerical parameter which cannot in general be determined analytically, nevertheless interesting properties are found and the functions are shown to be a kind of intermediary between the spherical polar and parabolic ones. They also turn out to be the so-called 'correct' zero-order functions to use when the atom is perturbed by a point charge, and the previous degeneracy is thereby removed.

### § 2. DEVELOPMENT OF THE WAVE FUNCTIONS

The general two-centre problem, with nuclei of charges  $Z_1$  and  $Z_2$  at A and B respectively, has been extensively studied in connection with  $H_2^+$  and other ions. Baber and Hassé (1935) gave a comprehensive account of the various solutions to the Schrödinger wave equation, which will separate in spheroidal coordinates. Wilson (1928) mentioned the special case of the hydrogen atom for which  $Z_2 = 0$  and  $Z_1 = 1$ , showing briefly how the well-known energy eigenvalues could be obtained, but he did not discuss the eigenfunctions sufficiently. We shall give an *a priori* derivation of the eigenvalues, and develop the wave functions as far as possible.

2.1. *Solution of the Wave Equation*

The spheroidal coordinates are  $\xi = (r_a + r_b)/R$ ,  $\eta = (r_a - r_b)/R$  and  $\phi$ , the angle between the plane PAB and some arbitrary fixed plane through AB; they form an orthogonal system with metric

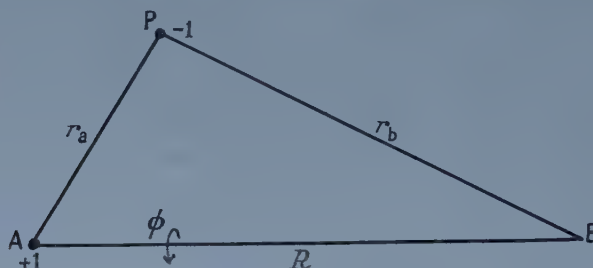
$$ds^2 = \frac{R^2}{4} \left( \frac{\xi^2 - \eta^2}{\xi^2 - 1} \right) d\xi^2 + \frac{R^2}{4} \left( \frac{\xi^2 - \eta^2}{1 - \eta^2} \right) d\eta^2 + \frac{R^2}{4} (\xi^2 - 1)(1 - \eta^2) d\phi^2$$

and volume element

$$d\tau = \frac{1}{8} R^3 (\xi^2 - \eta^2) d\xi d\eta d\phi.$$

In the general case with charges  $Z_1$  at A and  $Z_2$  at B, the Schrödinger wave equation for the electronic energy eigenvalues is, in atomic units,

$$\begin{aligned} \frac{\partial}{\partial \xi} \left[ (\xi^2 - 1) \frac{\partial \psi}{\partial \xi} \right] + \frac{\partial}{\partial \eta} \left[ (1 - \eta^2) \frac{\partial \psi}{\partial \eta} \right] + [(\xi^2 - 1)^{-1} + (1 - \eta^2)^{-1}] \frac{\partial^2 \psi}{\partial \phi^2} \\ + [\tfrac{1}{2} E R^2 (\xi^2 - \eta^2) + R(Z_1 + Z_2)\xi - R(Z_1 - Z_2)\eta] \psi = 0. \end{aligned}$$



We shall only consider bound states, so that  $E$  is negative. It is convenient to work in terms of the parameter  $p$ , defined by

$$p^2 = -\tfrac{1}{2} E R^2.$$

Then, if we set  $\psi(\xi, \eta, \phi) = X(\xi)Y(\eta)\Phi(\phi)$ , the following equations are obtained:

$$\frac{d}{d\xi} \left[ (\xi^2 - 1) \frac{dX}{d\xi} \right] + [A + R(Z_1 + Z_2)\xi - p^2\xi^2 - m^2(\xi^2 - 1)^{-1}]X = 0, \quad (1 \leq \xi \leq \infty) \quad \dots\dots (1)$$

$$\frac{d}{d\eta} \left[ (1 - \eta^2) \frac{dY}{d\eta} \right] - [A + R(Z_1 - Z_2)\eta - p^2\eta^2 + m^2(1 - \eta^2)^{-1}]Y = 0, \quad (-1 \leq \eta \leq +1) \quad \dots\dots (2)$$

$$\frac{d^2\Phi}{d\phi^2} + m^2\Phi = 0, \quad (0 \leq \phi \leq 2\pi). \quad \dots\dots (3)$$

Equation (3) is the usual  $\phi$ -equation, and the separation constant  $m$  must be zero or integral for a physically acceptable  $\Phi$ . We can consider  $m$  to be positive without loss of generality, and so avoid writing  $|m|$  in the analysis. We then have  $\Phi = \exp(\pm mi\phi)$ .  $A$  is a second separation constant whose eigenvalues will be investigated.

From now onwards, we consider the case of the hydrogen atom, with  $Z_1 = 1$  and  $Z_2 = 0$ . Equations (1) and (2) take exactly the same form, but we cannot say at once that the functions  $X(\xi)$  and  $Y(\eta)$  will be the same, because the ranges of the variables  $\xi$  and  $\eta$  are different. We treat the two equations in turn.

2.1.1. The  $\xi$ -equation.

Equation (1) becomes

$$\frac{d}{d\xi} \left[ (\xi^2 - 1) \frac{dX}{d\xi} \right] + [A + R\xi - p^2\xi^2 - m^2(\xi^2 - 1)^{-1}]X = 0, \quad (1 \leq \xi \leq \infty).$$

Let  $X(\xi) = e^{-p\xi}(\xi^2 - 1)^{m/2}f(\xi)$ . Then the equation for  $f(\xi)$  is

$$(\xi^2 - 1) \frac{d^2f}{d\xi^2} + 2[(m+1)\xi - p(\xi^2 - 1)] \frac{df}{d\xi} + [2p\sigma\xi + A - p^2 + m(m+1)]f = 0,$$

where  $\sigma = R/2p - (m+1)$ . This equation has regular singularities at  $\xi = \pm 1$ ; hence a series solution in powers of  $\xi - 1$  will be valid with a radius of convergence of at least 2. Putting  $\xi - 1 = t$ , so that  $0 \leq t \leq \infty$ ,

$$(t^2 + 2t) \frac{d^2f}{dt^2} + 2[-pt^2 + (m+1-2p)t + (m+1)] \frac{df}{dt} + (2p\sigma t + B)f = 0,$$

where  $B = A - p^2 + 2p\sigma + m(m+1)$ . A trial solution

$$f(t) = \sum_{s=0}^{\infty} a_s t^{c+s}$$

gives the indicial equation

$$2c(c+m)a_0 = 0, \quad (a_0 \neq 0).$$

Two cases now arise, depending on whether  $m$  is zero or a positive integer. First we suppose  $m$  to be a positive integer. Then  $c=0$  or  $c=-m$ , and the basic solutions are

$$f_1(t) = 1 + a_1(c)t + a_2(c)t^2 + \dots$$

with  $c=0$ , and

$$f_2(t) = t^{-m} + a_1'(c)t^{-m+1} + a_2'(c)t^{-m+2} + \dots$$

with  $c=-m$ . We have set  $a_0$  and  $a_0' = 1$  without loss of generality. The general solution is  $C_1 f_1(t) + C_2 f_2(t)$ , where  $C_1$  and  $C_2$  are arbitrary constants. So we have

$$f(\xi) = C_1 f_1(\xi - 1) + C_2 f_2(\xi - 1),$$

and  $X(\xi) = C_1 e^{-p\xi}(\xi^2 - 1)^{m/2} f_1(\xi - 1) + C_2 e^{-p\xi}(\xi^2 - 1)^{m/2} f_2(\xi - 1)$ .

At  $\xi=1$  the second term above is of order  $(\xi-1)^{-m/2}$ . We must therefore choose  $C_2=0$  if  $X(\xi)$  is to be physically acceptable.

If  $m$  is zero, however, the indicial equation has two equal roots  $c=0$ . In this case the basic solutions are  $f_1(t) = 1 + a_1(c)t + a_2(c)t^2 + \dots$  with  $c=0$ , as before, and  $f_3(t) = f_1(t) \ln t + (\partial/\partial c)f_1(t)$  with  $c=0$ . The general solution is  $C_3 f_1(t) + C_4 f_3(t)$ , and

$$X(\xi) = C_3 e^{-p\xi} f_1(\xi - 1) + C_4 e^{-p\xi} f_3(\xi - 1).$$

The term in  $C_4$  now has a logarithmic singularity at  $\xi=1$ , and so we must choose  $C_4=0$  for a physically acceptable  $X(\xi)$ .

We see therefore that whatever the value of  $m$ , the solution of the  $\xi$ -equation is expressible as

$$X(\xi) = K_1 e^{-p\xi}(\xi^2 - 1)^{m/2} f_1(\xi - 1),$$

where  $K_1$  is a constant.

2.1.2. The  $\eta$ -equation.

The  $\eta$ -equation (2) is

$$\frac{d}{d\eta} \left[ (1 - \eta^2) \frac{dY}{d\eta} \right] - [A + R\eta - p^2\eta^2 + m^2(1 - \eta^2)^{-1}]Y = 0, \quad (-1 \leq \eta \leq +1).$$

The argument now is parallel to that for the  $\xi$ -equation. If we let

$$Y(\eta) = e^{-\nu\eta}(1-\eta^2)^{m/2}g(\eta),$$

and then put  $u = \eta - 1$ , so that  $-2 \leq u \leq 0$ , we obtain

$$g(u) = C_5 f_1(u) + C_6 f_2(u)$$

as the general solution of

$$(u^2 + 2u) \frac{d^2 g}{du^2} + 2[-pu^2 + (m+1-2p)u + m+1] \frac{dg}{du} + (2p\sigma u + B)g = 0.$$

As before, we can show that  $C_6 = 0$  by considering the behaviour at  $\eta = 1$ , both when  $m \neq 0$  and when  $m = 0$ . Hence we may write the solution of the  $\eta$ -equation

$$Y(\eta) = K_2 e^{-\nu\eta}(1-\eta^2)^{m/2} f_1(\eta-1).$$

### 2.1.3. The series for $f_1(t)$ .

The coefficients of the power series for  $f_1(t)$  satisfy the recurrence formula

$$\alpha_s a_{s+1} + \beta_s a_s + \gamma_s a_{s-1} = 0 \quad (a_{-1} = 0), \text{ for } s \geq 0,$$

where

$$\alpha_s = 2(s+1)(s+m+1),$$

$$\beta_s = s^2 + s(2m+1-4p) + B,$$

$$\gamma_s = 2p(\sigma+1-s).$$

Now suppose that

$$\frac{a_{s+1}}{a_s} = b_0 + \frac{b_1}{s} + \frac{b_2}{s^2} + \dots,$$

then

$$\frac{a_s}{a_{s-1}} = b_0 + \frac{b_1}{s-1} + \frac{b_2}{(s-1)^2} + \dots = b_0 + \frac{b_1}{s} + \frac{b_1+b_2}{s^2} + \dots$$

On equating coefficients in

$$\alpha_s \frac{a_{s+1}}{a_s} + \beta_s \frac{a_s}{a_{s-1}} + \gamma_s = 0$$

we obtain

$$2b_0^2 + b_0 = 0,$$

$$4b_0 b_1 + 2b_0^2(m+2) + b_0(2m+1-4p) + b_1 - 2p = 0.$$

These conditions give either  $b_0 = 0$ ,  $b_1 = 2p$  or  $b_0 = -\frac{1}{2}$ ,  $b_1 = \frac{1}{2} - \frac{1}{2}m$ .

There are now three possibilities for the series  $f_1(t)$ :

$$(i) \quad a_{s+1}/a_s = 2p/s + O(1/s^2),$$

$$(ii) \quad a_{s+1}/a_s = -\frac{1}{2} - \frac{1}{2}(m-1)/s + O(1/s^2),$$

(iii) the series terminates.

A closer inspection of case (i) shows that it actually leads to the result

$$a_{s+1}/a_s = 2p/s - (R/2p + m+1)2p/s^2 + O(1/s^3),$$

which gives

$$a_s = \frac{(2p)^s}{s!} s^{-(R/2p+m)} l_s,$$

where  $l_s \rightarrow$  a limit  $l$  as  $s \rightarrow \infty$ .

Then

$$f_1(t) \sim l \sum_{s=0}^{\infty} \frac{(2pt)^s}{s!} s^{-(R/2p+m)} > l \sum_{s=0}^{\infty} \frac{(2pt)^s}{s! s^N} > l \sum_{s=0}^{\infty} \frac{(2pt)^s}{(s+N)!} = lL(t)$$



say, where  $N$  is any positive integer greater than  $R/2p+m$ .

We have 
$$L(t) = \frac{1}{(2pt)^N} \sum_{s=0}^{\infty} \frac{(2pt)^{s+N}}{(s+N)!} = \frac{1}{(2pt)^N} \left[ e^{2pt} - \sum_{s=0}^{N-1} \frac{(2pt)^s}{s!} \right] \sim \frac{e^{2pt}}{(2pt)^N},$$

and so  $X(\xi) \sim$  a function of  $\xi$  which is greater than

$$K_1 l (\xi^2 - 1)^{m/2} [2p(\xi - 1)]^{-N} e^{p(\xi - 2)}.$$

This itself tends to  $\infty$  as  $\xi \rightarrow \infty$ , so that case (i) cannot occur with physically significant wave functions.

Now consider case (ii). If  $m \neq 0$ , it follows that  $a_s = (-\frac{1}{2})^s s^{m-1} l'_s$ , where  $l'_s \rightarrow$  a limit  $l'$ . Thus

$$f_1(u) \sim l' \sum_{s=1}^{\infty} (-\frac{1}{2}u)^s s^{m-1} \sim l' (1 + \frac{1}{2}u)^{-m}$$

as  $u \rightarrow -2$ . So  $f_1(\eta - 1) \sim l' (\frac{1}{2} + \frac{1}{2}\eta)^{-m}$ . This would make  $Y(\eta)$  of order  $(1 + \eta)^{-m/2}$  at  $\eta = -1$  and therefore unacceptable.

If  $m = 0$ ,  $f_1(u) \sim -l' \ln(1 + \frac{1}{2}u)$  and  $Y(\eta)$  would have a logarithmic singularity at  $\eta = -1$ . Thus in both situations  $Y(\eta)$  is not an acceptable function, and therefore case (ii) cannot occur. We can also see that the series expansion in  $X(\xi)$  is not acceptable in this case either, because the series for  $f_1(t)$  will diverge when  $t > 2$ .

There only remains case (iii), and so the series for  $f_1(t)$  must terminate.

## 2.2. The Eigenvalues

Suppose  $a_{M-1}$  is the last non-zero coefficient in the series for  $f_1(t)$ , i.e.

$$a_M = a_{M+1} = a_{M+2} = \dots = 0.$$

Then since

$$\alpha_M a_{M+1} + \beta_M a_M + \gamma_M a_{M-1} = 0,$$

we must have  $\gamma_M = 0$ , i.e.  $\sigma + 1 = M$  and  $R/2p = M + m =$  a positive integer  $n$ , say. This is the principal quantum number, and  $E = -\frac{1}{2}n^2$ . In this way we retrieve the familiar energy eigenvalues for the hydrogen atom.

We now have a set of equations to determine the eigenvalues for the separation constant  $A$ :

$$\beta_0 a_0 + \alpha_0 a_1 = 0$$

$$\gamma_1 a_0 + \beta_1 a_1 + \alpha_1 a_2 = 0$$

$$\gamma_2 a_1 + \beta_2 a_2 + \alpha_2 a_3 = 0$$

$$\dots \dots \dots$$

$$\gamma_{\sigma-1} a_{\sigma-2} + \beta_{\sigma-1} a_{\sigma-1} + \alpha_{\sigma-1} a_{\sigma} = 0$$

$$\gamma_{\sigma} a_{\sigma-1} + \beta_{\sigma} a_{\sigma} = 0$$

where  $\sigma = n - m - 1$ , and

$$\alpha_s = 2(s+1)(s+m+1),$$

$$\beta_s = s^2 + s(2m+1-2R/n) - R^2/4n^2 + m(m+1) + R\sigma/n + A,$$

$$\gamma_s = R(\sigma+1-s)/n.$$



Let us suppose  $\Delta_s$  and  $\Delta_{s-1}$  have a common root  $\mu$ . Then

$$D_s(-\mu) = D_{s-1}(-\mu) = 0.$$

But  $D_s = \beta_s D_{s-1} - \alpha_{s-1} \gamma_s D_{s-2}$ , and so  $D_{s-2}(-\mu) = 0$  also. In turn we can show

$$D_{s-3}(-\mu) = \dots = D_1(-\mu) = D_0(-\mu) = 0.$$

It is clear that  $D_1(-\mu) = D_0(-\mu) = 0$  is impossible, for this would imply  $\alpha_0 \gamma_1 = 0$ , and so in fact  $\Delta_s$  and  $\Delta_{s-1}$  have no common characteristic root. We deduce that the characteristic roots of  $\Delta_0$  are all real and distinct, and hence that  $A$  has  $\sigma + 1$ , or  $n - m$ , real, distinct eigenvalues.

### 2.3. The Wave Functions

Let the  $n - m$  eigenvalues for  $A$  be  $A_k$ ,  $k = 1, 2, \dots, n - m$ . Then

$$\psi_{n,m,k} = \exp[-R(\xi + \eta)/2n] \{(\xi^2 - 1)(1 - \eta^2)\}^{m/2} f_k(\xi) f_k(\eta) e^{\pm mi\phi} \dots \dots (4)$$

where  $f_k(t) = 1 + a_1 t + a_2 t^2 + \dots + a_\sigma t^\sigma$  is the polynomial whose coefficients involve the eigenvalue  $A_k$ . There are  $n - m$  functions  $\psi$  for given  $n$  and  $m$ .

We have

$$a_1 = -\frac{\beta_0}{\alpha_0}, \quad a_2 = -\frac{\gamma_1}{\alpha_1} + \frac{\beta_0 \beta_1}{\alpha_0 \alpha_1}, \quad a_3 = \frac{\gamma_1 \beta_2}{\alpha_1 \alpha_2} + \frac{\gamma_2 \beta_0}{\alpha_2 \alpha_0} - \frac{\beta_0 \beta_1 \beta_2}{\alpha_0 \alpha_1 \alpha_2}, \text{ etc.,}$$

or the coefficients may be expressed in terms of continued fractions. It is only possible to find the  $A_k$  analytically in the simpler cases where  $n - m = 1, 2, 3$  or  $4$ ; otherwise numerical methods will be necessary to find the characteristic roots of  $\Delta_\sigma$ . As defined above,  $\psi$  is not normalized.

We can illustrate the above discussion by giving a few of the simpler wave functions. Thus in the cases where  $n$  equals 1, 2 and 3 they are as follows where  $A'$  is written for  $A - R^2/4n^2$ :

$$n=1, m=0: \exp[-\frac{1}{2}R(\xi + \eta)], \quad A' = 0.$$

$$n=2, m=0: \exp[-\frac{1}{4}R(\xi + \eta)](\xi - R/2A')(\eta - R/2A'), \quad A'(A' + 2) = R^2/4.$$

$$n=2, m=1: \exp[-\frac{1}{4}R(\xi + \eta)](\xi^2 - 1)^{1/2}(1 - \eta^2)^{1/2}e^{\pm i\phi}, \quad A' + 2 = 0.$$

$$n=3, m=0: \exp[-\frac{1}{6}R(\xi + \eta)]\{\xi^2 - 3(A' + 6)\xi/R + 1 + 8/A'\} \\ \times \{\eta^2 - 3(A' + 6)\eta/R + 1 + 8/A'\}, \quad A'(A' + 2)(A' + 6) = 4R^2(A' + 4)/9.$$

$$n=3, m=1: \exp[-\frac{1}{6}R(\xi + \eta)](\xi^2 - 1)^{1/2}(1 - \eta^2)^{1/2}\{\xi - R/3(A' + 2)\} \\ \times \{\eta - R/3(A' + 2)\}e^{\pm i\phi}, \quad (A' + 2)(A' + 6) = R^2/9.$$

$$n=3, m=2: \exp[-\frac{1}{6}R(\xi + \eta)](\xi^2 - 1)(1 - \eta^2)e^{\pm 2i\phi}, \quad A' + 6 = 0.$$

### § 3. ORTHOGONALITY

We shall now show that the functions obtained in the above manner are all orthogonal. The orthogonality of the  $\psi$ 's with different  $n$ -values follows from the inherent nature of Schrödinger's equation, while that of the  $\psi$ 's with different  $m$ -values is seen from the factor  $e^{\pm mi\phi}$ . It remains to prove that

$$\int \psi_{n,m,k_1}^* \psi_{n,m,k_2} d\tau = 0$$

unless  $k_1 = k_2$ , where, from equation (4)

$$\psi_{n,m,k} = X_k(\xi) Y_k(\eta) e^{\pm mi\phi}.$$

Here  $X_k(\xi)$  is defined by

$$\frac{d}{d\xi} \left[ (\xi^2 - 1) \frac{dX_k}{d\xi} \right] + \left[ A_k + R\xi - \frac{R^2 \xi^2}{4n^2} - m^2 (\xi^2 - 1)^{-1} \right] X_k = 0$$

and is entirely real; a similar equation holds for  $Y_k(\eta)$ .

This equation is of self-adjoint type, in which the parameter  $A_k$  plays the role of eigenvalue. Consequently, all its solutions are mutually orthogonal, provided only that the  $A_k$  are distinct. We have shown earlier in this paper that the  $A_k$  are all real and distinct. Consequently

$$\int_1^\infty X_{k_1} X_{k_2} d\xi = 0 = \int_{-1}^1 Y_{k_1} Y_{k_2} d\eta.$$

It follows that

$$\begin{aligned} \int \psi_{n,m,k_1}^* \psi_{n,m,k_2} d\tau &= \iiint X_{k_1} Y_{k_1} X_{k_2} Y_{k_2} \cdot \frac{1}{8} R^3 (\xi^2 - \eta^2) d\xi d\eta d\phi \\ &= \frac{1}{4} \pi R^3 \left\{ \int_1^\infty X_{k_1} X_{k_2} \xi^2 d\xi \left[ \int_{-1}^1 Y_{k_1} Y_{k_2} d\eta \right] \right. \\ &\quad \left. - \int_{-1}^1 Y_{k_1} Y_{k_2} \eta^2 d\eta \left[ \int_1^\infty X_{k_1} X_{k_2} d\xi \right] \right\} = 0, \end{aligned}$$

and so the  $n-m$  degenerate wave functions are mutually orthogonal. Hence if  $\psi_1$  and  $\psi_2$  are wave functions with any difference at all in their quantum numbers  $n, m$  and  $A_k$ , then  $\psi_1$  and  $\psi_2$  are orthogonal.

Another important consequence of the vanishing of the integrals

$$\int_1^\infty X_{k_1} X_{k_2} d\xi \quad \text{and} \quad \int_{-1}^1 Y_{k_1} Y_{k_2} d\eta$$

is that these spheroidal wave functions are the so-called 'correct' zero-order functions for the problem of a hydrogen atom perturbed by a point charge  $q$  placed at the dummy focus B. The additional term in the Hamiltonian is

$$V_{\text{pert.}} = q \left( \frac{1}{R} - \frac{1}{r_b} \right) = \frac{q}{R} \{ 1 - 2(\xi - \eta)^{-1} \},$$

and the off-diagonal elements such as

$$\int \psi_{n,m,k_1}^* V_{\text{pert.}} \psi_{n,m,k_2} d\tau$$

in the secular determinant all vanish. This follows from the fact that

$$\begin{aligned} \int \psi_{n,m,k_1}^* \left( \frac{q}{R} - \frac{2q}{R} (\xi - \eta)^{-1} \right) \psi_{n,m,k_2} d\tau \\ = 0 - \frac{2q}{R} \cdot \frac{R^3}{8} \cdot 2\pi \iint X_{k_1} Y_{k_1} X_{k_2} Y_{k_2} \left( \frac{\xi^2 - \eta^2}{\xi - \eta} \right) d\xi d\eta \\ = -\frac{1}{2} q R^2 \pi \int_1^\infty X_{k_1} X_{k_2} \xi d\xi \left[ \int_{-1}^1 Y_{k_1} Y_{k_2} d\eta \right] \\ - \frac{1}{2} q R^2 \pi \int_{-1}^1 Y_{k_1} Y_{k_2} \eta d\eta \left[ \int_1^\infty X_{k_1} X_{k_2} d\xi \right] = 0. \end{aligned}$$



Normal perturbation theory can therefore be applied to this problem, paying no further attention to degeneracy, provided that the functions  $\psi_{n,m,k}$  are used.

Coulson and Gillam (1947), when investigating the interaction between a proton and a hydrogen atom, incorrectly used parabolic wave functions for the zero-order ones. Parabolic functions are correct for the Stark effect in a uniform field, and it can be shown that as  $R \rightarrow \infty$ , i.e. as the influence of the point charge at  $B$  becomes equivalent to a uniform field at  $A$ , then the spheroidal functions become equivalent to the parabolic ones. (Cayrel (1955) has apparently also wrongly used the parabolic functions in a similar context.)

#### § 4. RELATIONS BETWEEN SPHEROIDAL, SPHERICAL POLAR AND PARABOLIC WAVE FUNCTIONS

With  $A$  as origin,  $AB$  as  $z$  axis,  $AP = r$  and angle  $BAP = \theta$ , the spherical polar solutions for the hydrogen atom are

$$\psi_{n,m,l} = e^{-\rho/2} \rho^l L_{n+l}^{2l+1}(\rho) P_l^m(\cos \theta) e^{\pm m i \phi} \quad (\rho = 2r/n),$$

and the parabolic solutions are

$$\psi_{S,T,m} = (uv)^{m/2} e^{-1/2(u+v)} L_{m+S}^m(u) L_{m+T}^m(v) e^{\pm m i \phi} \quad (S+T = n-m-1),$$

where  $nu = \lambda = r(1 - \cos \theta) = r - z$  and  $nv = \mu = r(1 + \cos \theta) = r + z$ . We have not given either of the normalizing factors, though they may be found, for example, in Schiff (1955). We can show that these two types of solution are the limiting cases of our spheroidal solutions as (i)  $R \rightarrow 0$ , (ii)  $R \rightarrow \infty$ .

##### 4.1. The Limit as $R \rightarrow 0$

It may be seen from the expression for  $D_\sigma(A)$  that as  $R \rightarrow 0$ , the eigenvalues for  $A \rightarrow -(s+m)(s+m+1)$ ,  $s = 0, 1, \dots, \sigma$ . This follows because  $\gamma_s \rightarrow 0$ , and

$$\beta_s \rightarrow s^2 + s(2m+1) + m(m+1) + A.$$

In the limit  $A = -l(l+1)$  where  $l = m, m+1, \dots, n-1$ .

For small  $R$ ,  $\xi \sim 2r/R$  and equation (1) becomes

$$\frac{d}{dr} \left( r^2 \frac{dX}{dr} \right) + \left[ -l(l+1) + 2r - \frac{r^2}{n^2} \right] X = 0,$$

(always considering the case where  $Z_1 = 1$ ,  $Z_2 = 0$ ), i.e.

$$\frac{d^2 X}{d\rho^2} + \frac{2}{\rho} \frac{dX}{d\rho} + \left[ \frac{n}{\rho} - \frac{1}{4} - \frac{l(l+1)}{\rho^2} \right] X = 0$$

where  $\rho = 2r/n$ . This is precisely the differential equation for the Laguerre function  $e^{-\rho/2} \rho^l L_{n+l}^{2l+1}(\rho)$ .

Also  $\eta \sim \cos \theta$  for small  $R$ , and equation (2) becomes

$$\frac{d}{d(\cos \theta)} \left[ \sin^2 \theta \frac{dY}{d(\cos \theta)} \right] + \left[ l(l+1) - \frac{m^2}{\sin^2 \theta} \right] Y = 0$$

which is the differential equation for the associated Legendre polynomial  $P_l^m(\cos \theta)$ .

4.2. The Limit as  $R \rightarrow \infty$ 

For the same reason that a parabola may be regarded as the limit of an ellipse when the second focus is removed to infinity, we may expect that as  $R \rightarrow \infty$  the limiting forms of our spheroidal wave functions should be the parabolic ones. This is indeed the case. Now the parabolic wave functions involve associated Laguerre polynomials, and so it is better here to appeal to the solutions of equations (1) and (2) which are available in terms of these polynomials. In this way we shall be able to develop an asymptotic form as  $R \rightarrow \infty$ .

With  $Z_1 = 1$  and  $Z_2 = 0$ , Hylleraas's general solution for (1) takes the particular form

$$X(\xi) = (\xi^2 - 1)^{m/2} e^{-x/2} \sum_{s=0}^{\sigma} \frac{b_s}{(m+s)!} L_{m+s}^m(x)$$

where  $\xi = 1 + nx/R$ , and the coefficients obey the recurrence relation

$$U_s b_{s+1} - V_s b_s + W_s b_{s-1} = 0.$$

Here

$$\begin{aligned} U_s &= (s+m+1)(s+1-n), \\ V_s &= 2s^2 - 2s\sigma + (2s-\sigma)R/n - (m+1)(n-1) + R^2/4n^2 - A, \\ W_s &= s(s+m-n) \end{aligned}$$

(see Baber and Hassé 1935 or Hylleraas 1931).

Similarly, it may be shown that a solution for (2) is

$$Y(\eta) = (1 - \eta^2)^{m/2} e^{-y/2} \sum_{t=0}^{\sigma} \frac{c_t}{(m+t)!} L_{m+t}^m(y)$$

where  $\eta = -1 + ny/R$  and

$$U'_t c_{t+1} - V'_t c_t + W'_t c_{t-1} = 0,$$

and where  $U'_t = U_t$ ,  $W'_t = W_t$  and

$$V'_t = 2t^2 - 2t\sigma + (\sigma - 2t)R/n - (m+1)(n-1) + R^2/4n^2 - A.$$

On account of the finite number of terms, the summations in  $X(\xi)$  and  $Y(\eta)$  lead to polynomials of degree  $\sigma$ , as we already know that they must do, from our studies in §2.1. Now since  $x + y = R(\xi + \eta)/n$ ,  $\psi$  may be written as

$$\begin{aligned} &\{(\xi^2 - 1)(1 - \eta^2)\}^{m/2} \exp[-\frac{1}{2}R(\xi + \eta)/n] \\ &\times \sum_{s=0}^{\sigma} \frac{b_s}{(m+s)!} L_{m+s}^m(x) \sum_{t=0}^{\sigma} \frac{c_t}{(m+t)!} L_{m+t}^m(y) e^{\pm m i \phi}. \end{aligned}$$

The consistency conditions for the sets of recurrence relations are that  $\Omega_{\sigma} = 0$  and  $\Omega_{\sigma}' = 0$ , where

$$\Omega_{\sigma} \equiv \begin{vmatrix} -V_0 & U_0 & & & & & & & \\ W_1 & -V_1 & U_1 & & & & & & \\ & W_2 & -V_2 & & & & & & \\ & & & \ddots & \ddots & \ddots & & & \\ & & & & \ddots & \ddots & \ddots & & \\ & & & & & \ddots & \ddots & \ddots & \\ & & & & & & \ddots & \ddots & \\ & & & & & & & \ddots & U_{\sigma-1} \\ & & & & & & & W_{\sigma} & -V_{\sigma} \end{vmatrix}$$

and  $\Omega'_\sigma$  is the corresponding determinant with primed elements. When  $R$  is large, the condition  $\Omega_\sigma = 0$  tends to the form  $V_0 V_1 \dots V_\sigma = 0$ , i.e.

$$\prod_{s=0}^{\sigma} \left[ \frac{R^2}{4n^2} + \frac{R(2s-\sigma)}{n} - A + 2s^2 - 2s\sigma - (m+1)(n-1) \right] = 0.$$

It is therefore necessary that for some  $s$ ,

$$A = \frac{R^2}{4n^2} + \frac{R(2s-\sigma)}{n} + 2s^2 - 2s\sigma - (m+1)(n-1);$$

similarly from the condition  $\Omega'_\sigma = 0$  we have

$$A = \frac{R^2}{4n^2} + \frac{R}{n} (\sigma - 2t) + 2t^2 - 2t\sigma - (m+1)(n-1)$$

for some value of  $t$ . If we let these critical values be  $s = S$  and  $t = T$ , and equate the two expressions for  $A$ , we get

$$\frac{R}{n} (2S + 2T - 2\sigma) + 2(S^2 - T^2) - 2\sigma(S - T) = 0.$$

In general this is only satisfied when  $S + T = \sigma$ .

Now  $V_S$  and  $V_{T'}$  are  $O(1/R)$ , while the other  $V_s$  and  $V_{t'}$  are  $O(R)$ . We may deduce from this that  $b_S$  and  $c_{T'}$  are the dominant coefficients in the series expansions, while  $b_{S\pm 1}$  and  $c_{\pm 1}$  are the next largest, and so on.

In terms of  $u$  and  $v$ ,  $x = u + nxy/2R$  and  $y = v - nxy/2R$ . We have also  $(\xi - 1)(1 - \eta) = 2nu/R$  and  $(\xi + 1)(1 + \eta) = 2nv/R$ , and so  $(\xi^2 - 1)(1 - \eta^2) = 4n^2 uv/R^2$  and  $R(\xi + \eta)/n = u + v$ . Hence in the limit as  $R \rightarrow \infty$ ,

$$\psi \rightarrow \text{constant} \times (uv)^{m/2} e^{-(u+v)/2} L_{m+S}^m(u) L_{m+T}^m(v) e^{\pm mi\phi}, \quad (S + T = \sigma),$$

which is precisely the parabolic solution.

We may further prove that when  $R$  is large, but not yet infinite, the normalized asymptotic form is

$$\begin{aligned} \psi_{S,T,m} = N [ & L_{m+S}^m(u) L_{m+T}^m(v) + n \{ (m+T)^2 (u-S+T-n) \\ & \times L_{m+S}^m(u) L_{m+T-1}^m(v) - (m+S)^2 (v-T+S-n) \\ & \times L_{m+S-1}^m(u) L_{m+T}^m(v) \} / 2R ] (uv)^{m/2} e^{-(u+v)/2} e^{\pm mi\phi} (2\pi)^{-1/2} + O(1/R^2), \end{aligned}$$

where  $N = 2n^{-2} \{ (m+S)! (m+T)! \}^{-3/2} \{ S! T! \}^{1/2}$ . It is not difficult to find the  $1/R^2$  term, but since it has contributions from five terms of the series for  $X(\xi)$  and  $Y(\eta)$ , it is rather unwieldy and will not be given here.

#### 4.3. Simple Relations between Solutions in Different Coordinates

The following simple relations are easily proved:

$$r_a = \frac{1}{2} R(\xi + \eta), \quad r_a \cos \theta = \frac{1}{2} R(1 + \xi\eta), \quad r_a \sin \theta = \frac{1}{2} R(\xi^2 - 1)^{1/2} (1 - \eta^2)^{1/2}.$$

We can therefore infer from

$$\psi(r_a, \theta, \phi) = e^{-\rho/2} \rho^l L_{n+l}^{2l+1}(\rho) P_l^m(\cos \phi) e^{\pm mi\phi} \quad (\rho = 2r_a/n)$$

that  $\psi(\xi, \eta, \phi)$  must be of the form

$$\exp [ -R(\xi + \eta)/2n ] (\xi^2 - 1)^{m/2} (1 - \eta^2)^{m/2} e^{\pm mi\phi} \chi(\xi, \eta),$$

where  $\chi(\xi, \eta)$  is a symmetric polynomial in  $\xi$  and  $\eta$ .

We also have the relations

$$\lambda = r_a(1 - \cos \theta) = \frac{1}{2}R(\xi - 1)(1 - \eta) \quad \text{and} \quad \mu = r_a(1 + \cos \theta) = \frac{1}{2}R(\xi + 1)(1 + \eta).$$

In easy cases the spheroidal wave functions can be obtained from either the spherical polar functions or from the parabolic ones, by taking the appropriate linear combinations of the degenerate functions with the same  $n$  and  $m$  values. For example with  $n=3$  and  $m=1$ , the spheroidal functions

$$\exp\left[-\frac{1}{6}R(\xi + \eta)\right](\xi^2 - 1)^{1/2}(1 - \eta^2)^{1/2} \left\{ \xi - \frac{R}{3(A' + 2)} \right\} \left\{ \eta - \frac{R}{3(A' + 2)} \right\} e^{\pm i\phi}$$

where  $A' \equiv A - R^2/36$  and  $(A' + 2)(A' + 6) = R^2/9$ , are equivalent to either

$$(6 - r)re^{-r/3} \sin \theta e^{\pm i\phi} + \frac{3(A' + 2)}{R} [r^2 e^{-r/3} \sin \theta \cos \theta e^{\pm i\phi}],$$

or to

$$[3(A' + 2) - R][(6 - \lambda)(\lambda\mu)^{1/2}e^{-(\lambda+u)/6}e^{\pm i\phi}] \\ + [3(A' + 2) + R][(6 - \mu)(\lambda\mu)^{1/2}e^{-(\lambda+u)/6}e^{\pm i\phi}]$$

apart from normalizing factors.

## § 5. DISCUSSION

It is interesting to discuss briefly why we can get simple solutions in spheroidal coordinates for the case  $Z_2 = 0$  but not otherwise. The essential feature of our present work is the termination of the power series for  $f_1(t)$  and the resulting simplification of the spheroidal solutions. This depends on the fact that  $\sigma$  can take integral values independently of the value of  $R$ .

In the general case with nuclei of charges  $Z_1$  and  $Z_2$  we get two different  $\sigma$ 's, one from the  $\xi$ -equation (1):  $\sigma_\xi = R(Z_1 + Z_2)/2p - (m + 1)$ , and one from the  $\eta$ -equation (2):  $\sigma_\eta = R(Z_1 - Z_2)/2p - (m + 1)$ . We also have two determinantal consistency conditions,  $D_1(A, \sigma_\xi, p) = 0 = D_2(A, \sigma_\eta, p)$ , which can be regarded as implicitly defining  $p$  in terms of  $\sigma_\xi$  and  $\sigma_\eta$  by means of some relation  $F(p, \sigma_\xi, \sigma_\eta) = 0$ .

If now  $\sigma_\xi$  and  $\sigma_\eta$  are predetermined as zero or positive integers to ensure termination of the two series, then  $p$  is fixed as a root of  $F(p, \sigma_\xi, \sigma_\eta) = 0$  and the terminating spheroidal solutions will only be valid for those particular values of  $RZ_1$  and  $RZ_2$  which are consistent with the expressions for  $\sigma_\xi$  and  $\sigma_\eta$ . For example, if we take the particular case of  $\sigma_\eta = 0$ , we can show that  $\sigma_\xi = 1$  or 2 leads only to  $p = 0$ , but with  $\sigma_\xi = 3$ , the following consistent set of values is obtained:  $A = p^2 = 10$ ,  $RZ_1 = 5\sqrt{10}$ ,  $RZ_2 = 3\sqrt{10}$ ,  $E = -20/R^2$ .

In general, therefore, as Wilson concluded, it will not be possible to have terminating series solutions in spheroidals for the two-centre problem. We might remark that if the series  $f_1(t)$  from the  $\xi$ -equation is not to terminate, then all three possibilities discussed in § 2.1.3 are ruled out and a solution for  $X(\xi)$  which is valid for the whole range  $1 \leq \xi \leq \infty$  is not available in this form. Fortunately, however, there are other satisfactory forms involving power series in  $(\xi - 1)/(\xi + 1)$  or  $L_{m+s}^m\{2p(\xi - 1)\}$  due to Jaffé (1934) and Hylleraas (1931) respectively. But in general these expansions are not terminating.

It is only in the hydrogen-like case, when  $Z_2 = 0$ , and  $RZ_1/2p = 1, 2, 3 \dots$  that terminating series solutions exist in spheroidals for all values of  $R$ . For then there is only one consistency condition, and  $p$  is free to vary with  $R$ .

The application of the spheroidal wave functions to the problem of a hydrogen atom perturbed by a point charge will be discussed in more detail in a future paper.



#### ACKNOWLEDGMENTS

We would very much like to thank Professor E. C. Titchmarsh for helpful discussions on the termination of the series occurring in the wave functions. One of us (P. D. R.) is grateful to the Department of Scientific and Industrial Research for a maintenance grant.

#### REFERENCES

- BABER, W. G., and HASSÉ, H. R., 1935, *Proc. Camb. Phil. Soc.*, **31**, 564.  
BARNARD, S., and CHILD, J. M., 1936, *Higher Algebra* (London : Macmillan), chap. 9.  
CAYREL, R., 1955, *C. R. Acad. Sci., Paris*, **240**, 603.  
COULSON, C. A., and GILLAM, C. M., 1947, *Proc. Roy. Soc. Edinb. A*, **62**, 362.  
HYLLERAAS, E. A., 1931, *Z. Phys.*, **71**, 739.  
JAFÉ, G., 1934, *Z. Phys.*, **87**, 535.  
MUIR, T., and METZLER, W. H., 1930, *Theory of Determinants* (New York : Albany), chap. 15.  
SCHIFF, L. I., 1955, *Quantum Mechanics*, 2nd edn. (New York : McGraw-Hill), chap. 4.  
SCHRÖDINGER, E., 1926, *Ann. Phys., Lpz.*, **80**, 437.  
WILSON, A. H., 1928, *Proc. Roy. Soc. A*, **118**, 617.

## Wave Functions for the Hydrogen Atom in Spheroidal Coordinates II: Interaction with a Point Charge and with a Dipole

By P. D. ROBINSON

Mathematical Institute, Oxford

*Communicated by C. A. Coulson; MS. received 30th December 1957, and in final form 12th February 1958*

**Abstract.** The interactions of a point charge and of a point dipole with a hydrogen atom are investigated. Interaction energies, dipole and quadrupole moments are calculated using exact perturbation theory. Spheroidal coordinates are necessary to solve the differential equations which arise, and wave functions for the atom in these coordinates are seen to be the correct zero-order ones to use. The exact form of the perturbing potential is employed, giving results with both polynomial and exponentially decreasing terms. These are compared with the simpler but less accurate results obtained when the expanded form of the perturbation is used.

### § 1. INTRODUCTION

IN Part I of this paper (Coulson and Robinson 1958) wave functions for the hydrogen atom were developed using spheroidal coordinates  $(\xi, \eta, \phi)$  in the form

$$\psi_{n,m,k} = \exp \left[ -\frac{1}{2} R(\xi + \eta)/n \right] \{ (\xi^2 - 1)(1 - \eta^2) \}^{|m|/2} f_k(\xi) f_k(\eta) \exp(\pm m i \phi),$$

$f_k(t)$  being a polynomial in  $t$  of degree  $n - |m| - 1$ ; the atomic nucleus was at one focus of the coordinate system ( $\xi = 1, \eta = -1$ ) while the second focus ( $\xi = 1, \eta = 1$ ) was chosen at an arbitrary point in space. It was seen that if a point charge was now placed at this second focus, then the resulting addition  $H'$  to the Hamiltonian had zero off-diagonal matrix elements with respect to the set of functions  $\{\psi_{n,m,k}\}$ , i.e.

$$\int \psi_{nm_1k_1}^* H' \psi_{nm_2k_2} d\tau = 0$$

unless we have  $m_1 = m_2$  and  $k_1 = k_2$ . This means that spheroidal wave functions, with foci at the nucleus and at the point charge respectively, are the correct zero-order ones for a perturbation investigation of the effect of a point charge on a hydrogen atom. Conventional non-degenerate perturbation theory can then be used with these functions, even for the degenerate excited states of the atom. In this way we avoid the difficulties of Coulson and Gillam (1947), who mistakenly used parabolic wave functions to study the interaction of a proton and an excited hydrogen atom. As was shown in Part I, the parabolic wave functions are the limiting cases of the spheroidal ones as the interfocal distance  $R \rightarrow \infty$ .

Dalgarno and Stewart (1956b, 1957) have made perturbation calculations of properties of  $\text{HeH}^{2+}$ , taking as their model a hydrogen-like atom with nuclear

charge  $\zeta$  perturbed by a point charge  $\zeta'$ . They set  $\zeta=1$ ,  $\zeta'=2$  for the  $1s\sigma$  state of the ion, and  $\zeta=2$ ,  $\zeta'=1$  for the  $2p\sigma$  state, each with the  $1s$  hydrogen-like wave function; for the  $2p\pi$  state they used the  $2p_x$  function with  $\zeta=2$ ,  $\zeta'=1$ , and so neither of their unperturbed wave functions was degenerate. Dalgarno and Stewart, like Coulson and Gillam, employ the form of the perturbation  $H'$  which is expanded in powers of  $1/R$ , i.e. they use

$$-\sum_{n=1}^{\infty} r_a^n P_n(\cos \theta)/R^{n+1}$$

instead of  $(1/R - 1/r_b)$  (see figure 1). This treatment leads to results given by series which are asymptotically divergent for all values of  $R$  (Dalgarno and Lewis 1956), and it also neglects the exponentially decreasing terms which arise with the unexpanded form of  $H'$ . To avoid these shortcomings spheroidal coordinates are necessary, not only to take care of any degeneracy but also to solve the differential equations which arise when exact second-order perturbation theory is used with the unexpanded form of  $H'$ .

The effects of a point charge (the energy of interaction and the dipole and quadrupole moments induced in the atom) are discussed in §§2 and 3, while in §4 the effects of a charge dipole are investigated. It is not easy to proceed using the exact form of  $H'$  if the hydrogen atom is in a general excited state, for we do not know the explicit form of the polynomial  $f_k$  occurring in  $\psi_{n,m,k}$ . In principle its coefficients can be found numerically for any given state, but for simplicity we will here content ourselves by considering only the cases of K- and L-shell wave functions.

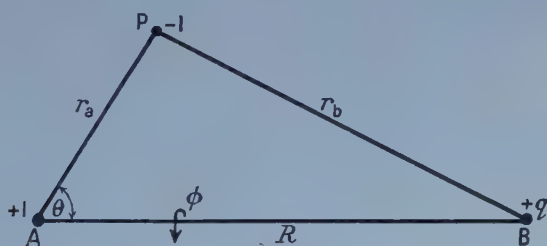


Figure 1.

## § 2. ENERGY OF INTERACTION WITH A POINT CHARGE

In figure 1, the atomic nucleus is at A, the electron at P and the point charge  $+q$  is at B. The spheroidal coordinates of P are  $\xi = (r_a + r_b)/R$ ,  $\eta = (r_a - r_b)/R$  and  $\phi$ , the azimuthal angle round the axis AB. The unperturbed wave functions considered are

(i) K shell,  $n=1$ ,  $m=0$ :

$$\exp[-\frac{1}{2}R(\xi + \eta)]/\sqrt{\pi} \text{ (the } 1s \text{ function),}$$

(ii) L shell,  $n=2$ ,  $|m|=1$ :

$$\frac{R}{16\sqrt{\pi}} (\xi^2 - 1)^{1/2} (1 - \eta^2)^{1/2} \exp[-\frac{1}{4}R(\xi + \eta)] \exp(\pm i\phi) \text{ (the } 2p_{\pm 1} \text{ functions),}$$

(iii) L shell,  $n=2$ ,  $m=0$ :

$$\frac{R}{16\sqrt{\pi}} \left(1 + \frac{2\alpha}{R}\right)^{-1/2} \exp[-\frac{1}{4}R(\xi + \eta)] (\xi - \alpha)(\eta - \alpha)$$

where  $\alpha^2 - 4\alpha/R - 1 = 0$ . (There are two degenerate functions for the same  $n$ - and  $m$ -values here, one from each root for  $\alpha$ . They are linear combinations of the 2s and  $2p_0$  spherical polar functions.) All these functions are correctly normalized, and in atomic units.

We can treat  $q$  as a parameter, writing the perturbation to the Hamiltonian as  $qH' = q(1/R - 1/r_b)$ , and we shall use the exact second-order perturbation theory of Dalgarno and Lewis (1955). If we set  $V = -1/r_b = -2/R(\xi - \eta)$ , and if  $F(\xi, \eta)$  is an acceptable solution of the differential equation

$$\nabla^2 F + 2 \text{grad } F \cdot \text{grad } (\ln \psi) = V - \int \psi^* V \psi d\tau \quad \dots\dots (1)$$

where  $\psi$  is the unperturbed wave function of the state considered, then this theory gives for the interaction energy

$$\Delta E = q(1/R + E^{(1)}) + q^2 E^{(2)} + O(q^3) \quad (\text{in atomic units}),$$

where 
$$E^{(1)} = \int \psi^* V \psi d\tau \quad \text{and} \quad E^{(2)} = 2 \left\{ \int \psi^* V F \psi d\tau - E^{(1)} \int \psi^* F \psi d\tau \right\}.$$

The notation  $\int \psi^* L \psi d\tau \equiv \langle \psi | L | \psi \rangle$  will be used, so that

$$E^{(1)} = \langle \psi | V | \psi \rangle, \text{ and } E^{(2)} = 2 \{ \langle \psi | V F | \psi \rangle - E^{(1)} \langle \psi | F | \psi \rangle \}. \quad \dots\dots (2)$$

The function  $F(\xi, \eta)$  is introduced as an ingenious means of summing the infinite series which normally occurs in the second-order energy term. Equation (1) can only be solved analytically if spheroidal coordinates are used, and so if we want to retain the exact form of  $V$  these coordinates are necessary even with the non-degenerate wave functions (i) and (ii).

### 2.1. Case (i), $n = 1, m = 0$

This is equivalent to the work of Dalgarno and Lynn (1957), but it is given here both for completeness and also because the results obtained are used later in §§ 3 and 4.

In this case we have  $\psi = \exp[-\frac{1}{2}R(\xi + \eta)]/\sqrt{\pi}$  and

$$E^{(1)} = \frac{1}{\pi} \int \exp[-R(\xi + \eta)] \left( \frac{-2}{R(\xi - \eta)} \right) d\tau = -\frac{1}{R} + \exp(-2R) \left( 1 + \frac{1}{R} \right).$$

Equation (1) for  $F$  becomes

$$\begin{aligned} \frac{\partial}{\partial \xi} \left[ (\xi^2 - 1) \frac{\partial F}{\partial \xi} \right] + \frac{\partial}{\partial \eta} \left[ (1 - \eta^2) \frac{\partial F}{\partial \eta} \right] - R \left[ (\xi^2 - 1) \frac{\partial F}{\partial \xi} + (1 - \eta^2) \frac{\partial F}{\partial \eta} \right] \\ = -\frac{1}{4} R^2 E^{(1)} (\xi^2 - \eta^2) - \frac{1}{2} R (\xi + \eta). \end{aligned}$$

This is separable in the form  $F(\xi, \eta) = F_1(\xi) + F_2(\eta)$ , and if we choose the arbitrary constants which arise so that  $F(\xi, \eta)$  is well-behaved along the axis where  $\xi = 1$  and  $\eta = \pm 1$ , then  $F(\xi, \eta)$  is uniquely determined as

$$\begin{aligned} \frac{1}{4} R E^{(1)} (\xi + \eta) + \frac{1}{2} \left[ \left( 1 - \frac{1}{R} \right) + \left( 1 + \frac{1}{R} \right) e^{-2R} \right] \ln(\xi + 1) \\ - \frac{1}{2} \left( 1 + \frac{1}{R} \right) [\ln(1 - \eta) + \text{Ei}\{R(1 - \eta)\}] \\ + \frac{1}{2} e^{-2R} \left( 1 + \frac{1}{R} \right) [\ln(1 + \eta) - \text{Ei}\{R(1 + \eta)\}]. \end{aligned}$$



Here

$$\text{Ei}(t) = \int_{-\infty}^t e^x/x \, dx$$

$$\text{and } \text{Ei}^*(t) = \int_t^{\infty} e^{-x}/x \, dx = -(\text{Ei} - t)$$

are the usual exponential integrals.

The following expression is finally obtained (from formula (2)):

$$\begin{aligned} E^{(2)} = & \frac{5}{2R^2} + \left(1 - \frac{1}{R}\right)^2 e^{2R} \text{Ei}^*(2R) - \left(1 + \frac{1}{R}\right)^2 e^{-2R} \text{Ei}(2R) \\ & + e^{-2R} \left[ 2 \left(1 + \frac{1}{R}\right)^2 (\gamma + \ln 2R) - \left(2 + \frac{4}{R} + \frac{5}{R^2}\right) - \left(1 + \frac{1}{R}\right)^2 e^{-2R} \text{Ei}(2R) \right] \\ & + e^{-4R} \left[ 2 \left(1 + \frac{1}{R}\right)^2 (\gamma + \ln 2R) + 2R + \frac{7}{2} + \frac{4}{R} + \frac{5}{2R^2} \right] \\ & + \text{Ei}^*(2R) \left[ 1 + \frac{2}{R} - \frac{3}{R^2} + \frac{4}{R} \left(1 + \frac{1}{R}\right) e^{-2R} \right] \end{aligned}$$

where  $\gamma$  is Euler's constant. This agrees with the result of Dalgarno and Lynn apart from a factor of 2 which arises from their use of the Rydberg rather than the strict atomic unit as unit of energy. If the asymptotically divergent series for the exponential integrals

$$\text{Ei}(2R) = e^{2R} \sum_{n=0}^{\infty} \frac{n!}{(2R)^{n+1}}, \quad \text{Ei}^*(2R) = e^{-2R} \sum_{n=0}^{\infty} (-)^n \frac{(n!)}{(2R)^{n+1}}$$

are substituted in the expression, and the exponentially decreasing terms are neglected, then

$$E^{(2)} = - \sum_{s=1}^{\infty} \frac{(2s-1)! (2s+1)(s+2)}{2^{2s} R^{2s+2}}$$

in agreement with Dalgarno and Stewart (1956b). Dalgarno and Lynn give a table to show the accuracy of this series expansion; it is very accurate for large  $R$  and quite useful for  $R$  as small as  $4a_0$ . The error arising from the asymptotically divergent nature of the series is small compared with that which arises from neglecting the exponentially decreasing terms.

## 2.2. Case (ii), $n=2$ , $|m|=1$

Here we have

$$\psi = \frac{R}{8\sqrt{2}} (\xi^2 - 1)^{1/2} (1 - \eta^2)^{1/2} \frac{\exp[-\frac{1}{4}R(\xi + \eta)] \exp(\pm i\phi)}{\sqrt{(2\pi)}};$$

it can be shown that

$$E^{(1)} = -\frac{1}{R} + \frac{6}{R^3} - \frac{1}{4} e^{-R} \left(1 + \frac{8}{R} + \frac{24}{R^2} + \frac{24}{R^3}\right)$$

and that the equation for  $F$  is:

$$\begin{aligned} \frac{\partial}{\partial \xi} \left[ (\xi^2 - 1) \frac{\partial F}{\partial \xi} \right] + \frac{\partial}{\partial \eta} \left[ (1 - \eta^2) \frac{\partial F}{\partial \eta} \right] + \left( \frac{2\xi}{\xi^2 - 1} - \frac{1}{2} R \right) (\xi^2 - 1) \frac{\partial F}{\partial \xi} \\ - \left( \frac{2\eta}{1 - \eta^2} + \frac{1}{2} R \right) (1 - \eta^2) \frac{\partial F}{\partial \eta} = -\frac{1}{2} R (\xi + \eta) - \frac{1}{4} R^2 E^{(1)} (\xi^2 - \eta^2). \end{aligned}$$

If, as before, the finiteness conditions are applied along the axis, we get

$$\begin{aligned}
 F(\xi, \eta) = & \frac{1}{2}RE^{(1)}(\xi + \eta) - \frac{1}{4}R \left[ 4E^{(1)} + 1 - K_1 \left( 1 - \frac{2}{R} \right) \right] (\xi + 1)^{-1} \\
 & + \frac{1}{2} \left( 1 + \frac{2}{R} \right) \left[ 4E^{(1)} + 1 - K_1 \left( 1 - \frac{2}{R} \right) \right] \ln(\xi + 1) \\
 & + K_2 \left[ \frac{2\eta e^{\frac{1}{2}R\eta}}{\eta^2 - 1} - \frac{e^{\frac{1}{2}R}}{\eta - 1} - \frac{e^{-\frac{1}{2}R}}{\eta + 1} \right] \\
 & + K_2 \left( \frac{1}{2}R - 1 \right) e^{\frac{1}{2}R} [\ln(1 - \eta) + \text{Ei}^* \{ \frac{1}{2}R(1 - \eta) \}] \\
 & + K_1 \left( \frac{1}{2}R + 1 \right) e^{-\frac{1}{2}R} [\ln(1 + \eta) - \text{Ei} \{ \frac{1}{2}R(1 + \eta) \}],
 \end{aligned}$$

where

$$K_1 \left( 1 + \frac{2}{R} \right) + 4E^{(1)} + 1 = 0 \quad \text{and} \quad K_2 = -\frac{2}{R} e^{-\frac{1}{2}R} \left( 1 + \frac{6}{R} + \frac{12}{R^2} \right).$$

Using this, we obtain the expression

$$\begin{aligned}
 E^{(2)} = & -\frac{1}{R^2} \left( 13 + \frac{260}{R^2} - \frac{2136}{R^4} \right) + \frac{1}{2} \left( 1 + \frac{12}{R} + \frac{56}{R^2} + \frac{96}{R^3} - \frac{96}{R^4} - \frac{576}{R^5} - \frac{576}{R^6} \right) e^{-R} \text{Ei}(R) \\
 & - \frac{1}{2} \left( 1 - \frac{12}{R} + \frac{56}{R^2} - \frac{96}{R^3} - \frac{96}{R^4} + \frac{576}{R^5} - \frac{576}{R^6} \right) e^{R} \text{Ei}^*(R) \\
 & + \text{exponentially decreasing terms.}
 \end{aligned}$$

If the series are substituted for the exponential integrals,  $E^{(2)}$  becomes

$$-\frac{78}{R^4} + \frac{2400}{R^6} + 2 \sum_{s=3}^{\infty} \frac{(2s-1)! (s+2)(2s^3+3s^2-13s-8)}{(s-1)(s-2)R^{2s+2}}$$

in agreement with Dalgarno and Stewart (1957), apart from the factor of 2. They obtained this series result using the expanded form of  $H'$ .

Table 1 shows the error caused by neglecting the exponentially decreasing terms in  $E^{(1)} + 1/R$ , and also the error resulting from the use of the series rather than the exact expression for  $E^{(2)}$ . The coefficients of the series increase rapidly, the next terms being

$$\frac{20400}{R^8} + \frac{1169280}{R^{10}} + \frac{106686720}{R^{12}} + \frac{14497781760}{R^{14}}.$$

It is convenient to sum the series for a given value of  $R$  by including terms up to but not including the smallest term, plus half the smallest term (Dalgarno and Lewis 1956, Jeffreys and Jeffreys 1956). We see from the table that serious errors arise if the series form of  $E^{(2)}$  is used for  $R < 9$ . It is to be expected that the error in neglecting the exponentially decreasing terms in the unexpanded form of  $E^{(2)}$  (the labour involved was thought too great to justify finding them) will be comparable with that in neglecting them for the  $q$  term. Consequently, for this L shell state of the hydrogen atom, with the electron generally further out from the nucleus than in the K shell, the error inherent in the series for  $E^{(2)}$  is of importance below  $R=7$ , and it is essential to use the exact form of the perturbation  $H'$ .

Table 1

(1)	(2)	(3)	(4)	(5)	(6)	(7)	(8)	(9)	(10)	(11)
0-071428	0-041680	0-025850	0-016877	0-011505	0-008162	0-005977	0-004500			
23-8	13-2	6-94	3-52	1-83	0-83	0-39	0-18			
0-112713	0-011881	-0-007346	-0-009871	-0-008576	-0-006705	-0-005076	-0-003815			
0-4368	0-0549	-0-002672	-0-010317	-0-008127	-0-006730	-0-005026	-0-003816			
287	362	63-6	-4-52	5-24	-0-38	0-99	0-02			

(1)  $R$  (units of  $a_0$ ); (2)  $E^{(1)} + 1/R$  (exact); (3) % error from neglecting  $e^{-R}$  terms; (4)  $E^{(2)}$  unexpanded; (5)  $E^{(2)}$  from series; (6) % error from using series.

Table 2

(1)	(2)	(3)	(4)	(5)	(6)	(7)	(8)	(9)	(10)	(11)
1-61803	1-47703	1-38742	1-32571	1-28078	1-24662	1-21980	1-19823			
0-116273	0-081336	0-060088	0-046188	0-036601	0-029710	0-024594	0-020692			
0-338	0-113	0-040	0-013	0-005	0-002	0-001	0-000			
-0-618034	-0-677033	-0-720754	-0-754286	-0-780776	-0-802180	-0-819804	-0-834598			
0-039342	0-063290	0-065519	0-058758	0-050407	0-041999	0-034804	0-028945			
87	64	43	27-6	16-0	9-0	4-9	2-56			

(1)  $R$  (units of  $a_0$ ); (2)  $\alpha_+$ ; (3)  $E^{(1)} + 1/R$  (exact); (4) % error\*; (5)  $\alpha_-$ ; (6)  $E^{(1)} + 1/R$  (exact); (7) % error\*. \* from neglecting the exponentially decreasing term.

Table 4

(1)	(2)	(3)	(4)	(5)	(6)	(7)	(8)	(9)	(10)
-0-012919	-0-002606	-0-000587	-0-000162	-0-000053	-0-000022	-0-000009	-0-000005		
234	68-7	28-9	11-6	4-3	1-3	0-4	0-1		
-0-003862	-0-001545	-0-000455	-0-000145	-0-000050	-0-000022	-0-000009	-0-000005		
-0-003086	-0-001442	-0-000443	-0-000141	-0-000051	-0-000022	-0-000009	-0-000005		

(1)  $R$  (units of  $a_0$ ); (2) Coefficient of  $\frac{1}{2}\mu^2$  (exact); (3) % error\*; (4) left-hand side of (3); (5) right-hand side of (3). \* from neglecting the exponentially decreasing terms.

(Tables of  $Ei(t)$  and  $Ei^*(t)$  for large values of  $t$  are given by Kotani, Amemiya, Ishiguro and Kimura 1955, and by Coulson and Duncanson 1942).

2.3. Case (iii),  $n=2$ ,  $m=0$ 

This time

$$\psi = \frac{R}{16\sqrt{\pi}} \left(1 + \frac{2\alpha}{R}\right)^{-1/2} \exp\left[-\frac{1}{4}R(\xi + \eta)\right](\xi - \alpha)(\eta - \alpha)$$

where  $\alpha$  satisfies the equation  $\alpha^2 - 4\alpha/R - 1 = 0$ , the two roots giving two different functions  $\psi$ . These functions, although degenerate, are the correct zero-order ones to use, as explained in § 1.

We obtain

$$E^{(1)} = -\frac{1}{R} + \frac{3}{R^2\alpha} + \left(\frac{1}{4} + \frac{1}{R} - \frac{3}{R^2\alpha}\right) \left(\frac{1-\alpha}{1+\alpha}\right)^2 \exp(-R).$$

The procedure for finding  $E^{(2)}$  is the same as in the previous cases, but the working involved is more tedious. The equation for  $F$  is

$$\begin{aligned} \frac{\partial}{\partial \xi} \left[ (\xi^2 - 1) \frac{\partial F}{\partial \xi} \right] + \frac{\partial}{\partial \eta} \left[ (1 - \eta^2) \frac{\partial F}{\partial \eta} \right] + \left( \frac{2}{\xi - \alpha} - \frac{1}{2}R \right) (\xi^2 - 1) \frac{\partial F}{\partial \xi} \\ + \left( \frac{2}{\eta - \alpha} - \frac{1}{2}R \right) (1 - \eta^2) \frac{\partial F}{\partial \eta} = -\frac{1}{2}R(\xi + \eta) - \frac{1}{4}R^2 E^{(1)} (\xi^2 - \eta^2) \end{aligned}$$

which has for its acceptable solution

$$\begin{aligned} F(\xi, \eta) = \frac{1}{2}RE^{(1)}(\xi + \eta) + \frac{2K_3}{R\alpha(\eta - \alpha)} - \frac{2K_4}{R\alpha(\xi - \alpha)} + (4E^{(1)} + 1) \ln(\xi + 1) \\ + \frac{R}{2} \left( \frac{12}{R^2\alpha} - \frac{4}{R} - 1 \right) (1 - \alpha)^2 \frac{e^{\frac{1}{2}R(\eta - 1)}}{\alpha(\eta - \alpha)} + 4 \left( E^{(1)} + \frac{1}{R} - \frac{3}{R^2\alpha} \right) \\ \times [\ln(1 + \eta) - \text{Ei}\{\frac{1}{2}R(1 + \eta)\}] + \left( \frac{12}{R^2\alpha} - \frac{4}{R} - 1 \right) [\ln(1 - \eta) + \text{Ei}^*\{\frac{1}{2}R(1 - \eta)\}] \end{aligned}$$

where

$$K_4 \left( 1 - \frac{2}{R\alpha} \right) = \alpha(1 + 6E^{(1)}) - 1 - 4E^{(1)} \quad \text{and} \quad K_3 = 2\alpha + \frac{12}{R} - K_4.$$

The expression for  $E^{(2)}$  is found to be

$$\begin{aligned} \frac{11}{2} + \frac{162}{R^2} + \frac{1798}{R^4} + \frac{7728}{R^6} - \frac{\alpha}{R} \left( \frac{R^2}{2} + 25 + \frac{340}{R^2} + \frac{1872}{R^4} \right) + \frac{240(1 - R\alpha/2)}{R^6(1 + \frac{1}{4}R^2)} \\ - \frac{1}{2} \left( 1 + \frac{4}{R} + \frac{48}{R^3} - \frac{12\alpha}{R^2} \right)^2 \left( \frac{1-\alpha}{1+\alpha} \right)^2 e^{-R} \text{Ei}(R) \\ + \frac{1}{2} \left( 1 - \frac{4}{R} - \frac{48}{R^3} + \frac{12\alpha}{R^2} \right)^2 \left( \frac{1+\alpha}{1-\alpha} \right)^2 e^R \text{Ei}^*(R) \end{aligned}$$

+ exponentially decreasing terms.

The expansion of  $\Delta E$  in powers of  $1/R$  starts

$$q \left[ \pm \frac{3}{R^2} - \frac{6}{R^3} \pm \frac{6}{R^4} \mp \frac{6}{R^6} \dots \right] + q^2 \left[ -\frac{84}{R^4} \pm \frac{1224}{R^5} - \frac{10368}{R^6} \dots \right] + O(q^3),$$

which agrees with the results of Coulson and Gillam (1947) (with  $q=1$ ) as far as the term in  $1/R^4$ .



Table 2 shows the importance of the exponentially decreasing terms in the first-order energy

$$E^{(1)} + \frac{1}{R} = \frac{3}{R^2\alpha} \left[ 1 - \left\{ 1 - \frac{1}{3}R^2\alpha \left( \frac{1}{4} + \frac{1}{R} \right) \right\} \left( \frac{1-\alpha}{1+\alpha} \right)^2 e^{-R} \right]$$

for the two values of  $\alpha$ , denoted by

$$\alpha_+ = 2/R + (1 + 4/R^2)^{1/2} \quad \text{and} \quad \alpha_- = 2/R - (1 + 4/R^2)^{1/2}.$$

It is clear from table 2 that the exponentially decreasing terms can only be safely ignored for  $R < 12$  when the positive root is taken for  $\alpha$ ; this is the case when the charge cloud is concentrated more between the nuclei. The exponentially decreasing terms arise from considering values of  $r_a$  greater than  $R$ , for they do not appear at all when the expansion

$$H' = - \sum_{n=1}^{\infty} r_a^n P_n(\cos \theta) / R^{n+1}$$

which is only valid for  $r_a \leq R$  is employed. Such a startling difference in the two cases however would not have been anticipated.

The formula for  $E^{(2)}$  with the positive root for  $\alpha$  should be accurate for quite small values of  $R$ .

### § 3. DIPOLE AND QUADRUPOLE MOMENTS INDUCED BY A POINT CHARGE

The presence of the point charge  $q$  in the neighbourhood of the hydrogen atom not only alters the energy of the system but also changes the shape of the charge cloud. Suppose the wave function is perturbed by  $q$  to

$$\psi = \psi^{(0)} + q\psi^{(1)} + q^2\psi^{(2)} + \dots$$

Then quantities like the dipole moment  $\langle \psi | r_a P_1(\cos \theta) | \psi \rangle$  and the quadrupole moment  $\langle \psi | r_a^2 P_2(\cos \theta) | \psi \rangle$  of the charge cloud will be different from their values with  $q=0$ . The differences in these values are the moments induced by the charge  $q$ , and these are investigated here.

According to conventional perturbation theory,

$$\psi^{(1)} = \sum_{r \neq 0} a_r \phi_r \quad \text{and} \quad \psi^{(2)} = \sum b_r \phi_r,$$

the summations being over the complete set of orthonormal eigenfunctions  $\{\phi_r\}$ , of which  $\psi^{(0)} = \phi_0$ . The coefficients  $a_r$  and  $b_r$  are given by

$$a_r = \frac{\langle r | H' | 0 \rangle}{E_0 - E_r} \quad r \neq 0, \quad a_0 = 0,$$

$$b_r = \sum_{s \neq 0} \frac{\langle s | H' | 0 \rangle \langle r | H' | s \rangle}{(E_0 - E_r)(E_0 - E_s)} - \frac{\langle r | H' | 0 \rangle \langle 0 | H' | 0 \rangle}{(E_0 - E_r)^2}, \quad r \neq 0,$$

$$b_0 = -\frac{1}{2} \sum_{r \neq 0} \frac{\langle r | H' | 0 \rangle \langle 0 | H' | r \rangle}{(E_0 - E_r)^2}.$$

$E_r, E_s, \dots$  are the energy eigenvalues corresponding to  $\phi_r, \phi_s, \dots$ , and  $\langle r | H' | s \rangle$  is written for  $\langle \phi_r | H' | \phi_s \rangle$ .  $\psi$  is now correctly normalized to order  $q^2$  (see for example Schiff (1955)).  $H' = 1/R - 1/r_b = 1/R + V$ , and  $H'$  may be replaced by  $V$  in the above formulae because of the orthonormal properties of the functions  $\phi_r$ . If the complete set of eigenfunctions  $\{\phi_r\}$  is taken to be the set in spheroidal coordinates, then we shall not be worried by questions of degeneracy.

We will consider the value of  $\langle \psi | J | \psi \rangle$ , where  $J$  will be put equal to  $r_a P_1(\cos \theta)$  or to  $r_a^2 P_2(\cos \theta)$ . Expanding in powers of  $q$ , we have

$$\langle \psi | J | \psi \rangle = \langle 0 | J | 0 \rangle + q \{ \langle \psi^{(1)} | J | 0 \rangle + \langle 0 | J | \psi^{(1)} \rangle \} \\ + q^2 \{ \langle \psi^{(1)} | J | \psi^{(1)} \rangle + \langle \psi^{(2)} | J | \psi^{(0)} \rangle + \langle \psi^{(0)} | J | \psi^{(2)} \rangle \} + O(q^3).$$

If now well-behaved functions  $F$  and  $G$  are defined as solutions of the differential equations

$$\nabla^2 F + 2 \text{grad } F \cdot \text{grad } (\ln \psi_0) = V - \langle 0 | V | 0 \rangle,$$

as in § 2, and

$$\nabla^2 G + 2 \text{grad } G \cdot \text{grad } (\ln \psi_0) = J - \langle 0 | J | 0 \rangle,$$

then using the summation methods indicated by Dalgarno and Stewart (1956 a), it can be shown that

$$\langle \psi | J | \psi \rangle = \langle 0 | J | 0 \rangle + 4q \{ \langle 0 | G V | 0 \rangle - \langle 0 | G | 0 \rangle \langle 0 | V | 0 \rangle \} \\ + 4q^2 \{ \langle 0 | F^2 J | 0 \rangle + 2 \langle 0 | F G V | 0 \rangle - 4 \langle 0 | F | 0 \rangle \langle 0 | G V | 0 \rangle \\ - 2 \langle 0 | V | 0 \rangle \langle 0 | F G | 0 \rangle + \langle 0 | J | 0 \rangle [\langle 0 | F | 0 \rangle^2 - \langle 0 | F^2 | 0 \rangle] \\ + 2 \langle 0 | G | 0 \rangle [2 \langle 0 | V | 0 \rangle \langle 0 | F | 0 \rangle - \langle 0 | F V | 0 \rangle] \} + O(q^3).$$

Matrix relations such as

$$\sum_{r \neq 0} \langle 0 | S | r \rangle \langle r | T | s \rangle = \langle 0 | S T | s \rangle - \langle 0 | S | 0 \rangle \langle 0 | T | s \rangle$$

have been employed. Equalities like  $\langle 0 | G V | 0 \rangle = \langle 0 | F J | 0 \rangle$  allow alternative forms and also serve as a useful check on results. As before, results will only be obtained for the K and L shells of the hydrogen atom.

### 3.1. Case (i), $n=1$ , $m=0$

#### 3.1.1. Induced dipole moment: value of $\bar{Z}$ .

Here  $J = r_a \cos \theta = z$ , and  $\phi_0 = \exp(-r_a)/\sqrt{\pi} = \exp[-\frac{1}{2}R(\xi + \eta)]/\sqrt{\pi}$ .

$\langle 0 | J | 0 \rangle = 0$  by symmetry.  $G(r_a, \theta) = -\frac{1}{2}r_a(1 + \frac{1}{2}r_a)\cos \theta$  and  $\langle 0 | G | 0 \rangle$  also vanishes. As in § 2.1,

$$F(\xi, \eta) = \frac{1}{4} R E^{(1)}(\xi + \eta) + \frac{1}{2} \left[ 1 - \frac{1}{R} + \left( 1 + \frac{1}{R} \right) e^{-2R} \right] \ln(\xi + 1) \\ - \frac{1}{2} \left( 1 + \frac{1}{R} \right) [\ln(1 - \eta) + \text{Ei}^*\{R(1 - \eta)\}] \\ + \frac{1}{2} \left( 1 + \frac{1}{R} \right) e^{-2R} [\ln(1 + \eta) - \text{Ei}\{R(1 + \eta)\}].$$

After fairly lengthy working the following result is obtained for the induced dipole moment:

$$\bar{Z} = \frac{q}{2R^2} \{ 9 - (2R^4 + 10R^3 + 18R^2 + 18R + 9)e^{-2R} \} + \frac{1}{2} q^2 \left\{ -2R - \frac{47}{R} - \frac{114}{R^3} \right. \\ + (R^2 - R) \left( 2 - \frac{12}{R} + \frac{27}{R^2} - \frac{33}{R^3} + \frac{18}{R^4} \right) e^{2R} \text{Ei}^*(2R) \\ + (R^2 + R) \left( 2 + \frac{12}{R} + \frac{27}{R^2} + \frac{33}{R^3} + \frac{18}{R^4} \right) e^{-2R} \text{Ei}(2R) \\ \left. + \text{exponentially decreasing terms} \right\} + O(q^3).$$

If the series are substituted for  $Ei(2R)$  and  $Ei^*(2R)$ , the first three terms in the expansion of the  $q^2$  term are

$$\frac{1}{2}q^2 \left\{ \frac{213}{R^5} + \frac{1620}{R^7} + \frac{104625}{R^9} \right\};$$

the first two agree with Dalgarno and Stewart (1956 b) who used the expanded  $H'$  but did not give the  $1/R^9$  term. Values of the  $q$  term as  $R$  varies are given in table 3.

### 3.1.2. Induced quadrupole moments, $Q$ .

Here  $J = \frac{1}{2}r_a^2(3 \cos^2 \theta - 1)$  for the  $Q_{zz}$  component, and  $\langle 0|J|0 \rangle = 0$ . We find that  $G = -\frac{1}{4}r_a^2(\frac{1}{2} + \frac{1}{3}r_a)(3 \cos^2 \theta - 1)$  and that  $\langle 0|G|0 \rangle = 0$ . The  $q$  term can be found quite easily, but the  $q^2$  term necessitates heavy integrations and was not evaluated. It would take a similar form to that in  $\bar{Z}$  above, and the expansion of it (without exponential terms) is given by Dalgarno and Stewart (1956 b).

We get

$$Q_{zz} = \frac{q}{R^3} \left\{ 15 - \left[ \frac{2R^6}{3} + \frac{11R^5}{3} + 10R^4 + 20R^3 + 30R^2 + 30R + 15 \right] e^{-2R} \right\} + O(q^2).$$

The other quadrupole moments can be deduced from symmetry considerations, for  $Q_{xx} = Q_{yy} = -\frac{1}{2}Q_{zz}$  and  $Q_{yz} = Q_{zx} = Q_{xy} = 0$ .

Table 3 compares the importance of the exponentially decreasing terms (which are not obtained by Dalgarno and Stewart) for the induced dipole and quadrupole moments. It is seen that the error involved in their neglect is more

Table 3

(1)	3	4	5	6	7	8	9	10
(2)	0.40952	0.28125	0.17723	0.12453	0.09176	0.07030	0.05556	0.04500
(3)	18.1	5.67	1.54	0.38	0.09	0.01	0.004	0.001
(4)	0.27077	0.17703	0.10854	0.06722	0.04333	0.02922	0.02056	0.01500
(5)	51.3	24.5	9.55	3.20	0.93	0.26	0.07	0.02

(1)  $R$  (units of  $a_0$ ); (2) coefficient of  $q$  in  $\bar{Z}$ ; (3) %error\*; (4) coefficient of  $q$  in  $Q_{zz}$ ; (5) %error\*

\* from neglecting the exponentially decreasing term.

serious with  $Q_{zz}$  than with  $\bar{Z}$ . This is because  $J$  has a factor of  $r_a^2$  in the  $Q_{zz}$  case, but only  $r_a$  in the  $\bar{Z}$  case, and the contributions to the integrals when  $r_a > R$  giving rise to the exponentially decreasing terms should therefore be greater for  $Q_{zz}$ .

### 3.2. Case (ii), $n=2$ , $|m|=1$

Here we have nothing to add to the work of Dalgarno and Stewart (1957), although the more reliable expressions involving exponential integrals could be derived using the function  $F(\xi, \eta)$  of § 2.2.

### 3.3. Case (iii), $n=2$ , $m=0$

The theory is illustrated by finding the  $q$  term of the induced dipole moment. This time

$$\phi_0 = \frac{R}{16\sqrt{\pi}} \left( 1 + \frac{2\alpha}{R} \right)^{-1/2} \exp \left[ -\frac{1}{4}R(\xi + \eta) \right] (\xi - \alpha)(\eta - \alpha)$$

$J=z=\frac{1}{2}R(\xi\eta+1)$  and  $\langle 0|J|0\rangle=3R/(2-\alpha R)$ , not zero as in the previous cases.  $F(\xi, \eta)$  is given in § 2.3 and after performing the integrations we obtain

$$\begin{aligned}\bar{Z} &= \langle \psi | z | \psi \rangle - \frac{3R}{2-\alpha R} \\ &= \frac{4q}{R^2} \left\{ 42 + \frac{1692}{R^2} - \frac{2\alpha}{R} \left( 153 + \frac{528}{R^2} \right) + \frac{468}{R^2(1+\frac{1}{4}R^2)} - \frac{1056\alpha}{R^3(1+\frac{1}{4}R^2)} \right. \\ &\quad \left. + \frac{15(1+2\alpha/R)}{(1+\frac{1}{4}R^2)^2} + \text{exponentially decreasing terms} \right\} + O(q^2).\end{aligned}$$

This expression can be expanded as a convergent power series if  $R > 2$ ; the first few terms are

$$q \left\{ \frac{168}{R^2} + \frac{4320}{R^4} \mp \left( \frac{1224}{R^3} + \frac{2448}{R^5} \right) + O\left(\frac{1}{R^6}\right) \right\}.$$

The minus sign is taken with the root  $\alpha_+ = 2/R + (1 + 4/R^2)^{1/2}$ . The exponentially decreasing terms can only be expected to be insignificant with this value of  $\alpha$ , as was the case in § 2.3.

The result for  $\bar{Z}$  in case (ii) is quoted for comparison; it is

$$\bar{Z} = q \left\{ \frac{156}{R^2} - \frac{4320}{R^4} + \text{exponentially decreasing terms} \right\} + O(q^2).$$

#### § 4. THE EFFECTS OF A PERTURBING POINT DIPOLE

Here we consider what happens when a hydrogen atom is in the presence of a charge dipole of strength  $\mu$ , distance  $R$  from the nucleus. In figure 2, the nucleus is at A, the electron at P, and the dipole is at B pointing along BB';  $\mathbf{k}$  is a unit vector along AB,  $\mathbf{i}$  is a unit vector perpendicular to  $\mathbf{k}$  in the plane ABB', and  $\mathbf{j}$  makes up the right-handed orthogonal triad.  $\phi$  is the angle between the planes APB and ABB', and  $r_a$ ,  $r_b$  and  $\theta$  have their previous definitions.

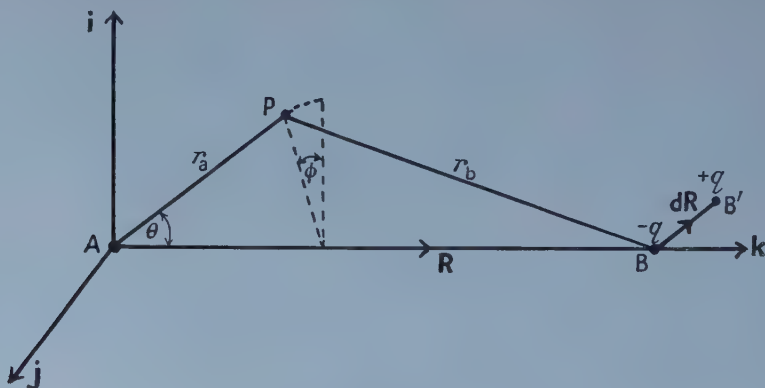


Figure 2.

The dipole can be thought of as the limiting case of charges  $-q$  at B and  $+q$  at B', provided that  $B' \rightarrow B$  and  $q \rightarrow \infty$  in such a way that  $q\overrightarrow{BB'} = qd\mathbf{R} \rightarrow \mu$ . Thus the effect of the dipole on the atom will be the same as the limiting case



of the sum of the effects of (a) a charge  $-q$  at B on an unperturbed state of the atom,  $\phi_0$  say, and (b) a charge  $+q$  at B' on the state perturbed by  $-q$  at B to

$$\phi_0 - q \sum_{r \neq 0} a_r \phi_r + O(q^2), \text{ where } a_r(\mathbf{R}) = \frac{\langle r | H'(\mathbf{R}) | 0 \rangle}{E_0 - E_r}.$$

The notation is that of § 3,  $\{\phi_r\}$  again being the set of eigenfunctions in spheroidal coordinates to take care of degeneracy.

As an example of this technique, the energy of interaction of the dipole with the hydrogen atom will be investigated. By conventional perturbation theory, the contribution from (a) is

$$-q \langle 0 | H'(\mathbf{R}) | 0 \rangle + q^2 \sum_{r \neq 0} \frac{\langle 0 | H'(\mathbf{R}) | r \rangle \langle r | H'(\mathbf{R}) | 0 \rangle}{E_0 - E_r} + O(q^3),$$

and that from (b) is

$$+q \langle \phi_0 - q \sum_{r \neq 0} a_r(\mathbf{R}) \phi_r | H'(\mathbf{R} + d\mathbf{R}) | \phi_0 - q \sum_{r \neq 0} a_r(\mathbf{R}) \phi_r \rangle \\ + q^2 \sum_{r \neq 0} \frac{\langle 0 | H'(\mathbf{R} + d\mathbf{R}) | r \rangle \langle r | H'(\mathbf{R} + d\mathbf{R}) | 0 \rangle}{E_0 - E_r} + O(q^3).$$

Adding the two contributions, we get the following expression for the interaction energy:

$$\Delta E = \lim_{qd\mathbf{R} \rightarrow \mu} q \langle 0 | \delta H' | 0 \rangle + q^2 \sum_{r \neq 0} \frac{\langle 0 | \delta H' | r \rangle \langle r | \delta H' | 0 \rangle}{E_0 - E_r} + O(\mu^3)$$

where  $\delta H' = H'(\mathbf{R} + d\mathbf{R}) - H'(\mathbf{R})$ . In terms of  $V$ ,

$$\langle 0 | \delta H' | 0 \rangle = \delta(1/R) + \langle 0 | \delta V | 0 \rangle,$$

and

$$\langle 0 | \delta H' | r \rangle \langle r | \delta H' | 0 \rangle = \langle 0 | \delta V | r \rangle \langle r | \delta V | 0 \rangle.$$

We can now re-introduce the function  $F(\xi, \eta; \mathbf{R})$  defined by equation (1), so that we finally obtain

$$\Delta E = \lim_{qd\mathbf{R} \rightarrow \mu} q \{ \delta(1/R) + \langle 0 | \delta V | 0 \rangle \} + 2q^2 \{ \langle 0 | \delta V \delta F | 0 \rangle - \langle 0 | \delta V | 0 \rangle \langle 0 | \delta F | 0 \rangle \} + O(\mu^3).$$

The integrations present some difficulty; for instance  $\langle 0 | \delta V | 0 \rangle \neq \delta \langle 0 | V | 0 \rangle$  unless  $n - |m| = 1$ , in which case  $\phi_0(\xi, \eta)$  is expressible in a form independent of  $R$ . Furthermore  $\langle 0 | \delta V \delta F | 0 \rangle$  can never be deduced from  $\langle 0 | V F | 0 \rangle$ ; both  $\delta V$  and  $\delta F$  will have to be found. For simplicity we will consider only the ground state of the hydrogen atom.  $\phi_0$ ,  $F(\xi, \eta; \mathbf{R})$  and  $E^{(1)}(\mathbf{R})$  are just as in § 2.1.

Now for any function  $g(R)$  of the magnitude of  $\mathbf{R}$ ,

$$\delta g = \frac{\partial g}{\partial R} \delta R = \frac{1}{R} \frac{\partial g}{\partial R} \mathbf{R} \cdot d\mathbf{R} = \frac{\partial g}{\partial R} \mathbf{k} \cdot d\mathbf{R}.$$

Using this we can show that

$$2\delta F = \mathbf{k} \cdot d\mathbf{R} \left\{ r_a \frac{\partial E^{(1)}}{\partial R} + \left[ \frac{1}{R^2} - e^{-2R} \left( 2 + \frac{2}{R} + \frac{1}{R^2} \right) \right] \ln(\xi + 1) \right. \\ + \frac{1}{R^2} [\ln(1 - \eta) + \text{Ei}\{R(1 - \eta)\}] - e^{-2R} \left( 2 + \frac{2}{R} + \frac{1}{R^2} \right) \\ \times [\ln(1 + \eta) - \text{Ei}\{R(1 + \eta)\}] \left. \right\} + \left[ 1 - \frac{1}{R} + e^{-2R} \left( 1 + \frac{1}{R} \right) \right] \frac{(\mathbf{b} - \xi \mathbf{k}) \cdot d\mathbf{R}}{R(\xi + 1)} \\ - \left( 1 + \frac{1}{R} \right) \frac{e^{-2R}}{R(1 + \eta)} [\{\eta + \exp[R(1 + \eta)]\} \mathbf{k} + \{1 - \exp[R(1 + \eta)]\} \mathbf{b}] \cdot d\mathbf{R} \\ - \left( 1 + \frac{1}{R} \right) \frac{1}{R(1 - \eta)} [\{\eta - e^{R(\eta - 1)}\} \mathbf{k} + \{1 - e^{R(\eta - 1)}\} \mathbf{b}] \cdot d\mathbf{R},$$

where  $\mathbf{b}$  is a unit vector along PB.

$$\text{Also} \quad \delta V = \delta \left( \frac{-1}{r_b} \right) = \frac{1}{r_b^2} \mathbf{b} \cdot d\mathbf{R} = \frac{4}{R^2(\xi - \eta)^2} \mathbf{b} \cdot d\mathbf{R}.$$

Since  $\phi_0$  is independent of  $R$  in this case, the first-order term of  $\Delta E$  can soon be found; it is

$$\lim_{q d\mathbf{R} \rightarrow \mu} q \delta \left\{ \frac{1}{R} + \langle 0|V|0 \rangle \right\} = - \left( 2 + \frac{2}{R} + \frac{1}{R^2} \right) e^{-2R} \mathbf{k} \cdot \mu,$$

(because  $1/R + \langle 0|V|0 \rangle = (1 + 1/R)e^{-2R}$ ).

The only case when the second-order term can be obtained at all easily is when the axis of the dipole is perpendicular to AB. Then  $\mathbf{k} \cdot d\mathbf{R} = 0$  as well as  $\mathbf{j} \cdot d\mathbf{R}$ , and  $\delta F$  simplifies considerably. In this case,

$$\mathbf{b} \cdot d\mathbf{R} = \mathbf{b} \cdot \mathbf{i} dR = -r_a \sin \theta \cos \phi \frac{dR}{r_b} = - \frac{(\xi^2 - 1)^{1/2} (1 - \eta^2)^{1/2}}{\xi - \eta} \cos \phi dR,$$

and

$$\delta V \delta F = (dR)^2 \frac{2(\xi^2 - 1)(1 - \eta^2)}{(\xi - \eta)^4} \cos^2 \phi \left[ \left\{ 1 - \frac{1}{R} + e^{-2R} \left( 1 + \frac{1}{R} \right) \right\} \frac{1}{\xi + 1} - \left( 1 + \frac{1}{R} \right) \left\{ \frac{1 - e^{R(\eta - 1)}}{1 - \eta} \right\} - e^{-2R} \left( 1 + \frac{1}{R} \right) \left\{ \frac{1 - e^{R(1 + \eta)}}{1 + \eta} \right\} \right].$$

$\langle 0|\delta V \delta F|0 \rangle$  is the only non-vanishing contribution, and after some long but fairly straightforward integrations the interaction energy is found to be

$$\Delta E = \frac{1}{2} \mu^2 \left[ \frac{1}{R^2} + \frac{1}{R^4} + \left( 1 - \frac{1}{2R} \right) e^{2R} \text{Ei}^*(2R) - \left( 1 + \frac{1}{2R} \right) e^{-2R} \text{Ei}(2R) - 2e^{-2R} \left( 1 + \frac{1}{R} \right) \left( 1 + \frac{1}{R} + \frac{1}{R^3} \right) + \frac{e^{-4R}}{R^2} \left( 1 + \frac{1}{R} \right)^2 \right] + O(\mu^3).$$

In the asymptotic series form,

$$\begin{aligned} & \frac{1}{R^2} + \frac{1}{R^4} + \left( 1 - \frac{1}{2R} \right) e^{2R} \text{Ei}^*(2R) - \left( 1 + \frac{1}{2R} \right) e^{-2R} \text{Ei}(2R) \\ & \sim - \frac{1}{16R^2} \sum_{s=0}^{\infty} \frac{(s+3)(2s+4)!}{(2R)^{2s}}. \end{aligned} \quad \dots\dots (3)$$

The right-hand side of (3) begins with

$$- \left( \frac{9}{2R^6} + \frac{45}{R^8} + \frac{1575}{2R^{10}} + \dots \right).$$

Table 4 shows how important the exponentially decreasing terms are, particularly when  $R < 7$ , and also gives values of the left-hand and right-hand sides of equation (3).

## § 5. DISCUSSION

The relative merits of the different forms of the various results should first be discussed. For the K shell, table 4 above and the table 1 of Dalgarno and Lynn (1957) both indicate that the error which arises from the use of an asymptotically divergent series is small compared with that arising from the neglect of the exponentially decreasing terms. These latter do not become negligible until  $R > 7$  or  $8a_0$ , when the series form might just as well be used. For the L shell, however, table 1 above shows that with the states  $n=2$ ,  $|m|=1$  it is the use of the series expansion which incurs the greater error, and that even

if the exponentially decreasing terms were neglected it would be still essential to use the unexpanded form for  $R < 7$ . As Coulson and Gillam (1947) observed, errors due to the divergence of the series will be far more serious with excited states of the atom. Even so, it is necessary to get some idea of the magnitude of the exponentially decreasing terms before neglecting them. With the degenerate states  $n=2$ ,  $m=0$ , table 2 shows that the second-order energy term will be subject to grave errors for  $R < 10$  with the negative root for  $\alpha$  unless the exponentially decreasing terms are found, but with the positive root for  $\alpha$  it should be accurate for quite small values of  $R$  without them.

We see, therefore, that it is desirable to use the unexpanded form of the perturbation  $H'$  and so obtain results free from asymptotically divergent series and complete with the exponentially decreasing terms. To do this, spheroidal coordinates are best employed, even when they are not necessary to take care of degeneracy, as they are with states where  $n - |m| \geq 2$ . The only limitations on these results now will be the errors arising from the neglect of third and higher order perturbation terms. A precise assessment of these further errors is not easy; an estimate of them which might be affected by the inherent faults in the use of the expanded form of  $H'$ , can be made from the work of Dalgarno and Stewart (1956b, 1957). It is not likely that they will be significant for  $R > 5$  with the K shell and for  $R > 7$  with the L shell.

The main drawback to the use of spheroidal coordinates lies in the heavy analysis involved in all but the simplest cases. This is contributed to appreciably by the complicated function  $F(\xi, \eta)$  which is vital to the exact second-order perturbation theory. Although it is preferable to persist with this function wherever possible and so obtain exact results, the use of the usual Unsold approximation (1927) for the second-order perturbation term would allow wider applications of the coordinates.

A word should be said about the results of §§ 2 and 3 in the special case when  $q=1$ , i.e. if the hydrogen atom is perturbed by a proton. Further degeneracy now arises because of the identity of the protons at A and B, and any theory not taking account of the existence of a centre of symmetry at the mid-point of the two nuclei is bound to be inaccurate (Dalgarno and Lewis 1956).

#### APPENDIX : THE INTEGRATIONS

The integrals can usually be broken down in a straightforward manner to depend on the basic functions

$$A_n(\lambda) = \int_1^\infty e^{-\lambda\xi} \xi^n d\xi, \quad B_n(\lambda) = \int_{-1}^1 e^{-\lambda\eta} \eta^n d\eta$$

and on the exponential integrals. The tables of Coulson (1941) and of Kotani, Amemiya, Ishiguro and Kimura (1955) were found useful, and in § 4 the reduction formula of Bartlett (1931) for

$$\int_1^\infty u(\xi) I(n, \xi) e^{-\lambda\xi} d\xi \quad \text{was employed where} \quad I(n, \xi) = \int_{-1}^1 \frac{e^{-\lambda\eta} d\eta}{(\eta - \xi)^n}.$$

#### ACKNOWLEDGMENTS

I would particularly like to thank Professor C. A. Coulson for proposing this work, and for his continued interest and many helpful suggestions. I am also grateful to the Department of Scientific and Industrial Research for a maintenance grant.

## REFERENCES

- BARTLETT, J. H., 1931, *Phys. Rev.*, **37**, 501.  
COULSON, C. A., 1941, *Proc. Camb. Phil. Soc.*, **38**, 210.  
COULSON, C. A., and DUNCANSON, W. E., 1942, *Phil. Mag.*, **33**, 754.  
COULSON, C. A., and GILLAM, C. M., 1947, *Proc. Roy. Soc. Edinb. A*, **62**, 362.  
COULSON, C. A., and ROBINSON, P. D., 1958, *Proc. Phys. Soc.*, **71**, 815.  
DALGARNO, A., and LEWIS, J. T., 1955, *Proc. Roy. Soc. A*, **233**, 70; 1956, *Proc. Phys. Soc. A*, **69**, 57.  
DALGARNO, A., and LYNN, N., 1957, *Proc. Phys. Soc. A*, **70**, 223.  
DALGARNO, A., and STEWART, A. L., 1956 a, *Proc. Roy. Soc. A*, **238**, 269; 1956 b, *Ibid.*, **238**, 276; 1957, *Ibid.*, **240**, 274.  
JEFFREYS, H., and JEFFREYS, B. S., 1956, *Methods of Mathematical Physics*, 3rd Edn (Cambridge : University Press), p. 502.  
KOTANI, M., AMEMIYA, A., ISHIGURO, E., and KIMURA, T., 1955, *Table of Molecular Integrals* (Tokyo : Maruzen).  
SCHIFF, L. I., 1955, *Quantum Mechanics*, 2nd Edn (New York : McGraw-Hill), p. 154.  
UNSOLD, A., 1927, *Z. Phys.*, **43**, 563.



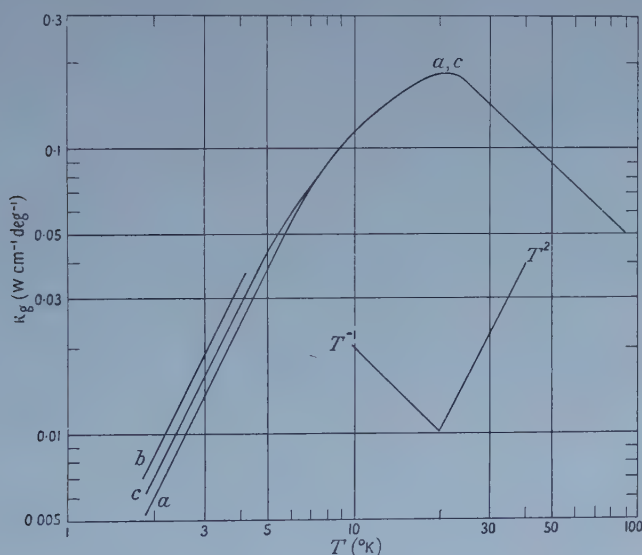
## RESEARCH NOTES

## The Lattice Thermal Conductivity of a Gold-Platinum Alloy

BY J. A. BIRCH, W. R. G. KEMP AND P. G. KLEMENS

Division of Physics, Commonwealth Scientific and Industrial Research Organization,  
Sydney*Manuscript received 17th December 1957*

IT is possible to deduce from the magnitude of the lattice thermal conductivity of monovalent metals at low temperatures the strength of the electron-phonon interaction and, by comparison with the electronic conduction properties, the nature of the coupling of the electrons with the lattice waves of various polarizations (Klemens 1954a, 1956). The lattice thermal conductivity of pure metals is overshadowed by a large electronic thermal conductivity and cannot be measured directly, but it can be deduced by interpolation from the lattice thermal conductivity of alloys. Thus, the lattice thermal conductivities of some



Lattice thermal conductivity of Au 98%<sub>0</sub>-Pt 2%<sub>0</sub>; curve *a*, specimen No. I; curve *b*, IIIa; curve *c*, IIIb.

silver alloys were derived from their measured thermal and electrical conductivities (Kemp, Klemens, Sreedhar and White 1954, 1956) and it was concluded that the interaction of the conduction electrons of silver with transverse waves was probably not much weaker, if at all, than with longitudinal waves. A similar conclusion was reached in the case of copper from a study of copper alloys (White and Woods 1955, Kemp, Klemens, Tainsh and White 1957). Such equal interaction with waves of all polarizations had been predicted from an intercomparison of the various electronic conduction properties for copper,

silver and gold (Klemens 1954b). To determine whether the lattice thermal conductivity of gold alloys also confirms this type of coupling, we have measured, as a preliminary step, the thermal and electrical conductivities of an alloy Au 98%–Pt 2% over a wide range of low temperatures, and deduced the lattice thermal conductivity  $\kappa_g$  from 2 to 90°K in a manner described previously (Kemp, Klemens, Tainsh and White 1957).

The specimen (No. I) was in the form of a polycrystalline rod, 0.3 cm in diameter, about 4 cm long, and had been annealed at 700°C. The electronic thermal conductivity was calculated from the measured residual resistivity  $\rho_0$  and from the intrinsic thermal resistivity, which was assumed to be the same as for gold, and had been measured by White (1953). The lattice component  $\kappa_g$ , which was then deduced by subtraction, is shown in the figure (curve *a*). As in other alloys,  $\kappa_g \propto T^2$  below about 6°K, indicating that the lattice thermal resistance  $W_g = 1/\kappa_g$  arises from the scattering of phonons either by electrons  $W_E$  or by dislocations  $W_D$ , since both  $W_E$  and  $W_D$  should vary as  $T^{-2}$ . Values of  $\rho_0$ ,  $W_g T^2$  at liquid helium temperatures and  $W_g/T$  at 90°K are given in the table.

Conduction Properties of Au 98%–Pt 2%

(1)	(2)	(3)	(4)	(5)
I	700	$1.85 \times 10^{-6}$	$6.5 \times 10^2$	0.2
II	900	$1.83 \times 10^{-6}$	$6.2 \times 10^2$	0.2
IIIa			$4.8 \times 10^2$	0.2
IIIb	1080	$1.95 \times 10^{-6}$	$5.6 \times 10^2$	
Theoretical value of $W_E T^2$				
(a) Makinson coupling scheme			$3.4 \times 10^2$	
(b) Bloch coupling scheme			$67 \times 10^2$	
Theoretical value of $W_g/T$				
(Leibfried and Schloemann)				0.03

(1) Specimen; (2) temperature of annealing (°C); (3)  $\rho_0$  (ohm cm); (4)  $W_g T^2$  (helium temperatures) ( $\text{w}^{-1} \text{cm deg}^3$ ); (5)  $W_g/T$  (oxygen temperatures) ( $\text{w}^{-1} \text{cm}$ ).

If  $W_D$  is negligible,  $W_g$  can be calculated from the intrinsic electronic thermal conductivity. If it is assumed that the electrons interact only with longitudinal waves (Bloch coupling scheme),  $W_E T^2 = 67 \times 10^2 \text{ w}^{-1} \text{cm deg}^3$ , while if they interact equally strongly with waves of all polarizations (Makinson coupling scheme),  $W_E T^2 = 3.4 \times 10^2 \text{ w}^{-1} \text{cm deg}^3$ . Since, however,  $W_D$  may not be negligible even in annealed materials, as for example appears from measurements on some copper alloys (Kemp, Klemens and Tainsh 1957), the observed values of  $W_g$  must be regarded as an upper limit for  $W_E$ .

Since the observed value of  $W_g T^2$  is only a factor 2 higher than the theoretical value of  $W_E T^2$  according to the Makinson coupling scheme, it may be concluded that the interaction with transverse waves is not appreciably weaker than with longitudinal waves, as expected from the electronic conduction data (Klemens 1954b) and from the similar behaviour of silver and copper alloys.

To test whether at least part of the discrepancy between  $W_g T^2$  and the theoretical value of  $W_E T^2$  is due to dislocations, the specimen was annealed at higher temperatures and measured again. After further annealing for four hours at 900°C the specimen (now No. II) showed a small decrease of  $\rho_0$ , but no significant change in  $\kappa_g$ —in particular the low temperature value of  $W_g T^2$  decreased by no more than about 5%. The specimen was then annealed again

for four hours at  $1080^{\circ}\text{C}$ , as high a temperature as was possible without melting. There had been considerable grain growth during this anneal, and the specimen had softened and changed its shape slightly. The specimen (now No. IIIa) was cooled slowly, mounted, and then measured.

The first measurements were made below  $4.2^{\circ}\text{K}$ . The residual resistivity  $\rho_0$  had increased by about 6%, probably due to some contamination during annealing, but more significantly,  $\kappa_g$  had increased by about 30% (see figure, curve b) so that  $W_g T^2$  now approached the theoretical limit to within a factor 1.4 (see table). This indicates that this high temperature annealing treatment had substantially reduced the dislocation density. Since the true value of  $W_E T^2$  is not known, and may differ from the theoretical value, it is not possible to estimate the residual dislocation resistance and dislocation density.

After these measurements the specimen was allowed to come to room temperature and observations above  $4.2^{\circ}\text{K}$  were continued a few days later. At these higher temperatures the curve of  $\kappa_g$  (curve c) gradually merges with the curve of specimen I, indicating that the imperfections responsible for the resistance at higher temperatures were not appreciably affected. However, when further measurements were made below  $4.2^{\circ}\text{K}$ , it was found that curve b could not be reproduced, but that  $\kappa_g$  of the specimen (now No. IIIb) had decreased to values intermediate between those of specimens II and IIIa.

Unless the first observations below  $4.2^{\circ}\text{K}$  on specimen III were in error, which in view of the internal consistency of these measurements we think to be unlikely, a change has occurred in the specimen which may be related to thermal cycling, although it is hard to believe that serious thermal stresses were set up, since the material is cubic. It is proposed to make further observations on the stability of the lattice thermal conductivity of highly annealed alloys.

The lattice thermal conductivity at oxygen temperatures, where  $\kappa_g \propto T^{-1}$ , is limited either by the scattering of phonons by point imperfections, or by the mutual interaction of phonons due to the anharmonicity of the lattice. The former may not be very important, since the platinum atoms have a mass and ionic radius similar to gold, so that they should not scatter phonons very strongly. Theoretical estimates of the resistivity due to the anharmonicity are not accurate, but there is an order of magnitude agreement with the theory of Leibfried and Schloemann (1954).

#### ACKNOWLEDGMENT

The authors wish to thank Mr. J. Middlehurst for his assistance with the high temperature annealing.

#### REFERENCES

- KEMP, W. R. G., KLEMENS, P. G., SREEDHAR, A. K., and WHITE, G. K., 1954, *Proc. Phys. Soc. A*, **67**, 728; 1956, *Proc. Roy. Soc. A*, **233**, 480.  
 KEMP, W. R. G., KLEMENS, P. G., and TAINSH, R. J., 1957, *Aust. J. Phys.*, **10**, 454.  
 KEMP, W. R. G., KLEMENS, P. G., TAINSH, R. J., and WHITE, G. K., 1957, *Acta Metallurg.*, **5**, 303.  
 KLEMENS, P. G., 1954 a, *Aust. J. Phys.*, **7**, 57; 1954 b, *Aust. J. Phys.*, **7**, 70; 1956, *Encycl. of Physics*, **14/4** (Berlin: Springer).  
 LEIBFRIED, G., and SCHLOEMANN, E., 1954, *Nachr. Akad. Wiss. Goettingen IIa*, No. 4, 71.  
 WHITE, G. K., 1953, *Proc. Phys. Soc. A*, **66**, 559.  
 WHITE, G. K., and WOODS, S. B., 1955, *Canad. J. Phys.*, **33**, 58.

## A New Absorption Band in Diamond and its Likely Cause

By F. A. RAAL

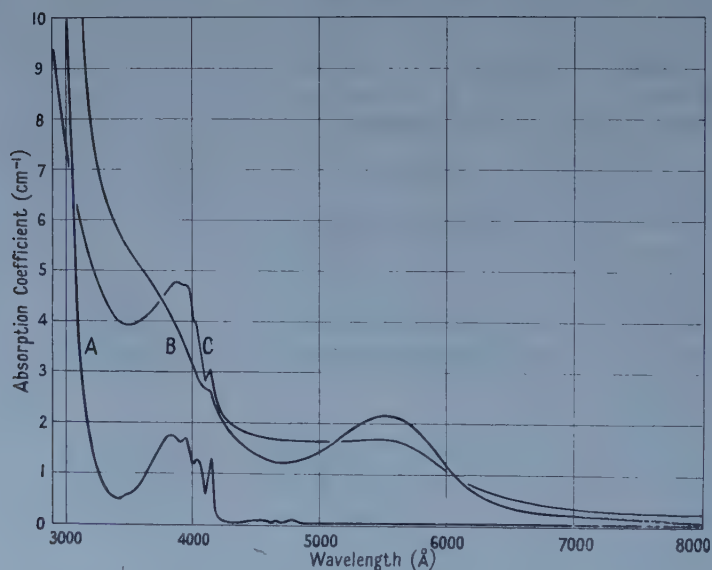
Diamond Research Laboratory, Johannesburg, South Africa

MS. received 9th December 1957, and in final form 20th January 1958

ON recording the absorption spectra of pink and mauve diamonds on an adapted Model DU Beckman spectrophotometer the existence of a new absorption band for diamond has been established. This band, which is very broad at room temperature, is located at approximately 5500 Å and cannot be resolved into component lines even at liquid oxygen temperature. It is found in all pink and mauve diamonds and is also observed in some brown diamonds in which a possible pink or mauve colour would be masked.

The fact that the absorption band is restricted to these distinctively coloured diamonds explains why it has not been detected by investigators such as Clark, Ditchburn and Dyer (1956) who made a very detailed study of the absorption spectra of the various diamond types. The strength of the band varies considerably and is correlated with the intensity of coloration of the diamond.

In the figure the absorption coefficients of white, pink and mauve diamonds are plotted as a function of the wavelength of the light. Curve A is that of the



white diamond and shows only those absorption bands found to be of general occurrence in Type 1 diamonds (Clark *et al.* 1956). Curves B and C are those of mauve and pink diamonds respectively and plainly show the new broad absorption band at about 5500 Å. This band must be due to a defect in the diamond which gives rise to an electronic energy level in the forbidden gap. The fact that the band, in that it has no sharp lines and is not temperature dependent, is not typical of those known to be associated with structural defects in diamond suggests that the absorption centre is a foreign atom impurity rather than a simple vacancy or dislocation,



A spectrographic analysis of some of the pink and mauve stones was made in order to identify this element.

The investigation was done on a qualitative rather than a quantitative basis since the minimum quantities of some of the transition or heavy elements which can be detected are sometimes comparatively high. These elements are of especial interest in view of their electronic configurations.

Analyses of three of the highly coloured specimens revealed the presence of Mn besides the impurities Si, Mg, Ca and Al normally found in diamond (Raal 1957). The most persistent lines of Mn were found to be more intense the deeper the colour. Since the strength of the 5500 Å absorption band is dependent on the depth of colour it can be inferred that the new absorption band is also correlated with the Mn concentration in diamond.

Some of the pale pink stones analysed did not show Mn as an impurity. Since the minimum concentration of Mn which can be detected is about ten parts per million this is probably due to Mn being present in a concentration such that its presence cannot be established spectrographically.

In their work on purple glasses Turner and Weyl (1935) have shown that Mn causes broad absorption at about 5000 Å. It appears, therefore, very likely that it is this element also which is responsible for the hitherto unknown absorption band. Since the characteristic band produced by the manganese is probably associated with a transition in an incompleated shell we would expect the wavelength of the band to be roughly the same for manganese in diamond and glass.

#### ACKNOWLEDGMENT

The author wishes to thank Messrs. Industrial Distributors (1946) Limited for permission to publish this note and is indebted to Dr. J. F. H. Custers, Director of Research, for his interest and co-operation.

#### REFERENCES

- CLARK, C. D., DITCHBURN, R. W., and DYER, H. B., 1956, *Proc. Roy. Soc. A*, **234**, 363.  
RAAL, F. A., 1957, *Amer. Min.*, **42**, 354.  
TURNER, W. E. S., and WEYL, W., 1935, *J. Soc. Glass Tech.*, **19**, 208.

---

### Some Observations on the Debye Effect in Electrolytes

By A. N. HUNTER

Physics Department, the University of Leicester

*MS. received 6th January 1958, and in final form 17th February 1958*

By the Debye effect we mean the existence of an electric potential wave accompanying the passage of an acoustic wave through an electrolyte. The purpose of this communication is to draw attention to some experiments, carried out in this laboratory, which indicate that an electric potential wave also results when a sound wave is passed through the purest available water (conductivity less than 1 micromho). This effect is not taken into account in

Debye's formula (Debye 1933) and suggests that experimental values for the Debye effect should be treated with caution.

The experiments were carried out by placing a small glass cell, containing the electrolyte sample, in a tank of castor oil at the end of an acoustic delay line (a metre-long tube filled with water). The castor oil was separated from the water by means of a piece of 'Styrafoil' plastic 0.003 in. thick, and the purpose of the castor oil was to absorb the sound emerging from the tube so as to avoid multiple reflections. A block diagram of the apparatus is given in figure 1.

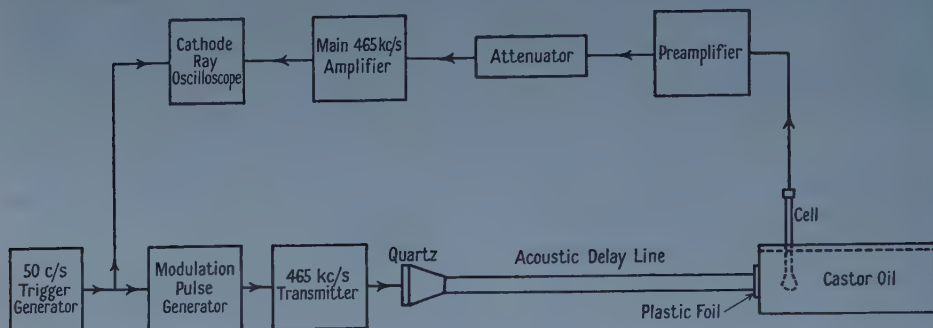


Figure 1.

The source was a  $2\frac{1}{2}$  in. diameter quartz plate pulsed at its resonant frequency of 465 kc/s, with a pulse length of about 1 millisecond and repetition rate of 50 c/s. The glass cell was similar in design to that described by Yeager, Dietrick and Hovorka (1953) and was fitted with twin probes consisting of a pair of 32 s.w.g. platinum wires each 1 cm long spaced approximately 1.5 mm apart (one half-wavelength of the sound). The details of the experimental arrangements will be given elsewhere, but the procedure consisted essentially of filling the cell with a given sample of electrolyte and then measuring the resistance between the probes with an a.c. bridge working at 1 kc/s. The sound field was then switched on and the signal from the cell adjusted to give a standard output on the cathode-ray oscilloscope by means of a calibrated attenuator. The experiment was repeated for different concentrations of solute etc. and it was found to be convenient to plot the attenuator setting in decibels against the cell resistance. This method of plotting shows the variation of output with concentration of solute and also emphasizes some similarities found between different solutes.

The Debye effect is small in electrolytes (of the order of microvolts) and it has been found difficult to obtain a sufficiently high signal-noise ratio for accurate determination of the variation of the effect with concentration of solute. In general the measurements indicate a small change with concentration over a wide range of concentrations of the order of 0.01 N. With high concentrations the signal is reduced and these results are in agreement with the predictions of Debye's equation. However, the Debye equation indicates zero effect for infinite dilution whereas we have consistently found that the signal in conductivity water is not much less than the maximum obtained for the solutes tried (a drop of not more than 6 dB in the case of NaI, NaCl and KCl). Because of the difficulty experienced in obtaining accurate results for these curves, and also in order to obtain more information about the behaviour of the cell, it was decided to try the effect of tuning out the capacitance of the cell,

The capacity between the probes, resulting from the high dielectric constant of water, is about 8 pF and has a reactance of about 30 000 ohms at 465 kc/s. This capacitance, together with that of the connecting cable and amplifier input circuit, was tuned by means of a parallel coil. The resulting signal was much larger than before and the improvement in signal-noise ratio such as to enable consistent results to be obtained. The curve for NaI given in figure 2 is typical

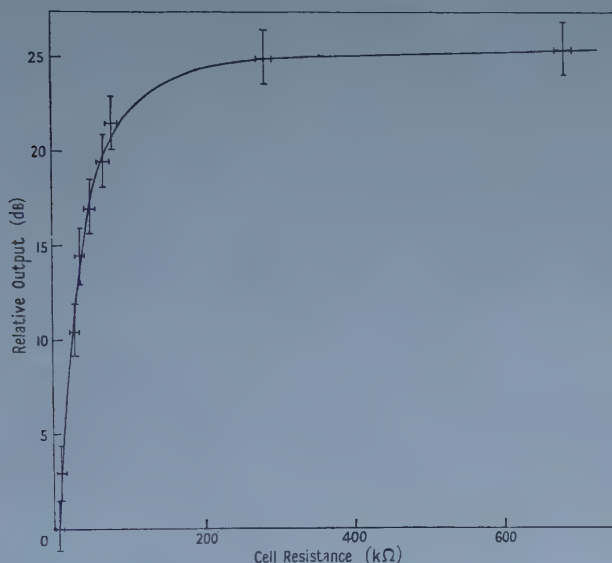


Figure 2. Signal plotted against cell resistance for NaI.

of the results obtained and shows that, under these conditions, the signal is largest for pure water and that the addition of solute reduces the signal. This effect has always been observed with all types of probes used and is unaltered by coating the probes electrolytically with platinum black. The signal vanishes if the sound is prevented from reaching the cell by insertion of a piece of sponge rubber or other similar obstacle and the measured delay time is correct for the acoustic path traversed. Rotation of the twin probe results in the signal passing through maxima and minima, corresponding to phase differences of  $\pi$  and 0 respectively between the two wires: measurements were always taken with the probe set to a maximum. It thus appears that the signal in water is not due to surface effects at the probes and that a large e.m.f. is generated in water by the passage of sound through the cell which is normally masked by the presence of a solute. The existence of an effect in pure liquids has been confirmed in a private communication by Professor Rutgers of the University of Ghent. One would like to know more about the mechanisms involved in order to apply a correction to Debye's formula. To this end an attempt is being made to establish an 'equivalent circuit' for the cell.

The following experiments have been tried with the tuning coil in position:

1. The cell was filled with conductivity water and exposed to the sound field with the capacity  $C$  tuned out. A variable shunt was connected across the cell and the attenuator setting for constant output recorded against the value of the



shunt resistance. The resulting curve fitted the curve of figure 2 for signal against cell resistance with varying concentrations of NaI.

2. The variation of attenuator setting for constant output with different values of cell resistance was found for the solutes KCl, NaI and NaCl. Again the curves were indistinguishable from each other and from that of 1 above.

3. Experiment 2 was repeated with chrome alum as the solute: in this case the curve differed from that obtained with the salts quoted above in that the signal was considerably less for a given cell resistance (about 12 dB at 60 000 ohms) except at very high dilution when the results for all salts extrapolate to those for water. This experiment showed that the effect observed was not spurious depending only on the resistive damping of the tuned circuit by the conductance of the electrolyte.

4. No signal could be detected with benzene in the apparatus which suggests that the effect may only occur in polar liquids.

5. Experiment 1, in which the cell was shunted by a variable resistance, was repeated with different electrolytes in the cell. The values of the shunt resistance were corrected for the finite  $Q$  of the tuning coil and the results were used to determine the effective output resistance of the cell.

6. A signal generator, operating on 465 kc/s, was connected to the cell through a variable non-inductive resistance. The output from the signal generator was adjusted to give a constant output from the cell (measured with the same amplifier used in the previous experiments) for each value of the series resistance. The experiment was repeated for different electrolytes and also with a capacitor substituted for the cell. The results were used to find the effective resistance of the tuned circuit and the internal resistance of the cell. The values of internal resistance so obtained agreed with these obtained in 5, although these two values did not agree with the a.c. bridge results to better than 50%.

#### SUMMARY

A potential wave appears to exist when a sound wave is passed through 'pure' water and the magnitude of this effect is comparable with that given by Debye's formula for solutions of simple salts. The effect has been observed over a period of years with different experimental arrangements and appears to be genuine. It does not occur with the non-polar liquid benzene and is unaltered by treatment of the electrodes with platinum black. The cell filled with water appears to act like a constant voltage generator with an e.m.f. of about 50 microvolts and having a high internal resistance of the order of 750 000 ohms (depending on the conductivity of the water) with the terminals shunted by a capacity of the order of 8 pF. The addition of solute results in a further conductance across the capacity and the modification of the e.m.f. In the case of the salts NaI, KCl and NaCl the shunting effect seems to be the more important. The apparatus has not been calibrated for sound amplitude but the signal in KCl, with the cell untuned, is a few microvolts; comparison with the results of Yeager, Dietrick and Hovorka (1953) indicates that the velocity amplitude should be about unity. Attempts are being made to improve the signal-noise ratio so that more complete curves can be taken for untuned cells and the measurements extended to other electrolytes and pure liquids.



## ACKNOWLEDGMENT

The author wishes to thank Professor E. A. Stewardson for his encouragement and for facilities to pursue the work.

## REFERENCES

- DEBYE, P., 1933, *J. Chem. Phys.*, **1**, 13.  
 RUTGERS, A., 1946, *Nature, Lond.*, **157**, 74.  
 YEAGER, E., BUGOSH, J., HOVORKA, F., and MCCARTHY, J., 1949, *J. Chem. Phys.*, **17**, 411.  
 YEAGER, E., DIETRICK, H., and HOVORKA, F., 1953, *J. Acoust. Soc. Amer.*, **25**, 456 (see also Yeager *et al.* 1949).

## Variation of Secondary Emission with Primary Electron Energy

BY BIPIN KUMAR AGARWAL

Physics Department, Allahabad University, Allahabad, India

*MS. received 7th January 1958*

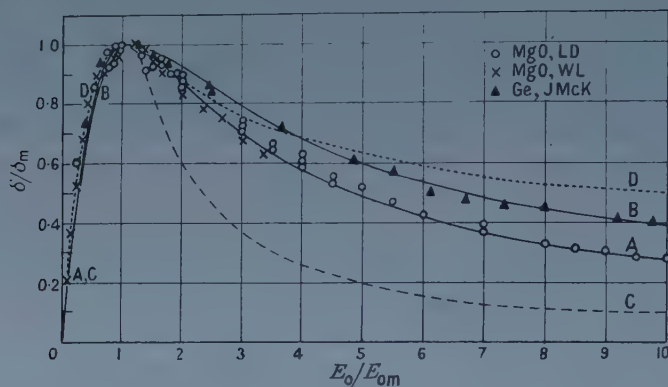
So far no experimentally satisfactory formula for the secondary yield of a given solid for a given initial energy of the primary beam has been developed from a theoretical standpoint. An accurate wave mechanical treatment is not possible at present because it requires a detailed knowledge of the momentum transfer between electrons and the lattice. However, avoiding these details, an elementary theory can be developed (Bruining 1954) by assuming that the production of secondaries per unit primary path is proportional to the rate of primary energy loss and that secondaries are absorbed exponentially. Baroody (1950) has shown that on the basis of these assumptions and Whiddington's law for primary energy loss a universal reduced curve between  $\delta/\delta_m$ , the secondary emission coefficient divided by its maximum value, and  $E_0/E_{0m}$ , the primary energy divided by the energy for maximum emission, can be deduced. But this curve deviates considerably from the experimental curve for metals. Recently Lye and Dekker (1957) have proposed that a better agreement between theoretical and experimental values can be obtained by replacing Whiddington's law by a power law of the form  $dE/dx = -A/E^n(x)$  for the energy loss of primaries. The power  $n$  is adjusted to yield a formula for the primary range in agreement with the empirical relation given by Young (1956) to fit his measurements on aluminium oxide. Although this improves the situation, the Lye and Dekker curve still remains unsatisfactory, particularly in the high energy region. Also, their formula is of little practical use because it gives one curve common to all materials when the experimental evidence is against it. In the present note a very simple formula is presented which reproduces the experimental results reasonably well.

The formula for the variation of secondary yield with primary energy can be written as

$$\delta/\delta_m = \frac{2(E_0/E_{0m})}{1 + (E_0/E_{0m})^{1.85(2Z/A)}} \quad \dots\dots (1)$$

where  $Z$  is the atomic number and  $A$  the atomic weight. This relation is plotted in the figure for MgO and Ge, together with the available experimental data.

For comparison the calculated curves due to Baroody (1950) and Lye and Dekker (1957) have also been included. It is observed that both these curves, C and D, lie away from the experimental points, while curves A and B calculated from relation (1) give a very good agreement even for higher primary energies.



Curve A, equation (1) for MgO; curve B, equation (1) for Ge; curve C from calculations of Baroody (1950); curve D from calculations of Lye and Dekker (1957). Experimental data shown by points as indicated. LD, Lye and Dekker 1957; WL, Whetten and Laponsky 1957; J. McK, Johnson and McKay 1954.

For lighter elements ( $Z \sim 10$ ) the value of  $2Z/A$  is 1, while for slightly heavier elements ( $Z \sim 30$ ) it is near 0.9. Therefore, according to equation (1) one would expect the experimental data on metals like Ni and Mo to fall closer to curve B than to A. This is confirmed by the measurements of Blankenfeld (1951).

#### REFERENCES

- BAROODY, E. M., 1950, *Phys. Rev.*, **78**, 780.  
 BLANKENFELD, G., 1951, *Ann. Phys.*, *Lpz*, **9**, 48.  
 BRUINING, H., 1954, *Physics and Applications of Secondary Emission* (New York: McGraw-Hill), Chap. 6.  
 JOHNSON, J. B., and MCKAY, K. G., 1954, *Phys. Rev.*, **93**, 669.  
 LYE, R. G., and DEKKER, A. J., 1957, *Phys. Rev.*, **107**, 977.  
 WHETTEN, N. R., and LAPONSKY, A. B., 1957, *J. Appl. Phys.*, **28**, 515.  
 YOUNG, J. R., 1956, *Phys. Rev.*, **103**, 292.

### Electron Traps Produced in KCl Crystals by Quenching or Pressure

By J. EWLES, S. C. JAIN† AND R. V. JOSHI

Department of Physics, University of Leeds

MS. received 12th November 1957, and in revised form 14th January 1958

#### § 1. INTRODUCTION

It is known that lattice defects created by mechanical or thermal strain in crystals can give rise to new optical and electrical properties. Kats (1950) found that grinding made sodium chloride thermoluminescent, Ewles and Lee (1953) reported luminescent effects in alkali earth oxides due to grinding

† I.C.I. Fellow, on leave of absence from the National Physical Laboratory of India, New Delhi.

and Ewles and Stead (1956) found luminescent centres produced in alkali halides by pressure or by quenching from a melt. Increased conductivity produced by quenching (Ewles and Stead 1956, Ewles and Jain 1957) has also been reported.

A brief account is now given of preliminary investigations by the well-known thermoluminescent method of Urbach on the electron traps produced by quenching or by pressure in KCl crystals and in fused and powdered 'specpure' KCl.

## § 2. EXPERIMENTAL ARRANGEMENTS

The sample to be studied was held against the upper flattened end of a thick rod of copper immersed in a Dewar flask. The upper flattened end of the rod projected about one inch beyond the mouth of the Dewar and was prevented from coming into contact with cold moist air by a quartz tube fitting snugly over the mouth of the Dewar and supplied with a continuous stream of dry nitrogen from another Dewar in which liquid nitrogen was kept boiling by an

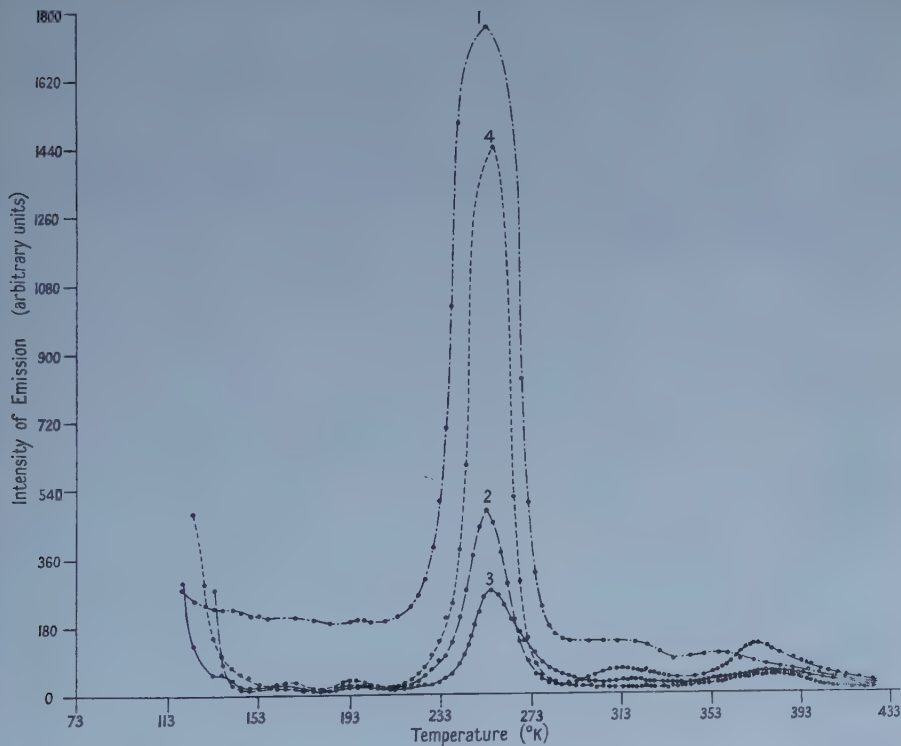


Figure 1. Glow curves. 1, KCl melt quenched in liquid nitrogen; 2, KCl melt quenched to room temperature in air; 3, KCl melt quenched to liquid nitrogen temperatures in vacuum of the order  $10^{-3}$  mm; 4, KCl melt quenched to liquid nitrogen temperatures in vacuum of better than  $10^{-5}$  mm.

electric heating coil. The copper rod and specimen were first cooled to about  $-190^{\circ}\text{C}$  by gradually pouring liquid nitrogen into the Dewar containing them. At this temperature the specimen was then excited to saturation by condensed sparks between aluminium rods. The copper rod and specimen were then

steadily heated by a current through a wire surrounding the lower end of the rod. The rate of heating used finally was  $0.12 \text{ deg sec}^{-1}$ . The thermoluminescence was measured by means of a photomultiplier connected to a d.c. amplifier and mirror galvanometer.

### § 3. EXPERIMENTAL RESULTS

#### 3.1. Effects of Quenching

The following effects of quenching were observed:

(a) Spectroscopically pure potassium chloride was melted in a platinum crucible and then poured into liquid nitrogen. A typical glow curve is shown in figure 1, curve 1.

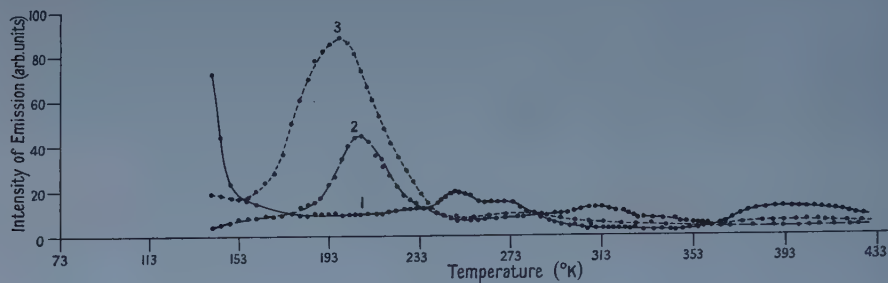


Figure 2. Glow curves. 1, KCl single crystal (Hilger); 2, KCl specpure powder compressed to tablet under pressure of  $4000 \text{ lb in}^{-2}$ ; 3, KCl single crystal (Hilger) after pressure of  $4000 \text{ lb in}^{-2}$ .

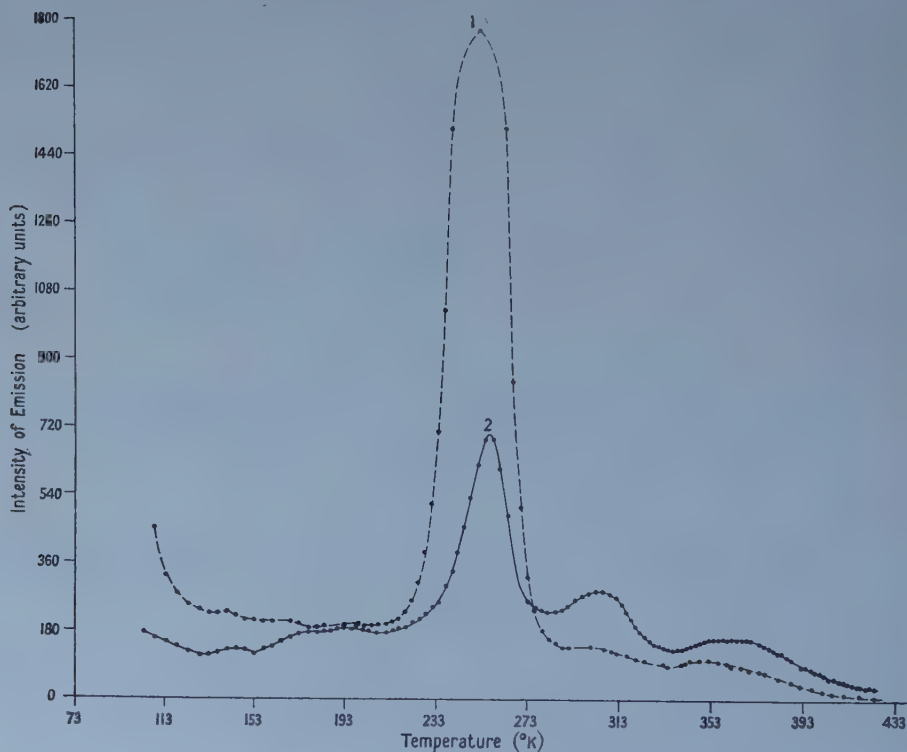


Figure 3. Glow curves. 1, KCl melt quenched in liquid nitrogen; 2, KCl melt quenched in liquid nitrogen and then compressed to tablet under pressure of  $4000 \text{ lb in}^{-2}$ .



(b) Another melt was poured from one platinum crucible into another (figure 1, curve 2).

(c) A specimen was prepared by quenching a melt rapidly *in vacuo* in the apparatus previously described (Stead 1956). Figure 1, curve 3, shows the glow curve for a vacuum of  $10^{-3}$  mm Hg and curve 4 for a vacuum of better than  $10^{-5}$  mm Hg.

(d) With KCl powder formed by subliming the vapour into a platinum crucible cooled to the temperature of liquid nitrogen no measurable glow peaks were obtained.

### 3.2. The Effect of Pressure

Figure 2, curve 2, shows the effect of pressure alone ( $4000 \text{ lb in}^{-2}$ ) on a tablet made from powdered 'specpure' KCl and figure 2, curve 3, the effect of pressure alone on a single crystal (supplied by Messrs. Hilger and Watts). Figure 3 shows the effect of pressure on quenched specimens. It is observed that the number of electrons in the  $253^{\circ}\text{--}255^{\circ}\text{K}$  trap has decreased while the number in the  $300^{\circ}\text{K}$  and  $350^{\circ}\text{K}$  regions has markedly increased.

### § 4. CONCLUSIONS

It is observed that the  $253^{\circ}\text{--}255^{\circ}\text{K}$  trap is present in all the quenched specimens except that produced by condensation of the vapour *in vacuo*. Since this trap is observed even when the quenching is not rapid enough to produce thermally 'frozen in' Schottky vacancies, figure 1, curve 2 (Stead 1956, Ewles and Jain 1957) it cannot be directly associated with such vacancies. This conclusion is also supported by the fact that it disappears, together with the other traps produced by quenching, upon heating to  $100^{\circ}\text{C}$  for a few minutes. The investigations of Jain (1957) and of Ewles and Jain (1957) showed that the mobility of the negative ion vacancies which controls the equilibrium number of positive ion vacancies, is such that it would take weeks of heating at  $100^{\circ}\text{C}$  to reduce the number of vacancies appreciably. Further Ewles and Stead showed that quenching from vapour to solid *in vacuo* produced a large number of Schottky vacancies—yet such a specimen showed no glow peaks. Thus it is concluded that the traps introduced by quenching are not connected directly with negative or positive ion vacancies. It is suggested that they are the result of plastic flow and dislocations set up by rapid cooling. The small peak at  $310^{\circ}\text{K}$  seen in the specimens not prepared *in vacuo* may be due to some adsorbed gas like the traps observed by Kats (1950) in NaCl heated in air. The traps at  $350^{\circ}\text{--}380^{\circ}\text{K}$  seen in all the specimens are not very 'sharp' or reproducible in position and may again be due to some adsorbed gas though the results shown in figure 3 suggest that they are connected with distortions or dislocations.

In the pressure treated specimens it is of considerable interest to observe that the trap at  $200^{\circ}\text{K}$  is at the same depth as one of the two prominent traps observed in  $\text{KCl}:\text{TlCl}$  and attributed by Johnson and Williams (1953) to a metastable level of the Tl ion. Since however it can be produced in 'specpure' material by pressure there is either a remarkable coincidence or it is not due directly to a Tl ion but to a structural defect which can be produced either by pressure or by the presence of an ion of different size from the cation of the host lattice. The implications of these points are now being investigated. Extensive investigations of traps in  $\text{KCl}:\text{TlCl}$  and in  $\text{KCl}:\text{Tl}$  have been in progress for some time here and will be reported later.

A comparison of figures 1, 2 and 3 shows that the effects of a pressure of  $4000 \text{ lb in}^{-2}$  are an order of magnitude smaller than those produced by thermal quenching in liquid nitrogen.

Further experiments on glow, decay and stimulation curves of thermally and mechanically strained crystals are in progress.

#### ACKNOWLEDGMENTS

Some of the apparatus used was purchased from funds supplied from the Government Grants Committee of the Royal Society.

One of us (S. C. J.) is grateful for the award of an I.C.I. Fellowship which made his part in the work possible.

#### REFERENCES

- EWLES, J., and JAIN, S. C., 1958, *Proc. Roy. Soc. A*, **243**, 353.  
 EWLES, J., and LEE, N., 1953, *Trans. Electrochem. Soc.*, **100**, 392.  
 EWLES, J., and STEAD, J. C., 1956, *Proc. Phys. Soc. B*, **69**, 392.  
 JAIN, S. C., 1958, *Proc. Roy. Soc. A*, **243**, 359.  
 JOHNSON, R. P., and WILLIAMS, F. E., 1953, *J. Chem. Phys.*, **21**, 125.  
 KATS, M. L., 1950, *J. Exp. Theor. Phys.*, **20**, 166.  
 STEAD, J. C., 1956, *Thesis*, University of Leeds.

## Expansion of the Regular Coulomb Wave Function in terms of Bessel Functions

By A. S. MELIGY

Faculty of Science, University of Alexandria, Egypt

MS. received 13th January, 1958

### § 1. INTRODUCTION

ABRAMOWITZ (1952) AND FRÖBERG (1955) have given reviews on the different treatments of Coulomb wave functions. Although extensive work has been done in this field, yet more simplified expansions suitable for certain ranges of the Coulomb parameters are still required. For particles of high energies, various expansions had been developed in series of Bessel functions of different orders (Abramowitz 1950, Meligy 1956, Morse, unpublished). In this communication a new expansion has been developed for the regular radial Coulomb wave function as a series of Bessel functions of integral orders.

### § 2. THE EXPANSION OF $F_L(\eta, \rho)$

The regular radial Coulomb wave function, in normalized form, can be expressed in terms of the confluent hypergeometric function of Whittaker and Watson (1927) as follows:

$$F_L(\eta, \rho) = \frac{1}{2} \frac{A_L(\eta)}{(2L+1)!} (i)^{-L-1} M_{i\eta, L+\frac{1}{2}}(2i\rho), \quad \dots\dots (1)$$

where

$$A_L(\eta) = \left\{ (1^2 + \eta^2)(2^2 + \eta^2) \dots (L^2 + \eta^2) \frac{2\pi\eta}{e^{2\pi\eta} - 1} \right\}^{1/2},$$

$L$  is the orbital angular momentum quantum number,  $\eta = ZZ'e^2/\hbar v$  and  $\rho = mvr/\hbar$ ;  $v$  is the relative velocity of the two particles,  $r$  is the distance between them and  $m$  is the reduced mass.

The function  $M_{i\eta, L+\frac{1}{2}}(2i\rho)$  can be represented by the contour integral

$$M_{i\eta, L+\frac{1}{2}}(2i\rho) = -\frac{1}{2i\pi} (2L+1)! e^{-i\rho} (2i\rho)^{L+1} \int_{\infty}^{(0+)} (-t)^{-2L-2} \left(1 + \frac{2i\rho}{t}\right)^{-1-L+i\eta} e^{-t} dt, \quad \dots\dots (2)$$

where the contour of integration starts at infinity on the real axis, encircles the origin in the positive direction and returns to plus infinity; on the contour  $|2\rho| < |t|$ .

Let the factor  $(1 + 2i\rho/t)^{-\frac{1}{2}-L+i\eta}$  in the integrand be expanded by the binomial theorem into the uniformly convergent series

$$\left(1 + \frac{2i\rho}{t}\right)^{-\frac{1}{2}-L+i\eta} = \sum_{n=0}^{\infty} \frac{(-)^n}{n!} \left(\frac{1}{2} + L - i\eta\right)_n \left(\frac{2i\rho}{t}\right)^n, \quad \dots\dots (3)$$

where  $(\frac{1}{2} + L - i\eta)_n = (\frac{1}{2} + L - i\eta)(\frac{3}{2} + L - i\eta) \dots (n - \frac{1}{2} + L - i\eta)$ . Substituting (3) in (2) and integrating term by term, it follows that

$$M_{i\eta, L+\frac{1}{2}}(2i\rho) = -\frac{1}{2i\pi} (2L+1)! e^{-i\rho} (2i\rho)^{L+1} \sum_{n=0}^{\infty} \frac{1}{n!} \left(\frac{1}{2} + L - i\eta\right)_n \times (2i\rho)^n \int_{\infty}^{(0+)} (-t)^{-2L-2-n} \left(1 + \frac{2i\rho}{t}\right)^{-1/2} e^{-t} dt.$$

The integral on the right-hand side of this equation can be expressed, according to (2), in terms of the function  $M_{s,s}(2i\rho)$ , thus having

$$M_{i\eta, L+\frac{1}{2}}(2i\rho) = (2L+1)! \sum_{n=0}^{\infty} \frac{(\frac{1}{2} + L - i\eta)_n}{n! (2L+1+n)!} (2i\rho)^{n/2} M_{s,s}(2i\rho), \quad \dots\dots (4)$$

where  $s = \frac{1}{2} + L + \frac{1}{2}n$ .

Applying the expansion of the confluent hypergeometric function given by Slater (1954), the function  $M_{s,s}(2i\rho)$  can be expressed in terms of Bessel functions as follows:

$$(2i\rho)^{n/2} M_{s,s}(2i\rho) = (2s)! 2^{3L+2n+2} (i)^{L+1+n} \rho^{-L} \sum_{\nu=0}^{\infty} \frac{(-i)^{\nu}}{\nu!} (4s)_{\nu} J_{2s+\nu}(\rho). \quad \dots\dots (5)$$

Substituting (5) in (4) and arranging the resulting expansion, which is easily seen to be absolutely convergent, as a series in Bessel functions one can express the Coulomb wave function (1) as follows:

$$F_L(\eta, \rho) = 2^{3L+1} A_L(\eta) \rho^{-L} \sum_{n=0}^{\infty} a_n J_{2L+1+n}(\rho), \quad \dots\dots (6)$$

where  $a_0 = 1$ ,  $a_1 = 4\eta$ ,  $a_2 = 8\eta^2 - 2L - 1$ , and in general, for  $n \geq 2$ ,

$$na_n = (4\eta)a_{n-1} - (4L+n)a_{n-2}. \quad \dots\dots (7)$$

This is the expansion of the regular Coulomb wave function as a series of Bessel functions of integral orders. As seen from (7), the expansion is convenient for the computation of  $F_L(\eta, \rho)$  for small values of  $\eta$ , that is for high energies.

#### REFERENCES

- ABRAMOWITZ, M., 1950, *J. Math. Phys.*, **29**, 303; 1952, *Tables of Coulomb Wave Functions*, *Appl. Math. Ser. U.S. Bur. Stand.* No. 17 (U.S. Gov. Printing Office, Washington, D.C.).  
FRÖBERG, C., 1955, *Rev. Mod. Phys.*, **27**, 399.

MELIGY, A. S., 1956, *Nuclear Phys.*, **1**, 610.

SLATER, L. J., 1954, *Proc. Camb. Phil. Soc.*, **50**, 628.

WHITTAKER, E. T., and WATSON, G. N., 1927, *Modern Analysis* (Cambridge: University Press).

## Polarization in Nuclear Reactions

BY J. N. LYNNESS

University of Malaya, Singapore

*MS. received 9th August 1957, and in revised form 28th January 1958*

THE square well optical model, discussed by Feshbach, Porter and Weisskopf (1954), has reproduced certain experimental results for the scattering of low energy neutrons by medium and heavy nuclei. In particular in the energy region up to 3 meV, the total elastic cross section  $\sigma_e$  agrees well with experimental results. At 1 meV, the shape-elastic differential cross section is in qualitative agreement, but there seems to be consistent disagreement for half-backward scattering. The model predicts a gradual minimum considerably lower than that experimentally observed. However, the authors point out that if favourable assumptions are made concerning the compound-elastic cross section  $\sigma_{ce}(\theta)$ , it is possible to predict a differential cross section which agrees well with observed measurements. The square well optical model used by these authors was of the form

$$\left. \begin{aligned} V(r) &= -V_0(1+i\zeta) & r < R = r_0 A^{1/3} \\ V(r) &= 0 & r > R \end{aligned} \right\} \quad \dots\dots (1)$$

with the parameters

$$V_0 = 42 \text{ meV}, \quad \zeta = 0.03, \quad r_0 = 1.45 \times 10^{-13} \text{ cm.}$$

In order to take into account polarization effects, this model has to be modified in some way. This can be done by adding to the potential a spin-orbit term  $\alpha(r)\mathbf{L} \cdot \mathbf{S}$ . This preserves the spherical symmetry and to each partial  $l$ -wave with total angular momentum  $j = l \pm \frac{1}{2}$  there can be ascribed an effective potential

$$\begin{aligned} V_l^{l \pm \frac{1}{2}}(r) &= -V_0(1+i\zeta) + \frac{1}{2}\alpha(r) \begin{cases} +l \\ -(l+1) \end{cases} & r < R, \\ V_l^{l \pm \frac{1}{2}}(r) &= \frac{1}{2}\alpha(r) \begin{cases} +l \\ -(l+1) \end{cases} & r > R. \end{aligned}$$

It can be shown by arguments based on the invariance properties of the Hamiltonian (Wolfenstein 1949) that the differential cross section is of the form

$$\sigma(\theta, \phi) = \sum_L A_L^0 P_L^0(\cos \theta) + \mathbf{n} \cdot \mathbf{p} \sum_L A_L^1 P_L^1(\cos \theta)$$

where  $\mathbf{p}$  is the polarization of the incident particles and  $\mathbf{n}$  is a unit vector perpendicular to the plane of scattering. Moreover, the polarization of outgoing neutrons after scattering is then given by

$$P(\theta) = \sum_L A_L^1 P_L^1(\cos \theta) / \sum_L A_L^0 P_L^0(\cos \theta).$$

Here  $A_L^m$  is independent of  $\theta$  and  $\phi$  and depends only on the elements of the scattering matrix (Blatt and Biedenharn 1952, Satchler 1955). Experimental



values for the polarization of 380 kev neutrons scattered by medium nuclei have been published and no satisfactory explanation in terms of the square well optical model with **L.S** term has been produced (Adair, Darden and Fields 1954, Okazaki 1955, Darden, Clements and Borelli 1957). It was considered useful to investigate the effect on the cross section and polarization in the first instance of two different simple forms of spin-orbit term with the square well optical model which were capable of exact solution. These were

$$\begin{aligned} \text{(i)} \quad & \alpha(r) = bA^{-2/3} & r < R = r_0 A^{1/3}, \\ & \alpha(r) = 0 & r > R, \end{aligned} \quad \left. \vphantom{\begin{aligned} \text{(i)} \quad} \right\} \dots\dots (2) \\ \text{(ii)} \quad & \alpha(r) = \frac{2Q}{R} \delta(r-R) & R = r_0 A^{1/3}. \quad \dots\dots (3) \end{aligned}$$

The parameters were chosen to give the best fit for energy level splitting due to spin for bound nucleons in the nucleus, and had the values  $b = 13$  mev,  $Q = 0.65$  (Blin-Stoyle 1955, Ross, Mark and Lawson 1956). Neither of these modifications made an appreciable difference to the differential cross section, and both predicted polarizations at a scattering angle of  $90^\circ$  of the same form as that given by Okazaki (1955) using  $\alpha(r) = 3$  mev;  $r < R$ . The peak in each case was too narrow and too high to fit the experimental results.

Secondly, a perturbation method was used in order to deal with the trapezoidal well. This involved a Green's function method (Mott and Massey 1949) and gave the general relation, to first order,

$$\eta_u - \eta_l = -\frac{1}{2ik} \int_0^\infty \{w_l(r')\}^2 v(r') dr'.$$

Here  $\eta_l$  is the  $l$ -wave reflection coefficient of Feshbach, Porter and Weisskopf (1954) for the potential  $V(r)$  given by (1) and  $w_l(r)$  is the  $l$ -wave radial wave function.  $\eta_u$  is the  $l$ -wave reflection coefficient corresponding to the potential  $V(r) + v(r)$ . This perturbation was used in the cases already solved rigorously, (2) and (3) above, and it gave results surprisingly close to the exact one.

The trapezoidal well

$$\left. \begin{aligned} V(r) &= -V_0(1+i\zeta) & r < R(1-t) \\ V(r) &= -V_0(1+i\zeta) + \frac{V_0}{Rt}(r-R(1-t)) + \frac{2Q}{Rtr} \mathbf{L.S} & R(1-t) < r < R \\ V(r) &= 0 & r < R \end{aligned} \right\} \dots\dots (4)$$

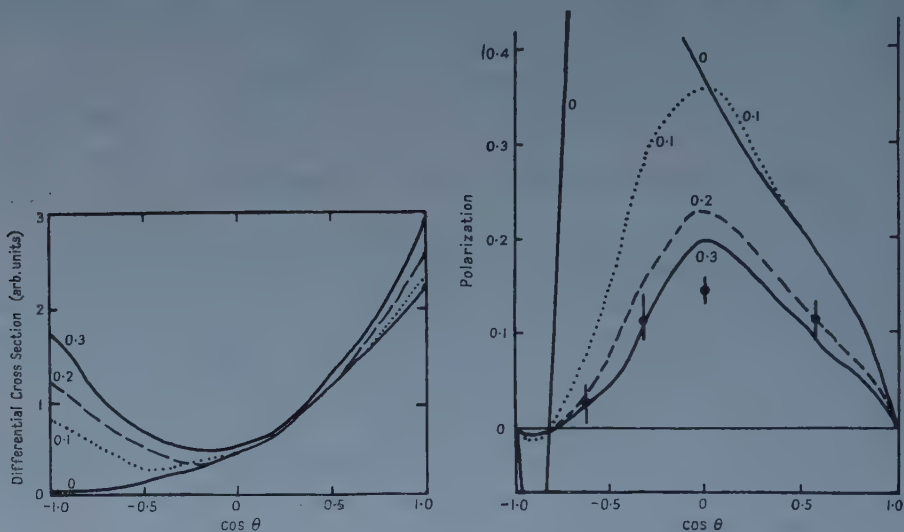
was then considered, treating the terms

$$\frac{V_0}{Rt}(r-R(1-t)) + \frac{2Q}{Rtr} \mathbf{L.S}$$

as the perturbation term  $v(r)$ . Here the coefficient of **L.S** is just the 'Thomas' term  $(1/r)(dV/dr)$  with a coupling constant. It was found that this does not give any very different result for the polarization at  $90^\circ$ . However, when applied to the differential cross section and the angular polarization distribution for the case in which  $kR = 0.90$  the use of a non-zero  $t$  does make the minimum less pronounced in the differential cross section, and gives more reasonable values for the polarization (see figure).

Before comparison with experiment can be taken seriously, there are several effects which should be taken into account. These include (i) compound elastic

scattering, which may be important at 380 kev, (ii) the ellipsoidal shape of the nuclei near Ag, shown by the  $J = 1/2, 3/2, 5/2$  rotational states and the low-lying spin  $7/2^+$  state in  $^{103}\text{Rh}$ ,  $^{105}\text{Ag}$  and  $^{107}\text{Ag}$ , (iii) the effect of second and higher order perturbation, (iv) the effect of rounding the well, which improves agreement with experiment at higher energies (Culler, Fernbach and Sherman (1956.)



The differential cross section and angular distribution of polarization of 380 kev neutrons for the case in which  $R = 6.4 \times 10^{-13}$  cm and  $t = 0, 0.1, 0.2$  and  $0.3$ , using potential (4). The experimental points refer to  $^{96}\text{Mo}$  (Darden, Clements and Borelli 1957) and were very kindly communicated to the author before publication.

However, the nuclear well is undoubtedly trapezoidal and it is useful to know the qualitative consequences of modifying the square well optical model in this way.

#### ACKNOWLEDGMENT

The author wishes to acknowledge the extensive help received from Dr. R. J. Blin-Stoyle and other members of the Theoretical Physics Department of the Clarendon Laboratory, Oxford, where this work was carried out.

#### REFERENCES

- ADAIR, R. K., DARDEN, S. E., and FIELDS, R. E., 1954, *Phys. Rev.*, **96**, 503.
- BLATT, J. M., and BIEDENHARN, L. C., 1952, *Rev. Mod. Phys.*, **24**, 25.
- BLIN-STOYLE, R. J., 1955, *Phil. Mag.*, **46**, 973.
- CULLER, G., FERNBACH, S., and SHERMAN, N., 1956, *Phys. Rev.*, **101**, 1047.
- DARDEN, S. E., CLEMENTS, J. P., and BORELLI, F., 1957, *Bull. Amer. Phys. Soc.*, **4**, 234.
- FESHBACH, H., PORTER, C. E., and WEISSKOPF, V. F., 1954, *Phys. Rev.*, **96**, 448.
- MOTT, N. F., and MASSEY, H. S. W., 1949, *Theory of Atomic Collisions* (Oxford: University Press).
- OKAZAKI, A., 1955, *Phys. Rev.*, **99**, 55.
- ROSS, A. A., MARK, H., and LAWSON, R. D., 1956, *Phys. Rev.*, **102**, 1613.
- SATCHLER, G. R., 1955, *Proc. Phys. Soc. A*, **68**, 1041.
- WOLFENSTEIN, L., 1949, *Phys. Rev.*, **75**, 1664.

## Low-Angle X-Ray Scattering from Cold-Worked Metals

By A. FRANKS AND K. THOMAS

Metallurgy Division, National Physical Laboratory, Teddington, Middlesex

*MS. received 25th February, 1958*

THE low angle x-ray scattering from cold-worked metals has been ascribed to various causes. In the classical theory developed by Guinier (1939), the scattering is caused by regions of differing electron density which are large compared with atomic dimensions. Blin and Guinier (1951) suggested that in metals the scattering was due to cavities, while Blin (1957) and Seeger (1957) have proposed that arrays of dislocations can account for the observed effects. Li and Smoluchowski (1955) have pointed out that variations in electron density caused by surface irregularities can also account for small-angle scattering. More recently, Beeman *et al.* (1957) have concluded that the cavity model is inadequate to explain the experimental results obtained with cold-worked foils. Experimental and theoretical evidence to support this view is contained in theses by Neynaber (1955), Brammer (1955) and Webb (1956). These authors favour a double Bragg reflection mechanism to account for low-angle scattering.

Double Bragg reflection can occur, for example, when a crystal is composed of sub-crystals. If one sub-crystal reflects the incident radiation, a 'Debye-Scherrer' pattern can be formed about the reflected beam by the other sub-crystals. For a small range of misorientations of the sub-crystals, the Debye-Scherrer pattern will consist of a short arc (or streak) passing through the origin (the intersection of the main beam and film), and in this region the radiation will also be highly polarized. Webb (1956) has found the predicted polarization for small deformations (up to 10%) but not for large deformations (approximately 50%). Although it might be expected that broadening of the reflections due to large deformations would tend to mask the polarization effect, he states that his experimental arrangements were such as to preclude this possibility. Webb concludes therefore that a double Bragg reflection mechanism is operative for small deformations but that for larger deformations some additional mechanism must be invoked.

Atkinson and Lowde (1957) have irradiated cold-worked specimens with neutrons of a wavelength sufficiently large to preclude the possibility of double Bragg reflection; i.e. the wavelength is such that the Bragg law cannot be satisfied. The intensity of the scattered radiation was so low that it was concluded that the bulk of the metal did not contain cavities. This experiment differs from the x-ray experiments in that thick specimens are used, so that surface effects are relatively unimportant.

The present authors have studied in detail the low-angle scattering from individual grains of a fatigued polycrystalline copper foil 0.002 in. thick, using a technique described previously (Franks 1955, Franks and Holden 1955), but with a camera (Franks 1958) in which the specimen can be accurately oriented with respect to the beam and in which both large-angle and small-angle photographs can be obtained on the same film. It has been found that a low-angle streak is associated with a large-angle Bragg diffraction spot, geometrically related to it as required by the double Bragg reflection theory. This effect might also be

accounted for by oriented cavities and in order to investigate this possibility the following experiments were performed.

A grain of a fatigued aluminium specimen, which gave a low-angle pattern with Cu K radiation was examined, *in vacuo*, in the same orientation with radiation from an Al target. Al K radiation precludes the possibility of Bragg reflection, but should merely alter the scale of the pattern caused by cavities. Although no pattern was detected the results were not considered conclusive because of the experimental difficulties.

A grain of a fatigued copper specimen was examined both with Cu K and Co K radiation in the same orientation. With the cavity model little change would be expected in the pattern. In fact, radical changes occurred: appearance and disappearance of Bragg spots was accompanied by the appearance and disappearance of the associated low-angle streaks.

It seems reasonable to conclude that in these experiments the low-angle scattering is caused by double Bragg reflection. In a copper specimen, which extended 10% on fatiguing, misorientations occurred of approximately  $10^\circ$ . The reflections so far observed are mainly from the {111} and {200} planes. Occasionally, breaks or peaks are observed in the streaks, which may be explained by a preferred orientation effect of the sub-grains. A full account of this work will be published elsewhere.

#### ACKNOWLEDGMENTS

The work described above has been carried out as part of the general research programme of the National Physical Laboratory and this paper is published by permission of the Director of the Laboratory.

#### REFERENCES

- ATKINSON, H. H., and LOWDE, R. D., 1957, *Phil. Mag.*, **2**, 589.  
 BEEMAN, W. W., KAESBERG, P., ANDEREGG, J. W., and WEBB, M. B., 1957, *Handbuch der Physik*, **32** (Berlin : Springer), p. 440.  
 BLIN, J., 1957, *Acta Met.*, **5**, 528.  
 BLIN, J., and GUINIER, A., 1951, *C. R., Acad. Sci., Paris*, **233**, 1288.  
 BRAMMER, W. G., 1955, *Ph.D. Thesis*, University of Wisconsin.  
 FRANKS, A., 1955, *Proc. Phys. Soc. B*, **68**, 1054 ; 1958, *Brit. J. Appl. Phys.*, in the press.  
 FRANKS, A., and HOLDEN, J., 1955, *Nature, Lond.*, **176**, 1022.  
 GUINIER, A., 1939, *Ann. Phys., Paris*, **12**, 161.  
 LI, Y. Y., and SMOLUCHOWSKI, R., 1955, *J. Appl. Phys.*, **26**, 128.  
 NEYNABER, R. H., 1955, *Ph.D. Thesis*, University of Wisconsin.  
 SEEGER, A., 1957, *Acta Met.*, **5**, 24.  
 WEBB, M. B., 1956, *Ph.D. Thesis*, University of Wisconsin.



# Direct Optical Transitions and Further Exciton Effects in Germanium

By G. G. MACFARLANE, T. P. McLEAN, J. E. QUARRINGTON  
AND V. ROBERTS

Royal Radar Establishment, Malvern, Worcestershire

*MS. received 24th March 1958*

RECENT work by us (Macfarlane, McLean, Quarrington and Roberts 1957, to be referred to as I) revealed fine structure in the optical absorption spectrum of Ge at low absorption levels ( $< 30 \text{ cm}^{-1}$ ) near the main edge. This structure was satisfactorily explained in terms of indirect optical transitions involving transitions in which not only were free electron-hole pairs produced, but also excitons with wave vectors lying at a  $\langle 111 \rangle$  direction zone edge. To obtain further evidence for the formation of excitons in Ge, we have investigated in detail the absorption around levels of about  $4000 \text{ cm}^{-1}$  where the absorption is thought to be due to direct optical transitions at the centre of the Brillouin zone (Dash and Newman 1955). We should expect direct transitions which produce excitons to show up clearly in the absorption curve as well-defined lines which would be broadened into sharp peaks. Elliott (1957) has investigated these effects in detail and has shown that, for direct optical transitions between spherical non-degenerate conduction and valence bands with extrema at the centre of the Brillouin zone, one would expect a series of absorption lines at photon energies

$$\hbar\nu = E_0 - E_{\text{ex}}/n^2, \quad n = 1, 2, 3 \dots \quad \text{..... (1)}$$

where  $E_0$  is the energy gap and  $E_{\text{ex}}$  is the binding energy of an exciton of zero wave vector, the intensities of the lines being proportional to  $1/n^3$ . These lines are followed by a region of continuous absorption beginning at  $\hbar\nu = E_0$  where the absorption coefficient

$$K \propto \frac{e^x}{\sinh x}, \quad x = \pi \left( \frac{E_{\text{ex}}}{\hbar\nu - E_0} \right)^{1/2} \quad \text{..... (2)}$$

When  $\hbar\nu - E_0 \gg \pi^2 E_{\text{ex}}$ , this expression gives  $K$  proportional to  $(\hbar\nu - E_0)^{1/2}$ , the result usually quoted for direct band-to-band transitions (Hall, Bardeen and Blatt 1954, Fan 1956). However, for smaller energies, the absorption departs significantly from this simple power law due to the effects on the wave functions of Coulomb interaction between the electron and hole and flattens off to a constant value close to the threshold  $E_0$ .

Using the same experimental technique as we described in I, we have made measurements of the absorption coefficient so far on two specimens, one approximately 10 microns and the other approximately 20 microns thick, at a series of temperatures from  $20^\circ\text{K}$  up to room temperature. These two specimens were prepared from completely different material but nevertheless showed identical structure in the absorption so that we believe this structure to be due to an intrinsic property of Ge and not due to the presence of some defect in the material. We show in figure 1 the experimental points obtained from the thinner specimen; both the energy and absorption scales in this figure have been adjusted at each temperature for clarity of presentation. The minimum in the absorption

at each temperature occurs roughly at the same absorption level of about  $3500\text{ cm}^{-1}$ . The rapid decrease in the absorption at the low energy end of our plots continues down to absorption levels of a few hundred  $\text{cm}^{-1}$  and joins smoothly on to our earlier measurements in that region. It is worth while noting that this decrease in absorption is so rapid that its shape is probably defined by the resolution of our spectrometer ( $\sim 4 \times 10^{-4}\text{ eV}$ ).

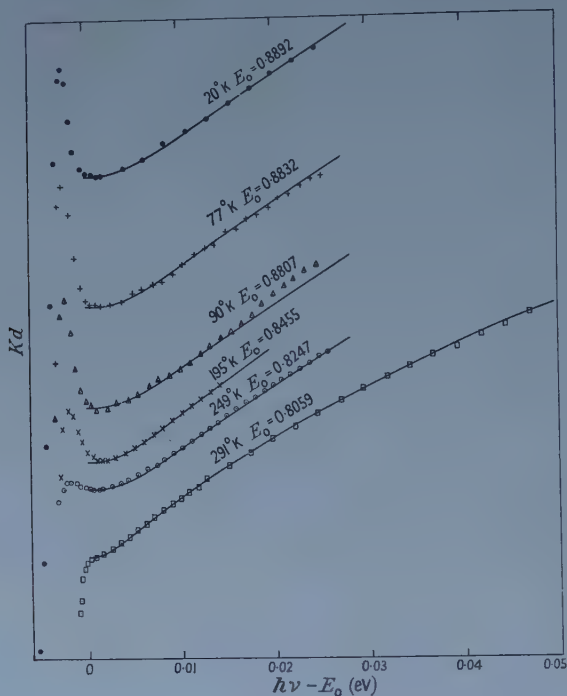


Figure 1. The variation of absorption  $Kd$  with incident photon energy  $h\nu$  at various temperatures. The points are the experimentally observed values and the full curves have been obtained from expression (2). The data at the various temperatures have been aligned in energy using the values of  $E_0$  given on the curves at each temperature and each set given an arbitrary vertical displacement. At each temperature, the value of  $Kd$  at  $E_0$  is about 3.5 and, at the lower temperatures, the peak value is about 0.6 above this. The data at room temperature have been plotted using a horizontal scale reduced by a factor of 2 from that shown.

The structure in the absorption shown by the experimental points clearly follows the predictions of Elliott, the rapid rise in absorption to a peak being an exciton line which broadens out and whose peak value decreases with increasing temperature; the following continuous absorption has apparently the energy dependence given by (2). With this interpretation of the structure in mind, we attempted to fit the shape given by (2) to the points in order to determine values for  $E_0$  and  $E_{ex}$  at each temperature. The value of  $E_{ex}$  is not expected to vary much, if at all, with temperature and, moreover, at each temperature it should be such that not only does it define the variable  $x$  in (2) so that the expression (2) fits the experimental points, but also it must correspond to the separation between the peak in the absorption and the beginning of the continuous absorption. Also, at these high absorption levels, the contributions to the

absorption from indirect transition processes can be neglected in a first approximation as they cannot form more than 10% of the total absorption at most. The continuous curves in figure 1 are derived from the expression (2) and represent the best fits we have been able to obtain to the experimental points. The value of  $E_0$  at each temperature is also given in the figure and has been used as the basis for lining up the curves in the figure. The values found for  $E_{ex}$  were

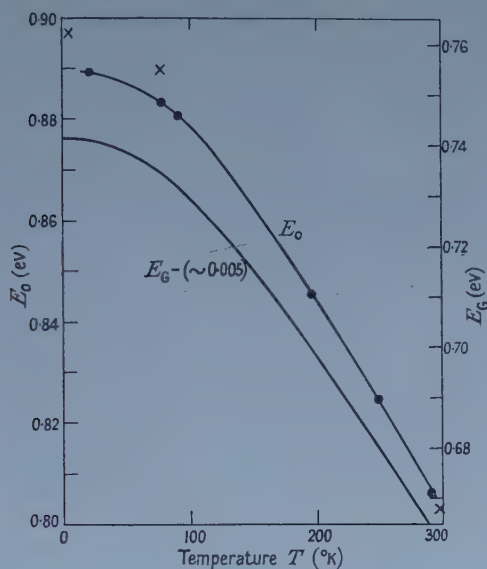


Figure 2. The variation of the direct gap  $E_0$  and the indirect gap  $E_G$  with temperature. The crosses indicate the values of the direct gap obtained by Zwerdling, Lax and Roth.

0.0012 eV at 20°K, 77°K and 90°K, 0.0010 eV at 195°K, 0.0011 eV at 249°K and 0.0009 eV at 291°K. The fitting at 291°K is difficult as the exciton peak has virtually disappeared; the low value of  $E_{ex}$  at this temperature and also the value given for  $E_0$  on figure 1 should be regarded as less reliable than the values at the lower temperatures where the exciton peak is well defined. Our values of  $E_{ex}$  are in excellent agreement with the binding energy of excitons in Ge at the centre of the Brillouin zone, estimated from effective mass values by Dresselhaus (1956). The fact that absorption lines corresponding to transitions into excited states of the exciton are not observed is not surprising in view of the fact that the absorption into these higher states is expected to decrease as  $1/n^3$ .

We show in figure 2 the variation of the direct energy gap  $E_0$  with temperature. For comparison, we have also shown the variation of the indirect gap  $E_G$  found from our earlier work (cf. I). We see from these two curves that as the temperature rises the energy difference between states in the conduction band at the centre of the Brillouin zone and at the band minima at the  $\langle 111 \rangle$  direction zone edges decreases. This variation is consistent with the increase in the effective mass at the minima with temperature discussed by us in I and the decrease of the effective mass at the centre of the zone with increasing temperature found by Zwerdling, Lax and Roth (1957) from their work on the oscillatory magneto-absorption effect. These workers also find from their analysis of this effect

values of the direct energy gap at various temperatures; their values are shown by crosses in figure 2. It is clear from this figure that there is a large discrepancy of about 0.007 eV between their values and ours at the lower temperatures. The apparent agreement at room temperature is not reliable as our value there is rather inaccurate. The discrepancy is also clearly seen from figure 1 where no significant changes in the behaviour of the absorption occur at energies equal to the energy gaps found by Zwerdling, Lax and Roth although one expects such changes to occur at these energies. The energy gap is obtained from the magneto-absorption effect by assuming that the maxima in the oscillations of the absorption coefficient occur at energies

$$E_n = E_0 + (n + \frac{1}{2}) \frac{e\hbar H}{m^*c} \quad \text{where } n = 1, 2, 3 \dots;$$

$H$  is the applied magnetic field and  $m^*$  is an effective mass associated with the two bands. As is shown in a forthcoming paper by Elliott, Macfarlane and McLean, this is certainly valid when one neglects the Coulomb interaction of the electron and hole, the absorption which rises as  $(\hbar\nu - E_0)^{1/2}$  from a threshold  $E_0$  in the absence of a magnetic field breaking up into a series of curves falling as  $(\hbar\nu - E_n)^{-1/2}$  from the energies  $E_n$ . However, as we see from (2), the inclusion of Coulomb field effects makes a significant change in the energy dependence of the absorption coefficient, when no magnetic field is on, especially in the region within about  $10E_{\text{ex}}$  of the threshold  $E_0$ , and, as we have seen, this expected change is borne out by the experimental points. A similar inclusion of Coulomb field effects in the presence of a magnetic field should produce significant changes in the expected energy dependence of the absorption coefficient and might be expected to alter the energies at which the maxima in absorption occur. Further investigations into the cause of this discrepancy are clearly necessary.

#### ACKNOWLEDGMENTS

The authors are indebted to Mr. P. J. Hoyland for the preparation of single crystals of Ge and to Mr. C. A. Wright and his staff for supplies of liquid hydrogen.

This paper is published by permission of the Controller, H.M. Stationery Office.

#### REFERENCES

- DASH, W. C., and NEWMAN, R., 1955, *Phys. Rev.*, **99**, 1151.  
 DRESSELHAUS, G., 1956, *J. Phys. Chem. Solids*, **1**, 15.  
 ELLIOTT, R. J., 1957, *Phys. Rev.*, **108**, 1384.  
 FAN, H. Y., 1956, *Rep. Progr. Phys.*, **19**, 107 (London: Physical Society).  
 HALL, L. H., BARDEEN, J., and BLATT, F. J., 1954, *Phys. Rev.*, **95**, 559.  
 MACFARLANE, G. G., MCLEAN, T. P., QUARRINGTON, J. E., and ROBERTS, V., 1957, *Phys. Rev.*, **108**, 1377.  
 ZWERDLING, S., LAX, B., and ROTH, L. M., 1957, *Phys. Rev.*, **108**, 1402.



## LETTERS TO THE EDITOR

**The Polarization-Asymmetry Equality**

In a recent note (Bell and Mandl 1958) we have reconsidered the polarization-asymmetry equality for the elastic scattering of spin- $\frac{1}{2}$  particles off unpolarized targets. The usual proofs (Dalitz 1952, Wolfenstein and Ashkin 1952) have assumed invariance under both space inversion and time reversal. We showed that the former assumption is unnecessary, provided that in the polarization experiment only components of polarization perpendicular to the final relative momentum are observed, and that in the asymmetry experiment the beam is polarized transversely to the initial relative momentum. It was then stated that the presence of a longitudinal component of initial polarization would not affect the asymmetry. This is incorrect, for reasons given below; we are indebted to Drs. A. Johansson, P. Hillman and T. Maris for pointing this out to us. In the absence of parity conservation, beams polarized by scattering would in general have such longitudinal components. This presents a difficulty in the application of the theorem; we will suggest how to overcome it, in principle at least.

Let  $\hat{\mathbf{k}}$  and  $\hat{\mathbf{k}}'$  be unit vectors in the direction of the initial and final relative momenta; let  $\hat{\mathbf{n}} = \hat{\mathbf{k}} \times \hat{\mathbf{k}}' / |\hat{\mathbf{k}} \times \hat{\mathbf{k}}'|$  and  $\hat{\mathbf{m}} = \hat{\mathbf{n}} \times \hat{\mathbf{k}}$ . Suppose that the initial polarization is

$$\mathbf{p} = p_1 \hat{\mathbf{n}} + p_2 \hat{\mathbf{m}} + p_3 \hat{\mathbf{k}}.$$

For spin- $\frac{1}{2}$  particles it can be shown that the scattered intensity  $I$  depends linearly on  $\mathbf{p}$  so that

$$I = I_0 + I_1 p_1 + I_2 p_2 + I_3 p_3$$

where for an unpolarized target  $I_0 - I_3$  are functions of  $k^2$  and of deflection angle  $\theta$ . The scattering in the opposite direction is obtained by reversing the transverse components  $p_1$  and  $p_2$ , and the difference between left and right scatterings is unaffected by the longitudinal component  $p_3$ . However, in the definition of fractional asymmetry the *sum* of the two scatterings also appears, as normalizing denominator, and this does depend on  $p_3$ . Now, by the use of a suitable magnetic field (the deflection by which of charged particles will have to be cancelled by repositioning of the apparatus, or possibly by a crossed electric field) the polarization can be rotated about the direction  $\hat{\mathbf{n}}$  through  $180^\circ$ . The intensity then becomes

$$I' = I_0 + I_1 p_1 - I_2 p_2 - I_3 p_3.$$

The average of intensities with and without the magnetic field is

$$\frac{1}{2}(I' + I) = I_0 + I_1 p_1,$$

which is just the intensity due to a beam of polarization  $p_1$  perpendicular to the scattering plane. So this averaging process provides, in effect, a beam of the kind assumed in the simple special case of the theorem proved in the first half of our original note.

We would mention finally two other consequences of reciprocity which can be derived, without any assumptions about parity conservation, by arguments like those of our original note.

Firstly, the longitudinal polarization (i.e. along the final relative momentum) produced by the elastic scattering of an unpolarized beam should equal the fractional difference of intensity for scattering through the same angle by beams initially polarized along and against the initial relative momentum.

Secondly, consider a double elastic scattering experiment with two different scatterers so heavy that recoil is negligible. For given and equal angles of deflection at the two targets, the final azimuthal distribution should be unaltered by interchanging the targets. The direct argument, which avoids discussion of the polarization of the intermediate beam, does not work when recoil is appreciable; the loss of energy by the incident particle then spoils the simple reciprocal relation between experiments with interchanged targets.

Always assuming the applicability of non-relativistic quantum mechanics, the experimental disproof of any of these consequences of reciprocity would disprove time reversibility (or else unitarity). In the case of spin zero targets it would indicate also the absence of parity conservation; for in this case the general parity conserving and rotationally invariant scattering matrix happens to satisfy also the reciprocity relation.

We are indebted to Drs. T. H. R. Skyrme and E. J. Squires for valuable discussions of this subject.

Atomic Energy Research Establishment,  
Harwell, Didcot, Berks.  
25th February 1958.

J. S. BELL.  
F. MANDL.

BELL, J. S., and MANDL, F., 1958, *Proc. Phys. Soc.*, **71**, 272.

DALITZ, R. H., 1952, *Proc. Phys. Soc. A*, **65**, 175.

WOLFENSTEIN, L., and ASHKIN, J., 1952, *Phys. Rev.*, **85**, 947.

### A Physical Interpretation of Impedance for Rectangular Waveguides

In a research note (Lane 1957) of the above title, the results of measurements on thin resistive strips in waveguides were adduced in support of the value  $Z_{\text{wv}} = 240\pi(\lambda_g b/\lambda a)$  for the characteristic impedance of a rectangular guide, to be used in preference to other values differing from it by the presence of a constant factor ( $\pi/4$ ,  $\pi^2/16$  and possibly other values). Since, as is well known,  $Z$  is only defined to within a constant factor, it is of some interest to note that the above expression, which is that obtained from a consideration of power flow in terms of maximum voltage across the guide, has some theoretical basis.

In a paper (Lewin 1957) on the impedance of probes in waveguides it has been shown that the equivalent circuit for a central probe, loaded at one end, consists of a transmission line feeding into an impedance comprising the probe inductance, in series with the loading impedance paralleled by the probe, and 'gap' capacities,  $Z = j\omega L + R/(1 + j\omega CR)$ . The line itself has an impedance  $Z_0 = 240\pi(\lambda_g b/\lambda a)$ , an expression which appears in the course of the calculation and involves no arbitrariness (except for the decision to call it the line impedance, a decision which is justified by the form of the resulting equivalent circuit). When the guide is narrow, or, alternatively, if the length of probe is reduced, the effects of both  $L$  and  $C$  decrease, the latter becoming very small, and we are

left with  $Z \simeq R + j\omega L$ , the situation described by Lane (1957). The two arrangements are therefore the same, and we deduce the value of characteristic impedance to be used for the waveguide, in confirmation of the results of the measurements.

Standard Telecommunication Laboratories Ltd.,  
Progress Way,  
Great Cambridge Road,  
Enfield, Middx.

L. LEWIN

31st January 1958.

LANE, J. A., 1957, *Proc. Phys. Soc. B*, **70**, 1173.

LEWIN, L., 1957, *Instn Elect. Engrs, Monograph* No. 259R.

## REVIEWS OF BOOKS

*Quantum Mechanics*, 2nd Edition, by F. MANDL. Pp. x+267. (London: Butterworths Scientific Publications, 1957.) 35s.

The task of conveying to the average experimental physicist sufficient knowledge of the principles of quantum mechanics for him to gain something by reading a modern theoretical paper is a difficult one. It is also an increasingly desirable one and it is surprising that so few of the standard treatises on the subject are really helpful in this respect. Dr. Mandl is familiar with the difficulties of experimentalists and his book goes a long way towards satisfying their requirements. Quantum mechanics is not an easy subject and its rigorous discipline cannot be avoided, but this book lightens its impact to a welcome degree and it should prove a popular and useful text.

The book opens with a brief mathematical introduction on vectors, Fourier series, function spaces and eigenfunctions. Chapter II gives a good physical introduction to wave mechanics and discusses the energy eigenfunctions of the Schrödinger operator. Several standard examples (one-dimensional barrier, three-dimensional square well, linear oscillator) are given in the following chapter, which also contains a particularly clear account of spherical harmonics and of the angular momentum operator.

Chapter IV is unavoidably hard; it erects the formal structure of quantum mechanics on the basis of observable quantities represented by Hermitian operators and sets out the properties of these operators. This approach is less familiar than that of wave mechanics, but it is more powerful and it is well presented here. The uncertainty principle, slit diffraction and the Breit-Wigner formula fall naturally into the discussion. The matrix representation of wave functions and operators follows in the next chapter and this method is largely used throughout the rest of the book. Chapter VI (systems of many particles) gives an excellent account of angular momentum, spin and the addition of angular momenta, in which the Clebsch-Gordan coefficients happily receive a prominence in accordance with their usefulness. The discussion of systems of identical particles would be improved by a note on isotopic spin. Time independent perturbation theory is given in Chapter VII with useful examples and the experimentally vital collision theory is extremely well treated in Chapter VIII. This section would be even better if some direct reference were made to examples such as deuteron stripping theory; resonant scattering is also apparently omitted.

Chapter IX gives an excellent account of group theory with specific reference to the symmetry properties of wave functions. The treatment of selection rules by this powerful method greatly clarifies this somewhat obscure subject. The final chapter is an extremely readable account of relativistic quantum mechanics; it is only to be regretted that it does not continue, at the same standard, well into the theory of beta decay. There is no treatment of field theory.

Quantum mechanics only becomes a reality to the student when he has had extensive practice in its manipulation. Dr. Mandl's book is generously provided with examples and with hints for their solution. These include many useful results which might be regarded as part of the text. The book on the whole covers its subject thoroughly, although some useful techniques such as the



W.K.B. method and the variation method are not treated. Both experimental and theoretical physicists, and particularly those working in nuclear physics, will find the book a valuable addition to their library.

W. E. BURCHAM.

*Glass*, by G. O. JONES. Methuen Monograph. Pp. 119. (London: Methuen; New York: John Wiley.) 8s. 6d.

This little book can be thoroughly recommended to all students of physics as a clear concise statement of the generally established ideas of the physics of the glassy state. As an introduction to the technology of glasses it is not so good; in fact, the subject is hardly given more than a glance. But what reasonable person could expect both the physics and technology of glasses to be treated adequately in such a small volume?

There is an introduction and five chapters dealing with the structural chemistry of glasses, crystallization and stability of glasses in relation to structure, properties of glasses near the transformation temperature, behaviour of glass under stress, properties of metallic ions in glass.

The first three chapters provide a short account of glass structure and formation which is at least as good as any available; it is therefore very pleasing to have such an account in the easily accessible form of this book.

Chapter 6 on metallic ions is the weakest of the book; the chapters dealing with the behaviour under stress and the transformation range are excellent. Professor G. O. Jones has made noteworthy contributions to the empirical study of visco-elastic effects in glasses, and to the thermodynamics of transformation range phenomena. A summary of this work is welcome.

R.W.D.

*Light, Colour and Vision*, by YVES LE GRAND. Pp. xiii + 512. (London: Chapman and Hall, 1957.) 63s. Approved translation by R. W. G. Hunt, J. W. T. Walsh and F. R. W. Hunt.

There can be little question that Professor Le Grand's three volume treatise *Optique Physiologique* is the best basic text on the subject since Helmholtz. The present English translation of volume two is a self-contained work dealing with those visual properties in which the behaviour of the eye as a receptor of radiation is the dominant factor. Thus all the sensitivities associated with the response to light and colour, the underlying principles of photometry and colorimetry, and the properties of normal and defective colour vision are included, but not the dioptrics of the eye, the fineness of vision and space perception. Chapters on the essentials of our present knowledge of the minute anatomy of the retina, its photochemistry and its electrophysiological response precede a concise discussion of theories of colour vision and of the visual threshold.

In almost all respects this is the ideal book for the student of the subject. It is authoritative and well balanced and is extremely well written. The exposition is logical, pithy, never blurred. The good qualities of the French text have been preserved in the translation which is excellent. An unusual feature in a book of this calibre is the inclusion of 'exercises' (with solutions).

Like most modern exponents, Professor Le Grand approaches trichromatic colour-matching after dealing with heterochromatic brightness-matching and the relative luminous efficiency function  $V_\lambda$ . He is thus led to make free use of luminance based on the  $V_\lambda$  function in introducing the trichromatic generalization.

Heterochromatic matching and the  $V_\lambda$  function are of course irrelevant to this generalisation, and nothing the author says is inconsistent with this fact. But I think he would have removed a familiar source of difficulty if he had made a more positive statement of the situation and had avoided luminance units in his first explanation of colour metamerism.

Some additions to the original text (1948) have been made by the author, but it was probably inevitable that several topics on which there has been important new work—human cone pigments and colour adaptation, in particular—receive less attention than one could have wished. Brindley's interesting discovery (1955) of the yellowing of the long-wave end of the spectrum and the theoretical follow-up by Lewis merit a mention. But it would be hard indeed to criticise for omissions or lack of detail a book so adroitly and tightly packed with essential material. Of the very few minor points calling for comment I shall mention two. It is said on p. 98 that the mydriatic, euphthalmine, paralyses the accommodation, but in fact it has little effect of that kind. The description of the flicker of alternating stimuli of different colours (p. 300) refers to the last trace of flicker as *colour flicker*. This differs from Anglo-Saxon descriptions which speak of colour flicker as disappearing first. A case can be made for either way of regarding the phenomenon, but perhaps in the translation an adjustment to our practice would have been better.

Although its value as a basic text has been stressed, Professor Le Grand's book is much more than a textbook. It is a stimulating, often a highly original and critical account of the subject from which everyone researching in this field will certainly have much to learn. A delightful feature is the occasional titbit from the limbo of visual theory, such as the suggestion that dichromats have a "flattening of the cranium near the eyebrows and a rather haggard expression".

When I reviewed the French original I complained of the bibliography. It is a pleasure to record that this is now all that could be wished. w. s. s.

*The Spectroscopy of Flames*, by A. G. GAYDON. Pp. ix+279. (London: Chapman and Hall, 1957.) 50s.

Flames present a variety of physico-chemical problems of both practical and theoretical interest. The attention which they are receiving is such that Dr. Gaydon's earlier book on *Spectroscopy and Combustion Theory* (1942, 1948) is now seriously out of date. In the new book are discussed the applications of spectroscopic techniques to the study of flames. Following outlines of methods and of the theoretical basis of spectroscopy, flames are discussed one by one—hydrogen flames, the carbon monoxide flame, flames of organic compounds, of ammonia, of the halogens and of other substances. There are also accounts of the measurement of effective temperatures and of flame spectrophotometry.

All this is primarily a work of description, but it is not by any means to be despised on that account, for it is full of interesting observations, many of which may well point the way to fruitful research work. The plan does lead unhappily to a degree of repetition which is sometimes tiresome. Thus, within five pages we are twice told that ground-state CO and O cannot give singlet CO<sub>2</sub>. One can also regret that the author is so brief in his discussion of flame structure and reaction processes. After all, this is really what we want to know. Spectroscopy is essentially a technique, and the general reader is more interested in the conclusions than in the observational minutiae. That the balance of the book

is on the latter rather than the former reflects less the prejudices of the author than the present state of our knowledge of the subject.

It must be admitted, too, that any book written to this title gives necessarily only part of the story, for as the author remarks "the visible and ultraviolet light from flames represents a very small fraction of the energy released, and this radiation comes from a very small fraction of very special molecules which are electronically excited and which may not be typical of the main bulk of the gas". Nevertheless, the spectra are there and their study must help in the elucidation of flames. Dr. Gaydon's book will help, too. The specialist will want to read it all: it is bound to stimulate, and it will serve him for reference (there is a bibliography of some 460 items). It is well produced, well illustrated, and apparently free from misprints (though 'stearic' for 'steric' on p. 181 reads oddly).

R. F. BARROW.

*An Introduction to Reactor Physics* (Second Edition), by D. J. LITTLER and J. F. RAFFLE. Pp. x+208. (London: Pergamon Press, 1957). 30s.

This second edition of Littler and Raffle's book differs very little from the first edition and therefore it is still essentially the early lectures given by the authors to the Harwell Reactor School. The differences between the editions are concerned more with arrangement than with material although the new edition does have a small extra section dealing with the Breit-Wigner formula and the Doppler broadening of nuclear resonances. Owners of the first edition need, in fact, have no worries about it being out-dated. The book is still the only British one in its field and there is no doubt that it has played a valuable part in introducing its readers to the sort of computations which enter the design of graphite-moderated reactors. Of course, reactor theory now goes well beyond the treatment given but nevertheless the middle chapters of Littler and Raffle still form a useful introduction to the subject although in certain sections one would like the advantage of attending a lecture and asking questions instead of merely reading. The section on the effect of a control rod is one of these; here specific mention is made of a control rod with radius small compared to the transport mean free path but the theory given seems inapplicable to this case. A cause for regret with this second edition is that it does not include features such as long-term changes in reactivity, types of fuel and fuel cycling which have become prominent and are certainly relevant to the subject matter covered by the book. It is, of course, impossible for any book to be kept completely up to date in a field developing as rapidly as this one, but a comparison between the two editions suggests that the authors have been too busy with other things to make a serious attempt, a situation which can arise very easily these days.

Looking for omissions in an introductory book of this type is always easy but in this case it does seem to point to the need for a British book with a different emphasis from Littler and Raffle and which could be made to some extent complementary to theirs. It could for example leave out the elementary information on atomic structure, the solid state and the detection and interactions of nuclear particles and give more information on reactor types and possibly also on the engineering ideas of design as well as the physical ones.

J. WALKER.



*Report on the Conference on Recent Developments in Cloud Chamber and Associated Techniques*, edited by N. MORRIS and M. J. B. DUFF. Pp. vi+227. (London: University College, 1956.) 30s.

The published record of the very successful conference held under this title in March 1955 at University College, London, bears witness to the vitality and versatility of cloud chamber techniques at a time when some sort of equilibrium has been established with the parallel application of emulsion methods. At the time of the conference no comparable equilibrium between cloud chamber applications and their own 'anti-technique', the bubble chamber, was in view, and it is appropriate that this exciting new tool should have been the subject of one group of papers.

The conference was organised in a series of sessions or half sessions on particular topics, each of these being introduced in a review paper. These review papers make a notable contribution to the value of the published volume, bringing their respective sections into perspective and enhancing the value of the more specialized papers that follow. Brief notes of discussion are included.

The first session, reported in a review and six other papers, dealt with diffusion cloud chambers. The theory of diffusion chambers is treated, design features of a range of chambers is reported in some detail, and a final paper describes observations on track distortion. The second session was divided between work with multiplate chambers and the applications of scintillation and Cerenkov counters to chamber selection systems. For reasons which are probably different, neither of these fields is covered as exhaustively as are diffusion chambers, although Peyrou's review of multiplate chamber work covers the more serious design features admirably. The important possibilities of combining fast timing techniques in light-emitting particle-detectors with identification in a controlled chamber is only represented by the reports of the Manchester group, which has done much of the pioneer work in this field.

The third session, covered in a review paper and eight other contributions, was devoted to high-pressure cloud chambers. It is largely concerned with the work of the Edinburgh and University College London group, and concentrates on operating techniques and interpretation.

The first half of the following session gives five papers concerning bubble chambers. Although this section is likely to date quickly, it provides a valuable introduction to the theory and basic design features of these chambers. The remainder of the session covers the extremely important problem of increasing the cycling rate of chambers by fast-recompression and by overcompression.

The fifth session, under the title of 'Interpretation of Cloud Chamber Photographs' is mainly concerned with the instrumentation of interpretation, and from the final session a succession of individualist contributions, all interesting, complete the record.

The economical, but quite excellent, presentation of this volume sets a standard which deserves to be widely followed.

J. G. WILSON.



*Observation and Interpretation—A Symposium of Philosophers and Physicists.* Edited by S. KÖRNER in collaboration with M. H. L. PRYCE. (Proceedings of the 9th Symposium of the Colston Research Society, Bristol, 1st–4th April, 1957). Pp. xiv+218. (London: Butterworths Scientific Publications; New York: Academic Press Inc., 1957.) 40s.

The generous support of the Colston Society made it possible to organize at Bristol a symposium in which physicists and philosophers met to discuss various aspects of the general problem of observation and interpretation. The experiment had all the success one could reasonably expect: the physicists got an insight into the problems and methods of the epistemologists, so surprisingly remote from their own preoccupations, while some of the latter were perhaps encouraged to realize the earnestness of the epistemological revolution brought about by quantum theory. If the confrontation of the two domains of enquiry did not help to bridge the gap between them, it was at least useful in emphasizing its existence. The book under review, which presents a very complete and faithful report of the proceedings of the symposium, excellently edited and produced, will enable everyone interested in these problems to follow the discussions from the standpoint of the spectator and draw his own conclusions. If he is a physicist, he will no doubt wonder at the tenuous subtlety of some points made by the philosophers and will at any rate be amused by the lively clashes which occurred among the physicists. Amateurs of paradoxes will find here the latest stage of the quickly moving ideas of the Bohmist sect. Serious students of the epistemological aspects of modern physics will especially enjoy the very original contribution of Professor Fierz, which throws most revealing light on the historical background of the ideals of classical physics, and the substantial analysis of the process of physical measurement in quantum mechanics by Professor Groenewold.

L. ROSENFELD.

*Tabellen der Elektronenphysik, Ionenphysik und Übermikroskopie*, Parts I and II, by M. VON ARDENNE. Pp. xvi+614; xii+754. (Berlin: Deutscher Verlag der Wissenschaften, 1956.) DM 75, 74.

M. von Ardenne, who is known by his early books on the cathode-ray tube (1933) and on the electron microscope (1940), has presented us here with a monumental work containing a comprehensive survey of the facts of electron physics and of all its neighbouring and auxiliary subjects. The information is given mainly in form of tables and diagrams, and the whole material is offered in two large volumes.

The first volume is divided into three approximately equal parts which deal substantially with: (i) Free electron, electron optics, electron emission and the production of electron beams, space charges, emission systems and beam intensities, deceleration and detection of electrons, x-ray production and electronic devices. (ii) Electron microscopes, their aberrations and resolution, techniques of specimen preparation. (iii) The free ion; ion optics, production and acceleration of ions, current densities in ion beams and ionic devices.

The second volume is devoted to auxiliary subjects and to the neighbouring fields of electron physics. This part contains 'excerpts' (Ausschnitte) from the kinetic theory of gases, high vacuum technique, gas discharges, plasma

physics, photography, high frequency techniques, stabilization of currents, nuclear physics, tables of constants and units.

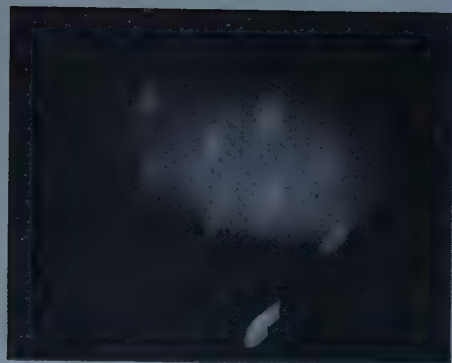
In the selection of the material preference is given to applied problems so that the book will be mainly useful to practical physicists concerned with the design of electronic apparatus. For instance, deflecting systems for beams in cathode-ray tubes are treated on thirteen pages while the important relations between electron velocity, voltage, momentum and wavelength are surveyed by a few curve diagrams on merely six pages. In contrast to this very brief treatment, it may be mentioned that the Electron Physics Tables issued by the U.S. Bureau of Standards present the above subject in eighty-six pages of formulae and exact figures.

The choice of material presented is not always well balanced. Though most of the German literature is adequately covered, various papers, in particular the author's own published and unpublished work, are reported with a detailed breadth quite out of proportion to the tabular character of the work. On the other hand, there are many gaps in the quotations from the Western European and American literature. There are negligibly few references to the Russian literature which has recently been published on subjects such as electron optics, photoelectricity or secondary emission. This is surprising since the author informs us in his preface that he has spent ten years working in the Soviet Union. The lack of adequate cover of the international literature is particularly evident in the second volume where nearly all the apparatus reported is of German manufacture and hardly any equipment not of German origin is mentioned.

In spite of these shortcomings, the book will find enthusiastic users and it will be helpful to many specialists. Its practical use is increased by a very elaborate index of 134 pages and by a summary of all signs and symbols used throughout the work. There is also a supplementary bibliography up to October, 1956. The book contains very few typographical errors, the printing is excellent and the figures are clear and well prepared.

The author must be admired for collecting nearly single handed this enormous amount of information. However, the conclusion cannot be avoided that a more balanced result could be accomplished by an adequately large staff of collaborators. The hope may be expressed that these tables of Electron Physics appear soon in a second edition containing all the wealth of information made available by international co-operation.

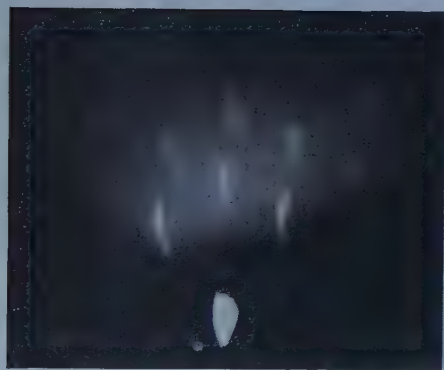
O. KLEMPERER.



(a)



(b)



(c)



(d)

Plate I

Figure 1. Primary beam limited by a  $25\ \mu$  aperture incident on the prism face in the direction of the hexagonal axis. Successive photographs taken with the aperture moved parallel to the edge of the face in steps of  $30\ \mu$ .

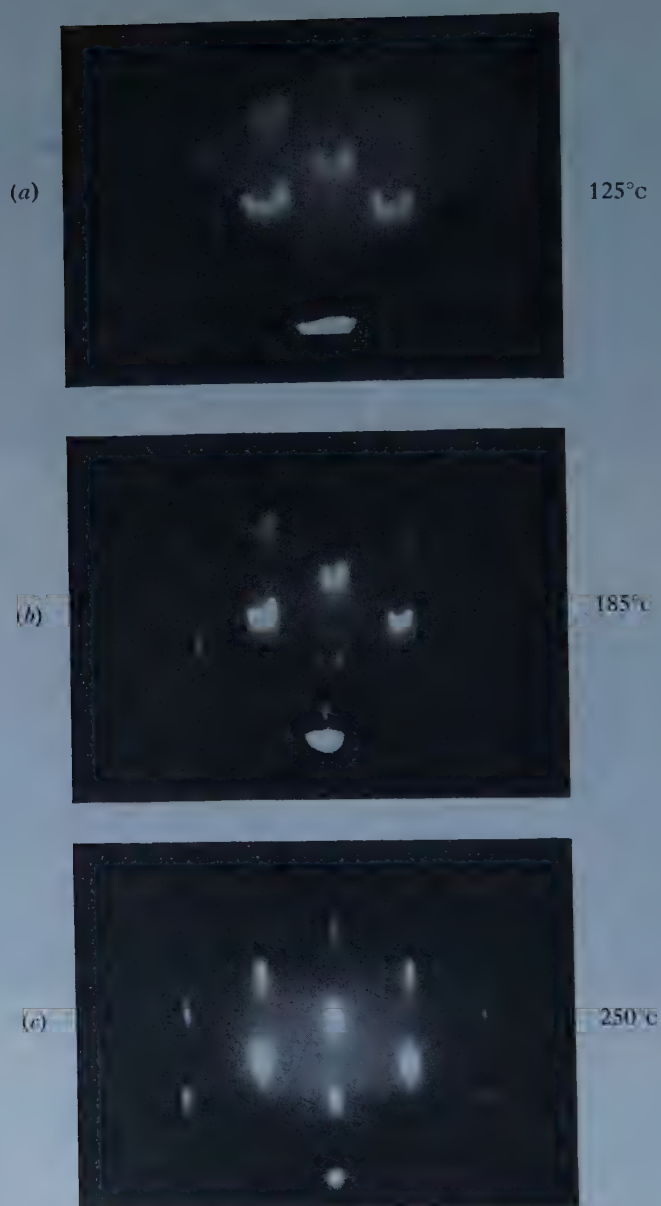


Plate II

Figure 2. Experimental arrangement similar to that of figure 1. Photographs taken at three different temperatures.





Figure 1.



Figure 2.

- Figure 1. Carbon replica of cleaved surface, showing a crack running vertically  $\times 15000$ .  
 Figure 2. Specimen in small normal field. Fine structure runs horizontally; large cracks run vertically  $\times 375$ .

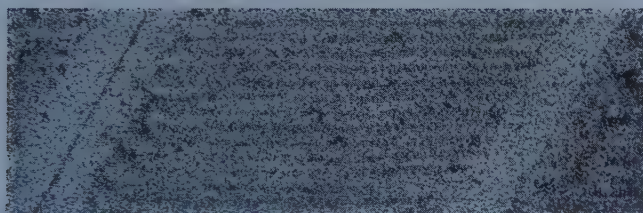


Figure 3. Electron micrograph of the extensive fine structure in zero field  $\times 5250$ .



Figure 4.



Figure 5.

- Figure 4. 'Fern' structure on cleaved surface, in small normal field  $\times 375$ .  
 Figure 5. Heavy wall structure on another part of the cleaved surface in small normal field  $\times 375$ .

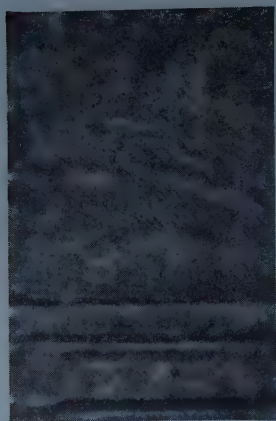


Figure 6.



Figure 7.

Figure 6. Fine structure with underlying 'fern' structure, in small normal field  $\times 750$ .  
 Figure 7. Electron micrograph of fine structure of figure 6. Note periodic intensification of the bands marked by arrows, showing effect of underlying 'fern' structure  $\times 1875$ .

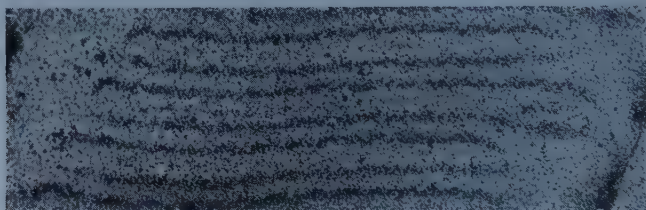


Figure 8. Electron micrograph of fine structure observed over a single small region  $\times 5250$ .

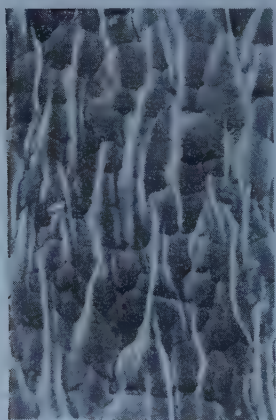


Figure 9.



Figure 10.

Figure 9. Carbon replica showing etch pattern  $\times 5250$ .  
 Figure 10. Unusual type of fine structure on new crystal surface in small normal field  $\times 750$ .

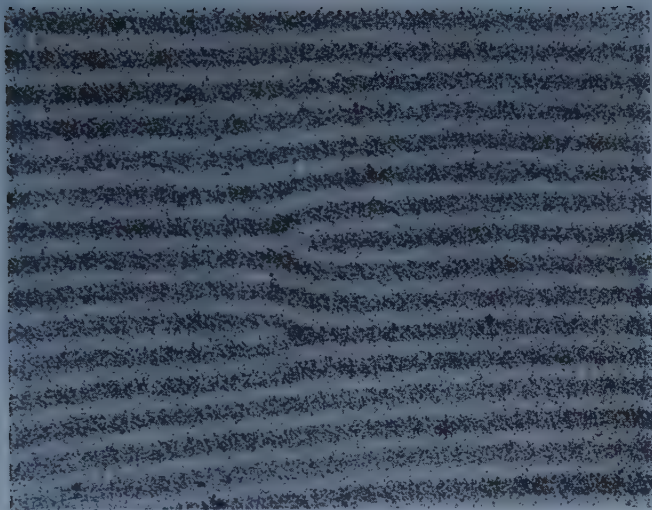


Figure 11. Electron micrograph of the extensive fine structure in small normal field, showing characteristic irregularities in otherwise parallel bands  $\times 5250$ .

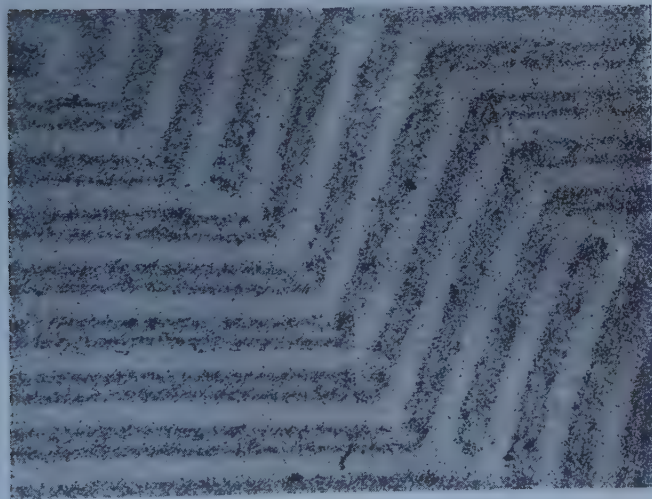


Figure 12. Electron micrograph of unusual tubular fine structure  $\times 5250$ .





Figure 13.

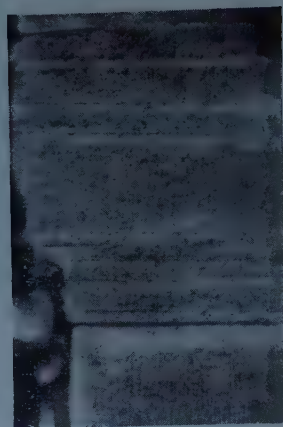


Figure 14.

Figure 13. Zigzag fine structure near edge of surface; small normal field  $\times 375$ .  
 Figure 14. Same region as figure 13, with small horizontal field  $\times 375$ .

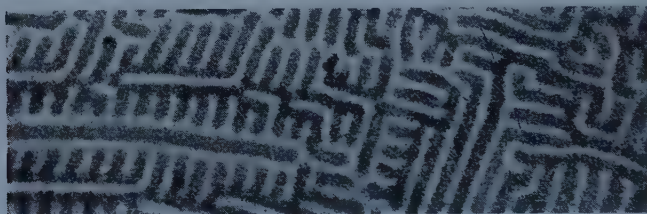


Figure 15. Electron micrograph of same region as figure 10 under same conditions  $\times 2625$ .

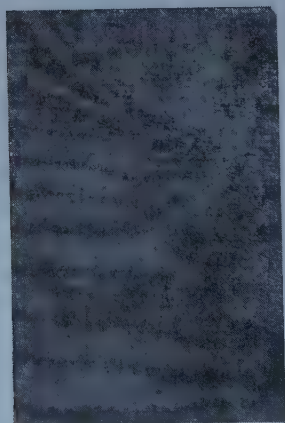


Figure 16.



Figure 17.

Figure 16. Pattern on etched surface; small normal field  $\times 750$ .  
 Figure 17. Pattern on polished surface (cf. cleaved surface of figure 10)  $\times 750$ .



# The Elastic Scattering of Slow Electrons by Hydrogen Atoms

By B. H. BRANSDEN†, A. DALGARNO‡, T. L. JOHN§ AND  
M. J. SEATON§

† Department of Natural Philosophy, The University of Glasgow

‡ Department of Applied Mathematics, The Queen's University of Belfast

§ Department of Physics, University College London

*MS. received 20th January 1958*

**Abstract.** Variational methods are used to calculate phases for the s- and p-wave scattering of electrons by hydrogen atoms. Full allowance is made for electron exchange and the influence of polarization is investigated. The derived elastic cross sections are compared with experimental results.

## § 1. INTRODUCTION

A PART from its importance in the development of approximate methods for the treatment of collision problems (cf. Mott and Massey 1949, Massey 1957), the theoretical description of the elastic scattering of electrons by hydrogen atoms has application in certain astrophysical contexts; in particular, the wave function describing the scattering is required for the determination of the bound-free and free-free transition probabilities of the negative hydrogen ion  $H^-$ , which largely controls the opacity of the solar atmosphere. Calculations of the s-wave scattering (MacDougall 1932, Morse and Allis 1933, Chandrasekhar and Breen 1946, Huang 1949, Kato 1950, Staver 1951, Massey and Moiseiwitsch 1951, Newstein 1955, Ochkv and Petrov 1957, Seaton 1957, Borowitz and Greenberg 1957) have been carried out to a high degree of refinement, though there is need for an improved treatment of the symmetric case at low energies, but the only calculations on p-wave scattering (Chandrasekhar 1944, Chandrasekhar and Breen 1946) are restricted to the 'one-body' approximation.

## § 2. SCATTERING THEORY

If  $\mathbf{r}_1$  and  $\mathbf{r}_2$  are the position vectors, referred to the nucleus, of the incident electron and the atomic electron respectively, then the Hamiltonian for the system is given in atomic units ¶ ( $m=e=\hbar=1$ ) by

$$\mathcal{H} = -\frac{1}{2}\nabla_1^2 - \frac{1}{2}\nabla_2^2 - \frac{1}{r_1} - \frac{1}{r_2} + \frac{1}{r_{12}} \quad \dots\dots(1)$$

where  $r_{12}=|\mathbf{r}_1-\mathbf{r}_2|$ . The wave functions  $\Psi_i^\pm(\mathbf{r}_1, \mathbf{r}_2)$  describing the scattering are solutions of the Schrödinger equation

$$(\mathcal{H} - E)\Psi(\mathbf{r}_1, \mathbf{r}_2) = 0, \quad \dots\dots(2)$$

having the symmetry properties

$$\Psi_i^\pm(\mathbf{r}_1, \mathbf{r}_2) = \pm \Psi_i^\pm(\mathbf{r}_2, \mathbf{r}_1), \quad \dots\dots(3)$$

the plus sign referring to the singlet state and the minus sign to the triplet state.

¶ The atomic unit of energy is 27.2 ev. Total cross sections are expressed in units of  $\pi a_0^2 = 8.806 \times 10^{-17} \text{ cm}^2$ .

It is convenient to write

$$\Psi_l^\pm(\mathbf{r}_1, \mathbf{r}_2) = \psi(\mathbf{r}_1)\chi_l^\pm(\mathbf{r}_2) \pm \psi(\mathbf{r}_2)\chi_l^\pm(\mathbf{r}_1) + \Phi_l^\pm(\mathbf{r}_1, \mathbf{r}_2) \quad \dots\dots (4)$$

where  $\psi(\mathbf{r})$  is the wave function of the ground state of the hydrogen atom,

$$\psi(\mathbf{r}) = (\pi)^{-1/2} \exp(-r), \quad \dots\dots (5)$$

and where

$$\chi_l^\pm(\mathbf{r}) = Y_{l0}(\hat{\mathbf{r}}) r^{-1} F_l^\pm(r), \quad \dots\dots (6)$$

$Y_{l0}(\hat{\mathbf{r}})$  being the normalized spherical harmonic

$$Y_{l0}(\hat{\mathbf{r}}) = \{(2l+1)/4\pi\}^{1/2} P_l(\cos\theta). \quad \dots\dots (7)$$

Then imposing the boundary conditions

$$r_1 r_2 \Phi_l^\pm(\mathbf{r}_1, \mathbf{r}_2) \rightarrow 0 \quad \text{as} \quad r_1 \rightarrow \infty \quad \text{and as} \quad r_2 \rightarrow \infty \quad \dots\dots (8)$$

and

$$F_l^\pm(r) \sim \sin(kr - \frac{1}{2}l\pi) + a_l^\pm \cos(kr - \frac{1}{2}l\pi), \quad \dots\dots (9)$$

where  $\mathbf{k}$  is the wave vector of the incident electron so that

$$2E = k^2 - 1, \quad \dots\dots (10)$$

it may be shown that for scattering through an angle  $\Theta$  (cf. Mott and Massey 1949) the amplitudes are given by

$$f^\pm(\Theta) = \frac{1}{2ik} \sum_{l=0}^{\infty} (2l+1) P_l(\cos\Theta) \{\exp(2i\eta_l^\pm) - 1\}, \quad \dots\dots (11)$$

the differential cross section by

$$I(\Theta) = \frac{3}{4} |f^-(\Theta)|^2 + \frac{1}{4} |f^+(\Theta)|^2 \quad \dots\dots (12)$$

and the total elastic scattering cross section by

$$Q = \frac{\pi}{k^2} \sum_{l=0}^{\infty} (2l+1) \{3 \sin^2 \eta_l^- + \sin^2 \eta_l^+\} \quad \dots\dots (13)$$

where

$$\eta_l^\pm = \arctan a_l^\pm, \quad \dots\dots (14)$$

and a summation over the final spin states and an average over the initial spin states have been performed. Throughout this formulation the influence of inelastic collisions has been ignored so that  $k^2$  is restricted to the range  $0 \leq k^2 \leq 0.75$ .

### § 3. THE CENTRAL FIELD MODEL

The elastic scattering of an electron by a hydrogen atom can be reduced to a central field problem if inelastic collisions and electron exchange are ignored. Then if  $V(r)$  represents the central field and  $G_l(r)$  are solutions of

$$\left\{ \frac{d^2}{dr^2} - \frac{l(l+1)}{r^2} - 2V(r) + k^2 \right\} G_l(r) = 0 \quad \dots\dots (15)$$

such that

$$G_l(r) \sim \sin(kr - \frac{1}{2}l\pi + \eta_l), \quad \dots\dots (16)$$

it may be shown that (cf. Mott and Massey 1949)

$$Q = \frac{4\pi}{k^2} \sum_{l=0}^{\infty} (2l+1) \sin^2 \eta_l. \quad \dots\dots (17)$$

If it is assumed that the scattered electron does not distort the atomic wave function then the average potential in which the electron moves is given by

$$V'(r) = \int |\psi(r')|^2 \left\{ -\frac{1}{r} + \frac{1}{|\mathbf{r} - \mathbf{r}'|} \right\} d\mathbf{r}', \quad \dots\dots (18)$$

evaluation of which gives

$$V'(r) = -\exp(-2r)(1+r^{-1}). \quad \dots\dots (19)$$

An estimate of the distortion may be made by supposing that the motion of the scattered electron is so slow that the distortion can be regarded as due to a point charge fixed at the position  $\mathbf{r}$ . Corresponding to these adiabatic conditions, the potential is given by

$$V(r) = V'(r) + V_p(r) \quad \dots\dots (20)$$

where  $V_p$  behaves asymptotically as a polarization potential. Thus for atoms in S states

$$V_p(r) \sim -\alpha/2r^4 \quad \dots\dots (21)$$

where  $\alpha$  is the polarizability of the atom (for H,  $\alpha=4.5$ ). The second-order perturbation expression for  $V_p(r)$  is

$$V_p(r) = - \sum_{n \neq 0} |V_{n0}(\mathbf{r})|^2 / (E_n - E_0) \quad \dots\dots (22)$$

where  $E_n$  is the energy of the  $n$ th excited state with wave function  $\psi_n(\mathbf{r}')$ ,  $\psi_0(\mathbf{r}') \equiv \psi(\mathbf{r}')$  and

$$V_{n0}(\mathbf{r}) = \int \frac{\psi_n^*(\mathbf{r}')\psi_0(\mathbf{r})}{|\mathbf{r} - \mathbf{r}'|} d\mathbf{r}' \quad \dots\dots (23)$$

and the corresponding first-order perturbed wave function is

$$\psi'(\mathbf{r}', \mathbf{r}) = \psi_0(\mathbf{r}') - \sum_{n \neq 0} \frac{V_{n0}(\mathbf{r})\psi_n(\mathbf{r}')}{(E_n - E_0)}, \quad \dots\dots (24)$$

which for atoms in S states behaves asymptotically as  $r^{-2}$ .

For atomic hydrogen, the limiting forms of (22) and (24) have been evaluated explicitly by Dalgarno and Lewis (1955) and more generally by Dalgarno and Stewart (1956). The resulting expressions are

$$V_p(r) = - \sum_{m \neq 0} \frac{1}{r^{2m+2}} \frac{(2m+2)!}{2^{2m}} \cdot \frac{(m+2)}{m(m+1)} \quad \dots\dots (25)$$

and

$$\psi'(\mathbf{r}, \mathbf{r}') = \psi_0(\mathbf{r}') + \sum_{m \neq 0} \frac{1}{r^{m+1}} \left( \frac{(r')^{m+1}}{m+1} + \frac{(r')^m}{m} \right) P_m(\cos \theta'). \quad \dots\dots (26)$$

These are valid in the limit of large  $r$ . The exact evaluation at all  $r$  of (22) and (24) has been achieved recently by Dalgarno and Lynn (1957) and the ratio of  $V_p(r)$  to  $-\alpha/2r^4$  is given in table 1 as a function of  $r$ . The general behaviour of the ratio, which initially increases to a value greater than unity before decreasing to zero, is similar to that found by Douglas (1956) in his analysis of optical spectra and may be understood classically by regarding the atom as a dielectric or conducting sphere (Hartree 1957). The contributions to  $V_p(r)$  from higher order perturbations have been discussed by Dalgarno and Lewis (1956).

Table 1. Polarization Potential  $V_p(r)$  calculated using the Adiabatic Theory

$r$	$-2r^4V_p(r)/\alpha$	$r$	$-2r^4V_p(r)/\alpha$	$r$	$-2r^4V_p(r)/\alpha$
0.0	0.000	5.0	1.137	10.0	1.037
1.0	0.089	6.0	1.111	15.0	1.017
2.0	0.500	7.0	1.082	25.0	1.007
3.0	0.925	8.0	1.061	35.0	1.004
4.0	1.112	9.0	1.047	45.0	1.002

To investigate the effect of polarization on the phase shifts  $\eta_l(k)$  it is convenient to write

$$\eta_l(k) = A_l k^{\nu_l} + O(k^{\nu_l+1}). \quad \dots\dots (27)$$

The exponent  $\nu_l$  does not depend upon the strength of the potential and accordingly may be determined from Born's approximation

$$\eta_l^B = -2k^{-1} \int_0^\infty \{j_l(kr)\}^2 V(r) dr \quad \dots\dots (28)$$

where

$$j_l(x) = \left(\frac{\pi x}{2}\right)^{1/2} J_{l+1/2}(x), \quad \dots\dots (29)$$

$J_{l+1/2}(x)$  being the regular Bessel function of order  $l + \frac{1}{2}$ . For small  $x$ ,

$$j_l(x) = \frac{l!}{2(2l+1)!} (2x)^{l+1} + O(x^{l+3}), \quad \dots\dots (30)$$

and therefore

$$\eta_l^B(k) = -2k^{2l+1} \left\{ \frac{l! 2^l}{(2l+1)!} \right\}^2 \int_0^\infty r^{2l+1} V(r) dr + O(k^{2l+3}) \quad \dots\dots (31)$$

provided the integral converges. Taking  $V(r) = V'(r)$ , (31) converges for all  $l$  and the corresponding phase shifts vary as  $k^{2l+1}$  as  $k$  tends to zero; in particular  $\eta_l/k$  tends to  $A_0$ , if  $l=0$  and to zero otherwise, so that the zero energy limit of the cross section  $Q(0)$  is  $4\pi A_0^2$  ( $A_0$  is the scattering length).

However, taking  $V(r) = V_p(r)$ , (31) converges only for  $l=0$  and the procedure leading to it is invalid for  $l>0$ . Returning to (28), for  $l>0$  and small  $k$  the main contribution to (28) arises from large values of  $r$  where it is legitimate to replace  $V_p(r)$  by its asymptotic form  $-\alpha/2r^4$ . Then

$$\eta_l^B \simeq \frac{1}{2} \pi \alpha k^2 \int_0^\infty x^{-3} \{J_{l+1/2}(x)\}^2 dx \quad \dots\dots (32)$$

which is convergent for  $l \geq 1$ . Thus, when account is taken of polarization  $\eta_l(k)$  for  $l \geq 1$  behaves as  $k^2$  in the limit of vanishing  $k$  in contrast to the variation as  $k^{2l+1}$  when polarization is ignored. This relative importance of polarization when  $l \geq 1$  is to be expected from classical considerations: slow collisions with finite angular momentum correspond to large distances of closest approach where the long range polarization forces are dominant. We shall say that allowance has been made for polarization only when some account has been taken of the long range polarization potential  $V_p$ .

#### § 4. VARIATIONAL METHODS

Defining the integral

$$L_l^{\pm(t)} = \int \Psi_l^{\pm(t)} [\mathcal{H} - E] \Psi_l^{\pm(t)} d\mathbf{r} \quad \dots\dots (33)$$

where  $\Psi_l^{\pm(t)}$  is a properly symmetrized trial wave function, which may be taken



as real and which obeys the boundary conditions (8) and (9), and considering small variations  $\delta\Psi_l^{\pm(t)}$  of  $\Psi_l^{\pm(t)}$  such that

$$\delta\Psi_l^{\pm}(\mathbf{r}_1, \mathbf{r}_2) \underset{r_2 \rightarrow \infty}{\sim} \psi(\mathbf{r}_1) Y_{l0}(\hat{\mathbf{r}}_2) r_2^{-1} \delta F_l^{\pm(t)}(r_2) \quad \dots\dots (34)$$

and

$$\delta F_l^{\pm(t)}(r) \sim \delta a_l^{\pm(t)} \cos(kr - \tfrac{1}{2}l\pi) \quad \dots\dots (35)$$

it may be shown (Hulthén 1944, 1948, Kohn 1948, Hulthén and Olsson 1950) that

$$\delta[L_l^{\pm(t)} - k a_l^{\pm(t)}] = 2 \int \delta\Psi_l^{\pm(t)} [\mathcal{H} - E] \Psi_l^{\pm(t)} d\mathbf{r} \quad \dots\dots (36)$$

to first order in  $\delta\Psi_l^{\pm(t)}$ . Since the right-hand side vanishes if  $\Psi_l^{\pm(t)}$  is a solution of the Schrödinger equation (2),

$$a_l^{\pm(K)} = a_l^{\pm(t)} - k^{-1} L_l^{\pm(t)} \quad \dots\dots (37)$$

gives an improved estimate for  $a_l^{\pm}$  the error in  $a_l^{\pm(K)}$  being of quadratic order in the error in the wave functions.

If  $\Psi_l^{\pm(t)}$  depends upon  $n$  parameters  $c_1, c_2, \dots, c_n$  in addition to  $a_l^{\pm(t)}$ , the variational method of Hulthén uses the equations

$$\left. \begin{aligned} \frac{\partial}{\partial c_i} L_l^{\pm(t)} &= 0 \\ L_l^{\pm(t)} &= 0 \end{aligned} \right\} \quad \dots\dots (38)$$

and that of Kohn the equations

$$\left. \begin{aligned} \frac{\partial}{\partial c_i} L_l^{\pm(t)} &= 0 \\ \frac{\partial}{\partial a_l^{\pm}} L_l^{\pm(t)} &= k \\ a_l^{\pm(K)} &= a_l^{\pm(t)} - k^{-1} L_l^{\pm(t)}. \end{aligned} \right\} \quad \dots\dots (39)$$

The exact wave functions satisfy the integral equation

$$a_l^{\pm} = -2k^{-1} \int \Psi_l^{\pm(t)} \left( \frac{1}{r_{12}} - \frac{1}{r_2} \right) \psi(\mathbf{r}_1) \chi_l^B(\mathbf{r}_2) d\mathbf{r}_1 d\mathbf{r}_2 \quad \dots\dots (40)$$

where

$$\chi_l^B(\mathbf{r}) = Y_{l0}(\hat{\mathbf{r}}) r^{-1} j_l(kr) \quad \dots\dots (41)$$

and for functions calculated by the Hulthén method the departure of the ratio

$$R_H = \frac{-2k^{-1} \int \Psi_l^{\pm(t)} \left( \frac{1}{r_{12}} - \frac{1}{r_2} \right) \psi(\mathbf{r}_1) \chi_l^B(\mathbf{r}_2) d\mathbf{r}_1 d\mathbf{r}_2}{a_l^{\pm(t)}} \quad \dots\dots (42)$$

from unity provides an indication of the accuracy of the wave function.

Wave functions calculated by the Kohn method automatically satisfy (40) but the departure of the ratio

$$R_K = a_l^{\pm(K)} / a_l^{\pm(t)} \quad \dots\dots (43)$$

from unity provides an indication in this case.

In the exchange approximation, the trial functions are restricted to the form

$$\Psi_l^{\pm(t)} = \psi(\mathbf{r}_1) \chi_l^{\pm(t)}(\mathbf{r}_2) \pm \psi(\mathbf{r}_2) \chi_l^{\pm(t)}(\mathbf{r}_1). \quad \dots\dots (44)$$

The requirement that the right-hand side of (36) should be stationary for

variation of  $\chi_l^{\pm(t)}$  yields the equations

$$\int \psi(\mathbf{r}_1)[\mathcal{H} - E]\Psi_l^{\pm(t)}(\mathbf{r}_1, \mathbf{r}_2) d\mathbf{r}_1 = 0; \quad \dots\dots (45)$$

$$\left\{ \frac{d^2}{dr^2} - \frac{l(l+1)}{r^2} - 2V_1(r) + k^2 \right\} F_l^{\pm(t)}(r) = \pm w_l(r) F_l^{\pm(t)}(r) \quad \dots\dots (46)$$

(cf. Seaton 1953) where  $V_1(r)$  is given by equation (19) and where the operator  $W_l(r)$  is defined by

$$W_l(r)F_l(r) = 2P(r) \left\{ -\frac{1}{2}(1+k^2)\Delta(PF_l)\delta_{l0} + \frac{1}{(2l+1)}y_l(PF|r) \right\}, \quad \dots\dots (47)$$

$$P(r) = 2r \exp(-r), \quad \dots\dots (48)$$

$$\Delta(PF_l) = \int_0^\infty P(r')F_l(r') dr' \quad \dots\dots (49)$$

and

$$y_l(PF_l|r) = r^{-l-1} \int_0^r P(r')F_l(r')r'^l dr' + r^l \int_r^\infty P(r')F_l(r')r'^{-l-1} dr'. \quad \dots\dots (50)$$

With exact solutions of (46),  $L_l^{\pm(t)} = 0$  and  $R_H = R_K = 1$ . The departures of  $R_H$  and  $R_K$  from unity indicate therefore the accuracy of the variational wave functions only within the limitations of the assumed form (44).

An improvement of the exchange approximation is the use of trial functions of the non-separable form (4) and some detailed results are given in § 5. It is worth remarking here that provided the energy is too low for inelastic collisions to occur, the adiabatic theory (cf. § 3) is valid in the limit of large  $r_1$  or  $r_2$  (Castillejo, Percival and Seaton, to be published), the asymptotic form of the exact wave function being

$$\Psi_l^{\pm}(\mathbf{r}_1, \mathbf{r}_2) \underset{r_2 \rightarrow \infty}{\sim} \psi'(\mathbf{r}_1, \mathbf{r}_2)\chi_l^{\pm}(\mathbf{r}_2) + O(r_2^{-4}), \quad \dots\dots (51)$$

where  $\psi'(\mathbf{r}_1, \mathbf{r}_2)$  is the perturbed wave function (24) and (26), and the asymptotic form of the equation satisfied by  $F_l^{\pm}(r)$  being

$$\left\{ \frac{d^2}{dr^2} - \frac{l(l+1)}{r^2} + \frac{\alpha}{r^4} + k^2 \right\} F_l^{\pm}(r) = 0. \quad \dots\dots (52)$$

Thus, the exact phases  $\eta_l^{\pm}(k)$  for  $l > 0$  vary as  $k^2$  for small  $k$ .

For the sake of completeness it should be mentioned that Newstein (1955) has applied the Schwinger variational method for the complete scattering amplitude to the problem of scattering of electrons by hydrogen atoms. Comparison of his results for the central field model with the corresponding exact solutions indicates that the method used does not compare in accuracy with the variational results described in the following section and it will therefore not be discussed further. Altshuler (1953) has obtained good results using the Schwinger method to calculate  $a_0$  in the central field approximation.

## § 5. CALCULATIONS FOR THE S-WAVE

Variational calculations of the s-wave scattering have been carried out by Massey and Moiseiwitsch (1951, where references to earlier work may be found), by Staver (1951) and in the low energy limit by Seaton (1957) and by Borowitz

and Greenberg (1957). These calculations all agreed in showing that phase shifts obtained in the exchange approximation differ markedly at low energies from those obtained in the central field approximation. Attempts to improve on the exchange approximation (Massey and Moiseiwitsch 1951, Seaton 1957, Borowitz and Greenberg 1957) have been made using trial wave functions of the form

$$\Psi_0^{\pm(t)}(\mathbf{r}_1, \mathbf{r}_2) = \psi(r_1)\chi_0^{\pm(t)}(r_2) \pm \psi(r_2)\chi_0^{\pm(t)}(r_1) + \Phi_0^{\pm(t)}(r_1, r_2, r_{12}) \quad \dots\dots (53)$$

but the trial functions chosen for  $\Phi_0^{\pm(t)}$  all tend exponentially to zero for large  $r_1$  or large  $r_2$ . Inclusion of such functions will be said to give an exchange-correlation approximation. To include polarization in the sense of § 3,  $\Phi_0^{\pm(t)}$  should vary as  $r_1^{-2}$  or  $r_2^{-2}$  for large  $r_1$  or  $r_2$ , Staver (1951) has attempted to allow for polarization by including a polarization potential in the exchange equations; whilst this allows explicitly for long range polarization effects, it is essentially empirical and cannot be obtained from the Schrödinger equation (2) by a consistent variational argument.

### 5.1. The *s*-Wave Exchange Approximation

Comparison of the phases obtained by Massey and Moiseiwitsch (1951) with those obtained from numerical integrations of the exchange equations for  $k=0$  (Seaton 1957) shows good agreement for the antisymmetric case and fair agreement for the symmetric case. The exact solution for  $F_0^{+(t)}$  behaves as

$$F_0^{+(t)}(r) \sim \sin kr + a_0^{+(t)} \cos kr - k\Delta(PF_0^{+(t)})P(r) \quad \dots\dots (54)$$

for moderate values of  $r$ , but the trial function used by Massey and Moiseiwitsch does not contain the last term in (54). In the limit of vanishing  $k$ , Seaton (1957) has shown that

$$F_0^{\pm(t)}(r) = \sin kr + a_0^{\pm(t)}\{1 - \exp(-2r)\} \cos kr + \frac{1}{2}kbP(r), \quad \dots\dots (55)$$

$b$  being a variational parameter, gives much better results and (55) has been adopted here for all energies. Since  $\psi(r) = P(r)/(4\pi)^{1/2}$ , the term  $\frac{1}{2}kbP(r)$  cancels in the complete antisymmetric wave function and (55) is reduced in this case to a single-parameter wave function.

It happens that in the calculation of  $L_0^{\pm(t)}$ , using (55), the coefficient of  $b^2$  vanishes at  $k=0.5$ , so that  $a_0^{\pm(t)}$  is determined by the single condition  $\partial L_0^{\pm(t)}/\partial b = 0$  and is presumably less reliable. Fortunately  $k=0.5$  is the value at which Staver (1951) performed his most elaborate calculations. The results of all the calculations are collected in tables 2 and 4.

### 5.2. The *s*-Wave Exchange-Correlation Approximation

For this approximation, Massey and Moiseiwitsch used the function

$$\Phi_0^{\pm(t)} = kp\psi(r_1)\psi(r_2)r_{12}\{r_2^{-1}[1 - \exp(-r_2)] \cos kr_2 \pm r_1^{-1}[1 - \exp(-r_1)] \cos kr_1\} \quad \dots\dots (56)$$

and Seaton (for  $k=0$  and the symmetric case only) the function

$$\Phi_0^{+(t)} = 2kp\psi(r_1)\psi(r_2) \exp(-r_{12}). \quad \dots\dots (57)$$

Results obtained using (57) at other energies are compared with previous calculations in tables 3 and 5.

Table 2. Symmetric case, s-wave Calculations Exchange Approximation

$k$	Kohn Method		Hulthén Method		St
	BDJS	MM	BDJS	MM	
	$\eta_0^+$	$R_K$	$\eta_0^+$	$R_H$	$\eta_0^+$
0	(-7.11)†	0.998	(-8.12)†	0.995	(-7.12)†
0.05	2.744	1.000	10.54	2.744	1.444
0.1	2.395	0.998	10.90	0.999	—
0.15	2.106	1.000	12.06	2.395	—
0.2	1.872	0.938	14.72	2.106	—
0.3	1.508	1.039	21.30	1.870	—
0.4	1.235	0.875	-69.46	1.508	—
0.5	1.024	0.920	-8.94	1.240	—
			—	complex	—
				1.074	1.513

Table 3. Symmetric Case, s-wave Calculations Exchange-Correlation Approximation

$k$	Kohn Method		Hulthén Method		St
	BDJS	MM	BDJS	MM	
	$\eta_0^+$	$R_K$	$\eta_0^+$	$R_H$	$\eta_0^+$
0	(-7.03)†	1.030	(-7.01)†	1.099	(-3.47)†
0.05	2.794	1.033	4.27	1.111	—
0.1	2.479	1.036	4.47	1.117	—
0.15	2.204	1.047	4.96	1.140	—
0.2	1.972	1.068	6.11	1.180	—
0.3	1.614	1.324	8.62	1.461	—
0.4	1.298	0.709	78.31	1.618	—
0.5	1.092	0.828	—	complex	—
			—	complex	—
				1.425	1.255

Table 4. Antisymmetric Case, s-wave Calculations Exchange Approximation

$k$	Kohn Method		Hulthén Method		St
	BDJS	MM	BDJS	MM	
	$\eta_0^-$	$R_K$	$\eta_0^-$	$R_H$	$\eta_0^-$
0	(-2.38)†	0.974	(-2.38)†	1.028	(-2.35)†
0.05	3.023	0.970	3.023	1.002	—
0.1	2.904	0.969	2.904	1.031	—
0.15	2.788	0.963	2.787	1.030	—
0.2	2.674	0.950	2.673	1.032	—
0.3	2.457	0.860	2.455	1.036	—
0.4	(2.383)	(-0.964)	complex	—	—
0.5	(3.034)	(-0.063)	complex	—	—
				2.257	2.072
				2.070	1.003



Table 5. Antisymmetric Case, s-wave Calculations  
Exchange-Correlation Approximation

Hulthén Method							
MM		$R_H$	St	MM		$R_H$	St
$k$	$\eta_0^-$		$\eta_0^-$	$k$	$\eta_0^-$		$\eta_0^-$
0	(-2.33)†	1.01	(-1.82)†	0.2	2.680	—	—
0.05	—	—	—	0.3	2.447	—	—
0.1	2.909	—	—	0.4	2.248	—	—
0.15	2.792	—	—	0.5	2.039	—	2.269

†, the scattering length  $A_0^-$ ; MM, Massey and Moiseiwitsch 1951; St, Staver 1951.

### 5.3. Discussion of Results

At lower energies the exchange values calculated using (55) in Hulthén's method and in Kohn's method are in excellent agreement with each other and  $R_H$  and  $R_K$  are very close to unity. Most of the values are also in very good agreement with those of Massey and Moiseiwitsch. It is noteworthy that where they differ significantly, the Hulthén and Kohn values of Massey and Moiseiwitsch also differ significantly and the ratio  $R_H$  is not close to unity. At the higher energies, the trial function (55) apparently becomes inadequate and the values of Massey and Moiseiwitsch are to be preferred.

The symmetric exchange-correlation values are less satisfactory for although Hulthén's method and Kohn's method give results in excellent agreement with each other,  $R_H$  is not so nearly unity as in the exchange case. However, the phase shifts should be accurate and at low energies should represent a slight improvement on the Massey and Moiseiwitsch values. The limiting value for zero energy also agrees quite well with the value  $A_0^+ = 7.67$  due to Borowitz and Greenberg (1957) who took  $\Phi_0^{\pm(t)}$  in the form of an approximate wave function of the negative hydrogen ion  $H^-$ .

For the antisymmetric exchange-correlation values, the Massey and Moiseiwitsch values were considered to be sufficiently accurate and no additional calculations were made.

The results differ significantly at low energies from the exchange-polarization values of Staver (1951) and further work is needed before it can be claimed that long-range polarization effects have been fully taken into account.

Table 6 gives the s-wave phase shifts adopted from the calculations reported here and those of Massey and Moiseiwitsch. There remains some uncertainty in their accuracy at least at low energies.

Table 6. Adopted s-wave Phases

$k$	$\eta_0^+$	$\eta_0^-$	$k$	$\eta_0^+$	$\eta_0^-$
0	(-7.02)†(-2.33)‡		0.4	1.42	2.25
0.05	2.795	3.02	0.5	1.25	2.04
0.1	2.48	2.91	0.6	1.09	1.91
0.15	2.21	2.79	0.8	0.86	1.42
0.2	1.98	2.68	1.0	0.71	1.40
0.3	1.64	2.45			

†, the scattering length  $A_0^+$ ; ‡, the scattering length  $A_0^-$ .

## § 6. CALCULATIONS FOR THE p-WAVE

There are no previous variational calculations of the p-wave scattering and it is of interest to report results for the 'one-body' approximation as well as the exchange approximation. In the 'one-body' approximation the trial functions are restricted to the form

$$\Psi_l^{(t)} = \psi(\mathbf{r}_1)\chi_l^{(t)}(\mathbf{r}_2). \quad \dots\dots (58)$$

Initially, attention was restricted to  $k=1$  and several forms of trial functions (58) were investigated. The final choice was

$$F_1^{(t)} = j_1(kr) - a_1^{(t)}\{1 - \exp(-2kr)\}^3 y_1(kr) + b(kr)^2 \exp(-3kr) \quad \dots\dots (59)$$

where

$$y_1(x) = \left(\frac{\pi x}{2}\right)^{1/2} J_{-3/2}(x). \quad \dots\dots (60)$$

This trial function has been used earlier by Bransden and Dalgarno (1956) in an investigation of autodetachment from  $H^-(2s2p)^3P$ . The function yields  $a_1=0.1119$  by both the Hulthén and Kohn methods compared to the exact value of 0.1120 computed by Chandrasekhar and Breen and the ratios  $R_H$  and  $R_K$  are very close to unity, being 1.001 and 1.006 respectively. For the exchange approximation, trial functions of the form (59) were employed in the appropriately symmetrized versions of (58).

The results of calculations for five different values of  $k$  between 0.5 and 1.0 are given in tables 7, 8 and 9 which include also values computed using the Born and Born–Oppenheimer approximations together with the exact central field phase shifts of Chandrasekhar and Breen (1946). The agreement between values derived by Hulthén's method and by Kohn's method is everywhere excellent, provided the parameter  $b$  is included, and the check provided by  $R_H$  suggests that the Hulthén wave functions may themselves be reasonably accurate, though  $R_K$  departs considerably from unity.

As for the s-phase, the central field values differ markedly from the exchange values. The Born and symmetric Born–Oppenheimer approximations are quite good, the antisymmetric Born–Oppenheimer approximation less so; for this case the phase shifts are larger.

The trial function (59) is unsatisfactory for small  $k$  for it varies as  $(kr)^2$  whereas it should vary as  $r^2 + 3A_1^\pm r^{-1}$  for vanishing  $k$  and  $r$  large but finite, where  $A_1^\pm$  is equal to  $\lim_{k \rightarrow 0}(\eta_1^\pm/k^3)$ . The region of small  $k$  has been studied instead by exact numerical integration at  $k=0$ ; for the central field case  $A_1=0.269$  and for the exchange cases  $A_1^+ = -1.16$  and  $A_1^- = +2.34$ . The quantity  $a_1/k^3$  is plotted in figure 1 as a function of  $k^2$  from which it can be seen that the calculated variational values extrapolate smoothly to the computed zero energy values.

An attempt to estimate the importance of polarization effects has been made using perturbation methods. As table 10 shows, the central field wave functions are not greatly different from the plane wave functions  $j_1(kr)$ . Hence  $a_1$  has been modified to include polarization by using the expression

$$a_1 = a_1^{(t)} - 2k^{-1} \int_0^\infty \{j_1(kr)\}^2 V_p(r) dr, \quad \dots\dots (61)$$

$a_1^{(t)}$  being the central field phase parameter. A family of polarization potentials

$$V_p(r) = -\alpha/2(r^2 + d^2)^2 \quad \dots\dots (62)$$

Table 7. P-wave Calculations, Central Field Model

$k^2$	Exact	Born $a_1^{(B)}$	$b=0$			$b \neq 0$			
			Hulthén $a_1$	$R_H$	Kohn $a_1$ $R_K$	Hulthén $b$ $a_1$	$R_H$	Kohn $a_1$ $R_K$	
0.25	0.02605	0.02314	0.02586	0.982	0.02520 0.615	0.043775	0.02602	0.02603	1.040
0.50	0.05845	0.05100	0.05812	1.013	0.05819 0.911	-0.054945	0.05827	0.05827	1.015
0.73	—	0.07383	0.08360	1.046	0.08446 0.771	-0.24696	0.08483	0.08483	1.000
0.80	0.09270	0.08013	0.09037	1.056	0.09164 0.740	-0.31353	0.09259	0.09260	1.041
1.00	0.1120	0.09657	0.1074	1.083	0.1102 0.672	-0.50878	0.1119	0.1119	1.006

Table 8. P-wave Calculations, Symmetric Case Exchange Approximation

$k^2$	Born- Oppenheimer $a_1^+$	$b=0$				$b \neq 0$			
		Hulthén $a_1^+$	$R_H$	Kohn $a_1^+$	$R_K$	Hulthén $a_1^+$	$d$	Kohn $a_1^+$	$R_K$
0.25	-0.07743	-0.07627	0.883	-0.07209	0.561	-0.07055	0.21973	-0.07054	7.057
0.50	-0.11505	-0.1598	0.618	-0.1129	0.302	-0.1131	0.57683	-0.1098	0.568
0.73	-0.1186	complex	—	-0.1175	0.164	-0.1192	0.96193	-0.1157	0.491
0.80	-0.1161	complex	—	-0.1155	0.128	-0.1179	1.02356	-0.1138	0.442
1.00	-0.1044	complex	—	-0.1044	-0.040	-0.1098	1.26372	-0.1034	0.230

Table 9. P-wave Calculations, Antisymmetric Case Exchange Approximation

$k^2$	Born- Oppenheimer $a_1^-$	$b=0$				$b \neq 0$			
		Hulthén $a_1^-$	$R_H$	Kohn $a_1^-$	$R_K$	Hulthén $a_1^-$	$b$	Kohn $a_1^-$	$R_K$
0.25	0.1237	0.1683	1.041	0.1691	0.877	0.1703	-0.17771	0.1704	1.068
0.50	0.2171	0.2670	1.186	0.2836	0.628	0.2877	-0.81529	0.2899	0.825
0.73	0.2663	0.3023	1.263	0.3347	0.535	0.3469	-1.66371	0.3486	0.845
0.80	0.2764	0.3075	1.280	0.3440	0.516	0.3570	-1.87268	0.3592	0.833
1.00	0.2976	0.3145	1.318	0.3606	0.470	0.3722	-2.28685	0.3764	0.783

has been considered. The results for various values of  $d$  are presented in figure 2 which shows also the result of evaluating (61) using the polarization potential obtained from the adiabatic theory (table 1). For the polarization correction to the exchange calculations the expression

$$a_1^{\pm} = a_1^{\pm(t)} - 2k^{-1} \int_0^{\infty} \{F_1^{\pm}(r)\}^2 V_p(r) dr, \quad \dots\dots (63)$$

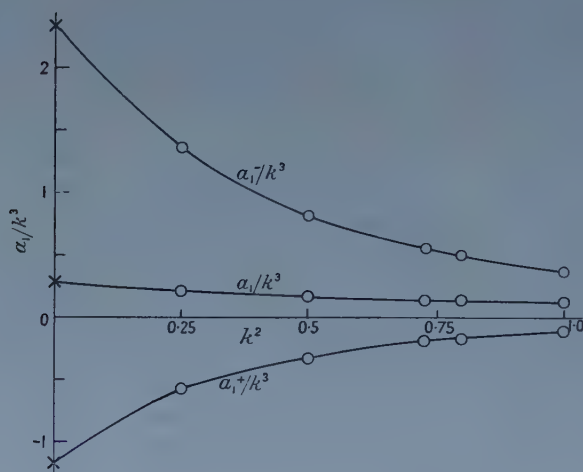


Figure 1. Values of  $a_1/k^3$  for p-wave calculations without polarization;  $a_1$  for central field,  $a_1^{\pm}$  for exchange cases. Circles give results of variational calculations, crosses give results obtained by numerical integration for  $k^2=0$ .

$a_1^{\pm(t)}$  being the exchange phase parameter and  $F_1^{\pm}(r)$  the exchange radial functions, has been used and the results are illustrated in figures 3 (a) and 3 (b).

Although there is considerable uncertainty in this method of allowing for polarization it seems that for the symmetric exchange case the phase shifts, when calculated with polarization, are small and the wave functions do not differ greatly from the plane wave or central field functions (cf. table 10). The symmetric wave functions are required for the calculation of the  $H^-$  bound-free absorption coefficients and it is possible therefore to understand the excellent agreement of the calculations by Chandrasekhar (1944), which were based upon

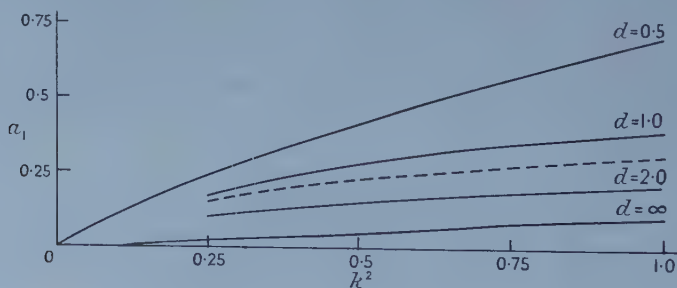


Figure 2. Effect of polarization on p-wave central field phases ( $a_1 = \tan \eta_1$ ). Full line curves for various values of  $d$  in the polarization potential (62), broken curve for the adiabatic polarization potential.

central field wave functions, with the observed solar opacity and with the measurements of Smith and Branscomb (1955).



For the antisymmetric case, the effects of potential, exchange and polarization all tend to give shifts of the same sign and the antisymmetric exchange-polarization phase shift is comparatively large. Indeed it cannot be excluded that a more complete treatment would yield a resonance-type effect ( $\eta_1^- \sim \frac{1}{2}\pi$ ) somewhere in the range  $0 \leq k^2 \leq 1$ .

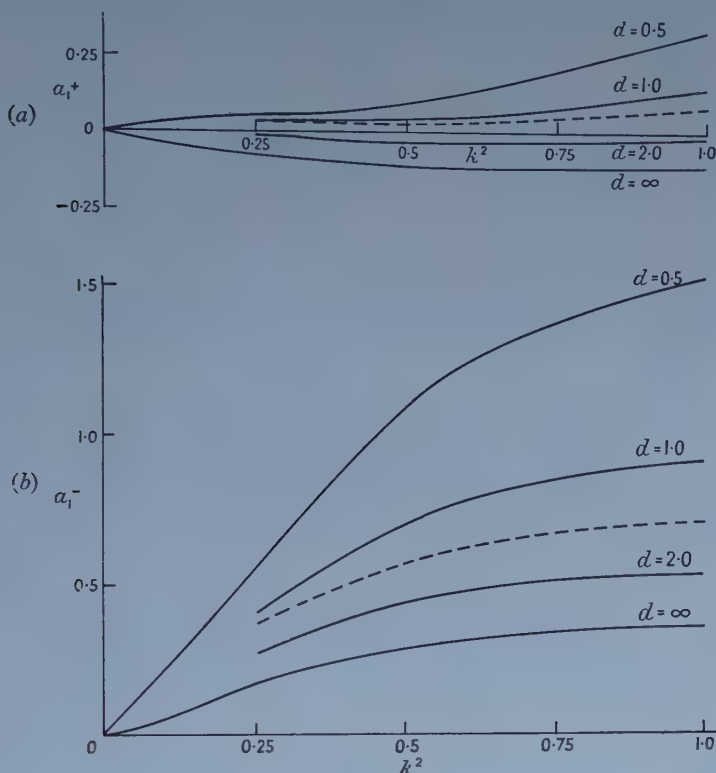


Figure 3. Exchange-polarization results for the p-wave. (a),  $a_1^+ = \tan \eta_1^+$ ; (b),  $a_1^- = \tan \eta_1^-$ . Full line curves for various values of  $d$  in the polarization potential (62), broken curves for the adiabatic polarization potential.

For the purposes of the following discussion, the values adopted for the p phase shifts are those obtained using the adiabatic polarization potential as shown by the broken curves of figures 3 (a) and 3 (b).

The contribution to  $Q$  from higher order partial waves is small; an elementary investigation using Born's approximation and the asymptotic form for  $V_p$  suggests that  $3k^2\pi a_0^2$  may be taken as an upper limit.

## § 7. DISCUSSION

Figure 4 illustrates  $Q_0$  as a function of  $k$ ,  $Q_0$  being computed using the phase shifts given in table 6, and also  $Q_1$  and  $Q_0 + Q_1$ ,  $Q_1$  being computed using the exchange-polarization phase shifts given in figure 3.

Bederson, Malamud and Hammer (1957) have reported measurements of  $Q$  of  $50\pi a_0^2$  at 4 eV ( $k^2 = 0.294$ ) and  $4\pi a_0^2$  at 12.5 eV ( $k^2 = 0.919$ ) whilst from measurements of the conductivity of an arc Maecker, Peters and Schenck (1955) obtained a mean cross section of  $150\pi a_0^2$  at a temperature of 12 000°K

Table 10. Comparison of p-wave Radial Functions for  $k=0.5$

$r$	Exact	Central field model		Exchange approximation			
		Born	Hulthén	Symmetric case		Antisymmetric case	
				Hulthén		Hulthén	
		$d=0$	$d \neq 0$	$d=0$	$d \neq 0$	$d=0$	$d \neq 0$
		$G_1$	$G_1$	$G_1^+$	$G_1^+$	$G_1^-$	$G_1^-$
0	$G_1$	$J_1(kr)$	0.0000	0.0000	0.0000	0.0000	0.0000
0.2	0.0000	0.0000	0.0000	0.0000	0.0000	0.0000	0.0000
0.4	0.0053	0.0033	0.0049	-0.0012	0.0007	0.0132	0.0120
0.6	0.0195	0.0133	0.0180	-0.0007	0.0052	0.0434	0.0399
0.8	0.0408	0.0297	0.0380	0.0053	0.0151	0.0524	0.0766
1.0	0.0682	0.0525	0.0641	0.0182	0.0313	0.1264	0.1188
	0.1010	0.0813	0.0958	0.0381	0.0536	0.1738	0.1651
1.5	0.2034	0.1772	0.1972	0.1176	0.1350	0.3037	0.2947
2.0	0.3297	0.3012	0.3242	0.2324	0.2485	0.4452	0.4381
2.5	0.4719	0.4439	0.4677	0.3719	0.3854	0.6002	0.5871
3.0	0.6200	0.5943	0.6172	0.5244	0.5352	0.7348	0.7319
3.5	0.7627	0.7405	0.7611	0.6772	0.6856	0.8638	0.8623
4.0	0.8886	0.8708	0.8877	0.8178	0.8241	0.9688	0.9681
4.5	0.9866	0.9740	0.9861	0.9345	0.9389	1.0405	1.0401
5.0	1.0474	1.0405	1.0472	1.0168	1.0195	1.0713	1.0709
6.0	1.0318	1.0370	1.0318	1.0483	1.0479	0.9915	0.9907
7.0	0.8199	0.8362	0.8200	0.8807	0.8776	0.7223	0.7208
8.0	0.4403	0.4644	0.4405	0.5330	0.5280	0.3054	0.3035
9.0	-0.0331	-0.0643	-0.0329	0.0715	0.0656	-0.1763	-0.1783
10.0	-0.4988	-0.4755	-0.4986	-0.4055	-0.4108	-0.6186	-0.6202

Note :  $G_1(r) = \cos \eta_1 F_1(r)$  has the asymptotic form  $G_1(r) \sim \sin(kr - \frac{1}{2}\pi + \eta_1)$ .

corresponding to a mean energy  $k^2 \simeq 0.08$ ; the latter measurement refers to the momentum loss cross section  $Q_d$  where

$$Q_d = \frac{\pi}{k^2} \sum_{l=0}^{\infty} (l+1) \{3 \sin^2(\eta_l^- - \eta_{l+1}^-) + \sin^2(\eta_l^+ - \eta_{l+1}^+)\}. \quad \dots (64)$$

Earlier measurements of the *total* cross section including inelastic collisions (Kuithof and Ornstein 1935, and Lindemann 1935 quoted therein) gave a value of  $4.7\pi a_0^2$  at  $k^2 = 1.0$ .

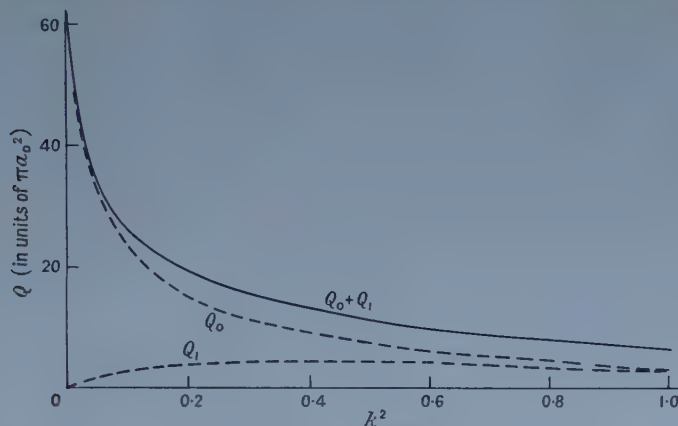


Figure 4. Cross sections in units of  $\pi a_0^2$ ,  $k^2$  in units of 13.60 eV. Broken curves give the partial cross sections  $Q_0$  (s-wave) and  $Q_1$  (p-wave). The full line curve gives the total cross section  $Q = Q_0 + Q_1$ .

The cross section measured at  $k^2 = 0.294$  is several times the calculated value and indeed is several times the maximum possible s-wave cross section  $13.6\pi a_0^2$ . It can only be explained if at least one partial cross section, other than  $Q_0$ , is much greater than that calculated. It has been remarked earlier that a resonance-type effect *might* occur for the antisymmetric p-wave case but it is not easy to reconcile a value of  $\eta_1^-$  near to  $\pi/2$  at  $k^2 = 0.294$  with the measured value of  $Q_d$  at  $k^2 \simeq 0.08$ . Further work is required in order to establish whether the experimental results of Bederson *et al.* (1957) are consistent with those of Maecker *et al.* (1955). The measured values at  $k^2 = 0.919$  and  $k^2 = 1.0$  are rather smaller than the theoretical value of about  $7\pi a_0^2$  but the discrepancy may not be serious for at these energies the calculations are in error because of the neglect of inelastic collisions.

The present results and also some earlier work on particular cases (Holtsmark 1930, Bates and Massey 1947, Hammerling, Shine and Kivel 1957) show that it is important to allow for both short and long range polarization effects in the calculation of low energy phase shifts and the development of a practical and less arbitrary method of allowing for polarization is very desirable. Progress in this direction has been made recently by Temkin (1957).

Accurate comparison data are required and further calculations are being carried out using an expansion of the wave function which includes the 2s and 2p states; the resulting integro-differential equations (cf. Percival and Seaton 1957) will be solved numerically. Further experimental work is also necessary†.

† *Note added in proof.*—Brackmann, Fite and Neynaber (1958) have recently obtained experimental results for  $Q$  that are in agreement with the theoretical calculations (illustrated in figure 4). We should like to thank Dr. W. L. Fite for communicating these results to us before publication.

If required, the phase shifts presented here can be used to obtain the differential scattering cross section, the momentum loss cross section and the cross section for the spin change process (cf. Purcell and Field 1956)

$$H(1s, F) + e \rightarrow H(1s, F') + e \quad \dots\dots (65)$$

where  $F$  is the resultant of the nuclear and electron spins.

#### ACKNOWLEDGMENTS

We are indebted to Dr. S. Borowitz for a discussion of the problem of electron scattering by hydrogen. We are also indebted to Mrs. J. B. G. Wallace of University College London for computational assistance. One of us (T. L. J.) acknowledges the receipt of a research grant from the Department of Scientific and Industrial Research. This work was supported partially by the Atomic Energy Research Establishment (Harwell), to whom we are indebted for permission to publish.

#### REFERENCES

- ALTSHULER, S., 1953, *Phys. Rev.*, **89**, 1278.  
 BATES, D. R., and MASSEY, H. S. W., 1947, *Proc. Roy. Soc. A*, **192**, 1.  
 BEDERSON, B., MALAMUD, H., and HAMMER, J., 1957, *Bull. Amer. Phys. Soc.*, **2**, 172.  
 BOROWITZ, S., and GREENBERG, H., 1957, *Bull. Amer. Phys. Soc.*, **2**, 172.  
 BRACKMANN, R. T., FITE, W. L., and NEYNABER, R. H., 1958, *Phys. Rev.*, in the press.  
 BRANSDEN, B. H., and DALGARNO, A., 1956, *Proc. Phys. Soc. A*, **69**, 65.  
 CHANDRASEKHAR, S., 1944, *Astrophys. J.*, **100**, 176.  
 CHANDRASEKHAR, S., and BREEN, F. H., 1946, *Astrophys. J.*, **103**, 41.  
 DALGARNO, A., and LEWIS, J. T., 1955, *Proc. Roy. Soc. A*, **233**, 70; 1956, *Proc. Phys. Soc. A*, **69**, 57.  
 DALGARNO, A., and LYNN, N., 1957, *Proc. Phys. Soc. A*, **70**, 223.  
 DALGARNO, A., and STEWART, A. L., 1956, *Proc. Roy. Soc. A*, **238**, 276.  
 DOUGLAS, A. S., 1956, *Proc. Camb. Phil. Soc.*, **52**, 687.  
 HAMMERLING, P., SHINE, W. W., and KIVEL, B., 1957, *J. Appl. Phys.*, **28**, 760.  
 HARTREE, D. R., 1957, *The Calculation of Atomic Structures* (London : Chapman and Hall).  
 HOLTSMARK, J., 1930, *Z. Phys.*, **66**, 49.  
 HUANG, S. S., 1949, *Phys. Rev.*, **76**, 477, 1878.  
 HULTHÉN, L., 1944, *K. Fysiogr. Sällsk. Lund. Förh.*, **14**, No. 21 ; 1948, *Ark. Mat. Astr. Fys.*, **35a**, 25.  
 HULTHÉN, L., and OLSSON, P. O., 1950, *Phys. Rev.*, **79**, 532.  
 KATO, T., 1950, *Phys. Rev.*, **80**, 475.  
 KOHN, W., 1948, *Phys. Rev.*, **74**, 1763.  
 KUITHOFF, H., and ORNSTEIN, L. O., 1935, *Physica*, **2**, 611.  
 MACDOUGALL, J., 1932, *Proc. Roy. Soc. A*, **136**, 549.  
 MAECKER, H., PETERS, TH., and SCHENCK, H., 1955, *Z. Phys.*, **140**, 119.  
 MASSEY, H. S. W., 1957, *Handbook der Physik*, Vol. 36 (Berlin : Springer).  
 MASSEY, H. S. W., and MOISEWITSCH, B. L., 1951, *Proc. Roy. Soc. A*, **205**, 483.  
 MORSE, P. M., and ALLIS, W. P., 1933, *Phys. Rev.*, **44**, 269.  
 MOTT, N. F., and MASSEY, H. S. W., 1949, *The Theory of Atomic Collisions* (Oxford : Clarendon Press), 2nd edn.  
 NEWSTEIN, M. C., 1955, *Technical Report No. 4*. Project for machine methods of computation and numerical analysis. M.I.T.  
 OCHKIV, V. I., and PETROV, I. V., 1957, *Soviet Physics, JETP*, **4**, 144.  
 PERCIVAL, I. C., and SEATON, M. J., 1957, *Proc. Camb. Phil. Soc.*, **53**, 654.  
 PURCELL, E. M., and FIELD, G. B., 1956, *Astrophys. J.*, **124**, 542.  
 SEATON, M. J., 1953, *Phil. Trans. Roy. Soc. A*, **245**, 469; 1957, *Proc. Roy. Soc. A*, **241**, 522.  
 SMITH, S. J., and BRANSCOMB, L. M., 1955, *J. Res. Nat. Bur. Stand.*, **55**, 165.  
 STAVER, T. B., 1951, *Arch. Math. Naturv. B*, **51**, 29.  
 TEMKIN, A., 1957, *Phys. Rev.*, **107**, 1004.



# Inelastic Scattering of High Energy Nucleons by Complex Nuclei I: Semi-Classical Formalism

BY G. P. McCAULEY AND G. E. BROWN

Department of Mathematical Physics, University of Birmingham

*Communicated by R. E. Peierls; MS. received 7th January 1958*

**Abstract.** A formalism is developed for treating scattering processes in the several hundred mev range in which the target nucleus is left in its ground state or in a low excited state. These processes will be described in terms of collisions between the incident particle and single nucleons of the nucleus, using approximations of a semi-classical nature. The inelastic processes can be regarded as single particle excitations, the effects of scattering by other nucleons being included in a distorting potential. The target nucleons are assumed stationary during the passage of the incident particle; it is demonstrated that this is a reasonable approximation.

## §1. INTRODUCTION

INELASTIC scattering of nucleons by complex nuclei at high energies is of interest, both because of the mechanism involved, and because some of the scattering to low excited levels is generally included in the elastic scattering experiments, and often must be corrected for before interpreting these. Very good energy resolution is needed to exclude the inelastic scattering experimentally at several hundred mev, since the energy loss is so small. It is therefore useful to develop a theory by which the inelastic scattering can be evaluated. We shall do this here using a semi-classical formalism, and allowing spin-dependent forces, since these are known to be important from the large polarizations observed in high energy scattering.

A particular example, which will be discussed in detail in part II, is the excitation of carbon to its first excited state. The excitation energy of 4.4 mev is sufficiently great for this process to be isolated experimentally in some high energy experiments (Tyrén and Maris 1957, Dickson and Salter 1957). We shall compare our method with others that have been applied to this particular excitation.

In §2 we outline a semi-classical approximation for the scattering of high energy particles by a potential that is smoothly varying, taking first the case of spinless particles and then extending the results to deal with spin-dependent cases. In §3 we show how short range forces may be characterized without the explicit use of a potential well, and consider the possible spin-dependent forms required for the most general nucleon-nucleon interaction. In §4 we give the formulae for multiple scattering of the incident nucleon inside the nucleus, and show that the elastic case is equivalent to an optical model with both a central and spin-orbit potential. In §5 we consider the excitation of single particle states corresponding to low excited states of the complex nucleus and show how the inelastic cross sections and polarizations can be calculated using a distorting potential to allow for the multiple scattering from the other (unexcited) nucleons.

## § 2. SEMI-CLASSICAL APPROXIMATION FOR POTENTIAL WELLS

In this section we review the basic formulae of the semi-classical approximation which are needed in later sections (Molière 1947, Shapiro 1955, Schiff 1956). We are concerned with energies which extend into the relativistic region, but not with specifically relativistic fermion effects (such as the creation of anti-particles). It is therefore convenient to start with a Klein-Gordon equation for spinless particles and to introduce the Pauli spin operators at a later stage. For a particle of mass  $M$  and total energy  $E$ , moving in a potential  $V(r)$  we have (setting  $\hbar = c = 1$ )

$$\left. \begin{aligned} \text{where} \quad & \left. \begin{aligned} \{\nabla^2 + k^2(\mathbf{r})\}\psi(\mathbf{r}) &= 0 \\ k^2(\mathbf{r}) &= \{E - V(\mathbf{r})\}^2 - M^2. \end{aligned} \right\} \end{aligned} \right\} \dots\dots (2.1)$$

Putting  $k^2 = E^2 - M^2$  we have

$$\left. \begin{aligned} \text{where} \quad & \left. \begin{aligned} k(\mathbf{r}) &= k + \delta k(\mathbf{r}) \\ \delta k(\mathbf{r}) &\simeq -\frac{E}{k} V(\mathbf{r}). \end{aligned} \right\} \end{aligned} \right\} \dots\dots (2.2)$$

Substituting  $\psi(\mathbf{r}) = e^{iS(\mathbf{r})} e^{i\mathbf{k} \cdot \mathbf{r}}$  in equation (2.1) with  $|\mathbf{k}| = k$  and taking the  $z$  axis along  $\mathbf{k}$ , we find

$$2k\delta k(\mathbf{r}) - 2k \frac{\partial S(\mathbf{r})}{\partial z} - (\nabla S)^2 + i\nabla^2 S = 0. \dots\dots (2.3)$$

An approximate solution to this equation is obtained by dropping the last two terms and using equation (2.2). Thus

$$S(\mathbf{r}) \equiv S(\mathbf{b}, z) \simeq \int_{-\infty}^z \delta k(\mathbf{b}, z') dz' \simeq -\frac{E}{k} \int_{-\infty}^z V(\mathbf{b}, z') dz'. \dots\dots (2.4)$$

The physical significance of this approximation is most clearly seen in a semi-classical picture. We have neglected the deflection of the incident particle by the potential well, but have allowed it to be speeded up so that the phase of the wave function on a plane  $z = \text{constant}$  varies with the position  $\mathbf{b}$  in the plane. This should give a good account of the situation on a plane  $z = z_0$  just beyond a potential, which is not so strong compared with  $k$ , or so discontinuous, as to give a large amount of large angle scattering.

Once clear of the scattering centre this distorted wave propagates as in free space, so that the distortion changes. Equation (2.4) does not allow for this, and is therefore a poor approximation in the region  $z > z_0$ . However, in this region we can use the Green's solution determined by the boundary conditions on  $z = z_0$  implied by equation (2.4). The resulting solution for large  $r$ , and  $z > z_0$ , is

$$\left. \begin{aligned} \psi(\mathbf{r}) &= e^{i\mathbf{k} \cdot \mathbf{r}} + \frac{1}{r} e^{ikrf(\theta)} \\ f(\theta) &= \frac{k}{4\pi i} (1 + \cos \theta) \int \exp(ikb \sin \theta \cos \phi) \\ &\quad \times \left\{ \exp\left(-i \frac{E}{k} \int_{-\infty}^{\infty} V(z, b, \phi) dz\right) - 1 \right\} b db d\phi \end{aligned} \right\} \dots\dots (2.5)$$

where  $(r, \theta, \phi)$  and  $(z, b, \phi)$  are the usual spherical and cylindrical polar coordinates.

The validity of equation (2.5) depends essentially on  $V$  being smooth, and small compared with  $k$ , and on  $\theta$  being small. A thorough discussion of the validity of formulae such as (2.5) has been given by Schiff (1956) and Shapiro (1955).

The extension of the formula (2.5) to spin-dependent cases is obtained by reinterpreting  $\psi$ ,  $f$  and  $V$  as operators in spin space. The derivation of equations (2.3) and (2.4) makes it clear that the exponential in the braces in equation (2.5) must be taken as an ordered product of infinitesimal operators  $1 - i(E/k)V dz$  when these do not commute for different values of  $z$ . In the particular case of spin-orbit forces we have to make the approximation  $\sigma \cdot \mathbf{l} \psi(\mathbf{r}) \simeq kb \sigma \cdot \mathbf{m} \psi$  where  $\mathbf{m} = (\mathbf{k} \times \mathbf{b})/|\mathbf{k} \times \mathbf{b}|$ , i.e. we assume  $\sigma \cdot \mathbf{l}$  to commute with  $S$  and operate only on  $\exp(i\mathbf{k} \cdot \mathbf{r})$ . We thus neglect derivatives of  $S$  here, as in going from equation (2.3) to equation (2.4).

### § 3. CHARACTERIZATION OF GENERAL SPIN DEPENDENT MATRIX

It is clear that within the scope of the semi-classical approach we can characterize the scattering from a smoothly varying potential by the function

$$\Gamma(\mathbf{b}) = \mathcal{P}_{(z)} \exp \left( -i \frac{E}{k} \int_{-\infty}^{\infty} V(\mathbf{b}, z) dz \right) - 1 \quad \dots\dots (3.1)$$

appearing in equation (2.5). (Here  $\mathcal{P}_{(z)}$  symbolizes the ordering required when  $V$  does not commute with itself, for different  $z$ .) In general it will be more direct to work with  $\Gamma(\mathbf{b})$  rather than explicit potentials, and obtain the scattered amplitude as

$$f(\theta) = \frac{k}{4\pi i} (1 + \cos \theta) \int \exp(ikb \sin \theta \cos \phi) \Gamma(b, \phi) b db d\phi. \quad \dots\dots (3.2)$$

As with  $V(\mathbf{r})$ ,  $\Gamma(\mathbf{b})$  will be an operator in spin space whose general form will be restricted by the number of invariants we can construct from the spin operators and other available physical quantities.

For the remainder of this section we consider the particular case of elastic nucleon-nucleon scattering. From the two spin operators  $\sigma_0$  and  $\sigma_1$  for incident and target nucleons and the three unit vectors  $\hat{\mathbf{k}}$ ,  $\hat{\mathbf{b}}$  (polar) and  $\mathbf{m}$  (axial) we can construct five independent invariants:

$$\left. \begin{aligned} &1, \quad (\sigma_0 + \sigma_1) \cdot \mathbf{m}, \\ &(\sigma_0 \cdot \hat{\mathbf{k}})(\sigma_1 \cdot \hat{\mathbf{k}}), \quad (\sigma_0 \cdot \mathbf{m})(\sigma_1 \cdot \mathbf{m}), \quad (\sigma_0 \cdot \hat{\mathbf{b}})(\sigma_1 \cdot \hat{\mathbf{b}}). \end{aligned} \right\} \dots\dots (3.3)$$

Other possible forms can be written as linear combinations of these, or will lead to a scattering matrix violating the usual invariance laws (in which we include charge independence). Apart from the directional dependence implicit in the forms (3.3),  $\Gamma(\mathbf{b})$  depends only on the magnitude of  $b$ , so we can write its general form as

$$\begin{aligned} \Gamma(\mathbf{b}) \equiv & \Gamma_{\alpha}(b) + (\sigma_0 + \sigma_1) \cdot \mathbf{m} \Gamma_{\beta}(b) + (\sigma_0 \cdot \hat{\mathbf{k}})(\sigma_1 \cdot \hat{\mathbf{k}}) \Gamma_{\delta}(b) \\ & + (\sigma_0 \cdot \mathbf{m})(\sigma_1 \cdot \mathbf{m}) \Gamma_{\epsilon}(b) + (\sigma_0 \cdot \hat{\mathbf{b}})(\sigma_1 \cdot \hat{\mathbf{b}}) \Gamma_{\eta}(b). \end{aligned} \quad \dots\dots (3.4)$$

With this form of  $\Gamma$ , equation (3.2) gives a completely general form for  $f(\theta)$ , unrestricted by our semi-classical approximations, since this  $\Gamma$ , which is essentially the wave function on the plane, includes all terms satisfying the necessary invariance laws. We will find it convenient, however, to use the

semi-classical treatment to connect the  $\Gamma$ 's with the nucleon-nucleon potential. We will work with two different functions  $\Gamma^{(+)}$  and  $\Gamma^{(-)}$ , defined to give the correct scattering for protons on protons or neutrons respectively when substituted in equation (3.2), rather than dealing explicitly with anti-symmetrized spin-isotopic spin equations.

As a particular case of equation (3.2) we note the connection between the expression (3.4) for  $\Gamma(\mathbf{b})$  and the general form of the nucleon-nucleon scattering amplitude (cf. Wolfenstein and Ashkin 1952).

$$f(\theta) \equiv \alpha(\theta) + (\boldsymbol{\sigma}_0 + \boldsymbol{\sigma}_1) \cdot \mathbf{n} \beta(\theta) + (\boldsymbol{\sigma}_0 \cdot \hat{\mathbf{k}})(\boldsymbol{\sigma}_1 \cdot \hat{\mathbf{k}}) \delta(\theta) \\ + (\boldsymbol{\sigma}_0 \cdot \mathbf{n})(\boldsymbol{\sigma}_1 \cdot \mathbf{n}) \epsilon(\theta) + (\boldsymbol{\sigma}_0 \cdot \mathbf{c})(\boldsymbol{\sigma}_1 \cdot \mathbf{c}) \eta(\theta) \quad \dots\dots (3.5)$$

where  $\mathbf{n} = \mathbf{k} \times \mathbf{k}' / |\mathbf{k} \times \mathbf{k}'|$ ,  $\mathbf{c} = (\mathbf{k}' - \mathbf{k}) / |\mathbf{k}' - \mathbf{k}|$ . This can be obtained by taking cartesian coordinates  $x, y, z$  along  $\mathbf{c}, \mathbf{n}, \mathbf{k}$  so that the usual orientation of polar coordinates gives

$$\hat{\mathbf{b}} = \mathbf{c} \cos \phi + \mathbf{n} \sin \phi, \quad \mathbf{m} = \hat{\mathbf{n}} \cos \phi - \mathbf{c} \sin \phi. \quad \dots\dots (3.6)$$

Direct substitution and integration over  $\phi$  give the relations

$$\left. \begin{aligned} \alpha(\theta) &= \frac{k}{2i} (1 + \cos \theta) \int_0^\infty J_0(kb \sin \theta) \Gamma_\alpha(b) b db \\ \beta(\theta) &= -\frac{k}{2} (1 + \cos \theta) \int_0^\infty J_1(kb \sin \theta) \Gamma_\beta(b) b db \\ \delta(\theta) &= \frac{k}{2i} (1 + \cos \theta) \int_0^\infty J_0(kb \sin \theta) \Gamma_\delta(b) b db \\ \epsilon(\theta) &= \frac{k}{2i} (1 + \cos \theta) \int_0^\infty [J_0 \cdot \frac{1}{2} (\Gamma_\epsilon + \Gamma_\eta) + J_2 \cdot \frac{1}{2} (\Gamma_\eta - \Gamma_\epsilon)] b db \\ \eta(\theta) &= \frac{k}{2i} (1 + \cos \theta) \int_0^\infty [J_0 \cdot \frac{1}{2} (\Gamma_\epsilon + \Gamma_\eta) + J_2 \cdot \frac{1}{2} (\Gamma_\epsilon - \Gamma_\eta)] b db \end{aligned} \right\} \dots\dots (3.7)$$

The results of §§ 4 and 5 will be found to involve integrals such as  $\int \Gamma_\alpha(b) b db$  from 0 to  $\infty$  which can be evaluated using the relations (3.7). In particular we note

$$\left. \begin{aligned} \int_0^\infty \Gamma_\alpha(b) b db &= \frac{i}{k} \alpha(0) \\ \int_0^\infty \Gamma_\beta(b) b^2 db &= -\frac{2}{k^2} \beta'(0) \\ \int_0^\infty \Gamma_\alpha(b) b^3 db &= \frac{4i}{k^3} \alpha''(0) \end{aligned} \right\} \dots\dots (3.8)$$

the primes denoting differentiation with respect to  $\theta$ .

#### § 4. MULTIPLE SCATTERING AND THE OPTICAL POTENTIAL

For high energy particles, collisions with the nucleons of the nucleus can be treated adiabatically, and the actual scattered amplitude obtained from the amplitude scattered by  $A$  scattering centres by taking a suitable average over the positions of these centres. This type of treatment has been extensively used for elastic scattering. We show in the Appendix that it can also be applied to the inelastic scattering which leaves the nucleus in a particular excited state.

The scattering from a complex system of  $A$  scattering centres at points  $\boldsymbol{\xi}_i$  can be characterized by a function  $G(\mathbf{b}; \boldsymbol{\xi})$  in the same way as the scattering



from a single centre. For scalar potentials  $V_i(\mathbf{r} - \boldsymbol{\xi}_i)$  equation (3.1) gives the relation

$$G(\mathbf{b}; \boldsymbol{\xi}) = \prod_{i=1}^A \{1 + \Gamma_i(\mathbf{b} - \mathbf{b}_i)\} - 1 \quad \dots\dots (4.1)$$

where  $\boldsymbol{\xi}$  stands for the set of all  $\boldsymbol{\xi}_i$ , and  $\boldsymbol{\xi}_i \equiv (\mathbf{b}_i, \zeta_i)$  and  $\Gamma_i(\mathbf{b} - \mathbf{b}_i)$  is obtained by putting  $V_i(\mathbf{r} - \boldsymbol{\xi}_i)$  in equation (3.1). For spin-dependent terms the ordering  $\mathcal{P}_{(z)}$  may be important and can be included by ordering the factors in equation (4.1) according to the  $\zeta_i$ , if there is no overlap between different scattering centres. In this case, when the incident particle does not interact simultaneously with two centres, the ordered form of equation (4.1) is valid even if no simple potential  $V_i$  is known. The functions  $1 + G$  and  $1 + \Gamma$  are essentially semi-classical approximations to  $T$ -matrices.

In the Appendix we employ an impulse approximation in which the interaction between a single particle of the nucleus and the remainder of the nucleus is neglected during that particle's interaction with the incident particle. The  $\Gamma_i$  of equation (4.1) can then be identified with the corresponding function for free nucleon-nucleon collisions; we work in the laboratory system of coordinates.

Since we will deal only with low excited states of the nucleus, we neglect the difference in magnitude of the initial and final momenta of the scattered particle. We find in the Appendix that both elastic and inelastic scattering can be obtained from equation (3.2) by replacing  $\Gamma(b, \phi)$  there by  $G(\mathbf{b})$  where

$$G(\mathbf{b}) = \int \Phi_f^*(\boldsymbol{\xi}) G(\mathbf{b}; \boldsymbol{\xi}) \Phi_0(\boldsymbol{\xi}) d\boldsymbol{\xi} \quad \dots\dots (4.2)$$

where  $\Phi_0(\boldsymbol{\xi})$  and  $\Phi_f(\boldsymbol{\xi})$  are the initial and final nuclear states.

We now evaluate equation (4.2) in the case of elastic scattering from an even-even (spin zero) nucleus, for which all terms in  $\Gamma_i$  involving  $\boldsymbol{\sigma}_i$  will cancel (cf. Bethe 1958). For a product wave function

$$\Phi_0(\boldsymbol{\xi}) = \prod_{i=1}^A \phi_i(\boldsymbol{\xi}_i)$$

each term in the product in equation (4.1) is averaged independently, and for large  $A$  the resulting product can be replaced by an exponential to give

$$G(\mathbf{b}) = \exp \left\{ \sum_{i=1}^A \int \phi_i^*(\boldsymbol{\xi}_i) \Gamma_i(\mathbf{b} - \mathbf{b}_i) \phi_i(\boldsymbol{\xi}_i) d\boldsymbol{\xi}_i \right\} - 1 \quad \dots\dots (4.3)$$

$$= \exp \left( A \int \bar{\Gamma}(\mathbf{b} - \mathbf{b}') \rho(r') dr' \right) - 1$$

Here  $\rho(\mathbf{r})$  is the nuclear density (normalized to 1), and  $\bar{\Gamma}$  is the mean of  $\Gamma^{(+)}$  and  $\Gamma^{(-)}$  with all terms in  $\boldsymbol{\sigma}_i$  omitted. Comparison of equations (4.3) and (2.5) shows that integration over  $\mathbf{b}'$  gives a description of the scattering equivalent to the use of a potential well. Corrections arising from the anti-symmetrization of the nuclear wave function seem to be small (Glauber 1956); they will be given explicitly for carbon in part II.

To obtain a specific form for the equivalent potential indicated by equation (4.3) we write

$$\left. \begin{aligned} \bar{\Gamma}(\mathbf{b} - \mathbf{b}') &= \bar{\Gamma}_\alpha(b'') + \boldsymbol{\sigma}_0 \cdot \mathbf{m}' \bar{\Gamma}_\beta(b'') \\ \mathbf{b}'' &= \mathbf{b} - \mathbf{b}', \quad \mathbf{m}' = \mathbf{k} \times \mathbf{b}'' / |\mathbf{k} \times \mathbf{b}''| \\ \text{and write also} \quad R(b') &= \int_{-\infty}^{\infty} \rho(b', z') dz' \end{aligned} \right\} \quad \dots\dots (4.4)$$

noting the symmetry of the product  $R(b')\bar{\Gamma}_\beta(b'')$  as a function of  $\mathbf{b}'$  about the line through the origin in the direction  $\mathbf{b}$ . Because of this symmetry, the integration over  $\mathbf{b}'$  will result in a scalar term and a term in  $\sigma_0 \cdot \mathbf{m}$  only, which are just the terms occurring in the exponent for a potential  $V_c(r) + \sigma_0 \cdot \mathbf{l} V_{so}(r)$ . The exponential can be linearized in  $\sigma_0 \cdot \mathbf{m}$ , since  $(\sigma_0 \cdot \mathbf{m})^2 = 1$ , to give

$$G(b) = A(b) + \sigma_0 \cdot \mathbf{m} B(b) - 1 \quad \dots\dots (4.5)$$

which will be used in § 5.

The equivalent potential can be related to the nucleon-nucleon scattering amplitudes by using an expansion in powers of the range of the nuclear forces (see Brown 1957), which is also useful for the inelastic case. This is obtained by expanding  $R(b')$  in a Taylor series about the point  $b$ ; thus

$$\left. \begin{aligned} \int \bar{\Gamma}(\mathbf{b} - \mathbf{b}') R(b') d\mathbf{b}' &= \int \{ \bar{\Gamma}_\alpha(b'') + \sigma_0 \cdot \mathbf{m}' \bar{\Gamma}_\beta(b'') \} d\mathbf{b}'' \cdot R(b) \\ &\quad - \int \{ \bar{\Gamma}_\alpha(b'') + \sigma_0 \cdot \mathbf{m}' \bar{\Gamma}_\beta(b'') \} \mathbf{b}_\lambda'' d\mathbf{b}'' \cdot \nabla_\lambda R(b) \\ &\quad + \frac{1}{2} \int \{ \bar{\Gamma}_\alpha(b'') + \sigma_0 \cdot \mathbf{m}' \bar{\Gamma}_\beta(b'') \} \mathbf{b}_\lambda'' \mathbf{b}_\mu'' d\mathbf{b}'' \cdot \nabla_\lambda \nabla_\mu R(b) \\ &\quad - \text{etc.} \dots \end{aligned} \right\} \quad \dots\dots (4.6)$$

The angular integrations can now be carried out using the relations

$$\left. \begin{aligned} \int \mathbf{b} F(b) d\mathbf{b} &= 0, \quad \int \mathbf{b}_\lambda \mathbf{b}_\mu F(b) d\mathbf{b} = \pi \delta_{\lambda\mu} \int_0^\infty F(b) b^3 db \\ \int \mathbf{b}_\lambda \mathbf{b}_\mu \mathbf{b}_\nu F(b) d\mathbf{b} &= 0, \quad \text{etc.} \end{aligned} \right\} \quad \dots\dots (4.7)$$

to get

$$\begin{aligned} \int \bar{\Gamma}(\mathbf{b} - \mathbf{b}') R(b') d\mathbf{b}' &= 2\pi \int_0^\infty \bar{\Gamma}_\alpha(b'') b'' db'' \cdot R(b) \\ &\quad - \pi \int_0^\infty \bar{\Gamma}_\beta(b'') b''^2 db'' \cdot \sigma_0 \cdot \mathbf{k} \times \nabla R(b) + \text{etc.} \dots \dots\dots (4.8) \end{aligned}$$

Now

$$\sigma_0 \cdot \mathbf{k} \times \nabla R(b) = \sigma_0 \cdot \mathbf{m} \frac{d}{db} R(b) = \sigma_0 \cdot \mathbf{m} \int_{-\infty}^\infty \frac{b}{r} \frac{d}{dr} \rho(r) dz$$

so that rewriting the first two terms of the exponent using equation (3.7) and comparing the result with equation (2.5) we obtain the equivalent potential  $V$  in the form

$$\left. \begin{aligned} V(\mathbf{r}) &= V_c(r) + \sigma_0 \cdot \mathbf{l} V_{so}(r) \\ \text{where} \quad V_c(r) &= -\frac{2\pi A}{E} \rho(r) \bar{\alpha}(0), \quad V_{so} = i \frac{2\pi A}{k^2 E} \frac{1}{r} \frac{d\rho}{dr} \bar{\beta}'(0). \end{aligned} \right\} \quad \dots\dots (4.9)$$

This conforms with the usual optical model choice of  $V_{so} \sim r^{-1} dV_c/dr$ . Results equivalent to these were derived by Risenfeld and Watson (1956) and Brown (1957) and used by Bethe (1958). We will now apply these methods to the inelastic scattering.

# § 5. SINGLE PARTICLE EXCITATIONS AND INELASTIC SCATTERING

We treat the inelastic case where each configuration in the excited state differs from the ground state configuration (assumed pure) in only one of its single particle components. For a spin zero ground state and spin  $J$  excited state there will be  $2J + 1$  possible transitions which combine incoherently when no observation of the orientation of the excited nucleus is made. We consider here the scattering matrix, or rather the corresponding function  $G(\mathbf{b})$ , for the excitation of a particular configuration.

Let us write the ground state configuration as a product of single-particle states  $|1\rangle, |2\rangle, \dots |A\rangle$  and the excited configuration as the (anti-symmetrized) product of these with  $|1\rangle$  replaced by  $|1'\rangle$ . Then each of the products in equation (4.1) which contribute to  $G(\mathbf{b})$  must contain a  $\Gamma_1$ , so we can write

$$G(\mathbf{b}; \xi) = \left\{ 1 + \sum_{\substack{i \neq 1 \\ \zeta_i > \zeta_1}} \Gamma_i(\mathbf{b} - \mathbf{b}_i) + \dots \right\} \Gamma_1(\mathbf{b} - \mathbf{b}_1) \left\{ 1 + \sum_{\substack{j \neq 1 \\ \zeta_1 < \zeta_j}} \Gamma_j(\mathbf{b} - \mathbf{b}_j) + \dots \right\} \dots \dots (5.1)$$

where there is a restriction (implicit in the inequalities on  $\zeta$ 's) that no particle of the nucleus can contribute to both braces. Thus the two expressions in the braces are not independent, but the approximation in which they are evaluated as such involves an error of relative order  $1/A$  in the triple scattering term. The leading single and double scattering terms are treated exactly, so this approximation should be quite good, and is consistent with those already made. In treating the events in the braces as elastic scattering events we ignore the possibility of a double scattering ( $2 \rightarrow 1', 1 \rightarrow 2$ ) in which one particle is excited, and then another is knocked into the newly vacant state. This process is essentially a two-particle excitation, and is assumed to be small compared with the direct single particle excitation.

The expressions in the braces still depend on  $\zeta_1$ , being equivalent to the distortions of the incident and scattered waves by the elastic scatterings which occur before and after the inelastic event. Thus, carrying out the integrations over  $\xi_i, i \neq 1$ , for the matrix element between the nuclear configurations we have

$$G(\mathbf{b}) = \langle 1' | \{ A^{(+)}(b, \zeta_1) + \sigma_0 \cdot \mathbf{m} B^{(+)}(b, \zeta_1) \} \Gamma_1(\mathbf{b} - \mathbf{b}_1) \times \{ A^{(-)}(b, \zeta_1) + \sigma_0 \cdot \mathbf{m} B^{(-)}(b, \zeta_1) \} | 1 \rangle \dots \dots (5.2)$$

where

$$\begin{aligned} A^{(+)}(b, \zeta_1) + \sigma_0 \cdot \mathbf{m} B^{(+)}(b, \zeta_1) &= \exp \left( -i \frac{E}{R} \int_{\zeta_1}^{\infty} V(\mathbf{b}, z) dz \right) \left\{ \dots \dots (5.3) \right. \\ &= A^{(-)}(b, -\zeta_1) + \sigma_0 \cdot \mathbf{m} B^{(-)}(b, -\zeta_1) \left. \right\} \end{aligned}$$

If we now integrate over  $\mathbf{b}_1$  we can write

$$\begin{aligned} G(\mathbf{b}) &= \int_{-\infty}^{\infty} \left\{ A^{(+)}(b, \zeta_1) + \sigma_0 \cdot \mathbf{m} B^{(+)}(b, \zeta_1) \right\} \left\{ A_1(b, \zeta_1) + \sigma_0 \cdot \mathbf{m} B_1(b, \zeta_1) \right. \\ &\quad \left. + \sigma_0 \cdot \hat{\mathbf{b}} C_1(b, \zeta_1) + \sigma_0 \cdot \hat{\mathbf{k}} D_1(b, \zeta_1) \right\} \left\{ A^{(-)}(b, \zeta_1) + \sigma_0 \cdot \mathbf{m} B^{(-)}(b, \zeta_1) \right\} d\zeta_1 \\ &= \left\{ A(b) + \sigma_0 \cdot \mathbf{m} B(b) \right\} \int_{-\infty}^{\infty} \left\{ A_1 + \sigma_0 \cdot \mathbf{m} B_1 \right\} d\zeta_1 \\ &\quad + \int_{-\infty}^{\infty} \left\{ A^{(+)} A^{(-)} - B^{(+)} B^{(-)} \right\} \left\{ \sigma_0 \cdot \hat{\mathbf{b}} C_1 + \sigma_0 \cdot \hat{\mathbf{k}} D_1 \right\} d\zeta_1 \\ &\quad + \int_{-\infty}^{\infty} \left\{ B^{(+)} A^{(-)} - A^{(+)} B^{(-)} \right\} \left\{ i \sigma_0 \cdot \hat{\mathbf{k}} C_1 - i \sigma_0 \cdot \hat{\mathbf{b}} D_1 \right\} d\zeta_1 \dots \dots (5.4) \end{aligned}$$

where the relations (5.3) and the fact that contributions to  $A_1$ ,  $B_1$  etc. are odd or even functions of  $\zeta_1$  as they come from odd or even  $\Delta m_1$  for the first particle imply the selection rule  $\Delta L_z$  odd for the first two terms of equation (5.4),  $\Delta L_z$  even for the third.

To evaluate (5.4) in any particular case, we use optical model results for the first term, and deal with the second term (matrix element of  $\Gamma_1$ ) by the expansion used in equations (4.6), (4.7) and (4.8). This can be done by expanding states in  $(\mathbf{l}, \mathbf{s})$  coupling so that the operators  $\sigma_i$  can be evaluated at once, leaving a sum of several terms of the form  $g(b, \zeta_1)e^{-i\mu\phi}$  in place of  $R(b)$  in (4.6). Here  $\phi$  is the angle in the plane of  $\mathbf{b}$ , and  $\mu$  will be  $M$  or  $M \pm 1$  ( $M = m_1, -m_1$ ). This programme will be carried out in part II for the  $1p_{3/2} \rightarrow 1p_{1/2}$  excitations. The final result of these evaluations is to produce a scattering amplitude  $f_M(\theta)$  for each orientation of the excited state of the form

$$f_M(\theta) = A_M(\theta) + \sigma_0 \cdot \mathbf{c} C_M(\theta) + \sigma_0 \cdot \mathbf{n} N_M(\theta) + \sigma_0 \cdot \hat{\mathbf{k}} K_M(\theta). \quad \dots\dots (5.5)$$

The  $A$ ,  $C$ ,  $N$ ,  $K$  will be sums of terms of the type

$$\gamma \int_0^\infty J(kb \sin \theta) \int_{-\infty}^\infty D(b, \zeta_1) g(b, \zeta_1) d\zeta_1 b db \quad \dots\dots (5.6)$$

where  $\gamma$  will be one of the expressions (3.8),  $J$  is a spherical Bessel function arising from the angular integration of equation (2.5),  $D$  is one of the distortion factors of equation (5.4), and  $g(b, \zeta_1)$  the product of appropriate orbital functions.

From equation (5.2) we get inelastic cross sections and polarizations given by

$$I(\theta) = AA^* + CC^* + NN^* + KK^* \quad \dots\dots (5.7)$$

$$I(\theta) \cdot (\mathbf{P}(\theta) \cdot \mathbf{n}) = AN^* + NA^* + i(KC^* - CK^*) \quad \dots\dots (5.8)$$

and permutations for  $\mathbf{c}$  and  $\hat{\mathbf{k}}$  components. If no attempt is made to observe the orientation of the residual nucleus (say by  $\gamma$ -ray coincidence), equations (5.7) and (5.8) should be summed over all possible  $M$ . In this case the polarization must be entirely along  $\mathbf{n}$ , so that cancellations must take place in the two expressions analogous to equation (5.8) for  $\mathbf{c}$  and  $\hat{\mathbf{k}}$  components. This does not necessarily mean that the term  $KC^* - CK^*$  will also vanish, so that the polarization may be different from the asymmetry in scattering a 100% polarized beam, which is given by

$$I(\theta) \cdot a_{(\mathbf{n})} = AN^* + NA^* - i(KC^* - CK^*). \quad \dots\dots (5.9)$$

Because of the complexity of the expressions involved in equation (5.5) it is difficult to draw any general conclusions about the inelastic scattering. However, the effect of the distortion factors  $D(b, \zeta_1)$  in (5.6) will generally be to cut off the lower limit of  $b$ -integration (corresponding to a short mean free path in nuclear matter), while  $g(b, \zeta_1)$  will fall rapidly beyond the nuclear radius. The cross section would then be dominated by a diffraction pattern similar to low-energy stripping and pick-up reactions. Near the diffraction minimum large polarizations, and very rapid fluctuations in the polarization, should be possible. If this does not occur at the same angle as the similar effect in the elastic scattering, it might have the effect of reducing the polarization observed in an experiment which did not clearly distinguish the two cases.

The combined effect of the distortion and the rapid decrease of the nuclear wave function beyond the nuclear radius, means that most of the contributions to the integrand come from the region of the nuclear surface. Thus, picturing the excitation as one of the collective model type (see Maris and Tyrén 1957),



where the interaction is localized at the surface, would be expected to give results similar to those from the method given here for transitions in which the angular momentum of the nucleus changes by an even amount. However, the manner in which the excitation arises is quite different in the two cases, and we believe that it is more natural to consider the process as one of single particle excitation in a nucleus as light as carbon.

One advantage of this approach is that the parameters of the inelastic excitation can be obtained in principle from the elastic nucleon-nucleon scattering, although, of course, a knowledge of the wave functions of the bombarded nucleus is necessary in order to evaluate the various integrals.

The particular merit of this method is that it allows evaluation directly in three dimensions without going to a partial wave analysis, which would be very lengthy at these high energies. Although approximate, it incorporates the essential features of a spin-dependent distortion and a spin-dependent excitation, which would seem to be necessary if one wants to describe the differential cross section and polarization of the scattered particle.

In a following paper it will be indicated that this method is practical for calculation. There it will be applied to the excitation of  $^{12}\text{C}$  to the first excited state.

#### ACKNOWLEDGMENTS

We would like to thank Professor R. E. Peierls for useful discussion and criticism. Several of the ideas in this paper originated in discussion with Professor R. Glauber. While this work was in progress we learned of a similar calculation using a central distorting potential by Benoist *et al.* (1957).

#### REFERENCES

- BENOIST, P., MARTY, C., and MEYER, P., 1957, *C. R. Acad. Sci., Paris.*, **245**, 1389.  
 BETHE, H. A., 1958, *Annals of Physics*, **3**, 190.  
 BROWN, G. E., 1957, *Proc. Phys. Soc. A*, **70**, 361.  
 DICKSON, J. M., and SALTER, D. C., 1957, *Nuovo Cim.*, (10) **6**, 235.  
 GLAUBER, R., 1956, *Physica*, **22**, 1185.  
 LIPPMANN, B. A., and SCHWINGER, J., 1950, *Phys. Rev.*, **79**, 469.  
 MARIS, TH. A. J., and TYRÉN, H., 1957, *Nuclear Phys.*, **3**, 35.  
 MOLIÈRE, G., 1947, *Z. Naturf.*, **2a**, 133.  
 RIESENFELD, W. B., and WATSON, K. M., 1956, *Phys. Rev.*, **102**, 1157.  
 SCHIFF, L. I., 1956, *Phys. Rev.*, **103**, 443.  
 SHAPIRO, I. I., 1955, *Thesis*, Harvard University.  
 TYRÉN, H., and MARIS, TH. A. J., 1957, *Nuclear Phys.*, **3**, 52.  
 WOLFENSTEIN, L., and ASHKIN, J., 1952, *Phys. Rev.*, **85**, 947.

#### APPENDIX

We show here that the scattering of a high energy particle by the  $A$  nucleons can be reduced, to a good approximation, to the scattering by  $A$  fixed centres, with a subsequent averaging over the positions of these centres. We shall further point out several features of this method.

We shall employ the Schrödinger equation here in order to avoid inessential complications introduced by the fact that the Klein-Gordon equation is not linear in the Hamiltonian. The generalization of the picture will be clear. The

wave function will be given by

$$\left\{ -\frac{\hbar^2}{2M} \nabla_r^2 - \frac{\hbar^2}{2M} \sum_i \nabla_i^2 + \sum_i V(\mathbf{r} - \boldsymbol{\xi}_i) + \sum_{i \neq j} V(\boldsymbol{\xi}_i - \boldsymbol{\xi}_j) \right\} \Psi(\mathbf{r}; \boldsymbol{\xi}) = E \Psi(\mathbf{r}; \boldsymbol{\xi}). \quad \text{..... (A1)}$$

Here  $\nabla_r$  denotes differentiation with respect to the  $r$ -coordinate,  $\nabla_i$  with respect to the  $\xi_i$ -coordinate,  $V(\mathbf{r} - \boldsymbol{\xi}_i)$  the interaction between the scattered particle and the  $i$ th nucleon, and  $V(\boldsymbol{\xi}_i - \boldsymbol{\xi}_j)$  the interaction between the  $i$ th and  $j$ th nucleons. To facilitate our approximations, we replace  $\Psi$  by

$$\Psi(\mathbf{r}; \boldsymbol{\xi}) = \Phi_0(\boldsymbol{\xi}) \exp\{i\mathbf{k} \cdot \mathbf{r} + iS(\mathbf{r}; \boldsymbol{\xi})\}. \quad \text{..... (A2)}$$

Inserting this in equation (A1) we obtain

$$\begin{aligned} \frac{\hbar^2}{M} k \frac{\partial S}{\partial z} + \sum_i V(\mathbf{r} - \boldsymbol{\xi}_i) + \frac{\hbar^2}{2M} (\nabla_r S)^2 - i \frac{\hbar^2}{2M} \nabla_r^2 S + \frac{\hbar^2}{2M} \sum_i (\nabla_i S)^2 \\ - i \frac{\hbar^2}{2M} \sum_i \nabla_i^2 S - \frac{\hbar^2}{M} \frac{1}{\Phi_0(\boldsymbol{\xi})} \sum_i \nabla_i \Phi_0(\boldsymbol{\xi}) \cdot \nabla_i S = 0. \end{aligned} \quad \text{..... (A3)}$$

It is clear that for large values of  $k$  (and smoothly varying potentials) the first two terms will be the dominant ones. Considering only these, we obtain

$$S \simeq -\frac{M}{k\hbar^2} \int_{-\infty}^z \sum_i V(\mathbf{r} - \boldsymbol{\xi}_i) dz. \quad \text{..... (A4)}$$

We can now employ this  $S$  in equation (A3) to find the magnitude of the other terms. The terms involving  $(\nabla_i S)^2$  and  $\nabla_i^2 S$  are seen to be of the same type as  $(\nabla_r S)^2$  and  $\nabla_r^2 S$ , which are neglected in the semi-classical treatment of scattering by a potential well. The ratio of the final term to the first term is seen to be of the order of that of the momentum in the nucleus to  $k$ . For large  $k$  this can be neglected. We are, of course, simply making an adiabatic approximation in which the momenta in the nucleus are neglected compared with that of the scattered particle. Combining (A4) and (A2) we find that the wave function is given by

$$\Psi \simeq \Phi_0(\boldsymbol{\xi}) e^{(i\mathbf{k} \cdot \mathbf{r})} e \left( -i \frac{M}{k\hbar^2} \int_{-\infty}^z \sum_i V(\mathbf{r} - \boldsymbol{\xi}_i) dz \right). \quad \text{..... (A5)}$$

Now, it is well known (Lippmann and Schwinger 1950) that the amplitude for leaving the nucleus in state  $f$  with the scattered particle having final momentum  $k'$  is just

$$f(\theta) = \frac{k}{2\pi i} \int \Phi_f^*(\boldsymbol{\xi}) \exp(-i\mathbf{k}' \cdot \mathbf{r}) \sum_i V(\mathbf{r} - \boldsymbol{\xi}_i) \Psi(\mathbf{r}; \boldsymbol{\xi}) d\mathbf{r} d\boldsymbol{\xi}. \quad \text{..... (A6)}$$

Employing our approximate  $\Psi$ , using the fact that

$$(\mathbf{k}' - \mathbf{k}) \cdot \mathbf{r} \equiv \Delta \mathbf{k} \cdot \mathbf{r} \simeq \Delta \mathbf{k} \cdot \mathbf{b} = kb \sin \theta \cos \phi,$$

and integrating over  $z$ , we find

$$\begin{aligned} f(\theta) = \frac{k}{2\pi i} \int e^{-ikb \sin \theta \cos \phi} \Phi_f^*(\boldsymbol{\xi}) \left\{ \exp \left( -i \frac{M}{k\hbar^2} \int_{-\infty}^{\infty} \sum_i V(\mathbf{r} - \boldsymbol{\xi}_i) dz \right) - 1 \right\} \\ \times \Phi_0(\boldsymbol{\xi}) d\boldsymbol{\xi} \cdot b db d\phi. \end{aligned} \quad \text{..... (A7)}$$

We see that the result is just as if we had calculated the scattering from potential wells at fixed points  $\boldsymbol{\xi}_i$ , and then weighted this with  $\Phi_f^* \Phi_0$ . The quantity in braces is just the non-relativistic counterpart of the  $G_1(\mathbf{b}, \boldsymbol{\xi})$  in equation (4.1),  $\exp \left( -i \frac{M}{k\hbar^2} \int_{-\infty}^{\infty} V(\mathbf{r} - \boldsymbol{\xi}_i) dz \right)$  being equal to  $1 + \Gamma_i(\mathbf{b} - \mathbf{b}_i)$ . Results equivalent to these have been obtained by Glauber (private communication).

We note several interesting features of this semi-classical treatment. The  $T$ -operator can be simply obtained from (A6) as

$$T(\mathbf{r}; \boldsymbol{\xi}) = \sum_i V(\mathbf{r} - \boldsymbol{\xi}_i) \exp(-iM/k\hbar^2) \int_{-\infty}^z \sum_i V(\mathbf{r} - \boldsymbol{\xi}_i) dz \quad \dots\dots (A8)$$

and it is seen to be a local operator in this approximation. Further, it is a function only of the difference of the coordinates  $\mathbf{b}_i$ ,  $\mathbf{b}$  and not of them separately. Since the change in momentum is, in our approximation, only in the transverse plane, and the  $T$ -operator is a function of only the difference of coordinates in this plane, momentum conservation in the process occurs in the same way as in Born approximation.

The calculations in this paper have been carried out in the laboratory system, handling the struck particle as if it were stationary during the collision and, therefore, might appear that it is treated as if it had infinite mass. If this were so it would be unreasonable to treat inelastic scattering, where the struck particle must change state, in this way. That the procedure is, in fact, reasonable can be seen from considering the collision first in the centre-of-mass system and then transforming to the laboratory system. In the former system the target nucleon is treated as moving with momentum equal, approximately, to  $k/2$ . (We neglect its momentum in the laboratory system for the present purpose.) Now, in equation (A7) the quantity in braces is a function of only the relative velocity  $M/k\hbar$ , which has the same value in the centre-of-mass system,  $M$  being replaced by the reduced mass  $M/2$  and  $k$  by  $k/2$ . The transformation of  $f(\theta)$  from the centre-of-mass system to the laboratory system then consists in changing the  $k$  in front of the integral, which gives the usual ratio of 2 for the amplitudes in the two systems. It is thus clear that we have not, in fact, treated the target nucleon as if it had infinite mass in any essential way.

# The Inelastic Scattering of 9.8 Mev Protons by Medium Weight Nuclei

By G. W. GREENLEES, J. LOWE, A. B. ROBBINS† AND P. M. ROLPH

Physics Department, University of Birmingham

*Communicated by W. E. Burcham; MS. received 24th February 1958*

**Abstract.** Recent experiments by Cohen on the inelastic scattering of protons by nuclei of medium  $Z$  have shown some unexpected effects, in particular, a pronounced increase in cross section at excitations of 2–3 mev in all elements with  $Z$  between 40 and 52. A search for this ‘anomalous scattering’ has been made in Sn, In, Cd, Ag, Pd, Mo, Nb, Zn, Cu and Ni, using 9.8 mev protons. The prominent effect at excitations of 2–3 mev was not found at 9.8 mev. In Cu, Zn and Ni an intense group corresponding to excitations of 1–1.4 mev was observed, in agreement with Cohen’s results.

## § 1. INTRODUCTION

MANY experiments have been reported in which the inelastic scattering of protons by light nuclei has been investigated. The spectra of protons scattered from the target show discrete groups corresponding to various excited states of the final nucleus. For heavier nuclei, however, the level spacing at high excitations in the final nucleus is much smaller and one would not expect to be able to resolve proton groups corresponding to individual levels using conventional scintillation counter techniques. The level spacing is expected to decrease rapidly with increasing excitation of the final nucleus, and at excitations of only a few mev in most nuclei of  $Z \geq 40$  a large number of levels would be contained within the resolution of the apparatus. Under these conditions the spectra of scattered protons should not show large fluctuations. Structure might be found, due to variations in the local level conditions, but this would be unlikely to reproduce from nucleus to nucleus. Such structure should be less marked in experiments using targets containing a mixture of isotopes.

Some recent experiments (Cohen 1957) using 23 mev protons, showed that these expectations were not fulfilled. At quite high excitations and in heavy nuclei, the proton spectra showed considerable structure. Often the spectra showed intense peaks, as if a single level or a small group of levels was excited much more strongly than other levels in that region. More surprisingly, some of these peaks seemed to occur at about the same excitation in many elements over limited ranges of  $Z$ , irrespective of whether the nuclei investigated were of even or odd  $Z$ , or had closed shells of neutrons or protons.

In the experiments reported here a search was made for similar effects using 9.8 mev protons.

## § 2. EXPERIMENTAL METHOD

A 9.8 mev external proton beam from the Nuffield cyclotron passed through a target foil at the centre of an evacuated chamber, and was collected in a Faraday

† On leave of absence from Rutgers University, New Brunswick, New Jersey, U.S.A.



cup and integrated. Protons scattered by the target nuclei were detected by a CsI (Tl) scintillation counter, mounted on the lid of the chamber, which could be set at any angle between  $15^\circ$  and  $165^\circ$  (lab.) to the incident beam. Pulses from the counter were amplified and displayed on a 60-channel pulse analyser. A more complete description of the experimental method has already been published (Greenlees *et al.* 1957a, b).

The linearity with energy of the response of the scintillation counter was checked by observing protons scattered inelastically from a thin Mg target. Groups corresponding to the well-known levels in  $^{24}\text{Mg}$  at 1.38 MeV, 4.14 and 4.24 MeV (not resolved), and 5.26 MeV (cf. Grant *et al.* 1955) were found. The outgoing proton energy was calculated for each of these groups and plotted against the pulse height on the pulse analyser. Further energy calibration points were obtained by repeating the experiment with an absorber of known thickness in the incident beam.

Inelastic scattering was investigated for ten elements of medium atomic number. The targets were in the form of metallic foils, of normal isotopic abundance, and of the following thicknesses in  $\text{mg cm}^{-2}$ : Sn, 4.58; In, 7.5; Cd, 6.87; Ag, 4.14; Pd, 8.0; Mo, 9.62; Nb, 12.6; Zn, 2.39; Cu, 2.42; Ni, 5.26.

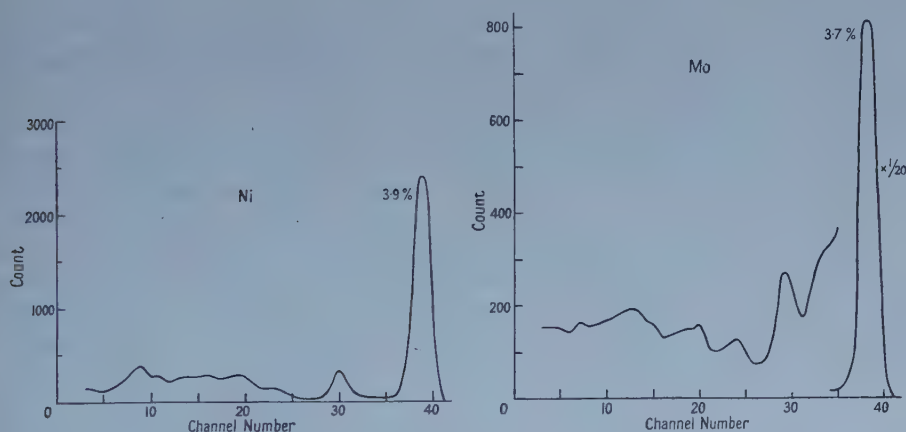


Figure 1. Two typical proton spectra obtained on the pulse analyser using Mo and Ni respectively. The elastic peak for Mo has been scaled down by a factor of 20. A bias equivalent to 14.5 channels was used in the pulse analyser in each case.

Figure 1 shows typical spectra obtained on the pulse analyser at a scattering angle of  $90^\circ$ . The intense group corresponding to elastically scattered protons is accompanied by a much lower yield at lower energies due to inelastic scattering. The resolution (full width at half maximum) of the elastic peak is given on each spectrum. The resolution of the apparatus depended on the target thickness, the outgoing proton energy, and the angular settings of the target foil and the counter, and was always between 2.5% and 5% for the elastic peak during the course of the experiments. Runs with no target in position confirmed that no background subtraction was necessary. The beam energy at the centre of the target foil was  $(9.78 \pm 0.07)$  MeV for Sn, In, Cd, Ag, Pd, Zn, Cu and Ni,  $(9.74 \pm 0.07)$  MeV for Mo and  $(9.71 \pm 0.07)$  MeV for Nb.

## § 3. RESULTS

Measurements were made at angular intervals of about  $10^\circ$ , and for each spectrum the pulse height scale was converted into a  $Q$  value scale using the elastic peak as an energy calibration. A knowledge of the integrator calibration, the target thickness, and the solid angle  $\omega$  of the counter enabled the ordinate scale to be converted to give the differential cross section  $\partial^2\sigma/\partial\omega\partial Q$  in mbn sterad $^{-1}$  mev $^{-1}$ .

For each element the spectra were integrated over a range of angles to give  $d\sigma/dQ$ . It might be expected that the dependence of  $d\sigma/dQ$  on  $Q$  would be best displayed by integration over a wide range of angles. It was found, however, that owing to the strong forward peaking of the elastic scattering, and the Gaussian nature of the elastic peak, some features of the spectra at low excitations could be seen more clearly if backward angles only were used in the integration. The results to be discussed are therefore based only on data taken between  $90^\circ$  and  $160^\circ$ , although observations were in fact made over a wider range of angles. In each case a detailed check was made to ensure that no features of the spectra were lost by this procedure. The absolute value of the cross section was found to depend on the range of angles used in the integration, and, since no data were available for the extreme forward angles, accurate absolute values could not be obtained. The values quoted below are the cross sections for scattering into the backward hemisphere.

Figure 2 shows a typical set of curves for one element, Mo, and also the integrated spectrum for the element. The curves in the figure have been drawn through the experimental points, without regard to the indicated statistical errors. The statistical errors in the integrated spectrum are about 1.5%. Uncertainties in the  $Q$ -values scales for individual spectra were always small compared with the resolution of the apparatus, and hence no features of the individual spectra were lost on integration.

Figures 3 and 4 show the integrated spectra for all the elements studied. The curves have been displaced in a vertical direction, and the scale on the right-hand side shows the point at which the cross section for scattering into the backward hemisphere is 25 mbn mev $^{-1}$  for each element. The relative errors at different  $Q$ -values are due only to statistics, and the statistical significance of all structure in these spectra has been carefully examined. The statistical uncertainty is about 2% in general. Errors in absolute cross sections arise from uncertainties in target thickness, integrator calibration, and dead time corrections, and from possible errors in the procedure for integrating the spectra. The absolute error is estimated at  $\pm 20\%$ .

3.1. Nuclei of  $Z=28-30$ 

These results are shown in figure 3. For nuclei in this region the level spacing is never very small in the range of excitations studied, so that the presence of structure in the spectra is not surprising. One is led therefore to look for features which are common to the three spectra. One such effect is the intense group at  $-Q=1-1.4$  mev in each spectrum.

In the case of Ni this can be accounted for by the first excited state in each of the two prominent isotopes (1.33 mev in  $^{60}\text{Ni}$  and 1.45 mev in  $^{58}\text{Ni}$ ). These states are known to be well separated from other levels (Spencer *et al.* 1957), in agreement with the spectra shown in figure 3. In both Zn and Cu, these groups are not the first excited states, which are known to lie below 1 mev. However, the level

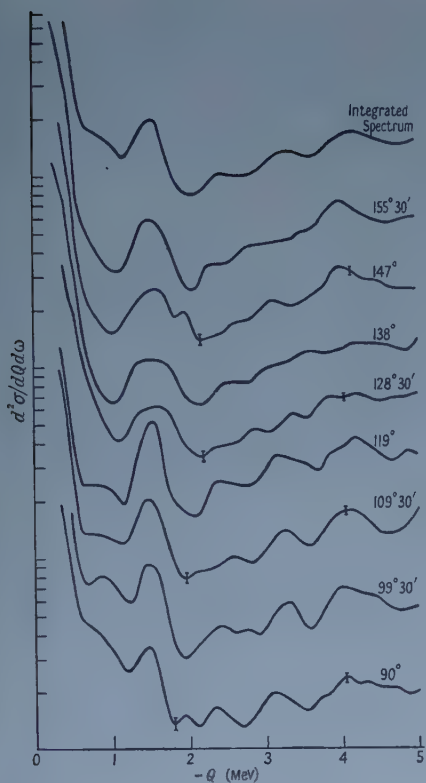


Figure 2. The curves obtained for Mo at all angles from  $90^\circ$ – $160^\circ$ . The integrated spectrum is also shown.

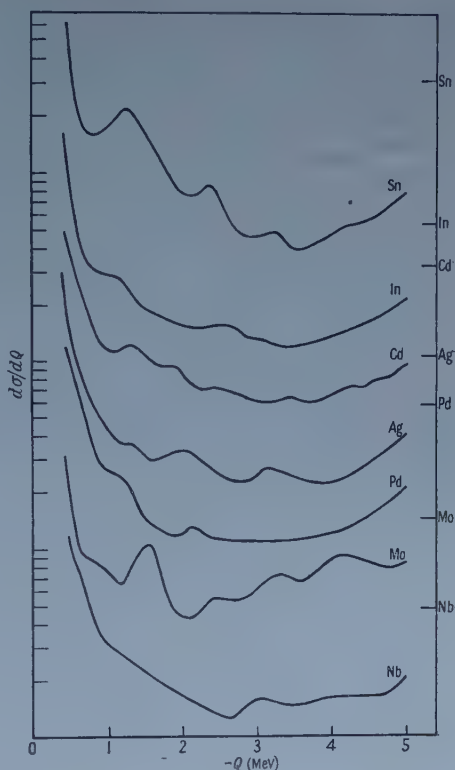


Figure 4. Results for  $Z = 41$ – $50$ .

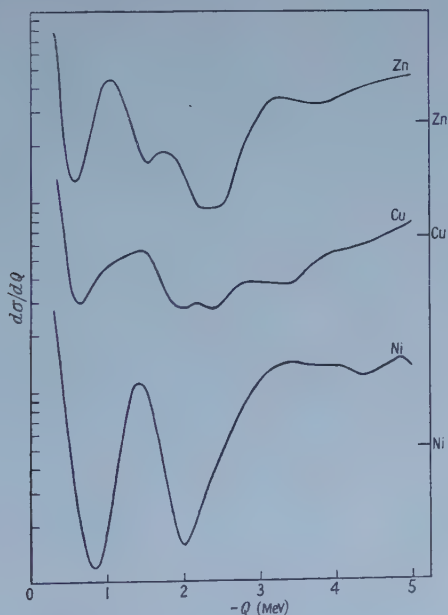


Figure 3. Results for  $Z = 28$ – $30$ .

The curves of figures 2, 3 and 4 have been displaced in a vertical direction, and the scale on the right-hand side in figures 3 and 4 shows the point at which the cross section for scattering into the backward hemisphere is  $25 \text{ mbn mev}^{-1}$ .

spacing is comparable with the resolution here and large fluctuations in the proton yield are not unexpected. Intense groups with  $-Q = 1.1\text{--}1.4\text{ MeV}$  were found by Cohen in these elements, and also in Co and Fe, at 23 MeV.

There are no other prominent features in the present results, but weak groups exist at  $-Q = 3.3\text{ MeV}$  in Zn and Ni, and at  $-Q = 2.9\text{ MeV}$  in Cu. These groups were found by Cohen to be strongly excited at 23 MeV.

### 3.2. Nuclei of $Z = 41\text{--}50$

The results are shown in figure 4. Structure exists in the spectra at excitations up to 5 MeV, but is not as marked as that found by Cohen.

The only persistent effect in these spectra is again a group at  $-Q = -1.1\text{--}1.4\text{ MeV}$  which occurs to a greater or less extent in all elements except Nb†, but is strong only in the magic number nuclei Sn ( $Z = 50$ ) and Mo (16%  $^{92}\text{Mo}$  with  $N = 50$ ). A group at about this excitation was found by Cohen, but with no special emphasis at the magic numbers.

## §4. DISCUSSION

The effects especially sought in these experiments were: (a) prominent structure in  $Q$ -value spectra at excitations of several MeV in medium weight nuclei, and (b) peaks in the spectra which persist from one element to another.

The first effect is not obvious in the present results; the fluctuations in proton yield corresponding to high excitations in the residual nuclei are not pronounced.

The only evidence for the second effect is the group at  $-Q = 1.1\text{--}1.4\text{ MeV}$  in the spectra for  $Z = 41\text{--}50$ . However, this is very weak in all nuclei except the magic nuclei (Sn and Mo) and cannot be regarded as a pronounced effect. In fact the increased cross section for magic nuclei suggests a different mechanism for the excitation of this level in these nuclei. Levels due to collective motion would be expected to be strongly excited, and the first collective level ( $2^+$  for these nuclei) could occur at this excitation. For non-magic nuclei the corresponding level would occur at much lower excitations (probably about 100 keV) and would be masked by the elastic peak in the present experiments.

The most striking feature of the present results in comparison with those of Cohen is the absence of any increase in cross section at  $-Q = 2\text{--}3\text{ MeV}$  in the nuclei with  $Z = 41\text{--}50$ . Cohen found an intense doublet at  $-Q = 2.3$  and 3 MeV, uniform in cross section and  $Q$ -value over the range  $Z = 40\text{--}52$ . There is no indication of any such effect at this excitation in the present results. The cross sections at excitations of a few MeV in these nuclei are higher in the present case than at an incident proton energy of 23 MeV. This can be attributed to a larger compound nucleus contribution, which might be expected at a lower incident energy. If the levels giving rise to the doublet were excited predominantly by direct interaction, the larger compound nucleus cross section would tend to mask the effect at  $9.8\text{ MeV}$ †. Moreover, if the excitation of these levels involved a high angular momentum transfer, the centrifugal barrier would reduce preferentially the scattering to these levels. A combination of these effects could account for the absence of the doublet in the present results.

† The Nb target was the thickest used and the consequent loss of resolution may have suppressed the peak in this element.

‡ The authors are grateful to Dr. A. M. Lane for drawing attention to this point.



In a recent paper, Tomasini (1957) has calculated the inelastic scattering which arises from perturbation of the average potential experienced by nucleons in the nucleus, when an extra proton enters the nucleus. His calculations describe Cohen's results at 23 meV well, but are unable to account for the absence of similar effects at 10 meV.

#### ACKNOWLEDGMENTS

The authors wish to thank Mr. O. N. Jarvis for assistance with the measurements. One of us (J. L.) also wishes to thank the Department of Scientific and Industrial Research for financial support.

#### REFERENCES

- COHEN, B. L., 1957, *Phys. Rev.*, **105**, 1549.  
GRANT, P. J., RUTHERGLEN, J. G., FLACK, F. C., and HUTCHINSON, G. W., 1955, *Proc. Phys. Soc. A*, **68**, 370.  
GREENLEES, G. W., HAYWOOD, B. C., KUO, L. G., and PETRAVIČ, M., 1957 a, *Proc. Phys. Soc. A*, **70**, 331.  
GREENLEES, G. W., KUO, L. G., and PETRAVIČ, M., 1957 b, *Proc. Roy. Soc. A*, **243**, 206.  
SPENCER, R. R., PHILLIPS, G. C., and YOUNG, T. E., 1957, *Phys. Rev.*, **108**, 69.  
TOMASINI, A., 1957, *Nuovo Cim.*, **6**, 927.

## Fluctuations in Slow Neutron Average Cross Sections

By P. A. EGELSTAFF

Atomic Energy Research Establishment, Harwell, Berks.

*MS. received 7th June 1957, and in revised form 22nd January 1958*

**Abstract.** The wide distribution in the values of the neutron widths and spacings of slow neutron levels leads to fluctuations in the cross section averaged over several levels. A method of deriving information on the properties of these distributions from observations on the fluctuations is described.

Fluctuations in total cross section measurements are analysed and agreement to order of magnitude is obtained with the predicted width and spacing distributions, but it does not appear that exact agreement is obtained at present. The  $^{235}\text{U}$  fission cross section also is analysed by this method, but the results do not agree with the theory of the method. It is probable that these discrepancies are due to the effect of correlations in the distributions.

### § 1. INTRODUCTION

A CONSIDERABLE body of data has been built up over the past few years on the parameters of slow neutron resonances (Hughes and Harvey 1955). These data have shown that both the values of the level spacing  $D$  and neutron width  $\Gamma_n$  have broad distributions, but the form of these distributions is not yet known precisely.

The usual method of studying these distributions is to measure the parameters of a number of individual resonances, but this method has two defects. First, the resolving power of neutron spectrometers decreases rapidly with neutron energy, and consequently the sample of neutron resonances of which the parameters can be obtained is small. And secondly, the problem of the analysis of a cross section curve into resonances is not always capable of a unique solution. It is therefore desirable both to increase the size of the sample and to make the method of analysis more reliable, and a method is described here which largely achieves these objectives.

The average value of the neutron total cross section over many resonances is dependent on the ratio  $\langle \Gamma_n \rangle / \langle D \rangle$  (Feshbach *et al.* 1954). If the number of resonances taken in the average is finite, the local value of  $\langle \Gamma_n \rangle / \langle D \rangle$  will vary with the sample of resonances taken because of the broad distribution of these quantities. Experimentally, this shows up as a fluctuation in the cross section as a function of energy, which is related to the distributions of  $\Gamma_n$  and  $D$ . To examine this point in detail it is necessary to work out the statistics of average cross sections taken over small energy regions. It will be shown that such a study can in principle yield information on the distribution of neutron widths and level spacings, on the actual values of  $\langle D \rangle$  and  $\langle \Gamma_n \rangle$ , on the spin dependence of the level spacings, and on the problem of whether these distributions are correlated.

The problem of obtaining this information from the experimental data will be considered here, and some of the existing data analysed in this manner.

## § 2. THE THEORY OF CROSS SECTION FLUCTUATIONS

In this section the statistical behaviour of a group of resonances will be discussed. The group will be defined as those resonances which fall into an energy interval of width  $W$ , and the value of  $W$  and the end points of the interval will be considered as variables. At first it will be assumed that  $W \gg \langle D \rangle$  and  $\langle \Gamma_\Delta \rangle$ , where  $\Gamma_\Delta$  is the total width (including Doppler effect) of the levels, and also that the widths and spacings are uncorrelated. For convenience the fluctuations in the total cross section will be considered in detail and in this treatment it will be assumed that  $\langle D \rangle$  is known. Subsequently, special cases of fluctuations in partial cross sections will be treated and the procedure for evaluating  $\langle D \rangle$  using the statistical methods developed here will be discussed.

The notation  $\langle a \rangle$  will denote an average of the quantity  $a$  taken over a very wide energy interval (infinite for the present purpose) and the notation  $\langle a \rangle_W$  to denote the average taken over an energy interval of width  $W$ .

### 2.1. Total Cross Sections

The average total cross section  $\langle \sigma_t \rangle$  for slow (i.e. zero angular momentum) neutrons may be approximated by (Feshbach *et al.* 1954)

$$\langle \sigma_t \rangle = 4\pi R^2 + \frac{2\pi^2}{k} \frac{\langle \Gamma_n/k \rangle}{\langle D \rangle} \quad \dots\dots (1)$$

where  $4\pi R^2$  is the shape elastic scattering, and  $k$  is the neutron wave number. Lane and Lynn (1957) have shown that the additional term  $-\pi^3 \langle \Gamma_n/k \rangle^2 / \langle D \rangle^2$  should be added to the right-hand side of equation (1) to represent the effects of interference between resonances. However, this term is very small and need not be considered in the present work.

Equation (1) may be rewritten in terms of averages over an energy interval of width  $W$ :

$$x(W) = \frac{k}{k_0} \langle \sigma_t - 4\pi R^2 \rangle_W = \frac{2\pi^2}{k_0^2} \frac{\Sigma \Gamma_n^0}{W} \quad \dots\dots (2)$$

where the subscript 0 denotes values at 1 ev, and the summation is over those levels falling in the interval selected. In what follows the distribution of a sequence of  $x(W)$  values will be discussed, where the sequence is obtained by allowing  $W$  to be measured from an energy  $E$  given by  $E = jW$ ;  $j = 0, 1, 2, \dots \infty$ . For convenience the symbol  $G$  will be used for the neutron width at 1 ev in place of the usual  $\Gamma_n^0$ .

Since at present consideration is being restricted to large values of  $W$ , the distribution of  $x(W)$  values will be nearly normal. Thus, the important quantity will be variance of the  $x(W)$  distribution, and Hammersley and Lane in the Appendix to this paper show that  $\text{Var } x(W)$  is related to the variances of the  $G$  and  $D$  distributions as (eqn (A 11))

$$\frac{\text{Var } x(W)}{\langle x \rangle^2} = \frac{\langle D \rangle}{W} \left[ \frac{\text{Var } G}{\langle G \rangle^2} + \frac{\text{Var } D}{\langle D \rangle^2} \right]. \quad \dots\dots (3)$$

Since the average value of  $x(W)$  over a very wide energy range is independent of  $W$ , it is written  $\langle x \rangle$  in this equation.

The quantity in the square brackets of equation (3) depends only on the shape of the distributions of  $G$  and  $D$  and hence should be independent of target mass and spin of the compound state formed by neutron absorption. We denote it by  $F$ .

Equation (3) is applicable to a target nucleus of zero spin. The extension to the case of non-zero spin is straightforward. The spin of the target nucleus is denoted by  $I$  and of the compound nucleus by  $J$ . The cross sections are weighted by a spin weighting factor  $g$  equal to  $\frac{1}{2}(2J+1)/(2I+1)$ , and we use the notation  $g_1$  and  $g_2$  for the two possible values of  $g$ . Similarly, the notation  $x_1(W)$  and  $x_2(W)$  refers to the value of  $x$  at equation (2) for the two systems of levels corresponding to the two values of  $J$ , and  $x(W)$  denotes the value of  $\langle k/k_0 \rangle \langle \sigma_t - 4\pi R^2 \rangle_W$  where  $\sigma_t$  is now the observable total cross section.

Now we may write, since the distribution of  $x(W)$  is approximately normal,

$$\text{Var } x(W) = g_1^2 \text{Var } x_1(W) + g_2^2 \text{Var } x_2(W) \quad \dots\dots (4)$$

which from equation (3) may be rewritten

$$W \text{Var } x(W) = F[g_1^2 \langle D_1 \rangle \langle x_1 \rangle^2 + g_2^2 \langle D_2 \rangle \langle x_2 \rangle^2]. \quad \dots\dots (5)$$

Since the ratio  $\langle G \rangle / \langle D \rangle$  is the same for the two systems of levels we may put

$$\langle x \rangle^2 = \langle x_1 \rangle^2 = \langle x_2 \rangle^2. \quad \dots\dots (6)$$

Further reduction of (5) depends upon the relation between the level spacing and  $J$  as follows. If  $\langle D \rangle$  is the average level spacing which can be observed we have

$$\frac{1}{\langle D_1 \rangle} + \frac{1}{\langle D_2 \rangle} = \frac{1}{\langle D \rangle} \quad \dots\dots (7)$$

and following Bethe (1937) we take the dependence of spacing on spin to be

$$\langle D_1 \rangle = \frac{C}{2J+1} \text{ etc.} \quad \dots\dots (8)$$

where  $C$  is a constant. This relation has recently received some support from experiments (Sailor 1956, Rae 1956). Equations (7) and (8) reduce to

$$\frac{\langle D \rangle}{\langle D_1 \rangle} = g_1; \quad \frac{\langle D \rangle}{\langle D_2 \rangle} = g_2. \quad \dots\dots (9)$$

From the relations (6) and (9) equation (5) reduces to equation (3). Thus, if the relation (8) is correct, equation (3) is valid for all target nuclei.

We now consider the case of a target consisting of a mixture of several isotopes. A relation analogous to (5) is valid, viz.

$$\frac{\text{Var } x(W)}{\langle x \rangle^2} = \frac{1}{W} F \sum_i a_i^2 \langle D_i \rangle \frac{\langle x_i \rangle^2}{\langle x \rangle^2} \quad \dots\dots (10)$$

where  $a_i$  is the abundance of the  $i$ th isotope. In most cases the mass of the several isotopes and their nuclear shape will be approximately the same, so that to a first approximation we can put

$$\langle x_i \rangle / \langle x \rangle \simeq 1. \quad \dots\dots (11)$$

Further reduction of (10) is not in general possible. However, when the abundances and level spacings of the isotopes are nearly the same equation (10) reduces to equation (3) to the second order of the small differences in these quantities.

## 2.2. Partial Cross Sections

The analogous relationships for the fluctuations in the partial cross sections (e.g. fission, capture) will be derived for two extreme situations only. These are: (a)  $\Gamma_n \ll \Gamma$ ; (b)  $\Gamma_n \simeq \Gamma$ , where  $\Gamma$  is the total width of a level.



The condition (a) would apply, for example, to the common fissile materials over the neutron energy range zero to 1 kev; it implies that  $\Gamma_n$  is not correlated with  $\Gamma$ . In this case the quantity  $x_f(W)$  used in this analysis is related to the fission cross section ( $\sigma_f$ ) by

$$x_f(W) = \frac{k}{k_0} \langle \sigma_f \rangle_W = \frac{2\pi}{k_0^2} \left[ \frac{g_1}{W} \Sigma \left( G \frac{\Gamma_f}{\Gamma} \right)_1 + \frac{g_2}{W} \Sigma \left( G \frac{\Gamma_f}{\Gamma} \right)_2 \right] \dots (12)$$

where  $\Gamma_f$  is the fission width of any level, and the sum extends over all the levels in the selected interval.

The average ratio of fission to total width  $\langle \Gamma_f/\Gamma \rangle$  may depend upon the spin of the compound state considered, and thus the result will be expressed in terms of the ratio

$$p = \frac{\langle \Gamma_f/\Gamma \rangle \text{ for state 2}}{\langle \Gamma_f/\Gamma \rangle \text{ for state 1}}. \dots (13)$$

Following the treatment used for the total cross section we find

$$\frac{\text{Var } x_f(W)}{\langle x_f \rangle^2} = \frac{\langle D \rangle [g_1(F_f)_1 + g_2(F_f)_2 p^2]}{W(g_1 + g_2 p)^2} \dots (14)$$

where

$$F_f = \frac{\text{Var } G}{\langle G \rangle^2} + \frac{\text{Var } D}{\langle D \rangle^2} + \frac{\text{Var } \Gamma_f/\Gamma}{\langle \Gamma_f/\Gamma \rangle^2}. \dots (15)$$

In cases where  $p=1$  and the fission width distributions for the two spin states are the same, the right-hand side of equation (14) reduces to  $\langle D \rangle F_f/W$ .

The condition (b) would apply to many nuclei in the kilovolt region; it implies a full correlation between  $\Gamma_n$  and  $\Gamma$ . As an example we consider the radiative capture cross section  $\sigma_r$ . The initial equation is now

$$x_r(W) = \frac{k^2}{k_0^2} \langle \sigma_r \rangle_W = \frac{2\pi^2}{k_0^2} \left[ g_1 \frac{\Sigma(\Gamma_\gamma)_1}{W} + g_2 \frac{\Sigma(\Gamma_\gamma)_2}{W} \right] \dots (16)$$

where  $\Gamma_\gamma$  is the capture width for any level and owing to the imposition of condition (b) the observed average capture cross section varies as  $k^{-2}$ . Again proceeding as for the total cross section we obtain equation (14) modified by putting  $x_r(W)$  in place of  $x_f(W)$ ,  $F_\gamma$  in place of  $F_f$  and  $q$  in place of  $p$  where

$$q = \frac{\langle \Gamma_\gamma \rangle \text{ for state 2}}{\langle \Gamma_\gamma \rangle \text{ for state 1}}; \quad F_\gamma = \frac{\text{Var } \Gamma_\gamma}{\langle \Gamma_\gamma \rangle^2} + \frac{\text{Var } D}{\langle D \rangle^2}. \dots (17)$$

For a zero spin target nucleus the right-hand side of the modified equation (14) reduces to  $\langle D \rangle F_\gamma/W$ .

Separate measurements of  $F$ ,  $F_f$  and  $F_\gamma$  provide a powerful method of determining the variances of the several distributions. We shall give some numerical examples in the next section.

### 2.3. Determination of $\langle D \rangle$

For the first application of this analysis the value of  $\langle D \rangle$  obtained from a study of well-resolved levels at low neutron energies could be used in equation (3). However, it is possible, in principle, to evaluate  $\langle D \rangle$  from the distribution of  $x(W)$ , and the methods which can be used for this step will be considered now.

As  $W/\langle D \rangle$  approaches infinity the distribution of  $x(W)$  approaches an exact Gaussian shape. But the actual shape of the  $x(W)$  distribution for finite values of  $W/\langle D \rangle$  is asymmetric (or skew); the ratio of the frequencies of finding large

values to small values of  $x(W)$  is greater than that for a symmetric distribution. The skewness  $\beta$  is measured by the ratio of the third moment of the distribution to the second moment raised to the power of  $3/2$ , and for certain distributions of  $G$  and  $D$  the skewness may be large for  $W$  within the range of validity of equation (3). This point will be considered for the total cross section case.

If the  $x(W)$  are statistically independent then it is easy to show that the third moment about the mean is proportional to  $(\langle D \rangle / W)^2 \langle x \rangle^3$ ; the constant of proportionality  $Q$  will depend upon the actual distribution of widths and spacings in a somewhat complicated fashion. Therefore the skewness of the distribution of  $x(W)$  is given by

$$\beta = \frac{Q}{F^{3/2}} \left[ \frac{\langle D \rangle}{W} \right]^{1/2}. \quad \dots\dots (18)$$

Hence we may either (i) choose the width and spacing distributions, calculate  $Q$  and  $F$  and find  $\langle D \rangle$  from equation (18) in order to test the chosen distributions via equation (3), or (ii) obtain a function of the distributions in terms of the experimentally determined quantities by substituting  $\langle D \rangle / W$  from (18) into equation (3), viz.

$$\frac{\text{Var } x(W)}{\beta^2 \langle x \rangle^2} = \frac{F^4}{Q^2}. \quad \dots\dots (19)$$

This type of analysis is useful when  $Q$  is of the same order of magnitude as  $F$ , but for distributions giving a small value of  $Q$ , an alternative approach is required. The relation between  $\text{Var } x(W) / \langle x \rangle^2$  and the moments of the distributions of widths and spacings may be expressed as a series. The right-hand side of equation (3) is the first term of this series. The second term (eqn. (A 11)) has the form

$$\left( \frac{\langle D \rangle}{W} \right)^2 \left[ \frac{1}{2} \left( \frac{\text{Var } D}{\langle D \rangle^2} \right)^2 - \frac{1}{3} \frac{\langle (D - \langle D \rangle)^3 \rangle}{\langle D \rangle^3} + \frac{1}{6} \right]. \quad \dots\dots (20)$$

If the distribution in  $D$  is symmetrical and wide this term will be important unless  $W / \langle D \rangle \gg \text{Var } D / \langle D \rangle^2$ . In this particular case the quadratic dependence of  $\text{Var } x(W) / \langle x \rangle^2$  on  $W$  may be used to estimate  $\langle D \rangle$ .

In general, however, the study of the behaviour of  $\text{Var } x(W)$  and  $\beta$ , for  $W / \langle D \rangle$  small, offers the only solution to this problem.

#### 2.4. Alternative Presentation of the Problem

The discussion so far has concerned the properties of the distribution of  $x(W)$ , that is the distribution of cross sections one observes by moving in steps of width  $W$  along the energy scale. Clearly the same data may be presented in an alternative form as a distribution of energies observed by moving in steps of width  $V$  along a scale of  $\Sigma G$ . The definition of this procedure is as follows in the case of the total cross section.

First rewrite equation (1) as

$$A(E) = \frac{k_0}{2\pi^2} \int_0^E k(\sigma_t - 4\pi R^2) d\epsilon = \Sigma G \quad \dots\dots (21)$$

where the sum is over the reduced neutron widths of all the levels occurring in the energy range  $0 \leq \epsilon \leq E$ . Let the energies  $E = E_j$  ( $j = 0, 1, 2 \dots \infty$ ) be defined as the points where  $A(E) = jV$ . Then the quantities  $y(V) = E_j - E_{j-1}$ , have the same properties as the  $x(W)$  defined at equation (2).

For  $V/\langle G \rangle$  large, the distribution of  $y(V)$  yields exactly the same information as  $x(W)$  for  $W/\langle D \rangle$  large. However, as  $V/\langle G \rangle$  and  $W/\langle D \rangle$  approach unity one can obtain additional relations between the distributions of  $G$  and  $D$ , which together with the relations discussed above enable some properties of the distributions of  $G$  and  $D$  to be obtained separately. Thus, for example, using the expression (20) the difference between  $\text{Var } y(V)/\langle y^2 \rangle$  and  $\text{Var } x(W)/\langle x \rangle^2$  is a first approximation:

$$\left. \begin{aligned} \frac{\text{Var } y(V)}{\langle y \rangle^2} - \frac{\text{Var } x(W)}{\langle x \rangle^2} &\simeq \left( \frac{\langle D \rangle}{W} \right)^2 L \\ L &= \frac{1}{2} \left( \frac{\text{Var } G}{\langle G \rangle^2} \right)^2 - \frac{1}{2} \left( \frac{\text{Var } D}{\langle D \rangle^2} \right)^2 - \frac{1}{3} \frac{\langle (G - \langle G \rangle)^3 \rangle}{\langle G \rangle^3} + \frac{1}{3} \frac{\langle (D - \langle D \rangle)^3 \rangle}{\langle D \rangle^3} \end{aligned} \right\} \dots (22)$$

if  $\langle G \rangle/\langle D \rangle = V/W$ . The latter condition can be imposed easily in a practical case since the value of  $\langle G \rangle/\langle D \rangle$  is found directly by the application of equation (1) to data averaged over very wide energy regions.

It will be shown in §4 that it is possible to measure  $L$  in certain cases. However, the main use of the combined  $x(W)$  and  $y(V)$  presentation of data is for an analysis in which  $W/\langle D \rangle$  is very small.

### § 3. SOME PREDICTIONS FOR THE VALUES OF $F$ , $F_f$ AND $F_v$ AND $Q$

There are some theoretical predictions for the distributions of  $G$  and  $D$ . Porter and Thomas (1956) suggest that the  $G$  distribution is the  $\nu=1$  member of the family

$$P(\alpha) = \text{const. } \alpha^{\nu/2-1} \exp \left( -\frac{\nu\alpha}{2\langle \alpha \rangle} \right) d\alpha. \quad \dots (23)$$

They find some support for this from an analysis of the measured parameters of a number of resonances. The family (23) has the property

$$\frac{\text{Var } \alpha}{\langle \alpha \rangle^2} = \frac{2}{\nu} \quad \dots (24)$$

so that Porter and Thomas predict  $\text{Var } G/\langle G \rangle^2 = 2$ .

A plausibility argument due to Wigner (1956) suggests that the distribution of spacings is of the form

$$\text{Const. } D \exp \left[ -\frac{\pi D^2}{4\langle D \rangle^2} \right]. \quad \dots (25)$$

In this case we have

$$\text{Var } D/\langle D \rangle^2 = 0.27. \quad \dots (26)$$

An analysis of experimental data on the level spacings in  $^{234}\text{U}$ ,  $^{236}\text{U}$  and  $^{238}\text{U}$  by Hughes (1956), suggests that the observed distribution is wider than that given by (25). Here  $\text{Var } D/\langle D \rangle^2$  could be about 0.5.

Thus, at present we might expect

$$F = \frac{\text{Var } G}{\langle G \rangle^2} + \frac{\text{Var } D}{\langle D \rangle^2} = 2.27 \text{ from theory} \quad \dots (27)$$

2.5 from resonance analysis.

Consequently, about four-fifths of the predicted value of  $F$  comes from the form of the distribution of neutron widths, and its measurement would provide an important test of the Porter-Thomas hypothesis concerning the neutron width distribution.



Next consider the fission width distribution, which is believed to belong to the family (23) (Porter and Thomas 1956). The value of  $\nu$  is expected to be small, perhaps about 2. If we put  $\nu=2$  and assume that the average fission, radiative capture and neutron widths are as given by Pilcher *et al.* (1956) for  $^{235}\text{U}$ , then the value of  $(\text{Var } \Gamma_f/\Gamma)/(\langle \Gamma_f/\Gamma \rangle^2)$  is  $2/5$ . The value of  $F_f$  (cf. eqns (14) and (15)) would then be predicted to be about 2.8.

Thus, again, the value of  $F_f$  should depend mostly upon the neutron width distribution. However, the difference  $F_f - F$  which could be measured in a very careful experiment would give the value of  $[\text{Var } (\Gamma_f/\Gamma)]/(\langle \Gamma_f/\Gamma \rangle^2)$  and hence test the hypothesis of the fission width distribution.

Now consider the value of  $F_\gamma$  (eqn (17)). The distribution of radiative capture widths is rather narrow compared with the distribution for the other width and the spacings (Porter and Thomas (1956) summarize the experimental and theoretical evidence for this). Consequently, we have

$$\frac{\text{Var } \Gamma_\gamma}{\langle \Gamma_\gamma \rangle^2} \ll \frac{\text{Var } D}{\langle D \rangle^2} \quad \dots\dots (28)$$

and the value of  $F_\gamma$  should be approximately equal to  $\text{Var } D/\langle D \rangle^2$  which is about 0.4. The difference  $F - F_\gamma$  may be used to find  $\text{Var } G/\langle G \rangle^2$ .

Thus if we measure  $F$ ,  $F_f$  and  $F_\gamma$  we can obtain the variances of the several distributions discussed above.

The value of  $Q$  has been calculated for some special cases. In order to cover the uncertainty over the distribution of  $D$ , we consider the  $G$  distribution discussed previously with each of three members of the family (23) for the  $D$  distribution. The chosen  $D$  distributions are those for  $\nu=2, 4$  and  $\infty$ . The third moments for the first two cases have been calculated by Lane and Lynn (1957). The results are shown in table 1.

Table 1. Value of  $Q$  and  $Q/F^{3/2}$  for Several Distributions  
(when  $W/\langle D \rangle$  is large)

Value of $\nu$ chosen for $D$ distribution	2	4	$\infty$
$Q$	15	11.6	8
$Q/F^{3/2}$	2.89	2.94	2.83

For these cases  $Q$  is large and hence it should be possible to determine the skewness  $\beta$  experimentally. Also since  $Q/F^{3/2}$  is almost constant the uncertainty in the distribution of  $D$  will introduce little error to a determination of  $\langle D \rangle$  from equation (18). This is due primarily to our choice of the neutron width distribution. Finally, the theoretically predicted value for the (non-dimensional) quantity at equation (19) is

$$\frac{\text{Var } x(W)}{\beta^2 \langle x \rangle^2} = 0.27. \quad \dots\dots (29)$$

#### § 4. SOME LIMITATIONS OF THE THEORY OF § 2

The theory given in § 2 rests upon the assumption of the statistical independence of the values of spacings and widths, and of the number of levels in  $W$  being large. Here we consider, for the total cross section case only, the modification to the theory to allow for correlations in widths and spacings and the limiting value of  $W/\langle D \rangle$  for which the theory is valid.



#### 4.1. The Effect of Correlations in $G$ and $D$

We shall consider only two simple types of correlation. First consider the possibility that each  $G$  is correlated with the preceding (or succeeding)  $D$  while the actual distribution of widths (or spacings) is an uncorrelated one. In this case the relation (3) can be generalized:

$$\frac{\text{Var } x(W)}{\langle x \rangle^2} = \frac{\langle D \rangle}{W} \left[ \frac{\text{Var } G}{\langle G \rangle^2} - 2r \left[ \frac{\text{Var } G}{\langle G \rangle^2} \frac{\text{Var } D}{\langle D \rangle^2} \right]^{1/2} + \frac{\text{Var } D}{\langle D \rangle^2} \right] \dots\dots (30)$$

where the correlation coefficient  $r$  is given by

$$r = \frac{\langle (G - \langle G \rangle)(D - \langle D \rangle) \rangle}{[(\text{Var } G)(\text{Var } D)]^{1/2}} \dots\dots (31)$$

If  $G$  varies in the same sense as  $D$  then  $r$  lies between 0 and +1, but if it varies in the opposite sense then  $r$  lies between 0 and -1. Also, if  $r=1$  then the distributions of  $G$  and  $D$  will be the same, apart from a displacement of origins, and the value of  $\text{Var } x(W)$  will depend upon the relative displacement of the origins.

At present there is no theoretical guidance on the likely values of  $r$ . It is generally assumed to be zero. However, since the absolute value of the cross section fluctuation depends upon the value of  $r$ , observations of the fluctuations can check this assumption.

The second type of correlation is that of the widths (or spacings) one with another. We shall consider only the case where the first serial correlation coefficient of the sequence of values of  $G$  (or  $D$ ) is non-zero, the higher coefficients being zero. If the  $G$  and  $D$  correlation coefficients are denoted by  $r_G$  and  $r_D$  respectively, equation (3) is modified as follows:

$$\frac{\text{Var } x(W)}{\langle x \rangle^2} = \frac{\langle D \rangle}{W} \left[ \frac{1}{1-r_G} \frac{\text{Var } G}{\langle G \rangle_\infty^2} + \frac{1}{1-r_D} \frac{\text{Var } D}{\langle D \rangle_\infty^2} \right] \dots\dots (32)$$

Again, the values of these two coefficients are usually assumed to be zero.

Now provided  $W/\langle D \rangle$  is large the correlations discussed above will not cause one member of the sequence of  $x(W)$  values to be correlated with another. But there are many types of correlation which would lead to this possibility, and therefore the sequence of  $x(W)$  values has to be tested for this feature by evaluating its serial correlation coefficients. If they are non-zero the analysis given above is invalid.

#### 4.2. The Theory for Small $W$

In the previous discussion we have assumed that  $W \gg D$  and  $\Gamma_\Delta$ , where  $\Gamma_\Delta$  is the observable (i.e. natural plus Doppler) width of the levels. The values of  $D$  found experimentally are generally much greater than  $\Gamma_\Delta$ , so that we need to find a lower limit to the ratio  $W/\langle D \rangle$  for which equation (3) is valid. The numerical value of this limit will depend upon the form of the distributions in  $G$  and  $D$ , and it will be estimated for distributions of the type discussed in the previous section. Again, we assume that both the distributions of  $G$  and  $D$  are members of the family (23), and because of the uncertainty about the actual distribution of  $D$  we consider the three cases  $\nu=1$  for the  $G$  distribution with  $\nu=2, 4$  or  $\infty$  for the  $D$  distribution. (The distribution (25) is intermediate between the distribution (23) with  $\nu=4$  and  $\infty$ .)

The quantity  $\text{Var } x(W)/\langle x \rangle^2$  as a function of  $W/\langle D \rangle$  has been calculated by Lane and Lynn (1957) for the first two cases. (These calculations as well as that for the third case assume that  $\Gamma_\Delta \ll W$ .) The limits are obtained from these functions and are given in table 2.

Table 2

Value of $\nu$ chosen for $D$ distribution	Remarks on range of validity of eqn. (3)
2	Exact for all values of $W/\langle D \rangle$
4	When $W/\langle D \rangle = 6$ , value of $F$ deduced from eqn (3) is 1% too large.
$\infty$	Exact for integer values of $W/\langle D \rangle$ . For $W/\langle D \rangle = 12.5$ value of $F$ deduced from eqn (3) is 1% too large.

From these results we see that for  $(W/\langle D \rangle)$  greater than 10 (say) equation (3) should be accurate for all cases, and this condition will define what is meant by large  $W$ .

Of the cases considered in table 2, the value of  $\nu=4$  for the  $D$  distribution gives a function closest to the theoretical distribution at equation (25). The first two terms alone of the expansion of  $\text{Var } x(W)/\langle x \rangle^2$  in powers of  $\langle D \rangle/W$  given in the Appendix (eqn (A 11)) are accurate, in this case, to better than 1% for  $\langle D \rangle/W=1$ . The approximate relation at equation (22) is satisfactory to a similar degree, and for the case being considered  $L = -5/8$ . Thus, for  $\langle D \rangle/W=1$ , the ratio  $L/F$  is  $-0.28$ , which implies that  $L$  should be a measurable quantity in this instance. These remarks are valid only if  $D \gg \Gamma_\Delta$ .

Finally, let  $W$  be of the order of  $\Gamma_\Delta$ . Here the values of  $x(W)$  will be correlated since the levels in any given region of width  $W$  will overlap the next region by a significant amount. The magnitude of this effect is measured through the serial correlation coefficient. This coefficient thus provides a test that we are satisfying the condition  $W \gg \Gamma_\Delta$ . On the other hand the range of  $W$  for which the correlation coefficients are non-zero will be related to the values of  $\langle \Gamma_\Delta \rangle$  and  $\langle D \rangle$ . In principle this will provide a new method of measuring  $\langle \Gamma_\Delta \rangle$  when  $\langle D \rangle$  is known.

The remainder of this paper is devoted to a discussion of the experimental determination of  $F$  and  $F_t$ . At the present time, the available experimental data are limited in quality and scope so that the methods described above cannot be fully employed.

## § 5. ANALYSIS OF EXPERIMENTAL DATA

The results available from neutron spectrometers are in the form of cross sections averaged over an energy range  $\Delta E$  equivalent to the width of the spectrometer resolution function. Because the neutron intensity from existing neutron sources is not independent of the neutron energy, it is necessary to make the width  $\Delta E$  sufficiently small that the neutron intensity is essentially uniform over the range  $E$  to  $E + \Delta E$ . If we have a sequence of cross section measurements over the interval  $W$ , then the value of  $x(W)$  will be given by

$$x(W) = \frac{1}{W} \sum_i \sigma_i \Delta E_i \quad \dots\dots (33)$$

where  $\sigma_i$  is the  $i$ th measurement in the interval  $W$  corrected according to equation (2). It is important to ensure that this averaging yields the cross section which would be measured with a neutron spectrometer which had a rectangular resolution function of width  $W$  and used a neutron source uniform with energy. This condition can be met, to a reasonable degree, if the number of measurements in the interval  $W$  is greater than 3.

In making total cross section measurements by the transmission method a true average cross section in  $\Delta E$  is not obtained because the samples used are thick and the front layers screen the rear layers. The method of correcting for this has been described by Gayther and Nicholson (1957). However, in our case, their method of correction must be applied to each experimental point in order to obtain the correct deviation of the points from the mean. This means that an approximate value of  $\langle \Gamma_n/D \rangle$  is obtained from the value of measurement itself and the correction applied through successive approximations. Partial cross section measurements are usually made on a very thin specimen. Thus a true average cross section is actually measured, and can be used directly for this analysis.

The standard deviation  $S$  due to errors of measurement on the values of  $x(W)$  is given by

$$S = \left[ \sum_i (\Delta\sigma_i \cdot \Delta E_i)^2 \right]^{1/2} \quad \dots\dots (34)$$

where  $\Delta\sigma_i$  is the standard deviation of  $\sigma_i$ . The relation between the observed and the true variance in  $x(W)$  is thus

$$\text{true variance} = \text{observed variance} - \Sigma S^2/n^2 \quad \dots\dots (35)$$

where  $n$  is the number of readings of  $x(W)$ .

The standard deviation in  $\text{Var } x(W)$  is composed of two terms, one coming from the subtraction in equation (32) and the other, which is the major contribution in practical cases, due to the size of  $n$ . The later term is equal to  $(2n)^{-1/2}$ .

## § 6. RESULTS

### 6.1. Total Cross Section Data

The total cross sections of a number of heavy elements have been measured on the Harwell fast chopper over the energy range 200 ev to 100 kev. (These data have been used by Gayther and Nicholson (1957) for the determination of  $\langle \Gamma_n \rangle / \langle D \rangle$ .) Corrections were applied in the manner outlined in the previous section. It was found that in most cases only the points between 400 and 2000 ev were suitable for the fluctuation analysis. Two values of the interval  $W$  were taken, 100 and 200 ev, agreement between the two analyses being satisfactory. In order to evaluate the quantity  $F$  a weighted average level spacing has to be used for results taken on polyisotopic elements. Comparison of equations (10) and (3) show that the average required is  $\sum_i a_i^2 \langle D_i \rangle$ . Since in general  $\langle D_i \rangle$  is unknown only a rough approximation to this average can be found, and in this work we have arbitrarily assumed that the level spacing for even-even isotopes is five times that for even-odd isotopes. (This ratio is of the order of magnitude observed experimentally.) Using the observed values for  $\langle D \rangle$  taken from the compilation by Hughes and Harvey (1955) we can then evaluate  $\sum_i a_i^2 \langle D_i \rangle$ . An exception to this is europium which consists of two even-odd nuclei for each of which the values of  $\langle D_i \rangle$  are known, so that an exact analysis is possible.

The results are shown in table 3. It can be seen that the values of  $F$  fluctuate about 1.7, although the errors are comparatively large. There does not seem to be any great dependence upon spin in agreement with the conclusion of § 2.

Table 3. Total Cross Section Results

(1)	(2)	(3)	(4)	(5)	(6)
Pu	239	1/2	1.8	—	$1.6 \pm 0.8$
Pt	194	0			
	195	1/2	15	29	$1.5 \pm 0.8$
	196	0			
	198	0			
Ta	181	7/2	4	—	$3.5 \pm 2$
Yb	171	1/2			
	172	0			
	173	5/2	3	7	$1.5 \pm 0.8$
	174	0			
	176	0			
Dy	161				
	162	0	1.5	3	$2.5 \pm 1.5$
	163				
	164	0			
Gd	155	3/2			
	156	0	2	4.3	$0.8 \pm 0.4$
	157	3/2			
	158	0			
	160	0			
Eu	151	5/2	0.9	0.6	$1.0 \pm 0.4$
	153	5/2	1.5		
Sm	147				
	148	0			
	149		1.8	3.8	$1.9 \pm 0.9$
	150	0			
	152	0			
	154	0			
Pr	141	5/2	80	—	$\sim 1$

(1) Element; (2) major isotopes; (3) spin; (4) assumed value of  $\langle D \rangle$  for element (ev); (5) calculated value of  $\sum a_i^2 \langle D_i \rangle$  (ev); (6) value of  $F$ .

### 6.2. The Fission Cross Section of $^{235}\text{U}$

Yeater *et al.* (1956) have measured the fission cross section of  $^{235}\text{U}$  from 5 to 2000 ev with high resolution. They observe fluctuations in the cross section over the whole of this energy range. Since the quantity of  $^{235}\text{U}$  used in these experiments was such that a 2000 barn cross section (larger than the peak cross section for low energy resonances in  $^{235}\text{U}$ ) was equivalent to 90% transmission, there is no correction for sample thickness.

Values of  $W$  equal to 8.1, 16.2, 32.5, 65, 130 and 260 ev were used in the analysis. An example of the distribution of  $x_1(W)$  is given in figure 1. It can be seen that the distribution is Gaussian within the limits of error. It was found, however, that  $\text{Var } x_1(W)$  was not proportional to  $W$  as indicated by equation (14). The actual results are shown in figure 2, compared with similar results for europium.



(data of § 6.1). Unlike the europium results the  $^{235}\text{U}$  data do not yield a constant of proportionality, although the range of  $W$  used for europium is not as large as for  $^{235}\text{U}$ . If we assume, following Pilcher *et al.* (1956), that  $\langle D \rangle = 0.65$  eV and  $p$  (eqn (13)) = 1, then we may derive the value of  $F_f$  as a function of  $W$ . For the lower values of  $W$  in figure 2 the result is about 1 and for the larger values it is about 3.

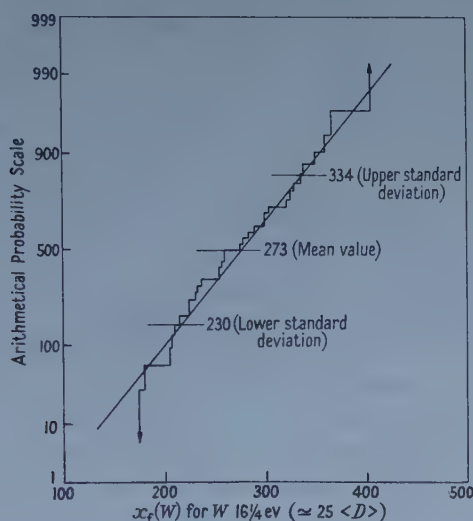


Figure 1. Distribution in  $x_f(W)$  for  $^{235}\text{U}$  fission cross section.

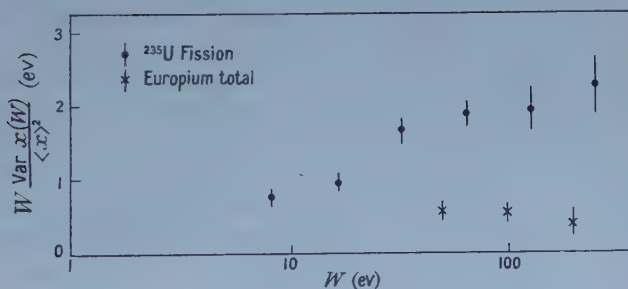


Figure 2. The dependence of  $\text{Var } x(W) / \langle x \rangle^2$  upon the value of  $W$  for  $^{235}\text{U}$  and natural europium.

## § 7. DISCUSSION OF RESULTS

First, we compare the total cross section results with the predictions of § 3. The values in table 2 are of the correct order of magnitude, and due to the large errors (which are partly systematic) it would be unwise to compare the average value of  $F$  in this table (i.e. 1.7) too closely with the predicted value ( $\approx 2.4$ ). However, in the case of europium the estimation of  $F$  should be reliable and the result is significantly less than the predicted value. This discrepancy suggests that either  $\nu=2$  for the distribution of  $G$ , or that the distributions of  $G$  and  $D$  are correlated. Suitable correlation coefficients in equation (30) or (32) would give  $F=1$ . Because of the limitations of the total cross section data a proper evaluation of their serial correlation coefficients has not been carried out. Hence

a firm conclusion is not yet possible. Secondly, consider the predicted value of  $F_f$  (i.e.  $\sim 2.8$ ) with the values obtained from figure 2. The prediction is consistent with the value found when  $W$  is very large—about 200 times the average level spacing—but inconsistent with the value for  $W \sim 20\langle D \rangle$ . This effect cannot be accounted for in terms of the correlation equations (30) and (32).

There is clearly a big discrepancy between the predictions of equation (3) and the fission cross section data of figure 2, which must be accounted for by a complicated type of correlation. The serial correlation coefficients for the  $x_f(W)$  values derived from these data have been calculated, and are found to be different from zero, and a preliminary analysis suggests a type of correlation leading to a periodic behaviour in the sequence of  $x_f(W)$  values. This would be consistent with the result shown in figure 2. Further work on this problem is in hand.

### § 8. SUMMARY AND CONCLUSIONS

The theory of cross section fluctuations has been developed for the case where the number of levels in the interval considered is large. It has been shown that from an analysis of the fluctuations one might hope to obtain the values of the variances of level width and spacing distributions. The method also allows one to test for correlations in these distributions. An important result of the theory is that the variation of  $\langle D \rangle$  with spin is directly related to the variation of  $\text{Var } x(W)$  with spin. The method may be extended to the determination of  $\langle D \rangle$ . In the region of small  $W$  the fluctuation analysis should be extended to find the actual distributions of  $G$  and  $D$  and the average total width.

A set of experimental average cross sections has been analysed by this method and agreement to order of magnitude only obtained with the predicted quantities.

In the absence of more detailed experimental information, it is concluded that because the experimental values of  $F$  and  $F_f$  disagree with the predicted values in certain cases, the assumptions on which equation (3) is based are not always valid. Correlations in the fission cross section of  $^{235}\text{U}$  are highly probable, and are possible in the total cross section of europium. The experimental data discussed here were not obtained with this method of analysis in mind and properly designed experiments could yield more complete and reliable information. If such experiments are combined with a more detailed theoretical treatment of the correlation problem, the experimental status of the spacing and width distributions will be substantially advanced.

### ACKNOWLEDGMENTS

I have benefited from the discussion of this method with Dr. A. Lane and Mr. E. Lynn who have made numerous suggestions. Miss B. R. Harrison and Mr. E. Fossey carried out the computations of the  $x(W)$ . I am indebted to Drs. Gaerttner and Yeater for kindly sending me a tabulation of their results prior to publication.

### APPENDIX

#### DERIVATION OF EQUATION (3)

BY J. M. HAMMERSLEY and A. M. LANE

In order to determine an expression for the variance of the total neutron width in a fixed energy interval, one must first determine the distribution of the

total width and then take the second moment of the distribution. It is not correct to use the well-known relation for the variance of a quotient:

$$\frac{\text{Var}(G/D)}{\langle G/D \rangle^2} = \frac{\text{Var } G}{\langle G \rangle^2} + \frac{\text{Var } D}{\langle D \rangle^2} \quad \dots\dots (A1)$$

because the variable  $G/D$  is not the same as the variable  $\Sigma G/W$  appearing in equation (2) with which we are concerned. The relation (A1), which happens to give the correct result, can only be used as the basis of a plausibility derivation of (3).

#### Derivation of probability distribution.

Suppose that the frequency functions for spacings and widths are  $f(D)$  and  $g(G)$  respectively. We assume throughout the following proof that there are no correlations, either between widths and widths, between spacings and spacings, or between widths and spacings.

It can be shown, although we will not prove it here, that the probability of finding the first and second levels within an interval  $D$  beyond a randomly chosen energy are

$$\left. \begin{aligned} A_1(D) &= \int_0^D \frac{dD'}{D} \int_0^{D'} f(D'') dD'' \\ A_2(D) &= \int_0^D A_1(D-D') f(D') dD'. \end{aligned} \right\} \quad \dots\dots (A2)$$

Let  $P_n(T, W)$  be the probability that there are  $n$  and only  $n$  levels in intervals  $W$  measured from random points and that the sum of their neutron widths is less than  $T$ . This satisfies the recursion relation

$$P_n(T, W) = \int_0^T \int_0^W P_{n-1}(T-t, W-w) f(w) g(t) dw dt \quad \dots\dots (A3)$$

for  $n > 2$  and

$$P_0(T, W) = 1 - A_1(W), \quad P_1(T, W) = g(T)[A_1(W) - A_2(W)].$$

If  $P(T, W)$  is the probability that the sum of the neutron widths in intervals  $W$  measured from random points is less than  $T$ , then

$$P(T, W) = \sum_{n=0}^{\infty} P_n(T, W) \quad \dots\dots (A4)$$

and, from (A3),

$$P(T, W) = P_0(T, W) + P_1(T, W) + \int_0^T \int_0^W [P(T-t, W-w) - P_0(T-t, W-w)] f(w) g(t) dw dt. \quad \dots\dots (A5)$$

This integral equation is the basic one of the present analysis and is most conveniently solved in terms of the Laplace transforms  $\rho(u, v)$ ,  $\gamma(u)$  and  $\phi(v)$  of  $P(T, W)$ ,  $f(D)$  and  $g(G)$ . Straightforwardly it follows that

$$\rho(u, v) - \frac{1}{uv} = - \frac{1}{uv} \frac{1 - \gamma(u)}{1 - \gamma(u)\phi(v)} \frac{1 - \phi(v)}{v \langle G \rangle}. \quad \dots\dots (A6)$$

Tables of Laplace transforms enable one to derive explicit forms for the distribution function  $P(T, W)$  for many commonly assumed forms for  $g(G)$  and  $f(D)$ .

*Extraction of the mean value and variance.*

The mean value  $M(W)$  and mean square value  $S(W)$  of the total width in intervals  $W$  are

$$\left. \begin{aligned} M(W) &= \langle \Sigma G \rangle = \int_0^\infty T \frac{dP}{dT} dT = \int_0^\infty \{1 - P(T, W)\} dT \\ S(W) &= \langle (\Sigma G)^2 \rangle = \int T^2 \frac{dP}{dT} dT = 2 \int_0^\infty \{1 - P(T, W)\} T dT \end{aligned} \right\} \dots\dots (A7)$$

where the sum in these equations is over all the levels in an energy interval of width  $W$ . Taking the Laplace transforms of these relations:

$$\int_0^\infty M(W) e^{-Wv} dW = \left[ \frac{1}{uv} - \rho(u, v) \right]_{u=0} \dots\dots (A8)$$

$$\int_0^\infty S(W) e^{-Wv} dW = 2 \left[ \frac{\partial}{\partial u} \rho(u, v) - \frac{1}{uv} \right]_{u=0} \dots\dots (A9)$$

It follows immediately from (A6) and (A8) that

$$\langle \Sigma G \rangle = \langle G \rangle \frac{W}{\langle D \rangle} \dots\dots (A10)$$

Assuming that  $W \gg \langle D \rangle$ , the expansion of the left-hand side of (A9) in powers of  $v$  along with standard Tauberian arguments for the moments gives, after some algebra:

$$\left. \begin{aligned} \frac{\text{Var } x(W)}{\langle x \rangle^2} &= \frac{\text{Var } \Sigma G}{\langle \Sigma G \rangle^2} = \frac{S(W) - M^2(W)}{M^2(W)} = \frac{\langle D \rangle}{W} \left[ \frac{\text{Var } G}{\langle G \rangle^2} + \frac{\text{Var } D}{\langle D \rangle^2} \right] \\ &+ \left( \frac{\langle D \rangle}{W} \right)^2 \left[ \frac{\frac{1}{2} \langle D^2 \rangle^2 - \frac{1}{3} \langle D^3 \rangle \langle D \rangle}{\langle D \rangle^4} \right] + O \left( \frac{\langle D \rangle}{W} \right)^3 \end{aligned} \right\} \dots\dots (A11)$$

## REFERENCES

- BETHE, H. A., 1937, *Rev. Mod. Phys.*, **9**, 84.  
 FESHBACH, H., PORTER, C. E., and WEISSKOPF, V. F., 1954, *Phys. Rev.*, **96**, 448.  
 GAYTHER, D. B., and NICHOLSON, K. P., 1957, *Proc. Phys. Soc. A*, **70**, 51.  
 HUGHES, D. J., 1956, *Proc. Gatlinburg Conference on Neutron Physics*.  
 HUGHES, D. J., and HARVEY, J. A., 1955, *Neutron Cross Sections*, BNL. 325.  
 LANE, A., and LYNN, E., 1957, *A.E.R.E. Report No. T/R 2210* (London: H.M. Stationery Office).  
 PILCHER, V. E., HARVEY, J. A., and HUGHES, D. J., 1956, *Phys. Rev.*, **103**, 1342.  
 PORTER, C. E., and THOMAS, R. G., 1956, *Phys. Rev.*, **104**, 483.  
 RAE, E., 1956, *Proc. Conference on Nuclear Reactions* (Amsterdam: North Holland Publishing Co.).  
 SAILOR, V., 1956, *Phys. Rev.*, **104**, 736.  
 WIGNER, E., 1956, *Proc. Gatlinburg Conference on Neutron Physics*.  
 YEATER, M. L., MILLS, W. R., and GAERTTNER, E. R., 1956, *Phys. Rev.*, **104**, 479.



# Gamma Rays from the 6.89 Mev Level in $^{10}\text{B}$

By R. D. EDGE AND D. S. GEMMELL

Research School of Physical Sciences, Australian National University, Canberra

MS. received 20th January 1958

**Abstract.** Use of a large NaI(Tl) crystal has permitted determination of the yield curves of each of the high-energy gamma rays arising from the  $^9\text{Be}(p, \gamma)^{10}\text{B}$  reaction for proton energies from 220 to 440 kev. The results indicate that all but the ground state gamma rays arise from the 6.89 mev level in  $^{10}\text{B}$ , and this confirms the postulated 20% isotopic spin impurity for this level. The ground state transitions arise from the broad 7.48 mev level and there is some evidence for part of this gamma radiation arising from direct transitions. The 6.89 mev level can also decay by gamma-ray emission to the 5.11 mev level.

## § 1. INTRODUCTION

It has been indicated by Wilkinson and Clegg (1956) that a large failure of the isotopic spin selection rules may occur for transitions from the 6.89 mev state of  $^{10}\text{B}$ .

The observed angular isotropy of the gamma radiation from this level, together with the fact that transitions to excited states are more probable than ground state transitions, indicates that the level has spin  $1^-$ .

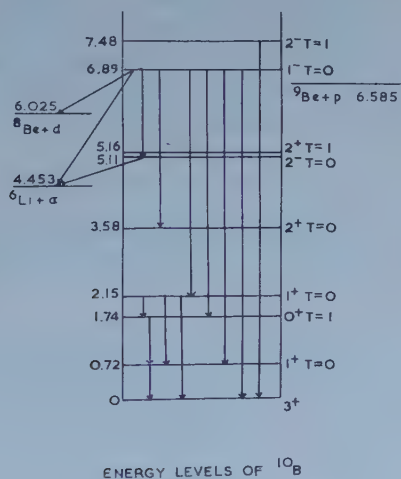


Figure 1. Relevant energy levels of  $^{10}\text{B}$ .

The isotopic spin of the level has been taken to be mainly  $T=0$  because of the intense E1 gamma-ray transition to the  $T=1$  state at 1.74 mev (see figure 1), and also because of the alternative modes of decay by deuteron or alpha-particle emission to the ground states of  $^8\text{Be}$  and  $^6\text{Li}$  respectively. However, if the assignment is correct, it is difficult to interpret the strong transitions to the  $1^+$ ,

$T=0$  states at 0.72 and 2.15 mev which are forbidden according to the isotopic spin selection rules for electric dipole transitions in self-conjugate nuclei. This would imply a  $T=1$  impurity of approximately 20% intensity, which is the largest impurity yet found in a light nucleus, and which is difficult to explain theoretically. Barker (1957) has shown that isotopic spin may be expected to remain a good quantum number up to quite high excitation energies in a light nucleus.

An alternative explanation which would resolve the difficulty is that, instead of the transitions occurring from a single state of  $^{10}\text{B}$  at 6.89 mev, they occur from two closely adjacent levels, one of which has  $T=0$ , and the other  $T=1$ . It was to test this possible explanation that the present experiments on the  $^9\text{Be}(p, \gamma)^{10}\text{B}$  reaction were performed.

## § 2. EXPERIMENTAL METHOD

It should be possible to distinguish two such levels by measuring the yield curves for the individual high-energy gamma rays as a function of proton energy. Transitions from the  $T=1$  state would be resonant at a proton energy differing from the resonance energy for transitions from the  $T=0$  state. It is also to be expected that the total widths would not be the same for the two resonances.

To determine these yield curves, accurate spectra of the high-energy gamma radiation from  $^{10}\text{B}$  were recorded at 10 kev intervals for proton energies between 220 and 440 kev. Thin beryllium targets were used, approximately 10 kev thick at 300 kev proton energy, and were prepared by evaporating beryllium metal on to a copper backing.

The protons were accelerated in a 1 mev Cockcroft-Walton h.t. set, and after deflection by a  $90^\circ$  analysing magnet, passed through a  $\frac{3}{8}$  in. diameter collimating stop, on to the target. A cylindrical electrode in front of the target was held at a negative potential to prevent the escape of secondary electrons from the beryllium. To reduce deposition of carbon, the target was held at a temperature of  $90^\circ\text{C}$  by passing water over the target backing, and a liquid air trap was inserted in the target tube to remove oil vapour.

## § 3. DETECTION OF GAMMA RAYS

The cross section for the  $^9\text{Be}(p, \gamma)^{10}\text{B}$  reaction is small (approximately  $20 \mu\text{bn}$  at the 336 kev resonance) and the gamma-ray spectrum is complex. Therefore, it was necessary to use a spectrometer which was both sensitive and of high resolution.

This was achieved by employing, as scintillator, a Harshaw NaI(Tl) crystal 5 inches in diameter and 4.5 inches in length, mounted on the 5-inch photocathode of a Dumont 6364 phototube. The combination of crystal and phototube was placed with its axis vertical and with the curved face of the crystal 6 inches from the beryllium target in line with the incoming protons. Gamma radiation from the target was collimated by a 1-inch diameter hole in a lead wall 3 inches thick, and by a similar hole in a large steel block in which the crystal was seated and which served to shield the crystal from scattered radiation. Pulses from the phototube passed through a non-overload amplifier into a 70-channel Sunvic pulse height analyser.

Irradiations of up to six hours at beam currents of  $200 \mu\text{A}$  were required at each of these proton energies in order to obtain spectra sufficiently accurate for

analysis. Figure 2(a) shows a typical spectrum for the high-energy gamma rays at a bombarding proton energy of 300 kev. The full-energy peaks and peaks corresponding to the escape from the crystal of one 511 kev positron annihilation quantum are marked.

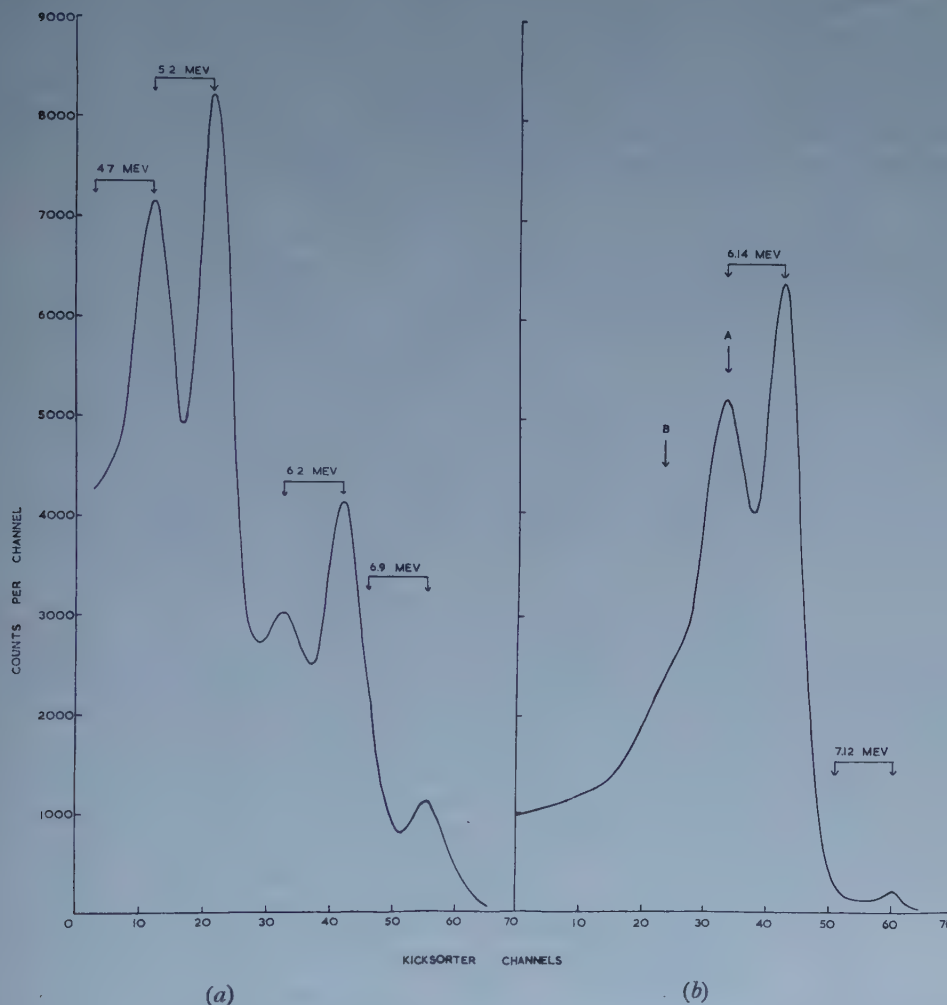


Figure 2. (a) Spectrum of  $^9\text{Be}(p, \gamma)^{10}\text{B}$  high-energy gamma rays at a proton energy of 300 kev.

(b) Spectrum of gamma rays from the 340 kev resonance in the reaction  $^{19}\text{F}(p, \alpha, \gamma)^{16}\text{O}$ .

The pulse height distribution produced by the 6.14 mev gamma rays arising from the 340 kev resonance in the  $^{19}\text{F}(p\alpha\gamma)^{16}\text{O}$  reaction is shown in figure 2(b). The lower intensity 7.12 mev radiation is also resolved. The size of the escape peak A could be further reduced and the resolution improved by collimation of the gamma rays into a narrower beam. However, in this experiment a 1-inch diameter collimator gave a satisfactory compromise between resolution and counting rate. The shoulder, marked B in figure 2(b), on the 6.14 mev spectrum is due to the peak corresponding to escape of both annihilation gamma rays.

This is greatly reduced relative to the single escape peak A because of the large dimensions of the crystal.

#### § 4. ANALYSIS

To determine the resonance width and energy of the transitions to the  $T=0$  and  $T=1$  states, each spectrum was analysed into the contributions from the constituent gamma rays. For the analysis, it was necessary to know the individual pulse height distributions produced by gamma rays of 4.7, 5.2, 6.2 and 6.9 mev energy. These were derived by interpolation between the distributions produced by a number of calibration gamma rays of known energy.

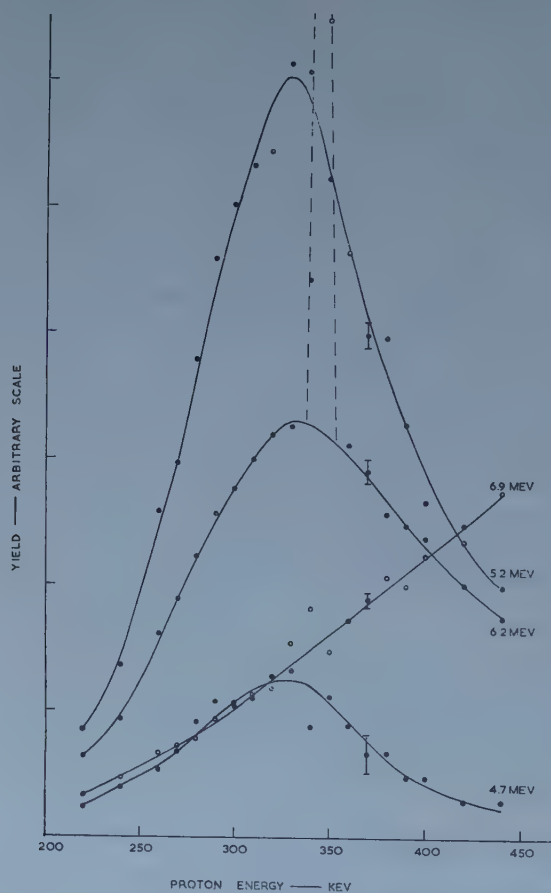


Figure 3. Yield curves of high-energy gamma rays. The probable errors are shown at a proton energy of 370 kev.

By substituting a  $^{13}\text{C}$  target for the beryllium one, the pulse height distribution produced by 8.1 mev gamma rays arising from the 550 kev resonance in the  $^{13}\text{C}(\text{p}, \gamma)^{14}\text{N}$  reaction was measured. Similarly, the 340 kev resonance in the  $^{19}\text{F}(\text{p}, \alpha \gamma)^{16}\text{O}$  reaction gave the distribution for 6.1 mev radiation. Pulse height distributions were also measured using the reaction  $^{11}\text{B}(\text{p}, \gamma)^{12}\text{C}$  at the 160 kev resonance; this gave two calibration gamma rays of 4.4 and 11.7 mev energy respectively. While measuring each calibration distribution, the geometry of



the experiment was kept exactly the same as that for the beryllium runs, in order to avoid any errors due to changes in resolution.

The analysis of each  $^9\text{Be}(p, \gamma)^{10}\text{B}$  spectrum was performed by successively subtracting the distributions due to the 6.9, 6.2, 5.2 and 4.7 MeV gamma rays. The resulting yield curves for the individual gamma rays are shown in figure 3, where the errors are calculated on the assumption that the distributions due to individual gamma rays are known exactly. The sharp peak in the 6.2 MeV curve, shown dashed in figure 3, is due to the 340 keV resonance in the  $^{19}\text{F}(p, \alpha\gamma)^{16}\text{O}$  reaction occurring in fluorine contamination of the beryllium. Several targets were prepared using beryllium from different sources, but each showed some degree of fluorine contamination. The fluorine gamma rays arise from a very narrow resonance, and it was possible to correct the yield curve for their effect.

It will be seen from figure 3 that, excluding the 6.89 MeV radiation, all the gamma rays are resonant at the same energy to within ten kilovolts, and have approximately the same width. This indicates that the explanation of two close states is untenable, and that the transitions to the  $T=1$  and to the  $T=0$  states do, in fact, come from the same state of  $^{10}\text{B}$ .

From the yield curves shown in figure 3, it is possible to derive the excitation function of the total resonant radiation. After using coulomb wave functions according to Christy and Latter (1948) to allow for the effect of barrier penetrability for S-wave protons, the curve shown in figure 4 was obtained. This could be fitted with a Breit-Wigner one-level dispersion formula with resonance energy 310 keV and a width of 135 keV.

### § 5. THE GROUND STATE TRANSITION

The good resolution obtainable with such a large crystal allows the 6.9 MeV gamma ray to be well resolved (figure 2(a)), and the yield curve to be determined. This transition is clearly non-resonant over the range of proton energies examined. The steadily increasing yield suggests that the 6.9 MeV gamma rays arise from the tail of the 993 keV resonance which is known to emit gamma rays predominantly to the ground state of  $^{10}\text{B}$  (Hornyak and Coor 1953). However, assuming the value of  $12 \pm 4 \mu\text{bn}$  given by Carlson and Nelson (1955) for the cross section for emission of 5.2 MeV gamma rays at the 336 keV resonance, one obtains a value of  $3 \pm 1 \mu\text{bn}$  for the cross section at 330 keV for emission of ground state gamma rays. This is approximately five times the cross section which is to be expected from the tail of the 993 keV resonance, using the data of Hornyak and Coor.

Evidence which confirms the existence of this difference was found by determining the excitation function of the ground state gamma rays in the range of proton energies between 300 and 1060 keV. It was found that while a dispersion formula gave a good fit to the experimental points in the region of the resonance peak at 993 keV, at lower proton energies the fit was not good. The yield at 330 keV was again found to be about five times that expected.

The difference between the experimental and theoretical yield curves could imply a contribution from a direct transition. It has been shown by F. C. Barker (private communication) that by analogy with the  $^7\text{Li}(p, \gamma)^8\text{Be}$  case, direct effects of the order of a few microbarns are to be expected for the  $^9\text{Be}(p, \gamma)^{10}\text{B}$  reaction at these proton energies.

Figure 5 shows that the resonant gamma rays do not bear quite the same ratios to one another over the resonance. It is possible that this might be caused by

a mixture of resonant radiation and direct transitions giving interference effects.

In addition, low-energy gamma-ray spectra were obtained at several bombarding energies. The low-energy spectra showed the variation with proton energy to be expected from the high-energy spectra, using the decay scheme of  $^{10}\text{B}$  shown in figure 1. To confirm that all the gamma radiation arose from S-wave protons incident on the nucleus, the resonance gamma-ray spectra at  $0^\circ$  and  $90^\circ$  to the incoming proton beam were closely compared. It was not possible to distinguish between the shapes of the spectra, and the yields at  $0^\circ$  and  $90^\circ$  did not differ by more than 2%.

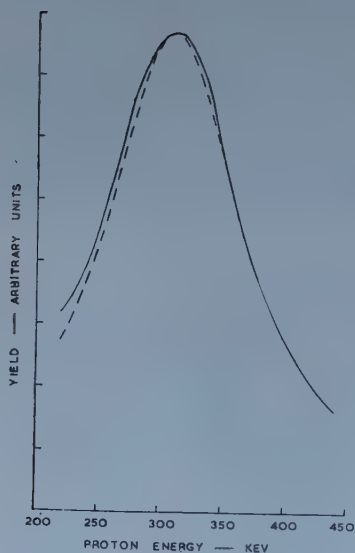


Figure 4. Excitation function of the total radiation resonant at 330 keV, after allowing for barrier penetrability and proton wavelength. The dashed line represents a single-level dispersion formula with a resonance energy of 310 keV and a width of 135 keV.

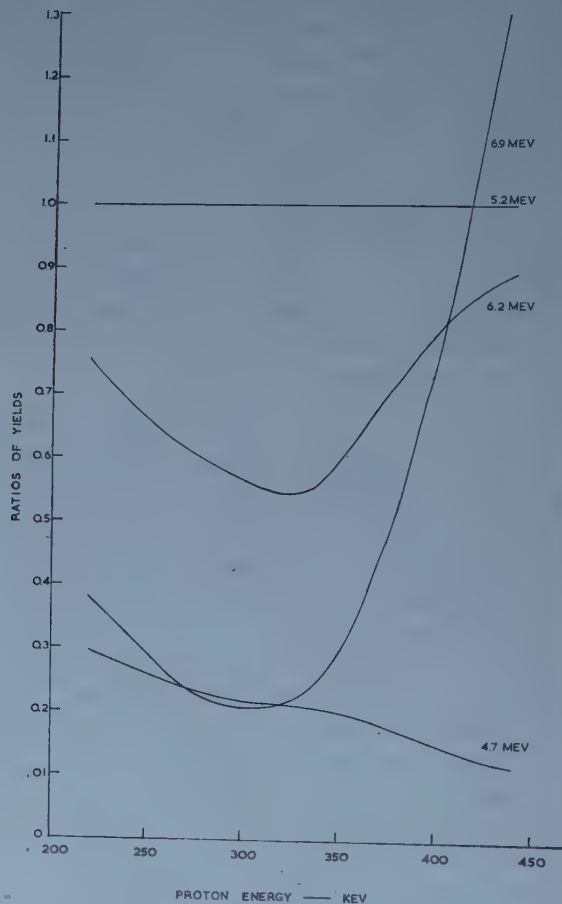


Figure 5. Ratios of yields of high-energy gamma rays to that of the 5.15 MeV gamma ray, as a function of proton energy.

#### § 6. THE 5.11 MEV STATE

It has been suggested by Clegg (1956) that a 1.7 MeV gamma-ray transition occurs from the 6.89 MeV level in  $^{10}\text{B}$  with an intensity 20% of that to the 1.74 MeV level. We have also observed a 1.7 MeV gamma ray and have performed a coincidence experiment to investigate possible cascades involving it and other gamma radiation.

A NaI(Tl) crystal 1.5 inches in diameter by 2 inches in length was used to examine the low-energy gamma rays. The spectrum from the small crystal was observed in coincidence with pulses from the big crystal which were larger than the pulse height corresponding to 3.5 MeV. From this, it is possible to say that less than 5% of the 1.7 MeV gamma rays are in coincidence with any gamma radiation of energy greater than 3.5 MeV.

This confirms that most of the 1.7 MeV gamma rays are caused by transitions to the 5.11 or 5.16 MeV states, because the only other way of generating gamma rays of this energy would be in transitions to the ground state from the 1.74 MeV level; this would imply a magnetic octopole transition, which is unlikely to occur. The absence of high-energy gamma rays in coincidence with the 1.7 MeV gamma ray indicates that ground state transitions from the 1.74 MeV state are, in fact, suppressed. Clegg's measurement of the energy of the 1.7 MeV radiation showed it to arise from transitions to the 5.11 MeV and not to the 5.16 MeV level in  $^{10}\text{B}$ . The present results show that whichever state is formed, it probably breaks up by alpha-particle emission to the ground state of  $^6\text{Li}$  since no high-energy gamma radiation is observed.

### § 7. CONCLUSIONS

The 6.89 MeV level in  $^{10}\text{B}$  has an abnormally large isotopic spin impurity which is difficult to explain theoretically. The ground state gamma-ray transition is not resonant at 330 keV in the  $^9\text{Be}(p, \gamma)^{10}\text{B}$  reaction, but may arise in part from the broad 7.48 MeV state which is known to emit gamma rays predominantly to the ground state; there may also be a possible contribution from direct transitions. A 1.7 MeV gamma-ray transition from the 6.89 MeV state produces a level of  $^{10}\text{B}$  which probably decays by alpha-particle emission.

### ACKNOWLEDGMENTS

The authors wish to thank Professor E. W. Titterton for his encouragement and interest in this investigation, and Dr. F. C. Barker for many instructive discussions of the results.

### REFERENCES

- BARKER, F. C., 1957, *Phil. Mag.*, **2**, 286.
- CARLSON, R. R., and NELSON, E. B., 1955, *Phys. Rev.*, **98**, 1310.
- CHRISTY, R. F., and LATTER, R., 1948, *Rev. Mod. Phys.*, **20**, 185.
- CLEGG, A. B., 1956, *Phil. Mag.*, **1**, 1116.
- HORNYAK, W. F., and COOR, T., 1953, *Phys. Rev.*, **92**, 675.
- WILKINSON, D. H., and CLEGG, A. B., 1956, *Phil. Mag.*, **1**, 291.

## Elastic Scattering of Pions at a Bound Nucleon

By E. W. LAING†

Natural Philosophy Department, University of Glasgow

*MS. received 16th September 1957, and in revised form 17th February 1958*

**Abstract.** In the approximation of the single nucleon model for the nucleus, the effect of nuclear binding on pion-nucleon scattering is estimated using a variational method and neglecting nucleon recoil in intermediate states. Results are compared with those of a simple p-wave phenomenological theory. Similar cross sections are obtained except in the region of the p-wave resonance of free nucleon-pion scattering, where the phenomenological theory leads to a cross section an order of magnitude smaller. This result is unaffected when nucleon recoil is taken into account, but may be sensitive to the choice of trial wave functions used in the variational calculation.

### § 1. INTRODUCTION

THE purpose of this work is to investigate the effect of nuclear binding on pion-nucleon scattering. Previous workers have adopted a phenomenological approach, making use of the fact that scattering by free nucleons of pions of medium kinetic energy (less than 200 mev) proceeds mainly through s and p meson waves. Peaslee (1952) has calculated scattering by  $^{12}\text{C}$  on the assumption of a p-wave resonance. Kisslinger (1955), following the methods of Watson (1953) and Francis and Watson (1953) and obtaining an optical model for the pion-nucleus interaction, employs free particle scattering amplitudes in order to obtain the relevant data for the optical model.

In the present paper, the Chew static p-wave interaction is assumed for the pion-nucleon interaction. For the nuclear binding, a simple model is assumed of a single nucleon moving in a central field  $V$ , representing the effect of the rest of the nucleus. With a one-nucleon model, there are no multiple scattering effects, though these will be present in a more realistic theory. To simplify matters,  $V$  is taken to be a square well potential, corresponding to approximately  $\alpha$ -particle data, so that there exists only one bound state. Only direct (non-spin flip) elastic scattering of positive pions by protons is considered. Even with these restrictions, it is possible for scattering to occur in all angular momentum states of the pion relative to the centre of nuclear potential, which is taken to be fixed. To evaluate the scattering, methods are used similar to those employed by Chew (1954 a, b) for pion scattering at free nucleons, which were based on a variational principle of Lippmann and Schwinger (1950). The scattering cross section is evaluated in the approximation of neglecting nucleon recoil in intermediate states. This is compared with results obtained from a phenomenological method. A discussion of effects of taking recoil into account is also given.

† Now at the Theoretical Physics Division, A.E.R.E., Harwell, Didcot, Berks.



## § 2. GENERAL FORMALISM

The total Hamiltonian for the pion-nucleon system is

$$H = K_n + K_m + V + H' \quad \dots\dots (1)$$

where  $K_{n,m}$  = kinetic energy operators for nucleon, meson respectively, the nucleon being treated throughout non-relativistically.  $V$  is the nuclear potential,  $H'$  is the Chew static p-wave interaction. In  $H'$ , the p-wave Galilean term and s-wave interaction terms are omitted, though these should be included in any subsequent refinement of the theory. An exact solution of the model proposed is impossible. It requires the solution of an integral equation for the reaction matrix  $K$  of the form

$$K = H' + H'P \frac{1}{E - K_m - H_0} K \quad \dots\dots (2)$$

where  $P$  indicates that a principal part of the denominator must be taken, and  $H_0 = K_n + V$  = nuclear Hamiltonian.

Lippmann and Schwinger have given variational methods which can be applied to this problem. To preserve the unitarity of the scattering matrix, it is more convenient to apply these methods to the reaction matrix  $K$ . This has been pointed out by other authors.

One requires the matrix element  $K_{ba}$  of  $K$  between the states  $a$  and  $b$ , given by

$$K_{ba} = (\phi_b, H' \psi_a) \quad \dots\dots (3)$$

where

$$\psi_a = \phi_a + P \frac{1}{E - H_0 - K_m} H' \psi_a \quad \dots\dots (4)$$

and  $\phi_a$  is an unperturbed state. Application of the variational techniques yields the result that

$$K_{ba}' = \frac{(\phi_b, H' \psi_a)(\psi_b, H' \phi_a)}{(\psi_b, H' \psi_a) - [\psi_b, H' P (E - H_0 - K_m)^{-1} H' \psi_a]} \quad \dots\dots (5)$$

is stationary for arbitrary small variations of  $\psi_a$  and  $\psi_b$  about the solutions of equation (4), and that the stationary value of (5) is  $K_{ba}$ . In (5),  $K_{ba}'$  is independent of the normalization of  $\psi_a$  and  $\psi_b$ . Suitable trial functions must be chosen to insert into (5) for  $\psi_a$  and  $\psi_b$ . It is assumed in this paper that  $\psi = [1 + P(E - H_0 - K_m)^{-1} H'] \phi$  is suitable. This immediately gives

$$K_{ba} = K_2^2 / (K_2 - K_4). \quad \dots\dots (6)$$

$K_2$  and  $K_4$  are the second- and fourth-order matrix elements of a perturbation expansion of  $K_{ba}$ .  $\phi_a$  and  $\phi_b$  are states containing a bound nucleon and a plane wave meson.  $K_{ba}$  may be written in the form

$$K_{ba} = \sum_l [4\pi(2l+1)]^{1/2} K_{ll}(k) Y_l^0(\theta) \quad \dots\dots (7)$$

where  $k$  = momentum of meson,  $l$  = angular momentum of meson,  $\theta$  = scattering angle.

Thus, the scattering is similar to that produced by a central field, with scattering phase shifts  $\delta_l$  related to  $K_{ll}(k)$  by the well-known expression,

$$\tan \delta_l = -K_{ll}(k) k \omega_k / 2\pi \quad \dots\dots (8)$$

where  $\omega_k$  = total meson energy.

For the no-recoil approximation,  $K_2$  and  $K_4$  are of the form

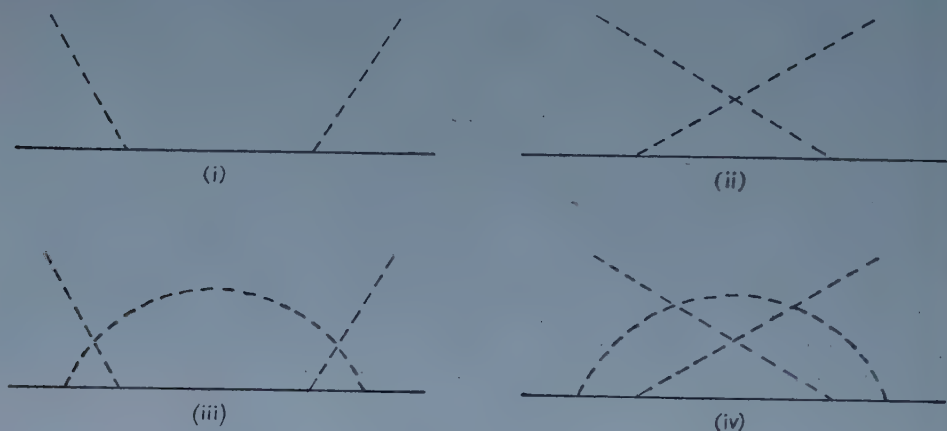
$$K_4 = \Delta(k)K_2 \quad \dots\dots (9)$$

$$K_2 = \sum_l [4\pi(2l+1)]^{1/2} A_l(k) Y_l^0(\theta)$$

so that

$$K_{ll}(k) = A_l(k)/(1 - \Delta(k)). \quad \dots\dots (10)$$

Finally,  $K_2$  and  $K_4$  correspond to the processes (i), (ii) and (iii), (iv), respectively (see figure).



In a charge-symmetric meson-nucleon theory, these processes carry the charge factors 0, 2, 4, 2 for (i), (ii), (iii), (iv) respectively, for the case of direct elastic scattering of positive pions on protons.

### § 3. NO-RECOIL APPROXIMATION

In the no-recoil approximation,  $H_0$  of equation (2) is set equal to zero. Calculations are performed in coordinate space. The nucleon bound state wave function is  $\psi_0(\mathbf{r}) = f(r)/(4\pi)^{1/2}$  for an s-state. The meson is initially and finally in the momentum states  $\mathbf{k}$  and  $\mathbf{k}'$  respectively (with  $k = k'$  and  $\mathbf{k} \cdot \mathbf{k}' = k^2 \cos \theta$ )

$$H'(\mathbf{k}) = \pm (if/\mu)(2\omega_k)^{-1/2} \boldsymbol{\sigma} \cdot \mathbf{k} \exp(\pm i\mathbf{k} \cdot \mathbf{r}) \quad \dots\dots (11)$$

where the plus sign is for pion absorption and the minus sign for emission.

Noting that, in this approximation, the Green's function for the propagation of a nucleon of energy  $E$  from  $\mathbf{r}$  to  $\mathbf{r}'$  is  $\delta(\mathbf{r} - \mathbf{r}')/E$ , the following expressions are obtained for  $A_l(k)$  of equation (10)

$$\begin{aligned} l=0, \quad A_0(k) &= B_1(k), \\ l \neq 0, \quad A_l(k) &= [lB_{l-1}(k) + (l+1)B_{l+1}(k)]/(2l+1) \end{aligned} \quad \dots\dots (12)$$

where

$$B_l(k) = -\frac{f^2 k^2}{\mu^2 \omega_k^2} \int_0^\infty j_l^2(kr) f^2(r) r^2 dr. \quad \dots\dots (13)$$

For  $\Delta(k)$  of equation (10) one obtains

$$\Delta(k) = f^2 \omega_k (2I + J)/4\mu^2 \pi^2 \quad \dots\dots (14)$$

where  $I$  and  $J$  are

$$\begin{aligned} I(k) &= P \int_0^{q_{\max}} \frac{q^4}{\omega_q^3 (\omega_q - \omega_k)} dq \\ J(k) &= \int_0^{q_{\max}} \frac{q^4}{\omega_q^3 (\omega_q + \omega_k)} dq. \end{aligned} \quad \dots\dots (15)$$

$q_{\max}$  is the cut-off required in PS(PV) theory. For definiteness, it is assumed that  $f^2=1$  and  $\omega_{q_{\max}}=5.6\mu$ , in accord with customary values employed in scattering at a free nucleon. For the square well nuclear potential  $V$ , suitable values for the depth and radius are  $V_0=30$  mev and  $r_0=2\times 10^{-13}$  cm. These values lead to a binding energy for the nucleon of 7 mev, which is neglected in the calculations of this section.

It should be noted that a resonance occurs in the scattering when  $\Delta(k)=1$ . However, the situation here is that all phase shifts pass through  $90^\circ$  at the same energy, a situation which is only slightly altered if recoil is taken into account. The consequence of this is that the scattering amplitude is zero except in the forward direction. This result is discussed further in §5.

Table 1. Differential Cross Section  $d\sigma/d\Omega$  (mbn) at  $20^\circ$ , as a function of Pion Energy

Pion energy (mev)	200	220	240	260	280	300	320	340
Calculated	1.2	2.8	6.3	13	28	62	153	377
Phenomenological	2.7	5.9	10.8	18	25	29	28	24

Table 2. Differential Cross Section  $d\sigma/d\Omega$  (mbn) at 260 mev and 320 mev, as a function of Pion Angle

Pion energy (mev)	Pion angle (deg.)									
	0	20	40	60	80	100	120	140	160	180
260 (calc.)	17	13	5.2	1.0	0.05	0.02	0.08	0.09	0.06	0.04
260 (phen.)	28	18	4.8	0.4	0	0.07	0.08	0.05	0.03	0.03
320 (calc.)	232	153	41	4.5	1.7	1.1	0.2	0	0.2	0.7
320 (phen.)	52	28	4.9	0.2	0	0	0	0	0	0

In table 1 the differential cross section at  $\theta=20^\circ$  is given for  $\omega_k$  in the range 200–340 mev. In table 2 two angular distributions are given for  $\omega_k=260, 320$  mev. These are compared with results obtained from a simple phenomenological theory, in which the scattering at a free proton, assumed at rest, is modified only by the inclusion of a form factor, which takes into account the fact that the nucleon is bound initially and finally, but allows the nucleon to be free in intermediate states. The differential scattering cross section in the phenomenological theory outlined above may thus be written as

$$\frac{d\sigma}{d\Omega} = |F|^2 \frac{d\sigma_f}{d\Omega} \quad \dots\dots (16)$$

where  $F = f\psi_0^2 \exp i(\mathbf{k} - \mathbf{k}') \cdot \mathbf{r} d\mathbf{r}$ .  $\mathbf{k} - \mathbf{k}'$  is the momentum transferred to the proton during the scattering. The free particle differential cross section,  $d\sigma_f/d\Omega$ , appropriate to direct scattering, is given by Bethe and de Hoffmann (1955), as

$$\frac{d\sigma_f}{d\Omega} = \frac{4 \sin^2 \delta \cos^2 \theta}{k^2},$$

where all quantities are to be evaluated in the centre-of-mass system of the pion and struck proton.  $\delta$  is the phase shift in the  $(\frac{3}{2}, \frac{3}{2})$  state as given by Orear (1955), all other phase shifts being negligibly small for the purposes of this calculation. Before inserting into equation (16),  $d\sigma_f/d\Omega$  must be transformed to the laboratory system.

## § 4. CORRECTIONS TO NO-RECOIL APPROXIMATION

In this section, the effect of taking into account the recoil of the nucleon is discussed, only in so far as it affects the energy denominators which occur in intermediate states. In § 3, the Green's function  $G_E(\mathbf{r}', \mathbf{r})$  is approximated by  $\delta(\mathbf{r} - \mathbf{r}')/E$ . This was the result of neglecting  $H_0$  of equation (2). The effect is now considered of taking  $H_0$ , (a) as  $K_n$ , and (b) as  $K_n + V$ . One introduces the complete set of eigenfunctions  $\psi_n$  satisfying  $H_0\psi_n = E_n\psi_n$ . For case (a), the  $\psi_n$  are plane waves; for case (b),  $\psi_0$  is the bound state and the remaining members of the set are positive energy distorted waves. The Green's function can be expanded in terms of the  $\psi_n$ :

$$G_E(\mathbf{r}', \mathbf{r}) = P \sum_n \frac{\psi_n(\mathbf{r}')\psi_n^*(\mathbf{r})}{E - E_n}. \quad \dots\dots (17)$$

The no-recoil approximation is recovered in cases (a) and (b) by neglecting  $E_n$  in equation (17) and using the completeness relation.

An expression has to be found for  $G_E(\mathbf{r}', \mathbf{r})$ , suitable for computation. This can be obtained in a similar way to that given by Mott and Massey (1949), where the outgoing wave condition at infinity is to be replaced by one of standing waves. The result is that

$$G_E(\mathbf{r}', \mathbf{r}) = \sum_{lm} g_l(E, r', r) Y_l^m(\mathbf{r}') Y_l^{m*}(\mathbf{r}) \quad \dots\dots (18)$$

where, for case (a) and  $E > 0$ ,

$$g_l(E, r', r) = 2Mqj_l(qr_<)n_l(qr_>) \quad \dots\dots (19)$$

where  $r_<, r_> = \min, \max(r, r')$ ,  $M$  is the nucleon mass and  $q^2/2M = E$ . Similar expressions occur for  $E < 0$  and for case (b). In case (b), a difficulty occurs at  $E = E_0$ , the eigenvalue of  $\psi_0$ , for the Green's function is then unbounded. This difficulty is removed by noting that  $G_E$  is in effect the propagator for a non-interacting system of one nucleon and any number of mesons, and applying the standing wave condition to the meson current.

To reduce the size of the computation, only the case of s-wave nucleons is investigated. That is, for  $l > 0$ , one replaces  $g_l$  in (18) by the no-recoil expression  $\delta(r - r')/r^2E$ . This approximation is expected to be valid for the following physical reasons. Variations from the no-recoil approximations are expected to be negligible except for small values of  $E$ ,  $r$  and  $r'$ , due to the rapid fall-off of the Green's function for  $q|\mathbf{r} - \mathbf{r}'|$  large and to the presence of bound state wave functions. The centrifugal repulsion experienced by all except s-wave nucleons will then produce the desired result. The result of this discussion is that the Green's function may be approximated by

$$G_E(\mathbf{r}', \mathbf{r}) = \delta(\mathbf{r} - \mathbf{r}')/E + \{g_0(E, r', r) - \delta(r - r')/r^2E\}/4\pi. \quad \dots\dots (20)$$

In  $K_2$ , only  $B_0(k)$  (expression (13)) is altered:

$$B_0(k) \rightarrow \frac{f^2 k^2}{\mu^2 \omega_k} \int_0^\infty j_0(kr) j_0(kr') f(r) f(r') g_0(-\omega_k, r', r) r^2 r'^2 dr dr'. \quad \dots\dots (21)$$

Ratios of  $B_0(k)$  in the various approximations are given in table 3.

Table 3. Ratios of  $B_0(k)$ 

Pion energy (mev)	200	260	300	340
Case (a)/no-recoil	1.04	1.06	1.07	1.03
Case (b)/no-recoil	—	—	1.15	—



In  $K_4$  an equivalent expression may be obtained, but is too involved for computation, leading to five-dimensional multiple integrals (including the summation over intermediate meson states). The results given in table 3 lead to the assertion that, in intermediate states, the nucleon propagator can be approximated by the no-recoil expression except when one, and only one, meson is also present. Thus, only corrections to graph (iii), in  $K_4$ , are required. Inserting expression (20) for the Green's function into  $K_4$ , one obtains the result that the following substitution must be made, for  $l=0$ ,

$$\begin{aligned}
 I(k) \int_0^\infty j_0^2(kr)f^2(r)r^2 dr &\longrightarrow I(k) \int_0^\infty j_0^2(kr)f^2(r)r^2 dr \\
 &+ \int_0^\infty j_0^2(kr)f^2(r)r^2 dr P \int_0^{q_{\max}} \frac{q^4 j_0^2(qr)}{\omega_q^3(\omega_k - \omega_q)} dq \\
 &- \int_0^\infty j_0(kr)j_0(kr')f(r)f(r')r^2 r'^2 dr dr' P \int_0^{q_{\max}} \frac{q^4}{\omega_q^3} g_0(\omega_k - \omega_q, r', r) j_0(qr)j_0(qr') dq.
 \end{aligned}
 \dots\dots (22)$$

Even this expression leads to lengthy numerical integrations. It was evaluated only for case (a),  $\omega_k = 300$  mev. It was found that, although a 50% correction to the nucleon s-wave contribution occurred, the major part of graph (iii) comes from high momentum and angular momentum components. This tends to smooth out the large s-wave correction, so that altogether only a 7% correction results. It seems reasonable to conclude that the same situation will arise at other meson energies and for case (b).

To investigate the effect of case (b) on  $K_4$ , it seemed that a good approximation would be to replace the positive energy states in equation (17) by plane waves. This gives

$$G_E(\mathbf{r}', \mathbf{r}) = \frac{\psi_0(\mathbf{r}')\psi_0^*(\mathbf{r})}{E - E_0} + G_E(\text{case (a)}). \dots\dots (23)$$

However, it can be shown by direct calculation in  $K_2$  that (23) is not reliable. Thus, for  $B_0(k)$  and  $\omega_k = 300$  mev, the contribution from the first term of (23) is 50% that of the second term, while direct calculation (see table 3) shows that the exact Green's function leads to only 8% more than the free particle case (a). This result is only to be expected, since the expansion (17) depends on the completeness of the set of functions  $\psi_n$ , which was disregarded in obtaining equation (23).

## § 5. DISCUSSION

In this paper, the effect of nuclear binding on pion-nucleon scattering has been investigated for the simple case of a one-nucleon model, in which the effect of other nucleons is represented by a square well potential. There were two reasons for carrying out this investigation; firstly, it seemed worth while to investigate the reliability of the phenomenological approach, which assumes that the scattering takes place as if the nucleon were free. Secondly, the simple model assumed afforded the possibility of investigating the validity of neglecting nucleon recoil.

On the first point, results indicate that, well below the resonance energy, the two methods yield similar results, but that near the resonance the method outlined in this paper leads to a much larger scattering cross section than the phenomenological approach. This is due to the fact that a large number of

partial waves participate in the scattering, while, in the phenomenological method, this effect is summed up in the form factor, which can never exceed unity. A large part of the effect may be artificial, due to the fact that the simple trial function assumed in the variational expression (5) automatically leads to a resonance denominator in (10) which is independent of the meson angular momentum. It is unlikely, physically, that all partial waves should resonate at the same energy. The possibility still remains that, since the nucleon can exchange momentum with the rest of the nucleus, in intermediate states, more states are available than in the corresponding free nucleon case. The phenomenological method does not permit this. It should be possible to investigate this situation by using a better trial function to feed into expression (5). Experimental results should also show if any effect exists, but effects of multiple scattering will obscure this, since they generally tend to reduce scattering cross sections.

Secondly, on the assumption that the main effect of nuclear recoil would be felt in nucleon s-waves, results indicate that the no-recoil approximation is reliable. In fact, the difference between the various approximations can be largely absorbed into the coupling constant, since there is little variation with energy. A more serious criticism of the results is the omission of an s-wave meson interaction and the Galilean term which should be added to the p-wave interaction when nucleon recoil is permitted. However, it is hoped that these effects will be small in the energy region in which results have been obtained, since they are also expected to be small in the free nucleon case.

#### ACKNOWLEDGMENTS

The author would like to thank Professor J. C. Gunn, Dr. R. G. Moorhouse and Dr. B. H. Bransden for valuable discussions.

#### REFERENCES

- BETHE, H. A., and DE HOFFMANN, F., 1955, *Mesons and Fields, Volume II* (Evanston, Illinois: Row, Peterson and Co.), p. 67.  
CHEW, G. F., 1954 a, *Phys. Rev.*, **93**, 341; 1954 b, *Ibid.*, **94**, 1755.  
FRANCIS, N. C., and WATSON, K. M., 1953, *Phys. Rev.*, **92**, 291.  
KISSLINGER, L. S., 1955, *Phys. Rev.*, **98**, 761.  
LIPPMANN, B. A., and SCHWINGER, J., 1950, *Phys. Rev.*, **79**, 469.  
MOTT, N. F., and MASSEY, H. S. W., 1949, *The Theory of Atomic Collisions* (Oxford: Clarendon Press).  
OREAR, J., 1955, *Phys. Rev.*, **100**, 288.  
PEASLEE, D. C., 1952, *Phys. Rev.*, **87**, 862.  
WATSON, K. M., 1953, *Phys. Rev.*, **89**, 575.

## Configurational Mixing in $\beta$ -Decay Theory

By C. A. CAINE

Clarendon Laboratory, Oxford

*MS. received 26th September 1957, and in revised form 20th February 1958*

**Abstract.** The effect of simple configurational mixing, within the  $j-j$  coupling shell model, on the nuclear matrix elements for allowed beta-transitions of odd  $A$  nuclei is considered. It is shown that such mixing could be responsible for the unfavoured nature of such transitions within the 2d and 1g shells.

### § 1. INTRODUCTION

THE  $j-j$  coupling shell model of the nucleus, in its extreme single-particle formulation, has had considerable success in systematizing and classifying the experimental beta-decay data (see, for example, Mayer and Jensen 1955). However, this success does not extend to a quantitative calculation of the lifetimes of beta transitions and in particular, for allowed decays, the model makes no distinction between the favoured transitions (between mirror nuclei) with  $\log ft$  less than 4 and the unfavoured transitions with  $\log ft$  greater than 4. A more correct application of the shell model involves the use of many-particle wave functions of lowest seniority (Flowers 1952) and the nuclear matrix elements for transitions between such states have been evaluated by Grayson and Nordheim (1956 a, b) who have made a detailed comparison of their results with experiment. The use of the many-particle wave functions considerably reduces the discrepancy between the experimental lifetimes and those predicted by the single-particle model, but it by no means explains the unfavoured nature of most of the allowed transitions. The situation is analogous to that regarding magnetic moments (in that we are now considering the off-diagonal matrix elements of  $\sigma$ ) where it has been shown, for odd- $A$  nuclei, that the deviations of these moments from the Schmidt lines, i.e. from the values predicted by the  $j-j$  coupling shell model, can be explained in terms of simple configurational mixing (Blin-Stoyle and Perks 1954, Arima and Horie 1954). It is natural, therefore, to suppose that such admixing could have considerable effect on the nuclear matrix elements for allowed beta-transitions. This problem has been considered in detail for the particular case of the  $^{19}\text{O}$  beta-decay branches by Elliott and Flowers (1955) where good agreement with experiment was obtained. The calculations described in the present paper, though much more crude, are an attempt to estimate such effects for the allowed beta-transitions in odd- $A$  nuclei for  $A$  greater than 40.

### § 2. NUCLEAR MATRIX ELEMENTS

The comparative half-lives for allowed beta-transitions are given by

$$ft^{-1} = G_F^2 |\langle 1 \rangle|^2 + G_{GT}^2 |\langle \sigma \rangle|^2 \dots\dots (1)$$

where, for the values of the interaction strengths, we take the values given by



Winther and Kofoed-Hansen (1953)

$$G_F^2 = G_{GT}^2 = 5300^{-1} \text{ sec}^{-1}. \quad \dots\dots (2)$$

The nuclear matrix elements are

$$\left. \begin{aligned} |\langle 1 \rangle|^2 &= \frac{1}{2J+1} \sum_{MM'} |(f| \sum_k \tau(k) |i)|^2 \\ |\langle \sigma \rangle|^2 &= \frac{1}{2J+1} \sum_{MM'} |(f| \sum_k \tau(k) \sigma(k) |i)|^2 \end{aligned} \right\} \quad \dots\dots (3)$$

where  $\tau$  is the isotopic-spin-flip operator normalized so that its eigenvalues are  $\pm 1$ , and where  $J$  is the total angular momentum and  $M$  its  $z$ -component of the initial state ( $i$ ), and similarly  $J'M'$  refer to the final state ( $f$ ).

We define the reduced matrix elements of a tensor operator  $T_q^{(k)}$  (Racah 1942) by

$$(\alpha'j'm'|T_q^{(k)}|\alpha jm) = (\alpha'j' || T^{(k)} || \alpha j)(jkj'm'|jkmq) \quad \dots\dots (4)$$

where the Wigner coefficient is defined as in Condon and Shortley (1935); it should be noted that (4) differs from the original (and more usual) definition of Racah. Moreover, in the following calculations we shall not work in the isotopic-spin formalism so that the term 'reduced matrix element' will be used throughout with reference to angular momentum operators. From (3) and (4) the nuclear matrix elements may now be written

$$\left. \begin{aligned} |\langle 1 \rangle|^2 &= \frac{2J'+1}{2J+1} |(f| \sum_k \tau(k) |i)|^2 \\ |\langle \sigma \rangle|^2 &= \frac{2J'+1}{2J+1} |(f| \sum_k \tau(k) \sigma(k) |i)|^2 \end{aligned} \right\} \quad \dots\dots (5)$$

where, of course, the usual selection rules apply.

As in the analogous calculations of magnetic moments, we assume that the nuclear states are basically those of the  $j$ - $j$  coupling shell model in the odd-group formulation, i.e. where the neutrons and protons are coupled up separately to states of lowest seniority. In this formulation it is necessary to consider two types of decay according as an odd or even nucleon makes the transition. Formally, the results for the second class of transitions may be deduced from those for the first by means of the theory of holes (Racah 1943), but the introduction of admixing, subject to the requirement that certain  $j$ - $j$  shells be filled, generally destroys this symmetry. Moreover, we would expect the isotopic spin to be a fairly good quantum number as long as both neutrons and protons end up in the  $1f_{7/2}$  shell or below. Consequently, the use of odd-group functions should restrict us to decays between nuclei of mass number greater than 50. However, we shall consider very briefly decays within the  $1f_{7/2}$  shell where odd-group functions are used, not from preference, but merely because the fractional parentage coefficients for the isotopic-spin eigenfunctions are not available, or at least not in simple algebraic form. In calculating the nuclear matrix elements we use the result of Nordheim and Yost (1937) that, for a decay  $n^m p^{m'} \rightarrow n^{m-1} p^{m'+1}$ , the reduced matrix element is  $[m(m'+1)]^{1/2}$  times that calculated by specifying that a particular nucleon has changed its state. Here  $m, m'$  refer to the total nucleon numbers. However, for the following shell model calculations, where all closed  $LS$  shells can be and are completely ignored,  $m$  and  $m'$  must be taken to be the numbers of nucleons outside such shells,



### § 3. CONFIGURATIONAL MIXING

As described in § 2, we assume that the nuclear states are basically those of the  $j$ - $j$  coupling shell model in the odd-group formulation and treat the residual two-body interactions as a perturbation, the effect of which is to mix in other states. Formally, for our purposes, this is the same as assuming that the central field arises from all nucleons within all closed  $LS$  shells, and that the perturbation is

$$V = \sum_{i < j} V_{ij} \quad \dots\dots (6)$$

where the summation includes all nucleons outside closed  $LS$  shells. We consider only those admixtures which will contribute linearly in their coefficients of admixing to the reduced matrix elements, and ignore all second-order terms.

The reduced matrix element of an operator  $T^{(k)}$  between states  $\Psi'$ ,  $\Psi$  corresponding to unperturbed shell model states  $\psi'$ ,  $\psi$  may then be written

$$\begin{aligned} \langle \Psi' || T^{(k)} || \Psi \rangle = & \langle \psi' || T^{(k)} || \psi \rangle - \sum_{\gamma} \frac{\langle \psi' || T^{(k)} || \phi_{\gamma} \rangle \langle \phi_{\gamma} | V | \psi \rangle}{\Delta E_{\gamma}} \\ & - \sum_{\gamma} \frac{\langle \psi' | V | \phi_{\gamma}' \rangle \langle \phi_{\gamma}' || T^{(k)} || \psi \rangle}{\Delta E_{\gamma}'} \quad \dots\dots (7) \end{aligned}$$

where  $\Delta E_{\gamma}$  is the energy difference between the admixture  $\phi_{\gamma}$  and the unperturbed shell model state  $\psi$ , and similarly  $\Delta E_{\gamma}'$ . We use a zero-range two-body force

$$V_{ij} = (a + b \boldsymbol{\sigma}(i) \cdot \boldsymbol{\sigma}(j)) \delta(\mathbf{r}_{ij}) \quad \dots\dots (8)$$

so that our results will be expressed in terms of the integrals

$$\left. \begin{aligned} \epsilon_s(l'l') &= \frac{(a-3b)}{4\pi} \int |R_l(r)|^2 |R_{l'}(r)|^2 r^2 dr \\ \epsilon_t(l'l') &= \frac{a+b}{a-3b} \epsilon_s(l'l') \end{aligned} \right\} \quad \dots\dots (9)$$

and following Pryce (1952) we take the ratio of the triplet to singlet strengths to be  $\epsilon_t : \epsilon_s = 3 : 2$ . (The use of a zero-range force is indeed crude, but is necessary to make the calculations practicable.)

It should be noted, also, that the energy denominators in (7) refer formally to the unperturbed states. In the cases where there are unfilled competing orbits it may happen that the residual two-body interactions produce an ordering of configurations which is different from that predicted by the single-particle model. Consequently, there exist configurations which, on the unperturbed model, are of lower energy than the configuration assumed for the nuclear ground state. However, in the application to specific nuclei, it is found that admixtures of such configurations have little effect on the beta-decay matrix elements.

### § 4. ALLOWED TRANSITIONS, $\Delta J = 0$

As a first example, we consider the decays for which  $\Delta J = 0$ , and we restrict ourselves to those decays within the  $1f_{7/2}$  shell so that we have not the additional complication of unfilled competing levels. (These decays form the greater part of the  $\Delta J = 0$  transitions for  $A$  greater than 40.) It is clear that configurational mixing of the type described in the preceding section can have no first-order effect on the Fermi element. In fact, for these decays, using odd-group functions, the Fermi element is sufficiently large to prevent us obtaining the large  $ft$  values

required by experiment. The Fermi element gives  $\log ft \lesssim 4.93$  irrespective of the value of  $|\langle \sigma \rangle|^2$  and since the decay  ${}_{20}\text{Ca}_{27} \rightarrow {}_{21}\text{Sc}_{26}$  with  $\log ft \sim 8.5$  is in this group, some further assumption is necessary. Clearly for these decays we should use isotopic-spin eigenfunctions as our unperturbed states, in which case  $|\langle 1 \rangle|^2 = 1$  for  ${}_{22}\text{Ti}_{21} \rightarrow {}_{21}\text{Sc}_{22}$ , but vanishes identically for the other known transitions in this region owing to selection rules. However, for the three decays involving calcium isotopes we might intuitively assume that the odd-group functions would be a reasonable approximation for the calculation of  $|\langle \sigma \rangle|^2$  (since the calcium functions are odd-group functions in any case) whilst taking  $|\langle 1 \rangle|^2 = 0$  as must be the case to first order. These transitions are of the form

$$\psi \equiv \{[k^{n_1}(k)][k^{n_2}(0)]\}_{(k)} \rightarrow \psi' \equiv \{[k^{n_1-1}(0)][k^{n_2+1}(k)]\}_{(k)}. \quad \dots\dots (10)$$

Here, and throughout, we let  $k = l + \frac{1}{2}$ ,  $j = l - \frac{1}{2}$ , where  $l$  is the orbital angular momentum. Thus in  $\psi$  there is an odd number,  $n_1$ , of neutrons (say), each of total angular momentum  $k$ , coupled to total angular momentum  $k$ ; there are  $n_2$  (even) protons coupled to zero total angular momentum; the resultant total angular momentum is  $k$ . States of the form  $k^n(k)$ ,  $k^n(0)$  are of seniority one and nought respectively, and, in the admixtures below, states of the form  $j^n(J)$  ( $n$  even) are of seniority two.

The possible contributing admixtures are to  $\psi$ :

$$\phi_J \equiv \{[k^{n_1-1}(0)j][k^{n_2}(J)]\}_{(k)}$$

and to  $\psi'$ :

$$\phi_{J'} \equiv \{[k^{n_1-1}(J)][k^{n_2}(0)j]\}_{(k)}. \quad \dots\dots (11)$$

In  $\phi_J$ , for example,  $[k^{n_1-1}(0)j]$  must be completely antisymmetrized. Using standard methods and equation (7) the total reduced matrix element is found to be

$$\frac{(k||\sigma||k)}{2(l+1)} [(2l+3-n_1)(2l+2-n_2)]^{1/2} \left\{ 1 + \frac{(l+1)(l+2)(n_1+n_2-1)}{2(2l+1)(2l+3)} \frac{(3\epsilon_t + \epsilon_s)}{\Delta E_l} \right\} \quad \dots\dots (12)$$

where  $(k||\sigma||k)$  is the single-particle matrix element,  $\Delta E_l$  the  $(l + \frac{1}{2}) - (l - \frac{1}{2})$  spin-orbit splitting, and  $\epsilon_s \equiv \epsilon_s(l)$ ,  $\epsilon_t \equiv \epsilon_t(l)$ . Defining

$$\xi_l \equiv \frac{\epsilon_s(l)}{\Delta E_l} \quad \dots\dots (13)$$

the reduced matrix element is of the form

$$(|\sigma|)_{JJ'} \{1 + B\xi_l\} \quad \dots\dots (14)$$

where  $(|\sigma|)_{JJ'}$  is the unperturbed (many-particle) reduced matrix element and where  $B$  is positive. Since  $\xi_l$  is necessarily negative, we see that we obtain a reduction in the single-particle model value firstly through the appearance of the many-particle element and secondly through the factor  $1 + B\xi_l$ . From the experimental  $ft$  value we can deduce the magnitude of the reduced matrix element, but not its sign, and hence there will be two possible values of  $\xi_l$  which will give agreement for a given decay. For each of the three decays mentioned above, we list in table 1 that value of  $\xi_l$  which is more consistent with the value  $\xi_{1f} \sim -0.3$  obtained from magnetic moments calculations. The experimental  $\log ft$  values given in table 1 are taken from the article by Mayer in Siegbahn (1955) (as are those in the later tables) with the exception of that for  ${}_{20}\text{Ca}_{27} \rightarrow {}_{21}\text{Sc}_{26}$  which is taken from King (1954). Our results, which are intended to be of heuristic

value only, do not depend acutely on the accuracy of the experimental results. We have also quoted the values of  $\log ft$  predicted by the unperturbed many-particle model. The values of  $\xi_l$  required, though of the correct order of magnitude, vary too much for the calculation to be taken seriously and in any case we had to assume the vanishing of  $|\langle 1 \rangle|^2$ . (A similar calculation for the remaining decays within the  $1f_{7/2}$  shell gives results which require unrealistic (usually positive) values of  $\xi_l$  for agreement with experiment.) However, it does indicate the manner in which configurational mixing could effect beta-decay matrix elements, and one might reasonably hope that the use of isotopic-spin eigenfunctions would permit a more quantitative estimate of this effect. As reported in Blin-Stoyle and Caine (1957), for the three-particle cases  ${}_{21}\text{Sc}_{22} \rightarrow {}_{20}\text{Ca}_{23}$  and  ${}_{22}\text{Ti}_{21} \rightarrow {}_{21}\text{Sc}_{22}$  the matrix elements can be correctly estimated using isotopic-spin eigenfunctions, and the required value of  $\xi_l = -0.31$  gives the magnetic moment of  ${}_{20}\text{Ca}_{23}$  to within the limits of relativistic and exchange effects.

Table 1

$A$	Decay	$(\log ft)_{\text{exp}}$	$(\log ft)_{jj}$	$\xi_l$
43	${}_{21}\text{Sc}_{22} \rightarrow {}_{20}\text{Ca}_{23}$	4.77	3.74	-0.398
45	${}_{20}\text{Ca}_{25} \rightarrow {}_{21}\text{Sc}_{24}$	5.94	3.92	-0.314
47	${}_{20}\text{Ca}_{27} \rightarrow {}_{21}\text{Sc}_{26}$	8.60	4.22	-0.192

### § 5. ALLOWED TRANSITIONS, $\Delta J = 1$

We now consider the allowed decays for which  $\Delta J = 1$  and which on the  $j$ - $j$  coupling shell model involve transitions between the two levels of a spin-orbit doublet. For most cases the situation is more complicated than for the  $1f_{7/2}$  transitions since we must now include all unfilled competing orbits. However, for medium  $A$ , when the neutron excess becomes large, we should expect the odd-group functions to give a better approximation, and also, of course, the Fermi element now vanishes automatically. We consider separately the two types of transitions mentioned in § 3.

#### 5.1. Odd Nucleon Decay

We write the transition for the case  $k \rightarrow j$  (i.e.  $l + \frac{1}{2} \rightarrow l - \frac{1}{2}$ )

$$\left. \begin{aligned} \psi &\equiv [k_1^{n_1}(0)j_1^{n_2}(0)k^{n_3}(k)][k_1^{n_4}(0)j_1^{n_5}(0)k^{n_6}(0)j^{n_7}(0)] \\ \rightarrow \psi' &\equiv [k_1^{n_1}(0)j_1^{n_2}(0)k^{n_3-1}(0)][k_1^{n_4}(0)j_1^{n_5}(0)k^{n_6}(0)j^{n_7+1}(j)] \end{aligned} \right\} \dots\dots (15)$$

where we specify that the subshell  $k^{n_6}$  be filled. The only admixtures which will contribute linearly to the reduced matrix element are

Admixtures to  $\psi$ :

$$\left. \begin{aligned} \phi_J &\equiv \{[k_1^{n_1}(0)j_1^{n_2}(0)k^{n_3-1}(0)j][k_1^{n_4}(0)j_1^{n_5}(0)k^{n_6}(0)j^{n_7}(J)]\}_{j(k)} \\ \theta_J &\equiv \{[k_1^{n_1}(0)j_1^{n_2}(0)k^{n_3}(k)][k_1^{n_4}(0)j_1^{n_5}(0)k^{n_6-1}(k)j^{n_7+1}(j)](J)\}_{j(k)} \\ \chi_J &\equiv \{[k_1^{n_1}(0)j_1^{n_2}(0)k^{n_3-1}(0)j][k_1^{n_4}(0)j_1^{n_5}(0)k^{n_6-1}(k)j^{n_7+1}(j)](J)\}_{j(k)} \\ \phi_J(1) &\equiv \{[k_1^{n_1+1}(k_1)j_1^{n_2}(0)k^{n_3-1}(0)][k_1^{n_4-1}(k_1)j_1^{n_5}(0)k^{n_6}(0)j^{n_7+1}(j)](J)\}_{j(k)} \\ \phi_J(2) &\equiv \{[k_1^{n_1+1}(k_1)j_1^{n_2}(0)k^{n_3-1}(0)][k_1^{n_4}(0)j_1^{n_5-1}(j_1)k^{n_6}(0)j^{n_7+1}(j)](J)\}_{j(k)} \\ \phi_J(3) &\equiv \{[k_1^{n_1}(0)j_1^{n_2+1}(j_1)k^{n_3-1}(0)][k_1^{n_4-1}(k_1)j_1^{n_5}(0)k^{n_6}(0)j^{n_7+1}(j)](J)\}_{j(k)} \\ \phi_J(4) &\equiv \{[k_1^{n_1}(0)j_1^{n_2+1}(j_1)k^{n_3-1}(0)][k_1^{n_4}(0)j_1^{n_5-1}(j_1)k^{n_6}(0)j^{n_7+1}(j)](J)\}_{j(k)} \end{aligned} \right\} (16)$$

Admixtures to  $\psi'$ :

$$\left. \begin{aligned} \phi_J'(1) &\equiv \{[k_1^{n_1-1}(k_1)j_1^{n_2}(0)k^{n_3}(k)](J)[k_1^{n_4+1}(k_1)j_1^{n_5}(0)k^{n_6}(0)j^{n_7}(0)]\}_{(j)} \\ \phi_J'(2) &\equiv \{[k_1^{n_1-1}(k_1)j_1^{n_2}(0)k^{n_3}(k)](J)[k_1^{n_4}(0)j_1^{n_5+1}(j_1)k^{n_6}(0)j^{n_7}(0)]\}_{(j)} \\ \phi_J'(3) &\equiv \{[k_1^{n_1}(0)j_1^{n_2-1}(j_1)k^{n_3}(k)](J)[k_1^{n_4+1}(k_1)j_1^{n_5}(0)k^{n_6}(0)j^{n_7}(0)]\}_{(j)} \\ \phi_J'(4) &\equiv \{[k_1^{n_1}(0)j_1^{n_2-1}(j_1)k^{n_3}(k)](J)[k_1^{n_4}(0)j_1^{n_5+1}(j_1)k^{n_6}(0)j^{n_7}(0)]\}_{(j)} \end{aligned} \right\} \quad (17)$$

The unperturbed  $k \rightarrow j$  reduced matrix element is

$$\left[ \frac{(2l+3-n_3)(2l-n_7)}{4l(l+1)} \right]^{1/2} (j||\sigma||k) \quad \dots\dots (18)$$

where  $(j||\sigma||k)$  is the single-particle element. The contributions from the above admixtures may easily be calculated and each has (18) as a factor.

Admixture	Contribution	
$\phi_J$	$\frac{n_7 l}{8(2l+1)} \frac{(3\epsilon_t + \epsilon_s)}{\Delta E}$	}
$\theta_J$	$\frac{n_6(l+2)}{8l(2l+1)} \left[ \frac{l(\epsilon_s + \epsilon_t)}{\Delta E} - \frac{(n_3-1)(3\epsilon_t + \epsilon_s)}{2\Delta E} \right]$	
$\chi_J$	$\frac{3n_6 l}{16(2l+1)} \frac{(\epsilon_s + \epsilon_t)}{\Delta E}$	

..... (19)

$\phi_J(1)$	$\frac{n_4(2l_1+2-n_1)(l_1+2)}{16(l_1+1)(2l_1+1)} \frac{(\epsilon_s + \epsilon_t)}{\Delta E}$	}
$\phi_J(2)$	$\frac{3n_5(2l_1+2-n_1)}{16(2l_1+1)} \frac{(\epsilon_s + \epsilon_t)}{(\Delta E - \Delta E_1)}$	
$\phi_J(3)$	$\frac{3n_4(2l_1-n_2)}{16(2l_1+1)} \frac{(\epsilon_s + \epsilon_t)}{(\Delta E + \Delta E_1)}$	
$\phi_J(4)$	$\frac{n_5(2l_1-n_2)(l_1-1)}{16l_1(2l_1+1)} \frac{(\epsilon_s + \epsilon_t)}{\Delta E}$	
$\phi_J'(1)$	$-\frac{n_1(2l_1+2-n_4)(l_1+2)}{16(l_1+1)(2l_1+1)} \frac{(\epsilon_s + \epsilon_t)}{\Delta E}$	
$\phi_J'(2)$	$-\frac{3n_1(2l_1-n_5)}{16(2l_1+1)} \frac{(\epsilon_s + \epsilon_t)}{(\Delta E - \Delta E_1)}$	
$\phi_J'(3)$	$-\frac{3n_2(2l_1+2-n_4)}{16(2l_1+1)} \frac{(\epsilon_s + \epsilon_t)}{(\Delta E + \Delta E_1)}$	
$\phi_J'(4)$	$-\frac{n_2(2l_1-n_5)(l_1-1)}{16l_1(2l_1+1)} \frac{(\epsilon_s + \epsilon_t)}{\Delta E}$	

..... (20)

where  $\Delta E$ ,  $\Delta E_1$  are the  $l$ ,  $l_1$  spin-orbit splittings respectively. In (19)  $\epsilon_s \equiv \epsilon_s(l)$  and in (20)  $\epsilon_s \equiv \epsilon_s(l_1)$ , and similarly for the  $\epsilon_t$ . For a transition  $j \rightarrow k$ , the results may be deduced from the above by first writing the transition in reverse order and then replacing  $(j||\sigma||k)$  in (18) by  $(k||\sigma||j)$ .

### 5.2. Even Nucleon Decay

We write the transition for the case  $j \rightarrow k$

$$\left. \begin{aligned} \psi &\equiv [k_1^{n_1}(0)j_1^{n_2}(0)k^{n_3}(0)][k_1^{n_4}(0)j_1^{n_5}(0)k^{n_6}(0)j^{n_7}(j)] \\ \rightarrow \psi &\equiv [k_1^{n_1}(0)j_1^{n_2}(0)k^{n_3-1}(k)][k_1^{n_4}(0)j_1^{n_5}(0)k^{n_6}(0)j^{n_7+1}(0)] \end{aligned} \right\} \quad \dots\dots (21)$$



where  $k^{n_6}(0)$  is completely filled. The possible admixtures are:

Admixtures to  $\psi$ :

$$\left. \begin{aligned} \phi_J &\equiv \{ [k_1^{n_1}(0)j_1^{n_2}(0)k^{n_3-1}(k)j](J)[k_1^{n_4}(0)j_1^{n_5}(0)k^{n_6}(0)j^{n_7}(j)] \}_{(j)} \\ \theta_J &\equiv \{ [k_1^{n_1}(0)j_1^{n_2}(0)k^{n_3}(J)][k_1^{n_4}(0)j_1^{n_5}(0)k^{n_6-1}(k)j^{n_7+1}(0)] \}_{(j)} \\ \chi_J &\equiv \{ [k_1^{n_1}(0)j_1^{n_2}(0)k^{n_3-1}(k)j](J)[k_1^{n_4}(0)j_1^{n_5}(0)k^{n_6-1}(k)j^{n_7+1}(0)] \}_{(j)} \\ \phi_J(1) &\equiv \{ [k_1^{n_1+1}(k_1)j_1^{n_2}(0)k^{n_3-1}(k)](J)[k_1^{n_4-1}(k_1)j_1^{n_5}(0)k^{n_6}(0)j^{n_7+1}(0)] \}_{(j)} \\ \phi_J(2) &\equiv \{ [k_1^{n_1+1}(k_1)j_1^{n_2}(0)k^{n_3-1}(k)](J)[k_1^{n_4}(0)j_1^{n_5-1}(j_1)k^{n_6}(0)j^{n_7+1}(0)] \}_{(j)} \\ \phi_J(3) &\equiv \{ [k_1^{n_1}(0)j_1^{n_2+1}(j_1)k^{n_3-1}(k)](J)[k_1^{n_4-1}(k_1)j_1^{n_5}(0)k^{n_6}(0)j^{n_7+1}(0)] \}_{(j)} \\ \phi_J(4) &\equiv \{ [k_1^{n_1}(0)j_1^{n_2+1}(j_1)k^{n_3-1}(k)](J)[k_1^{n_4}(0)j_1^{n_5-1}(j_1)k^{n_6}(0)j^{n_7+1}(0)] \}_{(j)} \end{aligned} \right\} \quad (22)$$

Admixtures to  $\psi'$ :

$$\left. \begin{aligned} \phi_J'(1) &\equiv \{ [k_1^{n_1-1}(k_1)j_1^{n_2}(0)k^{n_3}(0)][k_1^{n_4+1}(k_1)j_1^{n_5}(0)k^{n_6}(0)j^{n_7}(j)](J) \}_{(k)} \\ \phi_J'(2) &\equiv \{ [k_1^{n_1-1}(k_1)j_1^{n_2}(0)k^{n_3}(0)][k_1^{n_4}(0)j_1^{n_5+1}(j_1)k^{n_6}(0)j^{n_7}(j)](J) \}_{(k)} \\ \phi_J'(3) &\equiv \{ [k_1^{n_1}(0)j_1^{n_2-1}(j_1)k^{n_3}(0)][k_1^{n_4+1}(k_1)j_1^{n_5}(0)k^{n_6}(0)j^{n_7}(j)](J) \}_{(k)} \\ \phi_J'(4) &\equiv \{ [k_1^{n_1}(0)j_1^{n_2-1}(j_1)k^{n_3}(0)][k_1^{n_4}(0)j_1^{n_5+1}(j_1)k^{n_6}(0)j^{n_7}(j)](J) \}_{(k)} \end{aligned} \right\} \quad (23)$$

The unperturbed reduced matrix element is:

$$\left[ \frac{n_3(n_7+1)}{4l(l+1)} \right]^{1/2} (k||\sigma||j) \quad \dots\dots\dots (24)$$

and the following contributions have (24) as a factor:

Admixture	Contribution
$\phi_J$	$\frac{l}{4(2l+1)} \left[ (n_7-1) \frac{(3\epsilon_t + \epsilon_s)}{2\Delta E} - 2(l-1) \frac{\epsilon_t}{\Delta E} \right]$
$\theta_J$	$\frac{n_6(2l+2-n_3)(l+2)}{16l(2l+1)} \frac{(3\epsilon_t + \epsilon_s)}{\Delta E}$
$\chi_J$	$\frac{3n_6l}{16(2l+1)} \frac{(\epsilon_t + \epsilon_s)}{\Delta E}$

$$\left. \begin{aligned} & \dots\dots\dots (25) \end{aligned} \right\}$$

The contributions from the  $\phi_J(i)$  and  $\phi_J'(i)$  are as in equation (20). In (25)  $\epsilon_s \equiv \epsilon_s(l)$  and similarly for  $\epsilon_t$ . For a transition  $k \rightarrow j$  the results may be deduced from the above by rewriting the transition in reverse and then replacing  $(k||\sigma||j)$  in (24) by  $(j||\sigma||k)$ .

The admixtures given above for the two types of transition are the formal possibilities. In the application of these results to specific decays the fact that certain subshells are filled or empty will restrict the number of admixtures as is clear from the form of the contributions.

## § 6. APPLICATION TO EXPERIMENT

The results of § 5 are still somewhat unwieldy. In order to reduce the number of parameters we have proceeded as follows: for a given decay, using oscillator radial functions, we have estimated the various  $\epsilon_s(l_i)$  occurring in terms of  $\epsilon_s(l)$  and have also put  $\epsilon_t(l) = 1.5\epsilon_s(l)$ . The various energy denominators formally depend only on spin-orbit splittings and we have estimated the  $\Delta E_1$  in terms of  $\Delta E$  by means of the results of Blin-Stoyle (1956). On this basis, our results are given in terms of  $\xi_i \equiv \epsilon_s(l)/\Delta E_i$ . Roughly, we would expect  $\epsilon_s(l) \propto A^{-1}$  and  $\Delta E \propto A^{-2/3}$ , so that  $\xi_i \propto A^{-1/3}$ . Hence  $\lambda_i \equiv A^{1/3}\xi_i$  should be roughly

independent of  $A$ . From the form of the results, which are finally similar to (14) we see that the  $ft$  values will be extremely sensitive to the value of  $\xi_l$ . Hence, the most we may expect is that the values of  $\lambda_l$  necessary to fit the experimental results will be sensibly constant for a given shell and of a reasonable magnitude. The integrals  $\epsilon_s(l)$  may be estimated by considering the experimental data on pairing energies and give

$$\epsilon_s(l) \sim -\frac{25}{A} \text{ meV} \quad \dots\dots (27)$$

(see Arima and Horie 1954) where we have ignored any orbital dependence. Using this value, and also the results of Blin-Stoyle (1956) for the spin-orbit splittings, we would expect

$$\left. \begin{aligned} \lambda(2p) &\sim -1.5 \\ \lambda(1g) &\sim -0.4 \\ \lambda(2d) &\sim -0.8 \end{aligned} \right\} \quad \dots\dots (28)$$

## § 7. COMPARISON WITH EXPERIMENT

The results for decays within the 2d, 1g and 2p shells are given in tables 2, 3 and 4 respectively.

### 7.1. 2d Shell Decays

The unperturbed configurations used are based mainly on those of Klinkenberg (1952) and in three cases alternative configurations are considered. Some nine of these decays are included in those considered by Grayson and Nordheim (1956 b) in which cases the configurations used by these authors is indicated thus †. The values of  $\lambda$  required are given in the last column of table 2. These show a tendency to decrease with increasing  $A$ , but are reasonably constant and, moreover, are of the correct magnitude as indicated by equation (28).

### 7.2. 1g Shell Decays

For these decays, unfortunately, the choice of basic configurations is not so straightforward in view of the competition between the  $1g_{7/2}$  and  $2d_{5/2}$  neutron levels and between the  $2p_{1/2}$  and  $1g_{9/2}$  proton levels. We have therefore considered all the possible basic configurations for each of the six decays. In comparing the values of  $\lambda$  required to fit the experimental results we are forced to consider two possibilities.

The first possibility is that the estimate of  $\lambda = -0.4$  given in equation (28) is incorrect which is certainly possible in view of the crude method employed. In this case the values of  $\lambda$  given in the penultimate column of table 3 are applicable, and it is seen that all configurations (excepting the first given for the decay  ${}_{49}\text{In}_{58} \rightarrow {}_{48}\text{Cd}_{59}$ ) give essentially the same result, with  $\lambda \sim -1.1$ . This value of  $\lambda$  corresponds to that used by Blin-Stoyle and Perks (1954).

The alternative is to assume that the estimate of  $\lambda \sim -0.4$  is reliable, in which case the values of  $\lambda$  given in the last column of table 3 are appropriate. For the decays  ${}_{41}\text{Nb}_{54} \rightarrow {}_{42}\text{Mo}_{53}^{\times}$  and  ${}_{43}\text{Tc}_{58} \rightarrow {}_{44}\text{Ru}_{57}^{\times}$  we see that the configurations used by Grayson and Nordheim (1956 b) now require  $\lambda = -0.52$  and  $-0.50$  respectively, although for these decays there are other configurations for which the required values of  $\lambda$  are reasonable. For the decay  ${}_{41}\text{Nb}_{56} \rightarrow {}_{42}\text{Mo}_{55}$  all the configurations require similar values of  $\lambda$  although it is more probable that the actual basic configurations is one of the first three given in table 3. For the decay

$_{49}\text{In}_{58} \rightarrow _{48}\text{Cd}_{59}$ , however, only the first configuration requires a consistent value of  $\lambda$ , but this configuration, which implies a minimum pairing in the  $2d_{5/2}$  shell in preference to the  $1g_{7/2}$  shell, is quite reasonable. We are then left with the two decays  $_{43}\text{Tc}_{50} \rightarrow _{42}\text{Mo}_{51}^{\times}$  and  $_{50}\text{Sn}_{61} \rightarrow _{49}\text{In}_{62}$  for which the required values of  $\lambda$  are anomalously large.

In view of the primitive nature of our calculations we do not feel confident to make a definite choice between these alternatives.

### 7.3. 2p Shell Decays

These results are given in table 4 where for each decay we have considered two different unperturbed configurations. The first assumes that after the  $1f_{7/2}$  shell the order of filling for an odd number of protons is

$$p_{3/2}, \quad p_{3/2}^3, \quad p_{3/2}^3 f_{5/2}^2, \quad p_{3/2}^3 f_{5/2}^4, \quad \dots \quad \dots (29)$$

whilst in the second the order assumed is

$$p_{3/2}, \quad p_{3/2} f_{5/2}^2, \quad p_{3/2} f_{5/2}^4, \quad \dots \quad \dots (30)$$

For the first type of configuration the various contributions tend to interfere, so that in the final result  $(||\sigma||)_{jj}(1 + B\xi)B$  is usually small ( $|B| \lesssim 1$ ) and occasionally of the wrong sign to produce a reduction in the  $j-j$  reduced matrix element. For the second type of configuration, however, the values of  $\lambda$  required are of the correct sign and magnitude (as estimated in equation (28)) and are fairly constant. It is therefore somewhat unfortunate that from the evidence of the positive quadrupole moments of the odd-proton nuclei in this region (see, for example, Mayer and Jensen 1955) it appears that the first type of configuration is that which actually occurs, or at least is predominant. Where the quadrupole moment of the daughter nucleus is unknown we could assume a configuration of the second type, but this would appear unlikely.

We are thus forced to find reasons for the breakdown of our simple model. One possibility is that of an error in estimating the various contributions in terms of  $\xi_l \equiv \epsilon_s(l)/\Delta E_l$ . For the decays within the  $2d$  and  $1g$  shells it happened that the contributions which were initially given in terms of  $\epsilon_s(l)/\Delta E_l$  were of most importance. Hence, no great error would be introduced in expressing the remaining radial integrals and spin-orbit splittings in terms of  $\epsilon_s(l)$  and  $\Delta E_l$ . In the present case, however, when there is interference between contributions, this procedure can introduce a considerable uncertainty into the final result. It seems unlikely, though, that this explanation could account, in all the relevant decays, for the disagreement with experiment. A more probable explanation, in view of the competition between the  $1f_{5/2}$  and  $2p_{3/2}$  levels, especially for protons, is that the nuclear states contain a more fundamental admixing than is allowed in our simple model and that the hypothesis of basically pure configurations is untenable. For example, the analogous calculation of magnetic moments (Arima and Horie 1954) cannot explain the magnetic moment of  $_{33}\text{As}_{42}$  which has a deviation of 2.4 n.m. from the Schmidt value. Similarly, in the calculations of transition rates for the  $l$ -forbidden M1 transitions (Arima, Horie and Sano 1957) two outstanding discrepancies are the  $3/2^- \rightarrow 5/2^-$  decays in  $_{30}\text{Zn}_{37}$  and  $_{33}\text{As}_{40}$ . Further evidence arises from the regularities in level spacing of nuclei with 31–39 odd nucleons (see, for example, Nussbaum 1956) which cannot be interpreted as rotational bands because of their spin values but which do suggest some form of collective effect.

Table 2. 2d Shell Decays

<i>A</i>	Decay	log <i>ft</i>	Configuration of daughter nucleus	$\lambda$	
121	${}_{53}^{108}\text{I}_{08} \rightarrow {}_{52}^{106}\text{Te}_{09}^{\times}$	5.05	$\dagger [g_{9/2}^{10} g_{7/2}^2] [g_{9/2}^{10} g_{7/2}^8 h_{11/2}^4 d_{5/2}^6 d_{3/2}]$	-1.48 -1.05	-1.05
121	${}_{50}^{120}\text{Sn}_{71} \rightarrow {}_{51}^{120}\text{Sb}_{70}$	5.00	$\dagger [g_{9/2}^{10} d_{5/2}] [g_{9/2}^{10} g_{7/2}^8 h_{11/2}^6 d_{5/2}^6]$	-1.28 -0.95	-0.95
123	${}_{50}^{122}\text{Sn}_{73} \rightarrow {}_{51}^{122}\text{Sb}_{72}$	5.27	$\dagger [g_{9/2}^{10} d_{3/2}] [g_{9/2}^{10} g_{7/2}^8 h_{11/2}^8 d_{5/2}^6]$	-1.18 -0.95	-0.95
125	${}_{50}^{124}\text{Sn}_{75}^{\text{m}} \rightarrow {}_{51}^{124}\text{Sb}_{74}$	> 5.43	$[g_{9/2}^{10} d_{3/2}] [g_{9/2}^{10} g_{7/2}^8 h_{11/2}^{10} d_{5/2}^6]$	-1.10 -0.92	-0.92
127	${}_{52}^{126}\text{Te}_{75} \rightarrow {}_{53}^{126}\text{I}_{74}$	5.66	$\dagger [g_{9/2}^{10} g_{7/2}^2 d_{5/2}] [g_{9/2}^{10} g_{7/2}^8 h_{11/2}^{10} d_{5/2}^6]$	-1.14 -1.00	-1.00
131	${}_{55}^{130}\text{Cs}_{76} \rightarrow {}_{54}^{130}\text{Xe}_{77}$	5.30	$[g_{9/2}^{10} g_{7/2}^4] [g_{9/2}^{10} g_{7/2}^8 h_{11/2}^{12} d_{5/2}^6 d_{3/2}]$	-1.22 -0.94	-0.94
			$[g_{9/2}^{10} g_{7/2}^4] [g_{9/2}^{10} g_{7/2}^8 h_{11/2}^{10} d_{5/2}^6 d_{3/2}^3]$	-1.20 -0.83	-0.83
133	${}_{54}^{132}\text{Xe}_{79} \rightarrow {}_{55}^{132}\text{Cs}_{78}^{\times}$	5.58	$\dagger [g_{9/2}^{10} g_{7/2}^4 d_{5/2}] [g_{9/2}^{10} g_{7/2}^8 h_{11/2}^{12} d_{5/2}^6 d_{3/2}^2]$	-1.08 -0.87	-0.87
			$[g_{9/2}^{10} g_{7/2}^4 d_{5/2}] [g_{9/2}^{10} g_{7/2}^8 h_{11/2}^{12} s_{1/2}^2 d_{5/2}^6]$	-0.87 -0.75	-0.87



Table 2. 2d Shell Decays (continued)

$A$	Decay	$\log ft$	Configuration of daughter nucleus	$\lambda$	
133	${}^{54}_{81}\text{Te} \rightarrow {}^{53}_{80}\text{I}$	5.19	$[g_{9/2}^{10} s_{7/2}^2 d_{5/2}^1] [g_{9/2}^{10} s_{7/2}^{12} h_{11/2}^{12} s_{5/2}^2 d_{3/2}^2]$	-0.84 -0.60	-0.84
135	${}^{54}_{81}\text{Xe} \rightarrow {}^{53}_{80}\text{I}$	5.91	$^{\dagger}[g_{9/2}^{10} g_{7/2}^4 d_{5/2}^1] [g_{9/2}^{10} s_{7/2}^{12} h_{11/2}^{12} s_{5/2}^2 d_{3/2}^2]$	-0.80 -0.69	-0.80
139	${}^{59}_{80}\text{Pr} \rightarrow {}^{58}_{81}\text{Ce}$	$\geq 5.51$	$[h_{11/2}^{12} s_{7/2}^2 d_{5/2}^6 d_{3/2}^3]$	-0.93 -0.70	-0.93
139	${}^{60}_{79}\text{Nd} \rightarrow {}^{59}_{80}\text{Pr}$	$\geq 7.63$	$\left\{ \begin{array}{l} [d_{5/2}^1] [h_{11/2}^{12} s_{7/2}^2 d_{5/2}^6 d_{3/2}^2] \\ [d_{6/2}^1] [h_{11/2}^{12} d_{5/2}^6 d_{3/2}^4] \end{array} \right.$	-0.72 -0.70 -0.83 -0.81	-0.72 -0.83
141	${}^{61}_{80}\text{Pm} \rightarrow {}^{60}_{81}\text{Nd}$	$\geq 5.28$	$^{\dagger}[d_{5/2}^2] [h_{11/2}^{12} s_{7/2}^2 d_{5/2}^6 d_{3/2}^3]$	-1.35 -0.85	-0.85
141	${}^{60}_{81}\text{Nd} \rightarrow {}^{59}_{82}\text{Pr}$	$\geq 5.12$	$^{\dagger}[d_{5/2}^1] [h_{11/2}^{12} s_{7/2}^2 d_{5/2}^6 d_{3/2}^4]$	-0.81 -0.51	-0.81

Note to tables 2, 3, and 4.

The superscripts  $\times$ ,  $\times$ ,  $\times$ ,  $m$ , denote first excited state, second excited state, and metastable state respectively. Configurations marked  $^{\dagger}$  are those used by Grayson and Nordheim (1956 b). The fifth column of each table gives, for a given decay and given basic configuration, the two possible values of  $\lambda$  required for agreement with the experimental lifetime. Where the experimental  $\log ft$  value is a lower limit the values of  $\lambda$  given are calculated using this limit.

In table 2, the last column contains a set of values of  $\lambda$  consistent with each other and with the estimate of equation (28).

In table 3, the sets of values of  $\lambda$  given in the sixth and seventh columns are discussed in § 7.2.

In table 4, the values of  $\lambda$  are given only if of the correct sign, the values in the sixth and seventh columns referring to the first and second type of configuration discussed in § 7.3. The entries in the sixth column are restricted to those of the correct order of magnitude.

Table 3. 1g Shell Decays

A	Decay	log ft	Configuration of daughter nucleus	$\lambda$	
93	${}^{43}_{50}\text{Tc} \rightarrow {}^{42}_{51}\text{Mo}^{\times}$	4.64	$[g_{9/2}^2] [g_{7/2}^{10}]$	-1.94	-1.06
				-1.06	-1.06
			$^{\dagger}[p_{3/2}^4 g_{9/2}^4] [p_{3/2}^2 p_{1/2}^2 g_{9/2}^{10} g_{7/2}^3]$	-2.50	-1.24
				-1.24	-1.24
95	${}^{41}_{54}\text{Nb} \rightarrow {}^{42}_{53}\text{Mo}^{\times}$	5.08	$[g_{9/2}^2] [g_{7/2}^{10} g_{7/2}^3]$	-1.09	-0.36
				-0.36	-0.36
			$[g_{9/2}^2] [d_{5/2}^2 g_{9/2}^{10} g_{7/2}^3]$	-1.24	-0.22
				-0.22	-0.22
			$^{\dagger}[p_{3/2}^4 g_{9/2}^4] [p_{3/2}^2 p_{1/2}^2 g_{9/2}^{10} g_{7/2}^3]$	-1.09	-0.52
				-0.52	-0.52
			$[p_{3/2}^4 g_{9/2}^4] [p_{3/2}^2 p_{1/2}^2 d_{5/2}^2 g_{9/2}^{10} g_{7/2}^3]$	-1.21	-0.40
				-0.40	-0.40
97	${}^{41}_{56}\text{Nb} \rightarrow {}^{42}_{55}\text{Mo}$	5.35	$[p_{3/2}^4 g_{9/2}^4] [p_{3/2}^2 p_{1/2}^2 g_{9/2}^{10} g_{7/2}^5]$	-0.88	-0.58
				-0.58	-0.58
			$[p_{3/2}^4 g_{9/2}^4] [p_{3/2}^2 p_{1/2}^2 d_{5/2}^2 g_{9/2}^{10} g_{7/2}^3]$	-0.92	-0.54
				-0.54	-0.54
			$[p_{3/2}^4 g_{9/2}^4] [p_{3/2}^2 p_{1/2}^2 d_{5/2}^2 g_{9/2}^{10} g_{7/2}^3]$	-1.00	-0.47
				-0.47	-0.47
			$[g_{9/2}^2] [g_{7/2}^{10} g_{7/2}^5]$	-0.87	-0.47
				-0.47	-0.47
			$[g_{9/2}^2] [d_{5/2}^2 g_{9/2}^{10} g_{7/2}^3]$	-0.91	-0.42
				-0.42	-0.42
			$[g_{9/2}^2] [d_{5/2}^4 g_{9/2}^{10} g_{7/2}^3]$	-1.02	-0.32
				-0.32	-0.32

Table 3. 1g Shell Decays (continued)

A	Decay	log ft	Configuration of daughter nucleus	$\lambda$		
101	${}^{43}_{58}\text{Tc} \rightarrow {}^{44}_{57}\text{Ru}^{\times}$	4.52	$\dagger[p^4_{3/2}g^6_{9/2}][p^4_{3/2}p^2_{1/2}g^{10}_{9/2}g^7_{7/2}]$	-1.12	-1.12	-0.50
				-0.50		
			$[p^4_{3/2}g^6_{9/2}][p^4_{3/2}p^2_{1/2}d^2_{5/2}g^{10}_{9/2}g^5_{7/2}]$	-1.17	-1.17	-0.45
				-0.45		
			$[p^4_{3/2}g^6_{9/2}][p^4_{3/2}p^2_{1/2}d^4_{5/2}g^{10}_{9/2}g^3_{7/2}]$	-1.26	-1.26	-0.37
				-0.37		
			$[p^4_{3/2}g^6_{9/2}][p^4_{3/2}p^2_{1/2}d^6_{5/2}g^{10}_{9/2}g_{7/2}]$	-1.44	-1.44	-0.18
				-0.18		
			$[g^4_{9/2}][g^{10}_{9/2}g^7_{7/2}]$	-1.08	-1.08	-0.39
				-0.39		
107	${}^{49}_{58}\text{In} \rightarrow {}^{48}_{59}\text{Cd}$	> 4.99	$[g^4_{9/2}][d^2_{5/2}g^{10}_{9/2}g^5_{7/2}]$	-1.14	-1.14	-0.33
				-0.33		
			$[g^4_{9/2}][d^4_{5/2}g^{10}_{9/2}g^3_{7/2}]$	-1.23	-1.23	-0.24
				-0.24		
			$[g^4_{9/2}][d^6_{5/2}g^{10}_{9/2}g_{7/2}]$	-1.44	-1.44	-0.04
				-0.04		
			$[g^8_{9/2}][d^2_{5/2}g^{10}_{9/2}g^7_{7/2}]$	-4.20	-0.52	-0.52
				-0.52		
			$[g^8_{9/2}][d^4_{5/2}g^{10}_{9/2}g^5_{7/2}]$	-3.68	-1.06	-1.06
				-1.06		
111	${}^{50}_{61}\text{Sn} \rightarrow {}^{49}_{62}\text{In}$	4.69	$[g^8_{9/2}][d^6_{5/2}g^{10}_{9/2}g^3_{7/2}]$	-3.46	-1.31	-1.31
				-1.31		
			$[g^9_{9/2}][d^4_{5/2}g^{10}_{9/2}g^8_{7/2}]$	-1.43	-0.91	-0.91
				-0.91		
			$[g^9_{9/2}][d^6_{5/2}g^{10}_{9/2}g^6_{7/2}]$	-1.75	-1.04	-1.04
				-1.04		

Table 4. 2p Shell Decays

<i>A</i>	Decay	log <i>ft</i>	Configuration of daughter nucleus	$\lambda$	
69	${}_{30}\text{Zn}_{39} \rightarrow {}_{31}\text{Ga}_{38}$	4.37	$\dagger[f_{7/2}^8 p_{3/2}^3] [f_{7/2}^6 f_{5/2}^6 p_{3/2}^4]$	wrong sign	
			$\dagger[f_{7/2}^8 f_{5/2}^2 p_{3/2}^2] [f_{7/2}^8 f_{5/2}^6 p_{3/2}^4]$	-2.34 -1.29	-1.29
73	${}_{31}\text{Ga}_{42} \rightarrow {}_{32}\text{Ge}_{41}^{\times}$	5.93	$\dagger[f_{7/2}^8 p_{3/2}^4] [f_{7/2}^8 f_{5/2}^6 g_{9/2}^2 p_{3/2}^4 p_{1/2}]$	-3.17 -2.76	-2.76
			$[f_{7/2}^8 f_{5/2}^2 p_{3/2}^2] [f_{7/2}^8 f_{5/2}^6 g_{9/2}^2 p_{3/2}^4 p_{1/2}]$	-1.15 -0.95	-1.15
75	${}_{32}\text{Ge}_{43} \rightarrow {}_{33}\text{As}_{42}$	< 5.24	$\dagger[f_{7/2}^8 f_{5/2}^2 p_{3/2}^3] [f_{7/2}^8 f_{5/2}^6 g_{9/2}^4 p_{3/2}^4]$	wrong sign	
			$[f_{7/2}^8 f_{5/2}^4 p_{3/2}^2] [f_{7/2}^8 f_{5/2}^6 g_{9/2}^4 p_{3/2}^4]$	-1.88 -1.52	-1.52
77	${}_{32}\text{Ge}_{45}^{\text{m}} \rightarrow {}_{33}\text{As}_{44}$	> 4.73	$[f_{7/2}^8 f_{5/2}^2 p_{3/2}^3] [f_{7/2}^8 f_{5/2}^6 g_{9/2}^4 p_{3/2}^4]$	-40.1 -22.9	
			$[f_{7/2}^8 f_{5/2}^4 p_{3/2}^2] [f_{7/2}^8 f_{5/2}^6 g_{9/2}^4 p_{3/2}^4]$	-1.88 -1.28	-1.28
77	${}_{33}\text{As}_{44} \rightarrow {}_{34}\text{Se}_{43}$	5.76	$\dagger[f_{7/2}^8 f_{5/2}^2 p_{3/2}^4] [f_{7/2}^8 f_{5/2}^6 g_{9/2}^4 p_{3/2}^4 p_{1/2}]$	-3.23 -2.73	-2.73
			$\dagger[f_{7/2}^8 f_{5/2}^4 p_{3/2}^2] [f_{7/2}^8 f_{5/2}^6 g_{9/2}^4 p_{3/2}^4 p_{1/2}]$	-1.19 -0.94	-1.19
77	${}_{35}\text{Br}_{42} \rightarrow {}_{34}\text{Se}_{43}$	5.36	$\dagger[f_{7/2}^8 f_{5/2}^4 p_{3/2}^2] [f_{7/2}^8 f_{5/2}^6 g_{9/2}^4 p_{3/2}^4 p_{1/2}]$	wrong sign	
			$[f_{7/2}^8 f_{5/2}^6] [f_{7/2}^8 f_{5/2}^6 g_{9/2}^4 p_{3/2}^4 p_{1/2}]$	-2.10 -1.61	-1.61



Table 4. 2p Shell Decays (*continued*)

<i>A</i>	Decay	$\log ft$	Configuration of daughter nucleus	$\lambda$	
77	${}^{36}_{36}\text{Kr}_{41} \rightarrow {}^{35}_{35}\text{Br}_{42}$	5.40	$\dagger[f_{7/2}^8 f_{5/2}^4 p_{3/2}^3] [f_{7/2}^8 f_{5/2}^6 g_{9/2}^2 p_{3/2}^4 p_{1/2}^2]$	-4.51	-3.77
			$[f_{7/2}^8 f_{5/2}^6 p_{3/2}^2] [f_{7/2}^8 f_{5/2}^6 g_{9/2}^2 p_{3/2}^4 p_{1/2}^2]$	-1.34	-1.34
81	${}^{34}_{34}\text{Se}_{47} \rightarrow {}^{35}_{35}\text{Br}_{46}$	4.72	$\dagger[f_{7/2}^8 f_{5/2}^4 p_{3/2}^3] [f_{7/2}^8 f_{5/2}^6 g_{9/2}^2 p_{3/2}^4]$	-36.4	
			$[p_{3/2}] [g_{9/2}^4 p_{3/2}^4]$	-20.7	-1.29
83	${}^{34}_{34}\text{Se}_{40}^m \rightarrow {}^{35}_{35}\text{Br}_{48}$	5.22	$\dagger[f_{7/2}^8 f_{5/2}^4 p_{3/2}^3] [f_{7/2}^8 f_{5/2}^6 g_{9/2}^4 p_{3/2}^4]$	-14.0	
			$[p_{3/2}] [g_{9/2}^4 p_{3/2}^4]$	-10.2	-1.33
83	${}^{35}_{35}\text{Br}_{48} \rightarrow {}^{36}_{36}\text{Kr}_{47}^m$	5.13	$\dagger[f_{7/2}^8 f_{5/2}^4 p_{3/2}^4] [f_{7/2}^8 f_{5/2}^6 g_{9/2}^4 p_{3/2}^4 p_{1/2}^2]$	-3.09	-2.19
			$[p_{3/2}^2] [g_{9/2}^4 p_{3/2}^4 p_{1/2}^2]$	-2.19	-1.29
85	${}^{35}_{35}\text{Br}_{50} \rightarrow {}^{36}_{36}\text{Kr}_{49}^m$	5.17	$\dagger[f_{7/2}^8 f_{5/2}^4 p_{3/2}^4] [f_{7/2}^8 f_{5/2}^6 g_{9/2}^4 p_{3/2}^4 p_{1/2}^2]$	-1.29	-0.78
			$[p_{3/2}^2] [g_{9/2}^4 p_{3/2}^4 p_{1/2}^2]$	-2.75	-1.98
85	${}^{36}_{36}\text{Kr}_{49}^m \rightarrow {}^{37}_{37}\text{Rb}_{48}$	5.00	$\dagger[p_{3/2}^3] [g_{9/2}^4 p_{3/2}^4]$	-1.23	-1.23
			$[g_{9/2}^2 p_{3/2}^2] [g_{9/2}^4 p_{3/2}^4]$	-0.76	-1.31

§ 8. *l*-FORBIDDEN TRANSITIONS

Finally, we consider briefly the *l*-forbidden transitions which, whilst experimentally showing the characteristics of allowed transitions (with somewhat larger  $ft$  values), are forbidden on the pure shell model since a change of orbital angular momentum is involved. It is clear that into the nominal configurations we can mix states which will produce first-order contributions to the reduced matrix elements for beta-transitions. We have considered some seven such decays which are nominally  $1f_{5/2} \Rightarrow 2p_{3/2}$ . These decays are between nuclei with mass numbers  $61 \leq A \leq 69$ , and in view of the difficulties described in § 7.3 we should not expect a too quantitative agreement with experiment. One further difficulty is that the energy denominators which occur now involve the relative positions of the  $f_{5/2}$  and  $p_{3/2}$  levels. The calculations and results are analogous to those described in the previous sections and will not be presented here. However, assuming that the level spacing is that used by Arima and Horie (1955) and again using oscillator functions to estimate the various radial integrals in terms of  $\epsilon_s(p, p)$ , we can express the reduced matrix elements once again in terms of  $\xi_p \equiv \epsilon_s(p, p)/\Delta E_p$ . Assuming a reasonable value  $\xi_p \sim -0.3$ , we find that the calculated lifetimes are smaller,  $4.7 \leq \log ft \leq 6.0$ , than those found experimentally,  $4.9 \leq \log ft \leq 7.4$ . This lack of agreement is not too surprising in view of the crude nature of the calculations, but it is indicative that our model will permit lifetimes corresponding to allowed decays.

## § 9. DISCUSSION

On the basis of the *j-j* coupling shell model and first-order perturbation theory it has been shown that the nuclear matrix elements for allowed beta-decays can be written in the form  $|\langle \sigma \rangle|^2 = |\langle \sigma \rangle|_{jj}^2 \{1 + B\xi_l\}^2$  where  $|\langle \sigma \rangle|_{jj}$  is the unperturbed many-particle matrix element,  $B$  is known, and  $\xi_l$  is a parameter depending on the strength of the two-body interaction and the spin-orbit splitting for a given orbit  $l$ . The considerations leading to this result are crude and are presented only as an indication of the results which might be expected from a more realistic calculation. Our results, then, are of heuristic value only. Moreover, in order that our results should agree with the experimental lifetimes, we find that the factor  $\{1 + B\xi_l\}^2$  must usually be of the order of  $10^{-2}$ . Hence, the calculated lifetimes will be extremely sensitive to the value of the parameter  $\xi_l$ . For a given orbit the parameter  $\lambda_l \equiv A^{1/3}\xi_l$  should be roughly independent of  $A$ ; we have tabulated the values of  $\lambda_l$  required to make the calculated and experimental lifetimes agree. It is clear that the most we can expect is that, for a given orbit, these values should be sensibly constant and of the correct order of magnitude as estimated by some independent method; a rough estimate of the values of the  $\lambda_l$  is given in equation (28).

For more than three particles the calculation is not practicable using isotopic-spin eigenfunctions as basic states, so that we have had to use wave functions that are separately antisymmetric with respect to the neutrons and protons respectively. For the  $\Delta J=0$  transitions within the  $1f_{7/2}$  shell the agreement with experiment is poor, and there is every indication that it is necessary to use isotopic-spin eigenfunctions in order to account for the experimental results. For  $A=43$  it has been shown that, using such functions as unperturbed states, we obtain a good one-parameter fit for the lifetimes of the decays  ${}_{21}\text{Sc}_{22} \rightarrow {}_{20}\text{Ca}_{23}$ ,  ${}_{22}\text{Ti}_{21} \rightarrow {}_{21}\text{Sc}_{22}$  and the magnetic moment of  ${}_{20}\text{Ca}_{23}$ . We would expect our present calculations to be more valid for decays within higher shells.

For decays within the 2d shell our results are satisfactory. It is found that the experimental lifetimes can be accounted for using values of  $\lambda_i$  which do not vary greatly and which agree with the estimate in (28). Where alternative configurations have been considered it is found that the values of  $\lambda_i$  required do not vary significantly; our results give no indication as to the correct zero-order configuration.

For decays within the 1g shell our results are not so clear cut. For each decay there are several possible basic configurations. If the estimate (28) is reliable the choice of configurations is restricted. However, for four of the six decays in this group, agreement with experiment can be obtained using values of  $\lambda_i$  which agree with (28), and with reasonable basic configurations. For the remaining two decays the values of  $\lambda_i$  required are too large. This implies either a breakdown of the model or that the estimate (28) is at fault. Certainly, the derivation of (28) is crude. If we ignore this estimate then we find that the experimental results can be obtained for all six decays using values of  $\lambda_i$  which do not vary greatly. These values are not very sensitive to the choice of zero-order configuration, so that again our results would give no indication of the true basic configuration. There seems to be no obvious reason why the model should break down for the two decays mentioned above and, in view of the crude nature of (28), the evidence would appear to be inconclusive.

For decays within the 2p shell the model breaks down. The basic configurations in this region are determined from the measured quadrupole moments, and with these configurations we require unrealistic values of  $\lambda_i$  to obtain agreement with the measured beta-decay lifetimes. For the transitions within this region it is found that the contributions to the matrix elements from different admixtures tend to interfere. The difficulty of assessing the relative magnitudes of the contributions is such that, for five of the decays, the discrepancy might be due to inaccuracies in this part of the calculation. Also, in cases where the quadrupole moment of the daughter nucleus is unknown, we might assume a different basic configuration for which the lifetimes can be obtained using values of  $\lambda_i$  which agree with (28). A more likely explanation, however, is that the wave functions of nuclei in this region contain a more serious admixing than that assumed in the present model. There is evidence that this is the case and it is pointed out that in similar perturbation calculations the major disagreements with experiment occur for nuclei in this region. Finally, for the *l*-forbidden transitions which occur in this region, the perturbation calculation predicts lifetimes corresponding to allowed decays. However, the approximations involved in the calculation preclude a detailed estimate of lifetimes.

Throughout, we have stressed the approximate nature of our calculations. However, the results indicate that the unfavoured nature of the  $\Delta J = 1$  transitions could, to a large extent, be ascribed to the presence of admixed configurations within the basic shell model configuration.

#### ACKNOWLEDGMENTS

I should like to thank Dr. R. J. Blin-Stoyle for suggesting this problem and for his advice. This work was carried out during the tenure of a maintenance grant from the Department of Scientific and Industrial Research.

## REFERENCES

- ARIMA, A., and HORIE, H., 1954, *Progr. Theor. Phys., Japan*, **11**, 509; 1955, *Phys. Rev.*, **99**, 778.
- ARIMA, A., HORIE, H., and SANO, M., 1957, *Progr. Theor. Phys., Japan*, **17**, 567.
- BLIN-STOYLE, R. J., 1956, *Phil. Mag.*, **46**, 973.
- BLIN-STOYLE, R. J., and CAINE, C. A., 1957, *Phys. Rev.*, **105**, 1810.
- BLIN-STOYLE, R. J., and PERKS, M. A., 1954, *Proc. Phys. Soc. A*, **67**, 885.
- CONDON, E. U., and SHORTLEY, G. H., 1935, *The Theory of Atomic Spectra* (Cambridge : University Press).
- ELLIOTT, J. P., and FLOWERS, B. H., 1955, *Proc. Roy. Soc. A*, **229**, 536.
- FLOWERS, B. H., 1952, *Proc. Roy. Soc. A*, **212**, 248.
- GRAYSON, W. C., and NORDHEIM, L. W., 1956 a, *Phys. Rev.*, **102**, 1084; 1956 b, *Ibid.*, **102**, 1093.
- KING, R. W., 1954, *Rev. Mod. Phys.*, **26**, 327.
- KLINKENBERG, P. F. A., 1952, *Rev. Mod. Phys.*, **24**, 63.
- MAYER, M. E., and JENSEN, J. H. D., 1955, *Elementary Theory of Nuclear Shell Structure* (New York : John Wiley).
- NORDHEIM, L. W., and YOST, F. L., 1937, *Phys. Rev.*, **51**, 942.
- NUSSBAUM, R. H., 1956, *Rev. Mod. Phys.*, **28**, 423.
- PRYCE, M. H. L., 1952, *Proc. Phys. Soc. A*, **65**, 773.
- RACAH, G., 1942, *Phys. Rev.*, **62**, 437; 1943, *Ibid.*, **63**, 367.
- SIEGBAHN, K., 1955, *Beta- and Gamma-Ray Spectroscopy* (Amsterdam : North-Holland).
- WINTHER, A., and KOFOED-HANSEN, O., 1953, *K. Danske. Vidensk. Selsk., Mat.-fys Medd*, **27**, no. 14.



# Intensity Measurements on the $O_2^+$ Second Negative, CO Ångström and Third Positive and NO $\gamma$ and $\beta$ Molecular Band Systems

BY D. ROBINSON AND R. W. NICHOLLS

Department of Physics, University of Western Ontario, London, Canada

*MS. received 31st December 1957*

**Abstract.** Relative band intensities of the Second Negative system of  $O_2^+$ , the Ångström and Third Positive systems of CO, and the  $\gamma$  and  $\beta$  systems of NO have been measured. They have been interpreted with the aid of the Franck-Condon factors  $q_{v',v''}$  and the  $r$ -centroids  $\bar{r}_{v',v''}$  to show the variation of the electronic transition moment  $R_e(r)$  with internuclear separation  $r$ . Arrays of the relative vibrational transition probabilities  $p_{v',v''}$  and the intensities  $I_\infty$  at infinite temperature have thereby been derived for these systems.

## § 1. INTRODUCTION

As part of a programme to obtain accurate relative intensity measurements for band systems of astrophysical interest, results have been published for the First Positive (Turner and Nicholls 1954) and Second Positive (Wallace and Nicholls 1955) systems of  $N_2$ , the First Negative system of  $N_2^+$  (Wallace and Nicholls 1955) and the CN red system (Dixon and Nicholls 1958). Measurements which have now been made on the Second Negative system of  $O_2^+$ , the Ångström and Third Positive systems of CO and the  $\gamma$  and  $\beta$  systems of NO are reported here. They have been interpreted to derive the form of the electronic transition moment  $R_e(r)$  and hence to obtain more accurate values of the relative transition probabilities  $p_{v',v''}$ .

The procedure used has been described in detail elsewhere (Nicholls 1956 a, b) and thus it will suffice to include the basic equations only. The integrated intensity  $I_{v',v''}$  of the  $v' \rightarrow v''$  molecular band may be written

$$I_{v',v''} = DN_{v'} E_{v',v''}^4 p_{v',v''} \quad \dots\dots (1)$$

where  $D$  is a constant depending on the units and geometry of the system,  $N_{v'}$  is the population of the upper vibrational level  $v'$ ,  $E_{v',v''}$  is the energy difference of the transition and  $p_{v',v''}$  is the relative vibrational transition probability. Within certain limitations discussed by Fraser (1954 a), equation (1) may be rewritten

$$I_{v',v''} = DN_{v'} E_{v',v''}^4 q_{v',v''} R_e^2(\bar{r}_{v',v''}) \quad \dots\dots (2)$$

where  $q_{v',v''}$  is the overlap integral square,  $|\int \psi_{v'}(r) \psi_{v''}(r) dr|^2$  called the Franck-Condon factor and  $R_e(r)$  is the electronic transition moment. The value of the internuclear separation defined by

$$\bar{r}_{v',v''} = \frac{\int \psi_{v'}(r) r \psi_{v''}(r) dr}{\int \psi_{v'}(r) \psi_{v''}(r) dr} \quad \dots\dots (3)$$

is called the  $r$ -centroid and evaluated by the methods of Nicholls and Jarman (1956). Rearranging equation (2)

$$R_e(\bar{r}_{v',v''}) = \left( \frac{DN_{v'} I_{v',v''}}{E_{v',v''}^4 q_{v',v''}} \right)^{1/2} \quad \dots\dots (4)$$

In equation (4),  $I_{v'v''}$  is measured experimentally,  $E_{v'v''}$  is known from wavelength tables, and  $q_{v'v''}$  can be computed by the methods of Fraser and Jarman (1953). Then, for a given  $v''$  progression, ( $v' = \text{const.}$ ), a plot of the right-hand side of equation (4) as a function of  $\bar{r}_{v'v''}$  will show, after suitable scaling of the segments for each  $v''$  progression, the variation of  $R_e(r)$  with internuclear separation  $r$ .

## § 2. EXPERIMENTAL

The  $\text{O}_2^+$ , CO and NO  $\gamma$  systems were excited by flowing oxygen, carbon monoxide and nitric oxide, respectively, through a heavy current water-cooled capillary discharge tube of the Hunter-Pearse design (1936), modified with external electrodes by the application of du Pont 5504-A electrically conducting paint. A Hartley type radio-frequency oscillator provided the power supply.

The NO  $\beta$  system appears only weakly in the Hunter-Pearse discharge tube and is badly overlapped by the NO  $\gamma$  system. However, the reaction between the active nitrogen afterglow and excess oxygen produces the NO  $\beta$  system strongly and the NO  $\gamma$  system relatively weakly. An active nitrogen source was therefore constructed in the form designed by Benson (1951) in which prepurified nitrogen was passed at a pressure of a few millimetres Hg through three 15 kv condensed sparks equipped with secondary gaps. When oxygen was introduced into the active nitrogen stream, the NO  $\beta$  system was excited strongly.

Intensity measurements were made on the bands of the  $\text{O}_2^+$  Second Negative system by both photographic and photoelectric methods and on the CO and NO systems by the photoelectric method only. For the photographic results a Bausch and Lomb large quartz spectrograph was used with Kodak IN plates. A rotating 15 step sector of step ratio 1.5:1 gave an overall intensity variation of 350:1. With this sector and a standard lamp, the variation of the sensitivity of the photographic emulsion with incident intensity was obtained at any given wavelength by standard techniques (Forsythe 1937). The calibration and band intensity profiles were traced with a Leeds and Northrup recording densitometer. The photoelectric results were recorded on a Leeds and Northrup photoelectric recording spectrometer. This spectrometer was designed for photomultiplier detection over a range of 2100 to 7000 Å and uses an Ebert-type monochromator (Fastie 1952) with an aperture of f/10. It has a 3 inch replica grating with 30 000 lines per inch and gives a reciprocal dispersion of about 8 Å per mm in the first order at the exit slit.

Both the photographic and photoelectric recording systems were calibrated with a Philips standard tungsten lamp.

## § 3. RESULTS

### 3.1. $\text{O}_2^+$ Second Negative System

Intensity measurements have been made on sixteen bands by both photographic and photoelectric techniques. The results of these measurements, given in table 1 are in good agreement. The photoelectric values are considered to be more accurate than the photographic since the former do not have many of the sources of error inherent in the use of a photographic plate. In every case the integrated intensity of the whole band is measured. Table 1 also gives the  $r$ -centroids and wavelengths used for each band in the determination of  $p_{v'v''}$ .

Table 1. Measured Relative Intensities,  $r$ -centroids and Wavelengths for  $O_2^+$  Second Negative System

$v'$	$v''$	3	4	5	6	7
0				6.7 7.5 1.32 <sub>8</sub> 3421	7.6 6.9 1.34 <sub>6</sub> 3630	8.1 8.0 1.36 <sub>5</sub> 3860
1			— 4.5 1.30 <sub>1</sub> 3141	10.0 10.0 1.31 <sub>9</sub> 3323	8.5 8.9 1.33 <sub>6</sub> 3518	7.5 6.9 1.35 <sub>5</sub> 3734
2		4.5 — 1.27 <sub>7</sub> 2907	8.7 6.9 1.29 <sub>3</sub> 3063	9.7 9.6 1.31 <sub>0</sub> 3231	— — 1.32 <sub>7</sub> 3416	1.9 1.9 1.34 <sub>5</sub> 3620
3		8.8 — 1.26 <sub>9</sub> 2840	8.7 8.0 1.28 <sub>5</sub> 2988			
4		9.2 — 1.26 <sub>3</sub> 2777	— — 1.27 <sub>8</sub> 2920			

Order of entry  
 $I_{v'v''}$  (photoelectric)  
 $I_{v'v''}$  (photographic)  
 $r$ -centroid (Å),  
wavelength (Å).

$I_{v'v''}$  for the strongest band, (1,5), is normalized to 10.0.

Table 2. Relative Transition Probabilities of  $O_2^+$  Second Negative System

$v'$	$v''$	3	4	5	6	7	8
0				0.02 <sub>6</sub> 0.02 <sub>5</sub> 6.6	0.05 <sub>1</sub> 0.05 <sub>5</sub> 10.0	0.06 <sub>9</sub> 0.08 <sub>5</sub> 8.9	0.09 <sub>8</sub> 0.14 <sub>1</sub> 6.7
1			0.04 <sub>0</sub> 0.03 <sub>2</sub> 12.5	0.07 <sub>5</sub> 0.06 <sub>7</sub> 20.8	0.10 <sub>0</sub> 0.10 <sub>0</sub> 22.7	0.09 <sub>3</sub> 0.10 <sub>6</sub>	
2		0.03 <sub>8</sub> 0.02 <sub>6</sub> 11.7	0.07 <sub>8</sub> 0.05 <sub>9</sub> 24.5	0.10 <sub>3</sub> 0.08 <sub>7</sub> 30.6	0.08 <sub>2</sub> 0.07 <sub>7</sub> 20.9	0.03 <sub>1</sub> 0.03 <sub>3</sub> 6.1	
3		0.06 <sub>7</sub> 0.04 <sub>4</sub> 19.8	0.10 <sub>2</sub> 0.07 <sub>4</sub> 32.2				
4		0.09 <sub>1</sub> 0.05 <sub>8</sub> 26.3	0.09 <sub>7</sub> 0.06 <sub>7</sub> 30.1				

Order of entry  
 $p_{v'v''}$   
 $q_{v'v''}$   
 $I_\infty = p_{v'v''}/\lambda^4_{v'v''}$

$p_{v'v''}$  and  $q_{v'v''}$  made equal for (1,6) band.

$I_\infty$  for the strongest band of  $v'=0$  progression is normalized to 10.0.

Using these values of  $I_{v'v''}$  in equation (4), a quadratic function for the variation of  $R_e(r)$  with internuclear separation  $r$  was found by a least squares treatment to be

$$R_e(r) = \text{const.} \times (-1 + 1.5386r - 0.5872r^2) \quad \dots\dots (5)$$





A straight line of the form

$$R_e(r) = \text{const.} \times (-1 + 0.943r) \quad \dots\dots (7)$$

was fitted to the data for the CO Third Positive system over the range  $1.08 \text{ \AA} < r < 1.16 \text{ \AA}$ .

Since only the bands of the  $v' = 0, 1$  progressions are known for the two CO systems, no values of the anharmonicity constant  $\omega_e x_e$ , which is used in the calculation of the  $q_{v'v''}$  values were available. Pekeris' rule (Herzberg 1950) was therefore used to predict the values of  $\omega_e x_e$ , and perturbation corrected  $q_{v'v''}$  were thereby calculated. They were found to be insensitive to  $\omega_e x_e$  over a relatively wide range of values. Details of this work will be published elsewhere.

The smoothed relative transition probabilities  $p_{v'v''}$  and the perturbation corrected Franck-Condon factors  $q_{v'v''}$  (McEachran, private communication), together with the relative intensities  $I_\infty$  at infinite temperature are given in table 4

Table 4. Relative Transition Probabilities of CO Ångström and Third Positive Systems

Ångström System		0	1	2	3	4	5	6
$v'$	$v''$							
0		0.08 <sub>8</sub>	0.17 <sub>1</sub>	0.15 <sub>4</sub>	0.13 <sub>9</sub>	0.11 <sub>0</sub>	0.09 <sub>1</sub>	
		0.08 <sub>8</sub>	0.18 <sub>0</sub>	0.20 <sub>9</sub>	0.18 <sub>1</sub>	0.12 <sub>5</sub>	0.08 <sub>3</sub>	
		6.8	10.0	6.7	4.5	2.6	1.5	
1		0.40 <sub>2</sub>	0.20 <sub>2</sub>	0.02 <sub>8</sub>	0.00 <sub>2</sub>	0.03 <sub>4</sub>	0.07 <sub>0</sub>	0.09 <sub>3</sub>
		0.25 <sub>1</sub>	0.17 <sub>9</sub>	0.03 <sub>2</sub>	0.00 <sub>3</sub>	0.04 <sub>6</sub>	0.08 <sub>6</sub>	0.09 <sub>8</sub>
		4.4	1.7	0	0	0	0.2	0.2
Third Positive System		0	1	2	3	4	5	6
$v'$	$v''$							
0		0.05 <sub>4</sub>	0.08 <sub>2</sub>	0.06 <sub>6</sub>	0.03 <sub>5</sub>	0.01 <sub>3</sub>	0.00 <sub>2</sub>	
		0.05 <sub>4</sub>	0.12 <sub>9</sub>	0.17 <sub>9</sub>	0.17 <sub>6</sub>	0.14 <sub>9</sub>	0.11 <sub>9</sub>	
		8.0	10.0	6.6	2.8	0.8	0.1	
1		0.34 <sub>2</sub>	0.22 <sub>5</sub>	0.05 <sub>4</sub>	0.00 <sub>1</sub>	0.00 <sub>3</sub>	0.00 <sub>6</sub>	0.00 <sub>3</sub>
		0.21 <sub>2</sub>	0.20 <sub>2</sub>	0.07 <sub>4</sub>	0.00 <sub>3</sub>	0.01 <sub>1</sub>	0.05 <sub>2</sub>	0.08 <sub>0</sub>
		64.0	35.0	6.9	0.1	0.3	0.4	0.2

Order of entry

$p_{v'v''}$

$q_{v'v''}$

$I_\infty = p_{v'v''}/\lambda^4_{v'v''}$

$p_{v'v''}$  and  $q_{v'v''}$  are made equal for (0,0) bands.

$I_\infty$  for the strongest band in the  $v' = 0$  progression is normalized to 10.0.

for the Ångström and Third Positive systems. It will be noticed that there is close agreement between the  $p_{v'v''}$  and  $q_{v'v''}$  values for bands of the Ångström system for which  $R_e(r)$  is thus almost independent of  $r$ . There is a divergence between them for the Third Positive system, with a consequent significant dependence of  $R_e(r)$  upon  $r$  in that case.

3.3. NO  $\gamma$  and  $\beta$  Systems

Intensity measurements have been made on ten bands in the  $v'=0, 1, 2$  progressions of the NO  $\gamma$  system and on eight bands in  $v'=0$  progression of the NO  $\beta$  system. The results obtained are given in table 5. Also included are the values of the  $r$ -centroids and the wavelengths. With these values of  $I_{v'v''}$ , the variation of  $R_e(r)$  with internuclear separation was again obtained as described above.

Table 5. Measured Relative Intensities,  $r$ -centroids and Wavelengths for the NO  $\gamma$  and  $\beta$  Systems

NO $\gamma$ System		1	2	3	4	5	6	7	8		
$v''$	$v'$										
0			4.7	10.0	7.5	4.7	—	—			
			1.06 <sub>7</sub>	1.04 <sub>9</sub>	1.03 <sub>1</sub>	1.01 <sub>5</sub>	1.00 <sub>0</sub>	0.98 <sub>4</sub>			
			2471	2588	2713	2850	2998	3171			
1			—	—	3.5	5.1	4.4	—			
			1.09 <sub>2</sub>	1.07 <sub>2</sub>	1.05 <sub>4</sub>	1.03 <sub>7</sub>	1.02 <sub>0</sub>	1.00 <sub>5</sub>			
			—	2440	2550	2671	2801	2942			
2			—	—	—	—	2.2	2.1	1.6		
				1.09 <sub>7</sub>	1.07 <sub>7</sub>	1.06 <sub>0</sub>	1.04 <sub>3</sub>	1.02 <sub>6</sub>	1.01 <sub>0</sub>		
				2310	—	2516	2631	2755	2888		
NO $\beta$ System		4	5	6	7	8	9	10	11	12	13
$v''$	$v'$										
0		2.7	5.5	8.5	10.0	9.7	8.0	5.9	3.5	—	—
		1.33 <sub>4</sub>	1.35 <sub>2</sub>	1.37 <sub>1</sub>	1.39 <sub>0</sub>	1.41 <sub>1</sub>	1.43 <sub>0</sub>	1.45 <sub>3</sub>	1.47 <sub>5</sub>	1.50 <sub>0</sub>	—
		2627	2754	2893	3043	3207	3386	3584	3801	4042	—
1		—	—	—	—	—	—	—	—	—	—
			1.34 <sub>2</sub>	1.36 <sub>0</sub>	1.37 <sub>8</sub>	1.39 <sub>8</sub>	1.41 <sub>9</sub>	1.43 <sub>9</sub>	1.46 <sub>0</sub>	1.48 <sub>4</sub>	1.50 <sub>8</sub>
			2679	2809	2951	—	—	3457	3659	3881	4128
2		—	—	—	—	—	—	—	—	—	—
				1.34 <sub>9</sub>	1.36 <sub>7</sub>	1.38 <sub>6</sub>	1.40 <sub>6</sub>	1.42 <sub>7</sub>	1.44 <sub>7</sub>	1.46 <sub>9</sub>	1.49 <sub>2</sub>
				2732	—	3011	3168	3340	—	—	3963
Order of entry $I_{v''} v'$ (arb. units) $r$ -centroid (Å) Wavelength (Å)											

Order of entry  
 $I_{v'v''}$  (arb. units)  
 $r$ -centroid (Å)  
Wavelength (Å)

$I_{v'v''}$  for the strongest band (0, 3) for NO  $\gamma$  system, (0, 7) for NO  $\beta$  system is normalized to 10.0

For the NO  $\gamma$  system a straight line was fitted by a least-squares treatment and found to be

$$R_e(r) = \text{const.} \times (1 - 0.899r) \quad \dots\dots (8)$$

over the range  $1.01 \text{ Å} \leq r \leq 1.06 \text{ Å}$ .

A straight line was fitted to the results of the NO  $\beta$  system of the form

$$R_e(r) = \text{const.} \times (-1 + 1.607r) \quad \dots\dots (9)$$

over the range  $1.33 \text{ Å} \leq r \leq 1.50 \text{ Å}$ .

An array of Franck-Condon factors  $q_{v'v''}$  for the NO  $\beta$  system (Jarman, Fraser and Nicholls 1955) has previously been calculated from the molecular constants quoted by Herzberg (1950), one for each sub-band. These values are inaccurate (Kivel *et al.* 1957), as only one value of the equilibrium separation,  $r_e = 1.415 \text{ Å}$ , should be used for the whole band. A recalculation including perturbation has now been made (McEachran, private communication).

Table 6. Relative Transition Probabilities of NO  $\gamma$  and NO  $\beta$  systems

NO $\gamma$ System		1	2	3	4	5	6	7	8
$v'$	$v''$	0	1	2	3	4	5	6	7
	0	0.02 <sub>7</sub> 0.26 <sub>3</sub> 4.0	0.07 <sub>3</sub> 0.23 <sub>7</sub> 9.3	0.09 <sub>7</sub> 0.16 <sub>1</sub> 10.0	0.09 <sub>1</sub> 0.09 <sub>1</sub> 7.7	0.06 <sub>6</sub> 0.04 <sub>6</sub> 4.6	0.04 <sub>1</sub> 0.02 <sub>1</sub> 2.3	0.02 <sub>3</sub> 0.00 <sub>9</sub> 1.0	
1	1	0	0	0.01 <sub>7</sub> 0.07 <sub>1</sub> 2.3	0.06 <sub>9</sub> 0.13 <sub>4</sub> 7.5	0.11 <sub>5</sub> 0.13 <sub>4</sub> 10.4	0.12 <sub>8</sub> 0.09 <sub>9</sub> 9.6	0.10 <sub>8</sub> 0.06 <sub>2</sub> 6.7	
2	2	0	0	0.00 <sub>1</sub> 0	0.00 <sub>3</sub> 0.07 <sub>7</sub> 0.4	0.01 <sub>4</sub> 0.03 <sub>3</sub> 1.6	0.06 <sub>3</sub> 0.08 <sub>7</sub> 6.0	0.11 <sub>8</sub> 0.10 <sub>5</sub> 9.5	0.14 <sub>3</sub> 0.09 <sub>0</sub> 9.5
NO $\beta$ System		1	2	3	4	5	6	7	8
$v'$	$v''$	0	1	2	3	4	5	6	7
	0	0	0.01 <sub>9</sub> 0.02 <sub>5</sub> 2.6	0.05 <sub>2</sub> 0.05 <sub>7</sub> 5.2	0.08 <sub>8</sub> 0.10 <sub>2</sub> 8.0	0.13 <sub>2</sub> 0.14 <sub>7</sub> 9.9	0.16 <sub>6</sub> 0.17 <sub>4</sub> 10.0	0.17 <sub>0</sub> 0.17 <sub>0</sub> 8.3	0.14 <sub>6</sub> 0.13 <sub>3</sub> 5.6
1	1	0	0.08 <sub>8</sub> 0.11 <sub>1</sub> 10.9	0.09 <sub>4</sub> 0.11 <sub>3</sub> 9.6	0.06 <sub>0</sub> 0.06 <sub>9</sub> 5.1	0.06 <sub>0</sub> 0.03 <sub>4</sub> 0.00 <sub>1</sub>	0.01 <sub>3</sub> 0.01 <sub>4</sub> —	0.00 <sub>4</sub> 0.00 <sub>4</sub> —	0.05 <sub>2</sub> 0.05 <sub>1</sub> 2.3
2	2	0	0.02 <sub>6</sub> 2.4	0.02 <sub>1</sub> 0.02 <sub>6</sub> 2.4	0.00 <sub>1</sub> 0.00 <sub>1</sub> —	0.03 <sub>4</sub> 0.03 <sub>8</sub> 2.6	0.08 <sub>4</sub> 0.08 <sub>9</sub> 5.3	0.05 <sub>7</sub> 0.05 <sub>8</sub> 2.9	0.01 <sub>4</sub> 0.01 <sub>3</sub> —

Order of entry

 $p_{v'v''}$  $q_{v'v''}$  $I_{\infty} = p_{v'v''}/\lambda_{v'v''}^4$  $p_{v'v''}$  and  $q_{v'v''}$  are made equal for (0,4) band, NO  $\gamma$  system, and (0,9) band, NO  $\beta$  system.

— indicates unobserved bands

 $I_{\infty}$  for the strongest band in  $v' = 0$  progression is normalized to 10.0.

Table 6 gives the values obtained for the  $\gamma$  and  $\beta$  systems of the smoothed relative transition probabilities  $p_{v'v''}$  using the above forms of  $R_e(r)$ , the Franck-Condon factors  $q_{v'v''}$  and the relative intensities  $I_\infty$  at infinite temperature. The  $p_{v'v''}$  and  $q_{v'v''}$  are found to agree closely for the NO  $\beta$  system while for the NO  $\gamma$  system there is a wide divergence.

#### ACKNOWLEDGMENTS

The authors would like to acknowledge their indebtedness to Dr. P. A. Fraser for many helpful discussions and to Mr. R. P. McEachran for calculating the  $q_{v'v''}$  values used in this work.

This work was partly supported by the U.S. Air Force Cambridge Research Center under Contracts AF 19(122)-470 and AF 19(604)-1718, and partly by The Defence Research Board of Canada through grant no. DRBC 5001-15.

#### REFERENCES

- BENSON, J. M., 1951, *National Advisory Committee on Aeronautics Report*, TN 2293.  
 DIXON, R. N., and NICHOLLS, R. W., 1958, *Canad. J. Phys.*, **36**, 127.  
 FASTIE, W. G., 1952, *J. Opt. Soc. Amer.*, **42**, 9.  
 FORSYTHE, W. E., 1937, *Measurement of Radiant Energy*, 1st edn (New York: McGraw-Hill), p. 246.  
 FRASER, P. A., 1954 a, *Canad. J. Phys.*, **32**, 515; 1954 b, *Proc. Phys. Soc. A*, **67**, 939.  
 FRASER, P. A., and JARMAIN, W. R., 1953, *Proc. Phys. Soc. A*, **66**, 1145, 1153.  
 HERZBERG, G., 1950, *Spectra of Diatomic Molecules* 2nd edn (New York: Van Nostrand).  
 HUNTER, A., and PEARSE, R. W. B., 1936, *J. Sci. Instrum.*, **13**, 403.  
 JARMAIN, W. R., FRASER, P. A., and NICHOLLS, R. W., 1955, *Astrophys. J.*, **122**, 55.  
 KIVEL, B. MAYER, H. and BETHE, H., 1957, *Annals of Physics*, **2**, 57.  
 NICHOLLS, R. W., 1956 a, *The Airglow and Aurorae* (London: Pergamon Press), p. 302; 1956 b, *Proc. Phys. Soc. A*, **69**, 741.  
 NICHOLLS, R. W., and JARMAIN, W. R., 1956, *Proc. Phys. Soc. A*, **69**, 253.  
 TURNER, R. G., and NICHOLLS, R. W., 1954, *Canad. J. Phys.*, **32**, 468, 475.  
 WALLACE, L. V., and NICHOLLS, R. W., 1955, *J. Atmos. Terr. Phys.*, **7**, 101.



# Acoustomagnetolectric Effects in Metal and Semiconductor Filaments

By G. G. E. LOW

Naval Research Laboratory, Auckland, N.I., New Zealand

*MS. received 4th November 1957, and in revised form 26th January 1958*

**Abstract.** The interaction of a magnetic field and a compressional acoustic wave travelling in a conducting medium is considered and expressions for the electric current densities and fields in filamentary-shaped specimens are derived on the assumption of charge neutrality. Calculations appropriate to metals and to semiconductors are carried out, the latter materials being of interest as the presence of charge carriers of both signs makes possible changes in carrier concentration without violation of the neutrality assumption. In addition, second-order acoustomagnetolectric effects are discussed.

## § 1. INTRODUCTION

SEVERAL calculations concerning the electric currents resulting from the interaction of a static magnetic field and a compressional acoustic wave travelling in a conducting medium have been given (field applied in a direction perpendicular to the direction of wave propagation). In these calculations the mechanical reaction arising from the flow of induced current in the region of the field is evaluated and its effect on the propagation of the wave taken into account. It appears, however, that the changes in wave velocity and attenuation resulting from the application of physically realizable fields are likely to be small (Alpher and Rubin 1954) and consequently to a good approximation the electric current densities set up in infinite media are simply given by  $\sigma H v$ , where  $\sigma$  is the electrical conductivity,  $H$  is the magnetic field and  $v$  is the particle velocity of the medium in the absence of a field ( $H$  and  $v$  mutually perpendicular). Robey (1953) suggests that this type of expression (modified, if necessary, to take account of the mechanical reaction mentioned above) should also apply in the case of finite specimens, such as filaments, as the low drift velocity of charge carriers would not permit the building up, during any one cycle, of a significant amount of charge at the surfaces perpendicular to the direction of current flow. However, it seems clear that such would not be the case and that, as the period of any acoustic waves will be much longer than the dielectric relaxation time of the medium and their wavelength much greater than a Debye length, a far better assumption would be the common one of charge neutrality. On the basis of this approximation departures from charge neutrality involved in establishing electric fields are neglected. Thus, it is assumed that complete neutrality is maintained and further that the necessary electric fields are set up instantaneously. Consequently, the current flowing in a finite medium would not follow a rectilinear path in accordance with the simple expression quoted above. The purpose of this note, therefore, is to evaluate the current

flow in finite filaments on the basis of charge neutrality and also to determine the resulting potential difference produced across such specimens. In addition some second-order acoustomagnetolectric effects are discussed. It is assumed in the analysis that the magnetic field has negligible effect on the propagation of the acoustic wave.

Initially, a simple calculation is made giving an approximate description of conditions in a metal filament and then this treatment is extended so as to be applicable to semiconductors. The latter materials are of interest as the presence of charge carriers of both signs makes possible changes in carrier concentration without violation of the neutrality assumption. An additional refinement introduced in connection with semiconductors is the use of deformation potentials. These are used in their simplest form in which it is assumed that a particle has a potential energy which is proportional to the negative of the dilatation of the medium. The initial equations derived are similar to those used by Weinreich (1956) in discussing the acoustoelectric effect in semiconductors, and his nomenclature has been adopted. This allows comparison of the acoustoelectric effect with the corresponding second-order acoustomagnetolectric effect.

## § 2. METAL FILAMENTS

Consider a metal filament with its longitudinal axis lying in the  $x$  direction and one pair of its sides lying in the planes  $y = \pm a$ . Suppose that a uniform magnetic field of  $H$  units be applied in the  $z$  direction and that

$$\phi = \phi_0 e^{ik(x-ct)}$$

defines a plane compressional wave having a dilatation of  $\phi/c\rho^{1/2}$  ( $c$  is the velocity of sound and  $\rho$  the density of the medium). Let  $\sigma$  be the electrical conductivity and  $\mu$  the carrier mobility of the metal, then we may write for the current densities

$$\begin{aligned} i_x &= -\sigma \left\{ \frac{\partial}{\partial x} (\gamma_\kappa \phi) \pm \mu H \frac{\partial}{\partial y} (\gamma_\kappa \phi) \right\}, \\ i_y &= -\sigma \left\{ \frac{\partial}{\partial y} (\gamma_\kappa \phi) - \frac{H\phi}{\rho^{1/2}} \mp \mu H \frac{\partial}{\partial x} (\gamma_\kappa \phi) \right\}, \end{aligned}$$

where  $\gamma_\kappa \phi$  is the induced electric potential discussed above in connection with the charge neutrality assumption. It is assumed that this potential is proportional to the dilatation and that the constant of proportionality is a function of  $y$  and in general complex. The terms in  $\mu H$  are of either sign as shown depending on the sign of the Hall effect.

Also because of the assumption of neutrality the continuity equation for the present one-carrier system reduces to

$$\nabla \cdot \mathbf{i} = 0.$$

On substitution it is found that

$$\gamma_\kappa = A_1 e^{ky} + B_1 e^{-ky},$$

and as  $i_y = 0$  at  $y = \pm a$ , the constants  $A_1$  and  $B_1$  are given by

$$\begin{aligned} A_1 &= \frac{H/\rho^{1/2}k}{(1 \mp i\mu H)(e^{ka} + e^{-ka})}, \\ B_1 &= -\frac{H/\rho^{1/2}k}{(1 \pm i\mu H)(e^{ka} + e^{-ka})}. \end{aligned}$$

It follows that the potential difference across the filament is

$$\frac{2H \tanh(ka)}{\rho^{1/2}k(1+\mu^2H^2)}\phi$$

and that the current densities are given by

$$i_x = -\frac{i\sigma H (e^{ky} - e^{-ky})}{\rho^{1/2} (e^{ka} + e^{-ka})}\phi,$$

$$i_y = -\frac{\sigma H (e^{ky} + e^{-ky})}{\rho^{1/2} (e^{ka} + e^{-ka}) - 1}\phi.$$

Thus the current in a finite specimen no longer follows the rectilinear course corresponding to an infinite medium, but rather it circulates in closed paths. One set of concentric closed paths is included in each length of filament corresponding to half an acoustic wavelength. Adjacent sets of paths have opposite directions of flow and hence the period of the flow pattern is the period of the acoustic wave. For a sound intensity of  $1 \text{ w cm}^{-2}$  in a metal having an acoustic impedance  $\rho c$  of  $2 \times 10^6 \text{ g cm}^{-2} \text{ sec}^{-1}$ , the term  $\phi_0/\rho^{1/2}$  has a value of  $10^{1/2} \text{ cm sec}^{-1}$ . Thus, for a metal of high electrical conductivity and for a magnetic field of some thousands of oersteds, current densities of the order of  $100 \text{ amp cm}^{-2}$  may be expected. If conditions are such that  $ka < 1$ , the potential difference across such a specimen would be of the order of 1 mv for every cm of specimen width. The terms dependent on  $\mu$  are of little importance for even if  $\mu$  has a value of  $10^3 \text{ cm}^2 \text{ v}^{-1} \text{ sec}^{-1}$ , the term  $(\mu H)^2$  is still only  $10^{-2}$  when  $H$  is equal to  $10^4$  oersteds.

### § 3. SEMICONDUCTOR FILAMENTS

If  $n$  and  $p$  are the concentrations of electrons and holes respectively,  $\mu_n$  the Hall mobility for electrons and  $b$  the mobility ratio for electrons and holes (assumed equal for both drift and Hall mobilities), the *particle* current densities in a semiconductor may be written

$$j_{n,x} = \frac{nD_n}{kT} \frac{\partial}{\partial x} (e\gamma_\kappa\phi + q_n\phi) - D_n \frac{\partial n}{\partial x} - \mu_n H \left\{ \frac{nD_n}{kT} \frac{\partial}{\partial y} (e\gamma_\kappa\phi) - D_n \frac{\partial n}{\partial y} \right\},$$

$$j_{n,y} = \frac{nD_n}{kT} \left\{ \frac{\partial}{\partial y} (e\gamma_\kappa\phi) - \frac{eH\phi}{\rho^{1/2}} \right\} - D_n \frac{\partial n}{\partial y} + \mu_n H \left\{ \frac{nD_n}{kT} \frac{\partial}{\partial x} (e\gamma_\kappa\phi + q_n\phi) - D_n \frac{\partial n}{\partial x} \right\},$$

$$j_{p,x} = -\frac{pD_n}{bkT} \frac{\partial}{\partial x} (e\gamma_\kappa\phi - q_p\phi) - \frac{D_n}{b} \frac{\partial p}{\partial x} - \frac{\mu_n H}{b} \left\{ \frac{pD_n}{bkT} \frac{\partial}{\partial y} e(\gamma_\kappa\phi) + \frac{D_n}{b} \frac{\partial p}{\partial y} \right\},$$

$$j_{p,y} = -\frac{pD_n}{bkT} \left\{ \frac{\partial}{\partial y} (e\gamma_\kappa\phi) - \frac{eH\phi}{\rho^{1/2}} \right\} - \frac{D_n}{b} \frac{\partial p}{\partial y} + \frac{\mu_n H}{b} \left\{ \frac{pD_n}{bkT} \frac{\partial}{\partial x} (e\gamma_\kappa\phi - q_p\phi) + \frac{D_n}{b} \frac{\partial p}{\partial x} \right\},$$

where  $D_n$  is the diffusion constant for electrons,  $e$  is the electronic charge and  $kT$  is the product of the Boltzmann constant and the absolute temperature. The effects of deformation potentials are taken into account with the aid of  $q_n$  and  $q_p$  which are the deformation potentials for electrons and holes respectively, divided by  $\rho^{1/2}c$ . The appropriate continuity equations are

$$\frac{\partial n}{\partial t} + \nabla \cdot \mathbf{j}_n + \frac{1}{\tau} \left\{ n - n_0 \left( 1 + \frac{q}{1+s} \frac{\phi}{kT} \right) \right\} = 0,$$

$$\frac{\partial p}{\partial t} + \nabla \cdot \mathbf{j}_p + \frac{1}{\tau} \left\{ p - p_0 \left( 1 + \frac{sq}{1+s} \frac{\phi}{kT} \right) \right\} = 0$$

where  $s = n_0/p_0$  is the ratio of the equilibrium concentrations of electrons and

holes,  $\tau$  is the bulk lifetime and  $q = q_n + q_p$ . The last term in each equation expresses to a first-order approximation, the change in equilibrium concentrations corresponding to the energy gap variation resulting from dilatation.

Owing to the neutrality assumption the concentrations of electrons and holes may be written as

$$n = n_0 + n_1 e^{ik(x-ct)}$$

$$p = p_0 + n_1 e^{ik(x-ct)}$$

to a good approximation. On substitution of these expressions the continuity equations may be solved for  $n_1$  giving

$$n_1 = P^2 \frac{Q^2}{R^2} + C e^{Ry} + D e^{-Ry} = n_1' + n_1''$$

where

$$P^2 = \frac{n_0}{1+s} \frac{q\phi_0}{kT},$$

$$Q^2 = k^2 + \frac{1+sb}{D_n \tau (1+s)},$$

$$R^2 = k^2 + \frac{1+sb}{D_n (1+s)} \left( \frac{1}{\tau} - ikc \right).$$

$Q^2/R^2 = M$  in Weinreich's (1956) notation and the first term in the above expression for  $n_1$  corresponds to conditions prevailing in the absence of a magnetic field and in an infinite medium. This term is represented by  $n_1'$  while the terms dependent on  $y$  are written as  $n_1''$ . Similarly, it is found that

$$e\gamma_k = E e^{ky} + F e^{-ky} + \frac{U^2}{k^2} + \frac{V^2}{R^2 - k^2} n_1''$$

where

$$U^2 = \frac{Q^2 q}{R^2 D_n (1+s)} \left( k^2 D_n + \frac{1}{\tau} - ikc \right) - k^2 q_n - \frac{q}{D_n \tau (1+s)}$$

$$V^2 = \frac{kT s(b-1)(\tau^{-1} - ikc)}{n_0 D_n \phi_0 (1+s)}.$$

Boundary conditions must now be introduced in order to determine the values of the constants. If the surface recombination velocity at the surfaces  $y = \pm a$  is  $S_r$ , the appropriate relations, to a first-order approximation, are

$$j_{ny} = j_{py} = \pm S_r \left\{ n - n_0 \left( 1 + \frac{q}{1+s} \frac{\phi}{kT} \right) \right\} \quad \text{at} \quad y = \pm a.$$

(No variations in the  $z$  direction have been envisaged, so that it must be assumed that the medium extends infinitely in this direction, or equivalently that at the surfaces defining the filament in this direction  $S_r = 0$ .)

At this point the system above will be examined under two different simplifying assumptions. The first of these is that thermal equilibrium between electrons and holes is established instantaneously, i.e. that  $\tau = 0$ . In the second simplification the terms dependent on  $\mu_n$  are neglected.

For both these approximations it can easily be shown that if

$$\sigma = \frac{e^2 n_0 D_n}{kT} \left( 1 + \frac{1}{sb} \right),$$

the same expressions for the electric current densities are obtained as were found



in the case of a metal. Thus returning to the original expressions for the particle current densities it can be shown that

$$\nabla \times \mathbf{j}_n = \mathbf{z} \left\{ -\frac{n_0 D_n e H}{k T \rho^{1/2}} \frac{\partial \phi}{\partial x} + \mu_n H \nabla \cdot \mathbf{j}_n \right\}$$

and

$$\nabla \times \mathbf{j}_p = \mathbf{z} \left\{ \frac{n_0 D_n e H}{s b k T \rho^{1/2}} \frac{\partial \phi}{\partial x} - \frac{\mu_n H}{b} \nabla \cdot \mathbf{j}_p \right\},$$

where  $\mathbf{z}$  is a unit vector in the  $z$  direction. Now for both of the above simplifications

$$\mu_n H \nabla \cdot \mathbf{j}_n = \frac{\mu_n H}{b} \nabla \cdot \mathbf{j}_p = 0$$

(i.e.  $\nabla \cdot \mathbf{j}_n = \nabla \cdot \mathbf{j}_p = 0$  in the first case and  $\mu_n = 0$  in the second case). Thus, under this condition

$$\nabla \times \mathbf{i} = e(\nabla \times \mathbf{j}_p - \nabla \times \mathbf{j}_n) = \mathbf{z} \frac{\sigma H}{\rho^{1/2}} \frac{\partial \phi}{\partial x}.$$

This suggests that we may represent the electric current density by the sum of a purely irrotational vector  $\mathbf{i}_i$  and a purely solenoidal vector  $\mathbf{i}_s$ , the latter having components of 0,  $\sigma H \phi / \rho^{1/2}$ , 0. Furthermore, under the neutrality assumption, it is apparent from the continuity equation that

$$\nabla \cdot \mathbf{i} = e(\nabla \cdot \mathbf{j}_p - \nabla \cdot \mathbf{j}_n) = 0,$$

and consequently  $\nabla \cdot \mathbf{i}_i = 0$  as  $\nabla \cdot \mathbf{i}_s \equiv 0$ . Suppose that we put  $\mathbf{i}_i = \sigma \nabla(\gamma \phi)$  so that

$$\nabla \cdot \mathbf{i}_i = \sigma \nabla^2(\gamma \phi) = 0$$

where  $\gamma$  is a function of  $y$  only, then we have as a solution

$$\gamma = A_2 e^{ky} + B_2 e^{-ky}.$$

Thus, on adding the components of the irrotational and the solenoidal vectors we have

$$i_x = ik \sigma \gamma \phi \quad \text{and} \quad i_y = \frac{\sigma H \phi}{\rho^{1/2}} + \sigma \phi \frac{\partial \gamma}{\partial y}.$$

Use of the boundary conditions  $i_y = 0$  at  $y = \pm a$  shows that the above expressions for the electric current density are equal to those found in the case of a metal.

We shall now continue with the analysis in terms of the particle current densities and evaluate the constants dependent on the boundary conditions in the circumstances defined by the two simplifications described above. These results will be used in the next section and additionally they provide values under these approximations for the potential difference across a specimen. For the first simplification in which  $\tau = 0$ , the expressions for  $n_1$  and  $e \gamma_k$  reduce to

$$n_1 = P^2 = \frac{n_0}{1+s} \frac{q \phi_0}{k T}$$

and

$$e \gamma_k = E_1 e^{ky} + F_1 e^{-ky} + \frac{q p - s q n}{1+s},$$

and the boundary conditions to be satisfied are

$$j_{ny} = j_{py} \quad \text{at} \quad y = \pm a.$$

Using these relations it is found that

$$E_1 = \frac{eH/\rho^{1/2}k}{\{1 - i\mu_n HB\}(e^{ka} + e^{-ka})},$$

and

$$F_1 = - \frac{eH/\rho^{1/2}k}{\{1 + i\mu_n HB\}(e^{ka} + e^{-ka})}$$

where  $B$  has been written for  $(1 - sb^2)/b(1 + sb)$ . Thus, the potential difference across the filament is given by

$$\frac{2H \tanh(ka)}{\rho^{1/2}k[1 + \{\mu_n HB\}^2]} \phi$$

on the basis of the present approximation.

In the case of the second simplification the terms dependent on  $\mu_n$  are neglected when applying the boundary conditions in order to determine the values of the constants  $C$ ,  $D$ ,  $E$  and  $F$ . In these circumstances the values found are as follows

$$C_2 = D_2 = \frac{P^2(1 - Q^2/R^2)}{e^{Ra} + e^{-Ra} + \{D_n R(1 + s)/S_r(1 + sb)\}(e^{Ra} - e^{-Ra})}$$

and

$$E_2 = -F_2 = \frac{eH}{\rho^{1/2}k(e^{ka} + e^{-ka})}.$$

Hence, for this approximation the expression for the potential difference across the filament is simply

$$\frac{2H}{\rho^{1/2}k} \tanh(ka) \phi.$$

The constants evaluated above may also be used to find expressions for the particle current densities in the semiconductor. Besides the terms which go to make up the electric current density, these expressions contain terms which appear equally in the formulae for electrons and holes and thus do not contribute to the net transport of electric charge. Hence, under some conditions it is possible for the particle current densities to exceed the electric current density by several orders of magnitude. The electric current flow in a semiconductor is closely similar in character to that in a metal. Owing to differences in conductivity, however, the magnitudes of the current densities are much smaller in a material of the former type. The potential difference across a filament is much the same in both cases, i.e. of the order of 1 mv for a specimen width of 1 cm and a sound intensity of  $1 \text{ w cm}^{-2}$ . For a few semiconductors the terms dependent on  $\mu_n$  may be important. Thus, semiconducting compounds having carrier mobilities greater than  $10^4 \text{ cm}^2 \text{ v}^{-1} \text{ sec}^{-1}$  are known and in such cases  $(\mu_n H)^2$  will become a predominant term for magnetic fields of a few thousand oersteds.

#### § 4. SECOND ORDER EFFECTS

It will be noticed that summed over the cross section of the filament, the electric currents in the  $x$  direction evaluated in the previous section are zero. Thus, to a first approximation there is no net transport of electric charge along the filament. A second-order approximation shows the possibility of a direct current, however. This arises as a consequence of the fluctuations in carrier concentrations in regions of dilatation and compression. The product of the

resulting variations in conductivity and the fluctuating fields gives rise to d.c. terms in the current densities. We shall consider the case in which the terms in  $\mu_n$  are neglected and a further simplification will be effected by assuming that  $1/\tau = S_r = 0$ . The particle current densities may be evaluated to a second-order approximation with the aid of the expressions derived in the previous section. The direct current terms in the  $x$  direction are as follows

$$\begin{aligned}\bar{i}_{n_x} &= W^2 c \left\{ 1 + \frac{1+sb}{q} E_2(e^{ky} - e^{-ky}) \right\}, \\ \bar{j}_{p_x} &= W^2 c \left\{ s - \frac{1+sb}{qb} E_2(e^{ky} - e^{-ky}) \right\},\end{aligned}$$

where

$$W^2 = \frac{1}{2} \frac{n_0}{(1+s)^2} \left( \frac{q\phi_0}{kT} \right)^2 / \left[ 1 + \left\{ \frac{c(1+sb)}{kD_n(1+s)} \right\}^2 \right].$$

Thus, the resulting direct electric current density is

$$\begin{aligned}\bar{i}_x &= e(\bar{j}_{p_x} - \bar{j}_{n_x}) \\ e &= W^2 c \left\{ s - 1 - \frac{(1+sb)(1+b)}{qb} E_2(e^{ky} - e^{-ky}) \right\}.\end{aligned}$$

This transport of electric charge as a result of the action of an acoustic wave has been called the acoustoelectric effect. The term obtained above which is independent of  $y$  corresponds to the expression found by Weinreich (1956) in the absence of a magnetic field and for an infinite semiconducting medium. If the current is summed over the cross section of the filament, this is the only term that remains.

In a medium of infinite extent there will be corresponding second-order direct particle currents in the  $y$  direction, as follows

$$\begin{aligned}\bar{j}_{n_y} &= -W^2 \frac{D_n(1+s)eH}{q\rho^{1/2}}, \\ \bar{j}_{p_y} &= W^2 \frac{D_n(1+s)eH}{qb\rho^{1/2}}.\end{aligned}$$

In a filament, however, there cannot be any net flow in the  $y$  direction and steady electric fields and carrier concentration gradients will be established which will reduce such flow to zero. If these fields and gradients are denoted by  $\partial V_0/\partial y$  and  $\partial n_0''/\partial y$  respectively, the expressions for the direct particle current densities in a filament are given by

$$\begin{aligned}\bar{j}_{n_y} &= W^2 \frac{D_n(1+s)eH}{q\rho^{1/2}} \left( \frac{e^{ky} + e^{-ky}}{e^{ka} + e^{-ka}} - 1 \right) + \frac{n_0 D_n}{kT} \frac{\partial}{\partial y} (eV_0) - D_n \frac{\partial n_0''}{\partial y} \\ \bar{j}_{p_y} &= -W^2 \frac{D_n(1+s)eH}{qb\rho^{1/2}} \left( \frac{e^{ky} + e^{-ky}}{e^{ka} + e^{-ka}} - 1 \right) - \frac{n_0 D_n}{sbkT} \frac{\partial}{\partial y} (eV_0) - \frac{D_n}{b} \frac{\partial n_0''}{\partial y}.\end{aligned}$$

Application of the boundary conditions in connection with these expressions shows that

$$\begin{aligned}\frac{\partial V_0}{\partial y} &= -2W^2 \frac{skTH}{qn_0\rho^{1/2}} \left( \frac{e^{ky} + e^{-ky}}{e^{ka} + e^{-ka}} - 1 \right), \\ \frac{\partial n_0''}{\partial y} &= W^2 \frac{(1-s)eH}{q\rho^{1/2}} \left( \frac{e^{ky} + e^{-ky}}{e^{ka} + e^{-ka}} - 1 \right).\end{aligned}$$

Thus, as a second-order effect there exists across a filament a steady potential difference of

$$-4W^2 \frac{s\mathbf{k}TH}{qn_0\rho^{1/2}k} \{\tanh(ka) - ka\}.$$

On the basis of the above analysis the d.c. effects considered appear to be extremely small. However, if the simplification concerning the bulk lifetime is relaxed so that  $\tau$  becomes finite, the changes in carrier concentration are more pronounced and the d.c. effects increase in magnitude. The acoustoelectric currents along the filament reach a maximum and then diminish as  $\tau$  decreases, while the d.c. acoustomagnetolectric potential difference across the filament reaches a maximum for  $\tau=0$ . Under the latter condition the expression for the potential difference is

$$-\frac{s(1+b)q\phi_0^2H}{(1+s)(1+sb)\mathbf{k}T\rho^{1/2}k} \{\tanh(ka) - ka\}$$

so that values of the order of a microvolt per  $\text{w cm}^{-2}$  of sound intensity may be expected for strong magnetic fields and if other conditions are favourable.

#### REFERENCES

- ALPHER, R. A., and RUBIN, R. J., 1954, *J. Acoust. Soc. Amer.*, **26**, 452.  
 ROBey, D. H., 1953, *J. Acoust. Soc. Amer.*, **25**, 603.  
 WEINREICH, G., 1956, *Phys. Rev.*, **104**, 321.



## The Behaviour of a Vibrating Visco-elastic Cylinder

By N. B. TERRY

Mining Research Establishment, National Coal Board, Isleworth, Middx.

*MS. received 5th December 1957*

**Abstract.** The general differential equation of wave-motion for a Burgers body is used to express the attenuation and retardation time of a visco-elastic material in terms of the mechanical quality factor of a cylinder of the material set into forced vibration. It is assumed that the vibrations are induced by the action of a sinusoidal stress at one end of the cylinder.

### § 1. INTRODUCTION

A STANDARD method of measuring the internal damping of a solid is to set a cylinder of the solid into forced mechanical vibration and to measure its mechanical resonance curve. It is usual to define a parameter  $Q$ , known as the mechanical quality factor, which can be measured from the resonance curve by using the equation

$$Q = \frac{\omega_r}{\omega_2 - \omega_1} \quad \dots\dots (1)$$

where  $\omega_r/2\pi$  is the resonance frequency and  $\omega_1/2\pi$  and  $\omega_2/2\pi$  are frequencies corresponding to the vibration of the cylinder at half the mechanical power developed at resonance.  $\omega_1/2\pi$  and  $\omega_2/2\pi$  are therefore frequencies corresponding to velocity amplitudes  $(1/\sqrt{2})(\partial\xi/\partial t)_{0,r}$  where  $(\partial\xi/\partial t)_{0,r}$  is the velocity amplitude developed at resonance.

A general expression for the elastic wave configuration in a vibrating cylinder is given by

$$\xi_{(x,t)} = e^{j\omega t} (A_1 e^{rx} + A_2 e^{-rx}) \quad \dots\dots (2)$$

where  $\xi$  is the displacement,

$$r = \alpha + jk, \quad \dots\dots (3)$$

$k = \omega/c$ ,  $c$  is the velocity, and  $\alpha$  is the attenuation constant;  $A_1$  and  $A_2$  are arbitrary constants.

In order to relate  $Q$  to the attenuation constant  $\alpha$ , it is necessary to formulate and solve the differential equation of motion of the vibrating cylinder. The form of the equation of motion depends on the mechanical model which is chosen to describe the visco-elastic behaviour of the solid. In previous treatments, for example, those by Cady (1922), Pierce (1929), and Quimby (1925), it has been assumed that the solid is rheologically equivalent to the Voigt model shown in figure 1 (a). If a stress  $\sigma$  is applied to this model, then

$$\sigma_{(x,t)} = Es + \eta \frac{\partial s}{\partial t} \quad \dots\dots (4)$$

where  $s$  is the strain,  $E$  is the appropriate modulus of elasticity of the spring (Young's modulus or shear modulus depending on the mode of vibration)

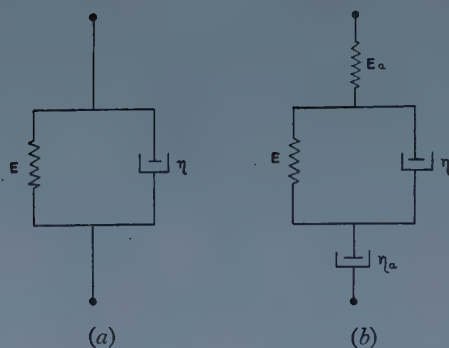


Figure 1. (a) Voigt model of a visco-elastic solid, (b) Burgers model of a visco-elastic solid.

and  $\eta$  is the appropriate coefficient of viscosity for the dashpot. Equating the force on an element to its mass acceleration, we obtain

$$\frac{\partial \sigma}{\partial x} = \rho \frac{\partial^2 \xi}{\partial t^2}, \quad \dots (5)$$

where  $\rho$  is the density, so that from equations (4) and (5), the equation of motion is

$$\frac{\rho}{E} \frac{\partial^2 \xi}{\partial t^2} = \frac{\partial^2 \xi}{\partial x^2} + \tau \frac{\partial^3 \xi}{\partial x^2 \partial t} \quad \dots (6)$$

where  $\tau$ , the retardation time, is defined as

$$\tau = \eta/E. \quad \dots (7)$$

From equations (2) and (6), after applying the appropriate boundary conditions,  $\alpha$ ,  $\tau$  and  $Q$  may be related.

Now if a static stress  $\sigma$  is applied to the Voigt model, from equation (4) we may show that

$$s(t) = \frac{\sigma}{E} (1 - e^{-t/\tau}). \quad \dots (8)$$

However, if the creep curve for a visco-elastic body is measured, it is found that the strain-time function is not that given by equation (8), but takes the general form

$$s(t) = \sigma[A + Bt + C(1 - e^{-t/D})] \quad \dots (9)$$

where  $A$ ,  $B$ ,  $C$  and  $D$  are constants of the solid. The simplest mechanical model which exhibits a strain-time relationship of the form given by equation (9) is the Burgers model, shown in figure 1 (b). It may be seen that the Burgers model is composed of two elements, the Voigt element already described, in series with a Maxwell element (i.e. the spring  $E_a$  and dashpot  $\eta_a$ ). Suppose a stress  $\sigma$  is applied to the Burgers model. The strain of the Maxwell element is given by

$$\frac{\partial s}{\partial t} = \frac{\sigma}{\eta_a} + \frac{1}{E_a} \frac{\partial \sigma}{\partial t} \quad \dots (10)$$

and since the total strain is the sum of the strains in the two component elements, from equations (4) and (10) we have

$$\frac{\partial s}{\partial t} = \frac{\sigma}{\eta_a} + \frac{\sigma}{\eta} + \frac{1}{E_a} \frac{\partial \sigma}{\partial t} - \frac{Es}{\eta} + \frac{E}{\eta\eta_a} \int \sigma dt + \frac{E\sigma}{\eta E_a}. \quad \dots (11)$$

If  $\sigma$  is a constant stress, applied at time  $t=0$ , equation (11) has the solution

$$s(t) = \sigma \left\{ \frac{1}{E_a} + \frac{t}{\eta_a} + \frac{1}{E} (1 - e^{-t/\tau}) \right\} \quad \dots\dots (12)$$

which is of the same form as equation (9).

Thus the Burgers model is more representative of a real visco-elastic solid than is the Voigt model, so that it follows that the dynamics of a vibrating cylinder should be based upon equation (11) rather than equation (6). Hillier (1949) and Kolsky (1953) have, in fact, considered the behaviour of travelling elastic waves along a modified Burgers solid. In the following section the behaviour of a cylinder, set into longitudinal or torsional vibration and represented by the Burgers model, is examined. For longitudinal vibrations, the cylinder is assumed to be thin so that the effects of lateral dilatation may be neglected and it is assumed that stresses are applied in the direction of the axis of the cylinder. For torsional vibrations, it is assumed that the cylinder is of circular cross section and that the axis of the cylinder is the axis of torsion.

## § 2. THEORETICAL TREATMENT

Differentiating equation (11) with respect to time, and remembering that  $s = \partial \xi / \partial x$ , we have

$$\left\{ \frac{1}{E_s} + \frac{\tau}{\eta_a} \right\} \frac{\partial \sigma}{\partial t} + \frac{\tau}{E_a} \frac{\partial^2 \sigma}{\partial t^2} + \frac{\sigma}{\eta_a} - \frac{\partial^2 \xi}{\partial x \partial t} - \tau \frac{\partial^3 \xi}{\partial x \partial t^2} = 0 \quad \dots\dots (13)$$

where

$$\frac{1}{E_s} = \frac{1}{E_a} + \frac{1}{E}. \quad \dots\dots (14)$$

$E_s$  is the modulus of the linear combination of springs  $E_a$  and  $E$  and therefore corresponds to the static modulus. At very high frequencies, the viscosity of the dashpot  $\eta_a$  prevents the deformation of spring  $E$ , so that the measured modulus corresponds to  $E_a$ .

Consider a thin cylinder of length  $l$  and let the origin  $x=0$  be at one end of the rod. Applying the general solution given by equation (2) to equation (13), the stress is found to be

$$\sigma_{(x,t)} = e^{j\omega t} r (A_1 e^{rx} - A_2 e^{-rx}) (E' + j\omega \eta') + A_3 e^{p_1 t} + A_4 e^{p_2 t} \quad \dots\dots (15)$$

where

$$E' = E_a^* E_s^* \left\{ \frac{E_a^* + \omega^2 \tau^2 E_s^*}{E_a^{*2} + \omega^2 \tau^2 E_s^{*2}} \right\}, \quad \dots\dots (16)$$

$$\eta' = \tau E_a^* E_s^* \left\{ \frac{E_a^* - E_s^*}{E_a^{*2} + \omega^2 \tau^2 E_s^{*2}} \right\}, \quad \dots\dots (17)$$

$$\frac{1}{E_s^*} = \frac{1}{E_s} + \frac{\tau}{\eta_a}, \quad \dots\dots (18)$$

$$\frac{1}{E_a^*} = \frac{1}{E_a} - \frac{1}{\eta_a \omega^2 \tau}, \quad \dots\dots (19)$$

$$p_1 = \frac{-E_a + (E_a^2 - 4E_s^{*2} \tau / \tau_a)^{1/2}}{2E_s^* \tau} \quad \dots\dots (20)$$

$$p_2 = \frac{-E_a - (E_a^2 - 4E_s^{*2} \tau / \tau_a)^{1/2}}{2E_s^* \tau}, \quad \dots\dots (21)$$

$$\tau_a = \eta_a / E_a \quad \dots\dots (22)$$

and  $A_3$  and  $A_4$  are arbitrary constants.

Several methods of setting the visco-elastic rod into vibration are available and have been described in the literature (Noltingk and Terry 1957). In general, the excitation is equivalent to the application of an alternating stress of constant amplitude at one end of the rod, whilst the mechanical resonance curve is obtained by measuring the velocity amplitude of the other end of the rod. Let us suppose that a stress  $Fe^{j\omega t}$  is applied at the end  $x=l$ . The following boundary conditions are applicable.

(i) At the free end of the rod, i.e. at  $x=0$ , the stress is zero for all values of  $t$ .

(ii) At the end  $x=l$ , the stress  $\sigma = Fe^{j\omega t}$  for all values of  $t$ . Applying the boundary conditions to equation (15), we have

$$A_3 = A_4 = 0 \quad \dots\dots (23)$$

and

$$A_1 = A_2 = \frac{F}{r(e^{rl} - e^{-rl})(E' + j\omega\eta')} \quad \dots\dots (24)$$

From equations (2), (3) and (24), a general solution for the displacement is

$$\xi_{(x)} = \frac{Fe^{j\omega t}(e^{rx} + e^{-rx})}{(E' + j\omega\eta')(\alpha + jk)(e^{rl} - e^{-rl})} \quad \dots\dots (25)$$

and at the free end of the rod, where  $x=0$ , the displacement is given by the real part of equation (25) as

$$\xi_{(x=0)} = \frac{F \cos(\omega t - \theta)}{[(E'^2 + \eta'^2\omega^2)(\alpha^2 + k^2)(\sin^2 kl + \sinh^2 \alpha l)]^{1/2}} \quad \dots\dots (26)$$

where

$$\tan \theta = \frac{(\omega\eta'\alpha + kE')(\cos kl \sinh \alpha l) + (E'\alpha - \omega k\eta')(\sin kl \cosh \alpha l)}{(E'\alpha - \omega k\eta')(\cos kl \sinh \alpha l) - (\omega\eta'\alpha + kE')(\sin kl \cosh \alpha l)}.$$

Differentiating equation (13) with respect to  $x$ , and applying equations (5) and (18) we have

$$\frac{\rho}{E_s^*} \frac{\partial^3 \xi}{\partial t^3} + \frac{\tau\rho}{E_a} \frac{\partial^4 \xi}{\partial t^4} + \frac{\rho}{\eta_a} \frac{\partial^2 \xi}{\partial t^2} - \frac{\partial^3 \xi}{\partial t \partial x^2} - \tau \frac{\partial^4 \xi}{\partial x^2 \partial t^2} = 0. \quad \dots\dots (27)$$

From equations (3), (25) and (27) we obtain, on equating real and imaginary parts,

$$2\omega\tau\alpha k - (\alpha^2 - k^2) - \frac{\rho\omega^2}{E_s^*} = 0 \quad \dots\dots (28)$$

and

$$\frac{\tau\rho\omega^3}{E_a^*} + 2\alpha k + \omega\tau(\alpha^2 - k^2) = 0. \quad \dots\dots (29)$$

From equations (28) and (29), remembering that  $k = \omega/c$ , we have

$$\frac{1}{c^2} = \frac{\rho}{2E_a^* E_s^*} \left\{ \left( \frac{E_a^{*2} + E_s^{*2}\omega^2\tau^2}{1 + \omega^2\tau^2} \right)^{1/2} + \left( \frac{E_a^* + E_s^*\omega^2\tau^2}{1 + \omega^2\tau^2} \right) \right\} \quad \dots\dots (30)$$

and

$$\alpha^2 = \frac{\rho\omega^2}{2E_a^* E_s^*} \left\{ \left( \frac{E_a^{*2} + E_s^{*2}\omega^2\tau^2}{1 + \omega^2\tau^2} \right)^{1/2} - \left( \frac{E_a^* + E_s^*\omega^2\tau^2}{1 + \omega^2\tau^2} \right) \right\}. \quad \dots\dots (31)$$

Equations (30) and (31) are similar to those derived by Kolsky (1953) for the propagation of continuous waves along a visco-elastic rod.



Differentiating equation (26) with respect to time, remembering that  $k = \omega/c$ , and using equations (16), (17), (30) and (31), we have

$$\frac{\partial \xi}{\partial t} = \left( \frac{\partial \xi}{\partial t} \right)_0 \sin(\omega t - \theta) \quad \dots\dots (32)$$

where

$$\left( \frac{\partial \xi}{\partial t} \right)_0 = P \{ \sin^2(\omega l/c) + \sinh^2 \alpha l \}^{-1/2} \quad \dots\dots (33)$$

and

$$P = F [E_a^* E_s^* \rho \{ (1 + \omega^2 \tau^2) / (E_a^{*2} + \omega^2 \tau^2 E_s^{*2}) \}^{1/2}]^{-1/2} \quad \dots\dots (34)$$

Equations (33) and (34) show the frequency dependence of the maximum velocity amplitude  $(\partial \xi / \partial t)_0$  at the free end of the rod. It is apparent from equation (33) that resonance occurs very nearly when  $\sin^2 \omega l/c = 0$ , i.e. when

$$\omega l/c = n\pi \quad \dots\dots (35)$$

where  $n$  is an integer denoting the harmonic number.

If we assume that the resonance is sufficiently sharp for  $P$  and  $\alpha$ , which are both functions of  $\omega$ , to remain sensibly constant as the pulsance changes from  $\omega_1$  to  $\omega_2$  (see § 1) it follows from equation (33) that a symmetrical resonance curve will be obtained, i.e.

$$\omega_r - \omega_1 = \omega_2 - \omega_r = \delta\omega \quad \text{say.} \quad \dots\dots (36)$$

The velocity amplitude at resonance  $(\partial \xi / \partial t)_{0,r}$ , is given by equations (33) and (35) as

$$(\partial \xi / \partial t)_{0,r} = \frac{P}{\sinh \alpha l} \quad \dots\dots (37)$$

and at pulsances  $\omega_1$  and  $\omega_2$ , by definition the velocity amplitude is given by

$$\left( \frac{d\xi}{dt} \right)_{0,1} = \left( \frac{d\xi}{dt} \right)_{0,2} = \frac{1}{\sqrt{2}} \left( \frac{\partial \xi}{\partial t} \right)_{0,r} \quad \dots\dots (38)$$

Thus from equations (1), (33) and (35) to (38), it follows that

$$\alpha = \frac{\sinh^{-1}(\sin n\pi/2Q)}{l} \quad \dots\dots (39)$$

Equation (39) expresses the attenuation constant in terms of the mechanical quality factor  $Q$ , and the harmonic number  $n$ . Thus from the resonance curve, using equations (1), (35) and (39) values may be obtained for  $c$  and  $\alpha$ . A value for  $\eta_a$  can be obtained from measurements of the linear portion of the creep curve, and the static modulus may be measured by one of the several available techniques. For most solids it is found that  $\tau/\eta_a \ll 1/E_s$  and except for very long cylinders, having very low resonance frequencies,  $\eta_a \tau \omega^2 \gg E_a$ . Thus from equations (18) and (19),  $E_s^* \simeq E_s$  and  $E_a^* \simeq E_a$ . A value for  $\tau$  may be obtained from equation (28) and a value for  $E_a$  from equation (29); in this way values may be obtained for all the parameters of the Burgers model at a given frequency (it is worth noting that for many substances,  $\tau$  is a function of frequency (Hillier 1949, Terry 1958). From equations (31) and (34), the variation of  $\alpha$  and  $P$  with frequency may be determined and the effect of this upon the accuracy of the measurements considered, bearing in mind the assumptions made that  $\alpha$  and  $P$  could both be regarded as sensibly constant over the frequency interval  $\delta\omega/\pi$ .

## ACKNOWLEDGMENTS

This communication describes work forming part of the research programme of the Mining Research Establishment of the National Coal Board and is published by permission of Dr. W. Idris Jones, Director General of Research. The views expressed are those of the author and not necessarily of the Board.

## REFERENCES

- CADY, W. G., 1922, *Phys. Rev.*, **29**, 1.  
HILLIER, K. W., 1949, *Proc. Phys. Soc. B*, **62**, 701.  
KOLSKY, H., 1953, *Stress Waves in Solids* (Oxford : University Press), p. 120.  
NOLTINGK, B. E., and TERRY, N. B., 1957, *Technical Aspects of Sound*, Ed. E. G. Richardson (Amsterdam : Elsevier), p. 147.  
PIERCE, G. W., 1929, *Proc. Inst. Radio Engrs, N.Y.*, **17**, 42.  
QUIMBY, S. L., 1925, *Phys. Rev.*, **25**, 558.  
TERRY, N. B., 1958, *Fuel*, in the press.

# Pressure Distributions beneath Spherical and Conical Shapes pressed into a Rubber Plane, and their Bearing on Coefficients of Friction under Wet Conditions

By B. E. SABEY

Road Research Laboratory, Harmondsworth, Middx.

*Communicated by G. Grime; MS. received 6th August 1957, and in revised form 6th March 1958*

**Abstract.** Investigations have shown that a high skidding resistance on wet roads is associated with the presence of sharp edges in the road surface: on these sharp edges high pressures are set up which assist in breaking through the lubricating water film between tyre and road. This paper gives some details of laboratory tests now being made to investigate further the dependence of skidding resistance on such localized pressures.

Pressure distributions beneath rigid spheres and cones pressed into rubber have been calculated, on the basis of the elastic theory, from measurements of their penetration into tyre-tread rubber under load. The experimental evidence confirms that under the conditions of test employed the rubber is behaving as an elastic material.

The effect of the pressures on friction under wet conditions has been investigated by sliding different shapes over wet rubber, using a laboratory friction machine designed to simulate conditions between tyre and road when skidding takes place. These tests indicate that the coefficient of friction recorded under wet conditions is closely related to the pressure over the contact area between slider and rubber, and that, to ensure a satisfactory skidding resistance in wet weather, the shape of individual projections in the road must be such that average pressures of the order of  $1000 \text{ lb in}^{-2}$  are set up on them. Ideally, what is required is that the individual projections in the surface of the road should have angles at their tips of  $90^\circ$  or less: the necessary pressures are unlikely to be obtained with rounded or polished projections, whatever their size or the load applied to them.

## § 1. INTRODUCTION

THE essential requirement for a road to be reliably non-skid under wet conditions is that the peaks of the small-scale projections in the road surface should be sharp. When a tyre passes over a wet road, localized high pressures are set up on these sharp projections, enabling the lubricating water film to be broken through rapidly, so that direct contact is established at these points between tyre and road (Grime and Giles 1954-5). The order of magnitude of the pressures necessary to ensure a satisfactory skidding resistance has not previously been determined, although it has been established, by making use of the pressure sensitivity of x-ray film, that, on the isolated peaks of the projections in a number of good non-skid surfaces, very high pressures may occur (Giles and Sabey 1951).

To investigate the relationship between skidding resistance under wet conditions and pressures on the peaks of projections on road surfaces in more detail, it is necessary to be able to estimate pressures on such peaks. But the difficulty of calculating pressures on projections as numerous and as irregular as those found in the road surface makes it impracticable to carry out such an investigation on a full scale. Work has therefore been carried out in the laboratory with a simple friction machine, using single sliders of regular shape to represent the projections in the road, and sliding them over a wet rubber track (Road Research Board 1954) under conditions of sliding similar to those experienced by projections in the road.

As a basis for this work, the pressure distributions between spherical and conical bodies penetrating rubber under load have been estimated from theories of elasticity relating to the loading of three-dimensional shapes on an elastic plane (Timoshenko 1934, Love 1939). This paper discusses these calculations of pressures and shows that, under the conditions considered, rubber appears to behave as an elastic material: the paper also gives an account of some measurements of friction made with spherical and conical sliders.

## § 2. CALCULATIONS OF PRESSURES SET UP BENEATH RIGID SPHERES AND CONES PENETRATING RUBBER UNDER LOAD

When a rigid body is pressed into rubber under load, the local deformation of the rubber and the magnitude of pressure set up within the contact area are greatly dependent on the mechanical properties of the rubber. Bearing in mind the anomalous behaviour of rubber under load, this immediately raises the problem as to whether, under the conditions used in the tests described here, rubber may be considered as a truly homogeneous and elastic material. Certainly, in tension, rubber does not obey Hooke's law. There is evidence however (Gough and Parkinson 1941-2) that over a certain range in compression the modulus of elasticity is independent of the applied stress.

In this section therefore, the pressure distributions have been calculated from measurements of the penetrations of spheres and cones into rubber under load, the calculations being based on the assumption that the rubber is behaving elastically: it is then shown from the experimental evidence to what extent this assumption is valid.

### 2.1. *Distribution of Pressure between a Rigid Sphere and an Elastic Plane*

The distribution of pressure between a rigid sphere and a semi-infinite elastic plane in contact under load has been dealt with by Timoshenko (1934). In this treatment the case where the radius of the area of contact is small compared with the radius of the penetrating sphere is considered, when the shape of the penetrating body approximates to a paraboloid. The results of this analysis are as follows: If a rigid sphere, radius  $R$ , is pressed into an elastic plane whose elastic constants are  $E$  (modulus of elasticity) and  $\sigma$  (Poisson's ratio) under a load  $W$ , there will be local deformations of the elastic material as indicated in figure 1, producing a circular surface of contact between sphere and plane.

Referring to figure 1, let  $Z$  be the penetration of the sphere into the plane, contact being made over a depth  $z_0$  and the radius of the projected area of contact being  $a$ .



The average pressure over the area of contact is given by

$$\bar{p} = \frac{8E}{3\pi(1-\sigma^2)} \times \frac{z_0}{a} \quad \dots\dots(1)$$

and  $\bar{p} = W/\pi a^2$ , where  $a^2 = z_0(2R - z_0)$ , and  $z_0 = Z/2$ .

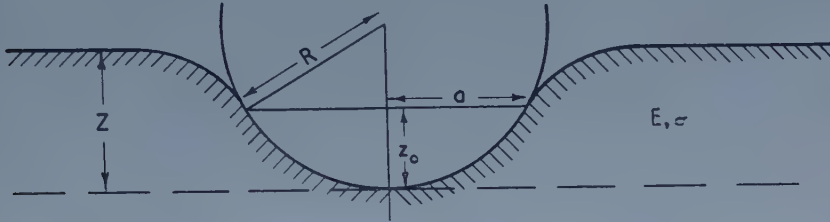


Figure 1. Penetration of a rigid sphere into an elastic plane under load.

The distribution of pressure  $p$  over the whole contact area is represented by the ordinates of a hemisphere of radius  $a$  constructed on the surface of contact: the peak pressure  $\hat{p} = 3\bar{p}/2$ .

## 2.2. Distribution of Pressure between a Rigid Cone and an Elastic Plane

The distribution of pressure between a rigid cone and a semi-infinite elastic plane has been dealt with by Love (1939).

Changing Love's notation to bring it into line with the analysis for spheres, the main results are as follows: Considering a rigid cone, semi-angle  $\alpha$  (figure 2),

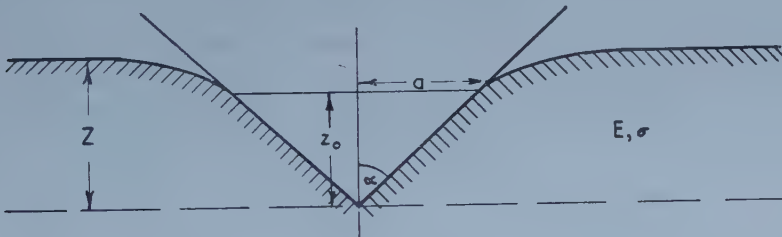


Figure 2. Penetration of a rigid cone into an elastic plane under load.

penetrating into an elastic plane under a load  $W$ , let the penetration of the cone into the plane be  $Z$ , contact being made over a depth  $z_0$  and the radius of the projected area of contact being  $a$ . The elastic constants of the material of the plane are  $E$  (modulus of elasticity) and  $\sigma$  (Poisson's ratio).

Love shows that for these conditions the average pressure is

$$\bar{p} = \frac{E}{2(1-\sigma^2)} \cot \alpha \quad \dots\dots(2)$$

where  $\bar{p} = W/\pi a^2$ , and  $a = 2Z \tan \alpha/\pi$ .

The pressure at any radius  $r$  within the contact area is given by

$$p = \frac{E}{4(1-\sigma^2)} \cot \alpha \ln \frac{1+\rho}{1-\rho}$$

where  $\rho = (1 - r^2/a^2)^{1/2}$ .

The pattern of the distribution of pressure over the contact area is illustrated in figure 3.

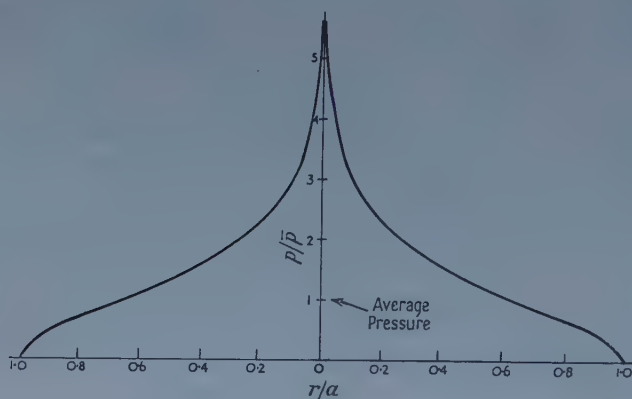


Figure 3. Pressure distribution over the area of contact of a rigid cone pressed into an elastic plane.

### 2.3. Experimental Results

Simple loading tests were made on tyre-tread rubber using steel spheres of diameters ranging from  $\frac{3}{16}$  in. to  $\frac{7}{8}$  in. and steel cones of semi-angles ranging from  $30^\circ$  to  $80^\circ$ , under loads from 5 lb to 15 lb. These sizes and loads were chosen to cover the main range of loading conditions likely to be encountered on projections in the contact area between tyre and road surface. The penetrations  $Z$  of the shapes into the rubber under load, i.e. the relative movement of the two surfaces in contact, were measured with a dial gauge, reading to 0.001 in. From corresponding values of penetration  $Z$  and load  $W$ , the area of contact between the surfaces and the pressure distribution over the contact area were calculated on the basis of the elastic theory. Corresponding values of penetration and pressure are given in the table.

The analysis for spheres is strictly applicable only in the case where the radius of the area of contact is small compared with the radius of the penetrating sphere, and the shape of the penetrating body approximates to a paraboloid. However, even for the greatest penetration of the smallest sphere (a sphere radius 0.094 in. under 15 lb load had radius of contact 0.075 in.), within the contact area, the spherical surface of contact is very little different in shape from the corresponding paraboloid passing through the vertex of the sphere and the extreme circle of contact. A plot (figure 4) of  $\bar{p} = W/\pi a^2$  and  $z_0/a$ , where  $a^2 = z_0(2R - z_0)$ , indicates that, within the limits of experimental error, the pressure  $\bar{p}$  is proportional to  $z_0/a$ . By comparison with equation (1), this implies that the elastic modulus is independent of the applied stress over the range of conditions of test used. It is also clear that the rubber is behaving homogeneously.



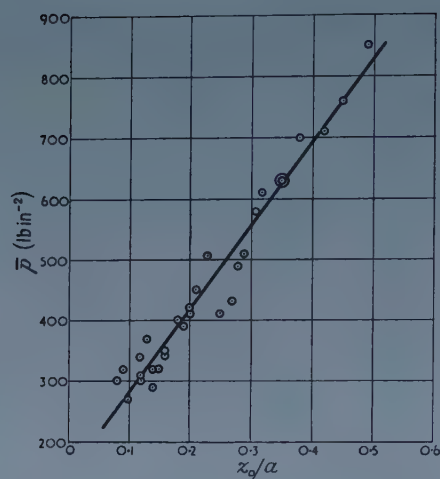


Figure 4. Pressure and penetration for spheres.

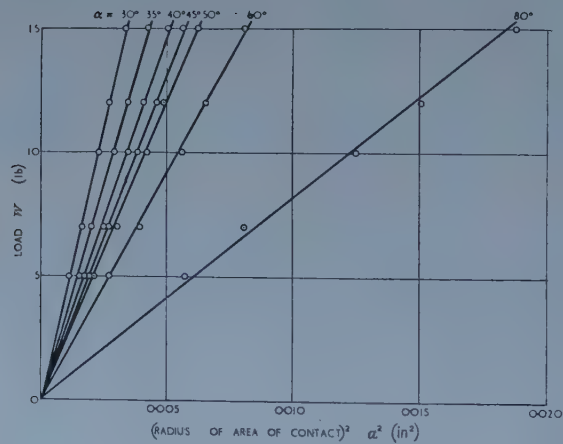


Figure 5. Load and radius of contact area for cones.

$\alpha$ (°)	30	35	40	45	50	60	80
$\bar{p}$ (lb in <sup>-2</sup> )	1400	1110	930	840	770	580	260

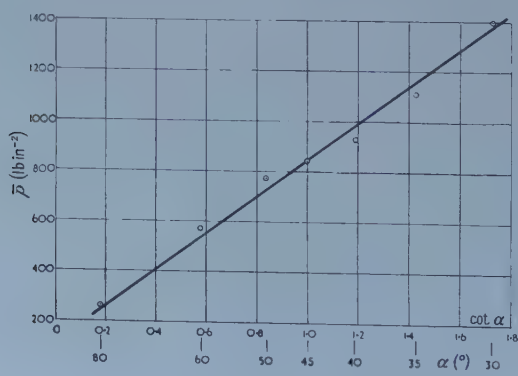


Figure 6. Pressure and angle of cone.



the conditions of test considered, the rubber is behaving homogeneously. From this plot, average pressures have been calculated from the slopes of the lines for all angles of cone: these values of pressures are tabulated in figure 5. Finally, figure 6, relating  $\bar{p}$  and  $\cot \alpha$ , shows that, within the limits of experimental error, the elastic laws are obeyed: from this figure the elastic constants may be found. Thus  $E/(1-\sigma^2)=1500 \text{ lb in}^{-2}$  and assuming  $\sigma=0.5$ , the modulus of elasticity for the tyre-tread rubber used in the experiments is  $E=1100 \text{ lb in}^{-2}$ . This value is in reasonable agreement with the value calculated from the results for spheres, assuming the laws of elasticity to be obeyed: it has therefore been established that, under the conditions considered, rubber in compression obeys the elastic laws, the modulus of elasticity calculated for the rubber used being of the order of  $1200 \text{ lb in}^{-2}$ .

From equations (1) and (2) given above it will be evident that the elastic constants of the rubber used are also important in determining the magnitude of the pressures set up; the harder the rubber, i.e. the larger the value of the modulus of elasticity, the higher is the pressure. The dependence of coefficient of friction on hardness of tyre-tread rubber is well known from full-scale experiments (Grime and Giles 1954-5) and this aspect has not been considered here: all tests were made using tyre-tread rubber of hardness  $75^\circ$ - $80^\circ$  B.S. hardness scale.

### § 3. LABORATORY FRICTION EXPERIMENTS

With this analysis as background, tests have been made to investigate the friction between a slider and a rubber track under wet conditions, and its dependence on the pressures set up beneath the slider. For this purpose a laboratory friction apparatus (Road Research Board 1954) has been developed, by means of which single sliders may be skidded over a wet rubber track under conditions comparable with those which obtain when a vehicle tyre skids over the projections in the road surface. The apparatus is shown in figure 7. The

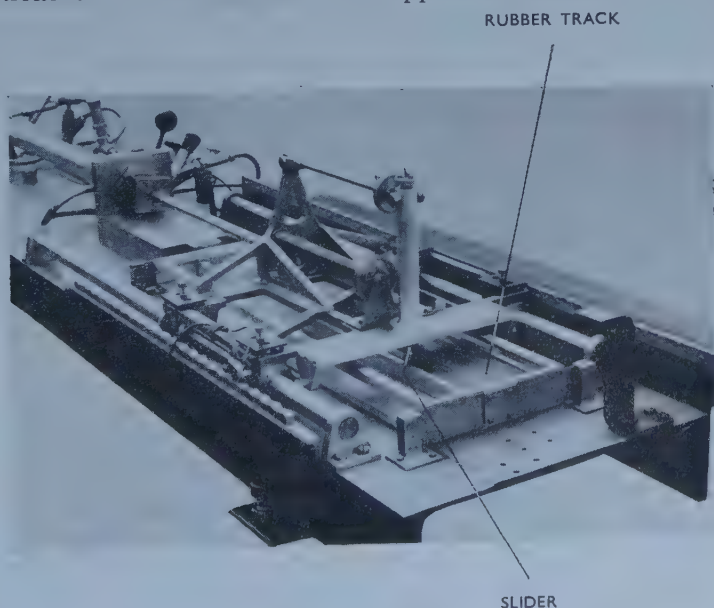


Figure 7. Laboratory friction apparatus.

frictional forces set up between slider and rubber are measured and recorded electrically, and the coefficient of friction (the skidding resistance) is calculated from measurements of the normal load on the slider.

Using the apparatus, coefficients of friction have been measured with the steel spheres and cones used in the penetration tests, for which pressure distributions under static loading conditions were therefore known. Results of the friction tests, in which the speed of sliding was of the order of  $6 \text{ ft sec}^{-1}$  are given in the table, along with values of pressure calculated from the static loading tests. Figure 8 shows that, within the limits of experimental error, there is a clearly defined relation between coefficients of friction and average pressures over the contact areas for the different sliders. Thus whether the sliders are spheres or cones the coefficients of friction are independent of loading conditions and size of sliders, except in as far as they affect the intensity of the pressures set up between sliders and track.

It should be noted that much of the scatter in figure 8 arises from the errors

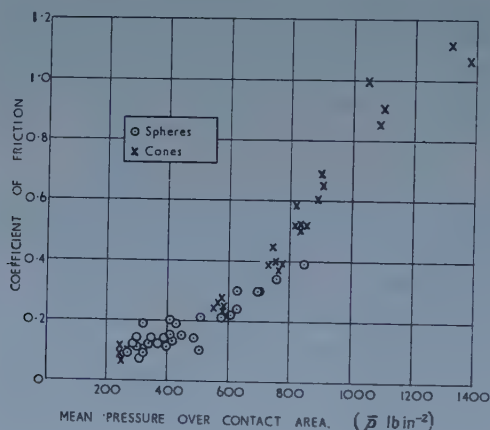


Figure 8. Coefficient of friction measured for spherical and conical sliders on wet rubber and the calculated pressure over the contact area.

in measurements of the normal load on the slider and the frictional force at low loads. For both spheres and cones, the average pressure under different loads depends only on  $z_0/a$ , the ratio of the penetration of the vertex of the sphere or cone into the rubber (measured from the circle of contact) to the radius of the circle of contact (see figures 1 and 2). Thus it is easy to see from the geometry of the shapes that high pressures are much more easily obtained with cones than spheres. Also, for spheres,  $z_0/a$  increases with load  $W$  and the mean pressure increases accordingly. On the other hand, for cones,  $z_0/a = \cot \alpha$  (where  $\alpha$  is the semi-angle of the cone). This is a constant for any particular cone; so that the average pressure over a given cone depends only on the angle and is independent of the loading conditions. As would be expected from these results and the observed dependence of the coefficient on pressure, the coefficients obtained increase with applied load for spheres, and are independent of the load for a given angle of cone. For the spherical sliders, although pressure and coefficient increase with increased load, there is a limit to the load which may be applied without the slider being completely embedded in the rubber. The limit has very nearly been reached with the 15 lb load on the smallest slider.

and thus it seems that coefficients greater than 0.4 are unlikely to be obtained with spherical sliders. For the conical sliders the angles of the cones are extremely important in determining the coefficients of friction. Under the same conditions of loading, the cones used, whose semi-angles ranged from  $80^\circ$  to  $30^\circ$ , gave results covering the whole range of coefficients from 0.1 to 1.1.

#### § 4. DISCUSSION OF THE RESULTS OF THE FRICTION TESTS AND THEIR PRACTICAL IMPLICATIONS

The general implication of these results with respect to road surfaces, in particular those of the rough coarse-textured type, is to emphasize the importance of the shape of the projections in the road surface rather than their size or the load applied to them. It is clear from figure 8 that the coefficient of friction of sliders on a wet rubber track is closely related to the average pressure set up beneath them under static loading conditions and, to obtain a high coefficient, it is necessary to have pressures averaging about  $1000 \text{ lb in}^{-2}$  over the contact area on individual projections.

It seems unlikely that pressures of this order can be obtained on spherical projections in the road whatever the loading conditions, although some small increase in skidding resistance may be obtainable by increasing the load between between tyre and road on surfaces in which the projections are rounded. On surfaces with sharp projections, pressures of the order of  $1000 \text{ lb in}^{-2}$  may easily be obtained: on conical shapes with tip angles of  $90^\circ$  or less pressures average at least  $1000 \text{ lb in}^{-2}$  over the contact area regardless of the loading conditions. It is evident from figure 3 that pressures over small areas at the peaks of these cones may rise to several thousand  $\text{lb in}^{-2}$ . However, a small degree of rounding of any cone (for example, values of  $r$  less than  $0.1a$ ) with the consequent reduction in peak pressure, will not change the average pressure over the contact area to any great extent: the overall angle of the projection is much more important in determining the average pressure. This result suggests that, if high average pressures of the order of  $1000 \text{ lb in}^{-2}$  can be obtained on individual projections by using sufficiently angular stones, a small degree of polishing of the tip might occur without appreciable loss of skidding resistance. Moreover, although the tests described here were made with steel sliders having highly polished surfaces, high coefficients were obtained simply by having sliders of suitable shapes.

It is also interesting to note from figure 8 how, between the values 0.4 and 0.6, the coefficient of friction rises sharply with increased pressure; this is the range of coefficient of friction considered as the critical range on the road between slippery and safe conditions. Thus in this range, small changes of pressure, that is, small changes in the shape of projections, will have an important bearing on the skidding resistance.

#### § 5. CONCLUSIONS

From considerations of the penetration of spheres and cones into tyre-tread rubber, it has been established that, within the limits covered by the tests, under compression, rubber obeys the elastic laws. Thus it has been possible to calculate pressures set up between spherical and conical shapes and rubber. With this knowledge, the relation between pressure and coefficient of friction under wet conditions may be investigated and preliminary tests have shown that such a relation does exist.



In their paper Greenwood and Tabor (1958) have suggested that this pressure dependence of coefficient of friction may be explained in terms of elastic hysteresis, combined in the case of the sharper cones with tearing of the rubber. However, their explanation assumes conditions of hydrodynamic lubrication, and the author believes that the sliding speed used in these tests is too low for hydrodynamic conditions to obtain, the time of contact between the slider and any point on the rubber being sufficiently long for the water film to be broken through to some extent. Measurements of coefficients of friction with skidding vehicles on road surfaces at different speeds (Giles and Lander 1956) give evidence to support this view, the coefficient decreasing steadily with speed and only tending to a minimum (presumably when hydrodynamic conditions have been reached) at very high speeds (of the order of 80 mile/hr). It does seem likely that the value of this minimum is determined by considerations of elastic hysteresis, but at lower speeds lubrication will be mixed and the value of the coefficient over and above the ultimate minimum will depend on the degree of dry contact between the sliding surfaces.

On individual projections on the road, it seems that pressures averaging  $1000 \text{ lb in}^{-2}$  are necessary to ensure a high resistance to skidding under wet conditions, and to obtain these pressures, the individual projections should have angles at their tips of  $90^\circ$  or less. The results stress the importance of the shape of projections in the road surface in determining the skidding resistance of wet roads.

#### ACKNOWLEDGMENTS

The work described in this paper was carried out at the Road Research Laboratory of the Department of Scientific and Industrial Research as part of the programme of the Road Research Board and is presented by permission of the Director of Road Research.

The author would like to thank Mr. C. G. Giles for his encouragement and Mr. G. N. Lupton for his assistance in the experimental work.

#### REFERENCES

- GILES, C. G., and LANDER, F. T. W., 1956, *J. R. Aero. Soc.*, **60**, 542, 83.  
 GILES, C. G., and SABEY, B. E., 1951, *Brit. J. Appl. Phys.*, **2**, 174.  
 GOUGH, V. E., and PARKINSON, D., 1941-2, *I.R.I. Trans.*, **17**, 168.  
 GREENWOOD, J. A., and TABOR, D., 1958, *Proc. Phys. Soc.*, **71**, 989.  
 GRIME, G., and GILES, C. G., 1954-5, *Proc. Instn Mech. Engrs, Lond. (Automobile Division)*, (1), **19**, 45.  
 LOVE, A. E. H., 1939, *Quart. J. Math.*, **70**, 161.  
 ROAD RESEARCH BOARD, 1954, *Report of the Road Research Board for 1953, Department of Scientific and Industrial Research* (London : H.M. Stationery Office), p. 23.  
 TIMOSHENKO, S., 1934, *Theory of Elasticity* (New York : McGraw-Hill), p. 339.



## The Friction of Hard Sliders on Lubricated Rubber: The Importance of Deformation Losses

By J. A. GREENWOOD AND D. TABOR

Research Laboratory for the Physics and Chemistry of Solids,  
Cambridge University

*MS. received 27th June 1957, and in revised form 18th October 1957†*

**Abstract.** A study has been made of the friction of hard spheres and cones on a well lubricated rubber surface under conditions where relatively large deformations are produced. It is found that with spheres the sliding friction is almost the same as the rolling friction. Earlier work has shown that in the latter case the friction arises primarily from hysteresis losses in the rubber and it is concluded that, under the experimental conditions described, the main source of friction in lubricated sliding arises from the same cause. With conical sliders it is not possible to make a direct comparison with rolling experiments, but a simple calculation suggests that here again the friction is largely due to deformation losses in the rubber. For cones of small semi-angle there is a large increase in friction but this is associated with penetration of the lubricant film and tearing of the rubber.

The friction results are in close agreement with measurements described by Miss Sabey for spheres and cones sliding on wet rubber at relatively high speeds ( $c. 6 \text{ ft sec}^{-1}$ ). This suggests that in her experiments the water film provides very effective lubrication and that the friction arises largely from hysteresis losses in the rubber itself.

As a general conclusion this study of the friction of lubricated rubber suggests that where interfacial adhesion is small and where relatively large local deformations occur the friction may well be dominated by deformation losses in the rubber. Under these conditions we may therefore expect the friction of hard spherical or conical sliders on rubber to be greater for rubbers of low Young's modulus and high hysteresis losses.

### § 1. INTRODUCTION

**I**N a paper by Miss Sabey (1958) the friction of steel sliders of various shapes on wet rubber is examined. It is found that for spherical and conical sliders the coefficient of friction is a function of the mean pressure between the slider and the rubber and is roughly the same for both types of indenters. The coefficient of friction increases approximately linearly with pressure but for high pressures (cones of small semi-angle) the friction rises markedly and values of  $\mu$  of the order  $\mu = 1$  are observed.

Miss Sabey very kindly showed us her paper before publication and the following account is an attempt to explain her results in a simple way. The first general observation is that with elastic materials such as rubber the coefficient of sliding friction generally increases as the pressure is *reduced* (Schallamach 1952) in marked contrast to Miss Sabey's results. On the other hand the coefficient of rolling friction which is due primarily to elastic hysteresis losses in the rubber

† Publication delayed to await preceding paper by Sabey.

increases with pressure (Tabor 1955 a). This suggests that in Miss Sabey's experiments there was little sliding friction in the conventional sense since at the high speeds of sliding used (*c.* 6 ft sec<sup>-1</sup>) the water film could behave hydrodynamically: the major source of frictional loss would appear to arise from the elastic deformation losses in the rubber itself. A similar effect has been observed by Attack in the frictional behaviour of wood.

## § 2. EXPERIMENTAL

The Eldredge friction apparatus (Eldredge and Tabor 1955) was used. With this apparatus both rolling and sliding friction measurements can be made. However, it is not possible to employ sliding or rolling speeds above about 1 cm sec<sup>-1</sup>. At these speeds water does not provide appreciable lubrication on rubber. A thin smear of wet soap, however, provides very effective lubrication and in the first experiments a direct comparison was made between the sliding friction  $\mu_s$  and the rolling friction  $\mu_r$  of a  $\frac{1}{8}$  in. and a  $\frac{1}{4}$  in. steel ball on a flat rubber surface. The rubber was a piece of the same material as that used by Miss Sabey in her work.

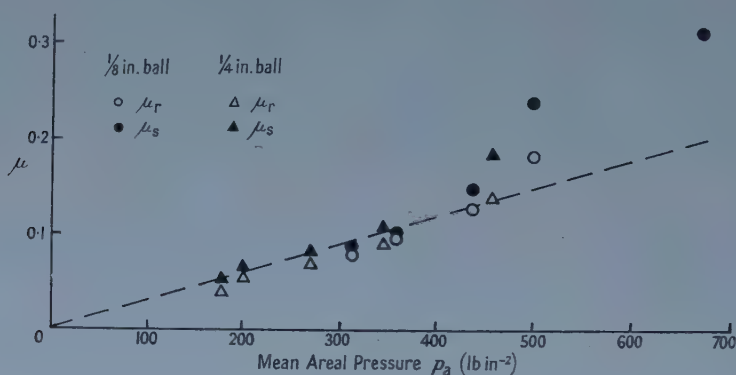


Figure 1. Coefficient of friction of steel spheres rolling and sliding on well lubricated rubber as a function of mean areal pressure  $p_a$  over the circle of contact. The broken line is the theoretical curve assuming the friction arises primarily from elastic hysteresis losses in the rubber.

Table 1. Rolling and Lubricated Sliding of Steel Sphere on Rubber

Sphere diameter	Load (lb)	$\mu_r$	$\mu_s$	Mean Pressure $p$ ( $\text{lb in}^{-2}$ )	
				from area	from depth (Sabey)
$\frac{1}{8}$ in.	0.88	0.08	0.09	320	440
	1.76	0.10	0.10	360	550
	3.52	0.13	0.15	440	700
	5.28	0.19	0.25	500	800
	6.16	0.20	—	540	840
	7.04	—	0.31	650	880
	—	—	—	—	—
$\frac{1}{4}$ in.	0.88	0.04	0.06	180	260
	1.76	0.06	0.07	200	300
	3.52	0.07	0.08	270	400
	7.04	0.09	0.11	350	510
	14.1	0.14	0.19	460	670

Simple loading experiments of the steel sphere on the rubber surface gave a clearly defined circular outline corresponding to the circle of contact: its diameter could be measured with a fair degree of accuracy. From this the mean pressure

over the region of contact (which we shall henceforth call the areal pressure) could be calculated. The pressure could also be calculated from the depth the ball sinks into the rubber using Hertz's equation. Such measurements gave values essentially the same as those quoted by Miss Sabey from her own *depth* measurements, but in general the pressures calculated from our *areal* measurements are about 30% less than those calculated from the depth. The coefficients of friction for rolling ( $\mu_r$ ) and for sliding ( $\mu_s$ ) are given in table 1 together with the mean pressures calculated in both ways.

In figure 1 the values of  $\mu_r$  and  $\mu_s$  are plotted against the mean areal pressure  $p_a$ . It is seen that  $\mu_s$  and  $\mu_r$  are very nearly the same and that for pressures below  $400 \text{ lb in}^{-2}$  both are almost linearly proportional to  $p_a$ .

### § 3. DEFORMATION LOSSES FOR SPHERICAL SLIDERS

The elastic work involved when spherical surfaces pass over an elastic surface has already been described (Tabor 1955 b), but since this paper contains a mistaken assumption which leads to a numerical error a brief account will be given here. The general idea is as follows. When a spherical indenter is pressed into rubber a certain amount of elastic work is performed. As the indenter moves forward elastic work is done in deforming the rubber in front of the indenter whilst elastic work is recovered from the rear. Since rubber shows a finite elastic hysteresis, energy is lost. In rolling this is the primary source of the frictional work. In sliding this is additional to any shearing work involved.

The elastic work done by a rolling or sliding sphere can be estimated from the forces involved in an infinitesimal forward movement of the ball (Greenwood and Tabor, in preparation). A somewhat simpler approach is to consider the forces exerted on the sphere and to resolve these into a vertical and horizontal component. The total vertical component supports the load, the horizontal component on the front half determines the work done when horizontal movement occurs. If the whole of the elastic energy were lost by hysteresis this would correspond to the force required to move the ball.

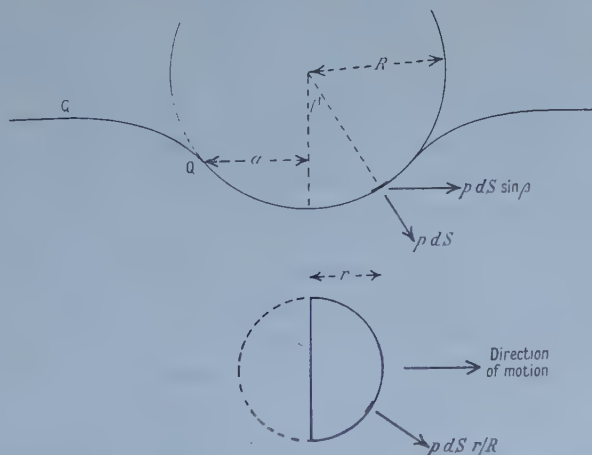


Figure 2. Calculation of the horizontal component of force over the front half of the circle of contact for a hard sphere indenting an elastic solid.

If the ball has radius  $R$  and is not deformed by the rubber and  $a$  is the radius of the circle of contact formed under a load  $W$  (see figure 2)

$$a^3 = \frac{3}{4} WR \frac{1 - \sigma^2}{E} \quad \dots\dots(1)$$

where  $\sigma$  is Poisson's ratio and  $E$  Young's modulus of the rubber. The Hertzian solution gives the pressure  $p$  at any point distant  $r$  from the centre as

$$p = \frac{3}{2} \frac{W}{\pi a^2} \left(1 - \frac{r^2}{a^2}\right)^{1/2} \quad \dots\dots(2)$$

If friction at the ball-rubber interface is negligible we may assume  $p$  at any point to be normal to the interface at that point†. The force on any element of area  $dS$  is  $p dS$ . The vertical component of this is  $p dS \cos \beta$  and contributes to the support of the normal load  $W$ . Since the Hertzian solutions are assumed to apply to small displacements,  $\cos \beta \simeq 1$  and  $\tan \beta = \sin \beta = \beta = r/R$ . The horizontal component of the force  $p dS$  is  $p dS \sin \beta$  or  $p dS r/R$ .

Consider an annulus at constant  $r$ . Then  $p$  will be the same at every point. Now consider the horizontal force on the front half of this annulus. The average value of  $p dS r/R$  around this region in the direction of motion is  $(2/\pi) p dS r/R$  whilst the area of the annulus  $dS = \pi r \sec \beta dr \simeq \pi r dr$ . Hence the total horizontal force in the direction of motion is

$$F = \int_0^a \frac{2}{\pi} \frac{p r}{R} \pi r dr = \frac{2}{R} \int_0^a p r^2 dr \quad \dots\dots(3)$$

Inserting the value of  $p$  from equation (2) we have

$$F = \frac{2}{R} \int_0^a \frac{3}{2} \frac{W}{\pi a^2} \left(1 - \frac{r^2}{a^2}\right)^{1/2} r^2 dr = \frac{3Wa}{16R} \quad \dots\dots(4)$$

In moving forward unit distance the elastic work  $\phi$  done in the horizontal direction is thus

$$\phi = \frac{3Wa}{16R} = \frac{9W^2}{64a^2} \frac{1 - \sigma^2}{E} \quad \dots\dots(5)$$

This value is one half the value given in an earlier paper (Tabor 1955 a). In the earlier derivation it was assumed that work was expended on every element of the rubber as it was dragged from the free surface (e.g. at Q in figure 2) to a point under the sphere. The present treatment implies that once the first indentation is formed work is expended only in dragging every element from the edge Q' of the circle of contact to a point under the sphere. This gives half the amount of work.

As the sphere moves forward it expends elastic energy on the rubber ahead of it of amount  $\phi$  per unit distance of travel. If the rubber were ideally elastic the rubber behind the sphere would yield up an identical amount and no net energy would be lost. If we now assume that, in fact, a constant fraction  $\alpha$  of the input elastic energy is lost as a result of elastic hysteresis in the rubber, the work lost per unit distance of sliding is  $\alpha\phi$ . This amount of work has to be provided by the frictional

† The Hertzian distribution is really a vertical distribution acting over an interface which is always horizontal. It is thus only strictly valid for infinitesimal displacements. In the present model this is equivalent to considering  $p \cos \beta = p$ . This does not, of course, imply that  $p \sin \beta = 0$ .



force  $F$ . Thus the contribution to the coefficient of friction due to hysteresis losses is,

$$\mu_{\text{hysteresis}} = \frac{\alpha \phi}{W} = \left[ \frac{9\pi}{64} \frac{1 - \sigma^2}{E} \right] \bar{p} \alpha \quad \dots\dots (6)$$

where  $\bar{p}$  is the mean pressure  $W/\pi a^2$ . It is seen that, provided  $\alpha$  is constant, the coefficient of friction arising from deformation losses is directly proportional to the mean pressure  $\bar{p}$  between the ball and the rubber and is independent of the ball radius.

From the size of the indentations formed under static loading and using Hertz's equation (equation (1)) connecting the load and the area of the indentation it may be shown that, assuming  $\sigma = \frac{1}{2}$ , the effective value of  $E$  is 900 lb in<sup>-2</sup>.

Thus  $\mu_{\text{hysteresis}} = 4 \times 10^{-4} p_a \alpha \quad \dots\dots (7)$   
where  $\bar{p}$  is now replaced by the areal pressure  $p_a$ .

Some cyclic static loading-unloading measurements similar to those described earlier (Tabor 1955 a) showed that for rates of deformation comparable to those occurring in the rolling and sliding experiments the first cycle involved an energy loss due to hysteresis which was about 0.35 of the total elastic energy of deformation, i.e.  $\alpha = 0.35$ . In the rolling and sliding experiments we may, however, expect a larger loss for the following reason. The hysteresis loss depends solely on the input elastic energy only when the rubber is subjected to isotropic strains. If, however, the *direction* of shear in the element is changed during the deformation process there is evidence (which we hope to describe in a later paper) that energy will be lost even if the energy in the rubber is kept constant. Consider now the deformation of the rubber as the ball rolls over it as shown in figure 3. (This is based on experiments in which a *cylinder* is rolled over a block of rubber and the distortion of grids painted on a lateral face of the rubber is photographed: similar distortions will occur for a sphere.) In the undisturbed part of the rubber is a square element A. As the ball rolls towards A the element is first distorted to

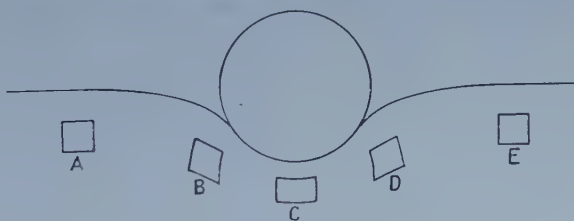


Figure 3. Deformation of elements during rolling.

the shape B, the greater part of the shear being parallel to the surface. When the element reaches the bottom of the ball it is under compression, the principle shear direction being at 45° to the surface. Between B and C there is little change in elastic energy but there is a 45° rotation in the direction of shear. In contrast, the static loading cycles used in determining  $\alpha$  subject each element to increasing strain as the load is applied, but there is very little change in the direction of strain on each individual element. Consequently, we may expect the losses during rolling to be greater than those deduced from static loading experiments†. A theoretical

† It may be noted that the element C after leaving the bottom of the ball goes through the reversed direction of shear, e.g. D compared with B. For metals which show a marked Bauschinger effect this reversal of shear direction could account for extremely large hysteresis losses in rolling compared with those that would be observed in comparable static loading experiments.

analysis for a *cylinder* rolling over a rubber surface (Greenwood 1957) suggests that the rolling losses may be more than twice as great as for static loading. Assuming a factor 2 to apply to the rolling of spheres the value of  $\mu_{\text{hysteresis}}$  becomes

$$\mu_{\text{hysteresis}} = 3 \times 10^{-4} p_a. \quad \dots\dots (8)$$

The theoretical curve for this is drawn on figure 1 and it is seen that it lies close to the observed values. Better agreement is not to be expected since  $\alpha$  is not strictly constant. In addition the occurrence of tangential forces which are a large fraction of the normal force modifies the Hertzian pressure distribution.

#### § 4. THE FRICTION OF CONICAL SLIDERS

With spherical sliders a direct comparison between rolling and sliding friction can be made. With conical indenters this is not possible so that there is no direct check on the assumption that interfacial adhesion is unimportant. Using wet soap as the lubricant sliding experiments were carried out with steel sliders of semi-angle  $\theta = 30^\circ, 45^\circ, 50^\circ, 60^\circ$  and  $80^\circ$ . It was found that, for any given indenter, the coefficient of friction was roughly independent of the load. The mean pressure

Table 2. Friction of Conical Sliders on Lubricated Rubber

Semi-angle of cone	$\mu_s$	Mean pressure $p_a$ from area (lb in <sup>-2</sup> )	Mean pressure $p_d$ from depth (Sabey) (lb in <sup>-2</sup> )
80	0.1	200	260
60	0.16	360	560
50	0.2	450	750
45	0.3	530	820
30	0.75	800	1400

over the circle of contact formed under static loading was also found to be roughly independent of the load. These values are, however, again appreciably lower than

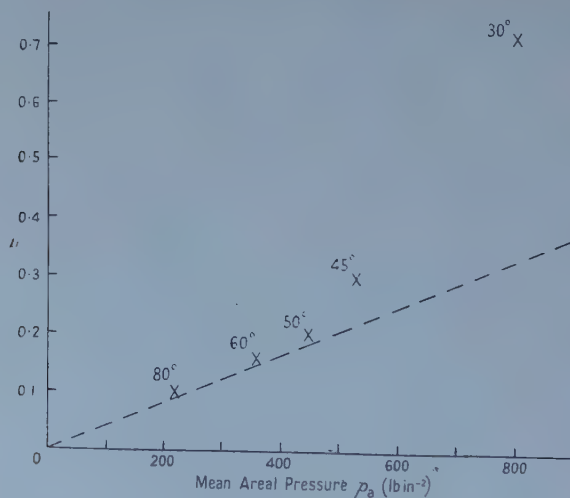


Figure 4. Coefficient of friction of steel cones of semi-angles  $80^\circ, 60^\circ, 50^\circ, 45^\circ$  and  $30^\circ$  sliding over a well lubricated rubber surface as a function of the mean areal pressure  $p_a$ . The broken line is the theoretical curve assuming that the friction arises primarily from hysteresis losses in the rubber.

those derived from depth measurements and for convenience both values are given in table 2. The plot of  $\mu_s$  against  $p_a$  (calculated from areal measurements) is given in figure 4.

### § 5. DEFORMATION LOSSES FOR CONICAL SLIDERS

We again assume that the cone is undeformed by the rubber (figure 5). Consider any element distance  $r$  from the centre where the pressure normal to the interface is  $p$ . The horizontal component on an element of area  $dS$  is  $p dS \cos \theta$ .

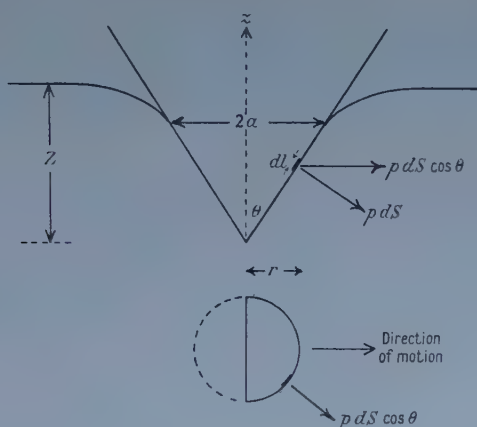


Figure 5. Calculation of the horizontal component of force over the front half of the circle of contact for a hard cone indenting an elastic solid.

On an annulus around the front half of the cone this has an average value  $(2/\pi)p dS \cos \theta$  in the direction of motion. Since the area of the band  $dS = \pi r dl$  and  $dl = \csc \theta dr$  the total horizontal force in the direction of motion is

$$F = \int \frac{2}{\pi} p \cos \theta \pi r dl = 2 \cot \theta \int_0^a p r dr. \quad \dots\dots(9)$$

But the total normal force  $W$  on the cone is

$$W = \int 2\pi r dl p \sin \theta = 2\pi \int_0^a p r dr. \quad \dots\dots(10)$$

Hence

$$F = \frac{W}{\pi} \cot \theta. \quad \dots\dots(11)$$

Thus  $\phi$ , the work done per unit distance of travel in the horizontal direction, is

$$\phi = \frac{W}{\pi} \cot \theta \quad \dots\dots(12)$$

and the coefficient of friction due to hysteresis losses becomes

$$\mu_{\text{hysteresis}} = \frac{\alpha \phi}{W} = \frac{\alpha}{\pi} \cot \theta. \quad \dots\dots(13)$$

This result is independent of the pressure distribution. If it is assumed that the mean pressure  $\bar{p}$  over the circle of contact is given by classical elastic theory (Love 1939), namely

$$\bar{p} = \frac{E}{2(1-\sigma^2)} \cot \theta \quad \dots\dots(14)$$

we may eliminate  $\cot \theta$  from equation (13). This gives

$$\mu_{\text{hysteresis}} = \frac{2(1-\sigma^2)}{\pi E} \bar{p} \alpha. \quad \dots\dots(15)$$

From the observed values of  $p_a$  given in table 2 and using equation (14) we obtain an average value for  $E$ , assuming  $\sigma=0.5$ , of about  $E=800 \text{ lb in}^{-2}$ . Inserting this value in equation (15) we obtain for a conical slider :

$$\mu_{\text{hysteresis}} = 5 \times 10^{-4} p_a \alpha. \quad \dots\dots(16)$$

Here again we may expect that in sliding the effective hysteresis loss will be greater than the quantity ( $\alpha=0.35$ ) determined from static loading experiments. Again we may expect an upper limit to the contribution from hysteresis losses of the order

$$\mu_{\text{hysteresis}} = 4 \times 10^{-4} p_a. \quad \dots\dots(17)$$

This is plotted on figure 4. It is seen that there is good agreement with experiment for cones of semi-angle greater than  $50^\circ$ . It is significant that the  $80^\circ$ ,  $60^\circ$  and  $50^\circ$  cones produced practically no damage on the rubber. The  $45^\circ$  cone produced a light tear and the  $30^\circ$  cone a very heavy tear along the centre of the region of contact. A similar increase in friction for these cones is also observed with unlubricated surfaces (see below).

#### § 6. UNLUBRICATED SLIDING

It is instructive to compare the sliding friction on lubricated rubber with that obtained on unlubricated surfaces. Typical results for a  $\frac{1}{4}$  in. ball and for the cones are reproduced in figure 6. There are two points of interest. For the spherical surfaces the coefficient of friction increases slightly with decreasing load or pressure. This is in agreement with the frictional behaviour generally observed with elastic solids: if the friction arises primarily from interfacial adhesion and shearing the friction will depend on the real area of contact. For a spherical indenter on smooth rubber this is roughly proportional to  $W^{2/3}$  so that the friction should vary in this way with load and the coefficient of friction should vary as  $W^{-1/3}$ . Since the mean areal pressure  $p_a$  is proportional to  $W^{1/3}$  this means that

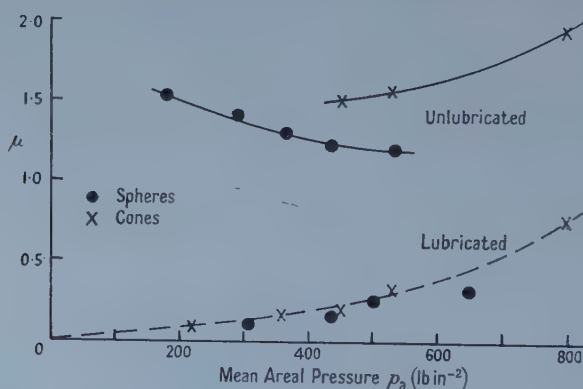


Figure 6. Coefficient of sliding friction of spheres (diameter  $\frac{1}{4}$  in.) and cones on rubber as a function of mean areal pressure  $p_a$ . Continuous line, unlubricated surfaces; broken line, well lubricated surfaces.



$\mu$  should vary as  $p_a^{-1}$ . For a rough rubber, if it is assumed that the roughnesses are of spherical shape the area of contact will be approximately proportional to  $W^{8/9}$  (Lodge and Howell 1954, Archard 1953) so that the coefficient of friction should vary as  $W^{-1/9}$ , that is as  $p_a^{-1/3}$ . The experimental results given in figure 6 are closer to the second value the coefficient of friction increasing as the pressure is reduced according to a power law of about  $p_a^{-0.25}$ . This behaviour is in marked contrast to that observed with lubricated surfaces where the friction is dominated by hysteresis losses and  $\mu$  increases with  $p_a$ .

With cones the area of elastic contact diminishes as the cone angle is reduced. One might therefore expect a decrease in friction with decreasing cone angle. This is not observed. Indeed there is a marked increase in  $\mu$  for cones of semi-angle less than  $45^\circ$ . This increase is associated with tearing of the rubber and it is interesting to note that an almost identical trend is observed for lubricated surfaces.

### § 7. THE SHEARING TERM IN LUBRICATED SLIDING

The results so far described suggest strongly that most of the friction observed in lubricated sliding arises from deformation losses in the rubber. The frictional force due to this effect for spherical sliders is approximately proportional to  $W^{4/3}$ . On the other hand any friction arising from shearing of the lubricant film will depend on the area of contact between the slider and the rubber and should, therefore, vary as  $W^n$  where  $n < 1$  assuming the shear strength of the lubricant film to be a constant. This suggests that as the load is reduced the shearing term should become increasingly more important. To examine this, experiments were carried out with the  $\frac{1}{4}$  in. ball on rubber lubricated with wet soap at loads down to 0.01 lb. The results are shown in figure 7, the frictional force being plotted against the load on logarithmic coordinates. It is seen that for loads greater than about 1 lb the rolling and sliding friction are almost equal. For loads below this the sliding friction is appreciably larger than the rolling friction, the effect becoming more

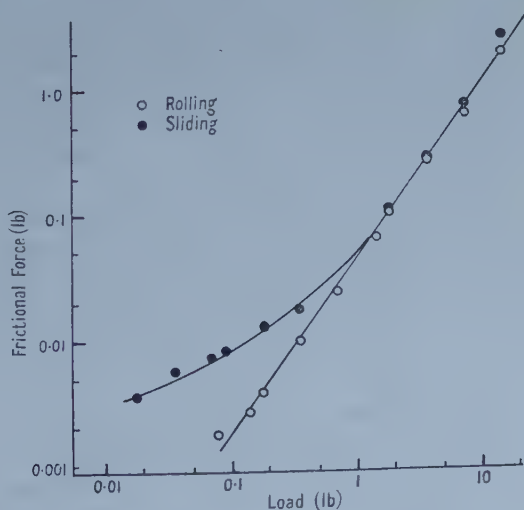


Figure 7. Log-log plot of frictional force against load for spheres (diameter  $\frac{1}{4}$  in.) rolling and sliding on well lubricated rubber. At very low loads the sliding friction is dominated by the shearing of the lubricant film.

marked the lower the load. These results are redrawn as  $\mu$  against  $p_a$  in figure 8 where the effect of the lubricant film at pressures below about  $100 \text{ lb in}^{-2}$  is very strikingly shown. At the other extreme, at very high pressures, the sliding friction is again greater than the rolling friction and this may be due to breakdown of the lubricant film and the occurrence of a small amount of metal-rubber contact.

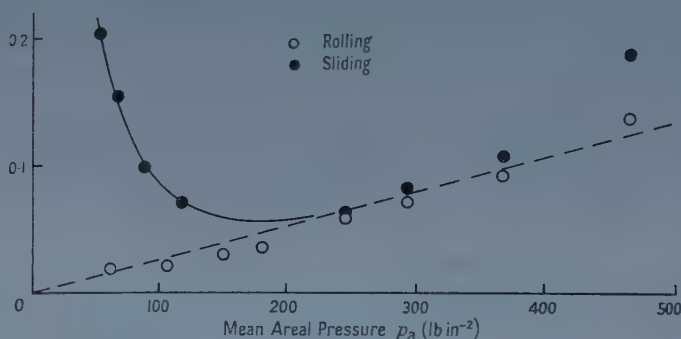


Figure 8. Results of figure 7 plotted as coefficient of friction against mean areal pressure  $p_a$ . Linear coordinates.

We may expect that the range over which these effects are important will depend on the nature and efficiency of the lubricant and also on the severity of the deformation to which the rubber is subjected. The effect of deformation on the magnitude of the hysteresis loss for spherical sliders is seen most clearly by using equation (5) where  $\phi = 3Wa/16R$  and combining it with the assumption that in effect  $\alpha = 0.7$ . This gives as an equivalent expression for equation (6)

$$\mu_{\text{hysteresis}} = 0.13a/R. \quad \dots\dots(6a)$$

Thus for  $\mu_{\text{hysteresis}}$  to exceed a value of say 0.05,  $a/R$  must exceed 0.4, i.e. the ball must penetrate the rubber to a considerable depth. For shallow indentations the value of  $\mu_{\text{hysteresis}}$  drops off and the observed friction is dominated by other factors. In the limit  $\mu_{\text{hysteresis}}$  will become extremely small either when the deformation is very slight or when it is restricted to a fixed portion of the rubber. This occurs, for example, when rubber slides over a smooth surface. Here, of course, apart from the effect of surface irregularities, the same part of the rubber remains distorted throughout the sliding process and very little friction can arise from deformation losses. However, even in this case, if the lubrication is extremely effective, and if surface roughnesses produce a fluctuating loading on small regions of the rubber within the geometric area of contact, hysteresis losses may not be a negligible part of the total friction observed.

#### § 8. CORRELATION WITH MISS SABEY'S RESULTS

At low speeds of lubricated sliding there is good agreement between the observed friction and that calculated on the assumption that 60–70% of the estimated input elastic energy is lost in hysteresis. In Miss Sabey's work the speed of sliding was very much higher, *c.*  $6 \text{ ft sec}^{-1}$ . This will lead to an increase in the effective elastic modulus of the rubber (Mullins 1950) which would imply a decrease in  $\phi$ ; on the other hand it will probably increase the hysteresis losses.

Unfortunately, it is not possible to estimate the relative importance of these effects. However, as a simplification we may assume that the elastic input work is the same as at slow sliding speeds and that, as an upper limit, the whole of this energy is lost. (This would, of course, involve a modification in the calculation of the input energy since it would imply that the load is carried only on the front half of the circle of contact. There is little point in considering this in greater detail since the other factors discussed above may be of comparable importance.) The results obtained for spheres and cones are shown in figure 9 together with the experimental results given in Miss Sabey's paper. The agreement is reasonable. For the more pointed cones the friction is very much greater than the theoretical values and the experiments described in this paper suggest that this is due to penetration of the lubricant and to tearing of the rubber.

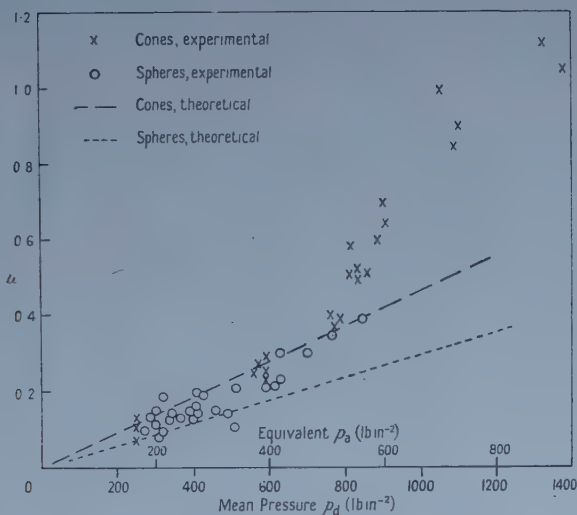


Figure 9. Results obtained by Miss Sabey for spheres and cones sliding on wet rubber at a speed of 6 ft sec<sup>-1</sup>. (The mean pressures given by Miss Sabey are based on depth measurements and the corresponding approximate pressures based on areal measurements have also been introduced.) The broken lines are theoretical curves assuming that the friction arises primarily from elastic hysteresis losses in the rubber. In this case it is assumed, as an upper limit, that the whole of the elastic energy is lost.

### § 9. DEFORMATION OF THE RUBBER

Miss Sabey's work has shown very clearly that when a spherical or conical indenter is pressed into the rubber used, the depth of penetration obeys the laws of elastic deformation surprisingly well. We may call the mean pressure calculated in this way  $p_d$ . Measurements carried out in this work show that the pressures derived from direct areal measurements ( $p_a$ ) also agree with the elastic equations: they are, however, always lower than those obtained from depth measurements the difference being more marked for cones than spheres. The reason is that the rubber is not truly elastic and the material surrounding the actual indentation is not dragged down as much as elastic theory demands. This is shown schematically in figure 10. It is clear from the derivations given for the sphere that, at a given load, the factor which determines the work of rolling is primarily the diameter of the circle of contact. This means that the

pressure derived from areal measurements is the parameter which determines the work of rolling rather than the pressure derived from depth measurements. For this reason the friction has been plotted in figures 1 and 4 against  $p_a$  rather than against  $p_d$ . For conical sliders either pressure may be used but it must be associated with the appropriate value of  $E$ .

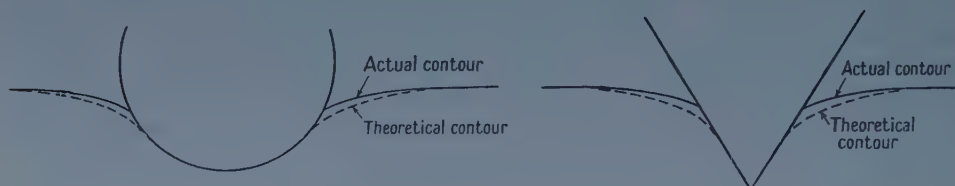


Figure 10. Deformation of the rubber under spherical and conical indenters as observed and as deduced from elasticity theory. The mean pressure deduced from areal measurements is consequently appreciably lower than that deduced from depth measurements.

### § 10. CONCLUSIONS

The experiments described here show that in the sliding of hard spheres or cones over well lubricated rubber the conventional shearing friction is very small. If the rubber has a poor resilience and the slider produces large strains, the major part of the friction arises from hysteresis losses in the rubber itself. Under these conditions, for example, the sliding friction of a sphere on a well lubricated rubber surface is almost the same as the rolling friction. For both spheres and cones the coefficient of friction under conditions of good lubrication is proportional to the mean pressure over the region of contact and there is good agreement between the observed experimental results and the simple theory attributing the friction to hysteresis losses. In these cases the friction may be considered as the work of grooving the rubber, although, of course, the groove disappears as a result of elastic recovery after the slider has passed.

These ideas may also be extended to explain the results obtained by Miss Sabey on wet rubber at sliding speeds of the order of  $6 \text{ ft sec}^{-1}$ . The results again suggest that for spherical sliders and for cones of semi-angle greater than  $50^\circ$  there is little 'shearing' friction. Apparently the water film at these speeds provides hydrodynamic buoyancy and the friction is mainly due to hysteresis or deformation losses in the rubber. For more pointed cones the friction is greatly in excess of the deformation losses. This is probably due to breakdown of the hydrodynamic film as a result of which there is a larger contribution from interfacial or shearing friction. In addition especially with the  $30^\circ$  cone there appears to be an appreciable amount of work expended in tearing the rubber. This suggests that pressures which are high enough to penetrate the water film and so give a large coefficient of friction are also likely to tear the rubber.

This study emphasizes the importance of deformation losses in the friction of surfaces which are subjected to large deformations and which show small interfacial adhesion. A similar effect has been observed by Attack, working in this laboratory, on the friction of wood (Bowden 1957).

It is clear from these observations that for hemispherical or conical sliders rubbing on well lubricated rubber the friction will be larger for rubbers possessing high hysteresis losses. In addition, with hemispherical sliders the effect will be more marked for rubbers with a small Young's modulus. If the surface of a



road may be considered to be covered with conical or spherical asperities, these conclusions may have a practical bearing on the selection of tyre materials required to show a high friction on wet or greasy road surfaces.

#### ACKNOWLEDGMENTS

We wish to thank Miss Sabey for showing us her report prior to publication and also for her kindness in making available specimens of the rubber used in her work. We also thank Mr. H. Minshall for making some of the friction measurements and Vauxhall Motors for a grant to the laboratory.

#### REFERENCES

- ARCHARD, J. F., 1953, *J. Appl. Phys.*, **24**, 981.  
BOWDEN, F. P., 1957, *Endeavour*, **16**, 5.  
ELDREDGE, K. R., and TABOR, D., 1955, *Proc. Roy. Soc. A*, **229**, 178.  
GREENWOOD, J. A., 1957, *Ph.D. Dissertation*, University of Cambridge.  
LODGE, A. S., and HOWELL, H. G., 1954, *Proc. Phys. Soc. B*, **67**, 89.  
LOVE, A. E. H., 1939, *Quart. J. Math.*, **70**, 161.  
MULLINS, L., 1950, *I.R.I. Trans.*, **26**, 27.  
SABEY, B. E., 1958, *Proc. Phys. Soc.*, **71**, 979.  
SCHALLAMACH, A., 1952, *Proc. Phys. Soc. B*, **65**, 657.  
TABOR, D., 1955 a, *Proc. Roy. Soc. A*, **229**, 198 ; 1955 b, *Brit. J. Appl. Phys.*, **6**, 79.

## Temperature Dependence of Carrier Lifetime in Silicon

By D. J. SANDIFORD†

Research Laboratory, The British Thomson-Houston Co. Ltd., Rugby

*Communicated by L. J. Davies; MS. received 25th September 1957, and in revised form 28th February 1958*

**Abstract.** Measurements of carrier lifetime have been made on both n- and p-type silicon crystals over the temperature range 0°C to 200°C. Results are given for both high and low values of injected carrier concentrations. A comparison is made with the Shockley-Read picture of carrier recombination. The results and theory may be reconciled on the assumption that the capture probabilities of the recombination centres are temperature dependent, and that the energy levels of the centres lie  $0.45 \pm 0.05$  eV above the valence band.

### § 1. INTRODUCTION

THE injection of excess carriers, electron-hole pairs, above thermal equilibrium concentration values in a semiconductor is followed by the eventual disappearance of such carriers due to recombination processes. It seems that an important type of recombination process in silicon is that involving localized states in the crystal structure with energy levels in the forbidden energy gap. Such a model for recombination has been treated mathematically by Shockley and Read (1952).

In this paper the results of lifetime measurements, over a range of temperature, on both p- and n-type silicon specimens are presented and a comparison is made with the Shockley-Read formula.

### § 2. EXPERIMENTAL DETAILS

#### 2.1. *The Method*

Carrier lifetime was measured by the method of photoconductivity decay using an air spark as radiation source (Haynes and Hornbeck 1955). The light output from the spark lasted about 1  $\mu$ sec.

The silicon specimens were filaments usually about 10 mm  $\times$  4 mm  $\times$  4 mm in size. They were obtained from slices cut transversely from silicon ingots which had been grown using the Czochralski technique (Czochralski 1917, Teal and Little 1950). Such crystals were grown with low rotation rates (about 3 rev min<sup>-1</sup>) and did not contain many temporary traps (Haynes and Hornbeck 1955, Hornbeck and Haynes 1955).

Contacts to the specimen were made by soldering to nickel or rhodium plated ends.

The light flash was focused on to the central 4 mm or so of the filament, and an iris diaphragm in the lens system gave control over the carrier injection level. Often, a silicon filter was used to remove the visible light radiation and so reduce

† Now at Sloane Physics Laboratory, Yale University.

the amount of electron-hole pair creation near the surface, with a subsequent reduction in surface recombination. On some of the p-type specimens a dichromate etch (Moore and Nelson 1956) was also used for this purpose. However, the geometry of all samples and the nature of the radiation were such that, even for high surface recombination velocities, the time constant of the dominant mode of the conductivity decay was negligibly affected by the surface. By 'dominant mode' we mean the portion of the decay at times after the initial fast recombination due to the surface. In practice this was the decay at least two lifetimes after the radiation flash.

The observed effect of a silicon filter was to remove almost all the initial fast decay and to reduce slightly the amplitude of the signal at longer times, but not to change the time constant of this latter exponential decay. This implies that a large proportion of the photons arriving at the specimen are of energies corresponding to the near infra-red such that electron-hole pairs are created throughout the bulk rather than at the surface. This, together with the short duration time, is why the air spark source is particularly convenient for this measurement.

Confirmation of the interpretation of the time constant of the dominant mode as Shockley's filament lifetime (Shockley 1950) was obtained empirically in the following way. The time constant of decay of a filament was measured both before and after the cross-sectional area was reduced by grinding on one of the faces. This was repeated until the filament was about 0.5 mm wide. On the assumption of infinite surface recombination, the changes of lifetime with cross-sectional dimensions were in excellent agreement with Shockley's formula and the known minority carrier diffusion constant. This demonstrated that for the cross-sectional dimensions chosen in the present experiment, measurements on the dominant mode of decay give values for the lifetime of carriers which are characteristic of the bulk.

There are two important effects to be controlled in this experiment. One is that of carrier trapping, discussed in detail by Haynes and Hornbeck (1955). To remove this effect, if it occurs, one must raise the steady injection level to saturate the traps. The other effect is that of injection level on lifetime itself (Bemski 1955). Most measurements were made at low injection levels, i.e. at a level sufficiently low that the lifetime did not alter with further reduction in injection level. Some measurements were also made at very high injection levels where, according to the Shockley-Read picture, lifetime is expected to approach a limiting value. To obtain this, a steady high injection background was provided by a 250 watt infra-red lamp at about 25 cm from the specimens. On some high resistivity samples such a high injection level could be provided by the spark source. According to theory no difference is expected between the time constant of the transient of a high injection level and the transient of a low injection level with a high injection level steady background, and none was found.

## *2.2. Experimental Results*

Figures 1 and 2 give typical results of lifetime measurements at low injection levels plotted against reciprocal temperatures for n-type and p-type material respectively. Figures 3 and 4 give results at both low and high injected densities for n- and p-type specimens respectively. Figure 5 gives the measurements on an n-type sample over a more extended temperature range.

None of the p-type specimens showed trapping effects in this experiment above room temperature; however, in some of the n-type specimens, trapping of time constant about 10 msec became important at temperatures of about 100°C. This was easily eliminated with steady illumination. Below room temperature trapping becomes important for both p- and n-type specimens and is difficult to remove.

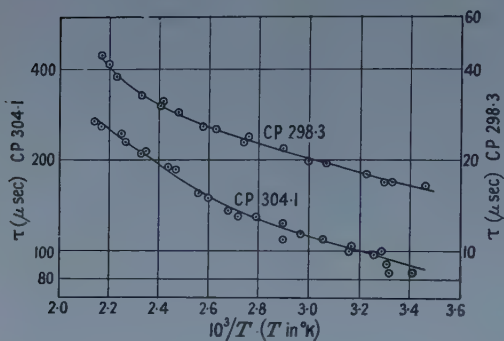


Figure 1. Lifetime results at low injection levels for n-type specimens CP.298.3 (5 ohm cm) and CP.304.1 (40 ohm cm).

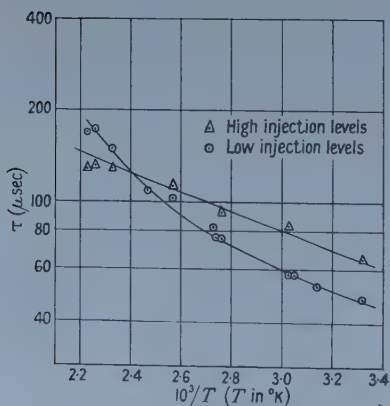


Figure 3. Lifetime results for n-type specimen CP.446.12 (20 ohm cm).

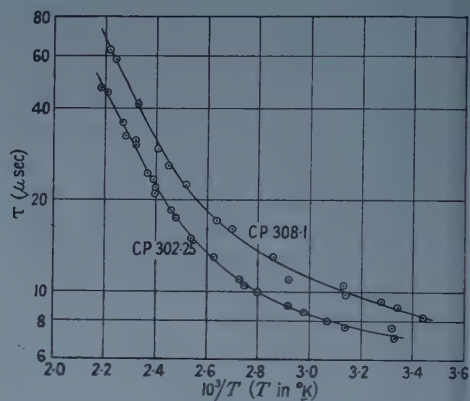


Figure 2. Lifetime results at low injection level for p-type specimens CP.302.25 (80 ohm cm) and CP.308.1 (65 ohm cm).

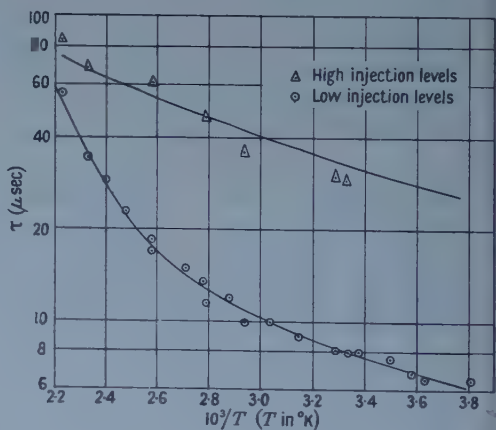


Figure 4. Lifetime results for p-type specimen CP.302.12 (100 ohm cm).

The crystals were in the 'as grown' state and had not been subjected to any heat treatment other than that experienced immediately after growth. The p-type crystals were doped with boron and the n-type crystals with phosphorus, otherwise there was no intentional addition of chemical impurities.

The results shown are typical of the majority obtained. There have been several exceptions, but these will not be discussed here.



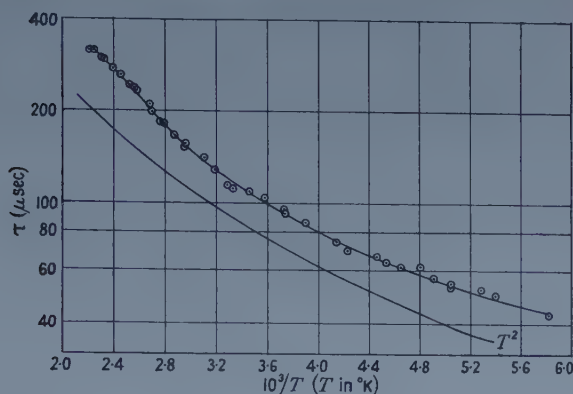


Figure 5. Lifetime results at low injection levels for n-type specimen CP.344.3 (105 ohm cm).

### § 3. DISCUSSION OF RESULTS

A single set of recombination centres of the Shockley-Read type gives rise to a low injection level lifetime, measured by a transient experiment such as that of conductivity decay, equal to (Sandiford 1957)

$$\tau_L = \frac{(\alpha_n N)^{-1} [p_0 + p_1 + N(1 + p_0/p_1)^{-1}] + (\alpha_p N)^{-1} [n_0 + n_1 + N(1 + n_0/n_1)^{-1}]}{n_0 + p_0 + N(1 + p_1/p_0)^{-1}(1 + n_1/n_0)^{-1}} \quad \dots\dots (1)$$

where  $p_0$  and  $n_0$  are the thermal equilibrium concentrations of holes and electrons,  $N$  is the concentration of recombination centres, and  $\alpha_p$  and  $\alpha_n$  are the probabilities for capture of holes and electrons respectively. When the occupation of the centres obeys simple Fermi statistics, which is the case if the centres are non-interacting,  $p_1$  and  $n_1$  are equal to the values of  $p_0$  and  $n_0$  for the Fermi level lying at the energy level of the recombination centre.

We will assume that  $N$  is small compared with any of the values  $p_0$ ,  $n_0$ ,  $p_1$ ,  $n_1$ . In that case we have the simple Shockley-Read expression

$$\tau_L = \frac{(\alpha_n N)^{-1}(p_0 + p_1) + (\alpha_p N)^{-1}(n_0 + n_1)}{n_0 + p_0} \quad \dots\dots (2)$$

At very high injected densities Shockley and Read (1952) show that, for a steady-state experiment

$$\tau_H = (\alpha_n N)^{-1} + (\alpha_p N)^{-1} \quad \dots\dots (3)$$

It may be shown that this also holds for the transient case.

At sufficiently low temperatures equation (2) shows that

$$\left. \begin{aligned} \tau_L &= (\alpha_n N)^{-1} \text{ for p-type material} \\ \tau_L &= (\alpha_p N)^{-1} \text{ for n-type material.} \end{aligned} \right\} \quad \dots\dots (4)$$

For the temperature range when equations (4) hold we have from equations (3) and (4)

$$\left. \begin{aligned} \frac{\alpha_n}{\alpha_p} &= \frac{\tau_H}{\tau_L} - 1 \text{ for p-type material} \\ \frac{\alpha_n}{\alpha_p} &= \left( \frac{\tau_H}{\tau_L} - 1 \right)^{-1} \text{ for n-type material.} \end{aligned} \right\} \quad \dots\dots (5)$$

Comparing the results of the last section with equations (2), (3), (4) and (5) we note the following features:

(i) Figures 3 and 4 show that at low temperatures ( $10^3/T > 2.8$ )  $\tau_L$  and  $\tau_H$  vary in a similar fashion with temperature for both the n- and p-type specimens. From equations (3) and (4) we may assume, therefore, that both  $\alpha_n$  and  $\alpha_p$  have a similar temperature dependence.

(ii) Confirmation of a temperature dependent  $\alpha_p$  is provided by figure 5 which gives measurements over a more extended low temperature range. The graph also shows a curve proportional to  $T^2$  which is similar in form to the lifetime curve, within experimental error. From equation (4) this leads to  $\alpha_p$  proportional to  $T^{-2}$ .

(iii) The application of equation (5) to the results of figures 3 and 4 leads to a ratio of  $\alpha_n/\alpha_p$  of about 3 for both the n- and p-type crystals.

(iv) Using equation (2) the results at high temperature are consistent with a set of recombination centres whose energy level lies  $0.45 \pm 0.05$  eV above the valence band. Also a ratio of  $\alpha_n/\alpha_p$  rather larger than unity explains the different behaviour of lifetime with temperature for the n- and p-type crystals.

We do not know what are the recombination centres whose description has just been given. There is evidence to show that room temperature lifetime in crystals similar to those measured may be determined by the crystal growing conditions, and is independent of the resistivity. This latter, of course, is in agreement with equation (4) and the model quoted, and the former point suggests some type of structural fault to be responsible. Allen (1956) has discussed the possibility of dislocations surrounded by an impurity atmosphere playing an important role in recombination processes in germanium. Such a situation might also be important in silicon.

There is very little published work on the capture probabilities with which to compare the possible dependence of  $T^{-2}$ . However, Burstein, Picus and Sclar (1956) show that such a temperature dependence is expected by the reverse impact-ionization process. At the least, this shows that such a temperature dependence is possible.

#### ACKNOWLEDGMENTS

The author would like to thank his colleagues of the British Thomson-Houston Research Laboratory for their encouragement and assistance, and in particular Mr. N. R. Howard and Mr. J. L. Parmee for the supply of single crystals, and Dr. F. W. G. Rose and Mr. I. Williams for helpful discussions.

#### REFERENCES

- ALLEN, J. W., 1956, *J. Electronics*, **1**, 580.  
 BEMSKI, G., 1955, *Phys. Rev.*, **100**, 523.  
 BURSTEIN, E., PICUS, G., and SCLAR, N., 1956, *Photoconductivity Conference* (New York: John Wiley).  
 CZOCHRALSKI, J., 1917, *Z. Phys. Chem.*, **92**, 215.  
 HAYNES, J. R., and HORNBECK, J. A., 1955, *Phys. Rev.*, **100**, 606.  
 HORNBECK, J. A., and HAYNES, J. R., 1955, *Phys. Rev.*, **97**, 311.  
 MOORE, A. R., and NELSON, H., 1956, *R.C.A. Review*, **17**, 5.  
 SANDIFORD, D. J., 1957, *Phys. Rev.*, **105**, 524.  
 SHOCKLEY, W., 1950, *Electrons and Holes in Semiconductors* (New York: Van Nostrand).  
 SHOCKLEY, W., and READ, W. T., 1952, *Phys. Rev.*, **87**, 835.  
 TEAL, G. K., and LITTLE, J. B., 1950, *Phys. Rev.*, **78**, 647.

# Anomalous Variation of Total Absorption of Radio Waves Reflected from the F2 Region of the Ionosphere Around Mid-day

By S. K. SHARMA

Radio Communication Laboratory, Engineering College, Banaras Hindu University,  
India

*MS. received 6th January 1958*

**Abstract.** The measurements of total absorption in the ionosphere have been made at vertical incidence by pulse technique on various frequencies during the day. It has been observed that at lower frequencies a single maximum is generally obtained after mid-day due to sluggishness of the lower absorbing layers as suggested by Appleton. At frequencies higher than the critical frequency of F1 layer, however, two such maxima are observed one before and the other after the local noon. This anomaly has been attributed to the thermal expansion of the F2 region of the ionosphere, the effect of which is usually observed before mid-day.

## § 1. INTRODUCTION

THE knowledge of total absorption of radio waves reflected from the F2 region of the ionosphere at different geographical latitudes is of great importance for maintaining long distance radio communication. As most of the absorption occurs during the passage of the waves through the ionosphere, attempts have been made by various investigators (Appleton 1937, Best and Ratcliffe 1938, Benner 1951, Appleton and Piggott 1954, Mitra and Mazumdar 1957) to study the amounts of absorption and its diurnal and seasonal variations in different regions of the ionosphere. It may, however, be mentioned that although the absorption measurements have been made at higher latitudes as referred to above, such observations at lower latitudes are still meagre. An attempt has therefore been made to study the diurnal variation of total absorption of radio waves reflected from the F2 region of the ionosphere at Banaras (Lat.  $25^{\circ}20'N$ , Long.  $83^{\circ}0'E$ ). It has been observed that besides the usual maximum of total absorption observed at lower frequencies after mid-day, another maximum is obtained before local noon at frequencies close to the critical frequency of the F2 region.

## § 2. METHOD OF MEASUREMENT

The total absorption of radio waves reflected from the ionosphere has been calculated from the measurement of apparent reflection coefficient after Appleton (1932) with subsequent modification suggested by Piggott (1953) as shown below.

The apparent reflection coefficient is calculated from the ratio of the amplitudes of the first and second order reflections at vertical incidence, given by

$$\rho_0 = \frac{2F''}{F'} \quad \dots\dots (1)$$

where  $\rho_0$  is the apparent reflection coefficient and  $F'$  and  $F''$  are the amplitudes of the first and second order reflections respectively.

It is, however, observed during the day that the variation of intensity of second and higher order of reflections are noticeably incoherent while that of the first echo is fairly steady. The reflection coefficients obtained during the day are therefore corrected (Piggott 1953) for incoherency associated with the second echo by the equation

$$\rho = \rho_0/1.3 \quad \dots\dots(2)$$

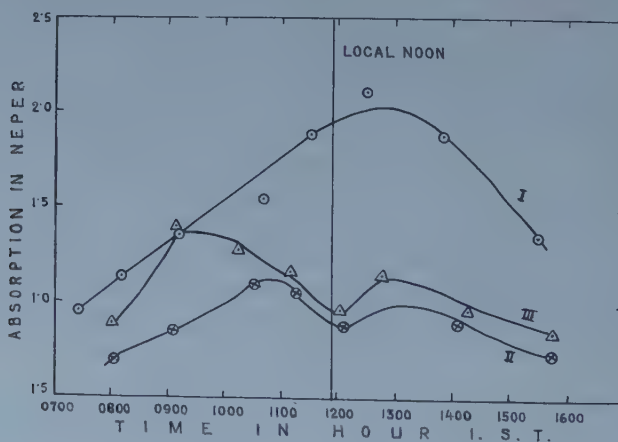
where  $\rho$  is the corrected reflection coefficient. The total absorption occurring in the ionosphere is then calculated by the equation

$$\eta = \ln \rho \quad \dots\dots(3)$$

where  $\eta$  is the total absorption in nepers.

### § 3. EXPERIMENTAL OBSERVATION

The observations were made at vertical incidence with a pulse transmitter having a peak power of about one kilowatt and a suitable receiver combined with a cathode-ray oscillograph. The amplitudes of the first and second reflected echoes were measured with a running average of twenty to fifty observations and  $\eta$  was calculated as mentioned above. The observations were made on two or three such frequencies that at least one of them might be reflected from the F1 region or just penetrate through it so that it may give information about the nature of variation of non-deviative absorption in the lower D, E and F1 regions of the ionosphere. The other frequencies were selected near the critical frequency of F2 layer in order to obtain the information regarding the nature of variation of deviative absorption in the F2 region. The observations were made in the



Diurnal variation of absorption. I, 6.5 Mc/s; II, 10.0 Mc/s; III, 11.5 Mc/s.

winter months (November to March) during 1955-57. The results given in the present communication are based on data which exclude the days on which sporadic E was present. The observations of a typical day in January 1957 recorded with the frequencies of 6.5, 10.0 and 11.5 Mc/s are shown in the figure. The critical frequencies of F1 and F2 layers at different hours on that day are given in table 1,



Table 1. Critical Frequencies of F1 and F2 Layers  
at different hours on 4th January 1957

Time (I.S.T.)	0800	0900	1000	1100	1200	1300	1415	1530
F1 (Mc/s)	5.8	6.2	6.3	6.6	6.8	6.6	6.4	6.3
F2 (Mc/s)	14.3	15.0	14.8	14.7	14.7	15.3	15.3	15.0

The curves in the figure show the variation of the observed total absorption around mid-day at different frequencies. Curve I shows the variation of total absorption with a single maximum occurring after local noon as is usually observed at lower frequencies. Curves II and III show the variation of total absorption at higher frequencies with two maxima, one in the forenoon and the other in the afternoon with a dip in the absorption at local noon. The occurrence of single maximum after mid-day at the lower frequency as shown in curve I has been attributed by Appleton (1953) to the sluggishness of the lower absorbing regions. It may be mentioned that the relaxation time due to the above cause obtained from our observations on such low frequencies is found to vary from 40 to 60 minutes, which is fairly close to that obtained by other investigators.

In connection with the anomalous occurrence of two maxima of total absorption at higher frequencies as shown by curves II and III, it may be mentioned that Mitra and Mazumdar (1957) working on 5 Mc/s at Delhi have also indicated a dip in the total absorption curve at local noon causing two maxima, one before and the other after the local noon, although the forenoon maximum was less pronounced. The critical frequencies of F1 and F2 layers during the period of their observations were near 4.0 and 10.0 Mc/s respectively.

#### § 4. DISCUSSION OF RESULTS

In order to find out the cause of the above anomaly, the absorptions likely to be suffered by the waves in different regions of the ionosphere may be considered and calculated for the frequencies used in the present investigations. It may be mentioned that for these frequencies the mode of propagation of these waves would be quasi-longitudinal in the D and E regions and quasi-transverse in the F1 and F2 regions. Considering the above modes of propagation and assuming all the layers to be of the simple Chapman type, we find the absorption for the ordinary wave after Appleton (1932) to be:

$$\text{non-deviative, D or E layer} = 4.13 \frac{4\pi e^2}{mc} \frac{N_0 \nu_0 H}{(p + p_L)^2} \cos^{3.2} \psi, \quad \dots\dots (4)$$

$$\text{non-deviative, F1 layer} = 4.13 \frac{4\pi e^2}{mc} \frac{N_0 \nu_0 H}{p^2} \cos^{3/2} \psi, \quad \dots\dots (5)$$

$$\text{deviative, F1 or F2} = \frac{4\pi e^2 H}{mc} \int \frac{N \nu}{p^2 (1 - 4\pi e^2 N / m p^2)^{1/2}} dz \quad \dots\dots (6)$$

where all the symbols are with usual notations.

Now using equations (4) and (5) for calculating the non-deviative absorption in the D, E and F1 regions for local noon in winter (4.1.57) at this latitude (for zenith angle  $\psi = 48^\circ 24'$ ) and equation (6) for the deviative absorption in the F1 or F2 region, the calculated values of the absorptions along with the assumed constants of the layers are shown in table 2.

Table 2. Calculated Values of Absorption in Different Layers for Local-Noon with the Assumed Values of the Constants of the Layers

(1)	(2)	(3)	(4)	(5)	(6)	(7)
D	$1.5 \times 10^4$	$1 \times 10^6$	8	1.387	0.645	0.485
E	$3 \times 10^5$	$1 \times 10^4$	10	0.362	0.160	0.120
F1	$6 \times 10^5$	$3 \times 10^3$	25	0.600	0.050	0.036
F2	$3 \times 10^6$	$2 \times 10^3$	50	0.012	0.300	0.415

(1) Layer; (2)  $N_0$  (electrons/cm<sup>3</sup>); (3)  $\nu_0$  (collisions/sec); (4)  $H$  (scale height, km); (5)  $\eta$  (nepers) for 6.5 Mc/s; (6)  $\eta$  (nepers) for 10.0 Mc/s; (7)  $\eta$  (nepers) for 11.5 Mc/s.

From this table it will be seen that the absorption of the wave at 6.5 Mc/s in the F2 region would be almost negligible compared with its absorption in the lower regions. On the other hand, the absorption suffered by waves at 10.0 and 11.5 Mc/s in the F2 region would be sufficiently large and comparable with their absorption in the lower layers. Therefore, the nature of variation of absorption in the F2 region may be expected to have observable effect on the variation of total absorption at these higher frequencies. It will be further observed that the two maxima of total absorption shown at higher frequencies in curves II and III are due to lowering of total absorption during mid-day. Now, as the absorptions in the D, E and F1 regions will continue to increase for sometime after mid-day due to sluggishness of these layers as mentioned above, the cause of decrease in the total absorption at mid-day seems to be associated with the lowering of deviative absorption in the F2 region at that time. The fact that the deviative absorption in the F2 region decreases with the advance of the day before noon is further evident from curves II and III, which show that the total absorption at higher frequency which suffers more deviative absorption, begins to decrease earlier than that at the lower frequency. It may be mentioned that the cause of lowering of the deviative absorption does not seem to be associated with the electron limitation in the F2 region as the electron density of the layer is found to remain almost constant throughout the hours of observations as will be evident from the values of critical frequencies of F2 layer shown in table 1. It is therefore concluded that the decreasing nature of deviative absorption in the F2 region with the advance of the day may be due to thermal expansion (Banerjee and Singh 1949, Appleton 1954) of the layer, the effect of which is usually observed before noon.

#### ACKNOWLEDGMENTS

The author is greatly indebted to Dr. S. S. Banerjee for suggesting the subject for investigation and constant guidance during the progress of the work. He also takes this opportunity to express his gratitude to the Government of Madhya Bharat for granting a scholarship to carry out the present investigations.

#### REFERENCES

- APPLETON, E. V., 1932, *J. Instn. Elect. Engrs*, **71**, 642; 1937, *Proc. Roy. Soc.*, **162**, 451.  
 1953, *J. Atmos. Terr. Phys.*, **3**, 283; 1954, *Ibid.*, **5**, 348.  
 APPLETON, E. V., and PIGGOTT, W. R., 1954, *J. Atmos. Terr. Phys.*, **5**, 141.  
 BANERJEE, S. S., and SINGH, R. N., 1949, *Nature, Lond.*, **164**, 925.  
 BENNER, A. H., 1951, *Proc. Inst. Radio Engrs, N.Y.*, **39**, 36.  
 BEST, J. E., and RATCLIFFE, J. A., 1938, *Proc. Phys. Soc.*, **50**, 232.  
 MITRA, S. N., and MAZUMDAR, S. C., 1957, *J. Atmos. Terr. Phys.*, **10**, 32.  
 PIGGOTT, W. R., 1953, *Proc. Instn Elect. Engrs*, Pt. III, **100**, 61.

## Crystal Reflectivity in Bent Crystal Spectrometers

By A. J. COCHRAN† AND M. A. S. ROSS‡

† Physics Branch, Royal Military College of Science, Shrivenham.

‡ Department of Natural Philosophy, University of Edinburgh.

*MS. received 13th January 1958*

**Abstract.** Previous work on the coefficient of reflection  $R$  of bent crystals used in transmission type focusing  $\gamma$ -ray spectrometers has shown a power law dependence on wavelength  $\lambda$  for  $\lambda$  less than  $0.5 \text{ \AA}$ . Theory is here presented which suggests that at longer wavelengths the power law does not hold and that  $R$  reaches a maximum. The wavelength corresponding to  $R_{\text{max}}$  depends on the assumptions made about the amount of secondary extinction occurring but could be about  $1 \text{ \AA}$ .

An experiment on a bent mica crystal shows that  $R$  is proportional to  $\lambda^{1.9}$  for  $\lambda$  less than  $0.5 \text{ \AA}$  and seems to confirm the existence of a maximum near  $1 \text{ \AA}$ .

### § 1. INTRODUCTION

WHEN a curved crystal spectrometer is used not merely for the measurement of the wavelength of  $\gamma$ -ray and x-ray spectrum lines, but also for the estimation of the relative intensities of such lines, allowance must be made for  $R$ , the coefficient of reflection of the crystal planes, since  $R$  is a function of  $\lambda$ .

The formula for  $R$  for the specially simple case of a single, perfect, non-absorbing crystal irradiated by a monochromatic parallel beam is (Compton and Allison 1935, p. 397)

$$R = 8F^2\delta(1 + \cos 2\theta)/3Z \sin 2\theta \quad \dots\dots (1)$$

where  $F$ , the crystal structure factor, is a function of  $\lambda^{-1} \sin \theta$  or  $n/2d$ , and thus is theoretically a constant for a given set of reflecting planes.  $1 - \delta$  is the real part of the refractive index of the crystal (the imaginary part having been assumed negligible);  $\delta$  is proportional to  $\lambda^2$ .  $\theta$  is the Bragg angle defined by the equation  $2d \sin \theta = n\lambda$ , where  $\lambda$  is the wavelength in air. As  $\sin \theta$  is in practice of the order of  $0.1$ , the trigonometrical factor in  $R$  is proportional to  $\lambda^{-1}$  and  $R$  is therefore proportional to  $\lambda$ .

For a mosaic crystal (the type usually encountered in practice) and otherwise the same conditions, Compton and Allison (1935, p. 414) give

$$R = (1 + \cos^2 2\theta)e^4\lambda^3 F^2 M^2 / 2 \sin 2\theta m^2 c^4 \text{ per unit volume} \quad \dots\dots (2)$$

where  $M$  is the number of unit cells per unit volume. This is proportional to  $\lambda^2$  on the assumptions mentioned above.

If the imaginary part of the refractive index is not neglected, the coefficient of reflection may be evaluated by numerical integration but cannot be expressed explicitly. To examine the dependence on  $\lambda$ , however, a rough approximation may be obtained by multiplying the previous expressions for  $R$  by  $\exp(-\mu x)$  where  $x$  is the distance travelled by the radiation in the crystal, and  $\mu$ , the effective absorption coefficient of the crystal, is given to a good approximation by  $C\lambda^\alpha + g\lambda^2$  where  $\alpha$  is about  $3$ , and  $C$  and  $g$  are constants. The first term of this expression



represents the absorption coefficient of the substance of the crystal in amorphous form; the second term represents the secondary extinction. We assume that the correction factor  $\exp(+C\lambda^2)$  is applied to the data to compensate for ordinary absorption. The correction for secondary extinction, however, cannot be made. It may be determined in favourable cases for the unbent crystal but its value is likely to be affected appreciably by the bending. Secondary extinction must therefore be incorporated in the expression for the coefficient of reflection. Thus for a mosaic crystal

$$R = K\lambda^2 \exp(-gx\lambda^2) \quad \dots\dots(3)$$

where  $K$  is independent of  $\lambda$ . Then

$$\frac{dR}{d\lambda} = K\lambda(2 - 2gx\lambda^2) \exp(-gx\lambda^2). \quad \dots\dots(4)$$

$R$  therefore reaches a maximum  $R_{\max}$  when

$$gx\lambda^2 = 1 \quad \dots\dots(5)$$

and for  $\lambda$  greater than the value satisfying (5)  $dR/d\lambda$  is negative and  $R$  diminishes.

In the rock-salt crystal the effect of secondary extinction is at least as great as that of ordinary absorption. If in other crystals, secondary extinction is comparable with ordinary absorption then  $\lambda$  for  $R_{\max}$  in such a crystal will be comparable with that given by substituting the known ordinary absorption of the crystal for the secondary extinction. Applying this in the case of a mica crystal 0.25 mm thick we find a maximum of  $R$  in the neighbourhood of 1 Å. We conclude therefore that it is essential to measure the value of  $R$  (including secondary extinction) for such a crystal if intensity measurements are to be made with it in the wavelength region  $\lambda > 0.5$  Å.

Jaffe *et al.* (1955) and Day (1955, 1956) have measured the intensities of  $\gamma$ -ray and x-ray lines following the disintegration of some heavy elements. They have applied a correction factor  $R$  but have used different powers of  $\lambda$  in their expressions for  $R$ . The background of this discrepancy is as follows. Lind *et al.* (1950) using a quartz crystal bent to 2 metres radius found  $R$  to be proportional to  $\lambda^2$  for  $0.5 \text{ Å} > \lambda > 0.095 \text{ Å}$  ( $25 \text{ kev} < h\nu < 1.3 \text{ mev}$ ). Browne (1952) observed that "lines widely spaced in energy" showed the same relative intensity when reflected from topaz and from quartz. Jaffe *et al.* (1955) relied on these observations and took  $R$  proportional to  $\lambda^2$  in their work with a topaz crystal bent to a radius of 10 inches. The lines measured by them include, however, the L x-rays of Np, the energies of which (13 to 22 kev) are lower than the low energy limit of the calibration by Lind *et al.* Day (1955) in his work on the Np L x-rays assumed  $R$  proportional to  $\lambda$  and later (1956) corrected this to  $\lambda^{1.35}$ . The latter expression was obtained by measuring, both with the topaz spectrometer and with a scintillation counter, the 84 kev  $\gamma$ -ray and the  $\sim 50$  kev K x-rays emitted in the disintegration of  $^{170}\text{Tm}$ . Here again, the power law deduced from calibration was applied far outside the energy range within which the calibration was made.

## § 2. EXPERIMENTAL METHOD AND RESULTS

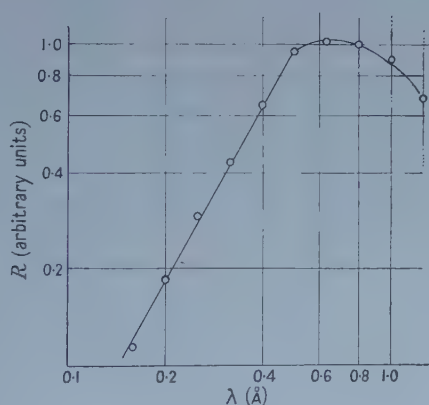
An experiment† has been conducted to measure, over a wide range of  $\lambda$ , the sensitivity of a photographic-recording curved crystal spectrometer. The

† The experimental work was carried out in the Physics Laboratory at the University of Edinburgh.



instrument was used with an extended source and a mica crystal 0.25 mm thick, bent to a radius of 20 cm. The real image formed by the spectrometer was focused on an Ilford G5 electron sensitive plate, the emulsion being  $200\mu$  in thickness. The experiment compared the observed sensitivity of the instrument with a calculated sensitivity. The calculation took into account the absorption of the radiation between the source and the surface of the nuclear emulsion (excepting, of course, the secondary extinction) and also all the processes of absorption occurring in the nuclear emulsion leading to the formation of developable silver bromide grains. The calculated sensitivity was evaluated in terms of the number of silver grains in the developed emulsion. The mean grain-number-energy calibration of Zajac and Ross (1949) was employed.

In the experimental determination of the sensitivity, the energy range from 8 keV to 40 keV ( $1.55$  to  $0.31\text{ \AA}$ ) was covered, using the K x-rays of 13 elements: 30 Zn, 33 As, 35 Br, 38 Sr, 42 Mo, 45 Rh, 47 Ag, 48 Cd, 49 In, 50 Sn, 53 I, 56 Ba and 58 Ce. The x-ray spectra were scanned by a microphotometer to determine the ratio of the blackening in the K ( $\alpha_1 + \alpha_2$ ) and  $K\beta_1$  lines, and the results were compared with the relative intensities measured by Williams (1933). Above 40 keV the calibration was continued by measuring, both with the crystal spectrometer and with proportional counter, the ratio of the intensities of the 82 keV  $\gamma$ -ray and  $\sim 31$  keV K x-rays emitted in the disintegration of  $^{133}\text{Xe}$ . Full details of the method (Cochran 1955) will be published.



The ratio of the observed sensitivity to the calculated sensitivity gives the coefficient of reflection of the (100) planes of the bent crystal. The graph shows  $R$  plotted as a function of  $\lambda$  on a log-log scale. In the short wavelength region,  $\lambda < 0.5\text{ \AA}$  ( $h\nu > 25$  keV), the curve is in general agreement with other experimental determinations,  $R$  being proportional to  $\lambda^{1.9}$ . For present purposes the important part of the curve is that for  $\lambda > 0.5\text{ \AA}$ . As  $\lambda$  increases, the gradient of the curve diminishes and appears ultimately to become negative. The exact form of the curve at the longer wavelengths cannot be determined with accuracy because the sensitivity of the instrument varies rapidly in this region on account of the increasing absorption in the path of the radiation and the decreasing photo-plate sensitivity. The errors, as indicated on the graph, are large but not large enough to justify the use of a constant power law over the whole range of observation.

If our interpretation of the form of the curve as given in § 1 is correct then, since the amount of secondary extinction depends on the type of crystal used, and possibly also on the radius of curvature, it will be essential to carry out a direct calibration over the actual range of wavelengths within which intensity measurements are to be made.

## REFERENCES

- BROWNE, C. I., 1952, *Ph.D. Thesis*, University of California, UCRL-1764.  
COCHRAN, A. J., 1955, *Ph.D. Thesis*, University of Edinburgh (account to be published).  
COMPTON, A. H., and ALLISON, S. K., 1935, *X-rays in Theory and Experiment* (New York : Van Nostrand).  
DAY, P. P., 1955, *Phys. Rev.*, **97**, 689; 1956, *Ibid.*, **102**, 1572.  
JAFKE, H., PASSELL, T. O., BROWNE, C. I., and PERLMAN, I., 1955, *Phys. Rev.*, **97**, 142.  
LIND, D. A., WEST, W. J., and DUMOND, J. W. M., 1950, *Phys. Rev.*, **77**, 475.  
WILLIAMS, J. H., 1933, *Phys. Rev.*, **44**, 146.  
ZAJAC, B., and ROSS, M. A. S., 1949, *Nature, Lond.*, **164**, 311.

## RESEARCH NOTES

**Configuration Interaction in the Ground State and Two Excited States, (1s, 2s)  $^1S$  and (1s, 3s)  $^1S$  of He Atom**

BY B. K. GUPTA AND V. S. R. RAO

Physics Department, Osmania University, Hyderabad, India

*MS. received 17th December 1957, and in final form 13th February 1958*

§ 1. SINGLET GROUND STATE

TAYLOR AND PARR (1952)<sup>†</sup> (TP), have made a detailed study of the ground state of He atom and they find that the calculated energy of the ground state improves substantially, firstly by the 'opening out' of the wave function  $\exp(-\delta r_1 - \delta r_2)$  into  $\exp(-\alpha r_1 - \beta r_2) + \exp(-\beta r_1 - \alpha r_2)$ , i.e. by changing (1s, 1s) into (1s, 1s'), and secondly by the inclusion of the 'angular configurations' (2p)<sup>2</sup>, (3d)<sup>2</sup>, etc., rather than the energetically much nearer configurations (1s, 2s), (1s, 3s), etc. The nature of the configurations (1s, 1s') of TP was reconsidered as follows leading to a comparison with one of the several Hylleraas functions for this state.

We can write  $\exp(-\alpha r_1 - \beta r_2) + \exp(-\beta r_1 - \alpha r_2)$  as

$$2 \exp[-\frac{1}{2}(\alpha + \beta)(r_1 + r_2)] \{1 + \frac{1}{8}(\alpha - \beta)^2(r_1 - r_2)^2 + \text{higher orders in } (r_1 - r_2)^2\}.$$

In the light of this we have tried a linear combination of the functions  $\phi_1 = \exp(-\delta r_1 - \delta r_2)$  and  $\phi_2 = (r_1 - r_2)^2 \exp(-\epsilon r_1 - \epsilon r_2)$  where  $\delta$  and  $\epsilon$  are chosen to give the lowest possible energy and the linear coefficient is used for minimization as usual.

We have found that  $\delta = \epsilon$  turns out to be the best choice and secondly that  $\phi_1$  and  $\phi_2$  give a slightly better energy value than (1s, 1s') of TP. When  $\delta = \epsilon$ , a linear combination of  $\phi_1$  and  $\phi_2$  gives one of the many functions which Hylleraas tried out in his exhaustive work on He atom. Our energy values differ from those of Hylleraas only in the fifth place and we have not been able to reproduce his values, as quoted by Pauling and Wilson (1935). We have found<sup>†</sup> that

$$\exp[-1.6850(r_1 + r_2)] \{1 + 0.14007(r_1 - r_2)^2\} \text{ gives } E = -5.75335$$

whereas the (1s, 1s') function of TP gives  $E = -5.75132$ .

The inclusion of (2p)<sup>2</sup> gives considerable improvement, as shown by TP. The following values of the energies were obtained on combining  $\phi_1$ ,  $\phi_2$  and (2p)<sup>2</sup>.

$$\phi_1, \phi_2 \text{ with } \delta = \epsilon = 1.6850 \text{ and } \phi_3 = (r_1^2 - r_1 r_2 + r_2^2) \exp(-\nu r_1 - \nu r_2),$$

$\nu = 2.450$  turns out to be the best value for  $\nu$ , giving  $E = -5.79219$ .

TP, using (1s, 1s') and  $\phi_3$  with  $\nu = 2.475$ , get  $E = -5.79037$ .

<sup>†</sup> Calculations were also made for all two electron systems up to C<sup>4+</sup> and the relative error in the calculated energy with respect to the experimental value decreases with increasing nuclear charge.

§ 2. EXCITED STATE (1s, 2s)  $^1S$ 

The experimental value of energy is  $-4.29198$ . We have computed with the following normalized functions which are respectively the functions (1s, 1s'), (1s, 2s) and (2p) $^2$  of TP:

$$\begin{aligned}\psi_1 &= N_1[\exp(-\alpha r_1 - \beta r_2) + \exp(-\beta r_1 - \alpha r_2)], \alpha = 1.19, \beta = 2.18365, N_1 = 2.23161/\pi \\ \psi_2 &= N_2[r_1 \exp(-\xi r_1 - \delta r_2) + r_2 \exp(-\delta r_1 - \xi r_2)], \delta = 2.00, \xi = 0.50, N_2 = 0.200987/\pi \\ \psi_4 &= N_4[(r_{12}^2 - r_1^2 - r_2^2) \exp(-\nu r_1 - \nu r_2)], \nu = 2.475, N_4 = 26.8093/\pi.\end{aligned}$$

We have found that

- (a)  $1.00582(\psi_1 - 0.015061\psi_2)$  gives  $E = -5.75160$ ,
  - (a')  $1.08621(-0.37789\psi_1 + \psi_2)$  gives  $E = -4.28342$ ,
  - (b)  $1.00587(\psi_1 - 0.020631\psi_2 + 0.063605\psi_4)$  gives  $E = -5.79093$ ,
  - (b')  $1.08602(-0.37292\psi_1 + \psi_2 - 0.011457\psi_4)$  gives  $E = -4.28481$ . $^\dagger$
- $^\dagger$  0.17% higher than the experimental value  $-4.29198$ .

The function (b') for the state (1s, 2s) seems to give a better energy value than the function proposed recently by Marriott and Seaton (1957) and seems at the same time to be slightly simpler in form than their function.

§ 3. EXCITED STATE (1s, 3s)  $^1S$ 

The experimental value of energy is  $-4.12256$ . Apart from  $\psi_1, \psi_2, \psi_4$  above, we have used for (1s, 3s),

$$\begin{aligned}\psi_3 &= N_3[r_1^2 \exp(-\lambda r_1 - \mu r_2) + r_2^2 \exp(-\mu r_1 - \lambda r_2)], \\ \mu &= 2.00, \lambda = 0.333, N = 0.0087031/\pi.\end{aligned}$$

Combining this with  $\psi_1, \psi_2, \psi_4$  we get

$$\begin{aligned}0.990962(\psi_1 - 0.026600\psi_2 + 0.0091759\psi_3 + 0.061261\psi_4), & \quad E = -5.79096. \\ 1.07714(-0.373516\psi_1 + \psi_2 + 0.011195\psi_3 - 0.011471\psi_4), & \quad E = -4.28482. \\ 1.36050(0.22422\psi_1 - 0.74003\psi_2 + \psi_3 + 0.0060114\psi_4), & \quad E = -4.11608.\end{aligned}$$

The accuracy of the calculated energy is, however, not the only criterion for considering the wave function as good, because the energy criterion controls only the regions of configuration space close to the nucleus and it is quite probable that a quantity which depends mainly on the electron distribution in the outer regions of the atom, if calculated by using wave functions constructed simply on the basis of the energy criterion, may lead to rather unexpected results. A good example of this appears in the computations of the polarizability of the  $H_2^+$  ion as has been pointed out with numerical details by Rahman (1953) where a criterion for the trustworthiness of the polarizability computed on the basis of approximate unperturbed wave functions has been developed.

## ACKNOWLEDGMENT

We are very grateful to Dr. A. Rahman for his inspiring guidance during this work.

## REFERENCES

- MARRIOTT, R., and SEATON, M. J., 1957, *Proc. Phys. Soc. A*, **70**, 296.
- PAULING, L., and WILSON, E. B., 1935, *Introduction to Quantum Mechanics* (New York: McGraw-Hill).
- RAHMAN, A., 1953, *Physica*, **19**, 377.
- TAYLOR, G. R., and PARR, R. G., 1952, *Proc. Nat. Acad. Sci., Wash.*, **38**, 154.



# Simple Method of Interpolation for Coulomb Wave Functions

By A. S. MELIGY

Faculty of Science, University of Alexandria, Egypt

MS. received 11th February 1958

THE regular radial Coulomb wave function, in standard form, is written as follows:

$$F_L(\eta, \rho) = C_L(\eta) \rho^{L+1} \phi_L(\eta, \rho), \quad \dots\dots (1)$$

where

$$C_L(\eta) = \frac{2^L}{(2L+1)!} \left\{ (1^2 + \eta^2)(2^2 + \eta^2) \dots (L^2 + \eta^2) \frac{2\pi\eta}{e^{2\pi\eta} - 1} \right\}^{1/2},$$

$$\phi_L(\eta, \rho) = e^{-i\rho} \left\{ 1 + \frac{1+L-i\eta}{1!(2L+2)} (2i\rho) + \frac{(1+L-i\eta)(2+L-i\eta)}{2!(2L+2)(2L+3)} (2i\rho)^2 + \dots \right\} \quad \dots\dots (2)$$

and the symbols have the usual meaning, viz.  $L$  is the orbital angular momentum quantum number,  $\eta = ZZ'e^2/\hbar v$  and  $\rho = mvr/\hbar$ ,  $v$  being the relative velocity of the two particles,  $r$  the distance between them and  $m$  the reduced mass.

The tables constructed by Abramowitz (1952) and Fröberg and Rabinowitz (1954) give the values of the function  $\phi_L(\eta, \rho)$  [or  $(2L+1)! 2^{-2L} C_L^2(\eta) e^{\pi\eta} \phi_L(\eta, \rho)$ ] for  $L=0, 1, 2, \dots$  and  $\eta=0, 1, 2, \dots$ . For the purpose of interpolating with respect to the parameter  $\eta$ , the tables also give the values of the reduced derivatives of  $\phi_L(\eta, \rho)$  with respect to  $\eta$ . The object of this communication is to present an expansion of  $F_L(\eta, \rho)$ , which provides a convenient method for interpolation with respect to  $\eta$  without using the tables of the reduced derivatives and thus eliminates the necessity of having such tables.

Let

$$f_L(\eta, \rho) = \rho^{L+1} \phi_L(\eta, \rho) \quad \dots\dots (3)$$

and assume the following expansion:

$$f_L(\eta, \rho) = \sum_{n=0}^{\infty} a_n f_{L+n}(\lambda, \rho), \quad \dots\dots (4)$$

where  $\lambda$  is arbitrary. The quantities  $a_0, a_1, \dots$  are determined by equating the coefficients of  $\rho^{L+1}, \rho^{L+2}, \dots$  on the two sides of this equation. They are given by  $a_0=1$ ,  $a_1=(\eta-\lambda)/(L+1)$ , and in general, for  $n \geq 2$ ,

$$a_n = \left[ 2(\eta-\lambda) + \frac{\lambda(n-1)(2L+n)}{(L+n-1)(L+n)} \right] \frac{a_{n-1}}{n(2L+1+n)} - \frac{(2L+n-1)(n-2)}{n(2L+2n-3)(2L+2n-1)(2L+n+1)} \left[ 1 + \frac{\lambda^2}{(L+n-1)^2} \right] a_{n-2}. \quad \dots\dots (5)$$

This expresses  $f_L(\eta, \rho)$  in terms of a series of functions of the same type. The interpolation with respect to  $\eta$  for a value of  $f_L(\eta, \rho)$  may now be performed with the aid of (4) by choosing the value of  $\lambda$  to be the nearest integer to  $\eta$  and taking the values of  $f_{L+n}(\lambda, \rho)$  from the tables of Coulomb wave functions. Thus,

if it is required to obtain  $f_0(1.2, 0.4)$ , take  $\lambda = 1$  and then from (5) and the tables of Abramowitz,

$n$	0	1	2	3	4
$a_n$	1	0.2	0.046667	0.002667	-0.000258
$f_n(1, 0.4)$	0.569107	0.191708	0.072224	0.028030	0.011010

giving  $f_0(1.2, 0.4) = 0.61089$ .

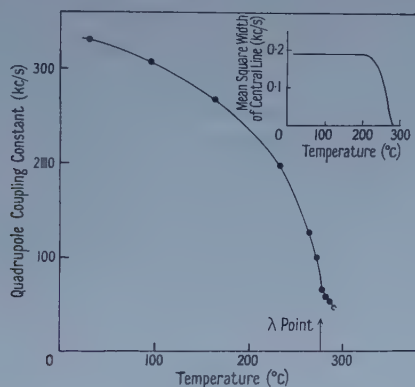
#### REFERENCES

- ABRAMOWITZ, M., 1952, *Tables of Coulomb Wave Functions*, National Bureau of Standards Applied Math. Series No. 17 (U.S. Govt. Printing Office, Washington, D.C.).  
 FRÖBERG, C., and RABINOWITZ, P., 1954, *Tables of Coulomb Wave Functions*, National Bureau of Standards, Report 3033.

## LETTERS TO THE EDITOR

The Nuclear Quadrupole Coupling Constant of  $^{23}\text{Na}$  in Sodium Nitrate

An unusually rapid variation of quadrupole coupling constant with temperature has been found for the  $^{23}\text{Na}$  nuclei in crystalline sodium nitrate. The quadrupole-split nuclear magnetic resonance spectrum has been measured for single crystals of sodium nitrate from room temperature to temperatures just below the melting point ( $309^\circ\text{C}$ ). The measurements were made using a modified Pound-Watkins spectrometer and a magnetic field of 6000 oersteds from a temperature-stabilized permanent magnet. The sodium nuclei lie on equivalent sites on the trigonal axis of the rhombohedral unit cell. For each



The variation with temperature of the electric quadrupole coupling constant  $e^2Qq/h$  of the  $^{23}\text{Na}$  nuclei in a single crystal of sodium nitrate.  $eQ$  is the nuclear electric quadrupole moment,  $eq$  is the electric field gradient along the crystal axis, and  $h$  is Planck's constant.

crystal orientation the three resonance lines were found to be narrow, symmetrical and approximately equal in width, indicating a freedom from crystalline defects affecting the electric field gradient. The frequencies of the lines were determined to a few parts in  $10^6$  and were found to follow accurately the predictions of perturbation theory carried to second order (Pound 1950, Bersohn 1952, Volkoff 1953). The variation of the electric quadrupole coupling constant with temperature is shown in the figure. The value at room temperature is in good agreement with that found by Pound (1950).

In most solids the quadrupole coupling constant declines slightly with increase of temperature on account of lattice expansion and increased vibrational amplitudes. The small temperature coefficient,  $-4.2 \times 10^{-4} \text{ deg}^{-1}$  for  $^{23}\text{Na}$  in sodium chlorate is typical (Gutowsky and Williams 1957). The rapid fall of the coupling constant for sodium nitrate by a factor of ten is in marked contrast, and is clearly associated with the changes in the crystal which bring about the second-order phase transition which is known to occur at  $276^\circ\text{C}$ .

Bersohn (1956) has been able to account for the quadrupole coupling constant measured at room temperature on the basis of a simple ionic model. We have

extended these calculations and have reached the following preliminary conclusions: (a) that lattice expansion can account for only a small part of the observed change of coupling constant; (b) that a co-operative re-orientation of the nitrate groups about their trigonal axes, of the kind proposed by Kracek, Posnjak and Hendricks (1931) to explain the phase transition, is unlikely by itself to account for the observed change of coupling constant; (c) that a co-operative disordering of the nitrate groups, of the kind proposed by Siegel (1949) to explain the phase transition, is also unlikely by itself to be sufficient to account for the observed change. If the simple ionic model is valid additional lattice movements seem to be required. Suitable movements might be the rocking and translatory vibration of the nitrate groups revealed by Raman work, together with movement of the sodium nuclei themselves. Evidence of motion of the sodium nuclei is indicated in the next paragraph. However, the ionic model may not be entirely adequate. The unperturbed resonance frequency is found to decrease by 850 c/s between 35°C and 295°C, representing a change in chemical shift of  $1.3 \times 10^{-4}$ .

Motion of the sodium nuclei is indicated by the narrowing of the central line of the spectrum at temperatures just below the phase transition (see inset of figure). The breadth of this line arises from nuclear dipole-dipole interaction. The reduction of its width to a very small value implies that above 276°C the sodium ions are migrating through the lattice at a rate of more than about  $10^3$  jumps per second, since the full line width is about 1 kc/s.

One of the crystals used came from the Harshaw Chemical Company, Cleveland, U.S.A. and the other was provided by Hilger and Watts Ltd., London, by courtesy of Mr. J. Skinner.

Physics Department,  
University College of North Wales,  
Bangor, Caernarvonshire.  
11th February 1958.

R. G. EADES.  
D. G. HUGHES.  
E. R. ANDREW.

- BERSOHN, R., 1952, *J. Chem. Phys.*, **20**, 1505; 1956, *Bull. Amer. Phys. Soc.* II, **1**, 215.  
GUTOWSKY, H. S., and WILLIAMS, G. A., 1957, *Phys. Rev.*, **105**, 464.  
KRACEK, F. C., POSNJAK, E., and HENDRICKS, S. B., 1931, *J. Amer. Chem. Soc.*, **53**, 3339.  
POUND, R. V., 1950, *Phys. Rev.*, **79**, 685.  
SIEGEL, L. A., 1949, *J. Chem. Phys.*, **17**, 1146.  
VOLKOFF, G. M., 1953, *Canad. J. Phys.*, **31**, 820.

---

### Electrical Properties of Clean Germanium Surfaces

Many investigations have been carried out recently on the properties of semiconductor surfaces. To increase understanding of the nature and origin of the surface states involved, it is desirable to study the properties of surfaces entirely free from contamination by foreign atoms. Farnsworth and co-workers (see Schlier and Farnsworth 1957) have employed bombardment techniques with this aim, but results obtained by the use of such a procedure without tests for its efficacy (Law and Garrett 1956) are always open to dispute.



Recent developments in vacuum techniques, particularly the use of the ionization gauge and pump designed by Alpert (1953) have made practicable the achievement of vacua in which freshly exposed surfaces would be expected to remain substantially uncontaminated for periods of hours. Using such a gauge in a system continuously evacuated by a mercury diffusion pump, we obtain pressures of the order of  $10^{-10}$  mm Hg in envelopes containing a specimen, electrodes and equipment for the fracturing process.

Surfaces freshly exposed under these conditions have been used for studies of field effect and of the photoconductance of the specimen. The nature of the measurement of field effect (the effective transverse mobility of induced surface charge) requires that the surface should be plane, and it has been found possible to obtain satisfactorily flat surfaces by cleavage on a (111) face using a magnetically operated system of levers. The final specimens so obtained have been in the form of rectangular filaments of dimensions about 2.5 cm by 0.3 cm by 0.1 cm, with a freshly exposed surface 2.5 cm by 0.1 cm, and with low resistance welded molybdenum contacts at the ends.

Measurements so far have been carried out on n-type (12 ohm cm) and near-intrinsic germanium. The field-effect studies have not shown the relaxation processes with time constants of the order of seconds which are normally attributed to slow surface states. The effective mobility measurements indicated a barrier height of less than  $2kT$  on the near-intrinsic material, and no inversion layer on the n-type specimens.

Values of surface recombination velocity on the clean surface were obtained from the measurement of d.c. photoconductance by a method involving calibration after contamination. The values observed were comparable with that of a well-etched surface.

As contamination of the surface by air takes place, the surface recombination velocity is found to increase monotonically to a value of several times that obtained immediately after cleavage. During this process, the field effect measurements indicate an initial movement towards a p-type surface condition, followed by a larger change towards an n-type state in the later stages of contamination. The interpretation of these results will be discussed in a future publication.

Physics Department,  
University of Reading.  
21st April 1958.

G. A. BARNES.  
P. C. BANBURY.

ALPERT, D., 1953, *J. Appl. Phys.*, **24**, 860.

LAW, J. T., and GARRETT, C. G. B., 1956, *J. Appl. Phys.*, **27**, 656.

SCHLIER, R. E., and FARNSWORTH, H. E., 1957, *Semiconductor Surface Physics* (Philadelphia: University of Pennsylvania Press).

## REVIEWS OF BOOKS

*Physical Optics*, by R. A. HOUSTOUN. Pp. 300. (London and Glasgow: Blackie, 1957.) 40s.

It is always pleasant to meet an old friend even if the years have greatly altered him. For forty-three years students have turned to Dr. Houston's *Treatise on Light* for a wealth of information, and the lineaments of this old friend may be recognized in the new guise. To be sure the new book is slimmer by half, but little of importance has been lost, and the new look is most becoming; few up-to-date developments have been omitted, though one is sorry to see no mention of Čerenkov radiation. It is good to find refractive index and the Brewsterian angle of maximum polarization described in terms of the fundamental process of scattering, although the student who has not already attained an advanced level of knowledge may find it puzzling that the origin of the phase lag of  $\frac{1}{2}\pi$  in the scattered wave is left unexplained. Geometrical optics is neatly and briefly treated, though the geometrical derivation of the formulae for lenses in combination is retained, perhaps to the advantage in understanding of principles, in place of the much shorter algebraical treatment. The chapters on diffraction are good.

Having acknowledged the pleasure with which the book is welcomed, a few criticisms may be permitted. Elimination of chromatic aberration by combining two lenses in contact is discussed, but no mention is made of the equally important achromatization of eyepieces used for telescopes and microscopes. Curvature of field is a lens aberration which should be considered with astigmatism, and not with distortion, with which students are apt enough to confuse it. It is surprising to see Rayleigh's experiment with two slits (on which his refractometer and Michelson's stellar interferometer are based), essentially a diffraction phenomenon of the Fraunhofer class, described as being a modification of Young's experiment, which is essentially a diffraction phenomenon of the Fresnel class. Jamin's interferometer is described but no explanation is given of the origin of the fringes, which are of the type of Brewster's bands. The Twyman and Green interferometer is mentioned in the section on Michelson's interferometer, but the reader might be misled into thinking it to be a modification without essential difference in principle. A spectrum is stated to be purest when the prism is in the position of minimum deviation, but this is not true if the instrument is in correct adjustment. The wavelengths, at which maximum emission of energy occurs, are given for the temperatures of boiling water and of the human body, but in such a way that the reader might imagine the emission restricted to these wavelengths alone.

Some errors have escaped the proof reader, but these are few indeed. On page 120 the phase is said to have increased, when it is the phase delay that has increased. On page 121 the scattered wavelets are erroneously stated to be "exactly out of phase with the incident wave" whereas, it is clear that in order to account for the change of phase velocity, they must be in quadrature. The reviewer has noticed no other misprints, in a well produced volume, adequately indexed, having many good diagrams and some interesting plates. A. M. TAYLOR,

*Semiconductor Surface Physics*, Edited by R. H. Kingston. Pp. xvi + 413. (Philadelphia : University of Pennsylvania Press, 1957.) 63s.

This volume is the record of a conference on the Physics of Semiconductor Surfaces held at Philadelphia in June 1956. It contains the invited papers and the discussion they stimulated. The contributors, who were internationally representative, were drawn approximately equally from industrial research laboratories, and from University and Government laboratories.

In his introduction the editor, R. H. Kingston, stresses the importance of the surface boundary on the properties of a semiconductor structure. However, the scope of the conference was much broader than this. The ambient atmosphere at a semiconductor surface affects the interior to the depth of the space charge region, and conversely the supply of carriers from the bulk can affect the reaction kinetics of the adsorbate. Catalysis and oxidation are therefore a natural complement to studies of conductivity and surface potential. The arrangement of the subject matter reflects this unity.

Part I is devoted to clean surfaces, and consists of only two papers describing the electron diffraction and conductivity of germanium surfaces cleaned by ion bombardment. Part II comprises half of the entire proceedings, and is concerned with the electrical properties of real surfaces, presumably in contradistinction to clean surfaces. There is a good deal of repetition, several authors reviewing the field effect on surface conduction and recombination. However, a large measure of agreement emerges concerning the roles of fast and slow states, and their location at the semiconductor-oxide interface and the oxide surface respectively. There are also noteworthy contributions by J. R. Schrieffer on the mobility in inversion layers, and by A. L. McWhorter on the origin of  $1/f$  noise.

Part III is concerned with adsorption and catalysis. An introduction by P. B. Weiss delineates the common ground of interest for physicist and chemist in the boundaries of a solid, and points out the analogy between the reactivity of a molecule and the charge distribution in a solid. This is followed by one theoretical and one experimental paper on catalysis at oxide surfaces. The section is closed by the work of G. W. Pratt and H. H. Kolm on field induced changes of contact potential, which are attributed to slow changes in the occupancy of traps associated with chemisorbed oxygen. N. Cabrera's review of the theory of oxidation of metals opens the final section on oxidation. The formation of an oxide film on an ideal surface and also the role of dislocations in the formation of oxide nuclei is discussed. The proceedings finish with several contributions on the oxidation of clean germanium surfaces.

It is not clear to what audience this collection will make the greatest appeal. Those actively engaged on the surface physics of silicon and germanium will already be familiar with much of the material. On the other hand, those who have only a general interest in the subject would probably find one or two comprehensive review articles more digestible than this sequence of papers, part review part original, with the inevitable repetition which results from multiple authorship. Despite this criticism the book contains a great deal to interest both solid state physicist and physical chemist.

O. SIMPSON.



*Handbuch der Physik*, Vol. 40, *Nuclear Reactions I*, edited by S. FLÜGGE. Pp. vi+553. (Berlin: Springer, 1957.) DM 128.

The growth of physics in the past 25 years or so, since the last appearance of the comprehensive *Handbuch der Physik*, has made the task of compiling an Encyclopaedia at the present time so obviously more elaborate and difficult a task that it needs no comment. In nuclear physics the growth has been, and still is, as great as in any other branch of the subject. Apart from the immense increase in the range of knowledge in this field, the change in the rate of development has been almost equally great; so that nowadays the couple of years that elapse between the initiation of an article of the encyclopaedia type and its actual publication and use, may see great changes in the subject. This applies to a particular article or volume of an encyclopaedia, let alone to the compilation as a whole.

The best that can be hoped for then, in such a comprehensive work at the present time, is that each volume should contain a full and coherent account of some branch of physics at the time of its preparation. To expect much more (for example, detailed inter-relation of neighbouring topics in different volumes) would be unduly optimistic; but to find less would be equally disappointing. In the case of the present volume, the subject matter—Nuclear Reactions—is one whose bulk has grown phenomenally in the past ten years. There have been major developments in both experimental methods and theoretical interpretation in this period. However, the real landmarks in the development are not so numerous, nor do they occur with such frequency, as to reduce the value of a thorough, if general, exposition of the basic methods and ideas at any one time, even allowing for the necessary period of preparation. The presentation of a complete account of the up-to-date detailed knowledge is of course a far more difficult problem—and one of more doubtful value. Most nuclear physicists find that some form of expandable card index is more useful in this connection than a handsomely bound volume, such as those of the *Handbuch* series.

In volume 40 of the *Handbuch*, which is the first of several dealing with Nuclear Reactions, the four contributors have tried to make a compromise between the presentation of basic principles and up-to-date compilation of facts, with the lion's share of the space devoted to the latter. As a consequence the volume teems with charts, tables and diagrams of collected data, and reproduction of experimental data. All this is very useful, but one can hardly express the hope that it will stay useful for many years!

The two articles by W. E. Burcham and B. B. Kinsey dealing with nuclear reactions in light and heavy nuclei respectively. (The border seems to be roughly at  $A=40$ .) Professor Burcham sketches briefly the background of the current theory (nuclear structure, types of reactions, interpretation of experiments), and follows with a brief survey of the different types of measurement and the experimental techniques involved. This is followed by an extensive account of the results of nuclear reaction studies classified according to increasing mass number of the nuclei involved ( $A=1$  to 40). The final section of this article is a compilation of the data, largely in diagrammatic form, of the spectra of energy levels for the same range of nuclei. There are ample detailed references in the text, and a substantial classified bibliography.

Dr. Kinsey's article has a somewhat more theoretical flavour, although there is little formal development of theory as such. The first few sections are devoted



to a general outline of the basic ideas of compound nucleus, statistical theory, direct interactions, etc. These are followed by an account of the results of the investigations of nuclear reactions, classified according to neutron reactions, proton reactions, etc. The second half of the article is devoted to an account of nuclear level densities and widths in the region of virtual levels, and finally an account of the spectrum and properties of the low lying levels of nuclei.

The article by J. Rainwater deals with a more restricted topic: "Resonance Processes by Neutrons". There is a short account of the basic methods of experiment and a very condensed treatment of the theory of the resonance dispersion formula and of the optical model. Most readers, I feel sure, would have liked to see the treatment of both these topics expanded considerably. The main content of this article are tables of neutron resonance parameters for individual nuclei, and numerous diagrams of neutron cross sections, and collected information about level widths and densities. A very large part of the extensive list of references deals with work done in the past year or two, since 1955, and each group of references ends with the inevitable entry: "Unpublished"!

The last article, by A. Wattenburg is less detailed and less precise than any of the others. It covers a wide field, "Nuclear Reactions at High Energies", in a rather discursive manner. At times the style of writing is more appropriate to a semi-popular review than to an authoritative *Handbuch* article. Experimental techniques of particle acceleration, analysis and detection, as well as brief references (often by name only) to the main theoretical interpretation are all dealt with. The article provides an easily read introduction to the subject, rather than a full account of its main developments. As such, a fuller *classified* bibliography would have enhanced its value.

The four separate articles differ from each other in style, scope and purpose, although the level of presentation is roughly comparable. They are united by a common broad title and a common subject index, and a single brief table of contents at the beginning of the volume. The distinct and self-contained nature of the four articles makes this attempt at unification of somewhat doubtful value. Certainly a more detailed list of contents at the beginning, or end, of each article would improve the usefulness of the book as a work of reference.

The quality of the printing and diagrams is, as one has come to expect of the publisher, first class.

S. DEVONS.

*Einführung in die Physik der magnetischen Werkstoffe*, by K. M. KOCH and W. JELLINGHAUS. Pp. vii+208. (Vienna: Deuticke, 1957.) DM 31.

This work is primarily a textbook intended for those concerned with the applications of magnetic materials. However, the authors' approach is not narrow and they have taken the proper view that an acquaintance with the fundamental processes and concepts is of importance in the efficient utilization of magnetic materials. The first half of the book is devoted to considerations of the physical background of magnetic phenomena, the relevant results where appropriate being summarized in vector notation. Chapters are devoted to the atomic theory of magnetism and the fundamental magnetization processes, leading to a brief discussion of domain theory. Then follows a section mainly concerned with technical magnetization phenomena in which such matters as the interpretation of the hysteresis cycle and theories of coercive force are considered.

The remainder of the book is concerned mainly with topics of technological interest including discussions of the behaviour of magnetic materials in alternating magnetic fields, the general properties of materials commonly available for magnetic applications and finally the standard methods of measuring the magnetic characteristics of such materials. There are appendices in which the properties of low coercivity materials are summarized. Owing to limitations of space in a book of this size no part of the wide subject covered can be treated thoroughly and the value of the book would have been increased if the authors had included many more references to original sources and review articles. Characteristically, the book is very well produced and contains many excellent diagrams. It is perhaps improbable that the book will have a wide appeal in this country as it certainly cannot be considered to supersede, either in content or presentation, the standard English texts already available on the subject.

R. STREET.

*Thermodynamics and Statistical Mechanics*, by A. H. WILSON. Pp. xv + 495. (Cambridge : University Press, 1957.) 50s.

This book is designed to provide chemists and physicists with a theoretically satisfying introduction to statistical thermodynamics. The reader must bring to it a grasp of non-relativistic quantum mechanics and considerable mathematical equipment; it is therefore beyond the reach of most undergraduates. The author deals with the fundamentals of thermodynamics (steam engines and Carathéodory) in the first four chapters, quantum statistical ensembles derivable from the microcanonical ensemble in the fifth chapter and selected applications of the theory in the remainder of the book.

A number of writers (e.g. Chandrasekhar, Born and Eisenschitz) have given partial expositions of Carathéodory's axiomatics in English. We have here the only *full* such account known to me. It is admirably done. Another welcome feature of the section on basic theory is a timely warning to enthusiasts against the indiscriminate use of grand canonical ensembles—especially for localized systems.

Passing to the applications, one finds careful accounts of the following topics: properties of gases and crystals; Fermi-Dirac and Bose-Einstein statistics; radiation; the Third Law; imperfect gases; phase transitions; gas mixtures; rubber elasticity; electrolytes; superlattices; electric and magnetic phenomena.

One might guess from this list that the selection of topics is 'classical', in the sense that it reflects the state of the subject about 20 years ago.

This would not be quite fair: there are excellent sections on Bose-Einstein condensation, ferroelectricity, antiferromagnetism and negative temperatures (with special reference to those induced by playing tricks on nuclear spins) which depend on recent work. Nevertheless, the overwhelming impression is that the bulk of this book could have been written (let us be charitable) twelve years ago with, say, a 10% addition to take care of more recent work.

Having said this, one can still maintain that the book constitutes the best *comprehensive* account of statistical thermodynamics available in English. Provided that the student eschews the Yang-Lee theory of condensation, ergodic theory, liquid helium, phase transitions in electrical systems and modern theories of solution, he will find clear, authoritative and elegant accounts of most parts of the subject.

R. O. DAVIES.

*Semiconductor Abstracts*, edited by E. PASKELL. Pp. viii + 322. (New York: J. Wiley; London: Chapman and Hall, 1957.) 80s.

This 1955 issue is the third volume of Abstracts collected by the staff of the Battelle Memorial Institute, and the first to appear in book form. The Abstracts are classified primarily in accordance with the materials to which the papers refer, under the principal headings of germanium, silicon, carbon and selenium, etc., intermetallics, sulphides, selenides and tellurides, oxides and halides, arsenates, phosphates and tungstates as well as organic semiconductors. A special section is devoted to reviews of theoretical papers and the volume includes a subject and an author index. The standard of the various entries is generally high. In length and character they are very similar to those published by *Science Abstracts* (I.E.E.) in this country, though some attempt has been made to include a greater number of numerical results. The collection covers semiconductors and phosphors, their preparation, properties and applications. This is a valuable reference book which many semiconductor laboratories will wish to have. Certain additions and improvements would add to its general usefulness. The journals abstracted are not explicitly listed and the reader who wishes to survey a particular subject remains uncertain as to how wide his net for specific information has been cast. In some cases it would be useful to know whether a particular entry is the author's own summary or the work of the abstractor. The section headings should appear on each page and the subject index could be usefully extended by multiple entries and cross-references. It would also be an advantage if future volumes in the series could be published with less delay.

H. K. HENISCH.

*Photosensors: A Treatise on Photo-Electric Devices and their Application to Industry*, by W. SUMMER. Pp. xvi + 675. (London: Chapman and Hall, 1957.) £5 5s. 0d.

The author begins by coining the word photosensor to cover devices which utilize photoemissive, photovoltaic or photoconductive effects. Elsewhere he provides a somewhat novel definition of a photosensor as a combination of two electrodes in an electrolyte! After a preamble of three chapters indicating the possible application of photoelectric instruments and a short dissertation on the human eye an attempt is made to provide a fundamental treatment of 'photosensors'. This is disappointing as a combination of confusions about physics, lack of appreciation of modern theories, experimental studies and development of photoelectric detectors and poor English usage decrease its value by a large factor. One can find many instances of these shortcomings. The author speaks of 'the impact of a watt of radiant energy', the 'wavelength of a photon', 'the number of electrons carried by one ampere', and he confuses work functions with potential.

Incompetence in use of English and of logic is made evident by the following examples:

- "Individual deviations... are due to causes at present not likely to be improved upon".
- "The liberation of secondary electrons by photoelectrons was shown to be of an undesirable nature".
- "... the velocity of the electrons is much greater than that of the ions due to their large mass and size",



It is certain that one manufacturer of photoelectric multipliers will be displeased to see a prime specimen of his production ascribed in figure 4. 10 to another manufacturer. The references for this first section of the book are not up to date and will fail to provide the present background for those who enquire further.

The last section of the book is concerned with the application of photocells to many different detailed industrial control systems. The material of the section is presented in peculiar combinations though it is handled in a more satisfactory way than that of the first section. However, some rather significant modern applications of photo-sensitive materials are omitted.

An expensive volume dealing with such a subject deserves to have the authorship of a leading worker in the field. One cannot recommend the present text and it is surprising that the publishers did not take expert advice on it before deciding to publish. A smaller edition limited to description of applications would have been preferable to such an expensive, encyclopaedic venture containing numerous scientific, logical and grammatical errors.

G. F. J. GARLICK.

*Basic Automatic Control Theory*, by G. J. MURPHY. Pp. xi+557. (Princeton: Van Nostrand, 1957.) 67s. 6d.

The spate of College textbooks on Control Theory from the presses in the U.S.A. continues and when each new one appears we hope to see something novel, some treatment of the field which the others have not got. This one seems to follow the same general pattern as the others.

It is essentially a Course book, based upon lecture notes, for advanced or post-doctorate students specializing in servo-mechanism theory and design. But like so many others it attempts to pack between its covers vastly too much material, too detailed and technical. Thus the first equation is  $v = R \cdot i$  and the final Appendices give lists of Laplace transforms and graphical aids to servo synthesis. There are whole worlds between, however, which the digest approach only conceals, and which one feels cannot have true educational value, cannot lead to broad understanding of the validity and application of scientific principles, nor launch the future research man into his trackless seas.

The author has clearly put many years of patient and detailed work into this book. The material is well laid out (though valid generalities are missed) and diagrams well prepared. There are numerous examples, both worked and unworked. A few references to other American texts are included, but references to original papers are almost non-existent.

COLIN CHERRY.



## PROCEEDINGS OF THE PHYSICAL SOCIETY

1958—VOL. 71

## SUBJECT INDEX

	PAGE
Aberration, spherical, systems with, geometrical-optical calculation of frequency response . . . . .	231
Absorption band, new, in diamond (R) . . . . .	846
Absorption coefficient, acoustic, of gases, from measurement of resonator decay time . . . . .	17
Acoustic absorption coefficient of gases, from measurement of resonator decay time . . . . .	17
Acoustomagnetolectric effects in metal and semiconductor filaments . . . . .	965
Air showers, cosmic-ray, extensive, lateral structure of ionizing component . . . . .	491
Alkali halides, stress birefringence relation in . . . . .	225
Alloy, gold-platinum, lattice thermal conductivity (R) . . . . .	843
Alloy, iron-chromium, in $\alpha$ and $\sigma$ phases, heat capacity between 1.8 and 4.2°K . . . . .	220
Alloys, liquid binary, of tin and zinc, physical properties . . . . .	88
Alloys, tin-indium, thermal conductivity in normal state . . . . .	597
Alpha particles, mean free path in nuclear matter (R). . . . .	126
Aluminium foils, transmission of electrons through . . . . .	201
Angular correlations with polarization, theory . . . . .	117, corr. 519
Angular correlations of $\gamma$ -rays in $^{103}\text{Rh}$ . . . . .	247
Antiferromagnetic crystal, nuclear magnetic interaction in (L) . . . . .	517
Band spectra, of AlH at 2173 and 2101 Å . . . . .	65
Band spectrum of SiF . . . . .	476
Band systems $\text{A}^3\Pi_{0+}$ , $\text{B}^3\Pi_1 - \text{x}^1\Sigma^+$ of TlF, rotational analysis (R) . . . . .	128
Band systems $\text{c}^3\Sigma$ , $\text{b}^3\Sigma - \text{a}^3\Pi$ of BF, rotational analysis . . . . .	61
Band systems, molecular, various, intensity measurements . . . . .	957
Beta decay of $^{185}\text{W}$ . . . . .	335
Beta-decay theory, configurational mixing in . . . . .	939
Binding energy of $^{16}\text{O}$ nucleus . . . . .	658
Bismuth telluride, electrical conductivity and thermoelectric power . . . . .	633
Bismuth telluride, n-type galvanomagnetic effects . . . . .	430
Boltzmann equation in theory of electrical conduction in metals . . . . .	585
Boron 10, gamma rays from 6.89 mev level . . . . .	925
Breakdown, electric, directional, in KCl (R) . . . . .	688
Cadmium oxide, characteristic temperature and effective electron mass for conduction processes . . . . .	109
Cadmium 110, excited levels of . . . . .	77
Carrier lifetime in silicon, temperature dependence . . . . .	1002
Cerenkov effect in composite (isotropic) media . . . . .	398
Colour centres, thermal and optical excitation . . . . .	761
Conduction, electrical, <i>see</i> Electrical conduction	
Conduction, ionic, <i>see</i> Ionic conduction	
Conduction processes in CdO, characteristic temperature and effective electron mass . . . . .	109
Conductivity, ionic, <i>see under</i> Ionic	
Conductivity, thermal, <i>see</i> Thermal conductivity	
Configuration interaction in ground and two excited states of He atom (R) . . . . .	1015
Configurational mixing in $\beta$ -decay theory . . . . .	939
Contact potential difference measurements by Kelvin method (L) . . . . .	703
Cosmic-ray air showers, extensive, lateral structure of ionizing component . . . . .	491
Cottrell atmospheres of solute atoms, theory of delayed yielding . . . . .	444
Cross sections, differential, for reactions $^{14}\text{N}(\text{d}, \text{p})^{15}\text{N}$ and $^{14}\text{N}(\text{d}, \alpha)^{12}\text{C}$ between 600 and 1000 kev . . . . .	325

	PAGE
Cross sections for electron attachment in air (L)	516
Cross sections, electron ionization, using chopped beams	351
Cross sections, nuclear, for 765 mev neutrons	293
Cross sections, slow neutron, fluctuations in average	910
Crystal, antiferromagnetic, nuclear magnetic interaction in (L)	517
Crystal, cobalt, magnetic effect on electron diffraction patterns	758
Crystal field effects in metals	33
Crystal reflectivity in bent crystal spectrometers	1011
Crystal structure, entropy of hausmannite to spinel transformation (R)	270
Crystals, KCl, electron traps, by quenching or pressure (R)	852
Crystals, with NaCl type of lattice, electronic structure	749
Crystals, single, calcium tungstate, trap distributions in	422
Crystals, single, of manganese ferrite, domain patterns on	789
Debye effect in electrolytes (R)	847
Diamond, infra-red spectrum	485
Diamond, new absorption band in (R)	846
Dielectric behaviour of magnesium manganese ferrite (R)	131
Diffraction theory, scalar, for restricted aperture	533
Discharge tubes, longitudinal pressure gradient in (R)	694
Dislocation regions in Ge, electrical methods of determining	647
Dispersion theory of direct photoeffect	733
Distorted wave approximation in reaction $P + P \rightarrow \pi^+ + D$	654
Domain patterns on single crystal of manganese ferrite	789
Eigenfunctions, $S^2$ , construction by method of spin operators: I—General theory	145
Eigenfunctions, $S^2$ , construction by method of spin operator: II—Six-electron systems	152
Eigenvalues, cellular, for titanium metal	383
Elastic cylinders, pulse propagation in, experimental study	608
Elastic scattering, <i>see</i> Scattering	
Elastic spheres, gas of, equation of state	238
Elastic wave propagation in semi-infinite solid medium	207
Electrical conduction in metals, Boltzmann equation in theory	585
Electrical conduction, <i>see also</i> Semiconductors and cross references	
Electrolytes, Debye effect in (R)	847
Electron attachment in air, cross sections for (L)	516
Electron capture decay energy determination for $^{198}\text{Au}$	330
Electron diffraction patterns from cobalt crystal, magnetic effects	758
Electron scattering, <i>see</i> Scattering	
Electron traps in KCl crystals by quenching or pressure (R)	852
Electrons, transmission through aluminium foils	201
Entropy of hausmannite to spinel transformation (R)	270
Equation of state of gas of elastic spheres	238
Equation of state of zinc, cadmium and magnesium	742
Excitation of 2p state of hydrogen by slow electrons: distorted wave treatment	574
Exciton effects and direct optical transitions in Ge (R)	863
Fermi level in Ge at high temperatures (R)	692
Fractures, controlled, experiments on (L)	136
Frequency response, geometrical-optical calculation for systems with spherical aberration	231
Friction, coefficients, effect of spherical and conical shapes pressed into rubber under wet conditions	979
Friction of hard sliders on lubricated rubber: deformation losses	989
Friction, <i>see also</i> Stick-slip	
Fusion of hydrogen and deuterium, muon catalysed, x-rays from	161

	PAGE
Gamma ray resonance, nuclear, in $^{49}\text{Ti}$ . . . . .	194
Gamma rays from muon catalysed fusion of H and D . . . . .	161
Gamma rays from 6.89 mev level in $^{10}\text{B}$ . . . . .	925
Gamma rays in $^{103}\text{Rh}$ , angular correlations . . . . .	247
Gas kinetics, symmetry effects in : II—ortho- and para-hydrogen . . . . .	457
Gas of elastic spheres, equation of state . . . . .	238
Gases, derivation of acoustic absorption coefficient from measurement of resonator decay time . . . . .	17
Germanium, direct optical transitions and further exciton effects in (R) . . . . .	863
Germanium, dislocation regions in, electrical methods of determining . . . . .	647
Germanium, Fermi level at high temperatures (R) . . . . .	692
Germanium surfaces, clean, electrical properties (L) . . . . .	1020
Heat capacity of iron-chromium alloy in $\alpha$ and $\sigma$ phases between 1.8 and 4.2°K . . . . .	220
Heat transport measurements of liquid helium II . . . . .	117
Helium atom, configuration interaction in ground and two excited states (R) . . . . .	1015
Helium II, liquid, heat transport measurements . . . . .	117
Hydrogen atom, wave functions in spheroidal coordinates : I—Derivation and properties . . . . .	815
Hydrogen atom, wave functions in spheroidal coordinates : II—Interaction with point charge and with dipole . . . . .	828
Hydrogen atoms, elastic scattering of slow electrons by . . . . .	877
Hydrogen, molecular, and x-ray and electron scattering . . . . .	2
Hydrogen, ortho- and para-, symmetry effects in gas kinetics . . . . .	457
Hydrogen, 2p state, excitation by slow electrons : distorted wave treatment . . . . .	574
Ice, strength, influence of imperfections on . . . . .	797
Indium antimonide, n-type, magnetoresistance at 4.2°K . . . . .	470
Indium antimonide, p-type, electrical properties . . . . .	676
Indium phosphide, semiconducting properties . . . . .	416
Infra-red spectrum of diamond . . . . .	485
Interactions, strong, invariance under time-reversal, double scattering experiments for (R) . . . . .	686
International Union of Pure and Applied Physics, information concerning (L) . . . . .	284, 519
Ionic conduction at high electric field strengths in $\text{Ta}_2\text{O}_5$ . . . . .	405
Ionic conductivity of potassium and rubidium chloride solutions at microwave frequencies (L) . . . . .	134
Ionization cross sections, electron, using chopped beams . . . . .	351
Ionosphere, F2 region, anomalous variation of absorption around mid-day . . . . .	1007
Ions, positive and negative, recombination coefficients . . . . .	341
Isotropic media, composite, Čerenkov effect in . . . . .	398
K Auger spectrum . . . . .	369
Kelvin method for contact potential difference measurements (L) . . . . .	703
Levels, excited, of cadmium 110 . . . . .	77
Liquid helium, <i>see</i> Helium	
Lithium, Li II spectrum (R) . . . . .	274
Lorentz-Einstein transformation, deduction from Maxwell's equations (R) . . . . .	512
Loss factor measurements in dry sand (L) . . . . .	135
Magnesium manganese ferrite, dielectric behaviour (R) . . . . .	131
Magnetic analysis for investigations of Mg(d, p) reactions . . . . .	49
Magnetic analysis, investigation of $^{16}\text{O}(\text{d}, \alpha)^{14}\text{N}$ reaction by . . . . .	252
Magnetic resonance, adiabatic fast passage experiment (R) . . . . .	497
Magnetoresistance measurements, source of error in (R) . . . . .	500
Magnetoresistance of n-type InSb at 4.2°K . . . . .	470
Mass-action laws in degenerate semiconductors (L) . . . . .	699

	PAGE
Maxwell's electromagnetic field equations, deduction of Lorentz-Einstein transformation from (R)	512
Metal, and semiconductor, filaments, acoustomagnetolectric effects	965
Metals, cold-worked, low-angle x-ray scattering from (R)	861
Metals, crystal field effects in	33
Metals, theory of electrical conduction, Boltzmann equation in	585
Microwave frequencies, ionic conductivity of potassium and rubidium chloride solutions at (L)	134
Microwave resonance in nickel at 35 Gc/s.	45
Molecular-orbital theory, and calculation of first order perturbation of eigenvector of finite matrix	724
Morse oscillator, Ta-You Wu's method of calculating overlap integrals for (R)	514
Muon catalysed fusion of H and D, $\gamma$ -rays from	161
Nernst effect in semiconductors, theory	82
Neutrons, 350 mev, elastic scattering by complex nuclei	552, 565
Nickel, microwave resonance at 35 Gc/s	45
Nitrogen, vapour pressure ratios of $^{14}\text{N}^{14}\text{N}$ , $^{14}\text{N}^{15}\text{N}$ and $^{15}\text{N}^{15}\text{N}$ (L)	701
Nuclear cross sections, <i>see</i> Cross sections	
Nuclear magnetic interaction in antiferromagnetic crystal (L)	517
Nuclear quadrupole coupling constant of $^{23}\text{Na}$ in sodium nitrate (L)	1019
Nuclear resonance, <i>see</i> Resonance	
Nucleons, high energy, inelastic scattering by complex nuclei: I—Semi-classical formalism	893
Optical systems, aplanatic	546
Optics, geometrical-optical calculation of frequency response for systems with spherical aberration.	231
Optics and signal analysis, reciprocity inequalities, coherence time and bandwidth in.	257
Overlap integrals for Morse oscillator, Ta-You Wu's method of calculation (R)	514
Oxygen, $^{16}\text{O}$ nucleus, binding energy	658
Paramagnetic impurities in NaF (R)	503
Penetration by rotating shaped charges (R)	508
Perturbation, first order, of eigenvector of finite matrix, and application to molecular-orbital theory.	724
Perturbed boundary condition in quantum mechanics	173
Photodisintegration of Na by $^7\text{Li}(p, \gamma)$ radiation	389
Photoeffect, direct, dispersion theory	733
Pions, elastic scattering at a bound nucleon	932
Polarization, angular correlations with, theory	177, corr. 519
Polarization-asymmetry equality (R), (L)	272, 867
Polarization in nuclear reactions (R)	858
Polarization in stripping reactions	627
Positrons, elastic scattering by atoms and molecules	38
Potassium chloride, directional electrical breakdown (R)	688
Protons, elastic and inelastic scattering by silicon	347
Protons, 9.8 mev, inelastic scattering by medium weight nuclei	904
Protons, <i>see also</i> Scattering	
Pulse propagation in elastic cylinders, experimental study	608
Quantum mechanics, perturbed boundary condition in	173
Radiation, $^7\text{Li}(p, \gamma)$ , and photodisintegration of Na	389
Radioactivity of $^{178}\text{Ta}$ , $^{179}\text{Ta}$ and $^{180}\text{Ta}$	618
Radio waves from F2 region of ionosphere, anomalous variation of absorption around mid-day	1007
Reaction $\text{P} + \text{P} \rightarrow \pi^+ + \text{D}$ , distorted wave approximation in	654
Reaction $^{16}\text{O}(d, \alpha)^{14}\text{N}$ , investigation by magnetic analysis	252



	PAGE
Reaction $^{24}\text{Mg}(\text{p}, \gamma) ^{25}\text{Al}$ at 418 kev resonance . . . . .	100
Reactions, nuclear, polarization in (R) . . . . .	858
Reactions, stripping, <i>see</i> Stripping reactions	
Reactions, $(\gamma, 2\text{n})$ and $(\gamma, 3\text{n})$ in $^{181}\text{Ta}$ . . . . .	613
Reactions, $^{14}\text{N}(\text{d}, \text{p}) ^{15}\text{N}$ and $^{14}\text{N}(\text{d}, \alpha) ^{12}\text{C}$ differential cross sections between 600 and 1000 kev . . . . .	325
Reactions $^{24}\text{Mg}(\text{d}, \text{p}) ^{25}\text{Mg}$ and $^{26}\text{Mg}(\text{d}, \text{p}) ^{27}\text{Mg}$ investigation by magnetic analysis . . . . .	49
Recombination coefficients for positive and negative ions . . . . .	341
Resistivity of ordered $\text{Au}_3\text{Cu}$ (R) . . . . .	506
Resonance, microwave, <i>see</i> Microwave resonance	
Resonance, nuclear $\gamma$ -ray, in $^{48}\text{Ti}$ . . . . .	194
Resonator, decay time, and acoustic absorption coefficient of gases . . . . .	17
Rotating shaped charges, penetration by (R) . . . . .	508
Rubber, lubricated, friction of hard sliders : deformation losses . . . . .	989
Rubber, pressure of spherical and conical shapes and effect on coefficients of friction under wet conditions . . . . .	979
Sand, dry, loss factor measurements in (L) . . . . .	135
Scattering, double, and invariance under time-reversal in strong interactions (R) . . . . .	686
Scattering, elastic and inelastic, of protons by silicon . . . . .	347
Scattering, elastic, of pions at a bound nucleon . . . . .	932
Scattering, elastic, of positrons by atoms and molecules . . . . .	38
Scattering, elastic, of slow electrons by hydrogen atoms . . . . .	877
Scattering, elastic, of 350 mev neutrons by complex nuclei . . . . .	552, 565
Scattering, elastic, of 380 mev protons by protons : I—Angles greater than $30^\circ$ . . . . .	770
Scattering, elastic, of 380 mev protons by protons : II—Angles less than $30^\circ$ . . . . .	781
Scattering, inelastic, of high energy nucleons by complex nuclei : I—Semi-classical formalism . . . . .	893
Scattering, inelastic, of high energy protons in carbon, direct interaction in . . . . .	717
Scattering, inelastic, of 9.8 mev protons by medium weight nuclei . . . . .	904
Scattering, neutron-proton, in energy range 70–170 mev . . . . .	305
Scattering, x-ray and electron, by molecular hydrogen . . . . .	2
Scattering, x-ray, low-angle, from cold-worked metals (R) . . . . .	861
Schrödinger equation, non-relativistic, $(2s)^2\ ^1\text{S}$ state solution for He and $\text{H}^-$ . . . . .	357
Secondary emission, variation with primary electron energy (R) . . . . .	851
Semiconducting indium phosphide, properties . . . . .	416
Semiconductors, degenerate, mass-action laws in (L) . . . . .	699
Semiconductors, magnetic field effects on electron populations in . . . . .	82
Semiconductor, and metal, filaments, acoustomagnetolectric effects . . . . .	965
Semiconductors, theory of Nernst effect . . . . .	82
Semiconductors, <i>see also</i> Bismuth telluride, Crystals, Indium antimonide	
Signal analysis and optics, reciprocity inequalities, coherence, time and bandwidth in . . . . .	257
Silicon monofluoride, band spectrum . . . . .	476
Silicon, temperature dependence of carrier lifetime . . . . .	1002
Sodium nitrate, nuclear quadrupole coupling constant of $^{23}\text{Na}$ (L) . . . . .	1019
Solid medium, semi-infinite, elastic wave propagation in . . . . .	207
Spectrometers, bent crystal, crystal reflectivity . . . . .	1011
Spectrum, band, <i>see</i> Band spectrum	
Spectrum, infra-red, of diamond . . . . .	485
Spectrum, K Auger . . . . .	369
Spectrum, Li II (R) . . . . .	274
Spin operators, construction of $S^2$ eigenfunctions by : I—General theory . . . . .	145
Spin operators, construction of $S^2$ eigenfunctions by : II—Six-electron systems . . . . .	152
Stick-slip process, intrinsic variables . . . . .	668
Stress birefringence relation in some alkali halides . . . . .	225
Stripping reactions, polarization in . . . . .	627
Tantalum, $^{178}\text{Ta}$ , $^{179}\text{Ta}$ and $^{180}\text{Ta}$ , radioactivity . . . . .	618
Tantalum, $^{181}\text{Ta}$ , $(\gamma, 2\text{n})$ and $(\gamma, 3\text{n})$ reactions in . . . . .	613

	PAGE
Thermal conductivity, lattice of gold-platinum alloy (R) . . . . .	843
Thermal conductivity of tin-indium alloys in normal state . . . . .	597
Thermoelectric power, <i>see</i> Semiconductors and cross references	
Titanium metal, cellular eigenvalues . . . . .	383
Trap distributions in calcium tungstate single crystals . . . . .	422
Two-electron wave equation, $(2s)^2\ ^1S$ state solution . . . . .	357
 Vapour pressure ratios of $^{14}\text{N}^{14}\text{N}$ , $^{14}\text{N}^{15}\text{N}$ and $^{15}\text{N}^{15}\text{N}$ (L) . . . . .	 701
Vibrating visco-elastic cylinder, behaviour . . . . .	973
Visco-elastic cylinder, vibrating, behaviour of . . . . .	973
 Wave function, Coulomb, expansion in Bessel functions (R) . . . . .	 856
Wave functions, Coulomb, simple method of interpolation (R) . . . . .	1017
Wave functions for hydrogen atom in spheroidal coordinates : I—Derivation and properties . . . . .	815
Wave functions for hydrogen atom in spheroidal coordinates : II—Interaction with point charge and with dipole . . . . .	828
Waveguides, rectangular, impedance, physical interpretation (L) . . . . .	868
Wave propagation, elastic, <i>see under</i> Elastic	
Wigner coefficients, expressions for . . . . .	corr. 519
 Yielding, delayed, in presence of Cottrell atmospheres of solute atoms, theory . . . . .	 444

# INDEX OF AUTHORS (WITH TITLES)

	PAGE
Agarwal, B. K.: Variation of secondary emission with primary electron energy (R)	851
Agu, B. N. C., Burdett, T., and Matsukawa, E.: Transmission of electrons through aluminium foils	201
Altmann, S. L., and Cohan, N. V.: Cellular eigenvalues for titanium metal	383
Andrew, E. R., with Eades, R. G., and Hughes, D. G.: The nuclear quadrupole coupling constant of $^{23}\text{Na}$ in sodium nitrate (L)	1019
Armitage, B. H., and Rosser, W. G. V.: The $\beta$ -decay of $^{185}\text{W}$	335
Asaad, W. N., and Burhop, E. H. S.: The K auger spectrum	369
Ashmore, A., with Brown, G. E., and Nordhagen, R.: Elastic scattering of 350 mev neutrons by complex nuclei	565
Ashmore, A., Mather, D. S., and Sen, S. K.: The elastic scattering of 350 mev neutrons by complex nuclei	552
Ashmore, A., Nordhagen, R., Strauch, K., and Townes, B. M.: The gamma rays from muon catalysed fusion of hydrogen and deuterium	161
Banbury, P. C., with Barnes, G. A.: Electrical properties of clean germanium surfaces (L)	1020
Banford, A. P., with Griffith, T. C., Uppal, M. Y., and Williams, W. S. C.: Neutron-proton scattering in the energy range 70 to 170 mev	305
Bansigir, K. G., and Iyengar, K. S.: The stress birefringence relation in some alkali halides	225
Barlow, G. S., and Standley, K. J.: Microwave resonance in nickel at 35 Gc/s (kMc/s)	45
Barnes, G. A., and Banbury, P. C.: Electrical properties of clean germanium surfaces (L)	1020
Barrie, R., with Hilsum, C.: Properties of p-type indium antimonide: I—Electrical properties	676
Barrow, R. F., Cheall, H. F. K., Thomas, P. M., and Zeeman, P. B.: Rotational analysis of bands of the $\text{A}^3\Pi_{0+}$ , $\text{B}^3\Pi_1-\text{X}^1\Sigma^+$ systems of thallous fluoride (R)	128
Barrow, R. F., with Johns, J. W. C.: The band spectrum of silicon monofluoride, $\text{SiF}$	476
Barrow, R. F., Premaswarup, D., Winternitz, J., and Zeeman, P. B.: Rotational analysis of bands of the $\text{c}^3\Sigma$ , $\text{b}^3\Sigma-\text{a}^3\Pi$ system of boron monofluoride, $\text{BF}$	61
Bassett, I. M., with Brown, R. D.: A method for calculating the first order perturbation of an eigenvector of a finite matrix, with applications to molecular-orbital theory	724
Bastin, J. A., with Wright, R. W.: The characteristic temperature and effective electron mass for conduction processes in cadmium oxide	109
Bates, L. F., Craik, D. J., and Griffiths, P. M.: Domain patterns on a single crystal of manganese ferrite	789
Baynham, A. C., with Hogarth, C. A.: Electrical methods for determining the positions of dislocations in germanium	647
Bell, J. S., and Mandl, F.: The polarization-asymmetry equality (R), (L)	272, 867
Berencz, F., and Pauncz, R.: Construction of $S^2$ eigenfunctions by the method of spin operators: I—General theory	145
Berz, F.: On the theory of surface recombination in semiconductors for large potential differences between surface and bulk (R)	275
Birch, J. A., Kemp, W. R. G., and Klemens, P. G.: The lattice thermal conductivity of a gold-platinum alloy (R)	843
Biswas, A. B., with Irani, K. S., and Sinha, A. P. B.: Entropy of hausmannite to spinel transformation (R)	270
Blackman, M., and Grünbaum, E.: Magnetic effects on the electron diffraction patterns from a cobalt crystal	758

	PAGE
Blakemore, J. S.: The Fermi level in germanium at high temperatures (R)	692
Booth, D. L., Price, F. V., Roaf, D., and Salmon, G. L.: The differential cross sections for the reactions $^{14}\text{N}(\text{d}, \text{p})^{15}\text{N}$ and $^{14}\text{N}(\text{d}, \alpha)^{12}\text{C}$ between 600 and 1000 kev.	325
Booth, N. E., Hutchinson, G. W., and Ledley, B.: Nuclear cross sections for 765 mev Neutrons	293
Boyd, R. L. F., and Green, G. W.: Electron ionization cross sections using chopped beams	351
Bransden, B. H., Dalgarno, A., John, T. L., and Seaton, M. J.: The elastic scattering of slow electrons by hydrogen atoms	877
Bray, A. R., Jacobs, P. W. M., and Young, L.: Ionic conduction at high electric field strengths in tantalum pentoxide	405
Brewer, D. F., and Edwards, D. O.: Measurements of the heat of transport of liquid helium II	117
Bromilow, N. S.: Geometrical-optical calculation of frequency response for systems with spherical aberration	231
Broom, R. F.: A source of error in magnetoresistance measurements (R).	500
Broom, R. F.: Magnetoresistance of n-type InSb at $4.2^\circ\text{K}$	470
Brown, G. E., Ashmore, A., and Nordhagen, R.: Elastic scattering of 350 mev neutrons by complex nuclei	565
Brown, G. E., and Levinger, J. S.: Dispersion theory of the direct photoeffect.	733
Brown, G. E., with McCauley, G. P.: Inelastic scattering of high energy nucleons by complex nuclei: I—Semi-classical formalism	893
Brown, R. D., and Bassett, I. M.: A method for calculating the first order perturbation of an eigenvector of a finite matrix, with applications to molecular-orbital theory	724
Bryant, T. H. E., and Grant, E. H.: Ionic conductivity of potassium and rubidium chloride solutions at microwave frequencies (L)	134
Buckingham, R. A., Davies A. R., and Gilles, D. C.: Symmetry effects in gas kinetics: II—Ortho- and para-hydrogen	457
Burdett, T., with Agu, B. N. C., and Matsukawa, E.: Transmission of electrons through aluminium foils	201
Burhop, E. H. S., with Asaad, W. N.: The K Auger spectrum	369
Caine, C. A.: Configurational mixing in $\beta$ -decay theory	939
Cairns, R. B., and Emeléus, K. G.: The longitudinal pressure gradient in discharge tubes (R)	694
Carter, C., March, N. H., and Vincent, D.: X-ray and electron scattering by molecular hydrogen	2
Carver, J. H., and Turchinets, W.: The $(\gamma, 2n)$ and $(\gamma, 3n)$ reactions in $^{181}\text{Ta}$	613
Carver, J. H., and Turchinets, W.: Radioactivity of $^{178}\text{Ta}$ , $^{179}\text{Ta}$ and $^{180}\text{Ta}$	618
Cheall, H. F. K., with Barrow, R. F., Thomas, P. M., and Zeeman, P. B.: Rotational analysis of bands of the $\text{A}^3\Pi_{0+}$ , $\text{B}^3\Pi_1-\text{X}^1\Sigma^+$ systems of thallos fluoride (R)	128
Cochran, A. J., and Ross, M. A. S.: Crystal reflectivity in bent crystal spectrometers	1011
Cohan, N. V., with Altmann, S. L.: Cellular eigenvalues for titanium metal	383
Cook, J. R.: Trap distributions in calcium tungstate single crystals	422
Cooke, A. H., and Edmonds, D. T.: Nuclear magnetic interaction in an antiferromagnetic crystal (L)	517
Cooper, R., and Fernandez, A.: Directional electric breakdown of KCl (R)	688
Coulson, C. A., and Robinson, P. D.: Wave functions for the hydrogen atom in spheroidal coordinates: I—The derivation and properties of the functions	815
Cowley, J. M., and Moodie, A. F.: A new formulation of scalar diffraction theory for restricted aperture	533
Craik, D. J., with Bates, L. F., and Griffiths, P. M.: Domain patterns on a single crystal of manganese ferrite	789
Dabrowski, J.: On the binding energy of the $^{16}\text{O}$ nucleus	658
Dalgarno, A., with Bransden, B. H., John, T. L., and Seaton, M. J.: The elastic scattering of slow electrons by hydrogen atoms	877



	PAGE
Dalton, A. W., Hinds, S., and Parry, G.: An investigation of the $^{16}\text{O}(\text{d}, \alpha)^{14}\text{N}$ reaction by magnetic analysis	252
Davies, A. R., with Buckingham, R. A., and Gilles, D. C.: Symmetry effects in gas kinetics: II—Ortho- and para-hydrogen	457
Dell, R. M., with Reynolds, W. N., and Lilburne, M. T.: Some properties of semi-conducting indium phosphide	416
Drabble, J. R., Groves, R. D., and Wolfe, R.: Galvanomagnetic effects in n-type bismuth telluride	430
Durney, B.: Distorted wave approximation in the reaction $\text{P} + \text{P} \rightarrow \pi^+ + \text{D}$	654
Eades, R. G., Hughes, D. G., and Andrew, E. R.: The nuclear quadrupole coupling constant of $^{23}\text{Na}$ in sodium nitrate (L).	1019
Edge, R. D., and Gemmell, D. S.: Gamma rays from the 6.89 mev level in $^{10}\text{B}$	925
Edmonds, D. T., with Cooke, A. H.: Nuclear magnetic interaction in an antiferromagnetic crystal (L).	517
Edmonds, P. D., and Lamb, J.: A method for deriving the acoustic absorption coefficient of gases from measurement of the decay-time of a resonator	17
Edwards, D. O., with Brewer, D. F.: Measurements of the heat of transport of liquid helium II	117
Egelstaff, P. A.: Fluctuations in slow neutron average cross sections	910
Emel�us, K. G., with Cairns, R. B.: The longitudinal pressure gradient in discharge tubes (R)	694
Ewles, J., Jain, S. C., and Joshi, R. V.: Electron traps produced in KCl crystals by quenching or pressure (R).	852
Farnsworth, H. E.: Comments on the paper by J. C. Riv��re 'Contact potential difference measurements by the Kelvin method' (L)	703
Fernandez, A., with Cooper, R.: Directional electric breakdown of KCl (R)	688
Flack, F. C., and Mason, P.: Angular correlations of gamma rays in $^{103}\text{Rh}$	247
Franks, A., and Thomas, K.: Low-angle x-ray scattering from cold-worked metals (R)	861
Gemmell, D. S., with Edge, R. D.: Gamma rays from the 6.89 mev level in $^{10}\text{B}$	925
Gilles, D. C., with Buckingham, R. A., and Davies, A. R.: Symmetry effects in gas kinetics: II—Ortho- and para-hydrogen	457
Goddard, K. F., with Wright, P.: The resistivity of ordered $\text{Au}_3\text{Cu}$ (R)	506
Goldsmid, H. J.: The electrical conductivity and thermoelectric power of bismuth telluride	633
Grant, E. H., with Bryant, T. H. E.: Ionic conductivity of potassium and rubidium chloride solutions at microwave frequencies (L)	134
Green, G. W., with Boyd, R. L. F.: Electron ionization cross sections using chopped beams	351
Greenlees, G. W., Kuo, L. G., Lowe, J., and Petravi�, M.: The elastic and inelastic scattering of protons by silicon	347
Greenlees, G. W., Lowe, J., Robbins, A. B., and Rolph, P. M.: The inelastic scattering of 9.8 mev protons by medium weight nuclei.	904
Greenwood, D. A.: The Boltzmann equation in the theory of electrical conduction in metals	585
Greenwood, J. A., and Tabor, D.: The friction of hard sliders on lubricated rubber: the importance of deformation losses	989
Griffith, T. C., Banford, A. P., Uppal, M. Y., and Williams, W. S. C.: Neutron-proton scattering in the energy range 70 to 170 mev	305
Griffiths, P. M., with Bates, L. F., and Craik, D. J.: Domain patterns on a single crystal of manganese ferrite	789
Grimley, T. B.: The electronic structure of crystals having the sodium chloride type of lattice	749
Groves, R. D., with Drabble, J. R., and Wolfe, R.: Galvanomagnetic effects in n-type bismuth telluride	430

	PAGE
Grünbaum, E., with Blackman, M.: Magnetic effects on the electron diffraction patterns from a cobalt crystal . . . . .	758
Gupta, B. K., and Rao, V. S. R.: Configuration interaction in the ground state and two excited states, (1s, 2s) <sup>1</sup> S and (1s, 3s) <sup>1</sup> S of He atom (R) . . . . .	1015
Gupta, R. K.: On the determination of the electron capture decay energy: <sup>196</sup> Au . . . . .	330
Harting, D., Holt, J. R., and Moore, J. A.: The elastic scattering of 380 mev protons by protons: I—At angles greater than 30°(c.m.) . . . . .	770
Hayes, W., and Jones, D. A.: Paramagnetic impurities in NaF (R). . . . .	503
Head, A. K.: A class of aplanatic optical systems. . . . .	546
Hilsum, C., and Barrie, R.: Properties of p-type indium antimonide: I—Electrical properties . . . . .	676
Hinds, S., with Dalton, A. W., and Parry, G.: An investigation of the <sup>16</sup> O(d, γ) <sup>14</sup> N reaction by magnetic analysis . . . . .	252
Hinds, S., Middleton, R., and Parry, G.: An investigation of the reactions <sup>24</sup> Mg(d, p) <sup>26</sup> Mg and <sup>26</sup> Mg(d, p) <sup>27</sup> Mg by magnetic analysis . . . . .	49
Hoare, F. E., and Matthews, J. C.: Heat capacity between 1·8 and 4·2°K of an iron—chromium alloy in the alpha and sigma phases . . . . .	220
Hogarth, C. A., and Baynham, A. C.: Electrical methods for determining the positions of dislocations in germanium . . . . .	647
Holeien, E.: The (2s) <sup>2</sup> S state solution of the non-relativistic Schrödinger equation for helium and the negative hydrogen ion . . . . .	357
Holt, J. R., with Harting, D., and Moore, J. A.: The elastic scattering of 380 mev protons by protons: I—At angles greater than 30° (c.m.) . . . . .	770
Holt, J. R., Kluyver, J. C., and Moore, J. A.: The elastic scattering of 380 mev protons by protons: II—At angles less than 30° (c.m.) . . . . .	781
Hsieh, D. Y., and Kolsky, H.: An experimental study of pulse propagation in elastic cylinders . . . . .	608
Hughes, D. G., with Eades, R. G., and Andrew, E. R.: The nuclear quadrupole coupling constant of <sup>23</sup> Na in sodium nitrate (L) . . . . .	1019
Hunter, A. N.: Some observations on the Debye effect in electrolytes (R) . . . . .	847
Hunter, A. N., Legge, R. D., and Matsukawa, E.: Loss factor measurements in dry sand (L) . . . . .	135
Hutchinson, G. W., with Booth, N. E., and Ledley, B.: Nuclear cross sections for 765 mev neutrons . . . . .	293
Irani, K. S., Sinha, A. P. B., and Biswas, A. B.: Entropy of hausmannite to spinel transformation (R) . . . . .	270
Iyengar, K. S., with Bansigir, K. G.: The stress birefringence relation in some alkali halides . . . . .	225
Jack, W., with Varma, J.: The reaction <sup>24</sup> Mg(p, γ) <sup>25</sup> Al at the 418 kev resonance . . . . .	100
Jacobs, P. W. M., with Bray, A. R., and Young, L.: Ionic conduction at high electric field strengths in tantalum pentoxide . . . . .	405
Jain, S. C., with Ewles, J., and Joshi, R. V.: Electron traps produced in KCl crystals by quenching or pressure (R). . . . .	852
Jellinek, H. H. G.: The influence of imperfections on the strength of ice. . . . .	797
John, T. L., with Bransden, B. H., Dalgarno, A., and Seaton, M. J.: The elastic scattering of slow electrons by hydrogen atoms . . . . .	877
Johns, J. W. C., and Barrow, R. F.: The band spectrum of silicon monofluoride, SiF . . . . .	476
Johns, T. F.: Vapour pressure ratios of <sup>14</sup> N <sup>14</sup> N, <sup>14</sup> N <sup>15</sup> N and <sup>15</sup> N <sup>15</sup> N (L) . . . . .	701
Jones, D. A., with Hayes, W.: Paramagnetic impurities in NaF (R) . . . . .	503
Jones, E. R., with Toye, T. C.: Physical properties of certain liquid binary alloys of tin and zinc. . . . .	88
Jones, R. V.: A possible infra-red detector using thermal expansion (R) . . . . .	280
Joshi, R. V., with Ewles, J., and Jain, S. C.: Electron traps produced in KCl crystals by quenching or pressure (R). . . . .	852
Kellermann, E. W., Shaw, T., and Walker, G. O.: On the structure of extensive cosmic ray air showers: lateral structure of the ionizing component . . . . .	491

	PAGE
Kemp, W. R. G., with Birch J. A., and Klemens, P. G. : The lattice thermal conductivity of a gold-platinum alloy (R) . . . . .	843
Khan, M. Aslam: AIH bands at 2173 Å and 2101 Å . . . . .	65
Khashaba, S., and Massey, H. S. W. : The excitation of the 2p state of hydrogen by slow electrons—distorted wave treatment . . . . .	574
Klemens, P. G., with Birch, J. A., and Kemp, W. R. G. : The lattice thermal conductivity of a gold-platinum alloy (R) . . . . .	843
Kluyver, J. C., with Holt, J. R., and Moore, J. A. : The elastic scattering of 380 mev protons by protons : II—At angles less than 30° (c.m.) . . . . .	781
Knapp, V. : Nuclear gamma ray resonance in <sup>48</sup> Ti . . . . .	194
Knipper, A. C. : Excited levels of cadmium 110 . . . . .	77
Kolsky, H., with Hsieh, D. Y. : An experimental study of pulse propagation in elastic cylinders . . . . .	608
Kuffel, E. : A note on the cross sections for electron attachment in air (L) . . . . .	516
Kuo, L. G., with Greenless, G. W., Lowe, J., and Petravić, M. : The elastic and inelastic scattering of protons by silicon . . . . .	347
Laing, E. W. : Elastic scattering of pions at a bound nucleon . . . . .	932
Lamb, J., with Edmonds, P. D. : A method for deriving the acoustic absorption coefficient of gases from measurement of the decay-time of a resonator . . . . .	17
Landsberg, P. T. : Magnetic field effects on electron populations in semiconductors . . . . .	69
Ledley, B., with Booth, N. E., and Hutchinson, G. W. : Nuclear cross sections for 765 mev neutrons . . . . .	293
Legge, R. D., with Hunter, A. N., and Matsukawa, E. : Loss factor measurements in dry sand (L) . . . . .	135
Leigh, R. S. : Crystal field effects in metals . . . . .	33
Levinger, J. S., with Brown, G. E. : Dispersion theory of the direct photoeffect . . . . .	733
Lewin, L. : A physical interpretation of impedance for rectangular waveguides (L) . . . . .	868
Lilburne, M. T., with Reynolds, W. N., and Dell, R. M. : Some properties of semi-conducting indium phosphide . . . . .	416
Louat, N. : A theory of delayed yielding in the presence of Cottrell atmospheres of solute atoms . . . . .	444
Low, G. G. E. : Acoustomagnetolectric effects in metal and semiconductor filaments . . . . .	965
Lowe, J., with Greenless, G. W., Kuo, L. G., and Petravić, M. : The elastic and inelastic scattering of protons by silicon . . . . .	347
Lowe, J., with Greenless, G. W., Robbins, A. B., and Rolph, P. M. : The inelastic scattering of 9.8 mev protons by medium weight nuclei . . . . .	904
Lyness, J. N. : Polarization in nuclear reactions (R) . . . . .	858
Macfarlane, G. G., McLean, T. P., Quarrington, J. E., and Roberts, V. : Direct optical transitions and further exciton effects in germanium (R) . . . . .	863
Mandl, F. : Double scattering experiments as a test for invariance under time-reversal in strong interactions (R) . . . . .	686
Mandl, F. : The theory of angular correlations with polarization . . . . .	177, corr. 519
Mandl, F., with Bell, J. S. : The polarization—symmetry equality (R), (L) . . . . .	272, 867
March, N. H., with Carter, C., and Vincent, D. : X-ray and electron scattering by molecular hydrogen . . . . .	2
Mason, P., with Flack, F. C. : Angular correlations of gamma rays in <sup>103</sup> Rh . . . . .	247
Massey, H. S. W., with Khashaba, S. : The excitation of the 2p state of hydrogen by slow electrons—distorted wave treatment . . . . .	574
Massey, H. S. W., and Moussa, A. H. A. : The elastic scattering of positrons by atoms and molecules . . . . .	38
Mather, D. S., with Ashmore, A., and Sen, S. K. : The elastic scattering of 350 mev neutrons by complex nuclei . . . . .	552
Matsukawa, E., with Agu, B. N. C., and Burdett, T. : Transmission of electrons through aluminium foils . . . . .	201
Matsukawa, E., with Hunter, A. N., and Legge, R. D. : Loss factor measurements in dry sand (L) . . . . .	135



	PAGE
Matthews, J. C., with Hoare, F. E. : Heat capacity between 1·8 and 4·2°K of an iron-chromium alloy in the alpha and sigma phases . . . . .	220
McCauley, G. P., and Brown, G. E. : Inelastic scattering of high energy nucleons by complex nuclei : I—Semi-classical formalism . . . . .	893
McLean, T. P., with Macfarlane, G. G., Quarrington, J. E., and Roberts, V. : Direct optical transitions and further exciton effects in germanium (R) . . . . .	863
Meligy, A. S. : Expansion of the regular Coulomb wave function in terms of Bessel functions (R) . . . . .	856
Meligy, A. S. : Simple method of interpolation for Coulomb wave functions (R) . . . . .	1017
Middleton, R., with Hinds, S., and Parry, G. : An investigation of the reactions $^{24}\text{Mg}$ (d, p) $^{25}\text{Mg}$ and $^{26}\text{Mg}$ (d, p) $^{27}\text{Mg}$ by magnetic analysis . . . . .	49
Mohr, C. B. O. : Direct interaction in the inelastic scattering of high energy protons in carbon . . . . .	717
Moodie, A. F., with Cowley, J. M. : A new formulation of scalar diffraction theory for restricted aperture . . . . .	533
Moore, J. A., with Harting, D., and Holt, J. R. : The elastic scattering of 380 mev protons by protons : I—At angles greater than 30° (c.m.) . . . . .	770
Moore, J. A., with Holt, J. R., and Kluyver, J. C. : The elastic scattering of 380 mev protons by protons : II—At angles less than 30° (c.m.) . . . . .	781
Mott, N. F. : International Union of Pure and Applied Physics (L) . . . . .	519
Moussa, A. H. A., with Massey, H. S. W. : The elastic scattering of positrons by atoms and molecules . . . . .	38
Mukhopadhyay, M., with Sen Gupta, S. : Problem of perturbed boundary condition in quantum mechanics . . . . .	173
Newns, H. C., and Refai, M. Y. : Polarization in stripping reactions . . . . .	627
Nicholls, R. W., with Robinson, D. : Intensity measurements on the $\text{O}_2^+$ second negative, CO ångström and third positive and NO $\gamma$ and $\beta$ molecular band systems . . . . .	957
Nordhagen, R., with Brown, G. E., and Ashmore, A. : Elastic scattering of 350 mev neutrons by complex nuclei . . . . .	565
Ophel, T. R., and Wright, I. F. : Photodisintegration of sodium by $^7\text{Li}$ (p, $\gamma$ ) radiation . . . . .	389
Parrott, J. E. : The theory of the Nernst effect in semiconductors . . . . .	82
Parry, G., with Dalton, A. W., and Hinds, S. : An investigation of the $^{16}\text{O}$ (d, $\alpha$ ) $^{14}\text{N}$ reaction by magnetic analysis . . . . .	252
Parry, G., with Hinds, S., and Middleton, R. : An investigation of the reactions $^{24}\text{Mg}$ (d, p) $^{25}\text{Mg}$ and $^{26}\text{Mg}$ (d, p) $^{27}\text{Mg}$ by magnetic analysis . . . . .	49
Pauncz, R., with Berencz, F. : Construction of $S^2$ eigenfunctions by the method of spin operators : II—Six-electron systems . . . . .	152
Peters, J., and Standley, K. J. : The dielectric behaviour of magnesium manganese ferrite (R) . . . . .	131
Petravić, M., with Greenlees, G. W., Kuo, L. G., and Lowe, J. : The elastic and inelastic scattering of protons by silicon . . . . .	347
Powles, J. G. : The adiabatic fast passage experiment in magnetic resonance (R) . . . . .	497
Premaswarup, D., with Barrow, R. F., Winternitz, J., and Zeeman, P. B. : Rotational analysis of bands of the $c^3\Sigma$ , $b^3\Sigma$ — $a^3\Pi$ system of boron monofluoride, BF . . . . .	61
Price, F. V., with Booth, D. L., Roaf, D., and Salmon, G. L. : The differential cross sections for the reactions $^{14}\text{N}$ (d, p) $^{15}\text{N}$ and $^{14}\text{N}$ (d, $\alpha$ ) $^{12}\text{C}$ between 600 and 1000 kev . . . . .	325
Quarrington, J. E., with Macfarlane, G. G., McLean, T. P., and Roberts, V. : Direct optical transitions and further exciton effects in germanium (R) . . . . .	863
Raal, F. A. : A new absorption band in diamond and its likely cause (R) . . . . .	846
Rabinowicz, E. : The intrinsic variables affecting the stick-slip process . . . . .	668



	PAGE
Rao, V. S. R., with Gupta, B. K. : Configuration interaction in the ground state and two excited states, (1s, 2s) $^4S$ and (1s, 3s) $^4S$ of He atom (R) . . . . .	1015
Refai, M. Y., with Newns, H. C. : Polarization in stripping reactions . . . . .	627
Reynolds, W. N., Lilburne, M. T., and Dell, R. M. : Some properties of semi-conducting indium phosphide . . . . .	416
Roaf, D., with Booth, D. L., Price, F. V., and Salmon, G. L. : The differential cross sections for the reactions $^{14}N(d, p)^{15}N$ and $^{14}N(d, \alpha)^{12}C$ between 600 and 1000 kev . . . . .	325
Robbins, A. B., with Greenlees, G. W., Lowe, J., and Rolph, P. M. : The inelastic scattering of 9.8 mev protons by medium weight nuclei . . . . .	904
Roberts, V., with Macfarlane, G. G., McLean, T. P., and Quarrington, J. E. : Direct optical transitions and further exciton effects in germanium (R) . . . . .	863
Robinson, D., and Nicholls, R. W. : Intensity measurements on the $O_2^+$ second negative, CO ångström and third positive and NO $\gamma$ and $\beta$ molecular band systems . . . . .	957
Robinson, P. D. : Wave functions for the hydrogen atom in spheroidal coordinates : II—Interaction with a point charge and with a dipole . . . . .	828
Robinson, P. D., with Coulson, C. A. : Wave functions for the hydrogen atom in spheroidal coordinates : I—The derivation and properties of the functions . . . . .	815
Robson, B. A. : The mean free path of alpha particles in nuclear matter (R) . . . . .	126
Rolph, P. M., with Greenlees, G. W., Lowe, J., and Robbins, A. B. : The inelastic scattering of 9.8 mev protons by medium weight nuclei . . . . .	904
Rose, F. W. G. : On the mass-action laws in degenerate semiconductors (L) . . . . .	699
Ross, M. A. S., with Cochran, A. J. : Crystal reflectivity in bent crystal spectrometers . . . . .	1011
Rosser, W. G. V., with Armitage, B. H. : The $\beta$ -decay of $^{186}W$ . . . . .	335
Sabey, B. E. : Pressure distributions beneath spherical and conical shapes pressed into a rubber plane, and their bearing on coefficients of friction under wet conditions . . . . .	979
Salmon, G. L., with Booth, D. L., Price, F. V., and Roaf, D. : The differential cross sections for the reactions $^{14}N(d, p)^{15}N$ and $^{14}N(d, \alpha)^{12}C$ between 600 and 1000 kev . . . . .	325
Sandiford, D. J. : Temperature dependence of carrier lifetime in silicon . . . . .	1002
Savadatti, M. I., with Tawde, N. R. : A note on Ta-You Wu's method of calculating overlap integrals for Morse oscillator (R) . . . . .	514
Sayied, A. M. : The Cerenkov effect in composite (isotropic) media . . . . .	398
Seaton, M. J., with Bransden, B. H., Dalgarno, A., and John, T. L. : The elastic scattering of slow electrons by hydrogen atoms . . . . .	877
Sen, S. K., with Ashmore, A., and Mather, D. S. : The elastic scattering of 350 mev neutrons by complex nuclei . . . . .	552
Sen Gupta, S., and Mukhopadhyay, H. : Problem of perturbed boundary condition in quantum mechanics . . . . .	173
Series, G. W., and Willis, K. : Note on the Li II spectrum (R) . . . . .	274
Sharma, S. K. : Anomalous variation of total absorption of radio waves reflected from the F2 region of the ionosphere around mid-day . . . . .	1007
Shaw, T., with Kellermann, E. W., and Walker, G. O. : On the structure of extensive cosmic ray air showers : lateral structure of the ionizing component . . . . .	491
Sherwood, J. W. C. : Elastic wave propagation in a semi-infinite solid medium . . . . .	207
Shiffman, C. A. : The thermal conductivity of tin-indium alloys in the normal state . . . . .	597
Shivananda Tolpadi, S. : Equation of state of zinc, cadmium and magnesium . . . . .	742
Simpson, J. H. : On the thermal and optical excitation of colour centres . . . . .	761
Singh, Sampooran : A note on penetration by rotating shaped charges (R) . . . . .	508
Sinha, A. P. B., with Irani, K. S., and Biswas, A. B. : Entropy of hausmannite to spinel transformation (R) . . . . .	270
Standley, K. H., with Barlow, G. S. : Microwave resonance in nickel at 35 Gc/s (kMc/s) . . . . .	45

	PAGE
Stephen, M. J. : The infra-red spectrum of diamond . . . . .	485
Stiegler, K. : On the deduction of the Lorentz-Einstein transformation from Maxwell's electromagnetic field equations (R) . . . . .	512
Stone, A. P. : Expressions for certain Wigner coefficients . . . . .	corr. 519
Strauch, K., with Ashmore, A., Nordhagen, R., and Townes, B. M. : The gamma- rays from muon catalysed fusion of hydrogen and deuterium . . . . .	161
Svensson, N. L. : Experiments on controlled fractures (L) . . . . .	136
Tabor, D., with Greenwood, J. A. : The friction of hard sliders on lubricated rubber : the importance of deformation losses . . . . .	989
Tawde, N. R., and Savadatti, M. I. : A note on Ta-You Wu's method of calculating overlap integrals for Morse oscillator (R) . . . . .	514
Temperley, H. N. V. : The equation of state of a gas of elastic spheres . . . . .	238
Terry, N. B. : The behaviour of a vibrating visco-elastic cylinder . . . . .	973
Thomas, K., with Franks, A. : Low-angle x-ray scattering from cold-worked metals (R) . . . . .	861
Thomas, P. M., with Barrow, R. F., Cheall, H. F. K., and Zeeman, P. B. : Rota- tional analysis of bands of the $A^3\Pi_{0+}$ , $B^3\Pi_1 - X^1\Sigma^+$ systems of thallos fluoride (R) . . . . .	128
Townes, B. M., with Ashmore, A., Nordhagen, R., and Strauch, K. : The gamma-rays from muon catalysed fusion of hydrogen and deuterium . . . . .	161
Toye, T. C., and Jones, E. R. : Physical properties of certain liquid binary alloys of tin and zinc . . . . .	88
Turchinets, W., with Carver, J. H. : The $(\gamma, 2n)$ and $(\gamma, 3n)$ reactions in $^{181}\text{Ta}$ . . . . .	613
Turchinets, W., with Carver, J. H. : Radioactivity of $^{178}\text{Ta}$ , $^{179}\text{Ta}$ and $^{180}\text{Ta}$ . . . . .	618
Uppal, M. Y., with Griffith, T. C., Banford, A. P., and Williams, W. S. C. : Neutron-proton scattering in the energy range 70 to 170 mev . . . . .	305
Varma, J., and Jack, W., The reaction $^{24}\text{Mg}(p, \gamma)^{25}\text{Al}$ at the 418 kev resonance . . . . .	100
Vincent, D., with Carter, C., and March, N. H. : X-ray and electron scattering by molecular hydrogen . . . . .	2
Walker, G. O., with Kellermann, E. W., and Shaw, T. : On the structure of extensive cosmic ray air showers : lateral structure of the ionizing com- ponent . . . . .	491
Williams, W. S. C., with Griffith, T. C., Banford, A. P., and Uppal, M. Y. : Neutron-proton scattering in the energy range 70 to 170 mev . . . . .	305
Willis, K., with Series, G. W. : Note on the Li II spectrum (R) . . . . .	274
Winternitz, J., with Barrow, R. F., Premaswarup, D., and Zeeman, P. B. : Rota- tional analysis of bands of the $c^3\Sigma$ , $b^3\Sigma - a^3\Pi$ system of boron monofluoride, BF . . . . .	61
Wolf, E. : Reciprocity inequalities, coherence time and bandwidth in signal analysis and optics . . . . .	257
Wolfe, R., with Drabble, J. R., and Groves, R. D. : Galvanomagnetic effects in n-type bismuth telluride . . . . .	430
Wright, I. F., with Ophel, T. R. : Photodisintegration of sodium by $^7\text{Li}$ (p, $\gamma$ ) radiation . . . . .	389
Wright, P., and Goddard, K. F. : The resistivity of ordered $\text{Au}_3\text{Cu}$ (R) . . . . .	506
Wright, R. W., and Bastin, J. A. : The characteristic temperature and effective electron mass for conduction processes in cadmium oxide . . . . .	109
Yeung, T. H. Y. : Recombination coefficients for positive and negative ions . . . . .	341
Young, L., with Bray, A. R., and Jacobs, P. W. M. : Ionic conduction at high electric field strengths in tantalum pentoxide . . . . .	405
Zeeman, P. B., with Barrow, R. F., Premaswarup, D., and Winternitz, J. : Rota- tional analysis of bands of the $c^3\Sigma$ , $b^3\Sigma - a^3\Pi$ system of boron monofluoride, BF . . . . .	61
Zeeman, P. B., with Barrow, R. F., Thomas, P. M., and Cheall, H. F. K. : Rota- tional analysis of bands of the $A^3\Pi_{0+}$ , $B^3\Pi_1 - X^1\Sigma^+$ systems of thallos fluoride (R) . . . . .	128

# INDEX TO REVIEWS OF BOOKS

	PAGE
von Ardenne, M. : <i>Tabellen der Elektronenphysik, Ionenphysik und Übermikroskopie</i> , Parts I and II . . . . .	875
Atkin, R. H. : <i>Mathematics and wave mechanics</i> . . . . .	522
Beck, C. K. : <i>Nuclear reactors for research</i> . . . . .	706
Birkhoff, G., and Zarantonello, E. H. : <i>Jets, wakes and cavities</i> . . . . .	707
Blackwood, O. H., Osgood, T. H., and Ruark, A. E. : <i>An outline of atomic physics</i> . (Third Edition) . . . . .	520
Bohm, D. : <i>Causality and chance in modern physics</i> . . . . .	529
Breckenridge, R. G., Russell, B. R., and Hahn, the late E. E. : <i>Photoconductivity conference</i> . . . . .	141
de Broglie, L. : <i>Propriétés et structure des noyaux</i> . . . . .	521
Cassirer, E. : <i>Determinism and indeterminism in modern physics</i> . . . . .	529
Dorfner, K. R. : <i>Dreidimensionale Überschallprobleme der Gasdynamik</i> . . . . .	524
Dunlap, W. Crawford : <i>An introduction to semiconductors</i> . . . . .	714
Ebert, H. : <i>Physikalisches Taschenbuch</i> . . . . .	705
Fast, J. D., Van Bueren, H. G., and Philibert, J. : <i>La diffusion dans les métaux</i> . . . . .	522
Flügge, S. : <i>Handbuch der Physik</i> . Vol. 20. <i>Electrical conductivity II</i> . . . . .	287
Függe, S. : <i>Handbuch der Physik</i> . Vol. 30. <i>X-rays</i> . . . . .	710
Flügge, S. : <i>Handbuch der Physik</i> . Vol. 35. <i>Atoms I</i> . . . . .	713
Flügge, S. : <i>Handbuch der Physik</i> . Vol. 40. <i>Nuclear reactions I</i> . . . . .	1024
Gaydon, A. G. : <i>The spectroscopy of flames</i> . . . . .	872
Gibson, A. F., Aigrain, P., and Burgess, R. E. : <i>Progress in semiconductors</i> . . . . .	288
Gorter, C. J. : <i>Progress in low temperature physics</i> . Vol. 2 . . . . .	706
Green, H. L., and Lane, W. R. : <i>Particulate clouds—dusts, smokes and mists</i> . . . . .	291
Harvey, E. N. : <i>A history of luminescence</i> . . . . .	141
Henisch, H. K. : <i>Rectifying semiconductor contacts</i> . . . . .	525
Houstoun, R. A. : <i>Physical Optics</i> . . . . .	1022
Institute of Metals : <i>The mechanism of phase transforms in metals</i> . . . . .	143
Jaeger, J. C. : <i>Elasticity, fracture and flow with engineering and geological appli- cations</i> . . . . .	144
Jones, F. Llewellyn : <i>The physics of electrical contacts</i> . . . . .	139
Jones, G. O. : <i>Glass</i> . . . . .	871
Kingston, R. H. : <i>Semiconductor surface physics</i> . . . . .	1023
Kittel, C. : <i>Introduction to solid state physics</i> . . . . .	716
Koch, K. M., and Jellinghaus, W. : <i>Einführung in die Physik der magnetischen Werkstoffe</i> . . . . .	1025
Körner, S. : <i>Observation and interpretation—A symposium of philosophers and physicists</i> . . . . .	875
Kramers, H. A. : <i>Quantum mechanics</i> . . . . .	532
Le Grand, Yves : <i>Light, colour and vision</i> . . . . .	871
Littler, D. J., and Raffle, J. F. : <i>An introduction to reactor physics</i> (2nd Edn.) . . . . .	873
Livesley, R. K. : <i>Digital computers</i> . . . . .	531
Lorentz, H. A. : <i>Impressions of his life and work</i> . . . . .	711

	PAGE
MacColl, L. A. : <i>Applied probability</i> (Proceedings of the seventh symposium in applied mathematics) . . . . .	290
Mandl, F. : <i>Quantum mechanics</i> (2nd Edn) . . . . .	870
Marton, L. : <i>Advances in electronics and electron physics</i> . Vol. 8. . . . .	139
Middlebrook, R. D. : <i>An introduction to junction transistor theory</i> . . . . .	528
Milnes, A. G. : <i>Transducers and magnetic amplifiers</i> . . . . .	292
Morris, N., and Duff, M. J. B. : <i>Report on the Conference on recent developments in cloud chamber and associated techniques</i> . . . . .	874
Murphy, G. J. : <i>Basic automatic control theory</i> . . . . .	1028
 Nye, J. F. : <i>Physical properties of crystals</i> . . . . .	 289
 Paskell, E. : <i>Semiconductor abstracts</i> . . . . .	 1027
Pfluger, A. : <i>Theorie der Riemannschen Flächen</i> . Vol. LXXXIX. . . . .	526
Prigogine, I. : <i>The molecular theory of solutions</i> . . . . .	713
 Reid, C. : <i>Excited states in chemistry and biology</i> . . . . .	 530
Richardson, E. G. : <i>Relaxation spectrometry</i> . . . . .	705
Robertson, A. J. B., Fabian, D. J., Crocker, A. J., and Dewing, J. : <i>Laboratory glass working for scientists</i> . . . . .	143
 <i>Scientific American</i> (sponsors) : <i>The physics and chemistry of life</i> . . . . .	 715
Société Française de Physique et la Faculté des Sciences de Bordeaux. <i>Colloque National sur l'optique moléculaire et la physiochimie structurale</i> . . . . .	291
Stevens, G. W. W. : <i>Microphotography, photography at extreme resolution</i> . . . . .	143
Summer, W. : <i>Photosensors : A treatise on photoelectric devices and their application to industry</i> . . . . .	1027
Synge, J. L. : <i>The hypercircle in mathematical physics</i> . . . . .	709
Synge, J. L. : <i>The relativistic gas</i> . . . . .	708
 Wilson, A. H. : <i>Thermodynamics and statistical mechanics</i> . . . . .	 1026
Wilson, J. G. : <i>Progress in cosmic ray physics</i> . Vol. 3 . . . . .	520
 Zeise, H. : <i>Thermodynamik</i> , Band III. 1, Tabellen. 2, Graphische Darstellungen und Literatur . . . . .	 521





